

Springer

Handbook

Petroleum
Technology

Hsu

Robinson

Editors



Springer

**Springer Handbook
of Petroleum
Technology**

Springer Handbooks provide a concise compilation of approved key information on methods of research, general principles, and functional relationships in physical and applied sciences. The world's leading experts in the fields of physics and engineering will be assigned by one or several renowned editors to write the chapters comprising each volume. The content is selected by these experts from Springer sources (books, journals, online content) and other systematic and approved recent publications of scientific and technical information.

The volumes are designed to be useful as readable desk reference book to give a fast and comprehensive overview and easy retrieval of essential reliable key information, including tables, graphs, and bibliographies. References to extensive sources are provided.

Springer Handbook of Petroleum Technology

Chang Samuel Hsu 許強, Paul R. Robinson (Eds.)

With 754 Figures and 282 Tables



Springer



Editors

Chang Samuel Hsu 許強
Department of Chemical & Biomedical Engineering
Florida A& M University – Florida State University
2525 Pottsdamer Street
FL 32310-6046 Tallahassee, USA

and

China University of Petroleum – Beijing
College of Chemical Engineering
Changping, China

and

Petro Bio Consulting LLC
Tallahassee, USA
chsu@fsu.edu

Paul R. Robinson
Katy Institute for Sustainable Energy
3418 Clear Water Park Drive
TX 77450 Katy, USA
pr.robinson@katysustain.org

ISBN: 978-3-319-49345-9 e-ISBN: 978-3-319-49347-3
DOI 10.1007/978-3-319-49347-3
Library of Congress Control Number: 2017960801

© Springer International Publishing AG 2017

This work is subject to copyright. All rights are reserved by the Publisher, whether the whole or part of the material is concerned, specifically the rights of translation, reprinting, reuse of illustrations, recitation, broadcasting, reproduction on microfilms or in any other physical way, and transmission or information storage and retrieval, electronic adaptation, computer software, or by similar or dissimilar methodology now known or hereafter developed.

The use of general descriptive names, registered names, trademarks, service marks, etc. in this publication does not imply, even in the absence of a specific statement, that such names are exempt from the relevant protective laws and regulations and therefore free for general use.

The publisher, the authors and the editors are safe to assume that the advice and information in this book are believed to be true and accurate at the date of publication. Neither the publisher nor the authors or the editors give a warranty, express or implied, with respect to the material contained herein or for any errors or omissions that may have been made. The publisher remains neutral with regard to jurisdictional claims in published maps and institutional affiliations.

Production and typesetting: le-tex publishing services GmbH, Leipzig
Typography and layout: schreiberVIS, Seeheim
Illustrations: le-tex publishing services GmbH, Leipzig
Cover design: eStudio Calamar Steinen, Barcelona
Cover production: WMXDesign GmbH, Heidelberg

Printed on acid free paper

This Springer imprint is published by Springer Nature
The registered company is Springer International Publishing AG
The registered company address is: Gewerbestrasse 11, 6330 Cham, Switzerland

Foreword

This *Springer Handbook of Petroleum Technology* could not have appeared at a more appropriate time. Petroleum and its close cousin, natural gas, continue to provide most of the energy we consume, and will undoubtedly do so for many decades to come. Oil and gas also serve as basic materials for manufacturing construction materials, fertilizers, and a panoply of chemicals.

We are now beginning to see a technology-driven transformation of global economics. Since the 1970s, the oil-rich countries of OPEC (Organization of the Petroleum Exporting Countries) have exerted disproportionate economic and political power by manipulating the availability of petroleum. But the balance of power is shifting.

Consider the United States (Fig. 1):

- In 2014, thanks to a creative combination of directional drilling and hydraulic fracturing, the US was the world's leading oil producer, pumping out an average of 12.3 million barrels per day [1].
- In 2007, the US imported 59% of its oil, but in 2014, US oil imports were down to 35% of consumption. Imports of natural gas had also dropped by 65% [2].
- The price of crude (West Texas Intermediate) reached \$146 per barrel in June 2008, fell to \$104 per barrel in May 2014, then crashed to below \$30 per barrel on January 12, 2016 before recent recovery [3].
- US CO₂ emissions have decreased, thanks to an ongoing shift in electricity production from coal to natural gas, solar, and wind. Another factor is higher efficiency automobiles, which are reducing gasoline consumption.

The net effect is that, compared to a couple of years ago, about \$320 billion per year stays in the US economy instead of enriching someone else. Lower prices for oil and gas are decreasing revenues from production and increasing margins for refining and petrochemicals. Upstream investments are being delayed or cancelled. Meanwhile, fuel-intensive industries, such as air transportation, are thriving [4]. Lower prices appear to be fueling renewed growth in non-OECD countries. (OECD is the Organization for Economic Cooperation and Development, which represents 14 of the world's richest countries in natural resources.) According to the US Energy Information Administration, in 2014 OECD consumed less than half the oil used in the world [5].

Other factors may influence the supply/demand picture. The recent US accord with Iran increased supply

when supply was already excessive. This further suppressed prices. Impact on prices also came from amending the 1975 Energy Policy Conservation Act and the 1979 Export Administration Act, which ban crude oil exports from the United States. Undoubtedly, light, sweet US crude will pour into the global oil pool, decreasing income in other producing countries, both by suppressing prices even more and by lowering how much the other producing countries can sell. The change will reverberate politically, perhaps in Russia, which has been using gas supply as a tool of diplomacy. It would raise strategic questions. Does America really want to drain itself first? Does it want to impoverish religiously restive North African countries, for which oil and gas are essentially the only source of external income? The US dollar is strengthening [6]. How would an even stronger dollar affect the US balance of trade with, for example, China?

Also consider the environment and worker safety. As Barry Commoner and others have said: There is no free lunch [7]. Despite tremendous profits, and well-publicized (and undoubtedly sincere) campaigns to improve work safety and protect the environment, catastrophic accidents continue to occur. Most are preventable, and most are due to poor training or lack of maintenance. As a colleague says, lessons have been learned, but not everyone has learned them, and many of those who have learned them have since forgot them or choose to ignore them. Major accidents include:

- On 23 March 2005, an explosion in an isomerization process unit at the BP Texas City refinery killed 15 people and injured 180 others. The official report [8] cited inadequate training and worker fatigue as root causes. BP declared profits of 3.68 billion for the fourth quarter of 2005 and \$5.62 billion for the first quarter of 2006 [9].
- On 20 April 2010, on the *Deepwater Horizon* drilling rig, a blowout killed 11 people and gushed 560 to 585 thousand tons of crude oil into the Gulf of Mexico. According to the official report [10], the blowout was preventable, and several poor decisions were made for economic reasons. Perhaps the most important were a lack of training, a lack of



Geoffrey E. Dolbear, PhD

American Chemical Society Fellow
Lifetime Achievement Award,
American Chemical Society Energy
and Fuels Division

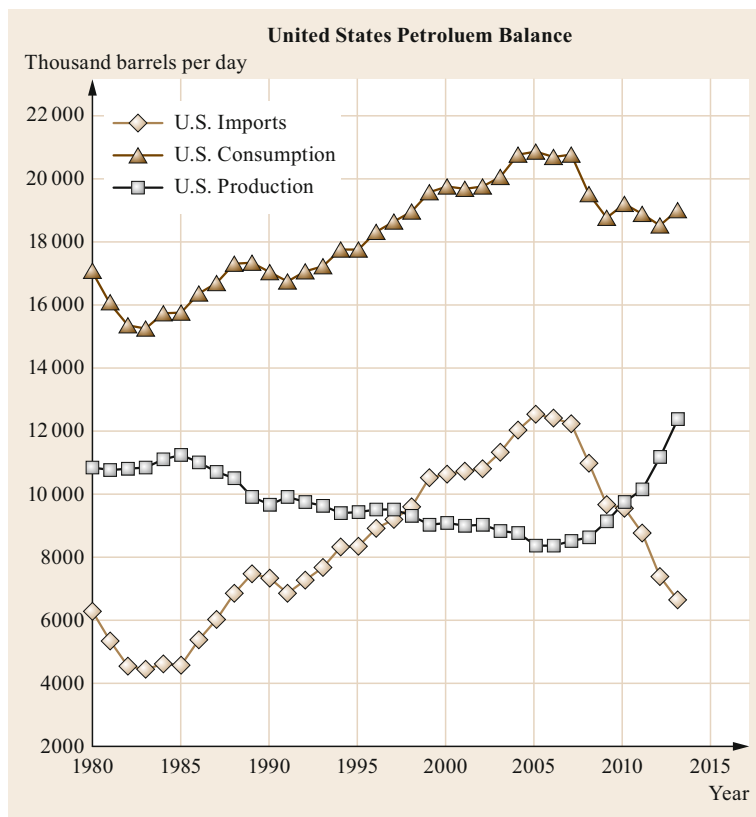


Fig. 1 Source: Energy Information Administration, <http://www.eia.gov>, retrieved 14 July 2015

technical supervision, and the use of only six centralizers instead of the recommended 21, apparently to save ten hours (page 97 of the report).

- The infrastructure for transporting *frack oil* from North Dakota was known to be limited and in poor condition, making problems inevitable. On 5 July 2013, a 74-car freight train carrying crude oil from the Bakken shale formation derailed and overturned in Lac-Mégantic, Quebec. The consequent fire and explosion killed 47 people and destroyed most of the town. The root cause was a known problem in a locomotive engine [11].

All of which brings me back to this *Springer Handbook*. It's a one-stop information shop. When I want to know something about any aspect of oil and gas, and related topics, I will look first in this book. If I can't find what I need in one of the 41 chapters written by more than 80 experts from ten countries, I will surely find a relevant reference among the book's roughly 2000 citations.

Here are some specific examples:

- I've heard that a lack of centralizers might have been largely responsible for the *Deepwater Horizon*

disaster. This book describes centralizers and explains why they are important. If I want to know how BP knew there was so much oil so deep under the sea in the Mississippi Canyon, I will consult the chapters on petroleum engineering and reservoir modeling.

- The Energy Independence and Security Act of 2007 exempts contaminated fluids associated with fracking from certain clean water regulations. If I want to know more about fracking, I will consult the chapters on advances in oil production technology. If I want to know how the exemptions might affect my drinking water, I will refer to the chapter on Safety and the Environment.
- I'm considered by some to be an expert in petroleum in the chemistry and catalysis of petroleum processing, obtaining chemicals from coal, and alternative energy. This book will update my knowledge of these topics, too.

I just wish something like this had been available when I entered the industry in the late 1960s.

I am proud to have contributed to this work and its predecessor, *Practical Advances in Petroleum Processing*, and I was honored to be invited to write a foreword

for this work, which promises to serve as a superb reference not just for students and industry professionals, but for people from many walks of life.

Geoffrey E. Dolbear

References

- [1] United States Energy Information Administration: *International Energy Statistics*. <http://www.eia.gov/cfapps/ipdbproject/IEDIndex3.cfm?tid=5&pid=53&aid=1>
- [2] United States Energy Information Administration: *U.S. Natural Gas Imports & Exports 2014*. <http://www.eia.gov/naturalgas/importsexports/annual/>
- [3] Macrotrends: *WTI Crude Oil – Historical Prices Since 1948*. <http://www.macrotrends.net/1369/crude-oil-price-history-chart>
- [4] A. Martyn-Hemphill: *Delta Benefits From Lower Fuel Costs, Profits Soar on Earnings*. The Street, <http://www.thestreet.com/video/13219639/delta-benefits-from-lower-fuel-costs-profits-soar-on-earnings.html> (July 15, 2015)
- [5] F. Norris: *U.S. Oil Production Keeps Rising Beyond the Forecasts*. The New York Times, <http://www.nytimes.com/2014/01/25/business/us-oil-production-keeps-rising-beyond-the-forecasts.html> (January 24, 2014)
- [6] G. Kristopher: *Crude Oil Prices: Downward Pressure from the US Dollar*. Market Realist, <http://marketrealist.com/> (July 17, 2015)
- [7] B. Commoner: *The Closing Circle*. (Alfred A. Knopf, New York 1971, 1974)
- [8] U.S. Chemical Safety and Hazard Investigation Board: *Refinery Explosion and Fire, BP Texas City Refinery (15 Killed, 180 Injured)*. Report No. 2005-04-I-TX (March 23, 2005)
- [9] http://www.bp.com/content/dam/bp/pdf/investors/bp_first_quarter_2006_results.pdf
- [10] National Commission on the BP Deepwater Horizon Oil Spill and Offshore Drilling: *Report to the President: Deepwater: The Gulf Oil Disaster the Future of Offshore Drilling* (January 2011)
- [11] https://en.wikipedia.org/wiki/Lac-Megantic_derailment (July 15, 2015)

Preface

The *Springer Handbook of Petroleum Technology* provides a comprehensive overview of the petroleum industry, and acts as a single reference touching on every important subject: the formation of oil and gas, characterization of petroleum and bitumen, exploration, production, upgrading, emerging technologies, and economics. It also covers special topics, such as catalytic production of lube base stocks and petrochemicals, optimization of hydrogen networks, process modeling, model-predictive control, online optimization, plasma applications, and renewable fuel/chemical processes. And lest we forget: safety, reliability, and pollution control.

The Times They Are a-Changin' is the title of a 1964 album by Bob Dylan, who won the 2016 Nobel Prize for literature [1]. For petroleum, it is far more apropos now than it was a decade ago, when we quoted the signature song in the preface to *Practical Advances in Petroleum Processing* [2].

1965–2005

We noted in our prior book, *Practical Advances in Petroleum Processing*, that in 1964, a wall divided Berlin. The Moon was free of footprints. In America, we said, *Fill 'er up with ethyl*, referring to the tetraethyl lead octane-number additive, as a team of uniformed fueling-station attendants hurried to check the oil level and wash the windows of our gasoline-thirsty Fords and Chevrolets. In the world of petroleum, natural gas, and petrochemicals, major changes began in 1962 with *Silent Spring*, the classic book by Rachel Carson on the global dangers of DDT (dichlorodiphenyl-trichloroethane), and with the efforts of Linus Pauling and other renowned scientists to publicize the dangers of radioactive fallout. The resulting public outrage led to the establishment of the Environmental Protection Agency (EPA) in the United States and the concurrent founding of similar agencies around the globe. In 1972, the EPA issued a general ban on DDT and strengthened the Federal Water Pollution Control Act, thereafter known as the Clean Water Act. In 1973, EPA began its stepwise program to remove tetraethyl lead from gasoline. More than anything else during this time, laws to protect the environment led to new research and development in the petroleum industry.

Crude oil prices leaped from US\$3 per barrel to nearly US\$12 per barrel during the Yom Kippur War in 1973–74, then leaped again during the Islamic Rev-

olution in Iran in 1978–79. Prices topped out at nearly \$40 per barrel – equivalent to more than \$100 per barrel in 2016 currency. The high prices motivated significant drops in worldwide oil consumption and opened automobile markets in Europe and the United States to fuel-efficient imports. Idle, non-OPEC oil and gas wells were reopened, and non-OPEC oil companies intensified efforts to find new reserves. World oil consumption dropped from 63.9 million barrels per day in 1979 to 57.6 million barrels per day in 1983 [3] due to significant conservation, especially in the United States and Europe, the world's major energy consumers. The drive to conserve created a market for rigorous models and advanced process control in refineries and petrochemical plants; advances which greatly improved energy efficiency and formed the foundation for online optimization.

A series of large-scale disasters intensified pressure to improve safety and protect the environment in the petroleum and petrochemical industries. Oil spilled from the *Amoco Cadiz*, the *Exxon Valdez* fouled coastlines and killed wildlife. Preventable refinery explosions at BP Texas City and Tosco Avon were deadly. The tragic release of MIC (methyl isocyanate) from a plant in Bhopal, India killed more than 3700 people and injured more than 550 000 others.

European Union directives and the US Clean Air Act Amendments (CAA) of 1990 again changed the industry. Both regulations required a phase-in of low-sulfur diesel with < 500 ppm sulfur, followed by ultralow-sulfur diesel (ULSD). (By 2017 in the EU, the UK, the United States, the most populous regions of China, and much of the rest of the world, ULSD must contain < 10 ppmw sulfur.) For gasoline, the CAA required the inclusion of oxygenates such as ethanol or methyl-*t*-butyl ether (MTBE), which is synthesized from methanol and isobutylene. Billions of dollars were spent building MTBE and methanol plants. Eventually, MTBE was banned in the United States, only to be replaced by a highly questionable ethanol mandate.

Meanwhile, the world economy boomed, especially in Asia, and the demand for fossil fuels increased accordingly.

2005–2015

When *Practical Advances in Petroleum Processing* was published in 2006, construction was underway in New York City on the new World Trade Center transportation

hub. Allied forces were bogged down in Afghanistan and Iraq. The US embargo of Cuba was still going strong. The US had just frozen the assets of individuals associated with Iran's nuclear program. Energy consumption and oil prices were approaching all-time highs. And Pluto was still a planet.

In *Practical Advances in Petroleum Processing*, we predicted that several ongoing trends would continue:

1. The industry would continue to consolidate.
2. Advances in automation would continue to improve efficiency and safety.
3. Consumption would continue increase in China and India, driving prices upward.
4. Environmental regulations would continue to tighten.
5. The world would continue to rely more heavily on heavier and heavier oil.

With one significant caveat, the first four predictions have come to pass. Consolidation continues, and automation is indeed improving efficiency and safety in our homes and factories [4]. Energy use in Asia is climbing, but – here is the caveat – oil prices have fallen precipitously. Prices dropped for the same reason that our fifth prediction was wrong: innovative technology.

In 2005, we tacitly assumed that United States oil reserves would continue to fall, and that the country would continue to import most of its oil and gas. We assumed that improvements in technology for hydrocarbon production and processing would be incremental, not revolutionary. We weren't quite as wrong as the person who wrote in 1899 that *Everything than can be invented has been invented* [5], but we were certainly surprised. (Contrary to popular lore, Charles H. Duell did NOT make that statement. The quote has been traced to a piece in *Punch or the London Charival*, entitled *The Coming Century*.)

By 2008, due to a creative meld of horizontal drilling and hydraulic fracturing, US producers tapped vast but previously unrecoverable reserves of oil and gas. Due to that technology, colloquially dubbed *fracking*, the United States is now the world's leading oil and gas producer. Instead of being heavy and sour, the new oil is light and sweet. Refineries thrive on frack oil, for which processing costs are reduced.

Eventually, overproduction of frack oil led to a glut, and prices for Brent crude fell from US\$110 per barrel in September 2013 [6] to less than US\$40 in December 2015. Prices for Brent clawed their way back to \$52 in October 2016 [7], but they were still less than half of their recent peak. Natural gas is now a glut in the United States; imports from Canada have dropped precipitously. In the US, exports of liquefied natural

gas (LNG) have begun, putting further downward pressure on energy prices. Thanks to cheap gas, for the first time in decades foreign companies are constructing huge petrochemical plants in the United States. The US Energy Information Administration predicts that the world's largest economy will be energy independent by 2025. As a colleague said, referring to these industry changes, *Oil is upside down*.

For the transportation and processing sectors, frack oil is a good- and bad-news story. Pipelines are the safest, most efficient way to move petroleum liquids long distances, but while pipeline construction is delayed, oil is being shipped by rail with sometimes-questionable rolling stock; the derailment of a poorly maintained frack-oil train led to an explosion in Lac-Mégantic Quebec on 6 July 2013 [8], killing 47 people.

More and more biomass-derived oil is being co-processed with conventional petroleum. Advances in other areas – characterization methods, reservoir modeling, process modeling, lubricants, petrochemicals, and safety systems – are enhancing the way the industry works.

Environmental regulations suffered a significant reversal when the US Energy Independence and Security Act of 2007 (EISA) exempted contaminated fluids associated with fracking from the Clean Air Act and certain Clean Water Act regulations. Arguably, the Energy Policy Act of 2005, in combination with EISA, delivered another setback by prompting the blending of vast amounts of corn ethanol into gasoline. Since Donald Trump became President of the US in 2017, there have been additional rollbacks of environmental regulations. Time will tell how significant and permanent the regulations will be.

Purpose of this Book

The issues above are complex, with significant worldwide impact, politically, economically, and technically. Our ultimate purpose is to provide a tool with which technically sound science-based opinions are developed. We hope that informed opinions will serve as the basis for sound decisions on energy policy.

Target Audience

Our target audience includes students, engineers, and scientists, including those who are experts in one area but want to learn about other fields.

Organization

The book is divided into four parts, except for the first two chapters: the introduction and the chapter on safety

and the environment, which are of general interest. Part 1 includes chapters on specific topics, including petroleum characterization. Part 2 covers the formation of fossil hydrocarbons, and the science and engineering of finding and recovering oil and gas. Part 3 focuses on upgrading technologies, with chapters on coking, fluid catalytic cracking (FCC), hydroprocessing, hydrogen production, catalytic reforming, and refinery-wide optimization. Part 4 provides enlightening information on lubricants, polymers, and novel and emerging technologies.

Contributors

We are pleased to have contributions from several sources, including integrated oil companies, catalyst suppliers, licensors, consultants, and academic researchers. Our 82 contributors hail from ten different countries on 3 continents.

Putting this book together has been a rewarding challenge. We trust that you, our readers, will find it useful and valuable.

Acknowledgements

We wish to thank our editors from Springer – Dr. Kenneth Howell and especially Dr. Judith Hinterberg – for their guidance and limitless patience. We also want to thank our many contributors for their time and effort. Obviously, without them, this book would be a lot shorter.

Most of all, we wish to thank our devoted, magnificent wives, Grace Miao-Miao Chen and Carrie Robinson, for putting up with our absences – mental if not physical – during so many nights and lost weekends throughout the past two years.

Chang Samuel Hsu
Paul R. Robinson

September 2016

References

- [1] B. Dylan: *The Times They Are a-Changin'*. (Columbia Records, 1964)
- [2] C.S. Hsu, P.R. Robinson (Eds.): *Practical Advances in Petroleum Processing*. (Springer, New York 2006)
- [3] *BP Statistical Review of World Energy 2015*. <http://www.bp.com/en/global/corporate/about-bp/energy-economics/statistical-review-of-world-energy.html>
- [4] <http://www.automationworld.com/safety>
- [5] D. Crouch: *Tracing the Quote*. Patentlyo, <http://patentlyo.com/patent/2011/01/tracing-the-quote-everything-that-can-be-invented-has-been-invented.html> (January 6, 2001)
- [6] <http://dailyreckoning.com/why-110-is-like-kryptonite-for-the-oil-price>
- [7] <http://www.investing.com/commodities/brent-oil-historical-data>
- [8] https://en.wikipedia.org/wiki/Lac-M%C3%A9gantic_rail_disaster

About the Editors

Chang Samuel Hsu 許強 had over 32 years' experience at ExxonMobil and BP before joining Florida State University in 2010 to establish the Future Fuels Institute. He also established the Refinery of the Future Lab at BP. Currently, he is an Adjunct Professor at the Department of Chemical and Biomedical Engineering at Florida A&M University/Florida State University, and also at the State Key Laboratory of Heavy Oil Processing of the College of Chemical Engineering at the China University of Petroleum in Beijing as *111 Plan* Professor sponsored by the Ministry of Education of People's Republic of China. He is also a visiting scholar at Guangzhou Institute of Geochemistry, Chinese Academy of Sciences. In 2012, he founded Petro Bio Oil Consulting, LLC.

Dr. Hsu was the first researcher to introduce ultrahigh resolution Fourier-transform ion cyclotron resonance mass spectrometry (FT-ICR MS) for in-depth molecular characterization of petroleum fractions, which has become common practice for analyzing resids/asphaltenes and other heavy oil fractions. He introduced a diophantine algorithm to eliminate the limitation encountered by the polynomial approach for calculating isotopic distribution, which has been used for very large molecules, such as high polymers and proteins. He was one of the pioneers of tandem mass spectrometry (MS/MS) at Exxon, which provides an additional dimension for the determination of the molecular structure of components in complex mixtures.

Dr. Hsu's research interests cover petroleum (both upstream and downstream), coal, shale and biomass oils. His current focuses are novel characterization of petroleum biomarkers for exploration and exploitation, and heavy hydrocarbon characterization for hydroprocessing, catalytic cracking, coking and fuels/lubes analysis. He also has extensive experience in environmental damage assessment and remediation for large scale oil spills. Dr. Hsu has published three books, 13 patents, ten book chapters and over 240 other publications and presentations prior to this handbook. He is a member of the American Chemical Society and American Society for Mass Spectrometry.



In 2016, **Paul R. Robinson** is a recognized expert on petroleum processing. During his 39 years in commercial energy, he visited more than 140 sites in 34 countries on 5 continents. At nearly half of these sites, he participated in project work or provided operations support. He started his career at the Oak Ridge National Laboratory, where his research focused on splitting water with thermochemical cycles. He then spent more than 30 years in various roles with Unocal, Aspen Technology Inc., Chevron, Shell, and KBR. At Unocal, he developed hydrotreating catalysts, studied conversion of syngas to alcohols, and became a Regional Manager for the technology licensing group. Along the way, he received three creativity awards and a patent achievement award. As a senior engineer at Chevron and Shell, he provided process monitoring, operations support, and troubleshooting for commercial hydroprocessing units. At AspenTech, he became Best Practice Leader for online optimization of hydrocracking units. In this role, he co-developed Aspen Hydrocracker, which was based on a model developed by Sun Oil Company and implemented online. At KBR, he was the Chief Technology Advisor for VCC technology, which converts vacuum residue and coal into clean diesel and gasoline.

In 2016, Dr. Robinson founded the Katy Institute for Sustainable Energy, a nonprofit organization devoted to stimulating science-based dialog on energy. KISE teaches courses and provides consultation on petroleum, hydroprocessing, climate change, and related topics.

Dr. Robinson earned BS (Honors) and MA degrees at the University of Missouri, Columbia. At the University of California, San Diego, he spent a year at the Scripps Institution of Oceanography before receiving a PhD in Chemistry. He has authored or co-authored more than 105 publications and presentations, including two books and 15 book chapters. He holds 11 patents, primarily on catalyst and process technology. He is Public Policy Chair for the Energy and Fuels Division of the American Chemical Society. He is most proud of his wonderful family and black belt in TaeKwonDo.



Contents

List of Abbreviations	XXIII
1 Introduction to Petroleum Technology	
<i>Paul R. Robinson, Chang Samuel Hsu</i>	1
1.1 Petroleum and Its Uses	3
1.2 People and Petroleum	8
1.3 The Oil Business	14
1.4 Macroeconomics	15
1.5 Origin of Fossil Hydrocarbons	18
1.6 Natural Gas, Coal, and Kerogen	19
1.7 Petroleum (Crude Oil)	20
1.8 Oil and Gas Exploration	25
1.9 Drilling and Production (Recovery)	27
1.10 Transportation and Storage	30
1.11 Refining	30
1.12 Petroleum Products	63
1.13 Characterization of Petroleum	72
1.14 Modeling	73
1.15 Petrochemicals	75
1.16 Alternatives to Petroleum	76
1.17 Protecting the Environment	77
1.18 Conclusion	80
References	81
2 Safety and the Environment	
<i>Paul R. Robinson</i>	85
2.1 Introduction and History	86
2.2 Pollution from Petroleum Production and Processing	89
2.3 Significant Accidents and Near-Misses	101
2.4 Agencies Protecting Safety and the Environment	126
2.5 Key Regulations	128
2.6 Pollution Control and Abatement Technology	135
2.7 Summary	143
References	143
Part A Petroleum Characterization	
3 Molecular Science, Engineering and Management	
<i>Chang Samuel Hsu</i>	151
3.1 Analytical Endeavors in the Petroleum Industry	152
3.2 Analytical Tools	153
3.3 Analytical Strategy	153
3.4 Chromatographic Systems	153
3.5 Mass Spectrometry	154
3.6 Petroleum Biomarker Analysis	155

3.7	Online LC-MS	158
3.8	Ionization for Molecules	160
3.9	Mass Analyzers	164
3.10	Data Interpretation and Management	166
3.11	Molecular Engineering and Management Through Science and Modeling	167
3.12	Conclusion	167
	References	168
4	Petroinformatics	
	<i>Manhoi Hur, Sunghwan Kim, Chang Samuel Hsu</i>	173
4.1	Petroleum Analysis and Statistical Approaches	175
4.2	Emerging Technologies for Storing, Visualizing, and Processing Crude Oil Data	190
4.3	Summary	194
	References	194
5	Separations in the Sample Preparation for Sulfur Compound Analysis	
	<i>Jan T. Andersson</i>	199
5.1	The Necessity of Sample Preparation	199
5.2	Separation	202
5.3	Chromatographic Methods	207
5.4	Conclusion	214
	References	215
6	Asphaltenes	
	<i>Oliver C. Mullins, Andrew E. Pomerantz, A. Ballard Andrews, Rudraksha Dutta Majumdar, Paul Hazendonk, Yosadara Ruiz-Morales, Lamia Goual, Richard N. Zare</i>	221
6.1	Overview of Asphaltenes	222
6.2	Reservoir Crude Oils	223
6.3	Asphaltenes and the Yen-Mullins Model	225
6.4	Asphaltene Molecules	226
6.5	Asphaltene Nanoaggregates	236
6.6	Clusters	240
6.7	Intermolecular Interaction of Asphaltenes	243
6.8	The Flory-Huggins-Zuo Equation of State	246
6.9	Conclusions	247
	References	247
7	Reservoir Evaluation by DFA Measurements and Thermodynamic Analysis	
	<i>Go Fujisawa, Oliver C. Mullins</i>	251
7.1	The Borehole Environment	252
7.2	VIS/NIR Spectroscopy of Hydrocarbon Reservoir Fluids	254
7.3	Implementation of DFA Hardware	257
7.4	Basic DFA Operations and Applications	260
7.5	Reservoir Evaluation via DFA and Thermodynamics	261
7.6	Reservoir Case Studies	262
7.7	Conclusions	270
	References	270

8 Phase Behavior and Properties of Heavy Oils	
<i>John M. Shaw, Marco A. Satyro, Harvey W. Yarranton</i>	273
8.1 Background	274
8.2 Phase Behavior and Phase Composition Measurement	277
8.3 Thermophysical Property Measurement	283
8.4 Heavy Oil Characterization	287
8.5 Phase Behavior Correlation and Prediction	294
8.6 Thermophysical Property Simulation and Prediction	303
8.7 Perspectives and Conclusions	311
References	311
Part B Exploration and Production	
9 Fundamentals of Petroleum Geology	
<i>Hendratta N. Ali</i>	321
9.1 The Petroleum Cycle	322
9.2 Historical Perspective	323
9.3 Geological Overview	326
9.4 How Petroleum Accumulates and Concentrates	343
9.5 Finding and Locating Petroleum	352
9.6 Future for Petroleum	356
References	357
10 Origin of Petroleum	
<i>Clifford C. Walters</i>	359
10.1 Historic Overview	360
10.2 The Petroleum System	361
10.3 Deposition of Organic-Rich Sedimentary Rocks	362
10.4 Kerogen Formation and the Generative Potential of Source Rocks ..	365
10.5 Generation and Expulsion of Oil and Gas	369
10.6 Composition of Produced Petroleum	371
10.7 Unconventional Resources	374
10.8 Summary	375
References	375
11 Basin and Petroleum System Modeling	
<i>Kenneth E. Peters, Oliver Schenk, Allegra Hosford Scheirer, Björn Wygrala, Thomas Hantschel</i>	381
11.1 Overview	382
11.2 Discussion	385
11.3 Conclusions	413
References	413
12 Seismic Explorations	
<i>Graham Ganssle</i>	419
12.1 Seismic Data Acquisition	420
12.2 Seismic Data Processing	423
12.3 Seismic Data Interpretation	426
12.4 Summary	431
References	431

13 Formation Evaluation	
<i>Donald G. Hill</i>	433
13.1 What Is Formation Evaluation?.....	435
13.2 The Need and Purpose of Formation Evaluation.....	435
13.3 Well Logs.....	436
13.4 Who Are Petrophysicists and How Do They Work?.....	443
13.5 How Wireline and MWD/LWD Logs Are Acquired.....	444
13.6 Uses of Well Logs.....	445
13.7 Petrophysics and Well Logging: Historical Development.....	445
13.8 The Schlumberger Legacy.....	457
13.9 Laboratory Measurements.....	458
13.10 Well Logging Environment.....	465
13.11 Well Logging Tools.....	471
13.12 Putting It All Together.....	492
13.13 Summary.....	498
References	498
14 Petroleum Production Engineering	
<i>Shengnan Chen</i>	501
14.1 Flowing Wells and Gas Lift.....	501
14.2 Artificial Lift.....	508
14.3 Well Stimulation.....	512
References	516
15 Offshore Production	
<i>Ekaterina V. Maksimova, Cortis K. Cooper</i>	517
15.1 Historical Overview.....	518
15.2 Ownership.....	520
15.3 Major Offshore Fields.....	521
15.4 Offshore Oil and Gas Platforms.....	522
15.5 Metocean Impacts on the Offshore Industry.....	525
15.6 Future Offshore Production and Drilling.....	529
References	529
Part C Refining Technologies	
16 Petroleum Distillation	
<i>Chang Samuel Hsu, Paul R. Robinson</i>	533
16.1 Overview.....	533
16.2 Distillation Theory.....	537
16.3 Crude Oil Distillation.....	541
16.4 Summary.....	549
References	549
17 Gasoline Production and Blending	
<i>Chang Samuel Hsu, Paul R. Robinson</i>	551
17.1 Gasoline Engines.....	552
17.2 Otto Engine Thermodynamic Cycle.....	558
17.3 Key Gasoline Properties.....	559
17.4 Gasoline Specifications.....	563

17.5	Gasoline Production	564
17.6	Production of Gasoline Blendstocks	567
17.7	Synthetic Gasoline.....	582
17.8	Reformulated Gasoline (RFG) in the United States	583
17.9	Gasoline Additives	584
17.10	Blending Optimization	585
	References	585
18	Catalytic Reforming	
	<i>Pierre-Yves le Goff, William Kostka, Joseph Ross</i>	589
18.1	Objective of Catalytic Reforming	589
18.2	Feedstock Characteristics and Treatment	592
18.3	Main Reforming Reactions.....	594
18.4	Reforming Catalyst Overview	602
18.5	Contaminants and Unit Troubleshooting	604
18.6	Reforming Evolution	607
18.7	Catalyst Regeneration	613
18.8	Conclusions	615
	References	615
19	Fluid-Bed Catalytic Cracking	
	<i>James G. Speight</i>	617
19.1	Catalytic Cracking Chemistry	619
19.2	Feedstocks and Products	622
19.3	Reactor Design.....	624
19.4	Catalysts.....	632
19.5	Process Options	639
19.6	Options for Heavy Oil and Residua	641
19.7	Environmental Aspects and the Future	644
	References	646
20	Sulfur Removal and Recovery	
	<i>Paul R. Robinson</i>	649
20.1	About Sulfur	650
20.2	Sulfur Sources.....	651
20.3	Sulfur from Petroleum and Natural Gas	654
20.4	Conversion of H ₂ S to Elemental Sulfur.....	659
20.5	Sulfur Uses	663
20.6	Pollution from Sulfur.....	665
20.7	Conclusion	671
	References	671
21	Modern Approaches to Hydrotreating Catalysis	
	<i>Joo-Il Park, Isao Mochida, Abdulazeem M. J. Marafi, Adel Al-Mutairi</i>	675
21.1	Overview	676
21.2	Hydrotreating Process	683
21.3	Bases for Hydrotreating	684
21.4	Deep Hydrodesulfurization of Diesel.....	699
21.5	Development Base of AR Hydrotreatment	700
21.6	Current Aims in Development of Residue Hydrotreatment.....	703

21.7	Role and Design of Catalyst Support for Residual HDM.....	704
21.8	Novel Hydrotreatment Processes for Residue Upgrading	705
21.9	Challenges in Hydrotreatment.....	707
	References	708
22	Hydrocracking	
	<i>Paul R. Robinson, Geoffrey E. Dolbear</i>	713
22.1	Role of Hydroprocessing in Petroleum Refining	714
22.2	Feedstock Molecules	719
22.3	Process Variables	722
22.4	Hydrotreating Chemical Reactions	725
22.5	Hydrocracking Chemical Reactions	731
22.6	Hydroprocessing Catalysts	736
22.7	Catalyst Cycles.....	740
22.8	Hydroprocessing Thermochemistry	745
22.9	Hydroprocessing Kinetics	747
22.10	Hydroprocessing Process Descriptions	754
22.11	Economics.....	762
22.12	Safety, Reliability, and Protection of the Environment.....	762
22.13	Conclusion	775
22.14	Additional Reading.....	775
	References	775
23	Hydroprocessing Reactor Internals	
	<i>F. Emmett Bingham, Douglas E. Nelson, Daniel Morton</i>	777
23.1	Elements of Hydroprocessing Reactor Design	777
23.2	Liquid Distribution Tray Design.....	778
23.3	Quench Mixing Chamber Design	781
23.4	Manway Access and Faster Access Options	782
23.5	Example of Reactor Internals Revamp.....	783
23.6	Conclusion	785
	References	786
24	Hydrogen Production	
	<i>M. Andrew Crews, B. Gregory Shumake</i>	787
24.1	Thermodynamics of Hydrogen.....	788
24.2	Technologies for Producing Hydrogen	790
24.3	Design Parameters for SMRs	800
24.4	Environmental Issues	804
24.5	Monitoring Plant Performance	807
24.6	Plant Performance Improvements	808
24.7	Economics of Hydrogen Production.....	809
24.8	Conclusion	814
24.9	Further Reading	814
25	Hydrogen Network Optimization	
	<i>Nick Hallale, Ian Moore, Dennis Vauk, Paul R. Robinson</i>	817
25.1	Background	817
25.2	Assets and Liabilities.....	819
25.3	It's All About Balance	820
25.4	Put Needs Ahead of Wants.....	821

25.5	Beyond Pinch	825
25.6	Investing versus Saving	828
25.7	Conclusion	830
	References	831
26	Model–Predictive Control Fundamentals	
	<i>Paul R. Robinson, Dennis Cima</i>	833
26.1	Useful Definitions	834
26.2	Overview of Economics	835
26.3	Sources of Benefits	836
26.4	Implementation	837
26.5	Costs versus Benefits	838
	References	839
27	Modeling Refining Processes	
	<i>Teh C. Ho</i>	841
27.1	Partition–Based Lumping	842
27.2	Composition–Based Modeling	843
27.3	Mathematical Reduction of System Dimension	849
27.4	Kinetics–Hydrodynamics Tradeoff	854
27.5	Total Lumping: Continuum Approximation	855
27.6	Conclusions	859
	References	860
28	Refinery–Wide Optimization	
	<i>Dale R. Mudt, Clifford C. Pedersen, Maurice D. Jett, Sriganesh Karur, Blaine McIntyre, Paul R. Robinson</i>	865
28.1	Overview of Suncor	865
28.2	Refinery–Wide Optimization (RWO)	866
28.3	Rigorous Models for Clean Fuels	868
28.4	Conclusion	876
	References	877
29	Rigorous Kinetics Modeling of Hydrogen Synthesis	
	<i>Milo D. Meixell Jr</i>	879
29.1	Steam Reforming Kinetics	880
29.2	Heat Transfer Rates and Heat Balances	887
29.3	Pressure Drop	890
29.A	Appendix: Simulation Results	895
29.B	Appendix: Case Study of Effects of Catalyst Activity in a Primary Reformer	897
	References	900
30	Delayed Coking	
	<i>Keith Wisecarver</i>	903
30.1	History of Thermal Processing	903
30.2	Delayed Coking Process	904
30.3	Other Thermal Processes	912
30.4	Future Challenges	913
	References	913

31	Transitioning Refineries from Sweet to Extra Heavy Oil	
	<i>Martin R. Gonzalez</i>	915
31.1	The Evolving Refinery	915
31.2	Characterization of Extra-Heavy Crudes	917
31.3	Crude Desalting	917
31.4	Aromatics Content Affecting Diesel and Jet Fuel Production	918
31.5	High Aromatics Content Affecting Gas Oil Conversion	918
31.6	Vanadium and Nickel in Crude and Gas Oil	919
31.7	Asphaltene and Clay Precipitation	920
31.8	Fouling in Gas-Oil Hydrotreaters	921
31.9	Sulfur and Nitrogen in Bitumen-Derived Crudes	922
31.10	Hydrodesulfurization and Hydrodenitrogenation of Gas Oils	923
31.11	Production of ULSD and Jet Fuel	924
31.12	Fouling in Naphtha Hydrotreaters	925
31.13	Sulfur and Nitrogen Removal from Naphtha	926
31.14	Choice of Resid Conversion Technology	927
31.15	Other Investment	927
31.16	Conclusion	928
	References	929
32	Carbon Dioxide Mitigation	
	<i>Sultan M. Al-Salem, Xiaoliang Ma, Mubarak M. Al-Mujaibel</i>	931
32.1	Main Sources of Carbon Dioxide (CO ₂) Emission in Petroleum Refineries	933
32.2	Case Study: CO ₂ Emission Estimation from a Refinery in the State of Kuwait	944
32.3	Challenges in Carbon Capture and Mitigation for Petroleum Refineries	950
32.4	Concluding Remarks	952
	References	952
 Part D Petrochemicals		
33	Conventional Lube Base Stock	
	<i>Brent E. Beasley</i>	957
33.1	Lube Base Stock Manufacturing	958
33.2	Key Base Stock Properties	959
33.3	Lube Oil Chemistry	960
33.4	Typical Lube Processes	960
33.5	Key Points in Typical Lube Plants	962
33.6	Base Stock End Uses	963
33.7	Lube Business Outlook	963
33.8	Feedstock Selection	963
33.9	Lube-Crude Assays	964
33.10	Vacuum Distillation	965
33.11	Pipestill Troubleshooting	970
33.12	Solvent Extraction	971
33.13	Corrosion in NMP Plants	978
33.14	Analytical Tests for Extraction	978

33.15 Dewaxing	978
33.16 The Role of Solvent in Dewaxing	979
33.17 Ketone Dewaxing Processes	980
33.18 Process Variable Effects	982
33.19 Solvent Composition	982
33.20 Scraped Surface Equipment	985
33.21 Filters	993
33.22 Cold Wash Distribution	997
33.23 Wash Acceptance	998
33.24 Wash Efficiency	998
33.25 Filter Hot Washing	1000
33.26 Dewaxed Oil/Wax–Solvent Recovery	1001
33.27 Solvent Dehydration	1001
33.28 Solvent Splitter	1002
33.29 Two–Stage Dewaxing	1002
33.30 Deoiling	1003
33.31 Propane Dewaxing	1005
33.32 Two–Stage Propane Dewaxing	1007
33.33 Analytical Tests in Dewaxing	1007
33.34 Dewaxing Aids	1007
33.35 DWA Mechanism	1008
33.36 Asphaltene Contamination	1009
33.37 Regulatory Requirements	1009
33.38 Glossary	1009
References	1013
34 Premium Lubricant Base Stocks by Hydroprocessing	
<i>Stephen K. Lee, John M. Rosenbaum, Yalin Hao, Guan–Dao Lei</i>	1015
34.1 Key Base Stock Properties	1016
34.2 Base Stock Categories	1018
34.3 Why the Need for Premium Base Stocks?	1019
34.4 Lube Base Stock Manufacturing Technologies	1020
34.5 All–Hydroprocessing Route for Lubricant Base Stocks	1021
34.6 Hydrotreating/Hydrocracking	1023
34.7 Dewaxing	1033
34.8 Hydrofinishing	1039
34.9 Integrating Hydroprocessing with Solvent Plants – <i>Hybrid Plants</i> ..	1040
34.10 GTL Base Oils	1041
References	1042
35 Synthetic Lubricant Base Stock	
<i>Margaret M. Wu, Suzzy C. Ho, Shuji Luo</i>	1043
35.1 Background	1043
35.2 Overview of Synthetic Base Stocks	1046
35.3 Synthetic Base Stock – Chemistry, Production Process, Properties, and Use	1047
35.4 Conclusion	1060
References	1060

36 Catalytic Processes for Light Olefin Production	
<i>Genquan Zhu, Chaogang Xie, Zaiting Li, Xieqing Wang</i>	1063
36.1 Fundamentals of the Cracking Mechanism for Light Olefin Production	1064
36.2 Catalysts	1066
36.3 New Technology	1068
36.4 Prospects	1077
References	1078
37 Polyolefins	
<i>David Fiscus, Antonios Doufas, Sudhin Datta</i>	1081
37.1 Olefin Feedstocks and Derived Polymers	1082
37.2 Polymerization Mechanism	1083
37.3 Polymerization Processes	1084
37.4 Postpolymerization Process	1085
37.5 The Structure of Polymers	1086
37.6 Synthesis and Processing of Polyethylene	1088
37.7 Polyethylene Process and Catalysts	1090
37.8 Structure of Polyethylene	1091
37.9 Polyethylene Processing	1091
37.10 Synthesis and Processing of Polypropylene	1094
37.11 Polypropylene Process and Catalysts	1094
37.12 Polypropylene Fabrication	1098
37.13 Synthesis and Processing of Elastomers	1105
37.14 Polybutadiene (BR)	1106
37.15 Styrene–Butadiene Rubber (SBR)	1107
37.16 Ethylene–Propylene Rubber (EPR/EPDM)	1109
37.17 Butyl (IIR) and Halobutyl Rubber	1112
37.18 Conclusion	1113
References	1113
38 Biomass to Liquid (BTL) Fuels	
<i>Gary Brodeur, Subramanian Ramakrishnan, Chang Samuel Hsu</i>	1117
38.1 Lignocellulosic Biomass	1119
38.2 Biomass Processing Routes	1120
38.3 Biomass Oil and Petroleum Oil Co-processing	1127
38.4 Conclusion	1130
References	1130
39 Renewable Diesel and Jet Fuels	
<i>Henrik Rasmussen</i>	1133
39.1 Processing Renewable Feeds: Consequences for Hydrotreating	1134
39.2 Renewable Diesel: Feeds, Products and Reaction Pathways	1135
39.3 Development of Catalysts for Conversion of Renewable Feeds	1137
39.4 Choosing the Right Main Bed Catalyst when Coprocessing	1138
39.5 Simplified Process Diagram	1138
39.6 Catalysts for Dewaxing of Renewable Diesel	1139
39.7 Conclusion	1140
References	1140

40 Small Scale Catalytic Syngas Production with Plasma	
<i>Adam A. Gentile, Leslie Bromberg, Michael Carpenter</i>	1141
40.1 Plasma	1142
40.2 Partial Oxidation Reformation Using Cold Plasma	1147
40.3 Cold-Plasma-Assisted Experimentation	1156
40.4 Analysis and Discussion.....	1159
40.5 Synergistic Benefits of Plasma.....	1160
40.6 Conclusion	1161
References	1162
41 Hydrocarbon Processing by Plasma	
<i>Robert J. Wandell, Bruce R. Locke</i>	1163
41.1 Historical Aspects.....	1164
41.2 Properties of Plasma – Thermal versus Nonthermal	1164
41.3 Commercial Viability of Plasma Processes	1165
41.4 Challenges in Performing Selective Organic Reactions with Plasma.	1165
41.5 Strategies to Induce Selectivity	1166
41.6 Radical Chemistry in Various Plasma Discharges.....	1167
41.7 Pure Organic Compounds in Direct Contact with Plasma Discharge .	1168
41.8 Functionalization of Hydrocarbons with Plasma-Generated Radical Species	1168
41.9 Functionalization of Liquid Hydrocarbons with Oxygen Plasma	1169
41.10 Functionalization of Liquid Hydrocarbons with Water Plasmas	1173
41.11 Conclusions and Future Trends	1174
References	1175
Important Conversion Factors in Petroleum Technology	1183
Glossary of Defining Terms	1185
About the Authors	1208
Subject Index	1220

List of Abbreviations

1-D	one-dimensional
2-D	two-dimensional
3-D	three-dimensional
4,6-DMDBT	4,6-dimethyldibenzothiophene
4-D	four-dimensional
4-MDBT	4-methyldibenzothiophene
5-D	five-dimensional

A

A/D	analog to digital
AARD	average absolute relative deviation
ABE	acetone-butanol-ethanol
ABS	acrylonitrile–butadiene–styrene terpolymer
ACDA	aminocyclopentene dithiocarboxylic acid
ACM	Aspen Custom Modeler
ADU	atmospheric distillation unit
AEBP	atmospheric equivalent boiling point
AED	atomic emission detector
AFR	air/fuel ratio
AGO	atmospheric gas oil
AGR	acid gas removal
AH-GO	Arabian heavy gas oil
AKI	anti-knock index
AL-GO	Arabian light gas oil
ALKY	alkylation
ALT	array laterolog tool
AM-GO	Arabian medium gas oil
AMD	acid mine drainage
AMW	average molecular weight
APC	advanced process control
APCI	atmospheric pressure chemical ionization
APCI MS	atmospheric pressure chemical ionization mass spectrometry
APGC	atmospheric pressure gas chromatography
API	American Petroleum Institute
APLI	atmospheric pressure laser ionization
APPI	atmospheric pressure photo ionization
APR	aqueous phase reforming
AR	atmospheric residue
ARC	advanced regulatory control
ARD	acid rock drainage
ARDS	atmospheric residue hydrodesulfurization
ART	asphalt residual treating
AS	acrylonitrile styrene
ASA	amorphous silica alumina
ASAT	aromatics saturation
ASO	acid-soluble oil
AST	array sonic log
ASTM	American Society for Testing and Materials
ATF	automatic transmission fluid
ATR	autothermal reforming

AVO	amplitude variations with offset
AVR	Athabasca vacuum residue

B

B-acid	Brønsted acid
BACT	best available control technology
BCF	bulked continuous filament
BDC	bottom dead center
BHC	borehole compensated
BHGM	borehole gravity meter
BHT	bottom-hole temperature
BHTV	borehole televiewer
BIIR	brominated butyl rubbers
BKB	brown coal briquettes
BO	butylene oxide
boe	barrel of oil equivalent
BPD	barrels per day
BPSM	basin and petroleum system modeling
BR	butadiene rubber
BSI	British Standards Institution
BSR	Beavon sulfur removal
BSW	basic sediment and water
BTL	biomass-to-liquid
BTU	British thermal unit
BTX	benzene, toluene, and xylene
BWR	boiling-water reactor

C

C–C	carbon–carbon
CAD	collisional activated dissociation
CAE	computer-aided engineering
CAL	caliper
CAP	combustion air preheat unit
CAST	circumferential acoustic scanning tool
CAT	catalyst average temperature
Cat-Ox	catalytic oxidation
cat/oil	catalyst/oil
CBA	cold-bed adsorption
CBM	coal bed methane
CCC	critical clustering concentration
CCD	carbonate compensation depth
CCR	Conradson carbon residue
CCS	carbon capture and storage
CDR	cold dilution ratio
CDU	crude oil distillation unit
CDW	catalytic dewaxing
CEOS	cubic equation of state
CFC	chlorofluorocarbon
CFD	computational fluid dynamics
CFR	combined feed ratio
CHNS	carbon–hydrogen–nitrogen–sulfur contents
CHOPS	cold heavy oil production with sand

CHPS	cold high-pressure separator	ECR	electron cyclotron resonance
CI	chemical ionization	EDP	emergency depressuring
CIIR	chlorinated butyl rubbers	EF	expanded fluid
CMI	compact microimager	EFI	electronic fuel injection
CMP	common midpoint	EG	ethylene glycol
CNAC	critical nanoaggregate concentration	EI	electron-impact ionization
CNL	compensated neutron logs	ELSD	evaporative low-angle light scattering detector
CNT	carbon nanotube	EMI	electrical microimaging
COC	Cleveland open-cup method	ENB	5-ethylidene-2-norbornene
COD	crude oil distillation	EO	ethylene oxide
COS	carbonyl sulfide	EoS	equation of state
COT	coil outlet temperature	EPDM	ethylene-propylene-diene terpolymer
CPI	carbon preference index	EPM	ethylene-propylene monomer
CPOX	catalytic partial oxidation	EPR	ethylene-propylene rubber
CPP	catalytic pyrolysis process	ES	electrical survey
CR	controlled rheology	ESI	electrospray ionization
CRU	catalytic reforming unit	ESP	electrical submersible pump
CSM	chloro sulfonated rubber	ESR	electron spin resonance
CSO	clarified slurry oil	ETBE	ethyl tertiary butyl ether
CSS	cyclic steam stimulation	EVA	ethylene vinyl acetate
CSTR	continuous stirred tank reactor	E&P	exploration and production
CTO	catalyst-to-oil		

D

DAFVA	dialkyl fumarate-vinyl acetate
DAO	deasphalted oil
DAWNT	dilute acid with NMMO treatment
DBD	dielectric barrier discharge
DBE	double-bond equivalent
DBT	dibenzothiophene
DCC	deep catalytic cracking
DCS	distributed control system
DCU	delayed coking unit
DDL	direct digital logging
DDT	dichlorodiphenyltrichloroethane
DEA	diethanolamine
DFA	downhole fluid analysis
DFT	density functional theory
DGA	diglycolamine
Dilbit	diluted bitumen
DIPA	di-isopropanolamine
DLA	diffusion limited aggregation
DMDBT	dimethyldibenzothiophene
DMDS	dimethyl disulfide
DME	dimethyl ether
DMR	dry methane reformation
DMT	dimethyl terephthalate
dP	pressure drop
DST	drill stem test
DWA	dewaxing aids
DWO	dewaxed oil

E

e-bed	ebullated bed
E-SBR	emulsion SBR
EAF	electric arc furnace
ECBM	enhanced coal-bed methane

F

F-theory	friction theory
F/E	feed/effluent exchanger
FAME	fatty acid methyl ester
FAR	fused aromatic ring
FCC	fluid catalytic cracking
FCE	flares carbon emission
FD	field desorption
FE	formation evaluation
FEA	finite element analysis
FF	feed-forward
FFR	filter feed rate
FHZ	Flory-Huggins-Zuo
FI	field ionization
FIC	flow-induced crystallization
FID	flame ionization detector
FLNG	floating liquid natural gas
FMI	formation micro-imager
FPS	floating production system
FPSO	floating production, storage and offloading
FPU	feed preparation unit
FSO	floating storage and offloading system
FT	Fischer-Tropsch
FT-ICR	Fourier-transform ion cyclotron resonance
FT-ICR MS	Fourier-transform ion cyclotron resonance mass spectrometry

G

GBS	gravity-based structure
GC	gas chromatography
GC×GC	comprehensive two-dimensional gas chromatography

GC-AED	gas chromatography-atomic emission detection	HTSC	high-temperature shift converter
GC-FID	gas chromatography-flame ionization detection	HTU	hydrotreating unit
GC-ICP-MS	gas chromatography-inductively coupled plasma-mass spectrometry	Hue-GRZ	Hue-gamma ray zone
GC-MS	gas chromatography mass spectrometry	HVGO	heavy vacuum gas oil
GC-MS-MS	gas chromatography-tandem mass spectrometry	HWEP	hot-water extraction process
GC-TOF	gas chromatography-time of flight		
GCD	gas chromatographic distillation	I	
GCU	gas concentration unit	I/O	isobutane-to-olefin
GHG	greenhouse gas	IBP	initial boiling point
GNT	gamma ray neutron tool	ICE	internal combustion engine
GOD	gas oil desulfurization	ICP-MS	inductively coupled plasma-mass spectrometry
GOHT	gas oil hydrotreater	IEA	International Energy Agency
GOR	gas-to-oil ratio	IFA	in situ fluid analyzer
GPC	gel permeation chromatography	IFO	intermediate fuel oil
GPR	general purpose rubber	IIR	isobutylene-isoprene rubber
GR	gamma ray	IMEP	instantaneous mean effective cylinder pressure
GTL	gas-to-liquid	IP	invasion percolation
		IPCC	Intergovernmental Panel on Climate Change
H		iPP	isotactic polypropylene
H/C	hydrogen-to-carbon	IPR	inflow performance relationship
H2OR	hydrogen-to-oil ratio	IR	infrared
HAP	hazardous air pollutant	IRR	internal rate of return
HC	hydrocracking	ISBL	inside-battery limits
HCA	hierarchical clustering analysis	ISIP	instantaneous shut-in pressure
HCC	Houdry cracking unit	ISO	International Organization for Standardization
HCFC	hydrochlorofluorocarbon	ISOM	isomerization
HCGO	heavy coker gas oil	K	
HCO	heavy cycle oil	KD	kerosene desulfurization
HCU	hydrocracking unit	KEC	Kuwait export crude
HDA	hydrodearomatization	KHT	kero hydrotreater
HDEO	heavy duty engine oil	KPS	permeability, porosity, saturation
HDM	hydrodemetalation		
HDN	hydrodenitrogenation	L	
HDO	hydrodeoxygenation	L ² MS	laser desorption, laser ionization mass spectrometry
HDPE	high-density polyethylene	L-acid	Lewis acid
HDS	hydrodesulfurization	LAB	linear alkyl benzene
HDT	hydrotreating	LAO	linear alpha-olefin
HECO	heterophasic copolymer	LC	liquid chromatography
HF	hydrofluoric acid	LCA	lube crude approval
HFA	hydrofluoric acid alkylation	LCB	long-chain branching
HHPS	hot high-pressure separator	LCGO	light coker gas oil
HI	hydrogen index	LCO	light cycle oil
HLPS	hot low-pressure separator	LDI	laser desorption ionization
HMS	high melt strength	LDI MS	laser desorption ionization mass spectrometry
HN	heavy naphtha	LDPE	low-density polyethylene
HOT	heavy oil treating	LDU	lube deasphalting unit
HPS	high pressure separator	LEC	ligand-exchange chromatography
HRTEM	high-resolution transmission electron microscopy	LFC	lower far crude
HSE	health, safety, environment	LFER	linear free energy relationship
HSQC	two-dimensional heteroatom single quantum coherence		
HSR	heavy straight run		
HTE	high-throughput experimentation		

LGO	light gas oil	MOR	middle-of-run
LGR	local grid refinement	MPC	model-predictive control
LHHW	Langmuir–Hinshelwood/Hougen–Watson	MPSG	mercaptopyryl silica gel
LHSV	liquid hourly space velocity	MRIL	magnetic resonance imaging log
LHV	lower heating value	MRM	multiple-reaction monitoring
LIAD	laser induced acoustic desorption	MRS	microresistivity scanner
LIAD-MS	laser induced acoustic desorption-mass spectrometry	MRT	maximum recording thermometer
LID	lithodensity identification	MRV	mini-rotary viscosity
LIFDI	liquid injection field desorption/ionization	MS	mass spectrometry
LL	laterolog	MSDS	material safety data sheet
LLDPE	linear low-density polyethylene	MSFL	microspherically focused log
LLV	liquid–liquid–vapor	MSSV	microscale sealed vessel pyrolysis
LN	light naphtha	MTBE	methyl <i>tert</i> -butyl ether
LNG	liquefied natural gas	MTG	methanol-to-gasoline
LOR	lean oil recovery	MTO	methanol-to-olefin
LPG	liquefied petroleum gas	Mtoe	million tonnes of oil equivalent
LPS	low-pressure separator	MUGC	makeup gas compressor
LSD	low-sulfur diesel	MV	manipulated variable
LSFO	low-sulfur fuel oil	MVGO	middle vacuum gas oil
LSV	liquid space velocity	MW	molecular weight
LTSC	low-temperature shift converter	MWD	molecular weight distribution
LVGO	light vacuum gas oil	MZCR	multizone circulating reactor
LWD	logging while drilling		
LWR	light-water reactor		

M

MABP	mean average boiling point
MALDI	matrix-assisted laser desorption/ionization
MCH	methylcyclohexane
MCHA	methylcyclo-hexylamine
MCHE	methylcyclohexene
MCHT	methylcyclohexanethiol
MCO	medium cycle oil
MCPBA	<i>m</i> -chloroperbenzoic acid
MCR	micro-carbon residue
MDEA	methyl diethanolamine
MDO	marine diesel oil
MDT	modular formation dynamic tester
MEA	monoethanolamine
MEK	methyl ethyl ketone
MFR	melt flow rate
MGO	marine gas oil
MIBK	methyl isobutyl ketone
MIC	methyl isocyanate
MID	metric matrix identification
MIR	mid-infrared spectroscopy
MLDW™	Mobil Lube Dewaxing
MLL	microlaterolog
MMSCFD	million standard cubic feet per day
MMT	methylcyclopentadienyl manganese tricarbonyl
MODU	mobile offshore drilling unit
MOF	metal–organic framework
MON	motor octane number

N

N slip	nitrogen slip
NA	nanoaggregate
NBR	natural butyl rubber
NCD	nitrogen chemiluminescence detector
NEO	net effective overburden
NHT	naphtha hydrotreater
NIM	nuclear instrument module
NIR	near-infrared
NKD	naphtha, kerosene and distillate fuel oil
NLL	neutron lifetime logs
NMAZ	NiMo/alumina-zeolite
NMI	nuclear magnetic imager
NMMO	<i>N</i> -methyl morpholine <i>N</i> -oxide
NMO	normal moveout
NMP	<i>N</i> -methylpyrrolidone
NMR	nuclear magnetic resonance
NO	nitric oxide
NOx	nitrogen oxides
NPD	nitrogen phosphorus detector
NPG	neopentylglycol
NR	natural rubber
NRTL	nonrandom two liquid
NSO	nitrogen, sulfur and oxygen

O

OBM	oil-based mud
OCC	olefins catalytic cracking
OCR	on-stream catalyst replacement
OCT	olefins conversion technology
OD	optical density
OECD	Organization for Economic Cooperation and Development

OGC	oil–gas contact
OHV	overhead valve
OP	opening position
OPEC	Organization of the Petroleum Exporting Countries
OPEX	operating cost
OSP	oil-soluble PAG
OWC	oil-water contact

P

PA	proton affinity
PAA	polyalkyl acrylate
PAG	polyalkyleneglycol
PAH	polycyclic aromatic hydrocarbon
PAMA	polyalkyl meth acrylate
PAN	peroxyacetyl nitrate
PAO	polyalphaolefin
PASH	polycyclic aromatic sulfur heterocycle
PBN	peroxybenzoyl nitrate
PBR	polybutadiene
PCA	principal component analysis
PCB	polychlorinated biphenyl
PCC	propylene catalytic cracking
PCR	principal component regression
PD	photodetector
PDF	process-derived fuel
PDH	paraffin dehydrogenation process
PDI	polydispersity index
PE	polyethylene
PEF	photo-electric factor
PEL	permissible exposure limit
PEM	polymer electrolyte membrane
PET	polyethylene terephthalate
PFR	plug flow reactor
PHWR	pressurized heavy-water reactor
PI	photoionization
PIB	polyisobutylene
PID	proportional-integral-derivative
PINA	normal paraffinic, branched paraffinic (iso-paraffins), naphthenic, and aromatic
PKN	Perkins–Kern–Nordgren
PM	particulate matter
PO	propylene oxide
PONA	paraffins, olefins, naphthenes, and aromatics
POX	partial oxidation
PP	polypropylene
PPE	personal protection equipment
PPM	proton precession magnetometer
PRT	power-recovery turbine
PS	polystyrene
PSA	pressure swing adsorption
PTA	purified terephthalic acid
PVC	polyvinyl chloride
PVT	pressure, volume, temperature
PWR	pressurized water reactor
PX	paraxylene

Q

QMS	quadrupole mass analyzer or spectrometer
QSRR	quantitative structure–reactivity relationship
QSSA	quasi-steady state approximation
QTOF MS	quadrupole time-of-flight mass spectrometer

R

RBOB	reformulated gasoline before oxygenate blending
RCC	reduced crude conversion
RDD	radiological dispersion device
REAC	reactor effluent air cooler
REL	recommended exposure limits
REMPI	resonance enhanced multiphoton ionization
RFCC	residue fluid catalytic cracking
RGC	recycle gas compressor
RHC	raffinate hydroconversion
RHG	Raymer–Hunt–Gardner
RI	refractive index
RIT	reactor inlet temperature
RLA	reaction limited aggregation
RON	research octane number
ROP	rate of penetration
ROT	riser outlet temperature
RPVOT	rotating pressure vessel oxidation test
RTO	real-time optimizer
RVP	Reid vapor pressure
RWO	refinery-wide optimization

S

S slip	sulfur slip
S-PAC	sulfur-containing polycyclic aromatic compound
SAA	sulfuric acid alkylation
SAFT	statistical associating fluid theory
SAGD	steam-assisted gravity drainage
SALDI	surface-assisted laser desorption ionization
SANS	small angle neutron scattering
SAOS	small angle oscillatory shear
SAPO	silica-alumina phosphate
SAPS	sulfated ash, phosphorus, and sulfur
SAR	Si–Al ratio
SARA	saturates, aromatics, resins, and asphaltenes
SAXS	small angle x-ray scattering
SBL	structure-based lumping
SBR	styrene–butadiene rubber
SC	shielding cone
SCAL	special core analysis laboratory
SCD	sulfur chemiluminescence detector

SCFOGIP	standard (temperature and pressure) original gas in place
SCR	selective catalytic reduction
SCWR	supercritical-water reactor
SDA	solvent deasphalting
SFC	supercritical fluid chromatography
SFE	supercritical fluid extraction
SimDist	simulated distillation
SLS	sodium lauryl sulfate
SM	styrene monomer
SMR	steam methane reforming
SNO	solvent neutral oil
SOL	structure-oriented lumping
SOR	start-of-run
SOx	sulfur oxides
SPA	solid phosphoric acid
SPD	slurry-phase distillate
SPI	single photon ionization
SPR	strategic petroleum reserve
SR	straight run
SR LGO	straight-run light gas oil
SRGO	straight run gas oil
SRU	sulfur recovery unit
SSC	scraped surface chiller
SSE	scraped surface exchanger
SSOT	single-stage once-thru hydrocracker
SSREC	single-stage with recycle hydrocracker
STG+	syngas-to-gasoline plus
STL	syngas-to-liquids
STOOIP	stock tank original oil in place
STP	standard temperature and pressure
SUS	Saybolt universal seconds
SWC	side wall core
SWS	sour-water stripper
syncrude	synthetic crude

T

TAME	<i>t</i> -amyl methyl ether
TAN	total acid number
TBP	true boiling point
TCC	Thermoform catalytic cracking
TCD	thermal conductivity detector
TD	total depth
TDC	top dead center
TDS	total dissolved solids
TEL	tetraethyl lead
TGTU	tail-gas treating unit
TI	temperature indicator
TIP	total isomerization process
TLC	thin-layer chromatography
TLP	tension-leg platform
TLV	threshold limit values
TMP	trimethylolpropane
TMT	tube metal temperature
TOC	total organic carbon
TOF	time-of-flight
TOF MS	time-of-flight mass spectrometry
TOST	turbine oil stability test

tpa	tons per annum
TPE	thermoplastic elastomer
TPO	thermoplastic olefin
TR	transformation ratio
TRFD	time-resolved fluorescence depolarization
TSP	thermospray
TSS	third-stage separator
TTR	truck tape recorder
TVD	true vertical depth
TWIM	thin-wall injection molding

U

UCO	unconverted oil
UHMWPE	ultrahigh molecular weight polyethylene
ULSD	ultra-low-sulfur diesel
US	ultra-stable

V

VAM	vinyl acetate monomer
VBI	viscosity blend index
VDU	vacuum distillation unit
VG	viscosity grade
VGO	vacuum gas oil
VI	viscosity index
VLDPE	very low-density polyethylene
VLE	vapor-liquid equilibrium
VLT	vapor-lift tray
VM	viscosity modifier
VOC	volatile organic compound
VPO	vapor pressure osmometry
VPS	vacuum pipestill
VR	vacuum residue
VSP	vertical seismic profiling
VSS	vortex separation system
VUV	vacuum-ultraviolet laser light

W

WABT	weighted average bed temperature
WART	weighted average reactor temperature
WAXS	wide angle x-ray scattering
WBM	water-based mud
WGS	water gas shift
WHR	waste heat recovery
WHSV	weight hourly space velocity
WPC	World Petroleum Council
WTI	West Texas intermediate

X

XRD	x-ray powder diffraction
XRF	x-ray fluorescence spectrometry

Z

ZSM-5	Zeolite Socony Mobil-5
-------	------------------------

1. Introduction to Petroleum Technology

Paul R. Robinson, Chang Samuel Hsu

When people consider petroleum, they first think of energy. Petroleum and other fossil fuels now provide more than 86% of the energy consumed by mankind. In addition, fossil resources, especially petroleum and natural gas, serve as the organic source of tens of thousands of consumer products, which enrich our daily lives.

To understand petroleum and the petroleum industry, one must be familiar with the technology used to find and recover crude oil and natural gas and transform them into useful products. These technologies can also be applied to gases and liquids from coal, shale, and renewable biomass. Research and development aimed at improving or modifying existing technologies and developing new ones usually require physical testing and chemical characterization.

Three-dimensional imaging exhibits geological formations most likely to contain oil and gas. Rigorous basin modeling optimizes exploration and production. Modern production technology includes enhancements in horizontal drilling and offshore platform design. The application of hydraulic fracturing to previously unrecoverable oil and gas from tight reservoirs has transformed the United States into the world's leading producer of oil and gas.

Midstream technology includes trading, shipping, and transportation, along with processing prior to transportation. Midstream processing includes froth treatment for upgrading bitumen from steam-assisted gravity drainage (SAGD) into synthetic crude oil (syncrude). Sophisticated planning models enable global energy companies to quickly decide logistics: which oils to buy, how to allocate them between numerous processing plants, and whether to resell them.

Crude oil goes to refineries, which use distillation, treating, conversion, extraction and blending processes to produce fuels, hydrogen, lubricants, waxes, coke products, asphalt, and sulfur. Some refinery streams are sent to petrochemical plants.

Ever-improving mathematical models enhance all aspects of petroleum technology. Model-predictive control (MPC) stabilizes operations and reduces product-quality giveaway, increasing profitability at relatively low cost. The simple return on investment for an MPC project can be 3–4 months. Process engineers rely on rigorous equipment and piping models to optimize designs, not just in the oil and chemical businesses, but in all process industries. With such models, energy consumption in processing plants has been reduced by up to 70% since the 1980s. Rigorous reaction models, based on molecular characterization, serve as the foundation for real-time online economic optimization, in some cases for entire refineries. Economic optimization uses an objective function to find the most profitable balance between equipment constraints, feed quality, product yields, product properties, and utilities costs.

One cannot over-emphasize the importance of safety and protection of the environment. Failure to understand technology fundamentals and process details is the root cause of many infamous industrial catastrophes. Lack of understanding of technology fundamentals occurs at all levels, from the control board to the board room. Corporate executives who insist that safety is Number One must invest in safety-enhancing infrastructure. They must ensure that operators are well-trained and equipment is well-maintained.

Petroleum will remain significant for decades to come. Hopefully, ever-advancing technology will continue to supply energy and raw materials while protecting workers and the environment.

1.1	Petroleum and Its Uses	3
1.1.1	Primary and Secondary Energy Sources ..	3
1.1.2	Oil and Gas as Primary Sources of Energy	4
1.1.3	Petroleum as a Source of Nonfuel Products	4
1.1.4	Advantages of Petroleum	4
1.1.5	How Long Will It Last?	6
1.1.6	Petroleum Composition	7

1.2	People and Petroleum	8	1.11.4	Petroleum Refining Processes	47
1.2.1	Petroleum in Ancient Times.....	8	1.11.5	Petroleum Refining Catalysts	59
1.2.2	Whaling.....	9	1.12	Petroleum Products	63
1.2.3	Modern Kerosene	10	1.12.1	Petroleum Gases.....	63
1.2.4	Major Oil Companies.....	11	1.12.2	Gasoline	64
1.2.5	Petroleum for Transportation.....	12	1.12.3	Naphtha	66
1.2.6	OPEC, Embargos and Conservation.....	13	1.12.4	Diesel	67
1.2.7	Recent Ups and Downs.....	13	1.12.5	Kerosene and Jet Fuel (Turbine Fuel)	68
1.3	The Oil Business	14	1.12.6	Heating Oils and Fuel Oils.....	69
1.3.1	Research and Development.....	14	1.12.7	Lubricant Base Oils, Wax, Grease, and Specialty Products.....	70
1.3.2	Upstream.....	14	1.12.8	Cokes.....	71
1.3.3	Downstream.....	14	1.12.9	Asphalt.....	72
1.3.4	Midstream	15	1.13	Characterization of Petroleum	72
1.3.5	Petrochemicals.....	15	1.13.1	Crude Oil Assay	72
1.4	Macroeconomics	15	1.13.2	Instrumental Analysis	73
1.5	Origin of Fossil Hydrocarbons	18	1.14	Modeling	73
1.6	Natural Gas, Coal, and Kerogen	19	1.14.1	Basin Modeling	74
1.6.1	Natural Gas.....	19	1.14.2	Design Models.....	74
1.6.2	Coal.....	19	1.14.3	Component Lumping	74
1.6.3	Kerogen.....	19	1.14.4	Real-Time Optimization	74
1.6.4	Heavy Oil and Bitumen	20	1.14.5	Planning and Scheduling	75
1.7	Petroleum (Crude Oil)	20	1.15	Petrochemicals	75
1.7.1	Bulk Physical Properties	20	1.16	Alternatives to Petroleum	76
1.7.2	Molecular Composition.....	24	1.16.1	Inexhaustible (Renewable) Energy Sources	76
1.8	Oil and Gas Exploration	25	1.16.2	Nuclear.....	76
1.8.1	Searching for Traps	25	1.16.3	Biomass (Renewable) Resources.....	77
1.9	Drilling and Production (Recovery)	27	1.17	Protecting the Environment	77
1.9.1	Drilling.....	27	1.17.1	Air Quality.....	77
1.9.2	Blowouts.....	27	1.17.2	Wastewater Treatment	79
1.9.3	Well Completion	28	1.17.3	Solid Waste Handling.....	79
1.9.4	Production (Recovery).....	28	1.17.4	Fugitive Emissions.....	79
1.9.5	Well Stimulation: Hydraulic Fracturing... ..	29	1.17.5	Improving Energy Efficiency and Safety with Automation	80
1.10	Transportation and Storage	30	1.17.6	Conservation	80
1.11	Refining	30	1.18	Conclusion	80
1.11.1	Refinery Configuration Overview	30	References		81
1.11.2	The Need for Conversion.....	34			
1.11.3	Petroleum Refining Chemistry.....	36			

When people consider petroleum, they first think of energy. Energy is the ability of a system to do work. Forms of energy include heat, light, magnetic, mechanical, chemical, nuclear, and gravitational. Importantly, energy can be transformed from one form into another. For example, burning petroleum converts the energy stored in chemical bonds into heat, light, and mechanical energy.

Figure 1.1 shows that in 2014, fossil resources – coal, petroleum and natural gas – provide more than 86% of the energy people consume in modern societies. As discussed in more detail below, in addition to sup-

plying energy, oil and gas serve as the organic source of tens of thousands of chemicals and consumer products, which enrich our daily lives.

Petroleum plays a crucial role in economics and politics. It has made small countries rich, and the wealth of large countries depends on its cost and availability. Petroleum has played a critical or decisive role in all major wars since the start of the twentieth century.

The petroleum industry is huge and complex. To understand the industry, one must gain familiarity with the underlying science and engineering, which are used to find and recover crude oil and natural gas and transform

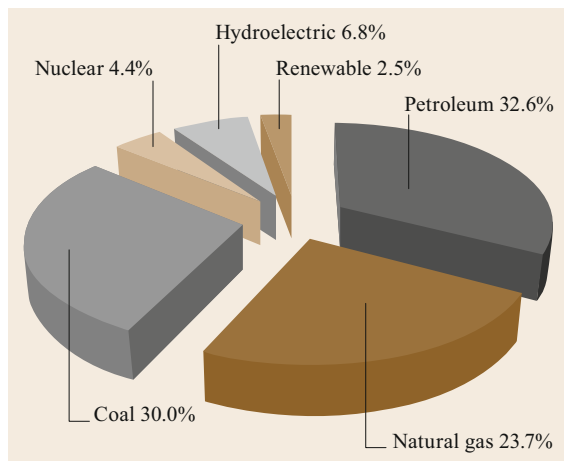


Fig. 1.1 World energy consumption by fuel type in 2014. (After [1.1]). The sum for fossil hydrocarbons is 86.3%, 1.4% lower than the 2013 total. Petroleum includes crude oil produced from tight formations with hydraulic fracturing. Gas includes co-produced petroleum gas, condensate, dry gas, and coal-seam gas. Renewable includes wind, solar, geothermal, and biomass (largely ethanol and oil from plants and animal fat). Data for the figure come from the BP Statistical Review of World Energy, 2015

them into useful products. These technologies can also be applied to gases and liquids from coal, shale, and renewable biomass. Research and development aimed at improving or modifying existing petroleum technologies and developing new ones starts with physical testing and chemical characterization.

Three-dimensional imaging exhibits geological formations most likely to contain oil and gas. Rigorous basin modeling optimizes exploration and production. Modern production technology includes enhancements in horizontal drilling and offshore platform design. Recently and significantly, hydraulic fracturing is recovering oil and gas from previously inaccessible reservoirs, transforming the United States into the world's leading producer.

1.1 Petroleum and Its Uses

1.1.1 Primary and Secondary Energy Sources

Petroleum, coal, and natural gas were formed from the remains of ancient organisms. Ultimately, they were created from the solar energy captured by plants, and the heat and pressure of the geological structures in which they were formed. But today, so far as we are concerned, fossil fuels are primary sources of energy.

Midstream technology includes transportation, trading and midstream processing, such as froth treatment for upgrading bitumen recovered by steam-assisted gravity drainage (SAGD) into synthetic crude oil (syn-crude).

Crude oil goes to refineries, which rely on distillation, treating, conversion, and blending to produce fuels, hydrogen, lubricants, solvents, sulfur, waxes, coke products, and asphalt. Refineries and natural gas plants supply raw petrochemicals. Refineries provide light olefins, aromatics (benzene, toluene, and xylenes) and petrochemical naphtha. Natural gas is transformed into light olefins and synthesis gas. From petrochemicals come thousands of vital materials – coatings, polymers, fibers, plastics, cosmetics, pharmaceuticals, and many others.

Ever-improving mathematical models enhance all aspects of petroleum technology. Sophisticated planning survey models enable global energy companies to quickly decide which oils to buy, how to allocate them between numerous processing plants, and whether to resell them.

Model-predictive control (MPC) stabilizes operations and reduces product-quality giveaway, increasing profitability at relatively low cost. The simple return on investment for an MPC project can be 3–4 months. Process engineers rely on rigorous equipment and piping models to optimize designs, not just for oil, gas, and petrochemicals, but for all process industries. With such models, energy consumption in processing plants has decreased by up to 70% since the 1980s. Rigorous reaction models, based on molecular characterization, serve as the foundation for real-time online process and economic optimization, in some cases for entire refineries.

One cannot overemphasize the importance of safety and protecting the environment. The root causes of many infamous industrial catastrophes were the failure of corporate executives, line managers, front-line engineers, and operators to learn and understand technology fundamentals well enough to respond properly to unusual situations.

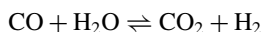
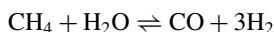
World energy sources compare different estimates of primary energy reserves from various government agencies [1.2]. It divides resources into three categories:

1. Fossil
2. Nuclear
3. Renewable.

Important sources of nonconventional fossil fuels include bitumen and oil shale. Renewable sources include solar, wind, hydroelectric, ocean waves, biomass, and waste. Biomass also serves as a source of biochemicals. Nuclear and renewable sources are carbon-neutral. They are not net producers of atmospheric CO₂. According to sources [1.2], proven, recoverable fossil sources total 39 ZJ, where 1 ZJ = 10²¹ J [1.3]. The International Atomic Energy Agency estimates that available nuclear power derived from uranium is 2500 ZJ, assuming the use of fast-breeder technology; breeder reactors create more fissile material than they consume. The Intergovernmental Panel on Climate Change (IPCC) estimates that reserves based on uranium are 1000 ZJ. Some estimates of available energy from uranium and fissile thorium are misleadingly low, because they neglect reprocessing and reuse of recovered isotopes. The safety of nuclear power is a huge concern. Nuclear accidents are rare, but when they occur, they are deadly and exceptionally difficult to contain, with planet-wide consequences.

Hydrogen and electricity are not energy sources. The US Energy Information Agency calls them secondary sources. Others prefer to call them energy vectors or energy transfer agents, because their main role is to move primary energy from power plants to consumers.

Now and then, hydrogen automobiles are touted to be pollution free, because hydrogen produces water when it burns. Most commercial hydrogen comes from steam/hydrocarbon reformers, which co-produce CO₂. Stoichiometry dictates that for every ton of produced H₂, 5.5 t of CO₂ are co-produced. The generation of requisite process heat via combustion yields additional CO₂. Natural gas is the primary feed to on-purpose hydrogen plants, in which methane reacts with steam to form CO, which reacts with addition water to form CO₂ and additional H₂ via *water gas shift* reactions. Converting heavier hydrocarbons co-produces even more CO₂.



Electrolytic hydrogen is co-produced in chlorine-manufacturing plants. Most often, the required electricity comes from fossil fuels.

Steam is a short-distance energy transfer agent. Generated from water vaporization in fired boilers or nuclear power plants, it drives turbines to generate electricity or run pumps and gas compressors. SE-TatWork [1.4] describes how Preem refineries near Lysekil and Goteborg, Sweden, deliver waste heat, as hot water, to nearby factories and homes. The corresponding reduction in CO₂ emissions is estimated to be 152 400 t/yr.

Major untapped energy *sources* are conservation and efficiency, for which the cost is far lower than building new facilities.

1.1.2 Oil and Gas as Primary Sources of Energy

Figure 1.2 shows how oil and gas consumption has grown since 1820. Figure 1.2 provides a breakdown of world consumption of energy from wind, biomass, and solar sources since 1965. Geothermal plays a minor role and is not shown. From these graphs, one can make the following observations:

- World consumption of energy has increased more than 500% since the end of World War II. Most of that increase came from coal, oil, and natural gas.
- In 1820, primitive biofuels directly from natural resources – mostly wood, peat, animal fat, and fodder consumed by draught animals – still provided most of our energy. In the graph, primitive and modern biofuels (mainly ethanol) are shown together.
- Near the end of the nineteenth century, coal consumption overtook primitive biofuels.
- In the 1950s, oil and gas overtook coal. Consumption of energy from all sources began to increase exponentially. The rate of increase slowed in the 1970s primarily due to turmoil in the Middle East.
- Energy from renewable sources, especially wind energy, continues to grow rapidly.

Table 1.1 presents a quantitative petroleum product breakdown in the United States for July and December 2014 [1.6]. Sulfur and other contaminants are excluded. Motor gasoline totals do not include ethanol. About 83 wt% (90 vol.%) of the products are fuels – gasoline, kerosene, jet, and fuel oils. Most refinery gases and petroleum coke are also used as fuels. In Europe, yields of motor gasoline and distillate fuel oil would be approximately reversed, and yields of petroleum coke would be lower.

1.1.3 Petroleum as a Source of Nonfuel Products

Petroleum not only provides transportation fuels, but it also supplies building blocks for the thousands of other chemicals and other materials that improve the quality of our daily lives (Tables 1.2 and 1.3).

1.1.4 Advantages of Petroleum

When wisely handled, petroleum can be safe and clean. Conventional crude oils are liquids at ambient temper-

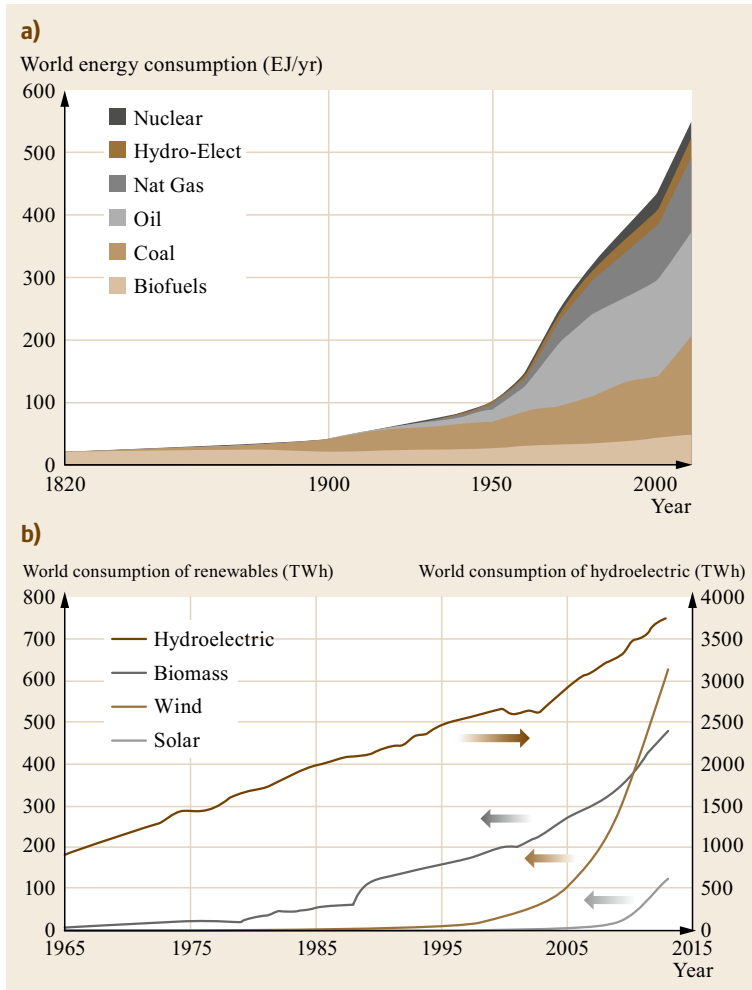


Fig. 1.2 (a) World energy consumption by fuel since 1820 (after [1.5], with kind permission from Gail Tverberg). **(b)** World consumption of renewable energy since 1965. Note that the scale for hydroelectric is 5× the scale for the other sources. Biomass includes both modern biomass, primarily fuel ethanol, and traditional biomass (wood, peat, animal fat, and fodder consumed by draught animals) (after [1.1])

atures; compared to solids and gases, liquids are easier to transport and process. Petroleum is noncompressible, so conventional pumps can push it through pipelines thousands of miles long or into and out of sea-going tankers. Bitumens are solids or goos at ambient temperature, but they can be liquefied by heating or by dilution with lighter oils.

Crude oils can be stored for months with minimal losses in above-ground tanks, or stored indefinitely simply by leaving them under-ground. (*Minimal losses* might include vaporization, leakage, oxidative degradation, and biodegradation. In certain cases, such losses are not so minimal). Fuels distilled from petroleum have high energy densities. 15 gal of gasoline can move a 3300pd automobile across 350 mi of flat road at 65 mi/h. (In metric units, those values are 57 l, 1480 kg, 565 km, and 105 km/h, respectively.)

Belying recent projections, petroleum still is abundant. On April 18, 1977, the US President Jimmy Carter

predicted that if the world consumption of oil kept rising by 5% per year, the world's proven reserves of petroleum would be used up by 1990 [1.7]. Carter then outlined an energy policy that encouraged conservation and stimulated the development of petroleum alternatives. Other countries, notably in Western Europe, already had implemented similar measures. In the years since, new technologies were developed for finding new petroleum deposits and improving production from known fields, including bitumen and oil shale.

While oil and gas are ubiquitous, they are not evenly distributed. In 2014, the top 10 countries held about 83% of world reserves of conventional petroleum and bitumen, led by Venezuela (17.5%), Saudi Arabia (15.7%), and Canada (10.4%). For natural gas, the top 10 countries held about 78% of world reserves, led by Russia (23.8%), Iran (16.4%), Qatar (12.1%), Turkmenistan (8.5%), and the United States (4.7%).

Table 1.1 Industry-average volume-percent yields from petroleum refineries in the United States

US refinery yields ^{a,b} (vol. % of feed)	Summer (Jul 2014)	Winter (Dec 2014)
Liquified petroleum gases (LPG) ^c	5.3	2.4
Motor gasoline ^d	44	46.5
Aviation gasoline	0.1	0.1
Kerosene-type jet fuel	9.7	9.7
Kerosene	0.1	0.2
Distillate fuel oil	29.1	30.7
Residual fuel oil	2.4	2.3
Petrochemical feed (naphtha)	1.3	1.4
Petrochemical feed (other)	0.7	0.5
Special naphthas	0.3	0.2
Lubricants	1	0.9
Waxes	0.1	0
Petroleum coke	5.5	5.3
Asphalt and road oil	2.3	1.7
Still gas ^c	4.2	4
Miscellaneous products	0.6	0.5
Volume gain ^e	6.7	6.4

^a After removal of sulfur, nitrogen, and other contaminants

^b Volumes of solids are expressed in fuel-oil equivalents

^c Still gas is largely methane but can also contain C2–C4 compounds

^d Does not include ethanol

^e The volume gain is due to cracking. Light cracked products have lower densities than crude oil

1.1.5 How Long Will It Last?

Petroleum as an energy source is slowly but surely being replaced, but no other single substance has all the same advantages. As already mentioned, in addition to serving as our major source of energy, oil and gas are the organic sources of thousands of consumer products with exceedingly different properties – from medicines

Table 1.2 Nonfuel petroleum products

Product class	Example	Some uses
Lubricants (including grease and industrial oils)	≫ 800 products	From <i>baby oil</i> to axle grease – all with stringent specifications
Asphalt and waxes	Asphalt Waxes	Paved roads, water-proofed buildings Coated paper packaging, water-proofing, candles
Carbon	Petroleum coke Needle coke Graphite	Fuel and making anodes for metal refining Electric arc anodes for aluminum and high-grade steel Metallurgy, specialty fibers, paints, pencils
Chemical plant feedstocks	Ammonia Aromatics C ₃ /C ₄ olefins Carbon dioxide Naphtha, UCO ^a Sulfur	Metal cleaning, fertilizer (Table 1.3) (Table 1.3) Dry ice, carbonated soft drinks Olefin production plants Sulfuric acid, fertilizers

^a UCO is highly upgraded unconverted oil from hydrocrackers

to pesticides, from golf club shafts to PVC pipes, from baby oil to asphalt, from adhesives to laxatives.

Deposits of petroleum and other fossil hydrocarbons were formed millions of years ago. They are finite. A commonly asked question is: How long will petroleum last?

It is common to see reports in which projections are made based on a simple ratio of present-day proven reserves by present-day rates consumption, using (for example) data from the US Energy Information Administration (EIA), the International Energy Agency (IEA), and the BP Statistical Review of World Energy (BP) [1.1]. With data from BP, we get the following results:

- Remaining oil, 52 years
- Remaining natural gas, 54 years
- Remaining coal, 110 years.

Fenton et al. [1.8] estimated that 1.3 trillion barrels of oil could be recovered from known reserves of kerogen-rich shale. This is equivalent to 40 more years of oil, bringing the total for oil to 92 years:

- Remaining oil + oil from shale, 92 years.

There are significant problems with using such ratios to predict how long fossil fuels will last. The problems include:

- *Failure to anticipate advances in technology.* While still theoretically finite, proven oil reserves are *increasing* – from 683 billion barrels in 1980 to 1690 billion barrels in 2014.
- *Market drivers.* As will be shown, consumption decreases, often dramatically, when prices rise.
- *Synthetic petroleum.* Synthetic petroleum is being generated from other fossil resources – natural gas, bitumen, and kerogen. Especially in China, coal is

Table 1.3 Chemicals derived from petroleum and uses

Family	Chemical	Used to make ...
Alcohols and derivatives (from natural gas processing)	Methanol	Methyl tertiary butyl ether (MTBE), acetic acid, formaldehyde, synthetic gasoline (MTG process)
	Acetic acid	Vinyl acetate ⇒ plastics, latex paints, cellulose acetate ...
	Cellulose acetate	Yarns, sheet plastic, films, lacquers
	Formaldehyde	Resins, butanediol, inks, nylon
	Ethyl alcohol (from ethylene)	Gasoline, solvents, personal care products, ethyl chloride ...
	Ethyl acetate	Solvent (e.g., nail polish remover)
	Isopropyl alcohol	Solvents, personal care products
Aromatics (from petroleum)	Higher alcohols	Solvents, plasticizers, detergents
	Benzene	Styrene, cumene, cyclohexane, maleic anhydride ...
	Toluene	Polyurethane
Aromatics derivatives	Xylenes	Polyester fibers, resins, plasticizers
	Cyclohexane	Nylon precursors
Olefins (from natural gas and petroleum)	Cumene and phenol	Phenolic resins, epoxy and polycarbonate resins
	Ethylene	Polyethylene, ethylene dichloride, ethylene oxide
	Ethylene dichloride	Polyvinyl chloride (PVC) ⇒ plastics
	Ethylene oxide	Polystyrene, ethylene glycol
	Ethylene glycol	Antifreeze, polyethylene terephthalate (PET) ⇒ plastic bottles
	Propylene	Polypropylene, propylene oxide ⇒ propylene glycol ...
	Propylene glycol	Antifreeze, polyesters, pharmaceuticals, hand sanitizers
	Butenes	Maleic anhydride
	Butadiene	Complex polymers, including synthetic rubbers
	Alpha olefins	Polymers, surfactants, synthetic lubricant oil and additives, fatty acids
Others	Acrylonitrile, acrylic acid	Polymers, including transparent polymers (Plexiglass, Lucite)
	Aldehydes and ketones	Acetic acid, acetone, other solvents
	Ethylbenzene and styrene	Polystyrene
	Isobutane	Methyl methacrylate resins
	Maleic anhydride	Polyesters, resins, plasticizers, dicarboxylic acids, nylon precursors

being converted into liquid fuels, chemicals, and syngas. Renewable plant-derived oils are being co-processed in existing oil refineries.

- *Energy efficiency.* Energy efficiency is improving. Significantly, driven by environmental regulations, the fuel efficiency of vehicles has been rising, slowly but surely, since the 1970s. To meet the regulations, vehicle manufacturers have improved engine design, vehicle body shape, materials, fuels, and lubricants. Rigorous design models have enabled significant energy reduction in many industries. In 10 US states, the energy cost of producing electricity has decreased by more than 70% [1.9].

M. King Hubbert's peak oil method [1.10] is sometimes used to predict how long oil will last. Once highly touted, Hubbert's approach has proven to be misleadingly pessimistic, due to its Malthusian assumptions. Hence, as with simple ratio calculations, Peak oil fails to account for advances in technology, which affect both availability and consumption.

1.1.6 Petroleum Composition

Petroleum is not a uniform substance. It can be present in nature as gas, liquid, or solid under ambient temperature and pressure. The gaseous form of petroleum in nature is also known as natural gas. The solid form of petroleum can be bitumen or tar. The petroleum fractions processed in the refineries are liquids (crude oils) or soluble/diluted viscous liquids or solids, such as syncrudes.

There are hundreds of different crude oils, and each one is a complex mixture of thousands, if not millions, of compounds. Some crude oils (crudes) are listed later in this chapter.

Petroleum is mainly composed of hydrocarbons, compounds of carbon and hydrogen; it also includes compounds containing heteroatoms, primarily sulfur, nitrogen, oxygen, and metals. The major classes of hydrocarbons are paraffins (normal and isoparaffins), cycloparaffins (naphthenes), aromatics (aromatic and naphthenoaromatic hydrocarbons), and heteroatom compounds (nonhydrocarbons). Most heteroatom compounds are harmful to upgrading equipment, processes,

the environment, and even human health, so they are removed during processing.

Petroleum crude oils can be broadly classified as paraffinic, asphaltic, and mixed crude oils. Paraffinic crude oils are composed of aliphatic hydrocarbons (paraffins), wax (long-chain normal paraffin), and high grade oils, but no or little asphaltic (bituminous) com-

ponents. On the other hand, asphaltic crude oils contain no or little paraffins. Some are naphthenic, i.e., they contain predominantly cycloparaffins, which can be feedstocks for making high viscosity lubricating oils. Most crude oils are mixed oils which include all three hydrocarbon types: paraffins, naphthenes, and aromatic hydrocarbons.

1.2 People and Petroleum

People were using petroleum tens of thousands of years ago. This section describes highlights of this long and interesting history, from the stone age to the space age.

1.2.1 Petroleum in Ancient Times

Spears and Baskets

Hafting is the process of attaching the heads spears, arrows, and axes to a shaft. The simplest technique, used in the Stone Age mostly for arrows, was to split the end of the wooden shaft and force the tapered base of the head into the resulting gap. For spears, the base of the head was notched, and leather strips were looped through the notches and wound around the shaft. In both methods, junctions were strengthened with mastic obtained from rendered animal hides or hooves, from tree resin, or from bitumen. According to *Boëda* et al. [1.11] people were hafting with bitumen more than 70 000 years ago near Umm el Tlel, in present-day Syria.

A book by *Jane McIntosh* [1.12] on the ancient Indus Valley describes how baskets were water-proofed with bitumen before 5500 BC in Mehrgarh, an ancient site located in present-day Pakistan between the cities of Quetta, Kalat, and Sibi.

Boats, Towers, and Mummies

Bitumen is described as *mankind's oldest engineering material* [1.13]. It is mentioned by some of the earliest known writing – transactions recorded in Cuneiform script on clay tablets found in the ancient city of Sumer [1.14, 15]. The Sumerian Empire, located in Mesopotamia between the Tigris and Euphrates rivers in present-day Iraq, lasted from about 3500 to 2500 BC. Pitch was used in mortar, for cementing eyes into carvings, building roads, caulking ships, and waterproofing, in general. Sumerian pitch came primarily from oil pits near the river Issus, one of the tributaries of the Euphrates.

Greek and Roman historians describe how Egyptians employed pitch for construction, to grease chariot wheels, and for mummification [1.16]. After they were thoroughly dried, mummies were coated with bituminous plaster and wrapped with bitumen treated cloth.

Molten pitch was poured into empty brain cavities. (One of the first steps in mummification was to remove and discard the brain.) Egypt's primary source of pitch was the Dead Sea, which the Romans called *Palus Asphaltites* (Asphalt Lake).

In Babylon (1900–1600 BC), bitumen was employed during construction of the famous Tower. Persians used bitumen and its fractions for lighting, topical ointments, and flaming projectiles.

By 500 BC, ancient civilizations knew that light petroleum fractions, such as naphtha, could be mixed with asphalt to make the latter easier to handle. The light fractions may have been recovered with alembics or simple batch distillation equipment such as that described by Zosimus of Panopolis, a Greek alchemist who lived at the end of the third century and beginning of the fourth century AD [1.16].

Early Natural Gas

Mark Kurlansky's book on the importance of salt tells a fascinating story about brine wells in the Sichuan region of China [1.17]. In 252 BC, a Qin Dynasty official named Li Bing ordered workers to drill brine wells after he discovered that brine pools on the surface were fed from underground. Occasionally, well diggers became weak or sick, and sometimes explosions killed an entire crew. By 100 AD, people understood that the source of their problems was an invisible, flammable gas, now called natural gas. They piped it into open sheds through leak-proofed bamboo tubes. In the sheds, using the gas as fuel, they boiled away the water, leaving behind crystallized salt. By the end of the second century AD, co-production of gas and brine was controlled by a system of leather valves, which resembled in many respects the valves used in certain modern wells.

By 347 AD, Chinese were drilling for gas with bamboo shafts. They collected bitumen, too, and employed it in unique ways. For example, they warmed it to drive off lighter fractions, leaving behind a thermoplastic material with which scabbards and other items were covered. Statuettes of household deities were cast with this material in Japan, and perhaps also in China.

Coal

Even before civilization took root in China 5000 years ago, people in the region had been using coal for about 1000 years [1.18, 19]. They carved it into ear ornaments, and they created the world's first coal mine. Ancient China's coal use enabled it to develop into a sophisticated economy and society.

Archeological evidence in China indicates surface mining of coal and household usage after approximately 3490 BC [1.20]. Iron artifacts, made between 2700 and 3000 BC, probably were manufactured with heat provided by charcoal.

By the first century AD, Romans were burning coal in hypocausts to heat homes and public baths, in smelters to recover iron from ore, and in forges to shape iron into weapons, ornaments, and other implements.

Greek Fire

Greek fire [1.3] was invented during the reign of Byzantine Emperor Constantine IV (668–685) by Callinicus of Heliopolis, a Jewish refugee from Syria. This formidable weapon was sprayed at enemy ships from siphons. It burst into flame on contact with air and could not be extinguished with water. Greek ships used the weapon to cripple an attacking Arab fleet, breaking the four-year siege of Constantinople (674–678). Experts are still debating the exact composition of Greek fire. Most believe it was comprised of naphtha, liquid petroleum, bitumen, and quicklime.

Early Kerosene

The great Persian scholar, Muhammad al-Razi (865–925 AD), wrote more than 200 books and articles, in which he documented fundamental contributions to medicine, alchemy, music, and philosophy [1.21]. He discovered numerous chemicals and compounds, including kerosene, which he recovered from petroleum. Kerosene has been used for heating ever since.

Early Lamps

Lamps were providing people with artificial illumination before 15 000 BC [1.22]. Lamps found in the Lascaux caves near Dordonis, France, were carved from stone; the Lascaux archaeological site is best known for its Paleolithic cave-wall paintings [1.23]. Ancient lamps found elsewhere were made from hollow stones, sea shells, coconuts, and even egg shells [1.24]. Oil for lamps came from olives and other oil-rich plants. Lard oils from animals were readily available, but they tended to burn with smoky, smelly flames.

Significantly, sea-faring folk discovered that the cleanest-burning animal oils came from whales.

1.2.2 Whaling

Rock carvings found at the Bangudae archaeological site near Ulsan, Korea, show that perhaps as early as 6000 BC, humans hunted whales from boats using harpoons and floats attached to lines [1.25]. Nearby, prehistoric caches of whale bones confirm that the creatures were an important resource for people in the area.

Thousands of years later, near-shore whaling was thriving in the Bay of Biscay near Bayonne, at the southwest corner of present-day France [1.26]. By the fourteenth century, Spanish whalers were venturing far into the north, hunting mainly the North Atlantic Right Whale. English, Dutch, French, and Scandinavian fleets dominated whaling in the eighteenth century. Especially prized was the sperm whale. Spermaceti, a clear, yellowish liquid that burns with a clear, bright flame, was harvested from the head cavity of this creature. Spermaceti sold at a premium, sometimes fetching up to 3 times more than other oils from whales.

In addition to fueling lamps, whale oil furnished lubricants for the machinery of the Industrial Revolution. Baleen from whales provided buggy whips, fishing poles, corset stays, and dress hoops [1.27].

Yankee Whaling

The American whaling industry started late in the eighteenth century. New Bedford, MA, was the hub, supplemented by major ports in Nantucket, MA, and New London, CT. Several important ships were built in Mattapoisett, MA. Yankee whaling flourished from 1783, when the Treaty of Paris ended the American Revolution, until the War of 1812, when the British navy (again) blockaded American ports. From 1814 to the 1870s, except during the American Civil War (1861–1865), Yankee whaling reached its height.

Due to overhunting, whales in the North Atlantic declined. To fill their holds, fleets ventured far and wide, sometimes skirting South America on years-long round trips between New Bedford and the North Pacific, all the way to the Bering Strait. Supplies fluctuated wildly due to world events and the *luck of the fleet*. In lean years, fleets ventured farther into the Arctic and stayed longer in dangerous, freezing waters. Consequently, the number of shipwrecks increased, and the number of whales decreased. By 1860, several species were almost extinct [1.28]. Prices reflected supplies, ranging from less than \$0.40/gal in 1830s to more than \$2.50/gal during and just after the American civil war [1.29]. Significant losses of ships during that war were devastating to whaling – but fortunate for whales. The *CSS Shenandoah*, a fully rigged Confederate ship with auxiliary steam power, captured or sank 38 Union merchant ships, 25 of which were unarmed New Bedford whale-

ships. *John Baldwin* wrote [1.30] that on or about June 23, 1865 – more than two months after Robert E. Lee surrendered his Confederate army to Ulysses S. Grant – the *Shenandoah* fired the last shot of the Civil War across the bow of a whaleship in the Aleutian Islands. In November 1865, to avoid the US Navy and reluctant to face an opponent that might shoot back, Commander James I. Waddell surrendered the *Shenandoah* to the British near Liverpool, England.

1.2.3 Modern Kerosene

More than 900 years after Muhammad al-Razi wrote about recovering kerosene from petroleum, the following occurred:

Gesner and Oakes

In 1846, Canadian geologist Abraham Gesner developed a distillation process to recover kerosene from coal, bitumen, and oil shale. In 1850, his company began installing lighting in Halifax, Nova Scotia, Canada [1.31]. Gesner was granted a patent for his recovery method in 1854. He did not invent kerosene per se.

In 1847, prior to the issue of Gesner's patent, James Oakes built a rock oil refinery in Riddings, Derbyshire, England, to recover oil for lamps [1.32].

Semyenov

In 1848, the *first modern oil* well was drilled by Russian engineer F.N. Semyenov [1.33] on the Aspheron Peninsula north-east of Baku. Eleven years later, a refinery was constructed near the well to convert raw petroleum into several products.

Łukasiewicz

In the 1850s, *Ignacy Łukasiewicz* [1.34] and Robert E. Dietz independently developed practical kerosene lamps [1.35]. Łukasiewicz was a pharmacist in Lvov, Poland. In 1852, he and his assistant, Jan Zeh, experimented with ways to improve the safety of burning seep oil from the Carpathian mountains. From a local peasant, they learned how to boil away the most volatile components. With their own experiments, they devised ways to remove heavy impurities. Working with a local tin smith, they developed a lamp that burned the purified fuel with a clean, steady flame. By 1858–1859, Łukasiewicz/Zeh lamps were replacing other forms of illumination in Austrian railway stations. In 1854, Łukasiewicz moved to Southern Poland, where he collaborated with a partner to develop an oil field near Bobrka. His first wells were dug with picks and shovels and reinforced by wood beams. The deepest was 150 m (480 ft). During subsequent years, he opened several more oil wells, and in 1859, he commissioned a refinery near Jasło.

Dietz

In 1840 in New York, Robert E. Dietz began selling lamps to burn whale oil and camphene. In 1859, he and his brother Michael patented a lamp with a flat-wick burner, one of the first designed specifically for kerosene. Due to their steady performance in windy weather, Dietz lanterns became known as *hurricane lamps*.

Williams

In July or August 1858, James Miller Williams struck oil while drilling a well for drinking water in Oil Springs, Ontario, Canada, near present-day Petrolia [1.36]. The well is often called the first oil well in North America.

The Drake Well

On August 27, 1859, Edwin L. Drake struck oil with a well near Titusville, in northwest Pennsylvania [1.37]. By today's standards, the well was shallow – about 69 ft deep (21 m) – and it produced only 35 bbl/day. The Drake well was not the first to produce oil, but it was the first on record to be drilled through rock with a powered rotary engine, specifically for oil.

The Drake well triggered the Pennsylvania oil rush. Owners of adjacent leases recognized that they and their neighbors were accessing the same large underground pool. The key to success, they believed, was to drill more wells faster than their neighbors. The result is illustrated in Fig. 1.3. Note the short distance between the two wells – the Phillips well and the Woodford well, which were among the most productive of the time. In the middle of the photo are wooden barrels in which the crude was stored and transported. The size of a barrel was not standardized yet, so the barrels shown are of different sizes.

At first, Drake was able to sell his oil for US\$20/bbl. The price of kerosene from the oil was slightly less than the price of lard oil and 50–70% less than the price of whale oil. But kerosene prices soon fell, largely due to overproduction. Another factor was the lack of infrastructure for transportation to population centers on the US East Coast. During the next few years, prices swung wildly, from \$10/bbl in January 1861 to \$0.10/bbl at the end of that year. Similar swings occurred in 1862. By September 1863, prices reached \$7.25/bbl.

After the Drake Well

Figure 1.4 shows important events subsequent to the Drake well. It includes annual average oil prices, both in money of the day and inflation-corrected dollars.

Russian crude became internationally significant when, starting in 1873, the Nobel brothers (Ludwig and Alfred) and then the Rothschild family invested heavily



Fig. 1.3 A Pennsylvania oil field in 1862. The two wells shown are the Phillips well and the Woodford well, among the most productive of the time. Note the small distance between them. In the middle of the photo are wooden barrels in which the crude was stored. The size of a barrel was not standardized yet, so the barrels shown are of different sizes

in developing Russian oil fields. These efforts led to the widespread use of tankers for transportation and to the Baku–Bantum railroad, which opened Western Europe to Russian Oil.

Significant discoveries in other countries include the following:

- Indonesia: Telaga Said well (1885)
- United States, East Texas: Spindletop well (1901)
- Iran (1908)
- Venezuela: Zumaque well (1914)
- Iraq: Kirkuk (1927)
- Bahrain (1932)
- Kuwait (1937)
- Saudi Arabia (1938)
- United States, Alaska: Prudhoe Bay (1967)
- North Sea: Brent field (1976)
- United States: Fracking in the Barnett Shale, Eagle Ford, and Bakken formations (starting in 1999).

1.2.4 Major Oil Companies

Standard Oil Company

In the mid-nineteenth century, John D. Rockefeller brought order to the US oil industry by monopolizing it. In 1865, his first major step was to acquire full ownership of a major refinery in Cleveland, OH, about 105 air miles from Titusville, PA [1.23]. By 1870, Rockefeller controlled several refineries in Cleveland. In that year, he led the formation of the Standard Oil company, which, at its peak, controlled 85–90% of the US oil industry and held significant interests in much of the rest of the world.

Rockefeller is vilified as the ultimate *robber baron*, but he probably saved the US oil industry from itself. His monopoly enabled him to hamper large price swings, largely preventing the boom/bust economics that plagued the industry elsewhere. In other parts of the world, notably Austrian Galicia, unrestrained overproduction, even when prices were very low, irreparably depleted one of the world's largest oil fields and damaged the nearby environment; evidence of that damage lingers even today, more than 100 years later [1.38].

In 1911, due to a ruling by the US Supreme Court, Standard Oil was split into 34 smaller companies. Among these were Standard Oil of New York (Mobil), Standard Oil of New Jersey (Exxon), Standard Oil of Ohio (Sohio), Standard Oil of Indiana (Amoco), Standard Oil of California (Socal), Continental Oil (Conoco), and The Ohio Oil Company (Marathon). Both Continental Oil and the Ohio Oil Company had been independent before. In the late 1990s, BP acquired Sohio and Arco (formerly Atlantic Richfield). In 1999, Exxon and Mobil merged into ExxonMobil. Socal is now Chevron, which grew significantly due to a series of mergers and acquisitions – notably of Gulf (1985), Texaco (2001), and Unocal (2005).

US oil companies that maintained independence from Standard Oil include Union Oil (Unocal), which was founded in California in 1890, and Pure, which was founded in 1895. A notable Pure accomplishment was to circumvent Standard's railroad monopoly by building a pipeline from the oil regions to the US east coast; the Pure advantage lasted only a short time – until Standard led the development of alternative pipelines. In 1901, Gulf and Texaco were spawned by the East Texas

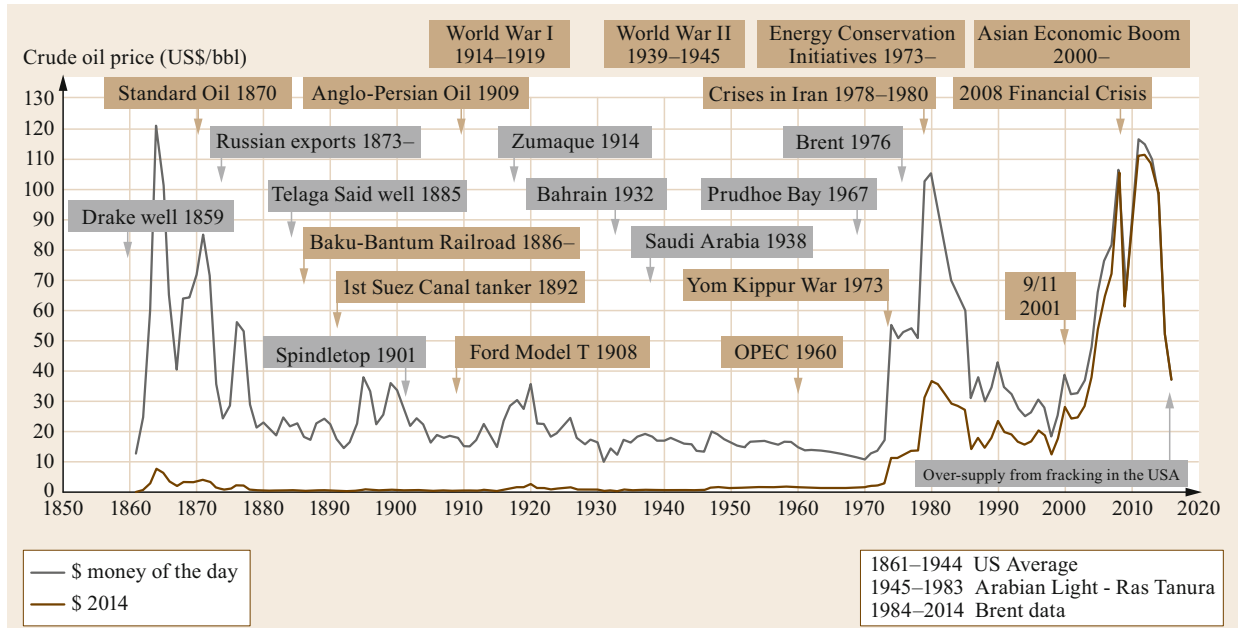


Fig. 1.4 Selected world events and crude oil prices in 1859–2015, prices are annual averages. Items in gray boxes indicate the start dates for major new production. The underlying format comes from the BP Statistical Review of World Energy (after [1.1]). Many events are described in Daniel Yergin’s book (after [1.39, Parts I and II]). Selected events and recent prices come from the US Energy Information Administration (after [1.40, 41])

oil boom. US companies founded after the Standard Oil breakup include Sinclair (1916), Phillips (1917), and Occidental (1920).

Major Multinationals

There are five major multinational oil and gas companies: ExxonMobil, Chevron, Royal Dutch Shell, BP, and Total. The Royal Dutch Petroleum company was formed in 1890 to develop an oil field in Sumatra, following up on discoveries at Telaga Said in 1885. In 1907, Royal Dutch merged with the Shell Transport and Trading Company to form the Royal Dutch Shell group, chartered in both the United Kingdom and the Netherlands. The British Petroleum Company (now BP) began in 1909 as the Anglo-Persian oil company. It grew through a combination of significant oil discoveries – notably the Prudhoe Bay field in Alaska and the Forties field off the coast of Scotland – and through mergers and acquisitions – notably with Sohio, Amoco, Arco, and Castrol. Total began in 1924, when France created the Compagnie Française des Pétroles (CFP). CFP was renamed Total in 1991. In 1999–2000, it merged with the Belgian company PetroFina and the French company Elf Aquitaine.

National Oil Companies

By establishing national oil companies, governments are better able to control the ways in which their re-

sources are exploited. Major national oil companies, some of which are more or less privatized, include the following: Agip Petroli (1926, Italy), ENI (established in 1953 from Agip), Saudi Aramco (1944, Saudi Arabia), KNPC (1960, Kuwait), NIOC (1951, Iran), Petronas (1974, Malaysia), Pertamina (1968, Indonesia), PTT (1978, Thailand), PetroChina (1999, China), Sinopec (2000, China), CNOOC (1999, China), CPC (1946, Taiwan), Ecopetrol (1951, Columbia), Pemex (1938, Mexico), PDVSA (1976, Venezuela), Petrobras (1953, Brazil), and Repsol (1987, Spain). Statoil was founded by the Norwegian government in 1972. In 2007, it was merged with the oil and gas division of Norsk Hydro.

1.2.5 Petroleum for Transportation

Initially, to improve the safety of kerosene, lighter more flammable fractions, such as naphtha, were driven off and burned. The heavier fractions – gas oil or residue – sometimes served as fuel oil and lubricants, but often they were simply incinerated.

In 1885–1886, Karl Benz and separately Gottlieb Daimler and William Maybach built the first automobiles whose internal combustion engines were powered with naphtha fuel [1.42]. Rudolf Diesel is credited for building a high-compression prototype engine in 1897, after Akroyd Stuart built the first working diesel en-

gine in 1892. The essence of Diesel's prototype was a gasoil-burning, 10 ft-long reciprocating iron cylinder with a flywheel at its base. Such engines burn fuels (gasoils) that are difficult to vaporize in a gasoline engine.

A major development was the switch from coal to oil in warships. In the 1890s, Germany openly discussed the merits of powering a new Navy with petroleum [1.43]. In the 1910s, Winston Churchill, who was then Great Britain's First Lord of the Admiralty, pushed the Royal Navy in this direction. With coal, he explained, storage bunkers closest to the boilers were emptied first. As the coal inventory decreased, the distance between the boilers and the supply increased, so it took more time and/or more sailors to bring coal to the boilers. This could handicap a ship in the heat of battle, when the need for both steam power and manpower were highest. Liquid petroleum could be pumped, so inventory did not affect the availability of fuel or fighters – unless of course the supply ran out. Britain's need to fuel its navy far from home led to the formation of the Anglo-Persian oil company, the precursor to British Petroleum.

The advent of the Model T Ford jump-started gasoline demand in 1908. By mass-producing the car, Henry Ford made automobiles affordable. Faced with high employee turnover and absenteeism, he increased wages to stabilize his work force. The benefits were immediate. Productivity surged, and profits doubled in less than two years. Ford later said that increasing wages was the best cost-cutting move he ever made. The higher pay scale expanded the American middle class which in turn expanded the market for automobiles and related consumer products [1.44].

Eventually, diesel engines replaced steam boilers in ships and railroad locomotives. Diesels became the norm for heavy-duty trucks, mining equipment, farm equipment, and stationary motors such as those that produce emergency electricity.

Today, transportation accounts for most of the world demand for petroleum, and 90% of the transportation fuel market is met by oil. Illumination is no longer the main use for kerosene. Most kerosene is refined into jet fuel.

1.2.6 OPEC, Embargos and Conservation

The Organization of Oil Exporting Countries (OPEC) was founded by five countries in 1960. OPEC now includes 13 members: Algeria, Angola, Ecuador, Indonesia, Iran, Iraq, Kuwait, Libya, Nigeria, Qatar, Saudi Arabia, United Arab Emirates, and Venezuela. Usually, OPEC – especially Saudi Arabia, which is the richest in reserves – strives to stabilize oil prices by

acting as a *swing* producer, raising production when prices are high and cutting production when prices are low.

In 1967, during the Six Days War with Israel, several Middle Eastern countries decreased or ceased oil shipments to the United States and the United Kingdom. This action had limited impact due to the lack of solidarity among exporters. The story was different after the Yom Kippur War in 1973–1974, when the Arab members of OPEC, along with Syria and Egypt, proclaimed an embargo against the United States, United Kingdom, Canada, Japan, and the Netherlands. World prices rose from \$3/bbl to \$10/bbl; US prices went up to \$12/bbl. Prices tripled again during 1978–1980 due to two crises in Iran – the Khomeini revolution and the subsequent war between Iran and Iraq.

Importing countries responded to the embargo with energy conservation measures, by stimulating domestic production, and by encouraging the development of alternatives to oil. In the United States, the Strategic Petroleum Reserve (SPR) was created in 1973 to counter sudden, severe supply interruptions. Short-term conservation initiatives included gasoline rationing, decreased speed limits, year-round daylight savings time, and simply turning off lights.

Long-term measures reaped long-term benefits. Factories invested in energy efficiency. People bought smaller vehicles with higher fuel efficiency. The measures worked. Demand dropped, and prices fell steadily, with occasional ups and downs, until 1998.

1.2.7 Recent Ups and Downs

In 1998, prices began to rise again, driven by rapid economic growth in India and China and OPEC's disinclination to increase supply. Except for a brief dip after the 9/11 attacks on the United States in 2001, prices continued to climb. Figure 1.4 illustrates this volatility.

Up

In June 2008, the weekly average spot price for Brent Crude reached \$141/bbl [1.45].

Down

After the failure of major US financial institutions in September 2008, the world economy suffered, oil consumption fell, and so did oil prices. On December 12, 2008, Brent was selling for \$40/bbl.

Up

In the next 6 years, economies and oil prices recovered. Brent sold for \$127/bbl on March 9, 2012, and on September 5, 2014, it sold for \$100/bbl.

Down

Then seemingly overnight, prices plummeted, hitting \$46/bbl in January 2015 and dipping below \$30/bbl in December 2015. Prices remained low through March 2016, bouncing between \$40 and \$50/bbl. There are several reasons for the dramatic drop in prices:

- *Fracking.* The industry has long known of seemingly inaccessible hydrocarbons trapped in shale formations, where the permeability of the reservoir rock is low. Hydraulic fracturing (*fracking*) increases permeability. First applied in 1947 in Grant County, KS [1.46], fracking involves pumping a slurry of water, sand, and chemicals at high pressure into a well. The pressure fractures the surrounding rock, and the sand props open the resulting passages. The chemicals can include acids, which dissolve particulates; silicones, which enhance flow; and surfactants. In the 1980s, George P. Mitchell, the founder of the Mitchell Energy and Development Corp., experimented with different fracking techniques in the depleted Barnett Shale formation in Texas. Shale is not uniform. Formations include cracks, and some sections are more dense than others. By drilling horizontal wells and fracking just beneath the denser sections, Mitchell got phenomenal results. By 1999, the Barnett Shale had been transformed into a major gas field. Since then, this combination of horizontal drilling and hydraulic fracturing has been improved and applied to several other formations, including the Eagle Ford in Texas, the Bakken in North Dakota, and the Marcellus in Ohio and Pennsylvania. By 2015, the United States once again was the world's leading producer of oil and natural gas. Domestic production displaced imports, creating worldwide oversupply.
- *US–Iran accord.* In 2015, an agreement between the United States and Iran diminished a long-standing embargo against Iranian oil. Exports from Iran poured more oil into an already glutted market.
- *Lower consumption in China.* An economic slowdown in China decreased oil demand.
- *OPEC restraint.* At the time we are writing this, OPEC has been refraining from decreasing its own production to prop up prices.

1.3 The Oil Business

Petroleum production and processing is a huge business. In terms of market capitalization, 9 of the world's 30 largest public corporations are oil and gas companies [1.47]. The oil business involves numerous functions within complicated organizations. The industry can be roughly divided into upstream, downstream, midstream, and petrochemical sectors.

1.3.1 Research and Development

Hydrocarbon production and processing employs cutting-edge technology. All of the main science and engineering disciplines are used. Hydrocarbon industries conduct and support fundamental R&D at an exceptionally high level. Internal R&D is augmented with university research, liberally supported by energy companies.

The sciences include geology, geophysics, oceanography, chemistry, geochemistry, microbiology, seismic imaging, satellite imaging, and more.

The engineering includes traditional disciplines, such as mechanical, civil, electrical and chemical; and special fields such as production engineering and reservoir engineering.

Technology used for petroleum can also be applied to, or integrated with, technologies for processing liq-

uids from coal, oil shale, and biomass to generate fuels and chemicals. Due to environmental considerations, the co-processing of biomass fuels with conventional refinery feedstocks is being intensively studied.

1.3.2 Upstream

The upstream sector deals with the discovery and recovery of petroleum resources, including natural gas, condensates, crude oils, and bitumen. The upstream processes may involve wellhead pretreatment to remove carbon dioxide and toxic hydrogen sulfide from natural gas prior to transportation. Natural gas plants also recover/remove noble gases, mainly helium, neon, and argon.

1.3.3 Downstream

In the downstream sector, refining processes can be divided into two main categories: fractionation/separation, which does not change molecules, and upgrading/conversion, which does change molecules. An important related activity is blending crude oils to meet refinery design constraints, and blending streams from individual processes to ensure that refinery products meet rigid specifications and achieve desired performance.

1.3.4 Midstream

Midstream involves all processes or procedures between upstream wellhead pretreatment and downstream desalting, including transportation and trading. One midstream process is the froth treatment of bitumen derived from oil sands. The treated bitumen is used to make *syncrudes*. The removal of carbon dioxide from natural gas prior to shipping LNG (liquefied natural gas) is also a midstream process.

Crude and product trading can be classified as a midstream technology. With advanced information technology, traders can make better decisions in a timely manner.

1.3.5 Petrochemicals

Non-fuel products from petroleum include lubricants, waxes, asphalts, and different grades of coke. Valuable by-products include sulfur, ammonia, and industrial CO₂; lubricants are discussed in several subsequent chapters, and sulfur and its uses are described in Chap. 20. One might think the term *petrochemical* means all chemicals derived from petroleum, but in practice it excludes by-products and includes chemicals made from natural gas.

Primary petrochemicals can be divided into three groups: olefins, aromatics and synthesis gas:

- Olefins include ethylene, propylene, butylenes and butadiene. They are manufactured with steam cracking from light paraffins from natural gas plants. Steam cracker feeds from refineries include naphtha and gas oils from primary distillation and upgraded vacuum gas oil from hydrocrackers. Many refinery fluid catalytic cracking (FCC) units are significant sources of propylene and C4 olefins. Polymer plants convert olefins into polyolefins such as polyethylenes, polypropylenes, and butyl rubbers. They also produce polyesters from oxygenated intermediates such as ethylene oxide. These

intermediates are transformed into various materials, such as Nylon 6 from adipic acid and hexamethylenediamine; acrylics from acrylonitrile; polyesters from ethylene oxide and terephthalic acid; polyvinyl chloride (PVC) from ethylene and chlorine; and so on. The polymers are converted into fibers, consumer plastics, and engineering plastics. Olefins also serve as sources of alcohols, ethylene glycol, and other simple but useful products.

- Aromatics include benzene, toluene and xylenes, which are mainly produced from catalytic reforming and as by-products of steam cracking.
- Synthesis gas is a mixture of carbon monoxide and hydrogen mainly produced from the steam reforming of methane and other light hydrocarbons from natural gas. It also is produced by gasification of coal and biomass. Synthesis gas is the major source of the hydrogen used in refineries and ammonia plants. It also is the major source for methanol and in a few locales for synthetic hydrocarbon fuels.

Methanol is the starting point for acetic acid and formaldehyde, which in turn are converted into adhesives, foams, and solvents. A growing use for methanol is production of mono-methyl esters of long-chain fatty acids, which are used as synthetic diesel.

Fine chemicals, which may be derived from petrochemicals, are pure chemicals manufactured during multistep processes. Important examples include the aforementioned adipic acid and hexamethylethylenediamine, of which 2.5 billion kg/yr and 1 billion kg/yr are consumed annually. Others include β -lactams, which are structural elements of penicillin and other antibiotics, and imidazoles, which are found in modern pesticides.

Pharmaceuticals are synthesized from fine chemicals and may include specialty waxes and solvents. Major pharmaceutical groups are based on pyrimidines, sulfanomides (most are antibiotics), and benzodiazepine (the starting point for Valium).

1.4 Macroeconomics

This chapter is about technology, but the development of technology is driven by economics. In this section, we provide an overview of macroeconomic trends in the energy industry. As we have witnessed, more than half of world's energy consumption comes from oil and gas.

Economic growth overrides all other macroeconomic trends in energy consumption. Figure 1.5 shows how world energy consumption has increased in dif-

ferent regions since 1965. Much of the recent increase comes from the Asia Pacific, China in particular.

Figure 1.6 shows that on a per capita basis, the Chinese consume far less energy than Europeans, North Americans, and Eurasians. In 2011, per capita consumption in the United States was still 4 times greater than that in China and 20 times greater than that in Africa. Per capita consumption has been falling in North America

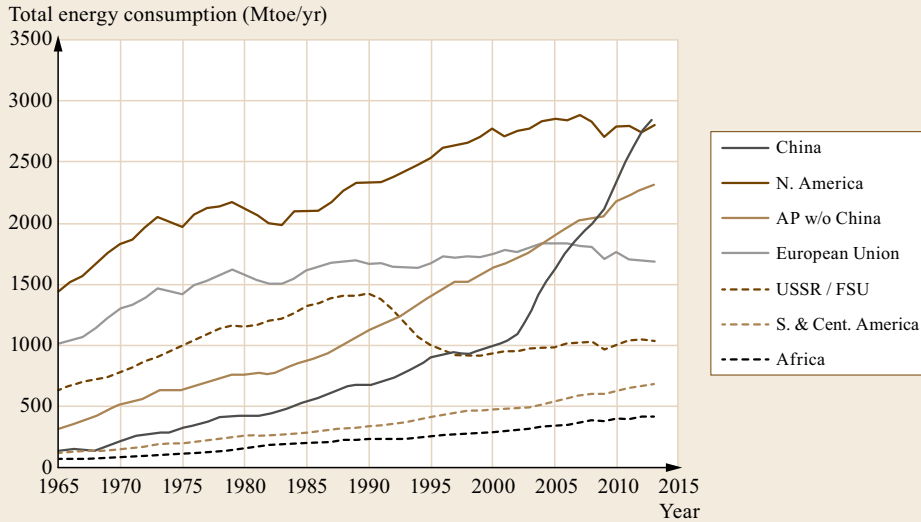


Fig. 1.5 Total energy consumption by region. AP = Asia Pacific (after [1.1])

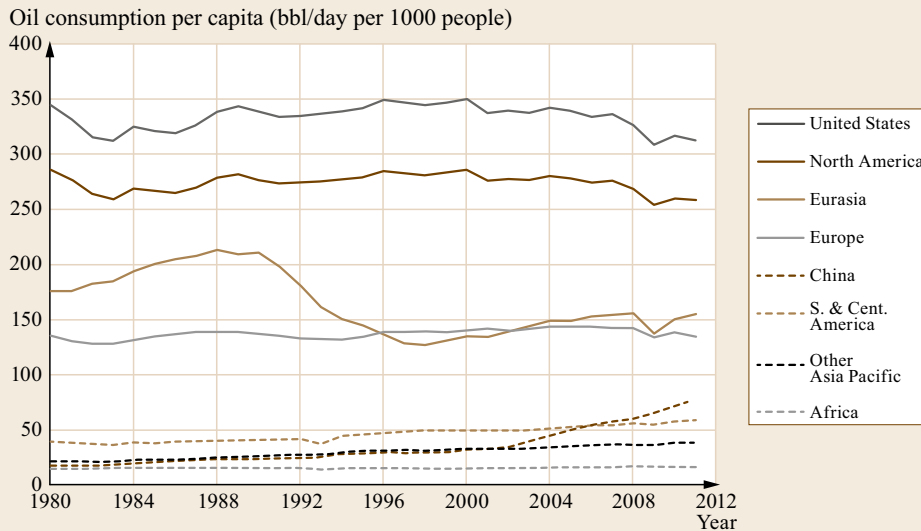


Fig. 1.6 Per capita energy consumption by region (after [1.1, 48])

and Europe since September 11, 2001, hitting a temporary low during the economic crisis of 2009. In Eurasia – in essence, the USSR until December 25, 1991 and the Former Soviet Union afterward – per capita consumption fell by 38% between 1989 and 1996, and then slowly increased to the present-day level, which is still 26% below 1989. In the rest of the world, per capita consumption has been increasing. It has increased by 262% in Asia and Oceania and by 148% in Central and South America, but only by 8% in Africa.

Figure 1.7 illustrates regional differences in present-day consumption of energy from different sources. Oil

and gas were important everywhere in 2013. Coal consumption varied considerably: from 4.3% in South and Central America to 52.3% in Asia-Pacific. In the European Union, 11.8% came from nuclear sources and 4.9% came from hydroelectric. In South and Central America, 0.7% came from nuclear and 23.5% came from hydroelectric.

As mentioned above, in recent years, fracking transformed the United States into the world's leading oil producer (Fig. 1.8). In 2015, the consequent increase in global supply dropped crude oil prices by more than 50%.

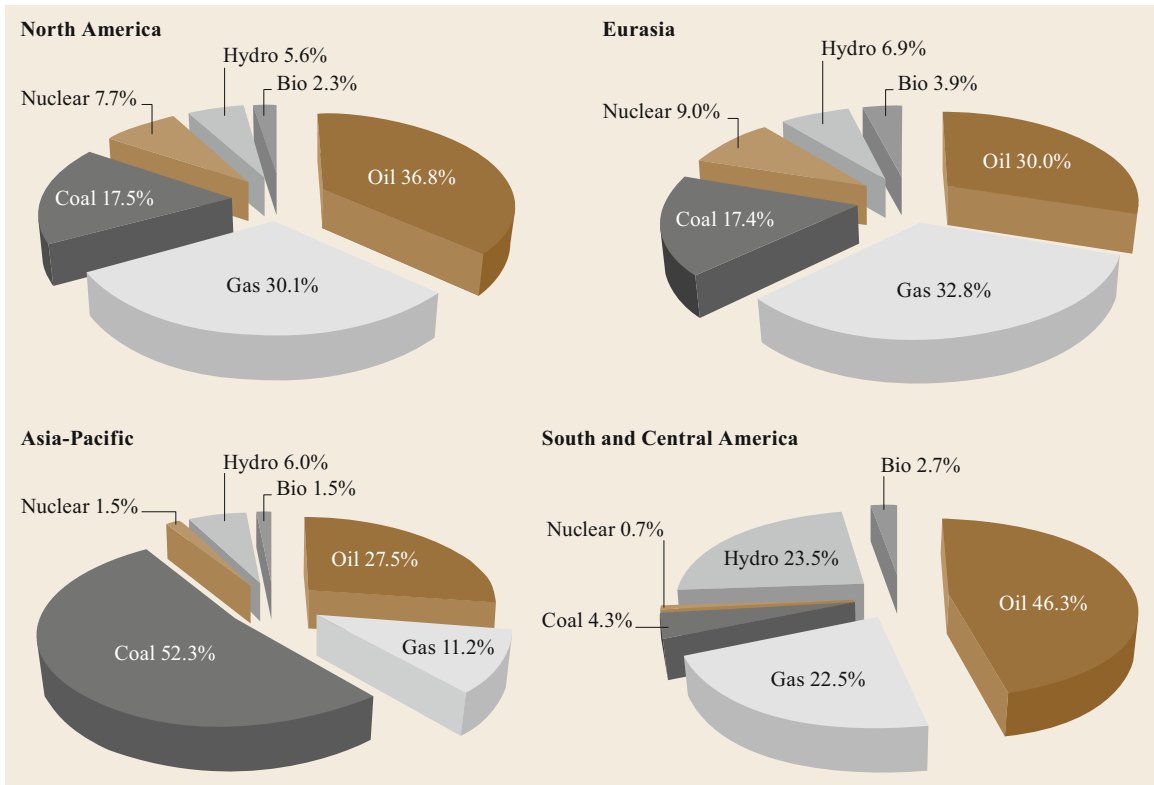


Fig. 1.7 Regional energy consumption by fuel in 2014 (after [1.1])

It is impossible to predict the future, but we're likely to see the following:

- Higher than world average economic growth is expected in the less developed regions of Asia, especially China and India.
- Production of frack oil and gas will continue, especially in the United States.
- If prices remain low, American oil and gas consumption will go up. Americans are already driving more than in recent years, due to abundant low-cost fuels; EIA expects average gasoline prices to reach the lowest level since 2004 [1.49]. In response to abundant low-cost frack gas, the US and non-US companies are investing in American petrochemical projects. Gas is replacing coal in electric power production plants, which is decreasing America's production of CO₂.
- Unforeseen events – political, financial, or technical – affect supply or demand in unexpected ways. Recent actions by the United States, which is both the world's largest producer and the world's largest consumer of oil, are especially significant. One such event occurred in December 2014, when the United States decided to allow several companies to export

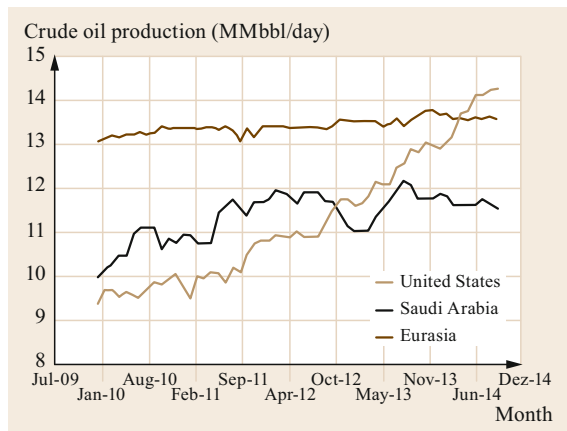


Fig. 1.8 Crude oil production during 2010–2014 by the United States, Saudi Arabia, and Eurasia (mostly Russia) (after [1.1, 2])

American crude oil beginning in August 2015; the ban had been in effect since 1973.

We can continue to generate pretty graphs and use them to extrapolate, but all we know for sure is that the landscape will change.

1.5 Origin of Fossil Hydrocarbons

Back in the eighteenth century, scientists concluded that coals were derived from plant remains (Chap. 10). Mikhailo Lomonosov gets credit for suggesting that petroleum and bitumen were produced underground from coal at high pressure and temperature. In the mid-nineteenth century, T.S. Hunt concluded that the organic matter in certain rocks comes from marine plants or animals.

In 1936, Alfred Treibs linked the chlorophyll in plants to the porphyrins in petroleum [1.50]. Even after millions of years, porphyrins and other biomarkers retain much of their original structures [1.51]. Biomarkers can be found in crude oil, rocks, sediments, and soil extracts. Figure 1.9 shows the resemblance between the core structure of chlorophyll *a* and porphyrins found in petroleum. The distribution of biomarkers can be correlated with the relative amounts of oil and gas in a source

rock, the age of a source rock, the environment in which organic matter was deposited, the maturity of a source rock, etc. Biomarker data are included in reservoir models of prospective oil fields.

Today, it is believed that petroleum is derived from ancient living microorganisms, such as plankton and algae, which escaped full oxidation upon death and accumulated at the bottoms of ancient lakes or seas, along with sand, clay, salts, and other material. Over time, tectonic movement, pressure, and heat transformed the deeply buried deposits into sedimentary rock through diagenesis and catagenesis. The origin of the organic matter, the depositional environment, age of the sedimentary deposit, and alteration (such as biodegradation) determined whether it became coal, kerogen (trapped in shale), bitumen, heavy oil, petroleum, or natural gas [1.52].

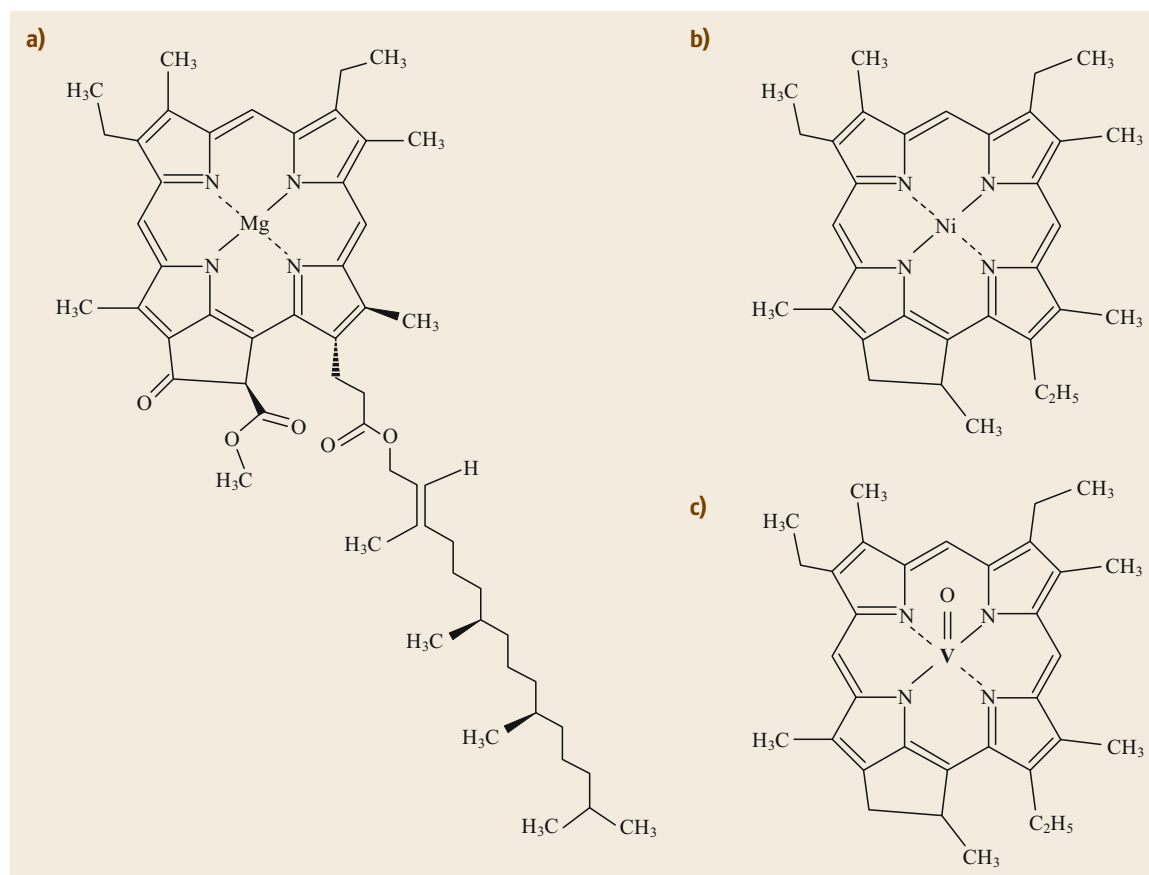


Fig. 1.9a–c Example of biomarkers: a comparison of chlorophyll *a* (a) with porphyrins found in petroleum (b,c)

1.6 Natural Gas, Coal, and Kerogen

Here we discuss natural gas, coal, and kerogen due to their impact on petroleum production and consumption. Crude oil reservoirs always contain some natural gas and vice versa, so oil and gas are coproduced. Like petroleum, natural gas and coal are major sources of energy and chemicals.

1.6.1 Natural Gas

Natural gas contains mostly methane (CH_4). It is called wet gas if it contains significant amounts of ethane, propane, butanes, pentanes, and heavier hydrocarbons, which can be separated from methane in natural gas processing plants. Dry gas includes only traces of higher hydrocarbons. Sour gas contains hydrogen sulfide, and acid gas contains carbon dioxide and/or hydrogen sulfide. Sour-gas-processing plants coproduce elemental sulfur, which is used to make sulfuric acid and fertilizers. According to industry reports [1.53], about 45–48% of world sulfur production comes from petroleum and natural gas. Natural gas can contain nitrogen and commercial quantities of inert gases – helium, neon and/or argon. Almost all commercial helium comes from natural gas plants [1.54].

Synthesis gas (syngas) is a mixture of carbon monoxide and hydrogen, usually derived from natural gas via steam-methane reforming (SMR) technology. Syngas can be converted into hydrogen and petrochemicals such as methanol. Worldwide, vast amounts of syngas-derived hydrogen are used to produce ammonia via the Haber–Bosch process.

1.6.2 Coal

Coal is a black or brown combustible rock composed mostly of carbon, hydrocarbons, oxygenates, and ash (metal oxides). Generally, coal is ranked as anthracite, bituminous, sub-bituminous, and lignite. Anthracite contains 86–97% carbon and has a high heating value. Anthracite is relatively rare. Bituminous coal is far more common. It contains 45–86% carbon and is burned to generate electricity. It is also extensively used in the steel and iron industries. Sub-bituminous coal, also called brown coal, contains 35–45% carbon. As shown in Sect. 1.1, coal is consumed on a large scale to produce heat, steam, and electricity.

Over the years, special circumstances have driven the large-scale conversion of coal into liquids, both directly and indirectly. Direct processes convert coal into various combinations of coal tar, oil, water vapor, gases, and char. The coal tar and oil can be refined into high-quality liquid fuels. Slurry-phase hydrocracking tech-

nology achieves very high direct conversion of coal into liquids; this technology was used extensively in Germany between 1934 and 1945 to make up for a lack of petroleum resources. Several coal conversion processes are described in a book by *James G. Speight* [1.55].

Developed in 1925, the Fischer–Tropsch (F–T) process is the main indirect route for converting coal into liquids. The coal is first gasified to make syngas with a balanced mixture of CO and hydrogen. Over F–T catalysts, syngas is converted into a full range of hydrocarbon products, including waxy paraffins, alcohols, naphtha, gas oils, and syncrude. The F–T process was used extensively in Germany before and during World War II.

In South Africa, the Sasol Slurry Phase Distillate Process (SPD) is the core of the gas-to-liquids (GTL) technology developed by Sasol. Synthesis gas for the SPD process can come from coal, natural gas or biomass. The process has been manufacturing chemicals and liquid fuels for more than 60 years.

1.6.3 Kerogen

Kerogen is the solid organic matter in sedimentary rocks. Unlike bitumen, it does not flow even when heated. But at high enough temperatures – e.g., 900 °F (480 °C) – it decomposes into gases, liquids, bitumen, and refractory coke. Huge amounts of kerogen are trapped in oil shale deposits. *Fenton et al.* [1.8] estimated that 1.3 trillion barrels of shale oil could be recovered from the world's oil shale reserves. Table 1.4 presents composition information on Green River oil shale from the western United States. About 91% of

Table 1.4 Typical composition of green river oil shale

Kerogen content: 15 wt% ^a	
Kerogen composition (wt%)	
Carbon	80.5
Hydrogen	10.3
Nitrogen	2.4
Sulfur	1
Oxygen	5.8
Total	100
Minerals (wt%)	
Carbonates	48
Feldspars	21
Quartz	15
Clays	13
Analcite and pyrite	3
Total	100
^a Equivalent to 25 gal oil per ton of rock	

the kerogen is hydrogen and carbon, but only 15% of the sample is kerogen. Shale oil – synthetic crude from thermally treated oil shale – tends to contain high amounts of arsenic and mercury, severe poisons for refinery catalysts and human health. Usually, the arsenic is removed with special high-nickel chemisorption catalysts, which trap the arsenic by forming nickel arsenides. Chemisorption is the most effective technique to remove mercury from oil and gas. The absorbent is comprised of a support (zeolite, activated carbon, metal oxide, or alumina) and one or more reactants (sulfur, metal sulfide, or iodide) [1.56].

1.6.4 Heavy Oil and Bitumen

As is often the case in the petroleum industry, the definitions of heavy oil and bitumen are functional and fuzzy. Heavy oils flow under most ambient conditions. They have densities greater than 1.0, so they sink in water. The viscosities of heavy oils range from about 5000 to 10 000 cP. Bitumens also have densities greater than 1.0, but their viscosities are higher: > 10 000 cP.

Natural bitumen is a tar or a solid, but when heated it softens and flows. Bitumen accounts for much of the world's recoverable oil. Large deposits are found in Venezuela, where in 2015, proven oil reserves totaled 298 billion barrels, mostly bitumen. Oil sands deposits in Alberta, Canada, contain 170 billion barrels. In addition, Alberta holds 1.4 billion barrels of conventional crude oil [1.57]. In oil sands, bitumen is

associated with sand and clay, from which it can be recovered with hot water or steam. In the United States, tar sands are found primarily in Eastern Utah, mostly on public lands. In comparison, reserves of conventional crude oil in the Middle East were 808 billion barrels [1.58].

For oil sand, froth treatment is applied to recover bitumen. In the froth treatment process, aqueous and solid contaminants are removed from the froth, which is diluted by a hydrocarbon solvent to reduce the viscosity and density of the oil phase. The solvent accelerates the settling of the dispersed phase by gravity or centrifugation. The solvent is recovered and recycled. The bitumen is mixed with light crude oil to form diluted bitumen, or *dilbit*, which flows more easily through pipelines to upgraders or refineries. There, the bitumen is converted into syncrude by means of a coker or a visbreaking unit, or in some cases a hydrotreater. A newer froth treatment developed in 1990 uses a paraffinic solvent to form aggregates composed of water droplets, mineral solid particles, and asphaltene precipitates for easy separation by conventional settlers with less energy [1.59]. In petroleum refineries, heavy oil and bitumen are blended with conventional petroleum crude oil and co-processed.

It is important at this point to distinguish between natural bitumen and refined bitumen. Refined bitumens are primarily used for paving and construction. They are special products with rather tight specifications.

1.7 Petroleum (Crude Oil)

There are hundreds of different crude oils with significantly different compositions. Crudes typically are named for their source country, reservoir, and/or some distinguishing physical or chemical property.

Day-to-day refineries base operations on:

1. Feed bulk properties, such as total acid number (TAN), total sulfur, specific gravity, distillation, and sometimes total nitrogen
2. Desired product properties
3. Analysis of waste streams.

Traders rely on crude assays to make buying/selling decisions.

Central laboratories pay attention to molecules. The identification of biomarkers is important for oil exploration. The development of processes and catalysts depends on in-depth knowledge of functional groups.

1.7.1 Bulk Physical Properties

Bulk properties are summarized in crude oil assay reports. Table 1.5 shows an example assay report template. The assays determine selected chemical and physical properties of whole crudes and several distilled fractions. The fractions correspond to boiling ranges for common fuels. Planners and oil traders select crudes by comparing their properties with refinery specifications. Sulfur content and TAN are common constraints, because they relate to corrosion in piping and process equipment. Traders might purchase off-spec crudes for subsequent trading.

Table 1.6 presents selected bulk physical and chemical properties for 21 crude oils. Athabasca is a heavy oil, with a specific gravity > 1.0. In the table, sulfur contents range from 0.14 to 5.3 wt%, and nitrogen contents range from nil to 0.81 wt%. Specific gravities range from 0.798 to 1.014. In sweet crudes

Table 1.5 Example crude assay report template (after [1.60])

	Whole crude	Light Naphtha	Medium Naphtha	Heavy Naphtha	Kero	AGO	LVGO	HVGO	VR	AR
True boiling point (°C)	Initial	10	80	150	200	260	340	450	570	340
True boiling point (°C)	Final	80	150	200	260	340	450	570	End	End
True boiling point (°F)	Initial	55	175	300	400	500	650	850	1050	650
True boiling point (°F)	Final	175	300	400	500	650	850	1050		
Yield of cut (wt% of crude)		✓	✓	✓	✓	✓	✓	✓	✓	✓
Yield of cut (vol.% of crude)		✓	✓	✓	✓	✓	✓	✓	✓	✓
Gravity (API)	✓	✓	✓	✓	✓	✓	✓	✓	✓	✓
Specific gravity	✓	✓	✓	✓	✓	✓	✓	✓	✓	✓
Sulfur (wt%)	✓	✓	✓	✓	✓	✓	✓	✓	✓	✓
Nitrogen (ppm)	✓		✓	✓	✓	✓	✓	✓	✓	✓
Viscosity at 50 °C (122 °F) (cSt)	✓			✓	✓	✓	✓	✓	✓	✓
Viscosity 135 °C (275 °F) (cSt)	✓			✓	✓	✓	✓	✓	✓	✓
Freeze point (°C)				✓	✓	✓	✓			
Freeze point (°F)				✓	✓	✓	✓			
Pour point (°C)	✓			✓	✓	✓	✓	✓	✓	✓
Pour point (°F)	✓			✓	✓	✓	✓	✓	✓	✓
Smoke point (mm)				✓	✓	✓				
Aniline point (°C)			✓	✓	✓	✓	✓	✓		
Aniline point (°F)			✓	✓	✓	✓	✓	✓		
Cetane index, ASTM D976				✓	✓	✓	✓	✓		
Diesel index		✓	✓	✓	✓	✓	✓	✓	✓	✓
Characterization factor (K)	✓	✓	✓	✓						
Research octane number, clear		✓	✓	✓						
Motor octane number, clear		✓	✓	✓						
Paraffins (vol.%)		✓	✓	✓	✓	✓	✓			
Naphthenes (vol.%)		✓	✓	✓	✓	✓	✓	✓		
Aromatics (vol.%)		✓	✓	✓	✓	✓	✓	✓		
Heptane asphaltenes (wt%)	✓								✓	✓
Micro carbon residue (wt%)	✓								✓	✓
Ramsbottom carbon (wt%)	✓								✓	✓
Vanadium (ppm)	✓								✓	✓
Nickel (ppm)	✓								✓	✓
Iron (ppm)	✓								✓	✓

Kero = kerosene, AGO = atmospheric gas oil, LVGO = light vacuum gas oil, HVGO = heavy vacuum gas oil, VR = vacuum residue, AR = atmospheric residue

such as Tapis, the sulfur content is low. Sour crudes have more sulfur, which gives them a tart taste; in the old days, prospectors did indeed characterize crude oil by tasting it.

Table 1.7 shows distillation yields for four common crudes. The naphtha content of Brent is twice as high as Ratawi, and its vacuum residue content is 60% lower. Bonny light yields the most middle distillate and the least amount of vacuum residue.

Crude assay fractions are defined primarily by distillation cutpoints. In commercial practice, cutpoints are not uniform or sharp, and product cutpoints can overlap (Fig. 1.10).

A refiner can adjust distillation yields to meet market demands, in part, just by adjusting cutpoints as shown in Table 1.8. Note that naphtha is not gasoline, kerosene is not jet fuel, and gas oil is not diesel unless they meet the tight specifications discussed below.

Table 1.6 Bulk properties of 21 natural crude oils (after [1.61])

Crude oil	API gravity ^a	Specific gravity	Sulfur (wt%)	Nitrogen (wt%)
Alaska north slope	26.2	0.8973	1.1	0.2
Arabian light	33.8	0.8560	1.8	0.07
Arabian medium	30.4	0.8740	2.6	0.09
Arabian heavy	28.0	0.8871	2.8	0.15
Athabasca (Canada)	8.0	1.0143	4.8	0.4
Beta (California)	16.2	0.9580	3.6	0.81
Brent (North Sea)	38.3	0.8333	0.37	0.10
Bonny light (Nigeria)	35.4	0.8478	0.14	0.10
Boscan (Venezuela)	10.2	0.9986	5.3	0.65
Ekofisk (Norway)	37.7	0.8363	0.25	0.10
Henan (China)	16.4	0.9567	0.32	0.74
Hondo blend (California)	20.8	0.9291	4.3	0.62
Kern (California)	13.6	0.9752	1.1	0.7
Kuwait export	31.4	0.8686	2.5	0.21
Liaohi (China)	17.9	0.9471	0.26	0.41
Maya (Mexico)	22.2	0.9206	3.4	0.32
Shengli (China)	13.8	0.9738	0.82	0.72
Tapis blend (Malaysia)	45.9	0.7976	0.03	nil
West hackberry sweet ^b	37.3	0.8383	0.32	0.10
West Texas intermediate	39.6	0.8270	0.34	0.08
Xinjiang (China)	20.5	0.9309	0.15	0.35

^a API gravity is related to specific gravity by the formula: $^{\circ}\text{API} = 141.5 / (\text{specific gravity at } 60^{\circ}\text{F} - 131.5)$

^b Produced from a storage cavern in the US strategic petroleum reserve

Table 1.7 Distillation yields for four selected crude oils. VGO = vacuum gas oil

Source field (Country)	Brent (Norway)	Bonny light (Nigeria)	Green canyon (USA)	Ratawi (Mid East)
API gravity	38.3	35.4	30.1	24.6
Specific gravity	0.8333	0.8478	0.8752	0.9065
Sulfur, wt%	0.37	0.14	2.00	3.90
Yields (wt% feed)				
Light ends	2.3	1.5	1.5	1.1
Light naphtha	6.3	3.9	2.8	2.8
Medium naphtha	14.4	14.4	8.5	8.0
Heavy naphtha	9.4	9.4	5.6	5.0
Kerosene	9.9	12.5	8.5	7.4
Atmospheric gas oil	15.1	21.6	14.1	10.6
Light VGO	17.6	20.7	18.3	17.2
Heavy VGO	12.7	10.5	14.6	15.0
Vacuum residue	12.3	5.5	26.1	32.9
Total naphtha	30.1	27.7	16.9	15.8
Total middle distillate	25.0	34.1	22.6	18.0
Naphtha plus distillate	55.1	61.8	39.5	33.8

Table 1.8 Optimizing product yields with cutpoint adjustment

	Max naphtha	Max kerosene	Max gas oil
Naphtha cutpoints (°C)	85–204	85–150	85–170
Kerosene cutpoints (°C)	No kero	150–274	No kero
Gas oil cutpoints (°C)	204–400	274–400	170–400

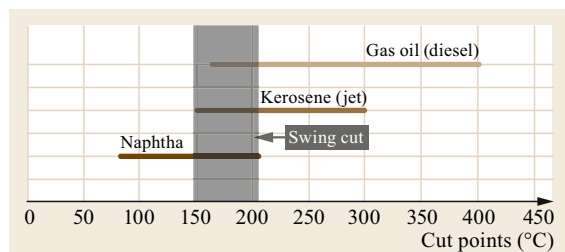
**Fig. 1.10** Distillation overlap for naphtha, kerosene, and gas oil. The swing cut from 150 to 205 °C can be blended into gasoline, kerosene, or gas oil

Table 1.9 leads to the next section on molecular composition. The table presents normal boiling points for selected pure compounds, illustrating how boiling point reduction can be due to hydrogen-consuming reactions that do not break C–C bonds. Such reactions include saturation of aromatics, hydrodesulfurization (HDS), and hydrodenitrogenation (HDN). The table also illustrates how changes in commercial cutpoints can include or exclude certain molecules. The boiling points of compounds in blends are not the same as their normal boiling points, and the compounds shown in the table comprise only a tiny percentage of the thousands of molecules in petroleum distillates.

In reaction 1, the desulfurization of 2-methylthiophene converts a gas oil contaminant into light naphtha. In reaction 5, the desulfurization of 4,6-dimethyldibenzothiohene, a heavy gas oil contaminant, gives dimethyl cyclohexyl benzene, a light-diesel or heavy-kerosene molecule. Total saturation of phenanthrene (reactions 9–12) yields a molecule that boils at 274 °C (525 °F).

Table 1.9 Boiling point reduction without breaking C–C bonds (after [1.62]). For comparison, Reactions 17 and 18 illustrate the greater extent of boiling point reduction by hydrocracking. For many compounds, normal boiling points cannot be measured experimentally. In such cases, boiling points were estimated with ACD lab correlations. HDS = hydrodesulfurization, ASAT = aromatics saturation, HC = hydrocracking

	Reaction	Formula	MW	Boiling point		Reaction type	Feed → Prod
				(°C)	(°F)		
1	Thiophene, 2-methyl → <i>n</i> -Pentane	C ₅ H ₆ S C ₅ H ₁₀	98.17 70.13	113 36	235 97	HDS	Gas oil → Naphtha
2	Benzo[<i>b</i>]thiophene → Ethylbenzene	C ₈ H ₆ S C ₈ H ₁₀	134.198 106.17	221 136	430 277	HDS	Gas oil → Naphtha
3	Dibenzothiophene →	C ₁₂ H ₈ S	184.26	333	631	HDS	Gas oil →
4	Dibenzothiophene, 1,2,3,4-tetrahydro → 1,1'-Bibylhexyl	C ₁₂ H ₁₂ S C ₁₂ H ₂₂	188.29 166.30	325 235	616 455		Gas oil Gas oil
5	Dimethyldibenzothiophene, 4,6- → Benzene, 1-methyl-3-(3-methyl cyclohexyl)	C ₁₄ H ₁₂ S C ₁₄ H ₂₀	212.31 188.31	365 273	689 524	HDS	Heavy gas oil → Gas oil
6	Quinoline → Benzene, <i>n</i> -propyl	C ₉ H ₇ N C ₉ H ₁₂	129.16 120.19	238 159	460 318	HDN	Gas oil → Naphtha
7	Naphthalene →	C ₉ H ₇ N	128.17	217	422	ASAT	Gas oil →
8	Tetralin → Decalin, <i>trans</i>	C ₁₀ H ₁₂ C ₁₀ H ₁₈	132.20 138.25	208 187	406 368		Naphtha → Naphtha
9	Phenanthrene →	C ₁₄ H ₁₀	178.23	336	637	ASAT	Gas oil
10	Phenanthrene, 9,10-dihydro →	C ₁₄ H ₁₂	180.25	315	598		
11	Phenanthrene, 1,2,3,4-,tetrahydro →	C ₁₄ H ₁₄	182.26	324	615		
12	Phenanthrene, octahydro → Phenanthrene, tetradecahydro	C ₁₄ H ₁₈ C ₁₄ H ₂₄	186.29 192.34	295 274	563 525		
13	Chrysene →	C ₁₈ H ₁₂	228.29	448	838	ASAT	VGO →
14	Chrysene, dihydro →	C ₁₈ H ₁₄	230.30	420	788		
15	Chrysene, 1,2,3,4,7,12-hexahydro →	C ₁₈ H ₁₈	234.34	369	696		Gas oil →
16	Chrysene, dodecahydro → Chrysene, perhydro	C ₁₈ H ₂₄ C ₁₈ H ₃₀	240.38 246.43	371 353	700 667		Gas oil → Gas oil
17	Tetraconane →	C ₂₄ H ₅₀	338.65	391	736	HC	Heavy gas oil →
18	<i>n</i> -Dodecane → <i>n</i> -Hexane	C ₁₂ H ₂₆ C ₆ H ₁₄	170.33 86.18	216 69	421 156		Gas oil → Naphtha

Total hydrogenation of chrysene transforms a residue molecule into diesel molecules (reactions 13–16). For comparison, Reactions 17 and 18 illustrate boiling point reduction by breaking C–C bonds via hydrocracking. Note that hydrocracking reduces boiling point to a far greater extent than do the other reactions.

Heavy naphtha goes to catalytic reforming, which generates aromatics and gasoline. The benzene content of gasoline is tightly controlled. The typical cutpoint between light naphtha and heavy naphtha is 180 °F (82 °C). This separates benzene and benzene precursors from C₇–C₁₁ compounds, keeping benzene out of gasoline. It also allows refiners to produce C₆ chemicals.

A typical heavy-naphtha/middle-distillate cutpoint is 400 °F (204 °C). This particular cutpoint improves gasoline by excluding naphthalene and tetralin, which have very low octane numbers. To maximize diesel, the cutpoint is lowered, perhaps to 302 °F (150 °C). For kerosene, limiting the upper boiling point to 525 °F (273 °C) excludes saturated 3-ring compounds, the presence of which would make it impossible to meet smoke-point specifications.

Diesel/VGO cutpoints depend on cold-flow properties, which are described in a subsequent section. Cutting at 650 °F (343 °C) keeps fully saturated 4-ring compounds out of diesel.

1.7.2 Molecular Composition

Prior to refining, crude oils contain some amount of dissolved gas, water, inorganic salts, and dirt. After these are removed, most of the remaining compounds are hydrocarbons, organic compounds which contain heteroatoms – sulfur, oxygen and nitrogen, or trace elements (Ni, V, Fe, Cu, As, Hg, etc.) – and inorganics such as H₂S and inorganic sulfur.

The hydrocarbon content may be as high as 97 wt% in paraffinic crude oil and as low as 50 wt% in heavy/asphaltic crude oil and bitumen. Nonhydrocarbons have characteristics of hydrocarbons with one or two heteroatoms. They are concentrated in higher boiling fractions and residua. More than any other element, carbon binds to itself to form straight chains, branched chains, rings, and complex three-dimensional structures. The most complex molecules are biological – proteins, carbohydrates, fats, and nucleic acids. This is significant, because petroleum was formed from the remains of ancient microorganisms – primarily plankton and algae.

In addition to normal- and isoparaffins (alkanes), petroleum contains a large number of mono- and poly-ring hydrocarbons, which may be saturated (naphthenes) or unsaturated (aromatics). Paraffin chains can

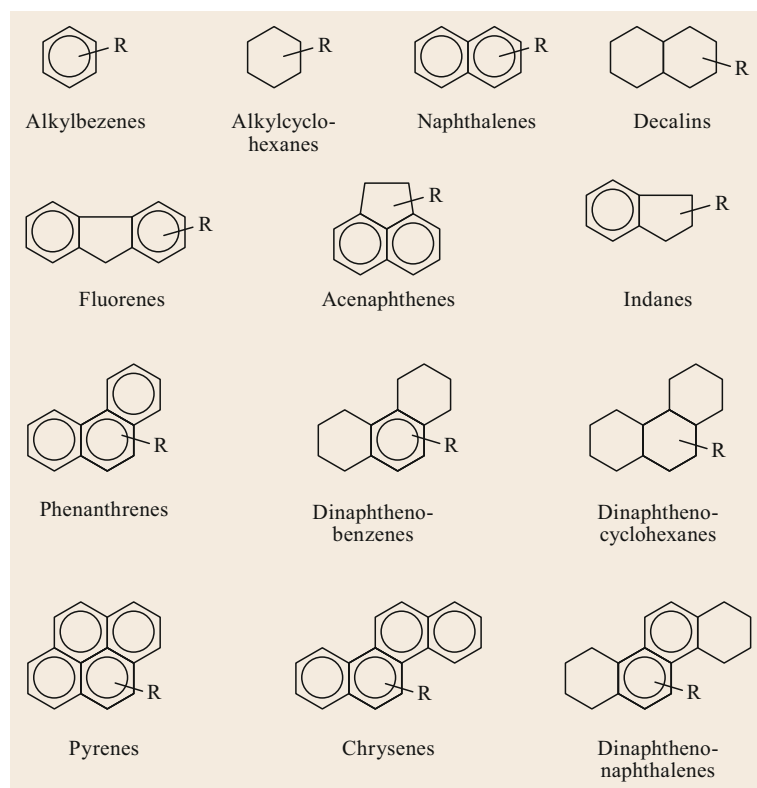


Fig. 1.11 Selected examples of hydrocarbon ring compounds

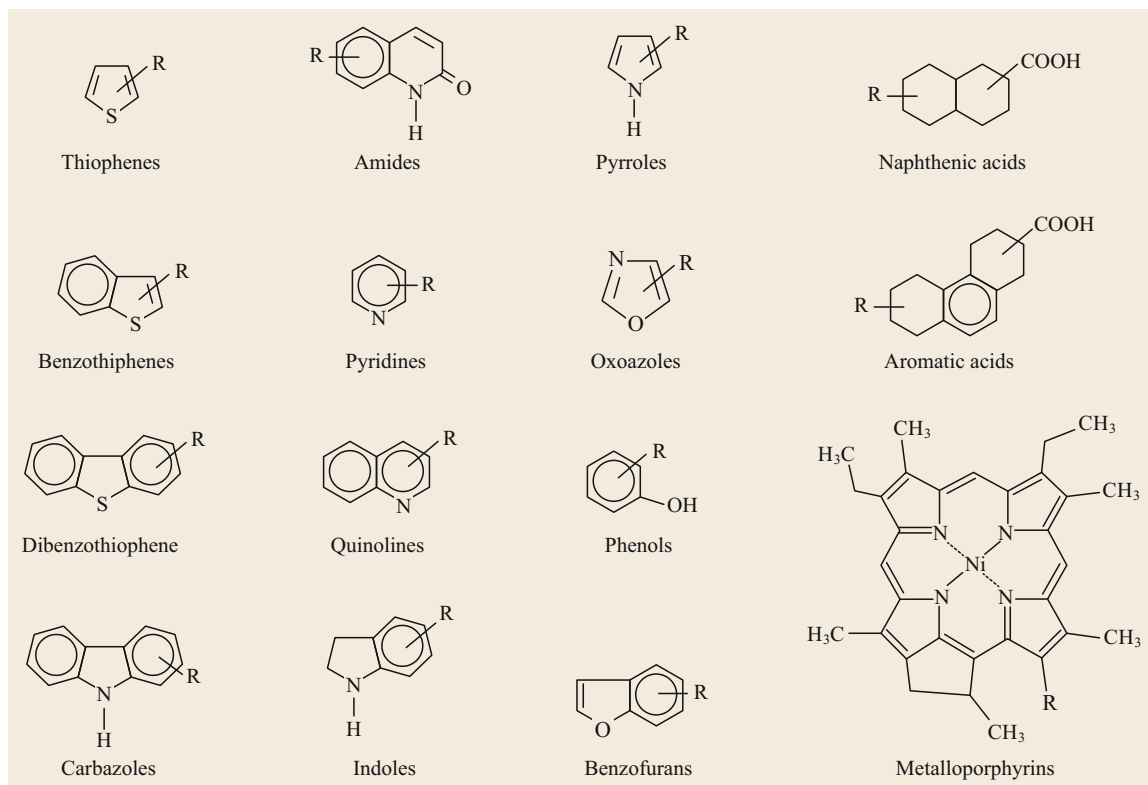


Fig. 1.12 Selected examples of ring compounds containing heteroatoms

be attached to the rings as substituents, as shown in Fig. 1.11. The long alkyl chains tend to be branched. Organic compounds containing sulfur, nitrogen, oxygen, and trace metals are illustrated in Fig. 1.12. Other sulfur compounds are naphthenic mercaptans (thiols), aliphatic sulfides and disulfides. The

R groups in the figures represent short or long alkyl chains.

Petroleum molecules can be lumped into groups, thereby allowing us to create manageable models for physical properties, chemical composition and reaction kinetics.

1.8 Oil and Gas Exploration

We search for oil and gas by looking for places where they might be trapped underground. Petroleum systems include the following:

- Organic-rich source rock in which oil and gas were formed.
- Pathways comprised of permeable rock such as sandstone and limestone, which allow oil and gas to migrate (secondary migration). Often, the movement of oil and gas is promoted by the flow of underground water.
- Porous, permeable reservoir rock to accumulate gas and oil capped by impermeable rock, which prevents fluids from migrating to the surface. Shale and salt domes are also common caps.

1.8.1 Searching for Traps

When petroleum geologists look for oil and gas, they rely heavily on reflection seismology. During seismic exploration, explosives or thumper devices send sound waves through the Earth's surface. Reflected sound waves are measured with hydrophones (in water) and geophones (on land). Different layers within different rock formations reflect sound in different ways. With the help of sophisticated software, geophysicists transform seismic data into detailed 3-D reservoir models that show the structure of subsurface rock formations. Measure-while-drilling (MWD) technology incorporates sound waves generated by drill bits to refine reservoir models as wells are being drilled.

Three common kinds of traps are illustrated in Fig. 1.13:

1. Anticline traps are like inverted bowls. They can be symmetrical or asymmetrical. A steep anticline

might be called a dome. Anticline traps hold much of the world's conventional crude oil.

2. Faults are formed at the boundaries of cracks in the Earth's crust. The four major kinds of faults are thrust, lateral, normal, and reverse. Thrust and lateral

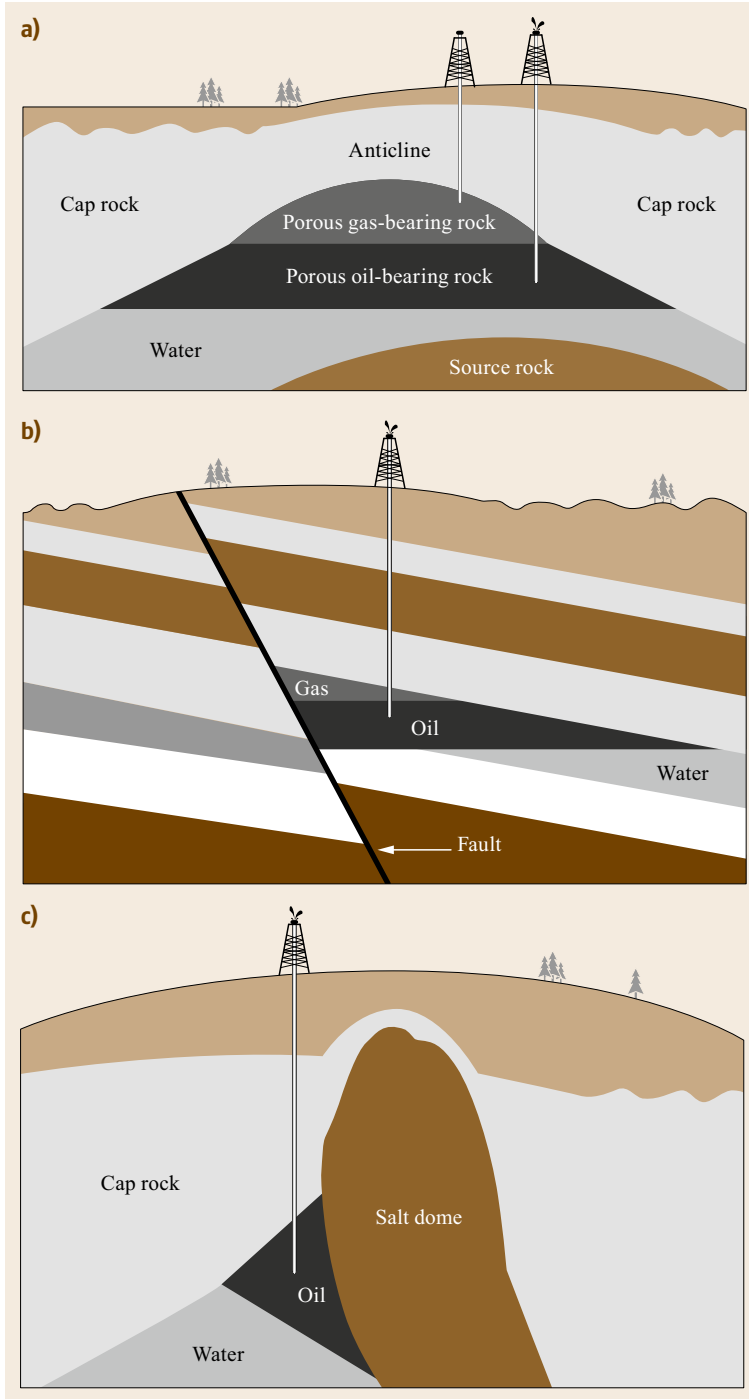


Fig. 1.13a-c Three types of hydrocarbon traps: anticline (a), fault (b), and salt-dome (c). As with oil and gas, the water layers are not pools, but water-saturated porous rock

faults are created by horizontal movement. The San Andreas Fault in California is a well-known example of a lateral fault. To be more specific, the San Andreas is a right-lateral, strike-slip fault. Normal and reverse faults are created by vertical movement and are more likely to create fault traps for petroleum.

3. A salt-dome trap is created when a mass of underground salt is pushed up by underground pressure into a dome. The salt dome breaks through layers of rock and pushes them aside as it rises. The salt is impermeable, and if it abuts porous rock, it can serve as a reservoir cap.

1.9 Drilling and Production (Recovery)

1.9.1 Drilling

Drilling is the primary method for recovering underground oil. Oil sand can be surface mined, and bitumen can be recovered by techniques such as SAGD [1.63].

The rotary drilling technique is commonly used. Key components of a rotary drilling rig are shown in Fig. 1.14. To drill a well, a bit is attached to the end of a drill string, which is built from sections of steel pipe that are 30 ft (9 m) long. The drill string is lengthened as the well gets deeper by attaching additional sections of pipe to the top. Drill collars are thick-walled sections of drill pipe at the bottom of the drill string; collars apply extra weight to the bit. As the bit cuts through rock,

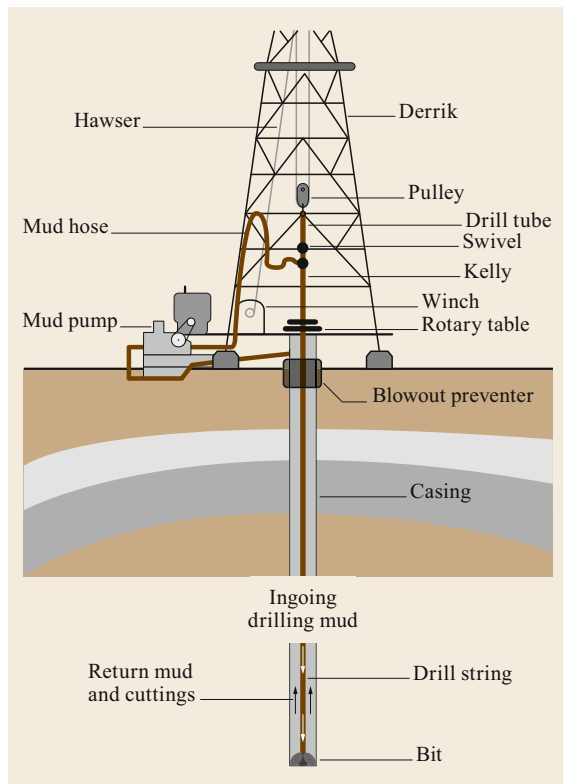


Fig. 1.14 Components of a typical drilling operation (after [1.64]). See also Fig. 13.1

mud is pumped down through the inside of the drill string, out the bit, and up through the annular space between the drill string and the well bore. Despite its dirty name, drilling mud is a specific blend of fluids, solids, and chemicals. It cools the drill bit and brings rock cuttings back to the surface. The cuttings are removed in shakers, and the fluid goes back to the mud pit, from which it is recycled.

The derrick must be tall enough to accommodate a 90 ft-long *triple* comprised of three pipe sections. The derrick, pulleys, and hawser must be robust enough to support the lifting and manipulation of the entire drill string. The kelly is the top joint of a drill string. It has flat sides that fit inside a bushing on the rotary table, which turns the drill string and bit. Note that not all drilling rigs use a kelly system.

In addition to vertical drilling, directional (horizontal) drilling can be used. First applied in 1934, directional technology allows many wells to be drilled from a single site. The technology can be applied all along the formation and is especially beneficial offshore, because it reduces the number of expensive platforms needed to develop large fields. In directional drilling, the section of pipe at the end of the drill string is bent, so that when the pipe is rotated, it moves to one side.

In percussion drilling, a drill bit is repeatedly raised and lowered, impacting rock on the down stroke, making a hole deeper. As with rotary drilling, circulating mud removes cuttings and cools the bit. Percussion drilling was used thousands of years ago in China.

Thanks to recent developments, offshore platforms do not have to be anchored to the ocean floor. Floating and semisubmersible platforms are kept in place with a combination of GPS and turbine-driven engines [1.65].

1.9.2 Blowouts

Blowouts are a common cause of well failures [1.66]. On April 20, 2010, the Macondo blowout, also known as the *Deepwater Horizon* disaster, killed 11 people and caused the largest accidental oil spill into the sea, spewing 210 million gallons into the Gulf of Mexico from April 20, 2010 until July 10, 2010. On land, the Iraqi soldiers intentionally released or burned 240 to 340 mil-

lion gallons during the 1991 Gulf War. The largest oil spill ever recorded was caused by the Lakeview blowout in Kern County, California. Lakeview gushed for 18 months – from March 1910 through September 1911 – spilling 380 million gallons onto the ground.

A *surface blowout* is a sudden loss of containment and uncontrolled flow of oil and gas into the atmosphere. The density of drilling mud is crucial. If the mud density is too low, a well is susceptible to a surface blowout. If the mud density is too high, it can cause an *underground blowout* – the rupture of the reservoir underground – which pushes drilling mud into another formation. Many surface blowouts begin as underground blowouts. Prompt, correct reaction to an underground event can prevent a dangerous and costly surface blowout.

Blowout prevention technology is a combination of procedures, hardware, monitoring, and control systems. The hardware includes *blowout preventers* (BOPs), which are stacks of valves that can be opened or closed to quickly reduce or stop sudden changes in pressure in oil and gas wells. BOPs are also called *preventers* or *preventer stacks*. The valves are stacked to provide redundancy. The sudden changes are called *kicks* and may signal impending loss of well control. BOPs on land wells are installed on the well head. On offshore rigs, they are often installed below the deck of the rig. Subsea BOPs are installed on the sea floor.

The two most common types of BOPs are *ram* and *annular*. Ram-type BOPs are similar in operation to gate valves. Common ram preventers are *pipe rams*, *sealing rams*, and *shear rams*. A BOP stack may include all three. Pipe rams restrict flow through the annular space between the well bore and the pipe but not through the pipe. Sealing rams can stop flow through both the annulus and the piping. Shear rams are used as a last resort. They compress the drill string and casing completely, sealing the well permanently. Rams can be actuated manually or hydraulically. An annular BOP operates like a wedge. It has a donut-like rubber seal, called the *packing*, which is reinforced with steel ribs. When actuated, a piston forces the packing to constrict like a sphincter, sealing the annulus and/or piping.

1.9.3 Well Completion

Wells are completed by casing the well bore with steel pipe and cementing the casing into place. Casing prevents the well from collapsing. The outside diameters of casing pipe range from 4.5 to 16 in (114–406 mm). Cementing is a key step. In a good cement job, the entire space between the casing and the well bore is filled with cement. Centralizers keep the casing from resting against the well bore and blocking the flow of cement to

the well bore below. In a poor cement job, cementing is incomplete or the cement itself is inadequate. Industry acquaintances say that poor cement jobs are the leading cause of post-completion blowouts. In open-hole completion, the last section of the well is uncased. Instead, the installation of a gravel pack stabilizes the casing and allows fluids to enter the well at the bottom. After cementing, perforation guns punch small holes through the casing and cement into the reservoir rock, providing a path for the flow of oil and gas into the well. After perforation, special acid-containing fluids are pumped into the well to increase porosity and stimulate production. Usually, a smaller diameter tube is inserted into the casing above the production zone and packed into place. This provides an additional barrier to hydrocarbon leaks, raises the velocity at which oil flows under a given pressure, and shields the outer casing from corrosive well fluids.

1.9.4 Production (Recovery)

In primary recovery, petroleum gas and/or oil flow out of reservoir due to reservoir pressure alone, propelled by gas and/or water drive. In gas drive, the drive comes from the excessive underground pressure of natural gas, dissolved gas evolving from oil, as well as liquid expansion. In water drive, oil is driven from the reservoir by hydrostatic pressure. Primary production often includes reinjection of recovered gas to maintain reservoir pressure. In the early days of the industry, operators believed that gas flow inhibited oil flow, so excess gas was flared. In addition to destroying valuable hydrocarbons and polluting the air, flaring substantially decreased the recoverability of oil in the reservoir.

Secondary recovery is applied when the natural pressure is low and not sufficient for primary recovery. Many older *stripper* wells require secondary recovery. Stimulation fluids are injected to push oil through the reservoir and disengage it from reservoir sands. Treated water is the most common stimulation fluid in secondary recovery. As mentioned in Sect. 1.6.1, the crude oil in a reservoir accumulates in permeable strata known as reservoir rock. For oil with higher viscosity, which adheres tightly to the rock, simple surfactants are added to the treatment water to free up the oil as tertiary recovery.

Figure 1.15 illustrates the use of an injection well to stimulate production with either secondary or tertiary treatment. Pumps located either above ground or submersed are used to pump the stimulation fluids.

For very viscous crude oil and impermeable carbonate reservoir rock, secondary recovery is not effective. Tertiary recovery, or enhanced oil recovery, is applied to reduce the viscosity of oil. The commonly used meth-

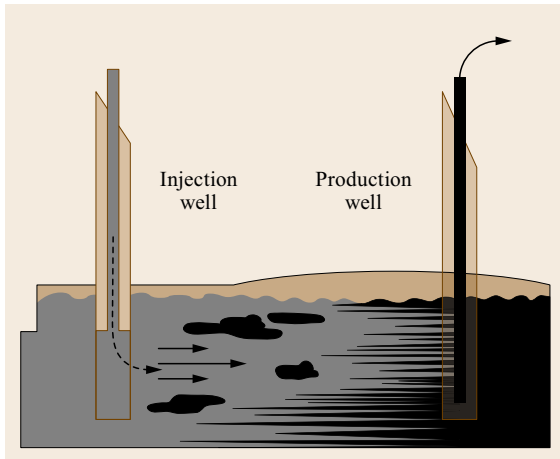


Fig. 1.15 Injection and production wells

ods are polymer-augmented flooding, surfactant flooding, and alkaline flooding. In these methods, chemicals are injected in the injection well and oil is recovered in the production well (Fig. 1.15). The most extensively used polymers in polymer augmented flooding are partially hydrolyzed polyacrylamines and a biopolymer, xanthan gum. Two steps are usually involved in surfactant flooding, or micellar flooding. A surfactant slug is injected into the well first followed by a large slug of water containing high molecular weight polymer, which pushes chemicals between the injection and production wells to improve mobility and sweep efficiency. Alkaline flooding is usually accompanied by surfactant and polymer flooding. Carbon dioxide has also been used in enhanced oil recovery. The injection of CO_2 is an effective way of achieving carbon capture and storage (CCS) for CO_2 sequestration. CO_2 stimulation and CCS are especially compatible with coal-bed methane production. When evaluating CCS for a particular application, CO_2 transportation and storage costs must be considered.

Production of bitumen is accomplished in several ways. It can be dug out with conventional mining techniques or liquefied by the injection of high-pressure steam. In so-called *huff and puff* operations, production is stopped, either naturally or on purpose. Hot steam is injected into the reservoir and left to soak, usually for a few days. During the soak, heat flows from the steam into the oil and surrounding rock, vaporizing hydrocarbons and increasing reservoir pressure. After the soak, the well is reopened and oil production resumes, at first by natural flow and then by artificial lift. Production decreases over time as the temperature and pressure of the reservoir go down. When the flow of oil drops below a certain limit, the process is repeated.

At surface facilities, notably in Venezuela and Canada, recovered bitumen is diluted with lighter

hydrocarbons. The resulting *Dilbit* (diluted bitumen) flows under ambient conditions, so it can be transported conventionally in pipelines and oil tankers.

Kerogen is recovered from oil shale by several methods. From 1985 to 1990, Unocal recovered some 4.6 million barrels of syncrude oil from oil shale in a complex mining and upgrading venture at Parachute Creek, CO [1.67]. The plant yielded roughly 40 gal of oil per ton of rock. In the vertical-shaft retort, crushed kerogen-containing shale was pumped up from the bottom of the retort vessel. Hot recycle gas flowed counter-currently downward, decomposing the rock and releasing hydrocarbons. Condensed shale oil was removed from the retort at the bottom. Part of the hot gas was recycled. The rest of the gas either was used to produce heat and hydrogen, or recovered as a product. The spent shale was removed from the top of the retort, cooled, and stored in pits or returned to the mine. In the reducing environment of the retort, sulfur and nitrogen were converted to H_2S and NH_3 , which were recovered from product gases by conventional means. The plant yielded high-quality syncrude oil suitable for further refining in conventional facilities.

Other oil shale processes involve partial combustion, either underground, at the surface, or in shafts drilled horizontally into kerogen-rich formations. From 1972 to 1991, Occidental Petroleum developed an in situ process, in which explosives were used to create underground chambers of fractured oil shale. The oil shale was ignited with external fuel, and air and steam were injected to support and control combustion. The hot rock fractured and released shale oil, which was pumped to the surface from a separation sump and collecting well. Bitumen derived from oil shale and many tar sands contain small but significant amounts of arsenic, which are severe poisons for catalysts in refineries.

1.9.5 Well Stimulation: Hydraulic Fracturing

For decades, hydraulic fracturing (*fracking*) has been used to restore production from depleted formations. Since 2008, fracking has dramatically increased new production of oil and gas in the United States, particularly in five areas: the Bakken Shale formation in North Dakota, the Eagle Ford shale formation in Texas, the Permian Basin in Texas and New Mexico, the Niobrara formation in Colorado and Wyoming, and the Marcellus Shale formation in Ohio and Pennsylvania. Several other US states have a significant fracking potential [1.68].

Fracking involves the injection of fluid (mainly water containing acids and other chemicals) and a proppant such as sand under controlled pressure inter-

mittently over 3–5 days. This creates fractures in a targeted rock formation permitting oil or natural gas to flow to the wellbore. As presently practiced,

fracking consumes considerable amounts of water, can contaminate ground water, and may cause earthquakes [1.69].

1.10 Transportation and Storage

Crude oils recovered from wells usually contain dissolved gases, salt, water, and even sand/dirt. Natural gas can contain significant amounts of nonhydrocarbon gases, such as CO₂, N₂, and toxic H₂S. Most of the production sites (gas/oil fields) are remote from the gas plants and refineries which convert natural gas and crude oils into useful products. Hence, the gas and oil must be transported by pipelines and tankers in large quantities and for considerable distances, or in barges, railroad tank cars, and trucks in smaller quantities and for shorter distances. Prior to shipment from gas/oil fields, the gas and oil must be treated. Treatments include gas/liquid/solid separation by gravity in a large vessel (*settler*). Gases are drawn off and treated as described in the next paragraph. In the settler itself, it may be necessary to use demulsifying agents to break oil/water emulsions. Solid materials accumulate in the bottom of the settler and must periodically be removed and disposed of as hazardous waste.

Strict specifications for the maximum water and salt contents of crude oils must be met for pipeline transportation. For heavier oils, viscosity, sulfur content, and nitrogen content are also specified. Similarly, CO₂ has to be removed from natural gas for transportation by specifically designed LNG tankers. H₂S in natural gas or petroleum gas is removed by amine scrubbing and converted into sulfur with the Claus process. Compat-

ible crude oils from several wells are usually blended for transportation. However, caution has to be taken for the characteristics of crude oil can change over time, even when the oil comes from the same well; the oil in a reservoir gets heavier over time as the reservoir is continuously depleted.

Trading revolves around transportation, and therefore is a midstream operation. The price negotiation will depend on the availability, market demand, and quality of different crude oils. The price differential from marker crudes, most commonly North Sea Brent and West Texas Intermediate (WTI), can be significant depending on the assessment of the crude oil by a crude assay.

Large quantities of crude oil arrive at marine terminals and refineries through pipelines and are stored in tanks, most of which are cylindrical with a moving roof under low vapor pressure. Partially refined products from other sites, such as atmospheric residue or vacuum gas oil, are stored in similar tanks. Reactive materials may require gas-blanketed tanks. Spherical tanks are used for high pressure substances such as liquefied petroleum gas; some high-pressure tanks are also thermally insulated. Crude oil can also be stored in salt domes underground, such as the US Strategic Petroleum Reserve (SPR) in Louisiana and Texas. Logistic management of tank farms is an integral part of refinery operations.

1.11 Refining

1.11.1 Refinery Configuration Overview

Modern petroleum refineries include several upgrading processes, such as the following:

1. Feedstock selection and blending
2. Separation:
 - Distillation
 - Solvent processes (extraction).
3. Treating:
 - Desalting
 - Hydrotreating
 - Mercaptan oxidation
 - Solvent scrubbing
 - Visbreaking.
4. Conversion:
 - Thermal cracking/steam cracking
 - Thermal hydrocracking
 - Catalytic cracking
 - Catalytic hydrocracking
 - Coking.
5. Catalytic reforming and isomerization
6. Recombination of light intermediates:
 - Alkylation
 - Oligomerization of C3 and C4 olefins.
7. Product treating and blending
8. Protecting the environment:
 - Gas treating
 - Sulfur recovery
 - SO_x and NO_x abatement

- Waste treatment.
- 9. Related operations:
 - Asphalt production
 - Lubricant base oil manufacturing

- Wax production
- Hydrogen production
- Hydrogen recovery and purification
- Production of petrochemicals.

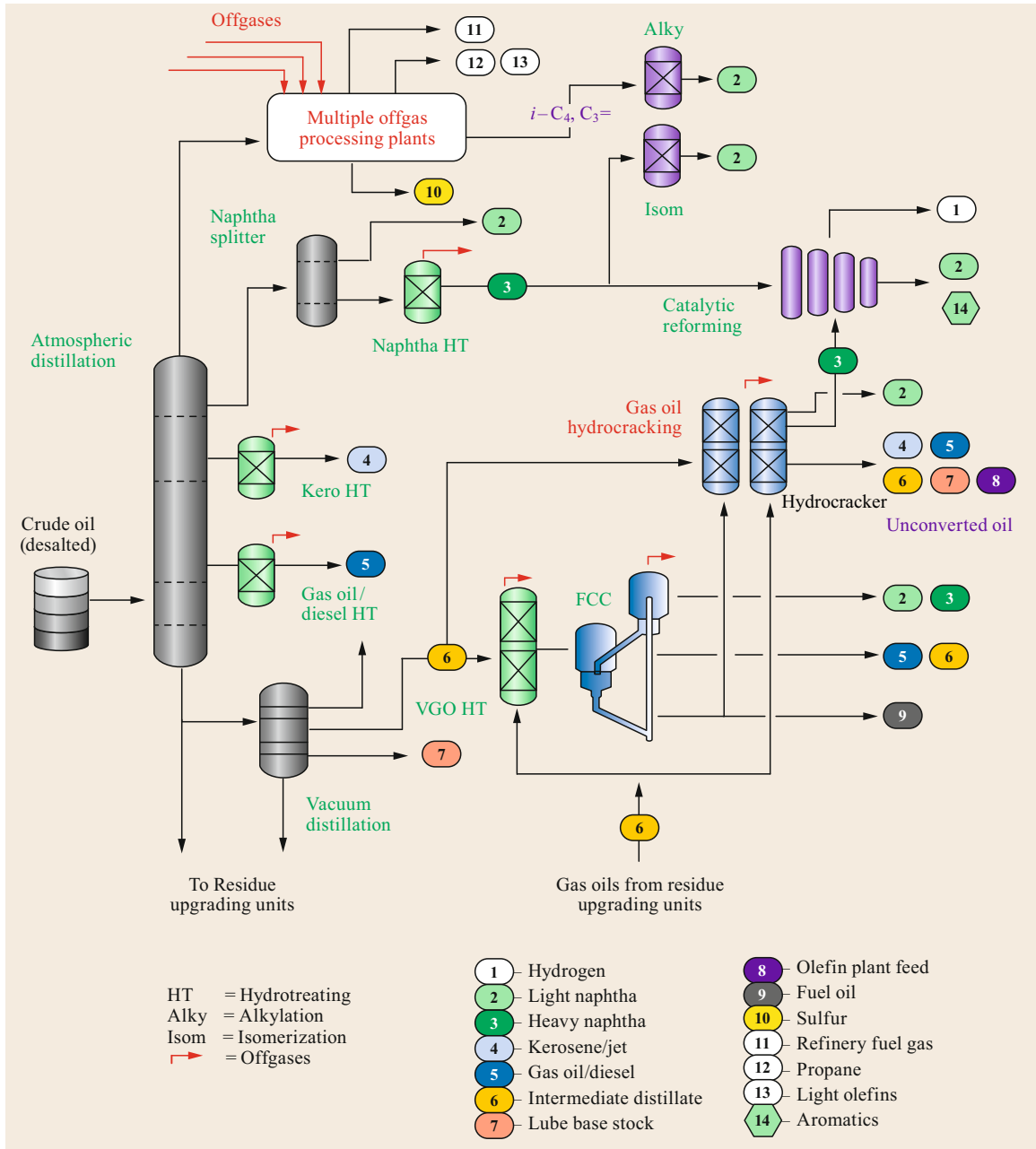


Fig. 1.16 Oil refinery process units: upgrading processes for top-of-the-barrel cuts – VGO and lighter – boiling below about 1050 °F (556 °C). Almost all processes generate offgas (represented by red arrows). Offgases are collected, purified, and separated into components in refinery gas plants. Usually there are two gas plants, one for saturated streams and another for streams containing olefins. HTU = hydrotreating unit, FCC = fluid catalytic cracking unit, Alky = alkylation unit, Isom = isomerization unit, VGO = vacuum gas oil. Not shown: olefin oligomerization to produce gasoline

No refinery refines a single crude. Different grades of crude oils and partially refined feedstocks are stored in an array of tanks prior to blending to meet refinery configuration and constraints. For example, sulfur constraints can be met by blending high sulfur with low sulfur crudes. Blended crudes must be compatible, i. e., it must be possible to mix them thoroughly and without risk of precipitating asphaltenes. LP (linear program) models are commonly used at refineries as tools for making crude purchase (term or spot) decisions, scheduling, planning, etc. The blended crude is sent to a desalter to remove contaminants prior to distillation.

While reading the remainder of this section, it will be useful to refer to Figs. 1.16–1.18. Figure 1.16

presents a simplified schematic diagram for the *light end* distillation units of high-conversion refineries. In this context, the *light end* includes processes which upgrade vacuum gas oil and lighter cuts with boiling points below 1050 °F (556 °C).

Figure 1.17 shows processes for upgrading vacuum residue, or bottom-of-the-barrel processes, which upgrade vacuum residue boiling above 1050 °F (556 °C). The processes in the figures are discussed individually in the remainder of this chapter.

Figure 1.18 gives an overview of product blending:

- Naphtha and gasoline components come from the following units: distillation, isomerization, alkyla-

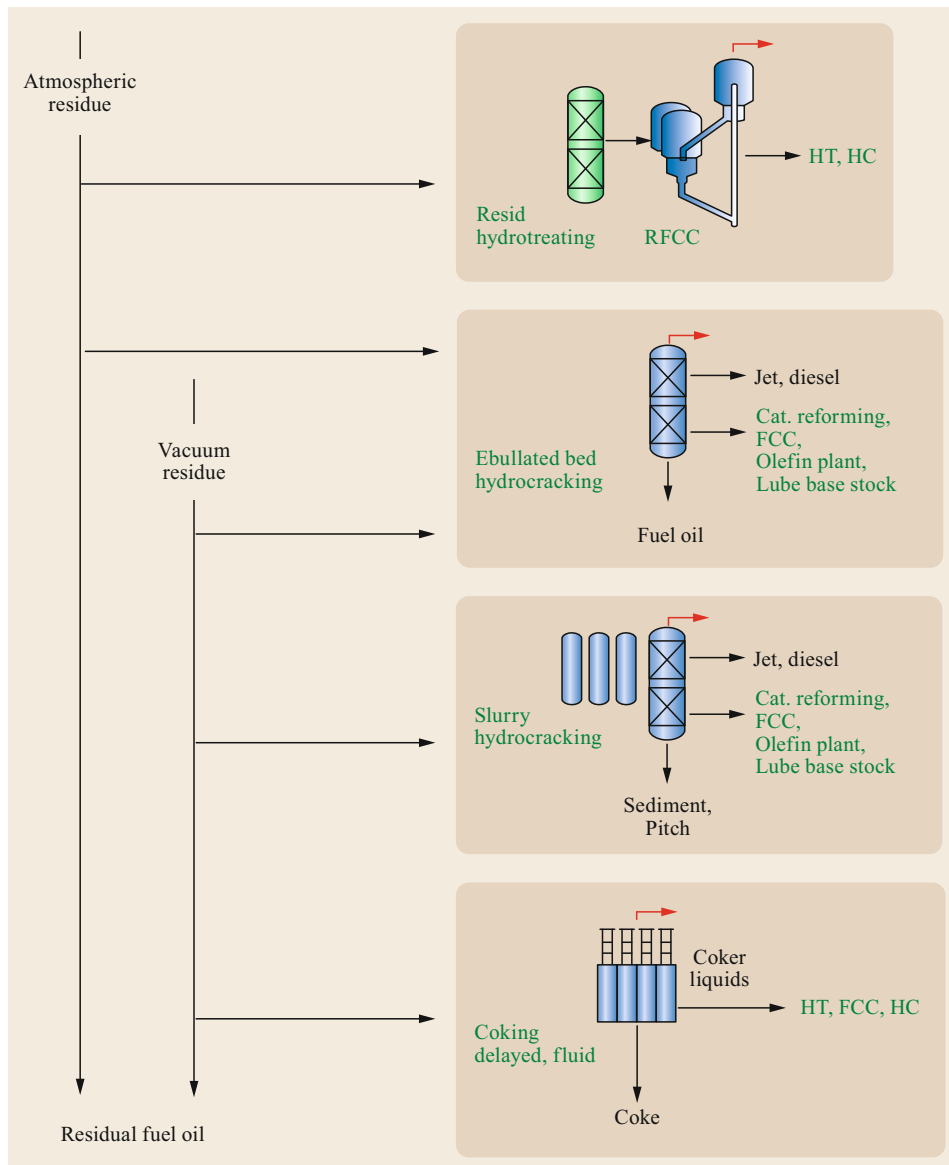


Fig. 1.17 Oil refinery overview: upgrading processes for bottom-of-the-barrel cuts – atmospheric residue, vacuum residue and extraction unit bottoms. The red arrows indicate offgas streams. Individual processes are discussed in the remainder of this chapter

tion, catalytic reforming, C3C4 olefin oligomerization, hydrocracking, catalytic cracking, and coking. Naphthas from different units have similar boiling ranges but may contain different components. Some naphtha molecules might end up in gasoline, some

might be sold as solvent, and others could go to thermal cracking in an olefins plant.

- Kerosene and jet fuel components come from the hydrocracker (HCU) and the kero hydrotreater (KHT).

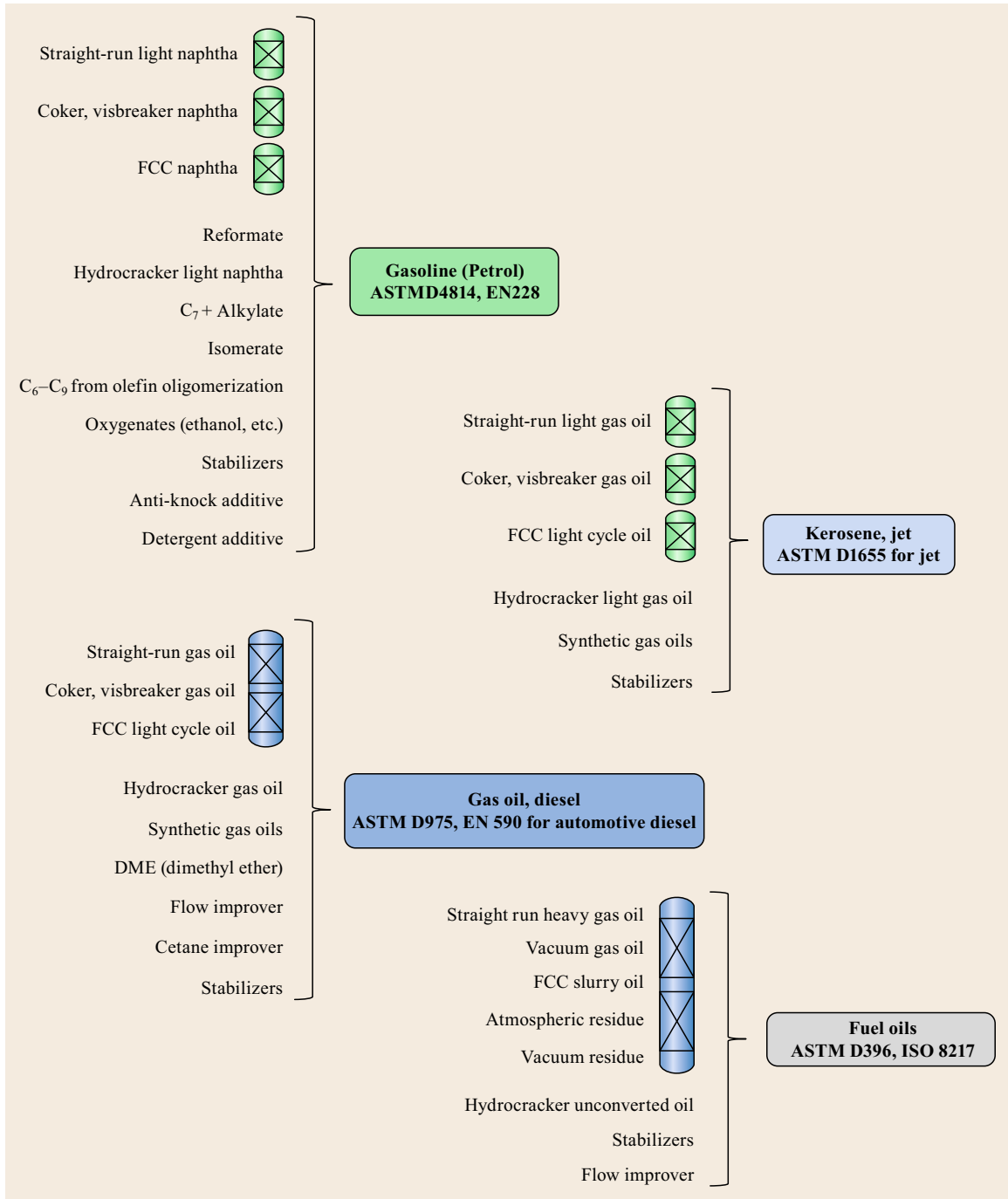


Fig. 1.18 Refinery product blending for gasoline, kerosene, turbine fuel (jet), and fuel oils

- Gas oil and diesel components come from the FCC, the HCU, the gas oil hydrotreater (GOHT), visbreaker, and coker. But in developed countries with tight product specifications, FCC gas oil does not meet specifications for diesel or other finished products. It often is used as *cutter stock* in residual fuel oil, but otherwise it must undergo further refining before it can be sold.
- Almost every unit makes offgas. For the most part, offgas streams are collected into a common system, desulfurized, and used for fuel gas. Propylene and C4 olefins are used in four major ways: to produce high polymers such as polypropylene, to produce epoxides for making polyesters, to react with isobutane in alkylation units, and to undergo oligomerization into C6 to C9 isoparaffins. The product from oligomerization units is commonly called, misleadingly, polymer gasoline.

Finished products are comprised of intermediate streams from different units, along with stabilizers, antioxidants, corrosion inhibitors, and other additives. To be products, the blends must meet specifications developed and published by international organizations such as the American Society for Testing and Materials (ASTM) and the International Organization for Standardization (ISO). ASTM and ISO specifications incorporate information from suppliers, users, government agencies, and equipment manufacturers.

A material in the kerosene boiling range is a jet fuel if it meets ASTM D1655-15 specifications no matter how it is made. Similarly, a material in the naphtha boiling range is gasoline if it meets the specifications of ASTM D4814-14b, no matter how it is made.

1.11.2 The Need for Conversion

To maximize profit, oil companies convert low value fractions into high value products. Throughout the world, 90% of vehicular transportation is powered by

petroleum products. Gasoline still accounts for most petroleum consumption in the United States. In Europe and Asia, diesel demand is relatively higher. Historically, in addition to increasing overall crude oil demand, the automobile increased demand for naphtha from which gasoline is derived.

Table 1.10 shows that in 2014, the United States consumed, on average, 79 wt% of its petroleum as naphtha, kerosene and distillate fuel oil (NKD); major destinations for NKD are gasoline, jet fuel and diesel, respectively. But the NKD contents of crude oil are lower than the demand. In Table 1.10, the NKD gaps range from 17.2 wt% to 45.2 wt% and the naphtha gaps range from 11.9 wt% to 26.2 wt%.

These gaps create a strong economic incentive to convert *other* into NKD. Here is a way to estimate the size of the incentive:

- The crack spread is the difference between the price of a crude oil and the wholesale prices of petroleum products extracted from it. Crack spread calculations are used to estimate refinery profit margins. The crack spread is expressed as $x : y : z$, where x is the price of X barrels of crude oil, y is the price of Y barrels of gasoline, and z is the price of Z barrels of distillate fuel oil (diesel, etc.). By convention $X = Y + Z$. Figure 1.19 shows that the 3 : 2 : 1 crack spread for Brent crude varied between 11 and \$22/bbl during June 2012 and May 2013.
- Assume the United States consumes 18 million barrels per day of oil.
- Assume the NKD gap is 23.9% – the same as for Brent in Table 1.9.
- Assume the crack spread is \$11/bbl.
- On this basis, the US conversion incentive is \$47.3 million per day.

In response to such huge incentives, refiners and licensors have developed an array of processes for converting heavy products into light ones.

Table 1.10 Conversion gaps for four crudes. N+K+D= the sum of naphtha, kerosene, and gas oil. Gaps are the difference between the consumption of a given product and the amount of that product in the crude before conversion

Product cut Becomes:	Naphtha Gasoline	Kerosene Jet	Dist. fuel oil Diesel	Other	NKD ^a	Gaps Naphtha ^b
US consumption (wt%)	42	9	28	21	–	–
Amount in crude (wt%)						
Brent	30.1	9.9	15.1	44.9	23.9	11.9
Bonny Light	27.7	12.5	21.6	38.2	17.2	14.3
Green Canyon	16.9	8.5	14.1	60.5	39.5	25.1
Ratawi	15.8	7.4	10.6	66.2	45.2	26.2

^a NKD gap = consumption of NKD – NKD in crudes

^b Naphtha gap = consumption of naphtha – naphtha in crudes

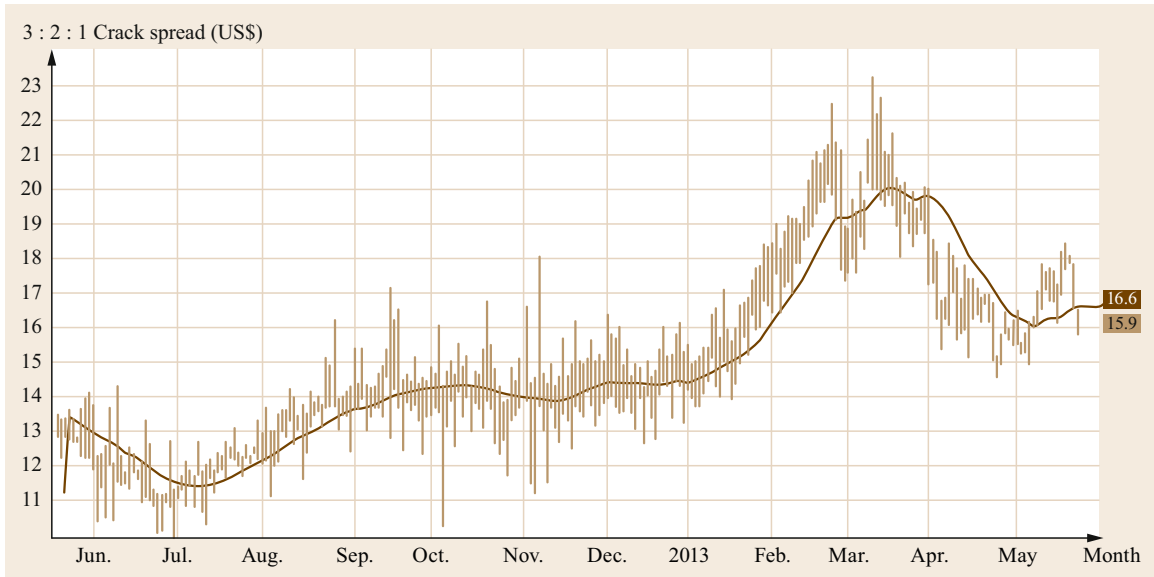


Fig. 1.19 The 3 : 2 : 1 crack spread for Brent crude date between June 2012 and May 2013 (after [1.70])

Table 1.11 Number of refineries and process unit capacities in different regions. VDU = vacuum distillation. Coking = both delayed and fluid coking. Thermal = thermal cracking, primarily visbreaking. FCC = fluid catalytic cracking unit. Cat. Ref. = catalytic reforming of all kinds. HC = catalytic and thermal hydrocracking. HT = all hydrotreating processes

Region	Plants	Total CDU (bbl/day)	CDU Avg. (bbl/day/plant)	Process unit feed rate (% of CDU rate)						
				VDU	Coking	Thermal	FCC	Cat. Ref.	HC	HT
Africa	48	3 518 950	73 311	16.3	2.4	2.7	6.0	13.9	2.5	26.0
Asia, dragons	40	8 816 140	220 404	27.0	2.2	0.2	17.4	14.5	6.2	77.9
China	56	7 542 000	134 679	5.4	3.2	0.0	9.5	3.7	4.5	7.7
India	23	4 642 761	201 859	17.5	3.7	1.6	11.0	1.1	3.6	4.4
Europe incl. Russia	169	22 716 485	134 417	38.8	2.5	9.0	12.4	14.4	7.1	58.7
Middle East	43	7 146 100	166 188	25.2	1.0	6.7	5.0	9.1	7.6	27.5
United States	123	18 024 750	146 543	44.8	14.9	0.2	30.9	19.3	10.6	80.5
North America excl. US	37	4 443 179	120 086	38.5	5.7	4.7	21.1	16.2	5.7	58.8
S. America	51	4 988 400	97 812	43.4	7.3	4.0	22.1	4.3	2.3	19.4

Table 1.11 shows average refinery configurations for different regions of the world. Within regions, configurations vary significantly based on crude availability and product demand. Feed rates for individual processes are shown as a percentage of crude distillation rate (CDU). For example, if the CDU throughput is 200 000 bbl/day and the FCC fraction is 50%, the throughput of the FCC is 100 000 bbl/day. The United States and Europe host 45% of the world's refineries and account for 46% of world's crude distillation capacity. The high usage of FCC in North and South America reflects the higher demand for gasoline in those regions.

Table 1.12 shows that four of the world's five largest refineries are Asian, led by 1.24 million bbl/day facility in Jamnagar; the five largest refining companies are ExxonMobil, Shell, Sinopec, BP, and Saudi Arabian Oil.

Table 1.12 Five largest refineries and five largest refining companies

Five largest refineries			
Company	Location	Country	1000 bbl/d
Reliance Industries	Jamnagar	India	1240
Petroleos de Venezuela	Paraguana	Venezuela	955
SK Innovation	Ulsan	South Korea	840
GS Caltex Corp.	Yoesu	South Korea	755
S-oil Corp.	Onsan	South Korea	669
Five largest refining companies			
Exxon Mobil Refining and Supply			5580
Royal Dutch Shell Group			4109
Sinopec			3971
BP PLC			2859
Saudi Arabian Oil co.			2855

1.11.3 Petroleum Refining Chemistry

Petroleum-refining processes include the chemical reactions and physical processes listed below:

- Distillation
- Extraction
- Desalting (removing entrained salt by dissolving it in water)
- Hydrogenation and generation of olefins
- Condensation and reversible saturation of aromatics
- Hydrotreating (removing sulfur, nitrogen, and oxygen):
 - Hydrodesulfurization (HDS)
 - Hydrodenitrogenation (HDN)
 - Hydrodeoxygenation (HDO)
 - Hydrodemetalation (HDM).
- Cracking (breaking carbon–carbon bonds):
 - Thermal cracking
 - Catalytic cracking
 - Hydrocracking (catalytic and thermal).
- Steam/hydrocarbon reforming/cracking (making hydrogen, olefins, and aromatics)
- Dehydrogenation, isomerization, reforming (no change in carbon number)
- Alkylation, olefin oligomerization (making carbon–carbon bonds)
- Acid/base reaction processes: amine treating, caustic scrubbing
- Mercaptan oxidation
- Blending, where molecular interactions change key properties.

Distillation

We mention distillation here, primarily because the rejection of heavy feed components from distillates prevents coking in processes designed for light feeds. At the very beginning (just after desalting), temperatures must be limited in atmospheric distillation units to avoid coking; vacuum distillation recovers VGO. VGO conversion units, such as conventional FCC and fixed-bed hydrocracking, choke to death on vacuum residue (VR). In FCC units, VR coking upsets the heat balance. In fixed-bed hydrocrackers, VR shortens catalyst life. Catalytic reforming catalysts deactivate quickly when the feed contains C12+ hydrocarbons.

Desalting. Desalting is a crucial pretreatment process for crude distillation feeds. By removing salts, acid, and inorganic particulates, desalting units preserve the functionality of other refinery units. Desalting entails mixing crude oil with water and treatment chemicals. Salts go into the water which is separated from the oil and purified for re-use.

Generation and Hydrogenation of Olefins

Olefins are produced by thermal cracking in the absence of excess hydrogen by processes such as coking (delayed or fluid), and FCC. Olefins are also produced from naphtha, gas oil, and light gases by thermal cracking in the presence of steam. A general mechanism for hydrocarbon thermal cracking is shown in Fig. 1.27. Hydrogenation of olefins in catalytic hydrotreating and hydrocracking units is rapid, essentially irreversible, and highly exothermic.

Condensation and Reversible Saturation of Aromatics

The saturation of aromatics and polyaromatics (Fig. 1.20) is common to several petroleum-refining processes. It is especially important in catalytic reforming, hydrotreating, hydrocracking, and cyclohexane production. Aromatics saturation is reversible, except when saturated C–C bonds are cracked or when polyaromatics condense to form larger polyaromatics. Carbon–carbon single bonds in polynaphthenes and

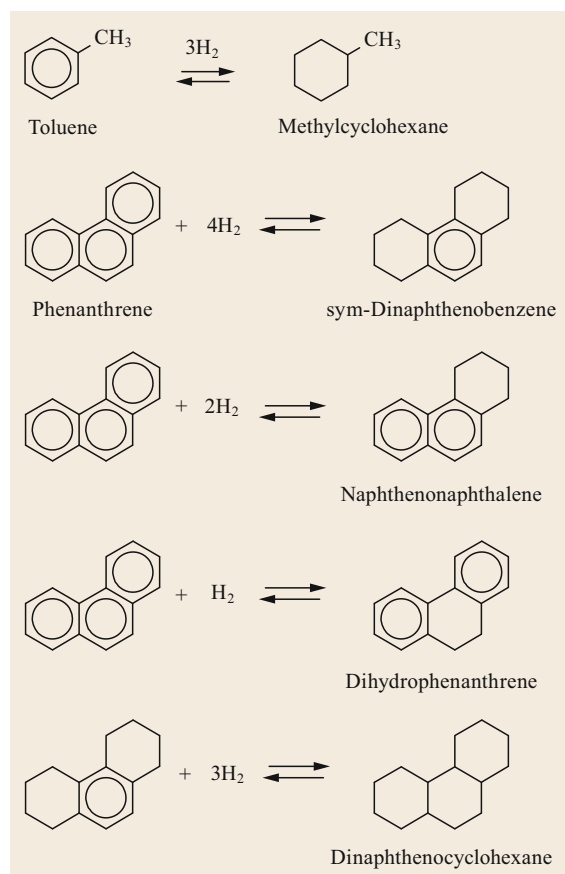


Fig. 1.20 Examples of saturation reactions of aromatics and polyaromatics (after [1.71])

naphthoaromatics can be broken irreversibly, but bonds within aromatic rings are more stable and difficult to break.

Figure 1.21 summarizes thermodynamic calculations for the competition between the saturation of naphthalene and the condensation of naphthalene with *o*-xylene to form chrysene. At high pressures and low temperatures, equilibrium favors saturation. At low pressures and high temperatures, equilibrium favors dehydrogenation. At high enough temperatures, equilibrium favors condensation. Fixed-bed catalytic hydrotreating and hydrocracking units operate in the aromatics crossover region between 315 and 425 °C (600–800 °F).

Figure 1.22 shows the so-called zig-zag mechanism for the production of large polyaromatics by adding 2- and 4-carbon species [1.72]. The condensation of large polyaromatics via the Scholl reaction [1.73] can lead eventually to coke formation and deactivation of the catalysts used in FCC, hydrotreating, and hydrocracking.

Figure 1.23 shows a mechanism for the one-at-a-time buildup of rings on a nucleus of coke [1.74]. The mechanism includes the following steps:

- Hydrogen abstraction by radicals
- Alkylation (olefin addition)
- Cyclization
- Dehydrogenation.

Hydrotreating: Sulfur Removal by HDS

Figure 1.24 shows representative hydrodesulfurization (HDS) reactions. For sulfur removal from the first three reactants, the mechanism is straightforward [1.76]. That is, the sulfur-containing molecule interacts with an active site on the catalyst, which removes the sulfur atom and replaces it with two hydrogen atoms. Additional hydrogen converts the sulfur atom into H₂S, which desorbs from the catalyst, leaving behind a regenerated active site.

For the fourth reactant – 4,6-dimethyldibenzothiophene (4,6-DMDBT), which has two methyl groups near the vicinity of the sulfur atom – HDS proceeds via both a direct and an indirect route. Overall, the indirect route is considerably faster. The 4,6-DMDBT molecule is planar, and the two methyl groups block the access of the sulfur atom to the catalyst surface, thereby inhibiting direct HDS. In the indirect route, saturating one of

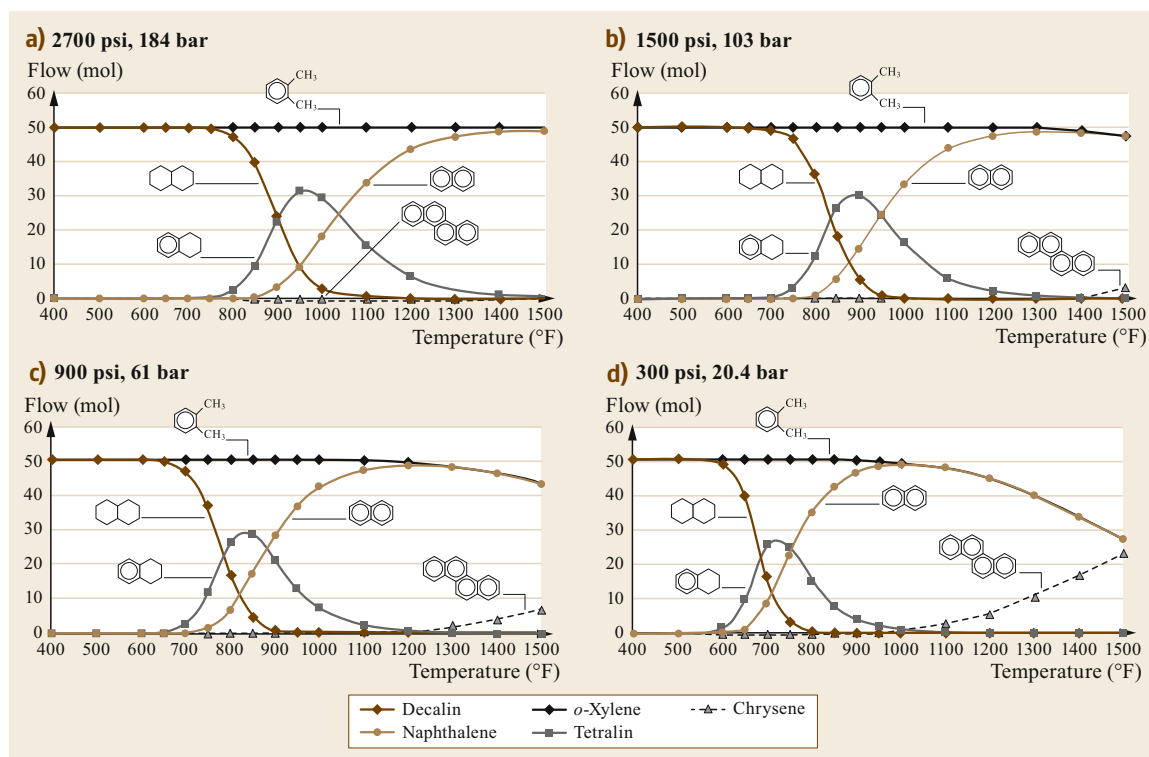


Fig. 1.21a-d Thermodynamic calculations illustrating the competition between saturation and condensation of polyaromatics. Data for the graphs were generated by Aspen Plus for a six-component system comprising naphthalene (C₁₀H₈), tetralin (C₁₀H₁₂), decalin (C₁₀H₁₈), *o*-xylene (C₈H₁₀), chrysene (C₁₈H₁₂), and hydrogen (not shown). The mol flow is the flow of a constituent at the reactor effluent (after [1.75])

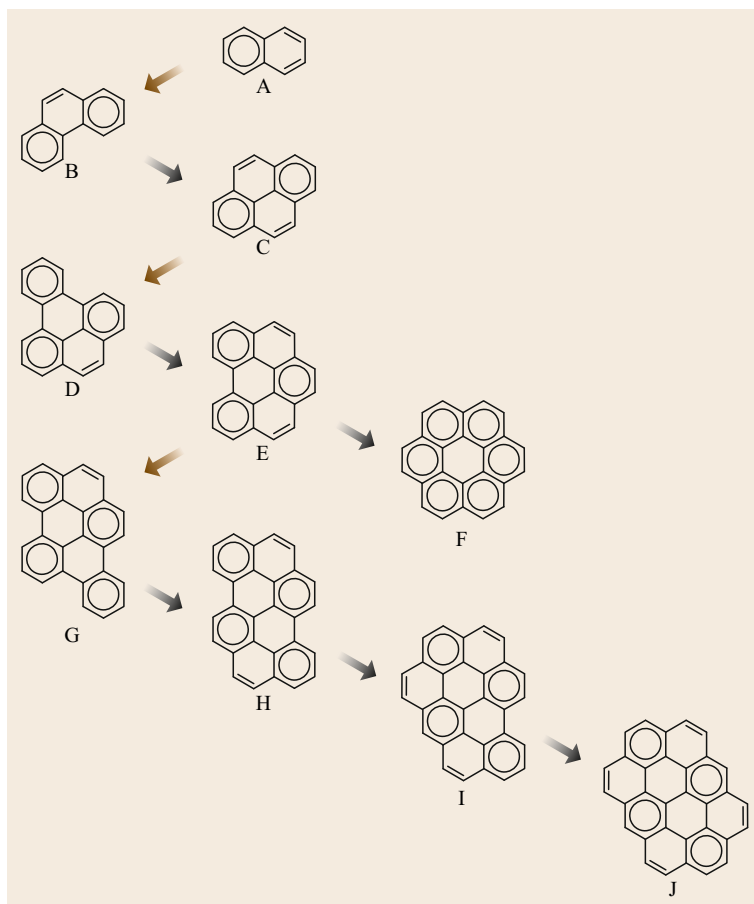


Fig. 1.22 Zig-zag mechanism for the condensation of polyaromatics by sequential addition of 2- and 4-carbon units. Formulas for isomers shown are (A) naphthalene, $C_{10}H_8$; (B) phenanthrene, $C_{14}H_{10}$; (C) pyrene, $C_{16}H_{10}$; (D) benzo[e]pyrene, $C_{20}H_{12}$; (E) benzo[ghi]perylene, $C_{22}H_{12}$; (F) coronene, $C_{24}H_{12}$; (G) dibenzo[b,pqr]perylene, $C_{26}H_{14}$; (H) benzo[pqr]naphtho[8,1,2-bcd]perylene, $C_{28}H_{14}$; (I) naphtho[2'.8',2.4]coronene, $C_{30}H_{14}$; and (J) ovalene, $C_{32}H_{14}$. Note that the H/C ratio goes down as condensation increases, from 0.8 for naphthalene (A) to 0.4375 for ovalene (J)

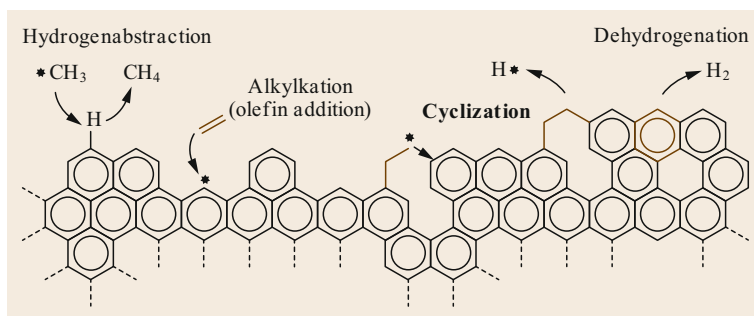


Fig. 1.23 Mechanism for the addition of rings to an existing layer of coke

the aromatic rings that flank the sulfur atom converts the planar structure into a puckered arrangement with tetrahedral C–C bonds. This puckering rotates one of the inhibiting methyl groups away from the sulfur atom, giving it better access to the catalyst.

Making ultra-low-sulfur diesel (ULSD), in which the sulfur content is less than 10–15 wppm, requires severe hydrotreating, after which the only remaining sulfur compounds are the above-mentioned 4,6-DMDBT and other di- and trimethyl dibenzothiophenes. Because

the removal of sulfur from these compounds is more facile after prior saturation, the crossover phenomenon affects the production of ULSD significantly, so much that it governs the design of commercial units.

Hydrotreating: Nitrogen Removal by HDN

Figure 1.25 shows representative HDN reactions, and Fig. 1.26 presents the simplified mechanism for the HDN of quinoline [1.77]. Simple amines are rarely found in natural petroleum. As with sulfur removal

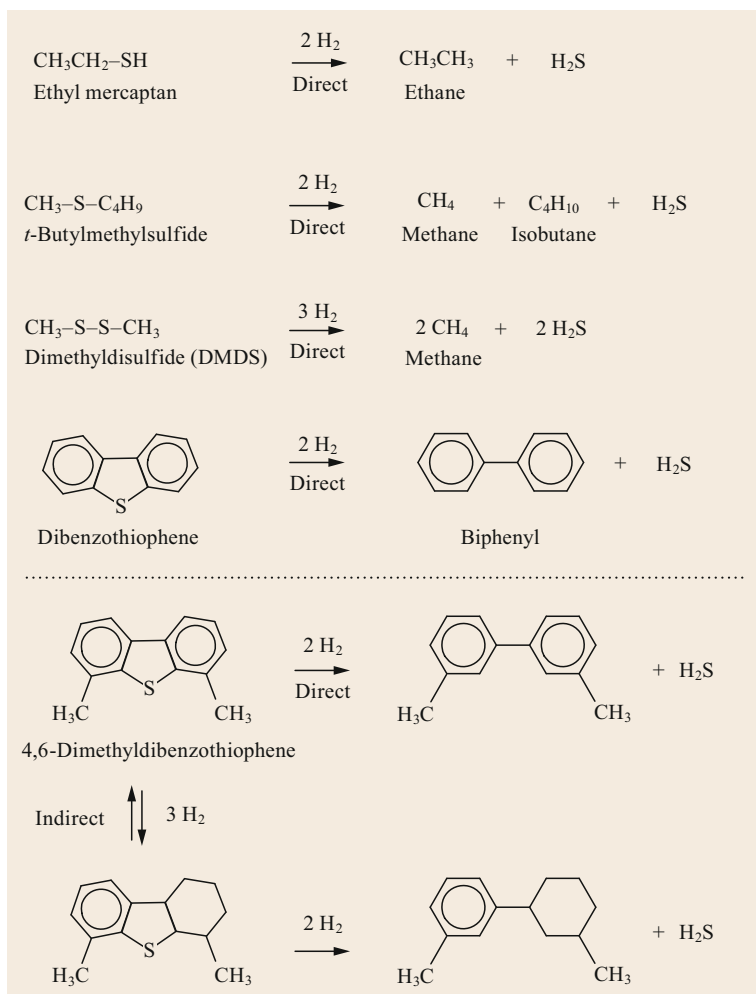


Fig. 1.24 Representative HDS reactions. For the hydrodesulfurization of 4,6-dialkylthiophenes, the indirect mechanism, which requires prior saturation, is preferred

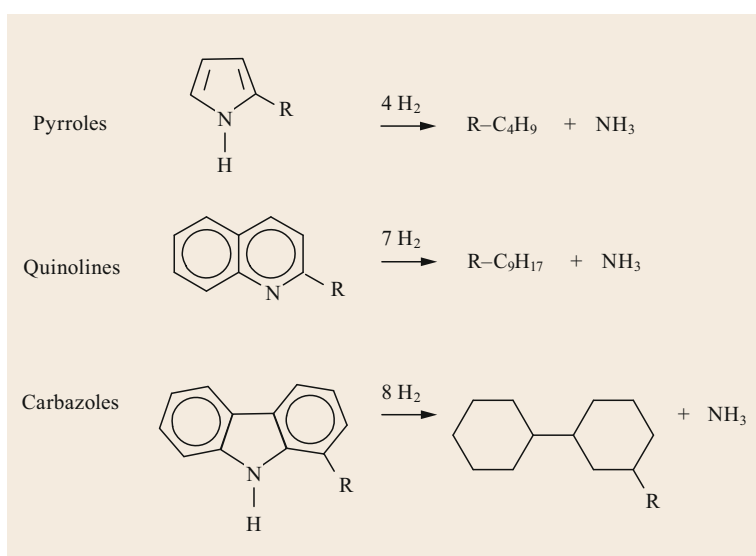


Fig. 1.25 Representative hydrodenitrogenation (HDN) reactions. R = any alkyl group. Simple amines are rarely found in petroleum

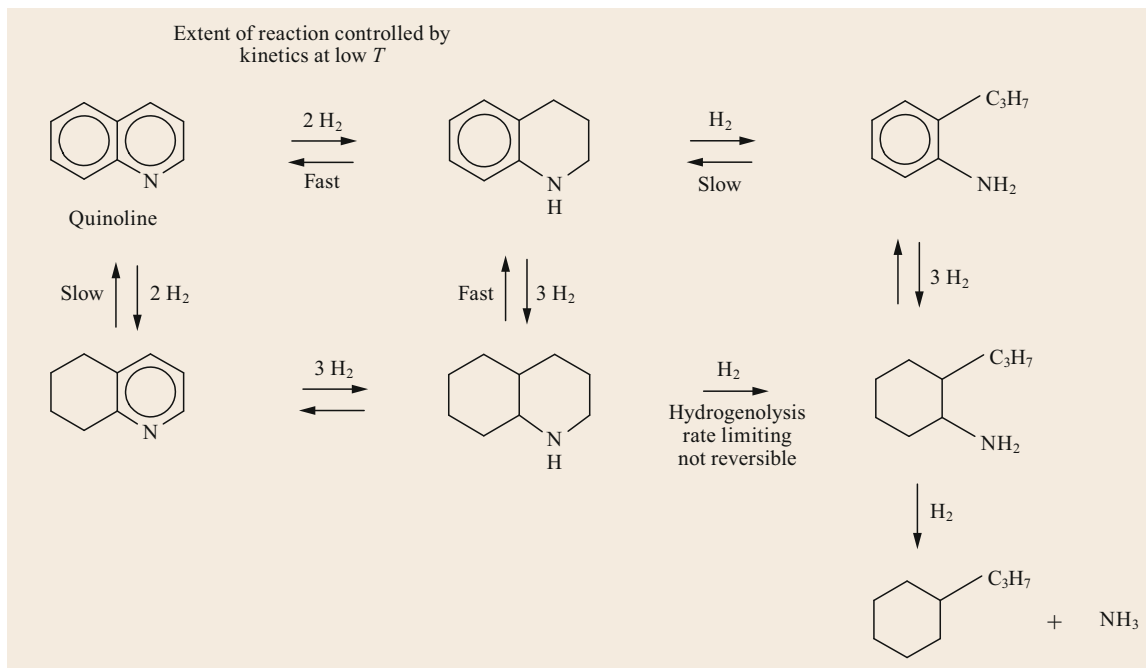


Fig. 1.26 Mechanism for the HDN of quinoline (simplified)

from hindered DMBTs, the crossover phenomenon is important for deep HDN because nitrogen removal requires prior saturation of an aromatic ring adjacent to the nitrogen atom.

Hydrotreating: Oxygen Removal by HDO

In feeds to industrial hydroprocessing units, oxygen is contained in furans, organic acids, ethers, peroxides, cresols, and other compounds. Some are formed by reacting with air during transportation and storage of crude oil, distillates, and cracked stocks generated by delayed coking and FCC units (see below). For compounds such as light furans, hydrodeoxygenation (HDO) proceeds rapidly, so rapidly that it can cause problems with excessive heat release. Other compounds, such as cresols, are less reactive, even refractory. Oxygen compounds can form gums and polymers, which inhibit flow and increase pressure drop.

Feedstocks from biomass contain considerably more oxygen than conventional crude oil and petroleum distillates. While a conventional vacuum gas oil may contain 0.5 wt% oxygen, a biomass-derived oil (bio-oil) in the same boiling range might contain > 2% oxygen. Producing fuels from bio oils in conventional oil refineries requires extra hydrogen and presents processing and storage challenges. Large-scale hydrogen production generates large quantities of CO_2 . When assessing the environmental impact of replacing conventional crude oil fractions with bio oils, it is crucial to consider the hydrogen required for upgrading.

Hydrotreating: Trace Metal Removal with HDM

Metals such as nickel and vanadium are present in high-boiling fractions, mostly in asphaltenes. Asphaltenes are mixtures of waxy solids with porphyrins. Corrosion generates soluble iron, and entrained salt brings in alkali and alkaline earth salts, primarily carbonates and bicarbonates of sodium and calcium. Synthetic crudes from oil sands and oil shale tend to contain significant amounts of arsenic – up to 10 ppm. For hydrotreating, 50 ppb is a typical upper limit for arsenic. Silicones are added to crude oil to facilitate flow through pipelines. Silicones are also used to control foaming in delayed coking units.

All of these metals poison refinery catalysts. In hydrotreating, they are removed with grading material, including special wide-pore guard catalysts. Guard materials remove some contaminants by chemisorption. Other contaminants, such as Ni, V, and soluble Fe, are removed by hydrodemetalation (HDM). The products of HDM are metal sulfides, which deposit inside catalyst pores, blocking active sites. They can also cause pore-mouth plugging.

Conversion

Table 1.13 compares compounds with different hydrogen content. For any given class of hydrocarbons, *light*

Table 1.13 Molecular weight, H/C and boiling points for selected hydrocarbons

Compound	Molecular weight	Formula	H/C	Boiling point	
				(°C)	(°F)
Paraffins					
Methane	16.04	CH ₄	4.0	−164.0	−263.2
Ethane	30.07	C ₂ H ₆	3.0	−88.6	−127.5
Propane	44.10	C ₃ H ₈	2.67	−42.1	−43.7
Butane (iso)	58.12	C ₄ H ₁₀	2.50	−6.9	19.6
Octane (iso)	114.23	C ₈ H ₁₈	2.25	99.2	210.6
Cetane (n)	226.44	C ₁₆ H ₃₄	2.13	287.0	548.6
Aromatics					
Benzene	78.11	C ₆ H ₆	1.0	80.1	176.2
Naphthalene	128.17	C ₁₀ H ₈	0.8	218.0	424.4
Benzopyrene	252.32	C ₂₀ H ₁₂	0.6	–	–

means a lower molecular weight, lower boiling point, lower density, and a higher hydrogen-to-carbon ratio (H/C). Methane, the lightest hydrocarbon, has an H/C ratio of 4.0. Benzopyrene has an H/C ratio of 0.6. The H/C ratio of common crude oils ranges from 1.5 to 2.0, while the H/C ratio for asphaltenes is about 1.15.

Hydrotreating and hydrocracking increase the H/C ratio by adding hydrogen. Other conversion processes – FCC, thermal cracking, and deasphalting – increase the H/C ratio by hydrogen reappportionment (also called coke rejection) in which both lighter molecules with higher H/C and heavier products with lower H/C ratios are formed at the same time. In coking and FCC, the heavier product is coke, in which the H/C ratio is < 1.0. It is common to hear *carbon rejection* instead of coke rejection, but *carbon rejection* is misleading; no elemental carbon is removed.

Distillation is central to refining operations; products are defined, first and foremost, by their boiling point ranges (cut points). The goal of a conversion process is to reduce boiling point. Conversion means transforming low value material that boils above a particular cutpoint into high value material that boils below that particular cutpoint. A typical cutpoint for naphtha-oriented conversion is 400 °F (204 °C), while a typical cutpoint for diesel-oriented conversion is 650 °F (343 °C). The equation for conversion is simple

$$\text{Conversion} = \frac{P}{FF} \cdot 100\%$$

where P is the amount of material in the product that boils below the chosen cutpoint and FF is the total amount of fresh feed. In *true conversion* calculations, the amount of P in the FF prior to conversion is subtracted from the numerator.

Table 1.9 shows how boiling point can be reduced without breaking C–C bonds. Saturation, HDS, and HDN can achieve perhaps 10% conversion of vacuum gas oil into diesel and lighter material. To achieve the

degree of conversion shown in Table 1.10, C–C bonds must be broken.

Conversion: Thermal Cracking

Figure 1.27 outlines a mechanism postulated by *Greensfelder* et al. [1.78] for the thermal cracking or steam cracking of hydrocarbons. This chain-reaction mechanism includes the following steps:

1. *Chain initiation*: Radicals are formed due to direct thermal rupture of a chemical bond. Common initiators are organic molecules that contain S, N, or O, which are present in delayed coker feeds. Epoxides, which can be formed by reaction with oxygen during transportation and storage, are potent initiators. In steam cracker feed, heteroatom initiators are absent, so the chain reaction is initiated by the high-temperature rupture of a C–C bond.
2. *Propagation*: A radical abstracts hydrogen from another compound, turning it into a different radical.
3. *Radical addition*: A radical attacks an olefin group, forming a C–C bond and a larger radical.
4. *Radical decomposition (cracking)*: A radical decomposes into an olefin and a smaller radical.
5. *Cyclization*: Radicals with five or more carbons and an olefin group react with themselves to form ring compounds. At the high temperatures at which thermal cracking occurs, aromatics and polyaromatics are thermodynamically favored, so saturated or partially saturated ring compounds readily undergo dehydrogenation and form aromatics.
6. *Chain reaction termination*: Two radicals react to produce a saturated product.

The radical mechanism is consistent with the fact that thermal cracking produces significant amounts of hydrogen, methane, ethane, ethylene, and higher olefins.

Feeds to delayed coking units contain organic sulfur, nitrogen, and oxygen compounds, which form radi-

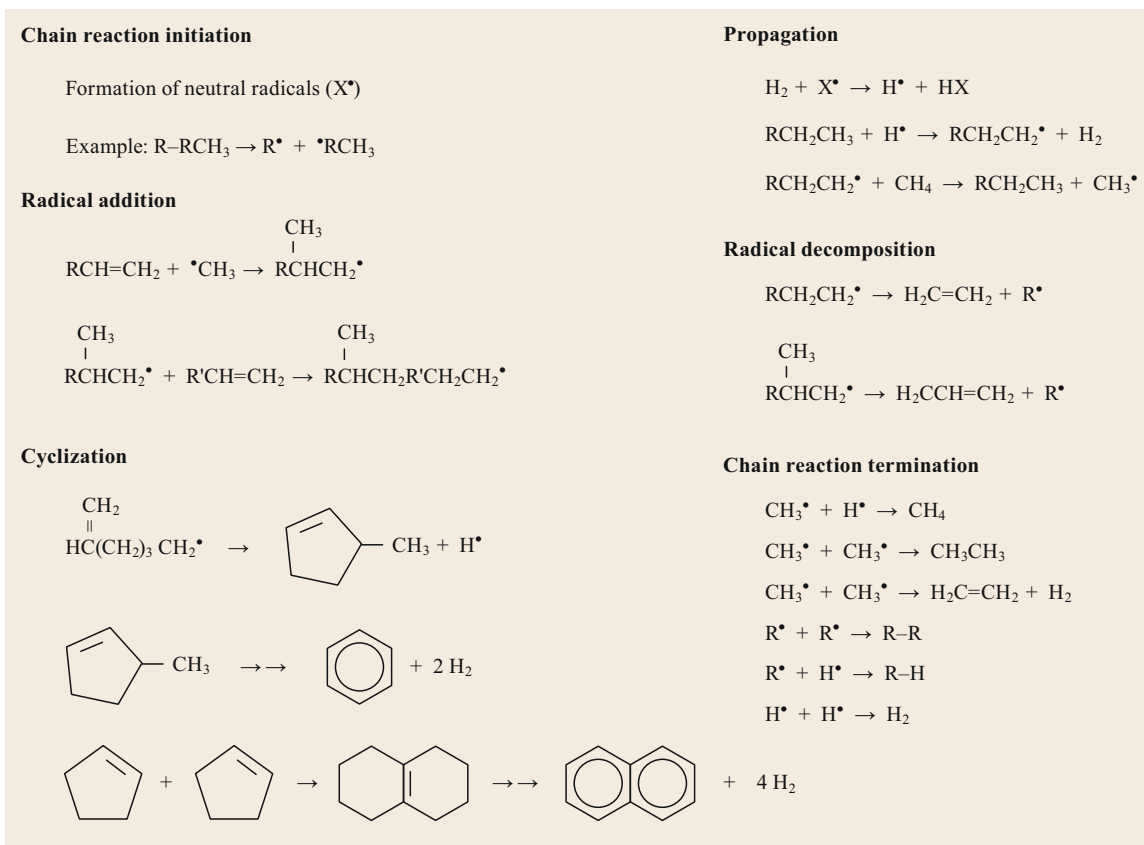
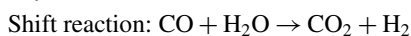
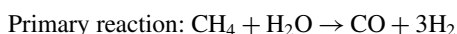


Fig. 1.27 Thermal cracking mechanism: radical chain reaction

cals more easily than hydrocarbons. These heteroatoms end up in two types of molecules – light ones (H_2S , ammonia, and water) and heavy ones, such as hindered dibenzothiophenes or carbazoles, from which they are harder to remove.

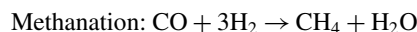
Steam-Hydrocarbon Reforming Chemistry

Steam-hydrocarbon reforming is commonly called SMR because methane is the most common feedstock. SMR produces hydrogen through the reaction of steam with light hydrocarbons at very high temperatures – around $1500^\circ F$ ($816^\circ C$). The product of the initial reaction is a mixture of H_2 , CO , CO_2 , residual methane, and traces of other hydrocarbons. The initial product goes to one or more shift reactors, where the reaction between H_2O and CO yields CO_2 and additional hydrogen



In older units, residual CO was removed by methanation over a nickel-based catalyst, and residual CO_2

was removed for example by adsorption with activated molten potassium carbonate (Benfield process). The product hydrogen contained up to 5% methane.



In newer units, pressure-swing adsorption (PSA) removes nearly all contaminants, yielding a product containing 99.99% hydrogen. A PSA unit employs a collection of solid adsorbents – molecular sieves, activated carbons, silica gels, and activated aluminas. For carbon, silica, and alumina, the separation is due to differential tendency to adsorb different gases. PSA cycles include pressurization, depressurization, and purging. The rejected gas, a low-BTU mixture containing methane, CO and CO_2 , is burned to provide some pre-heat duty.

Another important source of hydrogen is catalytic reforming.

Steam Cracking Chemistry

Olefin plants employ the steam-cracking process to produce ethylene and propylene feedstock for polymer plants. Steam cracking in olefin plants co-produces hydrogen. The reaction temperature is very high, at around

850 °C, and the residence time is very short, as fast as milliseconds, to improve yield and decrease oligomerization and coke formation. The reaction is stopped by rapid quenching. Steam cracking of heavier feed produces products rich in aromatic hydrocarbons suitable for blending into gasoline and fuel oil.

Conversion Chemistry: Catalytic Cracking

In refining, catalytic cracking falls into two categories: catalytic cracking in the absence of external hydrogen – primarily FCC – and catalytic cracking in the presence of external hydrogen – hydrocracking.

Catalysts for both kinds of catalytic cracking contain strong acid sites. The mechanism involves carbocations, also known as carbenium ions or carbonium ions. Acidity is provided by amorphous silica/alumina (ASA) or a crystalline zeolite. Hydrocracking catalysts are bifunctional because in addition to acid site, they contain metal sites, which catalyze hydrogenation.

Key features of catalytic cracking include a preponderance of branched-chain paraffin products and low yields of methane and ethane. Commercial catalysts for these and other processes are discussed in a subsequent section.

FCC units produce aromatics and other heavy products via cyclization, alkylation, and polymerization of intermediate olefins. As shown in Fig. 1.22, polyaromatics can grow into larger polyaromatics, which eventually can form coke. In hydrocracking units, abundant high-pressure hydrogen quickly saturates olefin intermediates, suppressing the growth of polyaromatic rings. For the hydrocracking of fluorene (C₁₃H₉), *Lapinas et al.* [1.79] proposed a mechanism that might apply generally to the hydrocracking of polyaromatics.

Figure 1.28 outlines the reaction sequence for hydrocracking a heptyl ethyl naphthalene isomer into lighter compounds. The reactions include:

- Removal of part of a side chain by dealkylation
- Saturation of an aromatic ring
- Isomerization of the saturated ring
- Opening the saturated ring
- Paraffin hydrocracking.

The first dealkylation reaction (1) removes hexanes through β -cleavage, leaving behind a methyl group. The ring itself remains intact due to resonance stabilization; one-ring aromatic compounds are especially stable. For mechanistic reasons, methyl and ethyl groups are not removed from aromatic rings by β -cleavage. This is consistent with the observation that acid-catalyzed cracking in hydrocracking and FCC units produces minimal methane and ethane. Hydrogenating aromatic rings (2) removes resonance, yielding a saturated ring which is susceptible to ring opening (3). Ring opening is followed by another dealkylation reaction (4), and paraffins are hydrocracked (5).

Comparison of Catalytic and Thermal Cracking

Table 1.14 compares catalytic and thermal cracking processes.

Alkylation Chemistry

In alkylation units, excess isobutane reacts with C₃–C₅ olefins to generate high-octane alkylate – a mixture of C₇–C₉ isoparaffins. Alkylate is a premium quality blend stock for gasoline. Alkylation reactions are catalyzed by strong Brønsted acids. Refineries employ either sulfuric acid alkylation (SAA) or hydrofluoric acid alkylation

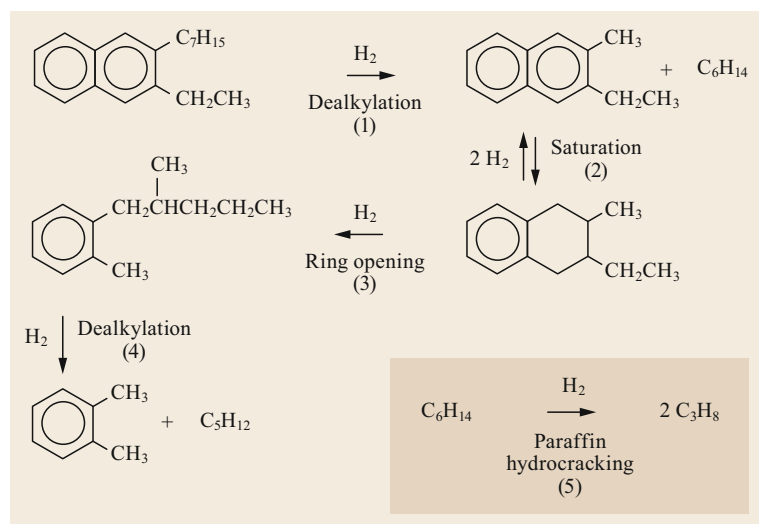


Fig. 1.28 Reaction sequence for the hydrocracking of polyaromatics

Table 1.14 Comparison of product yields for catalytic and thermal cracking processes (after [1.9])

Process	Type	Product characteristics
FCC	Catalytic cracking in the absence of external H ₂	C ₁ and C ₂ : low Iso/normal paraffin ratio: high C ₃ and C ₄ olefin yields: can be significant H ₂ production: moderate Aromatics: higher than feed Coke formation: high Alkyl aromatics: β -scission next to the ring
Catalytic hydrocracking	Catalytic cracking in the presence of external H ₂	C ₁ and C ₂ : low Iso/normal paraffin ratio: high Olefins: removed by hydrogenation Aromatics: significantly lower than feed Coke formation: minimal Alkyl aromatics: β -scission next to the ring
Slurry-phase hydrocracking	Thermal cracking in the presence of external H ₂	C ₁ and C ₂ : high Iso/normal paraffin ratio: similar to feed Olefin production: moderate Aromatics: depends on feed (VR versus coal) Coke formation: low Alkyl aromatics: scission within the side chain
Coking and visbreaking	Thermal cracking in the absence of external H ₂	C ₁ and C ₂ : high Iso/normal paraffin ratio: similar to feed Olefin production: high Aromatics: moderate Alkyl aromatics: scission within the side chain
Steam cracking	Thermal cracking in the presence of steam	Olefin production: high H ₂ production: high Aromatics: high (in the pyrolysis oil) Coke formation: low

(HFA). In both processes, unreacted isobutane is recycled to maintain a high isobutane-to-olefins ratio (I/O), which typically is around 10. In one recently developed process, acidity is provided by a specific zeolite. In another, acidity is provided by an ionic liquid.

Alkylation reactions are highly exothermic. Temperatures are kept low. They range from 0 °C (32 °F) for SAA to around 30 °C (86 °F) for HFA. In HFA, temperature is controlled with refinery cooling water, but SAA requires refrigeration. The excess isobutane moderates temperature increase by absorbing reaction heat. Excess isobutane is the source of *t*-butyl ions to propagate the reaction and also dilutes the olefins, suppressing olefin polymerization.

The mechanism for alkylating butenes is shown in Fig. 1.29. In commercial units, the butene stream is predominantly 2-butene, but it also can contain isobutylene, and 1-butene [1.80]. Olefins are initially ionized by strong acid to form stable *t*-butyl cation via rearrangement, as shown in reaction 1.

Reactions 2–4 are the *alkylation* (addition) reactions. In reaction 2, the *t*-butyl cation reacts with isobutylene to generate the 2,2,4-trimethylbutane cation. Reactions 3a and 4a occur when the *t*-butyl cation encounters 2-butene and 1-butene. The products of 3a and

4a are secondary carbocations. They undergo *methyl shift* in reactions 3b and 4b to generate 2,2,4-trimethylpentane, a more stable tertiary carbocation. Reactions 3b and 4b do not proceed to completion, as indicated by the presence of 2,2,3-trimethylpentane and 2,2-dimethylhexane in the finished product.

Reaction 5 shows the *hydride transfer* reaction that converts isobutane into the *t*-butyl cation while generating finished products – iso-C₈ paraffins (alkylate). Reaction 6 indicates that unwanted side reactions can occur. These include olefin polymerization and follow-on alkylation, both of which form larger molecules, including sludge and acid-soluble oil (ASO).

Catalytic Reforming Chemistry

Figure 1.30 summarizes the reactions of catalytic reforming, the purpose of which is to transform C₆ to C₁₁ naphthenes and paraffins into aromatic compounds. The aromatics can go to chemical plants (Table 1.3) or be used as high-octane gasoline blend stocks. The process yields considerable amounts of hydrogen; in Fig. 1.30, 4 mol of hydrogen are produced from 1 mol of hexane through cyclization (ring closure) and aromatization. The hydrogen is used in hydrotreaters, hydrocrackers, isomerization units, and others.

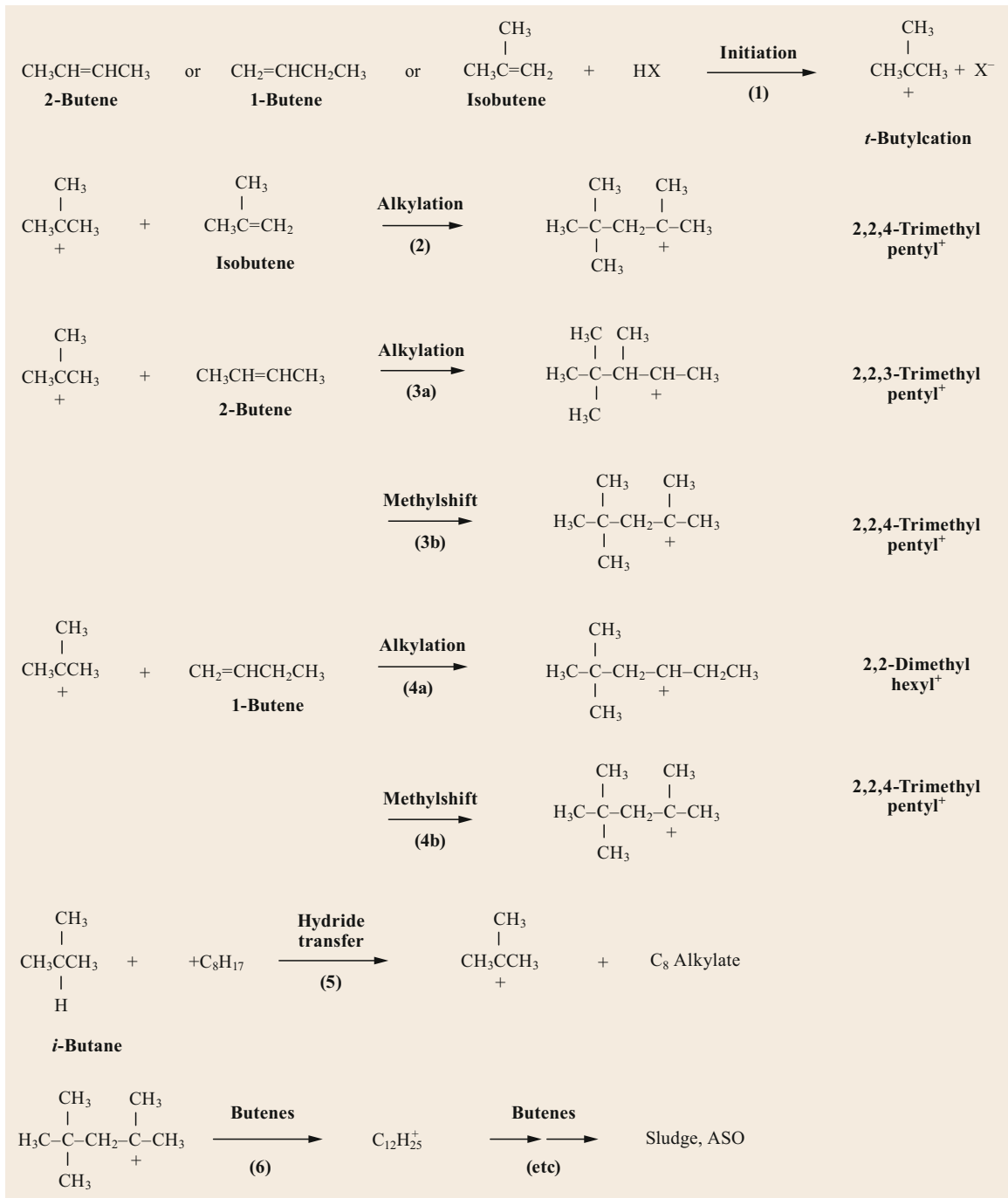


Fig. 1.29 Mechanism for acid-catalyzed alkylation of C₄ olefins, where X is HSO₄⁻ or F⁻

In contrast to hydrocracking, which operates at high hydrogen pressure and moderate temperature to saturate aromatics, catalytic reforming operates at low pressure and high temperature, which favors production of aromatics. In the example shown in Fig. 1.30,

low-octane *n*-hexane is isomerized over an acidic catalyst into 2-methylpentane (isohexane) of higher octane rating, which can further undergo cyclization to form methyl cyclopentane. The conversion of alkylcyclopentanes over a shape selective catalyst into cyclohexanes

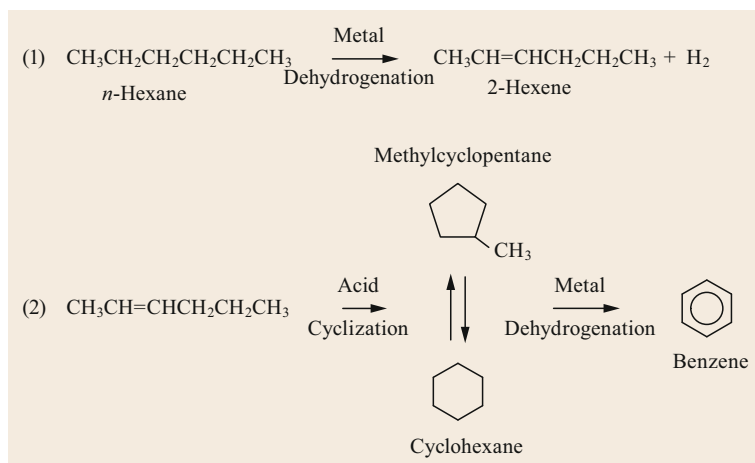


Fig. 1.30 Catalytic reforming reactions for *n*-hexane

is a key step in the production of benzene and alkylbenzenes.

Paraffin Isomerization Chemistry

Paraffin isomerization reactions transform *n*-paraffins into *iso*-paraffins. Paraffin isomerization occurs in many conversion units. It is especially important in FCC, hydrocracking, and hydroisomerization to make lubricant (lube) base stocks. In C_4 isomerization units, *n*-butane is converted to isobutane in a two-stage process, which employs HCl-promoted AlCl_3 for the 1st stage and a supported noble metal catalyst in the 2nd stage. The isobutane product is the key feedstock for alkylation units, which produce high octane alkylates. C_5/C_6 isomerization produces isopentanes and isohexanes, which are high-octane components of gasoline.

Heavy *n*-paraffins are waxy. They solidify in cold weather, so during lube base stock production, they must be removed, either by extraction, conversion, or isomerization. In isodewaxing units, they are transformed into isoparaffins, with minimal cracking, over silica-alumina-phosphate (SAPO)-based catalysts. Compared to *n*-paraffins, isodewaxed products have considerably lower cloud and pour points; they flow more readily at low temperature.

The impact of heavy paraffin isomerization on melting point is illustrated in Table 1.15 for $\text{C}_{18}\text{H}_{38}$. Going from the *n*-isomer to the 3-methyl isomer lowers the melting point by 34°C . The melting points of com-

Table 1.15 Melting points of three C_{18} paraffins (after [1.62])

Compound	Melting point ($^\circ\text{C}$)
<i>n</i> -Octadecane	28
2-Methylheptadecane	6
3-Methylheptadecane	-6

pounds in mixtures differ from pure-compound melting points, and melting point is not the same as cloud point or pour point. Even so, the magnitudes of the changes in melting point are consistent with the changes in cloud and pour points.

Olefin isomerization converts straight-chain C_4 – C_6 olefins into the corresponding *iso*-olefins, which can be used as feeds to alkylation units (Sect. 1.11.3, *Alkylation Chemistry*).

Acid/Base Reactions:

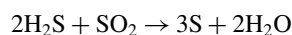
Amine and Caustic Scrubbing

Several processes entail seemingly simple acid–base reactions. Treating with alkanolamines removes acid gases – H_2S and CO_2 – from fuel gas and off-gas streams. In refineries, H_2S -laden amines go to the sulfur recovery unit. There, the H_2S is stripped off with steam, and the amine is recirculated. The H_2S goes to a modified Claus unit, where it is converted into elemental sulfur.

Caustic scrubbers are used in several ways, including removing the last traces of H_2S from the hydrogen used for processes in which the catalysts are highly sulfur sensitive.

Modified Claus Process Chemistry

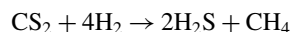
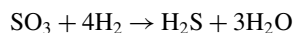
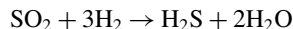
Modified Claus sulfur-recovery units burn hydrogen sulfide in enough air to form a mixture of H_2S and SO_2 in a 2 : 1 molar ratio. In downstream beds of alumina catalyst, H_2S reacts with SO_2 in the Claus reaction to form elemental sulfur and water. The product sulfur can include many different isomers of S_x



Claus Tail Gas Recovery Chemistry

Claus units achieve up to 96% conversion of H_2S into sulfur. The Claus tail gas contains SO_2 , SO_3 , COS , CS_2 ,

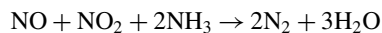
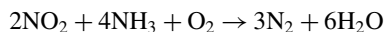
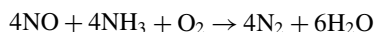
and volatile forms of sulfur. The carbon comes from CO_2 or methane, both of which can be present in the feed gas. Tail-gas treating units (TGTU) bring the total sulfur recovery up to $> 99.9\%$. Most tail-gas treating processes send the tail gas to a hydrotreater, which converts all sulfur-containing compounds into H_2S



In the SCOT process, offered by Shell Global Solutions, the H_2S is absorbed by an alkanolamine and returned to the front of the Claus furnace. In the LO-CAT process, offered by Merichem, H_2S is air oxidized to sulfur in an aqueous solution containing a chelated iron catalyst. For all tail-gas treatment processes, the last traces of unrecovered sulfur go to an incinerator, where they are converted by reaction with air into SO_2 and dispersed into the atmosphere.

Catalytic NO_x Removal Chemistry

Selective catalytic reduction (SCR) removes nitrogen oxides (NO_x) by reaction with ammonia to produce nitrogen via the following main reactions. Secondary reactions involve sulfur oxides and ammonium sulfates.



1.11.4 Petroleum Refining Processes

Separation

Separation processes in refineries are mainly based on volatility and solubility. They include distillation, extraction, and settling. Settling allows dirt and brine to disengage from the oil prior to shipment or processing.

Crude Oil Distillation

Figure 1.31 illustrates a crude oil distillation complex. As mentioned, when crude oil is extracted from underground, it is mixed with a variety of substances: gases, water, salt, and dirt. These must be removed before the crude can be transported effectively and refined without undue fouling and corrosion. Some cleanup occurs in oil fields and midstream processes such as the preparation of syncrudes. In refineries, crude desalting units provide subsequent cleanup.

A field separator at a well site is often no more than a large covered vessel that provides enough residence time for gravity separation into four phases: gases, crude oil, water, and solids. Generally, the crude oil floats on the water. The water is withdrawn from the bottom and is disposed at the well site. Gases are withdrawn from the top and piped to a natural gas processing plant or reinjected into the reservoir to maintain well pressure. Crude oil is pumped either to a refinery through a pipeline or to storage to await transportation by other means.

At the refinery, the crude is treated with hot water in one or more desalters. Desalters employ either chemical or electrostatic precipitators to remove dissolved salts and collect remaining solids. In chemical desalt-

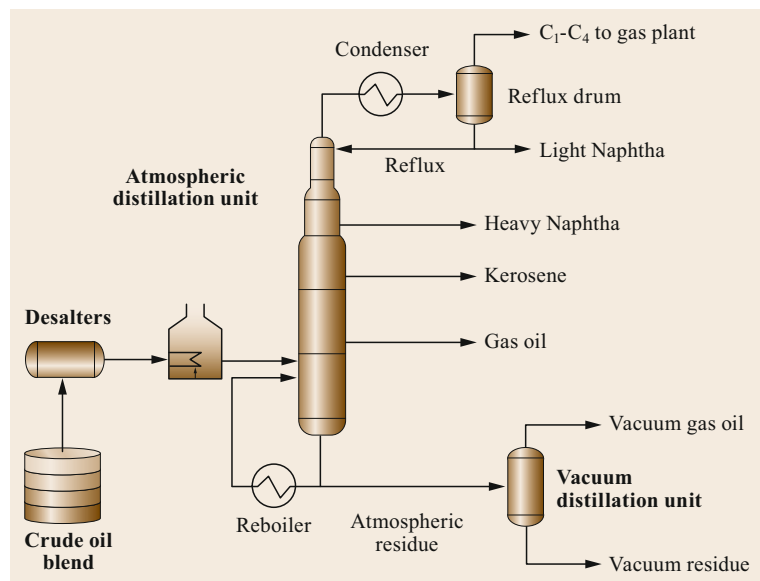


Fig. 1.31 Two-stage crude oil distillation unit with desalting, atmospheric distillation, and vacuum distillation

ing, water and surfactants are added to the crude, heated to dissolve salts and other impurities, and then sent to a settling tank, where the water and oil separate. In electrostatic desalting, chemicals are replaced with a strong electrostatic field at 12–35 kV, which drives the separation of water from oil. Coalescence is aided by passage through a tower packed with sand, gravel, and the like. Emulsion can be broken by adding chemicals, such as demulsifiers.

If the crude is not desalted, residual solids can clog downstream equipment and deposit on heat exchanger surfaces, thereby reducing heat-transfer efficiency. Salts can induce corrosion in major equipment and deactivate catalysts.

Before reaching the atmospheric distillation tower shown in Fig. 1.32, desalted oil goes through a network

of pre-heat exchangers to a fired heater, which brings the temperature up to 657–725 °F (347–385 °C). If the oil gets much hotter than this, it starts to crack, generating carbon. The carbon would deposit inside the pipes and equipment through which the oil flows.

As shown in Fig. 1.32, the hot crude enters the tower just above the bottom. Steam is added to enhance separation; it does so largely by decreasing the vapor pressure of hydrocarbons in the column. When it enters the tower, most of the oil vaporizes. Unvaporized oil drops to the bottom of the tower, from where it is drawn off. The vapors rise through the distillation trays, which contain perforations, bubble caps, downcomers, and/or modifications thereof. Each tray permits vapors from below to bubble up through the relatively cool condensed liquid on top of the tray. This vapor/liq-

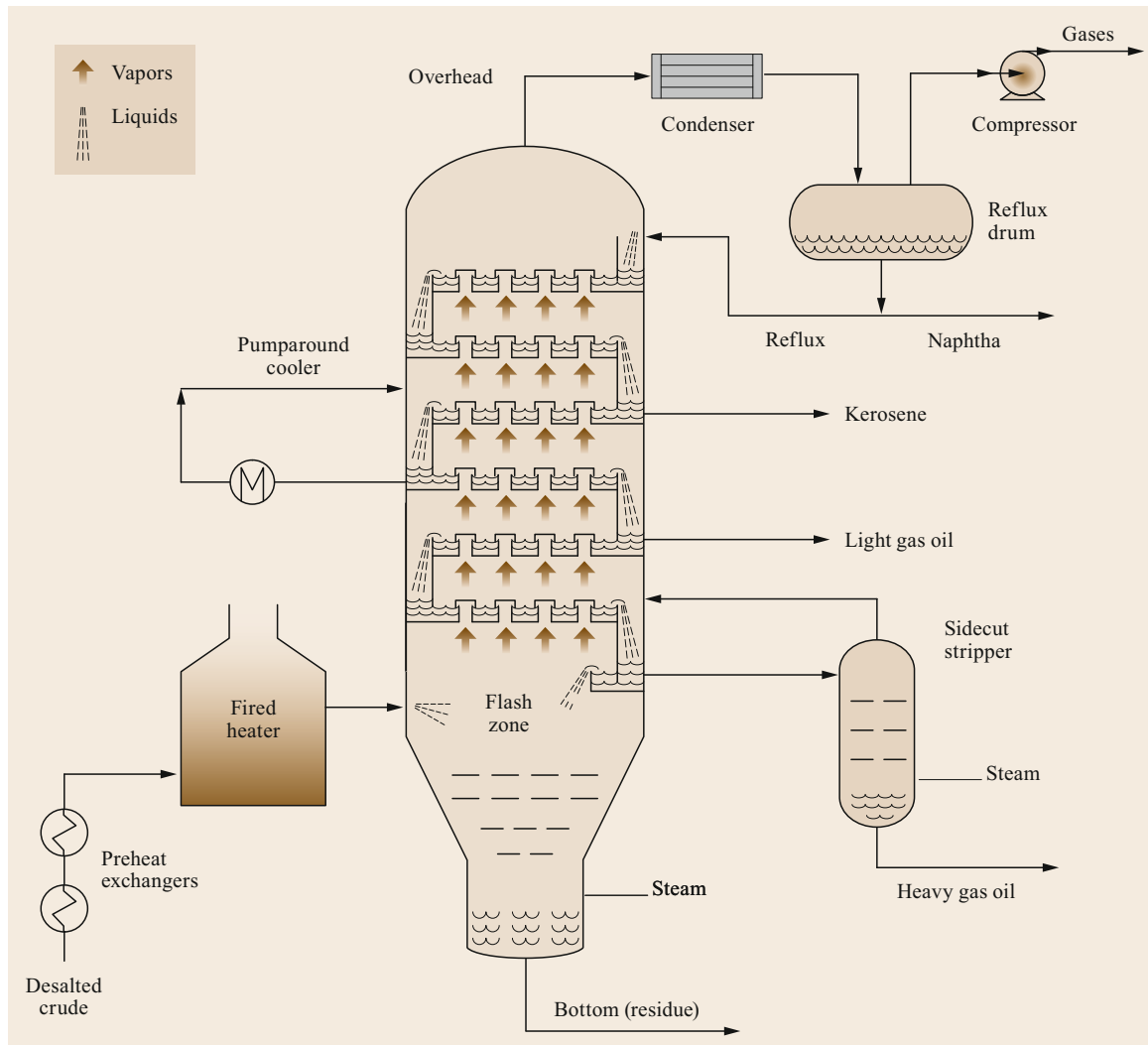


Fig. 1.32 Atmospheric distillation tower with bubble-cap trays, one pumparound, and three side draws

uid contact knocks heavy material out of the vapor. Condensed liquid flows down through a downcomer to the hotter tray below, where the higher temperature causes re-evaporation. A given molecule evaporates and condenses many times before finally leaving the tower.

Products are collected from the top, bottom, and side of the column. Side-draw products are taken from trays where the temperature corresponds to the cut-points for a desired product. Some of the side-draws can be returned to the tower as a pump-around or pump-back stream to control tower temperatures and improve separation efficiency. Reflux plays a major role in controlling temperature and enhancing separation at the top of the tower, where gases and light naphtha are drawn off overhead. Reflux ratio is the amount of reflux liquid returning to distillation tower to the amount of liquid withdrawn as product per unit time. With a higher reflux ratio, fewer theoretical plates are required. There is a reboiler at the bottom of tower to ensure that light components are not carried out of the bottom of tower.

Products from the crude distillation unit go to other process units, as shown in Table 1.16.

The bottom stream from the main fractionator (atmospheric distillation tower) is called atmospheric bottom, atmospheric residue, reduced crude, or long resid. It goes to a second fired heater, where the typical outlet temperature is about 750–775 °F (400–413 °C). From the second heater, the atmospheric residue goes to a vacuum distillation tower. Steam ejectors reduce the absolute pressure to about 7.0 psi (0.5 bar). Under this so-called vacuum, hydrocarbons vaporize at lower temperatures than atmospheric boiling points. For example, if the atmospheric equivalent boiling point of a com-

pound is ≈ 1050 °F (565 °C), then its boiling point under 40 mmHg vacuum is around 800 °F (427 °C). Hence, in a vacuum distillation unit, the molecule is far less likely to undergo thermal cracking and far more likely to undergo vaporization.

Solvent Refining

Solvent refining processes include solvent deasphalting, solvent extraction, and deoiling/dewaxing processes.

Solvent Deasphalting. Solvent deasphalting takes advantage of the fact that aromatic compounds are insoluble in paraffins. Unwanted deasphalting can occur during attempts to blend incompatible crudes and distillates.

Propane and *n*-pentane are used to precipitate asphaltenes from residual oils. The deasphalted oil (DAO) is sent to hydrotreaters, FCC units, hydrocrackers, or fuel-oil blending. In FCC units, DAO is easier to process than the corresponding straight-run residue. This is because the asphaltene content of DAO is very low. The asphaltenes in straight-run residue easily form coke and often contain catalyst poisons such as nickel and vanadium. Although DAO no longer contains asphaltenes, it still has a very high endpoint. Hence, DAO is harder to process than straight-run VGO and FCC cycle oils in hydrocrackers.

In traditional propane deasphalting, residual oil and propane are pumped to an extraction tower at 150–250 °F (65–120 °C) and 350–600 psig (2514–4240 kPa). Separation occurs in a tower, which may include a rotating disk contactor. Liquid products are evaporated and steam stripped to recover the propane solvent, which is recycled.

Table 1.16 Destinations for straight-run distillates. Resid is an abbreviation for residua, and 340+ etc. means everything that boils above 340 °C etc.

Fraction	Approx. boiling range		Next destination	Ultimate product(s) or subsequent destination
	(°C)	(°F)		
LPG	–42–0	–44–31	Sweetener	Propane fuel
Light naphtha	39–85	80–185	Hydrotreater	Gasoline, petrochemical plant
Heavy naphtha	85–200	185–390	Cat. reformer	Gasoline, aromatics
Kerosene	170–270	340–515	Hydrotreater	Jet fuel, No. 1 diesel
Gas oil	180–340	350–650	Hydrotreater	Heating Oil, No. 2 diesel
Atmos. resid	340+	650+	Visbreaker	FCC or hydrocracker feed, low-viscosity resid
			Resid hydrotreater	Resid FCC
			Ebullated bed hydrocracker	Naphtha, gas oils, FCC
Vacuum gas oil	340–566	650–1050	FCC	Gasoline, LCO, gases including C ₃ /C ₄ olefins
			Hydrotreater	Fuel oil, FCC, lubes
			Hydrocracker	Naphtha, jet, diesel, FCC, olefins, lubes
			Solvent refining	DAO, asphalt
Vacuum resid	540+	1000+	Coker	Coke, coker gas oil, coker naphtha, gases
			Solvent refining	DAO, asphalt
			Residue hydrocracker	Traditional hydrotreater, hydrocracker, heavy fuel oil

An advanced version of solvent deasphalting is *residuum oil supercritical extraction* or ROSE. The ROSE process was developed by the Kerr-McGee Corporation and is now offered for license by KBR. In this process, residue and solvent are mixed and the extractor temperature is typically maintained below the solvent's critical temperature. As the extraction temperature approaches the solvent's critical temperature, the DAO rapidly becomes less and less soluble in the solvent. Increasing the extraction temperature reduces the solubility of the heavier components of the feedstock, improving DAO quality but reducing DAO yield [1.81]. Liquid yields are higher under supercritical conditions, because the lighter part of the oil becomes more soluble. In addition to giving higher yields, the process is more energy efficient and has lower operating costs due to improved solvent recovery. The ROSE process can employ three different solvents, the choice of which depends upon process objectives:

- *Propane*: Preparation of lube base stocks
- *Butane*: Asphalt production
- *Pentane*: Maximum recovery of liquid.

Solvent Extraction. Solvent extraction removes aromatics and other impurities from lube base stocks and grease stocks. The feedstock is dried, and then contacted with the solvent in a counter-current or rotating disk extraction unit. The solvent is separated from the product stream by heating, evaporation, or fractionation. Remaining traces of solvent are removed from the raffinate by steam stripping or flashing. Electrostatic precipitators can enhance the separation of inorganic compounds. The solvent is then regenerated and recycled. Today, phenol, furfural, *N*-methyl-2-pyrrolidone (NMP) and cresylic acid are widely used as solvents. Liquid sulfur dioxide, chlorinated ethers, and nitrobenzene also have been used.

Solvent Dewaxing. This process removes wax (normal paraffins) from deasphalted oils. The main process steps include mixing the feedstock with the solvent, chilling the mixture to crystallize wax, and recovering the solvent. Commonly used solvents include toluene and methyl ethyl ketone (MEK). Methyl isobutyl ketone (MIBK) is used in a *wax deoiling* process to prepare food-grade wax, which is used to coat the paper used for milk cartons and other such products.

Visbreaking

Visbreaking is a mild form of thermal cracking that achieves about 15% conversion of atmospheric residue into gas oils and naphtha. At the same time, a low-viscosity residual fuel is produced. The main purpose of

visbreaking is not for conversion, but viscosity reduction for fuel oil. The two main types of visbreaking are *short-contact* and *soaker*. In short-contact visbreaking, the feed is heated to about 900 °F (480 °C) in furnace tubes (coils) and sent to a soaking zone reactor at 140–300 psig (1067–2170 kPa). The elevated pressure allows cracking to occur while restricting coke formation. To avoid over-cracking, the residence time in the soaking zone is short – several minutes (typically 1–3 min) compared to several hours in a delayed coker. The hot oil is quenched with cold gas oil to inhibit further cracking and sent to a vacuum fractionator for product separation. Soaker visbreaking keeps the hot oil at about 800 °F (430 °C) in a drum after the furnace for a longer time to increase the yield of middle distillates. Low-viscosity visbreaker gas oil can be sent to an FCC unit or hydrocracker for further processing, or used as heavy fuel oil.

Delayed Coking

Delayed coking is a cyclic process that employs more than two coke drums – typically at least four. The drums operate on staggered 18–24 h cycles. Each cycle includes preheating the drum, filling it with hot oil, allowing coke and liquid products to form, cooling the drum, and decoking the drum. As it is pumped into a drum, vacuum residue feed is heated to about 900–970 °F (487–520 °C). Thermal cracking begins immediately, generating coke and cracked products. Coke accumulates in the drum, while the vapors enter a product fractionator. Meanwhile, hot feed keeps flowing into the drum until it is filled with solid coke. At the end of a cycle, the top and bottom heads of the drum are removed. A rotating cutting tool uses high-pressure jets of water to drill a hole through the center of the coke from top to bottom. In addition to cutting the hole, the water also cools the coke, forming steam as it does so. The cutter is then raised, step by step, cutting the coke into lumps, which fall out the bottom of the drum.

Light products include coker naphtha, light coker gas oil (LCGO), and heavy coker gas oil (HCGO). All of these require further processing due to their high content of olefins, which makes them unstable and poorly suited for direct blending into finished products. The coker naphtha and LCGO are hydrotreated. The HCGO can go either to an FCC unit or a hydrocracker. Coke can account for up to 30 wt% of the product.

Fluid (Continuous) Coking

Fluid coking, also called continuous coking, is a moving-bed process for which the operating temperature is higher than the temperatures used for delayed coking. In continuous coking, hot recycled coke particles are combined with liquid feed in a radial reactor

at about 50 psig (446 kPa). Vapors are taken from the reactor, quenched to stop any further reaction, and fractionated. The hot coke goes to a surge drum, and then to a classifier where the larger coke particles are removed as product. The smaller coke particles are recycled to a surge drum (preheater), where they are mixed with fresh feed then sent to the reactor through a transfer line. Coking occurs both in the reactor and in the surge drum. Depending on the feed, 15–25% of the coke is burned with air to satisfy the heat requirements of the process, such as maintaining reactor temperature and sustaining thermal cracking reactions. Installation costs for fluid coking are higher than for delayed coking, but heat losses are lower. Fluid coking makes more fuel gas than delayed coking.

Flexicoking

Flexicoking is a version of fluid coking developed by ExxonMobil. Coke is gasified in an integrated steam air gasifier to produce clean CO and H₂ flue gas, instead of coke as product. Flexsorb hindered amine, also developed by ExxonMobil, is used to reduce H₂S to a low level.

Fluid Catalytic Cracking (FCC)

Fluid catalytic cracking (FCC) produces more than half the world's gasoline. It generates middle distillate streams (cycle oils) for further refining or blending. It also produces a large quantity of high-quality steam.

FCC Process Flow. A typical FCC unit (Fig. 1.33) comprises three major sections – riser/reactor, regenerator, and fractionation. In the riser/reaction section, preheated oil is mixed with hot, regenerated catalyst. The mixture acts as a fluid because the catalyst particles are quite small. The hot catalyst vaporizes the oil, and the vaporized oil carries the catalyst up the riser/reactor. The cracking reaction is very fast. It produces light gases, high-octane gasoline, and heavier products called light cycle oil (LCO), heavy cycle oil (HCO), slurry oil, and decant oil. It also leaves a layer of coke on the catalyst particles, rendering them inactive.

At the top of the riser, the riser outlet temperature (ROT) can reach 900–1020 °F (482–549 °C). The ROT determines conversion and affects product selectivity, so FCC operators control it as tightly as possible. Higher temperatures favor production of olefin-

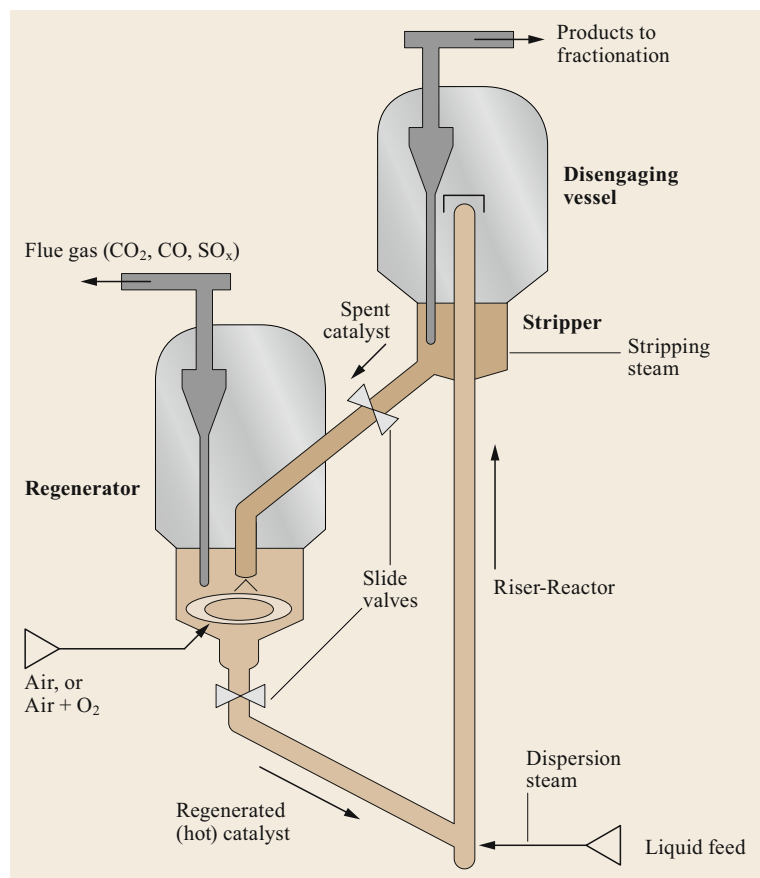


Fig. 1.33 FCC process flow

rich light gases, especially propylene, at the expense of gasoline; many FCC units maximize refinery-grade propylene for purification and use in nearby olefin plants. Moderate temperatures favor gasoline production. Lower temperatures decrease gasoline yields and increase heavier products – LCO and HCO.

In the disengaging section, steam helps separate the now-deactivated catalyst from the reaction products. The catalyst goes to the regenerator, where the coke is burned away by fluidized combustion in the presence of air or oxygen-enriched air. The regenerated catalyst is hot, with temperatures up to 1350 °F (732 °C). It returns to the riser/reactor, where the cycle begins again.

In a 60 000 bbl/day unit processing a typical mixture of vacuum gas oils, the total catalyst in the unit (the *inventory*) is 400–500 t. To maintain activity, about 0.5–1 wt% of the inventory is replaced each day. If the feed to the unit contains significant amounts of residue, the replacement rate is higher. The discharged catalyst is cooled and shipped either to a land fill for disposal or to another refiner, which might need *conditioned* FCC catalyst.

Table 1.17 Representative FCC heat duty

Factor	Portion of total
Heat up and vaporize fresh feed	40–50%
Heat recycled oil	0–10%
Heat of reaction (endothermic)	15–30%
Heat steam	2–8%
Heat losses	2–5%
Heat air to regenerator temperature	15–25%
Heat coke from the reactor to regenerator temperature	1–2%
Total heat duty	500–1000 BTU/lb 1160–2325 kJ/kg

Table 1.18 Feeds and products for hydroprocessing units

Feeds	Products from hydrotreating	Products from hydrocracking
Heavy naphtha	Catalytic reformer feed	LPG
Straight-run light gas oil	Middle distillate fuels	Naphtha
Straight-run heavy gas oil	Diesel fuel	Naphtha
Atmospheric residue	Lube base stock, low-sulfur fuel oil, RFCC ^a feed	Naphtha, middle distillates, FCC feed, lube base stock
Vacuum gas oil	FCC feed, lube base stock	Naphtha, middle distillates, FCC feed, lube base stock, olefin plant feed
Vacuum residue	RFCC ^a feed	See note ^b
FCC LCO	Diesel blend stocks, fuel oil	Naphtha
FCC HCO	Blend stock for fuel oil	Naphtha, middle distillates
Visbreaker gas oil	Diesel blend stocks, fuel oil	Naphtha, middle distillates
Coker gas oil	FCC feed	Naphtha, middle distillates, FCC feed, lube base stock, olefin plant feed
Deasphalted oil	Lube base stock, FCC feed	Naphtha, middle distillates, FCC feed, lube base stock

^a RFCC = *residue FCC* or *reduced crude FCC*. This process is designed for feeds that contain high concentrations of carbon-forming compounds, ^b Traditional fixed-bed hydrocrackers cannot process vacuum residue. However, ebullated-bed and slurry-phase hydrocrackers can. Products from the latter include naphtha, middle distillates, and FCC feed

FCC Heat Balance. FCC units must be heat balanced, or they would not run. The burning of coke deposited on the catalyst in the regenerator provides all of the heat required by the process. In fact, FCC units are significant sources of high-quality steam for other refinery units. Table 1.17 gives a representative breakdown of FCC heat requirements.

Residue FCC. Some FCC units process significant amounts of residue. These units use catalyst coolers (e.g., steam coils) in the regenerator or a second-regeneration zone to remove excess heat from the unit. This is because residue generates substantially more coke than conventional FCC feeds, and excess heat is generated when the extra coke is burned off the catalyst. Steam for other process units is generated from the excess heat. The trace-metal content of residues can be very high. Trace metals destroy FCC catalysts, so removing them – usually with hydrotreating or solvent deasphalting – is essential.

Hydroprocessing

Hydroprocessing includes hydrotreating and hydrocracking. In hydrocracking, C–C bonds are broken, but in hydrotreating, for the most part they are not. The flow schemes for fixed-bed hydrotreating and hydrocracking units are similar. Hydrotreating is an essential precursor to fixed-bed gas oil hydrocracking. Feeds and products for typical hydrotreaters and hydrocrackers are shown in Table 1.18.

Figure 1.34 shows a fixed-bed hydroprocessing unit with two reactors, four flash drums, an amine unit, and emergency depressuring (EDP). The unit shown is a hydrocracker, as indicated by hydrocracking catalyst in the second reactor (R2). Preheated feed mixes with hy-

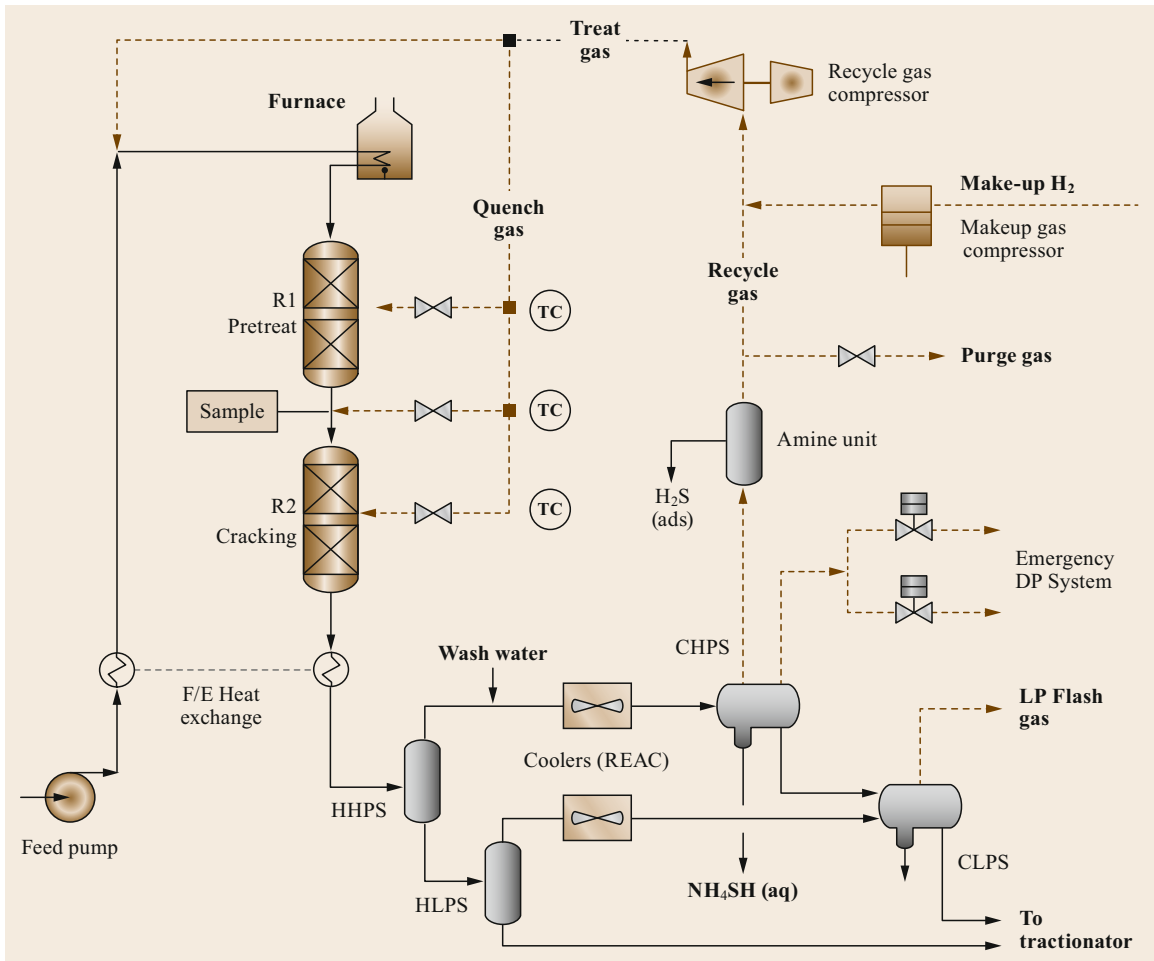


Fig. 1.34 Fixed-bed hydrocracking flow sketch with two reactors, four flash drums, amine unit, and emergency depressuring (EDP). F/E = feed/effluent, TC = temperature controller, HHPS = hot high-pressure separator, HLPS = hot low-pressure separator, CHPS = cold high-pressure separator, and CLPS = cold low-pressure separator. Hydrotreaters seldom include EDP

drogen and flows down through the catalyst-containing reactors. Some units mix hydrogen with oil and heat the mixture, as shown. In others, the hydrogen is heated first and mixed with preheated feed. Upon exiting the reactors, the reaction fluids go through a heat exchanger train to the separators (flash drum). Prior to the cold low-pressure separator, wash water is added to remove NH_3 which reacts with water and H_2S to form aqueous NH_4SH ; the aqueous NH_4SH is drained from the CHPS. The HHPS liquid flows to the HLPS, and then to the fractionator (not shown). The HLPS overhead goes to the CLPS. The CLPS overhead goes to a stripper, and the CLPS liquid goes to the fractionator. The emergency depressuring system, as shown, includes two independent lines. The hydrocracking chapter (Chap. 22) discusses process design in more detail.

Hydrotreating

Hydrotreating removes sulfur, nitrogen, and oxygen from organic sulfur, nitrogen, and oxygen compounds. The hetero atoms are transformed into H_2S , NH_3 , and H_2O , respectively. Under reaction conditions, these remain in the gas phase. But at lower temperatures, the H_2S and NH_3 combine and dissolve in process water to form aqueous ammonium bisulfide (NH_4SH). Ammonia also reacts with chlorides to form NH_4Cl ; chloride can come into the unit with makeup gas, feed, or wash water. These salts may deposit in air coolers and heat exchangers, blocking flow and – even worse – inducing corrosion. Fortunately, they are water-soluble, so they can be controlled by injecting wash water into the reactor effluent.

FCC Feed Pretreating. These days, most refiners pretreat FCC feeds in a fixed-bed hydrotreater. The hydrotreater removes trace metal contaminants such as nickel and vanadium. Nickel increases coke formation and decreases liquid yields. Vanadium reduces conversion, decreases liquid yields, and destroys the catalyst. In addition to removing Ni and V, the pretreater decreases concentrations of sulfur, nitrogen, and aromatics. In the FCC regenerator, sulfur on the coked catalyst is converted to sulfur oxides (SO_x) in the flue gas. Clean air regulations restrict SO_x emissions, which cause acid rain. Therefore, removing sulfur from the FCC feed – thereby reducing SO_x formation in the FCC regenerator – is highly beneficial. Removing nitrogen is beneficial, too, because basic feed nitrogen suppresses the activity of highly acidic FCC catalysts. Pretreating also saturates aromatics. As we have seen, saturating uncrackable aromatics converts them into crackable naphthenes, so pretreating increases FCC conversion, often by more than 10 vol.%.

FCC Gasoline Post-Treating. Conventional hydrotreating does a good job of removing sulfur from FCC gasoline. Unfortunately, it also does a good job of reducing octane by saturating C₆–C₁₀ olefins. In processes such as Prime-G+, offered for license by Axens,

full-range naphtha is split into light and heavy fractions. The light fraction contains most of the high-octane olefins but not much of the sulfur. After diolefins are removed via selective hydrogenation, the light cut is ready for gasoline blending. The heavy fraction contains most of the sulfur but not much of the olefins. It is hydrotreated conventionally. The ConocoPhillips S Zorb process uses selective adsorption to remove sulfur from FCC gasoline. The feed is combined with a small amount of hydrogen, heated, and injected into an expanded fluid-bed reactor, where a proprietary sorbent removes sulfur from the feed. A disengaging zone in the reactor removes suspended sorbent from the vapor, which exits the reactor as a low-sulfur stock suitable for gasoline blending. The sorbent is withdrawn continuously from the reactor and sent to the regenerator section, where the sulfur is removed as SO₂ and sent to a sulfur recovery unit. The clean sorbent is reconditioned and returned to the reactor. The rate of sorbent circulation is controlled to help maintain the desired sulfur concentration in the product.

Fixed-Bed Catalytic Hydrocracking

As with other conversion processes, hydrocracking breaks carbon–carbon bonds, thereby converting heavy hydrocarbons into lighter ones. An integral part of

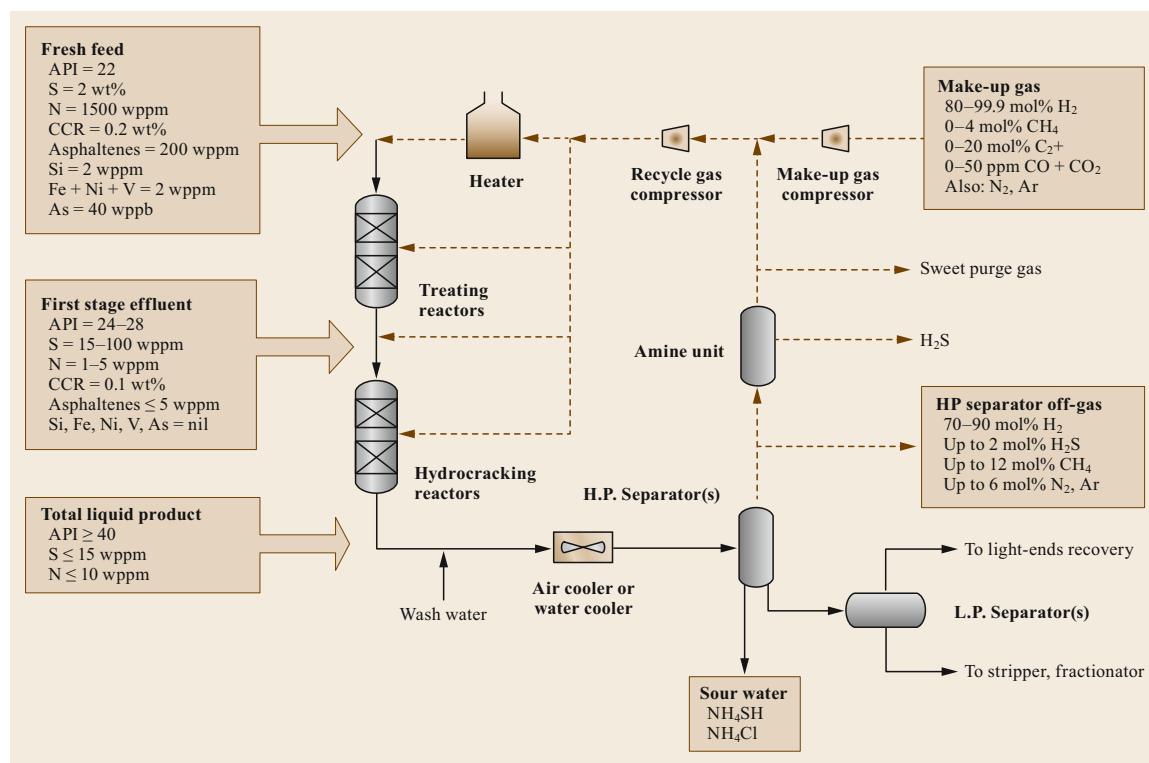


Fig. 1.35 Once-through hydrocracking process flow with selected stream properties

hydrocracking is hydrotreating, which in fixed-bed units removes almost all oxygen, sulfur, nitrogen, and trace elements from the feed before it reaches the cracking catalyst. Organic nitrogen poisons acidic cracking sites, so its removal is essential. Along the way, hydrocracking also isomerizes *n*-paraffins and saturates olefins and aromatics. With respect to equipment and process flow, fixed-bed hydrocrackers are similar to fixed-bed hydrotreaters.

Figure 1.35 shows a two-reactor once-through hydrocracker with four catalyst beds, along with some typical properties for feed and product streams. Figure 1.36 shows iconic examples of commercial hydrocracker configurations. The purpose of recycling unconverted oil is to increase overall conversion.

As shown in Table 1.19, a fixed-bed recycle hydrocracking unit can have significant product flexibility,

producing either large amounts of C₄-plus naphtha or large amounts of middle distillates in the same unit with the same catalyst, just by adjusting temperatures and cut points. In petroleum refining, this kind of process flexibility is unique.

Ebullated Bed Hydrocracking

In contrast to fixed-bed hydrocrackers, ebullated bed (e-bed) units can process large amounts of residual oils. Catalyst life does not limit these units, because fresh catalyst is added and spent catalyst is removed continuously. In such units, it is impossible to segregate catalysts, so the catalyst accomplishes both hydrotreating and hydrocracking. In e-bed reactors (Fig. 1.37), hydrogen-rich recycle gas is bubbled up through a mixture of oil and catalyst particles. This provides three-phase turbulent mixing, which is needed to ensure

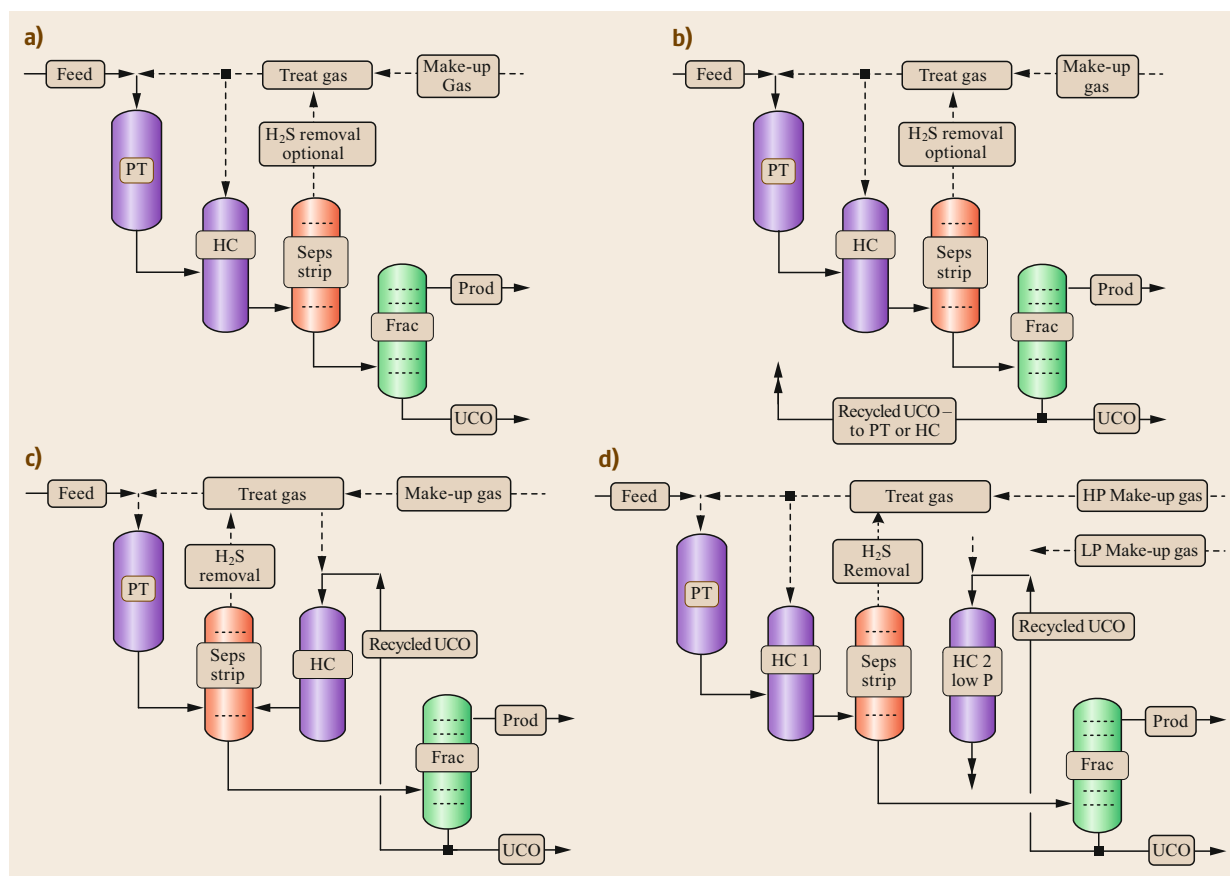


Fig. 1.36a–d Four simplified examples of hydrocracker flow configurations. (a) Once-through. (b) Series flow, in which reactants go directly from the pretreat section to hydrocracking section without intermediate stripping or fractionation, and in which unconverted oil (UCO) is recycled either to the first pretreat (PT) reactor or the first hydrocracking (HC) reactor. (c) Separate pretreat, where the products from the pretreat section are stripped and fractionated before going to the hydrocracking section. (d) Two-stage, in which UCO goes to a 2nd hydrocracking section. Some two-stage units have an independent recycle gas system, and hence can operate at lower pressure in a sweet environment free of H₂S, NH₃, and organic nitrogen

Table 1.19 Hydrocracking product flexibility

Feed	Straight-run vacuum gas oil		
Boiling range (°C)	340–550		
Boiling range (°F)	644–1020		
API gravity	22.0		
Specific gravity	0.9218		
Nitrogen (wppm)	950.0		
Sulfur (wt%)	2.5		
Primary product objective	Naphtha	Kerosene	Gas oil
Weighted average reactor temp (°C)	Base	–6	–12
Weighted average reactor temp (°F)	Base	–11	–22
Product yields, vol. % Fresh Feed			
Butanes	11	8	7
Light naphtha	25	18	16
Heavy naphtha	90	29	21
Kerosene or gas oil	–	69	77
Total C ₄ -plus	126	124	121
Chemical H ₂ consumption (Nm ³ /m ³)	345	315	292
Chemical H ₂ consumption (Scf/bbl)	2050	1870	1730
Product qualities			
Light naphtha (C ₅ –82 °C)			
RON (research octane number) Clear	79	79	80
Heavy naphtha			
P/N/A	45/50/5	44/52/4	–
RON clear	41	63	67
End point (°C) [°F]	216 [421]	121 [250]	118 [244]
Kerosene			
Flash point (°C) [°F]	–	38 [100]	–
Freeze point (°C) [°F]	–	–48 [–54]	–
Smoke point (mm)	–	30	–
FIA aromatics (vol.%)	–	7	–
End point (°C) [°F]	–	282 [540]	–
Gas Oil			
Cloud point (°C) [°F]	–	–	–15 [5]
API gravity	–	–	44
Cetane number	–	–	55
Flash point (°C) [°F]	–	–	52 [126]
End point (°C) [°F]	–	–	349 [660]

a uniform temperature distribution. The process can tolerate significant differences in feed quality, because in addition to manipulating temperature, operators can change catalyst addition rates. Catalyst consumption is determined by the concentrations of trace metals – particularly Fe, Ni, and V – in the feed.

At the top of the reactor, catalyst is disengaged from the process fluids, which are separated in downstream flash drums. Most of the catalyst is returned to the reactor. Some is withdrawn and replaced with fresh catalyst. When compared to fixed-bed processes, e-bed technology offers the following advantages:

- The ability to achieve more than 70 wt% conversion of atmospheric residue.

- Ample free space between catalyst particles, which allows entrained solids to pass through the reactor without accumulation, plugging, or build-up of pressure drop.
- Better liquid-product quality than delayed coking.

Disadvantages of e-bed technology versus fixed-bed processes include high catalyst attrition, which leads to high rates of catalyst consumption; higher installation costs due to larger reactor volume and higher operating temperatures; and sediment formation. Recent improvements include second-generation catalysts with lower attrition; catalyst rejuvenation, which allows the reuse of spent catalysts; improved reactor design leading to

higher single-train feed rates; and two-reactor layouts with inter-stage separation.

Slurry-Phase Hydrocracking

Slurry-phase hydrocracking can achieve up to 95 wt% conversion of vacuum residue, coal, or coal tar. Reaction temperatures are about 840 °F (450 °C) and pressures range from 2000 to 3000 psig (14 000–20 800 kPa). Slurry-phase hydrocracking employs finely divided solid additives, which are proprietary and not necessarily catalytic. Inside the reactor, the liquid/additive mixture behaves as a single phase due to the small size of the additive particles. The additives prevent bulk coking by providing highly dispersed nucleation sites for *micro coking*. The additive is not recovered. Instead, it ends up in a pitch fraction, which comprises roughly 5 wt% of the feed.

Slurry-phase hydrocracking has several advantages:

- It can achieve up to 95 wt% conversion of vacuum residue. It can also achieve high conversion of coal.
- In two-stage designs, which incorporate fixed-bed hydrotreating and hydrocracking, product quality is excellent.
- Feeds can include vacuum residue, FCC slurry oil, and even coal.
- The additive is low cost and disposable. Due to the micronic size of the additive, it flows like a liquid through the process.
- For a given volume of residue feed, total slurry phase reactor volume is lower than the reactor volume of e-bed processes.

A significant disadvantage is the production of low quality, refractory pitch. At high conversion, the pitch is so poor that it cannot be blended into bunker oil or asphalt; it has been blended with coal, sent to a metals reclaimer, or used in a cement plant as clinker.

LC-MAX Process

The LC-MAX process, developed by Chevron Lummus Global (CLG) and CB&I, is an innovative approach to residue hydrocracking. It combines two stages of LC FINING with solvent deasphalting (SDA). While the overall conversion of VR may be lower than that for slurry hydrocracking, all products, including the asphalt, can be sold conventionally. LC-MAX operates at lower pressures than slurry hydrocracking and therefore is less costly. LC-MAX also is more flexible: the product VGO is stable and can be sold as-is, sent to an FCC unit, sent to a conventional hydrocracking unit, etc.

Catalytic Reforming

The three major process flow schemes for catalytic reforming are:

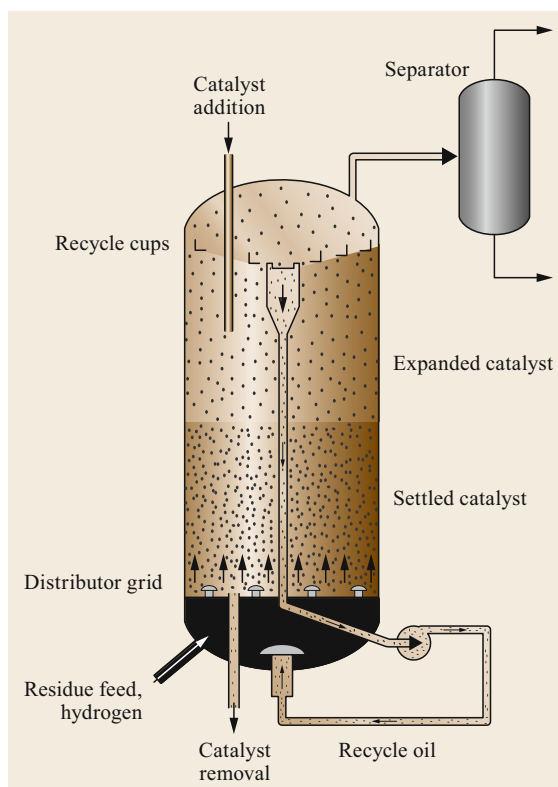


Fig. 1.37 Ebullated bed hydrocracking process flow

- Semiregenerative
- Cyclic
- Continuous catalyst regeneration (CCR).

Figure 1.38 shows a fixed-bed semiregenerative reformer. Catalyst cycles last from 6 to 12 months. A cycle ends when the unit is unable to meet its process objectives – typically octane number and overall C₅-plus yields. At the end of a cycle, the entire unit is brought down and coke is burned off the catalyst. Desulfurized naphtha is mixed with hydrogen, heated to > 900 °F (> 480 °C), and passed through a series of fixed-bed reactors. The feed is spiked with an organic chloride, which converts to hydrogen chloride in the reactors. This provides the required catalyst acidity and helps minimize catalyst coking.

The major chemical reactions – dehydrogenation and dehydrocyclization – are endothermic and the reactors are adiabatic. Consequently, the temperature drops as reactants flow through a reactor. Between reactors, heat from fired heaters brings the process fluids back to desired reactor inlet temperatures (RIT). The last reactor effluent is cooled and sent to a separator, from which hydrogen-rich gas is recovered. Part of the hydrogen is recycled to the reactors. The remainder –

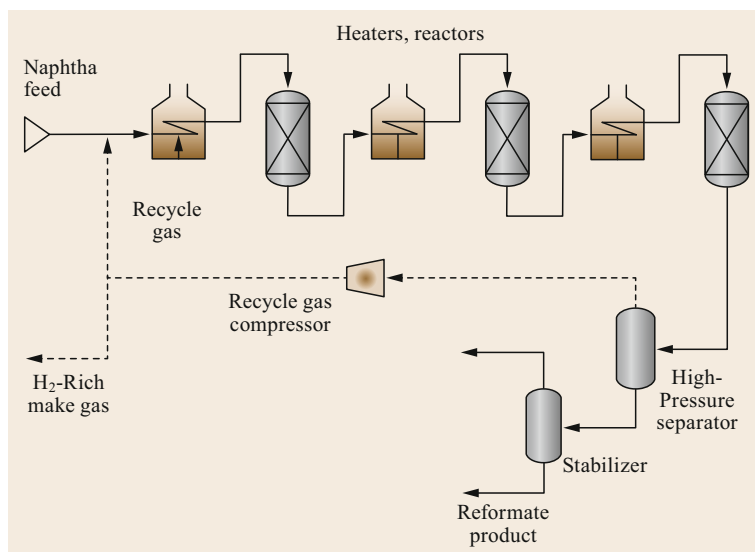


Fig. 1.38 Semiregenerative catalytic reforming process flow

the *net gas* – goes to a hydrogen header for distribution to hydrogen-consuming units. The liquid product flows to a stabilizer column, where entrained gases are removed, before going to the gasoline blender or aromatics plant.

A cyclic reformer has more reactors, and catalyst cycles are shorter, that is, 20–40 h. Shutdowns are staggered so that only one reactor is down at a given time.

The UOP Platforming process, which employed a platinum-based catalyst, was commercialized by UOP in 1949. In 1971, UOP commercialized the CCR Platforming process, shown in Fig. 1.39, which has several advantages. CCR means continuous catalyst regeneration. Hydrotreated feed mixes with recycle hydrogen and goes to a series of adiabatic, radial-flow reactors arranged in a vertical stack. Catalyst flows down the stack, while the reaction fluids flow radially through the catalyst beds. Heaters are used between reactors to reheat the reaction fluids to the required temperature. Flue gas from the fired heaters is typically used to generate steam.

A CCR reforming unit can operate at very low pressure (100 psig, 791 kPa). The low pressure improves yields of aromatics and hydrogen. It also accelerates coke formation, but that is okay in a CCR reformer, because the catalyst is continuously being regenerated.

Isomerization

As mentioned, isomerization units convert *n*-paraffins into isoparaffins and straight-chain olefins into isoolefins. Butane isomerization provides isobutane as the major feed for subsequent alkylation. Pentane/hexane isomerization improves the octane number of light naphtha for gasoline blending.

In butane isomerization, the feed contains *n*-butane, which typically contains some isobutane. The catalyst is highly sensitive to water, so the feed must be thoroughly dried. In the low-temperature first stage, the catalyst comprises aluminum chloride promoted by HCl. Hydrogen gas is added to inhibit olefin and coke formation. In the high-temperature second stage, the catalyst contains a noble metal such as platinum. Temperatures range from 230 to 340 °F (110–170 °C) and pressures range from 200 to 300 psi (14–20 bar). The reactor effluent goes to a flash drum, from which hydrogen is recovered and recycled. HCl is removed in a stripper column. The liquids go to a fractionator (deisobutanizer), which separates unconverted *n*-butane from the isobutane product. The *n*-butane is recycled and mixed with fresh feed.

In the Shell Hysomer process for pentane/hexane isomerization, the feed is combined with hydrogen-rich gas, heated to 445–545 °F (230–285 °C) and routed to the Hysomer reactor at 190–440 psi (13–30 bar). As with fixed-bed hydrotreating and hydrocracking, the process fluids flow down through the catalyst bed, where a part of the *n*-paraffins is converted into branched paraffins. The catalyst is comprised of a noble metal on a zeolite-containing support. The reactor effluent is cooled and sent to a flash drum, which separates hydrogen from the liquid product. The hydrogen is recycled. The liquid is fractionated, and the *n*-paraffins are recycled. The net conversion of *n*-paraffins into branched products can be as high as 97%, and the octane can be boosted by 8–10 numbers.

Often, the heat-exchanger and fractionation systems of isomerization units are integrated with those of other process units, such as catalytic reformers. In the

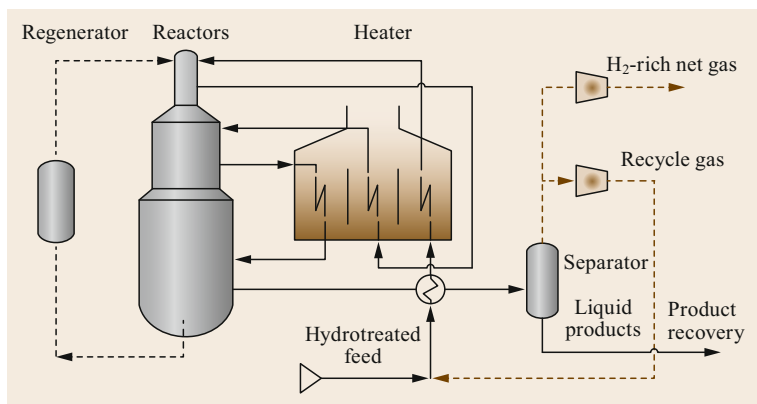


Fig. 1.39 CCR catalytic reforming process flow

Union Carbide total isomerization process (TIP), C₅/C₆ isomerization was integrated with molecular sieve separation, which provided complete conversion of *n*-paraffins. Other C₅/C₆ isomerization units presently used in the industry include the UOP Penex process, which improves octane ratings from 50–60 to 82–86 or higher.

The CDTECH ISOMPLUS process achieves near-equilibrium conversion of *n*-butenes into isobutylene, and *n*-pentenes into isoamylene over a zeolite catalyst.

Alkylation

During alkylation, an excess amount of isobutane reacts with light olefins such propylene, butylenes, and amylene in the presence of strong acids to form branched chain hydrocarbons. These hydrocarbons, often referred to as alkylate, have high octane values (motor octane number from 88 to 95 and research octane number from 90 to 98), nil benzene, nil olefins, nil sulfur, and low Reid vapor pressures (RVPs), making them an excellent contributor to the gasoline blending pool.

Alkylation employs either hydrofluoric acid or sulfuric acid. The process usually runs at low temperatures to avoid polymerization of the olefins. Temperatures for HF catalyzed reactions are approximately 100 °F (38 °C). For sulfuric acid, they are approximately 50 °F (10 °C). Figure 1.40 describes HF alkylation. HF is dangerous, and extra precautions are taken to ensure that it is always contained.

Both HF and H₂SO₄ require relatively expensive corrosion-resistant equipment. Safety in handling and operations is a major concern for both, which also face disposal issues associated with spent acids and acid-soluble oils. These problems can be diminished by two recently developed breakthrough processes: ionic-liquid alkylation and solid-acid catalyzed alkylation. The former (ionilkylation) was developed by China University of Petroleum – Beijing with PetroChina in

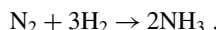
2006. The first commercial unit based on composite ionic liquid alkylation was started up in Dongying, Shandong, China in 2013. In 2016, Honeywell UOP announced commercialization of the ISOALKY process developed by Chevron. The latter (AlkylClean) was developed by CB&I, Albermarle Catalyst and Neste Oil, and the first commercial unit employing Albermarle's AlkylStar catalyst together with CB&I's novel reactor design was started up in Zibo, Shandong, China in 2015 (Chap. 17).

1.11.5 Petroleum Refining Catalysts

Several refining processes require catalysts. A catalyst is a material that facilitates and increases the rate of chemical reactions without being changed itself. Catalysts decrease energy requirements and reduce the size of process equipment.

In practice, catalysts do change as time goes by and more materials are processed. They degrade due to coking, attrition, feed contamination, and/or process upsets. Some catalysts last for years before they have to be replaced. In other processes, such as FCC and CCR catalytic reforming, they are regenerated and reused inside the process during normal operation (Sect. 1.9.3). In the FCC process, degraded catalyst is removed and replaced with fresh catalyst as needed. The chemistry of coke formation on catalysts is presented in Sect. 1.9.3.

Catalysts facilitate reactions by decreasing activation energies. Consider ammonia synthesis



The reaction is favored by thermodynamics, but molecular nitrogen is exceedingly stable due to the strength of the N≡N triple bond. To break the N≡N bond with heat alone requires 3000 °C (5400 °F). Before the catalytic Haber–Bosch process, ammonia was synthesized from

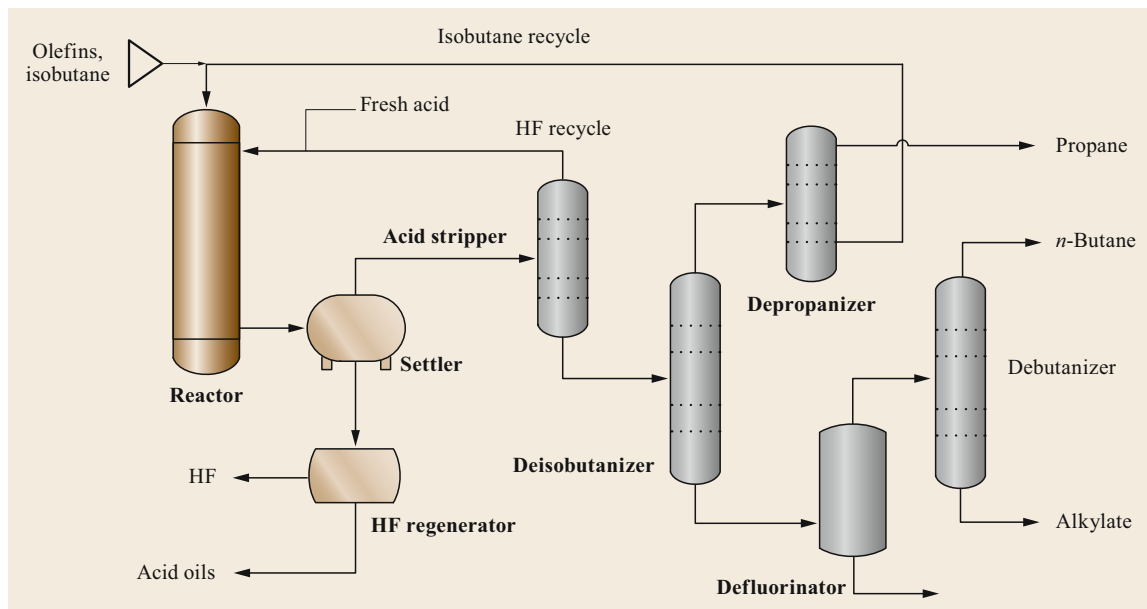


Fig. 1.40 HF alkylation process flow

nitrogen and hydrogen in electric arc reactors, which in essence generate mini-lightning bolts while consuming immense amounts of energy. In catalytic ammonia synthesis, the $\text{N}\equiv\text{N}$ bond is weakened when it adsorbs to the catalyst, allowing it to react with hydrogen at $< 750^\circ\text{F}$ ($< 400^\circ\text{C}$).

Most petroleum refinery catalysts are solids, with active metals supported on high-strength γ -alumina, silica, or aluminosilicates. The major exceptions are HF, H_2SO_4 , and ionic liquid alkylation catalysts, which employ liquid-phase acids. The separation of liquid and vapor products from solids is straightforward, so it is easier to recover the catalysts and regenerate or dispose of them.

FCC and hydrocracking employ solid-acid catalysts, primarily based on synthetic zeolites. Hydrocracking also employs amorphous silica-alumina (ASA) catalysts. Zeolites possess high surface area and high acidity, both of which contribute to their high activity. They also possess a mesopore structure, which affects feed flexibility and product selectivity.

Related materials are used in other processes. For example, metal-promoted silica alumina phosphates such as SAPO-11 are used to isomerize normal paraffins in catalytic dewaxing (CDW) units. Figure 1.41 shows six zeolite structures [1.12]. In cracking catalysts, HY zeolite is the most common, but beta and ZSM-5 are used as well. The building blocks of A, X, and other zeolites are tetrahedral units of Si and Al oxides. In the ultra-stable Y (USY) zeolites employed in cracking catalysts, the Si/Al ratio is > 10 .

The acidity of zeolites (and ASAs) comes from their structure [1.13]. Figure 1.42 shows how one can visualize these materials as a silica (SiO_2) superstructure, in which every so often an aluminum atom replaces a silicon atom. The silicon atoms have a valence of +4, and each one binds to four oxygen atoms.

The oxygen atoms in hydroxyl groups are Brønsted acids (proton donors). Replacing Si (+4) with Al (+3) creates electron-rich Lewis acid sites, which are associated with positive counter-ion such as Na^+ , K^+ , NH_4^+ , or H^+ . The counter ions can be swapped via ion exchange. For example, when Na-Y zeolite is exchanged with an ammonium salt, the Na^+ ion is replaced by NH_4^+ . When $\text{NH}_4\text{-Y}$ is heated to the right temperature, the ammonium ion decomposes, releasing NH_3 (gas) and leaving behind highly acid H-Y zeolite. A typical Si/Al ratio for a zeolite with high cracking activity is about 5. In hydrocracking catalysts with less activity but greater selectivity for production of middle distillates, the Si/Al might be about 30.

ZSM-5 is a shape-selective zeolite made by including a soluble organic template in the mix of raw materials. (Templates for this kind of synthesis include quaternary ammonium salts.) ZSM-5 enhances distillate yields in FCC units and CDW in hydroprocessing units, where due to its unique pore structure, it selectively cracks waxy *n*-paraffins into lighter molecules.

The ASA catalysts used for hydrocracking are less active, but they do a better job of converting straight-run VGO into diesel with minimal co-production of naphtha and lighter products. Figure 1.43 provides

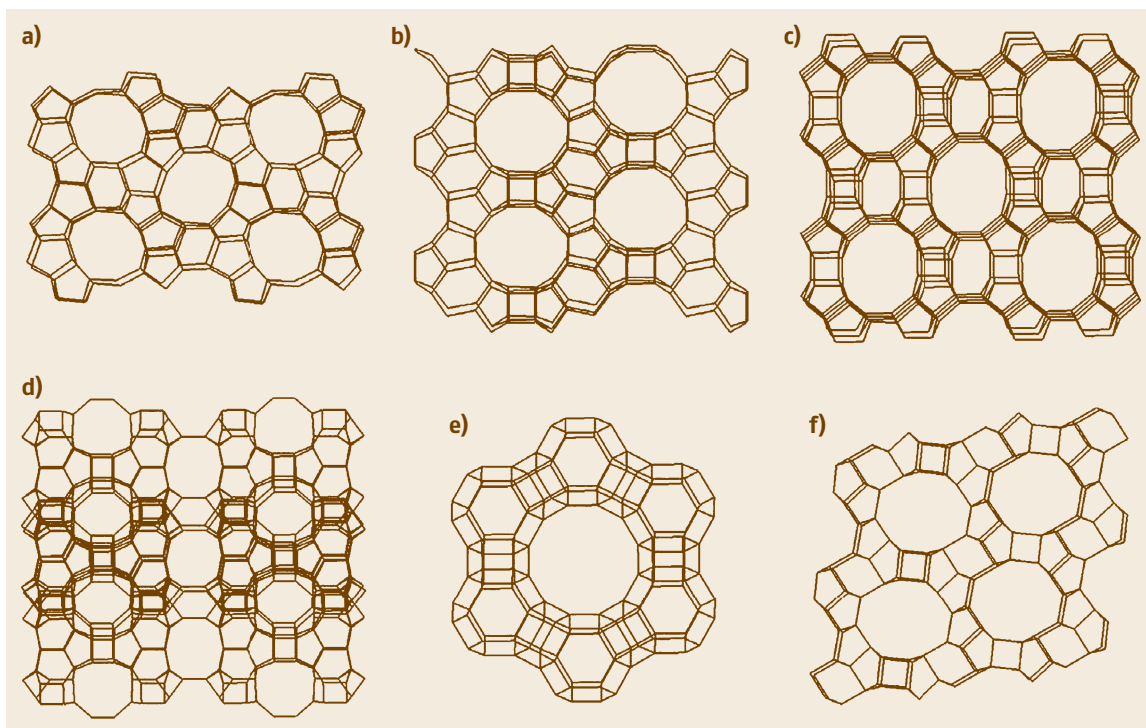


Fig. 1.41a–f Structures of zeolites ZSM-5 (a), mordenite (b), beta (c), MCM-22 (d), zeolite Y (e), and zeolite L (f)

a conceptual comparison of amorphous ASA catalysts with crystalline zeolite catalysts. The pore diameters of HY zeolite catalysts are uniform and relatively small – around 7.5 Å, give or take. Mesopores have larger diameters, which admit mid-sized molecules such as those found in vacuum gas oils. ASA catalysts include small, medium, and large pores. The width of ASA pores can exceed 100 Å. The larger pores can accommodate larger molecules. This explains why ASA catalysts do a better job of cracking feeds with very high endpoints. The pore diameter for ZSM-5 is 6.3 Å.

FCC Catalysts and Additives

Finished FCC catalysts are powders with the consistency of sifted flour. They are given their final form by spray drying, in which a slurry of catalyst components is converted into a dry powder by spraying into hot air. The method gives a consistent particle size distribution. The particles are roughly spherical, with bulk densities of 0.85–0.95 g/cm³ and average diameters of 60–100 μm.

The catalysts include four major components – one or more *zeolites* (up to 50%), a *matrix* based on non-crystalline alumina, a *binder* such as silica sol, and a clay-based *filler* such as kaolin. The zeolite is ultra-stable (US) H-Y (faujasite) or very ultra-stable (VUS) H-Y. The extra stability is provided by de-alumination

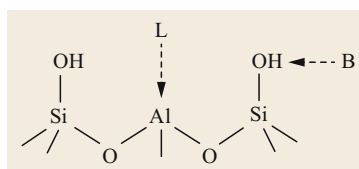


Fig. 1.42 Brønsted (B) and Lewis acid sites (L) in zeolites and ASAs

with hydrothermal or chemical treatment. The H-Y zeolite is sometimes augmented with ZSM-5 to increase propylene yield. To provide thermal stability and optimize the relative amounts of different active sites, a mixture of rare earths (RE) is incorporated into the zeolite structure by ion exchange. A lanthanum-rich mixture of RE oxides is added to provide thermal stability. The RE mixture can contain up to 8 wt% ceria, and up to 80% La₂O₃, up to 15 wt% Nd₂O₃, with traces of other RE.

Other components can be part of the core catalyst or introduced as external additives. The extra components can provide NO_x and/or SO_x reduction. Noble metal combustion promoters enhance the conversion of CO to CO₂ in the regenerator.

Catalysts for Fixed-Bed Reactors

Fixed-bed catalysts are shaped into spheres, cylinders, hollow cylinders, lobed extrudates, or pellets. Some look like small dog biscuits as shown in Fig. 1.44.

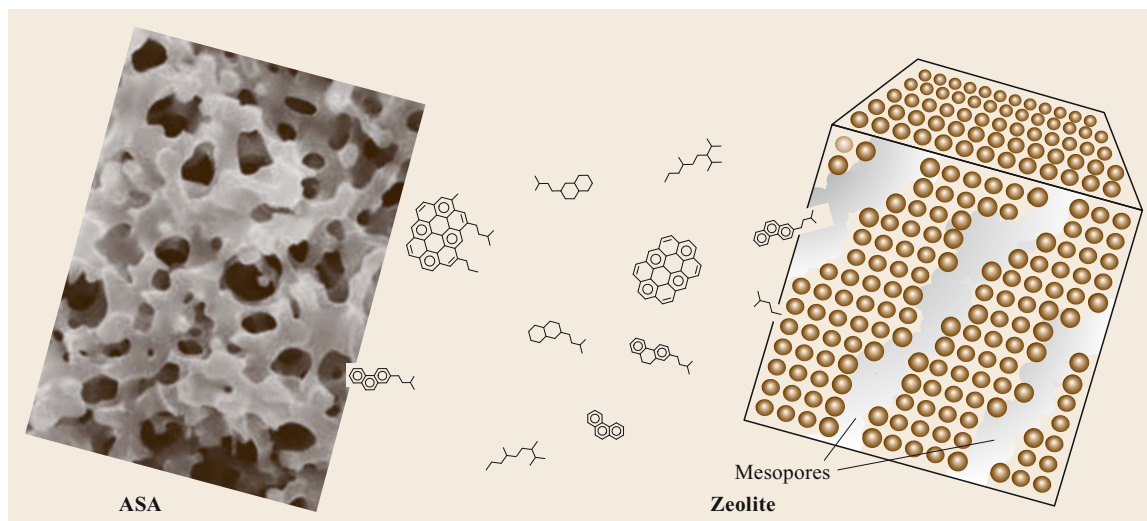


Fig. 1.43 Schematic comparison of amorphous alumina silica (ASA) and zeolite structures



Fig. 1.44 Catalyst loading scheme showing size/shape grading. Photo used with kind permission from Haldor Topsoe, Inc.

A cross-section of a lobed extrudate can look like a three-leaf or four-leaf clover without the stem. Compared to cylindrical extrudates, shaped extrudates have a higher surface-to-volume ratio, and the average distance from the outside of a particle to the center is shorter. This increases activity by decreasing the average distances traveled by molecules to reach active catalyst sites. To make extrudates, a paste of support material is forced through a die. The resulting spaghetti-like strands are dried and broken into short pieces with a length/diameter ratio of 2–4; for main-bed hydrotreating catalysts, diameters range from 1.3 to 4.8 mm. The particles are calcined, which hardens them and removes additional water and volatile molecules such as ammonia.

Spherical catalysts are made in one of several ways, including:

1. Spray-drying slurries of catalyst precursors
2. Spraying liquid onto powders in a tilted rotating pan
3. Dripping a silica–alumina slurry into hot oil. FCC catalysts are made by spray drying.

Pellets are made by compressing powders into dies.

Impregnation distributes active metals within the pores of a catalyst support. Like sponges, calcined supports are especially porous. Far more than 99% of the surface area is inside the pores. When the pores are exposed to aqueous solutions containing active metals, capillary action pulls the aqueous phase into them. After drying, the catalyst might be soaked in another solution to increase the loading of the same (or a different) active metal. Catalysts can also be made by co-mulling active metal oxides with the support. Co-mulling tends to cost less because it requires fewer steps. It also pro-

duces materials with different activities – sometimes higher, sometimes lower – than impregnation.

Eventually, refinery catalysts deactivate and must be replaced. The major causes of deactivation are process upsets, feed contaminants (trace metals, particulates, etc.) and catalyst coking; the latter is discussed above in some detail. In FCC, CCR processes, and

ebullated-bed hydrocracking, aged catalysts are continuously removed and replaced with fresh. But in fixed-bed units, catalyst replacement requires a shutdown. For a 40 000 bbl/day hydrocracker with an upgrade value of \$15–20/bbl, every day of down time costs \$600 000–800 000. Lost production during a 4-week catalyst changeout can amount to \$18–24 million.

1.12 Petroleum Products

Products from modern refineries comprise several individual streams, which are blended to meet specific requirements. Boiling ranges and carbon numbers for common petroleum products are summarized in Table 1.20. The values shown can vary from locale to locale, from refinery to refinery, and from season to season.

Developing petroleum product specifications involves cooperation between stakeholders, including equipment manufacturers, consumers, petroleum product suppliers, government agencies, environmental groups, and others. Specifications and test methods are published by ASTM International, the International Organization for Standardization (ISO), the European Union, Japanese Industrial Standards (JIS), and others. Many tests are developed by process licensors. For example, UOP's *Laboratory Test Methods* defines several hundred procedures for analyzing catalysts, chemicals, and fuels.

Table 1.21 lists some ASTM fuel specifications. Recent low-sulfur gasoline and diesel directives from the

US Environmental Protection Agency are incorporated into D975 and D4814, respectively.

Additives are essential components of finished fuels. They increase stability, improve flow properties, enhance performance, and reduce environmental impact. Cetane improvers are routinely added to diesel fuel, and additives that prevent intake-valve deposits are now required in all grades of gasoline in the United States.

1.12.1 Petroleum Gases

Methane, the main hydrocarbon ingredient of natural gas, is produced by certain refinery processes. It can be used as a refinery fuel and feedstock for hydrogen production by pyrolytic cracking and reaction with steam in SMR. Ethane is used as refinery fuel or as feedstock to produce hydrogen and ethylene, which is an important petrochemical. Propane is used as refinery fuel or as feedstock for propylene manufacturing. Liquefied refinery propane is called LPG (liquefied petroleum

Table 1.20 Boiling ranges and carbon numbers for petroleum distillates. Values vary seasonally and geographically

Product	Carbon number range	Boiling range (°C)	Boiling range (°F)	Primary uses
RFG (refinery fuel gas)	C ₁ and C ₂			Fuel
LPG (liquefied petroleum gas)	C ₃ (with some C ₄)			Fuel
Butanes, butenes	C ₄	–12 to –0.5	10–31	Fuel, chemicals, gasoline
Light naphtha	C ₅ (with some C ₄ and C ₆)	9–38	48–100	Gasoline, chemicals
Heavy naphtha	C ₇ –C ₁₂ (with some C ₆)	38–205	85–400	Gasoline, avgas, chemicals
Kerosenes	C ₉ –C ₁₈	180–280	300–540	Jet fuel, avgas, home heating
Gas oils	C ₁₆ –C ₂₆	121–370	250–700	Diesel fuel, fuel oil
Vacuum gas oils	C ₂₄ –C ₆₀	343 to > 593	650–1100	Fuel oil, lubricants
Residue	> C ₆₀	> 565	> 1050	Lubricants, asphalt, coke

Table 1.21 ASTM specification numbers for hydrocarbon fuels

Product	ASTM specification	Description
Gasoline	D4814	Standard specification for automotive spark-ignition engine fuel
Jet fuel	D1655	Standard specification for aviation turbine fuels
Kerosene	D3699	Standard specification for kerosene
Diesel	D975	Standard specification for diesel fuel oils
Fuel oil	D396	Standard specification for fuel oils

gas). LPG, which also contains minor amounts of butanes, can be used by other industries and domestic applications. Butanes can be blended into gasoline for regulating vapor pressure and promoting better starting in winter or cold weather areas.

Limited amounts of *n*-butane can be blended into gasoline or LPG. Significant amounts serve as feedstock to produce isobutane in isomerization units. Isobutane goes primarily to alkylation units, where it reacts with C₃–C₅ olefins to produce high-octane isoparaffins (isomerate) for gasoline blending. Isobutane is also converted into isobutylene for making polyisobutylenes, MTBE, ethyl tertiary butyl ether (ETBE), and various grades of butyl rubbers including chlorobutyl and bromobutyl rubbers for the tire industry.

1.12.2 Gasoline

Since the birth of modern automobile in 1886, the demand for gasoline to fuel automobiles with internal combustion engines has increased dramatically. The rate of the increase jumped in 1908, when the advent of the Model T made autos affordable for average people. It is estimated that the number of automobiles in the world exceeded 1 billion around 2010.

The typical boiling range of gasoline is from 100 °F (≈ 40 °C) to 400 °F (≈ 205 °C). The components have carbon numbers ranging from C₅ to C₁₂.

Octane and RVP

In a spark-ignition engine, some compounds start to ignite before the piston reaches the top end (highest compression ratio) near the spark plug. This premature ignition causes knocking, which reduces the power of the engine, increases engine wear, and can cause serious damage. Octane number or octane rating is a measure of the tendency of a fuel to knock. It is based

on a scale in which the octane number of *n*-heptane is designated as zero and the octane number of isooctane (2,2,4-trimethylpentane) is 100. When a fuel is tested in a standard single-cylinder engine, mixtures of isooctane and *n*-heptane of various percentages are used as reference standards for comparing the knocking of the test fuel with the percentage of isooctane in the mixture. ASTM D2699 and ASTM D2700 describe methods for measuring research octane number (RON) at 600 rpm to simulate low speed or city driving with load conditions and motor octane number (MON) at 900 rpm to simulate high-speed highway driving conditions.

In North America, the posted octane of gasoline is the arithmetic average of RON and MON: (R+M)/2. This is the number displayed on pumps at filling stations. Typical grades are *regular* with a posted octane of 87, *mid-grade* with a posted octane of 89, and *premium* with a posted octane of 91–93. In some locales, customers can dial in any octane they want between 87 and 93.

Another important property of gasoline is Reid vapor pressure (RVP) which is the vapor pressure of a motor gasoline measured at 100 °F in a volume of air four times the liquid volume. RVP indicates the ease of starting and vapor-lock tendency as well as explosion hazards and evaporation losses.

Gasoline Blend Stocks

Several refinery streams have the right vapor pressure, boiling range, sulfur content, and octane to end up in the gasoline pool. Table 1.22 shows properties for blend stocks from which gasoline might be made. Finished gasoline must have the proper octane while meeting RVP requirements. The octane of a particular grade is constant, but RVP requirements are seasonal.

In the summer, when outdoor temperatures can exceed 100 °F (38 °C), the RVP of gasoline must be low to avoid over-pressure in gasoline tanks, causing

Table 1.22 Gasoline blend stock composition and properties (after [1.82])

Component	API Gravity	RVP (psi)	Boiling range		RON	MON
			(°C)	(°F)		
<i>n</i> -Butane		52.0	−0.5	30	92.0	93.0
Light straight-run gasoline	78–79	11.0	30–80	85–176	61.6	66.4
Heavy straight-run gasoline	48	1.0	85–205	185–400	58.7	62.3
Light isomerate	80	13.5	30–80	85–176	81.1	83.0
Reformate	41–46	2.2–2.8	78–197	160–400	100.5	89.5
Hydrotreated FCC light gasoline	49.3	5.0	C ₆ –93	C ₆ –200	74.0	86.0
Hydrotreated FCC heavy gasoline	48.5	0.5	C ₅ –93	300–400	81.0	90.0
Alkylate, polymer gasoline	74	4.6	85–95	185–205	93.0	94.5
Ethanol	47.8	18.0	78	173	116.0	112.0
TAME ^a	53.5	1.5	86	187	112.0	98.0
MTBE ^b	59.7	8.0	55	134	115.0	97.0

^a *t*-Amyl methyl ether, ^b methyl-*t*-butyl ether. So-called polymer gasoline comes from oligomerization of C₃ and C₄ olefins.

vapor lock during ignition, and to limit hydrocarbon emissions; hydrocarbons react in the atmosphere with nitrogen oxides to produce ozone, a noxious component of photochemical smog. Summer RVP must be less than 6.9 psi in California; in urban areas along the east coast from Virginia to New Hampshire; and near Houston, Dallas, Chicago, and St. Louis. In other urban areas, the limit ranges from 7.0 to 7.8, and in most rural areas, the limit is 9.0. Summer RVP limits last from May 1 to September 15 for refineries and terminals, and from June to September 15 at filling stations; in California, switch-over dates start earlier and last longer. As weather gets colder, RVP must be higher; otherwise, engines might not start. Permissible winter RVP can reach 15 psi in especially cold and/or high-altitude areas.

A typical summer RBOB (reformulated gasoline before oxygenate blending) might contain 40% FCC gasoline, 25% straight run naphtha, 15% alkylate, 18% reformate, 0–2% butanes, and 0–2% other. During the winter, the butane content can be higher [1.83].

Aviation Gasoline

Gasoline used for piston-engine-powered aircraft is called aviation gasoline, or avgas, which has high octane number and low flash point to improve ignition characteristics on propeller aircraft. The flash point is the lowest temperature at which a liquid gives off enough vapor to ignite when an ignition source is present. As mentioned in the jet-fuel section, avgas can mean either Jet B or JP-4.

Gasoline Additives

A finished gasoline contains the base blend and small amounts of additives for corrosion inhibition, lubrication, and cleaning. Typical additives include metal deactivators, corrosion inhibitors, antioxidants, detergents, demulsifiers, anti-icing additives and oxygenates.

Table 1.23 lists additives used to prepare finished gasoline. Additive packages vary from season-to-season, region-to-region, and retailer to retailer. Aftermarket additives contain similar types of ingredients, and are more concentrated. They are packaged to be added by consumers to the gasoline in individual vehicles.

Reformulated Gasoline (RFG) in the United States

In the mid- to late twentieth century, making gasoline was a relatively simple task. If a mixture of components met specifications for volatility and octane, it could be shipped to retail outlets and sold as-was. If the octane was low, the problem could be fixed by adding a small amount of tetraethyl lead (TEL). Butanes could

Table 1.23 Additives used in gasoline

Additive type	Function
Oxygenates	Decrease emissions
Anti-oxidants	Minimize oxidation and gum formation during storage
Detergents	Clean fuel injector and minimize carbon deposit
Metal passivators	Deactivate trace metals that can accelerate oxidation
Corrosion inhibitors	Minimize rust and corrosion throughout the gasoline supply chain
Demulsifiers	Prevent the formation of stable emulsion
Anti-icing additives	Minimize ice in carburetors during cold weather
IVD control (detergent)	Control deposition of carbon on intake valves
CCD control	Control deposition of carbon in combustion chambers

be added or left out as needed to adjust volatility, especially during winter time or cold weather.

In 1970, gasoline blending became more complex. The US Clean Air Act required the phase-out of TEL because of its cumulative neurotoxicity and its damaging effect on catalytic converters, so refiners had to find other ways to provide octane. Regulations in other developed countries soon followed suit.

In 1990, the Clean Air Act (CAA) was amended. It empowered EPA to impose emissions limits on automobiles and to require reformulated gasoline (RFG). RFG was implemented in several phases. The Phase I program started in 1995 and mandated RFG for 10 large metropolitan areas. Several other cities and four entire States joined the program voluntarily. In the year 2000, about 35% of the gasoline in the United States was reformulated. Almost all US gasoline is now reformulated.

US Tier 1 reformulated gasoline regulations required a minimum amount of chemically bound oxygen, imposed upper limits on benzene and Reid vapor pressure (RVP), and ordered a 15% reduction in volatile organic compounds (VOC) and air toxics. VOC react with atmospheric NO_x to produce ground-level ozone. Air toxics include 1,3-butadiene, acetaldehyde, benzene, formaldehyde, and others.

The regulations for US Tier 2 gasoline, which took force in January 2000, were based on the EPA complex model, which estimates exhaust emissions for a region based on geography, time of year, mix of vehicle types, and – most important to refiners – fuel properties. As of 2006, the limit on sulfur in the gasoline produced by most refineries in the United States was 30 wppm. Tier 3 vehicle emission and fuel standards lowered the allowed sulfur content of gasoline to 10 wppm, beginning in 2017.

Oxygenates in Gasoline

In the United States, reformulated gasoline must include chemically bound oxygen. Initially, the oxygen could be supplied as ethanol or C₅–C₇ ethers. The most common were MTBE and *t*-amyl methyl ether (TAME). MTBE and TAME have excellent blending octanes and low vapor pressures. But due to leaks from filling station storage tanks, MTBE was detected in ground water samples in New York city, Lake Tahoe, and Santa Monica, California. In 1999, the Governor of California issued an executive order requiring the phase-out of MTBE. Eventually, ether blending was banned nationwide.

MTBE and ETBE still serve as high-value gasoline blend stocks in Europe, where ground water contamination is prevented by ensuring that tanks do not leak.

Now in the United States, ethanol must be added to automotive gasoline. In Brazil, obtaining fuel ethanol from sugar cane has been a highly successful, energy-efficient alternative to gasoline [1.84]. But in the United States, almost all fuel ethanol comes from American corn. All things considered, obtaining ethanol from corn is far less energy efficient than obtaining ethanol from sugar cane. According to one report [1.85], the energy balance for sugar cane ethanol is roughly four times greater than the balance for corn-based ethanol; energy balance is the difference between the energy expended to convert a crop into ethanol and the energy produced from burning the ethanol and flammable by-products such as corn stover. Getting ethanol from corn is more complicated. The starch in corn is first converted by enzymes into dextrose, which is then fermented by yeast into ethanol and CO₂. In contrast, the sucrose in sugar cane can be fermented directly. Land use is less for sugar cane ethanol. On average, an acre of sugar cane produces about twice as much ethanol as an acre of corn.

As a component of US gasoline, ethanol has some advantages. Its blended octane is high, and the corn ethanol requirement increases employment and farm income in corn-growing states. On the other hand, its high RVP reduces or even eliminates the blending of butane into gasoline. During the summer in urban areas, even pentane blending is limited by the ethanol requirement. It may or may not decrease American dependence on imported oil.

But ethanol in gasoline has significant disadvantages:

1. Ethanol increases the solubility of water in gasoline and also increases the solubility of polar hydrocarbons, additives, and lubricants in water. Spills of ethanol-containing gasoline are more likely to

introduce hydrocarbons into ground water. Water-contaminated gasoline is more likely to freeze, so aviation gasoline is exempted from the ethanol mandate.

2. Older motors are constructed with parts that degrade faster when exposed to ethanol.
3. The United States uses up to 45% of its corn crop to make fuel ethanol [1.86]. This has increased food costs, not just in the United States but also globally.
4. Water-use efficiency for corn ethanol production is improving dramatically [1.87], but the ethanol industry continues to impact ground-water levels, notably in the Ogallala aquifer, which spans eight Great Plains US states.
5. US Midwest farmers fertilize their fields extensively with ammonia, which reacts with air to form N₂O, a potent greenhouse gas. The ammonia is manufactured from hydrogen and nitrogen with the Haber–Bosch process; including the burning of natural gas to provide heat and steam for the process, making one ton of hydrogen produces up to 10 t of CO₂.

Butanol is a potential alternative to ethanol. Its heat content (i. e., fuel economy) is higher than for ethanol and only slightly less than conventional gasoline. Due to lower water solubility, butanol does not damage engines and has less tendency to separate polar additives from gasoline. It can be used directly as fuel without modification of vehicles designed for use with gasoline.

Gasoline (Petrol) in the EU

Transportation fuel specifications in the European Union are described by EN 228, *Specification for unleaded petrol (gasoline) for motor vehicles* (Table 1.24).

EU gasoline is cleaner than US EPA gasoline, it is easier to manufacture and regulate, and the allowed sources of oxygen are based on science rather than politics.

1.12.3 Naphtha

Light naphtha (LN) includes primarily C₅ and C₆ molecules and boils between 30 and 85 °C. The upper boiling point is lower if a refiner wishes to exclude benzene, which boils at 80 °C. Benzene is an air-toxic molecule, so its concentration in gasoline is limited to 1%. However, it is a valuable chemical and often undergoes purification in downstream units.

Heavy naphtha (HN) can include C₆–C₁₂ molecules. It boils between 80 and 210 °C. To exclude benzene and all other C₆ molecules, the initial boiling point is raised to 85 °C. Most HN goes to catalytic reforming or isomerization units.

Table 1.24 Specifications for unleaded petrol (gasoline) for motor vehicles in the EU (EN228)

Parameter	Limit
Octane	
RON (min)	95
MON (min)	85
Vapor pressure (kPa)	60.0 ^a
Volatility	
Vaporized at 100 °C (%)	46
Vaporized at 150 °C (%)	75
Hydrocarbon types	
Olefins	18 vol.% max
Aromatics	35 vol.% max
Benzene	1 vol.% max
Oxygen	3.7 wt%. Sources can include alcohols (with stabilizing agents) and ethers such as MTBE and ETBE
Sulfur	10 pmw max

^a Equivalent to RVP = 8.7 psi

Naphtha-range products – including reformates, isomerates, and alkylates – are high-octane gasoline-blend stocks. Straight-run naphtha is employed as a diluent in the bitumen mining industry, and as feed-stock for producing olefins via steam cracking. Naphtha serves as a solvent for paints, dry-cleaning, cutback asphalt, industrial extraction processes, and in the rubber industry.

1.12.4 Diesel

A diesel internal combustion engine uses heat from adiabatic compression to ignite a fuel/air mixture inside a piston. Wide-range diesel fuel boils between 150 and 410 °C (330–770 °F), and includes molecules with carbon numbers ranging from 8 to 21. The boiling range of automotive diesel is narrower, typically from 180 to 356 °C (365–680 °F). The initial boiling point is set by the flash point, which must be greater than 55 °C. The flash point corresponds to an initial true boiling point (TBP) of about 180 °C (356 °F). The upper distillation limit can be set by one of several properties. For Euro V diesel, the ASTM D86 95% boiling must be less than or equal to 360 °C (680 °F). This corresponds to a TBP final boiling point between 370 and 380 °C, depending on the nature of the blend components of the fuel and the other properties listed below.

Cetane Number and Cetane Index

The ignition quality of diesel fuels is related to cetane number, which is measured relative to standard mixtures of *n*-hexadecane (cetane), with a defined

cetane number = 100, and isocetane (2,2,4,4,6,8,8-heptamethylnonane), with a defined cetane number = 15. Previously, the low end of the scale was set by α -methyl naphthalene, with a defined cetane number = 0. Isocetane is preferred because it is less expensive and safer to handle.

Table 1.25 lists cetane numbers for selected pure compounds. As with octane, blended cetane numbers can differ significantly from those for pure compounds. Roughly speaking, there is an inverse, non-linear correlation between octane number and cetane number.

Cetane index is a number calculated from the average boiling point and specific gravity of diesel fuels. The results of cetane index calculations correspond to the results of cetane number measurements, but cetane index does not require an expensive engine test. Diesel engines can operate with fuels having cetane numbers between 40 and 55. For Euro V diesel, the minimum cetane *index* is 46 and the minimum cetane *number* is 51. The cetane number can be as high as 60 in premium diesel fuel (No. 1 diesel). Due to its higher heat content, the fuel economy of diesel is better than that for gasoline.

Other Important Diesel Fuel Properties

Other important diesel-fuel properties include flash point, cloud point, pour point, kinematic viscosity, lubricity – and of course sulfur. Cloud point and pour point indicate the temperatures at which the fuel tends to thicken and then gel in cold weather. In a diesel engine, viscosity not only measures the tendency of a fluid to flow but also indicates how well a fuel atomizes in spray injectors. Lubricity measures the fuel's quality as a lubricant for the fuel system, where it reduces friction between solid surfaces in relative motion. It indicates how the engine will perform when loaded.

Specifications for Euro V automotive diesel, as defined by EN 590, are presented in Table 1.26.

Diesel fuels used in railroad locomotives can have higher boiling final boiling points – up to 400 °C (752 °F) and lower cetane number (in the 1930s). Marine diesel oil contains some heavy fuel oil, unlike regular diesel fuels. Marine bunker fuels sometimes contain waste products such as used motor oil.

Diesel Additives

Diesel additives may contain a cetane number improver, such as alkyl nitrate, a lubricity agent, detergents to clean the fuel injectors and minimize carbon deposits, dispersants, and metal deactivators. Table 1.27 lists the common diesel additives and the reasons they are used.

Table 1.25 Cetane numbers for selected pure compounds

Compound	Type	Carbons atoms	Formula	Cetane No.
<i>n</i> -Decane	Paraffin	10	C ₁₀ H ₂₂	76
Decalin	Naphthene	10	C ₁₀ H ₁₈	48
α -Methylnaphthalene	Aromatic	11	C ₁₁ H ₁₀	0 ^a
<i>n</i> -Pentylbenzene	Aromatic	11	C ₁₁ H ₁₆	8
3-Ethyldecane	Paraffin (iso)	12	C ₁₂ H ₂₆	48
4,5-Diethyloctane	Paraffin (iso)	12	C ₁₂ H ₂₆	20
3-Cyclohexylhexane	Naphthene	12	C ₁₂ H ₂₄	36
Biphenyl	Aromatic	12	C ₁₂ H ₁₀	21
α -Butylnaphthalene	Aromatic	14	C ₁₄ H ₁₆	6
<i>n</i> -Pentadecane	Paraffin	15	C ₁₅ H ₃₂	95
<i>n</i> -Nonylbenzene	Aromatic	15	C ₁₅ H ₂₄	50
<i>n</i> -Hexadecane (cetane)	Paraffin	16	C ₁₆ H ₃₄	100 ^a
2-Methyl-3-cyclohexylnonane	Naphthene	16	C ₁₆ H ₃₄	70
Heptamethylnonane	Paraffin (iso)	16	C ₁₆ H ₃₄	15 ^a
8-Propylpentadecane	Paraffin (iso)	18	C ₁₈ H ₃₈	48
7,8-Diethyltetradecane	Paraffin (iso)	18	C ₁₈ H ₃₈	67
2-Octylnaphthalene	Aromatic	18	C ₁₈ H ₂₄	18
<i>n</i> -Eicosane	Paraffin	20	C ₂₀ H ₄₂	110
9,10-Dimethyloctane	Paraffin (iso)	20	C ₂₀ H ₄₂	59
2-Cyclohexyltetradecane	Naphthene	20	C ₂₀ H ₄₀	57

^a Used as standards for ASTM D976

Table 1.26 Specifications for Euro V automotive diesel, as defined by EN 590

Property	Units	Low limit	Upper limit	Test-method
Cetane index		46	–	ISO 4264
Cetane number		51	–	ISO 5165
Density at 15 °C	kg/m ³	820	845.0	ISO 3675, 12135
Polycyclic aromatic hydrocarbons	(wt%)	–	11.0	ISO 12916
Sulphur content	mg/kg	–	10.0	ISO 20346, 20347, 20334
Flash point	°C	55	–	ISO 20346, 20334
Carbon residue (on 90–100% fraction)	(wt%)	–	0.3	ISO 2719
Ash content	(wt%)	–	0.01	ISO 10370
Water content	mg/kg	–	200	ISO 6245
Total contamination	mg/kg	–	24.0	ISO 12937
Copper strip corrosion (3 h at 50 °C)	rating	Class 1	Class 1	ISO 12662
Oxidation stability	g/m ³	–	25.0	ISO 2160
LubriCity, wear scar diameter at 60 °C	pm	–	460	ISO 12205
Viscosity at 40 °C	mm ² /s	2	4.5	ISO 12156-1
Distillation recovered at 250 °C. 350 °C	(vol.%)	35	< 65.0	ISO 3104
95 vol.% recovered at	°C	–	360	ISO 3405
Fatty acid methyl ester content	(vol.%)	–	7.0	ISO 14073

1.12.5 Kerosene and Jet Fuel (Turbine Fuel)

Prior to the invention of automobiles, kerosene for lighting and fuel oil for ships were the most marketable products of petroleum. Today, while a small amount of kerosene is burned in lamps, most of it is consumed in domestic heaters or furnaces and in jet engines [1.88]. Significant amounts are used as solvents for greases and insecticides.

At the front of a jet engine, a turbine sucks in air with a fan. The pressure of the air is raised by a compressor, which is powered by a turbine. Fuel is injected, and the air/fuel mixture is burned, generating exhaust gases that push through the fans of the turbine and exit through a nozzle at the back of the engine. As the jets of gas shoot backward, the aircraft is propelled forward. Turbine engines can operate with a wide range of fuels. Fuels with higher flash

Table 1.27 Diesel fuel additives

Additive type	Function
Anti-oxidants	Minimize oxidation and gum formation during storage
Cetane improver	Increase cetane number
Dispersants	Improve behavior in fuel injectors for cluster/aggregate formation
Anti-icing additives	Minimize ice formation during cold weather
Lubricity agent	Compensate for poor lubricity of severely hydrogenated diesel fuels
Detergents	Control deposition of carbon in the engine and clean fuel injector
Injector cleanliness agents	Clean deposits from fuel and lubricant
Metal passivators	Deactivate trace metals (e.g., Cu, Fe) that can accelerate oxidation
Smoke suppressants	Reduce black smoke from incomplete combustion
Corrosion inhibitors	Minimize rust throughout the diesel fuel supply chain
Cold-flow improver	Improve flow characteristics in cold weather
Demulsifiers	Allow fuel and water to separate
Stabilizers	React with weakly acidic components
Biocides	Kill bacteria in fuel system that cause clogging

points are less flammable and safer to transport and handle.

Kerosene, jet fuel, and turbine fuel have similar boiling ranges. The key product properties are flash point, freezing point, sulfur content, and smoke point. The freezing point is especially important at high altitudes where the outside temperature is very low. If jet fuel freezes, it cannot be pumped to the engine(s). Without functioning engines, airplanes cannot fly. The sulfur content is important, because sulfur compounds induce corrosion.

Originally, smoke point was a measurement of fuel quality in kerosene lamps. To get more light from a flat-wick lamp, one can turn a knob to lengthen the wick. But if the wick is too high, it gives off smoke. Per ASTM D1322, smoke point is the maximum height of smokeless flame that can be achieved with a calibrated wick-fed lamp, using a wick of *woven solid circular cotton of ordinary quality*. The smoke point of a test fuel is compared to reference blends. A standard 40 vol.%/60 vol.% mixture of toluene with 2,2,4-trimethylpentane has a smoke point of 14.7, while pure 2,2,4-trimethylpentane has a smoke point of 42.8. Clearly, isoparaffins have better smoke points than aromatics.

The primary sources of jet fuels are hydrotreated straight-run kerosene from an atmospheric distillation

unit and hydrocracker products with the right volatility. The boiling range specifications for different jet fuels are shown in Table 1.28. Military jet-fuel grades are designated with JP followed by a number, where JP stands for jet propellant. Civil grades are designated with *Jet* followed by a letter.

JP-1 was specified for military jets in 1944. It was pure kerosene, having a freezing point of -60°C . JP-2 and JP-3 also were developed during World War II; all three are obsolete today. JP-2 had higher freezing point and JP-3 had higher volatility than JP-1.

JP-4 is a present-day wide-cut fuel with a carbon number range of $\text{C}_4\text{--C}_{16}$, for broader availability. JP-5 is specially blended kerosene. JP-6 has a higher end-point than JP-4 with fewer impurities. JP-7 is used in supersonic jets requiring high flash point. JP-8 is kerosene similar to the Jet A-1 fuels used in civilian aircraft.

For civilian jet fuels, Jet A and Jet A-1 are kerosene-type jet fuels. The primary physical difference between the two is freeze point. Jet A has been used in the United States since the 1950s. Today, specifications for Jet-A and Jet A-1 are the same as those published by the International Air Transport Association (IATA). The freezing points of Jet A and Jet A-1 are -40 and -47°C , respectively. Both have minimum flash points of 38°C (100°F) with autoignition temperatures of 210°C (410°F). Both have a carbon number distribution between 8 and 16, similar to JP-8.

Jet B, also called aviation gasoline, is a lower-boiling fuel used for its enhanced cold-weather performance. Naphtha-type jet fuel has a carbon number distribution between 5 and 15, similar to JP-4.

Jet fuel additives include antioxidants, which are usually based on alkylated phenols to prevent gumming, antistatic agents such as dinonylnaphthylsulfonic acid to dissipate static electricity and prevent sparking, corrosion inhibitors, fuel system de-icing agents, biocides to remediate microbial growth in the fuel system, and metal deactivators to remediate deleterious effects of trace metals on the thermal stability of the fuel.

Table 1.28 lists specifications for common turbine fuels.

1.12.6 Heating Oils and Fuel Oils

Both heating oil and fuel oil are liquid petroleum products burned in furnaces or boilers to heat buildings or in generators to produce power [1.89].

No. 1 fuel oil is a volatile distillate similar to kerosene, but with higher pour points and end points. It is intended for vaporizing pot-type burners. It has a carbon number range of 9–16. No. 2 fuel oil is similar to

Table 1.28 Turbine fuel specifications

Specification	Jet A	Jet B	JP-4	JP-5	JP-8
Flash point, min (°C)	38	–	–	60	38
Freeze point, max (°C)	–40 (Jet A) –47 (Jet A-1)	–50	–58	–46	–47
API gravity	37–51	45–57	45–57	36–48	37–51
Distillation, °C					
10% max	205	–	–	205	205
20% max	–	145	145	–	–
50% max	–	190	190	–	–
90% max	–	245	245	–	–
EP	300	–	270	290	300
Sulfur, wt% max	0.3	0.3	0.4	0.4	0.3
Aromatics, vol.% max	22	22	25	25	25
Olefins, vol.% max	–	–	5	5	5

No. 1 but can contain cracked stocks; it has a carbon number range of 10–20. No. 3 fuel oil is for burners requiring low viscosity heating oil; it is merged with No. 2 in specifications. No. 4 fuel oil is usually a light residual oil used in a furnace that can atomize the oil and is not equipped with a preheater. It has a carbon number range of 12–70. No. 5 fuel oil has higher viscosities than No. 4, requires preheating to 170–220 °F (≈ 76 –104 °C) for atomizing and handling, and has a carbon number range of 12–70. It is also known as Bunker B fuel oil. No. 6 fuel oil is a high viscosity residual oil that requires preheating to 220–260 °F (≈ 104 –126 °C) for storage, handling and atomizing. No. 6 has a carbon number range of 20–70. It is specified by navy as Bunker C oil for ships.

Marine Diesel Oils

The fuel oils used in marine diesel engines have different classifications. Marine gas oil (MGO) is made from distillates only. It is roughly equivalent to No. 2 fuel oil. Marine diesel oil (MDO) is a blend of heavy gas oil that may contain very small amounts of black refinery fuel oil stocks, but needs not be heated for use in internal combustion engines. Intermediate fuel oil (IFO) is a blend of gas oil and heavy fuel oil, with less gas oil than marine diesel oil. Marine fuel oil (HFO) is roughly equivalent to No. 6 fuel oil (Bunker oil).

Major seaports, including those in the United States and the European Union, are imposing tighter emissions limits on sea-going ships and the fuels they burn. In 2012, a global treaty (MARPOL Annex VI) capped SO_x emissions at 1% in coastal waters and extended the coastal zone to 200 mile offshore around Canada and the United States. The SO_x limit was decreased to 0.1% on January 1, 2015, requiring even tighter limits on the sulfur content of marine fuels. Meanwhile, changes in vessels and the use of larger, more fuel-efficient vessels have decreased marine fuel consumption.

1.12.7 Lubricant Base Oils, Wax, Grease, and Specialty Products

Lube Base Oils

Refiners prepare lube base stocks from different crude oils by removing asphaltenes, aromatics, and waxes [1.90, Chaps. 33, 35]. Lube base stocks are hydrofinished, blended with other distillate streams for viscosity adjustment, and compounded with additives to produce finished lubricants. In the past, solvent-based technology was used to prepare lube base stocks. Propane deasphalting removes asphaltenes. Furfural and related substances extract aromatics, and MEK or MIBK remove wax. Wax removal technology was introduced in Sect. 1.9.3. With the advent of catalytic dewaxing (CDW), some or all of these solvent-based methods can be replaced with hydroprocessing. The first process for catalytic dewaxing, called MLDW, was developed by Mobil (now ExxonMobil) in the 1980s. The Mobil process employs ZSM-5, which selectively converts waxy *n*-paraffins into lighter hydrocarbons. The Isodewaxing process was commercialized in 1993 by Chevron. Isodewaxing is a hydroisomerization process, in which conversion of *n*-paraffins into smaller molecules is minimized. Instead, it reduces wax catalytically by isomerising *n*-paraffins into isoparaffins. Isodewaxing includes prior high-pressure hydrotreating and post-treating, which removes sulfur and nitrogen and saturates aromatics. The products have a high viscosity index (VI), low pour point, and excellent response to additives.

It is important to distinguish among lubricant products. Base stocks are products produced from the lubricant plant without any additives in the oil. Base oils are blends of one or more base stocks. Finished oils or formulated oils are blends of base oils with special additives.

Lubricant base stocks can be categorized into 5 groups [1.91]. The first three groups (I–III) are derived from mineral oils. Group I oils are manufactured by solvent extraction and hydro-finishing processes. They contain < 90% saturates and > 0.03% sulfur with a VI of 80–120. Common group I base oils are 150N (solvent neutral), 500N, and 150BS (bright stock). Group II oils are manufactured by hydrocracking or other catalytic processes, such as MLDW. They contain over 90% saturates and under 0.03% sulfur with VI of 80–120. Group II oils have superior antioxidation properties since virtually all hydrocarbon molecules are saturated. They are clear and water-white. Group III oils are manufactured by special processes such as hydrosomerization such as Isodewaxing and from base oil or slack wax. They also contain > 90% saturates and < 0.03% sulfur, but their VI is more than 120.

Synthetic lubricant base oils also have VI > 120. Group IV is specific to the base oils derived from poly alpha olefins (PAOs). Group V includes other synthetic base stocks, such as dibasic esters, aromatic esters, polyol esters, etc. Chapter 35 is dedicated to the production of synthetic lubricant base oils.

Finished lubricant oils with additives can be used as engine oils, transmission fluids, gear oils, turbine oils, hydraulic oils, metal cutting oils, paper machine oils and mixed with soaps as greases. Finished lubricants are formulated with base oil and special additives [1.14]. Detergents and dispersants are the dominant performance additives in motor oils. The additives are typically 5–20% of formulated engine oil or 55–70% of performance-package oil. The remaining additives include antiwear agents, ash inhibitors, friction modifiers, etc.

Petroleum Wax

Petroleum wax (paraffin wax) can come from atmospheric or vacuum distillates, which form wax with large crystals or plates with molecular weights between 300 and 450 (C_{17} – C_{35}). Such wax contains mostly normal paraffins and small amounts of isoparaffins, cycloparaffins and minute amounts of aromatics. Another source of wax is vacuum residue, which forms microcrystalline wax with molecular weights between 450 and 800 (C_{35} – C_{60}). Such wax contains mostly cycloparaffins with *n*-alkyl and isoalkyl side chains. Microcrystalline wax is often used in tire and rubber industries, candles, cosmetics, and for other purposes. The blending of paraffin and microcrystalline waxes is practiced in the tire and rubber industries.

Greases

Greases are made by blending detergents (salts of long-chain fatty acids) into lubricating oils at 400–600 °F

(204–315 °C). Antioxidants are added to provide stability. Some greases are batch-produced, while others are made continuously. The characteristics of a grease depend to a great extent on the counter-ion (calcium, sodium, aluminum, lithium, etc.) in the fatty-acid salt.

Specialty Oils

Other specialty products include white oil and insulating (electrical) oils. Naphthenic crude oils give white oil products of high specific gravity and viscosity, suitable for pharmaceutical uses. Paraffinic crude oils produce oils with lower gravity and viscosity suitable for lubrication purposes. Technical grade white oils are employed for cosmetics, textile machinery lubrication, insecticides, vehicles, paper impregnation, etc. Pharmaceutical (medical) grade white oils may be employed as laxatives or for lubrication of food-handling machinery. Insulating oils are highly refined fractions of low viscosity; they are stable at high temperature and have excellent electrical insulating properties. They are used in transformers, circuit breakers, and oil-filled cables, and for impregnating the paper covering of wrapped cables.

1.12.8 Cokes

Coke is a carbonaceous solid derived from coking or other cracking processes. Undesirable coke is deposited on catalysts used in certain oil refining processes, such as catalytic reforming, hydrotreating, and hydrocracking. In the FCC process, coke is not undesirable, it is essential, because burning the coke in the catalyst regenerator provides heat to run the unit.

The coke directly out of delayed coking units is often referred to as green coke. The most common grades of coke are fuel grade coke and anode grade coke. If the green coke contains low metals and low sulfur it may be calcined to remove residual hydrocarbons. Sulfur recovery is required during calcination. The calcined coke can be processed in an anode baking oven to produce anode grade coke or needle coke. Needle coke, named for its needle-like structure, is a high-value product that has a low thermal expansion coefficient, making it suitable for conversion into graphite anodes for the electric-arc furnaces mainly used in the specialty steel and aluminum smelting industries.

If the metals and sulfur contents in the green coke are too high, it will not be calcined and is used as fuel grade coke for burning. Fuel grade coke has as either desirable sponge coke or undesirable shot coke morphology (see Fig. 30.3). The formation mechanisms of sponge coke and shot coke are not well understood. However, low temperatures and high pressures promote sponge coke formation.

Sponge coke is named for its sponge-like appearance. It is produced from coker feeds with low-to-moderate asphaltene concentrations. Fuel coke with high heat and low ash content is used for power generation. Low ash content is important, because ash can foul boilers. When burning fuel coke, some form of sulfur capture is required to meet current emission standards. Fuel grade coke can be a feedstock for gasification, during which it is converted into synthesis gas – a mixture of CO and H₂.

Shot coke is undesirable because it tends to be unstable. It forms when the coking reaction is too rapid, as when the concentration of feedstock asphaltenes and/or coke-drum temperatures are too high. A block of shot coke is a cluster of discrete mini-balls with diameters 0.1–0.2 in. (2–5 mm). The clusters can be as large as 10 in (25 cm) across. If a cluster breaks apart when the coke drum is opened, it can spray a volley of hot mini-balls in every direction. Adding aromatic feeds, such as FCC decant oil, can eliminate shot coke formation. Other methods of eliminating shot coke – decreasing temperature, increasing drum pressure, increasing the amount of product recycle – decrease liquid yields, which is not desired.

Specialty carbon products made from petroleum include recarburizer coke, which is used to make special steels, and titanium dioxide coke, which is used as a reducing agent in the titanium dioxide pigment industry.

1.12.9 Asphalt

Asphalt is a sticky, black, and highly viscous liquid or semisolid form of petroleum. Also known as bitumen, it may be found in natural deposits or may be produced in refineries.

Asphalt base stocks can be produced directly from vacuum residue or by solvent deasphalting. Vacuum residue is used to make road-tar asphalt. To drive off

light ends, it is heated to about 750 °F (400 °C) and charged to a vacuum column.

In road-paving, the asphalt serves as a binder for aggregate, which can include stone, sand, or gravel. The aggregate comprises about 95% of the final mixture. Polymers are added to the binder to improve strength and durability. The recommended material for paving highways in the United States is Superpave32 hot-mix asphalt. Superpave was developed in 1987–1993 during a US\$50 million research project sponsored by the Federal Highway Administration.

Roofing asphalt is produced by bubbling air through liquid asphalt at 260 °C (500 °F) for 1–10 h. During this *blowing* process, organic sulfur is converted to H₂S and SO₂. Catalytic salts such as ferric chloride (FeCl₃) may be used to adjust product properties and increase the rates of the blowing reactions, which are exothermic. To provide cooling, water is sprayed into the top of the blowing vessel, creating a blanket of steam that captures sulfur-containing gases, light hydrocarbons, and other gaseous contaminants. These are recovered downstream. Cooling water may also be sprayed on the outside of the vessel. The length of the blow depends on desired product properties, such as softening temperature and penetration rate. A typical plant blows 4–6 batches of asphalt per 24 h day. There are two primary substrates for roofing asphalt – organic (paper felt) and fiberglass. The production of felt-based roofing shingles consists of:

- Saturating the paper felt with asphalt
- Coating the saturated felt with filled asphalt
- Pressing granules of sand, talc or mica into the coating
- Cooling with water, drying, cutting and trimming, and packaging.

If fiberglass is used as the base instead of paper felt, the saturation step is eliminated.

1.13 Characterization of Petroleum

As mentioned earlier, petroleum is a very complex mixture. In order to determine its value and processability, a battery of analytical tools, instruments, and methods have been developed to measure bulk properties and to determine detailed chemical composition. In fact, petroleum analysis has played an important role in petroleum research and development.

1.13.1 Crude Oil Assay

Both physical and chemical properties of crude oils vary with location, depth, and age of the oil field. They

are measured by testing laboratories according to the requirements of a crude oil assay (or crude assay). The assay can be performed on the whole crude oil or its distillation fractions. The assay can be an extensive (full) assay, especially for new crude oils, or an inspection assay that includes only selected tests. Full assay analyses are done by combining atmospheric and vacuum distillation runs. High quality assay data are used by producers, oil traders, and refiners, enabling them to predict the true value of an oil for a specific facility. Considerations include compatibility, processability, processing options, potential problems,

and expected product quality. In addition to quality, crude oil price is determined by many factors, including supply and demand, oil reserves and inventory, and the effect of world events. Two commonly used benchmark crude oils are West Texas Intermediate (WTI) and Brent (from North Sea).

For a whole crude oil, one of the most important properties is the yields of distillation fractions. The yields can be determined by distillation laboratory or by simulated distillation (SimDist) using gas chromatography (GC). The ASTM D 2892 (15/5 distillation) method is designed for atmospheric distillation to determine accurate boiling point and yields of distillation fractions using a 15 theoretical plate fractionation column with a 5 : 1 reflux ratio. The ASTM D 5236 (Hivac distillation) method is developed for vacuum distillation in a vacuum potstill to produce gas oil and traditional lube oils as well as vacuum resid. True boiling point (TBP) curve, i. e., a curve of accumulated volume or weight percent of distillates versus temperature, is created by combining atmospheric (ASTM D 2892) and vacuum (ASTM D 5236) distillation runs. SimDist uses a nonpolar GC column with a temperature program, typically from -50 to 350°C at $8^{\circ}\text{C}/\text{min}$. Products are measured with a flame ionization detector (FID) which response is proportional to the number of carbon atoms present and closely approximates weight percent. SimDist data are compared with a full assay TBP curve to determine true distillation curve and predict distillate yields. It provides a quick and robust method for obtaining distillation data with much less sample, time, and effort.

The full assay contains a vast amount of data, including API gravity, sulfur content, nitrogen content, metal content, salt content, total acid number, micro carbon residue, viscosity, refractive index, aniline point, freeze point, cloud point, pour point, smoke point, and more. The refinery may set up a testing grid of the above tests for each distillation fraction. There is no standard testing grid. Requirements vary from refinery to refinery. The extent of assay depends on customer need and affordability.

For manufacturing lubricant base oils, assay is used for identifying economically attractive crude oils based on the yield and quality [1.15]. The assay processes

include atmospheric distillation, vacuum distillation, extraction, and dewaxing to produce lubricant base stocks. Modeling uses assay information to predict process response for desired lube products and to investigate process variables and operating optimization for distillation, extraction, and dewaxing. This allows refiners to assess manufacturing flexibility. Plant tests for products include blending into formulated lubes for further testing. Periodic re-evaluation is performed to assess lube quality variation over time. Important lube qualities include viscosity, VI, sulfur, density, oxidative stability, refractive index, etc. The yield in the lube boiling ranges is also determined for economic evaluation.

1.13.2 Instrumental Analysis

With advances in instrumentation, many tests have been replaced by analytical instruments. For example, high temperature simulated distillation of whole crude oil by gas chromatography has been used as a replacement for assessing distillation yields without the use of a large-scale distillation apparatus with time-consuming, tedious, and very costly procedures [1.92]. In addition, the sample quantity is reduced by several orders of magnitude for handling and cleaning. There are numerous analytical instruments for testing other petroleum properties [1.93, 94].

To determine the composition of complex petroleum mixtures, it usually requires a battery of analytical techniques to detect specific features of the molecules, such as mass, elemental composition, boiling point, solubility, vibrational frequencies, nuclear magnetic resonance frequencies, etc. Modern instrumentation used to determine the petroleum composition for upstream, downstream, chemical and environmental applications includes elemental analysis, chromatography, mass spectrometry (MS), nuclear magnetic resonance spectroscopy (NMR), infrared spectroscopy (IR), and x-ray absorption spectroscopy [1.16]. The robust versions of selected instruments are used for routine analysis of process streams and products at refinery and chemical plant laboratories. More sophisticated and difficult-to-operate instruments are used in research and development laboratories for the development of new and novel technologies and problem solving.

1.14 Modeling

Ever-improving mathematical models are enhancing all aspects of petroleum technology. Three-dimensional imaging identifies geological formations most likely to contain oil and gas. Rigorous basin modeling optimizes

exploration and production. Global energy companies employ sophisticated planning models to quickly decide which feedstocks to buy, how to use them in numerous processing plants, and whether to resell them.

Rigorous equipment and piping models serve as the basis for designing piping networks and upgrading facilities in gas plants, refineries, and petrochemical plants; the use of such models has improved energy efficiency by up to 70% at some sites. Rigorous process modeling, based on molecular characterization, serves as the foundation for real-time online process optimization. The modeling and automation of product blending reduce product-quality giveaway, increasing profitability at relatively low cost, especially when no new equipment is required.

1.14.1 Basin Modeling

Basin and petroleum system modeling in the upstream sector aids the prediction of petroleum occurrence, migration, accumulation, and preservation. This helps with reducing exploration risk and highlights prospective exploration areas [1.95]. The four-dimensional models track migration through time, along with the composition and volumes of the entrapped fluids. They incorporate a broad spectrum of geoscience data from seismic measurements, well logs, stratigraphy, structure geology, and geochemistry.

1.14.2 Design Models

Equipment models based on rigorous thermodynamics, fluid dynamics, and other fundamental principles are employed in all sectors of process industries for many purposes, starting with process design. For existing petroleum and gas processing plants, rigorous models can aid the selection of feedstocks and enable optimization of operation conditions to give the most profitable balance between feed rate, process severity, catalyst life, and product yields. The models include equipment constraints and product property specifications; as mentioned, naphtha is not gasoline unless it meets gasoline specifications. Design models enable evaluation of possible revamps. No unit runs exactly as designed, in part because feedstocks are never the same as the design feed, and their qualities and availability always change. Other reasons for revamps include unexpected process bottlenecks and changes in market conditions, which change the relative value of products. The simulation results are compared with data from pilot plants as well as commercial practice.

1.14.3 Component Lumping

Lumping reduces the complexity of the astronomical number of molecular components in petroleum mix-

tures to a manageable size [1.96]. Hence, it enables one to simulate the reaction chemistry of complex mixtures with a hundred or so mathematical proxies instead of thousands of individual molecules. The first publications on lumping came from researchers at Mobil Oil, where the technique was called structure-oriented lumping (SOL). Similar techniques were developed at roughly the same time by Shell Oil; developers from Shell later formed DMC Corporation, which for a long time was the leading provider of lump-based online optimization services to refining and petrochemical companies, including Mobil.

At present, process models for middle distillate, VGO, and resid processing units rely on lumping extensively, with heavy dependence on bulk composition measurements. Models for catalytic reformers make little if any use of lumping. Lumping is not needed, because such units process mixtures containing only a small number of light compounds with less than 12 carbon atoms.

1.14.4 Real-Time Optimization

Real-time optimizers (RTO) based on rigorous process models are found in just about every olefin production plant in first-world countries. They are found in other chemical plants and many refineries, especially refineries operated by ExxonMobil. For an olefin plant, net benefits can exceed \$10–20 per ton of product [1.97].

In a fully rigorous conversion model, the number of lumps affects almost every piece of equipment in a unit. A VGO hydrocracker model might contain > 100 pieces of equipment, including pumps, compressors, heat exchangers, reactors, quench valves, flash drums, strippers, and distillation trays. For each piece, in addition to component information, pressure, temperature, and flow rate must be specified or calculated. In conversion units, the number of components affects the number of reactions. One modern hydrocracker optimizer includes 116 lumps and 240 reactions (Chap. 28). Even with an advanced computer, the execution time for an online version can exceed 10 min.

An RTO model must include a feed blending model. Feed quality and availability change frequently and often significantly, several times per week. In real time, it is impossible to determine detailed molecular compositions and distribute them into lumps. Therefore, the RTO described in Chap. 28 includes a feed adjustment block. The feed adjustment block is crucial, because it determines the fidelity of the entire RTO.

A feed adjustment block compares measured bulk properties of a candidate feed to the bulk properties

of a library feed. Each library feed includes a distribution of lumps, each of which is associated with a set of chemical and physical properties. The feed adjustment model develops a lump distribution for the candidate feed by skewing the lump distribution of a library feed until its bulk properties match (within an acceptable error range) the measured properties of the candidate feed.

In each optimization cycle, the program executes twice. The first time, it determines whether the plant is steady and detects gross errors. If process measurements are grossly wrong or if key data are missing, the optimizer might not run. If the plant is steady and measurements are reliable, the RTO imports price information for every input stream, product stream, and all utilities. It uses a sophisticated solver, which computes and automatically downloads optimal settings for every valve in the unit.

For fixed-bed catalytic units, the RTO must include a catalyst deactivation model [1.18]. Without considering deactivation, the RTO would select the heaviest possible feeds and push conversion to the limit, even if so doing would deactivate the catalyst immediately.

1.14.5 Planning and Scheduling

Petroleum companies strive to operate safely, reliably, and in compliance with the law. If a company is not

producing and/or processing petroleum due to a terrible accident or violating a regulation, it cannot make any money.

After safety, reliability, and legal objectives are met, feed selection and allocation determine profitability more than any other activity. In advanced companies, corporate planning models are linked to linear program (LP) models for individual refineries, and the LP models are linked to individual process unit optimizers (if they exist). At every level, the models include feedstock costs, information on how feedstock properties affect process unit capability, and product yields and prices.

If gasoline prices suddenly go up and diesel prices drop, the company may or may not make changes. If it has long-term contracts for feeds and separate long-term supply contracts, it may not be able to make significant changes in operation. If it buys crude on the spot market and sells products to the open market, it might be able to change operation, but the changes cannot be instantaneous. It can take days to readjust operating conditions in a single process unit, weeks to process on-site inventories, and a month to obtain pipeline crudes. Other companies also will make changes, increasing supply and thereby affecting prices.

The best planning models strive to account for the impact of a large company's decisions on the world market.

1.15 Petrochemicals

Refineries produce a very large quantity of commodity petrochemicals, which are used in subsequent chemical and pharmaceutical production. Primary petrochemicals can be divided into three groups as olefins, aromatics, and synthesis gas. Olefins are major source of polyolefins, such as polyethylene, polypropylene, and ethylene/propylene co-polymers. Ethylene and propylene are sources of other polymers, too. Ethylene reacts with benzene to make ethyl benzene, which leads to styrene and polystyrene. Propylene is oxidized to acrylic acid, which is used to make polyacrylates. Oxidation of propylene in the presence of ammonia produces acrylonitrile, which leads to polyacrylonitrile and several derivatives (Chap. 36). Aromatics are mainly benzene, toluene, and xylenes. They are solvents and feedstocks for a variety of chemicals. *p*-Xylene is a major feed for polyester production. Synthetic gas is used for making methanol and ammonia as well as synthetic fuels. Butyl rubbers made from C₄ olefins are basic ingredients for tires. Bromobutyl

(and chlorobutyl) is the key ingredient for tubeless tires due to its excellent air impermeability, UV resistance, and ozone resistance properties. High polymers can be further processed into plastics and engineering plastics.

Table 1.29 lists some of the refinery process units which produce petrochemicals. Figure 1.45 provides an example of the synergies between a refinery and a petrochemical plant.

Table 1.29 Sources of petrochemical feedstocks

Process unit	Petrochemicals
Natural gas processing	CO-based chemicals (synthesis gas, methanol, detergent alcohols)
Naphtha hydrotreating	Clean naphtha → olefin plants → polymers
FCC	Propylene and butylene → polymers
Hydrocracking	Unconverted oil → olefin plants → polymers
Catalytic reforming	Aromatics → solvents, polymers

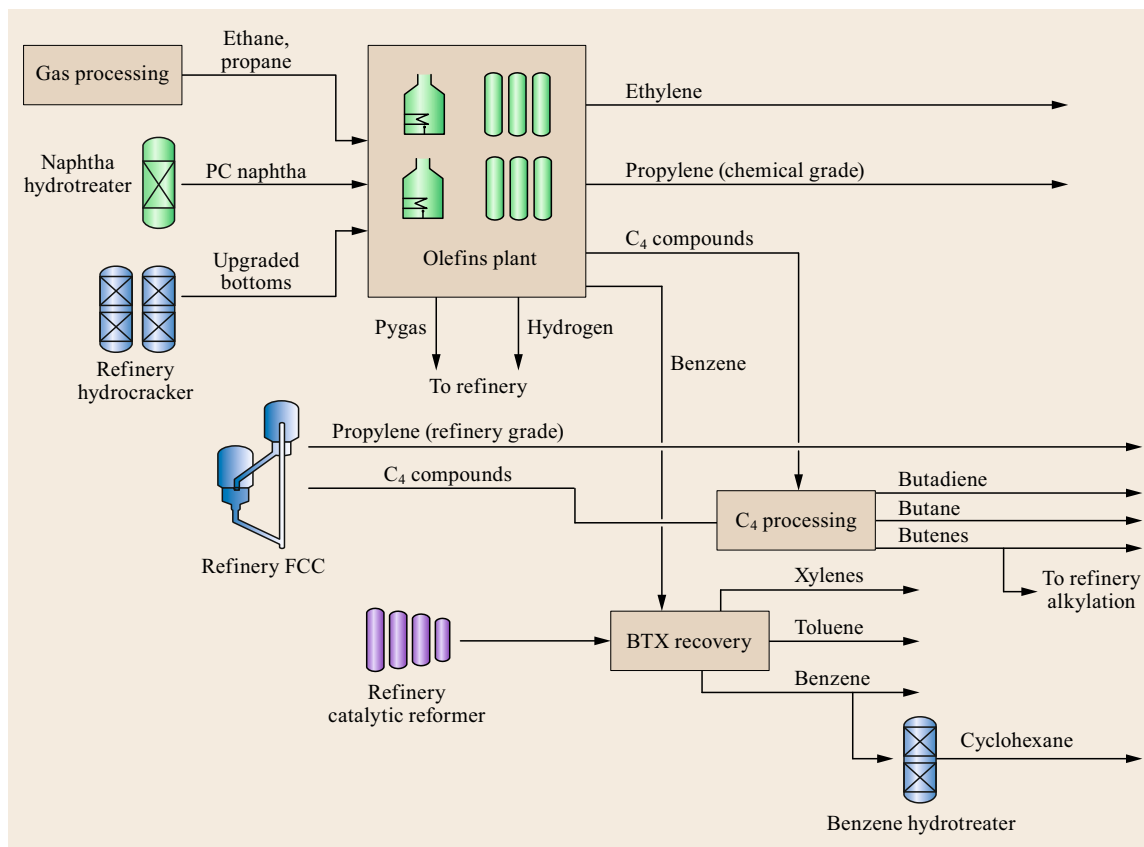


Fig. 1.45 Example showing interactions between a refinery and an olefins plant

1.16 Alternatives to Petroleum

Oil and gas reserves are finite. They are versatile, serving as sources of energy and raw materials for producing chemicals and consumer products. It will be difficult to replace them completely with any single alternative.

For decades, finding conventional crude oil has been getting harder. Even so, reserves are now increasing due to advances in technology, such as the recent advent of *fracking* technology to increase oil and gas production from tight formations and nonconventional reservoirs. Declining availability of conventional petroleum can be offset to some extent by nonfossil sources, but in the interim unconventional fossil resources are likely to carry most of the load. Liquid fuels are being produced from natural gas, bitumen, kerogen, and coal. Some of these, especially kerogen, contain daunting amounts of contaminants, so converting them into petroleum alternatives is costly and difficult.

1.16.1 Inexhaustible (Renewable) Energy Sources

Hydroelectric, wind, solar, and geothermal energy are carbon-neutral. They do not contribute to climate change, and they are practically inexhaustible. Importantly, capturing such energy is friendly to the environment, except perhaps when certain kinds of solar cells are employed. But, because they are carbon-neutral, they cannot serve as sources of carbon-containing chemicals.

1.16.2 Nuclear

Nuclear energy is finite, but with breeder technology, which converts ^{238}U and other nonfissile isotopes into useful nuclear fuel, it could provide our energy needs for thousands of years. Nuclear energy is carbon-

neutral. Hence, like the energy sources mentioned above, it cannot replace fossil resources as sources of petrochemicals.

1.16.3 Biomass (Renewable) Resources

Ethanol, cellulose, and vegetable oil do contain carbon, and already research is underway to develop bio-refineries [1.98].

Many countries offer incentives to add oils from plants to diesel fuels. Bio-oils, except biobutanols, are not suitable for direct use in existing gasoline engines, so they often are mixed in small amounts with conventional petroleum in existing refineries.

First-Generation Biofuel Technology

Brazil replaced most of its petroleum needs with ethanol from sugar cane, creating the world's first *biofuel economy* [1.84]. The key to Brazil's success was the demonstrated fact that the energy gain for ethanol from sugar is eight times; energy gain is the ratio of the energy obtained from product consumption divided by the non-solar energy required for manufacturing and collecting the product.

The United States now requires the blending of more than 10% ethanol into most of its gasoline. Most American fuel ethanol comes from corn, for which the energy gain ranges from 2.1 to 4.1 times [1.99]. Other aspects of corn ethanol are discussed in Sect. 1.12.2. First-generation biofuels derived from sugar cane or corn compete with food resources.

Another first generation biofuel is biodiesel consisting of methyl, ethyl or propyl esters of long-chain fatty acids. The esters are made by reacting lipids (vegetable oils, corn oil or animal fats) with an alcohol via transesterification.

Second-Generation Biofuel Technology

Second-generation biomass technology involves gasification or pyrolysis of nonfood sources. Raw materials for gasification technologies include forest and agricultural residues, waste wood, saw dust, energy crops, and black liquor from pyrolysis units. The product is syngas, which is converted via Fischer-Tropsch technology to alcohols and *n*-paraffins, which in turn are converted into gas oil, naphtha, and fuel gas.

Gasoline is produced from methanol through the MTG process developed at Mobil, now ExxonMobil. A useful byproduct is dimethyl ether (DME). Gas oil and naphtha can be converted into diesel and gasoline, respectively, with the conventional refining technology. Chemicals can be manufactured from methanol and DME. The fuel gas generates mechanical and electrical power via gas motors or gas turbines.

The same raw materials can be used for fast pyrolysis, which thermally decomposes organic material at elevated temperatures in the absence of oxygen. Pyrolysis oil is highly reactive and must be stabilized by hydrogenation prior to further processing in conventional crude oil refineries. The cost of hydrogenation is considerable, and producing the hydrogen in steam-methane reformers generates large amounts of CO₂.

1.17 Protecting the Environment

In addition to desired products, upstream, downstream, and petrochemical facilities produce wastes. If not contained or processed, these wastes can harm people and the environment. Waste control is a crucial consideration during process design and operation. Various treatment, capture, and disposal units are required, and emissions are constantly monitored.

As described in Chap. 2, despite concerted efforts to put safety first, preventable accidents still cause tremendous loss of life and environmental damage. Examples include the BP Texas City refinery explosion, the *Exxon Valdez* oil spill, and the recent *Deepwater Horizon* blowout in the Gulf of Mexico.

1.17.1 Air Quality

In the 1970s and 1980s, environmental laws compelled oil and gas companies to reduce emissions of SO_x,

NO_x, CO₂, and hydrocarbons. In the atmosphere, SO_x reacts with water vapor to make sulfurous and sulfuric acids, which return to Earth as dry or wet deposition (acid rain). Volatile hydrocarbons react with NO_x and sunlight to make ozone, a noxious component of photochemical smog. CO₂ is a major *greenhouse* gas responsible for climate change. To reduce these pollutants, the industry tightened its operations by:

- Reducing fugitive hydrocarbon emissions from valves and fittings
- Removing sulfur from refinery streams and finished products
- Adding tail-gas units to sulfur recovery plants
- Reducing the production of NO_x in fired heaters
- Scrubbing SO_x and NO_x from flue gases
- Reducing the production of CO₂ by increasing energy efficiency.

In several oil fields, companies keep CO₂ out of the atmosphere by pumping it into oil wells to maintain reservoir pressure, thereby enhancing production.

Sulfur Recovery

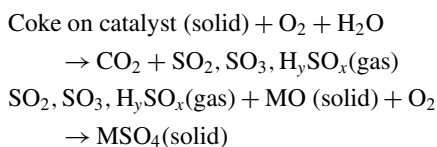
Natural gas can contain significant amounts of hydrogen sulfide. Some gas processing plants in Alberta, Canada, recover more than 2000 t of sulfur per day using the Claus process. Sulfur is recovered by a much smaller Selectox unit on Platform Irene off the coast of California [1.100]. For the most part, sulfur is recovered from petroleum in refineries. Conversion processes, hydrotreaters, and sweetening units remove chemically bound sulfur, which can end up as SO_x, H₂S, NH₄SH, or NaSH.

Fuel-oil fired heaters and the regenerators of FCC units are major sources of refinery SO_x and NO_x emissions. The most obvious solution to reduce SO_x emissions from a heater is to use low-sulfur fuels. Unfortunately, although that solution requires no investment in processing, it would probably be the most expensive due to the relatively high cost of buying low-sulfur crudes for the entire refinery and/or hydrotreated VGO just for the FCC.

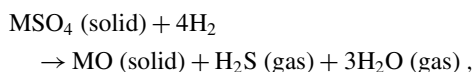
A large fraction of the sulfur in the feed to an FCC unit ends up in coke on the catalyst. SO_x are formed in the regenerator when the coke is burned away. Therefore, removing sulfur from the feed, usually by hydrotreating, decreases SO_x emissions. FCC feed pretreating has other substantial benefits. Removing basic nitrogen decreases deactivation of acid sites on the FCC catalyst, which allows the FCC to reach a given conversion at lower temperatures. The saturation of aromatics in the feed pretreater provides the biggest benefit, because it converts hard-to-crack aromatics into easier-to-crack naphthenes. This alone can justify the installation of an FCC feed pretreater.

SO_x transfer additives, first developed by Davison Chemical, react with SO_x in the FCC regenerator to form sulfates. When the sulfated additive circulates to the riser/reactor section, the sulfate is reduced to H₂S, which is recovered by amine absorption and sent to the sulfur plant. In some units, these additives reduce FCC SO_x emissions by more than 70%. Consequently, if a pre-treater or post-treater still must be installed, its size can be reduced. The chemistry of SO_x transfer is summarized below.

FCC Regenerator (Oxidizing Environment).



FCC Riser-Reactor (Reducing Environment).



where MO is a weakly basic metal oxide such as MgO or La₂O₃.

Flue-gas scrubbing is a refiner's last chance to keep NO_x and SO_x out of the air. In wet flue-gas desulfurization, gas streams containing SO_x react with an aqueous slurry containing calcium hydroxide Ca(OH)₂ and calcium carbonate CaCO₃. Reaction products include calcium sulfite (CaSO₃) and calcium sulfate (CaSO₄), which precipitate from the solution. NO_x removal is more difficult. Wet flue-gas scrubbing removes about 20% of the NO_x from a typical FCC flue gas. To remove the rest, chemical reducing agents are used. As mentioned above, in the SCR process, anhydrous ammonia is injected into the flue gas as it passes through a bed of catalyst at 500–950 °F (260–510 °C). The chemical reaction between NO_x and ammonia produces N₂ and H₂O.

When sulfur-containing feeds pass through hydrotreaters or conversion units, most of the sulfur is converted into H₂S, which eventually ends up in off-gas streams. Amine absorbers remove the H₂S, leaving only 10–20 wppm in the treated gas streams. H₂S is steam-stripped from the amines, which are returned to the absorbers. The H₂S goes to the refinery sulfur plant.

Claus Process

At the sulfur plant, H₂S is combined with sour-water stripper off-gas and sent to a Modified Claus unit. (The Modified Claus process includes a combustion furnace. The original Claus process did not. In common usage, both the modified and original versions are called Claus. Additional information is given in Chap. 20.) Almost every refinery in the world uses some version of this process to convert H₂S into elemental sulfur. H₂S and a carefully controlled amount of air are mixed and sent to a burner, where about 33% of the H₂S is converted to SO₂ and water. From the burner, the hot gases go to a reaction chamber, where the reactants and products reach equilibrium. In several units, the air is enriched with oxygen to increase plant capacity. Elemental sulfur is produced by the reversible reaction between SO₂ and H₂S. Ammonia comes in with the sour-water stripper off-gas. In the Claus process, it is thermally decomposed into nitrogen and water.

In the Claus burner, combustion temperatures reach 2200 °F (1200 °C). Much of the heat is recovered in a waste-heat boiler, which generates steam as it drops the temperature to 700 °F (370 °C). Next, the process gas goes to a condenser, where it is cooled to

about 450°F (232°C). At this temperature, sulfur vapors condense, and the resulting molten sulfur flows through a drain to a heated sulfur-collection pit. At the bottom of the drain, a seal leg maintains system pressure and keeps unconverted gases out of the pit. Uncondensed sulfur and other gases flow to a series of catalyst beds, which recover additional sulfur by promoting the Claus reaction between left over H₂S and SO₂. With fresh catalyst and a stoichiometric gas composition, the cumulative recovery of sulfur across four condensers is about 50%, 80%, 95%, and 96–98%, respectively.

Claus tail-gas treating units (TGTU) bring the total sulfur recovery up to > 99.9%. Most tail-gas treating processes send the tail gas to a hydrotreater, which converts all sulfur-containing compounds (SO₂, SO₃, COS, CS₂, and various forms of S_x) into H₂S. The carbon for CS₂ and COS comes from CO₂ and/or hydrocarbons in the feed gas. In the SCOT process, offered by Shell Global Solutions, the H₂S is absorbed by an amine and returned to the front of the Claus furnace. In the LO-CAT process, offered by Merichem, H₂S is air oxidized to sulfur in an aqueous solution containing a chelated iron catalyst. For all tail-gas treatment processes, the last traces of unrecovered sulfur go to an incinerator, where they are converted into SO₂ and dispersed into the atmosphere.

1.17.2 Wastewater Treatment

Wastewater treatment purifies process water, runoff, and sewage. Purified wastewater streams are re-used in the refinery as much as possible. Wastewater streams may contain suspended solids, dissolved salts, phenols, ammonia, sulfides, and other compounds. The streams come from just about every process unit, especially those that use wash water, condensate, stripping water, caustic, or neutralization acids.

Primary treatment uses a settling pond to allow most hydrocarbons and suspended solids to separate from the wastewater. The solids drift to the bottom of the pond, hydrocarbons are skimmed off the top, and oily sludge is removed. Difficult oil-in-water emulsions are heated to expedite separation. Acidic wastewater is neutralized with ammonia, lime, or sodium carbonate. Alkaline wastewater is treated with sulfuric acid, hydrochloric acid, carbon dioxide-rich flue gas, or sulfur.

Some suspended solids remain in the water after primary treatment. These are removed by filtration, sedimentation, or air flotation. Flocculation agents may be added to consolidate the solids, making them easier to remove by sedimentation or filtration. Activated sludge is used to digest water-soluble organic compounds, either in aerated or anaerobic lagoons. Steam-stripping is

used to remove sulfides and/or ammonia, and solvent extraction is used to remove phenols.

Tertiary treatment processes remove specific pollutants, including traces of benzene and other partially soluble hydrocarbons. Tertiary water treatment can include ion exchange, chlorination, ozonation, reverse osmosis, or adsorption onto activated carbon. Compressed oxygen may be used to enhance oxidation. Spraying the water into the air or bubbling air through the water removes remaining traces of volatile chemicals such as phenol and ammonia.

1.17.3 Solid Waste Handling

During drilling and production operations, oil-bearing cuttings from wells present environmental challenges. Onshore, the cuttings can be stored onsite in clay-lined pits. Offshore, contaminated cuttings may have to be shipped to shore for treatment. If the cuttings meet certain criteria, they are discharged to the seabed whenever possible but often are dumped into the sea. Other wastes are transported to waste treatment facilities. In the oil sands fields in Alberta, Canada, bitumen is washed away from the inorganic substrate with hot water. The water goes into huge tailings ponds. The ponds emit considerable amounts of CO₂, and they contain significant amounts of trace contaminants.

Refinery solid wastes may include spent catalyst and catalyst fines, acid sludge from alkylation units, and miscellaneous oil-contaminated solids. All oil-contaminated solids are treated as hazardous and sent to sanitary landfills.

Recently, supercritical extraction with carbon dioxide has been used with great success to remove oil from contaminated dirt, including cuttings from oil-well drilling.

1.17.4 Fugitive Emissions

Fugitive emissions are comparatively small amounts of gaseous, liquid, and solid wastes, which come from process equipment during industrial activities. Even small quantities of leaked gases, such as benzene, can cause serious damage to health and environment when the emissions are continuous or chronic. Flammable chemicals can accumulate to form explosion hazards. One recent study showed that fugitive emissions were equivalent to 0.17 wt% of a refinery's throughput.

Leaks from high-pressure equipment usually occur through valves, connections, or mechanical seals. Other emissions come from storage tanks and waste treatment facilities. Operators regularly check for leaks with gas detectors and take appropriate corrective action.

Fugitive emissions can be hard to detect, and the sizes of leaks can vary with processing intensity and ambient conditions. Work continues on developing improved methods for discovery and analysis. One new technology is differential absorption, which measures concentrations of atmospheric hydrocarbons hundreds of meters from a facility. Opacity meters measure particulate emissions, and IR imaging can detect otherwise invisible gases escaping from leak sources.

1.17.5 Improving Energy Efficiency and Safety with Automation

The ever-increasing development and use of better instruments and analyzers, engineering models, and real-time online optimization continue to improve the efficiency and safety of petroleum processing plants. Examples are provided on the websites of companies

1.18 Conclusion

The petroleum industry is huge and complex. It is one of the most important industries on planet Earth. To understand the industry, one must gain familiarity with the underlying science and engineering used to find and recover crude oil and natural gas and to transform them into useful products. These technologies can also be applied to gases and liquids from coal, shale, and renewable biomass.

Research and development aimed at improving or modifying existing petroleum technologies and developing new ones start with physical testing and chemical characterization.

Three-dimensional imaging exhibits geological formations most likely to contain oil and gas. Rigorous basin modeling optimizes exploration and production. Modern production technology includes enhancements in horizontal drilling, offshore platform design, and in-situ SAGD. The application of hydraulic fracturing to previously unrecoverable oil from tight reservoirs transformed the United States into the world's leading oil producer.

Midstream technology includes transportation, trading, and upgrading oil sand bitumen into syncrude. Sophisticated computer models enable global energy companies to quickly decide which oils to buy, how to allocate them between numerous processing plants, and whether to resell them.

such as Applied Manufacturing Technologies (AMT), Aspen Technology, Honeywell, Invensys, Yokogawa, and others. A paper by *Hampton* and *Robinson* provides an example of using advanced regulatory control to improve the safety of a hydrocracking unit [1.101].

1.17.6 Conservation

Conservation also decreases the demand for petroleum and other fossil hydrocarbons while reducing pollution. According to the Rocky Mountain Institute [1.102], with modest investment in proven, widely applied technology, the United States could increase the efficiency of power production by 30%.

Figure 1.6 demonstrates that prices have a tremendous effect on energy consumption. We can save energy not just by traveling less, turning off lights and driving less, but also through innovation.

Crude oil goes to refineries, which rely on distillation, treating, conversion, extraction, and blending to produce fuels, hydrogen, lubricants, construction asphalt, solvents, and bulk chemicals (sulfur, ammonia, and CO₂). Refineries supply raw materials for chemical and pharmaceutical plants, which generate thousands of materials we use to enrich our daily lives – coatings, polymers, rubbers, fibers, plastics, cosmetics, pharmaceuticals, and many others.

Ever-improving mathematical models enhance all aspects of petroleum technology. Model-predictive control (MPC) stabilizes operations and reduces product-quality giveaway, increasing profitability at relatively low cost, especially when no new equipment is needed. The simple return on investment for an MPC project can be 3–4 months. Rigorous reaction models, based on molecular characterization, serve as the foundation for real-time online economic optimization, in some cases for entire refineries.

One cannot over-emphasize the importance of safety and environment protection. The root causes of many infamous industrial catastrophes and accidents were the failure of corporate executives, line managers, front-line engineers, and operators to learn and understand technology fundamentals.

References

- 1.1 BP: Statistical Review of World Energy, <http://www.bp.com/en/global/corporate/energy-economics/statistical-review-of-world-energy.htm> (2016)
- 1.2 Wikipedia: World Energy Sources, http://en.wikipedia.org/wiki/World_energy_sources (2015)
- 1.3 Encyclopaedia Britannica: Greek Fire, Online, <http://www.britannica.com/technology/Greek-fire/> (2015)
- 1.4 SETatWork: Good practice: Use of waste heat from refining industry, Sweden, SETat Work Good Practice #20, <http://www.setatwork.eu/database/products/R179.htm> (2015)
- 1.5 G. Tverberg: Consumption of energy by source since 1820, Our Finite World, <http://ourfiniteworld.com/2012/03/12/world-energy-consumption-since-1820-in-charts/> (2015)
- 1.6 US Energy Information Administration: Petroleum & Other Liquids: Refinery Yield Data, http://www.eia.gov/dnav/pet/pet_pnp_pct_dc_nus_pct_m.htm (2015)
- 1.7 J. Carter: The president's proposed energy policy, Vital Speeches of the Day **43**(14), 418–420 (1977), <http://www.pbs.org/wgbh/americalexperience/features/primary-resources/carter-energy/>
- 1.8 D.M. Fenton, H. Hennig, R.L. Richardson: The chemistry of shale oil and its refined products. In: *Proc. Symp. Oil Shale, Tar Sands and Related Mater., ACS Annu. Fall Meet* (1980) pp. 102–109
- 1.9 N. Mims, M. Bell, S. Doig: *Assessing the Electric Productivity Gap and the US Efficiency Opportunity, Tech. Rep.* (Rocky Mountain Institute, Snowmass 2009)
- 1.10 Wikipedia: Hubbert peak theory, http://en.wikipedia.org/wiki/Hubbert_peak_theory (2016)
- 1.11 E. Boëda, S. Bonilauri, J. Connan, D. Jarvie, N. Mercier, M. Tobey, H. Valladas, H. al Sakhel, S. Muhesen: Middle Paleolithic bitumen use at Umm el Tiel around 70 000 BP, *Antiquity* **82**, 853–886 (2008)
- 1.12 J.R. McIntosh: *The Ancient Indus Valley. New Perspectives (Understanding Ancient Civilizations)*, 1st edn. (ABC–CLIO, Santa Barbara 2008) p. 57
- 1.13 UK Essays: The History of Bitumen, <http://www.ukessays.com/essays/engineering/the-history-of-bitumen-engineering-essay.php> (2015)
- 1.14 Wikipedia: Asphalt, <http://en.wikipedia.org/wiki/Bitumen> (2015)
- 1.15 H. Abraham: *Asphalts and Allied Substances: Their Occurrence, Modes of Production, Uses in the Arts, and Methods of Testing*, 4th edn. (Van Nostrand, New York 1938)
- 1.16 A. Lucas: The question of the use of bitumen or pitch by the ancient Egyptians in mummification, *J. Egypt. Archaeol.* **1**(4), 241–245 (1914)
- 1.17 M. Kurlansky: *Salt: A World History* (Penguin Books, London 2003) pp. 26–28
- 1.18 Government of Alberta: Early Coal History to 1990 – Unearthing Ancient Mysteries: Ancient China, <http://history.alberta.ca/energyheritage/coal/early-coal-history-to-1990/unearthing-ancient-mysteries/ancient-china.aspx> (2016)
- 1.19 E. Chan: Remarkable discovery shows humans were burning coal as fuel more than 3.500 years ago as world's earliest site of the activity is unearthed in China, Daily Mail, <http://www.dailymail.co.uk/news/peoplesdaily/article-3202104/Remarkable-discovery-shows-humans-burning-coal-fuel-3-500-years-ago-world-s-earliest-site-activity-unearthed-China.html> (2015)
- 1.20 J. Dodson, X. Li, N. Sun, P. Atahan, X. Zhou, H. Liu, K. Zhao, S. Hu, Z. Yang: Use of coal in the bronze age in China, *The Holocene* (2014) doi:10.1177/0959683614523155
- 1.21 Muhammad Ibn Zakariya al-Razi, Majzooban Noor, <http://www.majzooban.org/en/biography/1574-muhammad-ibn-zakariya-al-razi.html> (2016)
- 1.22 N. Papatzanankis: Ancient Oil Lamps, <http://www.epalladioartworkshop.com/OILLAMPS/HISTORY/index.htm> (2015)
- 1.23 The Field Museum: Scenes from the Stone Age: the Cave Paintings of Lascaux, exhibition at the Field Museum, Chicago, <http://lascaux.fieldmuseum.org/> (2013)
- 1.24 Oil Lamp: http://en.wikipedia.org/wiki/Oil_lamp#cite_note-1 (2015)
- 1.25 BBC News: Rock Art Hints at Whaling Origins, <http://news.bbc.co.uk/2/hi/science/nature/3638853.stm> (2004)
- 1.26 Wikipedia: History of Basque Whaling, http://en.wikipedia.org/wiki/History_of_Basque_whaling (2016)
- 1.27 Wikipedia: History of Whaling, [http://en.wikipedia.org/wiki/History_of_whaling#Yankee_open-boat-whaling](http://en.wikipedia.org/wiki/History_of_whaling#Yankee_open-boat_whaling) (2015)
- 1.28 San Joaquin Valley Geology: How the Oil Industry Saved the Whales, <http://www.sjvgeology.org/history/whales.html> (2005)
- 1.29 Fritz Funk: Early Years: The Whaling Era at Killisnoo, http://www.backwater.org/herring/history/whaling_era.html (2016)
- 1.30 J. Baldwin: *Last Flag Down: The Epic Journey of the Last Confederate Warship* (Random House, New York 2007)
- 1.31 Wikipedia: Abraham Pineo Gesner, http://en.wikipedia.org/wiki/Abraham_Pineo_Gesner (2015)
- 1.32 Somercotes Local History Society: James Oakes & Co – A Timeline, <http://www.somercoteshistory.co.uk/industryfeatured.asp?newsid+82> (2016)
- 1.33 San Joaquin Valley Geology: The history of the oil industry, <http://sjvgeology.org/history/index.html> (2015)
- 1.34 I. Lukasiewicz (Ed.): *Encyclopedia of World Biography* (The Gale Group, Farmington Hills 2008)
- 1.35 Crownplacebrands.com: *Dietz: The Greatest Lantern Invented*, <http://crownplacebrands.com/wp-content/uploads/2016/01/Dietz-History.pdf> (2016)

- 1.36 Wikipedia: James Miller Williams, http://en.wikipedia.org/wiki/James_Miller_Williams (2015)
- 1.37 Wikipedia: Drake Well, http://en.wikipedia.org/wiki/Drake_Well (2016)
- 1.38 A.F. Alison: *Oil Empire: Visions of Prosperity in Austrian Galicia* (Harvard Univ. Press, Cambridge 2007)
- 1.39 D. Yergin: *The Prize* (Simon Schuster, New York 1991)
- 1.40 US Energy Information Administration: Petroleum & Other Liquids, <http://www.eia.gov/petroleum/> (2015)
- 1.41 US Energy Information Administration: Energy Timelines – Oil (petroleum), http://www.eia.gov/kids/energy.cfm?page=tl_petroleum (2015)
- 1.42 L. Bruno: *Science and Technology First* (Detroit, Gale 1997) pp. 499–534
- 1.43 B.C. Black: *Crude Reality: Petroleum in World History* (Rowman Littlefield, New York 2012) pp. 58–61
- 1.44 S. Cwiek: The Middle Class Took Off 100 Years Ago: Thanks to Henry Ford?, Houston Public Media News 88.7 (2014)
- 1.45 US Energy Information Administration: Weekly Europe Brent Spot Price, <http://www.eia.gov/dnav/pet/hist/LeafHandler.ashx?n=PET&s=RB RTE&f=W> (2016)
- 1.46 B. Hicks: A Brief History of Fracking, Energy & Capital, <http://www.energyandcapital.com/articles/a-brief-history-of-fracking/2972> (2013)
- 1.47 Wikipedia: List of world's largest companies, http://en.wikipedia.org/wiki/List_of_largest_companies_by_revenue (2016)
- 1.48 United Nations Department of Economic and Social Affairs: Population and vital statistics report, <http://unstats.un.org/unsd/demographic/products/vitstats/> (2015)
- 1.49 United States Energy Information Administration: Summer Fuels Outlook: U S. Gasoline and Diesel Fuel Prices, <http://www.eia.gov/forecasts/steo/report/summerfuels.cfm> (2016)
- 1.50 A. Treibs: Chlorophyll and hemin derivatives in organic mineral substances, *Angew. Chem.* **49**, 682–686 (1936)
- 1.51 C.S. Hsu, C.C. Walters, G.H. Isaksen, M.E. Schaps, K.E. Peters: Biomarker analysis for petroleum exploration. In: *Analytical Advances for Hydrocarbon Research*, ed. by C.S. Hsu (Kluwer, New York 2003) pp. 223–245
- 1.52 B.P. Tissot, D.H. Welte: *Petroleum Formation and Occurrence* (Springer, Berlin, Heidelberg 1984)
- 1.53 Sulfur Information Service: Recovered Sulfur, <http://sulfur.nigc.ir/en/sulfurproductionprocess/recoveredsulfur> (2015)
- 1.54 Web Elements: Helium: The Essentials, <http://www.webelements.com/helium> (2015)
- 1.55 J.G. Speight: *The Chemistry and Technology of Coal, Part II: Utilization*, 2nd edn. (Marcel Dekker, New York 1994)
- 1.56 G.S. Sanchez: *Mercury in Extraction and Refinery Process of Crude Oil and Natural Gas*, PhD Thesis (Univ. of Aberdeen, Aberdeen 2013)
- 1.57 Natural Resources Canada: Froth Treatment, <http://www.nrcan.gc.ca/energy/oil-sands/5873> (2014)
- 1.58 US Energy Information Administration: International Energy Statistics, <http://www.eia.gov/cfapps/ipdbproject/IEDIndex3.cfm?tid=5&pid=57&aid=6> (2016)
- 1.59 Natural Resources Canada: Froth Treatment, <http://www.nrcan.gc.ca/energy/oil-sands/5873> (2016)
- 1.60 M.R. Watt, S.G. Roussis: Crude assay. In: *Practical Advances in Petroleum Processing*, ed. by C.S. Hsu, P.R. Robinson (Springer, New York 2006) pp. 103–112, Chap. 2
- 1.61 P.R. Robinson: Overview of petroleum processing. In: *Practical Advances in Petroleum Processing*, ed. by C.S. Hsu, P.R. Robinson (Springer, New York 2006) p. 6, Chap. 1
- 1.62 Royal Society of Chemistry: ChemSpider, <http://ChemSpider.com>
- 1.63 Wikipedia: Steam-assisted gravity drainage, http://en.wikipedia.org/wiki/Steam-assisted_gravity_drainage (2016)
- 1.64 R.H. Burroughs: Oil and gas deposits: extraction and uses. In: *Environmental Geology, Encyclopedia of Earth Sciences Series*, ed. by D.E. Alexander, R.W. Fairbridge (Springer Nature, New York/Philadelphia 1999) pp. 454–456
- 1.65 Offshore Technology: Floating Systems Fit for the Future, Offshore Technology, <http://www.offshore-technology.com/features/feature1585/> (2008)
- 1.66 B.A. Tarr, L. Flak: Underground blowouts, <http://www.jwco.com/technical-literature/p06.htm> (2015)
- 1.67 J.H. Duir, A.C. Randle, C.P. Reeg: Unocal's parachute creek oil shale project, *Fuel Process. Technol.* **25**(2), 101–117 (1990)
- 1.68 Wikipedia: Shale Gas in the United States, http://en.wikipedia.org/wiki/Shale_gas_in_the_United_States (2016)
- 1.69 Wikipedia: Hydraulic Fracturing in the United States, http://en.wikipedia.org/wiki/Hydraulic_fracturing_in_the_United_States (2016)
- 1.70 AlphaVN Research: Falling crack spreads cloud near term for refiners, <http://seekingalpha.com/article/1468771-falling-crack-spreads-cloud-near-term-for-refiners> (2013)
- 1.71 P.R. Robinson: Petroleum and its products. In: *Handbook of Industrial Chemistry and Biotechnology*, ed. by J.A. Kent (Springer, New York 2012)
- 1.72 R.F. Sullivan, M.M. Boduszynski, C.J. Fetzer: Molecular transformations in hydrotreating and hydrocracking, *Energy Fuels* **3**, 603–612 (1989)
- 1.73 R. Scholl, C. Seer: Abspaltung aromatisch gebundenen Wasserstoffs und Verknüpfung aromatischer Kerne durch Aluminiumchlorid, *Justus Liebig's Ann. Chem.* **394**(2), 111–177 (1912)
- 1.74 V.V. Speybroek, M.F. Reyniers, G.B. Marin, M. Waroquier: The kinetics of cyclization reactions on polyaromatics from first principles, *Chem. Phys. Chem.* **3**, 863–870 (2002)
- 1.75 P.R. Robinson: Deactivation of hydroprocessing catalysts: Thermochemistry of coke formation. In: *Proc. Int. Symp. Hydrocrack./Hydrotreat. Technol., 232nd Annu. Fall Meet.* (2006)

- 1.76 C.N. Satterfield: *Heterogeneous Catalysis in Industrial Practice*, 2nd edn. (McGraw-Hill, New York 1991) pp. 378–383
- 1.77 C.N. Satterfield: *Heterogeneous Catalysis in Industrial Practice*, 2nd edn. (McGraw-Hill, New York 1991) pp. 385–387
- 1.78 B.S. Greensfelder, H.H. Voge, G.M. Good: Catalytic and thermal cracking of pure hydrocarbons, *Ind. Eng. Chem.* **41**(11), 2573–2584 (1949)
- 1.79 A.T. Lapinas, M.T. Klein, B.C. Gates, A. Macris, J.E. Lyons: Catalytic hydrogenation and hydrocracking of fluorene: Reaction pathways, kinetics, and mechanisms, *Ind. Eng. Chem. Res.* **30**(1), 42–50 (1991)
- 1.80 K. Krantz: *Intro to Alkylation Chemistry: Mechanisms, Operating variables, and Olefin Interactions* (DuPont STRATCO Clean Fuel Technology: Leawood, Kansas 2008)
- 1.81 E.J. Houde, M.J. McGarth: When solvent deasphalting is the most appropriate technology for upgrading residue. In: *Proc. IDTC Conf., London* (2006) pp. 1–11
- 1.82 H.J. Gary, G.E. Handwerk: *Petroleum Refining: Technology and Economics*, 4th edn. (Marcel Dekker, New York 2001) pp. 246–247
- 1.83 US Energy Information Administration: Date of switch to summer gasoline approaches, Today in Energy, <http://www.eia.gov/todayinenergy/detail.cfm?id=11031#> (2013)
- 1.84 Wikipedia: Ethanol Fuel in Brazil, http://en.wikipedia.org/wiki/Ethanol_fuel_in_Brazil#cite_note-Wilson-2 (2016)
- 1.85 Wesleyan Economics Bio-energy: Sugarcane vs. corn based ethanol, <http://biowesleyan.wordpress.com/first-generation-biofuels/ethanol/case-study-brazil/sugarcane-vs-corn-based-ethanol> (2016)
- 1.86 D.K. Albino, K.Z. Bertrand, Y. Bar-Yam: Food for fuel: The price of ethanol, <http://necsi.edu/research/social/foodprices/foodforfuel> (2012)
- 1.87 University of Illinois Extension Water Use for Ethanol Production, <http://web.extension.illinois.edu/ethanol/pdf/wateruse.pdf> (2009)
- 1.88 Chevron Products Company: *Aviation Fuels: Technical Review* (Chevron Products, San Ramon 2007)
- 1.89 J.G. Speight: *Petroleum Chemistry and Refining* (Taylor Francis, Washington 1998) pp. 224–234
- 1.90 I.A. Cody: Selective hydroprocessing for new lubricant standards. In: *Practical Advances in Petroleum Processing*, Vol. 2, ed. by C.S. Hsu, P.R. Robinson (Springer, New York 2006) pp. 79–104
- 1.91 Noria Corporation: Machinery Lubrication: Understanding the Differences in Base Oil Groups, <http://www.machinerylubrication.com/Read/29113/base-oil-groups> (2016)
- 1.92 D.C. Villalanti, J.C. Raia, J.B. Maynard: High-temperature simulated distillation applications in petroleum characterization. In: *Encyclopedia of Analytical Chemistry*, ed. by R.A. Meyers (Wiley, Chichester 2000) pp. 6726–6741
- 1.93 C. Song, W.-C. Lai, M. Reddy, B. Wei: Temperature-programmed retention indices for GC and GC-MS of hydrocarbon fuels and simulated distillation GC of heavy oils. In: *Analytical Advances for Hydrocarbon Research*, ed. by C.S. Hsu (Kluwer, New York 2003) pp. 147–210
- 1.94 C.S. Hsu (Ed.): *Analytical Advances for Hydrocarbon Research* (Kluwer, New York 2003)
- 1.95 M.M. Al-Hajeri, M. Al Saeed, J. Derks, T. Fuchs, T. Hantschel, A. Kauerauf, M. Neumaier, O. Schenk, O. Swientek, N. Tessen, D. Welte, B. Wygrala, D. Kornpihl, K. Peters: Basin and petroleum system modeling, *Oilfield Rev.* **21**(2), 14–29 (2009)
- 1.96 R.J. Quann, S.B. Jaffe: Structure-oriented lumping: Describing the chemistry of complex hydrocarbon mixtures, *Ind. Eng. Chem. Res.* **31**(11), 2483–2497 (1992)
- 1.97 D. Geddes, T. Kubera: Intergration of planning and real-time optimization in olefin production, *Comput. Chem. Eng.* **24**, 1645–1649 (2000)
- 1.98 CHEManager: Designing the next generation of bio-refineries: The EuroBioRef project gets underway, CHEManager, <http://www.chemanager-online.com/en/news-opinions/headlines/designing-next-generation-bio-refineries> (2010)
- 1.99 P.W. Gallagher, W.C. Yee, H.S. Baumes: *2015 Energy Balance for the Corn-Ethanol Industry* (United States Department of Agriculture, Washington DC 2016) pp. 7–15
- 1.100 R.V. Bertram, P.R. Robinson: In selectox process for sulfur recovery offshore. In: *Proc. 68th Annu. Gas Process. Assoc. Meet., San Antonio* (1989)
- 1.101 G.W. Hampton, P.R. Robinson: Controlling hydrocracker temperature excursions. In: *Proc. NPRA Q&A Technol. Forum, PD-11-01, San Antonio* (2011)
- 1.102 N. Mims, M. Bell, S. Doig: *Assessing the Electric Productivity Gap and the US Efficiency Opportunity* (Rocky Mountain Institute, Snowmass 2009)

Safety and the Environment

2. Safety and the Environment

Paul R. Robinson

Introduction

Safety, reliability, and protecting the environment are inextricably linked. In modern industry, they are prerequisites to profit. Company executives frequently tout their strong commitment to worker health and safety. Their commitment derives to a large extent from strict legislation. Health and safety rules address personal protection equipment, toxic substances, equipment maintenance, worker training, and compliance monitoring. Environmental regulations fall into five main categories: air pollution, waste water, solid wastes, spills, and fugitive emissions. Harm from chronic exposure to pollutants accumulates with time. Harm from major accidents causes tremendous short-term destruction, which often is followed by damage that lingers for years. Many of the worst industrial incidents occur in the coal, oil, and chemical industries. This chapter describes and analyzes numerous examples, many of which are infamous. In most, human misbehavior is the root cause. Misbehavior by unit engineers and operators includes ignoring safety rules, changing procedures without proper management of change, and sabotage. Misbehavior by management includes failing to provide proper training, postponing maintenance, approving substandard equipment, distracting workers (sometimes just with their presence) during safety-sensitive tasks, and understaffing turnarounds with exhausted personnel. Accidents can teach hard lessons. But not everyone learns such lessons, and those who do learn sometimes forget. Others choose to ignore the lessons, because they got away with ignoring them before. Things have gotten better – in developed countries, coal mining companies no longer employ children – but there's still room for improvement.

2.1	Introduction and History	86
2.1.1	History of Labor Legislation and Decrees.....	87
2.1.2	History of Environmental Laws and Decrees.....	88
2.2	Pollution from Petroleum Production and Processing	89
2.2.1	Particulate Matter.....	89
2.2.2	Carbon Monoxide.....	89
2.2.3	Hydrogen Sulfide and Sulfur Oxides.....	90
2.2.4	SMOG: Nitrogen Oxides, VOC and Ozone..	90
2.2.5	Acid Deposition.....	91
2.2.6	Stratospheric Ozone.....	91
2.2.7	Greenhouse Gases and Climate Change .	91
2.2.8	Wastewater.....	100
2.2.9	Solid Waste.....	100
2.2.10	Oil Spills.....	100
2.2.11	Fugitive Emissions.....	100
2.2.12	Fracking.....	100
2.3	Significant Accidents and Near-Misses	101
2.3.1	Coal Mining: Explosions and Black Lung Disease.....	102
2.3.2	Lakeview Oil Well: Blowout (March 1910–September 1911) .	102
2.3.3	Texas City, Texas: Ammonium Nitrate Explosion (1947)	103
2.3.4	London: Killer Fog (1952, '56, '57, '62).....	103
2.3.5	Amoco Cadiz: Oil Spill (1978).....	103
2.3.6	Bhopal, India: Methyl Isocyanate Leak (1984).....	103
2.3.7	Nuclear Power Incidents: Context.....	104
2.3.8	Three Mile Island: Nuclear Reactor Meltdown (1979).....	106
2.3.9	Chernobyl: Nuclear Reactor Fire (1986) .	107
2.3.10	Sandoz, Switzerland: Chemical Spills and Fire (1986).....	108
2.3.11	Exxon Valdez: Oil Spill (1989).....	109
2.3.12	Arabian Gulf War: Intentional Oil Spill, Oil Well Fires (1991).....	109
2.3.13	Tosco Avon Hydrocracker: Deadly Pipe Rupture (1997).....	110
2.3.14	BP Texas City Isomerization Unit: Explosion (2005).....	114
2.3.15	Deepwater Horizon Offshore Drilling Rig: Blowout (2010).....	116
2.3.16	Lac-Mégantic Quebec, Canada: Oil Train Derailment (2013).....	118
2.3.17	Tianjin, China: Storage Station Explosions (2015).....	118

2.3.18	Personal Observations.....	119	2.5.9	Toxic Substances Control Act (TSCA)	133
2.3.19	Lessons.....	123	2.5.10	Asbestos School Hazard Abatement Act	134
2.4	Agencies Protecting Safety and the Environment	126	2.5.11	Control of Dumping at Sea.....	134
2.4.1	Environment Protection Agencies.....	126	2.5.12	Climate Control: Rio, Kyoto, and Paris.....	134
2.4.2	Worker Safety.....	127	2.6	Pollution Control and Abatement Technology	135
2.5	Key Regulations	128	2.6.1	Particulate Matter.....	135
2.5.1	Clean Air Acts	128	2.6.2	Carbon Monoxide and VOC.....	135
2.5.2	Rivers and Harbor Act, Refuse Act.....	130	2.6.3	Sulfur Oxides.....	135
2.5.3	Federal Water Pollution Control Act.....	131	2.6.4	Nitrogen Oxides.....	136
2.5.4	Clean Water Acts, Water Quality Act.....	131	2.6.5	Wastewater.....	137
2.5.5	Marine Protection, Research, and Sanctuaries Act.....	132	2.6.6	Cleaning Up Oil Spills.....	137
2.5.6	Safe Drinking Water Act.....	132	2.6.7	Solid Waste Recovery and Disposal.....	141
2.5.7	Resource Conservation and Recovery Act (RCRA).....	132	2.7	Summary	143
2.5.8	Superfund, CERCLA.....	133	References		143

Process knowledge is the key to ensuring safety and protecting the environment. The purpose of this chapter is to impart knowledge, with focus on the impact of hydrocarbon processing on workers, the public, and the planet we share.

Hopefully, after reading this chapter, managers will be less inclined to:

- Underfund training
- Postpone maintenance
- Purchase substandard equipment
- Understaff operations during critical periods
- Disregard procedures recommended by licensors, industry committees, and their own companies.

2.1 Introduction and History

In developed countries, the quality of human life revolves around the exploitation of coal, petroleum, and natural gas. In 2016 [2.1] these fossil resources provided about 86% of the nonfood energy consumed by people. Oil and gas also serve as organic sources of chemicals. Table 2.1 gives a high-level overview of how petroleum derivatives are transformed into thousands of consumer products [2.2].

The negative impact of exploiting fossil hydrocarbons is both obvious and subtle. Major disasters – mine explosions, oil well blowouts, toxic chemical spills, etc. – generate tremendous immediate damage with aftereffects that can linger for months. They get considerable attention, but as the aftereffects diminish, they tend to fade from memory. Less attention is

Due to lack of knowledge, elected officials seem to believe that there are no right answers. They make serious mistakes about building pipelines, forcing ethanol in gasoline, exempting the fracking industry from clean water legislation, eliminating funding for the cleanup of hazardous sites, and other important matters.

Due to lack of knowledge (and common sense) large numbers of people allow themselves to be convinced that water burns, that batteries can capture lightning, that ultrasound removes sulfur from gasoline, and other misbegotten assertions. Instead of asking challenging questions and checking references, they squander money on schemes that turn charlatans into billionaires.

Can one chapter in one book improve industrial safety and change the way decisions-makers view the environment? One can only hope.

given to long-term exposure to chronic leaks and fugitive emissions, which can cause even greater harm than spectacular accidents.

In developed countries, health, safety, reliability, and protecting the environment are inextricably linked. In today's litigious society, they are prerequisites to profit. Modern executives behave accordingly. Shrugging while saying *It's a dangerous business* has been replaced by Zero-Zero-Zero campaigns aimed at achieving zero injuries, zero loss of containment, and zero unplanned shutdowns. The slogan for ExxonMobil's program is Nobody Gets Hurt [2.3]. Shell preaches Goal Zero [2.4], and employees who violate Lifesaving Rules may be discharged. KBR promotes Zero Harm 24/7 [2.5]. Chevron's ten Tenants of Operation [2.6]

Table 2.1 Overview of the transformation of refinery products into consumer goods

Refinery products	Refinery products to petrochemical plants	Intermediates from petrochemical plants	Fiber precursors	Consumer goods (partial list)
Fuels	Propylene	Acetic acid	Acrylics	Adhesives and sealants
● Gasoline	Isobutane	Acrylonitrile (AN)	Graphite fibers	Antifreeze
● Jet fuels	Butadiene	Acrylonitrile butadiene styrene	Nylons	Carpets
● Diesel	Butenes	Acrylonitrile styrene (AS)	Polybutadiene (PBR)	Construction chemicals
● Fuel oils	Benzene	Alcohols	Polyesters	Corrosion control chemicals
Heating Oils	Xylenes	Cyclohexane	Polyethylene (PE)	Cosmetics
Lubricants	Naphthas	Dimethyl terephthalate (DMT)	Polyethylene terephthalate (PET)	Electronics
Solvents	Middle distillates	Ethanolamine	Polyvinyl chloride (PVC)	Fabrics
Cokes	Hydrocracker bottoms	Ethoxylate	Styrene butadiene resin (SBR)	Fertilizers
Asphalts	Vacuum residue	Ethylene glycol (EG)	Thermosetting resins	Fishing rods
Carbon dioxide		Ethylene oxide (EO)		Flavorings, fragrances, food additives
Sulfur		Formaldehyde		Inks, dyes and printing supplies
Ammonia		Linear alkyl benzene (LAB)		Kevlar
		<i>n</i> -Hexene		Life sciences chemicals
		Phenol		Packaging, bottles, and containers
		Polyol		Paint, coatings, and resins
		Polypropylene (PP)		Pesticides
		Polystyrene (PS)		Pharmaceuticals
		Propylene oxide		Polymers
		Purified terephthalic acid (PTA)		Specialty chemicals
		Styrene monomer (SM)		Surfactants and cleaning agents
		Vinyl acetate monomer (VAM)		
		Vinyl chloride monomer (VCM)		

are prefaced by two statements: *Do it safely or not at all. There is always time to do it right.* These particular companies have departments dedicated to health, safety, and the environment (HSE) led by executives who report directly to the CEO or COO, not just to someone in human resources. The 0-0-0 initiatives are not just for show. They reflect a sincere belief that the energy business doesn't have to be deadly. HSE rules are strictly enforced. This approach requires investment, but the return on such investments is enormous in many measurable ways.

Vox populi – the voice of the people – instigated the regulations that play such a critical role in protecting workers and the environment. Worker safety and environmental movements [2.7, 8] are international, with long and interesting histories.

2.1.1 History of Labor Legislation and Decrees

Worker-protection rules go back to 15th Century England, when provisions were made to prevent abuses in the *truck system* – the paying of wages in goods in-

stead of money. Similar reforms were implemented in Switzerland in the 17th Century.

Efforts to improve the plight of coal miners go back as far as 1775, when an Act of Parliament partially emancipated colliers, coal-bearers, and salters in Scotland [2.9]. According to the Act, the workers were in a *de facto state of bondage*. (They had been since 1606, when an Act of the Scottish Parliament bound them to the mines.) In 1799, another Act explained and amended the 1775 Act, abolishing bondage totally.

In 1802 in England, the Health and Morals of Apprentices Act limited working hours for apprentices to twelve per day and abolished night labor. It required basic education and the provision of clothing and adequate sleeping accommodations. The Factory Act of 1819 limited working hours to twelve per day and prohibited employment of children under nine years of age.

In 1841 in France, a law prohibited employing children under eight years of age and prohibited night labor for any child under 13. In 1848, the working day was limited to 12h for adults in factories. The law was amended in 1885 to include factories with motor power

or furnaces, and to workshops employing more than 20 people.

The first labor law in the Netherlands, passed in 1874, applied only to children working in factories; then as now, it was deemed appropriate for children to do chores on family farms. In 1889, the law was extended to all industries except agriculture, forestry, and fishing. It prohibited the employment of children under 12. In 1895, a law established standards for space, lighting, ventilation, and sanitation. And in 1897, a decree limited working hours according to age and sex, with special provisions for certain industries and pregnant women.

The American Colonies were largely agrarian. Slaves provided labor in southern plantations. Industry was conducted for the most part by master and journeyman craftsmen, supported by apprentices and indentured servants [2.10]. Recorded labor disputes included a 1636 fishermen's strike on an island near Maine, prosecution of strikers in 1677 in New York City, and a 1746 strike by carpenters in Savannah, Georgia.

The United States Congress passed the first federal law governing mine safety in 1891 [2.11]. The law established ventilation requirements for underground coal mines and prohibited owners from employing children under 12. Owners had resisted acting voluntarily, arguing that doing so would put them at a competitive disadvantage.

In 1910, after a decade in which coal mine fatalities exceeded 2000 annually, Congress established the Bureau of Mines to conduct research and reduce accidents in the coal mining industry. Violations of regulations were rampant until 1941, when Congress empowered federal inspectors to enter mines. Over the years, regulations improved, culminating in the Federal Mine Safety Act of 1977, which was amended by the MINER Act of 2006.

US child labor laws lagged the rest of the world by decades. According to the 1890 US Census, about 1.12 million children between six and ten years old were engaged in so-called *gainful occupations* out of a total population of 63 million [2.12–14]. According to the 1900 US Census, the number had increased to 1.75 million children out of a total population of 76.2 million. About 16.7% of children under ten were working, and 18% of children between 10 and 15 were employed full time. Child labor on family farms was expected, but the increase of 50% in under-ten employment for wages, mostly in factories, alarmed many Americans. Attempts at reform were thwarted by the Supreme Court. In 1912, a law established the United States Children's Bureau in the Department of Commerce and Labor. In 1916, the Keating–Owen Act prohibited interstate shipment of goods manufactured or processed by child labor. The

bill passed 337 to 46 in the House and 50 to 12 in the Senate. But in 1918, in a 5-4 decision, the law was ruled unconstitutional by the Supreme Court. In 1938 – after years of court decisions overturning attempts at labor reform – and 118 years after the first child labor law in England – Congress passed the Fair Labor Standards Act (FLSA) [2.15]. The FLSA banned oppressive child labor, set a minimum wage of 25 cent/h, and limited the work week to 44 h. After surviving several Supreme Court challenges, notably the *United States versus Darby Lumber Co.* case in 1941, the FLSA remains in force today.

2.1.2 History of Environmental Laws and Decrees

As humans living on an ever-more-crowded planet, our main reason for abating pollution is self-preservation. While addressing waste in *What Is Life? Margulis and Sagan* [2.16] remind us that *every species or organism produces wastes that are incompatible with its own existence.*

In *The Closing Circle* [2.17], Barry Commoner generalized this principle with his Four Laws of Ecology. The first two are especially relevant: (1) Everything is connected to everything else. What affects one organism affects all. (2) Everything must go somewhere. There is no *waste* in nature and there is no *away* to which things can be thrown.

Fallout from open-air nuclear testing appeared all across the planet. Radioactive isotopes showed up in food, water, and the bones of animals. For the first time, it became clear that certain events have long-lasting global impact. On January 15, 1958, Nobel Laureate *Linus Pauling* presented to the United Nations a petition protesting further nuclear testing [2.18]. The document was signed by 9235 scientists from many countries. The nuclear powers, including the Soviet Union, the United States, and the UK, voluntarily stopped open-air testing that same year. The Soviet Union announced the resumption of open-air testing in August 1961, adding urgency to efforts to conclude a test-ban treaty. In July 1963, the Nuclear Test Ban Treaty was signed, outlawing atmospheric testing but allowing underground testing.

In 1962, *Rachel Carson* published *Silent Spring* [2.19]. Among other things, she presented evidence linking dichlorodiphenyltrichloroethane (DDT) to declines in the bald eagle population, due to the thinning of egg shells. She used the DDT linkage to tell a broader story: what affects one organism can affect all. According to data recently cited by PAN [2.20], an antipesticide organization, DDT breakdown products are still being found in food supplies and human blood.

In response to the efforts of outspoken organizations and people such as Carson, Commoner, and Pauling, the United States formed the Environmental Protection Agency (US EPA). Signed into law by President Nixon in 1970 [2.21], EPA was an amalgamation of departments, bureaus, and agencies taken from the Interior Department; the Department of Health, Education, and Welfare; the Agriculture Department; the Atomic Energy Commission; the Federal Radiation Council; and the Council on Environmental Quality. One of the first actions promoted by EPA was the 1972 ban on DDT.

The history of environmental protection goes back (at least) to the 17th Century [2.22].

After the Great London Fire of 1666, King Charles II proclaimed that all buildings must be constructed from stone, and streets must be widened. The London Cooking Fire Bylaw of 1705 specifically prohibited open fires in the attics of thatched buildings [2.23].

In 1842, the Madras Board of Revenue started local forest preservation efforts in British India. In 1855, under Governor-General Lord Dalhousie, a large-scale, state-managed forest conservation program was established.

Other early examples of British legislation are the 1863 Alkali Acts [2.24], implemented to regulate emissions of hydrochloric acid from the Leblanc process, the leading process for making soda ash. Pressure for the Alkali Acts came from the urban middle class.

Parliament passed the Public Health Act of 1875 to combat the spread of diseases such as cholera and typhus, which percolated in the sewage that flowed

through public streets [2.25]. The Act required all new construction to include running water and internal drainage. It also regulated housing construction and required every public health authority to employ a medical officer and an inspector.

Previous attempts at reform were inhibited by the reluctance of factory owners to improve conditions voluntarily. The Act itself included a *grandfather* clause, which exempted existing facilities. Both factors – grandfather clauses and the reluctance of owners to seek ways to improve conditions voluntarily – continue to plague safety and environmental programs.

The emergence of great coal-burning factories and the concomitant growth in coal consumption increased air pollution in industrial centers enormously. Smoke, soot, and sulfur oxides led to the Great Smog of 1952, which is described in Sect. 2.2.

Conservation in the United States began with the establishment of national parks [2.26], such as the Hot Springs Reservation (1832) [2.27], Yellowstone (1872), Sequoia (1890), Yosemite Valley (1890), Mount Rainier (1899), and Crater Lake (1902).

Major US environment-related legislation includes the following:

- The National Park Service Organic Act (1916)
- Land and Water Conservation Act (1964)
- National Trails System Act (1968)
- National Wild and Scenic Rivers System Act (1968)
- National Environmental Policy Act (1969)
- Clean Air Acts and Amendments (1963 through 1970).

2.2 Pollution from Petroleum Production and Processing

This section describes the predominant gaseous, liquid and solid pollutants generated by the coal, petroleum, and petrochemical industries. It also explains why they can be harmful. Technology for abating these pollutants is described later.

2.2.1 Particulate Matter

The main sources of air pollution from petroleum refineries are listed in Table 2.2. Refineries can be significant sources of particulate matter (PM), which can irritate the respiratory tract. PM is especially harmful when it is associated with sulfur and nitrogen oxides (SO_x and NO_x).

PM from coal is coal dust. PM from refining comes mainly from two sources – delayed coking units and the regenerators of fluid catalytic cracking (FCC) units.

FCC regenerators also emit ammonia, which combines with SO_x and NO_x in the air to form ammonium sulfates and nitrates. According to the South Coast Air Quality Management District (AQMD) [2.28] in Southern California, 1 t of ammonia can generate 6 t of PM₁₀ – airborne particulates with particle diameters less than 10 μm. PM_{2.5} stands for airborne particulates with diameters less than 2.5 μm.

2.2.2 Carbon Monoxide

Carbon monoxide (CO) is formed by incomplete combustion in boilers, process heaters, power plants, and FCC regenerators. CO is toxic because it binds strongly to the hemoglobin in blood, displacing oxygen. It is colorless and odorless, so without a special analyzer, it is hard to detect. This adds to its danger. Un-

Table 2.2 Main sources of air pollution in hydrocarbon processing

Source	PM	SO ₂	CO	VOC	NOx	Hg	VTCs
Coal handling	✓	✓					
Coal combustion		✓	✓	✓	✓	✓	
Fluid catalytic cracking (FCC) units	✓	✓	✓	✓	✓		
Coking units	✓	✓		✓	✓		
Compressor engines		✓	✓	✓	✓		
Vapor recovery and flare systems		✓	✓	✓	✓		
Vacuum distillation unit and condensers				✓			
Sulfur recovery units		✓	✓		✓		
Waste-water treatment plants				✓			
Boilers and process heaters		✓	✓		✓		
Storage tanks				✓			
Petrochemical production			✓		✓		✓

PM = particulate matter

SO₂ = sulfur dioxide

CO = carbon monoxide

VOC = volatile organic compounds

NOx = nitric oxide (NO) and nitrogen dioxide (NO₂)

Hg = mercury

VTCs = volatile toxic chemicals

der particular conditions in refinery hydroprocessing units, the nickel on NiMo catalysts can react with CO to form nickel carbonyl, an exceptionally hazardous gas.

2.2.3 Hydrogen Sulfide and Sulfur Oxides

Hydrogen sulfide (H₂S) is a pervasive hazard in petroleum production, petroleum refining, and natural gas processing facilities. Sour natural gas can contain several percent H₂S, which is recovered by amine adsorption and converted into elemental sulfur. In developed countries, H₂S recovery must be more than 99% – more than 99.8% in some instances.

Workers are most likely to be exposed due to leaks or when taking samples of sulfur-containing gases or liquids. Sample-taking stations should be well ventilated and equipped with several fixed-in-place toxic-gas monitors. In addition to the fixed monitors, mobile pocket-sized monitors are worn by all workers. Sample-taking procedures include the buddy system: one person takes the sample while another watches. In the past, workers died when rushing forward to help a stricken companion, so the watchers stand at a safe distance with quick access to a radio and/or self-contained breathing apparatus (SCBA).

The impact of H₂S depends on its concentration and duration of exposure [2.29]. At 0.01–1.5 ppm, the characteristic rotten-egg odor is detectable. The odor becomes offensive at 3–5 ppm, where prolonged exposure causes nausea, tearing, asthma, and headaches. Above 20–30 ppm, the odor is said to be sweet or

sickly sweet. Above 100 ppm, olfactory nerves are paralyzed and H₂S can no longer be smelled. Exposure to more than 700–1000 ppm causes immediate collapse and death after one or two breaths.

H₂S is flammable. The explosive range is 4.5–45.5% in air.

Despite periodic training, some workers choose to ignore regulations. During a startup attended by the author in 2015, the buddy system was not used for taking samples of H₂S-containing gas, even though there were six or seven idle workers sitting in a lounge in the control center. The reason given for failure to follow procedure – i. e., to use the buddy system – was: *It is cold outside*.

Sulfur dioxide (SO₂) and sulfur trioxide (SO₃), collectively known as SOx, are produced by the burning of sulfur-containing coal and fuel oil. SOx also are produced by burning coke off of catalysts in FCC regenerators.

2.2.4 SMOG: Nitrogen Oxides, VOC and Ozone

NOx are formed in fired heaters, power plants, and FCC regenerators. NOx also damage respiratory tissues and contribute to acid rain.

Ozone (O₃), a nasty component of smog, is generated by reactions between oxygen, hydrocarbons and NOx. The reactions are initiated by sunlight. In the troposphere, ozone reacts with volatile organic hydrocarbons (VOC) to form aldehydes, peroxyacetyl nitrate (PAN), peroxybenzoyl nitrate (PBN) and a number of

other substances. PAN irritates nasal passages, mucous membranes, and lung tissue. Collectively, these compounds are called *photochemical smog*. They harm humans, animals, and plants, and they accelerate the degradation of rubber and construction polymers. In some areas, smog looks like a brownish cloud just above the horizon. It makes for spectacular sunsets, but nothing else about it is good.

2.2.5 Acid Deposition

In the atmosphere, SO_x and NO_x react with water vapor to make sulfuric and nitric acids. The acids return to Earth as dry particulates or dissolved in moisture – rain, fog, or snow. Acidic moisture, commonly called *acid rain*, poisons trees and contaminates lakes and rivers. In humans, gaseous SO_x and NO_x molecules are trapped by mucous in the upper respiratory track, but dry particulates can penetrate deep into lungs. Experts estimate that SO₂ can remain in the air for 2–4 days. During that time, it can travel 600 mi (1000 km) before returning to the ground. Consequently, SO₂ emissions have caused a number of international disputes. Before 1990, acid rain from neighboring countries caused the death of about a third of the trees in Germany forests. In the past, the United States and Canada argued bitterly about the cross-border impact of SO_x emissions from US power plants and copper smelters; the passage and enforcement of clean-air legislation in both countries has reduced the problem dramatically.

2.2.6 Stratospheric Ozone

The previous section mentions the harmful effects of ground-level ozone. But in the stratosphere, located about 6–30 mi (10–50 km) above the ground, an *ozone layer* protects organisms from harmful ultraviolet-B (UV-B) solar radiation [2.30].

In the 1980s, scientists noticed that the ozone layer over Antarctica was thinning [2.31]. Researchers linked several man-made substances to ozone-layer depletion, including carbon tetrachloride (CCl₄), chlorofluorocarbons (CFCs), halons, methyl bromide, and methyl chloroform. These chemicals leak from air conditioners, refrigerators, insulating foam, and some industrial processes. Winds carry them through the lower atmosphere into the stratosphere, where they react with strong solar radiation to release chlorine and bromine atoms. These halide atoms initiate chain reactions. Scientists estimate that a single chlorine atom can destroy 100 000 ozone molecules.

In 1987, 27 countries signed the Montreal Protocol, which recognized the international consequences of

ozone depletion and committed the signers to limiting production of ozone-depleting substances. Today, more than 190 nations have signed the Protocol, which now calls for total elimination of certain ozone-depleting chemicals.

The 1998 and 2002 scientific assessments of stratospheric ozone firmly established the link between decreased ozone and increased ground-level UV-B radiation. In humans, UV-B is linked to skin cancer. It also contributes to cataracts and suppression of the immune system. The effects of UV-B on plant and aquatic ecosystems are not well understood. However, the growth of certain plants can be slowed by excessive UV-B. Scientists suggest that marine phytoplankton, which are the foundation of the ocean food chain, are under stress from increased UV-B.

In the United States, production of halons ended in January 1994 [2.32]. In January 1996, production virtually ceased for several other ozone-depleting chemicals, including CFCs, CCl₄, and methyl chloroform. January 1, 2010 saw a ban on production, import, and use of HCFC-22 and HCFC-142b, except for continuing servicing needs of existing equipment. In 2015, the production, import, and use of all HCFCs were banned, except for continuing servicing needs. In 2020, there will be no production or imports of HCFC-22 and HCFC-142b, achieving a total reduction of 99.5%.

New products less damaging to the ozone layer are replacing chlorofluorocarbons. For example, computer makers now use ozone-safe solvents to clean circuit boards, and automobile manufacturers use HFC-134a, an ozone-safer refrigerant, for air conditioners in new vehicles.

Studies indicate that the Montreal Protocol has been effective. Stratospheric concentrations of methyl chloroform are falling. Concentrations of other ozone-depleting substances, such as CFCs, are also decreasing. According to the US EPA [2.33], the ozone layer has not grown thinner since 1998 and appears to be recovering. Antarctic ozone is expected to return to pre-1980 levels sometime between 2060 and 2075.

2.2.7 Greenhouse Gases and Climate Change

For a thorough but succinct overview of the technology and politics of climate change, please refer to *Energy and Climate: Vision for the Future*, by Michael B. McElroy [2.34].

According to the US Environmental Protection Agency [2.35]:

The Earth's climate is changing. Temperatures are rising, snow and rainfall patterns are shifting, and

more extreme climate events – like heavy rainstorms and record high temperatures – are already happening. Many of these observed changes are linked to the rising levels of carbon dioxide and other greenhouse gases (GHGs) in our atmosphere, caused by human activities.

The Inter-government Panel on Climate Change (IPCC) estimates that if present trends continue, sea level will rise by about 1 meter by 2100 [2.36]. That could displace up to 100 million people from coastal areas, contaminate ground water and increase storm-surge damage. By putting more thermal energy into the oceans and atmosphere, warming will strengthen storms and continue to distort weather patterns, threatening certain crops.

Two important climate-change concepts are radiative forcing and global warming potential (GWP) [2.37].

Radiative forcing is the change in net irradiance (expressed in W/m^2) due to a change in an external driver of climate change, such as a change in the concentration of carbon dioxide or the energy output of the Sun. Radiative forcing is computed with all other tropospheric properties held fixed at their unperturbed values. Typically, radiative forcing is defined as the change relative to conditions in 1750 or 1850 and usually refers to a global and annual average value.

Global Warming Potential (GWP) is an index based upon radiative forcing of a unit mass of a given well-mixed GHG in the present-day atmosphere integrated over a chosen time horizon, relative to that of carbon dioxide. The GWP calculation includes the combined effects of residence time in the atmosphere and the

relative effectiveness of a gas in absorbing outgoing infrared radiation.

How Do We Know Global Temperatures Are Rising?

We have been collecting direct temperature readings since the 1800s. At the behest of Alexander von Humboldt, ships from many nations began collecting temperature and salinity data before 1804. Land-based data are now being gathered from more than 4300 stations around the globe. Thousands of buoys and floats measure ocean temperatures, both at the surface and down to 4000 m. The Goddard Institute for Space Studies (GISS) estimates that the global mean temperature of the Earth's surface increased by about $1.2^\circ C$ between 1880 and 2016 (Fig. 2.1) [2.38]. The figure also shows, for subsequent discussion, atmospheric carbon dioxide (CO_2) data from Figure 2.5.

Temperatures for the past 2000 years are estimated from tree-ring measurements and coral growth. Ocean surface temperatures back to 800 000 BCE are inferred by measuring isotope ratios in ice cores [2.39]. When water evaporates, lighter molecules – those containing ^{16}O and simple hydrogen – vaporize more readily, enriching the remaining water in heavier molecules – those containing ^{18}O and/or deuterium. The extent of the difference depends on temperature. Evaporation is greater in equatorial regions. As air masses move poleward, water vapor condenses into rain. Condensation preferentially removes deuterium and ^{18}O , further enriching the remaining vapor in lighter isotopes. In higher-latitude regions, the deuterium/hydrogen and $^{18}O/^{16}O$ ratios in rain (and snow) are significantly lower than in equatorial rains. There is more ^{18}O and deuterium in ice

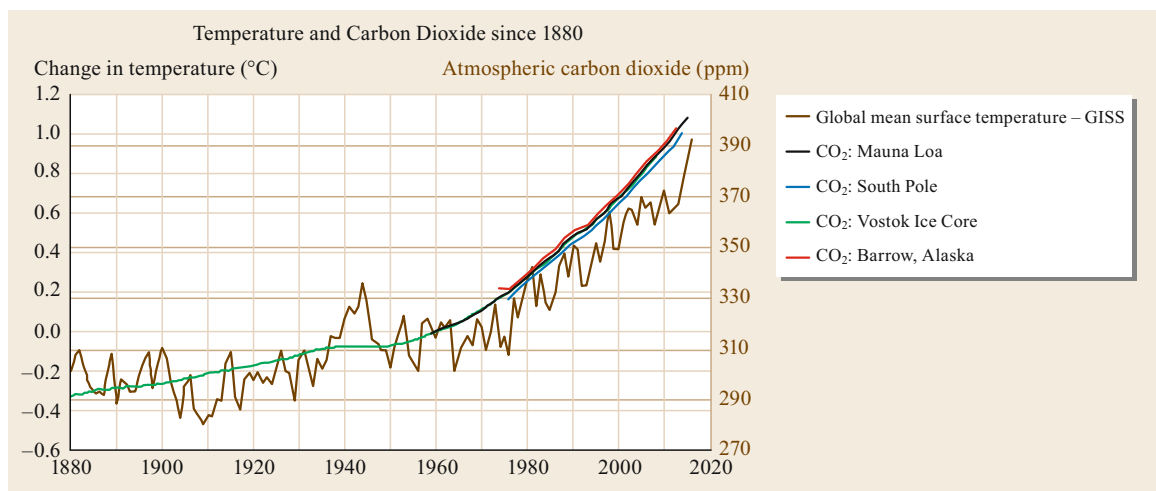


Fig. 2.1 Change in global mean surface temperature and concentration of atmospheric carbon dioxide since 1880. The base period for temperature is the average for 1951–1980

during warm periods, because higher temperatures put more water vapor into the air, and more water containing heavy isotopes reaches higher latitudes.

Rock cores provide another isotopic proxy for ancient temperatures. The $^{18}\text{O}/^{16}\text{O}$ ratio in surface water depends on temperature, and it determines the $^{18}\text{O}/^{16}\text{O}$ ratio in the shells of the foraminifera growing in that water. When the organisms die, their remains sink to the bottom and become incorporated into sedimentary rock. The cores are dated radiometrically, typically with the $^{234}\text{U}/^{230}\text{Th}$ method [2.40].

When coupled with information from other sources, isotope data from the EPICA Dome C ice core indicate the following:

- Around 125 000 years ago, when average surface temperatures were $4\text{ }^{\circ}\text{C}$ higher than now, the average global sea level was 4 m to 6 m higher.
- Around 20 000 years ago, when average surface temperatures were $12\text{ }^{\circ}\text{C}$ lower than now, the average global sea level was 120 m lower [2.41].

What Is the Greenhouse Effect?

Scientists have been discussing climate change and the greenhouse effect for more than 200 years. Humboldt postulated human-induced climate change in 1800. Jean Baptiste Joseph Fourier (1768–1830) recognized that the Earth's atmosphere retained solar radiation, likening the effect to that of a black box in which the top panel is replaced by a pane of glass.

In 1862, John Tyndall, a prominent Irish physicist, conducted experiments which showed that certain gases, including water vapor and CO_2 , absorb IR radiation [2.42]. He concluded that in the atmosphere, such gases helped to warm the Earth by capturing escaping heat. He wrote:

As a dam built across a river causes a local deepening of the stream, so our atmosphere, thrown as a barrier across the terrestrial rays, produces a local heightening of the temperature at the Earth's surface.

Visible light enters a greenhouse through transparent glass. Inside, the light is absorbed by plants and other objects and then reradiated as heat, i. e., infrared (IR) radiation. Ordinary glass is mostly opaque to IR, so reradiated heat is trapped inside the greenhouse, causing temperatures to go up.

An interesting analogy comes from the American Chemical Society [2.44]:

Think of yourself under a blanket in a cold room. You represent the Earth, a warm body giving off energy [...] The blanket represents the atmospheric layer of greenhouse gases. As the heat energy leaves your body it is absorbed by the innermost fibers of the blanket. As they give off some of that energy, they warm the next layer of fibers and so on and on until some energy leaves the outermost cold fiber layer and is lost to the room. Just as the Sun continually warms the Earth, you continually produce energy through respiration. You will finally reach a balance where the energy leaving the blanket is equal to the energy you produce and your skin will remain at a constant temperature, just like the surface of the Earth.

Greenhouse Physics

GHG molecules are analogous to fibers in our imaginary blanket. IR radiation causes them to vibrate. They re-radiate vibrational energy in all directions. Some is absorbed by other GHG molecules, some goes back to the Earth's surface, and some escapes into space.

The wavelengths of light emitted by an object depend on the object's temperature [2.45]. As shown by Figure 2.2, the effective temperature of solar radiation when it reaches the Earth is around $5800\text{ }^{\circ}\text{C}$. The Sun emits a broad spectrum of radiation with peak intensities at wavelengths in the visible range between 0.4 and $0.7\text{ }\mu\text{m}$. The Earth re-emits that energy into space at an average temperature of $-18\text{ }^{\circ}\text{C}$ as IR radiation with peak intensities at wavelengths above $10\text{ }\mu\text{m}$ [2.46].

Continuing with the blanket analogy: what if the blanket has gaps or holes? Water vapor is the most

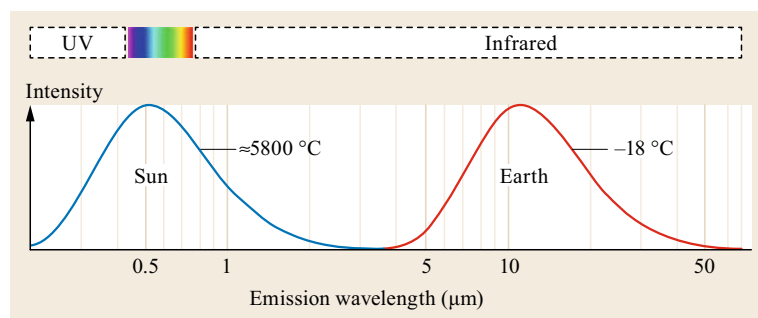


Fig. 2.2 Temperature and frequency of light emissions from the Sun and Earth (after [2.43])

abundant GHG and absorbs the most heat. It has gaps because it does not absorb at all IR wavelengths. Other GHGs reinforce absorption at wavelengths where water vapor absorbs, but in some cases they also fill the gaps left by water vapor. Figure 2.3 illustrates this plug-the-gap phenomenon for CO₂.

Which Gases Are Greenhouse Gases?

N₂ and O₂ are the main constituents of the Earth's atmosphere (see Table 2.3). They are not GHGs, because they are transparent both to visible and IR radiation. Other non-GHGs are H₂ and noble gases.

Table 2.4 presents current atmospheric concentrations, residence times, and 100-year global warming potentials for CO₂, CH₄, N₂O, and three selected fluorinated gases, all of which are significant GHGs [2.47]. The table also mentions water vapor, the most abundant GHG.

Table 2.5 gives a breakdown of anthropogenic GHG emissions.

Carbon Dioxide (CO₂). Figure 2.4 presents a simple view of the global carbon cycle. Most atmospheric CO₂ is natural. In the short-term carbon cycle, significant amounts of CO₂ are exchanged with the biosphere, soil and the hydrosphere.

Dissolved in water, CO₂ forms carbonic acid (H₂CO₃), bicarbonate (HCO₃⁻), and carbonate (CO₃²⁻). Sea water is slightly alkaline, with a surface pH of 8.2, so it readily reacts with H₂CO₃. Corals, foraminifera, and other marine organisms incorporate carbonates into aragonite shells. The extent to which H₂CO₃ forms inorganic bicarbonate (HCO₃⁻) and carbonate (CO₃²⁻) in deeper water depends on water acidity and depth [2.49]. The long-term carbon cycle includes silicate weathering, in which silicate rocks are dissolved by carbonic acid (H₂CO₃) or converted into carbonate rocks. Eventually, volcanic action releases CO₂ from carbonate rocks. The long-term cycle also includes fossil-fuel formation from dead organic matter, a process which takes hundreds of millions of years.

When something happens to upset the balance, exchange processes move the system toward a new steady state. But the movement is not instantaneous. Since the

advent of the industrial revolution in the mid-eighteenth century, humans have been upsetting the short-term carbon cycle by burning fossil fuels and biomass, by making cement, and by altering land use with deforestation, agriculture and soil degradation. It takes time for the biosphere and hydrosphere to take up excess CO₂. Uptake by surface waters is governed by equilibrium. It takes hundreds if not thousands of years for surface-ocean CO₂ to move into deeper waters. The ultimate CO₂ buffer is weathering, but weathering takes even longer.

During 2002–2011, about 46% of anthropogenic CO₂ remained in the atmosphere. The remainder went into terrestrial biomass (28%) and the oceans (26%) [2.50]. In recent years, humans sent as much as 7.4 Gt of carbon into the air, mostly as CO₂. This amount can be more than 80 times greater than the carbon from volcanic activity [2.51].

Says John Higgins of Princeton University [2.52]:

The earth can take care of extra carbon dioxide when it has hundreds of thousands or millions of years to get its act together. In contrast, humankind is releasing carbon dioxide today so quickly that silicate weathering can't possibly respond fast enough [...] The earth has these long processes that humankind has short-circuited.

Another CO₂-related concern is ocean acidification. Between 1751 and 1996, the pH of the surface ocean has dropped from about 8.25 to 8.14 [2.53]. This increase in acidity is dissolving coral reefs [2.54].

Methane (CH₄). Methane is emitted during the production and transport of coal, petroleum, and natural gas. Methane also is produced by termites, livestock, agricultural practices, and the anaerobic decay of mu-

Table 2.3 Average concentrations of non-greenhouse gases in dry air

Gas	Vol%
N ₂	78.08
O ₂	20.95
Argon	0.93
He, Kr, Xe, H ₂	Traces

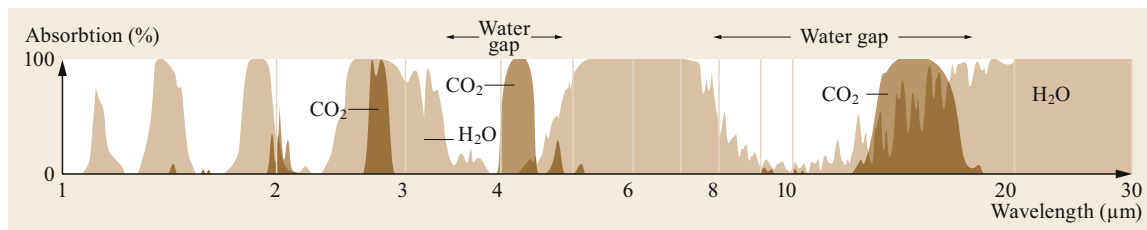


Fig. 2.3 Filling gaps in IR absorption by water vapor with CO₂

Table 2.4 GHG concentrations, residence times, and GWP for a 100-year horizon

Gas	Formula	Current atmos. concentration	Residence time (years)	GWP versus CO ₂ , 100-year horizon
Water vapor	H ₂ O	≈ 1% at sea level ≈ 0.4% throughout the troposphere	N/A	N/A
Carbon dioxide		400 ppm	^a	1
Methane ^b	CH ₄	1.8 ppm	12.4	28–36
Nitrous oxide	N ₂ O	320 ppb	121	265–298
HCF-134a	CH ₂ FCF ₃	0.01 ppb	14.6	1300
Halon 1301	CBrF ₃	0.003 ppb	65	7140
Sulfur hexafluoride	SF ₆	0.008 ppb	3200	23 900

^a CO₂ is not destroyed in the atmosphere. Instead, it cycles between the biosphere, soil, and hydrosphere. The global carbon dioxide cycle is illustrated in Fig. 2.4.

^b CH₄ has direct and indirect effects. It absorbs IR radiation and generates O₃, which itself is a GHG.

Table 2.5 Global anthropogenic emissions of greenhouse gases [2.48]

Gas	wt%
CO ₂ (fossil fuel combustion, cement, other industrial processes)	65
CO ₂ (forestry and other land use)	11
CH ₄	16
N ₂ O	6
Fluorinated gases	2

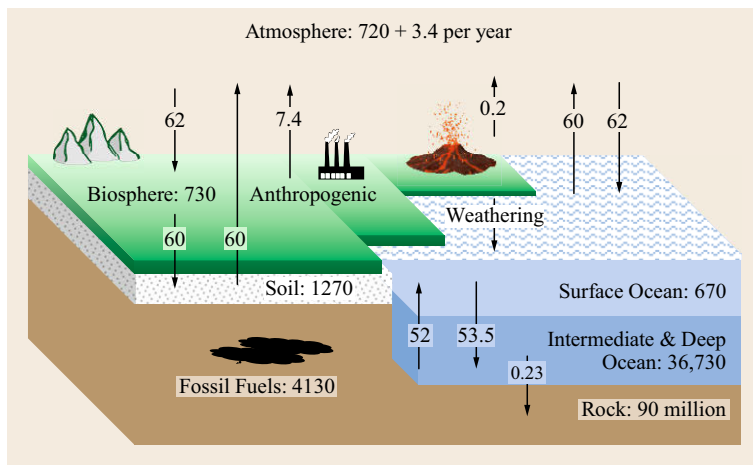


Fig. 2.4 Simple view of the global carbon cycle. Reservoirs include the atmosphere, biosphere, soil, oceans, and rocks. The unit of measure for reservoir size is Gt of carbon. The unit of measure for fluxes (exchanges between reservoirs) is Gt of carbon per year

nicipal wastes in landfills. Table 2.6 provides a breakdown.

Nitrous Oxide (N₂O). Nitrous Oxide is emitted by excessive use of ammonia fertilizers and by certain chemical manufacturing plants. It also is produced during combustion of fossil fuels and solid waste. Table 2.7 provides a breakdown.

Fluorinated Gases. Fluorinated Gases include hydrofluorocarbons, perfluorocarbons, sulfur hexafluoride, and other compounds. They are emitted during industrial, commercial and household use. They do

not occur naturally. Some are used as substitutes for ozone-depleting substances such as chlorofluorocarbons (CFCs).

How Do We Know Greenhouse Gas Concentrations Are Higher Now than Before?

We have been measuring atmospheric GHG concentrations in several stations at different latitudes since 1959, and we are measuring GHG concentrations in air bubbles trapped in ancient ice cores. Figure 2.5 shows atmospheric CO₂ measurements from several sources – from ice core samples that are as old as 800 000 years and, since 1959, from surface measurement stations.

Table 2.6 Sources of methane emissions [2.55]

Source	Percent
Anthropogenic	
Coal, oil, natural gas	19
Ruminants (cows, sheep, goats, other)	16
Rice cultivation	12
Biomass burning	8
Landfills	6
Sewage treatment	6
Animal waste	5
Natural	
Wetlands	21
Termites	4
CH ₄ hydrates, ocean	3

Table 2.7 Sources of nitrous oxide emissions

Source	Percent
Anthropogenic	
Agriculture	67
Industrial processes	11
Human sewage	3
Natural	
Biomass burning	10
Atmospheric deposition	9

Prior to the 1800s, the peak atmospheric CO₂ concentration was <280 ppm except for a brief excursion to nearly 300 ppm at around 331 000 BCE. In 1878, the concentration topped 290 ppm and has been rising ever since. In 2015, the annual average at the Mauna Loa station in Hawaii topped 400 ppm.

How Do We Know People Are Responsible for the Recent Increase in GHGs?

As shown, by 2015, atmospheric CO₂ had increased to 400 ppm compared with 280 ppm in pre-industrial times. The increase cannot be explained by natural causes. When we add the observed CO₂ increase in the atmosphere to the observed increase in the oceans, the sum is approximately equal to all of the coal, oil, and natural gas burned since the nineteenth century [2.57].

The ¹³C/¹²C ratio in atmospheric CO₂ has been dropping steadily. This shows that atmospheric CO₂ is being diluted with CO₂ that contains less ¹³C. Both fossil fuels and old trees are low in ¹³C; we have been burning the former and destroying the latter at unprecedented rates. The ¹³C/¹²C ratio for oceanic CO₂ has dropped, too, with the greatest depletion in surface water. Radioactive ¹⁴C in atmospheric CO₂ also is getting lower. Fossil fuels contain no ¹⁴C; the CO₂ produced from their use contains no ¹⁴C. The carbon in old trees does contain ¹⁴C. The conclusion is clear: the extra CO₂ in the air comes from fossil fuels.

Finally, the annual mean CO₂ abundance in the northern hemisphere is higher than in the southern hemisphere. The difference has increased in recent years. This is consistent with the fact that most fossil fuel burning occurs in the northern hemisphere.

Global Energy Balance

Ultimately, we are concerned about GHGs because they play a major role in the global energy balance. The

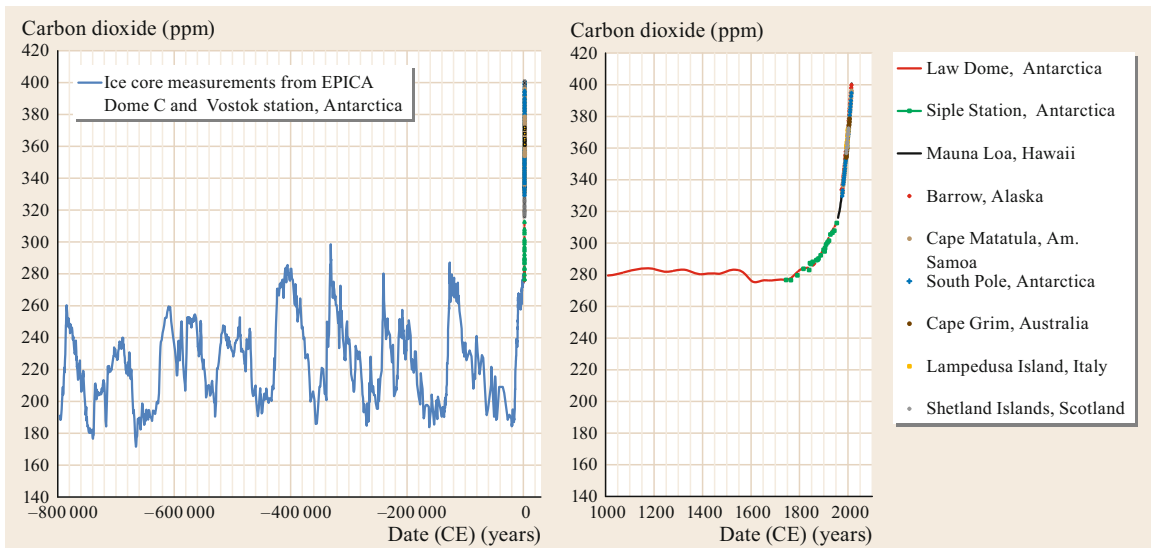


Fig. 2.5 Measurements of CO₂ in ice core air bubbles. Ice core data come from EPICA Dome C and Vostok Station, Antarctica (back to 800 000 BCE); Law Dome, Antarctica (back to 1010 CE), and Siple Station, Antarctica (back to 1744 CE) [2.56]

balance is affected by many phenomena, including the following:

- Solar irradiance: determined by the ellipticity and obliquity of Earth's rotation and the Sun's surface temperature
- Volcanic aerosols: direct and indirect effects
- Tropospheric aerosols: particulates produced by burning
- Cloud cover
- Greenhouse gases: water vapor, CO₂, CH₄, N₂O, fluorinated gases, ozone
- Oceans: composition and circulation
- Snow and ice albedo
- Black carbon: from forest and grass fires, burning biomass for fuel, and fossil fuels
- Plants: growth, death, decomposition
- Land use: deforestation, cultivation, ruminants.

Figure 2.6 illustrates the relative impact of various phenomena on global energy. For each factor, the starting point is the 1880 value. Data for the plots are from GISS CMIP5 simulations [2.58] with the following exception: black carbon is split into natural (40%) and human (60%) components per *Ramanathan and Carmichael* [2.59].

Section A shows the impact of solar irradiance. Black carbon is a highly absorptive component of fine particulate matter. About 40% comes from open burning (forest and grass fires), about 20% comes from burning wood and other biofuels, and about 40% comes from burning fossil fuels. Stratospheric aerosols come from volcanoes. Major eruptions hurl immense quantities of particulates (aerosols) into the stratosphere, where they cool the Earth by reflecting sunlight back into space. The figure does not show the impact of the 1815 eruption of Mt. Tambora in Indonesia, which caused the *year without a summer* (1816) in the northern hemisphere. But it does show the impact of Krakatoa (Indonesia, 1882), Mt. Agung (Indonesia, 1963–64), Mt. St. Helens (USA, 1980) and Mt. Pinatubo (Philippines, 1991). Volcanoes also emit CO₂, SO₂, and halogens. As mentioned, on average, global anthropogenic CO₂ emissions are ≈80 times greater than CO₂ from volcanic emissions.

Section B shows the impact of eight anthropogenic factors. Greenhouse gases include anthropogenic CO₂, CH₄, N₂O, and fluorinated gases. Black carbon is mentioned above. Tropospheric ozone forms with photochemical smog. Snow albedo is reduced when fouled by soot from coal combustion. Direct tropospheric aerosols reflect sunlight back into space. Indirect effects include inducing cloud formation.

Section C compares forcings for greenhouse gases with all forcings, all natural forcings and all human

forcings. The data come from models, but the models match enormous amounts of data from many sources with high fidelity. It is difficult to view Figure 2.6 without concluding that GHGs impact the global heat balance in a major way.

Figure 2.7 and Table 2.8 illustrate a representative energy balance for the Earth; the balance changes seasonally [2.60]. Incident solar radiation is 340.4 W/m². Of this, 77.0 and 22.9 are reflected directly back into space by the atmosphere and surface, respectively. The fraction of reflected light is called the albedo, which in this case is 0.29. Clouds and aerosols account for most atmospheric reflection. Ice, desert sands, and other light-colored materials account for most surface reflection.

Of the non-reflected portion (240.4 W/m²) 32% is absorbed by the atmosphere and 68% is absorbed by the surface. The surface receives 485.2: 163.3 from the Sun and 321.9 re-radiated from GHGs. The surface re-emits this energy as IR radiation, thermals and evaporation. Thermals are rising masses of air, which distribute heat in the troposphere. Evaporation includes transpiration from plants. It generates clouds, in which latent heat is released via condensation to form rain or snow.

Of the re-emitted energy, 40.1 goes directly to space and the remainder goes to the atmosphere. The atmosphere and clouds emit 199.8 into space and recycle 321.9 to the surface.

Total outgoing radiation is 239.9. This is 0.2% less than incoming radiation. The imbalance increases temperature. Temperature change is easy to measure, but it is moderated by the properties of water. That marvelous substance is present on Earth in three phases. Liquid water has a high heat capacity, and both evaporation and freezing absorb considerable latent heat without a change in temperature. Small changes in temperature can correspond to large changes in heat. It's the heat that matters.

What Can Be Done About Climate Change?

Climate always will be changing. The real questions are: do you believe the science, which implies that human behavior is accelerating global warming? If so, do you believe the problem warrants action? If so, what should we do to minimize the damage that our actions are likely to cause during the remainder of the twenty-first century?

The *we* in this case means individuals, not just governments or companies. Unlike other matters discussed in this chapter, the problem is not specific to one technology, one company, or one industry. Everyone has an impact. In metabolizing food, an average human consumes 100 W of energy – the same as a typical light bulb – just by being alive. But we consume far more

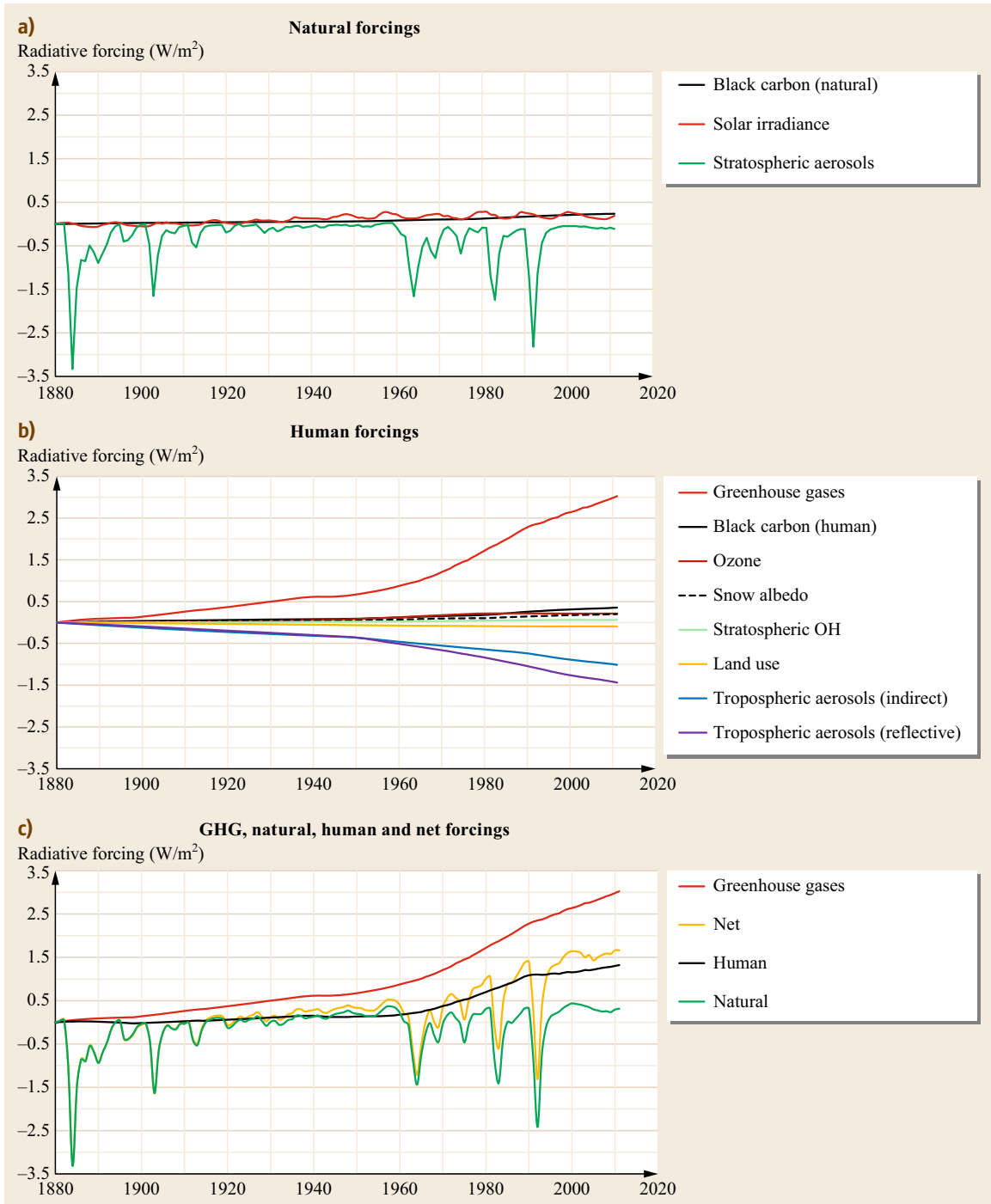


Fig. 2.6a–c Radiative forcings in W/m^2 for natural and human phenomena. with the following exception: black carbon is split into natural (40%) and human (60%) components per *Ramanathan and Carmichael* [2.59]

than a single light bulb. In 2013, average per capita energy consumption was 9210 W in the United States, 5150 W in Germany, 2965 W in China, 810 W in In-

dia, and 290 W in Bangladesh [2.61]. Especially in the United States, the world's 2nd-largest consumer, there is ample opportunity to conserve; Figure 1.5 in the

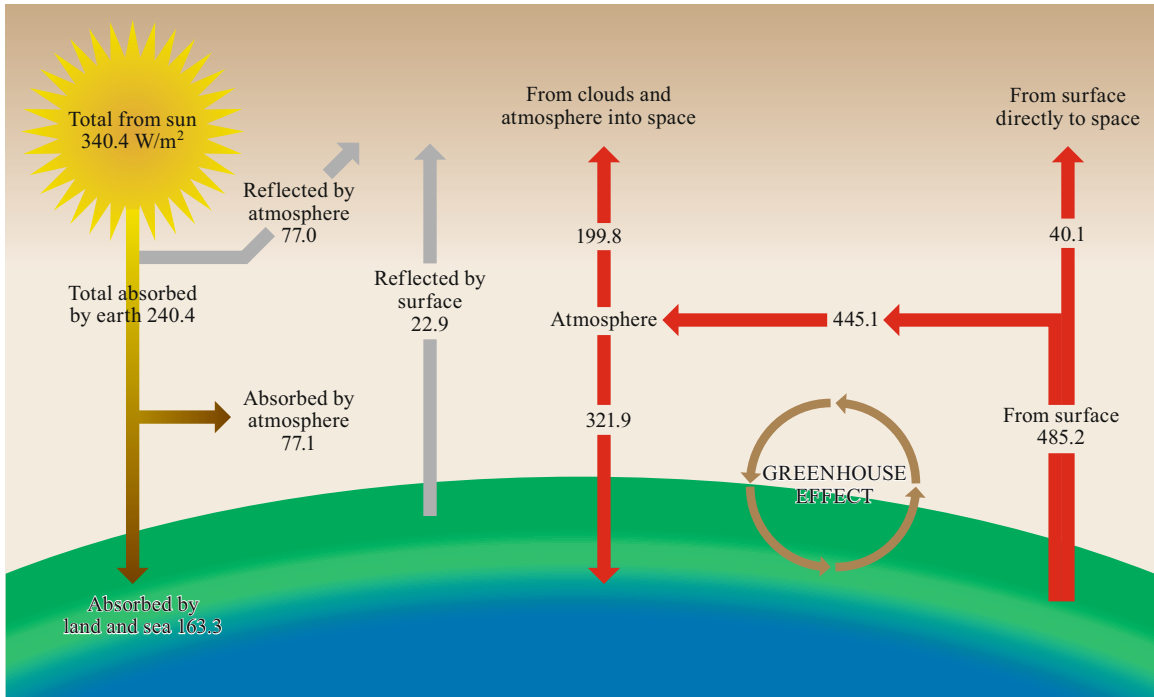


Fig. 2.7 Representative energy balance for the Earth. Accompanies Table 2.8. Incoming sunlight (340.4 W/m^2) exceeds outgoing radiation (339.8 W/m^2) by 0.21%

Table 2.8 Energy budget for the Earth. Accompanies Figure 2.7

	W/m^2		Percent of incoming	
Incoming sunlight (340.2 W/m^2)		340.4		100.00
Total reflected light:		99.9		29.35
● Reflected by clouds, aerosols, other	77		22.62	
● Reflected by the surface (ice, sand, other)	22.9		6.73	
	W/m^2		Percent of absorbed	
Absorbed by the Earth:		240.2		100.00
● By the atmosphere	77.1		32.07	
● By the surface	163.3		67.93	
IR Radiation				
Total outgoing IR radiation:		239.9		99.88
● From the atmosphere	169.9		70.73	
● From clouds	29.9		12.45	
● Directly into space	40.1		16.69	
From the surface to the atmosphere:		445.1		185.30
● GHGs	340.3		141.67	
● Hot-air thermals	18.4		7.66	
● Evaporation	86.4		35.97	
From the atmosphere to the surface		321.9		134.01
Net absorbed	0.5		0.21	

first chapter of this book describes how price shocks have led to significant reductions in energy consumption.

But the world population is rising and the economies of India and other developing countries are

growing. These factors alone are offsetting GHG reductions in developed countries. To make substantial long-lasting impacts will require low-cost infrastructure improvements, such as replacing consumption of fossil fuels – especially coal – with wind and solar energy.

More expensive endeavors – hydroelectric projects and nuclear power plants – also reduce fossil fuel consumption, but they have greater impact on other aspects of the environment.

Major projects require means but also will. In many quarters, will is lacking. Key decision-makers doubt the veracity of climate-change science. In the United States in 2017, the administration seemed to believe that the problem would go away if the terms *climate change* and *global warming* were deleted from government web sites.

In the end, regardless of whether you believe human-induced climate change is something to be concerned about, taking care of Planet Earth is the right thing to do. There is no Planet B.

2.2.8 Wastewater

Bitumen recovery processes such as SAGD (steam-assisted gravity drainage) and cyclic steam stimulation (CSS) require tremendous amounts of water [2.62]. SAGD produces wastewater contaminated with fines, trace metals, and hydrocarbons. At present, only a fraction of wastewater is recovered. Most goes to large tailing ponds, where the oil undergoes oxidation, generating significant amounts of CO₂ [2.63]. Environment Canada tolerates the tailings ponds.

Refineries and chemical plants generate contaminated process water, oily runoff, and sewage. Water is used by just about every process unit, especially those that require wash water, condensate, stripping steam, caustic, or neutralization acids. Contaminated process water may contain suspended solids, dissolved salts, water-soluble chemicals, phenols, ammonia, sulfides, and other compounds. As much as possible, wastewater streams are purified and reused. Present requirements ensure that the water going out of a U.S. or EU refinery processing plant is at least as clean as the water coming in.

Wastewater regulations and cleanup are described below.

2.2.9 Solid Waste

Solid wastes from coal and petroleum processing may include the following:

- Coal fines
- Cuttings from oil-well drilling
- Used drilling mud
- Spent catalyst and catalyst fines
- Acid sludge from alkylation units
- Sludge from the bottom of storage tanks
- Miscellaneous oil-contaminated solids.

Wastes that cannot be recycled are cleaned on site, sent to landfills, or transported to reclamation facilities. Some of the technology used for cleanup and reclamation is discussed in Sect. 2.6.

2.2.10 Oil Spills

Large spills of oil from tankers and pipelines can cause tremendous damage to the environment. Small spills come from leaks in tanks or mishaps during the loading or unloading of trucks, ships, or rail cars. Technology for cleaning up spills is discussed in Sect. 2.6.6.

2.2.11 Fugitive Emissions

Fugitive emissions are comparatively small amounts of gaseous, liquid, and solid wastes, which come from process equipment during industrial activities. Even small quantities of leaked gases, such as benzene, can cause serious damage to health and the environment when the emissions are continuous or chronic. Flammable chemicals can accumulate to form explosion hazards. One recent study showed that fugitive emissions were equivalent to 0.17 wt% of a refinery's throughput.

Leaks from high-pressure equipment usually occur through valves, connections, or mechanical seals. Other emissions come from storage tanks and waste treatment facilities. Operators regularly check for leaks with gas detectors and take appropriate corrective action.

Fugitive emissions can be hard to detect, and the sizes of leaks can vary with processing intensity and ambient conditions. Work continues on developing improved methods for discovery and analysis. One new technology is differential absorption, which can be used to measure concentrations of atmospheric hydrocarbons hundreds of meters from a facility. Opacity meters measure particulate emissions, and IR imaging can detect otherwise invisible gases escaping from leak sources.

2.2.12 Fracking

Fracking, discussed in Sect. 14.3.2, warrants a separate section in this chapter, because its widespread use is relatively recent, and because of unresolved questions about its impact on the environment. The economic impact of fracking is global. It dropped the price of oil, causing it to fall by more than 50% in less than two years while transforming the United States into the world's leading producer of oil and gas.

Fracking Technology

For decades, oil and gas companies knew of seemingly inaccessible hydrocarbons trapped in shale for-

mations with low permeability. Hydraulic fracturing (*fracking*) [2.64] increases permeability. Fracking involves pumping slurries of water, sand, and chemicals at high pressure into a hydrocarbon-containing formation. The pressure fractures the surrounding rock, and the sand props open the resulting passages. The chemicals can include acids, which dissolve particulates; silicones, which enhance flow; and surfactants.

Fracking isn't new. It was first applied in 1947 in Grant County, Kansas [2.65]. But now it is being employed in a new way. In the 1980s, George P. Mitchell started experimenting with different fracking techniques in the depleted Barnett Shale formation in Texas. By drilling horizontal wells and fracking directly under the densest rock, Mitchell got phenomenal results. His method transformed the Barnett Shale into a major gas field. Since then, similar methods have been applied to several other formations, including the Eagle Ford in Texas, the Bakken in North Dakota, and the Marcellus and Devonian, which at different depths underlay significant regions of Tennessee, Kentucky, Ohio, West Virginia, New York and Pennsylvania. The Marcellus shale alone contains around 500 trillion cubic feet of natural gas.

Fracking Exemption to the US Safe Drinking Water Act

Fracking requires immense amounts of water. In 2010, the US Environmental Protection Agency estimated that 70–140 billion gal of water are used to fracture 35 000 wells in the United States each year [2.66]. For coal-bed methane wells, fracturing uses 50 000–350 000 gal per well. For deeper horizontal shale wells, fracturing uses 2–10 million gal per well. In some cases, up to 90% of the water remains underground [2.67]. The rest comes back with the oil and gas, accompanied by natural underground water.

Typically, the wastewater is dark, thick, and smells of sulfur [2.68]. It contains dissolved minerals and chemicals. It tends to have high salinity, and sometimes it contains low levels of radiation. The wastewater goes

to a settling pit, where entrained oil disengages and floats to the surface. The oil is skimmed off and sold. The water is trucked to disposal wells and injected deep underground for permanent storage.

The Energy Policy Act of 2005 exempted fracking fluids from the United States Safe Drinking Water Act (SDWA) [2.69], except when diesel fuels are used. The Act did not exclude fracking wastewater, which is still covered by the SDWA. The *fracking loophole* was created, in part, so that service companies wouldn't have to disclose the chemical composition of their frack water. The problem is that if an incident forces chemicals into an aquifer, responders may be unprepared to take action. They won't know in advance what the contaminants might be, and they won't know at all until they analyze samples and/or get answers from the responsible company. Citizen's groups are deeply concerned. Several times between 2009 [2.70] and 2013 [2.71], legislation was introduced to close the fracking loophole. As of February 2017, the loophole was still open.

Fracking Induced Earthquakes

According to Scientific American [2.72], researchers at the United States Geological Survey (USGS) and other institutions have linked earthquakes to hydraulic fracturing and injecting wastewater from oil and gas operations into deep wells. Earthquake rates have skyrocketed in Oklahoma and Texas. Before 2008, not a single earthquake had been recorded by the USGS in the Dallas–Fort Worth area. Since then, nearly 200 quakes have shaken the cities and their immediate suburbs. The largest measured 5.6 on the Richter scale. Oklahoma has seen a 160-fold spike in quakes. Some damaged buildings and highways and sent people to hospitals. In 2014, Oklahoma's earthquake rate surpassed California's. Certain states have started to limit the amount of wastewater sent underground. But quakes could continue even if injections were stopped, because pressure changes can migrate for years, inducing changes in faults farther and farther away from the points of injection.

2.3 Significant Accidents and Near-Misses

As mentioned, safety, reliability, and protecting the environment are inextricably bound. The worst industrial accidents are deadly both to people and their surroundings. Several such accidents are reviewed in this section. Some are described by *Incidents that Define Process Safety* [2.73], a fine book assembled by John Atherton and Frederic Gil. At the front of that book is

a quote from Jesse C. Ducommun, a director of American Oil Company and a process safety pioneer. In 1961, he said:

It should not be necessary for each generation to re-discover principles of process safety which the generation before discovered. We must learn from the

experience of others rather than learn the hard way. We must pass on to the next generation a record of what we have learned.

George Santayana said: *Those who cannot remember the past are condemned to repeat it.* (Experience has taught me that there is truth in Kurt Vonnegut's rejoinder: *I've got news for Mr. Santayana: we're doomed to repeat the past no matter what.* In other words, there will always be people who ignore the past and others who don't care to learn.)

Reviewing incidents tells us that the following factors are common root causes:

1. *Absences of Regulations.* Workers and managers behave as they always have, either because they don't know there's a problem with a particular practice or there is no incentive to change.
2. *Design Flaws.* Flaws in design include flaws in procedures. Many are caused when equipment or procedures are exposed to a previously unknown physical phenomenon. Others result from willful misconduct – cutting corners to reduce costs or avoid delays.
3. *Poor Maintenance.* Poor or nonexistent maintenance plays a role in several of the incidents below, including one of the worst (Bhopal). According to the U.S. Coast Guard's National Response Center, equipment failure caused about half of the roughly 7600 accidental chemical releases reported by refineries during 2001 to 2010. Factories are scheduling fewer maintenance shutdowns, known as turnarounds, while increasing burdens on aging equipment. This is sometimes called *run to failure* – pushing equipment until it breaks [2.74].
4. *Ignorance.* The examples reveal two sources of ignorance: (a) an accident was the first of its kind and could not have been predicted by the people at hand, and (b) lack of training.
5. *Lack of Preparation.* Accidents can get worse when people are not prepared to respond.
6. *Willful misconduct.* Examples of willful misconduct abound. One of the most famous was the decision by senior managers to launch the Space Shuttle Challenger on January 28, 1986, despite vehement opposition from Roger Boisjoly and other engineers. Crucial O-ring seals failed, and the Challenger and its crew were destroyed. The Chernobyl nuclear reactor meltdown (see below) also was caused by willful misconduct.
7. *Did-it-before syndrome (DIBS).* People learn from experience. When they get away with shortcuts, with flouting rules over and over again, they come to

believe that flouting rules is acceptable. Eventually, they conclude that their way is better. They may be correct. If so, they are obliged to take proper steps to modify the rule.

8. *Malicious acts.* These include illegal midnight dumping; cover-ups; sabotage; and acts of war.

2.3.1 Coal Mining: Explosions and Black Lung Disease

Coal mine explosions and maladies such as black lung disease have plagued the energy industry since the start of the Industrial Revolution. In 1906, in a mine explosion in Courrières, France, 1099 people died, including children. Courrières was the worst mine accident in Europe. In April 1942, in a coal-mine explosion in Benxi, Liaoning, China, 1549 workers died in the worst coal-mine accident ever.

Mine explosions are caused by methane and/or coal dust. *Damp* is a catch-all term for gases other than air in coal mines. In addition to firedamp (methane), there is blackdamp (carbon dioxide), stinkdamp (hydrogen sulfide), and afterdamp (carbon monoxide). Firedamp is explosive in air at concentrations between 4 and 16%.

In May 1812, Sir Humphry Davy developed the Davy lamp, in which a low flame was surrounded by iron gauze. Due to the gauze, the lamp did not ignite ambient methane, but methane could pass into the lamp and burn safely within the flame. At first, the Davy lamp improved safety by eliminating open-flame lighting. But it led to the mining of areas that had previously been closed for safety reasons, sometimes with disastrous results [2.75].

Black lung disease is actually a set of maladies associated with coal dust [2.76]. It was not well understood until the 1950s. In the Federal Coal Mine Health and Safety Act of 1969, the US Congress set limits on coal dust exposure and created the Black Lung Disability Trust. Mining companies agreed to a clause that guaranteed compensation for workers or the families of workers who had spent 10 years doing mine work and could provide x-ray evidence of lung damage. Families of deceased miners were allowed to provide autopsy evidence. Financed by a federal tax on coal, by 2009 the Trust had distributed over \$44 billion in benefits to disabled miners or their widows.

2.3.2 Lakeview Oil Well: Blowout (March 1910–September 1911)

The Lakeview gusher [2.77] remains the largest accidental oil leak or spill in history. It released 1.2 million t of crude in 544 days. Drilling started in January 1909.

Initially, the only product from the well was natural gas. On March 14, 1910, pressurized oil blew through the well casing above the drill bit. At the time, blowout prevention technology didn't exist, so the well gushed unabated. The initial flow rate was 18 800 bbl/day. The peak flow rate was 90 000 bbl/day. The blowout created a river of crude, which crews contained with sand bag dams and dikes. About half of the oil was saved. The remainder seeped into the ground or evaporated. The Lakeview incident revealed the need for blowout prevention technology.

2.3.3 Texas City, Texas: Ammonium Nitrate Explosion (1947)

On April 16, 1947, the *SS Grandcamp* exploded in port at Texas City, Texas [2.78]. The ship was loaded with 7700 t of ammonium nitrate. The initial blast, together with fires and explosions on other ships and nearby oil-storage facilities, killed 581 people and injured up to 8000. The force of the blast was equivalent to 3.2 kt of TNT. At about 08:00 a.m., a fire was spotted in the cargo hold of the ship. For roughly an hour, attempts to extinguish the fire failed as a red glow returned after each effort to douse the fire. The cause of the initial fire remains unknown. The primary lesson from this disaster was to avoid storing large amounts of explosive chemicals in one place.

2.3.4 London: Killer Fog (1952, '56, '57, '62)

In December 1952, thick fog rolled across many parts of the British Isles. In the Thames River Valley, the fog mixed with smoke, soot and sulfur dioxide from the burning of coal, turning the air over London into a dense yellow mass. An unusual weather condition kept the air from moving. The smog was so thick that buses could not run without guides walking ahead of them carrying lanterns. Fog stayed put for several days, during which the city's hospitals filled to overflowing. According to the Parliamentary Office of Science and Technology [2.79], more than 3000 people died that month because of the polluted air. Similar, less-severe episodes occurred in 1956, 1957, and 1962. The 1956 event killed more than 1000 people.

London's deadly smog was caused by *usual-practice* pollution. Due to the widespread use of cheap, high-sulfur coal, London air had been bad for decades, but postwar growth made it worse than ever. In response to the incidents, Parliament passed Clean Air Acts in 1956 and 1962, prohibiting the use of high-sulfur fuels in critical areas.

2.3.5 Amoco Cadiz: Oil Spill (1978)

On March 16, 1978, the supertanker *Amoco Cadiz* was 3 mi off the coast of Brittany when its steering mechanism failed. The ship ran aground on the Portsall Rocks [2.80].

For two weeks, severe weather restricted cleanup efforts. The wreck broke up completely before any remaining oil could be pumped out, so the entire cargo – more than 1.6 million bbl of Arabian and Iranian crude oil – spilled into the sea.

The resulting slick was 18 mi wide and 80 mi long. It polluted 200 mi of coastline, including the beaches of 76 Breton communities. On several beaches, oil penetrated the sand to a depth of 20 in. Piers and slips in small harbors were covered with oil. Other polluted areas included the pink granite rock beaches of Tregastel and Perros-Guirec, and the popular bathing beaches at Plougasnou. The oil persisted for only a few weeks along exposed rocky shores, but in the areas protected from wave action, the oil remained as an asphalt crust for several years.

The *Amoco Cadiz* incident caused considerable loss of marine life. Cleanup activities on rocky shores, such as pressure washing, also caused harm. Two weeks after the accident, millions of dead mollusks, sea urchins, and other bottom-dwelling organisms washed ashore. Nearly 20 000 dead birds were recovered. About 9000 t of oysters died. Fish developed skin ulcerations and tumors.

Years later, echinoderms and small crustaceans had disappeared from many areas, but other species had recovered. Even today, evidence of oiled beach sediments can be seen in sheltered areas, and layers of subsurface oil remain under many impacted beaches.

From this disaster, the oil industry learned the need for prompt action and the relative efficacy of different techniques to sink, disperse, and recover spilled oil. It also gained experience in onshore cleanup.

2.3.6 Bhopal, India: Methyl Isocyanate Leak (1984)

In December 1984, up to 200 000 people were exposed to methyl isocyanate (MIC) in Bhopal, India and surrounding towns [2.81]. More than 2500 died. Thousands more suffered permanent lung and/or eye damage. All told, there were 524 000 personal injury claims, 2800 lost-cattle claims, 4600 business claims, and 3400 wrongful death claims. Eventually, Union Carbide, owner of the MIC plant, reached a US\$470 million settlement with the Parliament of India.

On December 2, 1984, a worker observed a buildup of pressure in a storage tank at the Union Carbide chem-

ical plant near Bhopal. The tank contained about 15 t of MIC, a chemical used to make pesticides. MIC is flammable, and at high concentrations it is deadly. At low concentrations, it causes lung damage and blindness. Several process and safety systems were out of service, any one which would have contained or destroyed the MIC:

1. The pressure increase was probably caused by water inside the storage tank. Water reacts with MIC to form methylamine and gaseous carbon monoxide. The reaction releases heat, which would have raised pressure by vaporizing MIC. Normally, a refrigeration unit would have controlled the temperature, but the cooler had been out of service for several months.
2. Eventually, the pressure rise popped a safety valve. When this happened, the vented gas should have been routed to a caustic scrubber, which would have absorbed and hydrolyzed the MIC, rendering it harmless. Instead, the vented gas went to the flare.
3. The flare should have converted the MIC into relatively harmless CO_2 , H_2O and N_2 . But the flare system failed, perhaps because it wasn't designed to handle such a large surge of gas.
4. If operators had noticed the leak immediately, they might have been able to stop the disaster before it did much damage. But the leak did not show up on control-room monitors because a critical panel had been removed. Instead, tons of MIC poured into the air and spread across the countryside, covering 25 mi^2 (65 km^2).

How did water get into the storage tank, where the MIC was kept under a blanket of dry nitrogen? Some experts suggest that the nitrogen was wet. Others guess that a water hose was inadvertently connected to the nitrogen line. A Union Carbide official suggested possible sabotage.

Even if the incident on December 2, 1984 was an act of sabotage, the MIC unit at Bhopal was a disaster waiting to happen. During a press conference, a Union Carbide executive acknowledged that the unit was in a state of sorry disrepair, and that its condition was so poor that it shouldn't have been running.

2.3.7 Nuclear Power Incidents: Context

This section sets the stage for descriptions of the incidents at Three Mile Island and Chernobyl. Table 2.9 provides a bare-bones introduction to relevant terminology.

Nuclear power plants generate heat from the enormous energy generated by nuclear fission. Two factors are essential to the success of nuclear power: generating

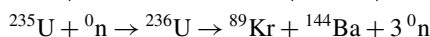
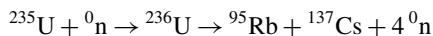
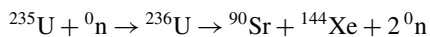
and controlling the heat, efficiently converting the heat into electrical power, and keeping radioactive isotopes inside the containment system.

Uranium and Its Hazardous Daughters

Modern nuclear plants are fueled by uranium-235 (^{235}U). Natural uranium is comprised of ^{235}U and two other isotopes, with the following abundances: ^{234}U (0.005–0.006%), ^{235}U (0.72%), and ^{238}U (99.274–99.275%). The isotopes contain 92 protons along with 142, 143, and 146 neutrons, respectively. Future plants may be fueled with plutonium (^{239}Pu) transmuted in nuclear reactors from ^{238}U , or with ^{233}U , transmuted from naturally occurring thorium (^{232}Th).

Many fission reactions produce more neutrons than they absorb. The extra neutrons can in turn induce fission in other fissile atoms, which generates more neutrons, and so on, in a chain reaction. Product isotopes are called *daughters*. Several daughters of ^{235}U fission are unstable and undergo subsequent nuclear reactions in *decay chains*. ^{90}Sr , ^{137}Cs , and ^{131}I are especially dangerous [2.82]. They are relatively abundant, comprising 4.5, 6.3, and 3 wt%, respectively, of all fission products in reactors.

Here are examples (excluding neutrinos) of primary fission reactions, including two which form ^{90}Sr and ^{137}Cs



In reactors, most ^{137}Cs is produced from three daughters: ^{137}Xe , ^{137}I , and ^{137}Te .

Decay of ^{90}Sr proceeds as follows



For ^{137}Cs , the decay is



Ba^* is an unstable version of Ba, which becomes stable after emitting a γ photon.

Carried aloft by dust, ^{90}Sr from the detonation of nuclear weapons in the atmosphere and from serious accidents was detected everywhere on the planet and continued to be found in soil and plants for more than 60 years afterwards. It goes from soil into growing plants and then into animal products, including milk. Chemically similar to calcium, strontium takes up residence in bones, where it can stay for years, greatly increasing the likelihood of cancer.

Table 2.9 A bit of nuclear physics

- By convention, the superscript which precedes the atomic symbol in nuclear notation is the *mass number* of the atom; it is not the *atomic mass*.
- The mass number is the sum of the number of *nucleons* – protons and neutrons.
- Atoms with the same number of protons but different numbers of neutrons are called *isotopes*. Isotopes of an element undergo the same chemical reactions.
- A *fissile* isotope is one which can undergo *nuclear fission*.
- Nuclear reactions can produce five types of radiation. Alpha (α) radiation is comprised of highly energetic helium nuclei (${}^4\text{He}$). Beta (β) radiation is comprised of highly energetic electrons (e^-). Gamma (γ) radiation is comprised of high-energy photons. Neutrons (${}^0\text{n}$) are released by many nuclear reactions. Neutrinos have no electric charge and are essentially massless; the nuclear reaction equations in this section do not show include neutrinos.
- In nuclear fission, a radioactive atom splits into two smaller atoms, all of which are heavier than an alpha particle (energetic ${}^4\text{He}$). The sum of the masses of all products (*daughter* atoms and neutrons) is less than the mass of the parent isotope. The difference is called the *nuclear binding energy*, which is released during the nuclear fission of heavy elements and the *nuclear fusion* of light elements.
- Binding energy is enormous. The amount can be calculated from the famous Einstein equation, $e = mc^2$, where e is energy, m is rest mass, and c is the speed of light. During the fission of one mole (235.043 g) of ${}^{235}\text{U}$, the products weigh about 0.2 g less than the uranium. The missing matter is converted into around 18 000 000 000 kJ of energy. In comparison, complete combustion of one mole of methane releases 810 kJ, about 222 billion times less energy!
- Half-life is the time it takes for half of a radioactive isotope to transform spontaneously into something else via radioactive decay.

${}^{137}\text{Cs}$ spreads more readily because much of it comes from gaseous ${}^{137}\text{Xe}$ and ${}^{137}\text{I}$. As it decays, ${}^{137}\text{Cs}$ emits an energetic – and mutagenic – gamma ray. It is chemically similar to sodium – its salts are highly soluble in water – so it can end up nearly everywhere. Most of the γ radiation at the Chernobyl and Fukushima accident sites came from the decay of ${}^{137}\text{Cs}$.

${}^{131}\text{I}$ is volatile because it finds its way into gaseous I_2 . As it decays to ${}^{131}\text{Xe}$, its half-life is 8.0 days, easily long enough to be spread hundreds of miles by winds. When inhaled or ingested it concentrates in the thyroid, where it can cause cancer.

Nuclear Power Plants. In natural uranium, chain-reaction fission does not occur. ${}^{238}\text{U}$ is mildly radioactive and relatively benign; it is present in nuclear power plants but does not undergo fission except indirectly. It also captures more neutrons than it releases. Most of the remaining neutrons are too fast to be captured by ${}^{235}\text{U}$. These challenges are met in two ways; isotopic enrichment and high-energy neutron moderation.

Most of the world's nuclear power plants employ light-water reactors (LWR). There are three kinds of LWR: pressurized water reactors (PWR), boiling-water reactors (BWR), and supercritical-water reactors (SCWR). Regular water (light water) is a preferred cooling medium and an excellent neutron-energy mod-

erator. But it also absorbs neutrons. Due to the latter, LWR require a higher concentration of fissile targets. This is accomplished by enriching uranium – increasing the ${}^{235}\text{U}$ content from the natural abundance (0.72%) to 3–5%. Chemical separation of isotopes is not possible, so separation is accomplished by mass-based techniques such as gas centrifugation.

Unenriched uranium fuels pressurized heavy-water reactors (PHWR) and graphite reactors. Heavy water is deuterium oxide (D_2O); it is a good coolant and neutron energy moderator, but it is a poor neutron absorber. In graphite reactors, such as the ones at Chernobyl, regular water is the coolant and graphite is the moderator. Graphite is flammable. At Chernobyl, graphite did not cause the incident, but burning graphite sent radioactive material into the atmosphere.

Most commercial land-based nuclear power plants, such as the one at Three Mile Island, contain pressurized-water reactors (PWR). PWR have multiple coolant loops as shown in Fig. 2.8. In the primary loop, nuclear heat generates super-heated water at 150–160 bar and 300°C . Through heat exchangers, heat from the primary-loop is transferred to the secondary loop, where it converts water into steam. The steam drives turbines to produce electricity. The primary and secondary loops exchange heat but not water; water in the secondary loop is not radioactive.

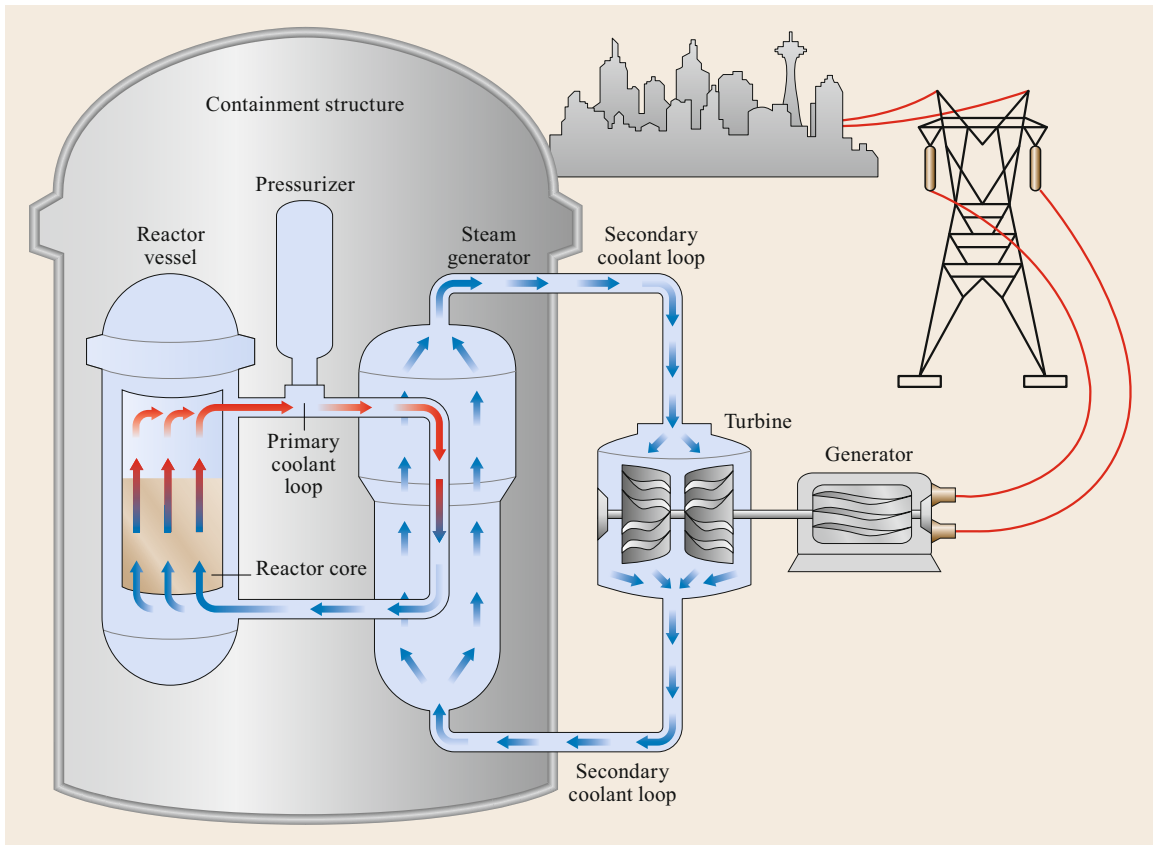


Fig. 2.8 Illustration of a pressurized large light water reactor (LWR) [2.83]

Fuel Elements. In reactors, fuel elements contain the uranium. Pellets of uranium dioxide (UO_2) are contained inside long tubes of zirconium (Zr) alloy.

Control Rods. In the reactor core, the fuel elements are surrounded by water or graphite and interspersed with control rods. The rods contain moderating elements, such as cadmium or boron, which regulate the chain reaction by absorbing neutrons. Operators control the reactor by raising or lowering the rods. The control rods can be attached to their hoist system by electromagnets. If electrical current is lost, the rods fall by gravity all the way into the core, completely shutting off fission.

Heat Control Is Crucial. There are two ways to control heat in a nuclear reactor – with control rods, which govern the production of heat, and with coolant. Both at Three Mile Island and Chernobyl, loss of coolant damaged equipment, which in turn led to loss of control of the nuclear reactions.

2.3.8 Three Mile Island: Nuclear Reactor Meltdown (1979)

On March 28, 1979, at the Three Mile Island PWR-based nuclear power plant near Middletown, Pennsylvania, the TMI-2 reactor partially melted down [2.84]. The accident began with failure of the reactor cooling system. The failure caused the turbine generator and the reactor to shut down automatically. Pressure began to rise in the nuclear portion of the plant. This activated a pressure relief valve, which should have shut automatically when the pressure returned to acceptable levels. But the valve failed to close, allowing water to bleed from the primary coolant loop. Alarms sounded, but due to lack of information, the operators did not know the reactor was losing water. They responded inappropriately, reducing the flow of water to the reactor core. The nuclear fuel overheated, and due to the high temperature, the zirconium alloy (zircalloy) fuel rod cladding ruptured, allowing the fuel pellets to melt.

Afterwards, inspections showed that half of the core had melted. In the end, things could have been much

worse. The reactor building remained intact and contained nearly all hazardous materials. A modest amount of radioactive gas was released, but due to dilution with air, ambient radiation levels hardly exceeded background.

After the accident, the US Nuclear Regulatory Commission (NRC) required several changes in the design and operation of US nuclear plants, which were implemented at all other PWR power plants.

The most significant health consequence of the Three Mile Island incident was its psychological impact, mostly on people in the surrounding area but also in the rest of the United States. Since the incident, the construction or expansion of nuclear power plants slowed to a crawl.

2.3.9 Chernobyl: Nuclear Reactor Fire (1986)

On April 26, 1986, a disaster occurred at the Chernobyl nuclear plant near Pripyat, Ukraine. According to official government figures, more than 4000 people who took part in the cleanup died, and 70 000 were disabled by radiation. About 3.4 million of Ukraine's 50 million people, including some 1.26 million children, were affected by the disaster [2.85].

The literature contains many summaries of the causes and lingering impact of the Chernobyl nuclear disaster. The International Nuclear Safety Advisory Group (INSAG) published a thorough report in 1986 and followed it with a revision in 1992 [2.86]. The INSAG documents remain the most generally accepted. The oft-vilified Anatoly Dyatlov, who was the Deputy Chief Engineer at the plant when the incident occurred, challenged the INSAG report. An English version of his perspective appeared in 1995 [2.87]. There are numerous summaries and timelines on the Internet, but they often disagree with each other and the INSAG document. A factual summary of health effects was published by the World Nuclear Association in 2009 [2.88]. Other articles on health effects are outlandish. For this chapter, choices had to be made. Please accept apologies for any errors, for which the author accepts complete responsibility.

SCRAM stands for *safety critical reactor axe man*. It is a term from the early days of nuclear power development, when graphite control rods were raised and lowered into the core of a reactor with a rope on a pulley. The axe man stood ready to cut the rope in an emergency, dropping all control rods all the way in, shutting down the reactor.

Before the accident, Anatoly Dyatlov was seeking ways to solve a nagging problem at the Chernobyl power plant. After a planned shutdown or emergency

SCRAM the cooling water pumps stopped due to lost electrical power. Backup power was supplied by diesel generators, but starting the diesels took almost a minute. During the delay, residual heat remained in the reactor. To Dyatlov, this delay was unacceptable. He thought of a solution. During the loss of power, the plant's steam turbines kept spinning for several minutes due to their massive inertia. Dyatlov calculated that, as the turbines slowed down, they could produce enough power to run the water pumps until the diesels were up and running. He designed a complex network of switches to keep the current steady as the turbines lost momentum.

Dyatlov talked to the Chief Engineer of the plant, who gave him permission to run his *electrical engineering* experiment. The test began on April 25, 1986, as Unit 4 was shutting down for long-delayed maintenance. With Dyatlov's approval, the operators decided to run the test manually instead of using the unit's *unimaginative automatics*.

At 02:00 p.m., in violation of one of the most fundamental nuclear power safety practices, the operators switched off the emergency cooling system. Just after midnight on April 26th, they switched off the reactor's power-density controls.

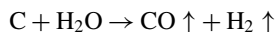
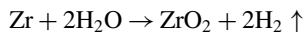
Under manual operation, the reactor became unstable. At 01:07 a.m., power output suddenly dropped to 0.03 GW, far less than the specified minimum of 0.70 GW. To generate more power, the operators increased heat by raising the graphite control rods to the maximum height allowed by regulations. Dyatlov ordered them to raise the rods further. When the operators balked, Dyatlov insisted, and the operators complied.

At 01:23 a.m., the power output seemed to be stable at 0.2 GW. The operators then violated THE most important nuclear power safety practice by disabling the emergency SCRAM. In this case, the SCRAM was not a man with an axe, but an automatic interlock designed to stop the reactor whenever the neutron flux exceeded a safe limit. (In today's nuclear power plants, it is physically impossible to disable this control.)

Now the experiment could begin. To see how long the electricity-generating turbine would spin without a supply of steam, operators closed the valve that channeled steam from the reactor to the turbine. Steam that should have been taking heat out of the reactor was now trapped inside.

In less than 45 s, the reactor started to melt. Super-hot pellets of uranium-oxide fuel deformed, rupturing their zirconium-alloy containers, and came into direct contact with cooling water. The water flashed into steam, causing the first of two explosions that blew the top off the reactor. The second blast was caused by a H₂-CO-air explosion. The H₂ and CO were generated

by reactions of zirconium and graphite with superheated steam



About 15 t of radioactive material from the reactor core rocketed into the atmosphere, where it spread across Europe. More than 36 h after the accident, plant personnel told local officials about the accident. About 14 h after that – 50 h after the accident – radiation from the explosion was detected by technicians at the Forsmark nuclear power plant in Sweden. That measurement was the first notification to the world outside the Soviet Union that something had happened in Pripjat.

At the site, more than 30 fires broke out, including an intensely hot graphite fire that burned for 14 days. About 250 people fought the various blazes. During 1800 helicopter sorties, pilots dropped 5000 t of lead, clay, dolomite and boron onto the reactor. Near term, the explosion and high-level radiation killed 31 people, including operators, firefighters, and helicopter pilots.

During a trial that ended in August 1987, the Chernobyl plant director (Brukhanov) was convicted and sentenced to 10 years in a labor camp. The Chief Engineer (Fomin), and Dyatlov received shorter sentences. The two operators were acquitted, but both of them died soon afterwards. More than 60 other workers were fired or demoted.

Long-Term Consequences

In June 1987, 14 months after the disaster, some 27 villages within the restricted zone were still heavily contaminated, because the cleanup operation had stopped. Nearby cities and towns were reporting dramatic rises in thyroid diseases, anemia, and cancer. Hardest hit were children.

According to Gernadij Grushevoi, cofounder of the Foundation for the Children of Chernobyl, the long-term danger is also critical in Belarus. In 1992, in testimony at the World Uranium Hearing [2.89], he said:

[...] 70 percent of the radioactive stuff thrown up by the explosion at Chernobyl landed on White Russian territory. There is not a centimeter of White Russia where radioactive cesium cannot be found.

The Rest of the Plant Kept Running for Nine Years

The three remaining nuclear reactors (Units 1, 2 and 3) continued to run. Despite ambient radiation levels nine times higher than widely accepted limits, workers lived in newly built colonies inside the *dead zone*. In 1991, Unit 2 was damaged beyond repair by a fire in the turbine room. That left Units 1 and 3, which kept going for

the next nine years. They kept going because the power was needed, and no funds were available to build a replacement.

On December 14, 2000, the plant was shut down. The shutdown was expedited by the European Commission, which approved a US\$585 million loan to help Ukraine build two new power plants, and by the European Bank for Reconstruction and Development, which provided US\$215 million.

2.3.10 Sandoz, Switzerland: Chemical Spills and Fire (1986)

On November 1, 1986, a fire broke out in a riverside warehouse at the Sandoz chemical plant in Schweizerhalle, Switzerland. While extinguishing the flames, firemen sprayed water over exploding drums of chemicals, washing as much as 30 t of pesticides, chemical dyes, and fungicides into the Rhine River. Up to 100 mi (160 km) downstream from Schweizerhalle, the Rhine was sterilized. All told, more than 500 000 eels and fish were killed. More than 50 million people in France, Germany, and The Netherlands endured drinking water alerts [2.90].

Afterwards, while checking the Rhine for chemicals as it rolled through Germany, officials discovered high levels of a herbicide (atrazine) that wasn't on the list provided by Sandoz. Eventually, Ciba-Geigy admitted that it had spilled atrazine into the river just a day before the Sandoz fire. As monitoring continued, more chemicals were discovered, alerting German authorities to the fact that many different companies were secretly discharging dangerous chemicals into the river. BASF admitted to spilling more than 1 t of herbicide, Hoechst discovered a chlorobenzene leak, and Lonza confessed to *losing* 2000 gal (4500 l) of chemicals.

Recovery

In response to the Sandoz disaster, companies all along the Rhine joined the Rhine Action Program for Ecological Rehabilitation, agreeing to cut the discharge of hazardous pollutants in half by 1995. Although many experts thought the target could never be reached, samples showed that from 1985 to 1992, mercury in the river at the German town of Bimmen-Lobith, near the Dutch border, fell from 6.0 to 3.2 t, cadmium from 9.0 to 5.9 t, zinc from 3600 to 1900 t, and polychlorinated biphenyls (PCBs) from 390 to 90 kg.

In December 1990, for the first time in 3 years, a large Atlantic salmon was fished from the Sieg River, a tributary of the Rhine in west-central Germany. The catch proved what officials had hoped: if you clean up your mess and clear the way, someday life will return. The event gave impetus to the Salmon 2000 project, and

further success followed. In 1994, researchers found recently hatched salmon in the Sieg, and in 1996 a salmon was hooked near Baden-Baden. In 1998, encouraged by the success of the Rhine Action Program, targets were set to designate a large protected ecosystem from streams in the Jura Mountains, the Alps, the Rhine mountains, the Rhineland-Palatinate, the Black Forest, and the Vosges to the mouth of the Rhine in The Netherlands. Meanwhile, not all of the Rhine's pollution problems have been solved. One of the most serious is a huge basin in the Netherlands, into which toxin-laden mud dredged from the Port of Rotterdam has been dumped since the 1970s. Contamination levels are falling, but several toxins are very stubborn.

All along the Rhine, the main source of remaining pollution comes from farm fertilizers, which seep into the river every time it rains.

2.3.11 Exxon Valdez: Oil Spill (1989)

On March 23, 1989, the 987-foot supertanker *Exxon Valdez* left port carrying more than 1.2 million bbl of Alaskan North Slope crude. The ship was headed south toward refineries in Benicia and Long Beach, California. At 10:53 p.m., it cleared the Valdez Narrows and headed for Prince William Sound in the Gulf of Alaska. To avoid some small icebergs, Captain Joseph Hazelwood asked for and received permission to move to the northbound shipping lane. At 11:50 p.m., just before retiring to his cabin, the captain gave control of the ship to the third mate, Gregory Cousins, instructing him to steer the vessel back into the southbound lane after it passed Busby Island.

Cousins did tell the helmsman to steer to the right, but the vessel didn't turn sharply enough. At 12:04 a.m., it ran aground on Bligh Reef.

Captain Hazelwood returned to the bridge, where he struggled to hold the tanker against the rocks. This slowed the rate of oil leakage. He contacted the Coast Guard and the Alyeska Pipeline Service Company. The latter dispatched containment and skimming equipment. According to the official emergency plan, this equipment was supposed to arrive at a spill within 5 h. In fact, it arrived in 13 h – 8 h late.

The *Exxon Baton Rouge* was sent to offload the spilled cargo and to stabilize the *Valdez* by pumping sea water into its ballast tanks. The oil transfer took several days. By the time it was finished, more than 250 000 bbl of oil had spilled into the Sound. Eventually, 33 000 birds and 1000 otters died because of the spill.

Eleven thousand workers treated 1200 mi (1900 km) of shoreline around Prince William Sound and the Gulf of Alaska, using 82 aircraft, 1400 vessels, and 80 mi (128 km) of oil-containing booms.

In response to the disaster, the US Congress passed the Oil Pollution Act of 1990. The Act streamlined and strengthened the ability of the US Environmental Protection Agency (EPA) to prevent and react to catastrophic oil spills. A trust fund, financed by a tax on oil, was established to pay for cleaning up spills when the responsible party cannot afford to do so. The Act requires oil storage facilities and vessels to submit plans to the Federal government, telling how they intend to respond to large oil discharges. EPA published regulations for above-ground storage facilities, and the US Coast Guard published regulations for oil tankers. The Act also requires the development of area contingency plans to prepare for oil spills on a regional scale.

Captain Hazelwood was tried and convicted of illegally discharging oil, fined US\$50 000, and sentenced to 1000 h of community service. Exxon spent US\$2.2 billion to clean up the spill, continuing the effort until 1992, when both the State of Alaska and the US Coast Guard declared the cleanup complete. The company also paid about US\$1 billion for settlements and compensation.

On July 10, 2004, USA Today reported [2.91]:

Not one drop of crude oil spilled into Prince William Sound from oil tankers in 2003 – the first spill-free year since the ships started carrying crude from the trans-Alaska pipeline terminal in 1977.

2.3.12 Arabian Gulf War: Intentional Oil Spill, Oil Well Fires (1991)

Mina Abdulla Spill

On January 25–27, 1991, during the occupation of Kuwait, Iraqis pumped 4–6 million bbl of oil from stations at Mina Al-Ahmadi into the Arabian Gulf. They did so to foil an expected beach invasion by allied troops. The size of the spill was 16–25 times greater than the *Exxon Valdez* spill. On January 27, allied bombers stopped the spill by destroying the pumping stations.

Ad Daffi Bay and Abu Ali Island experienced the greatest pollution. The spill damaged sensitive mangrove swamps and shrimp grounds. Marine birds, such as cormorants, grebes, and auks, were killed when their plumage was coated with oil. The beaches around the shoreline were covered with oil and tar balls.

Despite the ongoing war, the cleanup of the oil spill proceeded rapidly. Kuwaiti crude is rich in light ends, and water in the Arabian Gulf is relatively warm. For these reasons, about half of the spilled oil evaporated, leaving behind a thick emulsion, which eventually solidified and sank to the bottom of the sea. Another 1.5

million bbl were recovered by skimming. Operators of sea-water cooled factories and desalination plants were concerned that the oil might foul their intake systems. To prevent this, protective booms that extended 3 ft (1 m) below the surface were installed around intakes in Bahrain, Iran, Qatar, Saudi Arabia, and the United Arab Emirates.

Oil Well Sabotage

On February 23–27, 1991, retreating Iraqi soldiers damaged three large refineries and blew up 732 Kuwaiti oil wells. Fires started on 650 of the wells. Up to 6 million bbl of oil per day were lost between February 23 and November 8, 1991. Crews from 34 countries assembled to fight the oil-well fires. Initially, experts said the fires would rage for several years. But due to the development of innovative firefighting technology, the job took less than 8 months.

The oil-well fires burned more than 600 million bbl, enough to supply the United States for more than a month. The firefighting effort cost US\$1.5 billion. Rebuilding Kuwait's refineries cost another US\$5 billion. In all, Kuwait spent between US\$30 and US\$50 billion to recover from the Iraqi invasion.

2.3.13 Tosco Avon Hydrocracker: Deadly Pipe Rupture (1997)

On January 21, 1997 a temperature excursion led to the rupture of a reactor outlet pipe at the Tosco Avon Refinery in Martinez, California. The consequent release of hydrogen and hydrocarbons ignited on contact with air, causing an explosion and fire. One worker was killed and 46 others were injured. There were no reported injuries to the public [2.92].

Context

Fixed-bed catalytic hydrocracking converts vacuum gas oil, and other petroleum fractions with similar boiling ranges, into diesel, jet fuel, gasoline and other products. See Chap. 22 for detailed information. Commercial fixed-bed units employ two kinds of catalyst – hydrotreating and hydrocracking – which usually are loaded into separate reactors.

Hydrotreating catalysts remove sulfur, nitrogen and other contaminants, converting the organic sulfur and nitrogen into H_2S and NH_3 respectively. It is especially important to remove the organic nitrogen, because it neutralizes the acid sites of hydrocracking catalysts, suppressing their activity. Ammonia also inhibits cracking, but to a significantly lesser extent. Nitrogen slip (N-slip) is the amount of organic nitrogen remaining in the feed after it undergoes hydrodenitrogenation (HDN). For high-activity cracking catalysts, typical N-

slip targets range from 4 to 40 ppmw. Above about 200 ppmw, cracking catalysts might have nil activity.

Active catalyst particles have diameters ranging from 1.3 to 3.2 mm and lengths ranging from about 4 to about 12 mm with a median between 5 and 6. They are tiny compared to the reactors into which they are loaded. The diameters of large reactors can reach 6 m; reactor heights can exceed 30 m. Most reactors have multiple beds, with quench zones in between. In the quench zones, hot fluids from the bed above mix with relatively cold hydrogen-rich quench gas. The cooling is required, because hydrotreating and hydrocracking are highly exothermic. If not controlled, temperatures can run away, becoming high enough to melt through inches of steel.

Figure 2.9 compares hydrocracking with combustion. Combustion requires oxygen, fuel, and heat. Hydrocracking requires hydrogen, oil, and heat. If one of the three is removed, the reaction stops. A wood fire can be smothered with a blanket or carbon dioxide, or cooled with water or carbon dioxide. The fastest and most effective way to stop a hydrocracker temperature excursion is to remove hydrogen by depressuring the unit through emergency depressuring (EDP) valves. Typically, there are two EDP valves. One depressures the unit at an initial rate of 7 bar/min (100 psi/min). The other depressures the unit up to three times faster.

Either EPD valve can be activated manually. All hydrocracking process licensors specify automatic depressuring at low rate when a reactor temperature (or any two reactor temperatures) reaches some limit, typically 427–440 °C (800–825 °F). High-rate depressuring is activated automatically at some higher temperature. If temperatures exceed the metallurgical limit, typically 465 °C (870 °F), the steel degrades. Certain events, such as a power failure or loss of the recycle gas compressor, automatically initiate high-rate depressuring. Alert operators act before limits are reached, by adjusting quench flow and furnace firing. Early action forestalls emergency action.

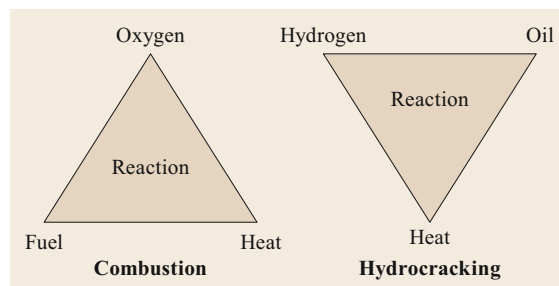


Fig. 2.9 Reaction triangles for combustion and hydrocracking, showing factors required for the chemical reactions. Removing any one factor stops the reactions

The Incident

Figure 2.10 shows the reactor layout for the Tosco Avon hydrocracker. The unit has three parallel Stage 1 hydrotreating reactors with six beds each, and three parallel Stage 2 cracking reactors with five beds each. The effluents from the Stage 1 reactors are combined and sent to a stripper. The stripper removes light gases, including methane, ethane, propane, and H_2S . The stripper liquids go to three parallel Stage 2 hydrocracking reactors. There are multiple temperature indicators (TI) at the top and bottom of each bed, spaced in a pattern that allows operators to evaluate horizontal temperature differences. Large differences indicate maldistribution of flow.

On January 19, two days before the fatal event, operators managed to defeat a temperature excursion in Reactor 1, without depressuring, by aggressively manipulating quench flow. The outlet pipe temperature indicator (TI) exceeded $482^\circ C$ ($900^\circ F$) versus the metallurgical limit of $465^\circ C$, and the center TI in Reactor 1 Bed 4 (R1B4) reached $537^\circ C$ ($998^\circ F$) versus a specified maximum of $440^\circ C$. Specifications have safety margins, but at such high temperatures, there is little doubt that the metal was compromised. During the ex-

cursion, an operator went outside to get TI readings from a field panel underneath the outlet pipe. The panel TIs could measure higher temperatures than the control-room readings.

Table 2.10 shows a timeline for the accident on January 21. The problem began several hours earlier when one of the Stage 1 hydrotreating reactors was brought down to repair a leak. Stories differ about whether the total unit feed rate was kept the same or reduced, and whether or not Stage 1 reactor temperatures were adjusted to compensate for the change in rate. Regardless, N-slip rose, and due to N-poisoning, cracking diminished. By 10:00 a.m., cracking had nearly stopped. Almost no light products were being formed, and the exotherms in the Stage 2 reactors were very low. Also, only a few quench flows were above 10% of full rate. The lab reported an N-slip of 352 ppmw versus a target of 15 ppmw. At 11:30 p.m., operators responded, appropriately, by increasing Stage 1 temperatures to decrease N-slip.

The second most dangerous decision of the day was taken at 01:10 p.m., when Stage 2 temperatures were raised to *burn off* the nitrogen from the Stage 2 catalyst.

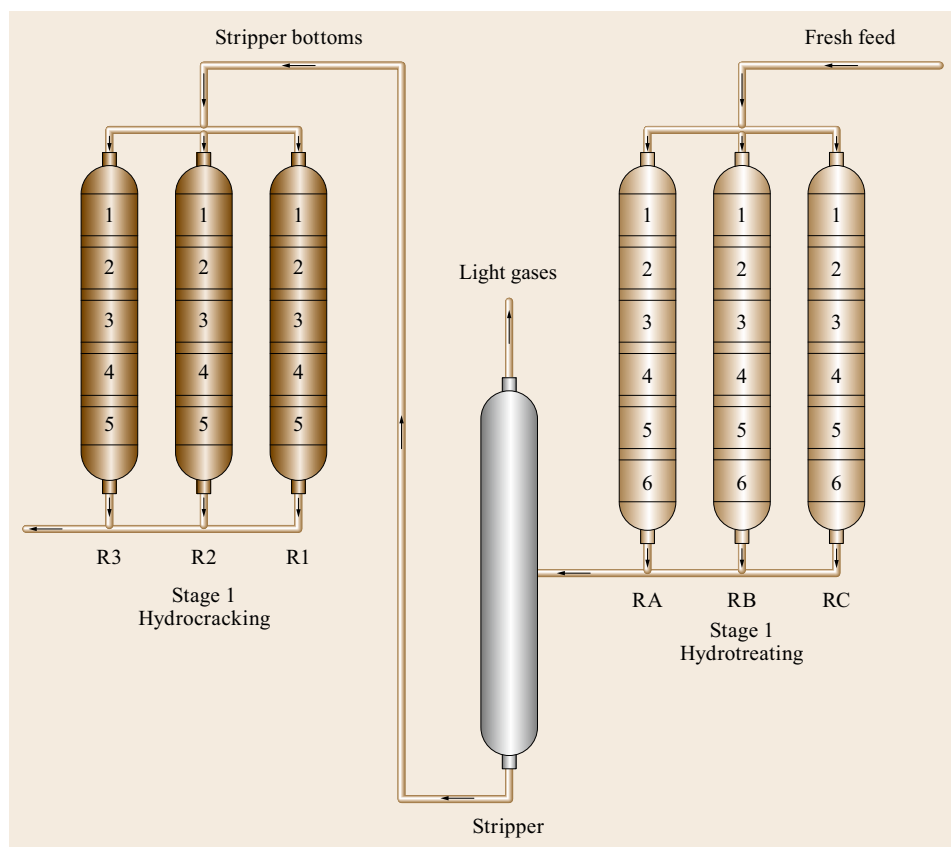


Fig. 2.10 Arrangement of reactors in the Tosco Avon hydrocracker

Table 2.10 Abbreviated timeline with comments for the Tosco Avon incident

04:50 a.m.	One of three Stage 1 hydrotreating reactors was brought down to repair a leak. Stories differ about whether the total unit feed rate was kept the same or reduced, and whether or not Stage 1 reactor temperatures were adjusted. Regardless, the extent of HDN was reduced.
10:00 a.m.	Nitrogen slip had risen from < 15 to 352 ppmw.
11:30 a.m.	Due to the high nitrogen slip and resulting inhibition of Stage 2 cracking activity, there was no temperature rise in one cracking reactor and very little rise in the other reactors. No light products were being formed. Stage 1 temperatures were raised to decrease nitrogen slip.
01:10 p.m.	Stage 2 hydrocracking reactor temperatures were raised to <i>burn off</i> inhibitory nitrogen. This was a horrendous mistake. Treating and cracking temperatures must never be raised at the same time. Figure 2.11 shows how very sensitive activity is to organic nitrogen.
05:38 p.m.	Nitrogen slip from Stage 1 was reported to be 47 ppmw. The actual nitrogen slip when the result was received was considerably lower than 47 ppmw. Since 10:00 a.m., the nitrogen slip had fallen 300 ppmw in 7.5 h, an average of 40 ppmw/h. If the lag time between taking a sample and getting results was 1 h as usual, the true nitrogen slip probably was < 10 ppmw at 05:38 p.m. and probably close to zero at 07:34 p.m.
07:34 p.m.	In Reactor 3, Bed 4 (R3B4), one TI jumped > 100 °C in 40 s, reaching 439 °C, 10 °C higher than allowed by procedure but not higher than in previous events.
07:34:20 p.m.	Quench to R3B5 opened 100%. Data logger temperatures cycled between –18, 649, and 343 °C. In well-run units, the associated uncertainty would have compelled operators to bring the unit down immediately (if it had not been depressured previously due to high temperature).
Before 07:37 p.m.	An operator went outside to verify temperatures at the field panel.
07:37–07:39 p.m.	All R3B5 outlet TIs were > 415 °C. One reached 679 °C.
After 07:40 p.m.	An operator phoned an instrument technician to work on the fluctuating data logger.
07:41:20 p.m. – 7 min after the first temperature jump	Explosion. The operator at the field panel died. A board operator activated the EDS.

Operating guidelines should have included the following prohibitions: During normal operation, never raise temperature in hydrotreating and hydrocracking catalysts at the same time. Never raise hydrotreating catalyst temperatures unless the cracking catalyst temperatures are at steady state, and vice versa. Figure 2.11 shows why. When concentrations of inhibitors are high, cracking reaction rates are not especially sensitive to modest changes. (Think of applying the brakes of an automobile, when the vehicle is stationary. Stepping harder on the brake pedal changes nothing.) However, at low inhibitor concentrations, small changes have a huge effect.

At 05:38 p.m., the reported N-slip was 47 ppmw. But surely the true N-slip at that time was considerably lower. How much lower we cannot know, but we can get an idea with a rough, linear approximation. On average, the N-slip had fallen 300 ppmw in 7.5 h, an average of 40 ppmw/h. If the lag time between taking a sample

and getting results was typical – say, about 1 h – the true nitrogen slip at 05:38 p.m. could have been < 10 ppmw, and it could have been close to zero at 07:34 p.m.

Recall: Due to the *burn off* decision, cracking reactor temperatures at 05:38 p.m. were higher and N slip was lower compared to conditions at 01:30 a.m. when the N-slip was 14 ppmw.

Figure 2.12 shows Reactor 3 temperatures during the Tosco temperature excursions. At 07:34 p.m., a temperature excursion struck R3B4 and cascaded into R3B5, peaking at 439 °C (823 °F). According to operating guidelines from the technology licensor, the unit should have been depressured when any bed TI reading reached 427 °C (800 °F). But instead of depressuring, operators made their most dangerous decision: to keep the unit running.

Instead, they did what they had done two days before and several times before that. They tried to control the excursion by cutting heater firing and manipulating

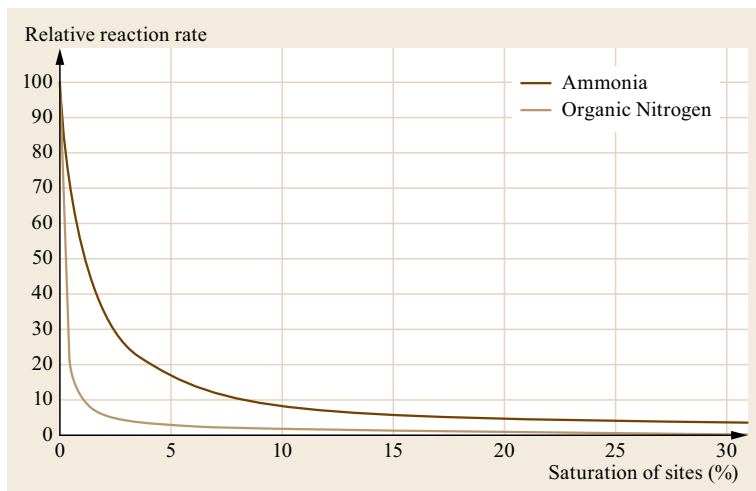


Fig. 2.11 Inhibition of hydrocracking by ammonia and organic nitrogen, where $K_{(\text{organic N})} = 7 \times K_{(\text{NH}_3)}$ by means of LHHW calculations. The trends are a function of percentage of inhibited catalyst sites at steady state, which is related to, but not the same as, the concentrations of ammonia or nitrogen in the feed

quench gas. As before, an operator went outside to get readings from the field panel beneath the reactor outlet pipe. Efforts to defeat the excursion with quench gas failed, the outlet pipe ruptured, and the operator died.

Surviving operators said they failed to depressure on January 21 because they didn't know whether or not an excursion was occurring. They had to reconcile temperature readings from three different sets of displays. Two sets were in the control room, and the other, as mentioned, was in the outside field panel. One control-room system was the data logger, which included most temperature readings. After the initial excursion, the data-logger readings started to fluctuate wildly, leading to further confusion.

In other refineries, uncertainty is not an excuse for unsafe behavior. Operators are told: Don't fly blind into a storm. When you don't know what's going on, assume the worse; bring the unit down.

Pipe Failure Analysis

Analysis of the ruptured pipe showed that the failure did not occur at weld, elbow or reducer. The pipe simply got too hot, reaching 1700 °F (927 °C). At the point of failure, the circumference of the 10 in (245 mm) diameter pipe expanded by 5 in (120 mm) before it failed. The wall thickness at the rupture was 0.3–0.4 in (7–10 mm), about 50% lower than the thickness of the rest of the pipe.

Root Causes and Recommendations

Root causes for the Tosco Avon accident include the following:

- *Management directives.* On July 23, 1992, the unit was depressured at low rate to stop an excursion. Due to a leak in the system, a grass fire started at

the flare. A source told the author that after this event in 1992, upper management strongly discouraged use of depressuring. A fire might spread into the nearby grassy hills and the John Muir Historic Site, creating a public relations nightmare. Fixing the flare would have required investment, which in those days at Tosco was not an option.

- *Confusion.* Operators used three different instrumentation systems to obtain temperature data. Not all the data were immediately accessible, and the data often disagreed. Monitoring points capable of reading the highest temperatures were underneath the reactors and not connected to the control room.
- *Inadequate supervision and process training.* Supervisory management and operator training were inadequate. Operators and engineers did not understand that a zero on the data logger indicated extremely high temperatures. They did not understand the sensitivity of cracking catalyst activity to changes in N-slip when the N-slip is very low.
- *Misunderstanding of sampling dynamics.* Operators and engineers did not comprehend the dynamics of sampling, i. e., the lag time between taking a sample, getting results, and what might have happened to the process in the meanwhile.
- *Poor procedure documentation.* Written procedures were outdated, incomplete, and contained in different documents in different locations.

The investigation team, led by EPA, developed recommendations for consideration by owners of all hydroprocessing facilities. These, with slight modifications by the author, are presented below:

- Management must ensure that operating decisions are not based primarily on cost and production.

	Bed 4	Bed 5	Bed 5	Bed 5	Bed 5	Bed 5	Rx 3	Rx 3
	Outlet	Inlet	Outlet	Outlet	Outlet	Outlet	Inlet	Outlet
	Temp (°F)	Temp (°F)	Temp (°F)	Temp (°F)	Temp (°F)	Temp (°F)	Temp (°F)	Temp (°F)
Time (pm)	Pt-133C2	Pt-140C3	Pt-134C1	Pt-134C2	Pt-134C4	Pt-134C5	Pt-125C	Pt-141C
7:33:00	628.3	636.9	648.6	646.3	656.8	645.9	632.2	641.3
7:33:20	628.3	636.9	648.6	646.3	656.8	645.9	632.2	641.3
7:33:40	636.5	658	648.6	646.3	656.8	645.9	632.2	641.3
7:34:00	823.2	720.7	648.6	646.3	656.8	645.9	632.2	641.3
7:34:20	732	859.5	648.6	646.3	656.8	645.9	632.2	641.3
7:34:40	732	859.5	648.6	646.3	656.8	645.9	632.2	641.3
7:35:00	637.3	792.4	624.2	627.7	633.4	645.9	632.2	641.3
7:35:20	637.3	715.7	624.2	627.7	633.4	615.4	632.2	641.3
7:35:40	637.3	664.4	624.2	640.3	633.4	615.4	632.2	641.3
7:36:00	637.3	633.4	650.3	647.9	623.6	615.4	632.2	649.9
7:36:20	637.3	633.4	663.9	667.7	623.6	615.4	632.2	649.9
7:36:40	637.3	660.7	672.9	667.7	623.6	625.6	632.2	658.9
7:37:00	637.3	660.7	681.1	676.8	656	645.8	632.2	658.9
7:37:20	637.3	660.7	681.1	676.8	672	673.5	632.2	760.7
7:37:40	637.3	660.7	697.3	707.5	690.7	673.5	640.2	760.7
7:38:00	637.3	660.7	717.2	876	690.7	673.5	640.2	684.6
7:38:20	637.3	660.7	1255.7	0	783	705.8	648.8	701.8
7:38:40	637.3	660.7	0	0	0	744	660	788.8
7:39:00	637.3	648	0	0	0	889	693	983.1
7:39:20	637.3	648	0	0	0	0	754.7	1219
7:39:40	637.3	655.6	0	0	0	0	826.5	0
7:40:00	637.3	655.6	0	0	0	0	889.1	0
7:40:20	637.3	655.6	0	0	0	0	960.7	0
7:40:40	637.3	645.7	0	0	1397.1	879.9	1233.5	0
7:41:00	637.3	645.7	0	0	1398.4	694.9	0	0
7:41:20	0.0 ????	0.0 ????	0.0 ????	0.0 ????	0.0 ????	0.0 ????	0.0 ??	0.0 ????
7:41:40	0.0 ????	0.0 ????	0.0 ????	0.0 ????	0.0 ????	0.0 ????	0.0 ??	0.0 ????

Fig. 2.12 Reactor 3 temperatures during the TOSCO Avon incident. Temperature indicator Pt-133C2 jumped by 104 °C (186 °F) in 20 s, reaching 439 °C (823 °F). The excursion cascaded through the quench section into the next catalyst bed, causing a jump of 223 °F (124 °C) in 40 s at Pt-140C3, reaching 460 °C (860 °F)

- Facility management must set safe, achievable operating limits and not tolerate deviations from these limits.
- Management must provide an operating environment in which operators can follow emergency shutdown procedures without fear of retribution.
- Process instrumentation and controls should be designed to consider human factors consistent with good industry practice. Hydroprocessing reactor temperature controls should be consolidated with all necessary data available in the control room. Backup temperature indicators should be used so that the reactors can be operated safely in case of instrument malfunction.
- Each alarm system should distinguish between critical alarms and other operating alarms.
- Adequate operator supervision is needed, especially to address critical or abnormal situations.
- Facilities should maintain equipment integrity and discontinue operation if integrity is compromised.
- Management must ensure that operators receive regular training on process operations and chemistry. For hydrocrackers, this should include training on reaction kinetics and the causes and control of temperature excursions.
- Operators should be trained on the limitations of process instruments and how to handle instrument malfunctions.
- Facilities should ensure that operators receive regular training on the use of the emergency shutdown systems and the need to activate these systems.

2.3.14 BP Texas City Isomerization Unit: Explosion (2005)

On March 23, 2005, an explosion in an isomerization unit at the BP Texas City, Texas refinery [2.93], along with related explosions and fires, killed 15 people and injured another 180. A shelter-in-place order was issued, requiring 43 000 people to remain indoors.

Houses were damaged as far away as three-quarters of a mile. Resulting financial losses exceeded \$1.5 billion.

Context

The isomerization process converts straight-chain *n*-pentane and *n*-hexane into branched isomers with higher octane. The resulting isopentane and isohexane are blended into gasoline. Raffinates from the process are mixtures of straight-chain hydrocarbons. A raffinate splitter separates the light raffinate from the heavy raffinate. During normal operation, an automatic level controller maintains liquid level in the splitter by sending heavy raffinate to a storage tank when the level is too high. The level controller depends on feedback from a level transmitter. As a backup, level can be measured manually with a sight glass. The tower overhead is cooled and drawn off or sent back to the splitter for temperature control. If the tower pressure gets too high, three pressure relief valves can open, one at a time or in combination, sending vapors and liquids to an emergency blowdown drum. In the unit at BP Texas City, the blowdown drum should have been connected to a flare, but instead, it vented to the atmosphere.

The Incident

The accident occurred during the restart of the isomerization unit, after maintenance on the raffinate splitter. Before the restart, there were several unresolved safety-critical issues, including a faulty pressure control valve, a defective high level alarm in the splitter, a defective (opaque) sight glass used for level measurement, and an uncalibrated level transmitter. During the morning of March 23, operators noticed that the heavy raffinate storage tanks were nearly full. Consequently, the night-shift supervisor agreed that the startup should not continue until some liquid was withdrawn from the tanks. But the day-shift supervisor arrived late and did not receive a full status report. He did not hear about the raffinate tank level. Under his direction, the startup resumed at 09:30 a.m. To reduce level in the raffinate splitter, the level control valve was opened, sending liquid to the already-nearly-full heavy raffinate storage tank. At about 10:00 a.m., the level control valve was closed. As the startup proceeded, more raffinate entered the tower. Without a way to withdraw product, the tower overflowed. But the uncalibrated level transmitter indicated that the level was below 100%. The opaque sight glass was useless, so it wasn't possible to confirm the level visually.

As the startup proceeded, burners in the furnace were started to heat the inflowing raffinate. The procedure specified that the temperature of return flow to the tower should be raised to 135 °C (275 °F) at 10 °C/h (18 °F/h), but this time the procedure was altered. The return flow temperature was allowed to reach 153 °C

(307 °F) with an increase rate of 23 °C/h (41 °F/h). The defective transmitter was indicating a high (but supposedly still-safe) level of 93%. Heat was increasing, causing expansion of the raffinate. Pressure started to build, but the operations team thought the increase was due primarily to overheating, which was a known startup issue. The pressure was relieved and the furnaces were turned down.

At 12:42 p.m., the faulty level transmitter showed 78% as liquid was overflowing into the pressure-relief system. At 01:13 p.m., all three pressure relief valves opened, sending liquid to the blowdown drum. An operator opened the level control valve and shut down the furnace completely. But he did not stop the inflow of raffinate. In the blowdown drum, a *geyser* of hot hydrocarbon liquid vented directly into the air, then flowed down the outside of the drum, where it hovered above the ground and drifted away from the unit. It soon reached a pickup truck about 9 m (30 ft) away. Investigators concluded that heat or a spark from the truck must have ignited the hydrocarbons. The 15 people who died were in or around a nearby row of contractor trailers.

I was scheduled to be participating in a hydrocracker startup in the refinery on the day of the explosion. The startup was delayed. Otherwise, I might have been in one of the destroyed trailers.

Root Causes

According to the investigation report, the Texas City disaster was caused by organizational and safety deficiencies at all levels of the BP Corporation. Warning signs of a possible disaster were present for several years and were reported to officials by employees. But company officials did nothing. The extent of the safety culture deficiencies was further revealed when the refinery experienced two additional serious incidents just a few months after the March 2005 disaster. In one, a pipe failure caused a reported \$30 million in damage. The other resulted in property loss worth \$2 million.

The report cited the following local deficiencies at the Texas City refinery:

- A work environment that encouraged operations personnel to deviate from procedure
- Lack of a BP policy or emphasis on effective communication for shift change and hazardous operations (such as during unit startup)
- Malfunctioning instrumentation that did not alert operators to the actual conditions of the unit
- A poorly designed computerized control system that hindered the ability of operations personnel to determine if the tower was overflowing
- Ineffective supervisory oversight and technical assistance during unit startup

- Insufficient staffing to handle board operator workload during the high-risk time of unit startup
- Chronic worker fatigue, due to the lack of a human fatigue-prevention policy
- Inadequate operator training for abnormal and startup conditions
- Failure to establish effective safe operating limits.

The industry learned from the BP Texas City disaster, but not everyone learned, and some who might have learned forgot. Events five years later showed that within BP itself, key people had failed to learn or had forgotten key lessons from Texas City.

2.3.15 Deepwater Horizon Offshore Drilling Rig: Blowout (2010)

On April 20, 2010, a blowout on the *Deepwater Horizon* drilling rig killed 11 people and gushed 560 000–585 000 t of crude oil into the Gulf of Mexico. On July 2, 2015, a settlement was announced between BP, United States, and five US states. BP agreed to pay up to US\$18.7 billion in penalties [2.94, 95].

Context

The offshore drilling rig *Deepwater Horizon* floated in 5000 f (1500 m) of water 41 mi (66 km) from the coast of Louisiana just beyond the continental shelf in the Mississippi Canyon. Below the seabed was a large reservoir of oil and gas. The Macondo well, drilled from the rig through sub-surface rock to the reservoir, was 2.5 mi long.

During drilling, operators compare the amount of drilling mud going into the well to the *returns* – the amount coming back out. For this well, the returns exceeded the input, indicating intrusion from the formation. Depending on the size of the difference and the depth (pressure) of the well, this is often a danger sign.

As a well is drilled, the well bore is cased with steel pipe. Casing prevents the well from collapsing. As BP was drilling the last section, Halliburton (the drilling contractor) recommended liner/tie-back casing with four redundant barriers to flow. BP opted for one liner with fewer barriers to save US\$7 to 10 million. Cementing fills the otherwise empty annular space between well bore and the casing. If the annular space is totally blocked, oil and gas can flow out of the formation only through the casing. At the top of the casing, valves, blowout preventers, and so on, control the flow of oil and provide a route for future activities, such as perforation and well stimulation.

Figure 2.13 illustrates how centralizers improve cementing. They keep the casing from resting against the surrounding rock, which possibly could block the

flow of cement and jeopardize the well-completion process. According to industry acquaintances, poor cement jobs are the leading cause of postcompletion blowouts. Among other things, poor cementing can result from using low-quality cement and not using enough centralizers. A Halliburton model called for 21 centralizers. But there were only six on the rig. In short order, 15 more could be flown to the rig. A BP engineer informed management that it would take 10 h to install the extra centralizers. BP decided to install just six.

Before cementing, cement mixtures are prepared and tested in a laboratory. Three tests conducted by Halliburton showed that the Macondo well cement did not meet Halliburton's best practices and might not set properly. During Coast Guard hearings, BP said it hadn't seen the testing results.

To prepare a well for cementing, it is typical to conduct one last *bottoms up*, in which drilling fluid is pumped through the annulus all the way from the bottom of the well to the top. A bottoms-up is a common way to improve the success of cementing by removing pockets of gas and debris. BP opted to circulate only a fraction of the usual amount of fluid.

To test the integrity of cementing, two important tests are conducted: a positive-pressure test and a negative-pressure test. During the positive-pressure test, the pressure is increased in the steel casing and seal assembly to see if they are intact. The negative-pressure test determines the integrity of the cement at the bottom of the hole. Pressure is reduced to below atmospheric, and then suction is stopped. If pressure remains low, the test is deemed successful. If flow occurs or the pressure increases, it is likely that reservoir fluids are entering

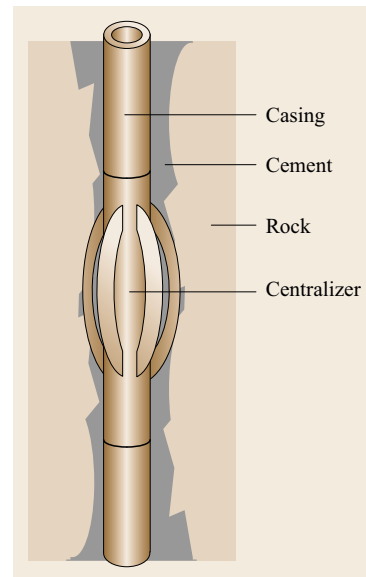


Fig. 2.13 Role of centralizers in oil well completion. The centralizer keeps the casing away from the rock while allowing cement to flow through. The drawing is, to say the least, not to scale

the well, probably through gaps in the casing and/or the cement. A failed negative pressure test requires remedial work to reestablish well integrity. If the remedial work is not done, the cement will fail and flow through the well will be impossible to control.

The Incident

At 7:00 a.m. on the day of the blowout, BP cancelled a scheduled *cement bond log*, a routine acoustical procedure which would have found spaces or weaknesses in the cement. The test would have taken 9 to 12 h and cost US\$128 000.

At about noon on the day of the blowout, the well had been cemented and other cement integrity tests were imminent. A helicopter arrived. Among its passengers were four VIPs from Houston – two from Transocean, the owner of the drilling rig, and two from BP. The executives were there to conduct a 24-hour *management visibility tour*. Their presence contravened two lessons that should have been learned from the BP Texas City disaster. During a highly critical activity, (1) nonessential personnel must be removed from the vicinity, and (2) supervisory oversight must be provided at all times by technically qualified personnel. Few activities are more critical than well completion, and few people are less essential than corporate executives. These particular VIPS were planning to stay on the rig overnight. They had to be fed, watered, and entertained. Their presence contributed to the flouting of Item (2) by monopolizing the time of highly capable experts, who otherwise might have been paying more attention to the drilling crew.

At 05:00 p.m., the rig crew began the negative-pressure test. The pressure repeatedly built back up after gases were evacuated. Between 06:00 and 07:00 p.m., the crew discussed how to proceed. A senior BP engineer insisted on another negative-pressure test. An assistant *tool pusher* said pressure could be measured through another line – the *kill line* – where the pressure did indeed stay low. For whatever reason, the crew decided that no flow through the kill line equaled a successful negative-pressure test.

The crew proceeded to replace dense drill mud, which had counteracted reservoir pressure during drilling, with sea water. Sometime later, people on the bridge of the rig felt a high-frequency vibration and heard a hissing noise. The senior BP engineer got a call from the assistant tool pusher, who told him that mud was coming out of the well and that gas was coming up too. The senior BP engineer grabbed his hard hat and stepped outside, where saw that mud and seawater were *blowing everywhere*. The assistant tool pusher called the senior tool pusher and said: *We have a situation [...] the well is blown out.*

Soon thereafter, at roughly 09:45 p.m., an explosion shook the rig, starting a fire. A second explosion followed, then several more. Meanwhile, people were being evacuated into life rafts. Others simply jumped into the water.

Eleven people died. Over the next several months, the blown-out well gushed 560 000–585 000 t of oil into the Gulf of Mexico, causing economic and ecological harm throughout the region, from Mexico to Florida.

Root Causes and Recommendations

The Presidential Commission appointed by President Barack Obama concluded with the following (author-abridged) observations:

- The explosion could have been prevented.
- The immediate causes were a series of mistakes made by BP, Halliburton, and Transocean. The mistakes revealed systematic failures in risk management. Tests and procedures were changed without consultation with technical experts.
- Deepwater energy exploration and production involves risks for which neither industry nor government was adequately prepared, but for which they can and must be prepared in the future.
- Regulatory oversight of leasing, energy exploration, and production require reforms, even beyond the significant reforms already initiated since the Deepwater Horizon disaster.
- Those in charge of oversight must have political autonomy, technical expertise, and authority to fully consider environmental protection concerns.
- Regulatory oversight alone will not be sufficient to ensure adequate safety, so the oil and gas industry will need to take its own, unilateral steps to increase safety throughout the industry, including self-policing mechanisms that supplement governmental enforcement.
- The technology, laws and regulations, and practices for containing, responding to, and cleaning up spills lag behind the real risks associated with deepwater drilling into large, high-pressure reservoirs of oil and gas located far offshore and thousands of feet below the ocean's surface. Government must close the gap, and industry must support rather than resist that effort.
- Scientific understanding of environmental conditions in sensitive environments in deep Gulf waters, along the region's coastal habitats, and in areas proposed for more drilling, such as the Arctic, is inadequate. The same is true of the human and natural impacts of oil spills.

2.3.16 Lac-Mégantic Quebec, Canada: Oil Train Derailment (2013)

At about 11:00 p.m. on July 5, 2013, a 74-car freight train carrying Bakken crude oil stopped in Nantes, Quebec. Nantes is about seven miles west of Lac-Mégantic. The train was owned by the MM&A, the Montreal, Maine and Atlantic Railway, for which Nantes is a crew-change point [2.96].

The train was named MMA-2. With a length of 1433 m (4700 ft), it stretched for almost a mile. Pulled by five locomotives, it weighed more than 11 000 tn sh. Each of the 72 tank cars carried about 30 000 gal (714 bbl) of crude oil. The oil was produced in North Dakota with hydraulic fracturing and was being shipped to the Irving Oil Refinery in Saint John, New Brunswick.

While riding in his usual taxi from the train to his usual hotel, the train engineer expressed concern about the lead locomotive, because it was smoking and leaking oil. Per MM&A policy, he had left the engine running, mainly to power the compressor that maintained pressure in the air brakes.

At about 11:45 p.m., the troubled engine caught fire. Local residents called 911, and within 5 min, firefighters and police arrived. They saw dark smoke coming from the engine, where a broken piston had started a *good sized blaze*.

After dousing the fire, a Nantes Fire Department member contacted the rail traffic controller for MM&A in Farnham, Quebec, 125 mi away. The controller sent two maintenance workers to the scene. The workers concluded that it wasn't safe to restart the damaged engine, so they decided to leave it off. They set hand brakes to augment the air brakes.

Without the compressor, the air brakes slowly released. The hand brakes alone couldn't restrain the 11 000-ton train. The train began to roll toward Lac-Mégantic down a 1.2% grade. When it arrived at about 01:15 a.m., the train was traveling at high speed. It derailed. The oil spilled out. The consequent fire and explosion destroyed the center of the town and killed 47 people.

The glut of oil being produced from the Bakken Shale in North Dakota is putting tremendous stress on truck and rail transportation. Old and poorly maintained rolling stock has been pressed into service. Until the equipment is replaced with new equipment or a pipeline the stage is well-set for future accidents.

2.3.17 Tianjin, China: Storage Station Explosions (2015)

On Wednesday, August 12, 2015, at around 22:50 LT, flames were reported in a warehouse in the Binhai dis-

trict of Tianjin, China. Situated on Bohai Bay 150 km southeast of central Beijing, the Binhai New Area is a Special Economic Zone (SEZ), similar to those in Shenzhen and Pudong in Shanghai. Several international companies, including Motorola and Airbus, have constructed facilities in the Binhai SEZ; in 2009, Airbus opened an assembly plant there for A320 airliners [2.97].

The warehouse was owned by Ruihai Logistics. It occupied 46 000 m² (500 000 sq ft) and included multiple areas for storing containers of hazardous chemicals. A regulation specified that such warehouses must be located at least 1 km away from public facilities, but in this case the regulation was ignored. Local officials, including emergency responders, did not know for sure what was stored at the site. The situation was aggravated by major errors, including errors of omission, in customs documents.

According to postmortem reports, the warehouse held more than 40 kinds of hazardous chemicals, including toluene diisocyanate, *vast quantities* of calcium carbide (CaC₂), 800 t of ammonium nitrate, 700 t of sodium cyanide, and 500 t of potassium nitrate. CaC₂ reacts with water to form calcium hydroxide and acetylene, a highly flammable gas. Sodium cyanide reacts with water to form sodium hydroxide and hydrogen cyanide gas, which is both toxic and flammable. Ammonium nitrate is the chemical responsible for the massive explosion in Texas City, Texas in 1947.

First responders to the fire were unable to keep it from spreading. Unaware of what they were facing, they tried dousing the flames with water. The consequent explosion, possibly due to acetylene formed from CaC₂, was equivalent to 3 t of TNT. Less than 1 min later, the ammonium nitrate detonated, causing a blast equivalent to 20 t of TNT. The blaze continued for several days, in part because of a pause in firefighting due to lingering uncertainty about the kinds and quantities of chemicals at the site. On August 15, the spreading flames triggered eight more explosions, which, fortunately, were relatively minor.

Photographs showed extensive destruction around the warehouse, with a massive crater at the center. Seven nearby buildings were destroyed, and others were rendered structurally unsafe. More than 17 000 nearby apartment units were damaged; 6000 people were evacuated.

On August 18, the first rain after the fire coated nearby streets with white chemical foam. People complained that contact with the rain caused burning sensations and rashes.

Also on August 18, the Central commission for Discipline Investigation (CCDI) initiated an investigation of Yang Dongliang. Yang was Director of the

State Administration of Work Safety. He was China's highest-ranking work safety official. He had been Tianjin's vice mayor for 11 years. In 2012, he had issued an order that loosened rules for the handling of hazardous substances. On October 16, he was expelled from the Communist Party for corruption and other offenses.

On August 20, tons of dead stickleback fish washed up on the land about 6 km from the explosion site.

On August 25, another rain brought more complaints of skin burns, and white foam again appeared on the streets. The director of Tianjin's environmental monitoring center claimed that the foam was *a normal phenomenon when rain falls. Similar things have occurred before.*

According to a report issued on September 12, the human toll at Tianjin was 173 killed, 797 hospitalized, and 8 still missing.

2.3.18 Personal Observations

During the past several years, in my role as a technology consultant, I have witnessed shutdowns, near-misses, and loss of containment due to known (but unamended) process design flaws, inadequate maintenance, inadequate training, lack of technical supervision, contravention of procedures, and worker fatigue.

DIBS – did-it-before syndrome – played a role in three of the examples in this section, and in many of the examples described above. DIBS leads workers and managers to disregard safety rules and procedures, because they got away with doing so before.

Hydrocracker Startup: Loss of Containment

The refinery in which this incident occurred was owned by a company known for its dedication to safety. Behind the hydrocracker area in the control room was a large sign that said, in effect, *All employees are obliged to stop any operation he or she believes is unsafe.*

The subject of this example was a two-reactor hydrocracker with multiple beds in each reactor. Catalysts had been loaded and warmed to drive off water. At midnight, it was time for the initial wetting of the catalysts with oil. Initial wetting occurs once and lasts about an hour, but it releases heat due to enthalpy of adsorption (see Chap. 22). In multiple-bed hydrocrackers, wetting causes the Bed 1 outlet temperature to rise, within minutes, by as much as 50 °C. Wetting exotherms can be just as high in subsequent beds. Oil adsorbs heat, so the oil rate is kept high, usually between 50% and 70% of the design maximum. If the oil rate is lower, the temperature rise is higher. Needless to say, controlling feed rate is very important.

Operators can prepare for the exotherms with postquench. When oil reaches the inlet to Bed 1, they

start sending cold gas into the quench deck between Bed 1 and Bed 2. It can take 5–8 min for oil to pass through the bed. When the oil arrives at the Bed 1 outlet, it mixes with the cold postquench gas, which quickly drops the temperature. Without postquench – that is, if operators didn't add cold gas until they saw the exotherm – the temperature wave would pass through the quench box to the inlet of Bed 2 unabated. The heat of adsorption in Bed 2 would increase the temperature by another 50 °C. The total increase across Beds 1 and 2 could be 100 °C. And so on.

Figure 2.14 compares wetting with and without postquench. Without postquench, wetting heat accumulates. Industry experience shows that temperatures can get high enough to initiate cracking and even temperature excursions. After the catalyst is wet, temperatures quickly fall to prewetting level.

Just after midnight in the subject refinery, the hydroprocessing Area Manager, unit engineer, and I were discussing how to proceed despite some known problems. As at BP Texas City, there were three known problems in a separation tower: the level transmitter wasn't working, the sight glass was foggy, and the off-gas compressor wasn't working. There was no way to observe level or control pressure in the tower. Repair work couldn't start before 08:00 a.m., and then it would take an unknown time to fix the compressor. An in-house technician probably could repair the level controller in parallel with other work.

Two VIPs – the refinery Engineering Manager and Operations Superintendent – appeared in the control room and immediately started firing questions. They were concerned that wetting was being delayed. They asked the lead operator to show panel displays irrelevant to the job at hand. Observing the operator's distress, I directed the VIPs to a nearby conference room. The room contained an observation-only display, on which the VIPs could browse without disturbing the startup team.

The Area Manager decided to proceed despite the known problems. He concluded that with postquench operation, the catalyst wouldn't get hot enough to induce hydrocracking. When wetting was over, oil could be circulated for a few hours to flush particulates out of the catalyst. By then, it would be 07:00 a.m. and the unit could be brought down for repairs.

Wetting started at about 03:00 a.m. When liquid feed was introduced, a fourth problem became apparent: the feed pump valve was *sticky*, taking up to 3 min to respond to a change in setpoint. Inability to control feed was crucial, due to the impact of feed on the size of exotherms. The operator called across the control room to the Area Manager. *This is not safe!* he said. *This is not safe!* he said again. According

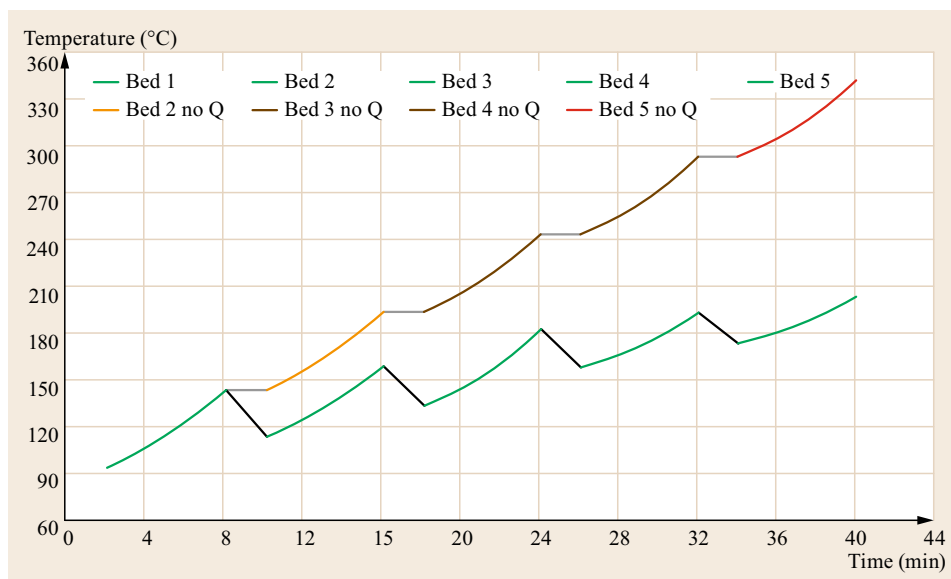


Fig. 2.14 Comparison of oil temperatures during initial catalyst wetting, with and without postquench. The black and gray segments are for temperatures in the quench boxes. The no Q trends do not include postquench

to company policy, instead of yelling, he should have brought the unit down immediately, without asking permission.

The Area Manager said: *We can't go back. It's okay. We've done this before.* During wetting, the oil flow was lower than specified. With less oil to pick up heat, exotherms were larger than ever before. Thanks to postquench operation, there was never any danger of a temperature excursion.

However, the tower overflowed, sending hydrocarbons to the flare. The flaring lasted 1 h or so, but it had to be reported to environmental authorities. The startup was delayed for days. Saving 5 h cost the refinery more than \$2 million.

The Area Manager had gotten away with operating the tower before without the overhead compressor. He had also gotten away with running without the tower level controller and without the sight glass. He had never run the unit before with all three problems at the same time, and he had never run before without reliable control of feed rate.

As for me: I was an outside consultant. I was consulted by the operator during the event, but not by the Area Manager. Later, I reported the event to my friend, a corporate subject matter expert. He was appalled.

Substandard Equipment.

Disabled Safety Interlock. Stagnation

A serious excursion was the latest of several in a new hydrocracker. The ultimate cause was a decision by the purchasing department to order substandard items for the associated hydrogen plant. One by one, the faulty items failed and were replaced with proper items. Dur-

ing its first 6 months of operation, the unit never ran continuously for more than 1 month.

Each hydrogen plant failure upset the hydrocracker. Some failures sent liquid into the suction of the hydrocracker recycle gas compressor (RGC), causing the RGC to shut down. The licensor's EDS interlock protocol gave operators 15 min to restart the compressor before automatically activating the low-rate depressuring valve. Each depressuring event shut the unit down for at least a day. To give themselves extra time to restart the RGC, the unit engineer and operators decided to disable the EDS/RGC interlock, assuming that temperature-triggered depressuring would be sufficient.

This demonstrated ignorance of several fundamental concepts. The most egregious were:

- Residence time has a significant impact on reaction rates.
- The flow of fluids is the only significant way to remove heat from a hydroprocessing reactor.
- With zero or low flow, bed outlet TI readings are meaningless.

It is crucial to understand the difference between TI readings and temperature. Chapter 22 explains why one never knows the highest or lowest temperature in a catalyst bed. When reactants are flowing through at 50–100% of design capacity, one sees how bed outlet TIs correspond to the temperatures above them. But when flow stops, no TI reading is relevant to any temperature more than a few inches away. Reactions do not stop when flow stops. Heat accumulates in catalyst beds, often without affecting the bed outlet TI readings. Without gas flow, hot oil pools due to gravity at

low points. Eventually, the pooling oil will reach one or more bed outlet TIs and/or reactor wall TIs, providing the first tangible indication that temperatures are too high. Undoubtedly, that is what happened in this unit. Table 2.11 shows a timeline for this incident. A visual representation is presented in Fig. 2.15.

After the first compressor failure, it took 144 min for some overheated oil to run down to the reactor outlet. At 17:38 LT, an upward spike in Reactor Outlet TI-3 triggered depressuring when it reached 440 °C.

TI-3 continued to rise until it reached 487 °C. Depressuring seemed to make things worse. It decreased TI-3, but as the pressure fell, the exiting gas pulled formerly stagnant hot oil through the reactor. Between 17:48 and 17:55 LT, Bed Outlet TI-1 jumped from 404 to 618 °C, an increase of 214 °C in 7 min.

The readings dropped after a restart of the RGC. But then, most likely due to the arrival of more overheated oil, TI-1 jumped back up to 618 °C, where it flatlined for more than 2.5 h. Actual temperatures were higher

Table 2.11 Timeline for personal observations, Example 2

16:14	Recycle gas compressor failed Pressure = 127 barg Maximum bed TI = 402 °C Reactor outlet TI = 398 °C
17:38	Reactor Outlet TI-3 exceeded 440 °C Automatic low rate depressuring
17:44	Reactor Outlet TI-3 continued up to 478 °C
18:00	Recycle gas compressor was restarted
18:27	A bottom reactor wall temperature reached 436 °C
19:17	Recycle gas compressor failed
18:20–20:54	Bed Outlet TI-1 jumped 214 °C in 7 min, stayed > 618 °C for 154 min
20:28	Recycle gas compressor was restarted successfully
18:56–22:30	Bed Outlet TI-2 reached > 618 °C, fell, rose to > 550 °C until 22:30

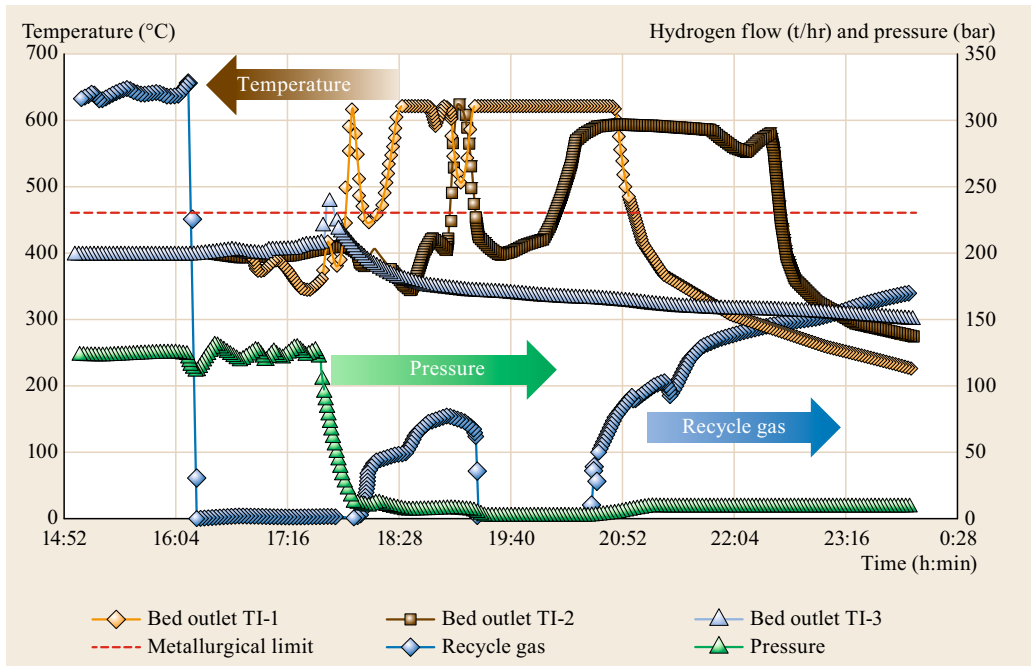


Fig. 2.15 Pressure, recycle gas flow, and selected temperatures. Bed Outlet TI-1 flatlined at 618 °C, because 618 °C is top-of-range. Actual temperatures were far higher, as evidenced by the fused catalyst in the bed when the reactor was unloaded

than 618 °C, which is top-of-range. It was thought that the TI-1 reading was faulty, but it wasn't; it returned to reading on-scale at 20:54 LT. A second attempt to restart the RGC succeeded. TI-1 readings started to fall. But as they did, Bed Outlet TI-2 rose above 550 °C and stayed there for another 2 h.

Afterwards, the unit ran at reduced rates for 6 months, with strict adherence to licensor-suggested temperature limits. The limits were kept lower than usual due to fears that the reactor outlet pipe had been compromised. During the subsequent turnaround, workers found that the reactor internals were damaged. They also found partially fused silica balls near the reactor wall. Pure silica melts at about 2000 °C. Impurities drop the fusion temperature considerably. But even so, it must have gotten incredibly hot in that reactor.

Botched Refinery Maintenance

Refineries schedule maintenance shutdowns for several units at once, often more than a year in advance. Each process unit depends on several others, serving as a destination for some streams or as a source of feedstock for other units. When a hydrocracker comes down, the need for hydrogen goes down, and major units normally fed by the hydrocracker have to be run differently. Product tanks are filled and arrangements are made with other refiners to maintain supply customers. Construction is scheduled to coincide with maintenance shutdowns. To minimize downtime, equipment replacements must be ready to install, catalysts must be on site, oil inventories must be adjusted, and maintenance contractors are hired to conduct repairs, provide maintenance, unload and load catalysts, and so on. An unplanned shutdown is far more expensive, because other units are not prepared for an outage, and arrangements have not been made with suppliers and customers. Restarting may be delayed because key subcontractor personnel are busy elsewhere.

The following instance was caused (mainly) by a decision to reduce the number of crews employed to service heat exchangers. In shell-and-tube exchangers, one gas or liquid stream is pumped through a bundle of parallel tubes. As it flows through a bundle, the *tube-side* fluid exchanges heat with *shell-side* fluid, which flows in the opposite direction, inside the shell but outside the tubes. During this turnaround, a key activity was the long-delayed cleaning or replacement of fouled tubes. Due to the shortage of people, exchanger maintenance was taking a lot longer than expected. It became clear that the preordained schedule could not be met, given the original scope of work. For a large and important set of exchangers at the hydrocracker, the feed/effluent exchanger (F/E), the crew cleaned only some tubes – the ones most badly fouled. Upon

restart, flow in the F/E followed the path of least resistance – preferentially through the just-cleaned tubes. Within weeks, under-performance of the F/E required an unplanned hydrocracker shutdown and caused costly changes in the operation of other units. The shutdown, service work, and subsequent restart required about two weeks at a cost of more than US\$1 million per day – a steep price to pay for saving less than \$50 000 by reducing tube-cleaning costs.

The decision to clean only some tubes in the F/E displayed fundamental ignorance. Not knowing about the crew's decision revealed slipshod management. No wonder. The refinery was chronically understaffed. During maintenance shutdowns, engineers had to work as many as 30 consecutive 14-hour days. Staffing decisions are made by refinery management, who are ultimately responsible for the consequences.

Fatigue-Related Near Miss

Despite the harsh comments in the BP Texas City report about worker fatigue and insufficient training, a small but significant number of US refineries remain understaffed, especially for shutdown and startup activities. Those refineries aren't alone. Many US service companies also are understaffed, especially during *turnaround season* in March through May. Refineries want to complete maintenance before June, so they can be up and running throughout the summer, when gasoline consumption is highest. A smaller turnaround season occurs near the end of the year.

Members of a vendor technical service team had been working long hours during the spring startup season, often more than 100 h per week. In addition to spending 12–14 h per day supervising startups, team members were required to handle questions from other customers, write proposals, and prepare for upcoming customer visits. Four hours of sleep per night was the rule, not the exception.

The group had always been busy, but the workload increased after the business unit was reorganized. The main reason was a switch from a VP of Technical Service who controlled the team's workload by screening sales-support work, to a non-technical GM of Sales who did not understand the service end of the business and insisted on chasing every apparent opportunity, no matter how unlikely.

One night, while driving from a refinery to his hotel, a team member fell asleep and drove off a country road. He wasn't injured. For that and other reasons, he didn't report the incident until several months later, when another member of the team persuaded him to complain.

In response to the complaint, which included mention of possible consequences, a high-level manager said: *What are you, a lawyer? Mister HSE?* followed

by *Why didn't you say something sooner?* The manager later admitted knowing about the overwork for several months. *We didn't add people*, the high-level manager said, *because we might have had to lay them off if business slowed down*. Within a year of the reorganization, 60% of the original team had left, primarily due to overwork.

The high-level manager's response to what could have been a fatal accident was completely inconsistent with company policy. Accidents and near-miss reports were supposed to be treated seriously, no matter how or when they were reported. The fact that the manager knew about the overwork for so long – and did nothing – is astounding.

2.3.19 Lessons

Lessons are learned from such events. But not everyone learns. Many of those who do learn forget. Or worse, they decide that the lessons don't apply to them.

DIBS

I believe that DIBS – did-it-before syndrome – is a fundamental characteristic of human behavior. People ignore safety rules because they got away with ignoring them before, not just in the workplace, but in homes and public places, especially on the highway.

Statistics on road accidents provide a down-to-Earth example, especially for North Americans. In the United States, the National Highway Traffic Safety Administration (NHTSA) conducts periodic surveys of speeding attitudes and behaviors. The most recent survey was conducted in 2011. The corresponding report was issued in 2013 [2.98]. Data were collected via telephone interviews with 6144 US households, with allowances made for land-line versus cell-phone use. The report classified 30% of US drivers as nonspeeders, 40% as sometime speeders, and 30% as speeders. About 9% had been stopped for speeding, and about 6% had received speeding citations. Here are a few survey results:

- 82% of respondents agreed that driving at or near the speed limit makes it easier to avoid dangerous situations.
- 79% agreed that driving at or near the speed limit reduces their chance of having an accident.
- 17% said that driving at or near the speed limit annoys them.

Other reports [2.99–101] provide the following statistics for the United States:

- Registered drivers = 212 million
- Registered vehicles = 269 million

- Crashes causing only property damage = 4.1 million
- Injury-causing crashes = 1.6 million
- Fatal crashes = 32 719
- Speeding-related fatalities = 9613
- Speeding related crashes in which the driver was alcohol-impaired = about 42%
- Speeding related crashes in which the people killed were wearing restraints = about 50%
- Average miles driven per year per vehicle = 13 476
- Average length of trip = 9.75 mi
- Average trips per year = 1360
- Speeding tickets per driver per year = 0.17
- Average speeding ticket cost = \$152.

Using these data, one can calculate the following:

- Accidents per trip = 0.156%
- Injuries per trip = 0.061%
- Deaths per trip = 0.00037%.

Speeding gets us where we want to be faster, and the risks are very low. The most likely negative consequence is a speeding ticket, for which the cost is tolerable. The average driver takes 460 trips without a fender-bender, 1640 trips without an injury, 80 000 trips without dying, and 270 000 trips without dying due to speeding. So we speed, even though we know speeding is dangerous.

In hydrocarbon industries, consequences of accidents can be far worse, threatening the lives, health and prosperity of thousands of people. In well-run facilities, the personal financial cost of breaking a rule can far exceed the cost of a speeding ticket; it can get a worker fired.

But as described in several of the examples above, workers, managers and executives – knowingly and willfully – continue to break critical rules. Why? Is it simply because the rules are inconvenient? Do they believe the rules don't apply to them? Or is it DIBS – concluding that their way is better, because they've behaved that way before with no negative consequences?

How can DIBS be diminished? Experience shows that threats are effective at decreasing DIBS. If people can lose a job or go to jail for violating a rule, they take the rule more seriously, whether or not they agree with it.

MOC

Perhaps a DIBS practitioner is correct. Maybe his/her way really is okay, or even better. Management of Change (MOC) [2.102] is a formal process by which procedures can be improved. With design models, a written document, and perhaps a formal presentation,

the originator presents an idea to everyone involved. For a minor, localized change in procedure, the MOC process can be quick, requiring approval from two or more colleagues and subsequent documentation. For a significant change in hardware or general operating procedures, an MOC committee is formed, which usually includes peers, supervisors, and internal experts. The committee might also include one or more outside consultants. Implementation might require detailed design, budget approval, and development and review of operating procedures.

Ineffective MOC is one of the leading causes of serious incidents, according to the US Chemical Safety and Hazard Investigation Board (CSB) [2.103]. CSB stated:

In industry, as elsewhere, change often brings progress. But it can also increase risks that, if not properly managed, create conditions that may lead to injuries, property damage or even death.

Changes subject to MOC procedures can include:

- Personnel changes, including reorganization, staffing, and training
- Equipment changes, including revamps, communications devices, control hardware, and control software
- Procedure changes, including maintenance schedules and procedures for normal operation, startup, and shutdown
- Material changes, including significant changes in catalysis, chemicals, and feedstock.

Comparison of Examples

The Lakeview blowout occurred before the advent of blowout-prevention technology. Blowouts were known before, but it's difficult to say what might have been done to prevent this one, other than not drilling the well at all.

The Texas City ammonium nitrate explosion also was due to ignorance. The dangers of having so much ammonium nitrate in one place were not then understood.

Lack of prompt official response to the London killer fog could be due in part to culture. In 1952, not very long after World War II, Londoners had learned to accept discomfort, including perhaps noisome smog, as minor compared the blitz.

In 1978, the world simply was not prepared for oil spills as large as the *Amoco Cadiz*. The main lesson learned there was that quick response is critical. By the time help finally arrived, the ship was destroyed and its entire cargo was in the sea.

At Bhopal, management was abysmal, as evidenced by the horrid lack of maintenance. As stated by a Union

Carbide executive, the plant should not have been running.

Chernobyl was caused by contravention of procedures by managers who didn't understand nuclear technology. Three major safety rules were violated when operators:

1. Shut off the emergency cooling water system
2. Raised the control rods too high
3. Disabled the emergency SCRAM.

Any one of the idled systems, if left in place, might have prevented the accident.

Chemical companies all along the banks of the Rhine secretly dumped wastes into the river to avoid having to spend money on proper disposal infrastructure.

On the *Exxon Valdez*, Captain Hazelwood violated a US Coast Guard guideline when he left the third mate in charge before the ship reached open water. Despite the eight-hour delay in expected response time, action by Alyeska and Exxon was relatively fast. Most of the oil stayed inside the ship until it was offloaded. Consequently, instead of losing the entire cargo of 1.2 million bbl, only 250 000 bbl spilled into the sea.

In the Gulf War, retreating Iraqis took *scorched earth* during a war to a new level. Due to strong incentives to develop new technology, putting out the oil fires took far less time than anyone expected.

The Tosco Avon disaster was caused by management-induced DIBS. Engineers and operators were not sufficiently trained. Management refused to invest in proper instrumentation. Management refused to fix the problem that had caused a fire during the 1992 depressuring event. Management strongly encouraged operators to avoid depressuring. Operators became so accustomed to defeating excursions without depressuring that it never occurred to them to act correctly, even when temperatures far exceeded metallurgical limits. Obviously, nobody understood the relationship between N-slip and hydrocracking catalyst activity.

At BP Texas City, operators proceeded with the startup despite the lack of reliable level measurement, reflecting a combination of inadequate training, inadequate technical supervision, and probably DIBS.

Similar factors played a role in the *Deepwater Horizon* incident. Fatal mistakes included the use of an insufficient number of centralizers and the assumption that pressure in the kill line was indicative of pressure in the well. The drilling crew did not understand the significance of several consecutive failed negative pressure tests. The visit of nonessential VIPs during the most critical phase of well completion distracted key tech-

nical personnel, who certainly would have understood the significance of the tests.

The train derailment in Lac-Mégantic was caused by faulty maintenance, the failure of the engineer to tell MM&A about the failing locomotive before it caught fire, and the failure of authorities to act to ensure that oil transportation infrastructure is safe. Government refusals to permit pipelines also are to blame. Pipelines are far more efficient – and thousands of times cleaner and safer – than railroad trains.

All four of my personal examples occurred during startups. All were influenced by cost-cutting and/or unreasonable schedules.

Of all the examples in this section:

- Seven occurred during a startup or shutdown.
- Nine were caused in large part by contravention of procedures. Of these, three involved willful disabling of safety interlocks.
- Eight were caused by shortcuts and cost-cutting understaffing, inadequate training, buying sub-standard equipment, or taking shortcuts to save time. In each case, the supposed savings were miniscule compared to the cost of the incident.
- All but three were due in part to management malfeasance.

General Observations

In this section, I mention other safety-related issues that are general and not related to a single event. Management of change is outlined above.

Whistleblowing. In the above examples, rogue managers would have been chastised (or fired) if their behavior had been reported and verified.

Over the years, the US Congress has passed at least seven laws to protect environmental whistleblowers from retribution from their employers. Even so, according to Seebauer [2.104]:

Studies confirm the intuitive perception that whistleblowers tend to face hostility within their organizations and commonly leave their jobs, either voluntarily or otherwise. Lengthy and costly litigation often follows.

Seebauer goes on to say:

Some employers are happy to hire workers who demonstrate such a strong commitment to high ethical standards. Nevertheless, there is no guarantee of employment, especially in a slow market. The whistleblower may lose seniority and retirement benefits, and must often move to another city. The needs of family members must be considered.

When faced with these realities, insiders are reluctant to report environmental wrongdoing.

Smart companies encourage whistleblowing. They send employees to courses that teach them about safety and environmental protection. They establish internal whistleblower hotlines and encourage employees to use them when they think their concerns haven't properly been addressed by the normal chain of command. They recognize that, in today's litigious society, whistleblowers can save a company billions of dollars in fines and cleanup costs.

Automation. Control systems aren't perfect. I have seen more than one process unit in which an advanced control application is so bad that the operators won't use it. On the other hand, safety-related interlocks must *never* be disabled. They are there for good reasons. Operators, engineers, and managers should be trained to understand exactly how the interlocks work and why they are critical.

Personal Protection Equipment. One of the first things a person learns in the oil and gas business is the importance of personal protection equipment (PPE). In the bad old days, it wasn't uncommon to see bare-headed workers in short-sleeved shirts building scaffolding in a refinery. That doesn't happen now. We are required to wear appropriate PPE at all times.

PPE includes fire-resistant clothing, hard hats, safety glasses, steel-toed shoes, gloves, and toxic gas detectors. Harnesses are used to protect against falls. Using fresh-air breathing equipment or self-contained breathing apparatus (SCBA) improves safety in confined spaces and in areas that might be contaminated by hazardous gases and particulates. In recent years, communication between outside and inside workers has been enhanced by allowing communication via inherently safe radios. Laboratory workers face unique hazards; hard hats are seldom needed in labs, but for some analytical procedures, special gloves and full-face shields protect against hazardous substrates, solvents, and acids.

Pocket-sized toxic gas detectors are important PPE. They sound an alarm when CO or H₂S reach dangerous levels. Some sites require all workers to wear H₂S monitors at all times when they are *inside the gate*. Four-gas monitors detect H₂S, CO, combustible hydrocarbons, and oxygen.

In the United States, the Occupational Safety and Health Administration (OSHA) sets standards for PPE [2.105, 106]. The first standards were adopted in 1971. A major revision was issued in 1994, after OSHA discovered gaps in the existing standards. Data indi-

cated that injuries were occurring at the same rate, whether or not employees were wearing PPE. Some regulations were so restrictive that they discouraged innovation. Present regulations are based on the effectiveness of PPE. Recent improvements are addressing the main cause of worker noncompliance before the revision: some PPE was cumbersome, uncomfortable, and even impractical.

Confined Spaces. People enter tanks, reactors, and other confined spaces to perform maintenance. Oxygen levels can become too low even if air is circulating. Required PPE for confined space entry includes fresh-air breathing equipment and a harness that allows colleagues to lift the worker out if necessary. Modern video technology enables outside personnel to monitor people inside directly.

2.4 Agencies Protecting Safety and the Environment

2.4.1 Environment Protection Agencies

This section focuses almost exclusively on US environment protection agencies and laws. Please understand that to include similar detail for other countries would have been infeasible in the space allotted for this chapter.

In 1970, the United States formed the Environmental Protection Agency (EPA) [2.21] and the Occupational Safety and Health Administration (OSHA). Together, these agencies are responsible for dramatic improvements in air and water quality and increases in workplace safety throughout the United States. EPA's mission is:

to enforce federal laws to control and abate pollution of air and water, solid waste, noise, radiation, and toxic substances. Other missions include administering the Superfund for cleaning up abandoned waste sites, and awarding grants for local sewage treatment plants.

After its creation, EPA quickly took the following actions:

- Established ten regional offices throughout the nation
- Established National Ambient Air Quality Standards, which specified maximum permissible levels for major pollutants
- Required each state to develop plans to meet air quality standards
- Established and enforced emission standards for hazardous pollutants such as asbestos, beryllium, cadmium, and mercury
- Required a 90% reduction in emissions of VOC and CO by 1975
- Published emission standards for aircraft
- Funded research and demonstration plants
- Furnished grants to states, cities, and towns to help them combat air and water pollution.

EPA's law-enforcement efforts are supported by the National Enforcement Investigation Center in Denver, Colorado, which gives assistance to federal, state, and local law enforcement agencies. This unit has clamped down on the *midnight dumping* of toxic waste and the deliberate destruction or falsification of documents.

Today, almost every US state has an environmental agency. Arguably, the most famous of these is the California Air Resources Board (CARB), which pioneered regulations to mitigate smog in Los Angeles. In addition to administering state programs for improving air and water quality, the Texas Commission on Environmental Quality (TCEQ) participates in making plans to prevent and react to industrial terrorism.

Most countries have environmental agencies. As shown in Table 2.12, some are combined with public

Table 2.12 Environmental agencies around the world

Country	Agency
Australia	Department of the Environment
Austria	Ministry for the Environment
Brazil	Ministry of Environment
Canada	Environment Canada
Europe	European Environment Agency
Finland	Ministry of the Environment
Indonesia	Kementerian Lingkungan Hidup
India	Ministry of Environment and Forests
Japan	Ministry of the Environment of Japan
Kuwait	Environment Public Authority
Malaysia	Department of Environment
Mexico	Secretariat of Environment and Natural Resources
Norway	Ministry of the Environment
Saudi Arabia	Presidency of Meteorology and Environment
Singapore	National Environment Agency
South Africa	Department of Environmental Affairs and Tourism
Thailand	Ministry of Natural Resources and Environment
United Kingdom	Environment Agency
United States	Environmental Protection Agency

health departments, some are combined with energy agencies, and at least one is coupled with tourism. In addition to handling internal issues, these agencies administer their country's participation in international treaties, such as the Kyoto Protocol [2.107].

2.4.2 Worker Safety

Pollution control and safety are two sides of the same coin. In the United States, the Occupational Safety and Health Administration (OSHA) is part of the US Department of Labor. Its legislative mandate is to assure safe and healthful working conditions by:

- Enforcing the Occupational Safety and Health Act of 1970
- Helping states to assure safe and healthful working conditions
- Supporting research, information, education, and training in occupational safety and health.

OSHA can levy fines against unsafe people and companies. Not surprisingly, a large percentage of the safety infringements cited by OSHA have caused environmental damage or put the environment at risk. For example, in 1993 OSHA fined the Manganas Painting Company for exposing workers and the environment to lead during sandblasting operations. The proposed fines totaled US\$4 million. The contractor appealed, but in February 2002, it pleaded guilty to dumping 55 t of lead-containing sandblasting material, in violation of the Resource Conservation and Recovery Act (RCRA) [2.108].

Under the Occupational Safety and Health Act, employers are responsible for ensuring a safe and healthy workplace. One key requirement is that all hazardous chemicals must be properly labeled. Workers must be taught how to handle the chemicals safely, and material safety data sheets must be available to any employee who wishes to see them.

Material Safety Data Sheets (MSDS)

Material safety data sheets (MSDSs) play a major role in improving worker safety by providing standardized and readily available information on potentially hazardous substances. MSDS include the following information.

Material Identification. The name of the product and the manufacturer's name, address, and emergency phone number must be provided.

Hazardous Ingredients. The sheet must give the chemical name for all hazardous ingredients comprising

more than 1% of the material. It must list cancer-causing materials if they comprise more than 0.1%. Listing only the trade name, only the Chemical Abstract Service (CAS) number, or only the generic name is not acceptable.

If applicable, exposure limits are listed in this section of the MSDS. The OSHA permissible exposure limit (PEL) is a legal, regulated standard. Other limits may also be listed. These include recommended exposure limits (REL) from the National Institute for Occupational Safety and Health (NIOSH) and threshold limit values (TLV) from the American Conference of Governmental Industrial Hygienists (ACGIH). Sometimes, short-term exposure and/or ceiling limits are shown. The ceiling limit should never be exceeded.

Physical Properties. These include the appearance, color, odor, melting point, boiling point, viscosity, vapor pressure, vapor density, and evaporation rate. The vapor pressure indicates whether or not the chemical will vaporize when spilled. The vapor density indicates whether the vapor will rise or fall. Odor is important because a peculiar smell may be the first indication that something has leaked.

Fire and Explosion Hazard Data. This section provides the flash point of the material, the type of extinguisher that should be used if it catches fire, and any special precautions.

The flash point is the lowest temperature at which a liquid gives off enough vapor to form an explosive mixture with air. Liquids with flash points below 100 °F (37.8 °C) are called flammable, and liquids with flash points between 100–200 °F (37.8–93.3 °C) are called combustible. Flammable and combustible liquids require special handling and storage.

The four major types of fire extinguishers are Class A for paper and wood, Class B for flammable liquids or greases, Class C for electrical fires, and Class D for fires involving metals or metal alloys.

Health Hazard Data. This section defines the symptoms that result from normal exposure or overexposure to the material or one of its components. Toxicity information, such as the result of studies on animals, may also be provided. The information may also distinguish between the effects of acute (short-term) and chronic (long-term) exposure. Emergency and first-aid procedures are included in this section.

Reactivity Data. This section includes information on the stability of the material and special storage requirements.

Unstable chemicals can decompose spontaneously at certain temperatures and pressures. Some unstable chemicals decompose when they are shocked. Rapid decomposition produces heat, which may cause a fire and/or explosion. It also may generate toxic gas. Hazardous polymerization, which is the opposite of hazardous decomposition; it can produce enough heat to cause a fire or explosion.

Concentrated acids and reactive metals are hazards when mixed with water. They should be stored separately in special containers.

Spill, Leak, and Disposal Procedures. This part of the MSDS gives general procedures, precautions and

methods for cleaning up spills and disposing of the chemical.

Personal Protection Equipment Requirements.

This section lists the protective clothing and equipment needed for the safe handling of the material. Requirements can differ depending on how the chemical is used and how much of it is used.

Protective equipment and clothing can include eye protection (safety glasses or face shields), skin protection (clothing, gloves, shoe covers), self-contained breathing equipment, and/or forced-air ventilation (fume hoods).

2.5 Key Regulations

In this section, important environmental legislation is described. Most examples come from the United States, but there is an excuse: for several decades, the United States has pioneered environmental regulations, and many countries have followed suit. Recently, the European Commission took the lead in promoting climate-control treaties, including the Rio and Kyoto Protocols.

2.5.1 Clean Air Acts

The first clear-air acts in the English-speaking world were implemented by Parliament in 1956, in response to the *deadly fog* incidents around London.

Since 1963, the United States government has passed several clean-air acts, including:

- Clean Air Act of 1963
- Motor Vehicle Air Pollution Control Act of October 20, 1965
- Clean Air Act Amendments of October 15, 1967
- Air Quality Act of November 21, 1967
- Creation of EPA: Clean Air Act of 1970
- Clean Air Act Amendments of 1975, 1977, and 1990.

For convenience, the entire package often is called just the Clean Air Act (CAA). A good source for general understanding is the Plain English Guide to the Clean Air Act, available from the US EPA web site [2.109]. The Guide shows how the CAA has led to significant improvements in human health and the environment. For example, since 1970:

- The six most commonly found air pollutants have decreased by more than 50%

- Air toxics from large industrial sources, such as chemical plants, petroleum refineries, and paper mills have been reduced by nearly 70%
- New cars are more than 90% cleaner and will be even cleaner in the future
- Production of most ozone-depleting chemicals has ceased.

At the same time, the US economy and associated energy consumption has grown significantly:

- The US GDP has tripled
- Energy consumption has increased by 50%
- Vehicle use has increased by almost 200%.

Under the CAA, EPA's role is to set limits on certain air pollutants, including ambient levels anywhere in the country. EPA limits emissions of air pollutants from point sources like chemical plants, utilities, and steel mills. Individual states or tribes may have stronger air pollution laws, but they may not have weaker pollution limits than those set by EPA.

EPA assists state, tribal, and local agencies by providing research, expert studies, engineering designs, and funding to support clean air progress. EPA must approve state, tribal, and local air pollution reduction plans. EPA can issue sanctions against states which fail to comply; if necessary, it can take over enforcing the CAA in noncomplying areas.

The CAA required EPA to set National Ambient Air Quality Standards (NAAQS) for pollutants considered harmful to public health and the environment. EPA set are two types of standards – primary and secondary. Primary standards protect against adverse health effects. Secondary standards protect against damage to

farm crops, vegetation, and buildings. Because different pollutants have different effects, the NAAQS are also different. Some pollutants have standards for both long-term and short-term averaging times. The short-term standards are designed to protect against acute, or short-term, health effects, while the long-term standards were established to protect against chronic health effects. NAAQS are shown in Table 2.13 [2.110].

Hazardous air pollutants (HAPs) are regulated, too. Table 2.14 lists 20 *core* compounds selected from the 188 HAPs regulated under Section 112 of the Clean Air Act.

Compliance with air quality standards is monitored by the Office of Air Quality Planning and Standards (OAQPS) [2.111]. OAQPS evaluates the status of the atmosphere as compared to clean air standards and historical information, using measurements acquired from many hundreds of monitoring stations across the United States.

Reformulated Gasoline (RFG) in the United States

In 1970, gasoline blending became more complex. The US Clean Air Act required the phase-out of tetraethyl lead, so refiners had to find other ways to provide octane. In 1990, the CAA was amended. It empowered EPA to impose emissions limits on automobiles and to require reformulated gasoline (RFG) [2.112]. RFG was implemented in several phases. The Phase I program started in 1995 and mandated RFG for ten large metropolitan areas. Several other cities and four entire States joined the program voluntarily. The current phase began in 2000. RFG is used in 17 States and the District of Columbia. In 2015, about 35% of the gasoline in the United States was reformulated.

Tier 1 reformulated gasoline regulations required a minimum amount of chemically bound oxygen, imposed upper limits on benzene and Reid vapor pressure (RVP), and ordered a 15% reduction in VOC and air toxics. Air toxics include 1,3-butadiene, acetaldehyde, benzene, and formaldehyde.

The regulations for Tier 2, which took force in January 2000, were based on the EPA Complex Model, which estimates exhaust emissions for a region based on geography, time of year, mix of vehicle types, and – most important to refiners – fuel properties. As of 2006, the limit on sulfur in the gasoline produced by most refineries in the US was 30 ppmw.

Initially, the oxygen for RFG could be supplied as ethanol or C₅–C₇ ethers. The ethers have excellent blending octanes and low vapor pressures. But due to leaks from filling station storage tanks, methyl-*t*-butyl ether (MTBE) was detected in ground water samples in New York City, Lake Tahoe, and Santa Monica, California. In 1999, the Governor of California issued an executive order requiring the phase-out of MTBE as a gasoline component. That same year, the California Air Resources Board (CARB) adopted California Phase 3 RFG standards, which took effect in stages starting in 2002. The standards include a ban on MTBE and a tighter cap on sulfur content. In the United States, Tier 3 vehicle emission and fuel standards lowered the allowed sulfur content of gasoline to 10 ppmw as of January 2017.

Conservation, Efficiency, and Renewable Fuel Mandates

The *Energy Policy Act of 2005* [2.113] was signed into law by President George W. Bush on August 8, 2005. The Act addresses energy production and use in the

Table 2.13 National Ambient Air Quality Standards (NAAQS) pollutants

Pollutant	Primary/secondary	Averaging time	Level	Form
Carbon monoxide	Primary	8 h	9 ppm	Not exceeded more than once/year
Carbon monoxide	Primary	1 h	35 ppm	Not exceeded more than once/year
Lead	Both	Rolling 3 month	0.15 μg/m ³	Not to be exceeded
Nitrogen dioxide	Primary	1 h	100 ppb	98th percentile of 1 h daily max concentrations, averaged over 3 years
Nitrogen dioxide	Both	Annual	53 ppb	Annual mean
Ozone	Both	8 h	0.075 ppm	Annual fourth-highest daily max 8 h concentration, averaged over 3 years
Particulates, PM _{2.5}	Primary	Annual	12 μg/m ³	Annual mean, averaged over 3 years
Particulates, PM _{2.5}	Secondary	Annual	15 μg/m ³	Annual mean, averaged over 3 years
Particulates, PM _{2.5}	Both	24 h	35 μg/m ³	Annual mean, averaged over 3 years
Particulates, PM ₁₀	Both	24 h	150 μg/m ³	Not to be exceeded more than once/year, on average, over 3 years
Sulfur dioxide	Primary	1 h	75 ppb	99th percentile of 1 h daily max concentrations, averaged over 3 years
Sulfur dioxide	Secondary	3 h	0.5 ppm	Not exceeded more than once/year

Table 2.14 Twenty of the hazardous air pollutants regulated by the Clean Air Act

Volatile organics (VOC)	Inorganics (Metals)	Aldehydes
Benzene	Arsenic	Formaldehyde
1,3-Butadiene	Beryllium	Acetaldehyde
Carbon tetrachloride	Cadmium	Acrolein
Chloroform	Chromium	
Propylene dichloride	Lead	
Dichloromethane	Manganese	
Perchloroethylene	Mercury	
Trichloroethylene	Nickel	
Vinyl chloride		

United States. It provides tax incentives and loan guarantees for specific types of energy production. Topics include:

- Energy efficiency
- Renewable energy
- Oil and gas
- Coal
- Tribal energy
- Nuclear matters and security
- Vehicles and motor fuels, including ethanol
- Hydrogen
- Electricity
- Energy tax incentives
- Hydropower and geothermal energy
- Climate change technology.

It authorized the following tax reductions:

- \$4.3 billion for nuclear power
- \$2.8 billion for fossil fuel production
- \$2.7 billion to extend the renewable electricity production credit
- \$1.6 billion in tax incentives for investments in *clean coal* facilities
- \$1.3 billion for energy conservation and efficiency
- \$1.3 billion for alternative fuels (bioethanol, biomethane, liquified natural gas, propane)
- \$500 million Clean Renewable Energy Bonds for government agencies for renewable energy projects.

The Energy Independence and Security Act of 2007 required improved vehicle fuel economy. It also increased production requirements for biofuels, specifically biomass-derived diesel. To be biomass-based diesel, the fuel must reduce emissions by 50% versus petroleum-derived diesel. It increased the total target volume for ethanol, and specified that a large portion should come from noncorn sources. The Act motivates energy savings with improved standards for appliances and lighting, and in industrial and commercial buildings.

Gasoline (Petrol) in the EU

Transportation fuel specifications in the European Union (EU) are described by EN 228, *Specification for unleaded petrol (gasoline) for motor vehicles*. The present version is sometimes called Euro IV gasoline. Key specifications include the following:

- Octane: minimum research octane number (RON) and motor octane number (MON) are 95 and 85 respectively.
- Volatility: minimum percent vaporized at 100 and 150 °C are 46 and 75 respectively.
- Hydrocarbon types: the maxima for olefins/aromatics/benzene are 18/35/1 vol%, respectively.
- Oxygen: The maximum oxygen content is 3.7%. Oxygenates can include different amounts of methanol, ethanol (with stabilizing agents), isopropyl alcohol, butyl alcohols, ethers such as MTBE, and other mono alcohols.
- Sulfur: 10 ppmw.

EU gasoline is just as clean if not cleaner than EPA gasoline, but it is easier to manufacture and regulate. The allowable sources of oxygen are based on science.

Ultra-Low-Sulfur Diesel

At present, the most advanced specification for diesel fuel is Euro V, which is described in Table 2.15. Severe hydroprocessing is required to make Euro V from difficult feedstocks.

2.5.2 Rivers and Harbor Act, Refuse Act

One of the first environmental laws in the US was the Rivers and Harbor Act of 1899. It was passed to control obstructions to navigation. The Act required congressional approval for the building of bridges, dams, dikes, causeways, wharfs, piers, or jetties, either in or over a navigable waterway. The Act also made it illegal to discharge debris into navigable water without a permit. In 1966, a court held that the River and Harbor Act made it illegal to discharge industrial waste without a permit, not just directly into navigable waters, but also into associated tributaries and lakes. This led to the Refuse Act Permit Program of 1970, under which specific kinds of pollution are allowed under permits issued by the Army Corps of Engineers. Every application for a permit is reviewed by EPA. If EPA concludes that the discharge described in the application will harm the environment, the Army Corp of Engineers denies the permit.

The penalties for violating permits are severe, including stiff fines and jail time. A corporation that employs the guilty person can be fined up to \$1 000 000. False reports also can be punished by fines or im-

Table 2.15 Clean fuels: Specifications for Euro V diesel, (EN 590)

Property	Units	Low limit	Upper limit	Test-method
Cetane index		46	–	ISO 4264
Cetane number		51	–	ISO 5165
Density (at 15 °C)	kg/m ³	820	845	ISO 3675, 12185
Polycyclic aromatic hydrocarbons	%(m/m)	–	11	ISO 12916
Sulfur content	mg/kg	–	10	ISO 20846, 20847, 20884
Flash point	°C	55	–	ISO 20846, 20884
Carbon residue (on 90–100% fraction)	%(m/m)	–	0.3	ISO 2719
Ash content	%(m/m)	–	0.01	ISO 10370
Water content	mg/kg	–	200	ISO 6245
Total contamination	mg/kg	–	24	ISO 12937
Copper strip corrosion (3 h at 50 °C)	Rating	Class 1	Class 1	ISO 12662
Oxidation stability	g/m ³	–	25	ISO 2160
Lubricity, wear scar diameter (at 60 °C)	µm	–	460	ISO 17705
Viscosity (at 40 °C)	mm ² /s	2	4.5	ISO 12156-1
Distillation, recovered at				ISO 3405
250 °C	%v/v	–	65	ISO 3405
350 °C	%v/v	85	–	ISO 3405
95 vol.% recovery at	°C	–	360	ISO 3405
Fatty acid methyl ester content	vol.%	–	7	ISO 14078

prisonment. In this context, *guilty person* refers to the corporate officer responsible for the facility from which the illegal discharge originates. In other words, a negligent act by a sloppy operator can send the Big Boss to jail.

2.5.3 Federal Water Pollution Control Act

The original Federal Water Pollution Control Act (FWPCA) was approved on July 9, 1956. The present Act includes the following:

- Pollution Control Act Amendments of July 20, 1961
- Water Quality Act of October 2, 1965
- Clean Water Restoration Act of November 3, 1966
- Water Quality Improvement Act of April 3, 1970
- Federal Water Pollution Control Act of 1972
- Clean Water Acts of 1977, 1981, and 1987.

The FWPCA of 1972 gave EPA greater authority to fight water pollution. While implementing the Act, EPA cooperates with the US Coast Guard and the Secretary of the Interior. Individual states have primary responsibility for enforcing water quality standards, but if the states fail to meet expectations, EPA can take civil or criminal action under the Refuse Act.

The FWPCA prohibits the discharge of harmful amounts of oil into navigable waters. If oil is spilled, the owner or operator is liable for cleanup costs. Initially, the bill authorized \$24.6 billion for water pollution control over three years. The goal of the law was to eliminate the pollution of US waterways by municipal and industrial sources by 1985.

2.5.4 Clean Water Acts, Water Quality Act

The main objective of the Clean Water Acts (CWA) of 1977, 1981 and 1987 is to maintain the *chemical, physical, and biological integrity of the nation's waters*. It seeks to have *water quality which provides for the protection and propagation of fish, shellfish and wildlife and provides for recreation in and on the water*. Under these Acts, each state is required to set its own water quality standards. All publicly owned municipal sewage treatment facilities are required to use secondary treatment for wastewater. To help states and cities build new or improved water treatment plants, Congress provides construction grants, which are administered by EPA. EPA allocates funds to states, which in turn distribute money to local communities.

Community programs are monitored by EPA. They must meet treatment requirements to obtain permits under the National Pollutant Discharge Elimination System (NPDES).

The Water Quality Act of 1987 requires discharge permits for all point sources of pollution. More than 95% of all major facilities now comply with five-year NPDES permits, which specify the types and amounts of pollutants that legally can be discharged. When permits are renewed, they can be modified to reflect more stringent regulations. Violators are subject to enforcement actions by EPA, including criminal prosecution.

The authority of the EPA was strengthened under the 1987 Water Quality Act. The allowable sizes of fines were increased, and violators found guilty of negligence could be sent to prison.

2.5.5 Marine Protection, Research, and Sanctuaries Act

The Marine Protection, Research, and Sanctuaries Act of 1972 gave authority to EPA to protect oceans from indiscriminate dumping. The Agency designates sites at which dumping is allowed and issues dumping permits. Fines can be imposed for illegal dumping.

2.5.6 Safe Drinking Water Act

Since the 1970s, the assurance of safe drinking water has been a top priority for EPA, along with individual states and over 53 000 community water systems (CWSs). The CWSs supply drinking water to more than 280 million Americans – about 90% of the population [2.114].

The Safe Drinking Water Act of 1974 was amended in 1977 and again in 1986. It empowered EPA to set national standards for drinking water from surface and underground sources. It also authorized EPA to give financial assistance to states, which are in charge of enforcing the standards. Aquifers are protected from wastes disposed in deep injection wells, from runoff from hazardous waste dumps, and from leaking underground storage tanks. In 1987, EPA also established maximum contaminant levels for VOC and 51 man-made chemicals. Standards for other chemicals were added as their toxicity was determined. At present, health and safety standards have been established for 91 microbial, chemical, and radiological contaminants.

2.5.7 Resource Conservation and Recovery Act (RCRA)

In the United States, solid wastes are regulated by the following:

- Solid Waste Disposal Act of 1965
- Resources Recovery Act of 1970
- Resource Conservation and Recovery Act of 1976 (RCRA).

In 1965, the Solid Waste Disposal Act provided financial grants to develop and demonstrate new technologies in solid waste disposal. The Resources Recovery Act of 1970 emphasized recycling and by-product recovery.

By 1976, problems caused by the accumulation of large quantities of hazardous waste prompted Congress to pass the Resource Conservation and Recovery Act (RCRA). This legislation gave EPA the responsibility of developing a *cradle to grave* approach to hazardous

waste, which culminated in the establishment of Hazardous Waste and Consolidated Permit Regulations (1980).

Under RCRA, hazardous waste is tracked from its source to every destination, including final disposal. Tracking is based on transportation manifests, other required records, and the issuance of permits.

EPA classifies wastes according to four measurable characteristics, for which there are standardized tests. The characteristics are:

- Ignitibility
- Corrosivity
- Reactivity
- Extraction procedure (EP) toxicity.

In 1980, the Waste Oil Recycling Act (WORA) empowered EPA to encourage the development of state and local programs for recycling waste motor oil. That same year, WORA was amended to strengthen its enforcement provisions.

A *generator* of hazardous waste is responsible for the following:

1. Determining if a waste is hazardous
2. Obtaining a facility permit if the waste is stored on the generator's property for more than 90 days
3. Obtaining an EP identification number
4. Using appropriate containers and labeling them properly for shipment
5. Preparing manifests for tracking hazardous waste
6. Assuring through the manifest system that the waste arrives at the designated facility
7. Submitting to EPA an annual summary of activities.

Prior to shipping hazardous waste, the generator must prepare a manifest which includes the following:

1. Name and address of the generator
2. Name of all transporters
3. Name and address of the facility designated to receive the waste
4. EPA identification number of all who will handle the waste
5. Department of Transportation (DOT) description of the waste
6. Amount of waste and number of containers
7. Signature certifying that the waste has been properly labeled and packaged in accordance with EPA and DOT regulations.

To send waste away from its site, the generator must use EPA-approved transporters. It must also keep records of all hazardous waste shipments and immedi-

ately report those that fail to reach the facility shown on the manifest.

A *transporter* of hazardous waste must:

1. Obtain an EPA identification number
2. Comply with the manifest system for tracking hazardous waste
3. Deliver the entire quantity of hazardous waste to the facility specified by the manifest
4. Retain copies of manifests for 3 years
5. Comply with Department of Transportation rules for reporting discharges and spills
6. Cleanup any spills that occur during transportation. All spills must be reported to both EPA and the DOT.

Any person who owns or operates a hazardous waste facility must receive a permit from the EPA. Standards for facilities that treat, store, or dispose of hazardous waste are designed to:

1. Promote proper treatment, storage, and methods of disposal
2. Provide states with minimum standards acceptable to EPA
3. Provide technical support to states that lack hazardous waste management programs.

The RCRA amendments of 1984 and 1986 extended the Act to cover underground storage tanks, especially those used for gasoline and other petroleum liquids. At the time, about 15% of the nation's 1.4 million gasoline storage tanks were leaking. Most of these leaks have since been repaired.

2.5.8 Superfund, CERCLA

Years ago, people were less aware of the dangers of dumping chemical wastes. On many properties, dumping was intensive and/or continuous. This created thousands of hazardous sites, many of which were uncontrolled and/or abandoned. On December 11, 1980, in response to public concern, Congress passed the Comprehensive Environmental Response Compensation and Liability Act (CERCLA) [2.115], which authorized EPA to locate, investigate, and remediate the worst of these hazardous sites.

CERCLA established the Superfund, which provides emergency cleanup funds for chemical spills and hazardous waste dumps. The Superfund allows the government to take immediate action to cleanup spills or dumps where the responsible party cannot be identified easily. The Superfund draws about 90% of its money from taxes on oil and selected chemicals. The remainder comes from general tax revenues.

Except in an emergency, state agencies are consulted before the federal government takes action. When it does so, it uses one of three approaches:

1. If the owner of the hazardous site cannot readily be identified, the federal government may proceed with the cleanup.
2. If the owner can be identified but refuses to clean the site, or if the owner's efforts are not up to par, the federal government can take charge of the cleanup. The owner must pay the cost, whatever it happens to be.
3. When the owner can be identified and decides to do the work, the federal government monitors the project and gives official approval when the work is completed according to standards.

CERCLA covers a wide range of sites. In addition to land-based dumps, it applies to spills into waterways, groundwater, and even the atmosphere. Initial funding for the Act was US\$1.6 billion over five years. In 1986, the Superfund Amendment and Reauthorization Act (SARA) extended the program by five years and increased the fund to US\$8.5 billion. It also tightened cleanup standards and enhanced EPA's enforcement powers. The Emergency Planning and Community Right-to-Know Act (EPCRA), also known as SARA Title III, encourages and supports emergency planning efforts at state and local levels. It also gives information to the public and local governments on potential chemical hazards in their communities. This legislation helped reduce pollution and improve safety all across the land.

In 1984, Hazardous and Solid Waste Amendments (HSWA) were passed because citizens were concerned about the potential contamination of groundwater by hazardous waste disposal sites.

In 1978, the Federal Insecticide, Fungicide, and Rodenticide Act (FIFRA) of 1947 was amended to give EPA authority to control pollution from DDT, mercury, aldrin, toxaphene, parathion, and related chemicals. About one billion pounds of pesticides, fungicides, and rodenticides are used every year in the United States. While they contribute enormously to the success of agriculture, they can be harmful to animals, birds and humans if not used properly.

2.5.9 Toxic Substances Control Act (TSCA)

The Toxic Substances Control Act (TSCA) of 1976 gave EPA the authority to regulate the development, distribution, and marketing of chemical products. Manufacturers, importers, and processors must notify EPA within 90 days before introducing a new chemical to the

market. Certain tests (e.g., fish-kill tests) must be conducted to determine toxicity. Approved chemicals must bear warning labels.

Many chemicals are restricted or banned under TSCA:

- The manufacture, processing and distribution of completely halogenated chlorofluorocarbons (CFCs) is banned, except for a small number of essential applications.
- Chromium(VI) may not be used as a corrosion inhibitor in comfort cooling towers (CCTs) associated with air conditioning and refrigeration systems.
- Nitrosating agents may not be mixed with metal-working fluids that contain specific substances.
- The import, manufacture, processing, or distribution of PCBs is banned unless EPA agrees that the PCBs will be *totally enclosed*.

2.5.10 Asbestos School Hazard Abatement Act

The Asbestos School Hazard Abatement Act (SHAA) of 1984 was passed to encourage the removal of asbestos from schools. In 1986, the Asbestos Hazard Emergency Response Act was passed to correct deficiencies in the previous Act. The final rule, issued in 1987, required local education agencies to:

1. Inspect school buildings for asbestos-containing materials
2. Submit asbestos management plans to state governors
3. Reduce or completely eliminate all asbestos hazards.

2.5.11 Control of Dumping at Sea

On November 13, 1972, the Convention on the Dumping of Wastes at Sea was agreed in London by representatives of 91 countries, including all of the world's principle maritime nations. The list of substances that may not be dumped includes biological and chemical warfare agents, certain kinds of oil, certain pesticides, durable plastics, poisonous metals and their compounds, and high-level radioactive waste. Enforcement is left to individual countries.

2.5.12 Climate Control: Rio, Kyoto, and Paris

Rio Earth Summit

In 1992, during the *Earth Summit* in Rio de Janeiro, 154 nations plus the European community signed the United Nations Framework Convention on Climate

Change (UNFCCC). At the time, the Earth Summit was the largest-ever gathering of Heads of State. Effective on March 21, 1994, the UNFCCC called on industrial nations to voluntarily reduce greenhouse gas emissions to 1990 levels by the year 2000. As of May 2015, there were 196 Parties (195 countries and one regional economic integration organization) to the Framework [2.116–118].

In many respects, the Rio Declaration resembled the Declaration on Human Environment issued by the Stockholm Conference in 1972. The 27 nonbinding principles of the Rio Declaration included the *polluter pays* concept and the *precautionary principle*. The latter recommends that, before a construction project begins, an impact study should be conducted to identify and forestall potential harm to the environment.

The declaration asserted that present-day economic development should not undermine the resource base of future generations. It also affirmed that industrial nations pollute more than developing countries. (For example, on a per capita basis, the United States emits 25 times more CO₂ than India.) On the other hand, industrial nations have advanced technology and greater financial resources, which enable them to contribute more to environmental protection.

Kyoto Protocol

The Kyoto Protocol extended the UNFCCC. Adoption committed countries to accept that global warming is a fact, and that anthropogenic CO₂ is the primary contributor. It was concluded in December 1997 and took force in February 2005. As of 2015, it was accepted by 192 countries. Significantly, Canada withdrew its support in 2012, and the United States never adopted it. The Protocol obliges developed countries to reduce current greenhouse gas emissions while giving allowances to transitional (developing) countries. It discusses intergovernmental emissions trading; to many interests in the United States, the emissions trading concept is especially onerous.

Paris Accord

The Paris Accord was signed in November 2016 by 194 members of the UNFCCC. As of December 2016, it had been ratified by 127 countries. The main differences between the Paris Accord and previous agreements are its bottom-up approach and its flexibility. Countries set their own targets voluntarily. Targets are not legally binding. No distinct difference is made between developed and developing economies. The goal of the Paris Accord is to limit the increase in global average temperatures to 1.5 °C above pre-industrial levels. The NASA GISS model predicts that if the temperature increase

reaches 2.0 °C more than 150 million people could be displaced.

According to *Hirtenstein* [2.119], green technology does more than keep the planet clean, it also generates

jobs. The green workforce in the US rose to 8.1 million in 2015, and solar energy jobs overtook those in the oil and gas extraction sector. Similarly, more people work in renewable energy than in oil and gas in China.

2.6 Pollution Control and Abatement Technology

In response to environmental regulation, the petroleum industry reduced pollution by:

- Reducing fugitive hydrocarbon emissions from valves and fittings
- Removing sulfur from refinery streams and finished products
- Adding tail-gas units to sulfur recovery plants
- Reducing the production of NO_x in fired heaters
- Scrubbing SO_x and NO_x from flue gases
- Reducing the production of CO₂ by increasing energy efficiency.

The technology behind these actions is explained below.

2.6.1 Particulate Matter

In petroleum refineries, coking operations and FCC regenerators are the main sources of particulate matter (PM) emissions. Coke-derived PM can be reduced by building enclosures around coke-handling equipment – conveyor belts, storage piles, rail cars, barges, and calciners.

For flue gas from FCC regenerators, many licensors offer scrubbing technology. ExxonMobil offers wet-gas scrubbing (WGS), which removes particulates, SO_x and NO_x [2.120]. UOP and Shell Global Solutions offer third-stage separator (TSS) technology, which removes PM in conjunction with flue-gas power recovery [2.121].

2.6.2 Carbon Monoxide and VOC

CO from partial combustion in FCC regenerators is converted to CO₂ in CO boilers. Flue gas from other boilers, process heaters, and power plants can also contain some CO, which can be diminished by the installation of high-efficiency burners and/or the implementation of advanced process control.

Fugitive emissions (leaks) from storage tanks, sewers, process units, seals, valves, flanges, and other fittings [2.122] can contain both CO and VOC. Floating roofs can be added to open tanks, and tanks that already have a roof can be fitted with vapor recovery systems. Open grates above sewers can be replaced with

solid covers. Emissions from seals, valves, and so on, can be pinpointed with portable combustible-gas detectors. Repairs can then be made at convenient times, for example during a maintenance shutdown.

2.6.3 Sulfur Oxides

In the petroleum industry, most sulfur oxide pollution comes from gas processing plants and crude oil refineries.

Sources of SO_x

Sour-gas processing, fuel-oil fired heaters and FCC regenerator units are major sources of SO_x and NO_x emissions. The most obvious way to reduce SO_x from a heater is to burn low-sulfur fuels. Switching fuels requires no capital investment, but it is probably the most expensive solution due to the relatively high cost of low-sulfur fuels.

A large fraction of the sulfur in the feed to an FCC unit ends up in coke on the catalyst. SO_x are formed in the regenerator when the coke is burned away. Removing sulfur from FCC feed with a pretreater decreases SO_x emissions.

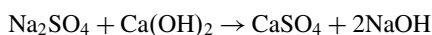
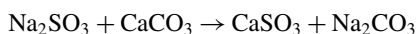
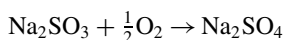
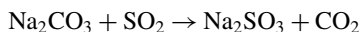
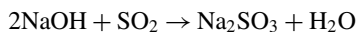
Flue Gas Desulfurization

Processes for removing sulfur oxides from stack gases include dry absorption, wet absorption, carbon adsorption, and catalytic oxidation.

Historically, wet flue-gas desulfurization processes used aqueous slurries of lime, dolomite, and/or sodium hydroxide. Sulfur oxides react with lime or limestone (CaCO₃) to produce calcium sulfate (CaSO₄) and calcium sulfite (CaSO₃), which precipitate from the scrubbing solution. The products move to a settling tank, in which the solid calcium salts separate from the solution as the scrubbed gas goes up the stack. After some time, the solids are removed and sent to a sanitary landfill. The solution is recycled, and fresh lime is added as needed.

The *dual alkali* approach starts with solutions or slurries of sodium hydroxide (NaOH), sodium carbonate (Na₂CO₃), or sodium bicarbonate (NaHCO₃). These compounds react with SO₂ to give sodium sulfite (Na₂SO₃) and sodium bisulfite (NaHSO₃), which

stay dissolved in the solution. Some of the sodium sulfite reacts with excess oxygen in the flue gas to give sodium sulfate. Sulfate and sulfite are removed by reaction with lime or limestone (CaCO_3). The sodium hydroxide solution is recycled. Makeup hydroxide is added as needed to compensate for losses. Selected dual-alkali reactions are shown below.



In a carbon adsorption process developed by Lurgi, hot flue gas first goes through a cyclone or dust collector for particulate removal. The gas is cooled with water and sent to an adsorption tower packed with activated carbon. The carbon adsorbs SO_x . Water is sprayed into the tower intermittently to remove the adsorbed gas as a weak aqueous acid. The scrubbed gas goes out the stack. The acid goes to the gas cooler, where it picks up additional SO_x by reacting with incoming flue gas. Cooler discharge is sold as dilute sulfuric acid.

In the Reinluft carbon adsorption process, the adsorbent is a slowly moving bed of carbon. The carbon is made from petroleum coke and activated by heating under vacuum at 1100°F (593°C).

Flue-gas scrubbing with catalytic oxidation (Cat-Ox) is an adaptation of the contact sulfuric acid process, modified to give high heat recovery and low pressure drop. In the Monsanto process, particulates are removed from hot flue gas with a cyclone separator and an electrostatic precipitator. A fixed-bed converter uses solid vanadium pentoxide (V_2O_5) to catalyze the oxidation of SO_2 to SO_3 . Effluent from the converter goes through a series of heat exchangers into a packed-bed adsorption tower, where it contacts recycled sulfuric acid. The tower overhead goes through an electrostatic precipitator, which removes traces of acid mist from the scrubbed gas. Liquid from the tower (sulfuric acid) is cooled and sent to storage. Some of the acid product is recycled to the absorption tower.

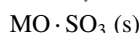
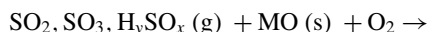
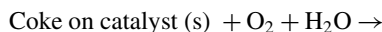
The Wellman-Lord process uses a solution of potassium sulfite (K_2SO_3) as a scrubbing agent. K_2SO_3 adsorbs SO_2 to give potassium bisulfite (KHSO_3). The bisulfite solution is cooled to give potassium pyrosulfite ($\text{K}_2\text{S}_2\text{O}_5$). This can be stripped with steam to release SO_2 , which is fed to a sulfuric acid plant.

FCC SO_x Transfer Additives

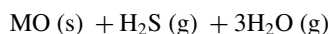
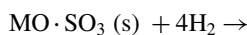
Arguably, SO_x transfer additives are the most cost-effective way to lower SO_x emissions from a full-

combustion FCC unit. These materials, first developed by Davison Chemical, react with SO_x in the FCC regenerator to form sulfates. When the sulfated additive circulates to the riser/reactor section, the sulfate is chemically reduced to H_2S , which is recovered by amine absorption and sent to a sulfur plant. Sulfur that would have gone up the stack as SO_x goes instead to the sulfur plant as H_2S .

FCC regenerator (oxidizing environment)



FCC riser-reactor (reducing environment)



In some units, SO_x additives can reduce FCC SO_x emissions by more than 70%. This can have a dramatic effect on the design and/or operation of upstream and downstream equipment – FCC feed pretreaters, FCC gasoline posttreaters, and flue-gas scrubbers for FCC regenerators.

Hydrogen Sulfide Removal

When sulfur-containing feeds pass through hydrotreaters or conversion units, some or most of the sulfur is converted into H_2S , which eventually ends up in off-gas streams. Absorbers containing aqueous solutions of alkanolamines, such as diethanol amine (DEA) or N-methyl diethanol amine (MDEA) remove the H_2S , leaving only 10–20 ppmw in the treated gas streams. H_2S is steam-stripped from the amines, which are returned to the absorbers. The H_2S is piped to the refinery sulfur plant, where it is converted into sulfur.

2.6.4 Nitrogen Oxides

In refineries and petrochemical plants, NO_x are formed in several ways. In high-temperature fired heaters, NO_x are produced by combustion. In FCC regenerators, NO_x are produced by combustion and from the nitrogen deposited with coke on spent catalysts. FCC NO_x emissions go up when:

1. The catalyst contains more combustion promoter
2. When oxygen in the flue gas goes up
3. At higher regenerator temperatures, and
4. At higher feed nitrogen contents.

Combustion promoter is a noble-metal material that accelerates the reaction between CO and O_2 to form CO_2 .

Dual-alkali flue-gas scrubbing as described in Sect. 2.6.3 only removes about 20% of the NO_x from a typical flue gas. Therefore, instead of simple scrubbing, chemical reducing agents are used. In selective catalytic reduction (SCR) processes, anhydrous ammonia is injected into the flue gas as it passes through a bed of catalyst at 500–950 °F (260–510 °C). The reaction between NO_x and ammonia produces N₂ and H₂O.

The MONO-NO_x process offered by Huntington Environmental Systems employs a nonnoble metal catalyst. For SO_x, NO_x and VOC removal, Ducon uses ceramic honeycomb or plate-type catalysts in which titanium dioxide is the ceramic and the active coatings are vanadium pentoxide and tungsten trioxide (WO₃). The working catalyst temperature ranges from 600–800 °F (315–427 °C). For NO_x abatement, Ducon provides complete ammonia injection systems with storage tanks, vaporizers and injection grids. Either anhydrous or aqueous ammonia can be used.

NO_x-removal catalysts are offered by Haldor-Topsøe, KTI, and others. The Thermal DeNO_x process offered by ExxonMobil is noncatalytic.

2.6.5 Wastewater

In large petroleum production operations and in refineries, the treatment of wastewater (Table 2.16) purifies process water, runoff from storms, and sewage. These may contain oil, suspended solids, dissolved salts, phenols, ammonia, sulfides, and other materials. They come from just about every process unit, especially those that use wash water, condensate, stripping water, caustic, or neutralization acids.

Primary Treatment

Primary treatment uses a settling pond to allow most hydrocarbons and suspended solids to separate from the wastewater. The solids drift to the bottom of the pond, hydrocarbons are skimmed off the top, and oily sludge is removed. Difficult oil-in-water emulsions are heated to expedite separation.

Acidic wastewater is neutralized with ammonia, lime, or sodium carbonate. Alkaline wastewater is treated with sulfuric acid, hydrochloric acid, carbon dioxide-rich flue gas, or sulfur.

Figure 2.16 shows a simplified sketch of an API oil-water separator. The large capacity of these separators slows the flow of wastewater, allowing oil to float to the surface and sludge to settle out. They are equipped with a series of baffles and a rotating endless-belt skimmer, which recovers floating oil. Accumulated sludge is removed through sludge hoppers at the bottom.

Secondary Treatment

A small amount of suspended solids remains in the water after primary treatment. These are removed by filtration, sedimentation or air flotation. Flocculation agents may be added to consolidate the solids, making them easier to remove by sedimentation or filtration. Activated sludge, which contains waste-acclimated bacteria, digests water-soluble organic compounds in either aerated or anaerobic lagoons. Steam-stripping is used to remove sulfides and ammonia, and solvent extraction is used to remove phenols.

Tertiary Treatment

Tertiary treatment removes specific pollutants, including traces of benzene and other partially soluble hydrocarbons. Tertiary processes include reverse osmosis, ion exchange, chlorination, ozonation, or adsorption onto activated carbon. Compressed air or oxygen can be used to enhance oxidation. Spraying water into the air or bubbling air through the water removes remaining traces of volatile chemicals such as phenol and ammonia.

2.6.6 Cleaning Up Oil Spills

Oil spills can be caused by natural seepage, leaky storage tanks, petroleum exploration and production ac-

Table 2.16 Refinery wastewater treatment

Designation	Source
Oil-free water	Oil-free storm runoff
	Steam turbine condensate
	Air-conditioner cooling water
	Cooling water from light-oil units
	Cooling-tower blowdown
Oily cooling water	Clean water from treatment plants
	Oily storm runoff
	Cooling water from heavy-oil units
Process water	Uncontrolled blowdown
	Desalter water
	Excess sour water
	Water drawn from oil-storage tanks
	Accumulator draws
	Treating plant waste
	Barometric condensers
	Slop-oil breaks
Ballast water	
Sanitary water	Employee locker rooms
	Cafeteria
	Office buildings
	Control rooms
Destination	
Oil-free water	Oil/water separator
Oily cooling water	Oil/water separator
Process water	API separator, activated sludge treatment
Sanitary water	Municipal water treatment plant

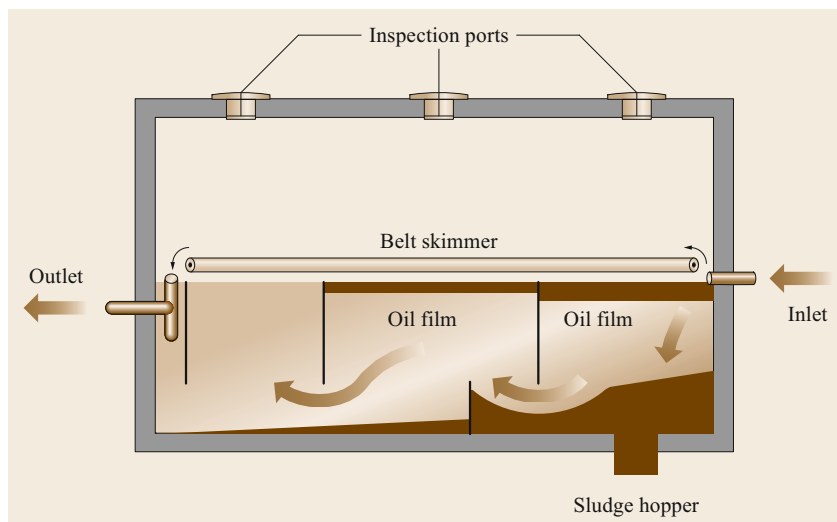


Fig. 2.16 API oil/water separator: simplified sketch

tivities, the on-purpose flushing of fuel tanks at sea, and accidents such as those described in Sect. 2.2.

The cleanup of oil spills includes containment, physical and mechanical removal, chemical and biological treatment, and natural forces. Land-based spills are easier to clean than spills onto open water, which are spread quickly by currents and winds.

Natural Forces

Several natural forces tend to remove oil spills. These include evaporation, spreading, emulsification, oxidation, and bacterial decomposition.

Evaporation. A large portion of an oil spill may simply evaporate before other methods can be used to recover or disperse the oil. Rates of evaporation depend on the ambient temperature and the nature of the oil.

Spreading. The fact that spilled oil spreads quickly across the surface of water is a *good news, bad news* story. The good news is that spreading increases rates of evaporation and air oxidation. The bad news is that the more dispersed the oil becomes, the harder it is to collect.

As with evaporation, rates of oil-spill dispersion depend upon ambient conditions and the nature of the oil. Not surprisingly, oil disperses best in fast-moving turbulent water.

Oxidation. Freshly spilled crude oil has a natural tendency to oxidize in air. Sunlight and turbulence stimulate the process. Oxidation products include organic acids, ketones and aldehydes, all of which tend to dissolve in water. As a spill ages, oxidation slows as *easy* molecules disappear from the mix. Compared to other

natural forces, oxidation plays a minor role in removing oil spills.

Emulsification. When crude oil spills at sea, it emulsifies rapidly. Two kinds of emulsions are formed – oil-in-water and water-in-oil. Oil-in-water emulsions, in which water is the continuous phase, readily disperse, removing oil from the spill. However, this kind of emulsion requires the presence of surface-active agents (detergents).

The composition of water-in-oil emulsions varies from 30% to 80% water. These are extremely stable. After several days, they form *chocolate mousse* emulsions, which are annoyingly unresponsive to oxidation, adsorption, dispersion, combustion, and even sinking. The most effective method for mousse emulsions is physical removal. After a 40–50% loss of light-ends through evaporation, a spill of 200 000 bbl of oil can form 400 000–500 000 bbl of mousse.

Containment and Physical Removal

Booms. When oil is spilled on water, floating booms may be used for containment. A typical boom extends 4 in (10 cm) above the surface and 1 ft (30 cm) below. Foam-filled booms are lightweight, flexible, and relatively inexpensive. Typically used for inland and sheltered waters, they are made from polyvinyl chloride (PVC) or polyurethane. Rectangular floats allow them to be wound onto a reel for storage.

Inflatable booms use less storage space and can be deployed from ships or boats in open water. Towed booms (Fig. 2.17) are good for preventing dispersion of oil by winds and currents.

Beach booms are modified for use in shallow water or tidal areas. Water-filled tubes on the bottom of the

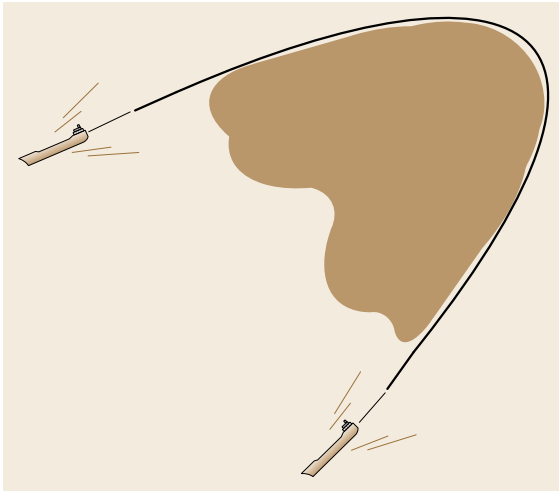


Fig. 2.17 Boom barrier towed by ships

boom elevate it above the beach when the water level is low and allow the boom to float when the water level rises.

Skimmers and Pumps. After a spill is contained, skimmers and pumps can pick up the oil and move it into storage tanks. Weir skimmers are widely used because they are so simple. Modern designs are self-adjusting and circular so that oil can flow into the skimmer from any direction. They can be fitted with screw pumps, which enable them to process many different types of oil, including highly viscous grades. Cutting knives keep seaweed and trash from fouling the pumps. Screw pumps can develop high pressure differentials, which gives them higher capacities than other kinds of pumps.

Another kind of skimmer is an oleophilic (*oil loving*) endless belt. The belt picks up oil as it passes across the top of the water. As the belt returns to its starting point, it is squeezed through a wringer. Oil recovered by the wringer flows into containers, where it is stored until it can be moved to a land-based processing facility.

Another method uses a subsurface impeller to create a vortex, similar to the vortex that forms as water flows out of a bathtub (Fig. 2.18). This funnels water down through the impeller and creates a bowl of oil in the middle of the vortex. A pump is used to remove oil from the bowl.

Adsorbents

Oil spills can be treated with absorbing substances or chemicals such as gelling agents, emulsifiers, and dispersants.

When applying adsorbents, it is important to spread them evenly across the oil and to give them enough

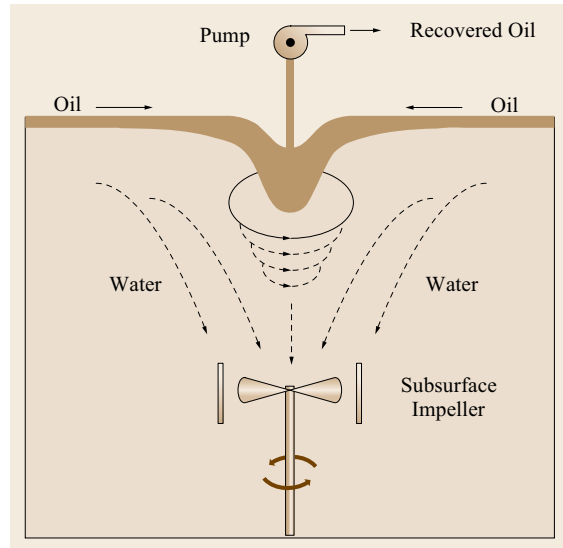


Fig. 2.18 Free vortex skimmer for oil recovery

time to work. When possible, innocuous substances should be used. Straw is cheap, and it can absorb between 8 and 30 times its own weight in oil. When it is saturated, the straw is loaded into boats with rakes or a conveyor system and transported to land. Oil can be recovered from the straw by passing it through a wringer.

Synthetic substances may also be used for adsorbing oil spills. Polymers such as polypropylene, polystyrene, and polyurethane have been used successfully. Polyurethane foam is especially effective. It can be synthesized onsite easily, even aboard a ship. It adsorbs oil readily and doesn't release its load unless it is squeezed. Best of all, a batch of polyurethane can be used again and again.

Dispersion Agents

Dispersion chemicals act like detergents. One part of the molecule is oil-soluble while the other is water-soluble. In effect, the oil dissolves in water and diffuses quickly away from the spill. Dispersants reduce the tendency of oil to cling to partly immersed solids, such as walls, docks, buoys and boats.

Nondispersive Methods

Nondispersive methods for removing oil spills include gelling, sinking, and burning.

Gelling. Fatty acids and 50% sodium hydroxide can be added to a spill to trigger a soap-forming reaction. The resulting gel does not disperse. Instead, it remains in place to block the spread of nongelled oil.

Oil Sinking. Sinking an oil spill keeps it from reaching shorelines, where it can devastate marine life. Sinking is best used in the open sea. In shallow water near the coast, it can cause more problems than it solves. Amine-treated sand is the most common sinking agent. To initiate sinking, a sand/water slurry is sprayed onto the oil slick through nozzles. The required sand/oil ratio is about 1 : 1. The oil sticks to the treated sand, which sinks toward the bottom of the sea; the oil-coated sand can remain in place for many years. According to others, it can damage fragile ecosystems on the ocean floor.

During a full-scale test 15 mi from the coast of Holland, Shell Oil used amine-treated sand to sink a 100-ton slick of Kuwaiti crude in less than 45 min. Oil removal exceeded 95%.

Other materials have been used for oil sinking. These include talc, coal dust, cyclone-treated fly ash, sulfur-treated cement, and chalk. In general, a 1 : 1 ratio of sinker weight to oil weight is needed to sink a fresh spill. If weathering takes place, the density of the oil increases and less sinking agent is needed. It has been estimated that the cost for sinking is similar to the cost for dispersion. However, in open seas under high winds and waves, it may be difficult to spread the sinking agent.

Burning. Freshly spilled crude oil in a confined area may be combustible. However, after several hours, the spill may have thinned due to spreading and the most volatile components may have evaporated. If so, it may not be possible to ignite the remaining material. The addition of gasoline or kerosene can restore combustibility.

Burning is not used much anymore. It seldom removes much oil, and it can generate concentrated, unpredictable pockets of atmospheric CO and SO₂, both of which are poisonous.

Cleanup of Oil-Contaminated Beaches

For cleaning oil from beaches, farm machinery and earthmoving equipment are used to good effect. In many cases, a layer of straw is spread across the oil. After a few days, the oil-laden straw is raked onto a conveyor, screened to drop out sand, and sent to a wringer. Recovered oil is trucked away to a refinery. The spent straw, which still contains some oil, can be blended with coal and burned in a power plant, or simply incinerated. The separated sand is washed and returned to the beach.

When beach pollution is severe, oily sand is removed with earthmoving equipment. When beach pollution is mild, sand removal may not be needed. Instead, detergents can be used. They must be used cautiously to minimize harm to marine life. Wave action does a great

job of mixing detergent into the sand. Usually, the detergent is applied about one hour before high tide. When the tide comes in, the washing begins. If high-tide washing is inappropriate, high-pressure hoses can be used. Hoses are also effective for cleaning oil off of walls and rocks.

Froth Flotation. In the froth-flotation process, oil-soaked sand from a polluted beach is poured into a vessel, where it is mixed with water and cleaned with a froth of air bubbles. Aided by chemical or physical pretreatment, the froth strips oil away from the sand. Due to its low density and the action of the bubbles, the oil floats to the top of the vessel, where it is drawn off and sent to a separating chamber, where entrained water is removed. Tests show that sand containing 5000 ppm of oil can be cleaned down to 130 ppm, generating effluent water with 165 ppm of oil. Usually, the cleaned sand is returned directly to the beach.

Hot Water Cleanup. When milder methods fail to give the desired degree of cleanup, hot water can mobilize some of the oil still trapped within the polluted sand. This method is used as a last resort because of the damage it does to intertidal ecosystems.

Amoco Cadiz Oil Spill Cleanup: A Case Study

As mentioned, for two weeks after the *Amoco Cadiz* ran aground off the coast of Brittany, severe weather restricted cleanup efforts. Eventually, the entire cargo – more than 1.6 million bbl of crude oil – spilled into the sea. The resulting slick was 18 mi wide and 80 mi long. The oil polluted 200 mi of coastline, including beaches, harbors and habitats for marine life.

A 2.5 mi permanent boom protected the Bay of Morlaix. Although it required constant monitoring, the boom functioned well because the bay was protected from severe weather and the brunt of the oil slick. In other areas, booms were largely ineffective due to strong currents, and also because they were not designed to handle such enormous amounts of oil. Skimmers were used in harbors and other protected areas. Vacuum trucks removed oil from piers and boat slips where seaweed was especially thick. *Honey wagons* – vacuum tanks designed to handle liquefied manure – were used to collect emulsified oil along the coast.

Oil-laden seaweed was removed from the beaches with rakes and front-end loaders. Farm equipment was used to plow and harrow the sand, making it more susceptible to wave and bacterial action. Prior to harrowing, chemical fertilizers and oleophilic bacteria were applied to the sand.

At first, authorities decided against using dispersants in sensitive areas and along the coastal fringe.

Meanwhile, the spill formed a highly stable water-in-oil emulsion (*mousse*). On the open sea, the French Navy applied both dilute and concentrated dispersants, but good dispersion was hard to achieve because in some places the mousse emulsion was several centimeters thick. If dispersants had been dropped from the air at the source of the spill – in days instead of weeks – the formation of mousse emulsion might have been prevented.

About 650 t of chalk was applied in an effort to sink the oil. But after one month at sea, the oil was so viscous that the chalk just sat on top of it. Rubber powder made from ground-up tires was applied to absorb the oil. The French Navy used water hoses to spread most of the powder. Some was applied manually from small fishing boats. Because it stayed on top of the oil, the rubber powder had little effect; wave action wasn't strong enough to mix it into the oil, most of which was trapped inside the chocolate mousse emulsion.

During the third and fourth months of the cleanup, high-pressure hot water (fresh water at 2000 psi, 80–140 °C) was very effective in cleaning oil from rocky shores. A small amount of dispersant was applied to prevent oiling of clean rocks during the next high tide. The mouths of several rivers contained oyster beds and marshes that required manual cleaning. Soft mud river banks were cleaned with low-pressure water. To improve oil-collection efficiency, a sorbent was mixed with water and poured in front of the wash nozzles. The oil was collected downstream by a local invention called an *Egmolap*. This device was good at collecting floating material in sheltered areas.

2.6.7 Solid Waste Recovery and Disposal

Contaminated solids are produced during the drilling of oil wells, the transportation of crude oil, and in oil refineries. All oil-contaminated solids are considered hazardous and must be sent to hazardous-waste landfills. The transportation and disposal of hazardous waste costs an order of magnitude more than the transportation and disposal of sanitary waste. Thus, there is a huge economic incentive to remove oil from contaminated solids before they leave a site.

Considerable amounts of solid wastes can be generated during oil drilling. Oil-contaminated cuttings must be cleaned before disposal. Table 2.17 shows the sources of solid wastes in a modern oil refinery. These data, provided by the American Petroleum Institute, are based on a typical 200 000 bbl/day high-conversion refinery. A plant this size produces about 50 000 t/yr of solid waste and about 250 000 t/yr of wastewater. As discussed above, all wastewater must be purified before it leaves the plant.

Table 2.17 Breakdown of refinery solid wastes

Solid Waste	Total (wt %)
Pond sediments	8.4
Sludge from biological treatment	18.9
Solid from DAF/IAF treaters	15.4
API separator sludge	13.2
Miscellaneous sludge	17.5
Off-grade coke	1.9
Spent catalysts	6.4
Slop oil emulsion solids	4.4
Spent solvents, chemicals	3.8
Contaminated soils and other solids	6.7
Heat exchanger cleaning sludge	0.1
Tank sludge	3.4

DAF = dissolved air flotation
IAF = induced air flotation

Supercritical Fluid Extraction

A supercritical substance exists as a single fluid phase. Simultaneously, it can have liquid-like solvating powers and gas-like diffusivity and viscosity; its surface tension is zero. Ammonia, argon, propane, xenon, water, CO, and CO₂ are used for supercritical fluid extraction (SFE). The phase diagram in Fig. 2.19 shows that the supercritical region for CO₂ lies above 88 °F (31 °C) and 1058 psig (7.4 MPa). The CO₂ triple point, where solid, liquid, and gas phases exist simultaneously, occurs at –69.9 °F (–56.6 °C) and 57.8 psig (0.5 MPa).

With nontoxic gases such as CO₂, the SFE process is simple. Untreated solids are placed in an extraction chamber and CO₂ is added. Pressurizing the CO₂ converts it into an effective solvent. By manipulating temperature and pressure, operators can extract the material of interest with high selectivity. After the extracted material dissolves in the CO₂, the mixture goes to a collection vessel, where the pressure is reduced. At low pressure, CO₂ loses its solvating power and separates from the extract. The CO₂ is recovered, condensed and recycled. In SFE with CO₂, no liquid solvents are used. The CO₂ is recycled, so the process is not considered to be a contributor to global warming.

SFE is common in the food, pharmaceutical and cosmetic industries, where it extracts caffeine from coffee beans, bitter from hops, tar and nicotine from tobacco, and other natural compounds from spices, flowers, aromatic woods, and medicinal plants.

Since about 1990, SFE with CO₂ has been used in oil fields to remove oil from drill cuttings. CO₂ is especially good for this purpose because it can be used on site. It is nontoxic (except when it suffocates), relatively unreactive, and it doesn't burn. On drill cuttings and other oil-contaminated soils and sands, it penetrates the mineral structure, removing both the free-oil phase and

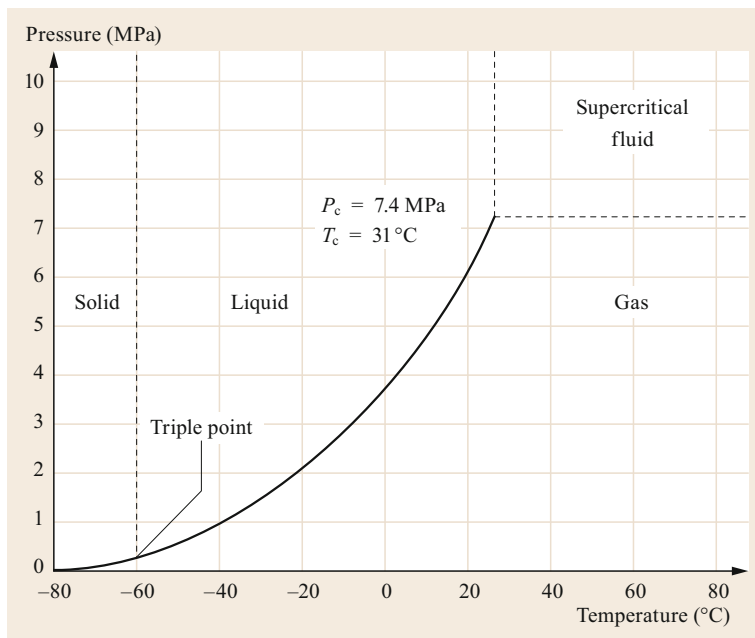


Fig. 2.19 Phase diagram for carbon dioxide

the oil trapped in the solid matrix. The process removes more than 99.9% of the oil, leaving no toxic residue. The required time is short – about 10–60 min/batch.

Sludge

According to RCRA, oil-containing sludge from storage tanks and refinery water treatment facilities is by definition hazardous, and should be sent to a hazardous landfill. In most cases, a lot of the sludge can be dissolved with detergents or solvents (such as hot diesel oil) and blended into crude oil. Alternatively, dissolved sludge can go to delayed cokers, asphalt plants, carbon black plants, or cement kilns.

In one method, hot water and a chemical are circulated through the tank. On top of the water, a hydrocarbon such as diesel is added. The density difference between warm water and the hydrocarbons in the sludge causes the sludge to rise, allowing the chemical to strip out water and solids. The method recovers good-quality oil, which can be processed in the refinery, and leaves behind a relatively clean layer of solids on the tank bottom.

Tanks associated with slurry oil from FCC units present an interesting challenge. It can be very expensive to take these tanks out of service, the sludge is loaded with finely divided FCC catalyst particles, and slurry-oil sludge is difficult to dissolve. Recently, a process called Petromax has been used to liquefy slurry-oil sludge, allowing it to be pumped out of tanks with ordinary equipment, even while the tanks are still in use [2.123].

Some service companies use robots, cutting wands, and other sophisticated devices to clean tanks completely without sending people inside. These methods are especially valuable when the tank contents are toxic. One such company is Petrochemical Services, Inc., which pioneered the use of robots in tank-cleaning operations.

Blending mobilized sludge into crude oil is limited by specifications on basic sediment and water. This seems equivalent to moving waste from one place to another, but it really isn't. The dissolution of tank sludge separates useful oil from inorganic solids (sand, clay, salts, and metal oxides) and refractory organics (asphaltenes, long-chain waxy paraffins, kerogen, and coke).

Spent Catalysts

Many refinery catalysts are regenerated several times. The regeneration of FCC catalysts occurs in the (aptly named) regenerator. Catalysts from fixed-bed units can be regenerated in place, but usually they are sent off site to a facility that specializes in catalyst regeneration.

Eventually, even the hardiest catalysts reach the end of their useful life. When this happens, they are sent to a metals reclaimer, which recovers saleable products such as alumina, silica, MoO_3 , V_2O_5 , nickel metal, and various forms of cobalt.

The reclamation company makes money on both ends of the plant – from the refiner who must dispose of the catalyst, and from the customer who buys reclaimed products.

2.7 Summary

Safety, reliability, and protecting the environment are inextricably linked. In modern industry, they are viewed as prerequisites to profit. Company executives frequently emphasize their strong commitment to worker health and safety. Their commitment derives to a certain extent from strict legislation.

Health and safety rules address personal protection equipment, toxic substances, equipment maintenance, worker training, and compliance monitoring. Environment regulations fall into four main categories: air pollution (particulate matter, volatile hydrocarbons, and harmful gases), waste water, spills and solid wastes. Harm from chronic exposure accumulates with time.

Harm from major accidents causes tremendous short-term destruction, which often is followed by damage that lingers for years. Many of the worst peace-time accidents occur in coal, oil, and chemical industries. Such accidents can teach hard lessons. But as the examples show, not everyone learns the lessons, and those

who do learn lessons sometimes forget or choose to ignore them.

Things have gotten better. Before the 1970s, black lung disease, dead forests downwind from coal-fired power plants, and pools of poison around abandoned strip mines were just part of the price we paid for cheap power and minerals. Smoky flares in refineries were the rule, not the exception. They *smelled like money*. More often than not, news of a river catching fire caused laughter instead of outrage. Climate change was derided as just another bogeyman imagined by academics.

Today a majority of us believe that our fundamental rights include clean air, clean water, and a safe and healthy workplace. We are products of the same social movement that created EPA, OSHA, and similar agencies around the world. Government regulations are providing the Big Stick. The Carrot for all is a safer, cleaner world. We all have one life and one planet. We must ensure the health of both.

References

- 2.1 BP: *BP Statistical Review of World Energy 2017*, <http://www.bp.com/en/global/corporate/energy-economics/statistical-review-of-world-energy.htm>
- 2.2 Wikipedia: *Petrochemical*, <https://en.wikipedia.org/wiki/Petrochemical>
- 2.3 ExxonMobil: *Our Safety Philosophy*, <http://corporate.exxonmobil.com/en/company/about-us/safety-and-health/our-safety-philosophy>
- 2.4 Shell Global: *Safety*, <http://www.shell.com/global/environment-society/safety.html>
- 2.5 KBR Code of Business Conduct, KBR Inc., Houston 2015
- 2.6 Chevron: *Operational Excellence Management System*, <http://www.chevron.com/about/operationalexcellence/tenetsofoperation/>
- 2.7 Wikipedia: *History of Labour Law*, https://en.wikipedia.org/wiki/Environmental_movement
- 2.8 Wikipedia: *Environmental Movement*, https://en.wikipedia.org/wiki/Environmental_movement
- 2.9 P. Mantoux: *The Industrial Revolution in Eighteenth Century: An Outline of the Beginnings of the Modern Factory System in England* (Routledge, Oxon 1961)
- 2.10 Wikipedia: *Labor History of the United States*, https://en.wikipedia.org/wiki/Labor_history_of_the_United_States
- 2.11 United States Department of Labor: *History of Mine Safety and Health Legislation*, <http://www.msha.gov/MSHAINFO/MSHAINFO2.HTM>
- 2.12 Wikipedia: *1900 United States Census*, https://en.wikipedia.org/wiki/1900_United_States_Census
- 2.13 Wikipedia: *Child Labor Laws in the United States*, https://en.wikipedia.org/wiki/Child_labor_laws_in_the_United_States
- 2.14 Wikipedia: *National Child Labor Committee*, https://en.wikipedia.org/wiki/National_Child_Labor_Committee
- 2.15 J. Grossman: *Fair Labor Standards Act of 1938: Maximum Struggle for a Mimimum Wage*, <http://www.dol.gov/dol/aboutdol/history/flsa1938.htm>
- 2.16 L. Margulis, D. Sagan: *What Is Life? The Eternal Enigma* (Univ. California Press, Berkeley 2000)
- 2.17 B. Commoner: *The Closing Circle: Nature, Man, and Technology* (Knopf, New York 1971)
- 2.18 Nobel Prize Organization: *Linus Pauling – Biographical*, http://www.nobelprize.org/nobel_prizes/peace/laureates/1962/pauling-bio.html
- 2.19 R. Carson: *Silent Spring* (Houghton Mifflin, New York 1962)
- 2.20 Pesticide Action Network: *The DDT Story*, <http://www.panna.org/issues/persistent-poisons/the-ddt-story>
- 2.21 United States Environmental Protection Agency: *EPA History*, <http://www2.epa.gov/aboutepa/epa-history>
- 2.22 Wikipedia: *Environmentalism*, https://en.wikipedia.org/wiki/Environmentalism#Early_environmental_legislation
- 2.23 Wikipedia: *History of Fire Safety Legislation in the United Kingdom*, https://en.wikipedia.org/wiki/History_of_fire_safety_legislation_in_the_United_Kingdom
- 2.24 Wikipedia: *Alkali Act 1863*, https://en.wikipedia.org/wiki/Alkali_Act_1863

- 2.25 Wikipedia: *Public Health Act 1875*, https://en.wikipedia.org/wiki/Public_Health_Act_1875
- 2.26 Wikipedia: *List of National Parks of the United States*, https://en.wikipedia.org/wiki/List_of_national_parks_of_the_United_States
- 2.27 National Park Arkansas: *History & Culture*, <http://www.nps.gov/hosp/learn/historyculture/index.htm>
- 2.28 South Coast AQMD: AQMD adopts regulation to reduce particulate emissions from oil refineries, AQMD Advis., November 7, 2003
- 2.29 United States Department of Labor: *Safety and Health Topics: Hydrogen Sulfide*, <https://www.osha.gov/SLTC/hydrogensulfide/hazards.html>
- 2.30 Environmental Protection Agency: *Air Trends: Stratospheric Ozone* (National Service Center for Environmental Publications, Cincinnati 2004)
- 2.31 U.S. Environmental Protection Agency: *Ozone Layer Protection*, <http://www.epa.gov/ozone/intpol>
- 2.32 United States Environmental Protection Agency: *Guidance for the EPA Halon Emission Reduction Rule (40 CFR Part 82, Subpart H)*, https://www.epa.gov/sites/production/files/2015-07/documents/guidance_for_halon_emissions_reduction_rule_40_cfr_part_82_subpart_h.pdf
- 2.33 United States Environmental Protection Agency: *Achievements in Stratospheric Ozone Protection: Progress Report*, https://www.epa.gov/sites/production/files/2015-07/documents/achievements_in_stratospheric_ozone_protection.pdf
- 2.34 M.B. McElroy: *Energy and Climate: Vision for the Future* (Oxford Univ. Press, New York 2016)
- 2.35 United States Environmental Protection Agency: *Climate change indicators in the United States*, <https://www.epa.gov/climate-indicators>
- 2.36 Intergovernmental Panel on Climate Change: *The Physical Science Basis. Working Group I Contribution to the IPCC Fifth Assessment Report*, <http://www.ipcc.ch/report/ar5/wg1> (2013)
- 2.37 Intergovernmental Panel on Climate Change: *Annex 1 Glossary*, <http://www.ipcc.ch/pdf/glossary/ar4-wg1.pdf>
- 2.38 GISTEMP Team: *GISS Surface Temperature Analysis (GISTEMP)*, NASA Goddard Institute for Space Studies: New York, <http://data.giss.nasa.gov/gistemp/graphs/> (2015)
- 2.39 L. Augustin, C. Barbante, P.R.F. Barnes, J.M. Barnola, M. Bigler, E. Castellano, O. Cattani, J. Chappellaz, D. Dahl-Jensen, B. Delmonte, G. Dreyfus, G. Durand, S. Falourd, H. Fischer, J. Flückiger, M.E. Hansson, P. Huybrechts, G. Jugie, S.J. Johnsen, J. Jouzel, P. Kaufmann, J. Kipfstuhl, F. Lambert, V.Y. Lipenkov, G.C. Littot, A. Longinelli, R. Lorrain, V. Maggi, V. Masson-Delmotte, H. Miller, R. Mulvaney, J. Oerlemans, H. Oerter, G. Orombelli, F. Parrenin, D.A. Peel, J.-R. Petit, D. Raynaud, C. Ritz, U. Ruth, J. Schwander, U. Siegenthaler, R. Souchez, B. Stauffer, J.P. Steffensen, B. Stenni, T.F. Stocker, I.E. Tabacco, R. Udisti, R.S.W. van de Wal, M. van den Broeke, J. Weiss, F. Wilhelms, J.-G. Winther, E.W. Wolff, M. Zucchelli: Eight glacial cycles from an Antarctic ice core, *Nature* **429**, 623–628 (2004), <https://www.nature.com/nature/journal/v429/n6992/full/nature02599.html>
- 2.40 J. Zhao, K. Yu, Y. Feng: High-precision 238U–234U–230Th disequilibrium dating of the recent past: a review, *Quaternary Geochronol.* **4**(5), 423–433 (2009)
- 2.41 V. Gornitz: *Sea Level Rise, After the Ice Melted and Today*, NASA Goddard Institute for Space Studies (GISS), https://www.giss.nasa.gov/research/briefs/gornitz_09/(2007)
- 2.42 J. Tyndall: *On radiation, the Rede Lecture delivered before the University of Cambridge* (Longman, Green, Longman, Doberts & Green, London 1865) pp. 54–55
- 2.43 Modified version of Figure 3 in R. Lindsey: *From NASA Earth Observatory: Climate and Earth's Energy Budget*, [http://earthobservatory.nasa.gov/Features/EnergyBalance\(2009\)](http://earthobservatory.nasa.gov/Features/EnergyBalance(2009))
- 2.44 American Chemical Society: *A greenhouse effect analogy*, <https://www.acs.org/content/acs/en/climatescience/climatesciencenarratives/a-greenhouse-effect-analogy.htm>
- 2.45 J.P. Peixoto, A.H. Oort: *Physics of Climate* (Springer, New York 1992) pp. 95–96
- 2.46 Q. Ma: *Greenhouse Gases: Refining the Role of Carbon Dioxide*, https://www.giss.nasa.gov/research/briefs/ma_01/(1998))
- 2.47 United States Environmental Protection Agency: *Climate Change Indicators: Greenhouse Gases*, <https://www.epa.gov/climate-indicators/greenhouse-gases#refl>
- 2.48 United States Environmental Protection Agency: *Global Emissions by Gas, Global Greenhouse Gas Emissions Data*, <https://www.epa.gov/ghgemissions/global-greenhouse-gas-emissions-data>
- 2.49 S.K. Lower: *Carbonate Equilibria in Natural Waters*, <http://www.chem1.com/acad/pdf/c3carb.pdf>
- 2.50 R. Monroe: *How much CO2 can the oceans take up?*, [https://scripps.ucsd.edu/programs/keelingcurve/2013/07/03/how-much-co2-can-the-oceans-take-up\(2013\)](https://scripps.ucsd.edu/programs/keelingcurve/2013/07/03/how-much-co2-can-the-oceans-take-up(2013))
- 2.51 S. Holloway, J.M. Pierce, T. Ohsumi, V.L. Hards: A review of natural CO2 occurrences and their relevance to CO2 storage. In: *Sustainable Energy and Geophysics Programme* (British Geological Survey, Nottingham, UK 2005), external report CR105/104
- 2.52 M. Kelly, *Ice Cores Reveal a Slow Decline in Atmospheric Oxygen over the Last 800,000 Years*, <https://blogs.princeton.edu/research/2016/09/23/ice-cores-reveal-a-slow-decline-in-atmospheric-oxygen-over-the-last-800000-years-science/>(2013)
- 2.53 M.Z. Jacobson: Studying ocean acidification with conservative, stable numerical schemes for nonequilibrium air–ocean exchange and ocean equilibrium chemistry, *J. of Geophys. Res.: Atmos.* (2005) doi:10.1029/2004JD005220
- 2.54 A.J. Andersson, K.L. Yeakey, N.R. Bates, S.J. de Puiron: Partial offsets in ocean acidification from changing coral reef biogeochemistry, *Nat. Clim.*

- Change 4, 56–61 (2014) doi:10.1038/nclimate2050
- 2.55 H. Augenbraun, E. Matthews, D. David: *The Global Methane Cycle*, NASA Goddard Institute for Space Studies, Institute on Climate and Planets, <https://icp.giss.nasa.gov/education/methane/intro/cycle.html> (1997)
- 2.56 United States Environmental Protection Agency: *Climate Change Indicators: Atmospheric Concentrations of Greenhouse Gases*, https://www.epa.gov/sites/production/files/2016-08/ghg-concentrations_fig-1.csv
- 2.57 US Department of Commerce, National Oceanic and Atmospheric Administration: *Climate Change, Frequently Asked Questions*, https://www.esrl.noaa.gov/gmd/outreach/faq_cat-1.html#3
- 2.58 J. Hansen, M. Sato, P. Kharecha, K. von Schuckmann: Earth's energy imbalance and implications, *Atmos. Chem. Phys.* **11**, 13421–13449 (2011) doi:10.5194/acp-11-13421-2011
- 2.59 V. Ramanathan, G. Carmichael: Global and regional climate changes due to black carbon, *Nat. Geosci.* **1**(4), 221–227 (2008) doi:10.1038/ngeo156
- 2.60 National Aeronautics and Space Administration: *Earth's Energy Budget*, https://science-edu.larc.nasa.gov/energy_budget/pdf/ERB_Litho_Edits_Percent_2016_v7.pdf
- 2.61 The World Bank: *Energy use (kg of oil equivalent per capita)*, <http://data.worldbank.org/indicator/EG.USE.PCAP.KG.OE>
- 2.62 Wikipedia: *Steam-Assisted Gravity Drainage*, https://en.wikipedia.org/wiki/Steam_assisted_gravity_drainage
- 2.63 I.D. Gates, S.R. Larter: Energy efficiency and emissions intensity of SAGD, *Fuel* **115**, 706–713 (2014)
- 2.64 Earthworks: *Hydraulic Fracturing 101*, https://www.earthworksaction.org/issues/detail/hydraulic_fracturing_101#.V3tHb7grLct
- 2.65 B. Hicks: *A Brief History of Fracking*, Energy & Capital, <http://www.energyandcapital.com/articles/a-brief-history-of-fracking/2972> (2013)
- 2.66 United States Environmental Protection Agency: *Draft Plan to Study the Potential Impacts of Hydraulic Fracturing on Drinking Water Resources*, EPA/600/D-11/001, February 2011. U.S. EPA, Washington
- 2.67 E. Hansen, D. Mulvaney, M. Betcher: *Water Resource Reporting and Water Footprint from Marcellus Shale Development in West Virginia and Pennsylvania: Final Report* (San Jose State University, San Jose 2013)
- 2.68 K. Galbraith, T. Henry: *As Fracking Proliferates in Texas, So Do Disposal Wells*, Texas Tribune, March 29, 2013
- 2.69 United States Environmental Protection Agency: *Understanding the Safe Drinking Water Act*, <https://www.epa.gov/sites/production/files/2015-04/documents/epa816f04030.pdf>
- 2.70 Earthworks: *Senators, Representatives Act to Close Halliburton Loophole in the Safe Drinking Water Act*, https://www.earthworksaction.org/media/detail/senators-representatives_act_to_close_halliburton_loophole_in_the_safe_drin#.V34mArfVxCo (2009)
- 2.71 S. Phillips: *Federal Legislation Aims to Close 'Fracking Loopholes'*, <https://stateimpact.npr.org/pennsylvania/2013/03/14/federal-legislation-aims-to-close-fracking-loopholes/> (2013)
- 2.72 A. Kuchment: Drilling for Earthquakes, *Sci. Am.*, **315**(1) 2016
- 2.73 J. Atherton, F. Gil: *Incidents that Define Process Safety* (Wiley, Hoboken 2008)
- 2.74 J. Morris, C. Hamby, M.B. Pell: *Regulatory flaws, repeated violations put oil refinery workers at risk*, Huffington Post, May 25, 2011
- 2.75 Wikipedia: *Davy Lamp*, https://en.wikipedia.org/wiki/Davy_lamp
- 2.76 Wikipedia: *Coalworker's Pneumoconiosis*, https://en.wikipedia.org/wiki/Black_lung_disease
- 2.77 Wikipedia: *Lakeview Gusher*, https://en.wikipedia.org/wiki/Lakeview_Gusher
- 2.78 Wikipedia: *Texas City Disaster*, https://en.wikipedia.org/wiki/Texas_City_Disaster
- 2.79 Parliamentary Office of Science and Technology: *Air Quality in the UK*, Postnote (188), November 2002
- 2.80 Proceedings of the Symposium: *Twenty Years after the Amoco Cadiz*, October 15–17, 1998, Brest (Univ. de Bretagne Occidentale, Brest 2000)
- 2.81 R. Varma, D.R. Varma: The Bhopal Disaster of 1984, *Bull. of Sci., Technol. and Soc.* **23**(10), 1–9 (2003)
- 2.82 S. Glasstone, P.J. Dolan: *Biological effects*. In: *The Effects of Nuclear Weapons* (Literary Licensing, Whitefish 1977), p. 605. Available as a PDF from LiteraryLicensing.com
- 2.83 Figure 3 from T.M. Persons, F.W. Rusco: *Nuclear Reactors: Status and Challenges in Development and Deployment of New Commercial Concepts*, 2015, U.S. Government Accountability Office, report GAO-15-652 (2015)
- 2.84 L. Stern, D. J. Balz, M.R. Benjamin, P. Brinkley-Rogers, W. Brown, V. Cohn, H. Craig, J. Freundel, J.R. Garreau, P. A. Masley, R. Mezsoly, P. Milius, T. O'Toole, B. Peterson, W. Pincus, W.C. Ross, M. Schram, W. Sinclair, J.P. Smith, T.R. Reid, B. Richards, E. Walsh: *What Happened: Crisis at Three Mile Island*, Washington Post, <http://www.washingtonpost.com/wp-srv/national/longterm/tmi/whathappened.htm> (1999)
- 2.85 S. Shargorodsky: *Ukraine to Mark 15th Anniversary of Chernobyl Nuclear Disaster*, Online Athens, Athens Banner-Herald, April 6, 2001, http://onlineathens.com/stories/042601/new_0426010039.shtml#.WJb_OfkrK1s
- 2.86 International Nuclear Safety Advisory Group: *The Chernobyl Accident: Updating of INSAG-1*, Safety Series No. 75-NSAG-7, (International Atomic Energy Commission, Vienna 1992)
- 2.87 A. Dyatlov: Why INSAG has still got it wrong, *Nucl. Eng. Int.*, September 1995
- 2.88 World Nuclear Association: *Chernobyl Accident-Appendix2 - Health Impacts*, <http://www.world-nuclear.org/information-library/safety-and-security/safety-of-plants/appendices/chernobyl-accident-appendix-2-health-impacts.aspx>

- 2.89 G. Grushevoi, I. Grushevaya: *Testimony from White Russia, Poison Fire, Sacred Earth – Testimonies, lectures, conclusions from the World Uranium Hearing*, <https://ratical.org/radiation/WorldUraniumHearing/GernadijGrushevoi.html>
- 2.90 U. Weber: *The Miracle of the Rhine*, UNESCO Courier, June 2000
- 2.91 Associated Press: *Tankers Have Spill-Free Year in Alaska*, July 11, 2004
- 2.92 U.S. Environmental Protection Agency: *EPA Chemical Accident Investigation Report: Tosco Avon Refinery, Martinez, California*, EPA 550-R-98-009, Washington (1998)
- 2.93 Chemical Safety and Hazard Investigation Board: *Refinery Explosion and Fire, BP Texas City Refinery (15 Killed, 180 Injured)*, Report No. 2005-04-I-TX, CASB: Washington (2005)
- 2.94 National Commission on the BP Deepwater Horizon Oil Spill and Offshore Drilling: *Report to the President: Deepwater: The Gulf Oil Disaster the Future of Offshore Drilling*, <https://www.gpo.gov/fdsys/pkg/GPO-OILCOMMISSION/pdf/GPO-OILCOMMISSION.pdf> (2011)
- 2.95 A. Nandakumar, R. Bousso, K. Finn: *BP Settles 2010 Gulf Oil Spill Claims for \$18.7 Billion*, Reuters: DailyFinance, <http://www.dailyfinance.com/2015/07/02/bp-pay-damages-water-pollution-gulf-oil-spill/> (2015)
- 2.96 Wikipedia: *Lac-Mégantic Rail Disaster*, https://en.wikipedia.org/wiki/Lac-Mégantic_derailment
- 2.97 Wikipedia: *2015 Tianjin Explosions*, https://en.wikipedia.org/wiki/2015_Tianjin_explosions
- 2.98 P. Schroeder, L. Kostyniuk, M. Mack: *2011 National Survey of Speeding Attitudes and Behaviors*, Report No. DOT HS 811 865: National Highway Traffic Safety Administration (U.S. Department of Transportation, Washington 2013)
- 2.99 N.H.T.S. Administration: *Traffic Safety Facts 2013: A Compilation of Motor Vehicle Crash Data from the Fatality Analysis Reporting System and the General Estimates System* (U.S. Department of Transportation, Washington 2013)
- 2.100 A. Santos, N. McGuckin, H.Y. Nakamoto, D. Gray, S. Liss: *Summary of Travel Trends: 2009 National Household Travel Survey*, Report No. FHWA-PL-11-022, Federal Highway Administration, (U.S. Department of Transportation, Washington 2011)
- 2.101 Federal Highway Administration: *Our Nations' Highways – 2000*, Publication No. FHWA-PL-01-1012, <http://www.fhwa.dot.gov/ohim/onh00/onh.htm> (2001)
- 2.102 ENLAR Compliance Services: *What is "Management of Change"?*, <http://ohsas18001expert.com/2007/07/18/what-is-management-of-change/> (2007)
- 2.103 U.S. Chemical Safety Board: *CSB Safety Bulletin Says "Managing Change" is Essential to Safe Chemical Process Operations*, <http://www.csb.gov/csb-safety-bulletin-says-managing-change-is-essential-to-safe-chemical-process-operations/> (2001)
- 2.104 E.G. Seebauer: *Whistleblowing: Is it always obligatory?*, Chem. Eng. Prog. **100**(6), 23–27 (2004)
- 2.105 United States Department of Labor, Occupational Safety and Health Administration: *Personal Protective Equipment for General Industry: Title 29 of the Code of Federal Regulations (CFR), Part 1910 Subpart I*, https://www.osha.gov/pls/oshaweb/owastand.display_standard_group?p_toc_level=1&p_part_number=1910
- 2.106 United States Department of Labor, Occupational Safety and Health Administration: *OSHA Fact Sheet – Personal Protective Equipment*, https://www.osha.gov/0shDoc/data_General_Facts/ppe-factsheet.pdf (2006)
- 2.107 J. Depledge, R. Lamb: *Caring for Climate: A Guide to the Climate Change Convention and the Kyoto Protocol* (Courir-Druck, Bonn 2003)
- 2.108 D. Heron: *Bridge Painting Company and Its President Plead Guilty to Federal Crimes Relating to the Dumping of Lead Waste*, <https://yosemite.epa.gov/opa/advpress.nsf/6427a6b7538955c585257359003f0230/fafbd6f7de051264852570d60070fce0!OpenDocument> (2002)
- 2.109 U.S. Environmental Protection Agency: *Overview of the Clean Air Act and Air Pollution*, <http://www.epa.gov/air/caa/peg/index.html>
- 2.110 U.S. Environmental Protection Agency: *NAAQS Table* <https://www.epa.gov/criteria-air-pollutants/naaqs-table>
- 2.111 U.S. Environmental Protection Agency: *Air Pollution Monitoring* <http://www.epa.gov/airquality/montring.html>
- 2.112 U.S. Environmental Protection Agency: *Gasoline Standards*, <http://www.epa.gov/otaq/fuels/gasolinefuels/rfg/index.htm>
- 2.113 U.S. Environmental Protection Agency: *Summary of the Energy Policy Act*, <http://www2.epa.gov/laws-regulations/summary-energy-policy-act>
- 2.114 Environmental Protection Agency: *2003–2008 EPA Strategic Plan. Goal 2: Clean and Safe Water* (U.S. Environmental Protection Agency, Washington 2003)
- 2.115 United States Environmental Protection Agency: *CERCLA Overview*, <http://www.epa.gov/superfund/policy/cercla.htm>
- 2.116 United Nations: *Kyoto Protocol to the United Nations Framework Convention on Climate Change* (UNFCC, Bonn 1998)
- 2.117 F. Pearce: *Kyoto protocol is just the beginning*, <https://www.newscientist.com/article/dn6494-kyoto-protocol-is-just-the-beginning> (2004)
- 2.118 United Nations: *The Paris Agreement*, <http://unfccc.int/2860.php>
- 2.119 A. Hirstenstein: *Clean-Energy Jobs Surpass Oil Drilling for First Time in US*, <https://www.bloomberg.com/news/articles/2016-05-25/clean-energy-jobs-surpass-oil-drilling-for-first-time-in-u-s> (2016)
- 2.120 Hamon Research-Cottrell: *Wet gas scrubbers*, <http://www.hamonusa.com/hrc/products/wgs>
- 2.121 K.A. Couch, K.D. Seibert, P. Van Opdorp: *Controlling FCC yields and emissions: UOP technology for a changing environment*, AM-04-45. In: *Proc. NPRA*

- 2.122 *Annu. Meet., San Antonio, March 23–25 (2003)*
BP Global: *Air Quality Brochure*, http://www.bp.com/content/dam/bp-country/en_au/about-us/what-we-do/air-quality-brochure.pdf
- 2.123 S. von Bergen: *Petromax Sand Sludge Conditioning* (Saxon Petrotechnologies, Nyon 2009), <https://www.youtube.com/watch?v=thAHde0KMyk>

Petroleum **Part A**

Part A Petroleum Characterization

3 Molecular Science, Engineering and Management

Chang Samuel Hsu, Tallahassee, USA,
Changping, China

4 Petroinformatics

Manhoi Hur, Ames, USA
Sunghwan Kim, Buk-Gu Daegu, Korea
Chang Samuel Hsu, Tallahassee, USA,
Changping, China

5 Separations in the Sample Preparation for Sulfur Compound Analysis

Jan T. Andersson, Münster, Germany

6 Asphaltenes

Oliver C. Mullins, Cambridge, USA
Andrew E. Pomerantz, Cambridge, USA
A. Ballard Andrews, Cambridge, USA
Rudraksha Dutta Majumdar, Toronto, Canada
Paul Hazendonk, Lethbridge, Alberta, Canada
Yosadara Ruiz-Morales, Mexico City, Mexico
Lamia Goual, Laramie, USA
Richard N. Zare, Stanford, USA

7 Reservoir Evaluation by DFA Measurements and Thermodynamic Analysis

Go Fujisawa, Cambridge, UK
Oliver C. Mullins, Cambridge, USA

8 Phase Behavior and Properties of Heavy Oils

John M. Shaw, Edmonton, Canada
Marco A. Satyro[†]
Harvey W. Yarranton, Calgary, Canada

3. Molecular Science, Engineering and Management

Chang Samuel Hsu

All organic materials, living and nonliving are made of molecules. Hence, the composition and structure of the organic molecules, either in pure compounds or different in complex mixtures, determine the properties, behavior, and reactivity of the compounds and mixtures. Chemistry is a science to study the changes of molecules and the relationship of those changes with physics, mathematics, biology, geology, and other disciplines. Chemistry controls how molecules can be used in exploration/production, refining engineering/processing, chemical production, drug discovery, disease controls, etc.

Molecular engineering is the science of manufacturing molecules through transformation and/or combination of molecules by engineering processes. It is especially valuable in petroleum, where it impacts chemical engineering (downstream) and petroleum engineering (upstream), the two major disciplines in which molecules are handled in large scales. Molecular engineering can be guided, controlled, or predicted through molecular-based modeling.

Through knowledge of chemistry and the understanding of chemical processes, we can manage molecules more economically, while minimizing harm to life and the environment. Waste molecules must be properly handled and disposed. Hence, science, engineering, and management should be an integral part of handling molecules from the beginning to the end of all chemical and biochemical processes.

Detailed information on molecules often requires the use of sophisticated analytical instrumentation. Analytical devices and instruments play key roles in providing information of existing, unknown, or new molecules for the design and control of chemical processes. Analytical research and development have been driven by business needs, market demands, and governmental regulations.

In the oil industry, regardless of sector – upstream, downstream, petrochemical, environmental or modeling, molecular understanding of

3.1	Analytical Endeavors in the Petroleum Industry	152
3.2	Analytical Tools	153
3.3	Analytical Strategy	153
3.4	Chromatographic Systems	153
3.5	Mass Spectrometry	154
3.6	Petroleum Biomarker Analysis	155
3.7	Online LC-MS	158
3.8	Ionization for Molecules	160
3.8.1	Ionization Under Vacuum and Reduced Pressure	160
3.8.2	Ionization Under Atmospheric Pressure	161
3.9	Mass Analyzers	164
3.9.1	Magnet Sector Mass Spectrometers	164
3.9.2	Quadrupole Mass Analyzers (QMS)	164
3.9.3	Time-of-Flight Mass Spectrometers (TOF MS)	165
3.9.4	Quadrupole Time-of-Flight Mass Spectrometers (QTOF MS)	165
3.9.5	Fourier-Transform Ion Cyclotron Resonance Mass Spectrometry (FT-ICR MS)	165
3.9.6	Other Mass Spectrometers	166
3.10	Data Interpretation and Management	166
3.10.1	Molecular Isotopic Pattern Computation	166
3.10.2	Compound Identification and Type Analysis	166
3.10.3	Integration of Molecular Characterization Data for Kinetic Modeling	166
3.11	Molecular Engineering and Management Through Science and Modeling	167
3.12	Conclusion	167
	References	168

petroleum and upgrading processes is important for science and technology development and the improvement of processes and products.

All organic materials, living and nonliving are made of molecules. Hence, the composition and structure of the organic molecules, either in pure compounds or different in complex mixtures, determine the properties, behavior, and reactivity of the compounds and mixtures. Physical properties include density, boiling point, melting point, mass (as aggregates of atoms), and energy (vibration, rotation, and intermolecular interaction). Chemical properties include reactivity, stability, and changes in molecules, and biological properties include toxicity, etc. Important behavior includes processability and disposal options of the feeds, intermediates, and products.

Chemistry is a science to study the changes of molecules and the relationship of those changes with physics, mathematics, biology, geology, and other disciplines. Chemistry controls how molecules can be used in exploration/production, refining engineering/processing, chemical production, drug discovery, disease controls, etc.

Molecular engineering is the science and technology of manufacturing molecules through transformation and/or combination of molecules by engineering processes. It encompasses chemical (including refining) and pharmaceutical research as well as material science. It is especially valuable for petroleum where it impacts chemical engineering (downstream) and petroleum engineering (upstream), the two major disciplines in which molecules are handled in large scales.

Through knowledge of chemistry and the understanding of chemical processes, we can manage molecules more economically, while minimizing harm to life and the environment. Waste molecules must be properly handled and disposed. Hence, science, engineering, and management should be an integral part of handling molecules from the beginning to the end of all chemical and biochemical processes.

Detailed information on molecules often requires the use of sophisticated analytical instrumentation. Analytical devices and instruments play key roles in providing information of existing, unknown, or new molecules for the design and control of chemical processes. Many physical and chemical devices can be used to monitor, analyze, and measure molecules in a pure form, bulk mixtures, or individual groups of components.

This chapter is derived mainly from the author's personal experience in and contributions to the development of petroleum mass spectrometry (MS). It is not intended to be an overview of all the molecular characterization techniques being developed and available. However, it provides evidence that molecular characterization can play important and critical roles in petroleum research and development. Many new technologies in molecular characterization and management (through modeling) continuously emerge, dealing with science understanding and leading to practical engineering improvements.

3.1 Analytical Endeavors in the Petroleum Industry

In the petroleum industry, the analytical endeavor can be generally divided into upstream and downstream applications. In upstream operations, the main goals are the discovery, recovery, and transportation of hydrocarbon resources. Certain individual molecules, most noticeably petroleum biomarkers, in crude oil or other fossil hydrocarbons (coal, oil shale, oil sands, tar sands, etc.) can provide key geochemical information to guide exploration and production. In downstream operations, refining processes involve large volumes of complex mixtures, such as crude oil or its distillation fractions. Molecular details are only obtained to assist the understanding or control of processes and their products.

In general, the higher the boiling point of the mixture, the more difficult it is to obtain the information of individual molecules due to the complexity of the mixtures. For example, it remains challenging to determine molecular compositions and structures of residua (*resids* in petroleum terminology) and asphaltenes reliably even using the most modern analytical techniques and instrumentation. But without an adequate or better understanding and knowledge of the molecules involved, existing refining or chemical processes cannot be optimized and new processes cannot be developed for upgrading resids and asphaltenes to high-value fuels and chemical products.

3.2 Analytical Tools

For pure compounds or simple mixtures, ^1H and ^{13}C nuclear magnetic resonance (NMR) spectroscopy and vibrational spectroscopy (infrared and Raman) can provide the unambiguous determination of molecular structures [3.1, 2]. When dealing with more complex mixtures, these spectroscopies can be coupled (hybridized) with chromatography (gas, liquid, or supercritical) either online or offline to separate individual components for molecular structural determination [3.1]. However, MS is much more convenient and effective when coupled with chromatography due to

its adaptability, sensitivity, and specificity. Therefore, MS has become the most commonly used analytical technology, either alone or coupled with chromatography, for detailed molecular characterization [3.1, 3]. Chromatography alone can also be used for identification purposes if authentic compounds are available for confirmation. Specific detectors are often used for the confirmation of the mass spectrometric identification of components containing heteroatoms, such as sulfur, nitrogen, oxygen, and phosphorus [3.1, 4].

3.3 Analytical Strategy

For complex crude oils, bulk properties such as distillation yield, density (API gravity), viscosity, CHNS (carbon-hydrogen-nitrogen-sulfur contents), metal content, ash content, and total acid number are measured by a series of physical tests, which are compiled into crude assays [3.5]. Overall functionalities are measured by spectroscopy on distillation fractions. Only in selected cases, when it is necessary to the understanding of crude oils or refining processes and/or identification of problem-causing materials, detailed molecular characterization is carried out.

In upstream, geochemists work with other geoscientists to study the paleotransformation of deeply buried organic deposits for local or integrated sedimentary basin assessment. A few target compounds, generally petroleum biomarkers, are analyzed in studies of geochemical processes to assist in exploration effort. Biomarkers are compounds that retain basic carbon skeletons of biological precursors and carry important geochemical information during organic sediment burial and subsequent transformation.

In downstream operations, crude oils are separated by distillation into different boiling fractions, including petroleum gas, naphtha, gasoline, jet fuel, diesel, gas oils, and resids. Lubricant base oils are produced through solvent-refining processes (deasphalting, extraction, dewaxing, etc.) of atmospheric or vacuum

resids, or by hydrorefining processes. The petroleum boiling fractions below gasoline have been well characterized. Hence, most of the refining research and developments today are in heavy hydrocarbon characterization for converting low-value residual oils and resids into high-value fuels and lubricant base oils to increase profit margins.

Many conversion processes involve the use of catalysts that are often expensive. Hence, modern research in the petroleum industry has also been on the development and application of novel catalysts to improve process performance, economic operations, and product quality. It is important for analytical scientists to cooperate with engineers or modelers for experimental design, information flow, and problem solving. Such cooperation leads to tool sharpening (development of new and improved analytical methodology or protocols).

The common problems of heavy petroleum fractions encountered in oil refineries include crude incompatibility, emulsions in desalters, corrosion, deposit/sediment formation in storage tanks and reactors, precipitation and fouling in heat exchangers, line blockage, carbon laydown, and catalyst fouling during upgrading processes, just to name a few. The characterization of foulants, undesired impurities, and off-specification products at the molecular level is a constant challenge to the scientists/engineers.

3.4 Chromatographic Systems

Several types of chromatographic systems are suitable for the analysis of organic molecules [3.6]. The most commonly used are gas chromatography (GC) and liquid chromatography (LC) [3.7]. Supercritical fluid

chromatography (SFC), which can have characteristics of GC and LC, is also used on many occasions. GC is generally used for separating nonpolar or low-polarity compounds with high and moderate volatility (boiling

points lower than 500°C) in gas and vaporized liquid mixtures, while LC is used for mixtures of polar compounds and high-boiling compounds in a liquid solution.

A GC system consists of an injector, an oven, and a detector. GC has become a mature, well-developed technology since the 1950s. The gaseous or liquid sample is introduced into an injector in a carrier gas like helium, hydrogen, or nitrogen. Injectors can be split/splitless, on-column, temperature programmable, etc. A dual injector is commonly available in modern GC systems. A single oven with a single column is usually used, but a dual oven with two columns can be found in comprehensive two-dimensional GC (GC×GC) [3.8]. Modern GCs use fused silica capillary columns typically 10–100 m long and ≤ 0.25 mm ID for the enhanced separation efficiency of the components based on diffusivity, although occasionally they use some packed columns for specific separation purposes. Other than for gas mixtures at room temperature, temperature gradient programs are often used for complex mixture analysis. However, the maximum temperature allowed for the column (and the oven) is generally not higher than 450°C due to the temperature limitations on stationary coatings for the separation of components based on diffusivity inside the column. There are many kinds of de-

tectors available. The most commonly used detectors in petroleum or petrochemical analysis include flame ionization (FID), sulfur specific (such as sulfur chemiluminescence, SCD), nitrogen specific (such as nitrogen chemiluminescence, NCD or nitrogen–phosphorus, NPD), and other element-specific (such as atomic emission, AED) detectors [3.4]. Since the 1960s, MS has been used as a GC detector, only for routine analysis without sophisticated instrument operations and spectral interpretations [3.9].

LC has been used for fractionating less volatile or nonvolatile complex mixtures based on solubility in different solvent systems [3.7]. Its separation efficiency is generally much less than GC for complex petroleum mixtures. Suitable detectors are also more limited. The detectors include mostly refractive index (RI), ultraviolet (UV), and evaporative low-angle light scattering (ELSD) for petroleum applications. The sample is generally dissolved in a solvent or solvent mixture that is compatible with the nonpolar or polar mobile phases. The column is packed with a suitable stationary phase. For petroleum fractions, the separation results in compound types grouped with numerous co-eluting components of various carbon numbers. When coupled with MS, it provides additional values for differentiating molecules with the same molecular formula but different functionalities [3.10].

3.5 Mass Spectrometry

Mass spectrometry (or spectroscopy) (MS) was invented, developed, and exclusively used by physicists at the turn of the last century for the studies of the basic properties of substances, which led to the discovery of elements and isotopes [3.11, 12]. After the first commercial instrument was delivered at Atlantic Richfield in 1942, it was used in the petroleum industry for the analysis of petroleum gases and light fuels during and after World War II. Since then, MS has become an indispensable and the most powerful analytical technique for molecular characterization [3.3, 13]. Its coupling with chromatography further enhances its capabilities in mixture analysis [3.9, 10, 14–16].

The four major components of a mass spectrometer are shown in Fig. 3.1 [3.17, 18]. A mass spectrometer is an analytical device for detecting and measuring vapor phase ions in vacuum, even though the ions can be generated in atmospheric pressure outside the mass analyzer. Hence, ion production in an ion source through various ionization techniques is essential. The sample can be introduced alone, such as in a batch inlet or in a direct insertion probe, or

through chromatography, most commonly GC and LC. A range of mass-resolving power is achievable by various types of mass analyzers, from unit mass resolution on a quadrupole mass spectrometer to ultrahigh resolution on a Fourier-transform ion cyclotron resonance mass spectrometer (FT-ICR MS). The ion detector is designed to be suitable or adaptable for the mass analyzer. For example, induced image current detection is associated with FT-ICR MS that is not suitable for electron multipliers for ion signal enhancement. Effective ion transmission between the components is also critical to a successful mass spectrometric experiment. There are numerous reference books for mass spectrometric operations. Although library or reference spectra are available for routine analysis, advanced data interpretation for much more complex high-boiling petroleum mixtures requires an in-depth training of professionals.

Petroleum is a mixture that is too complex for the characterization of individual molecules [3.19]. It is more practical to analyze distillation fractions, such as those produced during conventional refinery operations,

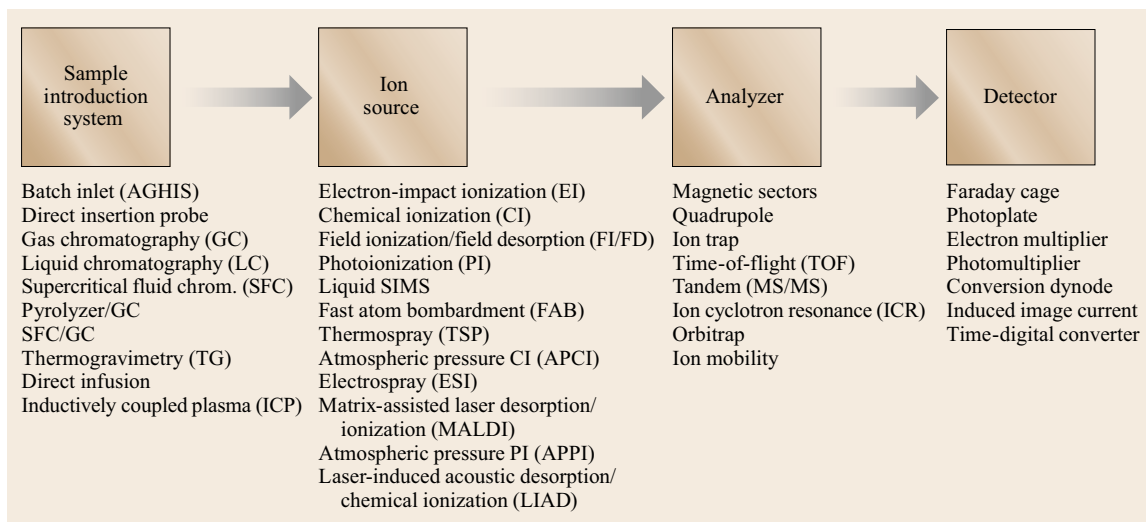


Fig. 3.1 An array of MS techniques has been developed for petroleum mass spectrometric analysis. (After [3.18])

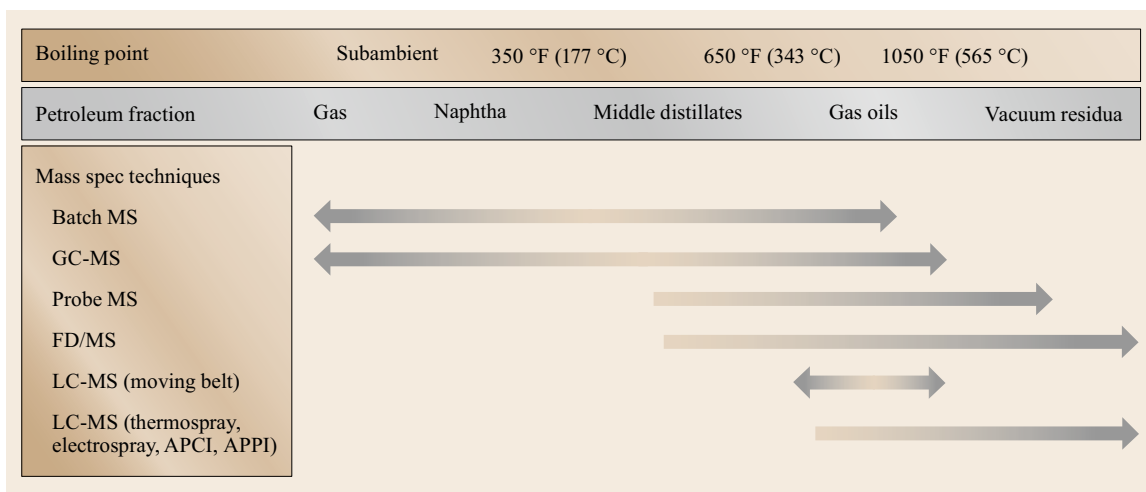


Fig. 3.2 Various petroleum fractions require different mass spectrometric modes of operation. (After [3.18])

namely, gas, naphtha, middle distillates, gas oils, and resids. For each fraction, various modes of mass spectrometric operations as shown in Fig. 3.2 are applied to obtain maximum molecular information [3.17, 18]. GC-

MS is the most powerful technique for mixture analysis including gas oils. For heavy fractions beyond gas oils, the use of direct insertion probe, direct liquid introduction, and field desorption (FD) is common.

3.6 Petroleum Biomarker Analysis

The most noticeable application of MS in upstream is petroleum biomarker analysis [3.18, 20–22]. As mentioned above, biomarkers are petroleum molecules that retain the basic carbon skeleton of biological origins through diagenesis. These molecules provide important geochemical information on source input (ma-

rine, lacustrine/terrestrial or paralic), age (Cretaceous, Jurassic, Devonian, etc.), maturity, alteration (such as biodegradation, oxidation and water washing), and depositional environment [3.23, 24]. They can be used for developing oil–oil and oil–source rock correlations for migration and accumulation studies, as well as en-

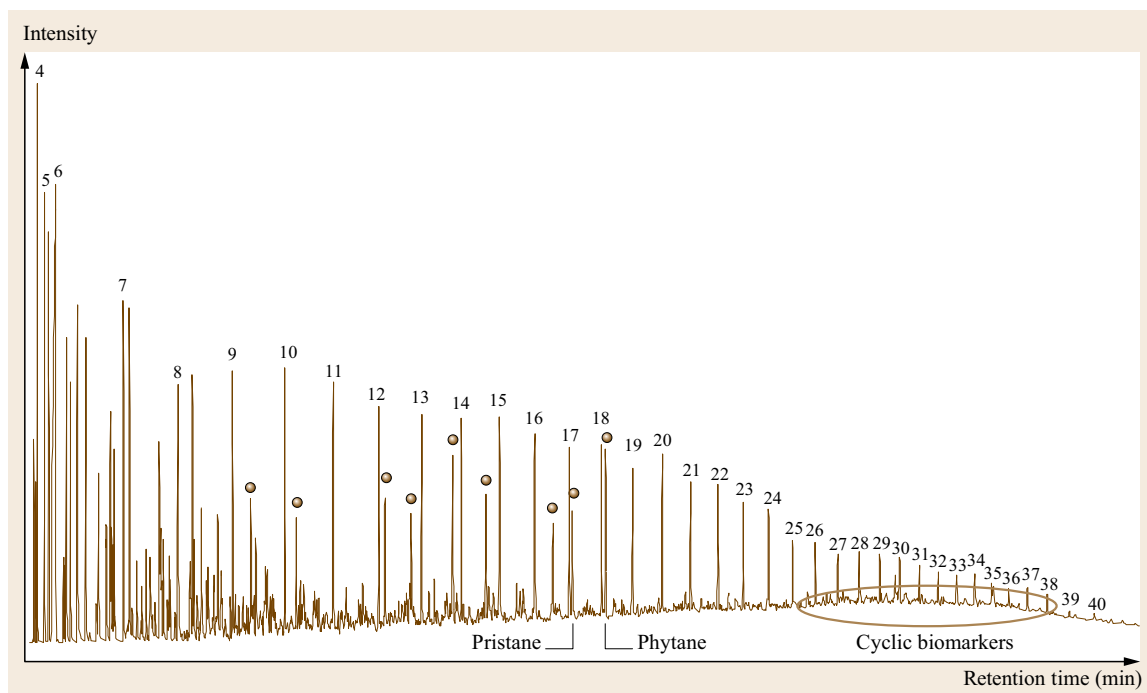


Fig. 3.3 Typical biomarker distributions in crude oils measured with GD-FID. (After [3.22]). The numbers on top of peaks are carbon numbers of *n*-paraffins, ●'s denote isoprenoid hydrocarbons

vironmental applications, including the identification of oil-spill sources, differentiation/correlation of oils, and monitoring the degradation process and weathering of oils under a wide variety of environmental conditions [3.25].

Limited analysis can be done by GC-FID, as shown in Fig. 3.3. The salient feature of the chromatogram is the presence of normal paraffins. Isoparaffins are also abundant. The ratio of C_{19} pristane (Pr) and C_{20} phytane (Ph) can be used as an indicator of whether the environment during deposition was reducing ($Pr/Ph < 1$) or oxidizing ($Pr/Ph > 1$). However, cyclic biomarkers that are rich in geochemical information cannot be analyzed with this method due to severe overlaps with other hydrocarbons and their low concentrations.

To detect the overlapping cyclic biomarkers as shown above, mostly 4-ring (steranes) and 5-ring (hopanes/triterpanes) cycloparaffins (see below), GC-MS is used [3.9]. Under 70 eV (high-energy) electron-impact ionization (EI) conditions, the 4-ring steranes yield a characteristic fragment ion at mass-to-charge ratio (m/z) at 217 while 5-ring hopanes (triterpanes) yield a characteristic m/z 191 ion. A mass spectrometer operated so as to record only these two masses

rather than a full scan from low to high masses can enhance the signals, yielding the m/z 191 and 217 mass chromatograms, as shown in Fig. 3.4. Hopanes (triterpanes) can be well resolved according to their carbon number. On the other hand, severe overlaps in carbon numbers are observed for steranes. However, the ratio of hopanes to steranes can be used as a source facies indicator [3.26]. In general, ratios below 4 generally indicate marine sources and greater than 15 indicate terrigenous/lacustrine sources. The medium ratios can be attributed to the paralic source inputs.

The overlapping steranes can be resolved by the use of tandem MS coupled with GC as GC-MS-MS [3.22]. Figure 3.5 shows the GC-MS-MS mass chromatograms displaying precursors (parents) of the m/z 217 ion characteristic to steranes. In the example shown, the second stage MS is fixed at m/z 217, while the first stage MS is stepped between m/z 372, 386, 400, and 414, the molecular ions of the C_{27} , C_{28} , C_{29} , and C_{30} steranes, respectively, to enhance the ion signals of fragmentation occurring between the two stages of MS. Not only steranes of different carbon numbers but also epimers of each carbon number are resolved for quantitation. The presence of trace amounts of C_{30} steranes as a marine source indicator that would be buried under C_{28} and

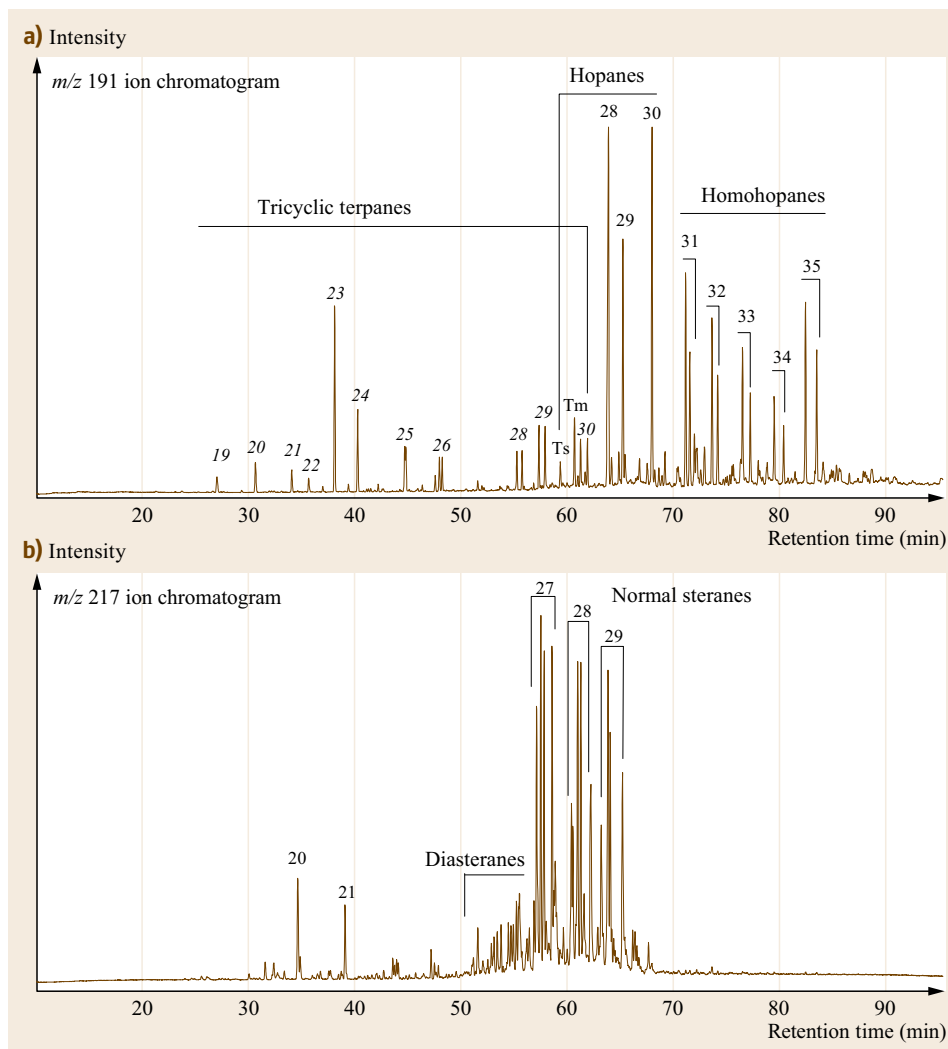


Fig. 3.4a,b GC-MS mass chromatograms of m/z 191 (a) and 217 (b) ions which display the distributions of hopanes and steranes, respectively. (After [3.22]). The *numbers* on top of the peaks are carbon numbers

C_{29} steranes in GC-MS runs can then be detected. For marine source oils and source rock extracts, the ratio of C_{28} -to- C_{29} steranes can be correlated with age reflecting different phytoplanktons appeared at different eras [3.22].

Instead of GC-MS-MS, comprehensive two-dimensional gas chromatography (GC \times GC) can also resolve the sterane and hopane biomarkers from co-eluting hydrocarbons appearing in the one-dimensional GC chromatograms. It was found that the reversed column arrangement, that is, a polar column as the first dimension and a nonpolar column as the second dimension would yield better results for acyclic and

cyclic paraffins, as shown in Fig. 3.6 as a contour plot of GC \times GC-FID chromatogram, than a normal column arrangement for which a nonpolar column is the first dimension and a polar column is the second dimension [3.27]. Steranes and hopanes are well resolved from each other and other paraffins and aromatics. Absolute quantitation is made possible by the use of a universal quantitation detector, FID [3.28]. However, the resolution of sterane epimers at each different carbon numbers still requires the use of MS. This may change when more polar GC columns that can withstand temperatures higher than 400 °C and resolve the epimers become available.

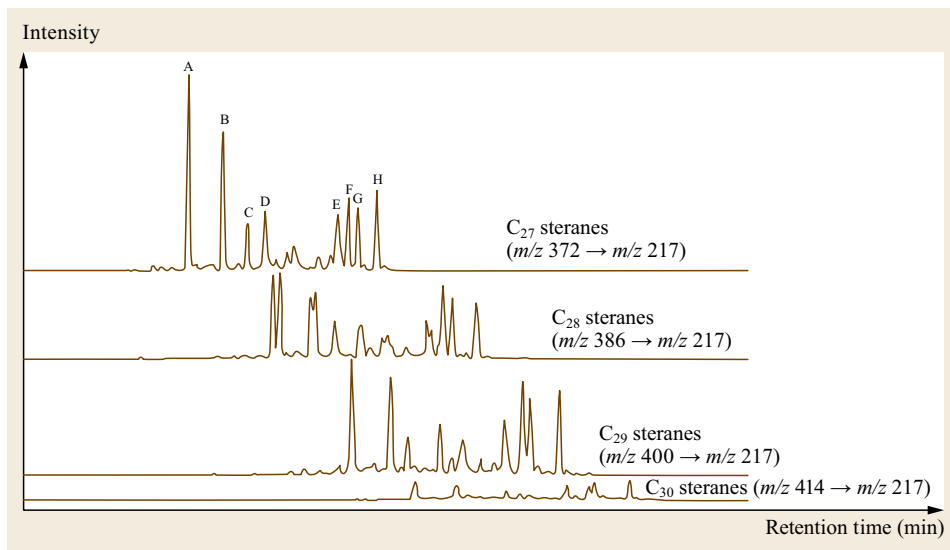


Fig. 3.5 GC-MS-MS mass chromatograms of precursor scans of m/z 217 ion resolve overlapping sterane epimers of different carbon numbers. (After [3.22]) A: C_{27} 13 β (H),17 α (H)-20*S*-diasterane; B: C_{27} 13 β (H),17 α (H)-20*R*-diasterane; C: C_{27} 13 α (H),17 β (H)-20*S*-diasterane; D: C_{27} 13 α (H),17 β (H)-20*R*-diasterane; E: C_{27} 5 α (H),14 α (H),17 α (H)-20*S*-cholestane; F: C_{27} 5 α (H),14 β (H),17 β (H)-20*R*-cholestane; G: C_{27} 5 α (H),14 β (H),17 β (H)-20*S*-cholestane; H: C_{27} 5 α (H),14 α (H),17 α (H)-20*R*-cholestane

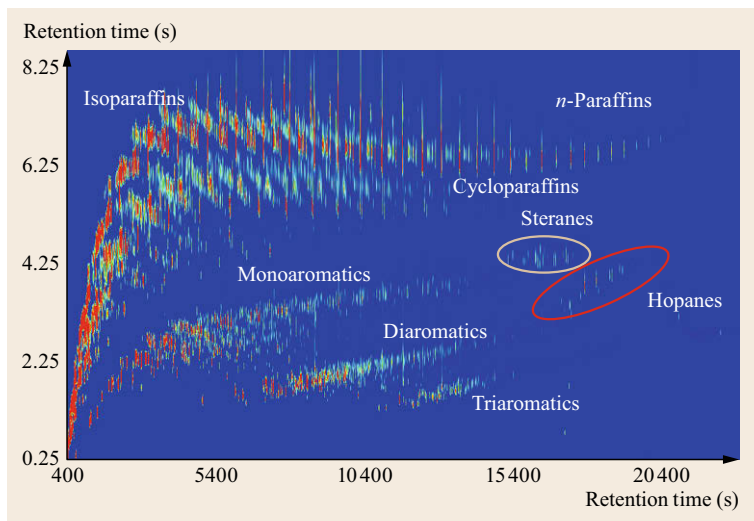


Fig. 3.6 GC \times GC-FID chromatogram of petroleum, showing the presence of steranes and hopanes. (After [3.27]). The x -axis is the first dimension retention time and the y -axis is the second dimension retention time. The intensities of the peaks are represented by colors, with red to be the most intense and blue the least

3.7 Online LC-MS

For simple low-temperature distillation fractions, detailed molecular characterization of mixtures is possible for thorough separation of individual components. It is possible to resolve individual isomers in distillation fractions up to naphtha by GC. With the perfection of interface technology in the 1970s, GC-MS has become

common practice for analyzing mixtures containing components having sufficient partial pressure up to 450 °C under carrier gas flow [3.9].

The prediction of the octane number by quantifying individual isomers in motor gasoline [3.29] is an early example of *petroleomics*, defined as the identification

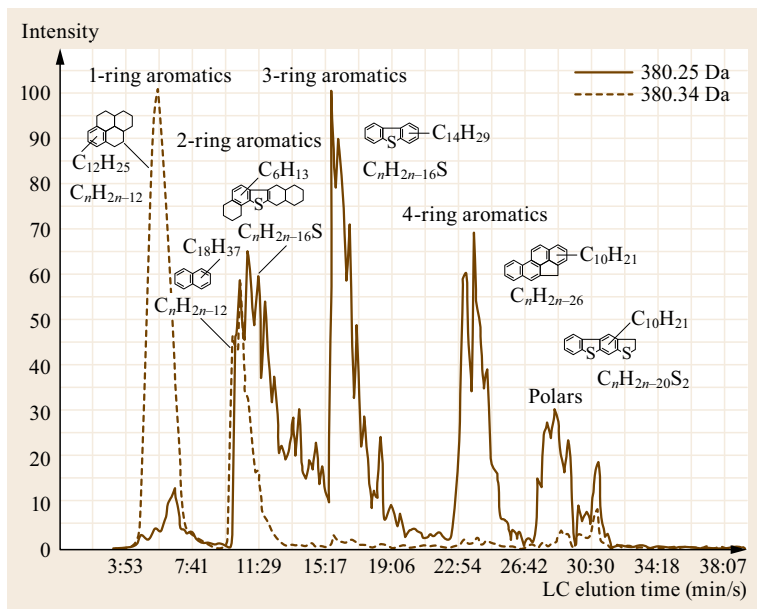


Fig. 3.7 Two m/z 380 mass chromatograms with a resolution window of 200 ppm by LC-MS. (Reprinted with permission from [3.31]. Copyright 1991 American Chemical Society)

of molecules in petroleum or its fractions for their contributions (roles) in properties and performance. The term was introduced at the *Hydrocarbon and Chemicals* workshop of 1999 American Society for Mass Spectrometry (ASMS) Conference and presented at 2003 Pittcon [3.30], to parallel *proteomics* as the identification of protein for their roles in physiological and pathophysiological functions. Beyond naphtha, the differentiation of isomers is less important because of their similarity in combustion characteristics as a transportation fuel (diesel and jet fuel).

For high-boiling complex mixtures with components having insufficient volatility under GC conditions, molecular characterization remains challenging. The separation of the components could rely on the difference in solubility. Hence, LC would become a logical choice [3.10, 32]. The separation of compound types according to the number of aromatic rings, as shown in Fig. 3.7, was performed with a solvent gradient program [3.31]. The pairs of C_nH_{2n-12} and C_nH_{2n-16}S compounds which have the same molecular formula, thus, exactly the same molecular weight, are not resolvable by any form of MS regardless how high the resolving power is, but they can be resolved by aromatic ring type LC separations. This approach was applied to look into the molecular transformation of feed and product for changes in compound types and carbon numbers through a hydrotreating process [3.33]. Due to poor resolving power inherent to LC for complex mixtures beyond naphtha, mass spectral analysis of sub-fractions within an LC peak by time slicing can provide elution characteristics of co-eluting compound types for

quantitation/estimation purposes [3.34]. This kind of analysis is commercially significant, because the results can be used to explain differences in the reactivity of feeds and the impact on the activity of catalysts in hydrotreating and hydrocracking units. Such differences cannot be explained only by looking at bulk properties, such as distillation behavior, density, and UV aromatics. Refiners who look only at bulk properties continue to make expensive feedstock and catalyst selection mistakes [3.35].

There are several interfaces available for coupling LC with MS [3.10]. Among them, the moving-belt interface, although difficult to operate and no longer commercially available, is the only LC-MS interface that has been able to analyze all types of hydrocarbons, including saturate hydrocarbons in middle distillates and gas oils online by EI [3.10, 31, 33] or field ionization (FI) [3.36, 37]. However, this interface is not suitable for distillate fractions beyond vacuum gas oil due to the temperature limitation of the polyimide belt that transport the analyte into the ion source. For resids and asphaltenes, a spray interface with atmospheric pressure ionization has been commonly used. However, challenges remain for their abilities of analyzing (ionizing) high-boiling saturated hydrocarbons. This is an active area of analytical research in the petroleum industry. In addition, repeatability and reproducibility of the results are of major concern.

For compound-type analysis, it is convenient to group members of homologous series. The adjacent members of a homologous series differ by a methylene group, CH₂. Hence, a mass scale in which the mass of

CH₂ defined as exactly 14, instead of the IUPAC mass of 14.01516 based on the ¹²C = 12.00000 mass scale, was proposed by *E. Kendrick* in 1964 [3.38]. Using the Kendrick mass scale, all members of a homologous series possess an identical mass defect regardless of the carbon number [3.34]. However, the use of the Kendrick mass scale suffered from measurement errors caused by the instability in mass measurements by high-resolution magnetic sector mass spectrometers that were com-

monly used until the 1990s [3.34]. The Kendrick mass scale has gained popularity after narrow measurement errors are obtainable with an ultrahigh resolution MS, such as FT-ICR MS. Through stable measurements in accurate mass for reliable elemental composition determination, compound distributions can then be conveniently expressed as double-bond equivalence (or *z*-number) versus the carbon number with peak intensity (ion abundance) as a third axis [3.18, 39].

3.8 Ionization for Molecules

MS is adapted for identifying and measuring individual components in a mixture based on their masses. However, it is only useful when the molecules can be ionized and subjected to electromagnetic separations for detection. Hence, ionization is an essential element of MS.

Ionization can be classified as universal and selective. Universal ionization, such as EI and field ionization (FI), ionizes all of the vaporized organic molecules. Chemical ionization (CI), photoionization (PI), and all of the atmospheric pressure ionization methods, including electrospray ionization (ESI), atmospheric chemical ionization (APCI), and atmospheric photoionization (APPI), selectively ionize certain classes of molecules, mostly aromatic, polar and metal-containing, for molecular weight and functional group studies.

Ionization can also be divided into vacuum and reduced pressure methods, such as EI, CI, FI, FD, and PI, and atmospheric pressure methods, such as ESI, APCI, APPI, and many others.

3.8.1 Ionization Under Vacuum and Reduced Pressure

Electron-Impact Ionization (EI)

EI was developed at the early stage of MS, replacing less controllable ionization by electrode discharge initially used in nascent MS [3.11]. It has been operated at high (50–70 eV) and low (10–12 eV) electron beam energies under vacuum ($\sim 10^{-6}$ torr). High repeatability and reproducibility can be achieved at electron beam energies greater than 50 eV, most commonly at 70 eV, also known as high-voltage EI (HVEI). Under carefully controlled ion source conditions with calibration reference materials, 70 eV EI mass spectra are highly reproducible, especially using magnetic sector instruments. Thus, over 200 000 HVEI mass spectra of pure compounds were compiled and are available in the data system of modern mass spectrometers for compound identification through a library search [3.40, 41]. A larger database of reference spectra for 662 000

spectra of 592 000 compounds with 565 000 searchable structures is available in McLafferty's book [3.42].

Low energy (< 15 eV) EI (low-voltage EI, LVEI) was used for aromatic and polar hydrocarbons that have a lower ionization potential than saturate hydrocarbons for differentiation between aromatics and overlapping cycloparaffins. For example, both tetracyclic paraffins and benzenes have identical molecular formulae at the same nominal mass. When EI is operated at proper low voltage, only benzenes are ionized, leaving tetracyclic paraffins unionized and not detected by MS. LVEI also produces fewer fragment ions than HVEI.

Chemical Ionization (CI)

For molecules that do not yield molecular ions under EI conditions, CI has been used. In CI, reactions between an excess amount of reagent gas ions and molecule generate molecular ions by charge exchange, or *pseudomolecular* ions through protonation, hydride abstraction, deprotonation (to form negative ions), and reagent ion adduction of the molecules under reduced pressure (~ 1 torr) [3.43]. Both positive and negative ions are generated at low internal energies, resulting in much less fragmentation compared to high-energy EI.

For hydrocarbon analysis, the most commonly used reagent gases are methane, isobutane, and ammonia for molecular weight determination [3.44]. Novel reagent gases, such as benzene [3.45], nitric oxide [3.46], carbon disulfide [3.47], and deuterated ammonia [3.48] were chosen for the studies of structure/functionality. The reagent gas ions are normally produced by a heavy-duty filament for nonoxidizing gases and Townsend discharge for oxidizing gases, such as oxygen and nitric oxide.

Field Ionization (FI)

Confusion in molecular weight can occur from the masses of pseudomolecular ions. For example, the protonated molecular ion, MH⁺, of a component will have the same mass as the hydride abstracted molecular ion, (M-1)⁺, of the component with molecular weight to

be two mass unit higher. Hence, it is often desirable to produce molecular ions by losing only one electron as surrogates of neutral molecules in a complex mixture for the determination of molecular weight distribution. This can be accomplished by FI, which uses a fine emitter or a sharp edge razor blade of the order of a few micrometers in diameter operated at 10–12 kV to create a high electric field of the order of 10^7 to several times 10^8 V/cm across the emitter and counter-electrode under vacuum ($\sim 10^{-6}$ torr) [3.49]. FI produces molecular ions from molecules at low internal energies through quantum tunneling [3.49, 50]. Figure 3.8 displays an FI mass spectrum of lubricant base oil containing only saturated hydrocarbons, yielding molecular ions at even masses, except for isoparaffins that yield a fragment ion unless lowering the emitter current [3.51, 52]. Based on the molecular ions, the distribution of saturated ring types (acyclic paraffins, 1-ring cycloparaffins, 2-ring cycloparaffins, etc.) can be discerned. Figure 3.9 shows the carbon number distributions of each ring type between a hydrotreating feed and its product. Since lubricant base oils are extracted from crude oil distillate without conversion thermally or catalytically, the distribution profiles of sterane and hopane biomarkers

remain visible. The red curves are for the feed and the blue curves are for the product. It is apparent that the production of acyclic alkanes and 1-ring cycloparaffins is at the expense of higher rings cycloparaffins.

Field Desorption (FD)

For high-boiling and nonvolatile petroleum fractions, such as resids and asphaltenes, vaporization for FI becomes difficult, if not impossible. The sample is dissolved in a suitable solvent to be deposited onto a fine emitter which is inserted into the ion source through a vacuum lock. The solvent is evaporated, and a high electric field, as FI, is applied to the emitter deposited with the sample (in condensed phase) to desorb molecules as ionic species (different than field evaporation) into the mass analyzer. This technique is called FD [3.49, 50, 53].

3.8.2 Ionization Under Atmospheric Pressure

Electrospray Ionization (ESI)

As mentioned previously, LC is a suitable technique for the separation of less volatile or nonvolatile mixtures.

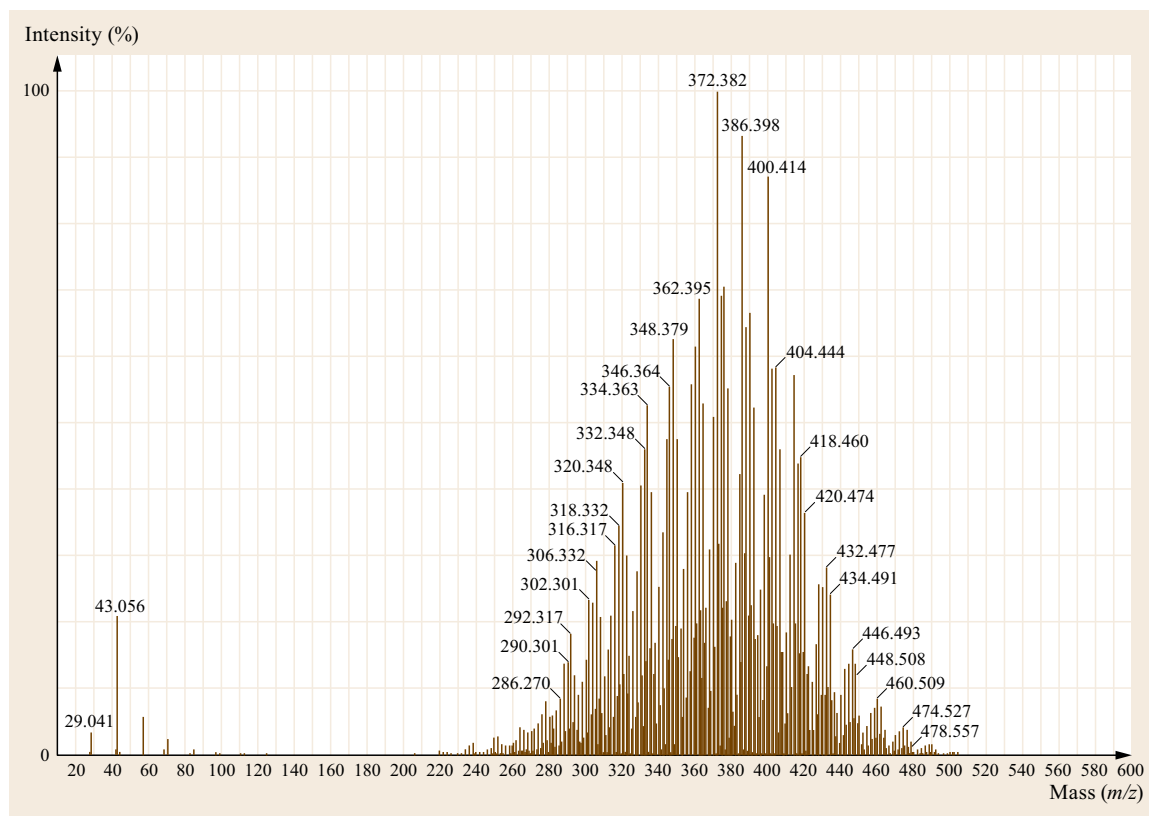


Fig. 3.8 Field ionization mass spectrum of a lubricant base oil

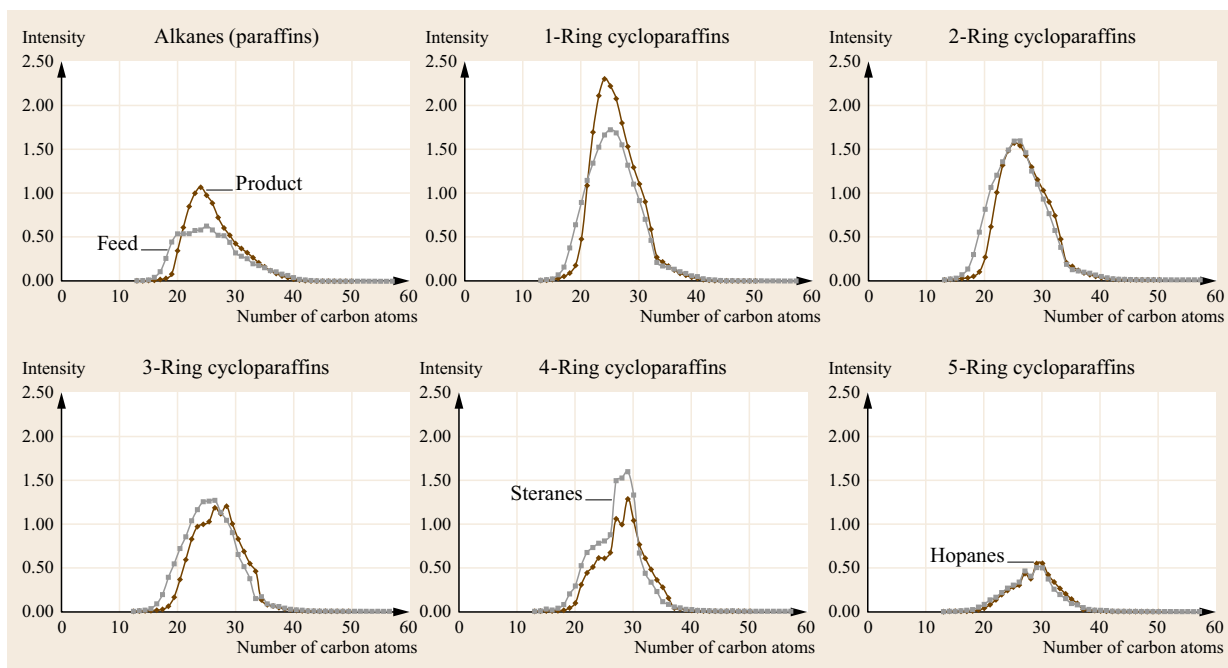


Fig. 3.9 Carbon number distribution of each saturated ring types can be obtained from molecular ions obtained in FI. The hydrotreating feed shown in gray, the product in brown

Many ionization methods, mostly gentle, were developed for the mass spectrometric coupling with LC. One example is ESI that was developed by Malcolm Dole in 1968 originally for the macromass analysis of high polymer (polystyrene) [3.54, 55] has become a common and convenient means of ionization for nonvolatiles. Electrospray also uses high voltage (> 10 kV) on a nebulizer but under nitrogen flow at atmospheric pressure, unlike FI and FD under mass spectrometric vacuum (on the order of 10^{-6} torr).

Although not successful in fully characterizing synthetic high polymers in Dole's effort [3.55], ESI has been adopted to biological systems for analyzing biomacromolecules as pioneered by late Nobel Laureate, *John Fenn* [3.56, 57]. Fenn's group also carried out exploratory experiments with ESI MS on crude oil, jet fuel, gasoline, and coal [3.58]. Their resulting mass spectra contain remarkable amounts of information on the composition and character of these sometimes very complex materials. Hence, it was suggested that ESI might have found a new arena in which to exercise its power [3.59]. Since then, ESI has also been popular in analyzing heavy petroleum resids (by distillation) and asphaltene (by solubility) fractions, including the derivatization of less polar or nonpolar compound classes to polar species suitable for ESI analysis [3.58, 60–64].

Because there is no effective chromatography to separate these extremely high-boiling mixtures into different classes or types of compounds, most of the LC ionization techniques are being used with direct liquid infusion. The resulting learning of detailed molecular composition comprises the basis for developing viable refining technologies. However, studies of resids that are fed to resid processing with resid fluidized catalytic cracking (RFCC) or resid hydrocracking have not yet been seen in the open literature. Such processes are strategically important, and it can be exceedingly profitable. Therefore, there are strong incentives to use the above-described analytical techniques to learn more about resids.

Thermospray (TSP)

There is another spray technique using heat without the use of an electric field, called thermospray (TSP), invented by *Marvin Vestal* in the early 1980s [3.65]. This can also be used for heavy petroleum fraction, as an example shown in Fig. 3.10 for the aromatic ring-type distributions in a 1120–1305 °F DISTACT fraction of a vacuum resid separated by LC [3.66–68].

The highest m/z value in typical spectra from the spray ionization of resids and asphaltenes is less than 2000 for ionic species confidently detected above noise threshold. Arguably, the heaviest molecule in petroleum

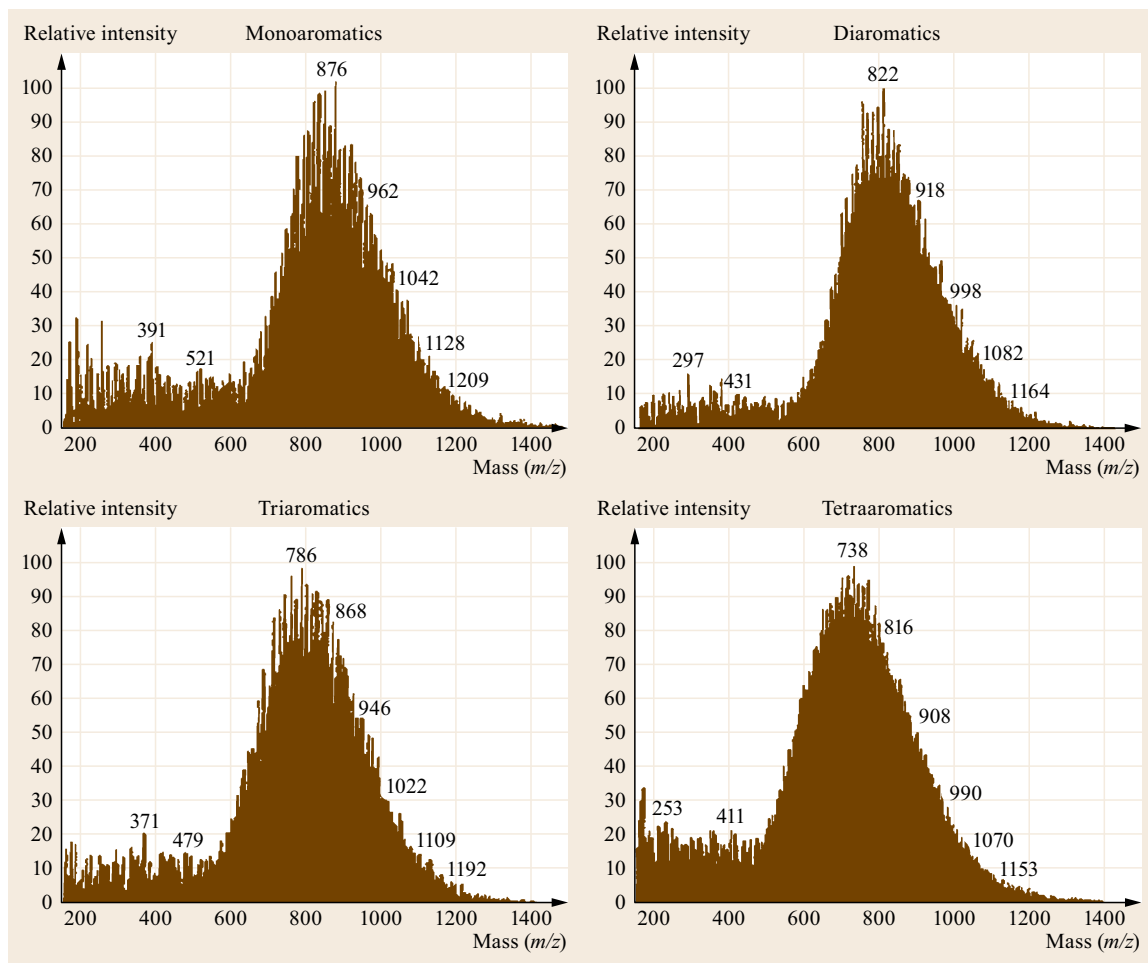


Fig. 3.10 Aromatic type distribution in the 1120–1305 °F DISTACT fraction of a vacuum resid by TSP. (After [3.68])

is less than 2000 without any possible aggregation in measurement, such as in vapor pressure osmometry (VPO). Mass spectrometric measurements, however, can suffer from deficiencies in ionization, ion transmission, and detection of heavier species. Some nonvolatile and nonionizable materials such as dissolved dust, coke, and tar particles will not be detected and analyzed by mass spectrometry. Under severe conditions, the sample can form char or coke or decompose preventing the analysis of heavy species.

Atmospheric Chemical Ionization (APCI)

With ever-increasing demand in proteomics, ESI has become commonly available in commercial instruments. However, ESI cannot be used to ionize all petroleum molecules unless they are aromatic or polar. Alternatively, atmospheric pressure chemical ionization (APCI) initially introduced by Horning for picogram-level detection [3.69] can provide an alternative for

analyzing the compounds [3.70] not amenable for ESI. For examples, the use of acetonitrile as a solvent for the APCI analysis of metalloporphyrins in the negative ion mode was found to be more sensitive than ESI [3.71, 72]. A recently developed version of APCI applying corona discharge at a high flow of nitrogen at atmospheric pressure, also called *atmospheric pressure gas chromatography* (APGC), provides a convenient ion source adaptable for both GC-MS and LC-MS operations. It has been demonstrated as an alternative ionization method for nonpolar sterane and hopane biomarkers [3.73].

Laser-Assisted Ionization

There are many other types of ionization methods performed under atmospheric pressure, most commonly laser-assisted ionization, such as APPI [3.74], matrix-assisted laser desorption/ionization (MALDI) [3.75], and laser induced acoustic desorption (LIAD) [3.76].

They are designed as selective ionization for specific compound types. APPI can be performed with or without dopants under vacuum-ultraviolet (VUV) laser light [3.77]. The most commonly used dopant for hydrocarbon analysis toluene that is added in excess is predominantly ionized by the laser. The analyte ions are formed by ion-molecule reaction between toluene ions and analyte molecules. Positive ions are formed through charge exchange, protonation, or hydride-abstraction, and negative ion are formed through deprotonation. Hence, APPI with dopants can be considered as laser-assisted APCI. MALDI and LIAD are performed with laser light before and after the sample matrix, respectively. They can produce interesting spectra depending on the matrix and gas environment. However, the reliability and applicability of the laser-

associated techniques, [3.78–81] particularly for repeatability and reproducibility in results, remain questionable.

Liquid Injection Field Desorption/Ionization

The incorporation of FI and FD operated under liquid flow, namely, liquid injection field desorption ionization (LIFDI), where the sample solution is delivered to the emitter inside the ion source without breaking the vacuum [3.82]. LIFDI should be capable of ionizing all types of hydrocarbon molecules, including nonpolar saturated hydrocarbons. Hence, this new method could be an ideal ionization technique for LC for overall molecular composition determination of resins and asphaltenes, compensates with other biased atmospheric pressure ionization (ESI, APCI, AAPI, etc.)

3.9 Mass Analyzers

Over the last 100 years, since the first mass spectrograph was constructed by Sir J. J. Thompson of the Cavendish Laboratory of the University of Cambridge, various types of mass analyzers were introduced (Fig. 3.1). They can be generalized as low- and high-resolution instruments. A high-resolution mass spectrometer consists of a mass analyzer capable of determining accurate masses of the components having the same nominal mass for the determination of elemental composition of the ionic species [3.83, 84]. The ability of elemental composition determination for molecular ions is of particular interest. The most commonly used mass spectrometers in the petroleum industry over the years for molecular characterization are briefly described below.

3.9.1 Magnet Sector Mass Spectrometers

Initial commercial single-focusing magnetic sector mass spectrometers were dominant in the 1940s and used in the petroleum industry during World War II for the quantitative analysis of organic gas and light fuel mixtures. In fact, it is the only type of mass spectrometer that provides data adopted by American Society for Testing Materials (ASTM) as standard quantitation methods, including ASTM D 2786 and ASTM D3239 for hydrocarbon mixtures up to gas oil [3.85]. Although obsolete, there are no substitute instruments for acceptable repeatability and reproducibility being manufactured.

For high resolution, a combination of electric sector with magnet in either Mattauch/Herzog or Nier/Johnson geometry provides double-focusing for sep-

arating overlapping components of the same nominal mass [3.11, 84]. The highest resolving power achievable by double-focusing mass spectrometers for a full scan mode is around 50 000. Reversed geometry double focusing-mass spectrometers are composed of the reversing Nier–Johnson geometry with a magnet (B) preceding the electric sector (E). They not only provide high resolution but also serve as a type of tandem mass spectrometers (MS/MS) to link between the precursor and product ions for structural determination and fragment ion kinetic energy release studies [3.86–89]. Due to high cost in maintenance and difficulty in construction and operation, double-focusing mass spectrometers have gradually been replaced by other types of high-resolution mass spectrometers capable of achieving resolving power up to several millions [3.18].

3.9.2 Quadrupole Mass Analyzers (QMS)

The quadrupole mass analyzer or spectrometer (QMS) consists of four hyperbolic rods parallel to each other with opposite rods connected electrically. When an oscillating radio frequency (RF) voltage is applied to one pair of rods and the other, both positive and negative ions are transmitted through the quadrupole rods with equal facility. When a direct current (DC) voltage is superimposed with the RF voltage, ions of different mass-to-charge ratios (m/z) are separated based on the stability of their trajectories by varying the DC and RF voltage ratio. At a certain value, only the stable ions can pass through and other ions with unstable trajectories colliding with rods. By scanning the DC/RF ratio, the

quadrupole can be used as a mass analyzer [3.90]. The resolving power of a QMS is as low as unit resolution (separated by nominal masses) accompanied with great sensitivity for the effective transmission of the ions. The coupling of GC with QMS has found great utility for mixture analysis from petroleum gas to gas oils.

A tandem triple-stage quadrupole mass spectrometer where the first (Q1) and third (Q3) quadrupoles function as mass scanning analyzers and the middle quadrupole (Q2) with RF serves only as a collision cell provides convenient MS/MS operations [3.91, 92]. Its operation modes can be: (1) precursor (parent) ion scan, (2) product (daughter) ion scan, (3) neutral loss scan (concurrent scan of Q1 and Q2 at a constant mass offset) and (4) full scan (with one of the Q1 and Q3 to be RF only as Q2). Triple-quadrupole MS/MS greatly improves the daughter ion mass resolution, which is poor in a reverse geometry double focusing MS due to kinetic energy release. The mass-scanning quadrupoles (Q1 and/or Q3) can be fixed at the nominal masses of interest, known as multiple-reaction monitoring, (MRM) to enhance the sensitivity of ion fragmentation pathways of interest. Unlike other types of MS/MS instruments, the precursor ion scan is unique to triple-quadrupole MS. When coupling with GC, precursor scans of triple quadrupole MS/MS greatly facilitate petroleum biomarker analysis, particularly for overlapping epimers, as described earlier for steranes [3.22].

3.9.3 Time-of-Flight Mass Spectrometers (TOF MS)

Time-of-flight MS (TOF MS) was developed in the late 1940s [3.93] and became prominent during the 1960s, but it was soon replaced by magnetic sector and quadrupole instruments with higher sensitivity and mass resolving power [3.11]. It regained popularity recently with greatly improved resolving power using orthogonal acceleration, reflectron technology and high-speed electronics [3.94]. It has an advantage of analyzing heavy molecules with no theoretical upper mass limit of ions.

In TOFMS, ions are separated by their velocities obtained from acceleration through an electric field (acceleration voltage) in the ion source. At a constant kinetic energy, the velocity of a singly charged ion is inversely proportional to the square root of its mass. Hence, the arrival time at the detector is proportional to the square root of m/z ratio of the ion. To reduce the energy spread, the ions into the mass analyzer are accelerated in a direction orthogonal to the ion path out of the ion source. To increase flight time for achieving higher resolution at a limited space inside the mass analyzer,

the ion flight path is lengthened using an ion mirror (reflectron) [3.95], multipath reflections [3.96], or spiral trajectory [3.97].

3.9.4 Quadrupole Time-of-Flight Mass Spectrometers (QTOF MS)

Quadrupole TOF MS (QTOF MS) can be considered as an instrument where the third quadrupole (Q3) of the triple quadrupole is replaced by the TOF mass analyzer. However, an additional quadrupole can be added for collision damping. With orthogonal injection (acceleration) of the ions, QTOF MS with a reflectron with two or more paths provides high-sensitivity and high-resolution/mass accuracy for both precursor and product ions with simplicity in operations [3.98, 99]. QTOF MS can be operated as a TOF MS by setting RF only on the quadrupole mass analyzer to transmit all ions through. Another advantage of QTOF MS is simultaneous high- and low-energy collisions producing similar mass spectra as HVEI and LVEI [3.73].

3.9.5 Fourier-Transform Ion Cyclotron Resonance Mass Spectrometry (FT-ICR MS)

The mass limitation encountered in high-resolution double-focusing magnetic sector instruments has been greatly reduced by using Fourier-transform ion cyclotron resonance mass spectrometry (FT-ICR MS). The resolving power of several millions, even capable of resolving mass difference less than an electron mass, can be achieved [3.18]. An ICR MS employs inherent resonance frequency of an ion in a fixed magnet field to determine m/z . The ions are introduced (transmitted) and trapped in electric trapping plates under the magnetic field. By applying an oscillating electric field orthogonal to the magnetic field, the ions are excited and rotated at their resonance frequencies. They circulate inside the trap as packets with larger radius to be closer to the detection electrodes, producing an induced current image from the induced decay detectable on a pair of electrodes. The frequency signals, which are sine waves on a time scale, are Fourier transformed to the frequency scale and then mass calibrated as a mass spectrum.

Modern FT-ICR MS was first recognized in 1994 as a powerful alternative to the high-resolution sector MS for resolving overlapping components, particularly hydrocarbons and their overlapping sulfur species of 3.4 mDa mass difference, in complex high-boiling mixtures that are of most interest in the petroleum industry [3.100]. Since then, numerous publications have appeared in the literature, mostly for asphaltene char-

acterization. Although previously unanalyzable polar species can be accurately mass measured for elemental composition determination, reliable and repeatable quantitation of the identified species remains a great challenge.

3.9.6 Other Mass Spectrometers

There are many other mass spectrometers, some of which are gaining popularity in the oil industry, such as the quadrupole ion trap [3.90] and the orbitrap [3.101]. Regardless of the type of mass spectrometer being used, the main purpose is to obtain the maximum molecular information and understanding in complex

petroleum mixtures for process and product improvements, problem solving, safety, and environmental compliance.

Recently, ion mobility analyzers have become commercially available associated with TOF and other types of mass analyzers [3.102]. They are improved versions of plasma chromatography [3.103] or ion drift MS to create mobility spectra, which was proposed for density measurements of gaseous ions [3.104]. Along with mass measurement by MS, ion mobility chromatography can be used for cross-sectional area measurements of ionic species [3.105, 106]. The cross-sectional area measurements are made by use of reference compounds with the known cross-sectional areas.

3.10 Data Interpretation and Management

The advent of modern high-speed computers greatly facilitates the instrument control and data acquisition of mass spectrometers and mass spectral data processing. Based on the needed information or desired results, a mass spectrometrists makes decisions of what instruments to be used and experiments to be performed. Data interpretation will be made to communicate with collaborative scientists and/or engineers to understand the underlying chemistry and evaluate/assess the process and/or products.

3.10.1 Molecular Isotopic Pattern Computation

The isotopes of elements were discovered by physicists in early mass spectroscopic studies [3.11]. Thus, MS is well suited for the isotopic pattern determination of molecules. Isotopic patterns can aid in compound identification and quantitation.

The earlier approach of calculating isotopic patterns of molecules involved the use of polynomial expressions to include probability theory and combinatorial analysis [3.11, 107]. For petroleum fractions containing components with the carbon number less than 90 and smaller numbers of heteroatoms including sulfur, nitrogen, and oxygen, the polynomial approach is adequate for isotopic distribution calculations. However, for much larger molecules, such synthetic polymers, the polynomial approach suffers from several limitations in the numbers of elements and carbon numbers being calculated. Another approach based on the Diophantine algorithm which can only have integer solutions was first proposed for eliminating the constraint in the number of elements and carbon numbers and providing simplicity in isotopic abundance calculations and monoisotopic

mass determinations of high-mass species [3.108]. This approach has been extended to polypeptides in proteomics [3.109] and biomedical research [3.110] dealing with biomacromolecules containing a larger number of carbon atoms and heteroatoms. No limitation in the number of elements has advantages of computing complex multielement catalysts or enzymes by mass spectrometric analysis.

3.10.2 Compound Identification and Type Analysis

A volatile component in light petroleum fractions can be analyzed by GC-MS. With EI, compounds can be identified individually by matching their mass spectra with reference spectra through library search. The best search system is published by *Pesyna* et al. [3.111] and *McLafferty* et al. [3.112]. If no matching spectrum can be found, the identification can be made by interpreting the mass spectral pattern based on the principles of organic chemistry [3.113, 114]. For higher boiling fractions, components are grouped together for characterization according to compound types. Several methods of compound-type analysis have been adopted by ASTM as semiquantitation methods of petroleum fractions.

3.10.3 Integration of Molecular Characterization Data for Kinetic Modeling

One of the ultimate goals for molecular characterization is its use in process control and performance assessment. It is desirable to develop process kinetic models based on the molecular information of the feed-

stock to predict processability and product yields under various refining conditions. A large volume of molecular characterization data are then integrated with the reaction chemistry network in the model for the prediction, control, and evaluation of the process and products. Hence, it can be considered as a form of molecular engineering for designing refining processes without a pilot plant. One successful example is the structural-oriented lumping (SOL) kinetic modeling method developed at ExxonMobil to describe molecular composition, reaction chemistry, and properties of complex hydrocarbon mixtures for predicting the yields of refinery processes [3.115]. Molecules are represented by structural vectors for computer manipulation. The method has been extended to molecules found in vacuum resid represented as multicore molecules

comprising single-core molecules found in lower boiling fractions. It includes two more vectors for nickel and vanadium, which poison the catalysts in VGO and resid conversion units [3.116]. SOL has been applied to steam cracking [3.117] and delay coking [3.118] processes to describe feedstock and reaction behavior for predicting product distributions. The predictions compare well with experimental results. SOL has been used for the prediction of the octane number of gasoline [3.119] and cetane numbers of diesel [3.120], providing true examples of petroleomics to relate molecular composition with properties, performance, and functions of refinery products [3.30]. Accurate quantitation is the key to the technical and economic success of molecular based models and this work is ongoing.

3.11 Molecular Engineering and Management Through Science and Modeling

Once the compounds in the petroleum mixture are identified, their physical and chemical properties that include thermodynamic and kinetic properties can be determined or predicted through science studies. Molecular composition in the petroleum fractions and process streams can be measured or estimated through quantitative analysis using sophisticated separation and analytical schemes. The molecular property database could be created for individual molecules, molecular groups, and structural types. Based on the property database of the molecules, all the possible reactions along with their rate constants of refining processes can be listed. To handle the huge amounts of data and information of the molecules involved in complex mixtures, model building based on modern sophisticated computers becomes necessary. To achieve this goal, the molecular structures need to be digitized as the digital expression for the

molecular composition model and the molecular level reaction network of every type (or group) of molecules for the kinetic model need to be established [3.115, 121]. Such kinetic modeling allows computers to perform dynamic calculations referring to the experimental conditions for the optimization and prediction of the yield and quality of products of the particular process. It can also be used for the development and application of new catalysts and new processes through the prediction on possible reaction routes. The visualization of the reaction network would also help users to understand and study the molecular conversion chemistry.

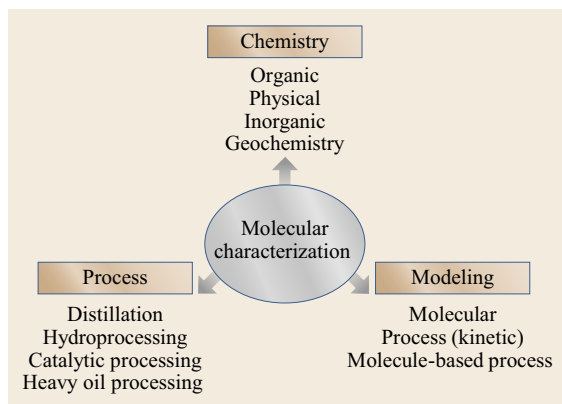
Molecular management for the overall optimization of the resource and refinery process would increase refinery profitability through feedstock selection, operation condition optimization, novel process development, product blending, and waste management.

3.12 Conclusion

In the oil industry, regardless of whether upstream, downstream, petrochemical, environmental, or modeling, molecular understanding of petroleum and upgrading processes is important for science and technology as well as the improvement of processes and products. Analytical devices and instruments play key roles in providing the information of existing, unknown or new molecules for the design and control of chemical processes. Analytical research and development have been

driven by business needs, market demands, and governmental regulations.

The value of molecular characterization is enhanced by integrating science (chemistry), engineering (processing), and management (modeling and chemometrics), as shown in Fig. 3.11. Molecule-based process kinetic modeling based on molecular characterization data and generalized rate constants in the reaction network for the simulation/optimization of refinery pro-



cesses and prediction of yields, properties, and performance of products has gained popularity, evidenced by

Fig. 3.11 Role of molecular characterization in molecular science (*chemistry*), molecular engineering (*process*) and molecular management (*modeling*) ◀

recent publications. Successful molecular engineering without a pilot plant studies would be a great savings for time and cost for designing new and improved processes. However, the calibration or correlation of the output with pilot plant results is always necessary to validate the process models.

Acknowledgments. The author would like to acknowledge valuable comments and suggestions from Fred W. McLafferty, R. Graham Cooks, and Paul Robinson. Discussion with Dr. Qing Wu of China National Offshore Oil Corporation (CNOOC) is also highly appreciated.

References

- 3.1 C.S. Hsu: *Analytical Advances for Hydrocarbon Research* (Kluwer Academic/Plenum Publishers, New York 2003)
- 3.2 G.J. Kennedy: Advances in NMR techniques for hydrocarbon characterization. In: *Analytical Advances for Hydrocarbon Research*, ed. by C.S. Hsu (Kluwer Academic/Plenum Publishers, New York 2003)
- 3.3 A. Mendez, J. Bruzual: Molecular characterization of petroleum and its fractions by mass spectrometry. In: *Analytical Advances for Hydrocarbon Research*, ed. by C.S. Hsu (Kluwer Academic/Plenum Publishers, New York 2003)
- 3.4 B. Chawla: Selective detection of sulfur and nitrogen compounds in low boiling petroleum streams by gas chromatography. In: *Analytical Advances for Hydrocarbon Research*, ed. by C.S. Hsu (Kluwer Academic/Plenum Publishers, New York 2003)
- 3.5 M.R. Watt, S.G. Roussis: Crude assay. In: *Practical Advances in Petroleum Processing*, ed. by C.S. Hsu, P.R. Robinson (Springer, New York 2006)
- 3.6 K.H. Altgelt, T.H. Gouw: *Chromatography in Petroleum Analysis*, Vol. 11 (Dekker, New York 1979)
- 3.7 L.R. Snyder, J.J. Kirkland: *Introduction to Modern Liquid Chromatography*, 2nd edn. (Wiley-Interscience, New York 1979)
- 3.8 F.P. Di Sanzo: Chromatographic analyses of fuels. In: *Analytical Advances for Hydrocarbon Research*, ed. by C.S. Hsu (Kluwer Academic/Plenum Publishers, New York 2003)
- 3.9 C.S. Hsu, D. Drinkwater: GC/MS in the petroleum industry. In: *Current Practice in GC/MS*, Chromatogr. Sci. Series Ser., Vol. 86, ed. by W.W.A. Niessen (Dekker Marcel, New York 2001)
- 3.10 C.S. Hsu: Coupling Mass Spectrometry with Liquid Chromatography for Petroleum Research. In: *Analytical Advances for Hydrocarbon Research*, ed. by C.S. Hsu (Kluwer Academic/Plenum Publishers, New York 2003)
- 3.11 R.W. Kiser: *Introduction to Mass Spectrometry and Its Applications* (Prentice-Hall, Englewood Cliff 1965)
- 3.12 M.A. Gayson: *Measuring Mass: From Positive Ray to Protein* (Chemical Heritage Press, Philadelphia 2002)
- 3.13 E. De Hoffmann, V. Stroobant: *Mass Spectrometry: Principles and Applications*, 3rd edn. (Wiley, Chichester 2007)
- 3.14 W.L. Budde, J.W. Eichelberger: *Organic Analysis Using Gas Chromatography Mass Spectrometry* (Ann Arbor Science, Ann Arbor 1979)
- 3.15 F.A. White, G.M. Wood: *Mass Spectrometry: Applications in Science and Engineering* (Wiley Interscience, New York 1986)
- 3.16 J.T. Watson: *Introduction to Mass Spectrometry*, 3rd edn. (Lippincott-Raven, Philadelphia 1997)
- 3.17 C.S. Hsu: Petroleomics: Composition/structure relationship with properties/performance of petroleum and its fractions, Keynote speech at Symposium on Heavy Hydrocarbon Resources: Characterization, Upgrading and Utilization, 240th American Chemical Society National Meeting, Boston (2010)
- 3.18 C.S. Hsu, C.L. Hendrickson, R.P. Rodgers, A.M. McKenna, A.G. Marshall: Petroleomics: Advanced molecular probe for petroleum heavy ends, *J. Mass Spectrom.* **46**, 337–343 (2011)
- 3.19 W.K. Robbins, C.S. Hsu: Petroleum: composition. In: *Kirk-Othmer Encyclopedia of Chemical Technology*, ed. by J. Kroschwitz, M. Howe-Grant (Wiley, New York 1996) pp. 352–370
- 3.20 K.E. Peters, J.W. Moldowan: *The Biomarker Guide: Interpreting Molecular Fossils in Petroleum and Ancient Sediments* (Prentice Hall, Englewood Cliffs 1993)

- 3.21 K.E. Peters, C.C. Walters, J.W. Moldovan: *The Biomarker Guide*, 2nd edn. (Cambridge Univ. Press, Cambridge 2005)
- 3.22 C.S. Hsu, C.C. Walters, G.H. Isaksen, M.E. Schaps, K.E. Peters: Biomarker Analysis for Petroleum Exploration. In: *Analytical Advances for Hydrocarbon Research*, ed. by C.S. Hsu (Kluwer Academic/Plenum Publishers, New York 2003)
- 3.23 B.P. Tissot, D.H. Welte: *Petroleum Formation and Occurrence*, 2nd edn. (Springer, Berlin 1984)
- 3.24 J.M. Hunt: *Petroleum Geochemistry and Geology*, 2nd edn. (W. H. Freeman and Co., San Francisco 1996)
- 3.25 Z. Wang, S. Stout, M. Fingas: Forensic fingerprinting of biomarkers for oil spill characterization and source identification, *Env. Forensics* **7**(2), 105–146 (2006)
- 3.26 G.H. Isaksen: Molecular geochemistry assists exploration, *Oil Gas J.* **89**(11), 127–131 (1991)
- 3.27 C.S. Hsu, J. Hu, J. Binkley, C. Fix, D. Alonso, M. Merrick: Comprehensive two-dimensional GC (GCxGC) for quantitation of petroleum biomarkers, *Proc. 36th Int. Symp. Capillary Chrom. and 9th GCxGC Symp.*, Riva Del Garda, Italy (2012)
- 3.28 C.S. Hsu, Q. Shi: Prospects for petroleum mass spectrometry and chromatography, *Sci. China Chem.* **56**(7), 833–839 (2013)
- 3.29 P.C. Anderson, J.M. Sharkey, R.P.L. Walsh: Calculation of research octane number of motor gasolines from chromatographic data and a new approach to motor gasoline quality control, *J. Inst. Pet.* **59**, 83 (1972)
- 3.30 C.S. Hsu: Petroleomics: Probing petroleum composition by mass spectrometry, Invited Speech, Symposium on Petroleomics, 2003 Pittsburgh Conference, Orlando (2003)
- 3.31 C.S. Hsu, K. Qian, Y.C. Chen, M.A. McLean, T. Aczel, S.C. Blum, W.N. Olmstead, L.H. Kaplan, W.K. Robbins, W.W. Schulz: On line liquid chromatography/mass spectrometry (LC/MS) for heavy hydrocarbon characterization, *Energy Fuels* **5**, 395–398 (1991)
- 3.32 W.W.A. Niessen, J. van der Greef: *Liquid Chromatography – Mass Spectrometry*, Vol. 58 (Marcel Dekker, New York 1992)
- 3.33 K. Qian, C.S. Hsu: Molecular transformation in hydrotreating processes studied by on line liquid chromatography mass spectrometry, *Anal. Chem.* **64**, 2327–2333 (1992)
- 3.34 C.S. Hsu, K. Qian, Y.C. Chen: An innovative approach to data analysis in hydrocarbon characterization by on line liquid chromatography mass spectrometry, *Anal. Chim. Acta* **264**, 79–89 (1992)
- 3.35 P.R. Robinson, G.E. Dolbear: Hydrotreating and hydrocracking: Fundamentals. In: *Practical Advances in Petroleum Refining*, ed. by C.S. Hsu, P.R. Robinson (Springer, New York 2006) pp. 177–218
- 3.36 Z. Liang, C.S. Hsu, P.B. Grosshans: Coupling field ionization mass spectrometry with liquid chromatography for the characterization of heavy saturated hydrocarbons, *Proc. 43rd ASMS Conf. Mass Spectrom. and Allied Top.*, Atlanta (1995) p. 1014
- 3.37 Z. Liang, C.S. Hsu: Molecular speciation of saturates by on-line liquid chromatography-field ionization mass spectrometry, *Energy Fuels* **12**(3), 637–664 (1998)
- 3.38 E. Kendrick: A mass scale based on $\text{CH}_2 = 14.0000$ for high resolution mass spectrometry of organic compounds, *Anal. Chem.* **35**(13), 2146–2154 (1963)
- 3.39 C.S. Hsu: Definition of hydrogen deficiency for hydrocarbons with functional group, *Energy Fuels* **24**, 4097–4098 (2010)
- 3.40 NIST/NIH/EPA, Mass Spectral Database – NIST 98
- 3.41 NIST/EPA/NIH, Mass Spectral Library with Search Program: <http://www.nist.gov/srd/nist1a.cfm>
- 3.42 F.W. McLafferty: *Registry of Mass Spectral Data* (Wiley-Blackwell, Hoboken 2009)
- 3.43 M.S.B. Munson, F.H. Field: Chemical ionization mass spectrometry. I. General introduction, *J. Am. Chem. Soc.* **88**, 2621–2630 (1966)
- 3.44 A.G. Harrison: *Chemical Ionization Mass Spectrometry*, 2nd edn. (CRC Press, Boca Raton 1992)
- 3.45 F.H. Field: Chemical ionization mass spectrometry, *Acc. Chem. Res.* **1**(2), 42–49 (1968)
- 3.46 I. Dzidic, H.A. Petersen, P.A. Wadsworth, H.V. Hart: Townsend discharge nitric oxide chemical ionization gas chromatography/mass spectrometry for hydrocarbon analysis of the middle distillates, *Anal. Chem.* **64**, 2227–2232 (1992)
- 3.47 C.S. Hsu, K. Qian: CS₂ charge exchange as a low energy ionization technique for hydrocarbon characterization, *Anal. Chem.* **65**, 767–771 (1993)
- 3.48 C.S. Hsu, K. Qian, W.K. Robbins: Nitrogen speciation of petroleum polars by compound class separation and on line LC/MS, *High Resolut. Chromatogr.* **17**(4), 271–276 (1994)
- 3.49 B.D. Beckey: *Principles of Field Ionization and Field Desorption in Mass Spectrometry* (Pergamon Press, Oxford 1977)
- 3.50 B.D. Beckey: Field ionization mass spectrometry, *Res./Dev.* **20**(11), 26–29 (1969)
- 3.51 C.S. Hsu, M. Green: Fragment-free accurate mass measurement of complex mixture components by gas chromatography/field ionization-orthogonal acceleration time-of-flight mass spectrometry: An unprecedented capability for mixture analysis, *Rapid Comm. Mass Spectrom.* **15**, 236–239 (2001)
- 3.52 C.S. Hsu, G.J. Dechert, H.S. Aldrich, G.D. Dupre: Method of producing molecular profiles of isoparaffins by low emitter current field ionization mass spectrometry, U.S. Patent 7 671 328 (2010)
- 3.53 L. Prokai: *Field Desorption Mass Spectrometry*, Vol. 9 (Marcel Dekker, New York 1990) p. 291
- 3.54 M. Dole, L.L. Mack, R.L. Hines, R.C. Mobley, L.D. Ferguson, M.B. Alice: Molecular beams of macroions, *J. Chem. Phys.* **49**, 2240–2245 (1968)
- 3.55 C. S. Hsu: National Science Foundation project as a Robert Welch Postdoctoral Research Fellow, Baylor University, Texas (1975)
- 3.56 M. Yamashita, J.B. Fenn: Electrospray ion source. Another variation on the free-jet theme, *J. Phys. Chem.* **88**(20), 4451–4459 (1984)
- 3.57 J.B. Fenn, M. Mann, C.K. Meng, S.F. Wong, C.M. Whitehouse: Electrospray ionization for mass

- spectrometry of large biomolecules, *Science* **246**, 64–71 (1989)
- 3.58 K. Qian, R.P. Rodgers, C.L. Hendrickson, M.R. Emmett, A.G. Marshall: Reading chemical fine print: Resolution and identification of 3000 nitrogen-containing aromatic compounds from a single electrospray ionization Fourier transform ion cyclotron resonance mass spectrum of heavy petroleum crude oil, *Energy Fuels* **15**, 492–498 (2001)
- 3.59 D. Zhan, J.B. Fenn: Electrospray mass spectrometry of fossil fuels, *Int. J. Mass Spectrom.* **194**, 197–208 (2000)
- 3.60 K. Qian, W.K. Robbins, C.A. Hughey, H.J. Cooper, R.P. Rodgers, A.G. Marshall: Resolution and identification of elemental compositions for more than 3000 crude acids in heavy petroleum by negative-ion microelectrospray high-field Fourier transform ion cyclotron resonance mass spectrometry, *Energy Fuels* **15**, 1505–1511 (2001)
- 3.61 S.G. Roussis, R. Proulx: Molecular weight distributions of heavy aromatic petroleum fractions by Ag⁺ electrospray ionization mass spectrometry, *Anal. Chem.* **74**(6), 1408–1414 (2002)
- 3.62 H. Müller, J.T. Andersson, W. Schrader: Characterization of high-molecular-weight sulfur-containing aromatics in vacuum residues using Fourier transform ion cyclotron resonance mass spectrometry, *Anal. Chem.* **77**, 2536–2543 (2005)
- 3.63 P. Liu, C. Xu, Q. Shi, N. Pan, Y. Zhang, S. Zhao, K.H. Chung: Characterization of sulfide compounds in petroleum: Selective oxidation followed by positive-ion electrospray Fourier transform ion cyclotron resonance mass spectrometry, *Anal. Chem.* **82**, 6601–6606 (2010)
- 3.64 X. Zhou, Q. Shi, Y. Zhang, S. Zhao, R. Zhang, K.H. Chung, C. Xu: Analysis of saturated hydrocarbons by redox reaction with negative-ion electrospray Fourier transform ion cyclotron resonance mass spectrometry, *Anal. Chem.* **84**, 3192–3199 (2012)
- 3.65 C.B. Blakley, M.L. Vestal: Thermospray interface for liquid chromatography/mass spectrometry, *Anal. Chem.* **55**(4), 750–754 (1983)
- 3.66 M.A. Mc Lean, C.S. Hsu: Aromatic hydrocarbons studied by thermospray liquid chromatography/mass spectrometry, *Proc. 38th ASMS Conf. Mass Spectrom.* Allied Top., Tucson (1990) pp. 1077–1078
- 3.67 C.S. Hsu, B.V. Kadtko, G.J. Dechert: Comparison of field desorption and thermospray mass spectrometry for the analysis of petroleum residues, *Proc. 41st ASMS Conf. Mass Spectrom.* Allied Top., San Francisco (1993) p. 212
- 3.68 C.S. Hsu, K. Qian: High-boiling aromatic hydrocarbons characterized by liquid chromatography-thermospray-mass spectrometry, *Energy Fuels* **7**, 268–272 (1993)
- 3.69 E.C. Horning, M.G. Horning, D.I. Carroll, I. Dzidic, R.N. Stillwell: New picogram detection system based on a mass spectrometer with an external ionization source at atmospheric pressure, *Anal. Chem.* **45**(6), 936–948 (1973)
- 3.70 I. Dzidic, D.I. Carroll, R.N. Stillwell, E.C. Horning: Comparison of positive ions formed in nickel-63 and corona discharge ion source using nitrogen, argon, isobutane, ammonia and nitric oxide as reagents in atmospheric pressure ionization mass spectrometry, *Anal. Chem.* **48**(12), 1763–1768 (1976)
- 3.71 E. Fukuda, Y. Wang, C.S. Hsu: Atmospheric pressure chemical ionization LC/MS for metalloporphyrins, *Proc. 44th ASMS Conf. Mass Spectrom.* Allied Top., Portland (1996) p. 1273
- 3.72 C.S. Hsu, G.J. Dechert, W.K. Robbins, E.K. Fukuda: Naphthenic acids in crude oils characterized by mass spectrometry, *Energy Fuels* **14**(1), 217–223 (2000)
- 3.73 D. Stevens, Q. Shi, C.S. Hsu: A novel analytical technique for petroleum biomarker analysis, *Energy Fuels* **27**, 167–171 (2013)
- 3.74 D.B. Robb, T.R. Covey, A.P. Bruins: Atmospheric pressure photoionization: An ionization method for liquid chromatography-mass spectrometry, *Anal. Chem.* **72**, 3653–3659 (2000)
- 3.75 C.S. Hsu, H.S. Aldrich, P.R. Geissler, E.E. Green: Time-of-flight MALDI for chemical oligomer analysis, *Proc. 53rd ASMS Conf. Mass Spectrom.* Allied Top., San Antonio (2005) p. A50684
- 3.76 L. Nyadong, J.P. Quinn, C.S. Hsu, C.L. Hendrickson, R.P. Rodgers, A.G. Marshall: Atmospheric pressure laser-induced acoustic desorption chemical ionization mass spectrometry for analysis of saturated hydrocarbons, *Anal. Chem.* **84**, 7131–7137 (2012)
- 3.77 T.J. Kauppila, T. Kuuranne, E.C. Meurer, M.N. Eberlin, T. Kotiaho, R. Kostianen: Atmospheric pressure photoionization mass spectrometry (APPI-MS) – Ionization mechanism and the effect of solvent on the ionization of naphthalenes, *Anal. Chem.* **74**, 5470–5479 (2002)
- 3.78 Y. Cho, J.M. Jin, M. Witt, J.E. Birdwell, J. Na, N. Roh, S. Kim: Comparing laser desorption ionization and atmospheric pressure photoionization coupled to Fourier transform ion cyclotron resonance mass spectrometry to characterize shale oils at the molecular level, *Energy Fuels* **27**, 1830–1837 (2013)
- 3.79 A.E. Pomerantz, M.R. Hammond, A.L. Morrow, O.C. Mullins, R.N. Zare: Two-step laser mass spectrometry of asphaltenes, *J. Am. Chem. Soc.* **130**, 7216–7217 (2008)
- 3.80 Y. Cho, M. Witt, Y.H. Kim, S. Kim: Characterization of crude oils at the molecular level by use of laser desorption ionization Fourier-transform ion cyclotron resonance mass spectrometry, *Anal. Chem.* **84**(20), 8587–8594 (2012)
- 3.81 Q. Wu, A.E. Pomerantz, O.C. Mullins, R.N. Zare: Minimization of fragmentation and aggregation by laser desorption laser ionization mass spectrometry, *J. Amer. Soc. Mass Spectrom.* **24**, 1116–1122 (2013)
- 3.82 H.B. Linden: Liquid injection field desorption ionization: A new tool for soft ionization of samples including air sensitive catalysts and non-polar hydrocarbons, *Eur. J. Mass Spectrom.* **10**, 459–468 (2004)

- 3.83 J.H. Beynon: Quantitative analysis of organic compounds by mass spectrometry, *Nature* **174**, 735–737 (1954)
- 3.84 J.H. Beynon: *Instruments in Mass Spectrometry and Its Applications to Organic Chemists*, 1st edn. (Elsevier, Amsterdam 1960)
- 3.85 ASTM: *Annual Book of ASTM Standards* (American Society for Testing and Materials, West Conshohocken 2014)
- 3.86 J.H. Beynon, R.G. Cooks, J.W. Amy, W.E. Baitinger, T.Y. Ridley: Design and performance of a mass-analyzed ion kinetic energy (MIKE) spectrometer, *Anal. Chem.* **45**, 1023A–1031A (1973)
- 3.87 R.G. Cooks, J.H. Beynon, R.M. Caprioli, G.R. Lester: *Metastable Ions* (Elsevier, Amsterdam 1973)
- 3.88 E. de Hoffmann: Tandem Mass Spectrometry: A Primer, *J. Mass Spectrom.* **31**, 129–137 (1996)
- 3.89 K.L. Busch, G.L. Glish, S.A. McLuckey: *Mass Spectrometry/Mass Spectrometry: Techniques and Applications of Tandem Mass Spectrometry* (VCH Publishers, New York 1988)
- 3.90 W. Paul, H. Steinwedel: Ein neues Massenspektrometer ohne Magnetfeld, *Z. Naturforsch.* **8a(7)**, 448–450 (1953)
- 3.91 R.A. Yost, C.G. Enke: Triple quadrupole mass spectrometry, *Anal. Chem.* **51(12)**, 1251A–1264A (1979)
- 3.92 R.A. Yost, C.G. Enke: Selected ion fragmentation with a tandem quadrupole mass spectrometer, *J. Amer. Chem. Soc.* **100(7)**, 2274–2275 (1978)
- 3.93 W.E. Stephens: A pulsed mass spectrometer with time dispersion, *Phys. Rev.* **69**, 691 (1946)
- 3.94 R.J. Cotter: *Time-of-Flight Mass Spectrometry: Instrumentation and Applications in Biological Research* (American Chemical Society, Washington 1997)
- 3.95 B.A. Mamyrin, V.I. Karataev, D.V. Shmikk, V.A. Zagulin: The mass-reflectron, a new nonmagnetic time-of-flight mass spectrometer with high resolution, *Sov. Phys. JETP* **37**, 45–48 (1973)
- 3.96 C.S. Hsu, J. Lu, V. Arteav, D. Alonso, K. McNitt, J. Binkley: High resolving power assessment for high resolution time-of-flight mass spectrometry, *Proc. 60th ASMS Conf. Mass Spectrom. Allied Top.*, Vancouver (2012)
- 3.97 T. Satoh: Development of JMS-S3000 MALDI-TOF/TOF utilizing a spiral ion trajectory, *JEOL* **45(1)**, 34–37 (2010)
- 3.98 G.L. Glish, D.E. Goeringer: Tandem quadrupole/time-of-flight instrument for mass spectrometry/mass spectrometry, *Anal. Chem.* **56**, 2291–2295 (1984)
- 3.99 I.V. Chernushevich, A.V. Loboda, B.A. Thomson: An introduction to quadrupole-time-of-flight mass spectrometry, *J. Mass Spectrom.* **36**, 849–865 (2001)
- 3.100 C.S. Hsu, Z. Liang, J.E. Campana: Hydrocarbon characterization by ultra-high resolution Fourier-transform ion cyclotron resonance mass spectrometry, *Anal. Chem.* **66**, 850–855 (1994)
- 3.101 A. Makarov: Electrostatic axially harmonic orbital trapping: A high-performance technique of mass analysis, *Anal. Chem.* **72**, 1156–1162 (2000)
- 3.102 M. Green, S. Pringle, H. Major, K. Giles: Ion mobility separation orthogonal acceleration time-of-flight mass spectrometry (IMS-0a-TOF-MS) for the analysis of small molecules and complex mixtures using an atmospheric solids analysis probe (ASAP), *Proc. 56th ASMS Conf. Mass Spectrom. Allied Top.*, Denver, Colorado (2008)
- 3.103 M.J. Cohen, F.W. Karasek: Plasma chromatography – a new dimension for gas chromatography and mass spectrometry, *J. Chromatogr. Sci.* **8**, 330–337 (1970)
- 3.104 C.S. Hsu: The use of plasma chromatography for density determinations, *Spectrosc. Lett.* **8(8)**, 583–594 (1975)
- 3.105 A. Ahmed, Y.J. Cho, M. No, J. Koh, N. Tomczyk, K. Giles, J.S. Yoo, S. Kim: Application of the mason-schamp equation and ion mobility mass spectrometry to identify structurally related compounds in crude oil, *Anal. Chem.* **83**, 77–83 (2011)
- 3.106 A. Ahmed, Y. Cho, K. Giles, E. Riches, J.W. Lee, H.I. Kim, C.H. Choi, S. Kim: Elucidating molecular structures of nonalkylated and short-chain alkyl ($n < 5$, $(CH_2)_n$) aromatic compounds in crude oils by a combination of ion mobility and ultrahigh-resolution mass spectrometry and theoretical collisional cross-section calculations, *Anal. Chem.* **86**, 3300–3307 (2014)
- 3.107 L. Li, J.A. Kresh, N.M. Karabacak, J.S. Cobb, J.N. Agar, P.A. Hong: Hierarchical algorithm for calculating the isotopic fine structures of molecules, *J. Am. Soc. Mass Spectrom.* **19**, 1867–1874 (2008)
- 3.108 C.S. Hsu: Diophantine approach to isotopic abundance calculations, *Anal. Chem.* **56**, 1356–1361 (1984)
- 3.109 M.T. Olson, A.L. Yergey: Calculation of isotope cluster for polypeptides by probability grouping, *J. Am. Soc. Mass Spectrom.* **20**, 295–302 (2009)
- 3.110 D.L. Hackey, W.W. Wong, T.W. Boutton, P.D. Klein: Isotope ratio measurements in nutrition and biomedical research, *Mass Spectrom. Rev.* **6**, 289–328 (1987)
- 3.111 G.N. Pesyna, R. Venkataraghavan, H.E. Dayringer, F.W. McLafferty: A probability based matching system using a large collection of reference mass spectra, *Anal. Chem.* **48**, 1362–1368 (1976)
- 3.112 F.W. McLafferty, M.-Y. Zhang, D.B. Stauffer, S.Y. Loh: Comparison algorithm and data bases for matching unknown mass spectra, *J. Am. Soc. Mass Spectrom.* **9**, 92–95 (1998)
- 3.113 F.W. McLafferty, F. Turecek: *Interpretation of Mass Spectra*, 4th edn. (Univ. Science Books, Sausalito 1993)
- 3.114 R.M. Smith, K.L. Busch: *Understanding Mass Spectra: A Basic Approach* (Wiley-Interscience, New York 1999)
- 3.115 R.J. Quann, S.B. Jaffe: Structure-oriented lumping: Describing the chemistry of complex hydrocarbon mixtures, *Ind. Eng. Chem. Res.* **31**, 2483–2497 (1992)
- 3.116 S.B. Jaffe, H. Freund, W.N. Olmstead: Extension of structure-oriented lumping to vacuum residua, *Ind. Eng. Chem. Res.* **44**, 9840–9852 (2005)

- 3.117 L. Tian, J. Wang, B. Shen, J. Liu: Building a kinetic model for steam cracking by the method of structure-oriented lumping, *Energy Fuels* **24**, 4380–4386 (2010)
- 3.118 L. Tian, B. Shen, J.A. Liu: Delayed coking model built using the structure-oriented lumping method, *Energy Fuels* **26**(3), 1715–1724 (2012)
- 3.119 P. Ghosh, K.J. Hickey, S.B. Jaffe: Development of a detailed gasoline composition-based octane model, *Ind. Eng. Chem. Res.* **45**, 337–345 (2006)
- 3.120 P. Ghosh, S.B. Jaffe: Detailed composition-based model for predicting the cetane number of Diesel fuels, *Ind. Eng. Chem. Res.* **45**, 346–351 (2006)
- 3.121 M.T. Klein, G. Hou, R. Bertolacini, L.J. Broadbelt, A. Kumar: *Molecular Modeling in Heavy Hydrocarbon Conversions* (CRC/Taylor & Francis, Boca Raton 2006)

Petroinformatics

4. Petroinformatics

Manhoi Hur, Sunghwan Kim, Chang Samuel Hsu

Studies on petroleomics have been focused on advanced molecular-level characterization of compounds that could not be analyzed by conventional techniques. The next stage of the development would be more discussions on the information obtained and relationships with the properties and functions. The relationship between molecular composition and bulk properties or functions can be explicitly expressed by *petroinformatics*, which utilizes statistics, mathematics, and computational visualization technology to interpret or correlate analytical results with bulk properties and experimental data. This provides explicit or implicit information for underlying science and engineering.

In this chapter, several examples of petroinformatics are presented. Statistical methods, such as principle component analysis (PCA) for dimensionality reduction in multivariate analysis, and hierarchical clustering analysis (HCA), have been applied to interpret complex petroleum mass spectra obtained by ultrahigh-resolution Fourier transform ion cyclotron resonance mass spectrometry (FT-ICR MS). The mass spectral peaks were statistically analyzed by Spearman's rank correlation, and by correlation diagrams showing relationships between composition and bulk properties. Additionally, the chapter demonstrates quantitative analyses for petroleum samples by PCA for multivariate analysis and *t*-tests for univariate analysis. Volcano plots are utilized to visualize the quantitative change or difference between samples in detail.

4.1	Petroleum Analysis and Statistical Approaches	175
4.1.1	Data Preprocessing for Statistical Analysis	175
4.1.2	Comparison of Multiple Crude Oil Samples by PCA and HCA.....	176
4.1.3	Correlation Between Chemical Composition and Physical Properties of Crude Oils.....	183
4.1.4	Quantitative Comparisons by Statistical Analysis	186
4.2	Emerging Technologies for Storing, Visualizing, and Processing Crude Oil Data	190
4.2.1	Development of a Data Analysis Platform with Mega Database	190
4.2.2	Integration of Traditional Methods and Statistical Methods	190
4.2.3	Development of Tools with Enhanced Visual Discrimination....	192
4.3	Summary	194
	References	194

The software platform, which integrates data from many samples obtained from different analytical instruments, is a very important tool to achieve more comprehensive understanding of complex analytes such as crude oils. The learnings from other research fields, such as metabolomics, genomics, and proteomics, are important and valuable for the next steps of petroinformatics development, i. e., standardization of data and retrieval of its metadata information.

In modern society, information is generated by studies, experiments, surveys, experience and other communications. Information technology, or informatics, vastly improves access to such information by people who support education, research, practice, development, and decision making. Thanks to advances in computer technology, a huge amount of information from various sources can be digitized, integrated, stored, and pro-

cessed by computers with high speed and efficiency. *Petroinformatics*, which utilizes statistics, mathematics, and computational visualization technology to interpret or correlate analytical results with bulk properties and experimental data, is particularly needed for very complex petroleum mixtures, ranging from light gas to solid residue that can contain millions of molecules. Sophisticated analytical techniques generate data that often

require noise rejection algorithms, statistical analysis, and other resolution enhancement tools for obtaining useful information. Models that employ advanced mathematics and statistics are being built and developed for handling critical physical and chemical data.

Since the beginning of the petroleum industry, various physical testing methods have been established to measure bulk properties of crude oils, exemplified by the Crude Assay [4.1]. Mass spectrometry for molecular characterization was pioneered at the Atlantic Richfield Company (ARCO) during World War II [4.2]. For complex mixtures even in light boiling ranges, such as petroleum gas and naphtha, sensitivity matrices were used for resolving the overlapping ionic species obtained by mass spectrometry. These enabled researchers to determine the distribution of hydrocarbon compound types for the properties and thus quality and performance of the fuels [4.2, 3]. Gas chromatography (GC) was advanced for accurate quantitative measurement of separated components using a universal flame ionization detection (FID) [4.4, 5]. An early application was the octane number prediction of naphtha, the main gasoline component [4.6]. The successful coupling of gas chromatography and mass spectrometry (GC-MS) greatly expands analytical capabilities in the oil industry for determining and monitoring the properties and behaviors of petroleum fractions at the molecular level, enabling identification of optimal processing conditions and product quality control or prediction [4.4, 7].

The term *petroleomics* [4.8–13] was first introduced at a hydrocarbon and chemicals workshop of the American Society for Mass Spectrometry (ASMS) conference in the late 1990s. The concept parallels proteomics for the physiological and pathophysiological functions related to molecular composition and functional groups [4.14]. It has been greatly practiced by a research group at the National High Magnetic Field Laboratory (NHMFL) using ultrahigh-resolution Fourier-transform ion cyclotron resonance mass spectrometry (FT-ICR MS) for heavy oils and fractions [4.15] to partially resolve problems associated with heavy components. Since its first introduction as a tool for petroleum analysis [4.16], FT-ICR MS has been evolved along with electrospray ionization (ESI) [4.17–26], atmospheric pressure photo ionization (APPI) [4.27–34], atmospheric pressure chemical ionization (APCI) [4.35–37] and laser desorption ionization (LDI) [4.38–42] as a principal tool to analyze compounds with higher molecular weights (e.g., 400–500 Da) and polar functional groups (e.g., –OH, thiophene, pyridine). It has played a critical role for petroleomics in which molecular-level understanding is pursued to find correlation between chemical compositions and reactivity/properties of crude oils. FT-ICR

MS is a powerful technique by which over 10 000 compounds can be detected and identified from a single spectrum [4.15, 18].

Elemental compositions (formulae) of the compounds are determined from accurate mass measurement, and relative abundance observed from spectra can be visualized and studied by various tools such as Kendrick mass defect analysis [4.43–46], van Krevelen diagrams [4.47–49], double bond equivalence (DBE) versus carbon numbers (C#) plots [4.10, 20, 23, 50–52], and statistical methods [4.53–60]. Planar limits (or compositional boundaries) [4.51], tandem mass spectrometry [4.61], and atmospheric pressure hydrogen-deuterium exchange mass spectrometry [4.62–65] have also been used to gain additional information on the molecular structures of compounds comprising crude oils.

Although ultrahigh-resolution mass spectrometry is a powerful tool for the analysis of crude oil components, it has limitations. Only limited information on molecular structures can be obtained by this technique because numerous isomeric compounds of various structures have the same elemental composition. One of the biggest obstacles for quantitative analysis by mass spectrometry is nonuniformity of the ionization processes, resulting in low repeatability and reproducibility. Two compounds with a small structural difference can have big difference in ionization efficiency, in addition to ion transmission and detection efficiencies. Therefore, it is difficult to directly correlate the amounts of components in solution with the amounts observed in the gas phase inside the mass spectrometer. There have been many studies devoted to understanding the ionization processes, but it would take more time and effort to further understand the quantitative aspects of the ionization processes. Despite the limitations listed above, ultrahigh-resolution mass spectrometry has been a powerful tool to study heavy molecules of crude oils in general. Research employing this technique has been active, leading to numerous publications.

In fact, considering the heterogeneity and complexity of crude oil's composition, it is obvious that no single analytical technique can determine the structural identities of all the compounds present in crude oils. The process of finding structural identities of the compounds can be compared to a group of men with blindfolds trying to find the shape of an elephant. Since the elephant is so big, each man can only cover a limited area. To find the overall shape of elephant, the information obtained from each man has to be coordinated and integrated by talking to each other. The areas covered by the men have to be well organized by being well spread out and wide enough to cover the whole elephant. At the same time, some overlaps of the covering areas would

be necessary to link information provided by each man. Care should also be taken to identify missing areas.

By analogy, all the available tools have to be used to characterize crude oil samples, since each technique can only cover a limited area of overall crude oil compositions. If petroleum is separated into traditional saturates, aromatics, resins, and asphaltenes (SARA) fractions, different techniques have to be used to characterize each fraction, as illustrated in Fig. 4.1. Combining and coordinating information obtained from different sources is not an easy task, but there have been a few attempts to achieve that goal. To combine the information, it is important to understand the capabilities and limitations of various analytical techniques. For each property measurement, each analytical method gives different information. The research effort has to be devoted not only to investigate what information can be obtained from each technique, but also how the information can be integrated to find ultimate and accurate information.

Therefore, it is clear that more research has to be carried out to devise methods for combining information obtained from each analytical technique. This information-driven research is called *petroinformatics*. The concept of *petroinformatics* was first introduced at a petroleomics workshop of a Pacificchem conference in 2010 [4.66]. The focus of petroinformatics is gathering

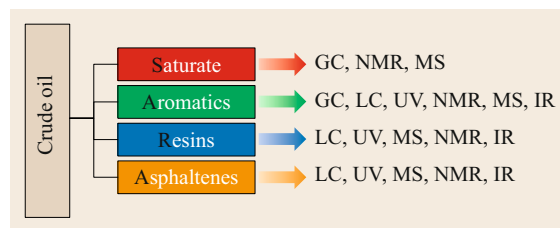


Fig. 4.1 Analytical strategy for the determination of chemical composition in a crude oil

and combining the chemical composition information on crude oils obtained from various traditional and new techniques, such as FT-ICR MS, quadrupole time-of-flight mass spectrometry, gas chromatography time-of-flight, and nuclear magnetic resonance spectroscopy (NMR), to strive for an integrated oil analysis. The gathered information can be statistically processed and correlated with reactivity and properties of the crude oils. The statistical data analysis techniques for a large amount of data have been actively investigated and evaluated. In the end, the overall information can be combined with theoretical simulation to understand and predict crude oil processing.

This chapter describes how petroinformatics can enhance the understanding and applications of petroleum science and technology.

4.1 Petroleum Analysis and Statistical Approaches

To analyze and mine information from large-scale datasets, statistical methods have successfully been applied in biological and biomedical fields, such as microarrays, transcriptomics, metabolomics, and proteomics. Similar statistical methods in crude oil studies could provide viable means of data analysis. The current chapter describes the application of principal component analysis (PCA), hierarchical clustering analysis (HCA) combined with the heatmap visualization method, and correlations between chemical composition and crude oil properties using correlational diagrams. In addition, it introduces a quantitative analysis method for using PCA to characterize heteroatom classes or samples, aided by the *t*-test and its visualization, called volcano plots.

4.1.1 Data Preprocessing for Statistical Analysis

PCA has been used as an effective statistical method for understanding crude oils [4.61]. Twenty oil samples were analyzed by FT-ICR MS utilizing both positive (+)

and negative (−) APPI modes. Triplicate measurements enabled determination of statistical significance. Hence, in this study, a total of 60 mass spectra were obtained from the 20 samples in each ionization mode. All peaks were generated by an automated peak picking algorithm with a moving window of data points [4.54, 67], which provided quicker and more reliable peak picking for analyzing crude oil samples. The relative abundance of individual peaks was normalized to the sum of abundances throughout the peak list. Assignments of molecular formulas were performed for more than 95% of the total number of peaks above a predetermined signal-to-noise ratio. For each ionization mode, the resulting peak lists with elemental formula assignments of 20 samples were aligned into a single table for statistical analysis. Normalized abundances and peaks with the same elemental formulas found in different samples were aligned into single lines. Peak alignment was performed on the basis of the assigned elemental formulas matching with theoretical mass-to-charge values. When aligning peaks, the relative abundance of peaks not detected in samples was assigned as zero [4.68].

4.1.2 Comparison of Multiple Crude Oil Samples by PCA and HCA

Conventionally, data interpretation and spectral comparison of complex datasets are carried out by Kendrick mass defect [4.16, 42, 43] and van Krevelen diagrams [4.46–48]. They have been applied to ultrahigh-resolution mass spectra of one sample at a time magnificently. Also, even though a pair of atomic abundance ratios of selected elements in molecular formulas, such as H/C, O/C, S/C, etc. is cross-plotted as a van Krevelen diagram to facilitate the visualization of changes or differences at the molecular level, the extraction of information out of complex mass spectra remains difficult when multiple samples must be analyzed and compared. A van Krevelen diagram of petroleum spectra, for instance, presents only one sample at a time. Since a detailed comparison of multiple samples, such as 20 in our example, would require the generation and manual examination of 20 individual van Krevelen diagrams and Kendrick plots, principal component analysis (PCA) and hierarchical clustering analysis (HCA) combined with the heatmap visualization method are utilized to simultaneously analyze APPI FT-ICR mass spectra from these crude oil samples.

PCA, discussed under *PCA Applications of Positive/Negative APPI Data*, is commonly explained in the literature [4.69–71] as the number of variables (eigenvectors) through linear combination of the original variables, e.g., the number of peaks observed in a mass spectrum to be transformed by PCA into principal components. Principal components (PCs) as the new variables are descriptive of the variance, or crucial difference, among the oil samples in question and those PCs are ordered by their contributions (eigenvalues) to the variance of peaks observed. Thus, the first PC generated by PCA describes more of the variation in the peaks observed than the second PC. Also, these PCs can be represented by two plots called loading and score. A loading plot contains the original variables and a set of coefficients, while a score plot can be described as a linear combination of PCs with a new set of coefficients. Both loading and score plots are frequently used to visualize the PCA results [4.61].

HCA, discussed under *Applications of HCA and Heatmaps to samples from Positive/Negative APPI Modes*, is one of the cluster analyses that generate clusters of related objects, in which a series of partitioning calculations are performed to group objects. In this study, both ward linkage [4.72] and Kendall rank correlations [4.73] were utilized to create clusters. A ward linkage is a least squares method, computed by the fol-

lowing equation

$$\sum_{i=1}^n (X_i - \bar{X})^2, \quad (4.1)$$

where X represents the value of an object and \bar{X} is the estimated mean value of the cluster. The Kendall tau (τ) is computed by the following equation

$$\tau = \frac{n_c - n_d}{\frac{1}{2}n(n-1)}, \quad (4.2)$$

where n_c and n_d are the concordant and discordant count numbers respectively, and n is the number of samples. Thus, two clusters in perfect positive correlation will be presented as $\tau = 1$. On the other hand, $\tau = -1$ represents a perfect negative correlation.

PCA Applications of Positive/Negative APPI Data
PCA Interpretation of Positive APPI Data. The score plot shown in Fig. 4.2a was constructed with PC-1 and PC-2 variables from each of the samples. The 20 samples were roughly split into three groups. In Fig. 4.2b, the loading variables for PC-1 and PC-2 are presented. For easy recognition and evaluation, the compound class distribution was color coded. In the loading plot as shown in Fig. 4.2b, N_1 class compounds are marked in gray, and HC class compounds are shown in dark green. Sulfur-containing classes such as S_1 , S_2 , and N_1S_1 are located mostly on the right side of the loading plot. It shows that the group I samples are rich in sulfur. Group II samples are rich in HC, O_1 and O_2 class compounds, and group III samples are rich in N_1 and N_1O_1 compounds. Thus, PCA can be used to describe the similarities and/or differences between complex spectra.

We use biplots, which superimpose score and loading plots, shown in the Figs. 4.3–4.5 for three groups of compound types, for easy visualization of the relationships between the samples and their observed peaks. Figure 4.3 is for HC, O_1 and O_2 class compounds, Fig. 4.4 is for N_1 and N_1O_1 class compounds, and Fig. 4.5 is for S_1 and S_2 class compounds. It can be seen that X01, X12 and X16 in Fig. 4.3 all contain high concentrations of nitrogen as shown in Table 4.1, while X02, X03, X11, X13, X17, X18 and X19 in Fig. 4.3 contain high concentrations of sulfur.

PCA can show good correlation between the spectral results and the bulk properties. For example, A.J.G. Barwise [4.74] previously reported a correlational relationship between bulk sulfur and vanadium contents in crude oil samples. Thus, the comparison of samples displayed in Figs. 4.3–4.5 (group I versus group II and III) and their properties listed in

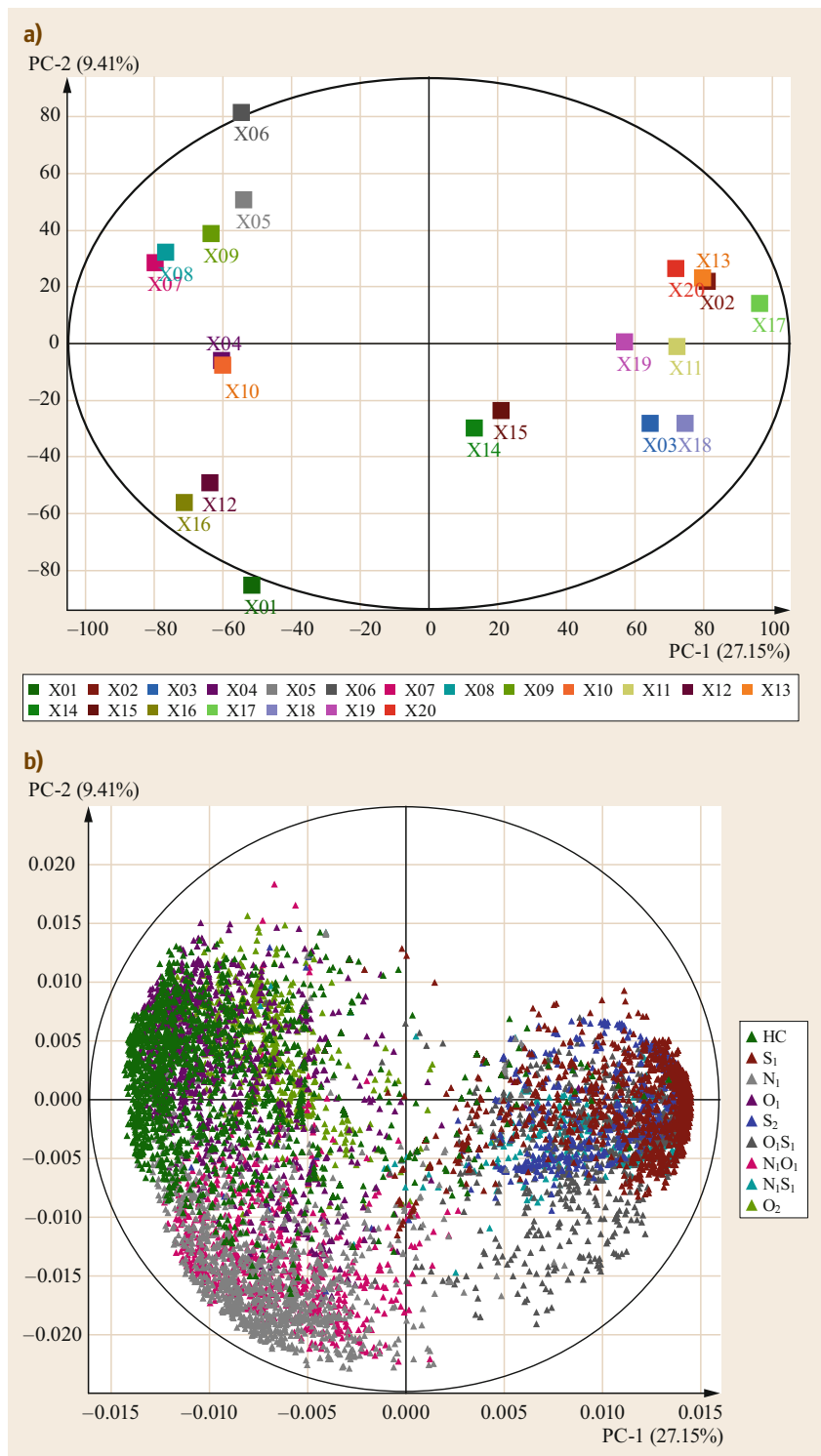


Fig. 4.2a,b PCA score (a) and loading (b) plots of positive APPI spectra of 20 oils. Reprinted with permission from [4.55]. Copyright (2010) American Chemical Society

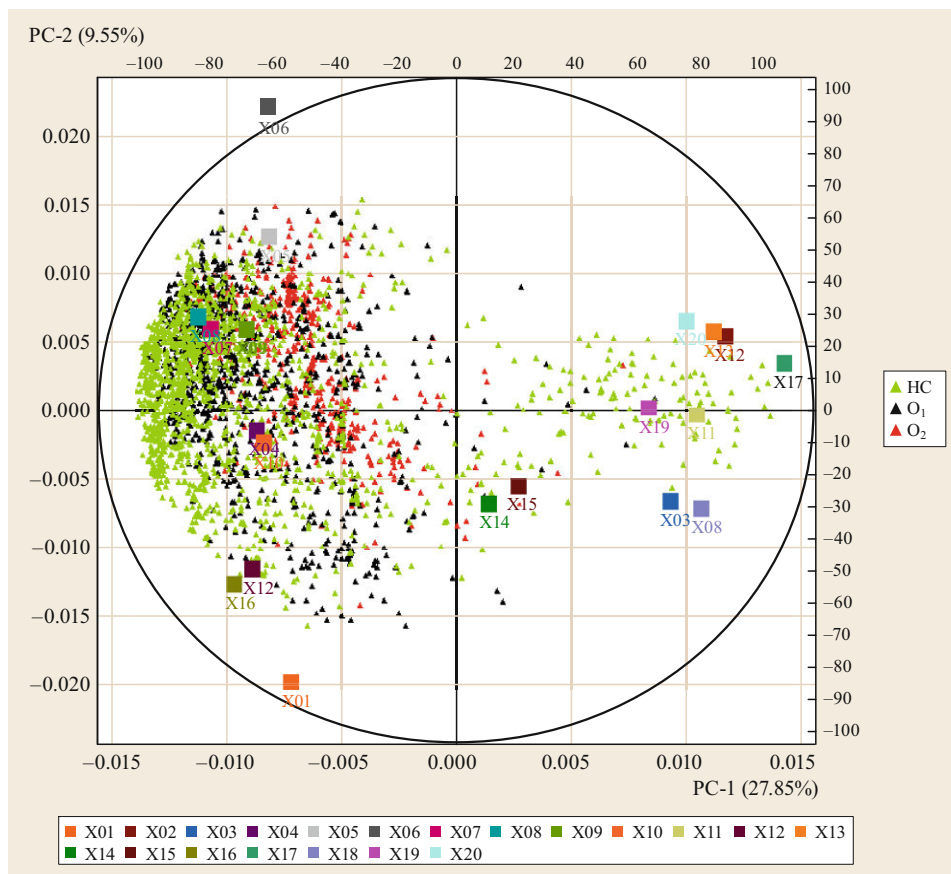


Fig. 4.3 Biplots of the score and loading plots displayed in Fig. 4.2 for HC, O₁ and O₂ class compounds. Reprinted with permission from [4.55]. Copyright (2010) American Chemical Society

Table 4.1 Bulk properties of samples used in this study (after [4.56])

Oil samples	Sulfur (%)	N (ppm)	TAN (mg KOH/g)	API	V (ppm)	Ni (ppm)	AR (wt%)
X01	0.61	3861	2.05	20.1	17.5	9.5	65.46
X02	2.87	1645	0.29	27.6	56.3	18.5	50.75
X03	4.5	–	3.5	8.0	105.6	–	–
X04	0.13	949	0.58	22.3	0	18.4	45.18
X05	0.09	–	0.54	39.57	–	–	29.12
X06	0.08	–	0.87	38.61	–	–	31.06
X07	0.08	2865	2.34	27.2	0	42.0	73.33
X08	0.11	1884	4.26	22.0	0	8.3	78.31
X09	0.2	3231	1.46	20.7	1.3	49.1	77.17
X10	0.13	1654	0.25	32.6	1.7	2.9	51.11
X11	4.79	2136	0.27	18.3	54.6	21.4	65.66
X12	0.18	3532	0.79	23.1	3.7	3.9	68.34
X13	2.71	1350	0.18	30.4	28.2	9.5	45.86
X14	1.85	3536	0.25	19.6	308.7	128.6	62.61
X15	2.01	4011	0.18	19.5	329.8	129.0	64.88
X16	0.25	4405	3.15	16.1	0	12.7	81.17
X17	3.77	1620	0.3	24.1	43.8	21.7	56.26
X18	3.57	4019	0.45	19.3	93.5	71.0	64.32
X19	3.53	3123	0.47	19.5	108.3	38.7	64.48
X20	1.91	900	0.38	34	11.5	10.6	41.18

– : Data not available

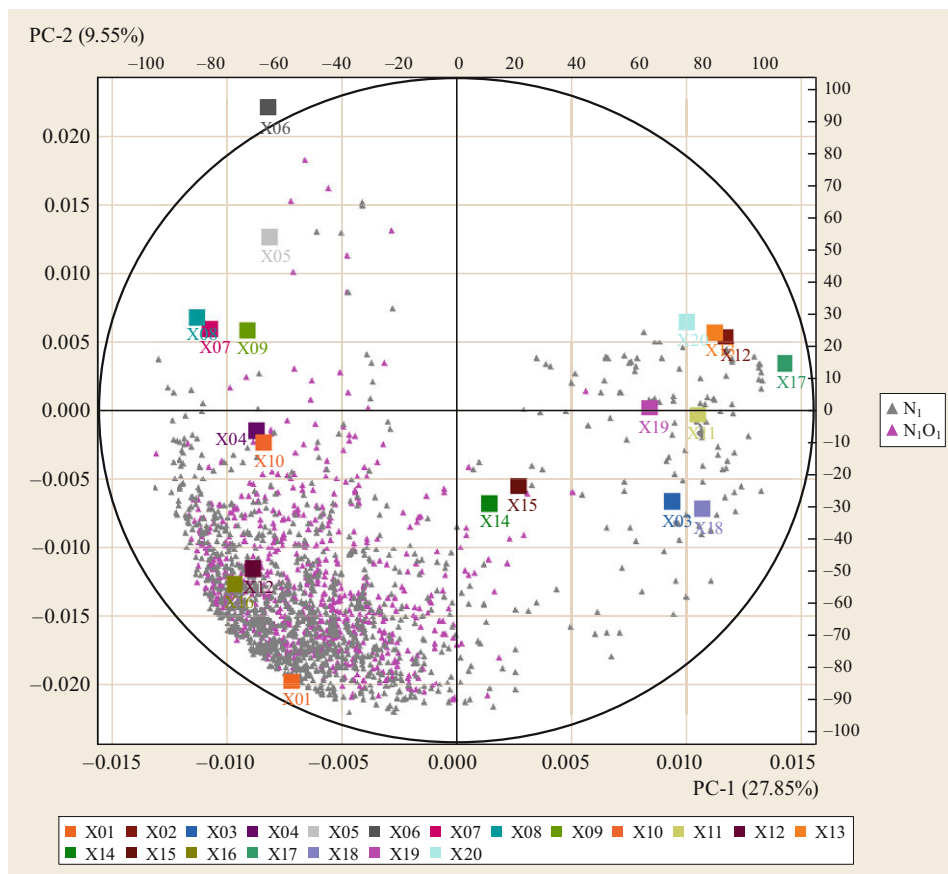


Fig. 4.4 Biplots of the score and loading plots displayed in Fig. 4.2 for N_1 and N_1O_1 class compounds. Reprinted with permission from [4.55]. Copyright (2010) American Chemical Society

Table 4.2 Sulfur and vanadium concentrations of the samples grouped in Figs. 4.3–4.5

	Sulfur (%)	Vanadium (ppm)
Group I		
X17	3.77	43.8
X11	4.79	54.6
X18	3.57	93.5
X13	2.71	28.2
X02	2.87	56.3
X15	2.01	329.8
X14	1.85	308.7
X03 ^a	4.5	— ^b
X20	1.91	11.5
X19	3.53	108.3

Table 4.2 indicates that some correlation might exist between vanadium- and sulfur-containing molecules as groups.

PCA Interpretation of Negative APPI Data. PCA was also performed on negative APPI spectra. The resulting score and loading plots for all 20 samples are presented

Table 4.2 (continued)

	Sulfur (%)	Vanadium (ppm)
Group II		
X10	0.13	1.7
X12	0.18	3.7
X04	0.13	0
X07	0.08	0
X09	0.2	1.3
X08	0.11	0
X05	0.09	— ^b
X06	0.08	— ^b
Group III		
X01	0.61	17.5
X12	0.18	3.7
X16	0.25	0

^a Unconventional, bitumen from oil sand

^b Data not available

in Fig. 4.6a,b respectively. The division between groups in the score plot was not as distinct as that observed for the positive APPI mode.

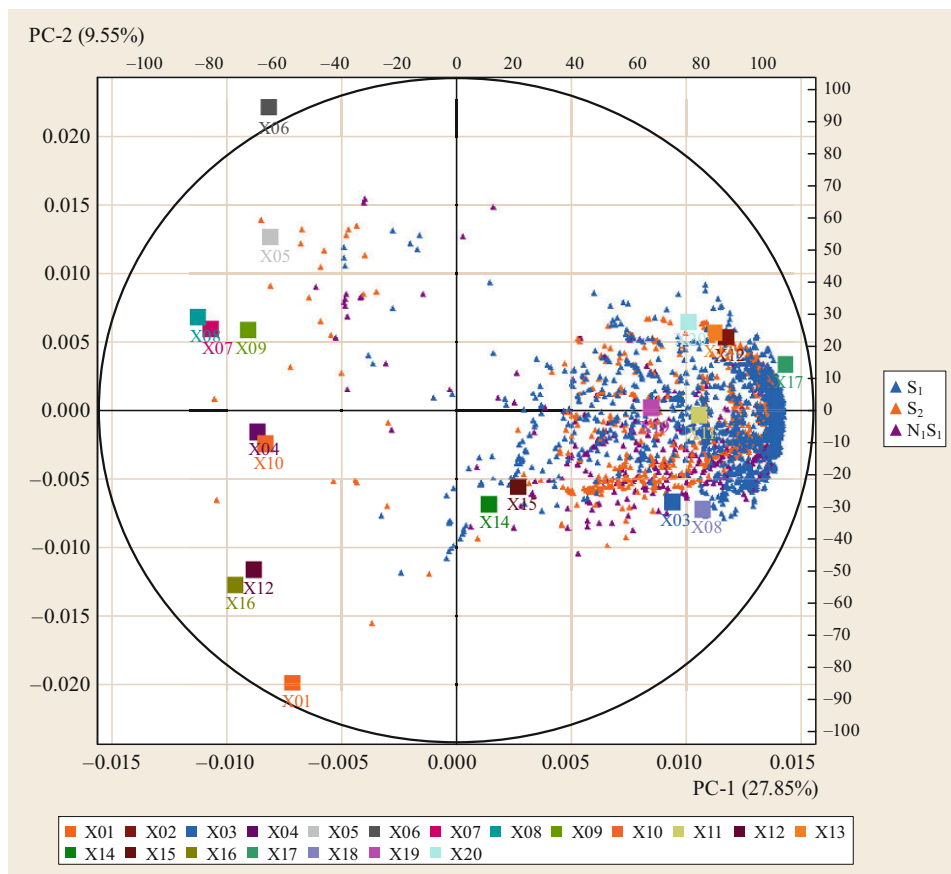


Fig. 4.5 Biplots of the score and loading plots displayed in Fig. 4.2 for S_1 and S_2 class compounds. Reprinted with permission from [4.55]. Copyright (2010) American Chemical Society

Among the 20 samples, X03 was the only unconventional oil that was a bitumen extracted from oil sands. It was well separated from all other samples in the score plot, situated at lower right corner. Comparing with the loading plot, it shows that S_xO_y ($x \geq 1$ and $y \geq 1$) compounds were uniquely abundant in X03. Hence, PCA can identify unique components in the samples.

By eliminating X03, the source and score plots of the remaining 19 conventional oils are shown in Fig. 4.7a,b. The division between three main groups becomes clear as shown in Fig. 4.7a. The distribution of compound classes can be seen in the loading plot of Fig. 4.7b. The group consist of sulfur-containing classes (N_1S_1 and S_1O_1) primarily located on the right side of the figure, nitrogen-containing classes (N_1 and N_1O_1) at the top, and oxygen-containing class such as O_2 class on the left side.

Applications of HCA and Heatmaps to Samples from Positive/Negative APPI Modes

HCA is useful to show relationships among samples based on selected clusters of peaks. The samples were divided into two main clusters, as shown in Fig. 4.8.

Each cluster can be further divided into several layers of subclusters.

Figure 4.8a displays the first layer of four subclusters: A, B, C and D of HC, O_1 and O_2 peaks shown in Fig. 4.3. The physical and chemical properties of the bulk oils corresponding to these clusters are listed in Table 4.1. The figure reveals that subclusters A and B contained higher amounts of vanadium and $> 1\%$ sulfur, while subclusters C and D contained lower or negligible amounts of vanadium and $< 1\%$ sulfur. All of the subcluster B samples contained no less than 90 ppm vanadium, and subcluster A contained samples with moderate amounts of vanadium ranging from 10 to 60 ppm. Thus, HCA can reveal relationships between crude oil samples by correlating the measured peaks to gross properties.

Similarly, Fig. 4.8b displays two first-layer subclusters, A' and B' of sulfur-containing S_1 , S_2 , and N_1S_1 classes shown in Fig. 4.5. Subcluster A' contained $> 1\%$ sulfur and significant amounts of vanadium, while subcluster B' contained less than 1% sulfur and small or negligible amounts of vanadium. Table 4.3 lists the oil samples in each of the subclusters.

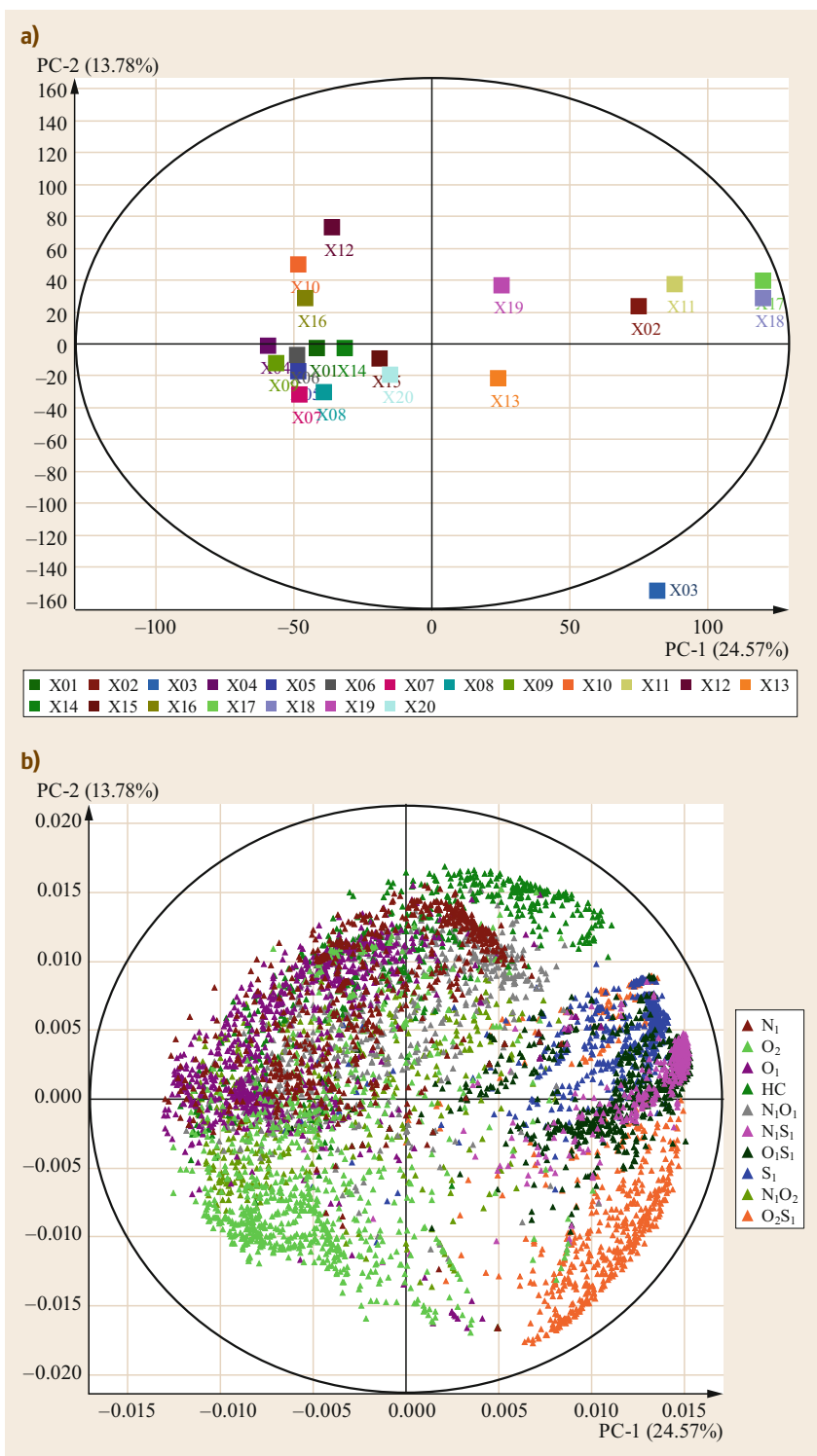


Fig. 4.6a,b PCA score (a) and loading (b) plots of negative APPI spectra of 20 oils. Reprinted with permission from [4.55]. Copyright (2010) American Chemical Society

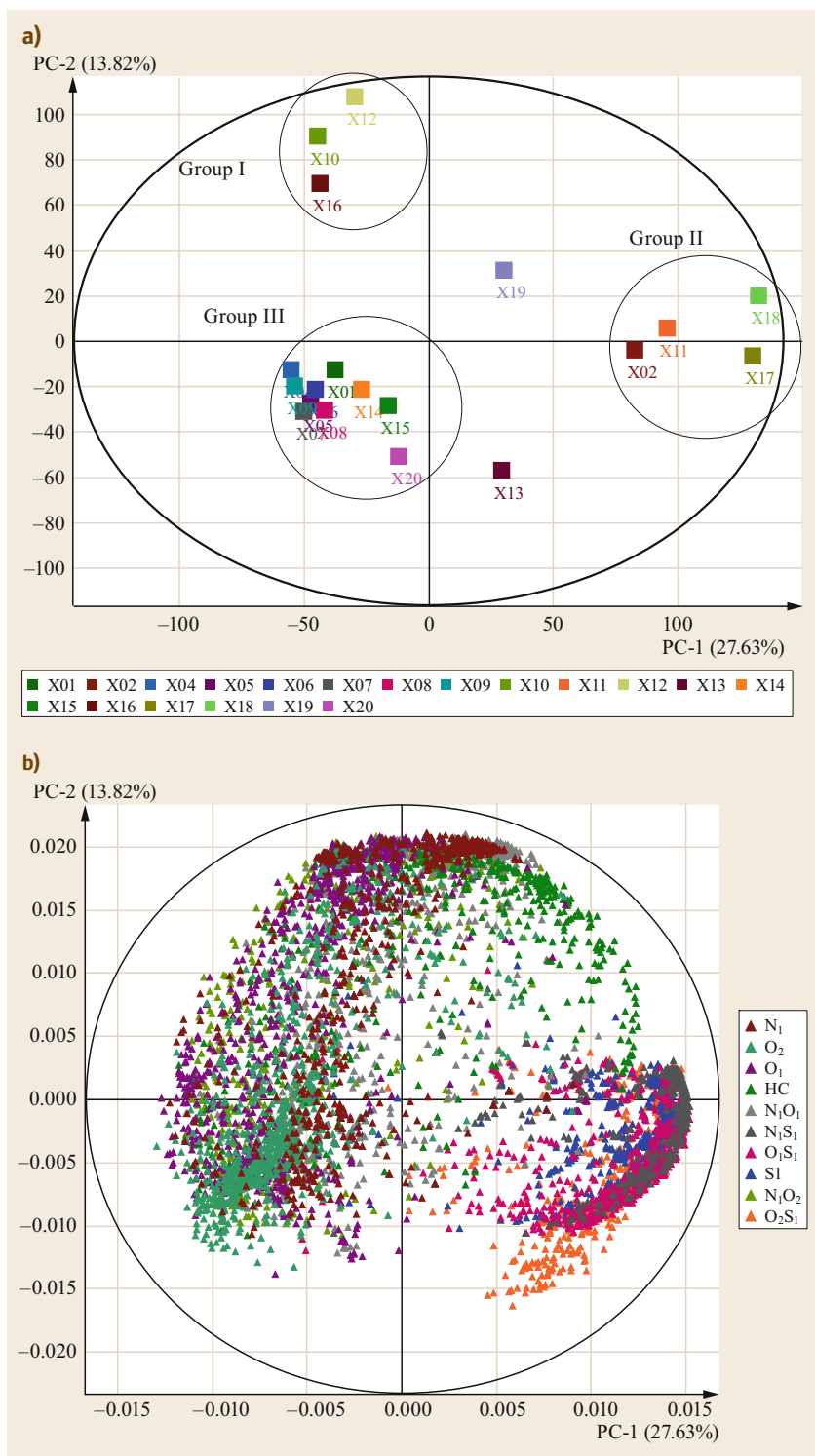


Fig. 4.7a,b PCA Score (a) and loading (b) plots of negative APPI spectra of 19 conventional oils (excluding X03 from oil sand). Reprinted with permission from [4.55]. Copyright (2010) American Chemical Society

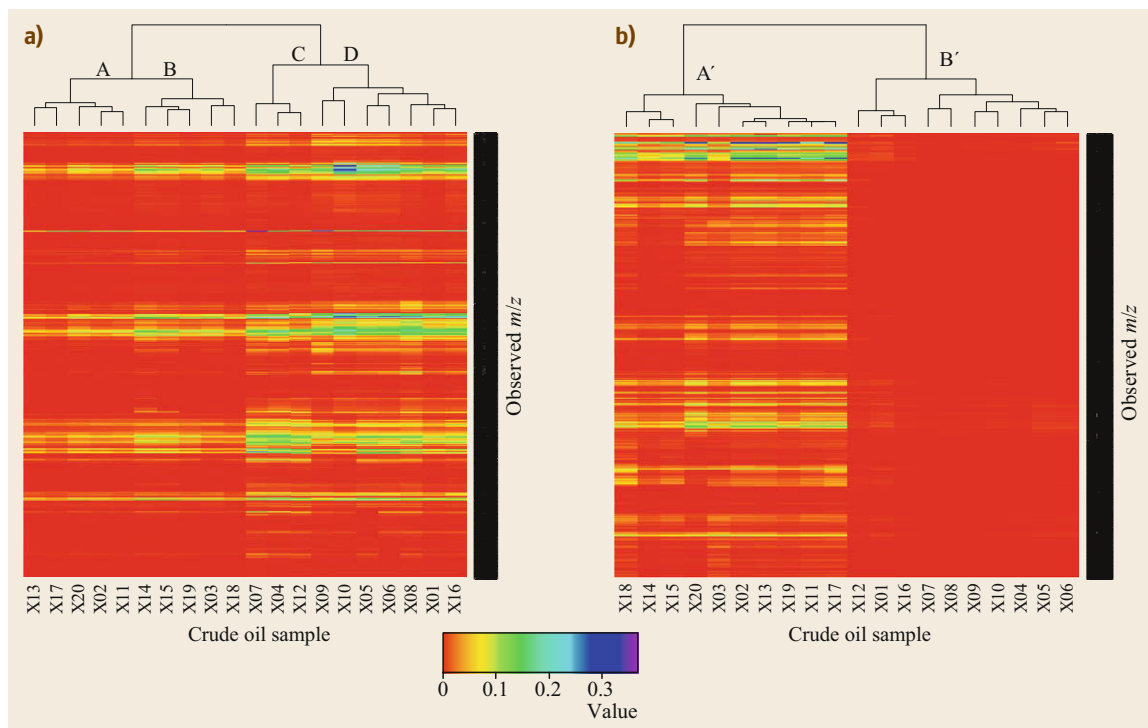


Fig. 4.8a,b Heatmaps and dendrograms showing the HCA results of the peaks presented in (a) Fig. 4.3 and (b) Fig. 4.5. Reprinted with permission from [4.55]. Copyright (2010) American Chemical Society

4.1.3 Correlation Between Chemical Composition and Physical Properties of Crude Oils

The following studies show the peaks measured by FT-ICR MS can be associated with chemical and physical properties of crude oils. The peaks were statistically analyzed by Spearman's rank correlation; utilized and graphically presented correlations are based on Circos diagrams [4.75]. Many peaks correlate strongly with sulfur, total acid number (TAN), and vanadium contents.

Statistical Analysis for Correlation Study

Prior to statistical analysis, peak lists with elemental formula assignments were aligned into a single table for each set of data. Further information can be found in Sect. 4.1.1. In this study, Spearman's rank correlation was utilized, [4.76] since the Spearman correlation does not require prior knowledge of a probability distribution. In the literature [4.76, 77], it is commonly explained that the original two variables were converted into ranks at the first step. After the ranks were determined based on size, variables were sorted by size and ranked according to their order. If a variable had

a smaller value, it had a lower rank, and if a variable had a larger value, it had a higher rank. When variables were of equal size, they had an equal rank. After ranking, a correlation value was then computed on the ranks. The first original variable was the relative abundance of peaks in the samples and the second original variable was a selected property of the crude oils. If there were no tied ranks, the correlation coefficient (ρ , Spearman's rho) was computed as follows

$$\rho = 1 - \frac{6 \sum_i (x_i - y_i)^2}{n(n^2 - 1)},$$

where x_i and y_i are the ranks of relative abundance and properties of crude oil respectively, for each set. If there were tied ranks, the following equation was used for the computation

$$\rho = \frac{\sum_i (x_i - \bar{x})(y_i - \bar{y})}{\sqrt{\sum_i (x_i - \bar{x})^2 \sum_i (y_i - \bar{y})^2}}.$$

Our correlation studies used bulk properties of samples shown in Table 4.2.

Table 4.3 Sulfur and vanadium concentrations of the samples in subclusters shown in Fig. 4.8

	Sulfur (%)	Vanadium (ppm)
Subcluster A		
X13	2.71	28.2
X17	3.77	43.8
X20	1.91	11.5
X02	2.87	56.3
X11	4.79	54.6
Subcluster B		
X14	1.85	308.7
X15	2.01	329.8
X19	3.53	108.3
X03 ^a	4.5	105.6
X18	3.57	93.5
Subcluster C		
X07	0.08	0
X04	0.13	0
X12	0.18	3.7
Subcluster D		
X09	0.2	1.3
X10	0.13	1.7
X05	0.09	– ^b
X06	0.08	– ^b
X08	0.11	0
X01	0.61	17.5
X16	0.25	0
Subcluster A'		
X18	3.57	93.5
X14	1.85	308.7
X15	2.01	329.8
X20	1.91	11.5
X03*	4.5	105.6
X02	2.87	56.3
X13	2.71	28.2
X19	3.53	108.3
X11	4.79	54.6
X17	3.77	43.8
Subcluster B'		
X12	0.18	3.7
X01	0.61	17.5
X16	0.25	0
X07	0.08	0
X08	0.11	0
X09	0.2	1.3
X10	0.13	1.7
X04	0.13	0
X05	0.09	– ^b
X06	0.08	– ^b

^a Unconventional, bitumen from oil sand
^b Data not available

Visualization/Interpretation of the Correlation Diagrams

Correlation diagrams were designed by Hur et al. [4.56] based on the Circos diagram [4.75], which was originally developed for comparative genomics. It is a very effective visualization tool for large amounts of data. Peaks with statistical significance (ρ -values < 0.05) were used to construct the diagram as shown Fig. 4.9, which serves as an example to explain how to interpret the diagrams. Correlation diagrams contain four bands: the chemical, or heteroatom, class band; the C# (number of carbon) versus DBE (rings plus double bonds to carbon) band for each class; the distribution of ρ band; and the correlation circle band. DBE values were calculated from chemical formulas using the following equation

$$\text{DBE} = c - h\frac{1}{2} + \frac{n}{2} + 1$$

(for the ions $\text{C}_c\text{H}_h\text{N}_n\text{O}_o\text{S}_s^+$ or $\text{C}_c\text{H}_h\text{N}_n\text{O}_o\text{S}_s^-$).

In Fig. 4.9, the peaks with the same C# are shown on a line in the band, and C# for the lines increased in a clockwise direction. In addition, the minimum and maximum values of C# are marked for each class. *Triangle dots* closer to the center have lower DBE values than outside *triangle dots*. The correlation circle is located at the center. The correlation circle shows not only the whole distribution of the correlation coefficient (ρ), but it also shows lines linking a property with observed peaks color-coded according to their ρ values. Colors in *red* and *orange* show a strongly positive correlation, *light green* a weak correlation, and *green* and *blue* a strong negative correlation. A more detailed distribution of the ρ band is presented in the band just outside of the circle.

Correlation with Sulfur and Vanadium Contents.

Correlation between peaks observed in (+) mode APPI spectra is presented in Fig. 4.9. The diagram shows that sulfur-containing classes such as S, S₂, OS, and NS were dominant. The correlation circle band was dominated by either *red* or *orange*, indicating a very strong positive correlation. This means that sulfur-containing compounds show a strong positive correlation with the sulfur content of the samples, which agrees with what is expected from crude oils. In Fig. 4.9, the classes that do not contain sulfur yield an apparently negative correlation with sulfur content. This could be due to the higher sensitivity of sulfur-containing compounds with (+) mode APPI detection. The negative correlation shown here could be the result of suppressed ionization when sulfur-containing compounds exist in large amounts in the sample. In addition, since a correlation

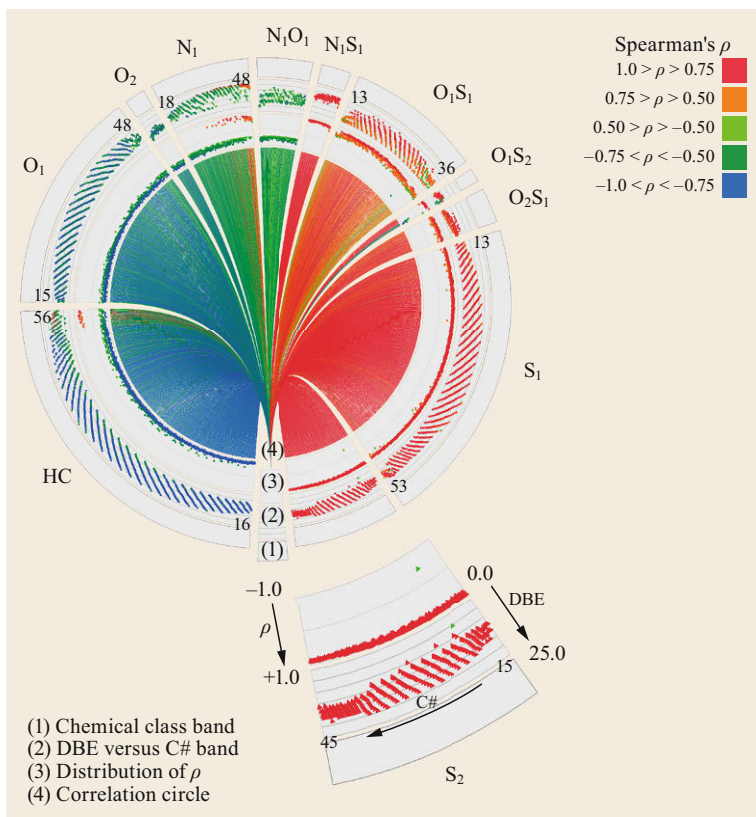


Fig. 4.9 A Circos diagram showing correlations with sulfur of oil components observed in (+) APPI FT-ICR mass spectra. Reprinted with permission from [4.56]. Copyright (2010) American Chemical Society

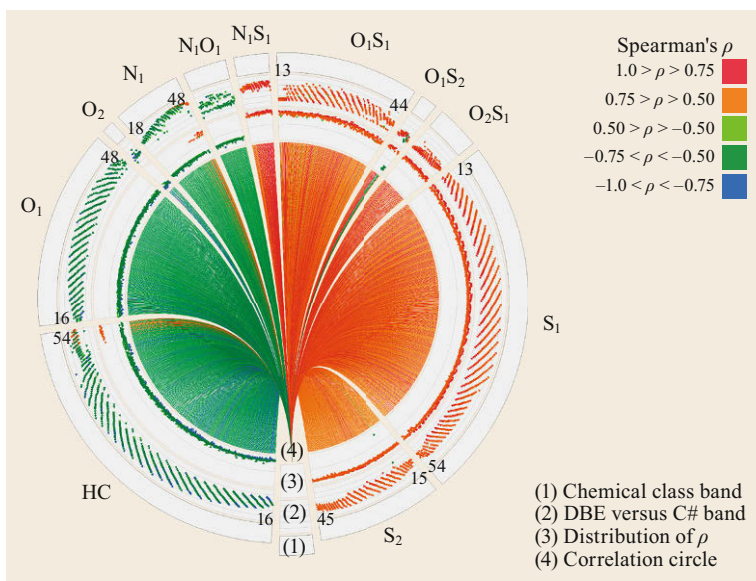


Fig. 4.10 Correlation with vanadium of oil components observed in (+) APPI FT-ICR mass spectra. Reprinted with permission from [4.56]. Copyright (2010) American Chemical Society

with SO class compounds showed DBE dependence, the SO compounds with relatively high DBE values had stronger correlation than those with lower DBE values in the *DBE versus C# band*. Hence, this result shows that information obtained from the ultrahigh-resolution mass spectra correlates well with sulfur contents of crude oils.

The vanadium contents were determined using the American Society for Testing and Materials (ASTM) method [4.78]. Figure 4.10 shows the correlations between peaks observed in (+) APPI mass spectra and the vanadium contents of the oil sample. A strong correlation between vanadium content and sulfur-containing compounds was observed. Clearly, the correlation diagram for vanadium content is very similar to Fig. 4.9 for sulfur-containing classes. This relationship has been previously reported [4.74]. The S_1 class compounds with relatively low DBE numbers presented stronger correlations with vanadium content in the *DBE versus C# band* of Fig. 4.8. The trend of a stronger correlation for lower DBE compounds was independent of C#. Table 4.4 presents the average DBE values of S_1 class compounds in two different ranges of Spearman coefficient values (ρ). The average DBE with a ρ value between 0.75 and 1.0 was computed to be 4, but those with a ρ value between 0.5 and 0.75 had an average DBE of about 11. It shows that S_1 class compounds with a lower degree of aromaticity and/or unsaturation were more strongly linked with vanadium content. Further studies are required to understand why this correlation exists.

Correlation with Total Acid Number (TAN). TAN values were commonly determined by titration [4.79],

Table 4.4 Average DBE values for S_1 class compounds in different ranges of ρ values

Spearman correlation coefficient (ρ)	$0.5 < \rho < 0.75$	$0.75 < \rho < 1.0$
Average DBE (\pm standard deviation)	4.0 (± 2.7)	10.8 (± 3.6)

which the oil industry uses to indicate the acidity of crude oils. The number is defined as the amount of KOH (in mg) needed to neutralize 1 g of crude oil. Since negative mode analysis is more suitable for acidic compounds, negative APPI spectra were used for the correlation with TAN as shown in Fig. 4.11. Strong correlations ($\rho > 0.5$) between TAN and O_2 and O_4 classes were observed. This is reasonable, since both naphthenic and aromatic acids contribute to the acidity of crude oils. The DBEs of the O_2 class correlated with the TAN widely from 1 to 17, with higher C# more strongly. The peaks in the O_4 class correlated positively with TAN at relatively low DBE values, 3–5. Hence, O_4 class compounds are likely to be dicarboxylic naphthenic acids. The DBE values ≥ 4 can also be aromatic.

4.1.4 Quantitative Comparisons by Statistical Analysis

Principle component analysis (PCA) for dimensionality reduction in multivariate analysis is useful to make grouped samples into score plots based on the molecular composition. Hierarchical clustering analysis (HCA) has been applied successfully to interpret complex petroleum mass spectra obtained by Fourier

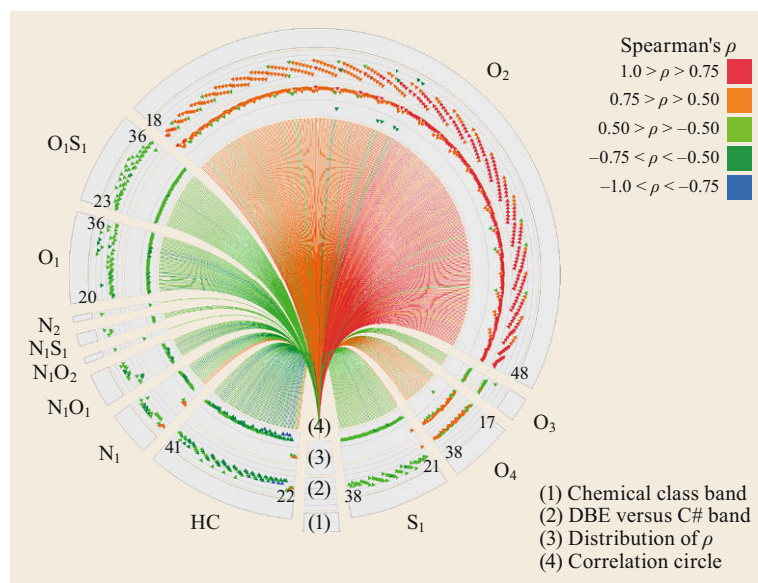


Fig. 4.11 Correlation with TAN of oil components observed in (–) APPI FT-ICR mass spectra. Reprinted with permission from [4.56]. Copyright (2010) American Chemical Society

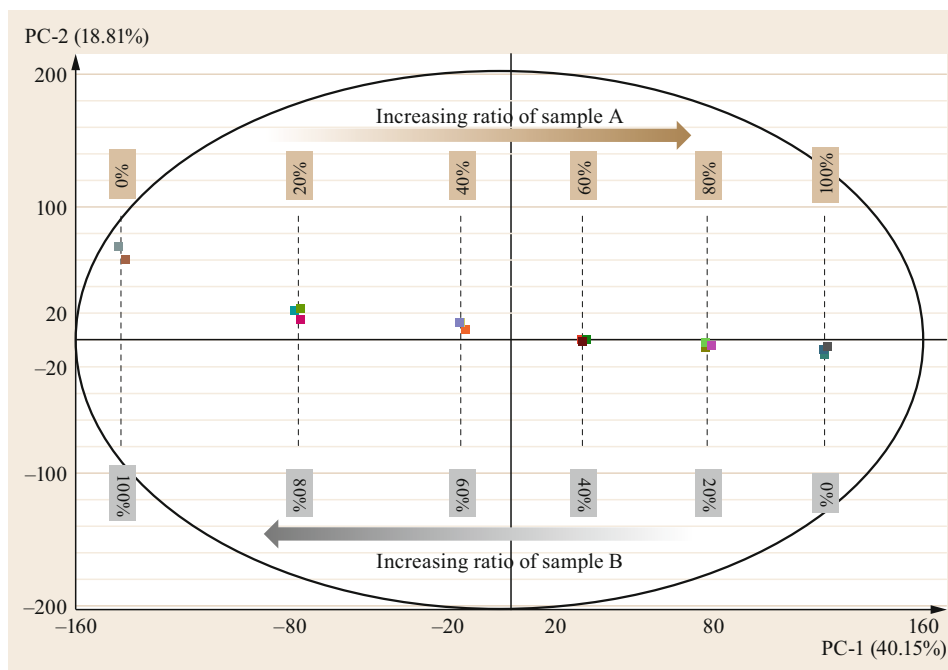


Fig. 4.12 Quantitative changes on PCA scores with changes in ratios of samples A and B, created by mzCruiser software

transform ion cyclotron resonance mass spectrometry (FT-ICR MS). This method has been used to group and compare samples based on the selected peaks that had been grouped by PCA. However, PCA and HCA have not been combined with conventional visualization methods such as DBE versus C# plot and van Krevelen diagram. Also, they do not explain how much difference in abundance there is between heteroatom classes or samples by quantitative analysis.

This section demonstrates a quantitative analysis for comparing two petroleum samples by PCA and *t*-test. As an illustration, two crude oils (samples A and B from North Sea offshore reservoirs provided by SINTEF in Norway) were mixed in different ratios from 0 to 100% of sample A (or sample B) at 20% increments. The resulting six crude oil mixtures were measured by Witt and Timm [4.80] in replicate using APPI positive ion mode for the determination of composition ratios in simulated binary and even ternary crude oil mixtures [4.80].

The six mixtures are separated on the score plot shown in Fig. 4.12. Each mixture was separated and changed constantly on PC-1 as *x*-axis and PC-2 as *y*-axis according to the ratio of samples A and B. This shows that the quantitative change of sample A or B is identified by PCA. It also indicates how the abundance of peaks is changed according to the change of ratio of samples A and B by 20%, because the PCA has the strongest linear trend along the principal component with the highest variance on PC-1.

Volcano plots are utilized to identify the quantitative change of samples in detail. Such graphics are generated by plotting statistical significance, called *p*-value, on the *y*-axis, and the degree of changes, called fold change (FC or \log_2 FC), on the *x*-axis. The degree of change between two samples can be determined by the abundance ratio of chemical components observed in the spectra.

For the pooled *t*-test analysis, the degree of change is generally computed with the \log_2 scale because the abundance of compounds can vary by orders of magnitude [4.81] and it has been commonly used to present spectral data for statistical analysis [4.54, 55, 82]. One of the reasons for using \log_2 scale rather than \log_{10} scale is to increase dynamic range of graphical presentation or statistical interpretation. If x_i is the abundance of the *i*-th compound in the spectra repeated for n_0 times and if y_i is the abundance of the *i*-th compound in the spectra repeated for n_1 times, then \bar{x}_i and \bar{y}_i are defined as

$$\bar{x}_i = \frac{1}{n_0} \sum_{j=1}^{n_0} x_{ij} \quad \text{and} \quad \bar{y}_i = \frac{1}{n_1} \sum_{k=1}^{n_1} y_{ik} \quad (4.3)$$

Thus, the degree of change of the *i*-th compound, \log_2 FC_{*i*}, in \log_2 scale is computed by (4.4), and FC_{*i*} is calculated by (4.5)

$$\begin{aligned} \log_2 \text{FC}_i &= \log_2(\bar{y}_i) - \log_2(\bar{x}_i) \\ \text{or } \log_2 \text{FC}_i &= \log_2\left(\frac{\bar{y}_i}{\bar{x}_i}\right) \end{aligned} \quad (4.4)$$

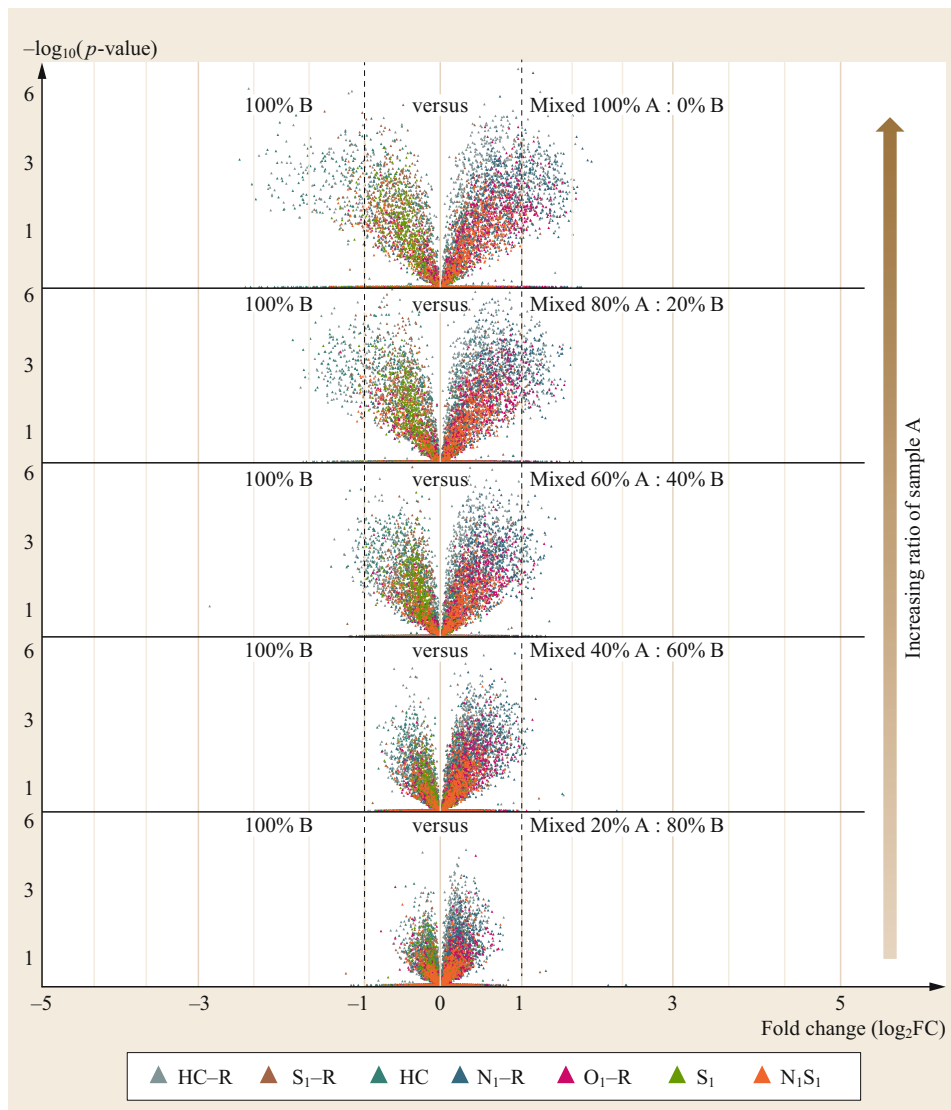


Fig. 4.13 Volcano plots and quantitative changes in major classes (HC-R, S₁-R, HC, N₁-R, O₁-R, S₁, and N₁S₁). As the ratio of sample A increases, the positive and negative fold change changed constantly in major classes. Volcano plots were generated by mzCruiser software

$$FC_i = 2^{\log_2 FC_i} \tag{4.5}$$

For the hypothesis testing, null and alternative hypotheses are stated in the following (4.6)

$$H_0 : \mu_x = \mu_y, \quad H_a : \mu_x \neq \mu_y, \tag{4.6}$$

where μ_x and μ_y are the population mean of x and y respectively. In the hypothesis testing, it is always assumed that $\mu_x = \mu_y$, and the sampling distribution is examined on the basis of this assumption. Within this sampling distribution, one will determine whether or not a sample statistic is unusual. Here it can be assumed that population standard deviations σ_x and σ_y have the

same value, therefore the sample variances s_x^2 and s_y^2 can be pooled to obtain an estimate of the common population variance σ^2 . The pooled estimate of σ^2 is denoted by s_p^2 and is a weighted average of s_x^2 and s_y^2 . The standardized test statistic can be then calculated by the following equation

$$t_i = \frac{(\bar{y}_i - \bar{x}_i) - (\mu_{\bar{y}i} - \mu_{\bar{x}i})}{\sqrt{s_{p,i}^2 \left(\frac{1}{n_1} + \frac{1}{n_0} \right)}}, \tag{4.7}$$

where $s_{p,i}^2$ is the pooled sample variance of the i -th compound x_{ij} and y_{ik} in (4.3); each n_0 and n_1 is the number of x and y replicate spectra obtained from the same sam-

ple. Then, the significance level (p -value) presented in ordinate (typically the $-\log_{10}$ of the p -value) is calculated by the following (4.8)

$$p\text{-value} = 2 \text{Prob}(T > |t|), \quad (4.8)$$

where T is a random variable, t is the standardized test statistic obtained from (4.7) and Prob is the probability. As a consequence, chemical components with statistical significance are located in the upper part of the volcano plot. Positive/negative \log_2 FC (4.4) was used as the abscissa for representing the degree of change on the volcano plots. Each dot that represents a chemical component can be color coded by its heteroatom class, DBE, or other parameters. This approach can be very effective for finding unique biomarkers or specific compounds in the samples.

Volcano plots based on \log_2 scale have been used for analyzing biological data since 2003 [4.83] (e.g., microarray [4.83, 84] and metabolomics [4.85]). Fold changes are the preferred quantification parameter (or variable) of differential expressions, which are basically the ratios of the measurement of the same species between two samples. However, the ratios are not symmetric around 1, making it problematic to perform statistical analysis. Thus, we choose logarithms (e.g., \log_2) because logs of the ratios are symmetric around 0.

Figure 4.13 shows the volcano plots that illustrate the quantitative changes or degrees of difference in peak intensity ratios of various compound types (in color codes shown on top of the figure) when sample B is mixed with sample A. Each dot represents a component that is present in both samples to be compared. Sample B if compared to itself would have both p -value and fold change of 0 for unity ratios. The components in sample B (100% B) having more statistical significance in abundance than sample A and its mixtures are in left-hand side with negative fold change values. On the other hand, the components in sample A and its mixtures with sample B having more statistical significance in abundance are in the right-hand side with positive fold change values. When more sample A is added into sample B in the mixtures, both p -value and fold change will be increased in absolute values due to increasing difference in intensities between the pairs to be compared.

As the ratio of sample A increases, the positive/negative fold change was changed constantly in the major classes of HC-R, S₁-R, HC, N₁-R, O₁-R, S₁, and

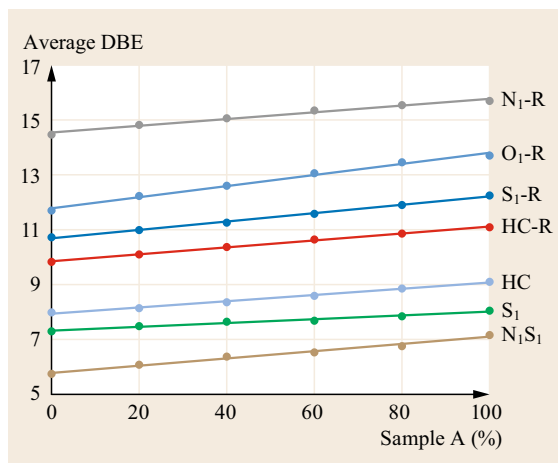


Fig. 4.14 Average DBE distribution and quantitative changes in major heteroatom classes (HC-R, S₁-R, HC, N₁-R, O₁-R, S₁, and N₁S₁) among mixtures

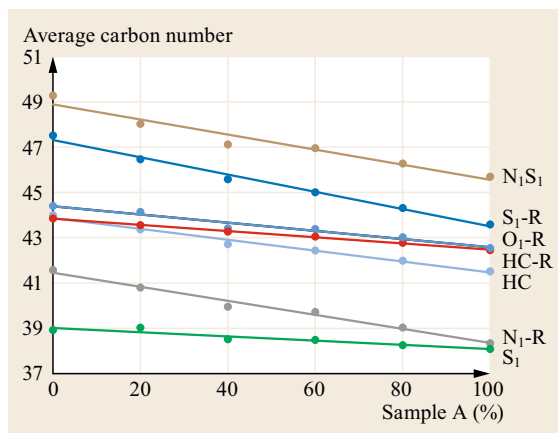


Fig. 4.15 Average carbon number (C#) distribution and quantitative changes in major heteroatom classes (HC-R, S₁-R, HC, N₁-R, O₁-R, S₁, and N₁S₁) among mixtures

N₁S₁ that appeared in positive APPI spectra, where the classes with -R represent radical molecular ions ($M^{+\bullet}$) and the ones without -R represent protonated molecular ions (MH^+). Also, average DBE as shown by Fig. 4.14 increased linearly, and average carbon number (C#) as shown Fig. 4.15 decreased linearly. There are big differences between molecular ions and protonated molecular ions, such as S₁ and S₁-R, due to the difference in ionization processes. In summary, the t -test and volcano plot can be used to present quantitative changes in crude oil samples.

4.2 Emerging Technologies for Storing, Visualizing, and Processing Crude Oil Data

Several key technical challenges in crude oil studies have been discussed. Researchers in other -omics studies have been developing a variety of analytical approaches and techniques to understand life phenomena, such as DNA sequencing, by integrating all the information obtained from experiments including analytical results [4.86]. Those approaches can be utilized for oil analysis.

4.2.1 Development of a Data Analysis Platform with Mega Database

Various analytical platforms provide a wealth of metadata for samples. Development of new techniques for extracting information from the metadata for relationships between crude oil and its properties can further enlarge our understanding of crude oils. Sect. 4.1.3 showed, for example, the studies of correlations between FT-ICR MS peaks and crude oil properties [4.56]. Due to their practical importance, bulk properties are perhaps the most significant metadata for oil samples. Therefore, correlation studies between a significant number of crude oil samples and their metadata are important for oil research [4.87]. However, the amount of data from different analytical instruments is massive, and the amount of corresponding metadata (chemical-physical properties) is equally massive. Consequently, manual evaluation is impossible. But, an efficient software platform for this task has not been developed at this point. Hence, developing such a platform is of utmost importance.

The first step for the platform is to develop an appropriate database system. The database should contain data and metadata obtained from different analytical platforms, and it should be designed to integrate data with metadata. A categorized model of a database for data integration should be considered. This categorized model should be able to incorporate data and metadata from several different platforms. It would be helpful to explain the difference of metadata and actual data among platforms.

Even though some tools are commercially available in petroleomics, the integrated analysis software with database does not exist at this point. Ideally, tools can be combined with the database to store experimental data and their associated metadata. The tools should also include conventional visualization methods and statistical methods now being developed.

The integrated analysis tools that combine with database technology are expected to make significant contributions to oil studies.

4.2.2 Integration of Traditional Methods and Statistical Methods

There have been recent attempts to integrate traditional analysis approaches with statistical methods in petroleomics. Kendrick mass defect analysis, van Krevelen diagrams, H/C versus carbon number (C#) plots, and DBE versus carbon number (C#) plots have been used in crude oil analysis. Meanwhile, varieties of statistical analysis have been combined with the conventional visualization methods [4.88–90]. *Sleighter et al.* [4.89] used this approach to interpret the complex mixtures. In the study, groups of PCA variables from loading plots were selected and further analyzed by van Krevelen diagrams.

The two FT-ICR mass spectra obtained by NHMFL of the S_1 -R ions shown in Fig. 4.16 for Arab Heavy and NIST2717a are obviously different from visual inspection. However, the visual difference needs to be quantified digitally to display the difference in abundance ratios quantitatively, as exemplified by the volcano plot shown in Fig. 4.17 to compare the S_1 -R ions of these two oils.

In Fig. 4.17, the quantitative difference in abundance is presented as fold change in x -axis and the statistical significance is presented as p -value in y -axis. Each dot in Fig. 4.17 represents a S_1 class component that is present in both oils, with carbon number coded on the right-hand side of the figure. The S_1 components in Arab Heavy having higher statistical significance in abundance are located in left-hand side with negative $\log_2 FC$ values. Arab Heavy has higher probability to contain S_1 species of carbon numbers < 40 and > 60 . On the other hand, the S_1 components having higher statistical significance in abundance in NIST2717a are located in right-hand side with positive $\log_2 FC$ values, with most components in the carbon number range of 30–60. Hence, the statistical difference in compound abundances between the two oils can be easily discerned from the volcano plot.

The quantitative comparison (QC) plots for DBE versus C# and H/C versus S/C in van Krevelen diagram are shown in Figs. 4.18 and 4.19 respectively, which were presented by *Hur* at a petroleomics workshop of a Pacificchem conference in 2015 to integrate traditional analytical approaches with statistical methods [4.91].

To be more specific, in the DBE versus C# QC plot shown in Fig. 4.18, the negative fold change area in blue where S_1 -R class components of smaller carbon numbers (C# < 40 and DBE < 15) and larger carbon numbers (C# > 60 and DBE 5–25) in Arab Heavy are more

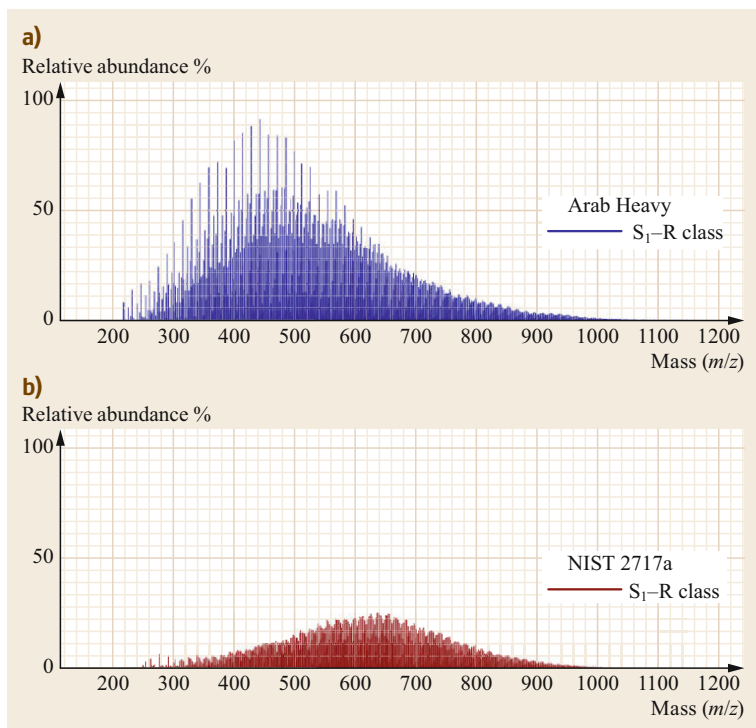


Fig. 4.16a,b Conventional comparison of two spectra of Arab Heavy (a) and NIST2717a (b) in S_1 -R class

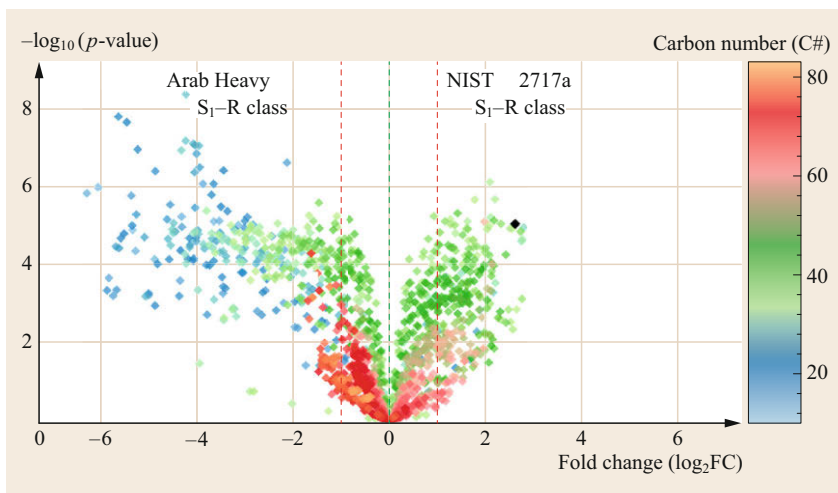


Fig. 4.17 Comparison of two samples using a volcano plot in S_1 -R class, with carbon numbers (C#) indicated by colored dots. Arab Heavy oil has more low C# (< 40) and high C# (> 60) components in the S_1 -R class. Components in Arab Heavy oil have negative fold change values while those in NIST2717a, mostly in the C# range of 30 and 60 have positive fold change values

statistically abundant than in NIST2717a. On the other hand, the positive fold change area in yellow shows S_1 -R class components of larger DBE (DBE > 18) and carbon number between 30 and 60 are more statistically abundant in NIST2717a than in Arab Heavy. The gray area indicates not much difference between the two samples.

Similarly, Fig. 4.19 shows that aromatic sulfur compounds of H/C less than 1.3 with relatively low sulfur-to-carbon ratio are more abundant in NIST2717a. On the other hand, sulfur compounds with H/C > 1.5 are

more abundant in Arab Heavy than in NIST2717a. This indicates that the sulfur components in NIST2717a are more aromatic than those in Arab Heavy.

Thus, QC plots can assist in visual inspection and quantitative determination of the differences of crude oils in compound type and carbon number distributions. It is therefore highly recommended to integrate traditional analysis approaches with statistical models for information retrieval. Volcano plots and QC plots in the section will be further discussed in detail [4.92].

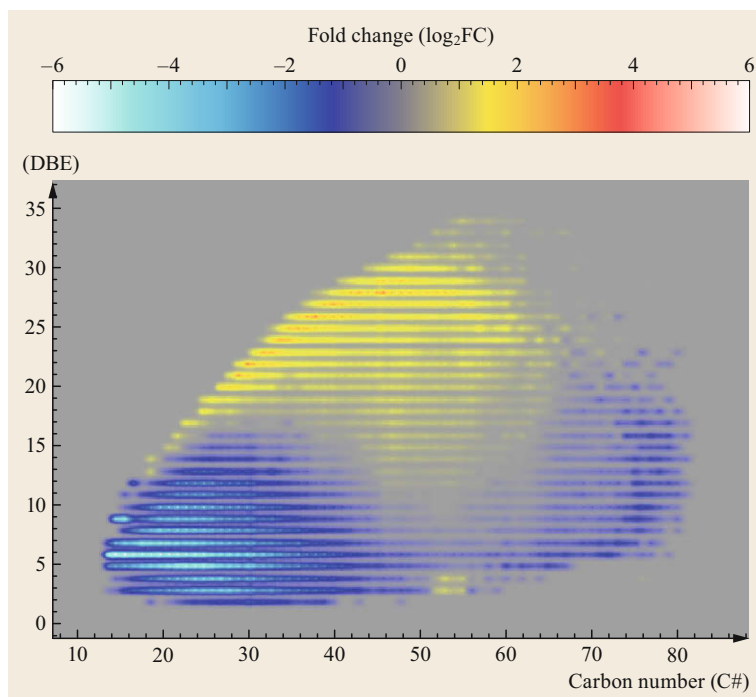


Fig. 4.18 A DBE versus C# QC plot in S₁-R class indicated by colored dots – fold change (\log_2 FC) from the volcano plot (Fig. 4.17). Blue indicates where S₁-R class compounds in Arab Heavy oil are more abundant than in NIST2717a. In the yellow area, S₁-R class compounds in NIST2717a are more abundant than in Arab Heavy. For S₁-R class compounds in gray between the blue and yellow areas, there is not much difference between oil samples

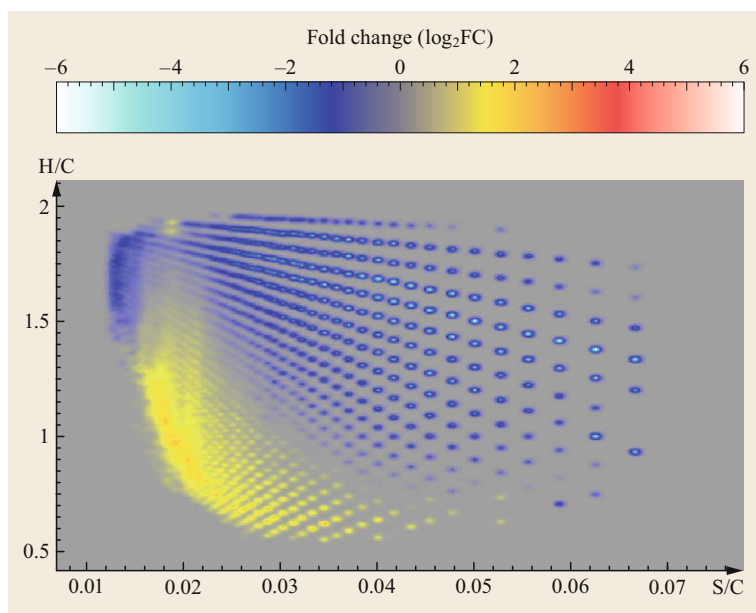


Fig. 4.19 A van Krevelen diagram QC plots in S₁-R class indicated by colored dots – fold change (\log_2 FC) from the volcano plot (Fig. 4.17). S₁-R class compounds in yellow represent higher fold change values for Arab Heavy oil. Conversely, S₁-R class compounds in blue reflect the higher fold change values for NIST2717a

4.2.3 Development of Tools with Enhanced Visual Discrimination

In crude oil analysis, investigators have been concentrating on using conventional methods combined with visual inspection/discrimination to extract significant features from analytical results. For large amounts of data and a large number of samples, statistical methods

have gradually been adopted. However, the development of tools with statistical methods requires visual discrimination, or color coding for heteroatom classes. Visual discrimination facilitates inspection of all the results from various analytical instruments. For example, when authors introduced the PCA technique [4.54] to analyze crude oil FT-ICR MS data, the PCA loading plot provides no significance, as shown in Fig. 4.20a.

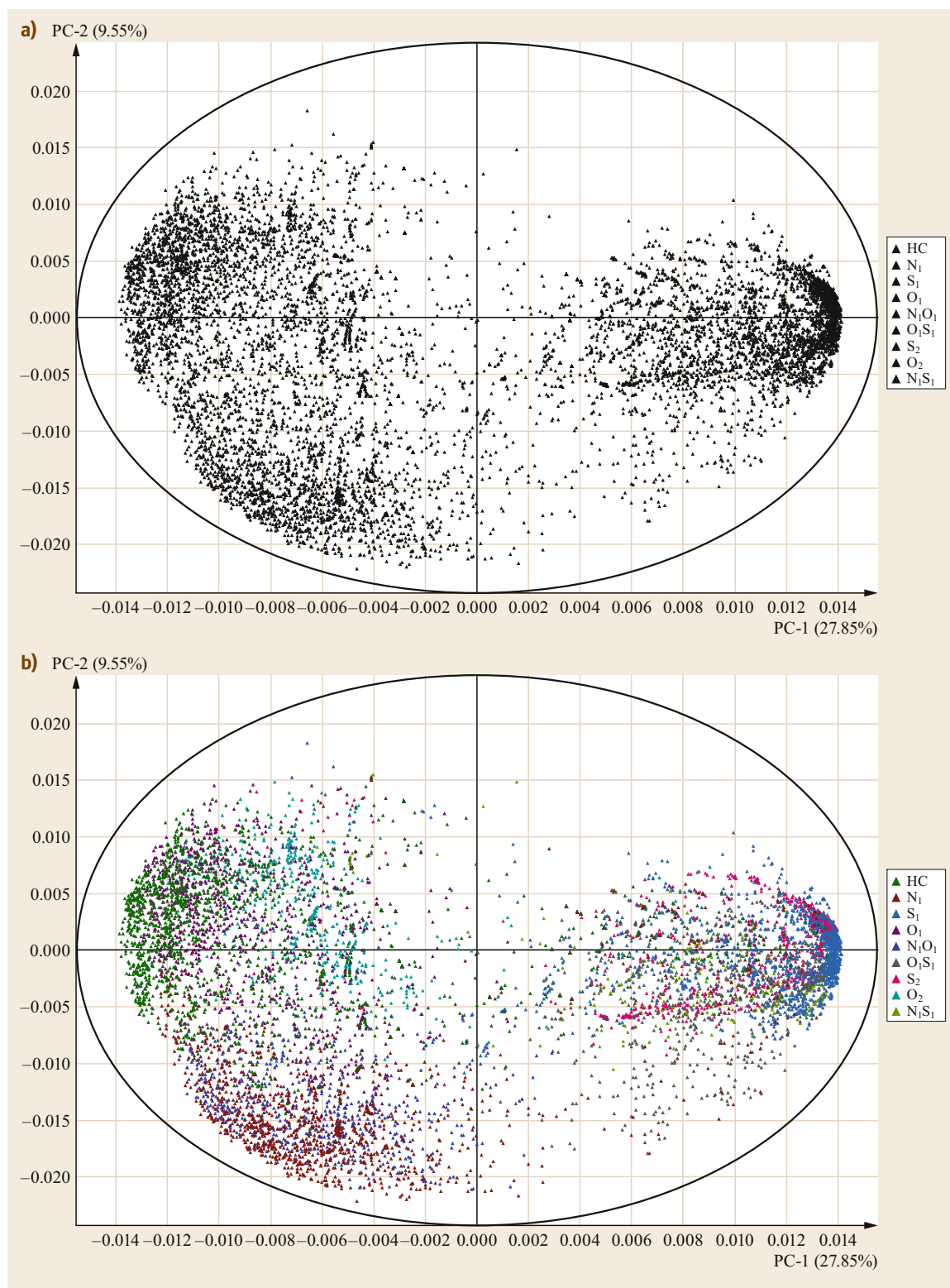


Fig. 4.20a,b Principal component analysis (PCA) plots – loading plot without a colored code (a) and loading plot with a colored code (b). Reprinted with permission from [4.55]. Copyright (2010) American Chemical Society

However, applying color coding to the loading plot for heteroatom classes reveals useful information, as shown in Fig. 4.20b. Therefore, when developing visualization tools for statistical methods, visual discrimination using colored codes should be actively adopted to enhance data interpretation information retrieval.

The tools for crude oil research should include dynamic data handling and visualization techniques to help researchers select areas of interest on the plots. A crude oil dataset could be much larger than the petroleomics dataset and others. Current petroleomics

has a lot of different visual diagnostic tools, which have played a significant role in petroleum research. However, the current tools for analyzing the data only generates static images. Researchers are hardly able to select data from the static images for comparing specific areas among oil samples. Also, it has been difficult to link the data on the conventional visualization with statistical results. Although tools are commercially available, researchers are not able to handle data freely across the existing data visualization programs. Such dynamic features are needed to be implemented for handling large datasets in crude oil studies.

4.3 Summary

Petroinformatics was defined at the beginning of this chapter and its components to be developed were discussed. Development of data interpretation methods, especially statistical approaches, is important for future petroinformatics development. In this regard, recent development and commercialization of PetroOrg [4.93] software, and highly interactive mzCruiser [4.87] software look very promising.

A software platform that can integrate data obtained from different analytical instruments among many samples is a very important step to achieve a more comprehensive understanding of crude oil, but quantitative analysis tools should also be combined with the software platform.

The next important step for *petroinformatics* is standardization of data and information. To achieve

this goal, we can learn from studies in other research fields. For example, there has been a lot of work devoted to the standardization of data and information in metabolomics [4.94–103], genomics [4.104], and proteomics [4.105–107]. Similar standardization is required in this field. Standardization helps to build a unified platform for a variety of devices and various researchers. It is also important to check reproducibility between data obtained from different laboratories. In addition, petroinformatics should have publicly available resources through cloud technology as a service (PaaS) [4.108]. The public resources should contain data from analytical instruments and metadata, including properties of a large number of crude oils in a wide variety of categories.

References

- 4.1 M.R. Watt, S.G. Roussis: Crude assay. In: *Analytical Advances for Hydrocarbon Research*, ed. by C.S. Hsu (Kluwer, New York 2003)
- 4.2 R.W. Kiser: *Introduction to Mass Spectrometry and Its Applications* (Prentice Hall, Englewood Cliff 1965)
- 4.3 A. Mendex, J. Bruzual: Molecular characterization of petroleum and its fractions by mass spectrometry. In: *Analytical Advances for Hydrocarbon Research*, ed. by C.S. Hsu (Kluwer, New York 2003)
- 4.4 C.S. Hsu: *Analytical Advances for Hydrocarbon Research* (Kluwer, New York 2003)
- 4.5 F.P. Di Sanzo: Chromatographic analyses of fuels. In: *Analytical Advances for Hydrocarbon Research*, ed. by C.S. Hsu (Kluwer, New York 2003)
- 4.6 P.C. Anderson, J.M. Sharkey, R.P. Walsh: Calculation of research octane number of motor gasoline from chromatographic data and a new approach to motor gasoline quality control, *J. Inst. Pet.* **59**, 83 (1972)
- 4.7 C.S. Hsu, D. Drinkwater: GC/MS in the petroleum industry. In: *Current Practice in GC/MS*, Chromatographic Science, Vol. 86, ed. by W.W.A. Niessen (Dekker Marcel, New York 2001)
- 4.8 A.G. Marshall, R.P. Rodgers: Petroleomics: The next grand challenge for chemical analysis, *Acc. Chem. Res.* **37**, 53–59 (2004)
- 4.9 O.C. Mullins, R.P. Rodgers, P. Weinheber, C.C. Klein, L. Wenkartaramanan, A.B. Andrews, A.G. Marshall: Oil reservoir characterization via crude oil analysis by downhole fluid analysis in oil wells with visible–near–infrared spectroscopy and by laboratory analysis with electrospray ionization Fourier transform ion cyclotron resonance mass spectrometry, *Energy Fuels* **20**(6), 2448–2456 (2006)
- 4.10 A.G. Marshall, R.P. Rodgers: Petroleomics: Chemistry of the underworld, *Proc. Natl. Acad. Sci. USA* **105**(47), 18090–18095 (2008)

- 4.11 M.P. Barrow: *Petroleomics: Study of the old and the new*, *Biofuels* **1**(5), 651–655 (2010)
- 4.12 A. Islam, Y. Cho, A. Ahmed, S. Kim: Data interpretation methods for petroleomics, *Mass Spectrom. Lett.* **3**(3), 63067 (2010)
- 4.13 Y. Cho, A. Ahmed, A. Islam, S. Kim: Developments in FT-ICR MS instrumentation, ionization techniques, and data interpretation methods for petroleomics, *Mass Spectrom. Rev.* **34**(2), 248–263 (2015)
- 4.14 C.S. Hsu: *Petroleomics: Probing petroleum composition by mass spectrometry*. In: *Proc. 2003 Pittsburgh Conf., Orlando* (2003)
- 4.15 C.S. Hsu, C.L. Hendrickson, R.P. Rodgers, A.M. McKenna, A.G. Marshall: *Petroleomics: Advanced molecular probe for petroleum heavy ends*, *J. Mass Spectrom.* **46**, 337–343 (2011)
- 4.16 C.S. Hsu, Z. Liang, J.E. Campana: Hydrocarbon characterization by ultra-high resolution Fourier-transform ion cyclotron resonance mass spectrometry, *Anal. Chem.* **66**, 850–855 (1994)
- 4.17 C.A. Hughey, C.L. Hendrickson, R.P. Rodgers, A.G. Marshall: Elemental composition analysis of processed and unprocessed diesel fuel by electrospray ionization Fourier transform ion cyclotron resonance mass spectrometry, *Energy Fuels* **15**(5), 1186–1193 (2001)
- 4.18 K. Qian, W.K. Robbins, C.A. Hughey, H.J. Cooper, R.P. Rodgers, A.G. Marshall: Resolution and identification of elemental compositions for more than 3000 crude acids in heavy petroleum by negative-ion microelectrospray high-field Fourier transform ion cyclotron resonance mass spectrometry, *Energy Fuels* **15**(6), 1505–1511 (2001)
- 4.19 G.C. Klein, S. Kim, R.P. Rodgers, A.G. Marshall, A. Yen: Mass spectral analysis of asphaltenes. II. Detailed compositional comparison of asphaltene deposit to its crude oil counterpart for two geographically different crude oils by ESI FT-ICR MS, *Energy Fuels* **20**(5), 1973–1979 (2006)
- 4.20 L.A. Stanford, S. Kim, R.P. Rodgers, A.G. Marshall: Characterization of compositional changes in vacuum gas oil distillation cuts by electrospray ionization Fourier transform-ion cyclotron resonance (FT-ICR) mass spectrometry, *Energy Fuels* **20**(6), 1664–1673 (2006)
- 4.21 L.A. Stanford, S. Kim, G.C. Klein, D.F. Smith, R.P. Rodgers, A.G. Marshall: Identification of water-soluble heavy crude oil organic-acids, bases, and neutrals by electrospray ionization and field desorption ionization Fourier transform ion cyclotron resonance mass spectrometry, *Environ. Sci. Technol.* **41**(8), 2696–2702 (2007)
- 4.22 S. Kim, R.P. Rodgers, G.T. Blakney, C.L. Hendrickson, A.G. Marshall: Automated electrospray ionization FT-ICR mass spectrometry for petroleum analysis, *J. Am. Soc. Mass Spectrom.* **20**(2), 263–268 (2009)
- 4.23 Q. Shi, C. Xu, S. Zhao, K.H. Chung, Y. Zhang, W. Gao: Characterization of basic nitrogen species in coker gas oils by positive-ion electrospray ionization Fourier transform ion cyclotron resonance mass spectrometry, *Energy Fuels* **24**(1), 563–569 (2009)
- 4.24 P. Liu, Q. Shi, K.H. Chung, Y.H. Zhang, N. Pan, S. Zhao, C. Xu: Molecular characterization of sulfur compounds in venezuela crude oil and its SARA fractions by electrospray ionization Fourier transform ion cyclotron resonance mass spectrometry, *Energy Fuels* **24**, 5089–5096 (2010)
- 4.25 S.K. Panda, K.-J. Brockmann, T. Benter, W. Schrader: Atmospheric pressure laser ionization (APLI) coupled with Fourier transform ion cyclotron resonance mass spectrometry applied to petroleum samples analysis: Comparison with electrospray ionization and atmospheric pressure photoionization methods, *Rapid Commun. Mass Spectrom.* **25**(16), 2317–2326 (2011)
- 4.26 X. Zhou, Q. Shi, Y. Zhang, S. Zhao, R. Zhang, K.H. Chung, C. Xu: Analysis of saturated hydrocarbons by redox reaction with negative-ion electrospray Fourier transform ion cyclotron resonance mass spectrometry, *Anal. Chem.* **84**(7), 3192–3199 (2012)
- 4.27 J.M. Purcell, C.L. Hendrickson, R.P. Rodgers, A.G. Marshall: Atmospheric pressure photoionization Fourier transform ion cyclotron resonance mass spectrometry for complex mixture analysis, *Anal. Chem.* **78**(16), 5906–5912 (2006)
- 4.28 K. Qian, A.S. Mennito, K.E. Edwards, D.T. Ferrughelli: Observation of vanadyl porphyrins and sulfur-containing vanadyl porphyrins in a petroleum asphaltene by atmospheric pressure photonionization Fourier transform ion cyclotron resonance mass spectrometry, *Rapid Commun. Mass Spectrom.* **22**(14), 2153–2160 (2008)
- 4.29 A.M. McKenna, J.M. Purcell, R.P. Rodgers, A.G. Marshall: Heavy petroleum composition. 1. Exhaustive compositional analysis of Athabasca bitumen HVGO distillates by Fourier transform ion cyclotron resonance mass spectrometry: A definitive test of the Boduszynski model, *Energy Fuels* **24**, 2929–2938 (2010)
- 4.30 K. Qian, K.E. Edwards, A.S. Mennito, C.C. Walters, J.D. Kushnerick: Enrichment, resolution, and identification of nickel porphyrins in petroleum asphaltene by cyclograph separation and atmospheric pressure photoionization Fourier transform ion cyclotron resonance mass spectrometry, *Anal. Chem.* **82**(1), 413–419 (2010)
- 4.31 Y. Cho, A. Islam, A. Ahmed, S. Kim: Application of comprehensive 2D GC-MS and APPI FT-ICR MS for more complete understanding of chemicals in diesel fuel, *Mass Spectrom. Lett.* **3**(2), 43 (2012)
- 4.32 J.M. Jin, S. Kim, J.E. Birdwell: Molecular characterization and comparison of shale oils generated by different pyrolysis methods, *Energy Fuels* **26**(2), 1054–1062 (2012)
- 4.33 H. Muller, F.M. Adam, S.K. Panda, H.H. Al-Jawad, A.A. Al-Hajji: Evaluation of quantitative sulfur speciation in gas oils by Fourier transform ion cyclotron resonance mass spectrometry: Validation by comprehensive two-dimensional gas chromatography, *J. Am. Soc. Mass Spectrom.* **23**(5), 806–815 (2012)
- 4.34 A. Sim, Y. Cho, D. Kim, M. Witt, J.E. Birdwell, B.J. Kim, S. Kim: Molecular-level characteriza-

- tion of crude oil compounds combining reversed-phase high-performance liquid chromatography with off-line high-resolution mass spectrometry, *Fuel* **140**, 717–723 (2015)
- 4.35 B.M. Kolakowski, J.S. Grossert, L. Ramaley: The importance of both charge exchange and proton transfer in the analysis of polycyclic aromatic compounds using atmospheric pressure chemical ionization mass spectrometry, *J. Am. Soc. Mass Spectrom.* **15**(3), 301–310 (2004)
- 4.36 D. Borton, D.S. Pinkston, M.R. Hurt, X. Tan, K. Azyat, A. Scherer, R. Tykwinski, M. Gray, K. Qian, H.I. Kenttämä: Molecular structures of asphaltenes based on the dissociation reactions of their ions in mass spectrometry, *Energy Fuels* **24**(10), 5548–5559 (2010)
- 4.37 Y.H. Kim, S. Kim: Improved abundance sensitivity of molecular ions in positive-ion APCI MS analysis of petroleum in toluene, *J. Am. Soc. Mass Spectrom.* **21**(3), 386–392 (2010)
- 4.38 A.S. Mennito, K. Qian: Characterization of heavy petroleum saturates by laser desorption silver cationization and Fourier transform ion cyclotron resonance mass spectrometry, *Energy Fuels* **27**(12), 7348–7353 (2013)
- 4.39 E. Lorente, C. Berrueco, A.A. Herod, M. Millan, R. Kandiyoti: The detection of high-mass aliphatics in petroleum by matrix-assisted laser desorption/ionisation mass spectrometry, *Rapid Commun. Mass Spectrom.* **26**(14), 1581–1590 (2012)
- 4.40 Y. Cho, M. Witt, Y.H. Kim, S. Kim: Characterization of crude oils at the molecular level by use of laser desorption ionization Fourier-transform ion cyclotron resonance mass spectrometry, *Anal. Chem.* **84**(20), 8587–8594 (2012)
- 4.41 Y. Cho, J.M. Jin, M. Witt, J.E. Birdwell, J.G. Na, N.S. Roh, S. Kim: Comparing laser desorption ionization and atmospheric pressure photoionization coupled to Fourier transform ion cyclotron resonance mass spectrometry to characterize shale oils at the molecular level, *Energy Fuels* **27**(4), 1830–1837 (2013)
- 4.42 Y. Cho, M. Witt, J.M. Jin, Y.H. Kim, N.S. Nho, S. Kim: Evaluation of laser desorption ionization coupled to Fourier transform ion cyclotron resonance mass spectrometry to study metalloporphyrin complexes, *Energy Fuels* **28**(11), 6699–6706 (2014)
- 4.43 E. Kendrick: A mass scale based on CH₂ 1/4 14.0000 for high resolution mass spectrometry of organic compounds, *Anal. Chem.* **35**, 2146–2154 (1963)
- 4.44 C.S. Hsu, K. Qian, Y.C. Chen: An innovative approach to data analysis in hydrocarbon characterization by on line liquid chromatography mass spectrometry, *Anal. Chim. Acta* **264**, 79–89 (1992)
- 4.45 C.A. Hughey, C.L. Hendrickson, R.P. Rodgers, A.G. Marshall: Kendrick mass defect spectrum: A compact visual analysis for ultrahigh-resolution broadband mass spectra, *Anal. Chem.* **73**, 4676–4681 (2001)
- 4.46 P.J. Roach, J. Laskin, A. Laskin: Higher-order mass defect analysis for mass spectra of complex organic mixtures, *Anal. Chem.* **83**(12), 4924–4929 (2011)
- 4.47 D. van Krevelen: Graphical-statistical method for the study of structure and reaction processes of coal, *Fuel* **29**, 269–284 (1950)
- 4.48 S. Kim, R.W. Kramer, P.G. Hatcher: Graphical method for analysis of ultrahigh-resolution broadband mass spectra of natural organic matter, the Van Krevelen diagram, *Anal. Chem.* **75**(20), 5336–5344 (2003)
- 4.49 Z. Wu, R. Rodgers, A. Marshall: Two- and three-dimensional van Krevelen diagrams: A graphical analysis complementary to the Kendrick mass plot for sorting elemental compositions of complex organic mixtures based on ultrahigh-resolution broadband Fourier transform ion cyclotron resonance mass measurements, *Anal. Chem.* **76**, 2511–2516 (2004)
- 4.50 Y. Cho, Y.H. Kim, S. Kim: Planar limit-assisted structural interpretation of saturates/aromatics/resins/asphaltenes fractionated crude oil compounds observed by Fourier transform ion cyclotron resonance mass spectrometry, *Anal. Chem.* **83**(15), 6068–6073 (2011)
- 4.51 C.S. Hsu, V.V. Lobodin, R.P. Rodgers, A.M. McKenna, A.G. Marshall: Compositional boundaries for fossil hydrocarbons, *Energy Fuels* **25**(5), 2174–2178 (2011)
- 4.52 V.V. Lobodin, A.G. Marshall, C.S. Hsu: Compositional space boundaries for organic compounds, *Anal. Chem.* **84**(7), 3410–3416 (2012)
- 4.53 H.P. Nguyen, I.P. Ortiz, C. Temiyasathit, S.B. Kim, K.A. Schug: Laser desorption/ionization mass spectrometry fingerprinting of complex hydrocarbon mixtures: Application to crude oils using data mining techniques, *Rapid Commun. Mass Spectrom.* **22**(14), 2220–2226 (2008)
- 4.54 A. Smaniotto, L. Montanari, C. Flego, A. Rizzi, E. Ragazzi, R. Seraglia, P. Traldi: Can crude oils be distinguished by different component distribution obtained by laser desorption ionization mass spectrometry and evaluated by chemometrics?, *Rapid Commun. Mass Spectrom.* **22**(10), 1597–1606 (2008)
- 4.55 M. Hur, I. Yeo, E. Park, Y.H. Kim, J. Yoo, E. Kim, M.H. No, J. Koh, S. Kim: Combination of statistical methods and Fourier transform ion cyclotron resonance mass spectrometry for more comprehensive, molecular-level interpretations of petroleum samples, *Anal. Chem.* **82**(1), 211–218 (2010)
- 4.56 M. Hur, I. Yeo, E. Kim, M.H. No, J. Koh, Y.J. Cho, J.W. Lee, S. Kim: Correlation of FT-ICR mass spectra with the chemical and physical properties of associated crude oils, *Energy Fuels* **24**, 5524–5532 (2010)
- 4.57 Y.E. Corilo, D.C. Podgorski, A.M. McKenna, K.L. Lemkau, C.M. Reddy, A.G. Marshall, R.P. Rodgers: Oil spill source identification by principal component analysis of electrospray ionization Fourier transform ion cyclotron resonance mass spectra, *Anal. Chem.* **85**(19), 9064–9069 (2013)
- 4.58 B.G. Vaz, R.C. Silva, C.F. Klitzke, R.C. Simas, H.D.L. Nascimento, R.C.L. Pereira, D.F. Garcia, M.N. Eberlin, D.A. Azevedo: Assessing biodegradation in the Llanos Orientales crude oils by electrospray ionization ultrahigh resolution and accuracy

- Fourier transform mass spectrometry and chemometric analysis, *Energy Fuels* **27**(3), 1277–1284 (2013)
- 4.59 S. Albisinni, C. De Nunzio, A. Tubaro, W.T. Barry, L.L. Banez, S.J. Freedland: Greater percent-free testosterone is associated with high-grade prostate cancer in men undergoing prostate biopsy, *Urology* **80**(1), 162–167 (2012)
- 4.60 I. Yeo, J.W. Lee, S. Kim: Application of clustering methods for interpretation of petroleum spectra from negative-mode ESI FT-ICR MS, *Bull. Korean Chem. Soc.* **31**(11), 3151–3155 (2010)
- 4.61 C.S. Hsu, C.C. Walters, G.H. Isaksen, M.E. Schaps, K.E. Peters: Biomarker analysis for petroleum exploration. In: *Analytical Advances for Hydrocarbon Research*, ed. by C.S. Hsu (Kluwer, New York 2003)
- 4.62 Y. Cho, A. Ahmed, S. Kim: Application of atmospheric pressure photo ionization hydrogen/deuterium exchange high-resolution mass spectrometry for the molecular level speciation of nitrogen compounds in heavy crude oils, *Anal. Chem.* **85**(20), 9758–9763 (2013)
- 4.63 A. Ahmed, S. Kim: Atmospheric pressure photo ionization hydrogen/deuterium exchange mass spectrometry – A method to differentiate isomers by mass spectrometry, *J. Am. Soc. Mass Spectrom.* **24**(12), 1900–1905 (2013)
- 4.64 T. Acter, Y. Cho, S. Kim, A. Ahmed, B. Kim, S. Kim: Optimization and application of APCI hydrogen-deuterium exchange mass spectrometry (HDX MS) for the speciation of nitrogen compounds, *J. Am. Soc. Mass Spectrom.* **26**(9), 1522–1531 (2015)
- 4.65 T. Acter, D. Kim, A. Ahmed, J.M. Jin, U.H. Yim, W.J. Shim, S. Kim: Optimization and application of atmospheric pressure chemical and photoionization hydrogen-deuterium exchange mass spectrometry for speciation of oxygen-containing compounds, *Anal. Bioanal. Chem.* **408**(12), 3281–3293 (2016)
- 4.66 S. Kim, M. Hur: In paving the way for understanding and predicting properties of crude oil based on molecular level information and statistical analysis: *Petroleum Informatics*. In: *Proc. PacificChem, Honolulu* (2010)
- 4.67 M. Hur, H.B. Oh, S. Kim: Optimized automatic noise level calculations for broadband FT-ICR mass spectra of petroleum give more reliable and faster peak picking results, *Bull. Korean Chem. Soc.* **30**(11), 2665–2668 (2009)
- 4.68 R. Pedreschi, M.L. Hertog, S.C. Carpentier, J. Lammertyn, J. Robben, J.P. Noben, B. Panis, R. Swennen, B.M. Nicolai: Treatment of missing values for multivariate statistical analysis of gel-based proteomics data, *Proteomics* **8**(7), 1371–1383 (2008)
- 4.69 R.A. Johnson, D.W. Wichern: *Applied Multivariate Statistical Analysis* (Prentice Hall, Upper Saddle River 2007) p. 773
- 4.70 T.W. Anderson: *An Introduction to Multivariate Statistical Analysis* (Wiley, New York 1958)
- 4.71 N.C. Giri: *Multivariate Statistical Analysis* (Marcel Dekker, New York 1996)
- 4.72 H. Joe, J. Ward: Hierarchical grouping to optimize an objective function, *J. Am. Stat. Assoc.* **58**(301), 236–244 (1963)
- 4.73 M.G. Kendall: A new measure of rank correlation, *Biometrika* **30**, 81–93 (1938)
- 4.74 A.J.G. Barwise: Role of nickel and vanadium in petroleum classification, *Energy Fuels* **4**(6), 647–652 (1990)
- 4.75 M. Krzywinski, J. Schein, I. Birol, J. Connors, R. Gascoyne, D. Horsman, S.J. Jones, M.A. Marra: Circos: An information aesthetic for comparative genomics, *Genome Res* **19**(9), 1639–1645 (2009)
- 4.76 C. Spearman: The proof and measurement of association between two things, *Am. J. Psychol.* **15**(1), 72–101 (1904)
- 4.77 J.S. Maritz: *Distribution-Free Statistical Methods* (Chapman Hall, New York 1981)
- 4.78 ASTM International: D5708–12 standard test methods for determination of nickel, vanadium, and iron in crude oils and residual fuels by inductively coupled plasma (ICP) atomic emission spectrometry. In: *Annual Book of ASTM Standards: Petroleum Products and Lubricants (II)*, Vol. 05(02) (ASTM, West Conshohocken 2014)
- 4.79 ASTM International: ASTM D974–08e1 standard test method for acid and base number by color-indicator titration. In: *Annual Book of ASTM Standards* (ASTM, West Conshohocken 2008)
- 4.80 M. Witt, W. Timm: Determination of simulated crude oil mixtures from the north sea using atmospheric pressure photoionization coupled to Fourier transform ion cyclotron resonance mass spectrometry, *Energy Fuels* **30**, 3707–3713 (2016)
- 4.81 B.M. Bennett: Note on power transformations which minimize skewness, *Biom. Z.* **9**(2), 73 (1967)
- 4.82 L. Ting, M.J. Cowley, S.L. Hoon, M. Guilhaus, M.J. Raftery, R. Cavicchioli: Normalization and statistical analysis of quantitative proteomics data generated by metabolic labeling, *Mol. Cell. Proteom.* **8**(10), 2227–2242 (2009)
- 4.83 X.Q. Cui, G.A. Churchill: Statistical tests for differential expression in cDNA microarray experiments, *Genome Biol* **4**(4), 210 (2003)
- 4.84 W.T. Li: Volcano plots in analyzing differential expressions with mrna microarrays, *J. Bioinf. Comput. Biol.* **10**(6), 1231003 (2012)
- 4.85 M. Hur, Y. Cho, S. Kim, E.S. Wurtele: An approach to analysis and visualization of crude oil samples. In: *Proc. 61st ASMS Conf. Mass Spectrom. Allied Topics, Minneapolis* (2013)
- 4.86 M. Hur, A.A. Campbell, M. Almeida-de-Macedo, L. Li, N. Ransom, A. Jose, M. Crispin, B.J. Nikolau, E.S. Wurtele: A global approach to analysis and interpretation of metabolic data for plant natural product discovery, *Nat. Prod. Rep.* **30**(4), 565–583 (2013)
- 4.87 M. Hur: *MzCruiser software* (iMass Consulting, South Korea 2010), <https://github.com/mhhur/PetroleumInformatics>
- 4.88 R.L. Slichter, Z.F. Lie, J.H. Xue, P.G. Hatcher: Multivariate statistical approaches for the characterization of dissolved organic matter analyzed by ultrahigh resolution mass spectrometry, *Environ. Sci. Technol.* **44**(19), 7576–7582 (2010)

- 4.89 R.L. Sleighter, R.M. Cory, L.A. Kaplan, H.A.N. Abdulla, P.G. Hatcher: A coupled geochemical and biogeochemical approach to characterize the bioreactivity of dissolved organic matter from a headwater stream, *J. Geophys. Res.-Biogeo.* **119**(8), 1520–1537 (2014)
- 4.90 A.M. Pohlabein, T. Dittmar: Novel insights into the molecular structure of non-volatile marine dissolved organic sulfur, *Mar. Chem.* **168**(20), 86–94 (2015)
- 4.91 M. Hur: Application of volcano plots for quantitative visualization and comparison of a set of two spectra obtained by high-resolution mass spectrometric analysis of crude oils. In: *Proc. PacifiChem, Honolulu* (2015)
- 4.92 M. Hur, L.R. Ware, M.A. McKenna, R.P. Rodgers, J. Park, S.E. Wurtele, S. Kim, A.G. Marshall: Statistically Significant Differences in Composition of Petroleum Crude Oils Revealed by Volcano Plots Generated from Ultrahigh Resolution Fourier Transform Ion Cyclotron Resonance Mass Spectra (in preparation)
- 4.93 Y.E. Corilo: *PetroOrg Software* (Florida State University, Tallahassee 2013), <http://software.petroorg.com>.
- 4.94 O. Fiehn, D. Robertson, J. Griffin, M. van der Werf, B. Nikolau, N. Morrison, L.W. Sumner, R. Goodacre, N.W. Hardy, C. Taylor, J. Fostel, B. Kristal, R. Kaddurah-Daouk, P. Mendes, B. van Ommen, J.C. Lindon, S.A. Sansone: The metabolomics standards initiative (MSI), *Metabolomics* **3**(3), 175–178 (2007)
- 4.95 L.W. Sumner, A. Amberg, D. Barrett, M.H. Beale, R. Beger, C.A. Daykin, T.W.M. Fan, O. Fiehn, R. Goodacre, J.L. Griffin, T. Hankemeier, N. Hardy, J. Harnly, R. Higashi, J. Kopka, A.N. Lane, J.C. Lindon, P. Marriott, A.W. Nicholls, M.D. Reilly, J.J. Thaden, M.R. Viant: Proposed minimum reporting standards for chemical analysis, *Metabolomics* **3**(3), 211–221 (2007)
- 4.96 J.L. Griffin, A.W. Nicholls, C.A. Daykin, S. Heald, H.C. Keun, I. Schuppe-Koistinen, J.R. Griffiths, L.L. Cheng, P. Rocca-Serra, D.V. Rubtsov, D. Robertson: Standard reporting requirements for biological samples in metabolomics experiments: mammalian/in vivo experiments, *Metabolomics* **3**(3), 179–188 (2007)
- 4.97 N.W. Hardy, C.F. Taylor: A roadmap for the establishment of standard data exchange structures for metabolomics, *Metabolomics* **3**(3), 243–248 (2007)
- 4.98 O. Fiehn, G. Wohlgemuth, M. Scholz, T. Kind, D.Y. Lee, Y. Lu, S. Moon, B. Nikolau: Quality control for plant metabolomics: reporting MSI-compliant studies, *Plant J* **53**(4), 691–704 (2008)
- 4.99 C. Ludwig, J.M. Easton, A. Lodi, S. Tiziani, S.E. Manzoor, A.D. Southam, J.J. Byrne, L.M. Bishop, S. He, T.N. Arvanitis, U.L. Gunther, M.R. Viant: Birmingham metabolite library: A publicly accessible database of 1-D ¹H and 2-D ¹H J-resolved NMR spectra of authentic metabolite standards (BML-NMR), *Metabolomics* **8**(1), 8–18 (2012)
- 4.100 J. Stanstrup, M. Gerlich, L.O. Dragsted, S. Neumann: Metabolite profiling and beyond: approaches for the rapid processing and annotation of human blood serum mass spectrometry data, *Anal. Bioanal. Chem.* **405**(15), 5037–5048 (2013)
- 4.101 K.A. Kouremenos, D.J. Beale, H. Antti, E.A. Palombo: Liquid chromatography time of flight mass spectrometry based environmental metabolomics for the analysis of *Pseudomonas putida* bacteria in potable water, *J. Chromatogr. B* **966**, 179–186 (2014)
- 4.102 S.A. Sansone, P. Rocca-Serra, D. Field, E. Maguire, C. Taylor, O. Hofmann, H. Fang, S. Neumann, W.D. Tong, L. Amaral-Zettler, K. Begley, T. Booth, L. Bougueleret, G. Burns, B. Chapman, T. Clark, L.A. Coleman, J. Copeland, S. Das, A. de Daruvar, P. de Matos, I. Dix, S. Edmunds, C.T. Evelo, M.J. Forster, P. Gaudet, J. Gilbert, C. Goble, J.L. Griffin, D. Jacob, J. Kleinjans, L. Harland, K. Haug, H. Hermjakob, S.J.H. Sui, A. Laederach, S.G. Liang, S. Marshall, A. McGrath, E. Merrill, D. Reilly, M. Roux, C.E. Shamu, C.A. Shang, C. Steinbeck, A. Trefethen, B. Williams-Jones, K. Wolstencroft, I. Xenarios, W. Hide: Toward interoperable bio-science data, *Nat. Genet.* **44**(2), 121–126 (2012)
- 4.103 S.A. Sansone, D. Schober, H.J. Atherton, O. Fiehn, H. Jenkins, P. Rocca-Serra, D.V. Rubtsov, I. Spasic, L. Soldatova, C. Taylor, A. Tseng, M.R. Viant: Metabolomics standards initiative: Ontology working group work in progress, *Metabolomics* **3**(3), 249–256 (2007)
- 4.104 D.M. Hendrickx, R.R. Boyles, J.C.S. Kleinjans, A. Dearry: Workshop report: Identifying opportunities for global integration of toxicogenomics databases, *Arch. Toxicol.* **8**(12), 2323–2332 (2014)
- 4.105 S.L. Seymour, T. Farrah, P.A. Binz, R.J. Chalkley, J.S. Cottrell, B.C. Searle, D.L. Tabb, J.A. Vizcaino, G. Prieto, J. Uszkoreit, M. Eisenacher, S. Martinez-Bartolome, F. Ghali, A.R. Jones: A standardized framing for reporting protein identifications in mzIdentML 1.2, *Proteomics* **14**(21–22), 2389–2399 (2014)
- 4.106 J. Teleman, A.W. Dowsey, F.F. Gonzalez-Galarza, S. Perkins, B. Pratt, H.L. Rost, L. Malmstrom, J. Malmstrom, A.R. Jones, E. Deutsch, F. Levander: Numerical compression schemes for proteomics mass spectrometry data, *Mol. Cell Proteom.* **13**(6), 1537–1542 (2014)
- 4.107 S. Orchard: Data standardization and sharing the work of the HUP0-PSI, *Biochim. Biophys. Acta – Proteins Proteom.* **1844**(1), 82–87 (2014)
- 4.108 Wikipedia: Platform as a service, http://en.wikipedia.org/wiki/Platform_as_a_service

5. Separations in the Sample Preparation for Sulfur Compound Analysis

Jan T. Andersson

Analytical chemists have been interested in the sulfur compounds found in petroleum for over 100 years. They have developed an impressive array of methods for separating the sulfur compounds from the matrix and for separating the several functional groups from each other. These separations greatly aid in molecular characterization of these materials, which is of fundamental importance in areas such as desulfurization, catalyst development, geochemical studies, etc. Here, such methods are reviewed from the methodological perspective. Chemical transformations have a prominent place in this area and can reversibly or irreversibly change the compounds. Chromatographic separations are shown to have contributed greatly to our knowledge of the composition of

5.1	The Necessity of Sample Preparation	199
5.1.1	Sulfur	200
5.2	Separation	202
5.2.1	Chemical Methods	203
5.2.2	Liquid–Liquid Extraction	206
5.3	Chromatographic Methods	207
5.3.1	Phases Nonselective for Sulfur	207
5.3.2	Phases Selective for Sulfur: Ligand–Exchange Chromatography	209
5.4	Conclusion	214
	References	215

petroleum. Areas where current methods fail are also pointed out.

5.1 The Necessity of Sample Preparation

Crude oils are exceedingly complex mixtures of hydrocarbons and heteroatom-containing compounds and are the basis for a large number of commercial products made from them in refineries and the petrochemical industry. The majority of hydrocarbons do not cause any problems during refining or storage, with the possible exception of the most polar compounds, the so-called asphaltenes, and nonaromatic unsaturated hydrocarbons (olefins). The asphaltenes have low solubility because of their chemical structure and sometimes precipitate in boreholes or pipelines. Olefins are rarely present in crudes but are formed in cracking processes and show enhanced reactivity because of the double bond. On the other hand, compounds containing heteroatoms are frequently found to be involved in deleterious processes such as corrosion, fouling, and catalyst deactivation, and this forms the background to many studies into the heteroatom-containing compounds in petroleum with a view to gaining information on their identity, distribution into different fractions, ease of removal, etc. Especially the sulfur compounds have been

studied also by organic geochemists to obtain information about the sources of a crude [5.1], its source rocks, depositional environment, maturity [5.2], oil migration distances [5.3], etc. In environmental chemistry, sulfur aromatic compounds can be used as sources of information for different kinds of problems [5.4], including source apportionment of air pollution (e.g., gasoline versus diesel) [5.5]. Forensic analytical chemists use heterocyclic compounds to provide evidence on questions such as the source of an oil spill [5.6, 7].

Studies of heteroatom-containing petroleum components can involve group-type analysis, which allows a whole group of compounds to be lumped together, e.g., acids as characterized by the total acid number (TAN). A more detailed investigation is molecular characterization, which attempts to obtain information on selected subgroups of compounds, for instance how the alkyl carbon substituents in an aromatic nucleus are distributed in a particular aromatic compound or how, starting with a given ring structure, more complex molecules can be constructed through annealing

more rings to it. Finally, the most informative but at the same time most difficult characterization is that of identification of individual compounds. According to IUPAC, speciation analysis is *the analytical activities of identifying and/or measuring the quantities of one or more individual chemical species in a sample*. Here, we limit use of the term *speciation* to identification of individual compounds, i.e., their qualitative analysis. With respect to quantification, suffice it to say that the quantity of individual compounds is rarely sought in the petroleum area. Frequently, determining the sum of all compounds sharing a certain property such as acidity, nitrogen content, unsaturation, etc., independent of the exact chemical structure, is attempted.

The ultimate goal when trying to understand the composition of fossil material cannot be complete speciation – such an undertaking would be illusory. Even putting a number on how many compounds can be found in petroleum is pure guesswork, but for a distilled fraction (a middle distillate, boiling range 150–370 °C) this number has been estimated to be far above one million [5.8]. As the number of carbon atoms increases, the number of isomers increases exponentially: There are only 75 isomers of decane ($C_{10}H_{22}$), but no fewer than 366 319 are found for eicosane ($C_{20}H_{42}$), and 4 111 846 763 for triacontane ($C_{30}H_{62}$), compounds found in any crude oil [5.9]. It is doubtful whether any useful information would be gained by such complete speciation, even if it were possible. Certainly, one would not expect every single one of all these isomers to occur in petroleum (although many of them would). The complexity is so high that petroleum has been described as a *supercomplex mixture* [5.10], meaning that it cannot be entirely separated (down to the detection limit) using any one technique or combination of techniques. Despite this, separation science and, above all, mass spectrometry (which basically is a separation technique) have made tremendous progress in the last decades, so that even for supercomplex mixtures, a considerable amount of information on groups of compounds can be obtained.

It is tempting to imagine that sample preparation should play less of a role with the advent of high-resolution techniques such as Fourier-transform mass spectrometry and comprehensive GCxGC/MS. However, experience tells a different story, and proper sample preparation pays off handsomely also for such techniques, despite the extra work involved. Matrix effects leading to ion suppression [5.11] can be so severe that ions known to be present are not recorded [5.12]. The benefit of some sample preparation is nicely illustrated by a North American crude oil that displayed 7884 exact masses when analyzed without sample preparation

with atmospheric-pressure laser ionization and Fourier-transform ion cyclotron resonance mass spectrometry (FT-ICR MS) in positive mode [5.13]. After a simple fractionation on alumina into four fractions, namely saturates, aromatics, resins, and asphaltenes (see below), a total of 29 180 exact masses were counted, 3.7 times as many as before fractionation.

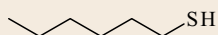
A similar experience was reported for the sulfur compounds in an analysis of a heavy gas oil [5.14]. A two-dimensional gas chromatographic system was used with a time-of-flight mass-selective detector. When the heavy oil was injected directly, without pretreatment, 9 sulfur compounds were recorded among the 7590 peaks detected. After isolation of the aromatic fraction on an alumina column, 135 peaks out of 8497 were assigned to sulfur compounds. Finally, after separation of the sulfur aromatic compounds from the hydrocarbons on a stationary phase containing Pd(II) ions (see below), the number of peaks for sulfur compounds increased to 317.

These results clearly show that, if detailed characterization of a petroleum sample is the goal, sample preparation that may involve several steps leads to much more information being obtainable. This is the perhaps surprising truth even today with the superior instruments available, as compared with the situation only 20 years ago, but it also shows that the analytical chemist with an intimate knowledge of both the instrumentation and the chemistry involved is not replaceable by expensive instruments.

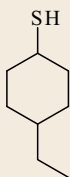
Sample preparation for determination of the total amount of a hetero element in a petroleum is not covered here; a recent review gives information on this topic [5.15]. Rather, we deal with how to isolate sulfur compounds from the matrix of a petroleum sample and, in many instances, how to separate the sulfur compounds according to their functional groups. This step may turn out to be necessary because there are isomers also among the different classes of compounds. For instance, a sulfide containing three saturated rings is isomeric with alkylated thiophenes, etc. Mass spectrometry alone would thus not be able to tell the difference between the two compounds. With the sample preparations described in this chapter, detailed analysis of the sulfur compounds should be greatly facilitated.

5.1.1 Sulfur

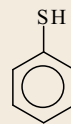
The heteroatoms most prominently found in crude oil are sulfur, nitrogen, and oxygen, although many others occur in smaller amounts, including metals (present as salts or in complexes, not as *organometallic* com-

Thiols


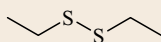
Hexanethiol



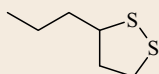
4-Ethylcyclohexanethiol

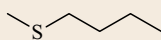


Thiophenol

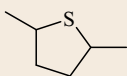
Disulfides


Diethyl disulfide

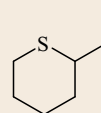

 3-Propyl-1,2-dithiacyclopentane
(3-propyl-1,2-dithiolane)

Sulfides


Butylmethyl sulfide



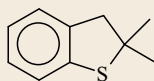
2,5-Dimethylthiacyclopentane



2-Ethylthiacyclohexane



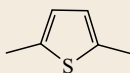
8-Thiabicyclo[3,2,1]octane



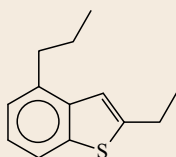
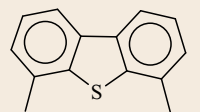
2,2-Dimethyl-1-thiaindane



2-Thiaadamantane

Thiophenes


Thiophene


 2-Ethyl-4-propylbenzo[*b*]thiophene


2-Ethyl-4-methylbenzothiophene

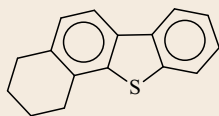
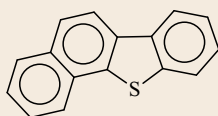
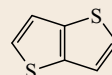

 1,2,3,4-Tetrahydrobenzo[*b*]
naphtho[2,1-*d*]thiophene

 Tetrahydrobenzo[*b*]
naphtho[2,1-*d*]thiophene

 Thieno[3,2-*b*]thiophene

Fig. 5.1 Different kinds of sulfur compounds, illustrating those that are common in petroleum

pounds – compounds that have a direct bond between the metal and a carbon atom – despite the frequent but erroneous use of this term in petroleum chemistry). Because of the noxious products formed on combustion of sulfur compounds, ultimately sulfuric acid, legislative efforts have mandated quite low sulfur limits in fuels today, in many countries 10 or 50 ppm ($\mu\text{g/g}$). This means that the sulfur content has to be lowered in the refinery from ca. 1–5% in most commercially important crudes, a factor of 1000. Another incentive to remove the element as far as possible is its affinity to many metals that are used as catalysts in refinery processes. Mainly noble metals are affected, leading to catalyst poisoning. For fuel cell applications, even lower sulfur limits are required [5.16]. This of course provides a strong incentive to reduce the concentration of the element as far as possible. Although a very large number of processes have been presented for removal of sulfur, hydrodesulfurization (HDS) dominates by far in industry. In a high-pressure hydrogen atmosphere, catalytic hydrogenation of the sulfur compounds takes place at a temperature around 350 °C, reducing the sulfur to hydrogen sulfide (as well as reducing many other functional groups in the crude, such as aromatic rings, ketones, phenols, etc.).

In petroleum, several kinds of sulfur functional group can be found, with quite different chemical and physical properties. The accepted view on the incorporation of sulfur in anoxic sediments into the organic precursors of petroleum invokes reduction of sulfate ions, originating in sea water, to reduced inorganic sulfur species that over time react with organic compounds [5.17]. Thiols can be formed, and in an intramolecular reaction these can form cyclic sulfides. If five-membered cyclic sulfides are dehydrogenated, a reaction that takes place during the maturation of the kerogen, a thiophene molecule arises. This may be subject to aromatic substitution, with the result that the

size of the aromatic system ultimately grows into polycyclic aromatic sulfur heterocycles (PASHs). Thus, the main sulfur species expected in petroleum are sulfides and thiophenes, accompanied by thiols, disulfides, and sulfoxides. Extensive alkylation of all these groups of compounds makes the total mixture of sulfur species extremely complex.

Different sulfur compounds show very different rates of hydrogenation. Thus thiols, disulfides, and sulfides are quite easily removed, but the aromatic sulfur compounds demand more severe conditions. Thiophenes and benzothiophenes (Fig. 5.1) are fairly easily hydrogenated, followed by ring systems containing four or more aromatic rings. The most difficult ones to desulfurize are the dibenzothiophenes (DBTs). Many studies on those DBTs that are particularly recalcitrant to HDS have shown that they possess alkyl groups in the positions closest to the sulfur atom, numbered 4 and 6. Speciation studies have revealed the identities of those DBTs that survive deep HDS [5.18].

Sample preparation involves all steps from sampling to ultimate analysis. In petroleum samples, most nitrogen compounds can be fairly easily separated from the matrix hydrocarbons based on their higher polarity. However, the carbon–sulfur bond is not polarized because the two elements have the same electronegativity, so that separation of sulfur compounds from hydrocarbons can be troublesome. Many efforts have been undertaken both to devise methods for separation of sulfur compounds from hydrocarbons (and other matrix components) as well as to separate sulfur compounds from each other based on their functional groups. It should be kept in mind that many compounds, especially in the heavier fractions of petroleum, can possess more than one heteroatom, such as two or three sulfur atoms. Furthermore, compounds with mixed heteroatoms such as N_1S_1 and N_1S_2 , are also well known. This contributes considerably to the difficulty of speciation.

5.2 Separation

Separation is needed to remove matrix components that interfere with qualitative and quantitative analysis of the compounds of interest. It is important to ensure that the ensemble of analytes is separated from the matrix as a group without losses; the selectivity in the separation step should be high versus matrix components but zero within the group of analytes. An early review discusses the techniques used in the 1980s [5.19], and a later one investigated separation methods for analysis of PASHs, especially in environmental samples that often are polluted by petroleum-derived material [5.20]. It should

not be overlooked that many reviews on petroleum analysis may be relevant to sulfur compound analysis even though they deal with general principles and not sulfur in particular [5.21, 22].

Many different approaches are reviewed here to show how analytical chemists have tried to use the chemical properties of their analytes for separation purposes. Although quite powerful techniques have resulted and are available today for routine use, it is still not possible to obtain clean class separations of all sulfur functional groups; For instance, disulfides remain

an unsolved problem, and no reliable separation principle exists for their analysis in fossil materials. This review also includes some methods described in fairly early works with the intention of illustrating that such approaches may stimulate thinking in new directions today when developing new sample preparation schemes. Some of these past attempts may be useful as a basis for continued method development in combination with modern analytical instrumentation – the field of sample preparation for heterocompounds in fossil materials is of basic importance and still a very fertile field for new work.

5.2.1 Chemical Methods

Chemical methods change an analyte through a – reversible or irreversible – reaction into a product that has more favorable properties for matrix separation than the analytes themselves do, thus enabling or at least facilitating sample preparation. Often this means making the analyte more polar so that it can be separated by chromatographic means from the unchanged matrix. Obviously, the chemistry should be as selective for, in this case, sulfur compounds as possible. The transformation leads to a product with quite different properties than the compounds had before; the matrix components retain their properties, enabling separation of the analytes from the matrix components in a subsequent step.

Oxidation

The sulfur atom is an obvious target for chemical transformations, since it is the chemical unit that distinguishes the analytes from the matrix components. Its reactivity allows for much chemistry to be carried out, and this has been used extensively in analytical chemistry. A scheme has been worked out for a visbroken naphtha that relies on selective oxidations of different sulfur-containing classes of compounds, namely thiols, sulfides, and thiophenes [5.23]. The thiols were oxidized to disulfides with iodine, and this increased their boiling point so much that in the gas chromatogram they appeared after the other sulfur species in the naphtha. The mercaptans and sulfides were oxidized with hydrogen peroxide in acetic acid to yield sulfonic acids and sulfones, respectively, which were removed by phase separation. The thiophenes were unreactive under these conditions and were easily analyzed by GC. The scheme was also applied to a jet fuel, and it was found that benzothiophene was lost to the extent of 16% [5.24]. It is well known that peracids (as formed by hydrogen peroxide in a carboxylic acid) oxidize condensed thiophenes to sulfones (see below), and although losses were ascribed to processing of

the solutions and considered to be of a physical nature, this oxidation requires more detailed investigation. The naphtha used was fairly low-boiling, meaning that the sulfur compounds are not too complex and reasonably soluble in the phase separation step. Higher-boiling materials are not likely to be amenable to this scheme.

Both sulfides and thiophenes can be selectively oxidized to either sulfoxides or sulfones (Fig. 5.2), but the course of the reaction is highly dependent on the oxidant and often on the reaction conditions to some extent. These products are considerably more polar than the original sulfur compounds, the sulfoxides more so than the sulfones, so that separation from nonoxidized compounds is easily carried out by using adsorption chromatography. The R_f values in thin-layer chromatography on silica were determined (unpublished) to be 0.71, 0.47, and 0.17 for dibenzothiophene, its sulfone, and its sulfoxide (benzene/acetone 9 : 1). In principle, the oxides should be analyzable without reduction to the starting compounds, e.g., by gas chromatography. However, the thermal stability differs appreciably between the two classes of compounds. Sulfones are stable and can easily be analyzed by GC, despite their polarity and often with better resolution than the nonoxidized compounds [5.25], but aromatic sulfoxides are commonly thermally degraded in the GC injector [5.26], although a scrupulously clean injection port liner can diminish this effect [5.27]. In an early work on identification of sulfur compounds in shale oils, the benzothiophenes were oxidized to the sulfones and the corresponding C_1 - and C_2 -isomers separated into individual compounds by either paper chromatography or preparative gas chromatography [5.28].

The two functional groups also differ in their ease of reduction. Sulfoxides are easily reduced back to the parent compounds, but the S=O bond in sulfones is much more stable and often resists reduction [5.29, 30]; other bonds in the molecule may be more reactive and be reduced, with the consequence that the identity of the analyte is lost. Unless the analytes can be analyzed as sulfones, this is a serious objection to

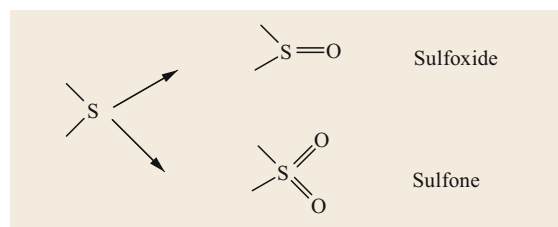


Fig. 5.2 Oxidation of organic sulfur compounds to sulfoxides and/or sulfones

use of oxidation to sulfones followed by reduction, as originally suggested for separation of condensed thiophenes [5.31].

Peracids. Peracids are well-known strong oxidants and form sulfones from sulfides and thiophenes when reacting in excess (as is done for an analytical sample). They can be produced in situ in an acid-catalyzed reaction from a carboxylic acid and hydrogen peroxide. In a work on the PASHs in shale oils and solvent-refined coals, the aliphatic sulfur compounds were first removed through liquid–liquid distribution between cyclohexane and dimethyl sulfoxide. Peracetic acid was then employed to oxidize the aromatic sulfur compounds to the corresponding sulfones [5.31]. The sample was boiled for 16 h in benzene solution with acetic acid and hydrogen peroxide. The sulfones were then separated by chromatography on silica gel, and the oxidized material reduced with LiAlH_4 . Criticism of this scheme centered on the oxidative changes to the matrix, which raised the suspicion that the analytes may also be changed (apart from sulfur oxidation), that the reduction back to the thiophenes is not clean, and that Diels–Alder condensation of the thiophene sulfones formed can take place, e.g., to yield benzonaphthothiophenes from benzothiophenes (Fig. 5.3) [5.30, 32]. The gas chromatogram of a test mixture of nine standard compounds showed little resemblance to that of the products from this procedure, so this procedure now seems obsolete.

A kinetic investigation showed that dibenzothiophene was completely converted to the sulfone after 65 min at 65 °C [5.33]. Despite some oxidation of dimethylphenanthrene, this reaction was judged more convenient than that involving *m*-chloroperbenzoic acid. The PASHs in a diesel (b.p. 190–360 °C) could be oxidized with or without preisolation of the aromatic fraction, and the products were analyzed qualitatively by reversed-phase LC with UV detection at 241 nm. The higher polarity of the sulfones than that of the unreacted hydrocarbons allowed them to elute so much earlier in the chromatogram that there was hardly any

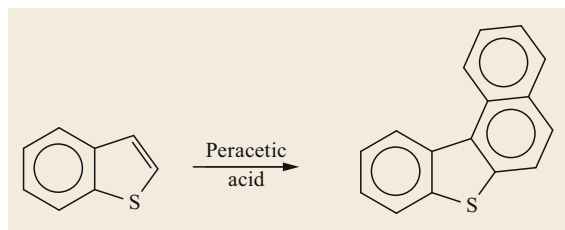


Fig. 5.3 Formation of benzonaphtho[1,2-*b*]thiophene on oxidation of benzothiophene with hydrogen peroxide in acetic acid

overlap between the two classes of compound. It would seem that this procedure is amenable only to distilled materials; in a whole crude oil or in material with a larger boiling range, the smaller and more hydrophilic polycyclic aromatic hydrocarbons (PAHs) will elute together with the larger, more hydrophobic sulfones. The low resolution of traditional high-performance liquid chromatography (HPLC) will also not resolve all the compounds present, although it would be interesting to investigate such separation on modern sub-2 μm particles.

A milder reagent that avoids the harsh oxidation conditions and the byproducts and allows for a faster reaction is *m*-chloroperbenzoic acid (MCPBA). It has been said that the recovery of PAHs was somewhat lower than with peracetic acid while the removal of recovered MCPBA and the product *m*-chlorobenzoic acid made an additional step necessary [5.33]. This oxidation was also performed on crude oils to obtain the sulfones [5.34]. On collision-activated dissociation in a triple quadrupole mass spectrometer, sulfones from PASHs but not from aliphatic sulfones lost sulfur dioxide as a fragment of 64 Da, and recording ions showing this difference produced a mass spectrum of the condensed thiophenes in the crude.

Periodate. A selective reagent that oxidizes sulfides quite cleanly to sulfoxides is tetrabutylammonium periodate ($\text{Bu}_4\text{N}^+\text{IO}_4^-$), dissolved in a toluene/methanol mixture [5.35]. The method has been used for sulfides in asphalt; the sulfoxides were determined by IR spectroscopy [5.36]. The oxides of the sulfides produced in this way from heavy oils and bitumens from Alberta, Canada were removed on silica gel from the nonoxidized material that contained the condensed thiophenes. The sulfur aromatics in the latter fraction were separated from the hydrocarbons through oxidation with *m*-chloroperbenzoic acid to produce sulfones. Finally, after chromatographic removal of nonpolar material, the sulfones were reduced with lithium aluminum hydride to the thiophenes. It was noted that not all thiophenes were cleanly regenerated in this step [5.35]. It was not clarified how disulfides react in this scheme. A similar scheme was used for analyzing sulfur compounds in a high-sulfur Boscan aromatic immature asphaltene. This macromolecular material was pyrolyzed to obtain smaller fragments that could be analyzed by GC [5.37]. The sulfides were oxidized to sulfoxides by periodate, separated from the remaining material, and regenerated by treatment with LiAlH_4 . Then, the thiophenes were oxidized with MCPBA, separated, and reduced with LiAlH_4 . This process gave low recovery of sulfur compounds, no doubt to a great extent because of the reduction steps not being clean. A large signal for

1-methyldibenzothiophene indicated a low maturity of the asphaltene.

If the analysis step involves liquid introduction of the sample into a mass spectrometer, reduction of the sulfoxides is not necessary, as these are easily ionized in an electrospray ionization chamber to yield positive ions through proton [5.38] or, advantageously, lithium ion adduction [5.39]. It should be ensured that the material does not contain sulfoxides to start with, since the analysis would then not discriminate between sulfides and sulfoxides. MS reveals that the oxidation is not complete even after 72 h [5.38]. The most abundant sulfides in the saturates fraction of an Athabasca oilsand bitumen contained two or three rings.

Singlet Oxygen. Photochemically generated singlet oxygen has been shown to oxidize sulfides to the exclusion of the thiophenes in high yield [5.40], and this reaction was employed to petroleum sulfides [5.41]. Methanol was essential as solvent. The drawbacks are that the reaction required 4–5 days, some dark sticky material was formed, and the oxidation of the sulfides went to ca. 90% completion only. The sulfoxide fraction was separated on silica gel and subsequently reduced with lithium aluminum hydride, and the recovered sulfides analyzed by gas chromatography.

Oxone (Potassium Hydrogen Persulfate). Oxone is a powerful but not frequently used commercial oxidant for sulfur, consisting of KHSO_5 admixed with KHSO_4 and K_2SO_4 from the production process. It was used in isolation of terpenoid derivatives, hexahydrodibenzothiophenes, from a deeply desulfurized diesel [5.42]. Sulfones were formed from the sulfides as well as the PASHs, necessitating both normal- and reversed-phase liquid chromatographic steps for isolation. The thermal stability of the sulfones produced was utilized in GC-MS analysis that helped assign structures to the sulfur compounds. The same terpenoids were later isolated in a simpler procedure using ligand-exchange chromatography on Pd(II) (see Sect. 5.3.2, *Palladium Ions*).

Since new reagents for oxidation to sulfoxides are constantly being developed [5.43], it may make sense to investigate more recently developed reagents for the selective oxidations needed here.

Methylation

Because of the nucleophilicity of the sulfur atom, it can quite easily be methylated to give a methyl sulfonium (methyl thiophenium) ion. Such ions are frequently found in biochemical systems, and they are more stable than may appear at first sight. They are eas-

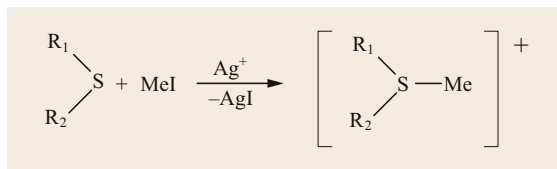


Fig. 5.4 Methylation of a sulfur compound with methyl iodide

ily formed on methylation with methyl iodide, aided by the presence of silver tetrafluoroborate. Silver iodide precipitates, facilitating the reaction (Fig. 5.4). Both sulfides and thiophenes react in this reaction, which is also used to ionize sulfur compounds for nuclear magnetic resonance (NMR) analysis [5.44], mass spectrometry, especially with electrospray ionization [5.45], and to impart electrophoretic mobility to PASHs for capillary electrophoretic analysis [5.46, 47]. The reaction is instantaneous, and there is no need to use an overnight [5.44] or 48 h reaction time as initially reported [5.45]. Although disulfides have been said to form similar ions with trimethyloxonium 2,4,6-trinitrobenzenesulfonate [5.48], experiments in the author's laboratory with commercial trimethyloxonium tetrafluoroborate failed to reproduce these results, and all disulfides were consistently recovered.

Methyl sulfonium ions are highly polar and precipitate in not too polar solvents such as dichloromethane, thus they can easily be separated from nonderivatized compounds by decantation. They are readily soluble in more polar solvents such as acetonitrile. After this separation, the sulfides and thiophenes can be recovered through demethylation with different nitrogen bases: 7-azaindole for the thiophenes, and 4-dimethylaminopyridine for the sulfides. This procedure was applied to a diesel and a vacuum gas oil [5.49] and crude oils [5.50]. Analysis of the separated sulfur compounds was done using both gas chromatography and mass spectrometry.

Reduction of Sulfides (Desulfurization)

The most drastic chemical procedure is surely complete removal of the sulfur atom. Sulfides can be desulfurized by treatment with nickel boride [5.50, 51], or Raney nickel [5.52] (Ra-Ni) in ethanol, and this reaction has been employed in studies of geochemical significance both to decompose large molecules into smaller ones that are amenable to GC analysis and to distinguish between different sulfide environments. The sulfides are recovered as hydrocarbons; naturally, it must be ensured that the hydrocarbons from the matrix do not interfere with the analysis of the hydrocarbons from this Ra-Ni reduction. The resins fraction of five crude

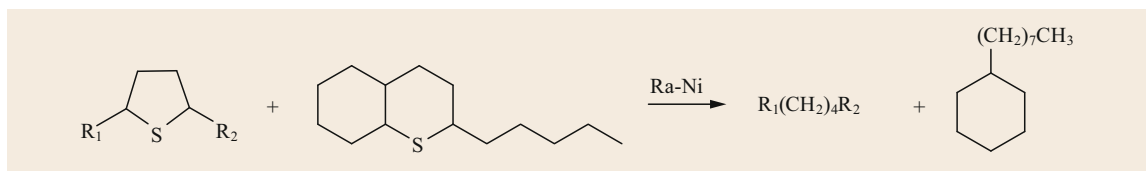


Fig. 5.5 Reduction with Ra-Ni of two sulfides

oils was treated in this manner, and the products analyzed by gas chromatography with flame ionization detection (GC-FID) [5.53]. *n*-Alkanes were the dominant products, mainly arising from reduction of cyclic sulfides (Fig. 5.5). They showed carbon numbers from 15 to ca. 44. Other important products were isoprenoid alkanes such as phytane, pristane, and norpristane, as well as tricyclic terpanes. Less dominant were *n*-alkylcyclohexanes, mid-chain methylalkanes, bicyclic terpanes, steranes, and hopanes.

Detailed information on cyclic terpenoid sulfides was obtained through desulfurization [5.41]. It turned out that the bicyclic and tetracyclic sulfides were reduced as expected, but that the tricyclic terpenoid sulfides resisted reduction unless forcing conditions were used. From these and other data, it was concluded that those tricyclic sulfides had the general structure shown in Fig. 5.6. This method has also been used to identify individual compounds in the hopane series [5.54] and of thiaindans (dihydrobenzothiophenes) in crude [5.55], showing how this sample preparation technique aids in speciation studies.

Thiols (mercaptans) are difficult to analyze due to the ease of their oxidation to disulfides. They can be added to electron-deficient olefins in a Michael addition, as is often done in bioanalytical work. Phenyl vinyl sulfone was recently introduced for thiols in crude oils and distilled fractions. Subsequent analysis of the resulting sulfones as sodium ion adducts was carried out by ESI FT-ICR MS [5.56].

5.2.2 Liquid-Liquid Extraction

Liquid-liquid extraction to separate sulfur compounds from hydrocarbons is not possible without using agents that selectively interact with the sulfur compounds. Sev-

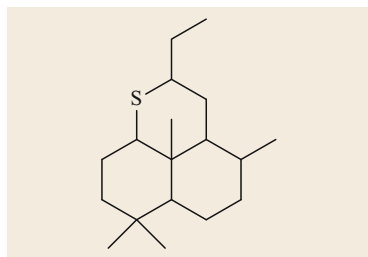


Fig. 5.6 General structure of tricyclic terpenoid sulfides that are difficult to reduce with Ra-Ni (after [5.41])

eral kinds of Lewis acid have been used as such agents that can form a complex with the Lewis base sulfur (Fig. 5.7). This complex and the (noncomplexed) matrix should have very different distribution coefficients for the two phases, enabling their separation. It is important that the complex formation is reversible so that the sulfur compounds can be released for further analysis.

Protons

Protons from Brønsted acids can attach themselves onto the lone electron pairs of the sulfur atom in sulfides ($A^{n+} = H^+$ in Fig. 5.7). Dimethylsulfide has proton affinity similar to that of ketones such as acetone and esters such as methyl acetate [5.57]. This methodology has been used to separate both open-chain and cyclic sulfides from hydrocarbons in petroleum for nearly 100 years [5.58]. Shaking petroleum with strong sulfuric acid will protonate the sulfides, which then become soluble in the acid. In this way, they can be separated from the nonprotonated hydrocarbons. In a second step, the sulfuric acid is diluted with water, which reverses the protonation so that the sulfides can be extracted from the aqueous solution into an organic solvent. The final separation of individual low-molecular-weight sulfides has been done by repeated fractional distillation or through fractional crystallization of the sulfide complexes with mercuric chloride [5.59], which of course is possible only with a large sample. It is not clear whether higher-molecular-weight sulfides would be extractable in this way, since the hydrocarbon part of these molecules would tend to increase the solubility of the ion in the organic phase and thus prevent extraction into the sulfuric acid. This method has recently been used for extraction of 234 sulfides in jet A-1 fuel, which were analyzed by GC-MS; some thiophenes were likewise extracted [5.60]. The sulfides were cyclic in nature with carbon number between 6 and 14.

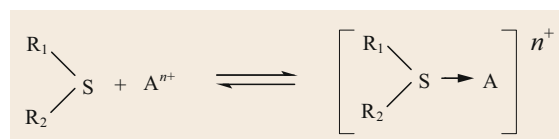


Fig. 5.7 Complexation/decomplexation of a sulfide with a Lewis acid (A^{n+})

Gasoline from fluid catalytic crackings was extracted with sulfuric acid with extraction efficiencies close to 100% for sulfides up to dipentylsulfide but very low efficiencies for mercaptans and thiophene [5.61]. However, thiophenes bearing several alkyl carbon atoms were efficiently extracted.

Hydroiodic acid dissolved in butane at -78°C has been used for the same purpose in crude oil analysis [5.55, 62].

Mercuric Ions

Lewis acids other than protons that have been employed for separation purposes are metal ions. It is expected that soft Lewis acids would interact better with the soft Lewis base sulfur, and indeed this seems to be the case. A set of metal ions of varying hardness was used in an attempt to extract sulfur compounds into complexing organic solvents, and the hard ones were shown to be less effective [5.63]. This was confirmed for the hard Lewis acid aluminum ion, which did not extract dibutyl sulfide to an appreciable extent [5.64]. The soft mercuric ions ($A^{n+} = \text{Hg}^{2+}$ in Fig. 5.7) were used to separate cyclic from dialkyl sulfides, the former complexes being more easily extractable into aqueous solution [5.65]. The sulfides were released through the action of hydrochloric acid on the mercuric complexes. Larger sulfides such as di-*n*-hexyl sulfide were not extractable. Mercuric acetate as complexing agent instead of the chloride led to complexes with higher aqueous solubility, so that also some larger sulfides were extractable [5.64]. A more detailed investigation of the influence of the counterions, cosolvents, release agent, time of extraction, etc. revealed that Na_2HgCl_4 worked well for the complexation with KCN and subsequent release of the sulfides from the complexes [5.66]. A peculiarity of the mercury(II) ion is its ability to form a direct C–Hg bond with aromatic compounds, particularly easily with thiophenes and benzothiophenes [5.67]. A serious objection to this scheme is the highly toxic nature of the salts of mercury,

which would seem to prevent this metal from being used in routine work.

In an early work, the $165\text{--}280^{\circ}\text{C}$ cut of a West Texas crude was treated with sulfuric acid to extract the sulfur compounds. When the extract was treated with aqueous mercuric chloride, the sulfides formed a paste-like complex, while the disulfides were found in the material that failed to form a complex [5.68]. This seems to be a rare example of separation between sulfides and disulfides, unfortunately involving toxic mercury salts.

Silver Ions

The silver ion looks like a good candidate for complexing sulfur atoms ($A^{n+} = \text{Ag}^+$ in Fig. 5.7), and its suitability for liquid–liquid extraction of sulfides has been investigated for standard substances [5.69]. Aliphatic and aromatic sulfides could be separated, albeit using a fairly elaborate extraction scheme, from unsaturated and aromatic hydrocarbons as well as from thiophenes and benzothiophenes. Silver nitrate extraction was employed to separate the sulfides in a shale oil, and they were found by gas chromatography to be alkylpentamethylene sulfides [5.70]. The sulfides were released from the complexes with ammonia. In view of the chromatographic separation of aromatic sulfur compounds on Ag^+ -modified phases (below), it is important to note that silver ions obviously do not interact with the sulfur atom in thiophenes, which is known to show lower Lewis basicity than the sulfur atom in sulfides. It has been found that many transition metals rather interact with the π -electrons of the benzo rings, e.g., in benzothiophenes, forming (η^6)-coordinated compounds [5.71].

A procedure in which sulfides and thiols in a naphtha were precipitated through treatment with a silver nitrate solution has been published [5.61]. The aromatic sulfur compounds were unaffected and could be analyzed by GC, free of interference from other classes of sulfur compound.

5.3 Chromatographic Methods

Chromatography is certainly the most important separation method used in analysis of petroleum, being used, in many variants, for both sample preparation and detailed analysis, including speciation. Here, we only consider chromatography in sample preparation. The stationary phases that have found use can be divided into those that separate the sample components with selectivity for sulfur and those that do not show this property. Both of these varieties are in very widespread

use and are treated here separately, beginning with such phases that are nonselective for sulfur.

5.3.1 Phases Nonselective for Sulfur

Silica and Alumina

The initial step in the sample preparation of crude oil and materials derived from it is very often a chromatographic separation of the components on a polar

stationary phase (silica, aluminum oxide) based on the ill-defined property known as polarity. SARA fractionation is widely used, leading to four fractions in order of ascending polarity:

- Saturates
- Aromatics
- Resins
- Asphaltenes.

The fractions are eluted using mobile phases of increasing solvent strength. It is important to realize that, in such systems, the compounds are not separated according to their functional groups but only based on the adsorptive strength of the whole molecule onto the stationary phase in the particular solvent used. Therefore, this fractionation does not deliver purified compound classes but mixtures of several compound classes of similar polarity. Aromatic sulfur compounds behave much like aromatic hydrocarbons and elute in the corresponding fractions, while sulfoxides are very polar and collect in the resins/asphaltenes fractions [5.72]. However, monoaromatic compounds can easily elute in the saturates fraction, especially if they are heavily substituted with alkyl groups. Thus, a series of terpenoid thiophenes were found in the saturates fraction from sulfur-rich Chinese oil samples [5.73].

Sulfides exhibit a more complex behavior. Experience shows that, although the C–S bond is not polarized (the electronegativity for carbon is 2.55 and for sulfur 2.58), sulfides do not as a class elute preferentially with the alkanes in the SARA fractionation, as might be expected, but are rather partially or fully distributed into the more polar aromatics and resins fractions [5.28, 41]. This occurs because of interactions of the free electron pairs on sulfur with the hydroxyl groups on the silica surface, as has been shown by IR spectrometry [5.74]. Such interactions between the analyte and the surface have been discussed for both silica and alumina [5.75]. Disulfides show smaller adsorption energies than sulfides [5.75]. This was shown in the separation of sulfur compounds in a fairly simple matrix, straight-run naphtha, on silica – the disulfides and most thiols were more weakly retained than the sulfides; both groups eluted with hexane:benzene, but with narrow cuts within the fraction, and the disulfides/thiols and sulfides could be separated [5.76].

The order of elution from silica gel has been given as [5.77]: aromatic hydrocarbons < thiophenes < alkanethiols < alkane disulfides < aromatic and cycloalkane thiols < alkane sulfides < cyclic sulfides.

Since nonaromatic sulfur compounds have been detected by mass spectrometry in the saturates, aromatics, and resins fractions of a heavy crude oil [5.78], a very basic question that arises is whether SARA fractiona-

tion is at all suitable for analysis of sulfur compounds or whether it would be more appropriate to develop a new separation scheme that is designed toward separating fossil material according to its sulfur functional groups.

Gel Permeation Chromatography

Gel permeation chromatography (GPC) is a technique in which the separation of the analytes depends on their hydrodynamic radius, with the consequence that larger molecules elute earlier than smaller ones. In the ideal case, the gel should not show any chemical interactions with the analytes, although in practice this is hard to avoid. In many cases, the gel is based on a mixed polymer of styrene and divinylbenzene and the aromatic groups can interact with aromatic rings in the analytes. It is desirable that the only role the gel should play is to provide pores that are used to sieve the molecules according to their size. Because of its low resolution, gel permeation (also called size-exclusion chromatography) has not been extensively used in sample preparation of materials derived from petroleum. Its main application has been for estimation of molecular weight distributions [5.79], but there is much debate about the accuracy of such data.

An early analysis involved GPC of an Alaska crude oil with detailed mass-spectrometric characterization [5.80]. A distilled fraction was subjected to a sample preparation scheme that started with an anion resin (removal of acids), a cation resin (removal of bases), treatment with ferric chloride (removal of neutral nitrogen compounds), and chromatography on silica + alumina to obtain the saturates, monoaromatics, diaromatics, and polyaromatics + polars fractions (with total consumption of 10 L of solvent in this latter step only). The final step was GPC (on a column with dimensions of 2.54 × 455 cm!) of the aromatic fractions, i. e., hydrocarbons and sulfur heterocycles, obtained from the normal-phase chromatography. A series of fractions were taken for offline MS analysis, and a large number of PASHs were detected with up to six aromatic rings. Benzothiophenes with 0–6 naphthene rings were detected in the diaromatic fraction. An alkyl chain carbon atom was found to contribute twice as much to the retention time in GPC as a carbon atom in a naphthene ring did, so that compounds of the same carbon number were separated to some degree.

The preisolated PASH fraction of a vacuum residue before and after hydrodesulfurization was separated by GPC followed by matrix-assisted laser desorption/ionization (MALDI) MS analysis [5.81]. It was verified that compounds of equal molecular weight but different degree of aromaticity showed strongly different retention times, depending on the mobile phase, as a result

of interactions with the polystyrene gel (Fig. 5.8). In the weaker solvent cyclohexane, the interactions were considerably stronger. Although narrow cuts were taken from the vacuum residue, the molecular weights within one cut differed by several 100 Da.

Although GPC has not been favored in sample preparation of fossil materials, modern phases allow sharper resolution than those used in earlier work. With careful attention to suppressing interactions between analytes and the gel and keeping in mind the possibility of association of analytes with each other (aggregation), the technique may find new uses in future work [5.82].

5.3.2 Phases Selective for Sulfur: Ligand-Exchange Chromatography

Some of the metal ions used in liquid-liquid extraction of sulfur compounds (Sect. 5.2.2) have also been deposited on a support material and used as stationary phases in liquid chromatography. A large range of metals have been evaluated for their interactions with different forms of sulfur compounds. Many of them have been studied with a view to complexing sulfur compounds and thus removing these from fossil fuels, as an alternative to hydrodesulfurization on a commercial scale. However, frequently only one or two sulfur compounds are used in such studies, so not enough data are available for estimating the usefulness of these methods for a general complexation scheme for analytical purposes. There are some metal ion systems that show selective properties for analytical separations and that can differentiate between sulfur and nonsulfur compounds, while others are useful for separating different kinds of sulfur functionalities. Since they all contain a metal ion of some kind, they are treated here according to the metal ion employed.

This form of chromatography is called ligand-exchange chromatography (LEC). A metal ion is incorporated into the stationary phase in liquid chromatography and used to form (reversible) complexes with sulfur compounds. The most frequent use involves such ions that allow the analytes to be eluted as groups of compounds that share some chemical feature. These groups are usually displaced by adding a component to the eluent that is strong enough to displace one group of compounds but weak enough to let other groups stay bonded. LEC has been called a *vital dimension for the reliable characterization of heterocycles in crude oils and refined products* [5.83].

In addition to sulfur compounds, nitrogen compounds also show strong interactions with these metal ions, and it would thus seem advisable to remove nitrogen compounds before separating the sulfur compounds. The nitrogen compounds will otherwise bind

to the metal and reduce its capacity for sulfur. Reconditioning of an LEC phase can be carried out by pumping a mobile phase with a strongly displacing eluent that does not elute the metal ions or by pumping a solution of the metal ion through the column [5.84].

LEC phases have received much attention also outside the petroleum area. Silver ions complex double bonds and thus can separate unsaturated from saturated compounds, e.g., fatty acids [5.85], and nickel ions are used in biochemical separations to separate proteins that have been tagged with the amino acid histidine, the so-called his-tag [5.86].

Mercuric Ions

Mercuric acetate deposited on silica gel is one of the very few systems that seem to allow a certain separation of sulfides and disulfides [5.87]. In thin-layer mode (TLC), a disulfide was more mobile than sulfides (and mercaptans) but exhibited considerable tailing. Dibenzothiophene and anthracene coeluted, indicating no particular interaction with a sulfur atom in a thiophene ring. By using two-dimensional TLC and scratching off the aromatic and sulfidic spots followed by extraction and GC-MS, series of alkyl thiophenols, alkyl hexahydrothiaindans, alkyl tetrahydrothiapyrans, and alkyl thiophenes were detected in a Kuwait crude oil.

A stationary phase containing 20% mercury(II) acetate deposited on silica was used to separate *n*-aliphatic sulfides [5.88]. They were not collected as a group but individually separated. Sulfides with carbon number up to ca. 18 could be efficiently separated from hydrocarbons; larger sulfides eluted with the hydrocarbons, as did the thiophenes. On the other hand, sulfides with carbon number below 10 were strongly adsorbed and could only be displaced as a group.

The ease of introducing Hg(II) into aromatic rings was the basis for the synthesis of a stationary phase containing mercuric ions bonded onto a phenyl group [5.89]. It was investigated for its selectivity towards sulfur aromatic compounds, but no such effect was seen [5.90]. However, it separated methyl-substituted aromatic compounds in the normal-phase mode very efficiently according to the number of methyl groups. Other sulfur compounds were not investigated.

Zinc Ions

Zinc(II) is a harder Lewis acid than mercury(II) and should therefore show weaker interactions with sulfur. Indeed, with a phase consisting of zinc chloride on silica, sulfides containing between two and six carbon atoms could be resolved while cyclic sulfides, being more nucleophilic than open-chain sulfides, were retained as strongly as a linear sulfide with two carbon atoms fewer [5.91].

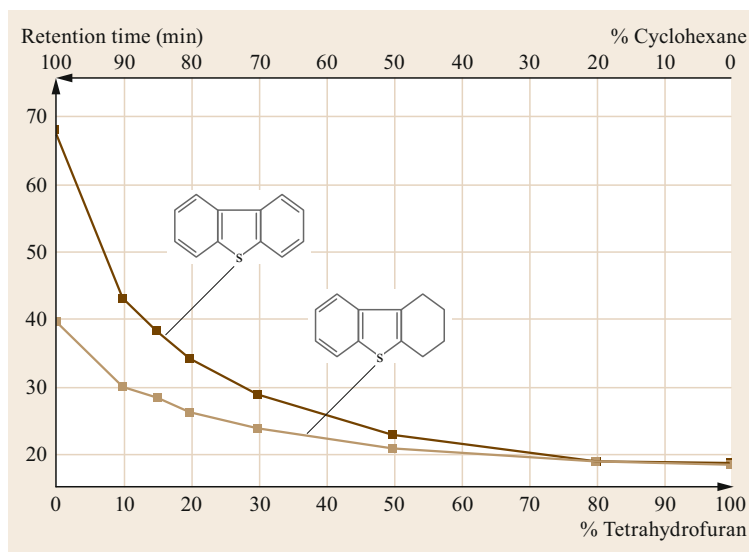


Fig. 5.8 Two PASHs of nearly identical size but quite different retention time in gel permeation chromatography in dependence on the eluent in a cyclohexane-tetrahydrofuran system. Reprinted from [5.81] with permission from Taylor & Francis, LLC

Nickel Ions

In many Russian papers, chromatographic separation on silica containing 5% nickel chloride has been used to obtain separation of sulfur species [5.92, 93]. In the three fractions eluted with hexane, benzene, and ethanol-chloroform (1 : 1), most sulfur compounds were detected in the benzene fraction, but the separation was not clean. Longer-chain sulfides were recovered in the hexane fraction, probably because of their stronger interaction with the mobile phase.

Copper(II) Ions

Copper ions have been employed in LEC in various configurations. The simplest way is to deposit CuCl_2 on silica gel for column chromatography [5.94]. With hexane, a first fraction was obtained from a crude oil that contained hydrocarbons, but also a large proportion of disulfides that were weakly retained. Sulfides were eluted in a second fraction with chloroform-ethyl ether (9 : 1), but the recovery was not quantitative for a set of standard sulfides. Isomeric butyl sulfides showed different strengths of interactions with Cu(II) : the *t*-butyl isomer was most strongly retained, and the *n*-butyl isomer the least. It should be noticed that ketones also eluted in this fraction. Alkyl phenyl disulfides were found to be major aromatic sulfur compounds (apart from PASHs) in Wilmington crude.

An ion exchange resin, loaded with Cu(II) , showed excellent separation properties for sulfides in a model mixture [5.95]. Sulfides that are crowded around the sulfur atom exhibited weaker bonding to the phase. The phase was applied to the fractions obtained from a Wilmington crude oil (370–535 °C) on silica/alumina with pentane as mobile phase for the hydrocar-

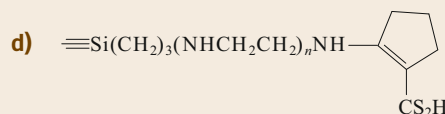
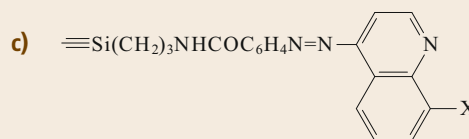
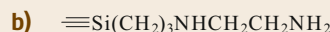
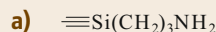


Fig. 5.9a–d Ligands bonded onto a silica surface for complexation with Cu^{2+} . (a) N1, (b) N2, (c) X = OH: 8-quinolinol-silica, X = SH: 8-quinolinethiol-silica, (d) $n = 0$: N1-ACDA, $n = 1$: N2-ACDA, ACDA = amino-1-cyclopentene-1-dithiocarboxylic acid

bons and backwashing with pentane–ethyl ether for the sulfides. The monoaromatic fraction from the Cu(II) column showed no sulfides in the hydrocarbon fraction by MS; the sulfides were abundant in the sulfide fraction, dominated by three-ring cyclic sulfides. The diaromatic fraction was more complex, and an intermediate fraction between hydrocarbons and sulfides contained large amounts of diphenyldisulfides. The final sulfide fraction was a mixture of one- to six-ring cyclic sulfides, diphenyl disulfides, and some oxygenated species.

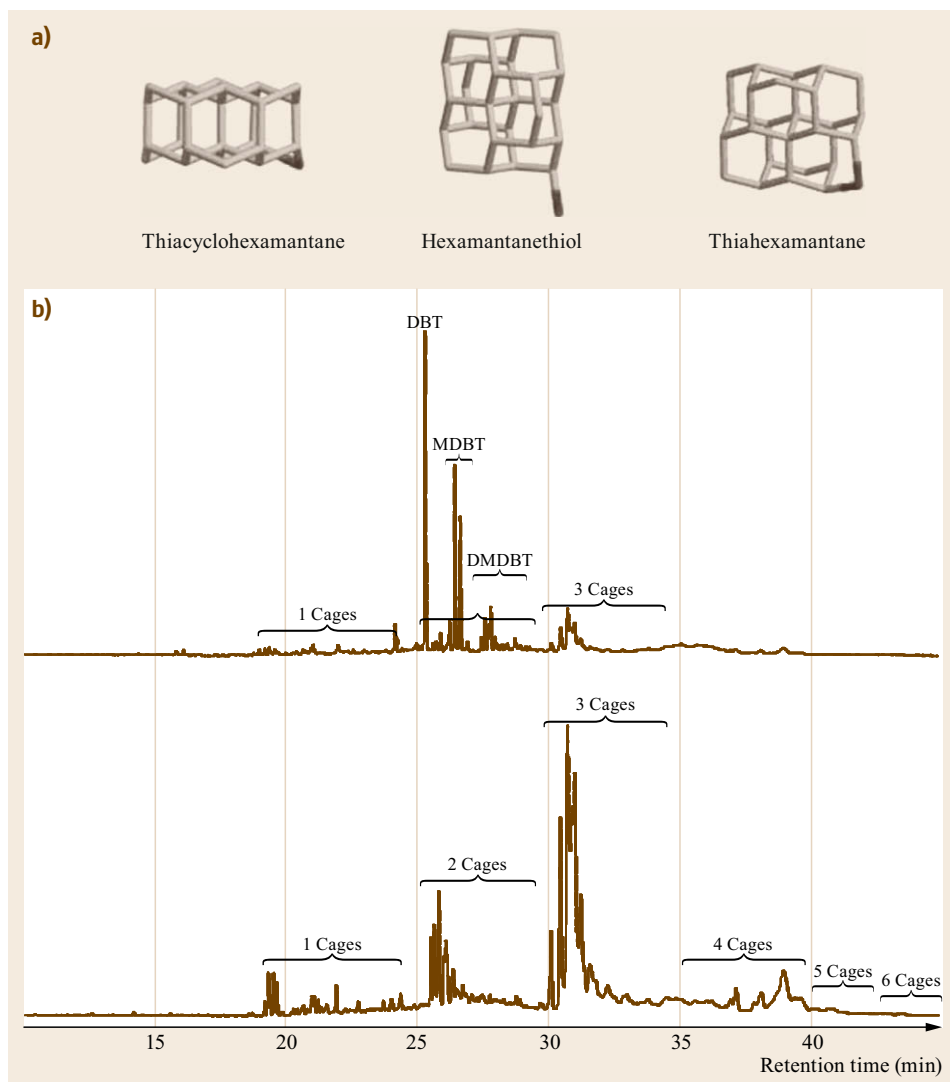


Fig. 5.10a,b GC trace with sulfur-selective detection of the (a) concentrated condensate, and (b) the third fraction from the chromatography on $\text{AgNO}_3/\text{silica}$. DBT: dibenzothiophene, MDBT: methyl dibenzothiophenes, DMDBT: C_2 -substituted dibenzothiophenes. One cage: thiaadamantanes and adamantane thiols; two cages: thiadamantanes and diamantane thiols; three cages: thiatriamantanes and triamantane thiols; four cages: thiatetramantanes and tetramantane thiols; five cages: thiapentamantanes and pentamantane thiols; six cages: thiahexamantanes, thiacyclohexamantane, and hexamantane thiols. The *black spots* in the structures indicate the sulfur atom (after [5.96], with permission from Elsevier)

A drawback with phases based on ion exchange is that their capacity is often fairly low, and thus the separation may not be optimal. A solution to this is to bind a ligand to a silica surface and form metal complexes with it, allowing considerably higher metal ion loading. A comparison of seven such ligands (Fig. 5.9) with Cu^{2+} as the metal ion showed that the N1-ACDA complex was superior to the others and that individual

sulfides could be separated in the normal-phase mode, with the smaller sulfides more strongly retained and the hydrocarbons much less strongly retained [5.97]. However, no petroleum sample was applied to these phases. Thiophenes were retained to the same extent as hydrocarbons, both on CuSO_4 deposited on silica in open column chromatography [5.98] and on CuCl_2 -impregnated silica in thin-layer chromatography [5.99];

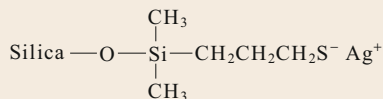


Fig. 5.11 Silver ions bonded onto silica through a mercapto group

in the latter case, sulfides displayed considerably lower R_f values on the impregnated than on the bare silica phase.

Silver Ions

Silver is also considered to be a soft Lewis acid, but there seems to be no selective interaction between the sulfur atom in aromatic compounds and silver metal in nanoclusters [5.100] or silver ions in the form of silver nitrate deposited on silica [5.101]. The retention coefficients in liquid chromatography were very similar for PAHs and PASHs. Thus, phenanthrene had a k value of 5.9 and dibenzothiophene 6.7. Sulfides in crude oils from a carbonate reservoir, however, interacted more strongly with AgNO_3 deposited on silica [5.102]. Hydrocarbons eluted with ethyl acetate, and the sulfides were displaced with diethyl sulfide in chloroform. A high abundance of polycyclic sulfides was indicated by GC-MS. Similar results were obtained with a middle distillate; here, the sulfide fraction could be collected using methanol/diethyl ether (1 : 1) from AgNO_3 deposited on alumina [5.103].

A similar system was used for isolating the thia-diamondoids from a gas condensate produced from a deep reservoir in the Gulf of Mexico [5.96]. The column was eluted with hexane (saturates fraction), dichloromethane (aromatics including PASHs), and acetone (organic sulfur compounds except the PASHs). Subsequent analysis by GC and sulfur-selective detection gave the chromatograms illustrated in Fig. 5.10. The top trace shows the fraction before the chromatography on the AgNO_3 column, the bottom one after, with the PASHs removed. Sulfides with up to six cages were indicated ($\text{C}_{25}\text{H}_{28}\text{S}$).

However, silver ions can also be bonded onto silica through a spacer containing a thiol group, in the simplest case mercaptopropyl (Fig. 5.11).

Ag^+ in this form shows quite useful interactions with the π electron cloud in aromatic compounds, which is considered to be a soft Lewis base. Indeed, many complexes of transition metals with benzothiophene have been described that contain an η^6 -BT ligand in which the heterocycle is bonded through the benzene π electron system to the metal ion [5.104]. This was utilized to separate the PASHs in Wilmington crude oil according to the size of the aromatic

system [5.105]. Compounds containing one, two, and three benzo rings (in addition to the thiophene ring) were very well separated, including the alkylated and naphtheno ring substituted aromatics (Fig. 5.12). It was shown mass spectrometrically that the PASH systems benzothiophene and dibenzothiophene are accompanied by derivatives containing up to five naphtheno rings.

Contrary results have been reported for the same silver system as in Fig. 5.11 [5.106]. Polycyclic aromatic sulfur heterocycles in a heavy gas oil could be separated from the PAHs, using a more polar solvent for the former, and then analyzed by GC \times GC-TOF MS.

Palladium Ions

A commonly used way to separate PASHs from PAHs and sulfides is LEC on a phase containing Pd(II) ions. Hydrocarbons do not interact with the metal ions and are eluted with cyclohexane, the PASHs show a medium bond strength, so that they can be easily eluted with a moderately strong eluent such as dichloromethane, and sulfides bind quite strongly and must be displaced with an agent that binds more tightly than the analytes. This technique has been widely applied to samples of varying origin and composition.

The simplest system involves depositing 5% PdCl_2 on silica [5.99], and this was used for isolating the PASHs from the preisolated aromatic fraction of a catalytically cracked petroleum bottom [5.107] and a catalytically cracked vacuum residue [5.108]. The PASHs eluted as a complex with PdCl_2 , and this complex needed to be destroyed in a separate step, e.g., with diethylamine. A closer study showed that many benzothiophenes as well as PASHs with a terminal thiophene ring are lost because they elute together with the hydrocarbons due to weak interactions with the Pd(II) [5.101, 109]. The decomplexation could be conveniently carried out online by incorporating some aminopropyl silica in the column [5.101, 109]. The procedure has been used for analysis of PASHs in samples such as a vacuum gas oil [5.110], a shale oil [5.111], and a diesel [5.112]. Sulfur compounds other than PASHs were isolated with this system, and three fractions were taken from a crude oil, a coal extract, and a hydrogenated coal liquid [5.113]. One PAH and one PASH fraction were collected, and a sulfur-containing polycyclic aromatic compound (S-PAC) fraction that contained sulfides. However, several compounds in a solution of standards were partially lost, and some compounds eluted in two fractions. A correlation between the elution behavior and the Hückel π electron densities of several thiophene benzologs was demonstrated.

To prevent elution of the palladium complex with the analytes, the Pd(II) ions can be incorporated into

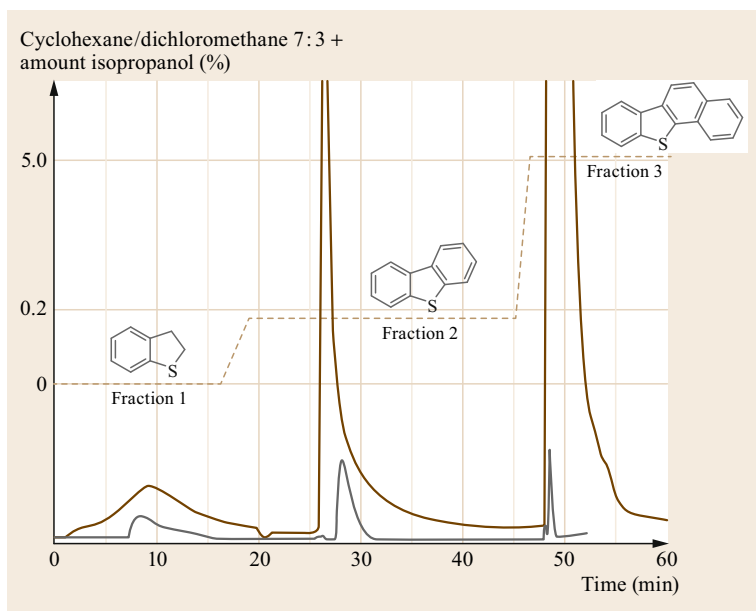


Fig. 5.12 Separation of a standard PASH mixture and a PASH fraction of Wilmington crude on a silver(I)-mercaptopropano silica gel stationary phase (250 × 4.6 mm). Conditions: mobile phase cyclohexane/isopropanol step gradient elution, 2.5 mL/min, room temperature, UV detection at 254 nm (after [5.105], with permission from Elsevier)

a complex that is bonded onto the silica surface. First successful attempts for isolation of PASHs [5.114] from middle distillates [5.115] and vacuum residues [5.45] were recorded for ACDA complexes (Fig. 5.9d, $n = 0$). With this isolation and through comparison with synthesized reference compounds, it was possible to identify the structures of 11 alkylidibenzothiophenes that were recalcitrant to deep hydrodesulfurization [5.18]. However, this ligand must be synthesized in the analytical laboratory, and thus there is some resistance to its use. A convenient alternative is offered by the simpler mercaptopropyl ligands that are bonded to the silica (MPSG, mercaptopropyl silica gel, Fig. 5.11 with Pd^{2+} instead of Ag^+); such phases are commercially available and need only to be treated with a solution of a palladium salt. As a stationary phase, it seems to have essentially the same separation properties as the Pd-ACDA complex and has been used extensively to isolate both a PASH fraction and, less commonly, a sulfide fraction. Although simple thiophenes are not retained and elute with the hydrocarbons [5.83, 114], this is not of great importance in many applications because such thiophenes are not present in relevant amounts.

Sample preparation using Pd-MPSG has been shown to greatly facilitate analysis of sulfur compounds in petroleum-related samples. In a comprehensive two-dimensional gas chromatographic study of heavy gas oils, 317 sulfur compounds were detected following this separation, but only 135 without it [5.14]. PASHs with two to five aromatic rings were recorded, as well as some hydrogenated PASHs.

A high-boiling Iranian vacuum gas oil (390–460 °C) was analyzed by atmospheric-pressure laser ionization (APLI) FT-ICR MS following separation of the PASHs on Pd-MPSG [5.117]. With atmospheric-pressure photoionization, a large number of OS and O_2S species were detected that were not found with APLI or electrospray ionization. Proper sample preparation removes sulfones and sulfoxides, so that the presence of such compounds in the mass spectrum is not necessarily an indication of their presence in the sample but probably of oxygenation in the instrument. However, it has been found that sulfides can oxidize to their sulfoxides also during sample separation [5.118]. On the whole, sample preparation should help avoid false assignments based only on mass-spectral data.

An example for the collection of a sulfide fraction from chromatography on a Pd complex is the elucidation of the structures of sulfides in a heating oil that are recalcitrant to deep hydrodesulfurization to 16 ppm S [5.116]. These compounds had the structures shown in the gas chromatogram in Fig. 5.13. The fraction shown was collected after removal of the hydrocarbons (fraction 1) and PASHs (fraction 2) with an eluent containing a 2 : 1 mixture of cyclohexane:dichloromethane with 1.5% ammonia-saturated isopropanol. The ammonia was needed to displace the strongly bonded sulfides from the complex with Pd^{2+} . The same separation technique was used to separate the sulfides from a crude oil. FT-ICR MS indicated double bond equivalents from 1 to 12. Obviously, this procedure is more convenient than the oxidation followed by several chro-

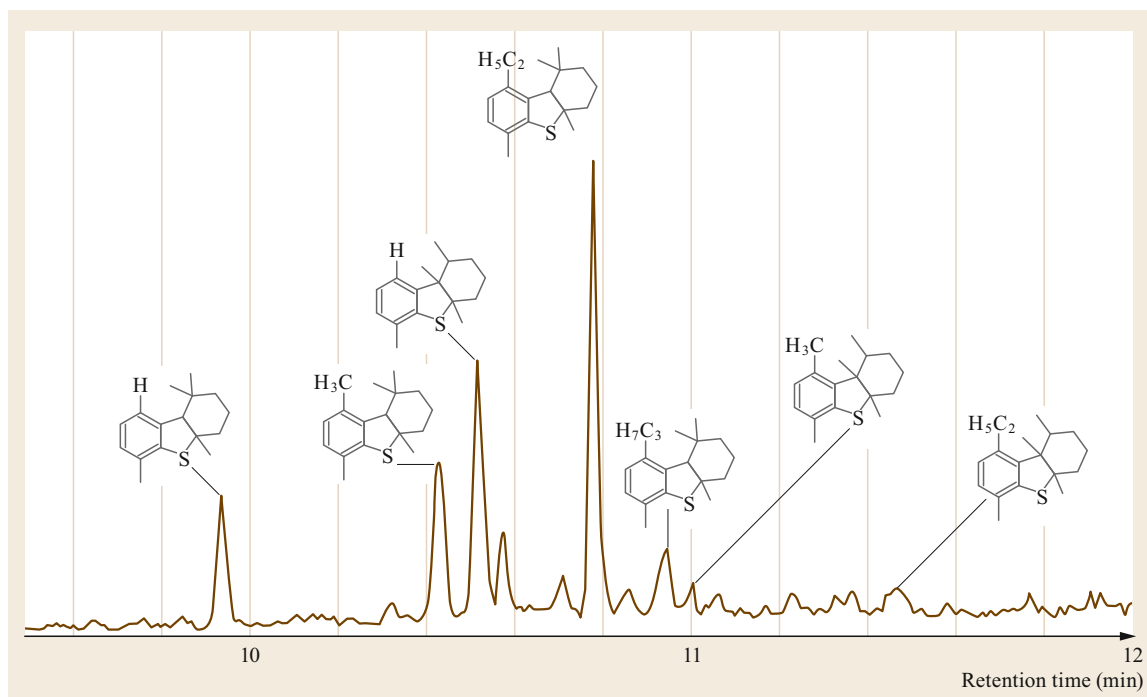


Fig. 5.13 Gas chromatogram with sulfur-selective atomic emission detection (AED) of the recalcitrant sulfides in a deeply hydrodesulfurized heating oil. This fraction was collected as fraction 3 from a Pd–MPSG column (after [5.116], Copyright 2009 American Chemical Society)

matographic steps as described above for the same compounds (Sect. 5.2.1, *Oxone (Potassium Hydrogen Persulfate)*) [5.42].

Quite a number of publications on various materials have now reported use of Pd(II) for separation. Heavy

oil [5.119], straight run diesel [5.120], Saudi Arabian heavy crude oil and its distilled fractions [5.83], residue fluid catalytic cracking diesel [5.121], coal tar [5.122], and vacuum gas oils [5.10, 123] are among the high-lights.

5.4 Conclusion

A large variety of separation methods have been presented here as applied to sulfur-containing compounds in fossil materials. Despite the very many approaches, it becomes clear that there is still much work left before sample preparation for molecular characterization of such compounds can be considered sophisticated enough to allow isolation of any desired functional group. Not even the first step in sample preparation, i. e., SARA fractionation, allows one functional group to elute cleanly in one fraction; such a result should be the goal of any initial separation. Here lies a vast land of useful discoveries to be made.

The next step in an analysis would often be separation of hydrocarbons from the sulfur compounds in such a fraction. Many of the techniques described

here approach this topic, but none are fully satisfactory. The oxidation/reduction schemes are laborious and not easy to automate, and the ligand-exchange chromatography methods suffer from some loss of analytes by too early breakthrough, as well as from binding some compounds so strongly that their removal presents problems. A displacer may be necessary for such compounds, which in turn binds so strongly that it may be impossible to regenerate the phase for another separation, necessitating the use of a fresh column for each application. Stationary phases based on noble metals such as palladium can be an expensive drawback for routine work.

One extension of any separation method would be to compounds containing mixed heteroatoms, presenting its own problems. Even if only heterocyclic compounds

are considered, this will be a challenge of its own. In all schemes, the mixed heterocycles would be expected to be distributed into the fraction of the *strongest* heteroatom, for instance OS compounds into the S fraction and NS compounds into the N fraction. To characterize these compounds in further depth than is possible by recording the molecular mass in MS, further separa-

tions would be needed that build on the presence of the other heteroatoms.

Despite these lacunae, it is impressive to see how far separations have come. The improvement in the analytical data with proper sample preparation provides strong motivation to continue such work and improve on current methods.

References

- 5.1 A.G. Requejo, R. Sassen, T. McDonald, G. Denoux, M.C.I.I.J.M. Kennicutt: Brooks: Polynuclear aromatic hydrocarbons (PAH) as indicators of the source and maturity of marine crude oils, *Org. Geochem.* **24**(10/11), 1017–1033 (1996)
- 5.2 L. Schou, M.B. Myhr: Sulfur aromatic compounds as maturity parameters, *Org. Geochem.* **13**(1–3), 61–66 (1988)
- 5.3 M.J. Li, T.G. Wang, S.B. Shi, K.Y. Liu, G.S. Ellis: Benzo[*b*]naphthothiophenes and alkyl dibenzothiophenes: Molecular tracers for oil migration distances, *Marine and Petroleum Geol.* **57**, 403–407 (2014)
- 5.4 J.T. Andersson, A.H. Hegazi, B. Roberz: Polycyclic aromatic sulfur heterocycles as information carriers in environmental studies, *Anal. Bioanal. Chem.* **386**(4), 891–905 (2006)
- 5.5 U.M. Sofowote, B.E. McCarry, C.H. Marvin: Source apportionment of PAH in Hamilton Harbour suspended sediments: Comparison of two factor analysis methods, *Environ. Sci. Technol.* **42**(16), 6007–6014 (2005)
- 5.6 A.H. Hegazi, J.T. Andersson: Characterization of polycyclic aromatic sulfur heterocycles for source identification. In: *Environmental Forensics: Spill Oil Fingerprinting and Source Identification*, ed. by Z. Wang, S. Stout (Elsevier, Amsterdam 2007) pp. 147–168
- 5.7 A.E. Bence, K.A. Kvenvolden, M.C.I.I. Kennicutt: Organic geochemistry applied to environmental assessments of Prince William Sound, Alaska, after the Exxon Valdez oil spill – A review, *Org. Geochem.* **24**(1), 7–42 (1996)
- 5.8 J. Beens, J. Blomberg, P.J. Schoenmakers: Proper tuning of comprehensive two-dimensional gas chromatography (GC × GC) to optimize the separation of complex oil fractions, *J. High. Resol. Chromatogr.* **23**(3), 182–188 (2000)
- 5.9 S. Kurz: Isomers of Alkane (C_nH_{2n+2}), <http://www.mathe2.uni-bayreuth.de/sascha/oeis/alkane.html> (2015) last accessed 1st September 2015
- 5.10 S.K. Panda, J.T. Andersson, W. Schrader: Characterization of supercomplex crude oil mixtures: What is really in there?, *Angew. Chem. Int. Ed.* **48**, 1788–1791 (2009)
- 5.11 H. Truffelli, P. Palma, G. Famigliani, A. Cappiello: An overview of matrix effects in liquid chromatography–mass spectrometry, *Mass Spectrom. Rev.* **30**(3), 491–509 (2011)
- 5.12 A. Alhassan, J.T. Andersson: Ketones in fossil materials – A mass spectrometric analysis of a crude oil and a coal tar, *Energy Fuels* **27**(10), 5770–5778 (2013)
- 5.13 A. Gaspar, E. Zellermann, S. Lababidi, J. Reece, W. Schrader: Characterization of saturates, aromatics, resins, and asphaltenes heavy crude oil fractions by atmospheric pressure laser ionization Fourier transform ion cyclotron resonance mass spectrometry, *Energy Fuels* **26**(6), 3481–3487 (2012)
- 5.14 M.E. Machado, L.P. Bregles, E.W. de Menezes, E.B. Caramão, E.V. Benvenutti, C.A. Zini: Comparison between pre-fractionation and fractionation process of heavy gas oil for determination of sulfur compounds using comprehensive two-dimensional gas chromatography, *J. Chromatogr. A* **1274**, 165–172 (2013)
- 5.15 P.A. Mello, J.S.F. Pereira, M.F. Mesko, J.S. Barin, E.M.M. Flores: Sample preparation methods for subsequent determination of metals and non-metals in crude oil – A review, *Anal. Chim. Acta* **746**, 15–36 (2012)
- 5.16 O. van Rheinberg, K. Lucka, H. Köhne, T. Schade, J.T. Andersson: Selective removal of sulphur in liquid fuels for fuel cell applications, *Fuel* **87**(13/14), 2988–2996 (2008)
- 5.17 W.L. Orr, J.S. Sinninghe Damsté: Geochemistry of sulfur in petroleum systems, *Proc. ACS Symposium Series Geochemistry of Sulfur in Fossil Fuels*, Vol. 429, ed. by W.L. Orr, C.M. White (American Chemical Society, Washington DC 1990)
- 5.18 J.T. Andersson, T. Schade: Speciation of alkylated dibenzothiophenes in a deeply desulfurized diesel fuel, *Energy Fuels* **20**(4), 1614–1620 (2006)
- 5.19 J.S. Sinninghe Damsté, J.W. de Leeuw: Analysis, structure and geochemical significance of organically-bound sulphur in the geosphere: State of the art and future research, *Org. Geochem.* **16**(4–6), 1077–1101 (1990)
- 5.20 J.T. Andersson: Separation methods in the analysis of polycyclic aromatic sulfur heterocycles. In: *Environmental Analysis, Handbook of Analytical Separations*, Vol. 3, ed. by W. Kleiböhmer (Elsevier, Amsterdam 2001)
- 5.21 K.D. Nizio, T.M. McGinitie, J.J. Harynuk: Comprehensive multidimensional separations for the analysis of petroleum, *J. Chromatogr. A* **1255**, 12–23 (2012)
- 5.22 M. Kamiński, R. Kartanowicz, E. Gilgenast, J. Namieśnik: High-performance liquid chro-

- matography in group-type separation and technical or process analytics of petroleum products, *Critical Rev. Analytical Chem.* **35**(3), 193–216 (2005)
- 5.23 A. Stumpf, K. Tolvaj, M. Juhász: Detailed analysis of sulfur compounds in gasoline range petroleum products with high-resolution gas chromatography-atomic emission detection using group-selective chemical treatment, *J. Chromatogr. A* **819**, 67–74 (1998)
- 5.24 D.D. Link, J.P. Baltrus, K.S. Rothenberger, P. Zandhuis, D.K. Minus, R.C. Striebich: Class- and structure-specific separation, analysis, and identification techniques for the characterization of the sulfur components of JP-8 aviation fuel, *Energy Fuels* **17**(5), 1292–1302 (2004)
- 5.25 J.T. Andersson: Gas chromatographic retention indices for all C₁- and C₂-alkylated benzothiophenes and their dioxides on three different stationary phases, *J. Chromatogr.* **354**, 83–98 (1986)
- 5.26 J.T. Andersson: Stability of dibenzothiophene oxides under gas chromatographic conditions, *J. High Resol Chromatogr Chromatogr Comm.* **7**(6), 334–335 (1984)
- 5.27 P.M. Fedorak, J.T. Andersson: Decomposition of two methylbenzothiophene sulphoxides in a commercial gas chromatography injection port liner, *J. Chromatogr.* **591**, 362–366 (1992)
- 5.28 M. Pailer, E. Simonitsch: Über die Zusammensetzung einer mittleren Siedefraktion des Seefelder Schieferöls, *Mh. Chem.* **98**(4), 1477–1491 (1967)
- 5.29 W.P. Weber, P. Stromquist, T.I. Ito: Observations on the mechanism of reduction of sulfones to sulfides, *Tetrahedron Lett.* **15**(30), 2595–2598 (1974)
- 5.30 J.T. Andersson: Polycyclic aromatic sulfur heterocycles I. Use of hydrogen peroxide oxidation for the group separation of polycyclic aromatic hydrocarbons and their sulfur analogs, *Intern. J. Environ. Anal. Chem.* **48**(1), 1–15 (1992)
- 5.31 C. Willey, M. Iwao, R.N. Castle, M.L. Lee: Determination of sulfur heterocycles in coal liquids and shale oils, *Anal. Chem.* **53**(3), 400–407 (1981)
- 5.32 W. Davies, N.W. Gamble, W.E. Savage: The direct conversion of thionaphthene into derivatives of 9-thiafluorene, *J. Chem. Soc.*, 4678–4683 (1952)
- 5.33 J. Bundt, W. Herbel, H. Steinhart: Determination of polycyclic aromatic sulfur heterocycles (PASH) in diesel fuel by high performance liquid chromatography and photodiode-array detection, *J. High. Resolut. Chromatogr.* **15**(10), 682–685 (1992)
- 5.34 D.F. Hunt, J. Shabanowitz: Determination of organosulfur compounds in hydrocarbon matrices by collision activated dissociation mass spectrometry, *Anal. Chem.* **54**(3), 574–578 (1982)
- 5.35 J.D. Payzant, T.W. Mojelsky, O.P. Strausz: Improved methods for the selective isolation of the sulfide and thiophenic classes of compounds from petroleum, *Energy Fuels* **3**(4), 449–454 (1989)
- 5.36 J.B. Green, S.K.-T. Yu, C.D. Pearson, J.W. Reynolds: Analysis of sulfur compound types in asphalt, *Energy Fuels* **7**(1), 119–126 (1993)
- 5.37 O.P. Strausz, T.W. Mojelsky, E.M. Lown, I. Kowalewski, F. Behar: Structural features of Boscan and Duri asphaltenes, *Energy Fuels* **13**(2), 228–247 (1999)
- 5.38 P. Liu, C. Xu, Q. Shi, N. Pan, Y. Zhang, S. Zhao, K.H. Chung: Characterization of sulfide compounds in petroleum: Selective oxidation followed by positive-ion electrospray Fourier transform ion cyclotron resonance mass spectrometry, *Anal. Chem.* **82**(15), 6601–6606 (2010)
- 5.39 V.V. Lobodin, P. Juyal, A.M. McKenna, R.P. Rodgers, A.G. Marshall: Lithium cationization for petroleum analysis by positive ion electrospray ionization Fourier transform ion cyclotron resonance mass spectrometry, *Energy Fuels* **28**(11), 6841–6847 (2014)
- 5.40 J.J. Liang, C.L. Gu, M.L. Kacher, C.S. Foote: Chemistry of singlet oxygen. 45. Mechanism of the photooxidation of sulfides, *J. Am. Chem. Soc.* **105**(14), 4717–4721 (1983)
- 5.41 J.D. Payzant, D.S. Montgomery, O.P. Strausz: Sulfides in petroleum, *Org. Geochem.* **9**(6), 357–369 (1986)
- 5.42 A. Charrié-Duhaut, C. Schaeffer, P. Adam, P. Manuelli, P. Scherrer, P. Albrecht: Terpenoid-derived sulfides as ultimate organic sulfur compounds in extensively desulfurized fuels, *Angew. Chem. Int. Ed.* **42**(38), 4646–4649 (2003)
- 5.43 M.B. Panda, M.B. Shaikh, P. Ghosh: Controlled oxidation of organic sulfides to sulfoxides under ambient conditions by a series of titanium isopropoxide complexes using environmentally benign H₂O₂ as an oxidant, *Dalton Trans.* **39**(9), 2428–2440 (2010)
- 5.44 T.K. Green, P. Whitley, K. Wu, W.G. Lloyd, L.Z. Gan: Structural characterization of sulfur compounds in petroleum by S-methylation and ¹³C NMR spectroscopy, *Energy Fuels* **8**(1), 244–248 (1994)
- 5.45 H. Müller, J.T. Andersson, W. Schrader: Characterization of high-molecular-weight sulfur-containing aromatics in vacuum residues using Fourier transform ion cyclotron resonance mass spectrometry, *Anal. Chem.* **77**(8), 2536–2543 (2005)
- 5.46 T. Nolte, J.T. Andersson: Capillary electrophoretic separation of polycyclic aromatic sulfur heterocycles, *Anal. Bioanal. Chem.* **395**(6), 1843–1852 (2009)
- 5.47 T. Nolte, T.N. Posch, C. Huhn, J.T. Andersson: Desulfurized fuels from Athabasca bitumen and their polycyclic aromatic sulfur heterocycles. Analysis based on capillary electrophoresis coupled with TOF MS, *Energy Fuels* **27**(1), 97–107 (2013)
- 5.48 G.K. Helmkamp, H.N. Cassey, B.A. Olsen, D.J. Pettitt: Alkylation of organic disulfides, *J. Org. Chem.* **30**(3), 933–935 (1965)
- 5.49 M. Wang, S. Zhao, K.H. Chung, C. Xu, Q. Shi: Approach for selective separation of thiophenic and sulfidic sulfur compounds from petroleum by methylation/demethylation, *Anal. Chem.* **87**(2), 1083–1088 (2015)
- 5.50 S. Schouten, D. Pavlovic, J.S. Sinninghe Damsté, J.W. de Leeuw: Nickel boride: An improved desulfurizing agent for sulphur-rich geomachromolecules in polar and asphaltene fractions, *Org. Geochem.* **20**(7), 901–909 (1993)

- 5.51 W.A. Hartgers, J.F. Lòpez, F.X.C.D. de las Heras, J.O. Grimalt: Sulphur-binding in recent environments. 1. Lipid by-products from Ni₂B desulphurization, *Org. Geochem.* **25**(5-7), 353-365 (1996)
- 5.52 M. Nagai, H. Urimoto, K. Uetake, N. Sakikawa, R.D. Gonzalez: The desulfurization of polynuclear aromatic sulfur compounds with a Raney nickel, *Bull. Chem. Soc. Jpn.* **62**(2), 557-562 (1989)
- 5.53 J.S. Sinninghe Damsté, W.I.C. Rijpstra, J.W. de Leeuw, G.W.M. Lijmbach: Molecular characterization of organically-bound sulfur in crude oils. A feasibility study for the application of Raney Ni desulfurization as a new method to characterize crude oils, *J. High Resolut. Chrom.* **17**(6), 489-500 (1994)
- 5.54 P. Schaeffer, P. Adam, E. Philippe, J.M. Trendel, J.-C. Schmid, A. Behrens, J. Connan, P. Albrecht: The wide diversity of hopanoid sulfides evidenced by the structural identification of several novel hopanoid series, *Org. Geochem.* **37**(11), 1590-1616 (2006)
- 5.55 C.J. Thompson, H.J. Coleman, R.L. Hopkins, H.T. Rall: Identification of thiaindans in crude oil by gas-liquid chromatography, desulfurization and spectral techniques, *Anal. Chem.* **38**(11), 1562-1566 (1966)
- 5.56 M. Wang, S. Zhao, X. Liu, Q. Shi: Molecular characterization of thiols in fossil fuels by Michael addition reaction derivatization and electrospray ionization Fourier transform ion cyclotron resonance mass spectrometry, *Anal. Chem.* **88**(19), 9837-9842 (2016)
- 5.57 E.A. Paukshtis, E.N. Yurchenko: Estimation of proton donor ability of surface hydroxy groups in terms of proton affinity, *React. Kinet. Catal. Lett.* **16**(2/3), 131-135 (1981)
- 5.58 E.H. Thierry: Sulphur compounds removed from a Persian petroleum by means of sulphuric acid. Part I, *J. Chem. Soc.*, 2756-2759 (1925)
- 5.59 W. Friedmann, C. Rodriguez: Sulfur Compounds from Pánzucu Gasoline II, *Petroleum Refiner.* **25**(2), 101-108 (1946)
- 5.60 L.C. Kelly, P. Rawson: *Detection and Identification of Sulfur Compounds in an Australian Jet Fuel* (Defence Science and Technology Organisation, Fishermans Bend 2010), www.dtic.mil/dtic/tr/fulltext/u2/a538148.pdf
- 5.61 C. Yin, D. Xia: A study of the distribution of sulfur compounds in gasoline produced in China. Part 3. Identification of individual sulfides and thiophenes, *Fuel* **83**(4/5), 433-441 (2004)
- 5.62 R.L. Hopkins, R.F. Kendall, C.J. Thompson, H.J. Coleman: Identification of alkyl aryl sulfides in Wasson, Texas, crude oil, *Anal. Chem.* **41**(2), 362-365 (1969)
- 5.63 R.S. Min, I.A. Savinova: Isolation of sulphur compounds of crude oil with solutions of metal chlorides in electron-donor organic solvents, *Petrol. Chem.* **37**(6), 537-545 (1997)
- 5.64 R. Emmott: Investigation of the sulphur compounds present in middle distillate SO₂-extracts, *J. Inst. Petrol.* **39**, 695-715 (1953)
- 5.65 S.F. Birch, D.T. McAllan: The separation of sulphur compounds by means of mercuric acetate, *J. Inst. Petrol.* **37**, 443-456 (1951)
- 5.66 M. Pailer, E. Simonitsch, W. Oesterreicher: Trennung schwefelhaltiger und schwefelfreier organischer Verbindungen mit Hilfe von Quecksilbersalzen, *Mh. Chem.* **96**(1), 48-68 (1965)
- 5.67 F. Challenger, S.A. Miller: The mercuration of thionaphthene, *J. Chem. Soc.* **0**, 1005-1008 (1939)
- 5.68 R.H. Brown, S. Meyerson: Cyclic sulfides in a petroleum distillate, *Ind. Eng. Chem.* **44**(11), 2620-2633 (1952)
- 5.69 M. Pailer, W. Oesterreicher, E. Simonitsch: Selektive Abtrennung von Thioäthern aus Gemischen schwefelhaltiger organischer Verbindungen mit Hilfe von Silbernitrat, *Mh. Chem.* **96**(3), 784-794 (1965)
- 5.70 M. Pailer, W. Oesterreicher, E. Simonitsch: Untersuchungen über die Geruchsträger des Seefelder Schieferöles, *Mh. Chem.* **96**(4), 1377-1406 (1965)
- 5.71 P.K. Das, A. Mukhopadhyay, S. Ray, S. Bhattacharya, S. Datta, A. De: Disorder in the structure of (λ⁶-benzo[*b*]thiophene)tricarboxylchromium(0), *Acta Cryst.* **C48**(2), 266-268 (1992)
- 5.72 P. Liu, Q. Shi, K.H. Chung, Y. Zhang, N. Pan, S. Zhao, C. Xu: Molecular characterization of sulfur compounds in Venezuela crude oil and its SARA fractions by electrospray ionization Fourier transform ion cyclotron resonance mass spectrometry, *Energy Fuels* **24**(9), 5089-5096 (2010)
- 5.73 H. Lu, Q. Shi, J. Lu, G. Sheng, P. Peng, C.S. Hsu: Petroleum sulfur biomarkers analyzed by comprehensive two-dimensional gas chromatography sulfur-specific detection and mass spectrometry, *Energy Fuels* **27**(12), 7245-7251 (2013)
- 5.74 C.H. Rochester, R.J. Terrel: Infrared study of the adsorption of sulphur compounds on silica and silica-supported nickel, *J. Chem. Soc. Faraday I* **73**, 596-608 (1977)
- 5.75 L.R. Snyder: Linear elution adsorption chromatography. XII. Functional group adsorption energies on the metal oxide adsorbents, *J. Chromatogr.* **23**, 388-402 (1966)
- 5.76 Y. Miki, M. Toba, Y. Yoshimura: Separation of sulfur compounds in straight-run naphtha, *Bull. Chem. Soc. Jpn* **80**(11), 2157-2160 (2007)
- 5.77 D. Haresnape, F.A. Fidler, R.A. Lowry: Separation of sulfur compounds by adsorption on silica gel, *Ind. Eng. Chem.* **41**(12), 2691-2697 (1949)
- 5.78 Y. Cho, J.-G. Na, N.-S. Nho, S. Kim, S. Kim: Application of saturates, aromatics, resins and asphaltenes crude oil fractionation for detailed chemical characterization of heavy crude oils by Fourier transform ion cyclotron resonance mass spectrometry equipped with atmospheric pressure photoionization, *Energy Fuels* **26**(5), 2558-2565 (2012)
- 5.79 A.A. Herod, K.D. Bartle, R. Kandiyoti: Characterization of heavy hydrocarbons by chromatographic and mass spectrometric methods: An overview, *Energy Fuels* **21**(4), 2176-2203 (2007)
- 5.80 H.J. Coleman, J.E. Dooley, D.E. Hirsch, C.J. Thompson: Compositional studies of a high-boiling 370-535 °C distillate from Prudhoe Bay, Alaska, crude

- oil, *Anal. Chem.* **45**(9), 1724–1737 (1973)
- 5.81 H. Müller, J.T. Andersson: Gel permeation chromatography of sulfur containing aromatics in vacuum residues, *Polycycl. Arom. Comp.* **24**(4/5), 299–308 (2004)
- 5.82 P.H. Arboleda, H.D. Dettman, C.A. Lucy: Hydrocarbon group type separation of gas oil resins by high performance liquid chromatography on hyper-cross-linked polystyrene stationary phase. *Energy Fuels* **29**(10), 6686–6694 (2015)
- 5.83 S.K. Panda, A.A. Al-Hajji, H. Müller, O.R. Koseoglu: Ligand exchange chromatography: A vital dimension for the reliable characterization of heterocycles in crude oils and refined products, *Anal. Bioanal. Chem.* **400**(5), 1231–1239 (2011)
- 5.84 D. Thomas, S.M. Crain, P.G. Sim, F.M. Benoit: Use of immobilized copper ion chromatography and on-line mass spectrometry with atmospheric pressure chemical ionization for the profiling of complex mixtures of polycyclic aromatic compounds, *J. Chromatogr. A* **695**, 1–9 (1995)
- 5.85 G. Dobson, W.W. Christie, B. Nikolova-Damyanova: Silver ion chromatography of lipids and fatty acids, *J. Chromatogr. B* **671**(1/2), 197–222 (1995)
- 5.86 J. Crowe, B.S. Masone, J. Ribbe: One-step purification of recombinant proteins with the 6×His tag and Ni-NTA resin, *Mol. Biotechnol.* **4**(3), 247–258 (1995)
- 5.87 T. Kaimai, A. Matsunaga: Determination of sulfur compounds in high-boiling petroleum distillates by ligand-exchange thin-layer chromatography, *Anal. Chem.* **50**(2), 268–270 (1978)
- 5.88 W.L. Orr: Separation of alkyl sulfides by liquid-liquid chromatography on stationary phases containing mercuric acetate, *Anal. Chem.* **38**(11), 1558–1562 (1966)
- 5.89 J. Chmielowiec: Organomercuric bonded phase for high performance liquid chromatographic separations of π -electron-, sulfur-, oxygen-, and nitrogen-containing compounds, *J. Chromatogr. Sci.* **19**(6), 296–307 (1981)
- 5.90 J.T. Andersson: Separations on a mercuric-acetate-substituted phenylsilica phase in normal-phase liquid chromatography, *Fresenius Z. Anal. Chem.* **326**(5), 425–433 (1987)
- 5.91 W.L. Orr: Aqueous zinc chloride as a stationary phase for liquid-liquid chromatography of organic sulfides, *Anal. Chem.* **39**(10), 1163–1164 (1967)
- 5.92 N. Gerasimova, E. Kovalenko, V. Sergun, T. Sagachenko, R. Min: Composition of heterorganic compounds in oils of middle Jurassic deposits, West Siberia, *Prog. Mining and Oilfield Chem.* **6**, 1–4 (2004), *Akadémiai Kiadó, Budapest*
- 5.93 V.P. Sergun, R.S. Min: Sulfur compounds in crude oils of the Jurassic-Paleozoic play in Western Siberia, *Petrol. Chem.* **52**(2), 68–73 (2012)
- 5.94 M. Nishioka, R.S. Tomich: Isolation of aliphatic sulfur compounds in a crude oil by a non-reactive procedure, *Fuel* **72**(7), 1007–1010 (1993)
- 5.95 J.W. Vogh, J.E. Dooley: Separation of organic sulfides from aromatic concentrates by ligand exchange chromatography, *Anal. Chem.* **47**(6), 816–821 (1975)
- 5.96 Z. Wei, P. Mankiewicz, C. Walters, K. Qian, N.T. Phan, M.E. Madincea, P.T.H. Nguyen: Natural occurrence of higher thiadiamondoids and diamondoidthiols in a deep petroleum reservoir in the Mobile Bay gas field, *Org. Geochem.* **42**(2), 121–133 (2011)
- 5.97 H. Takayanagi, O. Hatano, K. Fujimura, T. Ando: Ligand-exchange high-performance liquid chromatography of dialkyl sulfides, *Anal. Chem.* **57**(9), 1840–1846 (1988)
- 5.98 P.G. Sim, H. Perreault, F.M. Benoit, L. Ramaley, S.M. Crain, G.K. McCully, D. Thomas, R.K. Boyd: The use of copper immobilized on silica for compound class fractionation of polycyclic aromatic compounds in environmental samples, *Polycycl. Arom. Comp.* **8**(2/3), 105–116 (1996)
- 5.99 K.-D. Gundermann, H.P. Ansteeg, A. Glitsch: Ligand exchange chromatography of coal extracts and coal products, *Proc. Int. Conf. Coal Sci.* (Pittsburg Energy Technology Center, Pittsburg 1983) pp. 631–634
- 5.100 E.R. Webster, A. Park, M.B. Stratton, V.C. Park, A.M. Mosier, R.S. Shine, L. Benz: Adsorption of dibenzothiophene and fluorene on TiO₂(110) and supported Ag clusters, *Energy Fuels* **27**(11), 6575–6580 (2013)
- 5.101 J.T. Andersson: Ligand-exchange chromatography of polycyclic aromatic sulfur heterocycles on silica gel modified with silver nitrate or palladium chloride, *Fresenius Z. Anal. Chem.* **327**(1), 38 (1987)
- 5.102 M.F.M. Guadalupe, V.A. Castello Branco, J.C. Schmid: Isolation of sulfides in oils, *Org. Geochem.* **17**(3), 355–361 (1991)
- 5.103 A. Del Bianco, M. Anelli, A. Riva: Fractionation and characterization of sulfur compounds in petroleum distillates, *Fuel Sci. Technol. Int.* **10**(3), 323–334 (1992)
- 5.104 S.C. Hockett, L.L. Miller, R.A. Jacobson, R.J. Angelici: Ruthenium, rhodium, and iridium complexes of π -bound thiophene and benzo[*b*]thiophenes: Models for thiophene binding to HDS catalysts, *Organometallics* **7**(3), 686–691 (1988)
- 5.105 M. Nocun, J.T. Andersson: Argentation chromatography for the separation of polycyclic aromatic compounds according to ring number, *J. Chromatogr. A* **1219**, 47–53 (2012)
- 5.106 T.R. Bjerk, E.W. de Menezes, M.B. Pereira, E.B. Carmao, E.V. Benvenuto, C.A. Zini: Silver bonded to silica gel applied to the separation of polycyclic aromatic sulfur heterocycles in heavy gas oil. *J. Chromatogr. A* **1470**, 104–110 (2016)
- 5.107 M. Nishioka, R.M. Campbell, M.L. Lee, R.N. Castle: Isolation of sulfur heterocycles from petroleum- and coal-derived materials by ligand exchange chromatography, *Fuel* **65**(2), 270–273 (1986)
- 5.108 M. Nishioka, D.G. Whiting, R.M. Campbell, M.L. Lee: Supercritical fluid fractionation and detailed characterization of the sulfur heterocycles in a catalytically cracked petroleum vacuum residue, *Anal. Chem.* **58**(11), 2251–2255 (1986)
- 5.109 J.T. Andersson: Retention properties of a palladium chloride/silica sorbent for the liquid chromatographic separation of polycyclic aromatic sulfur

- heterocycles, *Anal. Chem.* **59**(17), 2207–2209 (1987)
- 5.110 X. Ma, K. Sakanishi, T. Isoda, I. Mochida: Determination of sulfur compounds in non-polar fraction of vacuum gas oil, *Fuel* **76**(4), 329–339 (1997)
- 5.111 J.T. Andersson, B. Schmid: Polycyclic aromatic sulfur heterocycles. IV. Determination of polycyclic aromatic compounds in a shale oil with the atomic emission detector, *J. Chromatogr. A* **693**(2), 325–338 (1995)
- 5.112 G. Michael, H. Al-Rabiah, R. Kadmi, M. Al-Mojbel: Separation of sulfur compounds from a diesel fraction by ligand exchange chromatography, *J. Liq. Chromatogr. Rel. Technol.* **30**(9/12), 1577–1601 (2007)
- 5.113 M. Nishioka: Aromatic sulfur compounds other than condensed thiophenes in fossil fuels: Enrichment and identification, *Energy Fuels* **2**(2), 214–219 (1988)
- 5.114 K. Sripada, J.T. Andersson: Liquid chromatographic properties of aromatic sulfur heterocycles on a Pd(II)-containing stationary phase for petroleum analysis, *Anal. Bioanal. Chem.* **382**, 735–741 (2005)
- 5.115 T. Schade, B. Roberz, J.T. Andersson: Polycyclic aromatic sulfur heterocycles in desulfurized diesel fuels and their separation on a novel palladium(II)-complex stationary phase, *Polycycl. Arom. Comp.* **23**, 311–320 (2002)
- 5.116 A. Japes, M. Penassa, J.T. Andersson: Analysis of recalcitrant hexahydrodibenzothiophenes in petroleum products using a simple fractionation process, *Energy Fuels* **23**(4), 2143–2148 (2009)
- 5.117 S.K. Panda, K.-J. Brockmann, T. Benter, W. Schrader: Atmospheric pressure laser ionization (APLI) coupled with Fourier transform ion cyclotron resonance mass spectrometry applied to petroleum samples analysis: Comparison with electrospray ionization and atmospheric pressure photoionization methods, *Rapid Commun. Mass Spectrom.* **25**, 2317–2326 (2011)
- 5.118 L.R. Snyder, B.E. Buell: Nitrogen and oxygen compound types in petroleum. A general separation scheme, *Anal. Chem.* **40**(8), 1295–1302 (1968)
- 5.119 M.E. Machado, E.W. de Menezes, L.P. Bregles, E.B. Caramão, E.V. Benvenutti, C.A. Zini: Palladium(II) chemically bonded to silica surface applied to the separation and identification of polycyclic aromatic sulfur heterocycles in heavy oil, *J. Sep. Sci.* **36**(9/10), 1636–1643 (2013)
- 5.120 N. Luna, L. Zelong, T. Songbai: Identification and characterization of sulfur compounds in straight-run diesel using comprehensive two-dimensional GC coupled with TOF MS, *China Petrol Process. Petrochem. Technol.* **16**(3), 10–18 (2014)
- 5.121 Q. Shi, C. Xu, S. Zhao, K.H. Chung: Characterization of heteroatoms in residue fluid catalytic cracking (RFCC) diesel by gas chromatography and mass spectrometry, *Energy Fuels* **23**(12), 6062–6069 (2009)
- 5.122 C.H. Marvin, C.-L. Lin, L.M. Allan, B.E. McCarry: Isolation and characterization of sulfur-containing polycyclic aromatic compounds (thia-arenes) from complex environmental mixtures, *Intern. J. Environ. Anal. Chem.* **77**(1), 15–28 (2000)
- 5.123 S.K. Panda, W. Schrader, J.T. Andersson: Fourier transform ion cyclotron resonance mass spectrometry in the speciation of high molecular weight sulfur heterocycles in vacuum gas oils of different boiling ranges, *Anal. Bioanal. Chem.* **392**(5), 839–848 (2008)

Asphaltenes

6. Asphaltenes

Oliver C. Mullins, Andrew E. Pomerantz, A. Ballard Andrews, Rudraksha Dutta Majumdar, Paul Hazendonk, Yosadara Ruiz-Morales, Lamia Goual, Richard N. Zare

Asphaltenes are the most enigmatic component of crude oil, and resolution of fundamentals such as asphaltene molecular weight and predominant molecular architecture has been required for the field to advance. Application of many sophisticated analytical methods to asphaltenes has recently given rise to a broad understanding. This chapter reviews many of the most important and recent studies of asphaltene molecular and nanocolloidal structures that have been codified in the Yen–Mullins model. Broad consistency across wide-ranging disciplines has been achieved, yielding robust interpretations. The result that a simple nanoscience model applies to chemically diverse asphaltenes is placed within the context of related similar findings of the gas and liquid components of crude oil. Implications are discussed for thermodynamic modeling of asphaltenes that are specifically treated in the next chapter. In addition to describing measurements of average molecular parameters, this chapter deals with the characterization of the width of certain asphaltene distributions, including molecular weight and the range of asphaltene polycyclic aromatic hydrocarbons (PAHs). The unique role of the asphaltene PAHs in intermolecular interaction is discussed within the context of structure–function relations, for example, for interfacial properties. With these advances, the concept of petroleomics, predictive petroleum science, is realized, even for the most complex fraction of petroleum.

6.1	Overview of Asphaltenes	222
6.2	Reservoir Crude Oils	223
6.3	Asphaltenes and the Yen–Mullins Model	225
6.4	Asphaltene Molecules	226
6.4.1	Time-Resolved Fluorescence Depolarization.....	226
6.4.2	Molecular Orbital Calculations and Optical Spectroscopy.....	227
6.4.3	Nuclear Magnetic Resonance (NMR) Spectroscopy.....	228
6.4.4	Pendant Drop Interfacial Studies.....	228
6.4.5	Laser Desorption, Laser Ionization Mass Spectrometry (L ² MS).....	229
6.5	Asphaltene Nanoaggregates	236
6.5.1	Surface-Assisted Laser Desorption Ionization Mass Spectrometry.....	236
6.5.2	Small Angle X-ray Scattering (SAXS) and Small Angle Neutron Scattering (SANS).....	236
6.5.3	NMR.....	237
6.5.4	High-Q Ultrasonics, DC Conductivity, and Centrifugation.....	238
6.6	Clusters	240
6.6.1	SAXS and SANS.....	240
6.6.2	Light Scattering and Flocculation Kinetics.....	240
6.6.3	DC Conductivity and Centrifugation.....	240
6.6.4	NMR Spectroscopy and Relaxometry.....	241
6.6.5	High-Resolution Transmission Electron Microscopy (HRTEM).....	242
6.7	Intermolecular Interaction of Asphaltenes	243
6.8	The Flory–Huggins–Zuo Equation of State	246
6.9	Conclusions	247
	References	247

6.1 Overview of Asphaltenes

Asphaltenes have long been the most enigmatic component of crude oil [6.1–3]. Almost every chemical and physical property of asphaltenes has been the subject of debate, spanning at least one order of magnitude except, mercifully, their elemental composition. For example, the debate regarding asphaltene molecular weight persisted for decades with published reports varying by two or more orders of magnitude [6.4]. Fortunately, this particular debate is settled. There is seemingly a paradox in asphaltene science; asphaltenes constitute a class of compounds with very broad ranges in molecular attributes such as molecular weight, size of polycyclic aromatic hydrocarbon (PAH), variability in heteroatom content, variable alkane type, etc. Nevertheless, there is substantial convergence of diverse studies resolving a wide variety of asphaltene molecular and colloidal properties. A very simple model of asphaltenes has emerged, the Yen–Mullins model, which accounts for the predominant molecular and colloidal structures of asphaltenes. The chemical polydispersity of asphaltenes is expected; the adherence of asphaltenes to a simple model is a positive surprise. Indeed, the overall uniformity of character for virgin (or chemically unaltered) crude oil asphaltenes is shown within this overarching construct. The current risk of misunderstanding asphaltenes is to overlook and underappreciate the overall simplicity of asphaltenes when investigating wide ranging attributes within this class of compounds.

To understand this paradox of tremendous polydispersity yet simplicity of asphaltenes, it is very instructive to consider the gas and liquid components of crude oil. With these compounds, there also exists huge chemical polydispersity. Advanced analytical methods such as two-dimensional gas chromatography (GC×GC) elucidate the complexity of the liquid phase of crude oils very clearly [6.5–7]. Nevertheless, many thermodynamic properties of live crude oil (containing the associated gas phase as in oil reservoirs) are very amenable to cubic equations of state, the simplest cubic equation of state (EoS) being the van der Waals EoS. The primary reason that a simple theoretical formalism is effective for a polydisperse chemical mixture, such as live crude oils, is that the corresponding dominant components, hydrocarbons, are nearly ideal. Moreover, there is largely a continuum of the chemical composition that obviates concerns of idiosyncratic behavior of specific components. The intermolecular interactions of alkanes are weak (per unit carbon) and the chemical population is a continuum; thus, simple mixing rules and *lumping* approaches work in the application of theory for this complex mixture.

For asphaltenes, the strength of interaction is certainly greater than that for alkanes. Nevertheless, the predominant intermolecular interaction for bulk asphaltenes is via dispersion forces, not hydrogen bonding and not polarity. Thus, although asphaltenes are not ideal (they do form nanocolloidal structures in oil), this intermediate strength of interaction does not preclude simple formalisms on its own. The important consideration is not whether asphaltenes are close to ideal, but whether they have moderate, simple intermolecular interactions on average, and whether they exhibit systematic behavior. In addition, asphaltenes also contain a chemical continuum similar to the alkanes. Moreover, for important applications such as understanding asphaltene gradients in reservoir fluids, simple polymer theory modified with a gravity term can be very useful. Naturally, the gravity term requires a (colloidal) size of the asphaltene particle. The asphaltenes have a predominant molecular architecture, which gives rise to a relatively well-defined nanoaggregate. In turn, with an increase in asphaltene concentration, these nanoaggregates can form clusters, again of relatively well-defined size. Consequently, asphaltenes are amenable to a simple molecular and colloidal construct, the Yen–Mullins model [6.8,9] which can then be used in a modified polymer theory, the Flory–Huggins–Zuo (FHZ) EoS [6.10–12] to treat asphaltene concentration gradients in reservoir crude oils. In addition, the Yen–Mullins model coupled with the Langmuir EoS has found significant utility associated with oil–water interfacial characterization [6.13–15]. This capability in the more demanding arena of interfacial science lends credence to the related formalisms applied to bulk crude oil.

In this chapter, simple, yet accurate descriptions of asphaltenes are emphasized, with congruence from diverse investigative studies. Consideration is given to the strength of intermolecular interactions of asphaltenes. A variety of bulk measurements associated with molecular and colloidal structures are discussed. Emphasis is placed on a variety of nuclear magnetic resonance (NMR) measurements. Laser mass spectrometry especially with unimolecular decomposition studies of asphaltenes is also considered and contrasted with bulk decomposition. A variety of other approaches from x-ray and neutron scattering to high-Q ultrasonics and direct current (DC) conductivity are also considered. Results for petroleum asphaltenes are compared with coal-derived asphaltenes as a means to understand structure–function relations in both types of asphaltenes. Important thermodynamic implications

associated with these simplifying ideas of asphaltenes are reviewed especially within the context of novel

applications associated with oilfield reservoir evaluation.

6.2 Reservoir Crude Oils

Reservoir crude oils consist of dissolved gases, liquids and dissolved solids, called as asphaltenes (Fig. 6.1). Although many carbonaceous materials contain an asphaltene fraction, it is for crude oils that asphaltenes are fundamental and key. Asphaltenes are defined by a chemical operational definition because (1) there had been such confusion about their chemical properties and (2) they remain a polydisperse class with many constituents. Consequently, any definition of asphaltenes delineating a chemical identity was precluded. Asphaltenes are defined by their solubility characteristics; typically, they are defined as the fraction of crude oil (or carbonaceous material) that is toluene soluble and *n*-heptane insoluble. This definition might seem arbitrary but it is not; this solubility fraction captures the heaviest, aromatic component of crude oil and largely captures the fraction of crude oil that is self-assembled in nanocolloidal particles under both reservoir and laboratory conditions. Also, this definition largely captures the fraction of crude oil that is (nonwax) solid.

It is instructive to consider the liquid and gas fractions of crude oil in order to guide thinking about asphaltenes. Analytic methods for gas analysis are well developed and accurate. For most gas phase components, gas chromatography (GC) yields reliable and unambiguous analyses [6.5, 16]. For reactive gases such as H₂S, Hg, and, to a lesser extent, CO₂, preservation of the sample from acquisition in the borehole to well site or laboratory represents a major challenge. In situ downhole fluid analysis in oil wells is a well-developed discipline [6.17] and is being extended to include labile crude oil components. The gas phase components of crude oils can consist of both hydrocarbon gases and nonhydrocarbon gases, including CO₂, H₂S, N₂ and to

a much lesser extent, Hg, and He (predominantly from α decay). The ratio of methane to other hydrocarbon gases depends explicitly on the origin of these gases, whether thermogenic or biogenic.

The liquid fraction of crude oils typically contains a very large number of components. Although methods such as gas chromatography-mass spectrometry (GC-MS), in principle, can be used to identify specific components unambiguously [6.6], the very large number of liquid components in crude oils precludes indiscriminant GC-MS application. For specific purposes, such as biomarker analysis, GC-MS has been very useful [6.18–20]. Comprehensive two-dimensional gas chromatography (GC×GC) is a powerful analytical tool for crude oil analysis [6.7]. In this method, two GC columns are used sequentially that perform separation based on different chemical attributes, such as volatility for the first column and polarizability for the second column. Each analyte in the sample is then characterized by two retention times, thereby, greatly expanding resolution. Although there are still many overlapping peaks in GC×GC, different chemical classes are much better resolved than in traditional GC and, in many cases, GC×GC achieves individual chemical resolution. Use of GC×GC-MS enables molecular structural characterization of many of the peaks in the GC×GC chromatogram. Figure 6.2 shows a typical GC×GC for a complex crude oil [6.21]. GC×GC provides much chemical specificity for crude oil composition of the liquid fraction of crude oil. The vision of petroleomics is to establish predictive petroleum science based on the composition of crude oil [6.1, 22]. This goal requires chemical resolution of the dominant components of any crude oil; GC×GC is an integral step in this process. As asphaltenes do not traverse GC columns, they cannot be analyzed by this method.

Figure 6.2 has been used to analyze the complex processes that have acted to give rise to this Colombian crude oil. The Llanos basin, east of the Andes Cordillera in Colombia, is known to have one of the more active aquifers on the planet. For certain fields in the Llanos basin, the putative claim is made that *production goes up when it rains*. The same conditions that form the Amazon river, the largest on Earth in terms of volumetric flow, also produce a large flux of water through aquifers adjacent to oil reservoirs in

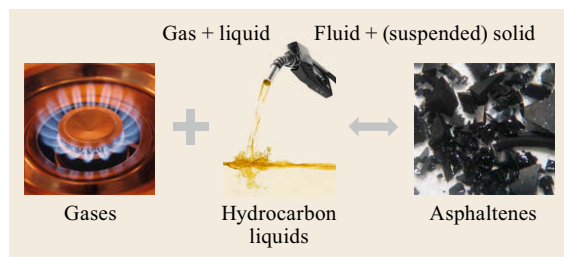


Fig. 6.1 Reservoir crude oils generally consist of dissolved gases, liquids, and dissolved (or nanocolloidally suspended) solids, called asphaltenes

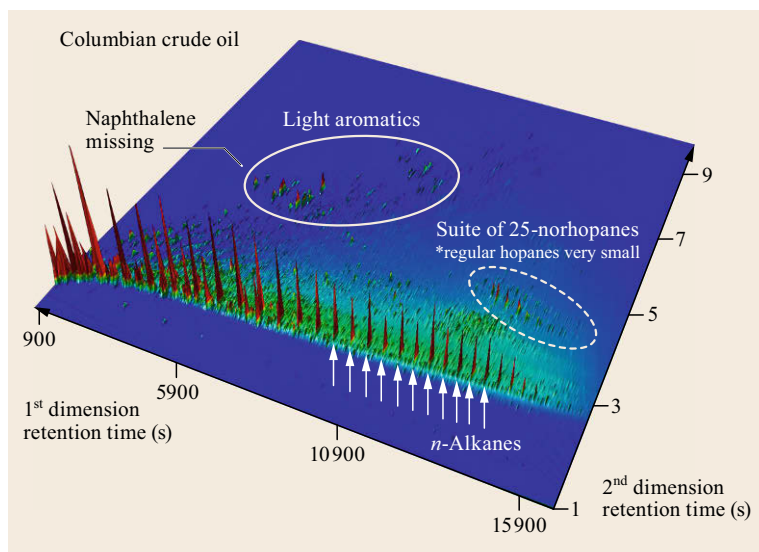


Fig. 6.2 GC×GC chromatogram of a Colombia crude oil. This chemical specificity enables identification of the complex processes that have acted on this reservoir crude oil including water washing (the lack of naphthalene), biodegradation (dominance of 25-norhopanes in the biomarker region), and multiple charging (presence of *n*-alkanes along with 25-norhopanes). Reprinted with permission from [6.21]. Copyright 2015 American Chemical Society

the Llanos basin. Figure 6.2 shows depletion of naphthalene as well as other water soluble components from this oil, which has been ascribed to water washing [6.21]. In addition, the dominance of 25-norhopanes over the hopanes in this oil shows that the oil has undergone extensive biodegradation, a level of 6 on the Peters–Moldowan scale [6.19, 20]. Moreover, the strong presence of *n*-alkanes in Fig. 6.2 shows that a large fraction of this oil is not biodegraded and is attributed to a process of reservoir paleopasteurization in the upper Miocene epoch, with a subsequent second crude oil charge into the reservoir. Moreover, a petroleum system analysis of the Llanos basin has confirmed all essential elements of the GC×GC analysis. Indeed, the vision of petroleomics is being realized in the analysis relying on GC×GC with specific geochemical processes being related to specific chemical composition of the crude oil.

Another significant advancement in petroleum science has been the application of high-resolution Fourier transform, ion cyclotron resonance mass spectrometry (FT-ICR MS) for its ability to resolve tens of thousands of components of unique elemental composition in typical crude oils [6.22, 23]. For example, long standing uncertainties about porphyrins in crude oils have been addressed in a very direct manner using these methods [6.24, 25]. In addition, examination of interfacially active components in complex carbonaceous materials can be isolated and characterized by FT-ICR MS [6.26]. Organic acids are particularly well suited to such analysis [6.27]. The combination of GC×GC with FT-ICR MS and downhole fluid analysis has proved very valuable in unraveling complexities of multiple charging, biodegradation, and reservoir connectivity [6.28].

It is also very important to perform thermodynamic analysis of reservoir crude oils for many fundamental purposes. It is necessary to maintain the pressure in the oil reservoir above the saturation pressure. If gas breakout occurs during oil production from the subsurface formation, then gas flows preferentially leaving the valuable liquids behind. The loss of gas removes a primary mechanism of pressure support in oil production. In addition, interfacial energy impedes a two-phase flow in porous media, thereby, reducing fluid mobilities. Thermodynamic modeling of the saturation pressure is required to understand pressure reduction limits, and thus oil (and cash) flow limits. In addition, understanding spatial variations of the gas–oil ratio (GOR) determines corresponding temporal GOR variations in production. There are major differences, particularly in cost, for gas versus liquid handling in oilfield facilities, hence accurate GOR analyses are required. There are many more issues that are addressed by thermodynamic modeling of crude oil [6.29].

Modified van der Waals EoS, the so-called cubic EoSs, have been very effective for modeling crude oils [6.29, 30] and are used in virtually every reservoir simulator that employs compositional analysis [6.31]. The Peng–Robinson EoS remains one of the most popular cubic EoSs to be used for crude oils. Requisite pseudo-critical constants can be obtained by simple mixing rules based on even a rough compositional analysis for crude oils. The long-term application of the cubic EoS to petroleum has led to acceptance of the seemingly implausible result that such a simple formalism works so well for gas–liquid equilibria of crude oils with their tens of thousands of components (or more).

For example, the cubic EoS is not well suited to handle simple mixtures of H_2O , CO_2 , and H_2S , yet can handle crude oil. Why? A significant part of the explanation is that saturated hydrocarbons and to a lesser extent aromatic hydrocarbons are nearly ideal, with very low energies of intermolecular interactions. Ideal solutions where simple mixing rules can apply are considered to consist of noninteracting components. Of course, to be a liquid, molecules must interact, but this minor discrepancy is overlooked.

The key point is that there is utility performing both the detailed compositional analysis of the gas and liquid components of crude oil and the simple thermodynamic modeling of these same components. The large number of chemical constituents does not preclude utility of either approach. The fact that both investigative di-

rections are successful makes petroleomics a reality. Nevertheless, for crude oil, it is required to incorporate asphaltenes into both types of analyses as best as possible. To treat asphaltenes in reservoir crude oils within a thermodynamic context, gravity is the key. Thus, a simple molecular and nanocolloidal description for asphaltenes is required. Projection of such a model to interfacial science is of interest. In addition, for a variety of purposes, it is important to characterize the specifics of asphaltene chemistry in a detailed manner. Phenomenological measurements such as surface tension might have chemical dependencies that are difficult to elucidate by the phenomenological method alone. Combining surface tension measurements with a detailed chemical characterization may lead to deep understanding.

6.3 Asphaltenes and the Yen–Mullins Model

Many characterization techniques have been applied to asphaltenes, and a clear picture of predominant structures has evolved. The predominant molecular and stable nanocolloidal structures of asphaltenes have been codified in the Yen–Mullins model and are shown in Fig. 6.3. In essence, this model is meant to represent the centroid of different species. Nevertheless, for some applications, the width to the distributions of these species is also very important. This model has been subjected to increasingly stringent tests in an expanding variety of ways, and the utility of the model has been established. Herein, we will review both key and recent results associated with this model of Fig. 6.3. In particular, a series of laser desorption, laser ionization mass spectral (L^2MS) studies have tested fundamental aspects of this model with strongly

supportive results [6.32–35]. In addition, recent NMR studies strongly support this model as well [6.36–39]. Combined studies of neutron and x-ray scattering also confirm this model [6.40–42]. Molecular orbital calculations combined with optical spectroscopy provide a clear picture of a range of sizes of asphaltene PAHs [6.43, 44]. Various other results such as combined TRFD, IR and NMR studies [6.45] and combined DC conductivity and centrifugation studies corroborate the Yen–Mullins model [6.46].

Each of these structures in Fig. 6.3 has been observed in reservoir crude oils; thus, each is stable for geologic time [6.12]. These structures have been employed with the Flory–Huggins–Zuo (FHZ) EoS to model asphaltene gradients in reservoirs. This novel approach of exploring the extent of thermodynamic

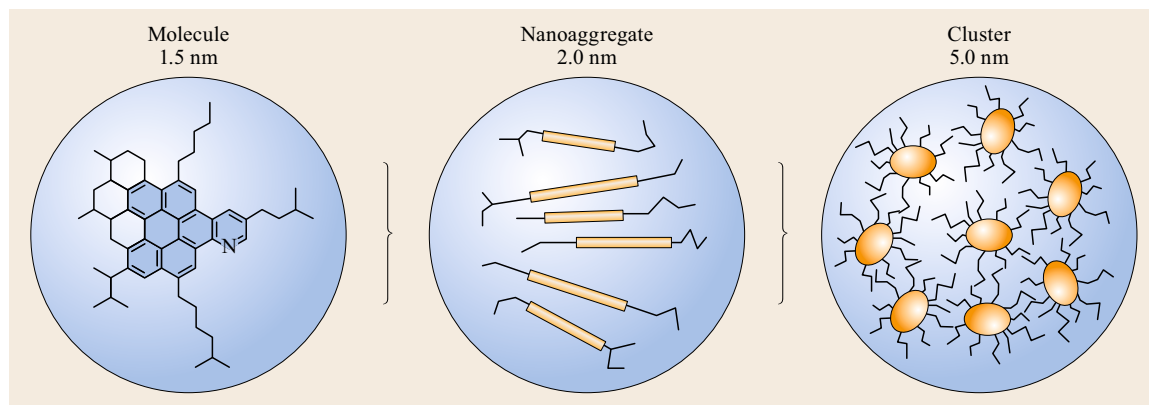


Fig. 6.3 The Yen–Mullins model depicts the dominant molecular and stable nanocolloidal species of asphaltenes [6.8, 9]. A molecule (*left*) with a single PAH with seven fused aromatic rings is shown. The nanoaggregate (*center*) consists of a disordered stack of approximately six molecules. The cluster (*right*) consists of approximately eight nanoaggregates

equilibrium of asphaltenes in reservoir fluids has been used to address many issues in production such as flow connectivity. In addition, the molecular and nanocolloidal species of asphaltenes are consistent with application of the Langmuir EoS applied to oil–water interfacial measurements, which will also be discussed below. The energetics of asphaltene intermolecular interactions is of considerable interest. This topic will also be addressed from several viewpoints. The importance of PAH polarizability is evident in many ways and plays a significant role in the applicability of the FHZ EoS.

In addition to bulk measurements and to centroid structures, there is great interest in specific molec-

ular structures that comprise asphaltenes. Unlike the liquid phase components, asphaltenes are not readily amenable to separation of individual molecular components, which of course precludes characterization of individual molecular structures. For example, ultrahigh resolution mass spectrometry applied to asphaltenes has been limited by the inability to break up asphaltene nanoaggregates in these studies [6.47]. In contrast, other mass spectral techniques such as L^2MS are readily able to disaggregate asphaltenes [6.35] but have only been employed in low resolution modes to date. Further improvement of various methods will be required to probe the very large number of individual chemical species of asphaltenes.

6.4 Asphaltene Molecules

The Yen–Mullins model starts with the predominant molecular structure. For many years, there had been no consensus regarding many fundamental properties of asphaltene molecular structure. For example, even such a basic property such as asphaltene molecular weight was unresolved, with disparities spanning several orders of magnitude [6.4]. The tendency of asphaltenes to aggregate negatively impacts a variety of experiments including mass spectrometry and colligative techniques such as vapor pressure osmometry (VPO). Today, these issues are understood and are addressed in the section below treating asphaltene nanoaggregates.

6.4.1 Time-Resolved Fluorescence Depolarization

Crucial early experiments that set the stage for resolution of many asphaltene molecular properties including molecular weight were the first experiments to determine asphaltene molecular diffusion constants, here, rotational diffusion, using time-resolved fluorescence depolarization (TRFD) [6.48–51]. Figure 6.4 shows the TRFD results on various asphaltene samples.

TRFD measurements determine the rotational correlation time of molecular species in dilute solution by measuring the rate of rotational depolarization. This is accomplished with an initial exciting laser pulse with laboratory z -polarization. The extent of polarization of fluorescence emission is measured versus time giving the rate of ensemble depolarization. The rotational correlation time is proportional to molecular volume, and thus molecular weight.

TRFD results show that virgin petroleum asphaltenes diffuse rapidly; thus, the molecules are fairly small. Comparison with known model compounds

shows that asphaltenes have a mean molecular weight of ≈ 750 Da. Asphaltenes extracted from vacuum distillation resid are smaller, as expected, in that their alkanes are cracked off reducing molecular weight. The larger PAHs that are formed in the refining process are part of the coke fraction, not the soluble asphaltenes. Coal asphaltenes are far smaller and are at the limit of TRFD correlation time measurements. Coal-derived asphaltenes have a very small alkane fraction and slightly smaller PAHs, so are roughly half-size compared to virgin crude oil asphaltenes [6.33, 48].

We use the term asphaltene to refer to virgin crude oil asphaltenes unless otherwise specified. The large range ($\approx 10\times$) of asphaltene correlation times reflects the expected large range of asphaltene molecular weight. However, the strong dependence of rotational correlation time on fluorescence emission wavelength is most instructive regarding asphaltene molecular architecture. The size of a PAH (i.e., the number of fused aromatic rings (FAR)) is related to its emission wavelength. This well-known result follows from the simple quantum description of a *particle-in-a-box*. Larger PAHs have longer wavelength π -electron orbitals, and thus lower energy transitions. For example, benzene is colorless with π -transitions only in the UV region, whereas graphite is black with π -transitions extending into the near-infrared (NIR) region [6.43, 44, 52]. Thus, the strong dependence of rotational correlation time versus fluorescence emission wavelength indicates that small asphaltene PAHs rotate $10\times$ faster than large asphaltene PAHs. This means they are not cross-linked. Thus, there is predominantly one asphaltene PAH per molecule. Exhaustive molecular orbital calculations were performed to check this logic [6.44].

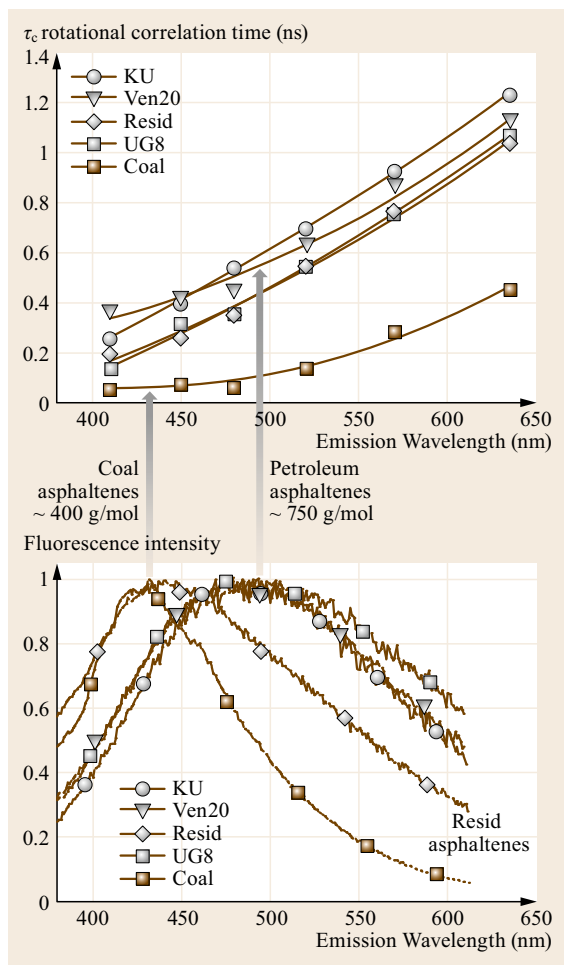


Fig. 6.4 Molecular diffusion measurements of asphaltenes by TRFD (after [6.48]). The rapid rotational diffusion indicates that petroleum asphaltenes are relatively small molecules (\leq kDa). The $10\times$ faster rotation of smaller, blue fluorescing PAHs versus larger, red fluorescing fluorophores indicates that different PAHs are not cross-linked; there is predominantly one PAH per asphaltene molecule. Centroids of the distributions of coal-derived asphaltenes and petroleum asphaltenes are indicated in the figure corresponding to the maxima in fluorescence emission spectra

6.4.2 Molecular Orbital Calculations and Optical Spectroscopy

In addition to size, PAH π -transitions are also dependent on the extent of aromatic sextet carbon versus isolated double bond carbon. Carbon x-ray Raman studies of asphaltenes show that they have more of the more stable sextet carbon in their PAHs [6.53]. Exhaustive molecular orbital calculations of PAHs confirm

Table 6.1 Number of compounds with differing numbers of FAR (fused aromatic rings) used in the absorption spectrum of Fig. 6.5. The weighting used for each FAR class is also given

FARs in PAH	Number of compounds used	Weighting in distribution
3FAR	2	0.20
4FAR	5	0.40
5FAR	28	0.60
6FAR	27	0.80
7FAR	41	1.00
8FAR	39	0.80
9FAR	71	0.60
10FAR	46	0.40
11FAR	41	0.20
12FAR	34	0.18
13FAR	61	0.16
14FAR	64	0.14
15FAR	64	0.12

that a distribution of PAHs spanning 3–15 fused rings with 7 fused rings most probable, largely reproduces the measured optical spectrum of asphaltenes as shown in Fig. 6.5. All π -electrons have unit oscillator strength, hence all PAHs appear in the absorption spectrum. For example, the proposed PAH distributions that have a preponderance of small ring systems would have too much absorption in the UV and not enough in the visible and NIR. Table 6.1 shows the PAH profile for the 523 PAHs used for the theoretical prediction in Fig. 6.5 [6.44]. The use of 523 PAHs acknowledges that there is significant chemical polydispersity in asphaltenes; nevertheless, it remains useful to identify centroids of distributions as shown in the Yen–Mullins model of Fig. 6.3. Interestingly, Table 6.1 shows that rather large PAHs had to be used to account for the significant NIR absorption of asphaltenes.

The first measurements of triplet state spectroscopy of asphaltenes in pump-probe experiments are consistent with the singlet state spectroscopy [6.54]. The chromophore population of asphaltenes obtained from spectral analysis indicates that asphaltenes have a preponderance of large PAHs.

There is a stringent consistency check with the TRFD predictions as confirmed by molecular orbital calculations. The TRFD results indicate that the mean molecular weight is 750 Da, and the PAH centroid has 7 fused rings. Knowing that asphaltenes are 50% aromatic carbon and 50% alkane carbon, the question arises whether these numbers are consistent. Coronene, a 7 fused ring PAH, has 24 carbons. This gives 48 carbons in total for the proposed molecule. Add \approx 58 hydrogens and 1 sulfur atom and obtains a molecular weight of 666 Da. A less symmetric distribution of 7

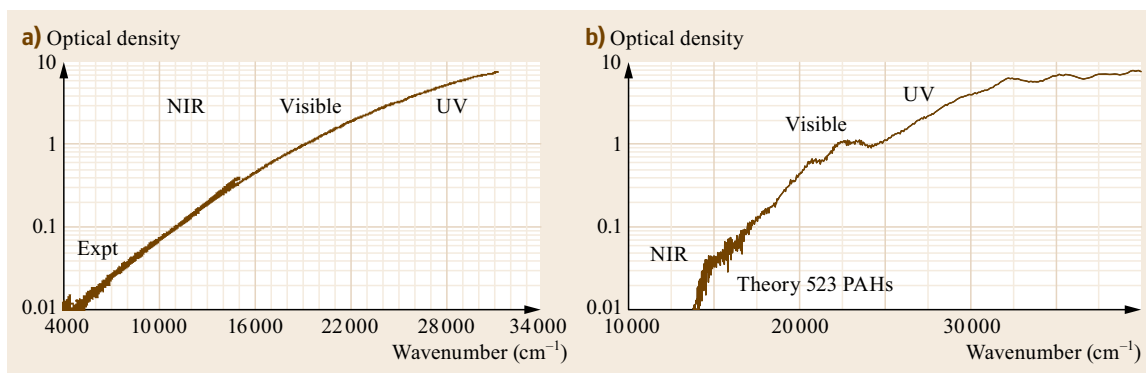


Fig. 6.5a,b Comparison of the measured and predicted absorption spectra of asphaltenes. The theoretical curve (right) utilized the sum of calculated spectra for 523 PAHs with a distribution shown in Table 6.1. A large distribution of PAHs including large PAHs is required to account for the absorption spectrum of asphaltenes. Reprinted (adapted) with permission from [6.44]. Copyright 2009 American Chemical Society

fused rings gives a larger number of carbon atoms. This is close to the measured mean of 750 Da, hence the TRFD results are internally self-consistent.

6.4.3 Nuclear Magnetic Resonance (NMR) Spectroscopy

Recent NMR experiments exploit both ^1H -NMR relaxometry as well as sophisticated 2D-HSQC (heteroatom single quantum coherence) NMR spectroscopy [6.38]. This work extends the previous NMR findings that are consistent with 6 fused ring PAHs as the mean for asphaltenes [6.36, 37, 55]. The latest NMR work provides a wealth of information about asphaltenes, not just on molecular architecture, but also regarding aggregate structures as well [6.38, 39]. A proposed molecule from this NMR work is shown that is consistent with the molecule shown in Fig. 6.3.

In Fig. 6.6, several fused alicyclic rings are shown in order to account for the measured large aromatic-aliphatic heteronuclear correlations [6.38]. Fused alicyclic groups were initially proposed for asphaltenes based on active asphaltene hydrogen similar to that to tetralin [6.56]. Again, similar conclusions from very different methods arrive at similar conclusions and reinforce each other. Unlike TRFD measurements, all of the asphaltene sample is interrogated in NMR studies.

6.4.4 Pendant Drop Interfacial Studies

Studies of the interface between asphaltene containing solutions and water have recently shown that a universal curve is obtained for surface tension versus (relative) asphaltene coverage at the interface, and is independent of surface aging time (between 0.5

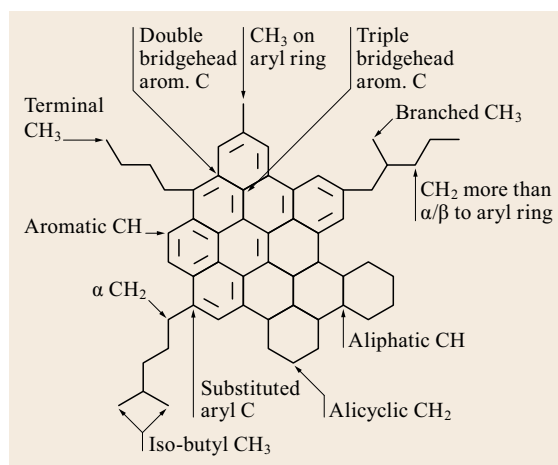


Fig. 6.6 A proposed *average* asphaltene molecule that satisfies many results from ^1H and ^{13}C NMR (after [6.38]). This structure is very similar to that in Fig. 6.3 showing consistency across many methods

and 12 h), asphaltene solution concentration, and viscosity (Fig. 6.7) [6.13, 14]. In addition, the elastic and loss moduli curves of the interface also exhibit universal curves dependent only on asphaltene surface coverage [6.13, 14]. The existence of universal curves lends credence to the analysis.

The Langmuir EoS (6.1) gives the surface tension $\gamma(\Gamma)$ at a particular surface coverage of asphaltenes Γ in terms of the clean surface interfacial tension γ_0 , kT (Boltzmann's constant k and temperature T), and the maximum surface coverage of asphaltenes Γ_∞ (in molecules per unit area)

$$\gamma(\Gamma) = \gamma_0 + kT\Gamma_\infty \ln \left(1 - \frac{\Gamma}{\Gamma_\infty} \right). \quad (6.1)$$

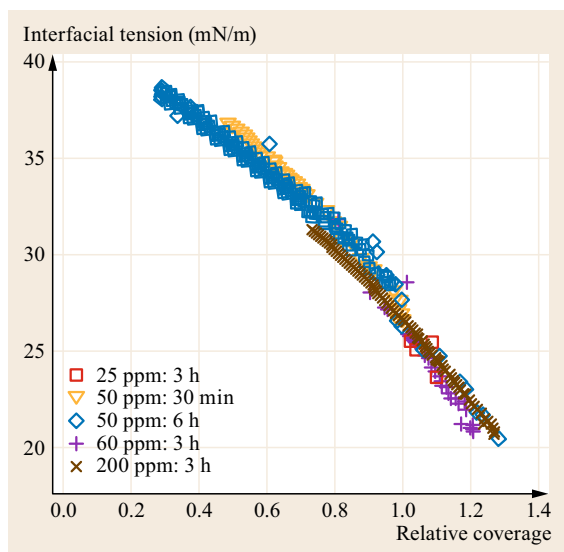


Fig. 6.7 Interfacial tension of oil–water versus (relative) coverage of the surface by asphaltenes (after [6.13, 14]). A universal curve is obtained that is given by the Langmuir EoS

Analysis of the universal curve in Fig. 6.7 with the Langmuir EoS gives an asphaltene molecular contact area of 6.2 ring PAH [6.13, 14]. This presumes an orientation of the asphaltene PAH in-plane and the alkanes out-of-plane; exactly this asphaltene molecular orientation was shown by sum frequency generation

experiments on Langmuir–Blodgett films [6.58]. In addition, recent pendant drop experiments on coal-derived asphaltenes, petroleum asphaltenes, and alkylhexabenzocoronene gave expected molecular contact areas over a range of a factor of 3, strongly validating these analyses [6.59]. These results are in excellent agreement with the molecular structures shown in Figs. 6.3 and 6.6. Moreover, these experiments show that the asphaltene nanoaggregate does not load onto the surface as expected due to its peripheral alkanes [6.13, 14].

6.4.5 Laser Desorption, Laser Ionization Mass Spectrometry (L^2MS)

A significant concern is that the TRFD studies are sensitive only to fluorescent asphaltene molecules. It is possible that fluorescent asphaltene molecules differ in molecular weight or architecture from nonfluorescent asphaltene molecules. What is needed is a method that can analyze molecular weight and molecular architecture and that is sensitive to the entire asphaltene sample. The method laser desorption, laser ionization mass spectrometry (L^2MS) satisfies all of these demanding constraints.

In L^2MS , an IR laser pulse desorbs asphaltenes from a surface with heating rates of 10^8 deg/s, creating a neutral plume of asphaltene molecules in the vacuum. A UV laser pulse then ionizes asphaltene molecules in this plume. An electric field is used to determine mass by time of flight. Figure 6.8 shows

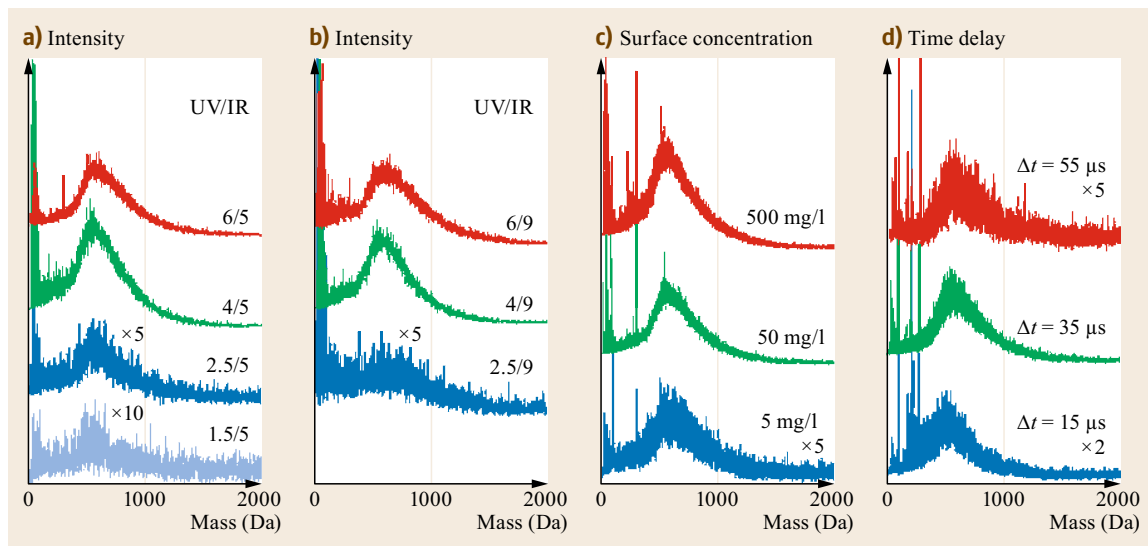


Fig. 6.8 L^2MS molecular weight determination for UG8 asphaltene (after [6.57]). The L^2MS results for asphaltenes are independent of UV laser power, IR laser power, surface concentration of asphaltene, and time delay for the ionization pulse, proving accuracy of this method. L^2MS and TRFD find comparable asphaltene molecular weights. Reprinted with permission from [6.57]. Copyright 2009 American Chemical Society

that L²MS molecular weight determination is independent of key experimental parameters, such as laser power, surface concentration of asphaltenes, and time delay of the ionization pulse [6.57]. Other methods such as laser desorption ionization (LDI) have shown acute sensitivity of molecular weight determination on laser power and surface concentration of asphaltenes in part associated with aggregation in the charged plume of asphaltenes. Carefully controlling for these factors does allow accurate asphaltene molecular weight determination with LDI [6.60]. The insensitivity of L²MS results to these experimental parameters establishes the accuracy of this method for molecular weight determination [6.35, 61].

In addition to molecular weight determination, L²MS has been crucial for the characterization of asphaltene molecular architecture [6.32]. There has been considerable debate regarding the number of isolated PAHs (not conjugated) in asphaltenes. When very high molecular weights were proposed for asphaltenes, the proposed number of PAHs was large [6.62]. Such a molecule has been termed the archipelago model. TRFD studies indicate that the predominant asphaltene molecular architecture has only one (maybe two) PAHs; this has been termed the island model [6.45, 48–50]. As the molecular weight of asphaltenes is now known to be rather small, the term archipelago is still even used for molecules containing two PAHs. Indeed, as noted in the original TRFD papers, a lesser fraction of molecules with two PAHs along with a dominant fraction of molecules with a single PAH is consistent with the TRFD data [6.48]. Some bulk decomposition studies have supported the presence of archipelago

molecules (possibly with two PAHs) [6.63]. Nevertheless, caution is advised as these decomposition methods are known to produce archipelago compounds [6.64].

Other mass spectral methods have yielded similar conclusion regarding asphaltene molecular weight and architecture. Molecular weights on a broad range of samples have been obtained by laser-induced acoustic desorption mass spectrometry (LIAD-MS) [6.65]. Fragmentation studies of asphaltenes from electron impact and collisional activated dissociation (CAD) indicated that island architecture was consistent with the results [6.66, 67].

The L²MS results in Fig. 6.9 indicate that, by comparing molecular stability of asphaltenes and model compounds, island molecular architecture dominates asphaltenes. This is consistent with the nondestructive TRFD studies. Of course, some smaller fraction of molecules with two PAHs is not inconsistent with this data. The L²MS decomposition study differs from bulk decomposition; the L²MS decomposition must be unimolecular, precluding the possibility of bimolecular reaction forming archipelago compounds. The L²MS results are particularly compelling in that the L²MS methods analyze all of the asphaltene sample with relatively uniform sensitivity for different molecular types [6.35].

Figure 6.10 shows that all of the asphaltene sample is placed in the vapor phase. No asphaltene remains on the sample plate where the IR laser has desorbed the sample (a line running from upper left to lower right in the figure) [6.35]. In addition, in the L²MS experiments, single photon ionization (SPI) with a single high energy UV photon accesses all molecules with a lower ioniza-

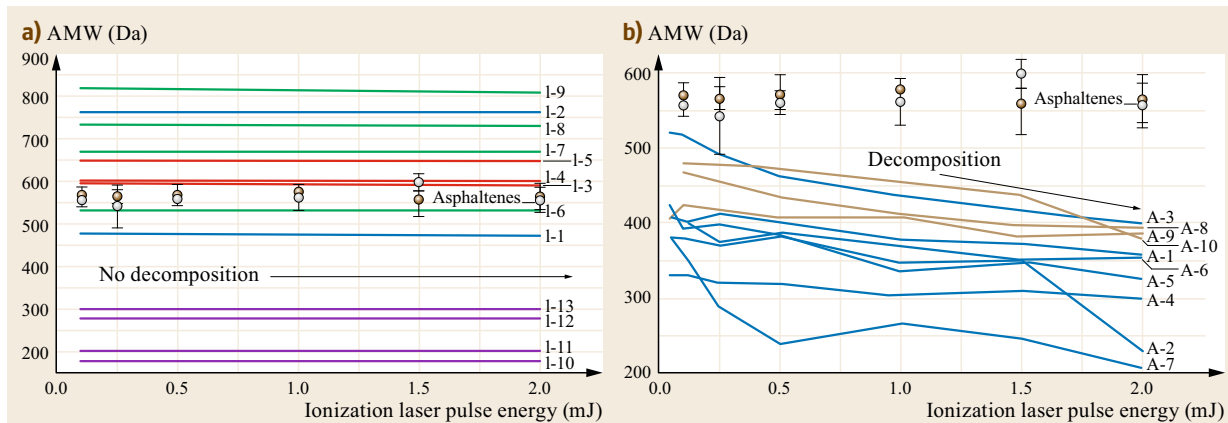


Fig. 6.9a,b L²MS average molecular weight (AMW) versus ionization laser pulse energy (after [6.32]). Fragmentation corresponds to a reduction of AMW. (a) All island model compounds measured and asphaltenes are resistant to decomposition at these laser energies. (b) All archipelago model compounds measured are labile and undergo decomposition at higher laser energies (AMW decreases with laser pulse energy). This indicates asphaltenes are predominantly island architecture. Tables 6.2 and 6.3 show the model compound structures (after [6.32])

Table 6.2 The model compounds for island and archipelago structures used for L²MS decomposition studies (after [6.68]). The greater stability of the island compounds and asphaltenes in L²MS indicates that asphaltenes are predominantly island structures. The asphaltene stability is consistent with these molecules being in oil reservoirs for geologic time

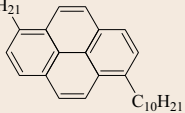
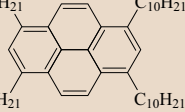
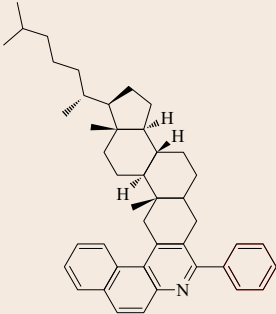
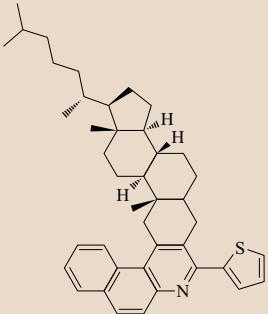
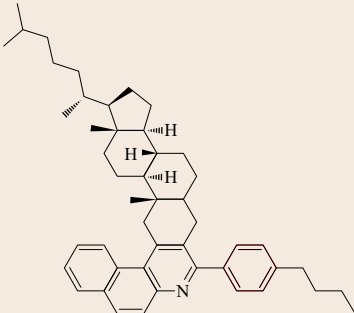
Island model compounds Name	Structure	MVV (g/mol)
1,6-Didecyl pyrene (I-1)	<chem>C10H21</chem>  <chem>C10H21</chem>	482
1,3,6,8-Tetradecyl pyrene (I-2)	<chem>C10H21</chem>  <chem>C10H21</chem>	762
MCR-cholestanone-phenyl (I-3)		597
MCR-cholestanone-thiophen (I-4)		603
MCR-cholestanone-phenyl- <i>n</i> -butyl (I-5)		653

Table 6.2 (continued)

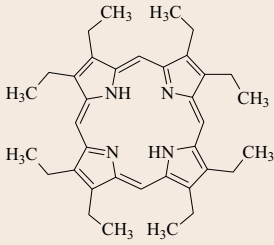
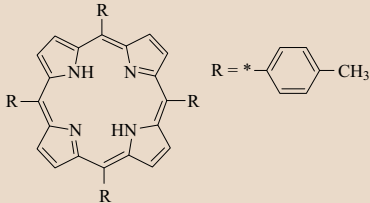
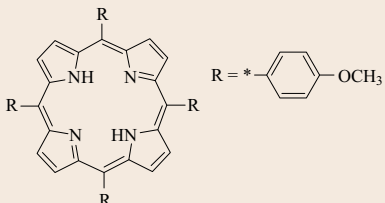
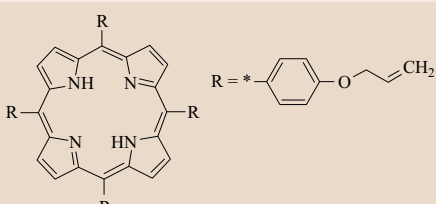
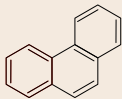

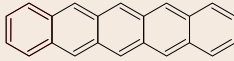

Island model compounds		
2,3,7,8,12,13,17,18-Octaethyl-21 <i>H</i> ,23 <i>H</i> -porphine (I-6)		534
5,10,15,20-Tetra- <i>p</i> -tolyl-21 <i>H</i> ,23 <i>H</i> -porphine (I-7)		670
5,10,15,20-Tetrakis(4-methoxyphenyl)21 <i>H</i> ,23 <i>H</i> -porphine (I-8)		734
5,10,15,20-Tetrakis[4-(allyloxy)phenyl]-21 <i>H</i> ,23 <i>H</i> -porphine (I-9)		839
Phenanthrene (I-10)		178
Pyrene (I-11)		202
Pentacene (I-12)		278
Coronene (I-13)		300

Table 6.3 The model compounds for island and archipelago structures used for L²MS decomposition studies (after [6.68]). The greater stability of the island compounds and asphaltenes in L²MS indicates that asphaltenes are predominantly island structures. The asphaltene stability is consistent with these molecules being in oil reservoirs for geologic time

Archipelago model compounds Name	Structure	MVV (g/mol)
1,4-Dipyren-1-yl-butane (A-1)		460
1,4-Bis(2-pyren-1-yl-ethyl)-benzene (A-2)		534
2,6-Bis(2-pyren-1-yl-ethyl)-pyridine (A-3)		535
2,5-Bis(2-pyren-1-yl-ethyl)-thiophene (A-4)		540
4,4'-Bis(2-pyren-1-yl-ethyl)-2,2'-bipyridine (A-5)		612
5,5'-Bis(2-pyren-1-yl-ethyl)-2,2'-bithiophene (A-6)		622
2,7-Bis(2-pyren-1-yl-ethyl)-9,9-diethyl-9H-fluorene (A-7)		678
3,5-Bis(2-phenanthr-9-yl-ethyl)-pyridine (A-8)		487

Table 6.3 (continued)

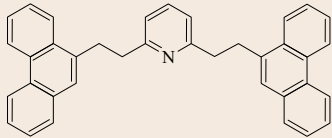
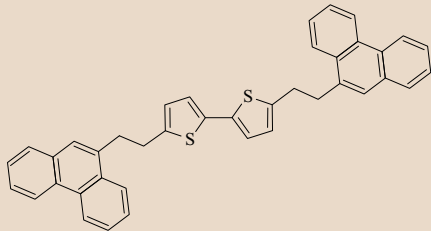
Archipelago model compounds		
2,6-Bis(2-phenanthr-9-yl-ethyl)-pyridine (A-9)		487
5,5'-Bis(2-phenanthr-9-yl-ethyl)-2,2'-bithiophene (A-10)		574



Fig. 6.10 All asphaltene sample is volatilized in L²MS experiments. The desorption IR laser track going from *upper left* to *lower right* establishes that bare metal remains after desorption. Reprinted from [6.35], Copyright 2015 American Chemical Society

tion potential than the photon energy. In the case of the L²MS SPI experiments, this includes all PAHs with two or more rings, thus, including virtually all the asphaltene fraction (Fig. 6.5 and Table 6.1). L²MS with SPI was shown to be relatively uniform in ionization and detection cross section using mixtures of model compounds [6.35]. These results compared favorably with L²MS results using resonance enhanced, multiphoton ionization (REMPI) [6.35].

Another concern is asphaltene aggregation. As mentioned previously, aggregation of asphaltenes greatly hinders application of specific molecular weight mea-

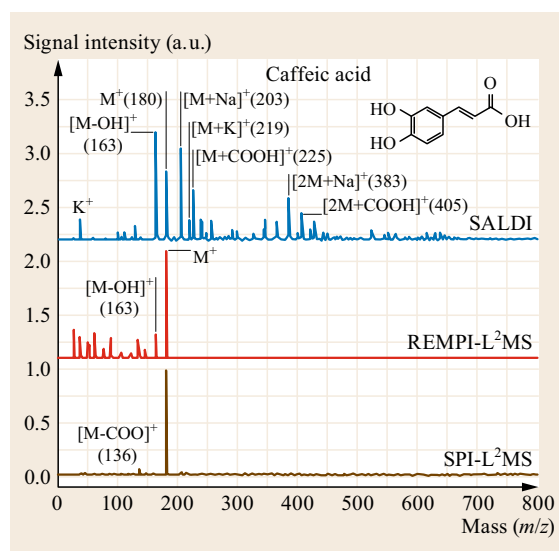


Fig. 6.11 Mass spectra of caffeic acid using several laser based techniques (after [6.61]). All techniques show the parent ion peak associated with caffeic acid. SALDI shows considerable aggregation. REMPI-L²MS shows no aggregation, but does show some fragmentation. SPI-L²MS shows no aggregation and almost no fragmentation (after [6.61])

surements such as VPO and LDI (unless care was taken to use low plasma concentrations) [6.4, 60]. A recent report noted that some mass spectra techniques are not able to disaggregate the asphaltene nanoaggregates, thereby limiting corresponding applicability to a smaller mass fraction of asphaltenes [6.47]. This might be considering a bit surprising because the strength of binding in the asphaltene nanoaggregate is only moderate (as discussed below). For example, asphaltene nanoaggregates fall apart in toluene at 10⁻⁴

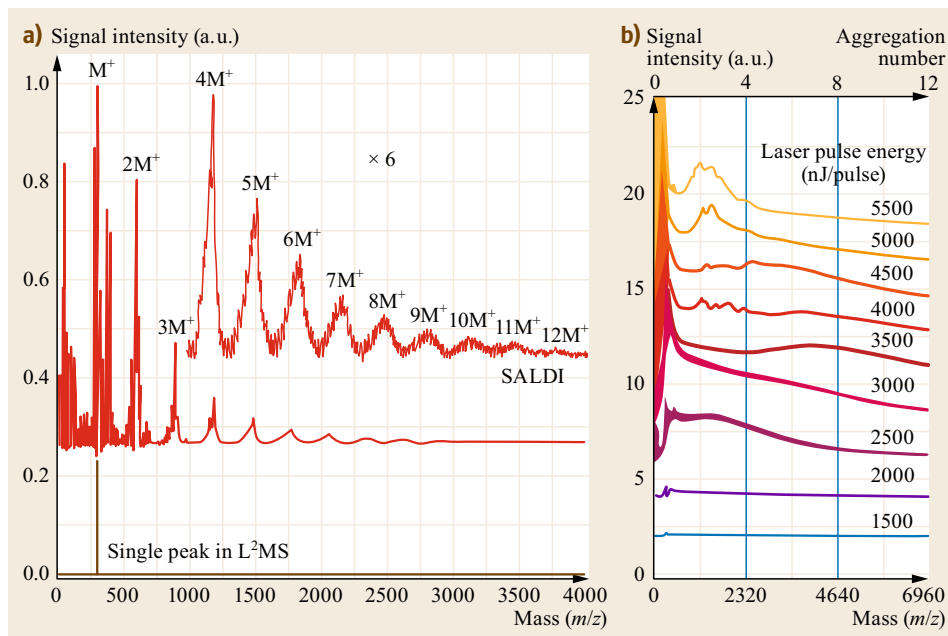


Fig. 6.12 (a) SALDI (3000 nJ/pulse) applied to coronene showing extensive aggregation with aggregates up to 12 monomers (M) (top) (after [6.34]) and L²MS applied to coronene showing a single peak without any aggregation (bottom). (b) SALDI applied to asphaltene with varying laser pulse energies (after [6.33]). At moderate laser power a peak corresponding to aggregation number of eight is observed. This corresponds to the asphaltene nanoaggregate. At increasing laser power, the nanoaggregate is broken up into decreasingly smaller multimers. Reprinted (adapted) with permission from [6.33, 34]. Copyright 2014 American Chemical Society

mass fraction as discussed below [6.69, 70]. Nevertheless, it is important to establish that laser-based mass spectral methods, especially L²MS, are able to disaggregate any asphaltene aggregates. First, model compound analysis is instructive. Figure 6.11 shows mass spectra of caffeic acid, a compound that has strong intermolecular interactions via the carboxylic acid and two hydroxyl groups (and is a matrix material for matrix-assisted LDI) [6.61].

Figure 6.11 shows that L²MS does not detect aggregates of caffeic acid with either REMPI or SPI. In contrast, this figure shows the surface-assisted laser desorption ionization (SALDI) exhibits considerable aggregation. REMPI-L²MS does show some fragmentation. This data shows that L²MS is much more efficient at breaking up aggregates than SALDI [6.61].

Figure 6.12a compares SALDI versus L²MS applied to coronene [6.34]. SALDI shows extensive aggregation, whereas L²MS detects a single peak corresponding to the parent ion. Figure 6.12b shows that SALDI applied to asphaltene detects aggregates. At

moderate laser power (3500 nJ/pulse), the asphaltene nanoaggregate is detected with an aggregation number of ≈ 8 . With increasing laser power, there is a reduction of the aggregation number [6.33, 34]. At 5500 nJ/pulse, the primary aggregate is the dimer. These data clearly show that even in SALDI where aggregates are easily detected, higher laser power can disaggregate asphaltene. L²MS, which is far more efficient at removing all vestiges of aggregates than SALDI, for example, with coronene, can clearly disaggregate asphaltene. For laser mass spectrometry, it is the preservation of the nanoaggregates that is difficult, not their disaggregation. Moreover, L²MS also has a relatively flat cross section for all types of asphaltene molecular structures [6.61]. Consequently, the fact that L²MS is sensitive to all fractions of asphaltene without problems of aggregation reinforces the validity of all L²MS results: Asphaltene molecular weight is ≈ 750 Da, the island molecular structure dominates and the aggregation of nanoaggregates is ≈ 8 (close to 6 depicted in Fig. 6.3).

6.5 Asphaltene Nanoaggregates

6.5.1 Surface-Assisted Laser Desorption Ionization Mass Spectrometry

SALDI in Fig. 6.12b shows a nanoaggregate aggregation number of ≈ 8 . Additional SALDI data on the aggregation number is shown in Fig. 6.13 where the baseline is subtracted. The petroleum asphaltenes all exhibit about the same aggregation number of ≈ 8 . The coal-derived asphaltene, with its very different character, has only a slightly different aggregation number of 6. The large difference in coal-derived asphaltenes with their very large aromatic carbon fraction ($\approx 85\%$) yields only a small difference in aggregation number. This is consistent with the same solubility of both types of asphaltenes. This also indicates that variation of aggregation numbers of virgin petroleum asphaltenes is minor. That is, the aggregation of coal-derived asphaltenes is similar to that of virgin petroleum asphaltenes. And all virgin petroleum asphaltenes are far more similar in chemical nature compared to coal-derived asphaltenes. Thus, the conclusion is that the aggregation properties of all virgin petroleum asphaltenes are similar, and thus dictated by their identical solubility constraints imposed by the definition of asphaltenes.

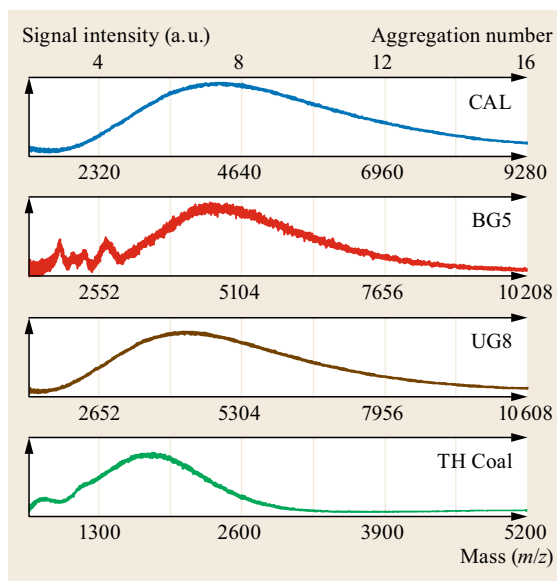


Fig. 6.13 SALDI measurements of aggregation numbers of asphaltene nanoaggregates for three petroleum asphaltenes, CAL, BG5, and UG8, and for a coal-derived asphaltene, TH Coal. The aggregation numbers for the petroleum asphaltenes are about 6–8 in agreement with Fig. 6.3 (after [6.33])

6.5.2 Small Angle X-ray Scattering (SAXS) and Small Angle Neutron Scattering (SANS)

SAXS and SANS have both been very informative with regard to asphaltenes. When combined into a single framework, they are most illuminating [6.40–42]. In asphaltenes, x-rays scatter preferentially from carbon, which is enriched in PAHs, whereas neutrons scatter preferentially from hydrogen, which is predominantly in alkane groups. The divergence of the SAXS versus SANS cross sections shown in Fig. 6.14 demonstrates that aromatic and saturate carbon groups are separately distributed in asphaltenes at the 1.4 nm length scale, the nanoaggregate. Analysis of this data shows that there is an aromatic carbon core and a periphery of

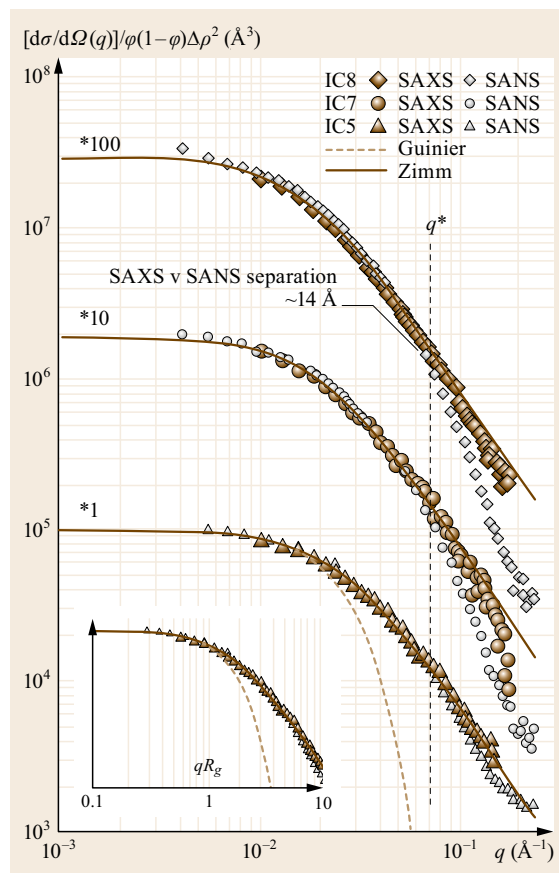


Fig. 6.14 Comparison of absolute cross sections of SAXS and SANS versus scattering vector q . The divergence at 14 \AA^{-1} (and smaller) shows that nanoaggregates have a core of aromatic carbon and a periphery of saturate carbon (Fig. 6.3) (after [6.40–42])

Table 6.4 Chemical shift assignments $\delta\{^1\text{H}\}$, line widths ($\Delta\vartheta_{1/2}$), and transverse (T_2) relaxation constants for the fitted peaks of solid-state ^1H -NMR spectrum at 8 kHz MAS, obtained with the 414 μs dipolar filter and variable delay spin-echo filter^a, corresponding to the spectrum in Fig. 6.15 (after [6.39])

Peak	$\delta\{^1\text{H}\}$ (ppm)	$\Delta\vartheta_{1/2}$ (Hz)	Assignment	T_2 (ms)
1	−0.18	76	−CH ₃ intercalated deep within the SC of its own NA or adjacent NA if on a long chain	0.11 (74.5%)
			−CH ₃ intercalated to a lesser extent within the SC of adjacent NA	24.25 (26.5%)
2	0.65	99	−CH ₃ on the cluster interior, ali. −CH ₂ intercalated within the SC	0.09 (70.0%)
			−CH ₃ on the cluster periphery	5.83 (30.0%)
3	1.06	167	ali. CH ₂ on the cluster interior, −CH ₃ attached to aro. ring	0.40 (21.1%)
			ali. CH ₂ on the cluster periphery	4.74 (78.9%)
4	1.29	90	ali. CH ₂ α to aro. core	3.33
5	1.56	653	alic. CH ₂ not α to aro. core	0.58
6	4.04	242	alic. CH/CH ₂ α to aro. core	1.11

^aaro. = aromatic, ali. = aliphatic, alic. = alicyclic, NA = nanoaggregate, SC = shielding cone. The values in parentheses represent the percentage of unfiltered signal having the corresponding T_2 . All the deconvolved peaks are Lorentzian

alkane carbon for asphaltene nanoaggregates. As noted by the authors, this geometry of the nanoaggregate is strongly supportive of the molecular architecture shown in Fig. 6.3 [6.40–42]. The length scale of the nanoaggregate in these combined SAXS and SANS studies led the authors to predict an aggregation number of 12, whereas an aggregation number of 6 is listed in Fig. 6.3. For such nanoscience determinations, this is largely considered agreement. For example, micelles and related structures often have aggregation numbers of 60 or 100. The central point is that asphaltene nanoaggregates have roughly an aggregation number of 10, with some spread in determination of the exact number. In any event, the structure and size of the nanoaggregate found in the combined SAXS and SANS study are in close agreement with the nanoaggregate shown in Fig. 6.3 and was predicted long before this observation based on simple steric repulsion arguments [6.69, 70]. The attractive central PAHs tend to form a stack, whereas peripheral alkanes interrupt stacking via steric hindrance [6.69, 70]. This simple argument predicts both a central PAH core with peripheral alkanes and small aggregation numbers as observed by SALDI [6.33, 34] and other methods.

6.5.3 NMR

The proposed disordered PAH stack of the nanoaggregate would yield some highly shielded alkane groups attached to these PAHs due to the familiar aromatic ring currents. The upfield peak at −0.18 ppm and other up-

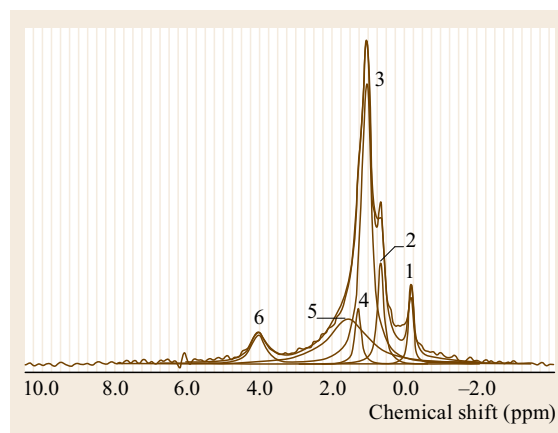


Fig. 6.15 ^1H -NMR spectrum of Athabasca bitumen asphaltene. The solid-state spectrum is shown at 8 kHz magic angle spinning after 414 μs dipolar filter and 125 μs Hahn-echo or T_2 relaxation filter showing the deconvolved peaks. The aromatic signals have been filtered out. The peak assignments are given in Table 6.4. The upfield peak (#1) corresponding to a −CH₃ group intercalated in a PAH stack is shown for the first time (after [6.39])

field peaks have been measured using solid-state magic angle spinning methods and, as the authors note, are consistent with the nanoaggregate and cluster structures shown in Fig. 6.3. This study also utilizes relaxation rates (Table 6.4) to discern inflexible alkane and aromatic groups, again lending support to fused alicyclic rings to the PAH as shown in Figs. 6.3 and 6.6 [6.39].

6.5.4 High-Q Ultrasonics, DC Conductivity, and Centrifugation

Other methods have shown the asphaltene nanoaggregate aggregation numbers to be quite small. These methods rely on measurement of properties above and below the critical nanoaggregate concentration (CNAC). The first determination of the CNAC where aggregate growth ceases was performed by high-Q ultrasonic studies [6.69, 70]. At that time, there was confusion about the value of the CNAC in part because it was not then recognized that there are two, not one aggregation thresholds for asphaltenes. Some studies were evidently sensitive to clustering, not nanoaggregate formation. For determination of asphaltene CNAC

in toluene, the high-Q ultrasonic results match with those of DC conductivity as shown in Fig. 6.16 [6.71]. The value of the CNAC, 10^{-4} mass fraction, is slightly larger than the onset of aggregation as determined by fluorescence measurements, as expected [6.72]. DC-conductivity measurements also confirmed that resins are unlikely to coat asphaltene nanoaggregates. Thus, the long-time-standing Nellensteyn hypothetical model, where resins adsorb on asphaltenes to provide a steric stabilizing layer, is not valid [6.73].

High-Q ultrasonics is sensitive to all asphaltenes in the corresponding solutions. The high precision in speed-of-sound determination allows the slight change of solution compressibility at CNAC to be detected. The speed of sound u is given by $u = \sqrt{1/(\beta\rho)}$, where β is

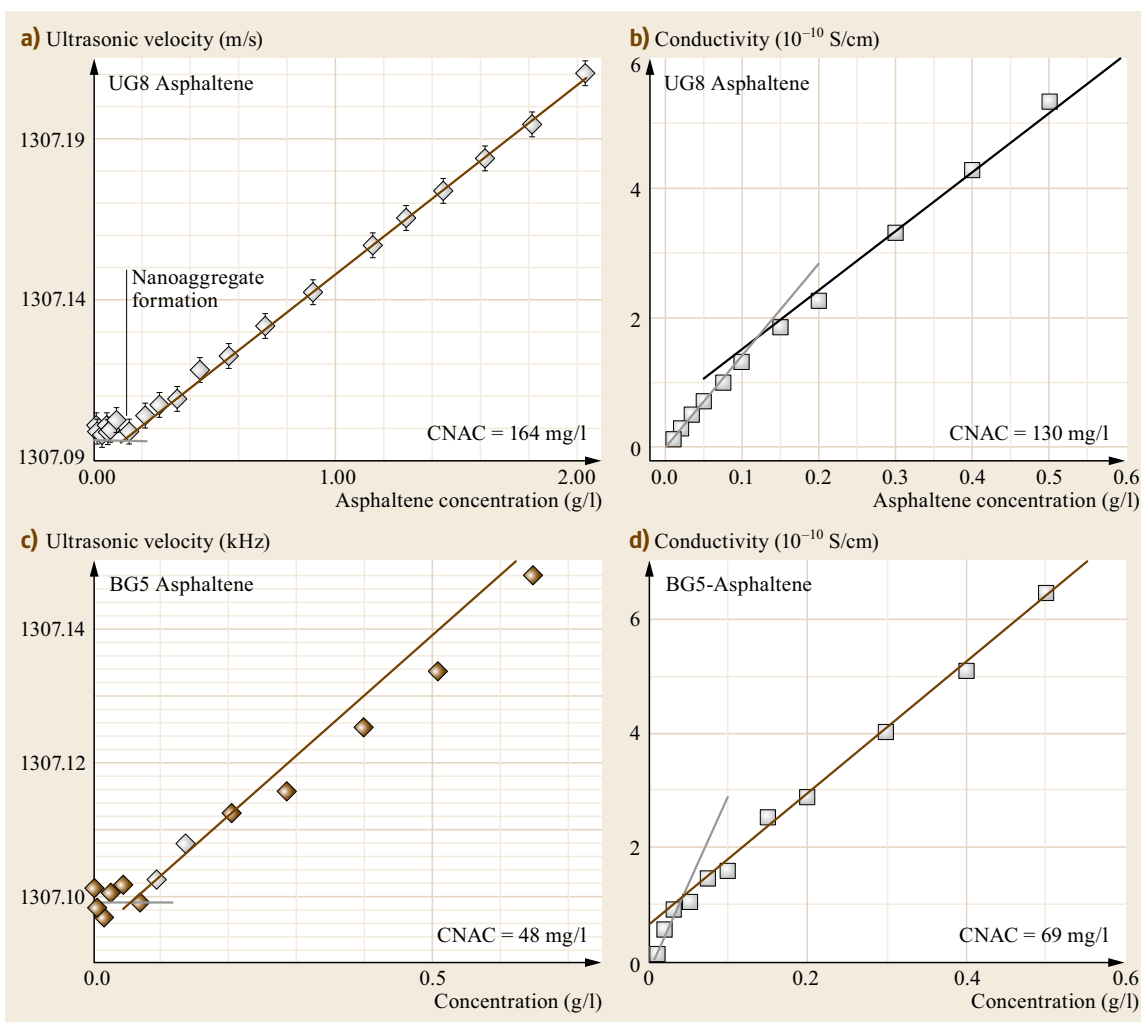


Fig. 6.16a–d Measurement of CNAC in toluene by (a,c) high-Q ultrasonics (after [6.69, 70]) and by (b,d) DC conductivity (after [6.71]) are in accord. The small increase in stokes drag at CNAC for DC conductivity indicates the aggregation number is small

compressibility and ρ is density. With the very small aggregation numbers, there is a range of concentrations corresponding to the CNAC; there is not one sharp, single CNAC [6.74]. These small variations require a very high quality factor Q of the resonator ($Q \approx 10\,000$), enabling speed of sound to be measured to a few parts per million (ppm). The DC conductivity depends on very different physics. In toluene, approximately one part in 10^5 of the asphaltene is ionized [6.71]. Thus, DC conductivity examines a small fraction of the sample. At CNAC, neutral molecules pack around the ion forming a nanoaggregate, thereby increasing the ion Stokes drag, which is linear in radius, yielding decreasing DC conductivity. The agreement between high- Q ultrasonics and DC conductivity validates the results. The change in Stokes drag at CNAC provides an estimate of the aggregation number. The obtained values for the aggregation number of the asphaltene nanoaggregate are always less than 10 by DC conductivity [6.71, 75, 76].

When homogeneous solutions of asphaltene nanoaggregates are centrifuged at a given speed, the nanoaggregates reach terminal velocities and, given time, will accumulate at the base of the centrifuge tube. By selecting centrifuge times that collect nanoaggregates, but not molecules, the CNAC can be determined. The centrifuge times are also dependent on nanoaggregate size as well. The sedimentation equation given below is applicable to these experiments

$$v_e = \frac{d^2 \Delta \rho g}{18 \eta}, \quad (6.2)$$

where v_e is the velocity of the colloidal particle in a gravitational or acceleration field of strength g , d is the particle diameter, $\Delta \rho$ is the discrete to continuous phase density difference, and η is the solvent viscosity. The sedimentation equation was previously shown to

Table 6.5 Calculated spin times for collection of corresponding asphaltene particles with diameter d . Time based on settling velocity from (6.2) (after [6.77])

Particle diameter (nm)	Settling velocity (m/s)	Spin duration
1.5	1.71×10^{-8}	21.8 days
2.5	4.75×10^{-8}	7.86 days
5	1.90×10^{-7}	1.96 days
10	7.59×10^{-7}	11.74 h
20	3.04×10^{-6}	2.93 h
50	1.90×10^{-5}	0.47 h

be applicable to asphaltene flocs of various sizes (in the order of $1 \mu\text{m}$), and these results were consistent with particle size determination from wavelength-dependent light scattering measurements [6.78]. Table 6.5 gives the spin times for the particular experimental configuration used versus asphaltene particle diameter in the toluene solutions.

In these asphaltene sedimentation experiments for nanoaggregates, centrifugation was carried out at fixed rotational frequency and temperature, 18 000 rpm and 298 K, respectively [6.77]. The settling field varied from 13 000 g near the top of the liquid surface to 37 600 g near the bottom so that the average settling field near the midpoint of the major axis of the tube was about 25 000 g. In these experiments, samples were spun for 7.86 days, corresponding to a particle size of 2.5 nm diameter. There is a variable collection efficiency dependent on where in the tube (vertically and laterally) the volume element is. Thus, centrifugation results are not precise in particle size, but the results are very robust, collecting asphaltene at the base of the tube.

Figure 6.17 shows that DC conductivity and centrifugation are in accord. DC-conductivity measurements rely on the increase of Stokes drag at CNAC. Centrifugation relies on the increased settling veloci-

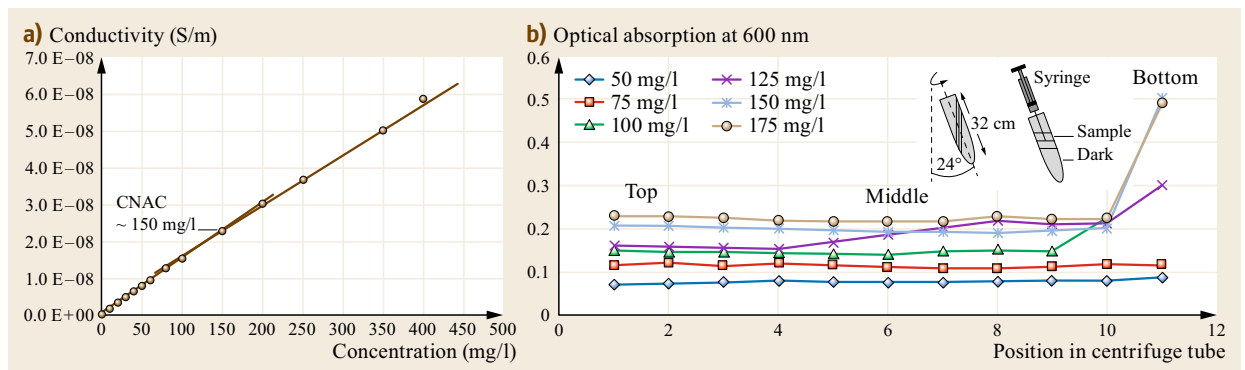


Fig. 6.17a,b Agreement of GOM asphaltene CNAC determination by (a) DC conductivity and (b) centrifugation (after [6.76, 77])

ties at CNAC. The CNAC determined by both methods are similar. The aggregation number determined by DC conductivity is less than 10. The nanoaggregate size determined by centrifugation is ≈ 2.5 nm, consistent with a small aggregation number. The temperature dependence of the CNAC is rather small [6.76, 79]; thus, the formation of the nanoaggregate has a significant entropic component. Nevertheless, the PAH stack in the nanoaggregate corresponds to the most stable energetics.

6.6 Clusters

6.6.1 SAXS and SANS

A second asphaltene nanocolloidal species can form: the asphaltene cluster. The combined SAXS and SANS studies show a fractal cluster with an aggregation number of 12 nanoaggregates [6.40–42]. This method is sensitive to nanoaggregate formation as discussed earlier, hence, the second level of aggregation found is robust and not due to confusion with nanoaggregate formation.

6.6.2 Light Scattering and Flocculation Kinetics

The critical clustering concentration (CCC) was first determined by examination of the kinetics of floc formation from different toluene solutions of asphaltenes upon *n*-heptane addition. Values of 2–5 g/l were obtained [6.80, 81]. Again, as with the CNAC, because the aggregation number of the cluster is small, there is a range of concentrations that corresponds to the CCC [6.74]. Below the CCC, the flocs are formed by diffusion limited aggregation (DLA); there is no barrier to floc formation from nanoaggregates. In contrast, above the CCC, the flocs are formed via reaction limited aggregation (RLA); clusters do not necessarily stick when colliding. A morphological change of the fractal cluster is required in order to stick, thus, RLA kinetics [6.81].

6.6.3 DC Conductivity and Centrifugation

Cluster formation has been probed by DC conductivity [6.46, 71] and centrifugation [6.46]. In DC conductivity, the increase in Stokes drag associated with cluster formation is recorded. In centrifugation, the settling velocity changes upon cluster formation essentially related to the change in Stokes drag and gravitational or cen-

trifugal force. Mass spectrometry has been used to measure CNAC; in a related solvent system [6.47], a CNAC of a little less than 10^{-4} mass fraction was obtained. NMR has also been used to obtain CNAC in toluene [6.79] and in a related solvent [6.13]. A somewhat lower CNAC was obtained in the less good solvent. The aggregation number of the mass spectral study was somewhat larger than 10 [6.47]; perhaps the different solvent system with a large methanol fraction accounts for this higher aggregation number.

The slight decrease in conductivity with cluster formation indicates that the aggregation number is less than 10. Likewise, the centrifugation spin conditions were set to detect a cluster size of 4 nm, corresponding to a spin time of about 3 days at 18 000 rpm (Table 6.5). This represents a lower limit for the clusters. If the particles are grown to 5 nm particle size, then the centrifugation experiments performed here (with longer spin times for smaller particles) would underestimate the CCC. The relevant spin parameters are the centrifugation speed and the time of spin. With these parameters fixed, and with changing concentration, Stokes drag determines whether asphaltenes can accumulate at the bottom of the centrifuge tube. As can be seen in Fig. 6.18, there is a large collection of asphaltenes in 1.5 g/l and above. Thus, the CCC is about 1.5 g/l.

In a related centrifugation study, a fixed asphaltene concentration of 3 g/l was used; this is above the CCC shown in Fig. 6.19. A large increase in asphaltene accumulation is observed at a spin time of 1.96 days, corresponding to 5 nm as shown in Table 6.5.

Figure 6.19 shows the spin time that corresponds to the accumulation of clusters toward the base of the centrifuge tube for this 18 000 rpm spin (Table 6.5). Most of the asphaltene gets accumulated at the base for a spin, corresponding to 5 nm particles for both the LC and HO asphaltenes [6.46].

The centrifugation experiments are robust in showing a change in aggregation occurring at the CCC and for showing the colloidal size. However, the centrifugation experiments are not as precise for showing CCC or particle size because there is variable centrifugation collection efficiency versus position in the centrifuge tube. The DC-conductivity measurements are perhaps more robust in determining the CCC. There is agreement in many studies that clusters are approximately 5 nm in diameter with an aggregation number of ≈ 8 nanoaggregates.

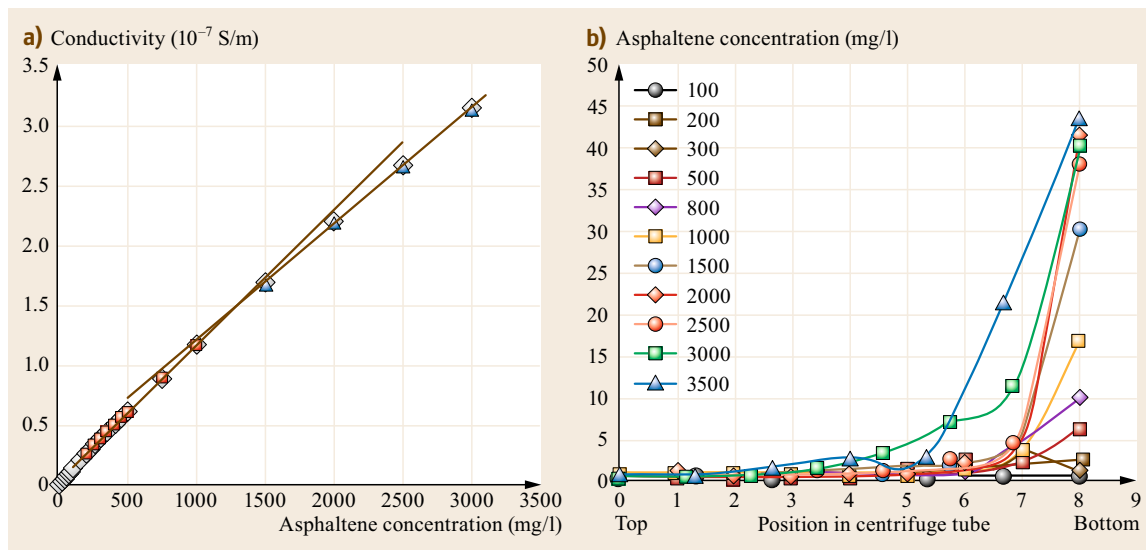


Fig. 6.18a,b Critical cluster concentration (CCC) measured by (a) DC conductivity and (b) centrifugation is in agreement, ≈ 1.4 g/l for this HO asphaltene. The small change in Stokes drag in both measurements indicates a cluster aggregation number less than 10 (after [6.46])

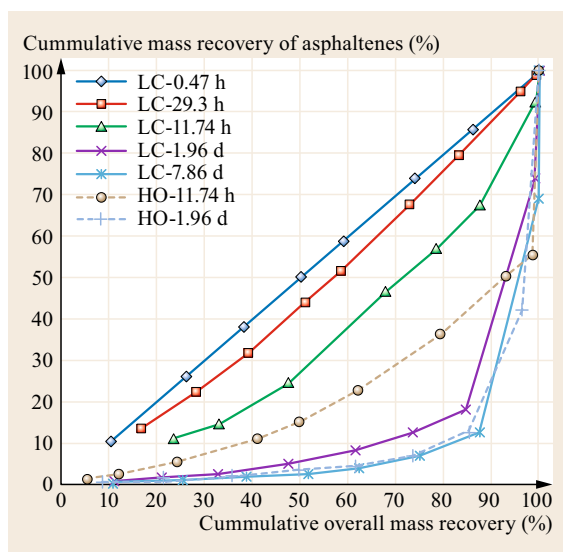


Fig. 6.19 Accumulation of asphaltene clusters versus spin time. Comparison with Table 6.5 and (6.2) shows that clusters are ≈ 5 nm in size (after [6.46]). Data for the asphaltenes, HO, and LC are shown

6.6.4 NMR Spectroscopy and Relaxometry

NMR measurements give a comparable cluster size by examining the diffusional motion of the peripheral alkane chains of asphaltenes. Figure 6.20 shows a schematic how T_1 and T_2 measurements of asphaltene alkanes at high concentration are used to evaluate

Table 6.6 Transverse (T_2) and longitudinal (T_1) relaxation times for the ^1H -NMR peaks in the solution state. The values in parentheses represent the percentage of protons having the corresponding T_2 (after [6.38])

$\delta \{^1\text{H}\}$ (ppm)	Assignment	T_2 (ms)	T_1 (s)
0.9	CH ₃ not attached to aromatic rings	33.3 (11.6%), 84.7 (88.4%)	0.73, 2.50
1.3	Aliphatic chain CH ₂	31.8 (9.7%), 59.5 (90.3%)	0.59, 1.50
1.6	Alicyclic CH ₂	24.9 (21.5%), 86.9 (78.5%)	0.35, 5.00
2.5	CH ₃ attached to aromatic rings	64.9	0.55, 7.10
2.8	Aliphatic chain/cyclic CH ₂ α or β to aromatics	24.4	0.42, 7.70
7.5	Aromatic CH	30.9 (15.6%), 75.2 (84.4%)	0.69, 2.90

cluster size. Estimates of the relative percentages of the rigid and mobile components of each signal were made by using the bi-exponential behavior of T_2 decay curves and are listed within parentheses in Table 6.6.

These percentages are indicative of the geometry and size of the nanoaggregates and their clusters. The low percentage of rigid aliphatic methyl and methylene groups (11.6 and 9.7%, respectively) indicates that the majority of the aliphatic chains remains on the periphery of the clusters [6.38]. This in turn implies that the clusters are made up of a small number of nanoaggregates. Moreover, the aromatic protons on the interior of

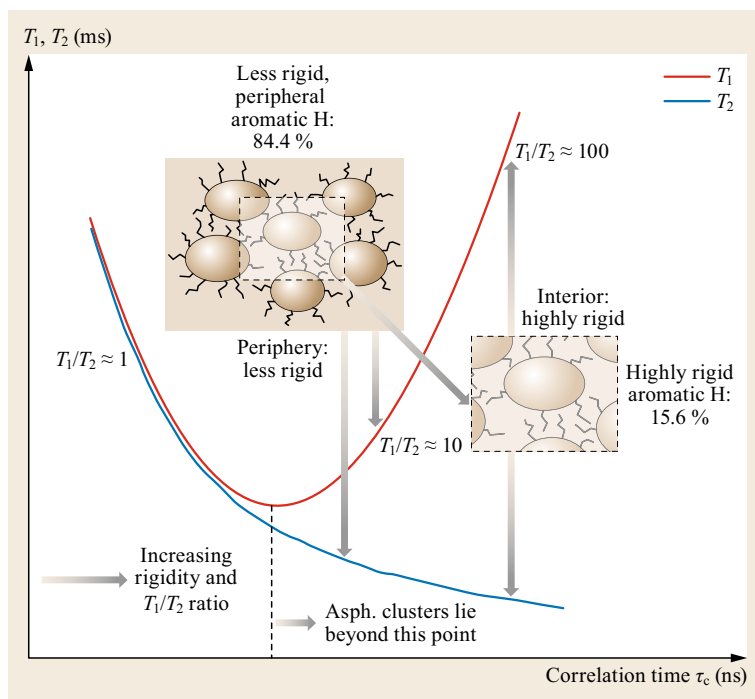


Fig. 6.20 (Not-to-scale) graphic showing that ^1H (T_1/T_2) ratios increase with rigidity of molecules (or their aggregates). Each oval with its side chains represents an asphaltene nanoaggregate. Higher correlation time (τ_c , x -axis) is an indicator of greater rigidity; all τ_c 's observed for Athabasca bitumen asphaltene protons at concentrations above the CCC lie beyond the T_1 -curve inflection point which is inversely proportional to the ^1H Larmor frequency. The aromatic protons on the interior of the clusters are significantly more rigid ($T_1/T_2 \approx 100$) than those on the periphery ($T_1/T_2 \approx 10$) and constitute $\approx 15.6\%$ of the total number of aromatic protons in the cluster, accounting for ≈ 1 in 6 or 7 nanoaggregates (after [6.38])

the clusters are significantly more rigid ($T_1/T_2 \approx 100$) than those on the periphery ($T_1/T_2 \approx 10$) and constitute $\approx 15.6\%$ of the total number of aromatic protons in the cluster. This fraction of highly rigid aromatic protons agrees with the cluster size of 6 or 7 nanoaggregates reported via other independent techniques (see above), where 15.6% would account for ≈ 1 rigid nanoaggregate at the center of the cluster. A cluster size larger than 6 or 7 would imply a larger fraction of these *interior* rigid protons. Therefore, the number of nanoaggregates per cluster can be predicted as 6–7, where the peripheral nanoaggregates have a higher mobility than the internal ones. This is in close agreement with the cluster aggregation number of 8 in the Yen–Mullins model (Fig. 6.3).

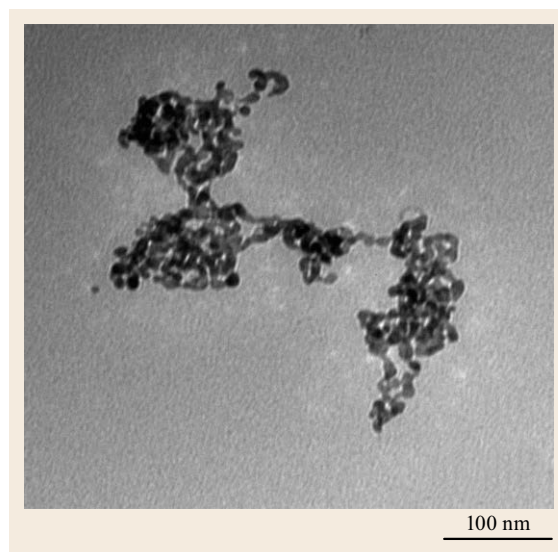
The 5 nm cluster of asphaltenes is stable for geologic time [6.82]. Many studies have been performed on asphaltene instability, and frequently, asphaltene flocs of greater than 1 μm are detected optically [6.78, 83]. As the instability is reduced, the rate of floc formation slows down essentially exponentially [6.84–86]. These slowly growing unstable asphaltene species have been shown to be in the range of 10 nm, which is close to the

Fig. 6.21 HRTEM micrograph of asphaltene flocculate in 70/30 toluene/heptane. The building blocks are clusters with an average size of 5 nm. Reprinted with permission from [6.87]. Copyright 2014 American Chemical Society ▶

size of the stable species, that is, the 5 nm asphaltene clusters.

6.6.5 High-Resolution Transmission Electron Microscopy (HRTEM)

Recent HRTEM studies on asphaltene aggregation in toluene/heptane solutions revealed that the onset of asphaltene flocculation was near 70/30 toluene/heptane.



At this ratio, clusters of clusters were no longer in colloidal stability and flocculated out of the solution. In these HRTEM images, small flocculates are globular in shape with an average diameter of 100 nm. Figure 6.21

presents a micrograph of small flocculates interacting with each other to form a larger one. The building blocks in this figure are clusters with an average size of 5 nm [6.87].

6.7 Intermolecular Interaction of Asphaltenes

In order to assess the range of applicability of any simple *universal* model of asphaltenes, it is important to understand their chemical interactions at the molecular level. Similar to the alkanes, weaker, simpler bonding is compatible with simpler asphaltene descriptions which may have broad applicability. Asphaltenes have been considered to be *strongly interacting*. However, the point of comparison to gauge asphaltene interaction is largely the other components of crude oil, the alkanes, which are very weakly interacting such that ideal solution formalisms are applicable. Moreover, intermolecular interaction yields aggregates of asphaltenes that are known to disrupt many molecular weight measurements such as laser desorption ionization mass spectrometry (LDI MS), atmospheric pressure chemical ionization mass spectrometry (APCI MS), and VPO [6.4, 35, 60]. However, mass spectrometry requires molecules to be in the vapor phase, and VPO necessitates the use of high concentrations; thus, these techniques accentuate issues related to intermolecular interactions. Nevertheless, asphaltenes are known to be predominantly molecularly dispersed in laboratory solvents at fairly high concentrations, 10^{-4} mass fraction, in toluene [6.69, 70], indicating that intermolecular interaction of asphaltenes is not that strong in comparison to a covalent bond.

The equilibrium constant K for aggregation depends on standard Gibbs free energy of nanoaggregate formation ΔG° as $K = \exp\{-\Delta G^\circ/kT\}$, where $\Delta G^\circ = \Delta H^\circ - T\Delta S^\circ$, ΔH° is the standard enthalpy of formation, and ΔS° is the standard entropy of formation. The temperature variation of the CNAC (in toluene) was determined to be smaller than error over a limited range of over the range 298–324 K [6.76]. Consequently, to zeroth order, the lack of temperature dependence of the CNAC means that the enthalpy of aggregate formation is zero as shown by van't Hoff equation

$$\frac{\partial \ln K}{\partial T} = \frac{\Delta H^\circ}{kT^2}, \quad (6.3)$$

where k is Boltzmann's constant and T is temperature. The important point is that the binding energy (enthalpy) of asphaltenes in solution is not high.

One should not confuse the role of minimum energy; the molecular configuration of the nanoaggregate

certainly minimizes the energy. An unfavorable configuration would require energy to form. With $\Delta H \approx 0$, ΔS° can be approximated. One can presume that the nanoaggregate forms in a process forming dimers, trimers, etc., and that the equilibrium constants of dimer formation, trimer formation, etc. are all presumed to be the same. At CNAC, the concentration of the monomer equals the dimer which equals the trimer . . . , and equals the CNAC, then $K = 1/[\text{CNAC}]$ and (6.4) follows

$$\Delta G_{\text{CNAC}}^\circ = -T\Delta S_{\text{CNAC}}^\circ = RT \ln(\text{CNAC}), \quad (6.4)$$

with the $\text{CNAC} = 150 \text{ mg/l} = 2 \times 10^{-4} \text{ mole/l}$, $\Delta S^\circ \approx 17 \text{ cal}/(\text{deg mol})$. This entropy is positive (intuition would naively suggest it should be negative). Evidently, the solvent positive change in solvent entropy more than compensates the negative change in asphaltene entropy upon aggregate formation. The magnitude of this entropy change at CNAC is comparable to the corresponding entropy change of critical micelle concentration for some aqueous surfactants when the enthalpy of formation is also zero [6.88]. This positive entropy of formation is larger than a previous determination for asphaltenes (8.3 cal/(deg mol)); this previous work also found a small negative enthalpy of formation (-3.6 kcal/mol) [6.79].

The Hildebrand solubility parameter, δ , is defined as the square root of the cohesive energy density, and provides a way to quantify intermolecular interaction. δ is very low for saturated hydrocarbons. For example, $\delta = 14.9 \text{ MPa}^{1/2}$ for *n*-hexane and $\delta = 16.0 \text{ MPa}^{1/2}$ for *n*-dodecane, whereas $\delta = 48 \text{ MPa}^{1/2}$ for water (Table 6.7). Alkanes are nearly ideal, whereas water is not. At room temperature, water, with one heavy atom, is a liquid, whereas for *n*-alkanes, it takes five heavy atoms to form a liquid (*n*-pentane). Regular solution theory such as Flory–Huggins theory accounts for some deviation from ideal solution theory, accounting for some limited intermolecular interaction. In particular, the applicability of simple regular solution theory depends on the types of intermolecular interactions. Projecting the Hildebrand solubility parameter, δ , into the composite Hansen solubility parameters of the three predominant intermolecular interactions, such as dispersion (or polarizability) δ_D , polarity δ_P , and hydrogen

Table 6.7 Hildebrand solubility parameters and the Hansen solubility parameters for asphaltenes and selected compounds

Compound	Hildebrand δ (MPa ^{1/2})	Hansen parameters		
		$\delta_{\text{Dispersion}}$	δ_{Polarity}	$\delta_{\text{H-bond}}$
Alkanes				
<i>n</i> -Pentane	14.5	14.5	0	0
<i>n</i> -Hexane	14.9	14.9	0	0
<i>n</i> -Heptane	15.3	15.3	0	0
<i>n</i> -Dodecane	16.0	16.0	0	0
Cyclohexane	16.8	16.8	0	0.2
Aromatics				
Benzene	18.6	18.6	0	2.0
Toluene	18.2	18.0	0	2.0
<i>o</i> -Xylene	18.0	17.8	1.0	3.1
Naphthalene	20.3	19.2	2.0	5.9
Chlorinated compounds				
Carbon tetrachloride	17.8	17.8	0	0.6
Chloroform	19.0	17.8	3.1	5.7
Methylene chloride	20.3	18.2	6.3	6.1
Chlorobenzene	19.6	19.0	4.3	2.0
Other hetero compounds				
Tetrahydrofuran	19.4	16.8	5.7	8.0
Acetone	20.0	15.5	10.4	7.0
Methyl alcohol	29.6	15.1	12.3	22.3
Ethyl alcohol	26.5	15.8	8.8	19.4
1-Propyl alcohol	24.5	16.0	6.8	17.4
1-Butyl alcohol	23.1	16.0	5.7	15.8
Phenol	24.1	18.0	5.9	14.9
Acetic acid	21.4	14.5	8.0	13.5
Ethylene glycol	32.9	17.0	11.0	26.0
Propylene glycol	30.2	16.8	9.4	23.3
Dimethyl sulfoxide	26.7	18.4	16.4	10.2
Carbon disulfide	20.5	20.5	0	0.6
Ethanethiol	18.6	15.8	6.6	7.2
Pyridine	21.8	19.0	8.8	5.9
Water	47.8	15.6	16.0	42.3
Asphaltenes [6.89]	20.4	19.5	4.7	4.2

bonding, δ_{H} , helps to clarify essential interactions and guide thinking on application of different solution theories.

The dependence of solubility on a comparison of the Hansen solubility parameters of the species in question is simply the manifestation of the well-known chemical axiom, *like dissolves like*. Table 6.7 provides a list of different classes of compounds (and asphaltenes) and the Hildebrand and Hansen solubility parameters

$$\delta = (\delta_{\text{D}}^2 + \delta_{\text{P}}^2 + \delta_{\text{H}}^2)^{1/2} \quad (6.5)$$

Small differences in the solubility parameters of two compounds indicate mutual solubility; large differences preclude solubility. If the two compounds are dominated by dispersion forces, then comparison of

Hildebrand parameters is sufficient. If the intermolecular interactions are complex including polarity and H-bonding, then the comparison must be made considering Hansen solubility parameters, with the root mean square of the distance in the Hansen space being the metric, along with the factor of two increase of the dispersion term difference. The latter point is that for compounds dominated by dispersion forces, subtler differences in δ_{D} can preclude solubility.

As noted earlier, alkanes are weakly interacting and water is strongly interacting. Table 6.7 quantifies these strengths. (The numerical value of the solubility parameter in MPa^{1/2} is 2.0455 times the value in (cal/cm³)^{1/2}). Alkanes are characterized by relatively small Hildebrand interaction parameters with the Hansen dispersion term dominating. In contrast,

water, alcohols, acids, and sulfoxides all have much larger Hildebrand parameters which have large contribution from the H-bonding parameter and from the polar term. Asphaltenes are intermediate in terms of their Hildebrand parameter, which, as with alkanes and aromatics, is dominated by the polarizability term. From the vantage of strongly interacting compounds listed in Table 6.7, asphaltenes are somewhat weak in their interaction. The relatively small heteroatom content of asphaltenes is also predominantly dominated by polarizability such as sulfide, thiophene, and aromatic nitrogen. This heteroatom content of asphaltenes does give rise to some dipolar charge separation; nevertheless, the dominant interaction is via polarizability. Solvents that dissolve asphaltenes likewise have comparable interaction parameters that are also dominated by polarizability, such as toluene and chlorinated solvents.

The fact that polarizability dominates the asphaltene solubility parameter [6.89] indicates that the central, large PAH of asphaltene molecules is the primary site of intermolecular attraction. The determination of molecular orientation at the oil–water interface in Langmuir–Blodgett films supports this conclusion. Sum frequency generation (SFG) experiments showed that asphaltenes orient with their PAH in-plane and their alkanes out-of-plane at the oil–water interface [6.58]. In contrast, PAHs with oxygen containing moieties along one side of the molecule or in pendant groups were shown to orient edge-on in the oil–water interface [6.58]. Evidently, asphaltene intermolecular attractive interactions are mediated by their PAH, not by heteroatom containing pendant groups. These results are also consistent with pendant drop experiments which obtain that the asphaltene contact area with the oil–water interface equals approximately 6 fused rings [6.13, 14]. These pendant drop experiments obtained three universal curves, lending credence to the results. One of the universal curves is the surface tension variation with relative asphaltene coverage. The Langmuir EoS was used to fit this curve, and one of two fitting parameters is the molecular contact area. The result of a 6-ring PAH for asphaltenes is consistent with the SFG results of direct determination of this same molecular orientation. Both the SFG and pendant drop experiments reinforce the idea that the asphaltene PAH dominates asphaltene intermolecular attraction.

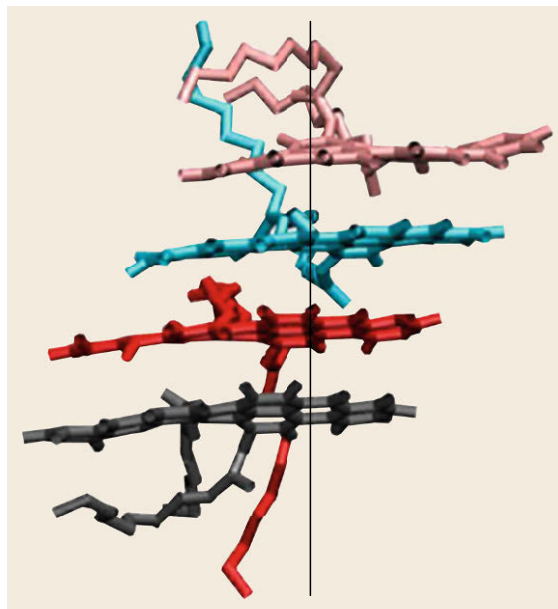


Fig. 6.22 Molecular dynamics simulation showing π -stacking of PAH-containing alkyl aromatic (with oxygen functions as well). Reprinted with permission from [6.90]. Copyright 2013 American Chemical Society

Molecular dynamics (MD) simulations have been performed on various model systems and frequently exhibit π -stacking, reinforcing the idea that the asphaltene PAH dominates intermolecular attraction (Fig. 6.22). In addition, the steric repulsion of long alkane chains was observed on the π -stacking as expected [6.90]. Asphaltenes have significant polydispersity that leads to some disorder in the π -stacking. In other MD studies, the interactions between aromatic cores of asphaltene molecules were the major driving force for association as the energy of association increased substantially with the number of aromatic rings. Moreover, heteroatoms attached to the aromatic cores had much more influence on the association free energy than to ones attached to the aliphatic chains. The length and number of aliphatic chains did not have a noticeable effect on asphaltene dimerization; however, they had a profound effect on asphaltene aggregation size since steric repulsion could prevent asphaltenes from forming T-shape configurations and therefore decrease the aggregation size of asphaltenes significantly [6.91].

6.8 The Flory–Huggins–Zuo Equation of State

Modeling reservoir crude oils necessitates knowing the effect of gravity. Prior to the Yen–Mullins model, the size of asphaltene particles and even molecules in crude oils or laboratory solvents was unknown. This precluded any modeling of asphaltene gradients in reservoirs. With the Yen–Mullins model, this size is resolved. Knowing the size of asphaltene particles in crude oil enables evaluation of the gravity term, an essential component of modeling reservoir fluids. The first theory introduced for asphaltene gradients is the FHZ EoS, which, of course, incorporates the effects of gravity. The gravity term is given by Archimedes buoyancy ($V\Delta\rho g$) of the asphaltenes in the Boltzmann distribution, where V is the size of the asphaltene particle, $\Delta\rho$ is the density contrast between the asphaltene particle and the oil phase, and g is Earth's gravitational acceleration. OD_i is optical density at height i in the reservoir, k is Boltzmann's constant and T is temperature

$$\frac{OD_h}{OD_o} = \exp\left(\frac{-V\Delta\rho gh}{kT}\right). \quad (6.6)$$

Replacing $V\Delta\rho$ with the weighted mass of nitrogen and oxygen molecules yields the barometric equation, which gives the atmospheric pressure gradient of planet Earth from the sea level to Mt. Everest and beyond. The weighted sum of atmospheric gases is used because compositional mixing from weather systems is far more rapid than the diffusive process that would lead to separate density gradients of the different gases. The Boltzmann distribution describes the counterbalance between excitation energy and temperature; gravity pulls objects with mass to lower elevation while thermal energy lifts objects to heights. For low GOR crude oils, the FHZ EoS largely reduces to this gravity term (6.6). The full FHZ EoS is listed below and applies to heavy ends in all crude oils [6.10–12].

By adding the gravity term to the Flory–Huggins polymer solution theory, the FHZ EoS is obtained. This theory combines simple regular solution theory of solubility with the effects of gravity to describe the distribution of dissolved (or nanocolloidally suspended) asphaltenes in reservoir fluid. The FHZ EoS is the first EoS for predicting asphaltene concentration gradients with depth in oil reservoirs [6.10–12]. It is the only proven EoS to describe asphaltene gradients in oil reservoirs for crude oils ranging from condensates to heavy oils [6.12]. Because of the simple form of the FHZ

EoS, it can use various measurements of reservoir fluid properties, in particular, by employing asphaltene concentration ratios or optical density ratios at two different depths in the reservoir. The FHZ EOS is given as

$$\begin{aligned} \frac{OD(h_2)}{OD(h_1)} &= \frac{\varphi_a(h_2)}{\varphi_a(h_1)} \\ &= \exp\left(\frac{v_a g (\rho - \rho_a)(h_2 - h_1)}{kT} \right. \\ &\quad \left. + \frac{v_a}{kT} [(\delta_a - \delta)_{h_1}^2 - (\delta_a - \delta)_{h_2}^2] \right. \\ &\quad \left. + \left[\left(\frac{v_a}{v}\right)_{h_2} - \left(\frac{v_a}{v}\right)_{h_1} \right] \right), \quad (6.7) \end{aligned}$$

where OD , k , ϕ , v , δ , T , g , ρ , and h are the optical density, Boltzmann's constant, volume fraction, molar volume, solubility parameter, temperature, gravitational acceleration, density, and depth (or height), respectively. Subscript a denotes the properties of asphaltenes; subscripts h_1 and h_2 stand for the properties at depths h_1 and h_2 , respectively. It should be pointed out that the crude oil solubility parameter, molar volume, and density of bulk fluids, temperature, pressure, and compositions are all dependent on depth.

In addition to the gravity term (the leading term in the argument of the exponential), the second term in the exponential is the solubility term. This term is the specific manifestation of the chemical axiom *like dissolves like*. If the solubility parameters of the asphaltene and the crude oil are not too dissimilar, then the energetics allow dissolution. Gaseous hydrocarbons are, well, gaseous and colorless. Hydrocarbon gases are colorless because asphaltenes do not partition (or dissolve) in this phase. Gaseous hydrocarbons are not *like* the dark brown solid, the asphaltenes. Consequently, high GOR crude oils have very limited capacity to dissolve asphaltenes, whereas low GOR fluids can dissolve asphaltenes. The variation of the solubility term in reservoir crude oils is dominated by GOR variations. For low GOR crude oils, the oils are incompressible; thus, there is very little GOR variation with depth. Consequently, the solubility term is constant, and the asphaltene variation is dominated by the gravity term.

The last term in the argument of the exponential in (6.7) is the entropy term. This term tends to be small and acts to yield distributions that are macroscopically homogeneous, that is, randomly distributed.

6.9 Conclusions

The confluence of results from very diverse, detailed studies on asphaltenes has led to the Yen–Mullins model to characterize the dominant molecular and nanocolloidal structures of asphaltenes. Original studies that gave rise to this model as well as recent studies that tested this model have been discussed herein and provide strong support for this model. The simplicities of the nanocolloidal structures of asphaltenes traces back in part to molecular architecture, with the single, attractive PAH in the molecular core and with peripheral alkanes involving steric hindrance. The dominant intermolecular interaction of polarizability also helps explain why simple concepts account for many obser-

vations associated with asphaltenes. The Yen–Mullins model provides a framework for understanding many asphaltene properties. It also serves as the foundation of the Flory–Huggins–Zuo EoS (discussed in the next chapter), which is now ubiquitously used for reservoir evaluation. It has long been known that the simplicity of crude oil gas and liquid components allows for broad applicability of the cubic EoS and simple mixing rules to account for many diverse properties of the gas and liquid phase equilibria of crude oils. The Yen–Mullins model coupled with the Flory–Huggins–Zuo EoS now extends these overarching concepts to solution and (dissolved) solid equilibria of crude oils.

References

- 6.1 O.C. Mullins, E.Y. Sheu, A. Hammami, A.G. Marshall (Eds.): *Asphaltenes, Heavy Oils and Petroleomics* (Springer, New York 2007)
- 6.2 O.C. Mullins, E.Y. Sheu (Eds.): *Structures and Dynamics of Asphaltenes* (Plenum, New York 1998)
- 6.3 O.C. Mullins: The asphaltenes, *Annu. Rev. Anal. Chem.* **4**, 393–418 (2011)
- 6.4 O.C. Mullins, B. Martinez-Haya, A.G. Marshall: Contrasting perspective on asphaltene molecular weight; this comment versus the overview of A.A. Herod, K.D. Bartle, R. Kandiyoti, *Energy Fuels* **22**, 1765–1773 (2008)
- 6.5 F.P. Di Sanzo: Chromatographic analysis of fuels. In: *Analytical Advances for Hydrocarbon Research*, ed. by C.S. Hsu (Kluwer/Plenum, New York 2003) pp. 113–146
- 6.6 C.S. Hsu, D. Drinkwater: Gas chromatography–mass spectrometry in the petroleum industry. In: *Current Practice in GC/MS*, *Chromatogr. Sci.*, Vol. 86, ed. by W.W.A. Niessen (Marcel Dekker, New York 2001) pp. 55–94
- 6.7 C. Eiserbeck, R.K. Nelson, C.M. Reddy, K. Grice: Advances in comprehensive two dimensional gas chromatography (GCxGC). In: *Principles and Practice of Analytical Techniques in Geoscience*, ed. by K. Grice (R. Soc. Chem., London 2015) pp. 324–365
- 6.8 O.C. Mullins: The modified Yen model, *Energy Fuels* **24**, 2179–2207 (2010)
- 6.9 O.C. Mullins, H. Sabbah, J. Eyssautier, A.E. Pomerantz, L. Barré, A.B. Andrews, Y. Ruiz-Morales, F. Mostowfi, R. McFarlane, L. Goual, R. Lepkowitz, T. Cooper, J. Orbulescu, J.M. Leblanc, J. Edwards, R.N. Zare: Advances in asphaltene science and the Yen–Mullins model, *Energy Fuels* **26**, 3986–4003 (2012)
- 6.10 D.E. Freed, O.C. Mullins, J.Y. Zuo: Asphaltene gradients in the presence of GOR gradients, *Energy Fuels* **24**(7), 3942–3949 (2010)
- 6.11 D.E. Freed, O.C. Mullins, J.Y. Zuo: Heuristics for equilibrium distributions of asphaltenes in the presence of GOR gradients, *Energy Fuels* **28**(8), 4859–4864 (2014)
- 6.12 J.Y. Zuo, O.C. Mullins, D.E. Freed, C. Dong, H. Elshahawi, D.J. Seifert: Advances of the Flory–Huggins–Zuo equation of state for asphaltene gradients and formation evaluation, *Energy Fuels* **27**, 1722–1735 (2013)
- 6.13 J.P. Rane, D. Harbottle, V. Pauchard, A. Couzis, S. Banerjee: Adsorption kinetics of asphaltenes at the oil–water interface and nanoaggregation in the bulk, *Langmuir* **28**, 9986–9995 (2012)
- 6.14 J.P. Rane, V. Pauchard, A. Couzis, S. Banerjee: Interfacial rheology of asphaltenes at oil–water interfaces and interpretation of the equation of state, *Langmuir* **29**, 4750–4759 (2013)
- 6.15 V. Pauchard, J.P. Rane, S. Banerjee: Asphaltene-laden interfaces form soft glassy layers in contraction experiments: A mechanism for coalescence blocking, *Langmuir* **30**(43), 12795–12803 (2014)
- 6.16 C. Song, W.-C. Lai, R. Madhusudan, B. Wei: Temperature-programmed retention indices GC and GC–MS of hydrocarbon fuels and simulated distillation GC of heavy oils. In: *Analytical Advances for Hydrocarbon Research*, ed. by C.S. Hsu (Kluwer/Plenum, New York 2003) pp. 147–210
- 6.17 O.C. Mullins: *The Physics of Reservoir Fluids; Discovery Through Downhole Fluid Analysis* (Schlumberger, Houston 2008)
- 6.18 C.S. Hsu, C.C. Walters, G.H. Isaksen, M.E. Schaps, K.E. Peters: Biomarker analysis in petroleum exploration. In: *Analytical Advances for Hydrocarbon Research*, ed. by C.S. Hsu (Kluwer/Plenum, New York 2003) pp. 223–245
- 6.19 K.E. Peters, C.C. Walters, J.M. Moldowan: *The Biomarker Guide: Biomarkers and Isotopes in Petroleum Systems and Earth History*, Vol. 1 (Cambridge Univ. Press, Cambridge 2005)
- 6.20 K.E. Peters, C.C. Walters, J.M. Moldowan: *The Biomarker Guide: Biomarkers and Isotopes in Petroleum Systems and Earth History*, Vol. 2 (Cam-

- bridge Univ. Press, Cambridge 2005)
- 6.21 A. Bartha, N. De Nicolais, V. Sharma, S.K. Roy, R. Srivastava, A.E. Pomerantz, M. Sanclemente, W. Perez, R.K. Nelson, C.M. Reddy, J. Gros, J.S. Arey, J. Lelijveld, S. Dubey, D. Tortella, T. Hantschel, K.E. Peters, O.C. Mullins: Combined petroleum system modeling, wireline formation sampling and GCxGC to improve understanding of the crude oil type in the Llanos Basin, Colombia, *Energy Fuels* **29**(8), 4755–4767 (2015)
 - 6.22 A.G. Marshall, R.P. Rodgers: *Petroleomics: Chemistry of the underworld*, *Proc. Nat. Acad. Sci.* **105**, 18090–18095 (2008)
 - 6.23 R.P. Rodgers, A.G. Marshall: *Petroleomics: Advanced characterization of petroleum-derived materials by Fourier transform ion cyclotron resonance mass spectrometry (FT-ICR MS)*. In: *Asphaltenes, Heavy Oils and Petroleomics*, ed. by O.C. Mullins, E.Y. Sheu, A. Hammami, A.G. Marshall (Springer, New York 2007)
 - 6.24 K. Qian, R.P. Rodgers, C.L. Hendrickson, M.R. Emmett, A.G. Marshall: Reading chemical fine print: Resolution and identification of 3000 nitrogen-containing aromatic compounds from a single electrospray ionization Fourier transform ion cyclotron resonance mass spectrum of heavy petroleum crude oil, *Energy Fuels* **15**, 492–498 (2001)
 - 6.25 A.M. McKenna, J.M. Purcell, R.P. Rodgers, A.G. Marshall: Identification of vanadyl porphyrins in a heavy crude oil and raw asphaltene by atmospheric pressure photoionization Fourier transform ion cyclotron resonance (FT-ICR) mass spectrometry, *Energy Fuels* **23**(4), 2122–2128 (2009)
 - 6.26 L.A. Stanford, R.P. Rodgers, A.G. Marshall, J. Czarnecki, X.A. Wu: Compositional characterization of bitumen/water emulsion films by negative- and positive-ion electrospray ionization and field desorption/ionization Fourier transform ion cyclotron resonance mass spectrometry, *Energy Fuels* **21**(2), 963–972 (2007)
 - 6.27 S.M. Rowland, W.K. Robbins, Y.E. Corilo, A.G. Marshall, R.P. Rodgers: Solid-phase extraction fractionation to extend the characterization of naphthenic acids in crude oil by electrospray ionization Fourier transform ion cyclotron resonance mass spectrometry, *Energy Fuels* **28**(8), 5043–5048 (2014)
 - 6.28 A.E. Pomerantz, G.T. Ventura, A.M. McKenna, J.A. Cañas, J. Auman, K. Koerner, D. Curry, R.L. Nelson, C.M. Reddy, R.P. Rodgers, A.G. Marshall, K.E. Peters, O.C. Mullins: Combining biomarker and bulk compositional gradient analysis to assess reservoir connectivity, *Org. Geochem.* **41**(8), 812–821 (2010)
 - 6.29 W.D. McCain: *The Properties of Petroleum Fluids* (PennWell, Tulsa 1990)
 - 6.30 D.Y. Peng, D.B. Robinson: A new two-constant equation of state, *Ind. Eng. Chem. Fundam.* **15**, 59–64 (1976)
 - 6.31 L.P. Dake: *The Practice of Reservoir Engineering* (Elsevier Science, Amsterdam 2001)
 - 6.32 H. Sabbah, A.L. Morrow, A.E. Pomerantz, R.N. Zare: Evidence for island structures as the dominant architecture of asphaltenes, *Energy Fuels* **25**, 1597–1604 (2011)
 - 6.33 Q. Wu, A.E. Pomerantz, O.C. Mullins, R.N. Zare: Laser-based mass spectrometric determination of aggregation numbers for petroleum- and coal-derived asphaltenes, *Energy Fuels* **28**, 475–482 (2014)
 - 6.34 Q. Wu, D.J. Seifert, A.E. Pomerantz, O.C. Mullins, R.N. Zare: Constant asphaltene molecular and nanoaggregate mass in a gravitationally segregated reservoir, *Energy Fuels* **28**, 3010–3015 (2014)
 - 6.35 A.E. Pomerantz, Q. Wu, O.C. Mullins, R.N. Zare: Laser-based mass spectroscopic assessment of asphaltene molecular weight, molecular architecture and nanoaggregate weight, *Energy Fuels* **29**(5), 2833–2842 (2015)
 - 6.36 A.B. Andrews, J.C. Edwards, O.C. Mullins, A.E. Pomerantz: A comparison of coal and petroleum asphaltenes by ^{13}C nuclear magnetic resonance and DEPT, *Energy Fuels* **25**, 3068–3076 (2011)
 - 6.37 R. Scotti, L. Montanari: Molecular structure and intermolecular interaction of asphaltenes by FT-IR, NMR and EPR. In: *Structures and Dynamics of Asphaltenes*, ed. by O.C. Mullins, E.Y. Shen (Springer, New York 1998)
 - 6.38 R.D. Majumdar, M. Gerken, R. Mikula, P. Hazendonk: Validation of the Yen–Mullins model of athabasca oil-sands asphaltenes using solution-state ^1H NMR relaxation and 2-D H 2 QC spectroscopy, *Energy Fuels* **27**(11), 6528–6537 (2013)
 - 6.39 R.D. Majumdar, M. Gerken, P. Hazendonk: Solid-state ^1H and ^{13}C nuclear magnetic resonance spectroscopy of athabasca oil sands asphaltenes: Evidence for interlocking π -stacked nanoaggregated with intercalated alkyl side chains, *Energy Fuels* **29**(5), 2790–2800 (2015)
 - 6.40 J. Eyssautier, P. Levitz, D. Espinat, J. Jestin, J. Gummel, I. Grillo, L. Barré: Insight into asphaltene nanoaggregate structure inferred by small angle neutron and x-ray scattering, *J. Phys. Chem. B* **115**, 6827–6837 (2011)
 - 6.41 J. Eyssautier, I. Heñaut, P. Levitz, D. Espinat, L. Barré: Organization of asphaltenes in a vacuum residue: A small-angle x-ray scattering (SAXS)-viscosity approach at high temperatures, *Energy Fuels* **26**(5), 2696–2704 (2012)
 - 6.42 J. Eyssautier, D. Espinat, J. Gummel, P. Levitz, M. Becerra, S. Shaw, L. Barré: Mesoscale organization in a physically separated vacuum residue: Comparison to asphaltenes in a simple solvent, *Energy Fuels* **26**(5), 2680–2687 (2012)
 - 6.43 Y. Ruiz-Morales, X. Wu, O.C. Mullins: Electronic absorption edge of crude oils and asphaltenes analyzed by molecular orbital calculations with optical spectroscopy, *Energy Fuels* **21**, 944 (2007)
 - 6.44 Y. Ruiz-Morales, O.C. Mullins: Measured and simulated electronic absorption and emission spectra of asphaltenes, *Energy Fuels* **23**, 1169–1177 (2009)
 - 6.45 E. Buenrostro-Gonzalez, H. Groenzin, C. Lira-Galeana, O.C. Mullins: The overriding chemical principles that define asphaltenes, *Energy Fuels* **15**, 972 (2001)
 - 6.46 L. Goual, M. Sedghi, F. Mostowfi, R. McFarlane, A.E. Pomerantz, S. Saraji, O.C. Mullins: Cluster size and critical clustering concentration by centrifuga-

- tion and DC-conductivity, *Energy Fuels* **28**(8), 5002–5013 (2014)
- 6.47 A.M. McKenna, L.J. Donald, J.E. Fitzsimmons, P. Juyal, V. Spicer, K.G. Standing, A.G. Marshall, R.P. Rodgers: Heavy petroleum composition. 3. Asphaltene aggregation, *Energy Fuels* **27**, 1246–1256 (2013)
- 6.48 H. Groenzin, O.C. Mullins: Asphaltene molecular size and structure, *J. Phys. Chem. A* **103**, 11237–11245 (1999)
- 6.49 H. Groenzin, O.C. Mullins: Molecular sizes of asphaltenes from different origin, *Energy Fuels* **14**, 677 (2000)
- 6.50 H. Groenzin, O.C. Mullins, S. Eser, J. Mathews, M.-G. Yang, D. Jones: Asphaltene molecular size for solubility subfractions obtained by fluorescence depolarization, *Energy Fuels* **17**, 498 (2003)
- 6.51 S. Badre, C.C. Goncalves, K. Norinaga, G. Gustavson, O.C. Mullins: Molecular size and weight of asphaltene and asphaltene solubility fractions from coals, crude oils and bitumen, *Fuel* **85**, 1 (2006)
- 6.52 Y. Ruiz-Morales, O.C. Mullins: Polycyclic aromatic hydrocarbons of asphaltenes analyzed by molecular orbital calculations with optical spectroscopy, *Energy Fuels* **21**, 256 (2007)
- 6.53 U. Bergmann, H. Groenzin, O.C. Mullins, P. Glatzel, J. Fetzer, S.P. Cramer: Carbon K-edge x-ray Raman spectroscopy supports simple yet powerful description of aromatic hydrocarbons and asphaltenes, *Chem. Phys. Lett.* **369**, 184 (2003)
- 6.54 T. Klee, T. Masterson, B. Miller, E. Barrasso, J. Bell, R. Lepkowitz, J. West, J.E. Haley, D.L. Schmitt, J.L. Flikkema, T.M. Cooper, Y. Ruiz-Morales, O.C. Mullins: Triplet electronic spin-states of crude oils and asphaltenes, *Energy Fuels* **25**, 2065–2075 (2011)
- 6.55 G.J. Kennedy: Advances in NMR techniques for hydrocarbon characterization. In: *Analytical Advances for Hydrocarbon Research*, ed. by C.S. Hsu (Kluwer/Plenum, New York 2003) pp. 369–384
- 6.56 K.A. Gould, I.A. Wiehe: Natural hydrogen donors in petroleum resids, *Energy Fuels* **21**, 1199–1204 (2007)
- 6.57 A.E. Pomerantz, M.R. Hammond, A.L. Morrow, O.C. Mullins, R.N. Zare: Asphaltene molecular weight distribution determined by two-step laser mass spectrometry, *Energy Fuels* **23**(3), 1162–1168 (2009)
- 6.58 A.B. Andrews, A. McClelland, O. Korkeila, A. Krummel, O.C. Mullins, A. Demidov, Z. Chen: Sum frequency generation studies of Langmuir films of complex surfactants and asphaltenes, *Langmuir* **27**, 6049–6058 (2011)
- 6.59 J.P. Rane, S. Zarkar, V. Pauchard, O.C. Mullins, D. Christie, A.B. Andrews, A.E. Pomerantz, S. Banerjee: Applicability of the Langmuir equation of state for asphaltene adsorption at the oil–water interface: Coal-derived, petroleum, and synthetic asphaltenes, *Energy Fuels* **29**(6), 3584–3590, (2015)
- 6.60 A.R. Hortal, P. Hurtado, B. Martinez-Haya, O.C. Mullins: Molecular weight distributions of coal and crude oil asphaltenes from laser desorption ionization experiments, *Energy Fuels* **21**, 2863–2868 (2007)
- 6.61 Q. Wu, A.E. Pomerantz, O.C. Mullins, R.N. Zare: Fragmentation and aggregation in laser desorption laser ionization and surface assisted laser desorption ionization mass spectrometry, *J. Am. Soc. Mass Spec.* **24**(7), 1116–1122 (2013)
- 6.62 O.P. Strausz, T.W. Mojelsky, E.M. Lown: The molecular structure of asphaltene, an unfolding story, *Fuel* **71**, 1355 (1992)
- 6.63 A. Karimi, K. Qian, W.N. Olmstead, H. Freund, C. Yung, M.R. Gray: Quantitative evidence for bridged structures in asphaltenes by thin film pyrolysis, *Energy Fuels* **25**, 3581–3589 (2011)
- 6.64 A.H. Alshareef, A. Scherer, X. Tan, K.M. Azyat, J.M. Stryker, R.R. Tykwinski, M.R. Gray: Formation of archipelago structures during thermal cracking implicates a chemical mechanism for the formation of petroleum asphaltenes, *Energy Fuels* **25**, 2130–2136 (2011)
- 6.65 D.S. Pinkston, P. Duan, V.A. Gallardo, S.C. Habicht, X. Tan, K. Qian, M. Gray, K. Muellen, H. Kenttamaa: Analysis of asphaltenes and asphaltene model compounds by laser-induced acoustic desorption/Fourier transform ion cyclotron resonance mass spectrometry, *Energy Fuels* **23**, 5564–5570 (2009)
- 6.66 M.R. Hurt, D.J. Borton, H.J. Choi, H.I. Kenttamaa: Comparison of the structures of molecules in coal and petroleum asphaltenes by using mass spectrometry, *Energy Fuels* **27**(7), 3653–3658 (2013)
- 6.67 D. Borton, D.S. Pinkston, M.R. Hurt, X. Tan, K. Azyat, R. Tywinsky, M. Gray, K. Qian, H.I. Kenttamaa: Molecular structures of asphaltenes based on the dissociation reactions of their ions in mass spectrometry, *Energy Fuels* **24**(10), 5548–5559 (2010)
- 6.68 H. Sabbah, A.L. Morrow, A.E. Pomerantz, O.C. Mullins, X. Tan, M.R. Gray, K. Azyat, R.R. Tykwinski, R.N. Zare: Comparing laser desorption/laser ionization mass spectra of asphaltenes and model compounds, *Energy Fuels* **24**, 3589–3594 (2010)
- 6.69 G. Andreatta, C.C. Goncalves, G. Buffin, N. Bostrom, C.M. Quintella, F. Arteaga-Larios, E. Perez, O.C. Mullins: Nanoaggregates and structure-function relations in asphaltenes, *Energy Fuels* **19**, 1282–1289 (2005)
- 6.70 G. Andreatta, N. Bostrom, O.C. Mullins: High-Q ultrasonic determination of the critical nanoaggregate concentration of asphaltenes and the critical micelle concentration of standard surfactants, *Langmuir* **21**, 2728 (2005)
- 6.71 H. Zeng, Y.Q. Song, D.L. Johnson, O.C. Mullins: Critical nanoaggregate concentration of asphaltenes by low frequency conductivity, *Energy Fuels* **23**, 1201–1208 (2009)
- 6.72 S. Goncalves, J. Castillo, A. Fernandez, J. Hung: Absorbance and fluorescence spectroscopy on the aggregation of asphaltene toluene solutions, *Fuel* **83**, 1823 (2004)
- 6.73 M. Sedghi, L. Goual: Role of resins on asphaltene stability, *Energy Fuels* **24**, 2275–2280 (2010)
- 6.74 S.E. Friberg: Micellization. In: *Asphaltenes, Heavy Oils and Petroleomics*, ed. by O.C. Mullins, E.Y. Sheu, A. Hammami, A.G. Marshall (Springer, New York 2007)

- 6.75 L. Goual: Impedance spectroscopy of petroleum fluids at low frequency, *Energy Fuels* **23**, 2090–2094 (2009)
- 6.76 L. Goual, M. Sedghi, H. Zeng, F. Mostowfi, R. McFarlane, O.C. Mullins: On the formation and properties of asphaltene nanoaggregates and cluster by DC-conductivity and centrifugation, *Fuel* **90**, 2480–2490 (2011)
- 6.77 F. Mostowfi, K. Indo, O.C. Mullins, R. McFarlane: Asphaltene nanoaggregates and the critical nanoaggregate concentration from centrifugation, *Energy Fuels* **23**, 1194–1200 (2009)
- 6.78 N.B. Joshi, O.C. Mullins, A. Jamaluddin, J.L. Creek, J. McFadden: Asphaltene precipitation from live crude oils, *Energy Fuels* **15**, 979 (2001)
- 6.79 D.E. Freed, N.V. Lisitza, P.N. Sen, Y.Q. Song: A study of asphaltene nanoaggregation by NMR, *Energy Fuels* **23**, 1189–1193 (2009)
- 6.80 M.A. Anisimov, I.K. Yudin, V. Nikitin, G. Nikolaenko, A. Chernoutsan, H. Toulhoat, D. Frot, Y. Briolant: Asphaltene aggregation in hydrocarbon solutions studied by photon correlation spectroscopy, *J. Phys. Chem.* **99**(23), 9576–9580 (1995)
- 6.81 I.K. Yudin, M.A. Anisimov: Dynamic light scattering monitoring of asphaltene aggregation in crude oils and hydrocarbon solutions. In: *Asphaltenes, Heavy Oils and Petroleomics*, ed. by O.C. Mullins, E.Y. Sheu, A. Hammami, A.G. Marshall (Springer, New York 2007)
- 6.82 O.C. Mullins, J.Y. Zuo, D. Seifert, M. Zeybek: Clusters of asphaltene nanoaggregates observed in oil reservoirs, *Energy Fuels* **27**, 1752–1761 (2013)
- 6.83 A. Hammami, J. Ratulowski: Precipitation and deposition of asphaltenes in production systems: A flow assurance overview. In: *Asphaltenes, Heavy Oils and Petroleomics*, ed. by O.C. Mullins, E.Y. Sheu, A. Hammami, A.G. Marshall (Springer, New York 2007)
- 6.84 T. Maqbool, A.T. Balgoa, H.S. Fogler: Revisiting asphaltene precipitation from crude oils: A case of neglected kinetic effects, *Energy Fuels* **23**, 3681–3686 (2009)
- 6.85 T. Maqbool, S. Raha, M.P. Hoepfner, H.S. Fogler: Modeling the aggregation of asphaltene nanoaggregates in crude oil-precipitant systems, *Energy Fuels* **25**, 1585–1596 (2011)
- 6.86 M.P. Hoepfner, H.S. Fogler: Multiscale scattering investigations of asphaltene cluster breakup, nanoaggregate dissociation, and molecular ordering, *Langmuir* **29**, 15423–15432 (2013)
- 6.87 L. Goual, M. Sedghi, X. Wang, Z. Zhu: Asphaltene aggregation and impact of alkylphenols, *Langmuir* **30**, 5394–5403 (2014)
- 6.88 F. Skrabal, F. Bangerter, K. Hamada, T. Iijima: Entropy contribution to an azo dye aggregation in aqueous solution, *Dyes and Pigments* **8**, 371–374 (1987)
- 6.89 S. Acevedo, A. Castro, E. Vasquez, F. Marciano, M.A. Ranaudo: Investigation of physical chemistry properties of asphaltenes using solubility parameters of asphaltenes and their fractions A1 and A2, *Energy Fuels* **24**(11), 5921–5933 (2010)
- 6.90 C. Jian, T. Tang, S. Bhattacharjee: Probing the effect of side-chain length on the aggregation of a model asphaltene using molecular dynamics simulations, *Energy Fuels* **27**, 2057–2067 (2013)
- 6.91 M. Sedghi, L. Goual, L. Welch, J. Kubelka: Effect of asphaltene structure on association and aggregation using molecular dynamics, *J. Phys. Chem. B* **117**, 5765–5776 (2013)

7. Reservoir Evaluation by DFA Measurements and Thermodynamic Analysis

Go Fujisawa, Oliver C. Mullins

Downhole fluid analysis (DFA) has enabled the cost-effective measurement in oil wells of a variety of chemical properties of reservoir crude oils. An immediate benefit of DFA is the improvement of the sample quality of the reservoir fluid in the subsurface environment. In addition, this early feedback on the nature of the reservoir fluid aids in understanding key reservoir challenges. DFA also enables the accurate determination of fluid gradients in the reservoir in both vertical and lateral directions. These gradients can then be analyzed in a thermodynamic equation of state (EoS) context; the gas-liquid properties can be modeled with the cubic EoS and the asphaltene gradients equilibrium can be modeled with the Flory-Huggins-Zuo (FHZ) EoS with its reliance on the Yen-Mullins model of asphaltenes. Time-dependent processes in geologic time can be modeled by adding appropriate dynamic terms to the EoS. Simple thermodynamic models can then be used to understand distributions of key fluid properties for reservoir crude oils and aid in simulating production. This thermodynamic analysis of the geodynamics of reservoir fluids fills a gap in the industry's modeling of reservoir fluids. Traditional basin modeling predicts what fluids enter

7.1	The Borehole Environment	252
7.2	VIS/NIR Spectroscopy of Hydrocarbon Reservoir Fluids	254
7.3	Implementation of DFA Hardware	257
7.4	Basic DFA Operations and Applications	260
7.5	Reservoir Evaluation via DFA and Thermodynamics	261
7.6	Reservoir Case Studies	262
7.7	Conclusions	270
	References	270

the reservoir. This new geodynamic modeling coupled with DFA measurements determines what transpired in geologic time in regards to fluid distributions within the reservoir. The output of this fluid geodynamic modeling can then be used as input for traditional reservoir simulation for production. This new understanding of reservoir fluid geodynamics is made possible by new DFA measurements coupled with new FHZ EoS with the Yen-Mullins model.

The volume and properties of hydrocarbon fluids (oil and/or gas) play a central role in establishing economic value of reservoirs and in developing production plans for those reserves [7.1]. For example, the gas-to-oil ratio (GOR) determines the fundamentally different requirements for handling high pressure gas versus oil. The asphaltene content has an enormous impact on viscosity, which impacts rates of fluid flow as well as economic value. The properties of the reservoir crude oil determine whether a deleterious phase transition will occur during production; transitions include asphaltene deposition, wax deposition, and organic scale, which can impede production and mandate costly solutions. Moreover, important fluid properties can vary dramatically vertically and laterally in reservoirs. Along the

lines of the ergodic theorem, spatial variation of fluid properties translates to temporal variation of fluid properties in production, and these variations need to be understood for production optimization.

In addition, the analysis of fluid gradients in the reservoir can address a variety of important issues. For example, the observations of thermodynamic equilibration of reservoir fluids is a strong indicator of reservoir connectivity, at least at some point in geologic time if not at the current time [7.2]. Disequilibrium of reservoir fluids often implies existence of a transient process in geologic time occurring in the reservoir. In turn, this aids in understanding complex reservoirs with simple formalisms enabling improved risk assessment of field development planning [7.3].

This analysis of reservoir fluids is best accomplished prior to production as production facilities, which represent significant capital expenditure and are designed to accommodate the specific reservoir fluid. Consequently, wireline logging and drilling tools have been developed to acquire fluid samples in openhole (or even cased hole) shortly after the well is drilled and long before production commences [7.4]. Nevertheless, it is not economical to blindly acquire fluid samples at all possible depths in the well to carry out this critical objective of reservoir fluid analysis. It is very important to be able to assess hydrocarbon reservoir fluid inside a wellbore in real time by the sample acquisition tool, so that informed and optimum decisions can be made regarding whether a fluid sample is required from any particular section of the well and if the current quality of fluid sample is sufficient [7.2]. Today, this important role is performed by downhole fluid analysis (DFA) and mostly by visible and near-infrared (Vis/NIR) spectroscopy [7.2]. Vis/NIR spectroscopy is a very powerful analytic tool and is utilized in many industrial settings. Vis/NIR spectroscopy has been the most powerful DFA measurement to analyze reservoir fluid in situ in oil/gas wells for more than 20 years. Today, DFA by Vis/NIR spectroscopy is widely accepted by upstream oil and gas companies as a valuable and indispensable method to understand their hydrocarbon fluids and reservoirs.

The capabilities of DFA have recently greatly expanded due to the ability to employ proper thermodynamic modeling of DFA data. Reservoir crude oils consist of dissolved gases, liquids and dissolved (or nanocolloidally suspended) solids, known as asphaltenes (Chap. 6). For decades, the dissolved gas and liquid properties of reservoir fluids have been treated by various cubic EoSs [7.1]. The effectiveness of this approach is well known and powerful for gas–liquid equilibria [7.1]. However, cubic EoSs, including the original cubic EoS the Van der Waals EoS, were never designed to handle colloidal solids. Crude oils contain (nanocolloidal) asphaltenes, and modeling of asphaltene gradients in reservoir crude oils has resisted proper

thermodynamic foundations until now. The problem was that nobody knew the size of asphaltene particles in crude oil. Even the asphaltene molecular weight had been the subject of debate spanning orders of magnitude [7.5]. This uncertainty precluded any understanding of the nanocolloidal structures of asphaltenes in crude oils. With the asphaltene size unknown, the corresponding gravitational force was unknown, and asphaltene gradient modeling was precluded. Fortunately, in recent years, the dominant molecular and colloidal structures of asphaltenes have been resolved and codified in the Yen–Mullins model [7.6]. With the gravity term resolved, a variation of a polymer regular solution theory, the Flory–Huggins–Zuo EoS has been used to great effect to model asphaltene gradients [7.7, 8].

In this chapter, we first describe measurement principles behind Vis/NIR spectroscopy of hydrocarbon reservoir fluids. Next, we explain some of the engineering challenges for implementing DFA hardware. Then, we explain the basic form of DFA operations and applications in a setting of formation testing and sampling tools to give clear views on how DFA is utilized in typical exploration and appraisal wells. The leading tool for sample acquisition in wireline logging is known as the modular formation dynamics tester (MDT), and we will refer to the MDT as the sample acquisition tool of interest. DFA is performed with specific DFA tools that are part of the MDT tool string. DFA data acquired by the MDT can then be analyzed using a thermodynamic basis. The cubic EoS is used for gas–liquid equilibria. The FHZ EoS along with the Yen–Mullins model is used for interpretation of DFA-measured asphaltene fluid gradients in oilfield reservoirs. Several case studies are shown that illustrate the power and capability of DFA and thermodynamic analysis to evaluate major reservoir concerns. A myriad of reservoir concerns are addressed such as connectivity, gas charging into oil reservoirs, tar mat formation and biodegradation. The combination of new asphaltene science and new DFA technology is leading to an explosion of applications in the oilfield.

7.1 The Borehole Environment

The borehole environment of oil wells presents several challenges for the objective of measurement of properties of fluids contained in the subsurface (rock) formations. Hydrocarbons can survive for geologic time at temperatures as high as 175 °C and at times above 200 °C so these temperatures set the specification for DFA measurements. These temperatures are associated

with pressures of 20 000 psi or at times 30 000 psi given normal temperature and pressure gradients in earth formations; thus setting the pressure specification for DFA measurements. Wellbore diameters can vary; frequently bit sizes are used in the hydrocarbon zones of interest that have diameters not much larger than 6 inches. Consequently, the tool housing, which must support the

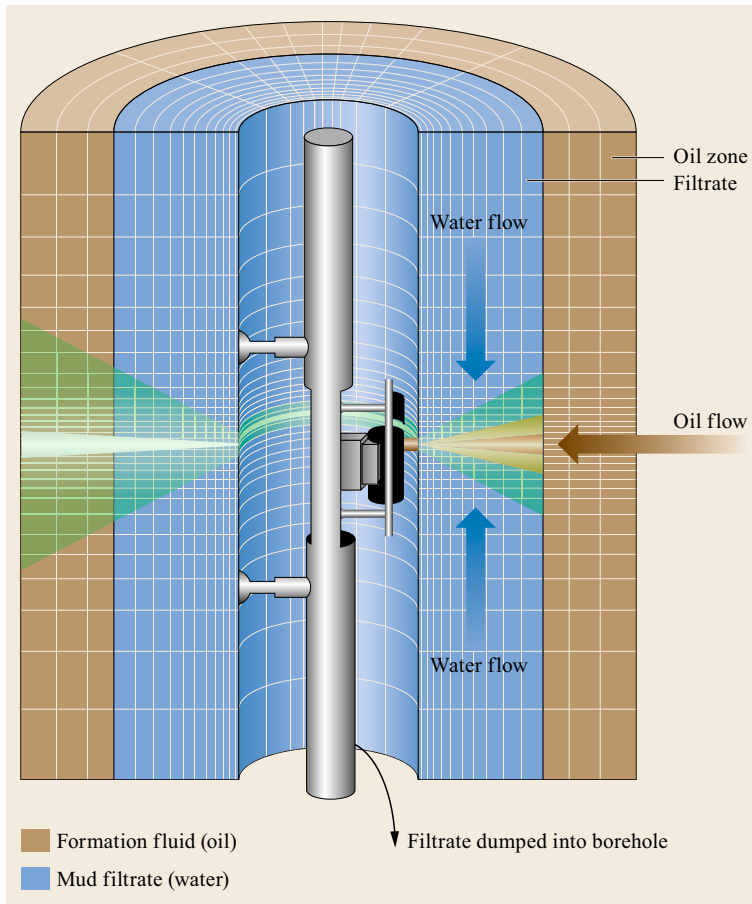


Fig. 7.1 A wellbore is depicted along with a formation sampling tool, the MDT. Oil wells are drilled with a drilling mud which can either be oil-based or water-based; the latter is depicted here. Some base fluid leaks into the formation giving an annulus of *mud filtrate* in an annular region in the formation. Clean sample acquisition of formation fluids requires good probe configurations and sufficient pumping times to drain the contaminating mud filtrate. DFA has the charter to monitor and quantify the filtrate contamination of the formation fluids (after [7.2])

large pressures just discussed, must not exceed 6 inches in order to be broadly used. The DFA measurement systems must be compact.

Oil wells are drilled with a drilling mud. The mud serves many purposes. The mud is pumped down the center of the drill string and flows back to surface along in the annular space between the drill string and borehole wall. This mud flow carries the rock cuttings out of the well. The mud is weighted with solids to maintain the fluid pressure in the borehole greater than that of the zones penetrated to prevent uncontrolled influx of formation fluids into the borehole. Such a blowout is extremely dangerous in all ways. The muds contain clays and bridging agents to build mud cakes on the borehole wall at permeable zones in order to prevent excessive fluid loss from the high pressure borehole to the lower pressure permeable zones. Excess fluid loss can lead to loss of well control due to loss of hydrostatic head pressure in the mud column. Excess fluid loss can also lead to formation damage hindering the eventual production of oil. The drilling muds can have either water or oil as the base fluid.

Figure 7.1 presents a clean view of the borehole, with an annulus of invaded mud filtrate that penetrates through the mud cake present on borehole wall at permeable zones. A sampling tool is depicted in the center of the borehole. The industry-leading fluid openhole sampling tool is the MDT, the modular formation dynamics tester tool [7.4]. Openhole refers to the condition of the wellbore prior to placement of casing, or cased hole. Thus, openhole sampling tools such as the MDT must establish hydraulic communication of the MDT probe with permeable formations in the presence of mud in the wellbore, and mud cake on the borehole wall of the permeable zone. A probe module with a strong tube is shown that contacts the borehole wall to make hydraulic communication with the formation fluids. Figure 7.1 correctly shows that the initial flow of fluid into the MDT will have significant contamination from the mud filtrate that has leaked into the permeable zones in the time between drilling the well and logging the well with the MDT [7.2]. Figure 7.1 depicts an oil-bearing formation with a water-based mud (WBM). Often oil bearing formations are drilled with oil-based

mud (OBM). One of the DFA objectives is to differentiate between the contamination mud filtrate versus formation fluids. This requires differentiating between oil and water for cases such as shown in Fig. 7.1. In addition, it is necessary to differentiate between OBM filtrate and crude oil. The OBM filtrate has little dis-

solved gas and no asphaltenes. Finally, there is interest in differentiating between WBM filtrate and formation water or connate water. Typically the WBMs are quite basic, thus pH measurements downhole using optical spectroscopy with litmus paper dyes become quite useful [7.9].

7.2 VIS/NIR Spectroscopy of Hydrocarbon Reservoir Fluids

Vis/NIR spectroscopy investigates molecules by spectral (electromagnetic) interrogation of various molecular modes. Typically, UV/Vis spectroscopy corresponds to valence electronic state transitions, infrared spectroscopy corresponds to vibrational modes and microwave spectroscopy to rotational modes. For downhole analysis in situ in oil wells, visible (Vis) and even near-infrared (NIR) spectral ranges are used to evaluate the electronic absorption edge of crude oils, specifically the asphaltenes and heavy resins of the oils. It is the large polycyclic aromatic hydrocarbons (PAHs) of asphaltenes that give rise to long wavelength absorption [7.5]. NIR is also used to examine the vibrational overtones of molecules. Mid-infrared spec-

troscopy (MIR) is of limited utility downhole because the large absorption strengths ensure nonlinear spectral response, thus it is error prone, and the requisite low photon energy sensitivity of MIR detectors yields large thermal noise at the elevated temperatures encountered downhole. In contrast, NIR spectroscopy is linear at pathlengths (2 mm) convenient for downhole flowlines, and the relatively high energy cutoff of NIR detectors minimizes thermal noise.

Figure 7.2 shows typical crude oil spectra in the Vis/NIR wavelength range for a 2 mm pathlength, which is operationally convenient downhole. OD is *optical density*, which accounts for attenuation from optical absorption and light scattering. There is no light

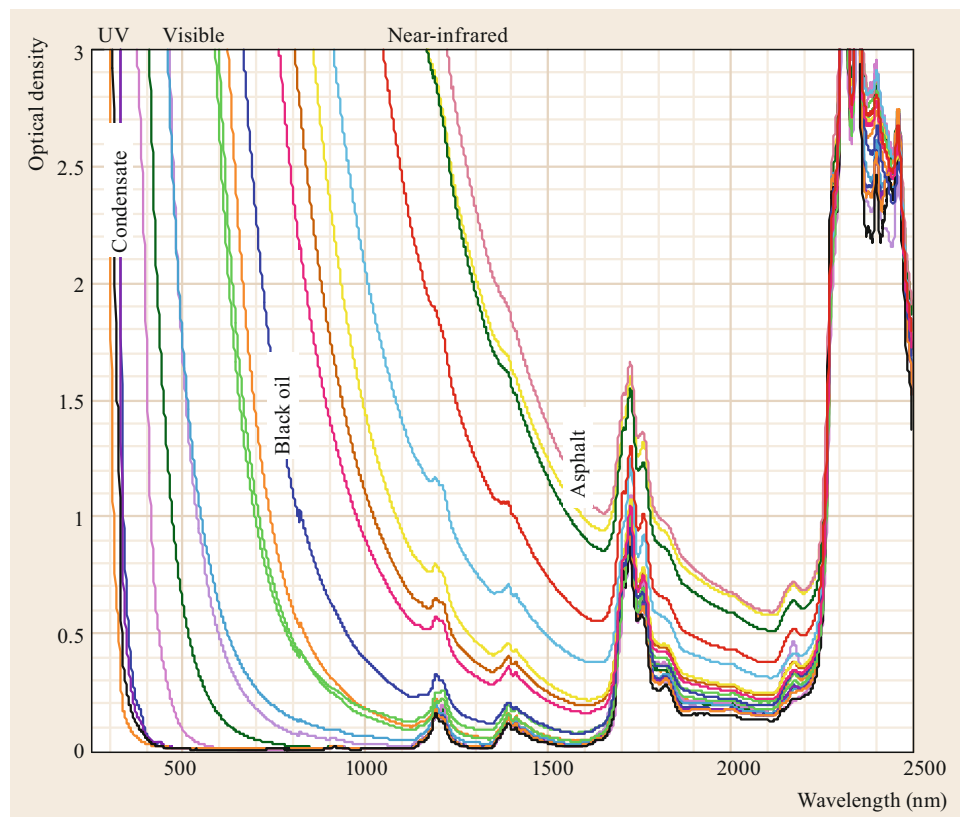


Fig. 7.2 Vis/NIR spectra of typical crude oils. The vibrational peaks can be used to differentiate oil versus water, while the differing, sloping electronic absorption edges can be used to differentiate amongst different oils (after [7.2])

scattering for the single phase fluids shown in Fig. 7.2. OD is defined as

$$OD = -\log_{10} \left(\frac{I}{I_0} \right), \quad (7.1)$$

where I_0 is the incident light intensity and I is the transmitted light intensity. OD is linear in the molecular extinction coefficient, concentration and pathlength. Both water and oil exhibit peaks associated with vibrational overtone and combination bands. The bands are (formally) forbidden, thus accounting for their small cross-section in comparison to the allowed fundamental vibrational bands in the MIR, which are roughly a thousand times larger in OD. The higher energy peaks (shorter wavelength) in Fig. 7.2 correspond to higher overtones and combination bands and are *more forbidden* accounting for their smaller size. These peaks offer the capability to differentiate water and oil in a robust manner. In addition, the oil spectra have differing electronic absorption spectra that are characterized by increasing absorption at shorter wavelengths. This variable, sloping absorption corresponds to the

electronic absorption edge of crude oils. Overall, the electronic spectrum of a crude oil is an incoherent sum of many contributing spectra from the numerous chemical constituents in crude oil. This valence shell electronic absorption increases continuously towards shorter wavelengths; towards the vacuum ultraviolet range (Chap. 6).

Identification of oil versus water is always key in oil well logging. Water has very distinctive absorption peaks around 1440 and 1940 nm. The peak at 1440 nm corresponds to the vibrational overtone of the O–H stretch mode (symmetrical and/or asymmetrical) of water, and the peak at 1940 nm corresponds to the combination of stretch plus bend mode of water. Oil has a group of absorption peaks around 1725 and 2350 nm. The peak at 1725 nm corresponds to the overtone of the stretch mode of the C–H bond (predominantly in methylene groups), and the peak at 2350 nm corresponds to the combination mode of the stretch plus bend of the C–H bond (again predominantly in methylene groups). The clear separation of water and oil peaks allows easy identification and quantification of water and oil in flowing fluid sample [7.10, 11].

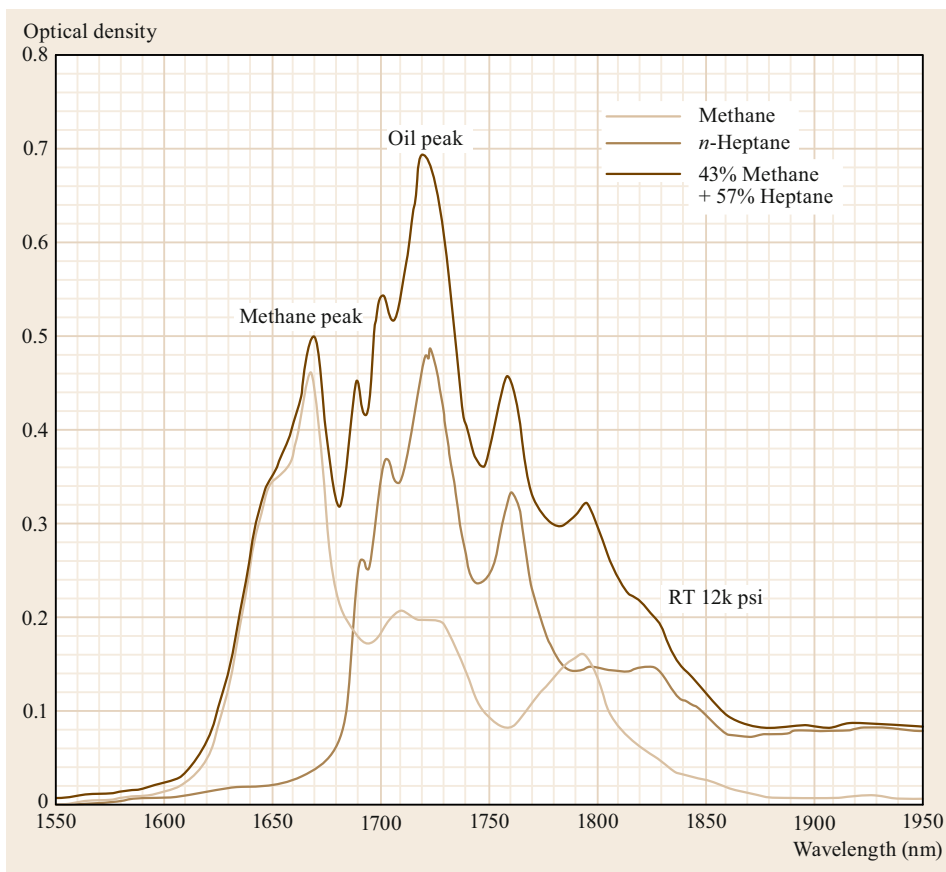


Fig. 7.3 The two-stretch overtone NIR spectra of methane, *n*-heptane, and a mixture of methane and *n*-heptane. The CH_4 two-stretch overtone is shifted to higher energy (1670 nm). The $-\text{CH}_3$ overtones appear as a doublet at 1690 and 1700 nm. The dominant $-\text{CH}_2-$ overtone is at 1725 nm; the so-called oil peak (after [7.10])

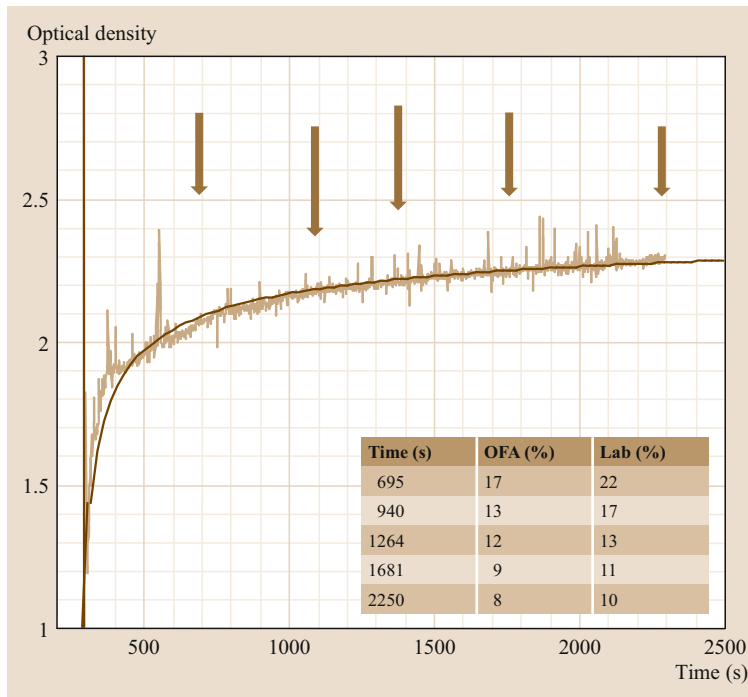


Fig. 7.4 The cleanup process for acquisition of crude oil in a well drilled with OBM. As MDT pumping time advances, the contamination of the flowline fluid is reduced enabling acquisition of clean formation crude oil. The OCM algorithm allows quantification of the time dependence of the color measurement or GOR (not shown) in real time during sample acquisition and is in agreement with subsequent lab contamination analyses (after [7.2])

Differentiation of different CH groups, CH_4 – CH_3 and $-\text{CH}_2-$ can be obtained by analysis of the two-stretch overtone at ≈ 1725 nm. (In crude oil, the methine contribution is very small and not useful.) Although all hydrocarbon molecules show absorption around 1725 nm, the exact absorption spectrum depends on the resonance frequency of each vibration mode. Since resonance frequency of carbon-hydrogen vibration is slightly different in methane (CH_4), methyl ($-\text{CH}_3$), or in methylene groups ($-\text{CH}_2-$), then some hydrocarbon compositional information can be obtained from the CH two-stretch overtone. Figure 7.3 shows relevant spectra and furthermore helps establish that the spectra are linear in composition [7.2].

For gaseous alkanes there are some further energy differences in the overtones enabling further spectral characterization of composition. This similarity of spectra among hydrocarbon molecules effectively sets a practical limit to a number of independently extractable compositional groups. We use a chemometric approach, principal components regression (PCR) [7.10] and partial least squares regression (PLS), to build interpretation models that map the measured spectrum into composition. The latest DFA spectrometer can determine methane (C_1), ethane (C_2), the C_3 – C_5 group, and C_{6+} groups in crude oil with reasonable accuracy [7.10]. In additions to these grouped hydrocarbon compositions, the CO_2 measurement is

also possible by measuring its peak around 2000 nm under some situations. These compositional analyses are useful by themselves, and furthermore, they also allow calculation of the GOR, which is one of the most important parameters for characterizing reservoir hydrocarbons [7.1].

In addition, differentiating between or among different oils is also essential downhole. In particular, oil wells are often drilled with oil-based muds (OBM) as discussed above (Fig. 7.1). Some of the OBM filtrate leaks into permeable zones. Differentiation of the OBM filtrate versus crude oil is essential. The OBM filtrates do not possess dissolved gas or asphaltenes. Thus, Vis-NIR spectroscopy can be used to differentiate drilling fluid versus subsurface formation crude oil. In particular, almost all reservoir crude oils contain dissolved gas, dissolved asphaltenes, or both. Using the NIR spectral analysis, the GOR of the flowline fluid is determined. Using the Vis-NIR measurement, the color of the flowline fluid is measured. Both GOR and color are measured as a function of pumping time. Using various algorithms such as the OCM algorithm [7.2], the measurement of color and GOR versus pumping time can be quantified as a percent contamination as shown in Fig. 7.4 [7.2].

In addition, to obtaining clean formation fluids, DFA is critical for understanding the spatial variation of formation fluid properties. Understanding the nature of crude oil variation throughout reservoirs is essen-



Fig. 7.5 Dead crude oils (at one atmosphere thus without their gas fraction) from a single oil reservoir, deepwater Gulf of Mexico. These oils have a huge, monotonic range of asphaltene content (courtesy of Hani Elshahawi, Shell)

tial for optimizing production. Figure 7.5 shows the type of variation of crude oil that can naturally occur in oil reservoirs. Some origins of these variations are discussed in case studies below.

Those working in the oil industry know that heavy oils have a black color and light condensates have a light brown to yellow color. Figure 7.3 shows a huge change in (dead) oil color in a single reservoir associated with dramatically differing asphaltene concentrations. The right side of Fig. 7.3 corresponds to the top of the reservoir and the left side corresponds to the base of the oil reservoir.

This color variation is caused by the variation in concentration of asphaltenes. Asphaltenes with their significant fraction of large PAHs absorb light in $\pi-\pi^*$ electronic transition of polycyclic aromatic hydrocarbons (PAHs). Larger fused ring systems of PAHs have greater π -orbital delocalization, thus lower energy transitions. Two extreme examples of π -electron excitation

are benzene and graphite. Benzene has just one aromatic ring with minimal π -electron delocalization, and requires relatively large energy (≈ 250 nm) to excite $\pi-\pi^*$ transitions. Graphite (or graphene), on the other hand, has essentially an infinitely large fused aromatic ring system with π -electrons that are completely delocalized; graphite is a two-dimensional electrical conductor and a zero bandgap semiconductor, thus readily absorbs across the Vis/NIR range. The number of fused rings in asphaltene PAHs can exceed 15 rings (Chap. 6) giving rise to red-shifted $\pi-\pi^*$ transitions. This explains why heavy oil, rich in large PAHs of asphaltene molecules, have very dark color. Crude oil color can be used as an indicator of oil weight (density). While this analysis has been mostly qualitative in nature in the past, recent developments provide a strong foundation in chemical physics and thermodynamics for quantitative interpretation of DFA data as will be discussed herein.

7.3 Implementation of DFA Hardware

While Vis/NIR spectroscopy is a common analytic method in laboratory settings, implementation of DFA hardware (downhole) has always been a challenging scientific and engineering task. This challenge can be understood by contrasting the environmental requirements of oil and gas wellbores versus laboratories. Figure 7.6 shows a range of pressure and temperature conditions encountered in hydrocarbon-bearing formations, and thus provides specifications for DFA tools. The temperature inside oil and gas wells can be above 175°C (347°F) or even over 200°C (392°F). Moreover, the temperature might not even be stable during the DFA measurements. The pressure inside oil and gas wells can reach 140 MPa (approximately 20 000 psi) or may reach 200 MPa in very deep wells, for example, in the Gulf of Mexico. DFA instruments may experience severe and continuous shock and vibration during transportation to a well site and descent in wells to the designated depths. The latter is particularly demanding if the DFA spectrometer is a part of a drill string. Other important hardware design considerations for

DFA spectrometers include hardware footprint, maintainability and reliability. We will briefly explain these factors in this section.

The most obvious and probably the most demanding environmental requirement for engineering any scientific measurement instrument is high temperature, which can exceed 175 or even 200°C . High temperature can affect DFA optical train design in several different ways. First, it may destroy or significantly reduce the functionality and/or lifetime of typical optoelectronic and electronic components. It is known through years of experiences that failure rates of typical plastic packaged components increase dramatically above 150°C . For reliable operation at higher temperature, packaging of optoelectronic and electronic components requires exotic high-temperature plastic, metal or ceramic packages, which almost certainly requires customization and increase of manufacturing cost.

High temperature may not destroy components but it may still significantly alter the characteristics of

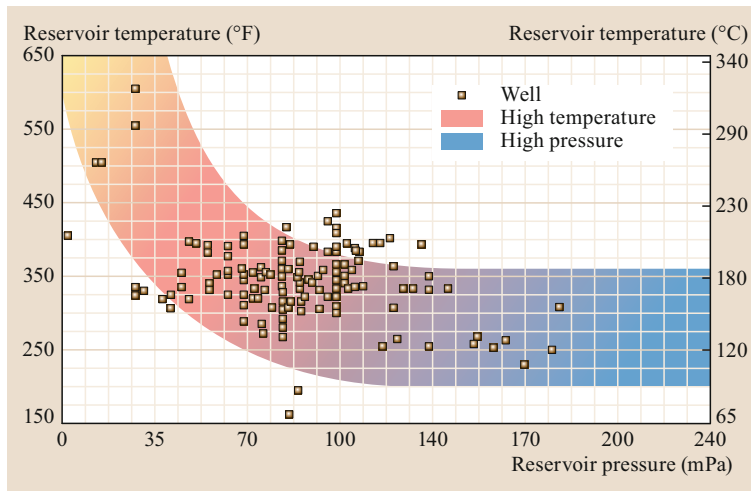


Fig. 7.6 Temperature and pressure conditions for selected wells (after [7.12]). The high temperatures are challenging for detectors and electronics. The high pressures mandate small devices

optoelectronic components. For example, lasers and light-emitting diodes (LEDs) may survive high temperature but their emission may be significantly altered, requiring significant compensation. For this reason, we have used a tungsten-halogen incandescent lamp operating around 3000 K for a light source for DFA spectrometers. A 3000 K black body radiator gives usable intensity in the entire Vis/NIR wavelength and tungsten-halogen lamps remain stable throughout a typical operating environmental range of room temperature to over 150 °C. Optical bandpass filters based on Fabry–Pérot interferometers may shift wavelength with temperature as high temperature causes thermal expansion and changing refractive index. High temperature can defocus and misalign optics by thermal expansion, particularly if the spectrometer is based on diffraction. These are some of the examples of engineering challenges for DFA spectrometer implementation.

Very high pressure, over 100 MPa (approximately 14 500 psi), is another common environmental requirement for measurement instruments used in oil/gas wellbores (Fig. 7.6). Realistically, the only way to design a DFA spectrometer in this setting is to seal the entire section of the spectrometer against pressure and only leave the optical window (or cell or probe) exposed to the high-pressure fluid. The optical window material needs to be strong enough to withstand high pressure, chemically stable against corrosive fluids, and transparent in the wavelength range used for spectroscopy. Sapphire is a perfect material satisfying all these requirements. For transmission geometry, we use a pair of sapphire windows separated by a flow channel enabling transmission spectroscopy.

Spectrometers generally are incompatible with mechanical shock and vibration, which is why most lab-

oratory spectroscopy often employs a shock absorbing table. Nevertheless, the DFA measurement setting requires that the DFA spectrometer will experience significant shock and vibration. Spectrometer hardware can achieve wavelength dispersion utilizing prisms and gratings, interferometry (e.g., FT-IR), or a set of (fixed wavelength) optical filters. Against mechanical shock and vibration, a spectrometer with fixed-wavelength optical filters (filter-array spectrometer) is the most robust design, although a high-resolution grating spectrometer is in use in a commercial DFA tool: the in situ fluid analyzer (IFA) [7.13].

A simplified schematic of a filter-array spectrometer is shown in Fig. 7.7. A 3000 K tungsten-halogen incandescent light source produces broadband radiation with a maximum output at roughly $\lambda = 1 \mu\text{m}$ and which covers the entire Vis/NIR wavelength range. A rotating chopper wheel selects the optical path and modulates the signal, reducing the noise floor. The modulated light source is selectively guided into a measurement cell or reference path via optical fiber bundles. The light transmitted out of a measurement cell and reference path are redistributed to individual photodetectors (PD) each coupled with a designated optical bandpass filter (only one of them is drawn in Fig. 7.7). The total number of optical bandpass filters (or channels) can be 10, 20, or any number decided by measurement requirements. With proper design customization, semiconductor-based PDs and optical filters can be reliable even over 150 °C.

Other important considerations for the DFA spectrometer design include the hardware size, maintainability and reliability. Space is a premium for downhole tools and the hardware needs to be designed to fit into a cylindrical tool string of typically 4 in or less in inner diameter. Once the DFA spectrometer is dispatched

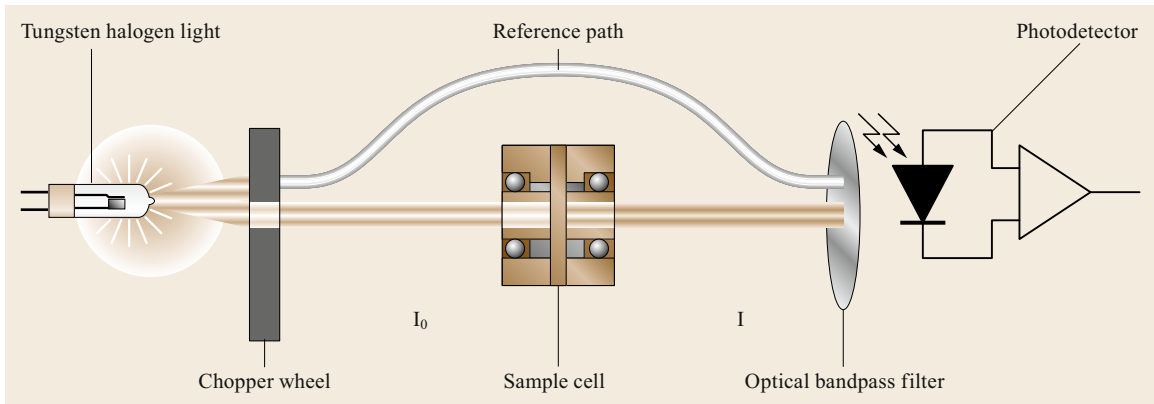


Fig. 7.7 A schematic of a DFA filter spectrometer. This figure is drawn for only one wavelength channel for simplicity

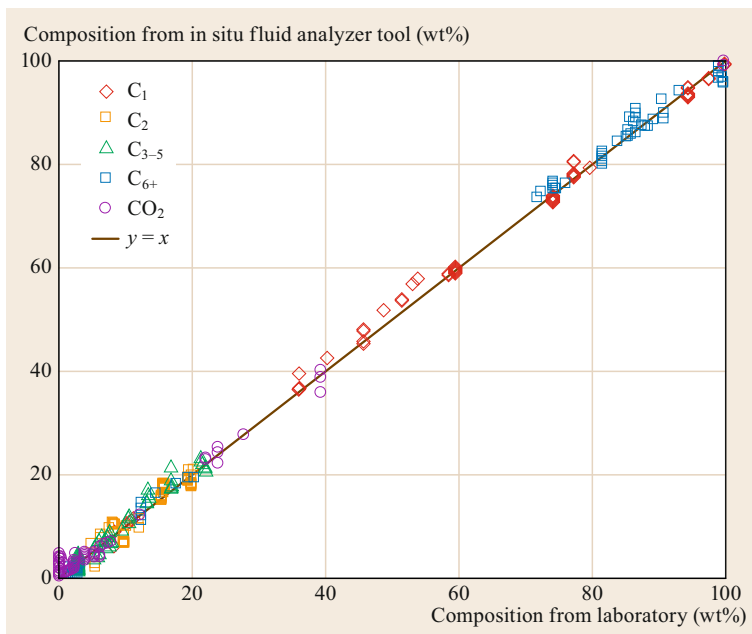


Fig. 7.8 Comparison of compositions obtained from a DFA spectrometer (in situ fluid analyzer) and laboratory (gas chromatography) (after [7.10])

to a wellsite for measurement, there is no further opportunity for calibration. The spectrometer calibration needs to be stable and can only be performed at the tool shop on a very intermittent basis. Reliability is critically important in an oilfield business setting. Rig costs can exceed \$ 1 million per day; lost time due to instrumentation failure is prohibitively expensive. Finally, the DFA tools must be economically viable. The cost of the DFA tools and DFA data must be commensurate with corresponding value. All these factors add to make DFA requirements most demanding.

DFA spectrometers schematically depicted in Fig. 7.7 have been successfully engineered, manufactured, and deployed to oil/gas wells all over the world and routinely provide vital measurements inside wellbores under these demanding conditions. By exploiting spectral overtone analysis, DFA spectrometers can achieve compositional analysis displayed in Fig. 7.8, which shows excellent agreement of between hydrocarbon compositions measured by a DFA spectrometer (Schlumberger in situ fluid analyzer [7.13]) and by laboratory gas chromatography [7.10].

7.4 Basic DFA Operations and Applications

When a wellbore is drilled and a hydrocarbon reservoir is penetrated, several measurements are made to understand the subsurface formation properties. These measurements include formation density, porosity, basic lithology, resistivity, and rock stress. To understand fluid properties and fluid distributions, a formation fluid sampling tool or *formation tester* is required. The lead-

ing formation tester tool in the industry is the MDT tool [7.4].

A typical MDT tool sting consists of one or more probe modules, pump modules, DFA modules, and sample chamber modules. Figure 7.9 shows an example formation tester. The main role of the probe module is to create a sealing contact at the wellbore wall, thus allowing formation fluid to flow into the MDT. The actual shape of probe can be a simple small tube surrounded by a sealing rubber flange, or two concentric tubes with two layers of sealing rubber flanges for more efficient sampling, or two sets of packers isolating a section of wellbore. Pump modules generate a differential pressure to move fluid from the formation to the formation tester. Typically, because of mud filtrate invasion into the formation, a large amount of formation fluid needs to be pumped and expelled into the wellbore before the desirable quality fluid is obtained. DFA modules analyze and evaluate the flowing fluid inside the MDT flowline in real time so that the operators can make necessary decisions such as whether and when to take fluid samples. Sample chamber modules are used to capture the fluid flowing inside the MDT if it is judged as worthy of detailed analysis in a laboratory.

DFA has many uses. As noted above, DFA is used to analyze the sample cleanup during acquisition of formation samples as shown in Fig. 7.4. By analysis of the types of formation fluids in real time, the sample program can be optimized. Of course, hydrocarbon fluids are desired (versus water). DFA can be used to determine when a high-pressure bottle should be filled with the formation fluid for laboratory analysis. The sampling quality assurance is the procedure to obtain representative reservoir fluids in a sample bottle for further analysis in the laboratory. It is vitally important that the sample fluid is captured under a single phase condition otherwise the differential flow rate of two phases (gas and liquid) will not yield a representative sample. To achieve this goal, the DFA spectrometer module continuously measures and monitors flowline contents to detect any indication of phase segregation [7.2]. If different subsurface permeable zones contain different hydrocarbons, more sample bottles can be filled and brought to the surface. A new and powerful use of DFA is to perform reservoir evaluation to address major production concerns.

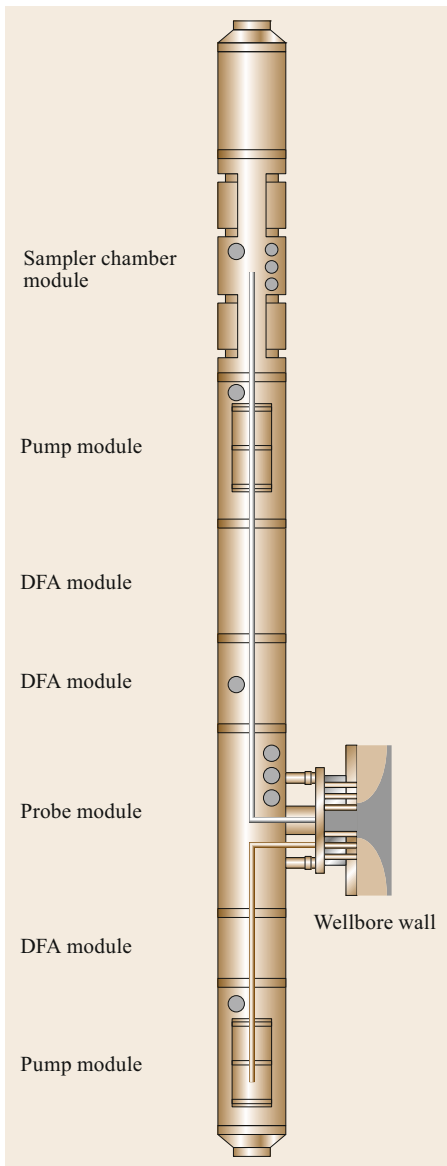


Fig. 7.9 A schematic example of the MDT sampling tool sting including DFA spectrometer modules, a probe module, pump modules and a sample chamber module

7.5 Reservoir Evaluation via DFA and Thermodynamics

DFA is the best method to measure fluid compositional gradients in oilfields. Figure 7.10 shows a schematic of the many uses of DFA measurement and thermodynamic analysis of reservoir fluid gradients. For measurements performed in single wells, many systematic errors cancel because DFA measurements at different points in the well have the same tool, almost the same time and temperature, the same calibration and same technologists. Thus, even subtle fluid gradients can be measured. With significant effort, tool-to-tool variation has been minimized in the latest generation of DFA tools such as the IFA; consequently, lateral variations of fluid properties can be measured accurately. In addition, the DFA data acquisition program can be matched to the complexity of the oil column. When large fluid differences are measured at two different depths in the well, DFA can be acquired at several intervening depths to clarify the type of fluid gradients.

In addition to the gravity term (the leading term in the argument of the exponential), the second term in the exponential is the solubility term. This term is the specific manifestation of the chemical axiom *like dissolves like*. If the solubility parameter of the asphaltene and the

crude oil are not too dissimilar, then the energetics allow dissolution. Gaseous hydrocarbons are gaseous and colorless. Hydrocarbon gases are colorless because asphaltenes do not partition (or dissolve) in this phase. Gaseous hydrocarbons are not *like* the dark brown solid, the asphaltenes. Consequently, high-GOR crude oils have very limited capacity to dissolve asphaltenes, while low-GOR fluids can dissolve asphaltenes. The variation of the solubility term in reservoir crude oils is dominated by GOR variations. For low-GOR crude oils, the oils are incompressible, thus there is very little GOR variation with depth. Consequently, the solubility term is constant, and the asphaltene variation is dominated by the gravity term (cf. Eq. (7.2)).

The last term in the argument of the exponential in (7.3) is the entropy term. This term tends to be small, and acts to yield distributions that are macroscopically homogeneous; that is randomly distributed.

Equation (7.3), mandates knowing the size of the asphaltene particle, explicitly the asphaltene size (or volume V). The inability to characterize asphaltene size previously precluded development of any EoS for asphaltene distributions. Without a known size, Newton's

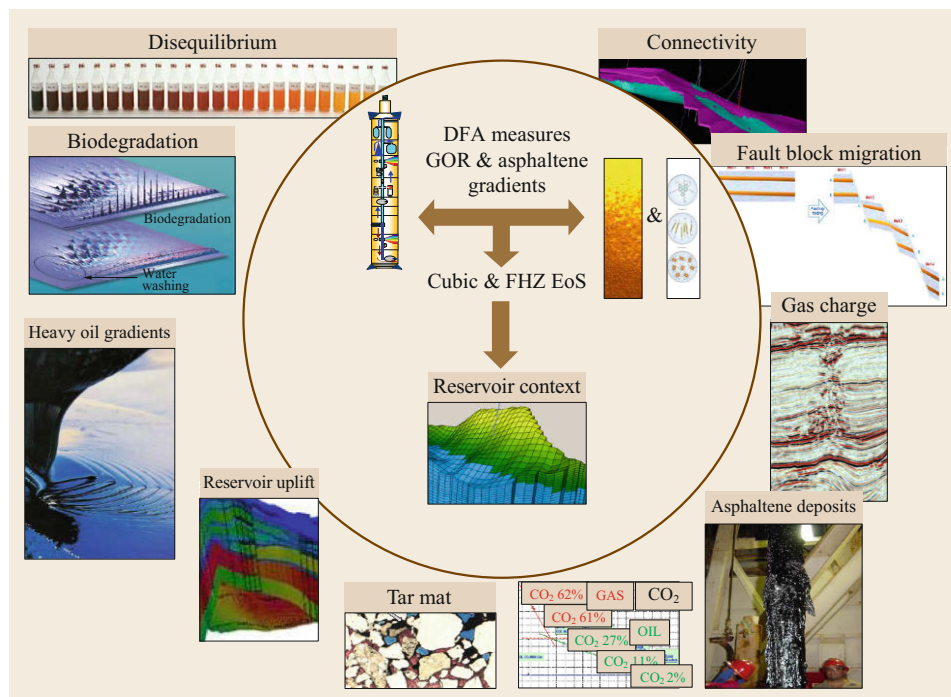


Fig. 7.10 The DFA workflow (after [7.3]). DFA measurements of fluid properties and gradients of fluid properties are made vertically and laterally in the reservoir. Thermodynamic analysis of the gas–liquid properties is performed with the cubic EoS. Asphaltene–fluid gradients are analyzed by the Flory–Huggins–Zuo equation of state (FHZ EoS) (after [7.8])

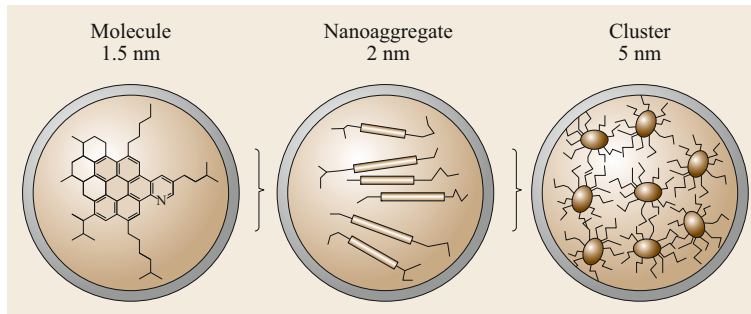


Fig. 7.11 The Yen–Mullins model depicting the predominant molecular and nanocolloidal structures of asphaltenes in crude oils and in laboratory solvents. At low concentrations such as in light oil, asphaltenes are dispersed as a true molecular solution (*left*). At higher concentrations such as in black oils, asphaltenes are dispersed as nanoaggregates (*center*). At yet higher concentrations such as in mobile heavy oils, asphaltenes are dispersed as clusters of nanoaggregates (*right*) (after [7.6]). All of these species are stable in the corresponding crude oils for geologic time

second law of motion, $F = ma$, remains undetermined for asphaltenes in a gravitational field. F is force, m is mass and a is acceleration; for a gravitational field $a =$

g . The size of asphaltenes has been resolved and codified in the Yen–Mullins model shown in Fig. 7.11 [7.6]. Chap. 6 treats this model in detail.

7.6 Reservoir Case Studies

The first reservoir to be studied linking the FHZ EoS and the Yen–Mullins model for reservoir evaluation was performed by Schlumberger and Chevron technologists for a reservoir in deepwater, Gulf of Mexico. Figure 7.12 depicts the upper and lower boundaries of the reservoir located at roughly 20 000 ft below sea level with a water depth of many thousand feet.

Fluid gradient data is essential in order to understand the thermodynamic context of the reservoir fluids. A single sample does not constrain the thermodynamic modeling. In contrast, fluid gradients provide a strin-

gent test for any thermodynamic modeling. The cubic equation of state (EoS) is used for modeling gas–liquid properties such as GOR and composition [7.1]. At this stage, this approach can be considered classic and is not reviewed here. In contrast, modeling asphaltene gradients is very new. Chapter 6 of this handbook describes the resolution of the molecular and colloidal structure of asphaltenes, which is now represented in the Yen–Mullins model. Knowing the size of asphaltene particles in crude oil enables evaluation of the gravity term, an essential component of modeling reservoir fluids. The first theory introduced for asphaltene gradients is the Flory–Huggins–Zuo EoS (FHZ EoS) which, of course, incorporates the effects of gravity. The gravity term is given by Archimedes buoyancy ($V\Delta\rho g$) of the asphaltenes in the Boltzmann distribution where V is the size of the asphaltene particle, $\Delta\rho$ is the density contrast between the asphaltene particle and the oil phase, and g is Earth’s gravitational acceleration. OD_i is optical density at height i in the reservoir, k is Boltzmann’s constant and T is temperature (cf. Eq. (7.2)).

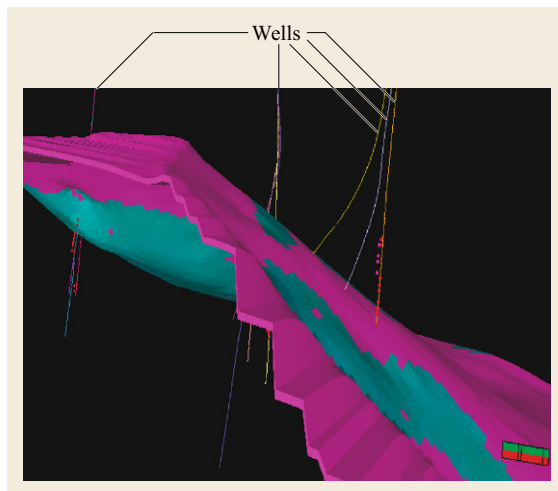


Fig. 7.12 The upper and lower surfaces of a reservoir are depicted: deepwater, Gulf of Mexico (after [7.2]). The reservoir contains two stacked sands at different pressures thus not in flow communication. The reservoir is tilted and faulted due to basin distortion. The primary risk in reservoir development is the extent of flow connectivity in each reservoir sand ◀

$$\frac{OD_h}{OD_o} = \exp \left\{ \frac{-V\Delta\rho gh}{kT} \right\}. \quad (7.2)$$

Replacing $V\Delta\rho$ with the weighted mass of nitrogen and oxygen molecules yields the barometric equation, which gives the atmospheric pressure gradient of planet Earth from sea level to Mount Everest and beyond. The weighted sum of atmospheric gases is used because compositional mixing from weather systems is far more rapid than the diffusive process, which would lead to separate density gradients of the different gases. The Boltzmann distribution describes the counterbalance between energy; gravity pulling objects with mass to lower elevation versus thermal excitation – thermal energy lifting objects above the lowest point. For low-GOR crude oils, the FHZ EoS largely reduces to this gravity term (7.2). The full FHZ EoS is listed below and applies to heavy ends in all crude oils [7.7, 8].

By adding the gravity term to the Flory–Huggins polymer solution theory, the Flory–Huggins–Zuo EoS is obtained. This theory combines simple regular solution theory of solubility with the effects of gravity to describe the distribution of dissolved (or nanocolloidally suspended) asphaltenes in reservoir fluid. The Flory–Huggins–Zuo (FHZ) EoS is the first EoS for predicting asphaltene concentration gradients with depth in oil reservoirs [7.7, 8]. It is the only proven EoS to describe asphaltene gradients in oil reservoirs for crude oils ranging from condensates to heavy oils [7.8]. Be-

cause of the simple form of the FHZ EoS, it can use various measurements of reservoir fluid properties in particular by employing asphaltene concentration ratios or optical density ratios at two different depths in the reservoir. The FHZ EoS is

$$\begin{aligned} \frac{OD(h_2)}{OD(h_1)} = \frac{\phi_a(h_2)}{\phi_a(h_1)} = \exp \left\{ \frac{v_a g (\rho - \rho_a) (h_2 - h_1)}{kT} \right. \\ \left. + \frac{v_a}{kT} [(\delta_a - \delta)_{h_1}^2 - (\delta_a - \delta)_{h_2}^2] \right. \\ \left. + \left[\left(\frac{v_a}{v} \right)_{h_2} - \left(\frac{v_a}{v} \right)_{h_1} \right] \right\}, \quad (7.3) \end{aligned}$$

where OD, k , ϕ , v , δ , T , g , ρ , and h are the optical density, Boltzmann's constant, volume fraction, molar volume, solubility parameter, temperature, gravitational acceleration, density and depth (or height) respectively. Subscript a denotes the properties of asphaltenes; subscripts h_1 and h_2 stand for the properties at depths h_1 and h_2 respectively. It should be pointed out that the crude oil solubility parameter, molar volume, and density of bulk fluids, temperature, pressure and compositions are dependent on depth.

For this low-GOR reservoir of crude oil, the GOR is largely homogeneous, and for asphaltene gradients the gravity term dominates. The measured asphaltene gradients versus true vertical depth (TVD) are shown in Fig. 7.13. In the following figures, TVD is arbitrarily offset to avoid using the actual depth which is proprietary.

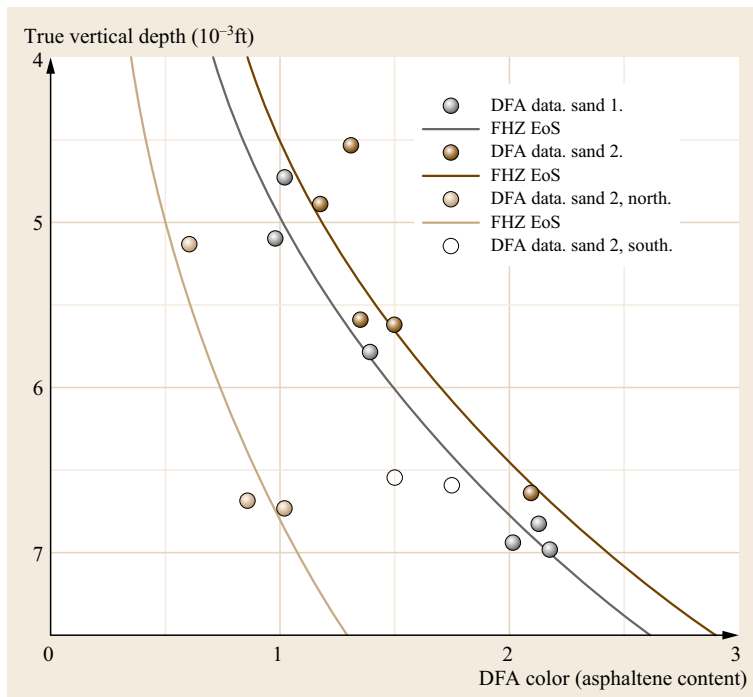


Fig. 7.13 Asphaltene (color) gradients versus true vertical depth. All three sands (grey, dark brown and light brown) are seen to fit (7.2) (lines) with a 1.6 nm asphaltene nanoaggregate size (after [7.2]). Thus, each sand individually shows equilibrated asphaltenes. Equilibrated asphaltenes indicate reservoir connectivity

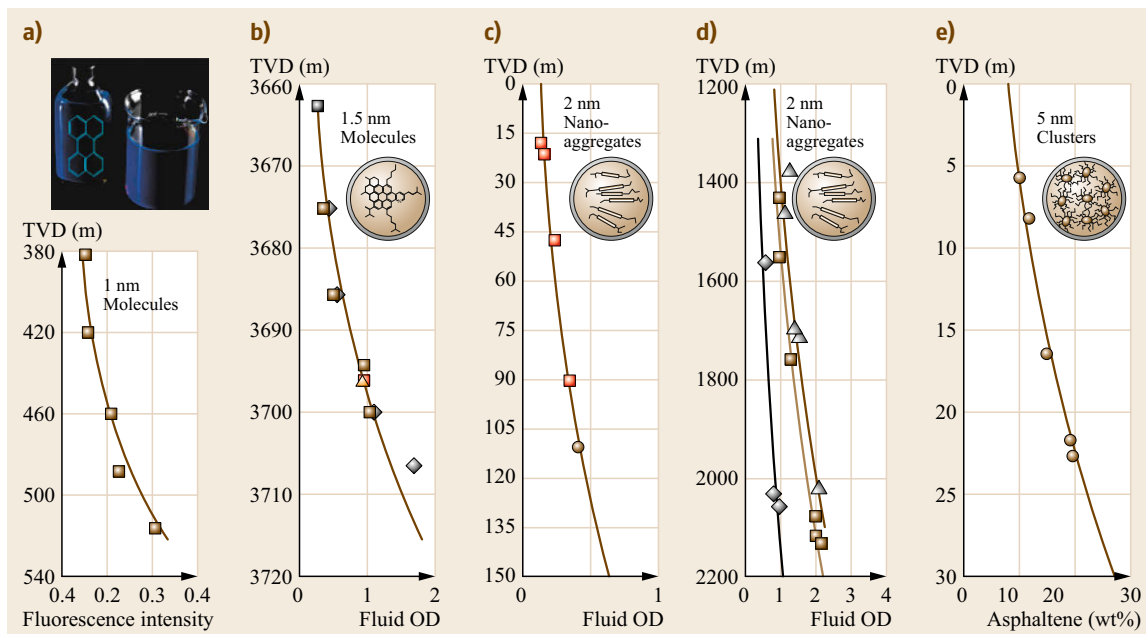


Fig. 7.14a–e The asphaltene (or heavy end) gradients in five reservoirs containing oil ranging from condensate (a) to heavy oil (e). (a) Condensate GOR = 600 m³/m³, (b) Volatile oil GOR = 350 m³/m³, (c) Black oil GOR = 180 m³/m³, (d) Black oil GOR = 90 m³/m³, (e) Heavy oil GOR = 12 m³/m³. In the light oil (a), the heavy ends are heavy resins such as perylene (inset), as this oil contains no asphaltenes (after [7.8]). For the other cases (b–e), the specific asphaltene structure from the Yen–Mullins model is shown (molecules, nanoaggregates and clusters). In all cases, the FHZ EoS fits the asphaltene gradients indicating equilibrated asphaltenes (or heavy ends). In all cases, the production established reservoir connectivity

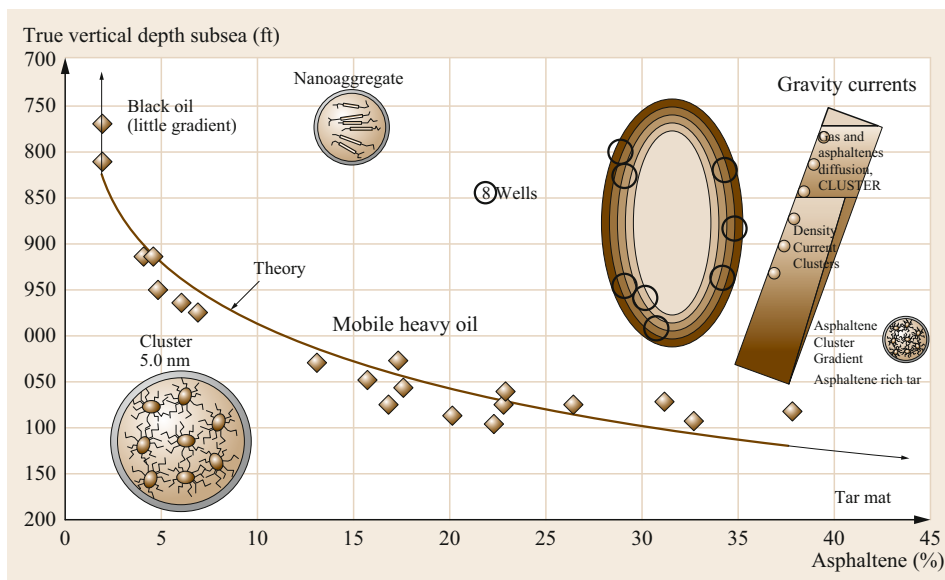


Fig. 7.15 A heavy oil rim of ≈ 100 km in length is accurately described by (7.2) using a 5.1 nm asphaltene cluster size, the only adjustable parameter, which is in excellent agreement with a nominal 5.0 nm cluster size (after [7.14]). The $10\times$ gradient of asphaltenes in ≈ 150 feet of height (≈ 50 m) over 100 km in length provides a very stringent test and positive result for fitting with (7.2). Reprinted with permission from [7.14]. Copyright 2013 American Chemical Society

For each of the two stacked sands, the grey sand and the dark brown sand, the asphaltene gradients are accurately fit by (7.2). The asphaltene particle size is the

only adjustable parameter in the fitting and the obtained size is 1.6 nm. The range of size of colloidal particles varies from 1 nm to 1 μ m. Any smaller and the system

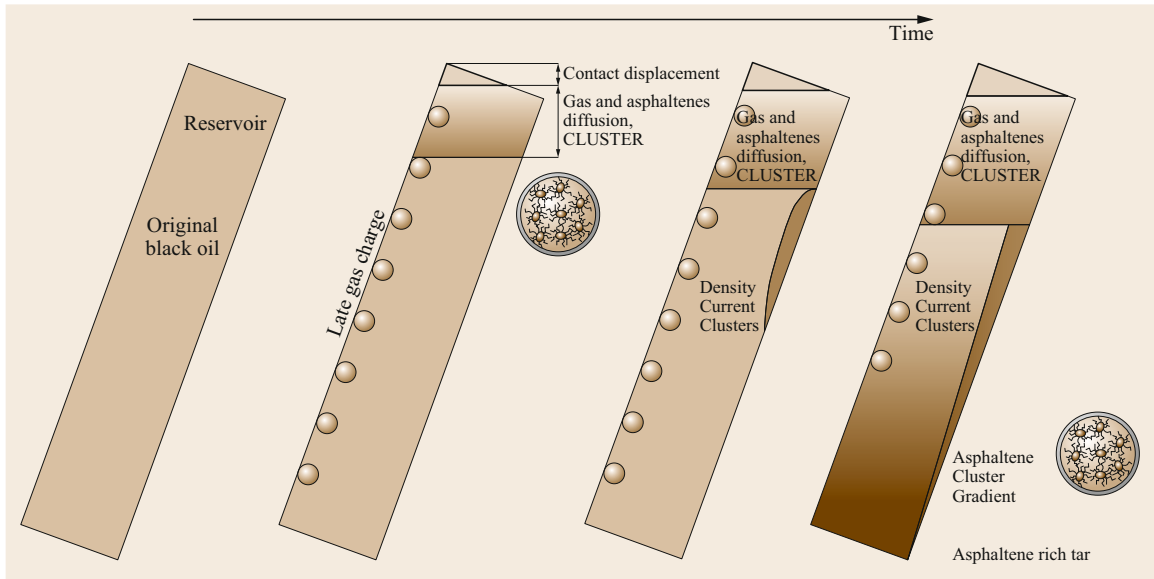


Fig. 7.16 The time sequence of a slow gas charge into an oil reservoir (after [7.3]). A diffusive front of gas entry into the oil column takes places thereby increasing solution gas at/near the GOC. Asphaltenes are expelled out of the high-GOR, upper regions of the oil column and diffuse in the form of asphaltene clusters ahead of the gas front. This causes a pileup of asphaltenes at the diffusive gas front, increasing the oil density there above the original oil. Convective currents follow and pump asphaltene-enriched oil to the base of the reservoir. This can cause formation of heavy oils at the base of the reservoir with large (asphaltene cluster) gravity gradients. With continued gas entry at the crest, asphaltene accumulation continues at the base causing formation of tar mats if sufficiently high concentrations of asphaltenes are attained

is molecular thus not colloidal, and any larger and the buoyancy forces cause rapid segregation. The nanoaggregate size obtained from Fig. 7.13 is within 20% of expected nanoaggregate size, thus is close to what is expected a priori.

The existence of equilibrated asphaltenes is a strong indicator of reservoir connectivity [7.15]. The separate equilibration curve shown in brown in Fig. 7.13 in the north of one of the sands indicates that this reservoir section is separate and not connected. One cannot have coffee color in one sand, tea color in another sand at the same depth and have all in equilibrium. All connectivity predictions made by DFA analysis here have been confirmed in production [7.2].

Figure 7.14 shows DFA data from five reservoirs with crude oils ranging from condensate to heavy oil. In all cases, the asphaltenes or heavy ends are equilibrated vertically and, in the cases with multiple wells, laterally, and in all cases in Fig. 7.14, connectivity has been established with production. In all cases, the FHZ EoS accurately accounted for the heavy end gradients [7.8].

The salient feature of Fig. 7.14 is the strong link between equilibrated asphaltenes (as determined by FHZ EoS analysis) and reservoir connectivity, established in production, a dynamic measurement. The lack of equilibration of asphaltenes does not mean there is no

connectivity; reservoir fluid geodynamics can preclude fluid equilibrium as shown below. In addition, there are cases where the asphaltenes equilibrated, then a subsequent geologic event sealed part of the reservoir. In such a case, asphaltene equilibration does not indicate connectivity. Nevertheless, the petroleum system is tightly constrained by the DFA data to have fluid equilibration followed by a sealing event.

In most cases in Fig. 7.14, the cubic EoS analysis of GOR gradients was not very instructive; thus the FHZ EoS analysis is key [7.8]. For low-GOR black oils (Fig. 7.14d) and heavy oils (Fig. 7.14e), the GORs are homogeneous, thus precluding effective connectivity analysis. The same fluid on both sides of a fault does not indicate the fault is hydraulically transmissive. Instead, it is a continuous gradient through a fault which indicates transmissivity (or connectivity). In addition, the error in GOR determination, lab or downhole, is often bigger than the corresponding gradient, thus giving an ambiguous connectivity analysis. This error problem generally applies to high-GOR black oils (Fig. 7.14c). In some cases, with late gas charge into the reservoir, the GOR can be in disequilibrium while the asphaltenes are equilibrated (Fig. 7.14b). As shown in production, the reservoir is connected proving the value of the FHZ EoS analysis. That is, fluid geodynamics in this

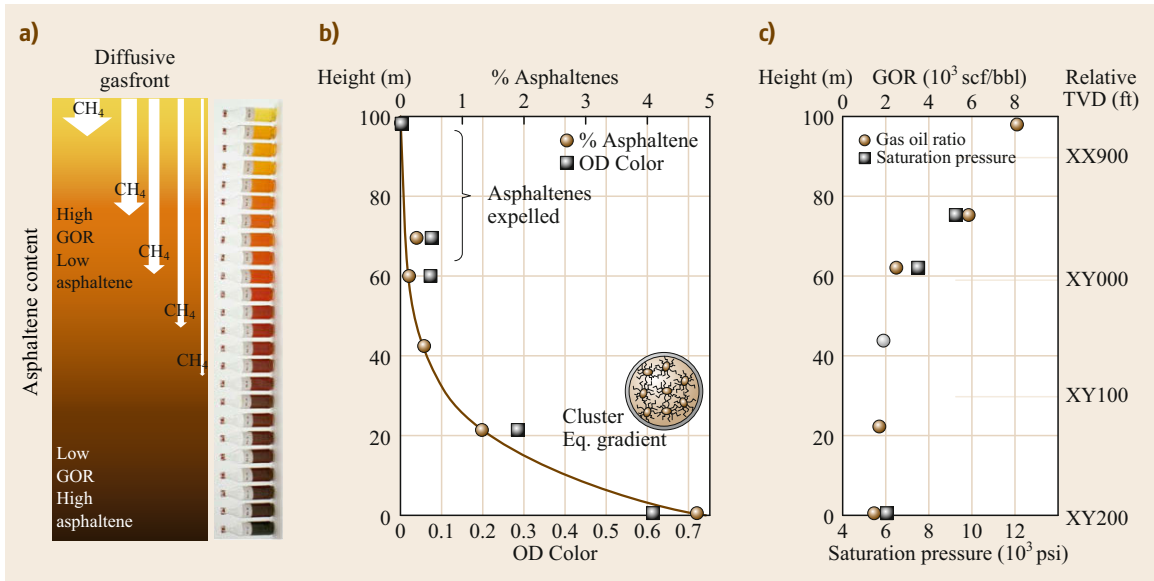


Fig. 7.17a–c A reservoir in the middle of a slow, late gas charge into oil (after [7.3]). **(a)** The color gradient of a series of dead oils from a single oil column (Fig. 7.5). Also shown is a cartoon of the process of diffusive methane entry into the oil column from the GOC. The solution gas gradient is diffusive as depicted in the cartoon. **(c)** Confirmation of a huge disequilibrium of solution gas in the top half of the oil column. XY is used to mark the leading numbers as the data shown is confidential. The GOR varies from 8000 to 2000 scf/bbl in 150 ft of height. The GOR in the bottom half of the oil column is equilibrated; the diffusion of methane has not had time to reach the bottom. **(b)** The asphaltenes have been expelled from the top of the oil column due to high GOR (the liquids possesses little color). Gravity currents of clusters pumped asphaltenes to the base of the reservoir yielding a gravitation gradient of asphaltene clusters. Copyright 2014, Society of Petroleum Engineers Inc. Reproduced with permission of SPE. Further reproduction prohibited without permission

reservoir precluded equilibration of the light ends but the perturbation was not sufficient to disturb the asphaltenes in this case [7.8].

Another reservoir, depicted in Fig. 7.15, in a four-way sealing anticline, has a fairly simple distribution of contained fluids. The crest of the field contains a black oil of low GOR and moderate asphaltene content. Around the 100 km rim of the field, there is ≈ 50 m height of heavy oil. This heavy oil is underlain by a tar mat of ≈ 10 m. As the GOR is low, the gravity term (7.2), dominates the distribution. The asphaltene particle in heavy oils is the asphaltene cluster. Figure 7.15 shows the data from seven of the eight wells that intersected this reservoir [7.14, 16]. A similar stacked reservoir in this field showed the same gradient.

The equilibration of the oil in Fig. 7.15 provides a strong indication of reservoir connectivity, as has been proven in production [7.16]. The only way to equilibrate fluids over such great distances is through convective currents, not diffusion. A diffusive process over a distance of 50 km would take a trillion years; while this reservoir is old, it is not 70 times the age of the universe! The origin of the convective currents is

associated asphaltene instability upon charging of a second light oil or gas into a black oil reservoir. Figure 7.16 shows a schematic of this process.

This same process occurs even if the second charge is not a slow gas charge, but instead is a slow, light liquid hydrocarbon charge. The light charge would migrate to the crest. The light components would diffuse into the oil column destabilizing asphaltenes, and the asphaltenes would diffuse down and away from oil enriched in light hydrocarbon components. For simplicity, we represent this second charge as a gas charge, but the same line of reasoning applies for a light hydrocarbon charge into an original column of black oil. Thus, a gas cap is not a prerequisite for the occurrence of this slow, late, light hydrocarbon charge into an oil column.

A key component in this process is the accumulation of asphaltenes at the base of the diffusive gas front. At greater times, expelled asphaltenes pile up ahead of the gas front similarly to the way snow piles up in front of a snow plow. Coupled diffusion equations between methane and asphaltenes in crude oil show this piling-up phenomenon [7.17].

The giant reservoir depicted in Fig. 7.15 shows the end result of this process. Figure 7.17 shows a reser-

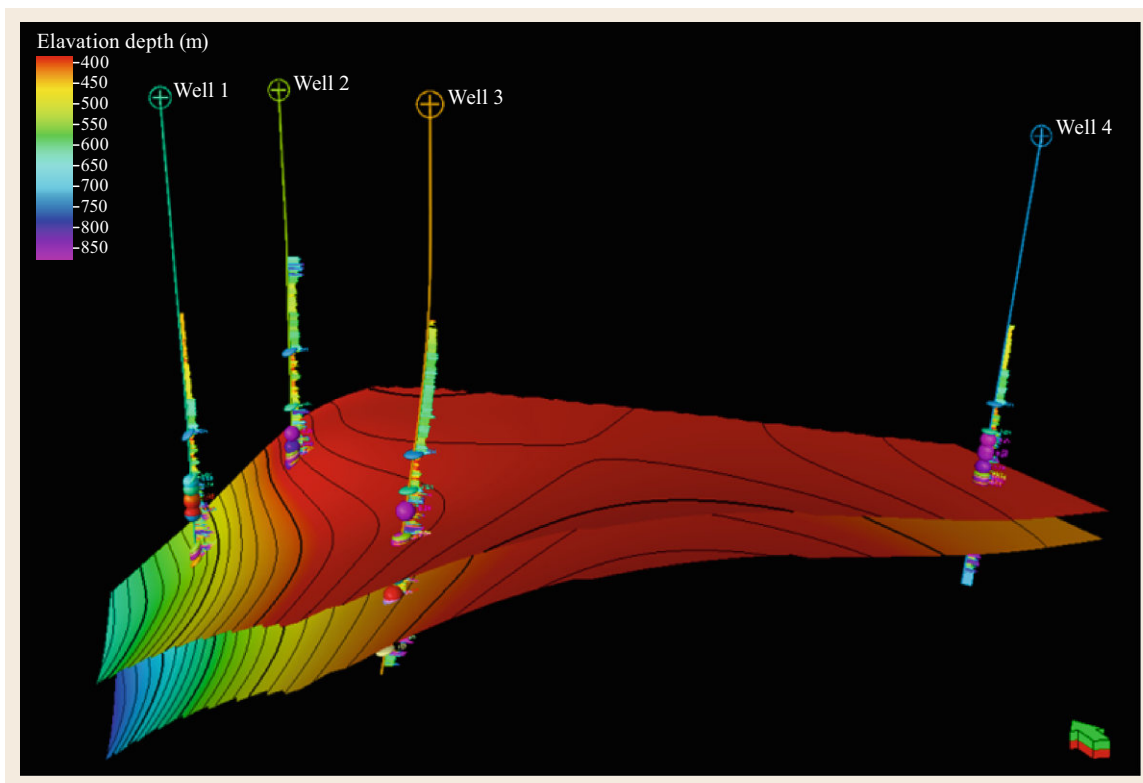


Fig. 7.18 The upper and lower horizons of the Bhagyam field. The field is only 300 m below surface and has been undergoing biodegradation since reservoir charging, which commenced in the lower Eocene. The rate-limiting step in the biodegradation is diffusion of labile alkanes to the oil-water contact at the base of the oil column. Reprinted with permission from [7.18, 19]. Copyright 2015 American Chemical Society

voir that is in the middle of gas diffusion and asphaltene convective currents. This reservoir fluid, particularly the light ends, is far from equilibrium even in this connected reservoir. Recent and ongoing reservoir fluid geodynamics can preclude equilibration as seen in Fig. 7.17.

Figure 7.17 shows the dramatic effects on oil properties associated with a slow gas charge into an oil reservoir. Both DFA and lab data show this effect. The gas charge into the oil reservoir migrates quickly to the top of the oil column, the so-called Stainforth charge mechanism [7.2]. In this deepwater field, the reservoir pressure is sufficiently high that the gas dissolves in the oil. The newly charged gas then diffuses down into the oil column. The GORs and saturation pressures for the top half of the oil column are grossly out of equilibrium (Fig. 7.17c). Instead the solution gas in the top half of the oil column is determined by the diffusion of methane from the top. The lower half of the oil column has equilibrated GOR and saturation pressure; diffusion of methane from the top has not had sufficient time to reach the bottom half of the oil column. For diffusion,

it is not the height that determines the requisite time, rather it is the distance along the reservoir (measured depth).

Figure 7.17 also shows that the asphaltenes have been expelled from the top of the oil column in accordance with the high solution gas; the higher the GOR, the less the asphaltene concentration. The bottom half of the oil column has equilibrated with solution gas exhibiting little variation with depth. Consequently, there was no perturbation of the asphaltene concentration in the lower half of the oil column from variations in solution gas. Nevertheless, there is a large asphaltene gradient matching a gravitation gradient of clusters. The most likely explanation for this observation is that the expelled asphaltenes from the top half of the oil column flowed in gravity currents to the base of the reservoir in the form of asphaltene clusters.

The gravity currents occur when the light hydrocarbon diffuses into the black oil and expels asphaltene [7.3]. These convective currents pump asphaltene from the crest of the field to the base of the field, giving rise to heavy oil at the base. If the asphaltene instability

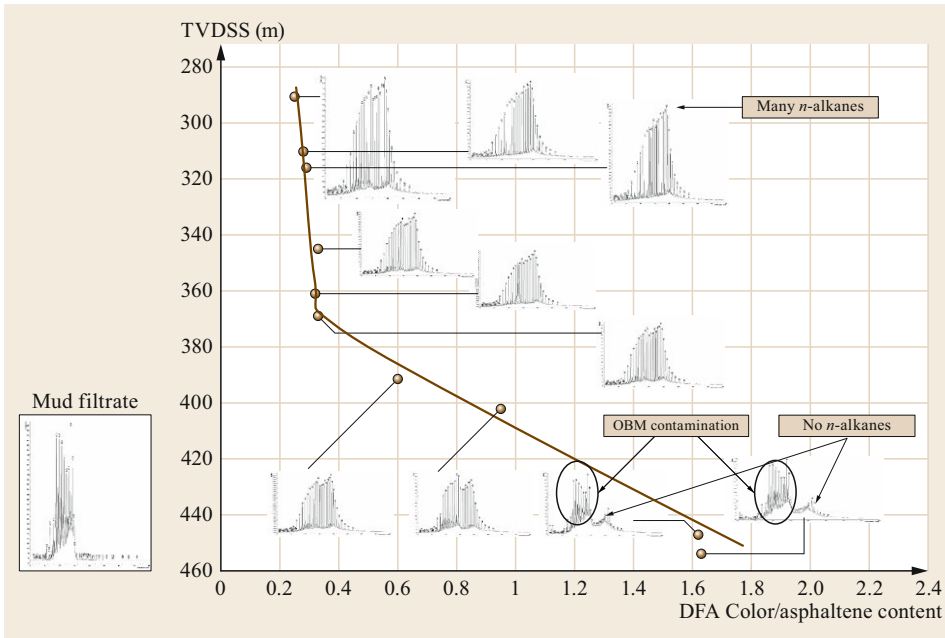
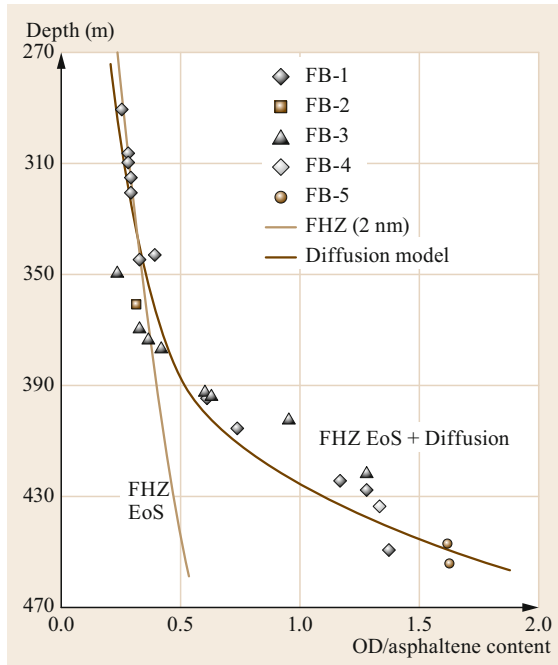


Fig. 7.19 The relative asphaltene content versus depth in the Bhagyam field, along with GC traces of selected samples. Approximately the top half of the oil column has GC traces exhibiting a full complement of alkanes (the tall regular *spikes*). The alkanes are seen to diminish with increasing depth (except the filtrate contamination). Reprinted (adapted) with permission from [7.18, 19]. Copyright 2015 American Chemical Society

process continues, enough asphaltene can be pumped to the base of the crude oil column to yield a tar mat [7.3]. The giant reservoir depicted in Fig. 7.15 had just this process. A cartoon showing the gas charging into the reservoir, gas diffusion into the oil column, along with an asphaltene-rich gravity current, is shown in the inset of Fig. 7.15 and in Fig. 7.16.



Other reservoir fluid processes can take place in geologic time that can preclude equilibration in addition to a late gas charge. An example of such a case is provided by the Bhagyam reservoir in the Rajasthan basin in India and shown in Fig. 7.18 [7.18]. There are five stacked sand reservoirs penetrated by four wells (in this study); all sands show identical fluid gradients.

The five-stacked sand reservoirs of the Bhagyam field commenced charging in the lower Eocene and ceased charging with uplift in the lower Miocene [7.20]. Figure 7.19 shows the DFA-measured fluid color (which gives the relative asphaltene content) versus depth in the field. In addition, the gas chromatograms (GCs) are shown for oils at various depths in the field. In addition, a GC of the OBM mud filtrate is also shown in Fig. 7.16 [7.18, 19].

The impact of biodegradation is readily observed in the GC traces in Fig. 7.19 towards the bottom of the oil column (the oil-water contact; OWC). The microbes live in the water and preferentially consume the alkanes. As the alkanes disappear, the asphaltenes become concentrated and the viscosity increases. The rate-limiting step is diffusion of alkanes higher in the oil column to the OWC; the biodegradation step is more rapid.

Fig. 7.20 Thermodynamic modeling and data from five-stacked sands (after [7.19]). The Bhagyam field is shown in Fig. 7.18, and the GC traces are shown in Fig. 7.19. Diffusion is the rate-limiting step; the analysis shows that the diffusive process initiated approximately 50 million years ago ◀

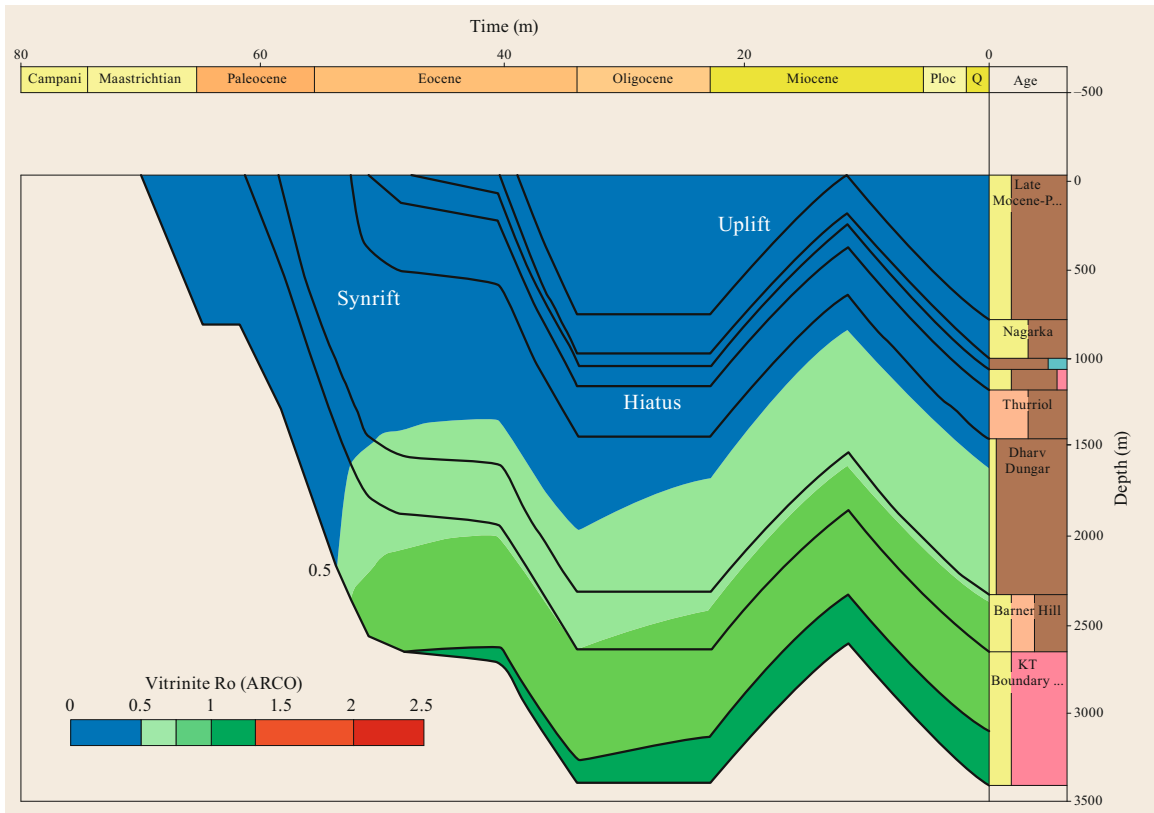


Fig. 7.21 Results from the Rajasthan basin modeling (1-D burial model) showing that the Bhagyam field commenced charging in the lower Eocene and terminated charging with uplift in the lower Miocene. Increasing thickness of the *dark and light green shaded areas* corresponds to source maturity and reservoir charging. The diffusion-biodegradation process has been taking place for ≈ 50 million years (after [7.20])

Figure 7.20 shows data from five separate sands; the DFA color (OD) all overlay. The top half of the oil column is well fit by the FHZ EoS using the 2 nm nanoaggregate from the Yen–Mullins model. The bottom half of the oil column increasingly diverges from the static FHZ EoS model with depth. Including a (time-dependent) diffusive term accounts for the gradient in asphaltenes and is also consistent with the GC traces in Fig. 7.19.

The data presented in Figs. 7.19 and 7.20 show that a diffusive gradient exists in the reservoir and accounts for the gross disequilibrium of the alkane distribution as well as the asphaltene distribution. The one-dimensional diffusion equation gives

$$2Dt = x^2, \quad (7.4)$$

where D is the diffusion constant, t is time, and x is the mean displacement. Using a reasonable value for the diffusion constant, $D = 4 \times 10^{-8} \text{ cm}^2/\text{s}$ (oil is $> 20 \text{ cP}$) and $\approx 100 \text{ m}$ for the vertical distance from the

OWC, a 13° reservoir dip angle, one obtains 40 million years as an approximate duration of this diffusion and biodegradation process [7.19].

The petroleum system analysis presented in Fig. 7.21 is consistent with the simple diffusion analysis of a ≈ 40 million year duration of the diffusion and biodegradation process. With a reduction of the alkane composition of the crude oil, the asphaltenes are concentrated. Biodegradation can consume approximately two thirds of the oil [7.21], thus the asphaltenes can concentrate by a factor of three, which is exactly the increase above FHZ EoS equilibration seen in Fig. 7.20. The asphaltenes tend not to diffuse up the column despite the high concentration of asphaltenes low in the column because the reduction of alkanes makes the remaining crude oil a better solvent for asphaltenes. Being able to model the asphaltene gradient, and thus the viscosity gradient, with a simple chemical physics model is important to optimize the field development plan.

7.7 Conclusions

Prior to DFA, there had been the presumption that reservoir crude oils are largely homogeneous at least for the purposes of field development planning. However, assumptions of reservoir fluid homogeneity often led to significant production inefficiencies. Moreover, DFA surveys of reservoirs have become increasingly popular in establishing that reservoir fluid complexities frequently prevail. Moreover, the cost structure of DFA is compatible with the routine evaluation of fluid complexities in order to manage risk in reservoir development. In addition, for the first time, the asphaltene gradients in reservoirs can be modeled from a first principles approach using the FHZ EoS and its reliance on asphaltene nanostructures described in

the Yen–Mullins model. The combination of new DFA technology and new petroleum asphaltene science has led to an explosion of applications for oilfield development. Many reservoirs are now being understood within simple chemical physics models. These models are being combined with petroleum system modeling to maximize reservoir evaluation. A new understanding of commonly misunderstood reservoir observations such as tar mats, heavy oil gradients, and GOR gradients are firmly within the purview of these new formalisms. Efficiencies in field development planning and production of crude oil follow from these growing insights. The enhanced role of science and technology continues unabated in the petroleum industry.

References

- 7.1 W.D. McCain: *The Properties of Petroleum Fluids* (PennWell, Tulsa 1990)
- 7.2 O.C. Mullins: *The Physics of Reservoir Fluids: Discovery Through Downhole Fluid Analysis* (Schlumberger, Houston 2008)
- 7.3 O.C. Mullins, K. Wang, D. Hernandez, A.E. Pomerantz, J.Y. Zuo, P.S. Hammond, C. Dong, H. Elshahawi, D.J. Seifert: Characterization of asphaltene transport over geologic time aids in explaining the distribution of heavy oils and solid hydrocarbons in reservoirs, SPE ATCE 170730 (2014)
- 7.4 T.H. Zimmerman, J.J. Pop, J.L. Perkins: Down hole tool for determination of formation properties, US Patent 4 860 581 (1989)
- 7.5 O.C. Mullins, E.Y. Sheu, A. Hammami, A.G. Marshall (Eds.): *Asphaltenes, Heavy Oil and Petroleumomics* (Springer, New York 2007)
- 7.6 O.C. Mullins: The modified Yen model, *Energ. Fuels* **24**, 2179–2207 (2010)
- 7.7 D.E. Freed, O.C. Mullins, J.Y. Zuo: Asphaltene gradients in the presence of GOR gradients, *Energ. Fuels* **24**(7), 3942–3949 (2010)
- 7.8 J.Y. Zuo, O.C. Mullins, D.E. Freed, C. Dong, H. Elshahawi, D.J. Seifert: Advances of the Flory–Huggins–Zuo equation of state for asphaltene gradients and formation evaluation, *Energ. Fuels* **27**, 1722–1735 (2013)
- 7.9 B. Raghuraman, G. Gustavson, O.C. Mullins, P. Rabbito: Spectroscopic pH measurement for high temperatures, pressures and ionic strength, *AIChE Journal* **52**, 3257 (2006)
- 7.10 G. Fujisawa, M.A. van Agthoven, F. Jenet, P.A. Rabbito, O.C. Mullins: Near-infrared compositional analysis of gas and condensate reservoir fluids at elevated pressures and temperatures, *Appl. Spectrosc.* **56**(12), 1615–1620 (2002)
- 7.11 A.R. Smits, D.V. Fincher, K. Nishida, O.C. Mullins, R.J. Schroeder, T. Yamate: In situ optical fluid analysis as an aid to wireline formation sampling, SPE Form. Evaluation **10**(2), 91–98 (1995)
- 7.12 C. Avant, S. Daungkaew, B.K. Behera, S. Danpanich, W. Laprabang, I. De Santo, G. Heath, K. Osman, Z.A. Khan, J. Russel, P. Sims, M. Slapal, G. Tevis: Testing the limits in extreme well conditions, *Oilfield Rev.* **24**(3), 4–19 (2012)
- 7.13 V. Achourov, A. Gisolf, A. Kansy, K.O. Eriksen, M. O'Keefe, T. Pfeiffer: Applications of accurate in-situ fluid analysis in the North Sea, SPE 145643, Aberdeen (2011)
- 7.14 O.C. Mullins, J.Y. Zuo, D. Seifert, M. Zeybek: Clusters of asphaltene nanoaggregates observed in oil reservoirs, *Energ. Fuels* **27**, 1752–1761 (2013)
- 7.15 T. Pfeiffer, Z. Reza, W.D. McCain, D. Schechter, O.C. Mullins: Determination of fluid composition equilibrium – A substantially superior way to assess reservoir connectivity than formation pressure surveys, Proc. SPWLA, Annu. Symp., SPWLA–2011–EEE, Colorado Springs (2011)
- 7.16 D.J. Seifert, M. Zeybek, C. Dong, J.Y. Zuo, O.C. Mullins: Black oil, heavy oil and tar mats, ADIPEC 161144, Abu Dhabi (2012)
- 7.17 K. Wang, Y. Chen, J.Y. Zuo, O.C. Mullins: The dynamic Flory–Huggins–Zuo equation of state, *Energy* **91**, 430–440 (2015)
- 7.18 R. Jackson, J.Y. Zuo, A. Agarwal, B. Herold, S. Kumar, I. De Santo, H. Dumont, C. Ayan, O.C. Mullins: Mapping and modelling large viscosity and asphaltene variations in a reservoir undergoing active biodegradation, SPE ATCE 170794, Amsterdam (2014)
- 7.19 J.Y. Zuo, R. Jackson, A. Agarwal, B. Herold, S. Kumar, I. De Santo, H. Dumont, M. Beardsell, O.C. Mullins, C. Ayan: Diffusion model coupled with the Flory–Huggins–Zuo equation of state and Yen–Mullins model accounts for large viscosity and asphaltene variations in a reservoir undergoing active biodegradation, *Energ. Fuels* **29**(3), 1447–1460 (2015)

- 7.20 B.N. Naidu, V. Kothari, N.J. Whitely, J. Guttormsen, S.D. Burley: Calibrated basin modelling to understand hydrocarbon distribution in Barmer Basin, India, Proc. AAPG Int. Conv. Exhib., Singapore (2012)
- 7.21 I.M. Head, D.M. Jones, S.R. Larter: Biological activity in the deep subsurface and the origin of heavy oil, *Nature* **426**, 344–352 (2003)

8. Phase Behavior and Properties of Heavy Oils

John M. Shaw, Marco A. Satyro[†], Harvey W. Yarranton

The phase behaviors and thermophysical and transport properties of heavy oils not only share numerous features with light oils and reservoir fluids, but also exhibit substantial differences because of their more complex chemistry and fluid physics associated with this chemistry. As a consequence, conventional understanding, experimental methods, and property/phase behavior computation tools are stretched to their limits. They often fail to provide needed data and insights for process development, design, and operation for production, transport, or refining applications. Heavy oils are inherently multiphase and exhibit time-dependent and polymorphic behaviors that depend not only on temperature and pressure, but also on thermal and shear history as well. Simple properties such as density at fixed temperature and pressure have irreducible uncertainty, and one must think in terms of rheological response rather than viscosity, particularly at low temperatures. Heavy oil characterization poses challenges as well because available analytical tools can provide composition information for less than 50 wt% of typical heavy oils and there is much guess work and correlation needed even to generate composition/property estimates with significant – and hard to quantify uncertainties. In this chapter, we draw upon our diverse experiences to survey the current state of the experimental and computational landscapes related to heavy oil thermophysical and transport properties and phase behavior. Differing and occasionally opposing approaches are presented. Limitations of experimental and computational methods and knowledge needs are discussed, and practical recommendations for specific calculations are noted, typically with caveats. There caveats arise because the landscape is changing rapidly and best practices are evolving continuously, even though we have been producing hydrocarbon resources, transporting, and refining them into diverse products at an industrial scale worldwide for more than a century.

8.1	Background	274
8.2	Phase Behavior and Phase Composition Measurement ..	277
8.2.1	Resources on Their Own.....	277
8.2.2	Heavy Oil and Diluent Phase Behavior ..	278
8.2.3	Heavy Oil and Water Phase Behavior.....	280
8.2.4	Equilibrium Compositions.....	282
8.2.5	Summary	282
8.3	Thermophysical Property Measurement	283
8.3.1	Density	283
8.3.2	Heat Capacity	284
8.3.3	Bitumen and Heavy Oil Rheology Measurement	285
8.3.4	Mutual Diffusion Coefficient Measurements	286
8.3.5	Summary	287
8.4	Heavy Oil Characterization	287
8.4.1	Heavy Oil Chemistry.....	288
8.4.2	Characterization Based on Distillation Data	290
8.4.3	Characterization Based on GC Data	290
8.4.4	Characterization Based on SARA Data	291
8.4.5	Characterization Based on Representative Molecules.....	292
8.4.6	Heavy Oil Characterization Summary.....	293
8.5	Phase Behavior Correlation and Prediction	294
8.5.1	Thermodynamic Model Selection	294
8.5.2	Essential Thermodynamic Equations.....	296
8.5.3	Cubic Equations of State (CEOS).....	297
8.5.4	Noncubic Equations of State	299
8.5.5	Activity Coefficient Models	301
8.5.6	Prediction of Water and Heavy Oil Phase Behavior	302
8.5.7	Phase Behavior Prediction Summary.....	303
8.6	Thermophysical Property Simulation and Prediction	303
8.6.1	Caloric Physical Properties – Enthalpy, Entropy, and Heat Capacities ..	304
8.6.2	Density Prediction.....	305
8.6.3	Heavy Oil Viscosity Prediction	307
8.6.4	Property Simulation and Prediction Summary	310
8.7	Perspectives and Conclusions	311
	References	311

8.1 Background

Crude oil has been produced, pipelined, and refined into transportation fuels and other products for more than a century on a global scale. Superficially, one would be excused for thinking that there is little new to report on the topic of oil characterization in what is increasingly perceived as a sunset industry. However, the nature of the resources now being produced, from shale oil to heavy oil and bitumen; the conditions under which they are produced, from mining to deep off-shore wells; the processes used for production and refining, from steam-assisted gravity drainage (SAGD) to solvent assisted processes; and the economic, environmental, and political constraints have changed radically during this period. The *newer* hydrocarbon resources are typically rich in undistillable fractions (500 °C+ equivalent atmospheric boiling fractions) that are difficult to characterize in detail. At the same time, environmental regulations and product specifications have become more stringent. Consequently, the need for accurate equilibrium phase behavior and phase composition data, transport property data, and models to support resource and product valuation, process design, process development and process optimization has intensified in an environment where conventional analytical tools and characterization schemes often fail. The knowledge demands arise at diverse length and relaxation time scales. Pertinent length scales range from the submolecular and molecular length scales to nano, micro, and larger length scales. Relaxation times in some heavy oil systems are so large that considerable care must be exercised before declaring that a physical property, as understood by classical thermodynamics, has been measured correctly.

This knowledge complexity is presented in the knowledge landscape, as shown in Table 8.1. Composition knowledge at the molecular and submolecular length scales is needed for resource valuation because the elements, functional groups, molecular sizes, and structures in the oil define the refining potential of a resource and the processes needed to transform it. Knowledge at this length scale also provides needed inputs for phase behavior modeling and operating condition selection for refining processes. At the supramolecular length scale, self-association and surface phenomena, arising from asphaltenes and waxes in particular, impact all stages of the production chain, including fluid extraction or production, transport, storage, and refining. At the micro scale, biphase liquid crystal domains have been identified in heavy hydrocarbon resources and resource fractions [8.1], and these materials have been shown to be inherently multiphase [8.2–4] over broad ranges of conditions. The supramolecular structures and microscopic and larger phase domains impact bulk fluid densities, transport properties (diffusivity, and Newtonian and non-Newtonian rheological behaviors), and the potential roles for solvents, for example, in production transport and refining operations. As many of these properties are irreversible to some extent within practical processing time scales, their values and impacts on production operations are affected by the actual thermal and shear histories of samples [8.1–5], and there are inherent limitations in property measurement reproducibility and repeatability that impose constraints on property certainty and consequently on property model development and the associated model quality.

Table 8.1 Heavy oil knowledge landscape

Length scale	Characterization	Motivations	Issues ^a
≈ 1 nm	Molecular and submolecular structures	Resource valuation, refining, phase behavior modeling	Molecular motif identification, species quantitation, tracking chemistry
≈ 10 nm	Self-associating and surface active species, <i>asphaltenes</i>	Avoid production and processing problems, source for refined products	(1) Dissonance regarding molecular structure and driving forces for assembly (2) Artifacts due to definitions (3) Disconnect between nanostructured materials studied in laboratories and those arising in situ.
≈ 20 μm	Liquid crystal domain	New category of materials, surface active	Composition, process and product implications
Bulk	Phase behavior, phase composition, transport properties, energy properties	Production and process models, new process development, transport models, roles of solvents, etc.	A priori prediction is infeasible. Correlation within narrow ranges of conditions is feasible, model breakdown, misuse and misconceptions are common.

^a Sampling and subsampling present challenges and create additional ambiguity at all length scales

Each of these length scales also presents challenges for measurement and theory. At the molecular and submolecular length scales, Fourier transform ion cyclotron resonance mass spectroscopy (FT-ICR MS) can provide a wealth of detail concerning the elemental composition and molar mass of molecules present in heavy oil samples [8.6, 7]. But this powerful technique has yet to yield quantitative composition information suitable for property prediction. This lack of quantification arises because, in spectroscopy, the relative sensitivities of the method to a specific molecular species are dependent on the chemical nature of constituents and mass fractions of all constituents present [8.8, 9]. So, the analysis of a sample as a whole, or as a series of subfractions prepared on the basis of a specific property such as polarity or boiling point range, can yield significantly different impressions as to the principal constituents of a sample from a mass or mole fraction perspective. The resolution of the issue of fluid composition quantitation based on FT-ICR MS analysis is a subject of intense research and the prize is significant. Alternate approaches targeting quantitative a hydrocarbon resource or resource fraction composition knowledge at this length scale based on combining various forms of spectroscopy such as ^{13}C and proton NMR, with elemental analysis, vapor pressure osmometry, and other more conventional techniques with subjective molecule construction algorithms are underconstrained mathematically and yield ambiguous outcomes at the molecular level [8.10, 11]. With additional constraints introduced from photo acoustic infrared and Raman analysis, this latter approach, offers the possibility of providing a limited number of characteristic molecular substructures, referred to here as molecular motifs, suitable for tracing the impact of chemical reaction on fluid composition and phase behavior and for providing practical inputs to production or refining process models based on a common characterization procedure. However, this potential is as yet unrealized. Consequently, conventional refinery characterization approaches continue to be extended to heavy oil composition assessment and modeling.

At the supramolecular length scale, there are divergent perspectives particularly regarding the properties and behaviors of the self-assembling *asphaltene* fraction. This divergence arises in part because of the structural ambiguity at the molecular and submolecular level. Diverse molecular prototypes are envisaged [8.12–15] and consequently diverse self-association mechanisms have been proposed [8.16–19]. These include the assembly of dense and open supramolecular or colloidal structures held together with noncovalent bonds of which acid–base interactions, hydrogen bonding, hydrophobic pockets, aro-

matic π – π stacking have all been proposed. Experimental validation of assembly mechanisms has so far proven to be elusive, and the assembly mechanisms and the nature of the resulting supramolecular structures continue to be subjects of ongoing research. Even defining the size range of aggregates poses numerous experimental challenges [8.20]. With further development, computational and experimental spectroscopy may provide both positive and negative controls [8.21, 22]. The second reason for divergence at this length scale arises because of the ambiguity of the definition of asphaltenes [8.23]. There are numerous pentane and heptane asphaltene definitions and variants to which differing mass fractions and presumably different chemical species of a crude oil report. Further, the link between the chemically separated asphaltene fractions, particularly any of the *heptane asphaltenes*, and the nanodispersed species in crude oils appears tenuous [8.24, 25]. With these caveats in mind, much of the research pursued at the nanometer length scale follows one of two radically different and incompatible paths. Along one path, asphaltene nanoaggregates are presumed to be soluble in toluene and in crude oils and to assemble/destabilize/precipitate from the solution by the addition of *n*-alkanes or systematic variation of intensive variables such as pressure. Pressure changes move solvent-like materials in or out of the oil phase and therefore significantly affect the oil stability and consequently the precipitation of asphaltenes. Along the other path, asphaltene nanoaggregates are presumed to be dispersed, rather than solubilized, in crude oils and even in toluene. Observed behaviors are then interpreted as a change in the nature or extent of aggregation. The difference between these perspectives is profound because the underlying physics and chemistry implied by them differ radically one from the other. As we will show, much of bitumen behavior can be explained with the former conventional approach, including phase behavior (via equations of state and regular solution theory) and physical properties (e.g., viscosity correlations based on Newtonian flow). However, there are instances where the conventional approach fails and these failures have begun to be probed systematically. For example, bitumen exhibits non-Newtonian behavior below approximately 300 K, indicating structure formation in the fluid [8.5]. Asphaltene + toluene + polystyrene mixtures have also been shown to exhibit fluid–fluid equilibrium, including a critical point [8.26]. This phase behavior is driven by a depletion flocculation mechanism that is only active if a significant fraction of asphaltenes are particulate in nature. Further, the application of conventional concepts of solubility such as regular solution theory to the behavior of asphaltene + solvent

mixtures has been challenged [8.27]. As asphaltene solubility concepts underlie deBoer plots [8.28] and so-called stability indices [8.29], this result may explain their high failure rate for predicting asphaltene deposition problems in industry. These examples demonstrate that the integration of the asphaltene self-assembly into phase behavior and property modeling is, at best, incomplete.

Bulk thermophysical and transport property measurement and prediction, and phase behavior measurement and prediction for heavy oil and bitumen, also present experimental and computational challenges, and many properties possess significant irreducible uncertainty. For example, normal boiling point, critical temperature and critical pressure, typical input parameters for phase behavior, and thermophysical property models are not accessible experimentally for heavy oils and along with mean molar mass become indirect fitting parameters for equation-of-state models. Thus, these fluids push the limits of traditional refinery-type fluid equilibria and property models. Alternative approaches based on group contributions from molecular pseudo-components selected to reflect the molecular structure and molar mass diversity of a sample that are identified using spectroscopic techniques and constrained by mass balance or carbon-type data are under development [8.30]. But for the moment these do not offer a significant advantage for property prediction over refinery models [8.31]. Both approaches are at the stage of data correlation, interpolation, and lim-

ited extrapolation rather than prediction. Simple to measure properties, such as density, possess large reproducibility uncertainties [8.32]. Heavy oils possess shear rate and thermal history-dependent viscosities, particularly at lower temperatures [8.33], which contribute to the reproducibility uncertainty of viscosity measurements [8.5]. Sample acquisition methodology, sample storage, subsampling, and handling methodologies for specific measurements are equally significant contributors to the apparent variability of measurements. Heavy oils are inherently multiphase and basic questions such as whether a subsample is representative or not are not readily answered.

From the foregoing, it is clear that there are few simple answers and there is much debate on the phase behavior and properties of heavy oils. The authors of this chapter do not always agree on specific methods or approaches, and have no doubt disagreed in print with one another over the years, but do share a vision of a structured and principled approach for moving measurement and modeling in this field from ambiguity toward certainty, as illustrated in Fig. 8.1, by integrating learning across all length scales. Our mandate is to be brief. Key thermophysical property and phase behavior topics are surveyed. Starting points and references for access to needed data, measurement methods, and computational tools are provided. We suggest tools that are usable, expose their limits, and discuss basic concepts and principles for when calculation or measurement methods fail.

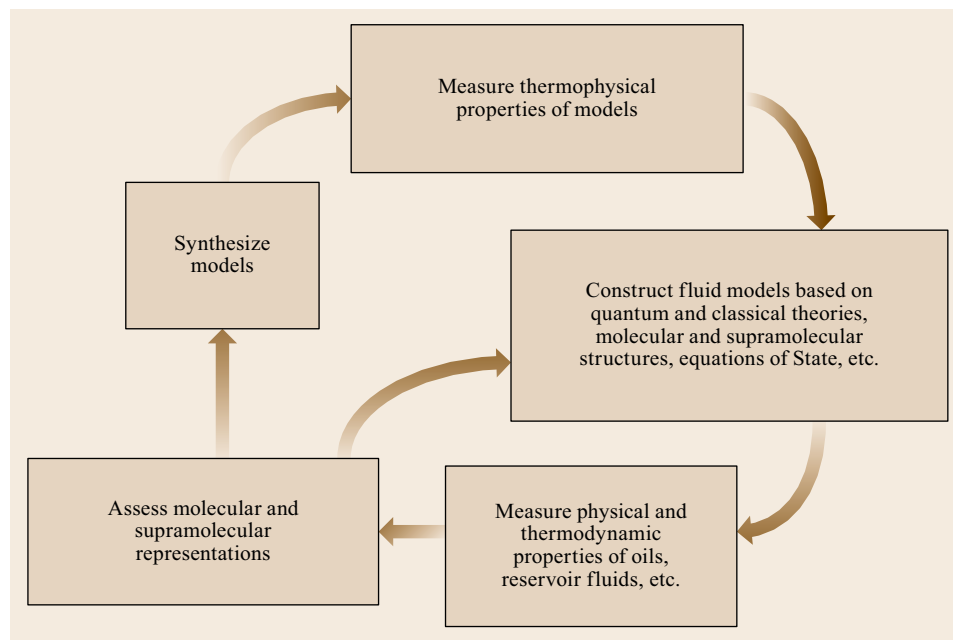


Fig. 8.1 Simultaneous validation of molecular structure, nanostructure, and thermophysical property prediction is required to transition from ambiguity toward certainty

8.2 Phase Behavior and Phase Composition Measurement

Phase behavior and phase composition measurement present numerous challenges not the least of which is the diversity of length scales that are active (nanoscopic, microscopic, bulk) and the complexity of the phase space itself both for the heavy oil and bitumen resources, which exhibit solid, liquid, and vapor behaviors, and for their mixtures with water, organic solvents, organic or inorganic gases, etc., that introduce added complexity because such mixtures are asymmetric and often polar from a thermodynamic perspective. Even simple binary asymmetric mixtures, such as ethane + tetracosane ($C_{24}H_{50}$), where one constituent tends to dominate on a mass fraction basis and the other on a mole fraction basis, can exhibit up to four phases in equilibrium [8.34]. Further, the diversity of conditions under which data are needed span reservoir, mining, pipelining, and in situ refining processing conditions. Thus, data are needed from below 270 K to above 700 K and from subatmospheric pressure to more than 20 MPa. This Herculean task is further complicated by the fact that there is not a coherent framework to describe the phase behavior of heavy oils and bitumen from a composition perspective and the concurrent development of experimental techniques targeting the observation of phase behaviors. Sample acquisition and integrity pose additional challenges. Consequently, the literature on this topic is fragmentary and episodic. Phase diagrams and phase composition data are incomplete and incompatible with one another. Researchers and engineers must exercise caution in the generation, interpretation, and use of phase behavior and phase composition results for process conceptual development, design, and optimization. Reliance on thermodynamic models and workflows that have been successful in the past must be tempered by the limited knowledge concerning material composition, diffusion and rheology, and the extreme nature of property values relative to databases on which conventional models and workflows are based.

8.2.1 Resources on Their Own

Heavy oil and bitumen are inherently multiphase materials and interact with reservoir rock. Use of pressure/heat to extract samples from cores leads to unrepresentative samples because materials not preferentially sorbed are over represented in the samples retrieved. An early contribution from *Henry and Fuhr* [8.35] who ultracentrifuged Athabasca oils and samples without adding solvent showed that the bitumen adhering to the sand grains was asphaltene deficient relative to the supernatant bitumen. Addition of solvents is also

problematic because they lead to preferential deposition of organic materials on acidic (FeS , SiO_2), and basic ($Fe_2O_3/FeOOH/FeO$, $Ni/NiO/NiOH$) substrates. On basic substrates, deposits are thinner and are enriched in sulfur [8.36]. On acidic substrates, deposits are thicker and are sulfur deficient relative to Athabasca vacuum residue (AVR), even though asphaltenes, which are rich in sulfur, sorb more strongly on acidic substrates in the absence of competition from other species. Solvents also contaminate phase behavior measurements by altering the phase behavior of condensed phases [8.1] and by altering bubble pressures and other phase behavior boundaries. Further, due to the costs associated with handling the so-called live oil samples, phase behavior data are largely available only for dead oils or at best reconstituted samples. So, phase behaviors observed in laboratory experiments approximate those arising in undisturbed reservoirs. For processed or partially processed heavy oils, the agreement is better because samples are more accessible and more representative.

The phase behavior topology of heavy oil and bitumen resources or their fractions can be presented in terms of a maltene-rich and a pentane asphaltene-rich pseudo-components partitioned directly from the parent sample using 5–100 nm nominal pore size filters to obtain subsamples with varying mass fractions of these two pseudo-components, without solvent addition. While the size of the asphaltene-rich domains varies significantly, their elemental compositions appear to be size independent other than for elements associated with clays that tend to be large [8.24]. Elemental analyses of these subsample are a linear function of pentane asphaltene content. For Maya crude oil, samples from 1.5 to 73 wt% pentane asphaltenes can be partitioned. For Athabasca bitumen, the range is 5–57 wt% and for Safaniya vacuum residue, the range is 5–56 wt%. The range of heptane asphaltene contents is narrower, for example, 0.7–36 wt% for Safaniya vacuum residue [8.4]. The calorimetric behavior of subsamples is then measured and analyzed in a framework that includes linear interpolation and extrapolation to 0 and 100% of each pseudo-component and comparisons with baseline heat capacities for solids and liquids with the same elemental composition [8.37–39]. In this way, the proof of the independence of the pseudo-component thermal behaviors, and phase transitions, corresponding to deviations from solid- or liquid-phase heat capacities, are identified. Rheological data are also obtained for each subsample, in order to detect the nature of transitions (solid–liquid or glass–liquid) found calorimetrically. For the hydrocarbon resource samples studied so far, these pseudo-components have been shown to be

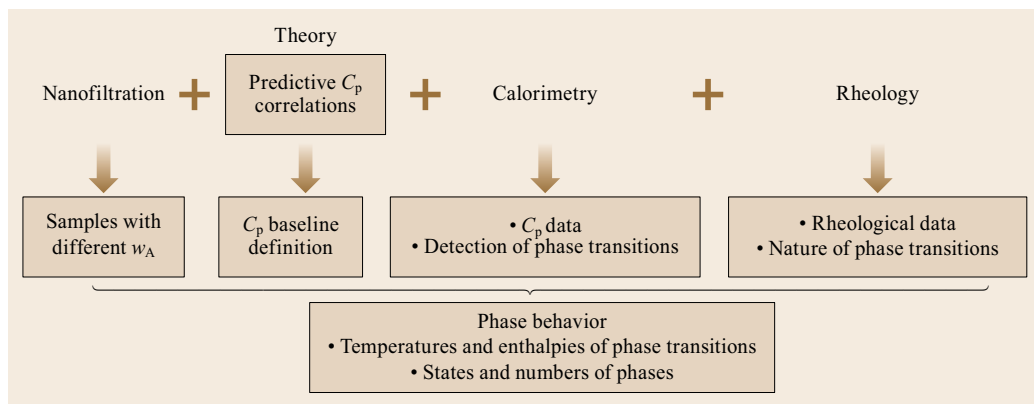


Fig. 8.2 Phase behavior assessment scheme for heavy oils (w_A is mass fraction of asphaltenes and C_p is isobaric heat capacity)

independent of one another, and to undergo phase transitions independently, within experimental error, over broad ranges of temperature [8.4]. The phase diagram construction framework is illustrated in Fig. 8.2. See Fulem et al. [8.2] for a detailed explanation of the method and experimental procedures.

Phase diagrams for individual resource samples arising from this framework are unique but share numerous features [8.4]. Figure 8.3 shows the phase diagram of Athabasca bitumen. Athabasca bitumen (Alberta, Canada) was obtained from Syncrude Canada Ltd. The sample was characterized as a coker feed. It is derived from mined bitumen subjected to warm water extraction, naphtha dilution, and naphtha recovery by distillation between 523 and 623 K. Some volatile constituents present initially were lost during sample preparation. Aliquots of this sample were nanofiltered at 473 K, and the subsamples were stored at 280 K for several weeks prior to phase diagram construction. To construct Fig. 8.3a, subsamples were cooled to 173 K prior to calorimetric and rheological measurements. For nanofiltered samples, a series of phase behaviors and phase behavior transition were observed. The maltene-rich component comprises crystalline (C_M) and glass (G_M) phases at low temperature and both phases undergo transitions to liquid (L_M) at higher temperatures. The asphaltene-rich component is solid (S_A) at low temperatures and undergoes a transition to liquid (L_A) at higher temperatures. The resulting phase diagram, Fig. 8.3a, is complex and includes three and four phase regions. Chemically separated pentane maltenes and asphaltenes undergo similar transitions, but the temperatures at which these transitions take place differ significantly from the nanofiltered subsamples. These sets of transitions are also shown in Fig. 8.3a – at the 0.0 and 1.0 w_A axes. The boundary at 350 K is particularly noteworthy, because the crystalline maltene phase is responsible for the non-Newtonian rheological behavior of heavy oils [8.4].

To construct Fig. 8.3b, subsamples were cooled to 258 K at a rate of 0.08 K/s followed by a repetition of the procedures used to construct Fig. 8.3. In this way, the impact of recent thermal history on observed phase behaviors was assessed. There is an indistinct transition of unknown nature in the maltene-rich material arising during the second heating cycle that is indicated by the x 's in Fig. 8.3b, and no transitions are detected in the asphaltene-rich material. At 400 K and above, maltene-rich and asphaltene-rich liquid phases are present. For chemically separated pentane maltenes, no transitions were detected and for chemically separated pentane asphaltenes, a glass transition (G_A) was detected at low temperature. Clearly, the phase behavior of heavy oils is sensitive to thermal history and transitions to solid or glass on cooling are kinetically slow. Impacts of thermal history on thermophysical and transport properties are significant and may account for the dissonance encountered among various types of measurements in the literature, particularly under conditions where solid and glass phases arise or persist and where their mass fractions are significant.

8.2.2 Heavy Oil and Diluent Phase Behavior

Two general types of phase behavior have been observed. Addition of low molar mass hydrocarbons such as n -alkanes or inorganic solvents such as CO_2 partition heavy oil and bitumen into diluent-rich and diluent-poor liquid phases and asphaltene aggregation is impacted concurrently. For this case, temperature plays a significant role in phase behavior because at low temperatures liquid–liquid and liquid–liquid–vapor regions arise over a range of compositions, while at temperatures significantly greater than the critical temperature of the diluent, a diluent-rich liquid phase does not arise. Addition of diluents such as 1-methylnaphthalene does not introduce additional bulk liquid phases, and impacts on asphaltene aggregation are not evident.

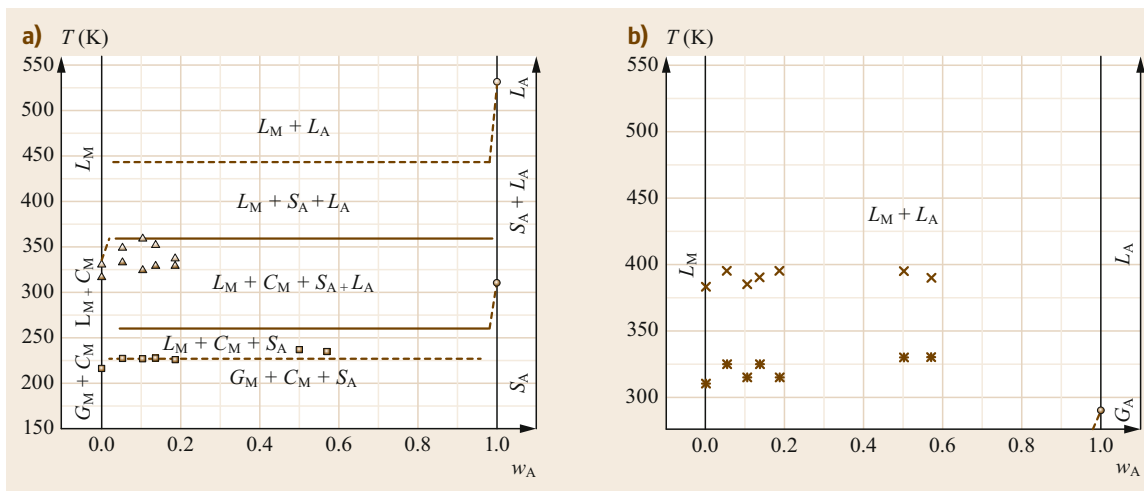


Fig. 8.3a,b Phase diagram for Athabasca bitumen: (a) heating cycle 1 and (b) heating cycle 2. (After [8.3])

However, at the microscopic scale, low molar mass hydrocarbons, such as toluene, and *n*-alkanes do disrupt microscopic liquid crystal domains in heavy oils and bitumen, including Athabasca bitumen [8.40]. So, from a processing perspective, nanoscale and bulk scale effects must be tackled simultaneously at a minimum. This is not feasible in general, and small and wide angle x-ray-scattering (SAXS/WAXS) measurements targeting nanoscale impacts must be performed separately from more conventional phase behavior studies performed in view cells.

Zou et al. [8.42] and Long et al. [8.43] provide a comprehensive and illustrative example for AVR + pentane mixtures where Zou et al. [8.42] report bulk phase behavior measurements, as shown in Fig. 8.4, and Long et al. [8.43] report nanoscale effects for the same mixtures at comparable pressures as shown in Fig. 8.5. At 433 K, AVR possesses a single bulk phase and a nano-dispersed asphaltene-rich phase. As pentane is added to the mixture, there is only one bulk liquid phase until the pentane content reaches ≈ 40 wt% (60 wt% AVR). However, in this composition range, level-2 (large) asphaltene-rich domains with leading dimensions exceeding 25 nm become more important and level-1 (small) asphaltene-rich domains become smaller, possess lower surface-to-volume ratios, and become more structured. At ≈ 45 wt% pentane (55 wt% AVR), a small mass fraction of a second bulk liquid phase appears, but along with it, there is large upward step change in the size, surface-to-volume ratio and the scattering coefficient of the level-1 and a downward step change in level-2 asphaltene-rich domains in the principal liquid phase.

While there are no other examples available with such detailed phase behavior data for mixtures con-

taining heavy oil at these three length scales, the complexity of the bulk phase behavior of reservoir fluids and heavy oils + low molar mass hydrocarbons or nonhydrocarbon gases such as CO₂ and hydrogen have been known for some time, and these behaviors have been placed in the context of phase diagram theory using model mixtures for both production and refining conditions [8.34, 44–46]. Such mixtures normally exhibit type-III pseudo-binary phase behavior where up to four phases in equilibrium (low-density liquid, high-density liquid, solid, and vapor) are observed at low temperatures. At higher temperatures, up to three phases (low-density liquid, high-density liquid, and vapor) are observed at approximately the vapor pressure of the added low molar mass component. At a temperature and a pressure exceeding the critical temperature of the added component, a three-phase critical point is observed where the low-density liquid and vapor phases become critically identical in the presence of a dense heavy hydrocarbon-rich liquid phase. This type of critical point is known as a K-point. Above the K-point temperature, only liquid, liquid vapor, and vapor phase behavior are possible. For example, heavy hydrocarbon + CO₂ mixtures exhibit this type of behavior, and the maximum observed K-point temperature and pressures are ≈ 320 K and 103 bar for heavy oil sample [8.46]. The critical temperature and pressure of CO₂ are 304 K and 74 bar, respectively. The maximum observed K-point temperature and pressure of AVR + pentane mixtures, which also exhibit type-III pseudo-binary phase behavior, are 486 K and 43 bar, respectively [8.47] versus the critical temperature and pressure of pentane, which are, respectively, 469 K and 34 bar. Retrograde behavior and other classical phenomena are also observed, and the

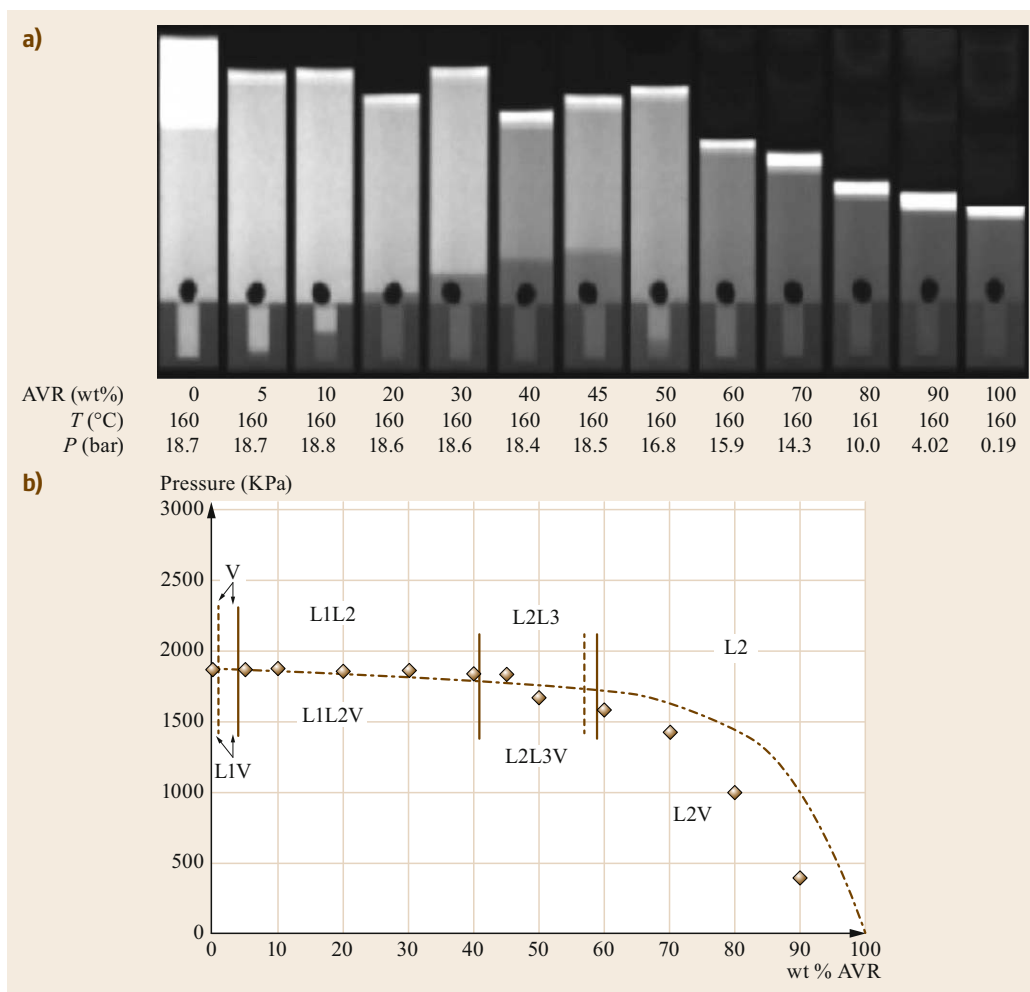


Fig. 8.4a,b Phase behavior for AVR + pentane mixtures at 433 K: (a) example x-ray images (after [8.41]) showing liquid–vapor phase behavior at 0 wt% AVR, liquid–liquid–vapor phase behavior from 5 to 60 wt% AVR, and liquid–vapor phase behavior from 60 to 100 wt% AVR (in these images the vapor phase is clear; the liquids designated L1, L2, and L3, are various shades of gray that link to their density; the black circle in the images is the stirrer); (b) partial phase diagram including only bulk phase behaviors, where the solid vertical lines and points denote experimental measurements and the dashed lines denote computed boundaries. (After [8.30])

phase behaviors of all heavy oil + all low molar mass hydrocarbons and nonhydrocarbons are qualitatively similar. The literature is replete with studies for specific petroleum + light hydrocarbons/nonhydrocarbons and model asymmetric mixtures. *Khaleghi* [8.48] reviewed the oil + CO_2 literature. The literature related to the appearance or deposition of large asphaltene-rich domains within the phase diagrams for specific oils or oils + light hydrocarbon/nonhydrocarbon mixtures is also well developed and this phenomenon is typically most pronounced at mixture bubble pressures [8.49].

8.2.3 Heavy Oil and Water Phase Behavior

Water + hydrocarbon mixtures may exhibit type-II, type-IIIa, or type-IIIb phase behavior. All binary water + hydrocarbon mixtures show similar LLV behavior at low temperatures. At high temperatures, the LLV three-phase behavior terminates at an L-point where the two liquid phases become critically identical (type II) or at a K-point where one of the liquid phases becomes critically identical to the vapor (type III). The distinction between types IIIa and IIIb is that, at high temperatures, the single liquid phase present in the phase diagram

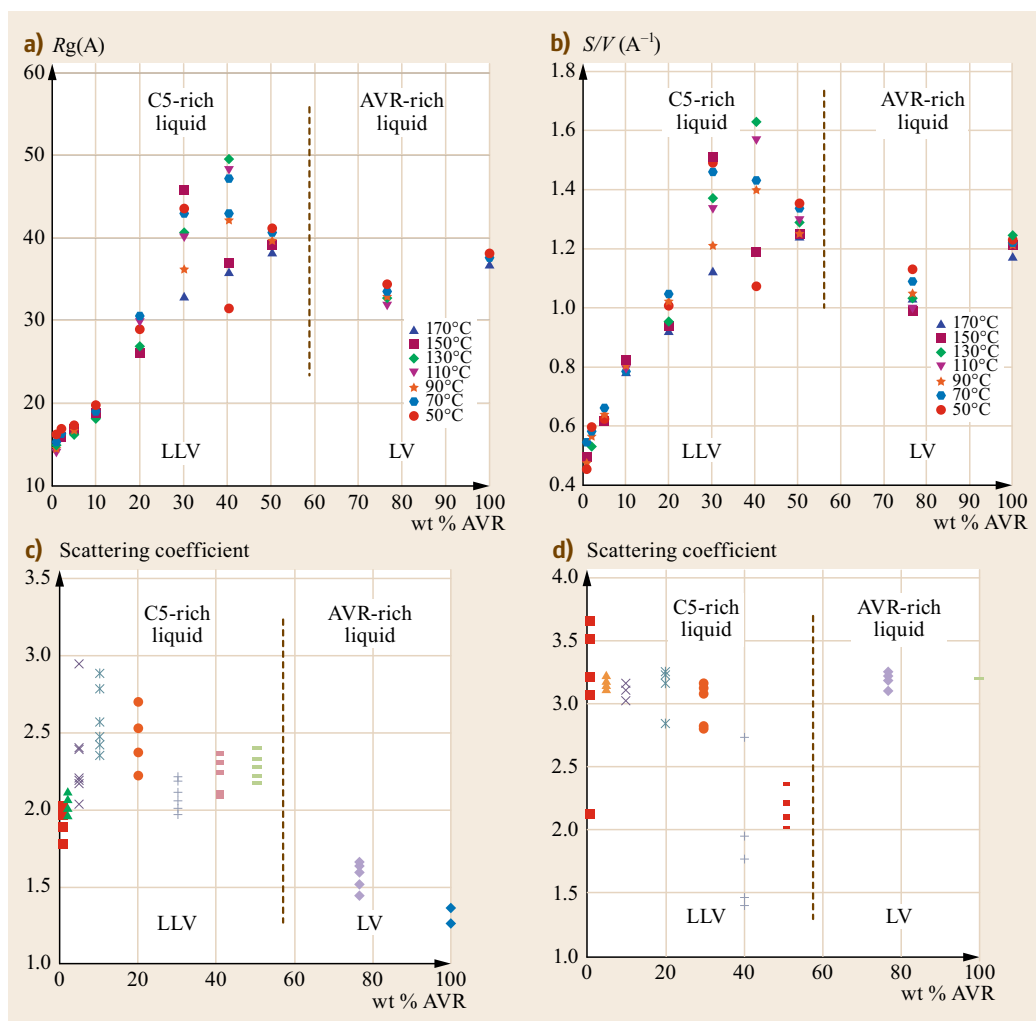


Fig. 8.5a–d Nanoscale behaviors arising in AVR + pentane mixtures: (a) radius of gyration, (b) surface-to-volume ratio, scattering coefficient for (c) level one (small) and large, (d) nanostructures. The vertical line is the approximate location of the liquid–vapor (LV) to liquid–liquid–vapor (LLV) phase transition. (After [8.43])

is water-rich for type-IIIa and hydrocarbon-rich for type IIIb. The solubility of water in the hydrocarbon phase, for all cases, tends to be in the order of a few parts per million at room temperature, and the solubility increases sharply with temperature. Mixtures of water + light hydrocarbons, where the critical temperature of the hydrocarbons is less than the critical temperature of water, exhibit type-IIIa phase behavior [8.50, 51]. Mixtures of water and heavy hydrocarbons, where the critical temperature of hydrocarbons are comparable to or exceed that of water, exhibit type-II or type-IIIb phase behavior [8.50, 51]. Water + Athabasca bitumen is an example of type-IIIb pseudo-binary phase behavior [8.52]. While water affects the enthalpy of solution of asphaltene in solvents [8.53], the impact of soluble

water on asphaltene precipitation is unresolved [8.54]. Tharanivasan et al. [8.54] demonstrated that emulsified water had no impact on the onset or amount of asphaltene precipitation at ambient conditions. However, water solubility is low at these conditions, and there may be more of an effect on asphaltene aggregation and precipitation at higher temperatures.

Composition measurements for hydrocarbon saturated water and water-saturated hydrocarbons present numerous challenges because hydrocarbon solubility values in water range over 11 orders of magnitude, while water in hydrocarbon solubility values range over four orders of magnitude. The solubility of hydrocarbons in water is also a strong function of molecular structure, where, for example, at fixed molar mass, aro-

matics exhibit higher solubilities than *n*-alkanes. For water solubility data in pure hydrocarbons and pure hydrocarbon solubility data in water, readers are referred to an extensive, critically evaluated series of papers on hydrocarbon + water solubility [8.55–65] which reviewed the previous extensive work done in the IUPAC Solubility Series, Volumes 37 and 38 [8.66, 67] but including corrections and new published work up to 2006. This recent work provides solubility data as a function of temperature for paraffins, naphthenes, aromatics, and other hydrocarbons ranging from C₅ to C₃₆. The available data points were individually examined and quality identifiers were assigned to them. Reference data are provided based on especially constructed correlation functions for specific chemical families. Experimental data differing from the reference data by less than 30% at similar temperatures from different sources are classified as *recommended*, while those that differ from the recommended data by more than 30% are classified as *doubtful*.

In addition to water solubility data in typically pure hydrocarbons and mixtures, water solubility results for five ill-defined heavy oils (Coalinga, Huntington Beach, Peace River, and Cat Canyon crude oil) reported by *Glandt* and *Chapman* [8.68] and Athabasca bitumen reported by [8.52] are available. In addition, water solubility data for Athabasca bitumen + toluene mixtures, comprising 44.3 and 66.8 wt% toluene, respectively, are also available [8.69]. The database is restricted to a narrow temperature range ≈ 400 –570 K. The lower temperature is restricted by the ability to make meaningful measurements and the upper temperature by the thermal instability of the hydrocarbons. The dataset provided by *Amani* et al. [8.52] attempts to compensate for the impact of thermal decomposition of Athabasca bitumen to provide approximate water-solubility values up to 644 K, which is close to the critical temperature of water. There are no data for water solubility in hydrocarbons above the critical temperature of water. In general, water in hydrocarbon and hydrocarbon in water-solubility data must be carefully scrutinized due to partial solidification of hydrocarbons at low temperature and thermal cracking at high temperatures.

8.2.4 Equilibrium Compositions

Equilibrium composition data for heavy oil containing mixtures is fragmentary at best. Some saturated single-phase composition data for light hydrocarbons or nonhydrocarbons in heavy oils or heavy oil fractions are available. Such data are available because they are more readily measured than multiphase data and are of specific importance. The solubility of inorganic gases such as hydrogen at high temperatures and pres-

ures is important for hydrotreating and hydrocracking. Fracking and in-situ combustion processes and the associated gases – carbon dioxide, hydrogen sulfide, and ammonia – are also important because they play roles in the oil phase as well as in the water phase where they form weak acid–base solutions. Heavy oil + CO₂ mixtures were reviewed by *Khaleghi* [8.48], heavy oil + water mixtures were reviewed by *Amani* et al. [8.69], and heavy oil + hydrogen mixtures were reviewed by *Saajanlehto* et al. [8.70]. Readers are referred to the literature for additional datasets and reviews of this type. Multiphase equilibrium data for heavy oil + light hydrocarbon liquids or gases or nonhydrocarbon gases are rare. *Zou* et al. [8.41–43] report on liquid–liquid partitioning of saturate, aromatic, resin, and asphaltene (SARA) fractions, and elements for AVR + pentane mixtures that include phase volume information and constitutes a comparatively complete dataset from this perspective. This is an underdeveloped topic, particularly in the public domain, and a subject of ongoing research from the perspective of multiphase visualization and sampling, and more intensively from the perspective of fluid characterization, the subject of Sect. 8.4.

8.2.5 Summary

The phase behavior complexity of heavy hydrocarbon resources and resource fractions is not encountered in conventional petroleum reservoirs. Many aspects of their phase behavior, including liquid crystals and solid maltenes, cannot be observed in conventional phase behavior experiments. Phase compositions, the subject of Sect. 8.4, fall largely outside the scope of conventional composition assays. Phase behavior and phase composition measurement for heavy oils and bitumen or mixtures that contain them impose a number of challenges including: the diversity of length scales at which phase behaviors arise and over which measurements must be made simultaneously, if at all possible; the time scales required to reach equilibrium, the need to develop new phase behavior measurement and fluid characterization techniques. A key concern is that the measured phase behavior of heavy oil and bitumen resources at a specific temperature and pressure is a function of sample thermal history. This suggests that there are likely to be significant differences between phase behaviors and hence properties encountered in the field or in processes, where thermal gradients are steep and timeframes are typically shorter than in laboratories where timeframes are typically much longer and where sample thermal histories arising from transport and storage differ qualitatively and quantitatively from those encountered in the field or in processes.

8.3 Thermophysical Property Measurement

As with phase behavior measurement, sampling and sample handling are sometimes the most challenging aspects of measurements. Heavy oil and bitumen deposits are heterogeneous even in oil properties. For example, *Larter et al.* [8.71] have reported viscosity variations of several orders of magnitude both vertically and laterally in a single reservoir. Some knowledge of this variation is required to obtain a set of representative samples.

Sample handling is particularly important when viscosity is to be measured because bitumen viscosity is very sensitive to even small amounts of contaminant [8.72]. Bitumen samples usually contain water and solids that must be removed for accurate property measurements. There are no guaranteed methods to remove water and solids without altering the sample. Heating and centrifugation can be an effective method for less viscous oils but heating can remove lighter components. Dilution and centrifugation are an effective means of removing water and solids, but it is impossible to remove all of the diluent afterward. Distillation and filtering are less intrusive methods particularly when any distilled hydrocarbons are recombined with the sample. While it can be argued that the most accurate results are obtained from samples squeezed from compressed cores if mud invasion is eliminated [8.73], such samples may not fully represent the fluid [8.35] because organic materials sorbed preferentially on the inorganic substrates are not removed during compression. Further, core samples are relatively rare and provide only small volumes of oil. Errors in viscosity measurements can arise from viscous heating and evaporation of light ends, and large variations in measured viscosity values can also arise from the thermal and shear prehistory of samples prior to measurement and the details of the measurement itself [8.5]. *Miller et al.* [8.74] noted viscosity differences in the order of 100% in blind tests on the same sample sent to different labs.

Live oil sample preparation is even more challenging. First, the correct solution gas composition must be determined and either a bubble point pressure or solution gas–oil ratio specified. Field data for these specifications are often unreliable because the gas volumes are small and production is not uniform. Second, equilibration times are long because the viscosity is high and mutual diffusion rates are low. It can take hours to days to reach an apparent equilibrium when mixing gases into bitumen or even when changing the pressure in an ongoing experiment. It is strongly recommended to evaluate the experimental procedures used in any heavy oil study before accepting the data. With this

proviso, the data available for heavy oil properties are outlined below.

8.3.1 Density

Apart from the everpresent challenge of sample handling, density measurements are straightforward and dead oil density is reported in most experimental studies. The AOSTRA handbook provides data for a number of dead heavy oils and bitumens [8.75]. By definition [8.76], the density of heavy oils lies between 934 and 1000 kg/m³ (°API from 20 to 10) and bitumen above 1000 kg/m³ at standard conditions (60°F and 1 atm). Bitumen densities as high as 1020 kg/m³ have been reported at standard conditions [8.32].

As expected for a hydrocarbon liquid, heavy oil density decreases as temperature rises and as pressure falls (Fig. 8.6). For dead oils, the trends are approximately linear over spans of a 100 K and tens of mega Pascals. Dead heavy oil density data [8.77] can be fit to within 1 kg/m³ with the following relationship

$$\rho = \rho_o[1 + c_o(P - 0.1)], \quad (8.1)$$

where ρ_o is the density in kg/m³ at atmospheric pressure, P is the pressure in MPa, and c_o is the oil compressibility in MPa⁻¹. The atmospheric density and oil compressibility are related to temperature as follows

$$\rho_o = A - BT, \quad (8.2)$$

$$c_o = C \exp(DT), \quad (8.3)$$

where T is the temperature in K, and A , B , C , and D are the fitting parameters.

Because heavy oil solution gas consists mainly of methane and some carbon dioxide, the solution-gas-to-oil ratio and therefore the live oil density are largely dictated by the solubility of these two components in the heavy oil at reservoir conditions. *Badamchizadeh et al.* [8.78, 79] showed that CO₂ molar solubilities in a broad range of crude oils fall on the same trend versus pressure. These CO₂ solubility data and data for methane solubility in bitumen [8.80] were fitted with Henry's law

$$x_i = \frac{y_i P}{H_i}. \quad (8.4)$$

For pure gases, $y = 1$, and for CH₄ and CO₂, Henry's constants are

$$\text{CH}_4: \ln(H) = 11.521 - \frac{500}{T} + \frac{0.1234P}{RT}, \quad (8.5)$$

$$\text{CO}_2: \ln(H) = 11.817 - \frac{872}{T} + \frac{0.1464P}{RT}, \quad (8.6)$$

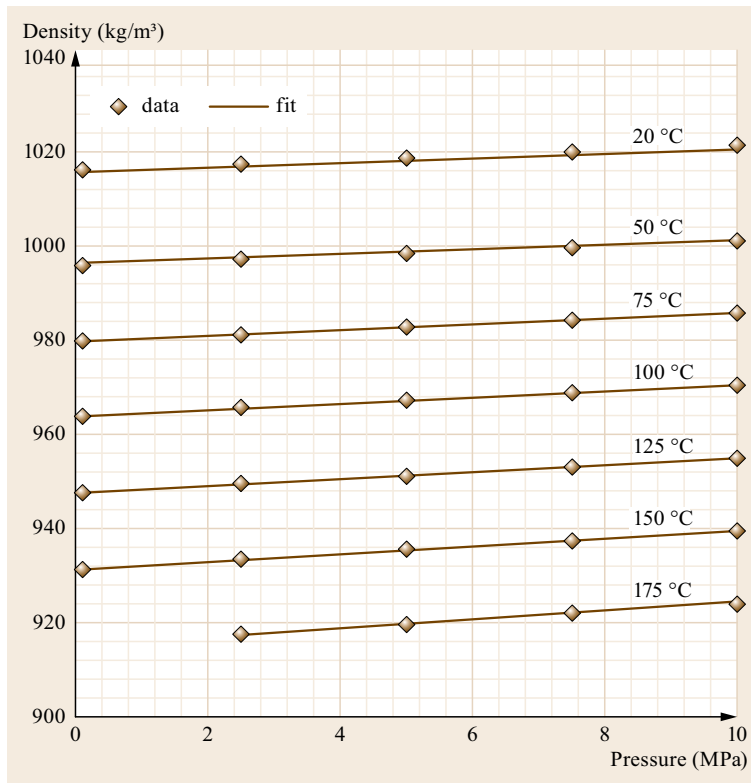


Fig. 8.6 Density of a Western Canadian WC-B2 bitumen as a function of temperature and pressure. Data fitted with (8.1). (After [8.77])

where x and y are the mole fractions in the gas and liquid phases of component i , respectively, H is Henry's constant in kPa, P is pressure in kPa, T is temperature in K, and R is the universal gas constant. When both gases are present, the solution gas composition must be specified and the solubilities in the oil are solved with a bubble point calculation. The density of the live oil can then be calculated from the liquid-phase composition and the mixing rules presented later in Sect. 8.6.

Heavy oil and bitumen are commonly diluted with solvents to reduce their density and viscosity. Typical solvents range from n -alkanes to condensate and naphtha. Densities of pure components are available from a number of sources, including the CRC chemistry handbook series and the NIST chemistry webbook database. Densities of multicomponent solvents can be estimated with an equation of state based on their compositional assays (Sect. 8.6), but measurements are required for accurate values. Experimental density and viscosity data for diluted bitumen are available for the following mixtures:

- Athabasca bitumen with methane, ethane, carbon dioxide, carbon monoxide, and nitrogen [8.80, 83]
 - Peace River bitumen with methane, ethane, carbon dioxide, carbon monoxide, and nitrogen [8.84]
 - Cold Lake bitumen with methane, ethane, carbon dioxide [8.85]
 - Bartlett heavy oil with carbon dioxide [8.85]
 - Athabasca bitumen with propane and propane+carbon dioxide [8.78, 79]
 - Western Canadian bitumen with ethane, propane, n -butane, n -pentane, n -heptane, and carbon dioxide [8.77, 86]
 - Western Canadian bitumen with solution gases and condensate [8.87].
- Diluted bitumen densities are well approximated with regular solution mixing rules remote from diluent critical points [8.32] but are more accurately predicted with excess volume-based mixing rules as discussed in Sect. 8.6.

8.3.2 Heat Capacity

Isobaric heat capacity values for heavy oils, and heavy oil fractions such as maltenes and asphaltenes are available in the literature from temperatures approaching absolute zero [8.37], where these materials are solid,

to over 600 K where they are liquid [8.38]. These data were obtained in order to test predictive correlations for heat capacity as described in Sect. 8.6. Data are also available for a variety of nanofiltered heavy oil and bitumen fractions as well that were obtained as part of the workflow related to phase diagram generation [8.2–4]. At room temperature, the values range from approximately 1.2 kJ/(kg K) for Athabasca pentane asphaltenes up to 1.6 kJ/(kg K) for Athabasca pentane maltenes. The corresponding range for Maya crude oil and for Safaniya vacuum residue is 1.3–2 kJ/(kg K). If the elemental composition and phase state of a fluid are known, isobaric heat capacity can be predicted with an absolute uncertainty of less than 0.1 kJ/(kg K) using the predictive correlations.

8.3.3 Bitumen and Heavy Oil Rheology Measurement

The Newtonian and non-Newtonian rheological behaviors of heavy oils and bitumens are key properties for production, transport, and refining. Conventional viscometers and viscosity measurement protocols do not detect shear-rate- and strain-rate-related non-Newtonian rheological effects that are important at and below ambient temperature for whole crudes, but which persist to up to 400 K for vacuum residues [8.4]. A whole crude example is shown in Fig. 8.7 where the apparent viscosity of Maya crude oil is a function of the shear rate at low temperature under steady shear conditions (Fig. 8.7a). Typical frequencies for viscometry measurements range up to more than 100 Hz, and it is clear that at low temperatures, orders of magnitude differences in apparent viscosity values result if the shear rate is not controlled. In oscillatory shear

measurements, varying the angular amplitude of the shear at fixed frequency also impacts the apparent viscosity (Fig. 8.7b) and suggests that Maya crude oil is thixotropic under these conditions. Care must be taken to ensure that a *viscosity* measurement is robust and not simply a condition specific rheological response.

With the caveat noted above, viscosity is arguably the most important property of heavy oil and bitumen because most processes for these fluids must include measures to reduce viscosity in their design. By definition [8.76], the viscosity of heavy oils lies between 100 and 100 000 mPa s and bitumen above 100 000 mPa s at room temperature. Bitumen viscosities of the order of a million mPa s have been reported at room temperature and, in practice, the most viscous bitumens are immobile at ambient conditions. The AOSTRA handbook provides data for a number of dead heavy oils and bitumens [8.75], but care must be taken with respect to their application unless the measurement temperature is significantly above ambient. Above approximately 298 K, whole crudes including Athabasca bitumen [8.5] may be treated as a Newtonian fluid and, like any other hydrocarbons, bitumen viscosity correlates with its density, illustrated in Fig. 8.8a. Bitumen density and viscosity decrease as temperature rises and pressure falls, as shown in Fig. 8.8b, but the effect of temperature is beyond exponential for viscosity. Correlations for dead bitumen viscosity are presented in Sect. 8.6.

Liquid solvents and dissolved gases dramatically decrease heavy oil and bitumen viscosity as shown in Fig. 8.9. Viscosities of pure components are available from a number of sources, including the CRC chemistry and chemical engineers handbook series, the NIST chemistry webbook and the NIST database [8.88]. Vis-

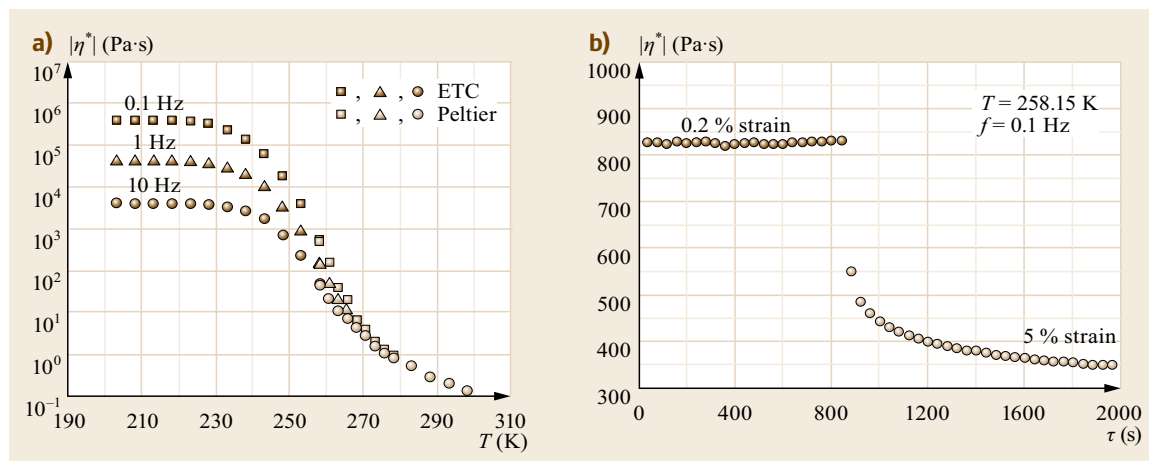


Fig. 8.7a,b Low-temperature steady shear (a) and oscillatory shear (b) rheological measurements for Maya crude oil, a heavy oil from Mexico. (After [8.33])

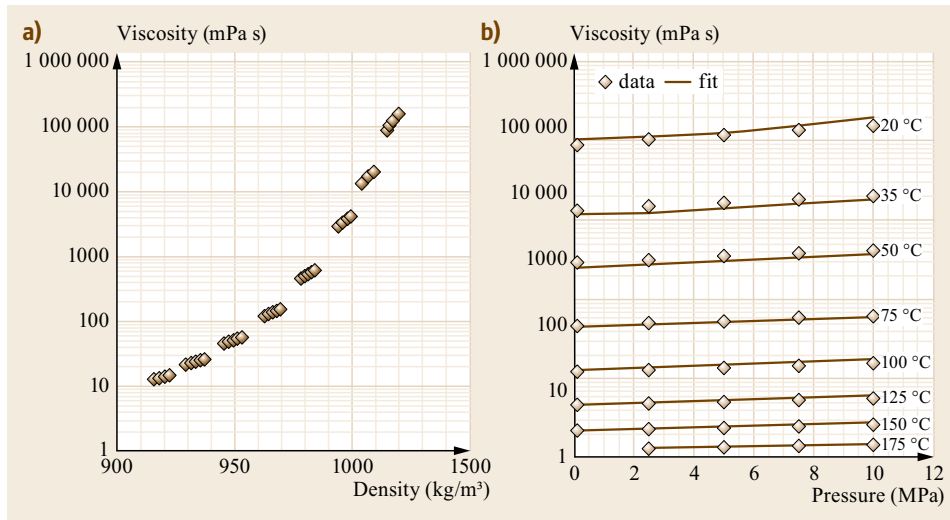


Fig. 8.8a,b Viscosity of Western Canadian WC-B2 bitumen at temperatures from 20 to 175 °C and pressures up to 10 MPa: (a) versus density; (b) versus pressure. Symbols are data from Motahhari et al. [8.86]; lines are EF model with two parameter tuning (Sect. 8.6)

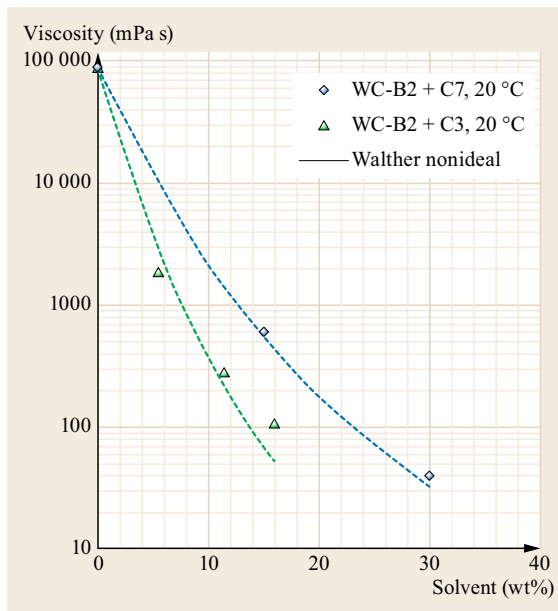


Fig. 8.9 Viscosity of Western Canadian WC-B2 bitumen diluted with *n*-heptane (C₇) and propane (C₃) 20 °C and atmospheric pressure. Symbols are data; lines are the non-ideal Walther model (Sect. 8.6). (After [8.20])

cosities of multicomponent solvents can be estimated with correlations based on their compositional assays (Sect. 8.6). But measurements are required for accurate values. Experimental viscosity data for diluted bitumen are available for the same mixtures reported in the density section. There are several correlations to

determine diluted bitumen viscosities as discussed in Sect. 8.6. Live oil viscosities can be estimated with the same methods based on solution gas compositions and/or liquid-phase densities as discussed for density measurements.

8.3.4 Mutual Diffusion Coefficient Measurements

Liquid-phase mutual diffusion coefficients are important parameters describing oil and gas reservoirs as they help define the time scale for secondary recovery processes such as miscible flooding with carbon dioxide or alkanes, or the SAGD + solvent production processes for heavy oil and bitumen. Normally, mixtures are treated as pseudo-binaries for the purpose of mutual diffusion coefficient determination, where the oil is lumped and the added hydrocarbon or nonhydrocarbon comprises the second component. Mutual diffusion coefficients are not measured directly but are inferred from experimental data. Diverse experimental methods and data interpretation techniques, including the computation of diffusion coefficients from measured composition profiles (preferred) or from pressure drops arising from the dissolution of a gas into a liquid (not recommended), are employed. There are a number of experimental and computational pitfalls related to mutual diffusion coefficient determination and care must be taken to avoid the misinterpretation of measurements that lead to unrealistic values, unrealistic trends in values with composition, and time-dependent values. Such artifacts arise in the applied literature, typically from

shortcomings in data interpretation. These issues are addressed elsewhere in detail [8.89–91]. Reported mutual diffusion coefficient values and trends must be used with care in design calculations, and it is important to note that liquid-phase mutual diffusion coefficient values fall between the self-diffusion coefficients of the constituents at the same temperature and phase state. Consequently, the values have defined upper and lower bounds that typically differ by no more than one order of magnitude [8.89]. So, for example, in mixtures of heavy oil + CO₂ at room temperature, the mutual diffusion coefficient values must be below the self-diffusion coefficient of *liquid* CO₂ at the same temperature. The most reliable lower bounds for whole heavy oils + low molar mass species, by analogy with polymers, place values at or above $\approx 3 \times 10^{-11} \text{ m}^2/\text{s}$ at room temperature. From mutual diffusion coefficient measurements for heavy oil + low molar mass species, constant values in the range $\approx 1\text{--}2 \times 10^{-10} \text{ m}^2/\text{s}$ are valid for the composition range 15–90 wt% heavy oil at room temperature. For atmospheric and vacuum residues, lower values, $\approx 5 \times 10^{-11} \text{ m}^2/\text{s}$, are valid over a comparable composition range [8.92]. Sharp increases in mutual coefficient values anticipated from theory close to the low molar mass constituent composition axis have not been observed, and measurements close to the heavy oil composition axis have yet to be reported. While further improvement in experimental measurement technique is needed, *Hosseini* et al. [8.93] recently reported on a promising microfluidics-based mutual diffusion coefficient measurement technique that greatly facilitates

the experimental acquisition of composition profiles, and *Sadighan* et al. [8.92] reported on forced versus diffusive mass transfer between immobile heavy oil and mobile low molar mass liquids. New data for Athabasca bitumen + solvents are also reported in these latter two publications.

8.3.5 Summary

There are a limited number of experimental thermo-physical property measurements available for heavy oils and bitumens. The measurements are of variable quality because the experimental techniques and data-processing approaches employed may not capture the physics and chemistry present (low-temperature rheology versus viscometry) or may indicate the presence of effects that are not real (mutual diffusion coefficients). Researchers may also not be aware of the limitations of the techniques employed or the impacts of these limitations. Measurement reproducibility as opposed to measurement repeatability is rarely reported. There is also a need for the use of measurement standards and standard calibration protocols, measurement method validation, and the use of control experiments during data acquisition. These along with the precise conditions of measurements and sample history are frequently lacking in publications. Finally, sample characterization presents challenges, and there is a pressing need for better characterization protocols so that the most productive use can be made of data as they become available.

8.4 Heavy Oil Characterization

Crude oils comprise innumerable molecular species [8.6, 7] encompassing a wide range of properties such as boiling point, molecular weight, density, and critical properties. Characterization involves representing the distribution of these properties in the oil in sufficient detail for modeling purposes. The amount of detail required depends on the application. For example, elemental analysis and phase state are sufficient for heat capacity calculations [8.38, 39, 94]. A compositional description is required for modeling phase behavior and for predicting the thermophysical and transport properties of each phase. A yet more detailed compositional description may be required to model reactions such as thermo- and hydrocracking. An extra level of sophistication is required if dispersed phases (hydrocarbon particulates such as asphaltenes, waxes, hydrates, water in oil, or oil in water emulsions) must be described in order to model the complex rheological behavior of dispersions or deposition phe-

nomena. Here, we focus on the characterizations used in phase behavior modeling whether for reservoir or refinery applications. Typically, a crude oil is characterized into a number of pseudo-components where each represents a narrow range of properties but collectively approximate the full distribution of properties of the oil. The most common choices of pseudo-components for heavy oils are based on boiling-point cuts (distillation or simulated distillation), and molecular weight ranges (gas chromatography, mass spectroscopy) plus residue fractions, and solubility cuts such as SARA fractions [8.95–98]. An alternate approach is to choose a set of representative molecules [8.30, 31] that reflect the molecular diversity of a fluid including residue fractions and can be used to populate group contribution-based models for fluid properties. Each of these methods is briefly presented below, but first some background in crude oil chemistry is provided.

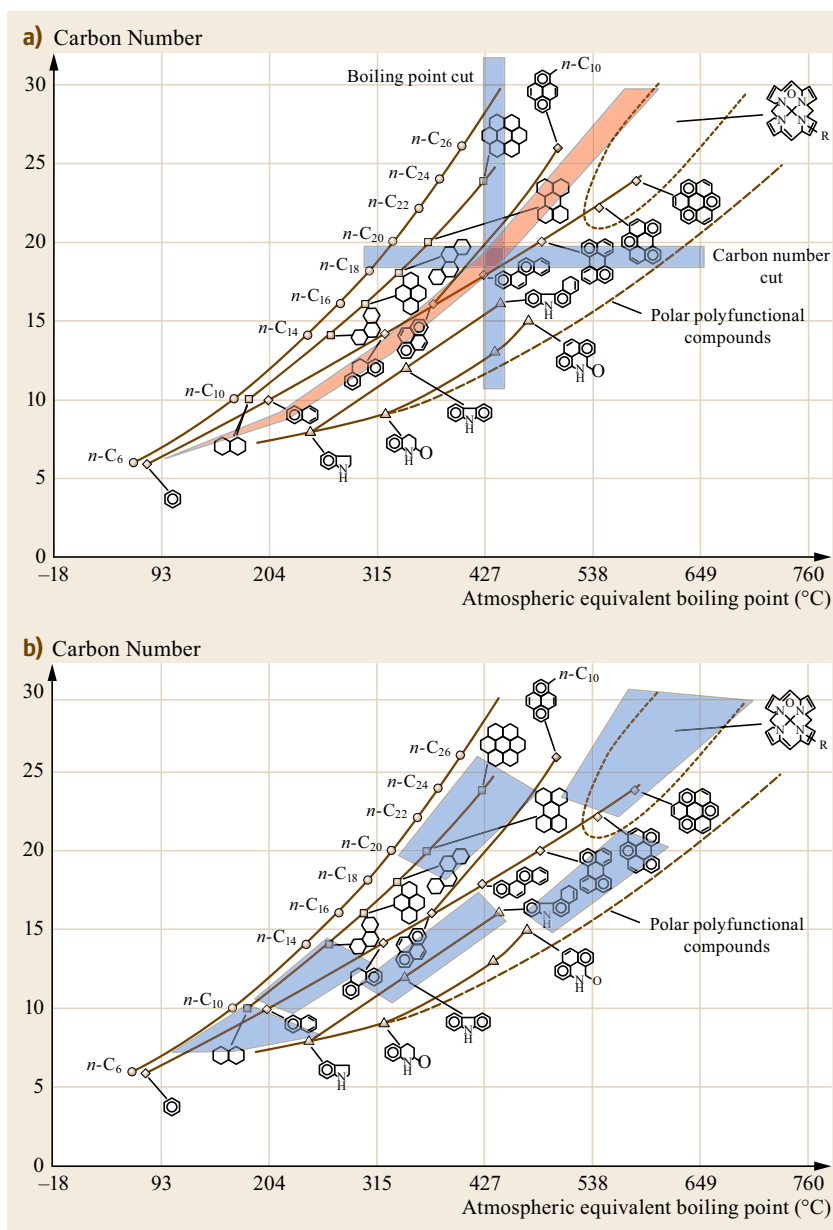


Fig. 8.10a,b Oil characterization approaches overlaying a graphic adapted from *Merdignac and Espinat* (after [8.99]) that shows the relationship between the carbon number and the boiling point for the components present in crude oils: **(a)** the highlighted vertical slice represents a boiling cut, the horizontal slice represents a carbon number cut, and the diagonal slice indicates the trajectory of average cut properties for a hypothetical crude oil; **(b)** highlighted and clear segments indicate components/properties encompassed by individual representative molecule pseudo-components

8.4.1 Heavy Oil Chemistry

In any crude oil, the variety and complexity of the constituent molecules increase with increasing boiling point and carbon number, as do the aromaticity, polarity, and heteroatom and metal content, as illustrated in a simplified manner in Fig. 8.10a [8.76, 99–101]. A single carbon number contains a wide variety of compound types with a wide range of boiling-points. For example, $C_{12}H_{26}$ has 900 possible isomers including stereoisomers with differences in boiling points of up

to approximately 30°C . The boiling-point difference is even greater with different hydrogen contents. For example, the boiling-point difference between acenaphthene, $C_{12}H_8$, and 2,2,7,7-tetramethyl octane, $C_{12}H_{34}$ is 94°C . These differences increase as the carbon number increases. Similarly, a boiling cut contains a wide variety of carbon number species. For example, the boiling point difference between octacosane, $C_{28}H_{58}$, and chrysene, $C_{18}H_{10}$, is only 8°C . In both cases, the representative fractions include diverse molecular species. Characterizations constructed on the basis of

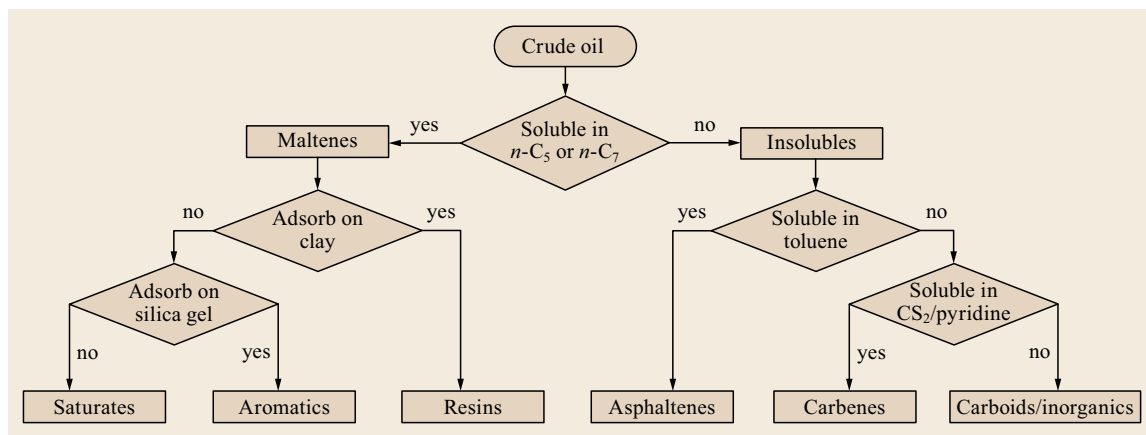


Fig. 8.11 Simplified representation of crude oil by solvent fractionation. (After [8.96, 98])

boiling or carbon number cuts have proven successful because the average properties of the cuts follow a consistent trend for naturally occurring hydrocarbon fluids, and consequently property estimation for a specific fluid requires limited tuning from properties linked to standard correlations for each cut. Issues arising with this characterization approach include uncertain extrapolation to undistillable fractions, and to processed hydrocarbon fluids found in refineries that can be prepared by blending in proportions that create materials which cannot be represented by a simple statistical distribution; no matter how it is defined. The property distributions as shown in Fig. 8.10a can also be considered as a large and complex collection of overlapping homologous series with increments in many structural elements, including ring number, side chain length and location, and heteroatom content and location. Note, for the sake of simplicity, the only homologous series shown in Fig. 8.10 is the *n*-paraffin series.

Group contribution methods attempt to represent these overlapping series with a set of representative molecules. In effect, individual molecules are used to reflect particular regions of the carbon number – boiling-point space. An illustrative subdivision is shown in Fig. 8.10b where each shaded and unshaded patches are represented by a representative molecule. To define sets of molecules and their representative mole/mass fractions for specific oils, measurable composition properties of the oil (aromatic carbon content, elemental analysis, gas chromatography with mass spectrometry (GC-MS), and physical properties (density, bubble pressure)) are fit numerically. A standard set of molecules or a customized set of molecules may be employed. In principle, it is possible to capture the chemical behavior of individual oils in production and refining environments and to provide composition models of varying but linked complexity. For example, more

constituents are desired for refinery models, where it is desirable to track fluid chemistry, and fewer constituents are needed for production models, where the emphasis is primarily on flow properties. This holistic approach to speciation requires more experimental research for its full potential to be realized, particularly for heavy oils, because of the uncertainty of the molecular level properties, and the distribution of properties of their undistillable fractions, but this characterization approach is already finding application in selected production and refining environments.

Solubility/adsorption-based fractionation methods also slice the distribution based on both size and chemical family. For example, a heavy oil can be divided into saturates, aromatics, resins, asphaltenes, carbenes, and carboids, as shown in Fig. 8.11. The saturate fraction consists mainly of long nonpolar carbon chains of linear, branched, and cyclic saturated hydrocarbons. Aromatics, resin, and asphaltenes consist of aromatic ring aggregates with aliphatic substitutions. The molecular weight, polarity, and heteroatom content increase from aromatics to resins to asphaltenes. Carbenes and carboids form a minor part of the heavy oil and include highly associated and condensed products that are insoluble in most of the solvents used for petroleum assays [8.102]. If the CS₂/pyridine separation is neglected, the diagram corresponds to the more common SARA fractionation. Asphaltenes are known to self-associate into nanometer-scale structures [8.20, 103] and their high molecular weight arises from dispersion forces rather than chemical bonding. Hence, a second distribution of nano-aggregate properties overlays the distributions, as shown in Fig. 8.10.

Conventional crude oils consist of relatively low carbon number species and most of the oil can be fractionated by distillation or characterized by gas chromatography (GC) [8.104]. However, only a rel-

atively small fraction of heavy oil (of the order of 30 wt%) is distillable or can be meaningfully assayed with gas chromatography. In addition, while conventional oils usually contain a low mass fraction of asphaltenes, whole heavy oils and bitumen can contain more than 20 wt% asphaltenes, and heavy oil fractions comprising more than 60 wt% asphaltenes have been reported [8.24]. Hence, heavy oil characterization is challenging for the two reasons:

1. Relatively little of the fluid can be assayed meaningfully using conventional distillation-based characterization.
2. The oil contains a significant fraction of asphaltenes which self-associate and may not follow the property trends observed for the lighter components.

8.4.2 Characterization Based on Distillation Data

Distillation data are obtained from direct measurements or GC data empirically converted to boiling points (simulated distillation or SimDist). Directly measured distillation assays are limited to temperatures below 330 °C [8.105] to avoid thermal cracking. Vacuum distillation (ASTM D-86, D-1160, D-2892, and D-5236) can fractionate to atmospheric equivalent boiling points up to approximately 838 K (565 °C). Typically, 80–95 wt% of a conventional oil, but only 20–30 wt% of heavy oil or bitumen, is distillable with these methods. SimDist can, in theory, be extended to atmospheric boiling points above 565 °C. However, the empirical conversion to boiling temperature cannot be validated above 565 °C and should be treated with caution. No standard methodology is yet available to extend a distillation assay above 565 °C [8.106].

There are two main options for crude oil characterization:

1. Extrapolate the boiling points based on measured trends and tune models with other parameters, such as binary interaction parameters, as outlined by *Whitson and Brulé* [8.97].
2. Adjust the extrapolated boiling point to optimize model fits similar to *Pedersen's* [8.95] approach for GC cuts.

One must also decide whether to include the asphaltenes in this extrapolation or to treat them separately. Once a complete boiling curve is constructed, it is divided into pseudo-components. The number of components is dictated by the needs of the model the characterization is intended for, computational effort, and data availability. For example, from 5 to 20 pseudo-

components are considered sufficient to define a crude oil for phase behavior modeling [8.97, 98, 107, 108]. For each pseudo-component, physical property correlations are then used to predict the critical constants and thermodynamic properties (the former are especially important when modeling the oil with an equation of state). Mixing rules are used to obtain the full characterization of the fluid.

Castellanos-Diaz et al. [8.107] recommended a characterization approach for heavy oil phase behavior modeling where the boiling-point distribution of the maltenes was extrapolated assuming a Gaussian distribution, as suggested by *Huang and Radosz* [8.108]. The asphaltenes were represented with a Gamma distribution of molecular weights (Fig. 8.12). The combined distribution was cut into 12 maltene and 6 asphaltene pseudo-components. Both the Lee–Kesler and modified Twu correlations were found to provide workable estimates of the critical properties. These methods provide reasonable fits when processing data from a characterization and are further used as inputs for the development of thermodynamic models for mixtures of interest. Other approaches may perform similarly if the *characterization* is modified and different extrapolations for maltenes and asphaltenes are used. *Characterizations and the model are intrinsically connected*. The connection between characterization and thermodynamic models is further explored in Sect. 8.5 and the equation-of-state model based on the above characterization is also presented there.

8.4.3 Characterization Based on GC Data

GC compound distributions are based on the retention times of the constituents of a crude oil sample carried over a carrier gas, such as helium or hydrogen through a fused silica capillary column after the sample is injected onto the injector (split/splitless, on-column, temperature-programmed vaporizer, etc.). A packed column is occasionally used. If a nonpolar-packed column, such as methyl silicone coated, is used, the retention times of the constituents are related to their boiling points. There are many types of detectors that can be chosen depending on the purpose of the analysis. The universal detector is a flame ionization detector (FID) in which the response is proportional to mass concentration. A fraction of the oil, the residue, does not vaporize or elute and stays in the injector or column head. The retention time is calibrated with *n*-paraffin standards. Apparent carbon number distributions of crude oils are reported relative to this standard and are used to characterize them. Actual carbon numbers and thus the molar masses at the same retention vary depending on the molecular structure. When a metal (such as aluminum)

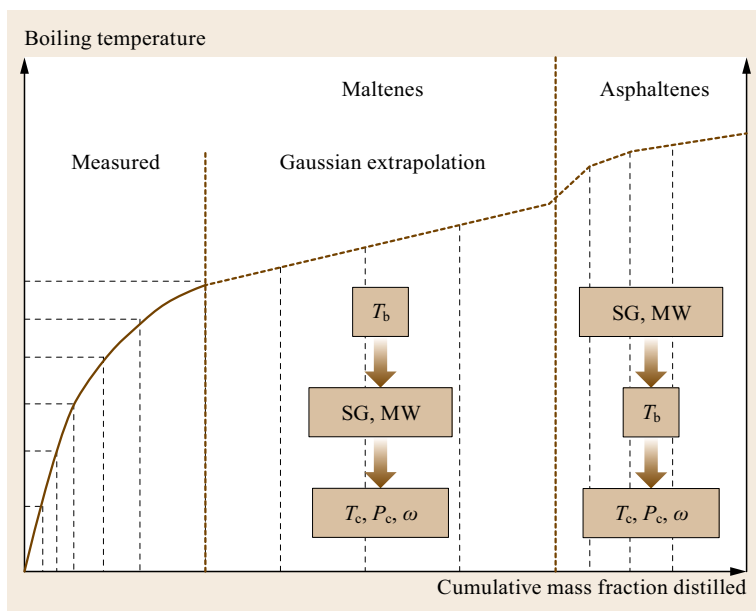


Fig. 8.12 A lumped characterization method for heavy oil based on extrapolating distillation data. The maltene fractions could also be based on SARA or liquid chromatography fractions. In this latter case, the maltene cuts would also represent a wide range of boiling points

column is used, the GC oven can be heated beyond 400 °C that would destroy the external polyimide coating of a fused silica column. Thus, it can be used for SimDist using a nonpolar column for boiling-point correlations. Hence, high-temperature GC is widely used as a rapid and inexpensive alternative to determine the distillation yields, including residues. Also, SimDist requires sample sizes in microliters, rather than liters as used in the distillation laboratory for a crude assay.

GC assays for crude oils include ASTM D-2887, ASTM D-3710, and ASTM D-7169. ASTM D-2887 is the most common procedure to provide carbon number data ranging from $< C_5$ to $\approx C_{44}$, corresponding to a maximum boiling point of 538 °C. ASTM D-3710 is recommended for gasolines with final boiling points less than 260 °C. ASTM D-7169 is the high-temperature SimDist procedure for a final boiling point up to 750 °C (equivalent to C_{120}). In general, the accuracy of the GC assay data above C_{25} is questionable because C_{25} is the upper limit of reliable true boiling point (TBP) distillation data for *n*-paraffins because TBP involves vacuum distillation [8.97]. In addition, based on the authors experience, the reproducibility of the residue determination (C_{30+} fraction) for bitumen is only ± 5 wt%.

Characterizations are constructed from GC data following the same steps as for boiling point data:

1. Extrapolate the carbon number (or calculated molecular weight) distribution
2. Divide the distribution into pseudo-components

3. Assign properties to the pseudo-component using correlations.

As with boiling point characterizations, tuning is accomplished by adjusting either the extrapolated molecular weight distribution or the binary interaction parameters in the phase behavior model [8.95, 97]. Tuning is essential because the characterization method does not include the molecule structure, and thermophysical properties and phase behavior are sensitive to the molecular structure.

The main challenge in the characterization of heavy oils is the large residue fraction. Figure 8.13 compares GC assays from a conventional oil and a bitumen. The residue (nonvaporized) fraction of the conventional oil was 33 wt%, compared to 70 wt% for the bitumen. The mass fractions of the higher carbon numbers in the conventional oil decrease following a clear and consistent trend. No clear trend is observed in the bitumen assay. With no trend to guide the extrapolation and relatively high uncertainty in the amount of residue, GC-based heavy oil characterization is not very reliable. The reliability can be improved when the characterization is constrained with other data such as the density and molecular weight of the oil and/or residue.

8.4.4 Characterization Based on SARA Data

SARA analyses possess a large number of operating definitions and a standard has not emerged [8.23]. The ASTM D2007 SARA assay of a crude oil starts by the separation of the asphaltenes using excess volumes of

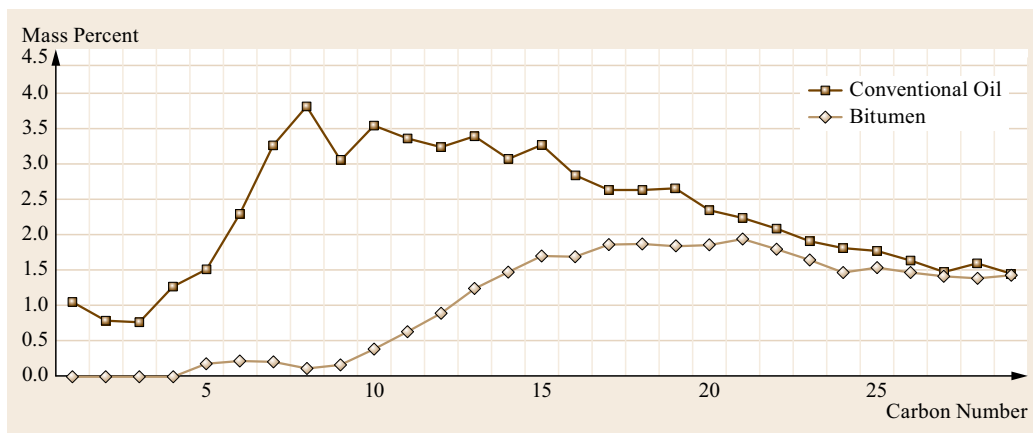


Fig. 8.13 Comparison of GC assays of a conventional oil and a bitumen. Their residue fractions were 33 and 70 wt%, respectively

a paraffinic solvent, commonly *n*-pentane or *n*-heptane (Fig. 8.11). The de-asphalted oil (DAO), also called maltenes, is recovered by evaporating the excess solvent. Then, the maltene fraction is further separated into saturate, aromatic, and resin fractions using liquid chromatography. The SARA composition is determined from the mass of the recovered SARA fractions and we stress that SARA-type components are distributed over boiling-point ranges as illustrated in Fig. 8.10. The resins and asphaltenes are present in the higher boiling ranges (middle distillates and above), while aromatics and saturates are concentrated in the lower boiling ranges.

SARA assays provide only four fractions and are coarse relative to distillation and GC assays. There is no standard method of constructing a TBP curve based on SARA components. Furthermore, there is no clear distinction between the properties of the aromatic, resin, and asphaltene fractions, and their relative amounts and properties depend on the details of the protocol used to separate them. SARA assays do provide an indication of the relative amount of saturated and aromatic components in an oil, and SARA assays are commonly used to characterize crude oils and for modeling asphaltene precipitation with regular solution theory-based models.

8.4.5 Characterization Based on Representative Molecules

Molecular level characterization of ill-defined hydrocarbons is a challenging task both experimentally and theoretically, and it leads to ambiguous outcomes because a broad range of pseudo-components can represent any of the subregions as shown in Fig. 8.10b and because the number of subregions may be chosen arbitrarily. Quantification of functional groups in molecules and the definition of mean molar mass for boiling fractions, or whole crudes, remain key challenges. For ex-

ample, *Jaffe* et al. [8.109] proposed more than 150 sub-molecular motifs in petroleum residues. These include chain and branched chain motifs of varying length, including chains with some double bonds; aromatic, naphthenic, and mixed naphthenic + aromatic motifs of various sizes; sulphur, nitrogen, oxygen, and metal substituted motifs. *Sheremata* et al. [8.110, 111] proposed molecular pseudo-components for the AVR using a Monte Carlo construction method. Only 10 motifs were used to build these molecules that respected elemental analysis, including heavy metals such as nickel and vanadium, and aromatic carbon content. Based on the same motifs, *Sheremata* [8.111] proposed an alternate set of molecules to represent the same fluid by respecting SimDist data as well. However, there is little agreement on the nature of the molecular motifs that comprise the AVR. Asphaltenes, for example, make up approximately 30 wt% of this residue, depending on the asphaltene definition employed. Both pericondensed [8.13, 112] (continental) and archipelago-type [8.14, 111] molecular pseudo-components [8.15, 113] have been proposed for Athabasca asphaltenes. The ambiguity appears to be linked to the molecule construction algorithms [8.10] because the pericondensed pseudo-components proposed by *Boek* et al. [8.112] were based on the same input data used by *Sheremata* et al. [8.110].

While the representative molecules, the motifs they comprise, and their molar masses remain ambiguous, there is greater agreement on the functional groups present and the types of carbon they comprise, because many of the groups are measured and quantified experimentally using more than one technique. These functional groups typically include one to a few atoms and range from specific carbon types to simple alkyl/aromatic groups, to sulfur, oxygen, and nitrogen containing groups. Therefore, group contribution methods based on pseudo-components are an emerging

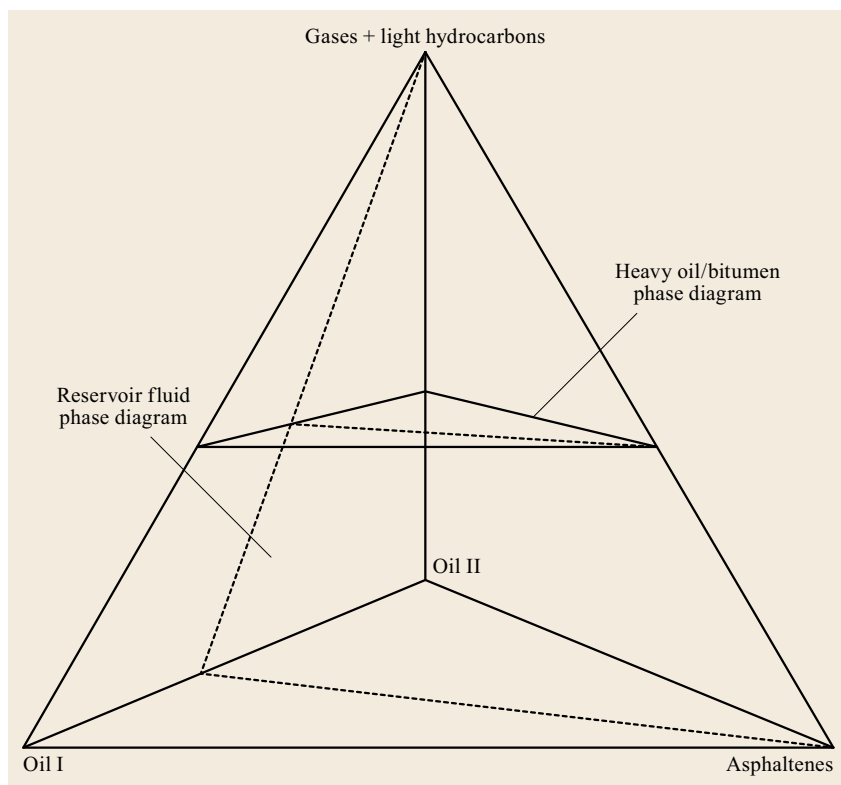


Fig. 8.14 Simplified characterization of heavy oils in reservoir and refining environments. (After [8.114])

alternative approach for characterizing thermophysical and transport and thermodynamic properties of individual fluids, as well as phase behavior and phase composition properties related to separations or mixing, whether in reservoirs or refineries. From the work of *Saber et al.* [8.30, 31, 115], the group contribution method proposed by *Marrero and Gani* [8.116] in combination with the Peng–Robinson cubic equation of state (CEOS) is a suitable basis for such calculations. In this approach, critical temperatures and pressures, and acentric factors for each pseudo-component that comprise required inputs for the equation of state are calculated on the basis of functional groups defined by the method. The approach was tested using simple ternary mixtures [8.115] where the results show that the Marrero and Gani group contribution method outperforms even the Peng–Robinson equation of state, even if critical temperatures, pressures, and acentric factors for the components are available exogenously. Illustrative phase behavior calculations with the AVR and *n*-alkanes are also available [8.30, 31]. While this approach offers advantages over refinery-type characterizations for thermophysical property and phase behavior calculations, a comparative study reveals that for the time being both approaches can be used for simulation but not prediction [8.114], as discussed in Sect. 8.5.

8.4.6 Heavy Oil Characterization Summary

Oil characterization, whether based on distillation or SimDist data, SARA analysis, spectroscopic data, direct measurement of specific properties, or a combination of these analyses, provides insights into the chemistry and physics of fluids. Characterizations of individual fluids do not exist in isolation, and are not an end in themselves. Characterizations provide bases for the generalization of properties and behaviors, and inputs tailored to specific types of calculations in diverse processing environments. The coexistence of primitive and sophisticated characterization schemes may at first glance appear to arise as an historical artifact, and one might imagine that more primitive schemes may disappear rapidly with advances in analytical chemistry. While both of these contentions are certainly true in the longer term, it is important to recognize that the diversity of the processing environments, and economic (analysis costs) and technological (computing power) constraints will continue to impose limits and permit diverse perspectives on this topic to flourish into the future. For example, in production environments, characterization relies primarily on GC analysis and focuses on low molar mass species (light hydrocarbons (C_1 – C_7), CO_2 , H_2S , etc.), while larger hydrocarbons are

lumped as maltenes and asphaltene fractions. These composition variables affect production rates, and only a limited number of parameters can be included in reservoir models due to computational constraints. Composition is frequently defined on the basis of five or fewer lumped components. In refining, low molar mass species are readily modeled. While these species are included in refining models, the focus is on fine-grained and high-cost speciation of the maltene fraction as these constituents affect process selection and design, process operation and product quality/value. Heavy oils are frequently represented by 50 or more components in refinery models. As illustrated in the simple schematic, Fig. 8.14, the compositions and hence the phase dia-

grams and properties are largely defined on the basis of vertical slices in composition space (reservoir models) and horizontal slices (refinery models). Currently, literatures related to phase behavior and property prediction, based on these divergent and in some respects incompatible characterization approaches, continue to co-exist as discussed in Sects. 8.5 and 8.6. The long-term goal of a single universal characterization approach, providing the required detail for refining but which can be systematically simplified to meet the computational constraints imposed by reservoir models, remains a work for the future. Currently, characterization approaches must be selected with care to ensure their relevance to a particular application.

8.5 Phase Behavior Correlation and Prediction

The successful correlation and prediction of phase behavior of hydrocarbon mixtures are dependent on good experimental assay data, good characterization, good thermodynamic models, and finally on a good flash algorithm for the proper determination of the numbers and natures of phases present, and the amount and composition of each phase at thermodynamic equilibrium. The definition of a good assay, notwithstanding the need of rigorous analytical procedures, reproducibility, and sample preparation, is its ability to characterize a fluid in such a way as to define a set of relevant and reliable inputs for a particular process model.

The definition of good characterization and good thermodynamics follow their ability to provide users with useful models that can be used to describe actual processes being designed or analyzed. Since the common denominator for modeling activity is the desire to simulate a process, and since processes of interest occur in widely different parts of the thermodynamic space (pressure, temperature, and composition), including areas where chemical reactions are important and where varying levels of details are required, no single set of experiments, characterization procedures, and thermodynamic models is sufficient. In this section, we assume that the characterization approach is selected and the data are collected in such a way as to provide meaningful information for the process of interest, and that the components are defined and lumped in such a way as to provide a reasonable basis for process modeling. Some examples and their limitations are discussed in Sect. 8.4.

8.5.1 Thermodynamic Model Selection

The number of available thermodynamic models appears to be almost unlimited. However, useful thermo-

dynamic models for the correlation and prediction of phase equilibrium behavior of interest for petroleum are, in practice, limited by the amount of useful information that can be provided as input to the model. For example, highly complex equations of state exist, but the determination of their parameters is essentially impossible due to the small amount of characterization data available, usually limited to a small set of average physical properties for the pseudo-components such as liquid density, molecular weight, and normal boiling point. From this small set of properties, critical properties and interaction parameters must be estimated. In other words, formal mathematical complexity does not equate to usefulness or accuracy. Further, petroleum is not simply a mixture of hydrocarbons. Petroleum also contains inorganic compounds such as water, carbon dioxide, and hydrogen sulfide, as well as trace materials such as metals and mineral fines. Any contribution of these components to the phase behavior, physical properties, and processing of petroleum must be accounted for. Meaningful thermodynamic models must also provide pertinent information for the computation of transport and other properties for process calculations such as viscosities. For high-pressure processes such as gas production, thermal upgrading, and hydrogenation, critical phenomena are important and the continuity of physical properties between gas and liquid phases is fundamental. It is useful to organize the key process questions we would like to answer in order to narrow modeling choices as suggested in Table 8.2. In general, model choices for the simulation of petroleum processes include equations of state (cubic, cubic plus association (CPA), statistical associating fluid theory (SAFT), and activity coefficient models (nonrandom two liquid (NRTL), regular solution theory).

Table 8.2 Matrix for model selection for typical hydrocarbon/petroleum-based processes

Main process to be modeled	Thermodynamic model	Example	Typical assay	Typical characterization
Gas processing	Cubic equations of state Corresponding states Reference equations	Gas plant, gas transportation in pipelines	C ₇₊ Chromatography	Lumped model Gamma distribution Pseudo-components
Refining, distillation	Cubic equations of state Modified Antoine	Atmospheric crude tower	Light ends Distillation assay SimDist	Curves to TBP Pseudo-components
Refining, reactors	Cubic equations of state	Hydrocracker, Hydrotreater, Coker, Upgrader	Light ends Distillation assay SimDist PNA	Curves to TBP PIONA Family pseudo components Surrogates
Heavy oil production	Cubic equations of state SAFT Activity coefficient	Bubble pressure calculations Determination of gas dissolved in oil	Light ends Distillation assay SimDist SARA	Curves to TBP Gaussian for maltenes, Gamma for asphaltenes Surrogates
Heavy oil treatment with solvents	Cubic equations of state Activity coefficient	Removal of asphaltenes from heavy oil	Light ends Distillation assay SimDist SARA high vacuum fractionation Yield versus solvent concentration	Curves to TBP Gaussian for maltenes, Gamma for asphaltenes Surrogates

After selecting an appropriate thermodynamic model, the importance of the representation of the physical-chemical properties of the fluids for the calculation of interest must be assessed. For example, if the primary concern is phase behavior, then good enough models can frequently be constructed using pseudo-components where the chemistry is only represented by average physical properties, such as liquid density and boiling point. For more detailed calculation of phase compositions or accurate modeling of chemical reactors, more detailed information about the chemical nature of the pseudo-components is necessary in order to capture the chemical transformations resulting from thermal or catalytic reactions, or the partitioning of specific species or species classes arising during liquid–liquid or liquid–vapor separation operations. This more detailed information can be expressed by using special pseudo-components determined using PIONA-type characterization [8.117] where specially determined family trends as a function of carbon number are used, or through the use of representative molecules that approximate the chemical characteristics of materials that constitute the different oil fractions [8.115]. The advantage of using surrogate molecules arises from their defined molecular structures that are amenable to modeling using group contribution methods [8.30, 118, 119].

It is important to recognize that the compositions of interest for a process being modeled may differ from the compositions defined through characterization. For

example, pseudo-components are defined on a water-free basis, but it is frequently necessary to estimate the mutual solubilities of water and hydrocarbons. Typically, the solubility of water in hydrocarbon streams is the main focus and this condition is not far from the original characterization. However, the solubility of hydrocarbons in water (e.g., contamination of water by trace hydrocarbons) at a composition vastly different (e.g., essentially pure water) from the original characterization may be needed. The simple equations of state used for refinery modeling are usually tuned to match the solubility of water in hydrocarbons, and the solubilities of hydrocarbon in water are not well modeled [8.120], and additional correlations, as noted in Sects. 8.2.3 and 8.5.6, are needed. Robust thermodynamic models must accommodate these compositional changes in a reliable and hopefully theoretical manner to provide a meaningful insight into the material and energy balances of interest.

The final selection of a thermodynamic model is then a function of intrinsic characteristics of the thermodynamic model and the type of derived information that can be obtained from the model given the inputs resulting from the assay and characterization data. Invariably, the outputs provided by the model comprise a small set of well-defined compounds (light ends, light portion of SimDist, solvents, water, inorganics such as ammonia, hydrogen sulfide, nitrogen, and carbon dioxide) and a set of pseudo-components (cuts or representative molecules) and their compositions. Based on this

information, thermodynamic models perform two major tasks. They define the necessary physical properties for the pseudo-components and the binary interaction parameters among all binary pairs present, and provide reliable fugacities for any phase composition of interest so that phase behaviors are adequately represented and that physical property calculations, for example, phase densities and enthalpies, and phase transport properties are supported by the thermodynamic model. These intermediate results are then used to compute viscosity, thermal conductivity, and other transport properties.

8.5.2 Essential Thermodynamic Equations

In order to model phase behavior, the most useful place to start is the equality of the chemical potential or equivalently the fugacity of each component in each phase at thermodynamic equilibrium given by

$$f_i^V = f_i^{LI} = f_i^{LII} = \dots f_i^{LN} = f_i^S = \dots, \quad (8.7)$$

where f is the fugacity of any component i , V stands for vapor, LI–LN denote the different liquid phases that may exist (light hydrocarbon, heavy hydrocarbon phases, aqueous phase, liquid carbon dioxide phase, etc.) and S stands for solid phases. While solids are important and may include hydrate phases, wax phases, ice phases, these comprise specialized topics and they are not discussed here.

For fluid phases, fugacity expressions can be written in two principal ways depending on whether activity coefficient or equation-of-state models, (8.8) and (8.9), are used

$$f_i = \gamma_i x_i f_i^{OL}, \quad (8.8)$$

$$f_i = \phi_i x_i P. \quad (8.9)$$

In (8.8), γ stands for the activity coefficient, x is the mole fraction, and f^{OL} is the standard state fugacity. At low pressures, the standard state fugacity is often represented by the vapor pressure or, for gases such as methane, hydrogen, nitrogen in the liquid phase, by a Henry constant which is solvent dependent. In (8.9), ϕ stands for the fugacity coefficient and P is the pressure. Formally, activity coefficients and fugacity coefficients are functions of pressure, temperature, and composition, and (8.8) and (8.9) can be freely applied to liquid and vapor phases. From a practical point of view, (8.8) is usually applied only to the liquid phase and due to small dependency on physical properties exhibited by liquids on pressure away from the mixture critical points. Consequently, liquid-phase activity coefficients are typically assumed to be pressure independent. Equation (8.9) can be applied to the vapor and liquid phases.

If an equation-of-state model is selected, liquid and vapor properties can be calculated formally to be consistent with critical phenomena. This choice improves the robustness of model predictions and facilitates interpolation and extrapolation of available data.

The formal relationship between fugacity coefficients and fugacities is given by

$$RT \ln \frac{f_i}{x_i P} = \int_V^\infty \left[\left(\frac{\partial P}{\partial n_i} \right)_{T,V,\bar{n}_j} - \frac{RT}{V} \right] dV - RT \ln Z, \quad (8.10)$$

where R is the universal gas constant, T is the absolute temperature, V is the volume, n is the number of moles, and Z is the compressibility factor defined as PV/RT . Equation (8.10) is basic for the modeling of natural gas processes where important phenomena such as retrograde condensation and other complex phase behaviors occur at high pressures and must be properly captured by the model. Heavy hydrocarbons are frequently processed at high temperatures and pressures, whether in situ, during deasphalting, or during hydrocracking where hydrogen is provided for the reforming of heavier materials into more useful lighter fractions. Thus, the ability to model high-pressure equilibria and to treat asymmetric mixtures, that is, mixtures comprising both light and heavy components that exhibit complex phase behaviors are important features of a model. Another benefit derived from using equation-of-state models is that they can be used to calculate residuals for enthalpy, entropy, heat capacity, and other physical properties, thus only requiring the availability of ideal gas heat capacities for the development of complete, self-consistent physical property calculation systems.

By contrast, activity coefficient models are semiempirical expressions derived from a model for the excess Gibbs excess free energy of mixing. Activity coefficient models require interaction parameters fitted against experimental data at each temperature of interest. Sometimes useful generalizations are possible, for example, for correlating solubility parameters [8.121]. However, activity coefficient models always require the development of separate procedures for the calculation of physical properties such as densities, enthalpies, and entropies. A separate model must also be selected for the gas phase. These separate phase models make activity coefficient models inherently inconsistent when extended to the mixture critical region. This significant disadvantage can be transformed into a formidable advantage. This is particularly true when modeling liquid–liquid equilibrium phenomena that arise from

the treatment of oils with solvents or water–oil phase equilibrium [8.69, 122, 123].

Effective use of equations of state is usually based on the use of van der Waals conditions at a critical point for a pure component, given by

$$\left(\frac{\partial P}{\partial v}\right)_T = 0, \quad (8.11)$$

$$\left(\frac{\partial^2 P}{\partial v^2}\right)_T = 0, \quad (8.12)$$

which define parameters appearing in equations of state based on the critical pressure and critical temperature. Equations-of-state parameters also must be adjusted to provide reasonable vapor pressure predictions. For example, by correlating the attractive parameter to the acentric factor [8.124, 125] or through the use of specialized functions [8.126]. Equations-of-state parameters are frequently tuned to liquid density data [8.127, 128]. In order to calculate enthalpies and entropies, ideal gas heat capacities are also required. Liquid-phase densities are frequently calculated using a form of the Rackett equation [8.129], and enthalpies and entropies are calculated using an equation of state for the gas phase and an empirical residual equation such as the Watson equation or generalized formulation of the corresponding states principle such as *Pitzer's* acentric factor [8.130].

A large number of methods are available for the estimation of pseudo-component physical properties [8.98, 131], but two methods that have been proven useful for widely different types of pseudo-components obtained

from oil characterization. These are the *Lee–Kesler* method [8.132] and the *Twu* method [8.133] for the calculation of critical properties for hydrocarbon cuts. For characterizations based on representative molecules, group contribution methods are required for the determination of critical properties [8.134, 135]. Thus, useful models for phase equilibrium and physical property calculations require, for each pseudo-component as well as defined components, the input properties summarized in Table 8.3.

8.5.3 Cubic Equations of State (CEOS)

Due to their simplicity, accuracy, robustness, and speed, models based on CEOSs are extensively used for the calculation of phase equilibria and physical properties for hydrocarbon mixtures. Although many CEO models exist, they all share some common characteristics. CEOS can be broadly categorized into two-parameter CEOS [8.124, 125, 136, 137], three-parameter CEOS [8.138–141], and four-parameter CEOS [8.142].

Two-parameter CEOS are by far the most commonly used type because only critical temperature, critical pressure, and acentric factor are necessary for the calculation of pure component properties. Since there are correlations for the critical properties and acentric factor that are functions of normal boiling point and liquid density, properties normally available through oil characterization, it is straightforward to build models based on exceptionally little data. However, correlation extrapolation to large molecules found in heavy oils in-

Table 8.3 Basic pure component properties required for thermodynamic model development—equations of state or activity coefficient based

Property	Data	Objective
Vapor pressure	Normal boiling point Acentric factor Antoine or Wagner coefficients Raw data	Calculate accurate vapor pressures.
Liquid density	Specific gravity Standard density at 60 °F Standard density at 25 °C Rackett coefficients Raw data	Calculate accurate liquid densities, in particular saturated liquid densities
Critical temperature	Correlations Raw data	Specify van der Waals conditions at critical point
Critical pressure	Correlations Raw data	Specify van der Waals conditions at critical point
Solubility parameter	Correlations Enthalpy of vaporization data	Used for regular solution activity coefficients
Ideal gas heat capacity	Correlations	Used for H , S , and C_p calculations and the associated energy balance calculations
Molar mass	Correlations Raw data	Material balance calculations

roduces uncertainty because the critical properties for large molecules cannot be measured experimentally due to their thermal instability. It is evident that equation-of-state parameters based on vapor pressure are at least ambiguous for pseudo-components that in many cases will be present in the solution at temperatures well below their melting point.

All two-parameter CEOSs suffer from the poor representation of liquid densities and usually this is corrected through the use of volume translation [8.128] where the volume computed from the cubic is empirically corrected through the addition of a constant. It is frequently found that, for high-accuracy liquid-density calculations, a constant volume translation is not enough and a correction that is a function of temperature is required. Although this type of correction makes the equation-of-state inconsistent from a thermodynamic point of view, it extends the range of usefulness considerably [8.143]. The vapor–liquid-phase equilibrium calculations for volume-translated equations of state are not changed by the volume translation, but computations related to hydrate phase formation or wax formation where accurate fugacities are required sometimes benefit from volume-translated equations of state. Some equations of state use a temperature-dependent volume translation or a temperature-dependent co-volume [8.142, 144] for accurate liquid density calculations, and significant improvements on the quality of the predicted fluid fugacity can be gained at the expense of thermodynamic consistency (either in the form of isotherm crossings, negative heat capacities at high pressures, or discontinuities at the critical point). These issues are well documented in the literature [8.145, 146].

Three-parameter equations of state provide better predictions for densities than two-parameter equations since the third parameter is frequently fit to liquid density data, but one often finds that the improvements are still not of sufficient accuracy for engineering calculations. Four-parameter equations of state are rarely used since the improvements over two- and three-parameter equations of state are unfortunately small from a phase equilibrium point of view, and it is difficult to justify the additional complexity versus the accuracy gained. These features are better illustrated through the examination of the actual model equations.

The typical structure for a CEOS is

$$P = \frac{RT}{v-b} - \frac{a_c \alpha(T)}{v^2 + ubv + wb^2}, \quad (8.13)$$

where v is the molar volume, a_c is the attractive term, b is the co-volume, $\alpha(T)$ is an empirical function designed to model vapor pressures, and u and w are the

numerical constants that define the actual shape of the equation of state. The term $\frac{RT}{v-b}$ represents a repulsive contribution to pressure to represent that the finite size molecules have and consequently the fact that fluids are not infinitely compressible. The term

$$-\frac{a_c \alpha(T)}{v^2 + ubv + wb^2}$$

represents the attractive forces between molecules. The terms a_c and b are determined based on the van der Waals conditions at the critical point (8.11) and (8.12). $\alpha(T)$ is frequently generalized for hydrocarbons [8.124, 125] as shown below, for the Peng–Robinson equation of state in (8.14) and (8.15)

$$\alpha(T) = \left[1 + f_w \left(1 - \sqrt{T_r} \right) \right]^2, \quad (8.14)$$

$$f_w = 0.37464 + 1.54226\omega - 0.26992\omega^2, \quad (8.15)$$

where T_r is the reduced temperature for a component and ω is the component acentric factor. Other general expressions for $\alpha(T)$ have been proposed [8.126] and as (8.14) and (8.15) are not accurate enough for the modeling of polar compounds frequently found in hydrocarbon processing, notably water and methanol, specialized $\alpha(T)$ have found extensive use [8.120, 147].

The volumes calculated from the equation of state are usually not accurate enough for technical calculations and the values are refined through the use of the volume translation technique briefly described above. The molar volume actually used for calculations is given by

$$v = v^{\text{EOS}} + s, \quad (8.16)$$

where v is the molar volume used for density calculations, v^{EOS} is the molar volume calculated from the equation of state, and s is the volume translation parameter. More elaborate forms of volume translation are also available [8.143, 148], including temperature-dependent forms.

Equations of state are usually extended to mixtures through the definition of mixing rules for the calculation of its parameters. For two-parameter equations of state, mixing rules are required for the calculation of the parameters a and b . The simplest mixing rules are the van der Waals rules and although too simple for accurate modeling of polar mixtures, they are useful for the modeling of hydrocarbon mixtures as well as mixtures of hydrocarbons with a series of important inorganic compounds for hydrocarbon processing, such as nitrogen, argon, carbon dioxide, and hydrogen sulfide. The

mixing rules are given by

$$a = \sum \sum (1 - k_{ij}) \sqrt{a_i a_j} x_i x_j, \quad (8.17)$$

$$b = \sum x_i b_i, \quad (8.18)$$

$$k_{ij} = k_{ij}^0 + \frac{k_{ij}^1}{T} + k_{ij}^2 \ln T. \quad (8.19)$$

The term k_{ij} is the interaction parameter and is an empirical term required for correcting the inaccuracies of the mixing rule for the a term (a similar formulation can be used for the b term, although really useful only when dealing with highly asymmetric mixtures such as hydrogen and heavy oils) and must be determined based on experimental vapor–liquid equilibrium data. Common values for k_{ij} can be found in the literature [8.149], although care must be exercised when using interaction parameters calculated by others due to inconsistencies between critical properties and acentric factors.

With multicomponent mixtures such as crude oils, the number of interaction parameters becomes large but experimental data are limited to determine their values. An attractive alternative is to correlate the interaction parameters with properties defined in the oil characterization such as critical volumes or temperatures [8.150]. The ability of a simple model to correlate and extend experimental data is remarkable as shown by Agrawal et al. [8.151] and illustrated in Fig. 8.15. Agrawal generalized the interaction parameters into binary classes (carbon dioxide/bitumen cuts, methane/bitumen cuts, ethane/bitumen cuts, n -pentane/bitumen cuts, and bitumen cut/bitumen cut binaries). For hydrocarbons characterized using representative molecules,

Saber et al. [8.30] showed that quantitative multiphase boundaries could be predicted using the Peng–Robinson CEOS, where parameters appearing in the model were defined using group contribution methods as shown in Fig 8.16. Use of boiling range characterization of the heavy oils and the same CEOS did not predict observed three-phase equilibria [8.152].

Notwithstanding their success, quadratic mixing rules are not satisfactory for liquid–liquid equilibrium calculations for highly asymmetric mixtures. While phase behavior is well represented, neither phase mass fractions nor their compositions are well represented [8.30], and it is necessary to relax the imposition of symmetric interaction parameters. Johnston et al. [8.153] illustrate this point clearly and show how a phase equilibrium model based on quadratic mixing rules fails to provide the quantitative representation of asphaltene precipitate yields, as shown in Fig. 8.17. Different methods for developing asymmetric mixing rules abound [8.154, 155], but the lack of complete mutual solubility data for oil–solvent mixtures limits the development of unambiguous models. Asymmetric mixing rules are an active area of research, but the accurate prediction of asphaltene yields with a CEOS has not yet been achieved.

8.5.4 Noncubic Equations of State

The theoretical weaknesses of CEOS are well known and many attempts to correct them have been reported. Sandler [8.154] provides an exhaustive review on equations of state. Here, we briefly examine the SAFT family of equations of state as these equations,

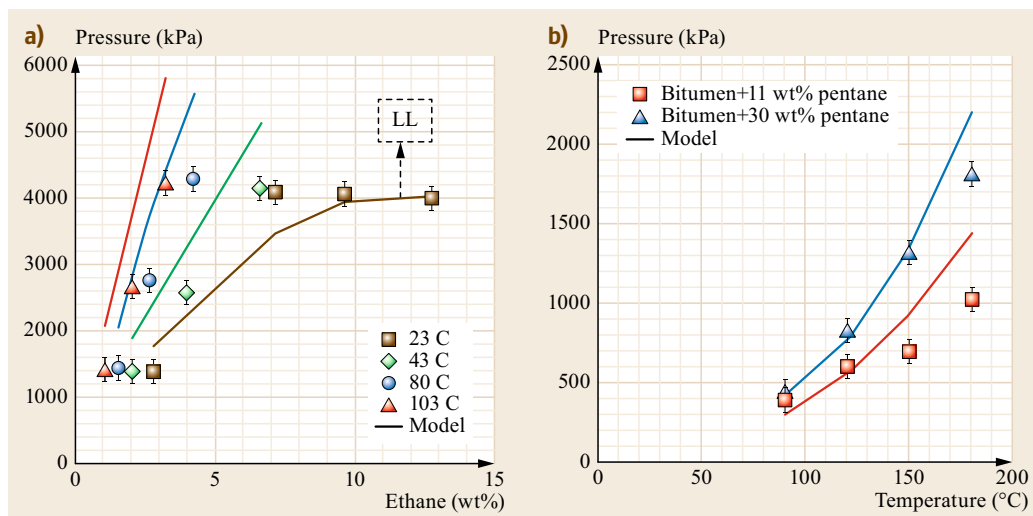


Fig. 8.15a,b Saturation pressures of ethane/bitumen (a) and n -pentane/bitumen, (b) mixtures. Symbols are experimental data and solid lines are APR model fits using independent interaction parameters

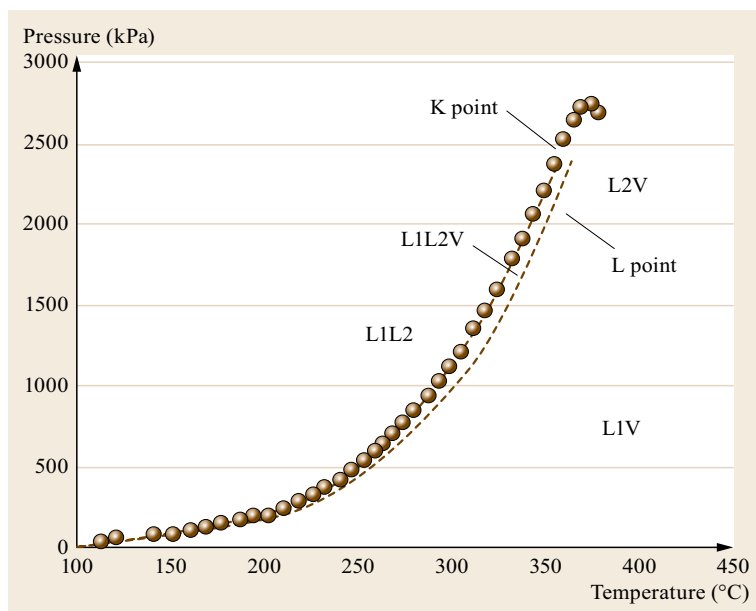


Fig. 8.16 Predicted and experimental liquid–liquid–vapor phase boundaries for 10 wt% AVR and *n*-decane mixture as a function of temperature. Red dots show the experimental L1L2V–L1L2 boundary, red lines values computed by the group-contribution CEOS. K ($L1 = V + L2$) and L ($L1 = L2 + V$) are three-phase critical points

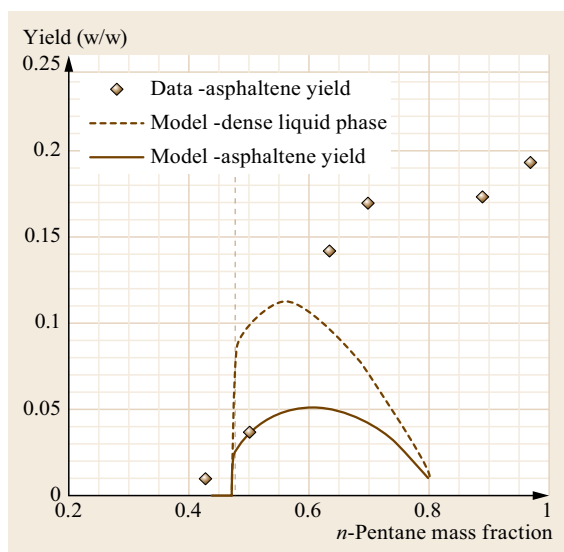


Fig. 8.17 Use of symmetric mixing rules to model asphaltene yields from oil diluted with *n*-pentane. Note that the onset is properly modeled but the yield of precipitate as a function of *n*-pentane concentration is not. An asymmetric mixing rule is likely required for proper model construction

based on statistical mechanics, have begun to be applied to petroleum processing. Although SAFT-derived equations of state are mathematically complex, the underlying concepts are straightforward. SAFT-based equations are constructed based on summing intra- and intermolecular contributions to the Helmholtz energy

(A) of components until all the major contributions are accounted for. With a complete Helmholtz energy expression, the pressure is calculated using (8.20)

$$p = - \left(\frac{\partial A}{\partial V} \right)_T \quad (8.20)$$

The expression for A is given by

$$A = A^{\text{ideal}} + m(A^{\text{HS}} + A^{\text{Disp}}) + A^{\text{Chain}} + A^{\text{Assoc}}, \quad (8.21)$$

where molecules are treated as chains of hard spheres. A brief explanation of each term in (8.21) is provided in Table 8.4

For nonassociating mixtures, the major parameters required for each component are the hard sphere diameter (σ), usually treated as a temperature-dependent term, the energy well depth (ϵ), and the number of segments (m). The hard sphere diameter and m model the fluid finite size and compressibility behavior at high pressures and the energy well models the intrinsic energy characteristics of the fluid such as vapor pressures and enthalpies of vaporization. In practice, these parameters are determined through simultaneous fitting of vapor pressures and saturated liquid densities. This simultaneous fitting and the better repulsive term used by SAFT vis-à-vis the simpler $\frac{RT}{v-b}$ term used by most CEOS are likely to provide better compressed density, especially when volumes calculated by the cubic results are not volume translated or are limited to two-parameter formulations. It is also found that the hard

Table 8.4 Main terms used for the construction of SAFT equations of state

SAFT term	Meaning
Ideal	Ideal gas contribution to the Helmholtz energy (ideal gas C_p)
HS	Hard sphere contribution, calculated using the Carnahan–Starling equation (1972)
Disp	Contribution from dispersion forces, that is, weak forces between hard spheres, usually modeled a simple energy well model like Lennard–Jones or square well
m	Spheres are joined tangentially to form chains and corresponding molecules. M is the number of segments required to build a molecule
Chain	Additional contribution for chain formation
Assoc	Contribution coming from association, for example, hydrogen bonding

sphere diameter and well depth energy can be correlated through group contribution methods and a theoretically based, predictive model can be constructed. For example, great regularity of SAFT parameters is observed for n -alkanes.

It is also frequently observed that SAFT-based equations of state can provide at least qualitative predictions when interaction parameters are set to zero and usually smaller interaction parameters are required than for CEOS used to model similar mixtures. This is undoubtedly linked to their more rigorous theoretical formulation. Interaction parameters are introduced through the energy well

$$\varepsilon_{ij} = \sqrt{\varepsilon_i \varepsilon_j} (1 - k_{ij}) . \quad (8.22)$$

The literature on SAFT has become large. For oil processing applications, the review by *de Hemptinne* et al. [8.155] is recommended. As noted in their review, promising results related to modeling heavy oils and solvents through SAFT have been obtained, for example, by *Chapman's* group at Rice University [8.156]. SAFT-based equations do provide a better theoretical platform for development than CEOS, and the use of a rigorous hard sphere reference allows for better modeling of compressed fluid behavior, an important factor for oil processing. At the same time, SAFT equations do not provide exact matches for the critical pressure and temperature as CEOSs do and sometimes exhibit unphysical behavior such as liquid–liquid de-mixing for pure components [8.157]. Perhaps more importantly, well developed and accepted characterization procedures using SAFT are not yet generally available, although there has been progress in this direction [8.158, 159].

SAFT-based theoretical enhancements, such as the explicit addition of association with model develop-

ment, are a potentially useful development for heavy oil modeling applications. The addition of explicit association terms is not necessarily limited to SAFT-like equations but rather can be applied to CEOSs as well, as shown by *Kontogeorgis* et al. [8.160] in the CPA equation of state. This model has a weaker theoretical basis than SAFT since it preserves the cubic equation framework as the reference for the Helmholtz energy calculation, but has the attractive feature of allowing engineers to work within the CEOS structure for hydrocarbon mixtures and to add complexity, and hence introduce noncubic EOS behavior into calculations only as needed, for example, for important polar compounds encountered in hydrocarbon processing, such as water, methanol, and glycols.

8.5.5 Activity Coefficient Models

While activity coefficient models do not provide many derived properties of interest for process calculations, they do provide an excellent platform for specific phase equilibrium challenges, especially for developing models for asphaltene precipitation from oils when in contact with light solvents. A useful, self-contained structure for modeling the behavior of heavy oils and their mixtures with diverse solvents is the model originally proposed by *Hirshberg* et al. [8.161] and elaborated by *Yarranton* and *Masliyah* [8.123]. The modeling approach is based on the Scatchard–Hildebrand theory extended to large asphaltene *molecules* through the Flory–Huggins term

$$\ln \gamma_i = 1 - \frac{v_i^1}{v_m} + \ln \left(\frac{v_i^1}{v_m} \right) + \frac{v_i^1}{RT} (\delta_m - \delta_i^1)^2 , \quad (8.23)$$

where v_i^1 is the molar volume of component i , v_m is the molar volume of the mixture, δ_i^m is the solubility parameter for component i , and δ_m is the solubility parameter for the mixture. The solubility parameter is defined using

$$\delta_i = \sqrt{\frac{\Delta U^{\text{vap}}}{v_i^1}} , \quad (8.24)$$

where ΔU^{vap} is the internal energy of vaporization, also expressed as $\Delta U^{\text{vap}} = \Delta H^{\text{vap}} - RT$.

The solubility parameters for asphaltenes and maltene fractions have been fitted as functions of liquid density and temperature, density being one of the key variables that are available from the oil characterization procedure. The molar volumes are functions of pressure and temperature, thus providing the model with additional accuracy and also the ability to estimate pressure effects on the solubility of asphaltenes

in oils [8.121]. The model has one adjustable parameter per pure component (δ_i) and is easily tunable if experimental data are available through changes in the statistical distribution describing the asphaltene nano-aggregate molecular weights. Figure 8.18 shows the model results for asphaltene yields upon contact with light solvents calculated for several heavy oils and bitumen. This model has also been successfully implemented in process simulators [8.162].

8.5.6 Prediction of Water and Heavy Oil Phase Behavior

Water is a permanent issue related to hydrocarbon processing, and accurate modeling of water composition in hydrocarbons and hydrocarbon composition in water are key factors for reliable process design and process simulation. Due to the low mutual solubility of water and hydrocarbon mixtures at temperatures and pressure removed from the critical point of water, simple models for engineering use have been developed and have found extensive use in process simulators through CEOSs. Perhaps the earliest general formulation for simple modeling of water and hydrocarbons is to use of a constant interaction parameter between water and hydrocarbons equal to 0.5 in CEOS [8.163]. This approximation provides a qualitative representation for

water solubility in hydrocarbon mixtures. Variants of this idea have been presented [8.164] and are included in process and reservoir simulation thermodynamic models. This approach does provide meaningful values for material and energy balances related to hydrocarbon phases, as long as water is modeled using a compound specific $\alpha(T)$ function [8.120].

However, modeling the mutual solubility of water and hydrocarbons with a single interaction parameter using a CEOS and quadratic mixing rules can only match one side of the solubility curve. Most process simulators are designed to provide meaningful values for refinery design and simulation, especially the simulation of crude distillation towers, and therefore the solubility of water in hydrocarbons is the key. This solubility is reasonably well modeled using a constant binary interaction parameter of the order of 0.5 and can be significantly improved if the interaction parameter is allowed to vary with temperature. However, this approximation causes the thermodynamic model to underestimate the solubility of hydrocarbons in the aqueous phase, typically by several orders of magnitude [8.120, 147], and the computed compositions cannot be used for the design of water-processing facilities.

Soreide [8.165] and *Kabadi and Danner* [8.166] proposed asymmetric mixing rules to better fit both sides of the solubility curve. Gibbs excess-based mixing

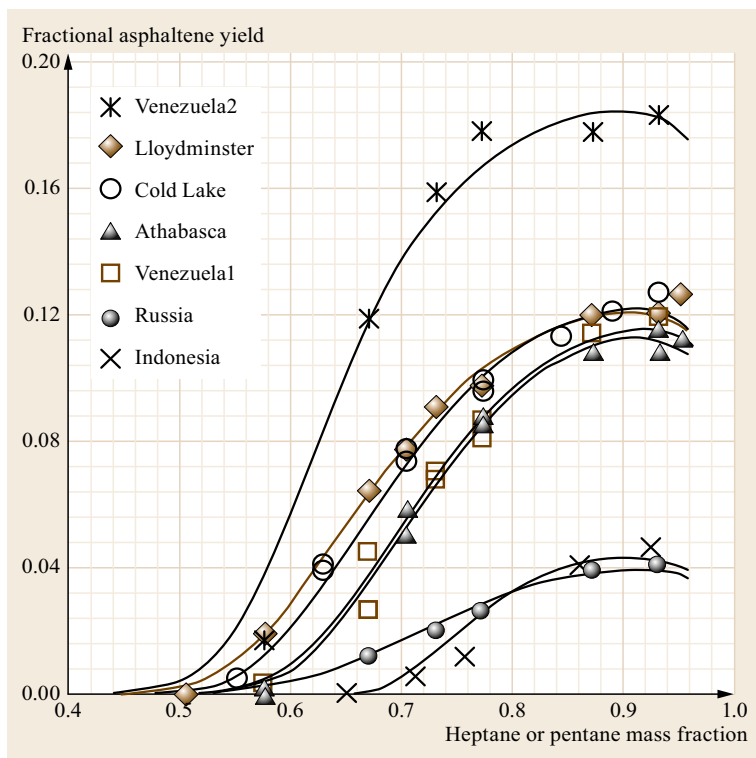


Fig. 8.18 Fractional asphaltene yield as a function of solvent wt% at 23 °C

rules, notably the Huron–Vidal mixing rule, can be used for very accurate modeling of water–hydrocarbon mixtures. Other models for water solubility have been applied, including density-dependent mixing rules [8.167] and the CPA model [8.160].

Notwithstanding the usefulness and convenience of having generalized interaction parameters for equations of state, it is useful to have methods independent from any specific thermodynamic model for the estimation of mutual solubility of hydrocarbons and water. These estimates then can be used directly for calculations or used to tune interaction parameters for specific thermodynamic models. Some of the more traditional models were reviewed by *de Hemptinne* et al. [8.155], and recent developments in this area include a method proposed by *Satyro* et al. [8.122], where mutual solubilities are estimated using only normal boiling points and specific gravities, properties commonly available when characterizing oils through pseudo-components. A method proposed by *Amani* et al. [8.69] for the estimation of water solubility in heavy oil and heavy oil + solvent mixtures is also available and offers advantages over other approaches, particularly at high temperatures near the critical temperature of water.

8.5.7 Phase Behavior Prediction Summary

Phase behavior prediction for heavy oils and heavy oils + hydrocarbon and nonhydrocarbon mixtures is based largely on the extension of methods with a long history of application for fluids well characterized by boiling fractions, carbon number fractions, individual molecules for which benchmark property data of most if not all components are available, and where time scales for systems to reach equilibrium are negligible compared to processing times. Computation approaches outlined in Sect. 8.5 all suffer from limited experimental data and consequently computed phase compositions, in particular, are poor. Phase behaviors can at best be simulated. Prediction remains infeasible. There are a number of possible explanations for this outcome and they comprise active areas for research.

8.6 Thermophysical Property Simulation and Prediction

Ideally, thermophysical properties should be calculated based on an equation of state to ensure consistency and adherence to exact boundary conditions determined by the first and second laws of thermodynamics and all ensuing relationships. Through careful parameterization and data fitting, accurate equation of state

With inherently high viscosities and low mass transfer rates, equilibration times may be orders of magnitude longer than process time scales, in some cases, and thermodynamic equilibrium may not be reached within time scales that are meaningful for certain process modeling problems:

1. Characterization is clearly a weak link because parameter identification is under constrained.
2. There is a small and growing body of literature that suggests that the molecular basis for phase behavior and property prediction implicit in the models may not capture all of the relevant physics and chemistry. This is particularly true for asphaltene-rich fractions which appear to form filterable nanoscopic phase domains with behaviors independent of the bulk fluids [8.25], and where depletion–floculation and other nonmolecular physical and chemical effects have been shown to drive phase behavior [8.26].
3. Interfacial phenomena may also play key roles in shaping fluid behaviors in specific processes [8.1]. So, even though classical thermodynamics is a powerful tool, it may not be the sole basis for the development of process and property models for heavy oils. In addition to the main thermodynamic variables for process engineering: pressure, temperature, and the number of phases present and their composition, other variables such as areas, interfacial tension, and surface coverage (e.g., for surface phenomena like adsorption) may play a role and the thermodynamic expressions – and associated need of more process engineering knowledge – must be augmented to include additional thermodynamic potentials.
4. At high temperatures, phase equilibrium thermodynamic models do not, in general, account for thermal cracking and although phase boundaries can be computed at arbitrarily high temperatures, they do not necessarily correspond to actual phase equilibria since the composition changes due to chemical reactions. The thermodynamic models are typically not corrected for reaction outcomes.

derived properties can be determined for many hydrocarbon mixtures [8.120] and extended, sometimes surprisingly, to highly nonideal systems using simple mixing rules [8.168].

For heavy oils, typically the thermophysical properties of most interest are, enthalpy, entropy, heat capac-

ity, density, and viscosity, and these are the properties discussed in this section. Density can be obtained directly from an equation of state or from independent correlations. Viscosity cannot be determined directly from an equation of state, although it can be linked to equation of state calculations, for example, by correlating viscosity to density. Nor can an equation of state directly determine thermal properties. Equations of state provide departures from the ideal gas state (residual property). Ideal gas properties must be known experimentally or estimated independently. These departures are defined through rigorous thermodynamic relationships [8.131] for caloric properties

$$\Delta A_{\text{res}} = A^{\text{real}} - A^{\text{ideal}} = \int_{\infty}^V \left(P - \frac{RT}{V} \right) - RT \ln Z, \quad (8.25)$$

$$\Delta S_{\text{res}} = - \frac{\partial \Delta A_{\text{res}}}{\partial T}, \quad (8.26)$$

$$\Delta H_{\text{res}} = \Delta A_{\text{res}} + T \Delta S_{\text{res}} + RT(Z - 1), \quad (8.27)$$

$$\Delta C_{p,\text{res}} = \int_{\infty}^V \left(\frac{\partial^2 P}{\partial T^2} \right) dV - T \frac{\left(\frac{\partial P}{\partial T} \right)_V^2}{\left(\frac{\partial P}{\partial V} \right)_T}, \quad (8.28)$$

where subscript “res” indicates a residual property.

So, for example, to determine the enthalpy of a real fluid at a fixed temperature and pressure (H), the ideal gas enthalpy (H_0), known exogenously, must be added to the residual enthalpy obtained from (8.27)

$$H = H_0 + \Delta H_{\text{res}}. \quad (8.29)$$

The enthalpy of an ideal gas is a simple integral of the ideal gas heat capacity from a reference temperature to the temperature of interest. Ideal gas heat capacities are pressure independent and the ideal gas heat capacity of a mixture is a weighted sum of the component heat capacities. Equations (8.25)–(8.29) underline the importance of hydrocarbon characterization methods and the associated estimation methods for physical properties. Ideal gas properties for pseudo-components, however defined, must be accessible, and critical properties and vapor pressure data are required by equations of state for the calculation of residual properties. Usually, the molar average normal boiling point, specific gravity, and mean molar mass are used for the estimation of ideal gas heat capacities. Comprehensive reviews of estimation methods for pure components are available [8.98, 131, 169], and they are usually adequate for hydrocarbon mixture simulation, although we stress that for important polar compounds associated with hydrocarbons, fitting to experimental data is frequently

necessary. Armed with an equation of state, and an ideal gas heat capacity model or data, and (8.25) to (8.29), volumetric and all caloric information for fluids and related processes can be obtained. The volumes obtained from the equation of state can be used along with temperature as inputs for viscosity calculations [8.170].

8.6.1 Caloric Physical Properties – Enthalpy, Entropy, and Heat Capacities

CEOSs are frequently used to estimate caloric departure functions for enthalpy, entropy, and heat capacity. Typically, the values obtained for fluid enthalpy, entropy, and heat capacity for both nonideal gases and liquids are in good agreement with data [8.171], particularly for light hydrocarbons and mixtures. The Lee–Kesler equation [8.131] in particular has been found useful for such applications. The common practice is to use CEOSs for the estimation of enthalpies, entropies, and heat capacities for hydrocarbon systems in general and rely on more complex equations of state [8.172] for high accuracy if the molecules/mixtures are simple. Although much data is available on excess enthalpies and excess heat capacities for binary hydrocarbon mixtures [8.173], there are no comprehensive reviews on the general accuracy of engineering equations of state related to the prediction of enthalpies and heat capacities and it is difficult, if not impossible, to provide comprehensive guidelines related to estimate’s accuracies. In general, enthalpy and entropy estimates from simple equations of state provide estimates within 10% of experimental values away from the critical point, but calculation outcomes should be checked against experimental data for detailed design and performance warranties as large errors arise. For example, CEOS, normally provide skewed fits vis-à-vis experimental values for isobaric liquid heat capacity, with systematic overestimation of values at low temperature and systematic underestimation at high temperature [8.174]. However, most calculations are performed in the $0.6 < \text{Tr} < 0.85$ region, where the fits are best and errors are typically small.

For heavy hydrocarbons, such as Athabasca bitumen, and high boiling fractions, little work has been done on the validation of generalized estimates of caloric properties other than isobaric heat capacity where a new approach for the estimation of ideal gas [8.94], liquid [8.37, 175], and solid [8.37, 38, 176] heat capacities based on atomic compositional analysis that are rooted in statistical thermodynamics have become available. The predictive equations comprising this new approach are based on the observation that the heat capacity of a molecule is primarily a function of the number of internal vibration per mass of molecule

captured by a similarity variable given by

$$\alpha = \frac{\sum_{i=1}^n v_i}{\sum_{i=1}^n v_i M_i}, \quad (8.30)$$

where w_i is the stoichiometric coefficient of element i in the molecule, and M_i is the molecular mass of element i . The value of the similarity variable, α , is easily determined from known molecular structures or elemental analysis. For methane, the numerator appearing in (8.30) is $5 = (4H + 1C)$ and the denominator is $16 = (4 \times 1.008 + 1 \times 12.08)$ and the similarity value is 0.311. The elemental analysis of an oil (or its fractions) should be part of the oil characterization procedure and the heat capacity is then correlated as a function of phase state, the value of α , and temperature. Pseudo-component chemical elemental analysis can be estimated [8.177] if values are not available from the oil assay.

The results from this new approach [8.94] compare well with ideal gas isobaric heat capacity estimates from the more complex Benson's method, a commonly used group contribution-based technique that requires detailed knowledge of a molecular structure [8.131] as illustrated in Fig. 8.19. *Dadgostar* and *Shaw* [8.39, 174] showed that elemental composition-based correlations make a priori predictions for liquid heat capacity values within 10% or 0.2 J/(g K) of experimental data even for

heavy oil and bitumen. This new approach was successfully adapted into oil characterization procedures available in a commercial process simulator [8.178].

8.6.2 Density Prediction

Vapor and liquid densities are usually estimated using simple equations of state, although complex, highly accurate equations of state [8.173] can be used for volumetric computations for specific pure compounds and mixtures of light hydrocarbons. Simple two-parameter CEOSs suffer from a simplistic repulsive term that makes them, in general, too *soft*, thus underestimating liquid densities. Vapor densities are typically more accurate away from critical points. For example, the Soave-Redlich-Kwong (SRK) equation of state provides reasonable estimates for liquid densities of light hydrocarbons (C_1 – C_2) but underestimates the liquid densities of other important hydrocarbons, typically by 15–25% making it unfit for design. The Peng–Robinson equation of state, designed to provide reasonable densities for liquid hydrocarbons in the gasoline range, attempts to correct this handicap related to liquid density calculation. The outcome is only partially successful, and it can be shown that no two-parameter CEOS provides good liquid densities. A third (or fourth) parameter is necessary [8.142].

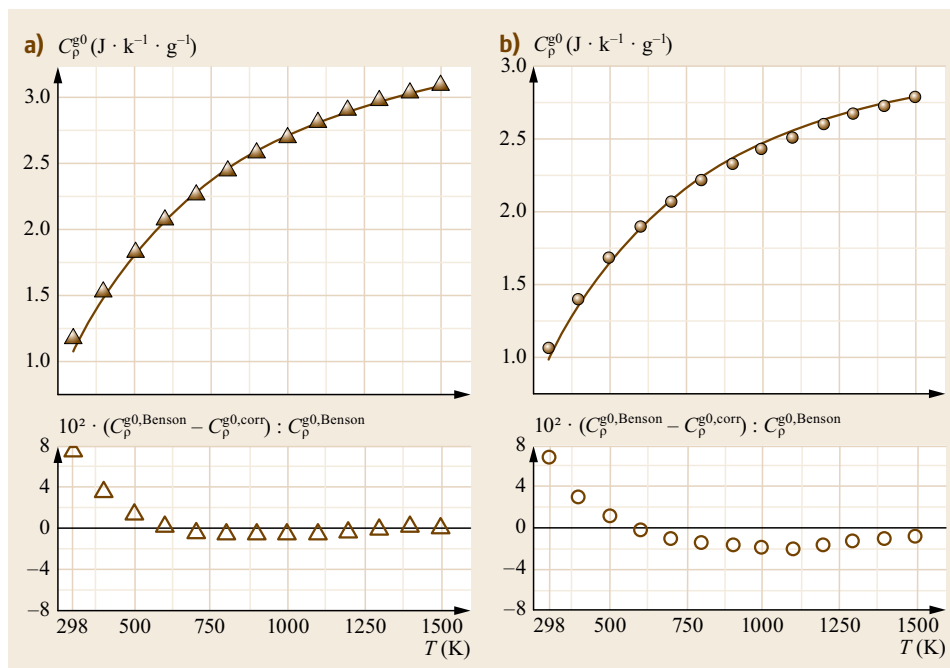


Fig. 8.19a,b Estimated c_p^{g0} values for: (a) $C_{283}H_{337}N_3O_4S_9$ ($M = 4133.3 \text{ g mol}^{-1}$, $\alpha = 0.1539 \text{ mol g}^{-1}$), (b) $C_{64}H_{52}S_2$ ($M = 885.2 \text{ g mol}^{-1}$, $\alpha = 0.1333 \text{ mol g}^{-1}$) evaluated from 298.15 K to up to 1500 K. Filled triangle Benson's group contribution method; filled circle, (after [8.94]); open triangle and circle relative deviations. (After [8.94])

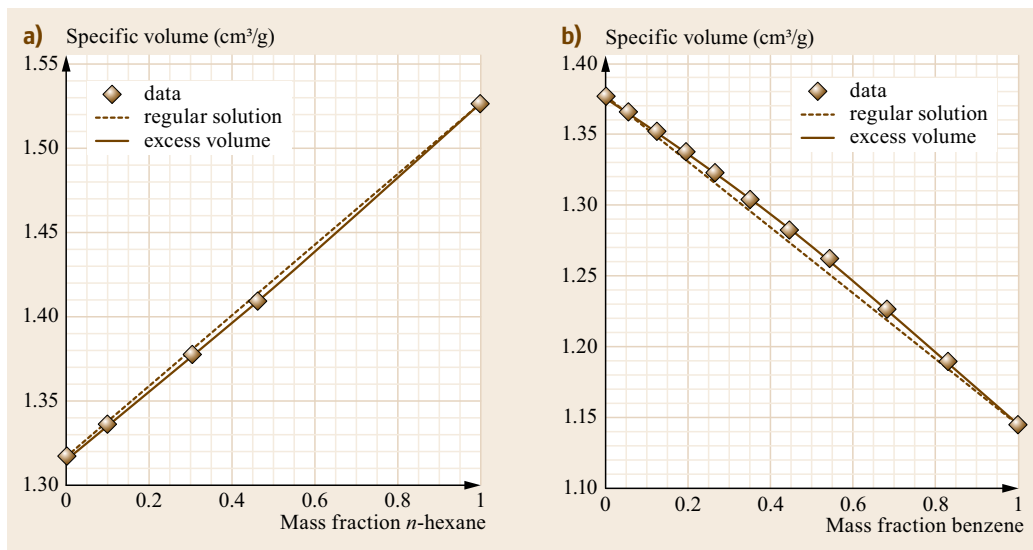


Fig. 8.20a,b
Specific volumes of mixtures of liquid hydrocarbons at 25 °C and 0.1 MPa modeled with regular solution mixing rules and excess volume mixing rules: (a) *n*-hexane and *n*-tetradecane; (b) benzene and *n*-decane. (After [8.77])

Three-parameter CEOSs do provide better liquid density estimates, the most famous being the *Patel–Teja* equation [8.138], but more commonly, this handicap of CEOS is addressed using volume translation as discussed in Sect. 8.5.

Some non-CEOSs do provide better density estimates than CEOS, notably the Lee–Kesler equation and the SAFT family of equations of state. The Lee–Kesler equation is particularly useful for light hydrocarbon mixtures. SAFT parameters are fitted to vapor pressure and liquid density data, and the equation of state benefits handsomely from this parameterization as well as from a more theoretically based repulsive term – the Carnahan–Starling expression for hard spheres. This comes at the cost of not reproducing the critical pressure and temperature of a compound, and the importance of this trade-off is always dependent on the objectives of the simulation at hand.

Vast amounts of data are available related to the excess volumes of liquid hydrocarbon mixtures but no comprehensive evaluation of this information is available, and it is impossible to provide guidelines related to the accuracy of density estimates for mixtures computed using equations of state. Some process simulation vendors recognized this handicap early on [8.178] and added an empirical correction to the volume translation parameter implemented as an excess function. This approach is useful when modeling highly asymmetric hydrocarbon mixtures such as light organic solvents and bitumen. While the additional term makes the equation of state inconsistent from a formal point of view, this is of no consequence for subcritical bitumen + solvent extraction process modeling.

For high-accuracy liquid density calculations for heavy oils and especially heavy oils and light hydrocarbon solvent mixtures important for upgrading via dilution through asphaltene precipitation, transportation, underground extraction through solvent injection and surface facility design, it is common to use a separate model for the calculation of liquid densities decoupled from the equation of state predictions

$$v = v^{\text{ideal}} + v^{\text{excess}}(T, \bar{x}), \quad (8.31)$$

where the liquid density is obtained as

$$\rho = \frac{MW_{\text{avg}}}{v}. \quad (8.32)$$

The excess term is small, but due to the large volumes of material usually processed, it may not be negligible. It is also important to note that the actual value of excess volumes (and even their *sign*) can be a function of the way the bitumen is processed and this apparently simple physical property exhibits an irreducible uncertainty and is not easily determined [8.32]. Also, for the calculation of actual densities, the average molecular weight of the material is required, thus underlining once more the importance of characterization methods.

Liquid mixture density calculation, independent of equation of state calculations, has a long history. Frequently, liquid densities for mixtures are well approximated by assuming ideal solution behavior

$$\rho = \sum_{i=1}^{nc} \frac{\omega_i}{\rho_i}, \quad (8.33)$$

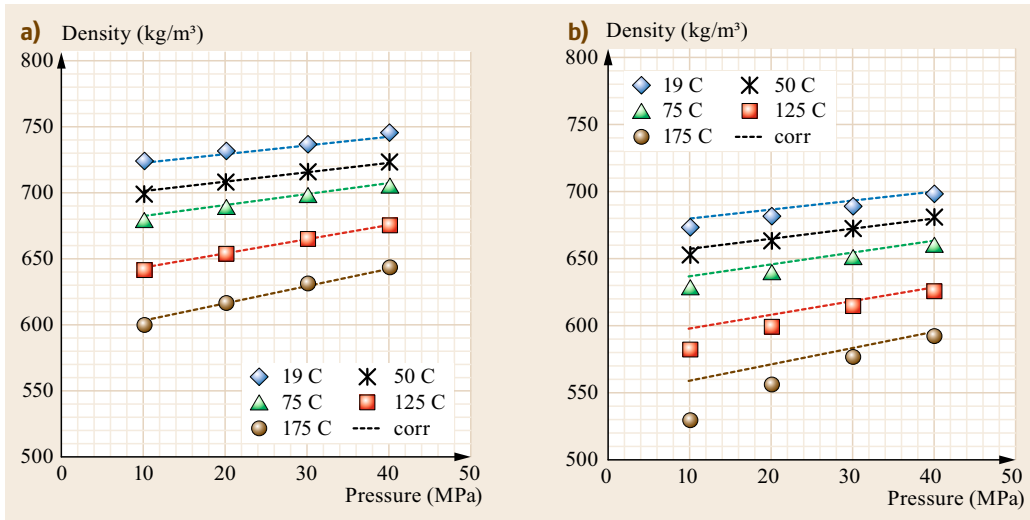


Fig. 8.21a,b Measured and predicted densities for mixtures of propane and *n*-decane: (a) 6.0 wt% propane; (b) 25 wt% propane. (After [8.77])

where the mixture density is simply a weighted sum of the component densities. Many hydrocarbon mixture densities are closely approximated on this basis as illustrated in Fig. 8.20. Nonideal mixing impacts can be introduced through the use of a mixing rule

$$\rho = \left[\sum_{i=1}^{nc} \sum_{j=1}^{nc} \frac{\omega_i \omega_j}{2} \left(\frac{1}{\rho_i} + \frac{1}{\rho_j} \right) (1 - \beta_{ij}) \right]^{-1}, \quad (8.34)$$

where β_{ij} is an adjustable parameter determined based on experimental mixture data.

For heavy oils and bitumen, the effect of dissolved gases and light solvents on mixture density can in principle be captured using (8.34) or a simple and accurate alternative approach reported by *Saryazdi et al.* [8.77] based on effective densities for light components that is illustrated in Fig. 8.21.

8.6.3 Heavy Oil Viscosity Prediction

While heavy oil fractions derived from the Safaniya vacuum residue have been shown to exhibit non-Newtonian rheological behavior up to more than 400 K [8.4], whole heavy oils such as Athabasca bitumen and Maya crude oil may be considered Newtonian fluids above ambient temperature. Below ambient conditions, non-Newtonian behaviors become important [8.5, 33, 179] and may impact pipeline and mixing operations. The transition from Newtonian to non-Newtonian behavior is governed by phase transitions

occurring in the maltene fraction and is not related to asphaltene content. Asphaltene content impacts the absolute value of the viscosity.

These two effects are frequently conflated and there is only limited work on parsing the distinct roles played by these two key components of heavy oils [8.180, 181]. Development and testing of computational approaches related to the rheological property prediction of complex fluids are ongoing fields of study and treatment of heavy oils as a combination of a Newtonian continuous fluid + a separate asphaltene-rich dispersed phase or as a combination of a structured non-Newtonian continuous phase + a separate asphaltene-rich dispersed phase to treat high- and low-temperature calculations is an open area of study.

For the moment, available viscosity correlations for heavy oil, and more broadly hydrocarbons, presume that they are single-phase Newtonian fluids, and viscosity simulation as opposed to pure prediction is targeted. Newtonian viscosity correlations for heavy oil can be divided into two groups, liquid-phase correlations and full phase correlations. *Monnery et al.* [8.182] and *Poling et al.* [8.131] provide extensive reviews of this class of viscosity models and the most relevant are reviewed below.

Liquid-Phase Newtonian Viscosity Correlations

Viscosity reduction by heating is a crucial aspect of many heavy oil processes, and therefore, it is a common practice to fit the temperature dependence of heavy oil viscosity. A simple correlation relating crude oil viscosity to temperature is the Arrhenius relationship [8.183]

given by

$$\log(\mu) = A + \frac{B}{T}, \quad (8.35)$$

where μ is viscosity, T is absolute temperature, and A and B are the fitted coefficients. This form of equation works well for conventional crude oils over small ranges of temperatures but provides poor predictions for broad ranges of temperature. For example, Fig. 8.22 shows the failure of the Andrade correlation to fit viscosity data from a Western Canadian bitumen over a temperature range from 20 to 175 °C. The accuracy of (8.35) is significantly improved by adding an extra term as shown in [8.184]

$$\log(\mu) = A + \frac{B}{T + C}. \quad (8.36)$$

Adding the third fitting parameter, C , provides an excellent fit to the data of Fig. 8.22 with an average absolute relative deviation (AARD) of 6%.

Amazingly, the best fit of viscosity to temperature is achieved with a simple linear relationship of double log viscosity to log temperature [8.185], given by

$$\log[\log(\mu + 0.7)] = A + B \log(T). \quad (8.37)$$

The value of 0.7 is added to the viscosity term to avoid negative logs at low viscosity; values of 0.8 and 1.0 have also been employed. With only two fitted parameters, the Walther correlation fit the viscosity of Western Canadian bitumen, as shown in Fig. 8.22, with an AARD of 4%. *Svrcek* and *Mehrotra* [8.186] correlated the slope with the intercept to reduce the correlation to one adjustable parameter, although with some loss of accuracy. Note that none of the above correlations include the effect of pressure.

Heavy oil viscosity is also reduced by dilution with a solvent and a variety of mixing rules have been employed to predict the viscosity of blends of oils and of heavy oils diluted with solvent. *Centeno* et al. [8.187] review many of these mixing rules. Some of the rules used for heavy oils are listed below.

Arrhenius [8.188]: molar

$$\log(\mu_{\text{mix}}) = \sum x_i \log(\mu_i), \quad (8.38)$$

Arrhenius [8.188]: mass

$$\log(\mu_{\text{mix}}) = \sum x_i \log(\mu_i), \quad (8.39)$$

Mehrotra [8.189]

$$\log(\mu_{\text{mix}}) = \sum \sqrt{x_i w_i} \log(\mu_i), \quad (8.40)$$

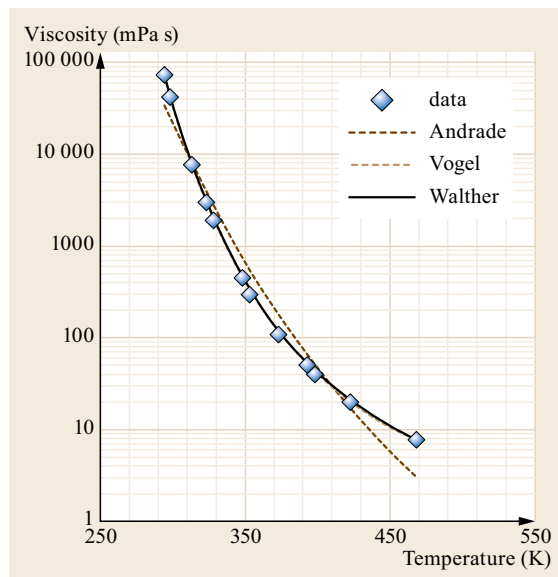


Fig. 8.22 The viscosity of a Western Canadian bitumen at 2500 kPa fitted with the Andrade, Vogel, and Walther correlations

Kendall and Monroe [8.190]

$$\frac{1}{\mu_{\text{mix}}^{1/3}} = \sum \frac{w_i}{\mu_i^{1/3}}, \quad (8.41)$$

Chirinos et al. [8.191]

$$\log[\log(v_{\text{mix}} + 0.7)] = \sum w_i \log[\log(v_i + 0.7)], \quad (8.42)$$

Yarranton et al. [8.20]

$$\log[\log(\mu_{\text{mix}} + 1)] = \sum w_i \log[\log(\mu_i + 1)], \quad (8.43)$$

where v is the kinematic viscosity.

Figure 8.23 compares the different mixing rules for a Western Canadian bitumen diluted with a condensate. Here, and in general, we have found that the double log mixing rule provides the best results for diluted heavy oils. Note, refiners use a variation of the double log mixing rule to predict blend kinematic viscosities such as in the Ruftas and Chevron methods where a viscosity blend index (VBI) is defined as a function of the double log of the viscosity and then mass-based mixing rules are applied [8.97, 192, 193]. Another option is to include adjustable parameters in a given mixing rule [8.194–200]. Most of these mixing rules use generalized fitting parameters based on a particular dataset of diluted crude oils.

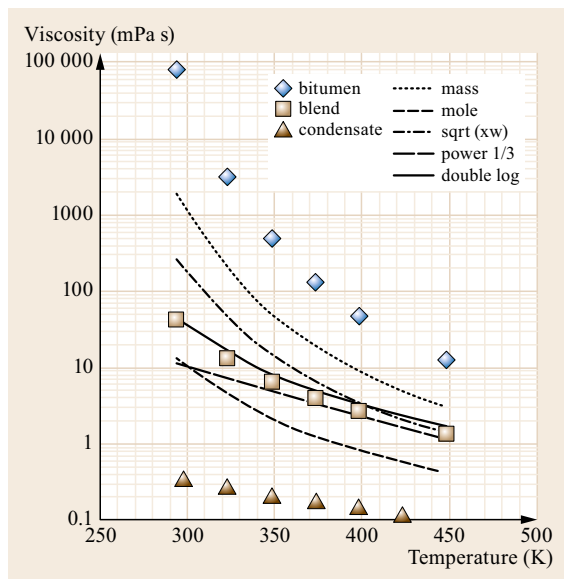


Fig. 8.23 Prediction of viscosity from different mixing rules for a mixture of 30 wt% condensate in dead Western Canadian bitumen at 2500 kPa. (After [8.20])

There are relatively few reliable methods available to predict heavy oil viscosity when no data are available. The viscosity of conventional crude oils is often predicted from correlations to temperature, API, and solution gas–oil ratio using the following steps:

1. Calculate the dead oil viscosity ($\mu_{od} = f(T, API)$)
2. Calculate the live oil viscosity at and below the bubble point based on the dead oil viscosity ($\mu_o = A\mu_{od}^B$, where A and B are the parameters that depend on the solution–gas–oil ratio)
3. Calculate the live oil viscosity above the bubble point based on the bubble point viscosity. ($\mu_o = f(\mu_{ob}, P - P_b)$).

The most well known of these correlations, such as the Standing, Beggs and Robinson, Bergman, and Glasø correlations, are reviewed by *Whitson and Brulé* [8.97]. These correlations are designed for black oil characterizations where viscosity is desired as a function of pressure at a fixed reservoir temperature. Each correlation was tuned to a regional dataset and does not necessarily provide accurate predictions for heavy oil. Since these correlations were designed for one specific temperature, they do not provide accurate predictions of the temperature dependence of oil viscosity. Finally, live oil viscosity prediction requires a gas–oil ratio and heavy oil–gas oil ratios are challenging to measure accurately and are often not available.

There are a number of correlations for the kinematic viscosity of crude oils characterized into boiling cuts, usually based on normal boiling point and specific gravity [8.201, 202]. *Yazdani and Maini* [8.203] have demonstrated the inadequacy of these models when applied to heavy oils despite their extensive use for light and medium reservoir fluids. The LBC correlation [8.204] relates the dense fluid viscosity to only the reduced density with a fourth degree polynomial. The correlation can be unreliable for heavy hydrocarbon fluids [8.205] and it is common to tune the correlation to the available experimental data by adjusting the critical volumes of the C_7+ fractions. The API [8.177] correlation for kinematic viscosity is a popular choice. This correlation has numerical problems depending on the Watson K and API gravity which arise when applied to heavy oils. These shortcomings were removed by *Loria* [8.206].

Yarranton et al. [8.20] developed a procedure to predict the viscosity of crude oils and their cuts solely from gas chromatography assays. They characterized the oil into molecular weight-based pseudo-components and correlated the Walther parameters with molecular weight. They calculated the parameters of the whole oil using a simple mass-based mixing rules. They also included pressure dependence in the correlation and were able to predict the viscosity of a variety of conventional and heavy crude oils over a range of conditions to within approximately 30%. A straightforward tuning procedure was also provided to fit available data including a binary interaction parameter for mixtures of bitumen and solvents (Fig. 8.8).

Full Phase Newtonian Viscosity Correlations

Full phase viscosity correlations encompass the gas, liquid, and supercritical regions and are usually designed to work with the fluid characterization used in process and reservoir simulation. Models which meet this criterion include corresponding states methods, friction theory, and the expanded fluid model.

The corresponding state models relate the reduced viscosity of the fluid to the reduced viscosity of a reference fluid at the same reduced temperature and either density or pressure [8.207, 208]. *Ely and Hanley* [8.209] used temperature and density for their reduced coordinates and introduced shape factors to correct for any noncorrespondence. Variations of their method are often used to model the viscosity of the light fraction of the crude oils. This model has been applied to heavier hydrocarbons, such as crude oil distillation cuts, using aromaticity corrections or mass shape factors [8.210, 211].

Pedersen et al. [8.208, 212] used temperature and pressure for their reduced coordinates and methane

as the reference fluid. Instead of shape factors, their model is tuned with a rotational coupling coefficient as well as an effective molecular weight of the mixture. Empirical correlations for these parameters were developed from a database of viscosity data, including pure components, characterized reservoir fluids, and petroleum distillation cuts. The model provides reliable viscosity predictions for most conventional reservoir fluids [8.205] but is not easily applied to heavy petroleum fluids since these fluids often correspond to methane at temperatures below its freezing point [8.213].

Friction theory or F-theory [8.214] relates the viscosity of the dense fluid to the friction between fluid layers. The friction force is related to the repulsive and attractive internal pressures of the fluid determined from the van der Waals pressure terms from the PR and SRK equations of state. A version of the model with one adjustable parameter per fluid component, called a characteristic critical viscosity, was developed for pure hydrocarbons and then extended to characterized crude oils [8.215]. The pseudo-component critical viscosity values were correlated with molecular weight and critical pressure and temperature through a single common proportionality factor which is tuned to match crude oil viscosity data. For heavier oils, those with molecular weights higher than 200 g/mol, a second tuning parameter was introduced to correct the estimation of the repulsive and attractive pressure terms [8.216]. Tuned one- or two-parameter models successfully fit experimental data above the saturation pressure and provided predictions at lower pressures to within experimental uncertainties. The two parameters were later made into functions of temperature to more accurately model the viscosity of the characterized oils at different temperatures [8.217].

The expanded fluid (EF) model [8.170, 218] is an empirical correlation of viscosity to density designed for modeling the viscosity of hydrocarbons. The inputs to the model are the gas viscosity from *Wilke's* [8.219] method, the fluid density, pressure, and three fluid-specific parameters. The fluid-specific parameters have been determined for a variety of hydrocarbons and are correlated with molecular weight for crude oil pseudo-components [8.220]. Predicted viscosities had an AARD of 50% and a maximum deviation of 100%. Tuning with a single multiplier applied to one parameter reduced the maximum deviation to less than 30% in all cases. Tuning two parameters reduced the deviation to within the experimental error, see Fig. 8.9. The EF model was successfully implemented in a process simulator [8.178], integrated with the oil characterization procedure and associate fitting procedures for heavy oil

and solvent interaction parameter estimation or regression.

8.6.4 Property Simulation and Prediction Summary

Property simulation and prediction are not normally done as standalone activities, and are best performed as part of an integrated package of cross-linked and cross-validated models embedded in process simulation software packages. Notwithstanding the sheer amount of work, creativity and time spent on the development of fluid characterization methods and thermodynamic models, few of the final users of this effort – process, production, and chemical engineers – are interested in the data or the models per se but rather on the results produced by the simulation software. This fact should never leave the minds of the data or model producers and no matter how much time is spent on the development of a technique or the mathematical prowess displayed when developing a model, if data or models cannot be used in a simulation their value is diminished. Simulations shape to a large extent production and refining process requirements, from strategies for field exploration, to the size of equipment, and the estimated capital and operating costs. They also deeply influence the financial decisions related to an engineering projects.

Users of property simulation and prediction software should not adopt a passive attitude toward the use of simulators and blindly accept values produced by them, even when pressed to *get the project moving*. The development of proper simulation models for heavy oil processing is not a cookie cutter type of activity and success arises from a combination of high-quality data, proper material characterization, understanding of the question models are required to answer and the questions they cannot answer. The greatest challenge physical property modelers face when addressing the needs associated with the understanding of heavy oil behavior is ignorance. Heavy oils are ill defined. More than 50 wt% of these materials are undistillable, and little quantitative information is available regarding their chemical makeup and composition.

With clever parameterization of undistillable fractions, simulation models for unit operations where property models are rooted in the behaviors of simple well-defined fluids can be quickly extended to cases where heavy oils and bitumen are principal constituents. However, fluid-specific properties are relevant and it is, for example, difficult to develop high-quality predictive models for heavy oil + solvent mixture viscosity.

8.7 Perspectives and Conclusions

Phase behavior and property measurement simulation and prediction for heavy oils and bitumens present sample handling and measurement challenges. Capturing the physics and chemistry at all of the relevant length scales required even for simple properties like density and viscosity not to mention phase equilibrium compositions can become Herculean tasks, especially at low temperatures, or where standard measurement techniques fail. Innovative and hypothesis-driven measurements that target the capture of underlying or overlooked aspects of thermophysical properties and phase behavior are needed in addition to essential but routine measurements that drive process design and development calculations.

Fluid characterization and property and process modeling present additional challenges because thermodynamic models are dependent on quantitative information about individual components and their mixtures. It is hard to develop meaningfully general models when little is known about components and their physical interactions. Consequently, the current state of the art of phase behavior and property calculation is driven by correlation and simulation rather than pure prediction, with few exceptions. We count these exceptions among the successes of a principled and rigorous approach involving simultaneous development and validation of

molecular structure, nanostructure, and thermophysical property concepts and models that will over time build toward prediction in other areas as outlined in Fig. 8.1.

Our specific recommendations are pragmatic and based on many years of helping people to get value from their investment in experimental data and simulation models. In our own work, we strive to keep models simple so that they can be tested and validated as clearly as possible and so that their range of application can be clearly delimited as we have done for viscosity and water in oil solubility models in this chapter.

Acknowledgments. Harvey W. Yarranton thanks the sponsors of the NSERC Industrial Research Chair in Heavy Oil Properties and Processing: CNOOC Nexen, Petrobras, Schlumberger, Shell, Virtual Materials Group, and the Natural Sciences and Engineering Research Council of Canada (NSERC). Marco A. Satyro thanks the Virtual Materials Group, Inc., and John M. Shaw thanks the sponsors of the NSERC Industrial Research Chair in Petroleum Thermodynamics: Alberta Innovates Energy and Environment Solutions, British Petroleum, ConocoPhillips Inc., NEXEN Inc., Shell Canada, Total E and P Canada, Virtual Materials Group Inc., and Natural Sciences and Engineering Research Council of Canada (NSERC).

References

- 8.1 S.R. Bagheri, A. Bazyleva, M.R. Gray, W.C. McCaffrey, J.M. Shaw: Test Observation of liquid crystals in heavy petroleum fractions, *Energy Fuels* **24**, 4327–4332 (2010)
- 8.2 M. Fulem, M. Becerra, A. Hasan, B. Zhao, J.M. Shaw: Phase behaviour of Maya crude oil based on calorimetry and rheometry, *Fluid Phase Equil.* **272**, 32–41 (2008)
- 8.3 A. Bazyleva, M. Fulem, M. Becerra, B. Zhao, J.M. Shaw: Phase behavior of Athabasca bitumen, *J. Chem. Eng. Data* **56**, 3242–3253 (2011)
- 8.4 A. Bazyleva, M. Becerra, D. Stratiychuk–Dear, J.M. Shaw: Phase behavior of Safaniya vacuum residue, *Fluid Phase Equil.* **380**, 28–38 (2014)
- 8.5 A. Bazyleva, M.A. Hasan, M. Fulem, M. Becerra, J.M. Shaw: Bitumen and heavy oil rheological properties: Reconciliation with viscosity measurements, *J. Chem. Eng. Data* **55**, 1389–1397 (2010)
- 8.6 A.M. McKenna, G.T. Blakney, F. Xian, P.B. Glaser, R.P. Rodgers, A.G. Marshall: Heavy petroleum composition 2. Progression of the Boduszynski model to the limit of distillation by ultrahigh resolution FT-ICR mass spectrometry, *Energy Fuels* **24**, 2939–2946 (2010)
- 8.7 C.S. Hsu, C.L. Hendrickson, R.P. Rodgers, A.M. McKenna, A.G. Marshall: Petroleomics: Advanced molecular probe for petroleum heavy ends, *J. Mass. Spectrom.* **46**, 337–343 (2011)
- 8.8 S. Lababidi, S.K. Panda, J.T. Andersson, W. Schrader: Deep well deposits: Effects of extraction on mass spectrometric results, *Energy Fuels* **27**, 1236–1245 (2013)
- 8.9 S. Lababidi, S.K. Panda, J.T. Andersson, W. Schrader: Direct coupling of normal-phase high-performance liquid chromatography to atmospheric pressure laser ionization fourier transform ion cyclotron resonance mass spectrometry for the characterization of crude oil samples, *Anal. Chem.* **85**, 9478–9485 (2013)
- 8.10 C. Obiosa–Maife, J.M. Shaw: Toward identification of molecules in ill-defined hydrocarbons using infrared, Raman and NMR spectroscopy, *Energy Fuels* **25**, 460–471 (2011)
- 8.11 C.S. Hsu (Ed.): *Analytical Advances for Hydrocarbon Research* (Kluwer, New York 2003)
- 8.12 T. Kuznicki, J.H. Masliyah, S. Bhattacharjee: Molecular dynamics study of model molecules resembling asphaltene-like structures in aqueous organic solvent systems, *Energy Fuels* **22**, 2379–2389

- (2008)
- 8.13 S. Zhao, L.S. Kotlyar, J.R. Woods, B.D. Sparks, K. Hardacre, K.H. Chung: Molecular transformation of Athabasca bitumen end-cuts during coking and hydrocracking, *Fuel* **80**, 1155–1163 (2001)
- 8.14 Y. Aray, R. Hernández-Bravo, J.G. Parra, J. Rodríguez, D.S. Coll: Exploring the structure–solubility relationship of asphaltene models in toluene, heptane, and amphiphiles using a molecular dynamic atomistic methodology, *J. Phys. Chem. A* **115**, 11495–11507 (2011)
- 8.15 J. Murgich, J.A. Abanero, O.P. Strausz: Molecular recognition in aggregates formed by asphaltene and resin molecules from the athabasca oil sand, *Energy Fuels* **13**, 278–286 (1999)
- 8.16 J.P. Dickie, Y.T. Yen: Macrostructures of asphaltic fractions by various instrumental methods, *Anal. Chem.* **39**, 1847–1852 (1967)
- 8.17 M. Agrawala, H.W. Yarranton: Measurement and modeling of the phase behavior of solvent diluted bitumens, *Ind. Eng. Chem. Res.* **40**, 4664–4672 (2001)
- 8.18 E. Rogel: Thermodynamic modeling of asphaltene aggregation, *Langmuir* **20**, 1003–1012 (2004)
- 8.19 M.R. Gray, R.R. Tykwinski, J.M. Stryker, X. Tan: Supramolecular assembly model for aggregation of petroleum asphaltenes, *Energy Fuels* **25**, 3125–3134 (2011)
- 8.20 H.W. Yarranton, J.J. van Dorp, M.L. Verlaan, V. Lastovka: Wanted dead or live – crude cocktail viscosity: A pseudo–component method to predict the viscosity of dead oils, live oils, and mixtures, *J. Can. Petr. Technol.* **52**, 178–191 (2013)
- 8.21 F. Alvarez-Ramírez, Y. Ruiz-Morales: Island versus archipelago architecture for asphaltenes: Polycyclic aromatic hydrocarbon dimer theoretical studies, *Energy Fuels* **27**, 1791–1808 (2013)
- 8.22 F. Spillebout, D. Bégué, I. Baraille, J.M. Shaw: On discerning intermolecular vibrations in experimental acene spectra, *Energy Fuels* **28**, 2933–2947 (2014)
- 8.23 D. Merino-García, J.M. Shaw, H. Carrier, H. Yarranton, L. Goual: Petrophase 2009 panel discussion on standardization of petroleum fractions, *Energy Fuels* **24**, 2175–2177 (2010)
- 8.24 B. Zhao, J.M. Shaw: Composition and size distribution of coherent nanostructures in Athabasca bitumen and Maya crude oil, *Energy Fuels* **21**, 2795–2804 (2007)
- 8.25 J. Eyssautier, D. Espina, J. Gummel, P. Levitz, M. Becerra, J.M. Shaw, L. Barré: Mesoscale organization in a physically separated vacuum residue: Comparison to asphaltenes in a simple solvent, *Energy Fuels* **26**, 2670–2687 (2012)
- 8.26 M. Khammar, J.M. Shaw: Liquid–liquid phase equilibria in asphaltene + polystyrene + toluene mixtures at 293K, *Energy Fuels* **26**, 1075–1088 (2012)
- 8.27 K. Nikooyeh, J.M. Shaw: On the applicability of the regular solution theory to asphaltene + diluent mixtures, *Energy Fuels* **26**, 576–585 (2012)
- 8.28 R.B. DeBoer, K. Leerlooyer, M.R.P. Elgner, A.R.D. Bergen: Screening of crude oils for asphaltene precipitation, *SPE Prod. Facil.* **10**(1), 55–61 (1995)
- 8.29 V.V. Likhatsky, R.Z. Syunyaev: New colloidal stability index for crude oils based on polarity of crude oil components, *Energy Fuels* **24**, 6483–6488 (2010)
- 8.30 N. Saber, X. Zhang, X.-Y. Zou, J.M. Shaw: Simulation of the phase behaviour of athabasca vacuum residue + *n*-alkane mixtures, *Fluid Phase Equil.* **313**, 25–31 (2012)
- 8.31 N. Saber, J.M. Shaw: On the phase behavior of athabasca vacuum residue + *n*-decane, *Fluid Phase Equil.* **302**, 254–259 (2011)
- 8.32 R. Stewart, C.V. Wood, S.J. Murowchuk, J.M. Shaw: Phase order inversion during heavy oil and bitumen production with solvent addition, *Energy Fuels* **28**(7), 4835–4848 (2014)
- 8.33 S. Mortazavi-Manesh, J.M. Shaw: Thixotropic rheological behavior of Maya crude oil, *Energy Fuels* **28**, 972–979 (2014)
- 8.34 J.M. Shaw, E. Behar: SLLV phase behavior and phase diagram transitions in asymmetric hydrocarbon fluids, *Fluid Phase Equil.* **209**, 185–206 (2003)
- 8.35 D. Henry, B. Fuhr: Preparation of bitumen from oil sand by ultracentrifugation, *Fuel* **71**, 1515–1518 (1992)
- 8.36 C. Xing, R.W. Hiltz, J.M. Shaw: Sorption of athabasca vacuum residue constituents on synthetic mineral and process equipment surfaces from mixtures with pentane, *Energy Fuels* **24**(4), 2500–2513 (2010)
- 8.37 V. Laštovka, N. Sallamie, J.M. Shaw: A similarity variable for estimating the heat capacity of solid organic compounds: Part I. fundamentals, *Fluid Phase Equil.* **268**, 51–60 (2008)
- 8.38 V. Laštovka, M. Fulem, M. Becerra, J.M. Shaw: A similarity variable for estimating the heat capacity of solid organic compounds: Part II application: Heat capacity calculation for ill-defined organic solids, *Fluid Phase Equil.* **268**, 134–141 (2008)
- 8.39 N. Dadgostar, J.M. Shaw: A predictive correlation for the constant–pressure specific heat capacity of pure and ill-defined liquid hydrocarbons, *Fluid Phase Equil.* **313**, 211–226 (2012)
- 8.40 R. Bagheri, M.R. Gray, J.M. Shaw, W.C. McCaffrey: In situ observation of mesophase formation and coalescence in catalytic hydroconversion of vacuum residue using a stirred hot-stage reactor, *Energy Fuels* **26**, 3167–3178 (2012)
- 8.41 X.-Y. Zou, J.M. Shaw: Dispersed phases and dispersed phase deposition issues arising in asphaltene rich hydrocarbon fluids, *Petroleum Sci. Technol.* **22**, 759–771 (2004)
- 8.42 X. Zou, X.H. Zhang, J.M. Shaw: The phase behavior of athabasca vacuum bottoms + *n*-alkane mixtures, *SPE Prod. Oper.* **22**, 265–272 (2007)
- 8.43 B. Long, M. Chodakowski, J.M. Shaw: Impact of liquid–vapor to liquid–liquid–vapor phase transitions on asphaltene-rich nanoaggregate behavior in athabasca vacuum residue + pentane mixtures, *Energy Fuels* **27**, 1779–1790 (2013)
- 8.44 J.M. Shaw, T. de Loos, J. de Swaan Arons: Prediction of unusual retrograde condensation in model reservoir fluids, *Fluid Phase Equil.* **84**, 251–266

- (1993)
- 8.45 S.J. Abedi, S. Seyfaie, J.M. Shaw: Unusual retrograde condensation and asphaltene precipitation in a model heavy oil systems, *Petroleum Sci. Technol.* **16**, 209–226 (1998)
- 8.46 E.A. Turek, R.S. Metcalfe, L. Yarborough, R.L. Robinson Jr.: Phase equilibria in CO₂-multicomponent hydrocarbon systems: Experimental data and an improved prediction technique, *SPE J.* **24**, 308–324 (1984)
- 8.47 X. Zou: *Selective Removal of Inorganic Fine Solids, Heavy Metals and Sulfur from Bitumen/Heavy Oils*, Ph.D. Thesis (Univ. Toronto, Toronto 2003)
- 8.48 K. Khaleghi: *Experimental PVT Study of the Phase Behavior of CO₂ + Heavy Oil Mixtures*, Ph.D. Thesis (Univ. Alberta, Edmonton 2011)
- 8.49 E. Béhar, P. Mougín, A. Pina: Integration of asphaltene flocculation modeling into a reservoir simulator, *Rev. IFP* **58**, 637–646 (2003)
- 8.50 E. Brunner: Fluid mixtures at high pressures IX. phase separation and critical phenomena in 23 (*n*-alkane + water) mixtures, *J. Chem. Thermodyn.* **22**, 335–353 (1990)
- 8.51 E. Brunner, M.C. Thies, G.M. Schneider: Fluid mixtures at high pressures: Phase behavior and critical phenomena for binary mixtures of water with aromatic hydrocarbons, *J. Supercrit. Fluids* **39**, 160–173 (2006)
- 8.52 M.J. Amani, M.R. Gray, J.M. Shaw: Phase behavior of athabasca bitumen + water mixtures at high temperature and pressure, *J. Supercrit. Fluids* **77**, 142–152 (2013)
- 8.53 K. Nikooyeh, J.M. Shaw: On enthalpies of solution of athabasca pentane asphaltene and asphaltene fractions, *Energy Fuels* **27**, 66–74 (2013)
- 8.54 A.K. Tharanivasan, H.W. Yarranton, S.D. Taylor: Asphaltene precipitation from crude oils in the presence of emulsified water, *Energy Fuels* **26**, 6869–6875 (2012)
- 8.55 A. Maczynski, D. Shaw, M. Goral, B. Wisniewska-Gocłowska, A. Skrzecz, Z. Maczynska, I. Owczarek, K. Blazej, M.-C. Haulait-Pirson, F. Kapuku, G.T. Hefter, A. Szafranski: IUPAC-NIST solubility data series. 81. Hydrocarbons with water and seawater-revised and updated part 1. C₅ hydrocarbons with water, *J. Phys. Chem. Ref. Data* **34**(2), 441–476 (2005)
- 8.56 A. Maczynski, D. Shaw, M. Goral, B. Wisniewska-Gocłowska, A. Skrzecz, I. Owczarek, K. Blazej, M.-C. Haulait-Pirson, G.T. Hefter, Z. Maczynska, A. Szafranski, C. Tsonopoulos, C.L. Young: IUPAC-NIST solubility data series. 81. Hydrocarbons with water and seawater-revised and updated. Part 2. Benzene with water and heavy water, *J. Phys. Chem. Ref. Data* **34**(2), 477–542 (2005)
- 8.57 A. Maczynski, D. Shaw, M. Goral, B. Wisniewska-Gocłowska, A. Skrzecz, I. Owczarek, K. Blazej, M.-C. Haulait-Pirson, G.T. Hefter, Z. Maczynska, A. Szafranski, C.L. Young: IUPAC-NIST solubility data series. 81. Hydrocarbons with water and seawater-revised and updated. Part 3. C₆H₈-C₆H₁₂ hydrocarbons with water and heavy water, *J. Phys. Chem. Ref. Data* **34**(2), 657–708 (2005)
- 8.58 A. Maczynski, D. Shaw, M. Goral, B. Wisniewska-Gocłowska, A. Skrzecz, I. Owczarek, K. Blazej, M.-C. Haulait-Pirson, G.T. Hefter, F. Kapuku, Z. Maczynska, C.L. Young: IUPAC-NIST solubility data series. 81. Hydrocarbons with water and seawater-revised and updated. Part 4. C₆H₁₄ Hydrocarbons with water, *J. Phys. Chem. Ref. Data* **34**(2), 709–713 (2005)
- 8.59 A. Maczynski, D. Shaw, M. Goral, B. Wisniewska-Gocłowska, A. Skrzecz, I. Owczarek, K. Blazej, M.-C. Haulait-Pirson, G.T. Hefter, F. Kapuku, Z. Maczynska, C.L. Young: IUPAC-NIST solubility data series. 81. Hydrocarbons with water and seawater-revised and updated. Part 5. C₇ Hydrocarbons with water and heavy water, *J. Phys. Chem. Ref. Data* **34**(3), 1399–1487 (2005)
- 8.60 D.G. Shaw, A. Maczynski, D. Shaw, M. Goral, B. Wisniewska-Gocłowska, A. Skrzecz, I. Owczarek, K. Blazej, M.-C. Haulait-Pirson, G.T. Hefter, Z. Maczynska, A. Szafranski: IUPAC-NIST solubility data series. 81. Hydrocarbons with water and seawater-revised and updated. Part 6. C₈H₈-C₈H₁₀ Hydrocarbons with water, *J. Phys. Chem. Ref. Data* **34**(3), 1489–1553 (2005)
- 8.61 D.G. Shaw, A. Maczynski, D. Shaw, M. Goral, B. Wisniewska-Gocłowska, A. Skrzecz, I. Owczarek, K. Blazej, M.-C. Haulait-Pirson, G.T. Hefter, F. Kapuku, Z. Maczynska, A. Szafranski: IUPAC-NIST solubility data series. 81. Hydrocarbons with water and seawater revised and updated. Part 7. C₈H₁₂-C₈H₁₈ Hydrocarbons with water, *J. Phys. Chem. Ref. Data* **34**(4), 2261–2298 (2005)
- 8.62 D.G. Shaw, A. Maczynski, D. Shaw, M. Goral, B. Wisniewska-Gocłowska, A. Skrzecz, I. Owczarek, K. Blazej, M.-C. Haulait-Pirson, G.T. Hefter, F. Kapuku, Z. Maczynska, A. Szafranski: IUPAC-NIST solubility data series. 81. Hydrocarbons with water and seawater-revised and updated. Part 8. C₉ Hydrocarbons with water, *J. Phys. Chem. Ref. Data* **34**(4), 2299–2345 (2005)
- 8.63 D.G. Shaw, A. Maczynski, D. Shaw, M. Goral, B. Wisniewska-Gocłowska, A. Skrzecz, I. Owczarek, K. Blazej, M.-C. Haulait-Pirson, G.T. Hefter, P.L. Huyskens, F. Kapuku, Z. Maczynska, A. Szafranski: IUPAC-NIST solubility data series. 81. Hydrocarbons with water and seawater-revised and updated. Part 9. C₁₀ Hydrocarbons with water, *J. Phys. Chem. Ref. Data* **35**(1), 93–151 (2006)
- 8.64 D.G. Shaw, A. Maczynski, D. Shaw, M. Goral, B. Wisniewska-Gocłowska, A. Skrzecz, I. Owczarek, K. Blazej, M.-C. Haulait-Pirson, G.T. Hefter, F. Kapuku, Z. Maczynska, A. Szafranski: IUPAC-NIST solubility data series. 81. Hydrocarbons with water and seawater – revised and updated. Part 10. C₁₁ and C₁₂ Hydrocarbons with water, *J. Phys. Chem. Ref. Data* **35**(1), 153–203 (2006)
- 8.65 D.G. Shaw, A. Maczynski, D. Shaw, M. Goral, B. Wisniewska-Gocłowska, A. Skrzecz, I. Owczarek, K. Blazej, M.-C. Haulait-Pirson, G.T. Hefter, F. Kapuku, Z. Maczynska, A. Szafranski: IUPAC-NIST solubility data series. 81. Hydrocarbons with water and seawater-revised and updated. Part 11. C₁₃-C₃₆ Hy-

- drocarbons with water, *J. Phys. Chem. Ref. Data* **35**(2), 687–784 (2006)
- 8.66 D. Shaw (Ed.): *IUPAC: Hydrocarbons with Water and Seawater. Part I: Hydrocarbons C₅ to C₇*, IUPAC Solubility Data, Vol. 37 (Pergamon, New York 1989)
- 8.67 D. Shaw (Ed.): *IUPAC: Hydrocarbons with Water and Seawater. Part II: Hydrocarbons C₈ to C₃₆*, IUPAC Solubility Data, Vol. 38 (Pergamon, New York 1989)
- 8.68 C.A. Glandt, W.G. Chapman: Effect of water dissolution on oil viscosity, *SPE Reserv. Eng.* **10**, 59–64 (1995)
- 8.69 M.J. Amani, M.R. Gray, J.M. Shaw: On correlating water solubility in ill-defined hydrocarbons, *Fuel* **134**, 644–658 (2014)
- 8.70 M. Saajanlehto, P. Uusi-Kyyny, V. Alopaeus: Hydrogen solubility in heavy oil systems: Experiments and modeling, *Fuel* **137**, 393–404 (2004)
- 8.71 S. Larter, J. Adams, I.D. Gates, B. Bennett, H. Huang: The origin, prediction and impact of oil viscosity heterogeneity on the production characteristics of tar sand and heavy oil reservoirs, *J. Can. Petr. Technol.* **47**, 52–61 (2008)
- 8.72 C.D. Jiang, B. Bennett, S.R. Larter, J.J. Adams, L. Snowdon: Viscosity and API gravity determination of solvent extracted heavy oil and bitumen, *J. Can. Petr. Technol.* **49**, 20–27 (2010)
- 8.73 B. Bennett, C. Jiang, L.R. Snowdon, S.R. Larter: A practical method for the separation of high quality heavy oil and bitumen samples from oil reservoir cores for physical and chemical property determination, *Fuel* **116**, 208–213 (2014)
- 8.74 K.A. Miller, L.A. Nelson, R.M. Almond: Should you trust your heavy oil viscosity measurement?, *J. Can. Petr. Technol.* **45**, 42–48 (2006)
- 8.75 L.G. Helper, C. His (Eds.): *Technical Handbook on Oil Sands, Bitumen and Heavy Oils* (AOSTRA, Edmonton 1989)
- 8.76 M.R. Gray: *Upgrading Petroleum Residues and Heavy Oils* (Marcel Dekker, New York 1994)
- 8.77 F. Saryazdi, H. Motahhari, F.F. Schoeggel, H.W. Yarranton: Density of hydrocarbon mixtures and bitumen diluted with solvents and dissolved gases, *Energy Fuels* **27**, 3666–3678 (2013)
- 8.78 A. Badamchizadeh, H. Yarranton, W. Svrcek, B. Maini: Phase behavior and physical property measurements for vapex solvents: Part I. Propane and athabasca bitumen, *J. Can. Petr. Tech.* **48**(2), 54–61 (2009)
- 8.79 A. Badamchizadeh, H.W. Yarranton, B.B. Maini, M.A. Satyro: Phase behavior and physical property measurements for vapex solvents: Part II. Propane, carbon dioxide, and athabasca bitumen, *J. Can. Petr. Tech.* **48**(3), 57–65 (2009)
- 8.80 W.Y. Svrcek, A.K. Mehrotra: Gas solubility, viscosity and density measurements for athabasca bitumen, *J. Can. Petr. Technol.* **21**, 31–38 (1982)
- 8.81 A.K. Mehrotra, W.Y. Svrcek: Measurement and correlation of viscosity, density and gas solubility for Marguerite Lake bitumen saturated with carbon dioxide, *AOSTRA J. Res.* **1**, 51–62 (1984)
- 8.82 A.K. Mehrotra, W.Y. Svrcek: Viscosity, density and gas solubility data for oil sand bitumens. Part III: Wabasca bitumen saturated with with N₂, CO, CH₄, CO₂, and C₂H₆, *AOSTRA J. Res.* **2**, 83–93 (1985)
- 8.83 A.K. Mehrotra, W.Y. Svrcek: Viscosity, density and gas solubility data for oil sand bitumens. Part I: Athabasca bitumen saturated with CO and C₂H₆, *AOSTRA J. Res.* **1**, 263–268 (1985)
- 8.84 A.K. Mehrotra, W.Y. Svrcek: Viscosity, density and gas solubility data for oil sand bitumens. Part II: Peace river bitumen saturated with N₂, CO, CH₄, CO₂, and C₂H₆, *AOSTRA J. Res.* **1**, 269–279 (1985)
- 8.85 A.K. Mehrotra, W.Y. Svrcek: Properties of cold lake bitumen saturated with pure gases and gas mixtures, *Can. J. Chem. Eng.* **66**, 656–665 (1988)
- 8.86 H. Motahhari, F.F. Schoeggel, M.A. Satyro, H.W. Yarranton: Viscosity prediction for solvent diluted live bitumen and heavy oil at temperatures up to 175°C, *J. Can. Petr. Technol.* **52**, 376–390 (2013)
- 8.87 H. Motahhari, F.F. Schoeggel, M.A. Satyro, H.W. Yarranton: The effect of solvents on the viscosity of an alberta bitumen at in situ thermal process conditions. In: *SPE Heavy Oil Conference, Calgary* (2013), SPE Paper 165548
- 8.88 NIST: NIST Standard Reference Database; NIST/TRC Source Database; Version 2008: WinSource (2008)
- 8.89 X. Zhang, J.M. Shaw: Liquid phase mutual diffusion coefficients for heavy oil plus light hydrocarbons, *Petr. Sci. Technol.* **25**, 773–790 (2007)
- 8.90 X.H. Zhang, M. Fulem, J.M. Shaw: Liquid-phase mutual diffusion coefficients for athabasca bitumen + pentane mixture, *J. Chem. Eng. Data* **52**, 691–694 (2007)
- 8.91 A.K. Tharanivasan, C. Yang, Y. Gu: Comparison of three different interface mass transfer models used in the experimental measurement of solvent diffusivity in heavy oil, *J. Pet. Sci. Technol.* **44**, 269–282 (2004)
- 8.92 A. Sadighan, M. Becerra, A. Bazyleva, J.M. Shaw: Forced and diffusive mass transfer between pentane and athabasca bitumen fractions, *Energy Fuels* **25**, 782–790 (2011)
- 8.93 F. Hossein, J.M. Shaw, D. Sinton: Bitumen-toluene mutual diffusion coefficients using microfluidics, *Energy Fuels* **27**, 2042–2048 (2013)
- 8.94 L.V. Lastovka, J.M. Shaw: Predictive correlations for ideal gas heat capacities of pure hydrocarbons and petroleum fractions, *Fluid Phase Equil.* **356**, 338–370 (2013)
- 8.95 K.S. Pedersen, A. Fredenslund, P. Thomassen: *Properties of Oils and Natural Gases* (Gulf, Houston 1989)
- 8.96 J.G. Speight: *The Chemistry and Technology of Petroleum*, 3rd edn. (Marcel Dekker, New York 1999)
- 8.97 C.H. Whitson, M.R. Brulé: *Phase Behavior*, Monograph Henry L. Doherty, Vol. 20 (Society of Petroleum Engineers, Richardson 2000)
- 8.98 M.R. Riazi: *Characterization and Properties of Petroleum Fractions*, 1st edn. (ASTM International, West Coughoocken 2005)
- 8.99 L. Merdrignac, D. Espinat: Physicochemical characterization of petroleum fractions: The state of the art, *Oil Gas Sci. Tech. Rev. IFP* **62**, 7–32 (2007)

- 8.100 K.H. Altgelt, M.M. Boduszynski: *Composition and Analysis of Heavy Petroleum Fractions* (CRC, Boca Raton 1994)
- 8.101 I. Wiehe: *Process Chemistry of Petroleum. Macromolecules* (CRC, Boca Raton 2008)
- 8.102 J. Read, D. Whiteoak: *The Shell Bitumen Handbook*, 5th edn. (Thomas Telford Publishing, London 2003)
- 8.103 O.C. Mullins, H. Sabbah, J. Eyssautier, A.E. Pomerantz, L. Barré, A.B. Andrews, Y. Ruiz-Morales, F. Mostowfi, R. McFarlane, L. Goual, R. Lepkowitz, T. Cooper, J. Orbulescu, R.M. Leblanc, J. Edwards, R.N. Zare: Advances in asphaltene science and the Yen-Mullins model, *Energy Fuels* **26**, 3986–4003 (2012)
- 8.104 C.S. Hsu, D. Drinkwater: Gas chromatography–mass spectrometry in the petroleum industry. In: *Current Practice of Gas Chromatography–Mass Spectrometry*, ed. by W.M.A. Niessen (Marcel Dekker, New York 2001)
- 8.105 H.-Y. Cai, J.M. Shaw, K.H. Chung: Hydrogen solubility measurements in heavy oil and bitumen cuts, *Fuel* **80**(8), 1055–1064 (2001)
- 8.106 C.B. Batistella, P. Sbaite, M.R.W. Maciel, R. Maciel Filho, A. Winter, A. Gomes, L. Medina, R. Kunest: Heavy petroleum fractions characterization: A new approach through molecular distillation. In: *Proc. Second Mercosur Congr. chem. eng. fourth mercosur congr. process syst. eng* (2005)
- 8.107 O. Castellanos-Díaz, J. Modaresghazani, M.A. Satyro, H.W. Yarranton: Modeling the phase behavior of heavy oil and solvent mixtures, *Fluid Phase Equil.* **304**, 74–85 (2011)
- 8.108 S.H. Huang, M. Radosz: Phase behavior of reservoir fluids III: Molecular lumping and characterization, *Fluid Phase Equil.* **66**, 1–21 (1991)
- 8.109 S.B. Jaffe, H. Freund, W.N. Olmstead: Extension of structure-oriented lumping to vacuum residua, *Ind. Eng. Chem. Res.* **44**, 9840–9852 (2005)
- 8.110 J.M. Sheremata, M.R. Gray, H.D. Dettman, W.C. McCaffrey: Quantitative molecular representation and sequential optimization of athabasca asphaltenes, *Energy Fuels* **18**, 1377–1384 (2004)
- 8.111 J.M. Sheremata: *Residue Molecules: Molecular Representations and Thermal Reactivity*, Ph.D. Thesis (Univ. Alberta, Edmonton 2008)
- 8.112 E.S. Boek, D.S. Yakovlev, T.F. Headen: Quantitative molecular representation of asphaltenes and molecular dynamics simulation of their aggregation, *Energy Fuels* **23**, 1209–1219 (2009)
- 8.113 J.M. Sheremata (MSc Thesis, University of Alberta, Edmonton Canada, 2001)
- 8.114 J.M. Shaw: Toward common generalized phase diagrams for asphaltene containing hydrocarbon fluids, *ACS Div. Petroleum Chem.* **47**(4), 338–342 (2002), Preprints
- 8.115 N. Saber, J.M. Shaw: Toward multiphase equilibrium prediction for ill-defined asymmetric hydrocarbon mixtures, *Fluid Phase Equil.* **285**, 73–82 (2009)
- 8.116 J. Marrero, R. Gani: Group-contribution based estimation of pure component properties, *Fluid Phase Equil.* **183**, 183–208 (2001)
- 8.117 H. Loria, G. Hay, M.A. Satyro: Thermodynamic modeling and process simulation through PIONA characterization, *Energy Fuels* **27**, 3578–3584 (2013)
- 8.118 J.N. Jaubert, F. Mutelet: Extension of the PPR78 model (predictive 1978, Peng–Robinson EOS with temperature dependent k_{ij} calculated through a group contribution method) to systems containing aromatic compounds, *Fluid Phase Equil.* **224**, 285–304 (2004)
- 8.119 E. Voutsas, K. Magoulas, D. Tassios: Universal mixing rule for cubic equations of state applicable to symmetric and asymmetric systems: Results with the Peng–Robinson equation of state, *Ind. Eng. Chem. Res.* **43**, 6238 (2004)
- 8.120 M.A. Satyro: The role of the thermodynamic modeling consistency in process simulation, *Proc. 8th World Congr. Chem. Eng., Palais des Congres, Montreal* (2009)
- 8.121 K. Akbarzadeh, H. Alboudwarej, W.Y. Svrcek, H.W. Yarranton: A generalized regular solution model for asphaltene precipitation from n-alkane diluted heavy oils and bitumens, *Fluid Phase Equil.* **232**, 159–170 (2005)
- 8.122 M.A. Satyro, J.M. Shaw, H.W. Yarranton: A practical method for the estimation of oil and water mutual solubilities, *Fluid Phase Equil.* **355**, 12–25 (2013)
- 8.123 H.W. Yarranton, J.H. Masliyah: Molar mass distribution and solubility modeling of asphaltenes, *AIChE J* **42**, 3533–3543 (1996)
- 8.124 G. Soave: Equilibrium constants from a modified Redlich–Kwong equation of state, *Chem. Eng. Sci.* **27**, 1197–1203 (1972)
- 8.125 D.-Y. Peng, D.B. Robinson: A new two-constant equation of state, *Ind. Eng. Chem. Fundam.* **15**, 59–64 (1976)
- 8.126 P.M. Mathias, T.W. Copeman: Extension of the Peng–Robinson equation of state to complex mixtures: Evaluation of the various forms of the local composition concept, *Fluid Phase Equil.* **13**, 91–108 (1983)
- 8.127 W.G. Chapman, K.E. Gubbins, G. Jackson, M. Badosz: A new reference equation of state for associating liquids, *Ind. Eng. Chem. Res.* **29**, 1709–1721 (1990)
- 8.128 A. Peneloux, E. Rauzy, R. Freze: A consistent correction for Redlich–Kwong–Soave volumes, *Fluid Phase Equil.* **8**, 7–23 (1982)
- 8.129 H.G. Rackett: Equation of state for saturated liquids, *J. Chem. Eng. Data* **15**, 514 (1970)
- 8.130 K.S. Pitzer, D.Z. Lippmann, R.F. Curl, C.M. Huggins, D.E. Petersen: The volumetric and thermodynamic properties of fluids. I. Theoretical basis and virial coefficients, *J. Am. Chem. Soc.* **77**, 3433 (1955)
- 8.131 B.E. Poling, J.M. Prausnitz, J.P. O’Connell: *The Properties of Gases and Liquids*, 5th edn. (McGraw-Hill, New York 2000)
- 8.132 B.I. Lee, M.G. Kesler: A generalized thermodynamic correlation based on three-parameter corresponding states, *AIChE J* **21**, 510 (1975)
- 8.133 C.H. Twu: An internally consistent correlation for predicting the critical properties and molecular weights of petroleum and coal-tar liquids, *Fluid*

- Phase Equil. **16**, 137–150 (1984)
- 8.134 K.G. Joback: *A Unified Approach to Physical Property Estimation Using Multivariate Statistical Techniques*, Ph.D. Thesis (MIT, Cambridge 1984)
- 8.135 J. Marrero–Morejón, E. Pardillo–Fontdevila: Estimation of pure compound properties using group–interaction contributions, *AIChE J* **45**, 615–621 (1999)
- 8.136 J.S. Rowlinson: On the continuity of the gaseous and liquid states. In: *Studies in Statistical Mechanics*, Vol. 14, ed. by J.D. van der Waals (North–Holland, Amsterdam 1988)
- 8.137 O. Redlich, J.N.S. Kwong: On the thermodynamics of solutions. V. An equation of state. Fugacities of Gaseous solutions, *Chem. Rev.* **44**, 233–244 (1949)
- 8.138 N.C. Patel, A.S. Teja: A new cubic equation of state for liquids and liquid mixtures, *Chem. Eng. Sci.* **37**, 463–473 (1982)
- 8.139 M. Cismondi: M.J.: Development and application of a three–parameter RK–PR equation of state, *Fluid Phase Equil* **232**, 74–89 (2005)
- 8.140 L.A.G. Forero, J.A.J. Velásquez: A modified Patel–Teja cubic equation of state: Part I – Generalized model for gases and hydrocarbons, *Fluid Phase Equil.* **342**, 8–22 (2013)
- 8.141 L.A.G. Forero, J.A.J. Velásquez: A modified Patel–Teja cubic equation of state. Part II: – Parameters for polar substances and its mixtures, *Fluid Phase Equil.* **364**, 75–87 (2014)
- 8.142 M.A. Trebble, P.R. Bishnoi: Development of a new four–parameter cubic equation of state, *Fluid Phase Equil.* **35**, 1–18 (1987)
- 8.143 P.M. Mathias, T. Naheiri, E.M. Oh: A density correction for the Peng–Robinson equation of state, *Fluid Phase Equil.* **47**, 77–87 (1989)
- 8.144 B. Schmid, J. Gmehling: The universal group contribution equation of state VTPR present status and potential for process development, *Fluid Phase Equil.* **302**, 213–219 (2011)
- 8.145 P.H. Salim, M.A. Trebble: A modified Trebble–Bishnoi equation of state: Thermodynamic consistency revisited, *Fluid Phase Equil.* **65**, 59–71 (1991)
- 8.146 M.A. Satyro, M.A. Trebble: On the applicability of the sandler–wong mixing rules for the calculation of thermodynamic excess properties – VE, HE, SE, CpE, *Fluid Phase Equil* **115**, 135–164 (1996)
- 8.147 R.K. Agarwal, Y.–K. Li, O.J. Santollani, M.A. Satyro: Cubic equations of state – the untold story, *Proc. AIChE Spring Meeting*, New Orleans (2002)
- 8.148 K. Frey, C. Augustine, R.P. Ciccolini, S. Paap, M. Modell, J. Tester: Volume translation in equations of state as a means of accurate property estimation, *Fluid Phase Equil.* **260**, 316–325 (2007)
- 8.149 H. Knapp, R. Doring, L. Oellrich, U. Plocker, J.M. Prausnitz: Vapor–liquid equilibria for mixtures of low boiling substances. In: Vol. **6** (DECHEMA, Frankfurt a.M. 1982)
- 8.150 G. Gao, J.L. Dadiron, H. Saint–Guirons, P. Xans, F.A. Montel: A simple correlation to evaluate binary interaction parameters of the Peng–Robinson equation of state: Binary light hydrocarbon systems, *Fluid Phase Equil.* **74**, 85–93 (1992)
- 8.151 P. Agrawal, F.F. Schoeggl, M.A. Satyro, S.D. Taylor, H.W. Yarranton: Measurement and modeling of the phase behavior of solvent diluted bitumens, *Fluid Phase Equil.* **334**, 51–64 (2012)
- 8.152 N. Saber, M. Satyro, H. Yarranton, J.M. Shaw: Multi–phase equilibrium prediction for ill–defined asymmetric hydrocarbon mixtures, *Hydrocarbon World* **6**, 51–57 (2011)
- 8.153 K.A. Johnston, M.A. Satyro, S.D. Taylor, H.W. Yarranton: Investigation of modeling asphaltene precipitation using a cubic equation of state with asymmetric mixing rules, *Proc. PetroPhase*, Houston (2014)
- 8.154 S.I. Sandler: *Models for Thermodynamic and Phase Equilibria Calculations* (Marcel–Dekker, New York 1994)
- 8.155 A. Barreau, J.–C. de Hemptinne, J.–M. Ledanois, P. Mougin: *Select Thermodynamic Models for Process Simulation* (Editions Technip, Paris 2012)
- 8.156 P.D. Ting, G. Hirasaki, W.G. Chapman: Modeling of asphaltene phase behavior with the SAFT equation of state, *Petr. Sci. Technol.* **21**, 647–661 (2003)
- 8.157 I. Polishuk: Addressing the issue of numerical pitfalls characteristic for SAFT EOS models, *Fluid Phase Equil.* **301**, 123–129 (2011)
- 8.158 K.S. Pedersen, S. Leekumjorn, K. Krebjerg, J. Azeem: Modeling of EOR PVT data using PC–SAFT equation. In: *Abu Dhabi Int. Petroleum Exhibition and Conf. 2012, ADIPEC 2012–Sustainable Energy Growth: People, Responsibility, and Innovation*, Vol. 5 (2012) pp. 3536–3546
- 8.159 X. Liang, W. Yan, K. Thomsen, G.M. Kontogeorgis: On petroleum fluid characterization with the PC–SAFT equation of state, *Fluid Phase Equil.* **375**, 254–268 (2014)
- 8.160 G.M. Kontogeorgis, G.K. Folas, N. Muro–Sune, N. von Solms, M.L. Michelson, E.H. Stenby: Modelling of associating mixtures for applications in the oil and gas and chemical industries, *Fluid Phase Equil.* **261**, 205–211 (2007)
- 8.161 A. Hirshberg: L.N.J. deJong, B.A. Schipper, J.G. Meijer: Influence of temperature and pressure on asphaltene flocculation, *SPE J* **24**, 283–293 (1984)
- 8.162 C. Landra, H. Loria, H. Yarranton: SARA regular solution method, *Inside VMG* November 2013; <http://www.mailoutinteractive.com/Industry/LandingPage.aspx?id=1395308&lm=16807768&q=658415008&qz=c25bb5875e0449e18f9bd3f4081c7d26>
- 8.163 R.A. Heidemann: Three–phase equilibria using equations of state, *AIChE J* **20**, 847–855 (1974)
- 8.164 C. Tsionopolous, J.L. Heidman: High–pressure equilibria with cubic equations of state, *Proc. 4th Conf. Fluid Properties and Phase Equilibria for Chem. Process Design*, Helsingor (1986)
- 8.165 I. Soreide: *Improved Phase Behaviour Predictions of Petroleum Reservoir Fluids from a Cubic Equation of State*, Ph.D. Thesis (The Norwegian Institute of Technology, Trondheim 1989)
- 8.166 V.N. Kabadi, R.P. Danner: A modified Soave–Redlich–Kwong equation of state for water–hydrocarbon phase equilibria, *Ind. Eng. Chem.*

- Proc. Des. Dev. **24**, 537–541 (1985)
- 8.167 J. Mollerup: Correlation of gas solubilities in water and methanol at high pressure, *Fluid Phase Equil.* **22**, 139–154 (1985)
- 8.168 M.A. Satyro, F. Schoeggl, H.Y. Yarranton: Temperature change from isenthalpic expansion of aqueous triethylene glycol mixtures for natural gas dehydration, *Fluid Phase Equil.* **305**, 62–67 (2011)
- 8.169 D.B. Robinson, D.-Y. Peng: *The Characterization of the Heptanes and Heavier Fractions for the GPA Peng–Robinson Programs* (Gas Processors Association, Tulsa 1978), Tech. Ref. RR–28
- 8.170 M.A. Satyro, H.W. Yarranton: Expanded fluid based viscosity correlation for hydrocarbons using an equation of state, *Fluid Phase Equil.* **298**, 1–11 (2010)
- 8.171 T. Daubert: *GPA Data Bank of Selected Enthalpy and Equilibria Values* (Gas Processors Association, Tulsa 1983), GPA Tech. Ref. RR–64C
- 8.172 E.W. Lemmon, M.L. Huber, M.O. McLinden: REFPROP Reference Fluid Thermodynamic and Transport Properties, <http://www.nist.gov/srd/nist23.cfm> (2013)
- 8.173 M. Frenkel, R. Chirico, V. Diky, K. Kroenlin, C.D. Muzny, A.F. Kazarov, J.W. Magee, I.M. Abdulgatov, E.W. Lemmon: *Thermo Data Engine Version 8.0*, NIST Standard Database #103b, 2013)
- 8.174 M. Dadgostar, J.M. Shaw: On the use of departure functions for hydrocarbon siobaric liquid phase heat capacity calculation, *Fluid Phase Equil.* **385**, 182–195 (2015)
- 8.175 N. Dadgostar, J.M. Shaw: Predictive correlations for liquid heat capacity – including the critical region, *Fluid Phase Equil.* **344**, 139–151 (2013)
- 8.176 V. Lastovka, J.M. Shaw: Predictive Correlation for cp of organic solids based on elemental composition, *J. Chem. Eng. Data* **52**, 1160–1164 (2007)
- 8.177 American Petroleum Institute: *Technical Data Book – Petroleum Refining*, 5th edn. (American Petroleum Institute, Washington 1992)
- 8.178 VMG: *VMGSim User's Manual*, Vol. 8 (Virtual Materials Group, Calgary 2014)
- 8.179 P. Abivin, S.D. Taylor: Thermal behavior and viscoelasticity of heavy oils, *Energy Fuels* **26**, 3448–3461 (2012)
- 8.180 M.A. Hasan, M. Fulem, A. Bazyleva, J.M. Shaw: Rheological properties of nanofiltered athabasca bitumen and maya crude oil, *Energy Fuels* **23**, 5012–5021 (2009)
- 8.181 M.A. Hasan, J.M. Shaw: Rheology of reconstituted crude oils: Artifacts and asphaltenes, *Energy Fuels* **24**, 6417–6427 (2010)
- 8.182 W.D. Monnery, A.K. Mehrotra, W.Y. Svrcek: Viscosity: A critical review of practical Predictive and correlative methods, *Can. J. Chem. Eng.* **73**, 3–40 (1995)
- 8.183 E.N.D.C. Andrade: A Theory of the viscosity of liquids, *Phil. Mag.* **17**, 497–511 (1934)
- 8.184 H. Vogel: The law of viscosity change with temperature, *Physik Z* **22**, 645–646 (1921)
- 8.185 C. Walther: The evaluation of viscosity data, *Erdol Teer* **7**, 382–384 (1931)
- 8.186 W.Y. Svrcek, A.K. Mehrotra: One parameter correlation for bitumen viscosity, *Chem. Eng Res Des* **66**, 323–327 (1988)
- 8.187 G. Centeno, G. Sánchez-Reyna, J. Ancheyta, J.A.D. Muñoz, N. Cardona: Testing various mixing rules for calculation of viscosity of petroleum blends, *Fuel* **90**, 3561–3570 (2011)
- 8.188 S.A. Arrhenius: Über die Dissociation der in Wasser gelosten Stoffe, *Z Phys. Chem.* **1**, 631–648 (1887)
- 8.189 A.K. Mehrotra: Development of mixing rules for predicting the viscosity of bitumen and its fractions blended with toluene, *Can. J. Chem. Eng.* **68**, 839–848 (1990)
- 8.190 J. Kendall, K.P. Monroe: The viscosity of liquids II: The viscosity–composition curve for ideal liquid mixtures, *J. Am. Chem. Soc.* **39**, 1787–1807 (1917)
- 8.191 M.L. Chirinos, I. Gouzalez, I.A. Layrisse: Rheological properties of crude oils from the orinoco oil belt and the mixtures with diluents, *Revista Tecnica Int-tep* **3**, 103–115 (1983)
- 8.192 J.M. Al-Besharah, O.A. Salman, S.A. Akashah: Viscosity of crude oil blends, *Ind. Eng. Chem. Res.* **26**, 2445–2449 (1987)
- 8.193 C.T. Baird: *Guide to Petroleum Product Blending* (HPI Consultants, Austin 1989)
- 8.194 E.L. Lederer: Viscosity of mixtures with and without diluents, *Proc. World Pet Cong.*, London (1933) pp. 526–528
- 8.195 V.M. Lobe: *A Model for the Viscosity of Liquid–Liquid Mixtures*, Ph.D. Thesis (Univ. Rochester, Rochester 1973)
- 8.196 C.S. Cragoe: Changes in the viscosity of liquids with temperature, pressure and composition, *Proc. World Pet Cong.*, London (1933) pp. 529–541
- 8.197 A. Miadonye, V.R. Puttagunta, R. Srivastava: Generalized oil viscosity model for the effects of temperature, pressure and gas composition, *J. Can. Petr. Tech.* **36**, 50–54 (1997)
- 8.198 A. Miadonye, N. Latour, V.R. Puttagunta: A correlation for viscosity and solvent mass fraction of bitumen–diluent mixtures, *Pet Sci. Technol.* **18**, 1–14 (2000)
- 8.199 W.R. Shu: A viscosity correlation for mixtures of heavy oil, bitumen, and petroleum fractions, *Soc. Petr. Eng. J.* **24**, 277–282 (1984)
- 8.200 M.A. Barrufet, A. Setiadarma: Reliable heavy oil–solvent viscosity mixing rules for viscosities up to 450 K, oil–solvent viscosity ratios up to 4×10^5 and any solvent proportion, *Fluid Phase Equil.* **213**, 65–79 (2003)
- 8.201 C.H. Twu: Internally consistent correlation for predicting liquid viscosities of petroleum fractions, *Ind. Eng. Chem. Process Des. Dev.* **24**, 1287–1293 (1985)
- 8.202 T.E. Daubert, R.P. Danner: *API Technical Data Book–Petroleum Refining*, 6th edn. (API, Washington DC 1997)
- 8.203 A. Yazdani, B.B. Maini: Measurements and modelling of phase behaviour and viscosity of a heavy oil/butane system, *J. Can. Petr. Tech.* **49**, 8–14 (2010)
- 8.204 J. Lohrenz, B.G. Bray, C.R. Clark: Calculating viscosities of reservoir fluids from their compositions, *J. Petr. Technol.* **16**, 1171–1176 (1964)

- 8.205 A. Danesh: *Developments in Petroleum Science 47: PVT and Phase Behaviour of Petroleum Reservoir Fluid* (Elsevier, Amsterdam 1998)
- 8.206 H. Loria: New API-VMG Correlation to Predict Liquid Viscosities of Petroleum Fractions, Inside VMG. Virtual Materials Group Inc., Calgary, Alberta, Canada <http://www.industrymailout.com/Industry/View.aspx?id=258092&q=356580263&qz=c96307> (2014)
- 8.207 H.J.M. Hanley: Prediction of the viscosity and thermal conductivity coefficients of mixtures, *Cryogenics* **16**, 643–651 (1976)
- 8.208 K.S. Pedersen, A. Fredenslund, P.L. Christensen, P. Thoassen: Viscosity of crude oils, *Chem. Eng. Sci.* **39**, 1011–1016 (1984)
- 8.209 J.F. Ely, H.J.M. Hanley: *A Computer Program for the Prediction of Viscosity and Thermal Conductivity in Hydrocarbon Mixtures (TRAPP)*, NBS Technical Note 1039 (National Bureau of Standards, Boulder 1981)
- 8.210 M.E. Baltatu, R.A. Chong, M.L. Huber: Viscosity of defined and undefined hydrocarbon liquids calculated using an extended corresponding-states model, *Int. J. Thermophys* **17**, 213–221 (1996)
- 8.211 M.E. Baltatu, R.A. Chong, M.L. Huber, A. Laesecke: Transport properties of petroleum fractions, *Int. J. Thermophys.* **20**, 85–95 (1999)
- 8.212 K.S. Pedersen, A. Fredenslund: An improved corresponding states model for the prediction of oil and gas viscosities and thermal conductivities, *Chem. Eng. Sci.* **42**, 182–186 (1987)
- 8.213 N. Lindeloff, K.S. Pedersen, H.P. Ronningsen, J. Milster: The corresponding states viscosity model applied to heavy oil systems, *J. Can. Petr. Technol.* **43**, 47–53 (2004)
- 8.214 S.E. Quiñones-Cisneros, C.K. Zéberg-Mikkelsen, E.H. Stenby: Friction theory (F-theory) for viscosity modeling, *Fluid Phase Equil.* **169**, 249–276 (2000)
- 8.215 S.E. Quiñones-Cisneros, C.K. Zéberg-Mikkelsen, E.H. Stenby: The friction theory for viscosity modeling: Extension to crude oil systems, *Chem. Eng. Sci.* **56**, 7007–7015 (2001)
- 8.216 S.E. Quiñones-Cisneros, C.K. Zéberg-Mikkelsen, A. Baylaucq, C. Boned: Viscosity modeling and prediction of reservoir fluids: From natural gas to heavy oils, *Int. J. Thermophys.* **25**, 1353–1366 (2004)
- 8.217 J.Y. Zuo, D.D. Zhang, J. Creek: Modeling of phase equilibria and viscosity of heavy oils, *Proc. World Heavy Oil Congress*, Edmonton (2008), Paper 2008-392
- 8.218 H.W. Yarranton, M.A. Satyro: Expanded fluid-based viscosity correlation for hydrocarbons, *Ind. Eng. Chem. Res.* **48**, 3640–3648 (2009)
- 8.219 C.R. Wilke: A viscosity equation for gas mixtures, *J. Chem. Phys.* **18**, 517–519 (1950)
- 8.220 H. Motahhari, M.A. Satyro, H.W. Yarranton: Extension of the expanded fluid viscosity model to characterized oils, *Energy Fuels* **27**, 1881–1898 (2007)

Explorati

Part B

Part B Exploration and Production

9 Fundamentals of Petroleum Geology

Hendratta N. Ali, Hays, USA

10 Origin of Petroleum

Clifford C. Walters, Annandale, USA

11 Basin and Petroleum System Modeling

Kenneth E. Peters, Mill Valley, USA,
Stanford, USA

Oliver Schenk, Aachen, Germany
Allegra Hosford Scheirer, Stanford, USA
Björn Wygrala, Aachen, Germany
Thomas Hantschel, Aachen, Germany

12 Seismic Explorations

Graham Ganssle, New Orleans, USA

13 Formation Evaluation

Donald G. Hill, Walnut Creek, USA

14 Petroleum Production Engineering

Shengnan Chen, Calgary, Canada

15 Offshore Production

Ekaterina V. Maksimova, St. Petersburg,
USA

Cortis K. Cooper, San Ramon, USA

Fundamentals

9. Fundamentals of Petroleum Geology

Hendratta N. Ali

This chapter provides an overview of the fundamental concepts, processes, and theories associated with petroleum exploration and exploitation. The content of this chapter is structured into four main topics. The first topic provides a brief history of the modern petroleum industry and the role that petroleum plays in the society today. The second topic covers the geological basis, and discusses the material, processes, time span, and conditions under which petroleum forms and migrates in rocks. The third topic discusses how petroleum accumulates and concentrates in economic quantities in rocks to warrant exploitation, and the last topic describes the sophisticated methods and techniques that are used in finding, locating, and extracting the petroleum that is found deep in the subsurface. Modern prospecting uses methods of exploration such as three-dimensional seismic surveying and geophysical well logging that have revolutionized how we explore and locate new petroleum reservoirs in the subsurface, to fuel today's fossil fuel addiction. Although petroleum and fossil fuel derivatives have been around for thousands of years, the dominance of petroleum as a global source of energy and petrochemicals products, only developed in the last couple of centuries. Extensive research has led to detailed understanding of the geological and geochemical processes that generate, migrate, and accumulate economic quantities of this essential resource. Additional studies on the source, nature, and composition of petroleum will continue to improve our ability to find, produce, refine, and utilize petroleum products. The chapter concludes with a look at the future of petroleum and its exploration in the world.

9.1	The Petroleum Cycle	322
9.2	Historical Perspective	323
9.2.1	Pre-Industrial Use of Petroleum	323
9.2.2	Early Industrial Exploration and Production	323
9.2.3	Measurements	324
9.2.4	Energy Equivalence	324
9.3	Geological Overview	326
9.3.1	Origin of Petroleum	326
9.3.2	Chemical Composition and Occurrence of Petroleum	326
9.3.3	Rocks in Which Petroleum Is Found	329
9.3.4	Some Common Rock-Forming Minerals Important in Petroleum Exploration	332
9.3.5	Sedimentary Rocks	334
9.3.6	When Petroleum Formed	337
9.3.7	Significance of Fossils in Petroleum Exploration	339
9.3.8	Summary of the Significance of Geologic Time in Petroleum Exploration	341
9.3.9	Significance of Time in Petroleum Exploration	343
9.4	How Petroleum Accumulates and Concentrates	343
9.4.1	Petroleum Accumulation	343
9.4.2	Petroleum Traps	347
9.4.3	Elements of Plate Tectonics and Petroleum Deposits	349
9.5	Finding and Locating Petroleum	352
9.5.1	Geological and Geochemical Methods of Exploration	353
9.5.2	Geophysical Methods of Exploration	353
9.5.3	Extracting and Producing Petroleum	354
9.6	Future for Petroleum	356
	References	357

Petroleum is comprised of diverse chemical compounds that are mostly made up of hydrogen and carbon, that is, hydrocarbons (HCs). It also contains minor amounts of hetero-atoms including sulfur, nitrogen, oxygen, and trace metal contaminants. Hydrocarbons are today's main source of energy and petro-chemicals, and will continue to be so for the foreseeable future. Fossil hydrocarbons occur as crude oil, natural gas (including gas hydrates), oil shale, oil sands, and coal. They are formed from the thermogenic transformation of ancient remains of organic material that was buried in sediments millions of years ago.

Petroleum geology is a branch of geology that studies how petroleum (and other fossil hydrocarbons) is sourced, generated, migrated, concentrated, and accumulated. Such studies enhance our ability to discover, map, and produce petroleum for economic benefit. Petroleum geology is a broad area of study, which integrates several basic sciences, technology, and engi-

neering. It touches on other areas including business, art, psychology, politics, and even speculation. However, the core subjects in the study of petroleum are found in the geological sciences: fundamental geology (physical and historical geology) and specialty areas like geophysics and geochemistry. These apply the basic sciences of physics and chemistry, statistics and probability, sedimentology, stratigraphy, structural geology, and subsurface mapping.

In our modern society, advances in technology have provided some major tools for the study of petroleum geology. Supercomputers have enabled the generation of specialty areas like seismic studies (acquisition, processing and interpretation), petrophysics, reservoir characterization, and subsurface modeling, to name a few. A petroleum geologist is someone who uses geologic information and studies geochemical processes to find, locate, and describe economic accumulations of petroleum for exploitation purposes.

9.1 The Petroleum Cycle

This section focuses on the petroleum cycle that describes the essential steps involved in the search, production, and use of petroleum products.

Several steps are required to transform petroleum into useful products and goods. First of all, professionals have to identify and locate parts of the Earth where the petroleum can be found and extracted from deep within the rocks before it can be processed and used. Figure 9.1 shows a schematic representation of the steps that constitute the cycle of petroleum:

- *Exploration* is a step that mostly involves the search for and location of petroleum in rocks. Once petroleum that is found underground has been located and assessed, it has to be brought to the surface of the Earth.
- *Production* involves the processes of drilling and extracting petroleum from the subsurface rocks. Once petroleum is extracted from the ground, *processing* and *refining* techniques are used to purify, separate, and reform components of the complex mixture into useful fractions.
- Products obtained from processing and refining may undergo *transformations* to further improve their quality, or these products may be used in the *manufacturing* of other products by reacting and blending them with other chemicals.
- End *products* are *distributed* and sold for public consumption.

At every stage in the cycle of petroleum from its hide-out in the bowels of the Earth to the use of its finished products, other resources are consumed or altered, and undesirable *waste products* are generated and have to be disposed of properly. A major challenge in the business of petroleum is dealing with and managing the waste products.

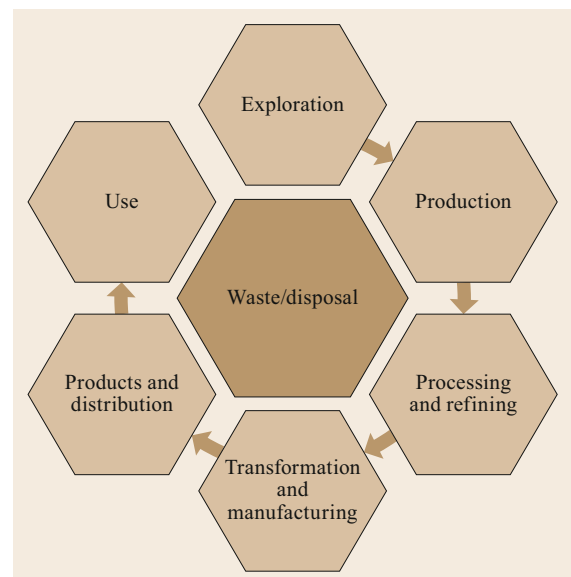


Fig. 9.1 Schematic of the cycle of petroleum in the modern world

9.2 Historical Perspective

Petroleum has been in existence for millions of years, well before the evolution of humans. However, the discovery of petroleum as a valuable product happened only in much more recent times (thousands of years ago) and its subsequent use as an energy source progressively developed over the last couple centuries. Long before petroleum was discovered, fire was the dominant source of energy, and came naturally from lightening, volcanic eruptions, and possible sparks from friction. After the discovery of fire, humans started using plant material such as wood, leaves, and grass, as well as animal material such as bones, fat, and dung to generate energy. In those days, it must have been a real challenge to keep a good fire going as is still the case in many developing countries and poor communities around the world today. In the quest to make hotter fires and keep them burning longer, humans through time discovered other material that could burn more easily and longer. By the 1800s, wood was the dominant source of heat energy and contributed more than 90% of the energy needed by humans. Gradually, the use of solid petroleum products like pitch/peat/bitumen and coal increased and became dominant toward the end of the nineteenth century, when kerosene from crude oil became the fuel of choice for illumination.

9.2.1 Pre-Industrial Use of Petroleum

Records from ancient Chinese, Persian, Mesopotamian, Greek, and Egyptian civilizations describe pre-industrial uses of petroleum components [9.1]. References in the Old Testament of the Christian Bible suggest that petroleum may have been used to waterproof Noah's boat and Moses' basket. In Persia (present day Iran) and Mesopotamia (present day Iraq), pitch was used for waterproofing the hanging gardens of Babylon (one of the seven wonders of the ancient world), boats for sailing, and for medicinal purposes to heal/cover wounds, etc. In ancient Egypt, some mummies were persevered with pitch and the ancient Chinese reportedly used flaming arrows in warfare.

9.2.2 Early Industrial Exploration and Production

The exploration for petroleum began late in the seventeenth century, when in about 1679, during the reign of King Charles II of Great Britain, the first patents to produce oil were issued. In 1745, the first well dug to find oil was sunk in France [9.2]. It is not clear how successful this search was. More than 100 years later, the industry began to see a boom in the pro-

duction and use of coal gas in the Eastern United States to light the streets of Maryland and Baltimore.

According to some sources [9.3–5], the big hit for the petroleum industry began in Canada around 1849, when Abraham Gesner first distilled kerosene from coal and later from crude oil. In 1857, the invention of the flat-wick kerosene lamp by Michael Dietz increased the demand for kerosene. Kerosene began to replace whale oil, which until then had been the most popular source of lamp fuel.

The rise in the demand for kerosene led to the scramble across the Western world to find new sources of petroleum. Around 1847, James Young discovered how to use heat to extract oil from shale [9.2], and opened a synthetic fuel plant to extract oil in Scotland. A couple of years later, Ignacy Lukasiewicz began to refine oil on an industrial scale, mainly to distill oil into kerosene. He set up his crude oil refinery in the city of Ulaszowice, Poland, in 1856. In 1859, in Titusville, PA, USA, W.A. Smith drilled a well using a spring pole, under the direction of Edwin Drake [9.5].

In 1863, J.D. Rockefeller and M.B. Clark financed a joint venture with a chemist Samuel Andrews to start an oil refinery in Cleveland, OH, USA. At the time, there were about 30 other refineries in Cleveland. After Clark sold out in 1865, the company became Rockefeller's and Andrews, which chartered the Standard Oil Company in 1870. By 1877, through mergers and acquisitions, Standard Oil grew to control 90% of petroleum refining in the United States [9.4, 5].

The demand for kerosene for lighting decreased due to the electric light bulb, which Thomas Edison patented in 1879 [9.6].

Meanwhile, the invention of the gasoline-powered internal combustion engine in France by Alphonse Beau De Rochas in 1862 [9.7] brought about a new market for petroleum. The German engineer Karl Friedrich Benz designed the first practical motorcar which is widely regarded as the first gasoline-powered automobile. By 1891, Daimler Motor Corporation was producing gasoline engines in the United States.

In 1908, the Ford Motor Company started the first mass production of cars, notably the Model T [9.8].

Meanwhile the production of petroleum continued to expand. In 1901, the giant spindle top gusher was drilled in east Texas. And in 1908, oil was discovered in Persia (present Iran), leading to the creation of the Anglo-Iranian Oil Company, which later became the British Oil Company [9.4, 9].

In 1911, citing violations of anti-trust laws, the US Justice Department ordered the breakup of Standard

Oil into 34 companies, including five regional *majors* (Fig. 9.2).

By 1920, there were seven major petroleum companies in the world (Fig. 9.3). Five of these companies were based in the United States – three of the spinoffs of Standard Oil (SOCONY, ESSO, and SOCAL) and two Midwestern companies (Texaco and Gulf Oil) – and two were based in Europe. The European companies were Royal Dutch Shell and British Petroleum.

Between 1920s and 1980s, the global search for new oil resources increased. Oil prices (Fig. 9.4) increased significantly and reserves were discovered in several parts of the world. Technology continued to develop, new inventions were made including wireline logging and seismic surveys, the Organization of Petroleum Exporting Countries (OPEC) was formed and oil became our dominant source of fuel.

Increased production, distribution, and use of hydrocarbons lead to increased awareness of the impact of the petroleum industry on the environment. In response to the issues, in 1970 the Nixon administration created the US Environmental Protection Agency (EPA), and the US Congress passed the Clean Air Act. For the petroleum industry, the Alaskan environmental catastrophe caused by the Exxon Valdez tanker in 1989 and the burning of the Kuwait oil fields in 1991 brought increased attention to the environmental issues associated with the activities of the petroleum industry into mainstream. These and other environmental disasters are discussed in another chapter. As a consequence, some tougher legislation was introduced in the United States, the country that consumes about a quarter of the world's fossil fuel energy, where in 2003–2004 the US Senate rejected oil exploration in the US Arctic National Wildlife Refuge, even though the country was importing 11.3 million barrels of oil per day. In 2005, Hurricanes Katrina and Rita struck the Gulf Coast of the United States, damaging some petroleum industry infrastructure. This led to increased hiring in the industry in 2006–2007, but the global financial recession in 2008 created another bust that affected the petroleum

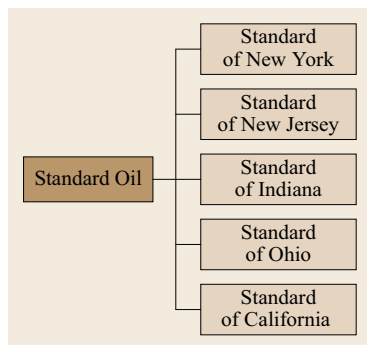


Fig. 9.2 Five major spinoff companies from Rockefeller's Standard Oil Co

sector. In 2010, the *Deepwater Horizon* oil disaster on the US Gulf coast added to the environmental concerns and increased activities from environmental and safety groups.

The present global petroleum dynamics is changing with the projections from the International Energy Agency (IEA), that the United States will lead global energy production and become energy independent by 2035. Emerging and high population economies like China and India are increasing their demand for global oil. This means that the search for petroleum will continue all over the world with the aide of new technologies and a skilled workforce.

Summary

Fossil fuels still represent the most important source of global energy today. The debate about the amount of oil that is available and how long it will last continues, but the search for more resources and improved technology to extract present reserves is essential to maintain the world's energy needs and sustain the global economy for the foreseeable future.

9.2.3 Measurements

Petroleum and other HC products in fossil fuels occur as solids, liquids, and gases under different temperature and pressure conditions. They are therefore measured and expressed in terms of mass, volume, energy content, viscosity, etc. Petroleum is measured differently depending on whether we are referring to gaseous components or liquid components. The common measurement expression for oil throughout the world is the US barrel (US bbl). 1 US bbl is equal to 42 US gallons (gal), which is approximately equivalent to 159 l, 5.62 cubic feet (ft³), 0.159 cubic meters (m³) and 34.97 UK gal. In most of the world, the common measurement of crude oil is metric tons (t). One metric ton (t) equals 1000 kg, 2204.6 lb, 1.102 tn sh used in the United States and 0.984 tn l used in United Kingdom. Volume in much of the world is expressed in cubic meter and liter. The mass of petroleum is expressed in kilogram (kg), pound (lb) and ton (t). Details of units and conversions for petroleum and other energy resources can be obtained from several sources such as <http://www.iea.org>, <http://www.bipm.org> among others.

9.2.4 Energy Equivalence

The bulk of petroleum and other fossil hydrocarbons are used to generate energy in different forms. For this reason, it is sometimes common to express petroleum products in terms of their heat content, calorific value,

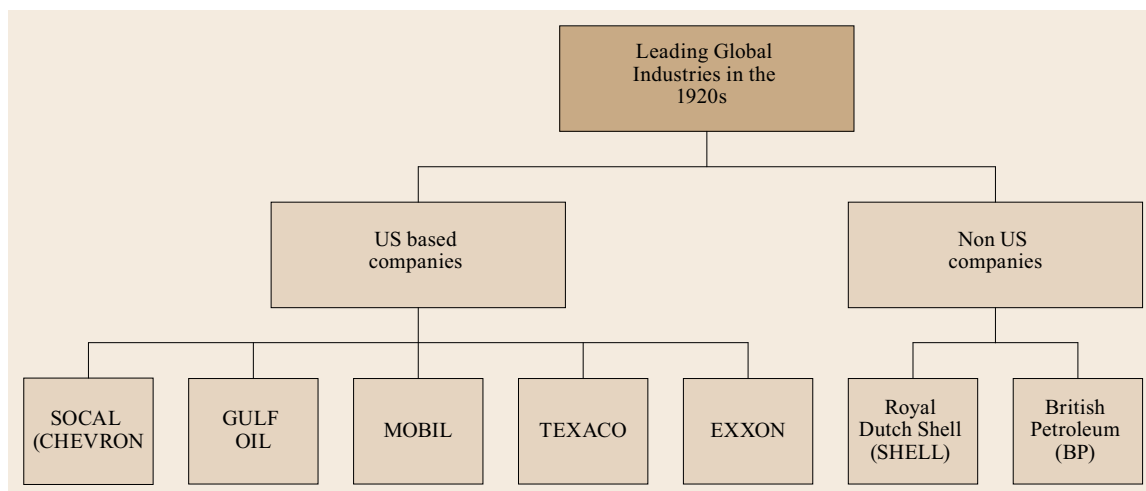


Fig. 9.3 Seven major global companies of the 1920s

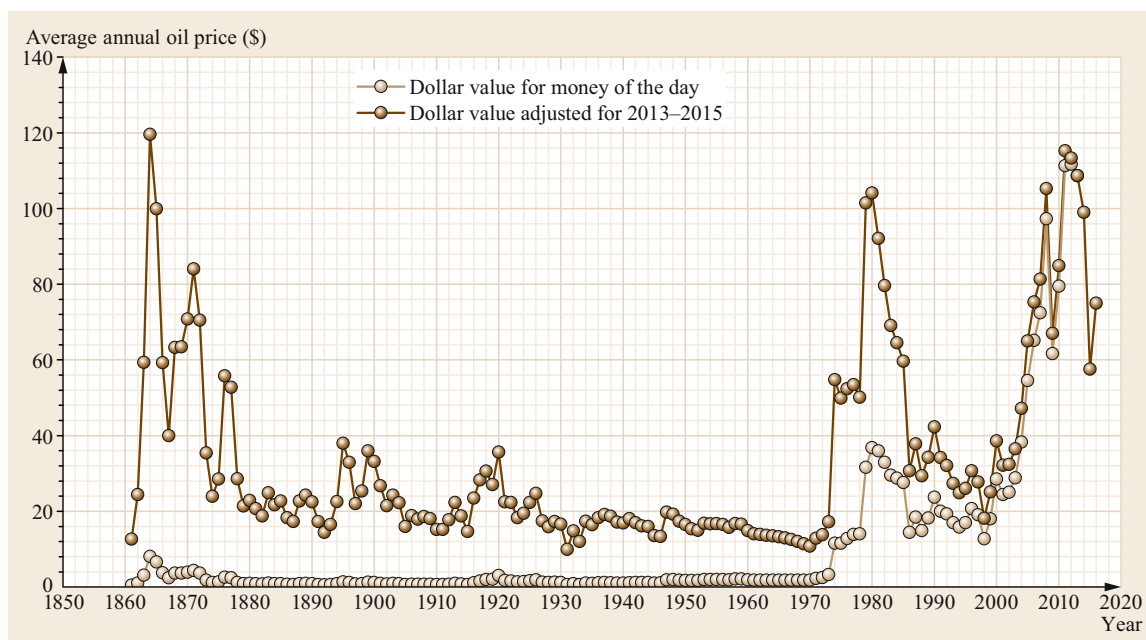


Fig. 9.4 Change in average annual oil prices from 1860–2016. (after [9.10, 11], courtesy of BP Statistical Review of World Energy)

electrical energy, or other terms of energy equivalence. The common expression of heat or energy content from petroleum is the British thermal unit (BTU), gigawatt-hour (GWh) and megatons of oil equivalent (Mtoe). The total energy (calorific) value of HCs refers to the amount of energy that can be produced from burning the HC molecules. For petroleum products, it is sometimes worthwhile to convert from mass or volume to heat in order to determine the equivalent amount of energy that

will be generated per unit quantity. For natural gas, the IEA calculates that 1 m^3 is equivalent to 37.912 BTU and 1 kg is equivalent to 54.40 MJ or 51 560 BTU. Oil and gas can be compared in terms of their energy content. This process helps us determine how much gas produces the same amount of energy as a given quantity of oil and vice versa. For example, 1 bbl of oil energy (boe) is equivalent to about 6300 standard cubic feet (scf) of gas.

9.3 Geological Overview

Petroleum geologists are mostly concerned with finding and locating petroleum resources that are buried underground in locations that are not directly visible to the eye. They must use proxies to *see* petroleum in these subsurface environments. The scientists study material from which petroleum formed, rocks in which petroleum is found, the way it appears and the state in which it occurs in the rocks, the changes that the presence of petroleum causes in the rocks and how these changes transform and alter the physical and chemical properties of rocks.

9.3.1 Origin of Petroleum

Petroleum originates from the chemical transformation of organic material that was deposited, trapped, and buried in sedimentary rocks millions of years ago. Several books and articles [9.12–14] have succinctly highlighted some evidence that confirms the predominantly organic source of petroleum. The evidence points to the composition of petroleum, the environments where petroleum forms, the rocks in which petroleum is found and even some experimental evidence. Petroleum mostly forms from microscopic plants and animals like algae, bacteria, spores, or planktons. Higher plant material, woody cellulosic plants, and cuticles mostly form coal. For petroleum to be formed from organic material, a series of conditions must be satisfied:

- *High productivity*: A lot of organic material must be produced from the demise of large amounts of micro organisms caused, for example, by massive kills due to anoxia, lack of nutrients, or natural hazards
- *Rapid burial*: The organic material must be trapped and buried very quickly to avoid decay.
- *Absence of oxygen*: The organic material must be buried under anoxic conditions deep enough so that trapping and burial excludes oxygen.
- *Pressure and heat*: The organic material must be buried deeply, typically with an overburden of more sediment above the organic rich layer to increase pressure and temperature.
- *Time*: There must be time for the geochemical transformation of the organic material into petroleum.

Once the organic material is buried, the next step is to transform and mature the organic material. The maturation process of organic material occurs through three main stages:

1. The first stage of *diagenesis* involves the early stages of anoxic burial of the organic matter-rich sediments. This step leads to the expulsion of wa-

ter, compaction, and cementation of the sediments containing the organic material. During this stage, kerogen (a type of disseminated organic material that is not soluble in most organic solvents) is formed.

2. The second stage, *catagenesis*, involves the transformation of kerogen to oil, gas or coal. This stage generates mostly large HC molecules in the early stages, and in the later stages it generates smaller HC molecules (including C₅ to C₁₂ molecules) and wet gas.
3. During the third stage, *metagenesis*, mostly dry gas (methane) is produced, followed by the onset of *metamorphism*.

9.3.2 Chemical Composition and Occurrence of Petroleum

As mentioned previously, although petroleum is dominantly composed of hydrogen and carbon, these atoms combine to form a variety of HC molecules that together occur as a very complex mixture to which may be associated non-hydrocarbon atoms commonly referred to as hetero-atoms occur in lesser amounts. The petroleum mixtures can contain gas, liquid and solid state components.

Gaseous Petroleum (Natural Gas)

The gaseous form of petroleum is generally referred to as natural gas. Natural gas can *occur* as associated (with oil) or non-associated gas. The *composition* of natural gas can be described as dry gas, and wet gas. Dry gas mostly contains methane molecules that are typically in the range of 85% or more. If natural gas is not dry, it is described as wet gas, which contains less than 85% methane and relatively more ethane and propane. Hydrocarbons that occur as gases in a well under bottom-hole temperatures and pressure, but condense to form liquids once brought to the surface are described as *condensates*. Natural gas can also be described based on the quantity of *impurities* that it contains. Thus, natural gas is described as *sweet gas* if it does not contain high amounts of impurities such as hydrogen sulfide (H₂S), and/or high amounts of carbon dioxide (CO₂(g)). This form of natural gas – sweet gas – is valued in the market. *Sour gas*, on the other hand, is natural gas that contains high amounts of H₂S(g) and a lot more CO₂(g). Sour gas is less economically valuable than sweet gas. Gas processing plants convert the H₂S in sour gas to sulfur for commercial purposes if the hydrogen sulfide occurs in significant amounts. Unrecovered H₂S(g) is burned in flares to form SO₂ and SO₃, com-

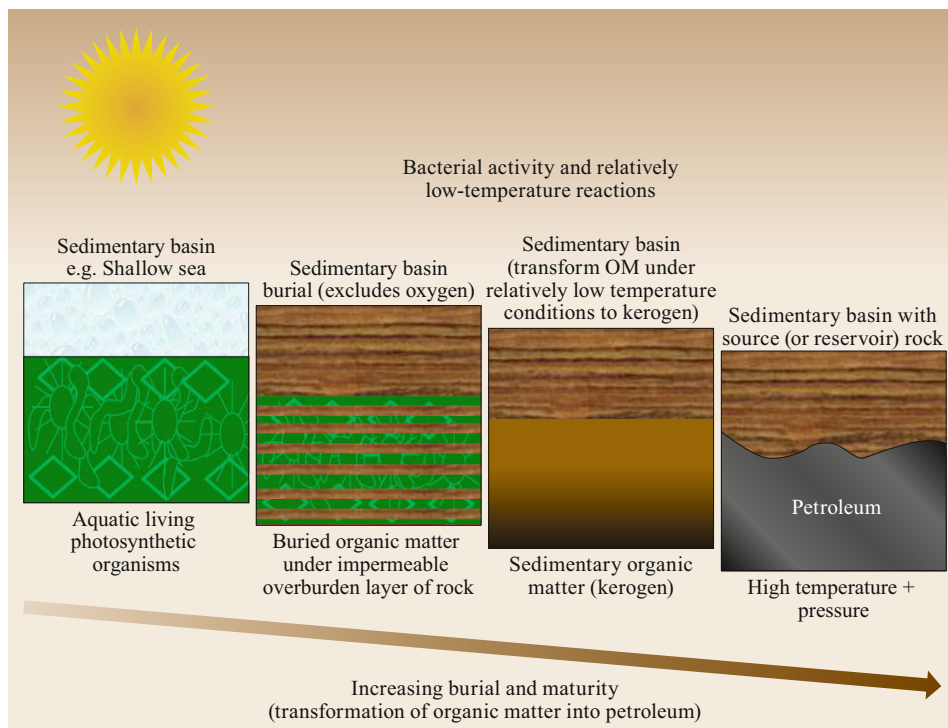


Fig. 9.5 Generation of petroleum from biological organism

monly known as sulfur oxides (SO_x). In many countries, environmental regulations restrict SO_x emissions from natural gas plants, usually to less than 0.5 mol%.

Natural gas plays a significant role during exploration because it has some properties that can be easily diagnosed using exploration techniques. Characteristics properties of natural gas are discussed in more detail later in this section. These properties are density, compressibility, acoustic velocity, composition, etc. These properties can help exploration geologists identify and map rocks and formations that contain petroleum. From an economic perspective, natural gas is more abundant and cleaner than liquid petroleum but it is more difficult to store and transport once it has been produced because of its high diffusivity.

Natural gas may also contain inert gases such as argon and helium, which are products of radioactive decay.

Liquid Petroleum (Crude Oil)

Unrefined crude oil has some distinctive characteristics which include viscosity, color, smell, flammability, fluorescence under UV (when some specific molecules are present), and immiscibility in water. These characteristics vary based on the size and type of molecules present in the crude oil. The *color* could be brown, black, straw, etc. The *smell* can be described as sweet, foul, weak, strong, fruity, etc. *Fluorescence* under UV oc-

curs when certain molecules (especially polyaromatics) are present. These characteristics are applied in identifying petroleum containing rocks samples during well site analysis while drilling an oil well. Typical components of liquid petroleum:

- Alkanes (paraffins) are chain structures in which the number of carbon atoms ranges from C_1 to C_{80} . The chains can be straight or branched with millions of possible structures. Generally, C_1 – C_4 molecules are gases and C_5 – C_{18} are liquids; C_5 – C_{11} are dominant in gasoline and C_{10} – C_{25} are dominant components in kerosene and diesel. Most alkanes with $> \text{C}_{20}$, are solids and waxes.
- Naphthenes (cycloalkanes) and polynaphthenes (Table 9.2) are fully saturated HCs which contain 5- and 6-membered carbon ring structures. Light naphthenes and polynaphthenes are liquids at standard temperatures and pressure and can occur in significant amounts (up to 50% or more) in some crude oils.
- Aromatics also contain 5- and 6-membered carbon ring structures, but they are unsaturated with conjugated double bonds. Polyaromatics can include several condensed rings. Due to a phenomenon called resonance, polyaromatics fluoresce (glow) under ultra violet light. Many polyaromatics are carcinogenic. Aromatics and polyaromatics are dense

molecules, so they are more common in heavy oils.

- Naphthoaromatics (Table 9.2) are partially saturated condensed-ring compounds. They are abundant in synthetic crudes and some naphthenic conventional crude.

As mentioned earlier, in addition to HCs, crude oil contains molecules with hetero-atoms, especially oxygen, nitrogen, and sulfur. Heavy asphaltics contain trace metals such as nickel (Ni) and vanadium (V). Sulfur compounds are the most abundant heteroatom compounds. They include mercaptans (thiols), sulfides, disulfides, thiophenes, and other cyclic compounds. As shown in Table 9.1, the sulfur content of a crude oil can range from 0.03 to nearly 5 wt%. Oxygen-containing compounds are common in young, immature, and biodegraded oils. Nitrogen compounds include amides, pyridines, indoles, and pyrroles (Table 9.3). The nitrogen content of a crude oil sample can range from less than 0.01–0.9 wt% (Table 9.1). Native sulfur is abundant in young shallow oils and reacts with hydrogen at temperatures above 100 °C to form H₂S(g). Heavy HC fractions include all of the above, plus asphaltics. Asphaltics contain trace metals like Ni and V. Ni and V are abundant in oils from young, shallow basins, and basins with degraded oil. They are rela-

tively rare in old deep basins, where mostly high API gravity crude occurs. During geochemical analysis, it is sometimes difficult to determine if trace and rare metals are produced from within reservoir rocks or introduced from elsewhere.

Crude oil can be described by its composition, impurity content, degree of viscosity and other physical characteristics. The density of crude oil is measured as the ratio between the specific gravity of the crude oil and the specific gravity of water. It is expressed in degrees of gravity units developed by the American Petroleum Institute (API) according to the formula

$$\text{API} = \frac{141.5}{\text{Specific gravity at } 60^{\circ}\text{F}} - 131.5 .$$

For example, the density of water is 1 g/cm³, and the gravity of water = 10° API. Crude oil floats on water when its gravity is greater than 10° API. In general, low API crudes have high density and high viscosity, while high API crudes have low density, and low viscosity. Light crude oil typically has an API gravity of more than 40° (Table 9.1).

Raw oil comes directly from the wellbore, before it is treated in a petroleum separation plant. Usually, raw oil contains contaminants, such as dissolved salt, sediment, metals and water, along with non-hydrocarbon

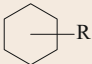
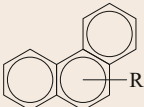

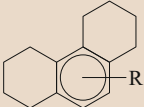
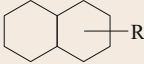
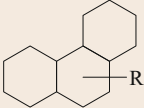

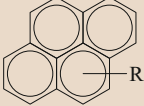
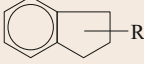
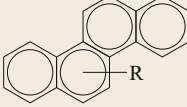

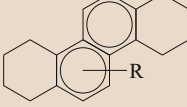

Table 9.1 Properties of 21 selected crude oils

Crude oil	API gravity ^a (deg)	Specific gravity	Sulfur (wt%)	Nitrogen (wt%)
Alaska North Slope	26.2	0.8973	1.1	0.2
Arabian Light	33.8	0.8560	1.8	0.07
Arabian Medium	30.4	0.8740	2.6	0.09
Arabian Heavy	28.0	0.8871	2.8	0.15
Athabasca (Canada)	8.0	1.0143	4.8	0.4
Beta (California)	16.2	0.9580	3.6	0.81
Brent (North Sea)	38.3	0.8333	0.37	0.10
Bonny Light (Nigeria)	35.4	0.8478	0.14	0.10
Boscan (Venezuela)	10.2	0.9986	5.3	0.65
Ekofisk (Norway)	37.7	0.8363	0.25	0.10
Henan (China)	16.4	0.9567	0.32	0.74
Hondo Blend (California)	20.8	0.9291	4.3	0.62
Kern (California)	13.6	0.9752	1.1	0.7
Kuwait Export	31.4	0.8686	2.5	0.21
Liaohi (China)	17.9	0.9471	0.26	0.41
Maya (Mexico)	22.2	0.9206	3.4	0.32
Shengli (China)	13.8	0.9738	0.82	0.72
Tapis Blend (Malaysia)	45.9	0.7976	0.03	nil
West Hackberry Sweet ^b	37.3	0.8383	0.32	0.10
West Texas Intermediate	39.6	0.8270	0.34	0.08
Xinjiang (China)	20.5	0.9309	0.15	0.35

^a API gravity is related to specific gravity by the formula: API gravity = 141.5/(specific gravity at 60 °F) – 131.5

^b Produced from a storage cavern in the US Strategic Petroleum Reserve

Table 9.2 Examples of HC ring compounds

Structural formula	Common name	Structural formula	Common name
	Alkylcyclohexanes		Phenanthrenes
	Alkylbenzenes		Dinaphthenobenzenes
	Decalins		Dinaphthenocyclohexanes
	Naphthalenes		Pyrenes
	Indanes		Chrysenes
	Acenaphthenes		Dinaphthenonaphthalenes
	Fluorenes		

gases. Processed oil has been treated, either at the well site or in a refinery. Sour crudes contain high amounts of sulfur. Sweet crude oil contains small amounts of sulfur. Typically, sour crudes are less valuable than sweet crudes.

Crude oil has several other characteristics that are measured and described for different purposes. For example, pour point describes the lowest temperature at which oil will flow before solidifying or becoming waxy as it cools. *Volatility* measures how easily oil can evaporate at standard temperature and pressure, and it is used to describe the tendency of oil to undergo shrinkage. Nonvolatile (black or low shrinking) oil has a low API gravity and contains relatively high amounts of long carbon chains (heavy) molecules. Low shrinking oils typically have a gravity significantly less than 40° API. Volatile (light or high shrinking) oil typically has a high API gravity, and has shorter carbon chain molecules than the low shrinking oil. A *flash point* describes the temperature above which crude oil or its components spontaneously ignite. The flash point is low for light oils and high for heavy oils. The viscosity in-

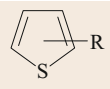
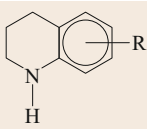
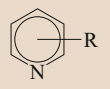
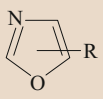
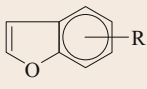
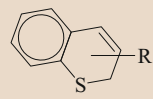
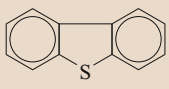
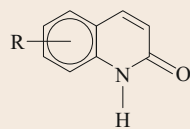
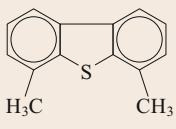

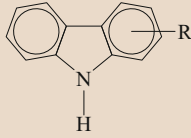
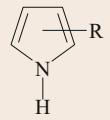
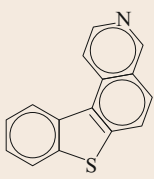
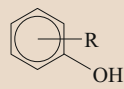
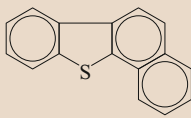
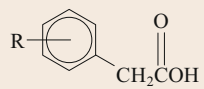
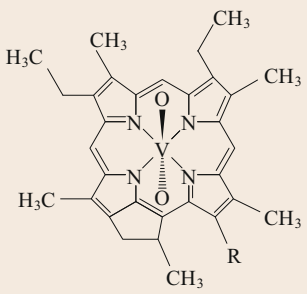
dex (VI) measures the extent of change in the viscosity of the oil as temperature changes.

The standard for measuring crude oil is the barrel (42 US gal), while gas is measured in standard cubic feet (scf). In addition to fuels, petroleum is used to produce numerous other products, from plastics to pharmaceuticals. These are described in the overview of petroleum processing section.

9.3.3 Rocks in Which Petroleum Is Found

Petroleum is typically found in rocks known as *reservoir rocks* and/or *source rocks*. Reservoir rocks are rocks in which petroleum can accumulate and concentrate. Source rocks are rocks in which petroleum was generated and mostly matures. The presence of petroleum in these rocks is caused by changes that occur inside the Earth, particularly increases in pressure and temperature. These changes can be biological or environmental, such as biological mass extinctions or climatic changes. To understand what happens in reservoir rocks and source rocks, it is important to take a step

Table 9.3 Examples of hetero-atom compounds

Structural formula	Common name	Structural formula	Common name
	Thiophenes		Indoles
	Pyridines		Oxazoles
RCH_2COOH	Carboxylic acids		Benzofurans
	Benzothiophenes		Dibenzothiophene
	Amides		4,6-Dimethyldibenzothiophene
	Quinolines		Carbazoles
	Pyrroles		Azathiophenes
	Phenols		Naphthobenzothiophene
	Naphthenic acids		Porphyrins

back and look at the geologic characteristics of rocks and minerals, so that we can better understand why petroleum will occur in these specific rocks and not other rocks.

Fundamentals of Rocks and Minerals

Rocks are dominantly made of minerals. Rocks form when a variety of minerals (discussed in Sect. 9.3.4) are *glued* together into a cohesive solid mass. When

we describe a rock, we are typically referring to a representative sample that contains a characteristic solid assemblage of minerals that comprises a large portion of the Earth. For this reason, geologists define a rock as an *aggregated solid of minerals*. As rocks form, other materials, such as trapped organic matter, smaller solid fragments, fossils and air bubbles, can be included. These are known as inclusions and may get integrated and consolidated in the rock and form valuable resources, for example, petroleum.

Major Categories of Rocks

There are three major categories of rocks that are found on Earth:

- Igneous rocks
- Metamorphic rocks
- Sedimentary rocks.

These categories have been extensively analyzed and described in various books and articles [9.15, 16]. In this section, we present the basic properties of these rocks that influence and affect petroleum exploration (Fig. 9.6).

Igneous rocks crystallize from molten or partially molten rock material called lava (when it is at the surface of the Earth) or magma (when it is still underground).

Metamorphic rocks form from the deformation of other rocks that are changed and transformed under high temperature and pressure without melting. This is called *solid-state transformation*. The process of metamorphism only occurs deep underground.

Sedimentary rocks form from weathered or altered particles and fragments of pre-existing rocks and other materials created by physical, chemical or biological action. This classification of rocks does not depend very

much on the material that the rock may contain, although in some cases some type of mineral or material may commonly occur in a particular category, for example, biogenic type material will most likely occur in sedimentary rocks because of the way in which, and environments where, sedimentary rocks form. How a rock forms, and the arrangement of the minerals that make up the rock will affect the generation and/or accumulation of petroleum in the rock. Therefore, you may have deduced that the category of rocks that is most valuable and significant in petroleum exploration is the *sedimentary rock category*. Another interesting aspect about these three major categories of rocks is that they are interrelated in what geologists call the *rock cycle*. Figure 9.7 represents a simplified diagram of the rock cycle showing some major processes that connect each category to the other.

Our discussion about rocks will not be fully complete if we do not discuss the nature of the minerals that are the building blocks of these rocks. A *mineral* is a naturally occurring inorganic crystalline solid substance that has a specific chemical composition and can be described by characteristic physical properties.

To break this definition down a little more, a *naturally occurring substance* comes from Earth's raw material and is not produced, engineered, or manufactured in a laboratory or factory. Today, due to technological and engineering advances, some engineered substances can have identical composition and characteristics as some naturally occurring minerals. For example, silica (SiO_2) is the molecule that makes up both glass and the mineral quartz. An *inorganic substance* (compound) that makes up the mineral cannot come from living things or be biogenic in nature (although an inorganic mineral like calcite (CaCO_3) is sometimes created by biological process). This raises a question for the

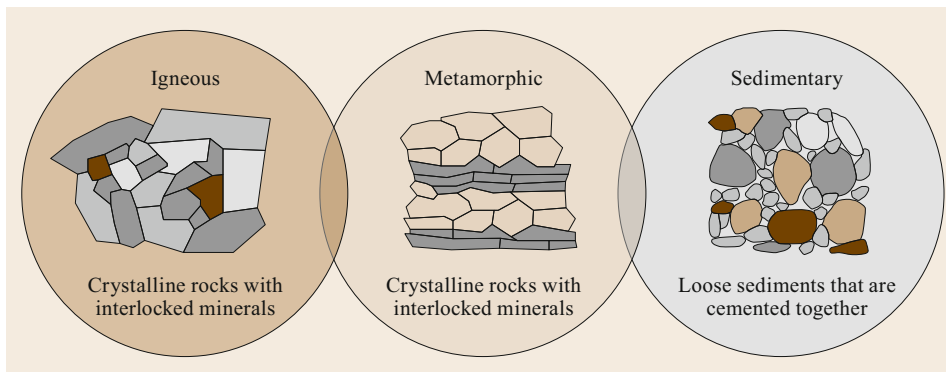


Fig. 9.6 The three major categories of rocks: igneous, metamorphic, and sedimentary. These categories are classified based on the processes that form the rocks and the determine the texture of the rock. The texture of rocks control the generation and accumulation of oil and gas in the rocks

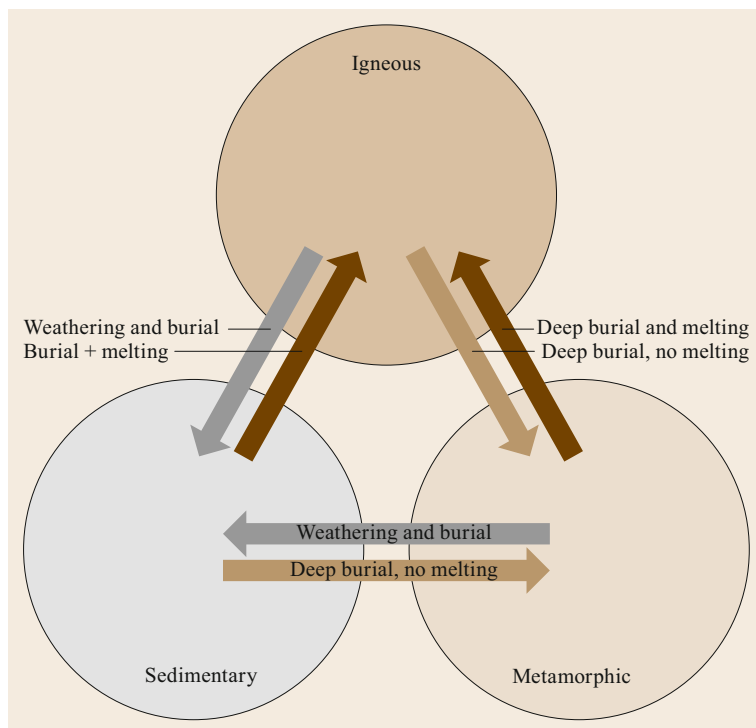


Fig. 9.7 Simplified diagram of the rock cycle showing major processes that connect the major categories of rocks and influence the generation of petroleum

material that makes up coal, which is widely considered a rock in its own right. (It is worth noting here that the material that makes up coal is called a *maceral* and not *mineral*). A *crystalline solid* must have an orderly, repetitive pattern of its molecules and create a unique crystal form. *Specific chemical composition* means that the substance has a unique or narrow range chemical formula and *characteristic physical properties* means that the mineral can be easily identified or recognized from its appearance. For this reason, minerals are typically described and classified on the basis of their physical and chemical properties. The more specific the properties the more easily the mineral can be identified and recognized in a sample.

9.3.4 Some Common Rock-Forming Minerals Important in Petroleum Exploration

There are several minerals that are of significance in petroleum exploration. Silicate minerals like *quartz* and *feldspar*, which are typically abundant in sandstones and conglomerates, will make good reservoir rocks. *Calcite* and *dolomite* are minerals that make up most carbonate rocks like limestone and dolostone. Carbonate rocks can make very good reservoir rocks, and to a lesser extent, source rocks, and other rocks known as overburden rocks. *Halite* (the mineral found in ta-

ble salt) makes up rock salt and salt domes and makes good seals and cap rocks. Clay minerals, for example, smectites, chlorites etc., iron oxides, and micas that are found in shales and some *mudstones* (but occur in lesser amounts in silicates, carbonates or evaporite rocks) make good source rocks, seal, and cap rocks. Oil shales are also unconventional reservoir rocks. Other minerals like anhydrite (CaSO_4), a mineral with high density, and gypsum ($\text{CaSO}_4 \cdot 2\text{H}_2\text{O}$) are sulfate minerals that form cap rocks on salt domes and other sedimentary layers. Examples of rock forming minerals are shown in Fig. 9.8.

The *chemical properties* of minerals depend on both the atomic composition and the arrangement of the atoms in the mineral. Atomic composition and arrangement are specific to each type of mineral. Consider for example, calcite (CaCO_3) the mineral in limestone. Because of its composition, calcite can easily react with acids to release calcium ions and carbon dioxide. This reaction can create cavities, vugs, channels, and pores in a calcite-containing rock. These cavities and pores are known as *secondary porosity* and are important for good reservoir rocks. Quartz (SiO_2) is abundant in most sandstone rocks, because it is very resistant to weathering and does not break down (or weather) easily when minerals are being transformed during sedimentary processes. It can therefore accumulate and creates good reservoir rocks. Magnetite is a magnetic oxide of iron.



Fig. 9.8 Examples of common minerals: Note the colors and distinctive appearance of some of the minerals

It forms during weathering processes or bacterial degradation of petroleum compounds in rocks.

Physical properties of minerals associated with the appearance of the mineral can be observed or measured relatively easily (Fig. 9.8). Common mineral properties are color (obvious and recognizable), luster (describes how *shiny* a mineral looks), cleavage (how the mineral breaks along surfaces), streak (describes the color of the powdered mineral), crystal form (describes the orderly, repeating pattern in the mineral, e.g., cubic crystal form), fracture (describes the indiscriminate cracks in the mineral), hardness (a measure of how easily the mineral can be scratched by other minerals or tools), smoothness (how the mineral feels to the touch), taste (not advisable), magnetic quality (e.g., attraction to a bar magnet), and density (the weight of the mineral).

Significance of Mineral Properties for Petroleum Exploration

The physical and chemical properties of a mineral directly control the role that mineral plays in the generation, accumulation, concentration, or trapping of petroleum. Hard minerals like diamond are hard enough to crush other minerals in rocks during drilling. Resistant minerals like quartz can be transported over long distances to sedimentary basins, where they accumulate and are cemented to form reservoir rocks. Other crystalline minerals like halite (NaCl) prevent petroleum from leaking out of a reservoir (i. e., they create a seal) and can be used in some cases to store oil and gas from refineries underground. Minerals like calcite dissolve readily in weak acids (carbonic acid, H_2CO_3 that form from dissolving carbon dioxide in water). The dissolution of calcite can create pores in rocks, making spaces where oil and water can accumulate. Tiny platy minerals in clays and shales can trap and hold other elements and organic matter between their sheets, thus creating ideal conditions for organic matter accumulation and the transformation of organic matter into oil.

Significance of Igneous and Metamorphic Rocks for Petroleum Exploration

In the previous section, we presented the major categories of rocks. In this section, we will summarize the role of igneous and metamorphic rocks in petroleum exploration. The significance of sedimentary rocks for exploration will be discussed in more detail in the next section.

Igneous rocks and metamorphic rocks tend to have interlocking (fused) crystals that contain little to no pore spaces for the accumulation of any oil or other fluids (Fig. 9.6). In addition, in igneous rocks the high temperatures of magma and volcanic lava exceed what is called the *oil and gas window*, which is the optimum tempera-

ture range at which oil and gas can form. In cases where igneous rocks are fractured and/or faulted, the fractures can provide pathways for oil and gas to migrate between different layers or accumulate in significant amounts. Igneous rocks are also important for the energy industry. When the magma chambers are shallow and hot enough, they can serve as sources that contribute heat for maturation in source rocks or as geothermal energy sources.

In metamorphic rocks, solid state transformation due to high pressure and temperature decrease pore spaces in the rock by compression and smelting. This alters reservoir rocks and source rocks by squeezing and fusing sediment grains and organic material. The high temperatures and pressures from metamorphism exceed oil and gas window. Similar to igneous rocks, metamorphic rocks may be fractured and/or faulted to provide pathways for oil and gas migration and possible accumulation in these rocks. They are also important for the overall energy industry because they can be sources of precious minerals, including radioactive substances like uranium.

9.3.5 Sedimentary Rocks

Sedimentary rocks make up only about 5% of the rocks in Earth's crust, but they represent up to 75% of all rocks exposed at the surface of Earth. This is because sedimentary rocks are formed from material that originates at or near Earth's surface before it is buried and transformed into a rock. Materials that form sedimentary rocks include fragments of pre-existing rocks, dissolved substances precipitated/evaporated from water, organic material that is trapped and buried in the Earth and other inclusions such as fossil remains. The materials that form sedimentary rocks are generally called *sediments* and can be grouped into 3 major types based on their source or process that formed them:

- Chemical sediment (typically dissolved ions)
- Detrital secondary particles and fragments or clasts
- Biogenic formed from or by organic processes.

Here are some common examples of rocks that are formed from these sediments. Sandstone forms from detrital material, limestone can form from biogenic or chemical substances, and evaporates from chemical substances. Detrital sedimentary rocks are the most widely distributed type of sedimentary rocks in the world. Billions of tons of detrital sediments are generated in all environments and transported to the world's oceans, lakes, ponds, and valleys. Detrital sediments are primarily classified based on their grain/particle size. The typical particle sizes are:

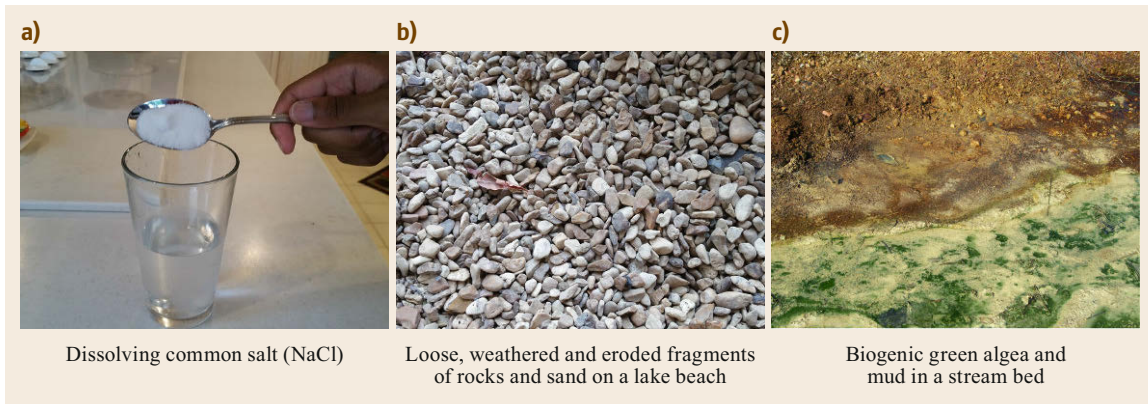


Fig. 9.9a–c Different types of sediments that can form sedimentary rocks: (a) Chemical sediments from dissolved substances, (b) detrital sediments from fragments and eroded remains of rocks, (c) biogenic sediments from microscopic algae

- Gravel (greater than 2 mm)
- Sand (2.00–0.0625 mm)
- Silt (0.0625–0.0039 mm)
- Clay (less than 0.0039 mm).

How Sediments Become Sedimentary Rocks

Sediments are loose unconsolidated materials or dissolved ions that form at the surface of the Earth. A group of sediments called clastic sediments occurs from the weathering and erosion (physical breakdown and loosening) of pre-existing rocks into smaller components. The loose fragments are displaced and *transported* by wind, water, glacier, or gravity and *deposited* into depressions known as sedimentary basins, where they accumulate and are buried through increasing deposition or other processes. Continuous burial creates higher, increasing pressure on underlying sediments, squeezing out fluids (water or air) and creating *compaction* of the sediments. The precipitation of dissolved minerals from the fluids bind and glue the sediments during compaction, leading to *cementation*. Common cement materials are composed of fine or amorphous calcite, silica, or iron oxides.

The process of compacting, cementing, and sometimes *crystallization* of similar sediments together is called *lithification*. This is the final process that transforms loose sediment material into a rock. Lithification is significant in petroleum exploration, because it leads to changes in the rock material that may affect the accumulation and concentration of oil and gas, altering the nature of reservoirs or source rocks by decreasing porosity and permeability.

Sedimentary Structures and Their Significance

When sedimentary rocks form, different types of features called sedimentary structures may form on, in, or

between the sedimentary layers at different times during the process. The two categories of sedimentary structures are *primary sedimentary structures* and *secondary sedimentary structures*, based on when they form.

Primary sedimentary structures provide stratigraphically relevant information about structures that formed when the layers of the rocks were deposited. Secondary sedimentary structures provide information about the changes that occurred after the rocks had been deposited such as the deformation processes that affect the rock layers and the types of structures that resulted from the deformation. Examples of primary sedimentary structures that form contemporaneously with the deposition of sediments are:

- Stratification
- Cross beds
- Ripple marks
- Mudcracks
- Fossil remains

Stratification (layering) is formed by the successive deposition of different sediments. Stratification is controlled by the geologic laws of original horizontality and superposition. Cross bedding is created by the changes in the direction or movement of currents and wind during deposition of sediments. Ripple marks are caused by flow and movement of water and wind on sediments. Mudcracks are formed when muddy surfaces dry up and contract from water loss. Mudcracks indicate drought conditions. Fossil remains are tracks, traces, prints, mold, casts, etc., of organisms that existed when the sediments were deposited.

Secondary sedimentary structures created after the rock is formed are known as post-depositional structures. These include fractures, folds, faults and secondary diagenetic features.

Categories of Sedimentary Rocks

Sedimentary rocks are categorized into three main groups based on the processes and/or the type of sediments (Fig. 9.10) that form the rock. The three main categories of sedimentary rocks are:

- Detrital sedimentary rocks
- Chemical sedimentary rocks
- Biochemical sedimentary rocks.

Detrital sedimentary rocks form from several types of material including:

1. Unaltered fragments of pre-existing rocks
2. Weathered remains of the fragments of pre-existing rocks
3. Secondary minerals that formed from the chemical transformation of the weathered substances from the fragments and composed of mostly clay minerals.

Chemical sedimentary rocks are typically salts, formed from either the precipitation of substances dissolved in water to form the rocks, or from the evaporation of water during droughts, leaving behind rocks known as *evaporites*. These rocks are mostly composed of one type of mineral. Examples include halite (NaCl), and anhydrite (CaSO₄).

Biochemical sedimentary rocks are formed from biogenic processes, which are caused by the action of living organisms. Biogenic sedimentary rocks can be chemical or detrital rocks. For example, limestone (a chemical sedimentary rock) may form from shells of

marine organisms, and coal forms from detrital material of woody plants.

Examples of Sedimentary Rocks

Sandstones are sedimentary rocks made from cemented sand sized sediments, mostly quartz and feldspars. Sandstones can be classified based on their textures, the environments where they are formed, and sometimes their composition.

The *texture* of a rock describes the size, shape and arrangements of the grains that make up the rock. Properties that describe the texture of these rocks are grain size, grain shape (sphericity), rock matrix or cement, grain smoothness (roundness), grain sorting, and grain orientation (fabric). The conditions under which sediments are transported and the environments where the sediments are deposited will affect the textural properties of the rock. *Sedimentary environments* where the rocks form represent the location (typically depressions), where sediment deposition occurs. Sandstone deposition occur in the following environments: deltaic (river deltas), aeolian (desert), fluvial (rivers and streams), marine (open oceans and seas), lacustrine (lakes), and glacial environments. Sandstone that forms in one environment can have characteristics that are different from sandstones formed in a different environment. For example, sandstones formed in desert environments will have different types of ripple structures than sandstones formed in deltaic or beach environments. The composition of sandstones can vary, although most sandstones are made of quartz. Other

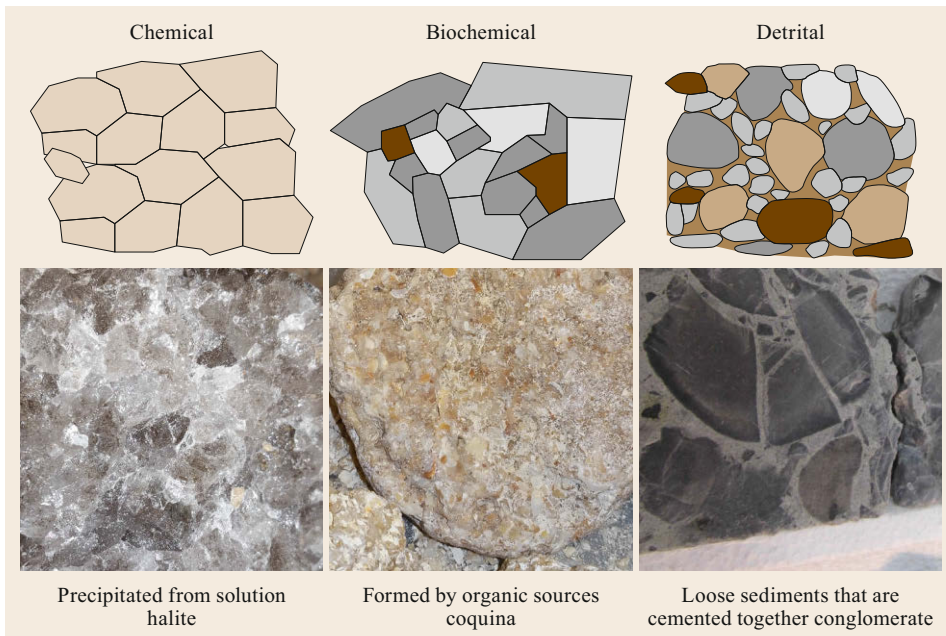


Fig. 9.10 Three categories of sedimentary rocks

components of sandstones are arkosic (feldspathic) minerals, nonsiliceous cements, and lithic (fragments of other rock) materials. The category of sandstones sometimes include breccia and conglomerates. Breccia and conglomerates are made of sediments that are typically larger (gravel) in size than grains in classic sandstones. Breccia mostly contains angular sediments, and conglomerates contain rounded (smooth) sediments. Sandstones are the most important *conventional reservoir rocks*.

Shales and *mudrocks* are formed from fine clay-sized grains either from weathered remains of detrital material or from secondary clay minerals. They occur in several colors (gray, black, red, green, etc.) based on their composition and may contain sufficient organic material to be petroleum source rocks. If organic material is absent from shales, they can form important seal and cap rocks, which prevent petroleum from leaking out of the rocks. Shales mostly contain clay minerals, and mudstones mostly contain siliciclastic minerals.

Carbonate rocks contain carbonate (CO_3^{2-}) ions in their minerals. They are formed by both biogenic and inorganic processes. Inorganic carbonate rocks are formed by the precipitation of carbonate minerals (like calcite) or by the reaction of calcite minerals with salt water. Biogenic carbonates are formed from skeletal materials of living organisms such as shells. *Marls* are fine grained carbonate and calcium rich rocks similar to mud rocks.

Evaporites form when water evaporates, leaving behind solute substances. Examples of common evaporites include salts like halite, gypsum, and anhydrite. Evaporites (like carbonate rocks) are mostly composed of one type of mineral, although varying traces of other minerals (impurities) maybe present in them.

Distribution of Sedimentary Rocks

Sedimentary rocks are formed in depressions on Earth's surface called sedimentary basins. For thick accumulations of sediments to occur, a source or supply of sediments and a depression to hold the sediments have to be available. Sedimentary basins can be created by plate tectonic activity, leading to subsidence, folding, faulting, and rifting of Earth material. These depressions can be any shape (bowl-shaped, irregularly shaped, elongated, polygonal), and they can be symmetrical or not. Sediments in basins typically come from detrital sources found on land masses or are created in situ by chemical and/or biological processes.

Sedimentary basins occur in all types of environments on Earth. These are:

- Continental environments (land masses)
- Ocean environments (aquatic)
- Transition or mixed environments.

These are the largest *megascopic* environments and each can be further subdivided into smaller environments to a *mesoscopic scale*, *macroscopic scale*, *microscopic scale*, *nanoscale*, etc. For example, *continental sedimentary environments* include large bodies like lakes, fluvial (river) valleys, and desert environments. These in turn can harbor smaller macroscopic (medium sized bodies) environments. For example, fluvial environments could contain a meandering river, a braided river, incised river valleys, etc. A meandering river environment in turn has a point bar, flood plains, river bed, and levees etc., where sediments are deposited. A braided river will include channel bars, floodplains, sand beds, channels, bed etc., where the sediments being moved by the rivers are deposited. Mixed or transitional sedimentary environments are areas under the influence of both land and ocean processes, such as deltas, bays, marshes, and barrier islands. The sediments and rocks that are formed in mixed or transitional environments will indicate the dominant processes that affected their deposition and formation as well as the source of the sediments. The ocean environments (Fig. 9.11) are areas that extend beyond the direct influence of land masses and continental sources or processes. The ocean environments can include the continental shelf, continental slope, continental rise, deep marine environments, and the abyssal plain.

Summary

Rocks are consolidated solids of minerals that can contain other material. Petroleum forms and occurs in rocks. The composition and arrangement of mineral crystals in rocks determines whether oil and gas can be formed, accumulated, and trapped in the rocks. Crystalline rocks (igneous and metamorphic rocks) do not create conditions that are favorable to generate, accumulate, and concentrate petroleum. Rocks that provide the ideal conditions favorable to the generation and accumulation of petroleum are sedimentary rocks. Sedimentary rocks in which petroleum is generated are called *source rocks* and sedimentary rocks in which petroleum accumulates and is concentrated are called *reservoir rocks*.

9.3.6 When Petroleum Formed

Petroleum formed millions of years ago, when a series of ideal conditions occurred all at the right times to generate and accumulate economic quantities of HCs. This ideal time span when favorable conditions occur to generate economic amounts of HC, is referred to as a *critical moment* (interval of time) in geologic history. The critical moment covers the time span when there was sufficient production and preservation of organic

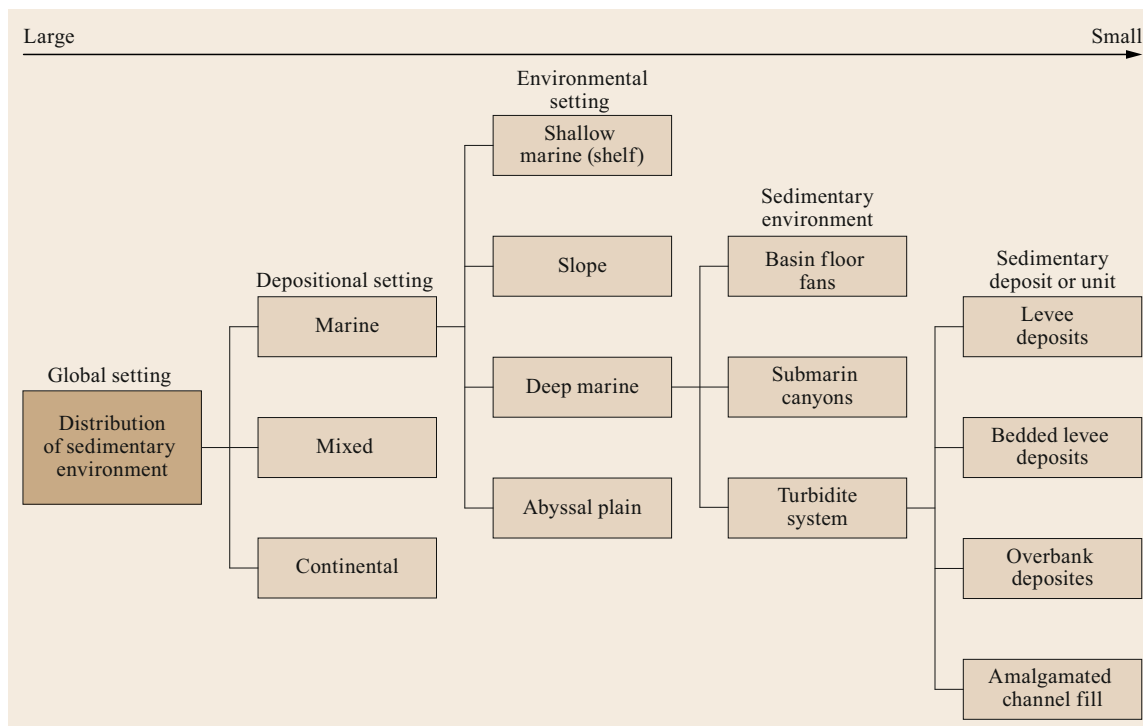


Fig. 9.11 Schematic representation of locations where sediments can be deposited in a marine environment

material, rapid burial of the organic material to ideal depths, ideal temperature, and ideal pressure to generate petroleum and enough time to migrate and accumulate the petroleum. The time period when petroleum formed can be determined by applying techniques of geologic dating. *Relative dating* establishes the sequential occurrence of events by establishing the order in which the events occurred with respect to the other events. This method of dating is based on and applies geologic laws and principles. Relative dating requires comparing at least two or more events.

Basis of Relative Dating

As mentioned earlier, geologic laws and principles are the basis of relative dating. Important geologic laws and principle used in relative dating are:

- *The law of original horizontality and lateral continuity* (Nicolaus Steno) [9.17]: Rocks that are formed from sediments are initially deposited horizontally and are laterally continuous. This law means that, in an environment where sediments are deposited (e.g., in a lake as illustrated in Fig. 9.12), the sediment layers (A, B, and C) that form the rock layers are stacked horizontally and continue laterally in all directions until they encounter a barrier.
- *The law of superposition* (Nicolaus Steno) [9.17]: In an undisturbed sequence of rocks in a sedimentary basin, the older layers are at the bottom and the younger layers are on the top. The older sediments are deposited first (found at the bottom of the lake), and successive layers above are younger with the top most layer being the youngest. In the example in Fig. 9.12, C is older than B, and B is older than A. Note that this order may change if the rocks are disrupted by tilting, bending or breaking.
- *Principle of cross cutting* (James Hutton) [9.17]: When a rock or an event cuts or intrudes through a sequence of rocks, for example, a dike (Fig. 9.13), it must be younger than the rock(s) through which it cuts. In the example illustrated in Fig. 9.12, the dike D is younger than layers C, B, and A.
- *Law of inclusions* (James Hutton) [9.17]: This law means that if a rock layer contains fragments of another rock or substance, then this rock layer must be younger than the fragments of other rocks or substance that it contains. In the illustration in Fig. 9.12, F is younger than the fragment E that it encloses. It is worth noting here that inclusions should not be confused with intrusions. Intrusions are younger and inclusions are older than the rocks they are in.

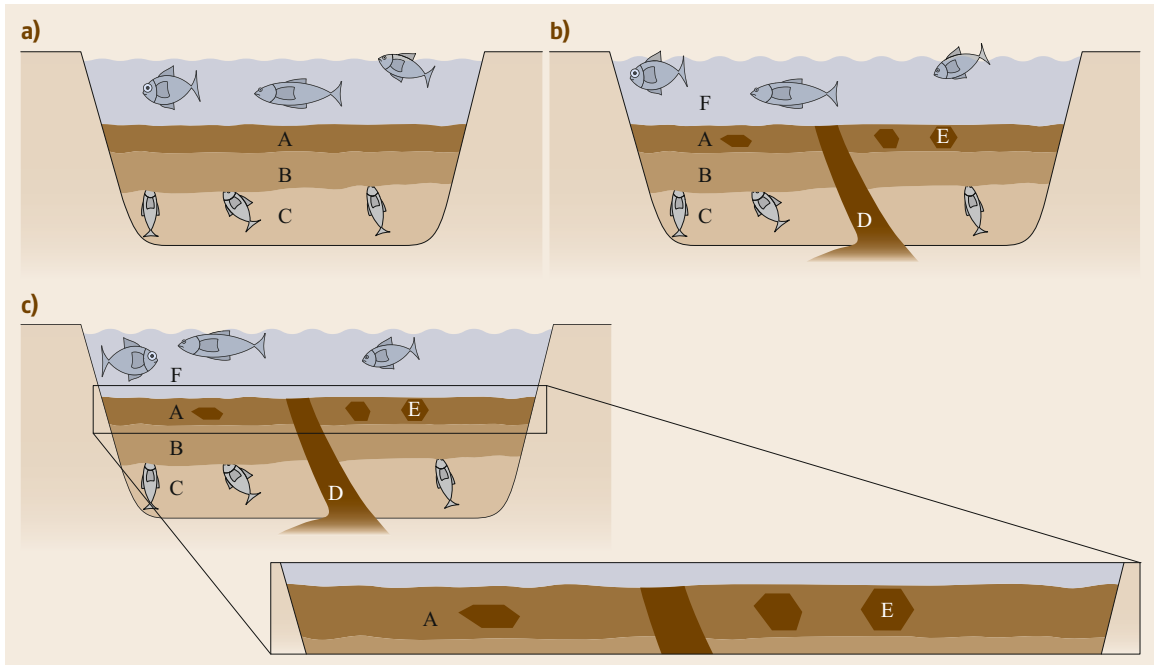


Fig. 9.12 (a) Schematic representation of original horizontality and lateral continuity in lake sediments, (b) schematic representation of cross cutting in lake sediments, and (c) the inclusion E is older than the surrounding rock F

- **Principle of Faunal succession** (William Smith) [9.17]: This principle states that sedimentary rock layers in any given location will contain a specific sequence of fossils that succeed each other through time. William Smith suggested that specific groups of fossils follow or succeed one another in the rock record over time, and that some fossils can thus be representative of the time when different types of rocks were deposited and formed. In terms of size, two classes of fossils exist. Macrofossils are large remains or traces of organisms distinctively visible to the human eye, and microfossils are tiny remains or traces of ancient organisms not distinctly visible to the human eye.

Fossils are evidence of past life in the rock record and can tell us something about the kind of organisms that lived when a group of rocks were formed, the type of environment that existed at the time, and climate conditions of the time. Thus, we can determine the paleo-environmental conditions from rocks and fossil records, for example we can tell, wet versus dry conditions, deep versus shallow water environments, hot versus cold temperatures, macro versus microscopic organisms, clear versus muddy waters and other climatic conditions that existed when the rocks formed. Fossils that help us to identify specific rocks and past conditions are termed index fossils.

Index fossils have to meet the following key conditions:

1. The fossilized organisms lived over a short time span
2. The fossils are geographically widespread around the world
3. The fossils are abundant
4. The fossils that are easily recognizable and identifiable
5. The fossils were easily preserved.

Fossils are important for dating rocks that have been deformed, overturned, or eroded and thus no longer obey fundamental geologic laws or principles, such as the laws of superposition and horizontality stated earlier. Another important point to remember is that because fossils are preserved from living organisms, they are also important in the generation of hydrocarbons.

9.3.7 Significance of Fossils in Petroleum Exploration

- **Microfossils:** These are tiny fossils that can only be identified with a microscope. They represent the important source material that generates petroleum. Microfossils are used in fingerprinting the source of oil in rocks. Some microfossils can also be useful as index fossils. Examples of microfossils

sils include planktonic organisms such as diatoms, foraminifera, radiolarian, and coccoliths.

- **Macrofossils** (Fig. 9.14): These are large fossils that are visible to the human eye or clearly visible with the aid of a hand lens. They are useful in subdividing layers of rocks into relative age and position in the geologic sequence. The subject of biostratigraphy studies rocks based on their fossil content. Macrofossils also aid in identifying depositional settings where rocks were formed. For example, fossils of woody plants will indicate an environment that was on or near land masses such as swamp and marshes.
- **Law of unconformities** (James Hutton) [9.17]: Unconformities are gaps in the geologic record of



Fig. 9.13 Intrusion in granitic rocks of the Rocky Mountains, USA



Fig. 9.14 Images of macroscopic fossils preserved in rocks

rocks (Fig. 9.16). They indicate time spans when rocks were missing from the sequence either because during that time span sediments were not deposited, an interruption occurred, or the rocks were removed by erosion or other processes. Missing rocks in the geologic sequence can be established from different fossil records in the succession of rocks, different types or categories of rocks that are side by side, and different orientation of the sequences rocks.

Four main types of unconformities are described based on the orientation, rock type and sequence of succession:

1. **Nonconformity** occurs when a sedimentary rock layers are in contact with metamorphic or igneous rocks, for example, intrusions of igneous dikes.
2. A **disconformity** occurs when rocks are missing between parallel layers of two different groups of sedimentary rocks. The formation of a disconformity is often due to the prior erosion of the older layers of rock before the younger layers of rocks are deposited.
3. **Paraconformity** occurs when sedimentary layers below and above the unconformity are parallel. Typically there is neither irregular erosional surface indicating erosion in a paraconformity, nor is there another visible change that occurs when no sediments were deposited over a long period.
4. **Angular unconformity** occurs when horizontal layers of sedimentary rock are deposited on tilted, folded and often eroded layers of older sedimentary rocks (Fig. 9.15).

Numeric (radiometric or absolute) dating relies on radioactivity, using the half-life of radioactive atoms to determine the age of an event. Unlike relative dating, it can be successfully applied to a single event or rock layer. Some common radioactive isotopes important to geology are uranium-238, thorium-232, potassium-40 and carbon-14 (Table 9.4).

For example, carbon-14 has a half-life of 5730 years. This is the number of years it will take the

Table 9.4 Table of parent atoms, daughter atoms, and half-lives of some common radioactive elements employed in petroleum geology

Parent	Daughter	Half-life (years)
^{238}U	^{206}Pb	4.6 billion
^{235}U	^{207}Pb	0.7 billion
^{232}Th	^{208}Pb	14.1 billion
^{87}Rb	^{87}Sr	47 billion
^{40}K	^{40}Ar	1.3 billion
^{14}C	^{14}N	5730

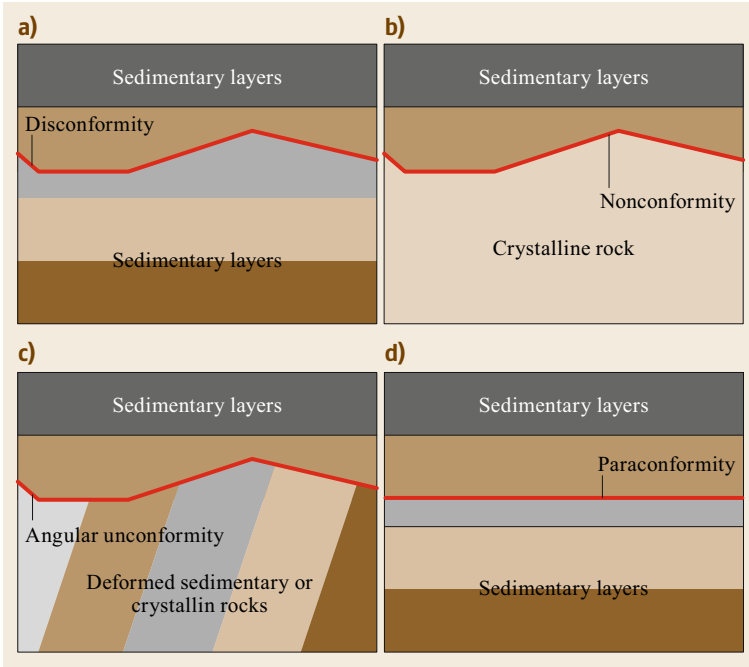


Fig. 9.15a–d Types of unconformities (shown as a *thick red line*): (a) disconformity, (b) nonconformity, (c) angular unconformity and (d) paraconformity

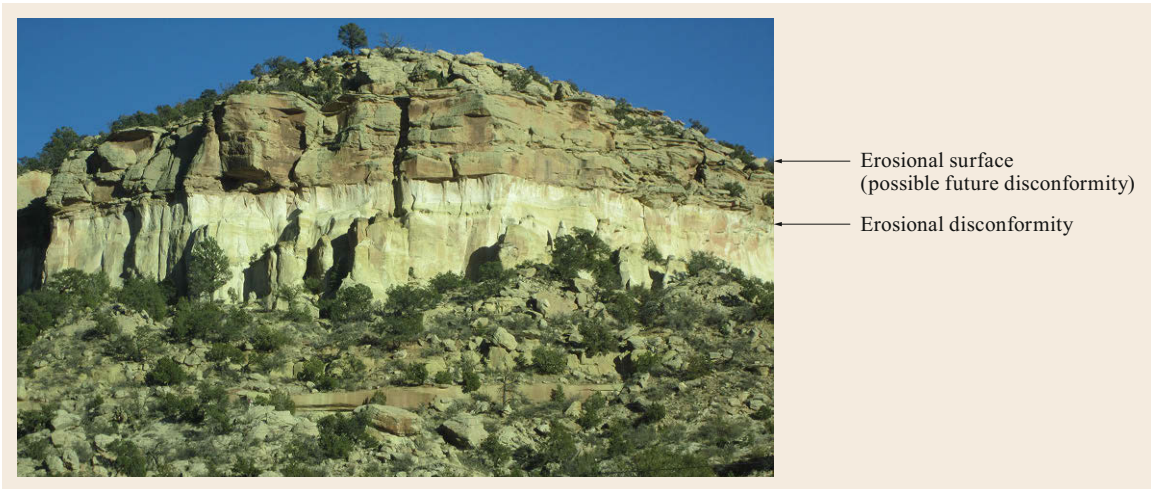


Fig. 9.16 Erosional unconformity in rocks of the Grand Canyon, USA

original number of atoms to decrease by half. When carbon-14 decays, it forms nitrogen-14 with the release of a β particle. This means that after 5 half-lives – 28 650 year – almost all the radioactive carbon-14 atoms would have dis-integrated into nitrogen-14 with the remaining carbon-14 being too low in concentration for detection. Due to its relatively short half-life, carbon-14 cannot be used to date rocks that are older than about 30 000 years. To date older rocks, a different isotope with a longer half-life has to be used, for example, uranium-238.

9.3.8 Summary of the Significance of Geologic Time in Petroleum Exploration

Dating rocks allows us to compare the age of one rock to that of other rocks. Relative dating establishes the order in which two or more rock units are formed. Relative dating techniques use geologic laws and principles, which are mostly applied to rocks in sedimentary environments, the most important category of rocks in petroleum exploration. Absolute dating is a technique

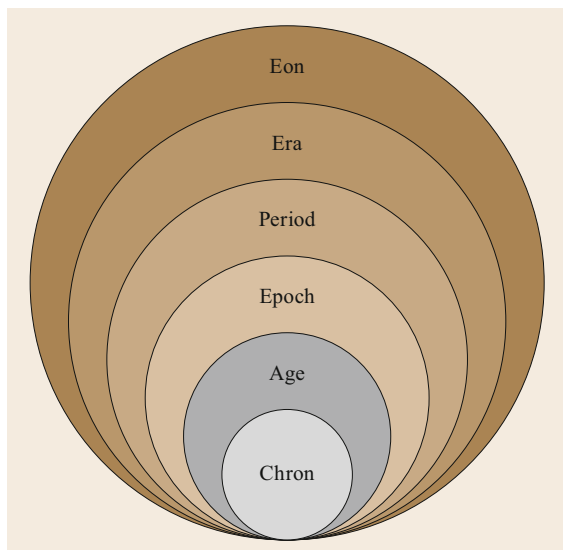


Fig. 9.17 Major divisions of the geologic time scale. In this case, the largest division is the Eon and the smallest is the Chron

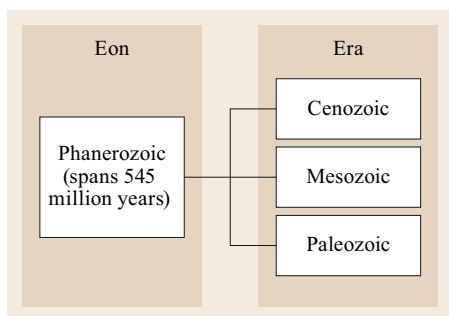


Fig. 9.18 The three Eras of the Phanerozoic Eon. Most oil and gas formed and accumulated during the Paleozoic through Mesozoic Eras

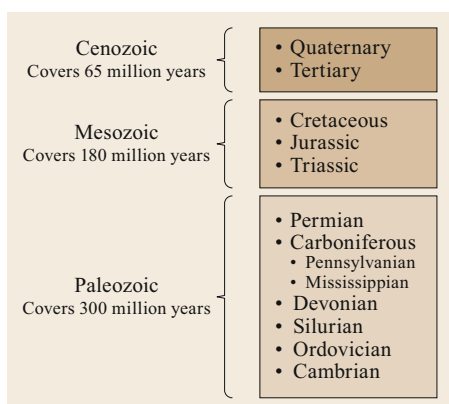


Fig. 9.19 Twelve subdivisions of the three geologic eras of the Phanerozoic

that uses the half-life of radioactive isotopes to determine numeric ages of rock units or events in the geologic record. By determining the numerical age of rocks, we can better understand the critical moment

in time when oil formed, when it migrated from the source, and when it became trapped in a reservoir rock.

The Geologic Timescale

Once the geologic sequence of rocks has been established and the numeric ages determined, combining these relative and numeric dating allows geologists to classify the 4.6 billion years of Earth's history into intervals of meaningful time segments on a chart that represents intervals of significant geologic events or processes of varying durations. Significant geologic events that occurred in the past, and can be used in subdividing the geologic record are events like the appearance and disappearance of unique life forms, mass and major extinctions, major climatic changes, catastrophic events, and the rise and fall in sea level glaciation, significant physical and chemical changes. Depending on the geologic subjects, different terminology for the divisions of the geologic timescale are used.

In geochronologic nomenclature, the *Eon* is the largest division of the geologic time scale, and covers time intervals of about 500 million years to more than a billion years long. There are four Eons in Earth history. These are listed below:

1. Phanerozoic: 545 million years–present
2. Proterozoic: 2.5 billion–545 million years
3. Archean: 3.8 billion–2.5 billion years
4. Hadean: 4.6 billion–3.8 billion years.

The most recent Eon, the Phanerozoic, represents the time interval when most of the petroleum formed and accumulated around the world. Henceforth, we will focus mostly on events that occurred during the Phanerozoic Eon.

Eons are subdivided into *Eras*. The events that delineate the Phanerozoic into 3 Eras (Fig. 9.18) are *major extinctions* of organisms that populated the Earth. For example, the boundary between the end of the Paleozoic Era and the beginning of the Mesozoic Era represents the time when about 90% of all marine species and about 70% of terrestrial species became extinct. Similarly, the boundary between the end of the Mesozoic Era and the beginning of the Cenozoic Era delineates the time when about 50% of all species on Earth went extinct, including the famous dinosaurs. The time span for each era covers tens of million to hundreds of millions of years (Fig. 9.19).

The Era is subdivided into smaller segments known as the *Period*. The Period is the most commonly used subdivision and the Fundamental unit of the geologic time scale. The Paleozoic Era has six Periods (or seven if you are using the United States-based classification), the Mesozoic has three Periods and the Cenozoic has two Periods as shown in Fig. 9.19. The most recent ge-

ologic Period is the Quaternary Period, which includes the industrial and technological age of humans and continues to the present time.

Periods cover time spans between thousands to tens of thousands of years. The geologic Periods are subdivided into smaller units known as the Epoch. The Epoch is subdivided into the Age and the Age into Chron representing successively smaller time spans in the geologic record of rocks.

9.3.9 Significance of Time in Petroleum Exploration

During the Paleozoic era, most hydrocarbon source rocks around the world were deposited mostly be-

tween the Devonian and Permian Periods. The mass demise of living things (including microscopic organisms) likely contributed to produce large amounts of organic material, and as a result led to the preservation of some of the organic matter in sedimentary rocks. Large accumulations caused the organic material to be buried deep enough to attain the oil and gas window for high temperatures and pressures to transform the organic matter to oil. The maturation process of organic matter into oil takes a long time. The accumulation of thick overburden layers of sediments buries the organic rich layer deeper and provides sufficient pressure and temperature to transform the organic matter into oil and gas (Fig. 9.5).

9.4 How Petroleum Accumulates and Concentrates

Once petroleum forms in source rocks, it may be moved from the source rock into other rocks known as *carrier beds* or *reservoir rocks*. The process of moving petroleum from source rocks to carrier beds or reservoirs rocks is called migration. *Primary migration* occurs when the petroleum leaves the source rock and migrate into a carrier or reservoir rock. *Secondary migration* occurs when petroleum leaves a carrier or reservoir rock and moves to another rock, or leaks and is lost to the surroundings. Migration of petroleum stops in *traps* where the petroleum is concentrated and accumulates.

The mechanism of how primary migration occurs from source rocks is not fully understood and several mechanisms have been proposed and described [9.12–14]. Secondary migration is controlled by oil viscosity, rock porosity, buoyancy and permeability of carrier beds.

9.4.1 Petroleum Accumulation

During *petroleum accumulation*, oil is concentrated and trapped in conventional reservoir rocks like sandstones. Petroleum *migrates* and *accumulates* in reservoir rocks because reservoir rocks can store and transmit fluids (liquids and gases). Rocks must have characteristic properties to qualify as good reservoir rocks. Important characteristics are:

- Temperature
- Pressure
- Porosity
- Permeability
- Fluid saturation

- Capillarity
- Wetting
- Trapping.

In the Earth, temperature increases with depth. Data from thousands of oil wells show that the surface temperature is always lower than the temperature measured at the bottom of a well. This increase in temperature with depth can also be observed in deep mines (the deeper you go the hotter it is). The sources of heat in the subsurface are varied but include heat that was trapped during the formation of the Earth, heat absorbed from sunlight, and heat that is converted or generated from other types of energy sources (mechanical energy, electrical, chemical, biological energy, and radioactivity). The rate at which temperature increases with depth is described as the *geothermal gradient*. Factors that affect temperature in the subsurface are fluid movement and type, drilling mud circulation, the type of rocks, depth, deformation, and radioactivity. Temperature is important for petroleum exploration and production because:

1. It controls oil and gas generation and maturation
2. It affects oil viscosity and flow
3. It affects the phase of the fluid (liquid or gaseous)
4. It influences pressure (generally high heat can cause expansion in gases, thereby increasing pressure)
5. It is useful in modeling, calibrations, and well-log interpretations.

There are three types of subsurface pressures, including *lithostatic pressure*, *hydrostatic pressure*, and *abnormal pressure*. The lithostatic pressure in the sub-

surface is caused by the weight of the sediments above a point under the sediments. Hydrostatic pressure is caused by the weight of the water column above a point underneath. In general, hydrostatic pressure is typically lower than lithostatic pressure (Fig. 9.20).

Porosity describes the ratio of total volume of pore space in a rock compared to the total volume of the rock. It can be expressed as a percentage or a fraction of the total volume

$$\text{Porosity (\%)} = \frac{\text{volume of pores}}{\text{total volume of rock}} \times 100 .$$

Porosity provides information about the amount of fluids (liquids and gases) a rock can hold. The common oil field symbol is the (ϕ). Three types of pores can be described in a rock based on how interconnected they are (Fig. 9.22).

Open or connected pores are linked to other pores creating a continuous connection between the pores. *Dead-ended pores* are open on only one side of the sediment creating a *cul-de-sac* on the other end. *Isolated pores* are not connected to other pores in the rock (they occur in isolation as one might see in bubble wrap). Geologists and engineers have different classifications of pores based on the pore size, when and how the pores form, or how the pores behave under different pressure conditions. The classification of pores directly relates to how the different groups of professionals interact with the information. Geoscientists (including petroleum geologists) are interested in understanding when, how, where and why rocks and pores are formed, while engineers are interested in the production conditions such as how well the pores are connected or the size of the pores and the capillarity. Geoscientists classify porosity as *primary porosity* if the pores were formed at the time

when the sediments were transformed into rocks. These are mostly the spaces that exist between the sediment grains in the rock after compaction and cementation have taken place. They describe *secondary porosity* as the porosity that forms after the rock was deposited. This may be formed by processes of boring, borrowing, fracturing, or dissolving rocks.

Geologists can also describe pores based on their *size*. Large pores that are visible to the eye or the aid of a hand lens are *macroscopic pores* (macroporosity). Tiny pores that are not visible to the eye are *microscopic pores* (micro-porosity).

Engineers classify porosity based on the connectedness of the pores and their response to pressure changes. *Total or absolute porosity* describes the total volume of pores in the rock. *Effective or open porosity* refers only to the volume of pores that are interconnected and can transmit fluids in the rock. *Dynamic porosity* refers to the amount of pores that can transmit fluids under a given pressure difference. In general, total porosity is always greater than effective porosity which is greater than dynamic porosity.

Generally, high-porosity rocks make better and more desirable reservoir rocks. The typical porosity ranges vary significantly for common reservoir rocks. In general, sandstone rocks that have less than 5% porosity are considered *very tight*. Rocks with 5–10% are considered *tight* (poor porosity), those with 10–15% have *fair*, those with 15–20% have *good*, and those with more than 20% have *excellent* porosity.

Permeability describes the ability of a rock to transmit fluids through porous media. It is commonly expressed in millidarcies (mD), a sub measure of the darcy (D). 1 D is equal to 1000 mD. A common symbol for permeability is *K*. Permeability depends on the connectedness of pores. This means that, although a rock must have porosity before it can have permeability, high porosity does not always mean good permeability. Permeability can occur in any direction within a rock layer depending on how the pores are formed. For example, vertical and lateral permeability in a rock sample can be significantly different due to the orientation of the sediments or minerals in the rocks. Rocks with layered minerals like clays will have preferentially more lateral permeability than rocks with spherical minerals like sandstones.

Permeability is classified into three main types:

1. *Absolute permeability* describes the ability of a rock to transmit a fluid when it is 100% saturated with the fluid, for example an aquifer filled with water.
2. *Effective permeability* describes the ability of a rock to transmit a fluid in the presence of another fluid

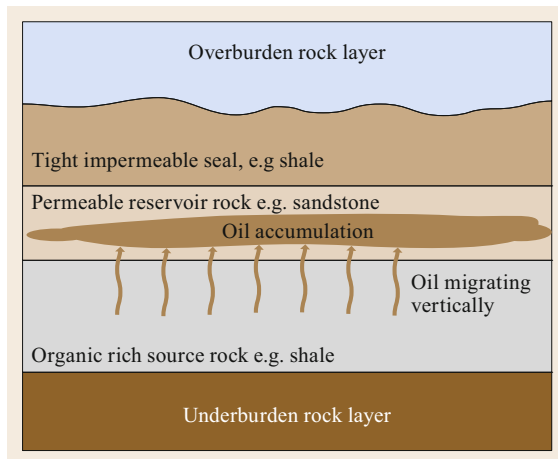


Fig. 9.20 During migration, oil and gas move from source rocks to carrier beds or reservoir rocks

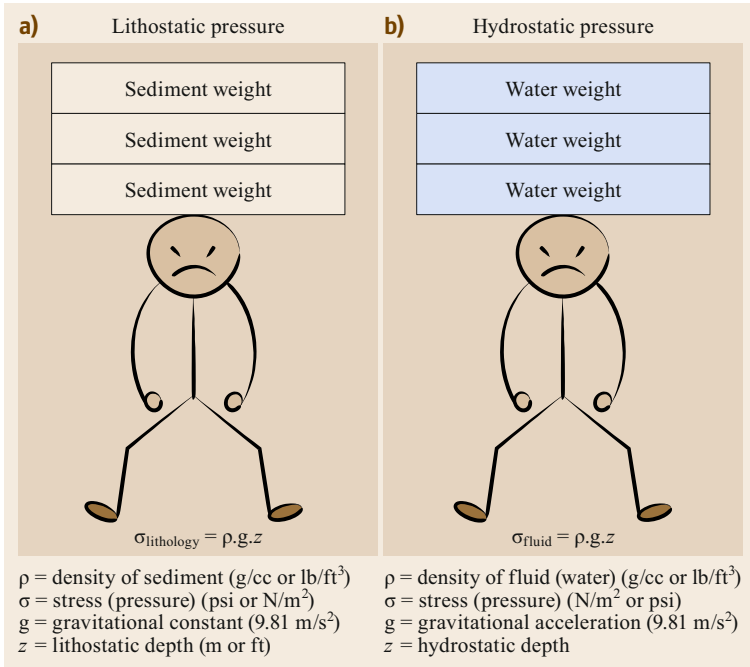


Fig. 9.21a,b Cause of lithostatic and hydrostatic pressure in the subsurface: **(a)** Lithostatic gradient (average rate at which lithostatic pressure increases) = 1 psi/ft **(b)** hydrostatic gradient (average rate at which hydrostatic pressure increases) = 0.43 psi/ft or 0.68 Nm²/ft

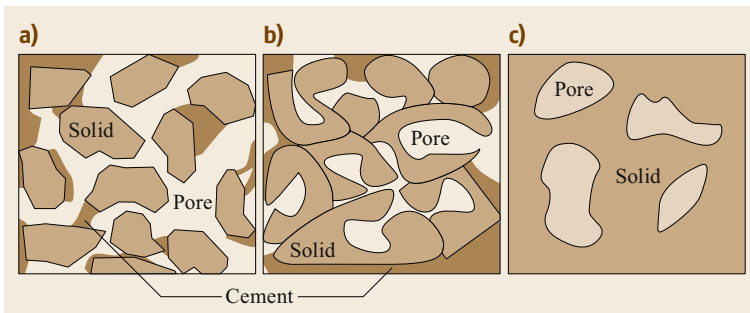


Fig. 9.22a-c Three types of pores based on their connectivity: **(a)** Connected or open pores, **(b)** dead-ended pores and **(c)** isolated pores

when the two fluids are immiscible such as oil and water in a reservoir.

3. *Relative permeability* describes the ratio between the effective permeability of a fluid at partial saturation and the absolute permeability of the fluid

$$\text{Relative } K = \frac{\text{Effective } K}{\text{Absolute } K}$$

Permeability in rocks is described as excellent when it is more than 100 mD, good when it is between 10–100 mD, and poor (tight rock) when it is less than 10 mD. It is worth remembering that a rock with low permeability could still have significant porosity.

Factors that Affect Porosity and Permeability

Textural characteristics of reservoir rocks will affect porosity and permeability. These sediment character-

istics are controlled by most of the processes that lead to the formation of the sedimentary rock as well as processes that affect the rock after it has been formed. Common textural characteristics of rocks include *shape, size, sorting, fabric, smoothness* and *packing* of the sediments in the rock (Fig. 9.25).

Primary porosity is affected by the processes that occur during the formation of the sedimentary rock. During the transport of sediments, *sorting* which is the redistribution of grains into similar sizes increases with increasing distance from sediment source. This increase in sorting can also enhance porosity. Sediment *packing*, which is the way the sediments are arranged and stacked in the rock relative to one another, also changes porosity. Efficient packing decreases porosity. The *compaction* of sediments squeezes the sediment grains close together and decreases porosity. The process of *cementation* that binds sediments together by

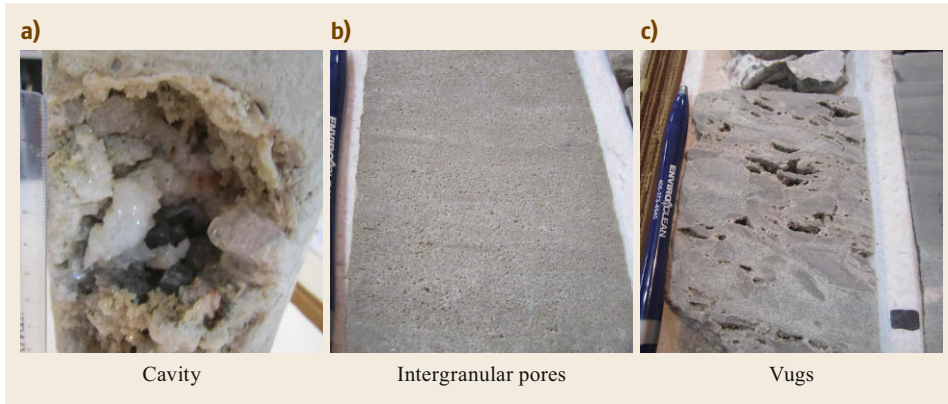


Fig. 9.23a-c Different types of macroporosity in core and slabs of Mississippian aged rock samples from Midwestern USA: (a) Large cavity, (b) intergranular pores and (c) vugs

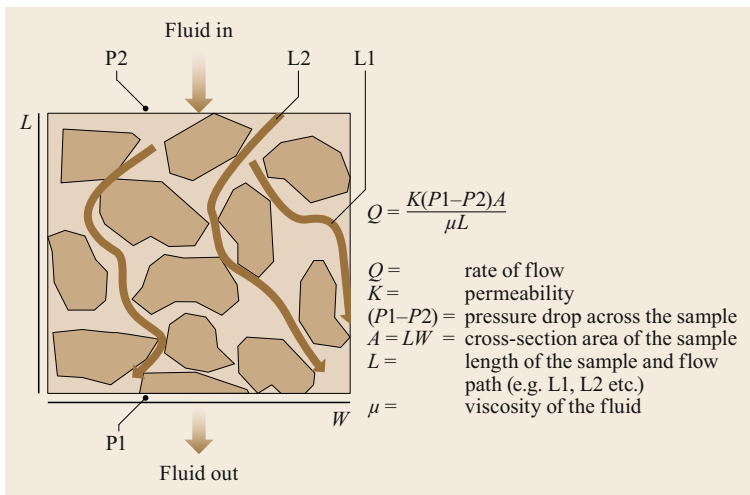


Fig. 9.24 Schematic of flow through a permeable rock sample

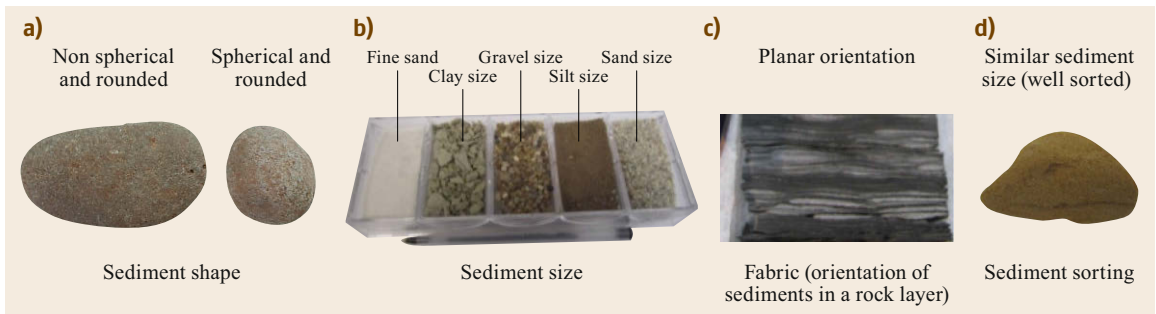


Fig. 9.25a-d Common textural characteristics of rocks: (a) shape (b) size (c) fabric (d) sorting

precipitating dissolved substances in spaces between the grains decreases porosity. Post-depositional processes like fracturing and dissolution tend to increase porosity and the connectedness of the pores and will thus increase permeability, while precipitation of solutes in fractures or vugs between sediments will decrease porosity as well as pore throat size, and thus decrease permeability.

Fluid Saturation, Capillarity and Wetting

Fluid saturation describes the relative amount of a given fluid (water, oil or gas) that occupies the pore spaces in a rock (Fig. 9.26). Saturation is expressed as a fraction or percentage of the volume of the fluid in the rock to the total pore volume. Generally, if the pore spaces in a sedimentary rock are not occupied by water, then they are probably occupied by oil or gas (which is

mostly hydrocarbon gas). Therefore, knowing the relative fraction of one fluid allows us to determine the fraction of the other. Thus the HC saturation (S_h) in the rock is simply computed as $S_h = 1 - S_w$ where S_w is the water saturation in the rock.

Capillarity measures the ability of a fluid to flow in very narrow pore spaces under the influence of forces of surface tension. Capillary pressure increases with decreasing pore throat diameter.

Wetting describes how a fluid interacts with the surface of sediments in the reservoir rocks (Fig. 9.27). Particularly, oil and water interact differently with the surfaces of different types of minerals in porous reservoir rocks. For example, sandstones are usually water wet (preferentially attract water to sand grain surfaces compared to oil) and carbonate rocks are typically oil wet. Generally in a reservoir, there is a continuum in wettability due to the presence of many different types of sediments.

Seals and Cap Rocks

Seals are rocks that prevent petroleum from leaking out of reservoir rocks and being lost. Important characteristics of seal rocks include low or no porosity, low or no permeability, and high ductility. Tightness is favorable in seal rocks because it prevents the accumulation and flow of petroleum into or out of them. Ductile rocks do not break and fracture readily when they are deformed thus minimizing connectivity between pores.

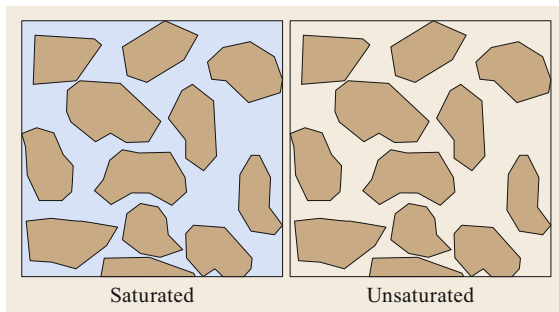


Fig. 9.26 Schematic of a medium that is completely (100%) saturated with water and the same medium with no visible water saturation (0–5%) or dry

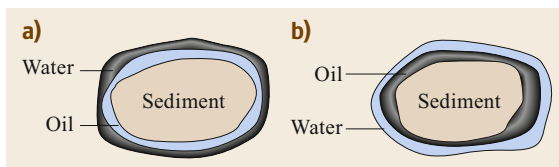


Fig. 9.27a,b Schematic illustrating two types of wetness: (a) Water wet sediment, for example, quartz grain and (b) oil wet sediment, for example, calcite grains

Seals rocks can cover large areas (regional seals) and as such can influence the migration pathways of oil and gas, or they can be limited (local seal) to a particular reservoir rock area and help in concentrating oil. Examples of common seal rocks are tight rocks e.g., shales, anhydrites, tight carbonates, and rock salt.

9.4.2 Petroleum Traps

A *petroleum trap* is a unique geometric arrangement of rocks and structural features that allow for economic quantities of HCs to be concentrated and contained in the reservoir unit [9.13]. This means that a trap does not only depend on the presence of reservoir rocks but also depend on the shape and how the rocks are arranged with respect to other rocks. Important components associated with a petroleum trap are:

1. A structural high
2. A geometric closure
3. Permeable rock containing oil/gas
4. Seal and cap rocks
5. Source rock/migration path (carrier bed)
6. Overburden rocks
7. Time.

Thus the key features of a petroleum trap (Fig. 9.28) include the reservoir, seals and cap rocks, underburden, closure, pay, zone, gas cap, crest, oil–water contact (OWC), oil–gas contact (OGC) (when there is a gas cap), and spill point. These features describe the relationship and the geometric arrangements of the trap elements and trap content.

Petroleum traps can be grouped into four categories based on the geologic processes that mostly influence the traps:

1. Structural traps
2. Stratigraphic traps
3. Hydrodynamic traps
4. Combination traps.

Structural traps are created during the deformation of rocks. Rock deformation is caused by stresses resulting primarily from tectonic activities and intrusions or other piecemeal features that cause local scale deformation on overburden rocks as a result of loading or differential compaction, bending, breaking, pulling and pushing. Bending leads to folds, breaking leads to faults and compaction or upward pushing causes piecemeal. *Fault-associated* traps are traps that are formed by, or because of, the occurrence of faults. Faults occur when rocks break and the rock blocks are displaced upward, downward or laterally relative to each other. Two main groups of faults can form when rocks are broken and displaced. These are (a) *dip-*

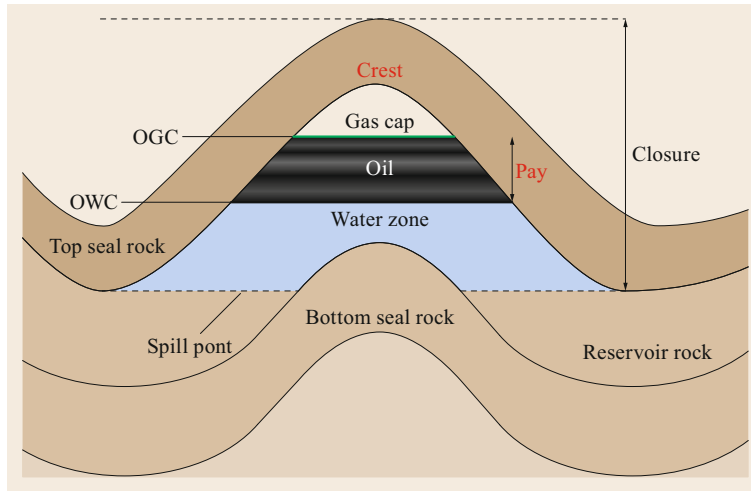


Fig. 9.28 Schematic of a simple anticlinal-type trap showing common trap features

slip faults that form when faulting is accompanied by vertical displacement. Examples of dip-slip faults are normal faults and reverse faults. (b) *Strike-slip faults* form when faulting is accompanied by lateral motion. Examples of strike-slip faults are right lateral and left lateral strike-slip faults. When rocks break without any accompanying displacement of the rock blocks, then fractures and joints form. Fractures are different from joints in that fractures have gaps and joints closed.

Faults can create or prevent leaks from a reservoir depending on whether the rock layers on the other side of the reservoir rock, along the fault, are permeable or not. *Fold-associated traps* are structural traps that form when rocks are compressed and folded. Folds form anticlines and synclines that may be symmetrical, asymmetrical, plunging, or not. Special forms of folds exist; these are domes/basins, diapiric doming, chevron, kinks etc.

Diapirs and *piercement* features deform overlying rocks. The deformation occurs when rocks that are buried underground are pushed toward the surface due to buoyancy, increasing compaction stress, or from rising intrusives. This can happen because rocks like salts and shales can only be compacted to a certain limit beyond which they tend to *flow*, pushing and doming the rocks above them. The upward movement of diapirs may induce fractures and faults to create a variety of traps that are associated with the fault, stratigraphic pinch outs, and doming around the intrusion.

Stratigraphic traps are formed from changes that are caused by sedimentary processes. Primary stratigraphic traps are caused by the depositional processes and the characteristic environment where the sediment is deposited. For example, point bar sands form in meandering river systems, when rivers bend and de-

posit sediments in the inner parts of the curves to create a pinch-out feature, carbonate reefs form in shallow clean seas or ocean water which are rich in ions and have high light levels. Primary stratigraphic traps can also be associated with unconformities. For example, channel fill sands form traps associated with unconformities in an ancient buried river channel. Secondary stratigraphic traps can form from diagenetic processes that occur after the rock has been formed (post-depositional alteration of the rock layer). Examples of diagenetic processes include cementation, dissolution and dolomitization.

Combination traps are traps that are formed from a combination of structural and stratigraphic traps. For example, angular unconformity traps develop when tilted or folded sedimentary layers are overlain by horizontal layers of rocks, to create a trap.

Hydrodynamic traps are traps that are modified and influenced by flowing water. These can also be considered combination traps because they are typically associated with a structure containing petroleum underneath which water flows. The movement of water modifies the shape and position of the oil accumulation and can also trap oil in a location where it would otherwise not accumulate. If oil and gas are present in the reservoir, the gas which is less dense (lighter) will be displaced ahead of oil and the overall fluid distribution in the reservoir will somewhat deviate from the conventional manner.

Petroleum trap assessment and evaluation is of prime importance in petroleum exploration. They help geologists and engineers to assess petroleum traps in order to evaluate their potential and their limitations. Assessing a trap from a three-dimensional perspective is essential for reservoir characterization. *Map or bird's eye views* provide additional information about

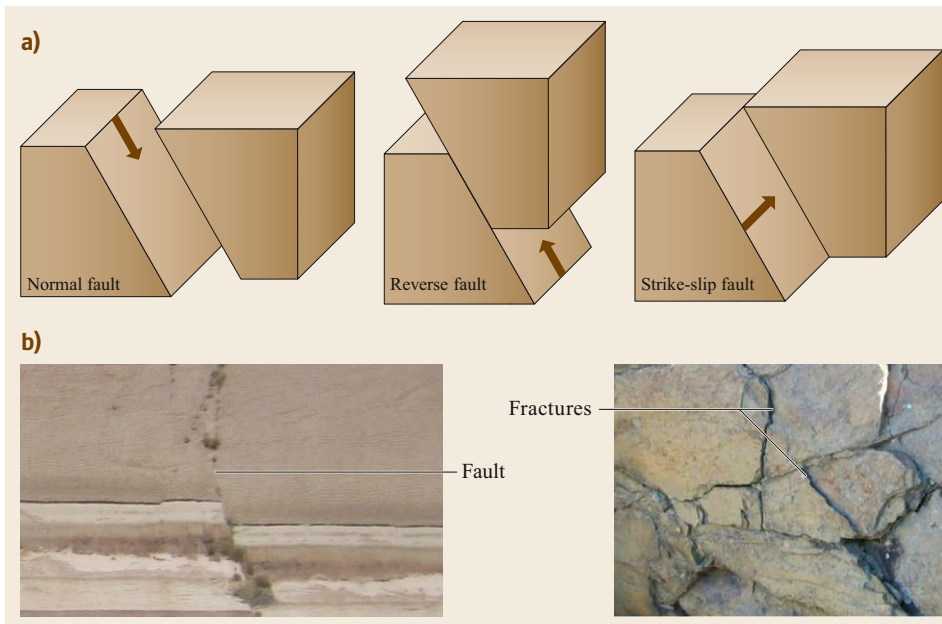


Fig. 9.29a,b
Faults and fractures: (a) types of faults (b) images of a normal fault and fractures in rock sample

areal extent and coverage of the reservoir within the trap. *Cross sections or vertical views* provide information about depth and thickness of a reservoir unit. Both views are essential in reservoir characterization and volumetric calculations for reserve estimation. During trap evaluation for reserve potential, it is important to keep in mind that traps can also have limitations. Sometimes very geometrically viable traps have no productive zones (i.e., the traps formed outside of the *critical moment*). The trap may contain multiple impermeable layers interbedded in the reservoir unit or very thin reservoir beds nested in impermeable units, or the trap could have some poorly productive transition zones and leak points caused by porous beds, faults, or diagenetic changes.

Overburden and underburden rock layers stacked above and below the trapped reservoir rock reinforce the seals and cap rock layers, and by virtue of their thickness provide increased temperature and pressure on the reservoir units. The ideal arrangement of a petroleum trap, reservoir rock, seal, cap rocks, and overburden rocks, together with source rocks generation, maturation, and migration pathways of petroleum, as well as the time that it takes for these processes to occur, constitute the elements of a *petroleum system*. Magoon and Dow [9.13] define the petroleum system as a *dynamic petroleum generating and concentrating system functioning in a geologic space and time*. A petroleum system is therefore critical for the creation of economic accumulations of oil and gas.



Fig. 9.30 Folded bed unit in the Ouachita outcrop in south central USA

9.4.3 Elements of Plate Tectonics and Petroleum Deposits

Plate tectonics is a theory that explains why fragments of Earth's outer solid layer (lithosphere) are in constant motion relative to one another. These motions are very slow and almost imperceptible. In plate tectonics, the lithosphere of the Earth is subdivided into a number of relatively thin and rigid fragments called *tectonic plates* that move very slowly relative to one another. The main processes that cause the motion of Earth's lithospheric plates are *seafloor spreading* and *subduction*. Seafloor spreading and subduction are caused by the movement of molten material in the mantle of the

Earth. The theory of plate tectonics began around 1912 when the German scientist, Alfred Wegener, hypothesized that approximately 200 million years ago, all the continents on Earth were joined together into one supercontinent called *Pangaea* (meaning *All Lands*) and over time the continents have drifted apart . . . and continue to do so today. This was called the *continental drift hypothesis*. Wegener pointed to several clues as evidence:

1. Some continents (e.g., the western portion of Africa and eastern portion of Latin America) appeared to fit like pieces from a puzzle.
2. The same type of fossils of land organisms have been found on different continents separated today by large oceans.
3. Similar rock types and structural features have been found on continents across opposite sides of the Atlantic Ocean. For example in the western edge of Africa and the eastern part of North America.
4. Paleoclimate evidence that shows that in present day tropical and subtropical parts of Africa, glaciers were present in the geologic past, indicating that continents were not always at their present location.

However, there were objections to Wegener's hypothesis because he could not provide evidence of a mechanism that caused these motions. Years later, evidence to support Wegener hypothesis was established when *seafloor spreading* was proposed and *paleomagnetism* was observed. Paleomagnetism is based on observations that:

- Earth's magnetic field is imparted onto iron-bearing minerals present in magma (e.g., magnetite) when it cools below a certain critical temperature known as the *Curie point temperature*.
- Earth's magnetic pole periodically reverses of over time. The reversal of Earth's magnetic field is called *magnetic reversal*.
- *Polar wandering* where Earth's magnetic pole appears to have shifted (wandered) over the past 500 million years.

In the 1960s, a US navy officer and geologist (Harry Hess) and others proposed and explained the concept of seafloor spreading that validated Alfred Wegener's continental drift hypothesis, and thus establishing plate tectonics theory. Seafloor spreading explains the spreading of Earth's crust at ocean ridges, where new crust is created as basaltic magma erupts out of Earth's interior. The seafloor spreads along relatively long narrow stretches called rift zones located in the middle part of the oceans where magma rises to the ocean floor cre-

ating elevated ridges. The spreading of the sea floor creates new crust on either sides of the spreading centers (rift zone). The continual spreading of sea floor is balanced by the destruction of lithospheric material at the other edge of these plates known as *subduction zones*, where older, colder, and denser lithospheric rocks collide with another plate, descend and melt in to Earth's mantle. The edges of tectonic plates, where subduction or spreading occur, form the plate boundaries. There are three types of plate boundaries that can exist between two different tectonic plates. *Divergent plate boundaries* form at constructive margins where new crust is being formed. *Convergent plate boundaries* form at destructive margins where the crust is damaged and *transform plate boundaries* form at strike-slip fault zones where no crust is formed or destroyed.

The movement of plates causes collisions, spreading, and deformations, which are responsible for major topographic features on Earth; like mountains, valleys, and ocean floor. Petroleum mostly formed in sedimentary depressions that contained water bodies some of which have disappeared today, and/or as in the case of present day oceans and seas where sediments continue to be deposited.

There are three major parts of the ocean environment:

1. Continental margins
2. Abyssal plain (deep-ocean basins)
3. Oceanic ridges.

Here is a brief description of these ocean environments and how they relate to petroleum. The oceanic ridges are the longest topographic features on Earth's surface. They extend over 70 000 km (43 000 mi) in length and cover about 20% of Earth's surface. They are relatively elevated deep ocean features with many faults, earthquakes and volcanic activities. Ocean ridges are present in all the major oceans of the world and have widths of 1000–4000 km. These oceanic ridges are not conducive to the formation, generation, or accumulation of petroleum, because of the depth and extremely high temperatures and associated volcanic activities. Abyssal plain and deep-ocean basins have been described as the most level places on Earth, with thick accumulations of sediments that were deposited into the basin over millions of years. They are also found in all oceans around the world. In portions of the deep-ocean basins that are close to the oceanic ridges, it is not uncommon to find isolated volcanic peaks that may emerge as an island above the ocean water surface to form volcanic island or stay below the water surface to form flat-topped seamounts called guyots. In addition, if large vast basaltic lavas oc-

cur on the ocean floor, they create extensive volcanic structures called oceanic plateaus. Due to the high temperatures and molten rock associated with volcanic activities these structures by themselves are not likely to host petroleum. In addition, due to the depth, and location of the deep-ocean basins (which are far from productivity sites for petroleum source material), little interest has been associated with these deep-ocean basins in the exploration for petroleum despite the massive amounts of sediments and associated sedimentary rocks.

The parts of the ocean closest to the continental land masses are known as the *continental margins*, and they separate the continents from the oceans. There are two types of continental margins: the active continental margins and the passive continental margins. The nature of the continental margins is closely dependent on whether tectonic activity is occurring at the margin. *Active continental margins* are mostly located around the Pacific Ocean. Parts of the active margin are the continental slope, deep-ocean trenches, and accretionary wedges. The *continental slope* is the dipping part that descends abruptly from continents into the deeper part of the ocean basin, including the oceanic trenches. The *deep-ocean trench* is a relatively long and narrow V-shaped depressions at subduction zones where plate boundaries occur. Trenches are currently known to be the deepest parts of the ocean. Most of the deep-ocean trenches in the world are located around the Pacific Ocean. The deep-ocean trenches contain accumulations of deformed sediments, fragments and scraps of ocean crust, scraped off of plates during subduction and known as accretionary wedges. It is not yet clear at this time if exploitable economic accumulations of HCs abound in deposits of the accretionary wedges. *Passive continental margins* are not directly associated with tectonic plate boundaries. A passive continental margin is made up of three parts that progress from the coastal environments into the deep ocean. The first part of the passive margin closest to land is the *continental shelf*, a more or less broad gently sloping, flooded extension of the continent that typically contains some of the largest deposits of clastic sediments, large accumulations of petroleum and important mineral deposits. The shelf steepens into the continental slope. The continental slope is a relatively steep surface found at the open sea/ocean edge of the continental shelf and can also contain important accumulations of sediments and HCs. The slope gently levels out onto the abyssal plain. The continental rise stretches into the abyssal plain. The continental rise contains thick accumulation of sediment made up of various types of deposits, including turbidity current deposits, slump deposits, and deep-sea fans. Passive continental mar-

gins are mostly associated with the Atlantic Ocean. There are no deep-ocean trenches in the passive ocean margins. Many petroleum accumulations around the world are found in passive margin basins, for example, there are large accumulations in the Atlantic Gulf coast of the United States, the Atlantic Coast of Brazil, Venezuela, and the Niger Delta region of west and southern Africa.

Tectonism and Rock Deformation

The relative motion of tectonic plates causes stresses that creates deformation to form sedimentary basins in which sediments can accumulate, if sediment sources are present. *Rock deformation* refers to all changes that affect the original form, shape, or size of a rock body after it formed. Deformations mostly occur along tectonic plate margins and are affected by temperature, pressure, rock type, and time. There are mainly two types of deformation that affect a rock body: *folding* (bending) or *faulting* (breaking). *Folds* are the result of bending rocks (without completely breaking) into wavy structures. Folds form when compressional stresses (pressure) are applied to rocks. Compression causes the rocks to be shortened and thickened forming arched or upfolded rocks called *antiform* and hollow or downfolded rock layers called *synforms*. Folds can be symmetrical or asymmetrical. Special types of folds are *domes* – circular, or slightly elongated, upward displacement of rocks with the oldest rocks in center of the fold, and *basins* – circular or slightly elongated downward displacement of rocks with the youngest rocks in the center of the fold. Faults form when rocks break under stress and are displaced. Two groups of faults can be described: dip-slip faults and strike-slip faults (Sect. 9.4.2).

Dip-slip faults are faults that show the vertical movement due to either compressional stress (reverse faults and thrust faults) or extensional stress (normal faults) resulting in movement along the inclination (dip) of the fault plane. The two main parts of the dip-slip fault on either side of the fault plane are known as the *hanging wall* – the rock above the fault surface and the *footwall* – the rock below the fault surface. In the normal fault, the hanging wall block moves downward. They are created by tensional forces or extensional stress regimes. The other types of dip-slip faults are reverse and thrust faults, where the hanging wall block moves upward. These are caused by strong compressional stresses. Reverse faults are high angled with dips greater than 45° and thrust faults are low angle faults with dips less than 45°.

Strike-slip (transform) fault are vertical or nearly vertical faults with dominant horizontal motion. Strike-slip faults are formed by shear stress. Transform faults

are large strike-slip faults that cut through the lithosphere and are often associated with plate boundaries. Two types of strike-slip faults are right-lateral strike slip and left-lateral strike-slip faults.

Tectonic Uplift and Reburial of Sediments and Rocks

Diagenetic processes are the primary processes responsible for the formation of sedimentary rocks that host oil and gas deposits. Subsequent uplift and reburial of these rocks and/or sediments can further transform and alter the rocks, obliterating the organic matter that is trapped in them, or they can create structures and cause the right temperature and pressure conditions, for the generation and accumulation of petroleum.

Plate tectonics has a big influence on the areas where oil and gas reservoirs are located around the globe. It also provides the logical explanation as to how present day arid and sometimes desolate environments came to host large accumulations of petroleum. For example, it can explain the presence of petroleum in present day glacial environments. The simple explanation is that these areas, which were underwater millions of years ago, were later uplifted and deformed by tectonic forces or moved to their present position.

Not all accumulations of petroleum are found in desert or arctic environments. Petroleum accumulations are also found in ancient rivers, lakes, coastal, and present day offshore environments. This is because several mechanisms are involved in the formation of sedimentary basins and the rocks in which petroleum forms or accumulates. For example, a basin can be formed by *crustal thinning*, which occurs when magma from deep within the Earth heats up the crust, causing it to stretch and thin as tectonic plates are pulled apart in a divergent setting, like you would pull a piece of hot plastic. *Lithospheric thickening* happens when molten material rising from the mantle pushes the overlying lithosphere to bulge and dome upward, resulting in depressions on the sides. *Sedimentary or volcanic loading* occurs when overburden sediments or volcanic structures create excessive weight that causes depressions around the sides of the structures. Compressional stresses that occurs at convergent boundaries during subduction can result in the uplift of sedimentary layers previously buried deep underground. Tectonic uplift

creates upfolded and downfolded rocks (anticlines and synclines), and may further overturn and bury these rocks by a process called reburial. The buckling and bending of stressed rocks creates conditions favorable for petroleum accumulation and concentration through folding and faulting. When brittle rocks are subjected to compressional stress, they break and form faults (reverse and thrust faults) that can create excellent conditions for petroleum accumulation and concentration (see the section on petroleum traps). When nonbrittle or ductile rocks are subjected to compressional stress, they too will buckle and create anticlines and synclines. Anticlines have been known to host some of the most prolific petroleum reservoirs in the world. *Tectonic loading* and *subsidence* are additional processes that can create sedimentary basins.

Implications of Plate Tectonics for Petroleum

Sedimentary rocks form in shallow and deep sedimentary environments. Tectonic activities make or break HC traps. Most of the world's major oil fields are found in present day ocean basins or ancient ocean basins. Most basins are created as a result of plate tectonic processes and a good understanding of the processes that create elements of a petroleum system, including plate tectonics, can help us to narrow our exploration focus.

Summary

All elements of the petroleum system are necessary for the accumulation of economic quantities of petroleum to occur. Time is one of the most essential components for the generation and accumulation of petroleum. This is because it takes time to produce sufficient amounts of organic source material, and it takes time to sufficiently bury and transform the organic material to generate petroleum. After generation, more time is required to expulse the petroleum from the source rock and accumulate sufficient amounts in reservoir rocks. Therefore, although the processes that produce, bury, transform organic matter, and generate petroleum are happening in the world today, the time component is not yet sufficient to allow for the accumulation and concentration of economic quantities of petroleum. The right conditions need to all happen at exactly the right times or *critical moment* to create economic traps.

9.5 Finding and Locating Petroleum

The methods and techniques used to search for and find petroleum have changed significantly since the early days of visual identification of seeps. Modern technol-

ogy and sophisticated equipment have revolutionized how we locate subsurface oil reservoirs. This section will summarize some of the methods and techniques

used for petroleum exploration. Methods of exploration can be organized into different categories, but it is important to remember that there is overlap in the use and exploitation of data obtained by any one of these methods during the exploration, extraction, production, and processing of petroleum products. Methods of exploration can be classified according to the techniques employed as follows:

- Geophysical methods
- Geochemical methods
- Geological methods
- Remote sensing/satellite imagery
- Drilling methods.

Most exploration projects start with an idea and prior knowledge that may or may not be exhaustive. Ideas and prior knowledge are typically followed by literature review, reading and some form of data collection.

9.5.1 Geological and Geochemical Methods of Exploration

These methods involve collecting samples, mapping, and analyzing data in/and from the field. They include active field work, sample handling, processing, analysis and interpretation. The goal of geological and geochemical exploration is to identify the types of rocks, minerals, structures, composition, and to identify outcrop analogs for the subsurface. The ultimate objective is to generate subsurface structural maps that show the rock units, how they were arranged when they formed and how they were deformed afterward during faulting or folding and variations in various subsurface geologic properties or characteristics.

Geological field methods and surface mapping involve the following activities:

- Data gathering
- Identifying structures
- Mapping strike and dip
- Identifying minerals and rock type
- Preparing sketches
- Analyzing photographs
- Collecting accurate location data etc.

The subsurface mapping of surfaces and structures is an essential part of geology and has been discussed in several classic publications [9.17–20].

Geochemical methods mostly involve the analysis of rock or fluid samples collected in the field or the interpretation of previously acquired data. The main objectives of geochemical methods are to determine chemical and mineral composition of rocks; identify anomalous (unusually) high or low concentrations of substances in the rocks; analyze composition and prop-

erties of samples to determine the quality and source material; and estimate quantities.

Structural methods determine how geologic units were arranged when they formed and after they were altered or deformed to generate a true representation of the subsurface arrangement and geometry of rocks. Structural methods are important to identify petroleum traps, to define trap geometry, and for reservoir characterization.

9.5.2 Geophysical Methods of Exploration

Geophysical methods of exploration are by far the most popular methods at present. These methods use physical science techniques to collect data from the subsurface. The data is then analyzed, interpreted, and converted into maps and models.

Several geophysical methods exist and can be grouped into two categories: the *noninvasive methods* like gravity and magnetics, and *invasive methods* like seismic and geophysical well logging. *Gravity methods* measure acceleration of Earth's gravity at a given location using an instrument called the gravimeter. The gravity method relates to density differences in rocks and is measured in Gals. *Magnetic methods* measure the strength of Earth's magnetic field in rocks at a location, to determine the magnetic properties of the rocks underground. Specific techniques can be used to determine how easily the rocks can be magnetized. The instrument used in magnetic surveys is the magnetometer and the measurements are expressed in gauss (G), nanotesla (nT) or other units depending on the magnetic property measured. Magnetic methods can be conducted on land, at sea or by air. For petroleum exploration, gravity and magnetic surveys are mostly applied at the early stages of exploration. *Geophysical well logging* is the collection of geophysical data in boreholes and plotting variations of the data with depth. It is used to interpret, qualify, and quantify the value of specific geophysical variables at specific depths. Geophysical well logging is also useful to correlate changes in different parameters at the same depth in a well. Common examples of geophysical logs are:

- Resistivity logs
- Spontaneous potential logs
- Porosity logs
- Nuclear magnetic resonance logs
- Gamma radiation (natural and induced) logs
- Acoustic wave interval transit time logs.

Several authors [9.21–23] have documented the types and applications of geophysical well logs used in exploration. The *seismic method* uses the propagation of natural or artificial seismic (elastic) waves in

the subsurface to measure the properties of rocks and fluids. The information obtained is used to *image* the subsurface. Seismic exploration uses the basic relationship between velocity and travel time to estimate the distance (depth) of subsurface structures and the variety of wave properties to characterize rocks and fluids. In the subsurface environment, the velocity of seismic waves varies with rock type and rock properties. The arrival times of reflected waves are measured at the surface and are used to locate underground structures conducive to oil accumulation, and to collect data for basin analysis, volumetric analysis, structure maps, etc. Over the years seismic exploration has progressed from 1-D to 4-D, time-lapse surveys and other variations.

Petroleum exploration aims to find oil and gas resources in the Earth. Applying the different methods of exploration allows the explorationists to narrow the search from a large to small scale as shown in Fig. 9.31. The ultimate goal is to identify the ideal location where a well can be drilled, in the acquired lease within a prospect in a good play in the sedimentary basin.

9.5.3 Extracting and Producing Petroleum

Drilling

Key components of a drilling rig are shown in Fig. 9.32. To drill a well, a bit is attached to the end of a drill string, which is comprised of sections of steel pipe that are 30 ft (9 m) long. The drill string is lengthened as the well gets deeper by attaching additional sections of pipe to the top. Drill collars are thick-walled sections of drill pipe at the bottom of the drill string; collars apply extra weight to the bit. As the bit crushes through rock, mud is pumped down through the inside of the drill string,

out the bit, and up through the space between the drill string and the well bore. Despite its dirty name, drilling mud is a designed blend of fluids, solids and chemicals. It cools the drill bit and brings rock cuttings back to the surface. The cuttings are removed in shakers, and the fluid goes back to the mud pit, from which it is recycled.

The derrick must be tall enough to accommodate a 90-ft-long *triple* comprised of three sections of pipe. The derrick, pulleys, and hawser must be robust enough to support the lifting and manipulation of the entire drill string. The kelly is the top joint of a drill string. It has flat sides that fit inside a bushing on the rotary table, which turns the drill string and bit. Note that not all drilling rigs use a kelly system.

A surface blowout is a sudden increase in well pressure resulting in loss of containment and uncontrolled flow of oil and gas into the atmosphere. The blowout preventer (BOP) is a safety valve or other device beneath the floor of the drilling rig. When activated, it stops a blowout by sealing off the top of the well.

The density of drilling mud is crucial. If the mud density is too low, a well is susceptible to a surface blowout. If the mud density is too high, it can cause an underground blowout – the rupture of the reservoir underground – pushing drilling mud into another formation. Underground blowouts are the most common of all well control problems. Many surface blowouts begin as underground blowouts. Prompt, correct reaction to an underground event can prevent a dangerous and costly surface blowout [9.22].

Completion

Wells are completed by casing the well bore with steel pipe and cementing the casing into place. Casing pre-

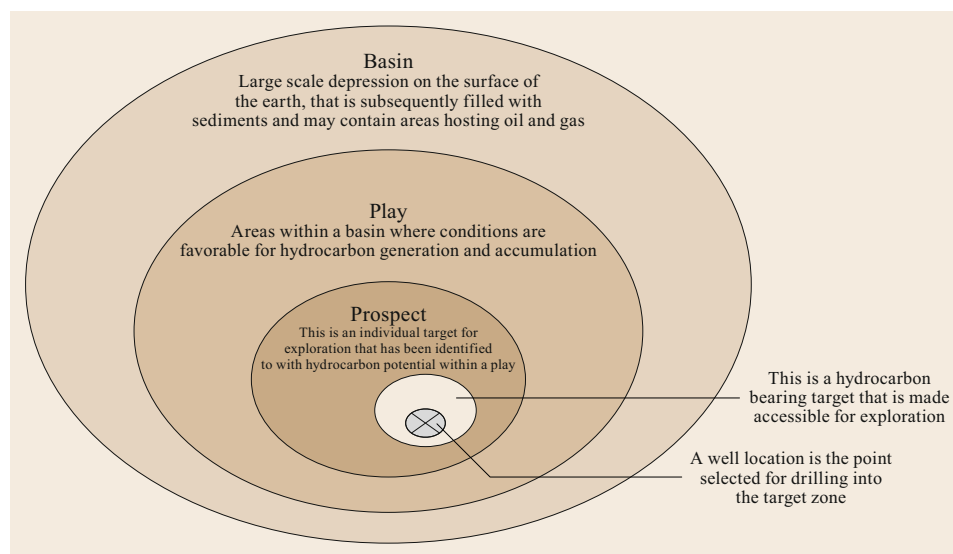


Fig. 9.31 Relationship between the scales of exploration. The basin scale is a largest scale, which progressively narrows to the well location, the smallest scale in this hierarchy

vents the well from collapsing. The outside diameters of casing pipe range from 4.5 to 16 in (114–406 mm). Cementing is a key step. In a good cement job, the entire space between the casing and the well bore is filled with cement. Centralizers keep the casing from resting against the well bore, which could block the flow of cement, resulting in a poor cement job and increasing the risk of a blowout.

After cementing, perforation guns punch small holes through the casing into the reservoir rock, providing a path for the flow of oil and gas into the well. In open-hole completion, the last section of the well is uncased. Instead, the installation of a gravel pack stabilizes the casing and allows fluids to enter the well at the bottom. After perforation, special acid-containing fluids are pumped into the well to increase porosity and stimulate production. Usually, a smaller diameter tube is inserted into the casing above the production zone and packed into place. This provides an additional barrier to HC leaks, raises the velocity at which oil flows under a given pressure, and shields the outer casing from corrosive well fluids.

Drilling and producing a well is the ultimate way to explore for petroleum. But they are the most expensive. If the well is successful, then oil will be produced and additional information is collected and analyzed to maximize oil recovery. If the well is unsuccessful, data

are collected and the well is plugged and abandoned. Unsuccessful wells may have no petroleum present in the reservoir, or contain petroleum but not in economic quantities.

During exploration, several steps lead up to the decision on the exact location where a well will be drilled. Before exploration, funding has to be arranged, and the land or lease has to be acquired. This involves understanding the rules and regulations that apply to each country or state. Contracts, staffing, and pricing, are all important arrangements prior to engaging in the drilling exercise. Once the preliminaries have been taken care of, the drill site is selected and a location picked, based on prior interpretations and studies. A surveyor is called to mark the exact location and collect elevation data. A site map is generated and the area is cleared, leveled where needed, and pits for muds and water are prepared before the drilling rig and equipment are put in place [9.24, 25].

Before modern day rotary drilling rigs, wells were drilled using various techniques including digging using picks, spades, shovels, etc., punching holes in the ground using large chisel-shaped devices, or with heavy duty ground-moving equipment, as in the strip mining of oil sands. Cable tool drilling is still used in specialized situations today, and rotary drilling is the most used drilling technique today.

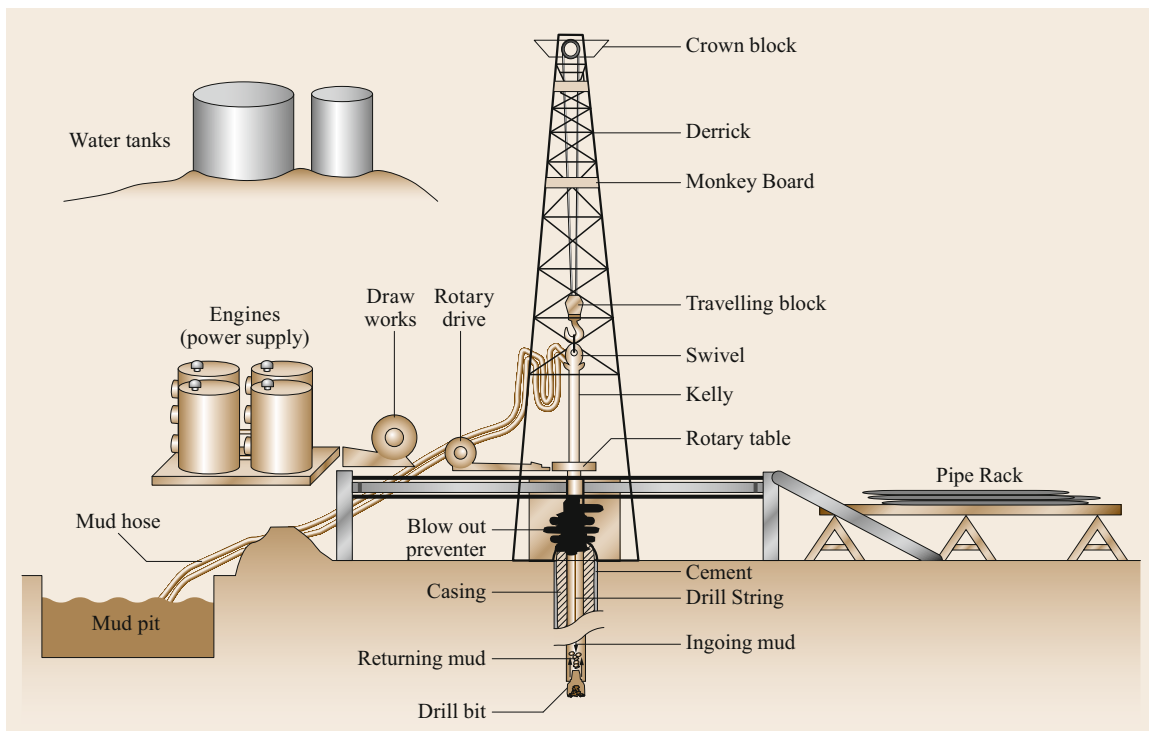


Fig. 9.32 Components of a typical drilling operation

The three ways of drilling wells are vertical drilling, deviated drilling, and horizontal drilling. During drilling, well completion begins and continues to the end of the project. The basic elements of well completion are casing and tubing, well head infrastructure, lifting, and well stimulation and/or treatment. Well casings are heavy metal pipes used to maintain the integrity of the hole and add strength to the sides of the hole, prevents seeps into and out of the hole, control and prevent blowouts, and isolate the hole from the groundwater system. The type of casing used depends on subsurface conditions. When drilling is complete and the well is declared successful, then completion in a stricter sense is carried out.

Completion is the process of finishing a well so that it is ready to produce petroleum. Several different types of completion techniques exist. They depend on whether or not casings are used in the producing zone, how the casings are made, and how many producing intervals are under consideration. Wells that are completed with no casing are open-hole completion wells and those that have casing are cased-hole completion wells. Several different types of completion techniques exist but the common method is the conventional perforated completion. The use of any completion method depends on the characteristics of the formations along the borehole, and the location and number of producible zones in the well. The last step of well completion is to install the well head which comprises the casing head, tubing head that is attached to the casing and production tubing, and the Christmas tree or lifting device if the well needs lifting.

9.6 Future for Petroleum

Quantifying HC reserves is a complex process that requires the use of approximations, extrapolations, and probabilistic analysis to various extents. It is also true that sociopolitical and economic considerations directly or indirectly filter into estimates of petroleum reserves. Results can depend on who does the calculations and why they do it.

The amount of petroleum still available on Earth is debatable. Most of the world's sedimentary basins have been identified, and estimates of reserves in these basins have been assessed. Large amounts of petroleum have already been produced from easily accessible reservoirs. The United States Geological Survey (USGS) [9.26] and other organizations and institutions like the International Energy Agency [9.27] provide assessments of the world petroleum resources.

Lifting Stimulation and Treatment

Lifting is the process of mechanically pumping or sucking oil or gas out of the well using artificial equipment. Different lifting techniques are used depending on the properties in the reservoir. Such techniques may include sucker rod pumps, hydraulic pumps, and fluid injections etc. In some cases, before installing the lifting equipment wells may need treatment or stimulation. Well *stimulation* is an artificial or engineered method that is used to increase the flow of fluids (permeability) in reservoirs drilled for oil. Some methods of stimulating a well include fracturing, acidizing, and an old technique called shooting. Well *treatment* involves adding chemical substances to reservoirs to increase the recovery of oil and minimize water. An example of a well treatment is the polymer treatment.

Before, during, and after production, wells can be tested and surveyed for different characteristics. Most formation tests are designed to provide information about fluid flow, pressure, oil-to-gas ratios, etc. For example, a drill stem test provides information about pressure conditions in a producing reservoir. Oil produced from successful wells is pumped into storage tanks or other holding facilities from which it is transported to refineries. Moving oil from the well head involves a network of flow lines, pipelines, trucks, and rail. Raw oil is first separated in the field in a separator tank in which the fluids are allowed to separate naturally by gravity. Water and heavy particulates sink to the bottom, oil floats on the water and gas is at the top. The oil is piped out and held in storage tanks for commercialization.

In the last couple of decades, the price of a barrel of crude oil has generally increased, making previously noneconomical petroleum resources like oil shale into valuable reserves. The continuing increase in petroleum reserves can be attributed to the improved exploration skills and technological development in computation, extraction and mapping.

It is undeniable that petroleum and its derivatives provide some of the greatest benefits in quality of life in society today. However, it is fully accepted that the problems associated with production, processing, distribution, and use of petroleum are unquestionable. Consumption of petroleum products continues to increase and it is debated whether this consumption is too much, too fast, and sustainable. Most scientists agree that petroleum is a finite, nonrenewable resource, but that it may continue to be available for several gener-

ations. The urgent question today is whether we have reached peak oil production. Although there is no con-

sensus on peak oil, the only certainty is that we will eventually reach peak oil if it is not yet the case.

References

- 9.1 E.W. Owen: *Trek of the Oil Finders: A History of Exploration for Petroleum*, AAPG Memoir 6 (American Association Petroleum Geologists, Tulsa 1975) p. 1647
- 9.2 R.C. Selley: *Elements of Petroleum Geology*, 2nd edn. (Academic, London 1998) p. 470
- 9.3 J.T. Henry: *The Early and Later History of Petroleum* (Rodgers, Philadelphia 1873)
- 9.4 L. Maugeri: *The Age of Oil: The Mythology, History, and Future of the World's Most Controversial Resource* (Globe Pequot, Guilford 2006)
- 9.5 I.M. Tarbell: *The History of the Standard Oil Company* (Cosimo, New York 2009) p. 462
- 9.6 J.L. Collier: *Electricity and the Light Bulb* (Marshall Cavendish, Tarrytown 2006) p. 112
- 9.7 G. De Holden-Stone: *The Automobile Industry* (Methuen, London 1904) p. 223
- 9.8 M. Burgan: *The Automobile* (Gareth Stevens, Milwaukee 2005) p. 48
- 9.9 A. Sampson: *The Seven Sisters: The Great Oil Companies and The World They Shaped* (Bantam Books, New York 1975)
- 9.10 <http://www.bp.com/>
- 9.11 U.S. EIA (Energy Information Administration): Short-Term Energy Outlook. http://www.eia.gov/forecasts/steo/pdf/steo_text.pdf (Washington 2017)
- 9.12 A.I. Levorsen: *Geology of Petroleum* (Vol. 8), ed. by F.A.F. Berry (WH Freeman, San Francisco 1967)
- 9.13 L.B. Magoon, W.G. Dow: *The Petroleum System – From Source to Trap*, AAPG Memoir 60 (American Association of Petroleum Geology, Tulsa 1994) pp. 3–24
- 9.14 R.C. Selley: *Elements of Petroleum Geology* (Academic, San Diego 1998)
- 9.15 E.J. Tarbuck, F.K. Lutgens, D. Tasa, R. Josephs: *Earth: An Introduction to Physical Geology* (Pearson/Prentice Hall, Upper Saddle River 2005)
- 9.16 F.K. Lutgens, E.J. Tarbuck, D. Tasa: *Essentials of Geology* (Pearson/Prentice Hall, Upper Saddle River 2009) p. 554
- 9.17 S. Boggs: *Principles of Sedimentology and Stratigraphy*, 4th edn. (Prentice Hall, Upper Saddle River 2006) p. 662
- 9.18 D.M. Ragan, Ragan: *Structural Geology – An Introduction to Geometrical Techniques*, 3rd edn. (Wiley, New York 1985)
- 9.19 J. Evenick: *Introduction to Well Logs and Subsurface Maps* (PennWell Books, Tulsa 2008) p. 236
- 9.20 J.W. Barnes, R.J. Lisle: *Basic Geological Mapping*, 4th edn. (John Wiley, Sussex 2004)
- 9.21 D.J. Tearpock, R.E. Bischke: *Applied Subsurface Geological Mapping with Structural Methods* (Prentice Hall, Upper Saddle River 2002)
- 9.22 G.B. Asquith, D. Krygowski, C.R. Gibson: *Basic Well Log Analysis: Methods in Exploration*, Vol. 16, 2nd edn. (American Association of Petroleum Geologists, Tulsa 2004)
- 9.23 D.V. Ellis, J.M. Singer: *Well Logging for Earth Scientists*, 2nd edn. (Springer, Dordrecht 2007)
- 9.24 M. Kobr, S. Mareš, F. Paillet: Geophysical well logging. In: *Hydrogeophysics*, ed. by Y. Rubin, S. Hubbard (Springer, Dordrecht 2005) pp. 291–331
- 9.25 N.J. Hyne: *Nontechnical Guide to Petroleum Geology, Exploration, Drilling, and Production*, 3rd edn. (PennWell Books, Tulsa 2012)
- 9.26 United States Geological Survey (USGS): <http://energy.usgs.gov/OilGas/AssessmentsData/WorldPetroleumAssessment.aspx>
- 9.27 International Energy Agency: <http://www.iea.org/>

Origin of Petroleum

10. Origin of Petroleum

Clifford C. Walters

Theories concerning the origin of oil on Earth fall into two camps: *biogenic*, where oil is generated by the thermal conversion of sedimentary organic matter derived from living organisms, and *abiogenic*, where oil is formed from mineral catalyzed reactions of nonbiological carbon deep within the Earth. Most geochemists believe that there are multiple and overwhelming lines of evidence supporting biogenic origins for petroleum. While there are known occurrences of abiogenic methane generated by geologic processes, these contribute little to petroleum resources. Economic reserves require all specific elements and processes occur within a sedimentary basin. The *Petroleum System* must contain: (1) at least one formation of organic-rich sediments (source rock) that has been buried to a sufficient depth by overburden rock such that petroleum is generated and expelled, (2) pathways (permeable strata and faults) that allow the petroleum to migrate, (3) reservoir rocks with sufficient porosity and permeability to accumulate economically significant quantities of petroleum, and (4) seal rock (low permeability) and structures that retain migrated petroleum within the reservoir rock. In the case of many unconventional resources, the source rock itself serves as source, reservoir, and seal.

Petroleum, composed of hydrocarbons and heteroatomic molecules, is the most complex mixture occurring in nature. The composition of petroleum generated within its source rock is influenced by the type of organisms that contributed organic matter, the environment of deposition, and thermal exposure. Most of the deposited biomolecules are chemically altered, broken apart,

10.1	Historic Overview	360
10.2	The Petroleum System	361
10.3	Deposition of Organic-Rich Sedimentary Rocks	362
10.4	Kerogen Formation and the Generative Potential of Source Rocks	365
10.5	Generation and Expulsion of Oil and Gas	369
10.6	Composition of Produced Petroleum ..	371
10.7	Unconventional Resources	374
10.8	Summary	375
	References	375

and reassembled into an insoluble carbonaceous material termed *kerogen*. Upon burial and heating, the kerogen reacts producing mostly compounds that have lost their biochemical signature; however, some of these generated molecules, termed *biomarkers*, preserve enough of their chemical structure that their original biological precursor can be identified. Expulsion from the source rock chemically fractionates the generated petroleum, with the expelled product enriched in gases and hydrocarbons, and retained bitumen enriched in heteroatomic polar species and asphaltenes. Petroleum composition can be further altered as it migrates and resides in reservoir rocks by physical, chemical, and biological processes. Collectively, these processes result in petroleum accumulations with a diverse range of compositions and physical properties.

10.1 Historic Overview

Man has used petroleum since Biblical time as a fuel, sealant, adhesive, construction material, or in medicinal and military purposes [10.1]. The earliest documented use of the term *petroleum*, derived from Latin *petra*+*oleum* or *rock-oil*, is by Constantinus Africanus (c. 1020–1087) [10.2]. Classical literature, however, is devoid of insight on the origin of oil and bitumen. Two theories on petroleum emerged during the Renaissance. In his 1546 text *De Natura eorum quae Effluunt ex Terra*, Georgius Agricola, a German physician, expanded on the Aristolian concept of exhalations from deep within the Earth [10.3] and proposed that bitumen, like other minerals, condensed from sulfur. Andreas Libavius, another German physician, theorized in his 1597 text *Alchemia* that bitumen formed from the resins of ancient trees. These early discussions mark the beginnings of one of the longest running scientific debates: whether petroleum is formed by abiogenic processes that occur deep within the Earth, or from sedimentary organic matter that was once living organisms.

As fossil evidence emerged during the eighteenth century that coals were derived from plant remains, many scientists proposed similar origins to explain petroleum. The historic record is somewhat questionable, but Mikhailo Lomonosov is credited by some to have proposed the theory that liquid oil and solid bitumen originate from coal through underground heat and pressure as early as 1757 [10.4] and certainly by 1763 [10.5]. Various biogenic theories emerged during the early nineteenth century suggesting that petroleum was derived directly from biological remains or through a distillation process [10.6].

Modern theories that petroleum originated from ancient sedimentary, organic-rich rocks emerged during the nineteenth century. T.S. Hunt of the Canadian Geological Survey concluded in 1863 that the organic matter in some North American Paleozoic rocks must be derived from marine vegetation or marine animals, and that the transformation of this organic matter to bitumen must be similar to the processes involved in coal formation [10.7]. *Leo Lesquereux*, the American father of paleobotany, reached similar conclusions after studying Devonian shales in Pennsylvania [10.8], as did *Newberry* in his study of Devonian shales in Ohio [10.9]. Early twentieth century field [10.10] and chemical [10.11] studies of the Monterey Formation by the US Geological Survey provided convincing evidence that oil was derived from diatoms in the organic-rich shales. Similar studies of organic-rich shales conducted in Europe during this time arrived at the same conclusion for the origin of associated oil [10.12, 13].

Full ascendancy of the biogenic hypothesis began in the mid-twentieth century with a convergence of scientific advances in paleontology, geology, and chemistry. In 1936, *Alfred Treibs* established a link between chlorophyll in living organisms and porphyrins in petroleum [10.14]. Additional geochemical evidence followed with the discoveries that low to moderate maturity oils still retained hydrocarbon fractions with optical activity [10.15], that the stable isotopes of carbon of petroleum bear a biological fractionation [10.16], and that oils contain in addition to porphyrins, a host of hydrocarbons that can be traced back to specific biological precursors [10.17]. Concurrent with these findings were field studies recognizing that organic-rich strata occur in all petroliferous sedimentary basins, that this sedimentary organic matter (kerogen) is derived from biota, that it has been chemically altered from its initial state [10.18, 19] and, that oil and gas is produced from kerogen as the sediments are buried and heated [10.20].

Although there is overwhelming evidence for a biogenic origin [10.21, 22], some still advocate abiotic theories. The development of the modern abiogenic concept is rooted in the mid-nineteenth century. The prolific French chemist *Marcelin-Pierre Berthelot* described in 1860 experiments where *n*-alkanes formed during the acid dissolution of steel [10.23]. *Dmitri Mendeleev* reasoned in 1877 that surface waters could percolate deep within the Earth, react with metallic carbides forming acetylene that could then condense further into larger hydrocarbons [10.24]. *Mendeleev's* abiotic theory, further refined in 1902 [10.25], was viewed initially as particularly attractive as it offered an explanation for the growing awareness of the widespread occurrence of petroleum deposits that suggested some sort of deep, global process.

Advocates of an abiotic origin for petroleum dwindled under the mounting evidence for a biogenic origin of petroleum. By the 1960s, there was little support for an abiotic origin, except among a small group within the Former Soviet Union. First proposed in 1951 by *Nikolai Kudryavtsev* [10.26] and advanced over the years in numerous Soviet publications, a modernized version of *Mendeleev's* hypothesis emerged. This theory relies on a thermodynamic argument, which states that hydrocarbons greater than methane cannot form spontaneously except at the high temperatures and pressures at the lowermost crustal depths. The theory ignores the fact that all of life relies on being in thermodynamic disequilibrium with its environment.

In the West, astronomers have been the most vocal advocates for abiotic petroleum. Carbonaceous chon-

drites and other planetary bodies, such as asteroids, comets, and the moons and atmospheres of the Jovian planets, certainly contain hydrocarbons and other organic compounds that were generated by abiotic processes [10.27]. *Sir Fredrick Hoyle* reasoned in 1955 that as the Earth was formed from similar materials, there should be vast amounts of abiogenic oil [10.28]. In more recent years, *Thomas Gold* was the strongest promoter for abiogenic petroleum [10.29, 30]. Against the advice of nearly all geochemists and petroleum geologists, Gold convinced the Swedish government to drill two deep wells (Gravberg 1 in 1986–1990 and Stenberg 1 in 1991–1992) into fractured granite under the Siljan ring, the site of an ancient meteorite crater. The wells failed to find economic reserves and evidence for

even trace amounts of abiogenic hydrocarbons is controversial [10.31].

Geochemists favoring biogenic origins for petroleum do not deny the existence of abiogenic hydrocarbons on the Earth [10.32]. Small amounts of abiogenic hydrocarbon gases are known to be generated by rock–water interactions involving serpentinization of ultramafic rocks [10.33, 34], the thermal decomposition of siderite in the presence of water [10.35], and during magma cooling as a result of Fischer–Tropsch-type reactions [10.36, 37]. However, the contribution of abiogenic hydrocarbons to the global crustal carbon budget is considered to be inconsequential [10.38]. The theory that abiogenic liquid hydrocarbon accumulations exist on Earth is considered to be invalid by most [10.39].

10.2 The Petroleum System

The accumulation of economic volumes of petroleum (oil and/or gas) in the subsurface requires that several essential geological elements and processes be present at specific time and space [10.40, 41]. *Source rocks* generate and expel petroleum when sufficient thermal energy is imparted to the sedimentary organic matter (kerogen) to break chemical bonds. This heating is usually induced by burial by *overburden rock*. Once expelled, petroleum migrates either along faults or highly permeable strata. Accumulations form only when high porosity strata (*reservoir rocks*) are charged by migrating petroleum that is prevented from further migration. These petroleum *traps* form when geologic movements result in subsurface topographies (structural) or changes in lithology (stratigraphic) block migration and when the reservoir rocks are covered by

low permeability strata (*seal rocks*). The mere presence of these geologic elements is insufficient to form petroleum reserves. Traps must be available at the time of oil expulsion and, once charged, their integrity must be preserved until exploited. These elements and processes constitute the *petroleum system* (Fig. 10.1).

As shown in Fig. 10.1, all petroleum systems contain:

1. At least one formation of organic-rich sediments that has been buried to a sufficient depth by overburden rock such that petroleum is generated and expelled.
2. Pathways (permeable strata and faults) that allow the petroleum to migrate.

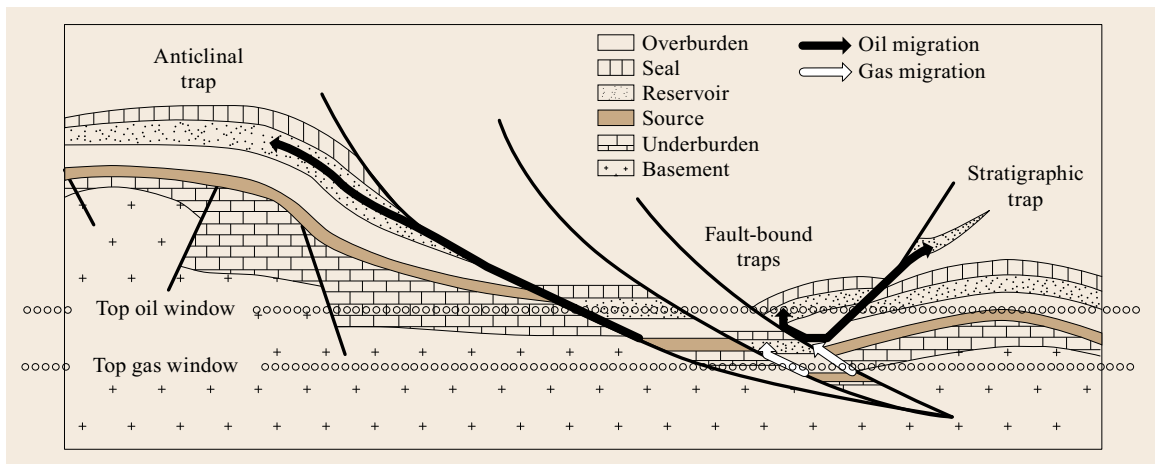


Fig. 10.1 Elements of a petroleum system

3. Reservoir rocks with sufficient porosity and permeability to accumulate economically significant quantities of petroleum and
4. Seal rock (low permeability) and structures that retain migrated petroleum within the reservoir rock.

The top and bottom of the oil window is approximated as a function of burial depth. In actual basins, these depths are not uniform and vary as a function of organic matter type, regional heat flow from basement, in thermal conductivity of the different lithologies, and burial history (e.g., deposition rates, uplift, erosion, and hiatus events).

A rigorous discussion of the origin of petroleum should encompass all of the interrelated elements of

the petroleum system. Such a discourse is beyond the scope of this review, which will focus only on the deposition of organic-rich strata and the generation of petroleum from these sources. The reader is referred to *Exploring for Oil and Gas Traps*, a publication of the American Association of Petroleum Geologists, for a complete discussion of all aspects involved with defining the petroleum system for effective exploration [10.42]. Books by *Tissot and Welte* [10.43] and *Hunt* [10.44] provide detailed discussions of the principles of petroleum geochemistry, and a publication by *Peters and Fowler* [10.45] is an excellent review of the application of modern geochemical techniques to exploration and production practices.

10.3 Deposition of Organic-Rich Sedimentary Rocks

Petroleum *source rocks* are water-deposited sedimentary rocks that contain sufficient amounts of organic matter to generate oil and/or gas when heated. The generated petroleum may be retained or expelled within the source rock matrix. Such organic-rich strata were deposited throughout Earth's history, in nearly all geologic environments, and in most sedimentary basins. Source rocks, however, typically represent only a minor amount of basinal strata and are formed only when specific conditions exist.

Three general factors control the deposition of organic-rich sediments: productivity, dilution, and preservation (Fig. 10.2) [10.46–48]. Biological productivity determines the amount of organic matter that is contributed to sediments. Dilution refers to the amount of inorganic minerals that mixes with the organic matter. Once deposited, the organic matter must be preserved in a form that may later generate petroleum. There was once an active debate as to which factor was the most important in forming organic-rich sediments [10.49]. It is now recognized that these three factors are interrelated in a highly complex, and variable manner.

Photosynthetic organisms, which include aerobic cyanobacteria, algae, phytoplankton, land plants, and some anaerobic bacteria, provide most of the initial organic matter by fixing CO₂ into biomass. The contribution of organic matter by nonphotosynthetic chemotrophs is minor, except in some unusual environments, such as the deep-sea hydrothermal vents. Most of the nonphotosynthetic biosystems, such as methanotropic communities [10.50], rely on recycled carbon that was fixed originally by photosynthetic organisms. Many factors moderate the biota and the primary pro-

ductivity (e.g., such as nutrient input from rivers and coastal upwellings, pCO₂, temperature, and turbidity) that are influenced by global climatic and tectonic conditions. Figure 10.3 shows generalized redox cycle for organic carbon.

Production of new organic matter by the photosynthetic fixation of CO₂ (primary productivity) can occur with (aerobic) or without oxygen (anaerobic) as a byproduct. Respiration and other processes result in the nearly complete oxidation of organic matter back to CO₂. A small amount of the organic matter in sediments escapes biological recycling and is preserved in rocks. Eventually, this carbon is recycled to the surface as CO₂ by geologic processes, such as subduction and venting, erosion and weathering, and more recently, by the combustion of fossil fuels.

Much of the primary organic matter created by photosynthetic or chemosynthetic autotrophs undergoes degradation by other organisms during the secondary production of organic matter. Heterotrophic organisms in the water column, sediments, and rock continually degrade and rework primary aquatic and terrigenous organic matter (Fig. 10.3). Aerobic respiration is very rapid and efficient and primary organic matter may pass through a chain of water and mud dwelling animals, protozoa, and bacteria, until fully consumed and returned to the atmosphere/hydrosphere as CO₂. Anaerobic microbes also degrade organic matter either by fermentation or respiration using terminal electron acceptors other than O₂ (e.g., nitrate, sulfate, iron). These microbial metabolisms are generally slower and may be curtailed by limited nutrients and electron acceptors within the sediment porewaters. Consequently, some of sedimentary organic matter, both from primary and

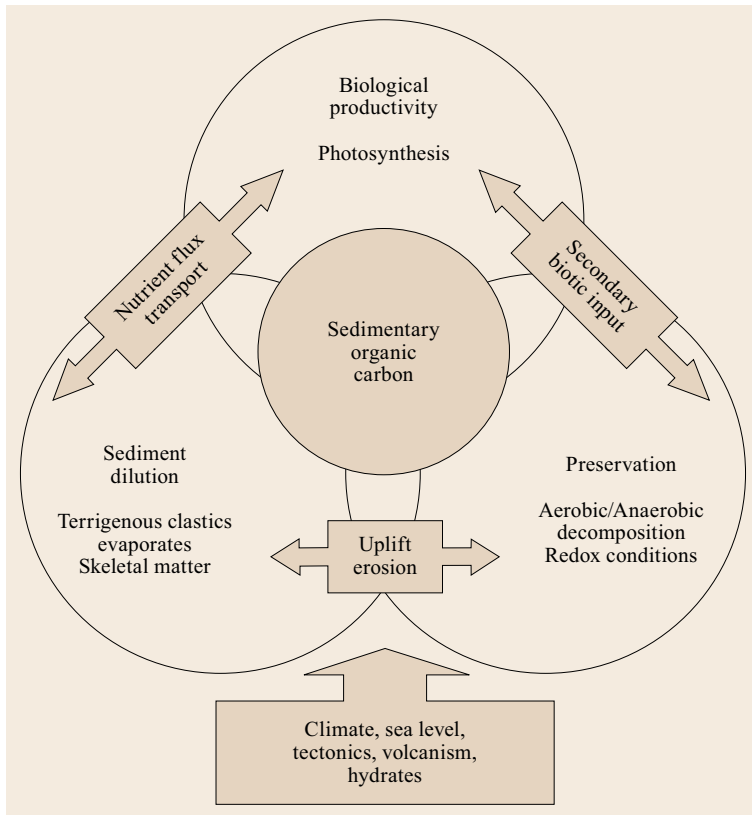


Fig. 10.2 Three major factors, primary productivity, preservation, and dilution, determine if organic-rich source rocks are deposited

secondary biogenic sources, may escape recycling and become preserved in lithified rock. Hence, anoxic conditions enhance the preservation of oil-prone organic matter and promote the deposition of potential source rocks (Fig. 10.4).

As shown in Fig. 10.4, oxic (a) and anoxic (b) depositional environments generally result in poor and good preservation of deposited organic matter, respectively [10.51]. The solid horizontal line separates oxic (above) from anoxic (below). In oxic settings, bottom dwelling metazoa bioturbate the sediments and oxidize most organic matter. In anoxic settings, especially where the oxic–anoxic boundary occurs in the water column, bottom-dwelling metazoa are absent and sediments are not bioturbated.

The amount of oxygen in bottom waters or sediments is determined by the rate of influx from the photic zone (via circulation and/or diffusion) and its rate of consumption (biological oxygen demand). Topographical barriers, currents, or water stratification due to temperature and salinity gradients may limit water circulation and diffusion. A high supply of primary organic matter raises the biological oxygen demand, rendering pore waters, and even the lower water column, anoxic. This mechanism is seen in terrigenous

environments with high input of land-plant material (e.g., swamps, and coastal plains), and in lake and marine environments with high nutrient influx (e.g., seasonal rains and stagnant water columns, and upwelling zones).

In anoxic marine environments, the most prevalent organisms are sulfate-reducing bacteria that produce H_2S . If not precipitated as pyrite by iron from clays and other clastic minerals, H_2S may react with organic matter, incorporating sulfur. If the production of H_2S is greater than the rate of sequestering, *euxinic* conditions (waters with free H_2S) occur. The transition between oxic and euxinic waters may occur within the sediments or water column. Some strata with excellent source potential were deposited where euxinic conditions extended into the photic zone [10.52]. Anoxia also occurs in hypersaline environments, such as playa lakes, lagoons, and restricted marine settings.

Sedimentation rate influences both the preservation and concentration of organic matter. The inorganic materials may be clastic (eroded clays and sands), chemical precipitates (carbonates, salts), or biogenic (siliceous and carbonate shells). Organic matter may be removed from biological recycling by rapid burial, such

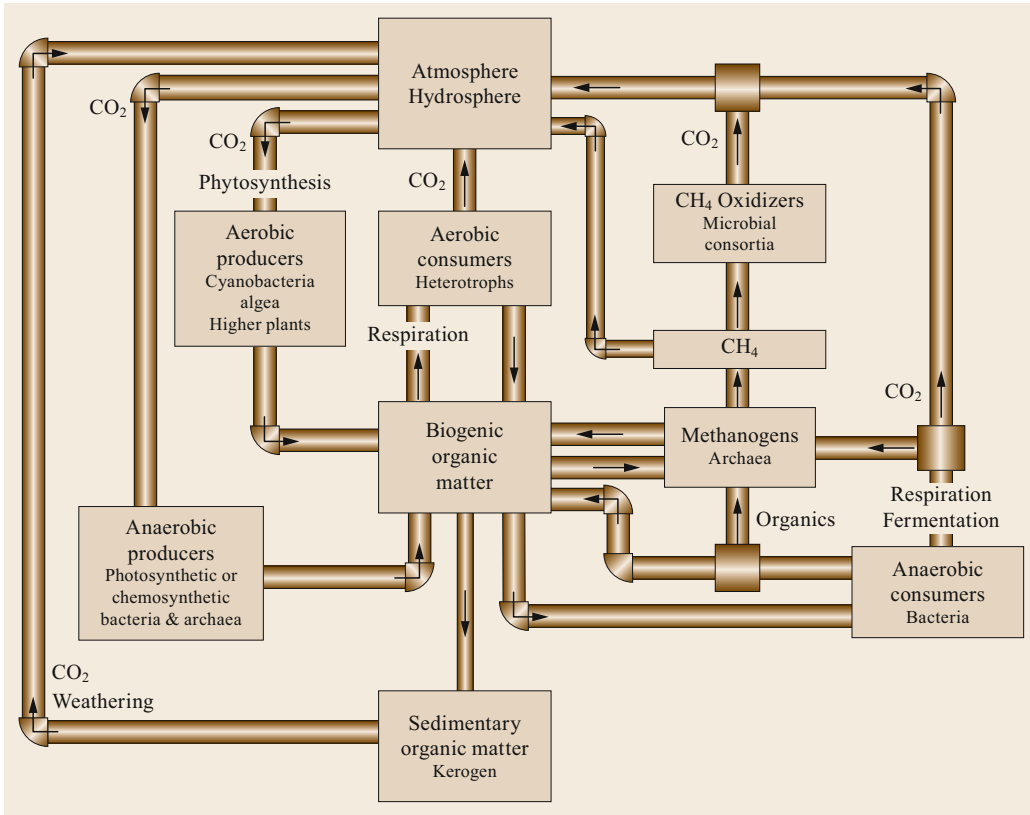


Fig. 10.3 Generalized redox cycle for organic carbon

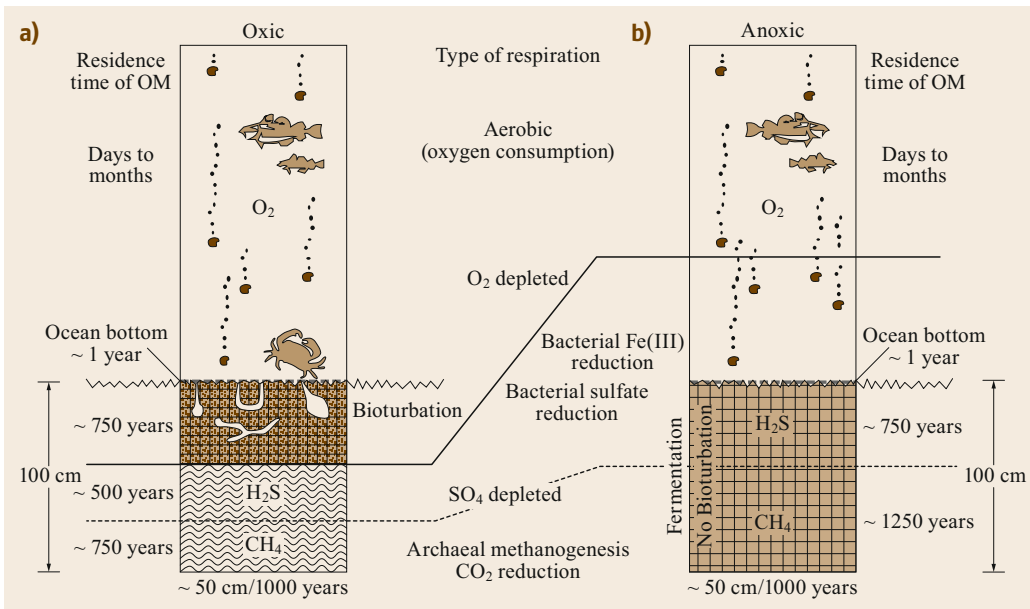


Fig. 10.4a,b Oxic (a) and anoxic (b) depositional environments

as in deltaic settings. However, preservation can be offset by dilution and the resulting rocks may be relatively low in organic carbon. This is why most deltaic shales do not exceed 4–5 wt% total organic carbon (TOC). Similarly, sediments resulting from high primary productivity, such as diatomaceous cherts, may have an

upper limit in organic carbon because of high autodilution. In general, sedimentary rocks with the highest concentrations of organic matter are deposited under conditions of moderate to high influx of primary organic matter, anoxic (possibly euxinic) bottom waters, and low sedimentation rates.

10.4 Kerogen Formation and the Generative Potential of Source Rocks

Although derived from biochemicals, the sedimentary organic matter in source rock is markedly different in chemical composition. Living organisms are composed mostly of proteins, carbohydrates, nucleic acids, and lipids. Structural materials, such as lignin and cellulose, and various resins are fairly well-defined biopolymers composed of a limited number of monomers. With the exception of some halophilic green algae and a few bacteria [10.53], only trace amounts of hydrocarbons are produced directly as biomass by most living organisms. In contrast, immature sedimentary rocks contain only low concentrations of the functionalized biomolecules. Most of the organic carbon is bound in a condensed, insoluble macromolecular material, termed kerogen, which has comparatively few functional groups. Kerogen has been called a *geopolymer* but this is a misnomer, as the term implies that there is a repetition of distinct monomers and some structural order. Kerogen has no unique molecular structure and can only be defined in terms of bulk elemental composition and average molecular distributions.

Optically, kerogen is often described as mixtures of amorphous organic matter and *macerals*, morphologically distinct particles from various organisms. Much of the terminology describing macerals is from organic petrography of coals where the macerals are mostly derived from land plants. The amorphous matter was once thought to be derived from the complete breakdown of biological macromolecules that then reassembled in a random fashion with low molecular-weight biomolecules (e.g., lipids) [10.55]. We now realize that there are biological macromolecules that are alkyl rich and resist microbial recycling [10.54]. These bio-macromolecules (e.g., cutan, sporopollenin, tannins, and algaenan) may constitute only a small fraction of the initial biomass, but are selectively preserved and enriched during early diagenesis (Fig. 10.5). They provide a core for the incorporation of functionalized low molecular-weight biomolecules, such as membrane lipids and the breakdown products of less resistant bio-macromolecules. A small fraction of this material may

remain soluble, which along with biogenic hydrocarbons and lipids that resist incorporation, becomes the bitumen that can be extracted from immature source rocks using organic solvents.

Kerogen formation begins at the point when living cells die and their biomolecules are exposed to the geologic environment. Microbial processes are mostly responsible for the breakdown of biological macromolecules and the recycling of lower molecular-weight biomolecules, resulting in the selective preservation of the more bio-resistant compounds. Low-temperature chemical reactions further alter kerogen through the loss of functional groups (e.g., $-\text{NH}_3$, $-\text{COOH}$), sulfur incorporation, condensation, cross-linking, and aromatization. The processes and thermal regime under which kerogen forms, termed *diagenesis*, occur under mild thermal conditions ($< 80^\circ\text{C}$).

As shown in Fig. 10.6, the quantity and quality of organic matter preserved during diagenesis of sediment determines the generative potential of the source rock and whether it will be prone to expel oil or gas. Quantity is determined by amount of organic input, the degree to which it is preserved (either as primary or secondary biogenic matter), and by its dilution with inorganic mineral matter. Typical oil-prone, marine source rocks contain 2–5 wt% TOC, but strata in the range of 10–20% are known to occur in high yield petroleum systems. Basins with world class reservoirs may contain source units with appreciably higher amounts of carbon. Expulsion of oil may be difficult from rocks with < 1 –2% TOC. Oil shales, many of which are lake deposits, contain over 10% TOC. Coals are $> 80\%$ TOC, and may be diluted by varying amounts of clastic minerals to yield coaly shales with a wide range of carbon content.

The hydrogen content of kerogen influences the quality of the expelled hydrocarbons (during metagenesis). Kerogens with high H/C ratios tend to generate oil, while those with low H/C ratios tend to generate gas. The hydrogen index (HI) is based on the Rock-Eval measurement. This pyrolysis method, commonly used by petroleum geochemists to rapidly screen rocks

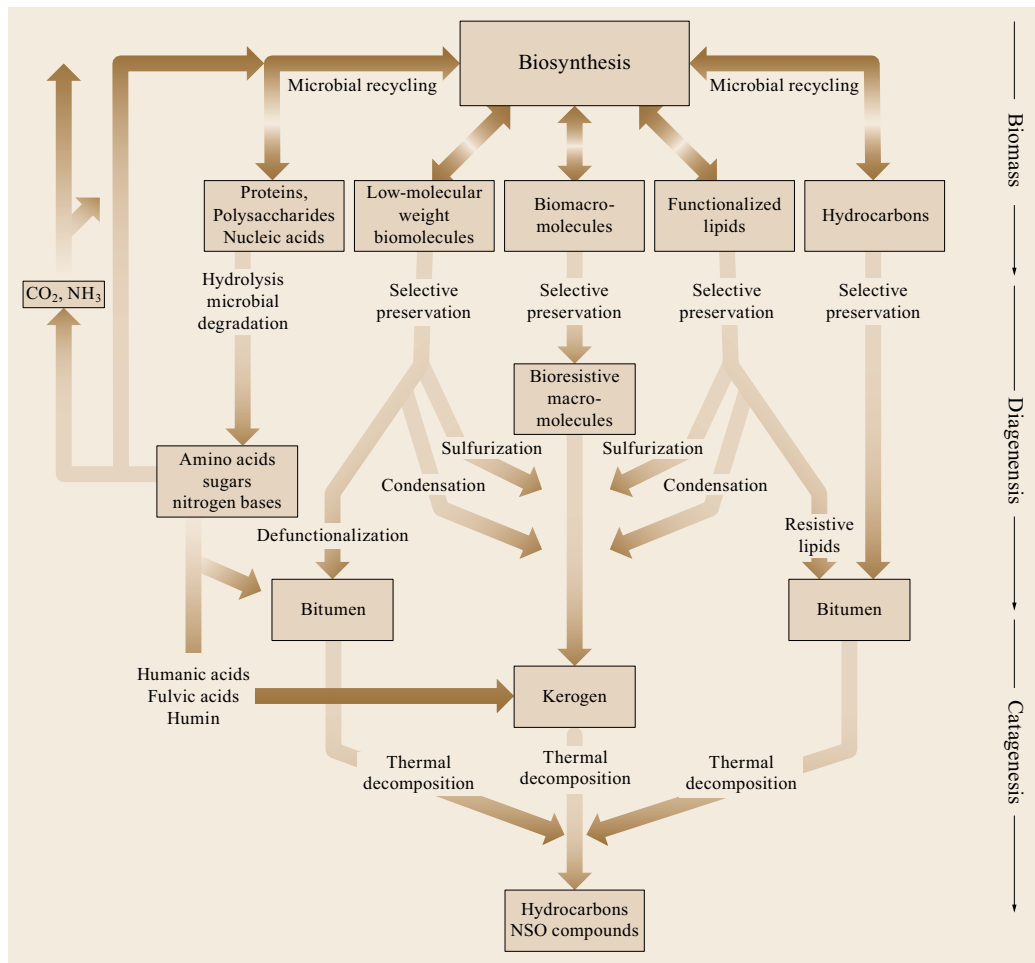


Fig. 10.5 Kerogen is formed during diagenesis by the selective preservation of bio-resistive macromolecules and from the incorporation of lower-molecular weight species (after [10.54])

for their generative potential, heats a ground sample and measures the pyrolyzate response using a flame ionization detector and the CO_2 response using an infrared detector [10.56]. These responses can be calibrated to a rough approximation of the kerogen H/C and O/C atomic ratios.

Kerogen quality is mainly a function of hydrogen content – kerogens with high H/C ratios (> 1.2) are oil prone, while those with lower H/C ratios (0.5–0.8) tend to generate mostly hydrocarbon gas. Biogenic input of organic matter and the manner of its preservation determine the hydrogen content of kerogen. Some algae and bacteria are extremely rich in membrane lipids and aliphatic biopolymers, such as algaenan. Sediments that receive this input have the potential to be hydrogen rich (kerogen H/C > 1.5). Conversely, land-plant lignins have low H/C ratios and sediments that received

only this input are hydrogen poor (kerogen H/C ratios < 1.0). The hydrogen, sulfur, and oxygen content of kerogen can be modified greatly during deposition and diagenesis. Oxidic conditions favor rapid and fairly complete heterotrophic consumption of primary organic matter. The organic matter remaining in the sediments tends to be oxidized or inert. Anoxic conditions conserve, or even enhance, the initial H/C ratio of the primary organic matter via selective preservation and/or contributions from secondary biota. Euxinic conditions promote the incorporation of sulfur, resulting in high S/C ratios [10.57].

There are many schemes that attempt to classify kerogen types by their morphology, maceral, and palynological assemblages, and/or bulk chemical composition. The most widely used is a modification of a method developed for coals [10.58], whereby the H/C

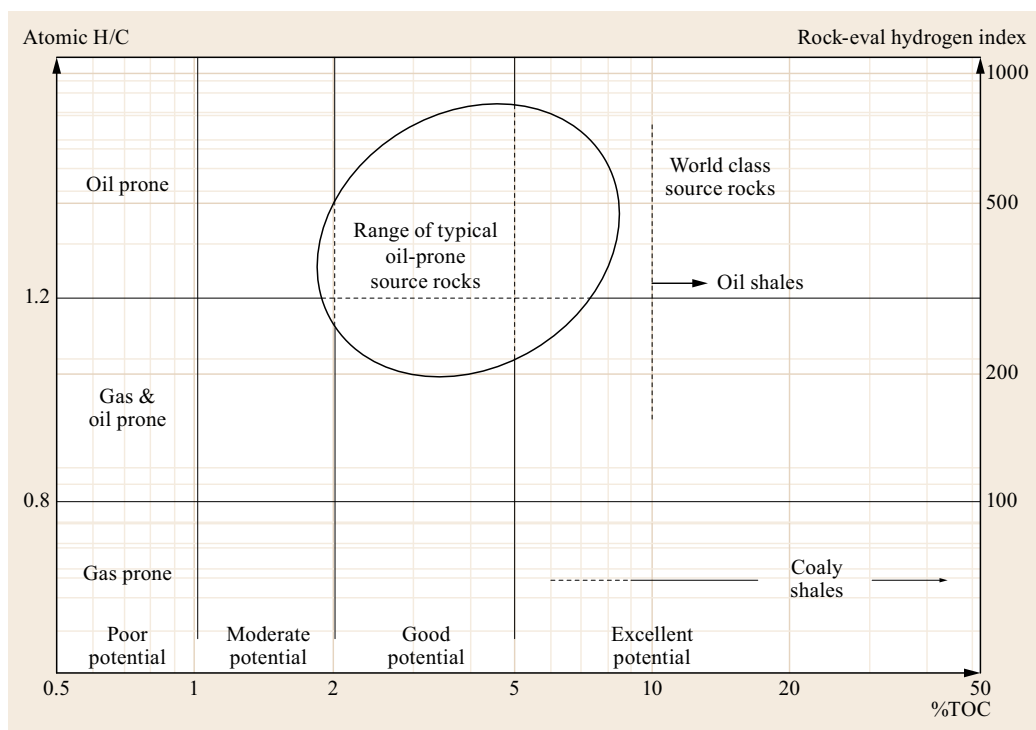


Fig. 10.6 The quantity and quality of kerogen determine the generative potential of source rock

Table 10.1 Kerogen types, their occurrence and bulk chemistry (at end of diagenesis)

Type	Depositional setting	Primary biotic input	H/C	O/C	S/C
I	Lakes, restricted lagoons	Green algae Cyanobacteria Dinoflagellates	> 1.4	< 0.1	< 0.02
IS	Lakes with a source of sulfate (rare)	Green algae Cyanobacteria	> 1.4	< 0.1	> 0.04
II	Marine shales	Marine algae, phytoplankton	1.2–1.4	~ 0.1	0.02–0.04
IIS	Marine carbonates, evaporites, silicates	Marine algae, phytoplankton	1.2–1.4	~ 0.1	> 0.04
III	Coals, coaly shales, deltas	Vascular land plants	0.7–1.0	> 0.1	< 0.02 ^a
IIIC	Coastal plains (oil-prone coals)	Vascular land plants, algae	1.0–1.2	> 0.1	< 0.02 ^a
IV	Inert carbon due to oxidation or advanced maturity	All possible	< 0.5	< 0.15	< 0.02 ^b

^a Coals generally are low in sulfur. Depositional settings with marine influence may result in coals with S/C > 0.02.

^b Some inert pyrobitumens may have higher S/C ratios as a result of secondary sulfur incorporation.

and O/C ratios are plotted (Fig. 10.7). Kerogens are assigned designations as being Type I, II, III, or IV depending where they fall on the plot. Type I and II are oil-prone, Type III is gas-prone, and Type IV is inert carbon. A substantial portion of the oxygen content is lost during diagenesis. Oil generation occurs during catagenesis, whereby the H/C ratios of the residual kerogens decrease. When the H/C ratio is < 0.5, the residual kerogens are capable of generating only methane.

This classification scheme can be subdivided further by considering the variation in sulfur content (Table 10.1). Since the incorporation of sulfur into sedimentary organic matter involves H₂S generated by sulfate reducing bacteria, kerogens with high S/C ratios (0.04 to > 0.10) are found mostly in marine (nonclastic) rocks where euxinic conditions prevail. Type I kerogens are deposited typically in continental lakes, which have no contact with marine waters and lack a ready supply of sulfate. Consequently, sulfur-rich Type IS kero-

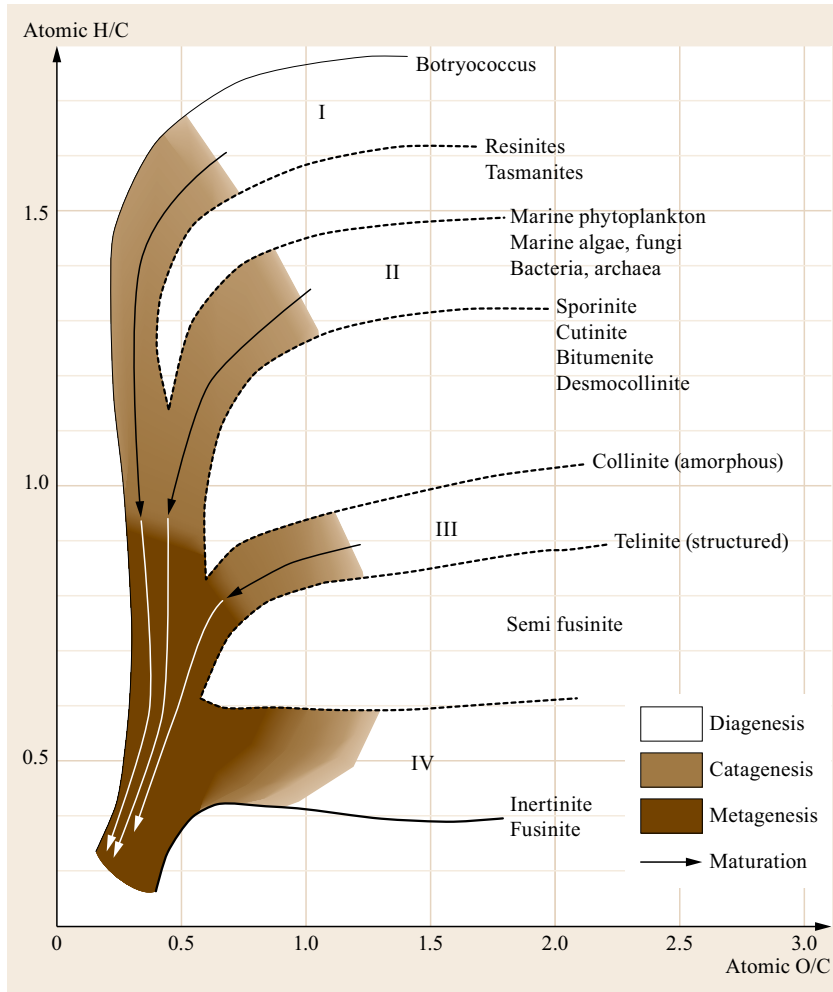


Fig. 10.7 van Krevelen-type diagram showing the distribution of kerogen types and some of their precursor macerals

gens arise only in unusual geologic settings where older evaporite beds (e.g., gypsum or anhydrite) are exposed and dissolved into normally fresh lake water [10.59, 60].

Type II kerogens are deposited primarily in marine settings dominated by photosynthetic organisms. During early diagenesis, this organic matter may react with H_2S produced by sulfate-reducing bacteria that thrive in marine, anoxic waters, and sediments. H_2S also reacts with iron and other metals, forming inorganic sulfides. Consequently, marine Type II kerogens may have varying sulfur content. Marine shales and mudstones, which contain iron oxides and iron-rich clays, yield low-sulfur Type II kerogens and pyrite. Carbonate, evaporite, and chert deposits, which are iron poor, commonly yield high-sulfur Type IIS kerogens.

Type III kerogens form in swamps and coastal plains. As these depositional environments may or may not have marine influence, the sulfur content of coals can vary, but is generally low. Type III kerogens are frequently allochthonous; that is, they are transported by fluvial systems into delta and nearshore marine sediments where they may mix with locally produced (autochthonous) Type II kerogens. Most Type III kerogens are dominated by vitrinite, a land-plant maceral that has a low H/C ratio and is gas-prone. Some coals, however, contain oil-prone materials (Type IIIC) that are derived from associated algae or from the selective preservation of cutinous macromolecules. Many oils from Southeast Asia are generated from Tertiary coaly shales that contain this type of kerogen.

10.5 Generation and Expulsion of Oil and Gas

During *catagenesis*, kerogen thermally cracks and produces bitumen. Weak C–S and C–O bonds break preferentially during the early stages of catagenesis producing bitumen that is highly enriched in polar (NSO) compounds. With additional heating (≈ 90 – 140°C), C–C bonds break within the evolved polar compounds and from residual kerogen, yielding a hydrocarbon-rich fluid that is then expelled from the source rock mineral matrix. With additional thermal stress, kerogen yields primarily condensate and then wet gas (C_1 – C_6). Catagenesis is complete when the kerogen has expended its capacity to generate C_{2+} hydrocarbons (≈ 150 – 175°C). *Metagenesis* may then take place under still more severe thermal alteration, where only methane is produced as methyl-groups are cleavage from highly condensed, aromatic structures.

Oil generation is a kinetic process – both time and temperature are critical [10.61]. The kinetic parameters of kerogen decomposition can be determined by artificially heating immature source rocks using relatively fast heating rates (≈ 300 – 550°C at ≈ 1 – $50^\circ\text{C}/\text{min}$) or lower isothermal temperatures (275 – 350°C for sev-

eral days) and measuring either product yield or the residual generative potential. Data fit to kinetic models defined by a series of parallel first-order reactions, usually at a single frequency factor. When geologic heating rates are applied (≈ 1 – $10^\circ\text{C}/\text{Ma}$), the derived kinetic models yield kerogen maturation results comparable to what is observed in petroliferous basins [10.62, 63]. More advanced models describe the fluid composition of the expelled products and include secondary cracking reactions (Fig. 10.8).

The rate of kerogen conversion is assumed to follow a series of parallel first-order kinetic reactions defined by the Arrhenius equation, $k = Ae^{-(E/RT)}$, where k is the rate coefficient, A is a constant termed the frequency factor, E is the activation energy, R is the universal gas constant, and T is the temperature. The kerogen model was derived by fitting the yield curves of pyrolyzates that evolved from a marine shale source rock containing Type II kerogen heated at several different heating rates under anhydrous conditions. In this case, the frequency factor was fixed at $A = 10^{14} \text{ s}^{-1}$. The evolved products are predicted from a more advanced model

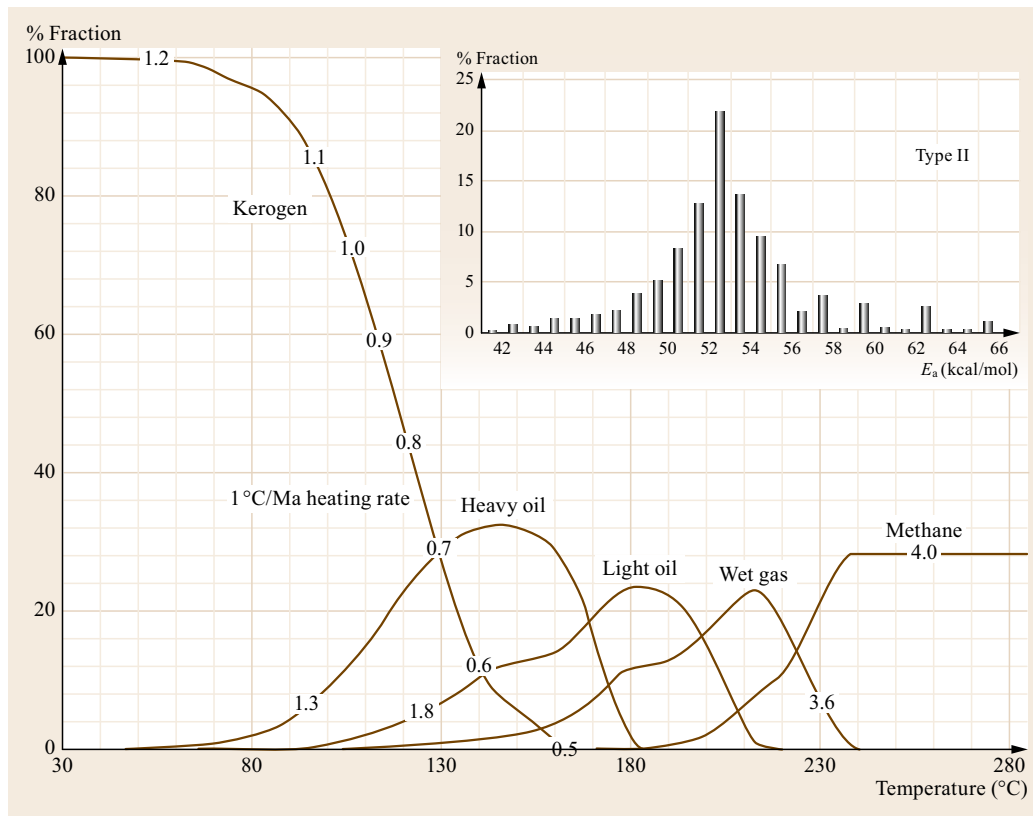


Fig. 10.8 Example of a kerogen decomposition kinetic model with predictions of expelled fluid composition

that accounts for expulsion and secondary cracking of retained bitumen and residual kerogen.

Although simple thermogenesis adequately describes petroleum generation, geocatalysis involving reactive mineral surfaces, clays, trace metals, or organic species has been proposed [10.64, 65]. Such processes are highly speculative, and it is difficult to image how inorganic agents would remain activated under subsurface conditions or how mass transport limitations inherent in solid–solid interactions could be circumvented [10.66].

Once generated from the kerogen, petroleum is expelled into mineral pore spaces (primary migration) and then through permeable rock and faults to the trap (secondary migration). Oil expelled from source rock is enriched in saturated and aromatic hydrocarbons relative to the bitumen that remains (Fig. 10.9). The factors that control primary expulsion and bitumen fractionation are largely unknown; and, although there is generally a lack of experimental or observational evidence for the underlying mechanisms, there is no shortage of hypotheses. Expulsion models that attempt to account for these chemical differences generally assume rate-limiting processes occur during the release of generated hydrocarbons from the kerogen or the movement of hydrocarbons within the mineral matrix.

Hypotheses based on kerogen–oil interaction postulate that the expulsion of oil is controlled by absorption or adsorption of the products onto the surface of the kerogen [10.67–69], diffusion of the hydrocarbons through the kerogen [10.70–73], and/or relative solubility [10.74]. These hypotheses attribute little importance to movement of petroleum within the source rock mineral matrix and the efficiency of the release of oil is controlled primarily by the amount of organic carbon and its composition (see [10.69] and references therein). Expulsion models based on interactions of generated products with the source kerogen have gained favor in recent years as they have the potential to account for compositional differences between bitumens and expelled oil and for expulsion efficiencies that depend on kerogen type and richness. This thinking can be traced to observations made on source rocks [10.75] and recognition of the absorptive capacity of solid organic matter as revealed by solvent swelling experiments [10.76–79]. It is now clear that Type I and II kerogens and Type III and IIIC coals have sufficient sorptive properties to explain residual oil concentrations in mature source rocks.

There are many expulsion models that target chemical or physical processes of oil moving within the source rock mineral matrix as the rate determining step.

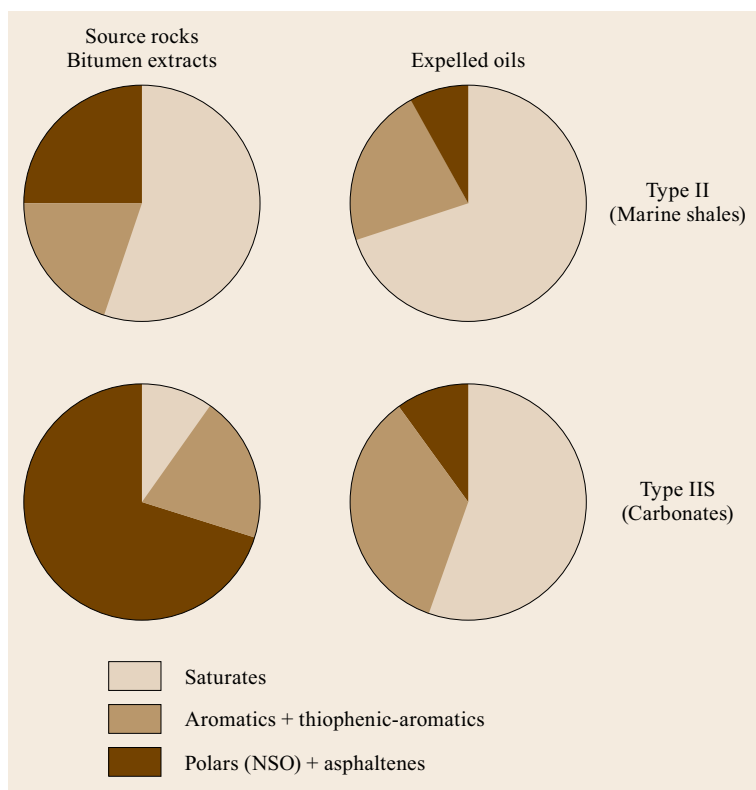


Fig. 10.9 Comparison of C_{15+} chemical group type distributions of expelled oil and retained bitumens for typical Type II (marine shale) and Type IIS (carbonate) source rocks (middle of the oil window)

Different aspects have been considered to be important in this movement. Some consider the amount and type of organic matter as being critical to generating sufficient bitumen to exceed a pore saturation threshold [10.80–82]. Others postulate that the establishment of effective and continuous migration pathways within the source rocks is critical [10.83–85].

Other factors suggested to be key elements in expulsion are: pressure build-up from generation and compaction and the failure of the rock fabric result-

ing in micro-fracturing [10.86], gas availability, and movement of oil in a gas or supercritical phase [10.87, 88], or movement of oil in an aqueous phase [10.89, 90]. For the most part, the conditions that determine these elements are controlled by the primary sedimentological conditions in the depositional environment of the source rock and secondary diagenetic processes. Consequently, the mechanisms that define oil movement differ according to the lithofacies of the source rock.

10.6 Composition of Produced Petroleum

Petroleum may be the single most complex chemical mixture that occurs in nature. As such, our knowledge of its molecular composition has advanced as new analytical methods become available. The first compositional study is attributed to *De la Rue and Miller*, who in 1856 identified several aromatic hydrocarbons by forming and crystallizing barium salts of sulfonic acids [10.91]. This was followed by several other studies in the second half of nineteenth century that relied on distillation and wet chemical methods [10.92]. In 1927, American Petroleum Institute Research Project 6 was launched to investigate the composition of petroleum. The collaborative program, which ran until 1959, was able to isolate and identify 169 individual hydrocarbons using laborious procedures involving distillation, selective solvent extraction, selective absorption, and finally crystallization [10.93, 94]. Characterization of the crystallized isolates advanced from elemental analysis to optical and mass spectrometric measurements. Gas chromatography provided the next advance in molecular characterization. Using pack columns, *Bray and Evans* in 1961 were able to separate individual *n*-alkanes and discover that their distribution changed with increasing maturation [10.95]. The separations were barely adequate to show pristane and phytane as shoulders on the nearly co-eluting *n*-C₁₇ and *n*-C₁₈. Starting in the 1970s improving hydrocarbon separation offered by capillary columns coupled to mass spectrometry launched an explosion of hydrocarbon characterization [10.96]. Today, all major and minor C₄₀-hydrocarbon species and many of the trace components, including a host of biomarkers are relatively easily characterized [10.21].

The same cannot be said for higher molecular-weight species, particularly the polar and asphaltene compounds. Only recently has *Petroleomics* emerged as a science that is attempting to provide a comprehensive molecular description of crude oil using advances in ultrahigh resolution mass spectrometry and ionization

methods [10.97, 98]. The number of distinct species detected by these methods is continually increasing and exceeds 100 000. The resolution and sensitivity of these instruments continue to improve and the petroporphyrins, discovered by *Treibs* in 1936 [10.14], can now be shown to be present in many forms, including sulfurized species [10.99]. These new techniques allow the distributions of these petroleum compounds to be described by their molecular formulae. There is now a consensus that asphaltenes have a centroid distribution of ≈ 750 Da with a full width half maximum of 500–1000 Da. However, structural configurations still remain mostly unknown. Some consider asphaltenes to be composed mainly of alkyl groups and other pendent moieties attached to a single large PAH core, the *Yen-Mullins* or *island* model [10.100]. Others consider asphaltenes to be multicore PAH structures with pendant groups that are linked together, the *archipelago* model [10.101]. It is likely that both types of species exist [10.102].

The molecular and isotopic composition of produced petroleum is determined by complex chemical, physical, and biological processes. As discussed above, the composition of petroleum is a function of the molecular nature of the source bitumen and kerogen, its thermal evolution and the fractional processes that occur during expulsion. Each source facies generates oil with distinct chemical composition that reflects biotic input, depositional setting, and thermal history (Fig. 10.10). For example, lacustrine and coaly source rocks generate waxy, low-sulfur crudes, while carbonate and evaporite source rocks generate asphaltic, high-sulfur crudes. These compositional differences are most apparent during the initial stages of oil expulsion and become less distinct as the source rock proceeds through catagenesis where secondary cracking reactions become prevalent.

Although petroleum is derived from biological matter, most of the individual compounds cannot be assigned to a specific biochemical precursor. Some

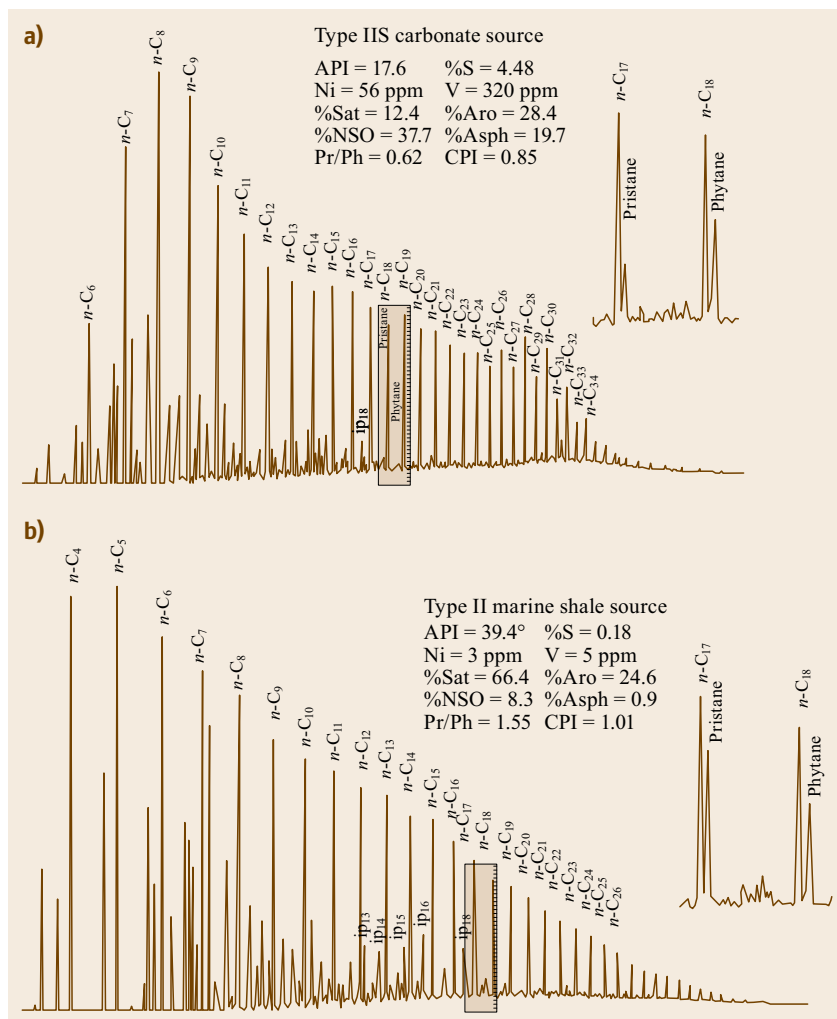


Fig. 10.10a-d Whole-oil gas chromatograms showing examples of oils from different source kerogens. The boxed area, showing the elution of n -C₁₇, pristane (Pr) and n -C₁₈, phytane (Ph), is enlarged. High pristane/phytane ratios (pr/ph) are associated with oxic depositional environments. Low pr/ph ratios are associated with evaporitic/anoxic environments.

petroleum hydrocarbons, termed *biomarkers*, retain enough of their original carbon skeleton structure that a likely biochemical precursor can be postulated [10.21]. The abundance and distribution of biomarkers allow geochemists to infer the origin and thermal history of oils and source rocks.

Once generated and expelled from the source rock, petroleum composition can be further modified during migration and entrapment within the reservoir. In most petroleum systems, the source formation is at greater temperature and pressure than the reservoir and migrating petroleum fluid may separate into gas and liquid phases that can then migrate independently [10.103–105]. Petroleum also interacts with water and the more soluble hydrocarbons may selectively partition into the aqueous phase [10.106].

Once in the reservoir, secondary processes can alter oil composition. Biodegradation, the consumption of

hydrocarbons by microorganisms, is likely to occur in shallow, cool reservoirs (< 80 °C) [10.107, 108]. This process selectively removes saturated hydrocarbons, enriching the residual crude oil in polar and asphaltic material. Biodegradation forms acids and biogenic CH₄, CO₂, and H₂S. Microbial alteration of crude oils is a relatively fast process and may occur naturally or result from poor production practices. Thermochemical sulfate reduction (TSR) is another reservoir alteration process that can affect oil quality and quantity. It is a chemical redox process that occurs at relatively high temperatures (> 120 °C), where hydrocarbons are oxidized to CO₂ and sulfate is reduced to H₂S [10.109, 110]. The residual oil is depleted in saturated hydrocarbons and enriched in sulfur-aromatic species. Reservoir charging and fill history can also alter oil composition. For example, mixing of gaseous hydrocarbons with oil can cause asphaltene to precipitate, forming a tar mat [10.111].

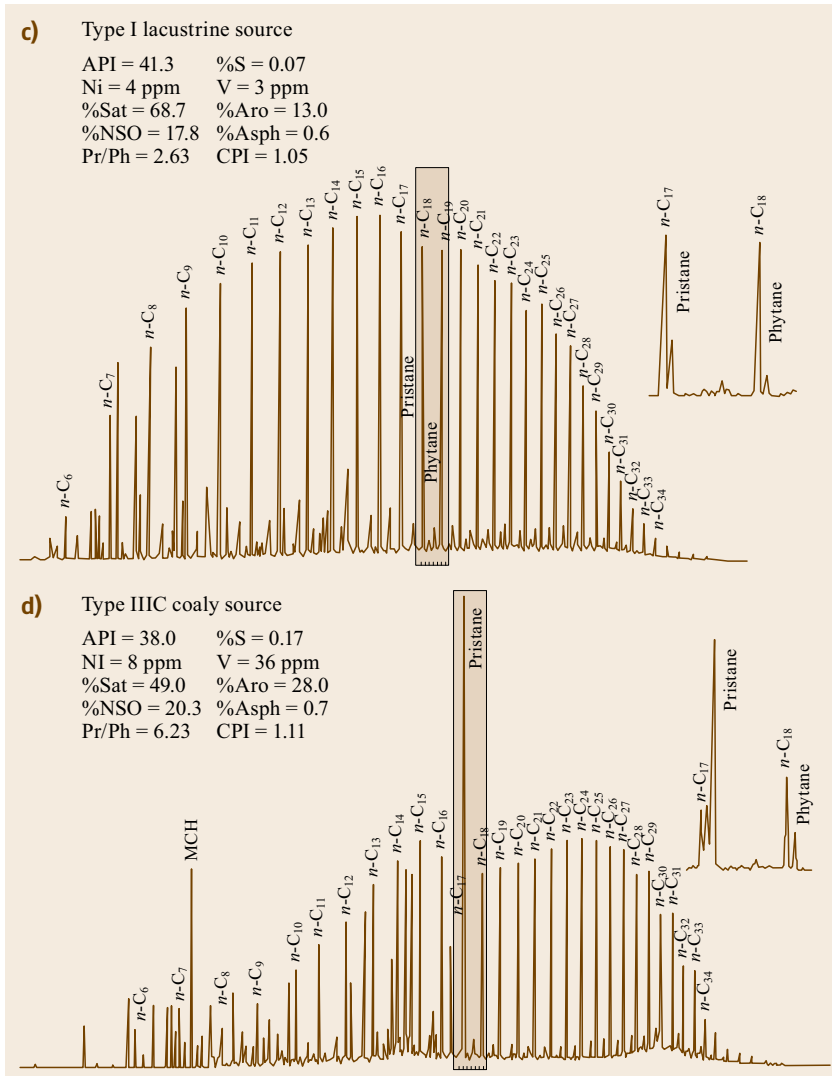


Fig. 10.10 (continued)

Figure 10.10 displays *whole-oil* gas chromatograms up to C_{44} of Types I, II, IIS and IIIC oils. Normal paraffins are predominant. The most noticeable isoprenoid hydrocarbons are pristane (Pr) and phytane (Ph), along with adjacent $n-C_{17}$ and $n-C_{18}$, enlarged in boxes. The pristane/phytane ratio, Pr/Ph, is used to infer the depositional environment (anoxic, hypersaline Pr/Ph < 1, oxic water column/anoxic sediments Pr/Ph 1~2, oxic deposition Pr/Ph > 2).

Carbon preference index (CPI) is defined as the ratio of sum of the C_{25} – C_{33} odd-carbon n -paraffins to the sum of C_{26} – C_{34} even-carbon n -paraffins [10.95]. A slightly modified version commonly used today is the ratio of twice of C_{25} – C_{33} odd carbon n -paraffins to the C_{26} – C_{34} plus the C_{24} – C_{32} even-carbon n -paraffins [10.112]. CPI is used to infer carbonate/evap-

orite source facies < 1, and higher land-plant input CPI > 1.

API gravity, the concentrations of sulfur (S), nitrogen (N), nickel (Ni), and vanadium (V) and the C_{15+} chemical group-type compositions are influenced by the organic matter, depositional environment, and thermal history of their source rocks and by reservoir alteration processes.

The composition of crude oil that arrives at a refinery is not identical to the original reservoir fluids. Gas and water is separated at the well head and emulsions are broken. Consequently, oils lose some light hydrocarbons (< C_6) by evaporation during production and transport. Pipeline and tanker oils are frequently blends of oils from multiple fields and reservoirs, which individually may be of varying composition and qual-

ity. In addition, refineries always blend many available crude oils, such as high and low acid as well as high and low sulfur crude oils, to meet the capacity and tolerance of refining operations. For these reasons, test-

ing of subsurface fluids, such as crude assay, from individual reservoirs is necessary to determine field economics and to design reservoir management practices.

10.7 Unconventional Resources

The petroleum system for conventional resources requires petroleum to migrate out of organic-rich source rocks and accumulate in reservoir rocks that are highly porous and permeable (Sect. 10.2). When sufficiently mature, source rocks generate and retain hydrocarbon gases, primarily methane. The source rock can also act as self-contained unconventional petroleum system where source, reservoir, and seal are contained within the same stratum. Unlike conventional reservoir rocks where the porosity is mainly in voids between mineral grains, the porosity within productive gas shale resides within the organic matter [10.113]. The potential for shale gas has long been known. Wells producing commercial quantities of gas from eastern US Paleozoic shales begin in the early 1820s and were developed as regionally, though minor, assets for decades [10.114]. The full resource potential of gas shales was finally recognized with the development of the Barnett Shale play starting in the 1980s [10.115]. Since 2000 when shale gas, mostly from the Fort Worth Basin, contributed only 2% of the total US production of natural gas, the use of horizontal drilling coupled with large scale, multi-stage hydraulic fracturing and rapid exploitation other US continental basins has increased its contribution to 30% in 2011 [10.116]. Shale gas production is currently mostly limited to the United States and Canada, but its global potential is now apparent and tests are being conducted worldwide [10.117].

Tight oil plays are unconventional in that their exploitation depends on the same technological advances in drilling and fracturing as shale gas; however, the successfully exploited plays geologically resemble conventional petroleum systems. For example, the Bakken Shale play, with reserves estimated at 2 billion bbl [10.118], produces primarily out of the middle member, a low permeability reservoir rock, which is sandwiched between two layers of organic-rich shale (avg. ≈ 12 wt% TOC [10.119]), and the basal Sanish/Pronghorn member and Three Forks Formation, which underlie the organic-rich lower member of Bakken shale. Eagle Ford shale, the conventional source rock for oil residing in overlying Austin Chalk, also is a self-contained petroleum systems producing oil and gas. However, the Eagle Ford is lithogenically heterogeneous with fossils, carbonates, sandstone laminae, and sand-filled bioturbation structures providing ample

internal porosity and permeability [10.120]. Tight gas plays are also considered by some as unconventional resources, but these too are really conventional petroleum systems where the gas is contained in low permeability reservoir rocks.

Methane desorbing from coal and associated water poses a constant safety issue in mines, where it is continually monitored (once by caged canaries) and vented to prevent explosive ignition. Long considered undesirable, coal bed methane (CBM) is now an economically exploitable resource. Spurred on by changes to the United States. Federal tax code in the 1980s, CBM has emerged as a global unconventional resource with the largest productive resources in the United States, China, Canada, Australia, and Russia [10.121, 122]. As lignite and coal matures it liberates organic nutrients that are consumed by microbial communities that produce biogenic methane [10.123]. At higher temperatures, the organic matter generates thermogenic methane. The methane is primarily absorbed within the organic matrix and storage capacity increases with thermal maturity. However, since CBM is typically produced from formations that have been uplifted and microbial activity can resume, it is not uncommon for CBM to have a mixed origin. The science and technology involved in shallow CBM production is fairly mature. Wells are drilled into coal beds that are fairly close to the surface (≈ 100 – 1500 m) and water and gas that are present in the cleats (fractures) are produced. As pressure is drawn down, methane desorbs from the coal matrix and is produced at comparatively low rates (typically $< 100,000$ m³ per day and well). The well performance depends on a number of factors, including cleat density, organic maceral composition and thermal maturity. Increased production and flow rates can be obtained using enhanced coalbed methane techniques that displace the sorbed methane while sequestering CO₂ [10.124].

Gas hydrates (clathrates) are ice-like crystalline solids that form when high concentrations of gases (e.g., CH₄, CO₂, C₂–C₄ hydrocarbons) and water contact at high pressures and low temperatures [10.125]. Occurring both onshore and offshore, methane hydrates represent a vast untapped reserve, with global estimates ranging from 10^{15} to over 10^{18} m³ (5×10^4 – 3.5×10^7 Tcf) [10.126]. However, most gas hydrates occurs

in low concentrations dispersed over large areas and are economically unrecoverable. It is likely that only deposits in Arctic and marine sands have sufficient resource density to ever be economic [10.127]. Several research programs have proven the occurrence and producibility of gas hydrates. Particularly notable are those conducted in the Nankai Trough, Mackenzie Delta, Gulf of Mexico, and Alaskan North Slope [10.128]. Gas can be liberated by destabilizing the hydrate structure through depressurization, heating, or chemical additives [10.129]. At present, the only commercially produced gas hydrates are those occurrences where a hydrate gas cap overlays a conventional gas reserve that has been drawn down in pressure [10.130].

Although the global abundance of abiotic hydrocarbons is inconsequential (Sect. 10.1), the occurrence of such gases is global and, in some local occurrences,

may contribute to minor amounts to economic reserves. Petroleum systems exist where fractured basement and igneous rocks are reservoirs [10.131, 132] and serpentinized rocks could contribute abiotic gases [10.133, 134]. The occurrence of minor amounts of abiotic gas in the economic accumulations in the Songliao Basin is supported by isotopic measurements of hydrocarbon gases and helium [10.135, 136]. Taking a larger view, the largest known hydrocarbon accumulations are not on the Earth, but on Titan, where lakes > 100 000 km² of liquid methane and ethane and pools have been found that exceed the known oil and gas reserves on Earth [10.137]. Considering the abiotic organic matter in comets, meteorites, and other planetary bodies, petroleum derived from biological sources is only tiny fraction of the total hydrocarbon inventory in the Solar System.

10.8 Summary

The theory that petroleum originates from sedimentary organic matter that was once living organisms is consistent with all natural observations, laboratory analyses and experiments, theoretical considerations, and basin simulations. The accumulation of economic quantities of petroleum (oil and gas) requires that a series of processes occur within sedimentary basins. Organic-rich sediments are deposited only under specific conditions that promote the production of biota and/or transport of biogenic organic compounds and the selective preservation of this material. The sedimentary organic matter converts to kerogen, an insoluble macromolecule with a composition that reflects the biotic input and chemical alterations (hydrogenation,

sulfurization, condensation, defunctionalization, and aromatization) that occur during diagenesis. These organic-rich strata have the potential to generate oil and gas when buried and heated to promote thermal cracking. Expelled petroleum migrates from the source rock through fractures and permeable strata. Economic reserves occur when geological conditions allow for the accumulation, retention, and preservation of significant volumes of migrated petroleum. The concept of source, reservoir, and seal applies to conventional petroleum systems, where each element may be a different formation, or to unconventional resources, where the elements exist within the same formation.

References

- | | | | |
|------|--|-------|--|
| 10.1 | Pliny the Elder: <i>Natural History</i> , Vol. XXXV.51, transl. by J. Bostock, H.T. Riley (Taylor Francis, London 1855) | 10.6 | R.H. Dott: Hypotheses for an organic origin. In: <i>Sourcebook for Petroleum Geology, Part 1. Genesis of Petroleum</i> , AAPG Memoir, Vol. 5, ed. by R.H. Dott, M.J. Reynolds (American Association of Petroleum Geologists, Tulsa 1969) pp. 1–244 |
| 10.2 | G.R. McDonald: Georgius Agricola and the invention of petroleum, <i>Bibl. d'Humanisme Renaiss.</i> 73 , 351–364 (2011) | 10.7 | T.S. Hunt: <i>Report on the Geology of Canada. Canadian Geological Survey Report: Progress to 1863</i> (Canadian Geological Survey, Calgary 1863) |
| 10.3 | Aristotle: Meteorology. In: <i>The Complete Works of Aristotle</i> , ed. by J. Barnes (Princeton Univ. Press, Princeton 1995) pp. 555–625 | 10.8 | L. Lesquereux: Report on the fossil plants of Illinois, <i>Ill. Geol. Surv.</i> 2 , 425–470 (1866) |
| 10.4 | J.F. Kenney: Considerations about recent predictions of impending shortages of petroleum evaluated from the perspective of modern petroleum science, <i>Energy World</i> 240 , 16–18 (1996) | 10.9 | J.S. Newberry: The general geological relations and structure of Ohio, <i>Ohio Geological Survey Report 1</i> , Pt. 1 (1873) p. 222 |
| 10.5 | F.E. Wellings: Geological aspects the origin of oil, <i>Inst. Petroleum J.</i> 52 , 124–130 (1966) | 10.10 | R. Arnold, R. Anderson: <i>Geology and Oil Resources of the Santa Maria Oil District, Santa Barbara County, California</i> , USGS Bulletin, Vol. 322 (U.S. |

- 10.11 Geological Survey, Washington 1907)
- 10.11 F.W. Clarke: *Data of Geochemistry*, USGS Bulletin, Vol. 616 (U.S. Geological Survey, Washington 1916)
- 10.12 J.F. Pompeckj: Die Juraablagerungen zwischen Regensburg und Regenstaufer, *Geol. Jahrb.* **14**, 139–220 (1901)
- 10.13 C. Schuchert: The conditions of black shale deposition as illustrated by Kupferschiefer and Lias of Germany, *Proc. Am. Philos. Soc.* **54**, 259–269 (1915)
- 10.14 A. Treibs: Chlorophyll and hemin derivatives in organic mineral substances, *Angew. Chem.* **49**, 682–686 (1936)
- 10.15 T.S. Oakwood, D.S. Shriver, H.H. Fall, W.J. Mcaleer, P.R. Wunz: Optical activity of petroleum, *Ind. Eng. Chem.* **44**, 2568–2570 (1952)
- 10.16 H. Craig: The geochemistry of the stable carbon isotopes, *Geochim. Cosmochim. Acta* **3**, 53–92 (1953)
- 10.17 G. Eglinton, M. Calvin: Chemical fossils, *Sci. Am.* **216**, 32–43 (1967)
- 10.18 J.P. Forsman, J.M. Hunt: Insoluble organic matter (kerogen) in sedimentary rocks of marine origin. In: *Habitat of Oil: A Symposium*, ed. by L.G. Weeks (American Association of Petroleum Geologists, Tulsa 1958) pp. 747–778
- 10.19 P.H. Abelson: Organic geochemistry and the formation of petroleum, *Proc. 6th World Petroleum Congr.* (1963) pp. 397–407
- 10.20 B. Tissot: Premières données sur les mécanismes et la cinétique de la formation du pétrole dans les sédiments. Simulation d'un schéma réactionnel sur ordinateur, *Rev. Inst. Fr. Pét.* **24**, 470–501 (1969)
- 10.21 K.E. Peters, C.C. Walters, J.M. Moldowan: *The Biomarker Guide*, Vol. 1/2 (Cambridge Univ. Press, New York 2005) p. 1155
- 10.22 K.E. Peters: Book review. The Deep Hot Biosphere by Thomas Gold, *Org. Geochem.* **30**, 473–475 (1999)
- 10.23 M.-P. Berthelot: *Chimie Organique Fondée sur la Synthèse* (Mallet-Bachelier, Paris 1860)
- 10.24 D. Mendeleev: L'origine du pétrole, *Revue Scientifique 2e*, Vol. VIII (1877) pp. 409–416
- 10.25 D. Mendeleev: *The Principles of Chemistry*, Vol. 1, 2nd edn. (Collier, New York 1902) p. 552, translated from the 6th Russian edn.
- 10.26 N.A. Kudryavtsev: Against the organic hypothesis of the origin of petroleum, *Petroleum Econ. (Nef. Khoz.)* **9**, 17–29 (1951)
- 10.27 J. Cronin, S. Pizzarello, D.P. Cruikshank: Organic matter in carbonaceous chondrites, planetary satellites, asteroids, and comets. In: *Meteorites and the Early Solar System*, ed. by J.F. Kerridge, M.S. Mathews (University of Arizona Press, Tucson 1988) pp. 819–857
- 10.28 F. Hoyle: *Frontiers of Astronomy* (Heinemann, London 1955)
- 10.29 T. Gold: The origin of natural gas and petroleum and the prognosis for future supplies, *Annu. Rev. Energy* **10**, 53–77 (1985)
- 10.30 T. Gold: *The Deep Hot Biosphere* (Copernicus, New York 1999)
- 10.31 R.A. Kerr: When a radical experiment goes bust, *Science* **247**, 1177 (1990)
- 10.32 G. Etiope, B. Sherwood Lollar: Abiotic methane on Earth, *Rev. Geophys.* **51**, 276–299 (2013)
- 10.33 B.S. Sherwood Lollar, S.K. Frape, S.M. Weise, P. Fritz, S.A. Macko, J.A. Whelan: Abiogenic methanogenesis in crystalline rocks, *Geochim. Cosmochim. Acta* **57**, 5087–5097 (1993)
- 10.34 T.M. McCollom, J.S. Seewald: A reassessment of the potential for reduction of dissolved CO₂ to hydrocarbons during serpentinization of olivine, *Geochim. Cosmochim. Acta* **65**(21), 3769–3778 (2001)
- 10.35 T.M. McCollom: Formation of meteorite hydrocarbons from thermal decomposition of siderite (FeCO₃), *Geochim. Cosmochim. Acta* **67**(2), 311–317 (2003)
- 10.36 J. Potter, A.H. Rankin, P.J. Treloar: The nature and origin of abiogenic hydrocarbons in the alkaline igneous intrusions, Khibina and Lovozero in the Kola Peninsula, *Hydrocarbons in Crystalline Rocks*, N.W. Geological Society London (2001)
- 10.37 T.M. McCollom: Laboratory simulations of abiogenic hydrocarbon formation in Earth's deep subsurface, *Rev. Mineral. Geochem.* **75**, 467–494 (2013)
- 10.38 B. Sherwood Lollar, T.D. Westgate, J.A. Ward, G.F. Slater, G. Lacrampe-Couloume: Abiogenic formation of alkanes in the Earth's crust as a minor source for global hydrocarbon reservoirs, *Nature* **416**, 522–524 (2002)
- 10.39 G.P. Glasby: Abiogenic origin of hydrocarbons: An historical overview, *Resour. Geol.* **56**, 83–96 (2006)
- 10.40 L.B. Magoon, W.G. Dow (Eds.): *The Petroleum System – From Source to Trap*, AAPG Memoir Ser, Vol. 60 (American Association of Petroleum Geologists, Tulsa 1994) p. 655
- 10.41 L.B. Magoon, E.A. Beaumont: Petroleum systems. In: *Handbook of Petroleum Geology: Exploring for Oil and Gas Traps*, ed. by E.A. Beaumont, N.H. Foster (American Association of Petroleum Geologists, Tulsa 1999) pp. 3–34
- 10.42 A. Beaumont, N.H. Foster: *Treatise of Petroleum Geology/Handbook of Petroleum Geology: Exploring for Oil and Gas Traps* (The American Association of Petroleum Geologists, Tulsa 1999)
- 10.43 B.P. Tissot, D.H. Welte: *Petroleum Formation and Occurrence* (Springer, New York 1984)
- 10.44 J.M. Hunt: *Petroleum Geochemistry and Geology* (W.H. Freeman, New York 1996) p. 743
- 10.45 K.E. Peters, M.G. Fowler: Applications of petroleum geochemistry to exploration and reservoir management, *Org. Geochem.* **33**, 5–36 (2002)
- 10.46 M.A. Arthur, B.B. Sageman: Marine black shales: A review of depositional mechanisms and significance of ancient deposits, *Annu. Rev. Earth Planet. Sci.* **22**, 499–551 (1994)
- 10.47 D.E. Canfield: Factors influencing organic carbon preservation in marine sediments, *Chem. Geol.* **114**, 315–329 (1994)

- 10.48 R.V. Tyson: *Sedimentary Organic Matter: Organic Facies and Palynofacies* (Chapman and Hall, London 1995) p. 615
- 10.49 T.F. Pedersen, S.E. Calvert: Anoxia vs. productivity: What controls the formation of organic-carbon-rich sediments and sedimentary rocks?, *Am. Assoc. Petroleum Geol. Bull.* **74**, 454–466 (1990)
- 10.50 W. Michaelis, R. Seifert, K. Nauhaus, T. Treude, V. Thiel, M. Blumenberg, K. Knittel, A. Gieseke, K. Peterknecht, T. Pape, A. Boetius, R. Amann, B.B. Jørgensen, F. Widdel, J. Peckmann, N.V. Pimenov, M.B. Gulin: Microbial reefs in the Black Sea fueled by anaerobic oxidation of methane, *Science* **297**, 1013–1015 (2002)
- 10.51 G.L. Demaison, G.T. Moore: Anoxic environments and oil source bed genesis, *AAPG Bulletin* **64**, 1179–1209 (1980)
- 10.52 M.P. Koopmans, S. Schouten, M.E.L. Kohnen, J.S. Sinninghe Damsté: Restricted utility of aryl isoprenoids as indicators for photic zone anoxia, *Geochim. Cosmochim. Acta* **60**, 4467–4496 (1996)
- 10.53 P. Metzger, C. Largeau, E. Casadevall: Lipids and macromolecular lipids of the hydrocarbon-rich microalga, *Botryococcus braunii*, *Prog. Chem. Org. Nat. Prod.* **57**, 1–70 (1991)
- 10.54 E.W. Tegelaar, J.W. De Leeuw, S. Derenne, C. Largeau: A reappraisal of kerogen formation, *Geochim. Cosmochim. Acta* **53**, 3103–3106 (1989)
- 10.55 B. Durand (Ed.): *Kerogen. Insoluble Organic Matter from Sedimentary Rocks* (Éditions Technip, Paris 1980)
- 10.56 J. Espitalié, J.L. Laporte, M. Madec, F. Marquis, P. Leplat, J. Paulet, A. Boutefu: Méthode rapide de caractérisation des roches mères, de leur potentiel pétrolier et de leur degré d'évolution, *Rev. Inst. Fr. Pet.* **32**, 23–42 (1977)
- 10.57 W.L. Orr: Kerogen/asphaltene/sulphur relationships in sulphur-rich Monterey oils, *Org. Geochem.* **10**, 449–516 (1986)
- 10.58 D.W. van Krevelen: *Coal* (Elsevier, New York 1961)
- 10.59 J.S. Sinninghe Damsté, F.X.C. de las Heras, P.F. van Bergen, J.W. de Leeuw: Characterization of Tertiary Catalan lacustrine oil shales; discovery of extremely organic sulphur-rich Type I kerogens, *Geochim. Cosmochim. Acta* **57**, 389–415 (1993)
- 10.60 K. Grice, S. Schouten, K.E. Peters, J.S. Sinninghe Damsté: Molecular isotopic characterisation of hydrocarbon biomarkers in Palaeocene–Eocene evaporitic, lacustrine source rocks from the Jianghan Basin, China, *Org. Geochem.* **29**, 1745–1764 (1998)
- 10.61 J. Connan: Time-temperature relation in oil genesis, *AAPG Bulletin* **58**, 2516–2521 (1974)
- 10.62 B.P. Tissot, R. Pelet, P. Ungerer: Thermal history of sedimentary basins and kinetics of oil and gas generation, *AAPG Bulletin* **70**, 656 (1986)
- 10.63 P. Ungerer, F. Bessis, P.Y. Chenet, B. Durand, E. Nogaret, A. Chiarelli, J.L. Oudin, J.F. Perrin: Geological and geochemical models in oil exploration; principles and practical examples. In: *Petroleum Geochemistry and Basin Evaluation*, ed. by G. Demaison, R.J. Murriss (American Association of Petroleum Geologists, Tulsa 1984) pp. 53–77
- 10.64 F.D. Mango: Transition metal catalysis in the generation of petroleum and natural gas, *Geochim. Cosmochim. Acta* **56**, 553–555 (1992)
- 10.65 R.W. Sabate, C.C. Baker: Synergetic catalysis in hydrocarbon generation, *Gulf Coast Assoc. Geol. Soc. Trans.* **44**, 657–661 (1994)
- 10.66 M.A.A. Schoonen, Y. Xu, D.R. Strongin: An introduction to geocatalysis, *J. Geochem. Explor.* **62**, 201–215 (1998)
- 10.67 C.D. McAuliffe: Oil and gas migration: Chemical and physical constraints. In: *Problems of Petroleum Migration*, AAPG Geological Studies, Vol. 10, ed. by W.H. Roberts, R.J. Cordell (American Association of Petroleum Geologists, Tulsa 1980) pp. 89–107
- 10.68 E.I. Sandvik, W.A. Young, D.J. Curry: Expulsion from hydrocarbon sources; the role of organic absorption, *Org. Geochem.* **19**, 77–87 (1992)
- 10.69 A.S. Pepper, P.J. Corvi: Simple kinetic models of petroleum formation; Part III, Modelling an open system, *Mar. Petroleum Geol.* **12**, 417–452 (1995)
- 10.70 M.M. Thomas, J.A. Clouse: Primary migration by diffusion through kerogen; I, Model experiments with organic-coated rocks, *Geochim. Cosmochim. Acta* **54**, 2775–2779 (1990)
- 10.71 M.M. Thomas, J.A. Clouse: Primary migration by diffusion through kerogen; II, Hydrocarbon diffusivities in kerogen, *Geochim. Cosmochim. Acta* **54**, 2781–2792 (1990)
- 10.72 M.M. Thomas, J.A. Clouse: Primary migration by diffusion through kerogen; III, Calculation of geologic fluxes, *Geochim. Cosmochim. Acta* **54**, 2793–2797 (1990)
- 10.73 J.G. Stainforth, J.E.A. Reinders: Primary migration of hydrocarbons by diffusion through organic matter networks, and its effect on oil and gas generation, *Org. Geochem.* **16**, 61–74 (1990)
- 10.74 U. Ritter: Solubility of petroleum compounds in kerogen: Implications for petroleum expulsion, *Org. Geochem.* **34**, 319–326 (2003)
- 10.75 A.S. Pepper: Estimating the petroleum expulsion behaviour of source rocks; a novel quantitative approach. In: *Petroleum Migration*, Geological Society of London Special Publication, Vol. 59, ed. by W.A. England, A.J. Fleet (Geological Society of London, London 1991) pp. 9–31
- 10.76 L.J. Shadle, M.R. Khan, G.Q. Zhang, R.A. Bajura: Investigation of oil shale and coal structures by swelling in various solvents, *Div. Petroleum Chem. Prepr.* **34**(1), 55–61 (1989)
- 10.77 J.W. Larsen, S. Li: Changes in the macromolecular structure of a Type I kerogen during maturation, *Energy Fuels* **11**, 897–901 (1987)
- 10.78 J.W. Larsen, S. Li: An initial comparison of the interactions of type I and III kerogens with organic liquids, *Org. Geochem.* **26**, 305–309 (1987)
- 10.79 J.W. Larsen, S. Li: Solvent swelling studies of Green River kerogen, *Energy Fuels* **8**, 932–936 (1994)

- 10.80 B. Tissot: Migration of hydrocarbons in sedimentary basins: A geological, geochemical and historical perspective, *Collect. Colloq. Sémin. Inst. Fr. Pétrole* **45**, 1–19 (1987)
- 10.81 P. Ungerer: State of the art of research in kinetic modelling of oil formation and expulsion, *Org. Geochem.* **16**, 1–25 (1990)
- 10.82 A.K. Burnham, R.L. Braun: Development of a detailed model of petroleum formation, destruction, and expulsion from lacustrine and marine source rocks, *Org. Geochem.* **16**, 27–39 (1990)
- 10.83 P.A. Dickey: Possible migration of oil from source rock in oil phase, *AAPG Bulletin* **72**, 337–345 (1975)
- 10.84 V.V. Palciauskas, P.A. Domenico: Microfracture development in compacting sediments: Relation to hydrocarbon-maturation kinetics, *AAPG Bulletin* **64**, 927–937 (1980)
- 10.85 U. Mann: Sedimentological and petrophysical aspects of primary migration pathways. In: *Sediments and Environmental Geochemistry*, ed. by D. Heling, P. Rothe, U. Förstner, P. Stoffers (Springer, New York 1990) pp. 152–178
- 10.86 S.J. Düppenbecker, D.H. Welte: Petroleum expulsion from source rocks; insights from geology, geochemistry and computerized numerical modelling, *Proc. 13th World Petroleum Congr.* (1992) pp. 165–177, WPC-24120
- 10.87 L.C. Price: Primary petroleum migration from shales with oxygen-rich organic matter, *J. Petroleum Geol.* **12**, 289–324 (1989)
- 10.88 D. Leythaeuser, H.S. Poelchau: Expulsion of petroleum from type III kerogen source rocks in gaseous solution; modeling of solubility fractionation. In: *Petroleum Migration*, Vol. 59, ed. by W.A. England, A.J. Fleet (Geological Society of London, London 1991) pp. 33–46
- 10.89 C. Barker: Aquathermal pressuring: Role of temperature in development of abnormal pressure zones, *AAPG Bulletin* **56**, 2068–2071 (1972)
- 10.90 K. Magara: Agents for primary hydrocarbon migration; A review. In: *Problems of Petroleum Migration*, ed. by W.H. Roberts III, R.J. Cordell (American Association of Petroleum Geologists, Tulsa 1980) pp. 33–45
- 10.91 W. De la Rue, H. Miller: Chemical examination of Burmese naphtha or Rangoon tar, *Proc. R. Soc. Lond.* **8**, 221–228 (1985)
- 10.92 F.D. Rossini, B.J. Mair: Composition of petroleum. In: *Progress in Petroleum Technology*, Vol. 5 (American Chemical Society, Washington 1951) pp. 334–352
- 10.93 F.D. Rossini, B.J. Mair: The work of the API Research Project 6 on the composition of petroleum, *Proc. 5th World Petroleum Congr.*, New York (1959) pp. 223–245
- 10.94 Y.M. Rabkin, J.J. Lafitte-Houssat: Cooperative research in petroleum chemistry, *Scientometrics* **1**, 327–338 (1979)
- 10.95 E.E. Bray, E.D. Evans: Distribution of *n*-paraffins as a clue to recognition of source beds, *Geochim. Cosmochim. Acta* **22**, 2–15 (1961)
- 10.96 C.S. Hsu, D. Drinkwater: GC/MS in the petroleum industry. In: *Current Practice in Gas Chromatography–Mass Spectrometry*, Chromatography Science Series, Vol. 86, ed. by W.W.A. Niessen (Dekker Marcel, New York 2001) pp. 55–94
- 10.97 A.G. Marshall, R.P. Rodgers: Petroleomics: Chemistry of the underworld, *Proc. Natl. Acad. Sci. USA* **105**, 18090–18095 (2008)
- 10.98 C.S. Hsu, C.L. Hendrickson, R.P. Rodgers, A.M. McKenna, A.G. Marshall: Petroleomics: Advanced molecular probe for petroleum heavy ends, *J. Mass Spectrom.* **46**, 337–343 (2011)
- 10.99 A.M. McKenna, J.T. Williams, J.C. Putman, C. Aeppli, C.M. Reddy, D.L. Valentine, K.L. Lemkau, M.Y. Kellermann, J.J. Savory, N.K. Kaiser, A.G. Marshall, R.P. Rodgers: Unprecedented ultrahigh resolution FT-ICR mass spectrometry and parts-per-billion mass accuracy enable direct characterization of nickel and vanadyl porphyrins in petroleum from natural seeps, *Energy Fuels* **28**, 2454–2464 (2014)
- 10.100 O.C. Mullins, H. Sabbah, J. Eyssautier, A.E. Pomerantz, L. Barré, A.B. Andrews, Y. Ruiz-Morales, F. Mostowfi, R. McFarlane, L. Goual, R. Lepkowitz, T.M. Cooper, J. Orbulescu, R.M. Leblanc, J.C. Edwards, R.N. Zare: Advances in asphaltene science and the Yen-Mullins model, *Energy Fuels* **26**, 3986–4003 (2012)
- 10.101 A.H. Alshareef, A. Scherer, X. Tan, K. Azyat, J.M. Stryker, R.R. Tykwinski, M.R. Gray: Formation of archipelago structures during thermal cracking implicates a chemical mechanism for the formation of petroleum asphaltenes, *Energy Fuels* **25**, 2130–2136 (2011)
- 10.102 F. Alvarez-Ramírez, Y. Ruiz-Morales: Island versus archipelago architecture for asphaltenes: Polycyclic aromatic hydrocarbon dimer theoretical studies, *Energy Fuels* **27**, 1791–1808 (2013)
- 10.103 A. Werner, F. Behar, J.C. de Hemptinne, E. Behar: Thermodynamic properties of petroleum fluids during expulsion and migration from source rocks, *Org. Geochem.* **24**, 1079–1095 (1996)
- 10.104 L.C. Kuo: Gas exsolution during fluid migration and its relation to overpressure and petroleum accumulation, *Mar. Petroleum Geol.* **14**, 221–229 (1997)
- 10.105 R. di Primio, V. Dieckmann, N. Mills: PVT and phase behaviour analysis in petroleum exploration, *Org. Geochem.* **29**, 207–222 (1998)
- 10.106 S.E. Palmer: Effect of water washing on C_{15+} hydrocarbon fraction of crude oils from northwest Palawan, Philippines, *AAPG Bulletin* **68**, 137–149 (1984)
- 10.107 J. Connan: Biodegradation of crude oils in reservoirs. In: *Advances in Petroleum Geochemistry*, Vol. 1, ed. by J. Brooks, D.H. Welte (Academic Press, London 1984) pp. 299–335
- 10.108 W.K. Seifert, J.M. Moldowan, G.J. Demaison: Source correlation of biodegraded oils, *Org. Geochem.* **6**, 633–643 (1984)

- 10.109 W.L. Orr: Changes in sulfur content and isotopic ratios of sulfur during petroleum maturation—Study of Big Horn Paleozoic oils, AAPG Bulletin **58**, 2295–2318 (1974)
- 10.110 H.G. Machel: Bacterial and thermochemical sulfate reduction in diagenetic settings – Old and new insights, Sediment. Geol. **140**, 143–175 (2001)
- 10.111 A. Wilhelms, S.R. Larter: Origin of tar mats in petroleum reservoirs: Part II: Formation mechanisms for tar mats, Mar. Petroleum Geol. **11**, 442–456 (1994)
- 10.112 R. Marzi, B.E. Torkelson, R.K. Olson: A revised carbon preference index, Org. Geochem. **20**, 1303–1306 (1993)
- 10.113 R.G. Loucks, R.M. Reed, S.C. Ruppel, U. Hammes: Spectrum of pore types and networks in mudrocks and a descriptive classification for matrix-related mudrock pores, AAPG Bulletin **96**, 1071–1098 (2012)
- 10.114 J.B. Roen: Introductory review – Devonian and Mississippian black shale, eastern North America. In: *Petroleum Geology of the Devonian and Mississippian Black Shale of Eastern North America*, USGS Bulletin, Vol. 1909, ed. by J.B. Roen, R.C. Kepferle (U.S. Geological Survey, Washington 1993) pp. A1–A8
- 10.115 D.B. Steward: *The Barnett Shale Play: Phoenix of the Fort Worth Basin: A History* (The Fort Worth Geological Society, Fort Worth 2007)
- 10.116 EIA: Natural Gas Annual 2011. (Energy Information Administration, Washington 2013) p. 201
- 10.117 EIA: World shale gas resources: An initial assessment of 14 regions outside the United States (U.S. Energy Information Administration, Washington 2011) p. 365
- 10.118 EIA: U.S. Crude Oil and Natural Gas Proved Reserves, 2012 (U.S. Energy Information Administration, Washington 2014) p. 43
- 10.119 J.W. Schmoker, T.C. Hester: Organic carbon in Bakken Formation, United States portion of Williston Basin, AAPG Bulletin **67**, 2165–2174 (1983)
- 10.120 W.C. Dawson, W.R. Almon: Eagle Ford Shale variability: Sedimentologic influences on source and reservoir character in an unconventional resource unit, Gulf Coast Assoc. Geol. Soc. Trans. **60**, 181–190 (2010)
- 10.121 A. Al-Jubori, S. Johnston, C. Boyer, S.W. Lambert, O.A. Bustos, J.C. Pashin, A. Wray: Coalbed methane: Clean energy for the world, Oilfield Rev. **21**, 4–13 (2009)
- 10.122 M. Mastalerz: Coal bed methane: Reserves, production and future outlook. In: *Future Energy*, 2nd edn., ed. by T.M. Letcher (Elsevier, Amsterdam 2014) pp. 145–158
- 10.123 D. Strąpoć, M. Mastalerz, K. Dawson, J. Macalady, A.V. Callaghan, B. Wawrik, C. Turich, M. Ashby: Biogeochemistry of microbial coal-bed methane, Annu. Rev. Earth Planet. Sci. **39**, 617–656 (2011)
- 10.124 R. Sander, L.D. Connell: A probabilistic assessment of enhanced coal mine methane drainage (ECMM) as a fugitive emission reduction strategy for open cut coal mines, Int. J. Coal Geol. **131**, 288–303 (2014)
- 10.125 S. Shahnazar, N. Hasan: Gas hydrate formation condition: Review on experimental and modeling approaches, Fluid Phase Equilib. **379**, 72–85 (2014)
- 10.126 A.V. Milkov: Global estimates of hydrate-bound gas in marine sediments: How much is really out there?, Earth-Sci. Rev. **6**, 183–197 (2004)
- 10.127 R. Boswell, T.S. Collett: Current perspectives on gas hydrate resources, Energy Environ. Sci. **4**, 1206–1215 (2011)
- 10.128 R. Boswell, K. Yamamoto, S.-R. Lee, T. Collett, P. Kumar, S. Dallimore: Methane hydrates. In: *Future Energy*, 2nd edn., ed. by T.M. Letcher (Elsevier, Amsterdam 2014) pp. 159–178
- 10.129 T. Collett, A. Johnson, C. Knapp, R. Boswell: *Natural Gas Hydrates – A Review*, AAPG Memoir, Vol. 89 (American Association of Petroleum Geologists, Tulsa 2009) pp. 146–220
- 10.130 Y. Makogon, V. Tsarev, N. Cherskiy: Formation of large natural gas fields in zones of permanently low temperatures, Dokl. Acad. Nauk SSR **205**, 700–703 (1972)
- 10.131 S.R. Schutter: Hydrocarbon occurrence and exploration in and around igneous rocks, Geol. Soc. Lond. Special Publ. **214**, 7–33 (2003)
- 10.132 S.R. Schutter: Occurrences of hydrocarbons in and around igneous rocks, Geol. Soc. Lond. Special Publ. **214**, 35–68 (2003)
- 10.133 P.D. Jenden, D.R. Hilton, I.R. Kaplan, H. Craig: Abiogenic hydrocarbons and mantle helium in oil and gas fields. In: *Future of Energy Gases*, USGS Professional Paper, Vol. 1570, ed. by D. Howell (U.S. Geological Survey, Washington 1993) pp. 31–35
- 10.134 P. Szatmari, T.C.O. da Fonseca, N.F. Miekley: Mantle-like trace element composition of petroleum – Contributions from serpentinizing peridotites. In: *Tectonics*, ed. by D. Closson (Intech, Rijeka 2011) pp. 332–358
- 10.135 Z. Jin, L. Zhang, Y. Wang, Y. Cui, K. Millae: Using carbon, hydrogen and helium isotopes to unravel the origin of hydrocarbons in the Wujiaweizi area of the Songliao Basin, China, Episodes **32**, 167–176 (2009)
- 10.136 Y. Ni, J. Dai: Geochemical characteristics of abiogenic alkane gases, Petroleum Sci. **6**, 327–338 (2009)
- 10.137 R.D. Lorenz, K.L. Mitchell, R.L. Kirk, A.G. Hayes, O. Aharonson, H.A. Zebker, P. Paillou, J. Radebaugh, J.I. Lunine, M.A. Janssen, S.D. Wall, R.M. Lopes, B. Stiles, S. Ostro, G. Mitri, E.R. Stefan: Titan’s inventory of organic surface materials, Geophys. Res. Lett. **25**(2), L2206 (2008)

11. Basin and Petroleum System Modeling

Kenneth E. Peters, Oliver Schenk, Allegra Hosford Scheirer, Björn Wygrala, Thomas Hantschel

Since the early 1970s, basin and petroleum system modeling (BPSM) has evolved from a simple tool, used mainly to predict regional source rock thermal maturity, to become a critical component in the worldwide exploration programs of many national and international oil companies for both conventional and unconventional resources. The selection of one-dimensional 1-D, 2-D or 3-D BPSM depends on available input data and project objectives. Organic richness and rock properties must be reconstructed to original values prior to burial. For example, in geohistory analysis each unit is decompacted to original thickness and corrected for paleobathymetry and eustasy. Boundary conditions for thermal evolution include heat flow and sediment-water interface temperature corrected for water depth through time. Default petroleum generation kinetics available in most software should be used only when suitable samples of the source rock organofacies are unavailable. Kinetic parameters are best measured using representative, thermally immature equivalents of the effective source rock. 3-D poroelastic and poroplastic rock stress modeling are significant advances over the 1-D Terzaghi method employed by most software. Calibration should start with the available pressure data, followed by thermal calibration (e.g., corrected borehole temperatures or vitrinite reflectance) and calibration to other measurements (e.g., petroleum composition). The dynamic petroleum system concept has proven to be a more reliable tool for exploration than static play fairway maps used in the past, partly because BPSM accounts for the timing of trap formation relative to generation-migration-accumulation. Tectonic activity and other processes can result in remigration or destruction of accumulations and more than one critical moment on the petroleum system event chart. Organoporosity within the kerogen and solid bitumen accounts for much of the petroleum in unconventional mudstone reservoirs, and secondary cracking of oil to gas is par-

11.1	Overview	382
11.1.1	BPSM Workflow	382
11.1.2	Introduction to Sedimentary Basins ...	382
11.1.3	Model Input	384
11.2	Discussion	385
11.2.1	One-Dimensional Models	385
11.2.2	Two-Dimensional Models	387
11.2.3	Three-Dimensional Models	387
11.2.4	Risk Analysis	388
11.2.5	Rock Stress and Pressure Prediction ...	388
11.2.6	Terzaghi Rock Stress Modeling	389
11.2.7	Compaction	389
11.2.8	Pore-Pressure Formation	391
11.2.9	Mixing and Upscaling Rules	391
11.2.10	Geohistory Analysis	392
11.2.11	Decompaction	392
11.2.12	Paleobathymetry	392
11.2.13	Eustatic Corrections	393
11.2.14	Backstripping	393
11.2.15	Original Organic Richness	393
11.2.16	Thermal Modeling and Temperature Prediction	393
11.2.17	Heat Conduction and Convection	394
11.2.18	Boundary Conditions	395
11.2.19	Petroleum Generation	395
11.2.20	Diagenesis, Catagenesis, Metagenesis	395
11.2.21	Petroleum Generation Kinetics	397
11.2.22	Petroleum Migration and Accumulation	399
11.2.23	Petroleum System Event Timing	403
11.2.24	Modeling Unconventional Resources ..	404
11.2.25	Poroelasticity Rock Stress Modeling	409
11.2.26	Rock Failure	410
11.2.27	Example of the North Slope 3-D Model	411
11.2.28	Continuing Developments	412
11.3	Conclusions	413
	References	413

ticularly important. Hybrid unconventional systems, which juxtapose ductile organic-rich and brittle, more permeable organic-lean intervals are typically the best producers.

11.1 Overview

Computerized basin and petroleum system modeling (BPSM) [11.1–3] is a quantitative outgrowth of the earlier, largely qualitative petroleum system concept. A petroleum system consists of four essential rock elements comprising source, reservoir, seal, and overburden; the two processes of trap formation and generation-migration-accumulation; and all crude oil and hydrocarbon gas that originated from one pod of thermally mature organic-rich source rock. BPSM developed as a quantitative tool to test and refine models of petroleum generation, migration, and accumulation for conventional resources [11.5]. The concept of the dynamic petroleum system represents a significant paradigm shift in the way that major national and international oil companies explore for conventional resources [11.6]. Recently, BPSM has expanded to include modules that account for new advances in understanding of geochemical processes, such as a biodegradation module to predict oil quality in conventional reservoirs, a thermochemical sulfate reduction (TSR) module to predict H₂S, and a saturate-aromatic-resin-asphaltene (SARA) module to predict the composition of petroleum remaining in unconventional source rocks [11.7,8]. An unconventional resource contains petroleum that requires some type of stimulation to achieve commercial rates of extraction because of low reservoir permeability and/or high fluid viscosity, e.g., tight gas, coal bed methane, shale gas, shale oil, oil sands or methane hydrate.

11.1.1 BPSM Workflow

BPSM begins with a well-defined conceptual model of the study area based on the sum of all available geologic information [11.9]. BPSM is a form of forward deterministic modeling, in which input data and interpretations are used to calculate the rock and fluid properties forward in time from an original state, typically basement rock emplacement prior to deposition of the overlying basin fill (Fig. 11.1). Simulations are performed on discretized numerical representations of a conceptual model. All practitioners of BPSM must recognize that it is a research tool that provides scenarios that can be tested. The value of the scenarios can be incrementally improved by additional high-quality data, but in the final analysis, no model exactly replicates nature. On the other hand, well-constructed models certainly reduce the uncertainty associated with exploration and exploitation of conventional and unconventional resources.

BPSM is commonly described as *basin modeling* or *petroleum system modeling*, although these two

terms actually differ in meaning [11.3]. Basin modeling utilizes mathematical algorithms to reconstruct the geohistory and thermal evolution of the rocks, whereas petroleum system modeling uses linked algorithms designed to reconstruct the evolution of the petroliferous fluids (oil and gas). Hydrocarbons consist of carbon and hydrogen and include thermogenic oil and gas, as well as biogenic methane. Common usage of the term hydrocarbons includes other petroleum fractions, such as polar compounds or asphaltenes, which contain additional elements, such as nitrogen, sulfur, and oxygen (NSO compounds) or metals (e.g., porphyrins). The petroleum industry is mainly interested in the discovery and exploitation of petroleum fluids, but to model petroleum systems, one must first understand the geologic and thermal evolution of the rocks. Scenarios from BPSM studies are of little value unless they are iteratively calibrated to various measured parameters from the study area, such as pore pressure, vitrinite reflectance, and corrected borehole temperature.

11.1.2 Introduction to Sedimentary Basins

Basin is one of the most common terms in geology, but it is seldom defined in publications. A sedimentary basin is a depression that accommodates sediments as a result of long-term subsidence. Basin subsidence may result from one or more of the following interrelated processes [11.10–12]:

1. Isostatic
2. Flexural
3. Thermal subsidence.

Isostatic subsidence is the result of physical changes in lithosphere thickness, e.g., if crustal thinning is the result of lithospheric stretching, isostatic compensation results in subsidence. In contrast, flexural subsidence depends on elastic plate rigidity and bending of the lithosphere. Thermal subsidence is the result of density changes during cooling of a thermally destabilized lithosphere, e.g., during postrift cooling.

Most classifications of basin type account for the underlying lithosphere (continental versus oceanic), the plate tectonic setting (plate margin or intracraton), and the principal tectonic stress (convergent, divergent, or transform). The lithosphere consists of the upper mantle and crust. The base of the lithosphere ($\approx 1333^\circ\text{C}$) [11.13] is thought to range from the sediment-water interface at midocean ridges to 100 km below cooler parts of the oceans and from 100 to

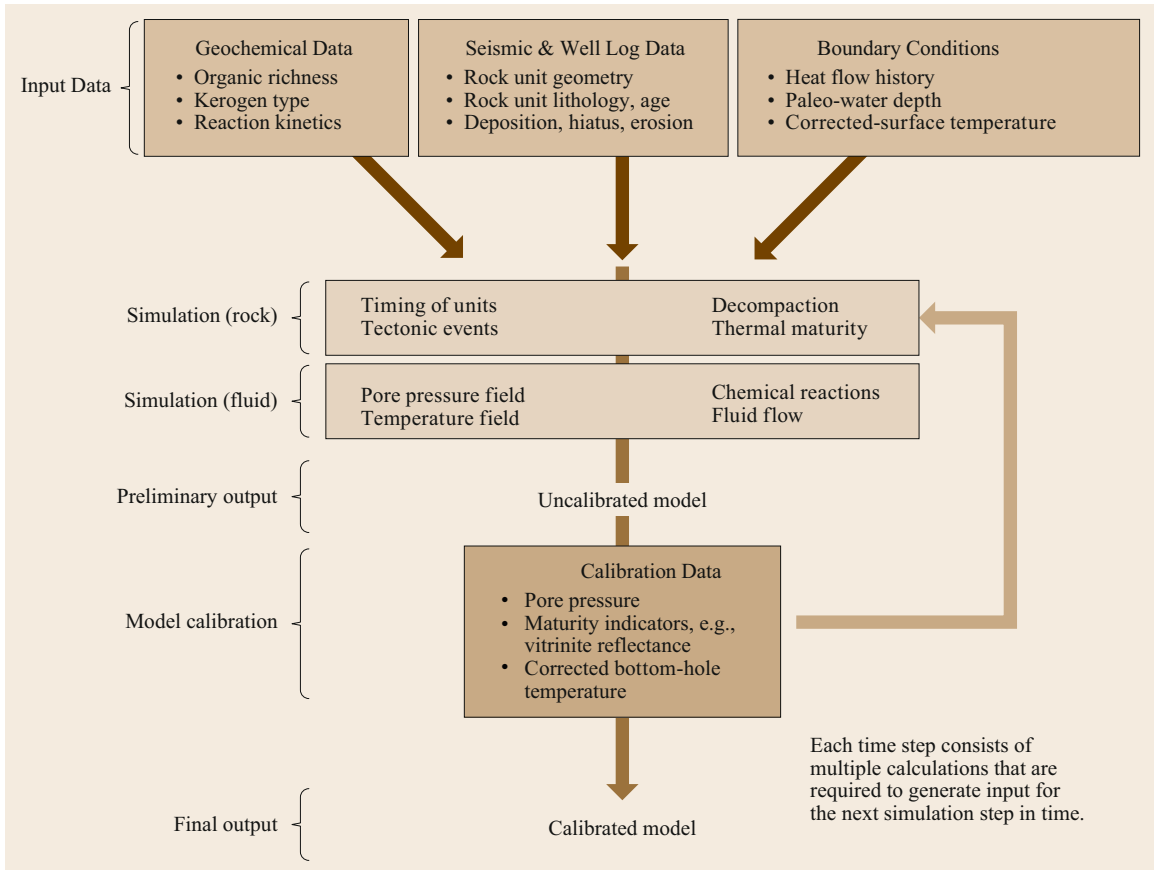


Fig. 11.1 Process workflow for basin and petroleum system modeling (BPSM) including simulation of the geohistory of the rock units and associated fluids. Modified from *Peters et al.* [11.4]

250 km under continents. Using the above criteria, six types of sedimentary basins were identified by *Dickinson* [11.14] and *Reading* [11.15]:

1. Oceanic
2. Rifted continental margins
3. Arc-trench
4. Suture
5. Intracratonic
6. Strike-slip.

Basin type is important in BPSM because it influences basal heat flow and the magnitude, timing, and distribution of temperature with depth (geothermal gradient). Understanding basin type allows the interpreter to narrow the range of possible heat flow scenarios. A simplified classification summarizes typical heat flow associated with extensional, compressional, and strike-slip sedimentary basins (Fig. 11.2) [11.11].

Although Fig. 11.2 is useful when no heat-flow data are available, it is best to determine heat flow for

each study area. Heat flow is the product of rock thermal conductivity and thermal gradient. Because thermal conductivity depends on mineralogy, texture, porosity, and fluid content of the rock, constant heat flow through heterogeneous rock units results in a piecewise linear geothermal gradient. For this reason, the temperature of a rock unit cannot be accurately estimated from average thermal gradients. *Peters and Nelson* [11.16] discuss various temperature measurements and their suitability for estimating heat flow. Thermal conductivities for a wide variety of lithologies were compiled by *Beardmore and Cull* [11.17, Table 4.2] and *Hantschel and Kauerauf* [11.1].

Acquiring accurate formation temperatures for BPSM calibration is laborious, but investigators must recognize the need for such data and they must rigorously exclude biased temperatures. Drill stem, production, or static tests provide generally reliable temperatures, but such measurements are rare. Most temperatures taken during drilling, logging, or well maintenance are inaccurate because drilling mud cools rock

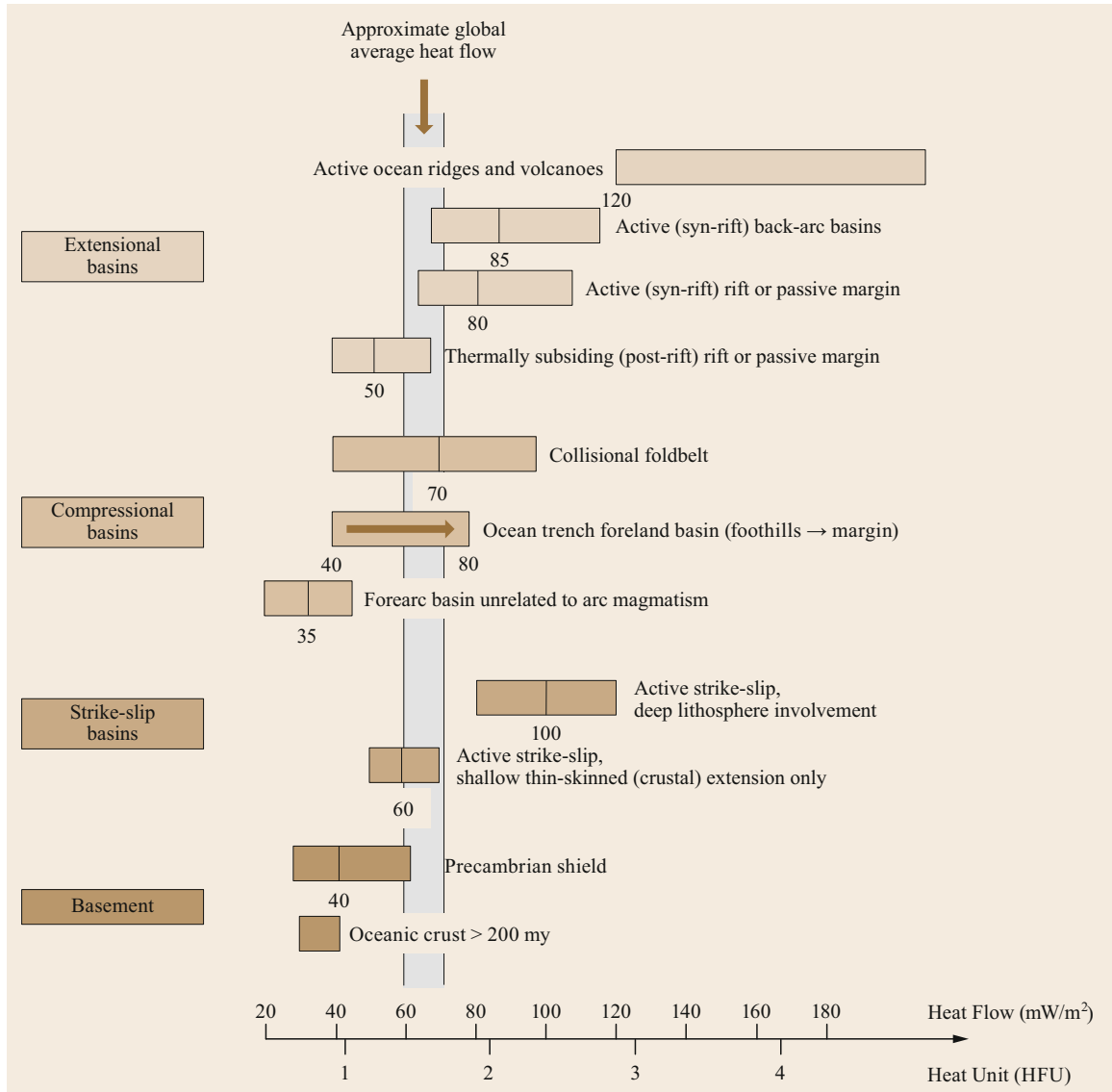


Fig. 11.2 Typical ranges of heat-flow values for extensional, compressional, strike-slip basins and basement rock (after [11.11])

adjacent to the borehole. Bottom-hole temperatures measured soon after circulation of drilling mud are common, but are generally biased to low values and require correction. Horner-corrected bottom-hole temperature (BHT) based on three time-temperature pairs measured at a single depth in a well can be useful for determining thermal gradients and for calibration of BPSM [11.16]. All interpretations of present-day thermal gradients based on temperature measurements must be constrained by the ranges of heat flow values for specific basin types in Fig. 11.2.

11.1.3 Model Input

BPSM describes the evolution of the rocks, kerogen, and generated petroleum throughout geologic history. Kerogen is the insoluble particulate organic matter in source rocks. Conceptual BPSM models can be constructed using minimal data, but abundant, high-quality input and calibration data, such as stratigraphy, subsurface structure, lithology, geochemistry, and age of the key rock units, can be used to enhance the predictive capabilities of BPSM. Geologic layers in BPSM are best

described as chronostratigraphic units in that each layer is constructed by combining time-equivalent units into a single layer [11.4] rather than lithostratigraphic units. The following is a list of recommended input data for conventional BPSM:

1. Maps of the study area, including location information (latitude, longitude) for all useful wells and culture data (e.g., block boundaries, field locations)
2. Key formations or other rock units expressed in a geologic column with standardized names across the study area that have been designated as source, reservoir, seal or non-source intervals
3. True vertical depth to formation tops relative to sea level
4. Formation ages, including diachronous units (i. e., strata having similar lithology, but differing in age at different locations); for salt basins, reconstructed salt movement through time and lithologic information
5. Age and duration of non-deposition (hiatus)
6. Amount of lost section and lithology; age and duration of erosion events
7. Lithofacies variations in maps, including porosity, permeability, capillary pressure, compaction behavior, thermal conductivity, and heat capacity
8. Structural elements, such as faults (including properties through time) and folds
9. Organofacies maps of original source-rock hydrogen index (HI, mg hydrocarbon/g TOC) and total organic carbon content (TOC, wt%) prior to thermal maturation
10. Kinetics of petroleum generation from laboratory analysis of thermally immature and representative source-rock samples
11. Boundary conditions, including sediment-water interface temperature (surface temperature corrected

for paleo-water depth) and basal heat flow through time (i. e., thermal events)

12. Calibration data, including present-day pore pressure, porosity, permeability, reservoir fluid properties (e.g., American Petroleum Institute (API) gravity, gas-oil ratio (GOR), petroleum composition, temperatures from drill stem tests (DST) or Horner-corrected BHT, vitrinite reflectance, Rock-Eval T_{max} and other maturity information, such as paleotemperatures from fluid-inclusion or fission-track analyses).

See Higley et al. [11.18] for a more comprehensive discussion of recommended input and the logistics of BPSM. Actual input can vary widely depending on the objectives of the study, including required turnaround time and availability of published information, commercial or in-house databases, seismic data, well logs, cross-sections, and lithology descriptions.

Additional input data are useful for unconventional shale plays. Although we use the term *shale* in this paper, it is important to recognize that source rocks for both conventional and unconventional petroleum consist of a wide variety of mudstones having distinct mineralogies. *Mudstone* is a general term that might be more appropriate than *shale* to describe the lithology of many source rocks, but the terms shale play, shale oil, and shale gas now represent common usage. Detailed organofacies maps of the source rock are particularly important for shale plays. Useful input for unconventional modeling includes Langmuir parameters (volume, pressure, isotherm temperature, sorption-desorption parameters), geomechanical parameters (e.g., Poisson's ratio, Young's modulus described later), and tectonic basin history (e.g., stress magnitude and direction).

11.2 Discussion

One-dimensional (1-D) BPSM reconstructs the geohistory at one location, commonly at the position of a well. Two-dimensional (2-D) BPSM reconstructs geohistory as projected along a plane. The plane is typically defined by a series of well positions, a seismic line, or a synthetic plane extrapolated from a three-dimensional (3-D) model. A 3-D BPSM reconstructs geohistory of an entire basin or portion of a basin. 3-D models are typically constructed from interpreted 3-D seismic data or multiple wells and seismic lines that are interpolated into a gridded (linear or nonlinear) array. True 2-D and 3-D models require that information, such as heat flow, fluid transport, and fluid properties, be communicated

between locations. Pseudo-2-D BPSM is simply a diagrammatic projection of 1-D results onto a plane with interpolation of information between the 1-D locations. Likewise, pseudo-3-D BPSM interpolates results from 1-D and/or 2-D models without complete information exchange within the study volume. Pseudo-3-D models can be helpful for maturity modeling in frontier areas.

11.2.1 One-Dimensional Models

1-D BPSM is based on burial histories constructed using formation tops from wells, seismic sections, outcrops, or extracts from 3-D models. Table 11.1 is an

Table 11.1 Example of input for a 1-D or 2-D basin and petroleum system model (after [11.19])

Age	Stratigraphic unit	Deposition (Ma) ^a		Thickness (m)	Erosion or hiatus (Ma) ^a		Erosion (m)	Lithology	Petroleum system element
		From	To		From	To			
Pliocene	Unnamed	0.6	0.2	0	0.2	0	25	Sandstone (typical)	Overburden
	Unnamed	2.5	2.0	0	2.0	0.6	381	Shale (typical)	
	San Joaquin	4.5	3.0	0	3.0	2.5	381	Shale (typical)	Seal
Miocene–Pliocene	Echeagoi	5.5	4.5	1570				Sandstone (typical)	Reservoir
Miocene	Monterey	13.0	5.5	0				Shale (typical)	Overburden
	Temblor	22.0	14.0	701	14.0	13.0	152	Sandstone (clay-poor)	Reservoir
Oligocene	Unnamed	37.0	30.0	0	30.0	22.0	610	Shale (typical)	Overburden
	U. Kreyenhagen	43.0	37.0	457				Sandstone (clay-rich)	
Eocene	L. Kreyenhagen	48.5	43.0	366				Shale (organic-rich)	Source
	Domengine	49.0	48.6	46	48.6	48.5	23	Sandstone (typical)	Reservoir
Paleocene–Eocene	Yokut	49.5	49.0	213				Sandstone (clay-poor)	
	Arroyo Hondo	51.5	49.5	183				Shale (organic-lean)	Seal
	Cantua	53.0	51.5	427				Sandstone (clay-poor)	Reservoir
	Cerros	55.5	53.0	107				Shale (organic-lean)	Seal
	San Carlos	58.5	55.5	274				Sandstone (clay-poor)	Reservoir
Cretaceous–Paleocene	Moreno	73.5	61.0	594	61.0	58.5	100	Shale (organic-rich)	Source
	Panoche	83.5	73.5	1000				Shale (organic-lean)	Underburden

^a Million years ago

example of input for typical 1-D or 2-D models. Based on the lithology assigned to each rock unit, porosity and permeability can be calculated at any point in the burial history using empirical compaction curves from the literature. Given present-day location, the paleolatitude of the 1-D site can be reconstructed based on plate tectonic movement through time. Paleowater depth can then be used to calculate sediment-water interface temperature [11.20]. 1-D models assess the extent of thermal maturation using a combination of paleowater depth, sediment-water interface temperature, and heat flow. Once the temperature history of the rock units has been reconstructed, 1-D models can be used to infer the extent of oil and gas generation from the source-rock interval(s) through geologic time. This requires laboratory assessment of kinetic parameters associated with the transformation of organic matter to petroleum and extrapolation to geologic time, as discussed later.

The main limitation of 1-D BPSM is that the output is at a single location and cannot account for lateral temperature and pressure gradients or 3-D fluid flow. Therefore, pseudo-2-D and -3-D visualizations built from multiple 1-D models are of limited accuracy and depend heavily on the map density of the 1-D locations. Other sources of uncertainty must also be considered, including thermal boundary conditions, accuracy of the assigned lithologies (e.g., thermal conductivity, heat capacity, compaction behavior) and calibration measurements (e.g., measured vitrinite reflectance or borehole temperatures).

11.2.2 Two-Dimensional Models

Two-dimensional models consider additional geologic factors not possible in 1-D. For example, 2-D models can include sealing or transmissible faults and can employ all of the migration methods used in 3-D models. Migration of petroleum from source rocks through carrier beds to the reservoir can be shown. Both 2-D and 3-D models offer Darcy flow, flow-path, invasion percolation, or hybrid migration methods to determine fluid flow. Multicomponent pressure-volume-temperature (PVT) calculations can be used to predict the quantity, composition, density, and viscosity of liquid, vapor and water phases throughout the burial history. 2-D models can be used to predict the composition of liquid and vapor hydrocarbon phases. However, 2-D models only allow relative comparisons between scenarios for GOR and API gravity. For example, a 14-component compositional scheme includes C_1 , C_2 , C_3 , iC_4 , nC_4 , iC_5 , nC_5 , nC_6 , C_7 – C_{15} , C_{16} – C_{25} , C_{26} – C_{35} , C_{36} – C_{45} , C_{46} – C_{55} , C_{55+} hydrocarbons [11.21]. Various time-dependent processes, such as open or closed

faults, igneous intrusions, allochthonous salt movement, and gas hydrate formation can be modeled.

The main limitation of 2-D BPSM is that the selected section may not capture the structural closure needed to register an accumulation. For this reason, careful selection of a 2-D line that passes from the depocenter to a structural high or known accumulation is recommended. Although data from wells used to build structure and isopach maps are generally proprietary, published 2-D sections that include these data are common. Volumes of petroleum in accumulations can be only approximated in 2-D models by assuming a thickness for each displayed unit. Despite this limitation, 2-D models can be used to compare the relative sizes of predicted accumulations resulting from different model scenarios.

11.2.3 Three-Dimensional Models

There are many advantages offered by 3-D models, including reconstruction of petroleum migration pathways to traps that may or may not have been previously identified by drilling. Maps of the pod of active source rock based on calculated transformation ratio (TR, extent of conversion of kerogen to petroleum) through time can be prepared. Volumes of petroleum generated, accumulated, and lost during migration can be estimated and flash calculations can be used to predict the properties of trapped petroleum at surface conditions during production. As discussed above, both 2-D and 3-D models can utilize Darcy flow, flow-path, invasion percolation, or hybrid migration methods. 3-D modeling is the only method for quantitative analysis of API gravity, GOR, pore pressures, or volumetrics of accumulations, although relative volumes can be compared using 2-D models.

An additional advantage of 3-D models is that they can be broken into smaller areas within the greater model and run using finer grid spacing than the large model might allow due to computing restraints. This so-called local grid refinement (LGR), allows improved resolution of key regions within the study area without the need to rerun the entire model (Fig. 11.3), but reservoir-scale spatial resolution of the input data is required.

The principal disadvantages of 3-D BPSM are an important consideration when deciding on a 1-D, 2-D, or 3-D modeling study. Although appealing, realistic 3-D models generally require more data and time to construct than 1-D or 2-D models, and necessary computer processing time may impede the progress of other studies having deadlines. Computing speed and available computer hardware specifications strongly influence the resolution that is possible for model processing and display. In addition, 3-D models that are inade-

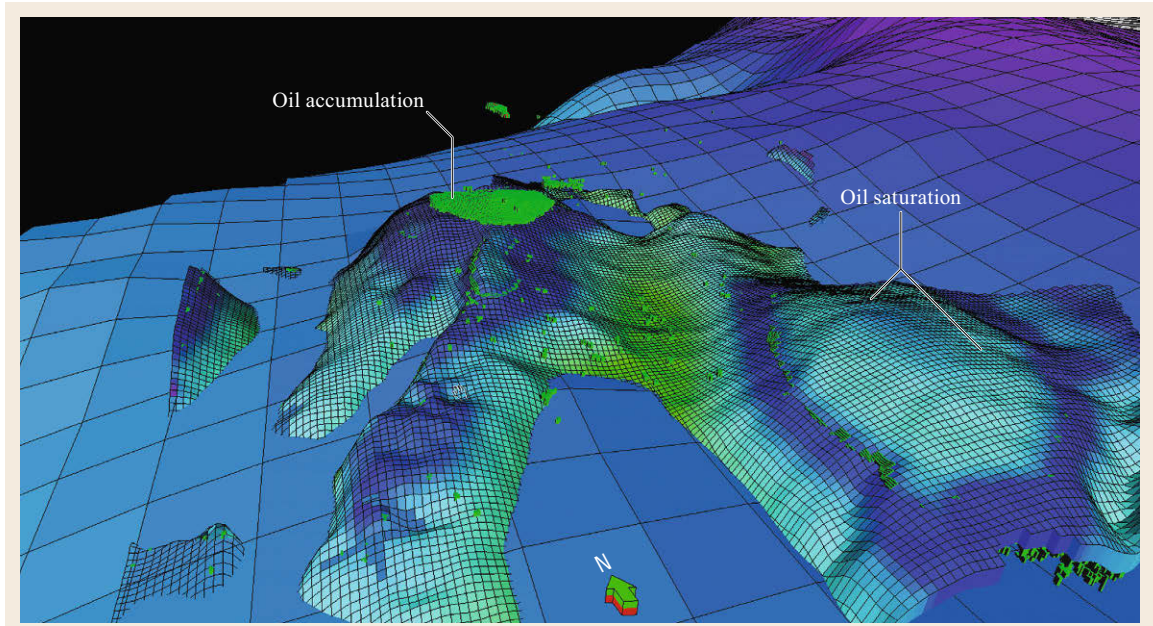


Fig. 11.3 Example showing a local grid refinement (LGR) within a larger discretized 3-D model. The oil accumulation (green cubes) initially modeled on the large grid ($3\text{ km} \times 3\text{ km}$) can be examined in more detail using the small grid ($200 \times 200\text{ m}$) in the LGR. Grid cell thickness varies, but is typically 400 m or less. Modified from *Al-Hajeri et al.* [11.2]. Figure copyright Schlumberger, used with permission

quately populated by measured data can be misleading compared to simpler 1-D or 2-D models that are better constrained.

11.2.4 Risk Analysis

A BPSM master run is based on input for each variable that is deemed to be the most accurate deterministic representation of nature. In effect, a master run assumes that uncertainties in the input data do not exist. However, every input variable in BPSM has associated uncertainty. The classical approach to address uncertainty is to run *high* and *low* scenarios in addition to the master run. For example, an uncertain temperature history might be addressed by low, master, and high heat-flow scenarios, while all other input variables are kept constant. Shortcomings of the classical approach are: (1) the choice of the most likely deterministic scenario depicted by the master run is at best a qualified guess, and (2) the approach is not systematic and it ignores the uncertainty associated with other input parameters.

Monte Carlo or Latin hypercube statistical sampling of the uncertainties associated with multiple input parameters can be used in BPSM to provide more quantitative assessment of risk. To perform such simulations, uncertainty distributions are assigned to key input parameters, such as heat flow, thermal conductivity, permeabil-

ity, capillary pressure, total organic carbon, hydrogen index, or kinetics. For most parameters, uncertainty distributions are based on measured variations from wells in the study area or modeled using normal, logarithmic normal, nominal, triangular, or uniform distributions. Other parameters, such as kinetics, can be modeled using two sets of kinetic parameters, which are alternately sampled during the simulation. Details of risk analysis are discussed in *Hantschel and Kauerauf* [11.1].

A tornado diagram (Fig. 11.4) compares the relative impact of risk among various input parameters. Tornado diagrams can be used to evaluate which parameters exert more influence on the calculated results and they are particularly useful to identify where further data acquisition might reduce model uncertainty. In the figure, source-rock HI, thermal gradient, and kinetics have the greatest impact on uncertainty for this model. A disadvantage of risk analysis is that long compute times and many simulations may be required for statistically meaningful results.

11.2.5 Rock Stress and Pressure Prediction

Subsurface pressure influences fluid expulsion and migration. Fluid-pressure modeling can be used to improve pore pressure prediction and reduce the drilling risk posed by unanticipated overpressures. Geomechan-

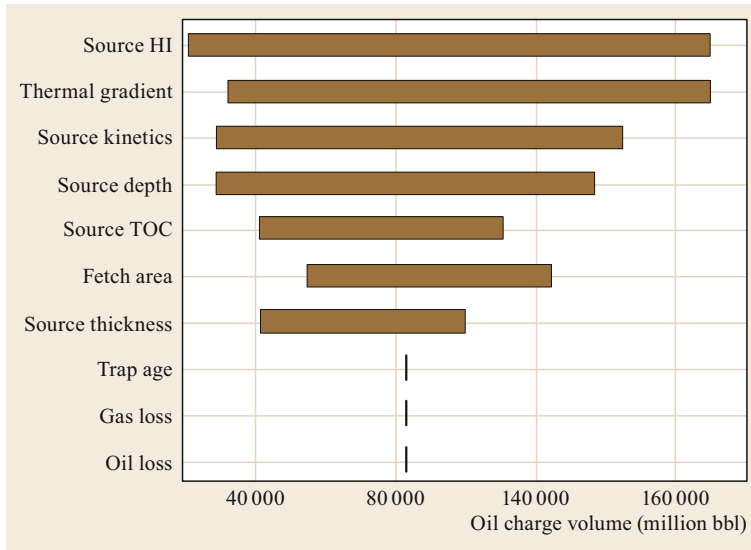


Fig. 11.4 Tornado diagram showing the relative impact of various input parameters on calculated prospect volumes (after [11.22], reprinted by permission of AAPG whose permission is required for further use)

ical modeling describes the response of rock to an external load and includes analysis of both fluid pressure and rock stress.

For pressure calculations, traditional BPSM generally treats dewatering as single-phase flow driven by changes in overburden weight caused by sedimentation (Fig. 11.5). Lithostatic pressure represents overburden weight. In contrast, hydrostatic pressure specifies the weight of the water column under equilibrium pressure conditions when there is no fluid flow. Fluid expulsion occurs as the sediments compact and overburden-induced pressure is reduced. The resulting pore pressure is usually less than lithostatic. The difference between lithostatic pressure and pore pressure is called effective stress, which specifies the amount of compaction. The difference between pore pressure and hydrostatic pressure is defined as overpressure (excess hydraulic pressure), which directly controls fluid flow. Rapid burial, which is common in deltaic settings, coupled with low permeability of fine-grained mudstones, results in the sediments being unable to dewater at rates in accordance with normal compaction. The resulting overpressure can retard compaction. Undercompaction also can be caused by fluid expansion during petroleum generation, as well as other generally less-important processes [11.23]. Compaction changes many lithologic properties, such as porosity, bulk density, thermal conductivity, and heat capacity, and this can be addressed in coupled pressure-temperature simulations.

11.2.6 Terzaghi Rock Stress Modeling

The traditional Terzaghi rock stress model [11.1] is based only on vertical stress. The vertical stress com-

ponent is the maximum principal stress (σ_1), which is identical to the overburden or lithostatic stress [11.1]. Extension of the Terzaghi model to a complete 3-D stress-strain poroelasticity model as originally formulated by *Biot* [11.24], or a 3-D poroplasticity model, allows improved predictions of stress-strain relationships, rock failure (fracture analysis), sealing capacity (fracture orientations and fault properties), and specific geomechanical effects caused by salt deformation and tectonic movement. Poroelasticity describes 3-D stress-strain relationships and can be used to differentiate subsurface regions that tend to be more strained and thus are more likely to fracture. Poroplasticity addresses rock failure based on the analysis of fractures and faults. Poroelasticity and rock failure are described in more detail later in the section on unconventional resources.

11.2.7 Compaction

Simple compaction modeling is based on assumptions that: (1) the volume of solids is conserved, i.e., mechanical compaction due to overlying water-sediment depends solely on porosity reduction, and (2) the sediments are normally (hydrostatically) pressured, i.e., water is free to be expelled from the pore space, while grain-grain contacts support the rock unit. Porosity-depth relationships based on laboratory and subsurface measurements can be expressed as negative exponential curves, which depend on the lithology of each rock unit. The porosity-depth relationship for normally pressured sediments is

$$\phi = \phi_0 e^{-cz}, \quad (11.1)$$

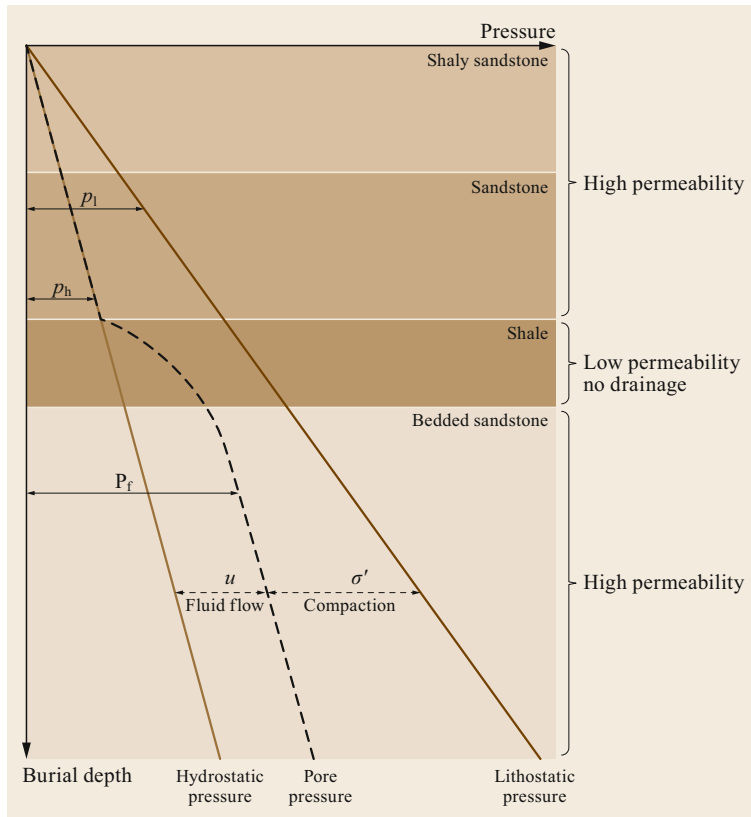


Fig. 11.5 Schematic of subsurface pressure conditions illustrating different types of pressure, fluid flow, and compaction. p_h = hydrostatic pressure, p_l = lithostatic pressure, u = excess hydraulic pressure (overpressure), σ' = effective stress. Pressures are commonly recorded in MPa (megapascal)

where ϕ is porosity at any depth z , ϕ_0 is depositional porosity at the surface, and c is a coefficient that depends on lithology and describes the slope of the porosity-depth curve.

Because (11.1) assumes that the volume of solids is conserved during compaction, the rate of compaction is mainly controlled by compressibility and porosity of the sediments and the expulsion rate of pore fluids. However, when fluids are trapped in sediments due to reduced hydraulic permeability, increased fluid pressure retards compaction. *Terzaghi's law* [11.25] describes the impact of fluid pressure on compaction by introducing the effective stress (σ') term

$$\sigma'_z = \sigma_z - p_f, \quad (11.2)$$

where σ'_z is the vertical component of the effective stress, σ_z is the vertical compressive (overburden) stress and p_f is the pore fluid pressure (Fig. 11.5). Assuming increased sediment load, the additional vertical stress is taken up by increased pore fluid pressure. Expulsion of pore water decreases fluid pressure and increases effective stress, resulting in compaction. Compaction can be formulated using effective stress (σ') instead of depth as follows

$$\phi = \phi_0 e^{-c\sigma'_z}. \quad (11.3)$$

Because the behavior of many rock types differs from ideal, variations of (11.3) for compaction have been published. *Hantschel* and *Kauerauf* [11.1] provide a list and description of various compaction models.

Muds generally compact faster with depth than sands as a result of their higher original porosity. However, the extent of compaction can be highly variable [11.26]. Therefore, it is best to use measured porosity to create a compaction model for each study area. If such data are unavailable, then a default compaction model can be used. Some popular default models for sediment compaction include *Sclater* and *Christie* [11.27], *Falvey* and *Middleton* [11.28], and *Baldwin* and *Butler* [11.29]. Wherever possible, measured porosity data should be used to validate the use of a default compaction model [11.17].

Bulk compressibility (C) is an important lithologic property for compaction and pore-pressure calculations. It describes the volumetric strain resulting from changes in rock stress, i. e., the ability of the rock framework to compact. For Terzaghi-type models, which are based on the lithostatic pressure concept, the compressibility is called Terzaghi-compressibility (C_T). It represents the ratio of volumetric strain to changes in vertical effective stress and defines the slope of the porosity-effective stress curve. Because mechanical compaction

is irreversible, porosity achieved during burial is largely retained, even when uplift reduces the effective stress. Therefore, effective stress is used for basins unaffected by uplift, whereas maximum effective stress is used for uplifted basins because the porosity was established prior to uplift.

Increased pore pressure with burial depth fails to completely counteract the effect of confining pressure. For this reason, *Biot* [11.24] established a more detailed poroelastic model that describes the decreasing effect of pore pressure with depth

$$\sigma'_z = \sigma_z - \alpha p_f, \quad (11.4)$$

where α is the Biot coefficient, which ranges between 0 and 1. For unconsolidated sediments, α is ≈ 1 and the Terzaghi effective stress formulation holds (compare to (11.2)). However, at greater depth and decreased porosity, α approaches 0, i. e., the effect of pore pressure is reduced.

Chemical compaction that accompanies cementation in sandstone and carbonate can be as important as mechanical compaction. This complex diagenetic process is mainly temperature-driven and becomes more important in deeply buried strata where porosity has already been reduced by mechanical compaction. Porosity reduction by chemical compaction may include dissolution, transport by diffusion, and precipitation. Chemical compaction can be described by an Arrhenius-type equation [11.30, 31], but it is also influenced by pore chemistry, effective stress, fluid viscosity, mineralogy, and rock fabric. Carbonate compaction is highly variable, and generally poorly understood. It depends mainly on cementation and pressure solution rather than mechanical compaction [11.32].

11.2.8 Pore-Pressure Formation

Pressure-driven fluid flow is the most efficient transport mechanism in sedimentary basins. The driving force for pore water flow is the overpressure gradient (Fig. 11.5). Overpressure formation couples fluid flow and compaction. Darcy's law describes this as a linear relationship between volume flux of the pore fluid (v) and the overpressure gradient

$$v = -\frac{k}{\nu} \left(\frac{dp}{dx} \right) = -\mu \left(\frac{dp}{dx} \right), \quad (11.5)$$

where dp/dx is the pressure gradient and μ is the mobility of the pore fluid, which depends on intrinsic permeability (k) and dynamic viscosity (ν). Fluid dynamic viscosity describes the resistance of the fluid

to flow depending on pressure, temperature, and fluid type. Intrinsic permeability is mainly affected by pore throat diameter and connectivity, which depend on the compaction state, and is thus a function of porosity. This exponential relationship must be adjusted for rock type. Multiphase pore fluids have different pressures in each phase. The pressure differences are represented by saturation-dependent capillary pressures, which can be significant in source and reservoir rocks. Rock permeability is also anisotropic, which is simplified in BPSM by introducing an anisotropy factor. Permeability is commonly derived from measurements on rock samples and needs to be upscaled for modeling (see below).

Overpressure can be caused by various processes, but the most influential are disequilibrium compaction due to rapid burial of fine-grained sediments [11.33] and hydrocarbon generation due to cracking [11.23]. Overpressure calibration can be complex. For basins in which sediments are affected mainly by mechanical compaction, the standard approach is to calibrate overpressure adjustments of compressibility (or effective stress versus porosity) and permeability in two steps: (1) the selected compaction law must be calibrated locally to measured porosity versus effective stress, and (2) permeabilities of the overpressured strata must be adjusted to fit calculated and measured pressures. Overpressure calibration can be difficult where the pressure regime is affected by other processes in addition to mechanical compaction, such as chemical compaction or fluid expansion. Because compaction causes changes in many lithologic properties, such as porosity, density, thermal conductivity, and heat capacity, overpressure calibration should be conducted prior to thermal calibration.

11.2.9 Mixing and Upscaling Rules

Most bulk properties in BPSM must be derived from measurements of mineral or fluid components using mixing or upscaling rules. For example, bulk densities, thermal conductivities, or heat capacities for rock units in the model must be calculated by averaging properties of the rock matrix and the pore fluid. Three basic methods for mixing and upscaling include arithmetic, harmonic, and geometric averaging. The mathematics for each method are given in *Hantschel and Kauerauf* [11.1, pp. 385–386] along with a table that identifies which mixing method applies for a given property. For example, arithmetic mixing is appropriate for calculations of bulk density, heat capacity, porosity, or critical oil saturation. Rock thermal conductivity or permeability are calculated using different mixture and upscaling rules, depending

on how the mineral grains are arranged in the rock unit:

1. Arithmetic for layering of the grains along flow direction
2. Harmonic for layering perpendicular to flow
3. Geometric for randomly oriented mineral grains.

11.2.10 Geohistory Analysis

Understanding of the dynamics of sedimentary basins and their associated fluids is required for evaluation of the timing of petroleum generation, migration, and accumulation in relation to trap formation. Geohistory analysis quantifies subsidence rates through geologic time [11.34] to visualize the vertical movement of each stratigraphic unit after deposition as an indicator of subsidence and uplift history. Geohistory analysis involves decompaction of each stratigraphic unit to its original thickness and corrections based on paleobathymetry and changes in eustasy. Several parameters are required for geohistory analysis:

1. Present-day thickness of stratigraphic units
2. Lithology
3. Stratigraphic age
4. Paleowater depth.

Additional data, such as porosity and maturity indicators, help to constrain and calibrate burial and thermal history. The resulting total subsidence can be expressed as a curve. To examine the tectonic contribution to subsidence, the effects of sedimentary loading must be removed from the total subsidence curve by backstripping, as discussed later.

Geohistory analysis of basins that have undergone minimal structural deformation involves four steps:

1. Plot sediment accumulation in the study area through time using present-day thickness of each stratigraphic unit
2. Decompact each unit to the thickness prior to burial and plot a corrected accumulation curve
3. Correct for depositional water depth through time, accounting for paleobathymetry and eustasy
4. Backstrip to reveal the tectonic component of subsidence (see below).

Sediment thickness can be obtained directly from well logs corrected to true vertical depth, or seismic data when accurate two-way seismic travel times are available. In addition, the geologic age of each formation top can be estimated by various methods, including biostratigraphy and radiometric dating.

11.2.11 Decompaction

To calculate decompacted thickness of a stratigraphic unit at any time in the past, the overlying rock units need to be removed sequentially. Using the basic assumption that the volume of solids is conserved, the decompacted thickness (d_0) can be calculated as follows

$$d_0 = d \frac{(1 - \phi)}{(1 - \phi_0)}, \quad (11.6)$$

where d is thickness and ϕ and ϕ_0 are the porosity and decompacted porosity respectively.

For clastic sediments, decompaction requires regional porosity-depth relationships. As described above, the porosity of normally pressured shale or sandstone typically decreases exponentially with depth (11.1). However, overpressure of pore fluids inhibits compaction. The porosity-maximum effective stress relationship (11.3) considers both pore fluid pressure and erosion.

Since pore pressure influences porosity evolution, depositional porosity can only be approximated from the relationships described above. Therefore, the first simulation run uses steady-state values for hydrostatic pressure conditions to decompact the sediments. Forward modeling that assumes that compaction is controlled by pore pressure then yields a present-day geometry that usually deviates from that of the input model. Model iterations using decompacted thickness allow improved optimization. Cementation, mineral transformations, fluid expansion (e.g., aquathermal or hydrocarbon generation), and chemical compaction by pressure solution are excluded in this decompaction approach, but modeling techniques can consider the effect of such processes on porosity evolution in iterative steps.

11.2.12 Paleobathymetry

Water depth changes through time during sediment deposition. To obtain the geohistory relative to a fixed reference level, the subsidence curve needs to be corrected for the effects of paleowater depth. Information on paleobathymetry can be obtained from biostratigraphy, sedimentary facies, and geochemical data [11.35]. For example, carbonate shells dissolve below the carbonate compensation depth (CCD) in the oceans [11.36]. If the sea floor is below the CCD, carbonate shells of calcareous plankton will dissolve. Depth to the CCD varies. For example, the present CCD occurs at about 5000 m in the temperate and tropical Atlantic Ocean and at about 4200–4500 m in the Pacific Ocean, except

near the equatorial upwelling zone where the CCD occurs at about 5000 m.

11.2.13 Eustatic Corrections

Eustasy describes global sea-level changes relative to a reference datum. Temporal changes in the sea-level datum can cause errors in calculations of basin subsidence history unless they are included in modeling. However, disagreement exists on details of global sea-level change, so it is advised to use only long-term eustatic fluctuations for modeling [11.11].

11.2.14 Backstripping

Decompaction and paleobathymetry determine the evolution of the basin floor and can be described by the total subsidence through time. Total subsidence is the sum of subsidence due to sediment loading and tectonic subsidence. Backstripping removes the isostatic effects of the sediment and water loads to reveal the tectonic component of subsidence. During successive removal of layers from the sediment column, densities, decompacted thicknesses, paleowater depths, and sea-level changes are used to calculate the hypothetical depth of the basin floor without isostatic response [11.10]. This is most commonly done using local (Airy) isostatic compensation. However, if the lithosphere supports the sediment load by regional flexure, backstripping is more complex [11.11].

Backstripping provides paleogeometries that are used again to forward-simulate deposition and compaction; such basin models are also called event-step models. This approach is satisfactory for basins that are characterized by simple sedimentary burial and subsidence with minimal structural deformation. However, complex tectonic events result in strongly deformed geometries that cannot be modeled by backstripping. Such settings include basins in compressional [11.37–39] or strike-slip tectonic regimes [11.40], and basins influenced by mobile salt [11.41]. To model such basins, predetermined paleogeometries are required as input. Structural restoration programs provide balanced and decompacted paleogeometries for individual tectonic phases. Forward modeling then interpolates from one paleostep to the next (paleostep model) and porosities are calculated from effective stress, whereas layer thicknesses are predefined [11.1].

11.2.15 Original Organic Richness

Petroleum generative potential depends on the original quantity and quality of organic matter in thermally

immature source rock. However, thermal maturation decreases generative potential. Thus, field measurements of the quantity and quality of organic matter in mature or postmature source rocks need to be corrected to original values for use in BPSM. By making some assumptions, the fractional conversion of source-rock organic matter to petroleum (f) and original TOC (TOC^0) can be calculated using the following equations (11.7) and (11.8) [11.42]

$$f = 1 - \frac{\text{HI}^x \left(1200 - \left[\frac{\text{HI}^0}{(1-PI^0)} \right] \right)}{\text{HI}^0 \left(1200 - \left[\frac{\text{HI}^x}{(1-PI^x)} \right] \right)} \quad (11.7)$$

PI^0 and PI^x are the original and measured Rock-Eval production indices ($PI = S1/(S1 + S2)$) respectively. PI^0 is assumed to be 0.02 for most thermally immature source rocks. The original hydrogen index (HI^0) can be estimated by various methods. For example, if thermally immature equivalents of a mature source rock are available and spatial variations in organic facies are minimal, measured HI^x is assumed to equal HI^0 . If no immature rock equivalents are available, then petrographic and paleoenvironmental information can be used to estimate HI^0 .

The original TOC in source rock prior to maturation is constrained by mass balance

$$\text{TOC}^0 = \frac{83.33(\text{HI}^x)(\text{TOC}^x)}{\text{HI}^0(1-f)(83.33 - \text{TOC}^x) + \text{HI}^x(\text{TOC}^x)} \quad (11.8)$$

where 83.33 is the percentage of carbon in the generated petroleum. For input to BPSM, maps of TOC^0 and HI^0 are superior to assuming constant TOC^0 or HI^0 in a given source rock.

11.2.16 Thermal Modeling and Temperature Prediction

Rocks achieve higher temperatures and pressures during progressive burial, which results in increased thermal maturity of kerogen. The most important parameters that control thermal maturity are temperature and time, as described by the Arrhenius equation (see later discussion). Thermal modeling of petroleum generation must account for heat provided by conduction, convection, and radioactive decay. The main thermal properties of rocks are conductivity, heat capacity, and radiogenic heat production. Details of these properties for various lithologies and fluids over wide temperature ranges are well known [11.1].

11.2.17 Heat Conduction and Convection

Heat conduction, the transfer of thermal energy by contact, is the primary thermal process in the shallow lithosphere [11.16]. The key parameter for thermal conduction is thermal conductivity, which depends on lithology, porosity, and temperature. Since rocks contain solid, liquid and vapor phases, bulk thermal conductivity, phase-behavior, and porosity need to be considered in the models. Simulations also need to take into account the influence of thermally anisotropic lithology. For example, thermal conductivity in shale is much higher parallel to rather than perpendicular to bedding.

Convection occurs when heat is transported by movement of solid or fluid. In sedimentary basins, heat convection generally involves the flow of pore water

and petroleum, which depends on fluid viscosity, temperature, rock porosity, and permeability. Convection can be more efficient than conduction when fluid flow rates are high, as might occur in foreland basins where water recharge from topographic highs displaces basin brines. A key parameter for heat convection is specific heat capacity, which describes the ability of the rock to store heat, and is largely controlled by lithology and porosity.

Radiogenic heat production can be significant when (1) the basin fill rests on relatively young granitic basement or (2) *hot shales* with abundant radioactive elements (uranium, thorium, potassium) occur within the basin fill. Radiogenic heat production is generally lowest in evaporite and carbonate rock, low to medium in sandstone, higher in shale and siltstone, and very high in black shale (organic matter) and granite (potassium)

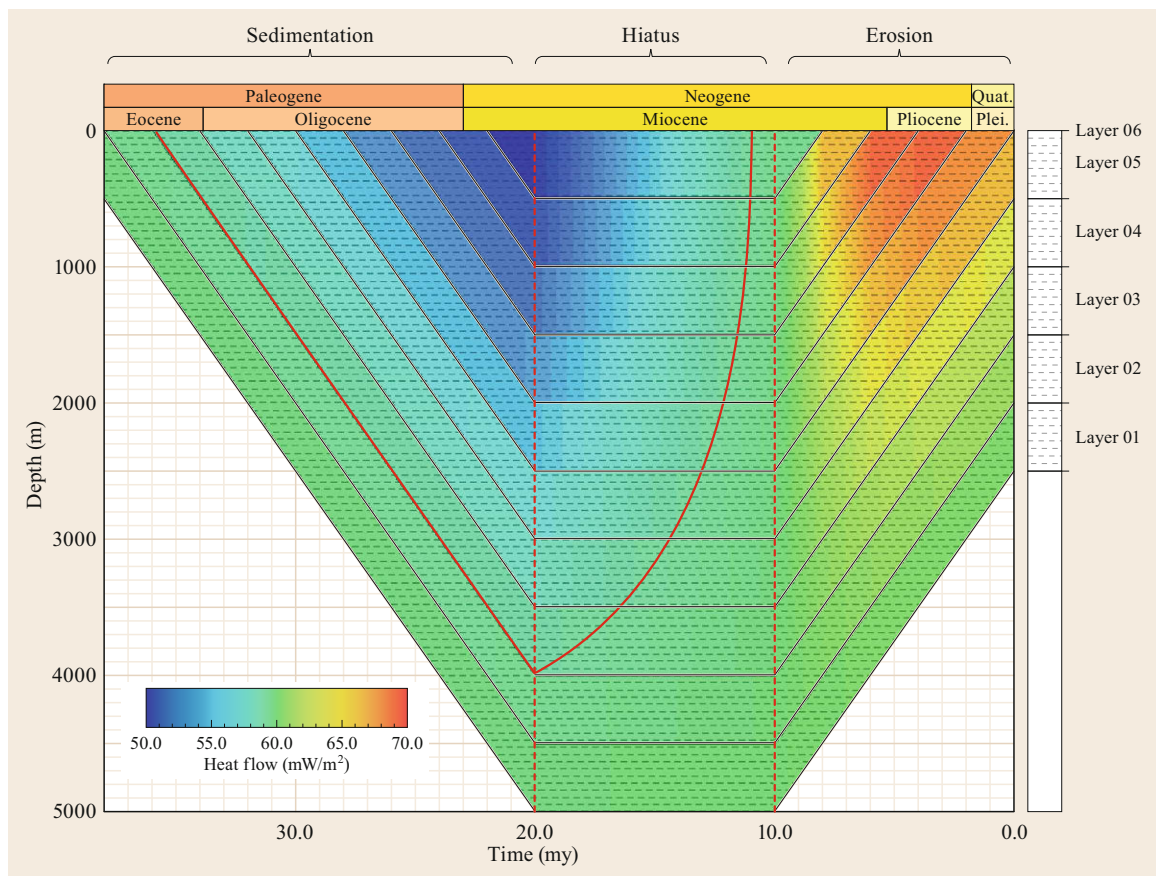


Fig. 11.6 Transient effects influence the timing of temperature and heat flow. This example shows the effect of rapid sedimentation of pure shale without compaction (*left*), where basal heat flow is fixed at 60 mW/m^2 . Unlike the steady-state condition (60 mW/m^2 through 5 km), heat flow decreases toward the surface because heat is absorbed by each layer. During the depositional hiatus (*center*) heat flow gradually returns to steady-state values (example assumes no radioactivity). During rapid erosion, heat flow is higher than the steady-state solution and increases toward the surface (after [11.1])

feldspars). Spectral gamma logs can be used to locally calibrate radiogenic input. However, in most cases, the radiogenic contribution can be approximated by selecting an appropriate default lithology in the BPSM software.

Because the main direction of heat flow in sedimentary basins is upward, it is possible to approximate the process using 1-D models. The steady-state heat flow solution is the simplest pattern where all temperatures are in equilibrium based on thermal conductivities and boundary conditions. Transient thermal effects caused by thermal inertia increase the complexity of heat-flow analysis (Fig. 11.6). Transient heat can be quantified by the time required for the rock to reach thermal equilibrium. Transient effects can occur during rapid deposition or erosion, or when thermal boundary conditions change, e.g., geologically rapid removal of an ice sheet. A measure of the transient effect is the ratio of specific heat capacity to thermal conductivity [11.1].

11.2.18 Boundary Conditions

BPSM requires thermal boundary conditions at the top and base of the sedimentary column. The top boundary condition is a temperature, which varies with latitude and water depth through geologic time. These temperatures can be related to geologic age and mean surface paleotemperature based on plate tectonic reconstructions [11.20]. Based on plate reconstruction, the paleolatitudes can be reconstructed and used to estimate paleosurface temperature. Together with the paleowater depth, the sediment surface temperature can be estimated (onshore, surface temperature; offshore, sediment–water interface temperature).

The basal thermal boundary condition can be either the assumed temperature at the base of the lithosphere (1333 °C) or the calculated basal heat flow. The heat-flow boundary condition is commonly used because it summarizes all uncertainties in one parameter, which simplifies calibration. Heat flow is one of the most critical input parameters for BPSM due to its impact on the amount, composition, and rate of petroleum generation. Although present-day heat flow may be known, paleo-heat flow is usually poorly constrained. Basal heat-flow values are often predicted by crustal models in separate preprocessing programs or they are interactively calculated for each geological event. Partly for this reason, model simulations use heat flow as a primary variable to calibrate calculated maturity and temperature curves with depth to measured maturity values (e.g., vitrinite reflectance) and corrected borehole temperatures from wells [11.16]. For extensional basins, many simulations use McKenzie's thermal model of subsidence [11.43] or variations of this thermal model.

11.2.19 Petroleum Generation

Figure 11.7 shows the generalized evolution of organic matter during and after sedimentation. Hydrocarbon gas can be created at shallow depth (biogenic) or deeper (thermogenic), when associated with oil generation from kerogen or secondary cracking of oil. Gas generation does not continue indefinitely with depth, as depicted in earlier profiles [11.44, Fig. II.7.1], but ends when the kerogen is depleted. Many biomarkers survive diagenesis and catagenesis prior to complete destruction during late catagenesis and metagenesis [11.42]. The depth scale varies depending on different factors, such as the geothermal gradient or kinetics of petroleum generation. The scheme is generally applicable, particularly for marine source rocks, which dominate the geologic record [11.45].

Oil and gas generation depend on deposition of organic-rich fine-grained sediments, preservation, and thermal alteration, usually due to burial [11.46]. Three stages in the evolution of sedimentary organic matter (Fig. 11.7) include:

1. Diagenesis, i.e., transformations that occur prior to significant thermal alteration (e.g., generation of microbial methane)
2. Catagenesis or thermal transformation of kerogen to petroleum in the approximate range 50–200 °C
3. Metagenesis or thermal destruction of petroleum at approximately 200 °C or higher, but prior to greenschist metamorphism.

11.2.20 Diagenesis, Catagenesis, Metagenesis

Pure methane (dry gas) can be generated by methanogenic archaea in shallow sediments (< 1 km) in an optimum temperature range of ≈ 35 –45 °C [11.47, 48] (Fig. 11.7). Subsurface biodegradation is mainly an anaerobic microbial process that generates dry gas over geologic time by two different mechanisms. Primary biogenic methane originates by microbial reduction of acetate or carbon dioxide liberated from thermally immature dispersed organic matter in source rock or coal. The source rock commonly serves as a shallow unconventional reservoir, although short-distance migration to conventional reservoir rocks also occurs. Several factors control primary biogenic gas generation, including source-rock organic richness, herbaceous vegetation, fast sedimentation of juxtaposed source and reservoir rock intervals, and low temperature (< 80 °C).

Primary microbial methane was believed to account for up to 20% of worldwide commercial gas accumula-

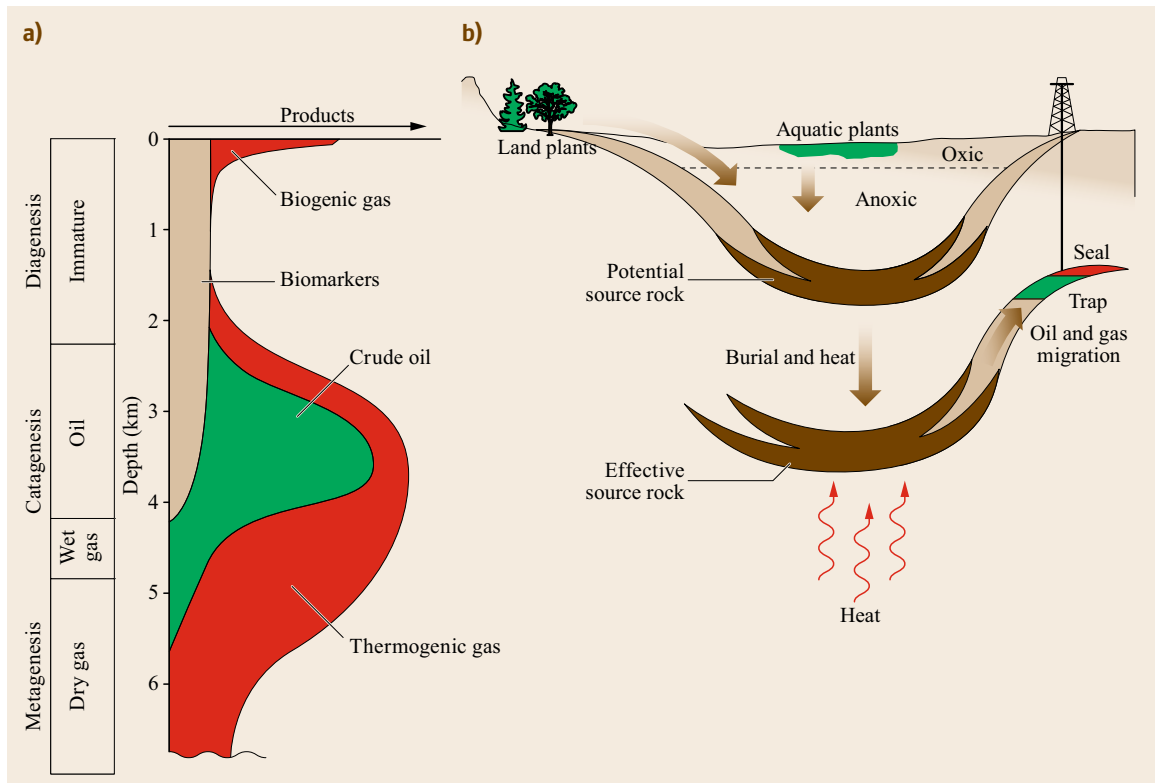


Fig. 11.7a,b Schematic stratigraphic column (a) depicts the generalized evolution of organic matter during and after sedimentation. The depths for top and bottom of the oil window vary depending on geothermal gradient and kerogen kinetics. Preservation of organic matter, especially under anoxic conditions during diagenesis, can result in potential source rock, which undergoes burial and thermal maturation to become effective source rock for migrated petroleum. (b) Unconventional petroleum remains in the source rock, which effectively becomes reservoir rock (after [11.42], reprinted with permission by ChevronTexaco Exploration and Production Technology Company, a division of Chevron USA Inc.)

tions [11.47], although evidence for secondary microbial methane generated by degradation of crude oil suggests a considerably smaller contribution [11.49]. Measurements of gas wetness and stable carbon and deuterium isotope ratios of the methane, carbon dioxide, and other gases allow biogenic and thermogenic gases to be differentiated [11.49, 50]. Stable carbon isotope ratios can also be used to estimate abundances of end members in two-component mixtures, i. e., biogenic-thermogenic gas mixtures [11.51]. Secondary biogenic gas originates by microbial degradation of thermogenic gas in conventional reservoirs at the oil-water contact, where heavier hydrocarbons are converted to methane and a heavy oil residuum. This process likely involves syntrophic bacteria and methanogenic archaea that ferment alkanes to hydrogen and acetate, oxidize the acetate to carbon dioxide and hydrogen, and then reduce the carbon dioxide to methane [11.52]. There are at least three different carbon-flow pathways employed by different methanogens [11.50]:

1. Hydrogenotrophic
2. Acetotrophic
3. Methylotrophic.

In BPSM, microbial gas can be calculated by defining a Gaussian distribution of temperatures governing microbial activity. Burial history is important because reservoirs are effectively pasteurized above 80 °C. For example, burial to this temperature followed by uplift of the reservoir commonly results in no further biodegradation of the trapped oil [11.53]. Other criteria that control secondary biogenic gas generation [11.42] include access to petroleum and nutrients (e.g., nitrate, phosphate) at the oil-water contact, low water salinity (< 100–150 ppm) and little or no sulfate (sulfate reducers outcompete methanogens).

Catagenesis begins at ≈ 50 °C and ends at ≈ 200 °C, when oil generation from labile kerogen is complete [11.54]. Much of the initial petroleum generated from oil-prone source rock is liquid that con-

tains dissolved associated vapor or components that would be gaseous at surface conditions. Above 150 °C, the remaining hydrogen-poor kerogen generates mainly thermogenic hydrocarbon gas, which may initially be enriched in dissolved condensate, but becomes drier (proportionally more methane) as generation nears completion. In the Gulf of Mexico Smackover Formation, complete fractional conversion of oil to gas corresponds to ≈ 200 °C and vitrinite reflectance (R_o) of 2.0% [11.42]. In contrast, Tian et al. [11.55] used pyrolysis of Triassic oil from the Tarim Basin and analysis of the resulting gas and residual hydrocarbons to show that complete cracking of wet gases to methane requires $R_o > 2.4\%$.

The extent of transformation of kerogen to petroleum within organic-rich source rock is commonly quantified in BPSM by the transformation ratio (TR) or vitrinite reflectance (R_o). TR expresses the converted mass fraction of the initial reactant, i. e., the ratio of petroleum formed from kerogen in source rock to the total amount of petroleum that could be formed from that kerogen [11.44]. R_o is the calibrated percentage of light that is reflected from a polished coal maceral called vitrinite that originates from higher plants. Accurate R_o may be difficult to obtain in organic-rich marine sediments having little or no land plant input. For this reason, R_o is normally measured in organic-lean shales above and below the source rock. In BPSM, vitrinite reflectance is calculated (EASY% R_o) for comparison with measured R_o using kinetics established by Sweeney and Burnham [11.56]. Although commonly used interchangeably, R_o and TR have different kinetics. R_o kinetics start at an activation energy (E_a) of 36 kcal/mol, whereas most hydrocarbon generation kinetics start at least 10 kcal/mol later [11.57]. Because the frequency factors are nearly the same, the difference in E_a explains the significant difference between R_o and TR during early maturation, when R_o increases but TR remains near zero [11.57]. It is important to recognize that the TR kinetics vary with kerogen type, as discussed later.

In BPSM, TR and R_o can be examined through geologic time to identify the onset of oil generation, typically defined as 0.6% R_o or 10% TR [11.4]. The critical moment of the petroleum system is the time between 50 and 90% TR that best depicts the generation-migration-accumulation of petroleum [11.5]. Many workers use 10, 50, and 99% TR for the start, peak, and end of oil generation. The end of oil generation occurs at $\approx 2\%$ R_o .

11.2.21 Petroleum Generation Kinetics

Increased burial and/or paleoheat flow can result in sufficient temperatures to crack kerogen to oil and

gas [11.58]. The Arrhenius equation quantifies the relationship between temperature (T , K) and the rate of a chemical reaction (k)

$$k = Ae^{-\frac{E_a}{RT}}, \quad (11.9)$$

where E_a is the activation energy (kcal/mol), R is the universal gas constant, and A is the frequency factor or pre-exponential constant (s^{-1}), which largely depends on vibrational frequencies of the chemical bonds that are broken. Most workers assume that kerogen converts to petroleum in a complex series of sequential and parallel first-order reactions described by the above equation. First-order reactions depend solely on the concentrations of each reactant and the rate constant k .

Three general methods commonly used to quantify petroleum generation kinetics are:

1. Bulk kinetics (Fig. 11.8), which account only for conversion of kerogen to petroleum and do not distinguish between petroleum fractions
2. Oil-gas kinetics, which account for light hydrocarbons (e.g., C_1 to C_5 hydrocarbon gases) and oil (C_{6+})
3. Multicomponent or compositional kinetics, which consider more than two hydrocarbon components.

Many variations of multicomponent kinetics are used, such as four components [11.59] or 14 components [11.21] based on boiling-point classes, which can be used to predict phase properties in reservoirs, such as API gravity, GOR, or saturation pressure [11.1].

Predictions of oil composition cannot be made using routine published kinetic parameters. Computation models need to account not only for the chemistry of the generated petroleum, but must also include aspects of expulsion, retention, and secondary cracking. For example, a new SARA (saturate, aromatic, resin, asphaltene) kinetic modeling method can be used to improve predictions of oil quality in unconventional targets [11.7]. It accounts for 11 components (four bitumen, three hydrocarbon gas, two oil, CO_2 , and H_2S) and includes additional features such as complex secondary cracking through a multistage reaction network for bitumen to oil, oil to gas, and bitumen to gas conversions, as well as a special adsorption model for the bitumen components. The components are lumped according to physicochemical properties to minimize processing time. The method can be used to predict asphaltene flocculation and tar mats as well as formation of CO_2 and H_2S .

Most BPSM software provides a selection of default kinetic parameters that can be used when representative

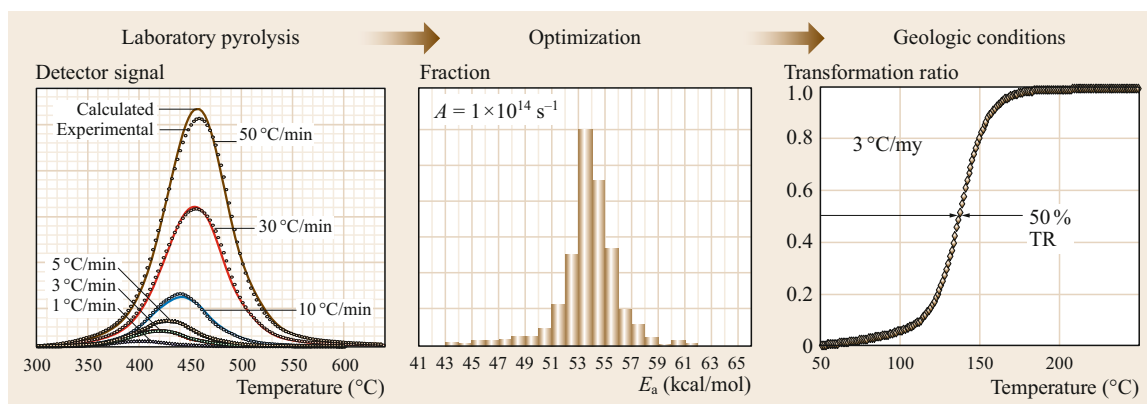


Fig. 11.8 A bulk kinetic model of a representative, thermally immature source-rock sample is obtained by optimizing (fitting) peaks from three or more programmed pyrolysis heating-rate experiments using software, such as Kinetics05 (after [11.60]). In the example, extrapolation to geologic conditions assumes a heating rate of 3 °C/my, but temperature history in the model may differ. TR = transformation ratio or extent of conversion of kerogen to petroleum

source-rock samples are unavailable [11.1]. However, default kinetics should be used cautiously. It is unwise to assume that kinetics for a specific source rock in the study area will be similar to default kinetics, unless both are from the same source rock at the same location. Kerogen type, as defined by Rock-Eval pyrolysis original HI, is not systematically related to kinetic response, and it is unwise to infer kerogen type or kinetics based on source-rock deposition environment [11.61]. Ideally, kinetic parameters should be determined on representative, organic-rich, unweathered source rock from the study area that has undergone diagenesis, but has yet to reach the early oil window (vitrinite reflectance equivalent ≈ 0.4 – 0.5%).

Various laboratory methods have been proposed to obtain E_a and A for conversion of source-rock kerogen to petroleum. These methods include closed-system isothermal pyrolysis, such as microscale sealed vessel pyrolysis (MSSV) [11.62], gold tube reactors [11.63], or hydrous pyrolysis [11.64, 65]. However, the most common approach is open-system programmed pyrolysis using Pyromat II, Rock-Eval VI, SRAnalyzer, Hawk, or similar systems and distributed reactivity kinetic modeling [11.66]. These calculations yield a range of E_a values that reflect the diversity of chemical bonds in the kerogen and an optimized value of A [11.67]. Pyrolyzate peaks for the conversion of kerogen to petroleum are optimized using standardized software, such as Kinetics05 (Fig. 11.8). Logarithms of E_a weighting factors and A are varied until the root mean squared discrepancy between observed and estimated rates of pyrolyzate yield reach a minimum [11.60]. Energy spacing of 1 kcal/mol through the E_a distribution is recommended because larger spacing (e.g., 2 kcal/mol) results in false minima [11.68].

Debate continues on the reliability of open- versus closed-system pyrolysis [11.65, 69–71]. Some consider that primary migration of petroleum through kerogen in the source rock is the rate-limiting step rather than cracking of carbon–carbon bonds [11.72]. More recently, some publications promote one-run open-system pyrolysis using a single heating rate and a fixed, universal A to determine petroleum generation kinetics [11.73]. However, based on analysis of 52 worldwide source rocks, Peters et al. [11.74] recommend at least three pyrolysis heating rates that span at least a 20-fold variation, where both E_a and A are optimized. Fast heating rates (e.g., 50 °C/min) may result in inaccurate temperatures due to the effects of thermal inertia. For these reasons, three or more heating rates in the range 1–30 °C (e.g., 1, 5, and 25 °C/min) are recommended, when the product of the heating rate and sample size is less than ≈ 100 mg °C/min.

The extrapolation of Arrhenius kinetic parameters determined in the laboratory to geologic time is based on three assumptions (Fig. 11.8):

1. The experimental data are accurate
2. The appropriate reaction model (e.g., distributed reactivity) is used to evaluate the data
3. The reaction mechanisms from experimental to geologic rates are similar [11.75].

Measured and predicted petroleum generation rate curves from open-system pyrolysis experiments are similar to those from natural maturation series, suggesting that laboratory experiments can be used to reliably predict maturation over geologic time [11.76]. However, distributed reactivity models fail for kerogens that have narrow activation energy distributions, and nucleation-growth models are necessary [11.74, 77].

11.2.22 Petroleum Migration and Accumulation

A key strength of BPSM simulators is the ability to model primary and secondary petroleum migration. Primary migration is expulsion of petroleum out of fine-grained, low-permeability source rocks, whereas secondary migration describes the transport of petroleum through coarser-grained, higher-permeability carrier beds and/or other conduits, such as faults, to the trap. Accurate modeling of primary and secondary migration efficiencies is needed to predict the volumes of petroleum in conventional accumulations and the amount that remains within the source rock. The latter capability is critical to evaluate unconventional resources.

Primary migration involves separate-phase transport of petroleum within the capillaries and pore throats of fine-grained, low-permeability source rocks. The driving force is internal pore fluid pressure during burial, but this also depends on source-rock richness and pore saturation. The initial expulsion is the release of generated petroleum from the kerogen into free pore space in the source rock. *Kelemen et al.* [11.78] used an extended Flory–Rehner regular solution theory to show that lower source-rock richness and cross-link density results in bitumen retention in the rock and enrichment of aliphatic components in the expelled fluid. Higher source-rock richness and cross-link density results in earlier fluid expulsion and enrichment of polar components. Two thresholds must be overcome before the petroleum becomes mobile: (1) the adsorption limit, and (2) the critical oil/gas saturation. Most light petroleum is first adsorbed onto the organic matter after generation, depending on TOC, temperature, and pressure. The excess amount is released as separate fluid phases of water, liquid petroleum, and gas, but must exceed the critical oil/gas and connate water saturation to allow fluid flow. These so-called saturation endpoints are lithologic parameters that are included in the relative permeability curves. Note that dissolved petroleum components can also be transported via diffusion within the phase, even if the phases remain immobile. Primary migration occurs over relatively short distances of less than 1 km [11.79].

Secondary migration is the subsequent transport of petroleum, driven by buoyancy, through coarser-grained, higher-permeability carrier beds or other conduits to the trap [11.44]. This may occur over tens or even hundreds of kilometers [11.79]. Finally, tertiary migration can occur when the trap for previous accumulations is reorganized, forcing the petroleum to move to another trap. Seeps can result from secondary or tertiary migration.

Petroleum migration is only relevant in 2-D and 3-D models. A limiting factor in migration modeling is that model paleoreconstructions may inadequately reflect the evolution of subsurface geometry or lithologic properties, i. e., the resolution of paleoreconstructions using available data seldom approaches that of nature.

A useful BPSM workflow is to first simulate without migration, for two main reasons: (1) this allows determination of the critical moment so that additional time steps can be added to the model if needed for better time resolution, and (2) because the model geometry is a reconstruction of the input basin geometry, it is prudent to check the reconstructed geometry before proceeding. Source-rock tracking allows the user to quantify the relative contribution of petroleum from different source rocks to a given accumulation. BPSM simulators also track the proportion of generated petroleum that seeps to the surface or beyond the edges of the model.

Depending on viscosity, rock permeability, and other factors, petroleum flows through permeable media at rates up to ≈ 100 m/yr and through fine-grained rocks at only 0.0001 m/yr [11.1]. This difference of seven orders of magnitude in flow rates suggests that different physics are required to model fluid flow. Because of the complexity of migration, several different modeling approaches are used, and no single method applies for all studies. The approaches include Darcy flow, flow-path (i. e., ray tracing), hybrid modeling and invasion percolation. Hybrid modeling combines two migration methods, as discussed below.

Darcy Flow Migration

Darcy flow migration is based on equations of flow through porous media where flow velocities are controlled by permeability and fluid viscosity (11.5). Like flow-path modeling, Darcy migration requires accurate definition of the carrier bed and seal rock in the model. Unlike flow-path modeling, Darcy migration accounts for complex transport processes, such as multiphase migration, gas diffusion, and the effects of pressure variations. Darcy migration balances all external forces within the petroleum system, i. e., capillary pressure, buoyancy, water pressure, and the viscous resisting force [11.1]. Accordingly, this method is especially suitable in BPSM when reservoir modeling, which also utilizes Darcy flow, will be employed.

Darcy migration modeling incorporates the full physics of the natural system and thus requires relatively long processing times, which limits use of detailed model geometries. Cell dimensions in complex models are commonly downscaled to allow the use of Darcy migration modeling, which entails loss of output resolution.

Typical analysis of a Darcy-flow BPSM model might involve visualizing the calculated vitrinite reflectance (EASY%R_o) or TR in the source rock and migration vectors and petroleum saturation in the reservoir rocks (Fig. 11.9). It may also be useful to examine the calculated pore pressure near faults to understand saturation behavior in those regions; faults can release pressure, thus focusing migration vectors toward them.

Flow-Path Migration

Flow-path migration modeling is the simplest of the migration methods to calculate and visualize in BPSM. The method is based on geometric analysis of the source-carrier-reservoir rock system: petroleum generated in source rock is expelled upward (only) into a carrier bed where fluid migrates by buoyancy to a geometric high below a seal rock [11.80]. Traps can fill with petroleum, which then spills to adjacent traps. Alternately, vertical leakage can take place through the seal or along faults. Within drainage areas, the uppermost portion of the carrier bed conducts petroleum to the reservoir rock. Thus, flow-path modeling encompasses migration path, drainage area, and accumulation analysis [11.1]. Flow-path modeling (and the flow-path domain in hybrid migration, below) does not account for the thickness of the carrier, reservoir, or non-reservoir rock between the pod of active source rock and trap. Petroleum is distributed below the top of the carrier bed or reservoir rock. Buoyancy pressure of the petroleum column and capillary pressure of the seal determine the volume of trapped petroleum, column height, and any loss through the seal.

Flow-path migration is rapid and highly focused using this approach. In effect, flow-path models produce inverted rivers of migrating petroleum (Fig. 11.10). BPSM flow-path output identifies discrete accumulations that are easily visualized and can be compared with maps of known oil and gas fields. It should be recognized that accumulations calculated in BPSM are approximations of existing fields and rarely match exactly. A typical output analysis might involve visualizing the flow paths and accumulations in carrier beds and some measurement of thermal maturity (e.g., saturations of residual petroleum) in the source rock.

Flow-path modeling has several advantages. The technique is most suitable where (1) petroleum is likely to occur in crestal structural traps that are well represented in the input basin geometry or (2) as an initial look at accumulation potential in frontier areas where little information about the subsurface exists. The method may be ideal where subsurface structure is imaged using high-resolution seismic data, which permit modeling of accurate reservoir geometries. Com-

puting times are short, thus allowing detailed model geometries, fine-scale model resolution (e.g., high accuracy of accumulation bodies, column heights, and seal losses), and rapid scenario testing of other model parameters. For this reason, it is also useful to employ flow-path modeling before other methods.

Flow-path modeling is generally unsuitable for study areas where petroleum occurs in stratigraphic traps or where subsurface structure is poorly known, e.g., some subsalt plays. However, when little subsurface data are available, flow-path modeling is commonly used to provide a quick look at potential accumulations. Flow-path modeling requires the user to predefine the carrier beds. Because geometric ray tracing is independent of any physical model of petroleum migration, it does not take into account interactions between the fluid and the layers between the source and reservoir rock. Physical processes that cannot be represented in flow-path modeling include overpressure generation, pressure-controlled petroleum migration, and pressure-driven downward expulsion [11.81]. Flow-path modeling also assumes instantaneous migration. Oil that arrives instantaneously in a trap based on flow-path modeling will experience a different thermal history than oil that migrates more slowly based on another migration method, resulting in predicted accumulations that may be compositionally distinct.

Hybrid Migration

Hybrid migration combines the two previously discussed methods, flow path and Darcy flow, into a hybrid scheme that distinguishes the mainly buoyancy-driven flow in carrier beds and reservoir rocks from pressure-dependent flow in the source and other non-reservoir rocks. In hybrid modeling, a predefined permeability threshold separates low-permeability (e.g., source rocks) from high-permeability lithofacies (carrier and reservoir rocks), which then are simulated by Darcy flow or flow-path migration, respectively. This so-called domain decomposition is applied throughout all model layers using the same grid size. However, the output can be sampled using grids of different size, i. e., Darcy flow and flow-path layers can be modeled at coarse and fine grid scales, respectively [11.1].

Hybrid migration modeling goes beyond domain decomposition to effectively handle each element of the petroleum system. Upward and downward expulsion from source rock is modeled using the Darcy equation. In the carrier bed leading to the reservoir rock, Darcy migration should be used for inefficient carriers, such as shale, when migration is slow. Flow-path migration is used for efficient carriers, such as sandstone. In the reservoir rock, the equilibrium state is treated with flow-path modeling, whereas breach of the seal and loss of

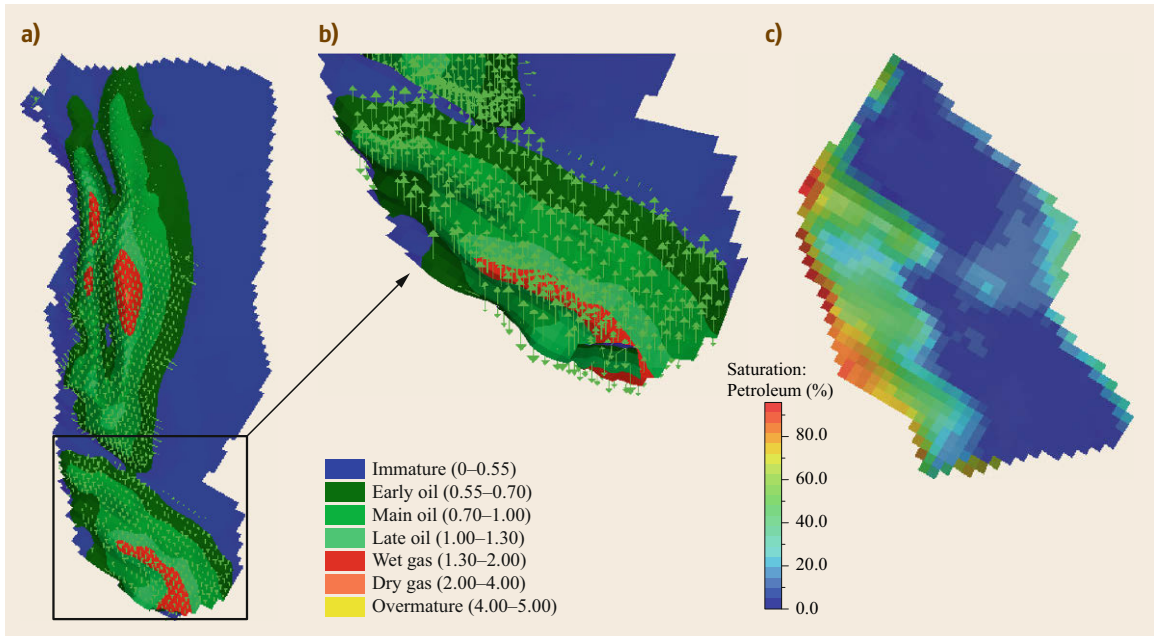


Fig. 11.9a-c Typical BPSM output based on Darcy migration showing EASY% R_o (after [11.56]) calculated in the source rock (a), migration vectors from the source rock to the overlying reservoir rock (b), and oil saturation in the reservoir rock (c). Note the coarse grid resolution in the reservoir rock (after [11.4])

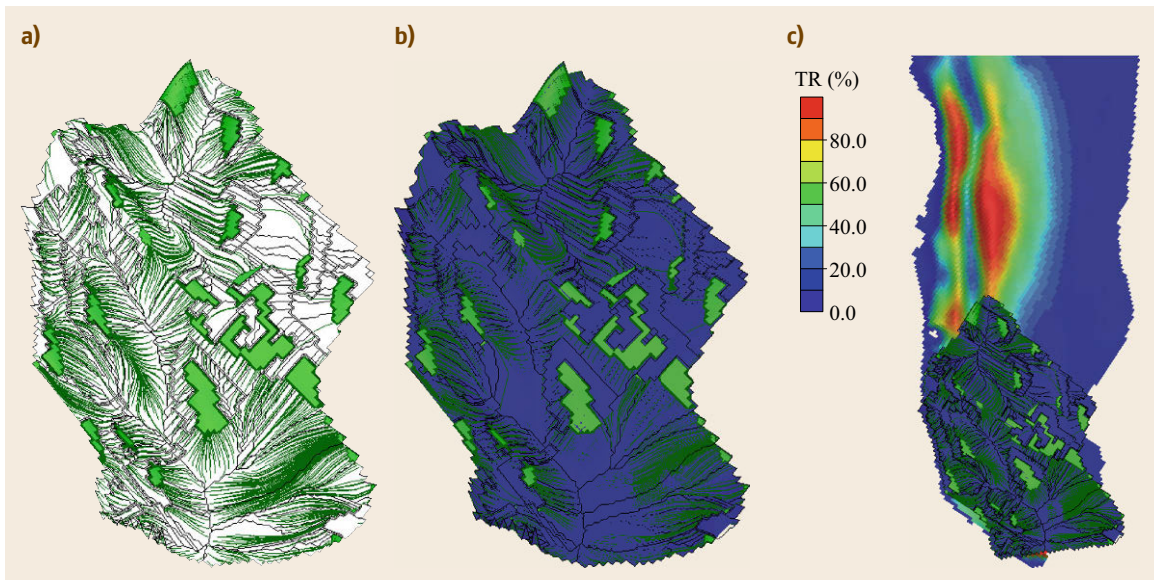


Fig. 11.10a-c Typical BPSM output based on flow-path migration showing drainage areas (*thin black lines*), migration pathways (*thin green lines*), and accumulations (*green polygons*) (a), the same view but with a superimposed reservoir rock depth map (b), and the same but with the source-rock depth map underlying the reservoir rock (c). The source rock is displayed as percent transformation ratio (after [11.4])

petroleum involves Darcy flow. Finally, flow velocities can be calculated using the Darcy equation in the overburden rock, depending on permeability.

As an example, a commonly used default value for the permeability threshold between the two domains is 10^{-2} mD at a porosity of 30% [11.1]. This threshold is

applied to model layers regardless of whether the porosity is 30% at a particular layer or event. In practice, the threshold that distinguishes Darcy from flow-path layers must be evaluated in context of the geology of each model unit. The 10^{-2} mD default means that only a few pure lithologies are treated as high-permeability layers (carrier beds and reservoir rocks). Once the user defines complex mixtures of lithologies for model layers, the consequent seal and reservoir layers may not behave as expected under the constraints of the domain decomposition. Thus, the user may need to adjust the threshold so layers that are known to be seals or reservoirs have permeabilities below or above the threshold respectively. In contrast, the user can also use in situ porosity to distinguish flow-path from the Darcy layers.

Invasion Percolation

Invasion percolation (IP) differs from the other migration mechanisms in that buoyancy is balanced against capillary entry pressure to determine where oil droplets move. The IP concept [11.81, 82], in which one fluid in a porous medium displaces the in situ fluid, was described earlier [11.83]. In petroleum migration, the invading fluid is petroleum, the in situ fluid is water, and the medium is a network of pores connected by narrow pore throats [11.84]. In IP calculations, the buoyancy force that drives migration is compared to the capillary entry pressure that retards it at these pore throats. Migration occurs as a front through the matrix of pore throats by accessing pores with the lowest threshold pressures. Initially, the choice of pathways by migrating petroleum is random, but later migration proceeds in preexisting pathways because the resisting force has already been reduced by petroleum saturations within the pore throats. In this way, the depth-dependent effect of gravity on the matrix concentrates the flow of the invading fluid into *stringers* within the porous medium. With increasing gravity gradient, stringers become confined and concentrated [11.85]. BPSM output for IP models consists of many stringers with physical properties that can be queried.

Determination of IP pathways relies on the relative distribution of permeability (i.e., capillary entry pressure) across the model domain. For IP to behave realistically in layers that are assigned homogeneous permeability in the model, heterogeneity is incorporated using a random distribution of permeability (noise) or by use of seismic attribute volumes to condition the flow pathways [11.84]. Some BPSM software permits capillary pressure variations (buoyancy forces for upward flow) and anisotropy (encourages lateral flow) to be specified. The challenge for the modeler is to choose the optimum combination of noise and

anisotropy to achieve the most realistic migration patterns.

As with flow-path modeling, IP compute times can be fast, allowing multiple charge scenarios to be tested quickly. Unlike flow-path migration, IP also allows consideration of fluid migration in non-reservoir layers, which do not need to be predefined by the model structure. However, IP can be slow to calculate when multicomponent kinetics and source-rock tracking are utilized in 3-D in conjunction with high-resolution seismic input.

BPSM output for models run with IP migration consists of hundreds to thousands of stringers with physical properties that can be queried. Stringer analysis, e.g., to query which pod of active source rock it derives from, is the reverse of flow-path analysis (Fig. 11.11). Accumulations in a model run with IP migration are actually probabilities of petroleum being present in a cell. Output is a series of discrete dots, but these can be displayed as bodies to determine column heights, as in flow-path modeling. It may be desirable to filter model output to reduce the many micro-accumulations that occur in low-permeability carriers.

Comparison of Migration Methods

Table 11.2 summarizes some features of the four main BPSM petroleum migration methods. The table is generalized, and comparisons may differ from model to model. Like flow-path modeling, IP assumes instantaneous flow and is suitable for modeling migration in high-resolution geometric models. Where charge timing is relevant, Darcy or hybrid flow methods are recommended over IP and flow path. For example, in cases where mixing or secondary oil cracking occur, time may be a relevant factor, so Darcy or hybrid migration should be used. In all methods except Darcy modeling, a high percentage of migrated petroleum is lost at the edges of the model if high-permeability layers are tilted to allow outflow [11.86]. Unlike flow-path modeling, IP is well suited for simulating complex migration paths and migration along faults in conjunction with seismic facies refinement. Compute times for IP migration can be as short as for flow-path modeling. However, if other numerically intensive routines are used, such as multicomponent kinetics and source-rock tracking, compute times for IP migration can be as long as those for Darcy flow modeling. Finally, all methods except flow-path migration can be used in areas of overpressure because capillary entry pressure can be modified by overpressure and the migration paths follow the direction of steepest ascent across the overpressure contours. In summary, no single migration modeling method is universally applicable. A useful approach for most BPSM studies is to compare results for

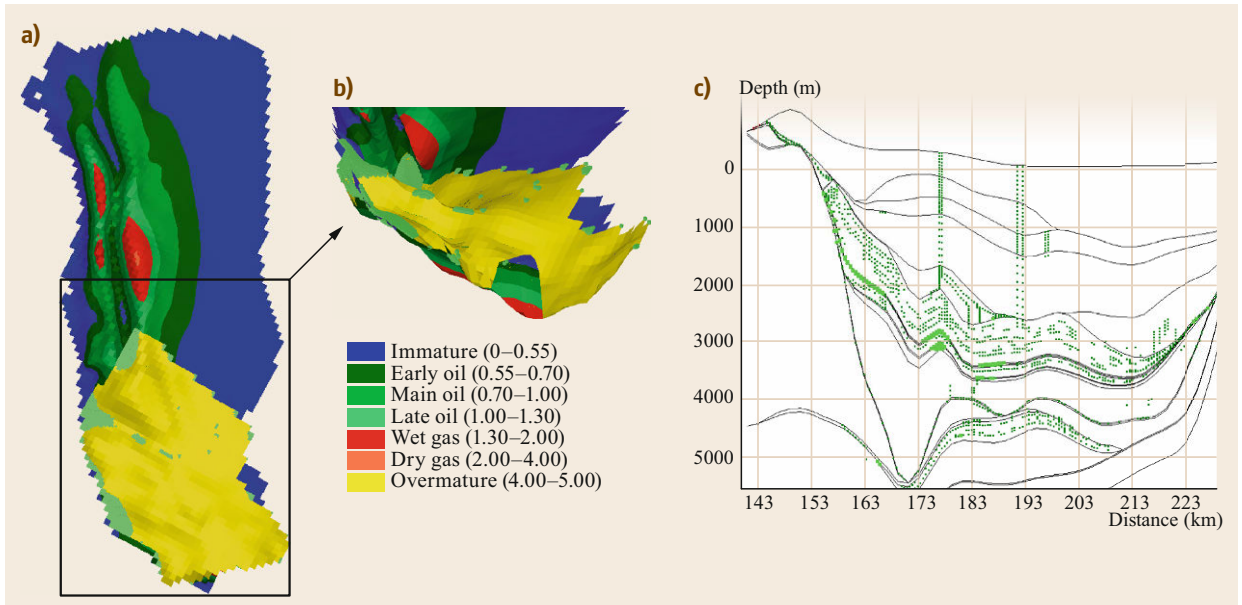


Fig. 11.11a-c Typical output from a BPSM model with IP migration showing EASY% R_o (after [11.56]) in the source rock overlain by IP accumulations in the reservoir rock (*green areas on yellow layer*) (a), discrete accumulation sites (*green areas*) in the reservoir rock (b), and a horizontal 2-D extraction from the 3-D model across the reservoir rock (c). *Smaller dark green dots* denote petroleum migration stringers and *larger green areas* denote accumulations (after [11.4])

Table 11.2 Comparison of features for Darcy flow, flow-path, hybrid migration, and invasion percolation modeling

	Darcy flow	Flow path	Hybrid migration	Invasion percolation
Compute time	Long	Short	Short/long	Short/long
Model resolution	Low	High	High (flow path) Low (Darcy)	High
Migration time	Timing of flow	Instantaneous	Instantaneous (flow path) Timing of flow (Darcy)	Instantaneous
Role of overpressure	Yes	No	Yes (Darcy) No (flow path)	Yes

all of the methods before focusing on the method that best addresses the study objectives [11.81].

11.2.23 Petroleum System Event Timing

Historically, most exploration was based on the simple play fairway concept in which the largest subsurface structures were drilled first. The petroleum system concept received little attention from industry until major exploration failures, such as the Mukluk wildcat well, Alaska [11.87], forced recognition of the need for a more systematic and comprehensive approach to exploration. A play consists of fields and prospects having similar trapping mechanisms (e.g., anticline, pinchout, or pinnacle reef plays). In play fairway exploration, previously discovered accumulations and their geology are used to risk undiscovered accumulations. For example, the Barrow Arch on the North Slope of Alaska contains

multiple structural-stratigraphic traps that were targeted for drilling mainly because of earlier discoveries in similar traps along the Arch, such as the Prudhoe Bay field. The spectacular and costly failure of the Mukluk well located along the Barrow Arch clearly demonstrated that play fairway maps are static present-day snapshots of subsurface geology that fail to account for the timing of petroleum system events. Unlike the play concept, modern BPSM is dynamic, accounts for the timing of petroleum system events, and can be used to better quantify the risk that traps are barren or the likelihood that they are filled with oil and gas.

The Alaska North Slope may contain much of the undiscovered oil and gas in the circum-Arctic [11.88]. A calibrated 3-D BPSM study of this area (Fig. 11.12) demonstrates the key role played by timing of petroleum expulsion from the source rock relative to trap formation [11.89].

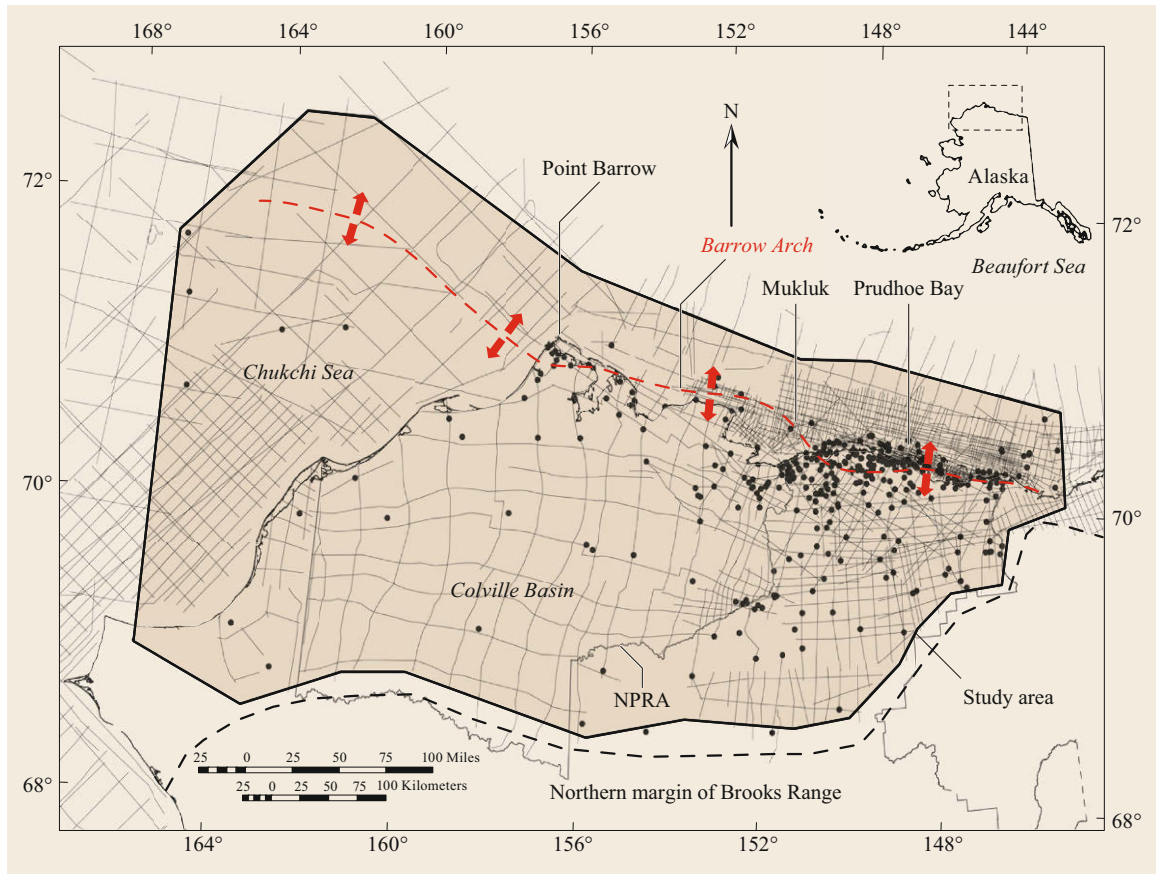


Fig. 11.12 A three-dimensional basin and petroleum system model of the Alaska North slope, which covers 275 000 km² (*polygon*) and is based on 48 000 km of seismic data (*gray lines*) in addition to stratigraphic and geochemical information from more than 400 wells. *Red dashed line* shows location of Barrow Arch (after [11.2], figure copyright Schlumberger, used with permission)

Trap formation at Prudhoe Bay preceded expulsion from the downdip thermally mature source rock, resulting in a giant accumulation. Chemometric (multivariate statistics) analysis of biomarker and stable isotope data shows that the Prudhoe Bay field contains a mixture of oil from the Triassic Shublik Formation and Cretaceous Hue-gamma ray zone (Hue-GRZ) with lesser input from the basal Jurassic Kingak Shale [11.90]. These results are consistent with the 3-D model, in which Shublik and Kingak source rocks started to expel petroleum during the Cretaceous, whereas the Hue-GRZ contributed later [11.89].

The reason for failure of the Mukluk wildcat well remains controversial. Prior to drilling, the Mukluk structure (Fig. 11.13) was estimated to contain 240 million m³ (\approx 1.5 billion bbl) of recoverable oil in a structural-stratigraphic trap, although permafrost impaired the quality of subsurface imaging and estimated seismic velocities. The 3-D model (Fig. 11.14) integrates the

hypothesis that so-called thief sands on the Lower Cretaceous unconformity (LCU) were responsible for remigration (tertiary migration) of hydrocarbons [11.91, 92]. Model results show that petroleum accumulated, but suggest significant risk of spillage from the structure through Kuparuk C-D thief sands overlying the LCU toward the Kuparuk River field to the southeast during Tertiary tilting (Fig. 11.15). A petroleum system event chart based on the 3-D model of the Mukluk area shows how the relative timing of these events impacted risk (Fig. 11.16). Drill cuttings from the completed well showed extensive oil stain in the target Ivishak Sandstone reservoir rock, but the well was uneconomic.

11.2.24 Modeling Unconventional Resources

BPSM software can be used to model both conventional and unconventional resources, and although there are differences (Table 11.3), they can be modeled simul-

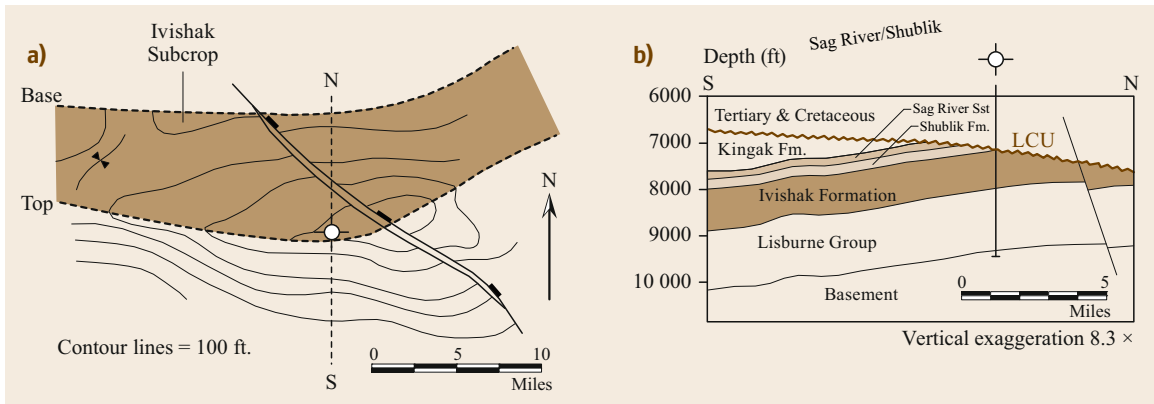


Fig. 11.13 (a) Seismic data indicated a four-way closure at the Mukluk prospect as depicted on the Ivishak Formation subcrop at the Lower Cretaceous unconformity (LCU; jagged line). The Mukluk structure is 32×14 km (≈ 20 mile long and 9 mile wide). The Ivishak Formation within the Permo-Triassic Sadlerochit Group is the main reservoir rock at Prudhoe Bay. (b) North-south cross-section through the well location shows the gentle Mukluk structure and truncation due to a normal fault to the north. The Sag River and Ivishak units contain carrier or reservoir facies, while the Shublik Formation is a major source rock on the North Slope (after [11.87], reprinted by permission of AAPG whose permission is required for further use)

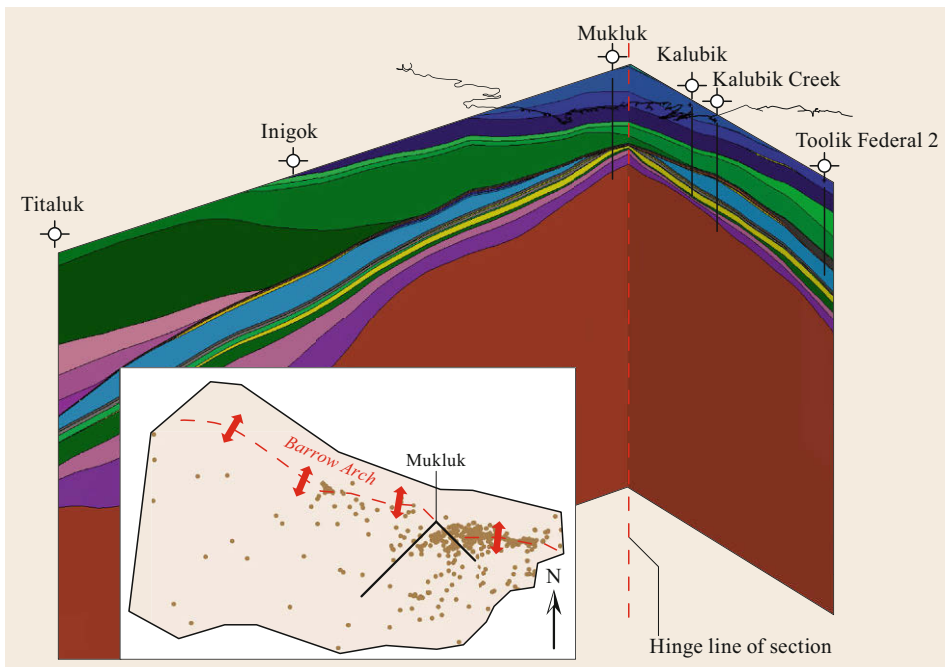


Fig. 11.14 Present-day cross-section extracted from the 3-D model showing location of the hinge line for the section (red dashed line) used for Fig. 11.15. Inset shows the location of the section extracted from the 3-D model through the Mukluk prospect

taneously. Conventional exploration targets petroleum that migrated from the source rock to traps. A principal objective of BPSM for conventional systems is to establish the relative timing of petroleum generation-migration-accumulation and the timing of trap formation. Unconventional exploration targets petroleum that remains within the source rock. In unconventional shale plays, the source rock is a key element because

it includes the charge, reservoir, trap, and seal. Secondary cracking of oil to gas is generally unimportant in shallow conventional traps. However, oil that remains in the source rocks in the oil window can be more deeply buried where it cracks to hydrocarbon gas. Conventional BPSM focuses on the reduction in porosity that occurs during burial, whereas unconventional BPSM also tracks the increase in organoporosity

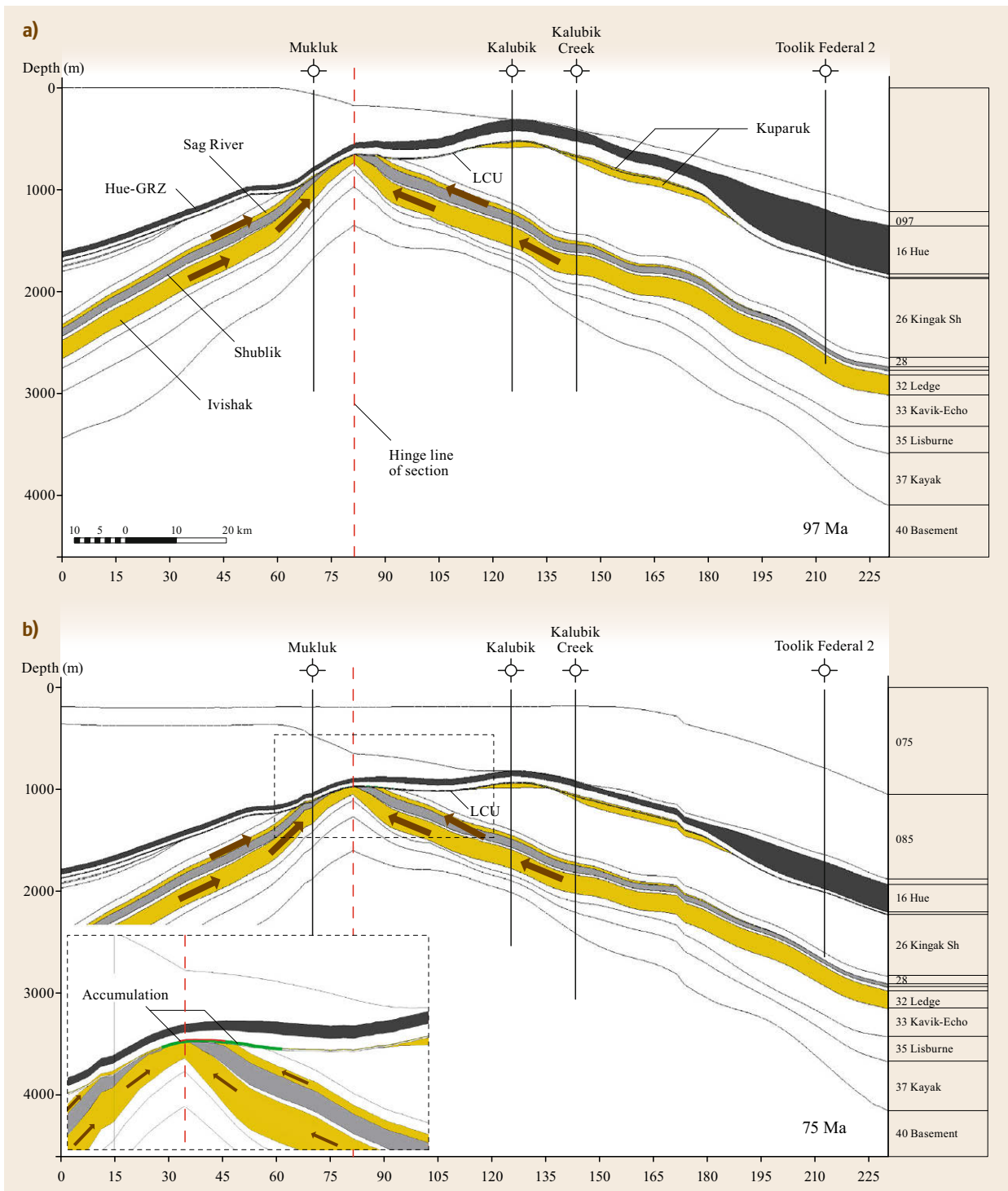


Fig. 11.15 (a) Cross-section from the 3-D model based on seismic data indicating four-way closure near the Mukluk prospect at 97 Ma. The section was opened to plane view along the hinge line from Fig. 11.14. (b) Cross-sections from the 3-D model showing closure at Mukluk at 75 Ma, although little oil accumulated due to erosion and early tilting (larger paleo-accumulations are predicted to the west of Mukluk along the Barrow Arch)

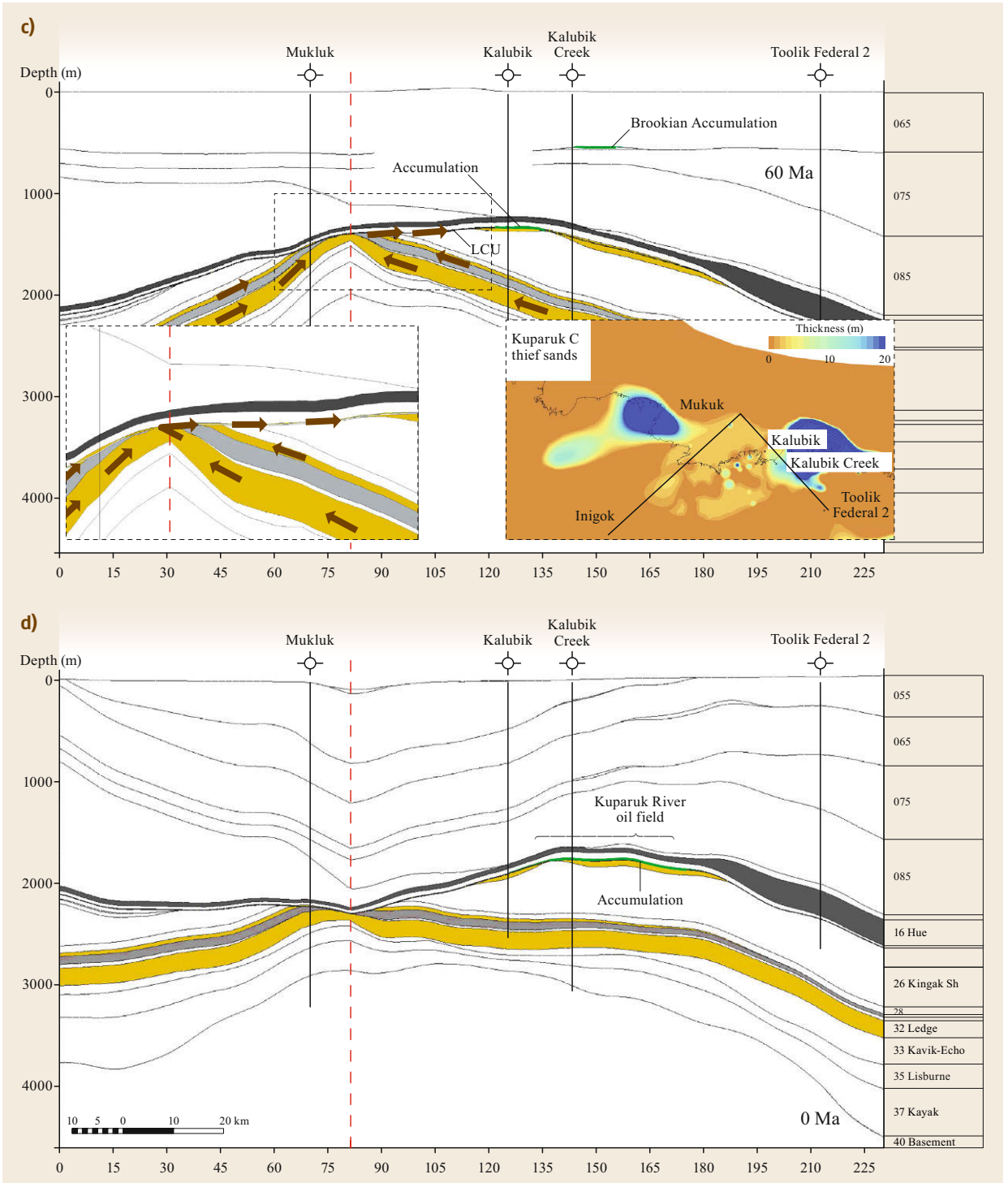


Fig. 11.15 (c) Continued Tertiary erosion at 60 Ma caused additional tilting and includes the possibility that Kuparuk C-D thief sands deposited on the LCU allowed remigration of oil to the southeast (*insets*) into small accumulations near the present-day Kalubik well at the LCU and in a sand lens in the shallower Brookian sequence. (d) Reversed tilting to present day (0 Ma) resulted in renewed closure at Mukluk, but most petroleum had already migrated toward the Kuparuk River field

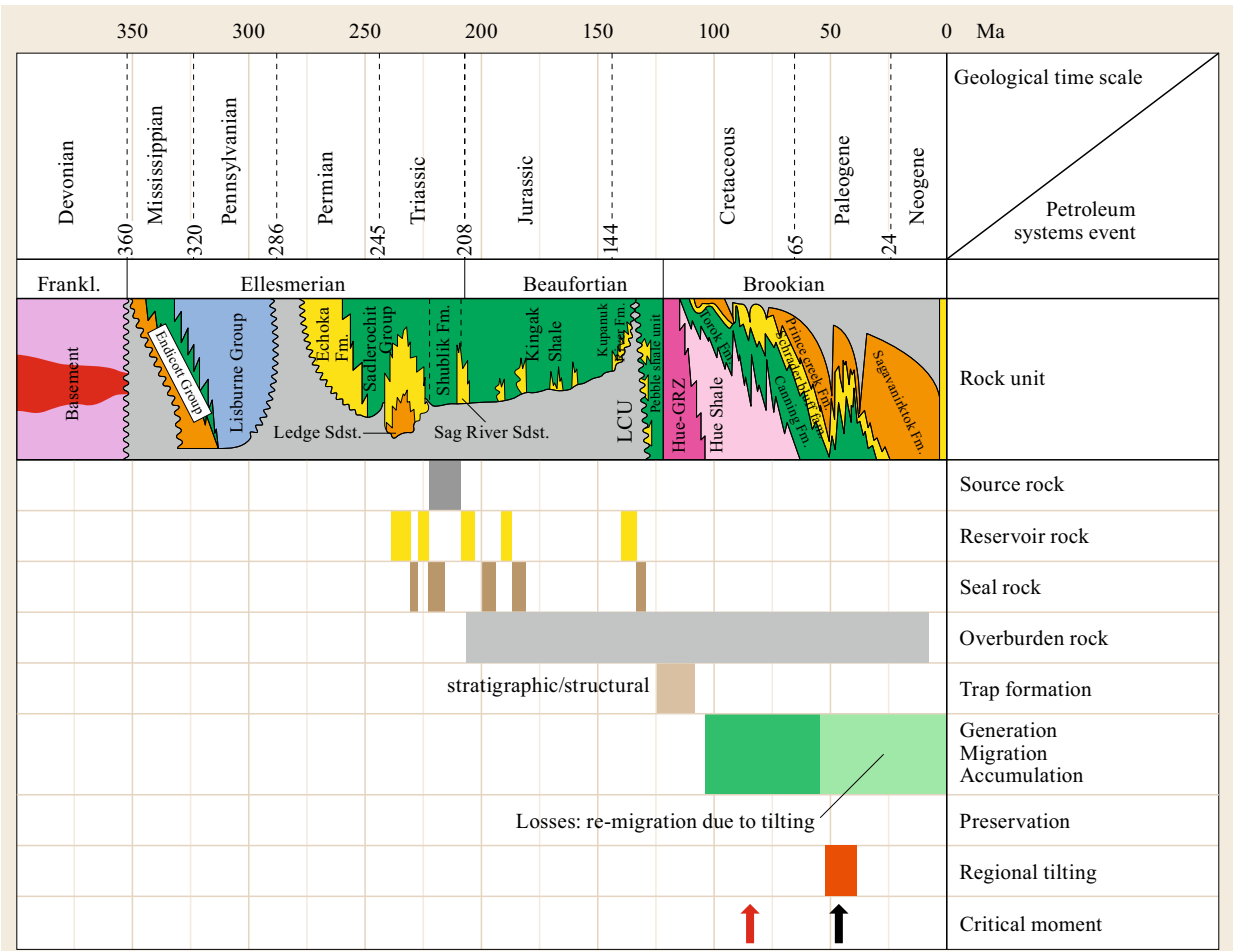


Fig. 11.16 Petroleum system event chart showing that tilting to a three-way closure during the Tertiary drained the Mukluk accumulation. *Light green part of bars* indicates estimated time of eastward migration of earlier trapped petroleum to traps in younger Cretaceous and Lower Tertiary reservoirs due to tilting. *Red arrow* points to the critical moment when the transformation ratio of the source rock in the adjacent depocenter is over 50%. *Black arrow* indicates the critical moment for the Mukluk well location in terms of geometry during regional tilting

Table 11.3 Some key differences between conventional and unconventional petroleum reservoirs

Conventional	Unconventional
Gas and oil migrate to the trap	Gas and oil remain in the source rock
Oil-to-gas cracking usually is unimportant	Oil-to-gas cracking is important
Reservoir storage in intragrain porosity	Conversion of kerogen creates reservoir porosity
Free gas is important	Proportions of free/adsorbed gas are important

that results from the conversion of kerogen to solid bitumen, oil and gas. Unlike conventional resources, which contain mainly free gas and oil in intragrain pore

spaces, production from unconventional resources depends on both free hydrocarbons in pore spaces and fractures and hydrocarbons adsorbed on the surface of the rock and trapped within the kerogen. An organic-rich source rock that contains 10 wt% TOC may have > 30 vol.% kerogen, which can provide substantial pore space for hydrocarbon gas and oil. As new porosity is created during kerogen cracking, hydrophobic hydrocarbons fill the pores in unconventional reservoirs.

Most unconventional petroleum systems have low porosity and permeability. Typically, these systems have at least 2 wt% TOC prior to thermal maturation, and some of the porosity occurs in pores that develop in the kerogen as it undergoes cracking to generate oil

and gas. *Jarvie* [11.93] divides organic-rich mudstones into:

1. Tight (no open fractures)
2. Fractured (open fractures)
3. Hybrid types (juxtaposed ductile organic-rich and brittle organic-lean facies).

Many tight shales show positive correlation between gas or oil saturation and TOC because much of the petroleum is trapped in pores that develop in the kerogen during cracking [11.94]. Organoporosity dominates the storage capacity of tight organic-rich mudstones, as in the Barnett (Texas) and Haynesville (Texas, Arkansas, Louisiana) formations. Clay minerals can also significantly contribute to the sorption capacity of shales [11.95].

Hybrid types of unconventional petroleum systems consist of intercalated fine- and coarse-grained units, so much of the generated oil and gas migrates short distances into the lean units, resulting in lack of correlation between gas or oil saturation and TOC. Hybrid types, such as the Bakken Formation in the Williston Basin, are generally the best-producing shale resource systems for two reasons: (1) matrix and fracture-related porosities are generally more significant in hybrid systems due to the juxtaposed organic-lean units, and (2) expulsion and short-distance migration from the organic-rich to the organic-lean units is favored.

Migration fractionation results in selective retention of heavy NSO compounds and asphaltenes in the tight organic-rich units and preferential migration of more mobile saturated and aromatic hydrocarbons to the organic-lean units, which increases their productivity. The Upper and Lower Members of the Bakken Formation are tight organic-rich mudstones with very low porosity and permeability and lack productivity, even when stimulated by hydraulic fracturing. However, the Middle Member of the Bakken Formation is organic-lean (low TOC), brittle (high carbonate content), and at the proper level of thermal maturity, and represents an excellent unconventional production target (Fig. 11.17).

A new play-based methodology provides a systematic approach to assess and explore for unconventional resources [11.96]. Use of this methodology with BPSM allows effective identification of *sweet spots* early in the exploration cycle. BPSM can be used to predict the amount and character of petroleum trapped in the mudstone. For example, BPSM can be used to assess high-grade portions of shale plays that contain oil or condensate in addition to hydrocarbon gas, which can differentiate commercial from noncommercial production. In addition, BPSM predicts the proportion of gas

adsorbed within kerogen pores or on mineral surfaces versus free gas in pore spaces or natural fractures. For example, implementation of a pressure-temperature-dependent Langmuir-type adsorption function allows reliable prediction of adsorbed gas in shale [11.95]. Ideally, Langmuir parameters should be measured on core or outcrop samples of the source rock.

In addition to the proportion of adsorbed hydrocarbons, geomechanical properties provide important information for unconventional resources, e.g., to differentiate between areas that are more or less likely to be naturally fractured as a result of stress-strain history. Three physical models are essential for BPSM: mechanical, thermal, and fluid flow. The mechanical model includes fluid pressure and rock stress predictions, which are closely coupled. Because the traditional Terzaghi model considers only the vertical stress component (discussed earlier), it is limited for predicting rock failure or fluid flow. Recent developments in BPSM simulators extend this concept to a 3-D rock stress model after *Biot* [11.24]. The 3-D rock stress model considers present-day geomechanical conditions and the evolution of basin-scale geomechanics through geologic time. Calculated stresses and strains can be used to improve evaluation of seal capacity and prediction of fracture orientations or fault properties, which are essential to assess unconventional resources.

Implementation of 3-D rock stress models in BPSM has the advantage that a complete data model can be directly used: the paleogeometries and cell grids; cell properties, such as porosity, compressibility and permeability; and physical values, such as temperature and fluid pressure. Pore fluid pressure is especially important because it is coupled with the solutions for rock stress.

11.2.25 Poroelasticity Rock Stress Modeling

BPSM can predict geomechanical properties that are key for hydraulic fracture stimulation of shale reservoirs. Geomechanical data are commonly combined with reservoir or borehole data to predict rock stress and strain for well completion design. Poroelasticity modeling of 3-D stress-strain can be used in BPSM to differentiate areas that are more or less likely to be naturally fractured due to stress-strain history. Hydraulic fracturing is likely to be more effective in previously naturally fractured unconventional targets.

The following poroelastic approach is based on Biot's effective stress equation, which relates stress to deformation of a porous and elastic medium. Stress and strain are bulk properties, i.e., stress is in equilibrium with boundary traction (tension or compression) and gravity load and strain represents deformation of the

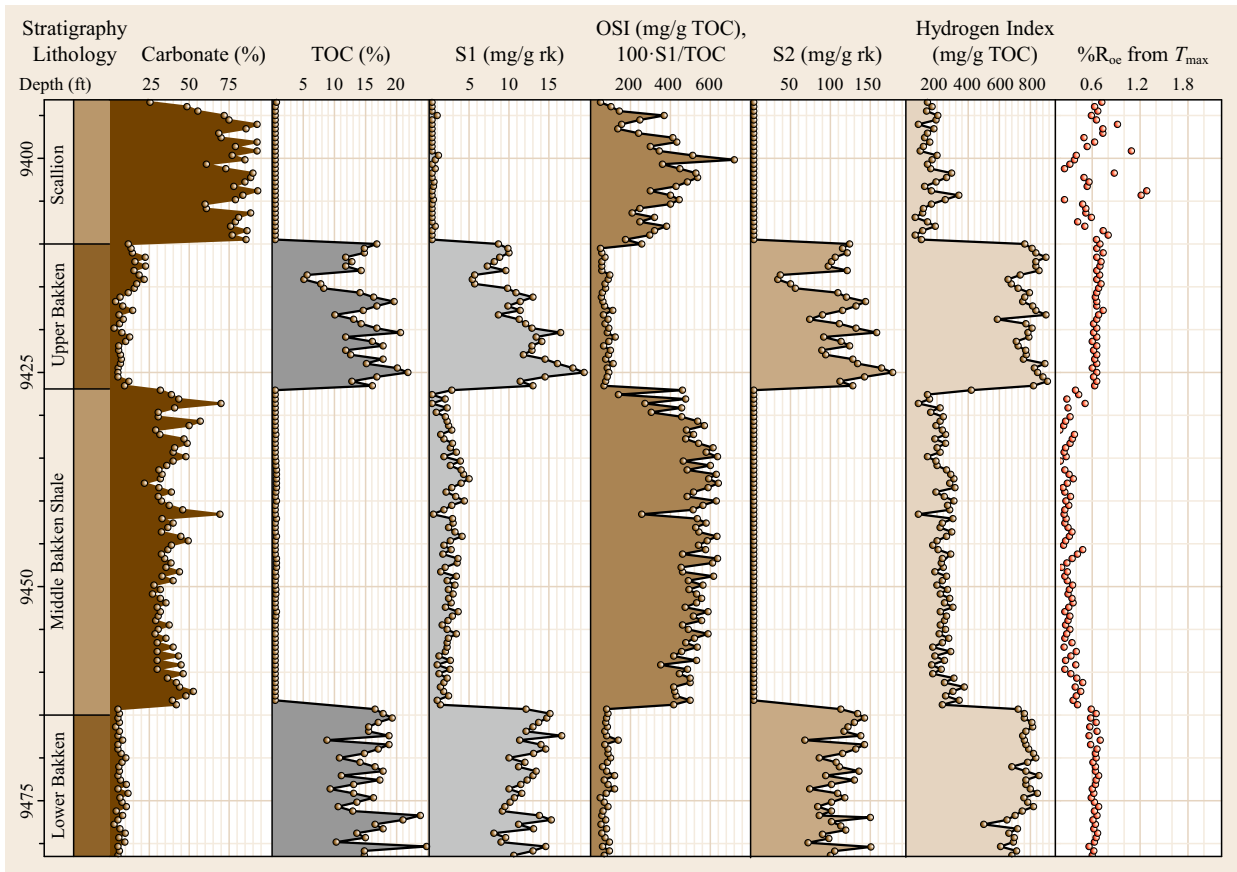


Fig. 11.17 Although the oil saturation index ($OSI = 100(S1/TOC)$) is apparently high for the Scallion Formation, both oil saturation (Rock-Eval pyrolysis $S1$ peak) and TOC are very low, resulting in unreliable OSI. $S1$ is high in the Upper and Lower Bakken, but the OSI is low. These zones do not produce petroleum, even when hydraulically stimulated, because $S2$ compensates for $S1$ and the kerogen adsorbs $S1$. However, the Bakken Middle Member in this well is productive because although $S1$ is lower than in the Upper and Lower Members, OSI is high (> 100 mg/g). Note that T_{max} (converted to vitrinite reflectance, R_o) is anomalously low in the Bakken Middle Member (after [11.93], reprinted by permission of AAPG whose permission is required for further use)

bulk volume

$$\sigma_{ij} - \alpha p \delta_{ij} = \sigma'_{ij} = \frac{E}{1 + \nu} \epsilon_{ij} - \frac{E\nu}{(1 - 2\nu)(1 + \nu)} \epsilon_{kk} \delta_{ij}, \tag{11.10}$$

where σ'_{ij} describes the effective stress tensor, σ_{ij} is the stress tensor, δ_{ij} is the Kronecker symbol, ν is Poisson's ratio, E is the bulk Young's elasticity modulus, and ϵ_{kk} is the strain. Poisson's ratio (ν) and the bulk elasticity modulus (E) can be derived from the Terzaghi compressibility (C_T) and simulation results using a traditional BPSM compaction law. Poisson's ratio is the negative ratio of transverse to axial strain, which describes how a rock that is compressed in one direction tends to expand perpendicular to this direction. Young's modulus, also called the elastic modulus, relates normal

stress to strain and measures stiffness of a rock (i. e., rock resistance to strain).

Commonly, boundary conditions include traction-free surfaces, fixed basin sides, and fixed basement. However, to handle compressional or extensional basins one can assign positive or negative displacements at the basin sides, respectively.

11.2.26 Rock Failure

The most common rock-failure models in BPSM are the Mohr–Coulomb [11.1] and Drucker–Prager [11.97] models in which differential stress or deviator stresses are the main controlling factors, respectively. Failure criteria are represented by envelopes that help to predict the stress conditions for rock failure and fracture type. The failure envelope is described by cohesion

and friction angle. Compaction can also be included when using a *cap* as an additional volumetric failure above the critical stress. Cap describes a strain regime that differs from brittle deformation. Increased normal stress beyond nonvolumetric plastic flow can result in compressive plastic flow and work hardening. In the Mohr diagram, this is described by an elliptical failure curve at high differential stress, e.g., see *Schutjens et al.* [11.98, Fig. 2].

The first step in failure analysis is to calculate failure risk, which is a measure of proximity of the stress to the failure envelope. The fracture directions and failure type (e.g., tensile, shear, or mixed-type fracture) can also be determined. The second step is a description of the effect of permeability increase on the stress-strain relationship. Implementation of these steps in forward modeling affects pore pressure and rock stress, and thus has implications for fluid flow. In addition, analysis of the basin-scale 3-D stress field allows prediction of fault transmissibility.

Failure analysis includes failure risk. The yield line distance (perpendicular distance between the failure envelope and the Mohr circle) is a measure of: (1) likelihood that fracturing will occur, and (2) the type of fracture. Rock failure depends on the fracture type and results in increased permeability. Implementation of failure analysis in BPSM results in pore-pressure variations and has implications for fluid flow. Finally, analysis of the basin-scale 3-D stress field allows prediction of the direction of fault planes. Note that alter-

native poroplastic solutions exist, such as the Cam–Clay model.

11.2.27 Example of the North Slope 3-D Model

The Alaska North Slope model provides a useful example of rock stress and failure analysis. Increasing awareness of unconventional shale gas and oil as a future long-term energy source has increased interest in its potential in northern Alaska. The Triassic Shublik Formation is a key source rock that contributes petroleum to the giant fields along the Barrow Arch (e.g., Kuparuk River and Prudhoe Bay). The Shublik Formation is considered to be a prime target for unconventional petroleum because of high organic carbon and carbonate (brittle) content, similar to the Eagle Ford Shale, which is a successful shale oil play in Texas. Key uncertainties for such unconventional systems include:

1. Rock properties and their vertical and lateral distribution
2. Geomechanical properties, such as brittleness
3. Organic content
4. Thermal maturity
5. Overpressure and its timing.

The distributions of horizontal stress tensors calculated in the Shublik Formation help to predict the directions of fractures (Fig. 11.18). Horizontal stress in

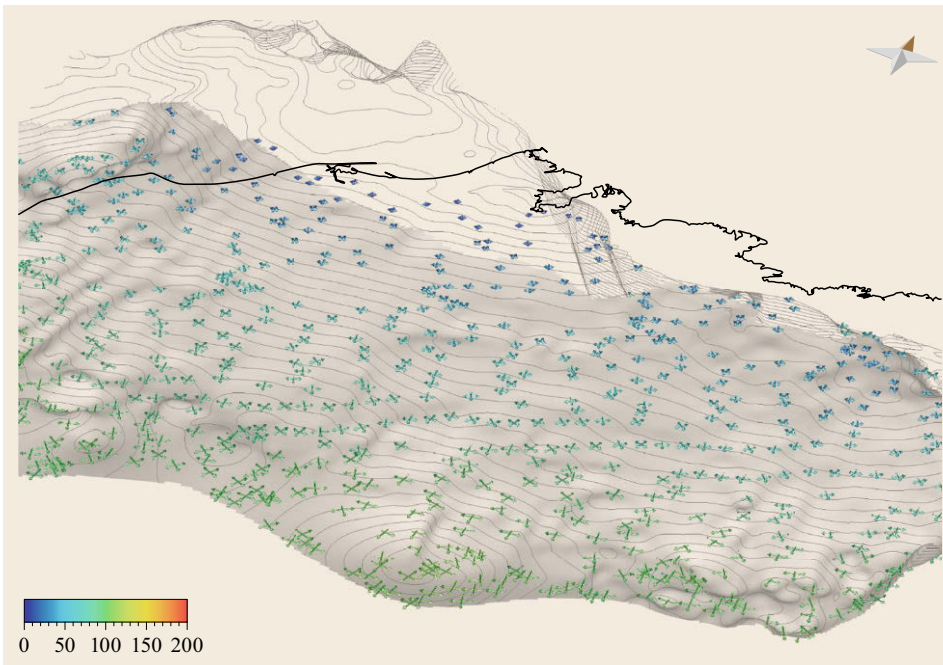


Fig. 11.18 Calculated horizontal total stress tensors (MPa) for the carbonate-rich, central portion of the Shublik Formation plotted on top of the basal unit of the Shublik Formation (gray). Length of tensors is scaled to total stress

the foothill region in the southern part of the model is higher than in shallow areas along the Barrow Arch. Different directions of the stress tensors indicate lateral variations of the stress pattern. Three-dimensional rock-stress modeling results indicate that there is less risk for brittle deformation in shallow regions along the Barrow Arch (Fig. 11.19). Mohr circle output is useful to compare the failure behavior of regions of interest. The first step in failure analysis is to examine whether the calculated Mohr circle for a specific location intersects the failure line. Figure 11.19 indicates that in the shallow region the Mohr circle fails to contact the failure envelope. However, farther downdip toward the center of the Colville Basin, the Mohr circle theoretically exceeds the failure envelope. Such a scenario is impossible in nature because when the Mohr circle touches the failure envelope, fracturing occurs and stress conditions shift the circle along the failure envelope toward the critical stress state to reach equilibrium conditions.

Once fracturing occurs, forward modeling in the second step of failure analysis considers the fracture-related permeability increase, which again influences

pore pressure, rock stress, and fluid flow. Figure 11.19 also shows the strong interrelationship of rock stress and pore fluid pressure. The horizontal red arrow points to an area where increased stress exceeds the failure line. This increased stress is related to Sag River Sandstone, which locally overlies the Shublik Formation. Elsewhere the Kingak Shale overlies the Shublik Formation. Because the compaction behavior of the Sag River Sandstone differs from that of the Kingak Shale, compaction of the underlying Shublik Formation is also affected, resulting in different pore pressures and rock stresses.

11.2.28 Continuing Developments

Continued advances in BPSM allow increasingly complex and accurate geologic studies. For example, the chemistry of migrating fluids affects the depth and temperature of silica phase transformations in biosiliceous rocks. These transformations change both the porosity and permeability of the rocks, which can influence the distribution of seals and traps. One recent advance in BPSM software is the ability to track the opal-

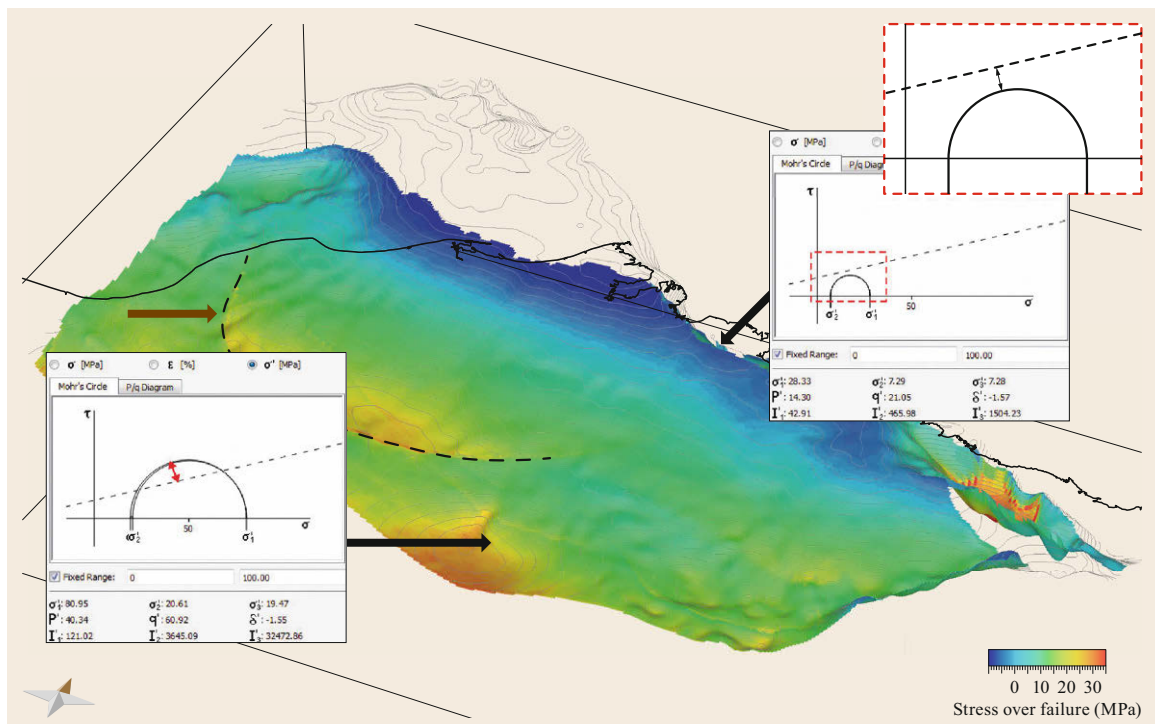


Fig. 11.19 Stress-over-failure overlay for the Shublik Formation showing Mohr circle output at two locations. *Insets* display the shortest distance from the Mohr circle to the dashed rock-failure line. Areas with negative values (*dark blue*) have little risk of natural fracture, whereas positive values (e.g., *red*; Mohr circle theoretically exceeds failure envelope) indicate high risk of fracture. *Horizontal red arrow* points to elevated stress-over-failure values that are related to the overlying Sag River Sandstone extending to the *black dashed line* (see text for details)

CT (cristobalite-tridymite) to quartz phase transition during burial history [11.99, 100]. This capability was used in a BPSM study of the Salinas Basin, California, to test the impact of silica diagenesis on generation timing due to differences in thermal properties of overburden rock and changes in bulk mechanical properties [11.40]. Some other examples of advances in BPSM focus on incorporating more sophisticated tec-

tonic histories. These include the role that structural thickening plays in the geologically rapid increase in overburden, the integration of strike-slip fault motion with 3-D BPSM [11.101], and the structural restoration of complex basin geometries due to thrusting via paleostep models [11.102]. Similar continued advances in BPSM software are vital to the success of petroleum exploration programs.

11.3 Conclusions

BPSM begins with a well-defined conceptual model based on discretized (gridded) input data to facilitate numerical simulation. Selection of 1-D, 2-D, or 3-D BPSM depends on available input data and the objectives and time constraints for each study. Recent advances in simulation software include 3-D poroelastic and poroplastic rock stress modeling, which are significant improvements over 1-D Terzaghi modeling. Because BPSM is forward deterministic modeling, organic richness and rock properties must be reconstructed to original values prior to burial. In geohistory analysis, each unit is decompacted to original thickness and corrected for paleobathymetry and eustasy. Boundary conditions for thermal evolution include heat flow and sediment-water interface temperature corrected for water depth through time. Measured petroleum generation kinetic parameters for representative, thermally immature equivalents of the effective source rock are generally superior to the default kinetics available in various software applications, which should be used only as a last resort. Calibration and risk analysis are vital parts of the modeling process. Because overpressure retards normal compaction, most calibrations start with the available pressure data, followed by thermal calibration using corrected borehole temperatures, vitrinite reflectance, or other maturity parameters, and calibration to other measurements, such as detailed compositions of petroleum in reservoirs.

The static play fairway concept uses a snapshot of the present-day geology of known accumulations

to risk undiscovered accumulations. Spectacular failures of the play fairway concept, such as the Mukluk wildcat well in Alaska, forced the industry to develop the quantitative petroleum system concept. Unlike the play fairway concept, the petroleum system concept is dynamic and can be used to reveal the relative timing of petroleum system elements and processes. Significant accumulations require trap formation prior to generation-migration-accumulation. Various processes, such as renewed tectonic activity, can result in remigration or destruction of accumulations and more than one critical moment. For unconventional resources, the source and reservoir rock are identical or closely associated, organoporosity is the container for much of the resource, and secondary cracking is particularly important. Hybrid systems, which juxtapose ductile, low permeability organic-rich with brittle and more permeable organic-lean intervals are typically the best producers. Finally, BPSM does not provide answers; it provides scenarios that can be tested or improved with more data to better understand and exploit each petroleum system.

Acknowledgments. We thank Schlumberger for permission to publish and the following reviewers who helped to improve the manuscript: Ian Bryant, John Dribus, Susan Duffield, Daniel Palmowski, Clifford Walters, Les Magoon, and Rodney Warford.

References

- 11.1 T. Hantschel, A.I. Kauer auf: *Fundamentals of Basin and Petroleum Systems Modeling* (Springer, Berlin 2009) p. 476
- 11.2 M.M. Al-Hajeri, T. Fuchs, T. Hantschel, A. Kauer auf, M. Neumaier, O. Schenk, O. Swientek, N. Tessen, D. Welte, B. Wygrala, D. Kornpohl, K. Peters: Basin and petroleum system modeling, *Oil-field Rev.* **21**, 14–29 (2009)
- 11.3 K.E. Peters, D.J. Curry, M. Kacewicz: An overview of basin and petroleum system modeling. In: *Definitions and Concepts, Basin Modeling: New Horizons in Research and Applications*, American Association of Petroleum Geologists Hedberg, ed. by K.E. Peters, D. Curry, M. Kacewicz (AAPG, Tulsa

- 2012) pp. 1–16
- 11.4 K.E. Peters, L.B. Magoon, C. Lampe, A. Hosford Scheirer, P.G. Lillis, D.L. Gautier: A four-dimensional petroleum systems model for the San Joaquin Basin, California. In: *Petroleum Systems and Geologic Assessment of Oil and Gas in the San Joaquin Basin Province, California*, ed. by A. Hosford Scheirer (USGS, Washington 2007) p. 35, US Geological Survey Professional Paper 1713, <http://pubs.usgs.gov/pp/pp1713/>
- 11.5 L.B. Magoon, W.G. Dow: *The Petroleum System – From Source to Trap*, American Association of Petroleum Geologists Memoir, Vol. 60 (AAPG, Tulsa 1994) p. 655
- 11.6 K.E. Peters, O. Schenk, B. Wygrala: Exploration paradigm shift: The dynamic petroleum system concept, *Swiss Bull. Appl. Geol.* **14**, 65–71 (2009)
- 11.7 K.E. Peters, T. Hantschel, A.I. Kauerauf, Y. Tang, B. Wygrala: Recent advances in petroleum system modeling of geochemical processes: TSR, SARA and biodegradation, *Proc. Annu. Meet.* (2013) p. 41261
- 11.8 B. Wygrala, O. Schenk, K.E. Peters: Assessment and exploration risking workflows for conventional and unconventional Arctic resources: Applications on the Alaska North Slope, *Lead. Edge* **32**, 564–572 (2013)
- 11.9 D.H. Welte, B. Horsfield, D.R. Baker: *Petroleum and Basin Evolution* (Springer, Berlin 1997) p. 535
- 11.10 C.L. Angevine, P.L. Heller, C. Paola: *Quantitative Sedimentary Basin Modeling*, American Association of Petroleum Geologists Continuing Education Course Note (AAPG, Tulsa 1990) p. 133
- 11.11 P.A. Allen, J.R. Allen: *Basin Analysis: Principles and Applications*, 2nd edn. (Blackwell Publishing, Malden 2005) p. 549
- 11.12 K. Stuewe: *Geodynamics of the Lithosphere*, 2nd edn. (Springer, Berlin 2007) p. 493
- 11.13 B. Parsons, J.G. Sclater: An analysis of the variation of ocean floor bathymetry and heat flow with age, *J. Geophys. Res.* **82**, 803–827 (1977)
- 11.14 W.R. Dickinson: Plate tectonics and sedimentation. In: *Tectonics and Sedimentation, Society of Economic Paleontologists and Mineralogists Special Publication*, Vol. 22, ed. by W.R. Dickinson (SEPM, Tulsa 1974) pp. 1–27
- 11.15 H.G. Reading: Sedimentary basins and global tectonics, *Proc. Geol. Assoc.* **93**, 321–350 (1982)
- 11.16 K.E. Peters, P.H. Nelson: Criteria to determine borehole formation temperatures for calibration of basin and petroleum system models. In: *Analyzing the Thermal History of Sedimentary Basins: Methods and Case Studies, SEPM Special Publication*, Vol. 103, ed. by N.B. Harris, K.E. Peters (SEPM, Tulsa 2009) pp. 5–15
- 11.17 G.R. Beardmore, J.P. Cull: *Crustal Heat Flow* (Cambridge Univ. Press, New York 2001) p. 324
- 11.18 D.K. Higley, M. Lewan, L.N.R. Roberts, M. Henry: *Petroleum System Modeling Capabilities for Use in Oil and Gas Resource Assessments*, US Geological Survey Open-File Report (USGS, Washington 2006) p. 18
- 11.19 M. He, S. Graham, A. Hosford Scheirer, K.E. Peters: A basin modeling and organic geochemistry study in the Vallecitos syncline, San Joaquin Basin, California, *Mar. Petroleum Geol.* **49**, 15–34 (2014)
- 11.20 B.P. Wygrala: *Integrated Study of an Oil Field in the Southern Po Basin, Northern Italy*, *Berichte Kernforschungsanlage Juelich*, Vol. 2313 (FZ Jülich, Jülich 1989) p. 217
- 11.21 R. di Primio, B. Horsfield: From petroleum-type organofacies to hydrocarbon phase prediction, *AAPG Bulletin* **90**, 1031–1058 (2006)
- 11.22 N.B. Schoellkopf: Quantitative assessment of hydrocarbon charge risk in new ventures: Are we fooling ourselves? In: *Basin Modeling: New Horizons in Research and Applications*, American Association of Petroleum Geologists Hedberg, ed. by K.E. Peters, D.J. Curry, M. Kacwicz (AAPG, Tulsa 2012) pp. 237–246
- 11.23 R.E. Swarbrick, M.J. Osborne, G.S. Yardley: *Comparison of Overpressure Magnitude Resulting from the Main Generating Mechanisms*, American Association of Petroleum Geologists Memoir, Vol. 76 (AAPG, Tulsa 2002) pp. 1–12
- 11.24 M.A. Biot: General theory of three-dimensional consolidation, *J. Appl. Phys.* **12**, 155–164 (1941)
- 11.25 K. Terzaghi: Die Berechnung der Durchlässigkeitssziffer des Tones im Verlauf der hydrodynamischen Spannungerscheinungen, *Sitz-Ber. Akad. Wiss. Vienna Math.-Naturwiss. Kl. Ila* **132**, 125–138 (1923)
- 11.26 H.S. Poelchau, D.R. Baker, T. Hantschel, B. Horsfield, B. Wygrala: Basin simulation and the design of the conceptual basin model. In: *Petroleum and Basin Evolution*, ed. by D.H. Welte, B. Horsfield, D.R. Baker (Springer, Berlin 1997) pp. 5–70
- 11.27 J.G. Sclater, P.A.F. Christie: Continental stretching: An explanation of the post Mid-Cretaceous subsidence of Central North Sea Basin, *J. Geophys. Res.* **85**, 3711–3739 (1980)
- 11.28 D. Falvey, M. Middleton: Passive continental margins: Evidence for a pre-breakup, deep crustal metamorphic subsidence mechanism, *Oceanol. Acta* **4**, 103–114 (1981)
- 11.29 B. Baldwin, C.O. Butler: Compaction curves, *AAPG Bulletin* **69**, 622–626 (1985)
- 11.30 F. Schneider, J.L. Potdevin, S. Wolf, I. Faille: Mechanical and chemical compaction model for sedimentary basin simulators, *Tectonophysics* **263**, 307–313 (1996)
- 11.31 O. Walderhaug: Modelign quartz cementation and porosity in Middle Jurassic Brent Group sandstones of the Kvitensjøen field, northern North Sea, *AAPG Bulletin* **84**, 1325–1339 (2000)
- 11.32 D. Croizé, K. Bjørlykke, J. Jahren, F. Renard: Experimental mechanical and chemical compaction of carbonate sand, *J. Geophys. Res.* **115**, B11204 (2010)
- 11.33 J.R. Allwardt, G.E. Michael, C.R. Shearer, P.D. Heppard, H. Ge: 2-D modeling of overpressure in a salt withdrawal basin, Gulf of Mexico, USA, *Mar. Petroleum Geol.* **26**, 464–473 (2009)
- 11.34 J.E. Van Hinte: Geohistory analysis-application of micropaleontology in exploration geology, AAPG

- Bulletin **62**, 201–222 (1978)
- 11.35 J.R. Dodd, R.J. Stanton: *Paleoecology, Concepts and Applications* (Wiley, New York 1981) p. 559
- 11.36 J.W. Morse, F.T. Mackenzie: *Geochemistry of Sedimentary Carbonates* (Elsevier, Amsterdam 1990) p. 707
- 11.37 F. Schneider: Understanding the diagenetic evolution of potential reservoirs in fold/thrust belts: An example from eastern Venezuela, *Petroleum Geology: North–West Europe and Global Perspectives – Proc. 6th Petroleum Geol. Conf.: Petroleum Geol. Conf. Ltd*, ed. by A.G. Dore, B.A. Vining (Geological Society, London 2005) pp. 1359–1366
- 11.38 F. Baur, M. Di Benedetto, T. Fuchs, C. Lampe, S. Sciamanna: Integrating structural geology and petroleum systems modeling – A pilot project from Bolivia’s fold and thrust belt, *Mar. Petroleum Geol.* **26**, 573–579 (2009)
- 11.39 M. Neumaier, R. Littke, T. Hantschel, L. Maerten, J.–P. Joonnekindt, P. Kukla: Integrated charge and seal assessment in the Monagas fold and thrust belt of Venezuela, *AAPG Bulletin* **98**, 1325–1350 (2014)
- 11.40 T. Menotti: *Petroleum System Evolution, Strike–Slip Tectonism, and Diagenesis of the Monterey Formation in the Salinas Basin, California*, Ph.D. Thesis (Geological and Environmental Sciences Department, Stanford Univ., Stanford 2014)
- 11.41 R. Gibson: A methodology to incorporate dynamic salt evolution in three–dimensional basin models: Application to regional modeling of the Gulf of Mexico. In: *Basin Modeling: New Horizons in Research and Applications*, American Association of Petroleum Geologists Hedberg, ed. by K.E. Peters, D.J. Curry, M. Kacwicz (AAPG, Tulsa 2012) pp. 103–118
- 11.42 K.E. Peters, C.C. Walters, J.M. Moldowan: *The Biomarker Guide* (Cambridge Univ. Press, Cambridge 2005) p. 1155
- 11.43 D. McKenzie: Some remarks on the development of sedimentary basins, *Earth Planet. Sci. Lett.* **40**, 25–32 (1978)
- 11.44 B.P. Tissot, D.H. Welte: *Petroleum Formation and Occurrence* (Springer, Berlin 1984) p. 699
- 11.45 T.S. Ahlbrandt, R.R. Charpentier, T.R. Klett, J.W. Schmoker, C.J. Schenk, G.F. Ulmishek: *Global Resource Estimates from Total Petroleum Systems*, American Association of Petroleum Geologists Memoir, Vol. 86 (AAPG, Tulsa 2005) p. 324
- 11.46 A. Hood, C.C.M. Gutjahr, R.L. Heacock: Organic metamorphism and the generation of petroleum, *AAPG Bulletin* **59**, 986–996 (1975)
- 11.47 D.D. Rice, G.E. Claypool: Generation, accumulation and resource potential of biogenic gas, *AAPG Bulletin* **65**, 5–25 (1981)
- 11.48 K. Wiese, K.A. Kvenvolden: Introduction to microbial and thermal methane. In: *The Future of Energy Gases*, US Geological Survey Professional, ed. by D.G. Howell (Reston, Virginia 1993) pp. 13–20
- 11.49 A.V. Milkov: Methanogenic biodegradation of petroleum in the West Siberian Basin (Russia): Significance for formation of giant Cenomanian gas pools, *AAPG Bulletin* **94**, 1485–1541 (2010)
- 11.50 M.J. Whiticar: Carbon and hydrogen isotope systematics of bacterial formation and oxidation of methane, *Chem. Geol.* **161**, 291–314 (1999)
- 11.51 M. Schoell, P.D. Jenden, M.A. Beeunas, D.D. Coleman: Isotope analyses of gases in gas field and gas storage operations, *Soc. Petroleum Eng.* **26171**, 337–344 (1993)
- 11.52 D.M. Jones, I.M. Head, N.D. Gray, J.J. Adams, A.K. Rowan, C.M. Aitken, B. Bennett, H. Huang, A. Brown, B.F. Bowler, T. Oldenburg, M. Erdmann, S.R. Larter: Crude oil biodegradation via methanogenesis in subsurface petroleum reservoirs, *Nature* **451**, 176–180 (2008)
- 11.53 A. Wilhelms, S.R. Larter, I. Head, P. Farrimond, R. di Primio, C. Zwach: Biodegradation of oil in uplifted basins prevented by deep–burial sterilization, *Nature* **411**, 1034–1037 (2001)
- 11.54 A.S. Mackenzie, T.M. Quigley: Principles of geochemical prospect appraisal, *AAPG Bulletin* **72**, 399–415 (1988)
- 11.55 H. Tian, Z. Wang, Z. Xiao, X. Li, X. Xiao: Oil cracking to gases: Kinetic modeling and geological significance, *Chin. Sci. Bull.* **51**, 2763–2770 (2006)
- 11.56 J.J. Sweeney, A.K. Burnham: Evaluation of a simple model of vitrinite reflectance based on chemical kinetics, *AAPG Bulletin* **74**, 1559–1570 (2006)
- 11.57 D.W. Waples, R.W. Marzi: The universality of the relationship between vitrinite reflectance and transformation ratio, *Org. Geochem.* **28**, 383–388 (1998)
- 11.58 J. Connan: Time–temperature relation in oil genesis, *AAPG Bulletin* **58**, 2516–2521 (1974)
- 11.59 M.A. Abu–Ali, J.G. Rudkiewicz, J.G. McGillivray, F. Behar: Paleozoic petroleum system of central Saudi Arabia, *GeoArabia* **4**, 321–336 (1999)
- 11.60 A.K. Burnham, R.L. Braun: Global kinetic analysis of complex materials, *Energy Fuels* **13**, 1–22 (1999)
- 11.61 K.E. Peters, C.C. Walters, P.J. Mankiewicz: Evaluation of kinetic uncertainty in numerical models of petroleum generation, *AAPG Bulletin* **90**, 1–19 (2006)
- 11.62 B. Horsfield, U. Disko, F. Leistner: The micro–scale simulation of maturation: Outline of a new technique and its potential applications, *Geol. Rundsch.* **78**, 361–373 (1989)
- 11.63 F. Behar, S. Kressman, J.L. Rudkiewicz, M. Vandenbroucke: Experimental simulation in a confined system and kinetic modeling of kerogen and oil cracking, *Org. Geochem.* **19**, 173–189 (1992)
- 11.64 M.D. Lewan, J.C. Winters, J.H. McDonald: Generation of oil–like pyrolyzates from organic–rich shales, *Science* **203**, 897–899 (1979)
- 11.65 M.D. Lewan, T.E. Ruble: Comparison of petroleum generation kinetics by isothermal hydrous and nonisothermal open–system pyrolysis, *Org. Geochem.* **33**, 1457–1475 (2002)
- 11.66 R.L. Braun, A.K. Burnham: Analysis of chemical reaction kinetics using a distribution of activation energies and simpler models, *Energy Fuels* **1**, 153–161 (1987)

- 11.67 A.K. Burnham, R.L. Braun, H.R. Gregg, A.M. Samoun: Comparison of methods for measuring kerogen pyrolysis rates and fitting kinetic parameters, *Energy Fuels* **1**, 452–458 (1987)
- 11.68 P. Sundararaman, P.H. Merz, R.G. Mann: Determination of kerogen activation energy distribution, *Energy Fuels* **6**, 793–803 (1992)
- 11.69 H.J. Schenk, B. Horsfield: Kinetics of petroleum generation from open versus closed system pyrolysis experiments, *Geochim. Cosmochim. Acta* **57**, 623–630 (1993)
- 11.70 U. Ritter, M.B. Myhr, T. Vinge, K. Aareskjold: Experimental heating and kinetic models of source rocks: Comparison of different methods, *Org. Geochem.* **23**, 1–9 (1995)
- 11.71 T. Barth, B.J. Smith, S.B. Nielsen: Do kinetic parameters from open pyrolysis describe petroleum generation by simulated maturation?, *Bull. Can. Petroleum Geol.* **44**, 446–457 (1996)
- 11.72 J.G. Stainforth: Practical kinetic modeling of petroleum generation and expulsion, *Mar. Petroleum Geol.* **26**, 552–572 (2009)
- 11.73 D.W. Waples, V.S. Nowaczewski: *Source–Rock Kinetics* (2013) <https://siriusdummy.files.wordpress.com/2013/11/perspective-on-sr-kinetics-ss.pdf>
- 11.74 K.E. Peters, A.K. Burnham, C.C. Walters: Petroleum generation kinetics: Single-versus multiple heating-ramp open-system pyrolysis, *AAPG Bulletin* **99**, 591–616 (2015)
- 11.75 R.L. Braun, A.K. Burnham, J.G. Reynolds, J.E. Clarkson: Pyrolysis kinetics for lacustrine and marine source rocks by programmed pyrolysis, *Energy Fuels* **5**, 192–204 (1991)
- 11.76 H.J. Schenk, B. Horsfield: Using natural maturation series to evaluate the utility of parallel reaction kinetics models: An investigation of Toarcian shales and Carboniferous coals, *Org. Geochem.* **29**, 137–154 (1998)
- 11.77 A.K. Burnham, R.L. Braun, T.T. Coburn, E.I. Sandvik, D.J. Curry, B.J. Schmidt, R.A. Noble: An appropriate kinetic model for well-preserved algal kerogens, *Energy Fuels* **10**, 49–59 (1996)
- 11.78 S.R. Kelemen, C.C. Walters, D. Ertas, H. Freund, D.J. Curry: Petroleum expulsion. Part 3. A model of chemically driven fractionation of petroleum from kerogen, *Energy Fuels* **20**, 309–319 (2006)
- 11.79 W.A. England, A.S. Mackenzie, D.M. Mann, T.M. Quigley, D. Robinson: The movement and entrapment of petroleum fluids in the subsurface, *J. Geol. Soc.* **144**, 327–347 (1987)
- 11.80 T. Hantschel, A.I. Kauerauf, B. Wygrala: Finite element analysis and ray tracing modeling of petroleum migration, *Mar. Petroleum Geol.* **17**, 815–820 (2000)
- 11.81 D.H. Welte, T. Hantschel, B.P. Wygrala, K.S. Weissenburger, D.J. Carruthers: Aspects of petroleum migration modelling, *J. Geochem. Explor.* **69–70**, 711–714 (2000)
- 11.82 D.J. Carruthers: Modeling of secondary petroleum migration using invasion percolation techniques. In: *Multidimensional Basin Modeling*, American Association of Petroleum Geologists Data-
pages Discovery, Vol. 7, ed. by S.J. Düppenbecker, R. Marzi (AAPG, Tulsa 2003) pp. 21–37
- 11.83 D. Wilkinson, J.F. Willemsen: Invasion percolation: A new form of percolation theory, *J. Phys. A: Math. Gen.* **16**, 3365–3376 (1983)
- 11.84 S.M. Clarke, S.D. Burley, G.D. Williams, A.J. Richards, D.J. Meredith, S.S. Egan: Integrated four-dimensional modelling of sedimentary basin architecture and hydrocarbon migration. In: *Analogue and Numerical Modeling of Crustal-Scale Processes*, Vol. 253, ed. by S.J.H. Buitter, G. Schreurs (Geological Society, Special Publications, London 2006) pp. 185–211
- 11.85 X. Luo: Simulation and characterization of pathway heterogeneity of secondary hydrocarbon migration, *AAPG Bulletin* **95**, 881–898 (2011)
- 11.86 A. Vayssaire: Simulation of petroleum migration in fine-grained rock by upscaling relative permeability curves: The Malvinas Basin, offshore Argentina. In: *Basin Modeling: New Horizons in Research and Applications*, American Association of Petroleum Geologists Hedberg, Vol. 4, ed. by K.E. Peters, D.J. Curry, M. Kacewicz (AAPG, Tulsa 2012) pp. 247–257
- 11.87 J.J. Hohler, W.E. Bischoff Alaska: Potential for giant fields. In: *Future Petroleum Provinces of the World*, American Association of Petroleum Geologists Memoir, Vol. 40, ed. by M.T. Halbouty (AAPG, Tulsa 1986) pp. 131–142
- 11.88 US Geological Survey: Circum-Arctic resource appraisal: Estimates of undiscovered oil and gas north of the Arctic Circle: US Geological Survey Fact Sheet 2008–3049 (2008) <http://pubs.usgs.gov/fs/2008/3049/fs2008-3049.pdf>
- 11.89 O. Schenk, K.J. Bird, L.B. Magoon, K.E. Peters: Petroleum system modeling of Northern Alaska. In: *Basin Modeling: New Horizons in Research and Applications*, American Association of Petroleum Geologists Hedberg, Vol. 4, ed. by K.E. Peters, D. Curry, M. Kacewicz (AAPG, Tulsa 2012) pp. 317–338
- 11.90 K.E. Peters, L.S. Ramos, J.S. Zumberge, Z.C. Valin, K.J. Bird: De-convoluting mixed crude oil in Prudhoe Bay Field, North Slope, Alaska, *Org. Geochem.* **39**, 623–645 (2008)
- 11.91 J.G. Gluyas, R. Swarbrick: *Petroleum Geoscience* (Blackwell Publishing, Hoboken 2004) p. 359
- 11.92 L.I. Dzou: Kuparuk oil field, Alaska, a mixture of Kektituk gas condensate and Shublik oil, *AAPG Bulletin* **94**, 1761–1778 (2010)
- 11.93 D.M. Jarvie: Shale resource systems for oil and gas: Part 2 – Shale-oil resource systems. In: *Shale Reservoirs – Giant Resources for the 21st Century*, American Association of Petroleum Geologists Memoir, Vol. 97, ed. by J.A. Breyer (AAPG, Tulsa 2012) pp. 89–119
- 11.94 Q.R. Passey, K.M. Bohacs, W.L. Esch, R. Klimentidis, S. Sinha: From oil-prone source rock to gas-producing shale reservoir – Geologic and petrophysical characterization of unconventional shale-gas reservoirs, *Int. Oil Gas Conf. Exhib. China, Beijing* (Society of Petroleum Engineers,

- 11.95 Houston 2010) doi:[10.2118/131350-MS](https://doi.org/10.2118/131350-MS)
 M. Gasparik, A. Ghanizadeh, P. Bertier, Y. Gensterblum, S. Bouw, B.M. Krooss: High-pressure methane sorption isotherms of black shales from the Netherlands, *Energy Fuels* **26**, 4995–5004 (2012)
- 11.96 A. Neber, S. Cox, T. Levy, O. Schenk, N. Tessen, B. Wygrala, I. Bryant: Systematic evaluation of unconventional resource plays using a new play-based methodology, *SPE Asia Pac. Oil Gas Conf. Exhib.*, Perth (Society of Petroleum Engineers, Houston 2012) doi:[10.2188/158571-MS](https://doi.org/10.2188/158571-MS)
- 11.97 T. Hantschel, M. Fuecker, T. Matava, A. Kauer-auf: Improving petroleum systems modeling with basin-scale 3-D stress-strain models, *AAPG Search Discov.*, article #120098 (2013)
- 11.98 P.M.T.M. Schutjens, T.H. Hanssen, M.H.H. Hettema, J. Merour, P. de Bree, J.W.A. Coremans, G. Helliesen: Compaction-induced porosity/permeability reduction in sandstone reservoirs: Data and model for elasticity-dominated deformation, *SPE Reserv. Eval. Eng. SPE* **88441**, 202–216 (2004)
- 11.99 D. Dralus, K.E. Peters, M.D. Lewan, O. Schenk, M. Herron, K. Tsuchida: Kinetics of the opal-CT to quartz phase transition control diagenetic traps in siliceous shale source rock from the San Joaquin Basin and Hokkaido, *Proc. AAPG Annu. Conv. Exhibit.*, Houston (2011), Article #40771
- 11.100 D. Dralus: Chemical Interactions Between Silicates and Their Pore Fluids: How They Affect Rock Physics Properties from Atomic to Reservoir Scales, Ph.D. Thesis (Stanford Univ., Stanford 2013)
- 11.101 T. Menotti: Investigations into burial history and petroleum system development in the Salinas Basin, California through 1-D modeling, *Geol. Soc. Am. Abstr. with Programs* **42(4)**, 78 (2010), 2010 AAPG Pacific section, joint meeting with west region SPE and GSA Cordilleran section, Anaheim
- 11.102 B. Burgreen: The Influence of Convergent Margin Structure on Deep-Water Stratigraphic Architecture, Pore Pressure Evolution, and Source Rock Maturation in the East Coast Basin, New Zealand, Ph.D. Thesis (Geological and Environmental Sciences Department, Stanford Univ., Stanford 2014)

Seismic Explorations

12. Seismic Explorations

Graham Ganssle

Geophysics is an extremely diverse subject including fields of study with backgrounds in chemistry, geology, biology, and physics. This chapter attempts to show the reader a broad cross section of the geophysics of petroleum exploration. Three fundamental steps exist in the workflow of geophysical petroleum exploration. First, there is the acquisition of seismic data by using initiating acoustic energy into the Earth's subsurface and recording the reflected energy. Second, this raw acoustic data is processed using the physical and mathematical principles of wave propagation and continuum mechanics. Finally the processed seismic data is interpreted. Interpretation endeavors

12.1	Seismic Data Acquisition	420
12.2	Seismic Data Processing	423
12.3	Seismic Data Interpretation	426
12.4	Summary	431
	References	431

to create a pseudo-geological model from the geophysical data for verification or update by purely geological data. The model is then iteratively updated by both geologists and geophysicists to form a complete risk assessment of a prospective drill location.

Seismic activity is an ongoing phenomenon. Earthquakes, caused by fault slip, are a recurring reminder of seismic activity in the Earth's subsurface. In reality, seismic activity is a result of the motion of any object. An object making contact with another object creates sound waves, especially when moving. These waves, in the case of earthquakes, can have very large amplitudes. Other seismic wave sources can create sound waves with quite small amplitudes. For example, every time a person walks down the street their footsteps on the pavement are creating very small seismic disturbances. The term *seismic* is used to describe the peak frequency of the resulting sound waves. Seismic waves are generally thought of as having low frequency (in the range of 5–8 Hz) and large amplitude. It is possible to measure seismic disturbances from earthquakes to footsteps on pavement using the right equipment. There are three major types of seismic waves. P-waves, also called primary or pressure waves, are familiar to everyone in the form of sound. Nearly all seismic exploration for petroleum uses p-waves. S-waves, also called secondary or shear waves, are slower and can only travel through solids. P-waves and s-waves are collectively called body waves because they pass through the Earth. Surface waves travel along the surface, similar to an ocean wave. Surface waves are not used for petroleum exploration, but they are extensively studied because

they cause most of the damage during earthquakes.

The velocity of body waves is related to the properties of the medium they pass through by the following equations

$$V_p = \sqrt{\frac{K + 4/3\mu}{\rho}} \quad V_s = \sqrt{\frac{\mu}{\rho}}, \quad (12.1)$$

where K is compressibility, μ is rigidity, and ρ is density. If we know both p-wave and s-wave velocities and can make some reasonable assumption about the density, we can determine the mechanical properties of the medium.

The measurement of seismic disturbances is carried out by measuring the motion of the ground for an extended period of time. This creates a record in time with each sample point being the magnitude of this motion. Recording from many locations arranged in a line or an array provides a record that approximates the local subsurface geology. When looking at a seismic data line the horizontal axis represents some spatial dimension, x , and the vertical axis represents the time dimension, t . At each (x, t) point the data is an amplitude. This amplitude is related to the reflection strength of the layer in the Earth's subsurface located at time t . In a perfect world, each reflection event on a seismic section would

represent one geologic bed, giving a perfect view of the Earth's subsurface.

Nowadays commercial seismic data is widely used in industry for the exploration of petroleum oil and gas. It is also used for the exploration of salt, certain hard-rock deposits, and engineering site investigation. The use of seismic data has proven to be so successful in petroleum exploration in the past 100 years that there are few prospects which have not had seismic shot over them at some point. Seismic data can be used in the exploration of new prospects, in the delineation of current targets, and in the classification of reservoirs. Therefore, it is extremely beneficial to use seismic data in any stage of target planning. However, the acquisition, processing, and interpretation of seismic data can be quite expensive. Because of this high cost, other techniques are employed. In large scale remote areas, gravity survey methods are often used to determine

where a seismic survey should be acquired. In areas with a large number of existing wells, the well data may be dense enough to eliminate the need for seismic data.

Inferring information about subsurface geology without going underground to take physical samples is a difficult task. Like all remote sensing problems, data is taken from a reference point far from the area of interest. There are many layers of interfering medium between the layer of interest and Earth's surface distorting the desired data. There are an incredibly large number of noise sources contaminating the data while it is being recorded. At the same time, the medium being recorded through is dispersing and absorbing the signal energy. These points demonstrate some of the reasons why a seismic survey is so expensive. They also fundamentally constrain the way seismic data must be acquired, processed, and interpreted after acquisition.

12.1 Seismic Data Acquisition

There are two major arenas of seismic geometry. The first is two-dimensional (2-D) seismic data. 2-D data is one line of data running in a direction of interest. The data looks like a panel of amplitudes, extending horizontally out in the direction of the line, and extending down in the direction of recording time. The second is three-dimensional (3-D) seismic data. 3-D data is a volume of data covering a lateral extent around the area of interest. The data looks like a 3-D volume of amplitudes, extending horizontally out in two directions, and extending down in the direction of recording time. 3-D data may be viewed on a computer in three dimensions or in cross section as a collection of 2-D lines. Seismic data specialists refer to increasing subsurface depth in terms of increasing recording time.

As with any specialty, the seismic industry has a wealth of nomenclature. In addition to 2-D and 3-D data there is four-dimensional (4-D) data. 4-D data does not implement a different recording geometry, like the difference between 2-D and 3-D, but is rather recorded repeatedly. 4-D data is recording a 3-D seismic survey, and then recording the same 3-D survey after some years to observe differences in the subsurface. The goal is to obtain information about the depletion of reservoirs and other time dependent processes. So, 4-D seismic is actually just two or more 3-D surveys acquired (preferentially in the same way) over the same area. There is also five-dimensional (5-D) terminology that is used in the seismic industry. 5-D is not a different recording geometry, but is a way of interpolating seismic data for special use in seismic data processing. By

means of these examples, it is realized that some of the nomenclature is overlapping and nonunique.

The initial requirement in recording seismic data is that there must be energy to record. Therefore, the acquisition of seismic data must start with a seismic source. In some cases, the seismic source is a natural one, as in the case of earthquakes. These scenarios are called passive seismic recording, as there is no operator controlled input energy. The acquisition of natural passive seismic activity is quite different than that of active seismic recording used in petroleum exploration. For example, the epicenter location of an earthquake is not known a priori, which creates a need for wide receiver spacing and continuous recording. After an earthquake has occurred, seismologists can look back in the seismic records from several stations to triangulate the signal to figure out the location of the epicenter.

Active seismic energy recording necessitates different acquisition parameters. In this case, the source position is known, so the receivers can be located according to signal requirements. The goal is to have a source that gives the best signal possible. A good seismic signal can be characterized by many features; several important ones are as follows. First, the source must transmit the bulk of its output energy into the ground. The energy that is not input into the ground is wasted for the purposes of subsurface imaging. Second, the source must input a signal of sufficient bandwidth to be used to image the strata in the exploration of petroleum. If the interpreters require a signal with a peak frequency of 40 Hz, for example, the source

may have to input a useable signal of up to 200 Hz depending on the geology. Third, the source must input enough energy into the ground that the signal is not degraded to the point of being undetectable. This parameter is a function of the absorption and dispersion characteristics of the local geology and the noise present in the area. There are many other constraints on sources, which in most cases can be controlled to an order of accuracy that is determined while planning the acquisition parameters.

There are three common ways to get the energy into the ground. These are dynamite, airgun, and vibroseis. If the survey is of an area on land, dynamite or vibroseis may be used. If the survey is over an area covered by water airguns are usually the preferred method, but in some shallow water instances dynamite may be used. Each of these three main types of sources has a huge variety of types, each meant for specific applications. Despite this large variety, dynamite, airgun, and vibroseis sources can be analyzed as groups with different signal characteristics.

Dynamite sources are used both on land and in shallow water surveys. The acquisition field crew drills holes into the ground where they place the dynamite. The holes are drilled to a depth sufficient to get the dynamite below the unconsolidated surface sediments, and into bedrock. This ensures good signal transmission from the dynamite into the ground. Unfortunately, dynamite does waste a good deal of energy in upward traveling waves going up into the air. However, dynamite is an excellent seismic source because of its desirable signal characteristics. The signal strength, or amplitude, can be very large. To get a larger signal amplitude, a larger charge or a combination of several charges can be used, or an array of charges can be laid out. Dynamite sources output an impulsive signal that has a large bandwidth. Short-duration, broadband inputs assist the seismic data processors in creating an accurate subsurface image.

Airguns are used in water surveys from shallow to ultra-deep water. The guns are towed behind a *shot boat* and are usually aligned in an array or linear pattern behind the boat. Airguns output less energy than dynamite, but can be very large in the case of deep water surveys. Because of the fluid coupling between the water and the seafloor, most of the energy the guns output is transferred into a usable signal. Some energy is lost to the atmosphere via transmission from the sea surface. Inputting more energy into the ground requires using a larger array of airguns, which can be costly. The signal from airguns is dependent on the design of the gun itself, the array design in which the guns are towed, and the timing of the individual guns. Just as dynamite, the signal is broadband impulsive.

The term Vibroseis came from an actual seismic acquisition company's brand name. Many other seismic acquisition companies now use similar designs, but the original name was so ubiquitous that it is generally used as a description of the process. The vibroseis method uses a heavy truck with a plate on the bottom attached to a vibrator driven by compressed air. The truck is moved into position, the plate is lowered to the ground and extended, lifting the truck off the ground. The plate then vibrates up and down in a specific pattern causing the ground to move as well. The vibration pattern is controlled by regulating the flow of compressed air with a servo. These trucks are usually lined up in arrays, and the vibrating pattern is decided very carefully to input a specific seismic signal. Of the three methods discussed, vibroseis inputs the smallest energy to the ground, making it ideal for use in populated areas where dynamite is not feasible. The signal obviously can be exactly specified, making it arguably the best signal shape of all of the seismic sources. The majority of vibroseis signals are called chirps. A chirp is a sinusoidal waveform that increases frequency as time increases. A simple chirp could be a sine wave with an argument of time squared; these signals sound a little like birds chirping to the human ear, hence the name. Chirps can be deconvolved with precision by the seismic processor, making vibroseis signals very useful.

Any of the three above mentioned sources inputs a seismic signal into the ground, where the signal is (among other things) reflected back to the Earth's surface. To gain any useful benefit from this system, receivers must be used to record the reflected signal. Two types of receivers are used: geophones and hydrophones. Geophones are used on land and hydrophones are used in water. Nowadays, geophones are sometimes used in the water as well. In deep water and ultra deep water plays, sometimes companies will use what are called ocean bottom nodes. Ocean bottom nodes are geophones placed on the seafloor by a remotely operated vehicle (ROV) robot. Airguns are used as a source in these instances. Ocean bottom node recording is extremely expensive, as thousands of geophones must be laid out by ROV operators and picked back up after recording is complete. The data quality however, is breathtaking.

Most geophones measure the vertical component of velocity only, although 3-component geophones are available. They record the motion at the Earth's surface as a function of time. Traditionally, only the vertical dimension of ground surface velocity is recorded to build a one-dimensional magnitude record. In some cases, all three dimensions are recorded separately to form what is called 3-component data. This data can be used to infer properties of the subsurface media by the motion of

shear waves. Geophones are laid out on the surface in groups, each of which is combined into a single trace. Each group may be an array or simply a cluster, and the groups may be laid out over an area for 3-D data or in a line for 2-D data. The location of each geophone group is recorded by a surveyor, or by a GPS unit attached to the geophone node.

Hydrophones are pressure vessels calibrated to record differences in the hydrodynamic pressure in the water in which they are towed. They are enclosed in long, flexible, oil-filled cables called streamers which are towed behind streamer boats at a depth of 5 to about 50 m. The streamers can be many miles long, so each streamer contains many hydrophones, several steering units capable of steering the streamer in depth and crosstrack (relative to the streamer boat's heading), and GPS units down the streamer to record position information. The streamer boats and the shot boats drive around in many different complicated patterns to accomplish an exact acquisition geometry decided in advance by a design team.

The geometry of the survey is of utmost importance. There is no point recording a seismic survey which does not most efficiently illuminate the subsurface area of interest so the geometry not only needs to be designed properly, but geometry also must be recorded in the field. The number one mishap in analyzing seismic data is incorrectly positioning the data relative to the original parameters. When seismic is recorded on land, the receivers and sources are laid out, their positions are recorded, and then the data recorded. In water, the shot boats and streamer boats both have GPS systems on the guns and the hydrophones to create a continuous record of position data along with the seismic data. During data processing, these positioning data are used to ensure that the final seismic section correctly indicates where to drill. The positioning data also constrains the way the seismic data must be handled during certain processing steps. If the recording locations for the seismic data are incorrect, not only will the resulting seismic section indicate incorrect locations to drill, it may also have erroneous structure and amplitude character as is demonstrated in Sect. 12.2.

When seismic data were first being recorded in the early twentieth century, the records were essentially the result of one source and one receiver being used at a time. This is called single density, or single-fold data. In modern seismic data, there are many receivers recording when a source goes off. The number of channels recording each subsurface location is the fold of the data. If the source and receiver spacings are equal, the fold will be one-half of the number of channels recorded from each shot. Today's seismic data is often recorded at up to 300-fold, an indication of why seismic

data sets are so large. In a typical land survey covering a 100 square mile area, you may have 10 000 sources with 300 records per source, for a total of three million records, also called traces. A typical sample interval is 2 ms, so if the trace lengths are (a typical) 8 s there would be 4000 samples per trace, for a total survey size of 12 billion sample points. This is hundreds of gigabytes of data even in a compressed format. The result is that it takes an incredible amount of computing power to deal with seismic data. Even still, the reason seismic data are recorded at such high fold is that data density is of paramount importance. As shown in Sect. 12.2, increasing the fold of the data input increases the quality of the data output.

In a hypothetical 3-D land survey, the recording acquisition geometry is a square. When shooting a source at the exact center of the square, which geophones should be recording? There are many answers to this question, depending on design parameters. One simple geometry, called split spread recording, would have 150 geophones recording in a line extending to the west of the source and a mirrored 150 geophones in a line to the east. This geometry would produce a fold of 300 if the shot spacing is one-half of the receiver spacing. This is very high fold and would hopefully produce a quality seismic section. The linear nature of this geometry however, means that there is only one direction, or azimuth, recorded. Azimuth is defined as a compass direction from source to receiver in the seismic survey.

The benefit of multiazimuthal acquisition geometries is to illuminate anisotropic properties of the rock. All subsurface beds are heterogeneous, meaning that they are inconsistent in lateral extent, for example, they have horizontally distributed inconsistencies. This is also true when looking in the vertical direction, as we have beds of varying rocks. Some rocks however exhibit anisotropy. Anisotropy is a change in seismic velocity as a function of direction. Nearly all sedimentary rocks have different seismic velocities in the vertical and horizontal directions. Fractured units often display azimuthal anisotropy. Multiazimuthal seismic data recording geometries can provide a characterization of the azimuthal anisotropy in subsurface beds. This happens because sound travels with different velocities through fractured and unfractured rock of the same composition. For example, imagine a shale with natural linear fracture planes oriented in the north-south direction. Sound waves would propagate with a certain speed through this shale in the north-south direction, but would be apparently slowed down in the east-west direction because of the interference created when propagating across the fractured layers. Because of this property, many modern acquisition geometries are laid out with a large azimuthal range.

Acquisition of seismic data is the first step in creating a seismic section that represents the subsurface geology. However, because of noise, waveform character, and geometrical considerations, a raw seismic record straight from the geophone does not look like a geologic section. It does look like a long record of

noise. Combining the large number of traces from the above hypothetical 3-D seismic example exhibits why the raw records of the full survey are incomprehensible. To get these noisy records to approximate anything resembling geology, seismic processing specialists must do an extremely large amount of number crunching.

12.2 Seismic Data Processing

Seismic data processing is more naturally accomplished in a different set of dimensions than that of the data acquisition dimensions. When acquiring seismic data, the directions to organize the data as it is streamed onto the hardware are the source, receiver, and time domains. This is because, as shown in Sect. 12.1, a source goes off while receivers are listening. The field crew records the live channels simultaneously as a function of time.

In many cases, it is more elegant mathematically to handle seismic data during processing in the offset, midpoint, and time domains. The offset domain is defined in terms of the linear distance between the source and the receiver. The midpoint domain is defined in terms of the imaginary distance halfway between source and receiver, at the surface. This domain is orthogonal to the offset domain. The time domain is the same as in the acquisition domains.

When the data comes in from the field it is often multiplexed, which means the bits from each channel are striped across one record. The seismic processor then must demultiplex the data, and sort it into midpoint, offset, time coordinates. This process is usually incorporated into the same steps as defining the geometry on the data. Each trace in a seismic data file includes a trace header which includes, among other information, the coordinates of the source and the receiver. Using the observer notes from the survey crew in the field, the data processor fills the geometry into each of these trace headers using any information available. This information may include the shotpoint, the record field ID number, or sometimes the actual GPS position of the stations themselves. Along with some other ancillary steps, these initial definitions and sorting are collectively named preprocessing.

There are many steps in the seismic data processing sequence that affect the data primarily in one of the three processing domains, midpoint, offset, and time. There are others that affect the data in more than one domain at a time, as they are intrinsically linked to the position of the data in both time and space. Each one of the dimensions can be discussed separately in many cases; however, the processing steps taken in an actual workflow can be in any order, and may be repet-

itive. A typical seismic data processing workflow can be thousands of steps long to get the data looking just right.

In the time domain among hundreds of processes that could be applied, there are three which stand out as being the categorical leaders. These are gaining, filtering, and deconvolution. All of these three processes affect the data only in the time domain, with no spatial effects in the midpoint or offset domains.

Gaining the data can be accomplished in many different ways. One of the first gain processes applied to seismic data is called geometrical spreading correction. Geometrical spreading correction gain is applied to correct for the natural absorptive effects of the Earth. As the acoustic waves propagate from the source to the receiver through rock, some of the energy is lost due to heat dissipation. The farther these waves must travel, the more energy is lost. Therefore, the late times on seismic records are always lower amplitude than the early times. Geometrical spreading correction gain is usually applied to the data as a time to the exponent gain. In many cases, a good starting guess for the exponent is two. Processors usually then scale the exponent up or down to make the records look even.

Filtering the data can be accomplished in thousands of ways. A common process uses a band-pass filter to allow a certain frequency spectrum of data to remain by eliminating everything else. For these types of filters, the data processor will apply Fourier transform to convert the data from the time domain to the temporal frequency domain, and then multiply some high and low frequency components by zero. The inverse Fourier transform is then applied, and the data is examined for content. Another filter is applied in frequency-wavenumber space, where a 2-D Fourier transform is applied and both dimensions are filtered. There are countless other 2-D filtering techniques, including methods in the time-space domain, the frequency-space domain, and the time-wavenumber domain.

Deconvolution of seismic data can be used to accomplish several things. Two major deconvolution processes are called spiking deconvolution and predictive error filtering. Spiking deconvolution aims to elimi-

nate the incoming signal waveform from the seismic source, called a wavelet, from the data. Spiking deconvolution generally tends to make the data appear to have sharper peaks and troughs on the waveform. Predictive error filtering deconvolution approximates and removes repetitive ringing from the waveform. This ringing could represent several things, but in many cases the ringing in a seismic record is produced by the propagation of multiple reflections, often simply called multiples. Multiples are caused by acoustic energy bouncing back and forth off a pair of reflectors, for example, the water bottom and the water surface in a marine seismic survey.

The offset domain is handled by many processes that affect the data only in the offset direction, but also some processes that also affect the data in the time and/or midpoint directions. The velocity of seismic wave propagation is of critical importance to the seismic data processor. The change in velocity and density between different regions in the Earth's subsurface is the cause of a seismic response. It is in the offset domain that seismic data processors estimate seismic wave propagation and correct for certain types of velocity changes.

When a source and a receiver are located at the same position, the acoustic energy measured propagates vertically. When we introduce a horizontal displacement, or offset, between the source and the receiver the acoustic energy measured has necessarily traveled not only in the vertical direction, but also in the direction of the offset. To see this, the seismic processor organizes the data traces into a group where all the energy has come from one source, and the traces increase in offset with respect to the horizontal axis. In many cases this offset is measured from the midpoint between the source and the receiver. In this case this group, or gather, of traces is called a common midpoint gather (CMP gather). CMP gathers are used to estimate the velocity with which acoustic energy propagates in the local media surrounding the midpoint in question.

Once the data is grouped into CMP gathers, the data processor begins to see a hyperbolic moveout response of the individual reflection events. Moveout is the increase in arrival time as a function of offset with each trace in a CMP (or other types of) gathers. The data processor can use the slope of the hyperbolas on the CMP gathers to estimate the velocity of the wave propagation. This is done by using a variable hyperbolic function as a function of time to sum, or stack, the traces in a CMP gather. The function's slope is varied many times and the semblance, or power average, is computed for each sample in time. Each semblance is then displayed as a function of velocity on a semblance panel. The data processor picks the highest semblance value,

which associates the velocity value at that time sample back to the data. The CMP gathers are then corrected in time according to the slope of each hyperbola so that the seismic events appear linear rather than hyperbolic. This process is called normal moveout (NMO) correction and is an integral part of seismic data processing.

Once the data has been corrected for normal moveout, the CMP gathers appear to have flat events. The traces in the gather are then summed and multiplied by some weighting function. This process is called stacking. Stacking a CMP gather creates one trace. This is done to reduce noise and increase signal quality. Every data trace in the seismic survey before this point has been sorted into CMP gathers. Each CMP gather is stacked, creating one trace per gather, and dramatically reducing the size of the data set.

The gathers in Fig. 12.2 correspond to the stacked section in Fig. 12.1. After normal moveout correction has been applied to a set of CMP gathers they are stacked. This means that every gather is summed into one trace on the stacked seismic section. In the example of Fig. 12.2, after stacking these six CMP gathers would become six traces in the stacked section of Fig. 12.1.

Assuming several other processes have been completed accurately, and that the geologic dips are not too steep, stacking the data approximates a zero offset section. Therefore the resulting seismic section after stack represents the subsurface geology. The data processor will output the data at this point, called a structure section, for a seismic data interpreter to look at to confirm whether or not the seismic data is on par with the subsurface model built from existing well data.

The midpoint domain processes are arguably the most interesting. There are several processes that affect the midpoint domain, but the most major of these is called migration. Migration processes strive to eliminate the effects of diffraction and sometimes refraction on the acoustic energy. There are a number of different migration algorithms, but all of them require a model of the seismic velocity throughout the survey area. Migration translates energy through the time, offset, and midpoint domains, although migration techniques are traditionally studied in the category of midpoint domain processes. Because of the movement of energy on the seismic section in the midpoint domain, the data processor must be very careful to apply the correct geometry before the migration inversion processes are implemented. Because the energy moves horizontally, the survey must extend a distance, called the migration aperture, beyond the area of interest. If the geologic dips are steep or lateral velocity variations are present, migration should be applied instead of the normal moveout correction before stacking. In the case of pre-stack migration inversion

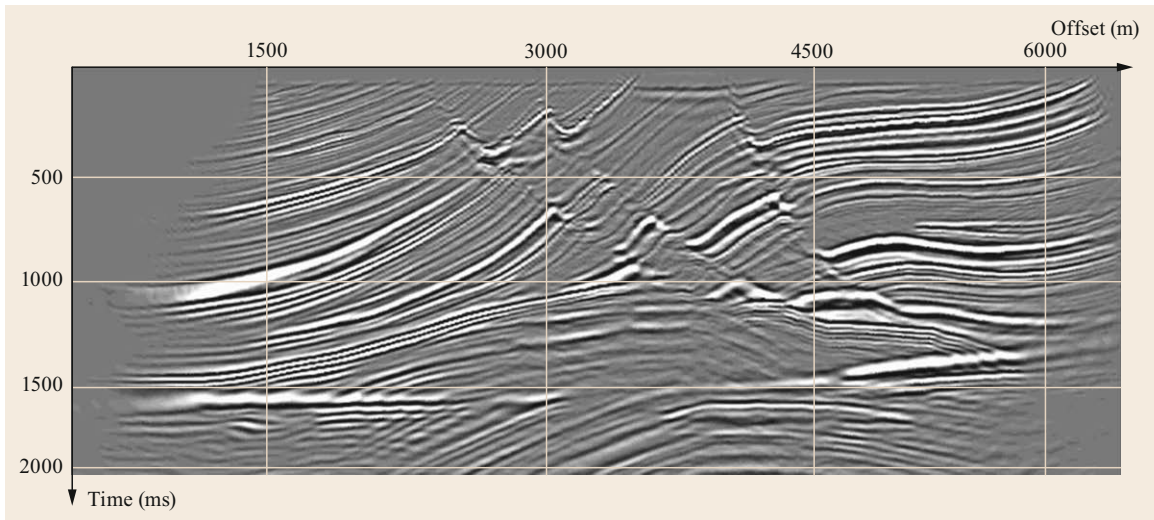


Fig. 12.1 A 2-D seismic cross section (Reprinted with permission after [12.1])

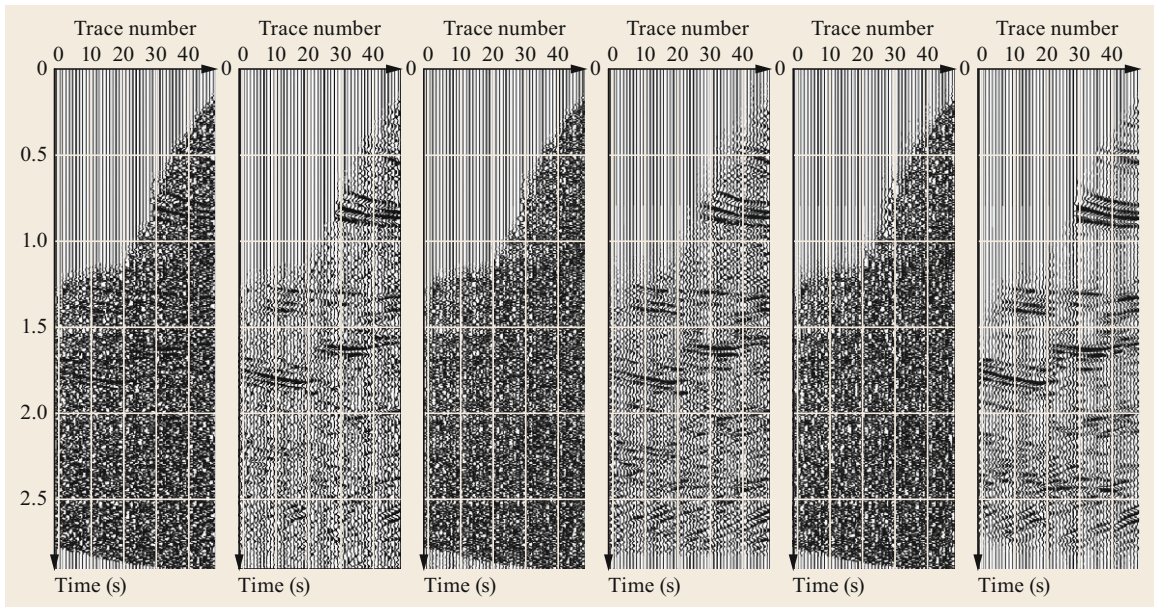


Fig. 12.2 A collection of CMP gathers corresponding to the seismic section in Fig. 12.1 (after [12.2])

techniques, the algorithm to complete the migration must in some cases apply geometry corrections to the trace headers.

Acoustic energy appears distorted on unmigrated seismic records. This distortion falls into several categories: first, approximate point reflectors in the subsurface cause acoustic energy to appear diffracted into hyperbolas, second, acoustic energy reflected off of dipping (sloped with respect to horizontal) reflectors appears to be translated in the down-dip direction with a smaller slope than reality, and third, all of this transla-

tion of energy creates an apparent change in amplitude of the seismic data. Migration processes work to fix all of these distortions. Migration is one of the largest subtopics of study in the seismic data processing arena, and as such there are many different approaches to implement migration. Before understanding how each of these processes works, a clear understanding of each distortion type is needed.

Diffraction of waves occurs in any wave dynamical system. The term diffraction describes the radial spreading of wave energy as it propagates away from

the spreading point. A simple analogy to the diffraction of seismic acoustic energy is a hole in a seawall off of a beach. Imagine there is a beach with a parallel seawall 100 m out from shore to stop waves. If there was a 1 m long section of seawall missing, when plane waves hit the seawall from the ocean side some of the waves would pass through the wall where the 1 m hole was. It is natural to automatically assume that beachgoers would see a flat sea with a wide wave hitting the shore. In point of fact, this is not the case. The energy from the incoming plane wave would be diffracted radially at the 1 m hole in the wall, causing a semicircular wavefront to propagate toward shore. If the beachgoers stood in a line down the beach and recorded the time at which the wavefront hit the shore in front of them, they would see a hyperbolic dependence in time with respect to their perpendicular distance from the hole in the seawall.

The same thing happens with seismic data. If there is a subsurface point diffractor the seismic receivers, which are laid out at even surface intervals extending away from the source, will record the diffracted energy with a hyperbolic dependence in time with respect to their offset from the diffractor. After stacking the data, the seismic section will show a hyperbola emanating from where the point diffractor is located in the subsurface. Assuming for the moment that the subsurface acoustic velocity is constant in the vertical and horizontal directions, the apex of the hyperbola will appear at the location of the diffractor.

The apparent shift in the location of seismic events along a dipping reflector is related to the diffraction response. The receivers only record acoustic energy as a function of time, therefore there is no directional component to their measurement. So the energy observed

after reflection from a dipping interface will appear skewed in the time and midpoint domains to be from a longer, less steep interface. This effect can also be accounted for by a process called dip moveout correction (DMO). DMO is similar to normal moveout correction with correction for dipping reflectors. Using DMO instead of normal moveout before stacking, followed by migration after stack, produces a result comparable to pre-stack migration if the lateral velocity variation is not too large. Because acoustic energy is diffracted and skewed in the subsurface, migration algorithms must also correct for an apparent loss of amplitude.

As was previously mentioned, there are many strategies for implementing migration algorithms. Some migration strategies use finite differencing methods, which can output a seismic section in depth or in time. Finite difference migration algorithms commonly use an approach to solving the wave equation by predicting the next sample point in the output section using the current sample point in the input section. Phase shift migration algorithms transform the input seismic section into frequency space to downward continue the wavefield by a specific interval for each step. After imaging has been completed, the output section is inverse transformed back into the time domain. Collapsing diffractions by a downward continuation and imaging strategy is analogous to using the focus ring on a camera. When the lenses are in the correct alignment the camera has focused the picture. When the continuation step in a migration algorithm has collapsed the diffractions to a point, the algorithm has imaged the data. While time migration corrects for diffraction, depth migration is necessary to correct for refraction effects such as the bending of seismic waves as they pass through an irregular salt body.

12.3 Seismic Data Interpretation

Once the data has been processed, a seismic data interpreter will analyze it to come up with recommendations on drilling target locations. The seismic data interpretation process is not as simple as point and shoot, however. There are six major subjects that fall under the umbrella of seismic data interpretation. These are: velocity profiling, structure interpretation, amplitude interpretation, well incorporation, attribute analysis, and analysis of amplitude variations with offset (AVO). Though there are many other subfields of work in the interpretation industry, it is essential to be familiar with these six.

Geophysicists have a litany of velocity definitions to deal with. In seismic data processing, there are stacking velocities, migration velocities, and many others. In

seismic data interpretation, there are sonic log velocities, checkshot velocities, and many others. Each type of velocity must be used in a particular circumstance. Stacking velocities are one measure of the acoustic velocity in the medium. Sonic logs use much higher frequencies than seismic surveys, typically thousands of hertz, and are not recorded all the way to the surface. Checkshot surveys approximate seismic acquisition in geometry and frequency and are thus the best velocity for depth conversion. If there are existing wells in the area, the first order of business when beginning interpretation of a new seismic survey is to vertically correlate the well data to the seismic data by creating a velocity function.

A velocity function in this case refers to a map from depth to time along a wellbore. The geophysicist must output a list of (time, depth) points increasing in depth down a well. This time–depth chart is discrete differentiated to come up with a set of velocity points with respect to depth in the well. These velocities are used by seismic data interpretation software to stretch or squeeze the projection of the wellbore on the seismic data to fit the geologic interpretation. When the velocity function for a well is correct the well should project on the seismic with the geologic interpretation in the same vertical position as known geophysical events.

In the simplest case, a geophysicist would create the time–depth chart by lining up geologic interpretation along the wellbore with known seismic events. For example, a geologist would provide the point at which a fault plane crosses the wellbore, so the geophysicist would find the fault plane on the seismic data. Now the depth (from the well data) and the time (from the seismic data) would be known at a single point. This would be done at several points along the wellbore to create the time–depth chart.

A sonic log is created by running an electric tool down the wellbore which creates acoustic energy at one end, and measures that energy at the other end. These tools can be very complicated, measuring different types of acoustic waves or directional acoustic energy, but overall the instrument simply measures the velocity (or slowness) of sound refracted in the borehole wall as the tool is passing through. Because of this dependence on the borehole wall, sonic logs produce questionable results in irregular boreholes as determined from the caliper log. The sonic log along with a formation density log is used to create a synthetic seismogram.

Acoustic impedance is the product of density and p-wave velocity. The reflection coefficient of a vertically incident p-wave is related to the difference in acoustic impedance across the reflecting interface by the following formula

$$RC = \frac{AI_1 - AI_2}{AI_1 + AI_2}, \quad (12.2)$$

where RC is the reflection coefficient, AI_1 is the acoustic impedance of the first medium and AI_2 is the acoustic impedance of the second medium. Reflection coefficients at non-normal incidence will be discussed later in the section on AVO. Because acoustic impedance contrasts are what cause variations in seismic waveforms, a simple synthetic waveform can be created in a clever way: first the density and sonic logs are multiplied to create a pseudo-acoustic impedance log. Next, an acoustic reflection coefficient series is generated

from the acoustic impedance. Then a seismic wavelet is created by either mathematical construct, or by approximation from real seismic data surrounding the wellbore. Finally, this wavelet is convolved with the reflection coefficient series to create the synthetic seismic trace (Fig. 12.3).

Once the synthetic data is created, it can be compared to the real data via the use of the time–depth chart. Recall that velocity is the derivative of the depth function with respect to time. By changing the velocity on individual intervals, the synthetic data can be stretched or squeezed vertically to match the real data. Usually a geophysicist will stretch/squeeze the synthetic data by eye next to the real data to correlate seismic events that look similar. The geophysicist will do this for many wells inside the area of the seismic survey. The benefit to all of this is that now the geologic interpretation will be qualitatively lined up to the seismic data via the projection of the wellbores on the seismic data. The next step in seismic data interpretation is to pick the seismic events that correspond to potential targets.

Picking seismic data is simply the process of selecting events in a seismic data volume by means of a colored marker so that a geophysical model can be built. There is no order in which the geophysicist must pick seismic data volumes, but there are some general guidelines to make orient the interpreter and build some structure into a large data set. When a seismic volume comes in from the processing shop, it can be overwhelmingly large. There are sometimes millions of data traces extending over many square miles of area. It is important to start picking a data set on the largest geophysical features and move toward the small scale.

First, the interpreter should pick major faults. Major faults are usually the easiest thing to see on seismic data, so beginning at one end of the data the interpreter picks a data line for the faults. Moving across the data set the interpreter picks seismic lines at some convenient interval. For a 100 square mile 3-D data set, a good gross fault picking interval may be every thirty lines. A computer program can be used to interpolate between picked lines, creating a full surface extending across the seismic data set which represents the fault scarp itself.

The next thing to pick on the seismic data should be important horizons of interest. A horizon is defined as a continuous, or discontinuous in some cases, seismic event extending in the lateral dimensions representing some geologic feature. If there is a large acoustic impedance contrast between, say, a dense limestone formation bottom and a porous sandstone bed top, the seismic data would have a large trough (or peak, depending on polarity) at the interface. This would be an

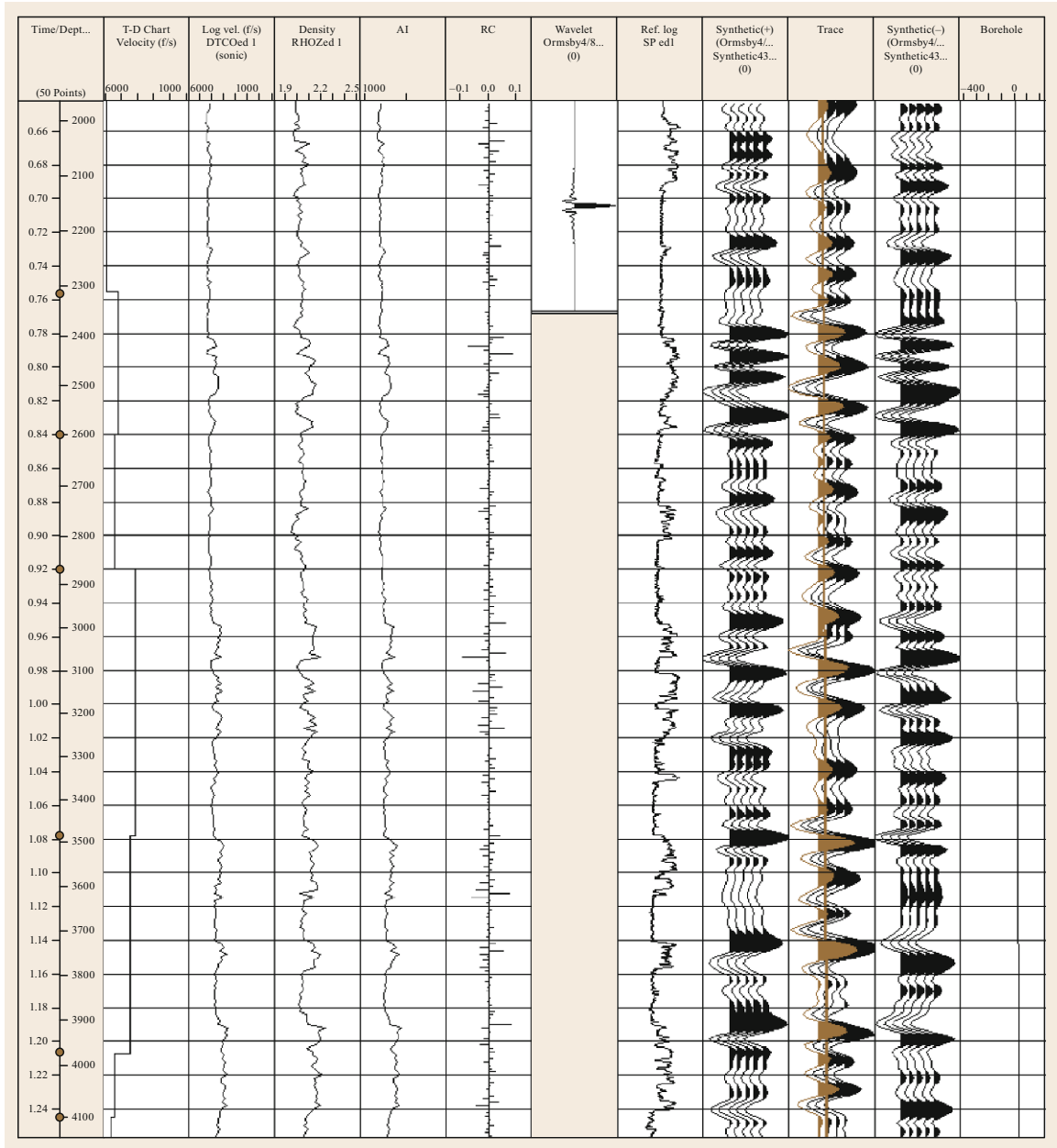


Fig. 12.3 A synthetic seismogram generated by convolution of the Ormsby wavelet shown on *right* with the reflection coefficient series shown on *left*

easy horizon of interest to pick as a starting point to make note of large scale geology–geophysical correlations.

After picking the major faults and horizons the interpreter will begin picking finer details in the data. The subtle structural features, geologic unconformities, and potential drilling target horizons should be picked at this point. In addition to these details, geobodies can

be picked during this step. A geobody is a 3-D seismic object of any construction picked in all three dimensions. Examples of geobodies can include erosional channels, fault blocks, or salt bodies. Software can be used to eliminate geobodies from a seismic volume, as to reconstitute a pseudo-stratigraphic section in time. Similar procedures to reconstruct stratigraphic slices from seismic data in time use flattening algorithms on

the horizons, which creates a (somewhat) geologically accurate image.

It is important when interpreting seismic data to recognize the difference between a seismic image and the subsurface reality. Seismic data is sometimes misunderstood as a picture of the subsurface. This could not be further from the truth. As was shown in the previous two chapters, seismic data not only undergoes many processes with apparent structure altering characteristics, but also acquired under noisy conditions miles away from target zones. Some seismic interpreters bet millions of dollars on seismic data alone. The reality is that the subsurface geologic interpretation is much more closely related to subsurface geologic reality. It is because of this fact that good seismic interpreters use geologic interpretations as a limiting case for the seismic interpretation. When interpreting, seismic always use real geologic data to test seismic-based hypotheses.

In any commercial software for seismic data interpretation, and in any other good interpretation software, there is the ability to input well data. These well data can be used in many ways. The above mentioned time–depth chart creation is one of the things seismic interpreters do with well data. Others include projecting geologic formation top interpretations on the seismic data to verify that the events being picked are close to geologic reality. The same thing can be done with well logs; an interpreter may use gamma ray, spontaneous potential, resistivity, neutron density, or many other well logs for geologic verification of geophysical picks. Well logs in some cases can also be used for qualitative comparison of areal coverage in a seismic data set.

The traces in a seismic data survey surrounding a wellbore are acoustic responses to the rocks surrounding that well. It follows then that seismic data anywhere in the survey bearing resemblance to the data around the well may be a response to similar rock characteristics. In this way, seismic data is used to create qualitative comparisons between well locations and prospective target locations. Well logs can be semi-quantitatively incorporated into this scheme by statistically analyzing the seismic response around many wells with similar log suites. Well logs can thereby be used to determine what causes seismic amplitude response.

In many introductions to geophysics courses, students are instructed to drill locations with bright spot seismic response. Bright spots, or isolated high amplitude anomalies within a low amplitude event, can be created due to the change in acoustic impedance of a formation because the pore spaces are filled with hydrocarbons rather than water. The bright spot phenomenon is certainly a good method to locate potential targets, but they are not necessarily always direct hydrocarbon indicators.

The amplitude of seismic data at a location is a function of a huge number of factors. Part of the interpretive geophysicist's job is to evaluate within each seismic survey what drives the amplitude response. In some areas, seismic amplitude may be very closely related to the presence of oil and gas. In these cases, the drilling company just puts the wells where the seismic data lights up!

Seismic amplitudes usually behave in a more complicated manner. In addition to hydrocarbons, seismic amplitudes can also respond to gross-to-net sand ratios, bed thickness, fracture orientation, etc. There are thousands of things that can cause seismic amplitudes to be artificially inflated or deflated in a location. When interpreting seismic amplitudes, one should always take a look at the processing sequence to be sure those amplitudes have been properly preserved. Statistically incorporating well logs into the seismic data can vastly improve the geophysicists' understanding of what is the greatest geologic contributor to seismic amplitude response. It is important to note that amplitude response may not have the same driving mechanisms throughout the entire seismic survey or from one target depth to another. Because of this, interpretation must be carried out separately from zone to zone and across the entire area.

Another type of seismic information that can help geophysicists understand potential drilling targets is called seismic attributes. A seismic attribute is anything represented at a point location in a seismic survey by a pair of spatial values, a time value, and the value of the attribute (x , y , time, attribute), for example, amplitude is a seismic attribute. Amplitude is one characteristic of a seismic waveform. Another characteristic, or attribute, of a seismic waveform would be velocity. In the seismic data processing chapter stacking velocities were defined. As was shown, every CMP gather location is analyzed and assigned a velocity for every time value in the stacked trace. Therefore, once this stacking procedure is complete the seismic data processor has a value of velocity at every point in the seismic survey. If desired the processor could output a seismic data volume of space, time, and velocity (x , y , time, velocity), this volume would be called the velocity attribute of the seismic survey.

As seismic attributes are derived from any mathematical operation on seismic data, there are an infinite number of attributes. Fortunately, due to the literature on the subject there are a finite number of categories into which these attributes fall. The major ones are geometrical, instantaneous, wavelet, and exotic attributes. The usefulness of seismic attributes varies with the geologic setting and the information, such as well data, available. The most important aspect to consider when deciding which attributes to use is that all attributes

come from recorded data. Performing mathematical operations on any data (seismic or otherwise) can provide a different view of that data, but once the data has been recorded no new information is available to that system. Seismic attributes do not create new information; they only bring out features of the data which are not accessible by the human eye in amplitude data.

The geometrical subset of seismic attributes includes several very useful attributes. They include curvature, dip characterizers, and coherence. Curvature attributes describe the shape of individual seismic events. Seismic interpreters can use attributes such as maximum curvature, Gaussian curvature, and most positive curvature to help tease out subtle structural details in seismic data or continuity in the bedding planes associated with their target prospects. The suite of dip characteristics includes dip azimuth, dip variance, and dip of maximum similarity. These attributes in areal cross section can help to delineate reservoirs or resolve geologically complex settings. Coherence, or similarity as it is also called, is an extremely helpful attribute which creates an image of the subsurface analogous to an MRI image. The discontinuities between seismic traces are assigned a low value of coherence, so continuous zones look blank. Coherence can be used in areal cross section or vertical cross section to delineate small faults or lineaments in the subsurface, for example, fluvial channels.

The instantaneous suite of seismic attributes is created using differential type operators which take only the surrounding samples into calculation, hence the name instantaneous rather than average. The major players in this category include instantaneous frequency, instantaneous phase, and relative acoustic impedance. The frequency and phase attributes are used to assist in quantifying geology–geophysical relationships. They can also be used to delineate the lateral extent of beds in some cases. Relative acoustic impedance is often touted as an attribute that shifts the seismic data from reflection coefficient amplitude data into a true geologic image. This is not quite the case, because there has not been any new information put into the system, but either way relative acoustic impedance gives the interpreter a phase shift and some scaling on the data which in some cases can, again, help delineate bedding.

In many cases the attributes of the wavelet attribute suite are used as intermediate products to create a final attribute based on several components. However, wavelet envelope and wavelet bandwidth can be used to assist in interpretation. These attributes can be viewed in vertical cross section to give the interpreter a better feel for the gross geologic structure under certain circumstances.

The term *exotic* attribute is used here to describe any attribute that does not appear in widespread use across the literature. As previously mentioned, there is an infinite number of attributes, so the exotic attribute category can include infinitely many attributes. One example that is used with great frequency is called sweetness. Sweetness is wavelet envelope over the square root of instantaneous frequency. Sweetness can be used to pick out areas of high net to gross sand ratio, which is important in in-field development projects and near-field exploration. If an interpreter recognizes which attributes work well in an area, he/she may be able to work together with a processor to create a custom exotic attribute. Just because this custom attribute works well in this one area does not mean it will work in any other setting.

Most beneficially, many seismic attributes will be used in concert with each other to create the best interpretation of the seismic data. One way to do this is by using a multivariate statistical approach. The seismic interpreter extracts traces of several seismic attribute volumes, including amplitude if valuable. The traces should be around wells that produce and wells that do not produce, as to build up a good sample set. Each of these trace data will be culled for samples around zones of interest. The interpreter then builds up a strong multivariate equation based on the attributes which seem to have clear response to the desired geological characteristic and builds a model zone for each real zone of interest. This can be done as a map-based (2-D) or volume based (3-D) process. When complete, the model zone should display a statistical likelihood of success for drilling as a function of time and/or space.

The last major tool in the interpretive geophysicist's toolbox is the analysis of amplitude with respect to offset. Amplitude versus offset (AVO) analysis can prove to be a powerful process for finding hydrocarbon rich target zones, and also for characterizing lithology in undeveloped regions. To perform AVO analysis, the interpretive geophysicist must have access to the processed CMP gathers from the processing geophysicist. The gathers may be processed to any point that the interpreter prefers, but should represent the final seismic section that is represented. All industry standard AVO analysis is done on NMO or, better yet, DMO corrected gathers, so that the interpreter can pick and observe flat events rather than hyperbolic events. Care must be taken at each pre-processing and processing step to preserve relative amplitudes. Amplitudes on land data are often affected by the near-surface, so surface-consistent amplitude balancing may be a necessary step. Pre-stack migration or DMO improves AVO response by moving energy between traces.

The interpreter will pick the gathers with a horizon of interest across an area of interest. This is usually performed with an autopicking software initialized with the normally incident traces in each gather. The picked event is analyzed by a simple algorithm on a per CMP basis and could output an AVO class for each. An AVO class (from class 1 to class 5) is an industry standard definition of the response characteristics in the gather. The Zoeppritz equations predict the amplitude of waves propagating away from an encounter with an interface with respect to angles from a normal. There are four Zoeppritz equations to give the amplitude of the reflected p-wave, the reflected s-wave, the transmitted p-wave, and the transmitted s-wave. All four equations use both p-wave and s-wave velocities, so the reflection amplitude behavior at non-normal

incidence contains information about mechanical properties such as compressibility of the formation that is not contained in the zero-offset trace. The presence of shallower interfaces means the transmission effects at each shallower interface must be modeled as well. There are a number of commercial AVO modeling packages available. The AVO characteristics can be displayed in a crossplot with the hopes of grouping outlying data. The outliers can be culled and their CMP locations displayed on a map. By way of example, if the interpreter knows that all CMP locations exhibiting an anomalously high Shuey three-term gradient to Shuey three-term curvature response are oil bearing, then this zone would be culled for this data response, and a possible location would present itself in areal cross section.

12.4 Summary

The seismic data interpretation procedures outlined above are used as a starting place for building a model. It is the interpreter's job to use the seismic data for verification of an Earth model. Sometimes the model only exists in the interpreter's head, but more explicit models are recommended. Seismic modeling software can create 3-D models from seismic interpretation. The interpreter will input his/her fault surfaces and horizon surfaces into the modeling software which will create 3-D volumes from this information. The 3-D models can be used to model reservoir drainage, to plan wells, or even to steer wells in real time as they are drilled.

The key to good modeling is iteration. The first model created will never be spot on, which is why the interpreter needs to rework the model as new information arrives. If for example a well is drilled on the initial model, the interpreter should have a new set of well logs to help quantify the seismic data. The iteration process continues from the initial model through the completion of the entire drilling program, and into any other projects of similar setting. Geophysicists also must iterate new geologic and engineering data into their models. Using all of the information at hand is crucial to continued success.

The initial and updated data must drive the model. It is a waste of money to come up with a hypothesis and then use the seismic data to prove that hypothesis. The correct order should be to look at the data and then come up with a hypothesis; if any new data comes in disproving that hypothesis, the hypothesis should be thrown out. A common mistake when building implicit Earth models that only exist in the head of the interpreter is following these incorrect hypotheses all the way to drilling a dry hole. In this way an explicit Earth model updated by the geophysicist, geologist, and engineer is the most accurate and successful way to complete a drilling program. The entire seismic data workflow is a procedure in risk mitigation. Any company can throw a dart at a map and drill that location, but the chance of success is low. Seismic data acquisition, processing, and interpretation reduce the risk of drilling to some point dependent on data and interpretation quality. If this reduced risk level is below whatever arbitrary threshold risk level the drilling company has decided on, then seismic exploration has done its job.

Acknowledgments. The author would like to acknowledge valuable comments from Dr. Greg Kroft and Professor Kent Pederson of the University of Calgary.

References

- 12.1 C.C. Ober: *Marmousi Model and Image* (Sandia National Laboratories, Albuquerque 1998), <http://www.cs.sandia.gov/~ccooper/seismic/marmousi.html>
- 12.2 J. Wang, M. Sacchi: Noise reduction by structure- and-amplitude-preserving multi-channel deconvolution, *CSEG Recorder* **34**(2), 24–27 (2009), Canadian Society of Exploration Geophysicists

Formation Evaluation

Donald G. Hill

Petrophysicists utilize laboratory and borehole geophysical measurements as input into petrophysical models to estimate reservoir hydrocarbon resources and recoverable reserves. Unlike surface and airborne geophysicists, who work with one to three scientific disciplines, petrophysicists comfortably work with eight or more scientific disciplines on a daily basis.

13.1	What Is Formation Evaluation?	435	13.7.1	The Schlumberger Brothers and Pros..	449
13.2	The Need and Purpose of Formation Evaluation	435	13.7.2	The Pechelbron Well	450
13.3	Well Logs	436	13.7.3	Archie's Equations	451
13.3.1	What Are Well Logs?	436	13.7.4	Continuous Velocity Logs and Jesse Wyllie's Relationship	452
13.3.2	Driller's Logs	436	13.7.5	Improvements in Recording the Results	452
13.3.3	Wellsite Geologist's Sample Description <i>Strip Logs</i>	436	13.7.6	Development of Formation Evaluation	457
13.3.4	Mud Logs	439	13.8	The Schlumberger Legacy	457
13.3.5	Wireline Logs	439	13.9	Laboratory Measurements	458
13.3.6	MWD/LWD Logs	441	13.9.1	Fluid Measurements	458
13.3.7	Who Uses Well Logs?	441	13.9.2	Rock (Core) Measurements	460
13.3.8	What Is Desired Versus What Can Be Measured	441	13.10	Well Logging Environment	465
13.4	Who Are Petrophysicists and How Do They Work?	443	13.10.1	Wellsite	465
13.5	How Wireline and MWD/LWD Logs Are Acquired	444	13.10.2	Logging Operations	466
13.6	Uses of Well Logs	445	13.10.3	Well Logs	466
13.7	Petrophysics and Well Logging: Historical Development	445	13.10.4	Borehole Model	469
			13.10.5	Subsurface Temperatures	471
			13.11	Well Logging Tools	471
			13.11.1	Porosity Tools	471
			13.11.2	Lithology Tools	480
			13.11.3	Saturation Tools	483
			13.11.4	Environmental Corrections	487
			13.11.5	Salinity (R_w) Tools	487
			13.11.6	Borehole Imagers	488
			13.11.7	Wireline Formation Testing	491
			13.12	Putting It All Together	492
			13.12.1	Western Australia Well	492
			13.12.2	Manual Analysis	492
			13.12.3	Computer-Aided Analysis	498
			13.13	Summary	498
			References		498

One of the most exciting things that an exploration and producing (E&P) company can do is to drill a well. Prior to *spud-in*, the drilling target is some type of model: an explorationist's dream for a *wildcat well*, or a reservoir model for a delineation or development well. The act of drilling a well serves to either confirm or reject that model.

Figure 13.1 shows a schematic of a modern rotary well drilling system. The rotary drill bit at the bottom of a long *drill string*, grinds away to *make hole*. A *mud system*, consisting of mud supply tanks/pits, and pumps at the surface, forces drilling mud down the center of the drill string to cool the bit and clear *drill cuttings* from the face of the drill bit and return them

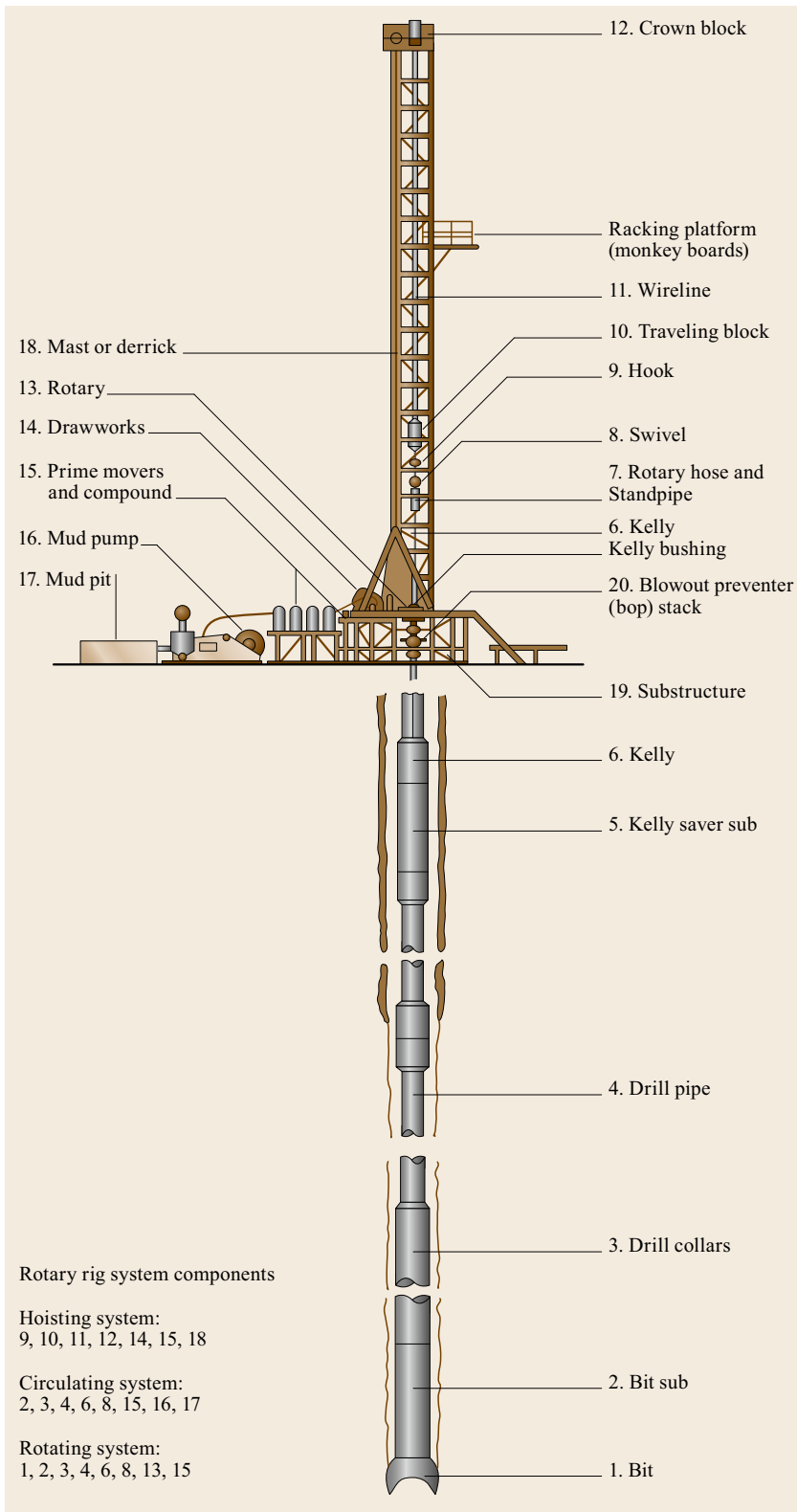


Fig. 13.1 Schematic drawing of a rotary well drilling system (courtesy of Petroleum Extension Service, The University of Texas, Austin)

to the surface, where they are removed, examined, and described. *Blowout preventers*, at the surface, can be closed to prevent high-pressure fluids and/or gases from escaping the well. The drill bit is rotated by a *down-hole drill motor, top drive, or rotary table* in the drill floor.

Heavy *drill collars*, above the bit and *bit subassembly*, provide weight on the bit to improve the *rate of penetration (ROP)*. The entire drill string is suspended by a *traveling block*, hung from a *crown block* at the top of the *derrick*. The crown block/traveling block assembly allows the driller to raise and lower the drill string

in the well and maintain the drill string under tension during the entire drilling process. The drill string must be maintained under tension to prevent it from twisting up, like so much wet spaghetti, during rotation.

The *drilling mud density (mud weight)* is maintained such that the borehole fluid pressure always slightly exceeds that of the formation pressure to prevent *blowouts*, which can be both dangerous and costly. Solids in the drilling mud form filter cake (*mudcake*) on the borehole walls opposite permeable formations, which protects the borehole prior to permanent protection via *casing and cement*.

13.1 What Is Formation Evaluation?

The terms, *formation evaluation, well log analysis, and petrophysics* are often used interchangeably, but do have slightly different meanings. Generally, however, they involve using core and fluid laboratory physical and chemical property measurements as well as wireline and logging while drilling (LWD) well logs to evaluate wells for potential hydrocarbon reservoir rocks and economic hydrocarbon accumulations, as well as mechanical properties of the rocks penetrated by a drilling well. The following types of information are all used to conduct formation evaluation (FE):

- Laboratory fluid property measurements
- Laboratory (rock) core physical property measurements
- Drill cuttings descriptions (strip log)
- Mud logs
- Wireline log measurements
- Measurements while drilling (MWD)
- Logging while drilling (LWD)
- Formation flow tests.

13.2 The Need and Purpose of Formation Evaluation

Without FE an oil or gas well is simply an expensive hole in the ground. Formation evaluation is used to establish the presence of potential reservoir rock, evaluate those reservoirs for potential hydrocarbons and to determine the value of those hydrocarbon reserves. It is also used to develop reservoir mechanical properties models for the drilling and producing departments. Figure 13.2 illustrates the interrelationships between FE and other disciplines within a petroleum exploration and production (E&P) operation.

To appreciate the economic role of formation evaluation in the operations of a modern petroleum company, look no further than the formula for calculating original oil (reserves) in place.

$$STOOIP = \frac{7758Ah\phi(1 - S_w)}{B_{oi}}, \tag{13.1}$$

where STOOIP is stock tank original oil in place (bbls), *A* is the reservoir closure area (ac), *h* is the average reservoir (net) thickness (ft), ϕ is the average reservoir decimal porosity, *S_w* is the average reservoir decimal

water saturation, *B_{oi}* is the initial oil formation volume factor, 7758 is the ac/ft to bbls conversion factor (different conversion constants will be required, for other units).

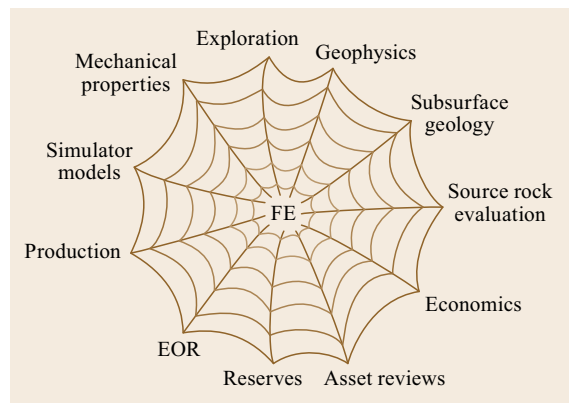


Fig. 13.2 Formation evaluation (FE) relationships in petroleum exploration and production (E&P)

A similar relationship also exists for gas reserves.

$$\text{SCFOGIP} = \frac{43\,560Ah\varphi(1 - S_w)}{B_{gi}}, \quad (13.2)$$

where:

- SCFOGIP is standard (temperature and pressure) ft³ original gas in place.
- A is the reservoir closure area (ac).
- h is the average reservoir (net) thickness (ft).
- φ is the average reservoir decimal porosity.
- S_w is the average reservoir decimal water saturation.
- B_{gi} is the initial gas formation volume factor.
- 43 560 is the ac/ft to SCF conversion factor (different conversion constants will be required, for other units).

Three of the five variables in (13.1) and (13.2), (h , φ , and S_w), are obtained from well logs via FE, well

13.3 Well Logs

To most people in the exploration and production (E&P), or *upstream* petroleum industry, *formation evaluation* means *well log analysis*. A good place to start, therefore, is to explain just what is meant by the term *well logs*.

13.3.1 What Are Well Logs?

Well logs are some record, as a function of depth, of what a well penetrates in the subsurface. They are endemic to the petroleum industry. The following quote says it all [13.1]:

Petroleum geologists as a whole spend much more of their time working on problems that arise after drilling has started than they do in finding structures and locating wildcat wells.

Most of this effort involves collection of data, preparation, and interpretation of well logs of various types.

The origin of the term *well log* seems to be lost in the antiquity of the petroleum industry. The most probable version, however, appears to be related to out of work whaler seamen after petroleum kerosene displaced whale oil for lighting.

13.3.2 Driller's Logs

Discussions with *E.C. Thomas* [13.2] and *Richard Bate-man* [13.3], at a recent Society of Petrophysicists and Well Log Analysts (SPWLA) meeting, however, provided some insight on this issue. According to Richard and E. C, the fallout from the Drake Well, in Pennsyl-

log analysis, or petrophysics. The closure area A comes from seismic mapping and/or subsurface geology. The formation volume factor B_{gi} comes from an analysis of rock and fluid measurements, by a *Qualified Reserves Engineer*.

In practice the terms h , φ and $(1 - S_w)$ in (13.1) and (13.2) are replaced by

$$\sum_{i=1}^n h_i \varphi_i (1 - S_{wi}), \quad (13.3)$$

where h_i can be as small as the sampling interval on the well logs. Obviously, because of the large values possible for A , small changes in φ_i and S_{wi} can result in very large changes in the reserves values. The remainder of this chapter will discuss how a petrophysicist uses FE to arrive at quantitative estimates of reservoir porosities and saturations, as well as estimates of permeabilities.

vania, decimated the previously lucrative whale oil industry, and displaced the crews of the whaling vessels. These unemployed seamen found work in the new Pennsylvania oil fields and, as a result, brought their seafaring vocabulary, including the use of *logs*, with them.

Most of us are familiar with the term *ship's log*, the diary, usually kept by the captain and/or first mate, of a ship's movement and activities when out of port. Just as the ship logs helped owners keep track of their property, *driller's logs* helped the owners of drilling rigs and developers drilling wells keep track of activities on a *drilling well*. Driller's logs are so common that most government agencies require *driller's logs* to be submitted for every oil, gas, geothermal and water injection, or environmental well drilled within their jurisdictions. Note that the driller's log examples, shown in Figs. 13.3 and 13.4 were submitted on a California Division of Oil and Gas form.

Driller's logs are considered to be *public domain* and unless the operator designates them to be *tight hole* (confidential), they are available to the general public as soon as they are received and recorded by the government agency. The driller's log header, shown in Fig. 13.3 details how the well was completed. Figure 13.4 shows the driller's account of what was encountered while drilling the well.

13.3.3 Wellsite Geologist's Sample Description Strip Logs

The science of stratigraphy, pioneered by English canal digger *William Smith* [13.4], showed that geological

FORM 100, 6-22-29 8-29 30M
REPLACES FORM 100 (REVISED)

SUBMIT LOG IN DUPLICATE
FILL THE BLANK IN WITH TYPERWRITER. WRITE ON ONE SIDE OF EACH SHEET ONLY.

STATE OF CALIFORNIA
DEPARTMENT OF NATURAL RESOURCES
DIVISION OF OIL AND GAS

LOG OF OIL OR GAS WELL

FIELD Santa Fe Springs COMPANY General Petroleum Corp. of Calif.

Sec. 6, T. 6, R. 11, S. B., B. & M., Elevation 160.22 Well No. Anderson 152-B

In compliance with the provisions of Chapter 718, Statutes of 1917, as amended, the information given herewith is a complete and correct record of the present condition of the well and all work done thereon, so far as can be determined from all available records.

Signed General Petroleum Corp. of Calif.

Date November 1, 1929

Title Burt Parsons
GENERAL AGENT
(President, Secretary, or Agent)

The summary on this page is for the ORIGINAL condition of the well

OIL SANDS

1st sand from.....to..... 4th sand from.....to.....
2d sand from.....to..... 5th sand from.....to.....
3d sand from.....to..... 6th sand from.....to.....

IMPORTANT WATER SANDS

1st sand from.....to..... 3d sand from.....to.....
2d sand from.....to..... 4th sand from.....to.....

CASING RECORD

Size of Casing	Where Landed	Where Cut	Weights Per Foot	Threads Per Inch	Kind of Shoe	Make of Casing	CEMENTED		Number of Sacks
							Yes	No	
20	1019		90			Hercules	X		1000
18-5/8	4048		61			Youngstown	X		600
9"	5536		45			"	X		400
6-5/8"	6245		26			"	X		150
4 1/2"	6980	6219	16					No	

CEMENTING OR OTHER SHUT-OFF RECORD

Casing Size	Sacks	Time Set	Method	Time and Results (Give water level and tubing results)
18-5/8"	600	5 days	Perkins	Balled to 1200'. No rise in 17 1/2 hours.
9"	400	5 days	"	Swabbed to 2030'. 18' drop in 3 1/2 hours.
6-5/8"	150	5 days	"	Swabbed to 2500'. No rise in 21 hours.

PLUGS AND ADAPTERS

Heaving Plug—Material.....Length.....Where set.....
Adapters —Material.....Size.....

TOOLS

Rotary Tools were used from.....0.....ft. to.....6980.....ft.
Cable Tools were used from.....ft. to.....ft.

PERFORATIONS

State clearly whether a machine was used or casing was drilled in shop

From	To	Size of Holes	Number of Rows	Holes Per Foot	Machine—Shop
6219 ft.	6980 ft.	140 Mesh Kobe	Slotted		
ft.	ft.				
ft.	ft.				
ft.	ft.				
ft.	ft.				

Thirty days after completion well produced 1512 barrels of oil per day.

Fig. 13.3 Driller's log header (courtesy of California Division of Oil, Gas, & Geothermal Resources)

The gravity of oil was 99.5 degrees Baumé. Water in oil amounted to 0.1 per cent.

NAMES OF DRILLERS: H. Wolf, G. F. Skaggs, H. E. Wiley
 NAMES OF TOOL DRIVERS: R. Robey, R. Frankenhager, J. Dodson

Date drilling started March 15, 1929 Date well was completed September 3, 1929

FORMATIONS PENETRATED BY WELL

DEPTH TO		Thickness	Name of Formation
Top of Formation	Bottom of Formation		
0	120		Sand & boulders
120	212		Sand & gravel & clay
212	337		Sand & gravel
337	420		Boulders
420	455		Sand
455	470		Hard sand
470	477		Boulders
477	485		Sand, hard
485	485		Hard sand
485	495		Boulders & sand
495	497		Boulders
497	510		Hard sand
510	561		Sand & gravel
561	582		Shell
582	583		Shell
583	595		Shell & gravel
595	656		Sandy shale
656	728		Sandy shale
728	749		Hard sand & boulders
749	760		Sand & boulders
760	929		Sand & boulders
929	949		Sand & boulders
949	1009		Sand & shale
1009	1018		Shale
1018	1132		Sandy shale
1132	1609		Sandy shale & sticky shale
1609	1625		Sticky shale
1625	1630		Hard shell
1630	1631		Shell
1631	1697		Sticky hard shale
1697	1913		Sticky shale
1913	2002		Sticky shale w/ streaks of hard sand
2002	2084		Sticky shale w/ streaks of hard sand
2084	2140		Sticky shale
2140	2271		Sandy shale
2271	2392		Sandy shale & boulders
2392	2394		Hard sand
2394	2475		Sticky shale
2475	2477		Shell
2477	2492		Hard sand
2492	2593		Sticky shale
2593	2635		Sticky shale
2635	2640		Hard shale
2640	2698		Sticky shale
2698	2715		Hard sand
2715	2730		Sandy shale

Fig. 13.4 Driller's log text (courtesy of California Division of Oil, Gas, & Geothermal Resources)

formations could be correlated between outcrops, road cuts, quarries, canal cuts, and building excavations. The specialty of subsurface geology took this tech-

nique down hole to materials encountered in drilling wells. The initial vehicles for subsurface correlation were driller's logs.

Fig. 13.5 Graphic drill cuttings sample description (*strip*) log ▶

Some drillers are very conscientious and, while not trained as geologists, their driller's logs can be used for subsurface correlation. Other driller's logs have been constructed from memory, after a well had been completed, and/or are not very descriptive of the material being drilled. These latter driller's logs are essentially useless for subsurface geology. They satisfied the legal requirement that a report be filed and that is about all.

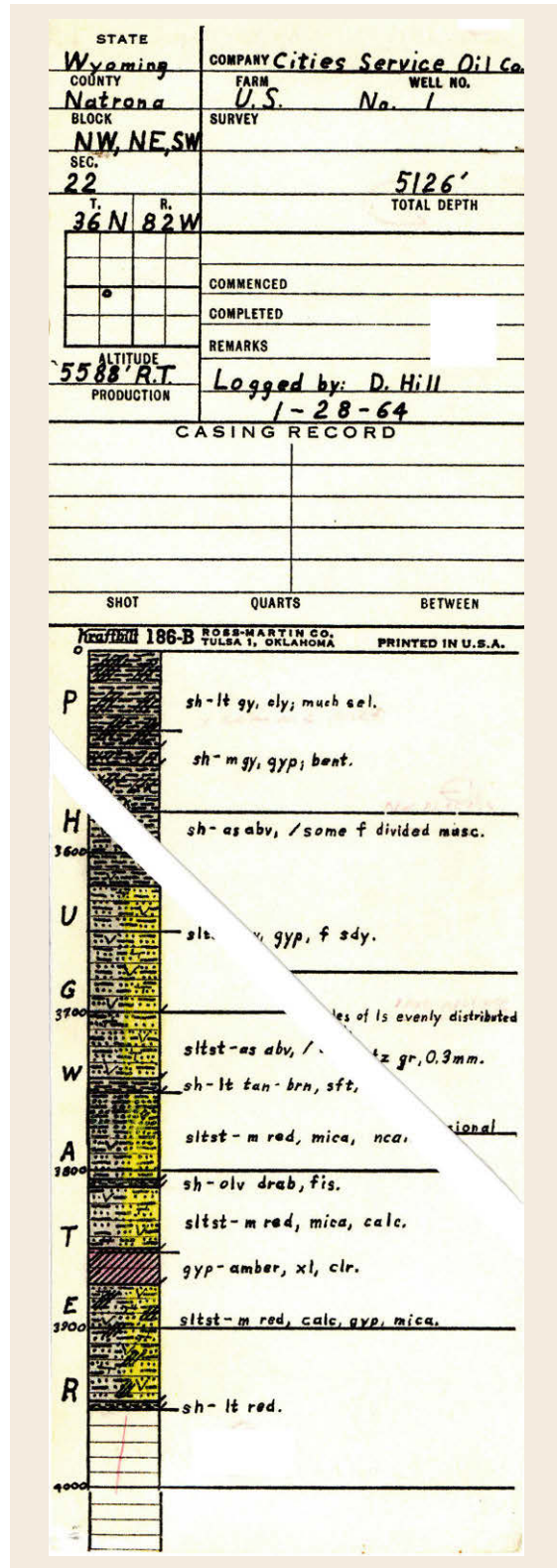
As soon as it became obvious that driller's logs were not that reliable, geologists became involved. The drill-site geologist's sample log initially consisted of descriptions of drill cuttings and/or cores cut as the well was drilled. Some operators (e.g., Standard Oil of California, now Chevron) required small drill cutting samples on their geologist's sample logs. Geologist's sample/core logs gradually evolved into a stylized graphical display, at standardized depth scales, with shorthand notations of the cuttings lithology. These records were often called *strip logs*, because the original preferred medium was 2" = 100 ft, depth scale, rolled card stock. Figure 13.5 is an example of a hand-drafted sample cuttings log.

13.3.4 Mud Logs

Mud logs incorporate simplified versions of geologist's sample logs, along with various drilling parameters. They are often used in lieu of geologist's sample description logs (contractors are cheaper than your own employees). They also provide an early warning of *pay zones*, as well as potential *blowouts*, *lost circulation*, as well as noxious and/or poisonous gases. Drillers utilize them to optimize their drilling operations. Mud logs were the first *real-time* logs available, as they are acquired as the well is being drilled.

13.3.5 Wireline Logs

Wireline logs are records of the physical and/or chemical properties of the materials penetrated by a drilling well. Open-hole wireline logs are acquired by suspending in instrument package (*sonde*) on a cable to make the measurements and are acquired after the well has been drilled (at least to a *casing point* depth), but before casing has been set to protect the well bore. They have evolved from simple station measurements, utilizing a jury-rigged surface electrical survey electrode array, to the current sophisticated system of continuously recorded multiple parameters, including quality control information available today. Figure 13.6 shows an open-hole wireline log through a sand-shale (clastic) section, with an initial geologic interpretation.



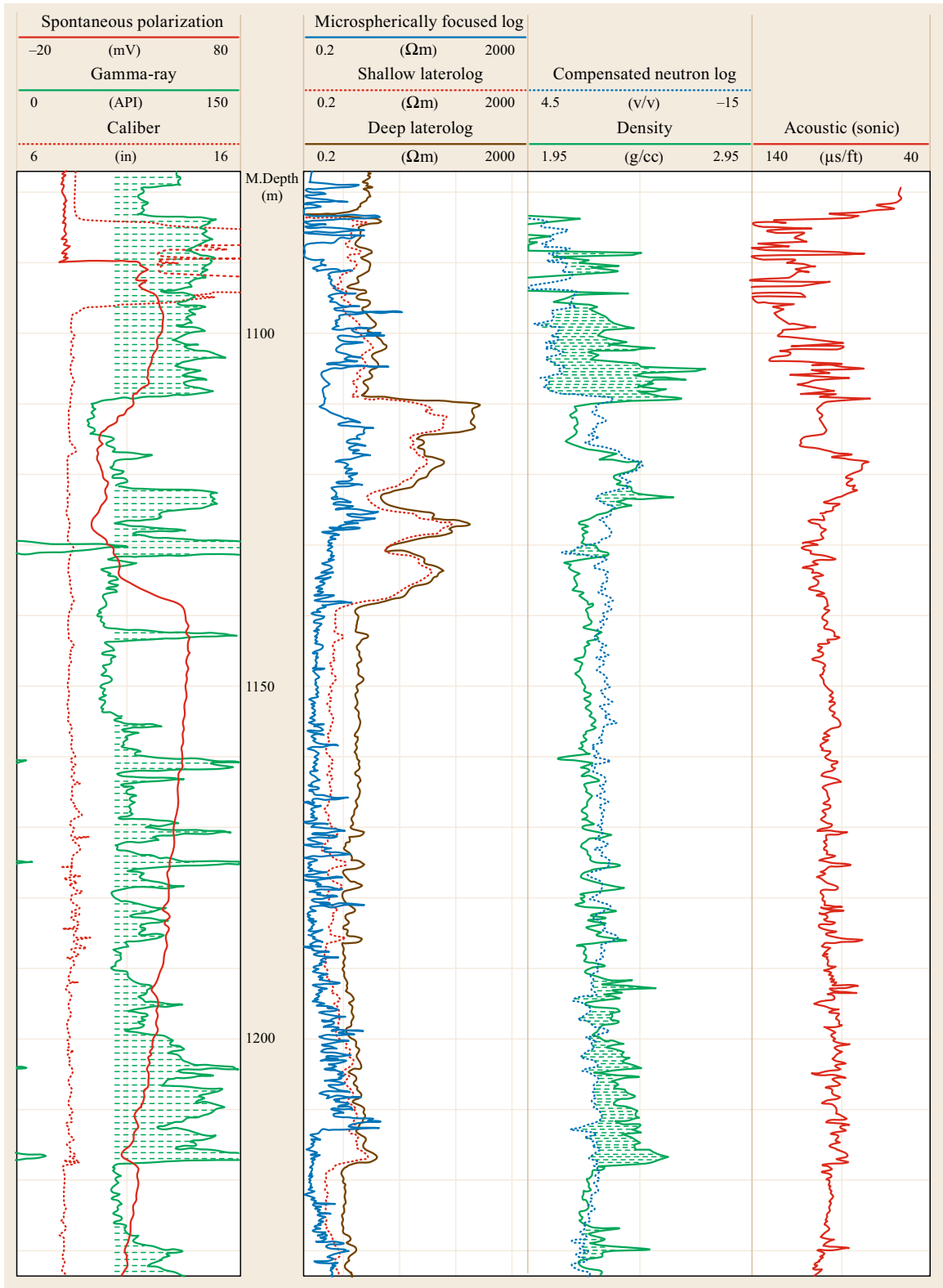


Fig. 13.6 Western Australia wireline log

Note that the different log curves not only have different colors, but also different curve types. This is so that the curves can still be differentiated, if the colored log display is sent via fax or copied in grayscale.

Cased-hole wireline logs are made after casing has been run. They are often used to evaluate the casing condition and effectiveness of cementation, monitor production operations and to identify remaining, or bypassed, reserves of producing fields.

13.3.6 MWD/LWD Logs

Measurements while drilling (MWD) and logging while drilling (LWD) logs utilize specialized drill collars and data telemetry systems that allow most (but not all) wireline measurements to be made as the well is being drilled. Because MWD/LWD systems use mud-pulse or electromagnetic (EM) telemetry, they are real time measurements, compared to wireline measurements, which are made only at casing points, or total depth (TD). They were developed for use in high-risk wells and for high angle deviated or horizontal wells, which are difficult to log with wireline methods.

The first vendors to offer MWD measurements were drilling and mud logging vendors and the measurements were unique to directionally drilled wells, where they were used for well steering control. With time, geological and formation evaluation measurements were added to the MWD subassemblies. The LWD designation was initially unique to a single vendor that used the term to distinguish its drill string measurements from those of other vendors. For a time, the two terms were used almost interchangeably.

Currently, MWD usually designates those measurements used to control directional drilling while LWD is used for those measurements that parallel wireline measurements. All of the major wireline vendors also now offer MWD/LWD services. In addition to duplicating most of the wireline measurements, there are also some FE measurements unique to MWD/LWD systems.

13.3.7 Who Uses Well Logs?

Petroleum E&P professionals can expect to encounter well logs and petrophysical analyses many times in the course of their careers:

- Completion Engineers utilize petrophysical results to establish completion intervals.
- Qualified Reserves Engineers utilize petrophysical results to establish recoverable reserves.
- Asset Review teams use petrophysical results to establish property values for property disposal and/or acquisition.
- Reservoir Engineers utilize petrophysical results to build simulator models and for depletion planning.
- Production Engineers utilize petrophysical results to help develop and operate fields.
- Enhanced Oil Recovery (EOR) Engineers utilize petrophysical results to plan EOR operations.
- Production Superintendents will decide budgets including petrophysical programs.

The most common users of well logs, however, are none of the above. *Geologists and geophysicists* are the petroleum E&P professionals that utilize well logs the most, to obtain seismic velocity information (geophysicists) and to make stratigraphic and structural correlations between wells (Fig. 13.7).

13.3.8 What Is Desired Versus What Can Be Measured

While three of the five variables in (13.1) and (13.2) are obtained from well logs, two of these three:

- Porosity φ
- Saturations:
 - Water saturation (S_w)
 - Oil saturation (S_o)
 - Gas saturation (S_g)

are not measured directly. Instead, well logs measure such things as:

- Acoustic interval transit time (Δt)
- Neutron porosity (φ_N)
- Bulk density (ρ_B), which depend upon:
 - Porosity (φ)
 - Water saturation (S_w)
 - Lithology
- Natural gamma radiation:
 - Total γ -ray
 - Potassium-Uranium-Thorium (K-U-T) spectral γ -ray
 - Photoelectric factor (PEF), which depend upon lithology
- Spontaneous polarization (SP), which depends upon:
 - Mud filtrate/formation water salinity contrast
 - Lithology
- Apparent resistivity R , which depends upon:
 - Porosity (φ)
 - Lithology
 - Water salinity
 - Water saturation (S_w)
- Nuclear Magnetic Resonance (NMR), which depends upon:
 - Porosity (φ)

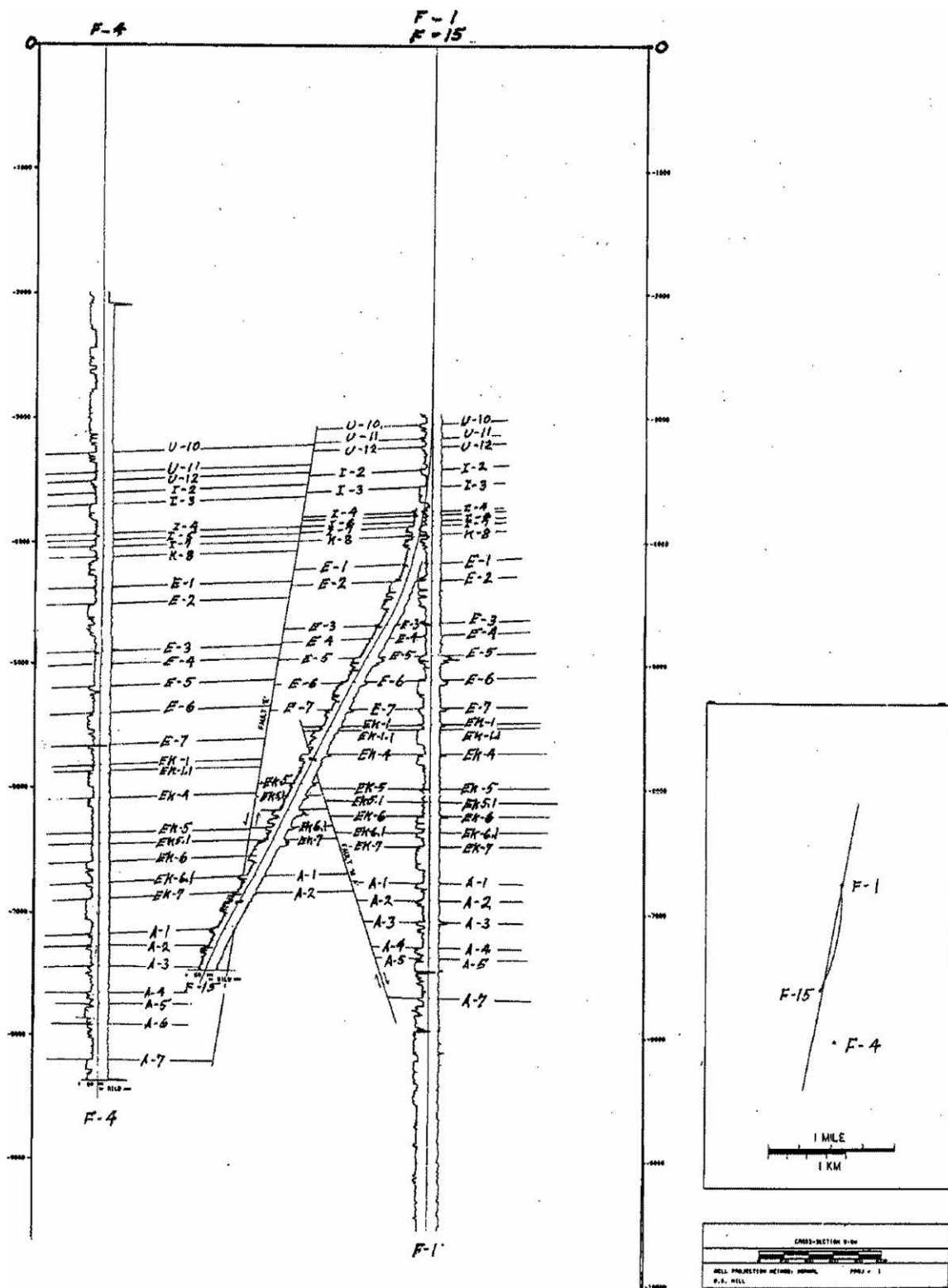


Fig. 13.7 Use of a well log cross-section to explain complex structure

Table 13.1 Open hole logging tools and techniques, with Schlumberger mnemonics (compiled from a variety of sources)

Primary purpose	Tool or technique
Lithology	Spontaneous potential (SP) Gamma ray (GR) Side wall cores (SWCs) Photoelectric factor (PEF) Tri-mineral, MID, and MN plots
Porosity	Density (RHOB) Nuclear magnetic resonance (NMR) Neutron (NPHI) Acoustic (ΔT) Cross-plots
Salinity/water resistivity	Spontaneous polarization (SP) R_{wa} analyses Hingle plots Pickett plots
Saturation	Resistivity (ES) Induction (IES, DIL) Laterolog (LL, LL3, DLL) Array induction (AIT)
Flushed zone saturation	Microspherically focused log (MSFL) Microlaterolog (MLL) Dielectric constant (EPT, DPT) Nuclear magnetic resonance (MRL)
Permeability	Nuclear magnetic resonance (MRL) Formation testers (FTs, RFT, MDT)
Fluid identification	Formation testers Density/neutron overplot FID plot S_w tools
Structural/stratigraphic information	Dipmeter (HDT, SHDT) Borehole televiewer (BHTV) Resistivity microscanners (FMS/FMI) Nuclear magnetic imagers (NMIs)
Borehole imaging	Borehole televiewer (BHTV) Resistivity microscanners (FMS/FMI) Nuclear magnetic imagers (NMI)
Borehole temperature	Temperature (TEMP)
Formation pressure	Formation testers (FT, RFT, MDT)
Borehole shape	Caliper (CAL)

- Fluid types
- Permeability
- Pore wall lining.

The desired porosities and saturations must be inferred from well-log measurements, using FE/petrophysical models and techniques. The petrophysical/FE models and techniques used to do this inference will be the subject of this chapter.

In spite of the overlapping responses of the various wireline and MWD/LWD tools, most of them are identified with specific applications. Table 13.1 lists some of the more common tools and interpretation techniques, by their primary purpose. Some tools and techniques (e.g., caliper) do have a single primary purpose. Many, however, really have multiple primary purposes. Almost all of them are used as components in various multiparameter petrophysical analysis techniques.

13.4 Who Are Petrophysicists and How Do They Work?

Petrophysicists may have formal training in any of several fields, including chemistry, physics, geophysics,

mechanical, electrical and petroleum engineering, geology, sedimentology, and stratigraphy. Regardless of

their formal training, good petrophysicists also have several years of experience, working with FE problems from a variety of geological settings throughout the world. Some specialize in specific techniques, specific geologic environments, and/or specific geologic basins. Some are generalists. Some have been practicing logging engineers. Others have gravitated to the field from research laboratories, or E&P operations.

The common characteristics among petrophysicists (if you can say there are such things) are curiosity, imagination, creativity, and a desire to make the best estimates of volumetric parameters given the information at hand. In short, a petrophysicist works much like a physician or detective, analyzing incomplete evidence to develop a logical analysis. Paul Worthington, former Petrophysics Director at the British Petroleum Sunbury E&P Research Laboratory, may have said it best [13.5]:

A petrophysicist is someone who, on a daily basis, is required to attempt the impossible and who almost pulls it off every time.

While this may be a little self-serving, it is not far off the mark. I know of few traditional scientists and engineers who would be willing to do what petrophysicists are asked to do, every day, given the sparse amount of information they usually have at their disposal.

Often (e.g., for discovery and older wells), not all of the information needed for a solid petrophysical interpretation is available. In these cases, the petrophysicist must make his/her best estimate of the missing information. Later, if the missing information becomes available, the petrophysical interpretation can be modified, using the new information. In a sense, *all petrophysical interpretations are preliminary*, subject to later revision as additional information becomes available.

13.5 How Wireline and MWD/LWD Logs Are Acquired

Table 13.1 lists common objectives for well log measurements, and the logging tools and/or petrophysical analysis techniques used to obtain them. The most effective approach to estimating the desired petrophysical parameters is to use multiple measurements and analysis techniques.

Figure 13.8 is a schematic drawing of a wireline logging system in operation. A measurement instrument package (sonde) is lowered to the bottom of the well to be logged and chemical/physical properties of the immediate borehole environment are measured as the sonde is slowly (1500–3600 ft/hr) retrieved from the well. A large winch, located in the (surface) logging unit, raises and lowers the sonde in the well via 1-9 conductor, double steel armor (also a conductor) wrapped cable. The logging cable also supplies power to the sonde and serves as the communications link between the measurement instruments in the sonde and the recording devices at the surface.

An alternative configuration (MWD/LWD) utilizes special instrument packages, contained in drill bit sub-assemblies, which make the log measurements, encode them, save them to downhole memory and/or transmit them to the surface via coded pressure pulses in the mud column or EM signals.

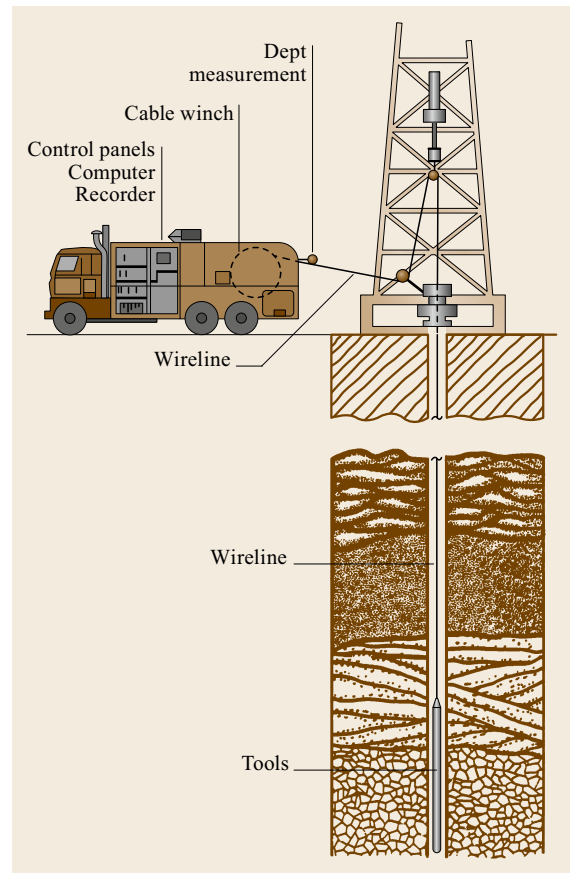


Fig. 13.8 Wireline logging system

13.6 Uses of Well Logs

The initial uses of wireline measurements were to correlate formations between boreholes. *William Smith* established that geologic formations could be correlated over great distances [13.4], by observing the character of the rocks and included fossils exposed in outcrops and in road cuts, canal cuts, quarries, and building excavations. Subsurface geologists carried this approach into the subsurface, by describing drill cuttings and cores.

The Schlumberger brothers established that wireline physical property measurements could be used for the same purpose. If the correlations are relative to (hung on) a specific formation, the results are called *stratigraphic cross-sections*. If the correlations are hung on subsurface depth, the result is called a *structural cross-section* (Fig. 13.7).

These (stratigraphic and structural) correlation uses of well logs are still the largest single use of wireline and MWD/LWD products.

Figure 13.7 shows a structural cross-section from a West African oil field. This cross-section was used to solve a perplexing field development problem. The F-15 (side-track) well was programmed *not* to cross Fault E. The well, however crossed the previously unknown Fault A, truncating the EK-4 Sand, and *floatated*, crossing Fault E in the A-3 Sand, bottoming out in the *hanging wall* of the fault structure, repeating the A-1 and A-2 Sands. The operator recognized that the well cut two faults, but interpreted the second fault to be antithetic, like Fault A, which would result in a missing section, and erroneously correlated the sands below the fault to deeper pay sands in the section of the horst, containing the oil field. The sands below the fault in the F-15 well were wet because they were off the structure containing the oil field. The structural cross-section of Fig. 13.7 shows the correct structural relationship of the F-15 well sands, to the F Structure and its pay sands.

Quantitative wireline measurement tools and laboratory measurements on core material led to the development of formation evaluation, well log analysis, or petrophysics (nearly interchangeable designations). Initially wireline measurements were calibrated using core measurements as standards. Current wireline and LWD tools, however, are sufficiently reliable and well calibrated that they can often identify core measurements, which are in error, and/or are biased by inhomogeneities (nugget effect).

Wireline measurement suites are now routinely used to scan wells to search for potential hydrocarbon-bearing intervals. Once hydrocarbon indications have been found, wireline measurements are used to quantify the reservoir thickness (net pay), pore space (porosity), and the type and amounts of fluids occupying that pore space (water, gas, and oil saturations). This basic reservoir information (net pay, porosity, and saturation) is used with structural and stratigraphic information to develop stock tank original oil in place (STOOIP) and standard cubic feet original gas in place (SCFOGIP) values for reserves estimates and depletion management ((13.1) and (13.2)).

In addition to volumetric measurements, modern wireline and MWD measurements also provide information on:

- Borehole volume
- Mechanical properties of the rocks penetrated by wells
- Temperatures and pressures of the subsurface
- Subsurface borehole path
- Images of the borehole wall
- Structural and stratigraphic information about the subsurface.

13.7 Petrophysics and Well Logging: Historical Development

Old well logs never die. They reside in records storage or well files and are repeatedly used by explorationists and engineers over time. The measurements currently being made, however, are much different from those that were done in the past. Because of this, it is worth a short history lesson. *Bateman* [13.6] and *Hill* [13.7] have more detailed historical reviews.

It is difficult to discuss the historical development of well logging without sounding like a promotion for Schlumberger, as the development of the industry and Schlumberger are so intertwined and this multinational integrated corporation so dominates the industry. While

exact figures are difficult to obtain, Schlumberger controls approximately 80%± of the world wireline, LWD and core laboratory industry. They do, however, have strong, though much smaller, competitors.

Schlumberger has not always been the first to introduce a new technology. Partially, this is because new technology introduction costs are generally much less for their smaller competitors, as vendors generally want to be able to offer any new services system-wide. Once a market has been established, however, Schlumberger has generally quickly covered the new (competitor) product and rapidly advanced the new technology, to

maintain their control of the market. In the few cases where Schlumberger did not have its own competing technology it has, in recent years, bought out startups with innovative technologies.

Tables 13.2–13.8 highlight some of the milestones in the logging/petrophysical industry. It has been com-

plied from a variety of sources, not all of which agreed upon the dates of when specific events happened. Most of the nonelectrical new technologies were introduced by organizations other than Schlumberger. Many of the significant improvements of these new technologies, however, did come from Schlumberger.

Table 13.2 Prelogging petrophysical milestones (from a variety of sources)

Date	Event
1830	First attempts to measure spontaneous polarization generated by metallic sulfide deposits
1900	Gamma ray discovered
1911	Conrad Schlumberger begins research in electrical prospecting techniques at Ecol des Mines, Paris Initial equipotential mapping field work by Conrad Schlumberger, at the family's Val-Richer estate, Normandy
1912	First observation of induced polarization First Schlumberger electrical prospecting patent filed
1913	First successful use of Mes a la Mass technique to outline a buried conductive ore body Conrad Schlumberger observed SP signals over buried sulfide ore bodies
1919	Paul Schlumberger underwrites Conrad Schlumberger's electrical prospecting research Brother Marcel joins the efforts Earl P. Halliburton founded New Method Well Cementing Co.
1923	Formation of Societe de Prospection Electrique, Precedes Schlumberger (Pros) Surface electrical surveys in Belgian Congo, Canada, Romania, Serbia and Union of South Africa

Table 13.3 Petrophysical milestones: 1927–1942 (from a variety of sources)

Date	Event
1927	First electric log (station measurements) at Pechelbronn Field, France
1928	Introduction of three-conductor logging cable
1929	<i>Electrical coring</i> paper presented at A.I.M.E meetings Electrical logging introduced to California, USSR, and Venezuela
1930	Introduction of SP log Electrical logging introduced to Indonesia
1931	Introduction of manual (hand-cranked) continuous pen recording
1932	Introduction of the normal electrode array resistivity log Introduction of directional surveys Introduction of temperature logs Introduction of bullet perforation Bill Land and Walt Wells form Lane-Wells Bullet Perforation Company Chadwick discovers the neutron
1933	First neutron log evaluation
1934	Schlumberger Well Surveying Corporation formed Introduction of automatic (galvanometer) recording
1935	Introduction of sidewall cores Introduction of photographic recording
1936	Introduction of dual galvanometer recording
1937	Introduction of three-galvanometer recording
1938	Introduction of four-conductor cable Introduction of neutron log Nuclear magnetic resonance discovered
1939	First gamma ray log publication
1940	Introduction of armored cable Introduction of gamma ray logs Jess Hall Sr. founded Weatherford Spring Co.
1941	Introduction of three-arm (SP) dipmeter
1942	Publication of Archie equations
1941	Introduction of three-arm (SP) dipmeter
1942	Publication of Archie equations

Table 13.4 Petrophysical milestones: 1945–1960 (from a variety of sources)

Date	Event
1945	Introduction of focused electrical logs Introduction of the R_{xo}/R_t (Rocky Mountain) Interpretation Technique
1946	Introduction of three-arm dipmeter with short (micro) resistivity pads and caliper logs
1947	Introduction of induction log Introduction of nine-pen galvanometers
1948	Schlumberger opens research center (later renamed Schlumberger-Doll Research Center) in Ridgefield, Connecticut Transistor invented
1949	Introduction of microlog, with caliper
1950	Introduction of guard resistivity logs, or Laterolog-3 (LL3). Introduction of gamma ray logs Introduction of gamma ray neutron log (GNT)–gamma ray log combination
1951	Introduction of continuous recording three-arm dipmeters, with microresistivity pads Introduction of microlaterolog
1954	Introduction of continuous velocity logs, later called acoustic or sonic logs. Introduction of powered downhole caliper arms Introduction of nuclear magnetic resonance (proton precession) magnetometer
1955	Introduction of wireline formation testing Introduction of compensated (dual detector) neutron log
1956	Introduction of five-coil induction Publication of Wyllie time-average equation Introduction of (single detector) density logs Establishment of American Petroleum Institute (API) calibration pits Publication of first nuclear magnetic resonance (NMR) logging paper
1957	Introduction of FORTRAN programming language Publication of first density logging paper
1958	Introduction of Laterolog-8 Introduction of cased-hole density logs for determining top of cement Sputnik launched Integrated circuits invented
1959	Introduction of six-coil induction logs Introduction of compensated (dual detector) density logs
1960	Introduction of chlorine logs

Table 13.5 Petrophysical milestones: 1961–1970 (from a variety of sources)

Date	Event
1961	Introduction of cement bond logging Introduction of production logging Introduction of (analogue) computer processed dipmeter data
1962	Introduction of sidewall neutron porosity logs First nuclear magnetic resonance (NMR) prototype tool Introduction of neutron-density cross-plot analysis
1963	Introduction of dual-induction logs Introduction of borehole compensated (BHC) sonic logs
1964	Introduction of compensated (dual detector) density logs Introduction of neutron lifetime logs (NLL) Introduction of IBM 360 computer series Introduction of punched paper teletype (TT) tape recording Introduction of BASIC programming language
1965	Schlumberger opens Clamart, France, Engineering Center The California Research Co. and Shell Development Co. begin laboratory studies of nuclear magnetic resonance First computerized seismic data processing
1966	Introduction of compensated (dual detector) neutron log Introduction of high-resolution dipmeter
1967	Introduction of borehole televiewer (BHTV)

Table 13.5 (continued)

Date	Event
1968	Introduction of truck quantizer (TQ5) Introduction of truck tape recorder (TTR) Publication of Waxman and Smitts Shaly-Sand Model
1969	Introduction of spectral (K-U-T) gamma ray logs Moon landing
1970	Introduction of triangular core slicer Introduction of first integrated digital FE sandstone analysis system (SARABAND™)

Table 13.6 Petrophysical milestones: 1971–1980 (from a variety of sources)

Date	Event
1971	Introduction of four-arm dipmeter Introduction of induction sonic combination stack Introduction of first complex mineralogy digital analysis FE analysis system (CORIBAND)
1972	Introduction of dual laterolog Introduction of cased-hole TDT neutron logs
1975	Introduction of direct digital logging (DDL), first in-truck digital computer system Introduction of quicklook computer log analysis system (Cyberlook)
1976	Introduction of carbon/oxygen logging Introduction of 5 1/4 in Floppy Disk recording media.
1977	Introduction of Cyber Service Unit (CSU) second in-truck digital computer system Introduction of dielectric constant logs Introduction of vertical seismic profiling (VSP) Introduction of dual water interpretation model SANDIA National Laboratory high temperature microcircuit project started
1978	Introduction of photoelectric effect density logs (LDT or Z-Logs) Introduction of Motorola 68000 microprocessor
1979	First commercial measurements while drilling (MWD) service First MWD log (gamma ray)
1980	Introduction of first reliable borehole gravity meter (BHGM) Introduction of 5 MB hard drives for microcomputers Introduction of over determine logic in FE

Table 13.7 Petrophysical milestones: 1981–1990 (from a variety of sources)

Date	Event
1981	Introduction of induced gamma ray spectrometry logs Introduction of MSDOS Introduction of 3 1/2 in floppy drives
1982	Introduction of array sonic logs (ASTs) Introduction of Cray XMP <i>supercomputer</i> Introduction of Commodore 64 microcomputer
1983	Introduction of improved dielectric constant (DPT™) logs Introduction of MS WORD word processor
1984	Introduction of six-arm dipmeter Introduction of Shiva dipmeter processing logic Introduction of array induction logs, with amplitude <i>and</i> phase measurements Introduction of Apple Macintosh microcomputer, with <i>mouse</i> cursor controller
1985	Introduction of formation micro-imager (FMI) Start of the Internet Evaluation of nonchemical density source (LINAC borehole accelerator)
1986	Introduction of Phasor (multiple frequency) induction logs Introduction of modern NMR logging tool Introduction of INTEL 386 (32 bit) microprocessor chip
1988	Introduction of acoustic dipole source
1989	Introduction of high-resolution (400 KHz) induction tools Introduction of INTEL 486 (62 Bit) microprocessor chip

Table 13.7 (continued)

Date	Event
1990	Introduction of MS WINDOWS microcomputer operating system Introduction of the Circumferential Acoustic Scanning Tool (CAST)

Table 13.8 Petrophysical milestones: 1991–2006 (from a variety of sources)

Date	Event
1991	Introduction of formation micro-imaging tool Introduction of Linux operating system Introduction of LWD array processing
1992	Introduction of array induction logs Introduction of in-cab color plotters
1993	Introduction of cross-dipole acoustic source Introduction of LWD focused resistivity logs Introduction of Intel Pentium microprocessor
1994	Introduction of LWD azimuthal gamma ray measurements Introduction of LWD acoustic imaging Introduction of LWD resistivity imaging
1995	Introduction of Platform Express, a compact complete measurement package Introduction of resistivity through casing measurements Introduction of LWD azimuthal density measurements
1996	Introduction of three-dimensional induction tools Introduction of improved NMR (CMR™) tools
1997	Introduction of multiradius NMR (CES™) tools
1998	Introduction of high-resolution laterolog array tools
1999	Introduction of horizontal production logging
2000	Introduction of LWD NMR tools
2002	Introduction of NMR diffusion tools Introduction of LWD spectral gamma ray tool
2004	Introduction of LWD wired pipe
2005	Introduction of elemental capture gamma ray spectroscopy Introduction of pulsed neutron tools
2006	Introduction of LWD directional resistivity tools

The first oil well was logged, using wireline techniques, in 1927, at Pechelbronn Field, Alsace-Lorraine, France (Fig. 13.9). The story, however, actually starts much earlier. R. W. Fox, a British scientist attempted to map spontaneous polarization (SP) anomalies generated by metallic sulfide deposits in Cornwall in 1830. Carl Barus, an American, utilized SP to study Nevada mines in 1880.

In 1900, Paul Schlumberger sold his interests in the family textile firm, Nicolas Schlumberger et Compagnie, to his brothers and emigrated from Alsace-Lorraine to Paris to be near his children. Two sons, Conrad and Marcel, became involved in minerals exploration and later started the first wireline company. Modern formation evaluation owes its heritage to these two men and the financial backing of their father.

13.7.1 The Schlumberger Brothers and Pros.

Conrad Schlumberger was a physics professor at l'École des Mines. He began experimenting with sur-

face electrical measurements to map geologic targets about 1911, commandeering his daughter's copper baby bathtub for his laboratory experiments [13.8]. Marcel Schumberger was a graduate mechanical engineer from l'École Centrale des Arts et Manufactures. He worked as a consulting mining engineer, based in Paris.

Conrad's first fieldwork involved surface equipotential mapping to locate buried inhomogeneities. Between 1912 and 1914, Conrad was able to successfully demonstrate his equipotential mapping techniques over several buried metallic ore bodies throughout Europe. Demonstrations, by Conrad and other geophysicists, utilized surface apparent resistivity profiling using centralized four-electrode current and potential arrays, also to identify buried subsurface features, such as shown in Fig. 13.10. These demonstrations had to be sandwiched in between his teaching and research at l'École des Mines.

In 1919, Paul Schlumberger pledged up to 500 000 Fr of his personal fortune to support his sons' *research study in view of determining the nature of*

the subsurface [13.8]. This, together with dowries from both of the brothers' wives, freed the Schlumberger brothers from the details of earning a living and allowed them to concentrate full time on commercializing Conrad's ideas of geoelectrical exploration techniques.

The Schlumberger brothers were ideally matched. Conrad was the dreamer and theoretician who developed conceptual techniques. Marcel was the practical engineer, who made these techniques work. In 1926, they felt confident enough in what they were doing to found l'Société de Prospection Électrique, Procèdes Schlumberger (Pros.).

Pros. offered surface electrical mapping services to the world. Electrical techniques were not utilized for petroleum exploration until 1923. Pros. would not attempt borehole measurements until the Pechelbronn well, in 1927. During this period (1919–1927) the Schlumberger brothers managed to exhaust most of their initial financial stake, without much return on their investment. They did, however, enjoy several technical, if not financial, successes.

13.7.2 The Pechelbronn Well

On 5 September 1927, Conrad Schlumberger's son-in-law Henry Doll, Roger Dost, and Charles Scheibli (all employees of Pros.) recorded the first well log, by dropping a surface electrical resistivity profiling electrode array down a well at Pechelbronn Field, Alsace-Lorraine, measured a resistivity profile of the formations intersected by the well [13.8]. This log (Fig. 13.11) was obtained with stationary readings, every 5 m. The purpose of the Pechelbronn well logging operation was to see if the Schlumberger brothers' surface resistivity profiling technique, dropped down a borehole, could be used to correlate subsurface geological formations between wells. While the resulting log (Fig. 13.11) does not look very impressive, compared to modern logging vendor products, it did demonstrate the concept that wireline measurements could be used for subsurface correlation.

The Schlumberger brothers were unlikely entrepreneurs. Pros. certainly had not been a money-making enterprise. While neither of them could have predicted it, at the time, that day at the Pechelbronn well allowed them to establish what would become one of the world's largest oilfield service companies. They only knew that someone was willing to pay them to run their resistivity profiling technique in a borehole. The Pechelbronn well logging operation allowed the Schlumberger brothers to rescue an intriguing, but struggling operation and turn it into a profitable one. Within three years, *Schlumberger electrical coring trucks* (Fig. 13.12) were logging wells throughout the world.



Fig. 13.9 First well logging operations: Pechelbronn Field, Alsace-Lorraine, France. Note multiple winches (from [13.10], courtesy of SPWLA)

In 1929, *E. G. Leonardon*, manager of Schlumberger Electrical Prospecting Methods, New York, convinced the Schlumberger brothers to publicize their well logging techniques via technical publications. The first wireline paper, *Electrical Coring: A Method of Determining Bottom-Hole Data*, presented in 1929 and published as A.I.M.E. Technical Publication 462, in 1932, established a tradition of stimulating technical disclosure via publication (if not complete) by Schlumberger, which has been followed by other wireline vendors [13.11].

Through the Great Depression, the logging arm of Pros., now named Schlumberger, grew steadily [13.10]. By WW-II Schlumberger could safely make the claim: *Where ever the oil bit goes, Schlumberger will follow.*

In 1931, the surface exploration arm of Pros. joined with another firm, l'Société Géophysique de Recherches Minières (specializing in electromagnetic and seismic refraction methods) to form *Compagnie Général de Géophysique (CGG)*. After World War II, CGG became a surface geophysical contractor, semi-independent of Schlumberger. Schlumberger Well Logging Services concentrated entirely on wireline measurements. There remained a rather loose connection between CGG and Schlumberger until Schlumberger

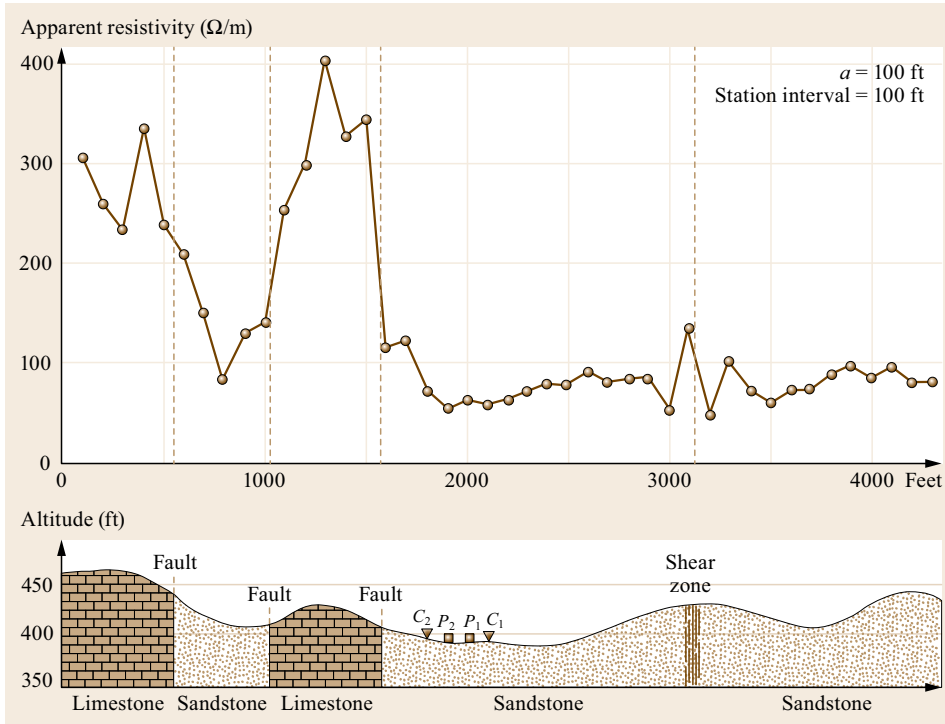


Fig. 13.10 Surface resistivity profile over a limestone fault block and a shear zone. The positions of current electrodes (C_i) and potential electrodes (P_i) are indicated (after [13.9])

acquired the geophysical contractors Western-GECO and PRAKLA-SEISMOS, while CGG acquired Davis Great Guns Wireline Services.

Conrad Schlumberger first observed spontaneous polarization (*polarisation spontanée*), over a buried pyrite ore body, in 1913. By 1931, SP (often called *porosity Log*) was being included with resistivity as part of the Schlumberger electrical logs (E-Logs) or electrical surveys (ES). The desire to obtain structural information stimulated the development of dipmeters. The desire to obtain rock samples (larger than cuttings) from wells, which had not been cored, led to sidewall core guns and, much later, rotary sidewall coring bits.

Through the end of World War II, wireline logging meant electrical logging and also meant Schlumberger. Logs were not often used quantitatively, but rather for correlation. After the war, other techniques and other vendors began to appear. Wireline measurements also began to be used in more quantitative ways. Early logging units (Fig. 13.12) looked much different from current models.

13.7.3 Archie's Equations

In 1942 and 1950, *G.E. Archie*, of Shell Oil Co., described the formation factor/porosity and resistivity index/water saturation relationships we now know as

Archie's equations [13.12, 13]

$$F = \frac{R_o}{R_w} = a\varphi^{-m} \quad (13.4)$$

$$F = \frac{R_t}{R_o} = S_w^{-n}, \quad (13.5)$$

where:

- F is the (dimensionless) formation factor.
- R_o is the electrical resistivity of a brine-saturated rock.
- R_w is the electrical resistivity of the brine saturating the rock.
- φ is the (decimal) porosity of the rock.
- a and m are coefficients determined by the data.
- I is the (dimensionless) resistivity index.
- S_w is the (decimal) water saturation of the rock.
- n is a coefficient determined by the data.

The empirical coefficient m is sometimes called the cementation exponent. The empirical coefficient a is sometimes called the tortuosity coefficient. The empirical coefficient n is sometimes called the saturation exponent.

Archie's equations ((13.4) and (13.5)) offered the opportunity to obtain quantitative reservoir information from wireline measurements. To do this, however, required wireline porosity tools. The failure of these (Archie) relationships, under certain circumstances, re-

quired the development of more complex petrophysical models.

The need for saturation tools for use in wells drilled with air and/or oil-based mud, led to the development of induction logs. Interest in uranium exploration stimulated the use of natural gamma radiation logging tools. The recently declassified nuclear technology (and

unemployed nuclear engineers, following the end of World War II) led to the development of density and neutron logs. The need for deep penetration, high-resolution resistivity information led to the development of guarded, or focused, laterologs. The need for detailed seismic velocity information led to the development of acoustic, or sonic, logs.

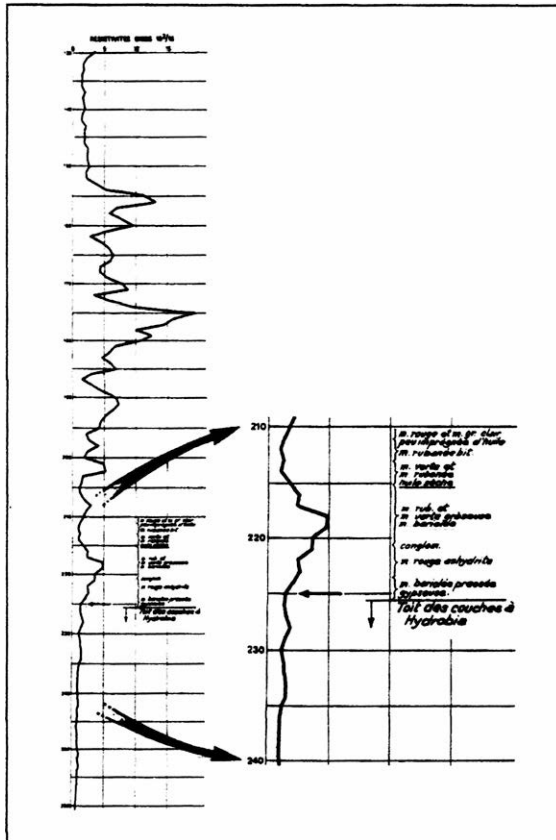


Fig. 13.11 First well log: Pechelbronn Field, Alsace-Lorraine, France (courtesy of SPWLA)



Fig. 13.12 Early Schlumberger logging unit in the California Desert (from [13.10], courtesy of SPWLA)

13.7.4 Continuous Velocity Logs and Jesse Wyllie's Relationship

Interest in better seismic velocity information led to the development of acoustic logs. The California Research Company (now part of Chevron Energy Technology Company, or ETC), Magnolia Petroleum (now part of EXXON-Mobil Exploration & Production Research, or EPR), and Shell Development (now part of Shell Upstream Technology) all developed operational acoustic tools in a dead heat. In 1956, *M.R.J. Wyllie* and associates, at Gulf Research and Development Company (now part of Chevron ETC), developed what we know as Wyllie's time-average equation [13.14]

$$\varphi_s = \frac{\Delta t - \Delta t_{ma}}{\Delta t_f - \Delta t_{ma}} \frac{1}{c}, \quad (13.6)$$

where:

- φ_s is the (Wyllie) sonic porosity.
- Δt is the observed rock interval acoustic transit time ($\mu\text{s}/\text{ft}$).
- Δt_{ma} is the rock matrix interval acoustic transit time ($\mu\text{s}/\text{ft}$).
- Δt_f is the fluid interval acoustic transit time ($\mu\text{s}/\text{ft}$).
- c is a coefficient, determined by the data.

The empirical coefficient c is sometimes called a compaction correction.

Most new logging techniques based upon applications of different branches of physics had occurred by the late 1960s. The development since then has been primarily in the areas of increased measurement accuracy, equipment reliability, data transmission and data processing techniques. In many ways, these last technological advances have been even more impressive than the initial technique developments.

13.7.5 Improvements in Recording the Results

The first logs were acquired as station measurements, like the Pechelbronn well. The logging array (or *sonde*) was suspended at the measurement depth, while instruments were adjusted and measurements recorded. Lore and legend has it that the first continuous logs were

obtained by using small boys who adjusted the instrumentation and called out the readings, as the sonde was slowly retrieved from the bottom of the well. A circa 1930s promotional movie, however, now called the *Schlumberger Melodrama* shows Schlumberger Engineers frantically balancing potentiometers, gang-linked to chart drive (linked to the logging cable winch) pen recorders as a well is logged (Fig. 13.12). The development of unbalanced bridge circuitry and pen chart recorders allowed faster continuous logging operations. The use of photographic film and light lever cameras with depth markers allowed the development of reproducible hard copy logs.

Manually adjusted bridges and other instrumentation were replaced by hand-wired (breadboard) analog computers. These, in turn, were replaced by specialized analog computer modules, called function formers, and standardized mounting racks, called NIM (for nuclear instrument module) BINS.

Initially, well logs were recorded only in hard copy mode (pen recorder charts and photographic film). At one point, the largest customer of Kodak continuous 8 in film was claimed to be Schlumberger. Film log prints made duplication easy, but if different instrument settings were desired the well had to be relogged.

Dresser Industries attempted, in the 1960s, to utilize multichannel FM magnetic tapes, similar to those used for recording seismic data. This soft copy data recording allowed playback with different function former settings, eliminating the need to relog the well. While technically successful, the system was so difficult and cumbersome to operate that it was never accepted by the petroleum industry and was eventually abandoned.

Schlumberger attempted to use paper Teletype tape. This recording system, however, proved to be not only overwhelmingly noisy, but the paper tape was often damaged by the elements under which wells were logged [13.6].

By the 1970s, fast and reliable multichannel analog to digital (A/D) systems and nine-track tapes were being used to record data in the field. Wireline vendors and several large petroleum companies began to utilize these field recordings as input to complex mainframe computer petrophysical analysis systems.

Gearhart Industries introduced the first use of a general-purpose minicomputer in a field logging system in the mid 1970s [13.15]. The use of an on-board minicomputer allowed not only digital recording of the data, but also some processing and analysis in the field. Other major wireline vendors quickly followed suit. Rumor has it that the Digital Electronics Co. (DEC) salesman that closed the deal for Schlumberger to install two DEC PDP-11 minicomputers in each logging unit was immediately promoted to Vice President, Marketing.

The final piece of the digital revolution involved replacing downhole analog electronics in the logging sonde, with miniaturized A/D and microprocessor chips. This advance was stimulated by two developments:

- Miniaturization was stimulated by the space program.
- Sandia National Laboratory sponsored a high-temperature/high-pressure logging tool component development program in the early 1980s, which completed the transition [13.16].

Table 13.9 Wireline vendor common wireline service mnemonics

Generic service type	Baker-Atlas (Western-Atlas) (Dresser-Atlas)	Halliburton (WELEX™) (Gearhart)	Schlumberger	Weatherford (Computalog) (Rives) (BPB™)
Surface unit	CLS	PLS, LOGIQ	CSU, MAXIX	?
Induction log	DIFL, HDIL	DIGL, DIL, HRI	DIL, DIT-E	STI
Array induction log	3DeX	HRAI, ARCT	AIT	MAI
Focused resistivity log	GL, DLL	GL, DLL, DLLT	LL3, LL8, DLL, SFL	DLL
Array focused resistivity log	RTeX	ACRT	HRLA	?
Microresistivity log	ML	MGL, MLL, MSFL	ML, MLL, MXFL, MCFL	MRT
Micro resistivity imager	?	XRMI, EMI	?	HMI
Spontaneous polarization	SP	SP	SP	SP
Acoustic log	AC, ACL, DAL, XMAC	AVL, FWST, BCS, LSS, BSAT	BHC, LSS	HBC
Array acoustic log	AAT	BSAT, Wave Sonic	AST	?
Downhole seismic	LRS, TOMEX	VIVSP	WST, DSA, SAT	VSP
Acoustic imager	?	CAST, CAST-I	BHTV	?
Total gamma ray	GR	GR, NGRT	GR	GR, UGR

Table 13.9 (continued)

Generic service type	Baker-Atlas (Western-Atlas) (Dresser-Atlas)	Halliburton (WELEX™) (Gearhart)	Schlumberger	Weatherford (Computalog) (Rives) (BPB™)
K-U-T spectral gamma ray	SL	CSNG, SGR	NGS, NGT	SGR
Neutron	NL, SNP, CN	GNL, SDN, NL, SNL, CNS, DSN, DSEN, DSNT	GNT, SNP, CNT	CNT
Density and PEF	CDL, ZDL	CDL, SDL	FDC, LDT	SPeD
Dip meter	DIP	HDT, FED, SAD, SED, XRMI	HDT	?
Dielectric constant	?	HFDT, HDFT-I	EPT, DPT	
Nuclear magnetic resonance	MReX	MRIL	CML	NMRT
Sidewall cores	SWC	SWC, ASCT, RSCT	CST, MCST	SCT, RSCT
Wireline formation tester	FMT	SFT, RDT	RFT, MDT	SFT, FRT
Cement evaluation	ACBL, SBT	MSGCBL, CBL, PET, CAST	CBL, CET	SB, URS, CIT
Pulsed neutron capture	NLL, PDK	TMD, TDL	TDT	PND
Geochemical	MSI/CO	PSGT, GEM	GST, GCL, AACT	?

Table 13.10 MWD/LWD vendor common logging service mnemonics

Generic service type	Baker-Atlas	Halliburton (Sperry)	Schlumberger (Anadrill)	Weatherford (Precision)
Surface unit	?	?	?	?
Induction log	AziTrak, EMR, DPR	EWR	ArcVision, CDR, ARC5	?
Focused resistivity log	ZoneTrak, DDG	ADR, AFR, RGD, LL3	RAB	?
Acoustic log	SoundTrak	QBAT, XBAT	?	ShockWave
Borehole imaging	?	ADR, AFR, ALD, GABI	?	
Total gamma ray	ZoneTrak G	ABG, DGR, GABI	?	HAGR
K-U-T spectral gamma ray	?	–	?	SAGR
Neutron	LithoTrak	CTN	EcoScope, adnVision, CDV, ADN	TNP
Density and PEF	LithoTrak	ALD	EcoScope, adnVision, CDN, ADN	AZD
Dielectric constant	?	HFDT	?	MFR
Nuclear magnetic resonance	MagTrak	NMR	ProVision	–
LWD formation tester	TesTrak, FasTrak	GEOTAP	?	?
Directional survey	NaviTrak	SOLAR	ArcVision	DMT, AMS

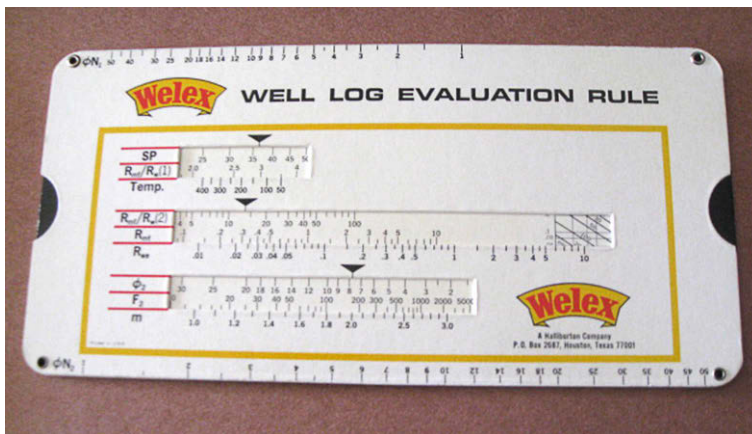
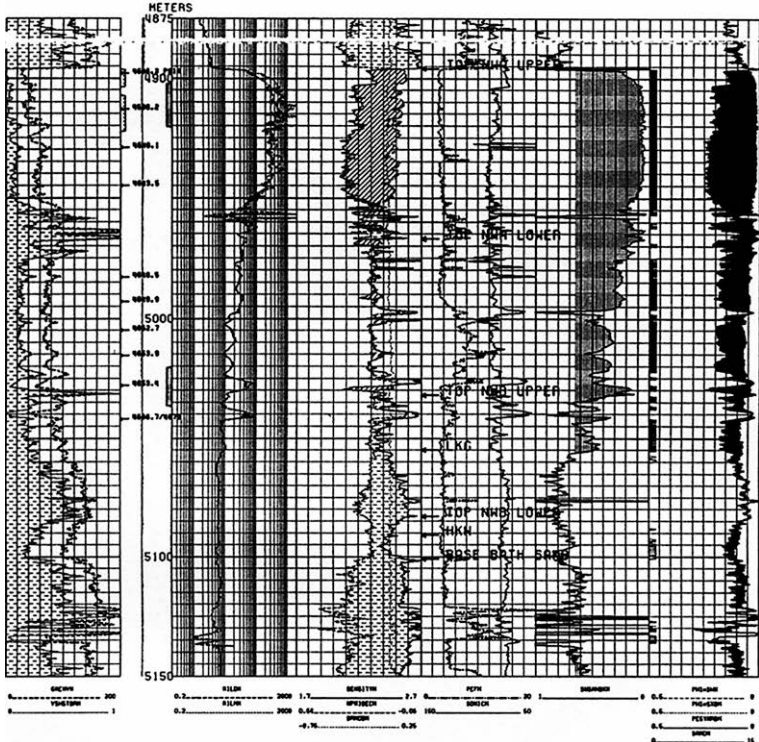


Fig. 13.13 Specialized formation evaluation slide rule (courtesy of WELEX)

CORRELATION	DEPTH	DIL/DLL	NEUTRON/DENSITY	SONIC/PEF	SATURATION	POROSITY
GRANITE	150	MSFL 2000	DENSITY 2.70	SONIC 50	SH 0	
SHALINESS		ILH 2000	NEUTRON 0.6	PEF 20	H.C. SATURATION BELOW SH CUT-OFF	
		ILD 2000	DRHO 1.25			



CORRELATION	DEPTH	DIL/DLL	NEUTRON/DENSITY	SONIC/PEF	SATURATION	POROSITY
GRANITE	150	MSFL 2000	DENSITY 2.70	SONIC 50	SH 0	
SHALINESS		ILH 2000	NEUTRON 0.6	PEF 20	H.C. SATURATION BELOW SH CUT-OFF	
		ILD 2000	DRHO 1.25			

Fig. 13.14 PNG well computer-aided multiple log formation evaluation analysis display

Downhole A/D sampling, storage and transmission meant more stable logging sondes and greater data transmission (i. e., broadband) speed and volumes to the surface. This allowed the development of more complex sondes, such as microresistivity borehole scanning tools, array acoustic, induction, and laterolog sondes, as well as shorter multitool stacks. Table 13.9 summarizes common wireline service mnemonics, by vendor.

A recent major technological development has been the introduction of specialized drill collars, with instrumentation packages, recording, and/or telemetry, which allow formation evaluation measurements during the drilling operation. Since the introduction of the first MWD (measurements while drilling) sub-assemblies in 1979, many wireline measurement capabilities have been duplicated by MWD (now called

Table 13.11 Precalculated S_w table for formation evaluation example. This worker saturation table should be used for $0.026 \leq R_w \leq 0.034$

Porosity (%)	True resistivity R_T																																					
	0.4	0.7	1.0	1.3	1.4	2.0	2.5	3	4	5	6	8	10	13	16	20	25	30	35	40	50	60	80	100	130	160	200	250	300	400	500	600						
3	-	-	-	-	-	-	-	-	-	-	-	-	-	-	-	-	-	-	-	94	84	76	66	59	52	47	42	37	34	30	26	24						
4	-	-	-	-	-	-	-	-	-	-	-	-	-	-	-	97	87	79	73	69	61	56	49	43	38	34	31	27	25	22	19	18						
5	-	-	-	-	-	-	-	-	-	-	-	-	-	95	85	76	68	62	58	54	48	44	35	34	30	27	24	22	20	17	15	14						
6	-	-	-	-	-	-	-	-	-	-	-	99	69	78	70	63	56	51	47	44	40	36	31	26	25	22	20	18	16	14	13	11						
7	-	-	-	-	-	-	-	-	-	-	97	84	75	66	59	53	48	43	40	38	34	31	27	24	21	19	17	15	14	12	11	10						
8	-	-	-	-	-	-	-	-	-	92	84	73	65	57	52	46	41	38	35	33	29	27	23	21	18	16	15	13	12	10	9	8						
9	-	-	-	-	-	-	-	-	-	91	81	74	64	57	50	45	41	36	33	31	29	26	23	20	18	16	14	13	11	10	9	8	7					
10	-	-	-	-	-	-	-	-	-	94	81	72	66	57	51	45	41	36	32	30	27	26	23	21	18	16	14	13	11	10	9	8	7	7				
11	-	-	-	-	-	-	-	-	-	93	84	73	65	56	47	42	37	33	29	27	25	23	21	19	16	15	13	12	10	9	8	7	6	6				
12	-	-	-	-	-	-	-	-	-	94	84	77	67	60	54	47	42	37	33	30	27	24	23	21	19	17	15	13	12	11	9	8	7	6	5			
13	-	-	-	-	-	-	-	-	-	97	86	77	71	61	55	50	43	39	34	31	27	24	22	21	19	16	14	12	11	10	9	8	7	6	5			
14	-	-	-	-	-	-	-	-	-	99	89	80	71	65	56	50	46	40	36	31	28	25	23	21	19	18	16	15	13	11	10	9	8	7	6	5		
15	-	-	-	-	-	-	-	-	-	92	83	74	66	61	52	47	43	37	33	29	26	23	21	19	18	17	15	14	12	10	9	8	7	6	5	4		
16	-	-	-	-	-	-	-	-	-	96	86	77	69	62	56	49	44	40	35	31	27	24	22	20	18	17	15	14	13	11	10	9	8	7	6	5	4	
17	-	-	-	-	-	-	-	-	-	92	80	72	65	58	53	46	41	37	32	29	25	23	20	18	17	15	14	13	12	10	9	8	7	6	5	4	4	
18	-	-	-	-	-	-	-	-	-	86	76	68	61	54	50	43	39	35	30	27	24	22	19	17	16	15	14	12	11	10	9	8	7	6	5	4	4	
19	-	-	-	-	-	-	-	-	-	97	81	71	64	57	51	47	41	36	33	29	26	23	20	18	16	15	14	13	11	10	9	8	7	6	5	4	4	
20	-	-	-	-	-	-	-	-	-	92	77	67	61	54	49	44	36	34	31	27	24	21	19	17	15	14	13	12	11	20	9	8	7	6	5	4	3	3
21	-	-	-	-	-	-	-	-	-	87	73	64	58	52	46	42	37	33	30	26	23	20	18	16	15	14	13	12	10	9	8	7	6	6	5	4	3	3
22	-	-	-	-	-	-	-	-	-	83	69	61	55	49	44	40	35	31	28	25	22	19	17	16	14	13	12	11	10	9	8	7	6	5	4	3	3	3
23	-	-	-	-	-	-	-	-	-	79	66	58	52	47	42	38	33	30	27	23	21	18	17	15	13	12	11	10	9	8	7	6	5	4	4	3	3	3
24	-	-	-	-	-	-	-	-	-	76	63	55	50	45	40	37	32	26	26	22	20	18	16	14	13	12	11	10	9	8	7	6	5	4	4	3	3	3
25	96	72	61	53	48	43	38	35	30	27	25	21	19	17	15	14	12	11	10	10	9	8	7	6	5	5	4	4	4	3	3	3	3	2	2	2		
26	92	69	58	51	46	41	37	34	29	26	24	21	18	16	15	13	12	11	10	9	8	7	6	6	5	5	4	4	4	3	3	3	3	2	2	2		
27	86	67	56	49	44	39	35	32	26	25	23	20	18	15	14	12	11	10	9	9	8	7	6	6	5	4	4	4	4	3	3	3	2	2	2	2		
28	85	64	54	47	42	38	34	31	27	24	22	19	17	15	13	12	11	10	9	9	8	7	6	6	5	5	4	4	4	3	3	3	2	2	2	2		
29	82	62	52	45	41	36	33	30	26	23	21	18	16	14	13	12	11	10	9	9	8	7	6	6	5	4	4	4	4	3	3	3	2	2	2	2		
30	79	59	50	44	39	35	31	29	25	23	20	18	16	14	12	11	10	9	8	8	7	6	6	5	4	4	4	4	4	3	3	3	2	2	2	2		
31	76	57	68	42	38	34	30	28	24	21	20	17	15	13	12	11	10	9	8	6	7	6	6	5	4	4	4	4	4	3	3	2	2	2	2	2		
32	73	55	46	41	37	33	29	27	23	21	19	16	15	13	12	10	9	8	8	7	7	6	5	5	4	4	4	4	3	3	3	2	2	2	2	2		
33	71	54	45	39	36	32	28	26	22	20	18	16	14	12	11	10	9	8	8	7	6	6	5	4	4	4	4	4	3	3	3	2	2	2	2	2		
34	69	52	43	36	34	31	28	25	22	19	18	15	14	12	11	10	9	8	7	7	6	6	5	4	4	4	4	3	3	3	3	2	2	2	2	2		
35	67	50	42	37	33	30	27	24	21	19	17	15	13	12	11	9	8	8	7	7	6	6	5	5	4	4	4	3	3	3	2	2	2	2	2	2		



Fig. 13.15 Microcomputer formation evaluation product

Table 13.12 Figure 13.15 microcomputer formation evaluation product summary

2873 ft sand		Petrophysical model parameters		DST #3	
Reservoir thickness	41.0 ft	Total porosity (φ_T)	Density/neutron	Perforations	2872–2880 ft MD-KB
Pay thickness	133 ft	Shale volume (V_{sh})	Linear GR	Choke size	16/64 in
Average porosity	30.0%	GR_{clean}	60 API	FARO	440 STOPD
Average water saturation	53.3%	GR_{shale}	140 API	Crude	30.8° API
		Effective porosity (φ_e)	$\varphi_T - V_{sh}\varphi_e$	BSW	0%
O/W contact	2888 ft MD-KB	φ_{sh}	25%	CO ₂	ND
		R_w	R_{wa}	H ₂ S	ND
Cut-off values		Water saturation	Simandoux	Permeability	Very high
$V_{sh} < 40\%$		a	1.13		
$\varphi > 15\%$		m	1.73		
$S_w < 70\%$		n	2.00		
		R_w	0.9 Ω m		
		R_{sh}	2.8 Ω m		

logging while drilling or LWD). Table 13.10 summarizes the several MWD/LWD vendors and their services.

13.7.6 Development of Formation Evaluation

Formation evaluation, or well log analysis, sophistication has kept pace with wireline and MWD hardware developments. Before calculators were readily available, log analysts utilized slide rules, such as shown in Fig. 13.13, *chart book* nomographs [13.17] and precalculated tables, such as Table 13.11. Worksheets were utilized to organize the process. Programmable calculators simplified this process and made more complex petrophysical models practical. Microcomputer spreadsheet calculations increased the speed and accuracy of

the process, once the log values were entered into the spreadsheet. Specialized formation evaluation software for mainframe and minicomputers (Fig. 13.14) made detailed well log analysis possible. Microcomputer FE software (Fig. 13.15) made it portable.

Wireline vendors can now telemeter data, via satellite, from the wellsite to processing centers or to client offices worldwide. This capability allows detailed digital well log analysis within hours of running the logs. Wireline vendors can also utilize on-board microcomputers to do complete log analysis, *in the cab* and will also download well log data, at the wellsite, to floppy disks or USB flash drives. This allows petrophysicists to conduct detailed digital well log analysis on laptop microcomputers at the wellsite utilizing the software similar to that available in vendor and client offices.

13.8 The Schlumberger Legacy

Many people and organizations have been responsible for the formation evaluation developments highlighted in the preceding section. The overwhelming contributors to these developments, however, have been the Schlumberger brothers and the organization they founded.

With their 1929 A.I.M.E. presentation, the Schlumberger brothers established an industry standard of using technical publications as a means of publicizing their capabilities. Much of the most valuable FE literature is from technical papers published by Schlumberger and their competitors.

Schlumberger developed an outstanding internal training program. The father of Russian and Soviet well logging, V.N. Dakhnov, was trained by Schlumberger in the 1930s. Many logging engineers currently working for competitors were originally trained by Schlumberger. Petroleum companies have eagerly hired Schlumberger-trained logging engineers as formation evaluation specialists.

Schlumberger has established the industry standard for client training. The rationale for this was that an informed client was more apt to purchase logging services than an uninformed one. Most petroleum explorationists and engineers have attended at least one Schlumberger-sponsored school.

Schlumberger's client publications provide excellent formation evaluation references. Most petroleum explorationists and engineers have at least one Schlumberger manual or chart book. Keeping up with modern technology, most of these documents are now available on CD, or as downloadable PDF files from Schlumberger and other vendor websites cited after the reference list.

Schlumberger has established industry standards for tool calibration, quality control, data recording, and

product presentation. The Schlumberger employees' technical pride is hard to match anywhere. Essentially all other wireline vendors have attempted to succeed by *looking like Schlumberger*.

In spite of this legacy, Schlumberger is not always the vendor of choice. Many of the petrophysical milestones, listed in Tables 13.2–13.8, were not introduced by Schlumberger. Whenever a competitor has introduced a new service, which appeared to be economically viable, however, Schlumberger has always been quick to introduce their own version of the service. Often, the new Schlumberger service has included significant technical improvements over the initial service offered by a competitor.

However, all vendors, shown in Tables 13.9 and 13.10, as well as several others, can deliver excellent products. The final criterion for wireline vendor selection is equipment availability, service, and competitive pricing.

All long-term logging service contracts should be written with performance clauses, which can, with cause, be exercised. No logging crew wants to be replaced by a competitor's unit, *in relief*.

13.9 Laboratory Measurements

All of the physical and chemical wireline and/or MWD/LWD measurements have their origin in laboratory measurements. In fact, most log measurements were originally calibrated by laboratory measurements on reservoir fluid samples and rock cores acquired from the wells, in which the logs were run. While modern log measurements and interpretation techniques are much more sophisticated than their ancestral versions, laboratory measurements still play a very important role in defining the petrophysical model parameters used in FE to convert what is measured via well logs into what is desired to evaluate petroleum reservoirs.

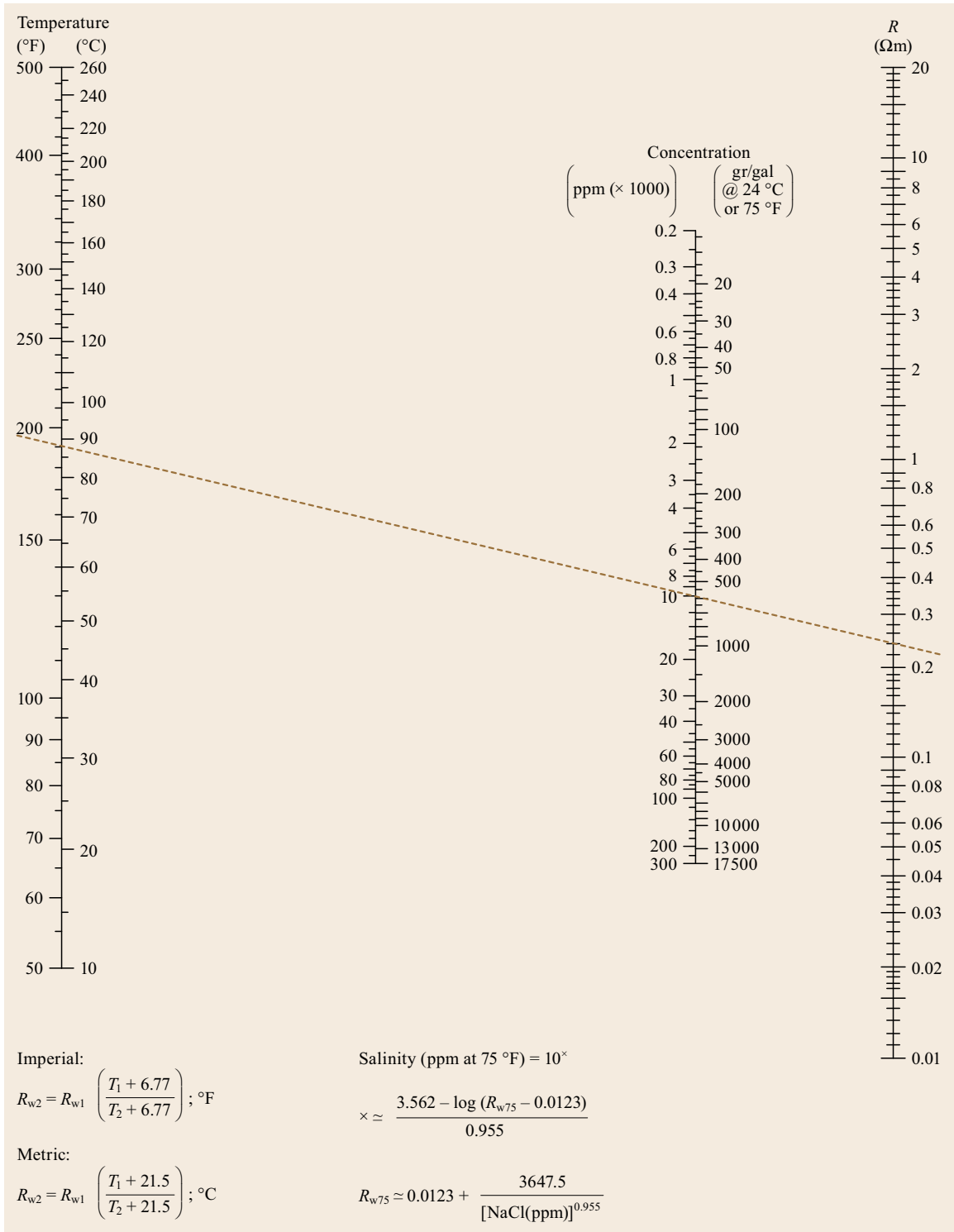
13.9.1 Fluid Measurements

In the simplest terms, petroleum reservoir rocks consist of fluid-filled pores, or *porosity* (ϕ) and solid rock, or *matrix* ($1 - \phi$). The pores, in turn, can be filled with air, hydrocarbon gases, other gases, liquid hydrocarbons, and/or water (*brine*) of various salinities and compositions. In typical FE fashion, we will start with the noneconomic (i. e., nonhydrocarbon) fluids, and then progress to what is desired (hydrocarbons).

Air and other gases, like (gaseous and liquid) hydrocarbons, are electrical insulators. As a result, oil-

and gas-filled porosity will have very high electrical resistivities. Like gaseous hydrocarbons, air and nonhydrocarbon gases will have very low density (i. e., close to zero gm/cc), resulting in very high apparent density porosities and low hydrogen indexes (density of hydrogen ion concentration), resulting in very low apparent neutron log porosities, and slow acoustic velocity, resulting in high apparent sonic porosities. Also, all gases absorb acoustic energy, resulting in sonic log *cycle skipping*. Unlike gaseous hydrocarbons and most other gases, however, air-filled porosity does not occur below the local water table. As a result, except for those areas with very shallow petroleum reservoirs, such as the US Appalachian Mountains and Mid continent, and/or with deep water tables, such as the California San Joaquin Valley, air-filled porosity is not a major concern for FE. Other nonhydrocarbon gases, such as nitrogen and CO₂, however can be a concern.

The chemical and physical properties of oil and gas field brines (waters) are critical to FE. This is because both oil and gas almost always coexist with brines in hydrocarbon reservoirs. Most quantitative volumetric hydrocarbon measures utilize the electrical resistivity contrast between the insulator hydrocarbons and con-



Part B | 13.9

Fig. 13.16 Arps empirical nomograph and equations. The nomograph allows a hands-on solution of the equations, as indicated by the *dotted line* (courtesy of Baker-Atlas)

ducting brines. As a result, laboratory measurements on reservoir brines are very common in FE.

J.J. Arps, of the British-American Oil Producing Co. (now Gulf Oil, Canada) conducted a series of experiments on the effects of salinity and temperature on the electrical resistivity of sodium chloride solutions [13.18]. Figure 13.16 shows empirical relationships and a nomograph for solving them, based on the Arps studies.

The Arps relationships of Fig. 13.16 are extremely useful for FE. Given the water resistivity R_w at one temperature T_1 it is very easy to estimate:

1. The apparent NaCl concentration
2. The water resistivity at any other temperature, T_2 .

The *fly in the ointment* of using the Arps relationships is that Na^+ and Cl^- are not the only ions in petroleum reservoir brines. Other cations and anions can and do behave differently from Na^+ and Cl^- . Several investigators [13.19–24] have investigated the electrical behavior of non-NaCl petroleum reservoir brines. Figure 13.17 is an empirical nomograph for multipliers to estimate *NaCl equivalent concentrations* of petroleum reservoir brines containing more than just Na^+ and Cl^- ions.

The concentration relationships, shown in Fig. 13.17, are very useful for two purposes:

1. They show which ions act much differently than Na^+ and Cl^- and how these effects change with total brine salinity.
2. They allow estimation of *equivalent NaCl salinity* from a chemical analysis of an unknown brine, by using the weighting factors from Fig. 13.17.

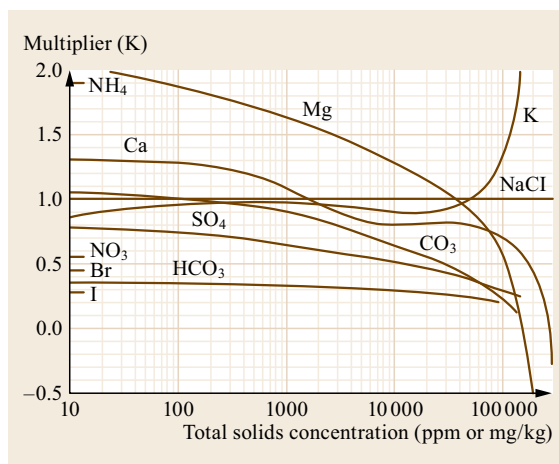


Fig. 13.17 Empirical equivalent NaCl salinity multipliers, for common petroleum reservoir anions and cations [13.25]

Fortunately, the relationships of Fig. 13.17 are not often needed. Most petroleum reservoir brines can usually be considered to be NaCl brines, without introducing significant error. Also, most modern brine chemical analyses usually include R_w measurements, which render the use of the Fig. 13.17 corrections unnecessary.

The density of water at standard temperature and pressure (STP) ranges from 1.00 gm/cc for distilled water to 1.146 gm/cc, for 200 000 ppm NaCl [13.21]. A good approximation for NaCl brine density ρ_w is a linear interpolation, i. e.,

$$\rho_w = 1 + 0.73 \frac{C}{1\,000\,000}, \quad (13.7)$$

where C is (NaCl) concentration, in ppm.

The most common hydrocarbon laboratory measurements are *pressure, volume, temperature* (PVT) measurements and are used to relate hydrocarbon volumes in place to their volumes at surface conditions. PVT measurements are the source of the formation volume factors, B_{oi} and B_{gi} , of (13.1) and (13.2).

The reported density of gaseous hydrocarbons is 0.4 g/cc, or less [13.26]. Oils and condensate densities range from 0.6–1.00 gm/cc [13.26]. Guerard [13.27] reports California heavy crude densities from 0.938 gm/cc (Wilmington Field, 19.4° API) to 0.982 gm/cc (Kern River Field, 12.6° API).

13.9.2 Rock (Core) Measurements

The original laboratory petrophysical measurements were conducted on cores, cut during drilling operations, and used to estimate reservoir properties. The cost of properly acquisition, preservation, transport, storage, and laboratory measurements on cores, compared to the relatively rapid (near real-time) wireline and MWD/LWD measurements have made core measurements less common. However, almost all major petroleum reservoir formation analyses include at least some core measurements.

Core acquisition can be accomplished via:

1. Percussion side wall cores (SWC)
2. Rotary sidewall coring devices
3. Rotary whole cores.

SWC are the simplest to obtain because they can be obtained, after the well has been drilled, using wireline SWC guns. Core material from SWC, however, is most appropriate for visual examination chemical analysis and grain density determinations only. The percussion coring operation shatters and/or compresses the rock fabric, making the resulting cores unsuitable for any physical measurements involving electrical or fluid flow and porosity.

Core material obtained via the other two methods can be used for all rock physical and/or chemical measurements.

Routine Core Analysis Measurements

Essentially all whole core (plugs) and rotary cores cut are subject to routine core analysis or permeability, porosity, and saturation (KPS) measurements:

1. Dean-Stark core (solvent) cleaning, and summation of recovered fluids, for estimation of porosity and *residual* (oil and water) saturations
2. *Ambient condition* helium Boyle's Law, or Archimedes, *effective* porosity ϕ_e measurement
3. *Ambient condition horizontal* (i. e., parallel to bedding) air permeability K_{ha} measurement.

The following are often also done at the same time as KPS measurements:

1. Whole core natural gamma ray, γ -ray, profile scan measurement
2. Whole core slabbing and *normal and ultraviolet light* core photography
3. Core *stratigraphic, mineralogical, and structural* description
4. Grain density ρ_g measurement
5. *Restored net effective overburden* air permeability and helium porosity measurements.

Because these additional services are at additional cost, they are not always done.

Whole core γ -ray scans allow proof positive depth matching between the core and wireline measurements. Core depths can, and often are, as much as 1–2 drill pipe joints different from the wireline measurement depth. Matching the whole core γ -ray scan and wireline γ -ray curves allow exact depth matching of the core and wireline measurements.

Whole core slabbing, photography and descriptions provide much more detailed information than available from either core measurement plugs or wireline measurements. The core photographs will last much longer than even preserved core. If the whole cores are to be slabbed and photographed, best practice is to do so *after* the core measurement plugs have been taken, as this provides a permanent record of the measurement plug locations.

Grain density measurements are the least expensive additional plug or rotary core measurements, as they usually constitute only an additional computation from the measurements made to calculate routine porosities.

Restored net effective overburden (NEO) ϕ and K_a values can be compared to wireline measurement estimates, which are taken at depth. Figure 13.18 shows a NEO transform for a Western Australia field.

Cross plots of core porosities have often been used to calibrate wireline porosity tools. Modern wireline porosity tools, however, are calibrated well enough that they can often be utilized to identify problems in laboratory core measurements, as shown in Fig. 13.19.

Special Core Analysis Laboratory (SCAL) Measurements

Special core analysis laboratory (SCAL) measurements are much more complex and time consuming and

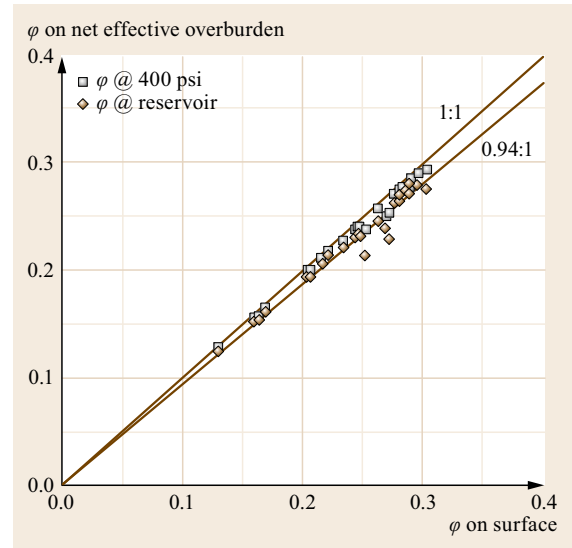


Fig. 13.18 Cross plot of surface versus restored net effective overburden (NEO) porosities and NEO model transform, from Western Australia field

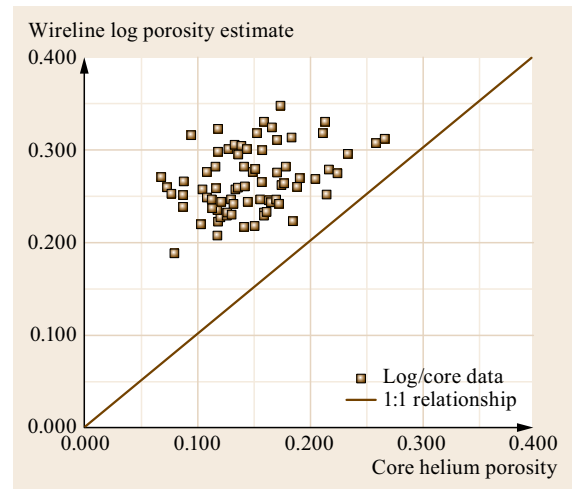


Fig. 13.19 Cross plot of core versus wireline log porosities, from Congo Basin field, illustrating the effects of small, interconnected vugs on core porosity

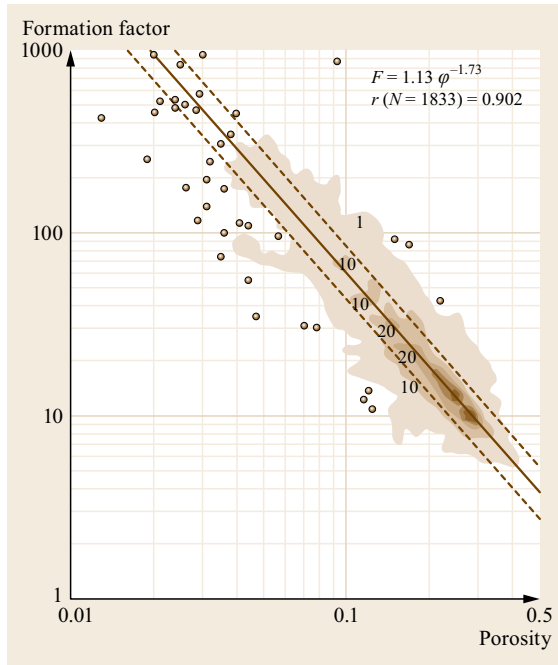


Fig. 13.20 Archie formation factor (1833 sample database) model for clean recent sandstones [13.28]

consequently much more expensive than routine core analysis measurements. As a result, while routine core analysis measurements may be taken every foot, or closer, SCAL measurements are usually conducted on a few locations within a cored interval, with these locations based on the routine measurements.

SCAL measurements include:

1. Single-phase liquid permeability k_l measurements
2. Dual-phase relative permeability k_r measurements
3. Capillary pressure P_c measurements
4. Formation factor F (see (13.4), Archie's first equation) measurements
5. Resistivity index I (see (13.5), Archie's second equation) measurements.

The most significant SCAL measurements for FE are the two responsible for the Archie equations ((13.4) and (13.5)).

In 1940, Gus Archie, a Petrophysicist with Shell Oil published a paper [13.12] based on his studies of the resistivities of water saturated rocks, their measured porosities, and the resistivity of the saturating brines (13.4), which is known as *Archie's first equation*.

Archie's initial values for the (13.1) constants a and m were 1.00 and 2.00 respectively [13.12]. As more and more formation factor measurements were made, it became clear that the a and m coefficients would vary from reservoir to reservoir. Figure 13.20 shows

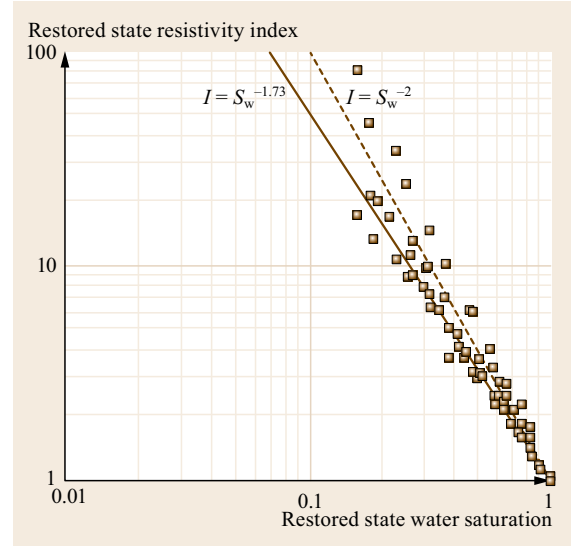


Fig. 13.21 Archie resistivity index for Congo Basin field reservoir

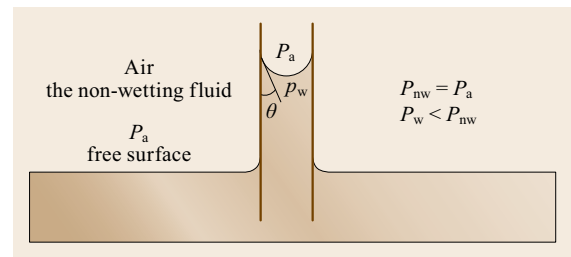


Fig. 13.22 Capillary pressure at atmospheric pressure (P_a) the indices indicate wetting (P_w) and nonwetting (P_{nw}) conditions (after [13.29])

a statistical analysis of 1833 sets of formation factor measurements collected from most of the major multinational and national oil companies, as well as research laboratories, of the time. This analysis returned values of $a = 1.13$ and $m = 1.73$, which are probably good default values for clean (i. e., low shale) recent (unconsolidated) sandstone reservoirs.

Archie also published a second paper [13.13] summarizing his studies of the resistivities of reservoir rocks with partial water saturations, which formed the basis of *Archie's second equation* (13.5).

Archie's initial value for the n coefficient was $n = 2.00$ [13.13]. As was the case for the Archie formation factor model, the n resistivity index coefficient is reservoir specific. Figure 13.21 shows the resistivity index for a Congo Basin reservoir. The reservoir, shown in Fig. 13.21 has at least two distinct reservoir n values: one (1.73) less than 2.00 and a second greater than 2.00. FE, in cases such as these, requires that the reser-

voir interval be first divided into those depth samples that satisfy each resistivity index model, prior to estimating water saturation S_w .

The third SCAL measurement most significant for formation evaluation is *capillary pressure* P_c the differential invasion of the wetting and nonwetting fluids into a pore throat or capillary (Fig. 13.22). Resistivity index measurements are conducted making repeat resistivity measurements on a core initially completely saturated ($S_w = 1.00$) with water, as the water is decreased by introduction of a nonwetting fluid. Since this is the same technique used to measure *capillary pressure*, the two measurements are often combined.

Capillary pressure data is often converted to the following normalized dimensionless quantity

$$J_{sw} = \frac{P_c}{\sigma \cos \theta} \sqrt{\frac{k}{\varphi}}, \quad (13.8)$$

where:

- J_{sw} is called the *Leverett J-function* [13.30]

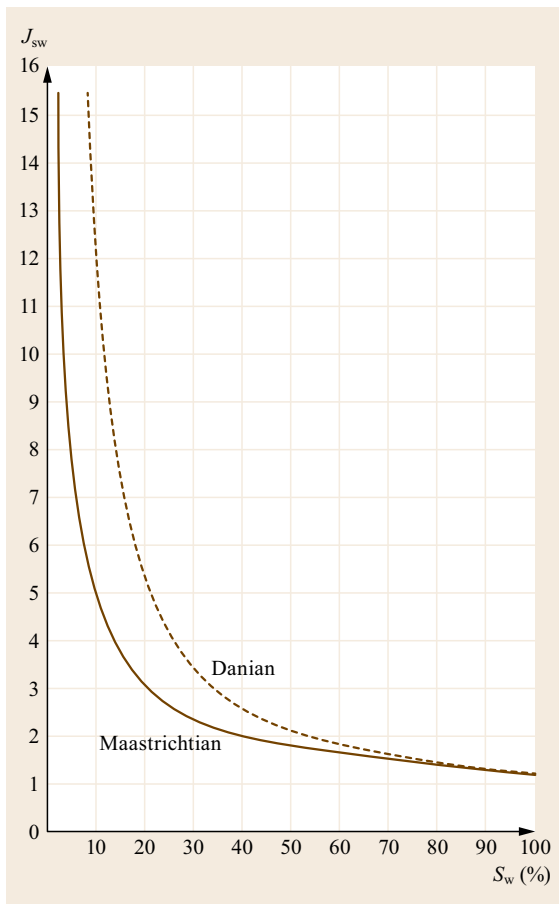


Fig. 13.23 Leverett J-functions for Danish North Sea field reservoirs

- P_c is (measured) capillary pressure
- σ is interfacial tension between the two fluids
- θ is the contact angle of the wetting phase
- k is the permeability of the sample
- φ is the porosity of the sample.

As was the case for the Archie equation a , m , and n coefficients and Leverett J-function models are reservoir specific (Fig. 13.23).

Once a Leverett-J function has been developed for a given reservoir, it can be used to independently verify wireline and MWD/LWD saturation results, as it is based entirely upon core measurements and height above a fluid contact. The Leverett J-function, shown in Fig. 13.24 was developed from capillary pressure measurements on core from a high-porosity, high-permeability Niger Delta field reservoir. Reservoir engineers responsible for developing this field did not believe the very low ($\approx 5\%$) wireline irreducible water saturation S_{wir} estimates obtained for this reservoir. The Leverett J-function for the reservoir (Fig. 13.24) confirmed the low wireline S_{wir} estimates.

Leverett J-function saturations can also be used to independently verify wireline and/or MWD/LWD S_w estimates through a transition zone between reservoir fluid phases. The P_c above a fluid contact is given by

$$P_c = \Delta\rho gh, \quad (13.9)$$

where:

- $\Delta\rho$ is fluid density difference
- g is gravitational acceleration
- h is height above the fluid contact.

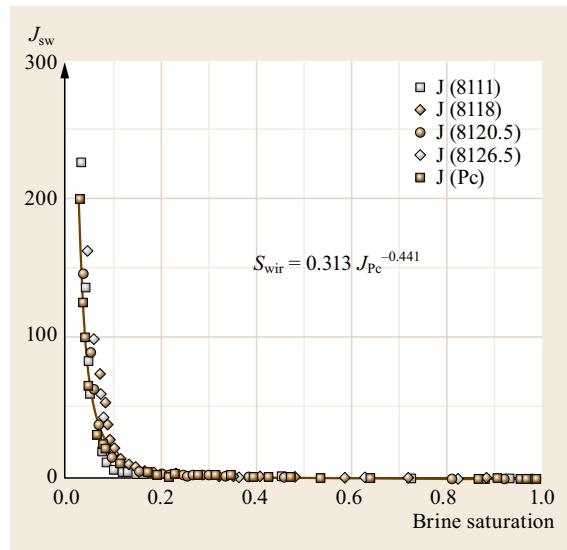


Fig. 13.24 Niger Delta field Leverett J-function illustrating very low S_{wir}

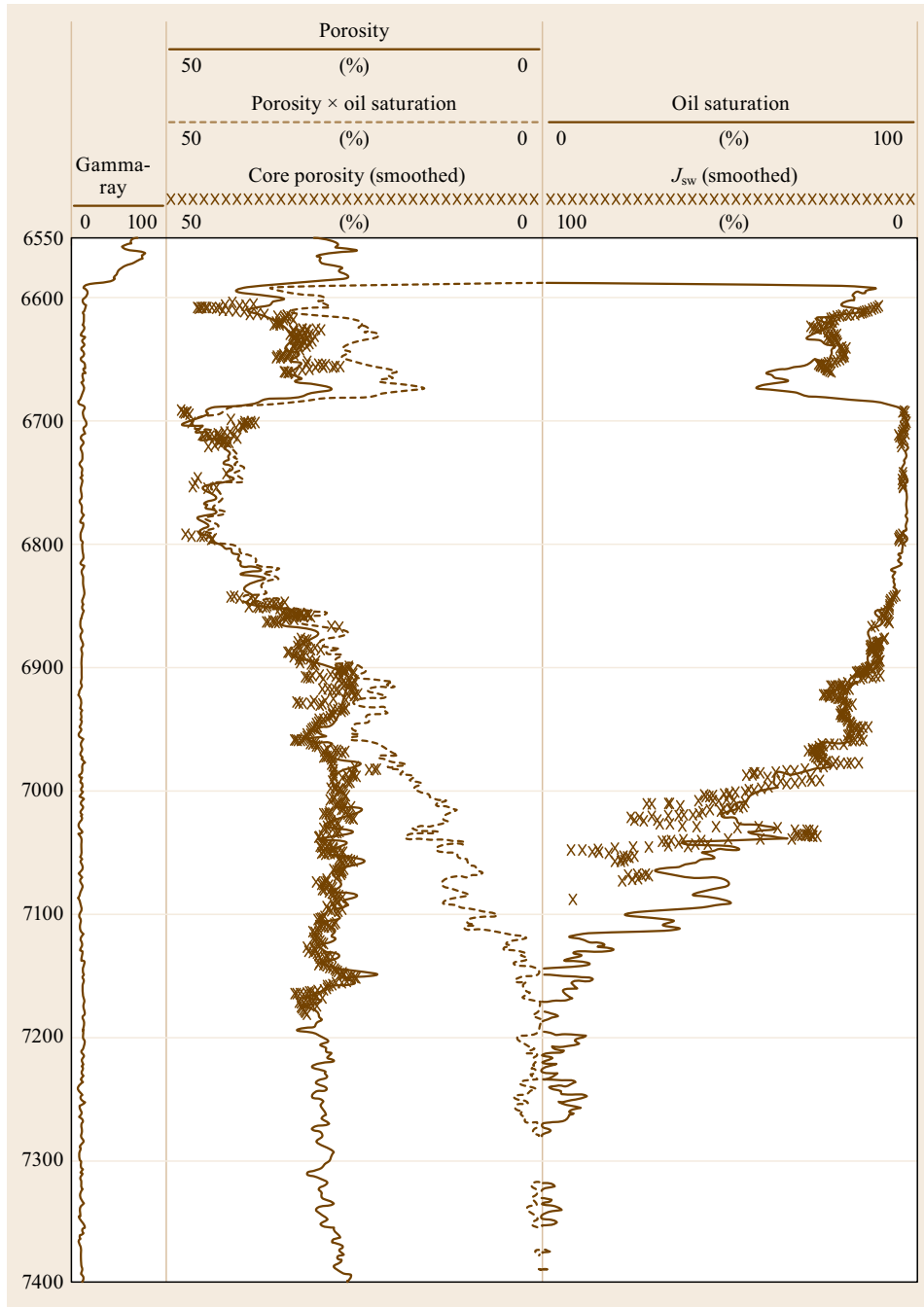


Fig. 13.25 Comparison of Leverett J-function J_{sw} (smoothed) and wireline s_w estimates for a Danish North Sea field well

Figure 13.25 shows a comparison between wireline and Leverett J-function saturation estimates for a Danish North Sea chalk reservoir. Considering that the J-function S_w are based on one-inch core plug measurements, at one foot sampling, while the wireline S_w are based upon 2–3ft average measurements sampled at 0.5 ft intervals, there is very close agreement.

Finally, Leverett J-functions, wireline porosity data, and O/W contact information can also be used in lieu of wireline saturation data, as was recently done for a major review of a world-class heavy oil resource in a third world country [13.31]. In this case, the reason for this approach was unreliable saturation log data.

13.10 Well Logging Environment

13.10.1 Wellsite

Most wireline and MWD/LWD quantitative measurements attempt to duplicate the results of similar laboratory measurements. In the laboratory, the sample measurement environment can be strictly controlled. All of this control changes when the measurements are taken from the laboratory to the wellsite.

The laboratory measurement sample (usually a 1 in \times 1 in core plug), is replaced by the earth and the laboratory sample holder is now the well. The measurement conditions, which can be strictly controlled in the laboratory, are now at whim of the downhole temperature, pressure and brine chemistry. The climate controlled laboratory recording instrument environment is replaced by the weather (dust, rain, mud, wind, snow, etc.) at the surface. In addition, getting the logging equipment to the wellsite can be an adventure in itself.

Figure 13.7 is a schematic of a modern wireline logging operation. The logging tool, or *sonde*, is suspended in the well by a multiconductor double steel armored cable, which passes over sheaves hung from the traveling blocks in the drill rig tower, and under a sheave anchored to the rig floor to the logging (truck or skid) unit. The wireline power and recording equipment are located at the surface. The multichannel double wrapped armored cable provides the means of delivering power to the sonde, serves as the strength member to retrieve the sonde, and the data transmission link from the sonde measurement, A/D sampling, preprocessing system and encoding systems are now on the sonde.

MWD/LWD systems *look* much like the schematic shown in Fig. 13.1, with the following exceptions:

1. The logging instrument package is part of a specialized bit subassembly (Item No. 2 of Fig. 13.1), which also includes a mud turbine that provides power to the measurement instrumentation, A/D sampling, preprocessing system and encoding systems.
2. The drill pipe and drill collars provide not only the weight on the bit, but also the strength to raise and lower the MWD/LWD instrument package.
3. Communication between the MWD/LWD instrument package and the surface is provided by a mud-pulse system in the bit subassembly (EM and drill pipe transmission systems are under development at time of writing, but are not yet fully commercial).
4. Sparse sampled log information is transmitted to the surface, during the drilling operation, via the mud-pulse system. Detailed logging data is recorded on

random access memory (RAM) storage in the logging instrument package and downloaded at the surface during bit change trips.

MWD/LWD data is acquired during the drilling operation. As a result the *sparse sampled* MWD/LWD data can be true *real-time* data preceding even mud log data to the surface, as the latter must wait for the mud to be circulated from the bit to the surface. Invasion and mud-borehole wall reactions should be at a minimum for all MWD/LWD data, as the sensors lag the bit by only a few feet. By contrast wireline data is acquired after the well has reached either total depth (TD), or a casing point, and the well has been circulated (*conditioned*) for the logging operation, which usually takes several hours. Consequently, wireline measurements are acquired a few hours to days after the bit has passed the measurement depths, allowing considerable invasion and mud-borehole reactions to occur. *Detailed* MW/LWD data does not usually reach the surface until the bit is retrieved, but the data acquisition occurs at the same time as the *sparse sampled* data.

Wireline data is normally acquired as the sonde is retrieved from the bottom of the well, so that the cable will be under tension. Exceptions to this protocol are temperature and pressure logs, which should be acquired with minimal disturbance to the mud column and to avoid hysteresis in the measurement sensors. MWD/LWD measurements can be acquired either during drilling or as the bit is retrieved from the borehole. The former protocol is preferred for the reasons given above.

Both wireline and MWD/LWD systems are subject to extreme temperature, pressure, chemical, and vibration conditions during data acquisition. At the surface the wireline and/or *sparse sampled* MWD/LWD data is retrieved via slip rings in the cable reel (wireline) or mud-pulse decoder (MWD/LWD). The *detailed* MWD/LWD data is retrieved from the bit subassembly RAM after they have been retrieved at the surface. The slip-ring or mud-pulse decoder systems may be noisy and/or fail. The RAM system can also fail due to the extreme operational conditions encountered in drilling super deep wells.

The logging crew is operating in a rather hostile environment. They may also be operating on little rest. The logging unit is office, workshop, mess hall, and sometimes even bunkhouse for the engineer and crew. The drillsite is usually remote from any support facilities. The drilling crew is openly suspicious that the logging vendor may *damage their hole*. Downtime while waiting for replacement equipment is simply not

tolerated by the client. That excellent physical measurements can, and usually are, obtained is a testimony to the ingenuity and dedication of the wireline and MWD/LWD tool designers, logging vendor crews, and operations base support shops.

13.10.2 Logging Operations

Table 13.13 summarizes the steps that *should* occur for all wireline and/or MWD/LWD logging operations. All logging tools, both wireline and MWD/LWD, must be calibrated according to vendor *shop calibration* standards at the vendor operations base prior to being delivered to the wellsite. *Shop calibrations* are a normal part of the logging vendor services and must not be negotiated away in return for reduced charges. There is an oft-quoted saying in the industry, attributed to an old time logging engineer: *If it wiggles, I can sell it.*

Poorly calibrated or uncalibrated logs are little more than *wiggly lines* and *are of no value* for quantitative, or even qualitative measurements.

Shop calibrations should be repeated at least monthly. With modern digital downhole circuitry, many logging vendors claim that that *shop calibrations* are good for 90 days. There is a significant problem with this reasoning. Even modern logging tools *do* fail and/or drift out of specifications.

If a logging tool fails to meet shop calibration standards, without significant adjustment, all logs run since the tool's last successful shop calibration are called into question.

For this reason, a good practice is to require successful shop calibration of all tools delivered to a wellsite *immediately* prior to leaving the vendor's operations base. Since logging vendors are continually running shop calibrations, *there should be no surcharge* for this service. Remote offshore and/or helicopter-accessed land drillsites do pose special problems. However, some operators address this situation by requiring the logging vendor to provide shop calibration facilities at these remote drillsites. This service may incur additional cost. However, it should be minor in light of the

Table 13.13 Typical wireline and MWD/LWD logging operations

Well logging operation order
Shop calibrations
Rig-up
Prelog calibrations and check against shop calibration
Logging
Postlog calibration checks
Rig down
Well-site processing and display
Transmission/transfer of log images and digital files to client

overall cost of a well costing several US\$ millions to drill.

Failure of a logging vendor to meet the above conditions should be cause for calling out another vendor, in relief, or cancellation of an extended logging contract. This only needs to happen once to get the attention of the logging vendor's upper management.

Delivery of logging tools with proper *shop calibrations* to the drillsite is only the first step in log quality assurance. The logging vendor must demonstrate that the tools can pass standard *prelog calibration checks*, referenced back to the most recent *shop calibration*, prior to putting them into the well. If the logging tools fail the *prelog calibration check*, they should be replaced by *backup tools*, which can pass the *prelog calibration check*. For this reason the logging vendor should *always* have sufficient *backup tools* at the drillsite to meet this contingency, without significant loss of rig time.

The logging witness must verify that the equipment used for the logging job is the same equipment used for the most recent shop calibration. Otherwise, the resulting logs are uncalibrated.

At the completion of the logging operation the logging vendor *must* perform *postlog calibration checks* to provide proof that the tool did not fail or undergo calibration drift during the logging job. While rare, this type of tool failure can happen. It took considerable persuasion to get the logging engineer to perform the *postlog calibration check* shown in Fig. 13.26. His shock was matched only by his chagrin when he learned that his supposedly stable tool had drifted 61 API units during a 2500 ft logging job.

13.10.3 Well Logs

Log Header

Figure 13.27 shows a typical well log header, which summarizes considerable information about the well and logging job. The logging vendor's logo and the log type (1) are always displayed across the top of the first page of the header. Below this, are: information about the well (2), consisting of operator name, well name, field name, country, state/province, location, and elevation. Information about the logging job, consisting of bit and casing size (3), logged interval (4), mud information (5), well bottom hole temperature and temperature buildup information (6), and who logged and

SGTE	TOOL CHECK			
	BEFORE	AFTER	UNITS	
GR	165	226	GAPI	+ 61 API

Fig. 13.26 Example of 61 API drift, between prelog gamma ray log calibration and postlog calibration check

1		DUAL INDUCTION SONIC GAMMA RAY SCALE 1:200 SUITE 1 1																																																																																																
2 2 2 2	FILE NO. _____ COMPANY _____ WELL _____ FIELD _____ COUNTY _____ STATE _____ Location: N : 9 405 600 M E : 176 980 M 05 22' 13.96" S 12 05' 04" W																																																																																																	
Permanent Depth: <u>MSL</u> ID _____ Log measured from: <u>RKB</u> ab. _____ Drilling measured from: <u>RKB</u>		Elev.: K.B. <u>80 FT</u> D.F. <u>79 FT</u> Q.L. <u>-65 FT</u>																																																																																																
<table border="1" style="width: 100%; border-collapse: collapse;"> <tr> <td>Date</td> <td colspan="3">19 APRIL 1981</td> </tr> <tr> <td>Run No.</td> <td colspan="3">ONE</td> </tr> <tr> <td>Depth - Driller</td> <td colspan="3">2026'</td> </tr> <tr> <td>Depth - Logger</td> <td colspan="3">2024'</td> </tr> <tr> <td>Bottom Logged Interval</td> <td colspan="3">2020'</td> </tr> <tr> <td>Top Logged Interval</td> <td colspan="3">145'</td> </tr> <tr> <td>Casing - Driller</td> <td colspan="3">13 3/8" @ 838'</td> </tr> <tr> <td>Casing - Logger</td> <td colspan="3">837'</td> </tr> <tr> <td>Bit Size</td> <td colspan="3">8 1/2", 12 1/4"</td> </tr> <tr> <td>Type fluid in hole</td> <td colspan="3">SW POLYMER</td> </tr> <tr> <td>Density</td> <td>Viscosity</td> <td colspan="2">ppm</td> </tr> <tr> <td>spH</td> <td>Fluid Loss</td> <td colspan="2">ppm</td> </tr> <tr> <td>Source of Sample</td> <td colspan="3">FLOWLINE</td> </tr> <tr> <td>Pen @ Meas. Temp.</td> <td>0.65 @ 73 ° F</td> <td colspan="2"></td> </tr> <tr> <td>Pen @ Meas. Temp.</td> <td>0.64 @ 73 °</td> <td colspan="2"></td> </tr> <tr> <td>Pen @ Meas. Temp.</td> <td>0.96 @ 73 °</td> <td colspan="2"></td> </tr> <tr> <td>Source: Pen / Pene</td> <td>PRESS / PRESS</td> <td colspan="2"></td> </tr> <tr> <td>Pen @ BHT</td> <td>0.486 @ 100 °</td> <td colspan="2"></td> </tr> <tr> <td rowspan="2">Circulation</td> <td>End Circulation</td> <td colspan="2">03:30</td> </tr> <tr> <td>Logger on bottom</td> <td colspan="2">08:26</td> </tr> <tr> <td>Meas. res. Temp.</td> <td colspan="3">100 °</td> </tr> <tr> <td>Equip. No.</td> <td>Location</td> <td colspan="2">1061-70 MAG</td> </tr> <tr> <td>Recorded by</td> <td colspan="3">P. SPOONER</td> </tr> <tr> <td>Witnessed by</td> <td colspan="3">A. LAOTA</td> </tr> </table>				Date	19 APRIL 1981			Run No.	ONE			Depth - Driller	2026'			Depth - Logger	2024'			Bottom Logged Interval	2020'			Top Logged Interval	145'			Casing - Driller	13 3/8" @ 838'			Casing - Logger	837'			Bit Size	8 1/2", 12 1/4"			Type fluid in hole	SW POLYMER			Density	Viscosity	ppm		spH	Fluid Loss	ppm		Source of Sample	FLOWLINE			Pen @ Meas. Temp.	0.65 @ 73 ° F			Pen @ Meas. Temp.	0.64 @ 73 °			Pen @ Meas. Temp.	0.96 @ 73 °			Source: Pen / Pene	PRESS / PRESS			Pen @ BHT	0.486 @ 100 °			Circulation	End Circulation	03:30		Logger on bottom	08:26		Meas. res. Temp.	100 °			Equip. No.	Location	1061-70 MAG		Recorded by	P. SPOONER			Witnessed by	A. LAOTA		
Date	19 APRIL 1981																																																																																																	
Run No.	ONE																																																																																																	
Depth - Driller	2026'																																																																																																	
Depth - Logger	2024'																																																																																																	
Bottom Logged Interval	2020'																																																																																																	
Top Logged Interval	145'																																																																																																	
Casing - Driller	13 3/8" @ 838'																																																																																																	
Casing - Logger	837'																																																																																																	
Bit Size	8 1/2", 12 1/4"																																																																																																	
Type fluid in hole	SW POLYMER																																																																																																	
Density	Viscosity	ppm																																																																																																
spH	Fluid Loss	ppm																																																																																																
Source of Sample	FLOWLINE																																																																																																	
Pen @ Meas. Temp.	0.65 @ 73 ° F																																																																																																	
Pen @ Meas. Temp.	0.64 @ 73 °																																																																																																	
Pen @ Meas. Temp.	0.96 @ 73 °																																																																																																	
Source: Pen / Pene	PRESS / PRESS																																																																																																	
Pen @ BHT	0.486 @ 100 °																																																																																																	
Circulation	End Circulation	03:30																																																																																																
	Logger on bottom	08:26																																																																																																
Meas. res. Temp.	100 °																																																																																																	
Equip. No.	Location	1061-70 MAG																																																																																																
Recorded by	P. SPOONER																																																																																																	
Witnessed by	A. LAOTA																																																																																																	

Fold Here

Fold Here

Changes in Mud Type or Additional Samples		Scale Changes			
Date	Sample No.	Type Log	Depth	Scale Up Hole	Scale Down Hole
Depth - Driller					
Type fluid in hole					
Density	Visc.				
spH	Fluid Loss				
Source of Sample					
Pen @ Meas. Temp.		Tool Type	Serial No.	Tool Position	Other
Pen @ Meas. Temp.		OIL-BA	84088	1 1/2" STAND-OFF	
Pen @ Meas. Temp.		SCB-FA	18075	1 1/2" STAND-OFF	
Source: Pen / Pene		SLD-SB	8061	ECCENTRICATED	
Pen @ BHT		CNT-HA	80073	ECCENTRICATED	
Pen @ BHT		UMR-HA	33246	ECCENTRICATED	
Pen @ BHT					
Remarks: MPT'S WERE 100, 100 AND 100 DEGREES F. Pen = 0.96 @ 96 DEG AND 0.94 @ 91 DEG F. LOG WAS CIRCULATED FROM 1796 FT TO TD. LAST CIRCULATION WAS FOR 15 MINUTES. SONIC THRESHOLD IS DIFFERENT ON REPEAT AND MAIN LOG TO TRY AND AVOID SKIPPING. SONO, SP AND BP WERE AT 1100FT AS 2 PASSES WERE MADE DUE TO SONIC SKIPPING. SKIPPING IS STILL PRESENT DUE TO VERY LOW AMPLITUDE SIGNAL. DT READING 82 US IN CASING AFTER LOG DUE TO THRESHOLD AND BIAS ADJUSTMENTS.					
HALLIBURTON LOGGING SERVICES, INC. (HLS) does not guarantee the accuracy of any interpretation of log data, conversion of log data to physical rock parameters, or recommendations which may be given by HLS personnel or which may appear on the log or in any other form. Any user of such data, interpretations, conversions, or recommendations agrees that HLS is not responsible, except where due to gross negligence or willful misconduct, for any loss, damages, or expenses resulting thereof.					

2

8

Part B | 13.10

Fig. 13.27 Modern well log header (courtesy of Halliburton)

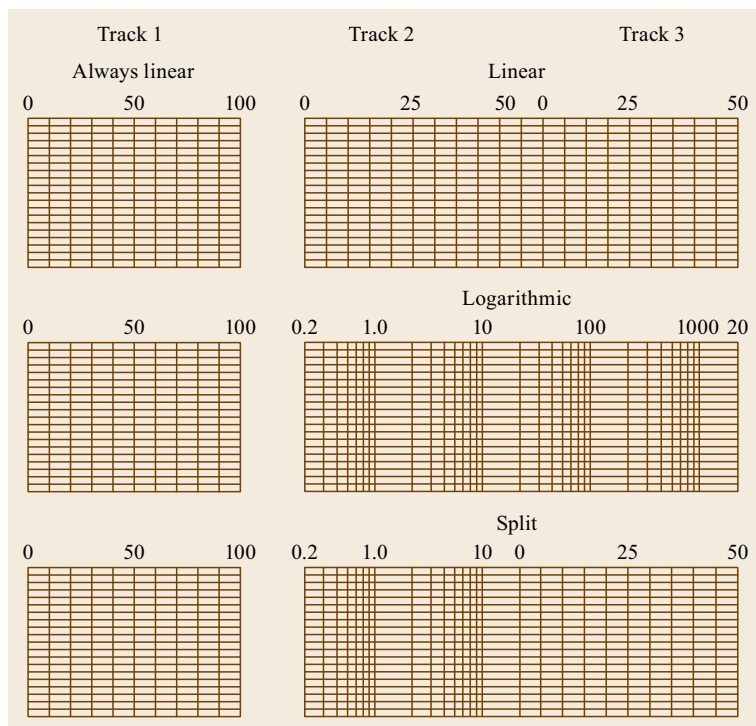


Fig. 13.28 Well log scales [13.26]

witnessed the logging job (7) are displayed on the lower half of the first page, and sometimes on the second page. Equipment data (8) and engineer's comments about the logging job (9) are located on succeeding pages of the header. Tool calibration records are also displayed below the header on detailed (1 : 200 or 5 in = 100 ft depth scale) log print headers and below the log. All detailed log prints should also contain a 200–300 ft *repeat section*, which documents the fact that the measurements can be repeated. This display standard was established by the American Petroleum Institute (API) over seventy years ago and survives to this day.

The *logging witness* is an extremely important part of the log documentation. Whoever signed the logging vendor's work order certifies that:

- The vendor's equipment was working properly.
- All logging sondes were properly calibrated.
- The shop calibrations were for the tools actually used for the job.
- The logging job was performed to the client's specifications.

From the client's standpoint, the *logging witness* is the most important person in the logging operation.

Logging witness *should not be an assignment for the most junior member of the office, or anyone else with little knowledge of proper logging protocol and calibration standards.*

Measurement Tracks

The API well log standard log display consists of three measurement tracks with a *depth track* between tracks one and two, as shown in Fig. 13.28. Linear scaled tracks usually have ten divisions per track and logarithmic scaled tracks usually have two or four logarithmic cycles per track (note that each cycle starts at deciles of two). Tracks 2 and 3 are often combined to give an expanded presentation (sometimes called *track 4*). This standard is followed even for complex tool stacks consisting of several measurements, resulting in multiple displays for all measurements taken at the same time. Wellsite and off-well computer analysis displays may have more log tracks than the API standard and the depth track may be moved to the left of track 1 or included on one of the display tracks.

Tool Stacks, Trips, Runs, and Suites

Wireline logs are run at well TD and at other intermediate depths where casing is set to protect the well bore. Detailed MWD/LWD are commonly organized along the same depth intervals. Depending upon the sophistication of the wireline vendor, not all log measurements may be made at the same time. Not all log measurements are conducted at each logging depth. All of these situations have resulted in some confusing nomenclature. Most large companies should have their own internal notations. The following nomenclature,

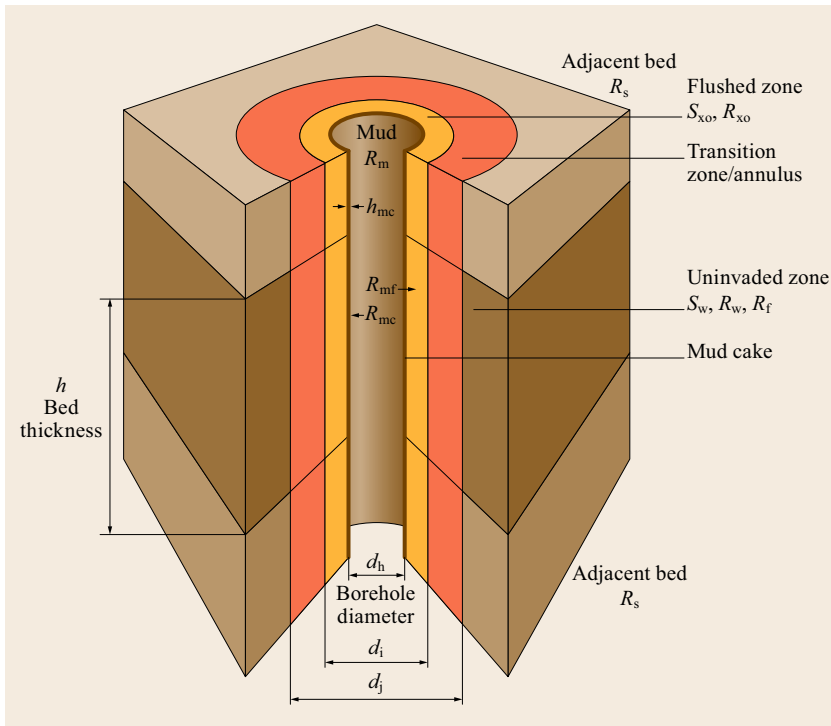


Fig. 13.29 Borehole model (courtesy of Baker-Atlas)

developed by Chevron, can serve as a good example:

- Tool stack: A combination of sondes capable of multiple types of measurements (e.g., density, neutron, gamma ray, and caliper all on a single combination tool stack)
- Trip: A single (tool stack) set of measurements (e.g., induction/sonic, on one trip, density/neutron on a second trip, borehole imager on a third trip)
- Run: Number of logging depths at which a single tool stack is run
- Suite: All logs run at a given depth.

Calibration Records and Logging Program Data

Detail (5 in = 100 ft, or 1 : 200 depth scale) log displays will have calibration records. Modern computer-driven log displays and Library ASCII Standard (LAS) files will also have several pages of information about the computer program input parameters and changes during the logging job and subsequent analysis. Three types of calibrations are documented on the detailed log displays:

1. Master, or shop calibrations
2. Prelog calibration checks
3. Postlog calibration checks.

It is critical that all three of these calibration records be attached to the detail log images and that the equipment serial numbers be the same. Calibration is the *only* time that anyone knows, for certain, that the tools are actually working properly.

13.10.4 Borehole Model

Figure 13.29 shows a generalized borehole model used for interpretation of wells drilled normal (*straight* or *vertical holes*) to formation bedding (satisfactory similar models for highly deviated and *horizontal wells* have yet to be developed) annotated with common FE notation.

Borehole Diameter

Bit and casing programs used for any given well will vary considerably. The actual bit and casing program used will depend drilling target depths, formation pressures, prior knowledge of the area, drilling costs, rate of penetration, borehole conditions, safety, and operational or casing and cement efficiency.

Each casing string represents a considerable investment. Because of this, well programs have bit and casing programs minimizing intermediate casing strings, consistent with safety and drilling target depth.

Bit and casing programs are extremely important to FE. The largest wireline sondes have 5.25 in diam-

eters and should not be run in boreholes drilled with ≤ 6.25 in bits, unless the rock is extremely competent.

Quantitative FE requires physical and chemical property measurements of the borehole rock. Logging tool measurements respond not only to the rock properties but also to the properties of the drilling fluid (*mud*) in the borehole, and *mudcake* lining the inside of the borehole, or casing and cement encasing the casing, for cased holes. The effects of the mud and mudcake or casing and cement between the sonde and borehole wall must be removed before quantitative FE parameters can be estimated.

Most wireline tools are calibrated for 8.5 in diameter boreholes, filled with freshwater (≈ 8.5 lb/gal) mud. MWD/LWD tools are calibrated for borehole sizes consistent with the bit size used with the individual MWD/LWD tools. If either type of tool is used in boreholes with conditions other than the design conditions, the measured results must be *corrected* to the design conditions. These corrections are called *environmental* or *borehole corrections*. Even borehole corrected log data is not very reliable for boreholes much larger than 6–12 in greater than the tool diameter.

Borehole Fluids

The primary purposes of drilling fluids are to:

1. Cool the drill bit
2. Lubricate the moving parts of a drill bit
3. Remove cuttings from the cutting face of the drill bit
4. Suspend the drill cuttings in the drilling fluid
5. Return the drill cuttings to the surface
6. Prevent well blowouts
7. Protect the borehole
8. Protect potential reservoirs.

Drilling engineers have a variety of drilling fluids and additives that help accomplish these goals. Many of these drilling fluid types and additives can effect log measurements and interpretation results. These drilling fluid effects must be accommodated for quantitative FE.

The final choice of drilling fluid types used is usually based upon drilling costs, drilling efficiency and anticipated drilling hazards.

Slightly *overbalanced* (i. e., pressure at a permeable bed slightly greater than the formation pressure) is often considered to be optimum, as this condition usually results in high rates of penetration (ROP), reduced formation damage, and boreholes closer to gage than those with highly overbalanced mud systems. Underbalanced muds risk blowouts. Dispersive mud additives (e.g., lignosulfonate) should not be used if expansive clays (e.g., montmorillonite) are prevalent in the formations to be

drilled. Tool sticking and borehole collapse is likely to occur in these situations. If swelling clays are expected, KCl-based and/or oil-based muds are preferred. Each of these mud types, however, must be accommodated during FE.

Heavy mud (e.g., mud weight greater than 16 lb/gal) used to contain deep high-pressure formations may result in severely overbalanced conditions at shallow permeable formations causing differential sticking of logging tools and drill pipe. Heavily overbalanced muds also risk driving mud additive chemicals deep into formations and causing unwanted reactions.

Mudcake

Mud weight additives are used in petroleum well drilling fluids to ensure that the pressure in the borehole, opposite permeable formations, is greater than that of the formation pressure. Fluid loss additives in the drilling fluid build up opposite permeable formations to stop the loss of drilling fluid into these formations, and also to protect the integrity of the borehole. The resulting solids buildup is called *mudcake*. Mudcake reduces the borehole diameter and displaces pad-type logging tools from the borehole wall. The resulting pad-type log data must be corrected for the effects of the mudcake. Mudcake buildup is usually greater for wireline tools than for MWD/LWD tools because the latter pass the formation to be logged within minutes of the drill bit and the mudcake does not have much time to form.

Flushed Zone

During the process of mudcake formation, drilling *mud filtrate* (liquor) is forced into the formation, flushing out most of the formation fluids. The resulting roughly cylindrical shell about the borehole is called the *flushed zone*. This mud filtrate invasion will alter logging tool responses. These invasion effects must be corrected before any quantitative FE is attempted.

Invaded Zone

Beyond the flushed zone is another roughly cylindrical shell of partially invaded formation, called the *invaded zone*. The flushed and invaded zone diameters, commonly called *invasion diameters* d_i will depend upon the mud/formation differential pressure, drilling and formation fluid viscosities and formation permeability.

Uninvaded Zone

The outermost portion of the Fig. 13.29 borehole model is called the *uninvaded zone*. It is the portion of the formation beyond any mud filtrate invasion. Usually only the deepest reading (induction or laterolog) resistivity

logs actually receive a significant response from beyond the invaded zone. The use of multiple resistivity tools with different investigation depths (the latest incarnations are the array induction and laterolog array tools) allow inversion of the measured values to a cylindrical shell resistivity model, defining the flushed, invaded, and uninvaded zones, which allows an estimate of true formation resistivity R_t .

13.10.5 Subsurface Temperatures

Geothermal Models

Knowledge of formation temperatures is very useful for FE and reservoir engineering. Electrical resistivities are highly temperature dependent. Temperature also figures heavily in reserve determination. Borehole temperatures are measured with temperature-sensitive devices attached to logging sondes. These can be maximum recording thermometers (MRTs) or continuously recording devices. Borehole temperatures, however, are generally *not* the same as the formation temperature at the same depth.

As a rule, subsurface temperatures increase with depth. Typical regional petroleum province geothermal gradients range from 1.0 to 3.0 °C/100 m (0.55 to 1.92 °F/100 ft). Detailed subsurface temperature gradients, however, are seldom linear. Rocks with low thermal transmissibility, such as dense impermeable rocks, have high geothermal gradients. Rocks with high thermal transmissibility, such as porous and permeable sands, have low geothermal gradients.

13.11 Well Logging Tools

The applications of well logging tools have greatly expanded, from the simple resistivity profiling used for the Pechelbronn well, to multiple specialized tools and tool stacks for measuring subsurface geology and physical properties.

13.11.1 Porosity Tools

What Are Porosity Tools?

In the simplest terms, a reservoir rock may be considered to be made up of two components:

- A solid (*matrix*)
- Void space (*porosity*).

Knowledge of porosity is extremely important for FE because without porosity, there would be no place to put liquid or gaseous hydrocarbons. Archie's equations

Fault zones often form permeable pathways, allowing deep, high-temperature fluids to circulate closer to the surface. A well encountering such a fault will exhibit shallow temperature highs and gradient reversals.

Heavy annual rainfall with outcropping permeable formations often result in deep flushing of reservoir rocks. Wells encountering such reservoirs may show low temperature excursions from the otherwise smooth geothermal gradient profiles.

Thermal Disturbances Due to Drilling

The act of drilling a well disturbs the local geothermal gradient. Abrasion at the bit face heats the rocks, while circulating drilling fluids cool the rocks at the bit face. The temperature of drilling mud pumped down the drill pipe is generally cooler than the mud returns coming back out of the well.

Temperature disturbances due to drilling can be predicted using a simple thermal model. This physical heat transfer problem was initially solved by the English Geophysicist, E.C. Bullard. Undisturbed temperatures can be estimated using semilogarithmic extrapolations of measured temperatures based on functions of the circulation and buildup times.

In 1951, D.R. Horner, a reservoir engineer with Shell Development, correctly recognized that the mathematical physics of transient pressure tests were the same as that of Bullard's drilling temperature disturbance problem. As a result, the petroleum industry usually refers to Bullard temperature buildup extrapolations as *Horner Plots*.

((13.1) and (13.2)) required knowledge of porosity to be able to estimate reserves. *Porosity tools* are borehole measurements that respond primarily to the porosity (void space) in the rock. Four established borehole measurements, *resistivity (conductivity)*, *density*, *acoustic (sonic) transit time*, and *hydrogen index (neutron porosity)*, as well as an emerging measurement, *nuclear magnetic resonance (NMR)*, all respond strongly to formation porosity.

Resistivity (Conductivity) Logs

Resistivity and induction (conductivity) logs are commonly known as *saturation logs* because formation resistivity (conductivity) is dependent upon both porosity and saturation. *Archie's equations* ((13.4) and (13.5)) relate formation resistivity to porosity and water saturation S_w . In the absence of hydrocarbons, $S_w = 1.00$, and Archie's first equation (13.4) can be solved for poros-

ity if the water resistivity R_w and Archie coefficients a and m are known. In these cases, Archie's first equation can be used to evaluate the reservoir qualities of water sands when only resistivity or induction logs are available. Resistivity (conductivity) logs were the first porosity tools available, when other porosity tools were yet to be developed.

Acoustic (Sonic) Logs

Measurement of Acoustic Interval Transit Time. An acoustic impulse will travel through a material at the speed of sound, characteristic of that material. The interval transit time Δt is the inverse of the acoustic velocity. Knowledge of Δt is useful, not only for estimating formation porosity, but also for estimation of seismic velocities for inversion of seismic data.

Acoustic (Sonic) Logging (Sonde) Tool. Figure 13.30 is a schematic drawing of a generalized borehole compensated (BHC) wireline acoustic logging tool. The measurement principle is analogous to a reversed seismic refraction profile. Two acoustic receivers, located beyond the critical refraction distance from an acoustic source, record the arrival time of an acoustic impulse, which has been refracted along the borehole wall.

To compensate for the effects of borehole diameter irregularities (rugosity) and sonde inclination, the process is reversed and the two arrival times averaged. The interval transit time Δt is this average divided by the dual receiver separation distance.

Different wireline and MWD/LWD vendors offer slight variations of the measurement concept shown in Fig. 13.30. Modern digital equipment allows specialized sources rich in compressive (longitudinal, or P) and/or flexural (shear or S) wave motion, as well as receiver arrays with automatic semblance picking logic to identify rock P and S wave inverse velocities. In all cases, however, the basic measurement concept is seismic refraction, as shown in Fig. 13.30.

Acoustic (Sonic) Porosity. Jesse Wyllie and associates at Gulf Research and Development Co. [13.14], Louis Raymer and associates at Schlumberger [13.32], and Jean Raiga-Clemenceau and associates at TOTAL [13.33] all developed empirical porosity/acoustic transit time relationships for sedimentary rocks. None of these relationships have any physical basis but do appear to fit observed data (some better than others).

Acoustic logs do not seem to be as severely affected by borehole washouts as some of the other porosity tools. For this reason, they are often preferred in rugose borehole situations. Acoustic logs are, however, affected by clay minerals and gaseous hydrocarbons and must be corrected for these effects.

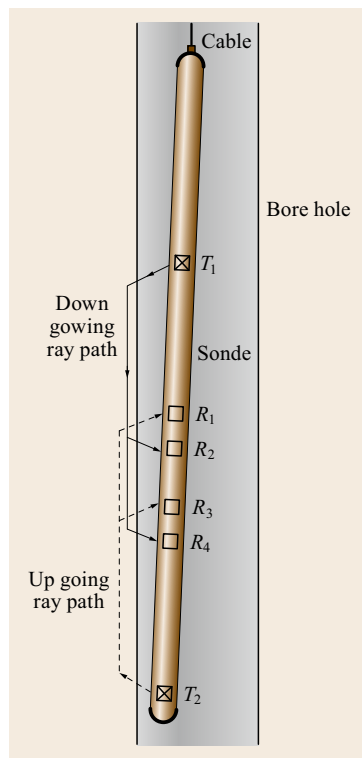


Fig. 13.30 Compensated acoustic sonde with transmitters (T) and receivers (R)

Density Logs

Borehole Measurement of Bulk Density. High-energy (1.17–662 KeV) γ -rays collide with electrons within the rock losing part of their energy to the electrons. The incident γ -ray does not disappear, but changes directions and does lose energy. This process is called *Compton scattering* and is the physical principle upon which γ - γ density logging is based. Eventually, after several collisions, the scattered γ -ray loses enough energy that it drops below the Compton scattering energy window. Lower density rocks will yield higher Compton energy window γ -ray count rates (*fluxes*) at the density sonde γ -ray detectors, than higher density rocks. This decrease in γ -ray flux is proportional to the *electron density* of the material through which the γ -rays pass. For most sedimentary rocks the *electron density* is proportional to the *bulk density*. *Compton scattering γ -ray flux* occurs for both rock solids (*matrix*) materials and (water and hydrocarbon) liquids, but much less so in gases.

γ - γ Density Logging (Sonde) Tool. The density logging sonde is a borehole wall contact tool. Figure 13.31 shows the progression of density log sondes over time.

Because γ -ray energies are attenuated with collisions with any electron, it is essential that the source and

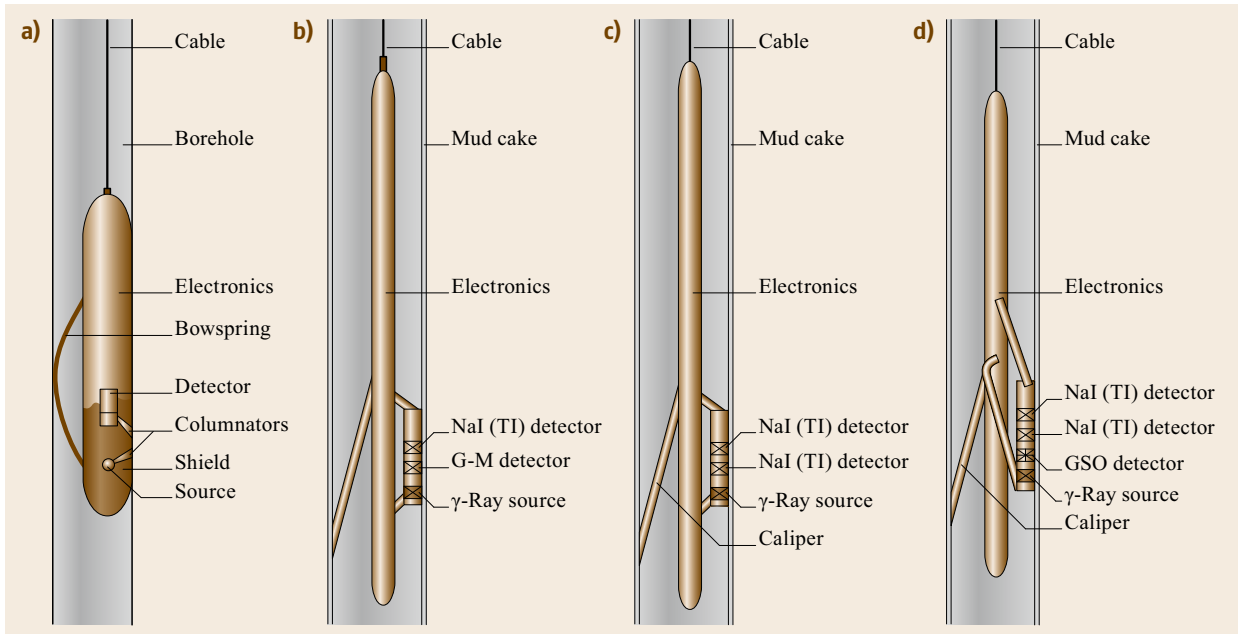


Fig. 13.31a–d Density sonde progression: (a) Original (single detector) sonde. (b) Compensated (dual detector) sonde. (c) Spectral (Compton scattering and photoelectric effect) sonde. (d) Three detector spectral sonde

detector(s) are placed in close contact with the borehole wall.

First-generation density log sondes (Fig. 13.31a) utilized a chemical γ -ray source and a single detector, encased in shielding material with columnating windows to the exterior of the source. The entire assembly was pressed against the borehole wall via a bowspring on the back of the tool. The tool actually measured the Compton scattering energy window γ -ray flux at a fixed distance from the source. Borehole wall density was estimated via calibration graticules, using mud weight and mudcake thickness from bit size and caliper measurements. Results of this sonde design were extremely susceptible to borehole rugosity and variations in mudcake thickness. These shortcomings almost doomed the technology before it even got started.

Addition of a second detector (Fig. 13.31b), however, made the density tool so reliable that it became the primary porosity tool, second only to the density-neutron combination. The dual detector compensated density log sonde mudcake correction was achieved by cross plotting the near and far detector fluxes, based upon empirically developed analogue borehole models (Fig. 13.32).

Modern density log sondes (Fig. 13.31c) record not only Compton scattering γ -rays, but also those within a lower, *photoelectric effect factor* (PEF), energy window. This latter measurement is useful for lithology identification, because *photoelectric effect* energy win-

dow γ -ray attenuation is nearly independent of porosity. Mudcake corrections for these sondes are based upon multivariable inversions of the Compton scattering and PEF window fluxes at the two detector distances. Unfortunately, *PEF* energy window γ -rays are highly attenuated by barite-weighted muds.

The most recent density log sondes (Fig. 13.31d) utilize a third spectral γ -ray detector adjacent to the γ -ray source. Information from the third detector helps stabilize the effects of barite-weighted mud and extend the utility of PEF measurements.

Compton energy window γ -ray attenuation is proportional to electron density, which for most sedimentary rocks, saturated with either water or oil, is roughly proportional to bulk density. PEF γ -ray energy window attenuation is less susceptible to porosity variations and thus more sensitive to variations in matrix types.

Different wireline and MWD/LWD vendors offer slight variations of the Fig. 13.31 sonde designs. Current MWD/LWD density tools use source-detector sets on four quadrants of the MWD/LWD subassembly to ensure that at least one of them is in wall contact as the drill string is rotated. In all cases, however, the basic measurement concept is based upon γ -ray attenuation physics.

Density Porosity. Unlike the sonic log, there is a theoretical basis for density log porosity estimates: mass balance. For a simple reservoir rock, consisting of

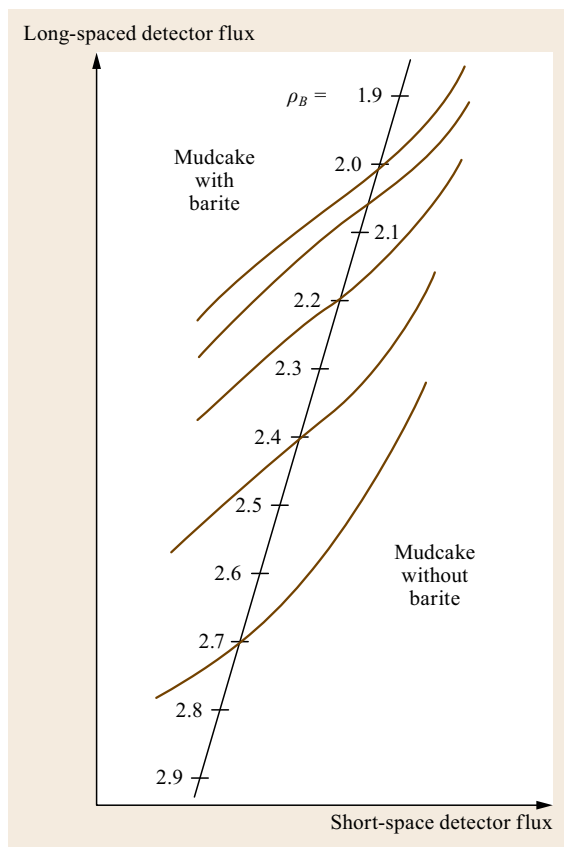


Fig. 13.32 Generalized rib and spine mudcake correction

a solid (matrix) of average density ρ_{ma} and porosity φ filled with a fluid of average density ρ_f , the bulk density ρ_B , is given by

$$\rho_B = \varphi \rho_f + (1 - \varphi) \rho_{ma} \quad (13.10)$$

which can be solved for φ as

$$\varphi_D = \frac{\rho_B - \rho_f}{\rho_{ma} - \rho_f} \quad (13.11)$$

Density logs are severely affected by borehole washouts, mudcake buildup, barite-weighted muds, clay minerals, and gas. Density log measurements must be corrected for these effects before (13.11) can be used for quantitative φ_D estimates. Severe borehole washouts may render density log data unusable.

Neutron Porosity Logs

Neutron logs were the first logging tool developed primarily to measure formation porosity.

Measurement of Hydrogen Index. When fast ($> 1.0 \text{ MeV}$) neutrons collide with nuclei within a rock

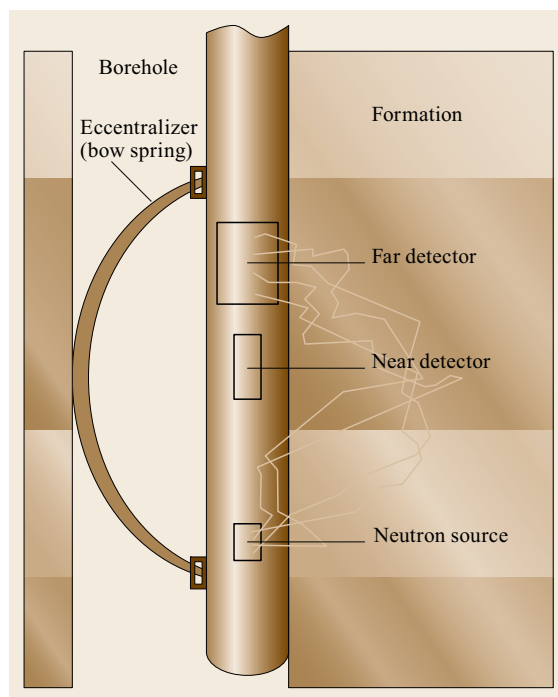


Fig. 13.33 Generalized compensated neutron sonde (after [13.34])

they are scattered (change trajectory direction) and lose part of their energy to the target nucleus. The amount of the energy loss is related to the relative masses of the neutron and the target nucleus. The greatest (i. e., near total) energy loss occurs when the mass of the target is close to that of the incident neutron (i. e., the hydrogen nucleus).

Within a few microseconds of introduction to a rock, fast neutrons are moderated (i. e., lose energy) to thermal ($< 0.1 \text{ eV}$) energy levels and the resulting moderated neutrons drift randomly until they are captured by chlorine, bromine, silicon, or hydrogen atoms. The capturing nucleus then becomes excited and emits a high-energy γ -ray of capture, whose energy is diagnostic of the capturing nucleus.

The hydrogen density of a material (often called the hydrogen index) can be estimated by counting either the thermal neutron or capture γ -ray flux at some distance from the fast neutron source. Both of these techniques have been used in neutron porosity tools.

Neutron Porosity (Sonde) Tool. Figure 13.33 is a schematic rendering of neutron porosity tool measurement principles [13.34]. The measurement principle is analogous to that of the density tool. A source of fast neutrons is introduced into the borehole wall, where they are scattered and the resulting moderated thermal

neutron and/or capture γ -ray flux is monitored at some distance from the neutron source.

The earliest neutron porosity tools (generically called GNT) used only a single detector, which measured the γ -ray of capture flux at a fixed distance from the source. This measurement was converted to apparent formation porosity via calibration gratitudes, which also utilized mud and borehole diameter information. The GNT results were extremely sensitive to borehole size, and usually had to be calibrated by core measurements on a field-by-field basis; a process which could be extremely time consuming, as each different sonde had to be calibrated for every borehole diameter in which it was run. *Swulius* [13.35] described the massive effort involved in calibrating over 70 GNT-type tools for the Kelly Snyder Field, West Texas, SACROC Unit Reservoir Description Project, which resulted in over 600 different core calibration neutron porosity transforms.

Modern Compensated Neutron Logs (CNL or CNT) utilize dual detectors and are much less sensitive to borehole variations. CNL porosity is empirically referenced to thermal neutron flux (detector count) ratios of prototype tools recorded in the American Petroleum Institute (API) limestone calibration pits, located on the University of Houston campus [13.36]. Each vendor has its own sandstone and dolomite calibration curves based on tests in their own calibration pits as shown in Fig. 13.34. *Ellis* [13.37] and *Ellis and Singer* [13.26] advocated a more basic calibration standard, based upon *slowing down length* for epithermal (0.1–100 eV) neutrons, and *moderation length* for thermal neutrons. While this approach has merit, the lithology-based calibrations appear to be too deeply entrenched in the industry for this change to happen.

Different wireline and MWD/LWD vendors offer slight variations of the measurement concept shown in Fig. 13.33. Current MWD/LWD neutron logs use source-detector sets on four quadrants of the MWD/LWD subassembly (i. e., similar to density subassemblies), to ensure that at least one of them is in wall contact as the drill string is rotated. In all cases, however, the basic measurement concept is the neutron attenuation physics, as shown in Fig. 13.33.

Neutron Porosity. Neutron porosity φ_N is based on the bulk *hydrogen index* (HI) HI_B (a fictitious parameter introduced by Schlumberger, specifically for neutron log interpretation), which is the ratio of hydrogen ions present in a rock to the number of hydrogen ions present in an equal volume of water. The bulk *hydrogen index* HI_B , for a simple reservoir rock, consisting of a solid (matrix) of average HI_{ma} , and porosity φ filled with

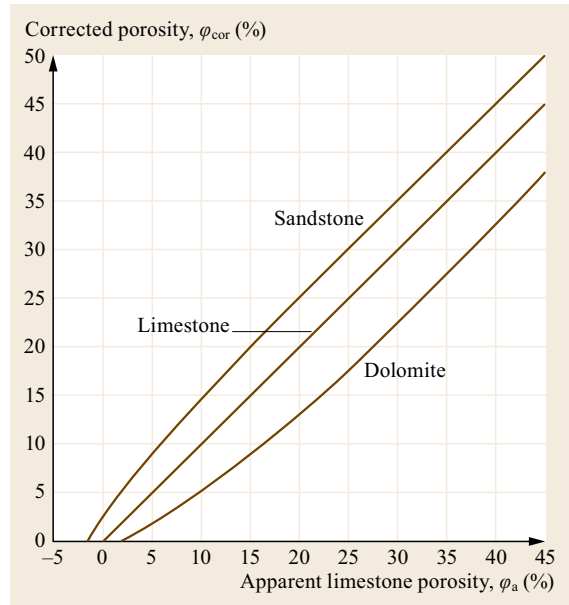


Fig. 13.34 Compensated neutron tool lithology based porosities (courtesy of Baker Atlas)

a fluid of average hydrogen index HI_f is given by

$$HI_B = \varphi HI_f + (1 - \varphi) HI_{ma} , \quad (13.12)$$

which is similar in form to (13.10), for bulk density. Because of the definition of HI, its value for water is $HI_w = 1.00$. The HI for most oils is usually assumed to be $HI_o \approx 1.00$. For most reservoir rocks, the average $HI_{ma} \approx 0.00$. With these assumptions and the HI definition, (13.12) can be simplified to

$$\varphi \approx HI_B . \quad (13.13)$$

The neutron empirical calibration standard is the API limestone test pits in Houston [13.36]. For this reason, neutron logs are often presented as limestone porosity, even if the dominant lithology penetrated by a well is not limestone. In these cases, transforms based on models such as that shown in Fig. 13.34 are used to convert the measured φ_{Nls} , to the appropriate lithology porosity. Cross-plot porosities and lithology analyses, such as that shown in Fig. 13.35, are all based on neutron data in limestone units.

Neutron logs are severely affected by borehole washouts, mudcake buildup, chlorine, boron, clay minerals, and gas. Neutron log measurements must be corrected for these effects before (13.13) or cross plots can be used for quantitative φ_D estimates. Severe borehole washouts may make neutron porosities unusable.

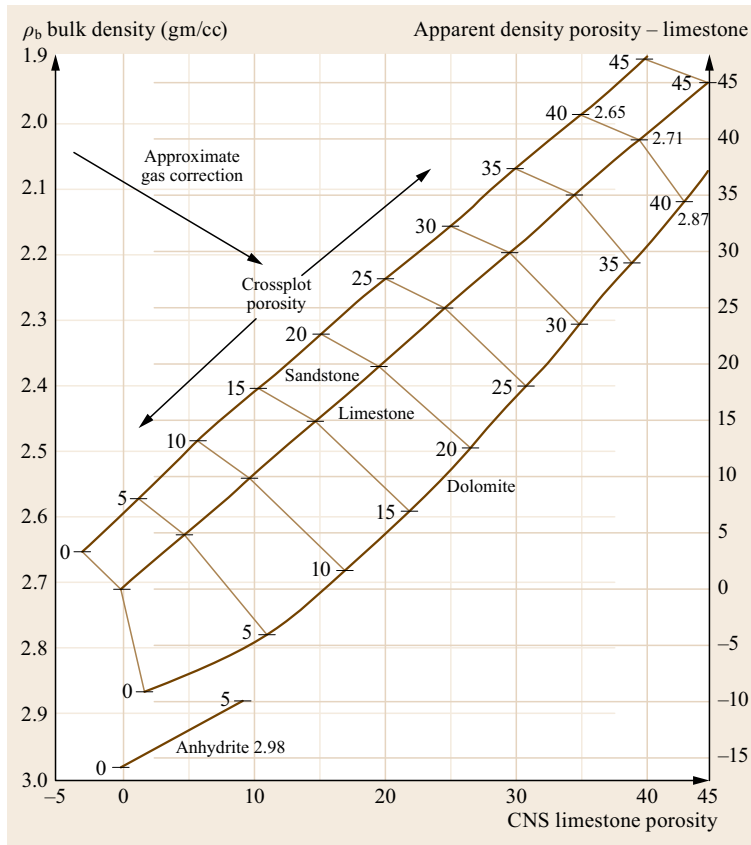


Fig. 13.35 Density-neutron cross-plot grid annotated for lithology and porosity

Advantages and Liabilities of Radioactive Porosity Tools

Since the introduction of compensated density and neutron tools, the combination of these two porosity tools has become the industry standard for both wireline and MWD/LWD porosity measurement. Not only do they provide excellent porosity measurements, they also provide information about reservoir rock lithology. In addition, the gas and clay mineral effects on these two measurements work in opposition:

- The effects of clay minerals increases apparent φ_N , but tend to decrease apparent φ_D .
- Conversely, the effects of gas increases apparent φ_D , but decreases apparent φ_N .

Consequently, if both density and neutron logs are available, good estimates of total porosity φ_T are

$$\varphi_T \approx \frac{\varphi_D + \varphi_N}{2}$$

or

$$\varphi_T \approx \sqrt{\frac{\varphi_D^2 + \varphi_N^2}{2}} \quad (13.14)$$

A second approach to estimating both φ_T is to use a *cross-plot* grid, such as Fig. 13.35.

Both the density and neutron tools are considered to be *radioactive porosity tools*, because they each use chemical radioactive sources. These chemical sources require special care and handling, because of health and safety (H&S) considerations. Density logs use either ^{60}Co or ^{137}Cs chemical radioactive sources. Neutron logs use either AmBe or ^{252}Cf chemical sources, or ^2H - ^3H neutron generators. All of these sources, including the tritium (^3H) target for the neutron generators, are considered to be hazardous materials and must be used under the direct supervision of a licensed radiological engineer.

Because of H&S, as well as environmental concerns, logging vendors using radioactive logging tools must provide secure storage and transport facilities, as well as keep extensive records of when and where the sources are taken. Sources lost must be recovered and, if abandoned in wells, must follow abandonment and notification protocols approved by the Nuclear Regulatory Commission (NRC) in the US or similar governmental agencies elsewhere. A recent breached density source accident in California's San Joaquin Valley resulted

in the well owner immediately instituting wellsite decontamination, hazardous waste disposal, shutting in wells within a defined exclusion zone with the loss of an estimated 60–100 BOPD production, and signing a Consent Order to monitor the field for 300 yr (10 half-lives) because of ^{137}Cs contamination.

Recent concerns about international terrorist activities have raised concerns about the security of all (medical, scientific, engineering and well logging) radioactive sources. US Homeland Security-commissioned studies have resulted in doomsday scenarios, such as the one depicted in Fig. 13.36. While Gilchrist et al. [13.38] stress that 3500 Ci of ^{137}Cs (used for the Fig. 13.36 scenario) would constitute close to the total of all density logging sources in the world, simulation maps, such that of Fig. 13.36, make it difficult to hold logical discussions of the costs and benefits of radioactive logging sources. The US National Academy Sciences (NAS) has recommended the phasing out of current well logging radioactive source technology, but has offered no timetable or alternatives. Two West African countries have also recommended phase-outs, but have not announced alternatives or timetables. The papers by Badruzzaman et al. [13.39] and Gilchrist et al. [13.38] provide very good summaries of the dilemma facing the industry.

Nuclear Magnetic Resonance (NMR) Logs

The utility of measuring NMR in reservoir rocks was recognized in the 1950s [13.40] and a prototype tool was developed the same decade [13.41, 42]. A reliable NMR logging tool was not developed, however, until the late 1980s [13.43]. It took 30 yr for the technology required to build a reliable MNR logging tool to catch up with the promise provided by scientific insight and laboratory measurements.

Measurement of Nuclear Magnetic Resonance (NMR). One of the subatomic particle quantum numbers is called *spin*, which generates a magnetic moment. The particle spin has two values $\pm\frac{1}{2}$ indicating parallel and antiparallel to the local magnetic field. Protons, neutrons, and electrons all have quantum spin numbers. Protons, however, have the largest NMR response [13.43].

For ions with multiple protons (i. e., $Z > 1$), protons pair up with protons of the opposite (spin) quantum number. Ions with odd atomic numbers have one unpaired proton and, thus, have greater NMR responses than those with even quantum numbers. The ion with the greatest NMR response is the hydrogen ion, with only one proton and no neutrons or electrons. Oxygen and carbon, by contrast, have only paired protons and a very low NMR response. Consequently, the primary

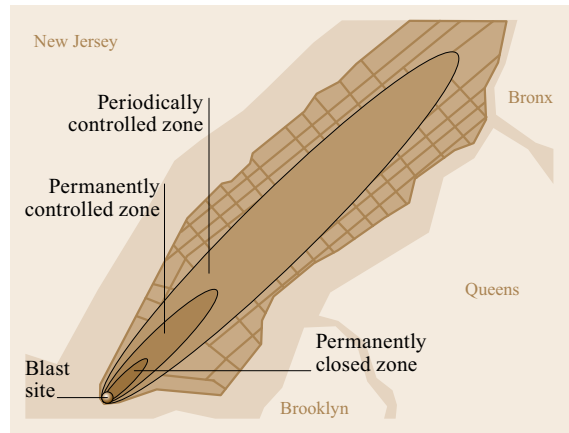


Fig. 13.36 Simulation of potential radiological contamination due to the hypothetical detonation of a radiological dispersion device (RDD, or dirty bomb) containing 50 lb explosive and 3500 Ci of ^{137}Cs , at the lower tip of Manhattan Island (after [13.38], courtesy of SPWLA)

source of NMR in reservoir rocks is due to the hydrogen ions in reservoir rocks, or to the hydrogen ions in water and hydrocarbon molecules. Unlike HI, the NMR response to clay minerals is negligible compared to that of water.

In the absence of any external magnetic field, proton spins have random orientations. In the presence of an external magnetic field, the proton spin moment will orient either parallel or antiparallel to the external field. If a larger (local) magnetic field is imposed, the proton spins will reorient, with their moments precessing (rotating) around the new net magnetic field, much like the gyroscope inertial field vector precessing around the Earth's gravitational field. This proton spin precession about the net external magnetic field vector is called *proton precession*, or (in the presence of a pulsed local field) *nuclear magnetic resonance (NMR)*. The frequency of the rotation is proportional to the magnetic field strength. The length of time for the precession to decay is related to the energy interaction between the spinning protons and material in the walls of vessels containing the water and/or hydrocarbons. The precession decay time for vessels of similar composition is thus the size of the vessels (i. e., pore sizes for reservoir rocks) and the composition of the vessel wall material (i. e., the pore throat lining).

In the mid 1960s, Varian Associates utilized the NMR phenomenon to develop a *proton precession magnetometer (PPM)*, which monitored the precession frequency of a fixed volume of water in a sealed container to measure spatial variations in the Earth's magnetic field [13.44].

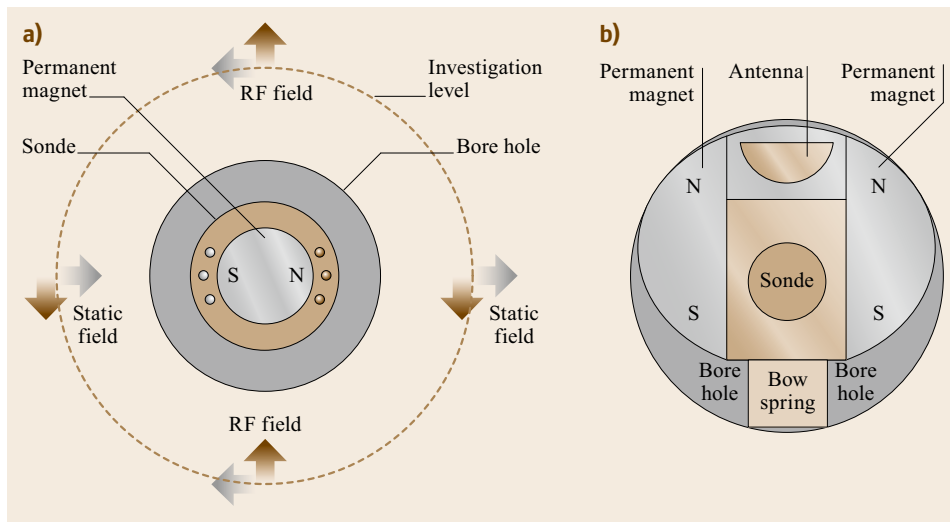


Fig. 13.37a,b Modern NMR logging sonde design cross-sections ((a) centralized sonde design, (b) eccentered sonde design)

Brown and Fatt [13.40] and Seevers [13.45] demonstrated that NMR precession times could be utilized to estimate volumes of *free fluid*, and consequently the pore space sizes in a reservoir rock. Brown and Gamson [13.41] used these concepts to design a prototype NMR logging tool.

Nuclear Magnetic Resonance Logging (NML) (Sonde) Tool. The first (NMR) logging tool was designed by Byron Jackson to Chevron specifications [13.41]. It used the Earth's magnetic field as the external field and Electromagnets for the locally imposed field. This tool was a technical success in that it did demonstrate that borehole NMR measurements were feasible. The original tool, however, was a prototype tool and subject to frequent failures. At the insistence of Chevron, Exxon, Mobil and Shell, Schlumberger and Dresser-Atlas (now Baker-Atlas) introduced their own NMR logging tools, which were also prototype tools. Because of the crude analog measurement circuitry used in all of these tools, the drilling mud had to be *poisoned* with steel filings to rapidly attenuate the borehole signals.

The initial target NMR log situations, for Chevron, Exxon, Mobil and Shell, were freshwater, heavy oil reservoirs, like those of California's San Joaquin Valley. This was just too small a potential market to justify the massive R&D effort needed to develop reliable NMR logging tools.

The NMR log situation remained at this level until the 1980s. By then new technologies (e.g., high temperature and pressure programmable microprocessors, and powerful new ferrite permanent magnets) had developed, which were favorable toward designing sophisticated and reliable NMR logging tools. NU-

MAR Corporation, a small Israeli startup, lured several NMR researchers and tool-design engineers from the major logging vendors and designed their own NMR tool, called *Magnetic Resonance Imaging Log (MRIL)* [13.46].

The NUMAR NMR tool incorporated:

- State-of-the-art ferrite technology
- Downhole high temperature and pressure digital circuitry, with microprocessors for A/D sampling, data processing, encoding and transmission
- Uphole data processing and interpretation.

NUMAR also worked closely with those oil companies requesting NMR logging services to ensure that their needs were met with the NUMAR tool. In less than 15 yr, NUMAR established NMR logging as a viable commercial market and themselves as a viable NMR logging vendor. With the NMR logging market established, Schlumberger introduced its own version of new NMR tools and Halliburton acquired NUMAR Corporation. All four major logging vendors now offer wireline NMR logs and three offer LWD versions. Two distinct designs have emerged: centralized and eccentered versions, as shown in Fig. 13.37. All current NMR sondes utilize *pulse echo magnetic resonance imaging*.

Nuclear Magnetic Resonance Porosity and Permeability. The original application of NMR logs was to estimate porosity and saturations in freshwater, heavy oil reservoirs. A second application was to estimate reservoir rock pore-size distributions, and thereby permeability. Figure 13.38 shows a comparison of laboratory core and NMR permeability analyses.

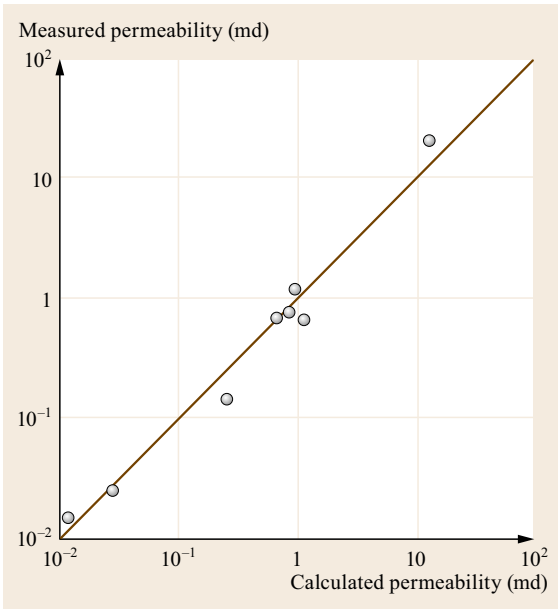


Fig. 13.38 Comparison of measured and NMR relaxation time predicted core permeabilities [13.45]

Figure 13.39 shows a comparison of wireline NMR and laboratory core porosity analyses.

Once major logging vendors had introduced reliable NMR tools, new applications were developed. Coates et al. [13.46] listed the following NMR log applications:

- Presence and quantities of different fluids (water, oil, and gas)
- Porosity and pore size distributions
- Bound and free water saturations
- Effective porosity and permeability
- Flushed zone saturation S_{xo} for wells drilled with oil-based mud (OBM).

Figure 13.40 shows a relationship between NMR T_2 relaxation time and light oil viscosity. Allen et al. [13.47] shows other examples of NMR Log versus core measurement comparisons.

Nuclear Magnetic Resonance and Lithology. Most NMR log vendors claim that NMR is independent of lithology, which is not completely true. While the NMR response to reservoir rock matrix material is not as strong as for the traditional porosity (acoustic, density and neutron) tools, the precession decay time, as indicated above, is related not only to the pore sizes, but also to the material lining the pore throats. To get the most reliable NMR log interpretations, an independent source of reservoir lithology is required. Kenyon [13.50] provides a very good summary of the

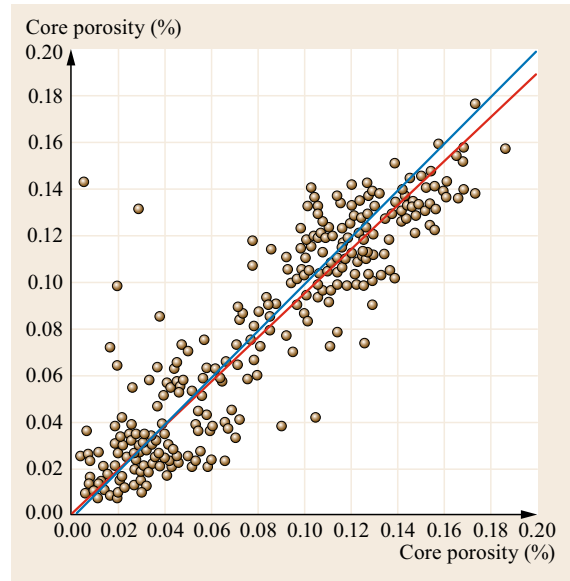


Fig. 13.39 Comparison of measured core porosities to those predicted from NMR Logs. The red line is a RMA fit to the data, while the blue line is the 1 : 1 correspondence (after [13.48])

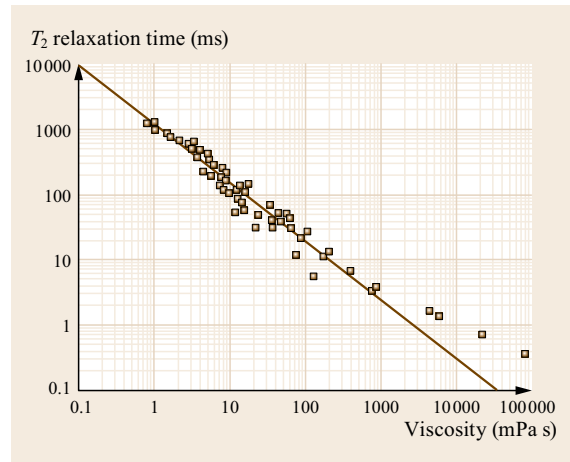


Fig. 13.40 Light and heavy oil have different viscosity versus NMR T_2 trends (after [13.49])

petrophysical principles behind NMR log applications, including the lithology aspects.

NMR Versus Conventional Porosity Logs. NMR logs are not simply the specialized tool for a limited (e.g., heavy oils and freshwaters) market, as was once thought. They are also not, however, the *magic bullet* or *Swiss army knife*, that many vendors claim. NMR logs are less sensitive to matrix lithology than conventional (acoustic, density, and neutron) tools. However,

they do require a good independent source of lithology and porosity information for best results. They also provide permeability estimates, which definitely fill a gap in the conventional porosity log tool kit.

NMR logs, however, are more expensive to run than conventional porosity tools, both in terms of logging charges and rig time. For best NMR log analysis results, conventional porosity tools also must be run, which makes them a luxury for many small oil and gas fields, as well as independent operators.

NMR logs do not require radioactive sources, like density and neutron logs. As indicated above, however, NMR logs are not a replacement for conventional porosity tools. Because of this, the petroleum industry (both operators and logging vendors) is mounting intense efforts to develop alternatives to chemical neutron and gamma-ray sources. These efforts have not been successful to date. As a result, the petroleum industry has been requesting extensions for using chemical density and neutron radioactive sources.

13.11.2 Lithology Tools

What Are Lithology Tools?

Essentially all wireline and MWD/LWD measurements respond to lithological changes in the borehole wall rock. *Lithology tools* are those tools, or combinations of tools, which have strong responses to these changes.

Single-Tool Methods

Single-tool methods utilize a single tool whose lithology response is unique enough that it can be used alone to determine the dominant lithology.

Natural Gamma-Ray Logs. There are three natural sources of γ -ray radiation as shown in Fig. 13.41:

- Potassium 40 (^{40}K)
- Thorium (^{232}Th) decay series
- Uranium (^{238}U) decay series.

Of these three sources, ^{40}K is the major contributor to sedimentary rock natural γ radiation, because potassium is a major constituent of feldspars, sylvite, micas and clay minerals.

Micas and clay minerals are major constituents in shales and contain large amounts of potassium: potassium 40 (^{40}K) is radioactive. Because potassium is not a constituent of quartz, calcite, or dolomite, the natural γ -ray log is often used as a shale indicator. Uranium and thorium salts are also often precipitated in reducing environments, such as organic shales (e.g., the Antrim Shale of the Michigan Basin).

Sand-shale lithologies are estimated by establishing a low- γ -ray *sand line* (100% sand) and a high- γ -ray

shale line (100% shale), for the interval of interest. Intermediate γ -ray values are assigned a shale volume V_{sh} by a variety of empirical γ -ray V_{sh} models. Similar V_{sh} estimates can be made for carbonate reservoir rocks.

The γ -ray log is not an infallible V_{sh} indicator. Arkosic sands contain large amounts of orthoclase and microcline (K-feldspars), which will generate high γ -ray responses. Zircon and sphene, often found in high-permeability, clean beach sand (good quality reservoir rock) deposits, commonly have thorium as contaminants, which will generate high γ -ray log responses. Apatite-rich sands often contain ^{212}Pb and/or ^{214}Pb , which are two of the radioactive daughter products of the uranium and thorium decay series, making them radioactive. Monazite sands are often mined for their thorium content, which makes them radioactive. Fractured carbonates and volcanics often have uranium and thorium contamination along fractures, which will also generate high γ -ray log responses. Sylvite and other potash minerals contain large amounts of potassium, which can generate high γ -ray log responses in evaporite sequences.

The γ -ray log works as a *shale* indicator often enough, however, it is commonly used to estimate V_{sh} .

Spontaneous Polarization (SP). Spontaneous polarization (SP) is an electrochemical phenomenon that occurs when the salinity of the drilling mud filtrate is different from that of the formation waters and high permeability rocks are bounded by low permeability shales (which form cation-selective membranes). When the formation waters and mud filtrate are not the same salinity, anions (negatively charged ions) and cations (positively charged ions) will migrate from the higher concentration fluid to the lower concentration fluid, in an attempt to equalize the salinities.

Shales act as cation-selective membranes, passing only cations and blocking anions, leaving a cation deficiency on the upstream (high permeability) and a cation surplus on the downstream (low permeability) fluid interfaces. The resulting electrical charge variations can be monitored by measuring the electrical potential, with respect to some fixed point, as a function of depth.

A *normal* SP occurs when the formation waters are more saline than the mud filtrate waters. In these cases, the SP opposite sands will be negative, compared to that opposite shales. A *reversed* SP occurs for the opposite situation.

Because the SP opposite (high-permeability) sands is different from that opposite (low-permeability) shales, the SP is often used as a sand-shale indicator. An SP *sand line* (100% sand) and a *shale line* (100% shale) are established for the interval of interest and the intermediate SP values are scaled linearly between 0 and 100% V_{sh} .

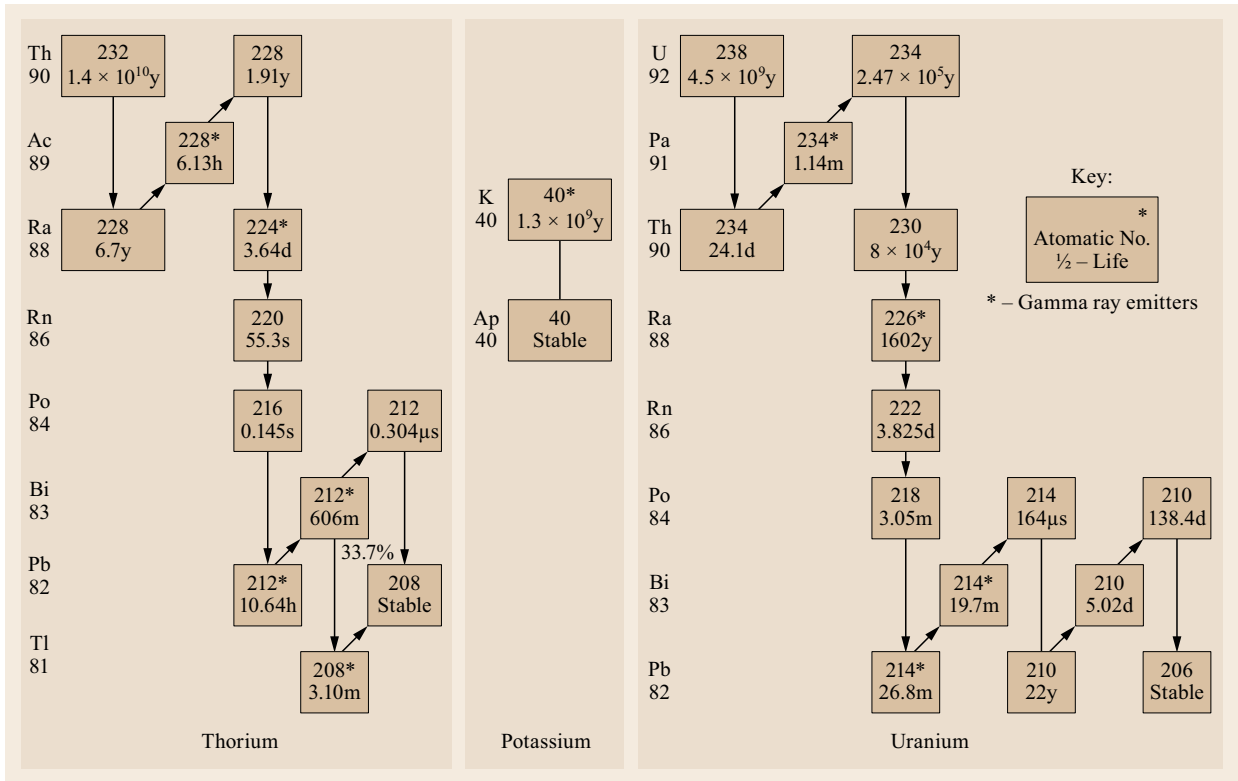


Fig. 13.41 Radionuclide decay for ⁴⁰K, ²³²Th series and ²³⁸U series (after [13.51])

There are many problems with using the SP as a quantitative V_{sh} indicator. If there is little or no salinity contrast between the mud filtrate and formation waters the SP will be flat and of little value. Because of formation water salinity variations, the SP can be reversed, flat, and normal, all in the same well. Clay minerals in sands will depress the SP sand deflections.

Photoelectric Factor (PEF). Low-energy (< 0.2 MeV) γ -rays are adsorbed by electrons within the rock increasing their energy level and releasing a photoelectron on impact. This process is called *photoelectric adsorption* and is the principal upon which the Z, or PEF, curve of modern density log tools is based.

Photoelectric absorption is dependent upon the atomic number (Z) of the target atom. Lithodensity, spectral density, or Z-logs use the near detector ratio of γ -ray flux in the Compton scattering and photoelectric absorption windows to estimate bulk photoelectric factor, PEF, which is largely independent of porosity. Because of this, the PEF curve can be an excellent lithology indicator.

The accepted matrix PEF values for common reservoir dominant minerals are:

- Calcite: 5.1
- Dolomite: 3.1
- Quartz: 1.8.

which provides sufficient separation for lithology identification in complex lithology environments, such as the Pinda Formation of the Congo Basin.

Less well known and appreciated is the fact that the accepted PEF values for common potassium feldspars are:

- Anorthoclase: 3.1
- Microcline: 2.8
- Orthoclase: 2.9.

which are all around the dolomite value. The reason this is significant is that arkosic sands, which have high potassium feldspar content, generally do not occur in carbonate environments. As a result, high- γ -ray responses in a clastic (sand and shale) environment, such as California's San Joaquin Valley, with PEF values near 3.0 may indicate arkosic sands, not shale or dolomite.

The PEF values for micas and clay minerals, the principal components of shales, range from 1.8 to 6.3,

which means that the PEF alone is not a good clay and mica mineral identifier. Because the PEF curves are based on low-energy γ -rays, they are very sensitive to barite mud additives and may not be useful for lithology identification in heavy mud situations.

Multiple Tool Methods

Multiple tool lithology determination methods utilize two or more measurements in either direct cross-plots, such as that of Fig. 13.35, or in computed parameter cross-plots, such as that of Fig. 13.42 or Fig. 13.43.

The techniques utilized to perform this type of analysis are collectively known as cross-plot techniques. There are many types of cross-plot techniques and their derivation can get rather tedious.

Single Versus Multiple Porosity Tools. Conventional (acoustic, density, and neutron) porosity tools work very well for estimating porosity if the dominant lithology is known and in the absence of gas or clay minerals. In cases of uncertain lithologies, clay minerals and/or gas, single porosity tools are not sufficient. Two, and often all three porosity tools are required to identify the lithology, as well as estimate porosity, in these cases.

Probably the most commonly used cross-plot technique is the density-neutron cross-plot, shown in Fig. 13.35. The Fig. 13.35 grid is actually a graphical nonlinear coordinate transform from neutron log limestone porosity $\varphi_{N_{ls}}$ versus density log bulk density ρ_B space to lithology-porosity space. Sandstone, limestone and dolomite (100% lithology) porosity curves are superimposed on a $\varphi_{N_{ls}} - \rho_B$ grid. Measured log values are plotted on the background ($\varphi_{N_{ls}} - \rho_B$) grid and the lithology and total porosity φ_T are interpolated between the matrix-porosity grid lines. Figure 13.35 also indicates the effect of gas. While not shown on the Fig. 13.35 grid, clays generally plot well below the dolomite line, toward high $\varphi_{N_{ls}}$ values. Similar grids exist for acoustic (sonic)-neutron and density-acoustic (sonic) cross-plot analyses.

Matrix Identification (MID) Plots. Figure 13.42 shows the metric matrix identification (MID) plot grid, which requires all three conventional (acoustic, density and neutron) porosity tools. Using the Fig. 13.42 MID grid is not as simple as the dual porosity grids. Use of this cross-plot analysis technique is a three-step process:

1. Plot the measured values from the three porosity tools on density-neutron and acoustic (sonic)-neutron dual porosity grids to obtain apparent (total) cross plot porosities for each pair.

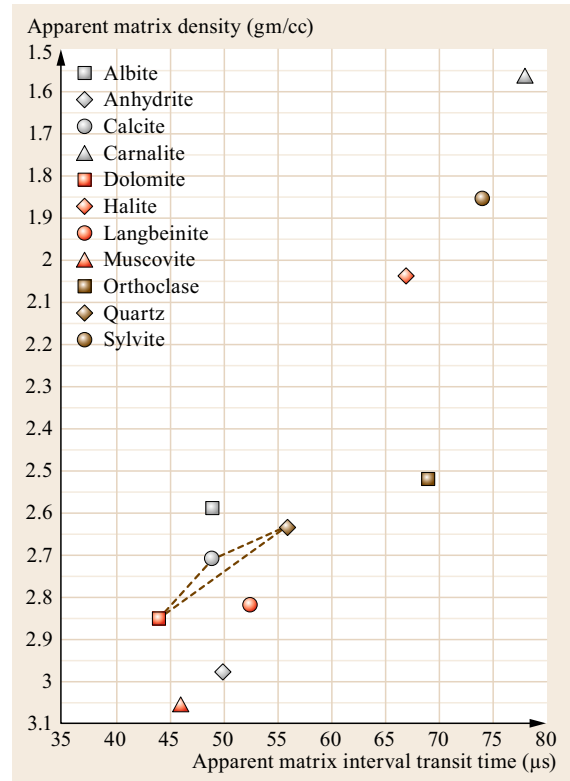


Fig. 13.42 Metric apparent matrix interval transit time t_{maa} versus apparent matrix density ρ_{maa} in a MID plot grid

2. Using the apparent total porosities, cross plot them and the measured density and acoustic (sonic) values on specialized cross-plot grids to obtain apparent matrix interval transit times, t_{maa} , and apparent matrix densities ρ_{maa} .
3. The resulting t_{maa} , and ρ_{maa} are then cross plotted on the MID grid of Fig. 13.42. Points falling between matrix points on Fig. 13.42 can be scaled linearly to obtain approximate mixture percentages (i. e., the quartz-calcite-dolomite triangle).

Manually, this is very tedious. Fortunately, however, most FE software will take care of the intermediate steps and plot the results on a grid, such as Fig. 13.42.

Lithodensity Matrix Identification (LID) Trimineral Plots. Figure 13.43 shows the lithodensity identification (LID) plot grid, which requires only lithodensity, spectral density, or Z-density ρ_B and PEF curves, along with neutron log $\varphi_{N_{ls}}$. Like the Fig. 13.42 MID grid, using the Fig. 13.43 LID analysis technique is a three-step process:

1. Plot the measured density and neutron porosity values on a density-neutron dual porosity grid to obtain

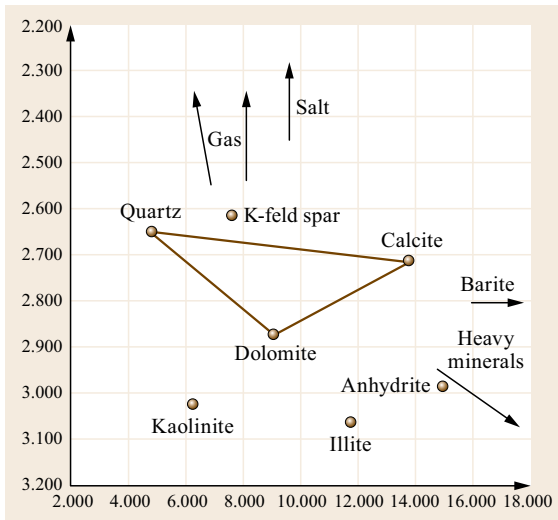


Fig. 13.43 Lithodensity matrix identification plot (LID) grid

apparent (total) cross-plot porosity ϕ_t and apparent matrix density ρ_{maa} .

2. Cross plot the PEF, bulk density, and total cross-plot porosity on a special nomograph to estimate the apparent volumetric photoelectric absorption factor U_{maa} .
3. Cross plot the resulting ρ_{maa} and U_{maa} on the Fig. 13.43 nomograph. Points plotting between the individual matrix points can be estimated as percentage mixtures.

Like the MID plot, this is very tedious to do manually. Again, most FE software will take care of the intermediate steps and plot the results on a grid, such as Fig. 13.43.

13.11.3 Saturation Tools

Saturation tools are those logging tools that are very sensitive to (gas, oil and water) saturation variations. Formation resistivity R_t estimated from these tools is used to estimate the uninvaded formation water saturation S_w . The hydrocarbon saturation, S_o or S_g , is then $1 - S_w$. There are four types of open-hole saturation tools:

- Resistivity tools, which use electrodes (e.g., laterologs)
- Resistivity tools, which use coils (e.g., induction Logs)
- Resistivity tools, which use antennas (e.g., dielectric or electromagnetic wave propagation logs)
- Nuclear magnetic resonance logs.

While three of these tools measure formation resistivity, they each interact with the formation differently.

Electrode Tools

Electrode tools utilize galvanic coupling between the sonde and the formation, so they require conductive fluid in the borehole.

Electrode tools should not be used in wells drilled with air, foam, mist, or oil-based mud (OBM).

Formation resistivity was the first borehole measurement that the Schlumberger brothers made. The Pechelbronn well was logged by dropping the then current Schlumberger surface resistivity electrode array down the borehole and making a series of (station) measurements at different depths similar to what had been previously been done on the surface, with a technique called resistivity profiling.

It soon became apparent that there were better borehole electrode array designs than those that had been used on the surface. As a result, several different electrode array designs have appeared over the years. The major purposes of the successive electrode designs were twofold:

- Enhance thin-bed resolution and quantitative measurement
- Decrease the influence of borehole fluids, mudcake, and invasion.

These two goals are essentially mutually exclusive. The initial response to this dilemma, continued to the present, has been to use multiple electrode arrays on the same sonde.

The current electrode tools of choice are array laterolog tools (ALTs). Schlumberger was the first vendor to offer this type of service, but most major vendors now offer it. The Schlumberger version, introduced in 1990, uses downhole microprocessors, multiple electrode arrays, all current electrodes on the sonde, multiple frequencies, and records both amplitudes (impedance), and phase shifts to provide six apparent resistivities, which can be inverted to provide two-dimensional (cylindrical) resistivity models (Fig. 13.44a). The Atlas Wireline version (Fig. 13.44b), introduced in 1995, uses downhole microprocessors, multiple guard or LL3 electrode arrays, multiple frequencies, and records both amplitudes (impedance), and phase shifts to provide six apparent resistivities, which can be inverted to provide two-dimensional (cylindrical) models [13.52].

Figure 13.45 shows the invasion effects for a Schlumberger HRLA tool in an 8 in borehole filled with conductive mud [13.53]. Laterolog-type tools work best when the borehole fluid resistivity R_m is less than that of the formation R_t . They are calibrated for 8 in boreholes filled with nominal (e.g.,

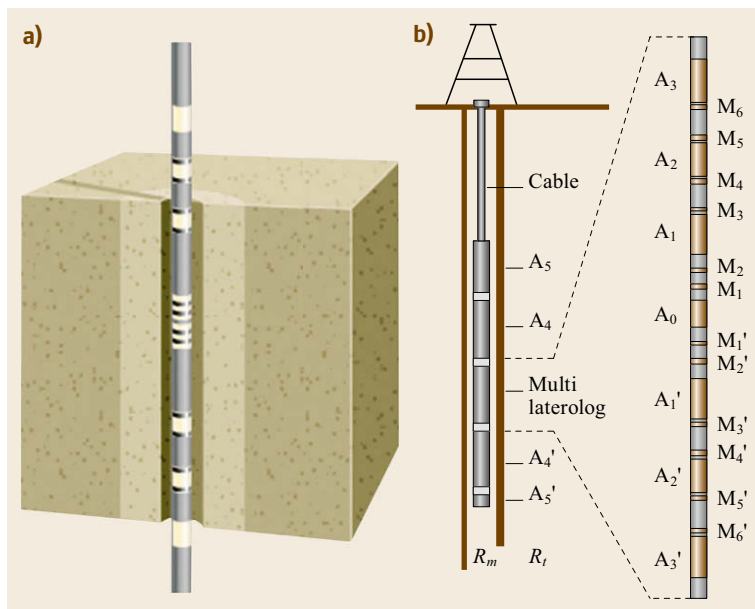


Fig. 13.44a,b Array laterologs: Atlas Wireline Multilaterolog with various antennas (A) and points of measurement (M). R_m represents the resistivity of the mud, R_t the (true) formation resistivity (after [13.52], courtesy of SPWLA)

15 000–25 000 ppm NaCl salinity mud. Significant departures from these conditions require borehole or environmental corrections before quantitative water saturation S_w estimates can be made. Array laterolog tool results are not measured resistivities, but ring resistivity model inversion results, and need no further environmental corrections. Figure 13.45 compares the Schlumberger array laterolog curve responses to other electrode tools.

Laterologs should not be used in air, mist, or oil-based mud filled boreholes.

Microelectrode Tools

Microelectrode tools are contact devices designed to provide flushed zone resistivities R_{xo} . In permeable formations there is usually significant flushing of formation fluids by the mud filtrate. This flushing, or invasion, is observable by separation of the micro- and deep resistivity curves and provides a qualitative indication of permeability. The resulting flushed zone water saturation S_{xo} is estimated from R_{xo} . The movable hydrocarbons (i.e., hydrocarbons that can be produced) are then estimated by $S_{xo} - S_w$.

Ballengee [13.54] describes several microresistivity pad designs, as shown in Fig. 13.46. The common goal of these different designs was to reduce the effects of the borehole mud and mudcake, while emphasizing the flushed zone resistivity measurement. The current microresistivity tools of choice are either the microspherically focused log (MSFL), shown in Fig. 13.46 or the microcylindrically focused tool (MCFT), shown in Fig. 13.47. Microelectrode tools are very sensitive to

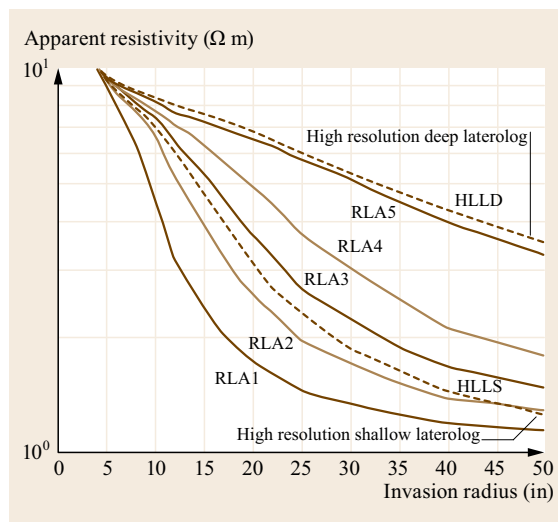


Fig. 13.45 Comparison of various high resolution laterolog array tool apparent resistivities (of five laterolog arrays RLA) versus invasion, for an 8 in borehole containing conductive mud (after [13.53])

mudcake thickness and must be corrected for it if accurate flushed zone resistivities are desired.

Microelectrode tools should never used in air, mist, or oil-based mud filled boreholes.

Coil Tools

Coil, or induction, resistivity tools were developed to be able to make formation resistivity measurements in air, mist, foam, or oil-based mud (OBM) filled bore-

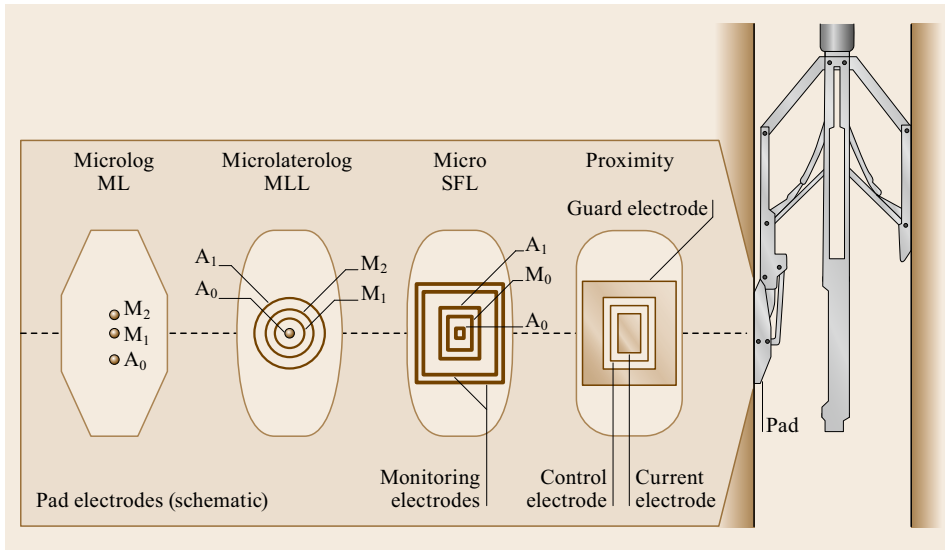


Fig. 13.46
Microresistivity sonde pads [13.54]

holes. They can also be used with freshwater mud-filled holes and modest formation resistivities, such as in the US Gulf of Mexico and Niger Delta. Induction tools really measure formation conductivity (the inverse of resistivity). The resolution of analogue induction tools is 5 Mho/m, which means that Induction resistivity values over $200 \Omega \text{ m}$ are highly suspect. Modern digital system induction tools, with downhole A/D conversion and microprocessors, can accommodate slightly higher formation resistivities, but are still not as reliable as laterolog tools for the highest formation resistivities.

Induction tools should not be used for situations with saline muds and/or high resistivity formations.

Figure 13.48 shows the operational principals of induction logging. A high-frequency (kHz) oscillating current is passed through a transmitter coil, which generates a primary oscillating dipole magnetic field. This primary magnetic field generates secondary oscillating currents in the formation surrounding the borehole (and in the borehole fluids), which generate secondary oscillating dipole magnetic fields. A receiver coil, coaxial with, but distanced from, the transmitting coil detects the combined primary and secondary magnetic fields and feeds this signal to software, which separates the primary and secondary signals and inverts them to apparent formation resistivity (conductivity). Analog induction tools only measured impedance, because the mutual induction in the long logging cables swamped the small signal phase shifts between the closely spaced transmitter and receiver coils. Modern digital system induction tools, with downhole A/D conversion and microprocessors, can measure both impedance and phase, providing more precise formation models [13.55].

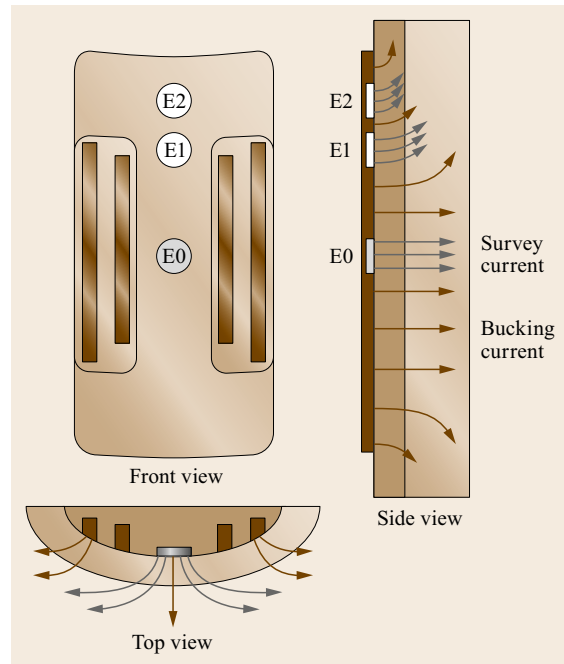


Fig. 13.47 Microcylindrically focused tool (MCFL) array with three electrodes (E) and operational schematic [13.26]

The original induction tools utilized only a single transmitter, emitting a single frequency signal and only one or two receiver coils. The current induction tools of choice are array induction tools, first introduced by BPB Oilfield Services (now Weatherford) [13.56]. Figure 13.49 shows two versions of array induction tools.

Recent AIT innovations involve tri-axial transmitter and receiver coils recording both amplitude and

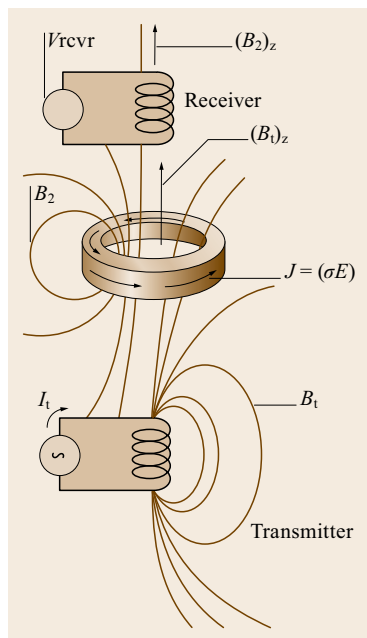


Fig. 13.48
Induction log
operational
schematic [13.26]

phase, which are inverted to define principal components of the formation resistivity tensors of anisotropic formations [13.57]. This configuration is very useful for dipping formations, deviated boreholes and/or horizontal wells.

Antenna (Dielectric) Tools

Antenna, or dielectric, resistivity tools were developed for use in situations with heavy, viscous, oils and very fresh waters. Water is one of the very few naturally occurring electrically polar molecules. As a result, freshwater has a very high (≈ 80) dielectric constant. Even saline waters have dielectric constants between 40 and 60 [13.58], depending upon salinity, temperature and signal frequency. By contrast oils and most reservoir rocks have dielectric constants less than nine (i. e., a factor of approximately ten or more below freshwaters) and oils have dielectric constants between 2–5.5 [13.58].

Dielectric constant logging measurements involve transmission of high (MHz–GHz) frequency electromagnetic (EM) waves through the borehole wall rock. At one time, all major logging vendors and some operating companies had versions of dielectric tools. The various tools fell into two the distinct styles, shown in Fig. 13.50. Low (MHz) mandrel-type tools had coils attached to nonconducting sondes and were centered in the borehole, while high (GHz) pad-type tools used slot antennas, pressed up against the borehole wall [13.60].

The original dielectric tools were so successful that they may have delayed development of NMR tools for

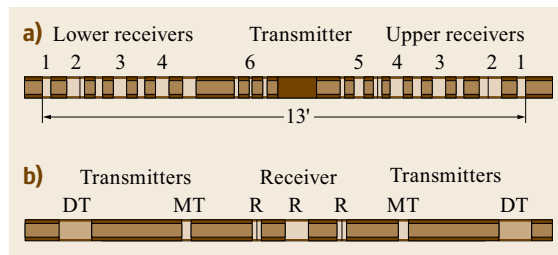


Fig. 13.49a,b Two array induction tool configurations. (a) An array of one transmitter and ten receiver units, (b) A single receiver with four transmitters (after [13.59])

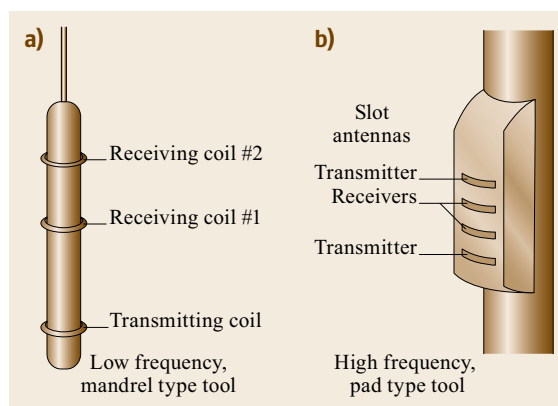


Fig. 13.50 Generic dielectric logging tools (after [13.60])

the heavy oil, freshwaters market. With the advent of the NUMAR MRIL tool and its successors, NMR tools displaced dielectric tools, because they were so versatile. As recently as early 2010, only a handful of operational dielectric tools remained, primarily in the San Joaquin Valley of California.

In late 2010 and early 2011, Schlumberger and Halliburton both introduced new-generation digital dielectric tools, which appear to be gaining market share. Discussions with several San Joaquin Valley operators indicate that the new generation dielectric tools are displacing NMR tools for freshwater, heavy oil reservoirs, leaving saline water, heavy oil reservoir and/or more complex situations to the NMR tools. The market for these new dielectric tools, however, appears to remain with heavy oils with fresh formation waters.

Modern dielectric constant tools utilize multiple transmitters, receivers, and frequencies to map dielectric dispersion [13.61, 62].

Nuclear Magnetic Resonance Logging Saturation

The original NMR logs were considered to be shallow measurement tools, useful only for flushed zone saturations, as well as porosity and permeability, and

could not distinguish between different fluid types. Current-generation NMR tools, however, with strong permanent magnets, utilizing magnetic pumping, and downhole digital circuitry, can discriminate between different fluid types, even though their depth of investigations is still very shallow [13.61, 62]. NMR logs can discriminate between clay-bound water, capillary-bound water, free water, and heavy oil. For best results, however, these NMR interpretations require supporting information from other porosity, lithology and saturation tools. Because of this and the additional costs of NMR, many operators still prefer to use traditional porosity tools.

13.11.4 Environmental Corrections

Petrophysical models are based on *true* formation physical properties. Unfortunately essentially all logging tool measurements, with the possible exception of acoustic measurements, include the effects of the borehole fluids, mudcake, and invaded zone. As a result, environmental or borehole corrections are required before the logging tool measurements can be used in petrophysical measurements. Petrophysical evaluations without first making environmental corrections risk sometimes expensive erroneous results.

Manual evaluation, using environmental corrections is tedious. As a result, experienced petrophysicists will often evaluate whether or not the borehole corrections are needed (i.e., will they make a significant difference), before applying them.

Petrophysical evaluations using FE software are relatively simple because the software does all of the tedious calculations and the analyst only needs to supply the correct input. For this reason petrophysicists will nearly always apply environmental corrections when using software. Then if questioned about whether or not environmental corrections were used, the simple answer is, *yes*.

The exceptions to universal environmental corrections are:

- Compensated acoustic log results
- Array laterologs
- Array induction logs.

Compensated acoustic logs only measure the acoustic transit time along the borehole wall. The transit times through the mud column and mudcake are canceled out by the measurement technique, so no correction is needed. The array laterolog and induction log curves are not measurements, but model inversions of the measured data. As a result, environmental corrections have effectively already been applied to these curves during inversion before they are presented.

13.11.5 Salinity (R_w) Tools

What Are Salinity Tools?

Archie's equations require porosity (from porosity tools), resistivity (from resistivity saturation tools) and formation water resistivity. Salinity tools provide the last element.

Wet Chemistry

If a formation water sample is available, its resistivity can be measured directly. Sometimes, particularly in older wet chemistry analyses, direct R_w measurements are not available. In those cases, equivalent NaCl salinities and R_w can be estimated from the individual ionic and total dissolved solids (TDS) concentrations [13.18–24]. Figure 13.17 is a nomogram based upon these empirical studies.

Spontaneous Polarization (SP)

The effects of cation-selective membranes in low permeability shales, adjacent to high permeability reservoir rocks, was described earlier in the *Lithology Tools* section. The potential differences created can be used to estimate formation water R_w , via the Nernst equation [13.63]

$$E = -\frac{RT}{F} \sqrt{\frac{a_w}{a_{mf}}}, \quad (13.15)$$

where E is the relative (i.e., from clay to sand) SP anomaly (mV), R is the universal gas constant, F is the Faraday constant, T is the absolute temperature ($^{\circ}\text{K}$). a_w and a_{mf} are the formation water and mud filtrate electrochemical activities, respectively.

The electrochemical activities are thermodynamic quantities independent of temperature, but not easily obtained. However, Doll [13.64] used a slightly different version of (13.14)

$$E = -\frac{RT}{F} \sqrt{\frac{R_{mf}}{R_{we}}}, \quad (13.16)$$

where R_{mf} and R_{we} are *equivalent* water resistivities, related to R_{mf} and R_w via laboratory determined empirical relationships. A good approximations for these relationships at 75°F are

$$R_{mf} = -0.032R_{mf}^2 + 1.069R_{mf} - 0.031$$

and (13.17)

$$R_w = -0.03R_{we}^2 + 0.0936R_{we} - 0.029,$$

which were obtained by fitting second-order polynomials to published nomograms. Equations (13.16)–(13.17) are presented in the normal R_{mf}/R_w order of usage. The terms R_w and R_{mf} are interchangeable.

A strong SP will develop opposite clean sands, bounded by clays, if the formation water salinity is significantly different than the mud filtrate salinity. In those cases, R_w can be estimated from the mud filtrate resistivity R_{mf} and the SP. Weak R_w/R_{mf} contrasts yield anemic SP deflections. The presence of clay minerals in the sand will also depress the SP deflection.

Spontaneous polarization (SP)-based R_w estimates tend to be less reliable than other estimates. As a result SP is often the R_w estimator of last resort. The SP, however, can be used to estimate R_w in oil and gas sands, with no water leg; something that other log-based R_w estimators cannot do.

Apparent Water Resistivity R_{wa}

In clean water sands, Archie’s equations can be solved for R_w , as $S_w = 1$. The resulting R_w estimate is called R_{wa} , or *apparent water resistivity*. This technique is extremely fast and may be one of the most commonly used means of estimating R_w . This technique will work only with environmentally corrected deep resistivity data and requires knowledge of the Archie a and m coefficients. It will not work, however, in the presence of clay minerals and/or hydrocarbons. It also requires the assumption that the same brine is present in the hydrocarbon zone as the water zone.

Cross-Plot Ratio R_w Estimators

Cross-plots of R_t versus porosity on various grids are also commonly used to estimate R_w . These techniques can also be used to estimate S_w . The Hingle plot (Fig. 13.51) requires prior knowledge of the a and m Archie coefficients to estimate R_w and also n to estimate S_w . Hingle plots require special grids unique to each a and m pair. The Pickett plot (Fig. 13.52) requires prior knowledge of the Archie a coefficient to estimate m and R_w and n to estimate S_w . Pickett plots use log-log grids. However, to be most effective, the x - and y -axes logarithmic cycles should be of equal lengths, as in Fig. 13.53. Then, not only is R_w , given by the 100% porosity, but the slope of the water line is the m exponent in Archie’s first equation.

13.11.6 Borehole Imagers

What Are Borehole Imagers?

Borehole imagers provide detailed (mm–cm scale) images of the borehole walls. Prior to the development of borehole imagers subsurface structural and stratigraphic information was obtained from four sources:

- Seismic reflection time and migrated depth sections, which provided both horizontal and vertical detail on a scale of tens of feet.

- Well-to-well log correlation, which provided vertical detail on a scale of feet, but very poor (well spacing scale) horizontal scale detail.
- Whole-core examination, which provided mm-scale vertical detail, but only over the interval of the core.
- Dipmeter interpretation, which provided inch-scale vertical resolution at the wells, but was clouded by the need to use statistical methods to make the determination. The geologic interpreter was distanced from the original data.

Borehole imagers provided whole-well mm–cm scale images of the borehole wall, which could be virtually manipulated and examined much like whole cores, but without the time and expense involved in obtaining oriented whole cores.

The two most successful borehole imagers have been:

- Acoustic borehole viewers (BHTV)
- Microresistivity scanners (MRSs).

Each of these imagers has its advantages and limitations. The real game changer for borehole imagers has been the image workstations. These are powerful mini- and/or microcomputer-based systems that allow the interpreter to manipulate and measure features on the borehole images, much like he/she would do with physical whole cores, and generate tables of dip and

Part B | 13.11

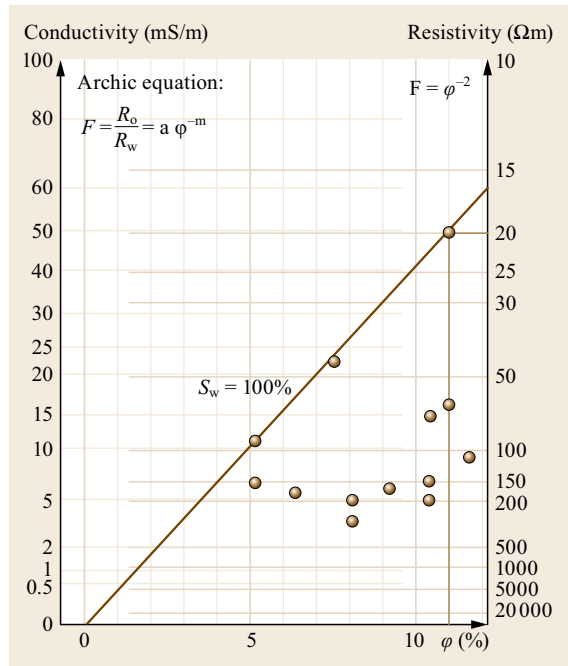


Fig. 13.51 Carbonate sequence Hingle plot example

strike information to present alongside other log data. While considerable creative software supports the data manipulation, analysis, and storage systems, the actual interpretation is done by the geologist or geophysicist manning the work station.

Acoustic Borehole Imagers

Acoustic borehole televiwers (BHTV), are really SONAR devices that emit ultrasonic (500 KHz–2 MHz) acoustic pulses into the mud column and measure the *reflected* amplitudes and (time-of-flight) reflection times. The first BHTV tools were developed by Mobil Field Research Laboratory (now EXXON-

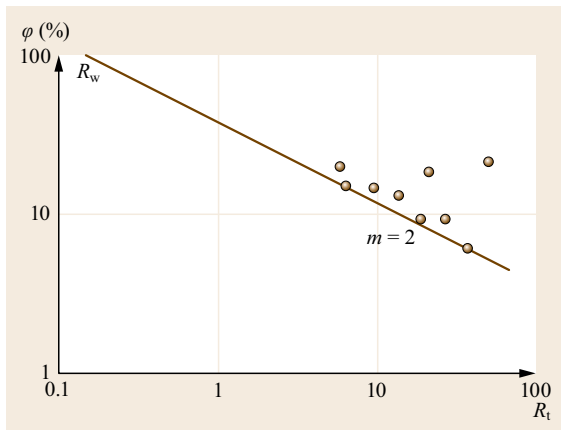


Fig. 13.52 Carbonate sequence Pickett plot example



Fig. 13.53 (a) Circumferential acoustic scanning tool (CAST) and (b) Three-dimensional pseudocore image of an openhole log (courtesy of Halliburton)

Mobil), in the late 1960s [13.65]. Early attempts to commercialize this tool, by Halliburton, Dresser-Atlas (now Baker-Atlas), and Schlumberger were plagued by poor performance (tool failures and poor resolution). The first truly successful commercialization was a re-engineered tool by Gearhart (now Halliburton), in the late 1980s [13.66], designated the circumferential acoustic scanning tool (CAST). Figure 13.53 shows the current CAST tool specifications and an example of a CAST pseudocore image.

Acoustic borehole televiwers require liquid-filled boreholes, but operate better in OBM than do microresistivity scanners, provide full 360° image coverage of the borehole walls, which microresistivity scanners generally do not, and operate better in rugose boreholes than do microresistivity scanners. The time-of-flight data also provide three-dimensional information about the borehole wall. Figure 13.54 shows four rotated pseudocore images of the same depth interval, from a Congo Basin well. The protrusions from the pseudocore are mud-filled vugs in the borehole wall, which were not measured in routine core analyses by two different laboratories, but which did effect the density and neutron logs run in the wells from this field.

Baker-Atlas, Halliburton, and Schlumberger now all offer modern digital system versions of BHTV.

Microresistivity Scanners

Microresistivity scanners were logical evolutions of dipmeters and were originally developed to overcome some of the shortcomings of early BHTV tools. Multiple button electrode arrays were added to dipmeter pads. The problem introduced with this approach is

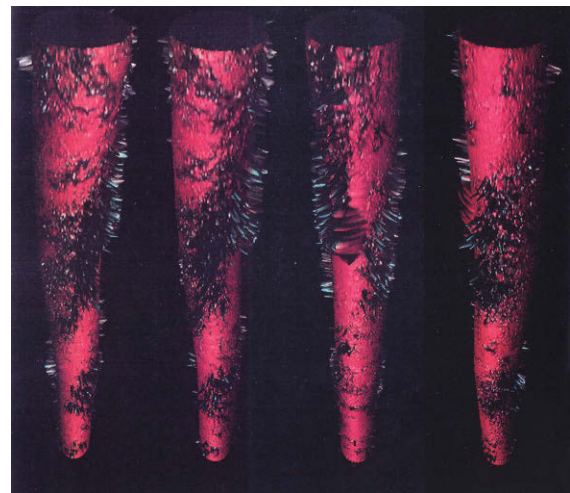


Fig. 13.54 Rotated CAST pseudocore images of the same depth interval, from a Congo Basin well, showing mud-invaded vugs in the borehole wall

that, as the borehole diameter increases, gaps in circumferential coverage between the dipmeter pads expand. The dilemma faced by logging vendors was how to distribute this loss in circumferential coverage to best describe the stratigraphy and structural patterns displayed on the borehole wall. Schlumberger uses four pads, Baker-Atlas and Halliburton use six and Weatherford uses eight.

The larger the number of pads, the smaller the circumferential coverage gap between each pad, but also the smaller the circumferential area covered by each pad. The smaller the number of pads, the larger the circumferential coverage on each pad, but also the larger the gap in coverage between pads.

Schlumberger, with only four pads, added side flaps to each of its pads to increase the circumferential coverage of each pad arm. While Schlumberger denies that this is a problem, there is always speculation that the pad flap may not have the same pressure against the borehole wall as the main pad, particularly with continued usage. Because all pads must be in good contact with the borehole wall, this can be a serious concern. Figure 13.55 shows an example of the Schlumberger FMI image, through vuggy carbonate [13.66]. The dark

portions indicated mud-filled vugs, while the bright yellow portions indicate hard carbonate. While Fig. 13.55 appears to show eight pad strips, there actually only four pads with their flap electrodes, making the appearance of two separate strips. The wide gaps indicate the separation between the pad/flap combos.

Baker-Atlas and Halliburton, with six pads, and Weatherford, with eight pads, staggered their pads into two slightly displaced rows of outsized pads, to maximize circumferential coverage on each pad and minimize the gaps between pad coverage. Figure 13.56 illustrates the Halliburton EMI pad arrangement [13.67]. Figure 13.57 shows a Weatherford CMI display.

Acoustic Versus Microresistivity Imaging Tools

Both imaging tools offer only images and neither deliver quantitative measurements. Acoustic imaging tools were developed, primarily, for fault and fracture identification. Microresistivity scanners were developed, primarily, for detailed stratigraphic evaluation.

The microresistivity scanners offer mm- to cm-scale image resolution, while the acoustic images offer only 2–3 cm scale resolution. The acoustic imagers gen-

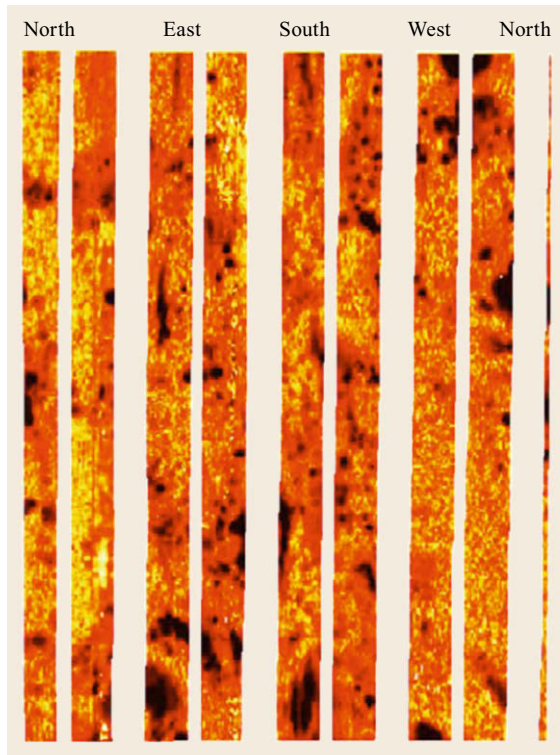


Fig. 13.55 Schlumberger fullbore formation microimager (FMI) images of a vuggy carbonate (from [13.65], courtesy of SPWLA)

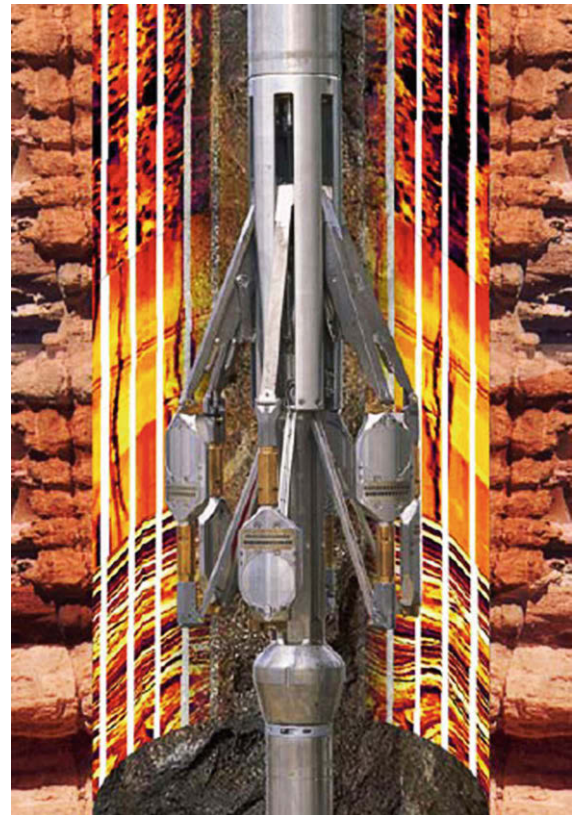


Fig. 13.56 Halliburton electrical microimaging (EMI) tool (courtesy of Halliburton)

erally work better in OBM-filled boreholes than do the microresistivity scanners, and offer full 360° borehole wall coverage, which the microresistivity scanners generally do not. Acoustic imagers also offer three-dimensional depth resolution, which the microresistivity scanners do not, and work better in rugose boreholes than the microresistivity scanners. Microresistivity scanners may work better in horizontal boreholes, because of the need for the acoustic imagers to be centered in the borehole. Acoustic imagers must be run at slower (1200 ft/hr) logging speeds than microresistivity scanners. Each tool has its niche market and the tools are not interchangeable.

13.11.7 Wireline Formation Testing

Wireline formation testers are special wireline tools, which allow one or more formation pressure measurement(s) and collection of one or more formation fluid sample(s), without having to conduct open-hole or cased-hole drill-stem tests. Modern versions of these tools include the ability to purge the sample chamber and to perform preliminary analysis of the sample fluid, to ensure that it is formation fluid and not mud filtrate. These tools are different from most wireline tools, in that they are used in fixed, or station logging, mode. Figure 13.58 shows one such tool. All major logging vendors offer similar services, for both wireline and LWD applications.

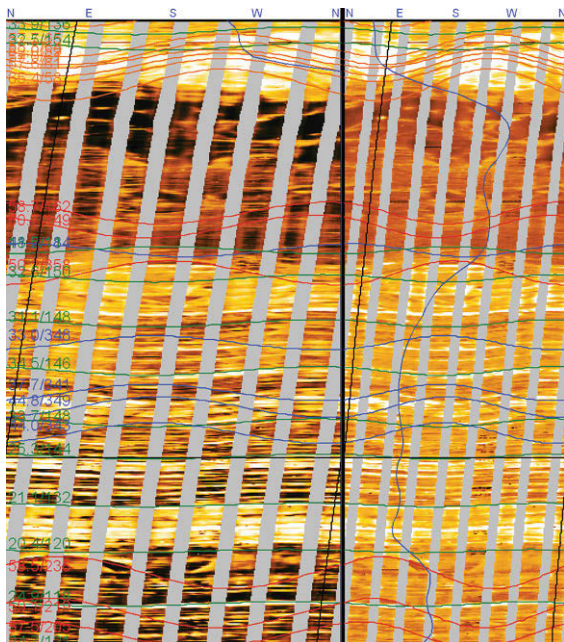


Fig. 13.57 Weatherford compact microimager (CMI) display

Wireline Formation Tester Applications

The principle applications for wireline formation testers are:

- Collecting formation-fluid samples for analysis
- Monitoring mud column and formation pressures
- Identification of formation-fluid pressure gradients and contacts

without having to run open-hole or cased-hole drill stem tests. Figure 13.59 shows a formation tester Pressure-depth plot for a Papua New Guinea well. Two gas

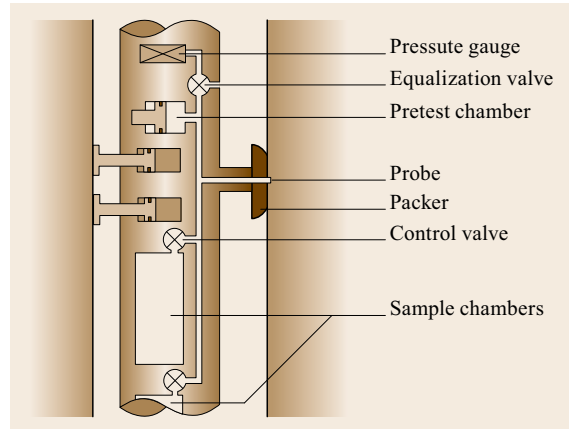


Fig. 13.58 Schematic of a wireline formation tester (after [13.68])

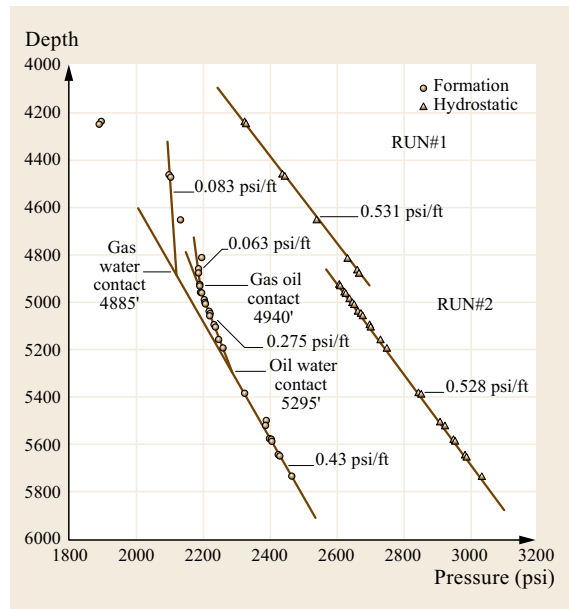


Fig. 13.59 Formation tester pressure-depth plot for a Papua New Guinea well, showing mud column and formation-fluid pressure gradients

gradients have been identified indicating isolated reservoirs, as well as an oil and water gradient in the second reservoir, which allows identification of the G/O and O/W contacts in this reservoir. Identification of fluid contacts from gradient intersections is critical for long

transition zones such as the Danish North Sea chalk reservoir, shown in Fig. 13.25. Formation tester pressure data have also been used to identify severely overbalanced mud situations, which could cause differential sticking.

13.12 Putting It All Together

To this point, we have covered the major pieces that make up formation evaluation. This section shows how they all fit together.

13.12.1 Western Australia Well

Figure 13.60 shows the dual laterolog/microspherically focused log (DLL/MSFL), with SP, gamma ray and caliper log display, for the pay interval of a Western Australia well. The well was the second, or confirmation well, for an off shore discovery. Track 1 of the log display contains the caliper, SP, gamma ray, and cable tension curves. Track 4 (combined tracks 2 and 3) displays the deep R_{LLD} and shallow R_{LLS} laterolog and micro-spherically focused log (MSFL) resistivity R_{xo} curves on logarithmic scales, with a four-cycle grid. The gross pay interval is from 1109.75–1130.0 m in depth. There appear to be shale breaks (nonreservoir rock) at 1122.50–1126.00 and 1130.00–1137.75 m depths.

Figure 13.60 shows the dual induction laterolog-3/borehole compensated sonic log (DIL/BCS), with SP, gamma ray and caliper log display, for the interval shown in Fig. 13.61. Track 1 contains caliper, SP, gamma ray, and cable tension curves, on linear scales. Track 3 contains the sonic interval transit time Δt and deep induction conductivity C_{ILD} curves on linear scales. Track 4 (combined tracks 2 and 3) contains the deep R_{ILD} and medium R_{ILM} induction and laterolog-3 R_{LL} resistivity curves on logarithmic scales, *even though the two-cycle logarithmic grid is only in track 2*. This DIL/BCS display is not typical for DIL/sonic (acoustic) log displays. The more common display is to use a two-cycle grid in track 2, with a 1 : 1 backup, for values over 20 Ω m.

Figure 13.62 shows the compensated neutron log/compensated density log (CNL/CDL), with gamma ray caliper and cable tension log display, for the interval shown in Fig. 13.61. Track 1 contains density caliper, neutron caliper gamma ray and cable tension curves on linear scales. Track 4 (combined track 2 and 3) contains density ρ_B and neutron limestone porosity φ_{CNS} curves on linear scales. Track 3 contains the density correction curve $\Delta\rho$ on a linear display.

The log displays in Figs. 13.60–13.62 were obtained on separate logging trips. Even though there is dupli-

cation of the SP, gamma ray, caliper, and cable tension curves, each curve is unique to the logging trip on which it was run.

13.12.2 Manual Analysis

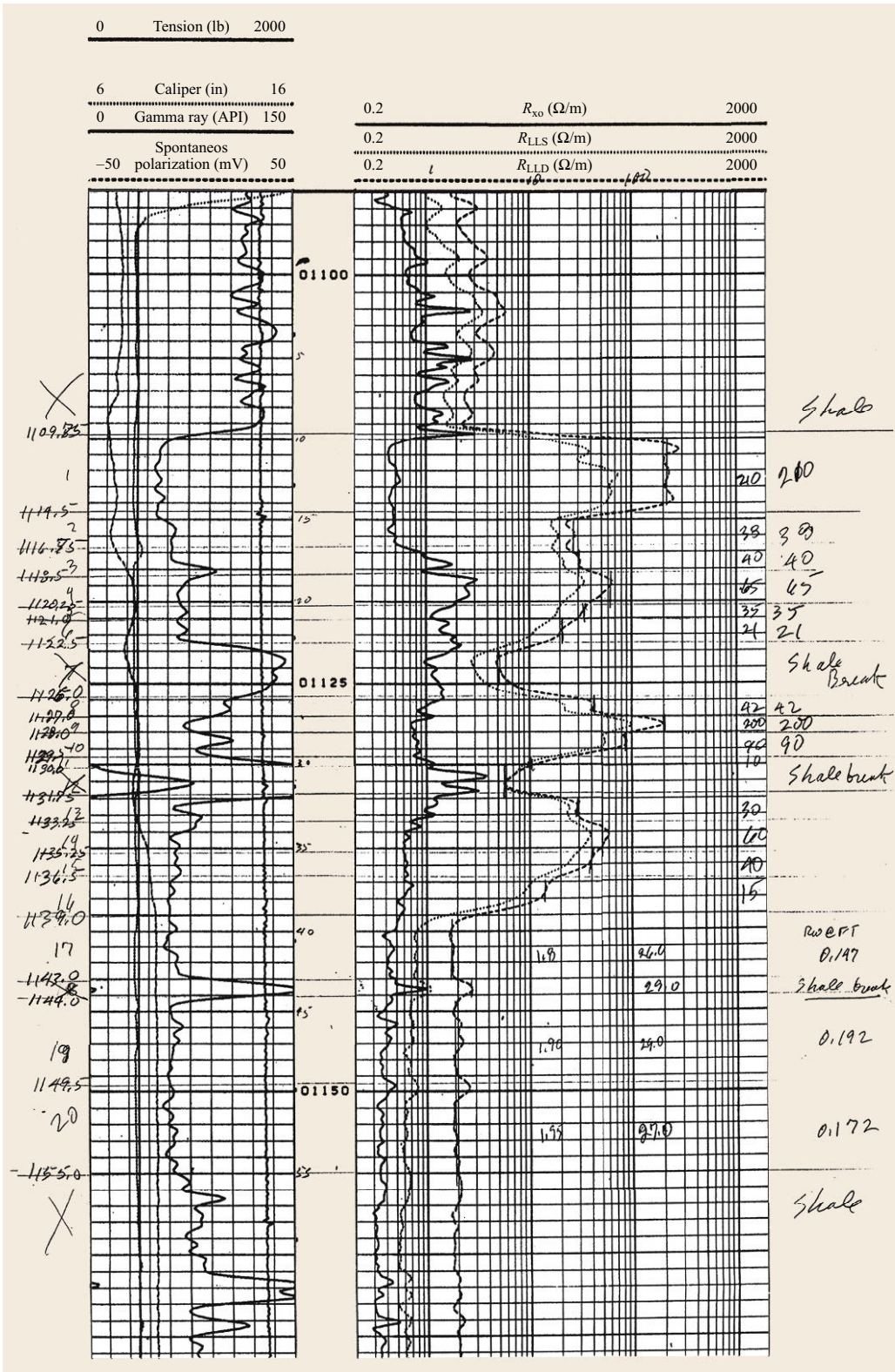
The pay zone in Figs. 13.60–13.62 has been broken into 14 separate analysis levels of essentially constant log values for manual analysis. Three additional analysis levels in the water leg, below the pay zone, are also included for estimating R_w . The deep laterolog resistivities have been annotated on Fig. 13.60, the acoustic interval transit times have been annotated on Fig. 13.61, and the bulk density and neutron porosities have been annotated on Fig. 13.62. Figure 13.63 shows the density-neutron cross-plot of the Fig. 13.63 density and neutron data and is used to obtain cross-plot porosities.

Table 13.14 shows R_{wa} estimate results for the 1139.00–1143.00, 1144.00–1149.00, and 1149.50–1155.00 m depth intervals in the water leg. Porosities are taken from the Fig. 13.63 density-neutron cross-plot. Raymer–Hunt–Gardner (RHG) porosities are also estimated from the sonic log data, as a check on the density-neutron cross-plot porosities. Archie a and m coefficients are from special core analysis laboratory (SCAL) results. Formation temperatures are estimated from a field-wide temperature-depth model. Formation water apparent NaCl salinities for the three R_{wa} estimates are also estimated as a check on the R_{wa} estimation.

Table 13.15 shows Archie S_w estimates for the 14 analysis intervals. Archie S_w is also estimated for the uppermost water leg analysis level, as a check on the S_w estimation. Density/neutron cross-plot porosities are used with RHG porosities estimated for verification. Deep laterolog resistivities (R_{LLD}) are used instead of the deep induction log resistivities because the well was drilled with high salinity (KCl) mud. The reservoir summary for this manual analysis is shown in the lower left-hand corner of Fig. 13.64, as:

- Gross pay: 29.25 m
- Net pay: 24.00 m
- Average porosity: 26.9%
- Average S_w : 17.0%.

Fig. 13.60
Western Australia well DLL/MSFL



0	Tension (lb)	2500	140	ΔT	40
-40	Spontaneous polarization (mV)	60	1000	C_{ILD} (mS/m)	0
6	Caliper (in)	16	0.2	R_{LL} (Ω/m)	2000
0	Gamma ray (API)	150	0.2	R_{ILM} (Ω/m)	2000
			0.2	R_{ILD} (Ω/m)	2000

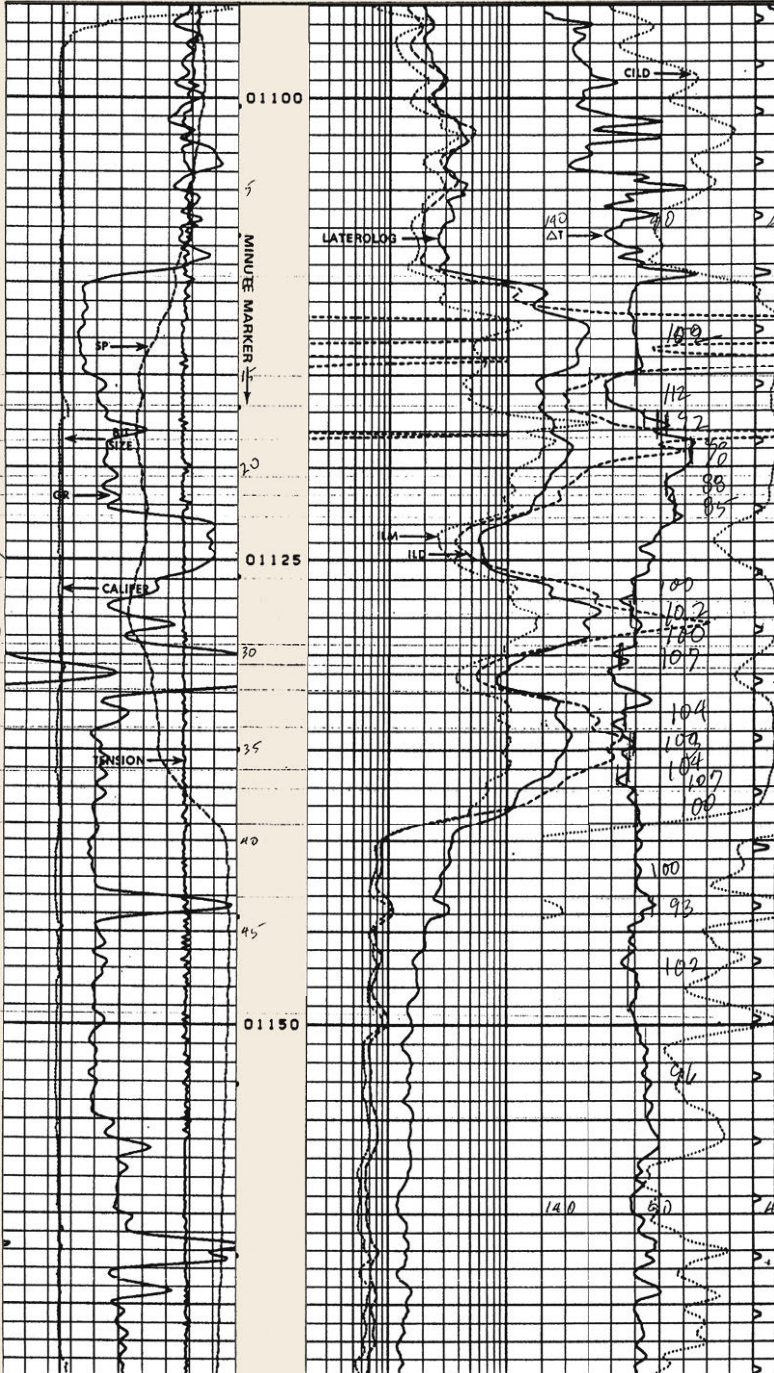


Fig. 13.61 Western Australia well DIL/BCS

0	Gamma ray (API)	150	1.95	-25	$\Delta\rho$	0.25
6	Caliper x (in)	16		ρ (B)		2.95
6	Caliper y (in)	16	45	ϕ_{CNS}		-15

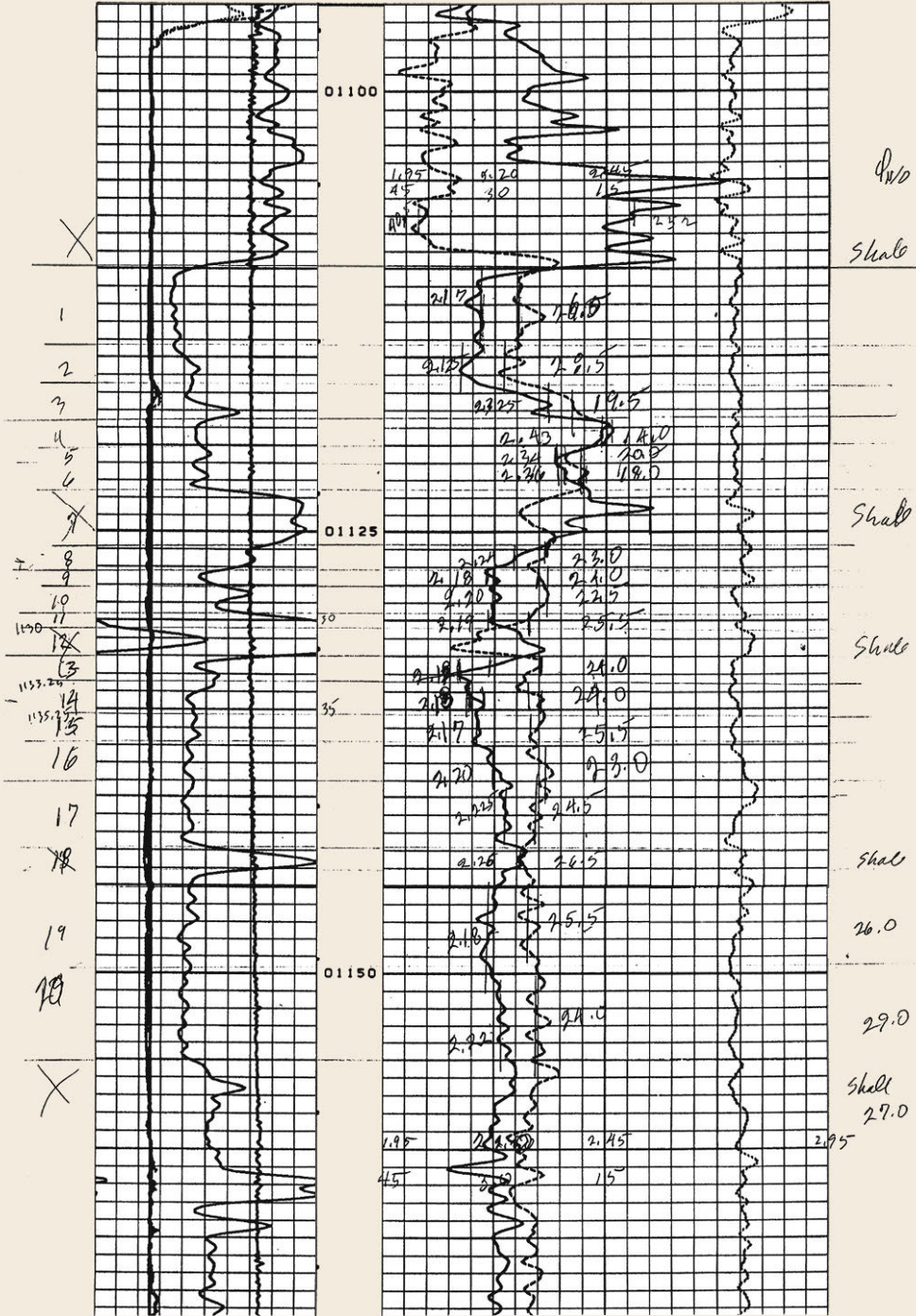


Fig. 13.62 Western Australia well CNL/CDL

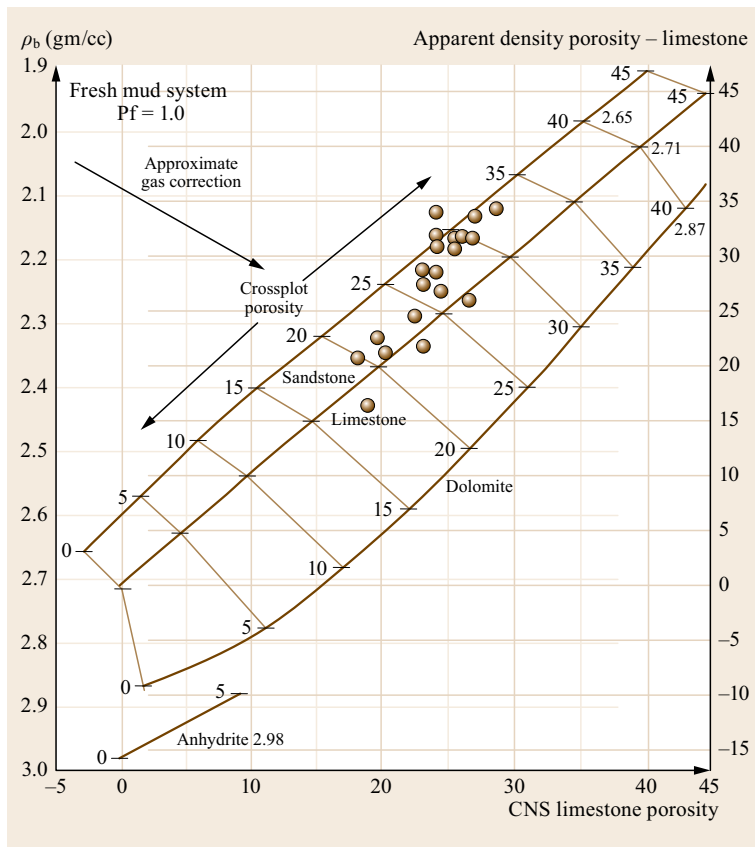


Fig. 13.63 Western Australia well density-neutron cross-plot

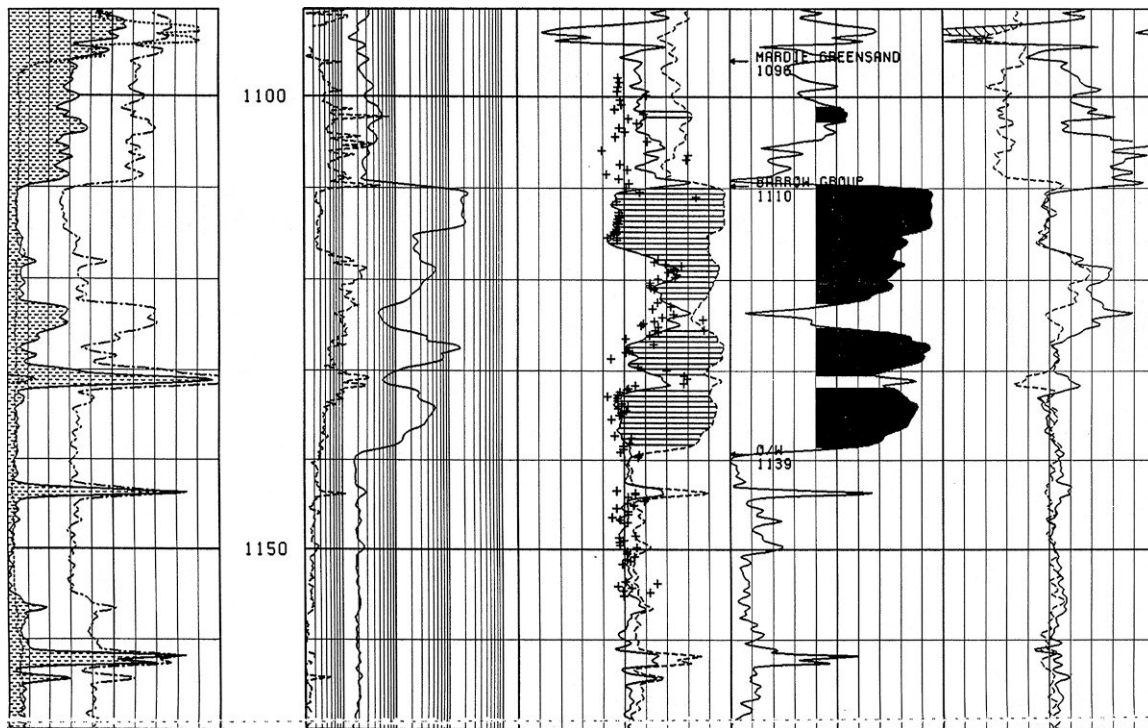


Fig. 13.64 Western Australia well, computer-aided log analysis

Table 13.14 Western Australia well, Excel R_{SUS} spreadsheet

R_{wa} determination															
Field name	Well name	Top MD (m)	Bottom MD (m)	Top TVD-SS (m)	Bottom TVD-SS (m)	ϕ_N	R_{hob} (gm/cc)	$\frac{\phi_N}{D}$	D_t ($\frac{\mu s}{ft}$)	ϕ_{RHG}	R_t ($\frac{\Omega}{m}$)	$R_{wa@FT}$ ($\frac{\Omega}{m}$)	Formation temperature (@ depth) ($^{\circ}F$)	$R_{wa@75^{\circ}F}$ ($\frac{\Omega}{m}$)	NaCl equivalent salinity (ppm)
		1139.00	1143.00	-1100.70	-1104.70	0.245	2.225	0.270	100	0.288	1.80	0.158	175	0.352	16616
		1144.00	1149.50	-1105.70	-1111.20	0.255	2.180	0.290	102	0.295	1.90	0.192	176	0.428	13465
		1149.50	1155.00	-1111.20	-1116.70	0.240	2.220	0.270	96	0.273	1.95	0.172	176	0.384	15126

Archie coefficients: $a = 0.92, m = 1.92$; RHG coefficients: $D_{ima} = 55 \mu s/ft, RHG = 0.64$

Table 13.15 Western Australia well, Excel Archie S_w spreadsheet

Archie S_w determination															
Well name	Top MD-KB (m)	Bottom MD-KB (m)	Top TVD-SS (m)	Bottom TVD-SS (m)	Formation temperature (@ depth) ($^{\circ}F$)	$R_w@FT$ ($\frac{\Omega}{m}$)	ϕ_N	R_{hob} (gm/cc)	ϕ_N/D	D_t ($\mu s/ft$)	ϕ_{RHG}	F	R_t ($\frac{\Omega}{m}$)	R_w/R_t	S_w
	1109.75	1114.50	-1036.75	-1041.50	168	0.160	0.270	2.170	0.300	102	0.295	9.28	210	0.0008	0.064
	1114.50	1116.75	-1041.50	-1043.75	168	0.160	0.285	2.125	0.325	112	0.326	7.96	38	0.0042	0.152
	1116.75	1118.50	-1043.75	-1045.50	169	0.160	0.195	2.325	0.220	92	0.257	16.84	40	0.0040	0.223
	1118.50	1120.25	-1045.50	-1047.25	169	0.160	0.140	2.430	0.180	78	0.189	24.76	65	0.0025	0.211
	1120.25	1121.00	-1047.25	-1048.00	169	0.160	0.200	2.340	0.210	88	0.240	18.41	35	0.0046	0.253
	1121.00	1122.50	-1048.00	-1049.50	169	0.160	0.180	2.360	0.200	85	0.226	20.22	21	0.0076	0.354
	1126.00	1127.00	-1053.00	-1054.00	170	0.160	0.230	2.240	0.260	100	0.288	12.22	42	0.0038	0.182
	1127.00	1128.00	-1054.00	-1055.00	170	0.160	0.240	2.180	0.285	102	0.295	10.24	200	0.0008	0.069
	1128.00	1129.50	-1055.00	-1056.50	170	0.160	0.225	2.200	0.265	100	0.288	11.78	90	0.0018	0.117
	1129.50	1130.00	-1056.50	-1057.00	170	0.160	0.255	2.190	0.290	107	0.311	9.91	10	0.0160	0.359
	1131.75	1133.25	-1058.75	-1060.25	170	0.160	0.240	2.180	0.285	104	0.302	10.24	30	0.0053	0.199
	1133.25	1135.25	-1060.25	-1062.25	171	0.160	0.240	2.180	0.290	103	0.298	9.91	60	0.0027	0.133
	1135.25	1136.50	-1062.25	-1063.50	171	0.160	0.255	2.170	0.300	104	0.302	9.28	40	0.0040	0.160
	1136.50	1139.00	-1063.50	-1066.00	171	0.160	0.230	2.200	0.270	100	0.288	11.36	15	0.0107	0.310
	1139.00	1143.00	-1066.00	-1070.00	171	0.160	0.245	2.225	0.270	100	0.288	11.36	2	0.0889	1.018

$a = 0.92, m = 1.92, n = 1.80, R_w@FT = 0.160, F = a\phi^{-m}, D_{ima} = 55.0, RHG = 0.64$

13.12.3 Computer-Aided Analysis

For comparison, Fig. 13.64 shows a computer-aided detailed log analysis for the Western Australia well. This

detailed evaluation utilized environmentally corrected log data, with more complex porosity and S_w models than the above manual analysis. Because of this, the results, though similar, are slightly different.

13.13 Summary

Wireline measurements have evolved from simple surface resistivity profiling arrays dropped down boreholes for well-to-well correlation to complex multimeasurement tool stacks, used to provide data for estimating reserves. Along the way specialized drill collars have been developed to duplicate wireline measurements and specialized tools developed for other useful downhole measurements.

Acknowledgments. This chapter is based on a one-day petrophysics review I developed for Chevron Overseas Petroleum, Inc. management and updated several times since. Anyone who attempts to do such a review stands on the shoulders of everyone who has gone before. In preparing this chapter, information has been collected from several sources. While many of the graphics and tabulations are my own, many oth-

ers have come from published sources, from in-house courses taught at Chevron, or from student presentations in classes taught at the University of Southern California, as well as the cited sources in the text and references. I would particularly like to express my gratitude to the Society of Petrophysicists and Well Log Analysts and the Petroleum Extension Service of the University of Texas, for permission to use graphics from their publications, as well as Baker-Atlas, Halliburton and Weatherford for permission to use some of their graphics. In many cases, these three vendors offered better examples than the graphics I originally asked to use. Finally, I appreciate the patience of Hsu Chang, the editor of this publication, for his patience while I tracked down permissions to use the third-party graphics I wanted to use to illustrate my thoughts.

References

- 13.1 W.L. Russell: *Principles of Petroleum Geology* (McGraw-Hill, New York 1960)
- 13.2 E.C. Thomas: personal communication (2009)
- 13.3 R.M. Batman: personal communication (2009)
- 13.4 S. Winchester: *The Map that Changed the World* (Harper Collins, New York 2001)
- 13.5 P.F. Worthington: personal communication (2011)
- 13.6 R.M. Bateman: Petrophysical data acquisition, transmission, recording, and processing: A brief history of change from dots to digits. In: *Trans. SP-WLA*, Vol. 50 (2009), Paper D
- 13.7 D.G. Hill: *Appendix A – Historical Review: Milestone Developments in Petrophysics* (Scrivener, Beverly 2012)
- 13.8 A.G. Schlumberger: *The Schlumberger Adventure* (Arco, New York 1982)
- 13.9 R.G. Van Nostrand, K.L. Cook: Interpretation of Resistivity Data, U.S. Geological Survey Professional Paper 499 (Washington, 1966)
- 13.10 D. Ross, R. Alger, D. Bishop, J. Dumanoir, J. Nawkins, F. Millard, J.T. Wall, D. Youngblood: *The Art of Ancient Log Analysis* (Society of Professional Well Log Analysts, Houston 1979)
- 13.11 C. Schlumberger, M. Schlumberger, E.G. Leonardon: Electrical coring – A method of determining bottom hole data by electrical measurements, *Trans. AIME* **110**, 503 (1932)
- 13.12 G.E. Archie: The electrical resistivity log as an aid in determining some reservoir characteristics, *Trans. AIME* **146**, 54–62 (1942)
- 13.13 G.E. Archie: Introduction to petrophysics or reservoir rocks, *Bulletin AAPG* **34**, 943–961 (1950)
- 13.14 M.R.J. Wyllie, A.R. Gregory, G.H.F. Gardner: An experimental investigation of factors affecting elastic wave velocities in porous media, *Geophysics* **23**, 459–493 (1958)
- 13.15 J.G. Burgen Jr.: Direct Digital Laserlogging. In: *SPE*, Paper 5506-MS (1975)
- 13.16 A.F. Veneruso, R.S. Simpson, C. Arnold (Eds.): *High Temperature Electronics and Instrumentation seminar Proceedings* (Sandia National Laboratory, Albuquerque 1979), SAND80-0834
- 13.17 R.P. Hoelscher, J.N. Arnold, S.H. Pierce: *Graphic Aids in Engineering Computation* (McGraw-Hill, New York 1952)
- 13.18 J.J. Arps: The effect of temperature on the density and electrical resistivity of sodium chloride solutions, *Pet. Trans. AIME* **198**, 327–330 (1953)
- 13.19 H.F. Dunlap, R.R. Hawthorn: The calculation of water resistivities from chemical analyses, *Trans. AIME* **192**, 373–375 (1951)
- 13.20 K.P. Desai, E.J. Moore: Equivalent NaCl determination from ionic concentrations, *The Log Analyst* **10**, 12–21 (1969)

- 13.21 J. Logan: Estimation of electrical conductivity from chemical analyses of natural waters, *JGR* **66**, 2479–2483 (1961)
- 13.22 E.J. Moore: A graphical description of new methods for determining equivalent NaCl concentration from chemical analysis. In: *Trans. SPWLA*, Vol. 7 (1968), Paper M
- 13.23 E.J. Moore, S.E. Szasz, B.F. Whitney: Determining formation water resistivity from chemical analysis, *Trans. AIME* **237**, 273–276 (1966)
- 13.24 A.W. Talash: An improved method for calculating water resistivities from chemical analyses, *JPT* **22**, 1396–1398 (1965)
- 13.25 Wireline Services Log Interpretation – Chart Book (Weatherford, Houston 2007)
- 13.26 D.V. Ellis, J.M. Singer: *Well Logging for Earth Scientists* (Springer, Dordrecht 2007)
- 13.27 W.F. Guerard: Heavy Oil in California (California Division of Oil and Gas, 1998) Publication TR28
- 13.28 A. Timur, W.B. Hemphkins, A.E. Worthington: Porosity and pressure dependence of formation resistivity factor for sandstones. In: *Trans. Canadian Well Logging Society*, Vol. 4 (1972), Paper D
- 13.29 R.M. Cohen, J.W. Mercer: *DNAPL Site Evaluation* (C.K. Smoley/CRC, Boca Raton 1992)
- 13.30 M.C. Leverett: Capillary behavior in porous solids, *Trans. AIME* **141**, 152–169 (1941)
- 13.31 D.M. Olson, W.R. Berry II: Deriving pseudo-capillary pressure curves from standard core analysis data in heavy oil reservoirs and their use in estimation of original Sw. In: *AAPG Joint Annual Meeting* (2015), Pacific Section
- 13.32 L.L. Raymer, E.R. Hunt, J.S. Gardner: An improved sonic transit time-to-porosity transform. In: *21st Annual Logging Symposium, SPWLA* (1980), Paper P
- 13.33 J. Raïga-Clemenceau, J.P. Martin, S. Nicoletis: The concept of acoustic formation factor for more accurate porosity determination from sonic transit time data, *The Log Analyst* **29**(1), 54–60 (1988)
- 13.34 D.V. Ellis, C.R. Chase, J.M. Chiaramonte: Porosity from neutron logs I: Measurement, *Petrophysics* **44**(6), 383–395 (2003)
- 13.35 T.M. Swulius: Porosity calibration of neutron logs, SACROC unit, *JPT* **38**, 468–476 (1986)
- 13.36 Anonymous: *Recommended Practice for Standard Calibration and Form for Nuclear Logs* (American Petroleum Institute, New York 1974), API RP-33
- 13.37 D.V. Ellis: *Well Logging for Earth Scientists* (Elsevier, New York 1987)
- 13.38 W.A. Gilchrist, I. Freyzi, L. Roberts: Nuclear source replacement – Promises and pitfalls. In: *Trans. SPWLA*, Vol. 52 (2011), Paper KKK
- 13.39 A. Badruzzaman, S. Barns, F. Blair, K. Grice: Radioactive Sources in Petroleum Industry: Applications, Concerns, and Alternatives. In: *SPE* (2009), Paper 123593-MS
- 13.40 R.J.S. Brown, I. Fatt: Measurements of fractional wettability of oilfield blocks by Nuclear Magnetic Relaxation method, *AIME Petroleum Trans.* **207**, 262–264 (1956)
- 13.41 R.J.S. Brown, W.B. Gamson: Nuclear magnetism logging, *AIME Petroleum Trans.* **219**, 201–209 (1960)
- 13.42 P. Hull, J.E. Coolidge: Field examples of nuclear magnetism logging, *JPT* **12**, 14–22 (1960)
- 13.43 G.R. Coates, L. Xiao, M.G. Prammer: *NMR Logging Principles and Applications* (Halliburton Energy Services, Houston 1999)
- 13.44 M.B. Dobrin: *Introduction to Geophysical Prospecting* (McGraw-Hill, New York 1960)
- 13.45 D.O. SeEVERS: A nuclear magnetic method of determining the permeability of Sandstones. In: *SPWLA Transactions*, Vol. 7 (1966), Paper L
- 13.46 G.R. Coates, M. Miller, M. Gillen, G. Henderson: The MRIL in CONOCO 33-1 An investigation of a new magnetic resonance imaging log. In: *SPWLA Transactions*, Vol. 32 (1991), Paper DD
- 13.47 D. Allen, C. Flaum, T.S. Ramakrishnan, J. Bedford, K. Castelijns, D. Fairhurst, G. Gubelin, N. Heaton, C.C. Minh, M.A. Norville, M.R. Seim, T. Pritchard, R. Ramamoorthy: Trends in NMR logging, *Oilfield Review* **12**, 2–19 (2000)
- 13.48 B. Sun, M. Skalinski, J. Brantjes, G.A. LaTorraca, G. Menard, K.-J. Dunn: The impact of T_1/T_2 ratio on porosity estimation. In: *SPWLA Transactions*, Vol. 49 (2008), Paper V
- 13.49 K.J. Dunn, D.J. Bergman, G.A. LaTorraca: *Petrophysical And Logging Applications*, Nuclear Magnetic Resonance (Pergamon/Springer, Amsterdam 2002)
- 13.50 W.E. Kenyon: Petrophysical principles of applications of NMR logging, *The Log Analyst* **48**(2), 21–43 (1997)
- 13.51 O. Serra, J. Baldwin, J. Quirein: Theory, interpretation, and practical applications of gamma ray spectroscopy. In: *SPWLA Transactions*, Vol. 21 (1980), Paper Q
- 13.52 H. Maurer, Y. Antonov, B. Corley, M. Rabinovich, Z. Zhou: Advanced processing for a new array laterolog tool. In: *SPWLA Transactions*, Vol. 50 (2009), Paper AA
- 13.53 R. Griffiths, J.W. Smits, O. Faivre, I. Duburg, E. Legendre, J. Doduy: Better saturation from new array laterolog. In: *SPWLA Transactions*, Vol. 40 (1999), Paper DDD
- 13.54 W.G. Ballengee: Resistivity logging. In: *Chevron Formation Evaluation Seminar, Laguna Beach* (1990)
- 13.55 B.I. Anderson, T.D. Barber: *Induction Logging* (Schlumberger Wireline and Testing, Sugarland 1996)
- 13.56 D.W. Martin, M.C. Spencer, H. Patel: Digital induction – A new approach to improving the response of induction measurement. In: *Trans. SPWLA*, Vol. 25 (2000), Paper C
- 13.57 J. Hou, L. Sanmartin, D. Wu, D. Torres, T. Celepcikay: A new multi-frequency triaxial array induction tool for enhancing evaluation of anisotropic formations and its field testing. In: *Trans. SPWLA*, Vol. 54 (2013), Paper CCC
- 13.58 M.G. LÜling, N. Seleznev, R. Chemali: Dielectric effects in petrophysics. In: *SPWLA Continuing Education Course, Cartagena* (2012)

- 13.59 R. Beste, T. Hagiwara, G. King, R. Strickland, G.A. Merchant: A new high resolution array induction tool. In: *Trans. SPWLA*, Vol. 41 (1984), Paper M
- 13.60 L.C. Shen: Problems in dielectric-constant logging and possible routes to their solution, *The Log Analyst* **26**(6), 14–25 (1985)
- 13.61 M. Bitter, J. Li, G. Kainer, R. Cherry, D. Torres, D. McCoy: Modern microwave formation evaluation sensor and its application in reservoir evaluation. In: *Trans. SPWLA*, Vol. 51 (2010), Paper B
- 13.62 J.D. Little, D.R. Julander, L.C. Knauer, J.T. Aultman, J.I. Hemmingway: Dielectric dispersion measurements in California heavy oil reservoirs. In: *Trans. SPWLA*, Vol. 51 (2010), Paper D
- 13.63 M.R.J. Wyllie: A quantitative analysis of the electrochemical component of the S.P. curve, *JPT* **1**, 17–26 (1949)
- 13.64 H.G. Doll: The SP Log: Theoretical Analysis and Principles of Interpretation, *Trans. AIME* **179**, 146–185 (1949)
- 13.65 T. Zhang, N.F. Hurley, W. Zhao: Numerical modeling of heterogeneous carbonates and multi-scale dynamics. In: *Trans. SPWLA*, Vol. 50 (2009), Paper JJJ
- 13.66 J. Zemanek, E.E. Green, L.J. Norton, R.L. Caldwell: Formation evaluation by inspection with the borehole televiewer, *Geophysics* **35**(2), 245–269 (1970)
- 13.67 J.F. Goetz, D.D. Seiler, C.S. Edmiston: Geological and borehole features described by the circumferential acoustic scanning tool. In: *Trans. SPWLA*, Vol. 31 (1990), Paper C
- 13.68 M.A. Proett, M.C. Waid, J. Heinze, M.W. Franki: Low permeability interpretation using a new wireline formation tester “Tight Zone” pressure transient analysis. In: *Trans. SPWLA*, Vol. 35 (1994), Paper III

Petroleum Production Engineering

Shengnan Chen

Petroleum production engineering focuses on producing hydrocarbons from well bottom-hole to surface through the wellbore. In this chapter, the terms inflow performance relationship, tubing performance relationship and choke performance relationship are firstly introduced, which relate the production rates with the in situ pressure along the flow path of the reservoir fluids in the wellbore. Different artificial lift techniques are then discussed to either resume production from a well where no flow is occurring or to achieve a higher production rate by lowering the well flowing bottom-hole pressure. Well stimulation methods, including matrix acidizing and hydraulic fracturing, are finally presented, which enhance the well production rate either by removing the skin from the well, or creating high conductive flow paths for the reservoir fluids to flow to the bottom-hole of the producers.

14.1 Flowing Wells and Gas Lift	501
14.1.1 Inflow Performance Relationship	501
14.1.2 Tubing Performance Relationship (TPR)	504
14.1.3 Choke Performance	506
14.1.4 Gas Lift	506
14.2 Artificial Lift	508
14.2.1 Sucker Rod Pumping	508
14.2.2 Other Artificial Lift Methods	509
14.3 Well Stimulation	512
14.3.1 Matrix Acidizing	512
14.3.2 Hydraulic Fracturing	514
References	516

The goal of petroleum production engineering is to maximize oil and gas production in a cost effective manner. It involves a series of techniques to ensure the inflow of oil and gas to the wellbore, to lift the fluids to the surface efficiently, and to separate produced oil, gas

and water on the surface. As an important subsystem of oilfield development engineering, petroleum production engineering is closely related to reservoir engineering and the storage and transportation engineering of oil and gas.

14.1 Flowing Wells and Gas Lift

Initial reservoir pressure and economic cost analysis determines what methods can be used to extract oil out of the reservoirs. In petroleum production engineering, engineers are concerned with transporting reservoir fluids from the well bottom-hole to the wellhead at surface. There are mainly two categories of production methods:

- Natural flow: reservoir fluids can flow to the surface naturally due to pressure in the formation.
- Artificial lifting: reservoir fluids must be lifted when there is insufficient pressure in the reservoir to lift the produced fluids to the surface.

Schlumberger claims that of the approximately one million oil and gas wells producing in the world, roughly 5% flow naturally – leaving nearly all of the world's oil and gas production reliant on efficient artificial lift operations.

14.1.1 Inflow Performance Relationship

The inflow performance relationship (IPR) is one of the most important methods for analyzing well production. IPR reflects the ability of fluids to flow from a reservoir to a well by quantifying interactions between well

production rate, well bottom-hole flowing pressure and reservoir pressure.

According to Darcy's law (14.1), well production rate can be expressed as

$$q_o = J (P_e - P_{wf}) , \quad (14.1)$$

where:

- q_o Well production rate (m^3/s)
- P_e Reservoir pressure (Pa)
- P_{wf} Well flowing bottom-hole pressure (Pa)
- J The productivity index ($\text{m}^3/(\text{Pa s})$).

The productivity index J , reflects the relationship of reservoir parameters, fluid properties, completion conditions, drainage area, and production rates.

IPR for Single-Phase Reservoirs

At initial reservoir conditions, the pressure of a reservoir may be above the bubble-point pressure of the hydrocarbon fluids. If so, it is referred as an undersaturated reservoir. Bubble-point pressure refers to the pressure (at a given temperature) at which the natural gas begins to come out of the oil and form bubbles. If well flowing bottom-hole pressure is also above the bubble-point pressure, then the reservoir only has single phase (hydrocarbon liquid) flow. For single-phase flow in the reservoir, the productivity index can be analytically calculated for different flow regimes.

Flow in a reservoir is often characterized as being one of two types: transient flow or boundary-dominated flow. The transient flow regime exists before the pressure wave created by well production has reached any reservoir boundary yet. Once the pressure wave reaches the boundary, steady-state or pseudosteady-state flow may appear in the reservoir, depending on the pressure condition at the boundary.

Transient Flow. Transient flow refers to a flow regime where the pressure wave has not reached the reservoir boundary. For a well located in the center of a circular reservoir, the productivity index equation for transient flow can be expressed as

$$J = \frac{q_o}{P_i - P_{wf}} = \frac{4\pi k_o h}{\mu_o B_o \ln \left(\frac{4k_o t}{\gamma \phi \mu_o c_t r_w^2} + S \right)} , \quad (14.2)$$

where:

- P_i Initial reservoir pressure (Pa)
- k_o Effective permeability (m^2)
- B_o Oil volume factor (m^3/sm^3)
- h Effective height (m)
- μ_o Oil viscosity (Pa s)
- r_w Wellbore radius (m)

- t Time (s)
- γ Euler's constant = 1.78
- ϕ Porosity
- c_t Total compressibility factor ($1/\text{Pa}$)
- S Skin factor, influenced by well completion, down-hole damage or well stimulation and obtained from build-up curve.

The flow time required for the pressure wave to reach a circular reservoir boundary can be expressed as

$$t_{\text{pss}} = 1200 \frac{\phi \mu_o c_t r_e^2}{k_o} , \quad (14.3)$$

where r_e is the radius of the drainage area (m).

Steady-State Flow. A steady-state flow regime may appear once the pressure wave reaches the boundary. In steady-state flow, all parameters including pressure, temperature and flow rate at any single point of the system do not change over time. Pressure at the boundary for steady-state flow is constant and could be maintained by a water injection well or an aquifer.

For a well located in the center of the circular reservoir with a constant pressure boundary, the productivity index of the production equation can be expressed as

$$J = \frac{q_o}{P_e - P_{wf}} = a \frac{2\pi k_o h}{\mu_o B_o \left(\ln \frac{r_e}{r_w} + S \right)} , \quad (14.4)$$

where a = unit conversion factor, which is $a = 1$ Darcy in SI units; $a = 86.4$ when units of measure are q (m^3/d), k (μm^2), μ (mPa s), h (m), p (MPa). If the unit of pressure is kPa, $a = 0.0864$.

Pseudosteady-State Flow. Pseudosteady-state flow may appear once the pressure wave reaches the boundary. In pseudosteady state flow, the pressure at any point in the reservoir declines at the same constant rate over time. For circular closed reservoirs, where there is no liquid flow at the boundary, the productivity index in the production equation at pseudosteady state can be expressed as

$$J = \frac{q_o}{\bar{P}_r - P_{wf}} = \frac{2\pi k_o h}{\mu_o B_o \left(\ln \frac{r_e}{r_w} - \frac{3}{4} + S \right)} , \quad (14.5)$$

where \bar{P}_r is the average reservoir pressure (Pa).

A shape factor needs to be used if the close drainage area is noncircular. Values of the shape factor for different shapes can be found elsewhere.

IPR Curves for Single-Phase Reservoirs. An IPR curve is a graphical presentation of the relationship between well production rate and well flowing bottom-hole pressure. IPR curves for single-phase reservoirs

are straight lines as shown in Fig. 14.1. The slope of the IPR curve is the productivity index, J , which is constant in a single-phase reservoir.

IPR for Two-Phase Reservoirs

Productivity index, J , presented in the previous section, is valid for reservoir pressure and well flowing bottom-hole pressure values as low as the bubble-point pressure, when single-phase flow exists in the reservoir. When the reservoir pressure drops below the bubble-point pressure, the dissolved gas escapes from the oil and becomes free gas. Both oil and gas will be flowing in the formation.

Vogel [14.1] proposed a dimensionless IPR equation for dissolved gas drive reservoirs

$$q_o = q_{o \max} \left[1 - 0.2 \frac{P_{wf}}{P_r} - 0.8 \left(\frac{P_{wf}}{P_r} \right)^2 \right], \quad (14.6)$$

$$q_{o \max} = \frac{J^* \bar{P}}{1.8}, \quad (14.7)$$

where J^* is the productivity index when reservoir pressure is above the bubble-point pressure.

IPR Curves for Two-Phase Reservoirs. An IPR curve for a two-phase reservoir is shown in Fig. 14.2. The productivity index, J , is not constant, but keeps decreasing as well flowing bottom-hole pressure decreases in a two-phase reservoir.

IPR for Partial Two-Phase Oil Reservoirs

Partial two-phase reservoirs refer to the cases where the reservoir pressure is above the bubble-point pressure,

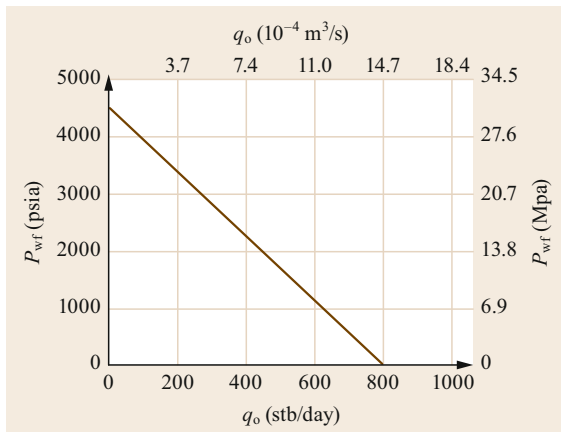


Fig. 14.1 A typical IPR curve for an oil well in a single-phase reservoir

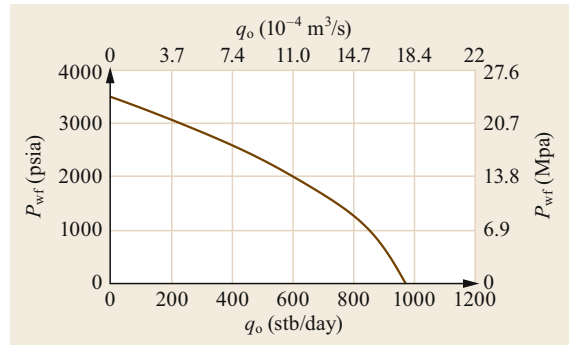


Fig. 14.2 A typical IPR curve for an oil well in a two-phase reservoir

while the well flowing bottom-hole pressure is below the bubble-point pressure. A generalized IPR model needs to be applied under such circumstance

$$q = J^* (\bar{P} - P_b) + \frac{J^* P_b}{1.8} \left[1 - 0.2 \left(\frac{P_{wf}}{P_b} \right) - 0.8 \left(\frac{P_{wf}}{P_b} \right)^2 \right], \quad (14.8)$$

where P_b is the bubble-point pressure of the reservoir fluids (Pa).

IPR Curves for Partial Two-Phase Reservoirs. An IPR curve for a partial two-phase reservoir is shown in Fig. 14.3. The productivity index, J is constant when well flowing bottom-hole pressure is larger than bubble-point pressure in a two-phase reservoir. When well flowing bottom-hole pressure is lower than bubble-point pressure, J is not constant, but decreases as well flowing bottom-hole pressure decreases.

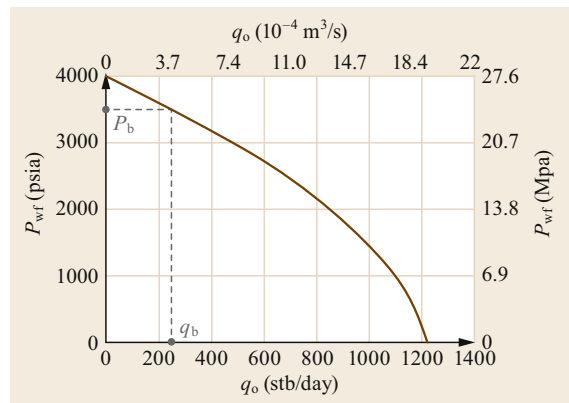


Fig. 14.3 A typical IPR curve for an oil well in a partial two-phase reservoir

14.1.2 Tubing Performance Relationship (TPR)

Flow Regimes

In the wellbore, the pressure of the reservoir fluid decreases as it flows from the well bottom-hole to the wellhead. If the pressure drops below the bubble point in the wellbore, the following four flow patterns may occur in a vertical wellbore (Fig. 14.4):

1. Bubble flow
2. Slug flow
3. Annular flow
4. Mist flow.

In bubble flow, small gas bubbles are dispersed in the liquid phase. Gas is the dispersed phase and liquid is a continuous phase. In slug flow, with expanding gas bubbles, small bubbles merge into large bubbles until

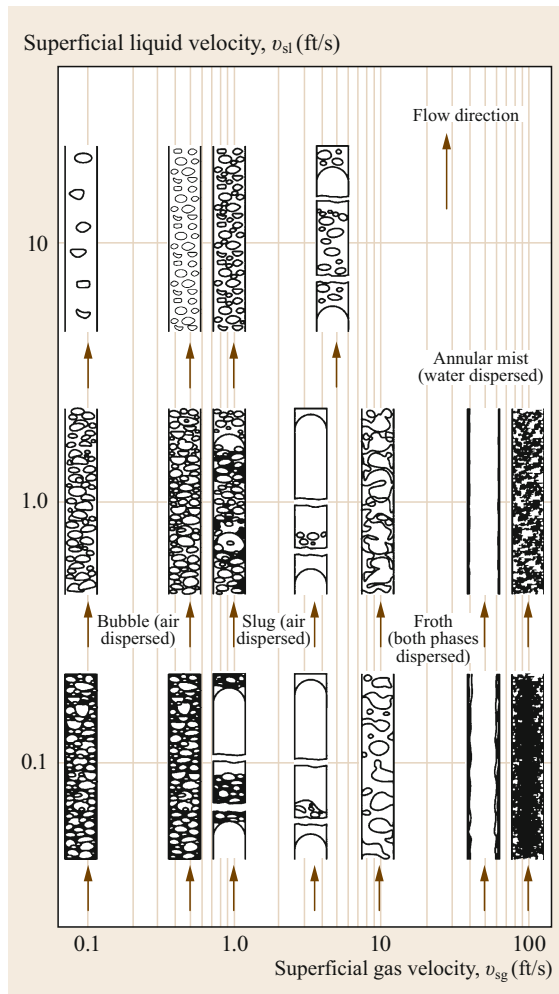


Fig. 14.4 Flow regimes in gas-liquid flow (after [14.2])

the entire cross-section is occupied by the gas phase. In annular flow, as the gas volume further increases, the continuous gas phase occupies the center of the tubing and the liquid phase appears as a ring flowing along the wall of the tubing. Gas and liquid phase are both continuous in annular flow. In mist flow, liquid exists as liquid droplets, which are dispersed in gas flow. The gas is the continuous phase and the liquid is dispersed phase.

Liquid Holdup

Due to the density difference between liquid and gas, and the low mixture flow rate, the gas phase rises faster than the liquid phase when oil and gas flow upward simultaneously in the wellbore. This phenomenon is called gas slippage. As a result of the slippage, the density of the in situ gas-liquid mixture will increase. The denser liquid phase is held up in the wellbore relative to the lighter gas phase. Thereby the hydrostatic head of the mixture, which is a function of gravity, also increases. Additional energy loss arising from slippage is called slippage loss.

TPR Models

Based on energy balance equations, the pressure gradient of multiphase flow along the vertical wellbore can be expressed as

$$\frac{dP}{dz} = \rho g + \rho v \frac{dv}{dz} + f \frac{\rho v^2}{2D}, \quad (14.9)$$

where:

P Pressure (Pa)

z Height of the fluid mixture calculated from the midpoint of pay zone (m)

ρ Fluid density (density of the mixture) (kg/m^3)

g Gravity acceleration (m/s^2)

v Mixture velocity (m/s)

f Darcy-Weisbach friction factor of mixture flow, which can be determined by Fig. 14.5

D Tubing diameter (m)

It can be seen from Fig. 14.5 that the friction factor is a function of Reynolds number and relative pipe roughness. Reynolds number is a dimensionless quantity in fluid mechanics used to determine whether a fluid flow pattern is laminar or turbulent flow. The relative pipe roughness is its absolute roughness divided by the internal diameter of the pipe.

Homogeneous Model. In 1952, *F.H. Poettmann* and *P.G. Carpenter* proposed a method to calculate a friction loss coefficient (or energy loss coefficient) for the pressure gradient of the gas-liquid vertical flow [14.4]. The features of this method are as follows:

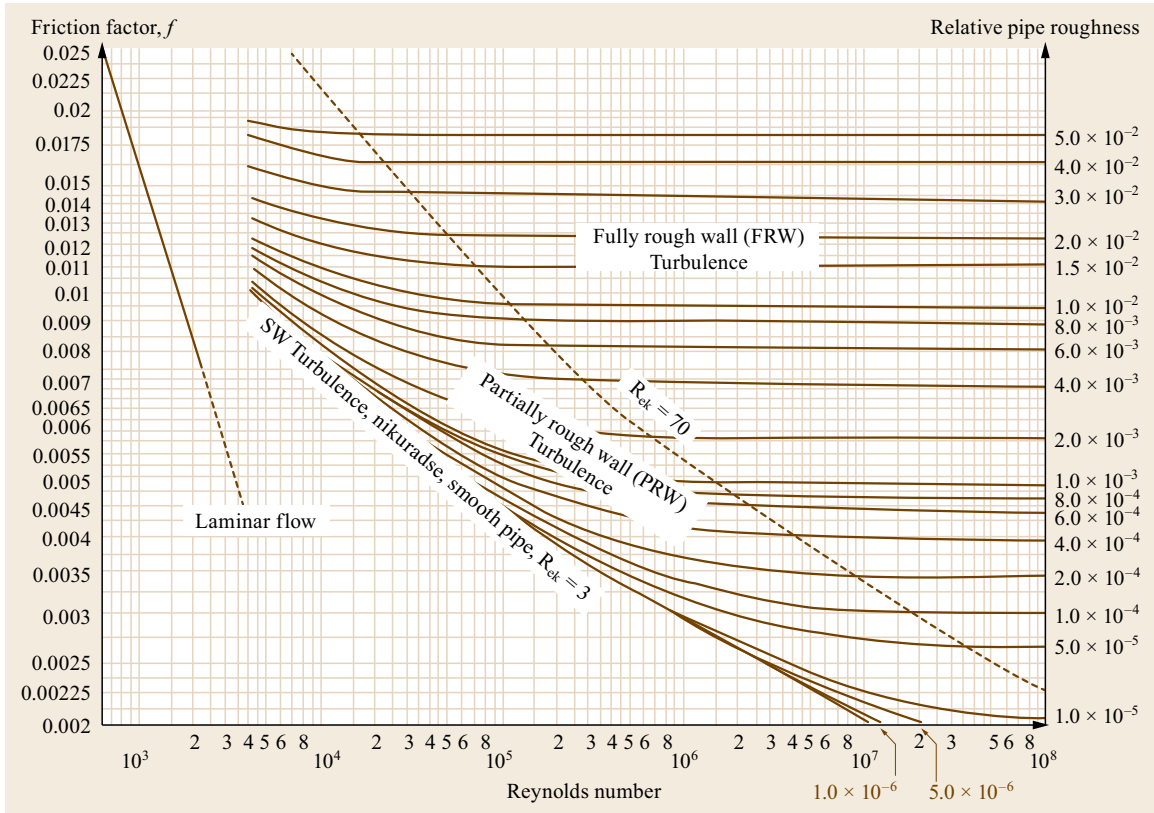


Fig. 14.5 Moody friction factor diagram (after [14.3])

1. The acceleration term is ignored in the pressure gradient equation, which is the second term on the right-hand side of (14.9)
2. No specific flow pattern description is used
3. Density calculations are done without considering slippage
4. Friction loss coefficients are calculated from the relationship curve of $f \approx Dv\rho$ based on the field data.

Because the curves of f are obtained from the field data, the impacts of the friction, slippage and acceleration are all taken into consideration. The calculation method for the loss resulting from these factors is similar to that of calculating friction loss. Obviously, the fluid viscosity and the liquid holdup are not considered in the homogeneous models.

Separated Flow Model. Separated flow models are more realistic than the homogeneous flow models. In situ density of the fluid mixture along the wellbore is calculated by determining the liquid holdup, and different flow regimes are also considered in the separated flow models. Many separated models are available for TPR calculations, and they all include empirical correlations in different models.

In 1967, *Orkiszewski* proposed a new method based on the analysis of previously published methods [14.5]. *Orkiszewski* compared previous methods with measured data and found that the *Griffith* and *Wallis* method [14.6] and the *Duns* and *Ros* method [14.7] were relatively accurate. The *Griffith* and *Wallis* method was more reliable in the low flow-rate range of slug flow, but it was not accurate at the high flow-rate range. The *Duns* and *Ros* method also shared a similar problem. *Orkiszewski* improved the *Griffith* equation of slug flow by extending it to the high-rate range, which increased the application range. When dealing with transitional flow patterns, *Orkiszewski* used the same approach with the *Duns* and *Ros* interpolation method. In *Orkiszewski*'s model, the retention rate (the ratio of one-phase volume to total volume in a pipe interval) was determined based on observed physical phenomena. The distribution pattern of gas and liquid phases should also be considered in calculating the pressure gradient of slug flow. Thus, calculation methods of retention rate and friction loss for each flow pattern (bubble flow, slug flow, transition flow and mist flow) were proposed in *Orkiszewski*'s model.

The method of calculating pressure gradients was similar to that of calculating friction loss coefficients

based on different flow patterns. The only difference was that the flow pattern needed to be determined in advance based on flow pattern boundaries before calculating mixture density and friction gradient.

14.1.3 Choke Performance

Once reservoir fluid reaches the surface of a flowing well, it will then pass through a choke, which is located on the wellhead. A wellhead choke controls the surface pressure and production rate from a flowing well. Chokes usually are selected so that fluctuations in the line pressure downstream of the choke have no effect on the production rate.

As shown in Fig. 14.6, the pressure difference through a choke is calculated based on the pressure before the choke (P_1) and the pressure after the choke (P_2). Due to the low tubing head pressure, gas expands at the wellhead and the gas flow rate increases significantly. The diameter of the wellhead choke is relatively small, and thus the flow rate of the mixture through the choke is extremely high and may reach the critical flow velocity. Critical flow occurs when the fluid flow rate reaches the propagation velocity of the pressure wave in the fluid media.

At this point, we can regard the gas–oil flow through the choke as nozzle flow at critical conditions. Under such conditions, the relationship between the mass flow through the choke and the pressure difference of the choke is shown in Fig. 14.6.

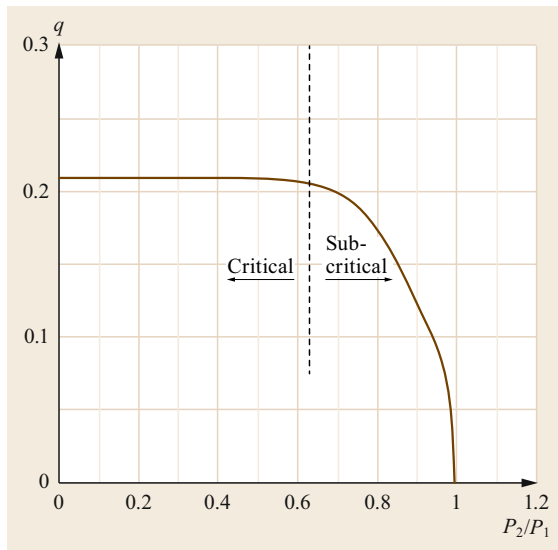


Fig. 14.6 Dependence of flow rate through a choke on the ratio of the upstream to the downstream pressure (after [14.8])

The critical pressure ratio is the pressure ratio P_c/P_1 at the maximum flow rate. Based on the thermodynamic calculation, the critical pressure ratio is

$$\frac{P_c}{P_1} = \left(\frac{k}{k+1} \right)^{\frac{k}{k-1}}, \quad (14.10)$$

where k = gas adiabatic exponent – for natural gas, k is 0.546.

The critical pressure ratio when air flows through the nozzle is

$$\frac{P_c}{P_1} \approx 0.528. \quad (14.11)$$

Based on (14.11), when the pressure ratio is equal to or less than 0.528, the flow rate is about equal to the speed of sound. Under the critical flow condition, that is, $P_2/P_1 = P_c/P_1 \leq 0.528$, the flow rate change is only affected by P_1 , i. e., the pressure before the choke.

The pressure before the choke is the tubing head pressure, which can be calculated by

$$P_t = \frac{cR^n q}{d^m}, \quad (14.12)$$

where:

- P_t Tubing pressure (Pa)
- R Oil gas ratio
- q Oil production
- d Choke diameter
- c, m, n Constant.

Due to the difference of fluid properties and mixture types of oil and gas, the constants c , m , and n may take different values, which are shown in Table 14.1.

14.1.4 Gas Lift

An oil well cannot flow naturally if the formation pressure is not high enough to push the reservoir fluids up to the surface. In order to maintain or increase the oil production rate, high-pressure compressed natural gas or air is injected into the lower section of the wellbore to propel the reservoir fluids to the surface. This is called gas lift. Besides pushing the liquid by its expansion energy, the high-pressure compressed gas aerates the liquid to reduce its effective density, thus facilitating the liquid reaching the surface.

Table 14.1 A summary of c , m , and n values given by different researchers

Correlation	c	m	n
Gilbert [14.9]	10.0	0.546	1.89
Ros [14.10]	17.4	0.5	2.0
Baxendell [14.11]	9.56	0.546	1.93
Achong [14.12]	3.82	0.65	1.88
Pilehviri [14.13]	46.67	0.313	2.11

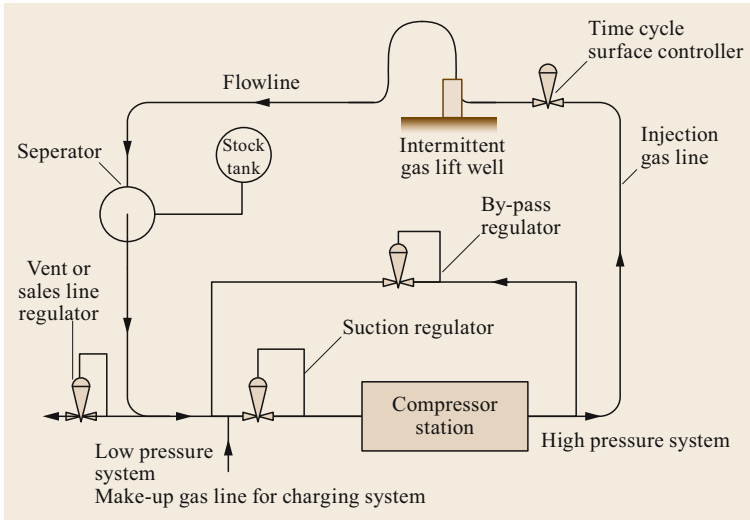


Fig. 14.7 A simplified flow diagram of a closed rotary gas lift system for a single intermittent well (after [14.8])

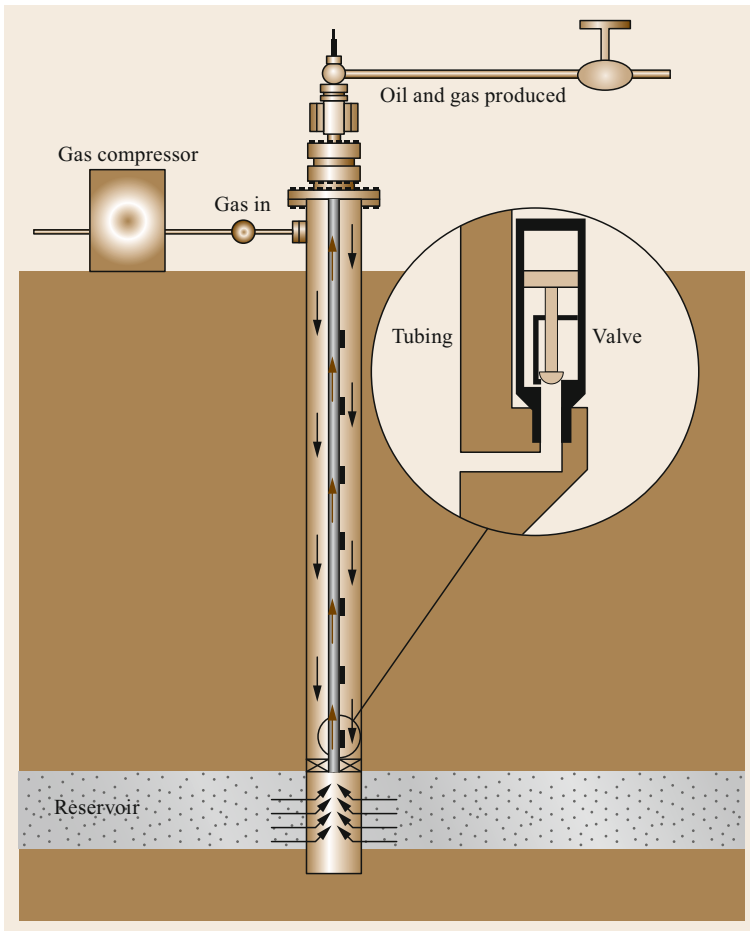


Fig. 14.8 Gas-lift concept (after [14.14])

Gas lift can be widely applied to high-productive and deep wells from which the fluids contain small

amount of sands, water, corrosive substances, and which have large gas-oil ratios. However, sufficient gas

sources, usually natural gas produced from nearby gas and oil wells, are the prerequisites to applying the gas lift method.

Based on the injecting operations, gas lift can be classified as continuous or intermittent. In continuous gas lift, high-pressure gas is continuously injected. Continuous gas lift is especially applicable to high-production wells with reasonable reservoir pressures. In intermittent gas lift, gas is injected periodically to lift the fluid plugs that form during injection intervals. Figure 14.7 depicts a simplified flow diagram of a closed rotary gas lift system for a single intermittent well. Intermittent gas lift operations have a start-and-stop gas

injection pattern, which is regulated by the time cycle surface controller. It is mainly used for low-production wells with low reservoir pressures.

Figure 14.8 illustrates the subsurface configuration of a gas lift well. Injected high pressure gas flows in the annulus and enters the tubing through the operating valve and gets mixed with the reservoir fluids. Multiple valves may be installed in a well during a gas lift operation. To obtain the maximum efficiency, the tubing end should reach the middle of the pay zone to produce fluids at the maximum submergence depth. Thus, even if reservoir pressure drops after a period of time, high efficiency gas lift can still be maintained.

14.2 Artificial Lift

Artificial lift increases production rates from a producing well. Generally this is achieved by the use of a mechanical device (e.g., pump) inside the well.

During development of oil fields, producing wells cannot always flow naturally. For some wells, natural flows can significantly reduce and eventually stop when there is insufficient pressure in the reservoir. For some other wells, natural flows cannot occur initially due to low formation pressure or high viscosity reservoir fluids. In these situations, artificial lift is required. Artificial lift may also be applied in naturally flowing wells to increase the oil production rate above what would flow naturally.

Artificial lift methods can be classified as gas lift and pumping. Commonly used well pumps include sucker rod pumps, hydraulic pumps, electrical submersible pumps, progressive cavity pumps, and plunger pumps. Although recent technology has facilitated the use of more and more electrical submersible pumps and hydraulic pumps, especially in deep wells, the majority of artificial lift pumps are still sucker rod pumps.

14.2.1 Sucker Rod Pumping

Sucker rod pumping (also known as beam pumping) consists of a pumping unit, a pumping rod and a downhole plunger pump. Figure 14.9 shows the schematic diagram of a working sucker rod pumping unit.

Pumping Unit

Pumping unit refers to the surface equipment. A beam pumping unit mainly includes a horsehead, polished rod, walking beam, crank arm, gear box, power, and assistive devices. When it is working, the speed rotary motions of the power machine are transferred to a crank shaft through a belt and a reducing gear box, in order to rotate the crank slowly. Such rotary motions are then

converted into the reciprocally up and down motions of the horsehead by the walking beam and a pitman. As a result, the horsehead drives the polished rod up and down to lift reservoir fluids.

Downhole Plunger Pump

A plunger pump is a downhole device used with a sucker rod pumping unit in the well. Normally, besides oil, the pumped reservoir fluids also contain sand, wax, gas, water and corrosive substances. As it usually works at hundreds or thousands of meters deep, the pump has to tolerate pressure of more than 20 MPa. The efficiency of the pump directly affects the production rate of the producing well.

The bottom of the pump barrel is installed with a sucking valve (also known as standing valve), which can only open in upwards movements. Using a polished rod, a plunger is put down into the pump barrel. A discharge valve (also known as traveling valve), which only opens in upwards movements, is installed on the plunger.

A stroke process includes an upstroke and a downstroke. In one cycle, reservoir fluids flow into plunger, and then into the tubing above the plunger. The maximum moving distance of polished rod in a cycle is called polished rod stroke.

Upstroke. In this process, the pumping rod drives the upward movement of the plunger and the traveling valve, as shown in Fig. 14.10. The traveling valve on the plunger is closed due to fluid pressure in the tubing. Meanwhile, the pressure below the plunger is reduced, and the standing valve is opened because of the pressure difference between fluid pressure and the pressure in the pump. The reservoir fluids pass the standing valve and enter the cylinder. If the tubing is filled with reservoir fluids, the produced fluid volume from the

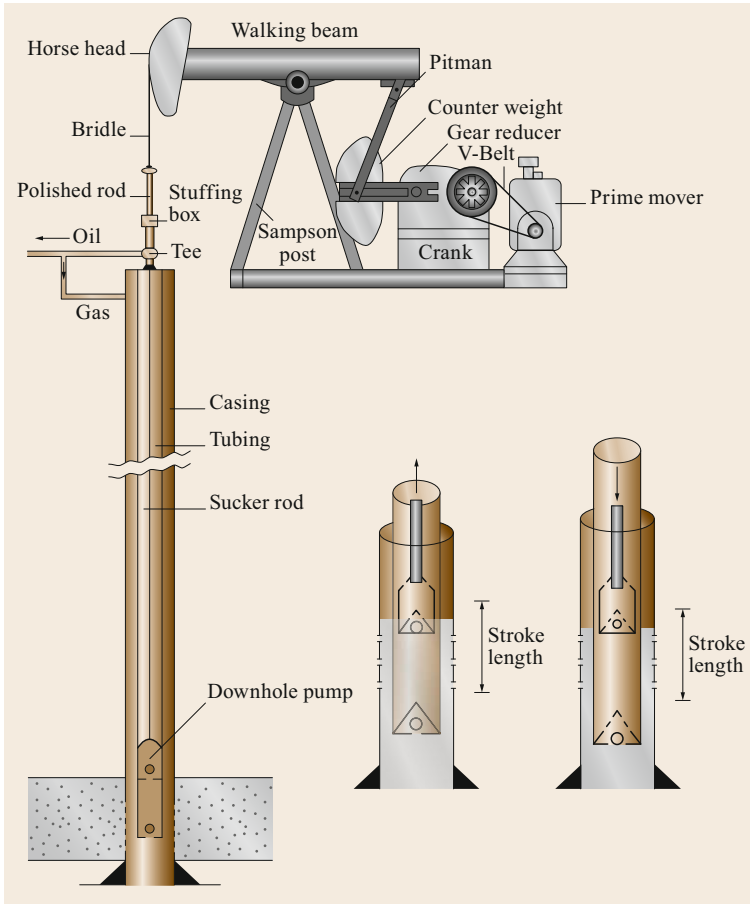


Fig. 14.9 Rod-pumped well (after [14.15])

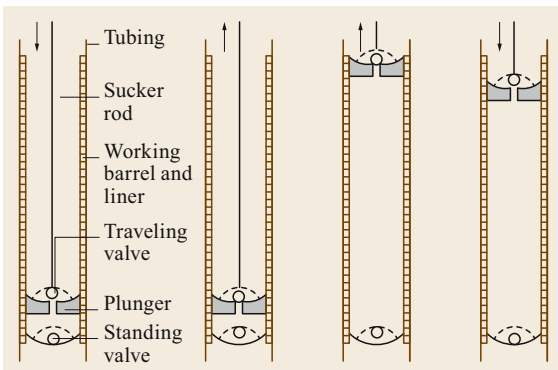


Fig. 14.10 Working principle of the plunger lift (after [14.16])

wellhead is equal to the volume corresponding with stroke length. Therefore, during the upstroke process, the plunger pump sucks in fluids, while the wellhead discharges fluids. To suck fluids into the pump, the pressure in the pump should be lower than a submergence pressure.

Downstroke. During this motion, the pumping rod drives the plunger and traveling valve downward, as shown in Fig. 14.10. The standing valve is closed. The traveling valve is opened once the pressure in the pump exceeds the pressure exerted by the liquid column above. As a result, liquids below the plunger flow upward into the tubing through the traveling valve. Fluids are discharged into the tubing from the plunger pump. To discharge fluids, the pressure in the plunger pump should be larger than the pressure of the liquid column above.

14.2.2 Other Artificial Lift Methods

In addition to sucker rod pumping and gas lift systems, other artificial lift systems are used in the oil field, including electrical submersible pumping, hydraulic jet pumping, hydraulic piston pumping, progressive cavity pumping and plunger lift systems.

Electrical Submersible Pump

As shown in Fig. 14.11, an electrical submersible pump (ESP) system consists of a motor, a protection box,

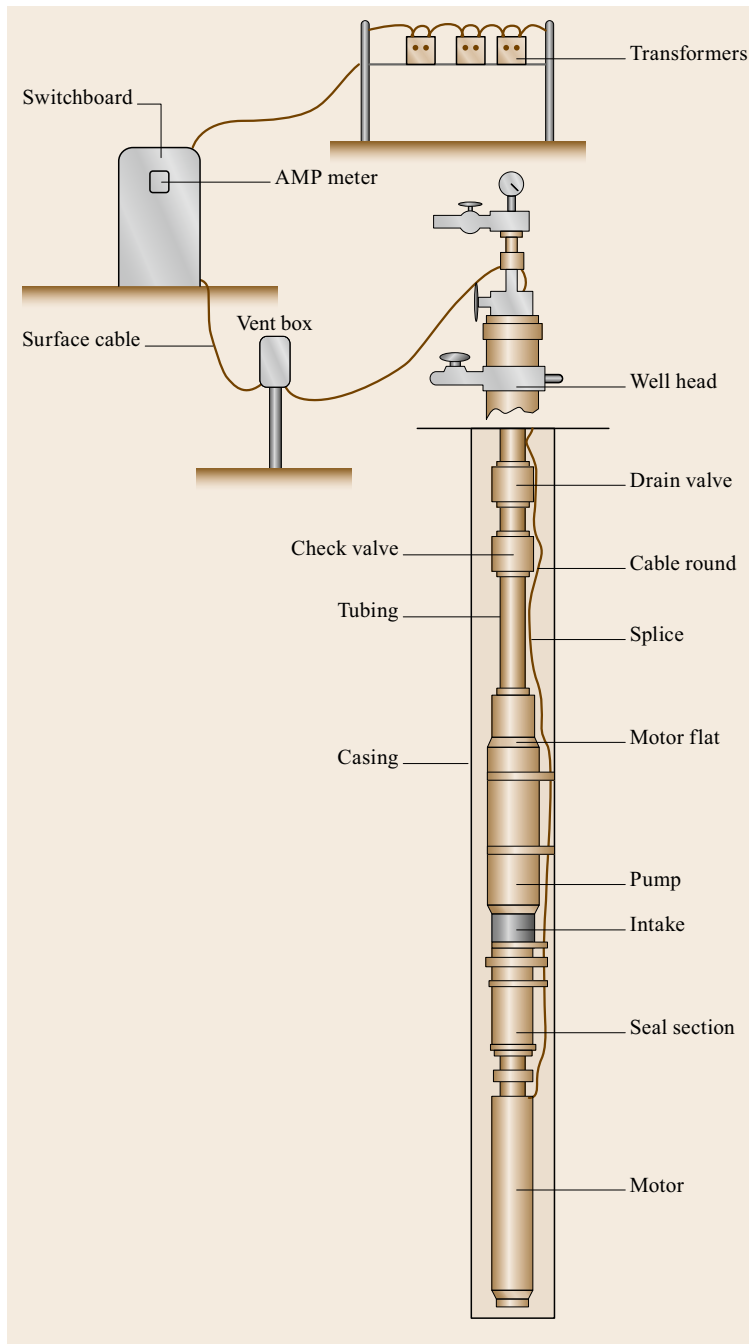


Fig. 14.11 Electrical submersible pump completion (after [14.17])

a gas-liquid separator, multistage centrifugal pumps, cables, junction boxes, a control panel, and transformers. In addition, some other small components are installed in this system, including single-direction flow valves, drain valves, centralizers, downhole pressure measuring instruments, and variable speed drive devices. ESPs used in the field are multistage centrifugal

pumps operating in a vertical position and utilizing centrifugal force to lift hydrocarbons to the surface, enabling high flow and enhanced production. Electrical power is transmitted to the downhole motor by cables to drive multistage centrifugal impeller and converted into kinetic energy via the downhole pump. Produced liquids, after being subjected to great centrifugal forces

caused by the high rotational speed of the impeller, lose their kinetic energy in the diffuser where a conversion of kinetic energy to pressure takes place, and are lifted up to the surface. ESPs are considered as a high-volume pump and are adaptable to highly deviated wells, up to horizontal, but must be set in straight sections. There are more than 130 000 ESPs installed globally.

Hydraulic Piston Pumping

A hydraulic piston pump is a device without rods. High-speed fluids are injected into the tubing to drive a motor up and down reciprocally. The fluids flow through the driven cylinder and valve to assist pumping. Hydraulic piston pumping is applicable to wells of high gas-oil ratio in which the oil has a high pour point, is sand-rich and/or waxy. It also is applicable to deep and inclined wells. It consists of a surface power tank, high pressure triplex pumps, a control manifold, wellhead control valves, and a downhole pump. The downhole pump is the core component in the system, which is typically double acting. All the surface pumps are high-pressure piston pumps. There are two operational types.

Open power fluid operation is a single-tubing structure using low-viscosity oil as the power fluid. Friction loss in the pipe is low for the power fluids. In addition, the fluids can reduce the viscosity of reservoir crudes by mixing them with the low-viscosity oil.

Closed power fluid operation utilizes light oil or water as power fluids. The power fluids are self-circulating, and do not mix with reservoir crudes. The power fluids can be recycled efficiently. Therefore, limited amounts of power fluids are required.

Hydraulic Jet Pumping

Hydraulic jet pumping is a special kind of hydraulic pumping. It injects high-pressure power fluid into the well through a nozzle-throat Venturi combination, mixes with produced fluids and by the Venturi effect creates a high pressure at the discharge side of the pump. Similar to a hydraulic pumping system, a jet pumping system consists of a surface tank, a high-pressure surface pump and a downhole jet pump.

Figure 14.12 demonstrates the working mechanism of a downhole jet pump. High-pressure power fluid is ejected at high speed from the nozzle, creating a low-pressure area that sucks reservoir fluids into the throat. Then, power fluids and reservoir fluids are mixed and exchange momentum. The kinetic energy of the reservoir fluid is increased, and converted to pressure energy through a diffuser.

Jet pumping does not have moving parts in the downhole. It is applicable to high-temperature, deep,

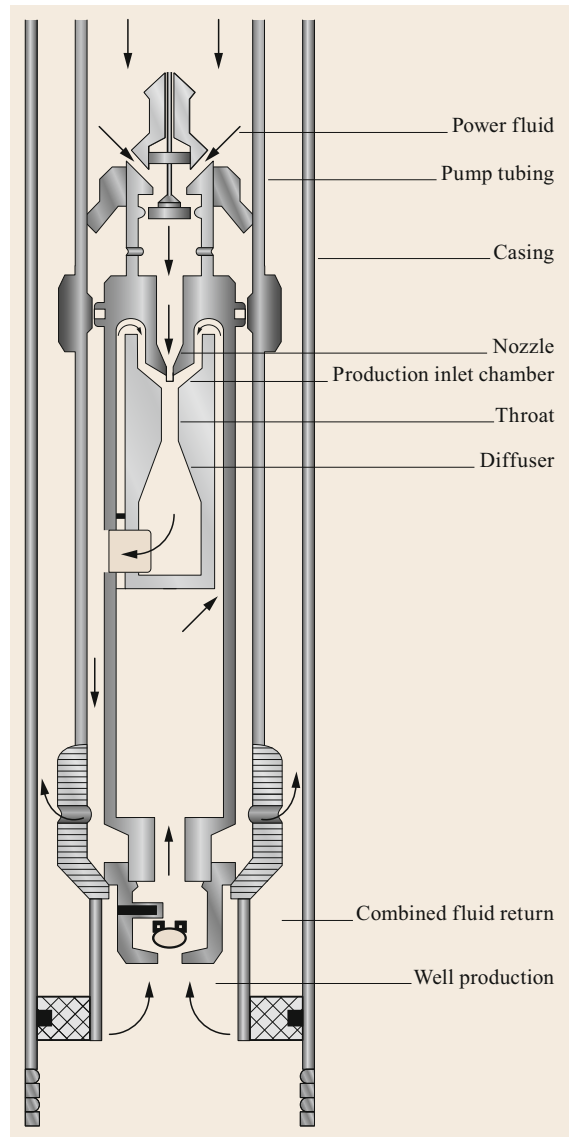


Fig. 14.12 Sketch of a hydraulic jet pump installation (after [14.8])

high-production wells, and to crudes that contain sand, corrosive substances and are viscous, and have a high gas-liquid ratio.

Progressing Cavity Pump

A progressing cavity pump is the fastest-evolving artificial lift technology in the petroleum industry. It consists of a stator with a double helix cavity and a rotor in the sleeve cavity, which can be engaged with the stator, as shown in Fig. 14.13. When the rotor moves around the stator in the cavity, the seal chamber between the rotor and the stator moves along the tubing axially to

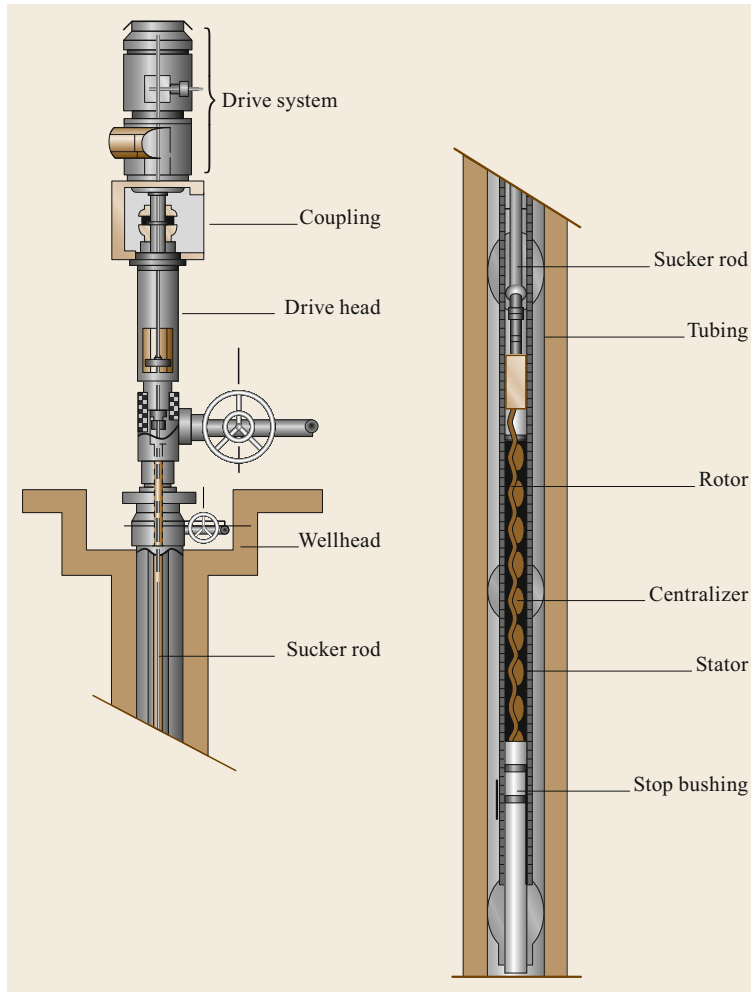


Fig. 14.13 Rod-driven PCP completion (after [14.18])

discharge fluids uniformly, continuously and steadily to the outlet. Progressive cavity pumps are advantageous because they are flexible, reliable, anti-abrasive and have high volumetric efficiency. With the develop-

ment of synthetic rubber and adhesive technology, the progressive cavity pump has become the major artificial lift method for cold heavy oil production with sand (CHOPS), as well as for polymer flooding.

14.3 Well Stimulation

Well stimulation refers to any well intervention performed on a production or injection well to enhance production or injection rates by improving the flow of the reservoir fluids from the drainage area into the well bore. Common well stimulation techniques include matrix acidizing and hydraulic fracturing.

14.3.1 Matrix Acidizing

Acidizing increases permeability of the formation matrix and removes skin near the wellbore. Matrix acidizing can be combined with hydraulic fractur-

ing procedures to further improve the flow capacity of the hydraulic fractures. In sandstone reservoirs, acid solution is injected into the formation to dissolve the cements in the matrix, and also to dissolve *skin* materials clogging the fractures. Such materials include clays, drilling muds and contamination of the formation during well completion. In carbonate reservoirs, acidizing is not used to recover the permeability of a damaged zone, but to create wormholes, which serve as low-resistance pathways for reservoir fluid to flow towards the production well.

Acidizing in Sandstone Formations

As with matrix acidizing, acidizing in sandstone formations dissolves the cements between sand grains and removes the damage near the wellbore. Acidizing can also dissolve materials clogging the pores or other scale to recover and improve formation permeability in the stimulated zone.

In sandstone formations, there is more argillaceous sandstone with less carbonate content. Ordinary hydrochloric acid (HCl) treatment can't achieve the desired performance improvement. For this application, the acid mixture includes 10–15% HCl, 3–8% hydrofluoric acid (HF) and additives. This mixed acid is usually referred as hydrofluoric-hydrochloric or mud acid.

The HF in mud acid is a strong acid and can dissolve all kinds of components in the sandstone (such as quartz, clay and carbonate). However, the HF cannot be used alone. The main role of HCl in the mud acid is to dissolve the carbonate and maintain a low-pH environment in the acid solution. This treatment will considerably recover and improve the permeability of the formation near the wellbore.

Acidizing in Carbonate Formations

Acidizing in carbonate reservoirs is used to create wormholes, through which reservoir fluids can flow after stimulation. Minerals in carbonate reservoirs mainly include calcite (CaCO_3) and dolomite ($\text{Mg}(\text{CO}_3)_2$). When the calcite content is more than 50%, the carbonate reservoirs are classified as limestone formations. On the other hand, when the dolomite content in the reservoirs is more than half, the carbonate reservoirs are classified as dolomite formations. In carbonate reservoirs, pores and fractures comprise the dominant pore space for the reservoir crude. Based on the type of pores and seepage channels, carbonate reservoirs can be classified into three categories:

1. Porous-type carbonate reservoirs
2. Fracture-porous carbonate reservoirs
3. Fractured carbonate reservoirs.

In the porous-type carbonate reservoirs, pores provide the primary crude storage space and seepage channels. In fracture-porous carbonate reservoirs, the main

seepage channels are fractures. However, the reservoir fluid storage space and seepage channels are different in fractured reservoirs. It is generally accepted that for a naturally fractured carbonated reservoir with high matrix porosity and low matrix permeability, matrix provides the dominant fluid storage space and fractures provide the seepage channels [14.19]. Acidizing in carbonate reservoirs mainly deals with the contaminations in the pores and fractures. In addition, it also can increase the intrinsic permeability by expanding the original fractures and pores.

Hydrochloric acid (HCl) plays an important role in acidizing treatment in carbonate reservoirs. When the HCl is injected into the reservoir pores or fractures, it will react with the fracture surface. HCl reacts with CaCO_3 to form CaCl_2 , CO_2 and H_2O . The acidizing parameters between the HCl and CaCO_3 at different concentrations of HCl are summarized in Table 14.2 [14.8].

Using appropriate acids and additives in matrix acidizing treatments is of crucial importance in enhancing oil production. The most commonly used acid for carbonate formations is HCl. Mixtures are used, including the formic acid, acetic acid, and multicomponent acid, which is a mixture of HCl, formic acid and acetic acid. Sulfamic acid can also be used in carbonate reservoir acidizing treatment. A wide variety of acids, such as oleic acid emulsions, concentrated HCl solutions and foamy HCl, are used to control reaction rates.

HCl is a strong acid, which can react with lots of metals, metal oxides, salts and other alkaline materials. When HCl reacts with carbonates, it produces highly soluble chlorides, such as CaCl_2 and MgCl_2 , leaving behind a residual acid solution without any precipitation. In the acidizing process, the higher extent of heterogeneous dissolution on the fracture face, the higher the fracture conductivity. In addition, the low cost of HCl makes it the most popular acidizing agent for stimulation treatment.

The advantages of high-concentration HCl treatment are:

1. When high-concentration HCl solutions are used for matrix acidizing, the reaction rate between acid and

Table 14.2 Acidizing parameters between HCl and CaCO_3 at different HCl concentration

HCl concentration (%)	5	10	15	20	28
HCl specific gravity	1.025	1.05	1.075	1.1	1.14
HCl content in 1 m ³ HCl solution (kg)	51	105	161	220	320
CaCO_3 corrosion ^a by 1 m ³ HCl solution (m ³)	0.026	0.053	0.081	0.111	0.162
Standard volume of generated CO_2/m^3	15.8	32	49.5	68	98
Weight percent of CaCl_2 solution (%)	7.3	14.1	20	26.3	35
Acid solution volume to dissolve 1 m ³ CaCO_3/m^3	38.4	18.9	12.4	9	6

^a The specific gravity of CaCO_3 is 2.71

rock matrix is relatively slow, which can increase the effective radius of acidizing.

2. The matrix acidizing process with HCl generates CO₂ gas, which leaves the formation and does not contribute to sludge formation. Hence, the amount of sludge is relatively low, which reduces sludge acid flow-back.
3. Usually, there is more calcium than magnesium in carbonate rocks. Therefore, acidizing will generate more calcium chloride and magnesium chloride. These chlorides increase the viscosity of sludge acid. Also, as chloride concentrations increase, they moderate the reaction rate between unreacted acid and the rock matrix. In addition, the higher viscosity improves the ability of the sludge acid to suspend solid particles and carry them out of the formation.
4. At high concentrations, HCl is less likely to be affected by reservoir water dilution. The disadvantage of HCl acidizing is that the initial reaction rate between the acid and limestone can be too fast, especially in deep wells with high temperature. As a result, acidizing mainly takes place near the wellbore. In addition, HCl will cause a lot of metal pitting, and even lead to severe corrosion. In wells with high H₂S content, HCl acidizing can lead to hydrogen embrittlement of steel.

14.3.2 Hydraulic Fracturing

Hydraulic fracturing uses a fracturing fluid (e.g., water) to transmit pressure to the formation around the well. A high pressure and large discharge pump is used on the surface. As large amounts of fracturing fluid are injected into the well, the well bottom-hole pressure increases. One or several fractures will be created near the wellbore once the well bottom-hole pressure exceeds the formation fracture threshold pressure. Fractures extend deep into the reservoir until the injection rate is equal to the rate at which the fracturing fluid seeps away. Proppants (such as sand) are added to the fracturing fluid to prevent the fracture from closing after stimulation, leaving behind multistage proppant-packed fractures with high flow conductivity.

Production after hydraulic fracturing stimulation is enhanced due to the following reasons:

1. *The flow resistance is decreased.* Before fracturing, the flow from the reservoir to well bottom-hole follows the rule of radial fluid flow. Pressure is mainly consumed in overcoming the flow resistance near the wellbore. The flow conductivity of the fractures is much higher than that of the unfractured matrix, and the flow area becomes larger too.
2. *Fractures break through near wellbore contamination.* Over time, various impurities accumulate near

the wellbore and form a blocked (contaminated) area, which reduces the well production rate. Fracturing breaks through the blocked area, allowing the reservoir fluids to flow through the blockages.

3. Fracturing expands the natural microfractures in the reservoir and connects them. This increases the effective reservoir volume, which significantly boosts the well productivity.

Fracturing Fluids

Commonly used fracturing fluids include water-based fluids, oil-based fluids, and emulsion-based fluids. Foam-based fracturing fluids are also used in the field.

Water-based fracturing fluid is a water-based solution with different chemical additives. Water-soluble polymers can improve the solution viscosity after dissolving in the water. Other commonly used additives include: demulsifiers, emulsion breakers, preservatives, antileaking agents, friction reducers, fungicides and stabilizers. Water-based fracturing fluid has high viscosity, can carry abundant proppants, and has good thermal stability and good rheological properties. But it may leak off to the formation and cause formation damage.

Oil-based fracturing fluids are usually crude oil or thickened crude oil acid-based fluids. Thickened crude oil will automatically break once encountering the formation brine. Oil-based fracturing fluid can prevent the swelling of the formation clay, which minimizes formation damage. However, oil-based fluids have low viscosity, poor thermal stability, low proppant carrying capability and low fracturing efficiency.

Emulsion fracturing fluids usually consist of oil and gelled water. The combination has the advantages of both constituents. Because the continuous phase is water, the friction of the emulsion is low, the viscosity is high, and the thermal stability is good. Also, the emulsion has high proppant carrying capability and low leak-off velocity. And it can prevent the swelling of clay.

Foam fracturing fluids are a mixture of liquid (e.g., water), gas (e.g., nitrogen) and chemical additives. Formation damage caused by such fluids is less due to the low leak-off rate into the formation.

Proppants

Currently, the mostly used proppants include ceramic proppants, resin-coated sands, and natural sands.

Natural sands have been widely used in shallow formations (less than 1500 m) and have a high success rate. Natural sands have high quartz contents, uniform particle sizes and high sphericity. In addition, natural sands are abundant and costs are lower compared to other proppant types. The main component of natural sand is coarse quartz without crystal cleavage. It will break into small pieces under high pressure, leading to lower

fracture conductivity. The highest stress quartz sand can stand is in the range of 21 and 35 MPa.

Ceramics are the most commonly used artificial proppants. The mineral constituents are alumina, silicates and iron-titanium oxide. Ceramic proppants have irregular shapes, with sphericities of around 0.65. Importantly, they have high strength. Ceramic proppants are suitable for deep reservoirs with high fracturing closure stress. Under 70 MPa fracturing closure stress, the permeability of ceramic pack is one order of magnitude higher than that of natural sand pack. The high density of the ceramic proppants requires high quality fracturing fluid, especially in deep high-temperature wells.

Resin-coated proppant has moderate strength, and can stand a fracture closure stress of between 56.0 and 70.0 MPa. Resin-coated proppant is produced by wrapping resin film on sand; the thickness of the resin film is about 0.0254 mm, accounting for about 5% of the weight or less.

Fracture Initiation and Propagation

Initiation pressure is the pressure at which fracture initiation starts in the formation rock. When the well bottom-hole pressure reaches initiation pressure, the fracture begins to propagate. This can be identified by a sudden pressure drop, shown as the breakdown pressure in Fig. 14.14. Figure 14.14 depicts the pressure change during fracturing operation of one stage. ISIP refers to the instantaneous shut-in pressure which equals the final injection pressure minus the pressure drop due to friction. Fracture closure pressure is equal to the minimum in-situ stress. Fracture will be closed once the pressure in the fracture is less than the fracture closure pressure. The fracture will continue to propagate into the formation if more fluid is injected. When the injection rate equals the leak-off rate, the propagation of fractures stops.

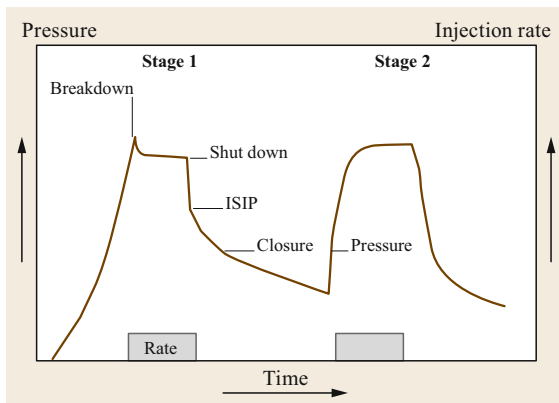


Fig. 14.14 Typical stress test pump-in/shut-in (after [14.20])

Fracture Model

There is still controversy about whether a single fracture or multiple fractures are created in a hydraulic fracturing job. The Perkins–Kern–Nordgren (PKN) model is one of the widely used models to predict the geometry of the fracture. It was developed by Perkins and Kern in 1961 [14.21]. In 1972, Nordgren [14.22] modified the Perkins and Kern model by adding terms for leak-off and storage within the fracture to the solution, thus, the model is commonly called PKN model. The PKN model assumes that fracture has a constant height and propagates along the horizontal direction. It can be used when the fracture length is much larger than the fracture height. A schematic view of the fracture geometry is shown in Fig. 14.15. In this figure, h_f is the fracture height, $w(x, t)$ is the fracture width, x_f is the fracture half length. $u(x)$ is the fluid flow rate within the fracture.

$$\bar{w} = 0.3 \left[\frac{2q_i \mu (1 - \nu)^2 x_f}{E} \right]^{\frac{1}{4}} \left(\frac{\pi}{4} \gamma \right), \quad (14.13)$$

where:

- \bar{w} Average width (in)
- q_i Pump rate (bpm)
- ν Poisson's ratio
- x_f Fracture half length (ft)
- E Young's Modulus (psi)
- μ Viscosity of the fracture fluid (cp)
- γ Constant ≈ 0.75 .

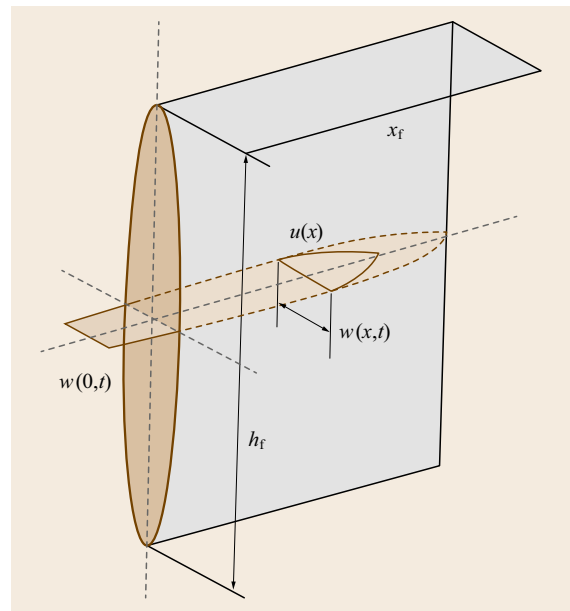


Fig. 14.15 The PKN fracture geometry (after [14.14])

References

- 14.1 J.V. Vogel: Inflow performance relationships for solution gas drive wells, *J. Petroleum Technol.* **20**, 83–92 (1968)
- 14.2 G.W. Goier, K. Aziz: *The Flow of Complex Mixtures in Pipes* (Robert E. Drieger, Huntington 1977)
- 14.3 L.F. Moody: Friction factor for pipe flow, *Trans. ASME* **66**, 671 (1944)
- 14.4 F.H. Poettmann, P.G. Carpenter: The multiphase flow of gas, oil, and water through vertical strings, *API Drill. Prod. Pract.* **1**, 257–263 (1952)
- 14.5 J. Orkiszewski: Predicting two-phase pressure drops in vertical pipe, *J. Petroleum Technol.* **19**, 829–838 (1967)
- 14.6 P. Griffith, G.B. Wallis: Two phase slug flow, *J. Heat Transf.* **83**, 307–320 (1961)
- 14.7 H. Duns Jr., N.C.J. Ros: Vertical flow of gas and liquid mixture in wells, *Proc. 6th World Petroleum Congr. Frankfurt* (1963), Paper WPC-10132
- 14.8 B. Guo, W.C. Lyons, A. Ghalambor: *Petroleum Production Engineering – A Computer Assisted Approach* (Elsevier, Burlington 2007)
- 14.9 W.E. Gilbert: Flowing and gas-lift well performance, *API Drill. Prod. Pract.* **20**, 126–157 (1954)
- 14.10 N.C.J. Ros: An analysis of critical simultaneous gas/liquid flow through a restriction and its application to flow metering, *Appl. Sci. Res. Sect. A* **9**, 374–389 (1960)
- 14.11 P.B. Baxendell: *Bean Performance – Lake Maracaibo Wells*, Internal Report (Shell Oil, Houston 1957)
- 14.12 I. Achong: *Revised Bean Performance Formula for Lake Maracaibo Wells*, Internal Report (Shell Oil, Houston 1961)
- 14.13 A.A. Pilehvari: *Experimental Study of Subcritical Two Phase Flow Through Wellhead Chokes* (Univ. Tulsa, Tulsa 1980), Fluid Flow Projects Report
- 14.14 M.J. Economides, A.D. Hill, C. Ehlig-Economides, D. Zhu: *Petroleum Production Systems*, 2nd edn. (Prentice Hall, Westford 2013)
- 14.15 M. Golan, C.H. Whitson: *Well Performance*, 2nd edn. (Prentice Hall, Englewood Cliffs 1991)
- 14.16 K.E. Brown: *The Technology of Artificial Lift Methods, Vol. 2b* (Petroleum, Tulsa 1980)
- 14.17 Centrilift: *Submersible Pump Handbook*, 4th edn. (Centrilift, Claremore 1987)
- 14.18 H. Cholet: *Well Production Practical Handbook* (Technip, Paris 2008)
- 14.19 J. Allen, S.Q. Sun: Controls on Recovery Factor in Fractured Reservoirs: Lessons Learned from 100 Fractured Fields, Paper SPE 84590 (2003)
- 14.20 J.D. Clegg: *Petroleum Engineering Handbook, Vol. IV*, Production Operations Engineering (Society of Petroleum Engineers, Richardson 2006)
- 14.21 T.K. Perkins, L.R. Kern: Width of hydraulic fracture, *J. Petroleum Technol.* **9**, 937–949 (1961)
- 14.22 R.P. Nordgren: Propagation of vertical hydraulic fractures, *J. Petroleum Technol.* **12**(4), 306–314 (1972)

Offshore Production

15. Offshore Production

Ekaterina V. Maksimova, Cortis K. Cooper

About 71% of the Earth's surface is under water. It is not surprising that exploration companies pay attention to the bedrock below oceans, treating it as a source of oil and gas. This chapter presents a brief overview of offshore drilling from oceanographic-meteorological, engineering, geological, legal, and historical perspectives. Some topics discussed are the types of rigs and platforms used for offshore drilling and effects of metocean conditions (such as currents, waves, and winds) on these structures and operations; the factors influencing the regions of hydrocarbon potential, and how the coastal state's ownership is defined; and finally, the history of offshore drilling, its current state, and prospects for the future are touched upon.

15.1	Historical Overview	518
15.2	Ownership	520
15.3	Major Offshore Fields	521
15.4	Offshore Oil and Gas Platforms	522
15.4.1	Jackets and Jack-Ups	522
15.4.2	Gravity-Based Structures (GBSS)	524
15.4.3	Tension-Leg Platforms (TLPs)	524
15.4.4	Semisubmersibles (Semis)	524
15.4.5	Spars	524
15.4.6	Floating Production, Storage and Offloading (FPSO) Units	524
15.4.7	Drillships	525
15.4.8	Subsea Systems	525
15.5	Metocean Impacts on the Offshore Industry	525
15.5.1	Winds	526
15.5.2	Waves Observed at the Ocean Surface ..	527
15.5.3	Ocean Currents	528
15.6	Future Offshore Production and Drilling	529
	References	529

So-called offshore drilling is nothing new – the first substantial offshore commercial production started in the 1960s. Figure 15.1 demonstrates that about one-third of the world's oil supply is currently produced

offshore – in shallow (< 500 m) or deep waters. Not only is the gap between onshore and offshore oil production increasing, but there is one distinct trend gaining steam in the offshore oil industry: compa-

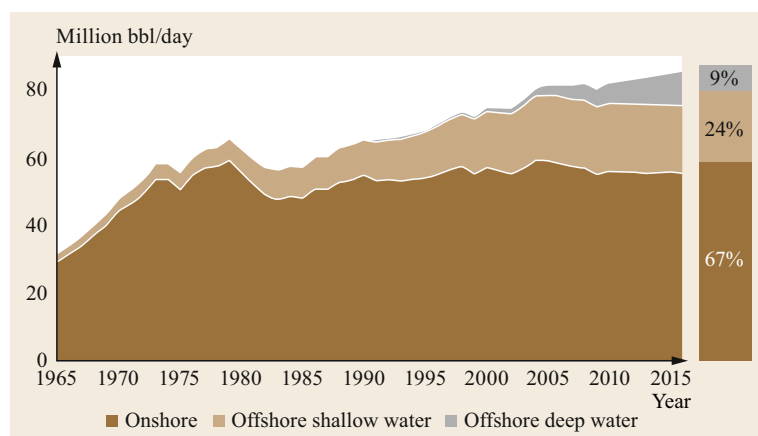


Fig. 15.1 Onshore versus offshore oil production (courtesy of Infield Systems, London)

nies are now forced to drill deeper than ever before. Total offshore oil production accounted for 22% of global production in 2000 – 1% of which (< 2 million bbl a day) was from deep water. In 2010 these figures rose to 33 and 7%, respectively. The

deep water production increased to 10 million bbl a day in 2014 and currently accounts for approximately 10% of the world's total production. Ultra-deep water (> 1500 m) production is gaining strength as well [15.1].

15.1 Historical Overview

How did it all begin? The oil production history can be divided into five main periods: pre-oil period (early history–1900), early onshore period (1900–1930), early offshore period (1930–1960), boom and bust (1960–1990), and deep water and reorganization period (1990–present).

In 1847, the first *onshore* oil well in the world was drilled using a primitive percussion drilling mechanism in Azerbaijan's Bibi-Heybet oil field under the direction and initiation of the Russian engineer V.N. Semenov. It was not until eleven years later that the first *onshore* oil well was drilled in Pennsylvania, US [15.4].

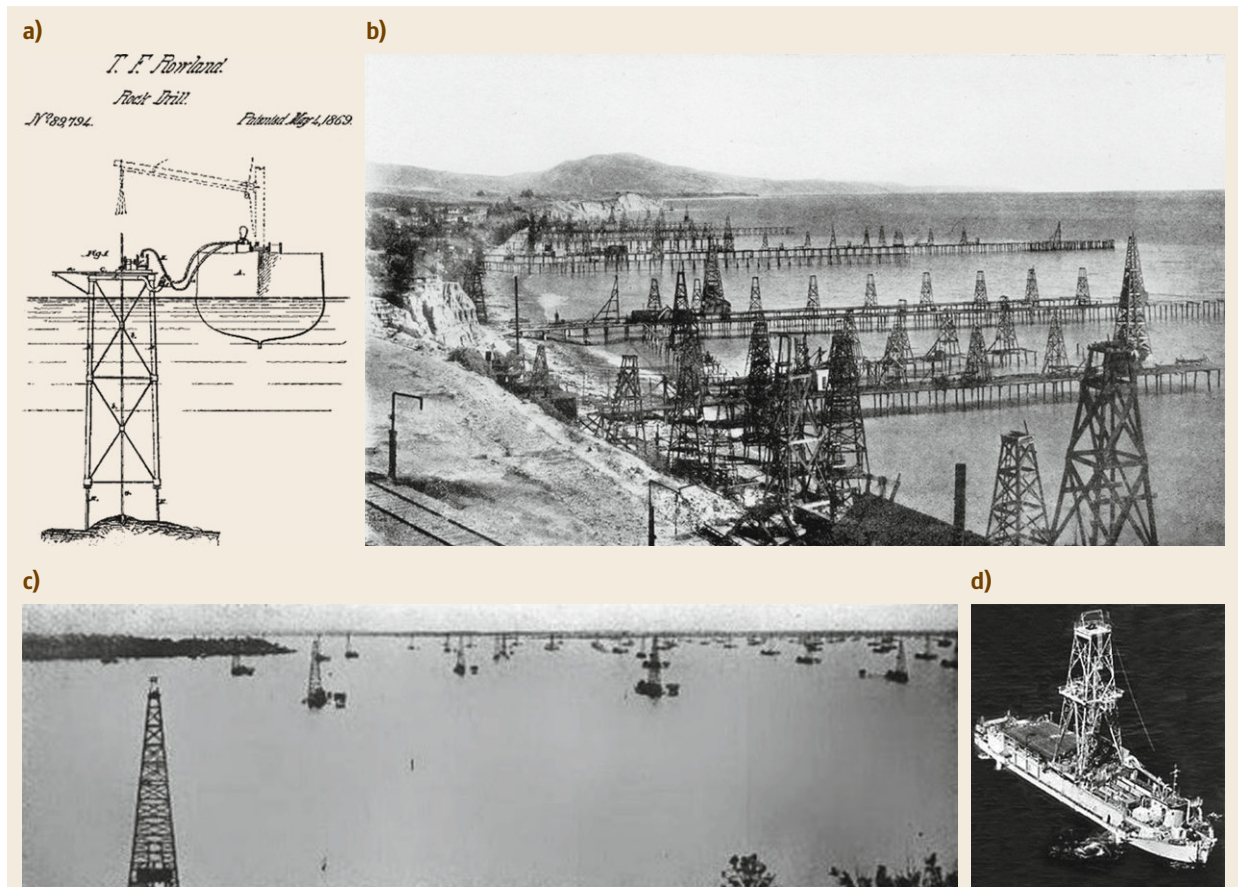


Fig. 15.2 (a) Although never built, Thomas Rowland's design for an offshore platform was far ahead of its time (US, 1869). (b) The people of Summerland, once a pleasure resort in California, are now successfully pumping oil out of the adjacent ocean bed (US, c. 1900s). (c) Cable-tool derricks on Louisiana's Caddo Lake (US, c. 1911). (d) CUSS I was one of the first vessels in the world capable of drilling in water depths up to 3600 m, while maintaining a position within a radius of 180 m (US, 1961) (after [15.2, 3], courtesy of US National Oceanic and Atmospheric Administration and US National Science Foundation)

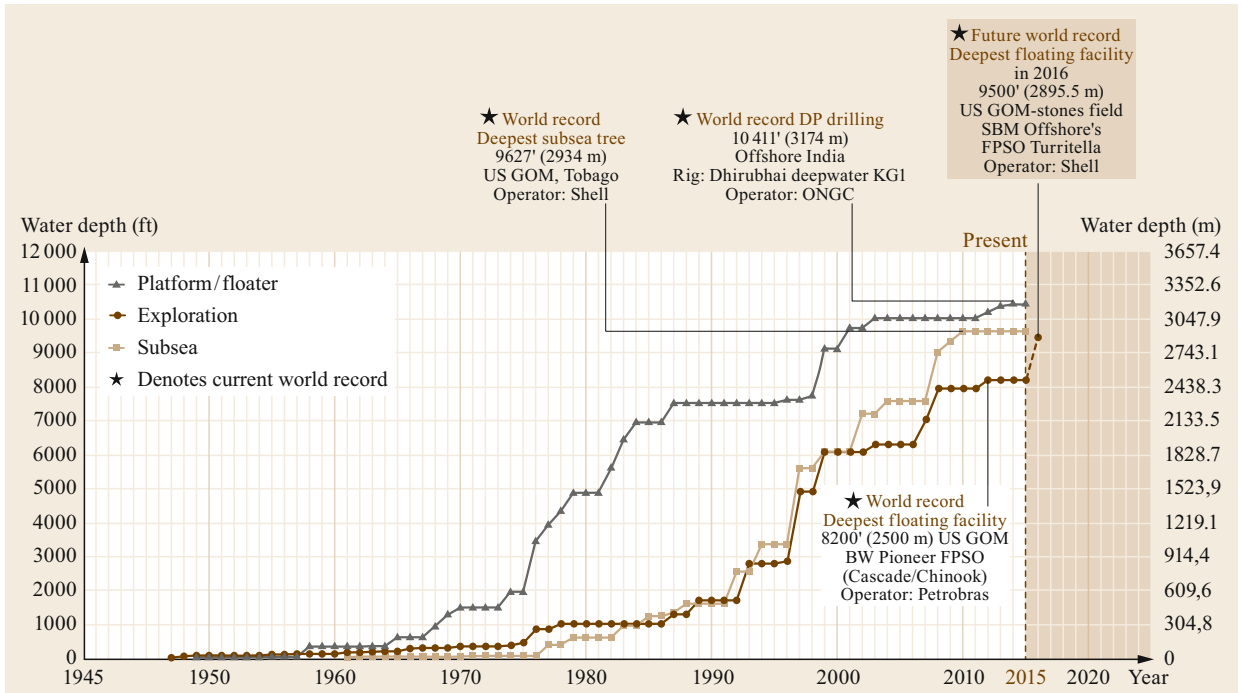


Fig. 15.3 Worldwide progression of water depth capabilities for offshore drilling and production as of March 2015 (courtesy of WoodGroup Mustang)

Oil and natural gas from the oceans and lakes have also been used for quite some time. Primitive methods of *offshore* oil collection existed in the 19th century in Azerbaijan (Caspian sea), US (California's coast), and Japan. Some historians say that the true beginning of the modern *offshore* industry can be traced to 1869, when Thomas Fitch Rowland of Greenpoint, New York, patented a *submarine drilling apparatus*. Rowland's design (Fig. 15.2a) included a fixed platform for drilling offshore to a depth of 15 m. The anchored four-legged tower resembled modern offshore platforms, but was never built.

Offshore petroleum production started in the US two decades later. The first *offshore* oil platform constructed from piles was done in *fresh* waters of Ohio's Grand Lake (St. Marys) in 1891. Small local companies produced oil there during the 1890s, ushering in the modern era of sea drilling [15.5]. The first offshore oil wells in *salt* water were drilled in the portion of the Summerland field extending under the Santa Barbara Channel off California in 1896. Closely resembling boardwalks in appearance (Fig. 15.2b), rows of narrow wooden piers extended up to 410 m from the shoreline with their piles reaching 11 m down to the floor of the Pacific. Using the same techniques as were used then on land, steel pipes were pounded 138 m below the seabed [15.6]. The Summerland ocean field pro-

duced for 25 years, fueling the growth of California's economy.

Other notable early offshore drilling activities occurred on the Canadian side of Lake Erie in the 1900s and Louisiana's Caddo Lake in the 1910s. The Caddo Lake wells – completed over water without a pier connection to shore (Fig. 15.2c) – have frequently been called America's first true offshore drilling [15.7]. Shortly thereafter, wells started to be drilled in tidal zones along the Texas and Louisiana coasts in the Gulf of Mexico. In the 1920s, drilling activities occurred from concrete platforms in Venezuela's Lake Maracaibo. One of the well-known offshore structures was a well in Azerbaijan, which came on stream in 1923 and was located on an artificial island in a shallow portion of the Bibi-Heybet bay in the Caspian Sea. Later, a solid milestone was achieved in 1947, when a productive well was first built beyond the sight of land – 17 km off the Louisiana coast in the Gulf of Mexico – but still in waters of only 5.5 m deep.

Rapid growth of the offshore oil and gas production began in the 1960s (Fig. 15.1). The process accelerated in 1970–1980s, as indicated by the number of countries that produced oil and natural gas on the continental shelf: in 1970, there were only about 20 countries, but more than 50 in the early 1990s [15.8]. The growth of offshore oil production was due to several factors.

First, the energy crisis of the mid-1970s brought a sharp rise in oil prices, which provided a financial incentive to take on the increased cost of drilling offshore. Second, large onshore fields started to decline – or were controlled by the Organization of the Petroleum Exporting Countries (OPEC). These factors drove innovation in offshore technology: the first mobile drilling ship, CUSS I, was developed under funding from the National Science Foundation’s Mohole Project in 1961 (Fig. 15.2d).

By the early 1990s, there were more than 40 000 offshore wells drilled [15.9], and the drilling depth was

steadily increasing (Fig. 15.3). In the early 1980s, 85% of offshore oil was produced at depths of less than 100 m, but already by the mid-1990s, developments from 200–400 m depths were no longer rare. The maximum production depth increased dramatically from 300 m in 1984 to 1000 m just ten years later, and to 2934 m in 2010 (Fig. 15.3). The offshore production also became more remote – in 1970, the installation location of the production platforms was only 10 km offshore. At present, the farthest installation – Husky’s SeaRose FPSO in Canada – is located 350 km away from the coast.

15.2 Ownership

How deep and far offshore can a country drill? The concept *freedom of the seas* was designed by the Dutch jurist Cornelius van Bynkershoek in 1702 and existed virtually unchanged for 300 years. According to this principle, the territorial waters of coastal states were limited by 3 nmi (5.6 km), which corresponded to the distance of a cannon shot, the state’s capacity of exercising an effective control over the offshore territory at that time. All waters beyond that distance were considered international waters and governed by the principle

of *mare liberum*, introduced by the Dutch jurist Hugo Grotius in 1609: free to all nations, but belonging to none of them.

In the early 20th century, most countries proposed updating the law of the sea and to define national waters with a broader interpretation – namely, to enable the use of mineral resources, create instruments for the protection of national fish stocks, and prohibit uncontrolled release of waste into the open sea. As a result, the United Nations held its first (1956), second (1960),

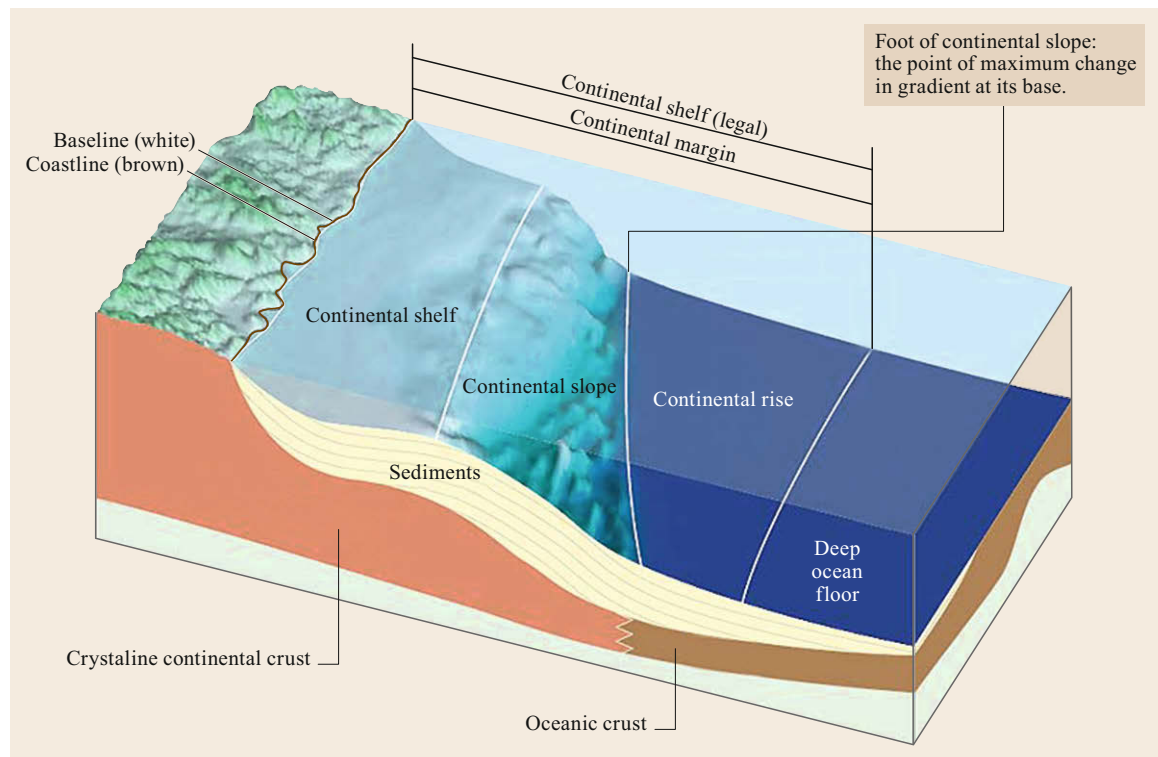


Fig. 15.4 Ocean zones near the coastline. Continental shelf delineation criteria (courtesy of GRID-Arendal)

and third (1967) conferences on the law of the sea. Currently, virtually all oil and gas offshore development is based on the use of United Nations Convention on Law of the Sea (UNCLOS) [15.10], and the possession issues are mostly resolved. The two main regions of disputes nowadays are the Arctic and the southern oceans. Under the UNCLOS article 76, the *legal continental shelf* is the part of the seabed (but not the water column itself) over which a coastal state exercises sovereign rights with regard to the exploration and exploitation of natural resources, including oil and gas deposits. The legal continental shelf (Fig. 15.4) extends as a natu-

ral prolongation of the land territory to the continental margin's outer edge, or 200 nmi (370 km; this zone is usually referred to as EEZ, or exclusive economic zone) from the coastal state's baseline, whichever is greater. The definition of the *legal* continental shelf should be distinguished from the *scientific* definition [15.11]: the continental shelf is the sea bed surrounding a continent at depths of up to 130–200 m, at the edge of which the continental slope drops steeply to the ocean floor (as also shown in Fig. 15.4). The UNCLOS article 76 gives further details of defining the borders of the *extended legal* continental shelf.

15.3 Major Offshore Fields

Would the continental shelf (UNCLOS definition) normally include any important coastal state locations with offshore hydrocarbon potential? Substantial oil and gas reservoirs typically require an organic-rich sediment layer, which is at least 1 km thick and overlaid by a geological *trap*. Common traps for hydrocarbons include shales, salt domes (evaporates), and anticlinal folds of permeable and nonpermeable strata. Continental shelves and rises (scientific definition in Fig. 15.4) usually contain the largest accumulations of sediments – often in excess of 10 km – with a high probability of including organic-rich source rocks deposited, when the

proto-ocean basins were narrow and had restricted circulation [15.13]. The abyssal plains probably contain insufficient thickness of sediments (< 1 km) to yield hydrocarbon accumulations. Parts of the deep trenches may be more favorable, as some foundered remnants of continental blocks may have broken off during early rifting processes [15.14].

Areas that contain wide legal continental shelves with thick sediments deposited in regions favorable for hydrocarbon formation are shown in Fig. 15.5 [15.12]. These occur throughout the Arctic Ocean (coasts of Greenland, Norway, Alaska, northern Canada, and Rus-

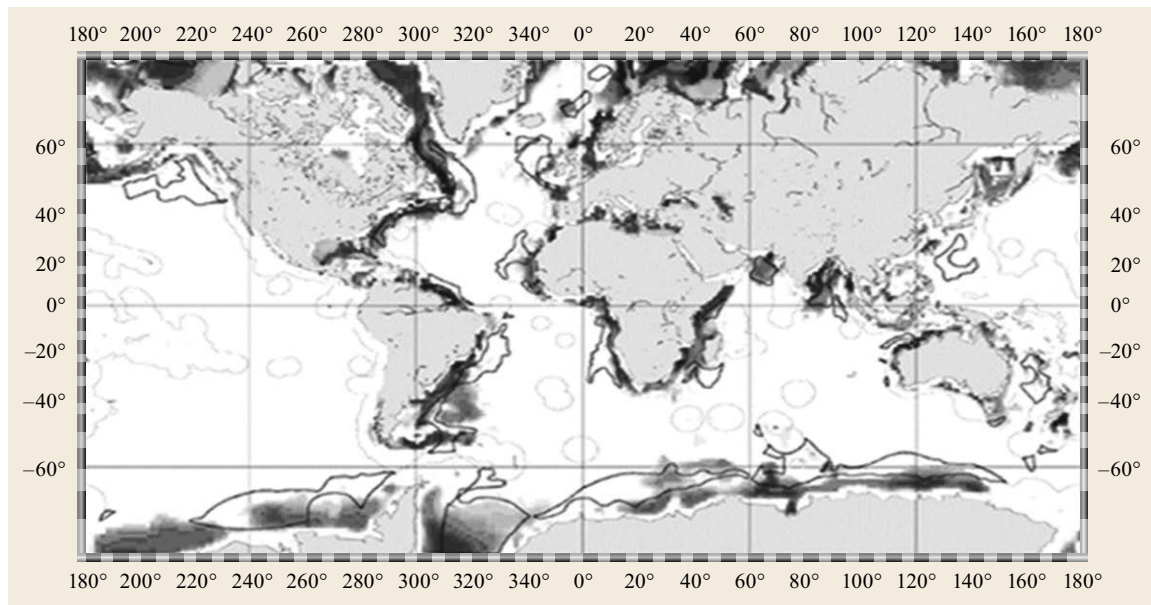


Fig. 15.5 Map showing conventional hydrocarbon potential based on sediment thickness and crustal age and type. High potential is represented by increasingly *darker grays* (qualitative and relative only), the extended legal continental shelf regions outlined in *black*, while the 200 nmi exclusive economic zone areas are outlined by *thin curved gray lines* (after [15.12])

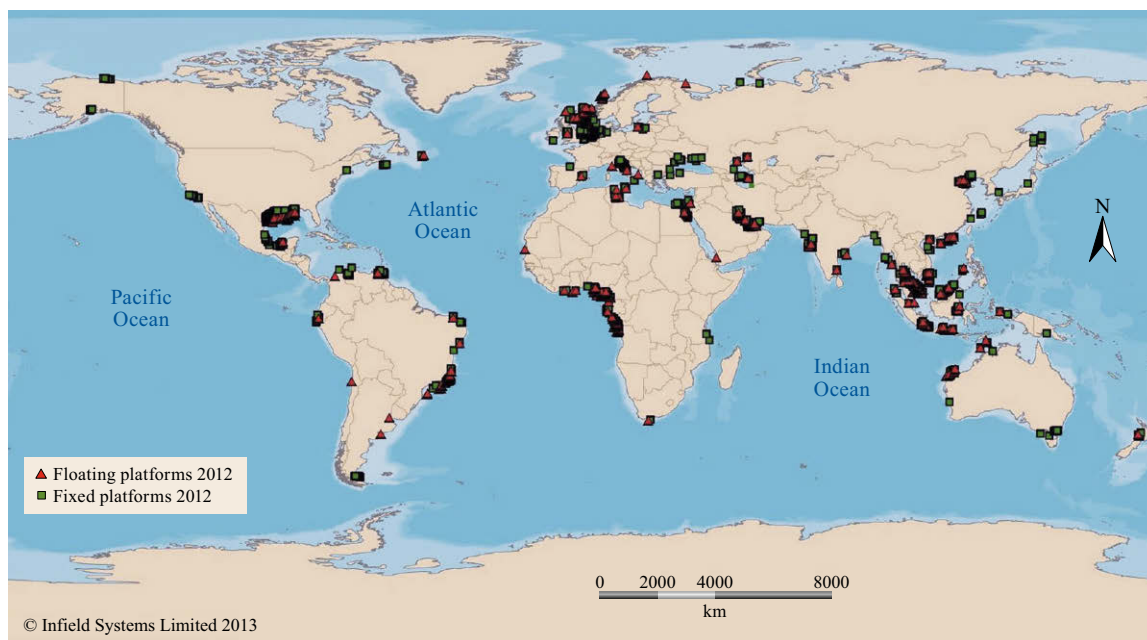


Fig. 15.6 Main offshore oil production regions as of 2012. *Triangles* and *squares* represent floating and fixed platforms, respectively (courtesy of Infield Systems Limited, London)

sia) and much of the continental margin of Antarctica. Favorable offshore conditions also occur along the Atlantic shores of North, Central, and South America (including Mexico, Trinidad-Tobago, Venezuela, Guyana, Suriname, French Guiana, Brazil, Uruguay, and Argentina), western Europe, around much of Africa, the northern margin of the Indian Ocean, Indonesia, and around Australia, New Zealand, off mainland China, Korea, Taiwan, and the Pacific shore of Russia (Sea of Okhotsk). Smaller basins include the Gulf of Mexico and the Caribbean Sea (2–6 km thickness), the Mediterranean Sea (up to 8 km), the Black Sea and the Caspian Sea (4 km), the Bering Sea, the Sea of Okhotsk, the Sea

of Japan, the South China Sea, and the seas within the Indonesian Archipelago (all 2–4 km). However, several of these favorable areas have water depths of as much as 5500 m and extend 1500 km or more from the shore, making hydrocarbon production there difficult. Out of these areas, ten shelves with the largest potential are off Antarctica, Canada, Brazil, US, Sri Lanka, India, Argentina, Madagascar, Russia, and Morocco. Figure 15.6 displays the actual global offshore production regions, which nowadays include the Persian Gulf, the Gulf of Mexico, Western Central Africa, Brazil’s coast, the North Sea, the Caspian Sea, and Southeast Asia [15.1].

15.4 Offshore Oil and Gas Platforms

As of 2014, there were roughly 9000 offshore production platforms [15.15] and 1020 mobile offshore drilling units (MODUs) [15.16] in service worldwide (approximate locations are as in Fig. 15.6). Figure 15.7 shows the major types of production platforms, while Fig. 15.8 is a montage of modern MODUs. MODUs drill exploratory (*wildcat*) wells and, in deeper water, are frequently used to drill development (production) wells prior to, but sometimes even after, the production facility is installed.

The choice of the type of production platform or MODU for a given field development depends on many

factors including water depth, ice coverage, soil conditions, and storminess. For production platforms, other important factors are production flow rate, hydrocarbon characteristics, and existing pipeline infrastructure.

15.4.1 Jackets and Jack-Ups

By far, the most prolific production platform is the *fixed platform* or *jacket* (left-most structure in Fig. 15.7), composed of a lattice of tubular steel held to the sea floor with long piles, also typically composed of steel

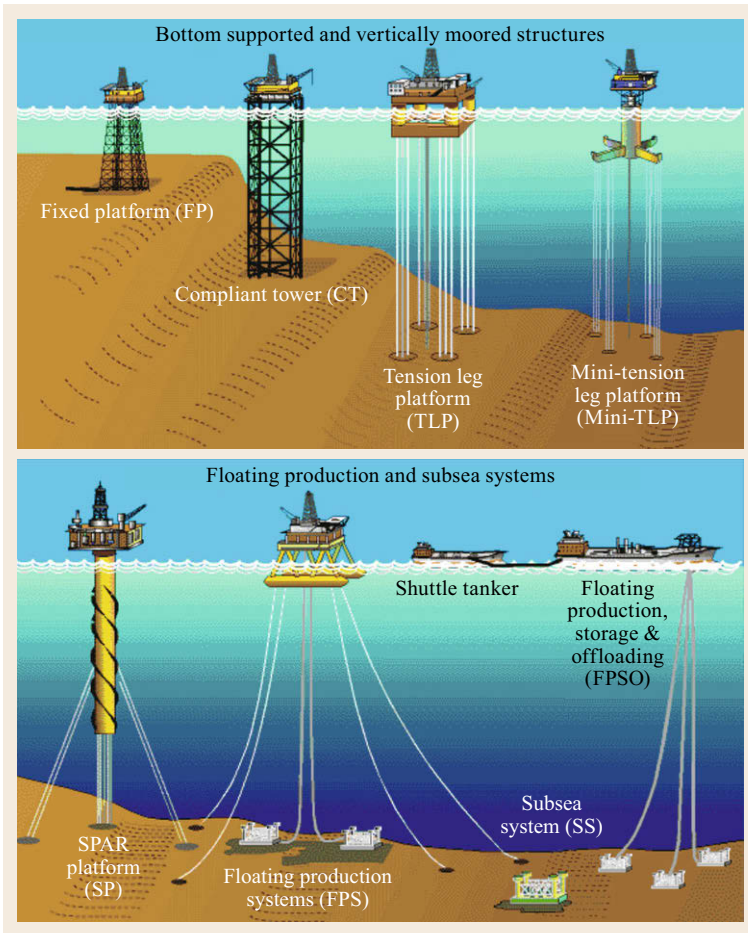


Fig. 15.7 Major types of offshore production systems (courtesy of US Bureau of Safety and Environmental Enforcement)

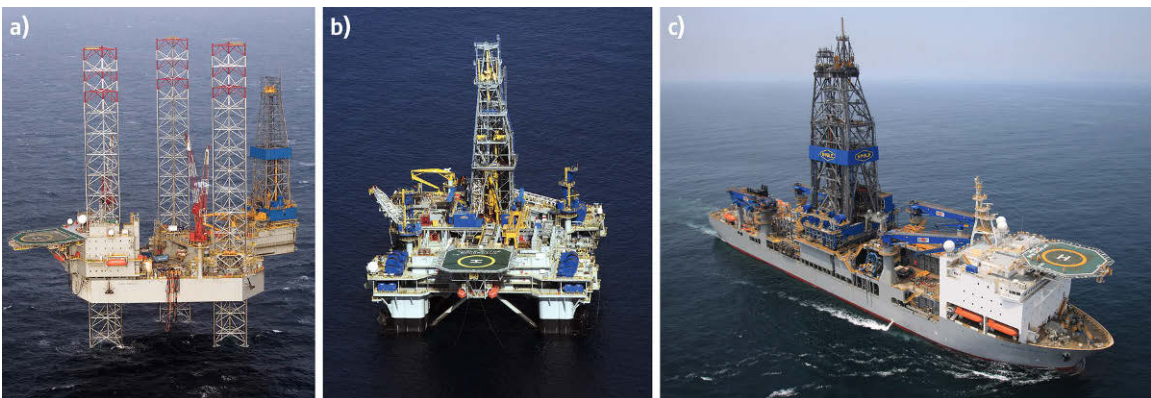


Fig. 15.8a–c Major types of offshore drilling systems. (a) Jack-up, (b) semi, (c) drillship (courtesy of Noble Corporation)

pipe pounded into the sea floor up to 50 m. Its analog for mobile drilling, known as a *jack-up*, is shown in Fig. 15.8a. Jack-ups are floated into place, and then the topsides are raised by extending the legs through a *jack-ing* mechanism.

The early precursor of modern jackets was first deployed off California in the 1930s, but it wasn't until the early 1950s that they began to proliferate in the Gulf of Mexico. Today there are 8000–8500 jackets in use around the world, the majority in the Gulf of

Mexico [15.15]. They are versatile and robust structures that can be easily scaled to the needed hydrocarbon production volume and built in many fabrication yards around the world. In shallower water regions with mild climates, a jacket might consist of just four legs and cost a few million US dollars. In deeper water, with a large number of producing wells, they can cost upwards of US \$100 million. Jackets have been deployed in many different environments, including mild low-latitudes like West Africa or Malaysia, more severe mid-latitudes affected by tropical cyclones (hurricanes), higher latitudes affected by frequent and severe extratropical storms, and even Arctic conditions with heavy first-year ice.

The chief constraint for jackets and jack-ups is water depth. At around 100–150 m, in harsh weather environments, a jacket's natural resonance period approaches the period of surface waves. In essence, the jacket begins swaying in rhythm with the wave forcing, resulting in metal fatigue, especially at the joints of the structure. The obvious solution is to stiffen the jacket with additional steel, but this, of course, increases cost. In milder climates, the economic cutoff is a bit deeper, but still only about 200 m. Designers have also tried extending the depth limit of the basic jacket design by purposely designing it to be more flexible, thus increasing the resonant period above the dominant waves. A few of these so-called *compliant towers*, or CTs (Fig. 15.7), have been built, but they are only economic in special circumstances.

15.4.2 Gravity-Based Structures (GBSs)

Another type of a fixed structure used for production is the so-called *gravity-based structure*, or GBS (not shown in Fig. 15.7). First deployed in the 1970s, almost all of the nearly 50 GBSs have been installed in the North Sea and were constructed of reinforced concrete. These are massive structures weighing up to one million tons and deployed in water up to 300 m, though most have been installed in 100–150 m. GBSs are well suited to stormy weather or heavy ice loads because of their mass, stiffness, resistance to overturning, and low foundation stresses. Their biggest weakness is that they must be built in a fjord; hence, they have only been used off Norway and the east coast of Canada.

15.4.3 Tension-Leg Platforms (TLPs)

One of the earliest floating production platforms was the *tension-leg platform*, or TLP (Fig. 15.7), which consists of a floating hull, usually composed of two large parallel pontoons, whose motion is constrained

by tendons made of tubular steel attached to the sea floor. As suggested by the name, the tendons remain in tension, essentially *pulling down* on the floating hull, and thus restraining its horizontal and vertical motions. A TLP experiences acceptable movement even in severe storms, yet is competitive with other alternatives in water depths ranging from roughly 500 m to at least 1500 m. As of 2015, there are 23 TLPs [15.17] in operation – all but eight in the Gulf of Mexico. Some of these are the so-called *mini-TLPs* (Fig. 15.7), which are inexpensive production-only platforms with no drilling capability.

15.4.4 Semisubmersibles (Semis)

By far, the most numerous deep water production and drilling platform is the *semisubmersible* (Fig. 15.8; a subtype of a semi, FPS, is shown in Fig. 15.7 as well). *Semis* are generally composed of two large sub-surface parallel pontoons connected to the upper deck by 4–6 columns, although triangular three-column versions have appeared more recently. Restrained by catenary moorings, semis were first used for drilling in the 1960s, but after about 20 years of stellar performance in the most severe ocean environments, the first purpose-built production semi was put into service in the North Sea. Semis are distributed widely, but primarily in the northeast Atlantic, Brazil, and the Gulf of Mexico. The deepest deployment is in the Gulf of Mexico at just over 2400 m. Semis are by far the most numerous floating drilling systems, with 273 in service in 2015 [15.17].

15.4.5 Spars

A *spar* (Fig. 15.7) is one of the more recently developed floating platforms, consisting of a long, large diameter cylinder (e.g., 30 m in diameter and 200 m in length) held vertically by heavy ballast at the base of the cylinder coupled with catenary mooring lines. Ballast and mooring lines keep the resonant period of the spar well above the period of wind waves. Hence, even in severe climates, spars deliver acceptable movement. As of 2015, 22 spars [15.17] had been installed in water depths ranging from 600 to 2400 m – all but two in the Gulf of Mexico.

15.4.6 Floating Production, Storage and Offloading (FPSO) Units

The prize for the most versatile floating production facility goes, without doubt, to the *floating production, storage and offloading* (FPSO, see Fig. 15.7) platform. First deployed in the 1970s using surplus oil tankers,

FPSOs are now purpose-built vessels with about 161 in service worldwide in 2015 [15.18]. They come in many different configurations, but are typically ship-shaped. In mild weather environments, they are simply spread moored with catenary lines in a fixed heading, but in moderate to severe climates, the FPSO is connected to a large buoy or a *turret* in the bow of the ship, which allows it to weather vane into heavy weather. FPSOs are economical in virtually any water depth, with systems having been installed in shallow water all the way out to 2500 m (Fig. 15.3). As the name implies, FPSOs include an offloading and storage capability, often making them the obvious choice for stranded fields where there is no existing pipeline infrastructure. FPSOs store oil, typically about one million barrels, and offload that oil to a tanker (also shown in Fig. 15.7), which is moored directly to the FPSO or from a nearby offloading buoy. Because the liquids ship directly, FPSOs are typically fitted with extensive onboard separation and processing equipment.

FPSOs are rarely equipped with the capability to drill or maintain wells and are frequently paired with subsea developments, the latter consisting of automated wellheads interconnected through flowlines and a flexible riser to the FPSO. Well expansion and maintenance must be done with a MODU.

There are many variants of FPSOs including floating storage and offloading systems (FSOs), floating production systems (FPSs), floating storage units (FSUs), and, most recently, floating liquid natural gas (FLNGs) units.

15.4.7 Drillships

As the name implies, *drillship* are ship-shaped MODUs, numbering 87 in operation worldwide [15.16] as of 2014. Typically used in very deep water, drillships (Fig. 15.8) are *dynamically positioned* by using thrusters or propellers. Thanks to the lack of moorings, drillships are capable of drilling to 3500 m (Fig. 15.3) and can quickly decouple from a well to avoid the most severe storms.

15.5 Metocean Impacts on the Offshore Industry

Metocean is an acronym for *meteorology and oceanography*, and is a term used in the offshore oil and gas industry to describe topics involving the quantification of winds, waves, currents, and related physical phenomena in the ocean and atmosphere. When engineers design a major facility or vessel to operate and survive in the sea, they must consider the loads, and other risks that may affect the facility. If the risks are under-

15.4.8 Subsea Systems

The fastest growing deep water offshore production system is the so-called *subsea system* (Fig. 15.7), consisting of wellheads, manifolds, and flowlines, placed on the sea floor and *tied back* to one of the surface-piercing systems described earlier. Subsea systems don't have to worry about severe weather, collisions, or ice, although these advantages are offset by the difficulty of maintaining equipment and a limited range of processing options. Nevertheless, subsea systems allow economic development of reservoirs that are thin but wide, meaning development of small uneconomic reservoirs that may be tens of kilometers away from an existing surface production or coastal facility.

The main component of a subsea system is a wellhead, which sits on the sea bed directly over the well. Wellheads are nicknamed *trees* because they contain many *branches* of pipes. Their complexity is partially a result of the many functions that they must execute, such as fluid monitoring, chemical injection for well maintenance, pressure boosting in the case of underpressurized reservoirs, and chemical injection to ensure unrestricted flow during the often long transit to the surface. Since most subsea systems are installed in deeper water (Fig. 15.3), they are generally serviced using remote operated vehicles (ROVs), further complicating their design.

Several hundred subsea systems have been installed [15.19], and many will follow in the future, as various constraints are removed with new technology. Arguably, the most serious constraint is the distance between the wellhead and the surface-piercing facility, the so-called *tieback*. As of 2015, the longest tieback was 150 km (Nobel Energy's Tamar gas field), but the average is closer to 20 km [15.17, 19]. The tieback constraints are driven largely by the difficulty in pumping a multiphase fluid (oil/gas/water) at low temperatures with high pressure drops and with limited available power. The discipline of *flow assurance* has become increasingly important in dealing with hydrate formation, slugging, wax deposition, and corrosion.

estimated, then damage can result, and lives may be lost. Conversely, if risks are overestimated, the costs may be too high, perhaps, to the point that the project cannot pass the financial hurdles and is never built. For instance, overestimating a design wave height for deep water floating production platforms could result in adding too many mooring lines. At several million US dollars per mooring, this is a substantial penalty.

But it doesn't stop there, since these additional lines would add hundreds of tons of static load, so a larger, more buoyant facility will be needed, thus, generating additional capital cost – well beyond the cost of the excess mooring lines. In short, an accurate quantification of air and sea parameters can have far-reaching effects on the safety and profitability of offshore facilities. For this reason, metocean risks are usually specified and described in a separate chapter in the project design documents.

In 2005, the American Petroleum Institute (API) recognized the influence of metocean criteria and began publishing a standalone set of recommended practices for the offshore industry [15.20]. Typical procedures include quantifying the so-called ambient air and sea *climatologies* on different time scales – hourly, daily, monthly, seasonally, annually, decadal, and so on. These include average and extreme statistics, exceedance probabilities and joint probability distributions, persistence information, and so on. The ultimate goal for offshore operations is to have accurate forecasts for the atmosphere and ocean states at any given time.

Metocean criteria are typically broken into two categories: operating and extreme. During *operating* conditions, the facility or vessel should be capable of achieving routine functions of its primary purpose, for example: drilling, pumping oil and gas, generating wind energy. Typical products used to quantify operational conditions are cumulative probability distributions of wave height, tables of wind speed persistence, average air and water temperatures, air moisture and pressure, water salinity, tidal amplitudes, and so on. These products are used in estimating the fatigue lives for structure components and operation down time. In contrast, *extreme* conditions are generated by episodic and, sometimes, poorly predictable events (e.g., storms, earthquakes, resonances in the basins) that occur *rarely*. During extreme conditions, normal operations are suspended – the vessel is slowed, oil or gas production is stopped, wind turbines are feathered, and so on. A common example of an often used extreme metocean parameter is the 100-year wave height – the largest wave expected over a 3 h period once in 100 years. Since both extreme and operating conditions are heavily affected by winds, waves, and currents, these phenomena are briefly discussed below, along with the processes that commonly control them and the impacts they can have on offshore facilities and operations.

15.5.1 Winds

In terms of raw speeds the most powerful storm in the marine environment is the *tropical storm*, commonly referred to as a hurricane, typhoon, or tropical

cyclone, depending on what part of the world they are in. These storms are *convective*, i.e., they are fundamentally driven by vertical movement of energy and humid air. Since they require warm, humid air and warm surface waters, tropical storms are creatures of summer and early fall. They can generate sustained winds around 200 km/h with horizontal scales of order 200 km. Because they move fairly fast, tropical storms pass over a site in a matter of hours. Tropical cyclones are strongest in latitudes of $30 \pm 10^\circ$ and most numerous in the eastern North Pacific, southern North Atlantic, and western Pacific.

Extratropical storms are large scale storms, sometimes affecting a 1000 km wide swath. They occur during the hemisphere's fall-winter-spring season, when strong horizontal temperature gradients are found in the mid- to higher-latitudes. Despite somewhat weaker wind speeds, extratropicals can still generate sustained winds of 120 km/h and do so over distances of order 500 km for a day or more. Because of their longer space and time scales, extratropicals hold the record for generating extreme waves. Figure 15.9 shows satellite images of Hurricane Katrina overlaid on the large extratropical storm. Note the circular, smaller scale of the hurricane in relation to the sprawling, more chaotic shape of the extratropical storm.

There are several types of other severe storms with small length scales that can generate strong winds. *Thunderstorms* (often called squalls) can generate winds up to 120 km/h, but individual cells have horizontal length scales of only a few km, so they affect a site for just a few minutes. *Water spouts* are small scale phenomena observed over water and are generally no stronger than a moderate squall, but tornadic water spouts can be generated by mesocyclones in a manner similar to terrestrial tornadoes. Another intense, small scale storm, known as the *polar low*, is only found at high latitudes in the presence of strong horizontal temperature gradients [15.21]. Because of their small size and isolated range, there are few direct wind measurements in polar lows. Indeed, they were not even fully recognized by meteorologists until the advent of satellite imagery in the mid-1960s.

When referring to the wind speed, it is always important to reference the time over which the speed is averaged. A wind *gust* is typically averaged over 3 s. For more sustained winds, typical averaging periods are 1 min and 1 h. The differences between averaging intervals can be substantial. For example the 3 s wind is typically about 300% less than the 1 min wind. Another important detail is the height of the wind above the mean sea level. The standard height is 10 m, but the most important winds for many platforms are at the level of the main decks, which can be 30–50 m above

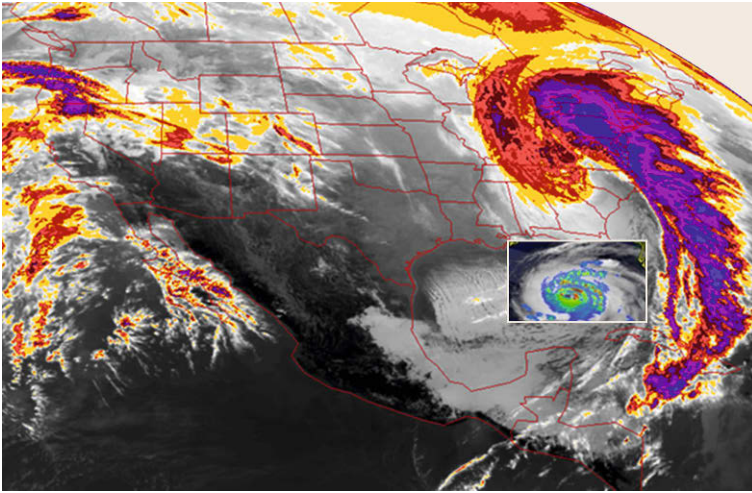


Fig. 15.9 Overlay of the so-called *storm of the century*, an extratropical storm affecting the Northeast US in March 1993, and hurricane Katrina as it approached New Orleans in August 2005 (courtesy of US National Oceanic and Atmospheric Administration)

the sea level. There, the winds will be of order 15% higher than at 10 m.

Strong winds impact the offshore industry in many ways: by making it difficult or impossible to perform certain operations, such as off- or on-loading of cargo using the on-board crane and installing or repairing facilities. Extreme wind loads dominate the environmental loads in several of the production and drilling concepts including TLPs, FPSOs, semis, and drillships. That is because these platforms have a relatively large portion of the structure above the sea, or because the platform has been carefully designed to minimize wave loads.

15.5.2 Waves Observed at the Ocean Surface

All motions in the ocean, just like in the atmosphere, can be ordered in terms of their periods space scales, as well as responsible generation mechanisms. Most readers are familiar with waves observed at the surface that are generated whenever the wind blows over open water. The longer the wind blows, the higher and the longer the period are the waves, all else being equal. Similarly, the longer the open-water distance over which the wind blows (*fetch*), the higher and longer period are the waves. *Storm surges* are massive waves with heights of up to 30 m that have periods shorter than those of the tides and are considered to be of a large scale external inertia-gravity wave type. They can flood the coastal areas when they surge onto the shore. The largest wave heights are generated by strong extratropical storms, where the winds can blow over a fetch of hundreds of km for several days. The small scale winds can generate waves with shorter periods. When dominated by gravity, they are called *surface gravity waves*; even smaller scale waves with periods

shorter than 0.25 s are affected by surface tension and are called *capillary waves*.

Surface gravity waves travel at speeds that are dependent on their period; though, in *shallow water* (compared to the half wavelength), the water depth also affects the wave speed. When the wind blowing in the direction of the surface gravity wave is faster than the wave speed, the wave is called the *wind wave*, and its height and period will continue to grow. If the wind drops below the wave speed, the waves are referred to as *swell*. Swell can travel for over 1000 km in the open ocean with little decay in energy. *Tides*, *tsunamis*, and *seiches* are other familiar types of waves that can propagate long distances. They originate independently of the wind forcing by predictable gravitational pull of other planets, intermittent earthquakes, and resonances in the basins respectively. Tsunamis and seiches typically have periods shorter than tides, and all show largest effects in shallower water.

Thus, waves in the ocean rarely have a single period but are composed of a spectrum of periods and are best quantified using statistical measures [15.22]. For example, the most common measure of surface gravity wave height is the so-called *significant wave height*, which is proportional to the total energy in the wave spectra, and for a typical wave field it can be shown to equal the average of the highest one-third of the waves. Significant wave height also corresponds to a wave height that a trained observer would notice when viewing a typical sea state during an interval of several minutes. The maximum wave height expected during a given period of time (e.g., an hour) can be calculated with a Forristall distribution [15.23], which shows that the largest wave expected during a 1 h time interval in a tropical or extratropical storm will be roughly 1.6–2.0 times the significant wave height depending on the wave period

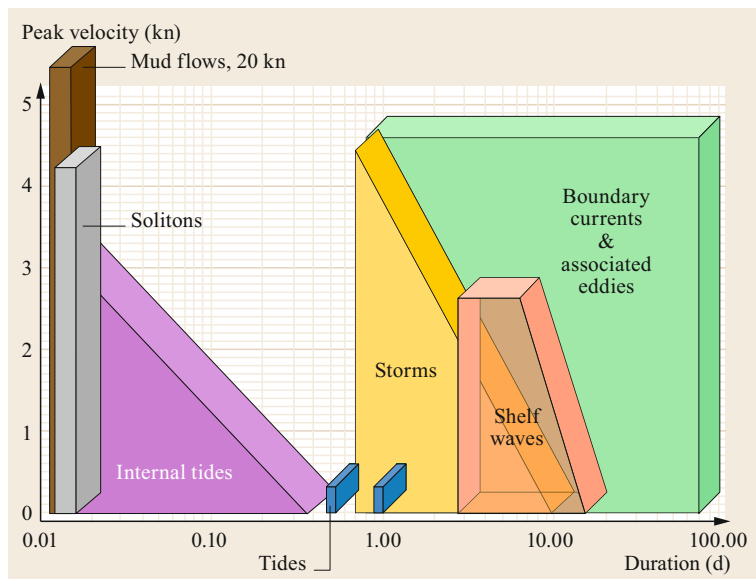


Fig. 15.10 Schematic summary of the characteristic duration and peak velocity of various types of deep water ocean currents

and how peaked the wave spectrum is. However, this distribution has no upper limit, which means that many of the so-called *rogue* or *freak* waves reported in the literature are, in fact, expected, as they lie well within the confidence limits of the Forristall distribution.

The large wave disturbances that one can easily observe at the ocean surface are often the dominant environmental loads on most offshore facilities, especially jackets, jack-ups, and GBSs. Waves, of course, also have a big effect on operations, including transferring of cargo, offloading of oil, installation, and repair.

15.5.3 Ocean Currents

The notion of *current* is usually used as a *common wisdom* term for either low-frequency (compared to tidal frequency) flow or higher frequency waves that appear to happen within the water column (e.g., tides in the deep water). Figure 15.10 shows the characteristic duration and maximum velocity scales of different types of energetic deep water ocean currents. For example, the figure shows that storm-generated currents have a broad range of magnitudes and periods, the latter being strongly related to the time scale of the generating atmospheric process. The strongest storm-driven currents with peaks of 4–5 kn (7.4–9.2 km/h) are driven by *tropical cyclones*. Cyclones are especially efficient generators of strong near-surface currents, in part because the storms typically translate at near-resonance to the inertial period of the ocean. Another factor is that tropical cyclones occur over regions of the ocean, topped by a relatively thin (30–60 m) layer of warmer water, which serves to concentrate the wind energy. *Ex-*

tratropical storms are the other type of atmospheric disturbance that generate substantial currents but of much longer time scales and lower magnitude – hence, the downward sloping trend of the curve in Fig. 15.10.

Other types of currents may include *internal tides* and *solitons* (internal inertia-gravity waves), *mud flows* (density-driven turbidity currents near the ocean bottom), *shelf waves* (also known as *coastally trapped waves*: large-scale waves due to the presence of the coast, density stratification, and bottom slope), and *boundary currents* and *eddies* (large scale ocean circulation patterns at mesoscale, subbasin, and basin scales). In an analog to Fig. 15.10 for shallower water of a continental shelf, the tidal curve would appear much higher, reaching something like 6 kn (11.1 km/h). Thus, the reader is reminded that a given site rarely, if ever, would be affected to the same extent by all the processes schematically depicted in Fig. 15.10, nor would the peak magnitude always reach the levels shown [15.24].

In the early years of offshore development, currents were completely neglected in the load calculations because the dominant structure types – jackets and jack-ups – have a small drag cross-section beneath the water level, and, hence, are dominated by wave and wind loads. However, as the industry expanded into deeper waters, currents have become much more important. That is due, in part, to the shift towards floating platforms, which are much more influenced by strong currents than jackets. For instance, in the case of a TLP, the current can push the TLP downstream, but, since the TLP is restrained vertically, this movement *knocks down* the TLP – lowers it in the water, bringing the deck closer to the waves. This, of

course, can be corrected in many different ways, but the bottom line is that currents are important to the TLP design. Ocean currents have similarly important impacts on spars and FPSOs, though for different reasons. Regardless of the surface platform type, ocean currents affect important subcomponents, such as drilling and

production risers. The former contain the drill string/mud, while the latter convey hydrocarbons from the sea floor to the surface platform. Ocean currents impose a drag load on the riser and can cause fatigue through *vortex-induced vibration* and other mechanisms.

15.6 Future Offshore Production and Drilling

What will the offshore oil and gas field of the future look like? There are at least two major unknowns that affect the outlook: the potential for a carbon tax on fossil fuels and the volume of production from onshore shale. If both are substantial, the demand for relatively costly production in the Arctic and ultra-deep water will be reduced. While these uncertainties will affect the pace of development, it probably won't affect the general direction. That direction is toward more subsea production in deeper water and in the Arctic. Such trend is driven by economics: the less expensive way is to install production equipment on the sea floor and to bring it ashore, if possible, or connect it to a preexisting surface facility. Such arrangements allow the development of relatively small reservoirs, which would not be economic if they required a new surface facility. In any case, the future of the offshore production, with no doubt, relies on the improved theoretical understanding of the ocean circulation and metocean criteria through physical observations, theory, and modeling efforts.

Because of the innate advantages of subsea production, major investments in engineering research are also underway to expand its capability. These efforts are focused on increasing tieback distances between the subsea wellheads and existing surface platforms, and putting more and more of the production activities on

the sea floor. Ultimately, the goal is to be able to develop reservoirs without any surface facility. This is a daunting challenge, since it requires new technology for subsea separation, well and flow line maintenance, and compression. Before these can become reality, progress will have to be made in generating large amounts of power (of the order 1 MW) on the sea floor [15.19]. In terms of new producing regions, it is likely that activity will continue to extend into deeper water. The main deep water play is in the Gulf of Mexico, but the US portion of this basin may be fully explored in another decade. Subsequently, deep water activity will likely increase in the deep waters off of Africa, Australia, and South America.

The Arctic is the last great region that may hold large reserves of hydrocarbons (Fig. 15.5), yet has not been much exploited (Fig. 15.6) because of high costs and environmental concerns. Decreasing ice cover will reduce costs and, to some degree, the environmental risks, so this could further spur production. That said, forecasts of increased offshore Arctic production have been made for at least four decades and yet have failed to materialize, because cheaper sources of hydrocarbons were discovered in the interim. Shale production may prove to be the next spoiler to advocates of Arctic drilling.

References

- 15.1 J. Ferentinos: *Global Offshore Oil and Gas Outlook* (Infield Systems, London 2013), www.gaselectricpartnership.com/HOffshore%20Infield.pdf
- 15.2 T.F. Rowland: Improved submarine drilling apparatus, US Patent US89794 (1869)
- 15.3 *Petroleum Age*, Vol. 7(4), (The Oil Publishing Company, Chicago 1920)
- 15.4 A. Ciarreta, S. Nasirov: Analysis of Azerbaijan oil and gas sector, Proc. 30th USAEE/IAEE Conf. (2010), www.usaee.org/usaee2011/submissions/OnlineProceedings/Ciarreta_Nasirov-Article1.pdf
- 15.5 K.L. Vogt, J.G. Wells: *Historic Oil and Gas Wells in and Adjacent to Grand Lake St. Marys* (The Ohio Department of Natural Resources, Division of Geological Survey, Columbus 2007), geosurvey.ohiodnr.gov/portals/geosurvey/PDFs/Energy/grandlakestmary_oil_wells.pdf
- 15.6 S. Curran: Summerland oil field, Proc. Calif. State Lands Comm. Meet. 20111, http://archives.slc.ca.gov/Meeting_Summaries/2011_Documents/09-01-11/Items_and_Exhibits/87ExhA.pdf (2011)
- 15.7 K.A. Franks, P.F. Lambert: *Early Louisiana and Arkansas Oil: A Photographic History 1901-1946* (Texas A&M Univ. Press, College Station 2000) p. 260
- 15.8 V. Maksakovskii: *Geographic Review of the World. Textbook for Colleges. Part 1: General Characteristics of the World. Global Problems of the Humanity*

- (Drofa, Moscow 2008), in Russian
- 15.9 Globalshift: Offshore drilled wells, <http://www.globalshift.co.uk/globoffdrill.html> (2015)
- 15.10 United Nations: United Nations Convention on the Law of the Sea, http://www.un.org/depts/los/convention_agreements/convention_overview_convention.htm (1982)
- 15.11 P.R. Pinet: *Essential Invitation to Oceanography* (Jones and Bartlett, Burlington 2014)
- 15.12 B.J. Murton: A global review of non-living resources on the extended continental shelf, *Rev. Bras. Geof.* **18**(2), 281–307 (2002)
- 15.13 P.A. Rona: Possible salt domes in the deep Atlantic off north-west Africa, *Nature* **224**(5215), 141–143 (1969)
- 15.14 E.D. Schneider: The deep-sea – A habitat for petroleum, *Undersea Technol.* **10**(10), 32–34 (1969)
- 15.15 Petrowiki: Offshore and subsea facilities, http://www.petrowiki.org/Offshore_and_subsea_facilities (2014)
- 15.16 OPL: Clarksons research services mobile drilling units of the world, <http://www.oilpubs.com/mdul> (2014)
- 15.17 C. Barton, H. Hambling, E.K. Albaugh, B. Mahlstedt, D. Davis: Deepwater solutions and records for concept selection. Going deeper with production technology, *Offshore Mag.*, <http://www.offshore-mag.com/content/dam/offshore/print-articles/volume-75/05/0515-DeepwaterPoster040815ADS.pdf> (2015)
- 15.18 C. Barton, H. Hambling, E.K. Albaugh, B. Mahlstedt, D. Davis: Worldwide survey of floating production, storage and offloading (FPSO) units, *Offshore Mag.*, <http://www.offshore-mag.com/content/dam/offshore/maps-posters/2015FPSO-072415-Ads.pdf> (2015)
- 15.19 L. Forster, T.M. Paes, R.J. Baker, R. Voight, S. Ionescu, J. Allen, M. Grund, D. Duke, E.K. Albaugh, D. Davis: Worldwide survey of subsea processing: Separation, compression, and pumping systems. Status of the technology, *Offshore Mag.*, http://www.offshore-mag.com/content/dam/offshore/print-articles/volume-75/03/1503off_SubseaposterDIG.pdf (2015)
- 15.20 American Petroleum Institute: *ANSI/API Recommended Practice 2MET, Derivation of Metocean Design and Operating Conditions*, 1st edn. (API, Washington 2014)
- 15.21 E.A. Rasmussen, J. Turner: *Polar Lows: Mesoscale Weather Systems in the Polar Regions* (Cambridge Univ. Press, Cambridge 2003)
- 15.22 L.H. Holthuijsen: *Waves in Oceanic and Coastal Waters* (Cambridge Univ. Press, Cambridge 2007)
- 15.23 G.Z. Forristall: On the statistical distribution of wave heights in a storm, *J. Geophys. Res.* **83**(C5), 2353–2358 (1978)
- 15.24 J.H. Steele, S.A. Thorpe, K.K. Turekian (Eds.): *Ocean Currents. In: Elements of Physical Oceanography – A Derivative of the Encyclopedia of Ocean Sciences* (Academic, London 2010)

Refining

Part C

Part C Refining Technologies

16 Petroleum Distillation

Chang Samuel Hsu, Tallahassee, USA,
Changping, China
Paul R. Robinson, Katy, USA

17 Gasoline Production and Blending

Chang Samuel Hsu, Tallahassee, USA,
Changping, China
Paul R. Robinson, Katy, USA

18 Catalytic Reforming

Pierre-Yves le Goff, Rueil-Malmaison,
France
William Kostka, Houston, USA
Joseph Ross, Princeton, USA

19 Fluid-Bed Catalytic Cracking

James G. Speight, Laramie, USA

20 Sulfur Removal and Recovery

Paul R. Robinson, Katy, USA

21 Modern Approaches to Hydrotreating Catalysis

Joo-II Park, Safat, Kuwait
Isao Mochida, Fukuoka, Japan
Abdulazeem M. J. Marafi, Safat, Kuwait
Adel Al-Mutairi, Safat, Kuwait

22 Hydrocracking

Paul R. Robinson, Katy, USA
Geoffrey E. Dolbear, Katy, USA

23 Hydroprocessing Reactor Internals

F. Emmett Bingham, Orange, USA
Douglas E. Nelson, Orange, USA
Daniel Morton, Houston, USA

24 Hydrogen Production

M. Andrew Crews, Houston, USA
B. Gregory Shumake, Tyler, USA

25 Hydrogen Network Optimization

Nick Hallale, Warrington, UK
Ian Moore, Stockport, UK
Dennis Vauk, Houston, USA
Paul R. Robinson, Katy, USA

26 Model-Predictive Control Fundamentals

Paul R. Robinson, Katy, USA
Dennis Cima, Houston, USA

27 Modeling Refining Processes

Teh C. Ho, Bridgewater, USA

28 Refinery-Wide Optimization

Dale R. Mudt, Sarnia, Canada
Clifford C. Pedersen, Sarnia, Canada
Maurice D. Jett, Houston, USA
Sriganesh Karur, Katy, USA
Blaine McIntyre, Calgary, Canada
Paul R. Robinson, Katy, USA

29 Rigorous Kinetics Modeling of Hydrogen Synthesis

Milo D. Meixell Jr, Houston, USA

30 Delayed Coking

Keith Wisecarver, Tulsa, USA

31 Transitioning Refineries from Sweet to Extra Heavy Oil

Martin R. Gonzalez, Naperville, USA

32 Carbon Dioxide Mitigation

Sultan M. Al-Salem, Safat, Kuwait
Xiaoliang Ma, Safat, Kuwait
Mubarak M. Al-Mujaibel, Safat, Kuwait

Petroleum Distillation

Chang Samuel Hsu, Paul R. Robinson

Crude oils are complex mixtures of numerous molecules with different boiling points. After removing solid particulates and salts by a desalting process, fractional distillation is the primary means for refineries to separate the molecules into fractions (cuts) continuously. A crude distillation unit includes an atmospheric distillation tower, a vacuum distillation tower, and associated equipment. The cuts can be further processed or upgraded in downstream units – hydrotreaters, catalytic reformers, fluid catalytic cracking units etc. The products of upgrading units often require further separations, usually by distillation for lighter cuts and extraction for heavy cuts.

16.1	Overview	533
16.2	Distillation Theory	537
16.2.1	Ideal Distillation	537
16.2.2	Vapor–Liquid Equilibrium (VLE)	538
16.2.3	Theoretical Stages	538
16.3	Crude Oil Distillation	541
16.3.1	Predistillation Processing	541
16.3.2	Desalting	542
16.3.3	Crude Distillation Overview	544
16.3.4	Atmospheric Distillation	545
16.3.5	Vacuum Distillation	546
16.3.6	Straight–Run Distillation Yields	548
16.4	Summary	549
	References	549

16.1 Overview

There are many phases of petroleum from gas to solid, including natural gas, condensates, crude oils, tar etc. Separating complex crude oils that contain thousands or millions of components is based on volatility by boiling point and solubility by various solvents. Fractional distillation is the primary means of separation of crude oils at refineries into fractions of different boiling ranges. The fractions are subsequently upgraded or converted into useful products in other units. For very heavy fractions, extraction becomes the method of choice for further separation. However, the crude oil distillation unit (CDU) is the first processing unit in virtually all petroleum refineries.

Crude oils are complex mixtures of numerous molecules with different boiling points. Refineries separate the molecules into fractions (cuts) primarily by continuous fractional distillation. Distillation separates mixtures of two or more substances, usually liquids, with the application of heat. The vapor over a boiling mixture is richer in components with lower boiling points. When this vapor is drawn away and condensed by cooling, the condensate will contain more of the more-volatile components. At the same time, the remaining liquid will contain more of the less-volatile components.

Distillation has an interesting history [16.1]. Aristotle wrote about the recovery of ethanol from wine, stating that *ordinary wine possesses a kind of exhalation, and that is why it gives out a flame* [16.2]. Recovering turpentine from tree sap is another example of ancient distillation [16.3]. In Alexandria, during in the first century AD, Greek alchemists used distillation to separate volatile spirits from many substances, including obtaining naphtha from bitumen. In China, distillation probably began during the Eastern Han 東漢 Dynasty (25–220 AD). Evidence indicates that distilled beverages were being consumed during the Jin 金 and Song 宋 Dynasties (907–1279 AD). A twelfth-century still was uncovered in Qinglong, Hebei province.

In 1500 AD, Hieronymus Braunschweig, a German alchemist, published the first comprehensive book on distillation [16.4]. The book is divided into three parts:

1. The first part describes the equipment and techniques used in batch distillation.
2. The second part is a list of plants and methods for distilling *spirits* from them.
3. The third part describes the medicinal uses for various spirits.

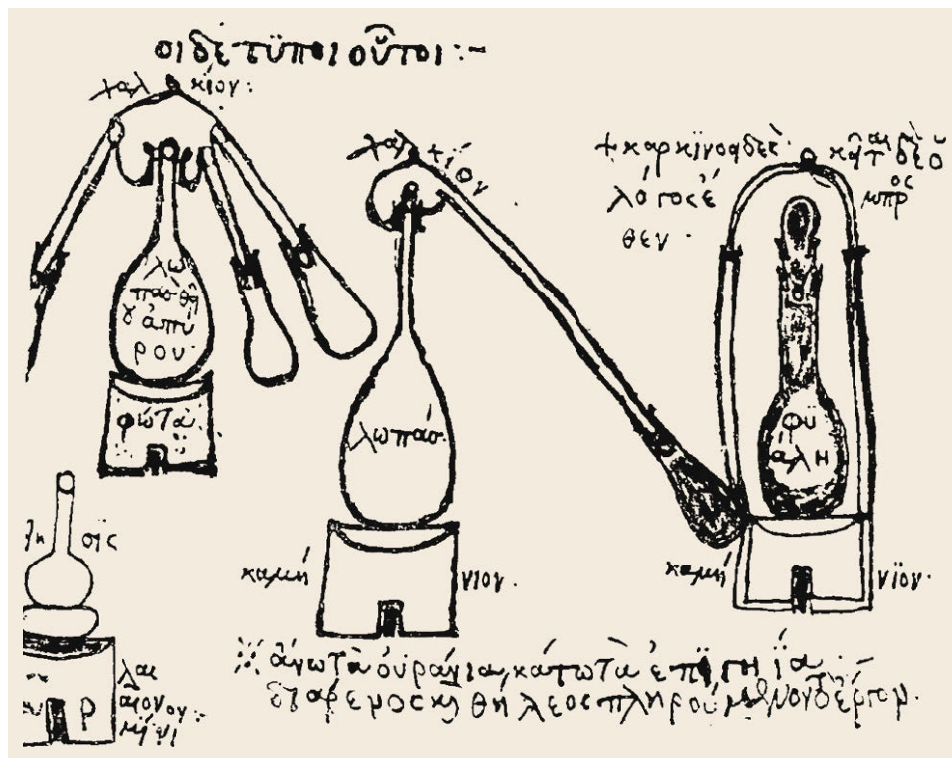


Fig. 16.1 Drawing of alembics by Zosimos of Paniplos (after [16.5])

Early batch-distillation gear included alembics and retorts, which are glass or ceramic flasks with long necks that point downward and to one side. Figure 16.1 presents drawings by Zosimos of Panopolis, a third-fourth century Greek alchemist and Gnostic scholar who was born in Egypt and may have traveled throughout the Middle East [16.6]. Figure 16.2 shows a retort assembly with a water-cooled receiver. As a mixture inside the main flask is heated, vapors rise and flow through the air-cooled neck. At the cooler temperature in the neck, the vapors condense and flow into a receiver, which collects the distillate. To improve separation (increase purity), the distillate is redistilled, usually in a different apparatus and sometimes several times.

Pot stills (Fig. 16.3) were fashioned from copper. Some included coiled water coolers, which improved separation efficiency. Today, pot stills are employed to produce cognac, Scotch whiskey, and tequila. The goal in distilling these products is not to achieve maximum purification of alcohol, but to prepare beverages with characteristic flavors.

Preheating and reflux emerged in the early nineteenth century. In reflux, cooled condensate is returned to the top of a column, from whence it flows downwards, pulling with it heavier molecules entrained in the upcoming vapor. Eventually, it reaches

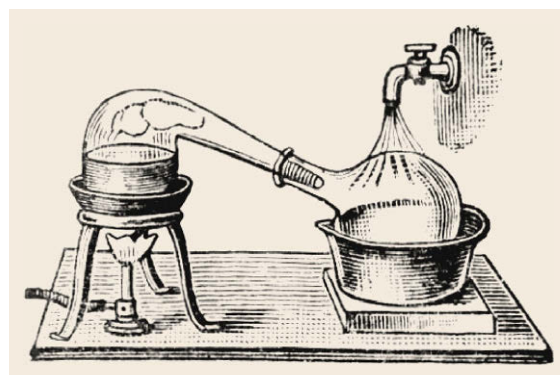


Fig. 16.2 Retort with water-cooled receiver (after [16.7])

a zone corresponding to its boiling point and vaporizes again.

Aeneas Coffey patented a single-column still in 1830, enhancing a previous design developed by Robert Stein in 1826. The *Coffey still*, also called the *Patent still*, operated continuously, producing spirits with more than 60 vol.% ethanol. The limit on alcohol purity is 95.6 vol.%, where ethanol and water form an azeotrope. An azeotrope is a constant-boiling mixture. The composition of the vapor is the same as the composition of the unboiled mixture. Further separation cannot be achieved by distillation alone.

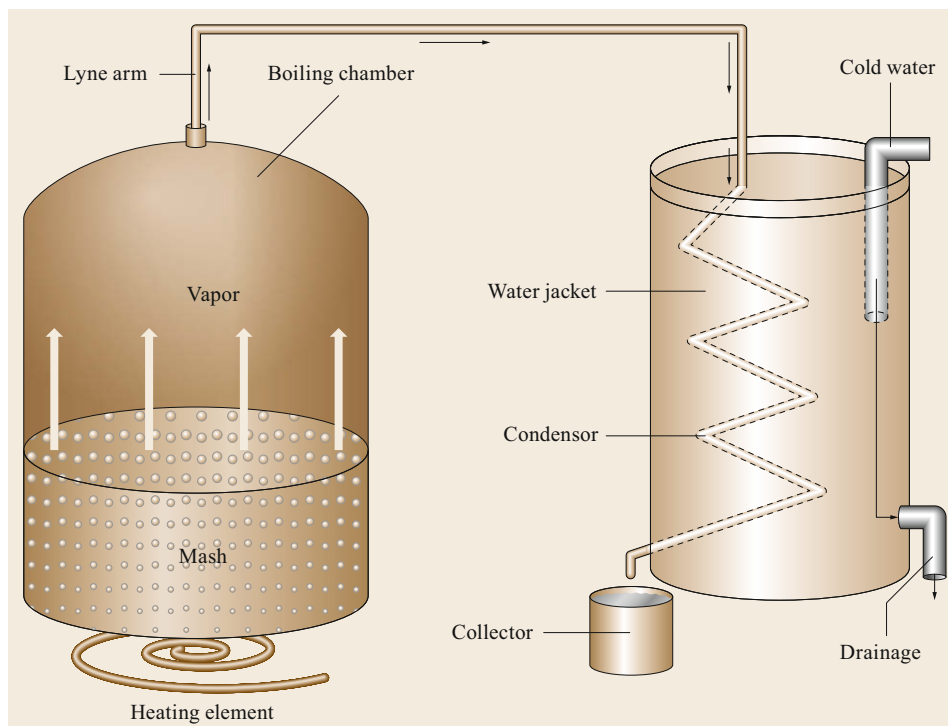


Fig. 16.3 A pot still for recovering alcohol-containing distillate from fermented mash. The condenser is a water-cooled coil. Cold water is added and hot water is removed to keep the condenser temperature constant

In 1877, Ernest Solvay obtained a US Patent for tray-column distillation, which he used to separate ammonia from water in his process for making sodium carbonate from limestone and brine.

Figure 16.4 shows a simple schematic for continuous fractional distillation, which is the primary separation method in oil refineries. Additional details are provided in subsequent sections. The preheated feed is a mixture of light and heavy liquids. It enters the column from the side.

In crude oil distillation, steam is injected into near bottom of the tower to improve separation. It does so by reducing the partial pressures of the hydrocarbon components while providing heat for vaporization. Steam is a key feature of crude distillation, but it may or may not be featured in other refinery distillation units.

Light components vaporize and flow up through several trays toward the top. Unvaporized feed flows down toward the bottom. At the top, vapors go to a cooler (condenser) into a reflux drum. Part of the light condensate is withdrawn as a product; the rest is returned to the top of the column as reflux to provide cooling. Reflux plays a major role in controlling temperature and enhancing separation at the top of the tower, where it shifts the mixture closer to vapor-liquid equilibrium and recovers more liquid products from vapor. The reflux ratio is the amount of liquid returning to the tower divided by the amount of liquid withdrawn

as product. With a higher reflux ratio, fewer theoretical plates are required.

At the bottom of the tower, the liquid residue goes through a reboiler. Part of the reboiled residue becomes product; the rest is returned to the tower to provide heating.

This combination of cooling at the top and heating at the bottom imposes a temperature gradient. One or more intermediate streams (middle distillates) are drawn as side cuts from the tower and cooled. The trays (plates) improve separation. At each tray, some of the vapor condenses and flows back down the column. When the condensed liquid reaches a zone that is hotter than its boiling point, it re-vaporizes. Temperatures are controlled by flow rates, and flows are adjusted with control valves (CVs).

Early distillation trays were perforated plates, which were relatively inefficient and very sensitive to deviation from horizontal; a tilt of just a few degrees could flood one side of the tray. With modern designs, separation efficiency has improved tremendously. Figure 16.5 illustrates a bubble-cap tray with downcomers. Condensed liquid flows down through a pipe (downcomer) to the hotter tray below, where the higher temperature causes re-evaporation of the lighter components. Ascending vapor flows up through the base of the cap, down through the lip, and into the liquid. The liquid level on the tray is set by the height of the

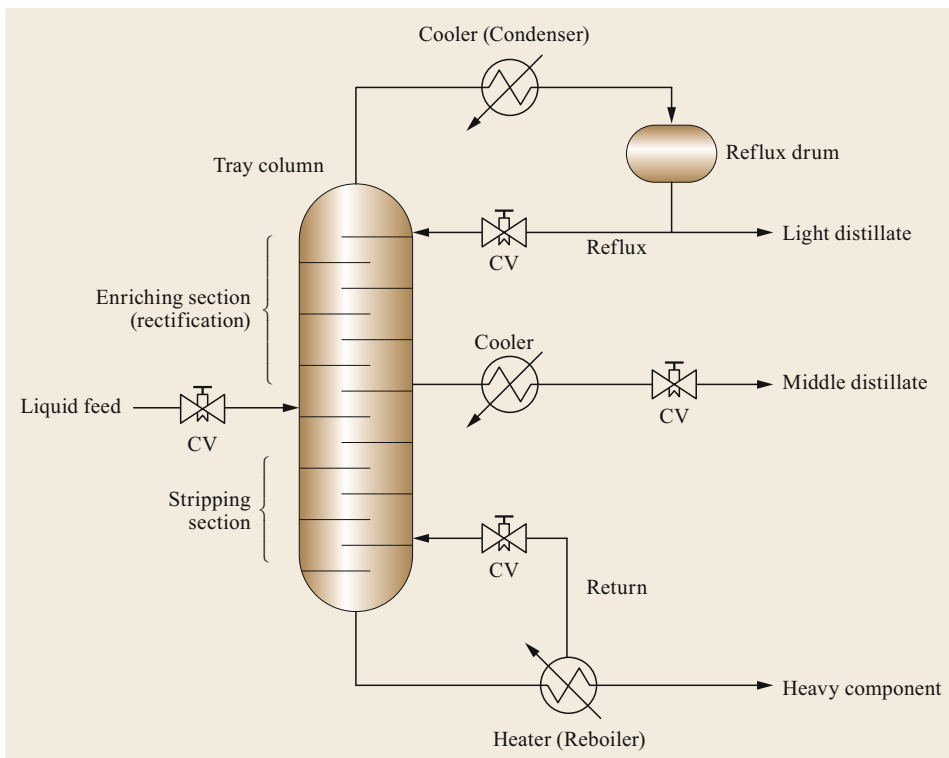


Fig. 16.4 Continuous distillation in a trayed column (tower)

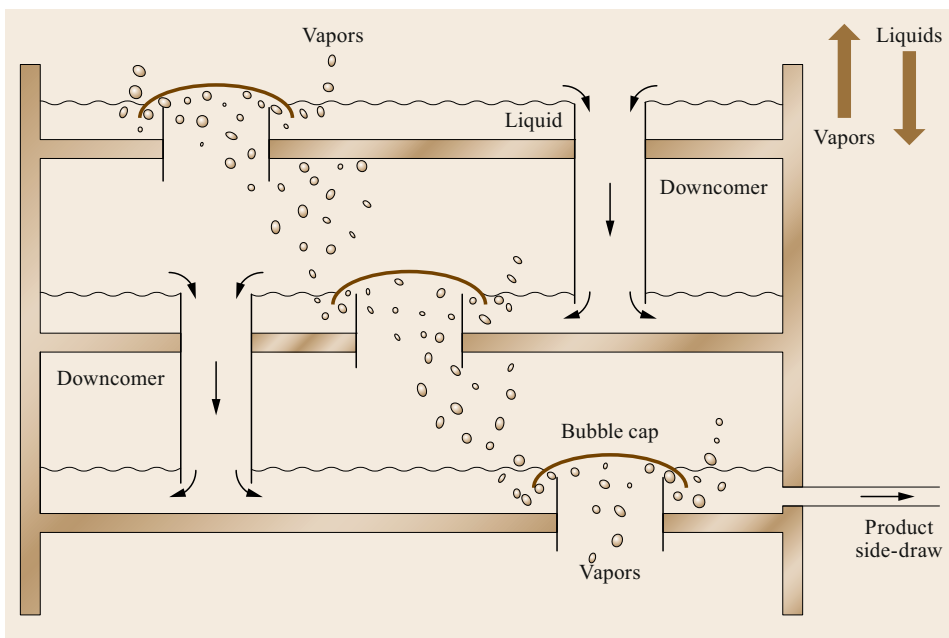


Fig. 16.5 Bubble caps and downcomers on distillation trays. The side-draw comes from a product tray (after [16.8])

downcomers. The level must be high enough to cover the outer lip of the bubble cap. A given molecule evaporates and condenses many times before finally leaving the tower. Bubble-cap trays provide good contact be-

tween downflowing liquid and upflowing vapor, which knocks heavy material out of the vapor.

Several other kinds of trays are available. On valve trays, bubble caps are replaced with chimneys topped

with a valve. When vapor flows up the chimney, the valve opens and vapor flows into the liquid on top of the tray. The direction of flow is horizontal, which provides superior mixing. If the vapor flow is too low, the valve closes, preventing *weeping* – the flow of liquid down the chimney.

Occasionally, refiners install inert packing, either structured or random, to improve liquid–vapor contact with minimal pressure drop. Adding packing can be equivalent to adding several trays. One type of random packing comprises unconnected metal rings. Figure 16.6 shows an example of structured packing.

Packing is bothersome during maintenance, because it can be hard to remove, especially if it is fouled or corroded.



Fig. 16.6 Structured packing for distillation (© Luigi Chiesa)

16.2 Distillation Theory

Distillation separates mixtures of two or more liquids with the application of heat. When heated, individual liquids either vaporize or decompose. The boiling point of a liquid is the temperature where the vapor pressure of the liquid equals the external pressure. For normal boiling, the external pressure is one atmosphere [16.9].

16.2.1 Ideal Distillation

Models for ideal distillation assume that the vapor and liquid phases are in equilibrium. Such models incorporate Raoult's law and Dalton's law. In Raoult's law, it is assumed that the vapor pressure of a solution is determined by the vapor pressures and mole fractions of solution components. In Dalton's law, it is assumed the total pressure is the sum of the partial pressures of each component. Combining Raoult's law with Dalton's law gives the following expression

$$P = P_A x_A + P_B x_B + \dots,$$

where P is the total pressure; P_A and P_B are the partial pressures of A and B respectively; and x_A and x_B are the mole fractions of A and B respectively. Figure 16.7 illustrates Raoult's law for an ideal solution with two components.

When a mixture is heated, the vapor pressure of each component rises, causing the total vapor pressure to rise. A mixture with a given composition has only one boiling point. Hence, lighter components don't really *boil first*. In an ideal system, all volatile components boil at the boiling point of the mixture. As mentioned, in continuous fractional distillation, there

is a temperature gradient in the tower. At each level, the compositions of liquids and vapors are different. Mixtures at the top of the column contain components with the lowest boiling points and the highest vapor pressures. Mixtures at intermediate draw points contain components with intermediate vapor pressures and intermediate boiling points.

Ideal distillation models are highly accurate for mixtures in which the components are similar, such as benzene and toluene or n -hexane and n -decane. Deviations from ideal are caused by molecular interactions, such as the formation of azeotropes.

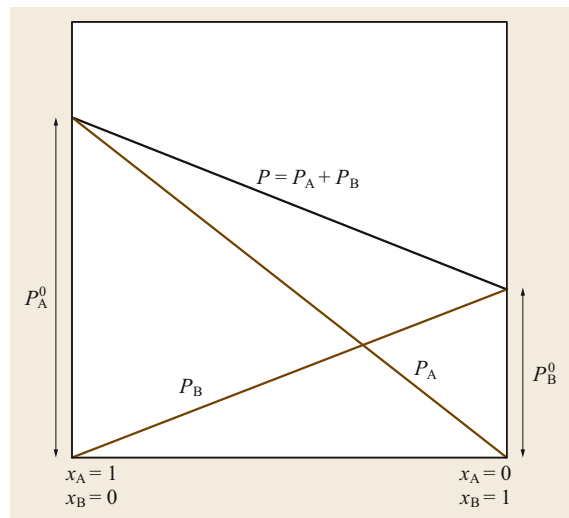


Fig. 16.7 Raoult's law for an ideal mixture of two components

In salt water, the vapor pressure of the salt is zero. In this case, boiling off the water is called evaporation.

16.2.2 Vapor–Liquid Equilibrium (VLE)

The difference between liquid and vapor compositions is the basis of distillation. Relative volatility is the difference between the boiling points of components. It indicates how easy or difficult a particular separation will be.

Boiling point diagrams show how equilibrium compositions of mixtures vary with temperature at a fixed pressure. Figure 16.8 shows a boiling point diagram for a mixture with two components, X and Y. The boiling point of X corresponds to temperature at which the mole fraction of X is 1.0 and Y is 0.0. Similarly, the boiling point of Y corresponds to temperature at which the mole fraction of X is 0.0 and Y is 1.0. In the figure, X is more volatile than Y.

The upper curve in the diagram is the dew-point curve, while the lower curve is the bubble-point curve. In the region above the dew-point curve, the vapor is superheated, while below the bubble-point curve, the liquid is subcooled. Consider a subcooled liquid in which the mole fraction of X = 0.4. When the mixture is heated from 80° (point A) to 90° (point B), the concentration of X remains constant until it reaches the bubble point (point B), where it starts to boil. At the bubble point, the mole fraction of X increases. The vapors evolved from the mixture have the equilibrium composition given by point C in Fig. 16.8, approxi-

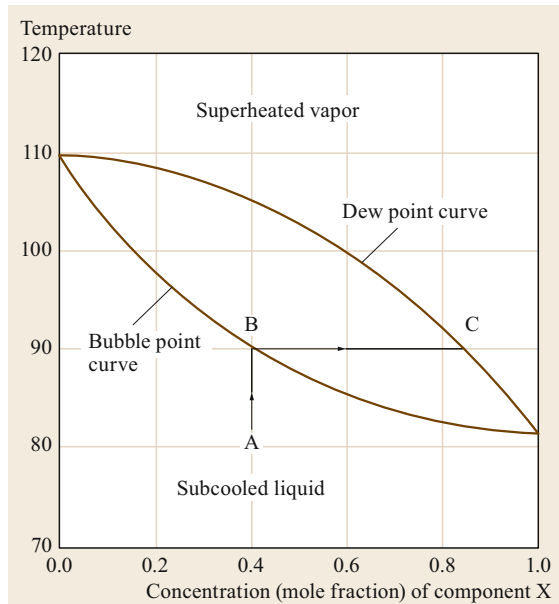


Fig. 16.8 Boiling point curve at constant pressure for a binary mixture

mately 0.85 mol fraction X. The vapor is more than 100% richer in X than was the original liquid.

Vapor–liquid equilibrium (VLE) is an important concept. For each component of a binary mixture, one can prepare a VLE equilibrium diagram, such as the one shown in Fig. 16.9. The liquid mole fraction is shown on a horizontal (x -) axis and vapor mole fraction on a vertical (y -) axis. These diagrams are square with a diagonal line running from the ($x = 0, y = 0$) corner to the ($x = 1, y = 1$) corner for reference.

16.2.3 Theoretical Stages

The design of a distillation column requires the estimation of several fundamental parameters, including the number of required stages (plates) and the reflux ratio.

McCabe–Thiele Method

The McCabe–Thiele graphical method [16.10, 11] relies on VLE plots to determine the number of theoretical stages required for a given service. The method assumes that the liquid on a tray and the vapor above it are in equilibrium, and it assumes constant molar overflow, which implies that the heats of vaporization of the components are roughly the same. It also assumes that heats of solution, heat losses to and from column etc. are negligible. Finally, it assumes that for every mole of vapor that condenses, 1 mol of liquid is vaporized.

Figure 16.10 illustrates the method for a binary mixture. With the VLE diagram of the mixture, operating lines are drawn. The operating lines define

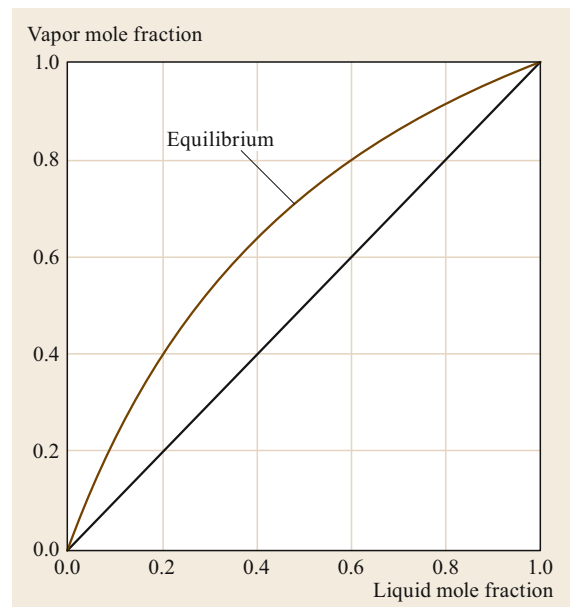


Fig. 16.9 Vapor–liquid equilibrium (VLE) curve

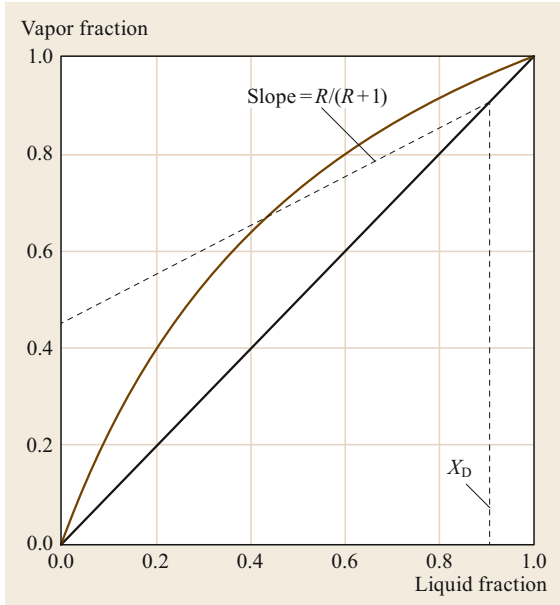


Fig. 16.10 Preparing a McCabe–Thiele diagram for the rectification section of a distillation column from a VLE diagram

the mass balance relationships between the liquid and vapor phases in the column. There is one operating line for the bottom (stripping) section and one for the top (rectification or enriching) section of the distillation tower (Fig. 16.4). For the rectification section, the desired top product composition (X_D) is located on the x -axis of the VLE diagram, and a vertical line is drawn to intersect a diagonal line that splits the VLE plot in half, shown in Fig. 16.10. An operation line with slope $R/(R+1)$ is then drawn from this intersection point where R is the reflux ratio – the ratio of reflux flow (L) to distillate flow (D). Hence, $R/(R+1)$ is equal to $L/(L+D)$, the portion of condensate from the condenser that returns to Tray n or the ratio of reflux liquid to vapor going into the condenser.

The operating line for the stripping section is constructed in a similar way. In this case, the starting point is the desired bottom product composition (X_B). A vertical line is drawn to the diagonal line as illustrated in Fig. 16.11. An operation line with slope L_S/V_S is drawn upward from the intersection point on the diagonal line, where L_S is the rate at which liquid flows down the stripping section of the column and V_S is the rate at which vapor flows up the stripping section of the column. The slope of the operating line is the ratio between the liquid and vapor flows.

As shown in Fig. 16.12, repeated application of the technique creates a number of corner sections, with

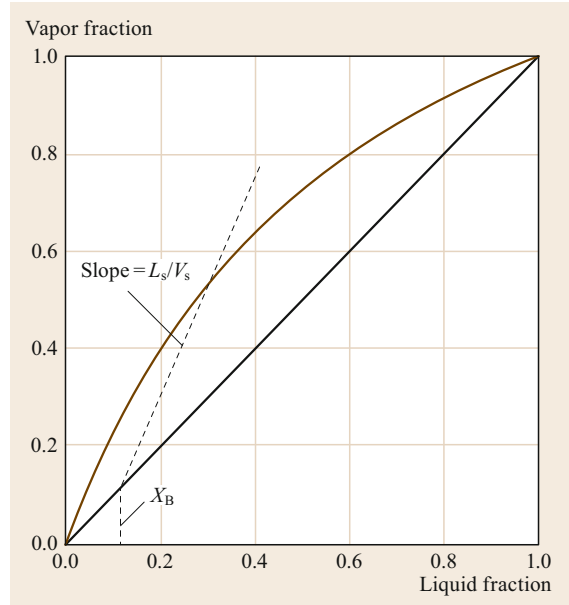


Fig. 16.11 Preparing a McCabe–Thiele diagram for the stripping section of a distillation column from a VLE diagram

each section being equivalent to a distillation stage. This is the basis of sizing distillation columns using the McCabe–Thiele graphical design method.

The required number of trays is one less than the number of stages, because the graphical construction includes the reboiler as a tray. Actual trays are not 100% efficient, so additional trays – more than the theoretical number – are used. Typical values for tray efficiency range from 0.5 to 0.7. Tray efficiency depends on the type of trays being used and internal liquid and vapor flow rates.

The Fenske Equation

The Fenske equation [16.13, 14] is used to calculate the minimum number of theoretical plates for continuous fractional distillation where the column is operated at total reflux.

For a binary mixture, the following equation is used

$$N = \frac{\log \left[\left(\frac{X_D}{1-X_D} \right) \left(\frac{1-X_B}{X_B} \right) \right]}{\log \alpha_{\text{avg}}}$$

where:

- N minimum number of theoretical plates
- X_D mole fraction of the more volatile component in the overhead distillate
- X_B mole fraction of the more volatile component in the bottom

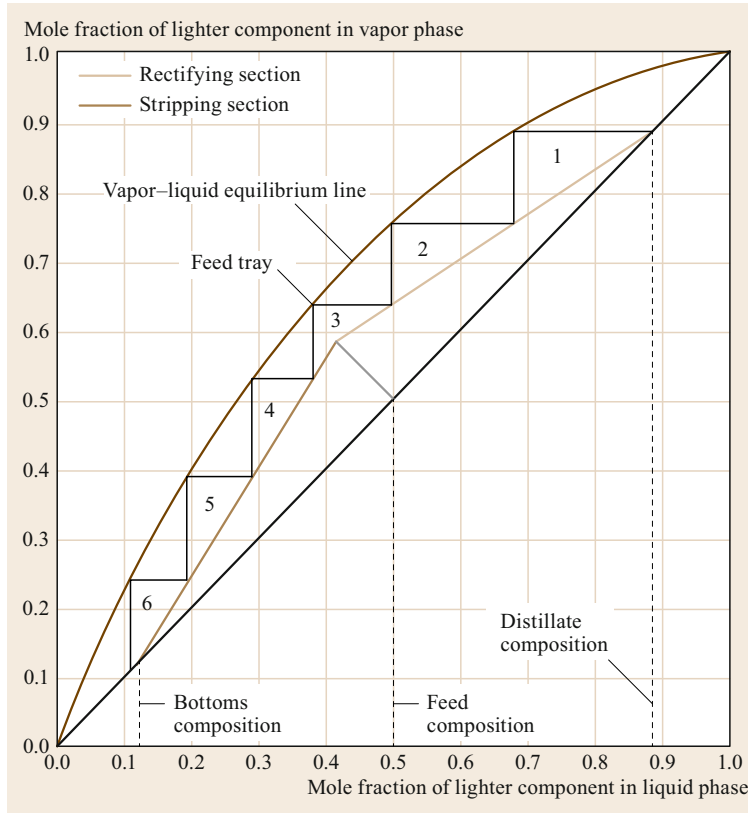


Fig. 16.12 Composite McCabe–Thiele diagram (after [16.12])

α_{avg} average relative volatility of the more volatile component to the less volatile component.

For a multicomponent mixture, the following formula holds

$$N = \frac{\log \left[\left(\frac{LK_D}{HK_D} \right) \left(\frac{HK_B}{LK_B} \right) \right]}{\log \alpha_{\text{avg}}}$$

where:

- N minimum number of theoretical plates
- LK light key = mole fraction of more volatile components
- HK heavy key = mole fraction of less volatile components
- α_{avg} average relative volatility of the LK and HK components.

If the relative volatility of the LK to the HK is constant from the column top to the column bottom, then $\alpha_{\text{avg}} = \alpha$. If the relative volatility is not constant from top (α_t) to bottom (α_b) of the column, then the following approximation may be used

$$\alpha_{\text{avg}} = \sqrt{(\alpha_t)(\alpha_b)}$$

The most challenging aspects of the Fenske method are (a) deciding which components in a complex, continuous mixture are LK and HK, and (b) estimating relative volatilities.

Versions of the Fenske equation are relevant to liquid–liquid extraction problems and gas chromatography, both of which can be treated as a series of equilibrium stages with solubility differences between liquids in a mixture.

Theory versus Practice

The actual number of trays needed for a particular separation duty depends on the efficiency of the plates. Anything that decreases tray efficiency diminishes column performance. Efficiencies degrade over time due to fouling, corrosion, and pressure pulses. Naphthenic acids are the main cause of corrosion in a crude distillation unit. High-acid feeds have dissolved most of the trays in a distillation tower in a matter of months.

Other entrained acids, such as hydrogen chloride, are volatile. Hydrogen chloride vapors are relatively innocuous. But at the distillation tower overhead, where the vapor goes from the top tray to the reflux drum, the temperature falls below the dew point of water. If HCl is present, it dissolves in the condensed wa-

ter to form highly corrosive hydrochloric acid, which rapidly corrodes metals. The problem can be minimized by injection of ammonia, morpholine, or higher-boiling neutralizing amines into the overhead, or by adding judicious amounts of caustic to the desalter effluent.

A major issue, of course, is that actual distillation units don't always operate with design feeds at design flow rates. Operational flexibility can be increased during design and construction by adding extra trays and/or installing extra return lines (pump-arounds and pump-backs) to manage the temperature profile in the tower. Some columns are designed with multiple feed injection points.

Operation is also affected by foaming, entrainment, flooding, and weeping.

Insufficient vapor flow causes weeping. Low vapor flow allows liquid to flow down through bubble caps, further blocking vapor flow. Excessive weeping leads

to dumping, where the liquid on all trays drops to the bottom of the column. When this happens, the column must be cleared and restarted. As mentioned, valve trays prevent weeping.

Excessive vapor flow causes flooding. Liquid becomes entrained in the vapor traveling up the column. When it disengages from the vapor, the excess liquid blocks the downcomers, causing the liquid level (holdup) on the trays to increase. This blocks the upward flow of vapor, building pressure in the tower. Eventually, vapor blows through in a pulse. Until action is taken, the cycle repeats. Separation efficiency drops precipitously, and product quality deteriorates. Flooding causes a sharp increase in column differential pressure and a sharp drop in separation efficiency.

Ambient conditions also affect performance. In hot weather, air coolers may not be able to provide sufficient temperature reduction. For uninsulated columns, extreme weather of any kind can degrade performance.

16.3 Crude Oil Distillation

A crude oil distillation unit (CDU) includes an atmospheric distillation unit (ADU) and a vacuum distillation unit (VDU) as shown in Fig. 16.13. The light products from a CDU are gases and naphthas. Middle distillates include kerosene, light gas oil, and heavy gas oil. The residue, or bottom, of the ADU is also known as reduced crude. It goes to the VDU to be fractionated into vacuum gas oil and vacuum residue (vacuum resid). The figure includes a desalter, which in some refineries is considered part of the CDU complex.

16.3.1 Predistillation Processing

As mentioned, when a crude oil emerges from underground, it is mixed with a variety of contaminants. These must be removed before the crude oil can be transported and refined. Some cleanup takes place in oil fields. A field separator at a well site is often no more than a large covered vessel that provides enough residence time for gravity separation into four phases: gases, crude oil, water and solids. Generally, the crude

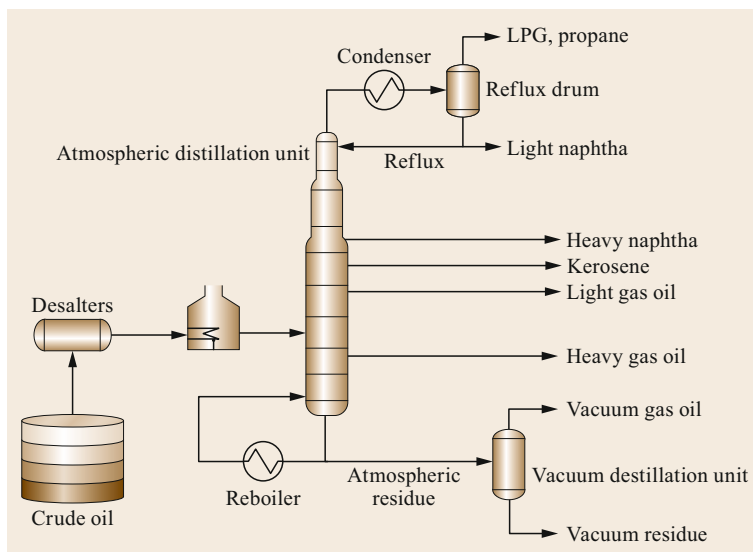


Fig. 16.13 A crude oil distillation complex includes three major operations: desalting, atmospheric distillation, and vacuum distillation

oil floats on the water. The water is withdrawn from the bottom; usually it is pumped into a wastewater injection well. Gases are withdrawn from the top and piped to a natural-gas processing plant or reinjected into the reservoir to maintain well pressure.

Crude oil is pumped to a refinery through a pipeline or to storage to await transportation by other means. Large quantities of crude oils are transported through pipelines or tankers. Others may be transported by barge, train or trucks. At the marine terminal, a cargo of crude oil may be routed through a pipeline directly to a storage tank in the refinery tank farm. Other tanks in a tank farm hold compressed gases, partially refined intermediate stocks, finished products, and chemicals for short- or long-term storage.

A refinery seldom refines single crude. Several crudes of similar characteristics are usually blended together. Incompatibilities between crude oils can occur, for example, between paraffinic crude oil and heavy asphaltic crude oil. Blending is used to maintain, as nearly as possible, constant feed quality suitable for the crude distillation unit. For example, high-acid crudes are mixed with low-acid crudes, and high-sulfur crudes are mixed with low-sulfur crudes to bring the acid or sulfur contents to a tolerable level for refinery operations.

16.3.2 Desalting

The impurities of most concern in crude oil include:

- The solid particulates (sand, clay, silt, rust etc.) or inorganic salts, which cause deposits and foul heat exchangers to pumps, pipelines etc. due to abrasion or erosion.
- The inorganic salts that can be decomposed in the crude oil heat exchangers and heaters. Salts that are most frequently present in crude oil are NaCl, $MgCl_2$ and $CaCl_2$. Formation of hydrogen chloride from chlorides by heat and hydrolysis can oc-

cur downstream. Hydrogen chloride gas condenses to aqueous hydrochloric acid at the overhead of distillation columns, causing serious corrosion of equipment. Hence, maintaining the ADU overhead temperature above the dew point of water vapor is important practice in distillation. Hydrogen chloride in gaseous form is not corrosive, which will be treated in the subsequent refining units.

- Sodium and calcium naphthenate compounds, which induce corrosion.
- Nickel, vanadium, iron, arsenic, and other metals in the crude, which can poison and deactivate catalysts.

At the refinery, many of these impurities are removed with hot water in one or more desalters. Two processes are used: dewatering and desalting. Dewatering removes water and constituents of brine that accompany the crude oil. Desalting is a water-washing operation that removes water-soluble minerals and entrained solids.

Desalters employ either chemical or electrostatic precipitators to expedite removal of dissolved salts and remaining solids. In chemical desalting, water and surfactants are added to the crude, heated to dissolve salts and other impurities, then sent to a settling tank, where the water and oil separate. In electrostatic desalting, chemicals are replaced with a strong electrostatic field at 12–35 kV, which drives the separation of water from oil. Coalescence is aided by passage through a tower packed with sand, gravel, and the like. Emulsion can be broken by adding chemicals, such as demulsifiers. Almost all refineries today use electrostatic desalters.

Figure 16.14 shows a flow diagram of a typical desalting unit. The blended crude is mixed with 3–10 vol.% water at 95–150 °C (200–300 °F) to dissolve salts and reduce viscosity and surface tension for easier mixing and subsequent separation of the water. The oil/water mixture is homogeneously emulsified.

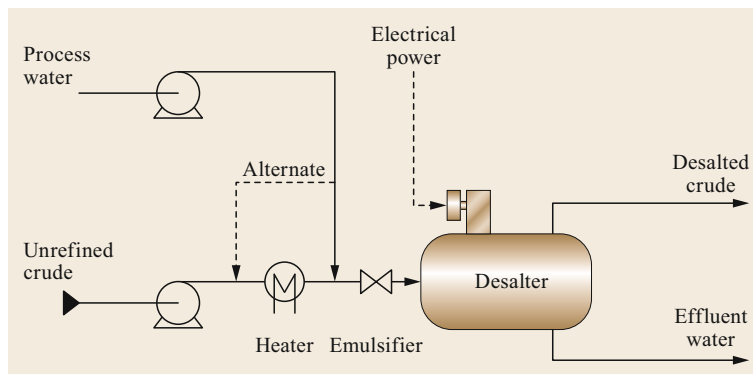


Fig. 16.14 Flow diagram of desalting involving an electrostatic desalter (after [16.15])

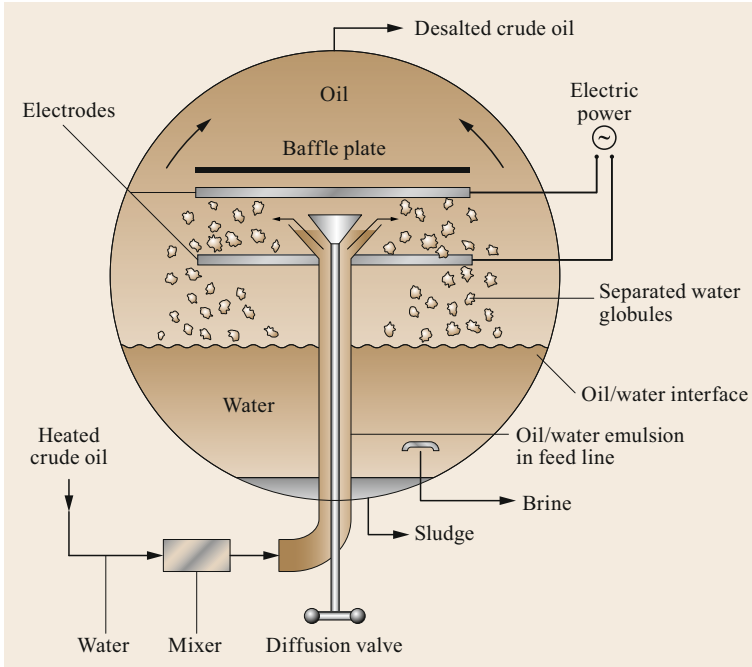


Fig. 16.15 Cross-section view of a desalter (after [16.16])

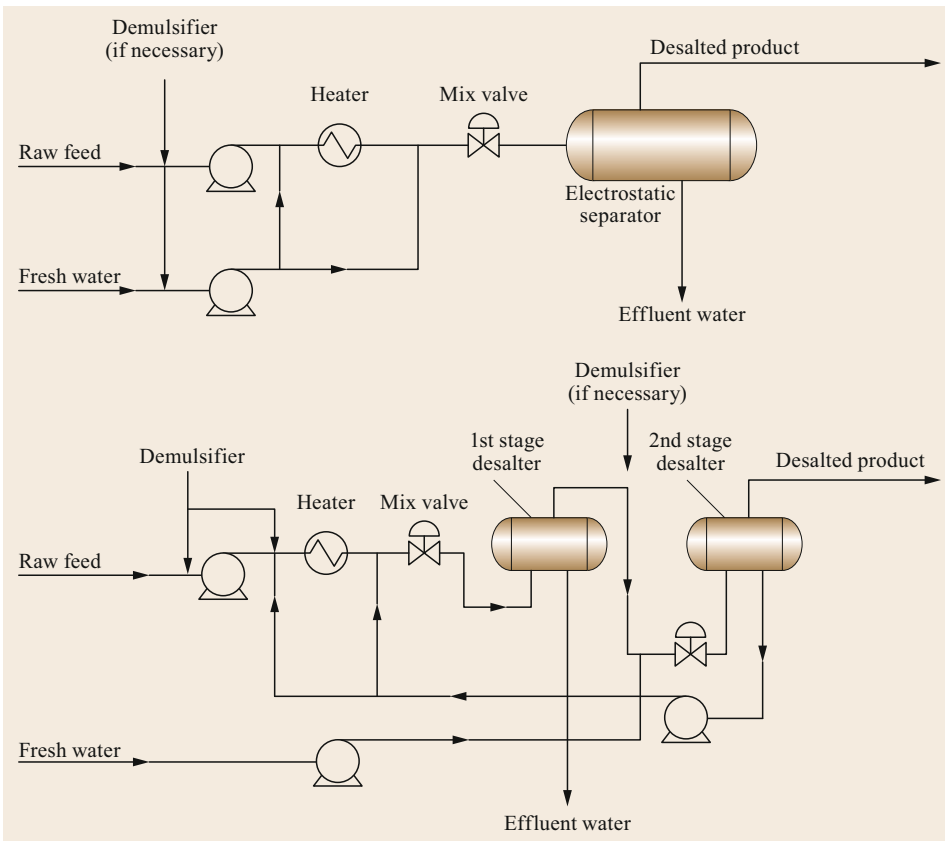


Fig. 16.16 Single- and two-stage electrostatic desalting systems (after [16.17])

The emulsion enters the desalter between a pair of electrodes of opposite polarity across which a high-potential electrostatic field (typically 12–35 kV) is imposed, where it separates into oil and water phases under the influence of electrostatic coalescence, shown in Fig. 16.15. The electrostatic field promotes coalescence with polarization of the droplets near the electrodes. Polarization of water droplets pulls them out from the oil/water emulsion phase. The droplets of opposite charges coalesce to form larger water droplets (globules) along with water-soluble salts, and settle to the bottom of the desalter to be withdrawn. Sediment is also settled at the bottom of desalter and withdrawn as sludge intermittently to prevent its blocking of the brine-water withdrawal outlet. Desalted crude oil exits at the top of desalter.

An emulsion between oil and water can be broken by adding chemicals or treating agents, such as soaps, fatty acids, sulfonates, long-chain alcohols or other demulsifiers.

A desalting unit can be designed with single stage or two stages, shown in Fig. 16.16. Refineries normally apply the two-stage desalting system with two electrostatic coalescers. Part of the brine water from the second stage can be recycled for use as wash water to the first

stage. For resid processing, three-stage desalting is used for some crudes. The two- or three-stage desalting can also be designed in a single vessel with multiple electrostatic coalescers.

16.3.3 Crude Distillation Overview

Crude oils contain numerous components with different boiling points. Continuous distillation is the simplest way to separate the components into fractions (cuts) with different boiling ranges. At atmospheric pressure, most, if not all, heavy molecules in crude oils decompose above 650 °F (≈ 350 °C).

To achieve additional separation of heavy fractions, the bottom cut from an atmospheric distillation unit (ADU) goes to a vacuum distillation unit (VDU), where additional distillates are recovered. The pressure in a VDU is typically 40 mmHg (5.3 kPa). Components that boil between 343 °C (650 °F) and 566 °C (1050 °F) at atmospheric pressure can be vaporized at less than 343 °C (650 °F) under 40 mmHg (5.3 kPa) vacuum without severe decomposition.

An important concept is the atmospheric equivalent boiling point (AEBP). The AEBP of a compound that boils at 260 °C (500 °F) at 40 mmHg

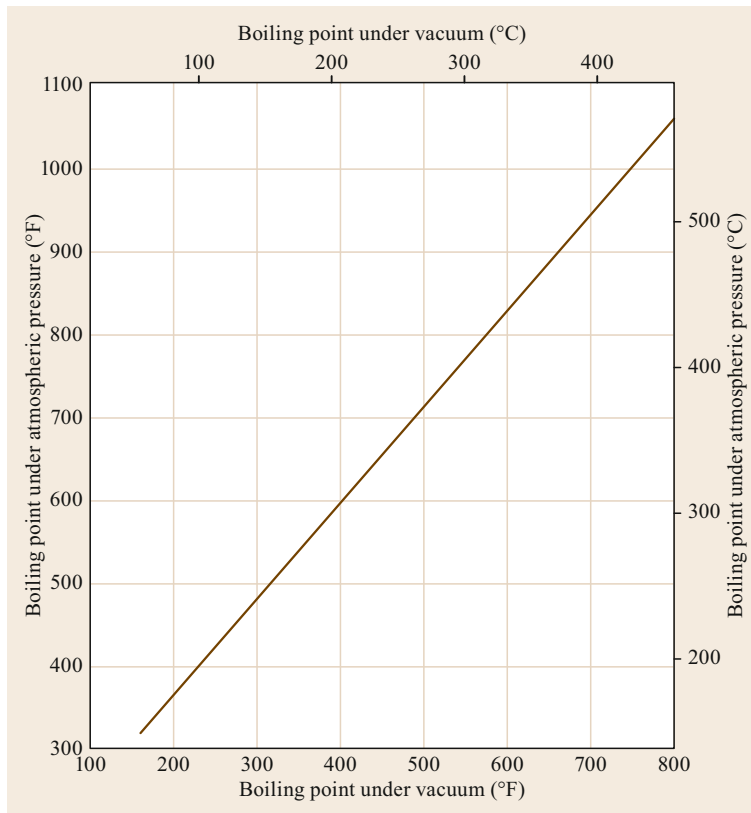


Fig. 16.17 Relationship between boiling points under atmospheric pressure (*y-axis*) and under 40 mmHg (5.3 kPa) vacuum (*x-axis*)

(5.3 kPa) vacuum is $\approx 400^\circ\text{C}$ (750°F). Similarly, the AEBP of a compound that boils at 343°C (650°F) at 40 mmHg (5.3 kPa) is $\approx 482^\circ\text{C}$ ($\approx 900^\circ\text{F}$). Figure 16.17 shows the relationship between boiling points under atmospheric pressure and under 40 mmHg (5.3 kPa) vacuum.

16.3.4 Atmospheric Distillation

A simplified diagram for atmospheric crude oil distillation is shown in Fig. 16.18. Desalted oil goes through a network of heat exchangers to a fired heater, which brings the temperature up to $347\text{--}385^\circ\text{C}$ ($657\text{--}725^\circ\text{F}$). If the oil gets much hotter than this, it starts to crack, generating coke. The coke would deposit inside the pipes and equipment through which the oil flows, increasing pressure drop and/or decreasing feed rate.

The hot crude enters the tower just above the bottom. Steam is added at the bottom to enhance separation; it does so largely by providing additional heat while decreasing the partial pressure of hydrocarbons in the column. When it enters the tower, most of the oil vaporizes. The steam flows upward with vaporized crude while the condensed liquid flows downward in a coun-

tercurrent fashion. The hottest trays are in the bottom section with the coolest at the top section. Unvaporized oil drops to the bottom of the tower, where it is drawn off.

Products are collected from the top, bottom and side of the column. Side-draw products are taken from trays where the temperature corresponds to the cut-points for desired products – naphtha, kerosene, light gas oil (diesel) and heavy gas oil. Some of the side-draws can be returned to the tower as pump-around or pump-back streams to control tower temperatures and improve separation efficiency. Side-cut strippers for naphtha and gas oil are shown in Fig. 16.18. There can be additional side-cut strippers for other distillates.

An atmospheric distillation tower usually contains 30–50 fractionation trays, and 5–8 trays for each product stream. Each stripper also has 5–8 trays to strip out the entrained light components and send them back to the distillation tower.

The boiling ranges of the distillation fractions are listed in Table 16.1. These numbers are only used as references. The actual cutpoints may vary at various refineries, depending on the season and market demands.

The distillation cuts obtained in refineries are not sharp. There are always overlaps between adjacent cuts.

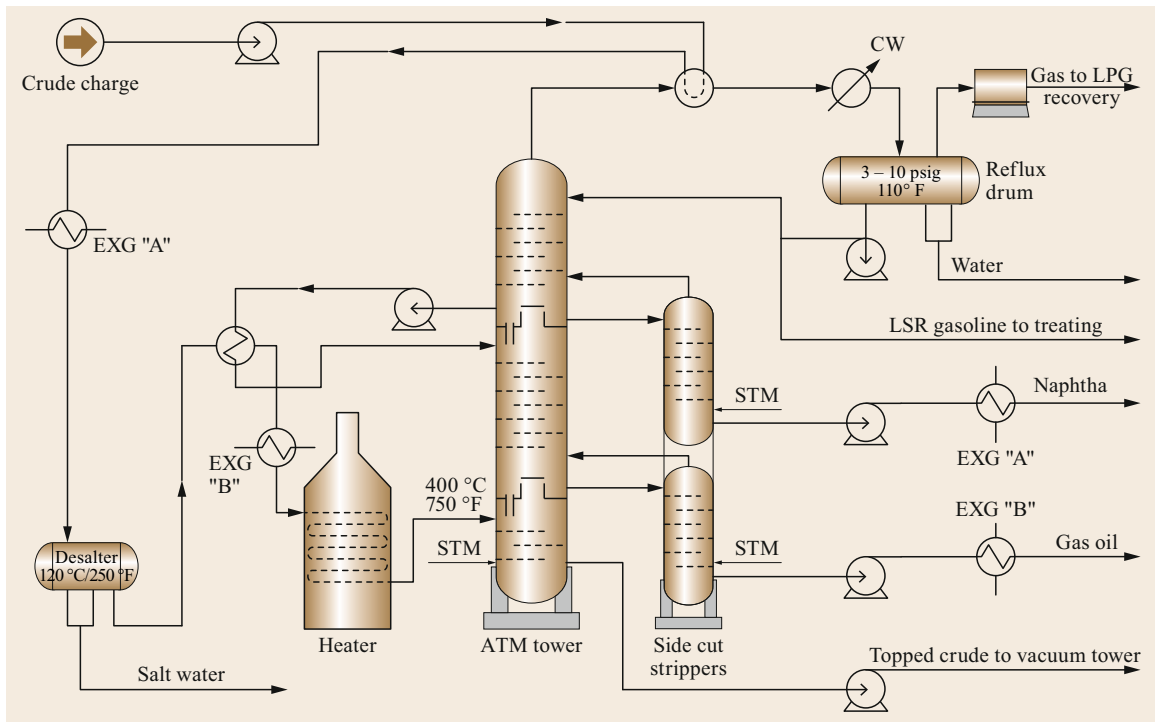


Fig. 16.18 Flow diagram of an atmospheric distillation tower (side cut strippers for kerosene and diesel between naphtha and gas oil are not shown). EXG: heat exchanger, CW: cold water, LPG: liquefied petroleum gas, LSR: light straight run, STM: steam (after [16.17])

Table 16.1 Boiling ranges of distillation fractions

Fraction	Boiling range ^a	
	(°C)	(°F)
Light naphtha	–1–150	30–300
Gasoline	–1–180	30–355
Heavy naphtha	150–205	300–400
Kerosene	205–260	400–500
Light gas oil	260–315	400–600
Heavy gas oil	315–425	600–800
Lubricating oil	> 400	> 750
Vacuum gas oil	425–600	800–1100
Residuum	> 510	> 950

^a For convenience boiling range are converted to the nearest 5°

The overlap between cuts can be *sharp* or *sloppy*, depending on several factors, especially oil flow rates, steam flow rate, and heat balance. Often nothing can be done to decrease overlap at maximum flow rate without making hardware changes.

Figure 16.19 shows distillation curves for the products from a 47 000 barrel/day commercial hydrocracking unit. The desired cutpoints for light naphtha, heavy naphtha, kerosene, and heavy diesel were 90 °F (32 °C), 190 °F (88 °C), 300 °F (149 °C), and 525 °F (274 °C) respectively. Due to operational constraints, the observed effective cutpoints were 99 °F (37 °C), 188 °F (87 °C), 302 °F (150 °C), and 523 °F (273 °C) respectively. The overlap between kerosene and heavy diesel is considerable. Instead of having an initial boil-

ing point (IBP) of 525 °F (274 °C), the IBP for the heavy diesel is 360 °F (182 °C). This indicated considerable entrainment of valuable kerosene into the far-less-valuable bottom product. Guided by a modeling project, operators learned how to lift an additional 2000 barrel/day of kerosene. This increased profit by \$20 000 per day at very low cost – about 80 h of an engineer's time.

16.3.5 Vacuum Distillation

Figure 16.20 shows a flow diagram of a vacuum distillation unit (VDU). The bottom stream from the main fractionator (atmospheric distillation tower) is called atmospheric bottoms, reduced crude, atmospheric residue (AR), or long resid. It goes to a second fired heater, where the typical outlet temperature is about 750–775 °F (400–413 °C). From the second heater, the AR goes to a vacuum distillation tower. Steam ejectors reduce the absolute pressure to 25–50 mmHg (3.3–6.6 kPa) vacuum, or about 7.0 psi (0.5 bar). As discussed, under vacuum, hydrocarbons vaporize at temperatures lower than their atmospheric boiling points (normal boiling point).

There are fewer trays in the VDU tower than in the ADU tower. Products from the VDU are light vacuum gas oil, heavy vacuum gas oil, and vacuum residuum (VR). Some gas and light components entrained or decomposed during heating in a furnace are carried out at the top of the tower.

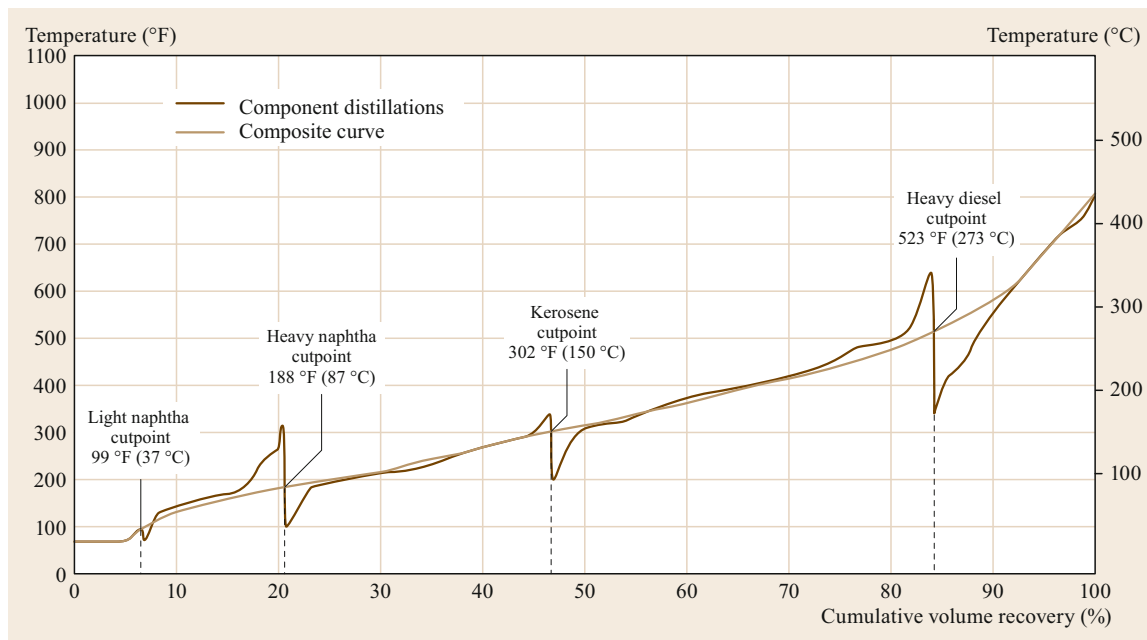


Fig. 16.19 Distillation curves for products from a 47 000 barrel/day commercial hydrocracking unit

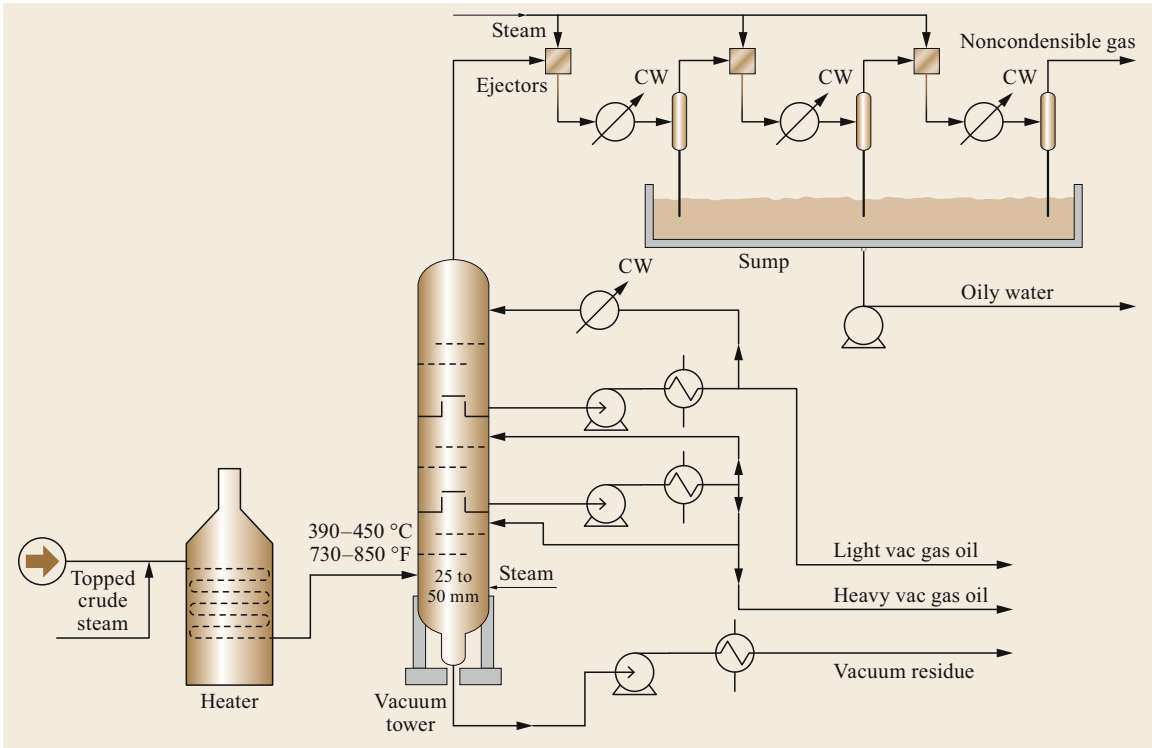


Fig. 16.20 Flow diagram of a vacuum distillation unit (after [16.17])

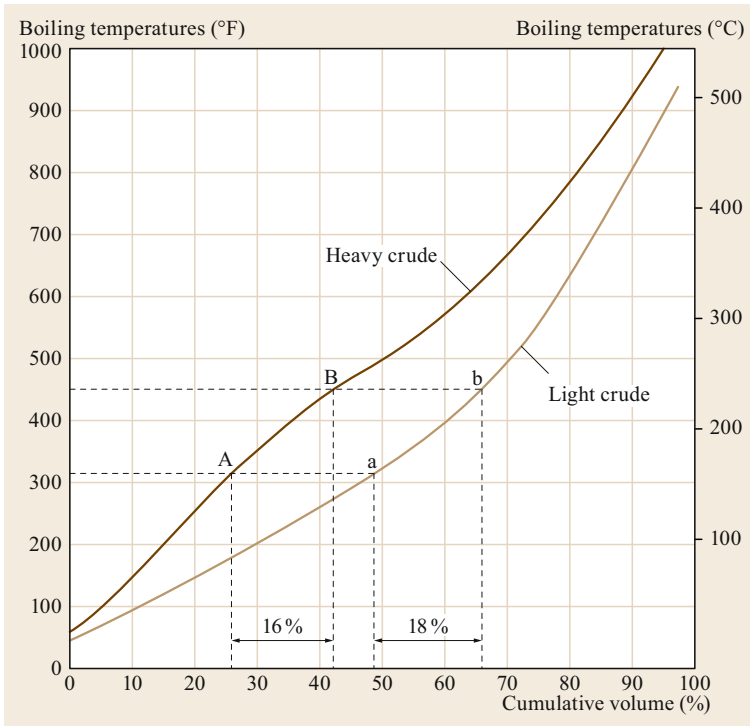


Fig. 16.21 Comparison of kerosene yields from light and heavy crude oils (after [16.8])

Table 16.2 Typical straight-run yields from various crudes

Source field Country	Brent Norway	Bonny Lt. Nigeria	Green Canyon USA	Ratawi Mid East
API gravity	38.3	35.4	30.1	24.6
Specific gravity	0.8333	0.8478	0.8752	0.9065
Sulfur (wt%)	0.37	0.14	2.00	3.90
Yields (wt% feed)				
Light ends	2.3	1.5	1.5	1.1
Light naphtha	6.3	3.9	2.8	2.8
Medium naphtha	14.4	14.4	8.5	8.0
Heavy naphtha	9.4	9.4	5.6	5.0
Kerosene	9.9	12.5	8.5	7.4
Atmospheric gas oil	15.1	21.6	14.1	10.6
Light VGO	17.6	20.7	18.3	17.2
Heavy VGO	12.7	10.5	14.6	15.0
Vacuum residue	12.3	5.5	26.1	32.9
Total naphtha	30.1	27.7	16.9	15.8
Total middle distillate	25.0	34.1	22.6	18.0

16.3.6 Straight-Run Distillation Yields

The products from the ADU and VDU directly are called straight-run products, such as straight-run naphtha or gas oil. The yields of different fractions depend on the crude oil being processed. Figure 16.21 shows the TBP distillation for a light and a heavy crude, comparing yields of kerosene with cutpoints between 157 and 232 °C (315 and 450 °F). The light crude yields more kerosene than the heavy crude, and hence has a higher value.

Table 16.3 Average US consumption of petroleum products, 1991–2003

Product	Consumption (barrel/day)	Percent of total
Gasoline	8032	43.6
Jet fuel	1576	8.6
Total distillates	3440	18.7
Residual fuel oil	687	4.8
Other oils	4501	24.4
Total consumption	18 416	100.0
Sum of gasoline, jet, distillates	13 048	70.8

Table 16.4 Destinations for straight-run distillates. Resid is an abbreviation for residua, and 340+ etc. means everything that boils above 340 °C etc.

Fraction	Approx. boiling range		Next destination	Ultimate product(s) or subsequent destination
	(°C)	(°F)		
LPG	−40–0	−40–31	Sweetener	Propane fuel
Light naphtha	39–85	80–185	Hydrotreater	Gasoline
Heavy naphtha	85–200	185–390	Catalytic reformer	Gasoline, aromatics
Kerosene	170–270	340–515	Hydrotreater	Jet fuel, No. 1 diesel
Gas oil	180–340	350–650	Hydrotreater	Heating oil, No. 2 diesel
Atmos. Resid	340+	650+	Visbreaker	FCC ^b or hydrocracker feed, low-viscosity resid
			Resid hydrotreater	Resid FCC ^b
			Ebullated bed hydrocracker	Naphtha, gas oils, FCC ^b
Vacuum gas oil	340–566	650–1050	FCC ^b	Gasoline, LCO ^a , gases including C ₃ /C ₄ olefins
			Hydrotreater	Fuel oil, FCC ^b , lubes
			Hydrocracker	Naphtha, jet, diesel, FCC ^b , olefins, lubes
			Solvent refining	De-asphalted oil (DAO), asphalt
Vacuum resid	540+	1000+	Coker	Coke, coker gas oil, coker naphtha, gases
			Solvent refining	DAO, asphalt
			Slurry-phase hydrocracker	Traditional hydrotreater or hydrocracker

^a Light cycle oil

^b Fluidized catalytic cracking

Table 16.2 lists a few crude oils and their typical straight-run yields. Total naphtha includes light, medium and heavy naphtha, and the middle distillates include kerosene and atmospheric gas oil. Naphtha is used for making gasoline and aromatics, kerosene for jet fuel and atmospheric gas oil for diesel. Table 16.3 shows that the demand for transportation fuels exceeds the straight-run yields for the crudes in Table 16.2.

The higher value crude oils have higher API gravity and tend to have less sulfur. The sulfur must be removed, so high sulfur content increases processing costs. Hence, the oil has lower value. Since sulfur is not removed during distillation, the straight-run products have to be treated for sulfur removal.

Products from the crude distillation unit i.e., the straight-run distillates, go to other process units, as shown in Table 16.4. The lightest cuts are gas and light naphtha. The gas goes to a gas processing plant or is liquefied into liquefied petroleum gas (LPG). The light

naphtha can be hydrotreated and sent to the motor gasoline blending pool. Heavy naphtha is a feed for catalytic reforming units. Kerosene can be used for lighting and for making jet fuel. In either case, it must first undergo hydrotreating. Light gas oil can go to diesel fuel (distillate fuel) blending. Heavy gas oil is a feed for fluid catalytic cracking (FCC), which converts it into olefin-containing gas, FCC gasoline, and cycle oil; sometimes the FCC gasoline must undergo mild desulfurization; the cycle oil is hydrotreated or hydrocracked to make diesel. The bottom stream (decant oil) boils in the atmospheric residue range. It can be processed as such in a delayed coker, or sent to a vacuum distillation tower for further fractionation. It contains large quantities of catalyst fines, which are difficult to remove.

Vacuum gas oil (VGO) and vacuum residue (VR) are of low value. They are normally converted into higher-value products through various upgrading processes, such as coking, FCC, hydrocracking or lube processing.

16.4 Summary

Crude oils are complex mixtures of numerous molecules with different boiling points. Virtually all refineries use continuous fractional distillation as the primary method to separate the molecules into fractions (cuts). Prior to distillation, a desalter is normally used to remove impurities that are harmful to the distillation unit. A crude distillation unit includes an atmospheric dis-

tillation tower, a vacuum distillation tower, and associated equipment. The cuts are processed in downstream units – hydrotreaters, catalytic reformers, fluid catalytic cracking units etc. The products of upgrading units often require further separation, usually by distillation.

Distillation is at the heart of a petroleum refinery as the most common separation technology.

References

- 16.1 Wikipedia: Distillation, <https://en.wikipedia.org/wiki/Distillation> (2016)
- 16.2 M.P.E. Berthelot: The discovery of alcohol and distillation, *Pop. Sci.* **43**(May), 85–94 (1893), https://en.wikisource.org/wiki/Popular_Science_Monthly/Volume_43/May_1893/The_Discovery_of_Alcohol_and_Distillation
- 16.3 Wikipedia: Turpentine, <https://en.wikipedia.org/wiki/Turpentine> (2016)
- 16.4 A. McLean: *The Book of Distillation: The First Book*, *Magnum Opus Hermetic Sourceworks*, Book 32 (A. McLean, Kilbirnie 1979–1986), <http://www.alchemywebsite.com/bookshop/mohs32.html>
- 16.5 Wikipedia: https://commons.wikimedia.org/wiki/File:Zosimos_distillation_equipment.jpg
- 16.6 Wikipedia: Zosimos of Panopolis, https://en.wikipedia.org/wiki/Zosimos_of_Panopolis (2016)
- 16.7 Unknown illustrator: Illustration from the 15th century Byzantine Greek manuscript *Parisinus graces*, https://upload.wikimedia.org/wikipedia/commons/1/17/Distillation_by_Retort.png (2015),
reprod. by M. Berthelot: *Collection des anciens alchimistes grecs*, 3 Vols. (Paris 1887–1888), p. 161
- 16.8 W.L. Leffler: *Petroleum Refining in Nontechnical Language*, 4th edn. (PennWell, Tulsa 2008)
- 16.9 A. Gumilar: Basic Theory: Distillation, <http://chemeng-processing.blogspot.com/2009/02/basic-theory-distillation.html> (2016)
- 16.10 W.L. McCabe, E.W. Thiele: Graphical design of fractionating columns, *Ind. Eng. Chem.* **17**, 605–611 (1925)
- 16.11 R.H. Perry, D.W. Green: *Perry's Chemical Engineers Handbook*, 6th edn. (McGraw-Hill, New York 1984)
- 16.12 Wikipedia: McCabe–Thiele method, https://en.wikipedia.org/wiki/McCabe-Thiele_method (2016)
- 16.13 M.R. Fenske: Fractionation of straight-run Pennsylvania Gasoline, *Ind. Eng. Chem.* **24**, 482 (1932)
- 16.14 D.S.J. Jones, P.P. Pujado (Eds.): *Handbook of Petroleum Processing*, 1st edn. (Springer, Dordrecht 2006)
- 16.15 Occupational Safety and Health Administration (OSHA), US Department of Labor: <https://www.osha>.

- 16.16 [gov/dts/osta/otm/otm_iv/otm_iv_2.html](http://www.dhs.gov/dts/osta/otm/otm_iv/otm_iv_2.html)
Citizendium: Crude oil desalter, http://en.citizendium.org/wiki/Crude_oil_desalter (2016)
- 16.17 J.H. Gray, G.E. Handwerk, M.J. Kaiser: *Petroleum Refining – Technology and Economics*, 5th edn. (CRC, Boca Raton 2007)

Gasoline Pro

17. Gasoline Production and Blending

Chang Samuel Hsu, Paul R. Robinson

Gasoline is a volatile, flammable mixture of liquid hydrocarbons primarily obtained from refining petroleum. Most gasoline is consumed as a fuel in spark-ignition engines, primarily those which power automobiles and certain airplanes. For engine performance, important gasoline properties include volatility (Reid vapor pressure), octane number and heat content. Reid vapor pressure (RVP) is one of the gasoline specifications for performance in engine. Reformulated gasoline laws now protect the environment by limiting smog precursors, banning tetraethyl lead (TEL) and regulating concentrations of sulfur, olefins, benzene and oxygenates in gasoline. Refineries produce gasoline from blendstocks derived from various processes – crude oil distillation, catalytic reforming, fluid catalytic cracking (FCC), thermal cracking, hydrocracking, alkylation, isomerization and catalytic polymerization. Finished products sold in the market include additives, which inhibit oxidation, inhibit corrosion, passivate trace metals, reduce deposition of carbon on intake valves and combustion chambers, and minimize the formation of ice in cold weather. Relative gasoline demand is highest in North America, while automotive diesel is preferred in most of the rest of the world.

17.1	Gasoline Engines	552
17.1.1	Fuel Delivery System.....	552
17.1.2	Air Induction System.....	553
17.1.3	Air-Fuel Mixing System.....	553
17.1.4	Sensor-Computer System.....	554
17.1.5	Ignition Control System.....	554
17.1.6	Piston Design.....	554
17.1.7	Four-Stroke Piston Engine.....	554
17.1.8	Lubrication.....	555
17.1.9	Engine Exhaust.....	555
17.1.10	Other Gasoline Engines.....	555
17.2	Otto Engine Thermodynamic Cycle ...	558
17.3	Key Gasoline Properties	559
17.3.1	Octane Number.....	559
17.3.2	Reid Vapor Pressure (RVP).....	561
17.3.3	Sulfur Content.....	562
17.3.4	Storage Stability.....	562
17.4	Gasoline Specifications	563
17.5	Gasoline Production	564
17.5.1	Refining Strategy.....	564
17.5.2	Gasoline Blending Stocks.....	567
17.6	Production of Gasoline Blendstocks	567
17.6.1	Distillation – Straight-Run Naphtha ..	567
17.6.2	Isomerization.....	568
17.6.3	Catalytic Reforming.....	571
17.6.4	Alkylation.....	575
17.6.5	Polymerization.....	579
17.6.6	Fluid Catalytic Cracking (FCC) Process ..	579
17.6.7	Other Processes.....	582
17.7	Synthetic Gasoline	582
17.8	Reformulated Gasoline (RFG) in the United States	583
17.9	Gasoline Additives	584
17.10	Blending Optimization	585
	References	585

Gasoline is a volatile, flammable mixture of liquid hydrocarbons obtained primarily from petroleum refining. Outside North America, *petrol* and *benzin* are synonyms for gasoline.

Historically, four events were particularly significant for gasoline production. The first was the drilling of the first oil well in the United States by Edwin L. Drake near Titusville, Pennsylvania in 1859. The well wasn't the first in the world and it was only 70 ft deep, but it triggered the Pennsylvania oil boom, the first great event in the American oil industry.

At that time, the most desired product from crude oil was kerosene for lamp lighting. For the most part, gasoline was discarded as a byproduct that in the 1870s was sold as a solvent by Carless, Capel and Leonard, a British wholesaling company. Carless et al. got much of the petrol from coal oil [17.1].

The second major event was the development of the four-stroke internal combustion engine in 1876 by Nikolaus Otto, a German engineer. Otto's compressed-charge engine burned gasoline, which became essential to the automobile industry.

The third event was the development of the light bulb by Thomas Edison. Over time, invention and the widespread use of light bulbs decreased the demand for kerosene as an illuminant. The first commercially viable bulbs worked with carbon filaments. These appeared on the market in 1882. In 1904, bulbs with tungsten filaments displaced those with carbon filaments.

The fourth event occurred in 1913, when Henry Ford rolled out the first moving assembly line to mass manufacture Model T automobiles. Before the Model T, automobiles were luxuries. Due to its lower cost, people of ordinary means could afford a Model T. In 1914, Ford began paying his workers US\$ 5.00 per day, more than twice the average wage for auto workers. In the 1926 book, *Today and Tomorrow*, Ford [17.2] said:

The owner, the employees and the buying public are all one and the same and unless an industry can so manage itself as to keep wages high and prices low it destroys itself, for otherwise it limits the number of its customers. One's own employees ought to be one's own best customers.

Against conventional wisdom, Ford was fond of saying that doubling workers' wages was the best cost-cutting move he ever made. The need for fueling automobiles shifted the market demand from kerosene to gasoline.

Since the birth of modern automobile, the demand for gasoline to fuel automobiles with internal combustion engines has increased dramatically. It is estimated the number of automobiles in the world exceeded one billion around 2010.

The development of modern refinery processes was driven by rapid growth in demand for transportation

fuels. Gasoline blendstocks come from a variety of refining processes, including straight-run distillation, catalytic reforming, catalytic cracking (FCC), thermal cracking, hydrocracking, isomerization, alkylation and polymerization. While cracking processes break large molecules into smaller molecules, alkylation and polymerization do the opposite. They were developed specifically to transform C_3 and C_4 molecules into C_6 to C_9 molecules suitable for gasoline. Blendstocks are mixed with each other and with additives to produce finished gasoline that meets volatility, octane rating and other requirements.

Ninety percent of the gasoline produced in the US is automobile fuel, with a very small percentage used to power agricultural equipment and aircraft. Gasoline for piston-engine powered aircraft is called aviation gasoline or avgas, which has a high octane number and low flash point to improve ignition characteristics. In the United States, automotive gasoline is specified by ASTM D4814. In Europe and urban China, automotive gasoline must meet EN 228 and China V respectively. Avgas is defined by specifications Jet B or JP-4.

US refineries are designed to maximize gasoline production, especially during the summer. Asian and European refineries emphasize diesel production. Due to tax incentives and superior vehicle performance, diesel demand in Europe has grown. As a result, Europe is importing diesel and exporting gasoline. US diesel demand is driven by heavy-duty applications (truck, train, ship and industry). Heavy-duty demand grows as economies grow.

Many other chapters in this book can serve as references for this chapter. A separate book (*Song, Hsu and Mochida*) discusses diesel in great detail [17.3].

17.1 Gasoline Engines

Motor vehicles are powered by internal combustion engines. Gasoline is the most common fuel for a spark-ignition engine. Figure 17.1 illustrates the route by which gasoline moves from a fuel to the engine. In modern automobiles, the entire process, including fuel pressure, fuel flow, air supply, air-fuel injection, piston timing and ignition is computer controlled. Typically, there is a great excess of air flow. Engine speed is controlled by fuel flow, which ultimately is controlled by the extent to which a driver presses the accelerator pedal.

Modern engines employ electronically timed fuel injection, also known as electronic fuel injection (EFI). An EFI system can be subdivided into the following:

- Fuel delivery system
- Air induction system
- Air/fuel mixing system
- Sensor/computer system
- Ignition control system.

17.1.1 Fuel Delivery System

The fuel delivery system includes an electric fuel pump, a fuel filter, a pressure regulator, the injector valves and the connecting lines and hoses. The fuel pump sends fuel from the tank to the pressure regulator. The pressure regulator controls fuel flow to the injector and valves. Pressure control is achieved with spill-back through the fuel-return line. The injector valves (and

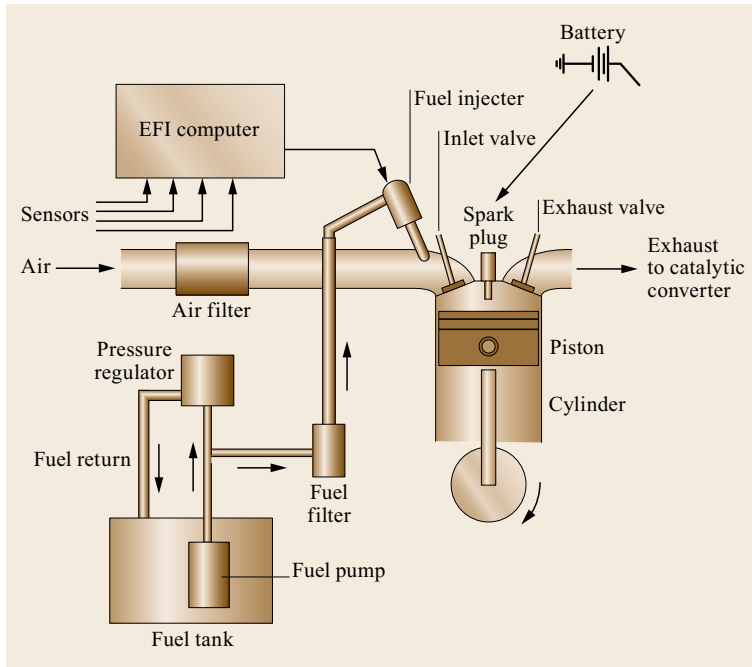


Fig. 17.1 Fuel system for a spark-ignition engine with electronically timed fuel injection, also known as electronic fuel injection (EFI)

exhaust valves as well) are controlled with solenoids. When a solenoid isn't energized, spring pressure keeps the valve closed. When energized, the solenoids open the valves.

17.1.2 Air Induction System

The air induction system includes a throttle valve, sensors, an air filter and connecting ducts. The throttle valve regulates air flow. Like the air-fuel mixing (carburetor) system, the air induction system is connected to the gas pedal. When the pedal is depressed, the throttle valve opens to allow more air into the engine.

17.1.3 Air-Fuel Mixing System

Prior to computer-controlled fuel injection, air was mixed with gasoline in carburetors. These devices followed Bernoulli's principle:

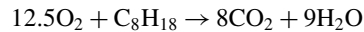
- Faster-moving air
- Lowers static pressure
- Increases dynamic pressure.

Controlling the throttle (accelerator) didn't directly control fuel flow. Instead, it controlled the carburetor, which changed the flow of air into the engine. Changing the air speed changed the air pressure, which changed the amount of fuel that was drawn into the airstream.

The *air/fuel ratio* (AFR) is the ratio between the mass of air and the mass of fuel in a combustible mix-

ture. The respective masses include all constituents, even those that do not react. For example, the air-mass calculation includes both oxygen and inerts – nitrogen, argon, CO₂ and water vapor.

For pure octane, the reaction stoichiometry is



The stoichiometric air/fuel ratio is about 14.7 wt/wt, depending on the exact composition of the air.

The *air/fuel equivalence ratio*, called λ (lambda), is the ratio of the actual AFR to the stoichiometric AFR. For stoichiometric mixtures, $\lambda = 1.0$. For rich mixtures, $\lambda < 1.0$ and for lean mixtures $\lambda > 1.0$. Naturally aspirated gasoline engines achieve maximum power at AFRs ranging from 12.5–13.3 ($\lambda = 0.850$ –0.9). The AFR for maximum fuel economy is about 16 ($\lambda = 1.09$). The composition of fuels changes, especially seasonally, so for many purposes, such as engine tuning, the industry prefers to use λ instead of AFR.

The *fuel/air equivalence ratio*, called ϕ , is defined as the ratio of the actual fuel-to-oxidizer ratio to the stoichiometric fuel-to-oxidizer ratio

$$\begin{aligned} \phi &= \frac{\text{fuel-to-oxidizer ratio}}{(\text{fuel-to-oxidizer ratio})_{\text{st}}} = \frac{m_{\text{fuel}}/m_{\text{ox}}}{(m_{\text{fuel}}/m_{\text{ox}})_{\text{st}}} \\ &= \frac{n_{\text{fuel}}/n_{\text{ox}}}{(n_{\text{fuel}}/n_{\text{ox}})_{\text{st}}}, \end{aligned}$$

where m represents the mass, n represents number of moles and st indicates stoichiometric. With ϕ , one can account both for mass and moles.

Most AFR sensors measure the amount of residual oxygen (for lean mixtures) or unburnt hydrocarbons (for rich mixtures) in the exhaust gas.

17.1.4 Sensor-Computer System

The sensor system monitors engine operating conditions and reports this information to the computer. Sensors include the following:

- Exhaust gas sensors
- Fuel oxygen sensor
- Manifold pressure sensor
- Throttle position sensor
- Engine temperature sensor
- Air flow sensor
- Inlet air temperature sensor
- Crankshaft position sensor.

Based on sensor readings, the computer optimizes fuel injection and the timing of spark-plug firing.

17.1.5 Ignition Control System

There is no need for manual tune-up for modern gasoline cars. Ignition timing in today's vehicles is controlled by computer, which measures the degree of crankcase rotation for the point at which the spark plug fires. Because it takes a fraction of a second to fire, the spark plug must fire a few degrees (such as 5°) when the engine is at idle speed) before the piston reaches the top dead center (TDC). Otherwise, the ignition of the mixture will not be complete when the piston reaches TDC and full power of explosion will not be utilized by the engine. The ignition timing is adjusted through electric signals from various sensors so that spark plugs ignite sooner when the engine speed increases. If the ignition is too far advanced, explosion will occur to push the piston down while it is still traveling up. If the ignition is too far retarded, the piston will be pushed down for only a portion of its travel, resulting in poor engine performance. However, the computer-controlled ignition is set in the factory and is not adjustable.

17.1.6 Piston Design

Figure 17.2 illustrates a typical piston assembly, including intake and exhaust valves, the spark plug and the cylinder. The piston itself is connected to the piston rod, crank shaft and wheel. The wheel is connected to the

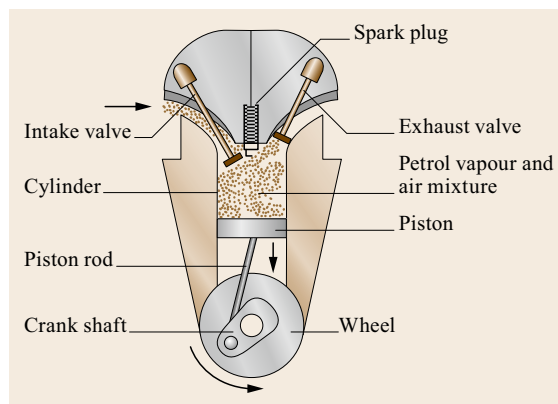


Fig. 17.2 Typical piston assembly

drive train, which transfers power from the engine to the wheels of a vehicle, a power generator, or other device.

17.1.7 Four-Stroke Piston Engine

The four-stroke Otto-cycle engine, invented by Nikolaus Otto in 1876, is still the most widely employed spark-ignition engine. Figure 17.3 illustrates the action of an Otto-cycle engine.

Intake stroke (Fig. 17.3a): The piston begins at the top of the cylinder. The intake valve is open. The exhaust valve is closed. As the piston moves down, the air-fuel mixture is injected into the cylinder. The stroke ends with the piston at the bottom of the cylinder – bottom dead center (BDC).

Compression stroke (Fig. 17.3b): The piston is at the bottom of the cylinder – just where it was at the end of the compression stroke. The intake valve closes. The exhaust valve remains closed. The piston rises, compressing the air-fuel mixture, until it reaches the top of the cylinder – top dead center (TDC).

Power stroke (Fig. 17.3c): The piston begins at the top of the cylinder – just where it was at the end of the compression stroke. Both the intake valve and the exhaust valve remain closed. The spark plug fires, igniting the compressed air-fuel mixture. The resulting explosion drives the piston to the bottom of the cylinder, providing power, via the crankshaft, to the wheel.

In a four-stroke engine, the crankshaft turns twice for each power stroke. In contrast, in a two-stroke engine (below) the crankshaft turns once for each power stroke.

The main combustion reactions include:

- Hydrocarbons + $O_2 \rightarrow CO_2 + CO +$ water
- Sulfur in hydrocarbons + $O_2 \rightarrow$ sulfur oxides
- $N_2 + O_2 \rightarrow$ nitrogen oxides.

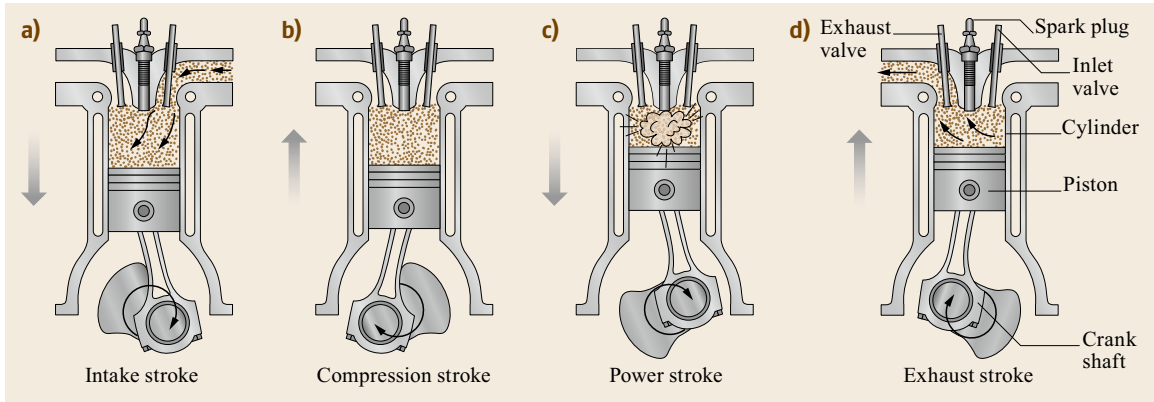


Fig. 17.3a–d Strokes of a four-stroke spark-ignition engine

Exhaust stroke (Fig. 17.3d): The piston is at the bottom of the cylinder – just where it was at the end of the power stroke. The intake valve remains closed. The exhaust valve opens. The piston returns to the top, expelling combustion products through the exhaust valve.

17.1.8 Lubrication

Compared to most of the designs mentioned below, in-line piston-driven engines have a significant advantage: only one side of a piston is exposed to fuel, so the cylinders can be lubricated with an independent system. For two-stroke, rotary, radial and Wankel engines, lubricating oil must be added to the fuel.

17.1.9 Engine Exhaust

Engine exhausts contain pollutants – sulfur oxides, nitrogen oxides, carbon monoxide, unburned hydrocar-

bons and volatile toxic compounds. These can be abated with reformulated fuels, catalytic converters and tighter engine design; issues which are discussed in a later section.

17.1.10 Other Gasoline Engines

Other gasoline engines include two-stroke, rotary, radial, Wankel and gasoline-powered turbine engines.

Two-Stroke Engine

The first practical two-stroke engine (Fig. 17.4) is attributed to A.A. Scott, who started making twin-cylinder water-cooled motorcycles in 1908 [17.4]. Two-stroke engines can be powered either by gasoline or diesel fuel. Gasoline-powered two-strokes require spark plugs, but in diesel-powered engines, the fuel-air mixture is ignited by the heat produced from adiabatic compression.

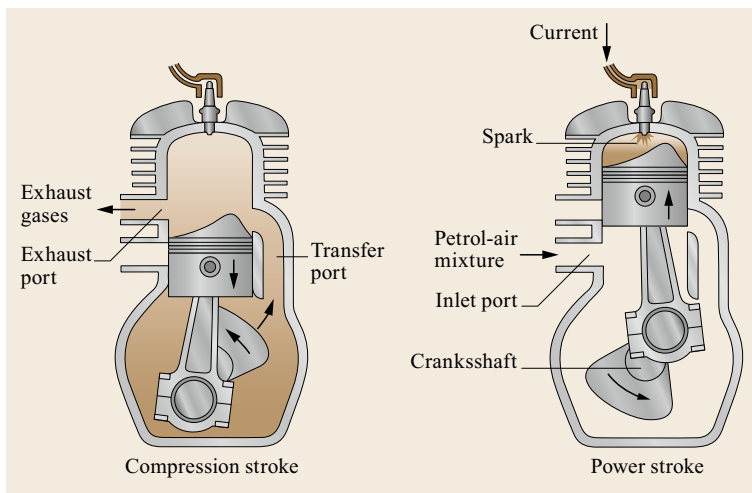


Fig. 17.4 Two-stroke engine cycle

The fundamental differences between two-stroke and four-stroke engines are lubrication and gas exchange – the removal of exhaust and the introduction of the fuel-air mixture. In the two-stroke engine, there is a power stroke in each cylinder during each revolution of the crankshaft. Exhaust and fuel introduction occur at the same time – when the piston is at the bottom of the cylinder.

In two-stroke engines, lubrication is supplied by the fuel. The lubricity of diesel fuel satisfies this need, but when gasoline is the fuel, it must be mixed with a small amount of lubricating oil. Compared to gasoline, lubricants are heavier and less likely to combust, so when they are burned in a two-stroke engine, they tend to generate smoke, an indication of incomplete combustion.

Two-stroke engines have fewer moving parts, are more compact and can be significantly lighter and more compact than four-stroke engines with equivalent power. Within a narrow range of engine speeds – the so-called *power band* – a two-stroke engine can have a relatively high power-to-weight ratio. This is because for each power stroke in a two-stroke engine, the crankshaft turns once, while for each power stroke in a four-stroke engine, the crankshaft turns twice.

Gasoline-powered two-stroke engines are common in lawn mowers and chain saws. In many countries, they are still common in motorcycles and *tuk-tuks*, the small, three-wheeled open-air carts found in India, Indonesia, Mexico, Thailand and other always-warm (tropical) countries. Due to air pollution caused by incomplete combustion of the lube oil that must be mixed with the gasoline, transportation vehicles powered by gasoline-burning two-stroke engines are almost impossible to find in Canada, the EU, the UK and the United States – countries with tight environmental regulations.

Rotary Engine

A rotary engine (Fig. 17.5) includes an odd number of cylinders arrayed radially around crankshaft inside a spinning crankcase. Some engines have multiple cylinder arrays. In aircraft, the crankshaft is bolted to the airframe and the propeller is bolted to the front of the crankcase. Piston firing alternates around the array. For most rotaries, fuel is mixed with air before entering a cylinder, as is the case in Otto engines.

Félix Millet built one of the first rotary engines, a five-cylinder affair, which he incorporated into a bicycle. He patented the engine in 1888 and displayed the bicycle at the Exposition Universelle in Paris in 1889 [17.5]. During World War I, rotary engines were preferred for high-speed aircraft, such as fighter planes, due to their high power-to-weight ratios. Rotaries ran smoothly because there are no reciprocating parts. Due

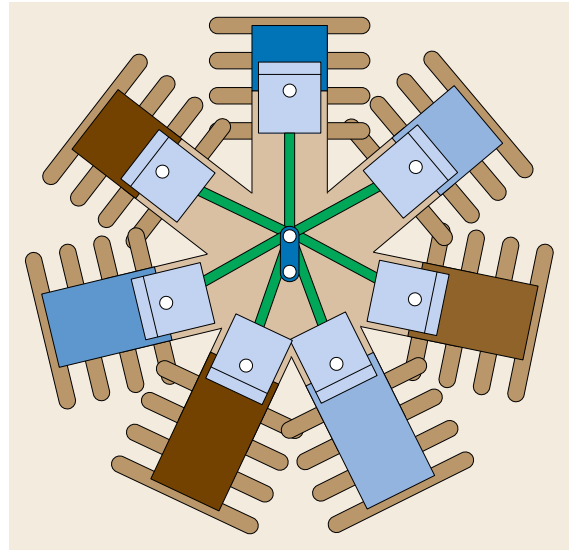


Fig. 17.5 Arrangement of cylinders in a seven-cylinder rotary engine

to their combined weight, the spinning crankcase and cylinders acted as a flywheel, decreasing the likelihood that the engine would stall. They were self-cooled, even when the airplane wasn't moving, which reduced their weight. On the other hand, fuel consumption was high. As with two-stroke engines, oil had to be mixed with the fuel, so oil consumption was high too. A major problem was the angular momentum of the heavy rotating crank case. It behaved like a gyroscope, causing problems with aircraft control.

Radial Engine

In a radial engine, the cylinders *radiate* outward from a central crankcase like the spokes of a wheel. Before the advent of jet engines near the end of World War II, air-cooled radials were commonly used for aircraft. At first glance, radial engines look like rotary engines, because in both cases cylinders are arranged in a circular array. But in radial engines, the crankcases don't rotate. They employ conventional rotating crankshafts in a fixed engine block. Compared to rotary engines, radial engines could achieve much higher engine speeds. The amount of rotating mass was reduced, so the gyroscopic effect and related control problems were significantly reduced.

Wankel Engine

The Wankel engine [17.6] is a pistonless internal combustion device, in which power is transferred by a rotor that resembles a Reuleaux triangle (Fig. 17.6). The concept was developed by Felix Wankel, who received the first patent for this kind of engine in 1929.

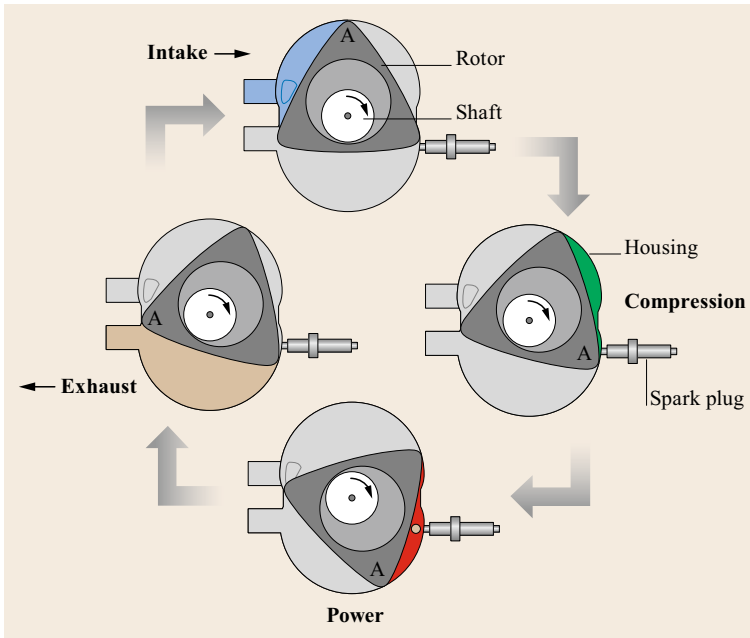


Fig. 17.6 Wankel engine cycles

In a Wankel, the four strokes of an Otto cycle occur in the spaces between the rotor and housing. The shape of the rotor is determined by a compromise between minimization of combustion chamber volume and maximization of compression ratio. The central drive shaft, called the *eccentric shaft* or *E-shaft*, passes through the center of the rotor and is supported by fixed bearings. One full orbit of the rotor equates to three turns of the E-shaft.

In theory, the Wankel engine has several advantages compared to engines with reciprocating pistons. The advantages are similar to those mentioned for rotary and radial engines, such as:

- Compact design
- Relative simplicity
- Smoother operation due to the lack of reciprocating parts
- Higher revolutions per minute
- A power-to-weight ratio that is two-thirds lower
- Less prone to engine knock
- Wider speed range.

Disadvantages include:

- Vastly different temperatures in the chambers. Metals expand when heated and the extent of expansion depends strongly on temperature. The thermal expansion phenomenon causes problems with sealing.
- Lubricating oil must be mixed into the fuel.
- Slower combustion due to the long, thin dimensions of the combustion chamber.

- Poor fuel economy due to seal leaks.
- Relatively high emissions.

Over the years, attracted by the Wankel's high theoretical power-to-weight ratios, General Motors, Mercedes-Benz, Mazda and other companies have conducted research and development on Wankel engines. Mazda has gone farther than most, achieving some success with its 12A engine at the Le Mans race in 1974. Mazda is the only company ever to win Le Mans with a nonpiston engine. At present, the emissions problems appear to be insurmountable. Until they are solved, Wankel-powered automobiles will not be approved for use on public highways.

Meanwhile, small Wankel engines continue to be sold for model airplanes, go-karts, personal motor boats and auxiliary power units.

Turbine Engine

Turbine engines, also known as gas turbines or combustion turbines, are pistonless internal combustion engines powered by kerosene-like jet fuel (avjet) or aviation gasoline (avgas). They include an upstream rotating compressor coupled to a downstream turbine, with a hot combustion chamber in between (Fig. 17.7).

Turbine engines provide power for aircraft, trains, ships, tanks and electricity generators. In a jet airplane, fresh air flows through the compressor, which brings it to high pressure. Fuel is sprayed into the air as it flows into the combustion chamber. Combustion produces tremendous heat and increases the system pressure.

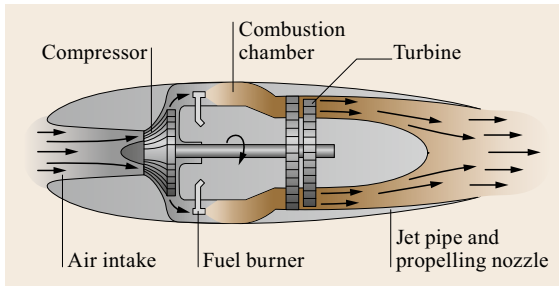


Fig. 17.7 Turbine engine

The high-temperature, high-pressure gas enters a turbine, expanding as it turns the turbine, which drives the compressor and other devices, including an electricity generator. The exhaust gases exit the turbine at high velocity, driving the airplane forward.

When a jet engine is started, the engine is *spun* until air is flowing at a desired speed. Fuel is added and igniters – similar to spark plugs – initiate combustion. From that point on, engine combustion is self-sustaining and igniters are then used only in unusual circumstances, such as:

- After a flame-out
- During heavy rain
- When air speed is very slow.

Turboprop engines often burn avgas. In this application, the turbine drives a propeller. The engine exhaust does not contain enough energy to provide much thrust. The propeller is coupled to the turbine with a gear that converts the high-RPM (RPM), low-torque output of the turbine into low-RPM, high-torque power for the propeller.

17.2 Otto Engine Thermodynamic Cycle

Figure 17.8 illustrates the thermodynamic cycle for a four-stroke Otto engine. Pressure and volume are exhibited on the two-dimensional plot [17.7]. Temperature is not shown. Note that automobile engines are not closed systems. External cooling is required and the heat capacity of the engine block is high. In combination, these factors keep the engine nearly isothermal.

At the intake stroke, the intake valve is open and the exhaust valve is closed. As the piston moves to the bottom of the cylinder, the fuel-air mixture expands in an isobaric fashion, shown by the green line from left to right at the bottom of the figure. At the compression stroke, both valves are closed. As the piston rises, it causes adiabatic compression with decreasing volume and increasing pressure and temperature (not shown). At the power stroke, both valves are still closed. The fuel is ignited and combusted. Initially, the system is isochoric. The product of heat and combustion products increases pressure for power. As the cylinder is driven downwards, the gases undergo adiabatic expansion with increasing volume and decreasing pressure and temperature (not shown). At the start of the final stroke, the exhaust stroke, both valves are closed. The pressure starts to fall isochorically. When the exhaust valve

opens, the exhaust gases expand isobarically. When the piston reaches the top of the cylinder, the exhaust valve closes as the intake valve opens and the cycle is repeated, starting with the intake stroke of the following cycle.

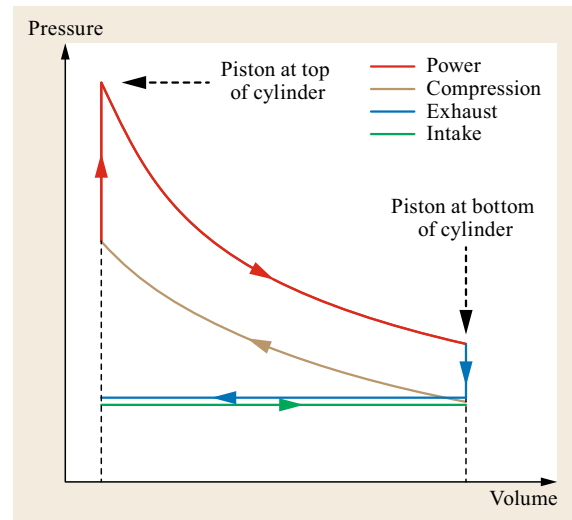


Fig. 17.8 Otto Cycle thermodynamics

17.3 Key Gasoline Properties

Petroleum products must meet certain specifications. For engine performance, key properties include octane number, volatility, sulfur and storage stability.

17.3.1 Octane Number

In the combustion chamber, vapor heats up during compression. Ideally, the mixture of gasoline vapor and air is ignited with a spark when the piston reaches a predetermined position near the top in the cylinder. However, some compounds tend to ignite before the spark plug fires at the end of the compression stroke. This is called self-ignition or premature ignition. It causes engine knock, which stops the ascent of the piston and pushes it in the opposite direction. Knocking reduces the power, increases engine wear and can cause serious damage.

Different gasoline components have different tendencies to knock. The compression ratio (V_1/V_2), shown in Fig. 17.9, is a factor related to knock behavior. Octane rating, or octane number, is related to the smallest compression ratio at which an engine starts to knock with a given fuel. It is based on a scale in which the octane number of *n*-heptane is designated as zero and the octane number of isooctane (2,2,4-trimethylpentane) is 100. When a fuel is tested in a standard single-cylinder engine, mixtures of isooctane and *n*-heptane of various percentages are used as reference standards for correlating the knocking of the test fuel with the percentage of isooctane in the mixture.

Thus, a gasoline with the same knocking characteristics as a mixture of 94% 2,2,4-trimethylpentane and 6% *n*-heptane has an octane rating of 94. A rating of 94 does not mean that the gasoline contains just isooctane and *n*-heptane in these proportions, but that it has the

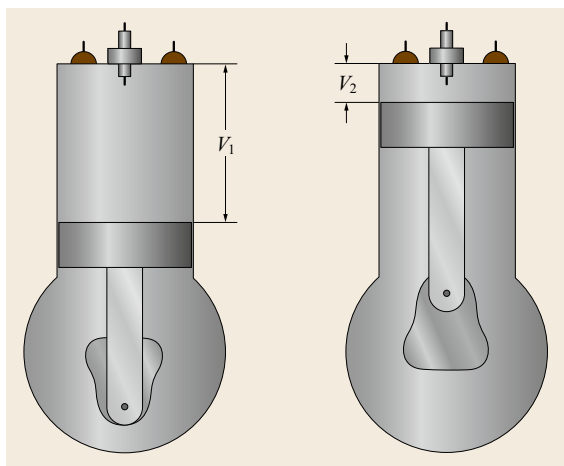


Fig. 17.9 Compression ratio V_1/V_2

same tendency to knock as this mixture. The blends of known octane ratings can also be used as references as shown in Fig. 17.10. The higher the number, the less likely is a fuel to pre-ignite.

A gasoline containing a high proportion of straight-chain alkanes has a greater tendency to knock. However, branched-chain alkanes, cycloalkanes and aromatic hydrocarbons are much more resistant to knocking. Straight-chain alkanes are converted into isoalkanes in several processes in the refinery. The gasolines available for octane rating of cars usually contain a mixture of alkanes (straight-chain, branched and cyclic) with aromatic hydrocarbons.

ASTM D2699 and ASTM D2700 describe respective methods for measuring research octane number (RON) at 600 rpm, which is most relevant to low-speed city driving with load conditions; and motor octane number (MON) at 900 rpm, which is most relevant to high-speed highway driving conditions.

In North America, the posted octane of gasoline is the arithmetic average of RON and MON: $(R + M)/2$. This is the number displayed on pumps at filling stations. Typical grades are *regular* with a posted octane of 87, *midgrade or medium* with a posted octane of 89 and *premium* with a posted octane of 91–93. In some locales, customers can dial in any octane they want between 87 and 93.

Table 17.1 provides data for 32 pure compounds that boil in the gasoline distillation range. Aromatics, olefins and branched paraffins have higher octane numbers than naphthenes and normal paraffins with similar carbon numbers. The trend is apparent especially for the C_6 and C_7 compounds shown:

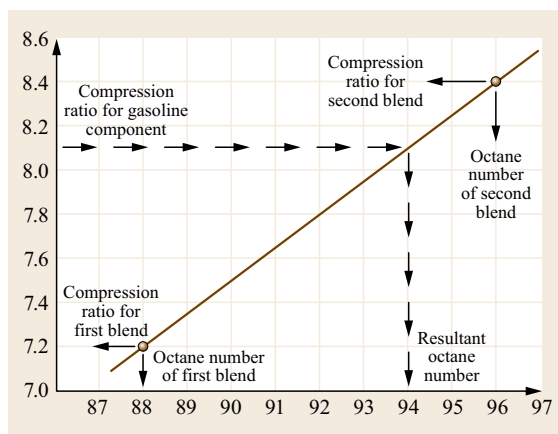


Fig. 17.10 Octane rating (octane number) is determined by comparing compression ratio causing knock using reference blends

Table 17.1 Octane numbers and other physical properties for selected pure compounds

Compound	Type	Formula	Normal boiling point		Specific gravity 60/60	API at 60 °F	Heat content ^a BTU/lb	RON	MON
			°F	°C					
<i>n</i> -Butane	<i>n</i> -Paraffin	C ₄ H ₁₀	31.1	−0.5	0.5840	110.79	19 657	93	90
Isobutane	Isoparaffin	C ₄ H ₁₀	10.8	−11.8	0.5629	119.89	19 589	110	98
<i>n</i> -Pentane	<i>n</i> -Paraffin	C ₅ H ₁₂	96.9	36.1	0.6311	92.70	19 495	62	62
Isopentane	Isoparaffin	C ₅ H ₁₂	82.1	27.8	0.6247	95.01	19 304	92	90
<i>n</i> -Hexane	<i>n</i> -Paraffin	C ₆ H ₁₄	155.7	68.7	0.6638	81.66	19 232	25	26
2-Methylpentane	Isoparaffin	C ₆ H ₁₄	140.5	60.3	0.6578	83.63	19 202	73	74
2,3-Dimethylbutane	Isoparaffin	C ₆ H ₁₄	136.4	58.0	0.6670	80.63	19 195	100	94
Methylcyclopentane	Naphthene	C ₆ H ₁₂	161.3	71.8	0.7540	56.17	18 768	91	80
Cyclohexane	Naphthene	C ₆ H ₁₂	177.3	80.7	0.7835	49.10	18 676	83	78
2-Methyl-2-pentene	Olefin	C ₆ H ₁₂	153.2	67.3	0.6909	73.32	18 970	98	83
Benzene	Aromatic	C ₆ H ₆	176.2	80.1	0.8829	28.77	17 258		103
<i>n</i> -Heptane	<i>n</i> -Paraffin	C ₇ H ₁₆	209.2	98.4	0.6882	74.11	19 158	0	0
2-Methylhexane	Isoparaffin	C ₇ H ₁₆	194.1	90.1	0.6823	75.88	19 135	42	46
3-Ethylpentane	Isoparaffin	C ₇ H ₁₆	200.3	93.5	0.7043	69.42	19 156	65	69
2,2-Dimethylpentane	Isoparaffin	C ₇ H ₁₆	174.6	79.2	0.6821	75.96	19 097	93	96
Methylcyclohexane	Naphthene	C ₇ H ₁₄	213.7	100.9	0.7748	51.13	18 642	75	71
2-Methyl-2-hexene	Olefin	C ₇ H ₁₄	203.7	95.4	0.7126	67.07	19 110	92	79
Toluene	Aromatic	C ₇ H ₈	231.1	110.6	0.8743	30.34	17 423	106	100
2,2,4-Trimethylpentane	Isoparaffin	C ₈ H ₁₈	210.6	99.2	0.6992	70.87	19 064	100	100
2,2,4-Trimethyl-1-pentene	Olefin	C ₈ H ₁₆	214.6	101.4	0.7193	65.22	18 916	101	86
Ethylbenzene	Aromatic	C ₈ H ₁₀	277.1	136.2	0.8744	30.32	17 595	101	98
<i>o</i> -Xylene	Aromatic	C ₈ H ₁₀	292.0	144.4	0.8849	28.40	17 546		100
<i>m</i> -Xylene	Aromatic	C ₈ H ₁₀	282.4	139.1	0.8694	31.26	17 542	104	103
<i>p</i> -Xylene	Aromatic	C ₈ H ₁₀	281.1	138.4	0.8666	31.78	17 546	103	101
2,2,3,3-Tetramethylpentane	Isoparaffin	C ₉ H ₂₀	284.5	140.3	0.7607	54.51	19 045	104	95
Isopropylcyclohexane	Naphthene	C ₉ H ₁₈	310.6	154.8	0.8064	43.97	18 775	63	61
1,3,5-Trimethylbenzene	Aromatic	C ₉ H ₁₂	328.5	164.7	0.8699	31.17	17 631	106	101
2,2,3,3-Tetramethylhexane	Isoparaffin	C ₁₀ H ₂₂	320.6	160.3	0.7684	52.65	19 011	102	92
<i>m</i> -Diethylbenzene	Aromatic	C ₁₀ H ₁₄	358.0	181.1	0.8683	31.45	17 791	103	97
1,2,3,4,-Tetrahydro-naphthalene ^b	Aromatic	C ₁₀ H ₁₂	405.8	207.7	0.9748	13.65	17 423	96	82
Ethanol	Alcohol	C ₂ H ₆ O	172.92	78.29	0.7967	46.11	11 530	109	90
Methyl- <i>t</i> -butyl ether	Ether	C ₅ H ₁₂ O	131.36	55.20	0.7459	58.20	15 119	116	101

^a Net liquid heat of combustion at 77 °F (25 °C)^b This compound is also known as tetralin

- MON values for *n*-hexane, 2-methylpentane and 2,3-dimethylbutane, are 26, 73.5 and 94.3 respectively. Of the three paraffins, the MON for 2,3-dimethylbutane is highest because it is the most highly branched. MONs for the two C₆ naphthenes (methylcyclopentane and cyclohexane) are lower than the MON for the olefin (2-methyl-2-pentene) and the aromatic compound (benzene).
- In the C₇ series, the MON for *n*-heptane is, by definition, equal to zero. MONs for the other paraffins increase with branching as they did for the C₆ series. Toluene has the highest value (MON = 100.3).

Octane does not blend linearly. The RON for pure 4-methyl-2-pentene is 99, but its blended RON can be as high as 130. Ethanol and MTBE show similar behavior. Blended octanes for ethanol can be 10–20 numbers higher than the octanes for pure ethanol. Table 17.2 compares measured pure-compound octanes with blended octanes. Values were selected from a compilation prepared by Texas A&M University [17.9]. Blended octane data for ethanol and MTBE come from the EIA-AFM website [17.10]. The blended values for olefins are exceptionally high, almost too high to be believed. Values may be skewed by the method(s) used to obtain such values, such as extrapolation, explained later.

Table 17.2 Comparison of pure-compound octane numbers with blending octane numbers. For olefins, blending octane numbers are exceptionally high, but this may be an artifact of the method used to obtain such values (after [17.8])

		Pure Compound		Blended	
		RON	MON	RON	MON
Paraffins					
<i>n</i> -Butane	C ₄	93	90	113	114
<i>n</i> -Pentane	C ₅	62	62	62	67
2-Methylbutane	C ₅	92	90	99	104
Dimethylpropane	C ₅	85	80	100	90
<i>n</i> -Hexane	C ₆	25	26	19	22
2,2-Dimethylbutane	C ₆	92	93	89	97
<i>n</i> -Heptane	C ₇	0	0	0	0
2,2-Dimethylpentane	C ₇	93	96	89	93
2,2,3-Trimethylbutane	C ₇	> 100	> 100	113	113
2,2,3-Trimethylpentane	C ₈	100	100	105	112
2,2,4-Trimethylpentane	C ₈	100	100	100	100
Olefine					
1-Pentene	C ₅	91	77	152	135
2-Methyl-2-butene	C ₅	97	85	176	141
3-Methyl-2-pentene	C ₆	99	81	130	118
4-Methyl-2-pentene	C ₆	99	84	130	128
2,2,4-Trimethyl-1-pentene	C ₈	> 100	86	164	153
2,2,4-Trimethyl-2-pentene	C ₈	> 100	86	148	139
Aromatic					
Benzene	C ₆	> 100	> 100	99	91
Toluene	C ₇	> 100	> 100	124	112
<i>o</i> -Xylene	C ₈	> 100	> 100	120	103
<i>m</i> -Xylene	C ₈	> 100	> 100	145	124
<i>p</i> -Xylene	C ₈	> 100	> 100	146	127
Ethylbenzene	C ₈	> 100	98	124	107
1,3,5-Trimethylbenzene	C ₉	> 100	> 100	171	137
Propylbenzene	C ₉	> 100	98	127	129
Isopropylbenzene	C ₉	> 100	98	132	124
Alcohols					
Ethanol		109	90	120–130	100–106
Methyl- <i>t</i> -butyl ether		116	101	115–123	98–105

Determining Octane Numbers Above 100

In Tables 17.1 and 17.2, several octane values exceed 100. To measure such numbers, one can extend the reference scale with standards that contain tetraethyl lead (TEL). Adding 3 ml of TEL per gallon of 2,2,4-trimethylpentane gives a reference with an octane of 125 [17.11]. This high-octane reference, which is toxic, can be purchased from the *Chevron Phillips Chemical Company* [17.12].

For octane numbers above 125, an experimenter must extrapolate. This method entails adding successively higher amounts of the sample to 100% isooctane and using the results to generate a plot.

Extrapolation is fraught with uncertainty. Results based on straight lines differ from results based on curves. This can explain the wide variation be-

tween published blending octane numbers for *i*-butane, toluene, xylenes and oxygenates.

So-called *performance numbers* provide an alternative to extrapolation. These are obtained by determining the instantaneous mean effective cylinder pressure (IMEP) for the fuel being tested at the highest boost that does not cause the engine to knock. The result is multiplied by 100 and divided by the IMEP for pure 2,2,4-trimethylpentane.

17.3.2 Reid Vapor Pressure (RVP)

Another important property of gasoline is Reid vapor pressure (RVP), which indicates the ease of starting a spark-ignition engine with the fuel.

RVP relates to vapor lock, which occurs when gasoline vaporizes while still in the fuel delivery system, resulting in too much vapor in the combustion chamber prior to ignition. A vapor-locked vehicle fails to start if a driver tries to restart a hot engine or if the outside temperature is too high. The engine won't run because vapor flow can't be controlled by injectors and pressure regulators designed to handle liquids. RVP is proportional to flash point, which indicates how likely it is for a fuel to explode spontaneously in open air.

Finally, regulations control RVP to limit evaporation of gasoline into the air, where the vapors react with ground-level ozone and nitrogen oxides to form photochemical smog.

RVP is defined as the vapor pressure measured at 100 °F (38 °C) in a volume of air four times the liquid volume. The parameter can be calculated from the composition of a fuel

$$M_t(\text{RVP})_t = \sum_{i=1}^n M_i(\text{RVP})_i ,$$

where M_t = total moles of blended product; $(\text{RVP})_t$ = specification RVP for product, psi or kPa; M_i = moles of component i ; and $(\text{RVP})_i$ = RVP of component i , psi or kPa.

Metal-Containing Octane Additives: TEL and MMT

Starting in the 1920s, adding tetraethyl lead (TEL) to gasoline substantially improved octane numbers and hence engine performance. It allowed engines to operate at higher compression. In addition to boosting power, TEL increased fuel economy.

But TEL causes cumulative neurotoxicity. Children are especially susceptible. TEL also deactivates the active metals in catalytic converters that convert unburned hydrocarbons and poisonous carbon monoxide in engine exhaust into carbon dioxide.

In the United States, the phase-out of TEL began in 1973. Except for a few low-volume specialty products, such as high-octane avgas for piston-engine aircraft, automotive gasoline was lead-free by 1986 in Japan, 1988 in Germany, 1992 in California, 1993 in Canada, 1996 in the rest of the United States, 2000 in the EU, China and India and 2002 in Australia and Russia. TEL was legal in Algeria and Iraq as recently as 2014 and illegal usage persists.

A less toxic alternative to TEL is MMT (methylcyclopentadienyl manganese tricarbonyl). MMT was common in Canadian gasoline starting in 1976. It is still permitted in small amounts in many regions, including China and the EU. Australia started using MMT in 2000. MMT is not allowed in the United States, due to concerns about as-yet-unquantified health risks.

17.3.3 Sulfur Content

Other than hydrocarbons, there are many heteroatom-containing hydrocarbons present in crude oils. The main heteroatom compounds include sulfur, nitrogen and oxygen, for which concentrations can reach 5 wt%; typically, the sulfur content is 5–10 times higher than nitrogen and oxygen. Trace metals, such as Fe, Ni, V, As and Hg are present at ppm levels. These contaminants are of concern to refining processes because they deactivate catalysts. Oxygen-containing hydrocarbons, such as naphthenic acids, can cause corrosion. Concentrations of heteroatom-containing compounds are highest in high-boiling fractions, but sulfur and nitrogen can be present in gasoline fractions.

Upon combustion, sulfur compounds form sulfur oxides (SO_x). When SO_x are released to the atmosphere, they form particulates and react with moisture to form acid rain. Hence sulfur-containing streams must be hydrotreated to remove sulfur and meet product sulfur limits. By 2017, the limit on sulfur in gasoline and diesel fuel in much of the world will be 10 ppmw.

17.3.4 Storage Stability

During storage in a fuel tank or other containers, gasoline can undergo oxidative degradation to form sticky gums, which can precipitate out of gasoline. These can cause fouling in the fuel system and engine components, reducing engine performance. Small amounts of antioxidants in gasoline additives can improve the storage stability and inhibit gum formation.

Reformulated gasolines in the United States contain ethanol, which is water soluble. At temperatures of 40 to 60 °F (4 to 16 °C), phase separation into a gasoline phase and an aqueous ethanol phase can occur when gasoline contains 10 vol.% ethanol and only 0.4 to 0.5 vol.% water. Thus, limiting water content in US reformulated gasolines can allow ethanol contents of more than 10 vol.% without phase separation.

17.4 Gasoline Specifications

Gasoline properties are specified by law or government agencies. Standard measurements for most properties are developed and published by organizations such as the American Society for Testing and Materials (ASTM) and the International Organization for Standardization (ISO). ASTM and ISO specifications incorporate information from suppliers, users, government agencies and equipment manufacturers. Except for sulfur and oxygen content, inter-

national gasolines specifications are similar in most respects for urban areas. Many countries follow ASTM D4814: Standard specification for automotive spark-ignition engine fuel. In Europe, the present specification is EN 228:2012. The Chinese specification is Gasoline V and Japanese specification is JIS K-2202.

Table 17.3 shows modern specifications for China, the EU and the United States.

Table 17.3 Gasoline specifications in China, the European Union and the United States (after [17.13])

	China V	Euro V 2009/30/EC	US RFG ^c	
			Summer	Winter
Research octane (RON), min	89–95	91–95	NS ^a	
Motor octane (MON), min	84–90	81–85	NS ^a	
Antiknock index (AKI), recommended	NS ^a	NS ^a	87-89-91 with seasonal and altitudinal variations	
Aromatics (vol.%) max	40	35	20.7 ^c	20 ^c
Olefins (vol.%) max	24	18	12 ^c	11
Benzene (vol.%) max	1	1	1	
Sulfur (ppm) max	10 as of 1-Jan-2017	10	10 as of 1-Jan-2017	
Gum content (mg/100 ml) max	5	5	5	5
Density at 15 °C (kg/m ³)	720–775 (20 °C)	720–775	NS ^a	
Distillation				
Percent recovered at 100 °C	46	46		
Percent recovered at 150 °C	75	75		
ASTM D4814 specifications, Class A				
10% evaporated (°C)			70 max	
50% evaporated (°C)			77 min, 121 max	
90% evaporated (°C)			190 max	
Endpoint (°C)			225 max	
RVP (kPa)	40–65 summer 45–85 winter	60/70 max	47.6 ^d	82
RVP (psi)			7	12
Lead (mg/l) max	5	5	ND ^b	
Manganese (mg/l) max	2	< 2 MMT	ND ^b	
Oxygen (% m/m)	2.7 max	2.7 max	2.5 ^d	2.4 ^d

^a Not specified

^b Must be nondetectable

^c US reformulated gasoline specifications vary regionally based on local situations. Values marked with (°) are averages from a 2005 national survey. Compliance is based on complex-model estimates of VOCs (VOCs), toxic compounds and NO_x emissions. The Clean Air Act (CAA) limits aromatics in RFG to 25 vol.%

^d US laws passed in 2005 and 2007 do not specify ethanol percentage. Instead, they specify a national target for consumption of ethanol as a gasoline blendstock, regardless of percentages. In 2016, discussions were being held on whether the ethanol percentage should exceed 15 vol.%

17.5 Gasoline Production

17.5.1 Refining Strategy

The typical gasoline boiling range is from 100 °F (≈ 40 °C) to 400 °F (≈ 200 °C) for adequate RVP. The components have carbon numbers ranging from C₅ to C₁₂.

The most straightforward gasoline blendstock is light straight-run naphtha from atmospheric pressure distillation. Heavier straight-run naphthas do not have high octane ratings. Without further processing to in-

crease octane rating, heavy naphtha can only be used as a solvent, diluent, or steam cracking feed.

As shown in Tables 17.1 and 17.2, octane numbers vary with hydrocarbon compound types. Linear normal paraffins have the lowest octane rating; for *n*-heptane as mentioned above, the octane number is 0. Isoparaffins, such as 2,2,4-trimethylpentane, have high octane numbers close to 100. Aromatic hydrocarbons, such as benzene and toluene, have octane numbers greater than 100. Cycloparaffins also have higher octane

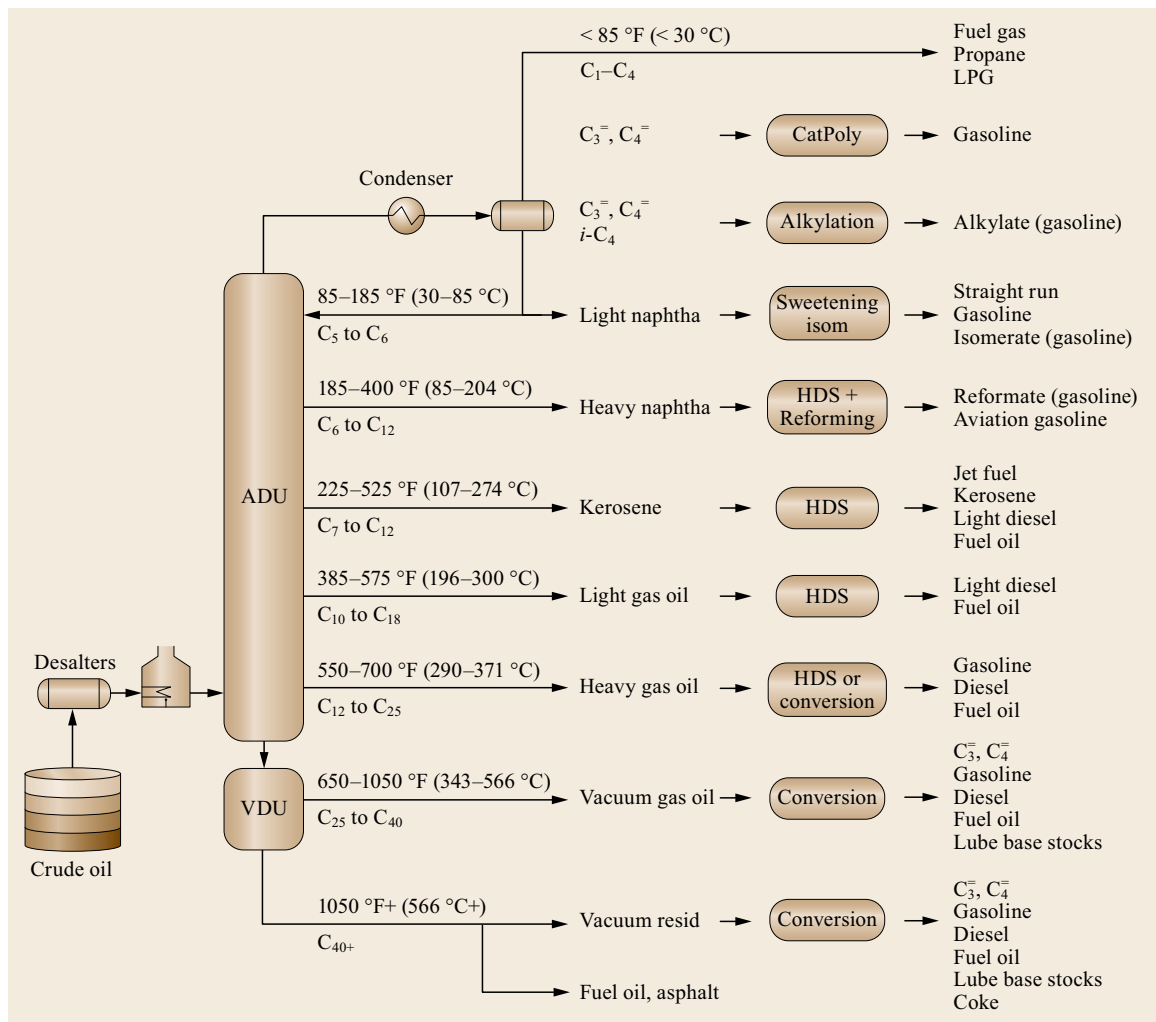


Fig. 17.11 Production of gasoline blendstocks in refineries. Fuel gas is mostly C₁C₂ compounds. All conversion processes produce at least small amounts of C₁C₂. LPG = liquefied petroleum gas, which is mostly C₃ and C₄ paraffins. Sweetening can involve mercaptan oxidation. Conversion processes include FCC, hydrocracking, delayed coking and other resid upgrading processes. C₃= and C₄= are propylene and butylenes respectively; these are converted into gasoline by catalytic polymerization. They also react with isobutane to make alkylate

Table 17.4 Properties of gasoline blendstocks

	iC ₄	nC ₄	iC ₅	nC ₅	iC ₆	Cyclohexane	2-Methyl-1-pentene	Benzene	Toluene	MTBE	Ethanol	Straight-run Light	FCC naphtha Full-range	Light	
API gravity	119.9	110.8	95.2	92.7	83.6	48.7	75.3	28.8	32.1	59.7	48.3	81.8	51.9	56.8	
Specific gravity	0.5629	0.5840	0.6241	0.6311	0.6578	0.7853	0.6844	0.8829	0.8650	0.7400	0.7870	0.6634	0.7715	0.7515	
Aromatics (vol.%)								100	100			2.2	35.9	17.6	
Olefins (vol.%)							100					0.9	25.4	44.9	
Saturates (vol.%)												96.9	38.8	37.4	
Benzene (vol.%)										0	0	0.73	1.23	1.24	
Bromine number												0.5	41.7	91.4	
RVP (psi)	71	52	19.4	14.7	6.4	3.3	2	3.2	1	8	18	11	4.6	9	
RVP (kPa)	490	358	134	101	44	23	14	22	7	55	124	76	32	62	
Boiling point (°F)	10.9	30.2	81.9	97	140	177.3	143.8	176.2	231.1	131.4	173.1				
Boiling point (°C)	-11.7	-1	27.7	36.1	60	80.7	62.1	80.1	110.6	55.2	78.4				
Distillation															
Initial boiling point													33 °C, 44 °C, 35 °C, 91 °F, 112 °F		
T10													45 °C, 68 °C, 51 °C, 113 °F, 155 °F	124 °F	
T30													49 °C, 87 °C, 59 °C, 121 °F, 189 °F	139 °F	
T50													56 °C, 115 °C, 73 °C, 132 °F, 239 °F	164 °F	
T70													65 °C, 150 °C, 93 °C, 149 °F, 302 °F	200 °F	
T90													84 °C, 193 °C, 125 °C, 184 °F, 379 °F	257 °F	
Endpoint													126 °C, 223 °C, 169 °C, 258 °F, 434 °F	337 °F	
RON	110.1	93.8	92.3	71.5	79.2	83	94.2	101	121	118	123	63.7	92.6	93.6	
MON	97.6	89.6	90.3	72.4	78.4	77.2	81.5	107	107	102	103	61.2	82.1	79.4	
Sulfur (ppmw)															
Nitrogen (ppmw)															
Lower heating value															
(Btu/lb)	19 287	19 466	19 454	19 484	19 213	18 680	19 260	17 270	17 450	15 094	11 587	18 400	17 300	18 700	
(MJ/kg)	44.86	45.28	45.32	45.32	45.32	43.45	44.80	40.17	40.59	35.11	27.0	42.8	40.2	43.5	

Table 17.4 (continued)

	Reformate			Alkylate		Isomerate C ₆	Hydrocrackate		Coker naphtha Full- range	Polymer		Pyrolysis Gasoline
	Full- range	Light	Mid	Heavy	Light		Heavy	Light		Heavy	Gasoline	
API gravity	44.2	72	32.8	29.8	72.3	55.8	83	79	49	58.0	59.5	36.6
Specific gravity	0.8054	0.6953	0.8612	0.8772	0.6943	0.7555	0.6597	0.6722	0.7839	0.7467	0.7408	0.8420
Aromatics (vol.%)	61.1	4.8	94.2	93.8	0.5	1	1.6	4	18	1.8	2	70
Olefins (vol.%)	1	1.5	0.6	1.9	0.2	0.9	0.1	<1	<1	50	4	20
Saturates (vol.%)	37.9	93.7	5.1	4.2	99.3	98.1	98.3	96	82	48	94	10
Benzene (vol.%)	1.17	4.01	0	0	0	0.01	0	<0.5	0	0.5	0	30–60
Bromine number	1.2	3.1	0.6	0.9	2.3	0.3	3.8	0.5	0	92	4	40
RVP (psi)	3.2	3.8	1	0.3	4.6	0.3	8	13	1.1	19	9	1
RVP (kPa)	22.1	26.2	6.9	2.1	31.7	2.1	55.2	89.6	7.6	131	62.1	6.9
Boiling point												
IBP	47 °C, 117 °F	59 °C, 138 °F	107 °C, 224 °F	156 °C, 313 °F	38 °C, 101 °F	148 °C, 299 °F	48 °C, 118 °F	C ₅	85 °C, 185 °F	C ₅	C ₅	13 °C, 56 °F
T10	89 °C, 192 °F	79 °C, 174 °F	111 °C, 231 °F	164 °C, 328 °F	72 °C, 162 °F	163 °C, 325 °F	57 °C, 134 °F					
T30	118 °C, 244 °F	83 °C, 182 °F	111 °C, 232 °F	168 °C, 335 °F	91 °C, 196 °F	171 °C, 340 °F	57 °C, 135 °F					
T50	132 °C, 270 °F	87 °C, 188 °F	112 °C, 234 °F	173 °C, 344 °F	99 °C, 211 °F	179 °C, 354 °F	58 °C, 136 °F					92 °C, 197 °F
T70	144 °C, 291 °F	89 °C, 192 °F	114 °C, 237 °F	181 °C, 358 °F	104 °C, 219 °F	189 °C, 373 °F	58 °C, 137 °F					
T90	161 °C, 322 °F	91 °C, 195 °F	122 °C, 251 °F	199 °C, 391 °F	115 °C, 239 °F	219 °C, 427 °F	59 °C, 139 °F					
EP	201 °C, 393 °F	103 °C, 218 °F	158 °C, 316 °F	252 °C, 485 °F	157 °C, 315 °F	269 °C, 517 °F	63 °C, 146 °F	85 °C, 185 °F	204 °C, 400 °F	210 °C, 410 °F	204 °C, 400 °F	180 °C, 356 °F
RON	97.3	57.6	109.3	104.3	93.2	65.9	8.6	82.8	67.6	88	96.9	107
MON	86.7	58.5	100.4	92.4	91.2	74.5	80.5	82.4	67.3	80	84	94
Sulfur (ppmw)	<5	<5	<5	<5	<5	<5	<5	<5	<2	860	0	400–700
Nitrogen (ppmw)	0	0	0	0	0	0	0	0	0	7	0	0
Lower heating value												
(Btu/lb)	16 800	18 200	15 500	17 300	18 400	18 100	18 500	18 400	18 100	18 600		
(MJ/kg)	39.1	42.3	36.1	40.2	42.8	42.1	43.0	42.8	42.1	43.3		

Shaded cells indicate high sulfur content or comparatively low heat content. Data source include the following: API data compiled by Texas A&M University [17.9], Gary and Handwerk [17.14], Jechura [17.15], the Oak Ridge National Laboratory [17.16], the NIST Chemistry WebBook [17.17], Lengyel et al. [17.18], Virid et al. [17.19]

numbers than normal paraffins, as with isoparaffins. Normal hexane has an octane number of 25. When it is cyclized to cyclohexane, the octane number will be improved to 83. Further dehydrogenation into benzene will increase the octane rating to 115. However, due to health concerns, refineries avoid or minimize the production of benzene in gasoline. Olefins also have high octane numbers. Hence, in hydroprocessing units designed to remove gasoline sulfur, conditions are optimized for minimizing hydrogenation of olefins to form corresponding paraffins of lower octane rating.

To increase gasoline yield in a crude oil, several refining processes have been developed to either increase the molecules in the lighter fractions or decrease the molecules in the heavier fractions. Alkylation and polymerization are developed to convert molecules of carbon number less than 5 to the range of 6–12. On the other hand, cracking and coking are developed to break down larger molecules into the gasoline range. Without changing carbon numbers, isomerization and reforming are developed to convert low-octane components into high-octane constituents. These processes will be discussed further in the following sections.

Catalytic cracking without hydrogen, such as occurs in FCC, yields gasoline and middle distillate cycle oils with high aromatic contents. Such middle distillates perform poorly in compression ignition (diesel) engines. On the other hand, hydrocracking provides high yields of the easily cracked components desirable in diesel engines. Hydrocracking also yields light and heavy naphtha, which can be transformed into gasoline components.

17.5.2 Gasoline Blending Stocks

Gasoline is blended from several refinery streams including straight-run light naphtha and products from upgrading processes – isomerization (isomerate), alkylation (alkylate), catalytic reforming (reformate), catalytic polymerization (cat poly gasoline), catalytic cracking (FCC gasoline), hydrocracking (hydrocrackate, see Chap. 22) and coking. Regardless of source, heavy naphthas go through a catalytic reformer, which increases octane by converting paraffins and naph-

thenes into aromatics. Figure 17.11 depicts the refinery streams that comprise modern gasoline.

Properties of typical blendstocks are shown in Table 17.4.

A representative summer gasoline blend in the United States might contain 40 to 50% FCC gasoline, 15 to 20% straight-run gasoline, 10 to 15% alkylate, 15 to 20% reformate, up to 2% butane, 10% ethanol and up to 10% other – isomerate and polymer gasoline. The RVP of the blend depends on the relative concentration of each component. *n*-butane is a relatively inexpensive ingredient, but it has the highest vapor pressure by far at around 52 psi (≈ 360 kPa) [17.20].

Table 17.4 shows RVP, octane and API gravity for common blendstocks. Blending changes the octane and RVP of individual stocks. An extreme case is ethanol, which has a pure-compound RVP of 2 psi (≈ 14 kPa) and blended RVP of 10 for gasoline containing 10 vol.% ethanol.

For octane, the best blendstocks are alkylate, reformate, FCC gasoline, polymer gasoline, *i*-butane, *i*-pentane and aromatics concentrate (i. e., raffinate from extraction of aromatics). Other high-octane blendstocks are ethanol and methyl-*t*-butyl ether (MTBE), with blended RONs of 130 and 118 respectively. MTBE is banned in the United States but remains a desired blend component in Europe. Much of the MTBE consumed in Europe is manufactured along the US Gulf Coast.

RVP restrictions range from 7.8–9.0 psi (≈ 53 –62 kPa). Depending on location, there can be a 1 psi (6.9 kPa) allowance when the ethanol content is 9–10 vol.% [17.21]. One can see from the table that for RVP, the most favorable blendstocks are reformate, alkylate, hydrocrackate and hydrogenated heavy FCC gasoline; untreated FCC gasoline contains excess sulfur, so it isn't suitable for direct blending. For RVP, the least desired blendstocks are butanes, pentanes and C₅C₆ fractions from straight-run distillation, FCC and hydrocracking. Present RVP regulations permit little if any butane content. In some urban areas during the summer, pentane content also is limited. Adding 10 vol.% ethanol increases blended RVP by 1.1–1.25 [17.22], further reducing the practical content of butanes and pentanes.

17.6 Production of Gasoline Blendstocks

17.6.1 Distillation – Straight-Run Naphtha

Crude oil introduced to refinery processing contains many undesirable impurities, such as sand, inorganic

salts, drilling mud, polymer, corrosion byproduct, etc. These undesirable impurities, especially salts and water, need to be removed by dewatering and desalting prior to distillation. Dewatering removes water and

constituents of brine that accompany the crude oil. Desalting is a water-washing operation that can be performed at the production field or at the refinery to remove water-soluble minerals and entrained solids.

Crude oils are made of numerous components of different boiling points. The simplest way to separate them is with continuous distillation into different fractions (distillates or cuts) of different boiling ranges. At atmospheric pressure, heavy molecules can decompose above $\approx 650^\circ\text{F}$ ($\approx 343^\circ\text{C}$). To achieve additional separation of heavy fractions, continuous distillation is carried out under *vacuum* – strictly speaking, at reduced pressure – in a vacuum distillation unit (VDU). The typical operating pressure for a VDU is 40 mmHg (≈ 5.3 kPa). In the VDU, additional components vaporize. Vacuum gas oil (VGO) goes either to conversion units or lubricant production plants.

Full-range naphtha, including light and heavy naphtha, boils in the same boiling range as gasoline, between $30\text{--}205^\circ\text{C}$. Carbon numbers range between 5–12. Light naphtha boils between $85\text{--}185^\circ\text{F}$ ($30\text{--}85^\circ\text{C}$) and consists of molecules with 5–6 carbon atoms. Some light naphthas, such as those from hydrocracking units, can be used as-is for gasoline blending. Light naphtha from an atmospheric distillation unit (ADU) with adequate octane rating can be blended into gasoline pool as *straight run gasoline* after sweetening to remove sulfur and other impurities. Others are sent to isomerization units. Heavy naphthas boil between $185\text{--}400^\circ\text{F}$ ($85\text{--}204^\circ\text{C}$) and consist of molecules with 6–12 carbons. Most heavy naphthas containing seven or more carbons are feeds for catalytic reforming. Naphtha from atmospheric distillation should contain no olefins that are not present in crude oil; however, if temperatures in the CDU are too high, light olefins can be formed. Most refinery olefins come from thermal processes, such as steam cracking, FCC and coking. Naphtha from catalytic hydrocracking does not contain olefins.

Naphtha boiling range products, including reformates, isomerates and alkylates, are used in high-octane gasoline. Straight-run naphtha with low octane ratings is used as a diluent in the bitumen mining industry, as feedstock for producing olefins via steam cracking and as solvents for paints (as diluents), dry cleaning, cut-back asphalt, industrial extraction processes and in the rubber industry.

17.6.2 Isomerization

Other than straight-run naphtha, a gasoline pool comes from various processes, including isomerization [17.24], polymerization, reforming, alkylation, catalytic cracking, hydrocracking and coking.

Normal paraffins of the lighter naphtha fraction, butanes, pentanes and hexanes, have poor octane ratings for gasoline engines. Isomers of normal paraffins have high octane ratings. Isomerization units convert *n*-paraffins into isoparaffins and straight-chain olefins into *iso*-olefins. Butane isomerization provides isobutane as the major feed for subsequent alkylation. Pentane/hexane isomerization improves the octane number of light naphtha for gasoline blending. During World War II, there was a demand for high-octane aviation gasoline (avgas) for propeller fighter planes and isomerization became an important process.

AlCl_3 was originally used as a catalyst in the isomerization of normal butane. Butane isomerization provides isobutane as the major feed for subsequent alkylation. Subsequently, *n*-pentane and *n*-hexane isomerization processes were developed, using supported acid catalysts that can stand high temperature ($370\text{--}480^\circ\text{C}$) and high pressure (300–750 psi; 2070–5170 kPa). A liquid-phase process employs a dissolved catalyst for C_5/C_6 isomerization. Pentane/hexane isomerization improves the octane number of light naphtha for gasoline blending. Carbon number is not supposed to change in the isomerization process.

In butane isomerization, *n*-butane is converted to isobutane normally in a two-stage process. The feed contains *n*-butane, typically mixed with other butanes. As shown in Fig. 17.12, mixed butane feed enters a deisobutanizer to separate isobutane followed by a debutanizer to separate butanes from C_5+ impurities. The purified butanes are mixed with hydrogen and heated to 230° to 340°F ($110\text{--}170^\circ\text{C}$) under a pressure of 200–300 psi (1380–2070 kPa). The catalyst is highly sensitive to water, so the feed must be thoroughly dried. In the low-temperature first stage, the catalyst comprises aluminum chloride promoted by HCl. Hydrogen gas is added to inhibit olefin formation and to control side reactions, such as disproportionation and cracking. In the high-temperature second stage, the catalyst contains a noble metal such as platinum. The reactor effluent goes to a flash drum, from which hydrogen is recovered and recycled. Make up gas is added to compensate for the loss, which is low because the isomerization reaction itself does not consume hydrogen. HCl is removed in a stripper column. The liquids go to a stabilizer that separates C_4 gases, which can be used as a fuel gas inside the refinery, from isobutene and unconverted *n*-butane. The C_4 compounds are recycled and mixed with fresh feed. Produced isobutane is collected at the top of the deisobutanizer. Isobutane is the key feedstock for alkylation units, which produce high-octane alkylates. The Butamer process developed by UOP specifically for the isomerization of *n*-butane to isobutane uses a platinum-containing catalyst [17.25].

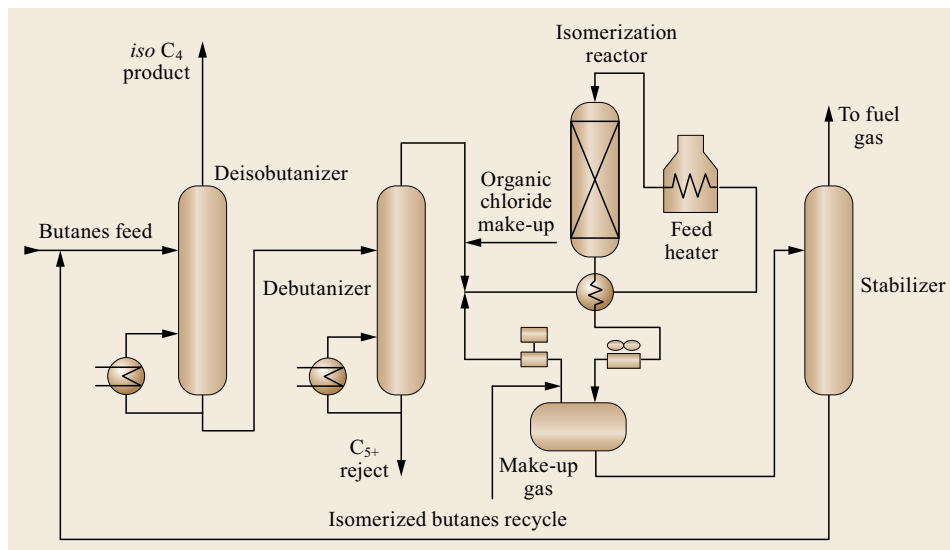


Fig. 17.12 Butane isomerization (after [17.23])

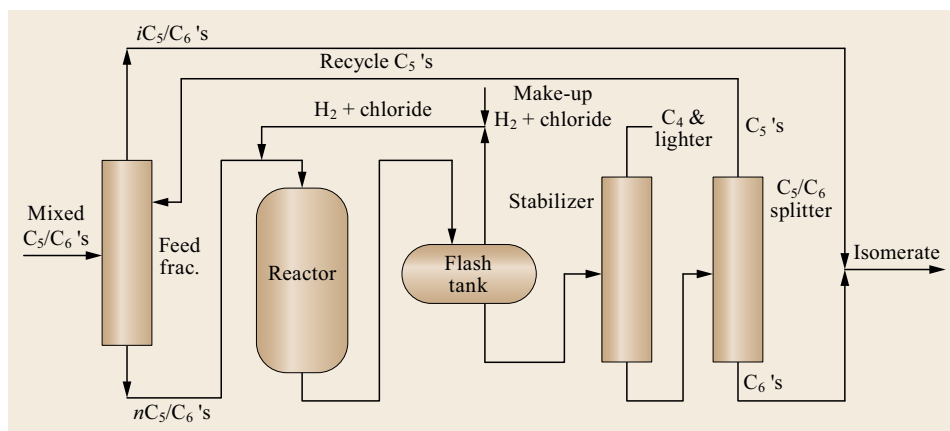


Fig. 17.13 C₅/C₆ isomerization

The C₅/C₆ isomerization process is shown in Fig. 17.13. The mixed C₅/C₆ feed enters a fractionator to separate *n*-C₅/C₆ from *iso*-C₅/C₆, which are the desired isomerization products. The purified *n*-C₅/C₆ is then mixed with hydrogen and hydrogen chloride and heated to 240–500 °C under 300–1000 psi (2070–6900 kPa) pressure before entering the reactor, which is packed with HCl-promoted AlCl₃ catalyst or a Pt-containing catalyst. The residence time is 10–40 min. Again, hydrogen is used to control side reactions (disproportionation and cracking). The product stream goes through a flash tank to recover hydrogen for reuse, then enters a stabilizer to separate C₄ and lighter impurities before entering a C₅ and C₆ splitter. The C₅ components are recycled back to the feed fractionator to recover *i*-C₅ into isomerate.

Another two-stage reactor scheme is shown in Fig. 17.14. The first reactor, using a Pt-catalyst, serves

as a hydrogenation reactor to convert organic chloride into HCl. The second reactor is packed with AlCl₃, which is promoted by HCl to perform isomerization.

Figure 17.15 shows the UOP Penex continuous isomerization unit with a similar design, first commercialized in 1958 [17.26]. Penex uses a dual-function platinum-alumina catalyst with 34 000 bbl per stream day of 85% *n*-pentane feed to produce 16 000 bbl per day of 95% isopentane. The UOP Penex process improves octane ratings from 50–60 to 82–86 or higher. The Penex-Platforming was introduced to convert unreacted *n*-pentane and *n*-hexane from platforming (a reforming process discussed later) into corresponding high-octane isoparaffins [17.25].

In the Shell Hysomer process for pentane-hexane isomerization [17.27], the feed is combined with hydrogen-rich gas, heated to 445–545 °F (230–285 °C) and routed to the Hysomer reactor at

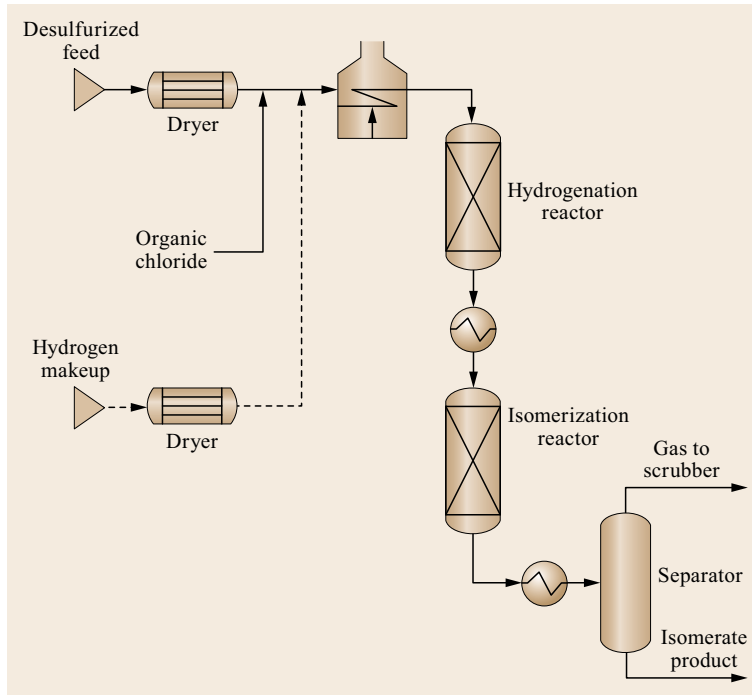


Fig. 17.14 C₅/C₆ isomerization with two reactors and once-through hydrogen

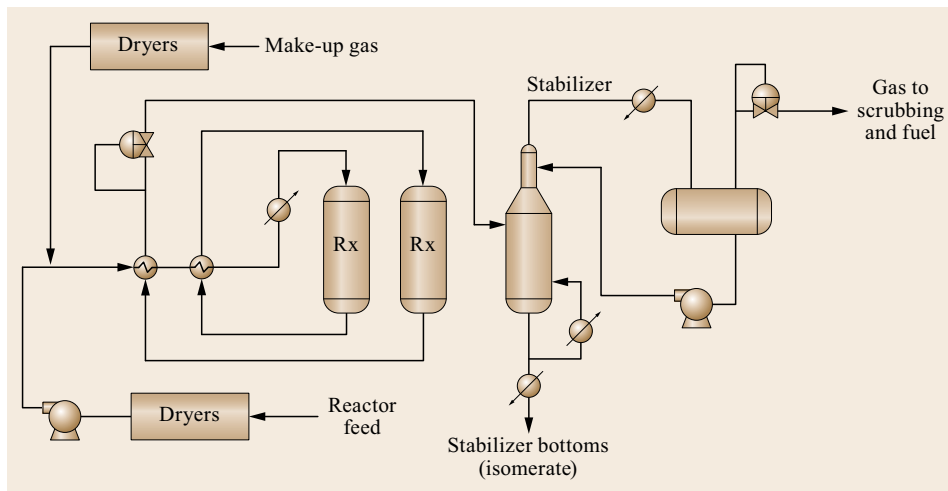


Fig. 17.15 UOP Penex isomerization unit

190–440 psi (1300–3030 kPa). As with fixed-bed hydrotreating and hydrocracking, the process fluids flow down through the catalyst bed, where a part of the *n*-paraffins are converted into branched paraffins. The catalyst is comprised of a noble metal on a zeolite-containing support. The reactions are exothermic and temperature rise is controlled by injecting relatively cold quench gas. The reactor effluent is cooled and sent to a flash drum, which separates hydrogen from the liquid product. The hydrogen is recycled. The liquid is fractionated and the *n*-paraffins are recycled. The net

conversion of *n*-paraffins into branched products can be as high as 97% and the octane can be boosted by 8–10 numbers.

The Iso-Kel process, developed by M.W. Kellogg (now KBR), is specifically for the isomerization of *n*-pentane and *n*-hexane, employing a nonplatinum precious metal catalyst operated at 700–850 °F (370–450 °C) and under 100–750 psi (690–5200 kPa) pressure [17.25]. Often, the heat-exchanger and fractionation systems of isomerization units are integrated with those of other process units, such as catalytic

reformers. In the Union Carbide total isomerization process (TIP) [17.28], C₅/C₆ isomerization was integrated with molecular sieve separation, which provided complete conversion to *n*-paraffins.

The CDTech Isomplus process achieves near-equilibrium conversion of *n*-butenes into isobutylene and *n*-pentenes into isoamylene over a highly selective zeolite catalyst [17.29]. It was developed when methyl *t*-butylether (MTBE) was in high demand for reformulated gasolines. Isobutylene is also an important feedstock for polyisobutylenes.

Olefin isomerization converts straight-chain C₄–C₆ olefins into corresponding *iso*-olefins, which can be used as alkylation feeds with an excess amount of isobutane for producing high-octane gasoline.

17.6.3 Catalytic Reforming

Straight-run gasoline (naphtha) from distillation has a very low octane number, i. e., high tendency to knock. Thermal reforming was initially developed from thermal cracking processes with naphtha as the feed. The feed with an end point of 400 °F (≈ 200 °C) is heated to 950–1100 °F (510–595 °C) under 400–1000 psi (2700–6900 kPa) pressure. The higher octane number is due to the cracking of long-chain paraffins into high-octane (65–80) olefins. Gases, residual oil or tar can be formed. Thermal reforming is less effective and less economical than catalytic reforming (Chap. 18). Catalytic reforming was commercialized during the 1950s to produce reformate with research octane numbers on the order of 90–95 [17.30]. Catalytic reforming now furnishes approximately 30–40% of US gasoline requirements.

Catalytic reforming is conducted in the presence of hydrogen over hydrogenation-dehydrogenation catalysts supported on alumina or silica-alumina. The first reforming catalysts were based on molybdena-alumina or chromia-alumina, but since the commercialization of the platforming process in 1949, noble metal catalysts have been used, either with supported platinum alone or with supported platinum-rhenium, platinum-rhenium-tin, or other trimetallics [17.31, 32]. Hydrogen chloride is a cocatalyst.

The noble metals catalyze reversible dehydrogenation reactions. Bimetallic catalysts bring the following advantages versus platinum-only catalysts:

- Better yield stability
- Lower temperature requirement
- Less hydrocracking at a given temperature
- Higher activity recovering after regeneration
- Longer ultimate life.

Table 17.5 Typical feed and product distributions in reforming

Component	Feed	Product
Paraffins	30–70%	30–50%
Olefins	0–2%	0–25%
Naphthenes	20–60%	0–3%
Aromatics	7–20%	45–60%

Fresh catalyst is chlorided (chlorinated) prior to use. Chlorinating the alumina support provides the acid sites needed for isomerization and cyclization. Acid sites also catalyze unwanted hydrocracking. Excessive chlorination depresses overall catalyst activity. Significantly, chlorination maintains dispersion of the active metals by inhibiting reductive agglomeration.

The operation conditions for modern catalytic reforming are: temperature at 840–965 °F (≈ 450–520 °C), pressure at 100–600 psi (690–4100 kPa). Continuous catalyst regeneration (CCR) reformers operate at the low end of the pressure range 100–150 psig (690–1030 kPa), where production of aromatics is more favored by thermodynamics.

Naphtha containing seven or more carbons is used as a reformer feed. There are four main hydrocarbon types in naphtha:

1. Paraffins
2. Olefins (rarely)
3. Naphthenes
4. Aromatics.

Organic sulfur and olefins must be removed by prior hydrotreating; the sulfur content must be < 1 ppmw. During the process, paraffins are cyclized into naphthenes and naphthenes undergo dehydrogenation to form aromatics. Aromatics left essentially unchanged. The preferred conditions for dehydrogenation are:

- High temperature
- Low pressure
- Low space velocity
- Low H₂/hydrocarbons ratio.

The dehydrogenation reaction in reforming is endothermic. Heat is required. Table 17.5 lists typical feed and product compositions in a reforming process.

Figure 17.16 summarizes the reactions of catalytic reforming, the purpose of which is to transform C₆ to C₁₁ naphthenes and paraffins into aromatic compounds. The aromatics can go to chemical plants or be used as high-octane gasoline blendstocks. For the paraffins in the feed, the acidic sites of the catalyst isomerize *n*-paraffins to isoparaffins. This is a key step for cyclization. It is followed by dehydrogenation to form

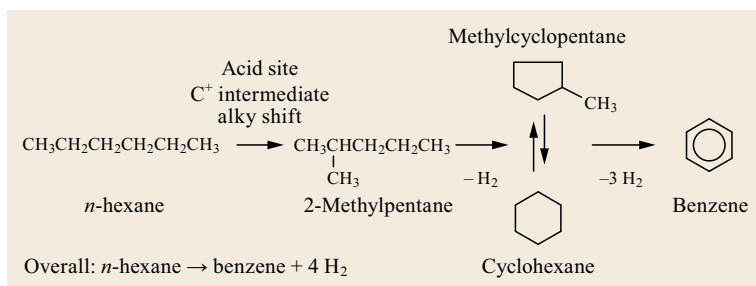


Fig. 17.16 Catalytic reforming reactions

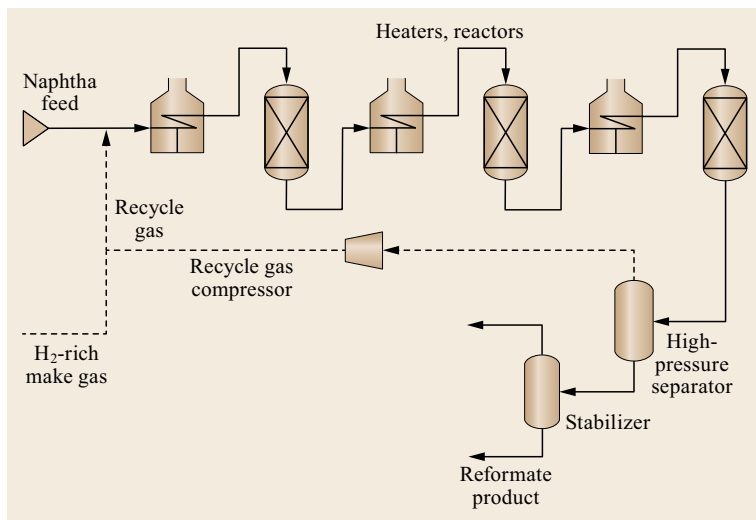


Fig. 17.17 Representative semiregenerative catalytic reforming process flow

aromatic compounds. The process yields considerable amounts of hydrogen; in Fig. 17.10, 4 mol of hydrogen are produced from 1 mol of hexane. The hydrogen is used in hydrotreaters, hydrocrackers, isomerization units and others.

In contrast to hydrocracking, which operates at high pressure, catalytic reforming operates at low pressure and high temperature, which favors production of aromatics by losing hydrogen. The isomerization of alkylcyclopentanes into cyclohexanes is a key step in the production of benzene and alkylbenzenes.

The three major process flows for catalytic reforming are:

1. Semiregenerative
2. Cyclic
3. Continuous catalyst regeneration (CCR).

Semiregenerative and Cyclic Catalytic Reforming

Figure 17.17 shows a process flow scheme for a semiregenerative catalytic reformer. Units can employ either traditional fixed-bed trickle-flow reactors (Fig. 17.18)

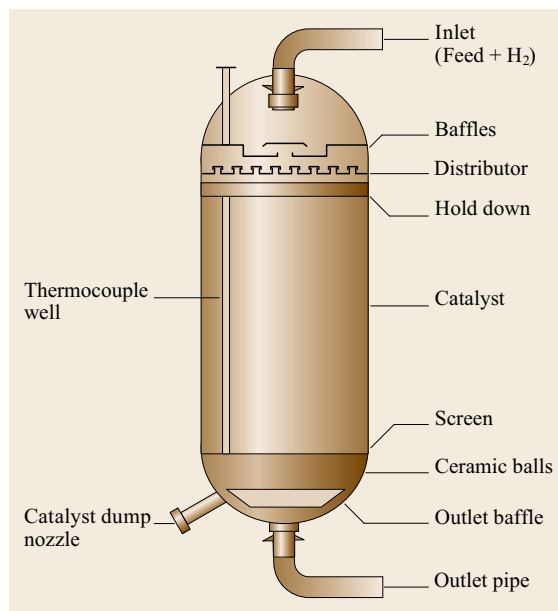


Fig. 17.18 Fixed-bed trickle-flow reactor with one bed. Not to scale

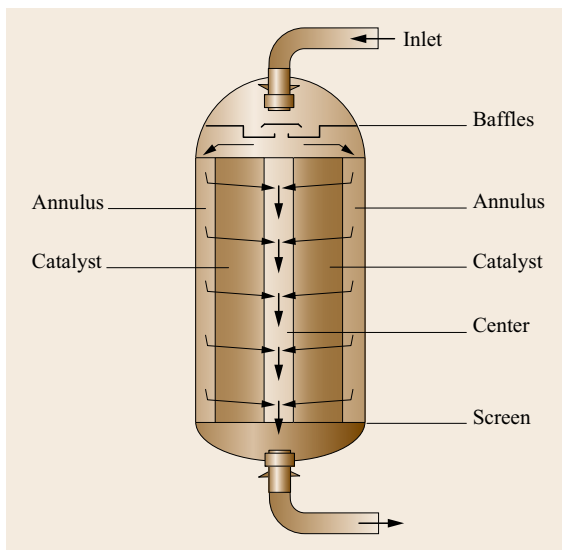


Fig. 17.19 Radial flow reactor. Not to scale. The direction of flow is shown in *black arrows*

or radial-flow reactors (Fig. 17.19). They are comprised of three cylinders. The catalyst is loaded between the two inner cylinders, both of which are slotted. The feed flows downward through the outer annular space, then inward through the catalyst to the center, where reaction products flow downward to the bottom of the reactor. Radial flow reactors are nearly isothermal. Compared to fixed-bed reactors, for a given average reactor temperature the peak temperature is lower. Undesired cracking is faster at higher temperatures, so in theory, radial reactors should make less gas and more liquid product. In practice, however, the difference in yields is low, and due to their complex design radial reactors are more difficult to operate and signifi-

cantly more expensive. They are still being used in older units [17.33], but almost all new catalytic reformers are CCR units, which are described below.

Catalyst cycles last from 6–12 months. A cycle ends when the unit is unable to meet its process objectives – typically octane number and overall C₅-plus yields. At the end of a cycle, the entire unit is brought down and coke is burned off the catalyst. Pentane and hexane are removed from desulfurized naphtha to be used as isomerization feeds, as discussed earlier. The depentanized/dehexanized naphtha is mixed with hydrogen and heated to > 900 °F (> 480 °C) and passed through a series of fixed-bed reactors. The feed is spiked with an organic chloride, which converts to hydrogen chloride in the reactors. This provides the required catalyst acidity and helps minimize catalyst coking. There are three reactors shown. One of them can be shut down in turn for catalyst regeneration, leaving the other two to continue the reforming operations.

The major chemical reactions – dehydrogenation and dehydrocyclization – are endothermic and the reactors are adiabatic. Consequently, the temperature drops as reactants flow through a reactor. Between reactors, fired heaters bring the process fluids back to desired reactor inlet temperatures (RIT). The product stream is cooled down by a heat exchanger and enters a high-pressure gas separator at 38 °C to collect hydrogen. A portion of hydrogen is recycled and other portions are used as hydrogen product. The liquid is then sent to a stabilizer to separate out gas from the final reformate product of octane number of 90–95. Like the distillation tower, both reflux and reboiler are used.

A cyclic reformer has more reactors and catalyst cycles are shorter – 20–40 h. Shutdowns are staggered so that only one reactor is down at a given time.

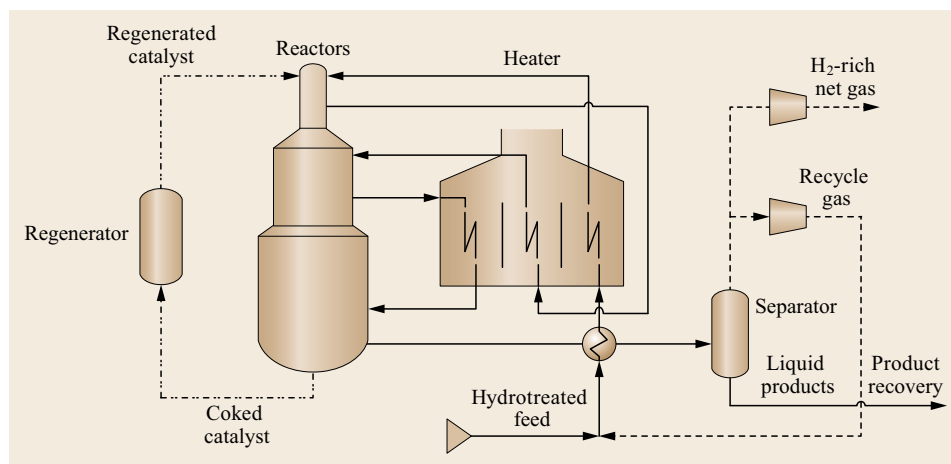


Fig. 17.20 CCR catalytic reforming process flow

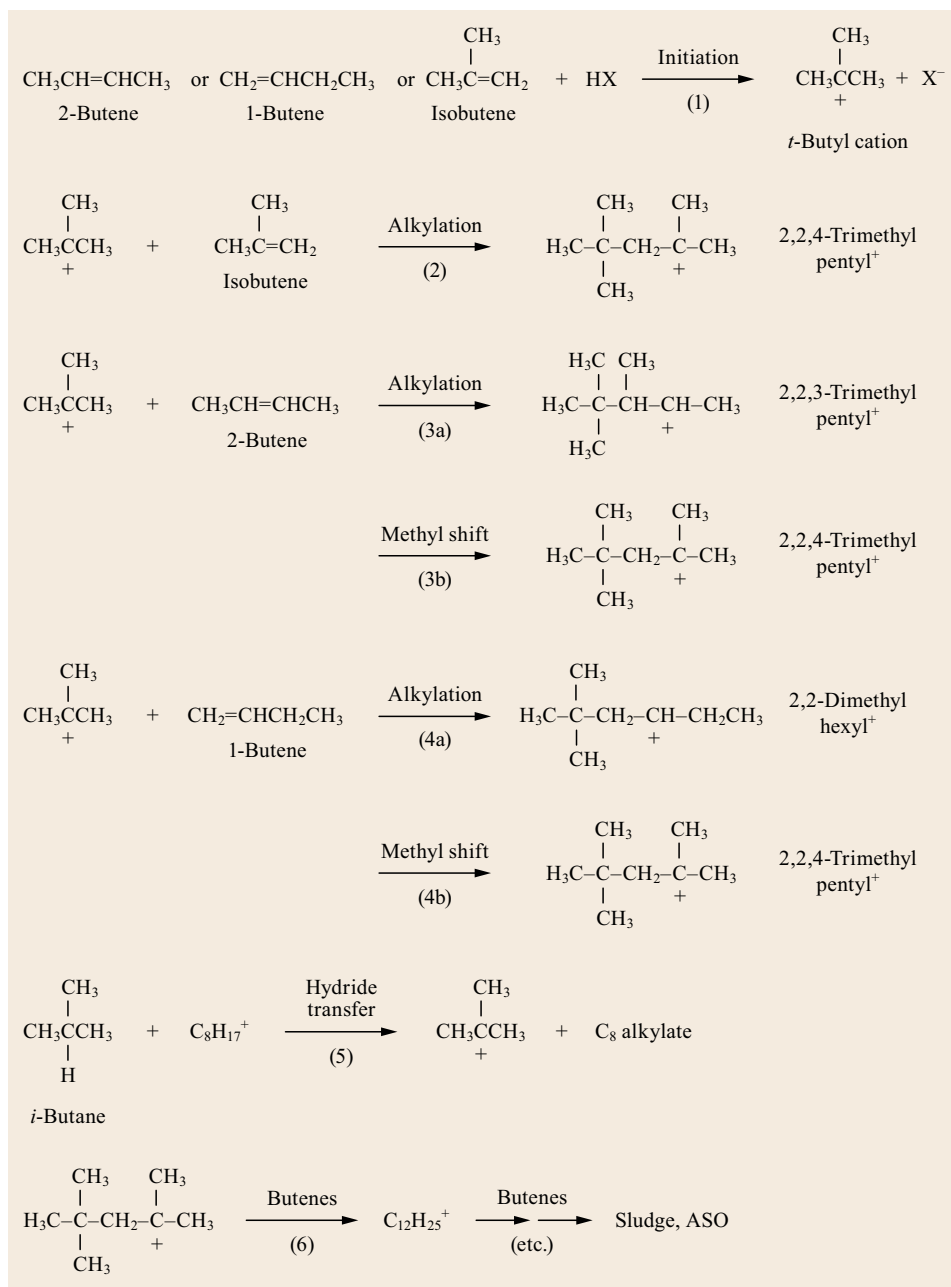


Fig. 17.21 Mechanism for alkylation of butenes in the presence of excess isobutane, where X = HSO₄ for sulfuric acid or F for hydrofluoric acid and ASO is acid-soluble oil

CCR Catalytic Reforming

While semiregenerative platforming employing regenerable platinum catalysts was commercialized by UOP in 1949 [17.29], the CCR platforming process (Fig. 17.20) was commercialized by UOP in 1971 (Chap. 18). CCR catalytic reforming also is licensed by IFP (now Axens). Hydrotreated feed mixes with recycle hydrogen and goes to a series of adiabatic, radial-flow reactors arranged in a vertical stack. Cat-

alyst flows down the stack, while the reaction fluids flow radially through the catalyst beds. Heaters are used between reactors to reheat the reaction fluids to the required temperature. Flue gas from the fired heaters is typically used to generate steam. A CCR can operate at very low pressure (100 psi; 791 kPa). This improves yields of aromatics and hydrogen, but it accelerates catalyst deactivation by increasing the rate of coke formation. However, faster coke forma-

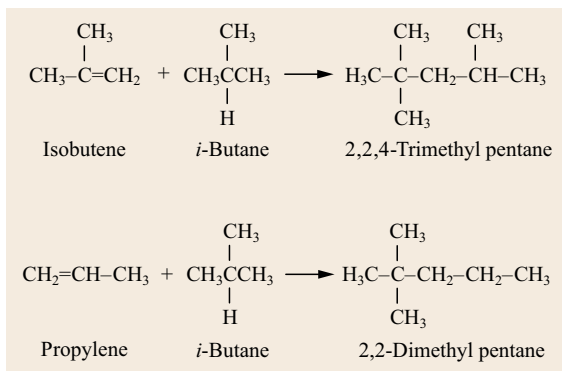


Fig. 17.22 Overall reactions for butylene and propylene alkylation

tion is acceptable in a CCR reformer because the catalyst is continuously being regenerated. The hydrogen recovery is superior to that for semiregenerative platforming and correspondingly product aromatics are higher.

Other catalytic reforming processes based on platinum catalysts include the following:

- Magnaforming, developed by Engelhard and Atlantic Richfield (now a part of BP). Magnaforming employs a manganese-containing catalyst for sulfur removal along with a platinum-containing catalyst for reforming [17.34].
- Powerforming, developed by Esso (now Exxon-Mobil). Powerforming uses a highly selective dual-function catalyst with atomically dispersed platinum to provide high activity for reversible dehydrogenation and chlorine on the alumina base to promote acidity for acid-catalyzed reactions [17.35].

- Ultraforming, developed by Standard Oil Indiana (Amoco, now a part of BP) in 1954. Ultraforming is a cyclic semiregenerative process [17.36].
- Rheniforming, developed by Chevron [17.25]. Rheniforming employs platinum-rhenium bimetallic catalysts where rhenium is combined with platinum to form more stable catalysts operated at low pressures [17.37]. The amounts of metal are very low, about 0.6 wt%, but they are highly dispersed. Acidity is provided by the support and dispersion is maintained by HCl.

Due to the high expense of the metals, such as platinum and rhenium, complete recovery of catalysts is emphasized, including dust and fines.

17.6.4 Alkylation

In alkylation [17.38], isobutane reacts with C_3 to C_5 olefins in the presence of strong acids to produce branched-chain hydrocarbons. The olefins come mainly from cracking units. Propylene and butylenes are gases. Alkylation with isobutane increases their carbon numbers to the gasoline range. The product hydrocarbons, often referred to as alkylate, have high octane values (motor octane number from 88–95 and research octane number from 90–98), with low Reid vapor pressures, no sulfur/aromatics/olefins and limited heavy ends, making them an excellent contributor to the gasoline blending pool.

Figure 17.21 shows the mechanism for the alkylation reaction of butenes with isobutane [17.39]. The process uses an excess of isobutane to control heat and minimize olefin polymerization. In reaction 1, butene is protonated by the acid catalyst, either hydrofluoric acid (HF) or sulfuric acid (H_2SO_4), to form a stable *t*-butyl

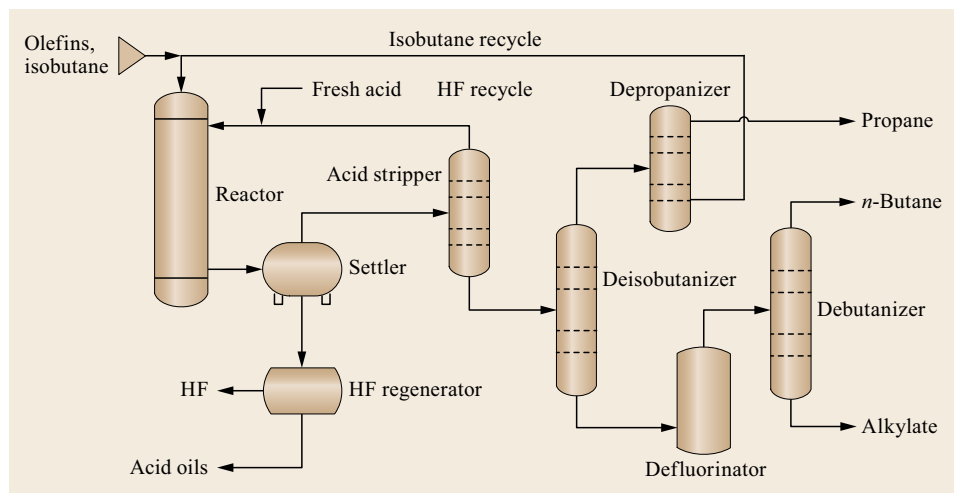


Fig. 17.23 HF alkylation process flow

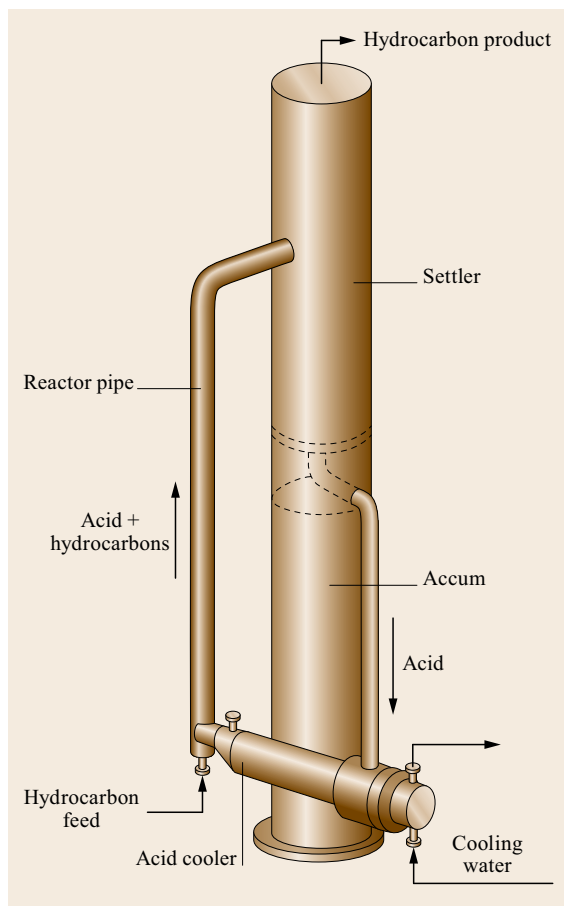


Fig. 17.24 Phillips HF alkylation reactor

cation as an initiation step. The *t*-butyl ion reacts with different butenes in the feed via reactions 2–4. The reaction with isobutylene forms a stable 2,2,4-trimethyl pentyl cation. The reaction with 2-butene forms a 2,2,3-trimethyl pentyl cation, which can undergo isomerization to form a more stable 2,2,4-trimethyl pentyl cation via methyl shift. Similarly, the reaction with 1-butene produces a 2,2-dimethyl hexyl cation, which can isomerize to a 2,2,4-trimethyl pentyl cation as well. The isomerization reaction will not reach completion due to thermodynamic equilibrium of reversible reactions, which is also evidenced by the presence of 2,2,3-trimethyl pentane and 2,2-dimethyl hexane in the final product (alkylate). The various C_8 cations are neutralized by extracting hydrogen (hydride transfer) from isobutane to yield *t*-butyl ion and propagate the alkylation reaction. The excess amount of isobutane is used to prevent polymerization of the olefins in great extent. However, some C_8 cations can proceed to react with olefins to form C_{12} cations, which could continue the polymerization and eventually produce sludge and

acid-soluble oil (ASO). Hence, temperature and space velocity control are important for limiting the extent of the reaction, ensuring maximum production of products in the gasoline range (C_5 to C_{12}).

Figure 17.22 summarizes the overall alkylation reaction. 2,2,4-trimethylpentane has been mistakenly called isooctane as a reference compound for which the gasoline octane rating is defined as 100.

Isobutane feed comes from a hydrocracker, an FCC unit, or a butane isomerization unit, as discussed earlier. Olefins are not present in crude oils, hence, they cannot come from distillation directly. There are many conversion units in the refinery, such as thermal cracking, catalytic cracking, hydrocracking, coking, etc. Except for hydrocracking, all these processes make olefins.

The alkylation reaction is highly exothermic, so the mixed feed of isobutene and cracked gas containing olefins need to be chilled to a low temperature before entering the reactor. The low temperature also decreases polymerization of the olefins. Alkylation is catalyzed by either hydrofluoric acid, as in a hydrofluoric acid alkylation unit (HFAU), or sulfuric acid, as in a sulfuric acid alkylation unit (SAAU). Temperatures for HF-catalyzed reactions are 70–100 °F (21–38 °C). For sulfuric acid they are 35–50 °F (2–10 °C), hence, it needs to be refrigerated.

After the reaction, the acid is recovered and recycled. The product is caustic-washed to remove the residual acid from the product. Then the product stream goes through the depropanizer to separate propane, to the deisobutanizer to recover isobutane for reuse, and to the debutanizer to separate butane from the desired product, alkylate.

Alkylate is an ideal gasoline component. It has high octane numbers in the 90s. It has zero sulfur, so it does not contribute to acid rain; zero benzene, so it does not contribute to air toxics; and zero olefins, so it does not contribute to gum formation. Its low Reid vapor pressure (RVP) reduces hydrocarbon emissions.

Hydrofluoric Acid Alkylation

Figure 17.23 describes a HF alkylation unit [17.40] (HFAU). HF is dangerous and extra precautions are taken to ensure that it is always contained. The feed is mixed with recycled isobutene to give an isobutene/olefin ratio of 15 : 1. The combination is introduced into the reactor at a temperature of 70–100 °F (\approx 20–38 °C). There it reacts in the presence of HF with purity > 88%. The product mixture is sent to a settler and an acid stripper to recover the acid, HF. The bottom of the stripper is sent to the deisobutanizer to recover isobutene. A depropanizer is used to purify the isobutene. The product stream is then enters a defluorinator for caustic wash the residual acid before entering

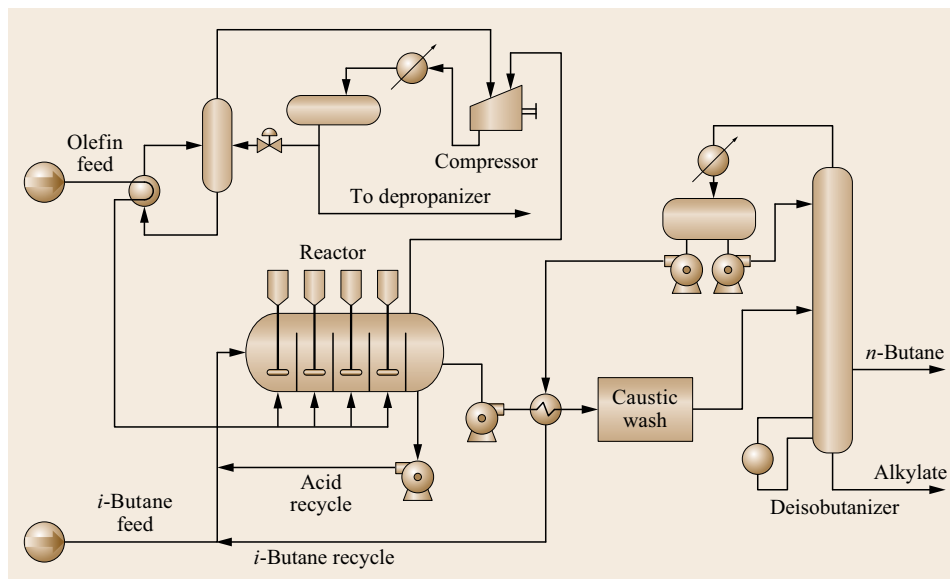


Fig. 17.25 Autorefrigeration sulfuric acid alkylation unit

a debutanizer for separating *n*-butane from the final product, alkylate.

Phillips developed a single-column HF alkylation reactor, shown in Fig. 17.24. The isobutene and olefin feed is mixed with acid in a reactor pipe at 70–80 °F ($\approx 20\text{--}25\text{ }^\circ\text{C}$), which leads to a settler to separate the product from the acid. Acid flows down a side pipe by gravity, without a pump, for returning to the reactor pipe after cooling.

A single tower can be used for fractionation of the product mixture. Propane comes off as an overhead. Isobutane recycles and is withdrawn at several trays above the feed tray. *n*-Butane is taken off as a vapor several trays below the feed tray. Alkylate flows off at the bottom.

Sulfuric Acid Alkylation

Figure 17.25 shows an autorefrigeration sulfuric acid alkylation unit [17.41]. The olefin feed is mixed with isobutane and acid and chilled to 35–45 °F ($\approx 2\text{--}7\text{ }^\circ\text{C}$) for minimizing redox reaction and preventing tar and SO_2 formation. A pressure at 5–15 psi (3–100 kPa) is applied to prevent vaporization. Propane and lighter gases are withdrawn at the top of the reactor. The gases are compressed and liquefied. A portion of this liquid is vaporized in an economizer to cool the olefin feed, as autorefrigeration, before it is sent to the reactor.

The C_4s and alkylate mixture is sent to debutanizer, after caustic wash to remove residual acid, to fractionate into isobutane for recycling with the isobutane feed, *n*-butane and alkylate.

A typical Stratco effluent refrigerated sulfuric acid alkylation unit is shown in Fig. 17.26. Stratco's effluent

refrigerated technology uses acid settler effluent as the refrigerant to provide cooling in the contactor reactor. The Stratco contactor reactor is a horizontal pressure vessel containing an inner circulation tube, a tube bundle to remove the heat of reaction and a mixing impeller. Hydrocarbon feed and recycle acid enter on the suction side of the impeller inside the circulation tube. As the feeds pass across the impeller, a fine emulsion of hydrocarbon and acid is formed by the extremely high shear forces induced by the impeller. Heat transfer from the reaction side of the tube bundle to the refrigeration side is aided by the high circulation rate, which also prevents any significant temperature differential within the contactor reactor. A portion of the circulating emulsion in the contactor reactor flows from the circulation tube, on the discharge side of the impeller, to the acid settler, where the hydrocarbon phase is separated from the circulating acid phase. Hydrocarbon leaves the settlers and is let down across a back-pressure control valve to the tube side of the contactor reactor bundle. The heat of reaction from the shell side is removed by further vaporization of the hydrocarbon effluent as it passes through the tubes.

HF Alkylation Process versus H_2SO_4 Alkylation Process

The HF alkylation process has several advantages over the sulfuric acid alkylation process:

1. Smaller and simpler reactor design
2. Less sensitive to temperature so that cooling water can be used instead of refrigeration
3. Smaller settling device for emulsions

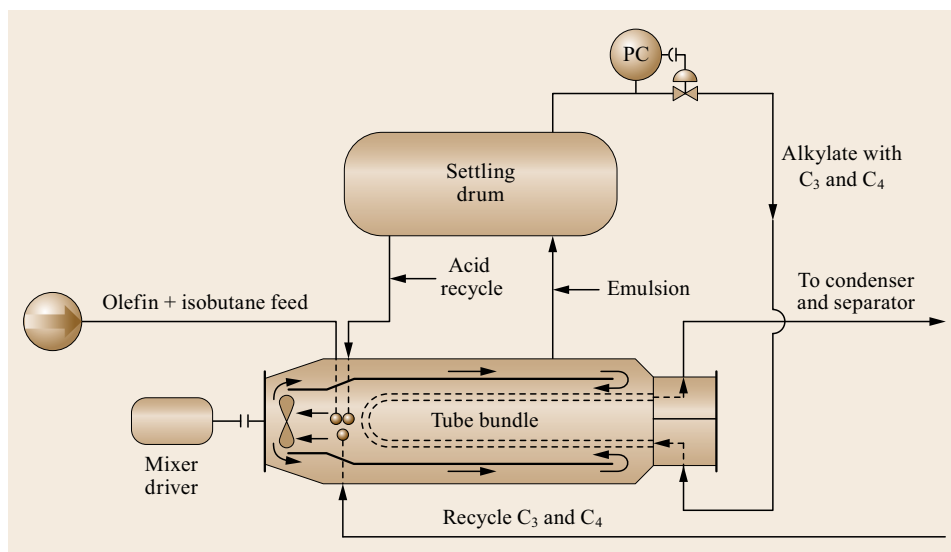


Fig. 17.26
Stratco effluent refrigeration process

4. HF consumption is low due to essentially complete regeneration
5. Disposal of acid is not necessary
6. Flexibility of operations in temperature and isobutane-to-olefin ratio and less need for turbulence or agitation.

On the other hand, the advantages of sulfuric acid alkylation process over HF alkylation process include:

1. Additional equipment, such as HF stripper, HF regeneration tower, etc. is needed for the HF process to recover or neutralize HF in various streams on-site. In the H_2SO_4 process, the entire HC stream is neutralized offsite.
2. Drying is not required for the H_2SO_4 process, while drying down to a few ppm water is needed for the HF process. In the H_2SO_4 process, only feed coalescers are used to remove the free water that drops out of the chilled feed.
3. Additional safety equipment is required for HF process, with greater costs.
4. Capital costs for HF process are higher.
5. Self-alkylation of isobutane occurs in the HF process.
6. H_2SO_4 alkylation works better for butylene.

However, due to their strong acidity in the liquid phase, both HF and H_2SO_4 require relatively expensive corrosion-resistant equipment. Safety in handling and operations is a major concern for both, which also face disposal issues associated with spent acids and acid-soluble oils (ASO). These problems can be diminished with ionic-liquid alkylation and essentially eliminated

by solid acid-catalyzed alkylation. These recently developed breakthrough processes are discussed below.

Ionic-Liquid Alkylation

Due to their lower vapor pressures, ionic liquids are easier to handle. The catalyst can be regenerated on-site, giving it a lower environmental footprint than HF and H_2SO_4 technologies.

The world's first composite ionic liquid alkylation (CILA) commercial unit, with a capacity 120 kt/a, was commissioned at the Deyang Petrochemical Plant in Dongying, Shandong in August, 2013. This followed a successful pilot plant test run and retrofitted into an existing 65,000 t/a sulfuric acid alkylation unit as *ionikylation* at a PetroChina Lanzhou Petrochemical plant starting in 2005. The technology was developed at the China University of Petroleum [17.42, 43]. The chemistry, alkylation of isobutylene, occurs in a strongly Lewis acidic ionic liquid based on aluminum(III) chloride. The retrofit not only increased the yield of the process (compared to sulfuric acid), but increased the process unit's capacity by 40% (to 248 tonnes per day), with attractive economics. This is by far the largest commercial usage of ionic liquids reported to date [17.44].

In the US, Honeywell UOP announced in 2016 the commercialization of ISOALKY, a new alkylation technology developed by Chevron USA [17.45]. Chevron proved the technology in a small demonstration unit at its Salt Lake City refinery, where it operated for five years. Due to the success of the small unit, Chevron committed to converting its hydrofluoric acid (HF) alkylation unit in Salt Lake City to ISOALKY technology. Construction is ex-

pected to commence in 2017, pending permit approvals.

The catalyst for the process is a highly acidic ionic liquid – a nonaqueous liquid salt. The process operates at temperatures below 100 °C. The net reactions are the same as for other alkylation processes: isobutane + C₃–C₅ olefins → alkylate. The ionic liquid catalyst performs as well or better than HF and H₂SO₄, but with lower volatility. Due to the lower vapor pressure, the ionic liquid is easier to handle. HF alkylation units can be cost-effectively converted to ISOALKY technology. Other advantages include the ability to produce alkylate from a wider range of feedstocks using a lower volume of catalyst. The catalyst can be regenerated onsite, giving it a lower environmental footprint than HF and H₂SO₄ technologies.

Zeolite Catalyzed Alkylation

AlkyClean is a solid-acid gasoline alkylation process developed by CB&I, Albemarle catalysts and Neste oil [17.46]. The process employs a robust zeolite catalyst. According to the developers, the total installed cost of an AlkyClean unit is significantly lower than current HF and H₂SO₄ units. No product posttreatment or acid disposal is required. Due to the lack of corrosive acids and the relatively mild operating conditions, carbon steel can be used for construction. The catalyst is much more tolerant to water and other feed impurities, such as oxygenates, sulfur compounds and butadiene. Deactivation from these impurities can be restored via gas-phase regeneration with hydrogen at 250 °C. The product quality from AlkyClean is comparable to that of liquid acid processes, with higher yields. This is because there are no acid-soluble oils produced.

The world's first solid acid catalyst alkylation unit employing Albemarle's AlkyStar catalyst, together with CB&I's novel reactor scheme, was started up at the Shandong, China, plant of Zibo Haiyi Fine Chemical Co., a subsidiary of Shandong Wonfull Petrochemical Group Co., on 18 August 2015. Without the use of liquid acid catalysts, the solid-acid catalyzed AlkyClean technology is not only safer but also more environmental friendly due to the reduction of waste streams, such as spent acids and acid-soluble oils. The alkylates produced consistently have high octane values between 96–98 [17.47].

17.6.5 Polymerization

Olefin gases can be polymerized [17.48] to liquid products that are suitable for gasoline in the carbon number range between 5–12. Polymer gasoline exhibits high octane values due to the branchiness of the hydrocarbon backbone. A typical reaction is shown in Fig. 17.27.

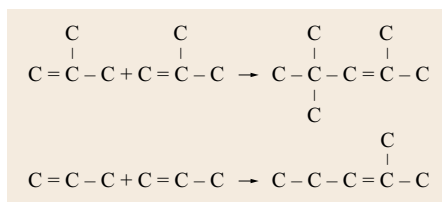


Fig. 17.27 Typical polymerization reactions

The usual feedstock is propylene and butylene from cracking processes. Catalytic polymerization came into use in the 1930s and was one of the first catalytic processes to be used in the petroleum industry.

Figure 17.28 shows a flow diagram of a UOP solid phosphoric acid (SPA) polymerization unit. The SPA catalyst is a combination of Kieselguhr and phosphoric acid [17.49]. The conditions can be varied to produce maximum polymer yield at almost complete conversion of the olefins. In the polymerization of butylenes the conditions can be carefully controlled to yield largely isoocenes, which on hydrogenation will yield isoocenes having an octane rating of 90–96. Pretreatment of feed for removal of sulfur compounds is accomplished by countercurrent contact with caustic solution. Removal of nitrogen compounds is accomplished by contact with a stream of water in a countercurrent packed tower. Water must be present in the feed to maintain the required equilibrium, i. e., to prevent the catalyst from becoming dehydrated.

17.6.6 Fluid Catalytic Cracking (FCC) Process

Fluid catalytic cracking (FCC) [17.50, 51] produces more than half of the world's gasoline (Chap. 19). It generates middle distillate streams (cycle oils) for further refining or blending. It also produces a large quantity of high-quality steam.

A possible mechanism is shown in Fig. 17.29 using *n*-octane as a representative molecule. The reaction is initiated by mild thermal cracking to form heptene with loss of a methyl radical. The acidic aluminosilicate catalyst promotes a proton transfer from a water molecule to heptane, forming a heptyl carbocation. A butyl carbocation is formed upon β -cleavage, which undergoes rearrangement to form more stable *t*-butyl carbocation. Isobutane is formed from hydrogen ion transfer.

A full range of smaller molecules are formed from the breakup of large molecules. Due to deficiency of hydrogen, significant amounts of olefins are formed via proton loss from the carbon adjacent to the carbon carrying the charge in carbocations. Since the feed contains large aromatic and naphthenic molecules with long side chains attached, side chain cleavage is common. The molecules after side-chain detachment have

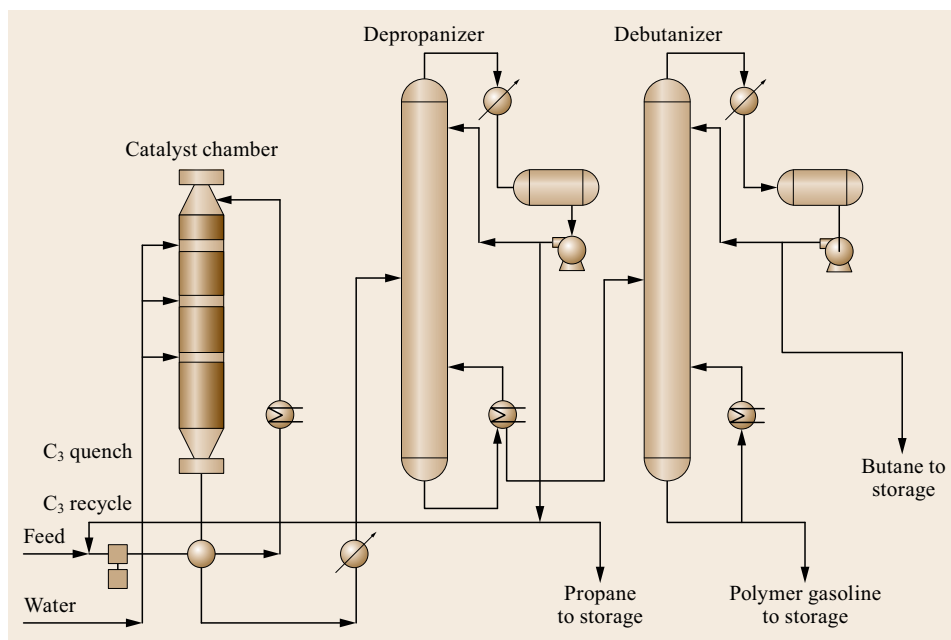
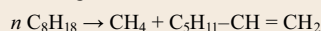
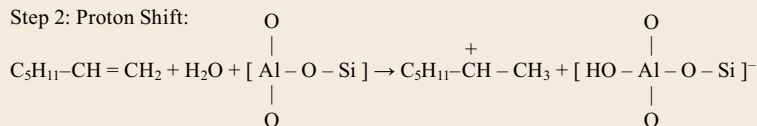


Fig. 17.28 UOP solid phosphoric acid polymerization unit

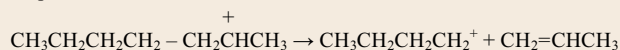
Step 1: Mild thermal cracking initiation reaction:



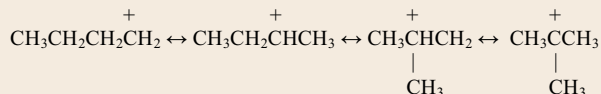
Step 2: Proton Shift:



Step 3: Beta scission:



Step 4: Rearrangement:



Step 5: Hydrogen ion transfer:

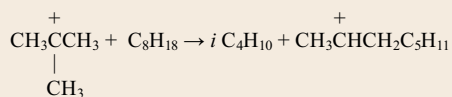


Fig. 17.29 Reaction mechanism for catalytic cracking

higher specific gravity, i.e., lower API gravity, with olefin formation. Coke is also formed due to there not being enough hydrogen to crack large molecules.

Coke is formed via aromatic ring growth by consecutive cyclization, polymerization and dehydrogenation. Hence, the catalyst needs to be regenerated by burning off the coke in order to restore activity. The thermo-

for catalytic cracking process (TCC) process, invented by E. Houdry, is a moving-bed catalytic cracking process [17.52]. The first TCC went on stream in 1937 at the Sun Oil refinery in Marcus Hook, Pennsylvania. The site is now a national historic monument [17.53]. Catalyst pellets were cycled between the reactor and regenerator. TCC is now obsolete, having been replaced

by more advanced fluidized bed units using greatly improved catalysts.

In fluidized catalytic cracking (FCC), finely powdered catalyst is circulated continuously between the reactor and regenerator [17.54]. The catalyst acts as a heat transfer vehicle, moving heat produced by combustion in the regenerator to the oil feed in the riser and reactor. There are two basic types of FCC units: *side-by-side*, where the reactor and the regenerator are adjacent to each other and the stacked type, in which the reactor is mounted on top of the regenerator.

A typical FCC unit (Fig. 17.30) comprises three major sections:

1. Riser-reactor
2. Regenerator
3. Disengaging vessel.

In the riser-reaction section, preheated oil is mixed with hot, regenerated catalyst. Cracking begins immediately. The mixture acts as a fluid because the catalyst particles are about the size of sifted flour. The hot catalyst vaporizes the oil and the vaporized oil carries the catalyst up the riser-reactor. The cracking reaction is very fast. It produces light gases, high-octane gasoline and heavier products called light cycle oil (LCO), heavy cycle oil (HCO), slurry oil and decant oil. It also leaves a layer of coke on the catalyst particles, rendering them inactive.

At the top of the riser, the riser outlet temperature (ROT) can reach 900–1020 °F (482–549 °C). The ROT determines conversion and affects product selectivity, so FCC operators control it as tightly as possible. Higher temperatures favor production of olefin-rich light gases, especially propylene, at the expense of gasoline; many FCC units maximize refinery-grade propylene for purification and use in nearby olefin plants. Moderate temperatures favor gasoline production. Lower temperatures decrease gasoline yields and increase heavier products – light cycle oil (LCO) and heavy cycle oil (HCO).

In the disengaging section, steam helps separate the now-deactivated catalyst from the reaction products. The spent catalyst goes to the regenerator by gravity, where the coke is burned away by fluidized combustion in the presence of air or oxygen-enriched air. The regenerated catalyst is hot, with temperatures up to 1350 °F (732 °C). It returns to the riser-reactor, where the cycle begins again.

In a 60 000 bbl/day unit processing a typical mixture of vacuum gas oils, the total catalyst in the unit (the *inventory*) is 400–500 t. To maintain activity, about 0.5–1 wt% of the inventory is replaced each day. If the feed to the unit contains significant amounts of residue, the replacement rate is higher. The discharged catalyst

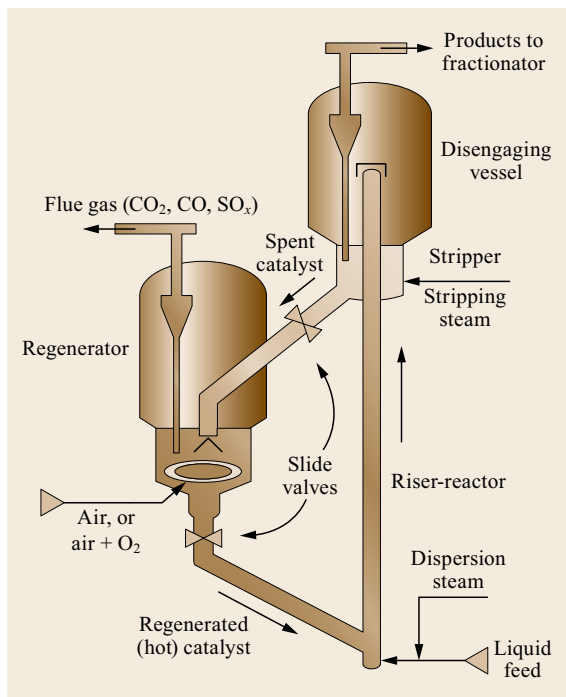


Fig. 17.30 FCC process flow

is cooled and shipped either to a landfill for disposal or to another refiner, which might need a *conditioned* FCC catalyst.

FCC Pretreating and FCC Gasoline Posttreating

Conventional hydrotreating does a good job of removing sulfur from FCC feed. This leads to lower sulfur in FCC products. Once-through mild hydrocracking does a much better job. During the run-up to ULSD, more than 100 hydrocrackers for pretreating FCC feed were commissioned worldwide. Collectively known as hydroprocessing, hydrotreaters and hydrocrackers also remove nitrogen and aromatics, improving FCC operation and greatly increasing gasoline yields [17.55, 56].

Unfortunately, despite feed pretreatment, FCC gasoline can still contain up to 150 ppmw sulfur – far more than the specification of 10–15 ppmw. Additional hydrotreating of the FCC gasoline removes additional sulfur, but if not conducted with care it also reduces octane by saturating C₆–C₁₀ olefins.

In processes such as Prime-G+ [17.57], offered for license by Axens, full-range naphtha is split into light and heavy fractions. The light fraction contains most of the high-octane olefins but not much of the sulfur. After diolefins are removed via selective hydrogenation, the light cut is ready for gasoline blending. The heavy fraction contains most of the sulfur but not much of the olefins. It is then hydrotreated conventionally.

The S-Zorb process [17.58], invented by ConocoPhillips, uses selective adsorption to remove sulfur from FCC gasoline. The feed is combined with a small amount of hydrogen, heated and injected into an expanded fluid-bed reactor, where a proprietary sorbent removes sulfur from the feed. A disengaging zone in the reactor removes suspended sorbent from the vapor, which exits the reactor as a low-sulfur stock suitable for gasoline blending. The sorbent is withdrawn continuously from the reactor and sent to the regenerator section, where the sulfur is removed as SO₂ and sent to a sulfur recovery unit. The clean sorbent is reconditioned and returned to the reactor. The rate of sorbent circulation is controlled to help maintain the desired sulfur concentration in the product.

Residue FCC

Some FCC units process significant amounts of residue. These units use catalyst coolers (e.g., steam coils) in the regenerator or a second regeneration zone to remove excess heat from the unit. This is because residue generates substantially more coke than conventional FCC feeds and excess heat is generated when the extra coke is burned off the catalyst. The trace-metal content of residues can be very high. Trace metals destroy FCC catalysts, so removing them – usually with hydrotreating – is essential (Chap. 21).

Residue FCC (RFCC) units, also known as heavy oil crackers, can process atmospheric residue (650 °F+, 340 °C+) and vacuum residue to produce gasoline and lighter components [17.59]. It generates substantially more coke than conventional FCC feeds. Excess heat

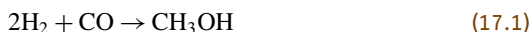
is generated when the extra coke is burned in the regenerator and residues contain high amounts of trace metals, particularly nickel and vanadium. Those metals destroy FCC catalysts. Residue FCC units must handle both challenges. The metals are removed in upstream hydrodemetalation (HDM) units. Catalyst coolers and supplemental regenerators recover the excess heat. The UOP two-stage stacked regenerator with catalyst cooler is an external vertical shell-and-tube heat exchanger [17.60]. Catalyst flows across the tube bundle in the dense phase. UOP's air lance distribution system ensures uniform air distribution within the tube bundle and a uniform heat transfer coefficient. The generation of steam (up to 850 psig; 5800 kPa) from the circulating water is used to remove heat from the regenerated catalyst. Three different styles of catalyst coolers – flowthrough, back-mix and hybrid – have been designed and commercialized to accommodate a wide range of heat removal duties as well as physical and plot-space constraints.

17.6.7 Other Processes

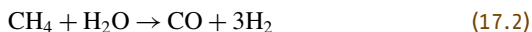
The above processes are specifically designed to increase gasoline yield. Other refining processes produce naphtha with low or high sulfur and/or low octane rating. For example, the light naphtha fraction from a hydrocracker can be blended directly into the gasoline pool, but the heavy naphtha must first go to a catalytic reformer for production of high-octane reformate. High-sulfur coker naphtha must be hydrotreated and maybe reformed before it can be blended.

17.7 Synthetic Gasoline

Gasoline can be synthesized from synthetic gas (syngas), a mixture of carbon monoxide and hydrogen, via conversion into methanol (17.1) followed by a methanol-to-gasoline (MTG) process. The overall process is also known as syngas-to-gasoline (STG+) or syngas-to-gasoline plus (STG+).



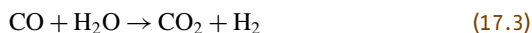
The source of carbon monoxide can be from steam reforming of natural gas to convert to syngas (17.2) or partial oxidation of heavy petroleum fractions, coal and biomass.



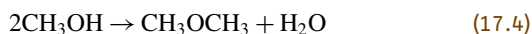
Syngas can also be converted into jet fuel, diesel and heavier linear alkanes through Fischer–Tropsch synthe-

sis. With proper selection of boiling range, these linear alkanes can be isomerized into gasoline or lubricant base oils.

Hydrogen can also be generated from carbon monoxide through water shift reaction (17.3).



Methanol-to-gasoline (MTG) technology was developed at Mobil (now ExxonMobil) in the early 1970s. In the process, methanol is first dehydrated to give dimethyl ether (DME) (17.4)



DME is then further dehydrated over a zeolite catalyst, ZSM-5, to yield a gasoline range of hydrocarbons,

including alkanes (paraffins), aromatics, naphthenes (cycloparaffins) and small amount of alkenes (olefins) of mostly C₆ to C₁₀. Over 80 wt% of the hydrocarbon products are C₅+

In converting methanol to gasoline, ZSM-5 is deactivated over time by a carbon buildup forming coke on the surface. The catalyst can be reactivated by burning off the coke in a stream of hot (500 °C; 930 °F)

air. However, the number of reactivation cycles is limited.

In the MTG+ process, the DME product is further treated by transalkylation and hydrogenation to reduce durene (1,2,4,5-tetramethylbenzene) and isodurene, which have high freezing points, leaving synthetic gasoline with high octane and desirable viscometric properties.

17.8 Reformulated Gasoline (RFG) in the United States

Gasoline blending used to be much simpler. As mentioned, deficiencies in octane could be compensated with TEL, sulfur wasn't regulated and other concepts – photochemical smog, volatile organic compounds (VOC) and air toxics – were ignored or not yet defined. But in the 1970s, smog had become a major problem in Los Angeles, the effects of acid rain had become unacceptable and the toxicity of TEL was verified and the carcinogenicity of benzene was recognized.

Gasoline blending became more complex in 1970, when the US Congress created the Environmental Protection Agency (EPA) [17.61] and passed the first of three amendments to the Clean Air Act of 1963. One of the main provisions required the phase-out of TEL. The amendments, passed in 1970, 1977 and 1990, also empowered the EPA to impose emissions limits on automobiles and to require reformulated gasoline (RFG). The titles of the Clean Air Acts that impact gasoline include the following:

1. Title I – Programs and activities:
 - Part A – Air quality and emissions limits
 - Part B – Ozone protection
 - Part C – Prevention of significant deterioration of air quality
 - Part D – Plan requirements for non-attainment areas.
2. Title II – Emission standards for moving sources:
 - Part A – Motor vehicle emission and fuel standards
 - Part B – Aircraft emission standards
 - Part C – Clean fuel vehicles.
3. Title IV-A – Acid deposition control.

Title II-A deals with RFG. It was implemented in several phases. The Phase I program started in 1995 and mandated RFG for ten large metropolitan areas. Several other cities and four entire states joined the program voluntarily. Phase II, the current phase, started on 1 January 2000.

Tier 1 RFG regulations required a minimum amount (2%) of chemically bound oxygen, imposed upper limits on benzene and Reid vapor pressure (RVP) and ordered a 15% reduction in volatile organic compounds (VOCs) and air toxics. VOCs react with atmospheric NO_x to produce ground-level ozone. Air toxics include 1,3-butadiene, acetaldehyde, benzene and formaldehyde.

The regulations for Tier 2, which took force in January 2000, were based on the EPA complex model, which estimates exhaust emissions for a region based on geography, time of year, mix of vehicle types and – most important to refiners – fuel properties. As of 2006, the limit on sulfur in the gasoline produced by most refineries in the US was 30 wppm. By 2017, the limit of sulfur in gasoline will be 10 wppm.

Initially, the oxygen for RFG could be supplied as ethanol or C₅–C₇ ethers. The ethers have excellent blending octanes and low vapor pressures. Methyl-*t*-butyl ether (MTBE) can be produced at refineries in low cost and was originally used. However, MTBE is extremely soluble in water, it moves farther and more rapidly through both groundwater and surface water than gasoline. Due to leaks from filling station storage tanks, methyl-*t*-butyl ether (MTBE) was detected in ground water samples in New York City, Lake Tahoe and Santa Monica, California. In 1999, the Governor of California issued an executive order requiring the phase-out of MTBE as a gasoline component. That same year, the California Air Resources Board (CARB) adopted California Phase 3 RFG standards, which took effect in stages starting in 2002. The standards include a ban on MTBE and a tighter cap on sulfur content – 15 wppm maximum. In the United States, Tier 3 vehicle emission and fuel standards will lower the allowed sulfur content of gasoline to 10 wppm, beginning in 2017.

Alcohols are alternatives to ethers. Methanol is not as compatible with engine fuel systems as ethanol, which is now required for US RFG. However, ethanol attacks rubber and some kinds of gasket materials. It

also attracts and holds moisture, accelerating corrosion in steel fuel tanks/lines/fittings.

RFGs have lower heating values than conventional gasoline. The BTU content of ethanol is 30% lower. That means lower fuel economy. Ethanol RFG has a considerably shorter shelf life than conventional gasoline (90 days is considered the practical limit) before phase separation occurs. It has been argued that the need for oxygenated fuels is unfounded in automobiles equipped with fuel oxygen sensors. Also, 75–85% of the smog in major cities is from nonautomobile sources and tailpipe emissions of new cars are 95% lower than they were in the 1960s [17.62].

Butanol is generally used as an industrial solvent. It can also be blended with gasoline and used as a transportation fuel as a possible alternative to ethanol. Isobutanol is especially suitable. Butanol is commonly produced using fossil fuels, but it can also be produced from biomass, in which case it is called biobutanol. Biobutanol is produced from the same feedstocks as ethanol—corn, sugar beets and nonfood sources, such as corn stalk, wood, leaves and switch grass.

Butanol has slightly a lower octane rating than ethanol. The RON and MON for butanol are 96 and 78 versus 107 and 89 for ethanol [17.63]. However, it

has a higher energy density – 32 MJ/l – only slightly less than conventional gasoline (also 32 MJ/l) but far higher than ethanol (19.6 MJ/l). Hence, butanol has better fuel economy than ethanol. Due to lower water solubility, it does not damage engines like ethanol. Also, it does not separate from gasoline in the presence of water. Hence, butanol has a longer shelf life. It can be blended at the refinery rather than at blending terminals.

Butanol may be used directly as a fuel because its longer hydrocarbon chain is nonpolar; more similar to gasoline than ethanol. Butanol has been demonstrated to work in vehicles designed for use with gasoline without modification.

Biobutanol has been produced by acetone-butanol-ethanol (ABE) fermentation using a bacterium, *Clostridium acetobutylicum*, from carbohydrates such as starch and glucose, invented 100 years ago [17.64]. However, the process produces too little butanol and too many unwanted products that have to be separated out. A family of new catalysts that convert ethanol to butanol in high yield and at large scale have been developed in the lab with 95% yield demonstrated. It is estimated that it will take another 10–15 years for butanol to replace ethanol economically.

17.9 Gasoline Additives

A formulated (or finished) gasoline contains base fuel and small amounts of additives. Typical additives include metal deactivators, corrosion inhibitors, antioxidants, detergents, demulsifiers, anti-icing additives and oxygenates. Table 17.6 lists the additives used to pre-

pare finished gasoline. Additive packages vary from season to season, region to region and retailer to retailer. After-market additives contain similar types of ingredients and usually are more concentrated. They are packaged to be added by consumers to their own vehicles.

Table 17.6 Additives used in gasoline

Additive type	Function
Oxygenates	Decrease emissions
Antioxidants	Minimize oxidation and gum formation during storage
Detergents	Clean fuel injector and minimize carbon deposit
Metal passivators	Deactivate trace metals that can accelerate oxidation
Corrosion inhibitors	Minimize rust and corrosion throughout the gasoline supply chain
Demulsifiers	Prevent the formation of stable emulsion
Anti-icing additives	Minimize ice in carburetors during cold weather
IVD control (detergent)	Control deposition of carbon on intake valves
CCD control	Control deposition of carbon in combustion chambers

17.10 Blending Optimization

Refinery product blending is a daunting task. It has evolved from a guessing game into a sophisticated model-based, price-driven optimization problem involving information from the entire refinery and beyond.

A major objective of blend optimization is to reduce product quality giveaway. This can be difficult if intermediate cuts are sloppy – if they are contaminated with heavy ends. The best place to limit giveaway is to improve fractionation and/or stripping within the process units.

Essential elements of product blending include:

- The number of finished products
- Storage infrastructure
- Analysis infrastructure
- Blendstock properties
- Product flexibility
- Blending frequency
- Transportation infrastructure
- Postblending considerations
- Product quality waivers
- Product certification method
- Advanced control and real-time database infrastructure.

It has been said that preparing low-octane *regular* blends offers greater blend-optimization opportunities

than preparing high-octane *premium* blends, because only certain components can go into high-octane products. This statement is incorrect. Greater benefits accrue when all grades are considered within the same optimization problem. Even greater benefits accrue when the quality and volume of jet and diesel production are included.

Blend optimization is relatively easy in refineries with ample storage for intermediate streams. Such is not always the case. Problems arise when, due to lack storage residence time, it is difficult to analyze streams before they are on their way to the blending complex. With modern instruments, the analysis problem can be minimized. Near-infrared (NIR), Raman or other spectroscopic techniques can serve as the basis for estimating RON, MON, distillation, benzene, olefins, aromatics and specific gravity. Online sulfur analyzers also are available.

The best place to start is with an organized library of successful recipes. With database software and a good regression program, the library can be quickly searched for the recipe that most closely matches available streams. Back-casting – comparing actual blend properties with ideal properties – can predict how small adjustments can improve profit. It is crucial to ensure that all analyses, including spectra, are correctly associated with individual blendstocks and the final blend.

References

- 17.1 P. Pugh: *Carless, Capel, Leonard plc – The Growth of a Family Firm into an International Oil Company* (Carless, Capel Leonard, Hackney Wick 1986)
- 17.2 J. Nilsson: Why did Henry Ford double his minimum wage?, *The Saturday Evening Post*, (2014)
- 17.3 C. Song, C.S. Hsu, I. Mochida (Eds.): *Chemistry of Diesel Fuels* (Taylor Francis, Philadelphia 2000)
- 17.4 J. Clew: *The Scott Motorcycle: The Yowling Two-Stroke* (Haynes, Newbury Park 2004)
- 17.5 A. Nahum: *The Rotary Aero Engine* (NMSI Trading, London 1999)
- 17.6 Wikipedia: Wankel Engine, https://en.wikipedia.org/wiki/Wankel_engine (2016)
- 17.7 Wikipedia: Otto cycle, https://en.wikipedia.org/wiki/Otto_cycle (2016)
- 17.8 G.D. Hobson (Ed.): *Modern Petroleum Technology Part II*, 5th edn. (Wiley, Chichester 1984) p. 786
- 17.9 M.A. Barrufet: Reservoir fluids petroleum engineering, http://www.pe.tamu.edu/barrufet/public_html/PETE310/APIDATA.XLS (2016)
- 17.10 International Energy Agency: Advanced motor fuels: Fuel formation, http://www.iea-amf.org/content/fuel_information/fuel_info_home (2016)
- 17.11 The Columbia Encyclopedia: Octane number, http://www.encyclopedia.com/topic/octane_number.aspx#1-1E:octanenu-full (2016)
- 17.12 Chevron Phillips LP: Safety data sheet for PRF isooctane + TEL, http://www.cpchem.com/msds/100000014063_SDS_EU_EN.PDF
- 17.13 TransportPolicy.net: Data from EN-228, ASTM D4814 and TransportPolicy.net, http://transportpolicy.net/index.php?title=Main_Page (2016)
- 17.14 J.H. Gary, G.E. Handwerk: *Petroleum Refining Technology and Economics*, 4th edn. (Dekker, New York 2001)
- 17.15 J. Jechura: Refinery feedstocks and products – Properties and specifications, Colorado School of Mines, http://inside.mines.edu/~jjechura/Refining/02_Feedstocks_&_Products.pdf (2016)
- 17.16 US Dept of Energy: Appendix A: Lower and higher heating values of gas, liquid and solid fuels. In: *Biomass energy data book 2011* (2016), http://cta.ornl.gov/bedb/appendix_a/Lower_and_Higher_Heating_Values_of_Gas_Liquid_and_Solid_Fuels.pdf
- 17.17 National Institute of Standards and Technology (NIST): NIST Chemistry WebBook, <http://webbook>.

- nist.gov/chemistry/ (2016)
- 17.18 A. Lengyel, S. Magyar, J. Hancsók: Upgrading of delayed coker light naphtha in a crude oil refinery, *Petroleum Coal* **51**(2), 80–90 (2009)
 - 17.19 H. Virdi, G. Sieli, D. Torchia: Impact of processing heavy coker gas oils in hydrocracking units, *Proc. Natl. Petrochem. Petroleum Refiners Assoc., Natl. Meet.*, Phoenix (2010)
 - 17.20 Energy Policy Research Foundation: A primer on gasoline blending, <http://eprinc.org/2009/06/a-primer-on-gasoline-blending/> (2009)
 - 17.21 US Environmental Protection Agency: Gasoline Reid vapor pressure: Gasoline standards, <https://www.epa.gov/gasoline-standards/gasoline-reid-vapor-pressure> (2016)
 - 17.22 J. Erwin: Vapor pressure and interactions of ethanol with butane and pentane in gasoline, *Proc. 207th Am. Chem. Soc. Natl. Meet.*, San Diego (1994)
 - 17.23 Occupational Safety and Health Administration: *OSHA Technical Manual, Sect. IV, Chap. 2 Petroleum Refining Processes* (US Dept. Labor, Washington), https://www.osha.gov/dts/osta/otm/otm_iv/otm_iv_2.html
 - 17.24 J.G. Speight: *The Chemistry and Technology of Petroleum*, 4th edn. (CRC, Boca Raton 2006)
 - 17.25 H. Connor: Platinum reforming catalysts – Production of high-octane fuels and of aromatic chemicals, *Platinum Metals Rev.* **5**(1), 9–12 (1961)
 - 17.26 L.E. Dean, H.R. Harris, D.H. Belden, V. Haensel: The penex process for pentane isomerization, *Platinum Metal Rev.* **3**(1), 9–11 (1959)
 - 17.27 Shell: *The Petroleum Handbook*, 6th edn. (Elsevier, Amsterdam 1986)
 - 17.28 T.C. Holcombe: *Total isomerization process*, US Patent (Application), Vol. 4210771A, 1980
 - 17.29 T. Zak, A. Behkish, W. Shum, S. Wang, L. Candela, J. Ruszkay: Isomerization of butenes: Lyondell-Basell's isomplus technology developments. In: *Proc. DGMK Conf.* (2009)
 - 17.30 N.J. Emms: Catalytic reforming, *Can. J. Chem. Engr.* **36**(6), 267–270 (1958)
 - 17.31 Honeywell UOP: Gasoline, <https://www.uop.com/processing-solutions/refining/gasoline/#naphtha-reforming> (2016)
 - 17.32 A. Poparad, B. Ellis, B. Glover, S. Metro: Reforming solutions for improved profits in an up-down world, UOP LLC, AM-11-59, 1–32 (2011). <https://www.uop.com/?document=uop-reforming-solutions-for-improved-profits-paper&download=1>
 - 17.33 P.-Y. Le Goff, J. de Bonneville, B. Domergue, M. Pike: Increasing semi-regenerative reformer performance through catalytic solutions, <http://www.axens.net/document/120/increasing-semi-regenerative-reformer-performance/english.html> (2016)
 - 17.34 T.J. Nelson: *Catalytic reforming process with sulfur removal*, US Patent (Application), Vol., Vol. 4225417A, 1980
 - 17.35 ChemPedia: The powerforming process, <http://chempedia.info/info/170935> (2016)
 - 17.36 J. Evans: *Ultraforming – 8 Years Later* (Petroleum, London 1955) pp. 419–424
 - 17.37 T.A. Albahri: Petroleum Refining – Course material, <http://www.albahri.info/Refinery/Ch11%20-%20Finishing.pdf> (2016)
 - 17.38 G. Stefanidakis, J.E. Gwyn: Alkylation. In: *Chemical Processing Handbook*, ed. by J.J. McKetta (CRC, Boca Raton 1993) pp. 80–138
 - 17.39 K. Krantz: *Alkylation Chemistry: Mechanisms, Operating Variables and Olefin Interactions* (STRATCO, Leawood 2003)
 - 17.40 M.B. Simpson, M. Kester: Hydrofluoric acid alkylation, *ABB Rev.* **3**, 23–26 (2007)
 - 17.41 J. Branzaru: Introduction to sulfuric acid alkylation unit process design, Stratco Inc. Leawood, http://www2.dupont.com/Clean_Technologies/en_US/assets/downloads/AlkyUnitDesign2001.pdf (2001)
 - 17.42 Z. Liu, R. Zhang, C. Xu, R. Xia: Ionic liquid alkylation process produces high-quality gasoline. *Oil and Gas J.* **104**(40), 52–56 (2006)
 - 17.43 Z. Liu, X. Meng, R. Zhang, C. Xu, H. Dong, Y. Hu: Reaction performance of isobutane alkylation catalyzed by a composite ionic liquid at a short contact time. *AIChE J.* **60**(6), 2244–2253 (2014)
 - 17.44 PetroChina Lanzhou Greenchem IIs (Center for Greenchemistry and Catalysis), Ionilkylation process: <http://www.ionicliquid.org/en/application/2014-04-24/40.html> (2014)
 - 17.45 Honeywell UOP: Honeywell UOP introduces ionic liquids alkylation technology, https://www.uop.com/?press_release=honeywell-uop-introduces-ionic-liquids (2016)
 - 17.46 CBI: AlkyClean solid acid catalyst alkylation technology, Rep. 02M082014H, <http://www.cbi.com/getattachment/61818074-13d9-4b08-9c5f-1261ccdefad2/AlkyClean-Solid-Acid-Catalyst-Alkylation-Technolo.aspx> (2016)
 - 17.47 Albemarle: Albemarle's alkyStar catalyst successfully employed in the world's first solid acid alkylation unit in Shandong, China, facility, <http://investors.albemarle.com/phoenix.zhtml?c=117031&p=irol-newsArticle&ID=2123306> (2016)
 - 17.48 V.N. Ipatieff, B.B. Corson, G. Egloff: Polymerization, a new source of gasoline, *Ind. Eng. Chem.* **27**(9), 1077–1081 (1935)
 - 17.49 E. Weinert: Polymerization with solid phosphoric acid catalyst, *Proc. 3rd World Petroleum Congr.*, The Hague (1951)
 - 17.50 R. Sadeghbeigi: *Fluid Catalytic Cracking Handbook*, 2nd edn. (Gulf, Houston 2000)
 - 17.51 P. O'Connor: Kinetics and mechanisms of fluid catalytic cracking. In: *Practical Advances in Petroleum Processing*, ed. by C.S. Hsu, P.R. Robinson (Springer, New York 2006) pp. 169–175
 - 17.52 S.C. Eastwood, C.V. Hornberg, A.E. Potas: Pilot plants – Thermoform catalytic cracking unit, *Ind. Eng. Chem.* **39**(12), 1685–1690 (1947)
 - 17.53 American Chemical Society: Houdry process for catalytic cracking, <https://www.acs.org/content/acs/en/education/whatischemistry/landmarks/houdry.html> (1996)
 - 17.54 P.R. Robinson: Petroleum processing overview. In: *Practical Advances in Petroleum Processing*, ed. by C.S. Hsu, P.R. Robinson (Springer, New York 2006)

- pp. 25–28, Chap. 1
- 17.55 M. Bhaskar, G. Valavarasu, K.S. Balaraman: Mild hydrocracking of FCC feeds yields more fuels, boosts margins, *Oil and Gas J.* **100**(23), 62–65 (2002)
- 17.56 A. Dahlberg, U. Mukherjee, C.W. Olsen: Consider using integrated hydroprocessing methods for processing clean fuels: New catalyst systems fine-tune cracking heavy refractory feeds for FCC and hydrocracking units, *Hydrocarb. Process.*, 111–120 (2007), http://www.chevrontechnologymarketing.com/Documents/HP_Sept2007.pdf
- 17.57 Axens Process Licensing: Prime-G+: The benchmark technology for ultra-low sulfur, Axens, Rueil-Malmaison
- 17.58 J.V. Laan: ConocoPhillips S Zorb gasoline sulfur removal technology, <http://www.icheh.com/Files/Posts/Portal1/S-Zorb.pdf> (2016)
- 17.59 P. Palmas: Traces the history of RFCC and provides guidelines for choosing the appropriate regeneration style, *Hydrocarb. Eng.*, <https://www.uop.com/?document=uop-25-years-of-rfcc-innovation-tech-paper&download=1> (2009)
- 17.60 Honeywell UOP: Residue upgrading, <https://www.uop.com/processing-solutions/refining/residue-upgrading/#resid-fcc> (2016)
- 17.61 United States Environmental Protection Agency: EPA history, <https://www3.epa.gov/aboutepa/epa-history> (2016)
- 17.62 M. Centrone: How the Environmental Protection Agency Became a Public Health Risk, National Center for Public Policy Research, National Policy Analysis 304, <http://www.nationalcenter.org/NPA304.html> (2000)
- 17.63 Wikipedia: Butanol fuel, https://en.wikipedia.org/wiki/Butanol_fuel (2016)
- 17.64 M.R. Wilkins, H. Atiye: Fermentation. In: *Food and Industrial Bioproducts and Bioprocessing*, ed. by N.T. Dunford (Wiley, Chichester 2012) p. 195

Catalytic Reforming

Pierre-Yves le Goff, William Kostka, Joseph Ross

Since the early 1940s, dual function catalysts have been converting lower octane, naphtha-range hydrocarbons into aromatics and higher octane blend stock for petrochemical and gasoline production while producing valuable hydrogen as a by-product. Early on, the associated technology became known as *catalytic naphtha reforming* to acknowledge that the desired products resulted from molecular rearrangement, reforming, of the reactants without alteration of their carbon number. Numerous improvements in catalyst and process technology have been commercialized over the past seven plus decades. Catalytic naphtha reformers remain key units in essentially every refinery and petrochemical plant throughout the world.

This chapter provides an overview of catalytic naphtha reforming with sections on the role of catalytic naphtha reforming in the refining and petrochemical industries, naphtha feedstock characteristics, reforming reactions, reforming catalysts, catalyst contaminants, process and catalyst evolution, and catalyst regeneration.

18.1	Objective of Catalytic Reforming	589
18.1.1	Role of Reforming in the Motor Gasoline Pool	590
18.1.2	Reforming for Aromatics Production	591
18.2	Feedstock Characteristics and Treatment	592
18.3	Main Reforming Reactions	594
18.3.1	The Role of the Catalyst	595
18.3.2	Desirable Reactions	595
18.3.3	Undesirable Reactions	597
18.3.4	Reaction Network	599
18.3.5	Parametric Effects	599
18.4	Reforming Catalyst Overview	602
18.4.1	Metallic Function	602
18.4.2	Acid Function	603
18.5	Contaminants and Unit Troubleshooting	604
18.5.1	Impact of the Main Temporary Poisons	604
18.5.2	Permanent Poisons	607
18.6	Reforming Evolution	607
18.6.1	Commercialization of Catalytic Reforming	607
18.6.2	Semiregenerative Catalytic Reforming ..	608
18.6.3	Cyclic Catalytic Reforming	608
18.6.4	Radial Flow Reactor Design	609
18.6.5	Evolution of Reforming Catalyst	610
18.6.6	Continuous Catalyst Regeneration Design	611
18.6.7	From High-Pressure to Low-Pressure CCR	612
18.7	Catalyst Regeneration	613
18.7.1	Combustion Step	613
18.7.2	Oxychlorination Step	614
18.7.3	Drying Step and Reduction Step	615
18.7.4	Chloride Control	615
18.8	Conclusions	615
	References	615

18.1 Objective of Catalytic Reforming

The major objective of catalytic reforming is to transform low-octane naphtha (C_6 – C_{10} hydrocarbons) into high-octane gasoline and by-product hydrogen. The principal means of obtaining the increase in octane is the conversion of paraffins and cycloparaffins (naphthenes) into aromatics (Fig. 18.1). Catalytic reforming accounts for a large share of the world's gasoline production and is the most important source of aromatics

for the petrochemical industry. Reforming is also a major source of refinery hydrogen, the demand for which is growing rapidly as a result of escalating hydrotreatment requirements.

In order to achieve these objectives, specialized multifunctional precious metal catalysts are employed in fixed bed or moving bed reactors. As a result of catalyst aging or deactivation by coke deposition, the

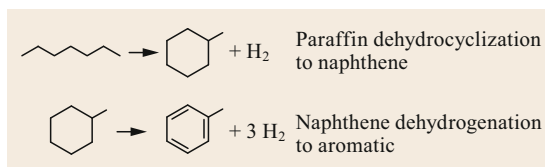


Fig. 18.1 Simplified main reactions in catalytic reforming

catalyst must be periodically or continuously regenerated in a process referred to as semiregenerative, cyclic, or continuous catalyst regeneration (CCR) catalytic reforming.

18.1.1 Role of Reforming in the Motor Gasoline Pool

The petroleum refining industry now processes almost 90 million barrels per day (BPD) of crude oil to supply the transportation motor fuels and other petroleum-based products to meet the world demands. The main transportation fuels are gasoline, jet, and diesel, and each has a set of specifications on physical and chemical properties for their efficient use in engines. Although motor gasoline demand accounts for about 25% of the crude oil processed, it is not found in the required amount or quality in the raw crude oil. The refining industry has, therefore, developed processes to transform and/or convert much of the crude oil into high-quality gasoline meeting engine and regulatory requirements.

There are over 600 petroleum refineries worldwide employing varying process configurations to produce gasoline and other products. Gasoline, like other fuels, is a composite of several blending components from within the refinery forming a product pool meeting both volume and quality requirements. An example of a refinery gasoline pool configuration is shown in Fig. 18.2.

Today there are over 700 catalytic reforming units in operation for fuels and aromatics production.

The catalytic reforming unit plays an important role in upgrading or reforming low octane material that boils in the gasoline range but does not meet finished product specifications. As shown in Fig. 18.2, the reforming unit is typically part of an integrated *naphtha complex* to upgrade not only *straight run* naphtha found in the crude oil, but also cracked naphtha produced by thermal or catalytic conversion of heavier crude components: delayed or fluid coking (Coker), distillate or resid hydrotreating (HDT) or hydrocracking (HC). Various local regulations on quality often require additional processing of gasoline components, such as hydrodesulfurization (HDS) of naphtha from fluid catalytic cracking (FCC), isomerization of light naphtha, and benzene saturation of the reformer product.

The gasoline pool must meet final product specifications, but individual blend components may not. In fact, each processing unit has certain product gasoline characteristics which complement each other to make a pool that meets specification. Table 18.1 shows a worldwide average gasoline composition with typical component property ranges and typical pool specification. Other specifications on fuel boiling range, sulfur content, stability, corrosion characteristics, and much more also apply.

The hydrocarbon liquid product from the reformer (reformate) is a vital gasoline blend component to meet pool octane requirements and is the only process unit with wide flexibility in product octane, typically 90 to 102. Higher severity operation is possible with octane greater than 102, but this is typically reserved for reformers dedicated to aromatics production as discussed later. On the other hand, reformer gasoline or reformate is the leading source of gasoline aromatics and benzene which are both subject to regulatory controls.

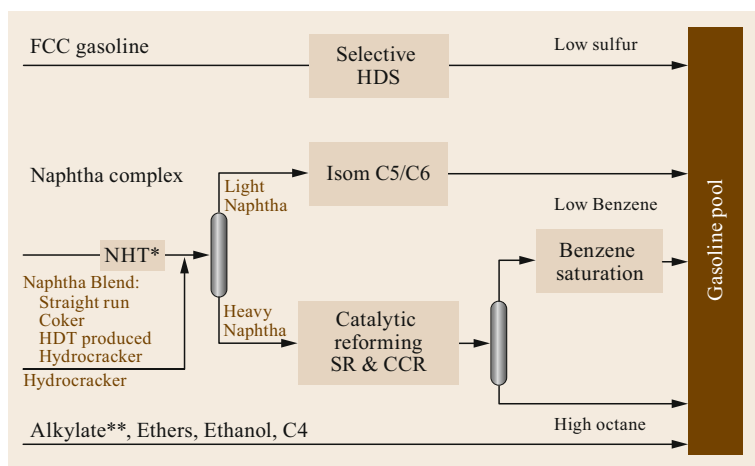


Fig. 18.2 Gasoline pool and naphtha complex, *NHT stands for naphtha hydrotreating unit; **Alkylation of FCC and Coker butenes with iso-butane

Table 18.1 Typical gasoline pool composition and properties

	Average (vol. %)	Octane RON ^a	Olefin (vol. %)	Aromatic (vol. %)	Benzene (vol. %)	RVP (psia)
Butane	5	93	0	0	0	52
Naphtha	16	65–70	0	1–10	1–10	11
Isomerate	5	83–87	0	0	0	13
Alkylate	9	95–98	0	0	0	5
Reformate	27	90–102	0–2	60–70	0.5–5+	3
FCC gasoline	30	90–94	20–40	20–35	0.5–1	5
MTBE ^b	2	118	0	0	0	9
Ethanol	6	132	0	0	0	11
Pool Specs ^c	100	90–100	< 10	< 35	0.6–1	6–9

^a Research octane number ASTM D2699. The United States (US) and Canada use the average of Research and Motor Octane, $(R+M)/2 \approx \text{RON}-5$ at retail locations

^b Banned in the United States

^c Regional variations apply and in the United States the Environmental Protection Agency (EPA) *Complex Model* may supersede specific limits

18.1.2 Reforming for Aromatics Production

The other major application for catalytic reforming is aromatics production for petrochemicals and polymers. The most important aromatics are the so-called BTX components: benzene, toluene, and xylenes. Historically, BTX has been readily available as a by-product mainly from ethylene plants (so-called steam crackers) that thermally convert feedstock into light olefins and by-product pyrolysis gasoline, or PyGas. When the ethylene plant feedstock is naphtha, the aromatics-rich PyGas yield can be on the order of 25–40% thereby supplying valuable aromatics for the petrochemical and polymer industry. In recent years, low-cost ethane from the Middle East and North American Shale-Gas has caused ethylene plants to shift toward ethane cracking which produces very little by-product PyGas. As the worldwide demand for BTX and particularly paraxylene (PX) has rapidly grown, on-purpose production of aromatics has become the norm in large aromatics complexes based on the catalytic reforming of naphtha.

Today, catalytic reforming has established itself as the most important process for the production of

aromatics with more than one-third of all worldwide reformers configured for maximum aromatics production. Figure 18.3 shows the worldwide demand for BTX and the strong dependence on reformate from catalytic reformers to supply BTX, particularly xylenes.

The demand for polyethylene terephthalate (PET) polymer accounts for the largest consumption of xylenes, and in particular PX. With worldwide growth

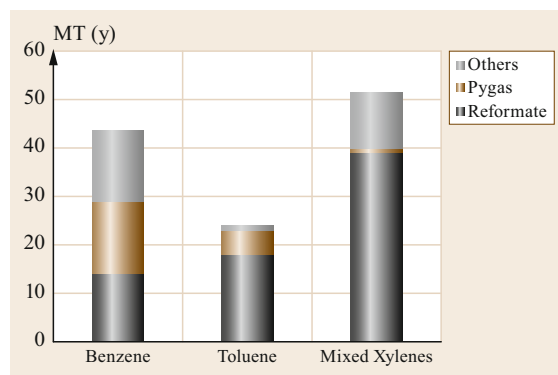


Fig. 18.3 Worldwide supply of BTX aromatics by source

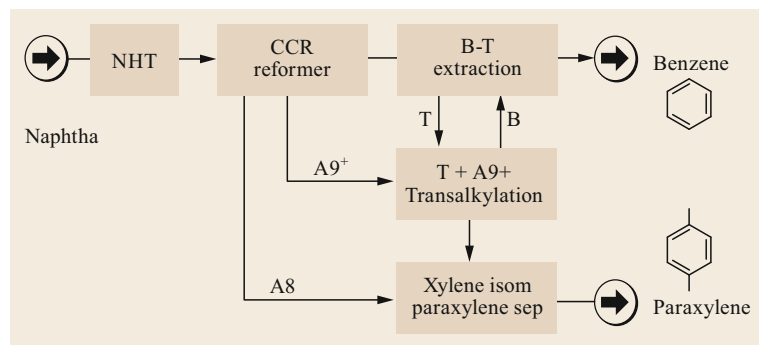


Fig. 18.4 Simplified scheme of an aromatic complex oriented to benzene and PX

of PET projected to be an impressive 6% per year, on-purpose aromatics production is growing rapidly. Highly integrated complexes with high-severity catalytic reformers coupled with aromatics transformation processes are able to produce BTX. When desired, such

complexes can be designed to selectively produce approximately 55–65% of PX from a typical naphtha feedstock.

Figure 18.4 provides a very simplified scheme for an aromatics complex.

18.2 Feedstock Characteristics and Treatment

The reforming unit processes a naphtha cut or petroleum fraction with an initial and final boiling point range from about 80 up to 200 °C, roughly corresponding to C₆–C₁₀ hydrocarbons.

In a straight-run naphtha cut, the main hydrocarbon types are paraffins, naphthenes (cycloparaffins), and aromatics. Naphtha originating from thermal or catalytic cracking (coking, visbreaking, pyrolysis, FCC) also contain olefinic hydrocarbons. An important characteristic of naphtha is the octane number as this relates to combustion performance in an engine, where a higher octane is preferred. Research octane numbers (RONs) for representative components in the C₆–C₈ range are shown in Table 18.2. Linear paraffins have the lowest RON and the aromatics have the highest [18.1, 2]. Paraffin-rich naphtha, therefore, has a low octane and requires reforming to increase the aromatics content and RON to meet motor gasoline requirements, typically over 90 RON.

A convenient measure of the quality of a reformer feed and indication of octane potential is its content of

aromatics (A) plus naphthenes (N) which are readily converted to aromatics in the reforming unit. A useful correlating parameter for feed quality is the combination N+2A in the feed, which represents the sum of the naphthene content and two times the aromatic content. Higher values of this parameter correspond directionally to more easily converted or reformed feeds resulting in higher reformate yield for a given octane.

The main sources of naphtha for catalytic reforming are as follows:

- Straight-run (SR) naphtha
- Naphtha produced in hydroprocessing units (HDT and HC)
- Coker naphtha (naphtha produced in delayed or fluid coking unit)
- VB naphtha (naphtha produced in a vis-breaker unit)
- Selected portions of FCC naphtha (naphtha produced in a FCC unit)
- PyGas from an ethylene plant or steam cracker.

These naphtha streams have widely different elemental and molecular compositions and contaminant levels as shown in Table 18.3. Sulfur, nitrogen, and silicon are harmful contaminants to the precious metal-reforming catalyst and, therefore, must be removed in an upstream naphtha hydrotreating unit (NHT). The limits on S and N are typically 0.5 ppm weight to limit precious metal catalyst inhibition and salt formation leading to corrosion and fouling in the catalytic reforming unit. Olefins are saturated to less than 0.5–1 wt% in order to minimize coke formation in the reforming unit.

Table 18.2 Research octane number, RON, for selected hydrocarbon according to API Research Project 45

Carbon Number	C ₆	C ₇	C ₈
Normal paraffin ^b	25	0	–19 ^a
Iso paraffin (single branch) ^b	74	52	25
Alkyl cyclopentane ^b	91	67–84	31–81
Alkyl cyclohexane ^b	83	75	46–81
Aromatics ^a	99	124	120–146

^a Blending octane

^b Pure octance

Table 18.3 Typical naphtha properties

Naphtha source	SR	Coker	Vis breaker	Hydrocracker	FCC	PyGas
S (ppm weight)	100–1000	> 5000	> 4000	< 1	100–3000	100–300
N (ppm weight)	< 10	50–1000	50–700	< 1	50–200	< 10
Si (ppm weight)	0	5–10	0	0	0	0
Paraffins & naphthenes (%)	80–90	35–55	40–55	95–100	25–55	5–20
Olefins (%)	< 1	30–40	30–40	0	20–40	15–20
Diolfins (%)	0	1–4	1–4	0	0.5–2	10–25
Aromatics (%)	10–20	15–20	15–20	5–10	25–35	55–70

Diolefin wt% \approx diene value/2 \approx maleic anhydride value/8

When comparing cracked naphtha to SR naphtha, the first obvious difference is that the sulfur and nitrogen levels can be much higher, especially in thermal cracked naphtha. The sulfur can be readily removed in the NHT, but the nitrogen compounds are more problematic with cracked stocks containing more basic, cyclic nitrogen compounds such as pyridines and anilines. These nitrogen species require a two-step reaction of ring saturation and opening followed by nitrogen removal as controlled by an overall equilibrium relationship that is favored by higher pressure. The combined effect of these compositional differences has a significant impact on the NHT design and pressure requirements.

Thermally cracked naphtha from vis-breaker or coking units, and FCC naphthas contain a high concentration of olefins, and some diolefins that require very specific NHT catalysts and designs to overcome gum and coke formation due to diolefin polymerization, and handle the high exotherm from diolefins and olefins saturation.

Additional precautions must be taken when processing coker naphtha that contains silicon from antifoaming additives injected in the coking process. Silicon is a poison to both the NHT catalyst and the downstream-reforming catalyst. A silicon guard bed at the inlet of the NHT, and in extreme cases a separate guard reactor, can be mandatory to protect the downstream catalyst. As seen in Figs. 18.5 and 18.6, the presence of these contaminants has a significant impact in NHT unit design.

In a straight-run NHT flow scheme, the feed and hydrogen are heated before entering the reaction section. The reactor effluent is cooled by preheating the feed in the feed-effluent exchanger and then in an air or water cooler before entering a separator drum. The hydrogen-

rich gas leaving the drum is recycled to the reactor, while the liquid phase is sent to the stripper where small amounts of light ends are removed. There is a make up of hydrogen (M/U H₂) to compensate for hydrogen consumption by chemical reaction and dissolution, while in the stripper section methane and ethane (FG – fuel gas) together with H₂S and NH₃ are removed.

When processing coker naphtha, a lead liquid phase diolefin reactor is used to saturate the diolefins present in the feed and avoid fouling, coking, and pressure drop in the downstream main hydrotreating reactor. The gas phase HDT reactor is more complex than the straight-run feed case with multiple catalyst beds to complete olefin saturation, trap silica contaminants, and finally remove sulfur and nitrogen.

In the case of a highly olefinic feed, a quench system can be added between catalyst beds to control the exotherm from olefin saturation.

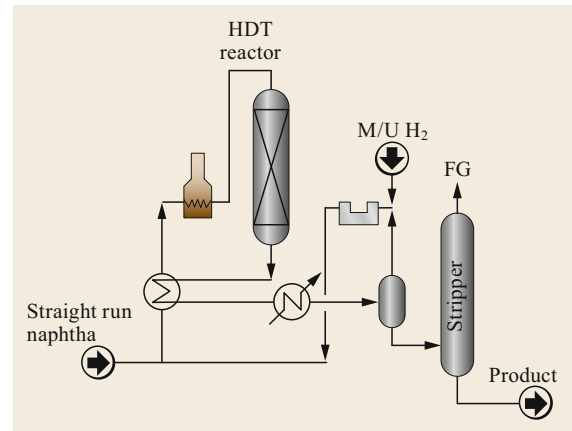


Fig. 18.5 Typical straight run naphtha hydrotreating unit

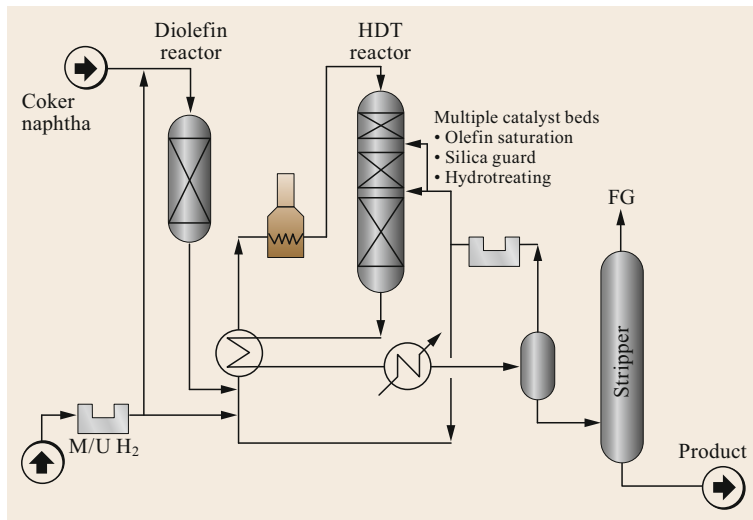


Fig. 18.6 Typical coker naphtha hydrotreating unit

Table 18.4 Impact of naphtha source on naphthene repartition

Ratio naphthenes with C ₆ ring/naphthenes with C ₅ ring (typical values)				
Carbon number	SR naphtha	Coker naphtha	Hydrocracking naphtha	FCC naphtha
6	1.5	0.5	0.3	0.1
7	1.7	0.3	0.5	0.3
8	2.0	0.6	1.5	0.5

After pretreatment in the NHT, the naphtha product should have essentially no sulfur, nitrogen, or olefins. The molecular composition in terms of paraffin, naphthene, and aromatics (PNA) will then determine the potential yield in the reforming unit subject to its design, catalyst type, and operation.

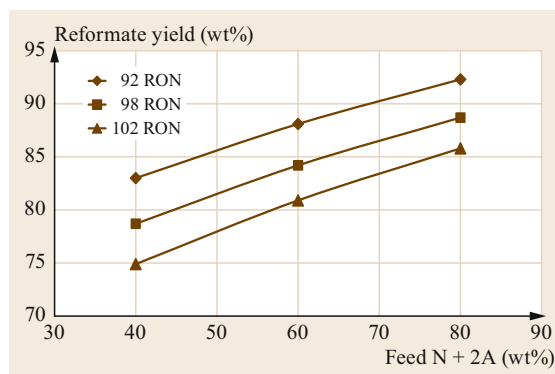
An illustration of the importance of feedstock quality on reformer performance is shown in Fig. 18.7. A feed rich in paraffins (low N+2A content) is more difficult to reform into high-octane aromatics than a low paraffin feed. When processing a paraffin-rich naphtha, the severity of the process (temperature and/or catalyst contact time) must be higher to attain the desired RON octane resulting in a higher yield loss to undesirable light by-products. Reformate RON octane is, therefore, the commonly used measure of overall unit severity. When the feed is rich in naphthene and aromatics (low in paraffins), milder operating conditions can be used to achieve the same RON and with a higher reformate yield.

An important concept is that the product reformate yield decreases as the severity of the unit is increased to produce a higher octane reformate. The economics based on feed quality determines the practical RON that can be obtained as balanced against yield loss and rate of coke formation that will limit unit operation.

18.3 Main Reforming Reactions

There are many possible chemical reactions in the reforming process. For any chemical reaction, thermodynamics dictates the possibility of its occurrence and the amount of products and unconverted reactants. Under certain conditions (pressure and temperature), some reactions are 100% completed, that is, all the reactants are converted into products. Others are in equilibrium, that is, only a part of the reactants are converted. Note that the thermodynamic equilibrium does not mention the time required to reach the equilibrium or the extent of a reaction.

Kinetics dictates the rate of a chemical reaction (i.e., the amount of feed that disappears in, say, 1 s). Kinetics (rate of reaction) is dependent upon operating conditions but can also be widely modified by using

**Fig. 18.7** Impact of N+2A and RON on reformate yield

Although N+2A is a convenient feed parameter and naphthenes are relatively easier to convert to aromatics than paraffin, the type of naphthenes are important in terms of reaction kinetics and potential products. Looking in greater detail into molecular composition, cracked naphthas have a much lower ratio of naphthenes with a six-carbon ring (cyclohexanes) to naphthenes with a five-carbon ring (cyclopentanes) than SR naphthas as shown in Table 18.4. The cyclohexanes are much more easily transformed into aromatics than the cyclopentanes. As a consequence, cracked naphtha is more difficult to reform.

properly selected catalysts. One reaction (or a family of reactions) is generally enhanced by a specific catalyst.

In other words, thermodynamics dictates the ultimate equilibrium composition assuming that the time is infinite. Kinetics enables the prediction of the composition after a finite time. Since time is always limited, when reactions are competing, kinetics is generally predominant.

As for all processes, the chemical reactions involved in reforming are of two types:

- *Desirable reactions*, that is, reactions that lead to an increased aromatics production and octane number as well as a high-purity hydrogen production. These are the reactions to promote.

- *Undesirable reactions*, that is, reactions that lead to a decreased octane number, a decrease in hydrogen purity, or a loss in desired products yield. These are the reactions to minimize.

Moreover, these chemical reactions can also be sorted in two other families:

- *Endothermic reaction*. These reactions require heat energy to proceed and according to Le Chatelier's principle are promoted at high temperature
- *Exothermic reaction*. These reactions give off heat and according to Le Chatelier's principle are thermodynamically hindered at high temperature.

In the case of catalytic reforming, most of the desirable reactions are endothermic while most of the undesirable reactions are exothermic.

18.3.1 The Role of the Catalyst

The role of the catalyst is to improve the rates of desirable reactions while reducing the rates of undesirable reactions, but it does not change the thermodynamics. In reforming dehydrocyclization, cycloparaffin dehydrogenation, and isomerization reactions are desirable as they increase RON, produce aromatics and hydrogen as shown in Fig. 18.1. The undesirable side reactions are mainly hydrogenolysis and hydrocracking which are to be avoided as they produce low-value gases and consume hydrogen [18.3]. Both reaction types are summarized in Fig. 18.8.

Reforming catalysts are composed of active metallic crystallites supported on an alumina (Al–OH) ma-

trix, which is acidic in nature and modified by the addition of chloride to achieve a complex catalyst system of metallic and acid reaction sites. The metallic catalyst particles can include one or more active catalyst components to achieve the desired activity and selectivity.

In the following sections, when a reaction is promoted by:

- The metallic function of the catalyst, (m) is written on the reaction scheme.
- The acidic function of the catalyst, (a) is written on the reaction scheme.

As a reminder, an acid is a compound which can donate a proton to a base. In the reforming system, the acid is an Al–OH group while the base is mostly an olefinic-type compound.

18.3.2 Desirable Reactions

Naphthene Dehydrogenation to Aromatics

Naphthenic compounds such as cyclohexane, methyl cyclohexane, dimethyl cyclohexane up to C₁₀ naphthenes are dehydrogenated, respectively, into benzene, toluene, xylenes, C₉ and C₁₀ aromatics with the production of 3 moles of hydrogen per mole of naphthene. The methyl cyclohexane reaction, for instance, proceeds as shown in Fig. 18.9.

Thermodynamically, the reaction is highly endothermic and is favored by high temperature and low pressure. In addition, higher carbon number cyclohexanes yield higher aromatics production at equilibrium [18.4].

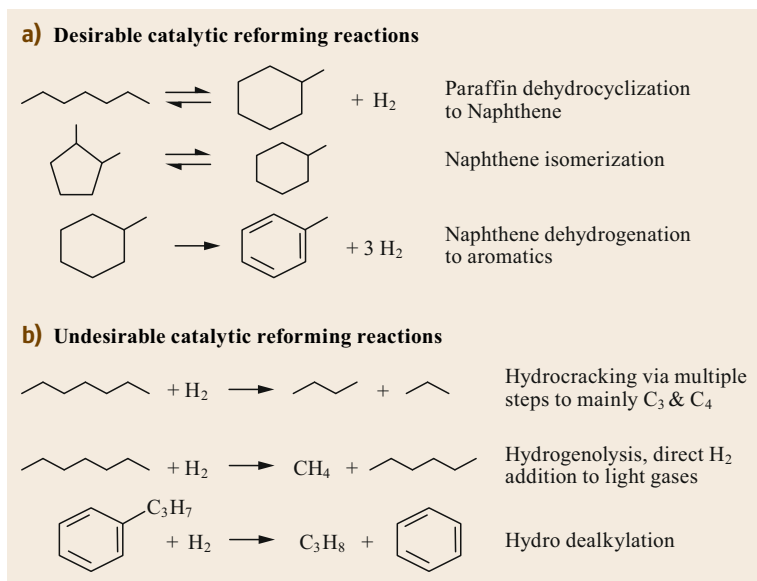


Fig. 18.8a,b Desirable (a) and undesirable (b) catalytic reforming reactions

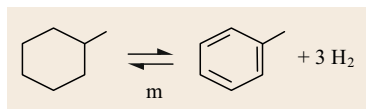


Fig. 18.9
Methylcyclohexane aromatization

From a kinetics view point, the rate of reaction increases with temperature and is not affected by the hydrogen partial pressure. The dehydrogenation reaction rate is high compared to other reforming reactions as discussed in Sect. 18.3.5.

The kinetic and thermodynamic effects are complex with adsorption and desorption of reaction intermediates influencing the reaction rate. The competing effects as influenced by the main parameters governing the dehydrogenation reactions are summarized in Table 18.5.

Under normal reformer operating conditions, the reaction is very fast and almost complete. It is promoted by the metallic function of the catalyst. Since it produces aromatics with a high octane, promoting this reaction is most desirable.

Paraffins Dehydrocyclization

The dehydrocyclization of paraffins is perhaps the most important reaction in reforming, and the most difficult. This is a multiple step process that applies to the normal paraffins (linear) and isoparaffins (branched). It involves a dehydrogenation with a release of one hydrogen mole followed by a molecular rearrangement to

Table 18.5 Impact of operating parameters on naphthene dehydrogenation

Increase of	Effect on dehydrogenation due to	
	Thermodynamics	Kinetics
Pressure	Decreases	Unaffected
Temperature	Increases	Increases
H ₂ /HC ratio ^a	Slightly decreases	Slightly decreases

^a Ratio of pure hydrogen (mol) to hydrocarbon feed (mol)

form a naphthene and the subsequent dehydrogenation of the naphthene. The molecular rearrangement to build a naphthene is the most difficult reaction to promote, however, the subsequent aromatization of the naphthene yields a noticeable octane increase [18.5]. It is important to note that most of the naphthenes initially formed are built on a five-carbon ring nucleus, which are thermodynamically favored.

The reaction can be summarized as shown in Fig. 18.10 [18.5].

The paraffin dehydrocyclization step becomes easier as the molecular weight of the paraffin increases; however, the tendency of paraffins to hydrocrack increases concurrently (discussed later related to Fig. 18.22).

Kinetically, the rate of dehydrocyclization increases with low pressure and high temperature (discussed later related to Figs. 18.20 and 18.21), but at typical operating conditions this rate is much lower than that of naphthene dehydrogenation by a factor of roughly 30:1. The reaction is promoted by both metallic and acidic functions of the catalyst with the formation of the naphthene being the rate-controlling step. Table 18.6 summarizes the impact of operating parameters on the dehydrocyclization reaction.

The positive impact of pressure and temperature on the thermodynamics is, as for the naphthenes, explained by Le Chatelier's principle. Contrary to naphthenes dehydrogenation, the pressure has a negative impact on the reaction rate due to a more complex reaction scheme and formation of specific intermediates.

Table 18.6 Effect of parameters on paraffin dehydrocyclization

Increase of	Effect on dehydrocyclization due to	
	Thermodynamics	Kinetics
Pressure	Decreases	Decreases
Temperature	Increases	Increases
H ₂ /HC ratio	Slightly decreases	Slightly decreases

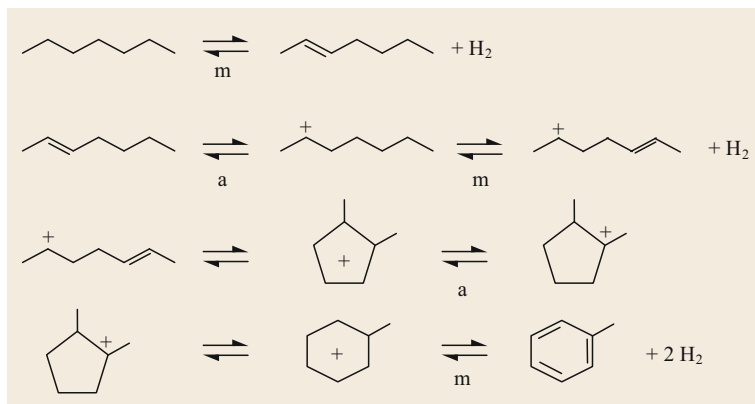


Fig. 18.10 Dehydrocyclization of paraffins

Linear Paraffin Isomerization

The acid-promoted isomerization reaction is important to convert linear paraffins into higher octane-branched paraffins. The reaction can be seen as shown in Fig. 18.11.

If the intermediates are taken into account, the actual scheme changes (Fig. 18.12).

These reactions are fast, slightly exothermic, and the number of carbon atoms does not change. The thermodynamic equilibrium of isoparaffins to normal paraffins depends mainly on the temperature (low temperature favorable) and increases with the carbon number of the paraffin as shown in Table 18.7. The pressure has no effect on the equilibrium.

The paraffins isomerization results in an increase in the octane number. From a kinetic view point (Figs. 18.20 and 18.21), high temperature favors isomerization but hydrogen partial pressure has no effect. These reactions are promoted by the acidic function of the catalyst support.

Naphthenes Isomerization

The isomerization of an alkylcyclopentane into an alkylcyclohexane involves a ring rearrangement and is desirable because of the subsequent dehydrogenation of the alkylcyclohexane into an aromatic. By virtue of the difficulty of the ring rearrangement, the risk of ring opening resulting in paraffin is high.

The reaction is slightly exothermic and is summarized in Fig. 18.13.

Theoretically, at typical reforming operating temperature (about 500 °C), thermodynamics limits the alkylcyclohexane formation. However, the subsequent dehydrogenation of the alkylcyclohexane into an aromatic is very fast and shifts the reaction toward the desired direction. This type of reaction is also easier for higher carbon number molecules.

The octane number increase is significant when considering the end product (aromatics) as shown in Table 18.8.

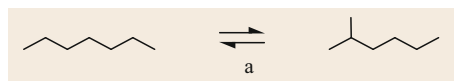


Fig. 18.11 Paraffin isomerization simplified scheme

Table 18.7 Impact on paraffin carbon number on equilibrium

Isoparaffin–normal paraffin equilibrium					
Carbon atom	C ₄	C ₅	C ₆	C ₇	C ₈
% Isoparaffin at 500 °C	44	58	72	80	88

Table 18.8 Octane number increase following aromatization: C₇ example

	RON	MON
Ethyl cyclopentane ^a	75	67
Methyl cyclohexane ^a	104	84
Toluene (blend octane) ^a	124	112

^a Blending octane

18.3.3 Undesirable Reactions

Hydrocracking

Hydrocracking affects either paraffins (normal or iso) or naphthenes. It involves both the acid and metallic functions of the catalyst. It is, to some extent, a parallel reaction to paraffin dehydrocyclization.

As shown in Fig. 18.14, hydrocracking can be represented schematically by a first step of dehydrogenation, which involves the metallic function of the catalyst, followed by a cleavage of the resulting olefin and the hydrogenation of the subsequent short-chain olefin. The second step of the reaction is promoted by the acidic function of the catalyst [18.6, 7].

At the selected operating conditions, hydrocracking reactions would be almost complete according to thermodynamics. Fortunately, however, the cracking reactions are somewhat limited by kinetics. Compared to its desirable concurrent reaction (dehydrocyclization), hydrocracking becomes even more significant as the temperature increases.

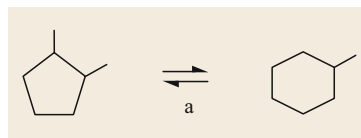


Fig. 18.13 Naphthene isomerization

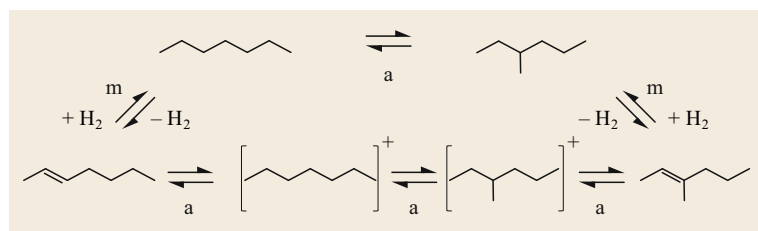


Fig. 18.12 Paraffin isomerization mechanism

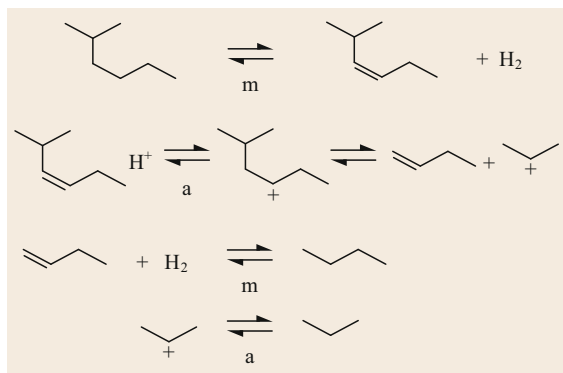


Fig. 18.14 Schematic representation of paraffin cracking

The main effects of hydrocracking are as follows:

- A decrease in paraffins in the reformat, which results in an increase in the aromatics by concentration, that is, an increase in octane and a loss of reformat yield.
- A decrease in hydrogen production.
- An increase in LPG production.

Hydrogenolysis

This undesirable reaction has some similarity with hydrocracking since it involves hydrogen consumption and cleavage of bonds. However, it is promoted solely by the metallic function of the catalyst and, as opposed to hydrocracking, leads to lighter $C_1 + C_2$ hydrocarbons, which are even less valuable than LPG ($C_3 + C_4$) (Fig. 18.15).

Hydrogenolysis also affects the naphthenes, mainly C_5 ring naphthenes. The carbon-carbon bond cleavage results in opening of the ring and formation of paraffinic products. The overall reaction is summarized in Fig. 18.16.

In this latter case, an increase in the hydrogen partial pressure has a positive effect on the reaction kinetics.

Alkylation and Dealkylation of Aromatics

Alkylation is a condensation reaction, which adds an olefin molecule on an aromatic ring (Fig. 18.17). It results in an aromatic with an increased molecular weight.

This reaction, promoted by the catalyst acid function, does not consume hydrogen, but it leads to heavier molecules that may increase the end point of the product. In addition, the high-molecular-weight hydrocarbons also have a high tendency to form coke that deposits on the catalyst and suppresses activity. This reaction must be avoided.

On the other hand, dealkylation, the reverse reaction, occurs mainly for alkyl chains having more than three carbon atoms on an aromatic ring and results

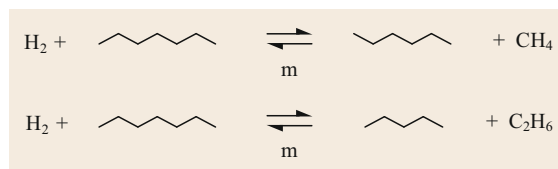


Fig. 18.15 Schematic representation of the hydrogenolysis of paraffin

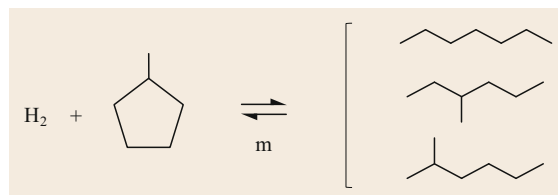


Fig. 18.16 Schematic representation of naphthene cracking

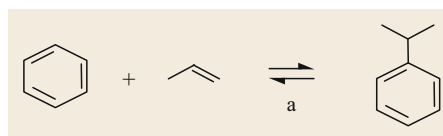


Fig. 18.17 Schematic representation of alkylation and dealkylation

in reduction of liquid and hydrogen yield and increased production of benzene (Fig. 18.17). Operation at higher pressure and temperature favors dealkylation and presents a challenge in meeting low benzene in gasoline regulations.

Coking

Coke formation on the catalyst results from a very complex group of chemical reactions, the detailed mechanism of which is not fully known. The coke has a negative impact on catalyst performance as it remains on the catalyst, covers the active surface area, and hence reduces catalyst activity.

In reforming, two types of coke can be distinguished according to their combustion temperature. The coke located on or nearby the metallic function contains relatively more hydrogen and burns at a low temperature of around 300°C , whereas coke on the alumina support contains relatively less hydrogen and requires a high temperature from 400°C to 500°C to oxidize during regeneration. Moreover, the coke deposited on the alumina is not homogenous, indeed even at high overall coke content on the catalyst, there are areas on the alumina support free of coke [18.8].

The coke is characterized by its hydrogen-to-carbon ratio, on a mole basis the ratio is around 1–1.2 indicating a polyaromatic deposit.

According to nuclear magnetic resonance (NMR) spectroscopy, coke is made from condensed aromatics rings with some methyl groups. A typical representation of a *high-temperature* coke is given in Fig. 18.18, with the stacking of aromatic rings.

Even if there is no detailed coke formation mechanism, coke formation is linked to the presence of heavy unsaturated products such as polynuclear aromatics resulting either from the feed or from the reforming reactions. Traces of heavy olefins or diolefins produced by the reforming reactions will promote coke formation.

The presence of cyclopentanes also promotes coke formation. At the light end of the feed spectrum, large quantities of methylcyclopentane and cyclopentane can promote naphthalene (diaromatic) formation via ring reorganization and condensation. At the other end of the spectrum, heavy molecules with more than nine carbon atoms can intracyclize to make indene type components, which are also coke precursors.

With their high ratio of five-carbon ring naphthenes versus six-carbon ring naphthenes, coker and FCC naphthas make more coke compared to straight-run naphthas. Straight-run naphtha and hydrocracked naphtha also contain five-carbon ring naphthenes, but their overall better reformability reduces operating tem-

perature requirement and results in less coke formation.

As mentioned earlier, coke is linked to the formation of heavily dehydrogenated compounds, therefore low hydrogen partial pressure and high temperature favor coke formation when all other parameters remain constant.

Other factors leading to coke formation include poor gas distribution that leads to stagnant zones in a reactor, and increased acidity from excessive moisture and chloride on the catalyst.

18.3.4 Reaction Network

As described above, many reactions take place in the reforming process. The resulting complex reaction network involves both metallic and acidic reaction sites. Hence, a reforming catalyst must be bifunctional.

Figure 18.19 summarizes the general reaction scheme in terms of acid-catalyzed and metal-catalyzed reactions. Reactions taking place in the horizontal direction are metal catalyzed and those taking place in the vertical direction are acid catalyzed.

18.3.5 Parametric Effects

The effects of the main operating conditions on the rate of the reactions involved in the reforming process are summarized below.

Effect of Hydrogen Partial Pressure

Figure 18.20 shows the relative rate of the various reactions as a function of hydrogen partial pressure on a logarithmic scale. The dehydrogenation rate of a naphthene to aromatic is used as reference and taken at 100 ($\log 100 = 2$). Other reaction rates are measured against this reference.

At lower hydrogen partial pressure (10 bar), the dehydrogenation of naphthene is about 10 times faster than isomerization, 30 times faster than the desired dehydrocyclization reaction of paraffins, and 50–60 times faster than the undesirable cracking reactions (hydrocracking and hydrogenolysis) (Table 18.9) [18.3]. Note that the main cause of increased cracking as the hydrogen partial pressure increases is linked to C₅ naphthene ring opening.

Figure 18.20 shows that there is an incentive to operate at low pressure where the cracking rate is relatively low and the slower dehydrocyclization of paraffin rate increases. Thermodynamics also favors low pressure for dehydrogenation and dehydrocyclization. The only drawback of low pressure is the higher coking rate, which is the reason why low-pressure reformers are equipped with a CCR system.

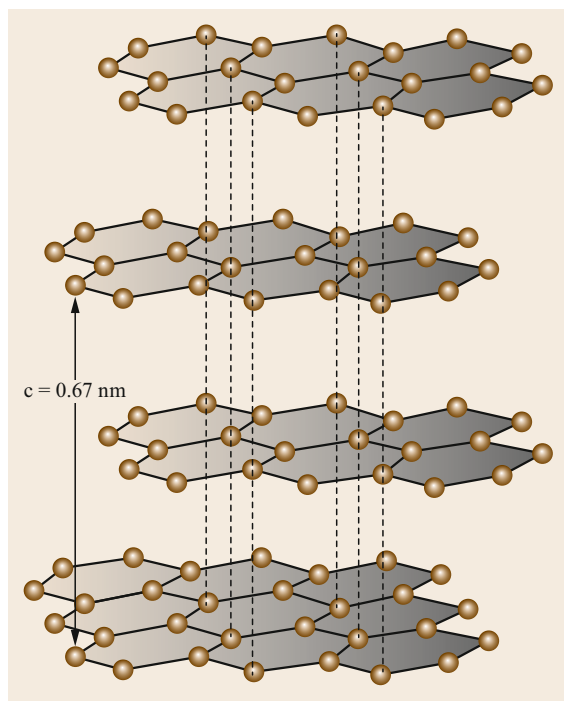


Fig. 18.18 Schematic representation of the high-temperature coke

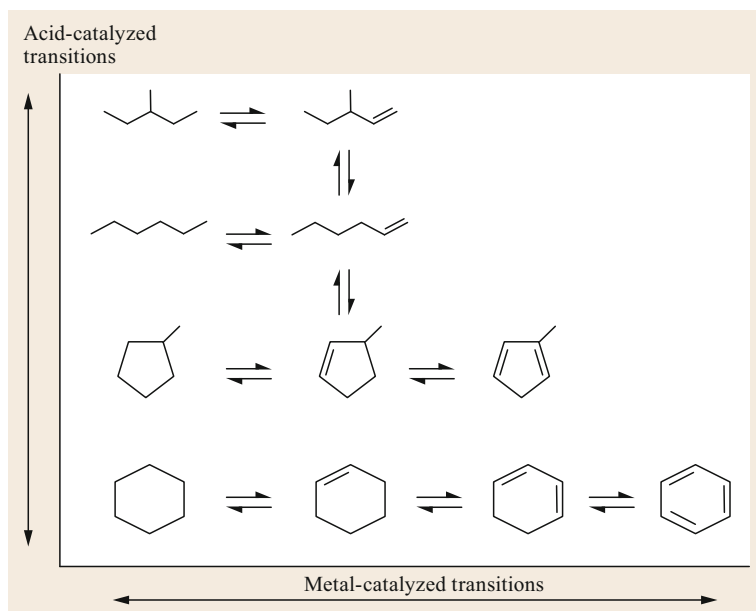


Fig. 18.19 Global reforming reaction scheme

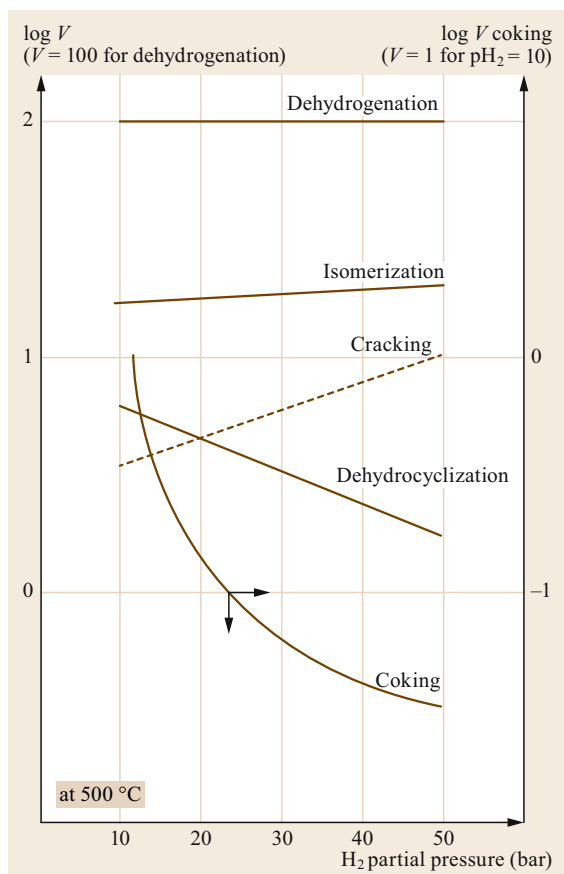


Fig. 18.20 Relative rate of reaction (V) versus hydrogen partial pressure

Table 18.9 Heat of reaction – relative rate of reaction (after [18.3, Chap. 4])

Reactions	Heat of reaction ^a (kcal/mol)	Relative rate ^b approx.
Naphthenes dehydrogenation	-50	30
Paraffin dehydrocyclization	-60	1 (base)
Isomerization: paraffins	+2	3
Naphthenes	+4	
Cracking	+10	0.5

^a If the heat of reaction is negative, the reaction is endothermic
^b For pressure below 12 bar

Effect of Temperature

Temperature influences the rate of the various reactions as shown in Fig. 18.21. The activation energy can be calculated from the slope of the curves. Dehydrogenation and isomerization have moderate activation energy (≈ 20 kcal/mol) and consequently temperature only slightly increases the rate of these reactions. Dehydrocyclization has a higher activation energy (≈ 35 kcal/mol) and consequently temperature has a greater impact on the rate of this reaction [18.9].

Cracking and coking have higher activation energies (≈ 45 and 35 kcal/mol, respectively). The rate of these undesirable reactions is more significantly increased by increasing temperature.

Considering the activation energy, highly active new or freshly regenerated catalyst and low severity permit lower temperature operation, which favors the desirable reactions over the side reactions. As the cat-

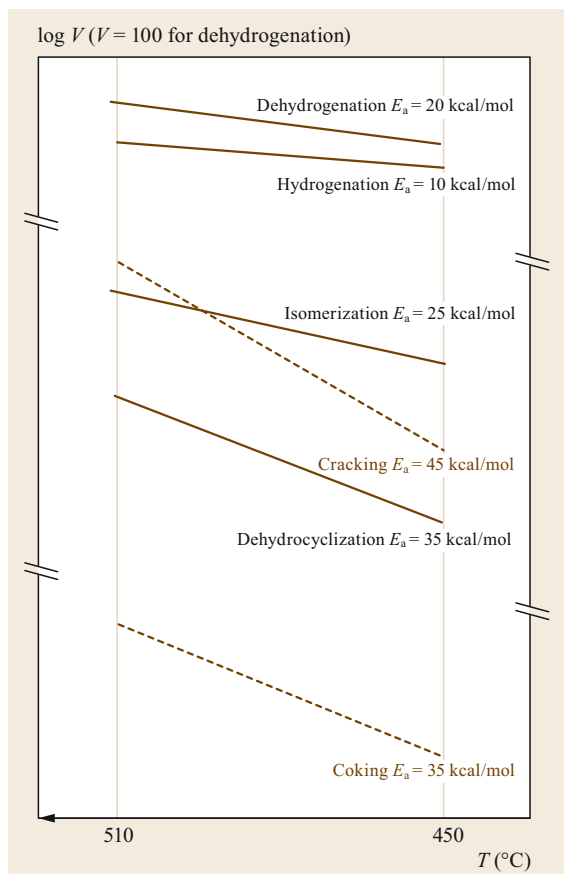


Fig. 18.21 Relative rate (V) of reaction versus temperature. E_a is the activation energy for the respective reaction

alyst deactivates or severity increases, higher operating temperature is required, which favors the undesirable reactions and yield selectivity to desired products declines.

Effect of Carbon Number

The kinetic study of the chemical reactions becomes even more complicated owing to the presence of molecules with different numbers of carbon atoms.

As is the case for thermodynamic equilibrium, the rates of the reactions are affected by the length of the carbon chain of the reactant. Figure 18.22 presents the rates of dehydrocyclization and cracking of C_6 to C_{10} paraffins relative to that of n -heptane.

Figure 18.22 shows that the cracking reaction rate (the curve represents the sum of hydrocracking and hydrogenolysis) increases regularly with the number of carbon atoms, whereas the dehydrocyclization rate exhibits a sudden sharp increase between hexane and heptane as well as between heptane and octane, while

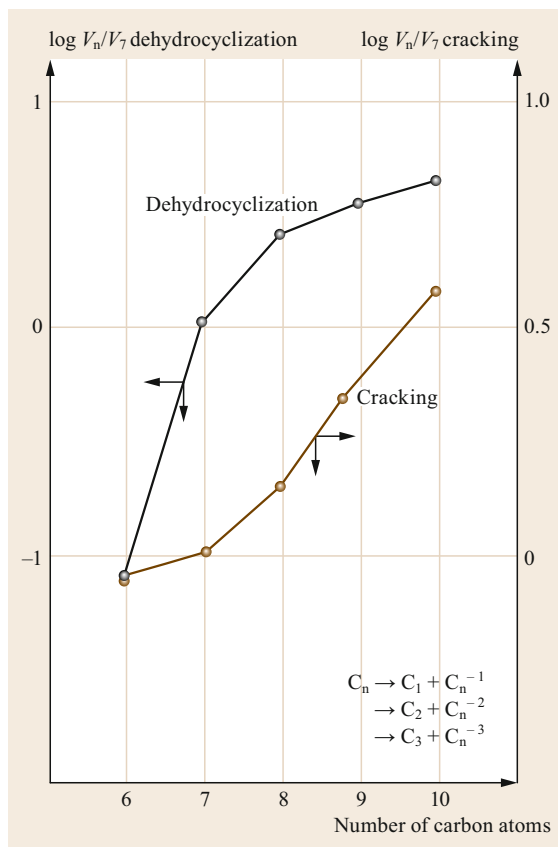


Fig. 18.22 Relative rate of reaction (V) versus carbon number. V_n/V_7 is the relative rate of dehydrocyclization of $C_nH_{2n} + 2VSC_7H_{16}$ cracking

the variation between the higher homologs remains relatively slight.

As a result, the dehydrocyclization of C_6 paraffins to benzene is more difficult than that of C_7 paraffin to toluene, which itself is more difficult than that of C_8 paraffin to xylenes. Accordingly, the most suitable reactive fraction to feed a reforming process is the C_7 – C_{10} fraction. Conversion of the C_6 paraffin to aromatics is one of the most difficult reactions in reforming.

Impact on Catalyst Distribution in Reactors

Thermodynamics and kinetics have shown that there is an optimum operating temperature range of approximately 480–535 °C in order to simultaneously favor the rate of the desirable reactions and limit the undesirable ones to an acceptable level.

Due to the highly endothermic nature of the most important and desirable reactions (naphthene dehydrogenation and paraffin dehydrocyclization), this optimum temperature cannot be sustained throughout

Table 18.10 Reactions distribution as a function of the reactor number

First reactor	Second reactor	Third and fourth reactors
Dehydrogenation	Dehydrogenation	Cracking
Isomerization	Isomerization	Dehydrocyclization
	Cracking	
	Dehydrocyclization	

the whole catalyst volume in an adiabatic system (Fig. 18.23). Upon entering the reactor and contacting the catalyst, the fast dehydrogenation reaction results in a rapid drop in process temperature. In order to restore the catalyst activity when the temperature has dropped below a critical level, the partially converted reactor feed must be reheated. To achieve this, the catalyst is distributed into several reactors (3 or 4 as shown in Fig. 18.23) and intermediate heaters are provided. The resulting conversion profile for the feed into products is also shown as a function of percentage of total catalyst contacted.

So, in a somewhat simplified but practical way, and for operational guidance, the main reactions that take place in the various reactors are represented in Table 18.10.

From the above analysis, it can be concluded:

- Dehydrogenation reactions are very fast, about one order of magnitude faster than the other reactions and produce high endotherm.
- Low pressure favors all desirable reactions and reduces cracking. To compensate for the detrimental effect of low pressure on coking, a low-pressure reformer requires CCR.
- An increase in temperature favors the kinetics of dehydrogenation, isomerization, and dehydrocyclization, but accelerates the degradation reactions (cracking, coking) even more. Consequently an increase in temperature leads to higher octane reformate product but is also associated with a decrease in reformate yield.
- The reaction rates of important reactions such as paraffins dehydrocyclization increase noticeably with the number of carbon atoms. Cyclization is faster for C_8 paraffin than for C_7 , and for C_7 than for C_6 . Consequently the C_7 – C_{10} fraction is the most reactive feed and C_6 paraffin is the last to be dehydrocyclized to aromatics in the last reactor.

18.4 Reforming Catalyst Overview

18.4.1 Metallic Function

As mentioned previously, reforming reactions require the presence of a metal function dehydrogenation cata-

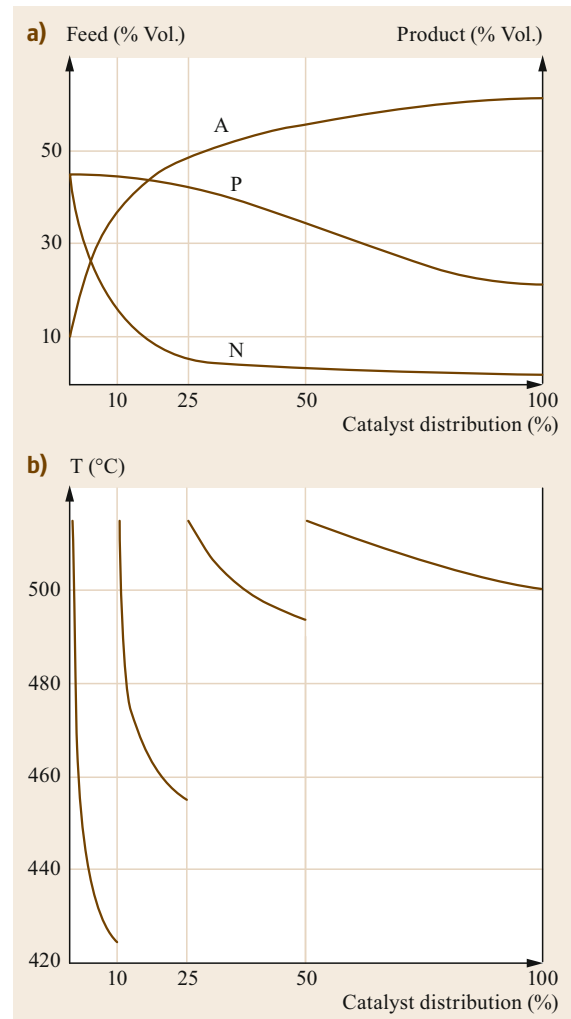



Fig. 18.23a,b Endotherm, catalyst distribution, and hydrocarbon conversion. *P*: Paraffin concentration profile, *N*: naphthene concentration profile, *A*: aromatic concentration profile

lyst and an acid function catalyst for dehydrocyclization and isomerization. Table 18.11 shows the relative dehydrogenation activity of several active metals. The most effective dehydrogenation catalyst is platinum and de-

Table 18.11 Relative catalyst naphthene dehydroisomerization activity (after [18.10])

Metal	Dehydrocyclization activity ratio	
Pt	1	
Ir	0.7	
Re	0.3	
Pd	0.15	

spite its high price, it is the metal of choice for the reforming application.

In order to efficiently utilize the precious metal, platinum is present as very small aggregates with a size close to or even below 1 nm as illustrated by the molecular model shown in Fig. 18.24 obtained by quantum calculations [18.11, 12].

18.4.2 Acid Function

The origin of the catalyst acidity comes from the carrier itself. The carrier is a high-purity γ -alumina doped with chlorine. At reforming conditions, the surface of the alumina is partially hydroxylated and partially chlorinated. These hydroxyl groups act as the acid sites. The strength of their Brønsted acidity is inversely related to their O–H bond strength: a stronger bond makes a weaker acid. By itself, this hydroxyl group does not exhibit sufficient acidity to catalyze the acid–base reac-

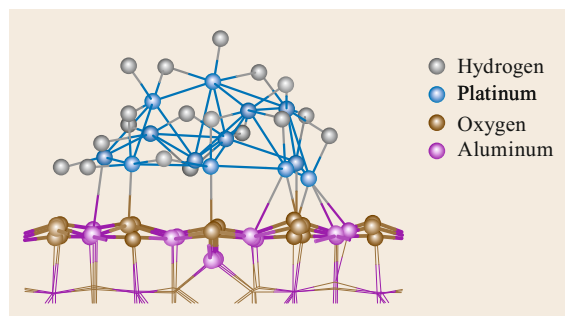


Fig. 18.24 Molecular model of Pt₁₃ particle supported on γ -alumina. Hydrogen pressure $p(\text{H}_2) = 10$ bar (platinum particle exhibits ≈ 1 H/Pt atom)

tions at a reasonable rate. Thus the addition of chloride to the catalyst promotes the required acidity since the chloride weakens the O–H bond strength by polarizing electron density away from it to help satisfy its nearly complete outer valence shell. Hence, the presence of chlorine induces a weakening of the hydrogen network of the OH groups on γ -alumina and makes them more available for protonation as shown by recent quantum simulations [18.13]. Catalyst acidity is controlled by the amount of chloride added to the support and the water partial pressure in the reactor. A schematic representation of a reforming catalyst is given in Fig. 18.25.

It is worth mentioning that chloride is also helpful to stabilize the platinum cluster.

Acidity Control

The relative balance between the Al–OH and Al–Cl groups is critical to ensure appropriate catalyst activity and selectivity [18.14]. The number of acid sites is controlled by the water partial pressure above the catalyst. Higher moisture level in the gas results in more acid sites on the surface. The water-to-chloride ratio of the gas above the catalyst determines the catalyst chloride content. Lower water-to-chloride ratios result in more chloride on the catalyst [18.13].

Catalyst surface area and temperature also impact the moisture and water-to-chloride ratio required to achieve the appropriate number and strength of acid sites. As catalyst surface area declines with age (number of regenerations), higher chloride partial pressure and lower water-to-chloride ratio are required to maintain appropriate acidity. As catalyst temperature is increased to increase reactivity, higher chloride partial pressure and lower water-to-chloride ratio are again required to maintain appropriate acidity.

As a basic rule, any increase in catalyst chloride content will increase the acidity and therefore the cracking; on the other hand, any increase in the water content in the feed without appropriate chloride increase to maintain the appropriate water-to-chloride ratio will strip chloride from the catalyst and consequently reduce the acidity and catalyst activity (Fig. 18.26).

In reforming, optimum acidity is typically obtained when the recycle gas moisture is in the range of

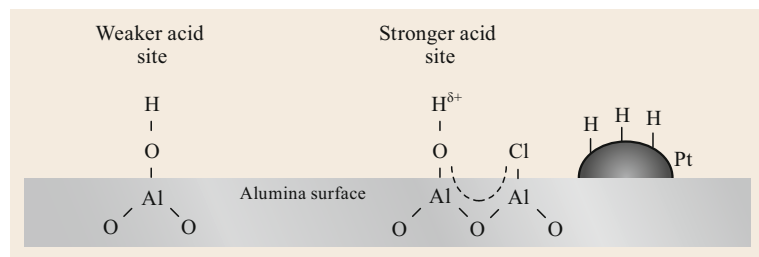


Fig. 18.25 Simplistic representation of reforming catalyst acidity

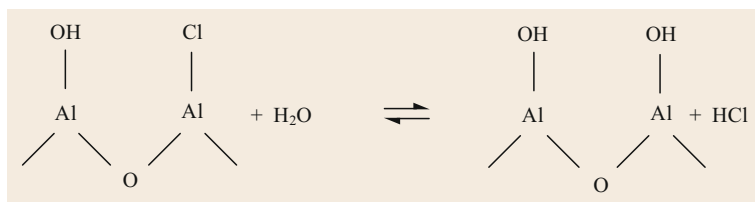


Fig. 18.26 Water and chloride balance

15–25 ppm volume. The associated recycle gas HCl content should be approximately 0.2–0.5 ppm volume depending on temperature, catalyst surface area, and contaminants.

Benefits of a Stable Surface Area

The catalyst carrier provides the surface area over which the acid and metal sites are distributed and the activity and selectivity controlled. As previously mentioned, the catalyst carrier is γ -alumina and has a fresh surface area on the order of 200 m²/g. As the catalyst ages and is subjected to regeneration cy-

cles, the surface area slowly declines primarily due to hydrothermal exposure during periodic regenerations. As the catalyst surface area drops with each successive regeneration cycle, catalyst acidity, Pt dispersion, and coke tolerance become progressively less effective. Thus, a catalyst with superior hydrothermal stability maintains its high surface area, which facilitates hydroxyl and chloride retention to provide the requisite acidity and Pt dispersion for superior performance. It has also been confirmed that chlorine itself improves the stability of small Pt particles [18.15].

18.5 Contaminants and Unit Troubleshooting

The importance of feed contaminants was discussed in general terms in Sect. 18.3. A more detailed review of the impact of contaminants on reforming catalysts is considered in this section.

Catalyst contaminants are classified into three categories: temporary (sometimes called inhibitors), semipermanent, and permanent poisons (Fig. 18.27) [18.16].

Temporary poisons are those that can be removed from the catalyst, either by dilution or release when the source of the contaminant is removed. Normal catalyst activity and selectivity is substantially or fully restored once the contaminant disappears.

The most common temporary poisons (inhibitors) of reforming catalysts are sulfur, organic nitrogen, water, and oxygenated organics. When the contaminant is no longer introduced, normal operation of the unit will return.

Coke is a type of temporary poison that requires interruption of unit operation to regenerate the catalyst and renew catalyst performance. As a result of this discontinuity in operation, it is considered to be a semipermanent poison.

Permanent poisons are those that induce a loss of performance which cannot be recovered, even with regeneration, and which is so severe that the catalyst must be replaced.

For conventional fixed-bed catalysts as well as for continuously regenerated catalysts, the main permanent

poisons are arsenic, lead, copper, iron, sodium, potassium, and silicon. Some of these, like silicon from coker naphtha, only become an issue once the upstream hydrotreater catalyst becomes overloaded with the contaminant.

Both the metallic and acidic sites on reforming catalyst are subject to poisoning. A summary of the main poisons and the type of site each impacts is shown in Fig. 18.28.

18.5.1 Impact of the Main Temporary Poisons

Sulfur

Sulfur is the most common impurity found in the feed of any reforming unit. The maximum allowable concentration is typically specified as 0.5 ppm weight expressed as S. Whenever possible, it is recommended to operate the NHT feed treater to attain an even lower sulfur content and provide additional catalyst stability and selectivity.

Poisoning is caused by H₂S, either contained in the unit feed or resulting from the decomposition of sulfur compounds contained in the feed. H₂S reacts with platinum according to the following equilibrium reaction (Fig. 18.29), and consequently it reduces the activity of the catalyst by decreasing the number of active metallic sites available to catalyze reactions as PtS is inactive for promoting dehydrogenation.

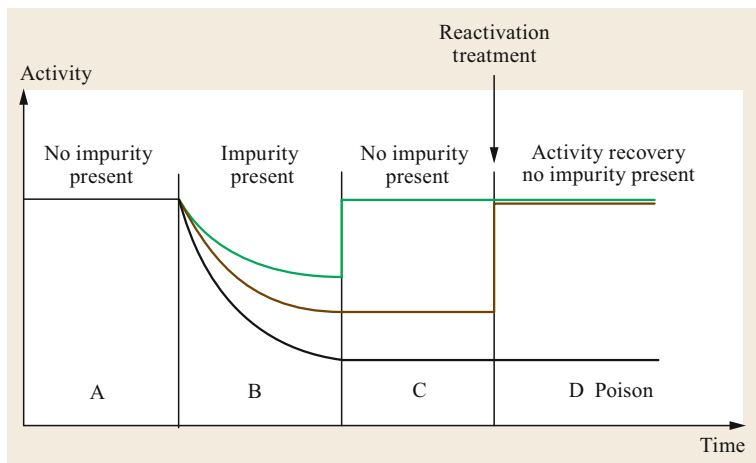


Fig. 18.27 Difference between inhibitors and permanent poisons. Temporary poison: *green curve*; semipermanent poison: *brown curve*; permanent poison: *black curve*

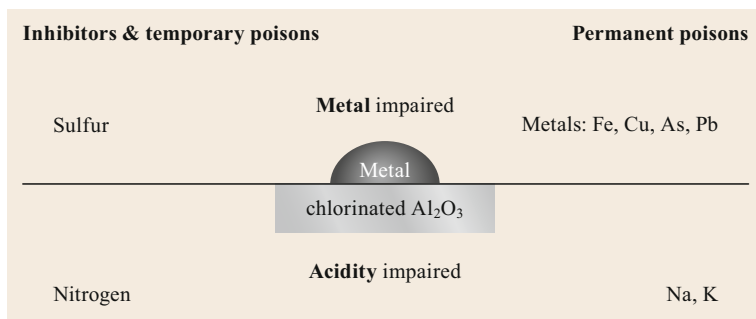


Fig. 18.28 Main reforming catalyst contaminants



Fig. 18.29 Interaction between sulfur and platinum

Catalyst contamination by sulfur is indicated by:

- A decrease in hydrogen yield
- A decrease in recycle gas purity (gas yield increase)
- An increase in hydrocracking (LPG yield increase)
- An increased coking rate
- A reduced temperature drop in the reactors, especially the first reactor where rapid naphthene dehydrogenation occurs, and sometimes an increase in temperature drop across the second reactor as this reaction shifts to the second reactor.

Normally, sulfur removal is achieved by pretreating the naphtha feed in a hydrotreating unit (NHT). Poor operation of the NHT or mechanical issues can result in sulfur breakthrough to the reforming catalyst. Possible causes for this breakthrough include the following:

- Low activity of the hydrotreater catalyst or low hydrogen partial pressure

- Change in NHT feed quality: higher final boiling point, sulfur or nitrogen content
- Excessive NHT temperature resulting in recombinant sulfur formation (H_2S reaction with olefins to produce mercaptans near the reactor outlet)
- A leak in the NHT feed-effluent heat exchanger that allows untreated naphtha to bypass the reactor
- Poor operation of the hydrotreater stripper resulting in dissolved H_2S and H_2O carryover to the reforming unit.

Whenever H_2S contamination is present, the reformer temperature should be maintained in the normal temperature range (despite a drop in octane) to avoid excessive coking of the catalyst. The recycle gas compressor rate should also be maximized to increase the sulfur stripping effect and minimize catalyst coke formation.

These conditions must be maintained until the cause of the upset has been found and corrected. High-severity operating conditions can be resumed once the H_2S content in the recycle gas is lower than 1–1.5 ppm volume.

Nitrogen

In contrast to sulfur, organic nitrogen is less frequently present in the reforming feed and scarcely present in straight-run naphtha. It is a common impurity of cracked naphtha and may also result from injection of amine-based corrosion inhibitors.

The maximum allowable concentration of organic nitrogen in the feed is typically specified at 0.5 ppm weight. Molecular nitrogen (N_2) has no detrimental effect.

Organic nitrogen is a problem because NH_3 forms by decomposition of organic nitrogen compounds in the presence of hydrogen on the reforming catalyst. In the reaction section, NH_3 , which is alkaline, reduces the acidity of the catalyst and increases its rate of chlorine loss. The increase in dechlorination is linked to the lower HCl partial pressure. Overall, these two effects reduce the catalyst activity. In the cold section of the unit, NH_3 reacts with chlorine to form NH_4Cl , which becomes solid below $80^\circ C$. The resulting salt deposition can foul downstream coolers, separators, recycle gas compressor, export gas compressor valves, and cold trays in the stabilizer creating mechanical problems. For a 25 000 BPD reformer, 0.5 ppm weight of organic nitrogen in the feed can lead to approximately 2 t/y of NH_4Cl deposition. Ammonium chloride deposits also raise the risk for under deposit corrosion with trace moisture present. Failure to replenish this lost chloride will reduce the acidic function of the catalyst and result in decreased catalyst activity.

Indicators of nitrogen contamination include:

- Decrease in octane
- Slightly increased hydrogen and C_5+ production.

Like sulfur, organic nitrogen removal is achieved by NHT pretreating of the feed; however, nitrogen removal is more difficult than sulfur removal and often requires the use of a Ni-Mo catalyst operating at higher hydrogen partial pressure than a typical NHT with Co-Mo catalyst. Naphtha with high nitrogen-content requires a NHT specifically designed for high nitrogen feed.

When nitrogen contamination is detected in the reformer:

- Avoid increasing reformer reactor temperature to compensate for lost catalyst chloride and the concomitant drop in reformate octane number as this will only increase the loss of chlorine.
- Take the necessary actions in the NHT to lower the nitrogen content down to the acceptable level of 0.5 ppm weight.
- Increase organic chloride injection into the reformer naphtha to compensate for the lost chloride.

- Reduce the end point of high nitrogen containing naphthas to the NHT to reduce nitrogen in the reformer feed.

Water Upset

The acidity of the catalyst is controlled by two main factors: the moisture in the feed and the chloride on the catalyst. An increase in the feed moisture without a compensating increase in the feed chloride content will strip chloride from the catalyst, thereby reducing its acidity. Conversely, too little moisture in the feed will severely dehydroxylate the catalyst, thereby reducing its overall acidity despite the fact that its chloride level may be building if no parallel adjustment has been made in feed chloride level. This phenomenon is most likely to occur in a fixed-bed reformer. Proper control of the water/chloride balance is crucial to maintain the correct metal/acid balance on the catalyst. Insufficient on-stream chloride, moisture addition, or both can ultimately compromise the acid function, and as a result, the metal function will become dominant producing increased formation of methane (C_1) and ethane (C_2) relative to propane (C_3) and butanes (C_4). Conversely, excess on-stream chloride addition, moisture addition, or both can ultimately increase catalyst acidity to the point where it begins to overwhelm the metal function, and as a result, C_3 and C_4 formation will overtake C_1 and C_2 production.

The water content of reformer feed is a combination of the intrinsic moisture found in the naphtha and the moisture added to the feed. Feed moisture should be controlled to achieve approximately 20 ppm volume in the recycle gas for typical conditions.

Water removal is usually achieved in the stripper of the NHT. Generally contamination by water results from poor operation of this equipment. Water can also be introduced indirectly in the form of oxygenates which will be reacted to form water in the reformer.

When feeding a reformer unit with low-sulfur naphtha from storage, the naphtha should be routed through the NHT stripper or splitter to remove excess water present.

If recycle gas water content exceeds 50 ppm volume, the reactor inlet temperature must be lowered to reduce the chlorine elution (leaching) from the catalyst and sintering of the metallic sites. The following guidelines are generally accepted:

- > 50 ppm volume water, limit reactor inlet temperature to $\leq 500^\circ C$
- > 100 ppm volume water, limit reactor inlet temperature to $\leq 480^\circ C$.

If recycle gas moisture drops too far below 10 ppm volume, the catalyst surface becomes sufficiently dehy-

droxylated to limit its acidity. Injection of 1 ppm weight water in the feed will increase recycle gas moisture by 2–5 ppm volume depending on the operating conditions.

Coke

The coke that deposits on the catalyst is a temporary poison since its detrimental effect is reversible through regeneration. Since coke formation is inherently associated with the reforming reactions, there is no real way to avoid it. One can only minimize coke formation.

Operating conditions directly impact coking rate. Higher severity (temperature) operation accelerates coke formation while higher hydrogen partial pressure and hydrogen recycle gas rate retards its formation due to coke's hydrogen deficiency.

The feed end boiling point can have a significant impact on coking rate. High-end-point naphtha, especially cracked naphtha, tends to accelerate coke formation due to the incremental presence of heavier aromatics and polyaromatic precursors.

Unfortunately, D86 final boiling point does not provide sufficient information in the case of mixed feeds. Each feed must be analyzed separately to know the true final boiling point of each stream to be able to specifically limit the heavy components in the cracked feeds. Very often mixed feeds are responsible for short catalyst cycle life, even though the final boiling point of the mixture stays within acceptable values.

18.5.2 Permanent Poisons

Permanent poisons have been defined as contaminants which irreversibly damage the catalyst.

Table 18.12 lists the main permanent poisons as well as their acceptable level in reformer feed and their most likely source.

Most metals poison the metal functions (platinum and promoter) of the catalyst. Their impact tends to progress sequentially through the reactors in a fixed-bed reformer. The first reactor is typically the reactor where the poisoning is first detected. In a CCR reformer unit with circulating catalyst, poisons can affect the whole catalyst inventory if the cause of pollution is not found.

Table 18.12 Main contaminant max level in feed and origin

Poisons	Maximum level (wt)	Source
Arsenic	5 ppb max	SR, cracked naphthas, or gas condensates
Lead	1 ppb max	Recycled slops
Iron	< Detection limit	Corrosion, metal dusting
Sodium	< Detection limit	Crude Fixed bed regeneration with caustic carryover
Silicon	< Detection limit	Additives (antifoaming)

Metal contamination is characterized by:

- A dramatic decrease in the ΔT (temperature drop) in the first reactor associated with an increased ΔT in the second reactor, then decrease in ΔT with the second reactor, etc.
- A decrease in octane number
- An increase in liquid product yield
- A decrease in hydrogen production and purity.

In addition to poisoning the catalysts functions, mechanical problems may result from the collection of corrosion products (scale, rust, etc.) in the top layer of the first catalyst bed in a fixed reactor system, or the accumulation of scale or rust in the stagnant zone of the first reactor.

The contaminants and the source of contamination are listed in Table 18.12. Prevention consists of adequate feed pretreatment in a NHT and appropriate material selection to limit corrosion. Metal poisons are generally partially retained on the upstream hydrotreating catalysts. However, their retention capacity is limited and breakthrough may occur. Such a breakthrough would result in a very harmful situation for the unit since these poisons would not be eliminated by the catalyst regeneration.

It is very important to periodically check the metal content of the hydrotreater feed and product. Monitoring the performance of the hydrotreater with regard to demetallization not only protects the reformer but also gives an indication of when the hydrotreatment catalyst needs to be replaced.

18.6 Reforming Evolution

18.6.1 Commercialization of Catalytic Reforming

Perhaps the earliest reference to catalytic reforming is found in US patent 2288336 entitled *Catalytic Re-*

forming of Naphthas filed in 1939 by Standard Catalytic Company, a subsidiary of Standard Oil. The process was developed as a means of producing aviation gasoline and toluene to meet the demands of World War II. The *Hydroforming* process was com-

mercialized in 1941 utilizing molybdenum-alumina and chromium-alumina catalyst in fixed-bed reactor systems. Rapid catalyst deactivation led to the development and commercialization of moving bed and fluid bed units by some of the major oil companies in the early 1950s.

The modern catalytic reforming process was first commercialized by UOP in 1949 using a bifunctional catalyst composed of platinum impregnated on a slightly chlorinated γ -alumina [18.17]. The process trademarked by UOP as Platforming represented a significant improvement in catalyst activity to produce high-octane gasoline. The process was widely applied for gasoline and aromatics production; however, frequent catalyst regeneration was required to maintain activity. Operation at relatively high pressure with recycle of product hydrogen was necessary to suppress coking reactions due to the poor stability of the catalyst system. Cyclic reformers with the capability to isolate and regenerate individual reactors while the remainder of the unit remained on oil were developed and commercialized by Standard Oil of Indiana (Ultraforming) and Standard Oil of New Jersey (Powerforming) in the early 1950s.

Development work on promoted or multimetallic catalyst formulations resulted in Chevron's commercialization of rhenium-promoted platinum catalysts in 1969 (Rheniforming). The significant improvement in catalyst stability (lower coke formation) obtained by using other metals, such as rhenium, in combination with the primary reforming catalyst metal, platinum, prompted a rapid development in catalyst formulations. With bimetallic catalysts, fixed-bed catalytic reforming processes could achieve cycle lengths of 1–2 years at higher severity operation before coke build-up on the catalyst reduced activity to the point where periodic shut down and catalyst regeneration was required. These units are referred to as semiregenerative, or Semi-Reg, reforming processes.

18.6.2 Semiregenerative Catalytic Reforming

A typical configuration of a fixed-bed semiregenerative reforming process is shown in Fig. 18.30.

In this flow scheme, hydrotreated naphtha feed is combined with hydrogen-rich recycle gas, preheated by heat exchange with the reactor effluent and then further heated in a fired heater before entering the first reactor. As the endothermic reforming reactions cool the feed and product mixture, the effluent from the first reactor must be reheated to the required reaction temperature in a fired heater before entering the second reactor, and similarly for the last reactor (refer also to Fig. 18.23).

The product liquid and gases are cooled and separated in a simple flash separator into a hydrogen-rich gas stream and a liquids product stream. Some of the hydrogen-rich gas is recycled to the reactors to suppress coke formation and the remaining product or *make gas* is sent to the refinery hydrogen system. The separator liquids are stabilized to recover a C_5+ reformatate product stream and LPG by-product stream, along with a small off-gas stream.

Over time, the catalyst in the fixed-bed reactors age (deactivate due to coke) and when the performance is no longer economic the unit is shut down and the catalyst regenerated on a periodic or semiregenerative basis. The catalyst may be removed for ex-situ regeneration and subsequent reloading, or regenerated in-situ. Catalyst regeneration can be a rather complex and precise operation as will be described later.

18.6.3 Cyclic Catalytic Reforming

A typical configuration for a fixed bed, cyclic reforming process is shown in Fig. 18.31.

This process scheme utilizes a *swing* reactor in addition to the 3–5 on-oil reactors and a separate re-

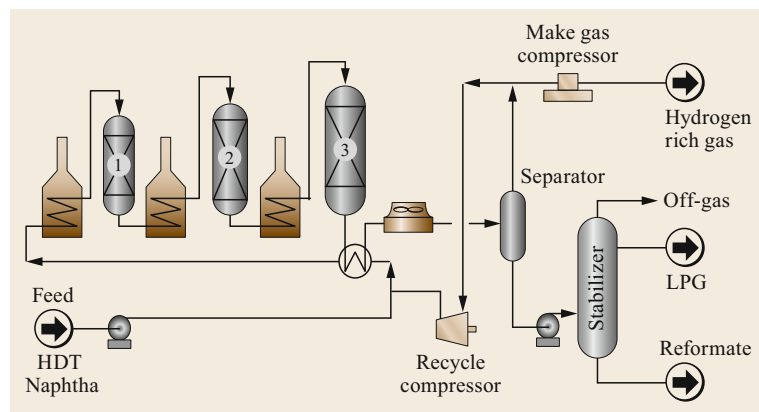


Fig. 18.30 Semiregenerative catalytic reforming process scheme

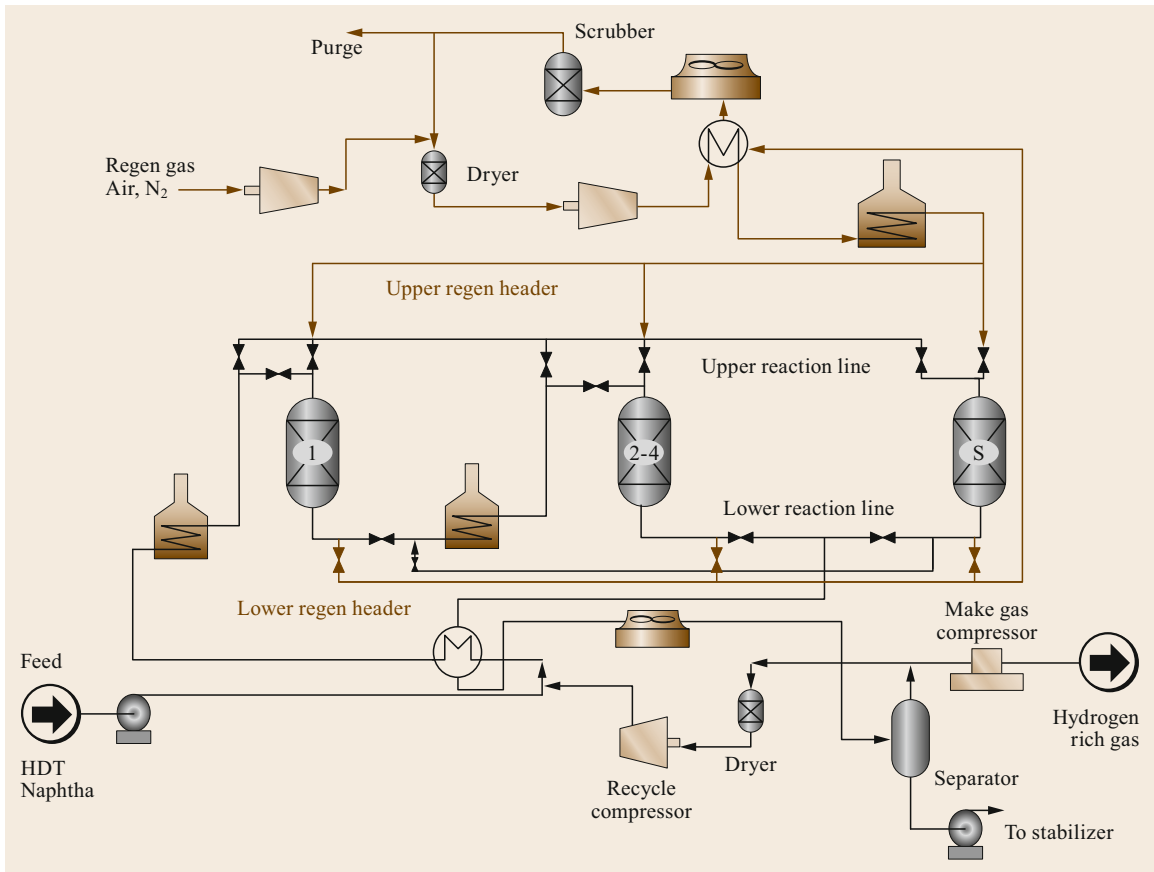


Fig. 18.31 Typical cyclic reforming process scheme. S: Swing reactor; regeneration process line *in brown*; reaction process line *in black*

generation system to maintain continuous operation of the reaction system, while individual reactors are regenerated in the regeneration system. As a reactor becomes sufficiently deactivated, the *swing* reactor replaces it in the on-oil reactor series through a sequence of valve movements in the reaction and regeneration headers. At the same time, a parallel sequence of valve movements transfers the deactivated reactor from the reaction header to the regeneration header for regeneration. The tail reactors are typically regenerated more frequently than the lead reactors, and the *swing* reactor is regenerated as often as needed to maintain on-oil performance. Units operating at high enough severity to require continuous operation of the regeneration section are said to be in full cyclic mode. As severity drops below the threshold for full cyclic operation, discontinuous use of the regeneration section becomes possible and the unit operates in semicyclic mode. At low enough severity, the unit operates more like a semiregenerative reformer, and occasionally regenerates the full complement of reactors one at a time.

In a cyclic reformer, reaction system H_2O and H_2S concentrations spike well above the desired operating target and catalyst performance declines for the duration of the disturbance every time a freshly regenerated reactor swings into on-oil service. Addition of a dryer in the recycle gas loop, regeneration loop, or both reduces the magnitude and impact of this disturbance.

18.6.4 Radial Flow Reactor Design

The first reforming reactors were spherical due to the high pressure of operation with monometallic catalysts. Catalyst loading and distribution problems associated with spherical reactors and thin reactor beds then led to cylindrical, axial flow fixed-bed reactors.

As the catalyst technology improved and lower pressure operation was possible for improved yield selectivity, the problem of catalyst bed pressure drop and recycle compressor duty led to the introduction of radial flow reactors (Fig. 18.32). The gas is introduced

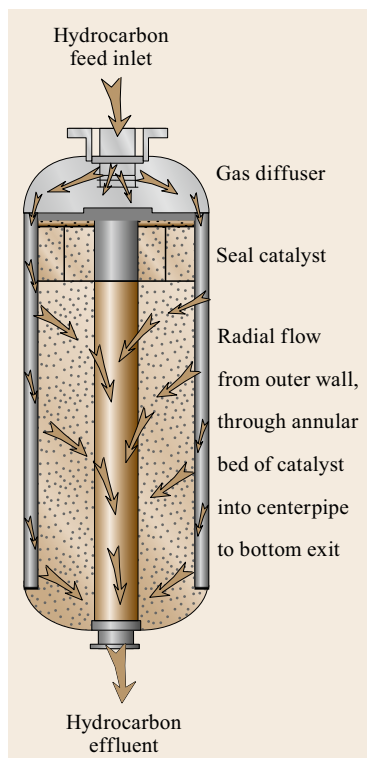


Fig. 18.32
Typical radial
flow reactor

through the top and flows down along the outer wall of the cylindrical reactor and then flows radially inward through the thin annular catalyst bed. Screens are used to contain the catalyst in the annular bed and allow reactants to enter from the wall, pass through the bed, and then enter a center pipe collection tube to exit the vessel at the bottom. This design provides intimate and controlled contact between the feed and catalyst with a low pressure drop across the thin bed of catalyst.

18.6.5 Evolution of Reforming Catalyst

The need to operate monometallic units at relatively high pressure and with high hydrogen recycle to suppress coke formation was at odds with the thermodynamically preferred low pressure. As noted above, catalyst development focused on ways to improve stability and therefore allow for operation at more favored lower pressure. The first step of combining promoter metals such as rhenium was very successful and Pt-Re catalysts are widely used today for fixed-bed reforming [18.18].

The explanation for the improvement obtained following the addition of rhenium can be understood by Fig. 18.33 [18.19].

As the reaction proceeds, the platinum accessibility reduces due to coke formation on the catalyst. When

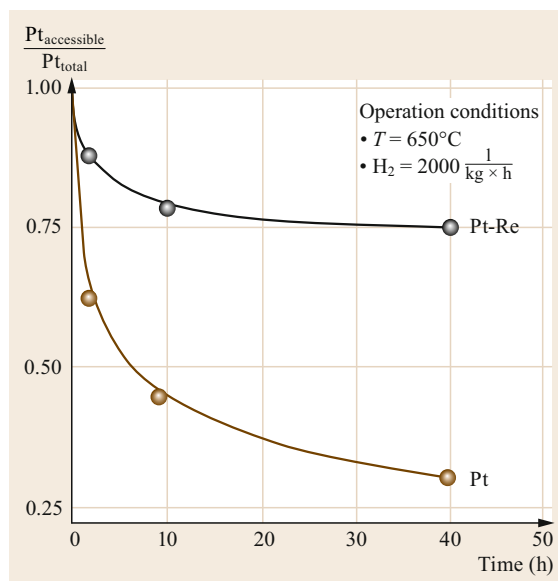


Fig. 18.33 Platinum stability improvement with Re addition

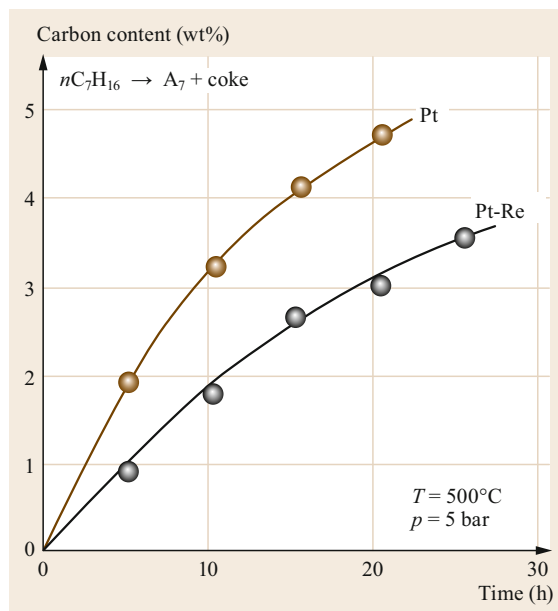


Fig. 18.34 Impact of rhenium on coke make (*n*-heptane feed)

only platinum is used, the activity or platinum accessibility declines rapidly. Note that recent quantum simulations have quantified the impact of H₂ partial pressure on the stability of hydrocarbon species present on the Pt nanoparticles: only high H₂ partial pressure may prevent the formation of undesired carbon species adsorbed on the Pt particle [18.20, 21]. When rhenium

is introduced along with the platinum, the platinum cluster is by far more stable with much more of the platinum accessible over a longer period of time.

Thus the desirable dehydrogenation/hydrogenation activity is more stable, which can be seen by the reduced coke make (Fig. 18.34) [18.19].

Further development work discovered other metal combinations with even greater yield selectivity and activity than either Pt alone or Pt-Re, as shown in Fig. 18.35. When Pt was combined with tin (Sn), the desired dehydrogenation reactions were greatly enhanced, but this benefit only occurred at low pressure. Indeed as seen in Fig. 18.35, Pt-Sn catalyst promotes the relative rate of aromatization of naphthene at the expense of their hydrogenolysis over a wide pressure range, but it is only at low pressure that their activity surpasses that of Pt or Pt-Re catalyst.

The challenge of lower pressure is that coke formation on the catalyst increases sharply and stability declines. This challenge was met with the introduction of CCR technology in the early 1970s.

18.6.6 Continuous Catalyst Regeneration Design

In order to realize the benefits of the new Pt-Sn catalyst, a means of operating at reduced pressure and with more frequent catalyst regeneration was required. A moving catalyst bed design was commercialized in the early 1970s so that a CCR scheme could be implemented. This innovation allowed for the development of more selective ultra-low pressure designs utilizing customized catalysts to achieve higher yields of C₅+reformate, aromatics, and hydrogen.

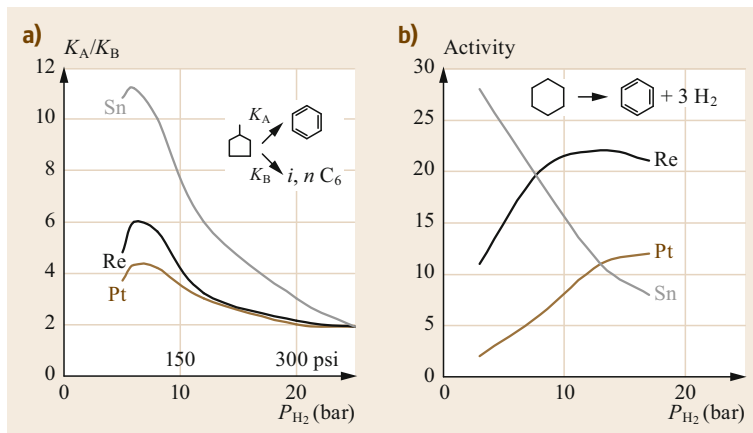


Fig. 18.35a,b Impact of metal complexes with Pt on selectivity (a) and activity (b)

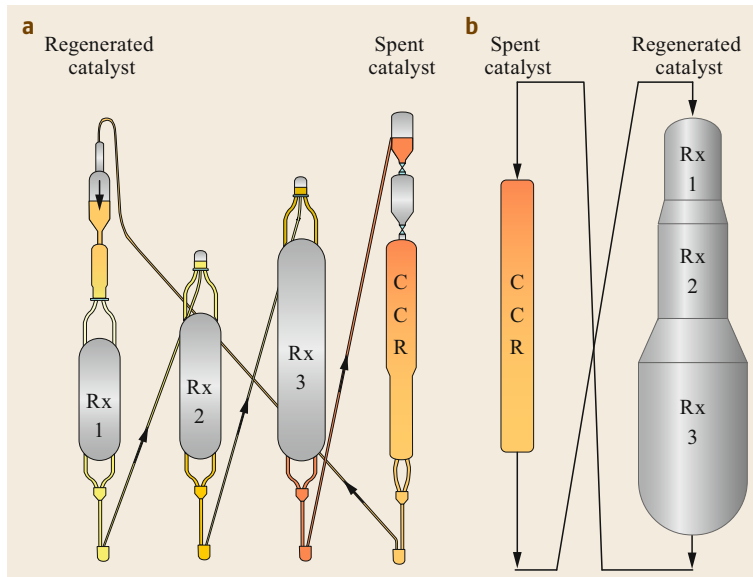


Fig. 18.36a,b Reactor configuration in CCR unit: (a) side-by-side (Axens), (b) stacked (UOP)

The CCR reforming process is offered by two licensors: Axens with a side-by-side reactor configuration (Fig. 18.36a) under the trade names Octanizing and Aromizing, and a stacked configuration offered by UOP under the trade name CCR Platforming (Fig. 18.36b).

A CCR reformer design is similar to a fixed-bed semiregenerative design with heaters between each reactor and a recycle gas compressor in order to reduce coke make. In order to ensure a continuous operation of the unit, the catalyst must move or circulate through the reactors and a regenerator so that coke is burned and the catalyst regenerated on a continuous basis.

The reactors (typically 3 or 4) can be configured in a side-by-side arrangement as practiced by Axens, or stacked in a tower as offered by UOP as shown above. In both cases, catalyst is circulated between the reactors and a regeneration section with catalyst flow within each reactor by gravity flow.

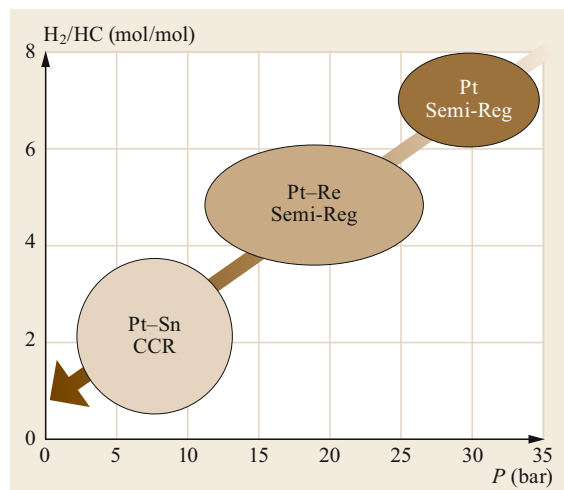


Fig. 18.37 Pressure trend in reforming and catalyst evolution

Like most modern fixed-bed designs, radial reactors are used in CCR designs to optimize catalyst and feed contact in a low pressure drop reactor design. However for CCR units, the catalyst moves slowly down and through the reactor and allowance must be made for the moving bed density. The CCR radial reactor design naturally also has special mechanical means for introducing, distributing, and removing catalyst from the annular radial bed.

In the regeneration section, four steps are performed on a continuous basis:

- Coke burning to remove coke deposits
- Oxychlorination to adjust catalyst chloride and re-disperse the active metals on the carrier support
- Calcination to dry the catalyst, and
- Reduction to convert Pt oxide to active metal.

18.6.7 From High-Pressure to Low-Pressure CCR

As was discussed in the Chemical Reaction section (Sect. 18.3), operation at high pressure causes a decline in gasoline and hydrogen production and thus has a negative impact on the overall economics. As new catalyst formulations allowed for greater stability, it was possible to reduce the reaction pressure and hydrogen recycle while still achieving an acceptable cycle length. When the CCR design was introduced, catalyst stability became less important and the operating pressure could be reduced as dictated by thermodynamics. Figure 18.37 illustrates the trend in operating pressure as catalyst formulations evolved.

As catalyst improvements allowed for a change in process configuration from high-pressure semiregenerative reforming to ultra-low-pressure CCR reforming, the yields improved dramatically. Figure 18.38 demonstrates the improvement in yields with 10 wt% more reformat and a 50% (relative) increase in hydrogen

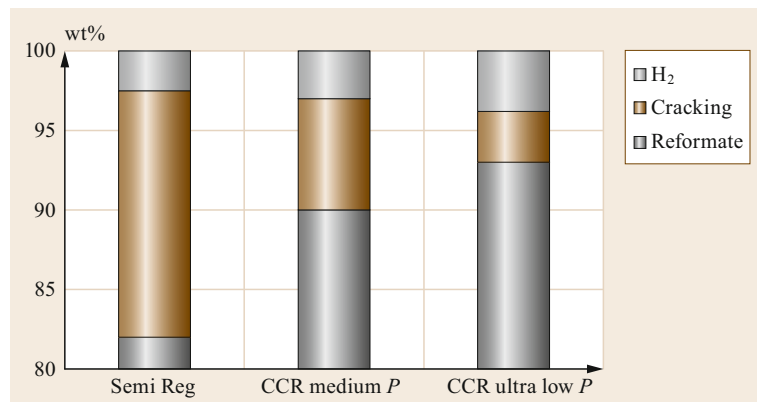


Fig. 18.38 Yields trend versus pressure (100 RON severity, feed PNA = 54/30/16w%)

production as the average reaction pressure is reduced from 20 bar(g) (275 psig), Semi-Reg case, to 3.5 bar(g) (50 psig) at a constant 100 RON severity. Typical operation pressure for semiregenerative units are around 20–25 bar(g) while for medium pressure CCR the operating range is around 6–8 bar(g). The ultra low pressure CCR operate close to 3 to 4 bar(g).

While the low-pressure CCR provides the highest yields and economic return, the trade-off is the need to circulate catalyst and operate a CCR system with a high regeneration frequency. In some ultra-low-pressure CCR units running at high severity for aromatics production, the entire catalyst inventory circulates through the unit and regenerator every 3–5 days

18.7 Catalyst Regeneration

As the feedstock is converted, some of the hydrocarbons will form coke which will accumulate on the catalyst as noted above. The lower the unit pressure and more severe the operation, the more rapidly will coke deposit on the catalyst. Therefore, the performance will decrease over time and at a given point the catalyst needs to be regenerated. The coke level on catalyst prior to regeneration may be 20–30 wt% in the case of fixed-bed semiregenerative catalysts and 3–7% for CCR catalyst.

Between a CCR and a fixed-bed unit, the regeneration steps are fundamentally the same, only the frequency and mechanical equipment are different. For a CCR, the regeneration can be every 3–7 days while for a fixed-bed unit it can be every 6 months up to 3 years.

There are four steps involved in the regeneration sequence:

- Combustion
- Oxychlorination
- Drying
- Reduction.

A block diagram of a regeneration scheme is shown in Fig. 18.39.

18.7.1 Combustion Step

The main objective of this step is to burn the coke. But in order to avoid a high exotherm from coke burning or localized hot spots, the burning gas is recycled to limit the oxygen content, which becomes progressively more diluted with nitrogen as it recirculates. A typical oxygen content of less than 1 vol.% is maintained to achieve a controlled burn of the coke without damaging the cat-

in order to maintain a coke on catalyst level below about 5 wt%.

Most of the new reforming units are based on ultra-low-pressure CCR design as it provides superior yields and the highest economic return. The frequent regenerations with a CCR subject the catalyst to severe conditions that reduce the carrier surface area and activity over time. Improvements in catalyst formulation and regeneration system design have been necessary to ensure long catalyst and equipment life.

Today, low-pressure reforming with moving catalyst beds and CCR technology is the norm to realize the benefits of new Pt catalysts using multiple promoter metals and optimized carrier systems [18.22].

alyst. The catalyst temperature during regeneration is generally limited to less than 600 °C. Staged oxygen addition is also implemented to limit the exotherm and protect the catalyst.

The regeneration process, consisting mainly of coke burning, has a negative impact on the surface area of the catalyst due to hydrothermal instability of the alumina and potential hot spots created by maldistribution. The reduction of the specific surface of the catalyst has

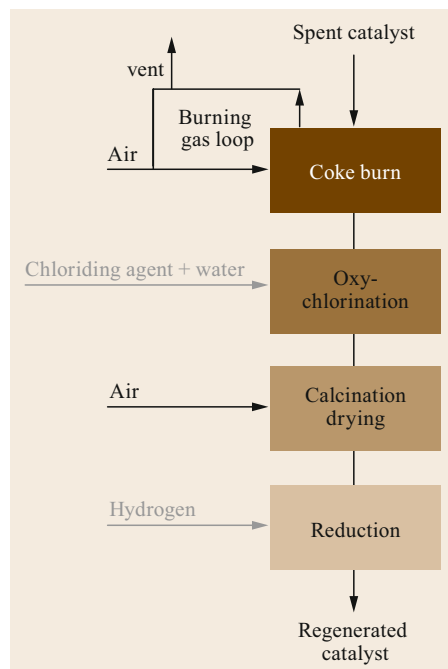


Fig. 18.39 Schematic representation of catalyst regeneration steps

a direct impact on the chloride retention of the carrier and acid function of the catalyst. This can have several drawbacks for the day-to-day operation of the unit. The activity of the catalyst will decline and this can lead to the formation of olefins and polymers called green oils. As chloride is lost, more must be injected resulting in downstream equipment corrosion and salt deposits that foul colder parts in the recovery section.

Thus the catalyst and regeneration system must be designed to limit surface area loss during regeneration, or an economic penalty of more frequent catalyst replacement will result.

The optimal design of the regeneration section is, therefore, of paramount importance for CCR applica-

tion with a high frequency of catalyst regeneration. Exposure to high temperature and particularly in the presence of steam is a well-known cause of surface area reduction in alumina systems. One means of reducing catalyst degradation as practiced in the Axens design, shown in Fig. 18.40, is to reduce the water partial pressure in the burning section by means of a dryer system and to implement staged combustion (air injection) to avoid localized hot spots. In addition to these process changes, the catalyst itself can be designed for high hydrothermal stability by the addition of promoters.

18.7.2 Oxychlorination Step

During the combustion step, the small platinum particles undergo sintering or agglomeration into larger clusters due to exposure to high temperature, moisture in the combustion gas, and elution or loss of chloride. As only the surface platinum atoms are active for re-

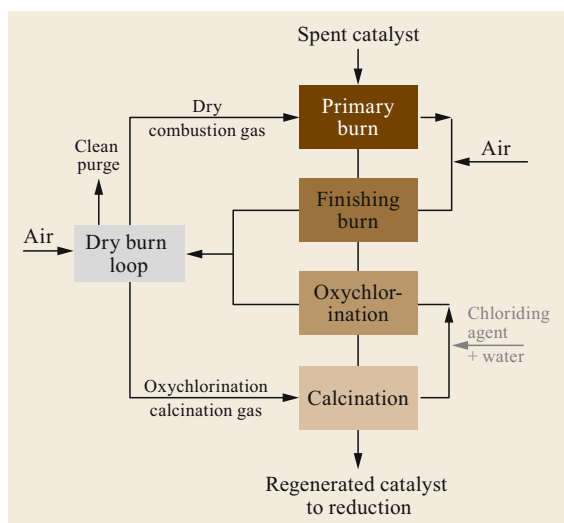


Fig. 18.40 Typical Axens regeneration loop



Fig. 18.41 Typical picture of an oxychlorinated catalyst

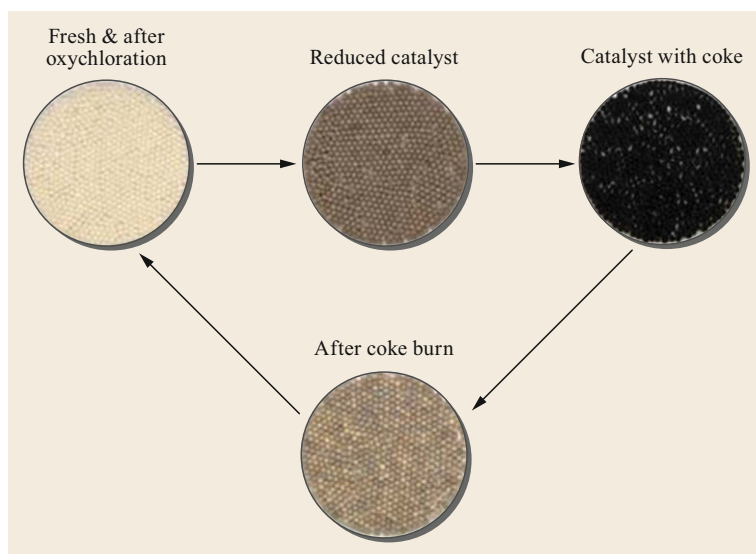


Fig. 18.42 Catalyst life cycle in a reforming unit

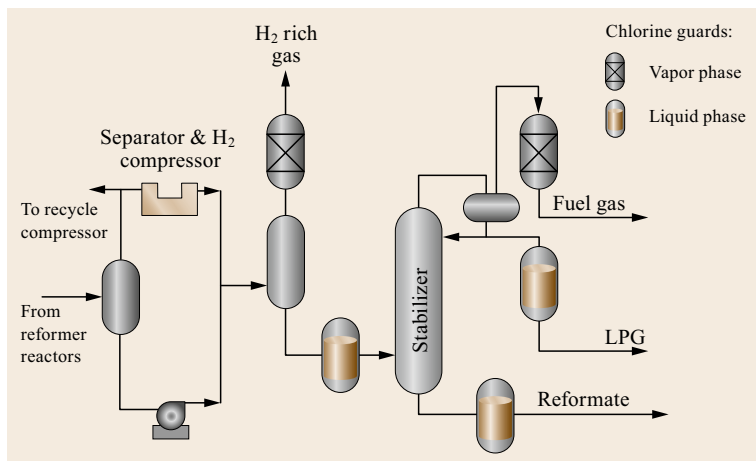


Fig. 18.43 Standard chloride trapping mass locations

forming reactions, larger clusters must be redispersed into smaller crystallites [18.23].

This redispersion is done under an oxygen atmosphere, typically above 5 vol.%, in the presence of chloride at temperatures typically above 480 °C. The proposed mechanism [18.24] assumes the formation of an oxychlorinated platinum complex. At the end of this oxychlorination step, the platinum is well dispersed as small clusters on the carrier and in an oxide form (PtO_xCl_y) (Fig. 18.41).

18.7.3 Drying Step and Reduction Step

The final regeneration step is the reduction to convert the oxide form of platinum to the active metallic form in order to ensure a good reduction. This catalyst needs to be dry and hence a calcination or drying step precedes the reduction step.

18.8 Conclusions

Since its development over 60 years ago, the reforming process and catalysts have significantly been improved.

Unit pressure has dropped from 40 bar(g) down to 3.5 bar(g) while reformat yields have been increased by more than 10 wt% (absolute). Catalyst and process developments continue to improve yield selectivity and

The transformation of the catalyst during regeneration is illustrated in Fig. 18.42, where the catalyst color goes from creamy white when oxychlorinated to gray under reduced form to black when coked.

18.7.4 Chloride Control

The control of chloride addition to the catalyst and loss to products and effluents is very important for reformer design and operation.

Since some chlorine loss from the catalyst always occurs, the products of reforming will be contaminated with chlorides. In order to protect process equipment in the reformer and downstream processes and catalysts, it is common to install a chlorine guard or trapping mass in one or more locations in the reforming unit. Figure 18.43 illustrates the possible locations of the trapping mass for vapor and liquid.

catalyst stability to provide greater operational flexibility and profitability.

From an economic stand point, reforming is still a key process in the refineries as it provides high octane components for the gasoline pool and hydrogen for hydrocracking and hydrotreating units. For the aromatics market, it is the main producer of xylenes.

References

- 18.1 C.A. Morley: Fundamentally based correlation between alkane structure and octane number, *Combust. Sci. Technol.* **55**, 115–123 (1987)
- 18.2 R. Bounaceur: Influence of the position of the double bond on the autoignition of linear alkenes at low temperature, *Combust. Flame* **142**, 170–186 (2005)

- 18.3 P. Le Prince (Ed.): *Conversion Process* (Technip Edition, Paris 2001)
- 18.4 A. Abeladim: Etude de la Transformation des Naphtenes en Présence de Catalyseurs de Reformage Catalytique, Ph.D. Thesis (Ecole Nationale Supérieure du Pétrole et des Moteurs, Rueil Malmaison 1982)
- 18.5 C. Alvarez Herrera: Etude Cinétique de la Déshydrocyclisation du N-heptane sur Catalyseur Platine sur Alumine, Ph.D. Thesis (Poitiers University, Poitiers 1977)
- 18.6 C. Marcilly: Chemistry of cabocations. In: *Acido-Basic Catalysis*, Vol. 1 (Technip Edition, Paris 2006),
- 18.7 C. Marcilly: Reactivity and conversion modes of the main hydrocarbon families. In: *Acido-Basic Catalysis*, Vol. 1 (Technip Edition, Paris 2006)
- 18.8 V.A. Mazzieri, C.L. Pieck, C.R. Vera, J.C. Yori, J.M. Grau: Analysis of coke deposition and study of the variables of regeneration and reju venation of naphtha reforming trimetallic catalysts, *Catal. Today* **133–135**, 870–878 (2008)
- 18.9 S. Marty: Influence de la Composition et de L'état de Vieillessement du Catalyseur sur L'évolution de sa Sélectivité en Déshydrocyclisation des Paraffines en Fonction des Conditions Opératoires, Ph.D. Thesis (Poitiers University, Poitiers 1986)
- 18.10 F. Humblot: Préparation par Voie Chimie Organométallique de Surface de Catalyseurs Bimétalliques, Application à la Déshydrogénation de L'isobutane, Ph.D. Thesis (Lyon University, Lyon 1995)
- 18.11 P. Raybaud, C. Chizallet, C. Mager-Maury, M. Digne, H. Toulhoat, P. Sautet: From γ -alumina to supported platinum nanoclusters in reforming conditions: 10 years of DFT modeling and beyond, *J. Catal.* **308**, 328–340 (2013)
- 18.12 C. Mager-Maury, G. Bonnard, C. Chizallet, P. Sautet, P. Raybaud: H₂-induced reconstruction of supported Pt clusters: Metal-support interaction versus surface hydride, *ChemCatChem* **3**, 200–207 (2011)
- 18.13 M. Digne, P. Raybaud, P. Sautet, D. Guillaume, H. Toulhoat: Atomic scale insights on chlorinated γ -alumina surfaces, *J. Am. Chem. Soc.* **130**, 11030–11039 (2008)
- 18.14 M. Paulis, H. Peyrard, M. Montes: Influence of chlorine on the activity and stability of Pt/Al₂O₃ catalysts in the complete oxidation of toluene, *J. Catal.* **199**, 30–40 (2001)
- 18.15 C. Mager-Maury, C. Chizallet, P. Sautet, P. Raybaud: Platinum nanoclusters stabilized on γ -alumina by chlorine used as a capping surface ligand: A density functional theory study, *ACS Catal.* **2**, 1346–1357 (2012)
- 18.16 J.P. Frank, G. Martino: Deactivation and regeneration of catalytic-reforming catalysts. In: *Progress in Catalyst Deactivation, NATO Advances Study Institute Series E*, ed. by J.L. Figueiredo (Springer, Dordrecht 1982) pp. 355–397
- 18.17 V. Haensel, C.G. Gerhold: Catalytic reforming of hydrocarbons in two stages utilizing a platinum-alumina-halogen catalyst composite (OCR), US Patent 2 659 692 (1953)
- 18.18 J.P. Bournonville: Etude de la Recristallisation du Platine Dans un Catalyseur de Reformage Influence de la Présence d'un Deuxième Métal, Ph.D. Thesis (Pierre et Marie Curie University, Paris 1980)
- 18.19 A. Bensaddik: *Etude EXAFS des Catalyseurs Bimétalliques Platine Rhénium* (Orsay University, Orsay 1995)
- 18.20 A.N. Jahel, P. Avenier, S. Lacombe, J. Olivier-Fourcade, J.-C. Jumas: Effect of indium in trimetallic Pt/Al₂O₃ SnIn-Cl naphtha-reforming catalysts, *J. Catal.* **272**, 275–286 (2010)
- 18.21 A.N. Jahel, V. Moizan-Basle, C. Chizallet, P. Raybaud, J. Olivier-Fourcade, J.-C. Jumas, P. Avenier, S. Lacombe: Effect of indium-doping of γ alumina on the stabilization of PtSn alloy clusters prepared by surface organostannic chemistry on platinum, *J. Phys. Chem. C* **116**, 10073–10083 (2012)
- 18.22 A.D. Silvana, R.V. Carlos, E. Florence, E. Catherine, M. Patrice, L.P. Carlos: Naphtha reforming Pt-Ge/ γ -Al₂O₃ catalysts prepared by catalytic reduction: Influence of the pH of the Ge addition step, *J. Catal. Today* **133–135**, 13–19 (2008)
- 18.23 F. Le Normand, A. Borgna, T.F. Garetto, R. Apesteguia, B. Moraweck: Redispersion of sintered Pt/Al₂O₃ naphtha reforming catalysts: An in situ study monitored by X-ray absorption spectroscopy, *J. Phys. Chem.* **100**(21), 9068–9076 (1996)
- 18.24 T. Cholley: Etude de la Redispersion de Phases Bimétalliques à Base de Platine Supportées sur Alumine Chlorée ou Neutralisée, Ph.D. Thesis (Paris 6 University, Paris 1997)

Fluid-Bed Ca

19. Fluid-Bed Catalytic Cracking

James G. Speight

Catalytic cracking is the thermal decomposition of petroleum constituents in the presence of a catalyst. Refineries use the process cracking to correct the imbalance between the market demand for gasoline and the excess of heavy, high boiling range products (as well as heavy oil and tar sand bitumen) resulting from the distillation of the crude oil.

The typical catalytic cracker that accepted a single-source gas oil feedstock is almost extinct and in the modern refinery is more inclined to be a blend of several high-boiling fractions – often with heavy oil and/or residuum as part of the blend, which has led to the development of residuum fluid catalytic cracking units. In addition to designing new units, as part of the evolutionary process many of the older catalytic cracking units were modified to accommodate more complex feedstocks as well as feedstock blends containing residua. Feedstocks to the modern units now range from blends of gas oil fractions (included in normal heavier feedstocks for upgrading) to residua (*reduced crude*), heavy oil, and even tar sand bitumen.

Fluid catalytic cracking is the most important conversion process used in petroleum refineries to convert the high-boiling feedstock constituents to more valuable naphtha, olefin gases, as well as other products and is likely to remain predominant in the refining industry for at least another three-to-five decades.

19.1	Catalytic Cracking Chemistry	619
19.1.1	General Chemistry	619
19.1.2	Coke Formation	621
19.2	Feedstocks and Products	622
19.2.1	Feedstock Quality	622
19.2.2	Pretreating and Contaminant Removal	623
19.3	Reactor Design	624
19.3.1	Fixed-Bed Processes	624
19.3.2	Moving-Bed Processes	625
19.3.3	Fluid-Bed Processes	626
19.3.4	Process Variables	627
19.3.5	Regenerator Temperature	631
19.3.6	Regenerator Air Rate	631
19.4	Catalysts	632
19.4.1	Catalyst Types	632
19.4.2	Catalyst Manufacture	634
19.4.3	Catalyst Activity and Selectivity	634
19.4.4	Catalyst/Oil Ratio	635
19.4.5	Catalyst Deactivation	635
19.4.6	Catalyst Stripping	636
19.4.7	Catalyst Treatment	636
19.5	Process Options	639
19.5.1	Fluid-Bed Processes	639
19.5.2	Moving-Bed Processes	640
19.6	Options for Heavy Oil and Residua	641
19.6.1	Asphalt Residual Treating Process	642
19.6.2	Residue Fluid Catalytic Cracking Process	642
19.6.3	Heavy Oil Treating Process	642
19.6.4	R2R Process	643
19.6.5	Reduced Crude Oil Conversion Process	643
19.6.6	Shell FCC Process	643
19.6.7	S and W Fluid Catalytic Cracking Process	643
19.7	Environmental Aspects and the Future	644
	References	646

Catalytic cracking is a conversion process that was originally designed for gas oil but can also be applied to a variety of hydrocarbonaceous feedstocks ranging from heavy oil, residua, and also to certain types of biomass-derived feedstocks [19.1–7]. The concept of catalytic cracking is the thermal decomposition of feedstocks constituents in the presence of a catalyst, which in theory, is not consumed in the process. Catalytic cracking is one of several practical applications used in a refinery that employ a catalyst to improve process efficiency and product slate.

The process – in the typical commercial sense in a refinery – involves contacting the feedstock with a catalyst under suitable conditions of temperature, pressure, and at a residence time that will reduce the amount of coke (carbonaceous residue) formed in the process. The goal of the process is to convert as much as possible of the feedstock into hydrocarbon gases (if needed), naphtha, and kerosene-type products [19.1–4, 7, 8]. However, if coking occurs, a carbonaceous material is deposited on the catalyst, which markedly reduces catalyst activity and efficiency. Removal of the deposit from the catalyst is usually accomplished by cleaning the catalyst through burn-off of the deposit in the presence of air until catalyst activity is reestablished.

This history of catalytic cracking started in the early-to-mid decades of the twentieth century as the need for gasoline arose – especially the need for higher octane gasoline than could be produced as a straight-run distillation product from petroleum which was accompanied by advances in catalyst science and technology (Table 19.1) [19.9]. This has been ongoing and as the technology moves into the 21st century there are both new and continuing challenges:

1. There is the continued use of heavy oil and tar sand bitumen as feedstock.
2. Biomass will become a more common feedstock for fluid catalytic cracking (FCC) units, possibly blended with petroleum-based feedstocks.
3. Feedstocks derived from waste – also blended with petroleum-based feedstocks – will see more common use.

In the beginning, the early (pre-1940s) thermal cracking units produced approximately 50 vol.% of the total gasoline manufactured with an octane number on the order of 70 (the octane number of straight-run naphtha was on the order of 60). The naphtha produced by thermal cracking and the straight-run product were then blended together and also with lower boiling fractions and sometimes with *polymer gasoline*, *alkylate*, and *reformate* to produce gasoline base stock with an octane number of about 65 [19.1–7]. Additives, such as *tetraethyl lead (ethyl fluid)* were used to increase the octane number to 70 for the *regular-grade* gasoline and 80 for *premium-grade* gasoline. The thermal reforming and polymerization processes that were developed during the 1930s could be expected to further increase the octane number of gasoline to some extent, but a different approach was needed to generate a product with a higher octane number in order to keep pace with the development of more powerful automobile engines.

This occurred with the introduction (in 1936) of the catalytic cracking process that brought about major improvements in process efficiency and product yields, and which continued to evolve along with the advances in the chemistry and physics of the catalysts as well as an understanding of the chemistry of catalytic cracking [19.10, 11]. Major advances in reactor design, such as the evolution of catalyst bed design, have led to different design innovations for the reactors currently in use – such as, for example, single-stage cracking and dual-stage cracking.

When cracking is conducted in a single stage, the more reactive constituents of the feedstock will be decomposed showing a high conversion to gas and coke in the reaction time necessary for reasonable conversion of the more thermally stable feedstock con-

Table 19.1 The evolution of catalytic cracking

Catalytic cracking process	
Batch reactor (1915)	Catalyst: aluminum chloride (AlCl_3) – a Lewis acid, electron acceptor Alkane – electron (abstracted by AlCl_3) to produce a carbocation (C^+) Ionic chain reactions to crack long chains Product: low-boiling distillate
Houdry process (1936)	Continuous feedstock flow with multiple fixed-bed reactors Cracking/catalyst regeneration cycles Catalyst: clay, natural alumina/silica particles
Thermoform (1942)	Continuous feedstock flow with moving-bed catalysts Catalyst: synthetic alumina/silica particles
Fluid (1942)	Continuous feedstock flow with fluidized-bed catalysts
New catalysts (1965)	Synthetic alumina/silica and zeolite catalysts

stituents. Conversely, in a two-stage process, gas and naphtha from a short-reaction-time high-temperature cracking operation (which may occur in a flow line or vertical riser with minimal coke formation) are separated before the main cracking reactions take place in a second-stage reactor. Cracked gases are separated and sent to a fractionator whereas the catalyst and noncracked feedstock material together with recycle oil from a second-stage fractionator are recycled to the main reactor for further cracking to

produce gas, naphtha, gas oil streams, and recycle oil.

Finally, and to avoid confusion in nomenclature, there is no one process in the modern refinery that produces gasoline – gasoline for sales is a blend of several streams, including additives [19.7]. Thus, the fraction of the requisite boiling range produced by the fluid catalytic cracking process is, in this chapter, referred to as *naphtha* (often called FCC gasoline, but not true sales gasoline).

19.1 Catalytic Cracking Chemistry

Catalytic cracking is the thermal decomposition of petroleum constituents in the presence of a catalyst (Table 19.2) and discussions still remain about the influence of thermal decomposition as well as catalytic decomposition during the reaction. It is, essentially, the role of the influence of free radical species (thermal decomposition) and the influence of ionic species (catalytic decomposition) that may be in competition. Nevertheless, the reactions that occur during catalytic cracking are complex but, as a result of advances in catalyst science with a better understanding of catalyst activity, there is a measure of predictability of the outcome of the process. Each type of constituent of the feedstock will undergo reactions that are specific to that type of chemical.

For example, the major catalytic cracking reaction exhibited by paraffins is carbon–carbon bond scission into lighter paraffins and olefins. Bond rupture occurs at specific locations within the paraffin molecule, rather than at random locations as occurs in thermal cracking. For example, paraffins tend to crack toward the center and branch points of the molecule, the long chains cracking in several places simultaneously. In either case, catalytic cracking tends to yield products containing three or four carbon atoms rather than the one-carbon or two-carbon atom molecules produced in thermal cracking.

19.1.1 General Chemistry

As in thermal cracking [19.1–5, 7], high molecular weight constituents usually crack more readily than small molecules, unless there has been some recycle and the constituents of the recycle stream have become more refractory and are less liable to decompose. Paraffins having more than six carbon atoms may also undergo rearrangement of their carbon skeletons before cracking, and a minor amount of dehydrocyclization also occurs, yielding aromatics and hydrogen.

Olefins are the most reactive class of hydrocarbons in catalytic cracking and tend to crack from 1000 to 10 000 times faster than in thermal processes. Severe cracking conditions destroy olefins almost completely, except for those in the low-boiling naphtha and gaseous hydrocarbon range and, as in the catalytic cracking of paraffins, *iso*-olefins crack more readily than *n*-olefins. Furthermore, olefins tend to undergo rapid isomerization and yield mixtures with an equilibrium distribution of double-bond positions and, in addition, the chain-branching isomerization of olefins is fairly rapid and often reaches equilibrium. These branched-chain olefins can then undergo hydrogen transfer reactions with naphthenes and other hydrocarbons. Other olefin reactions include polymerization and condensation to

Table 19.2 Comparison of thermal cracking and catalytic cracking

Thermal cracking	Catalytic cracking
No catalyst	Uses a catalyst
Free-radical reaction mechanisms	More flexible in terms of product slate
Moderate yields of gasoline and other distillates	Ionic reaction mechanisms
Gas yields feedstock dependent	High yields of gasoline and other distillates
Low-to-moderate product selectivity	Low gas yields
Low octane number gasoline	High product selectivity
Low to moderate yield of C ₄ olefins	Low <i>n</i> -alkane yields
Low to moderate yields of aromatics	High octane number
	Chain-branching and high yield of C ₄ olefins
	High yields of aromatics

yield aromatic molecules, which in turn may be the precursors of coke formation.

In catalytic cracking, the cycloparaffin (naphthene) species crack more readily than paraffins but not as readily as olefins. Naphthene cracking occurs by both ring and chain rupture and yields olefins and paraffins, but formation of methane and the C_2 hydrocarbons (ethane, CH_3CH_3 , ethylene, $CH_2=CH_2$, and acetylene, $CH\equiv CH$) is relatively minor.

Aromatic hydrocarbons exhibit wide variations in their susceptibility to catalytic cracking. The benzene ring is relatively inert, and condensed-ring compounds, such as naphthalene, anthracene, and phenanthrene, crack very slowly. When these aromatics crack a substantial part of their *conversion* is reflected in the amount of coke deposited on the catalyst. Aromatic systems containing attached alkyl groups (C_2 or longer chains) typically form benzene and the corresponding olefins, and the thermal sensitivity (susceptibility to cracking) increases with an increase in the size of the alkyl group.

Although thermal cracking is a free radical (neutral) process, catalytic cracking is an ionic process involving carbonium ions, which are hydrocarbon ions having a positive charge on a carbon atom. The formation of carbonium ions during catalytic cracking can occur by: (1) addition of a proton from an acid catalyst to an olefin and/or (2) abstraction of a hydride ion (H^-) from a hydrocarbon by the acid catalyst or by another carbonium ion. However, carbonium ions are not formed by cleavage of a carbon-carbon bond.

More generally, the chemistry of catalytic cracking is not random involving the generation of free radical species but involves the generation of charged species that are dictated by the interactions between the feedstock constituents and the catalyst [19.12]. Thus, carbonium ions can be generated by protonation of carbon-carbon or carbon-hydrogen bonds at specific Brønsted sites. In addition, carbenium ions can be generated by:

1. Elimination of alkane or hydrogen from carbonium ions
2. Protonation of olefins
3. Abstraction of hydride by Lewis sites (including sorbed carbenium ions).

The reaction products are largely determined by carbenium ion chemistry (isomerization, β -scission, H-transfer, oligomerization/alkylation) which is influenced by acid-site strength, density and distribution and also by pore/cage effects. Shape selectivity (both primary and secondary) can influence the product distribution and, at higher temperatures, at lower conversions,

and in reactions in smaller pore zeolites, product distributions over strongly acid catalysts increasingly reflect carbonium-ion chemistry. However, the participation of free radical intermediates – particularly at higher temperature régimes – cannot be excluded but there is little evidence for a major influence of free radicals on the product distribution [19.12].

In essence, the use of a catalyst permits alternate routes for cracking reactions, usually by lowering the free energy of activation for the reaction. The acid catalysts first used in catalytic cracking were amorphous solids composed of approximately 87% silica (SiO_2) and 13% alumina (Al_2O_3) and were designated low-alumina catalysts. However, this type of catalyst is now being replaced by crystalline aluminosilicates (zeolites) or molecular sieves.

Once the carbonium ions are formed, the modes of interaction constitute an important means by which product formation occurs during catalytic cracking; for example, isomerization either by hydride ion shift or by methyl group shift, both of which occur readily. The trend is for stabilization of the carbonium ion by *movement* of the charged carbon atom toward the center of the molecule, which accounts for the isomerization of α -olefins to internal olefins when carbonium ions are produced. Cyclization can occur by internal addition of a carbonium ion to a double bond which, by continuation of the sequence, can result in aromatization of the cyclic carbonium ion.

Like the paraffins, naphthenes do not appear to isomerize before cracking. However, the naphthenic hydrocarbons (from C_9 upward) produce considerable amounts of aromatic hydrocarbons during catalytic cracking. Reaction schemes similar to that outlined here provide possible routes for the conversion of naphthenes to aromatics. Alkylated benzenes undergo nearly quantitative dealkylation to benzene without apparent ring degradation below $500^\circ C$ ($930^\circ F$). However, polymethylbenzene derivatives undergo disproportionation and isomerization with very little benzene formation.

Catalytic cracking can be represented by simple reaction schemes. However, questions have arisen as to how the cracking of paraffins is initiated. Several hypotheses for the initiation step in catalytic cracking of paraffins have been proposed but the kinetics picture remains complex [19.13–16], as might be expected when dealing with such complex feedstocks as are used in refineries. The Lewis site mechanism is the most obvious, as it proposes that a carbenium ion is formed by the abstraction of a hydride ion from a saturated hydrocarbon by a strong Lewis acid site: a tri-coordinated aluminum species. On Brønsted sites a carbenium ion may be readily formed from an olefin by the addition of

a proton to the double bond or, more rarely, via the abstraction of a hydride ion from a paraffin molecule by a strong Brønsted proton. This latter process requires the formation of hydrogen as an initial product. This concept was, for various reasons that are of uncertain foundation, often neglected.

19.1.2 Coke Formation

Higher boiling feedstocks that contain substantial amounts of aromatic constituents typically produce higher yields of coke than feedstocks of lesser aromaticity. Furthermore, condensed polynuclear aromatic systems and aromatic ring systems containing heteroatoms (i. e., nitrogen, oxygen, and sulfur) are more facile coke makers than simpler nonheteroatom ring systems [19.17].

Coke formation is considered, with just cause to be a malignant side reaction of normal carbenium ions. However, while chain reactions dominate events occurring on the surface, and produce the majority of products, certain less desirable bimolecular events have a finite chance of involving the same carbenium ions in a bimolecular interaction with one another. Of these reactions, most will produce paraffin products and leave carbene/carboid-type species on the surface. This carbene/carboid-type species can produce other products but the most damaging product will be one which remains on the catalyst surface and cannot be desorbed and results in the formation of coke, or remains in a noncoke form but effectively blocks the active sites of the catalyst.

A general reaction sequence for coke formation from paraffins involves oligomerization, cyclization, and dehydrogenation of small molecules at active sites within zeolite pores:

- Alkenes → alkenes
- Alkenes → oligomers
- Oligomers → naphthenes
- Naphthenes → aromatics
- Aromatics → coke.

Whether or not these are the true steps to coke formation can only be surmised. The problem with this reaction sequence is that it ignores sequential reactions in favor of consecutive reactions. And it must be accepted that the chemistry leading up to coke formation is a complex process, consisting of many sequential and parallel reactions.

There is a complex and little understood relationship between coke content, catalyst activity, and the chemical nature of the coke. For instance, the atomic hydrogen/carbon ratio of coke depends on how the coke

was formed; its exact value will vary from system to system [19.13]. And it seems that catalyst decay is not related in any simple way to the hydrogen-to-carbon atomic ratio of the coke, or to the total coke content of the catalyst, or any simple measure of coke properties. Moreover, despite many and varied attempts, there is currently no consensus as to the detailed chemistry of coke formation. There is, however, much evidence and good reason to believe that catalytic coke is formed from carbenium ions which undergo addition, dehydrogenation and cyclization, and elimination side reactions in addition to the main-line chain propagation processes [19.13].

The major coke-formers are constituents of the asphaltene fraction. The reactions leading to the formation of coke typically involve thermolytic removal of alkyl chains from the aromatic nuclei to form olefins and lower molecular weight higher polar species (carbenes and carboids) which then react to form coke. Indeed, as opposed to the bimolecular approach, the initial reactions in the coking of petroleum feedstocks that contain asphaltene constituents appear to involve unimolecular thermolysis of asphaltene aromatic-alkyl systems to produce volatile species (paraffins and olefins) and nonvolatile species (aromatics) [19.17–20].

Nitrogen species also appear to contribute to the pattern of coke formation. For example, the hydrogen or carbon-carbon bonds adjacent to ring nitrogen undergo thermolysis quite readily, as if promoted by the presence of the nitrogen atom [19.21, 22]. If it can be assumed that heterocyclic nitrogen plays a similar role in the thermolysis of asphaltene constituents, the initial reactions therefore involve thermolysis of aromatic-alkyl bonds that are enhanced by the presence of heterocyclic nitrogen. An ensuing series of secondary reactions, such as aromatization of naphthenic species and condensation of the aromatic ring systems, then leads to the production of coke. Thus, the initial step in the formation of coke from asphaltene constituents is the formation of volatile hydrocarbon fragments and nonvolatile heteroatom-containing systems. Furthermore, models of petroleum asphaltene constituents (which, despite evidence to the contrary, invoked the concept of an average structure involving a large polynuclear aromatic system) offer little, if any, explanation of the intimate events involved in the chemistry of coking [19.7].

Thus, it is now considered more likely that molecular species within the asphaltene fraction, which contains nitrogen and other heteroatoms (and have lower volatility than the pure hydrocarbons), are the prime movers in the production of coke [19.17]. Such species, containing various polynuclear aromatic systems, can be denuded of the attendant hydrocarbon moieties and

are undoubtedly insoluble [19.23–25] in the surrounding hydrocarbon medium. The next step is gradual carbonization of such entities to form coke [19.26–29]. This type of chemistry is also applicable to catalytic decomposition of feedstock constituents, especially in the case of reactions between basic nitrogen species and acidic sites on the catalyst. The attraction between the nitrogen atom and catalyst base is strong

and decomposition of the organic species on the catalyst results in a coking reaction leaving a carbonaceous residue on the catalyst. This newer concept of the behavior of asphaltene constituents offers doorways to understanding the behavior of asphaltene constituents in the presence of catalysts and the potential to markedly reduce coke formation in catalytic cracking units.

19.2 Feedstocks and Products

Many of the older refinery fluid catalytic cracking units were designed for specific feedstocks, such as high-boiling gas oil fractions. As petroleum refining evolved into the era of heavy oil and more complex feedstocks, the ability of any single unit to accommodate wide variations in feedstock became an issue related to the flexibility of the process, particularly the ability of the catalyst to accommodate the notorious catalyst poisons that are part of such feedstocks. The typical single-source gas oil feedstock became (almost) extinct and in the modern refinery is more inclined to be a blend of several high-boiling fractions – often with heavy oil and/or residuum as part of the blend, which has led to the development of residuum fluid catalytic cracking (RFCC) units. In addition to designing new units, as part of the evolutionary process many of the older catalytic cracking units were modified to accommodate more complex feedstocks as well as feedstock blends containing residua [19.6, 7]. Feedstocks to the modern units now range from blends of gas oil fractions (included in normal heavier feedstocks for upgrading) to residua (*reduced crude*), heavy oil, and even tar sand bitumen.

19.2.1 Feedstock Quality

In addition to a series of standard test methods for determining feedstock quality [19.30], improving feedstock quality (by removal of catalyst poisons such as *metallic constituents* and *high-molecular weight nonvolatile materials*) is usually carried out through the application of any one of several other processes [19.31, 32]:

- Controlled coking-visbreaking
- Propane deasphalting
- Furfural extraction
- Vacuum distillation
- Hydrodesulfurization (HDS).

Vacuum gas oil (initial boiling point: 315–345 °C or 600–650 °F; final boiling point: 510–565 °C or 950–1050 °F), as produced by vacuum flashing or vac-

uum distillation, has typically been the feedstock of choice with final boiling point being limited by the presence of coke-forming constituents (measured by the Conradson carbon residue) or metals content, since both properties have adverse effects on cracking characteristics and catalyst activity. The vacuum residua (565 °C⁺ or 1050 °F⁺) are occasionally included in feedstocks for a fluid catalytic cracking unit – especially when the units (residuum catalytic crackers) are capable of handling such materials [19.1–4, 6, 7]. In such cases, the residua have either (1) low propensity to form coke and/or (2) low metals content (as, for example, a residuum from a waxy crude) so that the effects of these properties are relatively minor and do not shorten the catalyst life by any large amount compared to the unblended gas oil. Many units also use recycle slurry oil (455 °C⁺ or 850 °F⁺) and a heavy cycle oil stream as feedstocks. Gas oils from thermal cracking or coking operations, hydrotreated gas oil, and deasphalted oil are often included in the feedstock to a catalytic cracking unit [19.1–4, 6, 7]. In some cases, the higher boiling fraction of bio-oil (produced by conversion of biomass to liquids) may also be included as blend stock [19.5].

However, the high levels of contaminants in heavy oil, residua, and bitumen – such as carbon-forming constituents that yield high levels of (Conradson) carbon residue and the overall coke production (as carbon on the catalyst) is high. Burning this coke requires additional regeneration air that might be a constraint that limits the capacity of the unit. In addition, there is a near-quantitative deposition of metallic constituents on to the catalyst where two significant effects are caused: (1) the deposited metals accelerate certain metal-catalyzed dehydrogenation reactions, thereby contributing to light-gas (hydrogen) production and to the formation of additional coke, and (2) the deposition of the metals on to the catalyst causes a decline in catalyst activity because the deposited metals tend to block the active catalytic sites, which requires frequent (and expensive) catalyst makeup practices (addition of fresh catalyst and withdrawal of spent or poisoned catalyst).

Finally, the amount of sulfur and nitrogen in the products, waste streams, and flue gas generally increases when high-boiling feedstocks are processed because these feed components typically have higher sulfur and nitrogen contents than gas oil. However, in the case of nitrogen, the issue is not only one of higher nitrogen levels in the products but also (because of the feedstock nitrogen is basic in character) catalyst poisoning that reduces the useful activity of the catalyst [19.33, 34].

In order to offset the effects of feedstock contaminants on the efficiency of fluid catalytic cracking units (as well as on other refining units), considerable use has been made of the chemical and physical relationship to *estimate* feedstock quality. For example, general feedstock quality and the suitability of the feedstock can be indicated by characterization factor (K)

$$K = \frac{\sqrt[3]{(\text{MABP})}}{\text{specific gravity at } 60^\circ\text{F}/60^\circ\text{F}}$$

In this equation, MABP is the mean average boiling point expressed in degrees Rankin ($^\circ\text{R}$, which is $^\circ\text{F} + 460$). However, the mean average boiling point is a single physical parameter, which can only indicate a *general trend* in feedstock quality [19.6, 7] and the accuracy and meaningful nature of the data remain questionable. However, the characterization factor and the boiling range of the feedstocks are generally insufficient for anything other than *approximate comparisons*. A more detailed description of the feedstock is needed to reflect and predict the variations in feedstock composition and cracking behavior [19.1–4, 7].

On the more physical equipment-related aspects of the process, heat-balance control may be the most immediate and troublesome aspect of processing high-boiling feedstocks. As the contaminant carbon increases, the first response is usually to increase regenerator temperature. Adjustments in operating parameters can be made to assist in this control, but eventually, a point will be reached for heavier feedstocks when

the regenerator temperature is too high for good catalytic performance. At this point, some external heat removal from the regenerator is required and would necessitate a mechanical modification like a catalyst cooler.

19.2.2 Pretreating and Contaminant Removal

Feedstocks for catalytic cracking can be any one (or blends) of the following [19.7, 35]:

1. Straight-run gas oil
2. Vacuum gas oil
3. Recycle stock
4. Atmospheric residuum
5. Vacuum residuum
6. Heavy oil
7. Tar bitumen
8. And on occasion used lubricating oil.

However, when blends of the above-named feedstocks are employed, compatibility of the constituents of the individual blends must be assured or excessive coke will be laid down on the catalyst as a result of the incompatibility (phase separation) of the feedstock constituents.

As a result of any such potential issues that may arise and cause coke formation and/or catalyst deactivation, there are several pretreatment options for the feedstocks for catalytic cracking units and these are [19.1–4, 7, 31, 35–37]:

1. Deasphalting to prevent excessive coking on catalyst surfaces
2. Demetallization, i. e., removal of nickel, vanadium, and iron to prevent catalyst deactivation
3. Use of a short residence time as a means of preparing the feedstock
4. Hydrotreating or mild hydrocracking to mitigate the possibility of excessive coking in the fluid catalytic cracking unit.

Table 19.3 Feedstock and product data for the fluid catalytic process with and without feedstock hydrotreating

Feedstock (> 370 °C, > 700 °F)	No pretreatment	With hydrotreatment
API	15.1	20.1
Sulfur (wt%)	3.3	0.5
Nitrogen (wt%)	0.2	0.1
Carbon residue (wt%)	8.9	4.9
Nickel + vanadium (ppm)	51.0	7.0
Products		
Naphtha (C ₅ -220 °C, C ₅ -430 °F) (vol.%)	50.6	58.0
Light cycle oil (220–360 °C, 430–680 °F) (vol.%)	21.4	18.2
Residuum (> 360 °C, > 680 °F) (wt%)	9.7	7.2
Coke (wt%)	10.3	7.0

In fact, hydrotreating the feedstock to the fluid catalytic cracking unit improves the yield and quality of naphtha (Table 19.3) and reduces the sulfur oxide (SO_x) emissions from the unit, but it is typically a high-pressure process and, furthermore, manipulation

of feedstock sulfur alone may not be sufficient to meet future gasoline performance standards. Refineries wishing to process heavy crude oil and/or tar sand bitumen may only have the option to desulfurize the resulting high-sulfur naphtha produced in the process.

19.3 Reactor Design

The main design focus of any fluid catalytic cracking process is the reactor and regenerator which are considered to be the heart of the fluid catalytic cracking unit and the various options have evolved accordingly [19.10, 38, 39]. The reactor is the vessel in which the cracked product vapors are separated from the so-called *spent catalyst* by flowing the vapors through a set of two-stage cyclones within the reactor, after which the *spent catalyst* flows downward through a steam stripping section to remove any hydrocarbon vapors before the spent catalyst returns to the *catalyst regenerator*. The flow of spent catalyst to the regenerator is regulated by a control valve in the spent catalyst line.

The major process variables are temperature, pressure, catalyst-feedstock ratio (ratio of the weight of catalyst entering the reactor per hour to the weight of feedstock throughput on an hourly basis), and space velocity (weight or volume of the feedstock charged per hour per weight or volume of catalyst in the reaction zone). Wide flexibility in product distribution and quality is possible through control of these variables along with the extent of internal recycling necessary. Increased conversion can be obtained by applying higher temperature or higher pressure. Alternatively, lower space velocity and higher catalyst-feedstock ratio will also contribute to an increased conversion.

When cracking is conducted in a single stage, the more reactive hydrocarbons may be cracked, with a high conversion to gas and coke, in the reaction time necessary for reasonable conversion of the more refractory hydrocarbons. However, in a two-stage process, gas and naphtha from a short-reaction-time, high-temperature cracking operation are separated before the main cracking reactions take place in a second-stage reactor.

The several processes currently employed in catalytic cracking differ mainly in the method of catalyst handling, although there is an overlap with regard to catalyst type and the nature of the products. The catalyst, which may be an activated natural or synthetic material, is employed in bead, pellet, or microspherical form and can be used in *fixed-*, *moving-*, or *fluid-bed* configurations.

19.3.1 Fixed-Bed Processes

The *fixed-bed process* was the first to be used commercially and uses a static bed of catalyst in several reactors, which allows a continuous flow of feedstock to be maintained [19.40]. Thus, the cycle of operations include:

1. Flow of feedstock through the catalyst bed
2. Discontinuance of feedstock flow and removal of coke from the catalyst by burning
3. Insertion of the reactor on-stream.

Feedstocks may range from naphtha to atmospheric residuum (*reduced crude*). Feed preparation (to remove *metallic constituents* and *high-molecular weight non-volatile materials*) is usually carried out through any one of the following ways [19.31, 32]:

- Coking
- Propane deasphalting
- Furfural extraction
- Vacuum distillation
- Viscosity breaking
- Thermal cracking
- Hydrodesulfurization.

Historically, the Houdry fixed-bed process, which went on-stream in June 1936, was the first of the modern catalytic cracking processes [19.41]. It was preceded only by the McAfee batch process, which employed a metal halide (aluminum chloride) catalyst but has long since lost any commercial significance.

In a fixed-bed process, the catalyst in the form of small lumps or pellets is made up in layers or beds in several (four or more) catalyst-containing drums (converters). The feedstock is vaporized at approximately 450°C (840°F) and less than 7–15 psi (0.5–1 bar) pressure as it passes through one of the converters where the cracking reactions take place. Deposition of coke on the catalyst renders it ineffective, and using a synchronized valve system, the feed stream is directed to a neighboring converter while the catalyst in the first converter is regenerated by carefully burning the coke deposits with air. After about 10 min, the catalyst is ready to go on-stream again.

Although fixed-bed catalytic cracking units have been phased out, they represented an outstanding chemical engineering commercial development by incorporating a fully automatic instrumentation system which provided a short-time reactor/purge/regeneration cycle, a novel molten salt heat transfer system, and a flue gas expander for recovering power to drive the regeneration air compressor.

The requirement of complete vaporization necessarily limited feeds to those with a low boiling range and higher boiling feedstock constituents are retained in a separator before the feed is passed into the bottom of the upflow fixed-bed reactors. The catalyst consisted of a pelletized natural silica alumina catalyst and was held in reactors or *cases* about 11 ft (3.4 m) in diameter and 38 ft (11.6 m) length for a 15 000 bbl/day operation. Cracked products are passed through the preheat exchanger, condensed, and fractionated in a conventional manner. The reactors operated at about 30 psi (207 kPa) and 480 °C (900 °F).

The heat of reaction and some of the required feed circulating a molten salt through vertical tubes distributed through the reactor beds. The reaction cycle of an individual reactor was about 10 min, after which the feed was automatically switched to a new reactor that had been regenerated. The reactor was purged with steam for about 5 min and then isolated by an automatic cycle timer. Regeneration air was introduced under close control and carbon was burned off at a rate at which the recirculating salt stream could control the bed temperature. This stream comprised a mixture of potassium nitrate (KNO_3) and sodium nitrate (NaNO_3), which melts at 140 °C (285 °F), and was cooled in the reactors through which the feed was being processed. The regeneration cycle lasted about 10 min. The regenerated bed was then purged of oxygen and automatically cut back into cracking service. There were 3–6 reactors in a unit but naphtha yields decreased by up to 20 vol.% over the life of the catalysts (approximately 18 months).

Equilibrium was never reached in this cyclic process. The gas oil conversion, i. e., the amount of feed converted to lighter components, was high at the start of a reaction cycle and progressively diminished as the carbon deposit accumulated on the catalyst until regeneration was required. Multiple parallel reactors were used to approach a steady-state process. However, the resulting process flows were still far from steady state. The reaction bed temperature varied widely during reaction and regeneration periods, and the temperature differential within the bed during each cycle was considerable.

Since the catalyst in the reactor becomes contaminated with coke, the catalyst is continuously withdrawn

from the bottom of the reactor and lifted by means of a stream of air into a regenerator where the coke is removed by controlled burning. The regenerated catalyst then flows to the fresh feed line, where the heat in the catalyst is sufficient to vaporize the fresh feed before it reaches the reactor, where the temperature is about 510 °C (950 °F).

Fixed-bed processes have now generally been superseded by moving- or fluid-bed processes.

19.3.2 Moving-Bed Processes

The fixed-bed process had obvious capacity and mechanical limitations that needed improvement and, thus, was replaced by a moving-bed process in which the hot salt systems were eliminated. The catalyst was lifted to the top of the reactor system and flowed by gravity down through the process vessels.

The *moving-bed process* uses a reaction vessel in which cracking takes place and a kiln in which the spent catalyst is regenerated; catalyst movement between the vessels is provided by various means.

In the moving-bed processes, the catalyst is in the form of pelletized (approximately 0.125 in (3 mm) diameter) beads that flow by gravity from the top of the unit through a seal zone to the reactor that operates at about 10 psi (69 kPa) and 455–495 °C (850 to 92 °F). The catalyst then flows down through another seal and countercurrently through a stripping zone to the regenerator or kiln that operates at a pressure that is close to atmospheric.

Two advances in the technology of moving-bed catalytic cracking have greatly changed the operation compared to the early processes. The more important of these advances was the introduction of crystalline aluminosilicate cracking catalysts and the second advance was the development of techniques to reduce catalyst attrition and metal erosion in moving-bed cracking units.

The *airlift Thermofor catalytic cracking (Socony airlift TCC) process* is a moving-bed, reactor-over-generator continuous process for conversion of heavy gas oils into lighter high-quality naphtha and middle distillate fuel oil [19.42, 43]. Feed preparation may consist of flashing in a tar separator to obtain vapor feed, and the tar separator bottoms may be sent to a vacuum tower from which the liquid feed is produced.

The gas-oil vapor-liquid flows downward through the reactor concurrently with the regenerated synthetic bead catalyst. The catalyst is purged by steam at the base of the reactor and gravitates into the kiln, or regeneration is accomplished by the use of air injected into the kiln. Approximately 70% of the carbon on the catalyst is burned in the upper kiln burning zone and the remainder in the bottom burning zone. Regenerated,

cooled catalyst enters the lift pot, where low-pressure air transports it to the surge hopper above the reactor for reuse.

The *Houdrifiow catalytic cracking process* is a continuous, moving-bed process employing an integrated single vessel for the reactor and regenerator kiln [19.40, 44]. The charge stock, sweet or sour, can be any fraction of the crude boiling between naphtha and soft asphalt. The catalyst is transported from the bottom of the unit to the top in a gas lift employing compressed flue gas and steam. The reactor feedstock and catalyst pass concurrently through the reactor zone to a disengager section, in which vapors are separated and directed to a conventional fractionation system. The spent catalyst, which has been steam purged of residual oil, flows to the kiln for regeneration, after which steam and flue gas are used to transport the catalyst to the reactor.

The *Houdresid catalytic cracking process* is a process that uses a variation of the continuously moving catalyst bed designed to obtain high yields of high-octane naphtha and light distillate from reduced crude charge [19.45]. Residuum cuts ranging from crude tower bottoms to vacuum bottoms, including residua high in sulfur or nitrogen, can be employed as the feedstock, and the catalyst is synthetic or natural. Although the equipment employed is similar in many respects to that used in Houdrifiow units, novel process features modify or eliminate the adverse effects and catalyst and product selectivity usually resulting when heavy metals – iron, nickel, copper, and vanadium – are present in the fuel. The Houdresid catalytic reactor and catalyst-regenerating kiln are contained in a single vessel. Fresh feed plus recycled gas oil are charged to the top of the unit in a partially vaporized state and mixed with steam.

The *suspensoid catalytic cracking process* was developed from the thermal cracking process carried out in tube and tank units [19.46, 47]. Small amounts of powdered catalyst or a mixture with the feedstock are pumped through a cracking coil furnace. Cracking temperatures are 550–610 °C (1025–1130 °F), with pressures of 200–500 psi (14–34 bar). After leaving the furnace, the cracked material enters a tar separator where the catalyst and tar are left behind. The cracked vapors enter a bubble tower where they are separated into two parts, gas oil and pressure distillate. The latter is separated into naphtha and gases. The spent catalyst is filtered from the tar, which is used as a heavy industrial fuel oil. The process is actually a compromise between catalytic and thermal cracking. The main effect of the catalyst is to allow a higher cracking temperature and to assist mechanically in keeping coke from accumulating on the walls of the tubes. The normal catalyst employed is spent clay

obtained from the contact filtration of lubricating oils (2–10 pound/barrel of feed).

19.3.3 Fluid-Bed Processes

The application of fluidized solid techniques to catalytic cracking resulted in a major process breakthrough. It was possible to transfer all of the regeneration heat to the reaction zone. Much larger units could be built and higher boiling feedstocks could be processed. In fact, the improvements in catalysts and unit configurations have permitted the catalytic cracking of higher boiling (poorer quality) feedstocks such as residua. Presently, there are a number of processes that allow catalytic cracking of heavy oils and residua [19.1–4, 7, 35].

The *fluid-bed process* differs from the fixed-bed and moving-bed processes insofar as the powdered catalyst is circulated essentially as a fluid with the feedstock [19.48]. The several fluid catalytic cracking processes in use differ primarily in mechanical design [19.49, 50]. Side-by-side, reactor-regenerator configuration or the reactor either above or below the regenerator are the main mechanical variations. From a flow standpoint, all fluid catalytic cracking processes contact the feedstock and any recycle streams with the finely divided catalyst in the reactor.

The first fluid catalytic cracking units were model I upflow units in which the catalyst flowed up through the reaction and regeneration zones in a riser type of flow regime. Originally, the model I unit was designed to feed a reduced crude to a vaporizer furnace where all of the gas oil was vaporized and fed, as vapor, to the reactor. The nonvolatile residuum (bottoms) bypassed the cracking section. The original model I upflow design (1941) was superseded by the model II downflow design (1944) followed by the model III (1947) balanced-pressure design with the later introduction of the model IV low-elevation design (1952).

A typical modern fluid catalytic cracking process involves mixing a preheated hydrocarbon charge with hot, regenerated catalyst as it enters the riser pipe leading to the reactor. The charge is combined with a recycle stream within the riser pipe, vaporized, and raised to reactor temperature (485–540 °C; 900–1000 °F) by the hot catalyst. As the mixture travels up the riser pipe, the charge is cracked at 10–30 psi (0.7–2 bar). In the more modern fluid catalytic cracking process units, all cracking takes place in the riser pipe and continues until the oil vapors are separated from the catalyst in the reactor cyclones. The resultant product stream (cracked product) is then charged to a fractionating column where it is separated into fractions, and some of the heavy oil is recycled to the riser pipe. Spent catalyst is regenerated to get rid of coke that collects on the catalyst during the

process. Spent catalyst flows through the catalyst stripper to the regenerator, where most of the coke deposits burn off and fresh catalyst is added as spent catalyst is removed to optimize the cracking process.

The three main components of a fluid-bed catalytic cracking unit are:

1. The reactor
2. The stripper
3. The regenerator.

Thus, in the unit, the catalyst and the feed and product hydrocarbons are lifted up in the riser pipe to the *reactor* where the predominately endothermic cracking processes take place. Since the reactions are endothermic, reaction temperature declines from bottom to top. At the top, the mixture enters a solid-gas separator, and the product vapors are led away. Cracked gases are separated and fractionated; the catalyst and residue, together with recycle oil from a second-stage fractionator, pass to the main reactor for further cracking. The products of this second-stage reaction are gas, naphtha and gas oil streams, and recycle oil.

The coked catalyst enters the *stripper* where steam is added and unreacted-reacted hydrocarbons adsorbed on the catalyst are released. The stripped catalyst is then directed into the *regenerator* where air is added and the combustion of coke on the catalyst (and any hydrocarbons still adsorbed which were not stripped) occurs with the liberation of heat. Regenerator temperatures are typically 705–760 °C (1300–1400 °F). Heat exchangers and the circulating catalyst capture the heat evolved during regeneration to be used in preheating the reactor feed to appropriate cracking temperatures (usually in the range 495–550 °C (925–1020 °F)).

During operations, the entire catalyst inventory is *continuously* circulated through the unit. Catalyst residence time in the riser reactor section is typically 1–3 s (with current trends to even shorter residence times), and the entire reactor-stripper-regenerator cycle is less than 10 min. To achieve cycle times of this order, catalyst circulation rates as high as 1 T/s in large units are required. To withstand such movement, the catalyst must be sufficiently *robust* to withstand the operational stress.

Process temperatures are high, coke is repeatedly deposited and burned off, and the catalyst particles are moving at high speed through steel reactors and pipes. Contact between the catalyst particles and the metal walls and interparticle contact are unavoidable. Thus, catalyst loss from the unit caused by poor attrition resistance can be a serious problem, since the quantities lost must be replaced by fresh catalyst additions to maintain constant unit performance. Catalyst manufacturers work hard to prevent inordinate losses due to attrition,

and refineries keep a close watch on catalyst quality to be sure the product conforms to their specifications. Therefore, the robustness of the catalyst is carefully monitored and controlled to a high attrition resistance that is determined by rigorous test methods that place their focus on a semiquantitative evaluation of attrition resistance, which is generally related to breakdown with time in commercial units.

As intimated above, in some units cracking does not always take place in the reactor and reaction often occurs in the vertical or upwardly sloped pipe called the *riser* (giving credence to the name *riser reactor*, with this *riser pipe cracking*) forming products, including coke [19.51]. Preheated feedstock is sprayed into the base of the riser via feed nozzles where it contacts extremely hot fluidized catalyst at 1230–1400 °F (665–760 °C). The hot catalyst vaporizes the feed and catalyzes the cracking reactions that break down the high molecular weight oil into lighter components including liquefied petroleum gas (LPG), constituents, naphtha, and diesel. The catalyst-hydrocarbon mixture flows upward through the riser for just a few seconds and then the mixture is separated via cyclones. The catalyst-free hydrocarbons are routed to a main fractionator for separation into:

- Fuel gas
- Propane and butanes
- Naphtha
- Light cycle oils used in diesel and jet fuel
- Heavy fuel oil.

Since the catalyst in the reactor becomes contaminated with coke, the catalyst is continuously withdrawn from the bottom of the reactor and lifted by means of a stream of air into a regenerator where the coke is removed by controlled burning. The regenerated catalyst then flows to the fresh feed line, where the heat in the catalyst is sufficient to vaporize the fresh feed before it reaches the reactor, where the temperature is about 510 °C (950 °F).

19.3.4 Process Variables

The major process variables are temperature, pressure, catalyst-oil ratio (ratio of the weight of catalyst entering the reactor per hour to the weight of oil charged per hour), and space velocity (weight or volume of the oil charged per hour per weight or volume of catalyst in the reaction zone). Wide flexibility in product distribution and quality is possible through control of these variables along with the extent of internal recycling necessary [19.52]. Increased conversion can be obtained by applying higher temperature or higher pressure. Alternatively, lower space velocity and higher

catalyst/oil ratio will also contribute to an increased conversion.

All of the independent variables in catalytic cracking have a significant effect on conversion which is truly a dependent variable but can be shown as a function of API gravity as well as a variety of other functions [19.53]. The detailed effects of changing conversion depend on how conversion is changed, i. e., by temperature, space velocity, or catalyst/oil ratio, and catalyst activity. Increasing conversion increases yields of naphtha and all light products up to a conversion level of 60–80% by volume in most cases. At this high conversion level, secondary reactions become sufficient to cause a decrease in the yields of olefins and naphtha. However, the point at which this occurs is based on the feedstock, operating conditions, catalyst activity, and other parameters.

However, these variables are not always available for maximizing conversion since most fluid catalytic cracking units already operate at an optimum conversion level corresponding to a given feed rate, feed quality, set of processing objectives and catalyst under one or more unit constraints (e.g., wet gas compressor capacity, fractionation capacity, air blower capacity, reactor temperature, regenerator temperature, and catalyst circulation). Once the optimum conversion level is found, there are very few additional degrees of freedom for changing the operating variables.

Reactor Temperature

Increasing *reactor temperature* increases feedstock conversion, primarily through a higher rate of reaction for the endothermic cracking reaction and also through increased cat/oil (catalyst/oil) ratio. A 10 °F increase in reactor temperature can increase conversion by 1–2% absolute but, again, this is feedstock dependent. Higher reactor temperature also increases the amount of olefins in naphtha and in the gases. This is due to the higher rate of primary cracking reactions relative to secondary hydrogen transfer reactions which saturate olefins in the naphtha boiling range and lowers gasoline octane.

The principal effects of increasing reactor temperature at constant conversion are to decrease naphtha and coke yield and to increase methane (CH₄), ethane (C₂H₆), propane (CH₃CH₂CH₃), and total butane (C₄H₁₀) yield; yields of pentanes (C₅H₁₂) and higher molecular weight paraffins decrease while olefin yields are increased.

The effect of reactor temperature on a commercial unit is, of course, considerably more complicated as variables other than temperature must be changed to maintain heat balance. For example, in order to increase the temperature of a reactor at constant fresh feed rate, interrelated changes of recycle rate, space velocity, and

feedstock preheat are required to maintain heat balance in the unit by increasing circulation rate and coke yield.

The combined effects of higher reactor temperature and higher conversion resulted in the following additional changes:

1. Increased yields of butanes and propane
2. Increased yields of naphtha
3. Decreased yield of light catalytic cycle oil.

Thus, the effects of an increase in reactor temperature on an operating unit reflect not only the effects of temperature per se but also the effects of several concomitant changes such as increased conversion and increased catalyst/oil ratio.

Pressure

Higher conversion and coke yield are thermodynamically favored by higher *pressure*. However, pressure is usually varied over a very narrow range due to limited air blower horsepower. Conversion is not significantly affected by unit pressure since a substantial increase in pressure is required to significantly increase conversion.

Catalytic cracker pressures are generally set slightly above atmospheric by balancing the yield and quality debits of high pressure plus increased regeneration air compression costs against improved cracking and regeneration kinetics, the lower cost of smaller vessels, plus, in some cases, power recovery from the regenerator stack gases. Representative yield and product effects show, at the same conversion level, that coke and naphtha yields are increased marginally and light gas yields are reduced at the higher pressure – in addition, the sulfur content of the naphtha fraction is reduced.

Pressure levels in commercial units are generally in the range 15–35 psi (103–241 kPa). Lowering the partial pressure of the reacting gases with steam will improve yields somewhat, but the major beneficial effect of feed injection steam is that it atomizes the feed to small droplets that will vaporize and react quickly. If feed is not atomized, it will soak into the catalyst and possibly crack to a higher coke make.

Both pressure and partial pressure of the feedstock, or steam/feedstock ratio, are generally established in the design of a commercial unit and thus are usually not available as independent variables over any significant range. However, in some units, injector steam is varied over a narrow range to balance carbon make with regeneration carbon burn off.

Recycle Rate

With most feedstocks and catalyst, the yield of naphtha increases with increasing conversion up to a point, passes through a maximum, and then decreases. This phenomenon (*over-cracking*) is caused by the increased

thermal stability (*refractory character*) of the unconverted feed as conversion increases and the destruction of valuable naphtha constituents through secondary reactions, primarily cracking of olefins. The onset of secondary reactions and the subsequent leveling off or decrease in yield of naphtha can be avoided by recycling a portion of the reactor product, usually a fractionator product with a boiling point on the order of 345–455 °C (650–850 °F).

Furthermore, starting from the fractionator bottom, the slurry oil cooler is a very demanding position, where fouling is a major problem. Some of the suspended catalyst will go into the fractionator and end up in the unit bottom fraction (slurry oil), which has the potential to cause fouling and significant problems when cooled in a traditional shell-and-tube system. If the slurry oil is clarified (to become what is known as clarified slurry oil, CSO) it has a much lower tendency to cause fouling than the catalytic cracker bottom fraction.

Other tests have shown the following effects of increasing recycle rate when space velocity was simultaneously adjusted to maintain constant conversion:

1. Naphtha yield increased significantly
2. Coke yield decreases appreciably
3. Decrease in the yield of dry gas components, propylene, and propane
4. Butane yields decreased while butylene yields increased slightly
5. Light catalytic cycle oil and clarified oil yields increased, but heavy catalytic cycle oil yield decreased.

With the introduction of high-activity zeolite catalysts, it was found that in once-through cracking operations with no recycle, the maximum yield of naphtha was much higher. In effect, the higher activity catalysts were allowing higher conversions to be obtained at severity levels that significantly reduced the extent of secondary reactions (*over-cracking*). Thus, on many units employing zeolite catalysts, the recycle stream has been eliminated or reduced to less than 15 vol.% of the fresh feed rate.

Reaction Time and Space Velocity

An increase in *reaction time* available for cracking also increases conversion. Fresh feed rate, riser steam rate, recycle rate, and pressure are the primary operating variables that affect reaction time for a given unit configuration. Conversion varies inversely with these stream rates due to limited reactor size available for cracking. Conversion has been increased by a decrease in the rate of injection of fresh feedstock. Under these circumstances, over-cracking of naphtha to liquefied petroleum gas and to dry gas may occur due to the in-

crease in reactor residence time. One approach to offset any potential naphtha over-cracking is to add additional riser steam to lower hydrocarbon partial pressure for more selective cracking. Alternatively, an operator may choose to lower reactor pressure or increase the recycle rate to decrease residence time. Naphtha over-cracking may be controlled by reducing the availability of catalytic cracking sites by lowering cat/oil ratio.

The role of space velocity as an independent variable arises from its relation to *catalyst contact time* or *catalyst residence time*. Thus,

$$\Theta = \frac{60}{(\text{WHSV} \times \text{C/O})}$$

where Θ = catalyst residence time (min), WHSV = weight hourly space velocity on a total weight basis, and C/O = catalyst/oil weight ratio.

The catalyst/oil ratio is a dependent variable so that catalyst time becomes directly related to the weight hourly space velocity. When catalyst contact time is low, secondary reactions are minimized, thus naphtha yield is improved and light gas and coke yields are decreased. In dense bed units the holdup of catalyst in the reactor can be controlled within limits, usually by a slide valve in the spent-catalyst standpipe, and feed rate can also be varied within limits. Thus, there is usually some freedom to increase space velocity and reduce catalyst residence time. In a riser-type reactor, holdup and feed rate are not independent and space velocity is not a meaningful term. Nevertheless, in dense-bed and riser-type reactors, contact times are usually minimized to improve selectivity. An important step in this direction was the introduction of high-activity zeolite catalyst. These catalysts require short contact times for optimum performance and have generally moved cracking operations in the direction of minimum holdup in dense-bed reactors or replacement of dense-bed reactors with short-contact-time riser reactors.

Strict comparisons of short-contact-time riser cracking versus the longer contact time dense-bed mode of operations are generally not available due to differences in catalytic activity, carbon content of the regenerated catalyst, or factors other than contact time but inherent in the two modes of operation. However, in general, improvements in catalyst activity have resulted in the need for less catalyst in the reaction zone.

Many units are designed with only riser cracking, i. e., no dense-bed catalyst reactor cracking occurs and all cracking is done in the catalyst–oil transfer lines leading into the reactor cyclone vessel. However, in some of these instances the reactor temperature must be increased to the 550–565 °C (1020–1050 °F) range in order to increase the intensity of cracking conditions to achieve the desired conversion level. This is because

not enough catalyst can be held in the riser zone, since the length of the riser is determined by the configuration and elevation of the major vessels in the unit. Alternatively, superactive catalysts can be used to achieve the desired conversion in the riser.

Significant selectivity disadvantages have not been shown if a dispersed catalyst phase or even a very small dense bed is provided downstream of the transfer line riser cracking zone. In this case the cracking reaction can be run at a lower temperature, say 510 °C (950 °F), which will reduce light gas make and increase naphtha yield when compared to the higher temperature (550–565 °C or 1020–1050 °F) operation.

Heat Balance

In the operation of a fluid catalytic cracking unit where heat balance is necessary, increasing the temperature of the feedstock to the unit reduces the heat that must be supplied by combustion of the coked catalyst in the regenerator. Feedstock preheating is usually supplied by heat exchange with hot product streams, a fired preheater, or both. When feed rate, recycle rate, and reactor temperature are held constant as feed preheat is increased, the following changes in operation result:

1. The catalyst/oil ratio (catalyst circulation rate) is decreased to hold the reactor temperature constant.
2. Conversion and all conversion-related yield, including coke, decline due to the decrease in catalyst/oil ratio and severity.
3. The regenerator temperature will usually increase. Although the total heat released in the regenerator and the air required by the regenerator are reduced by the lower coke yield, the lower catalyst circulation usually overrides this effect and results in an increase in regenerator temperature.
4. As a result of the lower catalyst circulation rate the usual outcome is that residence time in the stripper and overall stripper efficiency is increased, liquid recovery is increased, and there is a corresponding decrease in coke. However, these effects must be weighed against the cost of the excess heat applied to the unit.

Thus, in order to maintain a dynamic heat balance in the process, hot regenerated catalyst supplying the net heat demand is required by the reactor. Finely sized solid catalyst continuously circulates in a closed loop between the reactor and the catalyst regeneration system (Fig. 19.1). The feedstock and catalyst are in intimate contact in the riser reactor in a controlled ratio and with the residence time and temperature required to achieve efficient conversion. The products are disengaged from the spent catalyst using a catalyst stripper

(Fig. 19.1) where any carbon product vapors entrained with the catalyst are removed and recovered. The regenerator (Fig. 19.1) system removes coke deposited on the catalyst and restores catalytic activity by combustion of the catalyst/coke in air. The system also provides heat of reaction and heat of vaporization (of the feedstock) by returning hot, freshly regenerated catalyst back to the reaction system.

The hot regenerated catalyst flows to the base of the reactor system riser where it is contacted with feed supplied through feedstock injectors. Vaporized feedstock and catalyst travel up the riser where catalytic reactions occur. The reacted vapor is rapidly disengaged from the spent catalyst in direct-coupled riser cyclones and routed directly to product fractionation, which minimizes the time available for nonselective, postriser cracking (typically, thermal cracking). The vapors from the reactor are quenched and fractionated in the product recovery system, which yields C₄ and lower molecular weight gases, naphtha (often called FCC gasoline, but not true sales gasoline), and middle distillate products (Fig. 19.1). The spent catalyst separated by the riser cyclones is degassed of most of the reaction vapor while flowing into the catalyst stripper, where the catalyst is steam-stripped to produce more hydrocarbon product.

The spent catalyst is transported from the stripper into the regenerator where the carbonaceous deposits on the coke start to react with the lift air at a lower combustion temperature relative to the regenerator dense-bed temperature, which reduces hydrothermal deactivation of the catalyst. The remainder of the carbonaceous deposit is burned off in the regenerator and the flue gas is routed through cyclones to minimize catalyst losses and then sent to energy recovery. Hot regenerated catalyst overflows into an external catalyst hopper where it is aerated to the necessary density before flowing back to the base of the riser. Furthermore, it is often considered to be advantageous to use any feedstock preheating effects, including the reduced air requirement, by increasing the total feed rate until coke production again requires all of the available air.

Additives

In addition to the cracking catalysts described above, a series of *additives* has been developed that catalyze or otherwise alter the primary catalyst's activity/selectivity or act as pollution control agents. Additives are most often prepared in microspherical form to be compatible with the primary catalysts and are available separately in compositions that:

1. Enhance gasoline octane and light olefin formation
2. Selectively crack heavy cycle oil

3. Passivate vanadium and nickel present in many heavy feedstocks
4. Oxidize coke to carbon dioxide
5. Reduce sulfur dioxide emissions.

Both vanadium and nickel deposit on the cracking catalyst and are extremely deleterious when present in excess of 3000 ppm on the catalyst. Formulation changes to the catalyst can improve tolerance to vanadium and nickel but the use of additives that specifically passivate either metal is often preferred.

19.3.5 Regenerator Temperature

Catalyst circulation, coke yield, and feedstock preheating are the principal determinants of regenerator temperature that is generally allowed to respond as a dependent variable within limits. Mechanical or structural specifications in the regenerator section generally limit regenerator temperature to a maximum value specific to each unit. However, in some cases the maximum temperature may be set by catalyst stability. In either case, if regenerator temperature is too high it can be reduced by decreasing feedstock preheat; catalyst circulation is then increased to hold a constant reactor temperature and this increased catalyst circulation will carry more heat from the regenerator and lower the regenerator temperature. The sequence of events is actually more complicated as the shift in catalyst/oil ratio and, to a lesser extent, the shift in carbon content of the regenerated catalyst will change coke make and the heat release in the regenerator.

19.3.6 Regenerator Air Rate

The amount of air required for regeneration depends primarily on coke production. Regenerators have been operated with only a slight excess of air leaving the dense phase. With less air, carbon content of the spent catalyst increases and a reduction in coke yield is required of air, burning of carbon monoxide (CO) to carbon dioxide (CO₂) above the dense bed will occur. This *after burning* must be controlled as extremely high temperature in the absence of the heat sink provided by the catalyst in the dense phase.

In terms of catalyst regeneration, higher stability catalysts are available and regenerator temperatures can be increased by 38–65 °C (100–150 °F) up to the 720–745 °C (1325–1370 °F) range without significant thermal damage to the catalyst. At these higher temperatures the oxidation of carbon monoxide to carbon dioxide is greatly accelerated and the regenerator can be designed to absorb the heat of combustion in the catalyst under controlled conditions. The carbon burning rate is improved at the higher temperatures, and there are usually selectivity benefits associated with the lower carbon on regenerated catalyst; this high temperature technique usually results in carbon on regenerated catalyst levels of 0.05% by weight or less. In addition, the use of catalysts containing promoters for the oxidation of carbon monoxide to carbon dioxide produce a major effect of high temperature regeneration, i. e., low carbon monoxide content regenerator stack gases and the resultant regenerator conditions may result in a lower carbon content regenerated catalyst.

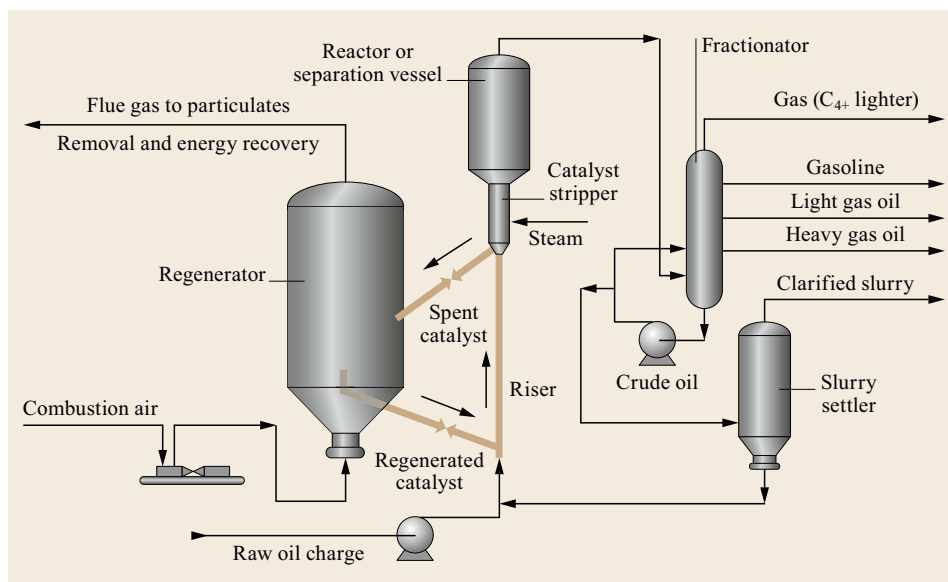


Fig. 19.1 Detailed schematic of a fluid catalytic cracking reactor (after [19.54])

19.4 Catalysts

Cracking of crude oil fractions occurs over many types of catalytic materials, but high yields of desirable products are obtained with hydrated aluminum silicates. These may be either activated (acid-treated natural clays of the bentonite type) or synthesized silica-alumina or silica-magnesia preparations. Their activity to yield essentially the same products may be enhanced to some extent by the incorporation of small amounts of other materials, such as the oxides of zirconium (zirconia, ZrO_2), boron (boria, B_2O_3 , which has a tendency to volatilize away on use), and thorium (thoria, ThO_2). Both the natural and the synthetic catalysts can be used as pellets or beads, and also in the form of powder; in either case replacements are necessary because of attrition and gradual loss of efficiency [19.55, 56].

The catalysts must be stable to physical impact loading and thermal shocks and must withstand the action of carbon dioxide, air, nitrogen compounds, and steam. They should also be resistant to sulfur compounds; the synthetic catalysts and certain selected clays appear to be better in this regard than average untreated natural catalysts. The silica-alumina catalysts are reported to give the highest-octane naphtha and silica-magnesia the largest yields, with the natural clays falling between them.

The catalysts are porous and highly adsorptive, and their performance is affected markedly by the method of preparation. Two catalysts that are chemically identical but have pores of different size and distribution may have different activity, selectivity, temperature coefficient of reaction rate, and response to poisons. The intrinsic chemistry and catalytic action of a surface may be independent of pore size, but small pores appear to produce different effects because of the manner and time in which hydrocarbon vapors are transported into and out of the interstices.

Commercially used cracking catalysts are *insulator catalysts* possessing strong acidic properties. They function as catalysts by altering the cracking process mechanisms through an alternative mechanism involving *chemisorption* by *proton donation* and *desorption*, resulting in cracked oil and theoretically restored catalyst. Thus, it is not surprising that all cracking catalysts are poisoned by proton-accepting vanadium.

The catalyst/oil volume ratios range from 5 : 1 to 30 : 1 for the different processes, although most processes are operated using a 10 : 1 ratio. However, for moving-bed processes the catalyst/oil volume ratios may be substantially lower than 10 : 1.

In addition to zeolite and matrix activity, many of the physical and chemical properties of the catalyst (*catalyst design*) contribute to increased conversion

through selectivity differences. These include zeolite type, pore size distribution, relative matrix to total surface area, and chemical composition.

Increasing the concentration of catalyst in the reactor, often referred to as cat/oil ratio, will increase the availability of cracking for maximum conversion, assuming the unit is not already operating at a catalyst circulation limit. This can be achieved by increasing reactor heat load or switching to a lower coke selective (i. e., lower delta coke) catalyst. Reactor heat load can be raised by increased reactor temperature or lower feed preheat temperature. This, in turn, increases the cat/oil ratio to maintain the unit in heat balance.

The lower the *carbon on regenerated catalyst* the higher the availability of cracking sites since less coke is blocking acid cracking sites. The carbon on the regenerated catalyst is reduced by increasing regeneration efficiency through the use of carbon monoxide oxidation promoters. Carbon on the regenerated catalyst can also be reduced by more efficient air and spent catalyst contact. Increased regenerator bed levels also reduce the amount of carbon on the regenerated catalyst through increased residence time but this must be traded off with reduced dilute phase disengager residence time and the possibility for increased catalyst losses.

19.4.1 Catalyst Types

The cracking of crude oil fractions occurs over many types of catalytic materials and cracking catalysts can differ markedly in both activity to promote the cracking reaction and in the quality of the products obtained from cracking the feedstocks [19.57–63]. Activity can be related directly to the total number of active (acid) sites per unit weight of catalyst and also to the acidic strength of these sites. Differences in activity and acidity regulate the extent of various secondary reactions occurring and thus the product quality differences. The acidic sites are considered to be Lewis-acid or Brønsted-acid sites, but there is much controversy as to which type of site predominates.

The first cracking catalysts were acid leached *montmorillonite clays*. The acid leach was to remove various metal impurities, principally iron, copper, and nickel that could exert adverse effects on the cracking performance of the catalyst. The catalysts first used in fixed-bed and moving-bed reactor systems were in the form of shaped pellets. Later, with the development of the fluid catalytic cracking process, the clay catalysts were made in the form of a ground, sized powder. Clay catalysts are relatively inexpensive and have been used extensively for many years.

The desire to have catalysts that were uniform in composition and catalytic performance led to the development of *synthetic catalysts*. The first synthetic cracking catalyst consisting of 87% silica (SiO_2) and 13% alumina (Al_2O_3) was used in pellet form and used in fixed-bed units in 1940. Catalysts of this composition were ground and sized for use in fluid catalytic cracking units. In 1944 catalysts in the form of beads about 2.5–5.0 mm diameter were introduced and comprised about 90% silica and 10% alumina and were extremely durable. One version of these catalysts contained a minor amount of chromia (Cr_2O_3) to act as an oxidation promoter.

Neither silica (SiO_2) nor alumina (Al_2O_3) alone is effective in promoting catalytic cracking reactions. In fact, they (and also activated carbon) promote hydrocarbon decompositions of the thermal type. Mixtures of anhydrous silica and alumina ($\text{SiO}_2 \cdot \text{Al}_2\text{O}_3$) or anhydrous silica with hydrated alumina ($2\text{SiO}_2 \cdot 2\text{Al}_2\text{O}_3 \cdot 6\text{H}_2\text{O}$) are also essentially noneffective. A catalyst having appreciable cracking activity is obtained only when prepared from hydrous oxides followed by partial dehydration (*calcining*). The small amount of water remaining is necessary for proper functioning.

Commercial synthetic catalysts are amorphous and contain more silica than is called for by the preceding formulae; they are generally composed of 10–15% alumina (Al_2O_3) and 85–90% silica (SiO_2). The natural materials, montmorillonite, a nonswelling bentonite, and halloysite, are hydrosilicates of aluminum, with a well-defined crystal structure and approximate composition of $\text{Al}_2\text{O}_3 \cdot 4\text{Si}_2\text{O} \cdot x\text{H}_2\text{O}$. Some of the newer catalysts contain up to 25% alumina and are reputed to have a longer active life.

In addition to synthetic catalysts comprising silica-alumina, other combinations of *mixed oxides* were found to be catalytically active and were developed during the 1940s. These systems included silica (SiO_2), magnesia (MgO), silica-zirconia ($\text{SiO}_2\text{-ZrO}$), silica-alumina-magnesia, silica-alumina-zirconia, and alumina-boria ($\text{Al}_2\text{O}_3\text{-B}_2\text{O}_3$). Of these, only silica-magnesia was used in commercial units but operating difficulties developed with the regeneration of the catalyst which at the time demanded a switch to another catalyst. Further improvements in silica-magnesia catalysts have since been made. High yields of desirable products are obtained with hydrated aluminum silicates. These may be either activated (acid-treated natural clays of the bentonite type) or synthesized silica-alumina or silica-magnesia preparations. Both the natural and the synthetic catalysts can be used as pellets or beads, and also in the form of powder; in either case replacements are necessary because of attrition and gradual loss of efficiency [19.55, 56].

During the period 1940 to 1962, the cracking catalysts used most widely commercially were the aforementioned acid-leached clays and silica alumina. The latter was made in two versions; *low alumina* (about 13% Al_2O_3) and *high alumina* (about 25% Al_2O_3) contents. High-alumina content catalysts showed a higher equilibrium activity level and surface area.

During the 1958 to 1960 period, *semisynthetic catalysts* of silica-alumina catalyst were used in which approximately 25–35% kaolin was dispersed throughout the silica-alumina gel. These catalysts could be offered at a lower price and therefore were disposable but they were marked by a lower catalytic activity and greater stack losses because of increased attrition rates. One virtue of the semisynthetic catalysts was that a lesser amount of adsorbed, unconverted, high molecular weight products on the catalyst were carried over to the stripper zone and regenerator. This resulted in a higher yield of more valuable products and also smoother operation of the regenerator as local hot spots were minimized.

Crystalline *zeolite catalysts* having molecular sieve properties were introduced as selective adsorbents in the 1955 to 1959 period. In a relatively short time period all of the cracking catalyst manufacturers were offering their versions of zeolite catalysts to refiners. The intrinsically higher activity of the crystalline zeolites vis-à-vis conventional amorphous silica-alumina catalysts coupled with the much higher yields of naphtha and decreased coke and light end yields served to revitalize research and development in the mature refinery process of catalytic cracking.

A number of *zeolite catalysts* have been mentioned as having catalytic cracking properties, such as synthetic faujasite (X-type and Y-type), offretite, mordenite, and erionite. Of these, the faujasite minerals have been most widely used commercially. While faujasite is synthesized in the sodium form, base exchange removes the sodium with other metal ions that, for cracking catalysts, include magnesium, calcium, rare earths (mixed or individual), and ammonium. In particular, mixed rare earths alone or in combination with ammonium ions have been the most commonly used forms of faujasite in cracking catalyst formulations. Empirically, X-type faujasite has a stoichiometric formula of $\text{Na}_2\text{O} \cdot \text{Al}_2\text{O}_3 \cdot 2.5\text{SiO}_2$ and Y-type faujasite $\text{Na}_2\text{O} \cdot \text{Al}_2\text{O}_3 \cdot 4.8\text{SiO}_2$. Slight variations in the silica-alumina ($\text{SiO}_2/\text{Al}_2\text{O}_3$) ratio exist for each of the types. Rare-earth-exchanged Y-type faujasite retains much of its crystallinity after steaming at 825 °C (1520 °F) with steam for 12 h; rare-earth form X-faujasite, while thermally stable in dry air, will lose its crystallinity at these temperatures in the presence of steam.

19.4.2 Catalyst Manufacture

While each manufacturer has developed proprietary procedures for making silica-alumina catalyst, the general procedure consists of:

1. The gelling of dilute sodium silicate solution ($\text{Na}_2\text{O} \cdot 3.25\text{SiO}_2 \cdot x\text{H}_2\text{O}$) by addition of an acid (H_2SO_4 , CO_2) or an acid salt such as aluminum sulfate
2. Aging the hydrogel under controlled conditions
3. Adding the prescribed amount of alumina as aluminum sulfate and/or sodium aluminate
4. Adjusting the pH of the mixture
5. Filtering the composite mixture.

After filtering, the filter cake can either be (1) washed free of extraneous soluble salts by a succession of slurring and filtration steps and spray dried or (2) spray dried and then washed free of extraneous soluble salts before flash drying the finished catalyst.

There are a number of critical areas in the preparative processes that affect the physical and catalytic properties of the finished catalyst. Principal among them are the concentration and temperature of the initial sodium silicate solution, the amount of acid added to effect gelation, the length of time of aging the gel, the method and conditions of adding the aluminum salt to the gel, and its incorporation therein. Under a given set of conditions the product catalyst is quite reproducible in both physical properties and catalytic performance.

During the period 1940 to 1962, a number of improvements were made in silica-alumina catalyst manufacture. These included continuous production lines versus batch-type operation, introduction of spray drying to eliminate grinding and sizing of the catalyst while reducing catalyst losses as fines, improving catalyst stability by controlling pore volume, and improved wash procedures to remove extraneous salts from high alumina content catalysts to improve equilibrium catalyst performance.

Zeolite cracking catalysts are made by dispersing or imbedding the crystals in a matrix. The matrix is generally amorphous silica-alumina gel and may also contain finely divided clay. The zeolite content of the composite catalyst is generally in the range of 5–16% by weight. If clay (e.g., kaolin) is used in the matrix, it is present in an amount of 25–45% by weight, the remainder being the silica-alumina hydrogel *glue* that binds the composite together. The zeolite may be pre-exchanged to the desired metal form and calcined to lock the exchangeable metal ions into position before compositing with the other ingredients. In an alternate scheme, sodium-form zeolite is composited with the other components,

washed, and then treated with a dilute salt solution of the desired metal ions before the final drying step.

As stated above, the matrix generally consists of silica-alumina, but several catalysts have been commercialized and contain (1) silica-magnesia, kaolin and (2) synthetic montmorillonite-mica and/or kaolin as the matrix for faujasite.

19.4.3 Catalyst Activity and Selectivity

The primary variables available to the operation of fluid catalytic cracking units for maximum unit conversion for a given feedstock quality include catalytic variables such as: (1) catalyst activity and (2) catalyst design, which includes availability of cracking sites and the presence of carbon on the regenerated catalyst.

Catalyst activity as an independent variable is governed by the capability of the unit to control the carbon content of the spent catalyst and the quantity and quality of fresh catalyst that can be continuously added to the unit. The carbon content of the regenerated catalyst is generally maintained at the lowest practical level to obtain the selectivity benefits of low carbon on the catalyst. Thus, catalyst addition is, in effect, the principal determinant of catalyst activity.

The deliberate withdrawal of catalyst over and above the inherent loss rate through regenerator stack losses and decant or clarified oil and a corresponding increase in fresh catalyst addition rate is generally not practiced as a means of increasing the activity level of the circulating catalyst. If a higher activity is needed, the addition of a higher activity fresh catalyst to the minimum makeup rate to maintain inventory is usually the more economical route.

The general effects of increasing activity is a reduction in severity and thus reduce the extent of secondary cracking reactions. Higher activity typically results in more naphtha and less coke. In other cases, higher activity catalysts are employed to increase the feed rate at essentially constant conversion and constant coke production so that the coke burning or regenerator air compression capacities are fully utilized.

In the catalytic cracking process, the most abundant products are those having 3, 4, and 5 carbon atoms. On a weight basis the 4-carbon-atom fraction is the largest. The differences between the catalysts of the mixed oxide type lie in the relative action toward promoting the individual reaction types included in the overall cracking operation. For example, silica-magnesia catalyst under a given set of cracking conditions will give a higher conversion to cracked products than silica-alumina catalyst. However, the products from a silica-magnesia ($\text{SiO}_2\text{-MgO}$) catalyst have a higher average molecular weight, hence a lower volatility,

lesser amounts of highly branched/acyclic isomers, but more olefins among the naphtha-boiling-range products ($C_4 - 220^\circ\text{C}$, 430°F) than the products from a silica-alumina catalyst. With these changes in composition, the naphtha from cracking with a silica-magnesia catalyst is of lower octane number.

These differences between catalysts may also be described as differences in the intensity of the action at the individual active catalytic centers. That is, a catalyst such as silica-alumina would give greater intensity of reaction than silica-magnesia as observed from the nature and yields of the individual cracked products and the gasoline octane number. Titration of these two catalysts shows silica-alumina to have a lower acid titer than silica-magnesia but the acid strength of the sites is higher.

While each of the individual component parts in these catalysts is essentially nonacidic, when mixed together properly they give rise to a titratable acidity as described above. Many of the secondary reactions occurring in the cracking process may also be promoted with strong mineral acids, such as concentrated sulfuric and phosphoric acids, aluminum halides, hydrogen fluoride, and hydrogen fluoride-boron trifluoride (BF_3) mixtures. This parallelism lends support to the concept of the active catalytic site as being acidic. Zeolites have a much higher active site density (titer) than the amorphous mixed oxides, which may account in large part for their extremely high cracking propensity. In addition, these materials strongly promote complex hydrogen transfer reactions among the primary products so that the recovered cracked products have a much lower olefin and higher paraffin content than are obtained with the amorphous mixed oxide catalysts. This hydrogen transfer propensity of zeolites to saturate primary cracked product olefins to paraffins minimizes the reaction of polymerizing the olefins to form a coke deposit, thus accounting in part for the much lower coke yields with zeolite catalysts than with amorphous catalysts.

Activity of the catalyst varies with faujasite content as does selectivity of the catalyst to coke and naphtha. As the faujasite content drops below 5% by weight the catalyst starts to show some of the cracking properties of the matrix, while for zeolite contents of 10% by weight or higher very little change in selectivity patterns is noted. The various ion-exchanged forms of the faujasite can result in slightly different cracking properties e.g., using high cerium content mixed rare earths improves carbon burning rates in the regenerator, use of H-form of faujasite improves selectivity to propane-pentane fractions, use of a minor amount of copper-form faujasite increases light olefin yield and naphtha octanes.

19.4.4 Catalyst/Oil Ratio

The dependent variable catalyst/oil ratio is established by the unit heat balance and coke make that in turn are influenced by almost every independent variable. Since catalyst/oil ratio changes are accompanied by one or more shifts in other variables, the effects of catalyst/oil ratio are generally associated with other effects. A basic relation, however, in all catalyst/oil ratio shifts is the effect on conversion and carbon yield. At constant space velocity and temperature, increasing catalyst/oil ratio increases conversion. In addition to increasing conversion, higher catalyst/oil ratios generally increase coke yield at a constant conversion. This increase in coke is related to the hydrocarbons entrapped in the pores of the catalyst and carried through the stripper to the regenerator. Thus, this portion of the catalyst/oil ratio effect is highly variable and depends not only on the catalyst/oil ratio change but also on the catalyst porosity and stripper conditions.

The following changes, in addition to increased coke yield, accompany an increase in the catalyst/oil ratio in the range of 5–20 at constant conversion, reactor temperature and catalyst activity:

1. Decreased hydrogen yield
2. Decreased methane to butane(s) yields
3. Minimal effect on the naphtha yield or octane number.

19.4.5 Catalyst Deactivation

A cracking catalyst should maintain its cracking activity with little change in product selectivity as it ages in a unit [19.64, 65]. A number of factors contribute to degrade the catalyst:

1. The combination of high temperatures, steam partial pressure, and time
2. Impurities present in the fresh catalyst
3. Impurities picked up by the catalyst from the feed while in use.

Under normal operating conditions, the catalyst experiences temperatures of $480\text{--}515^\circ\text{C}$ ($900\text{--}960^\circ\text{F}$) in the reactor and steam stripper zones and temperatures of $620\text{--}720^\circ\text{C}$ ($1150\text{--}1325^\circ\text{F}$) and higher in the regenerator accompanied by a substantial partial pressure of steam. With mixed oxide amorphous gel catalysts, the plastic nature of the gel is such that the surface area and pore volume decrease rather sharply in the first few days of use and then at a slow inexorable rate thereafter. This plastic flow also results in a loss in the number and strength of the active catalytic sites.

Zeolite catalysts comprising both amorphous gel and crystalline zeolite degrade from instability of the gel, as stated above, and also from loss in crystallinity. The latter also results from the combined effects of time, temperature, and steam partial pressure. When crystallinity is lost, the amorphous residue is relatively low in activity, approximating that of the amorphous gel matrix. The rate of degradation of the amorphous gel component may not be the same as that of the zeolite crystals e.g., the gel may degrade rapidly and through thermoplastic flow effectively coat the crystals and interfere with the diffusion of hydrocarbons to the catalytic sites in the zeolite. Catalyst manufacturers try to combine high stability in the matrix with high stability zeolite crystals when making zeolite catalysts.

Residual impurities in freshly manufactured catalysts are principally sodium and sulfate. These result from the use of sodium silicate and aluminum sulfate in making the silica-alumina gel matrix and subsequent washing of the composite catalyst with ammonium sulfate to remove sodium. Generally, the sodium content of the amorphous gel is < 0.1% by weight (as Na₂O) and sulfate < 0.5% by weight.

With zeolite catalysts the residual sodium may be primarily associated with the zeolite, so that sodium levels may range from about 0.2–0.80% for the composite catalyst. Sulfate levels in zeolite catalysts are still < 0.5%. An excessive amount of sodium reacts with the silica in the matrix under regenerator operating conditions and serves as a flux to increase the rate of surface area and pore volume loss. Sodium faujasite is not as hydrothermally stable as other metal-exchanged (e.g., mixed rare earths) forms of faujasite. It is most desirable to reduce the sodium content of the faujasite component to < 5.0% by weight (as Na₂O) with rare earths or with mixtures of rare earths and ammonium ions.

Finally, catalysts can degrade as a result of impurities picked up from the feed being processed. These impurities are sodium, nickel, vanadium, iron, and copper. Sodium as laid down on the catalyst not only acts to neutralize active acid sites, reducing catalyst activity, but also acts as a flux to accelerate matrix degradation. Freshly deposited metals are effective *poisons* to cracking catalysts because of the loss of active surface area by metal deposition. Zeolite catalysts are less responsive to metal contaminants than amorphous gel catalysts. Hence, equilibrium catalysts can tolerate low levels of these metals so long as they have enough time to become buried. A sudden deposition of fresh metals can cause adverse effects on unit performance. Metals levels on equilibrium catalysts reflect the met-

als content of the feeds being processed, typical ranges are 200–1200 ppm V, 150–500 ppm Ni, and 5–45 ppm Cu. Sodium levels are in the range of 0.25–0.8% by weight (as Na₂O).

19.4.6 Catalyst Stripping

Catalyst leaving the reaction zone is fluidized with reactor product vapors that must be removed and recovered with the reactor product. In order to accomplish this, the catalyst is passed into a stripping zone where most of the hydrocarbon is displaced with steam.

Stripping is generally done in a countercurrent contact zone where shed baffles or contactors are provided to insure equal vapor flow up through the stripper and efficient contacting. Stripping can be accomplished in a dilute catalyst phase. Generally, a dense phase is used, but with lighter feeds or higher reactor temperature and high conversion operations a significant portion of the contacting can be done in a dilute phase.

The amount of hydrocarbon carried to the regenerator is dependent upon the amount of stripping steam used per pound of catalyst and the pressure and temperature at which the stripper operates.

Probes at the stripper outlet have been used to measure the composition of the hydrocarbon vapors leaving the stripper. When expressed as percent of coke burned in the regenerator, the strippable hydrocarbon is only 2–5%. Very poor stripping is shown when the hydrogen content of the regenerator coke is 10% by weight or higher. Good stripping is shown by 6–9% by weight hydrogen levels.

The proper level of stripping is found in many operating units by reducing the stripping steam until there is a noticeable effect or rise in regenerator temperature. Steam is then marginally increased above this rate. In some units, stripping steam is used as a control variable to control the carbon burning rate or differential temperature between the regenerator bed and cyclone inlets.

In summary, the catalytic cracking unit is an extremely dynamic unit, primarily because there are three major process flow streams (the catalyst, hydrocarbon, and regeneration air), all of which interact with each other. Problems can arise in the equipment and flowing streams which are sometimes difficult to diagnose because of the complex effects they can create.

19.4.7 Catalyst Treatment

The latest technique developed by the refining industry to increase naphtha yield and quality is to treat the catalysts from the cracking units to remove metal poi-

sons that accumulate on the catalyst [19.66]. Nickel, vanadium, iron, and copper compounds contained in catalytic cracking feedstocks are deposited on the catalyst during the cracking operation, thereby adversely affecting both catalyst activity and selectivity. Increased catalyst metal contents affect catalytic cracking yields by increasing coke formation, decreasing naphtha and butane and butylene production, and increasing hydrogen production. The recent commercial development and adoption of cracking catalyst-treating processes definitely improve the overall catalytic cracking process economics.

For the last two decades, demetallized oil (produced by the extraction of a vacuum-tower bottoms stream using a light paraffinic solvent) has been included as a component of the feedstock in fluid catalytic cracking units. Modern solvent-extraction processes, such as the Demet process [19.66, 68], provide a higher demetallized oil yield than is possible in the propane-deasphalting process that has been used to prepare fluid catalytic cracker feedstock, as well as demetallized feedstocks for other processes. Consequently, the demetallized oil is more heavily contaminated. In general, demetallized oils are still good cracking stocks, but most feedstocks can be further improved by hydrotreating to reduce contaminant levels and to increase their hydrogen content thereby becoming more presentable and amenable for processing feedstock [19.69].

Demet

In the process, a cracking catalyst is subjected to two pretreatment steps [19.66, 68, 70]. The first step effects vanadium removal; the second, nickel removal, to prepare the metals on the catalyst for chemical conversion to compounds (chemical treatment step) that can be readily removed through water washing (catalyst wash step). The treatment steps include use of a sulfurous compound followed by chlorination with an anhydrous chlorinating agent (e.g., chlorine gas) and washing with an aqueous solution of a chelating agent (e.g., citric acid, $\text{HO}_2\text{CCH}_2\text{C}(\text{OH})(\text{CO}_2\text{H})\text{CH}_2\text{CO}_2\text{H}$, 2-hydroxy-1,2,3-propanetricarboxylic acid). The catalyst is then dried and further treated before returning to the cracking unit.

Met-X

This process consists of cooling, mixing, ion-exchange separation, filtration, and resin regeneration [19.70]. Moist catalyst from the filter is dispersed in oil and returned to the cracking reactor in a slurry. On a continuous basis, the catalyst from a cracking unit is cooled and then transported to a stirred reactor and mixed with an ion-exchange resin (introduced as slurry). The catalyst-resin slurry then flows to an elutriator for separation. The catalyst slurry is taken overhead to a filter, and the wet filter cake is slurried with oil and pumped into the catalytic system. The resin leaves the bottom of the elutriator and is regenerated before returning to the reactor.

Table 19.4 Standard test methods for determining catalyst properties, including catalysts for the fluid catalytic cracking process (after [19.67])

Designation	Title
Catalytic properties	
D3907/D3907M-13	Standard test method for testing fluid catalytic cracking (FCC) catalysts by microactivity test
D4463/D4463M-96(2013)	Standard guide for metals free steam deactivation of fresh fluid cracking catalysts
D5154-10	Standard test method for determining activity and selectivity of fluid catalytic cracking (FCC) catalysts by microactivity test
D7206/D7206M-06(2013)	Standard guide for cyclic deactivation of fluid catalytic cracking (FCC) catalysts with metals
Chemical composition	
D1977-03(2008)	Standard test method for nickel and vanadium in FCC equilibrium catalysts by hydrofluoric/sulfuric acid decomposition and atomic spectroscopic analysis
D3610-00(2010)	Standard test method for total cobalt in alumina-base cobalt-molybdenum catalyst by potentiometric titration method
D3943-10	Standard test method for total molybdenum in fresh alumina-base catalysts
D4481-10	Standard test method for total nickel in fresh alumina-base catalysts
D4642-04(2010)	Standard test method for platinum in reforming catalysts by wet chemistry
D4782-10	Standard test method for palladium in molecular sieve catalyst by wet chemistry
D5153-10	Standard test method for palladium in molecular sieve catalyst by atomic absorption
D7085-04(2010)	Standard guide for determination of chemical elements in fluid catalytic cracking catalysts by x-ray fluorescence spectrometry (XRF)
D7442-08a	Standard practice for sample preparation of fluid catalytic cracking catalysts and zeolites for elemental analysis by inductively coupled plasma-atomic emission spectroscopy

Table 19.4 (continued)

Designation	Title
Nomenclature and definitions	
D3766-08(2013)	Standard terminology relating to catalysts and catalysis
Physical–chemical properties	
D3663-03(2008)	Standard test method for surface area of catalysts and catalyst carriers
D3908-03(2008)	Standard test method for hydrogen chemisorption on supported platinum catalysts by volumetric vacuum method
D4222-03(2008)	Standard test method for determination of nitrogen adsorption and desorption isotherms of catalysts and catalyst carriers by static volumetric measurements
D4284-12	Standard test method for determining pore volume distribution of catalysts and catalyst carriers by mercury intrusion porosimetry
D4365-13	Standard test method for determining micropore volume and zeolite area of a catalyst
D4567-03(2013)	Standard test method for single-point determination of specific surface area of catalysts and catalyst carriers using nitrogen adsorption by continuous flow method
D4641-12	Standard practice for calculation of pore size distributions of catalysts and catalyst carriers from nitrogen desorption isotherms
D4780-12	Standard test method for determination of low surface area of catalysts and catalyst carriers by multipoint krypton adsorption
D4824-13	Standard test method for determination of catalyst acidity by ammonia chemisorption
D4926-06(2011)	Standard test method for gamma alumina content in catalysts containing silica and alumina by X-ray powder diffraction
Physical–mechanical properties	
C515-13	Standard specification for chemical-resistant ceramic tower packings
D4058-96(2011)	Standard test method for attention and abrasion of catalysts and catalyst carriers
D4164-13	Standard test method for mechanically tapped packing density of formed catalyst and catalyst carriers
D4179-11	Standard test method for single pellet crush strength of formed catalysts and catalyst carriers
D4180-13	Standard test method for vibratory packing density of formed catalyst particles and catalyst carriers
D4438-13	Standard test method for particle size distribution of catalysts and catalyst carriers by electronic counting
D4464-10	Standard test method for particle size distribution of catalytic material by laser light scattering
D4512-03(2013)	Standard test method for vibrated apparent packing density of fine catalyst and catalyst carrier particles and powder
D4513-11	Standard test method for particle size distribution of catalytic materials by sieving
D4699-03(2013)	Standard test method for vibratory packing density of large formed catalyst and catalyst carrier particles
D4781-03(2013)	Standard test method for mechanically tapped packing density of fine catalyst particles and catalyst carrier particles
D5757-11	Standard test method for determination of attrition and abrasion of powdered catalysts by air jets
D6175-03(2013)	Standard test method for radial crush strength of extruded catalyst and catalyst carrier particles
D6761-07(2012)	Standard test method for determination of the total pore volume of catalysts and catalyst carriers
D7084-04(2009)	Standard test method for determination of bulk crush strength of catalysts and catalyst carriers
Designation	
Zeolites	
D3906-03(2013)	Standard test method for determination of relative X-ray diffraction intensities of Faujasite-type zeolite-containing materials
D3942-03(2013)	Standard test method for determination of the unit cell dimension of a Faujasite-type zeolite
D5357-03(2013)	Standard test method for determination of relative crystallinity of zeolite sodium A by X-ray diffraction
D5758-01(2011)	Standard test method for determination of relative crystallinity of zeolite ZSM-5 by X-ray diffraction

Catalyst Testing

The American Society for Testing and Materials (ASTM) has a series of standard test methods that can be applied to catalysts (Table 19.4) as a means of testing and for chemical analysis of the various forms of catalysts and catalyst carriers used to increase the rate of specific chemical reactions. The test methods and techniques presented in these catalyst standards include hydrofluoric/sulfuric acid decomposition, atomic spectroscopic analysis, potentiometric titration method,

microactivity test, volumetric vacuum method, static volumetric measurements, mercury intrusion porosimetry, electronic counting, laser light scattering, nitrogen adsorption by continuous flow method, ammonia chemisorption, x-ray powder diffraction (XRD), x-ray fluorescence spectrometry (XRF), and elemental analysis by inductively coupled plasma-atomic emission spectroscopy. These standards are helpful in allowing catalyst users to examine and assess catalysts to ensure their safe handling and use.

19.5 Process Options

Fluid catalytic cracking processes exist in several different proprietary designs that have been developed over the past several decades. Each design was in response to the characteristics and peculiarities of different feedstocks as well as the need for a balanced product slate that was often (and still is) regionally dependent. Generally, the various designs can be separated into two main configurations: (1) the *side-by-side type*, in which the reactor and catalyst regenerator are in two separate vessels, and (2) the *stacked type*, in which the reactor and catalyst regenerator are contained in a single vessel with the reactor above the catalyst regenerator.

19.5.1 Fluid-Bed Processes

A typical fluid catalytic cracking reactor (Fig. 19.1) process involves mixing the preheated feedstock with hot, regenerated catalyst as it enters the riser pipe leading to the reactor after which the feedstock is combined with a recycle stream within the riser, vaporized, and raised to reactor temperature (485–540 °C or 900–1000 °F) by the hot catalyst. As the mixture travels up the riser pipe, the charge is thermally decomposed at minimal pressure (10–30 psi). In most modern units, cracking takes place in the riser (*riser pipe cracking*) and the reactor no longer functions as a reactor but serves as a holding vessel for the cyclones where the product vapors are separated from the catalyst. The resultant product stream (cracked product) is then charged to a fractionating column where it is separated into fractions – part of the high-boiling distillate recycled to the riser for further cracking (*cracking to extinction*).

The catalyst is typically in a form such that when the catalyst particles are *aerated* with air or feedstock vapor, the catalyst behaves like a liquid and can be moved through pipes – the flow patterns through the reactor may vary depending upon the precise reactor configuration. Coke deposits collect on the catalyst during the process and the spent catalyst (catalyst with deposits of

coke and metals) sent to a catalyst stripper and thence to the regenerator, where most of the coke deposits are burned off. A portion of the regenerated catalyst – the amount is subject to feedstock quality – is exchanged for fresh catalyst to maintain the efficiency of the process.

Model IV Fluid-Bed Catalytic Cracking

The *model IV fluid-bed catalytic cracking unit* involves a process in which the catalyst is transferred between the reactor and regenerator by means of U-bends and the catalyst flow rate can be varied in relation to the amount of air injected into the spent-catalyst U-bend [19.71]. Regeneration air, other than that used to control circulation, enters the regenerator through a grid, and the reactor and regenerator are mounted side by side.

The model IV low-elevation design was preceded by the model III balanced-pressure design (1947), the model II downflow design (1944), and the original model I upflow design (1941). The first commercial model IV installation in the United States was placed on-stream in 1952.

Orthoflow Fluid-Bed Catalytic Cracking

The *Orthoflow fluid-bed catalytic cracking process* uses the unitary vessel design, which provides a straight-line flow of catalyst and thereby minimizes the erosion encountered in pipe bends [19.9]. Commercial Orthoflow designs are of three types: models A and C, with the regenerator beneath the reactor, and model B, with the regenerator above the reactor. In all cases, the catalyst-stripping section is located between the reactor and the regenerator. All designs employ the heat-balanced principle incorporating fresh feed-recycle feed cracking.

This process uses the unitary vessel design, which provides a straight-line flow of catalyst and thereby minimizes the erosion (*impingement damage*, *erosion corrosion*) encountered in pipe bends. Commercial or-

thoflow designs are of three types: model A and model C, with the regenerator beneath the reactor, and model B, with the regenerator above the reactor. In all cases, the catalyst-stripping section is located between the reactor and the regenerator and all designs employ the heat-balanced principle incorporating fresh feed–recycle feed cracking.

Shell Two-Stage Fluid-Bed Catalytic Cracking

The *Shell two-stage fluid-bed catalytic cracking process* was devised to permit greater flexibility in shifting product distribution when dictated by demand. Thus, feedstock is first contacted with cracking catalyst in a riser reactor, that is, a pipe in which fluidized catalyst and vaporized oil flow concurrently upward, and the total contact time in this first stage is on the order of seconds. High temperatures 470–565 °C (875–1050 °F) are employed to reduce undesirable coke deposits on catalyst without destruction of naphtha by secondary cracking. Other operating conditions in the first stage are a pressure of 16 psi (110 kPa) and a catalyst/oil ratio of 3 : 1 to 50 : 1; volume conversion ranges between 20–70% have been recorded. All or part of the unconverted or partially converted gas oil product from the first stage is then cracked further in the second-stage fluid-bed reactor. Operating conditions in the second reactor are 480–540 °C (900–1000 °F) and 16 psi with a catalyst/oil ratio of 2 : 1 to 12 : 1.

Universal Oil Products (UOP) Fluid-Bed Catalytic Cracking

The *Universal Oil Products (UOP) fluid-bed catalytic cracking process* is adaptable to the needs of both large and small refineries [19.49]. The major distinguishing features of the process are:

1. Elimination of the air riser with its attendant large expansion joints
2. Elimination of considerable structural steel supports
3. Reduction in regenerator and in air-line size through use of 15–18 psi pressure operation.

Other Processes

The *residuum cracking unit* (M.W. Kellogg Co./Phillips Petroleum Co.) offers feedstock conversion up to 85% by weight of atmospheric resids (an atmospheric residuum is the fraction of the feedstock boiling above 650 °F/343 °C) or equivalent feedstocks. The unit is similar to the Orthoflow C unit but there are some differences that enhance performance on residua. The catalyst flows from the regenerator through a plug valve that controls the flow to hold the reactor temperature. Steam is injected upstream of the feed point to accel-

erate the catalyst and disperse it so as to avoid high rates of coke formation at the feed point. The feedstock, atomized with steam, is then injected into this stream through a multiple nozzle arrangement. The flow rates are adjusted to control the contact time in the riser since the effects of metals poisoning on yields are claimed to be largely a function of the time that the catalyst and oil are in contact. Passing the mix through a rough cut cyclone stops the reaction.

The *Gulf residuum process* consists of cracking a residuum that has been previously hydrotreated to low sulfur and metals levels. In this case, high conversions are obtained but coke yield and hydrogen yield are kept at conventional levels by keeping metals on catalyst low.

The *deep catalytic cracking (DCC)* process is designed for selective conversion of gas oil and paraffinic residual feedstocks to C₂ to C₅ olefins, aromatic-rich naphtha, and other distillates. There is also the *Flexicracking* process, which is designed for conversion of gas oils, residua, and deasphalted oils to distillates [19.50].

19.5.2 Moving-Bed Processes

In the moving-bed catalytic cracking process, the catalyst is in the form of pellets that are moved continuously to the top of the unit by conveyor or pneumatic lift tubes to a storage hopper, then flow downward by gravity through the reactor, and finally to a regenerator. The cracked product is separated into recycle gas, naphtha, distillate, and gas oil.

Airlift Thermofor Catalytic Cracking

The airlift Thermofor catalytic cracking process (Socony Airlift TCC process) is a moving-bed, reactor-over-generator continuous process that was originally designed for conversion of heavy gas oil into naphtha and middle distillate fuel oil. Feed preparation may consist of flashing in a separator to obtain vapor feed, and the separator bottoms may be sent to a vacuum tower from which the liquid feed is produced.

The gas oil vapor-liquid flows downward through the reactor concurrently with the regenerated catalyst (usually in bead form). The catalyst is purged by steam at the base of the reactor and gravitates into the kiln, or regeneration is accomplished by the use of air injected into the kiln. Approximately 70% of the carbon on the catalyst is burned in the upper kiln burning zone and the remainder in the bottom burning zone. Regenerated, cooled catalyst enters the lift pot, where low-pressure air transports it to the surge hopper above the reactor for reuse.

Houdresid Catalytic Cracking

Houdresid catalytic cracking is a process that uses a variation of the continuously moving (synthetic or natural) catalyst bed designed to obtain high yields of naphtha and light distillate from feedstocks such as residua, ranging from atmospheric residue to vacuum residua including residua high in sulfur or nitrogen. The process features modify or eliminate the adverse effects and catalyst and product selectivity usually resulting when metals (such as nickel, vanadium, copper, and iron) are present in the fuel. The Houdresid catalytic reactor and catalyst-regenerating kiln are contained in a single vessel. Fresh feed plus recycled gas oil are charged to the top of the unit in a partially vaporized state and mixed with steam.

Houdrflow Catalytic Cracking

The Houdrflow catalytic cracking process is a continuous, moving-bed process in which the reactor and regenerator kiln are integrated as a single vessel. The feedstock can be any fraction of the crude boiling between naphtha and atmospheric resid. The catalyst is transported from the bottom of the unit to the top in a gas lift employing compressed flue gas and steam.

The reactor feed and catalyst pass concurrently through the reactor zone to a disengager section, in which vapors are separated and directed to a conventional fractionation system. The spent catalyst, which has been steam purged of residual oil, flows to the kiln for regeneration, after which steam and flue gas are used to transport the catalyst to the reactor.

Suspensoid Catalytic Cracking

Suspensoid cracking was developed from the thermal cracking process carried out in tube and tank units [19.7] and, in the process, small amounts of powdered catalyst as a mixture with the feedstock are pumped through a cracking coil furnace – cracking temperatures are on the order of 550–610 °C (1025–1130 °F), with pressures in the range 200–500 psi. After leaving the furnace, the cracked material enters a separator where catalyst and high-boiling entrained material (*tar*) are left behind. The cracked vapors enter a bubble tower where they are separated into two fractions: gas oil and pressure distillate – the latter is separated into naphtha and gases. The spent catalyst is recovered from the higher boiling product, which is used as a heavy fuel oil.

19.6 Options for Heavy Oil and Residua

In recent decades, because of an increasing demand for low-boiling products such as naphtha, most refineries perform the operation by partially blending residua into vacuum gas oil. However, conventional fluid catalytic cracking processes have limits in residue processing, so *residue fluid catalytic cracking processes* (RFCC process) have lately been employed one after another. Because the residue fluid catalytic cracking process enables efficient naphtha production directly from residues, it will play the most important role as a residue cracking process, along with the residue hydroconversion process. Another role of RFCC is to generate high-quality gasoline blending stock and petrochemical feedstock. Olefins (propene, butene derivatives, and pentene derivatives) serve as feed for alkylating processes, for polymer gasoline, as well as for additives for reformulated gasoline.

The processes described below are the evolutionary offspring of the fluid catalytic cracking process and the residuum catalytic cracking process. Some of these newer processes use catalysts with different silica/alumina ratios as acid support of metals such as Mo, Co, Ni, and W. In general the first catalyst used to remove metals from oils was the conventional

hydrodesulfurization (HDS) catalyst. Diverse natural minerals are also used as raw material for elaborating catalysts addressed to the upgrading of heavy fractions. Among these minerals are: clays; manganese nodules; bauxite activated with vanadium, nickel, chromium, iron, and cobalt, as well as iron laterite, sepiolite, and transition metal sulfides supported on silica and alumina. Other kinds of catalyst, such as vanadium sulfide, are generated in situ, possibly in colloidal states.

In the past decades, in spite of the difficulty of handling heavy feedstocks, RFCC has evolved to become a well-established approach for converting a significant portion of the heavier fractions of the crude barrel into a high-octane naphtha blending component. RFCC, which is an extension of conventional fluid catalytic cracking technology for applications involving the conversion of highly contaminated residua, has been commercially proven on feedstocks ranging from gas oil-residuum blends to atmospheric resid, as well as blends of atmospheric and vacuum residua. In addition to high naphtha yields, the residuum fluidized catalytic cracking unit also produces gaseous, distillate and fuel oil-range products.

The product quality from the residuum fluidized catalytic cracker is directly affected by its feedstock quality. In particular, and unlike hydrotreating, the RFCC redistributes sulfur among the various products, but does not remove sulfur from the products unless, of course, one counts the sulfur that is retained by any coke formed on the catalyst. Consequently, tightening product specifications have forced refiners to hydrotreat some, or all, of the products from the resid catalytic cracking unit. Similarly, in the future the emissions of sulfur oxides (SO_x) from a resid catalytic cracker may become more of an obstacle for residue conversion projects. For these reasons, a point can be reached where the economic operability of the unit can be sufficient to justify hydrotreating the feedstock to the catalytic cracking unit.

19.6.1 Asphalt Residual Treating Process

The *asphalt residual treating* (ART) process is a process for increasing the production of naphtha and kerosene for transportation fuels by reducing the production of heavy fuel oil without hydrocracking [19.1, 7].

In the process, the preheated feedstock (heavy oil, atmospheric residuum, vacuum residuum, or tar sand bitumen) is injected into a stream of fluidized, hot catalyst where efficient mixing of the feedstock with the catalyst is achieved in the contactor which is operated within a pressure–temperature envelope to ensure selective vaporization. The vapor and the contactor effluent are quickly and efficiently separated from each other and entrained hydrocarbons are stripped from the contaminant (containing spent solid) in the stripping section. The contactor vapor effluent and vapor from the stripping section are combined and rapidly quenched in a quench drum to minimize product degradation. The cooled products are then transported to a conventional fractionator and spent solid from the stripping section is transported to the combustor bottom zone for carbon burn-off.

In the combustor, coke is burned from the spent solid that is then separated from combustion gas in the surge vessel. The surge vessel circulates regenerated catalyst streams to the contactor inlet for feed vaporization, and to the combustor bottom zone for premixing. The components of the combustion gases include carbon dioxide (CO_2), nitrogen (N_2), oxygen (O_2), sulfur oxides (SO_x), and nitrogen oxides (NO_x) that are released from the catalyst with the combustion of the coke in the combustor – these components of the gas stream can be removed by conventional gas treating processes [19.1–4, 7, 72]. The concentration of sulfur oxides in the combustion gas requires treatment for their removal.

19.6.2 Residue Fluid Catalytic Cracking Process

The residue fluid catalytic cracking process (RFCC process, also called the HOC process) is a version of the fluid catalytic cracking process that has been adapted to conversion of residua that contain high amounts of metal and asphaltene constituents.

The feedstocks for the process are rated on the basis of carbon residue and content of metals. Thus, *good-quality feedstocks* have less than 5% by weight carbon residue and less than 10 ppm metals. *Medium-quality feedstocks* have greater than 5 but less than 10% by weight carbon residue and greater than 10 but less than 30 ppm metals. *Poor-quality feedstocks* have greater than 10 but less than 20% by weight carbon residue and greater than 30 but less than 150 ppm metals. Finally, *bad-quality feedstocks* have greater than 20% by weight carbon residue and greater than 150 ppm metals.

In the process, the feedstock is desulfurized and the nonvolatile fraction from the hydrodesulfurization unit is charged to the residuum fluid catalytic cracking unit. The reaction system is an external vertical riser terminating in a closed cyclone system. Dispersion steam in amounts higher than that used for gas oils is used to assist in the vaporization of any volatile constituents of heavy feedstocks. A two-stage stripper is utilized to remove other products from the catalyst. Hot catalyst flows at low velocity in a dense phase through the catalyst cooler and returns to the regenerator. Regenerated catalyst flows to the bottom of the riser to meet the feed.

The coke deposited on the catalyst is burned off in the regenerator along with the coke formed during the cracking of the gas oil fraction. If the feedstock contains high proportions of metals, control of the metals on the catalyst requires excessive amounts of catalyst withdrawal and fresh catalyst addition – but use of a pretreatment option can reduce the amount of catalyst withdrawal and addition.

19.6.3 Heavy Oil Treating Process

The heavy oil treating process (HOT process) is a catalytic cracking process for upgrading heavy feedstocks such as topped crude oils, vacuum residua and solvent deasphalted bottoms using a fluidized bed of iron ore particles [19.1, 7]. The main section of the process consists of three fluidized reactors and separate reactions take place in each reactor (*cracker*, *regenerator*, and *desulfurizer*):

- $\text{Fe}_3\text{O}_4 + \text{asphaltene constituents} \rightarrow \text{coke/Fe}_3\text{O}_4 + \text{oil} + \text{gas}$ (in the *cracker*)

- $3\text{FeO} + \text{H}_2\text{O} \rightarrow \text{Fe}_3\text{O}_4 + \text{H}_2$ (in the *cracker*)
- $\text{Coke}/\text{Fe}_3\text{O}_4 + \text{O}_2 \rightarrow 3\text{FeO} + \text{CO} + \text{CO}_2$ (in the *regenerator*)
- $\text{FeO} + \text{SO}_2 + 3\text{CO} \rightarrow \text{FeS} + 3\text{CO}_2$ (in the *regenerator*)
- $3\text{FeS} + 5\text{O}_2 \rightarrow \text{Fe}_3\text{O}_4 + 3\text{SO}_2$ (in the *desulfurizer*).

In the *cracking section*, heavy oil cracking and the steam-iron reaction take place simultaneously under conditions similar to thermal cracking. Any unconverted feedstock is recycled to the cracker from the bottom of the scrubber. The scrubber effluent is separated into hydrogen gas, liquefied petroleum gas (LPG), and liquid products that can be upgraded by conventional technologies to priority products.

In the *regenerator section*, coke deposited on the catalyst is partially burned to form carbon monoxide in order to reduce iron tetroxide and to act as a heat supply. In the *desulfurizer*, sulfur in the solid catalyst is removed and recovered as molten sulfur in the final recovery stage.

19.6.4 R2R Process

The R2R process is a fluid catalytic cracking process for conversion of heavy feedstocks [19.1, 7, 73, 74]. In the process, the feedstock is vaporized upon contacting hot regenerated catalyst at the base of the riser and lifts the catalyst into the reactor vessel separation chamber where rapid disengagement of the hydrocarbon vapors from the catalyst is accomplished by both a special solids separator and cyclones. The bulk of the cracking reactions takes place at the moment of contact and continues as the catalyst and hydrocarbons travel up the riser. The reaction products, along with a minute amount of entrained catalyst, then flow to the fractionation column. The stripped spent catalyst, deactivated with coke, flows into the number 1 regenerator.

Partially regenerated catalyst is pneumatically transferred via an air riser to the number 2 regenerator, where the remaining carbon is completely burned in a dryer atmosphere. This regenerator is designed to minimize catalyst inventory and residence time at high temperature while optimizing the coke-burning rate. Flue gases pass through external cyclones to a waste heat recovery system. Regenerated catalyst flows into a withdrawal well and after stabilization is charged back to the oil riser.

19.6.5 Reduced Crude Oil Conversion Process

In the reduced crude oil conversion process (RCC process), the clean regenerated catalyst enters the bottom

of the reactor riser where it contacts low-boiling hydrocarbon *lift gas* that accelerates the catalyst up the riser prior to feed injection [19.1, 7]. At the top of the lift gas zone the feed is injected through a series of nozzles located around the circumference of the reactor riser.

The catalyst–oil disengaging system is designed to separate the catalyst from the reaction products and then rapidly remove the reaction products from the reactor vessel. Spent catalyst from the reaction zone is first steam stripped, to remove adsorbed hydrocarbons, and then routed to the regenerator. In the regenerator all of the carbonaceous deposits are removed from the catalyst by combustion, restoring the catalyst to an active state with a very low carbon content. The catalyst is then returned to the bottom of the reactor riser at a controlled rate to achieve the desired conversion and selectivity to the primary products.

19.6.6 Shell FCC Process

The Shell FCC process is designed to maximize the production of distillates from residua (Table 19.4) [19.1, 7].

In the process, the preheated feedstock (vacuum gas oil, atmospheric residuum) is mixed with the hot regenerated catalyst. After reaction in a riser, volatile materials and catalyst are separated after which the spent catalyst is immediately stripped of entrained and adsorbed hydrocarbons in a very effective multistage stripper. The stripped catalyst gravitates through a short standpipe into a single vessel, simple, reliable and yet efficient catalyst regenerator. Regenerative flue gas passes via a cyclone/swirl tube combination to a power recovery turbine. From the expander turbine the heat in the flue gas is further recovered in a waste heat boiler. Depending on the environmental conservation requirements, a *deNO_xing*, *deSO_xing*, and particulate emission control device can be included in the flue gas train.

Pretreatment of tar sand bitumen (by hydrogenation) prior to fluid catalytic cracking (or for that matter any catalytic cracking process) can result in enhanced yield of naphtha. It is suggested that mild hydrotreating be carried out upstream of a fluid catalytic cracking unit to provide an increase in yield and quality of distillate products. This is in keeping with earlier work [19.75] where mild hydrotreating of bitumen was reported to produce low-sulfur liquids that would be amenable to further catalytic processing.

19.6.7 S and W Fluid Catalytic Cracking Process

The S and W FCC process is also designed to maximize the production of distillates from residua [19.1,

7]. In the process, the heavy feedstock is injected into a stabilized, upward flowing catalyst stream whereupon the feedstock-steam-catalyst mixture travels up the riser and is separated by a high-efficiency inertial separator. The product vapor goes overhead to the main fractionator.

The spent catalyst is immediately stripped to minimize hydrocarbon carryover to the regenerator system. The first regenerator (650–700 °C or 1200–1290 °F)

burns 50–70% of the coke in an incomplete carbon monoxide combustion mode running counter-currently. This relatively mild, partial regeneration step minimizes the significant contribution of hydrothermal catalyst deactivation. The remaining coke is burned in the second regenerator (ca. 775 °C or 1425 °F) with an extremely low steam content. Hot clean catalyst enters a withdrawal well that stabilizes its fluid qualities prior to being returned to the reaction system.

19.7 Environmental Aspects and the Future

The future of many industries will continue to be guided by the various environmental regulations [19.63, 76, 77, 77] which will ensure that contamination of the various ecosystems is minimized – rather than halted altogether. Both sides of the environmental issue need to learn that in order to survive together there must be a balance between industrial preferences and environmental preferences. Industry cannot continue to pollute the environment as was the case in the first two thirds of the 20th century. At the same time, environmental advocates seem to fail to realize (or ignore) that shutting down industry means that we will all freeze together in the green darkness. Hence, there is a need for a balanced agreement where industrial advocates and environmental advocates work together for the betterment of all concerned. In this respect, the petroleum industry has taken considerable steps to reduce emissions from recovery operations and from refining operations – with the exception of notable accidental environmental disasters (not discussed here) that have occurred during the past four decades.

Fluid catalytic cracking is the most important conversion process used in petroleum refineries to convert the high-boiling feedstock constituents to more valuable naphtha, olefin gases, as well as other products and is likely to remain predominant in the refining industry for at least another 3–5 decades [19.1–7, 48, 78]. In terms of the environment [19.79], the feedstock supplied to a fluid catalyst cracking unit is usually that portion of the crude oil that has an initial boiling point in excess of 340 °C (645 °F) and contains most of the heteroatoms (nitrogen, oxygen, and sulfur) as well as the majority of the metals in the crude oil [19.7]. In fact, refineries use the cracking process to correct the imbalance between the market demand for gasoline and the excess of heavy, high-boiling range products (as well as heavy oil and tar sand bitumen) resulting from the distillation of the crude oil.

Thus, catalytic cracking is widely used in the petroleum refining industry to convert lower value

heavy feedstocks into higher value naphtha (a gasoline blend stock) and other high-value products. In order to improve the process, several innovations have been introduced in the form of varying process options that may well fit into the refinery of the future [19.6]. Examples, as they pertain to the fluid catalytic cracking process include (1) unit integration with sulfur removal to produce low-sulfur naphtha and (2) development of new catalysts.

Furthermore, recent enhancements made to units designed for the fluid catalytic cracking of residua and similar feedstocks for processing significant amounts of such feedstocks, while simultaneously improving yields and reducing emissions, have focused on improved feed injection and dispersion, reduced contact time of products and catalyst, improved separation of products and catalyst, and regenerator heat removal. Traditional technology has been modified in key areas including:

- Catalyst design to accommodate higher metals feed and to minimize the amount of coke formed on the catalyst
- Feed injection
- Riser pipe design and catalyst–oil product separation to minimize over-cracking
- Regenerator design improvements to handle high coke output and avoid damage to catalyst structure
- Overall reactor/regenerator design concepts as a means of reducing process emissions.

There is also the possibility of pretreating the feedstock by a process such as hydrodesulfurization [19.7, 31, 32]. The hydrodesulfurization pretreatment of the fluid catalytic cracker feedstock removes some of the metals and also reduces the sulfur content of the products – a boon to the environment. Conversely, increasing fresh catalyst addition will also serve to maintain or even increase the efficiency of the process and increasing the rate of such exchange lowers the level of metals in the circulating equilibrium catalyst, but (like the hy-

drodesulfurization option) this is also quite a costly option.

In addition, hydrotreating the feedstock to the unit not only increases feedstock conversion but reduces the sulfur content of the naphtha product (gasoline blend component stock) to levels low enough to meet the future low sulfur gasoline pool specifications. In fact, with the increasing focus on reducing sulfur content in fuels, the role of *desulfurization* in the refinery becomes more and more important. Currently, the process of choice is the hydrotreater, in which hydrogen is added to the fuel to remove the sulfur from the fuel. Some hydrogen may be lost to reduce the octane number of the fuel, which is undesirable. Thus, because of the increased attention on producing low-sulfur fuel stocks by desulfurization, various new process concepts are being developed with various claims of efficiency and effectiveness.

Finally, the nickel, vanadium, iron, copper and other metal contaminants, present in fluid catalysts cracking feedstocks, all have detrimental effects on catalyst activity and performance – nickel and vanadium are particularly troublesome. However, there are a number of methods for mitigating the effects of the contaminant metals, which include processing feedstocks with low content of metals – a virtual impossibility in view of the increase in heavy oil in refinery slates unless blending with lower metals feedstocks is viable without initiating incompatibility (sediment formation, fouling) of the constituents of the blend. However, having to choose low-metal feedstocks can seriously hamper the flexibility of a refinery to process various crude oils or purchased feedstocks for the catalytic cracking unit.

The commercial Demet process removes nickel and vanadium from the withdrawn spent catalyst and the two metals are converted to the respective chlorides which are then washed out of the catalyst and, after drying, the demetallized catalyst is recycled into the circulating catalyst – the removal of the majority of the nickel (approximately 95 wt%) and vanadium (67–85 wt%) is possible. As environmental regulations become more strict [19.63] the Demet and Met-X processes might become more common either in refineries and/or in catalyst manufacturing and regenerating operations. The final option for metals removal is *passivation* – certain materials can be used as additives which can be impregnated into the catalyst or added to the feedstock in the form of metallo-organic compounds. These compounds react with the metal contaminants and passivate the contaminants by forming less harmful compounds that remain on the catalyst. For example, antimony and bismuth are effective in passivating nickel and tin is effective in passivating vanadium.

Complete process technologies for residuum catalytic cracking units are the most comprehensive ap-

proach to improving resid processing operations, but present, as might be anticipated, the most expensive option and are subject to high emission factors. Product recycle and multiple reaction sections will be the prevalent technology trends to reduce emissions as will improving feedstock injectors, riser termination and catalyst separation devices, strippers, and regenerator components.

Finally, the use of bio-feedstocks (such as animal fats and vegetable oils) in fluid catalytic cracking will increase the yield of light cycle oil and also provide high-quality products in terms of cetane number. In fact, over the next two decades of the 21st century, fluid catalytic cracking units will take on two additional roles: (1) use of biomass feedstocks and (2) reduction in carbon dioxide emissions, which will help alleviate concerns not only related to energy security but also those related to global climate change.

The implementation of bio-feedstock processing techniques in petroleum refineries can result in competitive advantages for refiners while diminishing many environmental concerns for consumers, especially as development of clays evolves [19.80]:

1. The processes provide refineries with alternative feeds that are renewable and could be lower in cost than petroleum.
2. They can reduce the costs of producing fuels and chemicals from bio-feedstocks by utilizing the existing production and distribution systems for petroleum-based products and avoiding the establishment of parallel systems.
3. The use of bio-feedstocks provides a production base for fuels and chemicals that is less threatened by changes in government policies toward fossil fuel feeds and renewable energies.
4. The use of bio-feedstocks will replace the more environmentally challenging heavy feedstocks in the fluid catalytic cracking unit, because of the flexibility of the unit to accept changing feedstocks and adapt to changing product demands [19.6, 7, 81, 82].

Bio-feedstocks that are able to be processed in the fluid catalytic cracking unit can be categorized as biomass-derived oils (both lignocellulosic materials and free carbohydrates) or triglycerides and their free fatty acids. The operating conditions and catalysts used for each type of feed to achieve a desired product slate vary, and each feed comes with inherent advantages and disadvantages [19.5, 83]. Most of the research work completed to date has been performed on relatively pure bio-feedstocks as opposed to blends of bio-based materials with traditional catalytic cracker feedstocks. In fact, biomass constituents can be blended

with petroleum-based feedstock and fed to a fluid catalytic cracking unit to produce fuels [19.81, 82]. Use of various types of waste streams is also an option for the future [19.84].

In general, bio-feedstocks, catalytic cracker catalysts or blends thereof achieve acceptable product

yields and selectivity. As bio-feedstock use or waste use in the catalytic cracking units continues toward commercialization, the market potential will begin to allow catalyst manufacturers to allocate resources for more tailored catalyst development, greatly improving the yield and quality of desired products.

References

- 19.1 J.G. Speight, B. Ozum: *Petroleum Refining Processes* (Marcel Dekker, New York 2002)
- 19.2 C.S. Hsu, P.R. Robinson: *Practical Advances in Petroleum Processing*, Vol. 1 (Springer, New York 2006)
- 19.3 C.S. Hsu, P.R. Robinson: *Practical Advances in Petroleum Processing*, Vol. 2 (Springer, New York 2006)
- 19.4 J.H. Gary, G.E. Handwerk, M.J. Kaiser: *Petroleum Refining: Technology and Economics*, 5th edn. (CRC, Boca Raton 2007)
- 19.5 J.G. Speight: *Synthetic Fuels Handbook: Properties, Processes, and Performance* (McGraw-Hill, New York 2008)
- 19.6 J.G. Speight: *The Refinery of the Future* (Gulf Professional, Elsevier, Oxford 2011)
- 19.7 J.G. Speight: *The Chemistry and Technology of Petroleum*, 5th edn. (CRC, Boca Raton 2014)
- 19.8 D.S.J. Jones: *Elements of Petroleum Processing* (Wiley, New York 1995)
- 19.9 R.P. Fletcher: The history of fluidized catalytic cracking: A history of innovation: 1942–2008. In: *Innovations in Industrial and Engineering Chemistry*, ACS Symposium Series, Vol. 1000, ed. by W.H. Flank, M.A. Abraham, M.A. Matthews (American Chemical Society, Washington 2009) pp. 189–249
- 19.10 A.A. Avidan, R. Shinnar: Development of catalytic cracking technology. A lesson in chemical reactor design, *Ind. Eng. Chem. Res.* **29**(6), 931–942 (1990)
- 19.11 G. Wang, J. Gao, C. Xu: Evolutionary design on FCC reactors driven by the high temperature and short contact time demands, *Petroleum Sci. Technol.* **22**(11–12), 1581–1594 (2004)
- 19.12 J. Dwyer, D.J. Rawlence: Fluid catalytic cracking: Chemistry, *Catalysis Today* **18**, 487–507 (1993)
- 19.13 K.A. Cumming, B.W. Wojciechowski: Catalytic cracking: Catalysts, chemistry, and kinetics, *Catalysis Rev. Sci. Eng.* **38**, 101–157 (1996)
- 19.14 D.K. Liguras, D.T. Allen: Structural models for catalytic cracking. 2. Reactions of simulated oil mixtures, *Ind. Eng. Chem. Res.* **28**(6), 674–682 (1989)
- 19.15 L.L. Oliveira, E. Biscala: Catalytic cracking kinetic models. Parameter estimation and model evaluation, *Ind. Eng. Chem. Res.* **28**(3), 264–271 (1989)
- 19.16 S. Wang, H. Lu, J. Gao, C. Xu, D. Sun: Numerical predication of cracking reaction of particle clusters in fluid catalytic cracking riser reactors, *Chin. J. Chem. Eng.* **16**(5), 670–678 (2008)
- 19.17 J.G. Speight: Initial reactions in the coking of residua, *Am. Chem. Soc. Div. Petrol. Chem.* **32**(2), 413 (1987)
- 19.18 I.A. Wiehe: The pendant–core building block model of petroleum residua, *Energy Fuels* **8**, 536–544 (1994)
- 19.19 J.F. Schabron, J.G. Speight: An Evaluation of the delayed coking product yield of heavy feedstocks using asphaltene content and carbon residue, *Rev. Inst. Fr. Pet.* **52**(1), 73–85 (1997)
- 19.20 D.A. Storm, S.J. Decanio, J.C. Edwards, E.Y. Sheu: Sediment formation during heavy oil upgrading, *Petroleum Sci. Technol.* **15**, 77 (1997)
- 19.21 E. Fitzer, K. Mueller, W. Schaefer: The chemistry of the pyrolytic conversion of organic compounds to carbon, *Chem. Phys. Carbon* **7**, 237–383 (1971)
- 19.22 J.G. Speight: Thermal chemistry of petroleum constituents. In: *Petroleum Chemistry and Refining*, ed. by J.G. Speight (Taylor Francis, Washington 1998)
- 19.23 A. Bjorseth: *Handbook of Polycyclic Aromatic Hydrocarbons* (Marcel Dekker, New York 1983)
- 19.24 J.R. Dias: *Handbook of Polycyclic Hydrocarbons. Part A. Benzenoid Hydrocarbons* (Elsevier, New York 1987)
- 19.25 J.R. Dias: *Handbook of Polycyclic Hydrocarbons. Part B. Polycyclic Isomers and Heteroatom Analogs of Benzenoid Hydrocarbons* (Elsevier, New York 1988)
- 19.26 R.A. Magaril, E.L. Aksenova: Study of the mechanism of coke formation in the cracking of petroleum resins, *Int. Chem. Eng.* **8**, 727–729 (1968)
- 19.27 R.A. Magaril, L.F. Ramazaeva: Study of coke formation in the thermal decomposition of asphaltenes in solution, *Izv. Vyssh. Ucheb. Zaved. Neft Gaz* **12**(1), 61–64 (1969)
- 19.28 R.L. Magaril, L.F. Ramazaeva, E.I. Askenova: Kinetics of coke formation in the thermal processing of petroleum, *Khim. Tekhnol. Topliv Masel.* **15**(3), 15–16 (1970)
- 19.29 T.A. Cooper, W.P. Ballard: Thermal cracking, vis-breaking, and thermal reforming. In: *Advances in Petroleum Chemistry and Refining*, Vol. 6, ed. by K.A. Kobe, J.J. McKetta (Interscience, New York 1962) pp. 170–239
- 19.30 J.G. Speight: *Handbook of Petroleum Product Analysis*, 2nd edn. (Wiley, Hoboken 2015)
- 19.31 J.G. Speight: *The Desulfurization of Heavy Oils and Residua*, 2nd edn. (Marcel Dekker, New York 2000)

- 19.32 J. Ancheyta, J.G. Speight: *Hydroprocessing of Heavy Oils and Residua* (CRC, Boca Raton 2007)
- 19.33 C.M.d.L. Alvarenga Baptista, H.S. Cerqueira, E.F. Sandes: Process for fluid catalytic cracking of mixed feedstocks of hydrocarbons from different sources, US Patent 7736491 (2010)
- 19.34 C.M.d.L. Alvarenga Baptista, E.M. Moreira, H.S. Cerqueira: Process for fluid catalytic cracking of hydrocarbon feedstocks with high levels of basic nitrogen, US Patent 7744745 (2010)
- 19.35 J.G. Speight, D.I. Exall: *Refining Used Lubricating Oils* (CRC, Boca Raton 2014)
- 19.36 D.B. Bartholic: Preparation of FCC charge from residual fractions, US Patent 4243514 (1981)
- 19.37 D.B. Bartholic: Upgrading petroleum and residual fractions thereof, Patent US4263128 (1981)
- 19.38 L.M. Wolschlag, A. Couch: *UOP FCC Innovations Developed Using Sophisticated Engineering Tools, Tech. Rep. AM-10-109* (UOP LLC, Des Plaines 2010)
- 19.39 W. Reid: Recent Trends in Fluid Catalytic Cracking Patents, Part V: Reactor Section. Dilworth IP. <http://www.dilworthip.com/recent-trends-fluid-catalytic-cracking-patents-part-v-reactor-section/>
- 19.40 D.B. Ardern, J.C. Dart, R.C. Lassiat: Catalytic cracking in fixed- and moving-bed processes. In: *Progress in Petroleum Technology*, Advances in Chemistry, Vol. 5, ed. by R.E. Wilson (American Chemical Society, Washington 1951) pp. 13-29
- 19.41 ACS: *The Houdry Process for the Catalytic Conversion of Crude Petroleum to High-Octane Gasoline* (American Chemical Society and the Sun Company Washington DC and Marcus Hook, Pennsylvania 1996)
- 19.42 F.J. Van Antwerpen: Thermoform catalytic cracking, *Ind. Eng. Chem.* **36**(8), 694-698 (1944)
- 19.43 S.C. Eastwood, C.V. Hornberg, A.E. Potas: Thermoform catalytic cracking unit, *Ind. Eng. Chem.* **39**(12), 1685-1690 (1947)
- 19.44 H.D. Noll, J.C. Dart, R.E. Bland: The houdriflow catalytic cracking process today, Proc. 4th World Petroleum Congress, Rome (1955)
- 19.45 R. Smith, W. Schortman, G. Mills: Characteristics of a houdresid gasoline, *Ind. Eng. Chem. Chem. Eng. Data Ser.* **3**(2), 283-386 (1958)
- 19.46 J. Weikart: Production of motor fuels from petroleum oils, US Patent 2641573 (1953)
- 19.47 J. Van Pool: Catalytic cracking process, US Patent 3542668 (1970)
- 19.48 R. Sadeghbeigi: *Fluid Catalytic Cracking Handbook: An Expert Guide to the Practical Operation, Design, and Optimization of FCC Units*, 3rd edn. (Elsevier, Amsterdam 2012)
- 19.49 C.L. Hemler, L.F. Smith: UOP fluid catalytic cracking process. In: *Handbook of Petroleum Refining Processes*, ed. by R.A. Meyers (McGraw-Hill, New York 1997), pp. 3.47-3.70
- 19.50 P.K. Ladwig: *Handbook of Petroleum Refining Processes*, 2nd edn., ed. by R.A. Meyers (McGraw-Hill, New York 1997) Chapter 3.1
- 19.51 D.B. Bartholic: Process for upgrading tar sand bitumen, US Patent 4804459 (1989)
- 19.52 D. Stratiev, R. Dinkov: Evaluation of FCC unit process variables impact on yield distribution and product quality part I. Evaluation of FCC unit variables impact on yield distribution, *Petroleum Coal* **49**(3), 71-77 (2007)
- 19.53 R.E. Maples: *Petroleum Refinery Process Economics*, 2nd edn. (PennWell, Tulsa 2000)
- 19.54 Occupational Safety and Health Administration: OSHA Technical Manual, http://www.osha.gov/dts/osta/otm/otm_iv/otm_iv_2.html#2
- 19.55 D. DeCroocq: *Catalytic Cracking of Heavy Petroleum Hydrocarbons* (Editions Technip, Paris 1984)
- 19.56 J.F. Le Page, J. Cosyns, P. Courty, E. Freund, J.P. Franck, Y. Jacquin, B. Guiguin, C. Marcilly, G. Martino, J. Miguel, R. Montarnal, A. Sugier, H. von Landeghem: *Applied Heterogeneous Catalysis* (Editions Technip, Paris 1987)
- 19.57 B.C. Gates, J.R. Katzer, G.C.A. Schuit: *Chemistry of Catalytic Processes* (McGraw-Hill, New York 1979)
- 19.58 B.W. Wojciechowski, A. Corma: *Catalytic Cracking: Catalysts, Chemistry, and Kinetics* (Marcel Dekker, New York 1986)
- 19.59 M. Ocelli: *Fluid catalytic cracking: Role in Modern Refining*, Symposium, Vol. 375 (American Chemical Society, Washington 1988)
- 19.60 A.B. Stiles, T.A. Koch: *Catalyst Manufacture* (Marcel Dekker, New York 1995)
- 19.61 A. Cybulski, J.A. Moulijn: *Structured Catalysts and Reactors* (Marcel Dekker, New York 1998)
- 19.62 M.L. Ocelli, P. O'Connor: *Fluid Cracking Catalysts* (Marcel Dekker, New York 1998)
- 19.63 M.E. Ocelli: *Advances in Fluid Catalytic Cracking: Testing, Characterization, and Environmental Regulations* (CRC, Boca Raton 2010)
- 19.64 E. Tangstad, M. Bendicksen, T. Myrstad: Effect of sodium deposition on FCC catalysts deactivation, *Appl. Catalysis A* **150**(1), 85-99 (1997)
- 19.65 H.S. Cerqueira, G. Caeiro, L. Costa, F. Ramôa Ribeiro: Deactivation of FCC catalysts, *J. Mol. Catalysis A* **292**(1-2), 1-13 (2008)
- 19.66 M.A. Gerber, J.L. Fulton, J.G. Frye, L.J. Silva, L.E. Bowman, C.M. Wai: Regeneration of Hydrotreating and FCC Catalysts. US Department of Energy Contract No. DE-AC06-76RLO 1830, Tech. Rep. PNNL-13025 (Pacific Northwest National Laboratory, Richland 1999)
- 19.67 ASTM: *Annual Book of Standards* (ASTM International, West Conshohocken 2016)
- 19.68 S.F. González, J.L. Carrillo, M. Núñez, L.J. Hoyos, S.A. Giraldo: Modified design for vacuum residue processing, *CTandF - Ciencia, Tecnología y Futuro* **4**(2), 57-69 (2010)
- 19.69 S.W. Shorey, D.A. Lomas, W.H. Keesom: Use FCC feed pretreating methods to remove sulfur, *Hydrocarbon Process.* **78**(11), 43-51 (1999)
- 19.70 J.S. Yoo: Metal recovery and rejuvenation of metal-loaded spent catalysts, *Catalysis Today* **44**(1), 27-46 (1998)
- 19.71 R.C. McFarlane, R.C. Reineman, J.F. Bartee, C. Georgakis: Dynamic simulator for a model IV catalytic cracking unit, Proc. AIChE Annu. Meet (American Institute of Chemical Engineers, Washington 1990)

- 19.72 J.G. Speight: *Natural Gas: A Basic Handbook* (Gulf, Houston 2007)
- 19.73 G. Heinrich, J.-L. Mauleon: The R2R process: 21st century FCC technology, *Rev. Inst. Fr. Pet.* **49**(5), 509–520 (1994)
- 19.74 K. Inai: Operation results of the R2R process, *Rev. Inst. Fr. Pet.* **49**(5), 521–527 (1994)
- 19.75 J.G. Speight, S.E. Moschopedis: The production of low-sulfur liquids and coke from athabasca bitumen, *Fuel Process. Technol.* **2**, 295 (1979)
- 19.76 K.A. Couch, K.D. Seibert, P.J. Van Oordorp: Controlling FCC yields and emissions, *Proc. Natl. Petrochem. Refiners Assoc. (NPRA) Annual Meeting*, San Antonio (2004)
- 19.77 L.M. Wolschlag, K.A. Couch, X. Zhu, J. Alves: UOP FCC Design Advancements to Reduce Energy Consumption And CO₂ Emissions, *Tech. Rep. AM-09-35* (UOP LLC, Des Plaines 2009)
- 19.78 R. Sadeghbeigi: *Fluid Catalytic Cracking: Design, Operation, and Troubleshooting of FCC Facilities* (Gulf, Houston 1995)
- 19.79 RTI: *Petroleum Refineries: Catalytic Cracking Units, Catalytic Reforming Units, and Sulfur Recovery Units – Background Information for Promulgated Standards and Response to Comments. Final Report, EPA-453/R-01-011* (Research Triangle Institute, Center for Environmental Analysis and US Environmental Protection Agency, Office of Air Quality Planning and Standards, Waste and Chemical Process Group, Research Triangle Park 2001)
- 19.80 O.D. Mante, F.A. Agblevor, S.T. Oyama, R. McClung: The effect of hydrothermal treatment of FCC catalysts and ZSM-5 additives in catalytic conversion of biomass, *Appl. Catalysis A* **445/446**, 312–320 (2012)
- 19.81 G. Fogassy, N. Thegarid, G. Toussaint, A.C. Van Veen, Y. Schuurman, C. Mirodatos: Biomass derived feedstock co-processing with vacuum gas oil for second-generation fuel production in FCC units, *Appl. Catalysis B* **96**(3/4), 476–485 (2010)
- 19.82 G. Fogassy, N. Thegarid, Y. Schuurman, C. Mirodatos: From biomass to bio-gasoline by FCC co-processing: Effect of feed composition and catalyst structure on product quality, *Energy Environ. Sci.* **4**, 5068–5076 (2011)
- 19.83 J.G.E. Speight: *The Biofuels Handbook* (Royal Society of Chemistry, London 2011)
- 19.84 P.M. Hudec, M. Horňáček, A. Smiešková, P. Daučík: Chemical recycling of waste hydrocarbons in catalytic cracking, *Petroleum Coal* **51**(1), 51–58 (2009)

Sulfur Removal and Recovery

Paul R. Robinson

Petroleum, natural gas and other fossil fuels contain significant amounts of sulfur. When burned, the sulfur becomes sulfur oxides (SO_x), which can cause significant damage to the environment and human health. To minimize such damage and to ensure that finished products meet performance specifications, the sulfur is removed and transformed into useful chemicals, primarily sulfuric acid and fertilizers.

About 57% of the world's sulfur is a byproduct of oil and gas processing. The sulfur in natural gas is primarily H_2S , sometimes accompanied by mercaptans. The sulfur compounds in heavier fossil fuels include entrained H_2S , inorganic sulfur compounds and organic sulfur compounds. For natural gas and petroleum, the predominant sulfur recovery strategy is:

1. To convert all sulfur compounds into H_2S
2. To adsorb the H_2S into a solution containing an alkanolamine
3. To transport the H_2S -laden amine to a sulfur plant
4. To convert the H_2S into elemental sulfur with the modified Claus process
5. To employ Claus tail-gas treatment to increase overall recovery to $> 99.5\%$.

Sulfur removal and recovery protects the planet from pollution by sulfur oxides and acids, which continue to threaten our atmosphere, water, land, and inhabitants. The challenge is worldwide, and so must be the solution.

20.1	About Sulfur	650
20.1.1	Sulfur in Antiquity	650
20.1.2	Sulfur for Life	650
20.2	Sulfur Sources	651
20.2.1	Elemental Sulfur	651
20.2.2	Frasch Process	652
20.2.3	Sulfuric Acid from Metallurgy	653
20.3	Sulfur from Petroleum and Natural Gas	654
20.3.1	Sulfur Removal/Recovery Strategies	654
20.3.2	Natural Gas Processing	655
20.3.3	Sulfur from Refineries	656
20.3.4	Amine Treating	657
20.4	Conversion of H_2S to Elemental Sulfur	659
20.4.1	The Claus Process	659
20.4.2	Catalytic Oxidation Processes	661
20.4.3	Tail-Gas Treating	662
20.4.4	Mercaptan Conversion	662
20.5	Sulfur Uses	663
20.5.1	Elemental Sulfur and Inorganic Salts ...	664
20.5.2	Organic Sulfur	664
20.5.3	Sulfites, Sulfates and Oxides	664
20.5.4	Other Uses	664
20.6	Pollution from Sulfur	665
20.6.1	Acid Deposition (SO_x , NO_x and PM)	665
20.6.2	Open-Air Roasting	668
20.6.3	Volcanic SO_x : The Year Without a Summer	668
20.6.4	International Shipping	669
20.6.5	Acid Mine Drainage	669
20.6.6	Midnight Dumping	669
20.6.7	Lax Regulation Enforcement	670
20.7	Conclusion	671
	References	671

20.1 About Sulfur

Sulfur is essential to life. But certain sulfur compounds, such as hydrogen sulfide (H_2S) and sulfur oxides (SO_x), are poisonous and can devastate the environment. Hydrogen sulfide is a broad-spectrum poison affecting several different systems in the body, especially the nervous system. At 50–100 ppm in air, it causes eye damage, at 100–150 ppm it shuts off the sense of smell and above 320 ppm it is deadly.

Petroleum, natural gas and other fossil hydrocarbons contain significant amounts of inorganic and/or organic sulfur. To mitigate environmental damage and to ensure that refined products meet performance specifications, sulfur is removed from fossil hydrocarbons and converted into relatively innocuous elemental sulfur.

Sulfur (also spelled sulphur) is a chemical element for which the atomic number is 16, the atomic weight is 32.065 (± 0.005) and the IUPAC symbol is S. Elemental sulfur forms more than 30 allotropes, ranging from S_2 and S_3 gases to crystalline solids with up to 20 atoms per molecule. Amorphous, glassy sulfur is formed by rapidly quenching molten sulfur; the glasses readily revert to crystalline forms. At room temperature and pressure, the predominant allotrope is orthorhombic (or rhombic) sulfur (S_8), which has the puckered cyclic structure shown in Fig. 20.1. For thermochemical calculations, orthorhombic S_8 is taken as the standard state for sulfur. It melts at 115.2 °C (239.4 °F), boils at 444.6 °C (832.3 °F) and easily sublimates. The two other cyclic S_8 species are beta monoclinic sulfur, which is stable above 95.3 °C (203.5 °F) and gamma monoclinic sulfur.

20.1.1 Sulfur in Antiquity

Sulfur was known in ancient times, due to its abundance and unique properties [20.1]. Bright yellow sulfur deposits appeared near volcanic craters and at the edges of foul-smelling hot springs. Other deposits were embedded in limestone formations [20.2]. Ancient Greeks fumigated clothing and dwellings with sulfur [20.3]. In the *Odyssey*, Homer mentioned *pest-averting* sul-

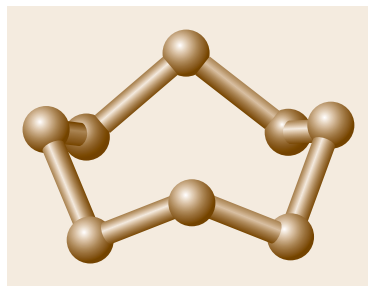


Fig. 20.1 Stick-and-ball structure of orthorhombic (rhombic) sulfur, S_8 , the standard state for elemental sulfur

fur [20.4]. Assyrian texts from the sixth century BC describe sulfur as a *product of the riverside*. In the first century AD, in his comprehensive *Natural History* [20.5], *Pliny the Elder* wrote that Melos was the best source of sulfur for medicine, fumigation and bleaching. Medicinal uses included ointments to alleviate scabies, ringworm and other epidermic ailments. Egyptians treated ocular maladies with a sulfur ointment. Roman soldiers mixed sulfur into pitch to increase the lethality of incendiary weapons.

Chinese writings indicate that sulfur was known in Hanzhong during the sixth century BC. In the third century AD, Chinese miners were recovering sulfur from pyrite. Black powder, a mixture of potassium nitrate, charcoal and sulfur, was invented during the Tang Dynasty (ninth century). Written recipes for black powder appeared in the 11th century during the Song Dynasty. The recipes arrived in Japan and Europe in the 13th century. Arab alchemists weaponized black powder by refining old formulations and standardizing production.

In Middle English texts, sulfur was called brimstone, brimston or bremston, which are corruptions of the old English brynstaen. Literally, *brimstone* means *stone that burns* or *burning stone*. The King James Bible associates *fire and brimstone* with hell, perhaps because sulfur so often is found near the mouths of active volcanoes. The German word *Bernstein* means *amber*, not brimstone; Schwefel is German for sulfur.

20.1.2 Sulfur for Life

Sulfur is essential to all life on Earth. It comprises about 0.03% of the Earth's crust and 0.3% of the human body (Table 20.1) [20.6]. In living organisms, it

Table 20.1 Elemental composition of the human body (after [20.6])

Element	Symbol	wt%
Oxygen	O	65.0
Carbon	C	18.5
Hydrogen	H	9.5
Nitrogen	N	3.2
Calcium	Ca	1.5
Phosphorus	P	1.0
Potassium	K	0.4
Sulfur	S	0.3
Sodium	Na	0.2
Chlorine	Cl	0.2
Magnesium	Mn	0.1
Trace elements	B, Cr, Co, Cu, F, I, Fe, Mn, Mo, Se, Si, Sn, V, Zn	< 1.0 (total)

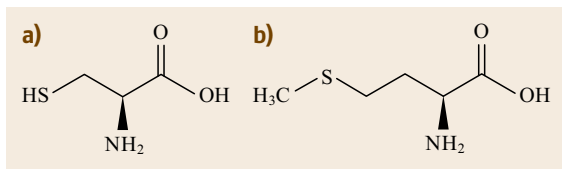
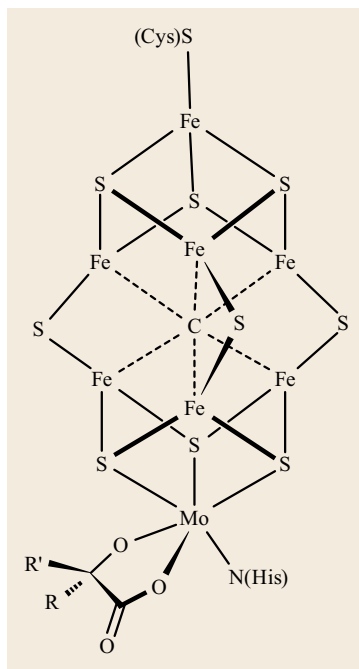


Fig. 20.2a,b Sulfur-containing amino acids, (a) L-cysteine and (b) L-methionine

Fig. 20.3 Iron-Molybdenum cofactor in the enzyme nitrogenase. Cys = cysteine, His = histone ►

appears primarily in two amino acids, cysteine and methionine (Fig. 20.2) and in the peptides and proteins that include those amino acids. In humans, methionine is an essential amino acid contained in food. Except for the vitamins biotin and thiamine, cysteine and all other sulfur-containing compounds in the human body can be synthesized from methionine. In animals, metabolism of methionine and cysteine requires sulfite oxidase. The enzyme nitrogenase, which catalyzes biological nitrogen fixation, includes Fe_4S_4 clusters and a $\text{Fe}_7\text{MoS}_9\text{C}$ cofactor (Fig. 20.3).



20.2 Sulfur Sources

Table 20.2 gives a breakdown of worldwide sulfur production by source in 2013 [20.7]. The values include direct production of sulfuric acid from metallurgy (roasting of sulfide ores). Petroleum and natural gas accounted for 57.2% of the total. Relative amounts vary considerably from country to country. For example, in the United States, 93.4% came from oil and gas and the remainder came from metallurgy. But in China, 56.2% came from pyrites; 32.4% came from oil, gas and metallurgy; and 11.4% came from elemental sulfur mines.

Table 20.2 Breakdown of worldwide sulfur production by source in 2012

Source	1000 t/yr	%
Elemental sulfur ^a	1700	2.4
Frasch	526	0.7
Pyrites	6500	9.2
Other metallurgy	13 200	18.8
Petroleum and natural gas	40 300	57.2
Unspecified ^b	7300	10.4
Total	69 500	

^a Elemental obtained by mining

^b Data from countries which provided total production without a detailed breakdown

20.2.1 Elemental Sulfur

During the 18th and 19th centuries, sulfur ore was mined from limestone deposits in Italy, especially Sicily. Sulfur was recovered from the ore by careful melting, at first with direct heating and later with steam. Italian sulfur dominated world markets until the advent of the Frasch process.

Sulfur from volcanoes is still mined today. A noteworthy example comes from Kawah Ijen [20.8], a volcano in East Java, Indonesia, which rises to about 2900 m above sea level. It is a favorite destination for adventuresome tourists. Two-day excursions start with a 5 h bus ride from Surabaya to a base camp. From the camp, it is a 4 km walk up to the edge of the caldera [20.9]. Along the way, tourists enjoy a unique panorama, which includes a beautiful turquoise lake. They also begin to smell (and taste) sulfur dioxide (SO_2). SO_2 is the product of the spontaneous combustion of sulfur vapor. At the end of the trek, the acrid odors intensify, stinging sensitive eyes and throats. If they can endure the gases until sunset, tourists marvel at the blue flames that flicker upwards from the ooze that emerges from the earth and creeps down the mountainsides (Fig. 20.4). The color isn't from lava, but from burning brimstone.



Fig. 20.4 Blue flames from spontaneous combustion of sulfur vapor to form sulfur oxides at the Ijen Crater, East Java, Indonesia (after [20.10], photo by Dodi Mulyana)

Inside the crater, the environment isn't so pleasant. The lake is sulfuric acid – aqueous H_2SO_4 with pH values that range from 0.5–1, depending on how and where measurements are taken. Air concentrations of SO_2 can exceed 30 parts per million, 15 times higher than the limit set by the US Occupational Safety and Health Administration (OSHA). Sulfur vapor that isn't burned condenses and floats back down to earth as a fine powder, forming thick deposits of beautiful yellow S_8 .

For miners working 1000 m down inside the crater, the powder is as dangerous as the SO_2 , because it penetrates deeply into lungs. The men defend themselves with paper masks or strips of cloth. They use torches and metal rods to pry out slabs of sulfur and break them into chunks that can be carried in baskets on poles across their backs. Miners retrieve and carry two loads

per day. For each load, they walk 8–10 km (4–5 km each way). Each load weighs between 70–90 kg – sometimes more than the men themselves [20.11, 12]. They are paid \$ 0.078 per kg, which translates to \$ 11–15 per day. The job is far more lucrative than other manual jobs in the area. PT Candi Ngrimbi employs about 100 registered full-time miners, who recover up to 15 t of raw sulfur per day. The sulfur is used locally, primarily for refining sugar.

20.2.2 Frasch Process

In 1900, domestic sulfur in the United States came from native deposits in Louisiana, Nevada, Texas and Utah, which were mined with conventional digging [20.13]. Virtually all elemental sulfur imports came from Sicily. In 1894, German-born American chemist *Herman Frasch* invented a method for recovering underground sulfur from the surface [20.14]. Sulphur, Louisiana is the site of the first large-scale Frasch facility, which began production in 1903. The second Frasch installation opened in 1912 in Brazoria County, Texas [20.15]. By about 1915, the United States had surpassed Italy as the world's leading producer of sulfur. From then until the middle of the 20th century, Frasch sulfur from Texas and Louisiana accounted for up to 90% of US sulfur production and comprised a significant portion of total world production. Frasch sulfur hit its peak in 1974, when 12 mines yielded eight million tons. The last US Frasch facility closed in 2000, but the process is still used in Mexico and Poland and under a different name in China.

Figure 20.5 illustrates the Frasch process. A well is drilled into a sulfur deposit and three concentric tubes are inserted into the bore hole. Under pressure, water is

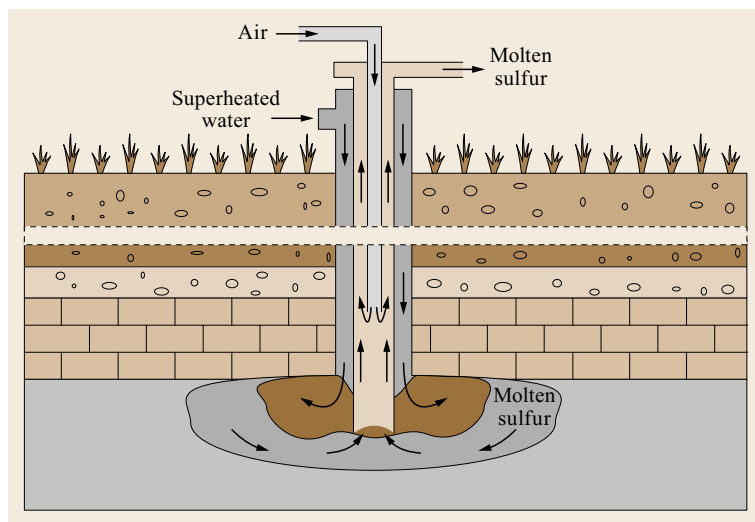


Fig. 20.5 The Frasch process. Superheated water is pumped into a deposit, where it melts elemental sulfur. The molten sulfur flows up the surface, propelled in part by hot air

superheated to about 165 °C and injected into the well through the outermost tube. The sulfur is liquefied and flows into the middle tube. Molten sulfur is viscous and dense and cannot be lifted with water pressure alone. Hot air is injected through the inner tube to froth the sulfur, decreasing its density and propelling it to the surface. The purity of Frasch sulfur tends to be very high – greater than 99.5%.

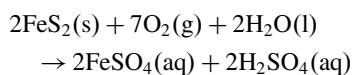
20.2.3 Sulfuric Acid from Metallurgy

The refining of sulfur-containing metal ores can produce sulfur, sulfuric acid and SO₂. Important sulfide ores include iron-containing pyrite (FeS₂); lead-containing galena (PbS); sphalerite, which contains both zinc and iron ([Zn,Fe]S); and copper-containing chalcocite (Cu₂S) and covellite (CuS).

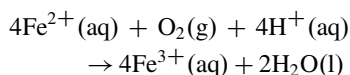
Pyrite Leaching

Pyrite leaching was generating sulfuric acid in classical times. In 15th century England, leaching became an alternative to making H₂SO₄ by burning sulfur and collecting the oxides in water. By the 19th century, leaching was much preferred [20.16].

In heap leaching, the ore is gathered into piles and allowed to weather. The net initial reaction is

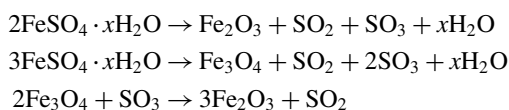


Green crystalline FeSO₄ · xH₂O is called ferrous sulfate, copperas, or green vitriol. Some of the aqueous ferrous ion is oxidized to ferric ion



The reactions occur spontaneously and they are expedited significantly by sulfur-oxidizing bacteria.

When heated, ferrous sulfate loses its water of crystallization. The green crystals become a brown amorphous solid. Additional heating to about 680 °C (1256 °F) generates sulfur oxides, leaving behind rust-colored hematite (Fe₂O₃). Magnetite (Fe₃O₄) also may be formed. Representative reactions (unbalanced) include



The iron oxides are reduced to iron metal by coke in a blast furnace or by electrolysis. The SO₂ is oxidized to SO₃ over a catalyst, such as supported vanadia [20.17].

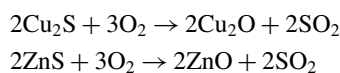
The SO₃ is dissolved in water or oleum to make sulfuric acid. Alternatively, in some locales, it is vented to the atmosphere.

Chemical Refining

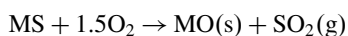
Prior to chemical refining, ores are sized by crushing, dry grinding and wet grinding (levigation). Methods for subsequent physical separation include hydraulic washing, gravity separation, magnetic separation and froth flotation. Levigation is commonly used for oxidic ores, froth flotation for sulfidic ores and magnetic separation for magnetic ores or impurities.

Preliminary chemical methods include leaching, calcining and roasting [20.18]. Pyrite leaching is described above. During calcination and roasting, ores are heated to drive off volatile impurities. Calcination decomposes carbonates, releasing CO₂ and leaving behind metal oxides.

Generally speaking, roasting involves reactions of solids and gases at elevated temperature. Roasting reactions can include oxidation, reduction, chlorination, sulfation and pyrohydrolysis. In the roasting of sulfide ores, the sulfides are converted to metal oxides and the sulfur is released as volatile sulfur oxides. For chalcocite (Cu₂S) and sphalerite (ZnS), the roasting reactions are



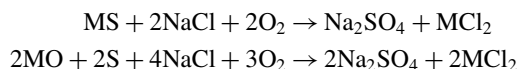
Oxidizing roasting is described above for zinc and copper oxides. The general reaction is



Complete or near-complete removal of sulfur gives a *dead roast*.

Volatilizing roasting is similar, except that the flow of air is carefully controlled. It is designed to remove volatile impurities without over-oxidizing the ore. This method is preferred for producing As₂O₃ and Sb₂O₃.

Chloriding roasting transforms certain metal compounds into chlorides. This method is preferred for uranium, titanium, beryllium and some rare earths. General reactions include



The first reaction represents chlorination of a sulfide ore of a divalent metal. The second reaction represents chlorination of an oxide ore in the presence of elemental sulfur. Chlorination of carbonate ores is preceded by calcination, which decomposes the carbonate into a metal oxide with effusion of CO₂.

Reduction roasting decomposes high-valent metal oxides into lower-valent oxides.

Magnetic roasting is a special case of reduction roasting. It converts nonmagnetic hematite (Fe_2O_3) into magnetic magnetite (Fe_3O_4).

Sinter roasting involves simultaneous oxidation and agglomeration of ores. Lead sulfide ores are refined with sinter roasting.

20.3 Sulfur from Petroleum and Natural Gas

Petroleum and natural gas provide 56% of the nonfood energy consumed by humans (Fig. 20.6) and they provide 57% of the world's industrial sulfur (Table 20.2).

Natural gas from commercial fields can contain more than 20% H_2S . Common crude oils contain up to 5 wt% sulfur. In contrast, sales-quality gas must contain less than 4 ppmv H_2S . In the United States and other countries, up to 90% of petroleum products are fuels and all but the heaviest products must be essentially sulfur-free. In the EU and the United States, the sulfur content of gasoline and diesel must be 10 ppmw or less by 1 January 2017. In much of China, similar limits will take effect in 2017.

Recovery of sulfur as a byproduct of natural gas processing and oil refining was first reported in 1938. Byproduct sulfur production grew steadily and in 1982 it surpassed Frasch sulfur in the United States. In 2000, US sulfur production totaled 10.3 million tons – 81% from recovery, 9% from one Frasch mine and 10% as

byproduct sulfuric acid from nonferrous metal smelters. Consumption was 12.5 million tons, including 2.8 million tons of imports.

20.3.1 Sulfur Removal/Recovery Strategies

For natural gas and petroleum, the choice of technology for removing and/or recovering sulfur depends on the nature of the sulfur compounds and their concentrations:

- If it is necessary to remove H_2S or SO_2 from a gas containing less than a few ppmv, caustic scrubbing may be sufficient. Flue-gas SO_x removal processes include both dry scrubbing with solid alkali and wet scrubbing. If only traces of H_2S are present, chemisorption onto zinc oxide (ZnO) may be preferred.
- Most crude oils contain between 0.5–2.5 wt% sulfur – some contain less, some contain more than 5 wt%. Many process units convert organic sulfur compounds into H_2S and sulfur-free hydrocarbons. The H_2S is adsorbed into a solution containing an alkanolamine and transported to a sulfur recovery unit (SRU).
- Sulfur appears in natural gas mostly as H_2S . Mercaptans are also present. Natural gas condensate is relatively sweet, with low concentrations of organic sulfur. It goes to a refinery, where it is blended with a suitable crude oil fraction and processed conventionally. As with offgas refinery gas, the H_2S in natural gas is adsorbed by an alkanolamine solution and transported to an SRU.
- SRUs oxidize the H_2S into elemental sulfur. With a few exceptions, oxidation is achieved by partial combustion in the modified Claus process. Alternatives employ direct catalytic oxidation instead of combustion. Examples include the Merichem LO-CAT process and the UOP Selectox process. Direct oxidation is preferred for small units or when open flames are dangerous, such as on oil production platforms or in remote locations where heat from a Claus furnace is a liability, not a benefit.
- Claus tail gas treatment units (TGTUs) bring the total sulfur recovery in an SRU up to > 99.5%. Examples include the Shell SCOT process, the Amoco cold-bed adsorption (CBA) process, the

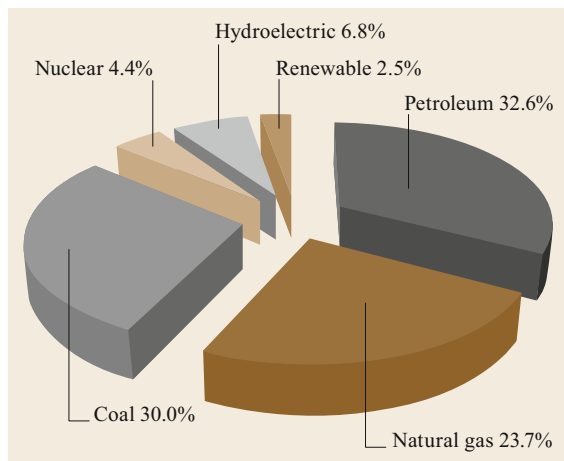


Fig. 20.6 World energy consumption by fuel in 2014 (after [20.19]). The sum for fossil hydrocarbons is 86.0, 1.7% lower than the 2013 total. From 2013 to 2014, renewables increased from 2.5–2.7%. Petroleum includes crude oil produced from tight formations with hydraulic fracturing. Gas includes coproduced petroleum gas, condensate, dry gas and coal-seam gas. Renewable includes wind, solar, geothermal and biomass (largely ethanol and oil from plants) (data for the figure come from BP Statistical Review of World Energy 2015)

UOP BSR/Selectox process and the Merichem LO-CAT process.

- Catalytic oxidation with a UOP Merox unit or a Merichem MERICAT unit removes mercaptans from gases.
- Chemisorption onto nickel-based catalysts removes ppm levels of mercaptans from naphtha.

20.3.2 Natural Gas Processing

Natural gas comprises methane and other light hydrocarbons, up to and beyond C₅+ paraffins. It often contains H₂S, CO₂ and/or other gases, such as mercury, nitrogen, argon and helium. The sulfur in natural gas is primarily H₂S, sometimes accompanied by mercaptans. The goal of natural gas processing is to separate components into salable products. The main steps in natural gas processing are outlined in Fig. 20.7. Figure 20.8 displays a photo of a pristine natural gas processing plant operated by PTT in Map Ta Phut, Thailand [20.21].

Here are some common industry terms:

- *Consumer gas*: In the consumer gas distributed by the Union Gas system, the typical sulfur content is

5.5 mg/m³. This includes the 4.9 mg/m³ of sulfur in *t*-butyl mercaptan, which is added as an odorant for safety reasons [20.22]. When people smell that odor, they instantly know there's a gas leak and can take appropriate action.

- *Sour gas*: Natural gas is considered sour if it contains more than 4 ppmv H₂S. About one-third of world natural gas reserves are sour [20.23]. Gas from the Charlotte (Buda) well in Atascosa County, Texas contains more than 8% H₂S [20.24]. Several wells in Alberta, Canada produce gas with more than 10% H₂S and a few yield gas with more than 50% H₂S [20.25]. Sour gas can also contain mercaptans (RSH), where "R" represents alkyl groups such as methyl-, ethyl-, and so on.
- *Wet gas*: Wet gas is mostly methane but also contains C₂–C₄ paraffins.
- *Condensate*: Condensate contains C₅+ paraffins. It is also called natural gasoline.
- *Liquefied natural gas* (LNG): LNG is a mixture of ethane and propane. In certain circumstances, refinery LNG might contain traces of propane and olefins.
- *Liquefied petroleum gas* (LPG): LPG is mostly propane but can contain some butanes.

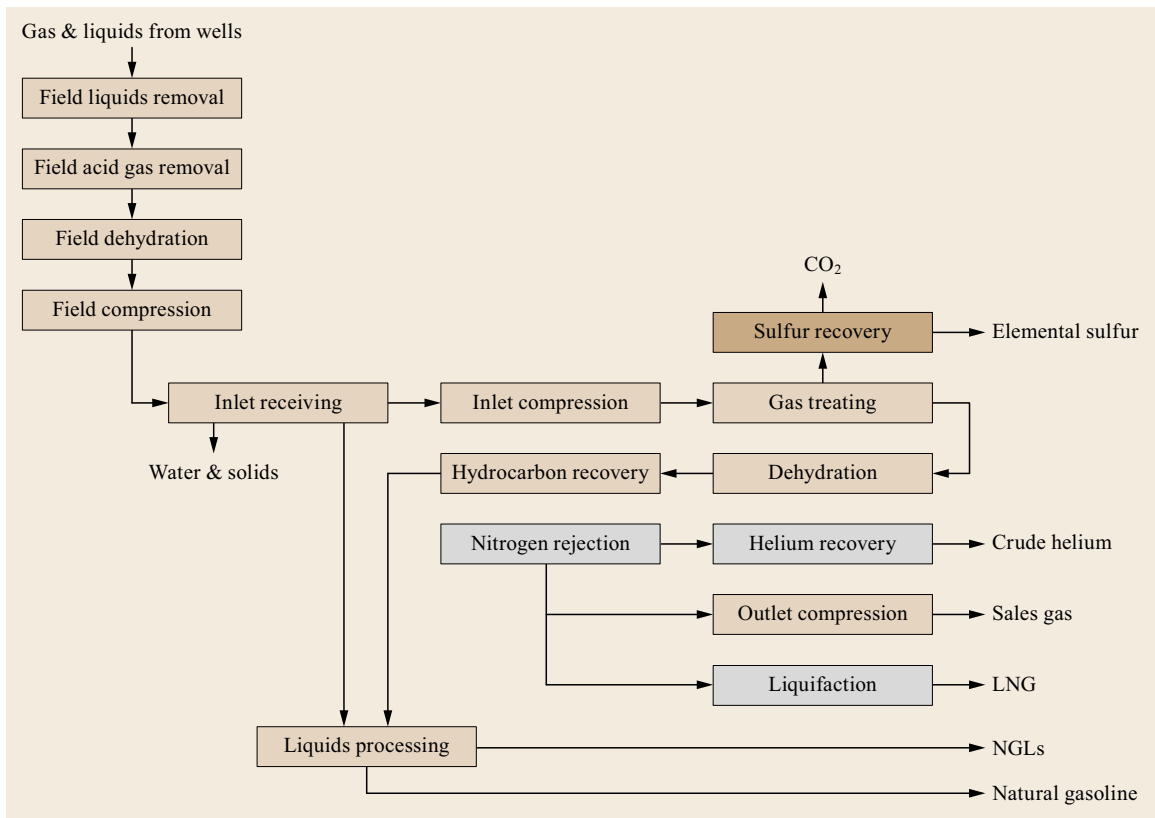


Fig. 20.7 Natural gas processing plant—block diagram (after [20.20])



Fig. 20.8 PTT natural gas processing plant in Map Ta Phut, Rayong, Thailand

- **Acid gas:** Acid gas from a natural gas process plant contains H_2S , CO_2 or a combination of CO_2 and H_2S . Acid gas goes to a sulfur plant, where the H_2S is oxidized to elemental sulfur.

Raw gas from wells contains water and condensate. These are removed in high- and low-pressure separators, as shown in Fig. 20.9. The separator overhead streams, which contain C_1 – C_4 hydrocarbons, light mercaptans, acid gas, mercury, and so on, are combined and piped to the acid gas removal section of the main plant. The water is treated and injected into disposal wells. The condensate is transported to a refinery for further processing.

Condensate production can be significant. The feed to a 90 000 barrel/day refinery in Borger, Texas includes up to 17 000 barrel/day of condensate from near-

by gas wells. The plant is owned by WRB Refining LP and operated by Phillips 66.

20.3.3 Sulfur from Refineries

The sulfur compounds in petroleum include entrained H_2S , inorganic sulfur compounds (sulfate salts and allotropes of elemental sulfur) and organic sulfur compounds including mercaptans. Most light gases – hydrocarbons, H_2S , mercaptans, nitrogen, etc. – effuse from liquid petroleum in settling tanks and are processed in upstream gas plants. When it reaches refineries, petroleum may still contain some of these contaminants. Salts are removed in refinery desalting units. Remaining light gases, entrained H_2S and remaining light mercaptans are recovered from the reflux drum at the top of the atmospheric distillation unit (ADU).

The ADU gases, along with gases from other refinery units, pass through an amine treater, which recovers H_2S and CO_2 . With few exceptions, CO_2 concentrations are very low in refineries. Amine treating does not remove mercaptans. These evil-smelling compounds are removed by special sweetening processes, such as the UOP Merox process and the Merichem MERCAT processes.

Typical refineries have more than one amine system. As in natural gas plants, H_2S is stripped from the amine in regenerator columns and conveyed to the sulfur plant.

Organic sulfur compounds are converted into H_2S by hydrotreaters and hydrocrackers. In fluid catalytic cracking (FCC) units, some organic sulfur is converted to H_2S in the riser-reactor. The remainder is converted to SO_x in the regenerator. In cokers, some sulfur is con-

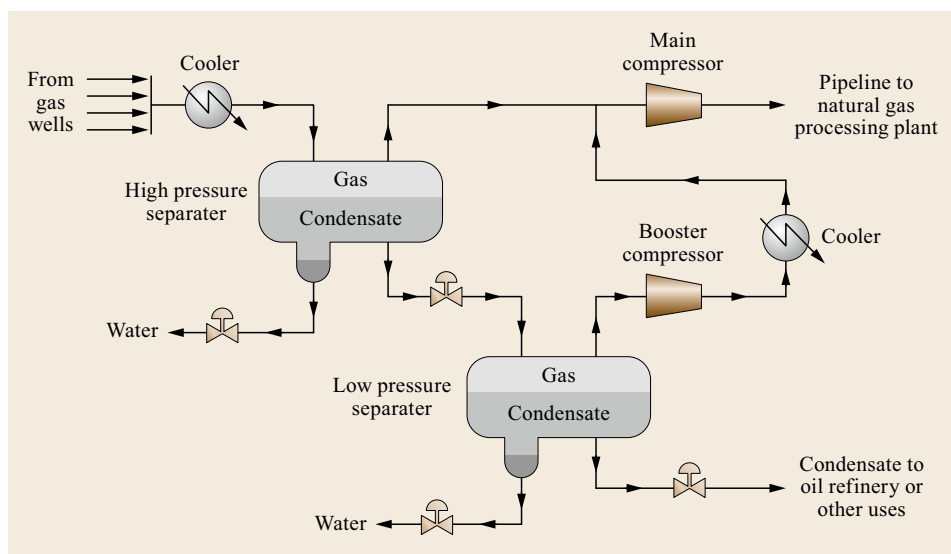


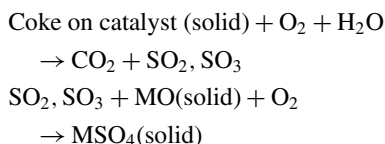
Fig. 20.9 Condensate and water removal from raw natural gas

verted to H_2S , but the remainder shows up in the liquid products. Coker liquids must be hydrotreated before they can be blended into finished products.

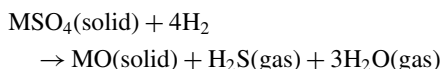
A large fraction of the sulfur in the feed to an FCC unit ends up in coke on the catalyst. SO_x are formed in the regenerator when the coke is burned away. Therefore, removing sulfur from the feed, usually by hydrotreating, decreases SO_x emissions. FCC feed pretreating has other substantial benefits. Removing basic nitrogen decreases deactivation of acid sites on the FCC catalyst, which allows the FCC unit to achieve higher, more selective conversion at lower temperatures. The saturation of aromatics in the feed pretreater provides the biggest benefit, because it converts hard-to-crack aromatics into easier-to-crack naphthenes. This alone can justify the installation of an FCC feed pretreater.

SO_x transfer additives, first developed by Davison Chemical, react with SO_x in the FCC regenerator to form sulfates. When the sulfated additive circulates to the riser/reactor section, the sulfates are reduced to H_2S , which is recovered by alkanolamine absorption and sent to the sulfur plant. In some units, these additives reduce FCC SO_x emissions by more than 70%. Consequently, if a pretreater or posttreater still must be installed, it can be smaller. The chemistry of SO_x transfer is summarized below:

- FCC regenerator (oxidizing environment)



- FCC riser-reactor (reducing environment)



Flue-gas scrubbing is a refiner's last chance to keep NO_x and SO_x out of the air. In wet flue-gas desulfurization, gas streams containing SO_x react with an aqueous slurry containing calcium hydroxide $\text{Ca}(\text{OH})_2$ and calcium carbonate CaCO_3 . Reaction products include calcium sulfite (CaSO_3) and calcium sulfate (CaSO_4), which precipitate from the solution. NO_x removal is more difficult. Wet flue-gas scrubbing removes about 20% of the NO_x from a typical FCC flue gas. To remove the rest, chemical reducing agents are used. In the selective catalytic reduction (SCR) process, anhydrous ammonia is injected into the flue gas as it passes through a bed of catalyst at 500–950 °F (260–510 °C). The chemical reaction between NO_x and ammonia produces N_2 and H_2O .

When sulfur-containing feeds pass through hydrotreaters or conversion units, most of the sulfur is converted into H_2S , which eventually ends up in offgas streams. Amine absorbers remove the H_2S , leaving only 10–20 wppm in the treated gas streams. H_2S is stripped from the rich alkanolamine, which is returned as lean amine to the absorbers. The H_2S goes to the refinery sulfur plant.

Another source of refinery sulfur is sour water. Wash water often is used to keep heat exchangers clean. In hydrotreaters and hydrocrackers, wash water is injected into the reactor effluent. When the effluent is cooled, the water reacts with the H_2S and NH_3 to form aqueous ammonium bisulfide (NH_4SH), which ends up in sour water streams. The H_2S and ammonia are removed in a sour water stripper and sent to the sulfur plant.

20.3.4 Amine Treating

Both in refineries and/or natural gas processing plants, H_2S and CO_2 are recovered by adsorption into aqueous solutions containing alkanolamine compounds, such as diethanol amine (DEA), monoethanol amine (MEA), methyldiethanol amine (MDEA) and diglycolamine (DGA). The structures of DEA and MDEA are shown in Fig. 20.10. Combinations of chemicals, such as MDEA plus sulfolane, also are employed. Light mercaptans are not removed by the kinds of amine treating employed by natural gas plants and refineries [20.26].

A typical layout for amine treating appears in Fig. 20.11. The absorber (contactor) is a trayed tower in which the lean amine solution mixes with natural gas. Acid gases (H_2S and CO_2) are adsorbed into the amine. The now-rich amine is withdrawn from the bottom of the tower and sent to the regenerator. Treated gas goes out the top.

In the trayed regenerator column, a steam-heated reboiler disengages the acid gases, which flow out the top through a condenser into a reflux drum. In this application, the reflux drum serves double duty as a cold low-pressure separator, from which the overhead acid gas is essentially liquid-free. Depending on the nature of the alkanolamine, the condensed solu-

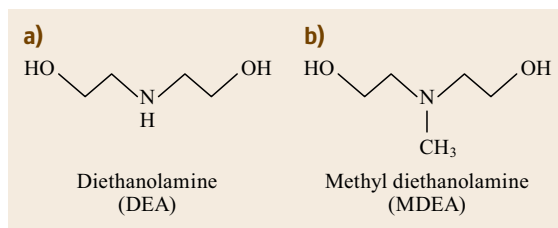


Fig. 20.10a,b Structures of DEA (a) and MDEA (b)

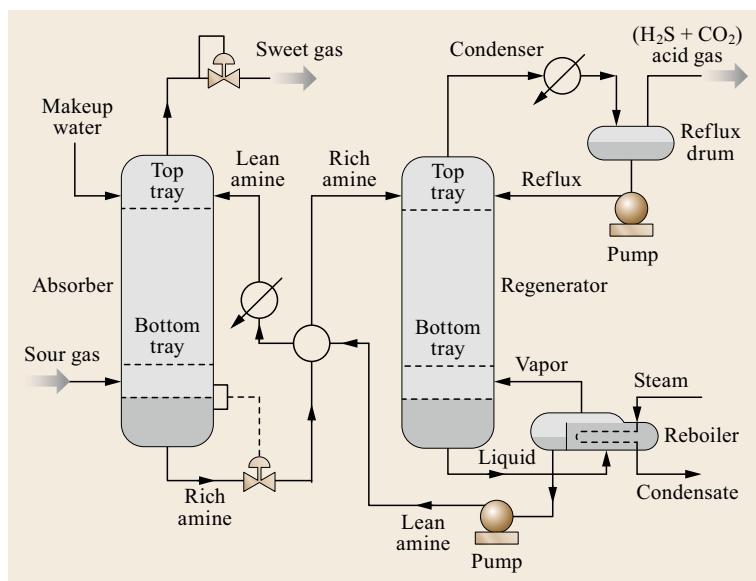


Fig. 20.11 Representative process flow sketch for removal of H₂S and CO₂ by alkanolamine adsorption

tion may still contain adsorbed gas. The solution is returned to the top of the tower. Lean amine is withdrawn from the bottom of the regenerator and returned to absorber.

The choice of amine and amine concentration depends on feed quality and process objectives. The systems used for high-CO₂ natural gas may not be optimal for refinery hydrotreaters, where the offgas is hydrogen-rich and contains nil CO₂. Some rough guidelines are given below [20.27]:

- MEA: About 20 wt% for removing H₂S and CO₂ and about 32 wt% for removing only CO₂
- DEA: About 20–25 wt% for removing H₂S and CO₂
- MDEA: About 30–55 wt% for removing H₂S and CO₂
- DGA: About 50 wt% for removing H₂S and CO₂.

According to the excellent review by *Goar and Nasato* [20.28]:

- MEA used to be the workhorse of the industry. It lost appeal because of its relatively large circulation rates, high energy consumption, high solvent vaporization losses and susceptibility to degradation by trace compounds often found in sour gas.
- DEA gained popularity due to its much lower circulation rates, lower energy consumption, lower vaporization losses and resistance to degradation. DEA is probably the most widely used gas treating solvent today.
- MDEA is popular now because it exhibits significant selectivity for H₂S in the presence of CO₂. It

is also very energy efficient. If the H₂S/CO₂ ratio in the sour gas is relatively low (say, less than 1 : 3), MDEA can be used to good advantage to absorb essentially all of the H₂S and only a small portion of the CO₂. Some CO₂ is removed indirectly by dissolution in water.

- DGA is well suited for gas processing in very hot climates, such as in the Middle East and when the gas contains appreciable trace contaminants. In many applications, it is very energy efficient. Disadvantages include the high cost of the solvent, the relatively high viscosity of DGA solutions and the tendency of solutions to absorb heavy or aromatic compounds.

The selectivity of MDEA can be explained as follows: With secondary alkanolamines, such as DEA, H₂S and CO₂ react directly and quickly with the alkanolamine by proton transfer. But MDEA is a tertiary amine. It does not have a proton attached to the nitrogen, so it cannot react directly with CO₂. When CO₂ dissolves in water, it forms a bicarbonate ion, which then reacts with the MDEA. The extent of adsorption of CO₂ by MDEA is therefore controlled by the extent of the conversion of CO₂(g) into HCO₃⁻(aq).

Separation of CO₂ from H₂S

In most existing operations, the entire acid gas stream, including both H₂S and CO₂, goes to the sulfur recovery plant. There, the H₂S is recovered, but the CO₂ is vented to the atmosphere. With the recent emphasis on CO₂ abatement, researchers are looking for ways

to recover the CO₂ for industrial use or sequestration.

Carbon Sequestration

At the Sleipner Field in the North Sea [20.29], the produced gas contains about 9% CO₂. But the sales specification limits CO₂ content to 2.5%. Sleipner-T, a special processing platform, separates and recovers the excess CO₂ for injection into a deep saline aquifer below the bottom of the sea. About one million tons of

pure CO₂ per year are captured this way. Sleipner-T is a laudable demonstration of carbon capture and sequestration (CCS) technology.

The UOP Benfield process is quite effective when feed gases contain a lot of CO₂ and very little H₂S. Benfield adsorbs CO₂ (and H₂S) into a hot potassium carbonate solution. More than 700 Benfield units have been installed primarily for hydrogen production plants. The process also is used in more than 50 natural gas processing plants.

20.4 Conversion of H₂S to Elemental Sulfur

20.4.1 The Claus Process

The Claus process was patented in 1883 by the Hesseborn chemist Carl Friedrich Claus. Educated in 1846–1848 at the University of Marburg, he moved to Liverpool, England in 1852. He became a British citizen in 1855 and lived in Liverpool, Warrington, Middlesbrough and London [20.30]. Over the years, he was granted several patents, including the ones that describe the process for which he is named [20.31, 32].

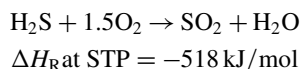
A paper by Linde Engineering North America (formerly Linde Process Plants, Inc.) provides a thorough description of H₂S conversion technology, including various versions of the Claus process [20.33]. Another good source is the presentation by *Prof. J. Jechura* of the Colorado School of Mines [20.20]. In the original Claus process, a mixture of hydrogen sulfide with air passed across a preheated catalyst bed. The end products were sulfur, water and heat. Reactions proceeded optimally at temperatures between 400–600 °F (93–204 °C). Heat recovery was poor, because heat was removed only by direct radiation. Only low concentrations of H₂S could be processed without overheating the reactor.

In 1938, engineers at I.G. Farben overcame these drawbacks by developing the modified Claus process. Modified Claus includes a combustion stage and a catalytic stage. The modified version serves as the basis of most modern sulfur recovery units (SRUs).

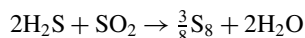
The feed gas to a Claus unit contains H₂S from alkanolamine treaters, along with CO₂, hydrocarbons and ammonia from a sour-water stripper (SWS). The treater gas can contain more than 75% H₂S.

A *straight-through* modified Claus unit, as shown in Fig. 20.12, works best when the H₂S concentration exceeds 60%. The feed gas is combined with a carefully controlled amount of air and sent to an open-flame burner, where 33% of the H₂S is converted to SO₂ and water at high temperature [20.34]. The standard heat of

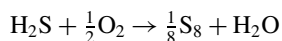
combustion is –518 kJ/mol of H₂S. This compares to –802.3 kJ/mol for combusting methane.



From the burner, the hot gases go to a reaction chamber, where H₂S reacts reversibly with SO₂ to form sulfur and water. The reaction is governed by equilibrium, so it is incomplete.



The overall Claus process equation is



When CO₂ and/or hydrocarbons are present, they react to form carbonyl sulfide (COS) and carbon disulfide (CS₂).

The degree of conversion of H₂S to sulfur is limited by thermochemistry. Figure 20.13 shows the maximum-possible conversion of H₂S to sulfur as a function of temperature. The maximum-possible conversion is 100% below the sulfur melting point. Between the melting and 1000 °F (538 °C), maximum-possible conversion decreases as temperature goes up.

Again quoting the Linde paper: The average temperature in the combustion chamber is 2200 °F (1200 °C). Much of the combustion heat is recovered in a waste-heat boiler, which generates steam as it drops the temperature to 700 °F (370 °C). The gas then goes to a condenser, which cools it to about 450 °F (232 °C) – well below the sulfur boiling point. The sulfur vapors condense, leaving behind unreacted H₂S and SO₂ and the liquid sulfur flows through a drain to a sulfur-collection pit. The pit is heated to keep the sulfur molten. At the bottom of the drain, a seal leg maintains system pressure and keeps gases out of the

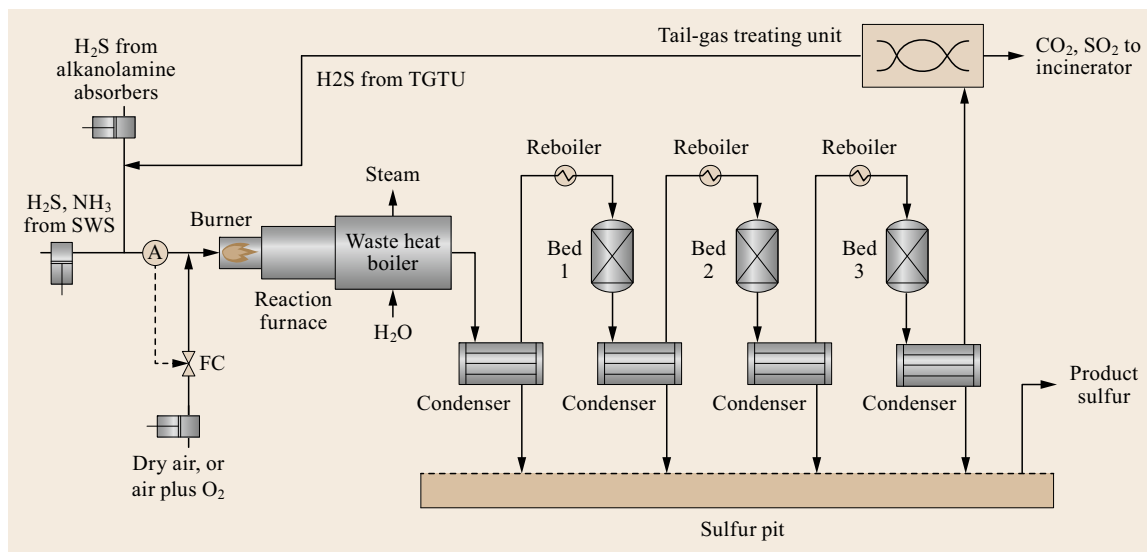


Fig. 20.12 Process flow sketch for the modified Claus process. SWS = sour water stripper. A = H₂S analyzer. FC = flow control valve. With fresh catalysts, a feed gas containing 75% H₂S and perfect flow control, the cumulative sulfur recovery at the four condensers can be approximately 50, 80, 95 and 98% respectively. Tail-gas treating brings the overall recovery to > 99.5%

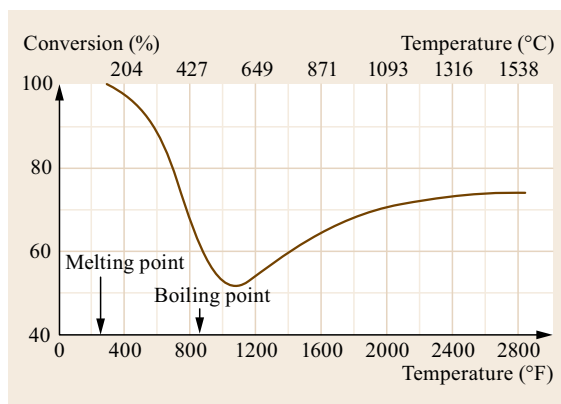


Fig. 20.13 Percent conversion of H₂S to sulfur as a function of temperature (after [20.20])

pit. Sulfur vapor and other gases flow to the catalytic section. The catalyst is alumina (Al₂O₃). In a series of beds with condensers in between, additional sulfur forms from reactions between remaining H₂S and SO₂. With fresh catalyst and a stoichiometric gas composition, the cumulative recovery of sulfur across four condensers is > 50, 80, 95 and up to 98% respectively.

The *straight-through* modified Claus process (Fig. 20.12) sends all the acid gas through the burner and reaction furnace. When the feed is *rich* – when it contains more than 60% H₂S – reaction heat keeps the flame temperature above 1200°C (2200°F). When

the gas is *leaner* – less than about 50% H₂S – the flame temperature drops. If the temperature falls below about 980–1090°C (1800–2000°F) the flame cannot be maintained. Preheating the air or feed gas can alleviate the problem, but only so much. When the H₂S concentration is less than 40%, the straight-through approach becomes impractical.

Split-flow enrichment can be applied to increase the H₂S concentration. Split-flow can handle gases with 15–50% H₂S. About one-third of the acid gas goes to the burner. The rest goes straight to the first catalyst bed. In the burner, all of the H₂S is converted to SO₂. Combustion can be maintained, because there is less unreacted gas to soak up the heat of reaction. At the inlet of the catalyst section, the burner gas is mixed with the bypass gas. Flows are adjusted so that the overall H₂S to SO₂ ratio is 2 : 1.

An attractive solution to low H₂S is *acid gas enrichment*. It entails installing an additional absorber to separate H₂S from unreactive gases. Using MDEA in the extra absorber is especially effective if the unreactive gas is CO₂, because MDEA can absorb nearly all of the H₂S while leaving behind almost all of the CO₂. *Acid gas enrichment* has increased H₂S concentrations by a factor of five or more. For a new design, incorporating enrichment allows the use of a smaller SRU and increases SRU reliability.

Oxygen enrichment can enhance both straight-through and split-flow configurations. Adding pure O₂ to the feed gas increases flame temperatures and de-

creases the amount of inert nitrogen going to the furnace. Retrofitting a plant for O₂ enrichment usually requires a different burner and also can require other modifications.

Ammonia destruction is required when gas from a sour water stripper (SWS) goes to a Claus unit. The practice is common in petroleum refineries. It is crucial to achieve complete destruction. A split-flow furnace design can increase ammonia destruction. All of the SWS gas and some of the acid gas goes to the Claus burner. The burner feed contains at least one-third of the total H₂S. Sufficient air is injected for complete combustion of all H₂S, hydrocarbons and ammonia. The remaining feed gas is injected into the middle of the reaction furnace. Residence time must be long enough for the SO₂ from the burner to react with the H₂S in the bypass gas. Operators use an optical pyrometer to monitor temperatures at the inlet to the furnace. If necessary, they adjust temperature by changing the amount of bypass acid gas.

20.4.2 Catalytic Oxidation Processes

Direct oxidation processes convert H₂S catalytically. Two such processes are the Merichem LO-CAT process and the UOP Selectox process.

UOP Selectox Process

The UOP Selectox process looks a lot like straight-through Claus with the furnace replaced by beds con-

taining a bismuth/vanadium selective oxidation catalyst. As in Claus, the oxidation section is followed by three beds of alumina Claus catalyst with condensers and reboilers in between. Selectox can handle a wider range of feed-gas qualities. There is no flame, so the process isn't affected by flame instability. Commercially, it processes gas with H₂S concentrations less than 5%.

Due to the absence of a flame, Selectox was deemed safe to recover sulfur from produced gas on an offshore oil platform – Platform Irene – near the coast of California [20.35]. Removing H₂S on the platform enabled the oil company to build a less-expensive product pipeline from the platform to the shore.

Other Selectox units are found in remotely located gas plants, where the total amount of recovered sulfur is low – less than about 30t/day. An example is discussed by Jones and Bertram [20.36]. They describe seven years of operation at the Lisbon gas plant in southeast Utah. The Lisbon Selectox unit processes acid gas containing 4% H₂S and 96% carbon dioxide (CO₂). It produces about 18 long ton/day of sulfur and achieves 94% sulfur recovery at the start of a catalyst cycle.

Selectox cannot be used for ammonia destruction.

Merichem LO-CAT Process

Another Claus alternative is Merichem's LO-CAT process [20.37]. LO-CAT is a patented, wet scrubbing, liquid redox system that uses a chelated iron solution to convert H₂S into elemental sulfur. Figure 20.14 pro-

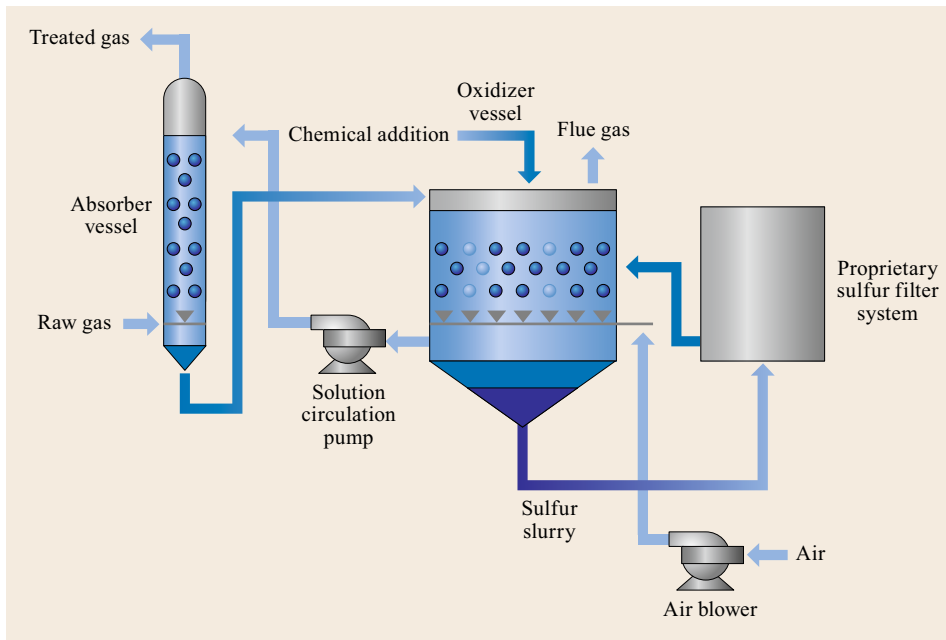


Fig. 20.14 LO-CAT process for direct oxidation of H₂S to elemental sulfur

vides a process flow sketch. LO-CAT does not require toxic chemicals and does not produce hazardous waste byproducts. Gas enters the unit through an absorber, where a chelated iron catalyst converts the H_2S directly into elemental sulfur. The sulfur travels with the solution into an oxidizer section where the catalyst is reactivated for reuse. The sulfur falls to the bottom of the reactor. From there, it is withdrawn and pumped to a pressure filter, which removes entrained liquids while forming a sulfur cake. The oxidized iron catalyst solution returns to the absorber for reuse by the process.

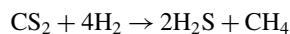
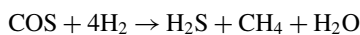
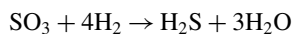
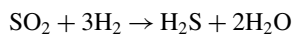
LO-CAT is applicable to all types of gas streams including air, natural gas, CO_2 , amine acid gas, biogas, landfill gas, refinery fuel gas, and so on. The liquid catalyst adapts easily to variations in flow and concentration. Flexible operation allows 100% turndown in H_2S concentrations. Units require minimal operator attention. More than 200 installations around the world employ the LO-CAT process to remove H_2S from gas streams.

20.4.3 Tail-Gas Treating

Claus tail-gas treating units (TGTU) can bring the total sulfur recovery up to $> 99.9\%$.

The cold-bed adsorption (CBA) process employs the same alumina catalysts as those used in Claus units, except that the catalysts operate below the sulfur dew point temperature. At the lower temperature, sulfur deposits on the catalyst. When the catalyst has adsorbed enough sulfur, the gas flow can be stopped or switched to a clean bed while the sulfur-laden bed is stripped with warm gas. CBA has achieved overall sulfur recoveries $> 99.0\%$.

The Shell Claus offgas treating (SCOT) process includes a front-end section to convert all of the sulfur compounds in the SRU tail into H_2S . This step is known as Beavon sulfur removal (BSR) – in honor of the inventor, David K. Beavon. The BSR reactions include



H_2S from the BSR step is absorbed by an amine and returned to the front of the Claus furnace. Utilities from the Claus section are used for preheating and other purposes. The SCOT process has given overall sulfur recoveries of 99.9% .

The UOP BSR Selectox tail-gas treating process also starts with BSR, reducing all tail-gas sulfur com-

pounds to H_2S . The H_2S is mixed with stoichiometric air and passed through a bed of Selectox catalyst for conversion to elemental sulfur. BSR Selectox can bring overall sulfur recovery up to 99.9% .

The LO-CAT technology also can be used for tail-gas treatment. One approach is to employ BSR technology to convert all sulfur to H_2S . The H_2S is then oxidized to elemental sulfur as described above by the LO-CAT liquid redox system. Sulfur is removed in a pressure filter and the liquid redox catalyst is recycled. The exit gas contains less than 10 ppmw H_2S . A LO-CAT TGTU can be designed to accept acid gas directly, bypassing the Claus unit entirely.

For all tail-gas treatment processes, the last traces of unrecovered sulfur go to a thermal oxidizer, where they are converted into SO_2 . Remaining CO_2 is vented to the atmosphere or sequestered and stored.

Transportation is an important aspect of sulfur recovery. Molten sulfur must be handled carefully in special equipment. So when regulations allow, the molten sulfur is transformed into powders or prills, which can be moved in bulk by rail or by sea.

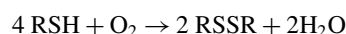
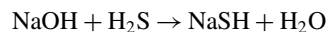
20.4.4 Mercaptan Conversion

Mercaptans are foul-smelling chemicals that must be removed from gas prior to shipment. Mercaptans are not easily removed with alkanol amines. Instead, they are adsorbed into caustic solution and oxidized catalytically.

Refiners have used caustic treating for decades to remove mercaptans and other impurities, including H_2S , CO_2 , COS and organic acids. Removing these impurities from LPG, gasoline, jet fuel, diesel, light crude and condensates ensures that the streams meet specifications for odor and corrosivity.

The UOP Merox process extracts low molecular weight mercaptans from refinery gas streams with a strong aqueous caustic solution [20.38]. The Merox process was commercialized over 50 years ago by UOP. It can eliminate the need to purchase expensive proprietary equipment, it is not susceptible to fouling and it does not require feed or caustic filters. In commercial service, it typically achieves greater than 99.5% on-stream availability. UOP has licensed more than 1700 Merox units worldwide.

Given below are the main Merox reactions, where RSH = mercaptan and RSSR = disulfide. The R can denote methyl, ethyl, propyl, etc. and can be different between mercaptan and disulfide.



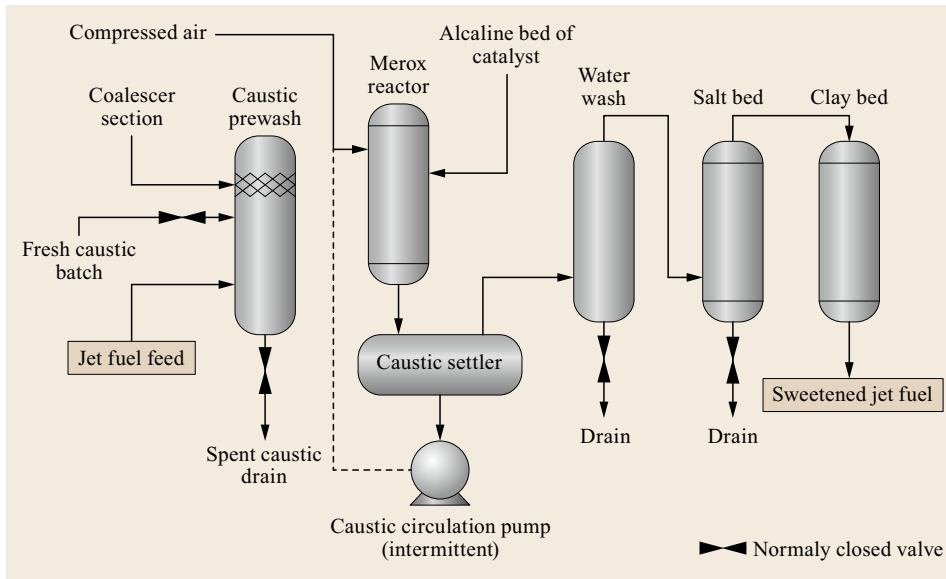


Fig. 20.15
Process flow
sketch for the
UOP Mercox
process

Figure 20.15 shows a process flow sketch. A high efficiency gas-liquid contactor enhances the design. The mercaptan-rich solvent, which contains the Mercox catalyst, goes to the regeneration section, where air is injected and the mercaptans are oxidized to disulfides. The disulfides are then separated from the solvent and the regenerated lean caustic is recycled back to the Mercox extractor. The disulfides are converted

to H₂S and hydrocarbons in a naphtha hydrotreater. Product mercaptan levels are reduced to less than 10 ppmw.

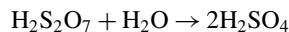
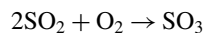
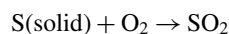
Merichem offers Mericat and Mericat C to remove H₂S and mercaptans from gasoline, naphtha, condensate and crude oil. The Mericat processes use a FIBER FILM Contactor for mass transfer and uses a caustic/catalyst/air mixture as the treating reagent.

20.5 Sulfur Uses

Elemental sulfur is used primarily to make sulfuric acid (H₂SO₄) [20.39, 40]. Before 1900, most sulfuric acid was made batch-wise with the *lead chamber* process. SO₂, steam and nitric oxides (NO and NO₂) were sprayed into large chambers lined with sheets of lead. The nitric oxides oxidized the SO₂ to SO₃, which dissolved immediately in the water to form H₂SO₄. The heat of reaction was controlled by running cooling water across the outside surface of the masonry chamber.

Modern processes do not require nitric oxides. In the *contact process*, sulfur is burned to form sulfur dioxide, which is then oxidized to sulfur trioxide (SO₃) over a vanadium oxide (V₂O₅) catalyst. The SO₃ is not directly dissolved in liquid water, because that interaction is highly exothermic and extremely difficult to control. Therefore, as an intermediate step, SO₃ is adsorbed into concentrated sulfuric acid to form oleum (H₂S₂O₇), also known as fuming sulfuric acid. The oleum then re-

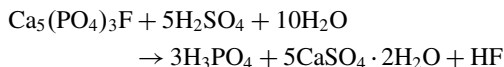
acts with water to give sulfuric acid.



In some respects, the *wet sulfuric acid* process is similar to the contact process: it employs a V₂O₅ catalyst to oxidize SO₂ to SO₃. But the wet process avoids the intermediate oleum step by hydrating SO₃ in the gas phase. Gas-phase hydration generates less heat, so it is easier to control. The condensation of gaseous H₂SO₄ gives highly concentrated liquid H₂SO₄. In the wet process, it is possible to start with gaseous H₂S instead of solid elemental sulfur.

The main industrial application for sulfuric acid is production of phosphoric acid from phosphate minerals such as calcium orthophosphate or apatite [20.41].

About 90% of manufactured phosphoric acid becomes fertilizer. Apatite has the general formula $(\text{Ca}_5(\text{PO}_4)_3)\text{X}$, where $\text{X} = \text{OH}, \text{F}, \text{Cl}$ or Br . Shown below is the reaction of H_2SO_4 with fluorapatite, the main component of tooth enamel.



The insoluble $\text{CaSO}_4 \cdot 2\text{H}_2\text{O}$ (gypsum) is removed by settling or filtration. To one extent or another, halides and other contaminants, such as arsenic, are removed to generate different grades of phosphoric acid. Near-complete removal of contaminants yields food-grade phosphoric acid. Most of the gypsum is mixed with water to form a plaster, which is pressed between two sheets of thick paper to form *drywall* for the construction industry.

Sulfuric acid is consumed by other industries, too, including metal refining, wastewater processing, petroleum processing, cement manufacturing and mineral extraction.

Sodium lauryl sulfate (SLS) is synthesized by reacting lauryl alcohol with SO_3 or oleum to generate hydrogen lauryl sulfate, followed by neutralization with a sodium salt. The chemical formula of SLS is $\text{NaC}_{12}\text{H}_{25}\text{SO}_4$. Widely used in cleaning supplies and personal hygiene products, the detergency of SLS is due to its amphoteric nature. The 12-carbon alkyl tail is oil-soluble and the sulfate group is water-soluble. Commercial formulations include sulfate surfactants derived from coconut and palm oils.

20.5.1 Elemental Sulfur and Inorganic Salts

Elemental sulfur candles consist of pure sulfur in blocks or pellets. In the past, they were burned to fumigate structures. They are no longer used in homes due to the formation of toxic and corrosive sulfur oxides.

Elemental sulfur is the only acceptable *green* fungicide and pesticide for organic farming. It is also an acceptable fertilizer. Dusting sulfur is a fungicide for grapes, strawberries, vegetables and other crops. Applied with a sulfur duster or from an airplane, it mitigates mildew, *black spot*, apple scab and other ailments. Wet sulfur is water miscible and hence can be easier to apply in certain cases. Sulfur powder, called *flow-*

ers of sulfur, can protect against ticks and mites when smeared onto clothing or bare skin.

Dilute solutions of lime sulfur, formed by mixing calcium hydroxide with elemental sulfur, is a dip to destroy ringworm fungus, mange and skin parasites on dogs and cats.

Hydrated crystals of magnesium sulfate, known as Epsom salts, can serve as a laxative, a bath additive, an exfoliant and a magnesium supplement for plants. In dry form, it is an excellent desiccant.

20.5.2 Organic Sulfur

Organosulfur compounds find uses in pharmaceuticals, dyes and agrochemicals. Sulfa drugs are sulfonamides. Sulfur is present in most β -lactam antibiotics, including penicillins, cephalosporins and monolactams.

20.5.3 Sulfites, Sulfates and Oxides

Adding small amounts of SO_2 (or potassium metabisulfite) to fermented wine produces traces of sulfurous acid or sulfite salts. This technique has been called *the most powerful tool in winemaking* [20.42]. After the yeast-fermentation stage in winemaking, sulfites absorb oxygen and inhibit aerobic bacterial growth that otherwise would turn ethanol into acetic acid, souring the wine. Without this preservative step, indefinite refrigeration of the product before consumption is usually required. Similar methods go back into antiquity. Written mentions go back to the 15th century. The practice is used by large industrial wine producers and small organic wine producers alike.

Sulfur dioxide and various sulfites have been used for their antioxidant antibacterial preservative properties in many other parts of the food industry also. The practice has declined since reports of an allergy-like reaction of some persons to sulfites in foods.

20.5.4 Other Uses

Other uses for sulfur include direct addition to alkaline soil and the vulcanization of black rubber. Sulfur is applied to plants as a fungicide and it is still a component of black gun powder. Sulfur reacts with methane to form carbon disulfide (CS_2), which is employed to make cellophane and fibers such as rayon.

20.6 Pollution from Sulfur

20.6.1 Acid Deposition (SO_x , NO_x and PM)

To paraphrase *Historica Canada* [20.43]:

Acid deposition is the wet or dry accretion of acidic substances and their precursors onto the Earth's surface. The acidic substances include sulfur oxides (SO_x) and nitrogen oxides (NO_x). Wet deposition refers to rain, snow, drizzle and other forms of precipitation. Dry deposition is the settling of particulates, especially sulfates.

Wet deposition may be acidic or alkaline. A clean water sample in equilibrium with atmospheric carbon dioxide has a pH value of 5.6. In the northern hemisphere, annual average measurements show that the pH of precipitation ranges from about 4.0–7.0. Low pH values occur over and immediately downwind of urban and industrial areas. High pH values are found over less industrial regions where the atmosphere contains significant amounts of alkaline dust. The primary cause of low pH is H_2SO_4 , which is produced in the atmosphere from the reactions between SO_x , water and oxygen. In like fashion, nitric acid (HNO_3) is generated from reactions of nitrogen oxides (NO_x) with moisture. NO_x are significant in urban areas, because they come primarily from transportation vehicles.

SO_2 comprises about 90% of ambient SO_x . Methods for reducing SO_2 emissions include:

- Using low-sulfur coal or cleaned coal for power plants

- Removing sulfur compounds from natural gas and petroleum before they are burned
- Removing sulfur from ores before they reach smelters
- Employing flue-gas desulfurization
- Consuming sulfur-neutral alternative energy sources.

Decades ago, I heard the CEO of an oil company say: *The solution to pollution is dilution.* Consistent with that philosophy, power plants and refineries installed taller emission stacks to increase the distance from the source to the ground. The taller stacks did indeed decrease ground-level SO_x and NO_x in the immediate vicinity, but they didn't solve the ultimate problem. Transported by winds, the pollutants can travel thousands of kilometers, affecting regions far away from their points of origin. In the 1980s, studies verified that 50% of the sulfate deposition in eastern Canada came from the USA.

Short-term exposure to SO_2 can impair human respiration and make breathing difficult. Children, the elderly and those who suffer from asthma are particularly sensitive. SO_x can react with other compounds in the atmosphere to form small particles. These particles contribute to particulate matter (PM) pollution. PM may penetrate deep into lungs to cause long-lasting health problems.

There are other potential adverse effects of acid rain on human health. Acid in water delivery systems accelerates the leaching of lead, copper and other metals,

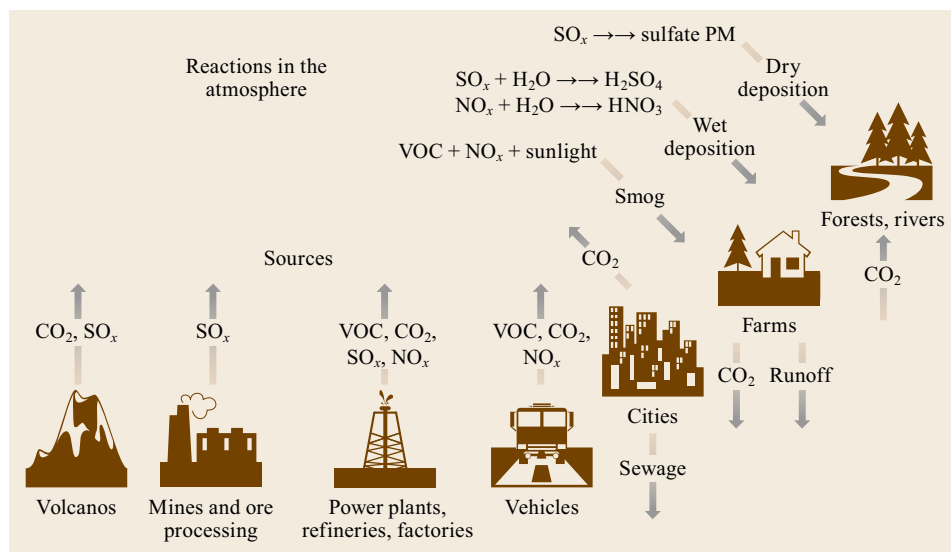


Fig. 20.16 Sources of SO_x , NO_x , CO_2 and volatile organic compounds (VOC). Generation of photochemical smog. Dry deposition of sulfate particulates, wet deposition of acids

increasing their levels in drinking water. A well-known example comes from Flint, Michigan where acid leaching due to orthophosphate led to high levels of lead in drinking water, affecting the health of thousands, including 6000–12 000 vulnerable children [20.44]. Officials became aware of the problem in April 2014, but hid the problem for more than a year. In the summer of 2015, Adam Rosenthal of the Michigan Department of Environmental Quality conspired with Patrick Cook and others to change data in lead and copper monitoring reports. The situation came to light in September 2015, when a team led Professor Marc Edwards of Virginia Tech University discovered and documented the problem. On 29 July, six officials, including Rosenthal and Cook, were officially indicted.

Increased concentrations of heavy metals in fish caught from acidified rivers and lakes could pose problems for people who consume significant quantities of these fish.

Figure 20.16 is a simplified illustration of the generation and disposition of SO_x , NO_x and other air pollutants. Ground-level ozone, chlorofluorocarbons (CFCs) and toxic metals are not shown.

In the United States, the clean air act (CAA) requires the US Environmental Protection Agency (EPA) to establish national ambient air quality standards (NAAQS) for harmful pollutants. EPA sets two types of standards – primary and secondary. Primary standards protect against adverse health effects. Secondary standards protect against damage to farm crops, vegetation and buildings. Some pollutants have standards for both long-term and short-term averaging times. The short-term standards are designed to protect against acute health effects, while the long-term standards protect against chronic health effects.

Table 20.3 lists NAAQS for six pollutants regulated by EPA.

Over time, ambient levels of SO_2 , NO_2 and other important pollutants have decreased considerably [20.45]. Table 20.4 shows percent reductions between 1990 and 2015. During the same period, the US economy grew, Americans drove more miles and overall energy use increased.

Similar improvements in pollution were achieved in the EU. Table 20.5 presents analogous data for EU nations during 1990 through 2012 [20.46].

Atmospheric sulfur oxides mostly come from fossil fuels, sulfide ores and volcanoes. Figure 20.17 plots worldwide SO_2 emissions by source from 1900–2014. Data for 1900–2005 come from *Smith et al.* [20.47]. Data after 2005 for China are from *Ma and Takeuchi* [20.48], using a normalization factor of 1.25 to match data reported by others. Data after 2005 for

Table 20.4 Percent reduction in concentrations of ambient pollutants in the United States, 1990–2015

Pollutant	Percent reduction
Carbon monoxide (CO), 8 h	77
Lead (Pb) three-month average	99
Nitrogen dioxide (NO_2) annual	54
Nitrogen dioxide (NO_2) 1 h	47
Ozone (O_3) 8 h	22
PM10 ^a , 24 h	39
PM2.5 ^b , annual	37
PM2.5 ^b , 24 h	37
Sulfur dioxide (SO_2) 1 h	81

^a PM10 = Particulate matter 10 μm mean diameter

^b PM2.5 = Particulate matter 2.5 μm mean diameter

Table 20.3 National ambient air quality standards (NAAQS) for six pollutants regulated by EPA

Pollutant	Primary/secondary	Averaging time	Level	Form
Carbon monoxide	Primary	8 h	9 ppm	Not to be exceeded more than once/year
Carbon monoxide	Primary	1 h	35 ppm	Not to be exceeded more than once/year
Lead	Both	Rolling three month	0.15 $\mu\text{g}/\text{m}^3$	Not to be exceeded
Nitrogen dioxide	Primary	1 h	100 ppb	98th percentile of 1 h daily max concentrations, averaged over three years
Nitrogen dioxide	Both	Annual	53 ppb	Annual mean
Ozone	Both	8 h	0.075 ppm	Annual fourth-highest daily max 8 h concentration, averaged over three years
Particulates, PM2.5	Primary	Annual	12 $\mu\text{g}/\text{m}^3$	Annual mean, averaged over three years
Particulates, PM2.5	Secondary	Annual	15 $\mu\text{g}/\text{m}^3$	Annual mean, averaged over three years
Particulates, PM2.5	Both	24 h	35 $\mu\text{g}/\text{m}^3$	Annual mean, averaged over three years
Particulates, PM10	Both	24 h	150 $\mu\text{g}/\text{m}^3$	Not to be exceeded more than once/year, on average, over three years
Sulfur dioxide	Primary	1 h	75 ppb	99th percentile of 1 h daily max concentrations, averaged over three years
Sulfur dioxide	Secondary	3 h	0.5 ppm	Not to be exceeded more than once/year

the United States come from EPA [20.49]. Table 20.6 gives reported total worldwide SO₂ emissions for 2005 and estimated emissions for 2014; the estimates include actual data from the USA and China and straight-line projections for other countries.

Figure 20.18 shows SO₂ emissions from five countries and international shipping. In 2005, these six sources accounted for nearly 58% of worldwide SO₂ emissions. SO₂ from shipping grew as oil refiners blended more high-sulfur components into bunker fuel. However, the trend will change in 2020, when the upper limit on ship-fuel sulfur outside sulfur emission control areas will drop from 3.5 wt% to 0.5 wt% [20.50].

Table 20.5 Percent reduction in concentrations of ambient pollutants in the EU, 1990–2012

Pollutant	Percent reduction
CO	66
NO _x	51
PM10 ^a	19
PM2.5 ^a	19
SO _x	84

^a Since 2000

From 1970 to 2000, worldwide emissions fell by 16%. In the USA, emissions decreased by 56% and in Germany, they plummeted by an astounding 93%. But in 2000, emissions began to rise. Steep declines in the USA, Russia, Germany and the rest of Western Europe were offset by precipitous rises in less developed countries, especially in China, where emissions rose by 58% in just five years. China's 11th five-year plan (2006–2010) included ambitious emission-reduction targets.

Table 20.6 Reported total worldwide SO₂ emissions for 2005 and estimated emissions for 2014. The estimates include actual data from the USA and China and straight-line projections for other countries and sources

	2005	2014 (est.)
Coal	52.2%	49.2%
Petroleum	18.4%	17.9%
Smelting	11.1%	10.1%
Int'l shipping	10.5%	13.5%
Fuel processing	3.1%	4.0%
Volcanic, other	3.9%	4.4%
Biomass	0.8%	0.9%
Total	100.0%	100.0%
Total tonnes	115 507	102 000

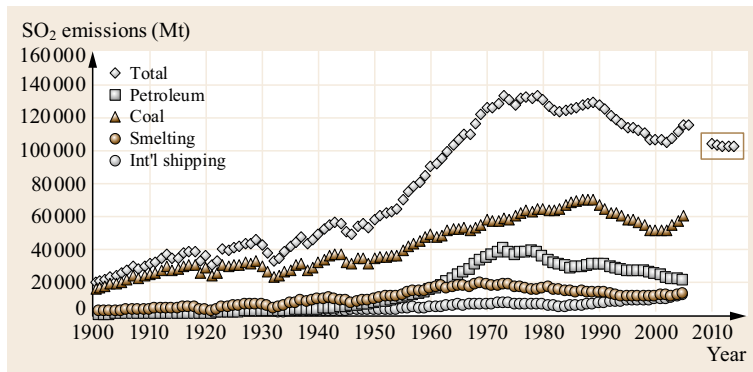


Fig. 20.17 Relative contributions of coal, petroleum, smelting and international shipping to worldwide SO₂ emissions from 1900–2014. The box surrounds values computed by a combination of recent data from the USA and China with projected values from other countries

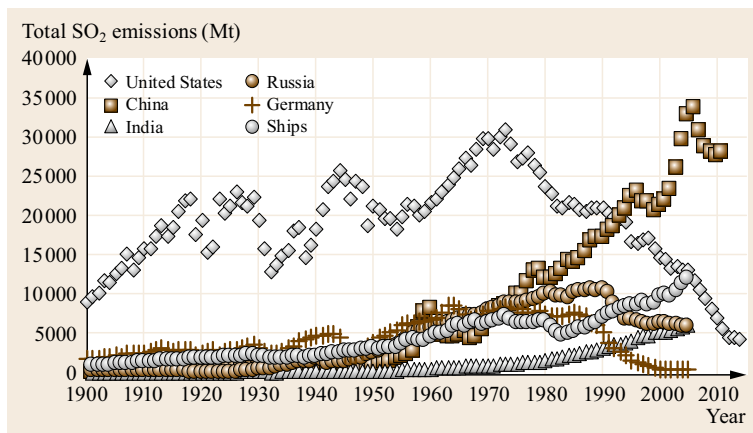


Fig. 20.18 Total SO₂ emissions for five countries and international shipping, 1900–2014

Between 2006 and 2010, total SO₂ emissions fell by more than 14% despite 10% annual economic growth.

Figures 20.19 and 20.20 compare SO₂ emissions by source for China and the United States. About 85% of Chinese SO₂ emissions are due to coal. Total emissions rose from 7300 thousand tons in 1970 to 32 700 thousand tons in 2005 – an increase of 450% – then fell by more than 14% between 2005 and 2010.

In the United States in 2005, about 72% of SO₂ emissions come from coal, compared to 62% in 1970, but overall emissions from coal were far lower in 2005. In 2005, 18% of emissions came from petroleum and less than 1% came from smelting. The remaining 9% came from other industrial activities, including shipping. Total US emissions fell from 29 800 thousand tons in 1970 to 4528 thousand tons in 2014, a decrease of roughly 85%. Much of the decline came from the implementation of ever-tighter restrictions on sulfur in fuels. A large percentage came from replacing sulfur-containing coal in power plants with sweet gas from shale produced by hydraulic fracturing [20.51].

20.6.2 Open-Air Roasting

Until the early 20th century, roasting was conducted in open-hearth roasters. The reaction was started by burn-

ing wood on top of a pile of ore. When the ore became hot enough, the sulfide oxidation reaction generated enough heat to keep the process going. The pile was stirred manually with rakes to expose unreacted ore to air.

For the health of workers and the environment, open-hearth roasting was disastrous. In addition to generating unrecovered SO₂, open-hearth roasting released toxic elements, such as arsenic and mercury. Even today, 80–100 years later, nothing grows near numerous open-hearth sites. Some dead zones occupy several square kilometers.

20.6.3 Volcanic SO_x: The Year Without a Summer

Volcanic activity, another significant source of SO₂, varies unpredictably. When SO₂ is injected into the stratosphere, it forms sulfuric acid, which condenses rapidly into fine sulfate aerosols [20.52]. The aerosols reflect sunlight back into space, cooling the lower atmosphere (troposphere). Several eruptions during the past century caused a decline in the average temperature at the Earth's surface of up to 0.5 °F for up to three years. The spectacular eruption of Mount Pinatubo on 15 June 1991 was one of the largest of the 20th cen-

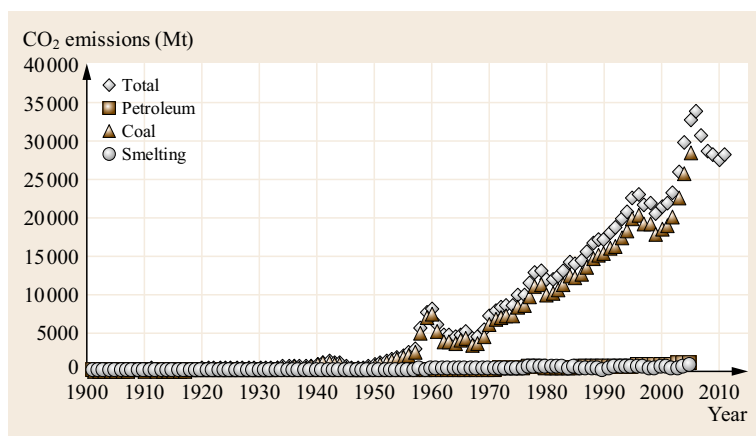


Fig. 20.19 SO₂ emissions in China by source, 1900–2005

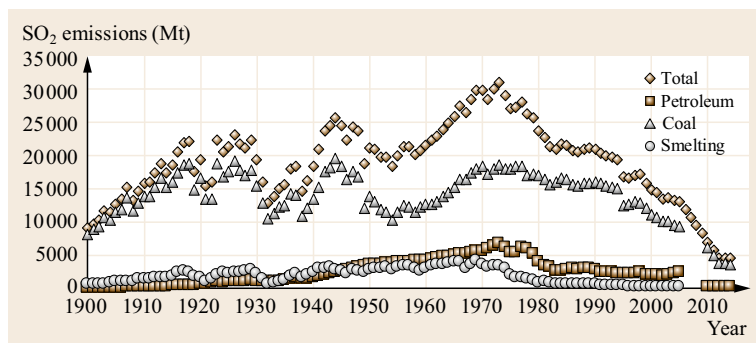


Fig. 20.20 SO₂ emissions in the USA by source, 1900–2005

ture. It blasted 20 million metric tons of sulfur dioxide into the stratosphere, where it reached an altitude of more than 20 miles (32 km). The Pinatubo SO₂ cloud was the largest since the beginning satellite observations in 1978. It caused what may be the largest injection of aerosols into the stratosphere during the 20th century. It cooled the Earth's surface for three years by as much as 1.3 °F at the height of the impact.

Pinatubo was probably smaller than the disturbances caused by Krakatau in 1883 and Tambora in 1815. The 1783–1784 Laki eruption in Iceland released six times more SO₂ than Pinatubo. Although the two eruptions were significantly different in length and style, the SO₂ caused regional cooling of Europe and North America by similar amounts for similar periods of time.

Tambora turned 1816 into the *year without a summer* [20.53, 54]. Volcanic ash and sulfate aerosols reddened and dimmed the sun, so much so that sunspots were visible to the naked eye. In northern regions of North America, Europe and China, summer frosts killed crops. In many parts of New England, killing frosts occurred in every summer month. Due to crop failures, food prices skyrocketed. In Germany, the crisis was especially severe. In India, the summer monsoon was delayed. When it finally arrived, it caused unusually severe floods. At higher elevations, the effects of Tambora lingered until the Spring of 1817.

Now-erupting volcanoes include Stromboli and Etna in Italy, Pavlof in Alaska, Kilauea and others in Hawaii, Colima in Mexico, Popocatepetl and others in Central America and several around the Pacific Rim in Western South America, Indonesia, the Philippines Japan and the Aleutians. All produce different amounts of SO₂, CO₂, H₂S, HF, HCl and HBr. An interesting example is the Kawah Ijen volcano. Instead of lava, it discharges molten sulfur.

20.6.4 International Shipping

MARPOL is the International Convention for the Prevention of Pollution from Ships.

As shown above, international shipping accounts for a significant percentage of world SO_x emissions. Starting on 1 January 2015, MARPOL Annex VI imposed tight limits on SO_x in emission control areas – the Baltic Sea; the North Sea; and the North American area, which includes designated coastal waters around the United States and Canada and the US Caribbean Sea around Puerto Rico and the US Virgin Islands. In 2020, outside the Emission Control Areas, the allowed

sulfur content of marine fuel oil will drop from 3.5 wt% to 0.5 wt%.

20.6.5 Acid Mine Drainage

Drainage from iron mines – and from copper, zinc, nickel and coal mines – is called acid mine drainage (AMD) or acid rock drainage (ARD). Simply exposing sulfur-containing ores to the elements, as in strip mining, creates conditions conducive to sulfuric acid formation. Uncontrolled AMD causes significant pollution. Acidity is the main problem. Runoff from the Iron Mountain Mine in California can have a pH as low as –3.6 [20.55]. Figure 20.21 shows the impact of pyrite leaching into the Rio Tinto in Spain.

20.6.6 Midnight Dumping

Surreptitious dumping continues to plague manufacturing industries. Recent examples include fouling of a Tennessee homeowner's yard by wastewater dumped at the side of a road [20.42], chronic illegal dumping of fracking wastewater in Ohio [20.56] and on-purpose dumping of waste oil into the sea [20.57]. Figure 20.22 shows a commonly reported method for waste-oil dumping – opening a flange to bypass pollution prevention equipment. This allows a slow, almost undetectable drip of the oil into the ocean [20.58, 59]. Waste oil (sludge) from ships typically contains up to 3 wt% sulfur and sometimes more, along with small amounts of toxic trace metals. The sludge comes from spilled fuel and oil-based lubricants.

Marine Defenders provides a succinct summary of the problem [20.60]. Almost all liquid wastes, including sludge, collect in bilge tanks at the bottom. The



Fig. 20.21 Uncontrolled acid runoff from pyrite leaching causes severe environmental damage to the Rio Tinto in Spain (photo by C. Stoke)

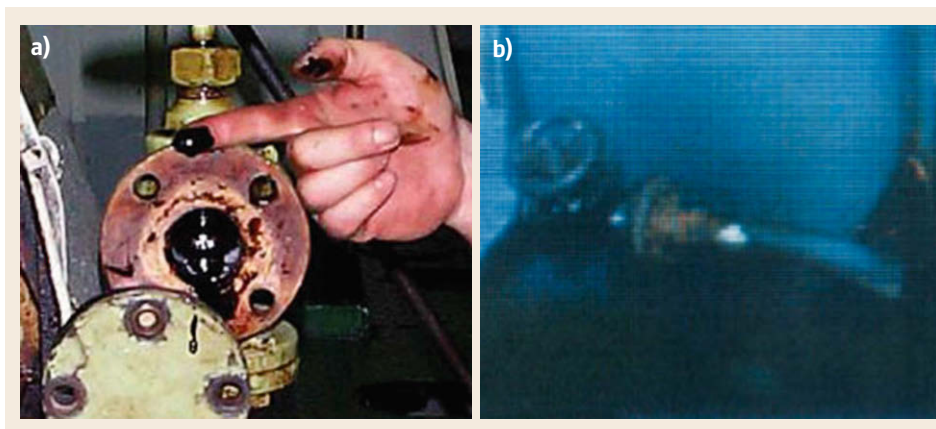


Fig. 20.22 (a) An illegal *magic pipe* used to bypass pollution prevention equipment on an open-sea ship. (b) Evidence photo taken with a whistleblower's cell phone. Photo credits: US Department of Justice

bilge tanks must be emptied regularly. Until the 1950s, ships pumped bilge water into the sea during a voyage and always just before reaching a port. However, as the environmental impact of oil pollution became clear, this practice was banned by MARPOL, the International Convention for the Prevention of Pollution from Ships in 1954. These rules were strengthened in the 1970s by the MARPOL treaty, after the wreck of the *Torrey Canyon* on the Cornish coast of England in 1967. The grounding and breakup of the supertanker was at that time the world's worst oil spill. It discharged 500 000–800 000 barrels of crude oil, fouling about 50 miles (80 km) of French coastlines and 120 miles (190 km) of Cornish coastlines. Some of the after-effects are visible even today in Guernsey, one of the Channel Islands.

The MARPOL treaty required that ships must use an oil/water separator to ensure that all wastewater pumped overboard has an oil content of less than 15 parts per million. It stated that all ships must carry functioning pollution control systems and maintain detailed and accurate oil record books. A 2002 report by the European Organization for Economic Cooperation and Development (OECD) estimated that the average annual cost of meeting the MARPOL regulations ranged from \$ 30 000 a year for an average cargo ship, to \$ 55 000 for a large container vessel, to \$ 150 000 per year for an oil supertanker. These values were equivalent to between 3.5–6.5% of a ship's overall operating expenses. In the case of a million-barrel supertanker, which may carry six or more cargoes per year, the cost of complying with MARPOL rules is about 0.05% of the value of the cargoes.

Interviews with crew members and ship owners indicate that saving time was the main reason for willful violations. It can take several hours to unload waste oil legally in a port.

20.6.7 Lax Regulation Enforcement

Based on work experience in 60 refineries worldwide, I can attest that regulation enforcement varies from country to country and, within countries, from region to region [20.61]. Enforcement is difficult when inspections are restricted or not allowed, when inspectors are less than diligent, or when enforcement agencies are understaffed.

In *Breakdowns in Air Quality*, Levin et al. [20.62] report that data from the Texas Commission on Environmental Quality (TCEQ) show that in 2015, 679 facilities emitted more than 34 000 t of SO₂, NO_x, benzene and other pollutants during 3421 shutdowns due to equipment failure or maintenance. Two instances stood out: Dow Chemical's plant in Freeport, which accounted for nearly 1.3 million pounds and the Keystone Gas Plant, which in 2014 emitted 11 million pounds of SO₂ versus a permit that limits SO₂ emissions to 1.6 million pounds.

The report says Texas is *well known for its hands-off approach to environmental enforcement*. In a statement, the director of Environment Texas said:

By their own admission, polluters in Texas are routinely and egregiously violating the law and endangering public health with unauthorized emissions. And too often regulators look the other way when polluters break the law. This lawlessness must come to an end.

In its own statement, the TCEQ calls the assertion [20.63]:

[...] patently untrue and misleading to the public. TCEQ consistently pursues administrative, as well as civil enforcement, against noncompliant regulated industries in accordance with a vigorous, clearly articulated regulatory framework.

Table 20.7 Budgets, staffing and workloads for environmental agencies in California and Texas

State	California	Texas
Agency	California Environmental Protection Agency (CalEPA)	Texas Commission on Environmental Quality (TCEQ)
Budget for 2016, \$ million ^a	1800	474
Employees	4550	2780
Number of oil refineries (2016)	18	29
Refining capacity, bbl/day (2016)	1 982 000	5 452 000
Oil production, thousand bbl, May 2016	15 816	99 168
Number of producing gas wells	1118	98 279
Gas production, million scf, May 2016	18 135	696 901
Petrochemical plants	Almost none	More than any other state in the USA

^a Includes permitting fees. In Texas, most of the budget comes from revenue collected from fees

Table 20.7 compares staffing, budgets and workloads for TCEQ and the California Environmental Protection Agency (CalEPA). Data on oil and gas facilities and production are from the *US Energy Information Administration* [20.64]. In both states, major activities include issuing permits and enforcing regulations. There are of course differences in purview, but it is clear

that with 40% fewer people and a budget that is 74% lower than that of CalEPA, the TCEQ has more work to do. At present in Texas, the number of new oil and gas wells and refinery expansions is unprecedented; most of the new wells employ fracking technology, for which the amount of wastewater disposal is unprecedented. TCEQ processes permits for all of those projects.

20.7 Conclusion

Petroleum, natural gas and other fossil fuels contain significant amounts of sulfur. When burned, the sulfur becomes SO_x, which can cause significant damage to the environment and human health. To minimize such damage and to ensure that finished products meet performance specifications, the sulfur is removed and transformed into useful chemicals, primarily sulfuric acid and fertilizers.

Sulfur oxides and acids continue to threaten our atmosphere, water, land, and inhabitants. I hope that the tremendous reductions in sulfur pollution in developed countries will serve as a guide to fast-growing but less-developed countries. To paraphrase Barry Commoner: On this beautiful planet we share, everyone is affected by the actions of everyone else.

References

- Wikipedia: Sulfur: Antiquity, <https://en.wikipedia.org/wiki/Sulfur#Antiquity> (2016)
- G.E. D'Aquin, R.C. Fell: Sulfur and sulfuric acid. In: *Handbook of Industrial Chemistry and Biotechnology*, 12th edn., ed. by J.A. Kent (Springer, New York 2012)
- G.R. Rapp: *Archaeomineralogy*, 2nd edn. (Springer, Berlin, Heidelberg 2009) p. 242
- WebElements: Sulfur: Historical information, <https://www.webelements.com/sulfur/history.html> (2016)
- J.F. Healy: *Pliny the Elder on Science and Technology* (Oxford Univ. Press, Oxford 1999) pp. 247–249
- R. Nave: Common elements important in living organisms, <http://hyperphysics.phy-astr.gsu.edu/hbase/tables/elabund.html> (2016)
- L.E. Apodaca: Sulfur, USGS minerals year-book, <http://minerals.usgs.gov/minerals/pubs/commodity/sulfur/myb1-2013-sulfu.pdf> (2013)
- Y. Kwok: Meet the sulfur miners of eastern Java, Time, March 3 2015, http://time.com/3709945/sulfur-miners_the-devils-gold_luca-catalano-gonzaga (2015)
- TripCanvas: How's it like to hike Ijen Crater, <https://indonesia.tripcanvas.co/kawah-ijen-crater-guide/#howitslike> (2016)
- D. Mulyana: Blue Fire!, <https://www.flickr.com/photos/dhodie/7961520680> (2016)
- M. Lane: Sulphur mining in an active volcano, BBC News, <http://www.bbc.com/news/world-asia-pacific-12301421> (February 9, 2011)
- Wikipedia: https://upload.wikimedia.org/wikipedia/commons/a/ac/Kawah_Ijen_-_East_Java_-_Indonesia_-_sulphur-31July2009.jpg
- J.A. Ober: Sulfur, 200 U.S.G.S Minerals Year-book, <http://minerals.usgs.gov/minerals/pubs/commodity/sulfur/640400.pdf> (2000)

- 20.14 Wikipedia: Frasch process, https://en.wikipedia.org/wiki/Frasch_process
- 20.15 D.J. Kleiner: Sulfur industry. In: *Handbook of Texas Online* (Texas State Historical Association, Austin 2010), <http://www.tshaonline.org/handbook/online/articles/dks04>
- 20.16 H.T. Wood: *Industrial England in the Middle of the Eighteenth Century* (John Murray, London 1910)
- 20.17 J.P. Dunn, P.R. Koppula, H.G. Stenger, I.E. Wachs: Oxidation of sulfur dioxide to sulfur trioxide over supported vanadia catalysts, *Appl. Catal. B* **19**, 103–117 (1998)
- 20.18 Wikipedia: Roasting (metallurgy), [https://en.wikipedia.org/wiki/Roasting_\(metallurgy\)](https://en.wikipedia.org/wiki/Roasting_(metallurgy))
- 20.19 BP: Statistical review of world energy, <http://www.bp.com/en/global/corporate/energy-economics/statistical-review-of-world-energy.html> (2014)
- 20.20 J. Jechura: Sulfur Recovery, Colorado school of mines, <http://inside.mines.edu/~jjechura/GasProcessing09.pdf>, based on a presentation by Prof. A. Kidnay (2016)
- 20.21 L. Krittaya: PTT natural gas processing plant in Map Ta Phut, Rayong, Thailand, https://commons.wikimedia.org/wiki/File:Natural_gas_separation_plants.jpg
- 20.22 Union Gas: Chemical composition of natural gas, <https://www.uniongas.com/about-us/about-natural-gas/Chemical-Composition-of-Natural-Gas>
- 20.23 Hydrocarbonds Technology: The sweet in the sour – Middle eastern gas, <http://www.hydrocarbons-technology.com/features/feature46255>
- 20.24 Railroad Commission of Texas: Hydrogen sulfide (H₂S) fields and concentrations listing, District 01, <http://www.rrc.state.tx.us/oil-gas/research-and-statistics/field-data/h2s/district-1>
- 20.25 G. Kutney: *Sulfur: History, Technology, Applications and Industry*, 2nd edn. (Chem Tec, Toronto 2013)
- 20.26 C.E. Jones, N.A. Hatcher, R.H. Weiland: Mercaptans removal from gases by absorption into amines and caustic, http://www.ogtrt.com/files/publications/65/Revised_2013_Brimstone_Vail_Mercaptans_Removal_from_Gases_Final.pdf (Optimized Gas Treating Inc., Buda)
- 20.27 Wikipedia: Amine gas treating, https://en.wikipedia.org/wiki/Amine_gas_treating
- 20.28 B.G. Goar, E. Nasato: Large plant sulfur recovery processes stress efficiency, *Oil Gas J.* (May 23, 1994) <http://www.ogj.com/articles/print/volume-92/issue-21/in-this-issue/general-interest/large-plant-sulfur-recovery-processes-stress-efficiency.html>
- 20.29 British Geological Survey: Removal of CO₂ from natural gas processing plant, <http://www.bgs.ac.uk/discoveringGeology/climateChange/CCS/RemovalCO2NaturalGas.html>
- 20.30 R. Steudel, L. West: Vita of Carl Friedrich Claus (1827–1900) – Inventor of the Claus process for sulphur production from hydrogen sulfide, https://www.researchgate.net/publication/270958109_Vita_of_Carl_Friedrich_Claus_inventor_of_the_Claus_Process (2015)
- 20.31 C.F. Claus: Neuerung bei dem Verfahren zur Gewinnung von Schwefel bzw. Schwefliger Säure aus Schwefelwasserstoff (Invention concerning the Production of Sulfur resp. Sulfurous Acid from Hydrogen Sulfide), German Patent 28758 (1883)
- 20.32 C.F. Claus: Process of obtaining sulfur from sulfureted hydrogen, British Patent 5958 (1883)
- 20.33 Linde Process Plants: Sulfur process technology, Linde Process Plants, Inc., Tulsa, http://www.linde-engineering.com/internet.global.lindeengineering.global/en/images/Sulfur%20Process%20Technology19_111155.pdf?
- 20.34 P.D. Clark, N.I. Dowling, M. Huang: Fundamental and practical aspects of the claus sulfur recovery process. In: *Proc. The Topsøe Catalyst Forum* (2007), <http://www.topsoe.com/sites/default/files/clark.pdf>
- 20.35 R.V. Bertram, P.R. Robinson: Selectox process for sulfur recovery offshore. In: *Proc. 68th Annual Gas Processors Assoc. Meet., San Antonio* (1989)
- 20.36 S. Jones, R.V. Bertram: Long-term operating data shed light on Selectox process, *Oil Gas J.* (August 27, 2001) <http://www.ogj.com/articles/print/volume-99/issue-35/processing/long-term-operating-data-shed-light-on-selectox-process.html>
- 20.37 Merichem Company: LO-CAT H₂S removal technology, <http://www.merichem.com/gas/upstream/natural-gas/lo-cat>
- 20.38 Honeywell UOP: Gas and LPG treating, <http://www.uop.com/processing-solutions/refining/gas-lpg-treating>
- 20.39 Wikipedia: Sulfur, <https://en.wikipedia.org/wiki/Sulfur>
- 20.40 Wikipedia: Sulfur: Applications, <https://en.wikipedia.org/wiki/Sulfur#Applications>
- 20.41 Wikipedia: Phosphoric acid, https://en.wikipedia.org/wiki/Phosphoric_acid
- 20.42 C. Ambriz: Truck dumps waste water, flooding Benton Co. homeowner's lawn. *WBBJ 7 Eyewitness News*, <http://www.wbbjtv.com/2016/05/09/truck-dumps-waste-water-flooding-homeowners-lawn> (2016)
- 20.43 H.L. Ferguson, D.S. Jeffries: Acid rain, *Historica Canada*, <http://www.thecanadianencyclopedia.ca/en/article/acid-rain> (2015)
- 20.44 R. Allen: Investigator: Workers changed reports, hid data in flint water crisis, *Detroit Free Press*, <http://www.freep.com/story/news/local/michigan/flint-water-crisis/2016/07/29/investigator-workers-changed-reports-hid-data-flint-water-crisis/87702870> (July 29, 2016)
- 20.45 US EPA: Our nation's air 2016, US Environmental Protection Agency, <https://gispub.epa.gov/air/trendsreport/2016>
- 20.46 European Environment Agency: Air Pollution: Key trends, <http://www.eea.europa.eu/soer-2015/europe/air/#figure-1-eu-28-emission-trends-for-the-main-air-pollutants> (EEA, Copenhagen February 18, 2015)
- 20.47 S.J. Smith, J. van Aardenne, Z. Klimont, R.J. Andres, A. Volke, A.S. Delgado: Anthropogenic sulfur dioxide emissions: 1850–2005, *Atmos. Chem. Phys.*

- 11(3), 1101–1116 (2011) doi:10.5194/acp-11-1101-2011
- 20.48 T. Ma, K. Takeuchi: Controlling SO₂ emissions in China: A panel data analysis of the 11th five-year plan, Graduate School of Economics, Kobe Univ., <http://www.econ.kobe-u.ac.jp/activity/graduate/pdf/316.pdf> (2016)
- 20.49 US EPA: Inventory of US greenhouse gas emissions and sinks: 1990–2014, US Environmental Protection Agency, <https://www3.epa.gov/climatechange/Downloads/ghgemissions/US-GHG-Inventory-2016-Main-Text.pdf> (2016)
- 20.50 Wikipedia: Sulfur Emission Control Area, https://en.wikipedia.org/wiki/Sulphur_Emission_Control_Area
- 20.51 Union of Concerned Scientists: Environmental impacts of natural gas, http://www.ucsusa.org/clean_energy/our-energy-choices/coal-and-other-fossil-fuels/environmental-impacts-of-natural-gas.html#bf-toc-1
- 20.52 US Geographical Survey: Volcanoes can affect the Earth's climate, http://volcanoes.usgs.gov/vhp/gas_climate.html
- 20.53 Wikipedia: Year without a summer, https://en.wikipedia.org/wiki/Year_Without_a_Summer
- 20.54 C. Oppenheimer: Climatic, environmental and human consequences of the largest known historic eruption: Tambora volcano (Indonesia) 1815, *Prog. Phys. Geogr.* **27**(2), 230–259 (2003)
- 20.55 D.K. Nordstrom, C.N. Alpers, C.J. Ptacek, D.W. Blowes: Negative pH and extremely acidic mine waters from iron mountain, California, *Environ. Sci. Technol.* **34**(2), 254–258 (2000)
- 20.56 Willisja: Jailed Ben Lupo sued again over OH wastewater dumping, Marcellus Drilling News, <http://marcellusdrilling.com/2016/06/jailed-ben-lupo-sued-again-over-oh-wastewater-dumping> (2016)
- 20.57 Pensacola New Journal: German companies fined locally for illegal oil dumping, <http://www.pnj.com/story/news/local/environment/2016/03/15/german-companies-fined-locally-illegal-oil-dumping/81830192> (2016)
- 20.58 Marine Defenders: Illegal dumping, <http://www.marinedefenders.com/oilpollutionfacts/illegal.php>
- 20.59 Marine Defenders: Rewards for whistleblowers, <http://www.marinedefenders.com/commercial/rewards.php>
- 20.60 Marine Defenders: <http://www.marinedefenders.com>
- 20.61 P.R. Robinson: Hydroprocessing: Tales from the trenches (P.R. Robinson, Katy) in preparation
- 20.62 I. Levin, K. Burkhart, L. Metzger, S. Smith: Breakdowns in air quality, Environmental Integrity Project and Environment Texas, <http://environmentalintegrity.org/wp-content/uploads/Breakdowns-in-Air-Quality.pdf> (2016)
- 20.63 K. Collier: Plants emitting pollutants illegally, Report claims, The Texas Tribune, <https://www.texastribune.org/2016/04/27/plants-emitting-pollutants-illegally-report-finds> (2016)
- 20.64 United States Energy Information Administration: <http://www.eia.gov>

21. Modern Approaches to Hydrotreating Catalysis

Joo-Il Park, Isao Mochida, Abdulazeem M. J. Marafi, Adel Al-Mutairi

Hydrotreating plays an important role in petroleum refining. Crude oil contains contaminants – sulfur, nitrogen, oxygen and trace elements – which must be removed to meet product specifications. Most refineries include at least three hydrotreating units for upgrading naphtha, middle distillates, gas oils, intermediate process streams, and/or residue. Hydrotreating catalysts are the core of the process.

This chapter reviews current progress in tackling the issues found in upgrading distillates and residues by hydrotreating and focuses on the chemistry of hydrodesulfurization (HDS), hydrodenitrogenation (HDN), hydrodeoxygenation (HDO) and hydrolytic demetalization (HDM). We discuss the composition and functions of hydrotreating catalysts, and we highlight areas for further improvement. The distillate molecules are accessed by gas chromatography–atomic emission detection (GC–AED) and gas chromatography–time of flight (GC–TOF) to identify and quantify all molecules in the feeds and hydrotreated products. Enhancement of reactivity and suppression of inhibition are discussed based on the molecular structure versus reactivity/inhibition correlations. A molecular approach towards the residue is progressed by applying ultrahigh–resolution Fourier–transform ion cyclotron resonance (FT–ICR) mass spectroscopy. Nevertheless, target molecules in resid HDS and HDN are not defined yet due to the polymeric and agglomerated nature of the molecules. Molecular images of sulfur– and nitrogen–containing species are still major targets of hydrotreating. However, porphyrinic metal compounds in the resid, even the asphaltene, can now be detected by GC–AED, gas chromatography–ionconductively coupled plasma–mass spectrometry (GC–ICP–MS) as well as FT–ICR, indicating that the porphyrinic metal compounds can be isolated for observation from the resid and asphaltene matrix under the analytical conditions. The carbon deposit on the catalyst in the HDM is reviewed to show its important influence on capacity and distribution of metal on the catalyst. The carbon deposit is the major issue in hydrotreating. The reactivity of feed molecules for

21.1	Overview	676
21.1.1	Hydrotreating Process	676
21.1.2	Chemical Composition of Distillates	676
21.1.3	Chemical Components in the Residues	679
21.2	Hydrotreating Process	683
21.3	Bases for Hydrotreating	684
21.3.1	Hydrotreating Catalysts	684
21.3.2	Chemistry of Hydrodesulfurization	687
21.3.3	HDN and HDO Reactions	694
21.3.4	Chemistry of HDM	694
21.3.5	Chemistry of Ring–Opening Hydrocracking	695
21.3.6	Catalyst Deactivation in Hydrotreatment of Residue	698
21.4	Deep Hydrodesulfurization of Diesel ..	699
21.5	Development Base of AR Hydrotreatment	700
21.5.1	Development of Catalyst and Reaction for AR Hydrotreatment	700
21.5.2	Kinetic Analysis	700
21.6	Current Aims in Development of Residue Hydrotreatment	703
21.7	Role and Design of Catalyst Support for Residual HDM	704
21.8	Novel Hydrotreatment Processes for Residue Upgrading	705
21.9	Challenges in Hydrotreatment	707
21.9.1	Analysis of Heavy Feedstocks	707
21.9.2	Coking	707
21.9.3	Polymerization and Aggregation of Feeds	707
21.9.4	Catalyst and Additive Improvements ...	708
	References	708

the carbon deposit includes the condensation and adsorption phase separation, which depend on reactivity and dissolution/antidissolution properties of surrounding species as well as the properties of particular molecules concerned. Further challenges in hydrotreating are also discussed concerning the issues picked up in the molecular structure reactivity/inhibition of distillates and residues.

21.1 Overview

21.1.1 Hydrotreating Process

There are a number of processes used in petroleum refining for upgrading petroleum fractions to produce valuable products, as shown in Fig. 21.1. These include:

- Isomerization
- Alkylation
- Reforming
- Thermal processes
- Catalytic cracking
- Hydroprocessing.

Hydroprocessing includes three major classes, namely:

1. Hydrotreating
2. Hydrocracking
3. Hydrofinishing.

Hydrotreating includes hydrogenative heteroatom removal and hydrogenation of olefins and aromatics. The heteroatoms include sulfur, nitrogen, oxygen and metals. Hydrocracking performs hydrogenation and cracking successively and simultaneously. There are differences between combined hydrotreating/catalytic cracking and hydrotreating/hydrocracking in terms of conditions and interactive reactions. Both have advantages and disadvantages. Hydrofinishing is really another form of hydrotreating that is used to achieve the final specifications of fuels.

Each process is individually optimized according to the boiling range and molecular composition of the specific petroleum fraction being processed [21.1]. Hence, when selecting a process or combination of processes for a particular application, it is very important to understand the feedstocks and process objectives, which determine process conditions, and costs. Before making such decisions, it is important to understand fully the underlying chemistry and reaction mechanisms associated with feedstocks, products and catalysts [21.2]. Most intermediate streams in a refinery are also hydrotreated.

This overview describes the remarkable progress in the detailed understanding of the chemistry of feeds, products, and the conversion mechanisms of hydrotreating at the molecular level, including the detailed structures of the reactants, their chemical and physical properties and conversion mechanisms. The roles of the detailed molecular interactions in the feed on reactivity and inhibition are also reviewed. The preparation, activation, composition and structure of catalysts are discussed, along with the associated causes of catalyst deactivation and ultimate catalyst lifetime in each pro-

cess. The approaches to new and improved catalytic processes and the production of more-active catalysts are also discussed.

Recently, some reviews on the hydrodesulfurization of gasoline and middle distillates have been published. *Song* [21.3] summarized the new aspects of deep HDS of diesel and gasoline fractions including a brief review of some commercial processes. *Moulijn* [21.4] also reported recent advances in deep HDS. His review described the conventional and nonconventional technology including adsorption and oxidation. French groups [21.5] summarized the chemical nature of HDS systems, including new acid catalysts and adsorption technology. Our previous chapter [21.6] is also referenced. For practical applications, new and improved catalysts have been developed and marketed by various companies such as Akzo Nobel, NEBULA, Criterion, Haldor-Topsøe, IFP, United Catalyst/Süd-Chemie, Advanced Refining Technologies, ExxonMobil, and Nippon Ketjen in Japan. These are well reviewed in *Song's* literature [21.3]. Recently, many efforts have been progressed by manufacturers. For example, Criterion developed a new CoMo ULSD catalyst, ASCENT DC-2534, for top-tier desulfurization performance in the low-to-medium pressure range, which may be designed for refiners that want to maximize diesel production while managing hydrogen consumption and operating cost [21.7]. New efforts for developing the desulfurization catalyst have been made by Haldor Topsøe with the detailed insight of interaction between support and type I/II sites in the catalyst [21.8]. The progress in fundamental HDS studies together with the elucidation of reaction pathways are expected to continue for the improvement of commercial catalysts.

21.1.2 Chemical Composition of Distillates

Figures 21.2 and 21.3 illustrate the diversity of composition by showing the elemental (C, S, N) distributions of some typical petroleum fractions, such as gasoline and light cycle oil LCO analyzed by gas chromatography with atomic emission detection (GC-AED) [21.9]. These figures also show the distributions of heteroatomic molecular species that must be converted into hydrocarbons by hydrotreating processes (HDS and HDN). AED can be replaced by other sulfur- and nitrogen-specific detectors, such as sulfur chemiluminescence (SCD) and nitrogen chemiluminescence (NCD) detectors [21.10], as well as inductively coupled plasma-mass spectrometry (ICP-MS) for high sensitivity.

Recently, comprehensive two-dimensional gas chromatography (GC×GC) has become avail-

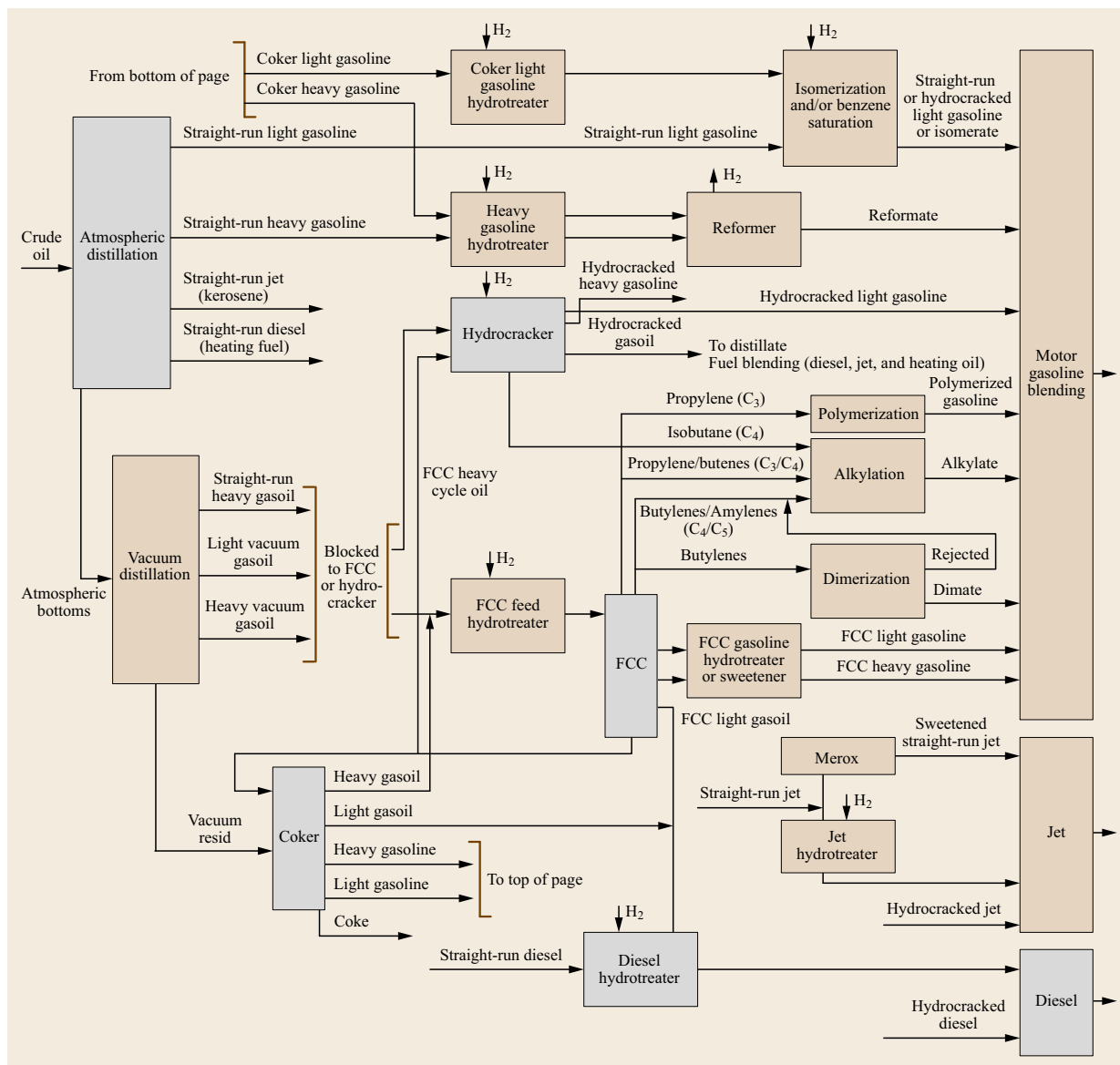


Fig. 21.1 Petroleum refining processes for production of transportation fuels

able [21.11]. A result of the GC×GC analysis of SRGO is shown in Fig. 21.3. With additional chromatographic separation the overlapping components encountered in one-dimensional GC can be resolved, resulting in sufficient resolution and sensitivity for identification and quantification of individual components. Thus, full analysis of molecular composition in petroleum distillates up to gas oils is now achievable.

An important feature of Fig. 21.3 is that the small amounts of thiophenic compounds having high retention time in second dimension are resolved from overwhelming amounts of saturated and aromatic hydrocar-

bons having lower retention time in second dimension even though they have the same retention time in the first dimension. Thus, it demonstrates the power of resolving thiophenes that are overwhelmed by co-eluting hydrocarbons in one-dimension GC and thus not able to be quantified.

Light (LCO) and medium cycle oils (MCOs) of the gas oil range in fluidized catalyst cracker (FCC) streams must be further hydroprocessed to yield high-quality fuels. The problems of high concentrations of aromatic hydrocarbons interfering with the measurement of small amounts of thiophenic compounds at

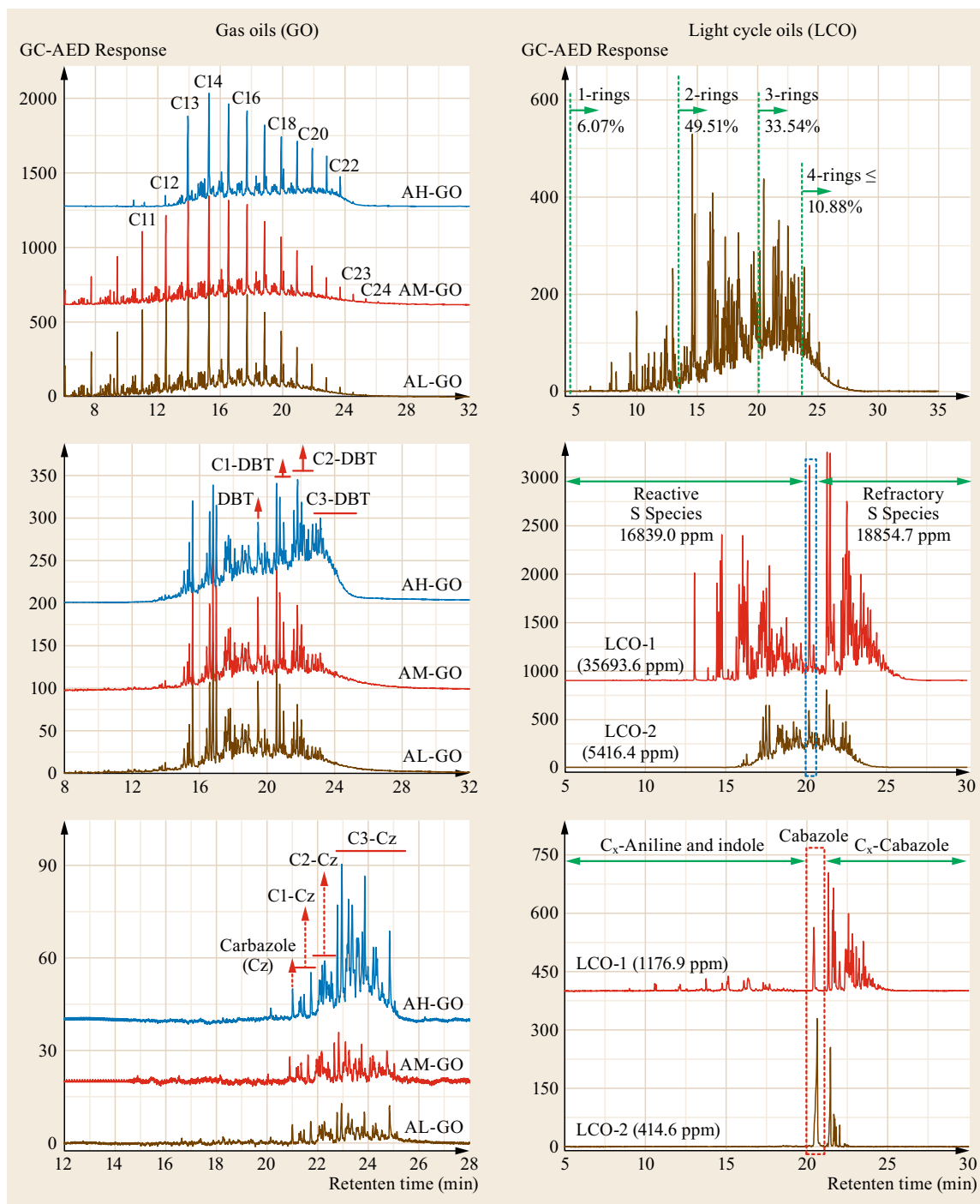


Fig. 21.2 AED chromatograms of various fuel oils. LCO: light cycle oil, AH-GO: Arabian heavy gas oil, AM-GO: Arabian medium gas oil, AL-GO: Arabian light gas oil. (C_n : paraffin with n carbons, T: thiophene, BT: benzothiophene, DBT: dibenzothiophene, Cz: carbazole)

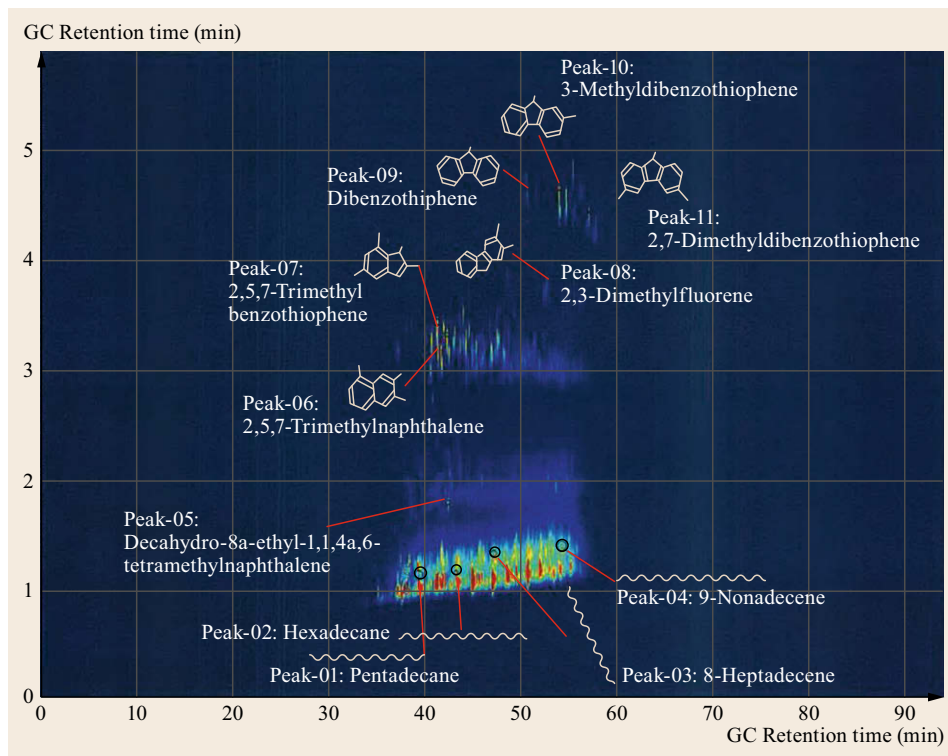


Fig. 21.3 Results on GC×GC assembled with TOF/MASS of a gas oil (cutting points of 260–340 °C)

one-dimensional GC systems for the deep HDS studies of LCO and MCO can now be resolved by using GC×GC or one-dimensional GC with an AED detection system. Thermally cracked products can contain fair amounts of olefins [21.12].

21.1.3 Chemical Components in the Residues

The heavier fractions such as atmospheric residue (AR) and vacuum residue (VR) are also target fractions for hydrotreatment. The vacuum residue consists of saturates, aromatics, resins and asphaltenes (SARA) as identified by liquid chromatographic separation. The molecular compositions including heteroatom-containing species in the first two fractions are analyzed by GC and high pressure liquid chromatography (HPLC). Specific chromatographic separations of heteroatomic species are very helpful for molecular characterization [21.13].

Remarkable progresses in Fourier-transform ion cyclotron resonance mass spectrometry (FT-ICR MS) provides very high resolution and accurate mass measurement, allowing the determination of elemental composition of individual species [21.11, 14, 15]. Some examples of analyzed molecular classes are illustrated in Fig. 21.4. Recently, commercially available spiral time-

of-flight TOF MS and multipath high-resolution TOF (HRT) MS have provided high resolution for millimass accuracy at lower cost, comparing to FT-ICR MS.

Although mass spectrometry-mass spectrometry (MS-MS) can provide structure information of particular species of interest, it fails to obtain any useful structural information for asphaltene molecules due to complexity and interference of other species.

The asphaltene in the residue is the actual ultimate target for both analysis and hydrotreatment. The fraction is believed to consist of three levels of the conceptual structure as follows:

1. Aggregate of polymeric molecules
2. Polymeric or macromolecules
3. Key structural units.

Aggregate

Yen's group proposed an aggregate model [21.16] that was modified by Mullins recently [21.17]. The molecular association is schematically illustrated in Fig. 21.5. The differences between the two models are as follows:

1. Priority of aggregation driving forces among:
 - a) Aromatic planner stacking
 - b) Polymeric entanglement including London force

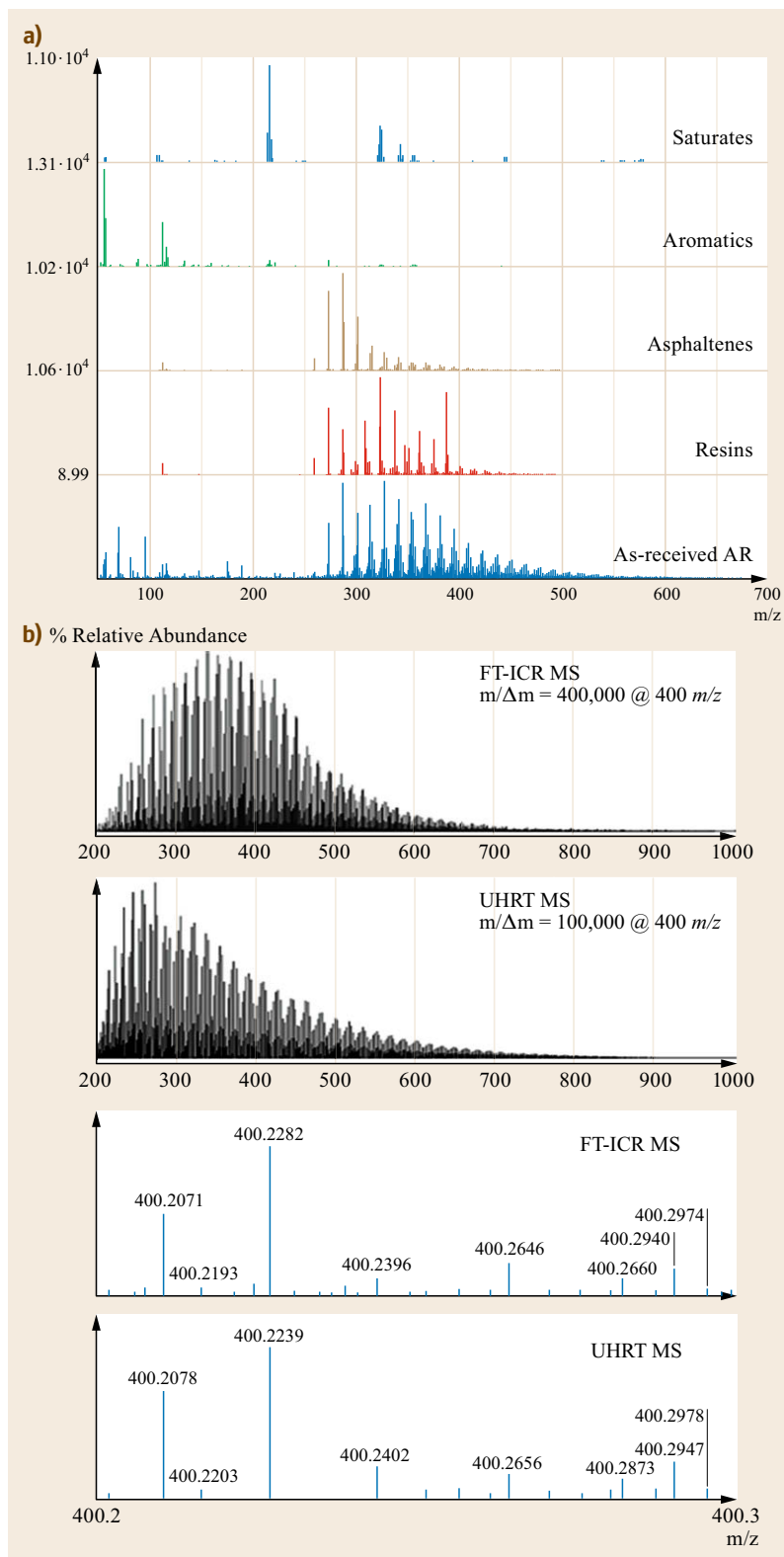


Fig. 21.4 (a) Spiral TOF-MS data for as-received AR and its fractionations of saturate, aromatic, resin and asphaltene (target plate: hairline 384 spots, mode: positive spiral, ionization: LDI, laser intensity: 40%) **(b)** ESI (+) typical broadband spectra of a representative crude oil with average levels of biodegradation and maturation obtained by FT-ICR MS and HRT MS analysis as well as expanded m/z 0.1 window views in the m/z 400.2–400.3 range (after [21.11]). (HRT system uses an innovative multipath-reflecting TOF with a folded flight path developed by Verentchikov et al. [21.14, 15])

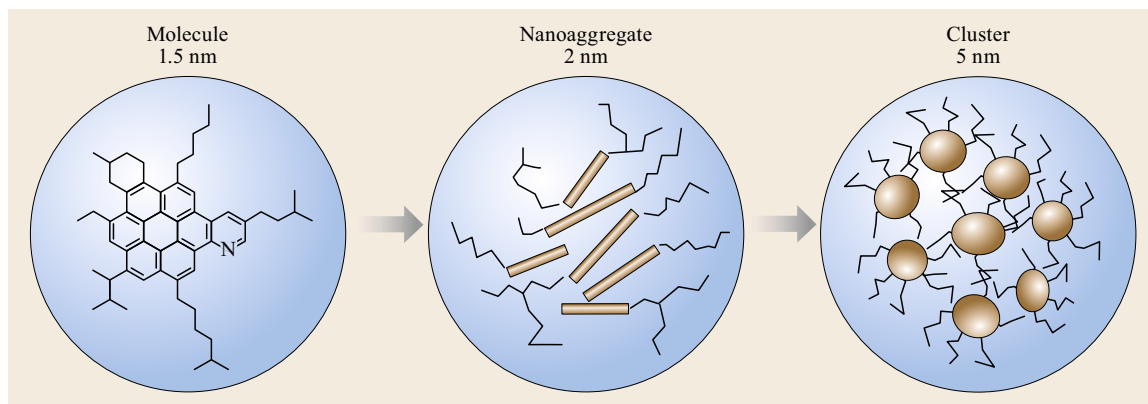


Fig. 21.5 The modified Yen model (or the Yen–Mullins model). *Left:* The predominant asphaltene molecular architecture contains a single, moderately large polycyclic aromatic hydrocarbon (PAH) with peripheral alkanes. *Center:* Asphaltene molecules form nanoaggregates with aggregation numbers of approximately six, with a single disordered PAH stack. *Right:* Asphaltene nanoaggregates can form clusters with aggregation numbers of approximately eight (after [21.17])

- c) Hydrogen bonding or polar–polar interaction including acid–base, and coordinative metallic bridge
- d) Donor acceptor interaction.
2. Aromatic units, multinuclear or single large ring forms. Molecules in Fig. 21.5 carry a fairly large ring with alkyl pendants.
3. Metallic components are bounded to the polymeric and located within aggregated units.

Such aggregation is believed to hinder the contact of its inner units with the surface of the heterogeneous catalysts that carry polar, acidic and hydrogenation sites.

Polymeric Molecules and Nuclear Units

Asphaltene polymers carry sulfur, nitrogen, oxygen in and on their polyaromatic rings. Hydrotreatment removes such elements, hydrogenates and even ring-opens the aromatic ring to refine VR to high-quality fuel and chemicals of lower molecular weight. Hence, we must clarify the image of how the catalyst contacts to the particular reaction sites of asphaltene polymers, for removal and the chemical modification of the target atoms or atomic groups. The basic reaction scheme and mechanisms have been clarified in the hydrotreatment of the distillate where the single molecular structure has been fully identified. Hence, the first objective is to clarify the unit structure concerning the asphaltene polymer. Currently, FT-ICR MS has been used to identify numerous atomic compositions of target species in the asphaltene by carbon number and double-bond equivalent (DBE) [21.18]. Mass-mass measurement can basically provide unit structure of concerned units. According to the knowledge of distillate hydrotreating, local structure surrounding the reaction site plays very

important roles in the reactivity of the target reaction site. The mechanism suitable for the target molecules depends on the molecular-level structure. At the moment, we do not have access to the level of understanding of the detailed structure of asphaltene molecules. Some approaches are described in detail in the later sections. Very roughly speaking, the skeleton of the unit may be similar to that of distillate. We must be concerned with the locations of the target atoms. Polymeric chain entanglement may be also taken into account. The separation and concentration of particular groups of the substrate are always very helpful for the molecular analysis. The location of heteroatoms in the asphaltene molecules is not identified yet, although some structures have been proposed [21.19].

The molecular weight of asphaltene components has been discussed extensively. Two extremes are already reported:

1. Very large molecular weight approaching 10 000–100 000 daltons (Da)
2. Rather small molecular weight less than 1500 Da.

Current mass spectrometry results using carefully controlled ionization conditions favor the second claim by excluding both fragmentation and oligomerization (condensation and coupling) at desorption/ionization stages.

Metals

Petroleum includes several metallic chemical forms:

1. Vanadium and nickel complexes
2. Naphthenic irons and iron sulfides
3. Salts derived from seawater.

Among them, vanadium, nickel, arsenic and silicon are a common cause of catalyst degradation and deactivation in hydrotreatment units. Salts are almost completely removed during desalting. But this process does not remove all of the As, Hg, and Si from crude, because of their status as nonpolar molecules. In addition, volatile alkyl arsenic is the worst of all trace contaminants, showing in VGO and HGO fractions mainly originated from Russia, West Africa and Canada. Alkyl mercury compounds with volatility are nearly as bad as arsenic. Silicones used as flow improvers in pipelines are applied to antifoam agents in delayed coking units, and a lot of silicones appear in naphtha-range fractions. Soluble iron, either from the raw feed or from corrosion of piping, can cause severe operating troubles. The vanadium and nickel complexes

are concentrated in the heavier fractions, while arsenic, silicon and mercury compounds can appear in all fractions. Their removal for refining becomes more important, as described later.

Two aspects of the metal complexes are of concern:

1. Molecular structure of the metal complex (described later in this section)
2. Location or binding of the metal complexes in the asphaltene aggregate and with its polymeric chains.

Certain metals, especially Ni and V, are believed to be present in the chelate forms [21.19]. Porphyrins are most common in the rather light crudes (Fig. 21.6). Nonporphyrins are present in the rather heavier crudes. Nonporphyrins are:

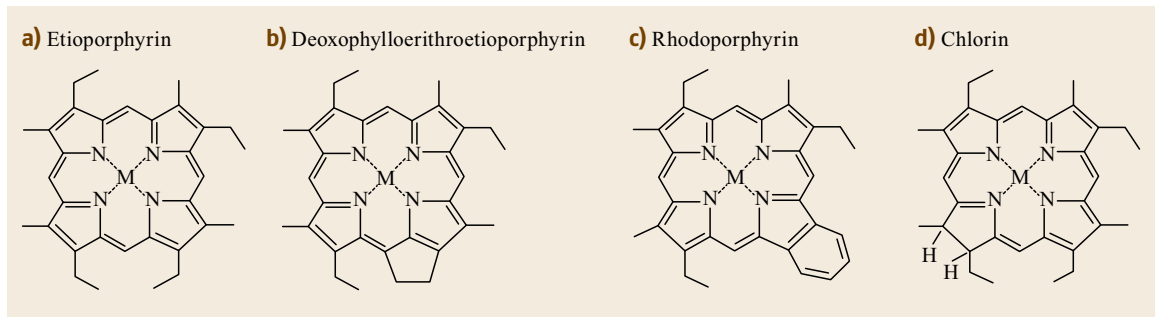


Fig. 21.6a-d Typical metal porphyrin structure in petroleum (a-c) and chlorin intermediate (d): M is Ni or V=O (after [21.20])

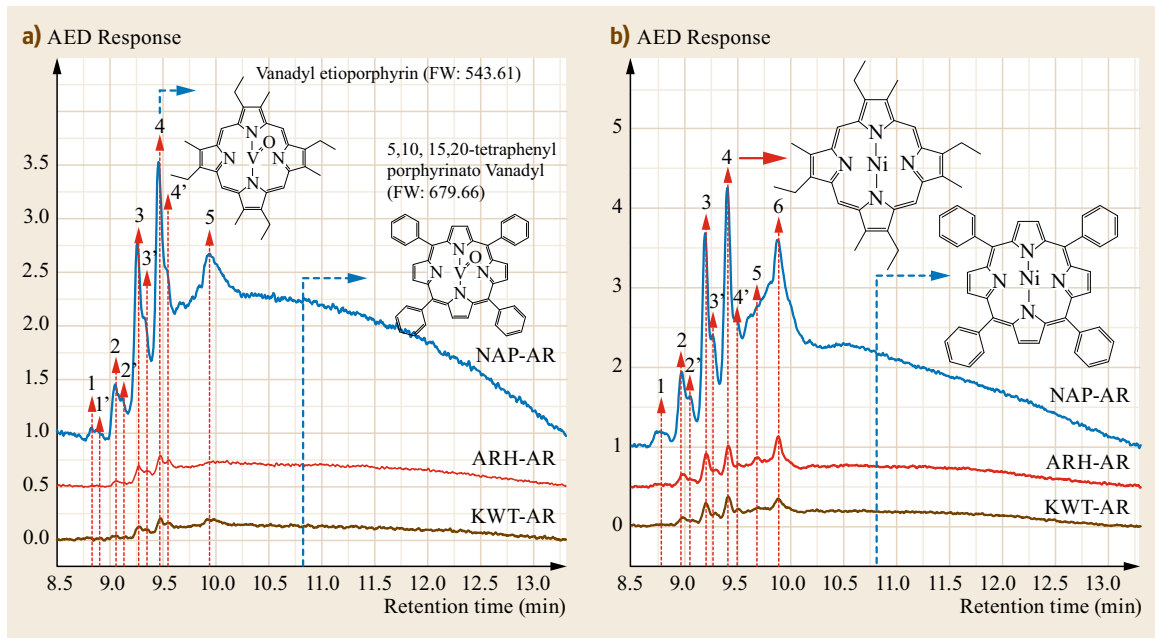


Fig. 21.7a,b The AED chromatograms on (a) V-species and (b) Ni-species in HT-GC-AED (after [21.21])

1. Hexagonal porphyrin-like complexes which carry fifth and sixth ligands in the planar porphyrins
 2. Nonnitrogen ligands in which the metals are bound to sulfur and/or oxygen.
2. Catalytic demetalization:
 - a) Direct metal extraction
 - b) Hydrogenation of the aromatic rings in the ligand, opening the coordination to liberate metal ions onto the catalyst.
 3. Sulfiding.

Currently porphyrins are identified by visible-ultraviolet (UV) spectroscopy [21.22], electron spin resonance (ESR) for vanadium [21.23, 24], GC-AED [21.21] (Fig. 21.7), GC-ICP [21.25], and FT-ICR [21.26, 27]. Nonporphyrins are detected by Visible-UV and ESR [21.23, 24]. The metal complexes are present principally in asphaltene and some in resin. According to Yen's group [21.16, 17], the metal complexes are bound with covalent bonds to the polymeric asphaltene molecules. The central metallic ion is coordinated to the ligand, which can be bound to the asphaltene molecules. Porphyrin rings are also included in the aromatic stacking of asphaltene.

Hydrodemetalation (HDM) is a hydrorefining reaction where the central metals are removed by HDM catalysts. The HDM reaction is assumed to proceed with:

1. Contact of porphyrins to the catalyst surface through their liberation from asphaltene aggregates

Metals may accumulate on the HDM catalysts as sulfides. H_2S is essential for HDM in hydrotreatment. Reactive sulfur may attack the metal ion present in the complex center or isolated on the HDM catalyst. Researchers at Chevron report that H_2S actually inhibits the rate of HDM reactions, and that without H_2S , HDM is too rapid. When HDM is too rapid, it prematurely chokes pore mouths.

Many researchers believe that some if not most of the asphaltene molecules simply plate out in large catalyst pores, where they age to form metal-containing hard coke. This explanation is plausible, because in addition to containing metals and sulfur, spent catalysts also contain significant amounts of carbon, and it is difficult to identify, on a molecular basis, how the metal atoms are bonded. Kinetics, detailed mechanisms and HDM catalyst design will be described later in this chapter.

21.2 Hydrotreating Process

The primary objectives of hydrotreating are:

1. To remove impurities, such as heteroatoms and metals from the feedstock
2. To increase the hydrogen content of the feedstock
3. To lower the molecular weight without a substantial loss in liquid product yield
4. To prepare feed for downstream processes (e.g., fluid catalyst cracking and product blending).

The impurities of concern basically depend on the molecular weight of the feedstock being processed. Lower molecular weight feedstocks such as naphtha, gasoline, middle distillates (atmospheric and light vacuum gas oils), diesel fuels and home heating oils (kerosene etc.) carry undesired impurities such as sulfur-containing compounds (S-compounds), nitrogen-containing compounds (N-compounds), oxygen-containing compounds (O-compounds), and polynuclear aromatic (PNA) compounds. Higher molecular weight feedstocks such as heavy vacuum gas oil, and atmospheric and vacuum residues, have metals in addition to the same impurities described above. In general, the concentrations of these impurities increase with their higher boiling ranges. Thus, the hydrotreating process of choice depends primarily on the boiling range of the feedstock. The boiling range is dictated by the molec-

ular weight distribution of the feedstock. The second-most important consideration in choosing a hydrotreating process is the product quality specifications, which are predominantly related to the total hydrogen content of the products that, in turn, are related to the PNA content.

O-compounds are generally not considered as major or environmental hazards in petroleum products. Nevertheless, some O-impurity compounds such as phenols and naphthenic acids lead to problems and corrosion in the transportation pipe and storage vessels [21.28]. Some crude oils that contain a large amount of naphthenic acids are classified as naphthenic crudes. Certain naphthenic crudes serve as lube base stocks. Iron dissolved by naphthenic acid in the crude causes plugging by forming FeS in the catalyst bed or on the feed filter. Finely dispersed FeS may enhance coking reactions, both in the hydrotreater and the FCC [21.29]. The O-compounds in the petroleum are much more reactive for removal than other impurities and, generally, hydrotreating is not developed specifically to remove O-compounds. However, less reactive O-compounds such as phenols and benzofurans are found in significant amounts in coal-derived oils. Hence, their removal is one of the major concerns in the hydrotreating of coal-derived oils [21.30].

S-compounds, N-compounds and M (metal) compounds have different reactivities and chemistry depending on the boiling ranges of fractions in which they are found. Thus, specific processes have been developed for the removal of each of these impurities. These are classified as hydrodesulfurization (HDS), hydrodenitrogenation (HDN) and hydrodemetallation (HDM) processes respectively. These are in turn subdivided into processes that are optimized for the boiling range of the particular feedstock being treated to achieve the highest activity, least hydrogen consumption and longest catalyst life.

In general, the sulfur impurity is of primary concern because S-compounds are major targets of environmental regulations and often are serious poisons and inhibitors for catalysts in secondary upgrading process, such as catalytic reforming and isomerization. Their combustion products create serious environmental hazards such as acid rain. Thus, the main hydrotreating processes that have been developed for distillable feedstocks are HDS processes. N-compound impurities are also removed during HDS processes. When subsequent processes employ acidic catalysts, extensive N-removal is required since the basic N-compounds poison the active site of those catalysts [21.31]. Lower-

ing aromatic content through hydrotreating is classified as hydrodearomatization (HDA). HDA reactions occur during HDS and HDN processes, but product quality often demands an HDA process that is conducted subsequently after HDS and/or HDN process. Future environmental regulations may emphasize HDA further [21.32]. Nevertheless, hydrogenation prior to HDS and HDN is often quite favorable for successive hydrotreatment.

Metal-compound impurities are found particularly in high boiling feedstocks, such as atmospheric and vacuum residues. Thus, HDM processes are tailored for high boiling and very viscous feedstocks [21.33]. Nevertheless, trace amounts of M compounds in the gas oil must not be overlooked since they cause catalyst deactivation in the long run.

The current crudes tend to be heavier and environmental regulation on petroleum fuel is becoming severer and severer. Hence, hydrotreatment becomes more important and should perform deeper refining of highly contaminated feed at acceptable cost. The future processes and catalysts must be improved to achieve the targeted product quality under milder conditions at higher productivity and long continuous operation.

21.3 Bases for Hydrotreating

21.3.1 Hydrotreating Catalysts

For Co(Ni)Mo(W) sulfide catalysts, recognition and control of the shape and size of catalyst sulfides, and their active sites for HDS and hydrogenation, are important topics for the understanding of the hydrotreatment catalysts. The basic principles can be found in [21.6].

Hydrotreating Catalyst for Residue

Hydrotreating for residue consists of HDM, HDS, HDN and hydrocracking. The commercial catalysts for the residue hydrotreatment contain MoS₂ promoted by sulfides of Co and/or Ni on an alumina support.

A support must meet several important criteria. It must be strong enough to bear the weight of tons of catalyst and the force exerted by the flow of fluids. Another important property of an alumina support is the pore size distribution to optimize the access of large molecules in the residue to the number of active sites or surface area. Dual distribution, which carries large and small pores on the same alumina, is designed for better and more effective access of large molecules and small molecules produced in the large pores and small pores respectively.

The kind and amount of sulfide catalysts depend on the target reaction: HDM catalysts carry a small amount of MoS₂, while HDS and HDN catalysts also contain sulfides of Co, Ni or both. In general, CoMoS catalysts are preferred for HDS, and NiMoS catalysts are preferred for HDN. The properties of the support and the amount of active sulfide are optimized to the feed, its sulfur and nitrogen content, and reactivity. The aromaticity and heaviness of the asphaltenes are very influential on the difficulty of HDM, HDS and HDN.

Hydrocracking after the impurity removal requires both hydrogenation and acidity, hence the catalyst must enhance both. Acidity tends to accelerate coking of the heaviest fraction on the catalyst, shortening the catalyst life. Hydrogenation suppresses the coking of adsorbed species on the acidic site, but too much hydrogenation suppresses cracking. The relative amounts of hydrogenation activity and acidity must be carefully balanced.

Progress in Support Materials for More Active HDS Catalysts

Enhancement of catalytic activity on CoMoS and NiMoS has been intended particularly for the HDS of refractory sulfur species in the gas oil, and has been

targeted to find more active support materials. Some oxides and carbon materials have shown superiority to alumina in HDS reactions, although the superiority could not be generalized due to the wide variation of reaction conditions and feed characteristics in HDS. The catalyst support influences the catalytic activity in HDS through two ways: modifying the active species itself and participating in the HDS reaction as a cocatalyst.

Acidic supports, such as zeolites, have been tested by many researchers and show superiority in the HDS reaction. Acidic zeolite was reported to facilitate isomerization and transalkylation of alkylated DBT, resulting in the enhanced HDS activity of refractory alkylated sulfur species [21.34].

Acidity has been recognized as important in deep HDS to improve resistivity against inhibition by H_2S or to enhance hydrogenolysis. Strong acidity can be inhibited by basic and polar nitrogen species, such as NH_3 , pyridines, and carbazoles. Nevertheless, HDN is also accelerated by adsorption and C–N bond fission. A series of CoMo and NiMo catalysts supported on alumina, silica-alumina, and alumina-zeolite were examined [21.10] in the deep HDS of straight run gas oil to evaluate enhanced activity by such supports in the presence of H_2S and NH_3 . Although H_2S and NH_3 inhibit the HDS of refractory sulfur species over all catalysts examined, a catalyst of high acidity achieved deep HDS even under such conditions. Adsorption of gas-phase inhibitors on the acidic sites and weakening of the metal-sulfur bond in the active sulfide caused by acidity of the support are believed to improve the resistivity against H_2S . Inhibition by NH_3 is moderate because of rather high reaction temperature where the adsorption of NH_3 is limited.

The functions of zeolite, as a representative acidic support, have been discussed from the viewpoint of enhanced hydrogenation and isomerization. In addition, zeolite itself has been found to desulfurize some sulfur species, such as thiophene. Acidic C–S bond breakage and hydrogen transfer can be postulated over the acidic zeolite. More research is needed.

In spite of the above advantages in using zeolite as a support material, an inevitable problem is present in such an acidic catalyst system: fast coking. Strong acidic sites cause extensive coking, which shortens the life of the catalyst by covering the strong acid sites, making them nonacidic. Although such behavior cannot be discussed in detail now due to the lack of information, a disadvantage such as fast coking may be moderated by blocking particular acidic sites with a third ingredient. We examined CoMoS and NiMoS catalysts supported on ultra-stable Y-zeolite (USY), modified by an alumina coating. Acidity, measured by NH_3 des-

orption, was lowered on the modified USY. However, its activity toward refractory sulfur species contained in the gas oil was basically maintained. Furthermore, cracking occurring on acid sites was much less over the alumina-coated zeolite catalyst. It is also important to locate the hydrogenation active site in the vicinity of the acidic site to hydrogenate strongly adsorbed species on the acidic site for desorption before coking.

Another issue with a zeolite support is the poor dispersion of active sulfide due to dominant coverage of SiO_2 on the zeolite surface. Incorporation of mobile composition of matter No. 41 (MCM-41) into alumina provided higher activity for the CoMo catalyst in dibenzothiophene (DBT) HDS [21.35]. MCM-41 was reported to reduce the interaction of Co and Mo with the support. As a result, it enhances the formation of polymeric Mo octahedral species, which are regarded as an active form on alumina [21.35]. Furthermore, it modifies the dispersion of Co to suppress the formation of an inactive $CoAl_2O_4$ phase. Such results indicate the importance of the acidic nature of the support in modifying active sites. Such a function can be ascribed generally to finer particles of alumina among the matrix with poor affinity for the active oxides such as SiO_2 , B_2O_3 and P_2O_5 . It is intended to incorporate active species in the pores of the zeolite. Difficulty for diffusion of large refractory species into the narrow pores of the zeolite must be considered.

Amorphous $SiO_2-Al_2O_3$ is also an acidic support like zeolites. HDS activity toward 4,6-dimethyldibenzothiophene (DMDBT) was reported to increase by the mixing of the conventional NiMo/ Al_2O_3 catalyst with $SiO_2-Al_2O_3$ [21.36]. Such an observation is believed to be caused by enhanced hydrogenation and isomerization by the acidic component in the catalyst. However, there are many questions on the fundamental aspects of HDS catalysts supported on $SiO_2-Al_2O_3$. First of all, the difference in MoS_2 morphology on Al_2O_3 and $SiO_2-Al_2O_3$ must be clarified. It is generally accepted that SiO_2 can't disperse MoO_3 well in a monolayer due to very weak interaction with MoO_3 [21.37]. However, Al_2O_3 incorporation alters the nature of surface to increase the monolayer capacity. Hence, the form of active species may be different from that observed on Al_2O_3 supports. Higher activity of $SiO_2-Al_2O_3$ -supported catalysts may come from a more favorable form of active species in addition to the stronger acidity of the support, but definite evidence has not been found yet.

The addition of P_2O_5 , ZrO_2 , and B_2O_3 to Al_2O_3 was reported to increase the acidity of catalysts and as a result enhanced the HDS of refractory sulfur species [21.38]. Other roles of P_2O_5 and B_2O_3 in the dispersion of MoS are described above. On alumina-

supported catalysts, phosphorus has been present in numerous commercial catalysts, where it stabilizes the active metals and provides acidity, for more than 25 years [21.39]. Catalysts containing NiP are a new type of species active for hydrodesulfurization [21.40]. The roles of acidic supports in HDS by sulfide catalysts are summarized in Table 21.1.

TiO₂ was evaluated as an active support material for HDS. Its main drawback, low surface area, was reported to be overcome by a kind of sol-gel process, giving as high a surface area as 120 m²/g [21.41]. It could carry a higher loading of Mo (19 wt% as MoO₃) than conventional TiO₂ supports, allowing well-dispersed Mo species. This catalyst showed higher HDS activity for 4,6-DMDBT than the alumina-supported one. An Al₂O₃-TiO₂ composite support was also tested to provide higher surface area. It showed higher activity than Al₂O₃ and TiO₂ alone in HDS of 4,6-DMDBT while its activity for the HDS of DBT was inferior to the alumina support [21.42–44]. Such binary oxides carry more Brønsted acidic sites and as a result have rather high activity. This gives another increase in the activity for 4,6-DMDBT HDS. It should be also noted that TiO₂ is believed to have much less interaction with active species than Al₂O₃, inducing a more easily reducible oxide phase of Mo and Co(Ni) due to the partial sulfidation of TiO₂ [21.45].

Carbon has been regarded as a promising catalyst support due to its very high surface area, peculiar pore structure, and surface-functional groups [21.46]. HDS catalysts supported on carbon can provide higher activity than alumina-supported ones [21.47–49]. Presumably, weak interaction of carbon with sulfide precursors provides more sulfidable species on carbon than on alumina, resulting in the more active sites for HDS. The very large surface area of carbon supports must be also helpful although the acidic contribution is not expected. Acidic or polar additives can be designed in carbon black as used in the rubber industry. The mechanical strength of carbon supports is of concern. Further development is expected.

The life of catalysts due to the sintering of active species must be carefully tested since such supports interact weakly with active species.

Deactivation and Regeneration of Hydrotreating Catalysts

Hydrotreating catalysts lose their activity in several ways [21.50]:

1. Process upsets
2. Deposition of trace contaminants such as V, Ni, Fe, As and Hg
3. Deposition of other impurities such as salts and silica
4. Covering of the active sites by reactants and/or products including coke
5. Degradation of the active phase, including degradation of sulfided forms
6. Sintering of the active phase into large crystal units.

The deactivation in HDS catalysts usually occurs in three steps: initial rapid deactivation, intermediate slow but steady deactivation, and rapid deactivation at the end of the reaction. Commercial processes usually are operated at constant conversion. This constant conversion is achieved by gradually heating the reactor to higher temperatures to compensate the slow but steady catalyst deactivation.

The initial rapid deactivation phase is believed to be due to rapid coking on active sites having very high acidity [21.50]. Deposited carbon can be characterized by temperature-programmed combustion and Raman spectroscopy [21.51]. The slow but steady deactivation is associated mainly with coking but also with metal deposition and sintering during the course of the process period. A higher reaction temperature applied at the end of the reaction may cause rapid deactivation by coking at the final stage. To avoid the rapid deactivation, the proper grading should be made both with respect to size, shape and catalyst properties in order to optimize the performance, and to obtain the desired product quality and longest catalyst life.

Table 21.1 Role of acidic supports in HDS by sulfide catalyst

Influences on the active species (catalyst–support interaction)	Catalytic functions of support (bifunctional catalysts)	Influence of active species on the substrate adsorbed on the supports
(1) Acidic modification on the natures of active sulfides – long- and short-range interaction	(1) Acidic activation of substrate-cracking, isomerization, transalkylation	(1) Hydrogen spillover for sulfide to oxide support
(2) Restriction of the area (site) for dispersion of active oxide precursors	(2) Acidic adsorption of substrate in σ - and π -coordination-spillover of coordinated substrate to active sulfide	
(3) Reverse spillover of proton from support to active sulfides		

The current design to suppress the coking is to control the pore size for no plugging at the pore mouth. Thus, the availability of the active site on the entire pore can stay through a longer time of continuous operation. Currently, adequate or optimized acidic supports are utilized to achieve high activity, hence coking deactivation appears important in current processes. Such deactivation schemes suggest that catalysts may be regenerable if suitable methods can be developed. Commercially, carbon-containing material is removed during regeneration by combustion. During regeneration of the catalyst, the active sulfide form is into the oxide form and the resulfidation must subsequently regenerate the activity. The combustion must be moderate to minimize sintering and to maintain the dispersion of active metals on the support. For some catalysts, a process called rejuvenation is used to redisperse the active metals prior to reloading and resulfidation.

One of the important points in the design of the catalyst is to improve the hydrogenation activity in the vicinity of acidic sites. This could hydrogenate the coke precursors to make them more susceptible to cracking or to be more soluble in the reaction matrix, so that they can be removed from the catalyst surface. The hydrogenative pretreatment as well as removal of asphaltenes can be attempted before the hydrotreatment of the heavy feed to reduce the coking tendency of the asphaltene. Another achievement can be used with catalyst grading [21.52].

21.3.2 Chemistry of Hydrodesulfurization

Distillate

The removal of sulfur from a petroleum stream depends greatly on the structure of the sulfur compound being treated. The rates of sulfur removal can vary by several orders of magnitude. Generally, acyclic sulfur compounds such as thiols and disulfides are highly reactive and can be removed under very mild HDS conditions. Saturated cyclic sulfur compounds and aromatic systems in which sulfur is present in six-membered rings are also highly reactive. However, compounds in which the sulfur atom is incorporated into a five-membered aromatic ring structure (such as thiophene) are much less reactive and the reactivity decreases as the ring structure becomes increasingly condensed (e.g., 1 ring > 2 rings > 3 rings) [21.2]. For highly condensed ring structures (four or more rings), the reactivity trend reverses and reactivity tends to increase slightly as the ring structure increases in size [21.2] as described later. A reason for such behaviors is that there are several different chemical pathways through which sulfur can be removed from a molecule and the preferred pathway

changes for different sulfur compound structures as shown Fig. 21.8, where 4,6-dimethylbenzothiophene is selected as the substrate of very low reactivity (refractory sulfur species).

In this scheme, there are three major pathways to desulfurized products. The first is called direct hydrodesulfurization, in which the sulfur atom is removed from the structure and replaced by hydrogen, without hydrogenation of any of the other carbon-carbon double bonds. The rate constant associated with this direct route is shown as k_{D0} in Fig. 21.8. Because of the steric hindrance by two methyl group adjacent to the sulfur atom, direct HDS becomes very hard. The second route is called the hydrogenative route and assumes that at least one aromatic ring adjacent to the sulfur-containing ring is hydrogenated before the sulfur atom is removed and replaced by hydrogen. The associated rate constants for hydrogenation and hydrodesulfurization routes are shown as k_{HS1} and k_{D1} in Fig. 21.8. In addition to hydrogenation of an aromatic ring before sulfur is removed, an aromatic ring may be hydrogenated after sulfur removal, and the associated rate constant for this reaction is shown as k_{HP1} in Fig. 21.8. Hydrogenation of one or two phenyl rings liberates the steric hindrance due to the nonplanar structure. This often leads to confusion in interpreting the results of experimental data as both routes can produce the cyclohexylbenzene final product.

It should also be noted that the hydrogenation pathways are subject to thermodynamic equilibrium constraints. Thus, the partially hydrogenated intermediates (such as tetrahydrodibenzothiophenes) have lower

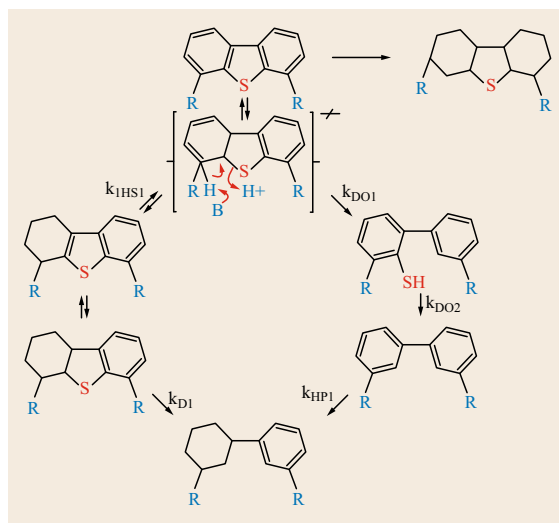


Fig. 21.8 Reaction mechanism of 4,6-dialkyl DBT (assuming the formation of dihydro-intermediate) for HDS (after [21.5])

equilibrium concentrations at higher temperatures. This results in a maximum in the observed rates of HDS via the hydrogenative routes, as a function of temperature. Thus, the hydrodesulfurization via the hydrogenative route becomes limited at low pressures and high temperatures.

Another route includes the isomerization and transmethylation of methyl groups at 4- and/or 6-positions, which reduce the steric hindrance as shown in Fig. 21.8. The direct pathway is believed to involve the insertion of a metal atom on the surface of the catalyst into a sulfur-carbon bond in the sulfur-containing compound [21.2]. This insertion can occur even for fully aromatic sulfur compounds, such as thiophene, benzothiophene and dibenzothiophene. Such a pathway is possible because the resultant metal-sulfur bond is energetically favorable. After the insertion, several other steps occur in which the sulfur is expelled as hydrogen sulfide and the catalyst is restored to its original state.

The hydrogenative pathway involves the initial hydrogenation of one or more of the carbon-carbon double bonds adjacent to the sulfur atom in the aromatic system. Hydrogenation destabilizes the aromatic ring system, weakens the sulfur-carbon bond and provides a less sterically hindered environment for the sulfur atom. Metal insertion is thus more facile.

There are two active sites (functions) postulated on HDS catalysts based on the above discussion, S-extrusion and hydrogenation. The active center is a coordinatively unsaturated metal site where the S ligand is facile. Sulfur in aromatic rings can coordinate to the active center of both functions. It is believed that the initial adsorption of the S-compound is through σ -bonding, in the case of direct S-extrusion. However, in the hydrogenative function, S-compound coordination is through π -bonding. Neighboring S-H groups are believed to be involved in the hydrogen transfer for both S-extraction and hydrogenation. Differences in the active sites for S-extraction and ring hydrogenation are not yet clear although they appear to be interconvertible.

H₂S-, NH₃- and nitrogen-containing compounds can also coordinate to the active center, inhibiting the S-extraction and hydrogenation as discussed later.

The direct pathway becomes more difficult as the ring structure becomes larger because the aromatic structures become increasingly more stable and because the insertion becomes more hindered for the more condensed rings. To illustrate these factors, Table 21.2 provides examples of hydrodesulfurization reactivities of sulfur compounds having different ring structures [21.53, 54]. For ease of discussion, all of the rate constants in this and following illustrations have been normalized relative to dibenzothiophene having a value of 100.

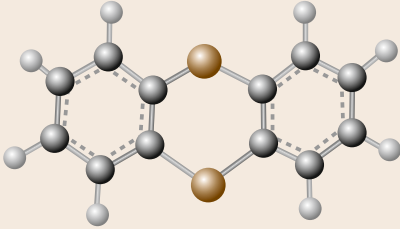
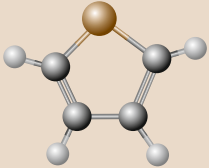
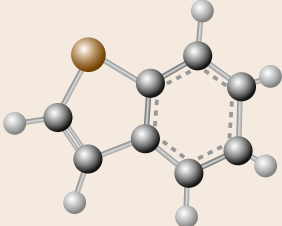
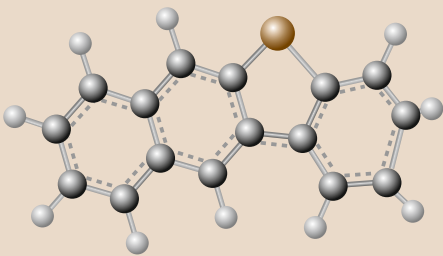
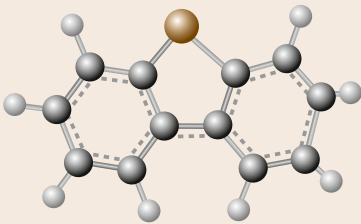
In Table 21.2, the overall hydrodesulfurization reactivity of the sulfur compounds decreases with increasing ring condensation from one ring to two rings to three rings, but then increases significantly for the four-ring system. As mentioned above, increasing ring condensation is detrimental to the insertion step in the direct route. However more ring condensation beyond four may not further hinder the insertion while the adsorption becomes stronger to facilitate the insertion. A switch in the preferred pathway from the direct route to the hydrogenative route must be also taken into account. Hydrogenation becomes more facile with increasing ring number.

Another complicating factor in reactivity is the proximity of the alkyl group to the sulfur atom in the aromatic ring structure. Generally, as the sulfur atom becomes more crowded by adjacent alkyl groups the reactivity decreases. This has been attributed to steric crowding around the sulfur during adsorption on the catalyst surface or at the some transition state in the desulfurization. This steric crowding affects the direct hydrodesulfurization route most severely. Table 21.3 illustrates this factor for several alkyl-substituted benzothiophenes and dibenzothiophenes. In Table 21.3, the reactivity for hydrodesulfurization decreases as the number of substituents around the sulfur atom increases [21.53]. Alkyl groups that are not close to the sulfur atom have little effect. Recently, migration of alkyl groups before the hydrodesulfurization was proved to enhance the direct hydrodesulfurization on the catalysts of strong acidity.

The hydrogenative routes are not significantly affected by alkyl substitution on the aromatic rings, while the rate of the direct route becomes lower when alkyl groups are adjacent to the sulfur atom. Thus, the relative rate changes summarized in Table 21.3 are primarily due to loss in the ability for hydrodesulfurization to proceed via the direct route. For this reason, the catalyst, which is preferred for hydrodesulfurization, is often different for light and heavy feedstocks, as the numbers of alkyl groups and of condensed aromatic rings in the sulfur-containing compounds increases markedly with boiling point.

Refractory sulfur species in distillates contain alkyl groups. Alkyl groups are especially inhibitory when they are neighboring the S-atom in the dibenzothiophene core. Compounds containing additional or larger alkyl groups, such as methylethyl dibenzothiophenes and trimethyl dibenzothiophenes, appear in the heavier fractions and are even more refractory. The addition of a cyclohexyl group to the two alkyl groups at the 4,6-positions on the dibenzothiophene make it extremely difficult to remove the sulfur by HDS due to strong steric hindrance. It resembles the nitrogen species of

Table 21.2 Desulfurization reactivities of compounds having different ring structures (after [21.53, 54])

Sulfur compound structure	Compound type	Relative reactivity
	Thianthrene	Very fast
	Thiophene	2250
	Benzothiophene	1300
	Benzo[b]naphtha[2,3-d]thiophene	100
	Dibenzothiophene	100

similar structure in vacuum gas oil, which has been identified as the most refractory species for HDN of distillates [21.56].

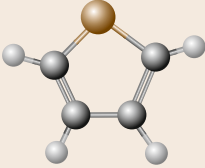
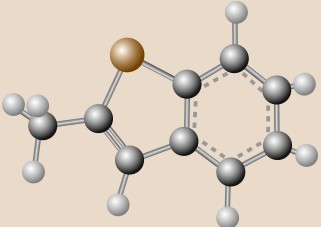
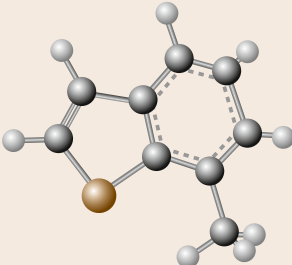
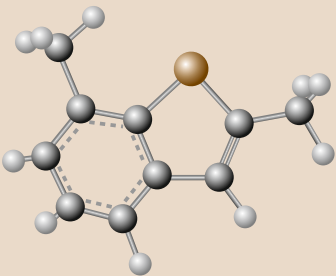
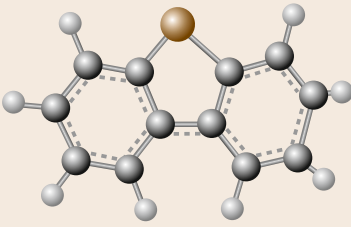
Residue

HDS of the residue is different in terms of its polymeric and aggregate structure from that of distillates where the macromeric sulfur species must approach the active sites of HDS (hydrogenation and hydrogenolysis C–S bond breakage). In the aggregate structure, poly-

meric components are entangled together around the sulfur species in the aggregate. The polymeric structure may carry more than one sulfur-containing unit as well as nonsulfur-containing units [21.57]. The units neighboring the particular target sulfur-containing unit in the polymeric chain may inhibit the HDS of the unit – a kind of polymeric intramolecular inhibition must be taken into account.

The sulfur species must be liberated to approach to the active sites over the solid catalyst. The sulfur to be

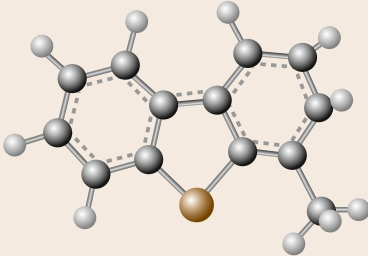
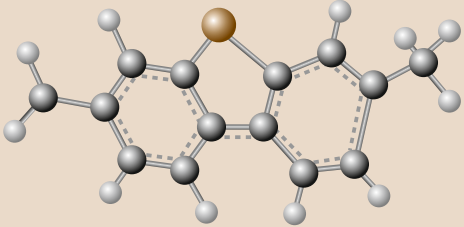
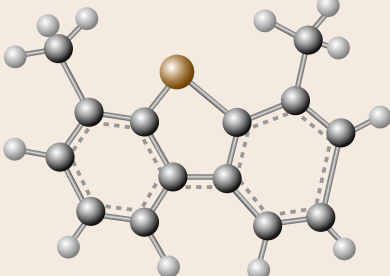
Table 21.3 Desulfurization reactivities of alkyl-substituted aromatic compounds (after [21.55])

Sulfur compound structure	Compound type	Relative reactivity
	Thiophene	1330
	2-Methyldibenzothiophene	596
	7-Methyldibenzothiophene	466
	2,7-Dimethyldibenzothiophene	310
	Dibenzothiophene	100

removed is located in a variety of unit structures with various alkyl substitutes. Some of them found in the aromatic fraction are listed in Table 21.4 according to Anderson et al. [21.58]. Their procedure for enhancing the measurement of the sulfur species using a Pd complex is very helpful for the detailed molecular analysis of sulfur compounds in complex mixtures by FT-ICR MS.

The sulfur-containing species are mostly either in benzothiophene or dibenzothiophene type, even if the connecting aromatic units are of a wide variety. Their HDS reactivity may not be very different as far as the unit structure is concerned. Their reactivity can be influenced by the alkyl substitution as observed with the sulfur species in the distillates. The IFP group reports a structure of sulfur species in the asphaltene

Table 21.3 (continued)

Sulfur compound structure	Compound type	Relative reactivity
	4-Methylthiophene	38
	3,7-Dimethylthiophene	90
	4,6-Dimethylthiophene	11

based on the stochastic reconstruction as shown in Fig. 21.9 [21.59].

The chains connecting cores provide the polymeric molecule where SH and dibenzothiophene are indicated as sulfur-containing parts. Neighboring alkyl and cyclopentyl groups may influence the reactivity sterically. The numbers of cores in the polymers, benzene and cyclohexane rings in the core are shown in Fig. 21.9.

Recent FT-ICR MS analyses reported the presence of multiple heteroatoms, such as S and N, S and O, as well as N and O, in the same molecules [21.60]. Since these compound types are very rare in the distillate, their HDS reactivity must be studied for residue.

The HDS mechanism and reactivity in residue appear basically similar to those of the distillates as far as those of unit structures. The different aspects are present as the polymeric and aggregated molecules in the residue. At least, steric effects due to coiled polymer and aggregation must be involved. The HDN, HDO, HDM and coking reactivities of the residue are in the same situation as those of HDS.

The catalysts for the distillate and the residue should have different diameters and depths of optimum pores

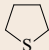
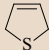
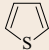
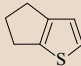
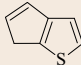
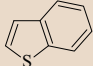
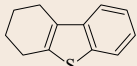
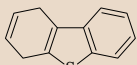
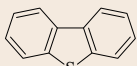
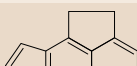

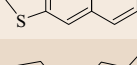
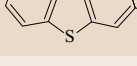
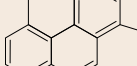
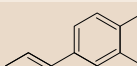
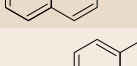
because their substrates must have different molecular size and degree of aggregation. More chemical factors must be emphasized with the catalysts for the residue, since coking takes place more easily. Liberation of polymeric entanglement aggregation is another chemical issue in the catalysts.

Inhibition of HDS

The active sites postulated for HDS catalysts promote sulfur extraction, hydrogenation and acid-catalyzed reactions regardless of whether the feed is distillate or residue. Such active sites are all commonly or selectively subject to occupancy by the inhibitors in the feed.

As mentioned above, several species in the feed and product are inhibitors for HDS. Reactive sulfur species appear to be less inhibited than the refractory species. This is because the naked S atom in the reactive species can easily or preferentially undergo metal insertion to break the C–S bond via the direct HDS route. They are also the major S-compounds present and can compete effectively with inhibitors for the active sites on the catalysts. Their concentrations become lower while H₂S and NH₃ inhibitors increase their concentration during

Table 21.4 Examples of typical sulfur-containing compounds in crude oil (after [21.58])

Possible structure	DBE	Compound type	Nominal mass
	1	Tetrahydrothiophene	88
	2	Dihydrothiophene	86
	3	Thiophene	84
	4	Naphthenothiophene	124
	5	Cyclopentenothiophene	122
	6	Benzothiophene	134
	7	Tetrahydrodibenzothiophene	188
	8	Dihydrodibenzothiophene	186
	9	Dibenzothiophene	184
	10	Acenaphthenothiophene	210
	11	Acenaphthylenothiophene	208
	12	Benzonaphthothiophene	234
	13	Naphthenophenathrenothiophene	246
	15	Chrycenothiophene	284
	16	Cholanthrenothiophene	296
	17	Benzopyrenothiophene	308

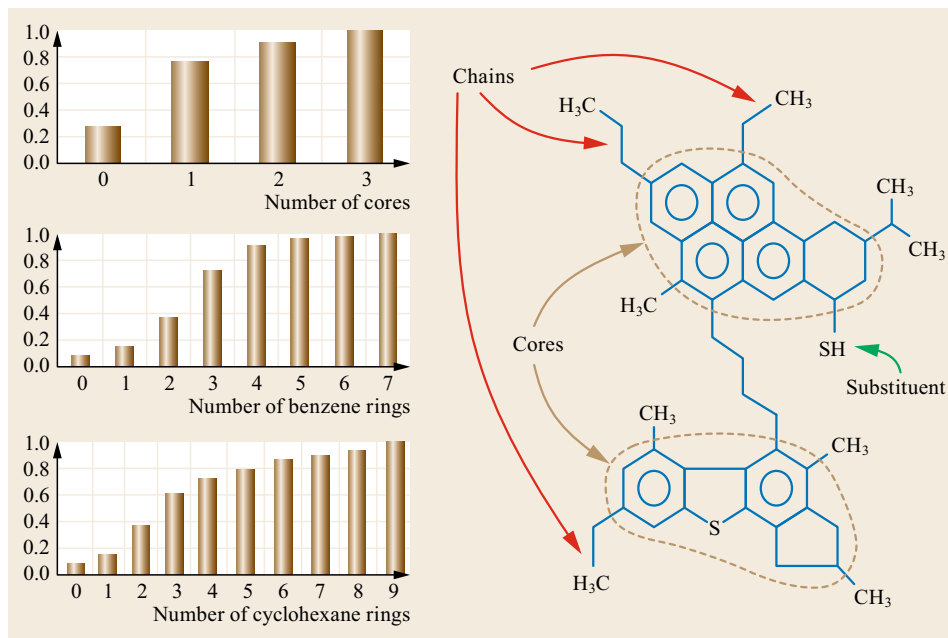


Fig. 21.9 Stochastic reconstruction to estimate S-containing species (after [21.59])

the initial stage of the HDS process, while the refractory species of very low content must be desulfurized for the deep HDS. It must be recognized that the initial and last stages of the HDS of refractory species are very different in their rates. Some processes have been developed that remove H_2S and NH_3 between stages to minimize this problem in the later stage as described above. Inhibition of H_2S for the direct HDS is very significant unless the H_2S desorption from the active site is very much accelerated. Neighboring acidity is proved to enhance H_2S desorption as described above.

Inhibition of H_2S on the hydrogenation site is not straightforward. An optimum amount of H_2S is necessary to maintain the hydrogenation site activity by keeping proper coordination of sulfur in $\text{Co}(\text{Ni})\text{MoS}$, particularly under conditions where the sulfur is replaced by other ligands such as oxygen and nitrogen. Strong acidity of the catalyst is often favorable for HDS of both mechanisms, whereas NH_3 can be an inhibitor. However, the acidity in the catalyst for the residue is lost almost immediately before the feed is cleaned up.

Other feed impurities such as N-compounds, especially heavy gas oil and LCO with high contents of N (over 500 ppm), are severe inhibitors for the HDS of both routes. N-compounds are basic or polar (acidic or neutral) to coordinate through their lone pair to the sulfur deficient site for the direct HDS and the acid site, and form strong π -bonding to hydrogenation sites and neighboring adsorption sites. The basic N-compound is a stronger inhibitor than the polar one. The nitrogen species are removed during the HDS, reducing their

concentration through concurrent HDN. The basic one is removed first due to its strong occupancy against the active sites. Hence, its inhibition is strong, but its removal takes place earlier in the initial stage. In contrast, polar nitrogen species are moderate inhibitors but, because of rather low reactivity for HDN, tend to stay in the feed and to continue the inhibition, until the refractory sulfur species remain to be desulfurized. Hence, their behaviors during HDS are very problematic for deep HDS.

The overall HDS process is much more facile when nitrogen species in the feed are removed prior to HDS. However, their removal is not practically feasible in any form even if a number of procedures have been proposed [21.61–64].

Aromatic species are also inhibitors for the HDS (hydrogenative HDS of refractory sulfur species) because aromatic species compete for the hydrogenation site with the refractory sulfur species. In theory, selective hydrogenation of sulfur species in the presence of the π -sulfur coordination. So far, such a catalyst has not been developed. Aromatic species, particularly multi-ring aromatics, are highly concentrated in some feeds such as FCC cycle oil and heavy fractions. The problem is that they survive in the last stages of HDS to inhibit the HDS of refractory sulfur species. The hydrogenation to reduce their inhibition cannot be practical in industrial processes because of the required increase of hydrogen consumption. To overcome this difficulty is not easy. Direct HDS is not so much inhibited by aro-

matic species, since σ -coordination of sulfur at the direct HDS site is much stronger than that of the aromatic species. The thermal moderation of steric hindrance of the sulfur species at higher temperature can provide another path for the solution [21.65] if the coking deactivation and excess cracking are avoided. However, this may be offset by the fact that removal of difficult sulfur requires saturation prior to hydrogenolysis, and saturation is more difficult at higher temperature.

21.3.3 HDN and HDO Reactions

The removal of nitrogen (HDN), oxygen (HDO) and metals (HDM) is also important to purify petroleum products. Such reactions progress concurrently together with HDS. Activated hydrogen can break C–X bonds over the same catalyst, although the affinity to the active site, the necessity of hydrogenation in the ring structure, and C–X bond reactivity are very different according to their individual mechanisms. In general, the ease of reactions are HDM < HDS < HDN < HDO, although the HDS and HDN of refractory sulfur and nitrogen species are comparable at the deepest levels of removal.

HDN of the nonbasic carbazoles is completed before HDS reaches the 10 ppm level. Basic nitrogen species compete for active sites with sulfur compounds. HDN of aromatic nitrogen species proceed through the initial hydrogenation of aromatic rings, because the aromatic C–N bond is too strong to be fissioned by hydrogenolysis. In contrast, the aliphatic C–N bond is easily broken. Thus, NiMoS and NiWS catalysts are often applied for HDN due to their higher hydrogenation activities. Due the required prior saturation, high hydrogen consumption is inevitable. An acidic support helps HDN on NiMoS by accelerating hydrogenation, although it also enhances the chance of deactivation due to coking on the acidic site. There is a competition between hydrogenation and acidic reactions on the same catalysts for nonheavy oil fractions.

Recently, the C–N bond cleavage was proposed by Prins et al. [21.66, 67] to be associated with H₂S in the formation of C–SH and NH₃. The C–SH bond is easily eliminated under hydrotreating conditions. They reported that 2-methylcyclo-hexylamine (MCHA) is hydrodenitrogenated through three ways:

1. Direct elimination of ammonia
2. Nucleophilic substitution of the NH₂ group by H₂S followed by removal of the SH group
3. Direct hydrogenolysis of the C–N bond.

They estimated the contribution of each pathway as shown in Fig. 21.10 [21.67]. Such a contribution of nucleophilic substitution is dependent on H₂S partial pressure. The natures of the catalysts are also impor-

tant since a variety of catalysts are now available. The involvement of aromatic C–N, especially alkylated derivatives from carbazoles, is not definite yet in such a mechanism, since it would be desired to reduce hydrogen consumption. Moreover, it should be considered by the fact that even if HDN requires more H₂ on a per-atom basis, the overall impact on H₂ consumption is relatively low.

Gas oils and LCOs from particular crudes have high nitrogen contents. Their extensive HDN is required because nitrogen species often inhibit the deep HDS. If significant amounts of nitrogen go to an FCC, it could increase NO_x emissions from the FCC regenerator if the FCC is not equipped with NO_x reduction technology.

HDO of dibenzofuran is very slow. An acidic support is helpful for the HDO of dibenzofuran species.

HDN and HDO of residue are not well studied yet. Some crudes are found to carry higher nitrogen and oxygen contents than those imagined before. Their problematic behaviors in upgrading must be overcome through extensive HDN and HDO. More research is needed. A certain amount of research on the catalytic decomposition of naphthenic acids in the petroleum products has been reported [21.68].

21.3.4 Chemistry of HDM

Removal of metals is the primary challenge for the fixed-bed hydrotreating of residue. Many commercial units are designed based on the capacity of catalysts to hold metals.

The metals in the petroleum are removed after the deposition of metal-containing molecules around or inside catalyst pores. Subsequent removal of metals from the coordinated forms in porphyrins and analogous ligands through two routes [21.57]:

1. Stepwise ring-opening of the cyclic ligand leading to the liberation of the metal ion onto the HDM catalyst.
2. Direct metal ion extraction from the complex onto the HDM catalyst.

The sulfiding of the liberated metal ion by H₂S in the surrounding atmosphere always follows the above elimination. The monomeric metal sulfides meet each other over the catalyst surface to form the bulk metal sulfide.

In commercial units, a small amount of MoS₂ or another sulfide catalyst is certainly favorable for initial HDM. But some catalysts acquire HDM activity as they remove metals removed from the feed. This could be seen as supporting route 2. Acidic sites on alumina and silica-alumina can remove metal ions from

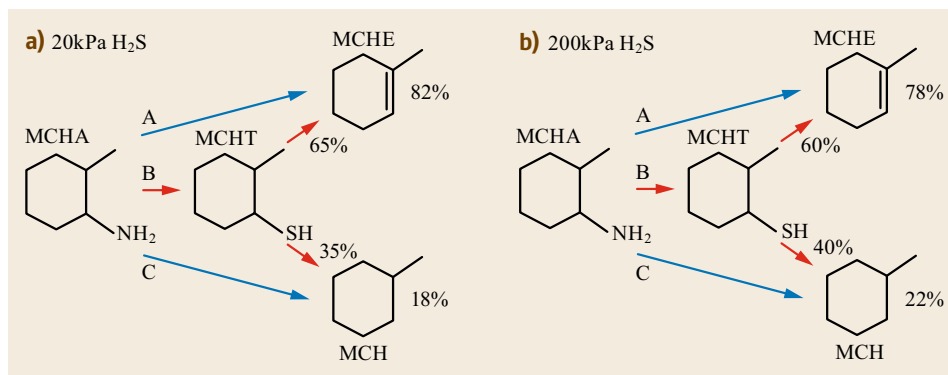


Fig. 21.10a,b Selective for elimination (A), nucleophilic substitution (B), and hydrogenolysis (C) in the HDN of 2-methylcyclohexylamine (MCHA), and the observed selectivities of methylcyclohexene (MCHE) and methylcyclohexane (MCH) in the HDN of 2-ethylcyclohexylamine and in the HDS of 2-methylcyclohexanethiol (MCHT) (20 and 200 kPa H₂S (after [21.67]))

the complex [21.21]. More acidic surfaces are more effective than alumina for the elimination. Again, there must be a balance between the relative activities of acid components for HDM and coking. Sometimes acidity is supplied by phosphorous. Liquid acid is known to be also effective for the extraction [21.69].

The role of hydrogenation is principally to suppress the coking of heavy components, which can cover the surface or plug the pore, killing the effective sites. Thus, hydrogenation activity is very important to maintain the HDM capacity of a catalyst. For this reason, process upsets involving the loss of hydrogen are particularly damaging to fixed-bed residue hydrotreating units.

Hydrogen sulfide is very essential for HDM, at least to form a metal sulfide. Desulfurization of reactive sulfur species in the feed provides sufficient H₂S for HDM. With some low-sulfur feeds, such as coal liquids, sulfur must be added to the process.

The nonporphyrin forms of metals in residue can show the different reactivity for removal, depending on the strength of coordinative bonds within the metal-containing compound [21.70]. At this moment, no direct information can be found. Other heteroatomic ligands appear to slow down HDM, as observed with the very heavy asphaltenes such as those in the Mayan crude, which contains metal ions in nonnitrogen ligands [21.71, 72].

The metal complexes are principally located in resin and asphaltene fractions [21.73]. Hence, the metal complex is believed to be bound or surrounded by polymeric constituents in the aggregate. The metal complex must contact with the HDM catalyst through the liberation from such locations in the aggregate. Thus the hydrogenation can accelerate such liberation although some metal complexes can be thermally isolated from the aggregate on the surface as observed in GC

columns as shown in the GC-AED chromatogram of Fig. 21.7 [21.21].

Acidic crudes often carry naphthenic iron, which is a concern when the acidic crude is refined [21.74–77]. Naphthenic iron easily reacts to form very fine FeS, which precipitates on the walls of the reactors, in transfer lines and in heat-exchange tubes. Hence, removal of Fe is particularly important. Naphthenic acids liberated by HDFe are also of concern because they may cause corrosion.

21.3.5 Chemistry of Ring-Opening Hydrocracking

Catalytic Access for the Selective Hydrocracking

The selective hydrocracking of light cycle oil (LCO) has attracted researchers to produce value-added (alkyl) benzenes, benzene, toluene, and xylene. The selective catalysis proposed here uses noble metals or molybdenum sulfide supported on suitable zeolites [21.78–81]. However, nonselective cracking of LCO leads to excess hydrogen consumption and excessive conversion into gaseous hydrocarbons, with coke deposition on the catalyst surface.

Extensive HDS is necessary for the noble metal catalyst. To avoid excessive hydrogen consumption, an HDS catalyst with low activity for saturating aromatics is used.

Achieving higher dispersion of supported NiMoS over the zeolite is another issue to be solved since the zeolite is a poor support, particularly when the alumina content is decreased to preserve its thermal stability. Hence, alumina is often blended as a binding component for the mixed support to disperse mainly NiMoS on its surface. In this case, NiMoS on alumina and acidic sites of zeolite must be geometrically separated.

The acidity of the catalysts in hydrocracking is very important for maximizing the yield of the desired products. This is why the catalysts are generally modified to control their acidity. Alumina has been an excellent support for CoMoS and NiMoS hydrotreating catalysts for aromatics saturation, HDS and HDN. But their acidity is not enough to promote the selective cracking of the hydrogenated aromatic ring.

The functions of the catalyst for the hydrocracking of naphthalene are as follows:

1. Selective hydrogenation of one of the aromatic rings
2. Immediate ring-opening of tetralin produced through the carbonic dealkylation mechanism
3. Selective fission of the alkyl side chain
4. A strong adsorption of aromatic rings leading to condensation (and possible coking)
5. Partial hydrogenation or hydrogenolysis of the strongly adsorbed species to avoid further condensation or coking.

The points to be considered for preparing the best support by the alumina/USY zeolite combination for the selective and active hydrocracking are:

1. Alumina is the good support for NiMoS.
2. Zeolite is expected to modify alumina through enhancing the hydrogenation activity of NiMoS on the alumina surface.
3. Acidic zeolite must not directly interact with hydrocarbon molecules, since too much hydrocracking may take place and coke formation on the zeolite quickly reduces its acidity.
4. Zeolite acidity must be modified to a moderate level for the selective cracking of hydrogenated aromatic rings.
5. Alumina is known to induce very strong acidity in amorphous or crystalline aluminasilicates.

Such catalytic functions are provided by a combination of hydrogenation and acid catalytic species. NiMo and USY zeolite can be selected as the catalyst components to achieve these functions. NiMo must be highly dispersed in the adequate crystal form. Alumina is much better support for NiMo than USY of high silica. Thus the first choice is a physical mixture of NiMo supported by Al_2O_3 and USY zeolite (NiMo/alumina-zeolite, NMAZ). Nevertheless, acidic and hydrogenation sites are separated on the different particles. The acidity of USY is not controlled by this combination, as it can expose the bare acidic sites of zeolite.

The second attempt is to coat USY with alumina and to support NiMo on the coated alumina. Acidic sites can be a part of uncoated USY or alumina modified by underlying USY through Al_2O_3 - SiO_2 contact. Thinner

coating of alumina is favorable to achieve this objective. Thus, very intimate cooperation of hydrogenation and acidic sites is expected. Acidic sites thus induced are moderated from that of the original zeolite or much enhanced from that of pure alumina. Hence optimum characteristics for the selective cracking of cyclohexyl group in tetralin can be expected.

In an earlier publication, alumina-modified USY zeolite for the hydrocracking of 1-methyl naphthalene (1-MN) as a model compound in LCO was been proposed by the present authors [21.82]. The selective hydrocracking activity of NiMoS supported on the alumina-coated USY zeolites varies with the coating amounts as illustrated in Fig. 21.11, since the thickness of alumina coating controls the balance between acidity and hydrogenation activity.

In detail, the least-alumina-coated USY zeolite (NMACZ-2) provides the highest production of alkyl benzenes among a series of the alumina-coated USY zeolites (NMACZ series). More hydrocracked alkyl benzenes were produced over NiMo supported on alumina coated with a thinner layer of zeolite, while NiMo supported on alumina coated with a thick layer of zeolite resulted in more hydrogenated products. In addition, a noncoated USY zeolite-supported NiMo catalyst (NMAZ) showed smaller yields of alkyl benzenes compared to the NMACZ-2 catalyst, which appears to be caused by the excess hydrocracking into gas hydrocarbons over the naked acid site.

Reaction Scheme: Chemistry of Selective Ring-Opening of 1-MN

Figure 21.12 summarizes the chemistry of principal and side-reactions for the selective ring-opening of 1-MN under the reaction temperature of 360°C and H_2 pressure of 6 MPa. The first step is the hydrogenation of one ring in naphthalene. According to the scheme, one-ring hydrogenation is preferred since the full hydrogenation produces many equivalent carbon-carbon bonds in the hydrogenated ring, which would be fissioned nonselectively or thermally on the acidic surface. Hydrogenation of one ring in 1-MN produces two isomers of methyl tetralin (1-methylcyclohexyl benzene; II_1 , and cyclohexyl-1-methyl benzene; I_1) in which the C-C bonds possess different reactivities. C-C bonds adjacent to the phenyl ring in the methyl-tetralin are most reactive when fissioned through the acidic dealkylation scheme, since the methyl group is located on the α -carbon of the cyclohexane ring to induce the secondary carbenium ion on the cyclohexyl ring over the acidic catalyst, as shown in Fig. 21.12. In contrast, I_1 produces a primary carbenium ion (I_2) over the same catalyst. I_2 provides C_4 alkenyl-toluene, which further reacts over the acidic catalyst to give

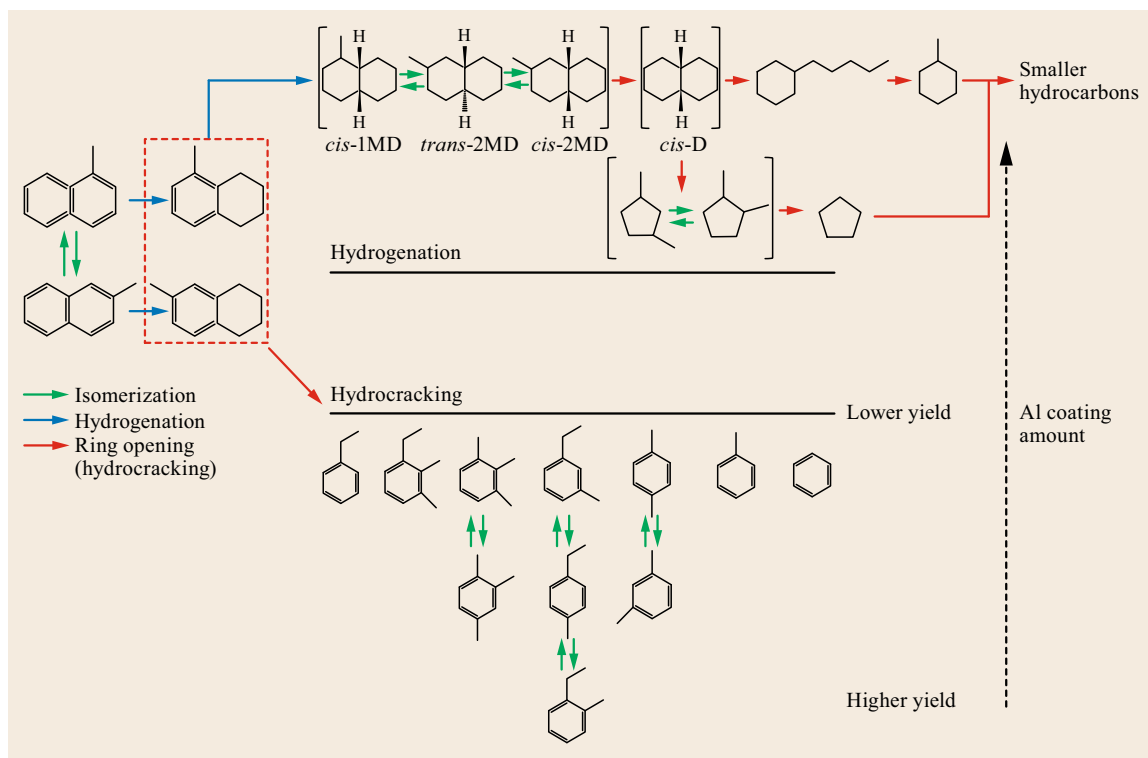


Fig. 21.11 Hydrocracking reaction pathway of 1-methyl naphthalene over the alumina coated USY zeolite (after [21.82])

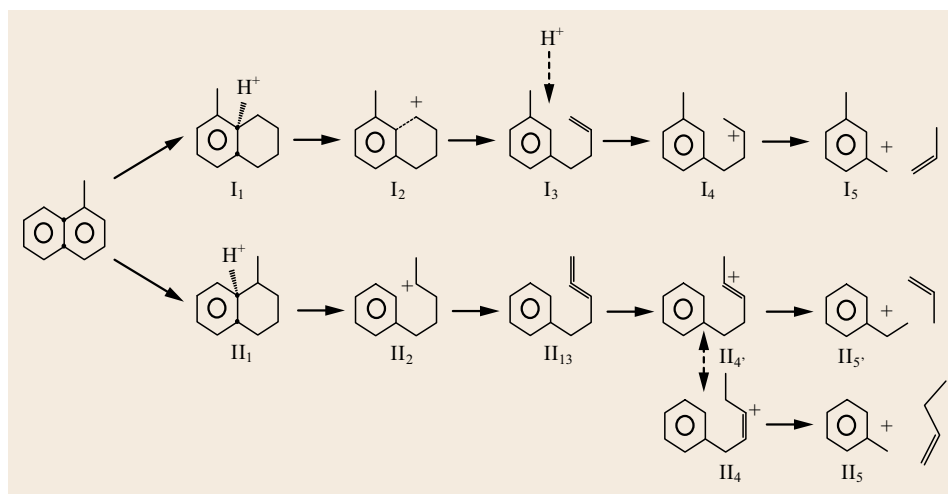


Fig. 21.12 Reaction scheme for selective hydrocracking of 1-MN through dealkylation

β -fission, giving xylene and propylene. II_2 gives C_5 alkenyl-benzene, which is successively β -fissioned into toluene (II_5) or ethylbenzene (II_5') according to the positions of the carbenium ion (II_4 and II_4') derived from II_3 .

Strong adsorption of aromatic species on the strong acidic site allows their extended stay over the catalyst, leading to condensed aromatic hydrocarbons (soft coke)

and hard coke on the acidic site. Hydrogen spillover from the NiMoS in the neighbor of acidic sites or from hydrogen donors (hydrogenated product) may partially hydrogenate the strongly adsorbed species into products that are volatile or are easier to crack further. Hydrogenation-assisted removal of coke precursor from the acidic site is important for the reduction of coke in the hydrocracking of aromatic hydrocarbon.

21.3.6 Catalyst Deactivation in Hydrotreatment of Residue

The catalyst used in the hydrotreatment is more or less deactivated during the period of use. Heavier feed tends to lead to deactivation more rapidly. The life of the catalyst for residue is usually 8–12 months, whereas it can be two to three years for the straight run gas oil from the light crude.

The residue hydrotreatment performs HDM where metal sulfide derived from the feed must accumulate on the catalyst. Hence, the life of the catalyst before the saturation is limited but it is not defined the deactivation, while the slipping of metal ions or sulfide from the HDM bed may deactivate the downstream catalysts as described later.

Carbon Deposition

Carbon deposition can be the primary cause for the deactivation of the hydrotreatment catalyst. Basic polar and high boiling compounds, typically nitrogen compounds, are the precursors for the coke through the strong adsorption by acid–base and polar–polar interactions. Some of such compounds are hydrogenated or hydrodenitrogenated over the hydrotreatment catalyst and liberated from the catalyst surface. Heavy aromatics such as asphaltenic compounds less soluble in the feed matrix are also strongly adsorbed over the polar surface of the catalyst, to be coked in a certain period of time. Thus, at the initial stage of adsorption, the adsorbed species is still a tar-like substance that can be hydrogenated and/or cracked to be soluble in the feed matrix or still soft to adhere with the similar substance on another catalyst particle. More adsorption of such organic substances may lead to covering of the catalyst surface, adhering to the catalyst particles and plugging the catalyst bed.

The coke precursors tend to be adsorbed on the polar/acidic parts of the catalyst, which are dominantly located on the support surface. Alumina, silica-alumina and zeolite commercially used as the supports for Co(Ni)MoS are more acidic in the order. In contrast, adsorbed species on the Co(Ni)MoS can be preferentially hydrogenated and not converted into heavier aromatics or final coke.

The carbon produced on the outer surface can be located near the pore mouth, plugging the pore and prohibiting the substrate from penetrating into the active site in the pore. The carbon deposited on the support can grow larger to cover the Co(Ni)S and/or reduce the

acidic properties of support, which are believed to enhance the catalytic activity of Co(Ni)MoS.

Alumina is the most common support for hydrotreatment catalysts. A less polar support is favorable for less carbon deposition from the heavy and polar commercial feed. Hence, when mechanical strength and dispersion power are sufficient, such supports have been examined, although supports other than alumina and silica-alumina are very rare in commercial catalysts. Some trials by the present authors are introduced in the later part of the review.

Metal Deposition

Typically, HDM catalysts are stacked on top of the main HDS and HDN catalysts, which are poisoned by V and Ni species. NiS is a component of NiMoS catalysts, but the NiS that slips through HDM catalysts does not provide additional activity for HDS or HDN by depositing on MoS₂ because it cannot always occupy the right location on MoS₂ or because it is accompanied by coke precursors and accelerates the coking of surrounding precursors. VS₂ is not expected to be active for hydrogenation. Hence, V and Ni deposition deactivates the HDS/HDN catalysts downstream of HDM.

Sintering of Sulfide Catalyst

The sulfide nanoparticles on the support are thermally sintered and/or degraded. The reactor must be designed carefully to prevent high temperatures during the operation, since high dispersion of the catalyst particles in a particular formulation is quite important for high activity. Hence, the reaction temperature must be strictly controlled not to exceed a certain temperature, typically 450 °C. As discussed in other chapters, the main reason for controlling temperature is to prevent loss of containment due to the rupture of piping or even the reactor. Exothermic hydrogenation/condensation reactions may cause local heating in the catalyst bed. Channeling of hydrogen and feed in the catalyst bed must be avoided to prevent local heating and heat accumulation as well as lower conversion. The way to control channeling is to use effective reactor internals and to load catalysts carefully, as described elsewhere.

Oxidation, Sulfur Deficiency or Excess Sulfiding

Sulfiding the catalyst is one of keys to obtaining optimal catalyst activity. Optimal sulfiding is obtained by controlling temperatures, heat-up rates, and the reaction atmosphere.

21.4 Deep Hydrodesulfurization of Diesel

Deep HDS of diesel fuel is currently a very important topic in refining [21.83]. Basically, deep HDS of diesel involves the extensive elimination of refractory sulfur species such as 4-methyl dibenzothiophene (4-MDBT), 4,6-DMDBT, and 4,6,X-TMDBTs. Such deep HDS is difficult because of the lower reactivities of these compounds and strong inhibition by coexisting species such as H_2S , NH_3 , nitrogen species and even aromatic species, especially when the sulfur level must be lowered to < 10 ppm. H_2S and NH_3 are derived from more reactive sulfur and nitrogen species contained in the same feed. It is always true that the fast HDS of reactive sulfur species is also important for deep HDS since the HDS active site is available for the refractory sulfur species soon after the disappearance of reactive sulfur species.

There are four approaches for achieving deep HDS:

1. Preparing catalysts in novel ways to maximize the concentration of type II sites.
2. Introduction of more active sites by impregnating more active metals on the catalyst
3. Removal or reduction of inhibitors in the process by adsorption
4. Stacking a series of catalysts in two successive layers to remove reactive sulfur species in the first layer, and to remove remaining refractory sulfur species to less than 10 ppm in the second layer under the presence of H_2S , NH_3 and other remaining inhibitors, such as nitrogen species and aromatic compounds
5. Novel catalyst designs to introduce new mechanistic pathways that are less subjective to inhibition.

Currently the first method is the major commercial approach.

In the third approach, the nitrogen species are removed prior to HDS with silica gel, silica-alumina or active carbon. The present authors suggest the high efficiency of active carbon for nitrogen species removal [21.84]. Some refractory sulfur species in the heavy oils are also removed by active carbon, which significantly helps deep hydrodesulfurization. Removal of sulfur species after hydrodesulfurization can also be used to lower the total sulfur content below 10 ppm. However, the capacity for sulfur removal is rather limited, compared to the removal of nitrogen species. In addition, loss of feed among the adsorbents in the adsorptive removal is never negligible. Removed substances must be recovered for regeneration and their utilization must be considered. Hence the application of this approach is rather restricted to the preparation of

ultraclean hydrocarbon fuels for fuel cells where very little removal is required.

The fourth approach has been proposed as a two-stage HDS process. Figure 21.13 shows the efficiency of two-stage HDS, in which the produced H_2S and NH_3 in the first stage are purged before the second stage [21.10].

The fifth approach is based on a novel way of thinking. The appropriate use of acidic supports can be a third approach since the acidity can enhance catalyst activity by methyl group migration and lowering H_2S inhibition. However, coking and NH_3 inhibition also must be reduced at the same time. As mentioned above, TiO_2 is an interesting support to produce higher activity to its supporting catalyst. A unique interaction between the sulfide and partially reduced TiO_2 is claimed for the higher activity. High surface area TiO_2 is now available [21.41]. Deeper sulfiding is proposed necessary for the higher activity, since the strong interaction between active oxides and the support is postulated preferably for better dispersion of active species, but may hinder the sufficient sulfiding. Reactive sulfide is recommended for such sulfidation.

Carbon inclusion in the active sulfide species during the sulfiding stage is claimed to give higher HDS activity. Some metals are reported to give higher HDS

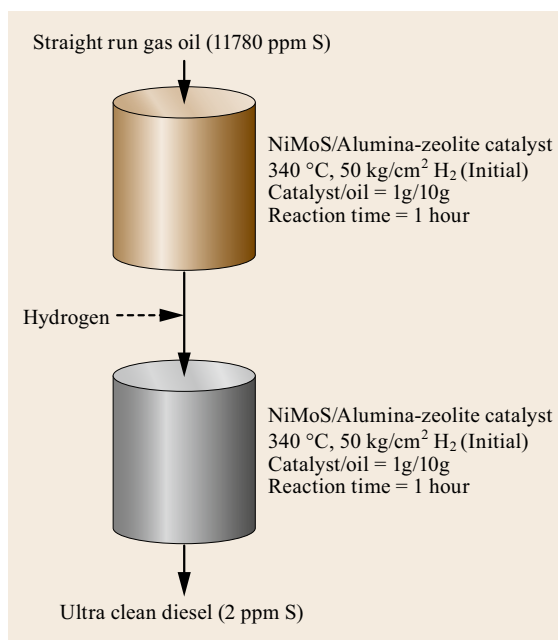


Fig. 21.13 Schematic diagram and performance of two-stage reaction concept

activity. Precise evaluation is still necessary by comparing the activity of catalysts currently lined up in the real process.

Highly aromatic feeds such as LCO and MCO appear now to require more severe conditions for deep HDS because they contain large amounts of refractory sulfur species. Catalytic species having higher affinity for sulfur than for olefins and aromatic hydrocarbons are currently targets of extensive research for achieving deep HDS of aromatic diesel. A sulfur atom can be an anchor to the soft acid site of the catalyst for the preferential hydrogenation of neighboring aromatic rings.

The present authors attempted deep HDS of aromatic-rich LCO with rather low nitrogen content by applying different supports to operate at rather high temperature [21.85]. The direct HDS of refractory sulfur species is enhanced at higher temperature, where the sulfur atom needs to approach the sulfur elimination site on the catalyst by overcoming the steric hindrance. Such direct HDS with larger activation energy is favored at higher reaction temperatures. On the other hand, the higher temperature promotes cracking and coking. Hence, high acidity is not preferred, whereas HDS activity must be enhanced by such supports. Generally, CoMo accelerates the direct HDS more selectively than NiMo and hydrogenolytic HDS

may play a minor role in the HDS of refractory sulfur species at a higher temperature [21.86].

Less polar TiO₂ and PAC (an activated carbon) supports may achieve deep HDS at 350–360 °C [21.85]. The amount of cracked products of lower boiling range was sufficiently lower on such supports under these conditions. CoMo/PAC shows the best results to achieve 12 ppm at 350 °C. The NiMo/TiO₂ catalyst was slightly better than CoMo/TiO₂, which indicates that hydrogenolytic HDS contributes to some extent even at this temperature. The higher activity of the PAC-supported catalyst can be attributed partly to its larger surface area. The chemistry of carbon surfaces and its effects on CoMoS are topics of further study. The mechanical strength of carbon supports must also be improved, perhaps by combining it with some oxide supports.

The pre-HDS of reactive species and hydrogenation of very heavy aromatic fractions before the high-temperature HDS over CoMo catalyst on nonpolar support (three stages) can be more efficient by choosing optimum catalysts and temperatures for the respective stages.

HDN, which occurs together with HDS, is hopefully much more enhanced. C–N bond breakage after adequate hydrogenation should be studied further.

21.5 Development Base of AR Hydrotreatment

21.5.1 Development of Catalyst and Reaction for AR Hydrotreatment

Petroleum companies are increasing production of heavier and more contaminated crude oils [21.87–90]. As a step toward refining these heavier crudes into low-sulfur products, some refining companies are hydrotreating atmospheric residues (ARs). These ARs often carry larger amounts of aromatics, sulfur, vanadium, and nickel, and some also are rich in nitrogen. Therefore, it is very important to understand these contaminants' reactivities, catalyst dependence, deactivation, and metal deposition profiles during hydrotreatment reactions [21.91–98].

Li et al. [21.91] suggested HD-Ni over a NiMo/ γ -Al₂O₃ catalyst by a one-pot method through the controlled precipitation of precursors using urea and ammonium carbonate as additives, and showed the influence of the urea/Al ratio on the catalytic activity for HDM. CoMo catalysts supported on the various materials (Al, Al-Ti, Al-Si, C) have been studied as heavy crude oil hydroprocessing catalysts for the early stage of deactivation by Maity et al. [21.92]. Marafi et al. [21.93, 94] reviewed spent catalyst waste manage-

ment and reported a real example through preparation of a heavy oil hydrotreating catalyst from spent residue hydroprocessing catalysts. They also reported the comparative study of the different heavy feeds over the catalyst [21.95, 96]. Interestingly, the comparative investigation on heavy oil hydroprocessing catalysts according to reactor type was studied by Rana et al. [21.97]. Long et al. [21.98] showing the mechanistic behaviors on initial decay of the HDM catalyst, which is very important to understand the phenomenon of metal adsorption on the catalyst.

A more direct comparison among reactivities of HDM and HDS of ARs from a series of crudes is informative over set of catalysts [21.99–101]. Kinetic and catalyst characterizations can further clarify their reactivity and reaction profiles. The present authors attempted to correlate the kinetic parameters of these feeds with their structural analyses.

21.5.2 Kinetic Analysis

The present authors tested catalysts in a flow reactor setup that consisted of HDM and HDS stages with two ARs from Kuwait export crude (KEC) and lower fars

(LFC) crudes [21.57]. The study aimed to accomplish the following three goals:

1. Examine the HDS performance of AR from a new and highly contaminated heavy crude oil (LFC-AR)
2. Compare the HDS and HDM reactivities of the ARs on the same catalysts in the same reactors
3. Measure the accumulation of metals on the catalysts.

A combination of commercial HDM and HDS catalysts in a series of reactors was used on the same catalyst by switching the feeds successively. The reaction temperatures were varied by 10 °C while maintaining all other conditions the same to compare the reactivities of the two ARs.

Through comparing the reactivities of these two ARs, the chemistry behind their HDS and HDM pro-

cesses can be discussed, since the metal, sulfur, and asphaltene contents are so different. Two comparisons were performed:

1. Correlations among the HDS and HDM reactions of the two ARs
2. Comparison of their kinetic parameters.

The HDS and HDM reactions were analyzed by assuming and confirming 1.0- and 1.2-order reactions, respectively, in both reactors. HDS of each AR progressed significantly in both stages with conversions reaching 47–60% in the first reactor and 80–90% in the second reactor (as shown in Figs. 21.14–21.16). Essentially, the reactive sulfur species are removed in the first reactor, and the refractory portion of sulfur species was principally removed in the second reactor. These phenomena justify the assumed 1.0-order HDS

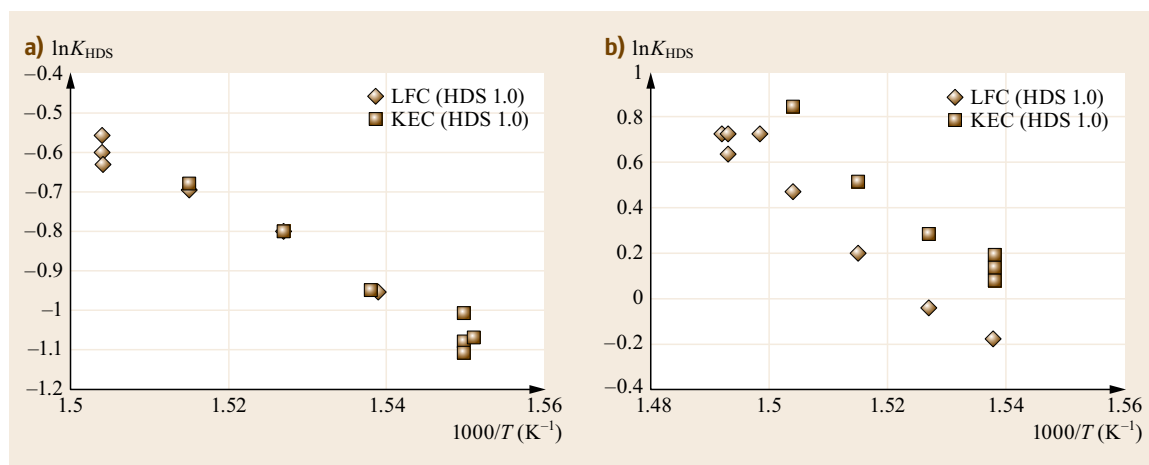


Fig. 21.14a,b Arrhenius plots of HDS rate constants of KEC- and LFC-AR in (a) first and (b) second reactors (after [21.57])

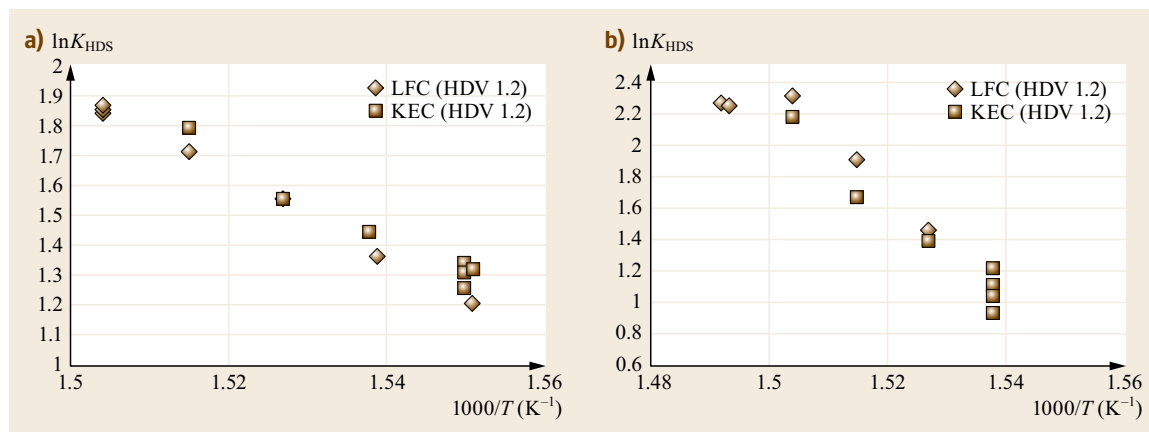


Fig. 21.15a,b Arrhenius plots of HDV rate constants of KEC- and LFC-AR in (a) first and (b) second reactors (after [21.57])

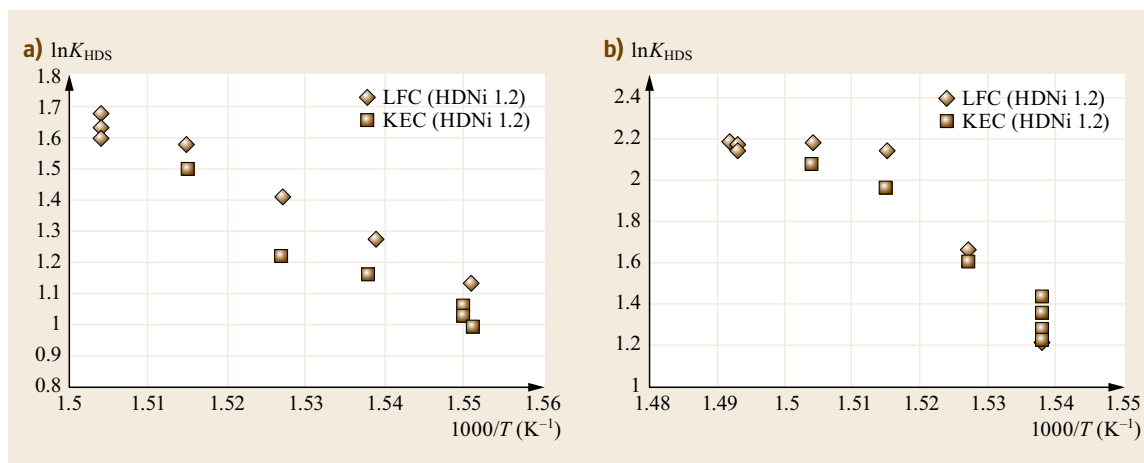


Fig. 21.16a,b Arrhenius plots of HDNi rate constants of KEC- and LFC-AR in (a) first and (b) second reactors (after [21.57])

reactions for both stages. First-order analyses of both KEC- and LFC-ARs in the first reactor provided their rate constants, which were plotted based on the Arrhenius equation; the two ARs have nearly the same rate constants at the same reaction temperatures and activation energies even though their sulfur contents were very different. The rate constants for the removal of highly reactive sulfur species of both ARs are the same despite inherent differences in the surrounding environment between the ARs. Therefore, we propose that the reaction environment of two residues does not interfere with the HDS of reactive sulfur species in the first reactor.

LFC-AR contains relatively more reactive sulfur species than KEC-AR to be desulfurized. Therefore, LFC-AR requires either longer reaction times (having the same rate constant at a given temperature) or higher temperatures than KEC-AR to achieve the same sulfur level and conversion in the first reactor.

In contrast, the rate constant of HDS for KEC-AR was certainly larger than that of LFC-AR in the second reactor. The higher reactivity of the particular sulfur species at this stage suggests that the environment of KEC-AR is less inhibitive. LFC-AR contains relatively more asphaltene, which may result in a more inhibiting environment since the refractory sulfur species in the asphaltene may be removed during this stage.

When we intend to achieve the same sulfur level at the same temperature and time, we must develop a more active catalyst via increased active sites in either the first or second stage (the latter must overcome the inhibition). Alternatively, the inhibiting environment can be overcome through the solvolysis and/or hydrogenation of inhibiting molecules and/or by liberating molecular assemblies in the asphaltene.

Rate analyses of HDV and HDNi (the removal of vanadium and/or nickel by hydrotreatment) of the ARs, giving 1.2-order reactions, provide similar rate constants and activation energies at both stages, even though the contents and environments of the ARs are very different. The rate constants of HDV and HDNi at the respective stages are also similar despite the higher activation energy and saturation of demetalization taking place at the second stage. Demetalization appears to progress very similarly regardless of the AR and metallic species, though the respective metals may have reactive and refractory species that are removed principally in the first and second reactors respectively. First-order kinetics has been often applied to HDM, but a 1.2-order reaction provided more reasonable Arrhenius plots in this study.

HDM has been proposed to progress via hydrogenation at the pyrrole rings of metal porphyrins, and hydrogenation over active HDM catalysts has been developed for enhanced HDM performance [21.57]. Another proposal has been suggested: that the hydrogenation of the resin in SARA matrix makes the asphaltene insoluble, so they simply precipitate on the catalyst. However, acidic catalysts can also remove metals from AR without any hydrogenation in H_2S and H_2 environments [21.21], which suggests direct metal extraction from the porphyrin ring and the formation of metal sulfide on the HDM catalyst. The hydrogenation may increase the contact of porphyrin rings with the surface of the catalyst through their facile liberation. Participation of such factors may take place more with feeds having higher metals. There is a higher reaction order in the metal content.

Metal porphyrins are primarily located within the asphaltenes of ARs as postulated from Yen's

group [21.16]. They can come into contact with the acidic catalyst surfaces through their liberation from the asphaltene and/or being exposed by following the deoagulation of asphaltene. Once the porphyrins are exposed during the HDM reaction, it may be easier to remove their coordinated V and Ni in the center. Given this postulation, the inability to remove the remaining refractory V and Ni species may reflect the difficulty in liberating porphyrin from the asphaltene matrix. Such species are treated in the second stage. A higher activation energy may be indicative of the bond breakage of the refractory species from the asphaltene molecules.

More V was deposited onto the catalyst than Ni, but the amounts of V and Ni are expectedly proportional to their initial content as governed by the same kinetics with similar reactivity. Previous reports have indicated a relatively high reactivity of the V species and its preferential deposition onto the surface of the HDM catalyst [21.90]. However, such overwhelming reactivity of the V species was not observed in our study. The metal content accumulated on our used catalyst was around 10%, which is much lower than that of the maximum metal capacity, and this may be one reason why preferential deposition was not observed. In order to clarify the deposition behaviors of V and Ni on the HDM catalysts, studying the used catalyst at the later stage or at the end of a long run is necessary.

This study achieved commercially required levels of HDM and HDS. However, further research of both elements may be required for commercial relevance. Refractory metals and sulfur species appear to exist in

the residue. Their studies are the target of deeper analyses and kinetics development.

The HDN process is another remaining aspect in the refining of AR. The present catalyst and conditions reached 50–60% conversion with both ARs, but the kinetics were not included in this study.

Nevertheless, we can claim the following:

1. The HDM catalyst is ineffective in its promotion of HDN.
2. HDN reactivities of KEC-AR and LFC-AR were not so different in terms of conversion (nitrogen contents of these ARs were very similar, which markedly contrasts to the differences in their sulfur and metal contents).
3. Higher temperatures are favorable for HDN.
4. There was a more apparent deactivation of the catalyst for HDN when it was compared to HDS and HDM.
5. Nitrogen elimination during both HDS and HDM reactions was not definite.

The HDS and HDM processes responsible for removing sulfur from heavy sulfur species and metals from the heavy metal porphyrins respectively progressed rather steadily, whereas HDN progressed rather slowly; this is most likely due to their limited contents (3000 ppm) as compared to those of sulfur and metals. A more active HDN catalyst must be explored to achieve deep HDN of ARs from the particular crudes with high nitrogen contents.

More study on residue HDN is expected, since some crudes are known to carry rather high nitrogen content.

21.6 Current Aims in Development of Residue Hydrotreatment

The feeds for the hydrotreatment become, in general, heavier and heavier except for shale oil. Nonconventional feeds of high metal, high sulfur, high nitrogen and even high oxygen contents must be also hydrotreated effectively and efficiently. On the other hand, environmental regulations become more stringent.

Higher activity and longer continuous operation of the catalytic reaction are always pursued. First of all, the continuous long operation requires the large capacity of metal removal. At the initial stage in the HDM process, carbon deposits must be minimized because carbon deposits may hinder HDM and restrict the metal capacity. Large capacities of the HDM catalyst for metal deposition or on-stream catalyst replacement processes are being pursued [21.102]. Deeper HDM is also expected to extend the life of HDS catalysts through less metal deposition downstream of HDM.

High activity for HDS and optimum hydrocracking are obtained commonly by high dispersion of Ni(Co)MoS on the catalyst supports. Acidic supports tend to be deactivated by rapid carbon deposition. The high catalyst dispersion is often canceled by sintering. Hence, particular catalyst materials for higher dispersion, and additives to stabilize the dispersion, are the aims of research and development in our laboratories. The selection and structural control of the support are another basic approach for better performance of the catalyst. The better materials and their better form are always looked for to achieve higher performance.

HDN and HDO become indispensable in hydrotreatment of some unique feeds.

Hydrogenation catalysts of particular performance can be a target of development for the pretreatment of particular feeds, since carbon deposition from the heavy

fraction is a large issue in the resid hydrotreatment in terms of catalyst life, aggregation of catalyst particles, plugging and fouling for pressure drop, as well as reduced yields of the light products.

Thus, better catalysts for respective objectives, and their combination in optimum amounts in the process scheme, are current aims and approaches for residue hydrotreatment.

21.7 Role and Design of Catalyst Support for Residual HDM

Concentrations of vanadium and nickel tend to be higher in heavier crudes and crude oil fractions. Unless they are removed, they may deposit on the catalysts in upgrading processes. The slipping of metals from HDM catalyst layers or beds may deactivate HDS/HDN and RFCC catalysts through deposition. They can also induce unwanted reactions, especially coking. Thus HDM can define the life of refining processes while increasing the ability of refineries to process low-cost heavy crudes.

Slippage of metals through HDM catalysts is an important phenomenon. Slippage is determined by both the capacity and completeness of metal removal at the HDM step. The removed metals on spent HDM catalysts are high-quality Ni and V ores, because they contain more Ni and V than conventional ores.

The HDM catalyst performs multiple roles: hydrogenation, metal ion extraction, HDS and accumulation of metals. Nevertheless, work is underway to reduce the amount of molybdenum on the support of alumina, both to reduce costs and provide more room for metal adsorption.

Another aim is to control the pore size of the support, which must be large enough to allow the easy access of large asphaltene molecules and metal complexes; nonasphaltic complexes are believed to behave together with the asphaltene heavy molecules. Particularly, the pore mouth must have large diameter, otherwise the coking at the mouth can plug the whole pore, reducing the capacity of the catalyst to contact with the metallic substrates.

Such approaches can be reexamined and revised from more flexible views based on the current research results.

The roles of hydrogenation have been accepted as follows:

1. Hydrogenation of ligand ring to be opened
2. Extraction of metal ion over the hydrogenation site
3. Generation of H₂S
4. Partial hydrogenation of the aggregated asphaltenes, which mobilizes metals for their better access to the pores and reduces their coking reactivity.

The current results indicate two mechanisms for the metal extractions:

1. Extraction of metal ion from the porphyrin ring on the polar catalytic surface by the aid of H₂S
2. Breakage of N–metal bonds in the porphyrin ring through the hydrogenation of ligand rings to facilitate the metal ion extraction.

Unpromoted supports, polar solvents and acids extract significant amounts of metal ions from isolated porphyrin complexes [21.103]. The hydrogenation of ligand rings has been proved with model porphyrins; however, ligand saturation has never been proposed as an exclusive mechanism.

Some industrial research has shown that H₂S inhibits HDM, but H₂S is certainly essential, at least to stabilize metal sulfides on the HDM catalyst. The various roles of H₂S are not fully elucidated. The mobility of metal ions or single sulfides from the metal extraction site to the other parts of the catalyst surface, like an open the extraction site, can make room for metal complexes coming in with fresh feed. This would increase the holding capacity of the HDM catalyst. H₂S is certainly produced from the reactive sulfur species in the HDM bed. H₂S is allowed to accumulate in the process recycle gas. Its concentration is controlled by bleeding recycle gas from the high-pressure loop to the refinery sulfur collection and recovery system.

Asphaltene deaggregation and/or dissolution is important to increase the capacity and completeness of metal removal, since the coking on the catalyst may take place in the pore mouth, preventing access to the rest of the pore. Metal porphyrins in the coke cannot be extracted from the catalyst surface.

Nitrogen species can be strongly adsorbed on the surface of the support. Hydrogenation of asphaltenes on the catalyst surface in the neighborhood of the hydrogenation site is very favorable and essential for optimum HDM capacity, through inhibiting the coke formation from the asphaltene.

Some metal porphyrins have recently been proved by GC and MS to be liberated into the gas phase from VR, as described above. Such metal porphyrins can

contact with HDM catalysts without extensive modification of the asphaltene aggregate and polymeric structure. Thermal or dissolving liberation of metal complexes can occur during HDM reactions. The acceleration of such liberation is worthwhile for further study.

The metals in the porphyrin complexes in AR have been extracted to a considerable extent on alumina and silica-alumina surfaces [21.21]. The acidic support appears more active for metal extraction than the nonacidic one. Then, the metal complexes tend to liberate metal ions according to their coordination strength to the support. The support can thus eliminate the metal ions according to its extraction activity.

The reactivity of metal complexes and the activity of the support surface interact to control the demetalation site on the solid catalyst surface. In an optimal situation, reactive metal can start by depositing at the bottom of the pore and then fill the pore completely. This can be achieved to a certain extent by layering.

In a multilayered HDM catalyst loading scheme, layering particles can be designed by arranging the weaker site on the surface and the stronger site at the bottom of the pore. Hydrogenation and some HDS are needed before HDM. The HDS before HDM is required to produce H_2S and segregate the asphaltene where easy HDM is not expected. The hydrogenation before HDM is to suppress the coking on the HDM catalyst, particularly polar metal elimination site. Thus, two layers for the first hydrogenation slight HDS and second HDM catalysts can be designed respectively. Such a catalyst concept can be applicable for both fixed and moving beds by taking the characteristics of such reactor design and performance into the consideration. The issues of moving beds are described in the next section.

So far, the reactivity of nonporphyrin metal complexes is not elucidated yet, although they appear less reactive than porphyrins. Analysis for the behavior of nonporphyrin complexes is strongly needed for understanding the upgrading of very heavy crudes [21.104].

21.8 Novel Hydrotreatment Processes for Residue Upgrading

Fixed-bed hydrotreatment process for atmospheric residue are widely used. Typically, these units look like fixed-bed gas oil or VGO hydrotreaters with two or more fixed beds of HDM, HDM/HDS/HDN and HDS catalysts to achieve targets for product metals, sulfur, nitrogen, asphaltenes and CCR. Catalyst cycles can last for 6–12 months, depending on the feedstock and process configuration. For better economics, refiners always want longer continuous operation with heavier residue containing more metal, more S- and N-species, and asphaltenes or CCR. As described previously in this chapter, each type of catalyst continues to be extensively studied to improve its performance. The major approach is to design the pore structure of the alumina support. Support materials other than alumina have also been explored. Nevertheless, alumina with well-designed shape and pore structure is most used for the practical catalyst described above.

Larger metal capacity for HDM and higher but stable activity for HDS are the keys to a longer effective operation. The intrinsic performances and smaller inhibition/deactivation of performances are both important for better catalysts. The major causes of inhibition/deactivation of HDS and HDN catalysts are leakage of metals from the HDM catalyst and deposition of carbonaceous materials. Hence, less appearance of carbon deposits and less slip of metals must be considered to improve the performance of these catalysts.

The life of HDM catalysts is first defined by metal holding capacity. In order to operate continuously within the limits of metal holding capacity, Chevron developed the OCR process, where OCR means on-stream catalyst replacement [21.102]. As illustrated in Fig. 21.17, the fresh catalysts are charged at the top of the OCR reactors and used catalysts are discharged at the bottom of the OCR reactors. The feed is charged at the bottom of the reactor and flows upward, fluidizing the catalyst. The aged catalyst, which has removed most of the metals from the feed, reaches the top of the conical screen, then slides down outside the screen to the bottom, where the metal-rich catalyst is discharged. The demetalized feed is hydrotreated and to some extent cracked. Contact time and sufficient modification of the adsorbed feed are important for the catalyst to stay dried in the charged feed. Otherwise, the catalyst particles to be discharged carry soft as well as hard carbon and adhere to each other before arriving at the cone bottom for discharge. Problems of plugging and sticking at the bottom have been reported to be important for a stable operation for a long time. The catalyst surface, catalyst transportation in the reactor and feed adjustment can be designed to avoid the adhesion. How to eliminate the adhesive nature of the soft carbon among the adsorbed fractions on the catalyst before encountering similar catalyst particles can be a key for smooth discharge. Solvents, such as FCC cycle oil, can be added

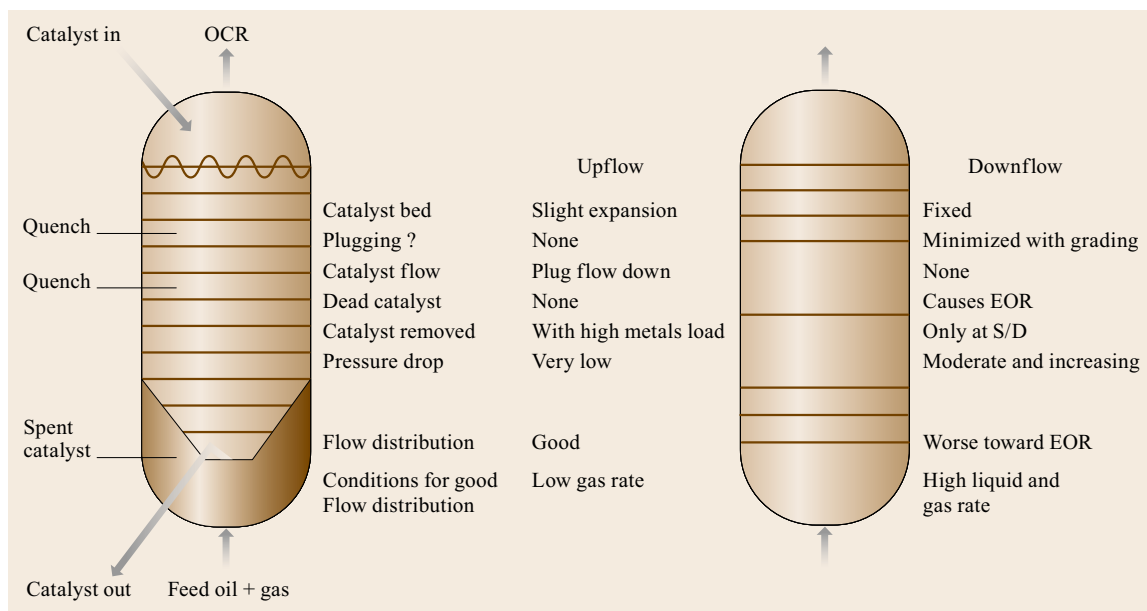


Fig. 21.17 Upflow versus downflow reaction

to this region to extract the adhesive fraction from the spent catalyst particles.

Higher hydrogenation and cracking activity of the outer layers of the catalyst can solve its adhesion issue. The separation of aged catalysts into fully deactivated and still-alive portions is another interesting topic to be studied.

A process based on p-flow reactors has been proposed by Chevron and recently commercialized by SINOPEC. Details have not been disclosed. Upflow can solve the plugging and adhesion problems seen with OCR and utilize more uniformly the HDM catalyst. Continuous charge and discharge are not clearly described in the published documents. Uniform contact of the feed with the differently aged catalyst particles in the reactor may not be favorable for deeper removal of the metal in the feed. Uniform fluidization requires the larger volumes of reactor and upflow hydrogen.

Slurry phase resid hydrocracking, such as the VCC process licensed jointly by KBR and BP, along with processes offered by ENI and UOP, can achieve < 95 wt% conversion of vacuum residue into diesel and lighter fractions. The VCC process can be used to upgrade coal. Four VCC units have been licensed. Two were completed in China (or will be as of March 2015) and another is under construction in Russia. In the VCC slurry-phase hydrocracking process, coal or VR is mixed with an additive or catalyst and hydrogen and bubbled upwards through the reactors, where they are thermally cracked. Slurry-phase hydrocracking is discussed in another chapter. The VCC process employs a noncatalytic

additive. The VCC process is based on coal liquefaction processes developed in the early 20th century [21.105]. ENI [21.106] announced its commercial process using a micro-MoS₂ catalyst. Excellent performances are reported. UOP applies a fine iron catalyst for its uniflex process [21.107]. In the VCC process, a noncatalytic additive is used. Recovery of additives or catalysts and the destination of removed metals may present problems in some locales, but as with fixed-bed residue hydrotreating, the pitch from these processes can be a high grade ore for Ni, V, and other metals.

Supercritical water at very high pressure and temperature is also applied in the treatment of the residue [21.108]. The erosion and corrosion of the reactor wall and let-down valves by the supercritical water that carries fine polar solids, dissolved CO₂ and salts, as well as the destination of removed metals, are the main concerns in this process.

We have proposed multistage catalyst beds as the process and design concept of each catalyst in the successive beds. The beds consist of:

1. Hydrogenative treatment without HDM with slight HDS to moderate coking properties of the heavy feed.
2. The catalyst of low activity for HDM to remove the reactive metals at the deeper site in its pore while HDM of refractory metals takes place anyway in the deeper pore. Such a design is expected to allow the homogeneous deposition of the metal through the whole pore wall.

3. The catalyst with high activity of HDM for deep and complete removal of the metals in the feed.
4. More active sulfides loading, larger surface area and selected supports can be still possible approaches as described above.

21.9 Challenges in Hydrotreatment

The foremost challenges for progressing hydrotreatment processes are the molecular characterization of feeds up to asphaltenes. Thus, the reaction mechanisms/schemes in every step of hydrotreatment process and catalyst designs best fitted to the feeds, intermediates and products can then be elucidated on a molecular basis. The advances in effective characterization of solid catalysts, spent and fresh, is another challenge.

Process improvements such as combining HDS with adsorption and staged configurations to accomplish the deep HDS of very difficult gas oils are issued with great importance. In addition, process and catalyst flexibility should be significantly considered. Depending on circumstances, refiners process different feeds at different severities. A catalyst that can achieve both high HDS and high HDM can provide such flexibility, even though it may not be optimal for a single type of operation.

In the case of biofeeds, traditional MoS₂-based catalysts may not be best for them, as they carry low sulfur content. Hence, nonsulfur-containing catalysts for such applications have been studied and developed.

Brainstorming ideas to improve catalyst activation procedures are also issued. Wet sulfidation preserving the activity of type II catalysts (Akzo) showed the nearly double activities compared to commercial HDS and HDN catalysts.

21.9.1 Analysis of Heavy Feedstocks

As described above, all molecules in the petroleum fractions can be analyzed by modern MS at least at the level of chemical formulae of desorbed and ionized species [21.109]. Careful MS/MS analysis of the respective MS peak can provide structural information based on the fragmentation pattern. However, MS coupling with GC would be necessary for the determination of isomers in feed, intermediates and product for the reaction mechanism studies and the effectiveness of catalyst and process conditions in hydrotreatment. However, this GC-MS technique is limited to fractions up to gas oils.

For deep HDS and other hydrotreatment beyond gas oils, such as resid refining, the use and development of liquid chromatography or effective class fractionation

schemes would benefit the studies of refractory species and the effectiveness of catalyst systems. On the other hand, ultrahigh resolution mass spectrometry, such as FT-ICR, orbitrap and multipath TOF, can provide compound type and carbon number distributions, but not information on isomeric structures.

However, the identification of the matrix molecules is necessary to clarify their inhibiting roles. The molecules adsorbed on the catalysts can be extracted for the analysis to find their roles in the reaction mechanisms and inhibiting schemes.

21.9.2 Coking

The coking of catalysts should be also studied, even if the coke in various forms and the substrates just before coke formation may be difficult to extract and analyze. The identification of locations of adsorbed species and the coke on the catalyst could lead to the design of better supports and placement of the catalytic species on the support.

Another challenge is to identify remaining species, intermediates and product molecules. Clarification of competing and inhibiting species may overcome the problems and solve difficulties in the hydrotreatment of particular feeds. The identification of reaction steps and schemes can be thus better understood on a molecular basis.

21.9.3 Polymerization and Aggregation of Feeds

The remaining issues in residue hydrotreatment involve the analysis of particular substrates found in the polymeric and the aggregate structures. The presence of a polymeric structure indicates that the reactive part of the substrate must approach the active site on the solid catalyst and overcome the inhibition by the other part of the same polymeric chain. The polymeric structure must fit the pore in its size and avoid unwanted side reactions before the molecule arrives on the active site in the pore.

The first point is the diffusivity of the substrate to active sites in the pore. The size and wall chemistry of the pore, as well as the size and all functional groups on the polymer substrates, must be considered. The cok-

ing of the polymeric chains is the largest issue in their catalytic reaction over a solid catalyst.

The aggregate structure of the heavy fraction in petroleum is now being studied extensively. Its behaviors under hydrotreating conditions are to be clarified. The effects of temperature and surrounding solvent-like fractions on the dissolution of the aggregate structure may be the remaining question. The solvent fractions can be present in the original feed, produced through the hydrotreatment, or added or induced from the added solvent. The solvent fraction, thus, can be the key to controlling the hydrotreatment of the heavy fraction in the aggregate dissolution, polymeric diffusivity and the structural modification of reactive unit. The minor amount of the target or problematic molecules must also be of concern in the aggregate.

The aggregate structure includes a variety of non-covalent bonding among the constituents. Some of bonding may be quite weak to release molecules or units rather easily from the aggregate and even polymeric structure. The authors believe some porphyrins in the asphaltene to behave so. It is quite important to design the HDM by taking account of such behaviors as described above.

21.9.4 Catalyst and Additive Improvements

The hydrotreating catalysts in the respective catalytic steps are now optimized and/or designed to enhance the wanted reaction, selectively reduce the difficulties of the wanted reaction with the particular feed and moderate the unwanted reaction.

So far, with one exception, catalysts for fixed-bed hydrotreating are limited to Mo and W sulfides promoted by Ni and/or Co sulfides. The exception is NEBULA, which uses a base metal support instead of alumina. Iron sulfide of lower price may play a role, particularly in the moving bed. There is still active research

on the use of nonalumina supports. For all supports, the uses of different materials, pore sizes, and their combination continue to be investigated. The multilayered concept of designing a catalyst particle consisting of an outer surface, mouth, intermediate wall and bottom of the pore may hold promise. It must have the right size and right materials for the intended functions in order to provide optimum activity for treating the coming feed components.

For HDM and HDS catalysts designed for the heavier feeds, the surface coking issue remains important for efficiency and long life without losing the catalyst performance. For HDM, it is also important to improve utilization of pore volume and decrease slippage of metals. The goal is to achieve complete removal of the metal before the feed leaves the HDM catalyst layer.

HDS catalysts for heavy fractions must be able to overcome the difficulty coming from the aggregate, polymeric, multihindered and multi-inhibiting substrates. At this moment, refractory sulfur units in the polymeric chains are not well defined. However, we have well-defined refractory sulfur species in the distillates. We can thus apply the principles of effective and deep HDS from the distillate by taking account of aggregate and polymeric difficulty with the residue.

Finally the authors claim the multibeds carrying a series of respective optimum catalysts with respective unique functions are strongly expected to realize the deep refining.

Acknowledgments. We would like to thank the Japan Cooperation Center, Petroleum (JCCP) for funding our research project on the refining of Kuwait Crudes through the support of Japan Ministry of Economy, Trade and Industry (METI), through which this chapter has been prepared. The authors would like to express gratitude to Dr. M. Marafi, ED/PRC at the Petroleum Research Center for her continued managerial support.

References

- | | | | |
|------|---|------|--|
| 21.1 | H. Topsøe, B.S. Clausen, F.E. Massoth: <i>Hydrotreating Catalysis</i> (Springer, Berlin 1996) | 21.5 | M. Breyse, G. Djega-Maridassou, S. Pressayre, C. Geantet, M. Vrinat, G. Pérot, M. Lemaire: Deep desulfurization: Reactions, catalysts and technological challenges, <i>Catal. Today</i> 84 , 129–138 (2003) |
| 21.2 | D.D. Whitehurst, T. Isoda, I. Mochida: Present state of the art and future challenges in the hydrodesulfurization of polyaromatic sulfur compounds, <i>Adv. Catal.</i> 42 , 345 (1998) | 21.6 | I. Mochida, K.H. Choi: <i>Practical Advanced in Petroleum Processing</i> (Springer, New York 2006) |
| 21.3 | C. Song: An overview of new approaches to deep desulfurization for ultra-clean gasoline, diesel fuel and jet fuel, <i>Catal. Today</i> 86 , 211–263 (2003) | 21.7 | Criterion Catalysts and Technologies: ASCENT DC-2534: Performance that delivers great value for your investment, http://www.criterioncatalysts.com/content/dam/shell/static/criterion/downloads/pdf/ascent-dc-2534-brochure.pdf |
| 21.4 | I.V. Babich, J.A. Moulijn: Science and technology of novel processes for deep desulfurization of oil refinery streams: A review, <i>Fuel</i> 82 , 607–631 (2003) | | |

- 21.8 H. Topsøe, R.G. Egeberg, K.G. Knudsen: Future challenges of hydrotreating catalyst technology, *Prepr. Pap.-Am. Chem. Soc., Div. Fuel Chem.* **49**(2), 569–560 (2004)
- 21.9 T. Kim, S.A. Ali, K. Alhooshani, M. Al-Yami, J.I. Park, S.H. Yoon, I. Mochida: Analysis and deep hydrodesulfurization reactivity of Saudi Arabian gas oils, *J. Ind. Eng. Chem.* **19**, 1577–1582 (2013)
- 21.10 B. Chawla: Selective detection of sulfur and nitrogen compounds in low boiling petroleum streams by GC chromatography. In: *Analytical Advances for Hydrocarbon Research*, ed. by C.S. Hsu (Kluwer/Plenum, New York 2003)
- 21.11 C.F. Klitzke, Y.E. Corilo, K. Siek, J. Binkley, J. Patrick, M.N. Eberlin: Petroleomics by ultra-high-resolution time-of-flight mass spectrometry, *Energ. Fuels* **26**, 5787–5794 (2012)
- 21.12 J.-M. Schweitzer, C. López-García, D. Ferré: Thermal runaway analysis of a three-phase reactor for LCO hydrotreatment, *Chem. Eng. Sci.* **65**, 313–321 (2010)
- 21.13 L. Boursier, V. Souchon, C. Dartiguelongue, J. Ponthus, M. Courtiade, D. Thiébaud: Complete elution of vacuum gas oil resins by comprehensive high-temperature two-dimensional gas chromatography, *J. Chromatogr. A* **1280**, 98–103 (2013)
- 21.14 A.N. Verentchikov, M.I. Yavor, Y.I. Hasin, M.A. Gavrik: Multireflection planar time-of-flight mass analyzer. I: An analyzer for a parallel tandem spectrometer, *Tech. Phys.* **50**, 73–81 (2005)
- 21.15 A.N. Verentchikov, M.I. Yavor, Y.I. Hasin, M.A. Gavrik: Multireflection planar time-of-flight mass analyzer. II: The high-resolution mode, *Tech. Phys.* **50**, 82–86 (2005)
- 21.16 J.P. Dickie, T.F. Yen: Macrostructures of the asphaltic fractions by various instrumental methods, *Anal. Chem.* **39**, 1847–1852 (1967)
- 21.17 O.C. Mullins: The modified Yen model, *Energ. Fuels* **24**, 2179–2207 (2010)
- 21.18 G.C. Klein, S. Kim, R.P. Rodgers, A.G. Marshall: Mass spectral analysis of asphaltenes. I. compositional differences between pressure-drop and solvent-drop asphaltenes determined by electrospray ionization Fourier transform ion cyclotron resonance mass spectrometry, *Energ. Fuels* **20**, 1965–1972 (2006)
- 21.19 Q. Shi, D. Hou, K.H. Chung, C. Xu, S. Zhao, Y. Zhang: Characterization of heteroatom compounds in a crude oil and its saturates aromatics, resins, and asphaltenes (SARA) and non-basic nitrogen fractions analyzed by negative-ion electrospray ionization Fourier transform ion cyclotron resonance mass spectrometry, *Energ. Fuels* **24**, 2545–2553 (2010)
- 21.20 E. Furimsky: Chapter 2: Properties of heavy feeds. In: *Catalysts for Upgrading Heavy Petroleum Feeds*, Studies in Surface Science and Catalysis, Vol. 169, ed. by E. Furimsky (Elsevier, Amsterdam 2007) pp. 5–22
- 21.21 T. Kim, J. Ryu, M.J. Kim, H.J. Kim, Y.G. Shul, Y. Jeon, J.I. Park: Characterization and analysis of vanadium and nickel species in atmospheric residues, *Fuel* **117**(A), 783–791 (2014)
- 21.22 M. Zeinali, M. Jamal: Biocatalytic activity of methyl-modified microperoxidase-11 in transformation of nickel- and vanadium-porphyrins, *J. Mol. Catal. B* **79**, 21–26 (2012)
- 21.23 P.C.H. Mitchell, C.E. Scott: Interaction of vanadium and nickel porphyrins with catalysts, relevance to catalytic demetallization, *Catal. Today* **7**(4), 467–477 (1990)
- 21.24 P.I. Premović, I.R. Tonsa, M.T. Pajović, L. Lopez, S.L. Monaco, D.M. Đorđević, M.S. Pavlović: Electron spin resonance study of the kerogen/asphaltene vanadyl porphyrins: Air oxidation, *Fuel* **80**, 635–639 (2001)
- 21.25 J. Ellis, C. Rechsteiner, M. Moir, S. Wilbur: Determination of volatile nickel and vanadium species in crude oil and crude oil fractions by gas chromatography coupled to inductively coupled plasma mass spectrometry, *J. Anal. At. Spectrom.* **26**, 1674–1678 (2011)
- 21.26 A.M. McKenna, J.T. Williams, J.C. Putman, C. Aeppli, C.M. Reddy, D.L. Valentine, K.L. Lemkau, M.Y. Kellermann, J.J. Savory, N.K. Kaiser, A.G. Marshall, R.P. Rodgers: Unprecedented ultrahigh resolution FT-ICR mass spectrometry and parts-per-billion mass accuracy enable direct characterization of nickel vanadyl porphyrins in petroleum from natural seeps, *Energ. Fuels* **28**, 2454–2464 (2014)
- 21.27 X. Zhao, Y. Liu, C. Xu, Y. Yan, Y. Zhang, Q. Zhang, S. Zhao, K. Chung, M.R. Gray, Q. Shi: Separation and characterization of vanadyl porphyrins in Venezuela Orinoco heavy crude oil, *Energ. Fuels* **27**, 2874–2882 (2013)
- 21.28 E. Furimsky: Catalytic hydrodeoxygenation, *Appl. Catal. A* **199**, 147–190 (2000)
- 21.29 O. Yépez: Influence of different sulfur compounds on corrosion due to naphthenic acid, *Fuel* **84**, 97–104 (2005)
- 21.30 S.D. Sumbogo Murti, K. Sakanishi, O. Okuma, Y. Korai, I. Mochida: Detail characterization of heteroatom-containing molecules in light distillates derived from Tanito harum coal and its hydrotreated oil, *Fuel* **81**, 2241–2248 (2002)
- 21.31 F.E. Massoth, S.C. Kim: Polymer formation during the HDN of indole, *Catal. Lett.* **57**, 129–134 (1999)
- 21.32 T.G. Kaufmann, A. Kaldor, G.F. Stuntz, M.C. Kerby, L.L. Ansell: Catalysis science and technology for cleaner transportation fuels, *Catal. Today* **62**, 77–90 (2000)
- 21.33 J. Wei, L.L. Hegedus: *Catalyst Design – Progress and Perspective* (Wiley, New York 1987)
- 21.34 I. Isoda, S. Nagao, X. Ma, Y. Korai, I. Mochida: Hydrodesulfurization pathway of 4,6-dimethyldibenzothiophene through isomerization over Y-zeolite containing CoMo/Al₂O₃ catalyst, *Energ. Fuels* **10**, 1078–1082 (1996)
- 21.35 J. Ramírez, R. Contreras, P. Castillo, T. Klimova, R. Zárate, R. Luna: Characterization and catalytic activity of CoMo HDS catalysts supported on alumina-MCM-41, *Appl. Catal. A* **197**, 69–78 (2000)

- 21.36 P. Michaud, J.L. Lemberton, G. Pérot: Hydrodesulfurization of dibenzothiophene and 4,6-dimethyldibenzothiophene: Effect of an acid component on the activity of a sulfide NiMo on alumina catalyst, *Appl. Catal. A* **169**, 343–353 (1998)
- 21.37 M.S. Rana, S.K. Maity, J. Ancheyta, J. Murali Dhar, T.S.R. Prasada Rao: TiO₂-SiO₂ supported hydrotreating catalysts: Physico-chemical characterization and activities, *Appl. Catal. A* **253**, 165–176 (2003)
- 21.38 E. Lecrenay, K. Sakanishi, I. Mochida, T. Suzuka: Hydrodesulfurization activity of CoMo and NiMo catalysts supported on some acidic binary oxides, *Appl. Catal. A* **175**, 237–243 (1998)
- 21.39 P.R. Robinson, H.D. Simpson: Ni-P-Mo catalyst and hydroprocessing use thereof, US Patent (Application) 4738944 (1988)
- 21.40 T.I. Koranyi: Phosphorus promotion of Ni(Co)-containing Mo-free catalysts in thiophene hydrodesulfurization, *Appl. Catal. A* **239**, 253–267 (2003)
- 21.41 S. Dzwigaj, C. Louis, M. Breyse, M. Cattenot, V. Bellière, C. Geantet, M. Vrinat, P. Blanchard, E. Payen, S. Inoue, H. Kudo, Y. Yoshimura: New generation of titanium dioxide support for hydrodesulfurization, *Appl. Catal. B* **41**, 181–191 (2003)
- 21.42 E. Lecrenay, K. Sakanishi, T. Nagamatsu, I. Mochida, T. Suzuka: Hydrodesulfurization activity of CoMo and NiMo supported on Al₂O₃-TiO₂ for some model compounds and gas oils, *Appl. Catal. B* **18**, 325–330 (1998)
- 21.43 E.Y. Kaneko, S.H. Pulcinelli, V.T. Silva, C.V. Santilli: Sol-gel synthesis of titania-alumina catalyst supports, *Appl. Catal. A* **235**, 71–78 (2002)
- 21.44 C. Pahal, F. Kameda, K. Hoshino, S. Yoshinaka, K. Segawa: Hydrodesulfurization of dibenzothiophene derivatives over TiO₂-Al₂O₃ supported sulfide molybdenum catalyst, *Catal. Today* **39**, 21–32 (1997)
- 21.45 J. Ramirez, L. Cedenio, G. Busca: The role of titania support in Mo-based hydrodesulfurization catalysts, *J. Catal.* **184**, 59–67 (1999)
- 21.46 T.M. Mata, R.L. Smith, D.M. Young, C.A. Costa: Life cycle assessment of gasoline blending options, *Environ. Sci. Technol.* **37**, 3724–3732 (2003)
- 21.47 H. Farag, D.D. Whitehurst, K. Sakanishi, I. Mochida: Carbon versus alumina as a support for Co-Mo catalysts reactivity towards HDS of dibenzothiophenes and diesel fuel, *Catal. Today* **50**, 9–17 (1999)
- 21.48 E. Auer, A. Freund, J. Pietsch, T. Tacke: Carbons as supports for industrial precious metal catalysts, *Appl. Catal. A* **173**, 259–271 (1998)
- 21.49 D.D. Whitehurst, H. Farag, T. Nagamatsu, K. Sakanishi, I. Mochida: Assessment of limitation and potentials for improvement in deep desulfurization through detailed kinetic analysis of mechanistic pathways, *Catal. Today* **45**, 299–305 (1998)
- 21.50 E. Furimsky, F.E. Massoth: Deactivation of hydroprocessing catalysts, *Catal. Today* **52**, 381–495 (1999)
- 21.51 M. Amemiya, Y. Korai, I. Mochida: Catalyst deactivation in distillate hydrotreating. (Part 2) Raman analysis of carbon deposited on hydrotreating catalyst for vacuum gas oil, *J. Japan. Petro. Ins.* **46**, 99–104 (2003)
- 21.52 P.R. Robinson: Petroleum and its products. In: *Handbook of Industrial Chemistry and Biotechnology*, ed. by J. Kent (Springer Science+Business Media, New York 2012), Chap. 18
- 21.53 M.J. Girigis, B.C. Gates: Reactivities, reaction networks, and kinetics in high-pressure catalytic hydroprocessing, *Ind. Eng. Chem. Res.* **30**, 2021–2058 (1991)
- 21.54 N.K. Nag, A.V. Sapre, D.H. Broderick, B.C. Gates: Hydrodesulfurization of polycyclic aromatics catalyzed by sulfide CoO-MoO₃/γ-Al₂O₃: The relative reactivities, *J. Catal.* **57**, 509–512 (1979)
- 21.55 X. Ma, K. Sakanishi, I. Mochida: Hydrodesulfurization reactivities of various sulfur compounds in diesel fuel, *Ind. Eng. Chem. Res.* **33**, 218–222 (1994)
- 21.56 P. Wiwel, B. Hinnemann, A. Hidalgo-Vivas, P. Zeuthen, B.O. Petersen, J.Ø. Duus: Characterization and identification of the most refractory nitrogen compounds in hydroprocessed vacuum gas oil, *Ind. End. Chem. Res.* **49**, 3184–3193 (2010)
- 21.57 T. Kim, A. Al-Mutairi, A.M.J. Marafi, J.I. Park, H. Koyama, S.H. Yoon, J. Miyawaki, I. Mochida: Hydrotreatment of two atmospheric residues from Kuwait export and lower Fars crude oils, *Fuel* **117(A)**, 191–197 (2014)
- 21.58 A.H. Hegazi, E.M. Fathalla, S.K. Panda, W. Schrader, J.T. Andersson: High-molecular weight sulfur-containing aromatics refractory to weathering as determined by Fourier transform ion cyclotron resonance mass spectrometry, *Chemosphere* **89**, 205–212 (2012)
- 21.59 L. Pereira de Oliveira, J.J. Verstraete, A. Trujillo Vazquez, M. Kolb: Molecular reconstruction of petroleum fractions: Application to vacuum residues from different origins, *Energ. Fuel* **77**, 3622–3641 (2013)
- 21.60 H. Muller, F.M. Adam, S.K. Panda, H.H. Al-Jawaad, A.A. Al-Hajji: Evaluation of quantitative sulfur speciation in gas oils by Fourier transform ion cyclotron resonance mass spectrometry: Validation by comprehensive two-dimensional gas chromatography, *J. Am. Soc. Mass Spectrom.* **23**, 806–815 (2012)
- 21.61 R. Prins: Catalytic hydrogenation, *Adv. Catal.* **46**, 399–464 (2001)
- 21.62 H. Topsøe, B.S. Clausen, F.E. Massoth: Hydrotreating catalysis. In: *Catalysis – Science and Technology*, Vol. 11, ed. by J.R. Anderson, M. Boudart (Springer, Berlin, Heidelberg 1996)
- 21.63 T. Kabe, A. Ishihara, W. Qian: *Hydrodesulfurization and Hydrodenitrogenation Chemistry and Engineering* (Kodansha, Tokyo 1999)

- 21.64 E. Furimsky, F.E. Massoth: Hydrodenitrogenation of petroleum, *Catal. Rev. Sci. Eng.* **47**, 297–489 (2005)
- 21.65 T. Song, Z. Zhang, J. Chen, Z. Ring, H. Yang, Y. Zheng: Effect of aromatics on deep hydrodesulfurization of dibenzothiophene and 4,6-dimethyldibenzothiophene over NiMo/Al₂O₃ catalyst, *Energ. Fuels* **20**, 2344–2349 (2006)
- 21.66 M. Egorova, Y. Zhao, P. Kukula, R. Prins: On the role of β -hydrogen atoms in the hydrodenitrogenation of 2-methylpyridine and 2-methylpiperidine, *J. Catal.* **206**, 263–271 (2002)
- 21.67 F. Rota, R. Prins: Role of hydrogenolysis and nucleophilic substitution in hydrodenitrogenation over sulfide NiMo/ γ -Al₂O₃, *J. Catal.* **202**, 195–199 (2001)
- 21.68 A. Zhang, Q. Ma, K. Wang, X. Liu, P. Shuler, Y. Tang: Naphthenic acid removal from crude oil through catalytic decarboxylation on magnesium oxide, *Appl. Catal. A* **303**, 103–109 (2006)
- 21.69 O.D. Onukwuli, I.M. Onyia, E.O. Ekumankama, S.I. Okeke: Solvent demetallization of atmospheric and vacuum residues, *Petro. Sci. Tech.* **17**, 37–49 (1999)
- 21.70 J.T. Miller, R.B. Fisher: Structural determination by XAFS spectroscopy of non-porphyrin nickel and vanadium in maya residuum, hydrocracking residuum, and toluene-insoluble solid, *Energ. Fuels* **13**, 719–727 (1999)
- 21.71 C.D. Pearson, J.B. Green: Comparison of processing characteristics of Mayan and Wilmington heavy residues: 1. Acid–base–neutral fractionation and characterization, *Fuel* **68**, 456–464 (1989)
- 21.72 C.D. Pearson, J.B. Green: Comparison of processing characteristics of Mayan and Wilmington heavy residues: 2. Characterization of vanadium and nickel complexes in acid–base–neutral fractions, *Fuel* **68**, 465–474 (1989)
- 21.73 Y.Y. Gao, B.X. Shen, J.C. Liu: Distribution of nickel and vanadium in Venezuela crude oil, *Pet. Sci. Tech.* **31**, 509–515 (2013)
- 21.74 L. Carbognani, J.C. Arambarri, H. Molero, P. Pereira-Almao: High temperature simulated distillation of bitumen fractions with open tubular capillary depleted silicone/siloxane stationary phases, *Energ. Fuels* **27**, 2033–2041 (2013)
- 21.75 G.C. Laredo, C.R. López, R.E. Álvarez, J.L. Cano: Naphthenic acids, total acid number and sulfur content profile characterization in Isthmus and Maya crude oil, *Fuel* **83**, 1689–1695 (2004)
- 21.76 B.S. Huang, W.F. Yin, D.H. Sang, Z.Y. Jiang: Synergy effect of naphthenic acid corrosion and sulfur corrosion in crude oil distillation unit, *Appl. Surf. Sci.* **259**, 664–670 (2012)
- 21.77 B.M.F. Ávila, V.B. Pereira, A.O. Gomes, D.A. Azevedo: Speciation of organic sulfur compounds using comprehensive two-dimensional gas chromatography coupled to time-of-flight mass spectrometry: A powerful tool for petroleum refining, *Fuel* **126**, 188–193 (2014)
- 21.78 L. Ding, Y. Zheng, Z. Zhang, Z. Ring, J. Chen: Hydrotreating of light cycle oil using WNi catalysts containing hydrothermally and chemically treated zeolite Y, *Catal. Today* **125**, 229–238 (2007)
- 21.79 L. Ding, Y. Zheng, H. Yang, R. Parviz: LCO hydrotreating with Mo–Ni and W–Ni supported on nano- and micro-sized zeolite beta, *Appl. Catal. A* **353**, 17–23 (2009)
- 21.80 W. Li, Z. Wang, M. Zhang, K. Tao: Novel Ni₂Mo₃N/zeolite catalysts used for aromatics hydrogenation as well as polycyclic hydrocarbon ring opening, *Catal. Comm.* **6**, 656–660 (2005)
- 21.81 X. Liu, K.J. Smith: Acidity and deactivation of Mo₂C/HY catalysts used for the hydrogenation and ring opening of naphthalene, *Appl. Catal. A: Gen.* **335**, 230–240 (2008)
- 21.82 J.I. Park, J.K. Lee, J. Miyawaki, Y.K. Kim, S.H. Yoon, I. Mochida: Hydro-conversion of 1-methyl naphthalene into (alkyl) benzenes over alumina-coated USY zeolite-supported NiMoS catalysts, *Fuel* **90**, 182–189 (2011)
- 21.83 A. Stanislaus, A. Marafi, M.S. Rana: Recent advances in the science and technology of ultralow sulfur diesel (ULSD) production, *Catal. Today* **153**, 1–68 (2010)
- 21.84 Y. Sano, K.-H. Choi, Y. Korai, I. Mochida: Adsorptive removal of sulfur and nitrogen species from a straight run gas oil over activated carbons for its deep hydrodesulfurization, *Appl. Catal. B* **49**, 219–225 (2004)
- 21.85 N. Azizi, S.A. Ali, K. Alhooshani, T. Kim, Y. Lee, J.I. Park, J. Miyawaki, S.H. Yoon, I. Mochida: Hydrotreating of light cycle oil over NiMo and CoMo catalysts with different supports, *Fuel Process. Technol.* **109**, 172–178 (2013)
- 21.86 S.A. Ali, S. Ahmed, K.W. Ahmed, M.A. Al-Saleh: Simultaneous hydrodesulfurization of dibenzothiophene and substituted dibenzothiophenes over phosphorus modified CoMo/Al₂O₃ catalysts, *Fuel Process. Technol.* **98**, 39–44 (2012)
- 21.87 H. Topsøe, B.S. Clausen, F.E. Massoth: Hydrotreating catalysis. In: *Hydrotreating Catalysis – Science and Technology*, Vol. 11, ed. by J.R. Anderson, M. Boudart (Springer, New York 1996)
- 21.88 D.A. Pappal, F.L. Plantenga, W.J. Tracy, R.A. Bradway, G. Chitnis, W.E. Lewis: Stellar improvement in hydroprocessing catalyst activity. In: *Proc. NPRA, Annu. Meet., San Antonio* (2003)
- 21.89 M.R. Gray: *Upgrading Petroleum Residues and Heavy Oils* (Marcel Dekker, New York 1994)
- 21.90 M.S. Rana, V. Sámano, J. Ancheyta, J.A.I. Diaz: A review of recent advances on process technologies for upgrading of heavy oils and residua, *Fuel* **86**, 1216–1231 (2007)
- 21.91 Z. Li, Z. Xia, W. Lai, J. Zheng, B. Chen, X. Yi, W. Fang: Hydrodemetallation(HDM) of nickel-5,10,15,20-tetraphenylporphyrion (Ni-TPP) over NiMo/ γ -Al₂O₃ catalyst prepared by one-pot method with controlled precipitation of the components, *Fuel* **97**, 504–511 (2012)
- 21.92 S.K. Maity, E. Blanco, J. Ancheyta, F. Alonso, H. Fukuyama: Early stage deactivation of heavy

- crude oil hydroprocessing catalysts, *Fuel* **100**, 17–23 (2012)
- 21.93 M. Marafi, A. Stanislaus: Preparation of heavy oil hydrotreating catalyst from spent residue hydroprocessing catalysts, *Catal. Today* **130**, 421–428 (2008)
- 21.94 M. Marafi, A. Stanislaus: Spend catalyst waste management: A review: Part 1–Development in hydroprocessing catalyst waste reduction and use, *Resour. Conserv. Recy.* **52**, 859–873 (2008)
- 21.95 A. Hauser, A. Marafi, A. Almutairi, A. Stanislaus: Comparative study of hydrodemetallization (HDM) catalyst aging by boscan feed and Kuwait atmospheric residue, *Energ. Fuels* **22**, 2925–2932 (2008)
- 21.96 A. Al-Mutairi, D. Bahzad, M.A. Halabi: A comparison study on the performance of a catalyst system for the desulfurization of two kinds of atmospheric residues, *Kuwait Export and Eocene residual oils*, *Catal. Today* **125**, 203–210 (2007)
- 21.97 M.S. Rana, J. Ancheyta, P. Rayo: A comparative study for heavy oil hydroprocessing catalysts at micro-flow and bench-scale reactors, *Catal. Today* **109**, 24–32 (2005)
- 21.98 F.X. Long, B.S. Gevert, P. Abrahamsson: Mechanistic studies of initial decay of hydrodemetallization catalysts using model compounds—effects of adsorption of metal species on alumina support, *J. Catal.* **222**, 6–16 (2004)
- 21.99 A.T. Jarullah, I.M. Mujtaba, A.S. Wood: Kinetic model development and simultaneous hydrodenitrogenation and hydrodemetallization of crude oil in trickle bed reactor, *Fuel* **90**, 2165–2181 (2011)
- 21.100 F.X. Long, B.S. Gevert: Kinetic parameter estimation and statistical analysis of vanadyl etioporphyrin hydrodemetallization, *Comput. Chem. Eng.* **27**, 697–700 (2003)
- 21.101 F.X. Long, B.S. Gevert: Kinetics of vanadyl etioporphyrin hydrodemetallization, *J. Catal.* **200**, 91–98 (2001)
- 21.102 Chevron Technical Marketing: OCR, <http://www.chevrontechnologymarketing.com/CLGtech/ocr.aspx>
- 21.103 K. Sakanishi, N. Yamashita, D.D. Whitehurst, I. Mochida: Depolymerization and demetallation treatments of asphaltene in vacuum residue, *Catal. Today* **43**, 241–247 (1998)
- 21.104 G. Caumette, C.P. Lienemann, I. Merdrignac, B. Bouyssiere, R. Lobinski: Element speciation analysis of petroleum and related materials, *J. Anal. At. Spectrom.* **24**, 263–267 (2009)
- 21.105 I. Mochida, O. Okuma, S.H. Yoon: Chemicals from direct coal liquefaction, *Chem. Rev.* **114**, 1637–1672 (2014)
- 21.106 A. Delbianco: Eni slurry technology: A new process for heavy oil upgrading. In: *Proc. 19th World Petroleum Congress* (2008)
- 21.107 A. Bhattacharyya, B. Mezza: Nano-catalysts for advanced slurry hydrocracking of heavy oil, special feature in process news, *Catal. Rev.* **24**, 6–11 (2011)
- 21.108 Z.M. Cheng, Y. Ding, L.Q. Zhao, P.Q. Yuan, W.K. Yuan: Effects of supercritical water in vacuum residue upgrading, *Energ. Fuel.* **23**, 3178–3183 (2009)
- 21.109 C.S. Hsu: *Analytical Advances for Hydrocarbon Research* (Kluwer/Plenum, New York 2003)

Hydrocracking

22. Hydrocracking

Paul R. Robinson, Geoffrey E. Dolbear

Hydrocracking converts heavy petroleum fractions into lighter products by breaking C–C bonds in the presence of hydrogen. It is in fact a collection of processes which transform a variety of feedstocks into both finished products and streams for further upgrading by downstream units. Hydrocrackers with fixed-bed reactors process straight-run VGO and/or streams with similar boiling ranges – FCC (Fluid catalytic cracking) cycle oils, coker gas oils, deasphalted oils, etc. Hydrocrackers designed for residue conversion employ ebullated bed (e-bed) reactors or slurry-phase reactors. All commercial units consume hydrogen at high pressure, typically 100–200 bar and generate considerable heat.

Fixed-bed and e-bed hydrocrackers employ dual-function hydrocracking catalysts, which contain both acid sites and hydrogenation sites. Acidity comes from amorphous aluminosilicates (ASA), crystalline zeolites, and related materials such as silica-alumina phosphates (SAPO). Hydrogenation activity comes either from noble metals (Pd or Pt) or metals sulfides (MoS_2 or WS_2). The acid sites catalyze C–C bond cleavage and the resulting fragments are stabilized by hydrogenation on the metal sites. In fixed-bed units, feed contaminants are removed first in a separate catalytic hydrotreating (pretreat) section. The most critical contaminant is organic nitrogen, which inhibits cracking by neutralizing cracking-catalyst acid sites.

In slurry-phase processes, the cracking is thermal and the cracked fragments are hydrogenated on highly dispersed additives. Some slurry-phase processes use noncatalytic additives. Additives for other processes are infused with catalytic metal compounds to enhance the conversion. Conversion of vacuum residue can exceed 95 wt%.

Products contain only ppm levels of nitrogen and sulfur and low amounts of olefins. Product aromatics are considerably lower than feed aromatics. From fixed-bed units, the heavy naphtha is a preferred feed for catalytic reformers. With some

feedstocks under appropriate process conditions, middle distillates meet sales-quality specifications for jet and/or diesel fuels without further treatment. The unconverted oil (UCO) is a premium feedstock for FCC units. UCO also can go to olefin production plants or lube base stock plants. The UCOs from e-bed and slurry-phase units can go to FCC units, but they tend to contain high concentrations of poly-ring compounds, which makes them less suitable for producing olefins and lube base stocks.

Safe operation requires tight control of reaction heat. This is achieved with proper design and effective training of operators, engineers, and managers. Poor decisions based on inadequate understanding of process dynamics and reaction chemistry have caused serious accidents, dozens of injuries, and at least one fatality.

22.1	Role of Hydroprocessing in Petroleum Refining	714
22.1.1	Overview of Petroleum Refining	714
22.1.2	Removal of Nonhydrocarbon Contaminants	717
22.2	Feedstock Molecules	719
22.2.1	Hydrocarbons	719
22.2.2	Sulfur, Nitrogen, and Oxygen	719
22.2.3	Trace Contaminants	720
22.2.4	Iron	720
22.2.5	Salts	721
22.2.6	Nickel, Vanadium, Silicon, Mercury, Arsenic	721
22.3	Process Variables	722
22.3.1	Liquid Composition	722
22.3.2	Liquid Feed Rate Parameters	722
22.3.3	Conversion Parameters	722
22.3.4	Gas-Related Parameters	723
22.3.5	Reactor Temperature Parameters	723
22.4	Hydrotreating Chemical Reactions ...	725
22.4.1	Hydrogenation of Olefins	725
22.4.2	Aromatics, Naphthenes, and Naphthenoaromatics	725

22.4.3	Hydrodesulfurization (HDS)	727	22.10	Hydroprocessing Process Descriptions	754
22.4.4	Hydrodenitrogenation (HDN)	730	22.10.1	Fixed-Bed Hydrocracking: Process Flow Schemes	754
22.4.5	Hydrodeoxygenation (HDO)	730	22.10.2	Fixed-Bed Hydrocracking: Design Considerations	758
22.4.6	Hydrodemetalation (HDM)	730	22.10.3	Fixed-Bed Hydrocracking: Product Flexibility in Recycle Units ...	760
22.4.7	Conversion Due to Hydrotreating	730	22.10.4	Ebullated Bed Hydrocracking	761
22.5	Hydrocracking Chemical Reactions ...	731	22.10.5	Slurry Phase Hydrocracking	761
22.5.1	Conversion by Hydrogen Addition versus H/C Rearrangement	731	22.10.6	Hybrid Processes for Residue Hydrocracking	762
22.5.2	Hydrocracking Reaction Sequence	731	22.11	Economics	762
22.6	Hydroprocessing Catalysts	736	22.12	Safety, Reliability, and Protection of the Environment	762
22.6.1	Hydroprocessing Catalyst Overview	736	22.12.1	Procedures	763
22.6.2	Catalyst Preparation	738	22.12.2	Management of Change	763
22.7	Catalyst Cycles	740	22.12.3	Personal Protection Equipment (PPE)	763
22.7.1	Catalyst Cycle Life	740	22.12.4	Confined Space Entry	763
22.7.2	Catalyst Selection and Loading	742	22.12.5	Toxic Gases: Hydrogen Sulfide and Carbon Monoxide	763
22.7.3	Activation of Non-Noble-Metal Catalysts in Fixed-Bed Units	743	22.12.6	Catalyst Handling	764
22.7.4	Activation of Noble-Metal Hydrocracking Catalysts	744	22.12.7	Erosion-Corrosion Around Reactor Effluent Air Coolers (REAC)	764
22.7.5	Catalyst Regeneration and Rejuvenation	744	22.12.8	Temperature Excursion Fundamentals	764
22.7.6	Catalyst Reclamation	745	22.12.9	Temperature Excursion Examples	766
22.8	Hydroprocessing Thermochemistry ..	745	22.12.10	Preventing Temperature Excursions ...	771
22.9	Hydroprocessing Kinetics	747	22.12.11	Stopping a Temperature Excursion ...	772
22.9.1	Pseudo First-Order Approximation (PFOA) Models	747	22.12.12	No DIBS	774
22.9.2	Temperature Dependence	748	22.13	Conclusion	775
22.9.3	Langmuir-Hinshelwood/Hougen-Watson Kinetics	749	22.14	Additional Reading	775
22.9.4	Structure-Based Lumping	750	References		775

22.1 Role of Hydroprocessing in Petroleum Refining

22.1.1 Overview of Petroleum Refining

Hydrocracking processes convert heavy petroleum fractions into lighter products by cracking C–C bonds in the presence of high-pressure hydrogen, while removing essentially all nonhydrocarbon contaminants. Catalytic hydrocracking units (HCUs) with fixed-bed reactors process straight-run VGO and/or streams with similar boiling ranges – FCC cycle oils, coker gas oils, deasphalted oils, etc. Units designed for residue conversion employ ebullated bed (e-bed) reactors or slurry-phase reactors. Ebullated bed units employ formed catalysts, while slurry-phase units, in which the hydrocracking is thermal, use finely divided proprietary additives; the additives may be catalytic or non-catalytic.

Commercial units operate at high pressure, typically 120–200 bar with H₂ purity > 70 vol.%. They generate considerable heat.

Process flow schemes for fixed-bed hydrotreaters and fixed-bed hydrocrackers are similar and much of the chemistry is the same. For this reason, industry professionals use the term *hydroprocessing* when discussing them together. The difference is the cracking part. Hydrocracking breaks carbon–carbon (C–C) bonds, but hydrotreating does not.

Figures 22.1 and 22.2 illustrate the role of hydroprocessing in a representative high-conversion petroleum refinery. Figure 22.1 includes processes for upgrading distillates that boil below about 595 °C (1100 °F), temperatures which mark the somewhat fuzzy boundary between vacuum distillates and vacuum residue. Fig-

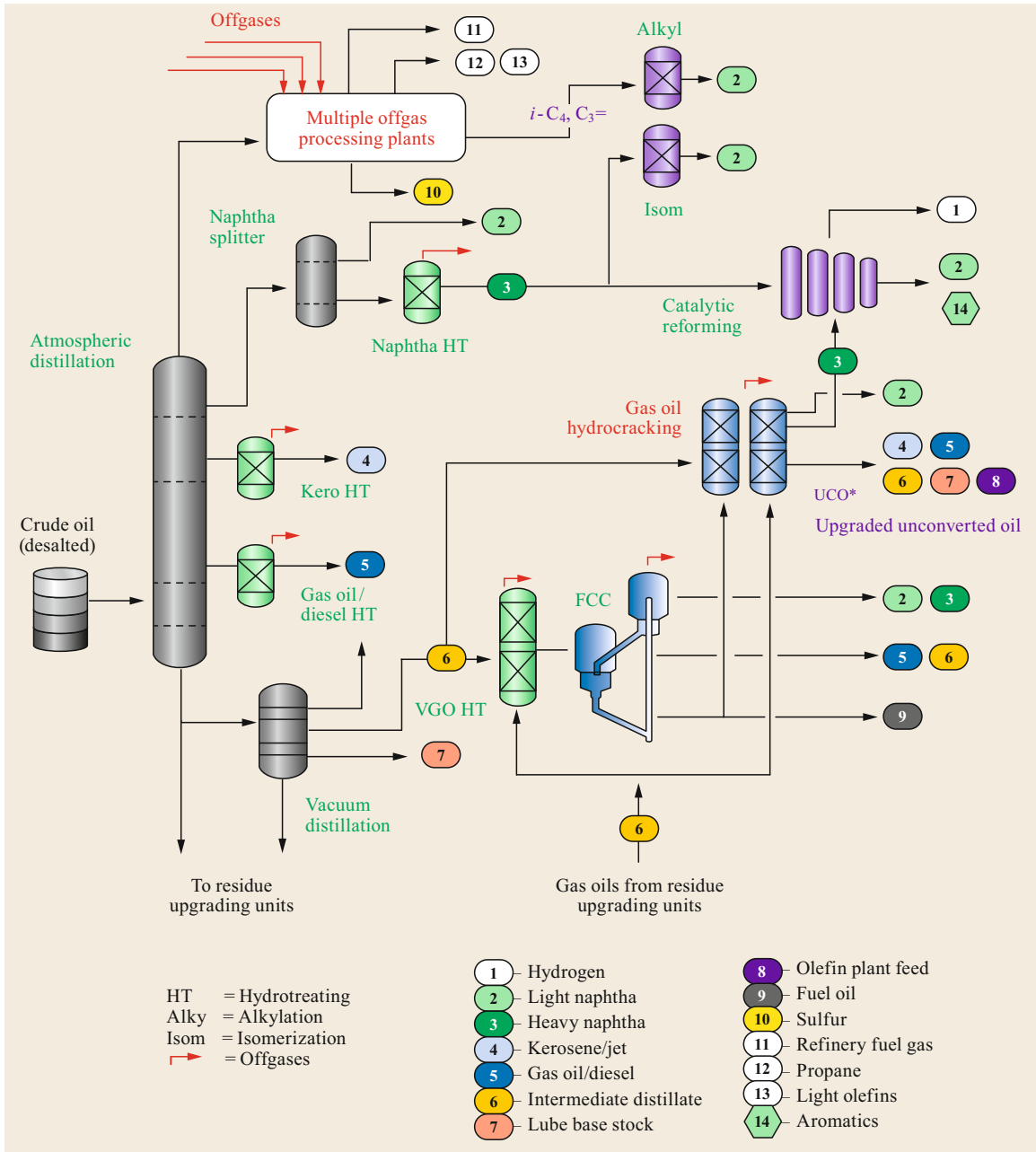


Fig. 22.1 Top part of a representative petroleum refinery

ure 22.2 shows residue conversion processes, including residue hydrocracking. Feeds to residue FCC (RFCC) units are hydrotreated to remove metals. In locales with restrictions on sulfur in gasoline, jet fuel and diesel, all liquid products from delayed cokers are hydrotreated or hydrocracked.

Most refineries were built between the 1940s and 1970s. Over time, they have evolved (or gone out of

business) due to changes in feedstock price, quality, and availability – and also due to changes in product demand and regulations. Since the mid-1990s, ever-tightening restrictions on product sulfur have increased the need for hydroprocessing. Figure 22.1 includes five hydroprocessing units – four hydrotreaters and one hydrocracker. These days, it is rare to find a refinery with less than three hydrotreaters.

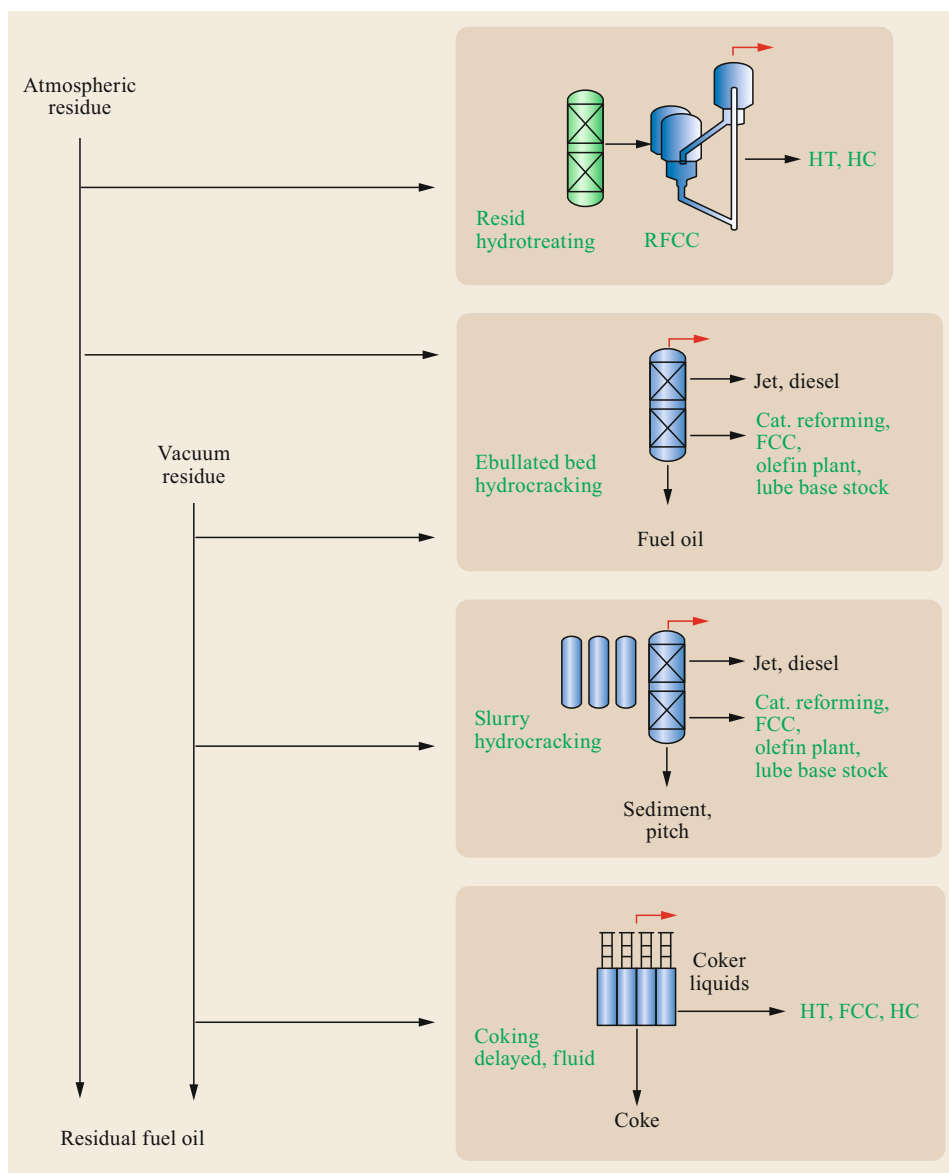


Fig. 22.2 Vacuum residue upgrading options for petroleum refining

Refining entails five major kinds of molecule manipulation:

- Removing contaminants (desalting, hydrotreating, amine treating, mercaptan oxidation)
- Separation (distillation, extraction)
- Conversion (hydrogenolysis in hetero-atom compounds and C–C bond cleavage)
- Isomerization, saturation, and reforming (no change in carbon number)
- Recombination (alkylation, polymerization).
- Feedstock management – selection, storage, blending, and transportation
- Product management – blending, storage, and distribution
- Hydrogen manufacturing, purification, and recovery
- Utilities – power, steam, water, instrument air, and industrial gases
- Waste processing and disposal.

Related activities, which may occur either inside or outside the refinery proper, include:

Soft activities – those which don't require steel – include software for design, simulation, automation, and optimization; laboratory services; planning and scheduling; training; management; and R&D.

The first major process unit in a refinery is the desalter, which removes dirt, water, salt, and other water-soluble contaminants from blended crude oils. From the desalter, the crude(s) go to an atmospheric distillation unit (ADU), which produces several streams. These include refinery fuel gas (RFG) containing mostly methane and ethane, liquefied petroleum gas (LPG) containing mostly propane and butanes, one or two straight-run naphtha streams, one or two straight-run middle distillates streams, and atmospheric residue (AR).

22.1.2 Removal of Nonhydrocarbon Contaminants

Figure 22.3 illustrates the importance of hydroprocessing for fuel production. All ADU products contain sulfur, either as H_2S , inorganic sulfur, or organic sulfur compounds. Heavier fractions also contain nitrogen, oxygen, and trace elements (Fe, Ni, V, Cu, Si, As, and Hg). Hydrotreating removes organic sulfur and the other contaminants from most C_5+ liquids. Sulfur can be removed from relatively sweet naphtha with mercaptan oxidation technology.

Nonfuel uses for straight-run petroleum distillates include the following:

- Streams heavier than naphtha – from kerosene through vacuum residue – are used to make lubricants. Hydrofinishing is an important step in base stock preparation. Hydrocracking and catalytic dewaxing are used to make group II base stocks and hydroisomerization is used to make group III base stocks.
- Light olefins (ethylene, propylene, and butylenes) are recovered and sent directly to olefin production plants. Olefins are produced from paraffin gases, petrochemical naphtha, and hydrocracker unconverted oil. Figure 22.4 illustrates how refineries interact with olefin plants.

Here are the main destinations for individual streams from atmospheric distillation units, from the bottom of the tower to the top:

- The AR goes to a vacuum distillation unit (VDU), which produces vacuum gas oil (VGO) and vacuum residue (VR). Refiners allocate VGO based on business requirements. Common VGO destinations include an FCC, a hydrocracker, a lube base stock facility, and fuel-oil blending.
- Either before or after hydrotreating, straight-run middle distillates are divided into light and heavy

fractions, which become kerosene or gas oil, respectively. Both can serve as fuel oil. If it meets specifications, the kerosene can be blended into jet fuel and the gas oil can be blended into diesel. Certain refineries produce just one middle distillate stream, typically wide-range gas oil.

- Naphtha is split into light and heavy fractions. Desulfurized light naphtha (LN) includes C_5 molecules along with differing amounts of C_4 and C_6 . LN can be blended into gasoline or separated into constituent components. Small amounts of mixed butanes can be blended into gasoline. *N*-Butane is sold as such or isomerized into *i*-Butane. *i*-Butane goes to alkylation (ALKY) units or is dehydrogenated to C_4 olefins for chemical plants. Heavy naphtha (HN) includes C_6 – C_{12} molecules; sometimes also C_{12} molecules. Catalytic reforming (CRU) and isomerization (ISOM) units are common HN destinations. C_6 compounds may be excluded from CRU feeds if a refiner wants to minimize benzene production. C_9 – C_{12} molecules can be blended into aviation gasoline.
- H_2S is removed from RFG by adsorption in alkalamine units. The H_2S is converted to elemental sulfur in Claus process units. Sweet RFG serves as fuel gas throughout the refinery. LPG is sold or exported to a chemical plant, either before or after segregation into individual components.
- Thermal cracking units, such as cokers and slurry-phase hydrocrackers, produce significant quantities of methane and ethane. In catalyst-based conversion units – FCCs and fixed-bed hydrocrackers – C_1C_2 production is low and for paraffins, the iso/normal ratio is high. Processes that operate without external hydrogen – FCC and coking – generate olefins, aromatics, hydrogen, and coke. FCC is a primary source of propylene and butylenes for downstream chemical plants. In hydrocracking units, which operate with large amounts of external hydrogen, olefins and coke are low and product aromatics are lower than feed aromatics.
- As much as anything else, VR conversion determines refinery profitability. The cost of crudes depends on their sulfur and VR content. High-sulfur, high-VR crudes cost less, so refineries configured to handle them tend to be more profitable. VR is a source of asphalt, bright-stock lubricants, greases, waxes, and specialty carbon products. To a certain extent, VR can be blended into No. 6 fuel oil (bunker fuel). Processes for converting AR and VR into lighter products include delayed coking, visbreaking, modified versions of FCC and either ebullated bed or slurry-phase hydrocracking.

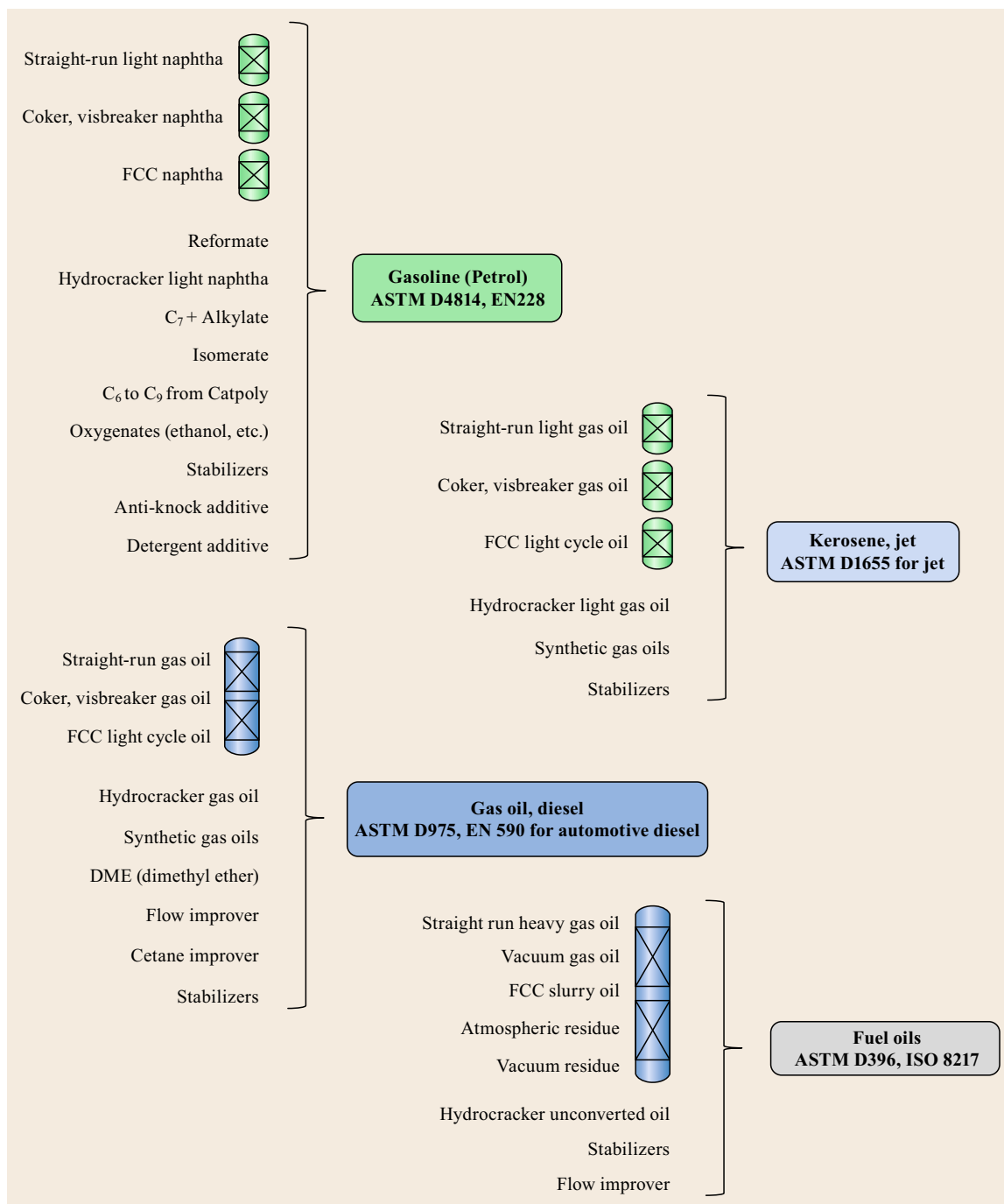


Fig. 22.3 Hydroprocessing for fuel production. Almost all C₅+ liquid streams are hydroprocessed – somewhere and to some extent. Components are shown for four types of liquid fuels: Naphthas (including gasoline), kerosenes (including jet fuel), gas oils (including diesel), and fuel oils. Destinations of key products are specified, along with approximate TBP (true boiling point) boiling ranges

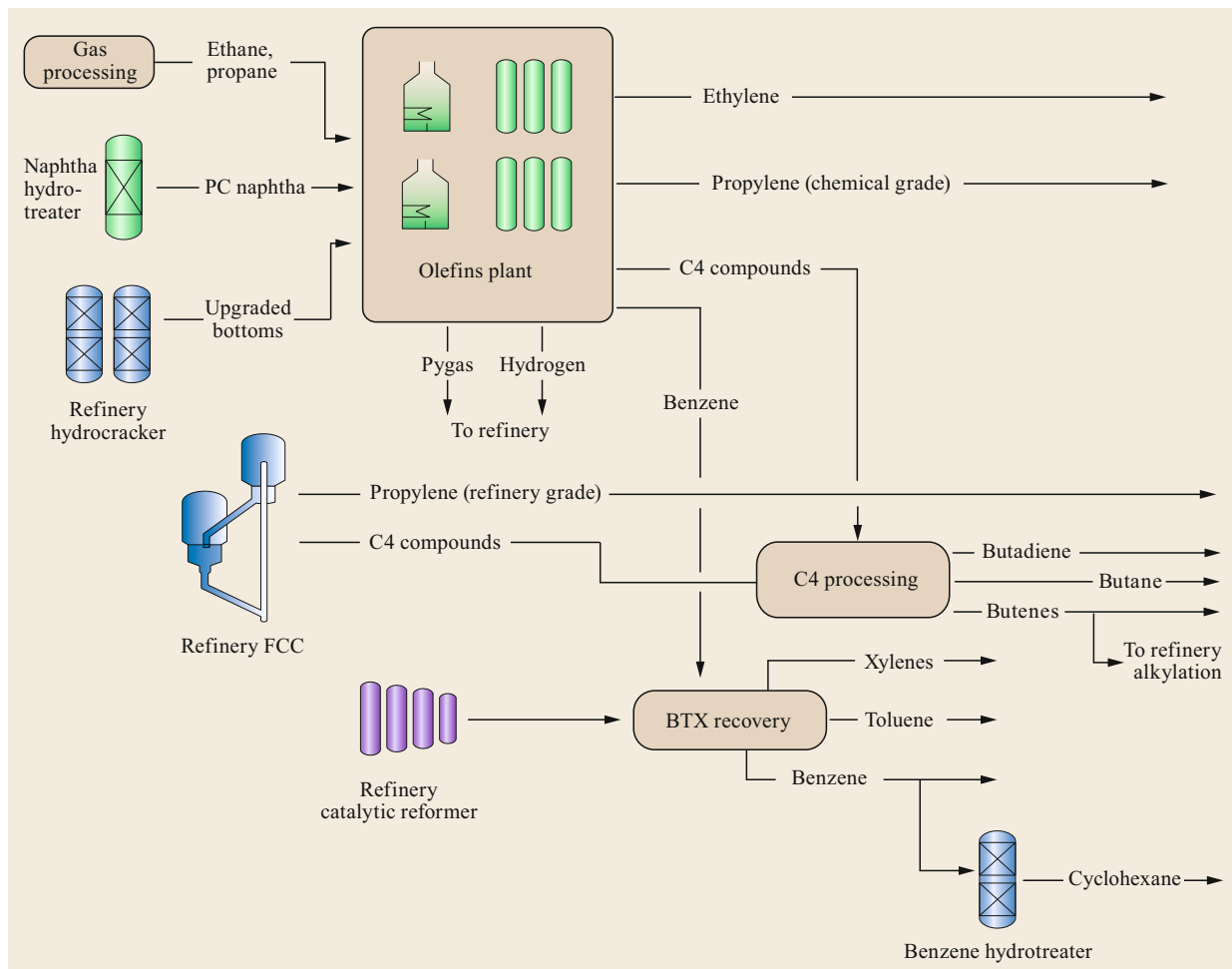


Fig. 22.4 Role of hydroprocessing in the petrochemical industry

22.2 Feedstock Molecules

First and foremost, feedstock properties determine the selection and performance of molecule manipulation technology. The properties of straight-run hydroprocessing feedstocks depend directly on the properties of the crude oils from which they are distilled.

22.2.1 Hydrocarbons

The preponderance of molecules in hydroprocessing feedstocks are hydrocarbons – alkanes (normal and isoparaffins), olefins (alkenes), and ring compounds. Figure 22.5 shows examples of hydrocarbon ring compounds that might appear in feeds to hydroprocessing units. Up to 80% of the carbon atoms in some feeds are part of a ring compound.

22.2.2 Sulfur, Nitrogen, and Oxygen

The major contaminants in feeds to hydroprocessing units are sulfur, nitrogen, and oxygen. Figure 22.6 shows some examples of hetero-atom compounds.

The sulfur content can range from < 0.2 wt% to > 4 wt%. Sulfur can be inorganic – dissolved H_2S and elemental sulfur – but mostly it is organic – sulfides, disulfides, thiophenes, benzothiophenes, and dibenzothiophenes.

The nitrogen content can range from 100 wppm to > 4000 wppm. Coal-containing feeds to residue hydrocrackers can contain > 1 wt% nitrogen. Amines are rare, but pyrroles, quinolines, and carbazoles are common.

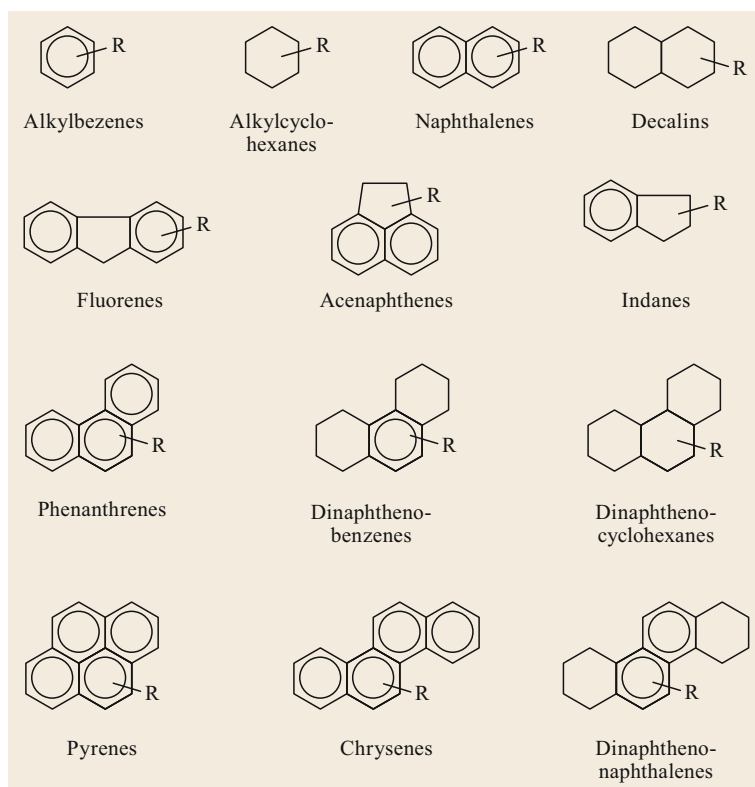


Fig. 22.5 Examples of hydrocarbon ring compounds

Nonwater oxygen comes from a variety of sources. Feedstocks from biomass contain considerably more oxygen than conventional crude oil and petroleum distillates. While a conventional vacuum gas oil may contain 0.5 wt% oxygen, a bio-derived oil in the same boiling range might contain > 2% oxygen. Organic oxygen compounds include furans, naphthenic acids, carboxylic acids, ethers, peroxides, and ring compounds that contain both oxygen and nitrogen or sulfur. Peroxides form when crude oil and heavy petroleum distillates are exposed to air during transportation and storage.

22.2.3 Trace Contaminants

The major trace contaminants in as-produced crude oil are iron, nickel, vanadium, and sometimes arsenic and mercury. Ni and V concentrations can range from < 2 to > 1000 wppm. Water and salts are entrained in many crudes. By the time they reach a refinery, oils might also contain silicon and corrosion-product iron. All trace contaminants degrade the performance of catalytic hydroprocessing units, usually by poisoning catalyst sites but sometimes by weakening catalyst supports. As and Hg are 100× more poisonous on a weight basis than Fe, Ni, and V. Weakened parti-

cles can disintegrate into chips and dust; in fixed-bed units, these accumulate in the space between intact particles, thereby blocking flow and increasing pressure-drop buildup (dP+).

Limits on feed metal content for fixed-bed VGO hydrocrackers are considerably tighter than those for residue hydrotreaters, e-bed hydrocrackers, and slurry-phase hydrocrackers. For the catalytic units (residue hydrotreating and e-bed hydrocracking), feed metals are a major concern. Fixed-bed residue hydrotreaters are loaded with wide-pore metals-removal catalysts, which can pick up > 100% of their weight in metals. In e-bed units, adjustments in the catalyst addition rate are based largely on feed metals content.

In slurry-phase units, which operate without catalysts, feed metals do not inhibit performance. Higher metals can in fact enhance conversion.

22.2.4 Iron

Both particulate and dissolved iron can impair the performance of refineries. Organometallic iron can be a constituent of as-produced crudes, but most of the soluble iron in refineries is generated by corrosion. Corrosion can be accelerated by naphthenic acids, halide salts, and hydro-halic acids. Polythionic acids cause

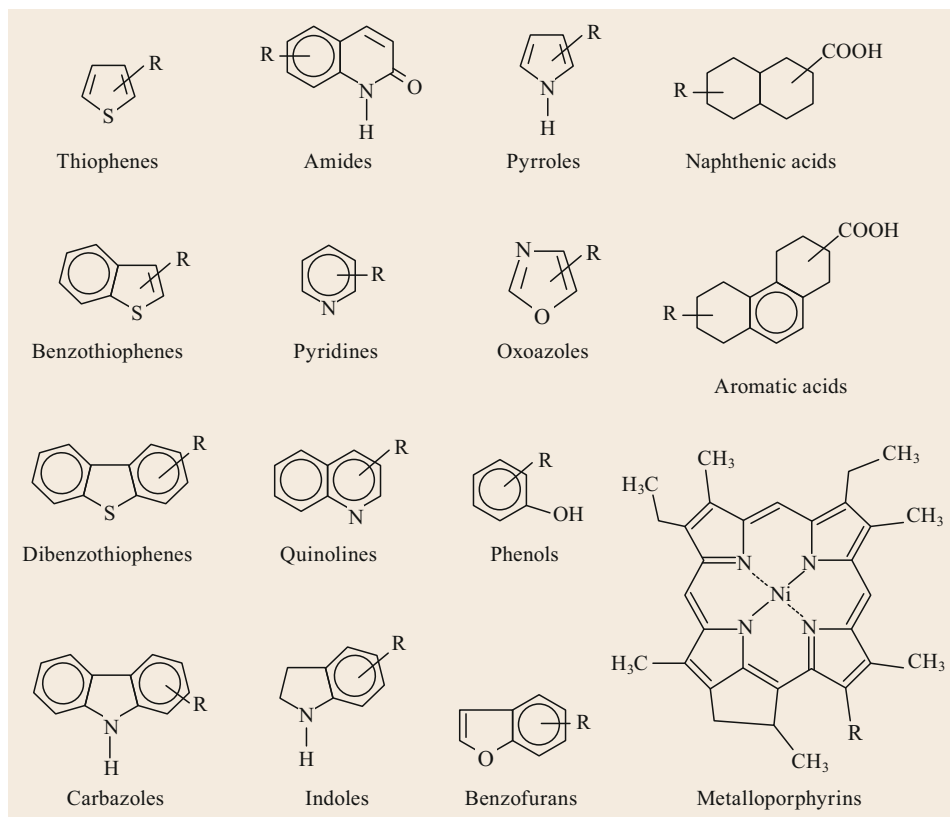


Fig. 22.6 Ex-amples of ring compounds containing hetero-atoms

stress corrosion cracking in certain steels. During hydroprocessing, H_2S reacts with stainless steel to form thin layers of metal sulfides. The sulfides are converted to polythionic acids when the steel is exposed to air during a maintenance shutdown. The acids are removed by washing or spraying exposed surfaces with aqueous soda ash (Na_2CO_3).

22.2.5 Salts

During production, shipment and storage, petroleum might be exposed to salt water, which becomes entrained. Salts include chlorides and sulfates of sodium, magnesium, and calcium. Bromine is especially corrosive. A major source of Br is drilling brine, which is co-produced with oil and can end up in the VGO feed to a hydrocracker.

22.2.6 Nickel, Vanadium, Silicon, Mercury, Arsenic

Good nickel, as nickel sulfide, is a promoter for hydroprocessing catalysts. In other forms, Ni is a serious contaminant. Organic Ni and V are encapsulated in porphyrins, which are constituents of asphaltenes. Inorganic Ni and V may also be present.

Organic silicon compounds are added to crude oil as flow improvers. They are also added to delayed cokers to mitigate foaming.

Mercury appears primarily in natural gas and gas condensate. Hg is especially abundant in gas and condensate produced from offshore Thailand fields.

Arsenic is relatively abundant in synthetic crudes from Canada, heavy shale oil and in crudes from West Africa and the Ukraine.

22.3 Process Variables

Hydrotreating and hydrocracking have their own jargon. In this section, we describe and define common process-specific terms.

22.3.1 Liquid Composition

Two general classes of measurements define the liquid streams in hydroprocessing units: bulk properties and molecular composition.

Bulk Properties

Bulk properties of crude oils and imported intermediate streams include distillation, specific gravity (or API gravity), TAN (total acid number), BSW (basic sediment and water), salt content, and total sulfur. For hydroprocessing, additional bulk properties are important. These include total nitrogen, CCR (Conradson carbon residue) or MCR (microcarbon residue content), UV aromatics, asphaltenes, heptane insolubles and trace elements. The ASTM methods for determining these properties are presented in Chap. 1.

Molecular Composition

Process development and/or the formulation of models for real-time optimization require determination of *molecular composition*. But middle distillates contain hundreds of molecules and vacuum gas oils and residues contain hundreds of thousands – perhaps even millions. It is impractical (and unnecessary) to measure each and every one. It is sufficient to split the feed into cuts – light and heavy naphtha, light and heavy oil, light and heavy vacuum gas oil and vacuum residue – and to determine for each cut, concentrations of the following:

- Paraffins – normal and iso-
- Aromatics – mono-, di-, tri- etc.
- Naphthenes – mono-, di-, tri- etc.
- Olefins
- Alkyl aromatics
- Sulfur compounds – sulfides, disulfides, mercaptans, thiophenes, benzothiophenes etc.
- Nitrogen compounds – amines, pyroles, quinolines, carbazoles etc.
- Oxygen compounds – naphthenic acids, cresols etc.
- Trace elements.

Composition variables specific to hydrocracking include:

- Nitrogen slip (N slip) = organic nitrogen (ppmw) in the pretreater effluent liquid
- Sulfur slip (S slip) = organic sulfur (9 ppmw) in the pretreater effluent liquid.

For Aspen Hydrocracker, a rigorous model for on-line optimization, this approach generated 113 reactive *lumps*. Section 22.9.4 presents additional information on the use of lumping in rigorous models.

While the bulk properties of blended feeds might be measured every day – or at least after every crude switch – the molecular composition of individual blend stocks is typically measured only once.

22.3.2 Liquid Feed Rate Parameters

Space velocity corresponds to the inverse of residence time. The term enables one to compare kinetics for commercial units of different absolute size:

- Space velocity (once-through) = ratio of fresh feed rate to catalyst volume
- Space velocity (combined feed) = ratio of total feed rate (fresh feed + recycle oil) to catalyst volume
- Liquid hourly space velocity (LHSV) = feed volume (specified as once-through or combined feed)/(catalyst volume)/h. The unit of measure (UOM) is h^{-1} .
- Weight hourly space velocity (WHSV) = feed weight (specified as once-through or combined feed)/(catalyst volume)/h. The UOM is $\text{kg}/\text{m}^3/\text{h}$.

Combined feed ratio (CFR) = (total amount of feed to a specific reactor)/(total fresh feed to the first reactor). CFR is relevant to units which recycle unconverted oil or accept varying amounts of external feeds between the hydrotreating and hydrocracking sections of a unit.

22.3.3 Conversion Parameters

Measurements and calculations important for quantifying conversion include the following:

- *Conversion cut point* (CCP) in a hydrocracker = cutpoint (TBP) of unconverted oil. Refiners sometimes employ the term RCP for recycle units.
- *True conversion* (weight) = $[1 - (\text{weight of cutpoint-plus material in the product})/(\text{weight of cutpoint-plus in the feed})] \cdot 100\%$
- *Apparent conversion* (volume) = $[1 - (\text{volume of liquid product})/(\text{volume of liquid feed})] \cdot 100\%$.
- *True conversion* (volume) = $[1 - (\text{volume of liquid product})/(\text{volume of unconverted oil in the feed})] \cdot 100\%$. The volume conversion in a fixed-bed hydrocracker operating to make C_4+ naphtha can exceed 125 vol.%. Economically, this so-called *volume swell* is significant, because gaso-

line and diesel are sold by volume, not weight. Higher volume is worth more, regardless of weight.

22.3.4 Gas-Related Parameters

- *Reactor average pressure* = [(reactor inlet pressure) + (reactor outlet pressure)]/2
- *Bed pressure drop* (Bed dP) = (bed outlet pressure) – (bed inlet pressure)
- *Reactor pressure drop* (Reactor dP) = (reactor outlet pressure) – (reactor inlet pressure)
- *Pressure-drop buildup* (dP+) = rate of change pressure drop. UOM can be psig/month or kPa/month
- *Hydrogen partial pressure* (p_{H_2}) = (reactor average pressure) · (hydrogen purity). UOM can be psig or kPa.
- *Hydrogen purity* (vol.% H_2) = average hydrogen purity in the reactor(s), based on analyses of the reactor inlet gas and the CHPS overhead gas (purge gas prior to amine treating)
- *Gas-to-oil ratio* (GOR) = (volume of gas to the reactor)/(volume of liquid feed to the reactor). UOM can be scf/bbl or Nm^3/m^3
- *Hydrogen-to-oil ratio* (H2OR) = (volume of hydrogen to the reactor)/(volume of feed to the reactor,

including recycle oil if any). UOM can be scf/bbl or Nm^3/m^3

- *Gas composition* = mole percent of each component in a gas stream.

22.3.5 Reactor Temperature Parameters

Scores of temperature indicators (TIs) are associated with modern hydrocracking reactors. There can be more than 20 per bed, a dozen or so *skin TIs* affixed to the outside of the reactor wall underneath the insulation, two or three on each quench line and two or three on each pipe leading into or out of the vessel. Refiners rely on calculations to translate all that data into useful information.

Some temperature calculations include catalyst weight, catalyst volume, and gas or liquid flow rates. It is important to know whether or not catalyst weights or volumes should include grading material; it is not surprising to see a catalyst loading scheme in which all available volume in the first bed of a 4- or 5-bed reactor is occupied by particulate traps, low-activity chemisorbents for taking out trace elements, and additional activity grading.

Figure 22.7 serves a basis for illustrating reactor temperature calculations for a two-bed hydroprocess-

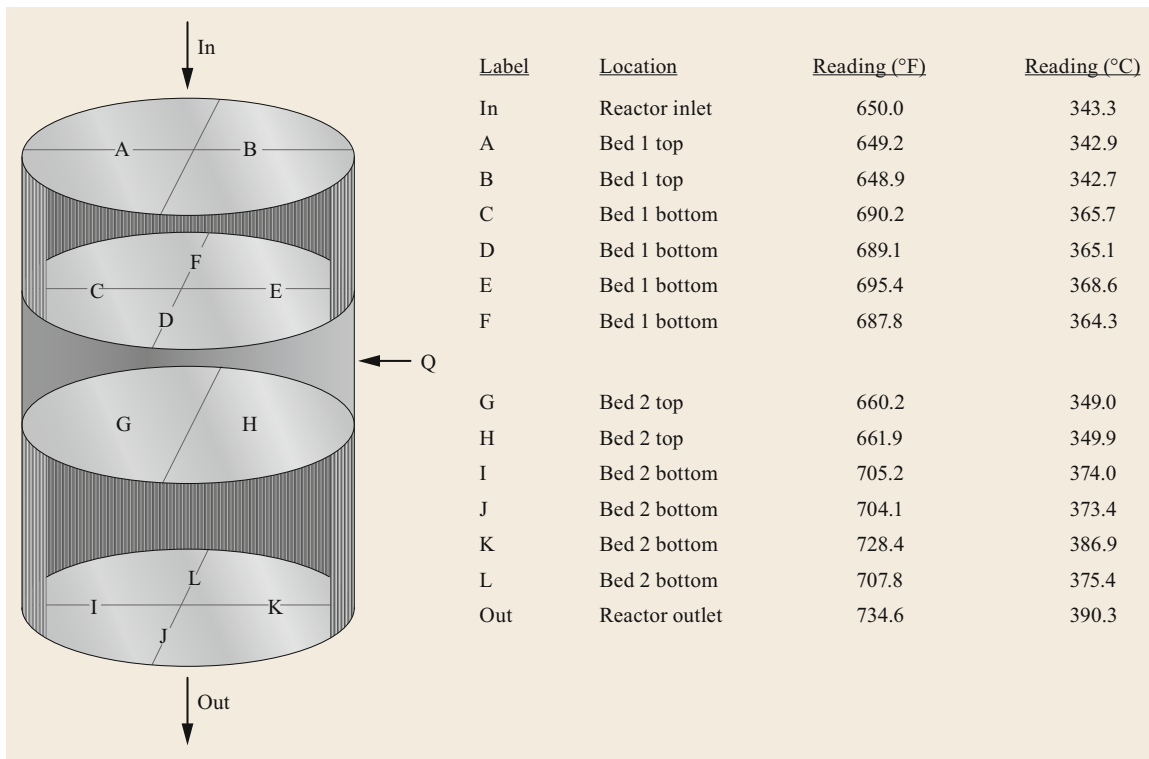


Fig. 22.7 Basis for temperature calculations

ing reactor. There are multiple temperature indicators (TIs) in horizontal planes at the top and bottom of each bed. Differences in coplanar TIs reveal uneven flow of fluids. In the figure:

- The arrows indicate the direction of flow
- Q represents quench gas flow into the deck between the beds; quenching controls the inlet temperature of bed 2
- Bed 1 contains 40% of the active catalyst. Bed 2 contains 60% of the active catalyst.

- (a) *Average bed top temperature* = average of all TI readings in a horizontal plane at the top of a given bed.
- (b) *Average bed bottom temperature* = average of all TI readings at the bottom of a given bed.
- (c) *Catalyst average temperature (CAT)* = average of Calculation (a) and Calculation (b). CAT is specific to units designed and/or licensed by Chevron Lummus Global (CLG).
- (d) *Weighted average bed temperature (WABT)* = $(1/3) \cdot (a) + (2/3) \cdot (b)$. More weight is given to the bed outlet temperature, because temperatures are higher at the outlet and reactions are faster at higher temperatures. The one-third, two-thirds weighting is arbitrary, but it has become a standard and it reflects commercial performance.
- (e) *Bed axial temperature rise (average)* = average T rise = $(b) - (a)$.
- (f) *Bed axial temperature rise (max)* = max T rise = (maximum TI reading at the bed bottom) – (a).
- (g) *Radial temperature difference (radial dT)* = (highest TI reading in a horizontal plane) – (lowest TI reading in the same horizontal plane).

- (h) *Quench temperature difference (quench dT)* = temperature difference across a quench section = $[(b) \text{ for the bed above the quench deck}] - [(a) \text{ for the bed below the quench deck}]$.
- (i) *Temperature gain* (as in a T -pulse test) = change in a TI reading at a bed outlet after a change in the bed inlet temperate, calculated after the bed outlet reaches steady state.
- (j) *Time to steady state* (as in a T -pulse test) = time required for a TI reading at a bed outlet to reach steady state after a change in the bed inlet temperate. UOM is minutes.
- (k) *Reactor axial temperature rise (reactor dT)* = sum of (e) for all beds.
- (l) *Reactor CAT* = $(\text{CAT for Bed 1}) \cdot (\text{fraction of active catalyst in bed 1}) + (\text{CAT for Bed 2}) \cdot (\text{fraction of active catalyst in bed 2}) + (\dots)$.
- (m) *Reactor WABT* = $(\text{WABT for Bed 1}) \cdot (\text{fraction of active catalyst in bed 1}) + (\text{WABT for Bed 2}) \cdot (\text{fraction of active catalyst in bed 2}) + (\dots)$.
- (n) *Required CAT or WABT* = the reactor CAT or reactor WABT required to achieve a specific process target, such as product sulfur, product nitrogen, or conversion.
- (o) *Catalyst deactivation rate* = average rate of change in required CAT or WABT ($^{\circ}\text{F}/\text{month}$).
- (p) *Catalyst cycle life* = length of time between the initial startup after catalyst loading and the final shutdown to remove catalysts.

Table 22.1 presents the results of the calculations just defined, based on the data in Fig. 22.7.

Note: The reactor outlet TI reading is higher than any TI reading inside bed 2. This indicates the presence of a hot spot, a subject discussed in some detail in Sect. 22.12.9.

Table 22.1 Results of calculations based on the data in Fig. 22.7 rounded to the nearest 0.1 degree

No.	Calculation	Bed 1 ($^{\circ}\text{F}$)	Bed 2 ($^{\circ}\text{F}$)	Reactor ($^{\circ}\text{F}$)	Bed 1 ($^{\circ}\text{C}$)	Bed 2 ($^{\circ}\text{C}$)	Reactor ($^{\circ}\text{C}$)
	Reactor inlet			650.0			343.3
	Reactor outlet			734.6			390.3
a)	Average top	649.1	661.1		342.8	349.5	
b)	Average bottom	690.6	711.4		365.9	377.4	
c)	CAT	669.8	686.2		354.4	363.5	
d)	WABT	676.8	694.6		358.2	368.1	
e)	Bed axial rise (average)	41.6	50.3		23.1	28.0	
f)	Bed axial rise (max)	46.4	67.4		25.8	37.4	
g)	Radial difference top	0.3	1.7		0.2	0.9	
h)	Radial difference bottom	7.6	24.3		4.2	13.5	
	Quench T difference		29.6			16.4	
l)	Reactor CAT			679.7			359.8
m)	Reactor WABT			687.5			364.1

22.4 Hydrotreating Chemical Reactions

Satterfield [22.1], Topsøe et al. [22.2], and Prins [22.3] describe the chemistry of hydrotreating in great depth. In this chapter, we provide an overview.

Hydrocracking breaks C–C bonds, but strictly speaking, hydrotreating does not. Hydrotreating converts compounds containing hetero-atoms into hydrocarbons, plus H₂S, NH₃, H₂O, or adsorbed trace elements. It also saturates olefins and aromatics. Removal of hetero-atoms often requires prior saturation of an aromatic ring followed by hydrogenolysis of the bonds between the heteroatom and one or more carbon atoms. Fixed-bed hydrocracking of polyaromatics also requires prior ring saturation. Hydrotreating reactions fall into six broad categories:

- Saturation of olefins
- Saturation of aromatics
- HDS
- HDN
- HDO
- HDM.

HDS = hydrodesulfurization, HDN = hydrodenitrogenation, HDO = hydrodeoxygenation, and HDM = hydrodemetalation.

Within each category, relative reaction rates depend on process conditions, feed quality, inhibitors, and catalyst type. In practice, it is more meaningful to consider extents of reaction. During the HDS of straight-run gas oil in a representative deep desulfurization unit, most of the light olefins will be gone before the feed has traveled through 10–20% of the active catalyst. Roughly halfway through the catalyst, 70–80% of the total sulfur will be gone. At the reactor outlet, depending on catalyst type, catalyst age, and reaction conditions, the sulfur content will be 15 wppm and the aromatics content will be 50–70% less than the aromatics in the feed. The extent of HDN, relative to HDS, varies with feed types, PH₂ and catalyst loading. Higher pressure and NiMo catalysts favor HDN. At lower pressure, a CoMo catalyst (or alternating layers of NiMo and CoMo catalysts) improves HDS.

22.4.1 Hydrogenation of Olefins

Olefins are rare in straight-run distillates, but they can be produced in atmospheric distillation towers if the towers are too hot. Thermal cracking generates olefins in abundance, even in slurry-phase hydrocrackers where the PH₂ is very high. Hydrogenation of olefins in catalytic hydrotreating and hydrocracking units is rapid,

essentially irreversible at low-to-moderate temperatures and highly exothermic.

Conjugated diolefins can polymerize into gums, which increase pressure drop (dP). The impact of diolefins can be minimized with catalyst activity grading.

22.4.2 Aromatics, Naphthenes, and Naphthoaromatics

The equilibrium between saturated and unsaturated ring compounds (Fig. 22.8) is an important phenomenon in several petroleum refining processes. It is central to catalytic reforming, hydrotreating, and hydrocracking. Equilibrium is destroyed by the breaking or forming of C–C bonds; both are locally irreversible. Saturated C–C bonds can be broken by ring opening. C–C bonds can be formed by the condensation of polyaromatics to form larger polyaromatics.

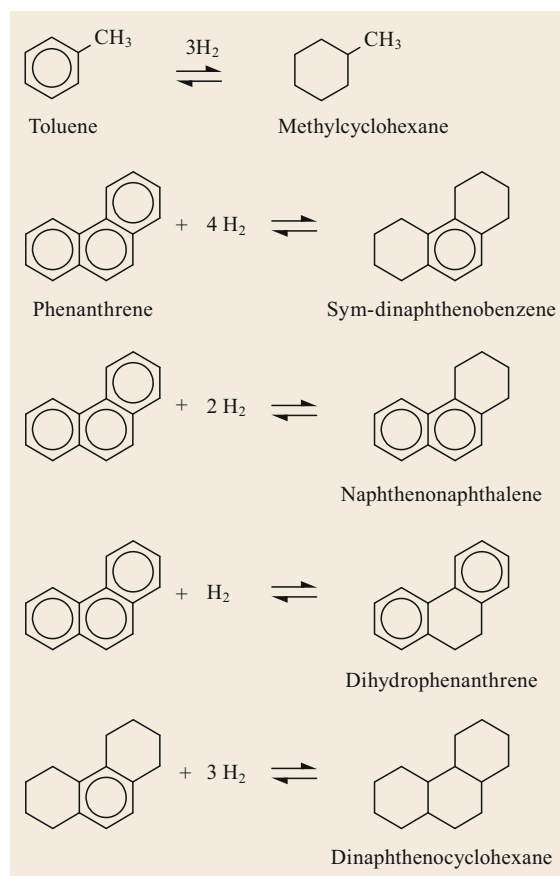


Fig. 22.8 Examples of saturation reactions of aromatics and polyaromatics

Figure 22.9 summarizes thermodynamic calculations for the competition between the saturation of naphthalene and the condensation of naphthalene with *o*-xylene to form chrysene [22.4]. At low temperatures, the extent of aromatics saturation increases with temperature. As the temperature goes up, saturation becomes more and more difficult. Above about 750 °F (400 °C), raising temperature decreases the extent of

saturation. Hydrogen partial pressure and feed composition determine the temperature range through which this *crossover* phenomenon occurs. At high-enough temperatures, net saturation becomes impossible. At very high temperatures, equilibrium favors condensation, even at very high pressures.

Figure 22.10 shows the so-called zig-zag mechanism for the production of large polyaromatics by

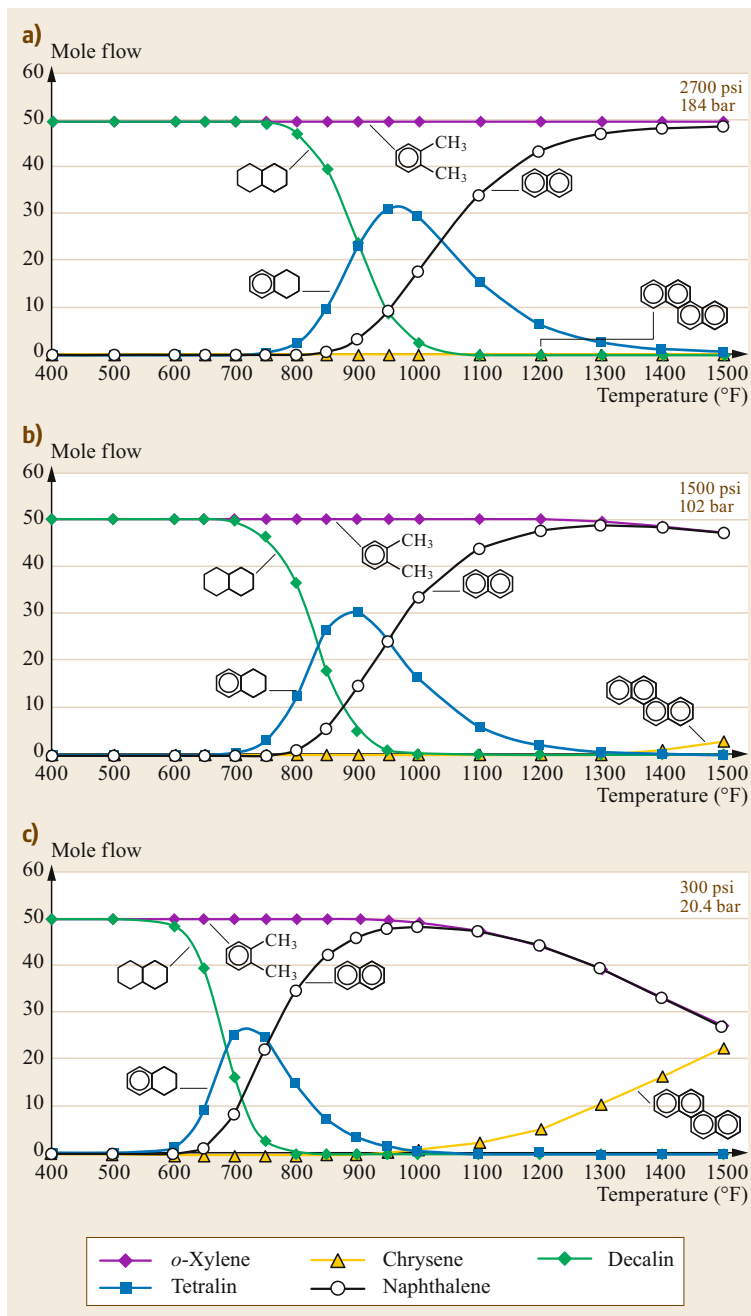


Fig. 22.9 Thermodynamic calculations showing competition between naphthalene saturation and condensation. Data for the graphs were generated by Aspen Plus for a 6-component system comprising naphthalene ($C_{10}H_8$), tetralin ($C_{10}H_{12}$), decalin ($C_{10}H_{18}$), *o*-xylene (C_8H_{10}), chrysene ($C_{18}H_{12}$), and hydrogen (not shown)

adding 2-carbon and 4-carbon species [22.5]. Note how the H/C ratio goes down as condensation increases, from 0.8 for naphthalene to 0.4375 for ovalene. The condensation of large polyaromatics via the Scholl reaction [22.6] can lead eventually to coke formation and coke-induced deactivation of catalysts.

Figure 22.11 shows a proposed mechanism for the one-at-a-time buildup of rings on a nucleus of coke [22.7]. The mechanism includes the following steps:

- Hydrogen abstraction by a radical
- Olefin addition (alkylation) to a radical on the surface
- Cyclization
- Dehydrogenation.

22.4.3 Hydrodesulfurization (HDS)

Figure 22.12 shows representative hydrodesulfurization (HDS) reactions. Per *Topsøe et al.* [22.2, p. 114], HDS

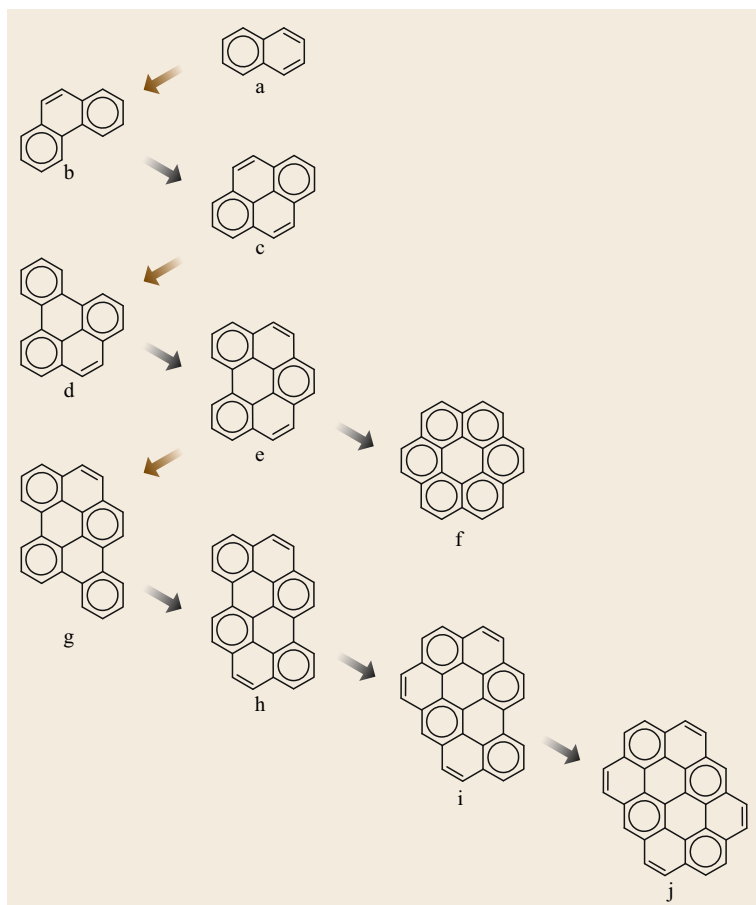


Fig. 22.10 Zig-zag mechanism for the condensation of polyaromatics by sequential addition of 2-carbon and 4-carbon units. Each reaction produces hydrogen. The isomers shown are (A) naphthalene, $C_{10}H_8$; (B) phenanthrene, $C_{14}H_{10}$; (C) pyrene, $C_{16}H_{10}$; (D) benzo[*e*]pyrene, $C_{20}H_{12}$; (E) benzo[*ghi*]perylene, $C_{22}H_{12}$; (F) coronene, $C_{24}H_{12}$; (G) dibenzo[*b,pqr*]perylene, $C_{26}H_{14}$; (H) benzo[*pqr*]naphtho[8,1,2-*bcd*]perylene, $C_{28}H_{14}$; (I) naphtho[2'.8'.2.4]coronene, $C_{30}H_{14}$; and (J) ovalene, $C_{32}H_{14}$

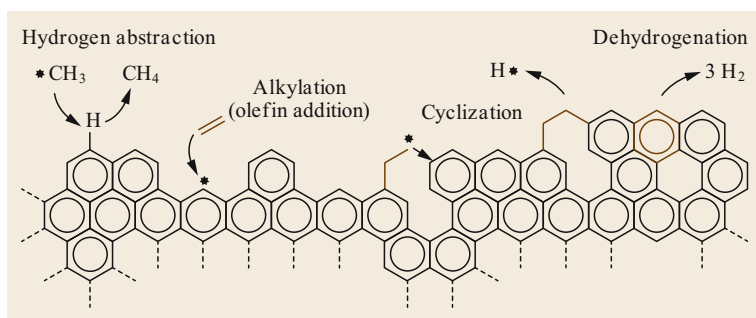


Fig. 22.11 Mechanism for adding rings to an existing layer of coke

rates vary as follows: sulfides \approx mercaptans $>$ thiophenes $>$ benzothiophenes $>$ dibenzothiophenes $>$ substituted dibenzothiophenes. In the figure, for removing sulfur from the first three reactants, the mechanism is straightforward. The sulfur-containing molecule interacts with an active site on the catalyst, which abstracts the sulfur atom. The sulfur-free fragment is hydrogenated and desorbs. The adsorbed sulfur is con-

verted to H_2S , which also desorbs, leaving behind a regenerated active site. The fourth reactant – 4,6-dimethyldibenzothiophene (4,6-DMDBT) – has two methyl groups near the sulfur atom. The reaction proceeds via both a direct and an indirect route. In this case, the indirect route is favored. The 4,6-DMDBT molecule is planar and the two methyl groups block the access of the sulfur atom to the catalyst surface,

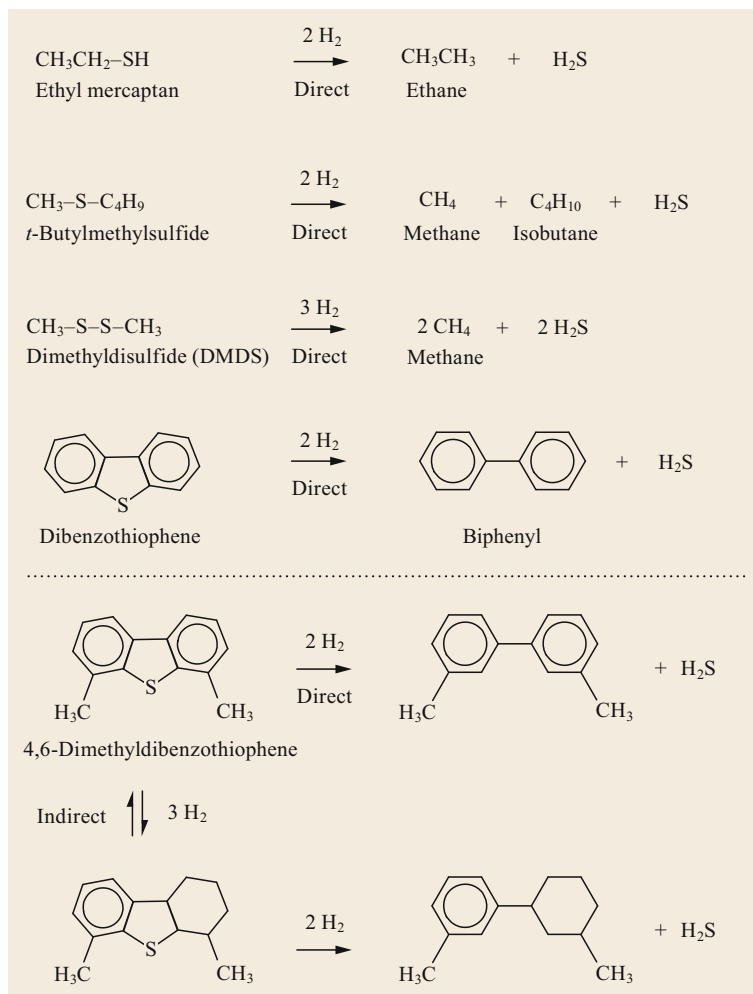


Fig. 22.12 Representative hydrodesulfurization (HDS) reactions

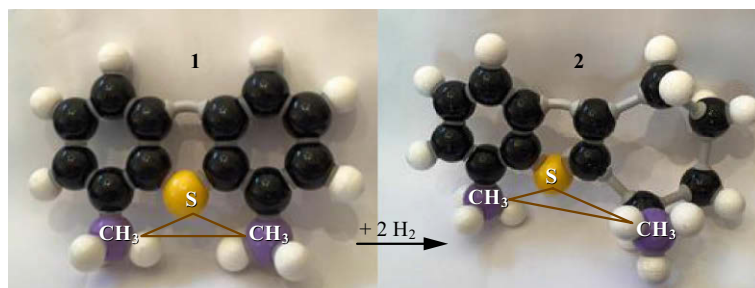


Fig. 22.13 Hydrogenation of one of the aromatic rings in 4,6-dimethyldibenzothiophene. Not to scale

thereby inhibiting direct HDS. In the indirect route, one of the aromatic rings flanking the sulfur atom is saturated. Hydrogenation removes resonance stabilization and changes the geometry around the carbon atoms from planar to tetrahedral. This rotates a methyl group away from the sulfur atom, diminishing steric hindrance. Figure 22.13 provides a not-to-scale illustration of this phenomenon.

In ultra-low-sulfur diesel (ULSD), for which the sulfur content is less than 10–15 wppm, the only remaining sulfur compounds after hydroprocessing are alkyl-substituted dibenzothiophenes. Catalysts with an abundance of edges and corners, such as the BRIM products offered by *Haldor Topsøe* [22.8], are good for removing sterically hindered compounds such as these.

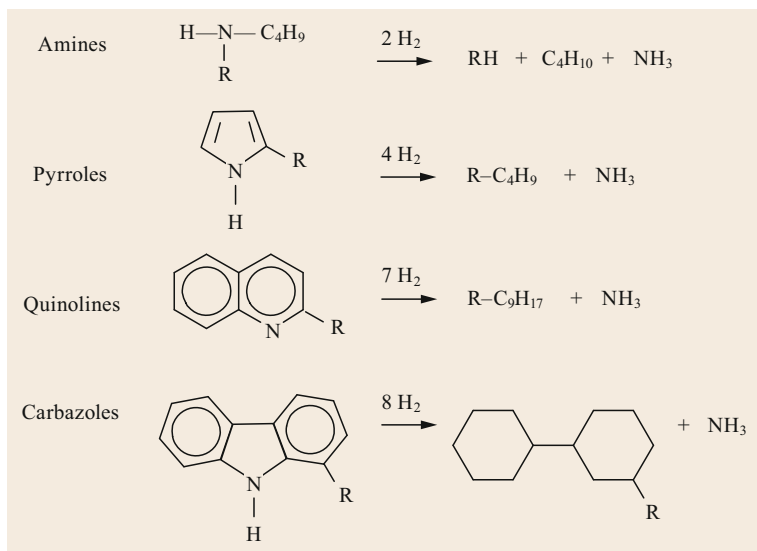


Fig. 22.14 Representative hydrodenitrogenation (HDN) reactions

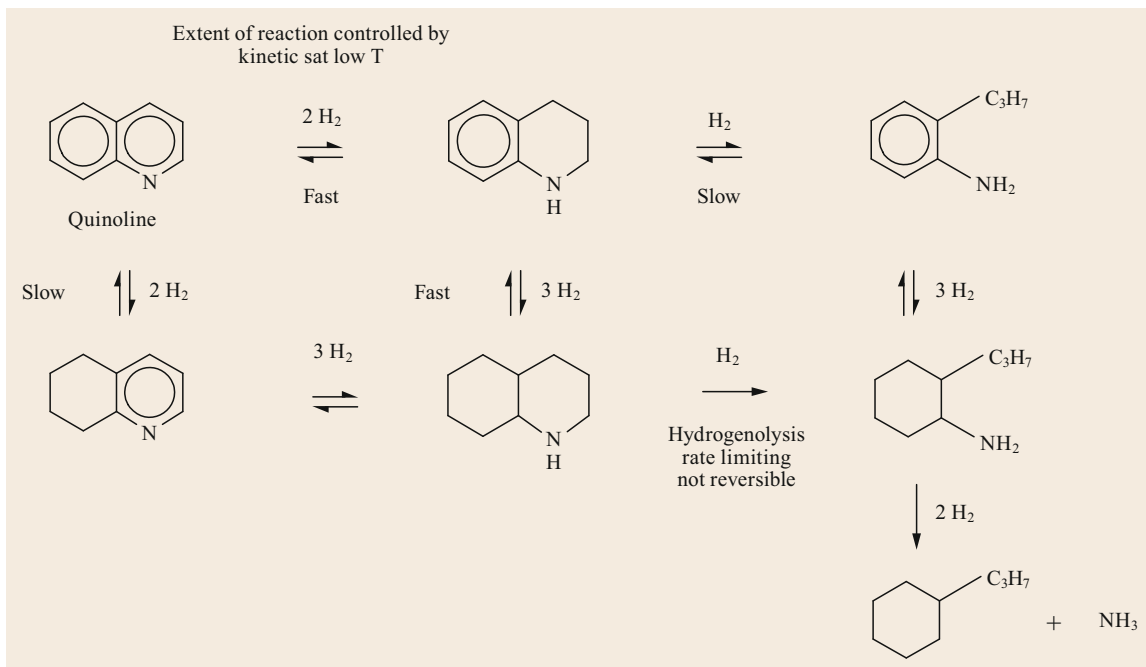


Fig. 22.15 Mechanism for the HDN of quinolone

22.4.4 Hydrodenitrogenation (HDN)

Figure 22.14 shows representative HDN reactions. Relative reaction rates are: amines > pyrroles > pyridines > quinolines > carbazoles. Figure 22.15 presents a simplified version of the Satterfield mechanism for the HDN of quinoline [22.9]. As with sulfur removal from hindered DMBTs, nitrogen removal requires prior saturation of an aromatic ring adjacent to the nitrogen atom.

22.4.5 Hydrodeoxygenation (HDO)

As mentioned, in feeds to industrial hydroprocessing units, oxygen is contained in furans, cresols, phenols, naphthenic acids, other organic acids, ethers, peroxides etc. Peroxides are formed by reaction with air during the transportation and/or storage of crude oil, imported distillates, and refinery intermediate streams. Peroxides induce the formation of flow-inhibiting gums, which cause buildup of pressure drop. For some oxygen compounds, hydrodeoxygenation (HDO) proceeds rapidly, causing excessive heat release. This problem is mitigated by catalyst activity grading. Other oxygen compounds, such as phenols and cresols, are exceedingly difficult to hydrotreat.

22.4.6 Hydrodemetalation (HDM)

Soluble trace metals are removed with special guard materials. For arsenic, high-nickel adsorbents are used. Other contaminants, such as Ni, V and soluble Fe, are removed by hydrodemetalation (HDM) reactions in catalyst pores that are wide enough to admit large molecules, such as the ones in which these metals are found.

22.4.7 Conversion Due to Hydrotreating

In practice, conversion means boiling-point reduction

$$\text{Conversion} = \frac{P}{FF} \cdot 100\%$$

where P = the amount of product and FF = is the amount of fresh feed. Product is defined as the amount of material boiling below a specified distillation cut-point. In *true conversion* calculations, the amount of P in the FF prior to conversion is subtracted from the numerator.

Boiling-point reduction comes from breaking carbon-carbon bonds, but it also comes from heteroatom removal and saturating aromatic rings. Table 22.2 compares normal boiling points for reactant/product

Table 22.2 Impact of sulfur removal and aromatics saturation on normal boiling point. Reactions 6 through 8 are reversible. Temperatures for diesel-range molecules are marked in (), temperatures for naphtha-range molecules are marked in [] and temperatures for residue are marked in {}. Reactions 3, 5, and 8 convert diesel into naphtha. Reaction 6 converts VGO into diesel. Reaction 9 shows that rupturing a decalin C-C bond gives an additional boiling point shift relative to naphthalene (after [22.10, 11]). Some values are estimated by Advanced Chemistry Development (www.acdlabs.com) via [22.10])

	Reaction	Formula	MW	Boiling point		Delta	
				(°C)	(°F)	(°C)	(°F)
1. HDS	Dibenzothiophene, 4,6-dimethyl → benzene, 1-methyl-3-(3-methylcyclohexyl)-	C ₁₄ H ₁₂ S	212.31	(364.9)	(688.8)	–	–
		C ₁₄ H ₂₀	188.31	(273.4)	(524.1)	91.5	164.7
2. HDS	Dibenzothiophene → biphenyl	C ₁₂ H ₈ S	184.26	(332.6)	(630.6)	–	–
		C ₁₂ H ₁₀	154.21	(253.9)	(488.9)	78.7	141.7
3. HDS	Benzo[b]thiophene → ethylbenzene	C ₈ H ₆ S	134.20	(221.1)	(429.9)	–	–
		C ₈ H ₁₀	106.16	[136.2]	[277.1]	84.9	152.8
4. HDS	Thiophene, 2-methyl → <i>n</i> -Pentane	C ₅ H ₆ S	98.17	[113.0]	[235.4]	–	–
		C ₅ H ₁₀	70.13	[36.1]	[96.9]	76.9	138.5
5. HDN	Quinoline → benzene, <i>n</i> -propyl	C ₉ H ₇ N	129.16	(237.9)	(460.1)	–	–
		C ₉ H ₁₂	120.19	[158.9]	[317.9]	79.0	142.2
6. SAT	Chrysene ⇌ chrysene, dodecahydro-	C ₁₈ H ₁₂	228.29	{448.0}	{838.4}	–	–
		C ₁₈ H ₂₄	240.38	(371.0)	(699.8)	77.0	138.6
7. SAT	Naphthalene ⇌ tetralin	C ₁₀ H ₈	128.17	(216.9)	(422.3)	–	–
				(207.9)	(406.1)	9.0	16.2
8. SAT	Tetralin ⇌ <i>t</i> -decalin	C ₁₀ H ₁₂	132.20	(207.9)	(406.1)	–	–
				[186.9]	[368.3]	21.0	38.7
9. HC	<i>t</i> -Decalin → <i>t</i> -butyl cyclohexane	C ₁₀ H ₁₈	138.25	[186.9]	[368.3]	–	–
		C ₁₀ H ₂₀	140.23	[171.3]	[340.3]	15.6	28.1

sets. The boiling points of the products are lower, in some cases considerably so. For the reactions 1–4 (HDS), reaction 5 (HDN) and reaction 6 (complete saturation of chrysene), boiling point drops are greater than 76 °C (138 °F). Reactions 3, 5, and 8 convert diesel molecules (in ()) into naphtha molecules (in []). Reaction 6 converts a VGO molecule into a diesel molecule.

The hydrogenation reactions are (usually) reversible. Dehydrogenation has the opposite effect –

converting naphtha molecules into diesel and diesel molecules into VGO. Such reactions, which can eventually lead to coke formation, play a significant role in catalyst deactivation [22.4]. Industrial experience shows that for feeds with high aromatics and sulfur, conversion due to hydrotreating reactions can reach 15%. An example is saturating a fraction that is rich in diaromatics, as might come from a coking unit, into a fraction that is rich in alkyl decalins.

22.5 Hydrocracking Chemical Reactions

Van Veen et al. [22.12] and Scherzer and Gruia [22.13] review hydrocracking reaction fundamentals in detail. Highlights from those works and others, are presented in this section.

22.5.1 Conversion by Hydrogen Addition versus H/C Rearrangement

In hydrocrackers, conversion consumes hydrogen during C–C bond cleavage and also during the saturation of aromatics and olefins, including reaction intermediates.

In delayed cokers and FCC units, conversion is due to H/C redistribution. In reactions that form compounds with higher H/C, paraffins are cracked and naphthene rings are opened. The side chains of alkyl aromatics are clipped, generating paraffins and leaving behind methyl-substituted aromatics. Reactions that decrease H/C generate olefins and polyaromatics. Polyaromatics condense, with release of hydrogen, to form larger polyaromatics. Successive condensation reactions eventually lead to coke.

Coke formation also occurs in hydrotreating and hydrocracking, but only to a small degree. This is due to the large excess of hydrogen, which keeps the catalyst surface clean.

22.5.2 Hydrocracking Reaction Sequence

Catalytic hydrocracking does not open aromatic rings, which are stabilized by resonance energy. The rings must be saturated before they can be opened via C–C bond cleavage. The hydrocracking of ring compounds follows the sequence illustrated in Fig. 22.16 for hydrocracking a heptyl ethyl naphthalene isomer:

- Removal of part of a side chain by dealkylation
- Saturation of an aromatic ring
- Isomerization of the saturated ring
- Opening the saturated ring
- Paraffin hydrocracking.

The ring itself remains intact due to resonance stabilization. One-ring aromatics are especially stable. The

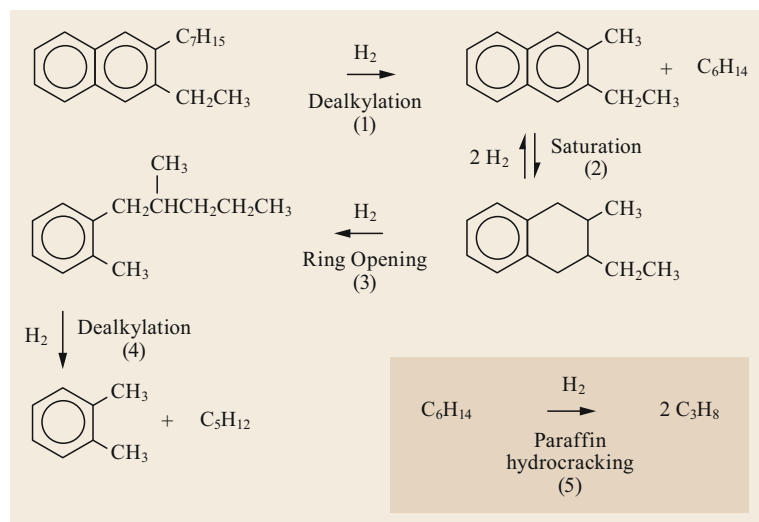


Fig. 22.16 Reaction sequence for the hydrocracking of a heptyl ethyl naphthalene isomer

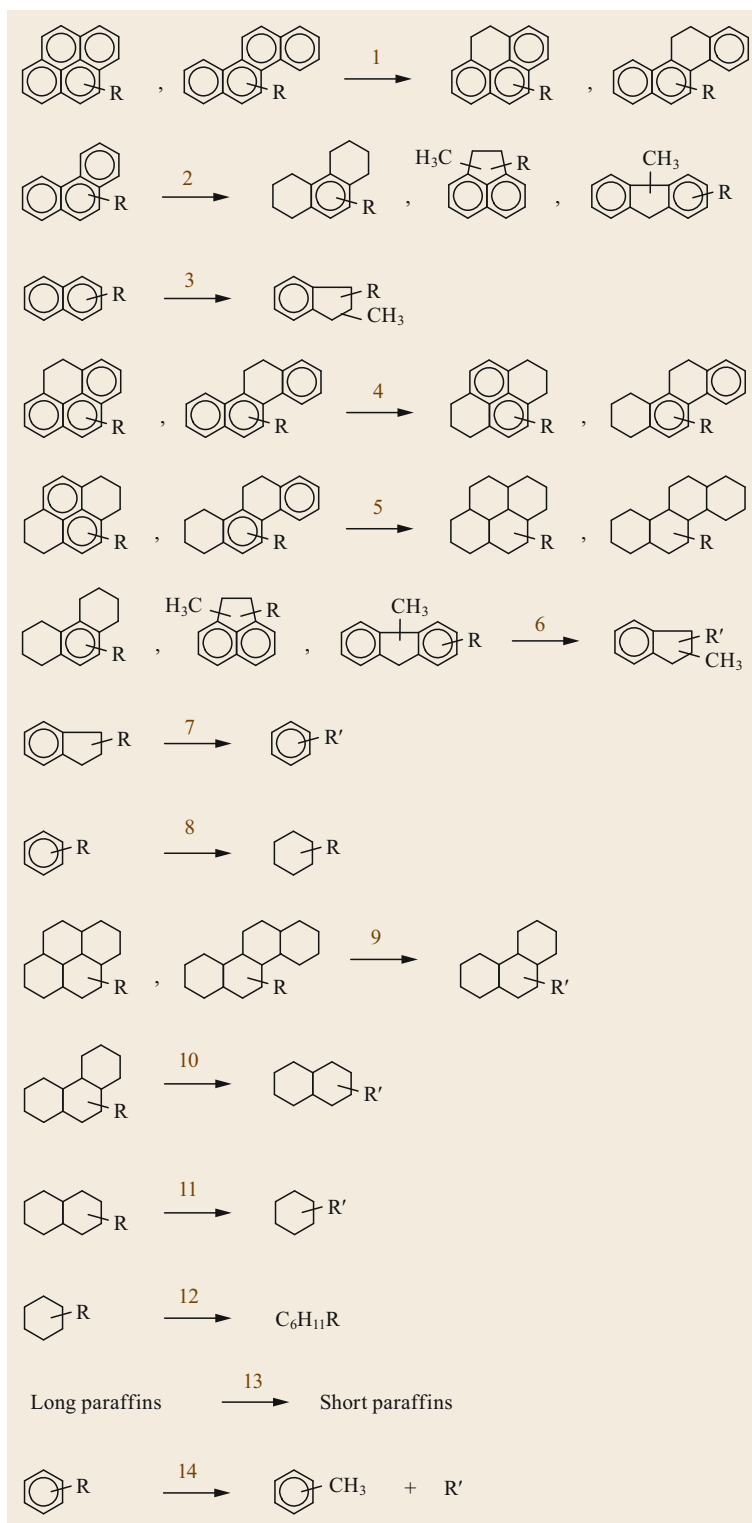


Fig. 22.17 Sequence of reactions for hydrocracking poly-ring compounds. Reactions 1–5 and 8 show saturation. In 2 and 3, saturation is accompanied by ring isomerization. Ring-opening reactions include 6–7 and 9–12. Any of the compounds in 1–11 might undergo dealkylation if R or R' contain four or more carbons. Hydrogen stoichiometry isn't shown

first dealkylation reaction (1) removes hexane isomers through β -cleavage, leaving behind a methyl group still attached to the ring. Rings do not give up methyl and ethyl groups with β -scission during catalytic cracking and catalytic hydrocracking. This is consistent with the observation that acid-catalyzed cracking in hydrocracking and FCC units produces minimal methane and ethane. Hydrogenating aromatic rings (2) removes resonance, yielding a saturated ring which is susceptible to ring opening (3). Ring opening is followed by another dealkylation reaction (4) and paraffins are hydrocracked (5).

In Sect. 22.8, we discuss how reaction rates in the absence of external inhibitors depend on a molecule's affinity to adsorb to the catalyst surface. According to *Scherzer and Gruia* [22.13, p. 190], adsorption affinity decreases as follows: heteroaromatics > polyring aromatics > monoaromatics > polyring naphthenes > mononaphthenes > paraffins. Larger molecules adsorb more strongly. But more than adsorption is involved.

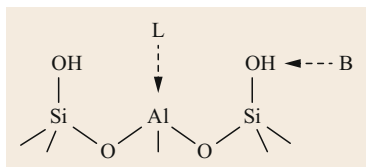


Fig. 22.18 Brønsted (B) and Lewis acid sites (L) in zeolites and amorphous silica–aluminas. Brønsted sites donate a proton (H^+). Lewis sites remove a hydride ion (H^-)

Dealkylation of adsorbed polyaromatics is quite facile, but the rings themselves do not react, not until they are saturated. The net effect on the relative reaction rates for hydrocarbon molecules with similar carbon numbers is as follows: dealkylation > ring opening > paraffin hydrocracking.

Figure 22.17 gives a more general illustration of ring hydrocracking [22.14]. The figure shows ring carbons only, except for methyl groups associated with isomerization of 6-carbon saturated rings into 5-carbon saturated rings. Hydrogen is consumed in each reaction, but the stoichiometry isn't shown. Reactions 1–5 and 8 show saturation. In 2 and 3, saturation is accompanied by ring isomerization. Ring-opening reactions include 6–7 and 9–12. Any of the compounds in 1–11 might undergo dealkylation if R or R' contain four or more carbons.

Catalytic cleavage of C–C bonds requires powerful acids. Hydrocracking catalysts are bifunctional, with both acid and metal sites. The metal sites catalyze both saturation and dehydrogenation. It is important to achieve a proper balance between cracking and hydrogenation activity. For a given conversion target, too much hydrogenation activity suppresses olefin intermediates, thereby suppressing the extent of cracking. With too little hydrogenation activity, over-cracking occurs.

In commercial catalysts, hydrogenation is catalyzed by noble metals (widely dispersed palladium metal) or non-noble metal sulfides (nickel-promoted MoS₂ or

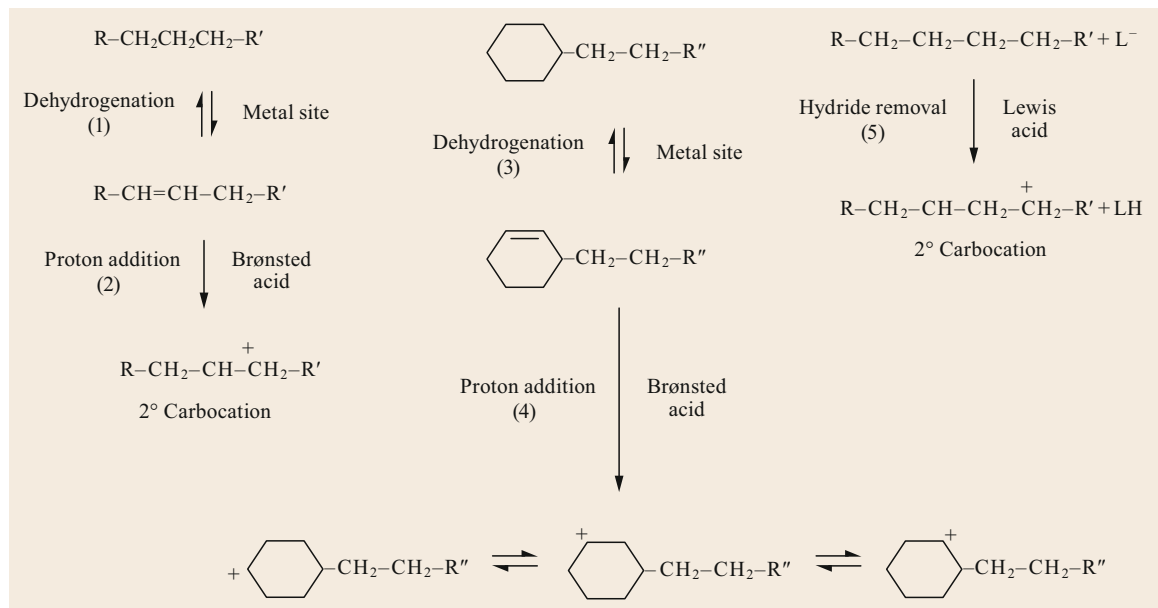


Fig. 22.19 Carbocation mechanism for hydrocracking: Initiation reactions. Reaction 4 gives three products, which are in equilibrium

WS₂). The acidity comes from zeolites and/or amorphous silica-alumina (ASA). Zeolites occur naturally, but the ones used for catalysis are synthetic. Zeolites serve as drying agents, ion-exchangers, and molecular sieves for gas separation. Their microporosity provides them with high surface area, a highly desirable characteristic.

Figure 22.18 shows how one can visualize acid sites as part of a silica (SiO₂) superstructure, in which every so often an aluminum atom replaces a silicon atom [22.15]. The silicon atoms have a valence of +4 and

each one binds to four oxygen atoms. Replacing Si (+4) with Al (+3) creates Lewis acid sites. Hydration generates hydroxyl groups, which are Brønsted acids (proton donors). Counter ions can be swapped via ion exchange. For example, when Na-Y zeolite is exchanged with an ammonium salt, the Na⁺ ion is replaced by NH₄⁺. When NH₄-Y is heated to the right temperature, the ammonium ion decomposes, releasing NH₃ (gas) and leaving behind highly acidic H-Y zeolite.

The relative acidity of zeolites depends on their Si/Al ratio (SAR). The SAR for a zeolite with high

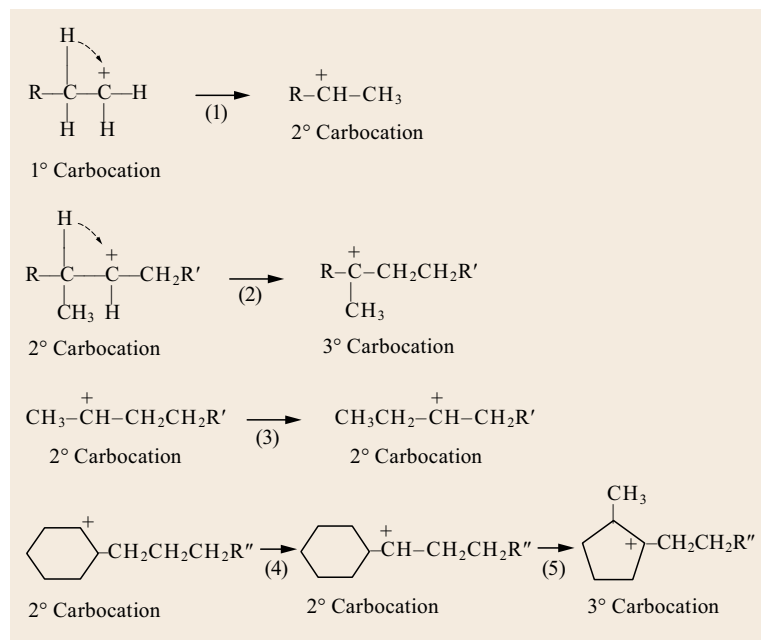


Fig. 22.20 Carbocation mechanism for hydrocracking: Hydride shift and skeletal isomerization

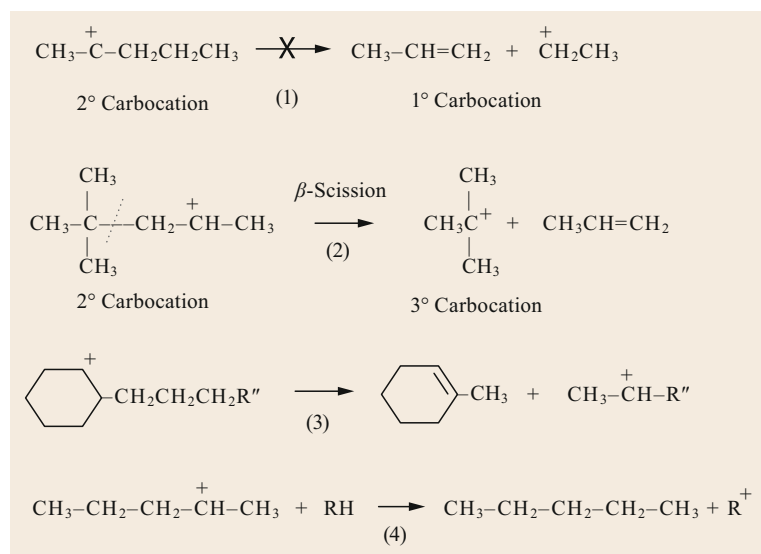


Fig. 22.21 Carbocation mechanism for hydrocracking: β -scission and hydrogen transfer. Scission occurs two carbons away from the positively charged carbon (C⁺), because scission beside the C⁺ would entail going from a relatively stable 3° or 2° carbocation to a less stable 1° carbocation

cracking activity can be < 10 . In hydrocracking catalysts with less activity but greater selectivity for production of middle distillates, the SAR might be > 100 .

Figures 22.19–22.22 illustrate the carbocation mechanism of catalytic hydrocracking at a more fundamental level [22.16]:

- Figure 22.19 shows how carbocations are formed, starting with generating an olefin by reversible dehydrogenation (reactions 1 and 3), forming a carbocation by proton addition at a Brønsted acid site (reactions 2 and 4), and hydride (H^-) abstraction at a Lewis acid site (reaction 5). Reaction 4 gives three products, which are in equilibrium.
- Figure 22.20 illustrates hydrogen shift and skeletal isomerization (alkyl shift) steps, which are driven by the relative stability of carbocations: $3^\circ > 2^\circ > 1^\circ$. In reaction 4, there are three canonical forms for the alkylcyclohexenyl cation.
- In Figure 22.21, we see cracking via β -scission, which means that scission occurs two carbons away from the positively charged carbon (C^+). Scission beside the C^+ does not occur, because it would entail going from a relatively stable 3° or 2° carbocation to a less stable 1° carbocation.
- Figure 22.22 shows how addition reactions generate larger molecules, including polyaromatics, which can condense to form coke. Such reactions are suppressed in hydrogen-rich environments, (i. e., in hydroprocessing units), but they become more significant at high temperatures, where olefins and especially aromatics are more thermochemically stable.

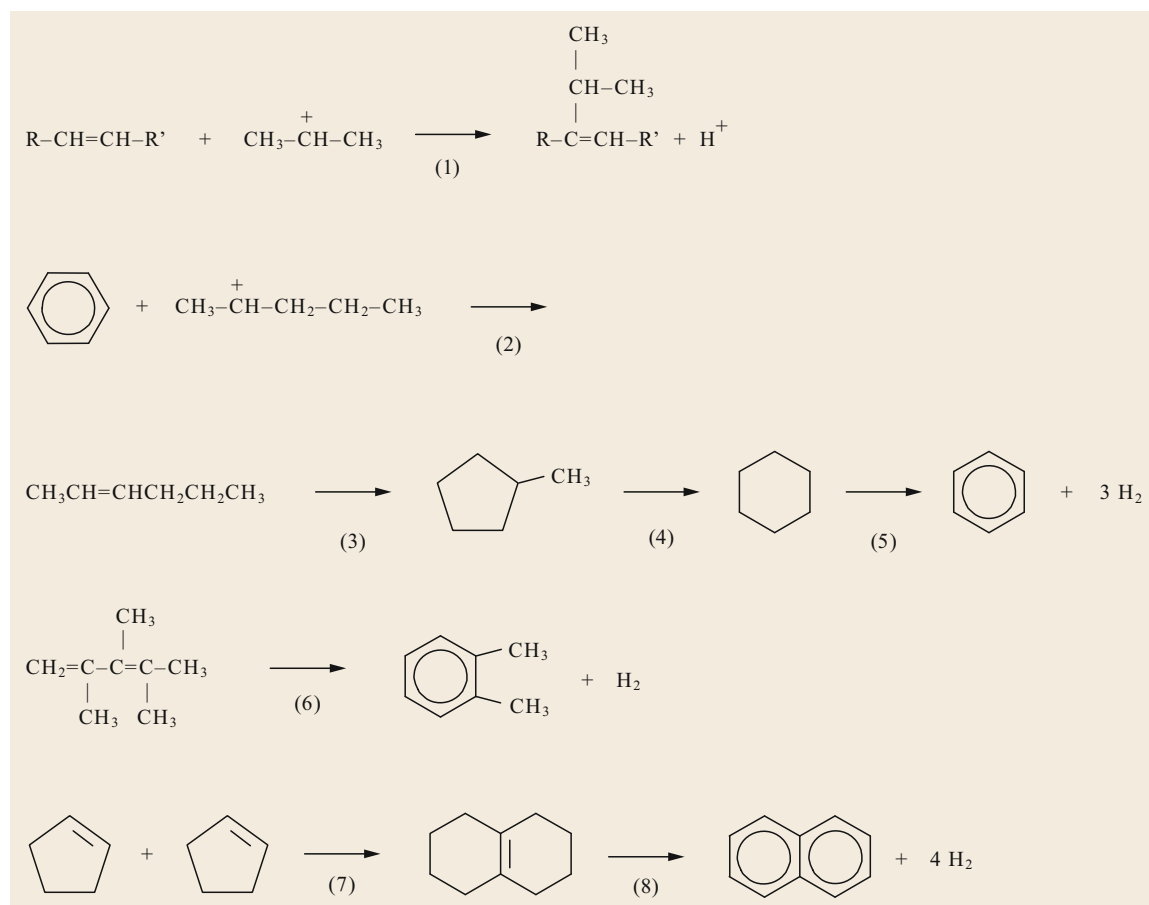


Fig. 22.22 Carbocation mechanism for hydrocracking: Ring formation and ring growth

22.6 Hydroprocessing Catalysts

22.6.1 Hydroprocessing Catalyst Overview

In fixed-bed hydroprocessing units, catalysts must be able to drive the desired reactions, and they also must possess a high surface area and great physical strength, enough strength to resist crushing under the forces imposed by rapidly flowing high-pressure fluids and the weight of the catalyst itself. A single bed can contain more than a hundred tons of catalyst.

Chemical reactions take place inside small pores, which account for almost all of the catalyst surface area. In hydrotreating catalysts, average pore diameters range from 75 to 85 Å for catalysts that process light and heavy gas oils. For catalysts that process residue, the average pore diameters range from 150 to 250 Å.

Catalyst Composition and Activation (Sulfiding)

Commercial hydrotreating catalysts comprise sulfides of either Mo or W promoted by Co or Ni on a support such as γ -alumina (Table 22.3). In a few tri-metallic catalysts, both Ni and Co are included. The Mo content ranges from about 16 to 24 wt% as the trioxide and the Ni or Co content ranges from 2.0 to 4.5 wt% as the oxides.

With noteworthy exceptions, the oxides are activated after loading by reductive sulfidation. (The exceptions include the use of Eurecat's Totsucat technology [22.17], which activates catalysts prior to delivery).

Nebula catalyst was jointly discovered and developed by ExxonMobil and Albemarle. Nebula is supported by base-metal oxides. Overall, it possesses higher activity than alumina-supported hydrotreating catalysts. It is especially good for HDN and saturation of aromatics [22.18].

Table 22.3 Supports used in hydroprocessing catalysts

Support	Major use	Acidity
γ -Alumina	Hydrotreating catalysts	Low
Amorphous aluminosilicates	Distillate-selective hydrocracking catalysts	High
Zeolites (H-Y and others)	High-activity hydrocracking catalysts	Very high

Table 22.4 Active metals used in hydroprocessing catalysts

Metals	Major use	Activation method	Hydrogenation activity
CoMo	HDS	Sulfiding	Moderate
NiMo	HDN, hydrocracking	Sulfiding	High
NiW	HDN, hydrocracking	Sulfiding	Higher
Pd, Pt ^a	Hydrocracking	Reduction by H ₂	Highest

^a Pd and Pt are poisoned by sulfur and are used in low-H₂S environments

Table 22.4 lists the active metals in hydrocracking catalysts. As with hydrotreating catalysts, hydrocracking catalysts are delivered as low-activity oxides and activated after loading. PdO is activated via reduction by hydrogen to the metal, and oxides of Ni, Mo and W are activated by reductive sulfidation.

Shown below are sulfiding chemical reactions. Reaction 5 shows the reductive decomposition of dimethyl disulfide (DMDS), which is the most common sulfiding agent. The exact compositions of the cobalt and nickel sulfides are not well established, but the reactions shown below are consistent with sulfur uptake [22.19]:

- $\text{MoO}_3 + 2\text{H}_2\text{S} + \text{H}_2 \rightarrow \text{MoS}_2 + 3\text{H}_2\text{O} + \text{heat}$
- $\text{WO}_3 + 2\text{H}_2\text{S} + \text{H}_2 \rightarrow \text{WS}_2 + 3\text{H}_2\text{O} + \text{heat}$
- $3\text{NiO} + 2\text{H}_2\text{S} + \text{H}_2 \rightarrow \text{Ni}_3\text{S}_2 + 3\text{H}_2\text{O} + \text{heat}$
- $9\text{CoO} + 8\text{H}_2\text{S} + \text{H}_2 \rightarrow \text{Co}_9\text{S}_8 + 9\text{H}_2\text{O} + \text{heat}$
- $\text{H}_3\text{C}-\text{S}-\text{S}-\text{CH}_3 + 3\text{H}_2 \rightarrow 2\text{H}_2\text{S} + 2\text{CH}_4 + \text{heat}$

Note that reactions 1 to 4 consume H₂ and H₂S, produce water, and generate heat. Reaction 5 consumes H₂ and produces methane and heat. The progress of sulfiding is monitored by observing these variables or the consequences thereof.

ASA Versus Zeolite

Figure 22.23 shows six zeolite structures [22.20]. In cracking catalysts, H-Y zeolite is the most common, but beta and ZSM-5 are used as well. ZSM-5 is a shape-selective zeolite made by including a soluble organic template in the mix of raw materials. Templates for this kind of synthesis are quaternary ammonium salts. ZSM-5 enhances distillate yields in FCC units. In hydroprocessing units, because of its unique pore structure, it selectively cracks waxy *n*-paraffins.

Related materials are used in other processes. For example, metal-promoted silica alumina phosphates such as SAPO-11 are used to isomerize normal paraffins in catalytic dewaxing units.

Figure 22.24 provides a conceptual comparison of amorphous ASA catalysts with crystalline zeolite catalysts. The pore diameters of H-Y zeolite catalysts are uniform and relatively small – around 7.5 Å, give or

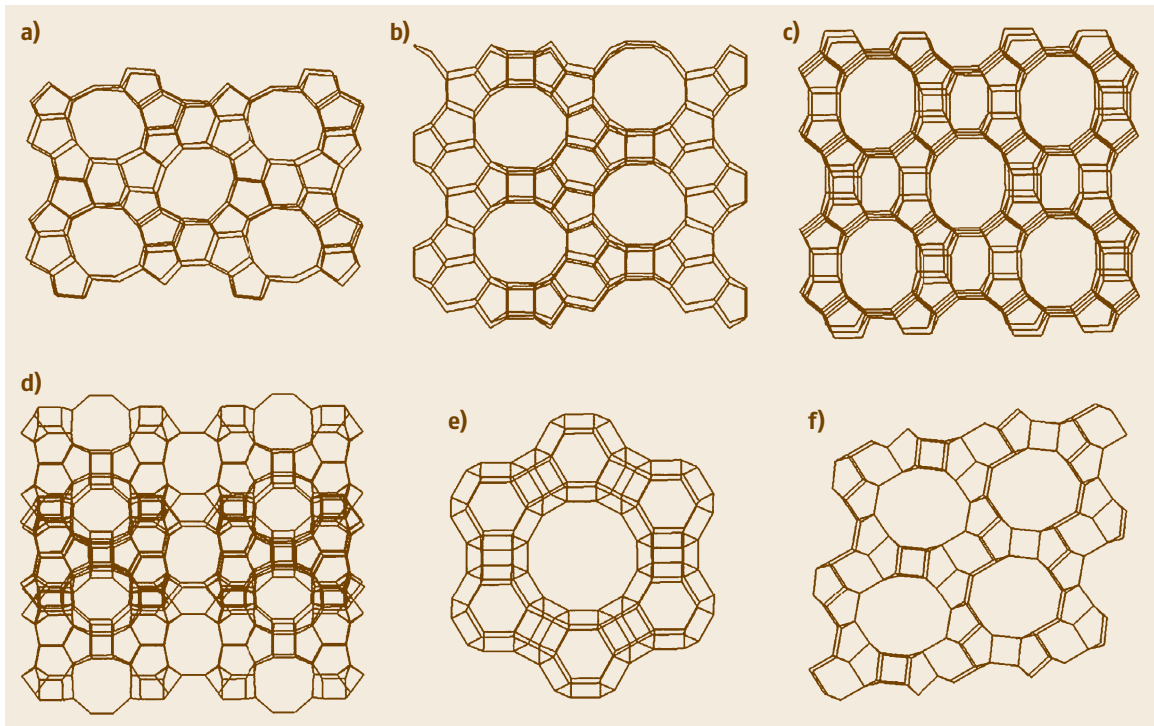


Fig. 22.23a–f Structures of zeolites ZSM-5 (a), mordenite (b), beta (c), MCM-22 (d), zeolite Y (e) and zeolite L (f)

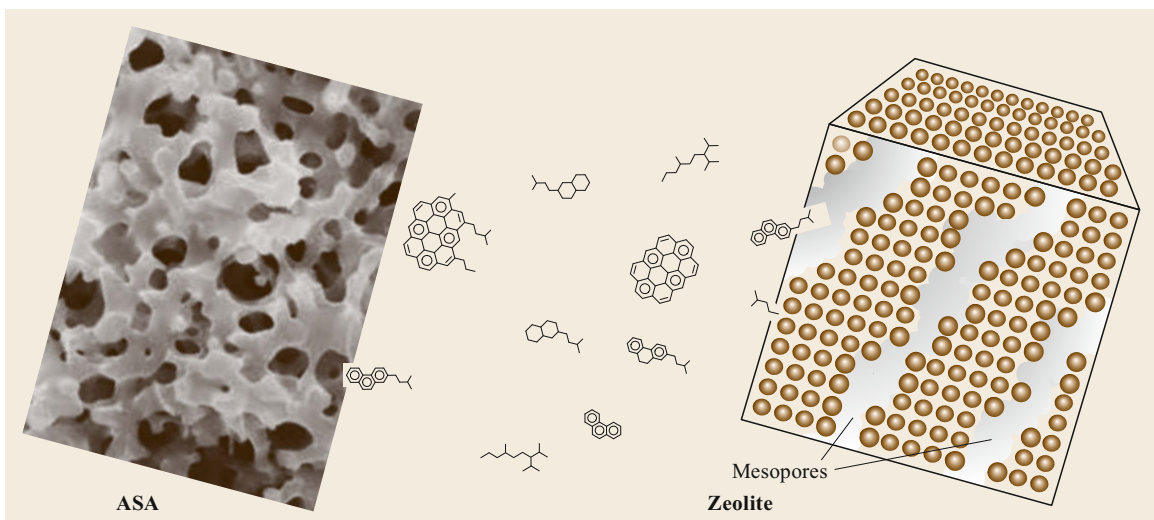


Fig. 22.24 Schematic comparison of amorphous alumina silica (ASA) and zeolite structures. ASA structure courtesy of Yabuki et al. [22.21]. Used with permission

take. The pore diameter for ZSM-5 is 6.3 Å. The mesopores of zeolites have larger diameters, which admit mid-sized molecules such as those found in vacuum gas oils.

ASA catalysts include small, medium, and large pores. The width of ASA pores can exceed 100 Å.

This explains why ASA catalysts do a better job of cracking feeds with higher endpoints. The larger pores can accommodate larger molecules. Recently, Chevron patented a method for making highly homogeneous ASA catalysts, which provide significantly better middle-distillate selectivity [22.22].

22.6.2 Catalyst Preparation

The following steps may be involved in preparing supported metal catalysts for fixed-bed hydrotreaters and hydrocrackers [22.23]:

- Precipitation
- Filtration (or centrifugation), washing, and drying

- Forming
- Calcining
- Comulling or impregnation
- Drying and final calcining.

For some catalysts, one or more of the above-listed steps are eliminated or additional steps are added. Figure 22.25 outlines possible procedures for synthesiz-

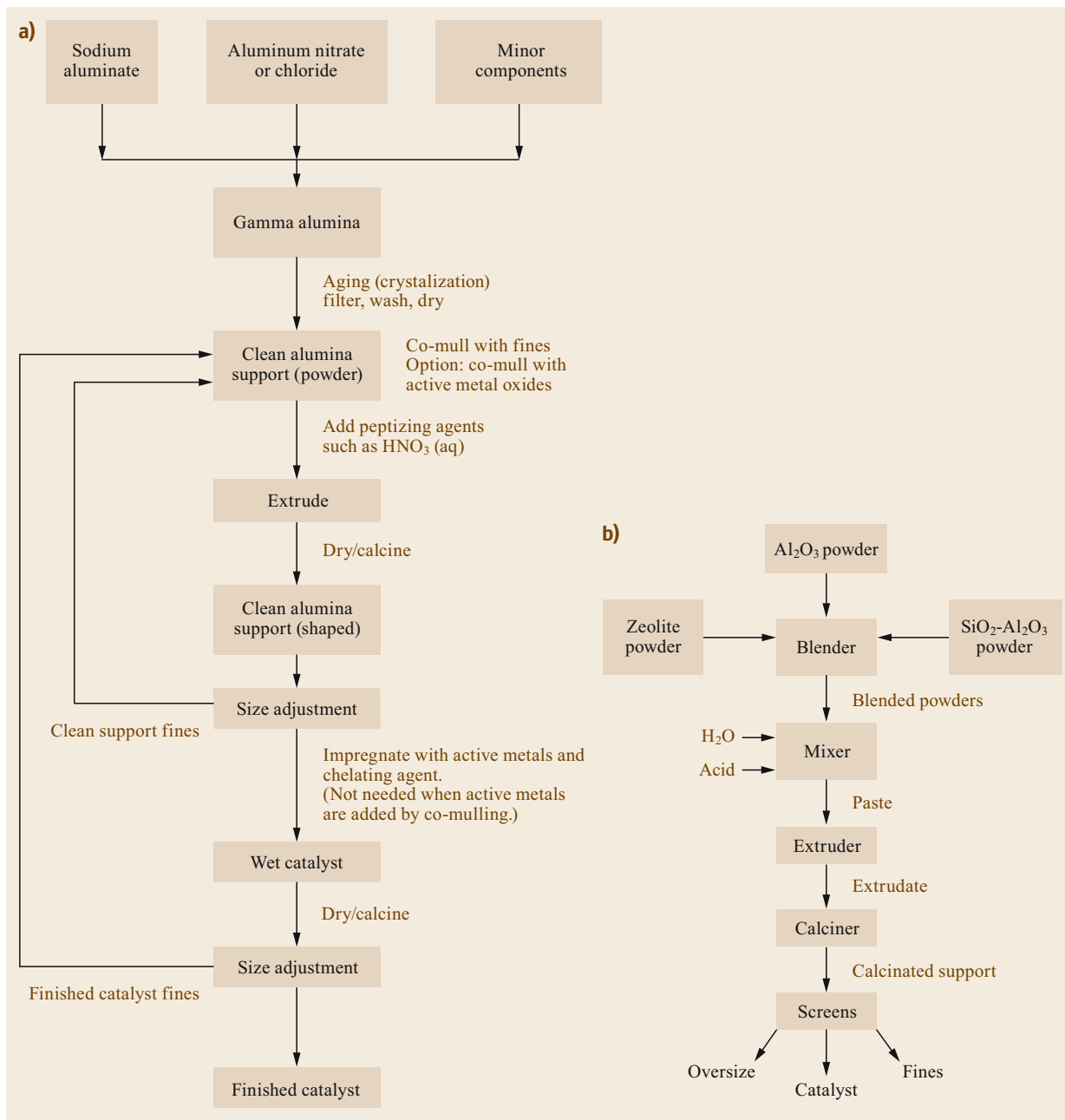


Fig. 22.25 (a) A synthesis procedure for hydrotreating catalysts. (b) A synthesis procedure for zeolite-containing hydrocracking catalysts

ing hydrotreating and hydrocracking catalysts, respectively.

Precipitation

The preferred alumina for hydrotreating catalyst supports is γ -alumina. In its final form, γ -alumina has a high surface area, great physical strength, and a well-defined pore size distribution. Its synthesis begins with mixing an aqueous solution of aluminum nitrate, $\text{Al}(\text{NO}_3)_3$, with sodium aluminate, $\text{Na}_2\text{Al}_2\text{O}_4$, to form aluminum hydroxide, $\text{Al}(\text{OH})_3$ and sodium nitrate. The $\text{Al}(\text{OH})_3$ forms a microcrystalline gelatinous solid. As the gel ages, crystals grow larger and the pore structure develops. Crystals are collected by filtration or centrifugation, then washed and dried.

Synthetic zeolites are prepared by precipitation from amorphous silica, sodium aluminate, and sodium hydroxide. The addition of seed crystals to the gel ensures that the right zeolite is formed and speeds up crystallization. The resulting Na-Y zeolite is exchanged with an ammonium salt to replace Na^+ with NH_4^+ . When $\text{NH}_4\text{-Y}$ is heated to the right temperature, the ammonium ion decomposes, releasing $\text{NH}_3(\text{gas})$ and leaving behind highly acid H-Y zeolite.

Filtration, Washing, and Drying

Filtration and washing removes undesired impurities. Subsequent air- and oven-drying removes most of the water and other volatile material. Washing requires tremendous amounts of water, because the finished product must be essentially sodium-free. Water treatment facilities can be costly to build and operate in locales with tight environmental regulations. Nearby chemical plants can accept offgases and waste water from catalyst plants and convert them into sales quality chemicals, such as nitric acid, sodium nitrate, and others.

Forming

Catalyst supports can be formed into pellets, powders, spheres, cylinders, hollow cylinders, shaped extrudates, and other forms. To make extrudates, pastes are formed from powders by mixing them with acids and solvents. The powders are either pure supports or supports commulled with active metal oxides. The pastes are forced through a die, from which they emerge as long strands that resemble spaghetti, but with a cross-sectional shape that resembles a 3-leaf or 4-leaf clover. The resulting spaghetti-like strands are dried and broken into short pieces with length-diameter ratios (L-D) ranging from 2 to 20. Screening rejects the longs and shorts, leaving behind material with L-Ds between 3 and 6. The long and short are returned to a previous step. The extrusion pressure, the acid strength, and the choice of

solvent affect the catalyst surface area and average pore size.

Multilobe extrudates have a higher surface-to-volume ratio than cylindrical extrudates and the average distance from the surface to the center of a particle is substantially shorter. If all else is constant, multilobe catalysts can be 40% more active than cylindrical. *Topsoe* et al. [22.2, p.23] present a description of the impact of shape on catalyst activity, pressure drop, and diffusional restrictions.

Figure 22.26 shows some common shapes for catalysts and supports. The shaped extrudate in the figure is a trilobe. Extrudate diameters range from 1.3 to 6 mm (1/20–1/4 in). For hydrocracking catalysts, Criterion Catalysts and Technologies offers a modified trilobe that gives lower pressure drop. Diameters for pellets, such as the wagon wheel shown in the figure, tend to be larger – up to 25 mm (1 in). Diameters for spherical silica support balls range from 3 to 25 mm (1/8–1 in).

Fine powders are made by spray-drying. To produce spherical catalysts, liquids are sprayed onto powders in a tilted rotating pan, or slurries are dripped into hot oil. Pellets, medallions, bow ties etc. are made by extrusion or by compressing powders in a dye.

Sizing

Figure 22.25 (above) identifies two size-adjustment steps. Sizing is a key step. High pressure drop results from loading shaped extrudates with a wide range of L-Ds.

Calcining

Calcination decomposes any remaining ammonium and nitrate. It also hardens the particles and increases surface area. If the calcination temperature gets too high, γ -alumina transforms into α -alumina or β -

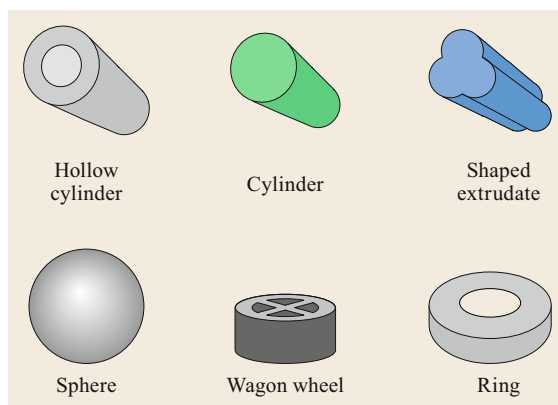


Fig. 22.26 Common shapes for supports and catalysts. NiMo catalysts are light green, while CoMo catalysts are deep blue

alumina, for which physical properties are far less desirable; specifically, the surface area is significantly lower.

Impregnation

During impregnation, the pores of a calcined support are filled with a metal-containing solution. Pores in the support suck up the solution with capillary action. In the *incipient wetness* method, precise amounts of solution are added – just enough to leave the support dry to the touch. After a drying step, the nascent catalyst may

be treated with more solution to increase metals loading.

During dip impregnation, supports are soaked in a solution of metal salts for several minutes.

Comulling

Catalysts can be made by comulling metal oxides with the support prior to extrusion. Comulling costs less because it requires fewer steps. The method provides formulation flexibility, because it is not limited by the solubility of metal salts.

22.7 Catalyst Cycles

Catalysts in fixed-bed process units, including hydrotreaters and hydrocrackers, do not last forever. Over time, because of feed contamination, routine coking and process upsets, the catalysts lose activity. In hydrotreaters and hydrocrackers, temperatures are increased to compensate for activity loss. When the required catalyst temperature nears the safe maximum, refiners can shut the unit down and change the catalyst during a so-called turnaround. In some cases they elect to extend a run for a short time by lowering the feed rate, switching to easier feeds and decreasing conversion. But at some point, a turnaround becomes necessary.

A planned turnaround seldom includes just one single unit. At a refinery in Louisiana, turning around the hydrocracking unit (HCU) affects at least seven other units. Liquid feed to the HCU comes from the vacuum distillation unit (VDU) and the delayed coking unit (DCU). The HCU takes hydrogen from a catalytic reforming unit (CRU), the onsite steam-methane reformer (SMR), and an offsite supplier. Light naphtha from the HCU goes through a sulfur absorber to the gasoline blending pool. The heavy naphtha goes to the CRU. The HCU unconverted oil goes to the FCC unit.

Before a planned turnaround, measures are taken to minimize business disruption. Inside the plant, operators build inventories of intermediate streams, such as heavy naphtha for the CRU and hydrotreated VGO for the FCC. Product storage tanks are filled. In some cases, exchange contracts are executed with other companies; the refinery arranges to purchase products from another plant to meet its sales commitments. If revamps or new construction are planned to coincide with the turnaround, equipment must be onsite and ready to install. Orders are placed for catalysts and chemicals. Arrangements are made to accommodate the hundreds of contract personnel who will be doing most of the work.

During a planned turnaround, spent catalysts are unloaded and shipped offsite for regeneration or dis-

posal. Reactors and other equipment are inspected and serviced. Maintenance work is performed. Piping and other connections are made between new and existing equipment. In hydrotreaters and hydrocrackers, catalysts are loaded and activated, which may require large amounts of chemicals such as ammonia or dimethyl disulfide.

An unplanned HCU shutdown often costs several times more than a planned turnaround. The impact on other units is sudden and unexpected. It is relatively easy to put an SMR into hot standby, but units that normally get feed from the HCU may have to shut down or limp along at half rate for weeks. The refiner might have to delay or default on commitments to customers. Weeks can be lost waiting for catalysts, chemicals, and maintenance teams. In a recent instance, an emergency shutdown lasted 28 days. Lost HCU production amounted to \$1 million per day. Throughout the refinery, business interruption losses were even greater.

22.7.1 Catalyst Cycle Life

In turnaround planning, predicting catalyst cycle life is crucial. Cycles can be as short as 12 months and we have seen a few that lasted > 40 months. Two-year cycles are typical.

At the start of a cycle, average reactor temperatures are low – about 315–360 °C (600–680 °F). As the cycle proceeds, the catalyst deactivates and refiners must raise temperatures to maintain product qualities or conversion.

A catalyst cycle is terminated for one or more of the following reasons:

1. *Planned shutdown.*
2. *Temperature limits:* To ensure safe operation, licensors specify limits on average reactor temperature, maximum peak temperature, and maximum bed temperature rise. *Note:* For high-zeolite catalysts,

typical values are 415 °C (780 °F) (max average) and 427 °C (800 °F) (max peak). For less-active catalysts, the limits may be higher: 427 °C (800 °F) (max average) and 440 °C (825 °F) (max peak). As hydrocrackers approach these limits, process economics may suffer. High temperatures increase yields of low-value C₁–C₄ and light naphtha. Middle distillate quality suffers from high aromatics, which decrease smoke point and cetane. Units approach temperature limits gradually, so usually there is ample warning that end-of-run is approaching. Possible responses are to extend the cycle by operating at reduced feed rate or with an easier feedstock, or change the turnaround schedule.

3. **Excessive dP:** The overall pressure drop (dP) in a hydroprocessing unit is the difference in pressure between the recycle compressor suction and the recycle compressor discharge. It includes dP through high-pressure pipes and heat exchangers. At start-of-run (SOR), the dP across the reactor is low – 3–10 psi (0.2–0.7 bar) for each bed. As a run proceeds, dP across the catalyst increases. If the dP exceeds the design limit, little can be done to keep the unit running without damaging reactor internals. Most often, dP and dP+ are greatest in the first catalyst bed, which is most susceptible to fouling by trace metals, particulates, and gum formation. But we have seen instances where, due to a combination of high operating temperature and hydrogen starvation, the dP in the last bed of a hydrotreating reactor was higher than the dP in the top bed. Hydrogen starvation occurs when the hydrogen–oil (H₂OR) ratio is too low – less than about 1000 scf/bbl (175 Nm³/m³) in a hydrotreating bed and less than about 5000 scf/bbl (875 Nm³/m³) in a hydrocracking bed. A related parameter is hydrogen availability – the ratio of circulating hydrogen to hydrogen consumption. Guidelines for hydrogen availability vary from source to source, but typical recommendations are > 3 for hydrotreaters processing straight-run feedstocks and > 5 for hydrocrackers and hydrotreaters processing reactive feedstocks. While it's possible to operate at lower H₂OR, minor process upsets, including small changes in feed quality, have a larger impact. The flow distribution degrades and coke formation increases.
4. **Process upset:** Upsets include equipment failure, power failure, and sudden changes in feed quality. For a fixed-bed VGO hydrotreater, a *burp* in an upstream VDU can send a slug of residue to the unit, fouling it with particulates, asphaltenes, and/or refractory carbon. This can poison large amounts of catalyst or increase dP beyond the design limit. If the fouling is confined to the top few feet of the first

catalyst bed, the ruined catalyst can be vacuumed out and replaced within a week or so. With modern instrumentation, diligent process monitoring and proactive maintenance, most equipment problems can be detected before a failure occurs.

5. **Emergency shutdown of a related unit:** Related units include upstream hydrogen sources, sources of liquid feed, downstream units for which the hydroprocessing unit supplies feed and refinery utilities. Hydroprocessing units which get feed from intermediate tankage might be able to keep running despite temporary feed disruptions. Hydroprocessing products can be traded if they can't be used in the usual way. If hydrogen supply is reduced or lost, it may be possible to operate briefly in standby mode, by continuing to run the recycle gas compressor and lowering temperatures to reduce conversion.

Process variables with significant impact on catalyst deactivation are shown in Table 22.5.

Hydrogen keeps catalysts clean by inhibiting coke formation. This explains why increasing the hydrogen partial pressure decreases the rate of catalyst deactivation. Raising the temperature increases the rates of most hydrocracking reactions, including coke formation. Raising the H₂OR increases heat removal, which limits temperature rise. If the feed rate goes up and targets for HDS, HDN, or conversion remain the same, the temperature must go up. If the feed rate goes up and the temperature does not, then HDS, HDN, or conversion

Table 22.5 Factors affecting catalyst cycle life

	Impact	Comment
Higher H ₂ partial pressure	+	
Higher recycle gas rate	+	Increases H ₂ partial pressure
Higher makeup gas purity	+	Increases H ₂ partial pressure
Increased purge of recycle gas	+	Increases H ₂ partial pressure
Higher fresh feed rate	–	
Higher conversion	–	
Higher fresh feed endpoint	–	Increases catalyst coking. Also can increase dP and dP+
Higher fresh feed impurities ^a	–	Related to feed type and feed endpoint
Process upsets ^b	–	

^a For cycle life, the worst feed impurities are refractory carbon, asphaltenes, trace elements and particulate matter (coke fines, FCC catalyst fines)

^b Process upsets include *burps* in upstream units that feed the hydrocracker, equipment failures, or temperature excursions requiring depressuring

will decrease. Increasing the feed endpoint and/or density tends to increase the amount of coke precursors in the feed. The precursors include asphaltenes, refractory carbon, and poly-ring compounds.

An important aspect of turnaround planning is projecting catalyst life for fixed-bed process units. For decades, refiners have accomplished such projections with average catalyst temperature calculations, such as CAT and WABT.

22.7.2 Catalyst Selection and Loading

Designing catalyst loading schemes for a fixed-bed hydroprocessing unit is more sophisticated than ever. In the 1970s, refiners tended to use one main catalyst in each bed, supported by inert ceramic balls at the bottom and held down by a thin layer of inert balls at the top. A bed might contain a layer of regenerated catalyst or left-over catalyst from the warehouse. So-called trash baskets were embedded at the top to catch particulates. Post-treat catalyst was loaded at the bottom of the last hydrocracking bed to remove light mercaptans.

The historical approach to hydrotreating catalyst selection was to use CoMo catalysts for HDS and NiMo catalysts for HDN. NiMo catalysts were also preferred for saturation of aromatics.

Today, suppliers offer arsenals of guard materials that improve removal of particulates and capture specific contaminants. Figure 22.27 shows an example. Five layers of inerts and catalysts protect the main catalysts from particulates, soluble contaminants, and products of unwanted reactions. The top layer is comprised of inert particles with considerable void volume. It filters out large particulates, allowing smaller particles into the second layer. Second-layer particles are smaller, have a different shape and possess a bit of activity. The low activity removes peroxides and diolefins gradually with low gum formation. Layers may be contaminant-specific. Special high-nickel catalysts remove arsenic. Wide-pore catalysts remove Ni, V, and CCR. High-surface-area catalysts remove Si. Successive layers contain smaller and smaller particles with higher and higher activity.

It is common to see two or more main catalysts in a diesel hydrotreater. An effective configuration is a sandwich – CoMo/NiMo/CoMo. The top CoMo layer takes out easy sulfur without excessive heat release from aromatics saturation. The NiMo then provides saturation, which is a prerequisite for deep HDS. The bottom CoMo layer completes the job.

The main job of the pretreat section in a hydrocracker is nitrogen removal. Section 22.4.4 explains why saturation of aromatics is important for HDN. Pretreat



Fig. 22.27 Catalyst grading scheme for the first bed of a fixed-bed catalytic hydrotreater (courtesy of Haldor Topsøe A/S)

process conditions are catalysts are selected according to process objectives. The PH₂ is relatively high – with few exceptions it is greater than 1400 psi (95 bar) – the main catalyst is NiMo. Criterion used to recommend a low-activity hydrocracking catalyst for the bottom of pretreat sections, purportedly to enhance HDN by opening saturated rings. CLG offers hydrotreating catalysts into which cracking activity can be added as needed.

Options for hydrocracking catalysts have also expanded. Today's catalysts might contain both ASA and Y zeolite, SAPO and a dewaxing component. Non-noble active metals can be NiMo or NiW.

To get the best from any vendor, a customer must develop clear objectives and explain them clearly. It is important to know the following:

- *Operating conditions and constraints:* Expected feed rate, feed rate limitations, mechanical pressure,

hydrogen availability, hydrogen composition, temperature limitations

- *Physical and chemical properties for each feedstock:* Density, distillation, sulfur, nitrogen, oxygen, aromatics, carbon residue (CCR), trace contaminants
- *Product objectives:* Maximum diesel, maximum naphtha, maximum conversion etc.
- *Desired flexibility:* For seasonal changes, batch operation etc.
- *Information from previous catalyst cycles*
- *Product property specifications.*

Arguably, the last two points are the most important. If pressure-drop buildup (dP+) has always limited catalyst cycles, it is more important to mitigate dP+ than to maximize catalyst activity. When asked for product property requirements for a particular unit, an engineer might say, for example, *maximize Euro 5 diesel*. This is an easy answer to give, but it may not be the best. On the one hand, with a moderate-activity diesel-selective catalyst, it may not be feasible to convert high-density FCC heavy cycle oil into low-density Euro 5 diesel at full feed rate. On the other hand, with a higher-activity catalyst, it might be possible to meet the density spec., but diesel yields would suffer due to over-conversion. Refinery products are blends of streams from several sources. Not all streams must meet every specification. If the hydrocracker product meets all specifications but density with a diesel-selective catalyst, the engineer should consider a density deviation, which would increase hydrocracker diesel yields and maximize Euro 5 diesel for the entire refinery.

Poor catalyst loading limits the capability of any fixed-bed process unit. In hydroprocessing, loading affects flow distribution, dP, and dP+. Uneven flow distribution shortens catalyst life and can degrade product quality. Poor distribution can create hot spots, which have caused temperature excursions and loss of containment.

Cylindrical catalysts and shaped extrudates can be loaded in one of two ways – sock loading and dense loading. A chapter by A. Gruia describes the two and provides a useful comparison [22.24]. In either case, to ensure that loading is safe and goes according to plan, considerable pre-work is required. A simple but important task is to mark desired loading heights on the inside reactor wall. When the catalyst reaches a loading mark, the loading is paused, either to measure level, measure the loaded density, or switch to a different catalyst. The loading is then resumed.

In sock loading, a canvas sleeve conveys the catalyst from a funnel at the top of the reactor down to the loading point. At the loading point, a worker moves the sock

around to distribute the catalyst as evenly as s/he can. The worker must wear a harness, carry a supply of fresh air for breathing and should (but doesn't always) wear weight-distribution shoes (snow shoes) to minimize catalyst crushing. The orientation of sock-loaded particles is random – horizontal, vertical and in between – leaving a lot of void space. During subsequent operations, under pressure from considerable mass flux, the bed settles and the void space shrinks.

In dense loading, a special device lines up the catalyst particles as they fall, either freely or propelled by air or nitrogen. The particles land with a much more uniform orientation [22.25]. One can visualize the difference between dense and sock loading by comparing a new box of toothpicks, in which all the toothpicks are lined up in parallel, versus the pile created by spilling the toothpicks into a tall jar. Dense loading can increase the amount of catalyst in a bed by up to 17%. It can improve flow distribution during operation. Arguably, dense loading leads to safer operation, because generally it is more uniform and less likely to create maldistribution of flow. It doesn't require a person inside the reactor to level the catalyst periodically with a rake or broom. Dense loading does increase SOR dP, so despite the many advantages of dense loading, several customers sock-load reactors in which they have experienced cycle-limiting dP+ in previous cycles.

Support balls and top-of-bed grading are sock loaded. Experience shows that good sock loading can be better than poor dense loading, which can be very bad indeed. If dense-loaded catalyst is uniformly bowed or domed, flow distribution will be poor during subsequent operation. Poor distribution only gets worse as catalyst cycle proceeds.

22.7.3 Activation of Non-Noble-Metal Catalysts in Fixed-Bed Units

Chapter 2 shows that an inordinately large percentage of accidents occur during maintenance shutdowns. Why? Because turnarounds are infrequent, occurring during a month or two every two or three years. Engineering managers assign inexperienced engineers to lead the effort. Under relentless pressure from executive management, planning managers push hard to cut maintenance, purchase cheap materials and substandard equipment. Staffing plans are inadequate, prepared without accounting for delays, which are inevitable when planning is done by poorly managed people.

In this section, we discuss some tricks of the startup trade, tricks which might be useful to the inexperienced. Our information is general. For specific catalysts in specific units, it is best to follow the guidance of your licenser or catalyst vendor.

Throughout the startup of a hydroprocessing unit, the makeup and recycle gas compressors are critical. Operators should monitor compressor vibration and power consumption. *High amps* correspond to high recycle-gas molecular weight. The molecular weight can be reduced by purging recycle gas.

Sulfiding is conducted either by dry or wet procedures. In dry sulfiding, no oil is added until sulfiding is complete. In wet sulfiding, oil is flushed through the catalyst before sulfiding begins. Because of heat of adsorption, wetting the catalyst with oil generates exotherms; we have seen wetting-induced temperature rises of 55 °C (130 °F). Fortunately, wetting is a one-time physical process, not an ongoing chemical reaction. The temperature drops within minutes after the heat wave passes.

Many modern hydrotreating catalysts require wet sulfiding. As delivered, these *type II* catalysts contain organometallic compounds, which encourage the stacking of MoS₂ slabs on the catalyst during activation. The slabs are stabilized by startup oil. After wetting, the catalyst temperature is raised to just above the decomposition temperature of the sulfiding agent, which is > 205 °C for DMDS (dimethyl disulfide). DMDS is injected at a rate determined by observations, primarily temperature rise. Injection continues at 205–210 °C (400–420 °F) until breakthrough – the point at which significant amounts of H₂S appear in the recycle gas. After a hold, during which breakthrough is verified, the heating resumes until the catalyst temperature reaches the target specified by the supplier, somewhere between 330 and 345 °C (625–650 °F). Sulfiding is done when the catalyst stops consuming H₂S.

During *dry sulfiding*, a mixture containing 0.5–2 vol.% H₂S in hydrogen is circulated through the catalyst. The temperature is increased slowly to the temperature at which the unit is expected to operate. The process continues until the exit gas contains the same amount of H₂S as the inlet gas. During dry sulfiding, no liquid is present to soak up reaction heat. Consequently, controlling exotherms can be quite a challenge.

Preactivated catalysts [22.26] are available for a small surcharge. Using such catalysts can shorten a startup by a day or so. The biggest advantage is a decrease in nuisance. The smell associated with sulfiding agents can cause complaints in urban areas.

Older pre-sulfurized catalysts were only partially activated prior to loading. Additional sulfur was included as elemental sulfur, which reacted with H₂ to form H₂S inside the reactor. Such catalysts tended to auto-ignite when exposed to air, with unpleasant consequences.

22.7.4 Activation of Noble-Metal Hydrocracking Catalysts

Noble-metal hydrocracking catalysts contain small amounts of highly dispersed platinum or palladium. These metals are expensive, but their concentrations are low – 0.6–1.0 wt%. Their superior hydrogenation activity often justifies the extra cost. The metals are added to the catalysts by impregnation with tetra ammine complexes – Pt(NH₃)₄²⁺ or Pd(NH₃)₄²⁺. When the catalysts are heated in air to about 840 °F (450 °C), the complexes decompose, giving off ammonia and leaving behind divalent metal oxides.

In commercial hydrocrackers, catalysts containing noble-metal oxides are activated by direct reduction with high-pressure hydrogen at 700 °F (350 °C).

22.7.5 Catalyst Regeneration and Rejuvenation

After working 24/7 for years in a fixed-bed hydroprocessing unit, a catalyst is spent, in part due to trace element poisoning and in part due to agglomeration of active metals, but mostly due to coking. The entire unit is shut down and the catalyst is removed. It takes several days to unload catalysts, a few weeks to inspect, service and repair equipment and a week to load and activate replacement catalysts. Most refiners reload hydrocrackers with fresh catalysts. Spent catalysts go to an off-site facility, where they are disposed of or regenerated by controlled combustion. During combustion, accumulated coke is converted to CO₂ and CO plus small amounts of SO₂ and NO_x, which are formed from the sulfur and nitrogen in the coke. Typical temperatures for regeneration in air are 400–500 °C (750–930 °F).

The regenerated catalyst may also undergo rejuvenation, a wet process in which the active metals are chemically re-dispersed. A combination of regeneration and rejuvenation can restore a catalyst to more than 95% of its original activity.

Inevitably, some particles break apart during the unloading, transportation, regeneration, and rejuvenation of spent catalysts. If part of the catalyst is contaminated with excessive amounts of trace elements, that part is sent to a catalyst reclamation company or a hazardous waste disposal company. Losses due to fragmentation and fouling can exceed 10%.

In the bad old days, regeneration meant burning coke off the catalyst while it was still inside the reactor. Today, in situ regeneration is rare because it is hard to control. A poor regeneration is costly, because afterwards the unit's performance will be poor. With a crippled catalyst, the unit may have to limp along for several months at lower feed rates and/or lower severity.

Worst of all, the catalyst won't last long, which means that it will have to be regenerated or replaced sooner rather than later.

22.7.6 Catalyst Reclamation

Even though noble-metal hydrocracking catalysts contain only small amounts of Pd or Pt, these metals are so valuable that recovering them is cost-effective. Other hydroprocessing catalysts contain Mo, W, Ni, and/or Co. Spent hydrotreating catalysts – especially those used to hydrotreat residue – can be very rich in nickel and vanadium, richer than natural ores.

Reclamation companies convert these materials into salable products using different combinations of oxidation, pyrolysis, dissolution in acid or alkali, precipitation, extraction, or ion exchange. Depending on the reclamation procedure, the salable products may include the materials shown in Table 22.6.

Table 22.6 Partial list of materials sold by catalyst reclamation companies

Material	Formula
Palladium metal or chloride salt	Pd or Na ₂ PdCl ₄
Platinum metal or chloride salt	Pt or Na ₂ PtCl ₄
Molybdenum trisulfide	MoS ₃
Molybdenum oxide	MoO ₃
Ammonium molybdate	(NH ₄) ₂ Mo ₄ O ₁₃ · 2H ₂ O
Sodium molybdate	Na ₂ MoO ₄ · 2H ₂ O
Tungsten trioxide	WO ₃
Ammonium para-tungstate	(NH ₄) ₁₀ W ₁₂ O ₄₁ · 5H ₂ O
Sodium tungstate	Na ₂ WO ₄ · 2H ₂ O
Vanadium pentoxide	V ₂ O ₅
Sodium (meta) vanadate	NaVO ₃
Nickel metal or chloride	Ni or NiCl ₂
Cobalt metal or chloride	Co or CoCl ₂
Nickel-cobalt concentrate	Ni _x Co _y
Iron-molybdenum concentrate	Fe _x Mo _y
Alumina hydrate	Al ₂ O ₃ · 3H ₂ O

22.8 Hydroprocessing Thermochemistry

Hydrotreating and hydrocracking generate heat. For hydrocracking, the first reaction step requires bond breaking, which is endothermic. The reactive intermediates undergo rearrangement, hydrogenation, and other reactions, which in toto are highly exothermic. The design and operation of commercial hydroprocessing units revolve around heat control. Loss of heat control can cause a temperature excursion. Minor excursions can lead to lost production and decreased catalyst life. Major excursions have caused loss of containment, consequent explosions, and, in at least one case, a fatality.

Fully rigorous reaction thermochemistry would be based on pure-component heats of formation, molar heat capacity, and heats of vaporization. Correc-

tions would be made for molecular interactions and temperature-dependent enthalpies of formation. But typical hydrocracker feeds contain hundreds of thousands of different molecules. It may never be possible to identify all of them. To isolate them and determine their individual properties is inconceivable. But with far less analytical rigor, we have done a decent job of designing and operating hundreds of commercial hydroprocessing units, some of which are more than 50 years old. With judicious assumptions and thermochemical data for selected model compounds, we can predict commercial performance with adequate fidelity.

The next three tables quantify heat release for the major hydroprocessing reactions, with pure-compound reactions as examples. Table 22.7 shows enthalpies of

Table 22.7 Calculated enthalpies of reaction at standard temperature and pressure for representative hydrotreating and hydrocracking reactions

No.	Reaction type	ΔH_R at STP (kJ/mol)	per H ₂ consumed
Olefin saturation		Average =	-116.3
1.	Propylene + H ₂ → propane	-125.0	-125.0
2.	2,2-Dimethyl-3-hexene + H ₂ → hexane, 2,2-dimethyl	-106.6	-106.1
3.	Styrene + H ₂ → ethylbenzene	-117.0	-117.0
Aromatics saturation		Typical =	-66.6
4.	Benzene + 3 H ₂ ⇌ cyclohexane	-207.5	-69.2
5.	Naphthalene + 2 H ₂ ⇌ tetralin	-120.0	-60.0
6.	Tetralin + 3 H ₂ ⇌ decalin	-212.2	-70.7

^a Intermediate step, no H₂S or NH₃ produced

Table 22.7 (continued)

No.	Reaction type	ΔH_R at STP (kJ/mol)	per H ₂ consumed
Hydrodeoxygenation of ethers (HDO)		Typical =	-52.4
7.	<i>n</i> -Butylether + 2 H ₂ → 2 <i>n</i> -butane + H ₂ O	-104.8	-52.4
Hydrodesulfurization (HDS)		Average =	-52.0
8.	Dibutylsulfide + 3 H ₂ → 2 <i>n</i> -butane + 2 H ₂ S	-150.2	-50.1
9.	Thiophene + 2 H ₂ → tetrahydrothiophene ^a	-150.0	-75.0
10.	Tetrahydrothiophene + 2 H ₂ → <i>n</i> -butane + H ₂ S	-112.1	-56.1
11.	Benzothiophene + 3 H ₂ → ethylbenzene + H ₂ S	-156.6	-52.2
12.	Dibenzothiophene + 2 H ₂ → biphenyl + H ₂ S	-53.3	-26.7
Hydrodenitrogenation (HDN)		Average =	-62.9
13.	Dipropylamine + 2 H ₂ → 2 propane + NH ₃	-119.3	-59.7
14.	Pyridine + 3 H ₂ → piperidine ^a	-187.4	-62.5
15.	Piperidine + 2 H ₂ → <i>n</i> -pentane + NH ₃	-145.9	-72.9
16.	Quinoline + 2 H ₂ → quinoline, 1, 2, 3, 4-tetrahydro ^a	-118.5	-59.3
17.	1,2,3,4-Tetrahydroquino + 2 H ₂ → benzene,propyl- + NH ₃	-120.4	-60.2
Hydrocracking		Average =	-51.2
18.	Eicosane + H ₂ → 2 nonane, 2-methyl	-64.6	-64.6
19.	<i>n</i> -Hexadecane + H ₂ → 2 isoctane	-56.1	-56.1
20.	Ethylcyclohexane + H ₂ → heptane, 2-methyl	-42.4	-42.4
21.	Butylbenzene + H ₂ → toluene + propane	-41.8	-41.8
Isomerization		Average =	-9.6
22.	<i>n</i> -Butane → isobutane	-8.6	
23.	<i>n</i> -Decane → nonane, 2-methyl	-10.5	
Other			
24.	CO ₂ + 4 H ₂ → methane + 2 H ₂ O(g)	-56.5	-14.1
25.	CO + 3 H ₂ → methane + H ₂ O(g)	-151.9	-50.6

^a Intermediate step, no H₂S or NH₃ produced

reaction for several hydroprocessing reactions at standard temperature and pressure (STP), organized by reaction type. Reactions 18 through 21 are hydrocracking reactions, in which C–C bonds are broken. All others are hydrotreating reactions. Reactions 9 and 16 are saturation reactions. They appear in the HDS and HDN categories, respectively, because they are mechanistic intermediates. The first column of numbers shows the results of heat-of-reaction calculations per mole of hydrocarbon reactant. The second column shows re-

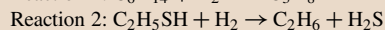
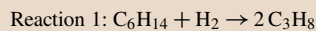
sults per mole of H₂ consumed. Isomerization does not consume hydrogen, but it does release heat because branched isomers are more stable than straight-chain isomers. At STP, saturation of olefins generates the most heat per mole of hydrocarbon. Saturation of aromatics generates the most heat per mole of reactant and more heat per mole of H₂ than HDS, HDN, and hydrocracking. In the absence of cracking and at mod-

Table 22.8 Selected average bond lengths and energy

Bond	Length (pm)	Energy (kJ/mol)	Bond	Length (pm)	Energy (kJ/mol)
C–H	109	413	H–H	74	436
C–C	154	348	H–N	101	391
C=C	134	614	H–O	96	366
C≡C	120	839	H–S	–	347
C–N	147	308	N–N	145	170
C–O	143	360	N≡N	110	945
C=O	–	745	O–O	148	145
C=O	in CO ₂	803	O=O	121	498
C–S	182	272	S–S	–	266

Table 22.9 Heats of reaction (kJ/mol) calculated from bond energies compared to heats of reaction calculated from heats of formation. Reaction 1 shows the hydrocracking of *n*-hexane and reaction 2 shows the HDS of ethyl sulfide

Reaction	Bonds broken	Bonds formed	Net bond energy	Calc. from ΔH_f
1.	C–C, H–H	2 C–H	-42	-42.3
2.	C–S, H–H	C–H, S–H	-52	-58



erate temperatures, aromatics saturation is reversible. Saturation becomes more difficult thermochemically as temperatures go up.

Table 22.8 presents selected average bond energies and Table 22.9 compares the results of bond-energy-based heat-of-reaction calculations for HDS and hydrocracking.

Reaction enthalpies calculated from bond energies come reasonably close to the averages in Table 22.7, which were calculated from heats of formation. The results are nearly identical for the hydrocracking reaction, but differ by about 10% for the HDS reaction.

22.9 Hydroprocessing Kinetics

For process design and safe operation, reaction rates are just as important as thermochemistry. It is not enough to understand how much heat is generated by various chemical reactions. One must know how fast the heat is generated, how and where the heat is controlled, and how temperature increase depends on related process parameters – the feed rate, catalysts, catalyst loading, system pressure, and chemical–physical properties of the reactants.

Operators and unit engineers might use simple first-order models to normalize plant data to a reference point; to estimate the impact of changes in feedstock quality; to estimate how to vary temperatures to meet different process objectives; and to monitor catalyst deactivation.

At the other end of the spectrum, steady-state models for real-time online optimization (RTO) do all of that and much, much more. RTO reactor models employ rigorous kinetics developed from detailed feedstock characterization. They incorporate ambient condition temperature measurements and prices for feedstocks, utilities, and products. They determine the actual capability of equipment by comparing design values with actual performance. Every hour or so, they calculate optimal setpoints for dozens of valves and automatically download the results to the DCS system.

Dynamic models calculate the rates at which reactors and other equipment respond to setpoint changes. They can be excellent vehicles for operator training. Complete dynamic models can be suitable for simulating startup, shutdown, and emergency procedures.

22.9.1 Pseudo First-Order Approximation (PFOA) Models

The simplest approach to kinetic modeling is the pseudo first-order approximation (PFOA) method. In a pseudo first-order experiment, all aspects of a system are held constant except one. The usual approach is to make the concentrations of everything else so high, that they don't change when the component of interest reacts.

For hydroprocessing, PFOA assumptions include the following:

- *Temperature assumption: The reaction environment is isothermal.* Real units are adiabatic. Hydroprocessing reactions generate heat and in a steady-state system at constant volume and pressure, adding heat increases temperature. In commercial units, reaction heat can induce considerable exotherms. More than a few times, we have seen steady-state temperature rises $> 50^\circ\text{C}$ across a hydrotreating catalyst bed. PFOA models account for adiabatic temperature rise by averaging TI measurements into isothermal equivalents, such as CAT or WABT.
- *Feed composition assumption: The feed contains only four reactive components – sulfur, nitrogen, aromatics, and unconverted oil.* We know this isn't true, but we are constrained by the fact that refiners routinely measure only distillation, density, acid number, total sulfur, and total nitrogen. Sometimes, if there is a perceived need, they measure bromine number, and trace metals. Olefins are related directly to bromine number. Aromatics are inferred from density, distillation, and sulfur. Oxygen can be estimated from acid number. For pilot plant studies, licensors and catalyst vendors measure additional feed and product properties, including aromatics, polyaromatics, and PNA ratio. The rigorous version of PNA ratio is the $C_P C_N C_A$ ratio, which is the ratio of carbon atoms in paraffins, naphthenic rings, and aromatic rings. Refractive index and the distribution of sulfur compounds might also be measures, both in feed and product samples.
- *Inhibitors:* Hydrocracking models include the impact of nitrogen and ammonia on total catalyst activity and HDS models include inhibition by H_2S .
- *Reaction reversibility assumption: All reactions are irreversible.* As discussed in Sect. 22.3, this assumption is wrong for the saturation of aromatics. Above the *crossover* temperature, the extent of saturation is determined by thermochemistry, not kinetics. In this region, the results of kinetic calculations are misleading.
- *Consecutive reaction assumption: All reactions are single-step.* As also discussed in Sect. 22.3, HDN

and the indirect mechanisms for the HDS of alkyl dibenzothiophenes, require initial saturation of an aromatic ring. When thermochemistry inhibits saturation, HDN and deep HDS are inhibited too. Again, we see how the results of PFOA kinetic calculations can be misleading.

- *Reaction environment assumption: All reactions occur in a single liquid phase.* This isn't true for naphtha hydrotreating at high temperatures, when the feed is completely vaporized.

First-order kinetic relationships [22.27] are derived from (22.1), where F is the concentration of a reactant X in the feed at time $= t$, k is the rate constant, and n is the reaction order. Rearrangement gives (22.2). For $n = 1$, integration from time $= 0$ to time $= t$ gives (22.3). In this context, reaction order is a tuning constant with limited physical significance. Having $n > 1$ does not indicate that a component reacts with itself.

$$\text{Rate}_{(t)} = -\frac{dX_t}{dt} = -kX_t^n, \quad (22.1)$$

$$\frac{dx}{X_t^n} = -kdt, \quad (22.2)$$

$$\text{If } n = 1, \text{ then } k = \left(\frac{1}{t}\right) \ln \left(\frac{X_t}{X_0}\right). \quad (22.3)$$

We can assume that the average residence time $= 1/LHSV$. If $t =$ residence time, we get (22.4), which is useful for predicting the impact of feed rate on reaction rates

$$k = -(LHSV) \ln \left(\frac{X_t}{X_0}\right) = (LHSV) \ln \left(\frac{X_0}{X_t}\right). \quad (22.4)$$

22.9.2 Temperature Dependence

The Arrhenius relationship, (22.5), quantifies the impact of temperature on reaction rate. The rate constant k , is the same as the rate constant in (22.1) through (22.4). T is the temperature, R is the gas constant, and E_a is the activation energy. A is the pre-exponential factor, a catch-all for temperature-independent factors. A bit of manipulation gives (22.6). One can determine E_a experimentally by plotting $\ln k$ versus $1/T$. The slope is E_a/R and the intercept is $\ln A$.

The assumption that E_a and A are constant at all temperatures leads to (22.7) and (22.8), which one can use to calculate rate-constant ratios at different temperatures. Equation (22.7) is especially useful for predicting the impact of temperature changes on reac-

tion rates.

$$k = Ae^{\frac{-E_a}{RT}}, \quad (22.5)$$

$$\ln k = \ln A - \frac{E_a}{RT}, \quad (22.6)$$

$$\ln \left(\frac{k_1}{k_2}\right) = \frac{E_a}{R} \left(\frac{1}{T_2} - \frac{1}{T_1}\right), \quad (22.7)$$

$$\frac{k_1}{k_2} = e^{\left[\frac{E_a}{R} \left(\frac{1}{T_2} - \frac{1}{T_1}\right)\right]}. \quad (22.8)$$

Table 22.10 presents commonly accepted activation energies for the main hydroprocessing reactions [22.28, 29].

Experiments demonstrate the futility of trying to use irreversible first-order kinetics to model reversible saturation of aromatics and by extension, reactions that require prior saturation of aromatics; mechanisms for HDN and deep HDS include indirect routes requiring initial reversible saturation of an aromatic ring adjacent to the hetero atom. To achieve a reasonable data fit for saturation, one must change either the activation energy or the reaction order for different temperature ranges. Both strategies are flawed. A temperature-dependent E_a conflicts with Arrhenius's primary assumption – that E_a is constant. Assigning a reaction order > 1.0 implies that the saturation mechanism requires some interaction of two aromatic molecules which is exceedingly improbable. Above about 440 °C (825 °F), saturation cannot occur and the calculated E_a for saturation is zero or negative.

The aromatics conundrum can be handled by adding a separate dehydrogenation reaction, with its own A and E_a . At equilibrium, the rates of saturation and dehydrogenation are equal. Knowing this enables one to derive (22.9). The system must mass-balance, so the solution requires solving simultaneous equations,

Table 22.10 Arrhenius activation energies for the main hydroprocessing reactions

Reaction	E_a (kcal/(mol K))
Bulk HDS of gas oils	16–20
Bulk HDS of VGO and AR	30–36
ULSD	12 ^a
Bulk HDN	30
Aromatics saturation	< 0–18
ASA-catalyzed hydrocracking	30
Zeolite-catalyzed hydrocracking (moderate activity)	45–50
Zeolite-catalyzed hydrocracking (high activity)	55
Thermal hydrocracking	62

^a Depends on which reaction order is being used

which is readily accomplished in programs such as MATLAB or the Solver add-in of Microsoft Excel.

$$\ln k_1 = \ln k_2 = \ln A_1 - \frac{E_{a1}}{RT} = \ln A_2 - \frac{E_{a2}}{RT}$$

$$\ln A_1 - \ln A_2 = \frac{E_{a1}}{RT} - \frac{E_{a2}}{RT}$$

$$R(\ln A_1 - \ln A_2) = \frac{E_{a1} - E_{a2}}{T}$$

$$\frac{E_{a1} - E_{a2}}{T} = \text{Const.} \quad (22.9)$$

Figures 22.28 and 22.29 illustrate the impact of activation energies on relative reaction rates as a function of temperature. The curves are based on (22.8), with $k_1 = 1$ and $T_1 = 380^\circ\text{C}$. T_2 is specified and k_2 is calculated. Figure 22.28 shows just two curves, one for ULSD and another for three reactions:

- Bulk HDS
- HDN
- ASA-catalyzed hydrocracking.

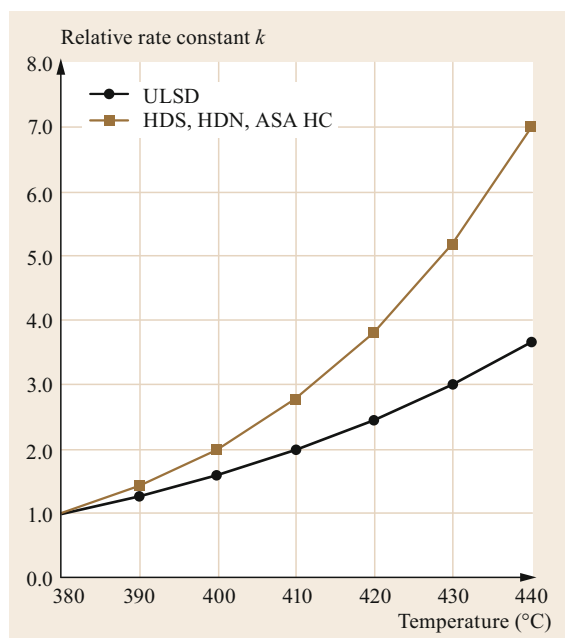


Fig. 22.28 Curves showing relative rate constant versus temperature for hydrotreating and ASA-catalyzed hydrocracking. Curves are calculated with (22.8), with $k_1 = 1$ and $T_1 = 380^\circ\text{C}$. For bulk HDS, HDN and ASA hydrocracking, E_a is 30 kcal/(mol k). Experiments show that E_a for deep desulfurization to make ULSD can range from 12–30 kcal/(mol k). For this graph, E_a for ULSD = 20 kcal/(mol k)

For the ULSD, $E_a = 20$ kcal/(mol k). In Fig. 22.29, three curves are added:

- Hydrocracking with a moderate-zeolite catalyst ($E_a = 45$)
- Hydrocracking with a high-zeolite catalyst ($E_a = 55$)
- Thermal hydrocracking ($E_a = 62$).

At 470°C , thermal hydrocracking is twice as fast as high-zeolite hydrocracking and 20 times faster than bulk HDS.

22.9.3 Langmuir–Hinshelwood/Hougen–Watson Kinetics

Researchers make limited use of PFOA models, because of their inherent drawbacks. Instead, they employ the LHHW (Langmuir–Hinshelwood/Hougen–Watson) mechanism, which was derived specifically for modeling heterogeneous catalysis [22.30]. For each component, an LHHW equation captures inherent reactivity and temperature effects, along with the impact of other reactants, inhibitors and catalyst characteristics. LHHW models are somewhat more complex than PFOA models, but they are far more informative. An

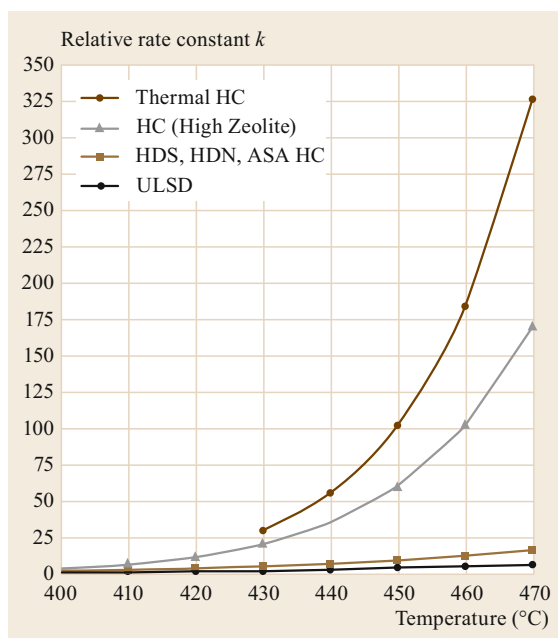


Fig. 22.29 PFOA kinetics: Similar to Fig. 22.28, $k = 1$ at 380°C with the addition of high-zeolite hydrocracking and thermal hydrocracking. Activation energies for the added curves are 45 kcal/(mol K), 55 kcal/(mol K), and 62 kcal/(mol K)

eight-component system (hydrogen, sulfur, H_2S , nitrogen, NH_3 , unconverted oil, aromatics, and saturates) can be solved with simple macros in programs such as Microsoft Excel, or by powerful solvers from MathWorks, Mathematica, and others.

The main LHHW steps are:

- Adsorption of reactants to the catalyst surface
- Reactions of adsorbed molecules
- Desorption of products.

Equation (22.10) summarizes the constituents of the equation

$$\text{rate} = \frac{(\text{kinetic factor}) \cdot (\text{driving force})}{(\text{adsorption terms})} \quad (22.10)$$

Adsorption terms include:

- Molecular: $K_A P_A$
- Dissociative: $(K_A P_A)^{0.5}$
- Includes adsorption terms for inhibitors.

Kinetic factors include:

- k = Reaction rate constant, including Arrhenius temperature effects
- N_T = Number of available adsorption sites (proportional to surface area)
- Turnover number = Max number of molecules that can be converted per active site per second (Michaelis–Menton kinetics).

Driving forces include: P_A , P_B , P_C , K_{eq} etc. The exponent n is an integer: $n = 0, 1, 2, \dots$ = Number of surface species involved, including inhibitors.

Equation (22.11) corresponds to a system with a single reactant, one type of active site, and multiple inhibitors. A molecule adsorbs to only one site and molecules do not combine with each other so

$$\text{Rate} = \frac{k N_T K_A P_A}{(1 + K_A P_A + \sum K_i P_i)} \quad (22.11)$$

where:

- k = Rate constant for conversion of A
- K_A = Adsorption constant for A
- P_A = Partial pressure of A
- $K_i P_i$ = Adsorption factors and partial pressures of inhibitors.

Catalytic hydrocracking employs bifunctional catalysts and hydrogen is a reactant, so the expression grows to

$$\text{Rate} = \frac{K N_T K_A P_A K_{H_2} (P_{H_2})^n}{(1 + K_A P_A + \sum K_i P_i) (1 + K_{H_2} (P_{H_2})^n)} \quad (22.12)$$

When several reactions are modeled at once, there is an (22.12) for each. The sets of equations are solved simultaneously. Inhibitors are generated by reactions, so their concentrations change as reaction fluids move through the unit.

When the adsorption factor for an inhibitor is considerably greater than the adsorption factor for a reactant, then (22.12) is essentially equivalent to (22.13)

$$\text{Rate} = \frac{k_A N_T K_A P_A}{(1 + K_i P_i)} \quad (22.13)$$

Equation (22.13) was used to generate Fig. 22.30 for the inhibition of hydrocracking by ammonia and organic nitrogen. The figure is based on pilot plant data. The test showed that the K_i for organic nitrogen is about $7 \times$ greater than the K_i for ammonia. The figure demonstrates that activity is very sensitive to small changes in inhibition at very low concentrations of inhibitor.

It is said that the poisoning of hydrocracking catalysts by organic nitrogen is reversible. Indeed, if a catalyst is poisoned by a high-nitrogen feed and if that feed is replaced by a low-nitrogen feed, much of the prior catalytic activity returns. But the molecules that leave have changed and they go away for different reasons. The light ones might simply be displaced, but the heavy ones undergo hydrocracking or coking. As a nitrogen-poisoned hydrocracking catalyst reacquires activity, activity remains low until the degree of inhibition is very low. Then, a small change in nitrogen has a huge effect on activity. As discussed in Sect. 22.11, failure to understand this phenomenon has been deadly.

22.9.4 Structure-Based Lumping

Rigorous process optimization relies on models with structure-based lumping (SBL), also known as structure-oriented lumping (SOL). High-fidelity SBL models can serve as the basis for closed-loop, real-time, online optimization. Examples include the models used for online refinery-wide optimization at Suncor Sarnia [22.31]. An SBL model might include < 30 to > 100 kinetic components. Table 22.11 shows one way to group hydrocarbons into structure-based lumps. Note that the sum of poly-ring compounds is 43 wt%.

For each type of structure, physical and chemical properties vary monotonically with carbon number. Figure 22.31 illustrates how density changes as carbon numbers increase. As molecules get heavier, they behave less like alkyl-substituted ring compounds (or hetero-atom compounds) and more like large paraffins. This makes sense, because each increment in carbon number comes from adding a methylene (CH_2) group.

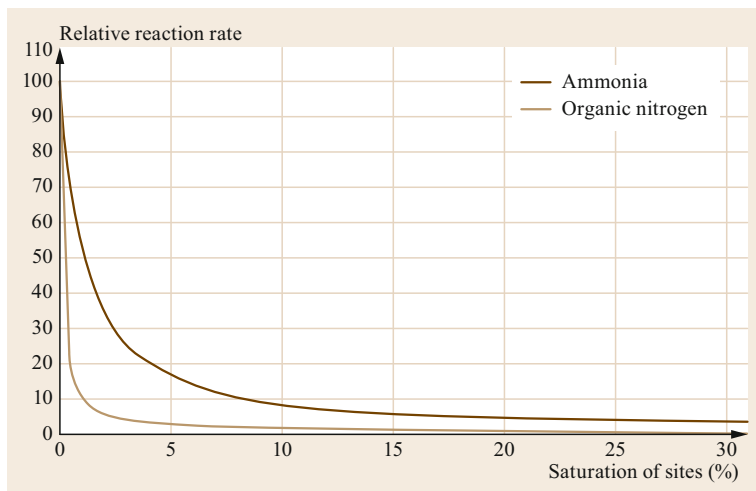


Fig. 22.30 Langmuir–Hinshelwood inhibition of hydrocracking by ammonia and organic nitrogen, where $K_{(\text{organic N})} = 7 \times K_{(\text{NH}_3)}$. The trends are a function of inhibited catalyst sites at steady state, which is related to, but not the same as, the content of ammonia or nitrogen in the feed

Online optimization models include a representation for every piece of equipment in a unit and contain tens of thousands of equations. In open-equation parlance, the number of nonzero elements in the model matrix for each unit can be more than a million. The equations are solved simultaneously with dynamic optimization software provided by companies such as AspenTech, ABB, Schneider Electric, Honeywell, and others.

The reaction model used for real-time optimization at the Suncor Sarnia hydrocracker includes 116 components and 195 reactions. The components are organized into seven cuts, which correspond to the boiling ranges of desired products – unconverted oil, heavy VGO, light VGO, heavy gas oil, light gas oil, C_5 – C_{10} hydrocarbons, and C_4 hydrocarbons. H_2 , H_2S , and NH_3 are included. The components and reaction network are patterned after Figs. 22.16 and 22.17. In addition to hydrocarbon lumps, the model includes 13 sulfur and 10 nitrogen components – at least one per cut. Each component has an integer CHSN ratio. Physical properties include density, heat capacity, standard ΔH_f , heat of vaporization, and normal boiling point. Heat balance is calculated rigorously. Equilibrium-like behavior is captured with separate forward and reverse reactions. To simulate adiabatic behavior, each catalyst bed has six collocation points, at which composition, heat release and vapor–liquid equilibria are re-computed and passed to the next collocation point. Figure 22.32 illustrates the kind of reactor information obtainable from such a model. Four of more than sixty process variables are tracked as they flow through four beds of hydrotreating catalyst. Between each bed, quench gas is added to control temperature. At the top of bed 1, temperature jumps quickly

due to saturation of olefins. Nearly all of the sulfur is gone at the end of bed 4, while nitrogen removal is 70% and removal of total aromatics is 60%. Graphs were prepared with Aspen Hydrocracker software, a product of Aspen Technology, Inc. With the open-equation mathematics underlying the model, one can specify bed inlet temperatures and calculate the outlet temperatures; or specify conversion and desired bed outlet temperatures and calculate what the bed inlet temperatures must be to meet those specifications.

A key to commercial success is the feed-adjust block, which decreases the need for detailed analysis of every new feed. This is important, because feeds in commercial units change frequently, sometimes several times per week. Feed bulk properties can be calculated with reasonable fidelity from the model component distribution and vice versa. When the feed is different, the feed-adjust block compensates by skewing the component distribution for a known feed to match the bulk properties of the different feed.

Another important feature is the composition-based deactivation model, which adjusts for catalyst activity online. It has been used off-line for *what-if* predictions of the impact of process changes (including feed changes) on catalyst deactivation rates [22.32].

Online optimization models are superb tools for process monitoring. During every execution cycle, they calculate differences between the expected and actual performance of pumps, furnaces, heat exchangers, distillation towers etc. It is a straightforward exercise to generate trends which show how the plant/model mismatch changes with time. With that information, engineers can identify equipment fouling and opportunities for process improvement.

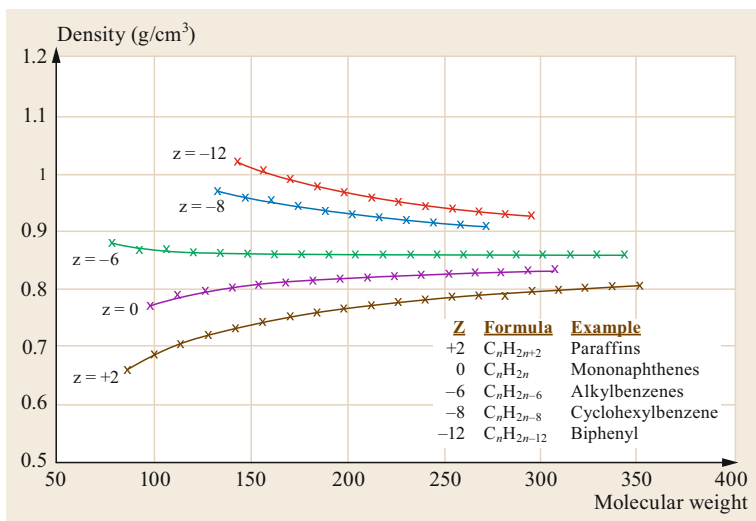


Fig. 22.31 Density versus molecular weight for hydrocarbons with different Z numbers at 20°C. Z represents the degree of saturation in hydrocarbons. It comes from the subscript for hydrogen in composition general formulas. For paraffins, C_nH_{2n+2} , $Z = +2$. For alkyl benzenes, C_nH_{2n-6} , $Z = -6$ (courtesy of J.W. Bunger)

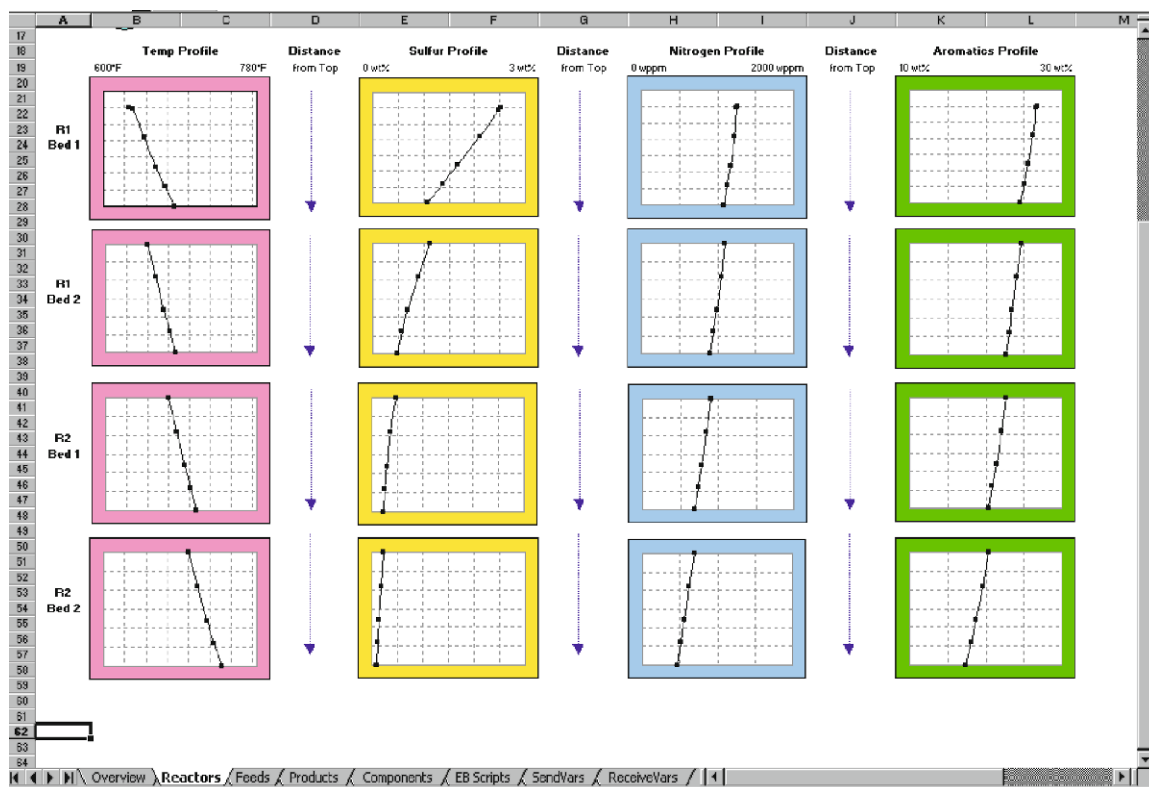


Fig. 22.32 Example output from an adiabatic SBL hydrocracking model. Four variables are tracked as they flow through four beds of hydrotreating catalyst. Between each bed, quench gas is added to control temperature. At the top of bed 1, temperature jumps quickly due to saturation of olefins. Nearly all of the sulfur is gone at the end of bed 4, where nitrogen removal is 70% and removal of total aromatics is 60%. Graphs were prepared with Aspen Hydrocracker software, a product of Aspen Technology, Inc.

22.10 Hydroprocessing Process Descriptions

22.10.1 Fixed-Bed Hydrocracking: Process Flow Schemes

In fixed-bed hydroprocessing units, the flow of reactants can be modeled with trickle-bed kinetics, with concurrent downflow of liquid and gas across a packed bed of catalyst particles. Trickle-bed kinetics [22.33] are based on plug flow of well-mixed fluids with no back-mixing or wall effects.

Figure 22.33 presents a process flow scheme for a two-reactor fixed-bed hydrocracker with four catalyst beds – two for pretreat catalysts and two for cracking catalysts. Four separators are shown:

1. HHPS = Hot high-pressure separator
2. CHPS = Cold high-pressure separator
3. HLPS = Hot low-pressure separator
4. CLPS = Cold low-pressure separator.

The emergency depressuring system (EDS) might be configured as shown or with two independent lines from the CHPS. Quench valves are moved by temperature controllers. The recycle gas compressor, as shown, is centrifugal with steam-drive. The amine unit is optional. The reactor effluent air cooler (REAC) is safety-critical because it is susceptible to erosion-corrosion induced by the deposition of $\text{NH}_4\text{SH}_{(\text{aq})}$ and $\text{NH}_4\text{Cl}_{(\text{aq})}$.

Fresh feed and hydrogen-rich gas are heated by heat exchange and a fired furnace. Liquid and gas might be mixed before entering the furnace. Alternatively, the furnace might heat just the recycle gas, which heats the oil when the two are mixed. The mixture enters the reactor and flows down through the catalyst beds in trickle-flow fashion. Commercial units contain up to six reactors and commercial reactors contain two to seven beds. Hydroprocessing reactions generate heat, which

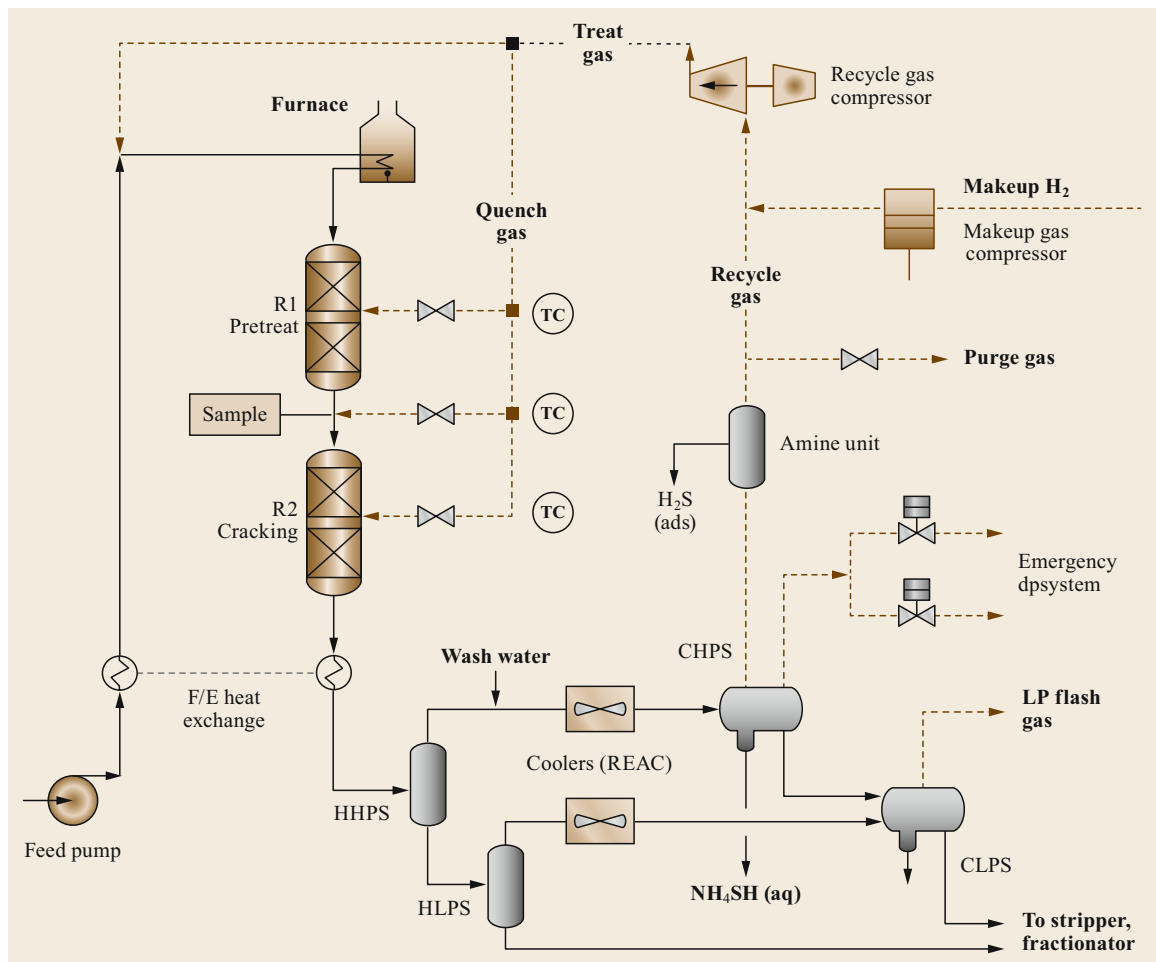


Fig. 22.33 Representative fixed-bed once-through hydrocracker

is controlled by the injection of relatively cold quench gas between catalyst beds. Quench valves are manipulated in cascade by temperature controllers, but they can also be operated manually.

In a two-separator design, the reactor effluent is combined with wash water and cooled in the feed/effluent changer. In the cold high-pressure separator, the wash water removes ammonia as aqueous NH_4SH . The CHPS overhead is recycled, sometimes after first going through an amine unit for H_2S removal. The CHPS bottom goes through a stripper to the fractionator.

HPLS liquid can go directly to the fractionator, avoiding the need to cool and reheat the product liquid. In the figure, the centrifugal recycle gas compressor (RGC) is steam-driven; sometimes the RGC is motor-driven. Units that process relatively sweet feeds may not require an amine unit. A gas-only furnace is less subject to tube fouling, especially during a sudden change in operation.

Products can include the following:

- Purge gas comprised of hydrogen, methane, ethane, and H_2S . Depending on the hydrogen source, it can also contain molecular nitrogen, argon.
- Propane.
- Butanes.
- Light naphtha (primarily C_5 paraffins).
- Heavy naphtha, which usually goes to a catalytic reformer.
- Kerosene, which often meets jet fuel specifications.
- Gas oil, which often meets specifications for ultra-low-sulfur diesel (ULSD).
- Unconverted oil, which can be recycled to achieve higher conversion, or forwarded to an FCC unit, an

olefin production plant, or a lubricant production plant.

Operating condition ranges at start-of-run (SOR) and end-of-run (EOR) are set during design and construction. They are based on specified feed qualities and process objectives. Approximate ranges are presented in Table 22.12.

Compared to hydrotreating, the LHSV for hydrocracking is higher (the residence time is shorter) due to concerns about temperature excursions. Low-pressure hydrotreaters are used to treat naphtha and straight-run light gas oil. Higher pressure is required for residue hydrotreating, lube-stock hydrofinishing, and hydrocracking. 2000 psig (135 bar) is a common pressure for VGO hydrocracking. Temperatures at SOR and middle-of-run (MOR) are situational.

During normal operation of an existing unit:

- Fresh feed rate is kept as high as possible.
- Pressure is relatively constant, as it must be to maintain hydraulic stability.
- It is tempting to try to save power or steam by automatically changing recycle gas compressor speed to maintain a constant H_2OR . Such a control scheme is risky, of questionable benefit, and difficult to implement. A high flow of recycle gas keeps a unit safe by removing process heat. The high flow provides a buffer against disturbances. Hydrocracking units are tightly integrated, so process parameters are exceedingly interactive, and they respond to changes with disparate dynamics because so many variables are so interdependent. For example: A change in feed rate often is accompanied by a change in feed

Table 22.12 Fixed-bed hydroprocessing: Approximate operating condition ranges. Exceptions are common

Process variable	Approximate range	
	Hydrotreating	Hydrocracking (zeolite catalyst)
LHSV, $\text{h}^{-1\text{a}}$	0.4 to > 2.0	1.0 to > 2.0
Metric units		
Pressure at the reactor inlet (bar)	40–200	85–200
SOR catalyst average temperature ($^{\circ}\text{C}$)	315–390	315–390
EOR catalyst average temperature ($^{\circ}\text{C}$)	427	415
Peak operating temperature ($^{\circ}\text{C}$)	440	427
Hydrogen–oil ratio (H_2OR) at reactor inlet (Nm^3/m^3)	> 360	880–1425
Treat gas ratio, recycle H_2 flow/makeup H_2 flow	> 3	> 5
American units		
Pressure at the reactor inlet (psi)	600–3000	1200–3000
SOR catalyst average temperature ($^{\circ}\text{F}$)	600–735	600–735
EOR catalyst average temperature ($^{\circ}\text{F}$)	800	780
Peak operating temperature ($^{\circ}\text{F}$)	825	800
Hydrogen–oil ratio (H_2OR) at reactor inlet (scf/bbl)	> 2000	5000–8000
Treat gas ratio, recycle H_2 flow/makeup H_2 flow	> 3	5

^a LHSV = liquid hourly space velocity = (volume of liquid feed)/hour/(volume of catalyst)

quality. If the feed rate drops but the feed is more reactive, temperatures will increase for two reasons – greater heat of reaction and longer residence time. If the recycle gas compressor slows to maintain a constant H₂OR, temperature will rise for a third reason: reduced flow of heat-removing gas. So: in a well-run hydrocracker, the recycle gas compressor is operated at a high, constant speed.

- When feed rate, pressure and H₂OR are constant, unit performance depends on temperature.

To respond to changes in feed quality, process objectives, or catalyst activity, operators manipulate temperature. For most of a catalyst cycle, temperature can be altered at will, subject to safety limits. Temperatures at EOR are constrained by metallurgy.

In the pretreat catalyst beds, sulfur and nitrogen are removed by HDS and HDN, respectively. Oxygen, olefins, and trace elements are also removed, accompanied by significant saturation of aromatics. Removing organic nitrogen is especially important, because it passivates acid sites on hydrocracking catalysts. Samples of liquid are collected at the line between the pretreating and cracking reactors and analyzed for nitrogen. On the basis of these measurements, pretreat reactor

temperatures are adjusted to maintain N slip i.e., the nitrogen content of the pretreat reactor effluent liquid. Targets for N slip are situational and can range from 5–50 wppm. HDN generates ammonia, which also passivates cracking catalyst acid sites. However, ammonia is significantly less inhibitory than organic nitrogen. The pretreated feed flows to the cracking catalyst beds, where conversion due to C–C bond cleavage occurs.

Under reaction conditions, the H₂S and NH₃ from hydrotreating are gases. But at temperatures below the sublimation temperature for ammonium bisulfide (NH₄SH), that salt can deposit and accumulate, blocking flow. It can also induce serious erosion–corrosion. In addition to reacting with H₂S, ammonia reacts with chlorides to form NH₄Cl, which also forms deposits below its sublimation temperature. Both NH₄SH and NH₄Cl are water-soluble. They can be controlled by injecting wash water into the CHPS feed. There are two guidelines for water injection: at least 25–30% of the water must remain liquid and the salt content of the CHPS sour water should not exceed a specified value. Licensor recommendations vary, but the limit usually is somewhere between 4–8 wt%.

Unconsumed hydrogen from the cold high-pressure separator (CHPS) might or might not be scrubbed with

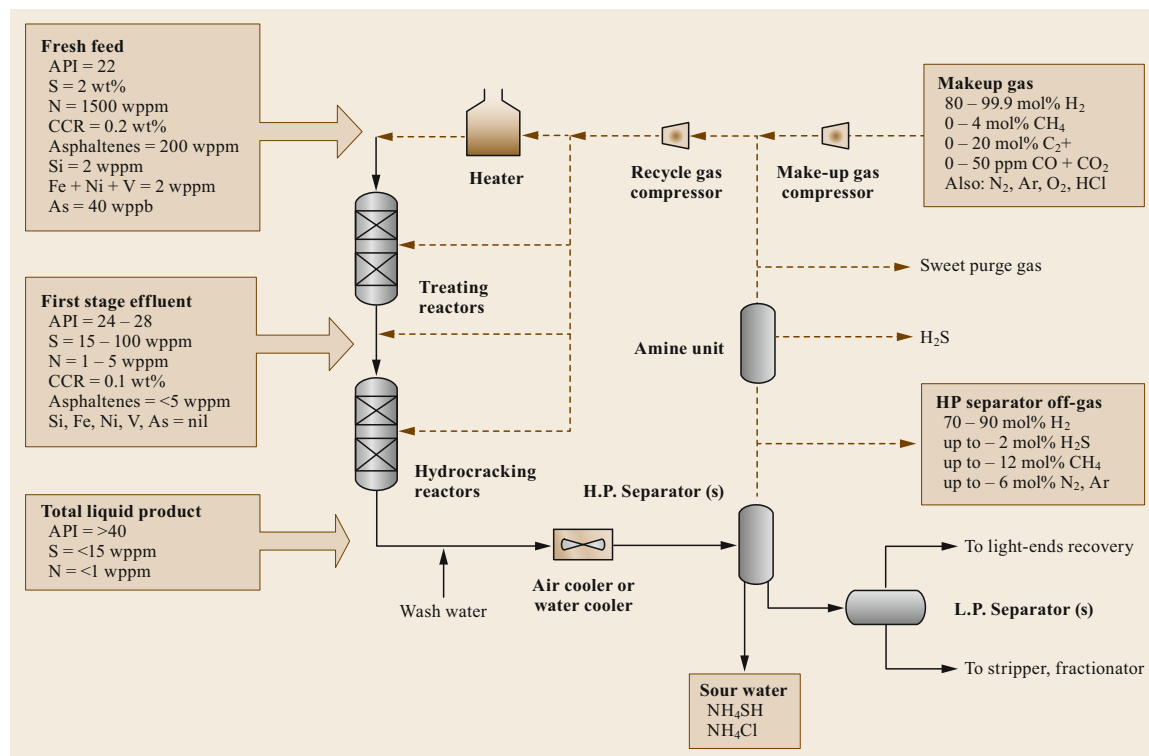


Fig. 22.34 Once-through hydrocracking process flow with representative stream compositions. Actual values differ from unit to unit and for different feeds and modes of operation

amine to remove H_2S . To control buildup of methane and nitrogen in the recycle gas, some gas can be purged to fuel gas or another process unit. The remaining gas is augmented with makeup hydrogen and recycled to the reactors.

In hydrocrackers, emergency depressuring systems quickly drop pressure when temperatures get out of control. As discussed in Sect. 22.11, in one case an excursion increased a bed TI reading by $188^\circ F$ ($104^\circ C$) in 20 s. In another, the temperature jumped $214^\circ C$ in 7 min. EDS stops excursions by removing hydrogen, an essential reactant and by pulling heat out of the unit. Failure to depressure has led to loss of containment, injuries and at least one fatality. API Recommended Practice 521 presents guidelines for pressure-relief and depressuring systems [22.34]. The document recommends sizing the system to give an initial depressuring rate of 100 psi/min (7 bar/min). Designs by hydrocracking technology licensors include two independent EDS lines, one sized for an initial rate of 100–150 psi/min (7–10 bar/min) and another with initial rates of 200–300 psi/min (14–20 bar/min). The

EDS valves are triggered automatically by high temperature or certain equipment problems. Both can be opened manually at any time. At least one licensor designs units for manual-only opening of the high-rate valve. The goal of high-rate pressuring is to reduce pressure by 50% within 15–20 min. For certain non-traditional hydrocrackers, such as integrated units comprised of a high-temperature slurry-phase section followed directly by a moderate-temperature fixed-bed section, depressuring alone may not be sufficient to abate a temperature excursion.

Figure 22.34 shows representative stream properties for a once-through hydrocracker. Actual values differ for different units, different feeds, and different types of operation.

Figure 22.35 gives a bird's-eye view of several hydrocracking process flow options. For all flow sketches, there can be either two, three, or four flash drums. Figure 22.35a shows a once-through unit in which the oil flows in series through the pretreat catalysts directly to the cracking catalysts. Figure 22.35b shows two options for recycle of unconverted oil (UCO).

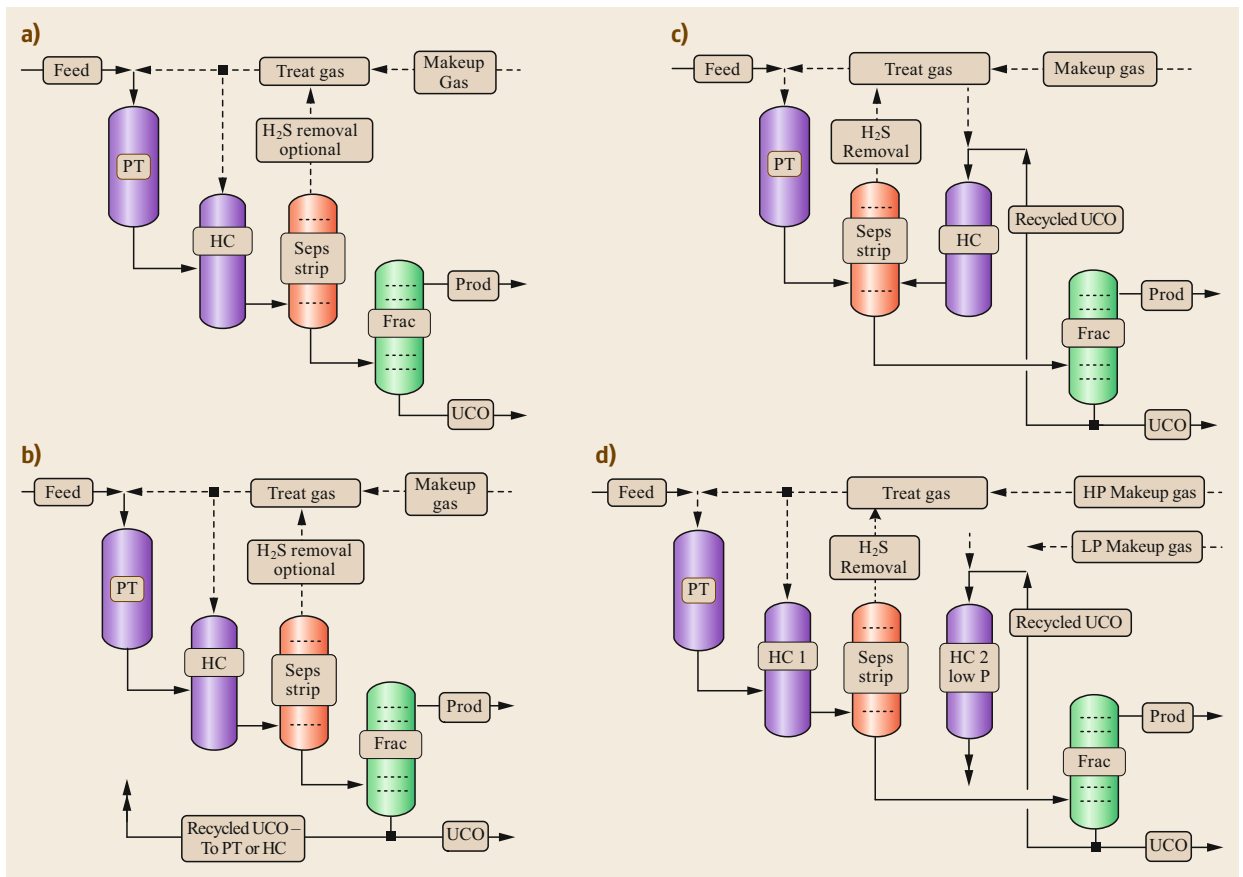


Fig. 22.35a–d Hydrocracking process configuration options

The UCO can go either to R1 or R2. Figure 22.35c shows a unit in which the pretreated oil is stripped or fractionated before moving on to a hydrocracking reactor. Figure 22.35d shows a unit with two independent recycle gas loops, one for R1 and R2 and another for R3. This configuration has two major process advantages: in R3, the pressure can be lower and the environment is nearly sweet – sweet because H_2S and ammonia are stripped and almost all of the nitrogen and sulfur are removed in R1 and R2. Temperatures required by uninhibited sweet hydrocracking are lower. This leads to increased saturation of aromatics, which improves the quality of middle distillate products. Some refiners still use noble-metal catalysts, due to the higher activity and lower gas production over such catalysts. The Fig. 22.35d option seems like it would be more expensive, because it contains additional equipment. But in one recent head-to-head comparison, due to the lower pressure and less expensive metallurgy, the estimated installation cost of a Fig. 22.35d unit was nearly the same as that for a Fig. 22.35b unit.

22.10.2 Fixed-Bed Hydrocracking: Design Considerations

Unit design starts with the definition of feed rate, feedstock qualities, the expected availability and composition of makeup hydrogen, desired product yields and qualities, and desired catalyst cycle life. With this input, reaction models generate mass-balanced yields and product qualities for different combinations of catalyst type and operating conditions. The results include estimates of reaction enthalpy. On the basis of the model results and various constraints, designers select a process configuration. The constraints include local limits on the weight and dimensions of vessels (particularly reactors), rotating equipment, and fractionators. Limits on catalyst-bed temperature rise determine the number and location of reactor quench zones. Mass flux guidelines set reactor diameters and heat exchanger design.

Startup requirements should (but don't always) determine furnace duty. A common design mistake is to size fired heaters based on normal operation, where

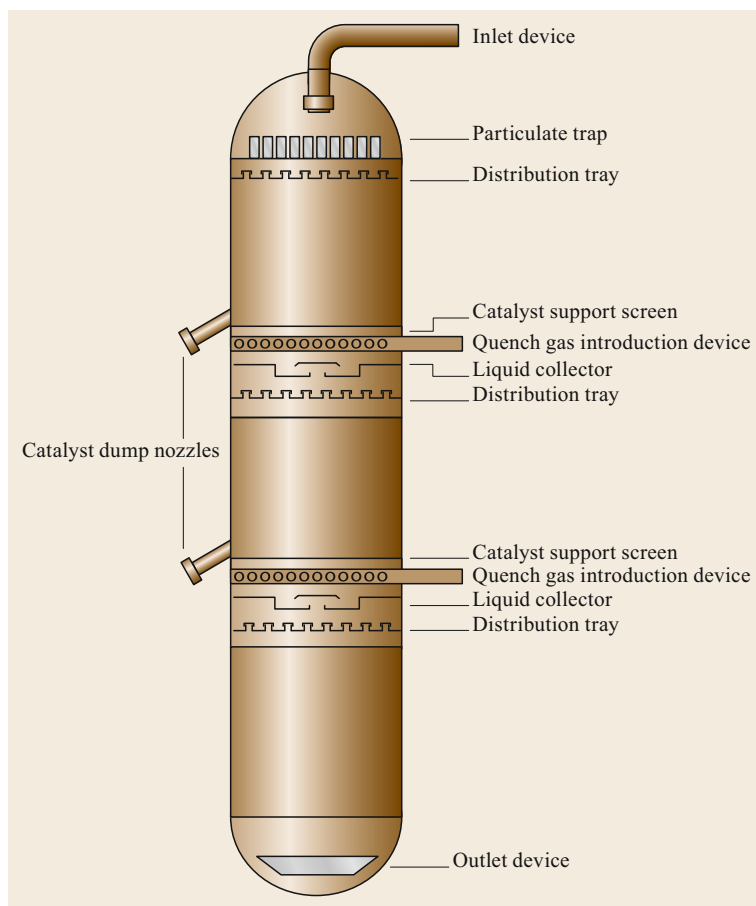


Fig. 22.36 Fixed-bed hydrocracking reactor internals. Alternatives to dump nozzles include intra-reactor dump tubes, through which catalysts can be conveyed from an upper bed to a lower bed. Dump tubes decrease the number of holes in the reactor wall and they make it easier to reposition quench decks if needed

a significant percentage of the required heat is supplied by chemical reactions, then adding an arbitrary margin for the extra duty required during catalyst activation. But the required startup margin strongly depends on unit-specific parameters, such as ambient temperature and piping. A 25% margin on furnace duty might be enough for some units but not enough for others.

It is common to have two feed pumps, each with 50–60% of design capacity.

The capacity of the makeup gas compressors (MUGC) is determined by expected hydrogen consumption. Units include at least two MUGCs. It is not unusual to see two MUGCs, each with 100% of design capacity, or three with 60% each. MUGCs are reciprocating, with electric or steam drive. They might draw from a dedicated hydrogen plant or from a header common to other hydroprocessing units.

The recycle gas compressor (RGC) is the single most important safety device in the plant. A high flux of recycle gas promotes plug flow for transporting heat through the reactors. Licensors recommend designing for at least 30% reserve quench. In addition, they say that the ratio of recycle gas to makeup gas, also known as the treat-gas ratio, should range from 4 : 1 for hydrotreating reactors to more than 8 : 1 for hydrocracking reactors. Different suppliers calculate treat-gas ratios in different ways. Some include 100% of the quench gas. Others include only 2/3 of the quench gas

because the top beds of catalyst don't see any quench at all. There is only one RGC. Almost always it is centrifugal. Licensors recommend steam drive, because the RGC is so safety critical. If power fails, an electric-drive machine stops immediately, while a steam-driven machine might continue to run for a while, maintaining all-important flow.

The best way to stop a temperature excursion is to depressure the unit by venting recycle gas through special valves at the CHPS. This decelerates all hydrocracking reactions by rapidly reducing H_2 partial pressure in the reactors and carrying heat out of the unit. The emergency depressuring valves and lines are sized to ensure that the flow rate does not exceed Mach 0.7 to 0.9.

Figure 22.36 shows the key elements of a fixed-bed hydrocracking reactor. The inlet device breaks the horizontal momentum of incoming reaction fluids and directs them vertically downwards. Shell Global Solutions offers particulate-trapping technology comprised of radial-flow elements. The elements stand on a deck at the top of the reactor, extending upwards into space which is usually empty. The distribution tray provides intimate mixing of oil with gas and distributes the mixture as a fine, even spray to the top of the catalyst bed underneath. The catalyst support screens, in conjunction with layers of spherical balls loaded just on top of them, keep catalysts from meandering from the bed above into the quench assembly below. Several types

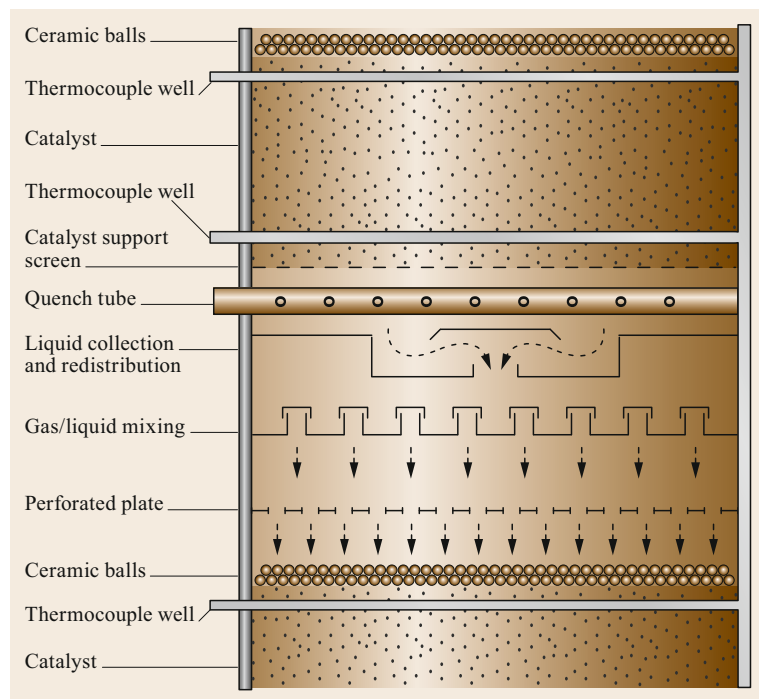


Fig. 22.37 Elements of a quench section for a fixed-bed catalytic hydrocracker (after [22.23]). Quench sections mix relatively cold quench gas with hot reactants from the catalyst bed above and distribute the mixture to the top of the catalyst bed below

of quench gas introduction devices are used commercially. Six are mentioned by *Scherzer and Gruia* [22.35, p. 186]. Configurations include rings with multiple slots, spiders and slotted tubes. The goal is to distribute quench gas evenly throughout the quench deck, not just at a single point. An outlet device at the bottom of the reactor decreases bottle-necking. Catalyst dump nozzles allow catalyst beds to be unloaded independently. Simultaneous dumping of beds is possible but seldom practiced. Figure 22.37 shows additional detail for quench sections.

A typical hydroprocessing hot-wall reactor is constructed from stainless steel containing 2.25 wt% Cr and 1 wt% Mo, with a 3 mm weld overlay of 347

stainless steel on the inside wall. Reactors can be enormous, with diameters up to 6 m (18 ft), with wall thicknesses up to 0.33 m (1 ft) and with weights greater than 1400 mt.

Cold-wall reactors, such as those used for residue hydrocracking, can be just as wide. The steel shells are thinner, but they are lined on the inside with refractory up to 0.66 m (2 ft) thick.

22.10.3 Fixed-Bed Hydrocracking: Product Flexibility in Recycle Units

As shown in Table 22.13, a fixed-bed recycle hydrocracking unit can have significant product flexibility,

Table 22.13 Product flexibility with fixed-bed recycle hydrocracking

Feed	Straight-run vacuum gas oil		
Boiling range (°C)		340–550	
Boiling range (°F)		644–1020	
API gravity		22.0	
Specific gravity		0.9218	
Nitrogen (wppm)		950	
Sulfur (wt%)		2.5	
Primary product objective	Naphtha	Kerosene	Gas oil
Weighted average reactor temp (°C)	Base	–6	–12
Weighted average reactor temp (°F)	Base	–11	–22
Product yields (vol. % fresh feed)			
Butanes	11	8	7
Light naphtha	25	18	16
Heavy naphtha	90	29	21
Kerosene or gas oil	–	69	77
Total C ₄ -plus	126	124	121
Chemical H ₂ consumption (Nm ³ /m ³)	345	315	292
(scf/bbl)	2050	1870	1730
Product qualities			
Light naphtha (C ₅ -82 °C)			
RON clear	79	79	80
Heavy naphtha			
P/N/A	45/50/5	44/52/4	–
RON clear	41	63	67
End point (°C), [°F]	216 [421]	121 [250]	118 [244]
Kerosene			
Flash point (°C), [°F]	–	38 [100]	–
Freeze point (°C), [°F]	–	–48 [–54]	–
Smoke point (mm)	–	34	–
FIA aromatics (vol.%)	–	7	–
End point (°C), [°F]	–	282 [540]	–
Gas oil			
Cloud point (°C), [°F]	–	–	–15 [5]
API gravity	–	–	44
Cetane number	–	–	55
Flash point (°C), [°F]	–	–	52 [126]
End point (°C), [°F]	–	–	349 [660]

producing either large amounts of C₄-plus naphtha or large amounts of middle distillates. In the table, SOR yields are shown. As the catalyst cycle proceeds, temperatures are increased. At higher temperatures, light-product yields go up and aromatics in heavier liquid products increase.

22.10.4 Ebullated Bed Hydrocracking

In contrast to fixed-bed hydrocrackers, ebullated bed (e-bed) units can process large amounts of residual oils. More than 20 units are now in operation. Catalyst life is not limiting, because fresh catalyst is added and spent catalyst is removed continuously. An H-Oil e-bed reactor is shown in Fig. 22.38. In operation, hydrogen-rich recycle gas is bubbled up through a mixture of oil and catalyst particles. E-bed reaction kinetics are fundamentally different from fixed-bed kinetics. The three-phase turbulent flow ensures a uniform temperature distribution. Substantial back-mixing and considerable liquid recycle cause the reactor to behave like a continuous stirred-tank reactor (CSTR). At the top of the reactor, catalyst is disengaged from

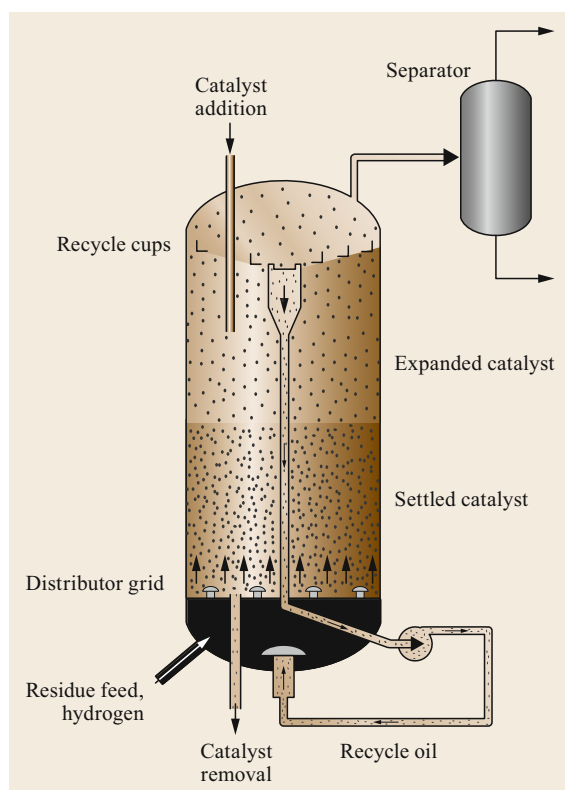


Fig. 22.38 Ebullated bed hydrocracking reactor (after [22.33])

the process fluids, which are separated in downstream flash drums. Most of the catalyst is returned to the reactor. Some is withdrawn and replaced with fresh catalyst.

When compared to fixed-bed processes, e-bed technology offers the following advantages:

- Catalyst life does not limit operation.
- Conversion of atmospheric residue can exceed 70 wt%.
- Operation can be flexible, with high-conversion and low-conversion modes.
- There is more free space between catalyst particles. This allows entrained solids to pass through the reactor without building up pressure drop.
- Smaller catalyst particles decrease diffusion limitations.
- Product selectivity is constant.

E-bed disadvantages versus fixed-bed hydrocracking include the following:

- Higher catalyst attrition, which leads to higher catalyst consumption.
- Higher installation costs due to larger reactor volume and higher operating temperatures.
- High sensitivity to feed metals, which determine catalyst addition rate.
- The formation of difficult-to-handle sediment comprised of degraded catalysts, metals from the feed, and precipitated asphaltenes.

Recent improvements include second-generation catalysts with lower attrition; catalyst rejuvenation, which allows the reuse of spent catalysts; improved reactor design leading to higher single-train feed rates; and two-reactor layouts with interstage separation. The design improvements will lead to substantial increases in conversion.

22.10.5 Slurry Phase Hydrocracking

In slurry-phase processes, finely divided additives are mixed with feedstock – vacuum residue, FCC slurry oil, coal, etc. – prior to contact with hydrogen. Additives for some modern processes are noncatalytic, while others employ catalytic additives. The technology began with the Bergius process in 1913 [22.36]. From 1933–1944, several units in Germany used modified versions to generate fuels and lubricants from coal.

The VCC process includes a slurry-phase and a fixed-bed section. The VCC additive is noncatalytic. The slurry-phase section converts vacuum residue, coal,

FCC slurry oil and other feeds into VGO and a spectrum of lighter products. The conventional fixed-bed section upgrades the VGO and distillates into finished products.

22.10.6 Hybrid Processes for Residue Hydrocracking

Chevron Lummus Global (CLG) offers a process in which CBI's LC-Slurry technology is integrated with solvent deasphalting. The asphalt can be handled conventionally. The deasphalted oil can go to an FCC unit, a separate hydrocracker or some other process unit. The activity of the catalytic ISOSLURRY™ additive enables operation at less than 3000 psig while achieving 100 wt% conversion to salable products, including asphalt. In 2016, the integrated technology was selected by Beowulf Energy and Preem for a large residue upgrading complex in Sweden [22.37].

22.11 Economics

Hydrocracker economics are determined by installation costs, operating costs, and product value. Here are some representative inside-battery limits (ISBL) estimates for the US Gulf Coast, 2012. Throughput, operating pressure, and process configuration – once-through or recycle of unconverted oil – are the major factors affecting construction costs for hydroprocessing units, which range from US\$ 3000 to US\$ 6000 per daily bbl. These estimates do not include costs for a hydrogen plant and off-site utilities.

For hydrotreaters, operating costs are roughly US\$ 1.7 per bbl. The cost of producing and compressing hydrogen accounts for 60–70% of this. For high-conversion hydrocrackers, operating costs are roughly US\$ 4.0–4.5 per bbl, of which 75–80% is due to hydrogen.

Eventually, refinery catalysts deactivate and must be replaced. In fixed-bed units, catalyst replacement requires a shutdown. For a 40 000 bbl/day hydrocracker with an upgrade value of US\$ 15–20 per bbl, every day of down time costs US\$ 600 000–800 000. Lost pro-

The advantages of slurry-phase processes include:

- The ability to achieve more than 90 wt% conversion of low-value vacuum residue, FCC slurry oil and even coal
- Insensitivity to trace metals in the feed
- Good product quality in two-stage designs, which incorporate fixed-bed hydroprocessing
- Feedstock flexibility
- For a given volume of residue feed: Lower reactor volume than e-bed processes.

Disadvantages of slurry-phase hydrocracking include high installation costs and the difficulty of getting rid of highly refractory pitch.

In this respect, the LC-SLURRY process has a tremendous advantage, because all products can be sold.

duction during a 4 week catalyst change-out can amount to US\$ 18–24 million.

For fixed-bed units, catalyst cycle life dominates economics. Catalysts can't be changed if the units are operating, so shorter catalyst cycles mean decreased production. In a given unit, higher feed rates and higher conversion are desirable economically, but they increase consumption of hydrogen and decrease catalyst cycle life. In units that can recycle fractionator bottoms, higher recycle oil rates can increase selectivity, but they may impose limits on fresh feed rate.

For many recycle hydrocrackers, switching to once-through (zero recycle) operation is attractive economically if the unconverted oil (i. e., the fractionator bottoms) goes to an FCC, olefins plant, or a lube plant for further upgrading. Conversion goes down in the hydrocracker, but it may be possible to increase fresh feed rates without decreasing catalyst cycle life. Operating costs may go down due to decreased hydrogen consumption.

22.12 Safety, Reliability, and Protection of the Environment

Safety, reliability, and protection of the environment are prerequisites to profit in modern industry. Executives know this and strive to behave accordingly. In hydrocarbon production and processing, we have learned from

tragic mistakes. But unsafe behavior continues and tragic incidents still occur, even in companies where the first priority of management really is the health and safety of its workers.

In this section, we discuss safety-related aspects of the following, especially as they apply to hydroprocessing:

- Procedures
- Management of change (MOC)
- Personnel protection equipment (PPE)
- Confined space entry
- Toxic gases: Hydrogen sulfide and carbon monoxide (CO)
- Catalyst handling
- Erosion–corrosion in reactor effluent air coolers (REAC)
- Temperature excursions
- Examples.

22.12.1 Procedures

Nothing in this chapter is a recommendation. The authors accept no responsibility for the operation of any commercial unit.

Process licensors, equipment suppliers, and catalyst vendors provide guidelines and procedures for operation. Many of the accidents and near-misses described below resulted from failure to follow procedures. Hydrocracking is mature technology, with procedures for operation that are decades old. That doesn't mean the procedures are perfect and general procedures may not apply exactly to a certain unit. Significant incidents have led to industry-wide changes. But changes must be managed properly, case-by-case.

22.12.2 Management of Change

A key concept is management of change (MOC) [22.38]. Ineffective MOC is one of the leading causes of serious incidents, according to the US Chemical Safety and Hazard Investigation Board (CSB) which said [22.39]:

In industry, as elsewhere, change often brings progress. But it can also increase risks that, if not properly managed, create conditions that may lead to injuries, property damage or even death.

Changes subject to MOC procedures can include:

- *Personnel changes*, including reorganization, staffing, and training.
- *Equipment changes*, including revamps, maintenance schedules, communications devices, control hardware, and control software.
- *Procedure changes*, including procedures for normal operation, startup, shutdown, and MOC.

- *Material changes*, including significant changes in catalysts, chemicals, and feedstock.

22.12.3 Personal Protection Equipment (PPE)

The PPE worn by workers includes fire-proof clothing, hard hats, safety glasses, steel-toed shoes, gloves, and toxic gas detectors. Harnesses are used to protect against falls. Using fresh-air breathing equipment or self-contained breathing apparatus (SCUBA) improves safety in confined spaces and in areas that might be contaminated by hazardous gases and particulates. In recent years, communication between outside and inside workers has been enhanced by allowing the use of inherently safe radios. Laboratory workers face unique hazards; hard hats are seldom needed in labs, but for some analytical procedures, special gloves and full-face shields protect against hazardous substrates, solvents, and acids.

Pocket-sized toxic gas detectors are important PPE. They sound an alarm when CO or H₂S reach dangerous levels. Some sites require all workers to wear H₂S monitors at all times when they are *inside the refinery gate*. Four-gas monitors are preferred during catalyst unloading. They detect H₂S, CO, combustible hydrocarbons, and oxygen.

In the United States, the Occupational Safety and Health Administration (OSHA) sets standards for PPE [22.40, 41]. The first standards were adopted in 1971. A major revision was issued in 1994, after OSHA discovered gaps in the existing standards. Data indicated that injuries were occurring at the same rate, whether or not employees were wearing PPE. Some regulations were so restrictive that they discouraged innovation.

Present regulations are based on effectiveness. Recent improvements are addressing the main cause of worker noncompliance before the revision: PPE could be cumbersome, uncomfortable, and even impractical.

22.12.4 Confined Space Entry

Empty hydroprocessing reactors are confined spaces. Workers enter reactors during maintenance and catalyst loading. Oxygen levels can become too low even if air is circulating. Required PPE for confined space entry includes fresh-air breathing equipment and a harness that allows colleagues to lift the worker out if necessary. Modern video technology enables outside personnel to monitor people inside directly.

22.12.5 Toxic Gases: Hydrogen Sulfide and Carbon Monoxide

Gaseous hydrogen sulfide (H₂S) is a pervasive hazard around hydroprocessing units. It is generated during

normal operation by HDS reactions and it is used during startups to activate catalysts. Workers are most likely to be exposed when taking samples of gases or liquids. It is common for gas samples to contain more than 5000 ppm H₂S – far above toxic levels.

The impact of H₂S depends on its concentration and duration of exposure [22.42]. At 0.01–1.5 ppm, the characteristic rotten-egg odor is detectable. The odor becomes offensive at 3–5 ppm, where prolonged exposure causes nausea, tearing, asthma, and headaches. Above 20–30 ppm, the odor is said to be sweet or sickly sweet. Above 100 ppm, olfactory nerves are paralyzed and H₂S can no longer be smelled. Exposure to more than 700–1000 ppm causes immediate collapse and death after one or two breaths.

H₂S is flammable. The explosive range is 4.5–45.5 percent in air.

Toxic carbon monoxide can be generated from partial oxidation of hydrocarbons during catalyst unloading; even after thorough stripping with hydrogen during a shutdown, catalyst pores can still contain traces of oil. Under particular conditions, the nickel on NiMo catalysts can react with CO to form nickel carbonyl, an exceptionally hazardous gas.

In hydroprocessing units, sample-taking stations should be well ventilated and equipped with several in-place toxic-gas monitors. Sample-taking procedures include the buddy system: one person takes the sample while another watches. In the past, workers died when rushing forward to help a stricken companion, so the watchers stand at a safe distance with quick access to a radio and SCUBA.

22.12.6 Catalyst Handling

As-delivered catalysts can be dusty. The dust can choke or suffocate workers during handling, especially during reactor loading.

During the dumping of spent catalysts, possible problems include dust, spontaneous combustion, and nickel carbonyl. If the catalysts haven't been sufficiently stripped of hydrocarbons during shutdown, they can ignite spontaneously when exposed to air. Catalysts should be cooled below about 50 °C (120 °F) before dumping, or they should be unloaded under flowing nitrogen and kept in nitrogen-blanketed containers until they are cool enough to handle in air.

22.12.7 Erosion–Corrosion Around Reactor Effluent Air Coolers (REAC)

In hydroprocessing units, erosion–corrosion in REACs can cause leakage and tube failure, leading to loss of hydrocarbon containment and catastrophic explosions.

Examples include the explosion in a German hydrocracker on December 10, 1991, which injured five people and shut the unit down for 8 months; the explosion at the Texaco refinery in Wilmington, California on October 8, 1992, which injured 16 and shut the unit down for 8 months; and more-recent events at Chinese refineries in Zhenhai and Yangzi [22.43].

HDS and HDN reactions convert organic sulfur and nitrogen into H₂S and NH₃, respectively. At reaction temperatures, they are gases. When the reactor effluent is cooled, they form ammonium bisulfide, NH₄SH, which can form solid deposits in REAC tubes. In addition to blocking flow, they induce erosion–corrosion in carbon steel. Wash water is added to the reactor effluent before it reaches the REAC. This mitigates deposition, because NH₄SH is highly soluble in water. The corrosion rate is accelerated, when the flow velocity of the NH₄SH solution is increased.

The piping areas most vulnerable to corrosion are upstream of the REAC but after water injection, between the REAC and the cold separator, and in the REAC itself. Before 1992, it was industry practice to specify carbon steel piping both upstream and downstream of the REAC. After the accidents in Germany and at Texaco, licensors started recommending the use of NH₄SH-resistant alloys.

Other recommendations include:

- Piping should be symmetrical.
- Linear velocity should be 10 to 20 ft/s.
- 30% of the injected water should be liquid.
- The salt content of the sour water should be limited. One licensor recommends < 8 wt%. Others recommend < 4 wt%.
- Corrosion and fouling should be monitored with test coupons and other appropriate means.

A personal recommendation is: Track the difference between ideal and actual performance for heat exchangers (and other equipment as well). This is an excellent way to see which exchangers are limiting unit performance, which ones need maintenance, and which ones can do without maintenance for a time; in certain cases, to opening a well-performing piece of equipment and exposing it to air is riskier than keeping it running. At least one operating company plans maintenance rigorously with design models.

22.12.8 Temperature Excursion Fundamentals

Hydroprocessing is exothermic. In hydrocrackers, loss of heat control causes temperature excursions, in which temperatures suddenly jump by as much as 104 °C (186 °F) in less than 20 s. One excursion ruptured a re-

actor wall. The excursion at Tosco Avon on January 21, 1997, ruptured a reactor outlet pipe, releasing a hot oil/hydrogen mixture, which ignited upon contact with air. The resulting explosion and fire killed one worker, injured 46 others, and shut the unit down for more than 6 months.

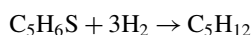
One can describe the fundamentals of temperature excursions by addressing the following observation and question: Per hydrogen consumed, hydrocracking releases a little less heat than HDS and 20% less heat than aromatics saturation. So why do temperature excursions occur in hydrocrackers but rarely in hydrotreaters?

The easy answer is: because hydrocracking doesn't occur in hydrotreaters. That's true, but not very instructive. It's more informative to examine additional observations as follows.

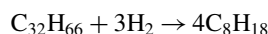
Relative Amounts of Reactants

If a feed contains 2 wt% sulfur and 86 wt% carbon, the C–S atom ratio is about 198 : 1 (Table 22.14).

Most sulfur compounds have two C–S bonds and HDS requires both to be broken with consumption of at least 2 moles of H₂. Paraffin hydrocracking breaks one bond with consumption of one mole of hydrogen. Assume that all sulfur is present as methyl thiophene isomers and that HDS entails the following reaction



Now assume that the rest of the feed is composed entirely of isomers of C₃₂H₆₆, which boil between 440 and 467 °C and have 31 crackable C–C bonds. Breaking all 31 C–C bonds would produce methane. Breaking just three bonds (10% of the total) could form four naphtha molecules



In this scenario, after correcting for the C–C bonds in sulfur compounds, hydrocracking heat production is 18.6 times greater than HDS heat production.

Disrupting Ring–Compound Equilibria

In the previous paragraph, we ignored ring compounds. In real feeds, the percentage of carbon atoms in ring compounds can range from 30% to more than 80%. Figure 22.8 shows equilibria between naphthalene, tetralin, and decalin at different temperatures and pressures. Saturation of aromatics and dehydrogenation of naphthenes involves 1 to 3 hydrogen molecules per ring. At low temperatures, exothermic saturation releases more heat per H₂ consumed than HDS, but above about 415 °C (780 °F), the reverse reaction, endothermic dehydrogenation becomes important.

At true equilibrium, there is no net heat consumption or production. As temperatures go higher, the equilibrium shifts further toward aromatics until

Table 22.14 Heat release for HDS, HDN, and HC reactions for a representative hydrocracker feed. Breaking 10% of the C–C bonds in the feed would release 18.6 times more heat than HDS

TBP distillation, IBP/50%/99.5%			
°C	200/346/520		
°F	393/655/968		
C _P /C _N /C _A /C _O ^a	54.8/25.9/15.3/4.0		
Sulfur (wt%)	1.16		
Nitrogen (wt%)	0.147		
Oxygen (wt%)	0.013		
Carbon (wt%)	86.26		
Hydrogen (wt%)	12.42		
	Mole ratio	Corrected for the C in thiophene	
S	1	–	
N	0.29	–	
C	198.2	≈ 190	
Reaction type	ΔH_R^c (kJ/mol)	ΔH_R (relative to HDS)	Heat production (relative to HDS)
HDS	–52.0	1	1
HDN	–62.9	1.21	0.8
HC: All C–C bonds broken ^b	–51.2	0.98	186.0
HC: 10% of C–C bonds broken	–51.2	0.98	18.6

^a Ratio of carbon atoms in paraffin chains, naphthene rings, aromatic rings and olefin groups

^b Complete conversion of C₃₂ into CH₄, all 31 of the C–C bonds are broken

^c Per mole of H₂ consumed

naphthenes are nearly nonexistent. In this way, the saturation/dehydrogenation equilibrium mitigates heat release. It has been said that dehydrogenation reactions *apply the brakes* to temperature rise. Removing saturated rings, e.g., by breaking saturated C—C within rings, or by clipping off alkyl side chains, disrupts equilibria, thereby *releasing the brakes*. Breaking C—C bonds replaces heat-neutral equilibrium with irreversible exothermic hydrocracking. The net difference in ΔH_R is -42 kcal/mol of H_2 consumed.

Hydrocracking is More Temperature Sensitive Than Hydrotreating

Please refer to Fig. 22.29, which is based on Langmuir–Hinshelwood kinetics and experimentally determined Arrhenius activation energies. It shows that if reaction rates for HDS and hydrocracking are the same at 380°C , then hydrocracking over high-zeolite catalysts is 20 times faster than HDS at 470°C . The hotter it gets, the faster it gets hotter. Activation energies for hydrocracking over amorphous silica-alumina (ASA) catalysts are slightly higher than those for HDS. Excursions over ASA catalysts do occur, undoubtedly for the first two reasons described above, but probably not due to activation energy.

Thermal Hydrocracking

Refer again to Fig. 22.29. It shows that around 470°C , thermal hydrocracking becomes $2\times$ faster than catalytic hydrocracking. Thermal cracking proceeds by a different mechanism, in which far more than 10% of C—C bonds are broken. An increase in methane production is a sure sign of thermal hydrocracking. Catalytic hydrocracking produces only small amounts of methane and ethane; typical yields of C_1C_2 are <0.2 wt% of fresh feed at SOR and <0.6 wt% at EOR. In contrast, thermal hydrocracking often produces more than 4 wt% C_1C_2 .

22.12.9 Temperature Excursion Examples

Example 1: Stagnation

Flow of fluids accounts for almost 100% of heat removal. Even in a hydrotreater, stagnation can be unsafe. A serious temperature excursion occurred in a stagnant, low-pressure hydrotreater. The reactor had been blocked in pending the completion of maintenance activity elsewhere in the refinery. To save time, the reactor wasn't drained before it was isolated by closing inlet and outlet valves. Temperatures were near-ambient, at least at first. Nobody imagined that a reaction could occur. The reactor contained oil, hydrogen, and (of course) hydrotreating catalyst. Initial reactions might have involved just a few molecules, with minuscule

heat release. But without flow, reaction heat accumulates. Accumulated heat raises local temperatures, which increase local reaction rates. Faster reactions generate more heat etc. The thermochemical driving force was strong. The residence time and supply of reactants were essentially limitless. In retrospect people agreed, after the fact, that an excursion was inevitable.

Example 2: Sudden Feed Switch

A feedstock change can trigger a temperature wave, which can cascade through several catalyst beds, growing as it goes. The temperature can get high enough to trigger an excursion. If operators know that a different feed is coming to the unit, they prepare by decreasing temperatures in advance, especially if they know the new feed is more reactive.

If the change is unexpected, the resulting temperature wave won't be noticed until it reaches the outlet of the 1st bed and (less than a minute later) the inlet of the 2nd bed. An automatic feedback control loop will drop the inlet temperature of the 1st bed, but that action won't stop the wave in the 2nd bed. Intercepting the wave requires adding quench to the outlet of the 2nd and 3rd beds. If alerted by alarms, operators have plenty of time to respond appropriately. But they must respond quickly and decisively. If the wave isn't stopped before it reaches the first bed of cracking catalyst, it will trigger an excursion.

Over-response to a heavier, less-reactive feed can also cause an excursion. When a bed outlet temperature falls, the temperature controller for that bed reduces quench to increase the inlet temperature. If the increase is too large, the bed outlet temperature – and the inlet temperature for the next bed – will be too high.

A feed-switch excursion occurred in a European hydrocracker during a change from one feed tank to another. There wasn't much difference between the oils in the two tanks, but the pipe between the new tank and the hydrocracker contained flush oil – light cycle oil from an FCC unit. LCO is lighter and far more reactive than the usual heavy VGO feed. When the LCO exited the first catalyst bed, the bed outlet temperature was significantly higher than usual. Operators responded immediately and appropriately by adding quench to all downstream beds. But they didn't add enough quench. The inlet temperature for the 1st bed of cracking catalyst was just a few degrees higher than usual. But due to the higher reactivity of the feed and also due to the fact that the light feed was mostly vapor by then, the bed outlet temperature jumped, exceeding the prescribed limit. The unit depressured automatically. Three days of production were lost, but no other negative consequences were observed.

Example 3: Hot Spots

During normal operation, flowing fluids – and practically nothing else – removes reaction heat from hydrocracking reactors of all kinds. For the paragraphs above, we assumed that flow distribution through reactors is perfect from top to bottom. In real units, there is always some mal-distribution of flow. Mal-distribution starts with poor reactor design, poor installation of reactor internals, improper catalyst loading, or a process upset.

The mal-distribution shows up as a *radial temperature difference* (radial dT), defined as the difference between highest and lowest TI readings in a horizontal plane.

Figure 22.39 and Table 22.15 show how mal-distribution of flow might affect measured temperatures, true maximum and minimum temperatures and critical calculations. The measured temperatures are from a commercial unit. The *real* maximum and minimum temperatures are made up, but they are consistent with hydrodynamic calculations.

Here are some observations based on the TI readings:

- All radial dT s are higher than usual. With modern reactor internals, SOR radial dT values are $< 1^\circ\text{C}$ at the bed inlet and $< 2^\circ\text{C}$ at the bed outlet. Typically at EOR, the inlet radial dT s haven't changed and the outlet radial dT s range from $4\text{--}6^\circ\text{C}$.

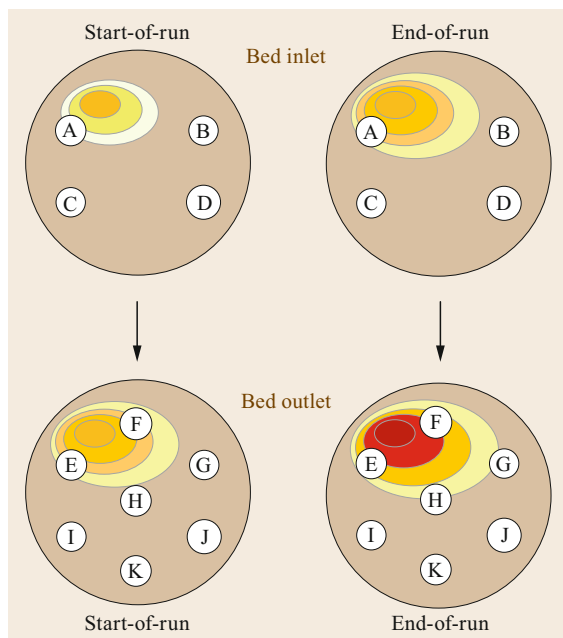


Fig. 22.39 Example: Impact of flow mal-distribution on TI measurements. This figure is associated with Table 22.14

- At EOR, the average axial dT is 14.5°C . For high-zeolite catalysts, this is slightly greater than max axial dT guidelines from some licensors (13.7°C) but lower than guidelines from another licensor (16.7°C).
- The EOR radial dT is almost the same as the average axial dT and the max axial dT is nearly $2\times$ higher than the average axial dT . Both are clear indications of severe mal-distribution of flow.

One never knows the true minimum and true maximum temperatures in a catalyst bed. If an operator sees the danger signs noted above, s/he knows there is a problem but not the severity of the problem:

- The inferred maximum temperature is 490°C and is associated with a hot spot
- 490°C is 51°C higher than the apparent maximum temperature and it is 35°C above the metallurgical limit for this particular reactor
- 490°C is $30\text{--}50^\circ\text{C}$ higher than the temperatures at which thermal cracking becomes dominant.

The customer was advised to look for other signs of a hot spot, such as off-color products and increasing methane in the recycle gas. Product color had indeed degraded since SOR and methane was indeed high. However, the refiner had not measured methane before, so it was impossible to know if there had been an increase.

A temperature pulse test was recommended but not conducted. In a pulse test, the bed inlet temperature is dropped quickly by at least 2.5°C . For each bed outlet TI, the response time is measured. When flow distribution is poor, the difference in bottom-of-bed TI response time can be more than 7 min. The leading explanation for the hot spot was poor catalyst loading, but there was no way to prove it.

Example 4: Wrap-Around Heat

The heat exchangers in hydrocrackers are highly integrated. An upset far from the reactors can cause problems. In September 2009 a temperature excursion occurred in the hydrocracker at CITGO Petroleum Company in Lake Charles, Louisiana, when a sudden loss of preheat caused a hydrogen heater to fire aggressively [22.44]. In response to the suddenly higher heater temperature, quench valves quickly opened to control a high bed inlet temperature, then quickly closed when the high bed inlet temperature was resolved. The quick closing of the quench valve permitted an even higher inlet temperature in the following bed, which led to a bed outlet temperature greater than the limit of 427°C (800°F). This initiated low-rate

Table 22.15 TI readings and process calculations for Fig. 22.39, plus calculations for inferred *true* values

TI designation	Start-of-run		End-of-run	
	Bed inlet	Bed outlet	Bed inlet	Bed outlet
A	372		420	
B	370		415	
C	369		413	
D	370		413	
E		384		439
F		383		438
G		379		425
H		380		428
I		379		426
J		379		426
K		380		426
Calculations based on TI measurements				
Average bed T		376.8		424.5
Max	372	384	420	439
Min	369	379	413	425
Radial dT	3	5	7	14
Average axial dT (avg Out–avg In)		10.3		14.5
Max axial dT (max Out–min In)		15		26
Calculations based on inferred but unmeasurable values				
Average bed T		377.3		437.8
Max	374	388	425	490
Min	369	378	412	424
Radial dT	5	10	13	66
Average axial dT (avg Out–avg In)		11.5		38.5
Max axial dT (max Out–min In)		19		78

depressuring at 7 bar/min (100 psig/min). The results were:

- A flaring event
- Production disruption lasting 3–4 days
- Loss of catalyst life.

Afterwards, an investigation team determined what had happened and suggested appropriate corrective action. Changes were made to the control system, including the following:

- Use setpoint tolerance and output tolerance to limit the size of changes that can be entered at the control board without a warning
- Make heater controls less aggressive
- Override feedback-based control of quench when a bed outlet temperature exceeds its setpoint
- Make the override more aggressive when the bed outlet is rising faster than 1 °F/min
- Limit how quickly the quench valves can close, but do not limit how fast they can open
- Limit how quickly heater firing can increase, but do not limit how quickly it can decrease.

Mr. Gregory Hampton developed an advanced regulatory control (ARC) application to capture the suggestions. Implementation was straightforward, except for the rate-of-rise limit. This was handled with a unique quench-demand calculation, which executes once per second in the ARC. According to enthusiastic unit operators, the application works well to detect and mitigate impending temperature excursions. It then automatically returns the unit to automatic control. The Hampton approach is now being implemented elsewhere around the world.

Example 5: Substandard Equipment, Disabled EDS Interlock, Stagnation

A serious excursion was the latest of several in a new hydrocracker. The ultimate cause was a decision by the purchasing department to order substandard items for the associated hydrogen plant. One by one, the substandard items failed and were replaced by proper ones. Each failure upset the hydrocracker. Some failures sent liquid into the suction of the recycle gas compressor (RGC), causing the RGC to shut down. The licensor's EDS interlock gave operators 15 min to restart the compressor before automatically activating the low-rate depressuring valve. Each depressuring event shut

the unit down for at least a day. To give themselves extra time to restart the RGC, the unit engineer and operators decided to disable the EDS–RGC interlock. It was acceptable, they assumed, to depressure only if the unit reached a temperature limit. These assumptions demonstrated ignorance of several fundamental concepts:

- The flow of fluids is the only significant way to remove heat from a hydroprocessing reactor.
- With zero or low flow, TI readings become meaningless.

Example 3 showed that one never knows the highest or lowest temperature in a catalyst bed. But when reactants are flowing, one can be confident that bed outlet TIs correspond to the temperatures above them. When flow stops, no TI reading is relevant to any temperature more than a few inches away.

Reactions do not stop when flow stops. Heat accumulates in catalyst beds, often without affecting the bed outlet TI readings. Hot oil sinks into pools at low points. Eventually, the pooling oil will reach one or more bed outlet TIs and/or reactor wall TIs, providing the first tangible indication that something is wrong. Undoubtedly, that is what happened in this unit. A timeline is shown in Table 22.16. A visual representation is presented in Fig. 22.40.

After the first compressor failure, it took 144 min for overheated oil to reach reactor outlet TI-3. The reading spiked at 17:38 local time (LT), initiating depressuring when it reached 440 °C. TI-3 continued to rise until it reached 487 °C. Depressuring seemed to make things worse. It decreased TI-3, but as the pressure fell, the exiting gas pulled hot, formerly stagnant

Table 22.16 Example 5 timeline

Local time	
16:14	Recycle gas compressor failed Pressure = 127 bar Maximum bed TI = 402 °C Reactor outlet TI = 398 °C
17:38	Reactor outlet TI-3 exceeded 440 °C Automatic low rate depressuring
17:44	Reactor outlet TI-3 continued up to 478 °C
18:00	Recycle gas compressor was restarted
18:27	A bottom reactor wall temperature reached 436 °C
19:17	Recycle gas compressor failed
18:20–20:54	Bed outlet TI-1 jumped 214 °C in 7 min, stayed > 618 °C for 154 min
20:28	Recycle gas compressor was restarted successfully
18:56–22:30	Bed outlet TI-2 reached > 618 °C, fell, rose to > 550 °C until 22:30

oil through the reactor. Between 17:48 and 17:55 LT, Bed Outlet TI-1 jumped from 404–618 °C, an increase of 214 °C in 7 min. The readings fell after a restart of the RGC. But then, most likely due to the arrival of more overheated oil, TI-1 jumped back up to 618 °C, where it flat-lined for more than 2.5 h. Actual temperatures were higher than 618 °C, which is top-of range. A second attempt to restart the RGC succeeded. TI-1 started to fall. But as it did, Bed Outlet TI-2 rose above 550 °C and stayed there for another 2 h.

Afterwards, the unit was operated at reduced rates for 6 months, with strict adherence to licensor-suggested temperature limits. The limits were tighter due to fears that the reactor wall and outlet pipe had been compromised. During the subsequent turnaround, workers found partially fused silica balls near the reactor wall. Pure silica melts at about 2000 °C. Impure silica melts at lower temperatures, but even so, it must have been incredibly hot near the wall of that reactor.

Example 6: Tosco Avon

On January 21, 1997 a temperature excursion led to the rupture of the reactor 3 outlet pipe at the Tosco Avon Refinery in Martinez, California [22.45]. Reactor 3 was one of three parallel Stage 2 reactors, each of which contained five beds of hydrocracking catalyst. The consequent release of hydrogen and hydrocarbons ignited on contact with air, causing an explosion and fire. One worker was killed and 46 others were injured. There were no reported injuries to the public.

Figure 22.41 shows the arrangement of the reactors in the Tosco unit. Figure 22.42 shows selected TI readings during the event. The initial excursion began in reactor 3 bed 4 (R3B4) and cascaded into R3B5 (reactor 3 bed 5). It may have started at a hot spot in R3B4. It peaked at 439 °C (823 °F). According to licensor-recommended procedures, the unit should have been depressured when TI readings reached 427 °C (800 °F). But instead of depressuring, the operators did what they had done several times since July 1992: they tried to control the excursion by manipulating quench gas. Two days earlier, on January 19, 1997, they had managed to defeat an excursion in reactor 1, but not before the outlet pipe TI exceeded 482 °C (900 °F) and the center TI in R1B4 reached 537 °C (998 °F). Along the way, an operator went outside to get a reading from a panel underneath the outlet pipe. On January 21, the operator who died went to the same place and was underneath the outlet pipe when it ruptured.

Operators said they failed to act on January 21, because they didn't know whether or not an excursion was occurring. They got readings from three different temperature systems, two in the control room and another in

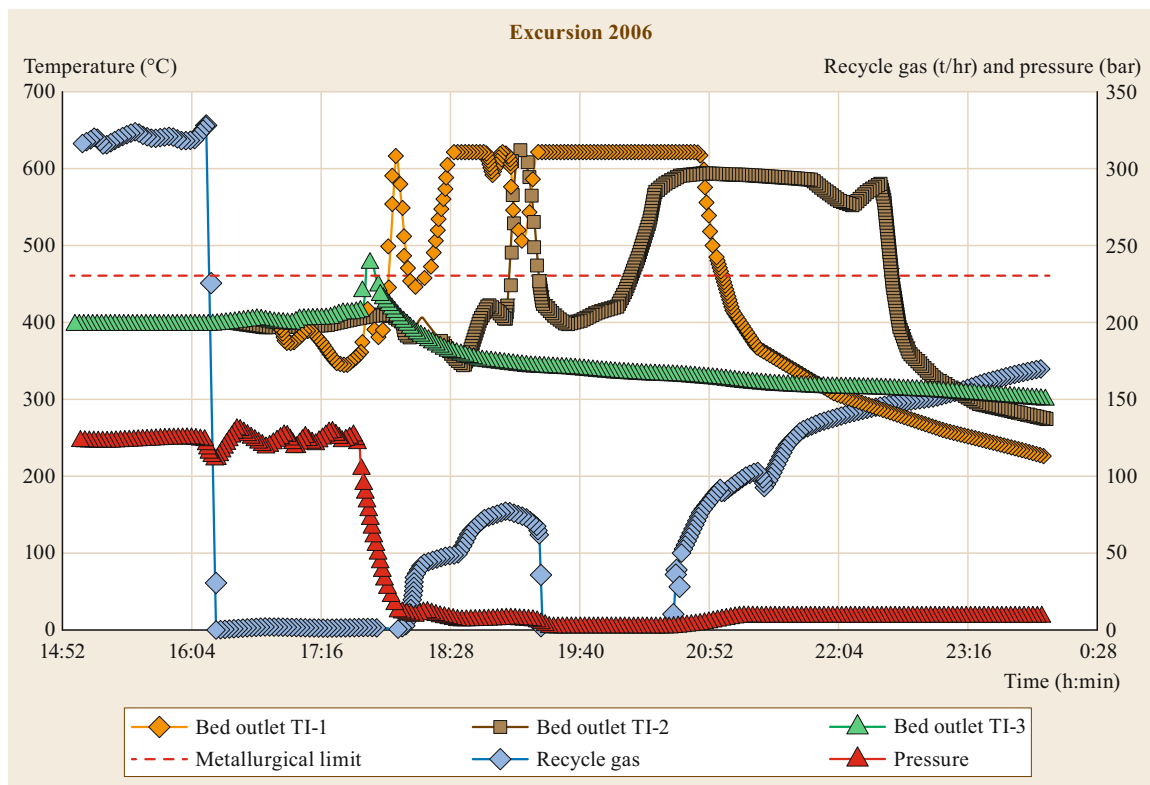


Fig. 22.40 Pressure, recycle gas flow, and selected temperatures for Example 5. Bed outlet TI-1 flat-lines at 618 °C, because 618 °C is top-of-range. Actual temperatures were far higher, as evidenced by the fused catalyst in the bed when the reactor was unloaded

the outside field panel. The systems in the control room gave different information. The data logger, with most of the reactor temperature information, was fluctuating wildly. Because of sudden changes in quench flow, the makeup compressor shut down.

In other refineries, uncertainty is not an acceptable excuse for unsafe behavior. Operators are told: When in doubt, assume the worse; bring the unit down.

Root causes for the Tosco Avon accident include the following:

- When the unit was depressured at a low rate to stop an excursion on July 23, 1992, a grass fire started at the flare. A worker told the lead author of this chapter, in a private conversation, that from that time on, upper management strongly discouraged use of depressuring, fearing the consequences of a fire spreading into the nearby grassy hills and the John Muir historic site.
- Operators used three different instrumentation systems to obtain temperature data. Not all the data were immediately accessible and they often disagreed. Monitoring points capable of reading the

highest temperatures were underneath the reactors and not connected to the control room.

- Supervisory management and operator training were inadequate. Operators were not taught to understand that zero default values on the data logger might mean extremely high temperatures. They did not understand the tremendous sensitivity of cracking catalysts to organic nitrogen. They did not understand the dynamics of sampling i.e., the lag time between taking a sample, getting results, and what might have happened to the process in the meanwhile (see Table 22.17).
- Written procedures were outdated, incomplete, and contained in different documents in different locations.

The investigation team developed the following recommendations for consideration by owners of all hydroprocessing facilities:

- Management must ensure that operating decisions are not based primarily on cost and production. Facility management must set safe, achievable op-

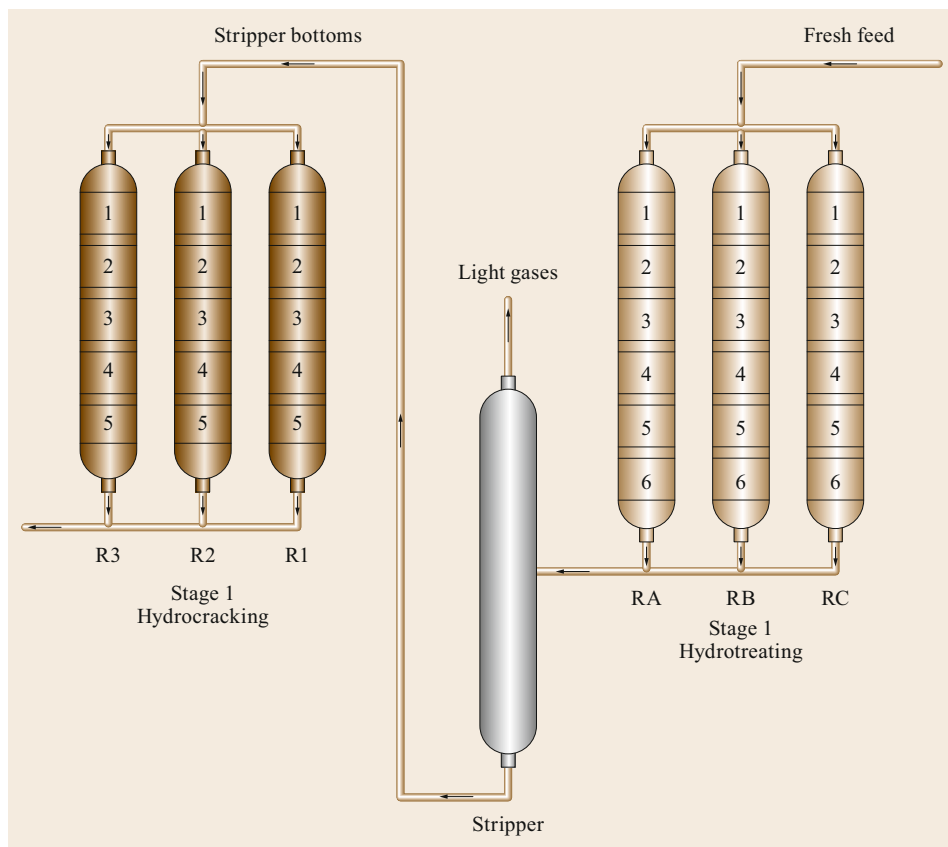


Fig. 22.41 Arrangement of reactors in the Tosco Avon hydrocracker

erating limits and not tolerate deviations from these limits. Management must provide an operating environment in which operators can follow emergency shutdown procedures without fear of retribution.

- Process instrumentation and controls should be designed to consider human factors consistent with good industry practice. Hydroprocessing reactor temperature controls should be consolidated with all necessary data available in the control room. Backup temperature indicators should be used so that the reactors can be operated safely in case of instrument malfunction. Each alarm system should distinguish between critical alarms and other operating alarms.
- Adequate operator supervision is needed, especially to address critical or abnormal situations.
- Facilities should maintain equipment integrity and discontinue operation if integrity is compromised.
- Management must ensure that operators receive regular training on the unit process operations and chemistry. For hydrocrackers, this should include training on reaction kinetics and the causes and control of temperature excursions.

- Operators need to be trained on the limitations of process instruments and how to handle instrument malfunctions.
- Facilities need to ensure that operators receive regular training on the use of the emergency shutdown systems and the need to activate these systems.

22.12.10 Preventing Temperature Excursions

Honor Temperature Limits

To ensure safe operation, licensors specify limits on average reactor temperature, maximum peak temperature, and maximum bed temperature rise (Table 22.18). For high-zeolite catalysts, typical values are lower than for less-active catalysts. The limits provide ample cushion between operating temperatures and the actual metallurgical limit, which is 455 °C for typical hot-wall reactors constructed from stainless steel containing 2.25% chromium and 1% molybdenum.

As temperatures approach these limits, process economics may suffer. High temperatures increase production of low-value C₁–C₄ and light naphtha. Middle distillate quality suffers from high aromatics, which de-

	Bed 4	Bed 5	Bed 5	Bed 5	Bed 5	Bed 5	Rx 3	Rx 3
	Outlet	Inlet	Outlet	Outlet	Outlet	Outlet	Inlet	Outlet
	Temp (°F)	Temp (°F)	Temp (°F)	Temp (°F)	Temp (°F)	Temp (°F)	Temp (°F)	Temp (°F)
Time (pm)	Pt-133C2	Pt-140C3	Pt-134C1	Pt-134C2	Pt-134C4	Pt-134C5	Pt-125C	Pt-141C
7:33:00	628.3	636.9	648.6	646.3	656.8	645.9	632.2	641.3
7:33:20	628.3	636.9	648.6	646.3	656.8	645.9	632.2	641.3
7:33:40	636.5	658	648.6	646.3	656.8	645.9	632.2	641.3
7:34:00	823.2	720.7	648.6	646.3	656.8	645.9	632.2	641.3
7:34:20	732	859.5	648.6	646.3	656.8	645.9	632.2	641.3
7:34:40	732	859.5	648.6	646.3	656.8	645.9	632.2	641.3
7:35:00	637.3	792.4	624.2	627.7	633.4	645.9	632.2	641.3
7:35:20	637.3	715.7	624.2	627.7	633.4	615.4	632.2	641.3
7:35:40	637.3	664.4	624.2	640.3	633.4	615.4	632.2	641.3
7:36:00	637.3	633.4	650.3	647.9	623.6	615.4	632.2	649.9
7:36:20	637.3	633.4	663.9	667.7	623.6	615.4	632.2	649.9
7:36:40	637.3	660.7	672.9	667.7	623.6	625.6	632.2	658.9
7:37:00	637.3	660.7	681.1	676.8	656	645.8	632.2	658.9
7:37:20	637.3	660.7	681.1	676.8	672	673.5	632.2	760.7
7:37:40	637.3	660.7	697.3	707.5	690.7	673.5	640.2	760.7
7:38:00	637.3	660.7	717.2	876	690.7	673.5	640.2	684.6
7:38:20	637.3	660.7	1255.7	0	783	705.8	648.8	701.8
7:38:40	637.3	660.7	0	0	0	744	660	788.8
7:39:00	637.3	648	0	0	0	889	693	983.1
7:39:20	637.3	648	0	0	0	0	754.7	1219
7:39:40	637.3	655.6	0	0	0	0	826.5	0
7:40:00	637.3	655.6	0	0	0	0	889.1	0
7:40:20	637.3	655.6	0	0	0	0	960.7	0
7:40:40	637.3	645.7	0	0	1397.1	879.9	1233.5	0
7:41:00	637.3	645.7	0	0	1398.4	694.9	0	0
7:41:20	0.0 ????	0.0 ????	0.0 ????	0.0 ????	0.0 ????	0.0 ????	0.0 ??	0.0 ????
7:41:40	0.0 ????	0.0 ????	0.0 ????	0.0 ????	0.0 ????	0.0 ????	0.0 ??	0.0 ????

Fig. 22.42 Reactor 3 temperatures during the TOSCO Avon incident. Temperature indicator Pt-133C2 jumped by 104 °C (186 °F) in 20 s, reaching 439 °C (823 °F). The excursion cascaded through the quench section into the next catalyst bed, causing a jump of 223 °F (124 °C) in 40 s at Pt-140C3, reaching 460 °C (860 °F)

crease smoke and cetane. Units have been shut down for a catalyst change due to poor selectivity.

Move Slowly

It can take more than an hour for changes to travel completely through a hydrocracker. For this reason, licensors recommend limits on heat-up rates.

Decrease Temperature Before Making Changes

One never really knows how a feedstock change will affect unit performance. To be safe, it is best to lower temperatures to protect against incidents such as the one discussed in Example 1.

Trends

Trends are an early warning system, indicating from history what is likely to happen next, providing time to back off before a limit is reached. Early warning also provides time to alert other units in the refinery

that a change might be coming. At a Shell refinery in Canada, the philosophy is SSS: slow down, stabilize, and (if necessary) shut down.

Software

Hampton et al. describe an advanced regulatory control (ARC) application that detects impending excursions and mitigates them with quench overrides [22.44].

22.12.11 Stopping a Temperature Excursion

Figure 22.43 shows how hydrocracking is analogous to combustion. In both cases, three factors are needed for a reaction. Combustion requires oxygen, flammable fuel, and heat. Hydrocracking requires hydrogen, oil, and heat. In both processes, removal of one factor stops the reaction.

Table 22.19 presents a qualitative overview of heat balance and heat removal in a hydroprocessing unit

Table 22.17 Abbreviated timeline with comments on nitrogen slip measurements for the Tosco Avon incident

Local time	
4:50 AM	One of three Stage 1 hydrotreating reactors was brought down to repair a leak. Stories differ about whether the total unit feed rate was kept the same or reduced and whether or not Stage 1 reactor temperatures were adjusted. Regardless, the extent of HDN was reduced.
10:00 AM	Nitrogen slip had risen from < 15 to 352 ppmw.
11:30 AM	Because of the high nitrogen slip and resulting inhibition of Stage 2 cracking activity, there was no temperature rise in one cracking reactor and very little rise in the other reactors. No light products were being formed. Stage 1 temperatures were raised to decrease nitrogen slip.
1:10 PM	Stage 2 hydrocracking reactor temperatures were raised to <i>burn off</i> inhibitory nitrogen. This was a horrendous mistake. Treating and cracking temperatures must never be raised at the same time. As discussed, catalytic cracking activity is highly sensitive to organic nitrogen.
5:38 PM	Nitrogen slip from Stage 1 was reported to be 47 ppmw. The actual nitrogen slip when the result was received was considerably lower than 47 ppmw. Since 10:00 AM, the nitrogen slip had fallen 300 ppmw in 7 ½ h, an average of 40 ppmw/h. If the lag time between taking a sample and getting results was 1 h as usual, the true nitrogen slip was < 10 ppmw at 5:38 PM and probably close to zero at 7:34 PM.
7:34 PM	In reactor 3, bed 4 (R3B4), one TI jumped 108 °C in 40 s, reaching 439 °C, 10 °C higher than allowed by procedure but not higher than in previous events.
7:34:20 PM	Quench to R3B5 opened 100%. Data logger temperatures cycled between –18 °C, 649 °C, and 343 °C. In well-run units, the associated uncertainty would have compelled someone to bring the unit down immediately (if it had not been depressured previously due to high temperature).
Sometime before 7:37 PM	An operator went outside to verify temperatures at the field panel.
7:37–7:39 PM	All R3B5 outlet TIs were > 415 °C. One reached 679 °C.
After 7:40 PM	An operator phoned an instrument technician to work on the fluctuating data logger.
7:41:20 PM	7 min after the first temperature jump. Explosion. The operator at the field panel died. A board operator activated the EDS.

Table 22.18 Common limits on temperatures in fixed-bed hydrocrackers

	High-zeolite catalyst (°C (°F))	Low-activity catalyst (°C (°F))	Hydrotreating (reference only) ^a (°C (°F))
Max WABT	415 °C (780 °F)	427 °C (800 °F)	–
Max temperature (any TI or any two)	427 °C (800 °F)	440 °C (825 °F)	440 °C (825 °F)
Max T-rise per bed	17 °C (30 °F)	19 °C (35 °F)	50 °C (70 °F)
Max deviation from setpoint	28 °C (50 °F)	28 °C (50 °F)	28 °C (50 °F)
Rate of change of T-rise	^b	^b	–

^a Hydrotreaters do not require depressuring systems. The numbers here are shown for reference only
^b Rate of change in T-rise can serve as the basis for an alarm

during normal operation and Table 22.20 compares stopping combustion with stopping hydrocracker temperature excursions.

Depressuring is immediate and always stops temperature excursions in fixed-bed hydrocrackers. As mentioned, guidelines for designing EDS are provided by API Recommended Practice 521. Emergency depressuring, especially high-rate depressuring, disrupts a unit. It has deformed reactor internals and disturbed catalyst beds, creating or aggravating flow-distribution problems.

Temperature-related EDP interlocks should never be disabled, as they were in Examples 5 and 6. Operators should never hesitate to depressure manually if necessary.

Depressuring must continue until the pressure is as low as possible, usually to just above the CLPS pressure. Operators who attempt to re-pressure sooner usually do so when the pressure is 50% of design. They don't realize that flow must be zero at some point during the switch from depressuring to repressuring and that even after extensive hydrogen stripping, some oil is still present inside catalyst pores. In our experience with two units, early repressuring led to a second excursion.

Early action prevents or mitigates excursions before they require depressuring. All of the non-depressuring actions in Table 22.20, including reduction of feed rate, can decrease the chance of an excursion before limits are reached. For these reasons, operators should be encouraged to manipulate quench valves and heater

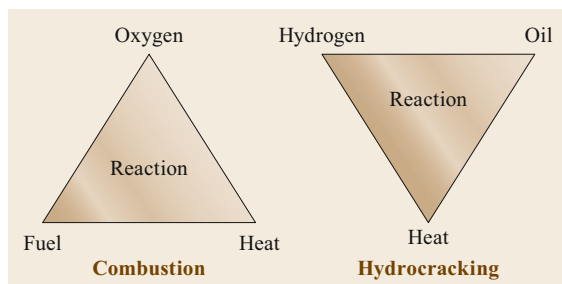


Fig. 22.43 Comparison of combustion with hydrocracking (after [22.44])

controls promptly and decisively at the first sign of an impending excursion.

22.12.12 No DIBS

We have come a long way since 1984, when the CEO of an oil company said, in response to a question about a fatal explosion: *What can I say? It's a dangerous business.* He was truly distraught about the incident, which had killed people he knew. He took care of the families of the victims. But his old-school attitude may have been part of the problem. In 2017, *It's a dangerous business* has been replaced by Zero-Zero-Zero campaigns – to achieve zero injuries, zero loss of containment, and zero unplanned shutdowns. These campaigns are not just for show. They reflect a sincere belief that it doesn't have to be a dangerous business. They require investment, but the return on that investment in today's litigious society is enormous in many measurable ways.

Accidents do still happen. The two worst examples in this section were caused by DIBS – Did It Before

Table 22.19 Heat sinks, heat sources, and heat removal in fixed-bed hydroprocessing units

Heat sources	Proportion
Chemical reactions	Major
Feed heater	Moderate ^a
Heat sinks	
Feed heat capacity	Major
Feed vaporization	Major
Hydrogen	Major
Catalysts	Minor ^a
Reactor walls	Minor ^a
Heat removal mechanisms	
Flow of fluids	Major
Heat exchangers and coolers	Major

^a Major during startup and shutdown

Syndrome. People did the wrong things, over and over again, knowing full well that they were ignoring procedures. Eventually, they came to believe that their way was sort of okay. But as Master Michael Reade says in martial arts classes, *Practice makes permanent. Only perfect practice makes perfect.*

We know first-hand that Tosco workers wanted to operate safely and pleaded for better equipment, only to be denied by profit-obsessed executives. In that environment, executive DIBS was more responsible for the fatality than worker DIBS.

We see DIBS everywhere in our personal lives. Motorists run stop signs and drive too fast. Children are allowed to ride bicycles without helmets. DIBS, it seems, is a fundamental aspect of human behavior. We might achieve Zero-Zero-Zero, but not before we zero in on DIBS.

Table 22.20 Comparison of stopping combustion with stopping hydrocracker temperature excursions

Combustion	Action	Speed	Effectiveness
Remove air	Smother with a blanket or foam, add CO ₂	Immediate	Very
Remove fuel	Set back fires around the main fire	Slow	Moderate
Remove heat	Add water or CO ₂ from a fire extinguisher	Immediate	Very
Hydrocracker temperature excursions			
Remove hydrogen	Depressure	Fast	Very
Remove fuel	Cut feed pump	Slow	^a
Remove heat	Depressure	Fast	Very
	Add quench gas	Immediate	Moderate
	Cut furnace firing	Slow	Moderate
	F–E exchanger bypass	Slow	Very

^a Decreasing feed rate increases residence time and removes a significant heat sink. Both factors might increase the severity of an excursion. For this reason, one licensor recommends keeping the feed pump running, at least for a time. When coupled with F–E exchanger by-pass, early action to send cold feed to the furnace and reactors can be quite effective in reducing reactor temperatures

22.13 Conclusion

Hydroprocessing plays a central role in petroleum refining. Advances in hydroprocessing are driven by competitive forces, clean-fuel regulations, the advent of different feedstocks, and the ongoing need to im-

prove process safety. Improved catalysts, more-flexible reactor design, advanced process control, and online optimization will continue to enhance the safety and capability of new and existing units.

22.14 Additional Reading

For additional information, we recommend the books by Satterfield [22.1], Topsøe et al. [22.2], Gary and Handwerk [22.46], Marcilly [22.47], Scherzer and Gruia [22.13], Speight [22.48], Ancheyta and Speight [22.33], Magee and Dolbear [22.49], and Hsu and Robinson [22.50]. Satterfield's book covers most aspects of heterogeneous catalysis and serves as a source of information for many subsequent works. Topsøe's book gives a thorough overview of the fundamentals of hydrotreating. Gary and Handwerk still sets the standard for textbooks on petroleum refining. In considerable

depth, Marcilly's work describes the fundamentals of acid/base catalysis in the refining and petrochemical industries. The Speight and Speight/Ancheta books focus on hydroprocessing fundamentals, heavy oil upgrading, reactor design, and related topics. Scherzer and Gruia provide useful information on hydrocracking chemistry and catalysis. The Magee/Dolbear book covers refining catalysis in general terms and the Hsu/Robinson books include chapters by several authors on all aspects of petroleum refining, including many areas not addressed in other publications [22.50].

References

- 22.1 C.N. Satterfield: *Heterogeneous Catalysis in Industrial Practice*, 2nd edn. (McGraw Hill, New York 1991)
- 22.2 H. Topsøe, B.S. Clausen, F.E. Massoth: Hydrotreating catalysis. In: *Catalysis – Science and Technology*, Vol. 11, ed. by J.R. Anderson, M. Bondast (Springer, Berlin, Heidelberg 1996) p. 114
- 22.3 R. Prins: Hydrotreating. In: *Handbook of Heterogeneous Catalysis*, ed. by G. Ertl, H. Knözinger, F. Schüth, J. Weitkamp (Wiley, New York 2008) pp. 2695–2718, Part 13.2
- 22.4 P.R. Robinson: Deactivation of hydroprocessing catalysts: Thermochemistry of coke formation. In: *Proc. 232nd Am. Chem. Soc. Annu. Meet., Int. Symp. Hydrocracking/Hydrotreating Technol., San Francisco* (2006)
- 22.5 R.F. Sullivan, M.M. Boduszynski, C.J. Fetzer: Molecular transformations in hydrotreating and hydrocracking, *Energy Fuels* **3**, 603–612 (1989)
- 22.6 R. Scholl, C. Seer: Abspaltung aromatisch gebundenen Wasserstoffs und Verknüpfung aromatischer Kerne durch Aluminiumchlorid, *Justus Liebig's Annalen der Chemie* **394**(2), 111–177 (1912)
- 22.7 V.V. Speybroek, M.-F. Reyniers, G.B. Marin, M. Waroquier: The kinetics of cyclization reactions on polyaromatics from first principles, *Chem. Phys. Chem.* **3**, 863–870 (2002)
- 22.8 L. Skyum, H. Topsøe: Next-generation BRIM catalyst technology, Digital Refining, http://www.digitalrefining.com/article/1000059,Next_generation_BRIM_catalyst_technology.html#.VVWj8s3WVGv5 (2009)
- 22.9 C.N. Satterfield, C.N. Smith: Effect of water on the catalytic reaction network of quinoline hydrodenitrogenation, *Ind. Eng. Chem. Process Des. Dev.* **25**(4), 942–949 (1986)
- 22.10 ChemSpider Search and Share Chemistry, continuously updated by the Royal Society of Chemistry: <http://www.chemspider.com>
- 22.11 NIST Chemistry WebBook, continuously maintained and updated by the National Institute of Standards and Technology on behalf of the U.S. Secretary of Commerce: <http://webbook.nist.gov/chemistry>
- 22.12 J.A.R. van Veen, J.K. Minderhoud, L.G. Huve, W.H.J. Stork: Hydrocracking and catalytic dewaxing. In: *Handbook of Heterogeneous Catalysis*, ed. by G. Ertl, H. Knözinger, F. Schüth, J. Weitkamp (Wiley, New York 2008) pp. 2778–2808, Part 13.6
- 22.13 J. Scherzer, A.J. Gruia: *Hydrocracking Science and Technology* (Dekker, New York 1996) p. 190
- 22.14 V.A. Filimonov, A.A. Popov, V.A. Khavkin: Perezhigina IYa, Osipov LN, Rogov SP, Agafonov AV: The rates of reaction of individual groups of hydrocarbons in hydrocracking, *Int. Chem. Eng.* **12**(1), 21 (1972)
- 22.15 G.A. Olah: My search for carbocations and their role in chemistry, *Angewandte Chemie Nobel Lecture* **34**, 1393–1405 (1995)
- 22.16 R. von Ballmoos, D.H. Harris, J.S. Magee: Catalytic cracking. In: *Encyclopedia of Catalysis*, ed. by G. Ertl, H. Knoezinger, J. Weitkamp (Wiley, Hoboken 1995) pp. 1955–1985
- 22.17 Eurecat US Inc.: Totsucat sulfiding and passivation (2015) <https://www.eurecat.com/pdf/totsucat->

- with-passivation-overview.pdf
- 22.18 S. Eijsbouts, F. Plantenga, B. Leliveld, Y. Inoue, K. Fujita: STARS and NEBULA – New generations of hydroprocessing catalysts for the production of ultra low sulfur diesel, Prep. Pap. Am. Chem. Soc. Div. Fuel Chem. **48**(2), 494 (2003)
- 22.19 F. Humblot, V. Srinivas: Activation of hydroprocessing catalysts: An in depth understanding of dimethylsulfide (DMS) decomposition chemistry on hydroprocessing catalysts during their activation via sulfiding. In: *Proc. AIChE Spring Meet. 9th Global Congr. Process Safety* (2013)
- 22.20 L. Ma and W. Lin: Designing metal-organic frameworks for catalytic applications. In: *Functional metal organic frameworks: Gas Storage, Separation and Catalysis*, ed. by M. Schroder **293**, 175–205 (Springer, Berlin, Heidelberg 2010)
- 22.21 M. Yabuki, R. Takahashi, S. Sato, T. Sodesawaa, K. Oguraa: Silica-alumina catalysts prepared in sol-gel process of TEOS with organic additives, Phys. Chem. Chem. Phys. **4**, 4830–4837 (2002)
- 22.22 H.K. Timken, M.M. Habib: *Highly homogeneous amorphous silica-alumina catalyst composition*, US Patent, Vol. 6995112, 2006)
- 22.23 P.R. Robinson, G.E. Dolbear: Hydrocracking fundamentals. In: *Practical Advances in Petroleum Processing*, ed. by C.S. Hsu, P.R. Robinson (Springer, New York 2006)
- 22.24 A. Gruia: Hydrotreating. In: *Handbook of Petroleum Processing*, ed. by D.S. Jones and P.R. Pujada (Springer: Dordrecht 2008) pp. 340–341
- 22.25 Densicat new generation: Petroval Refining and Petrochemical Process Solutions, Saint-Romain de Colbosc (2017) <http://www.petroval.com/PETROVAL-Corporate.pdf>
- 22.26 Eurecat US Inc.: Totsucat with passivation overview – load and go, pp. 1–2. <https://www.eurecat.com/pdf/Totsucat%20with%20Passivation%20Overview%20-%20LOAD%20AND%20GO.pdf>
- 22.27 R. Curtis, C. Nguyen, S. Lower: First order reactions (2015) http://chemwiki.ucdavis.edu/Physical_Chemistry/Kinetics/Reaction_Rates/First-Order_Reactions
- 22.28 What-when-how: In depth tutorials and information: Fundamentals of hydrotreating Part 1: <http://what-when-how.com/petroleum-refining/fundamentals-of-hydrotreating-part-1/>
- 22.29 J. Scherzer, A.J. Gruia: *Hydrocracking Science and Technology* (Marcel Dekker, New York 1996) p. 189
- 22.30 M.T. Klein, Catalytic Kinetics: *Cycles and the LHHW Formalism* (Delft University of Technology, Delft) <https://sites.udel.edu/kleinresearchgroup/files/2015/09/LHHW-Models-and-the-KSSA-1h6gbxo.pdf>
- 22.31 D.R. Mudt, C.C. Pedersen, M.D. Jett, S. Karur, B. McIntyre, P.R. Robinson: Refinery-wide optimization with rigorous models. In: *Practical Advances in Petroleum Processing*, ed. by C.S. Hsu, P.R. Robinson (Springer, New York 2006)
- 22.32 P.R. Robinson: Catalyst life management with a predictive deactivation model. In: *Proc. NPRA Plant Automation Decis. Support Conf* (2004) p. PD-04–171
- 22.33 J. Ancheyta, J.G. Speight: *Hydroprocessing of Heavy Oils and Residua* (Taylor Francis, New York 2007)
- 22.34 American Petroleum Institute: *Pressure-Relieving and Depressuring Systems*, 6th edn. (American Petroleum Institute, Washington 2014) API Recommended Practice 521
- 22.35 J. Scherzer, A.J. Gruia: *Hydrocracking Science and Technology* (Marcel Dekker, New York 1996) p. 186
- 22.36 R.J. Morley, A.W. Scaroni, S.V.L.N. Pisupati: *Coal utilization: Liquefaction processes: The Bergius process*. In: *Encyclopaedia Britannica Online*: <https://www.britannica.com/topic/coal-utilization-122944/Gasification#ref623935>
- 22.37 CB&I: Press release, Announces Technology and Development Contract for Residue Upgrading Complex in Sweden (2016) <https://www.sn1.com/IRWebLinkX/file.aspx?iid=4234612&fid=34777474>
- 22.38 ENLAR Compliance Services Inc.: What is management of change? (2007) <http://ohsas18001expert.com/2007/07/18/what-is-management-of-change/>
- 22.39 US Chemical Safety Board: CBS Safety Bulletin says managing change is essential to safe chemical process operations (2001) <http://www.csb.gov/csb-safety-bulletin-says-managing-change-is-essential-to-safe-chemical-process-operations/>
- 22.40 United States Department of Labor: Occupational safety and health administration, personal protective equipment for general industry: Title 29 of the code of federal regulations (CFR), Part 1910 Subpart I
- 22.41 US Department of Labor: OSHA fact sheet personal protective equipment (2006) https://www.osha.gov/OshDoc/data_General_Facts/ppe-factsheet.pdf
- 22.42 US Department of Labor: Hydrogen Sulfide, <https://www.osha.gov/SLTC/hydrogensulfide/hazards.html>
- 22.43 G. Ou, Z. Zheng, H. Jin, J. Bao: Investigation of the flow-induced erosion-corrosion failure of hydrocracking air cooler systems and optimization study. In: *Proc. ASME Press. Vessel and Piping Div. Conf., Prague* (2009)
- 22.44 G.W. Hampton, P.R. Robinson: Controlling hydrocracker temperature excursions. In: *Proc. NPRA Q and A and Technol. Forum, Plant Automation Decis. Support Session, San Antonio* (2011) p. PD-11–01
- 22.45 US Environmental Protection Agency: EPA Chemical Accident Investigation Report (Tosco Avon Refinery, Martinez 1998)
- 22.46 J.H. Gary, G.E. Handwerk: *Petroleum Refining: Technology and Economics*, 4th edn. (Marcel Dekker, New York 2001)
- 22.47 C. Marcilly: *Acido-Basic Catalysis* (Technip, Paris 2006)
- 22.48 J.G. Speight: *Petroleum Chemistry and Refining* (Taylor Francis, New York 1998)
- 22.49 J.S. Magee, G.E. Dolbear: *Petroleum Catalysis in Nontechnical Language* (Penn Well, Tulsa 1998)
- 22.50 C.S. Hsu, P.R. Robinson: *Practical Advances in Petroleum Processing* (Springer, New York 2006)

Hydroprocess

23. Hydroprocessing Reactor Internals

F. Emmett Bingham, Douglas E. Nelson, Daniel Morton

As discussed in other chapters, catalytic hydrotreating upgrades petroleum fractions by saturating olefins and aromatics with hydrogen, and by converting contaminants such as sulfur, nitrogen and sometimes oxygen into H₂S, NH₃, and H₂O respectively. Hydrotreating also remove trace elements such as Ni, V, Fe, Si, As and Hg. Catalytic hydrocracking converts heavy hydrocarbons into lighter material by breaking carbon-carbon bonds.

The hydroprocessing process is exothermic, and thus produces heat as the process stream and treat gas are reacted in the catalyst bed. Controlling temperature rise is a major concern during design and operation. Flow distribution is also important. Inside reactors during normal operation, fluid flow is the only significant way to remove process heat. Uneven fluid flow can impair performance. It can lead to hot spot formation, which can jeopardize process safety and catalyst life.

While proper catalyst loading and grading is very important, reactor design, specifically the internals, is the key to controlling both the exotherm and fluid flow.

This chapter provides an overview of essential components of reactor internals, with emphasis on the relative performance of different designs.

Since the introduction of fixed-bed hydroprocessing technology in the early 1950s, catalyst suppliers have made significant advances in improving the relative activities of hydroprocessing catalysts. As illustrated in Fig. 23.1, the activities of current commercial hydrotreating catalysts are an order of magnitude higher than those initially just a few decades ago.

23.1	Elements of Hydroprocessing Reactor Design	777
23.2	Liquid Distribution Tray Design	778
23.2.1	Spacing Density	780
23.2.2	Sensitivity to Levelness	780
23.2.3	Operating Stability	780
23.3	Quench Mixing Chamber Design	781
23.3.1	Advanced Reactor Internals for Hydroprocessing Units.....	781
23.4	Manway Access and Faster Access Options	782
23.5	Example of Reactor Internals Revamp 783	
23.5.1	Reactor Internals Performance (Prerevamp)	783
23.5.2	New Reactor Internals Modifications and Improvements	784
23.5.3	Performance Improvement Results	784
23.5.4	Radial Temperature Differences.....	784
23.5.5	Weighted Average Bed Temperature	784
23.6	Conclusion	785
	References	786

In the mid-1990s it became apparent that the design of hydroprocessing reactors had not advanced at the same pace as the development of hydroprocessing catalysts and the existing reactors were not capable of taking full advantage of the potential benefits of the high-activity catalysts. As a result, licensors began to develop high-performance reactor internals to address the demands of ultralow sulfur diesel production.

23.1 Elements of Hydroprocessing Reactor Design

The following describes the reactor internals elements that should be considered in the design of internals for hydroprocessing reactors:

- *Inlet diffuser device*: The purpose of this device is to diffuse the velocity profile of the fluids entering the reactor inlet nozzle and create an even pattern of

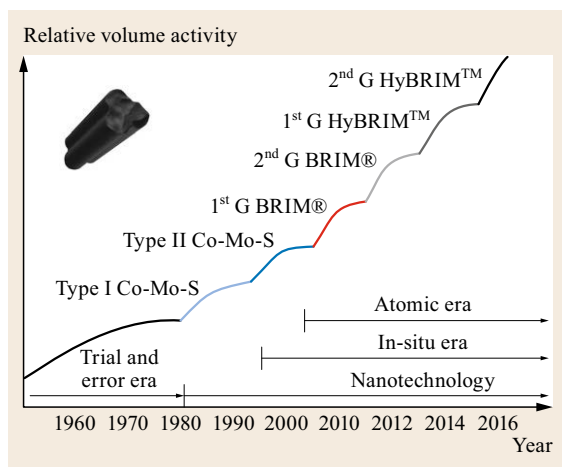


Fig. 23.1 Development of hydrodesulfurization catalysts

liquid dispersion across the top liquid distribution tray.

- **Top liquid distribution tray:** The top liquid distribution tray evenly distributes the liquid charge across the surface of the top catalyst bed.
- **Catalyst support:** Multiple beds are often utilized in reactors that have high temperature rises or would benefit from redistribution of the reactants. These reactors would have catalyst support grids and beams to carry the weight of each catalyst bed.
- **Quench injection device:** In multibed reactors, quench gas or liquid is introduced into a quench zone through a quench distributor for cooling purposes or replenishment of depleted reactants. Typically, the quench injection is a slotted pipe system. Although some units employ hydrocarbon liquids

for quenching, hydrogen-rich gas is used most often. The injection is typically part of and incorporated into the entire quench chamber.

- **Quench mixing chamber:** In multibed reactors, the mixing chamber ensures that hot liquid and vapor phases from above the catalyst bed are adequately mixed with relatively cold quench gas or liquid injection. The mixing chamber ensures that all fluids reach an equilibrium temperature and composition upon exiting the mixing zone. The mixing chamber also has the job of correcting any radial spreads from the catalyst bed above. The temperatures leaving the quench chamber should be uniform and if quenching is also performed, much cooler to meet the next catalyst bed's inlet temperature requirements.
- **Liquid redistribution tray:** The redistribution tray evenly distributes the quenched liquid and vapor exiting the mixing chamber across the surface of the subsequent catalyst bed.
- **Thermocouples:** Thermocouples monitor the temperature of the fluids reacting throughout the catalyst bed. They should be located to provide sufficient data to indicate that the reaction and radial temperatures in each section of the catalyst bed is even.
- **Outlet collector:** The outlet collector supports the bottom catalyst bed and is designed to promote even flow in the bottom of the reactor.

Although the entire reactor internals elements listed above are important to the performance of the hydroprocessing reactor, the distribution trays and mixing chambers are critical to ensuring the efficient utilization of the hydroprocessing catalyst.

23.2 Liquid Distribution Tray Design

Liquid distribution trays are typically used to establish good flow distribution in hydroprocessing reactors. By obtaining even distribution of the liquid reactants over the entire reactor cross-sectional area, all the catalysts at a given level are evenly wetted, giving the catalyst bed what is called a proper *plug flow*. Thus, all the catalysts at a given level operate at the same efficiency, which optimizes the overall efficiency of the reactor. Additionally, even liquid distribution minimizes the radial temperature profile across the reactor. This minimizes the occurrence of hot spots which, over time, cause coking and high rates of catalyst deactivation. Consequently, the reactor operates more efficiently, which enables a longer cycle length. Better distribution trays increase value by reducing catalyst

requirements, improving processing capability and/or longer cycle lengths. It should be noted that all the extremely detailed and complex process calculations used to determine the catalyst type, size, loading, depth, cycle length, etc., assume a plug flow regime inside the catalyst bed(s). So when a catalyst is selected and guarantees are given, there is no way to accurately predict the cycle life and efficiency inside a new catalyst bed if the distribution and mixing are not ideal.

Most liquid distribution devices are proprietary designs developed by process licensors and internals fabricators. Most of the known designs fall into one of four categories.

The first is a series of troughs and overflow weirs that systematically subdivide the liquid into multiple

streams before it contacts the bed. This type is often used in liquid contactors or countercurrent absorbers. The trough-type distribution device is mechanically complex and very sensitive to levelness. Depending on the design of the troughs, the quality of the distribution may be susceptible to fouling. An example of this type is US Patent 5192465 by *Petrich* and *Martinengli* assigned to Glitsch, Inc. [23.1].

A second type of liquid distribution device is a perforated tray. This may or may not have notched weirs around the perforations. The tray may also have chimneys for vapor flow. This type of distribution device is often used for rough liquid distribution in conjunction with a more sophisticated final liquid distribution tray. A perforated tray is possibly the least expensive design with regards to materials and fabrication cost, and it can offer a large number of distribution points. However, it is not an efficient primary distribution device because it must be absolutely level to provide even distribution of liquids, and it is very prone to plugging by debris collecting on the tray. Examples of this type are described in US Patent 4836989 by *Aly* et al. assigned to Mobil Oil Co. [23.2] and US Patent 3824080 by *Smith* et al. assigned to Texaco [23.3].

A third common type of liquid distribution device is a chimney tray. This device uses a number of standpipes laid out typically on a regular square or triangular pitch pattern on a horizontal tray. The standpipes typically have holes or notches cut through the sides for the passage of liquid. The tops of the standpipes are open to allow vapor flow down through the center of the chimneys. Some designs use special vapor chimneys to handle the bulk of the vapor flow. Functionally, the chimney tray design is very similar to the perforated tray design, except the holes or perforations are elevated above the surface of the tray to allow some capacity to maintain a liquid level and hold debris that may collect off the tray. The chimney design is an improvement over a perforated tray, since it can be designed for a wider range of liquid/vapor loadings. However, the spacing of the chimney risers typically reduces the number of distribution points compared to a perforated tray. A properly designed chimney must either become taller or have smaller holes drilled in the side to maintain a liquid level on the tray as the liquid rate changes. At turndown, it is possible that some holes will be covered with liquid and others will not. This results in uneven liquid distribution over the surface below the tray. The key issue with chimney trays is that the liquid level is completely independent of the gas rates, as the gas flows through the center tube. As there is very little pressure at the liquid flow holes on the sides of the tubes, they are susceptible to fouling as well and are not very flexible over

a wide range of operating conditions, if these holes get plugged or the tray is uneven due to out-of-level or sagging over time. Examples of this type are US Patent 4126540 by *Grosboll* et al. assigned to ARCO [23.4] and US Patent 3353924 by *Riopelle* assigned to Shell Oil Co. [23.5].

The fourth type of liquid distribution device is a bubble-cap tray, originally designed for application in fractionation towers. This device employs a number of bubble caps laid out on a regular pitched pattern on a horizontal tray. The bubble-cap distributor works on a vapor-assist principle that offers a relatively stable operation compared to a chimney device. The bubble cap is a cap centered concentrically over a standpipe. The sides of the cap are slotted for vapor flow. Liquid flows under the cap and is aspirated by the vapor, flowing upward in the annular area between the cap and the standpipe, and then down through the standpipe.

The advantage of a bubble-cap device over a chimney-type design is the wider turndown range possible with the bubble cap. As the liquid charge rate drops the level drops on a bubble-cap tray and the slot area increases resulting in a reduced vapor velocity through the slots. The reduced vapor velocity pulls less liquid through the distributor, and the liquid level is reestablished. Another advantage of the bubble cap over the chimney-type design is that the bubble cap is less sensitive to an out-of-level tray. Due to fabricating tolerances, installation difficulties and deflection due to operating load, not all of the distribution devices will be at the same level in the vessel. With proper design, the bubble-cap device will minimize the liquid flow differences between bubble caps at different elevations better than can be achieved with a chimney-type design. A final advantage of the bubble cap over the chimney-type design is the increased contacting of the liquid and vapor phases. The intimate contacting that occurs in the upflow portion of the device provides closer approaches to thermal and compositional equilibrium than would be achieved in the chimney tray.

The primary disadvantage of a bubble-cap tray is the comparatively large size of the bubble caps relative to a chimney device. The large size and necessary wider spacing of the bubble caps reduces the number of distribution points over the cross-section of the tray and catalyst bed below. The wide spacing and pitched array of the bubble-cap tray also results in poorer distribution coverage adjacent to the reactor wall, further reducing catalyst utilization. An example of this type is US Patent 5158714 by *Shih* and *Christolini* assigned to Union Oil Co. [23.6].

A comparison of the performance characteristics of a typical multipoint chimney-type distributor and a standard bubble-cap distributor is illustrated in Fig. 23.2.

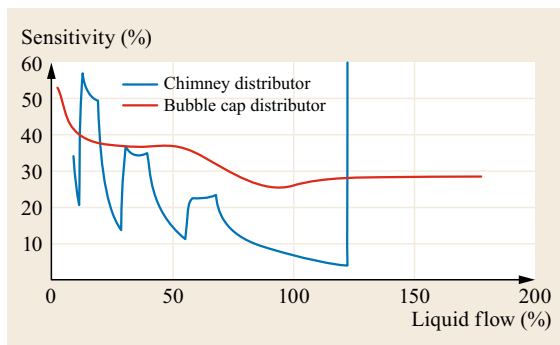


Fig. 23.2 Liquid distributor sensitivity to levelness as a function of liquid flow. Sensitivity of liquid flow to 10 mm elevation difference

The performance parameter, sensitivity %, is a measurement of the difference in the liquid delivered by adjacent distributors at different elevations. This parameter is described by the following formula

$$S = \left[\frac{(F_l - F_h)}{[F_{ave}]^*} \right] 100,$$

where:

- S performance sensitivity
- F_l liquid flow through low distributor
- F_h liquid flow through high distributor
- F_{ave} average flow through all distributors.

Figure 23.2 illustrates the deterioration in performance of a nonlevel chimney-type tray as the liquid rate is reduced and the liquid level drops. Each time the liquid level reaches the nominal elevation of one of the chimney's holes, holes of the low chimneys may be covered with liquid while holes of the high chimneys are dry. Thus some distributors deliver more liquid. This causes flow maldistribution across the catalyst bed. The same sensitivity is seen on dirty or fouled chimney trays, as their small holes will tend to plug up, thus affecting how much flows through each chimney in an uneven manner.

When Haldor Topsoe began to investigate the design of a high-performance distribution tray, several parameters were recognized as critical to achieve the desired performance efficiency. These are as follows:

23.2.1 Spacing Density

Because of the difficulty in visualizing the performance of the distribution devices under actual operating conditions of a hydroprocessing reactor, assumptions as to the effectiveness of overlapping spray patterns, or deflection splash patterns should be discounted. The only

positive approach to ensure adequate liquid distribution is to achieve a high number of liquid drip points across the surface of the catalyst by reducing the spacing of the distribution devices as much as is practically possible. Increasing the spacing density also enables a greater number of distribution points in the area adjacent to the reactor wall. This is very important for improved catalyst utilization, because over 35% of the catalyst in the reactor is contained within an annular ring between the reactor wall and 80% of the reactor diameter.

23.2.2 Sensitivity to Levelness

When first installed, reactor distribution trays are never perfectly level. Deviations from level can increase over time, in part due to thermal expansion and retraction as reactors are heated and cooled. Also trays can sag due to long life or upset in the reactors during operation. Trays should be designed so that an out-of-level condition has a very low impact on the operation of the tray. As described earlier, a distributor device operating on a vapor-assist principle will have a greater tolerance to levelness compared to a chimney-type distributor device. In addition, the geometry of the distributor device can further improve the sensitivity to levelness. Leveling devices can also be incorporated into the tray design to compensate for out-of-levelness due to ring warpage, beam deflection, or plumbness of the reactor.

23.2.3 Operating Stability

A distribution tray may have very good performance at the design conditions. However, as the operation diverges from the design point due to changes in the charge rate or changes in vaporization due to temperature or feed quality, the performance of the distribution tray can deteriorate rapidly. A high-performance tray should be capable of maintaining a relatively level height of liquid and an even flow rate through the distributor devices as the operation of the reactor changes.

The distribution device developed through the research and development efforts undertaken by Haldor Topsoe is a combination of bubble-cap and chimney devices referred to as a vapor-lift tray, or VLT. The VLT device has an operating concept similar to a bubble-cap device but has several advantages. The VLT device has a smaller footprint and closer spacing, which enables an increase in the number of liquid distribution points across the tray area. Furthermore, since the spacing pattern is square rather than triangular in pitch, gaps in liquid distribution coverage along beams and near the vessel wall are minimized. Overall wetting efficiency of the catalyst below the tray is improved when the liquid

distributors have a smaller pitch compared to a larger pitch.

A standard bubble-cap tray design is limited by the relatively large spacing, so modifications have been attempted to improve the dispersion pattern of the liquid exiting from the cap, e.g., the shear plate described in the Shih patent or the turbine baffles described in the Jacobs patent. Increasing the number of bubble caps by reducing the spacing would increase the number of distribution points. However, doing so would negatively impact the liquid/vapor flow relationships through each cap. Smaller bubble caps with fewer slots will not be as efficient as a VLT due to the geometry of the concentric caps. The geometry of the VLT enhances the stability over a wide operating range compared to a bubble cap. A further advantage for the VLT device is that its simplicity makes it easier and less costly to fabricate in the optimal size prescribed by the process conditions. The performance characteristics of a VLT compared to bubble caps and chimney tray designs are illustrated in Fig. 23.3.

Sensitivity is, as described previously, a gage of the difference in the liquid flow measured from adjacent liquid distributors positioned at different elevations. These plots show that the percentage difference in the liquid flow from VLT distributors is much smaller com-

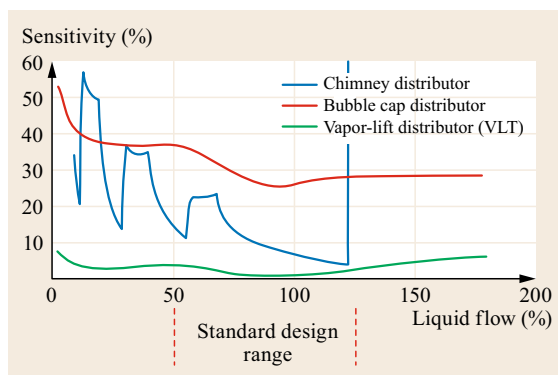


Fig. 23.3 VLT distributor performance relative to chimney and bubble-cap distributors. Sensitivity of liquid flow to 10 mm elevation difference

pared to other distributor types. This ensures an even distribution of liquid over a broad range of operations, even though the tray may not be perfectly level. Poorly designed distributor devices can become very unstable and sensitive to differences in elevation as the liquid level on the tray drops. At very low liquid levels, a poorly designed distributor can actually cause maldistribution of liquid across the catalyst bed beneath the tray.

23.3 Quench Mixing Chamber Design

The catalyst in hydroprocessing reactors with high temperature rises or large catalyst volumes is separated into multiple catalyst beds. A quench section separating catalyst beds is designed to mix the reactants and introduce a quenching medium to typically reduce the equilibrium temperature before the reactants are distributed over the following catalyst bed. Since distributor trays are basically plug-flow devices, an apparatus is needed to mix the liquid into a homogeneous blend before it is delivered onto the distribution tray. Several different mixing chamber designs have evolved during the development of hydroprocessing reactor internals.

23.3.1 Advanced Reactor Internals for Hydroprocessing Units

Baffle mixer designs such as ribbon blenders and disc-and-donut-type mixers promote mixing by changing the direction of the fluid streams. These designs can be effective mixing devices, but they usually have comparatively high differential pressures to achieve mixing and they can be comparatively tall, requiring more

reactor shell length to accommodate the quench section.

Impingement-type quench boxes promote mixing by injecting or directing separate portions of the reactant fluids and impinging them against one another in a small area. This type of mixer can be designed with a reduced height. However, test work has shown that it is difficult to achieve an equilibrium temperature with an impingement-type mixer. In a low-pressure drop design, the vapor and liquid phases typically follow separate paths through the mixing chamber and can segregate and inhibit the mixing of liquid collected from different quadrants of the reactor.

A preferred type of mixing chamber is a centrifugal or vortex-type design, typical of the design introduced by US Patent 4836989 by Aly et al. assigned to Mobil Oil Co [23.2]. This mixer collects liquid and vapor from all quadrants of the reactor and introduces them close to the perimeter of a circular chamber where they make several rotations before being ejected out through a central exit port. This design can have a comparatively shallow depth, a very low pressure drop, and can

achieve an equilibrium temperature of the liquid passing through the mixer. Several licensors skilled in the design of hydroprocessing reactors employ a vortex-type mixing chamber.

The next generation of mixer design would have to expand upon the advantages of the success of the vortex type, while trying to minimize the side effects of the extreme velocities inside these mixer sections. The gas and liquid rates exiting these mixers can sometimes affect the distributor tray below, if not managed properly with additional hardware and baffle plates. This is especially the case in hydrocracker service. There are many challenges when trying to mix two-phase flows with very high space velocities through a small device. The process of getting the liquid and gas to mix completely usually involves increasing the pressure drop by creating significant amounts of turbulence. However, turbulence and wave action can cause as much as a 4–6 mm difference in liquid height on the distributor

tray below, which can lead to issues with differential pressure and liquid distribution. Additional baffles and/or rough cut trays are needed to offset these issues, which will in turn increase the height of the mixing device and thus be counterproductive. This also adds to the complexity and space of the manways. Haldor Topsoe has developed a new mixer design where all this additional hardware and associated issues are completely eliminated. Called the Torus mixer, this design mixes the liquid and gas in the outer chamber close to the vessel wall, and redistributes the mixture slowly onto the tray below, with a series of radial turning blades that are incorporated into the structure and angled in such a way so as to eliminate the need for further baffling hardware. The final outflow has low pressure and low velocity, while further improving on the manway access. Furthermore this concept is very compressed leaving more space for more catalyst in a given reactor.

23.4 Manway Access and Faster Access Options

Recent improvements have been made to make installation and turnaround times faster and safer, with less parts and easier fastening of the tray and manways. First-generation reactor internal trays were fastened together completely with bolts and nuts, designed to go together as one solid assembly. This included the manway panels, typically a removable center panel in each tray that can be detached so that maintenance personnel can enter the reactor during a shutdown to change the catalyst and/or inspect the vessels. The main problem with this design is that stainless steel threads will more often than not bind up when you try and remove them. Standard industry practice is to use an antiseize paste on all threaded connections when you assemble the trays, which prevents this from happening during the first assembly. But after some time in the reactor, especially under long service over the years, unfastening the threaded manway is not possible. Often most or all of the threaded bolt connections will seize and need to be cut out by torching, grinding or some other manner. This is a process that is to be repeated at each and every manway, at each turnaround. Users must then still replace the threaded connections to resecure and seal the manways for the next cycle. All of this can take hours as you can well imagine.

More recent designs have changed the manways so that they are fastened with a wedge pin device, an an-

gled piece of thin steel that can be wedged into place around the manway perimeter to secure and seal it into place, while not causing it to seize up as stainless steel does on threaded connections. This is a very effective practice and has been working now for several years. This can even be implemented and installed on current older bolted manways, at little cost compared to the time it usually takes with threaded connections. Check with the original tray licensor to see if this is an option.

Wedge pins are an easy and less expensive alternative to bolted manways. However they sometimes get damaged during removal and can be lost or broken. Additional spares are required to be ready for these issues. Also they can be hard to access and need to be hammered in place and set correctly. Topsoe has improved on this design even further with a top-access latch system that requires no spare parts like wedge pins, nor any tools to operate. This has improved the access time even further, made installation faster and time spent inside the reactor was reduced making it safer. Aside from replacement sealing gasket, there are no spare parts needed for each turnaround, and no readjustment is needed of the manway fastening hardware. The type of manway access on your internals should be considered when scheduling downtime for maintenance.

23.5 Example of Reactor Internals Revamp

The following is an example of improved performance that has been realized by replacing a classic reactor internals design with a recently developed high-performance design.

The original reactor internals included bubble-cap liquid distribution trays and impingement-type, quench mixing chambers similar to those described in US Patent No. 3218249 and US Patent No. 3502445, *Balard and Hines* [23.7, 8] assigned to Union Oil of California (Fig. 23.4). The original thermometry comprised three vertical thermowells running the length of the reactors and horizontal thermowells traversing the top and bottom of each of three catalyst beds.

23.5.1 Reactor Internals Performance (Prerevamp)

Due to changes in the plant operation subsequent to the initial installation, the performance of the impingement-type quench mixing chambers deteriorated and the distribution trays could no longer maintain an even flow distribution across the catalyst beds. The degradation in performance of the reactor internals resulted in wide radial temperature variations ranging from 7–10 °C at the catalyst bed inlets to 15–40 °C and the catalyst bed outlets. The flow/temperature maldistribution is documented by temperature profiles plotted from thermocouple measurements (Fig. 23.5).

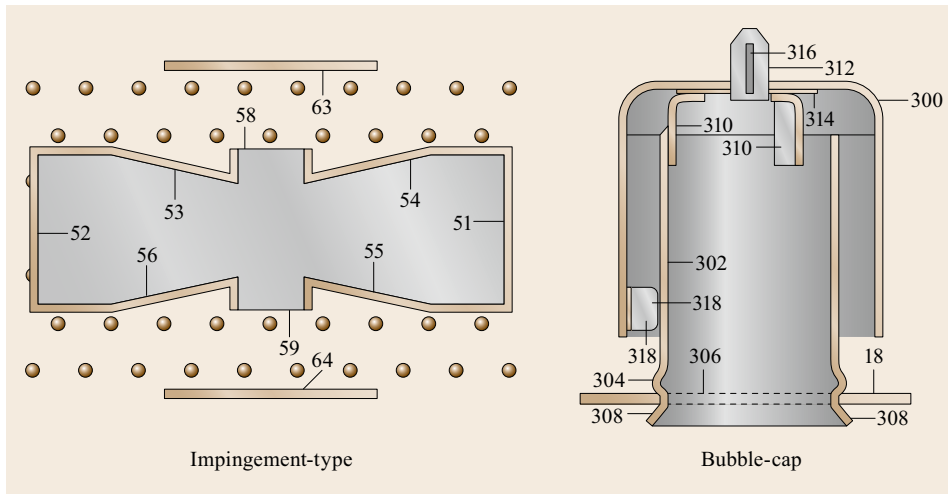


Fig. 23.4 Pre-revamp reactor internals

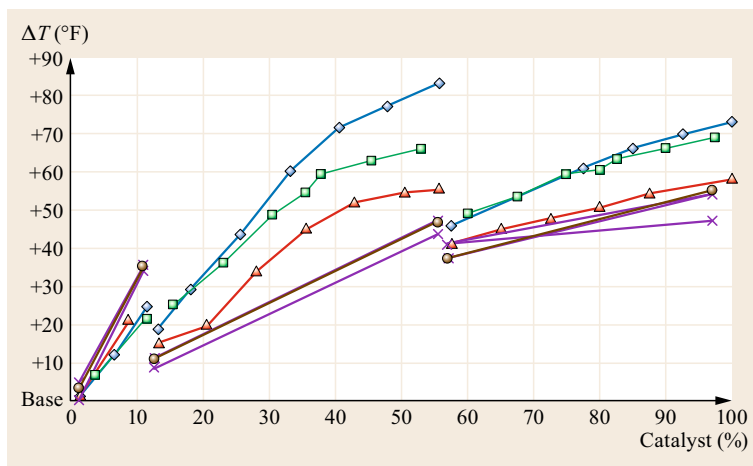


Fig. 23.5 Prerevamp performance

As seen, significant radial temperature differences were measured by the thermocouples in the vertical thermowells, especially at the bottom of the second catalyst bed in the reactor. The temperature difference measured at the top of the middle and lower catalyst beds is an indication that the quench boxes were not adequately mixing the liquid to an equilibrium temperature before passing it on to the redistribution trays. Further, the vapor-liquid mixing through the distributors was not sufficient to evenly quench the liquid before it was distributed onto the next bed. In addition to the temperature maldistribution, the original redistribution trays were not providing an even liquid flow onto the following catalyst beds. This flow maldistribution is indicated by the widening of the radial temperature differences measured by thermocouples descending through the beds.

Large radial temperature differences are problematic because they reduce the length of the operating cycle between turnarounds. High peak temperature areas adjacent to the reactor wall lead to premature unit shutdown as the temperature approaches the reactor design limit. Furthermore, because of limited thermocouple coverage, there is real concern that the existing temperature indicators might not record the actual hot spot in the catalyst bed, and that damage to the reactor wall could occur unknowingly.

23.5.2 New Reactor Internals Modifications and Improvements

To improve unit performance, the existing reactor internals were replaced by high-performance vortex-type mixing chambers to optimize liquid-liquid mixing and VLT distribution trays to increase the number of drip points and minimize the dead flow zones adjacent to the reactor wall (Fig. 23.6). The VLT distribution trays also offered low sensitivity to tray levelness and improved stability over a wide operating range.

To improve monitoring of the temperature profiles, the existing thermocouple arrangement was replaced by 84 flexible-type thermocouples in the catalyst beds.

23.5.3 Performance Improvement Results

Following the restart of operations, the temperature profile across the reactor with the new internals is plotted in Fig. 23.7. The improved performance of the new internals is readily seen when comparing this plot with that previously shown in Fig. 23.5.

Several observations from such a comparison are immediately apparent.

23.5.4 Radial Temperature Differences

The radial temperature spreads for the revamped operation are significantly improved compared to the original equipment. At the start of the operating cycle conditions, the actual deviation in bed inlet temperature is approximately 1 °C. With the old internals, the temperature deviation at the bed inlets ranged from 7–10 °C. The radial temperature spread at the bed outlets ranges from 2–4 °C. This is significantly lower than the 15–40 °C bed outlet temperature deviation experienced with the old internals.

23.5.5 Weighted Average Bed Temperature

A reduction in the temperature required to achieve process objectives is typically observed when less efficient distribution trays are replaced. This is due to more efficient utilization of the catalyst resulting from improved liquid flow distribution. It appears that a directional 2–4 °C reduction in weighted average bed temperature (WABT) may have been achieved. However, it is dif-

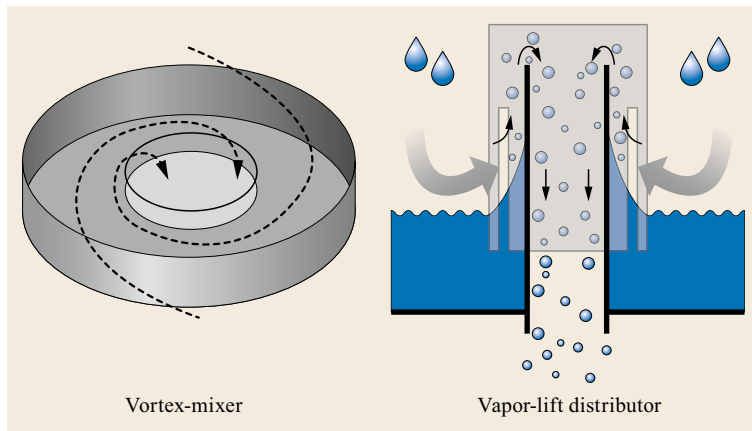


Fig. 23.6 High-performance reactor internals

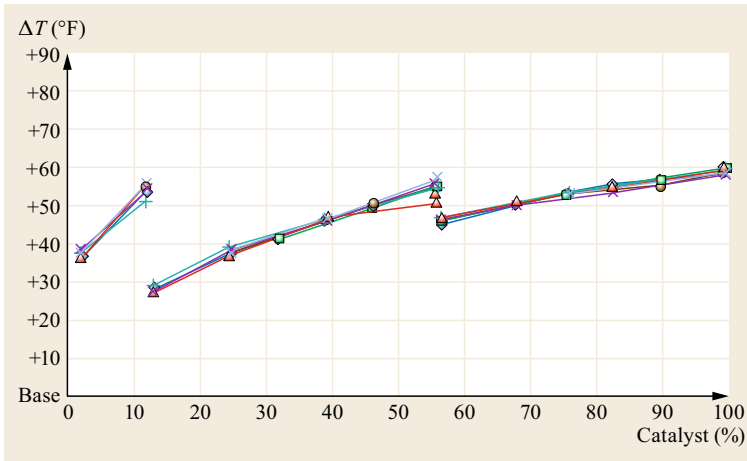


Fig. 23.7 Revamped reactor performance

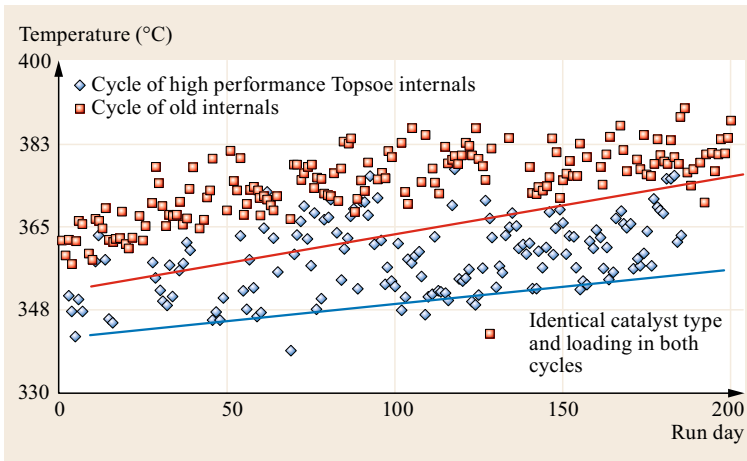


Fig. 23.8 Graph comparing WABT, before and after new internals. Normalized WABT is reduced by more than 10°C ($\approx 18^{\circ}\text{F}$)

difficult to estimate the degree of improvement with any precision because the widely divergent temperatures measured by the three vertical thermowells during the prevamp operation make estimating the actual WABT very speculative.

Figure 23.8 shows another example of a diesel hydrotreater, where the internals were replaced while the process objectives and catalyst types remained the same. The data shows that the operating WABT is reduced significantly.

23.6 Conclusion

Hydroprocessing reactors originally designed for low-severity service typically are not adequate to handle increased severity with high-activity catalysts or to achieve the operating efficiency demanded by the current and future fuel specifications.

High-performance reactor mixing chamber and distribution tray designs developed by some licensors can often be incorporated into existing reactors to improve

their performance. If large radial temperature spreads are observed in the catalyst bed, replacing older internals with newer technology will result in lower operating temperatures with associated longer cycle length or higher production rates. The time savings obtained in a single turnaround by the implementation of the new manway plates can in many cases justify the entire cost of the reactor internals.

References

- 23.1 T. Petrich, P. Martinenghi: Method of and apparatus for liquid distribution, US Patent (Application) 5 192 465A (1993), Glitch, Inc.
- 23.2 F.A. Aly, R.G. Graven, D.W. Lewis: Distribution system for downflow reactors, US Patent (Application) 4 836 989A (1989), Mobil Oil Co.
- 23.3 R. Smith, J. Strickland, J. Sanwald: Vertical reactor, US Patent (Application) 3 824 080A (1974), Texaco, Inc.
- 23.4 M.P. Grosboll, R.R. Edison, T. Dresser: Apparatus and process for distributing a mixed phase through solids, US Patent (Application) 4 126 540A (1978), Atlantic Richfield Co.
- 23.5 J.E. Riopelle: Bed reactor with quench deck, US Patent (Application) 3 353 924A (1967), Shell Oil Co.
- 23.6 C.-C.J. Shih, B.A. Christolini: Vapor-liquid distribution method and apparatus, US Patent (Application) 5 158 714A (1992), Union Oil Co. of California
- 23.7 J.H. Ballard, J.E. Hines, Jr.: Vapor-liquid distribution method and apparatus for the conversion of hydrocarbons, US Patent (Application) 3 218 249A (1965), Union Oil Co. of California
- 23.8 J.H. Ballard, J.E. Hines, Jr.: Apparatus for mixing fluids in concurrent downflow relationship, US Patent (Application) 3 502 445A (1970), Union Oil Co. of California

Hydrogen Production

M. Andrew Crews, B. Gregory Shumake

Many petroleum refining processes require hydrogen. Some is generated as a by-product from other units, such as catalytic reformers, but additional on-purpose production is required to meet increasing demands to process heavier feeds and meet tighter fuel and lubricant base oil specifications. In this chapter, we describe technology for on-purpose H₂ production, which is accomplished by four different processes – steam methane reforming (SMR), SMR with oxygen enrichment (SMR/O₂R), autothermal reforming (ATR), and thermal partial oxidation (POX). Designs can be adjusted to produce hydrogen, pure carbon monoxide, or mixtures of H₂ and CO (synthesis gas). All aspects of SMR, SMR/O₂R, and ATR are described: chemistry and thermodynamics, process design parameters and options, hydrogen purification, environmental protection, operation, process monitoring, processes improvements, safety, and economics.

24.1	Thermodynamics of Hydrogen	788
24.2	Technologies for Producing Hydrogen	790
24.2.1	Steam Methane Reforming (SMR) Technologies	790
24.2.2	Oxygen-Based Technologies	792
24.2.3	Technology Comparison	796
24.2.4	Hydrogen Purification	799
24.3	Design Parameters for SMRs	800
24.3.1	Function	800
24.3.2	Feedstocks	801

24.3.3	Fuels	801
24.3.4	Design	801
24.3.5	Pressure	801
24.3.6	Exit Temperature	802
24.3.7	Inlet Temperature	802
24.3.8	Steam/Carbon Ratio	802
24.3.9	Heat Flux	802
24.3.10	Pressure Drop	803
24.3.11	Catalyst	803
24.3.12	Tubes	803
24.3.13	Burners	804
24.3.14	Flow Distribution	804
24.3.15	Heat Recovery	804
24.4	Environmental Issues	804
24.4.1	Flue Gas Emissions	804
24.4.2	Process Condensate (Methanol and Ammonia)	805
24.4.3	Wastewater	806
24.5	Monitoring Plant Performance	807
24.6	Plant Performance Improvements	808
24.7	Economics of Hydrogen Production	809
24.7.1	Overall Hydrogen Production Cost	810
24.7.2	Overall Production Cost Comparisons	810
24.7.3	Evaluation Basis	811
24.7.4	Utilities	811
24.7.5	Capital Cost	811
24.7.6	<i>Life of the Plant Economics</i>	811
24.7.7	Sensitivity to Economic Variables	813
24.7.8	Feed and Fuel Price	813
24.7.9	Export Steam Credit	813
24.8	Conclusion	814
24.9	Further Reading	814

Hydrogen is a key feedstock in many refining operations associated with the production of cleaner gasoline and diesel products, as well as high-quality premium lubricant base oils. There are several drivers for the increase in hydrogen demand in the refining industry. Crude oil continues to become heavier with higher amounts of sulfur, nitrogen, and metal species. As the demand for heavy fuel oil abates, additional upgrading of the *bottoms* is required to produce a high-

value marketable fuel. More stringent environmental regulations have reduced the level of sulfur in both gasoline and diesel products. The combined result of these trends is that refineries must add hydrogen production capacity to meet the increasing demands in hydrotreating, hydrocracking, and other hydroprocessing processes.

There are many routes to the production of hydrogen. In particular, several refinery unit operations, espe-

cially catalytic reforming and olefins production, yield hydrogen as a by-product. In order to focus the scope of discussion, this chapter will only cover on-purpose hydrogen production. The technologies discussed will be limited to those that can produce hydrogen in sufficient quantities to satisfy typical refinery operations, i. e., from 5 to 200 MMSCFD.

Hydrogen can be produced from a variety of feedstocks and technologies. Feedstocks for hydrogen production can range from natural gas to coal and includes

all hydrocarbons in-between. The availability of specific feedstocks will limit the number of technology options for the production of hydrogen. The conversion of hydrocarbons to hydrogen requires significant heat input and produces excess (waste) heat resulting from the high temperatures required for sufficient feedstock conversion. This excess heat is typically recovered to produce steam and can also be recovered to improve the overall efficiency of the technology chosen, but with a significant capital cost.

24.1 Thermodynamics of Hydrogen

The production of hydrogen from hydrocarbons can be broken down into three key sets of chemical reactions:

- Steam methane reforming
- Partial oxidation
- Water gas shift.

Strictly speaking, steam methane reforming (SMR) should be called steam/hydrocarbon reforming, because the feed gas may contain higher hydrocarbons other than methane.

The use of the term *reforming* in a refinery environment can be confusing as there are several *catalytic reforming* operations that are used to improve the oc-

tane numbers of gasoline. In the context of a hydrogen plant, a reformer is a furnace or vessel associated with the steam/hydrocarbon reforming reaction, usually called steam methane reforming (SMR) because the most common hydrocarbon feed is methane. The reaction produces hydrogen (H₂), carbon monoxide (CO), carbon dioxide (CO₂), and un-reacted methane (CH₄) from hydrocarbons and water based on the following chemical reaction

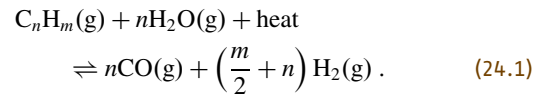


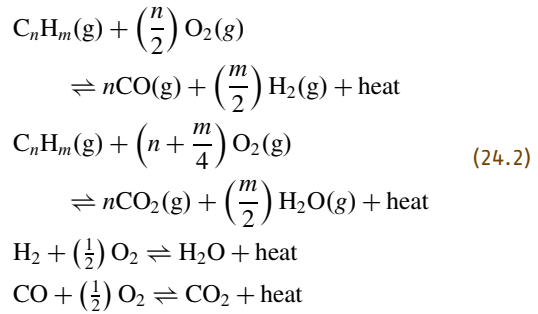
Table 24.1 Reaction and equilibrium constants (used with permission of Sud-Chemie)

Temperature (°F)	Temperature (°C)	CO + H ₂ O ⇌ CO ₂ + H ₂			CH ₄ + H ₂ O ⇌ CO + 3H ₂		
		ΔH° (Btu/(lb mol))	ΔH° (kJ/(kg mol))	K _p	ΔH° (Btu/(lb mol))	ΔH° (kJ/(kg mol))	K _p
200	93	-17 570	-40 868	4523	90 021	209 389	7.813 × 10 ⁻¹⁹
300	149	-17 410	-40 496	783.6	91 027	211 729	6.839 × 10 ⁻¹⁵
400	204	-17 220	-40 054	206.8	91 957	213 892	7.793 × 10 ⁻¹²
500	260	-17 006	-39 556	72.75	92 804	215 862	2.173 × 10 ⁻⁹
600	316	-16 777	-39 023	31.44	93 566	217 635	2.186 × 10 ⁻⁷
700	371	-16 538	-38 467	15.89	94 252	219 230	1.024 × 10 ⁻⁵
800	427	-16 293	-37 898	9.03	94 863	220 651	2.659 × 10 ⁻⁴
900	482	-16 044	-37 318	5.61	95 404	221 910	4.338 × 10 ⁻³
1000	538	-15 787	-36 721	3.749	95 880	223 017	4.900 × 10 ⁻²
1100	593	-15 544	-36 155	2.653	96 283	223 954	0.4098
1200	649	-15 299	-35 585	1.966	96 628	224 757	2.679
1300	704	-15 056	-35 020	1.512	96 922	225 441	0.1426 × 10 ²
1400	760	-14 814	-34 457	1.202	97 165	226 006	0.6343 × 10 ²
1500	816	-14 575	-33 901	0.9813	97 378	226 501	2.426 × 10 ²
1600	871	-14 344	-33 364	0.8192	97 545	226 890	8.166 × 10 ²
1700	927	-14 117	-32 836	0.697	97 655	227 146	2.464 × 10 ³
1800	982	-13 892	-32 313	0.6037	97 741	227 346	6.755 × 10 ³
1900	1038	-13 672	-31 801	0.5305	97 786	227 450	1.701 × 10 ⁴
2000	1093	-13 459	-31 306	0.4712	97 818	227 525	3.967 × 10 ⁴
2100	1149	-13 246	-30 810	0.4233	97 812	227 511	8.664 × 10 ⁴
2200	1204	-13 041	-30 333	0.3843	97 791	227 462	1.784 × 10 ⁵

The reforming reaction is endothermic and is favored by high temperature and low pressure. In other words, as the net reaction temperature is increased, the higher the conversion of methane, and as the pressure at which the reaction takes place is decreased, the methane conversion is increased. Another variable in the reforming reaction is the steam-to-carbon ratio. As the amount of water increases above the stoichiometric requirement, the amount of methane conversion also increases. Conversely, as the ratio of water to steam decreases, the greater the possibility of forming carbon precursors (coking) through alternative reaction pathways. This is an undesirable condition because the formation of carbon can destroy the reforming catalyst, increase the pressure drop through the reformer, increase the reformer tube-wall temperature, and consequently require an unscheduled plant shutdown to repair these problems. See Table 24.1 for equilibrium constant information on the steam methane reforming reaction.

Partial oxidation refers to a chemical reaction where hydrocarbons react with oxygen in a substoichiometric burn reaction to produce carbon monoxide and hydrogen. Partial oxidation technologies require oxygen as a feedstock. Several other reactions take place in the partial combustion zone and contribute to the overall

heat provided by the partial oxidation reaction.



The partial oxidation (POX) reaction is highly exothermic and provides the heat required for the steam methane reforming reaction that occurs following the conversion of hydrocarbons to carbon monoxide and hydrogen. The partial oxidation reaction is favored by high temperature and high pressure. However, the higher the pressure, the more likely are alternative reactions that will lead to the formation of carbon.

The water gas shift (WGS) reaction is where carbon monoxide is *shifted* on a mole per mole basis to hydrogen by the following reaction

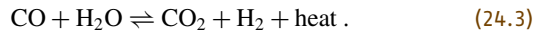


Table 24.2 Equilibrium constants and heats of reaction (used with permission of Sud-Chemie)

CO ⇌ 0.5CO ₂ + 0.5C _(s)				
Temperature (°F)	Temperature (°C)	ΔH° (Btu/(lb mol))	ΔH° (kJ/(kg mol))	K _p
100	38	-37 130.24	-86 364.94	7.5489 × 10 ⁹
200	93	-37 244.17	-86 629.94	4.7479 × 10 ⁷
300	149	-37 313.43	-86 791.04	1.1237 × 10 ⁶
400	204	-37 345.16	-86 864.84	6.3291 × 10 ⁴
500	260	-37 346.08	-86 866.98	6.4858 × 10 ³
600	316	-37 321.90	-86 810.74	1.0223 × 10 ³
700	371	-37 277.30	-86 707.00	2.2190 × 10 ²
800	427	-37 216.05	-86 564.53	6.1052 × 10 ¹
900	482	-37 141.19	-86 390.41	2.0628 × 10 ¹
1000	538	-37 055.16	-86 190.30	8.0522
1100	593	-36 959.90	-85 968.73	3.5533
1200	649	-36 856.96	-85 729.29	1.7338
1300	704	-36 747.60	-85 474.92	9.1957 × 10 ⁻¹
1400	760	-36 632.77	-85 207.82	5.2304 × 10 ⁻¹
1500	816	-36 513.23	-84 929.77	3.1565 × 10 ⁻¹
1600	871	-36 389.57	-84 642.14	2.0036 × 10 ⁻¹
1700	927	-36 262.22	-84 345.92	1.3284 × 10 ⁻¹
1800	982	-36 131.47	-84 041.80	9.1460 × 10 ⁻²
1900	1038	-35 997.52	-83 730.23	6.5074 × 10 ⁻²
2000	1093	-35 860.48	-83 411.48	4.7655 × 10 ⁻²
2100	1149	-35 720.36	-83 085.56	3.5799 × 10 ⁻²
2200	1204	-35 577.17	-82 752.50	2.7506 × 10 ⁻²
2300	1260	-35 430.71	-82 411.83	2.1563 × 10 ⁻²
2400	1316	-35 280.92	-82 063.42	1.7210 × 10 ⁻²
2500	1371	-35 127.58	-81 706.75	1.3960 × 10 ⁻²

The water gas shift reaction is favored by low temperature and is mildly exothermic. The WGS reaction is typically the final reaction step that produces hydrogen in a multiple reactor train. Since the WGS reaction is fa-

vored by low temperature, it is typically included in the heat recovery train downstream of the high-temperature reactors. See Table 24.2 for thermodynamic and equilibrium data.

24.2 Technologies for Producing Hydrogen

24.2.1 Steam Methane Reforming (SMR) Technologies

Steam methane reformers generate the majority of the world's on-purpose hydrogen. A steam methane reformer (SMR) is a fired heater with catalyst-filled tubes. Hydrocarbon feedstock and steam react over the catalyst to produce hydrogen. The reacted process gas typically exits the reformer at about 1600 °F (≈ 870 °C). The flue gas leaving the reformer radiant section is typically about 1900 °F (≈ 1040 °C).

The flue gas at 1900 °F (≈ 1040 °C) must then be cooled to about 300 °F (≈ 150 °C) to achieve efficient heat recovery. This heat is recovered in the convection section of the SMR. The process gas at 1600 °F (≈ 870 °C) must then be cooled to about 100 °F (≈ 38 °C) before final product purification.

Maximum Steam Export

A maximum export steam plant (Fig. 24.1) is defined as a plant that makes the maximum prac-

tical quantity of export steam, without auxiliary firing.

Table 24.3 gives a typical feed and utility summary for a maximum export steam plant, as defined above.

Limited Steam Export

A limited export steam plant (Fig. 24.2) is defined as a plant that makes some export steam but significantly less than the maximum. This is typically achieved by adding a combustion air preheat unit (CAP). This unit consists of a modular heat exchanger that heats the combustion air to the SMR by heat exchange with the flue gas from the SMR. The hot combustion air reduces the fuel requirement for the SMR, which in turn reduces the steam production.

A typical combustion air preheat temperature for this type of plant is approximately 750 °F. This permits use of carbon steel ducting in the air preheat distribution system. Table 24.4 gives a typical feed and utility summary for a limited export steam plant, as defined above.

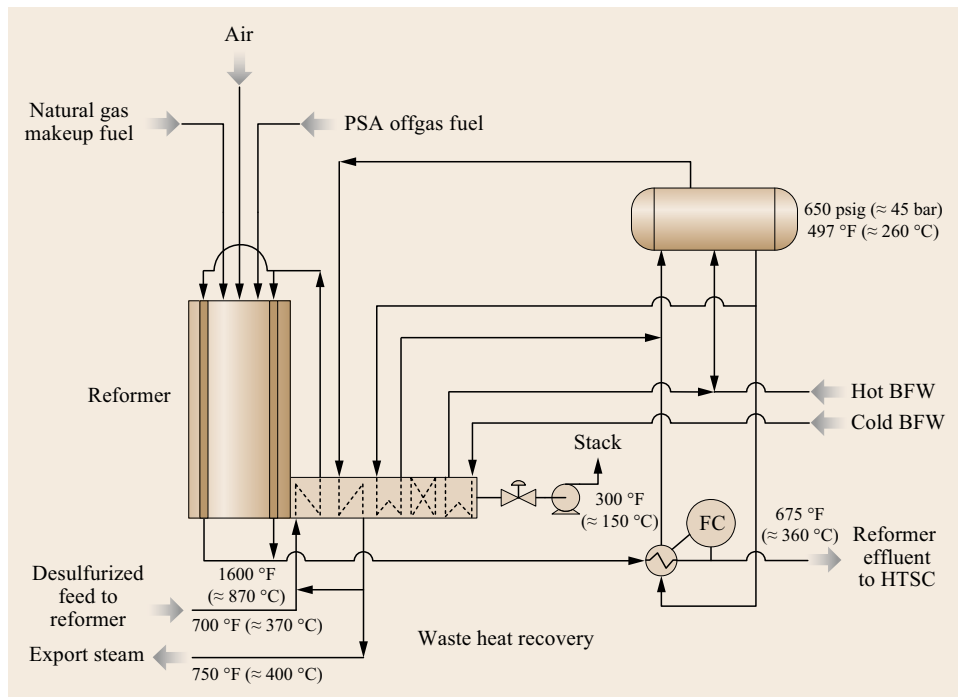


Fig. 24.1 Steam methane reforming with maximum steam export

Table 24.3 Maximum export steam feed and utility summary

	Units	H ₂ product (Units/MSCF)	H ₂ product (Units/MNCM)
Natural gas	MMBtu LHV	0.45	–
	GJ LHV	–	17.72
Export steam	lbs	86.80	–
	kg	–	1470.68
Treated water	lbs	117.00	–
	kg	–	1982.36
Power	kWh	0.55	–
	kWh	–	20.53
Cooling water circ	gal	12.70	–
	m ³	–	1.79

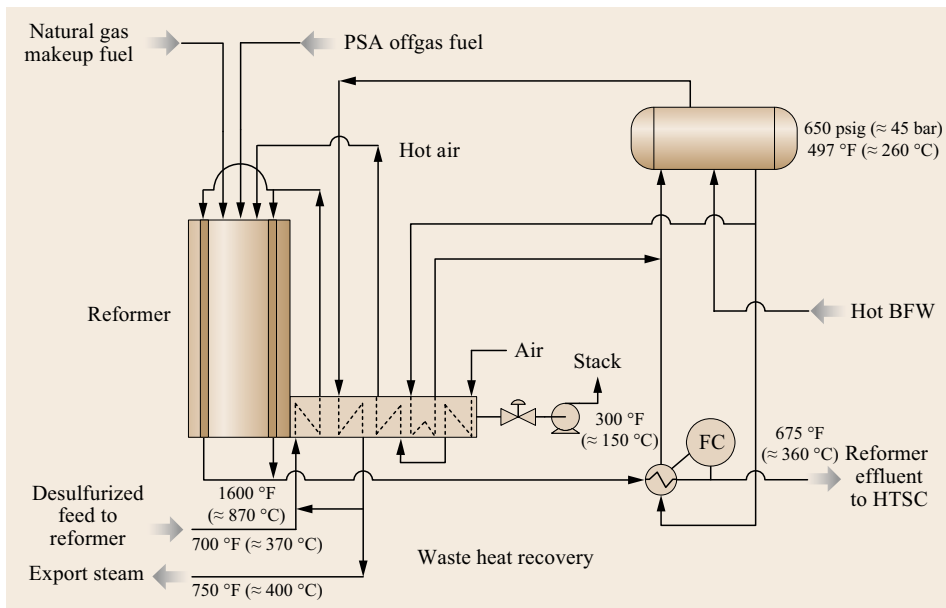

Fig. 24.2 Steam methane reforming with limited steam export

Table 24.4 Limited export steam feed and utility summary

	Units	H ₂ product (Units/MSCF)	H ₂ product (Units/MNCM)
Natural gas	MMBtu LHV	0.386	–
	GJ LHV	–	15.20
Export steam	lbs	38.0	–
	kg	–	643.84
Treated water	lbs	67.7	–
	kg	–	1147.06
Power	kWh	0.58	–
	kWh	–	21.65
Cooling water circ	gal	13.1	–
	m ³	–	1.85

Note that the limited export steam plant makes less than half as much export steam as the maximum steam export case, but also uses less natural gas. At

the same time, the limited steam export plant capital cost is higher, because of the addition of the air preheat unit.

Steam versus Fuel

The steam value and fuel price typically determine which of these two cases is the most economic. A high steam value (relative to fuel price) favors the Maximum Steam Export Case. A high fuel price and a low steam value (relative to fuel price) favor the Limited Steam Export Case.

Figure 24.3 is a plot of natural gas price versus steam value. For a given natural gas price, if the steam value is above the curve, then maximum steam export is favored. But if the steam value is below the curve, then CAP (limited steam export) is favored. For example, for a natural gas price of 3.00 US\$/MMBtu LHV (lower heating value), Fig. 24.3 indicates that if the steam value is above 3.30 US\$/Mlbs, then steam generation is favored. But if the steam value is below 3.30 US\$/Mlbs, then CAP (limited steam export) is favored.

Minimum Export Steam

A minimum export steam plant optimizes heat recovery to the maximum extent possible. This is often done when the value of steam is essentially zero or the price of the feedstock and fuel are exceptionally high. Minimum steam export is often achieved by first increasing the SMR process gas inlet temperature and then the combustion air preheat temperature, both of which reduce the fired duty of the SMR. Typical temperatures are 1150 °F (≈ 620 °C) for the process gas and 900 °F (≈ 480 °C) for the air preheat. These changes reduce the export steam to a low level, but typically not completely to zero. Additional modifications are required to reduce the export steam to an absolute minimum.

Adding reaction steps to the process can further reduce the amount of feed and fuel required by the hy-

drogen plant. The first reaction step that can be added is a prereformer. The prereformer is an adiabatic reactor where the feed is heated to approximately 900 °F (≈ 480 °C), and the gas is partially reformed over a catalyst bed and hydrocarbon components of ethane and heavier are converted to methane. The conversion of ethane plus components to methane is exothermic. If the feedstock is essentially methane (i. e., natural gas), the amount of heat required to drive the steam methane reforming reaction to equilibrium will produce a temperature decrease across the reactor. However, if the feedstock is butane or heavier, the methane conversion reaction produces more heat than is required by the steam methane reforming reaction and there is a net temperature increase across the reactor.

The prereformer is an excellent way to produce a consistent feed to a steam methane reformer. Heavier feedstocks to the SMR increase the potential for carbon formation. The ultimate in energy recovery can be achieved by utilizing a heat recuperative reforming step in the process. Since the steam methane reforming occurs at high temperature, the reformed gas is typically cooled by generating steam. However, if the heat can be recovered by utilizing it in an additional reforming step, the net heat input required to complete the reaction is reduced and, therefore, the quantity of fuel required to operate the furnace is reduced. The reformer effluent gas is passed through the shell side of a tubular heat exchanger with catalyst-filled tubes.

24.2.2 Oxygen-Based Technologies

Steam methane reforming (SMR) has been the conventional route for hydrogen and carbon monoxide

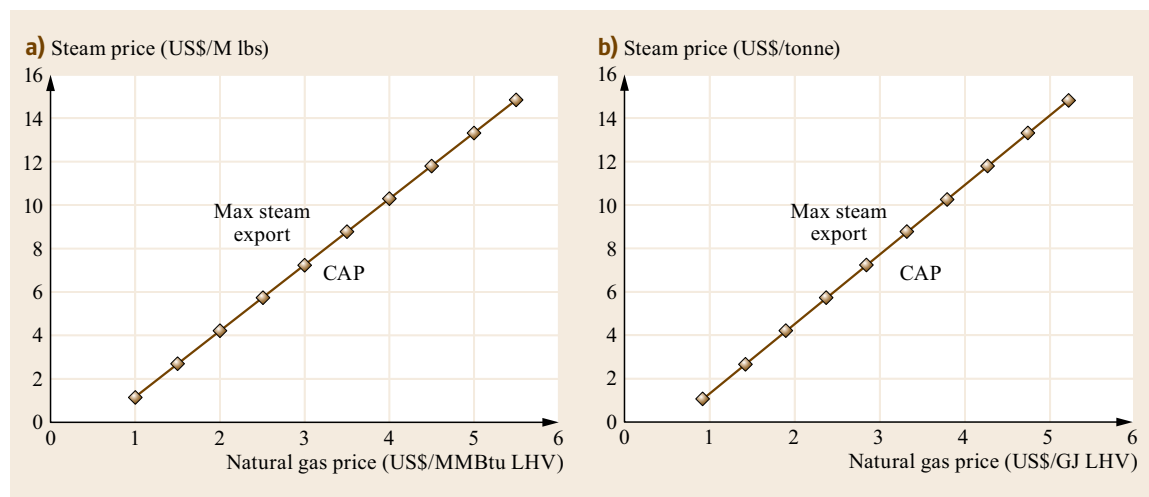


Fig. 24.3a,b Steam price versus natural gas price

production from natural gas feedstocks. However, several alternative technologies are currently finding favor for an increasing number of applications.

These technologies are:

- SMR/O₂R: Steam Methane Reforming combined with Oxygen Secondary Reforming
- ATR: Autothermal Reforming
- POX: Thermal Partial Oxidation.

Each of these alternative technologies uses oxygen as a feedstock. Accordingly, if low-cost oxygen is available, they can be an attractive alternative to an SMR for natural gas feedstocks. Low-cost oxygen is now available in many large industrial sites where a large air separation plant already exists or can be economically installed to serve the needs of the area. (Note that unlike ammonia plant technology, air cannot be used in place of oxygen since the contained nitrogen would dilute the hydrogen/carbon monoxide product.)

A brief description of each technology follows.

SMR/O₂R

An SMR/O₂R essentially consists of an SMR followed by an oxygen secondary reformer (Fig. 24.4). The oxygen reformer is a refractory-lined vessel containing catalyst and a burner. The reaction mixture from the SMR is fed to the top of the oxygen reformer, where it is mixed with oxygen fed through the burner. Partial oxidation reactions occur in a combustion zone just below the burner. The mixture then passes through the catalyst bed where reforming reactions occur. The gas exits at about 1900 °F.

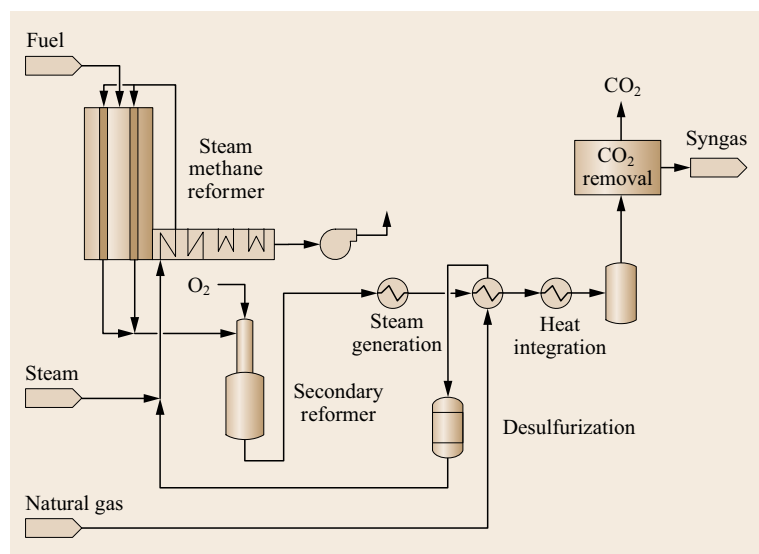


Fig. 24.4 SMR/O₂R plant

ATR

An ATR is similar to an oxygen secondary reformer except that it does not receive feed from an SMR. Instead, it is fed directly with a natural gas/steam mixture, which is mixed directly with oxygen from a burner located near the top of the vessel (Fig. 24.5). Again, partial oxidation reactions occur in a combustion zone just below the burner. The mixture then passes through a catalyst bed where reforming reactions occur. The gas exits at about 1900 °F (≈ 1040 °C).

POX

A POX (Fig. 24.6) is similar to an ATR except that it does not contain a catalyst and does not require steam in the feed. It is fed directly with a natural gas stream, which is mixed directly with oxygen from a burner located near the top of the vessel. Partial oxidation and reforming reactions occur in a combustion zone below the burner. The gas exits at about 2500 °F (≈ 1370 °C).

Products

The exit gas from each of the above reactors consists of hydrogen, carbon monoxide, carbon dioxide, steam, and residual methane. Small quantities of nitrogen and argon from the original feedstocks may also be present. This gas mixture is then typically processed to yield one or more of the following products:

1. High-purity hydrogen
2. High-purity carbon monoxide
3. A hydrogen/carbon monoxide gas mixture.

If only hydrogen is required, the plant becomes a hydrogen plant. If only CO is required, the plant becomes a carbon monoxide plant. If both hydrogen and

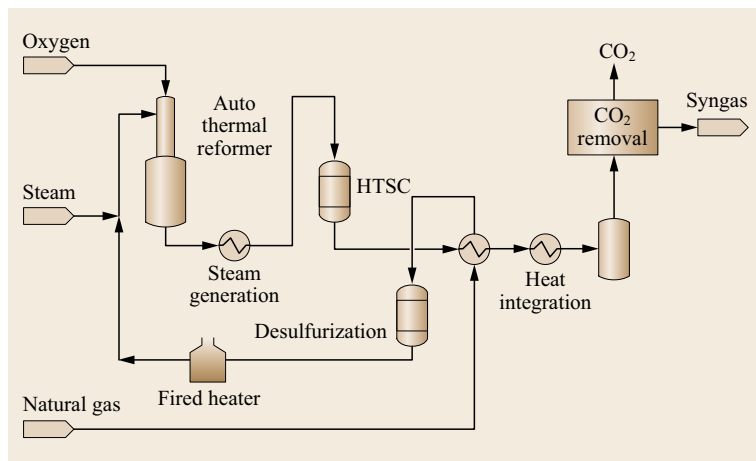


Fig. 24.5 ATR plant

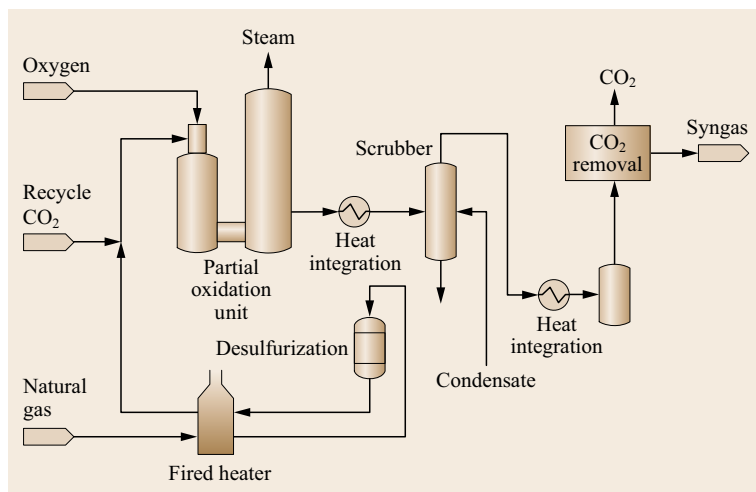


Fig. 24.6 POX plant

carbon monoxide are required as separate streams, the plant is typically known as a hydrogen and CO co-production (HYCO) plant. If only a hydrogen/carbon monoxide mixture is required, the plant is typically known as a synthesis gas (or syngas) plant. If all three products are required, the plant is considered a combination (hydrogen/carbon monoxide/syngas) plant.

H_2/CO Ratio

A key variable in the design of these plants is the product H_2/CO ratio. For HYCO and syngas plants, the product H_2/CO ratio typically varies from 1.0 to about 3.0. But for hydrogen plants, the ratio is almost infinite. And for carbon monoxide plants, the ratio is essentially zero.

Natural Ratio Range

Each of the above technologies makes products with inherently different H_2/CO ratios. The natural ratio range

is defined herein as the range of ratios that can be achieved when varying only the CO_2 recycle. The natural ratio ranges for each technology are shown in Table 24.5, as applicable to natural gas feedstocks. (Other feedstocks will produce a different set of natural ratios).

As seen in Table 24.5, the natural ranges for natural gas are as follows: For the SMR: 3.0–5.0. For the SMR/ O_2R : 2.5–4.0. For the ATR: 1.6–2.65. And for the POX: 1.6–1.8. Note that some ranges are broader than others, and that some of the ranges do not overlap.

The technology that offers a natural ratio that spans the required product ratio is considered to have an inherent advantage and merits careful consideration.

CO_2 Recycle

CO_2 recycle is the typical means of tailoring the natural ratio span to meet the desired H_2/CO product requirement.

Table 24.5 Hydrogen to CO ratio summary

	Membrane or import CO ₂	Total CO ₂ recycle	No CO ₂ recycle	Increase steam	Add shift converter
AMR	< 3.0	3.0	5.0	> 5.0	Infinity
SMR/O ₂ R	< 2.5	2.5	4.0	> 4.0	> 5.0
ATR	< 1.6	1.6	2.7	> 2.7	> 3.0
POX	< 1.6	1.6	1.8	> 1.8	> 2.0

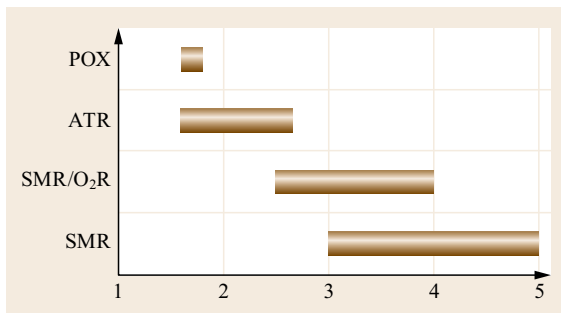
As noted earlier, carbon dioxide is present in all the reactor effluents. Since CO₂ is considered an impurity, it must typically be eliminated. In most designs, the CO₂ is removed from the process gas by selective adsorption in a suitable solvent such as an amine solution. The CO₂ is then stripped from the solvent as a separate stream.

(Note: synthesis gas for methanol plants typically retains some or all of the carbon dioxide. This is a special case, which is outside the scope of this discussion.)

The separate CO₂ stream can be removed from the system or it can be recycled back to the reactor. If it is recycled, the CO₂ can be converted to CO in the reactor by the reverse water gas shift reaction. This reduces the final H₂/CO ratio because the carbon atoms in the original CO₂ are converted to CO. Conversely, if the CO₂ is not recycled, the H₂/CO ratio is increased, because the carbon atoms in the original CO₂ are not converted to CO. (CO₂ that is not recycled is typically vented to the atmosphere. However, sometimes it is sold as a by-product).

The natural H₂/CO range for each technology represents the spread between full CO₂ recycle and no CO₂ recycle (Fig. 24.7). By operating with partial recycle, any H₂/CO ratio within the natural range can be achieved.

But as noted earlier, some of the natural ratio ranges do not overlap; hence, for a given product H₂/CO ratio, at least some of the technologies will require additional ratio adjustment to meet the product requirements. Fortunately, a number of process techniques are available to do this. The viability of the technology will depend on the economics of using these techniques.


Fig. 24.7 Natural range of H₂/CO ratio adjustment

To decrease the ratio below the natural range, common techniques include importing CO₂; use of a membrane; or use of a cold box. To increase the ratio, common techniques include increasing the quantity of steam in the reactor feed or adding a shift converter. These techniques, along with CO₂ recycle, are summarized in Table 24.6.

Import CO₂

The H₂/CO ratio can be decreased by importing CO₂ as a feed to the reactor. The import CO₂ is added to the CO₂ already being recycled. The carbon atoms in the import CO₂ can then be converted to CO by the reverse water gas shift reaction.

Membrane

The H₂/CO ratio can also be decreased by use of a membrane unit. Hydrogen is removed from the membrane as a permeate stream, which reduces the H₂/CO ratio of the main process stream.

Cold Box

A cold box is often used to separate the hydrogen and carbon monoxide into a high-purity CO stream and a H₂-rich stream. This reduces the ratio to near zero with respect to the CO stream. The H₂-rich stream may undergo further purification (typically in a pressure swing adsorption (PSA) unit to yield a high-purity H₂ stream. This increases the ratio to near infinity with respect to the H₂ stream.

Steam

Adding steam to the reactor converts CO to H₂ by the water gas shift reaction. This increases the H₂/CO ratio.

Table 24.6 Techniques for H₂/CO ratio adjustment

	Decreases ratio	Increases ratio
Recycle CO ₂	✓	
Import CO ₂	✓	
Use membrane	✓	
Remove CO ₂		✓
Increase steam		✓
Add shift converter		✓
Use cold box	See note	

Note: A cold box decreases the ratio with respect to CO and increases the ratio with respect to H₂

Shift Converter

A shift converter is a catalytic reactor that catalyzes the conversion of CO to H₂ by the water gas shift reaction. This step can be used to increase the H₂/CO ratio to a very high value. It is widely used in hydrogen plants.

Table 24.6 summarizes the ranges achievable by each technology by inclusion of these techniques. Typically, the viability of the technology decreases with the magnitude of the added steps necessary to achieve the required product H₂/CO ratio.

Other Considerations

As stated above, these ratios are based on natural gas feedstocks. If heavier feedstocks are used, the ratios will be lower because the hydrogen-to-carbon ratio of the feed will be lower.

The above ratios are based on typical reformer outlet temperatures and pressures for each technology. The reformer outlet temperature is typically set by the residual methane requirement. The reformer outlet pressure is typically set by compression requirements. Some design flexibility often exists between these limits. However, within the normal range of flexibility, the H₂/CO ratio does not change appreciably with the reformer outlet temperature or pressure. Hence, for a given design, it is normally impractical to achieve a significant change in H₂/CO ratio by varying the reformer outlet tem-

perature or pressure. Instead, the techniques discussed above should be utilized.

If it is impractical for a given technology to achieve the desired ratio by the techniques discussed above, then excess hydrogen- or carbon monoxide-containing gas can be burned as fuel in the SMR (for SMR and SMR/O₂R plants) or in the Process Heater (for ATR or POX plants). If necessary, the Process Heater can be expanded to include a second radiant section to permit burning of excess product by generating steam. Alternatively, a package boiler can be used to burn excess gas and generate steam.

Thus far, considerable discussion has centered on the H₂/CO ratio, since as noted above, the technology that can most easily achieve the required product H₂/CO ratio has an inherent initial advantage. But there are other considerations that could override this advantage. These are outlined below.

24.2.3 Technology Comparison

Table 24.7 is a comparison of some key process advantages and disadvantages for the technologies under consideration for hydrogen/carbon monoxide plants with natural gas feedstock. Please note that while the oxygen requirement is shown as a disadvantage, it may not be a disadvantage in cases where low-cost oxygen is available.

Table 24.7 Technology comparison

SMR	ATR
Advantages: <ul style="list-style-type: none"> ● Most commercial experience ● Does not require oxygen ● Reforming temperature relatively low ● Best natural H₂/CO ratio for hydrogen product Disadvantages: <ul style="list-style-type: none"> ● Natural ratio high for CO product ● Highest atmospheric emissions 	Advantages: <ul style="list-style-type: none"> ● Natural H₂/CO ratio often favorable ● Lower reforming temperature than POX ● Low residual CH₄ ● Tailor residual CH₄ Disadvantages: <ul style="list-style-type: none"> ● Limited commercial experience ● CO₂ cycle higher than POX ● Require oxygen
SMR/O ₂ R	POX
Advantages: <ul style="list-style-type: none"> ● Smaller than SMR ● Low residual CH₄ ● Tailor residual CH₄ Disadvantages: <ul style="list-style-type: none"> ● Two-step reforming ● Higher reforming temperature ● Require oxygen 	Advantages: <ul style="list-style-type: none"> ● Does not require feedstock desulfurization ● Does not require oxygen ● Low residual CH₄ ● Low natural H₂/CO ratio Disadvantages: <ul style="list-style-type: none"> ● Narrow H₂/CO ratio ● Cannot tailor residual CH₄ ● Require oxygen ● Makes carbon (soot) ● Complex heat recovery section ● Licensed process ● Significant third-party involvement

Process Parameters

Key process parameters and feedstock requirements for each technology include the following:

- **Pressure:** Most SMR plants run at reformer furnace outlet pressures between 150 and 400 psig (≈ 10 and 28 bar). The maximum pressure is about 550 psig (≈ 38 bar), due to metallurgical considerations in the SMR outlet piping. The same applies to SMR/O₂R plants. This limits the final product gas pressure to about 500 psig (≈ 34.5 bar). Above this, product gas compression is required. ATR and POX plants can run at much higher pressures. For example, some plants require synthesis gas at about 800 psig (≈ 55.2 bar); this can be supplied directly from an ATR or POX without synthesis gas compression.
- **Temperature:** SMR plants typically run at reformer outlet temperatures of 1550–1700 °F (≈ 840 –930 °C). SMR/O₂R and ATR plants typically run at outlet temperatures of 1750–1900 °F (≈ 950 –1040 °C). POX plants typically run at about 2500 °F (≈ 1370 °C). This high temperature is needed to maintain low residual methane without a catalyst.
- **Steam/carbon:** Steam is typically required to prevent carbon formation on the reformer catalyst. The steam requirement is generally expressed as the steam/hydrocarbon-carbon ratio (steam/hcc). This is the ratio of the moles of steam to moles of hydrocarbon-carbon in the feed (the carbon in any CO₂ recycle is not included in computation of the ratio).
Both the SMR and SMR/O₂R plants typically use a 2.5–5 steam/hcc ratio for no CO₂ recycle, and a 2 : 1 steam/hcc ratio when all the CO₂ is recycled. (A lower ratio can be used with the CO₂ recycle since the CO₂ makes some H₂O by the water gas shift reaction). For a partial recycle, a ratio between 3 : 1 and 2 : 1 is typically used.
ATR plants can operate at a lower ratio, often about 1 to 1.5 with or without CO₂ recycle.
POX plants require no steam. Some soot is formed, but since there is no catalyst, there is obviously no possibility of catalyst bed plugging. With proper design and operation, the soot can be processed and removed in the downstream equipment without affecting plant on-stream time.
- **Methane slip:** The exit gas from each reactor contains some residual methane, which corresponds to unreacted natural gas feed. This is typically referred to as the methane slip. A low methane slip increases the purity of a synthesis gas product. It also reduces the natural gas requirement.

An SMR typically has a relatively high methane slip (3–8 mol %, dry basis). This is primarily because the SMR operates at a lower outlet temperature. The other technologies operate at higher outlet temperatures and typically have low slips (0.3–0.5 mol %, dry basis).

If a methane-wash cold box is used, typically a methane slip of at least 1 to 2 mol % is required to maintain the methane level in the box. This is not a problem for an SMR design because its methane slip is considerably more than this. It is also easily achieved by the SMR/O₂R and ATR designs by simply reducing the reactor outlet temperature. However, this methane level is more difficult to achieve with a POX, since in the absence of a catalyst, a high temperature and corresponding low methane slip should be maintained to ensure consistent performance.

- **Raw materials:** Natural gas and oxygen are the two major raw materials. For each technology, the quantities required must be considered on a case-by-case basis, since they depend on the H₂/CO requirement for each application.

For example, the product H₂/CO ratio may require that CO₂ be either recycled or vented, depending on the ratio and the technology.

If the required H₂/CO product ratio is 2.0, all the CO₂ would be recycled in an SMR or SMR/O₂R design; part of the CO₂ would be recycled in an ATR design; and no CO₂ would be recycled in a POX design.

The extent of CO₂ recycle changes the raw material requirements for a given technology, because if CO₂ is vented, its contained carbon and oxygen is not recovered.

To provide a basis of comparison, a design can be considered wherein all the CO₂ is recycled for each technology. This would normally occur in designs for a H₂/CO product ratio less than 1.6.

A typical design meeting this requirement would be a carbon monoxide only plant (H₂/CO ratio of zero). For such a design, we have compared all four technologies for a proposed plant on the US Gulf Coast. For this plant, the natural gas and oxygen requirements are given in Table 24.8. The natural gas requirement shown is the net requirement on a heating value basis and includes credit for excess hydrogen at fuel value. (For this plant, all the technologies produce excess hydrogen since CO is the only required product and there is no requirement for product hydrogen).

For the following discussion, the SMR and SMR/O₂R are called SMR-based technologies because the SMR is the dominant component. And the ATR

Table 24.8 Feedstock requirements

	SMR ^a	SMR ^b	SMR/O ₂ R ^a	SMR/O ₂ R ^b	ATR ^a	ATR ^b	POX ^a	POX ^b
Net natural gas* (MMBtu LHV)	0.729	–	0.724	–	0.531	–	0.509	–
Net natural gas* (GJ LHV)	–	28.70	–	28.51	–	20.91	–	20.04
Oxygen import (lb)	0	–	14.2	–	56.5	–	58.7	–
Oxygen import (kg)	–	0.0	–	240.6	–	957.3	–	994.6

^a Units per 1000 SCF CO Product, ^b Units per 1000 NCM CO Product

* Includes credit for excess hydrogen at fuel value

All cases based on full CO₂ recycle

and POX are called oxygen-based technologies because the partial oxidation reactor is the dominant component.

From Table 24.8, note that the natural gas requirements for the SMR-based technologies are about the same. Note also that the natural gas requirements for the oxygen-based technologies are about the same. But also note that the oxygen-based technologies require only about 70% as much natural gas as the SMR-based technologies.

The natural gas requirement is lower for the oxygen-based technologies because most of the oxygen in the feed reacts with carbon in the natural gas to form carbon monoxide. The oxidation reaction is therefore more efficient for the formation of carbon monoxide, which is the desired product for the referenced plant.

Another reason for the lower natural gas requirement is that for the oxygen-based technologies, the heat required for the reaction is applied directly to the process gas in the reactor vessel. This is more energy efficient than the SMR-based technologies, which require a temperature driving force between the combustion gas and the in-tube process gas.

With respect to oxygen consumption, the oxygen requirement for the SMR is obviously zero. For the SMR/O₂R, the oxygen requirement is about 25% of that for the ATR or POX.

The ATR and POX oxygen requirements are about the same. This is to be expected, since both technologies use the same direct combustion process, and for the referenced plant, both technologies recycle all the CO₂ and produce essentially the same H₂/CO product ratio.

Export Steam

For the referenced plant, the export steam is relatively low since the excess hydrogen is not burned within the plant to make export steam. Accordingly, the export steam for the SMR, SMR/O₂R, and POX averaged only about 150 lbs per 1000 SCF (2541 kg per 1000 NCM) of carbon monoxide and any differences were not considered significant. However, the ATR export steam was

less than half this value because the energy requirement for the CO₂ removal system is larger.

Economic Considerations

The economics of each technology depend on the conditions and requirements of each project and must be studied on a case-by-case basis. Some of the most important considerations are as follows.

Oxygen Availability

The availability of oxygen is obviously a key parameter. Since the SMR requires no oxygen, it is the obvious choice if oxygen is unavailable or prohibitively expensive. Studies indicate that the oxygen-based technologies can be attractive if oxygen is available at less than about US\$25 per short ton. If oxygen is greater than about US\$30 per ton, the SMR is favored.

The oxygen price can be less than US\$25 per ton in large industrial sites where a large air separation plant already exists or can be economically installed to serve the needs of the area. Hence, in such cases the oxygen-based technologies merit serious consideration.

Hydrocarbon Feedstock

This section is based on natural gas feedstock. With natural gas, all technologies are technically viable. However, if the feedstock is a heavy hydrocarbon (such as fuel oil or vacuum bottoms), the POX is the only viable technology. This is because the other technologies cannot process feedstocks heavier than naphtha (to avoid carbon deposition on the catalyst).

H₂/CO Ratio

The importance of the product H₂/CO ratio has already been discussed extensively. As previously stated, the technology that offers a natural ratio spanning the required product ratio is considered to have an inherent advantage and must be seriously considered.

Natural Gas Price

Since the SMR-based technologies directionally require more natural gas, they are favored by low natural gas prices.

Capital Cost

The SMR-based technologies typically have a somewhat higher capital cost because the SMR furnace with its high alloy tubes and large flue gas heat recovery section is inherently more expensive than the ATR or POX technologies, which use refractory-lined carbon steel vessels without external flue gas heat recovery.

An SMR has a lower capital cost than an SMR/O₂R when the operating pressure is relatively low. Since low pressure favors the reforming reaction, under such conditions most of the reforming occurs in the SMR, and the O₂R does not significantly reduce the size of the SMR. But at higher pressures, an SMR/O₂R can cost less, because more of the reforming is done in the O₂R, and the size of the SMR can often be significantly reduced.

The ATR and POX technologies have offsetting capital costs, depending on the extent of CO₂ recycle.

For full CO₂ recycle, the CO₂ removal system is much larger for the ATR than the POX, and the added capital cost associated with this difference tends to make the ATR more expensive overall.

However, for no CO₂ recycle, the ATR tends to cost less than the POX because its reaction and heat recovery section is inherently less expensive and it does not carry any third-party royalty.

Section Conclusions

On the basis of the above, the following conclusions can be drawn:

1. The SMR/O₂R, ATR, and POX technologies can be attractive if low-cost oxygen is available.

2. For competing technologies, the H₂/CO product ratio is typically the most important process parameter.
3. For low methane slip, the SMR/O₂R, ATR, and POX technologies are favored.
4. For full CO₂ recycle, the POX is typically better than the ATR.
5. Relative to the POX, the ATR is a nonlicensed technology which avoids third-party involvement.
6. The economics of each technology is dependent on the conditions and requirements for each project and must be evaluated on a case-by-case basis.
7. The technology with the most favorable H₂/CO ratio for producing hydrogen is the SMR.

24.2.4 Hydrogen Purification

Old Style

Many refiners are still operating hydrogen plants that were designed and built 20 or more years ago. These older plants were generally designed with the best available technology of the time. These plants typically consist of a steam methane reformer (SMR) to convert the hydrocarbon feed to a syngas mixture followed by a high-temperature shift converter (HTSC) and low-temperature shift converter (LTSC) to shift most of the CO to hydrogen. This hydrogen-rich gas is purified by a CO₂ removal unit where a hot potassium carbonate or monoethanolamine (MEA) solution removes the CO₂ and then a methanator is used to convert the remaining CO and CO₂ to methane and water. The final product gas is typically about 95–97% hydrogen. Figure 24.8 shows a typical layout for an Old Style hydrogen plant.

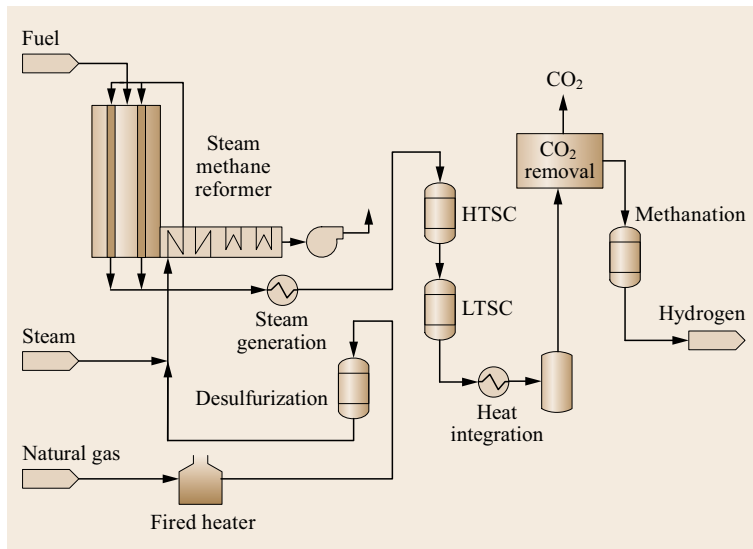


Fig. 24.8 Old style hydrogen plant

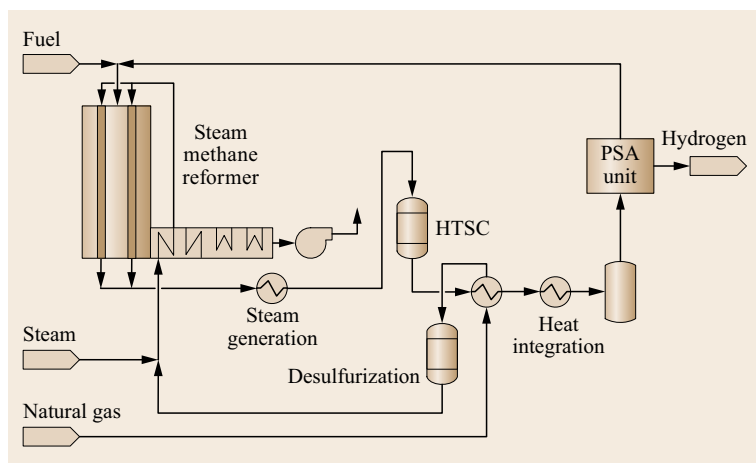


Fig. 24.9 Modern hydrogen plant

Modern

The main process difference between a Modern hydrogen plant and an Old Style hydrogen plant is the hydrogen purification technology. A Pressure Swing Adsorption (PSA) unit replaces both the CO₂ removal unit and the methanator, enabling the Modern plant to produce hydrogen product with a much higher purity, more than 99.9%. In addition, many significant improvements in technology and design allow the Modern plant to operate at much higher efficiency and with substantially lower operating costs.

A PSA unit employs a collection of solid adsorbents – molecular sieves, activated carbons, silica gels, and activated aluminas. For carbon, silica, and alumina, separation is due to their differential tendency to adsorb different gases. PSA cycles include pressurization, depressurization, and purging. The rejected gas, a low-Btu

mixture containing methane, CO, and CO₂, is burned to provide some preheat duty.

A Modern hydrogen plant includes an SMR followed by an HTSC. A PSA unit purifies the syngas effluent from the HTSC. The final product gas is typically 99.99% hydrogen. Since the PSA unit removes the impurities from the syngas, an LTSC is not required to further reduce the CO content.

The PSA unit produces an offgas stream that can be used by the SMR as the primary fuel source. In addition, the increase in product purity from the PSA unit has potential benefits in downstream units. For example, the higher purity hydrogen makeup to a hydrotreater increases reactor hydrogen partial pressure, lowers the recycle flow, and potentially reduces compression costs, and/or increases hydrotreater performance and catalyst run life. Figure 24.9 shows a typical layout for a Modern hydrogen plant.

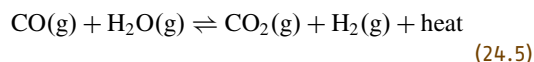
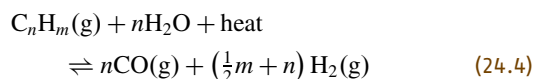
24.3 Design Parameters for SMRs

Steam reformers are used in hydrogen generation plants throughout the refining and petrochemical industries and are expected to remain the most cost-effective approach for on-purpose hydrogen production. The steam reformer for hydrogen plants consists of a fired heater containing catalyst-filled tubes. This article discusses process design considerations for a modern reformer of this type.

24.3.1 Function

The primary function of a steam reformer is to produce hydrogen. Hydrocarbon feed gas is mixed with steam and passed through catalyst-filled tubes. Hydrogen and

carbon oxides are produced by the following reactions.



The first reaction is the reforming reaction, and the second is the shift reaction. Both reactions produce hydrogen. Both reactions are limited by thermodynamic equilibrium. The net reaction is endothermic. These reactions take place under carefully controlled external firing, with heat transfer from the combustion gas in

the firebox to the process gas within the catalyst-filled tubes.

The carbon monoxide in the above product gas is subsequently shifted almost completely to hydrogen in a downstream catalytic reactor by further utilization of (24.5).

24.3.2 Feedstocks

Typical hydrocarbon feedstocks for the reformer include natural gas, refinery gas, propane, LPG, and butane. Naphtha feedstocks with final boiling points up to about 430 °F (220 °C) can also be processed.

24.3.3 Fuels

Typical fuels for the reformer are light hydrocarbons such as natural gas and refinery gas, although distillate fuels are sometimes used. Residual fuels are not utilized since trace metals in the fuel oil can damage the reformer tubes.

In most hydrogen plants, a pressure swing adsorption (PSA) system is used for hydrogen purification. In such plants, a major portion of the reformer fuel is PSA offgas, with the makeup fuel being a hydrocarbon stream as discussed above.

24.3.4 Design

Reformers are fired to maintain a required process gas outlet temperature. Most modern reformers are top-fired. In this design, the burners are located in the top of the furnace, and fire downward. The process gas flows downward through the catalyst-filled tubes in the same direction.

Accordingly, the top-fired design features co-current flow of process gas and flue gas. The co-current flow permits use of (1) the highest flue gas temperature when the in-tube process gas temperature is lowest, and (2) the lowest flue gas temperature when the in-tube process gas temperature is highest. This in turn provides tube-wall temperatures that are quite uniform over the length of the tube. Because of this uniformity, the average tube-wall temperature is lower. And lower tube-wall temperatures reduce tube cost and increase tube life.

Another advantage of co-current flow is that as the flue gas cools, it sinks in the same direction as its normal flow. This provides an inherently stable furnace operation. In particular, it avoids flue gas back-mixing that inherently occurs in alternative designs. Since there is no back-mixing, the flue gas outlet temperature tends to more closely approach the process gas outlet temperature than in alternative designs. This improves the furnace efficiency.

Note that the highest tube-wall temperature occurs at the outlet, which is quite common for this type of furnace. Also note that at the tube outlet, the tube-wall temperature is very close to the required process gas outlet temperature. This is because the heat flux at the outlet is quite low, having fallen steadily for the last two-thirds of the tube.

Therefore, the tube-wall temperature is minimized for the required process gas outlet temperature, which in turn minimizes the required tube-wall thickness.

In addition, note that the flue gas temperature falls off steadily for the last two-thirds of the tube, and is at a minimum at the tube outlet. Since the furnace must be fired to provide the necessary flue gas outlet temperature, the fact that the flue gas outlet temperature is relatively low means that the fuel requirement is minimized.

The burners are housed at the top of the reformer by an enclosure commonly referred to as a penthouse. This housing provides a convenient shelter for the burners and for the inlet piping and valving.

The flue gas is collected at the bottom of the reformer in horizontal fire-brick ducts, often referred to as *tunnels*. The flue gas then exits horizontally into a waste heat recovery (WHR) unit. The combustion gas is drawn through the WHR unit by an induced draft fan and the gas is then discharged to the atmosphere through a stack. The WHR unit and fan are essentially at grade, which facilitates operation and maintenance.

When the above features of the top-fired design are considered and weighed against alternative arrangements, the consensus of the industry favors the top-fired design.

The remainder of this section will therefore focus on the top-fired design.

The process considerations discussed below focus on steam reformer parameters specifically related to hydrogen plant design. However, many of these parameters also apply to steam reformers for other types of plants (such as syngas, ammonia, and methanol plants).

24.3.5 Pressure

The shift reaction equilibrium is independent of pressure. However, the reforming reaction equilibrium is favored by low pressure. Therefore, for the overall reaction, the lower the pressure, the higher the conversion of hydrocarbon to hydrogen. Accordingly, from the reaction standpoint, it is best to operate at low pressure.

However, there are other considerations. For example, modern hydrogen plants typically use a pressure swing adsorption (PSA) unit for hydrogen purification. PSA units are more efficient at higher pressure. The

minimum pressure for acceptable operation is typically 150–200 psig (≈ 10 –14 bar). The optimum pressure may be 300–450 psig (≈ 20 –30 bar). Therefore, to accommodate the PSA unit, the reformer pressure will need to be adjusted accordingly.

Another consideration is product hydrogen pressure requirements. In many applications, the hydrogen product from the hydrogen plant requires subsequent compression to a much higher pressure, for example for refinery hydrotreating applications. In such cases, the compression cost can be reduced considerably if the hydrogen from the hydrogen plant is produced at a higher pressure.

As discussed below, hydrogen plant reformers typically operate at process gas outlet temperatures up to 1700 °F (≈ 930 °C). At these temperatures, metallurgical considerations for the outlet piping typically limit the reformer outlet pressure to about 550 psig (≈ 38 bar). This corresponds to a hydrogen product pressure of about 500 psig (≈ 35 bar).

Many hydrogen plant reformers are designed consistent with a hydrogen product pressure of about 300–350 psig (≈ 20 –24 bar). Although this decreases the reforming reaction conversion, the overall plant economics often favors the higher pressure.

Conversely, if the product pressure requirement is low, then the PSA unit will typically determine the minimum pressure.

Therefore, for hydrogen plants, the reformer outlet pressure typically runs between 150–550 psig (≈ 10 –38 bar).

24.3.6 Exit Temperature

The reforming reaction equilibrium is favored by high temperature. At the pressure levels used in hydrogen plants, the reformer process gas exit temperature typically runs between 1500 and 1700 °F (≈ 815 –930 °C). Lower temperatures give insufficient conversion. Higher temperatures increase metallurgical requirements, tube-wall thickness, and fuel consumption.

24.3.7 Inlet Temperature

The reforming reaction rate becomes significant at about 1000 °F (≈ 540 °C), so it is usually advantageous to design for an inlet temperature near this value. This is typically achieved by preheating the reformer feed against the hot flue gas in the WHR section of the reformer.

A higher reformer inlet temperature decreases the absorbed duty requirement and therefore decreases the number of tubes, the size of the furnace, and the fuel re-

quirement. It also decreases the steam generation from the waste heat recovery unit.

If steam has a high value relative to fuel, it may be economical to reduce the reformer inlet temperature somewhat in order to maximize steam generation. In many such cases, the optimum inlet temperature is about 1050 °F (≈ 565 °C). This is low enough to maximize steam generation, but high enough to keep the furnace size down.

If steam does not have a high value, the optimum reformer inlet temperature is often about 1100 °F (≈ 590 °C). Above this, metallurgical considerations with the inlet piping become a factor.

Up to 1050 °F (≈ 565 °C), 2-1/4 Cr-1 Mo material is satisfactory for the inlet piping. At higher temperatures, stainless steel would ordinarily be used, but stainless steel is generally considered unacceptable because of the possibility of chloride stress cracking. Such cracking can occur if the steam in the feed has chloride-containing water droplets carried over from the steam drum. Incoloy is considered the next step up in metallurgy and is not subject to chloride stress cracking, but its cost typically prohibits its use. Accordingly, for metallurgical reasons the maximum inlet temperature should remain at about 1050 °F (≈ 565 °C).

24.3.8 Steam/Carbon Ratio

The feed must contain sufficient steam to eliminate carbon formation. The relationship between steam and hydrocarbon is typically expressed as the steam-to-carbon ratio. This corresponds to the moles of steam per mol of carbon in the hydrocarbon. The design steam-to-carbon ratio is typically about 3.0 for all hydrocarbon feedstocks. Lower values (down to about 2.5) can be used for some feedstocks, but there is a higher risk from potential operating upsets that might occur which could drop the ratio down to where carbon formation could occur.

For heavier feedstocks, carbon formation is more likely, and an alkali-based catalyst must be used to suppress carbon formation. Such catalysts are readily available, and it is understood that the 3.0 steam-to-carbon is applicable only if the proper catalyst is chosen. Otherwise, higher steam-to-carbon ratios are required.

24.3.9 Heat Flux

The reformer heat flux is typically defined as the heat input per unit of time per area of inside tube surface. For a given absorbed duty, the heat flux is therefore determined by the amount of tube surface.

A low heat flux provides extra catalyst volume and lower tube-wall temperatures. This provides sev-

eral advantages: The extra catalyst volume increases the reforming reaction conversion. The lower tube-wall temperature reduces the tube-wall thickness, which in turn reduces the cost per tube and increases the tube life. The lower tube-wall temperature also reduces the fuel requirement.

A high heat flux has the opposite effect, but has the advantage of reducing the number of tubes.

Because of these trade-offs, commercial heat fluxes typically vary from about 20 000 to 28 000 Btu hr⁻¹ ft⁻² (63 000–88 000 W/m²). A conservative design will typically run from 20 000 to about 25 000 Btu hr⁻¹ ft⁻² (63 000 to about 79 000 W/m²).

The above fluxes are average values for the entire furnace. The point flux is highest in the zone of maximum heat release, and then falls off to a relatively low value at the tube outlet. The maximum point flux is often 35 000–40 000 Btu hr⁻¹ ft⁻² (110 000–126 000 W/m²).

24.3.10 Pressure Drop

The reformer pressure drop depends primarily on the number of tubes, the tube diameter, and the catalyst selection. Typically, the overall design pressure drop will range from 40–60 psi.

24.3.11 Catalyst

Reforming catalysts are typically manufactured in a ring or a modified ring form. The modified ring forms have increased surface area and a higher activity for about the same pressure drop, but they cost more.

Reforming catalysts use nickel as the principal catalytic agent. For heavier feedstocks, an alkali promoter is typically used to suppress carbon formation. For heat fluxes above about 25 000 Btu hr⁻¹ ft⁻², modified ring shapes are needed to maintain the reforming reaction conversion.

The reaction conversion is typically measured in terms of *approach to equilibrium*. A typical design approach to reforming equilibrium is 20 °F (≈ -7 °C). This means that the reforming reaction (24.1) is at equilibrium corresponding to a temperature 20 °F (≈ -7 °C) lower than the actual temperature. This corresponds to a typical end-of-life catalyst condition. Fresh catalyst typically runs at essentially a 0 °F (≈ -18 °C) approach to reforming equilibrium (that is, for fresh catalyst the reforming reaction is essentially at equilibrium at the actual temperature). The shift reaction (24.3) is rapid and is considered in equilibrium at all times.

Typical catalyst life is 4–5 yr. To obtain the performance discussed above over this time frame, the

appropriate catalyst must be selected, consistent with the design heat flux and allowable pressure drop.

For higher flux reformers, a dual charge of catalyst is typically used. The top half of the tube is loaded with a high activity catalyst that prevents carbon formation in the zone of maximum flux. The bottom half of the tube can be a more conventional, less expensive catalyst.

Catalyst pressure drop is also an important consideration. Fortunately, the modified ring catalysts, with high void space, can provide higher activity for about the same pressure drop. If significantly higher activity is needed, a higher pressure drop must be accepted.

24.3.12 Tubes

Reformer tubes typically operate at maximum temperatures of 1600–1700 °F (≈ 870–930 °C) and are designed for a minimum stress-to-rupture life of 100 000 operating hours. Today's preferred metallurgy is a 35/25 Ni/Cr alloy modified with niobium and microalloyed with trace elements including titanium and zirconium.

Smaller tube diameters provide better in-tube heat transfer and cooler walls. The cooler walls reduce tube-wall thickness, which reduces tube cost and increases tube life. The cooler walls also decrease fuel consumption. However, more tubes are required and the pressure drop is higher. On the basis of these parameters, the optimum inside tube diameter is typically 4–5 inches (≈ 10–13 cm).

Thin walls increase tube life because secondary stresses are minimized during thermal cycling on startups, shutdowns, and upsets. Accordingly, the tube-wall thickness should be minimized consistent with meeting the tensile strength requirement. For many applications, the minimum sound wall (MSW) can be as low as 0.25 inches (≈ 0.6 cm).

Longer tubes provide a longer co-current heat transfer path in the reformer, and thereby reduce the flue gas exit temperature, which conserves fuel. Longer tubes also reduce the number of tubes. However, the pressure drop is higher. The optimum tube length is typically 40–45 feet (≈ 12–14 m).

Increasing the tube pitch (the center-to-center spacing) reduces the shielding effect between tubes and lowers the peak temperature around the tube circumference. This improvement is significant for short tube pitches, but falls off at longer pitches.

If the pitch is too short, the design must be modified to avoid overlapping the tube inlet flanges. The optimum pitch is typically 2–3 tube diameters.

The lane spacing between tube rows must be sufficient to avoid flame impingement from the burners. Typical spacing ranges from 6 to 8 feet (≈ 1.8–2.4 m).

24.3.13 Burners

The burners are located between the tube rows. Increasing the number of burners reduces the heat release per burner, which permits a smaller flame diameter and reduced lane spacing. The number of burners varies with the design, but a ratio of one burner for every 2–2.5 tubes will provide a very uniform heat release pattern and is considered good design practice.

For most hydrogen plants, the burners are a dual-fired design, which will fire both PSA offgas and the supplemental makeup gas. Lo-NO_x burners are typically used to meet modern environmental requirements. In some burner designs, the makeup gas is used to induce flue gas into the flame, thereby reducing the flame temperature and the NO_x level. With a properly designed burner, NO_x levels of as low as 0.025 lbs/MM Btu LHV (0.011 kg/GJ) of heat release can be expected.

24.3.14 Flow Distribution

It is important to obtain good flow distribution for all reformer streams. The piping should be designed such that the variation in gas flow to the reformer tubes and to the burners does not exceed $\pm 2.5\%$. Otherwise, the tube-wall temperatures may not be sufficiently uniform.

Special consideration must be given to the PSA offgas flow since it is typically available to the burners at only about 3 psig. Even greater consideration must be given for preheated combustion air (if used), since the differential air pressure across each burner is typically no more than 2 inches (≈ 5 cm) H₂O.

To help ensure good distribution, the piping should be as symmetrical as possible, and detailed pressure drop computations should be made and analyzed.

It is especially important that the flue gas tunnels be properly designed. The tunnels are rectangular fire-

brick structures located at the bottom of the reformer which serve as horizontal ducts for flue gas removal. Selected bricks are removed along the bottom of the tunnels to provide openings for the flue gas. To ensure plug flow of flue gas down the box, these openings must be designed for uniform flow distribution of the flue gas from the box into the tunnels. To ensure proper design, detailed hydraulic calculations should be made and analyzed.

24.3.15 Heat Recovery

The flue gas typically exits the radiant box at 1800–1900 °F (≈ 980 – 1040 °C). A waste heat recovery (WHR) unit is provided to recover heat from this gas. Typically, this consists of a package unit containing a reformer feed preheat coil, followed by a steam superheat coil (if applicable), followed by a steam generation coil, followed by a boiler feedwater preheat coil. If combustion air preheat is used, the air preheat unit typically replaces the boiler feedwater coil. The flue gas typically exits the WHR unit at about 300 °F (≈ 150 °C).

On this basis, and with a typical heat loss of 3% of the absorbed duty, the overall efficiency of the reformer (radiant plus WHR) is about 91% on an LHV basis.

Steam is also generated in a process steam generator, which extracts heat from the reformer outlet process gas. The WHR unit and the process steam generator typically share a common steam drum.

Steam generation pressure must be sufficient to provide steam to the reformer. Typically, the minimum required pressure is 100–150 psig above the hydrogen product pressure, depending on the plant pressure drop. Significantly higher steam pressures can easily be accommodated, and reformers generating 1500 psig steam are not uncommon in some industries.

24.4 Environmental Issues

The federal government's passage of the Clean Air Act in 1970 set national limits on industrial emissions to reduce air pollution and acid rain. Since 1970, the Clean Air Act has been amended and some states, such as California, have set even stricter limits on several of these emissions. Therefore, a major point of emphasis when designing a hydrogen plant is the reduction of plant emissions. A typical hydrogen plant has three sources of emissions:

- Flue gas from the combustion chamber of the reformer

- Condensate from the process
- Wastewater from the steam generation system.

24.4.1 Flue Gas Emissions

There are five primary pollutants found in the flue gas: nitrogen oxides, carbon monoxide, sulfur oxides, unburned hydrocarbons, and particulates. These components are formed during the combustion process.

The majority of the flue gas emissions consist of the nitrogen oxides (NO_x). NO_x is an environmental concern because it can cause photochemical smog and

acid rain. The nitrogen oxides from a hydrogen plant primarily consist of nitrogen oxide (NO) and nitrogen dioxide (NO₂). There are three types of NO_x formation: prompt NO_x, fuel NO_x, and thermal NO_x. Prompt NO_x is formed when fragments of hydrocarbons in the fuel combine with nitrogen in the combustion air. This form of NO_x is considered to be negligible as compared to thermal NO_x in hydrogen plant applications. Fuel NO_x is formed when nitrogen-containing hydrocarbons in the fuel are burned. However, this is typically not a concern for hydrogen plants because the makeup fuel is usually natural gas. Thermally produced NO_x represents the largest contributor to NO_x formation in a hydrogen plant. Thermal NO_x is produced by N₂ and O₂ in the combustion air reacting in the hottest part of the burner flame. The rate of thermal NO_x formation is based on the burner flame temperature, the amount of combustion air, and residence time. As the flame temperature increases, the amount of NO_x formed increases. Issues such as type of fuel gas, amount of excess air and combustion air temperature affect the amount of thermal NO_x formation. Therefore, to reduce the flame temperature, many burner manufacturers have developed burner designs that incorporate staged combustion and flue gas recirculation. The recirculation of the flue gas cools the flame thus lowering the amount of thermal NO_x formation. The recirculation will also lower the amount of CO exiting the burner, as a portion of it will be recycled and combusted.

A NO_x removal system may be required to meet a site's emission requirements. The typical system used for this case is a Selective Catalytic Reduction unit (SCR). The SCR unit reduces NO_x by reacting ammonia with the flue gas over a catalyst, which yields nitrogen and water vapor. An SCR unit can reduce the NO_x emission from a hydrogen plant by approximately 90%. There is a small slipstream of ammonia, approximately 10 ppmv that will exit with the flue gas. This unit adds additional capital costs as well as operating costs and ammonia handling issues but is sometimes required as the best available control technology (BACT) for NO_x removal.

The CO, combustion-produced particulates, and the unburned hydrocarbons are all related to the amount of excess air, type of fuel, and the amount of mixing of the

fuels within the burner. Insufficient air and inadequate mixing can result in incomplete combustion thus raising the amount of CO and unburned hydrocarbons in the flue gas. Particulates formed in the combustion process are very low for gaseous fuels but will increase with the use of liquid fuels.

The sulfur oxides that are formed are directly related to the amount of sulfur found in the fuel. These emissions are typically low when PSA offgas is burned with natural gas. The PSA offgas is sulfur-free due to feedstock pretreatment to protect catalyst beds within the hydrogen plant. Natural gas also typically contains very low levels of sulfur. However, if refinery fuel gases are used as a makeup fuel to the reformer, then the sulfur emissions can increase dramatically as these streams often contain large amounts of sulfur.

Burner manufacturers will have typical values of these emissions for their burners based on actual tests of their burner design. The emission limits of the CO, sulfur oxides, unburned hydrocarbons, and particulates are generally met since light gaseous fuels are typically used as the fuels for the reformer. Table 24.9 below contains some typical emission values for a standard hydrogen plant utilizing Low-NO_x burners when burning PSA offgas with natural gas.

24.4.2 Process Condensate (Methanol and Ammonia)

The process condensate from a standard hydrogen plant contains impurities such as dissolved gases, ammonia, methanol, and traces of other organic compounds. The dissolved gases that are found in the process condensate consist of the components in the syngas (CO, CO₂, H₂, CH₄, and N₂). Henry's Law can be used to calculate the amounts of these gases that are in the condensate

$$P = Hx, \quad (24.6)$$

where P is partial pressure of a component, H is Henry's Law constant, x is mole fraction of component in solution.

The CO₂ represents the largest amount of dissolved gas in the condensate, typically in the range of several 1000 ppmw. The dissolved H₂, CO, and CH₄ are typ-

Table 24.9 Typical emission values for a standard hydrogen plant

Emission	Units	Value
NO _x	lb/(MMBtu LHV)	0.03
	kg/GJ LHV	0.013
CO	ppmv (3% O ₂ dry basis)	25
Unburned hydrocarbons	ppmv (3% O ₂ dry basis)	5
Particulates	lb/MMBtu LHV	0.005
	kg/GJ LHV	0.002

ically in lower concentrations of less than a hundred ppmw each.

In a hydrogen plant, ammonia is produced in the reformer. The steam methane reformer's operating conditions are similar to that of an ammonia synthesis reactor. The amount of ammonia produced is based on the amount of nitrogen in the feed. Feedstocks with negligible amounts of nitrogen will not produce an appreciable amount of ammonia. Ammonia formation depends on the reaction equilibrium and the residence time inside the reformer. The ammonia equilibrium reaction is given below.

$$[\text{NH}_3] = K_{\text{PNH}_3} [\text{N}_2]^{0.5} [\text{H}_2]^{1.5} P_T, \quad (24.7)$$

where [] is mole fractions, K_{PNH_3} – Equilibrium constant, P_T – Total pressure (atm).

Ammonia formation is lessened due to the fact that the residence time of the steam methane reformer is designed for hydrogen production not ammonia production with recycle. In an NH_3 plant, the ammonia is considered to be at equilibrium in a secondary reformer that is operating approximately 300–500 °F (≈ 140 –260 °C) higher than a traditional steam methane reformer. Therefore for calculations, the worst case for ammonia production in a hydrogen plant can be assumed to be equilibrium at the reformer outlet temperature plus an additional 300 °F (≈ 140 °C).

Methanol is produced as a by-product in the shift converters within the hydrogen plant. In High-Temperature Shift Converters (HTSC), the formation of methanol is an equilibrium reaction similar to that of ammonia formation in the reformer. The equilibrium reaction for methanol is given below.

$$[\text{CH}_3\text{OH}] = \frac{K_{\text{PCH}_3\text{OH}} [\text{CO}_2] [\text{H}_2]^3 P_T^2}{[\text{H}_2\text{O}]}, \quad (24.8)$$

where [] is mole fractions, $K_{\text{PCH}_3\text{OH}}$ – Equilibrium constant, P_T – Total pressure (atm).

The typical concentrations of methanol in an HTSC application are approximately 100–300 ppmw. In a Low-Temperature Shift Converter (LTSC) application, the methanol production is greater than that of an HTSC application. The formation of methanol is not just related to equilibrium for an LTSC but also to the catalyst characteristics and kinetics. Therefore, the catalyst vendor should be contacted in reference to calculating the expected amount of methanol from an LTSC application.

In the majority of hydrogen plants today, the process condensate is used as makeup water to the steam generation system of the plant. Typically, boiler feedwater makeup is mixed with the process condensate and

sent to a deaerator. The deaerator uses steam to strip the dissolved gases, namely O_2 and CO_2 , and the other contaminants from the boiler feedwater. These contaminants can be harmful to downstream equipment and boiler operation. These contaminants are then emitted to the atmosphere. Since there are large amounts of CO_2 , the type of deaerator for hydrogen plant use typically has a vertical stripping section consisting of either trays or packing located on top of the deaerator. To calculate the amount of each contaminant leaving the deaerator's stripping section, one can use the equations below.

Mole Fraction Remaining

$$\frac{(Lx_{\text{OUT}})}{(Lx_{\text{IN}})} = \frac{(S-1)}{(S^{n+1}-1)} \quad (24.9)$$

and Mole Fraction Stripped

$$\frac{(Gy_{\text{OUT}})}{(Lx_{\text{IN}})} = \frac{S(S^n-1)}{(S^{n+1}-1)}, \quad (24.10)$$

where G & L are Molar Flow Rates, S – Stripping Factor (KG/L), n – Number of Equilibrium Stages, K – Vapor-liquid distribution coefficient, ($y/x = H/P_T$).

As methanol emissions continue to be monitored more closely, there are some methods for reducing the methanol in the deaerator vent. The vent stream could be condensed and sent to the reformer or the steam system. Catalytic combustion could be used to reduce the methanol. A scrubber system could be added to remove the methanol. In some instances a condensate stripper is added instead of the deaerator to remove the ammonia, methanol, and other contaminants from the condensate. This system recycles the vent stream to the reformer as process steam and the bottoms are mixed with the incoming boiler feedwater makeup. However, this system adds considerable capital cost to a project.

24.4.3 Wastewater

The wastewater from a hydrogen plant typically consists of only the blowdown from the boiler system. The boiler feedwater that feeds the steam generation system has small amounts of impurities such as sodium, chlorides, silica, and organic carbons. These impurities will accumulate within the boiler system and create sludge, scaling of the boiler tubes, and possible carryover of solids into the process steam. Blowdown of the boiler water is performed to prevent these issues from affecting the operation of the steam system. The blowdown is typically sent to the sewer or the on-site waste treatment plant for treatment and disposal.

24.5 Monitoring Plant Performance

There are several areas of focus when monitoring the performance of a hydrogen plant. The first area of focus is the performance of the catalyst beds employed in the hydrogen plant. The Hydrotreater, which converts sulfur compounds to H_2S , should be checked periodically for pressure drop through the bed. The hydrotreating catalyst life is approximately 3 yr. If the catalyst bed's pressure drop exceeds design then it may be time to change the catalyst out due to catalyst degradation and activity loss.

The next typical catalyst bed in a hydrogen plant is the desulfurizer bed. The desulfurizer uses zinc oxide to remove traces of H_2S from the feed gas. The desulfurizer catalyst bed design is based on the loading of the sulfur compounds. Therefore, the gas exiting from the desulfurizer bed should be checked to ensure that the sulfur levels are below 0.1 ppmv. If the original design life of the catalyst bed is known, then periodic feedstock analysis can be used to forecast when the bed may require change out.

Since the reforming reaction constitutes the majority of the hydrogen production in the plant, it is important to monitor the reforming catalyst. The reforming catalyst is typically designed for a 5 yr life. Pressure drop measurements should be taken across the catalyst-filled tubes in the reformer. If the pressure drop increases as time goes by, this could be an indication that catalyst attrition or possible carbon formation on the catalyst could be taking place. The activity of the catalyst can be checked by comparing the outlet composition of the reformer to the expected composition at the design approach to equilibrium conditions. If the pressure drop increases or the activity has decreased, then it is probably time to change out the reforming catalyst.

The examination of the high-temperature shift catalyst is similar to that of the reforming catalyst. The catalyst life for the high-temperature shift catalyst is approximately 5 yr. Pressure drop readings should be taken to check for possible catalyst attrition. The outlet composition should be validated with the expected composition with the design approach to equilibrium conditions.

The pressure swing adsorption (PSA) system has a catalyst life of approximately 20 yr or equal to the expected plant life. However, hydrogen purity and recovery should be recorded periodically to watch for possible catalyst poisoning. The amount of nitrogen in the feedstock also has an effect on these two operating parameters and should be checked. A higher nitrogen content in the feed gas than design could lower the hydrogen recovery in the PSA unit.

The reformer tubes are one of the most important pieces of equipment in a hydrogen plant. These tubes are built from microalloyed materials in order to handle the extreme environment to which they are exposed. The industry standard for reformer tube design is for 100 000 h life. To ensure that the tubes will last the designed 100 000 h life, the reformer tube-wall temperature readings should be taken on a regular basis. An optical pyrometer is the instrument of choice for this task. In order to obtain the correct tube-wall temperature reading, the tube-wall and the furnace background should be measured for each tube reading. The background temperature is required to correct for background radiation. The equation below can be used to correct the tube-wall temperature readings (Please note that the temperature scale is Rankine). The emissivity on the pyrometer should be set to 1 before taking the readings.

$$T_t = \left[\frac{(T_{MT}^4 - (1 - e)T_{MB}^4)}{e} \right]^{1/4}, \quad (24.11)$$

where T_t is True Tube Temperature ($^{\circ}R$), T_{MT} is Measured Tube Temperature ($^{\circ}R$), T_{MB} is Measured Background Temperature ($^{\circ}R$), e is average furnace emissivity (typical = 0.82).

The maximum allowable tube stress will need to be calculated in order to calculate the actual reformer tube life. This is accomplished by using the Mean Diameter Formula given below.

$$S = \frac{PD_M}{2t_{MIN}}, \quad (24.12)$$

where S is tube stress (psi max), P is tube inlet pressure (psig), D_M is tube mean diameter = $(D_O + D_I)/2$, D_O is tube OD, as cast (in), D_I is tube ID = $D_O - 2t_{MIN} - 2CA$, CA is casting allowance (typically 1/32 in on outside wall, 0 in on inside wall), t_{MIN} is minimum sound wall (in).

The Larson–Miller equation correlates the stress-temperature to life of the tubes. The equations below are for Manaurite XM material tubes.

$$S = 0.145B \times 10^{(-0.0062P^2 + 0.2955P - 1.5426)} \quad (24.13)$$

$$P = T[22.96 + \log(t)] \times 10^{-3} \quad (24.14)$$

where S is minimum stress to rupture (ksi), B is ratio of minimum to average stress (typical temperature range, $B = 0.85$), P is Larson-Miller parameter (dimensionless), T is tube-wall temperature (K), t is tube life (hours).

If the measured temperature is less than design, then the reformer tubes should last their expected life. However, if the measured temperature is greater than the design temperature, then the reformer tube life will be shortened. If the actual life of the reformer tubes is below the expected life, then the operating conditions of the reformer should be further investigated.

The steam system is an area that requires constant attention to ensure proper operation of the hydrogen plant. If the steam quality decreases, it can lead to solids carryover from the steam drum. These solids will plate out in the feed preheat coil of the convection section and subsequently lead to an equipment failure and plant shutdown. To reduce the probability of an upset, the steam drum should be manually blown down on a regular basis to reduce the amount of dissolved solids and other impurities in the steam drum. Next, the boiler feedwater should be analyzed on a regular basis to ensure that the treatment it is receiving is adequate for the desired steam generation conditions.

Cooling water is generally used for the final trim cooling of the process gas before the hydrogen purification step. In most instances, the cooling water is considered to be a dirty medium. Therefore, it is recommended to develop a temperature profile of the cooling water side of the exchanger based on design data. Ad-

ditional temperature profiles should be developed based on data from the operation of the plant and compared to the original profile. This data can be used as a means to check for fouling of the cooling water side of the exchanger and improper heat transfer through the exchanger.

Another means of monitoring the performance of the hydrogen plant is to check the pressure drop through the entire plant. If the pressure drop is higher than design, then individual pieces of equipment should be checked for excess pressure drop. This may signify several things such as catalyst attrition, excessive exchanger fouling, or equipment failure.

The final method of checking the performance of the unit is to calculate the overall utility consumption of the plant and compare it to the design summary or previous summaries. The feed and fuel flows are typically converted to energy since their utility cost are typically on an energy basis (for example: MM Btu/hr LHV). These numbers as well as the other utility quantities are divided by the hydrogen product flow. This method allows for calculating the total price of hydrogen on a US\$/M SCF H₂ basis. Once the summary has been created, comparisons to earlier summaries and analysis of major cost areas can be investigated. The effects of process improvements can be evaluated on this basis.

24.6 Plant Performance Improvements

The most common method of improving plant profitability is to increase the capacity of the hydrogen plant. The plant design should be evaluated as to its capability to handle an increased load before this is attempted. The process design specifications should be retrieved on all of the relevant plant equipment and compared to the vendor's design specifications. If there are any significant differences between the two sets of specifications, investigation into the cause of the difference is warranted. From this comparison, a final set of equipment design data should be developed for each piece of equipment.

The operating data of the equipment should then be compared to the design capabilities of the equipment in order to set the available capacity increase for each piece of equipment. Compressors should be checked for capacity versus design flow, spillback design, inspection of valves, and motor requirements. The fans should be checked for operating versus design capacity, vane inspection, and motor requirements. The pumps should be checked for operating versus design capacity, inspection of screens and impellers, and motor requirements.

The next area of evaluation consists of the pressure profile of the plant. The operating pressure profile should be compared to the design pressure profile. Any significant differences should be investigated and possibly corrected. An acceptable capacity increase for the equipment should be used to set a proposed capacity increase for the plant. The pressure drop for this raised capacity case should be calculated and compared to design pressure profile. Depending on the results of this calculation, investigation into the available feed pressure may be warranted. Relief settings for the raised capacity case should be evaluated to ensure proper operation. Some pieces of equipment may have to be checked to determine if they can be re-rated for a higher operating pressure than design.

The reformer tubes will need to be evaluated as to their capability of handling an increase in capacity. Temperature readings should be taken at several plant capacity increments (50%, 75%, 100%). This data should be compared with the maximum design tube-wall temperature. If the tube-wall temperature is approaching the maximum design tube-wall temperature, there are several things that can be considered.

The catalyst vendor should be contacted about the possibility of a more active reforming catalyst. The burners could be revamped or replaced. The burner pressure drop should be monitored and compared to design data. The excess air used for the combustion should be checked to ensure proper operation. If the burners were to be replaced, it would affect firing capacity, flame pattern, and NO_x emissions. The reformer tube metallurgy should be checked to see if it could be upgraded. An upgrade in tube metallurgy would affect the tube ID and the design tube-wall temperature.

Most hydrogen plants utilize a PSA system for their hydrogen purification. This system should be checked for H_2 purity, and a corresponding H_2 recovery should be calculated. This data should be compared to the original design data of the unit. The cycle times should be compared to the design cycle time. To check the available capacity increase for the PSA unit, the adsorption time should be increased in small increments until the maximum permissible impurity breakthrough occurs. The cycle time should be adjusted and the H_2 recovery calculated. The purge time in this cycle should be compared with the design purge time. The additional purge time is a measure of the additional capacity that is available in the PSA unit. If the PSA unit is capacity limiting, then the following options should be considered: reduction of offgas drum back pressure, improvement of feed conditions, relaxation of purity specifications, setting unit on automatic purity control, change cycle (equalizations), adsorbent change out, or addition of additional vessels.

The reduction of the utility consumption of the plant is another method of improving plant performance. It is important to make certain that the plant is not using an excessive amount of utilities. The reformer is a key target area for this investigation. The burners should be checked to ensure that they are using the correct amount of excess air (typically 10%, 20% for heavier fuels). For example, if the burners were using 20% versus 10% excess air, this would translate to an approximate increase in reformer firing of 10%. Therefore, using the correct amount of excess air does not waste fuel. The bridge-wall temperature should also be checked. For every 20°F ($\approx 7^\circ\text{C}$) above the required bridge-wall temperature, there is a 1.5% increase in reformer firing. The bridge-wall temperature should be set at the temperature required to obtain the process outlet temperature that yields the proper CH_4 slip through the reformer. As discussed above, the PSA recovery should be maximized. For every 1% increase in recovery, there is an approximate saving of 0.5% of feed and fuel. The deaerator vent and steam system blowdowns should be checked. Excessive blowdown adds additional treating chemicals and boiler feedwater flow while reducing the export steam quantity.

Another option is to debottleneck an existing hydrogen plant by revamping or upgrading portions of it. However, these cases should be evaluated on a case-by-case basis as different sites have different utility and/or plot considerations. Some of the upgrades are discussed in Sect. 24.7.

24.7 Economics of Hydrogen Production

There is a growing focus in the refining industry on hydrogen capacity. Hydrogen is generally required for deep sulfur removal from hydrocarbon products. As sulfur restrictions on gasoline and diesel become increasingly stringent, the refining demand for hydrogen continues to grow.

By evaluating the hydrogen utilization in their facilities, refiners are coming to the realization that they need additional hydrogen supply. There are a number of options available to address this need. Refiners may be able to meet the increased demand by improving operations of their existing hydrogen plants. They may choose to separate hydrogen from waste or offgas streams or even purchase hydrogen from third parties. As an alternative, after careful technical and economic evaluation, they may conclude that the best solution to optimize the economic benefit to them over the longer term is to build a new hydrogen plant.

In recent years, many advances have been made in hydrogen plant technology. Substantial improvements have been incorporated into hydrogen plant design to significantly improve overall life cycle costs. On the basis of experience with hydrogen plant benchmarking, it has become clear that the optimum economic solution in some cases may be to replace an existing hydrogen plant with a new modern hydrogen plant.

There are a number of options available to refiners to meet the increase in hydrogen demand. Before deciding to proceed with any option, refiners should conduct a comprehensive technical and economic evaluation of their existing operations and evaluate the technical and economic benefits of the options available to them. The option that provides the optimum economic and operations benefits will be different for each situation and will depend on such things as the existing steam balance, the cost and availability of utilities,

plot limitations, and the condition of existing hydrogen plants.

The first option for refiners who are operating Old Style (Sect. 24.2.4) hydrogen plants is to consider ways to increase the capacity of these plants. Following an evaluation of the condition and efficiency of the existing plant, they may be able to effectively increase the capacity by either tightening up on operations or selectively upgrading portions of the old plant.

In many refineries, hydrogen is treated like a utility. There may not be much of a focus on the details of the actual production and the plants are sometimes operated *loose*. In this case, simple operational changes could significantly increase production and efficiency. Refiners could also debottleneck an existing hydrogen plant by revamping or upgrading portions of it. Debottlenecking options can also have a positive efficiency impact. Some of these potential upgrades may include:

- Replacing reformer tubes with upgraded metallurgy and thinner walls will allow for more throughput and a higher heat flux, which would increase capacity.
- Adding a Preformer would unload the primary reformer so capacity can be increased.
- Adding a Secondary Reformer would increase methane conversion, which increases capacity.
- Adding Combustion Air Preheat would lower the fuel requirement and potentially unload the waste heat recovery unit and fluegas fan, resulting in a capacity increase.
- Upgrading the CO₂ removal unit would minimize hydrogen loss in the Methanator, resulting in a potential capacity increase.
- Adding a PSA unit would decrease hydrogen production, but would typically produce more cost effective and higher purity hydrogen.

A second option is to separate hydrogen from a waste stream or an offgas stream that is currently being sent to fuel. This would typically require the addition of separation equipment and possibly some compression. In addition, separating hydrogen out of the fuel system will usually result in additional makeup fuel. This could change the heating value of the refinery fuel system and possibly have an impact on other fuel-burning equipment.

A third option is to buy hydrogen from a third party. Various industrial gas suppliers are willing to sell hydrogen to refiners either by pipeline or, depending on location, by a stand-alone plant. This option requires a minimal capital investment by the refiner but the delivered hydrogen will probably be more expensive per unit than if self-produced.

The last option is to build a new hydrogen plant. Building a Modern hydrogen plant is typically the most capital intensive of the options available. However, the capital investment could pay off if there is a significant gain in efficiency. Below we will analyze and compare the typical overall production cost of hydrogen between a Modern and an Old Style hydrogen plant.

24.7.1 Overall Hydrogen Production Cost

The most significant economic factor in evaluating options to increase hydrogen capacity is the overall production cost of hydrogen. The overall production cost can be estimated over the life of the hydrogen plant by using the different cost parameters of constructing, operating, and maintaining the hydrogen plant. This overall production cost reflects a complete picture of the hydrogen plant economics over the life of the plant.

The efficiency of producing hydrogen and by-products are very important in minimizing the production cost of hydrogen. Utility costs are the major operating cost in hydrogen production. Utilities typically include usage of feed, fuel, boiler feed water, power, and cooling water, and generation of export steam (steam is typically a by-product of the hydrogen production process). Of these, feed and fuel make up the largest portion of the utility costs. In addition, the credit for export steam can have a significant impact on utility costs, especially when refinery utility costs are favorable for steam production. The remainder of the utilities combined typically make up less than 10% of the total operating cost.

These utility costs, together with other economic parameters applicable to the plant being evaluated, can be incorporated into a cash flow model and the overall production costs of hydrogen can be evaluated. The other economic parameters include such things as capital cost, start-up cost, other operating costs (including catalyst replacement and tube replacement), and maintenance costs. From this model, the internal rate of return (IRR), net present value (NPV) at various rates of return, net cash flow, and a generated income statement can also be developed.

24.7.2 Overall Production Cost Comparisons

Building a new hydrogen plant is typically not the most appealing alternative to refiners. A new hydrogen plant requires a significant capital investment, and although hydrogen is required to support many of the refinery unit operations, it is generally not viewed as a direct *money maker*. However, once all factors are taken into account and a total production cost of hydrogen over the life of the plant is determined, the best economic solu-

tion may be replacing an Old Style hydrogen plant with a new Modern hydrogen plant. The following evaluation illustrates this potential.

24.7.3 Evaluation Basis

To demonstrate the economics of building a Modern hydrogen plant versus continuing to operate an Old Style plant, two representative plants each producing 90 MMSCFD of contained hydrogen from a natural gas feed will be compared. Natural gas will also be used for fuel, and both plants will export 600 psig superheated steam. The Old Style plant will consist of the major processing units described above and will produce hydrogen with a purity of 95%. Other parameters for the Old Style plant will be based on typical observed values. The Modern plant will consist of the major processing units described above and will produce hydrogen with a purity of 99.99%. The Modern plant design will be based on producing maximum export steam.

This evaluation could be done based on a variety of other plant configurations, but for demonstration purposes, this evaluation is limited to the plant types described. For comparison purposes, the cost of utilities will be based on the following:

- Natural Gas US\$4.00 per MMBtu (US\$3.79 per GJ)
- High pressure (HP) Steam US\$5.00 per 1000 lbs (US\$11.02 per ton)
- Boiler Feedwater US\$0.50 per 1000 lbs (US\$1.10 per ton)
- Power US\$0.05 per kWh
- Cooling Water US\$0.10 per 1000 gals (US\$0.026 per m³).

24.7.4 Utilities

As previously discussed, the utility costs of a hydrogen plant are among the most important economic factors in determining the overall production cost of hydrogen. Simulation models were built for both the Old Style and Modern plants to calculate utility costs. The Old Style plant utilities are based on a simulation model built to reflect typical plant performance. The Modern plant utilities are based on a simulation model for the design of a typical new plant. Table 24.10 shows the utilities and utility cost of hydrogen for each plant.

Table 24.10 clearly illustrates a lower total utility cost for producing hydrogen in the Modern Plant than in the Old Style plant. The Modern plant produces hydrogen at a rate of US\$1.409 per MSCF of contained hydrogen, while the Old Style plant produces at a rate of US\$1.908 per MSCF of contained hydrogen. For

a plant producing 90 MMSCFD of contained hydrogen, this difference results in annual utility savings for a Modern plant of US\$16.4 MM. Of course, the utility cost alone does not complete the picture of the overall production cost of hydrogen. We must also evaluate a number of other economic and operating factors.

24.7.5 Capital Cost

Capital must be invested to build the new plant in order to capture the utility savings of the Modern plant. A total capital investment of about US\$55 MM would be expected for a new typical 90 MM SCFD hydrogen plant. This approximate installed sales price is based on inside battery limits, natural gas feed, no compression, no buildings, no water treatment units, no SCRs or MCCs, industry engineering standards, and delivery to the US gulf coast. For purposes of comparison, no capital investment is considered for the Old Style plant.

24.7.6 Life of the Plant Economics

A cash flow economic model can be generated using the utility costs developed for each plant, the capital cost required for the Modern plant, as well as a number of other economic factors. These other economic factors, along with their associated values are listed below:

- New Plant construction time – 2 years
- Escalation Rate 1.5% for all feed, product, and utilities
- Labor – two operators per shift
- Overhead – 50% of labor
- Maintenance – 2% of plant cost per year
- Other Misc – 1% of plant cost per year
- Catalyst costs accrued in year of change out
- Reformer tube replacement – every 10 years
- On Stream Time – 98.5%
- Working Capital – 45 days
- Debt Level – Borrow 75% for New Plant
- Cost of Capital – 8%
- Debt Length – 7 years
- Depreciation Life (of Capital Cost) – 10 years
- Tax Rate – 34%
- Project Life – 25 years (includes 2 years of construction)
- Internal Rate of Return – 0% to obtain actual cost of hydrogen production.

The resulting average overall production cost of hydrogen, calculated for the life of the plant, is shown in Table 24.11.

The evaluation shows that taking all relevant economic factors into consideration, the overall production

Table 24.10 Utility cost of hydrogen production

Utilities per 1000 SCF contained hydrogen		
	Old Style	Modern
Natural gas feed (MMBtu LHV)	0.275	0.317
Natural gas fuel (MMBtu LHV)	0.200	0.126
Total feed + fuel (MMBtu LHV)	0.475	0.443
HP export steam (lbs)	20	90
Boiler feedwater (lbs)	45	120
Power (kWh)	0.65	0.52
Cooling water (gal)	530	8
Cost (US\$) per 1000 SCF contained hydrogen		
	Old Style	Modern
Natural gas feed (MMBtu LHV)	1.100	1.268
Natural gas fuel (MMBtu LHV)	0.800	0.504
Total feed + fuel (MMBtu LHV)	1.900	1.772
HP export steam (lbs)	− 0.100	− 0.450
Boiler feedwater (lbs)	0.023	0.060
Power (kWh)	0.033	0.026
Cooling water (gal)	0.053	0.001
Total utility cost (US\$)	1.908	1.409
Utilities per 1000 NCM contained hydrogen		
	Old Style	Modern
Natural gas feed (GJ LHV)	10.83	12.48
Natural gas fuel (GJ LHV)	7.87	4.96
Total feed + fuel (GJ LHV)	18.70	17.44
HP export steam (kg)	338.87	1524.90
Boiler feedwater (kg)	762.45	2033.19
Power (kWh)	24.26	19.41
Cooling water (m ³)	74.88	1.13
Cost (US\$) per 1000 NCM contained hydrogen		
	Old Style	Modern
Natural gas feed @ US\$3.79/GJ LHV	41.05	47.32
Natural gas fuel @ US\$3.79/GJ LHV	29.86	18.81
Total feed + fuel @ US\$3.79/GJ LHV	70.91	66.13
HP export steam @ −US\$11.02/tonne	− 3.74	− 16.81
Boiler feedwater @ US\$1.10/tonne	0.84	2.24
Power @ US\$0.05/kWh	1.21	0.97
Cooling water @ US\$0.0264/m ²	1.98	0.03
Total utility cost (US\$)	71.204	52.563

Table 24.11 Overall production cost of hydrogen

	Old Style	Modern
Plant capacity (MM SCFD) contained	90	90
Plant capacity (NCMH) contained	100 482	100 482
Capital cost (MM US\$)	–	55
Average H ₂ production cost (US\$/1000 SCF)	1.996	1.602
Average H ₂ production cost (US\$/1000 NCM)	74.491	59.787
Average H ₂ production cost (US\$/yr)	65 568 600	52 625 700
Average annual production cost savings (US\$)	–	12 942 900

cost of hydrogen is lower for the Modern plant. The Modern plant produces hydrogen at a rate of US\$1.602 per M SCF of contained hydrogen while the Old Style plant produces hydrogen at US\$1.996 per M SCF of contained hydrogen. This lower overall production cost

results in an annual savings for the Modern plant of about US\$12.9 MM per year. This evaluation proves that for the cases analyzed, it is economically feasible and potentially advantageous to build a new, more efficient hydrogen plant.

24.7.7 Sensitivity to Economic Variables

Economic parameters for each refinery are different. The major parameters that can significantly alter these results are the efficiency of the existing plant, the feed and fuel price, and the export steam credit. The efficiency of the existing plant can span a wide range and is specific to each plant. For the remaining evaluations, the Old Style plant utilities will be held constant. The overall production cost of hydrogen will be analyzed as a function of the other two major factors, feed and fuel price and export steam credit.

24.7.8 Feed and Fuel Price

The cost of feed and fuel is typically the largest component of the overall production cost of hydrogen. Feed and fuel usually account for more than 80% of the total before the steam credit is taken. The overall operating cost changes significantly as the natural gas price varies. Figure 24.10 shows the effect of varying the natural gas price

price. For this evaluation, the export steam credit to natural gas price ratio was held constant.

As the price of natural gas increases, the Modern plant becomes more favorable. This is due to the overall feed and fuel efficiency advantage of the Modern plant. For example, if the natural gas price were changed from US\$4 to US\$8 per MMBtu (double the base case credit), the overall production cost would increase by US\$1.326 per MSCF of hydrogen for the Modern plant and US\$1.804 for the Old Style plant. The higher natural gas price would increase the average annual savings for the Modern plant from US\$12.9 MM to US\$28.6 MM.

24.7.9 Export Steam Credit

The export steam credit also has a significant effect on the overall production cost. The value a refinery places on steam depends on utility factors and the existing steam balance in the refinery. For example, during the winter, steam tracing is generally used more heavily

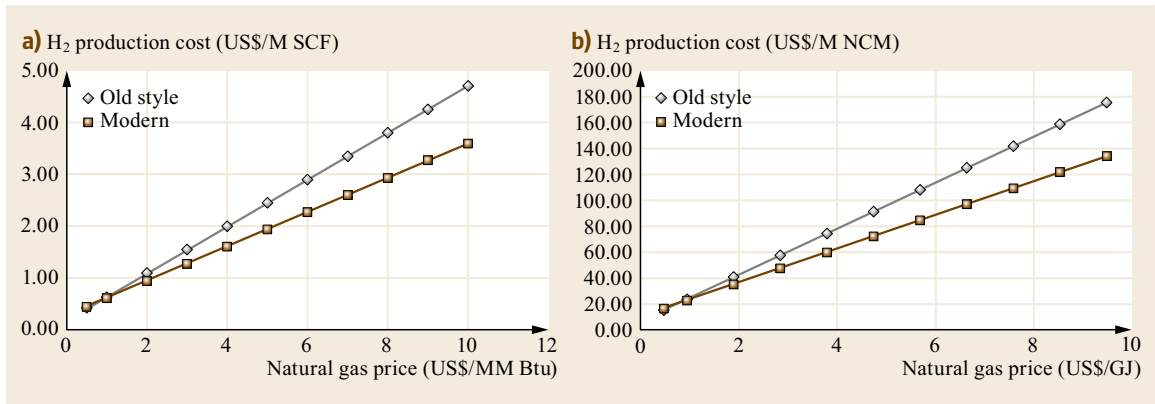


Fig. 24.10a,b H₂ production versus natural gas price

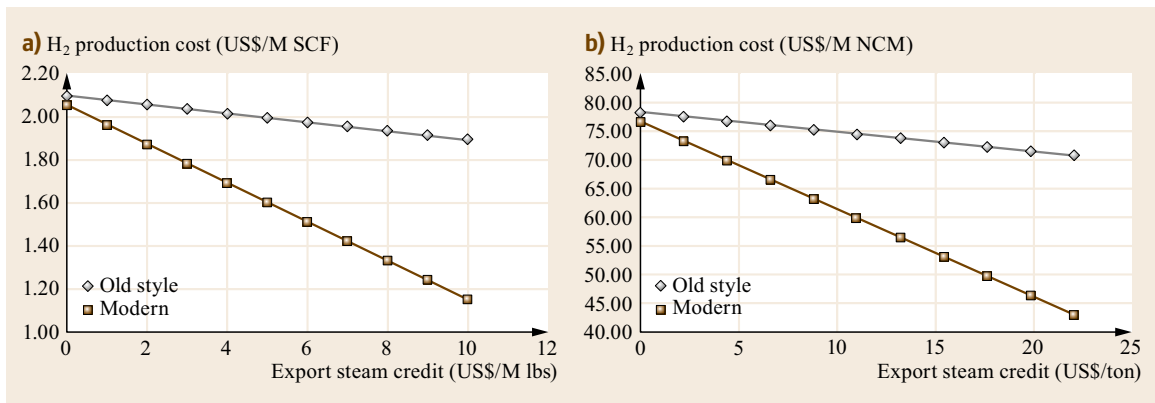


Fig. 24.11a,b H₂ production cost versus steam credit

and the value of steam could be higher than average. Conversely, in the summer, when less steam tracing may be utilized, steam may have a lower than average value. Modern hydrogen plants typically export much more steam due to the fact that they are more efficient and have a CO₂ removal regeneration requirement. Figure 24.11 shows the effect of varying the export steam credit. For this evaluation, the natural gas price remained the same.

24.8 Conclusion

Refiners have a number of different options to consider in addressing the demand for additional hydrogen. A comprehensive technical and economic evaluation of existing operations is required to determine the optimum solution for each specific application. The optimum solution for each refinery will be different due to site-specific items such as the cost and availability of utilities, plot limitations, refinery steam balance, emission requirements, and the condition of any existing hydrogen plants. The rising cost of utilities, and particularly natural gas, has placed a premium on the overall

As the export steam credit increases, the economics for the Modern plant become more favorable. For example, if the export steam credit were changed from US\$5 to US\$10 per Mlbs (double the base case credit), the overall production cost would drop by US\$0.450 per MSCF of hydrogen for the Modern plant and US\$0.100 for the Old Style plant. The higher steam credit would increase the average annual savings for the Modern plant from US\$12.9 MM to US\$24.4 MM.

plant efficiency. Therefore, the overall plant efficiency has not only become a key factor in determining the economics of what option to pursue, but also in the performance enhancement of existing hydrogen plants.

Today's Modern hydrogen plants take advantage of numerous technological improvements and offer a much more efficient plant with a lower overall life cycle cost. Once technical and economic evaluations are performed, it should not be surprising that the most economically attractive and most feasible approach may be to build a new hydrogen plant.

24.9 Further Reading

- B.M. Tindall, D.L. King: Design steam reformers for hydrogen production, *Hydrocarbon Process.* **73**(7), 69–75 (1994)
- B.M. Tindall, M.A. Crews: Alternative technologies to steam-methane reforming, *Hydrocarbon Process.* **74**(11), 75–84 (1995)
- D.L. King, C.E. Bochow: What should and owner-operator know when choosing an SMR/PSA plant, *Hydrocarbon Process.* **79**(5), 39–48 (2000)
- K. Hoitsma, P. Snelgrove: Effective reformer design and erection, *World Refin.* **July/August**, 24–28 (2002)
- B.M. Tindall, M.A. Crews: Economics of export steam for hydrogen plants, *Hydrocarbon Eng.* **8**(2), 39–41 (2003)
- C. Boyce, R. Ritter, M.A. Crews: Is it time for a new hydrogen plant, *Hydrocarbon Eng.* **9**(2), 68–70 (2004)
- W.S. Ernst, S. Venables, P.S. Christensen, A.C. Berthelsen: Push syngas production limits, *Hydrocarbon Process.* **79**(3), 100-C (2000)
- H. de Wet, G. Shaw, F. Hohmann: Commissioning of world's largest oxygen blown secondary reformers. In: *Ammonia Plant Safety & Related Facilities*, Vol. 35, (American Institute of Chemical Engineers, New York 1995) pp. 315–335
- I. Dybkjaer: Tubular reforming and autothermal reforming of natural gas, *Fuel Process. Technol.* **42**, 85–107 (1995)
- T.S. Christensen, I.L. Primdahl: Improve syngas production using autothermal reforming, *Hydrocarbon Process.* **73**(3), 39–46 (1994)
- A. Lowson, I. Primdahl, D. Smith, S.-I. Wang: Carbon Monoxide Production by Oxygen Reforming, Air Products and Chemicals, Inc., 2-21 1475H (1990)
- F.C. Jahnke, M. Ishikawa, T. Rathbone: High efficiency IGCC using advanced turbine, air separation unit, and gasification technology, *Proc. 1998 Gasif. Technol. Conf.* (1998), <http://www.gasification-syngas.org/uploads/eventLibrary/gtc9814p.pdf>
- P.S. Wallace, M.K. Anderson, A.I. Rodarte, W.E. Preston: Heavy oil upgrading by the separation and gasification of asphaltenes, *Proc. 1998 Gasif. Technol. Conf.* (1998), <http://www.gasification-syngas.org/uploads/eventLibrary/gtc9817p.pdf>

- W. Liebner, N. Hauser: *The Shell Oil Gasification Process (SGP) and its Application for Production of Clean Power* (Lurgi and Shell 1990)
- T.D. Corporation: *Texaco Gasification Process for Gaseous or Liquid Feedstocks* (Texaco Image Services, Tulsa 1993)
- D.L. Heaven: Gasification converts a variety of problem feedstocks and wastes, *Oil Gas J.* **May**, 49–54 (1996)
- W.F. Fong, L.F. O’Keefe: Syngas generation from natural gas utilizing the Texaco gasification process, Proc. 1996 NPRA Annu. Meet. (1996), paper AM-96-68
- R.J. Stellaccio: Partial oxidation process for slurries of solid fuel, U.S. Patent 4 443 230 (1984)
- N. Hauser, C. Higman: The use of the Shell gasification process (SGP) in refining heavy crude and tar sands, Proc. 6th UNITAR Int’l. Conf. Heavy Crude Tar Sands, Houston (1995)
- Lurgi Corporation: *Integrated Gasification Combined Cycle Process (IGCC)* (1995)
- C. Jigman: Perspectives and experience with partial oxidation of heavy residues, *Tale Ronde – Assoc. Francaise des Tech. du Petrole*, Paris (1994), <http://www.higman.de/gasification/papers/paris.pdf>
- C.L. Reed, C.J. Kuhre: Make syn gas by partial oxidation, *Hydrocarbon Process.* **58**(9), 191–194 (1979)
- P.E.J. Abbott: *Advanced Steam Reforming Technology in GTL Flowsheets*, Syntex (ICI) (1999)
- T. Hicks: A Decade of Gas Heated Reforming, *FINDS*, Vol. XI, Number 3 (1996)
- J.B. Abbishaw, B.J. Cromarty: The use of advanced steam reforming technology for hydrogen production, Proc. 1996 NPRA Annu. Meet. (1996), paper AM-96-62
- P.W. Farnell: Commissioning and operation of ICI Katalco’s leading concept methanol process, Proc. *AIChE Ammon. Saf. Symp.* (1995)
- P.W. Farnell: Commissioning/operation of leading concept methanol process. In: *Ammonia Plant Safety & Related Facilities*, Vol. 36, (AIChE, New York 1996) pp. 268–277
- E. Goudappel, A.H. Herfkens, T. Beishuizen: Gas Turbines for crude oil heating and cogeneration, *PTQ 2000 Q2*, pp. 99–109
- G. Shahani, L. Garodz, B. Baade, K. Murphy, P. Sharma: Hydrogen and utility supply optimization, *Hydrocarbon Process.* **77**(9), 143–150 (1998)
- D. Hairston: Hail hydrogen, *Chem. Eng.* **103**(2), 59–62 (1996)
- P.W. Farnell: Investigation and resolution of a secondary reformer burner failure, Proc. 45th Annu. Saf. Ammon. Plants Relat. Facil. Symp. (2000), Paper no. 1D
- G.H. Shahani, H.H. Gunardson, N.C. Easterbrook: Consider oxygen for hydrocarbon oxidations, *Chem. Eng. Prog.* **92**(11), 66–71 (1996)
- C.S. Jung, K.K. Noh, S. Yi, J.S. Kim, H.K. Song, J.C. Hyun: MPC improves reformer control, *Hydrocarbon Process.* **74**(4), 115–122 (1995)
- W.F. Baade, N. Patel, R. Jordan, S. Sekhri: Integrated hydrogen supply-extend your refinery’s enterprise, Proc. NPRA 2001 Annu. Meet. (2001), paper AM-01-19
- M.D. Grant, N.R. Udengaard, R. Vannby, C.P. Cavote: New advanced hydrogen plant in California refinery by the Topsoe process, Proc. NPRA 2001 Annu. Meet. (2001), paper AM-01-27
- Howard, Weil, Labouisse, Friedrichs Inc., Fischer-Tropsch Technology: *GAS-TO-LIQUIDS, SOLIDS-TO-LIQUIDS, LIQUIDS-TO-LIQUIDS* (1998)
- D. Sanfilippo, E. Micheli, I. Miracca; L. Tagliabue: Oxygenated Synfuels from Natural Gas, *PTQ 1998 Q2*, pp. 87–95
- J.J. Barba, J. Hemmings, T.C. Bailey, N. Horne: Advances in hydrogen production technology: The options available, *Hydrocarbon Eng.* **3**(1), 48–54 (1997/98)
- I. Dybkjaer, S.W. Madsen: Advanced reforming technologies for hydrogen production, *Hydrocarbon Eng.* **3**(1), 56–65 (1997/98)
- P.L. DaPrato, H.H. Gunardson: Selection of optimum technology for CO rich syngas, *Hydrocarbon Eng.* **September/October**, 34–40 (1996)
- G.J. Hutchings, J.R.H. Ross, S.K. Kunchal: *Methane Conversion* (1994–97) pp. 1–81
- ICI Group: *ICI Catalysts for Steam Reforming Naphtha*, ICI Group 72W/033/1/CAT46, pp. 1–19, 46. Series
- F.C. Brown: *Alternative Uses for Methanol Plants*, *PTQ 2000 Q2*, pp. 83–91
- T. Mii, K. Hirotsu: Economics of a World Class Methanol Plant, *PTQ 2000 Q2*, pp. 127–133
- J. Carstensen: Reduce methanol formation in your hydrogen plant, *Hydrocarbon Process.* **77**(3), 100–C (1998)
- J.R. LeBlanc, R.V. Schneider III, R.B. Strait: *Production of Methanol* (Marcel Dekker, New York 1994) pp. 51–132
- S.B. Parks, C.M. Schillmoller: Improve alloy selection for ammonia furnaces, *Hydrocarbon Process.* **76**(10), 93–98 (1997)
- B. Cromarty: Effective steam reforming of mixed and heavy hydrocarbon feedstocks for production of hydrogen, Proc. NPRA 1995 Annu. Meet. (1995)

- R.P. Martin: Nitrogen oxide formation and reduction in steam reformers, Proc. Int. Fertilizer Ind. Assoc. Conf. (1994)
- L. Clark: Controlling NO_x, Posted on <http://www.JohnstonBurner.com>, April 1, 2002, article no longer posted online
- A. Garg: Reducing NO_x from fired heaters and boilers, Proc. Chem. Eng. Expo (2000), paper ESL-IE-00-04-46
- R.G. Kunz, D.D. Smith, N.M. Patel, G.P. Thompson, G.S. Patrick, Air Products and Chemicals, Inc. Control NO_x from gas-fired hydrogen reformer furnaces, Proc. NPRA Annu. Meet. (1992), AM-92-56
- Yokogawa: Boiler Blowdown, Analytical-SIC4900-02, Posted on <http://www.Yokogawa.com>
- G. Harrell: Boiler blowdown energy recovery, Energy Eng. **101**(5), 32–42 (2005)

Hydrogen Ne

25. Hydrogen Network Optimization

Nick Hallale, Ian Moore, Dennis Vauk, Paul R. Robinson

Plantwide systems impact every process unit in a petroleum refinery. All units require electrical power, water, steam and instrument air. Units with fired heaters burn fuel oil or fuel gas from a common pool. Many units require hydrogen and most produce offgas streams, which are collected and treated in common facilities. In addition to methane and other light hydrocarbons, offgas may contain H₂ and toxic H₂S. Most modern refineries can benefit from hydrogen recovery and purification. Keeping hydrogen out of fuel gas is beneficial for many reasons. Recovery decreases the required amount of on-purpose hydrogen. Hydrogen burns hotter than other gases, so it raises the temperature of fuel gas combustion, which can limit fired heaters constrained by tube temperature limits. Hydrogen network optimization is more complex than other utility optimization efforts, because in addition to flow and pressure, one must consider the impact of gas composition on the units to which hydrogen gas might be sent. The benefits of hydrogen network optimization with the technology described in this chapter range from US\$ 1 mil-

25.1	Background	817
25.1.1	Hydrogen Production	818
25.1.2	Other Hydrogen Sources	818
25.1.3	Hydrogen Purification and Recovery	818
25.1.4	Hydrogen Consumption and Losses	818
25.2	Assets and Liabilities	819
25.3	It's All About Balance	820
25.4	Put Needs Ahead of Wants	821
25.5	Beyond Pinch	825
25.5.1	Multicomponent Methodology	825
25.5.2	Hydrogen Network Optimization	826
25.6	Investing versus Saving	828
25.7	Conclusion	830
	References	831

lion per year for low- or no-cost recovery and purification projects to more than US\$ 15 million per year for modest-investment projects, with payback times measured in months.

25.1 Background

Plantwide systems impact every process unit in a petroleum refinery. To one extent or another, all units require electrical power, water and steam. Units with fired heaters burn fuel oil or fuel gas from a common pool. Many require hydrogen and most produce offgas streams, which are collected and treated in common facilities. Optimizing plantwide hydrogen networks can provide considerable benefits, ranging from US\$ 1 million per year for low- or no-cost recovery and purification projects [25.1, 2] to more than US\$ 15 million per year for modest-investment projects with paybacks measured in months [25.3].

These days, you can't be involved in the oil refining industry without coming across something on hydrogen management. However, most articles and presentations follow the same route, namely discussing

stricter sulfur and aromatics specifications, such as Euro V and perhaps the need to upgrade heavier oil. They then move on to say that more hydroconversion will be required. The conclusion? Refineries are going to need more hydrogen. But are they telling the refiners anything they didn't already know? An obvious option, of course, is to build or revamp a hydrogen plant, or buy more hydrogen from an offsite supplier in the future.

This chapter aims to be different. Instead of focusing on the problems, we will look at the opportunities. The intention is to get refiners thinking of their hydrogen as an asset not a liability.

Before proceeding, here is some background information on hydrogen production, purification and consumption in the petroleum processing industry.

25.1.1 Hydrogen Production

- *Catalytic reforming* converts treated heavy naphtha into aromatics while generating hydrogen. Hydrogen purities range from 75–90 vol. %.
- *Steam-methane reforming* (SMR) converts mixtures of steam and light hydrocarbon gases into hydrogen and CO₂ via the water-gas shift reaction. Product hydrogen may contain traces of CO and, depending on the process, 0.0001–4 vol. % CH₄.
- *Partial oxidation* (POX) produces CO and H₂ from natural gas or heavier feeds, such as vacuum residue or coal. POX does not require a catalyst or external steam. Design and operation can be varied to maximize production of hydrogen or synthesis gas. Chemicals are manufactured from the latter. Co-generation (*co-gen*) POX plants also generate steam for power production.
- *Olefin production plants*, also known as steam crackers, convert a wide variety of feeds, ranging from ethane to unconverted oil from hydrocrackers, into ethylene, propylene, higher olefins and aromatics. Hydrogen is a by-product, which can be consumed in the plant or exported. The hydrogen stream may contain around 4% CH₄.
- *Chlorine plants* generate hydrogen and chlorine from aqueous hydrochloric acid. The hydrogen may contain unwieldy amounts of Cl₂, which must be removed before the hydrogen is exported.
- *Lean oil recovery* (LOR) recovers C₃–C₆ hydrocarbons, mostly C₃–C₄, from offgas streams. The hydrocarbon-rich oil goes to a stripper, where the hydrocarbons are covered. LOR is one of the most cost-effective hydrogen purification units.
- *Pressure-swing adsorption* (PSA) prepares hydrogen with 99.99% purity, recovering 75–90% of the hydrogen in the feed gas. Modern SMR units include a PSA. In newer units, pressure-swing adsorption removes nearly all contaminants, yielding a product containing 99.99% hydrogen. A PSA unit employs a collection of solid adsorbents – molecular sieves, activated carbons, silica gels and activated aluminas. For carbon, silica and alumina, separation is due to their differential tendency to adsorb different gases. PSA cycles include pressurization, depressurization and purging. The rejected gas, a low-Btu mixture containing methane, CO and CO₂, is burned to provide some preheat duty.
- *Membrane units* employ semipermeable membranes to purify hydrogen, providing hydrogen with 85–98% purity, typically 95%. H₂ recovery ranges from 80 to 99%, typically 90%. The driving force is pressure differential across the membrane. There is a tradeoff between H₂ recovery and product purity. Higher recovery is associated with lower purity and vice versa.
- *Cold box* units can be designed to separate H₂ and CH₄ from other gases, to separate H₂ and N₂ from CO, etc., at cryogenic temperatures.

25.1.2 Other Hydrogen Sources

- *Purge streams from hydrogen consumers* often contain recoverable hydrogen. Hydrogen may be purged to manage the purity of recycle gas, or improve operability, or occasionally for pressure control.
- *Wet gas from cracking units* contains significant amounts of hydrogen. In a few studies, we saw that the fluid catalytic cracking (FCC) produced nearly as much hydrogen as the catalytic reformer. But the economics of hydrogen recovery were poor, due to the low pressure of the stream – recovery would have required an expensive compressor – and contaminants such as olefins and H₂S.

25.1.3 Hydrogen Purification and Recovery

- *Amine units (scrubbers)* remove H₂S (and in certain instances CO₂) from offgas streams and transport the H₂S to a sulfur recovery plant. Scrubbed gases often contain recoverable hydrogen. Hydrogen may be purged to manage the purity of recycle

- gas, or improve operability, or occasionally for pressure control. Scrubbed gas contains < 20 ppm H₂S.

Table 25.1 provides a rough comparison between PSA, membrane and cold-box technology for hydrogen purification.

25.1.4 Hydrogen Consumption and Losses

- *Hydroprocessing* units – hydrotreaters and hydrocrackers – consume hydrogen chemically.
- *Isomerization* units consume less hydrogen – just enough to keep the catalysts clean.
- *Entrainment and dissolution* losses occur in flash drums, which reduce the pressure of process fluids. Flash-drum overhead vapors are recycled and/or cooled and flashed again. Flash-drum liquids contain dissolved or entrained hydrogen, which eventually is stripped away at low pressure. Stripper hydrogen usually ends up in the fuel gas system.
- *Purging to fuel gas* accounts for most of the hydrogen lost in refineries. Purging can be intentional or unintentional. Unintentional purging can be surprisingly significant.

Table 25.1 Comparison of common hydrogen purification processes

Variable	PSA	Membrane	Cold box
H ₂ product purity	> 99.9%	85–95%	90–99%
H ₂ recovery	75–90%	80–90%	98–99%
H ₂ product pressure	10 psi less than feed	200–1400 psi less than feed	Design variable
Feed H ₂ content	> 40 vol. %	> 30 vol. %	> 20 vol. %
Feed pressure	250–900 psig	Up to 2500 psig	Design variable
Pretreatment	Liquids removal	Liquids removal	H ₂ O, H ₂ S, CO ₂ removal
Modular?	Yes	Yes	No

Speaking of losses: during hydrogen network optimization studies, we talked with people who believed that hydrogen leaks are common, significant and undetectable. This is simply not true. The auto-ignition range

for hydrogen in air is wide – from 18.3 to 59 vol. % at standard conditions – wider by far than the range for any other pure substance. Hydrogen leaks – even small leaks – cause fires.

25.2 Assets and Liabilities

As we will show, refiners will never get the most value from their hydrogen unless they have the correct view of it. For the most part, refiners tend to view hydrogen as a necessary evil – often expensive – that has to be supplied in order for them to operate, just like fuel, electricity and water. In other words, it is a liability.

Hydrogen – if properly managed – can be an asset, something that *makes* money for the refinery. Just as there are good and bad investments, there are good and bad ways to use hydrogen in a refinery. The secret is in finding the good ways. To do this requires a willingness to question conventional wisdom and to take a wider view of the issues. This chapter will discuss some of the important tools that will help to do this. It will also discuss some of the lessons learned from studies and industrial projects conducted by AspenTech and Air Liquide as part of their alliance called PRO-EN Services [25.4].

Refineries generally fit into one of three situations with respect to hydrogen:

Type 1: Hydrogen long: The refinery has an excess of hydrogen, which is routed to the fuel gas system. Refinery operations are not constrained by hydrogen. The price of hydrogen is based on its fuel gas value. Direct pressure-control let-downs to fuel gas have no economic penalty. In process units, high-pressure purge rates can be increased to increase hydrogen partial pressure in reactors without penalty. In some cases, catalytic reformer hydrogen is the only source of hydrogen supply.

Type 2: Hydrogen short: The refinery often needs more hydrogen. In locales where diesel is preferred over gasoline, the catalytic reformer acts as the *swing* hydrogen producer. Refinery operations and profitability are constrained by hydrogen. Key process units *compete* for hydrogen, which is priced in the refinery linear pro-

gram (LP) model based on plantwide profitability (e.g., gasoline over-production). Direct pressure-control let-downs have a high economic penalty. In process units, high-pressure purges are minimized, reducing hydrogen partial pressure in the reactors. In these cases, catalytic reformer hydrogen may still be the only source of hydrogen supply, although Type 2 also applies when on-purpose generation or import capacity is limited and operating at maximum.

Type 3: Hydrogen available on demand: The refinery can meet changes in hydrogen demand through *on-purpose* hydrogen production (e.g., with an SMR) or through external import. These are the refinery *swing* hydrogen producers. Refinery operations are not constrained by hydrogen. Hydrogen is priced based on its marginal production cost or import value. Direct pressure control letdowns have an economic penalty based on the value of hydrogen as a reactant in process units relative to its value as fuel. In process units, high-pressure purge rates are optimized to balance the value of higher hydrogen partial pressures (better yields, increased capacity, longer catalyst life) against the cost of purge losses. The value of hydrogen depends on whether or not the cost of capital is included in the price. For a refinery that has pre-invested in a hydrogen plant, the marginal production cost could be 500 €/t (2003 prices, which were considerably higher than present prices in most locales). If hydrogen is imported from an external supplier, the cost is more likely to approach 900 €/t.

Most refiners have completed the journey from type 1 to type 2. Larger and more profitable refineries are developing and implementing plans that take them to type 3, while a small number may choose to stay within type 2 because major new investment simply cannot be justified.

25.3 It's All About Balance

Accountants talk about balance sheets. Chemical engineers talk about mass balances. The principle is the same: what goes in must be accounted for. When we are dealing with hydrogen systems, the total amount of hydrogen produced and/or supplied must equal the total hydrogen that is chemically consumed, exported, burned as fuel or flared. Unfortunately, it is very rare to find a refinery where all hydrogen is accounted for. There is usually a poor hydrogen balance – poor not in reality but on paper – to begin with. Streams, flow rates and compositions are often not measured, and when they are the data may contain significant inconsistencies. In many cases, large imbalances are often accepted and attributed to *leaks*, *distribution losses*, *meter error* and *unaccounted flow*. If actual currency were involved, the accountants would probably use less euphemistic terms, such as *embezzlement*, *fraud*, *misappropriation* and *theft*. If we take the view that hydrogen is a valuable asset, not having a decent hydrogen balance is tantamount to throwing money away or letting someone steal it. It has been our experience that significant benefits – hundreds of thousands of dollars or more per year – can be achieved by examining the hydrogen balance and finding no-cost *housekeeping* improvements.

Simple as this may sound, it can only be realized by understanding the overall hydrogen system and this in turn needs systematic analysis and modeling capabilities.

To give an example, we performed a hydrogen system study for a US refinery, in which the hydrogen generated by its two catalytic reformers is supplemented with purchased hydrogen. Flow rate and composition data were collected from the refinery and used to set up a flow sheet balance with surprising results. We found that hydrogen worth \$2 million per year was being lost to flare and fuel gas through three specific areas, one of which was a leaky valve. We also found other opportunities, including reducing the amount of hydrogen purged for pressure control and avoiding the needless recompression of rather large gas streams.

So what is needed to set up a hydrogen balance? Firstly, flow rates, compositions and pressures must be determined at certain key points in the hydrogen system. Flow diagrams of the hydrogen-consuming processes are also needed so that reactor and separator configurations as well as recycle locations can be determined.

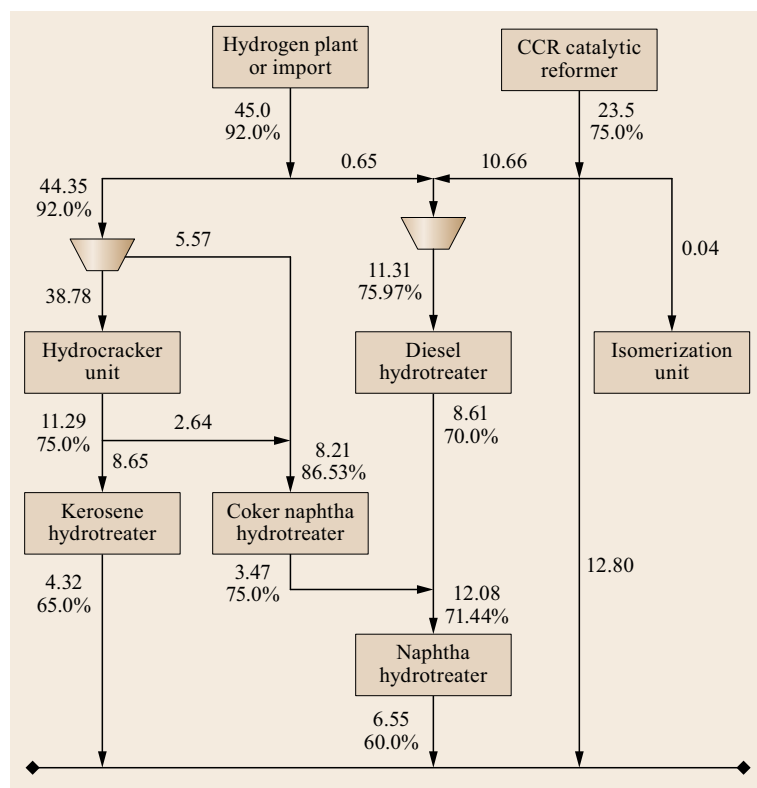


Fig. 25.1 A typical refinery H₂ balance (flows in million standard cubic feet per day (MMSCFD), H₂ purity in mol%)

Secondly, models of the consumers are required. These models need not be totally rigorous ones because configuring the models might take far too long in the early stages of a project. However, they should be sufficiently detailed to capture the important operating features of the units as well as to predict their performance. AspenTech developed such models using software that generates fit-for-purpose simplified models for reactors, flash drums and separation columns, which can be used as building blocks for the entire hydrogen network.

Thirdly, data correction and reconciliation tools are required. During this process, many refiners are surprised to discover that their hydrogen-system flow meter readings, if properly corrected, aren't so bad after all. Think of currency exchange rates. No semidecent accountant would try to convert South African rands into US dollars at the exchange rate used in the 1970s. However, it is surprising to see how often people are happy to trust flow meters calibrated with molecular weights that are now quite different from present op-

eration. Because the molecular weight of hydrogen is so low, small changes in stream composition can affect the stream molecular weight significantly. For example, a mixture consisting of 99% hydrogen and only 1% ethane has a molecular weight 14% greater than that of pure hydrogen. Refiners typically correct flow meter readings for temperature and pressure, but not for composition. In other words, if hydrogen were currency, they would be using outdated exchange rates. The software mentioned above can automatically correct measured stream flow rates for deviations from the calibration point. It can also carry out a data reconciliation whereby the user can enter whatever data are available and then specify how much confidence he or she has in each value. For example, a flow rate can be an accurate measurement (within 5%), an accurate estimate (within 20%), a rough estimate (within 50%) or a guess (within 500%). The software will then reconcile the values to achieve a balance while staying within the confidence bounds. Figure 25.1 shows what a completed hydrogen system balance might look like.

25.4 Put Needs Ahead of Wants

We believe that refiners should question whether certain units actually need to be fed with hydrogen of very high purity. If there is a supply of hydrogen at 99% purity available, chances are that engineers or operators will claim that their unit *needs* to have 99% pure hydrogen. It is this mindset that needs to be challenged. Once we break away from this, the scope for reusing and recycling hydrogen becomes a lot greater and benefits can be substantial.

One European refinery used a significant flow rate of very pure hydrogen for drying purposes. When questioned about this, the refinery engineers replied that this was the way it had always been done. That made sense because until recently, the refinery had a large surplus of hydrogen. Then, however, that hydrogen was worth several hundred thousand dollars per year. It would be far more sensible to use the offgas from another consumer, accomplishing the same job for free!

Admittedly, most refineries do not have such obvious savings. Most hydrogen consumers require a certain flow rate of gas and hydrogen purity in order to operate properly. The flow rate is needed to maintain a gas to oil ratio high enough to prevent coking, while the purity is required to maintain the required hydrogen partial pressure for effective kinetics. With fixed flow rate and purity demands, it may not look like there is any scope for improvement. However, the opportunities are still there if we know where to look for them.

The secret is simple: look at reactor inlets, not makeup streams. Figures 25.2 and 25.3 illustrate this point. Figure 25.2 is a diagram of a hydrogen consumer showing the makeup hydrogen and the high pressure and low pressure purges. Looking at it in this way, it is very easy to be misled into thinking that the unit requires 10 000 sm³/h of hydrogen at 99% purity. However, this is wrong. In order to find the real requirement, one needs to look at the internal workings of the consumer as shown in Fig. 25.3.

As can be seen, the hydrogen makeup stream is mixed with hydrogen recycle before being fed to the reactor inlet. Therefore, the purity that the reactor actually sees is only 83%. Recognizing this immediately opens

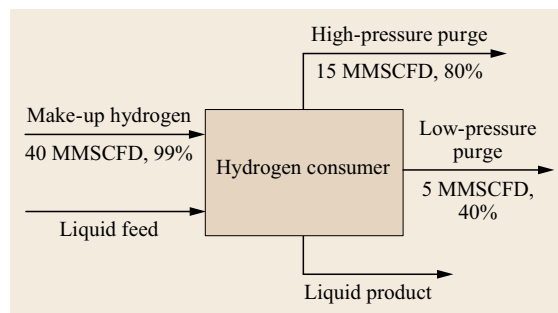


Fig. 25.2 A black-box view can mislead us to think the consumer needs 99% pure hydrogen

up the scope for reusing other gases in the makeup stream and using less of the 99% hydrogen. As long as the flow rate and purity of the hydrogen going into the reactor do not change, the makeup purity is not that important. Put another way, the consumer may *want* 99% purity in the makeup, but it really needs 83% purity at the reactor inlet.

A simple example is shown in Figs. 25.4 and 25.5. Two hydrogen consumers are both taking makeup hydrogen from an external supplier at 99% purity, with a total demand of 20 000 sm^3/h . If we make the mistake of saying that the makeup purity must be fixed, there is clearly no scope at all for reusing hydrogen (Fig. 25.4).

However, if we do the correct thing and focus on the reactor inlet, Fig. 25.5 shows that it is possible to reuse the purge from Consumer A as part of the makeup of Consumer B. This allows the demand from the external supplier to be reduced by 1710 sm^3/h or 8.7%. With typical hydrogen costs, this could be worth between half a million and a million US dollars per year. The flow rates being compressed by B's makeup and recycle compressors are lower, giving power-cost savings too. Pretty good value for the cost of a pipe! Notice that consumer B still has exactly the same flow rate and hydrogen purity at the reactor inlet as before. All that has changed are the makeup and recycle flow rates.

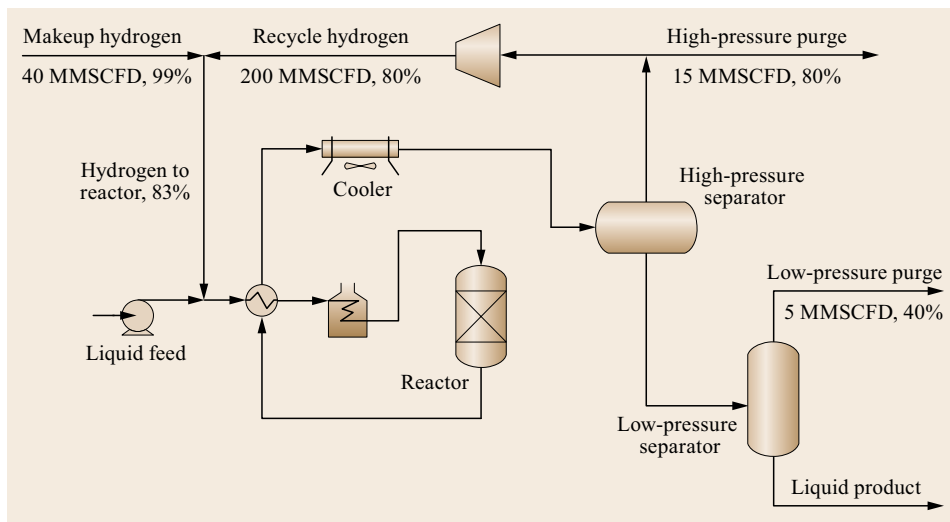


Fig. 25.3 The true reactor inlet purity requirement is only 83%

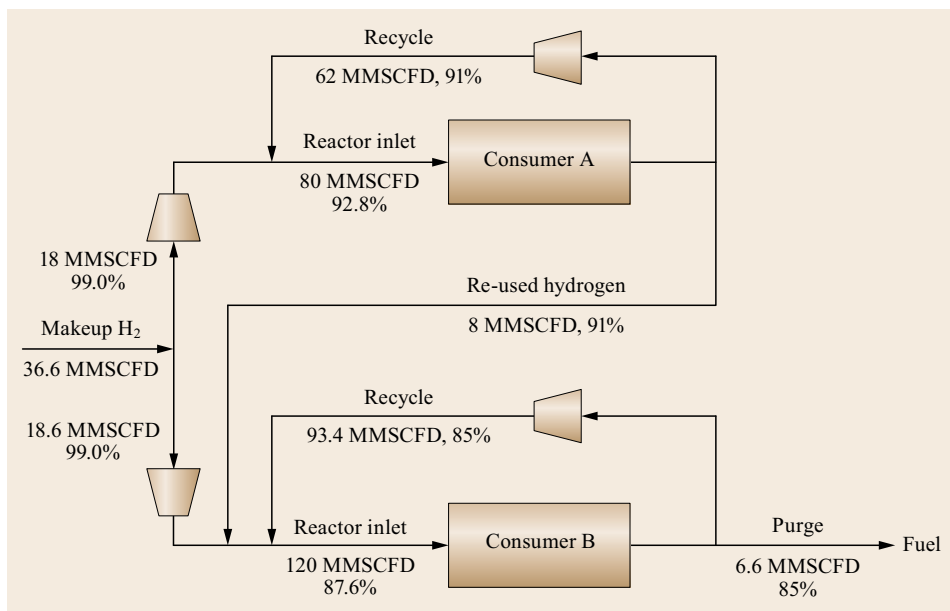


Fig. 25.4 If the makeup purities are fixed, there is no way to reduce the makeup flow rate

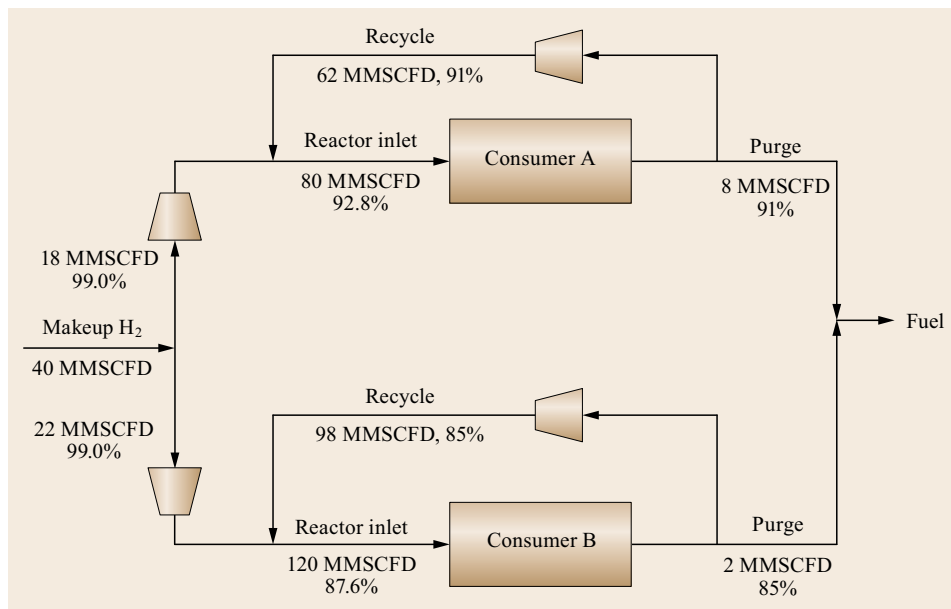


Fig. 25.5 Focusing on reactor purity allows about 87.6% at constant reactor inlet purity

Real refineries have to consider a lot more than two units at once. Should we use hydrocracker offgas to feed the diesel hydrotreater, or should we send it to the naphtha hydrotreater? Maybe we should use cat reformer hydrogen instead of imported hydrogen, but should we use it directly or blend it with hydrogen from elsewhere? Maybe that hydrocracker offgas should be used as fuel instead? Or maybe we could purify it in a PSA. Or why not a membrane? Since we're thinking of PSAs and membranes, maybe we should purify the naphtha hydrotreater offgas as well? Where should we send the purified product?

Hydrogen pinch analysis is a quick and systematic way of knowing immediately what the maximum hydrogen recovery achievable is. The method is similar to the well-known energy pinch analysis used for designing heat exchanger networks [25.5]. Instead of looking at enthalpy and temperature, though, we concern ourselves with gas flow rate and hydrogen purity. The method in its original form aims at maximizing the in-plant reuse and recycling of hydrogen to minimize *on-purpose* or *utility* hydrogen production [25.6]. Later in this article we will discuss whether this is, in fact, the correct thing to do in all cases.

The first step in the pinch analysis is to plot hydrogen composite curves (Fig. 25.6). These are plots of hydrogen purity versus flow rate for all the sources and all the demands for hydrogen in the refinery. Sources are streams containing hydrogen that potentially could be used. They include catalytic reformer hydrogen, *on-purpose* hydrogen as well as the overhead gases from high and low pressure separators in the various consum-

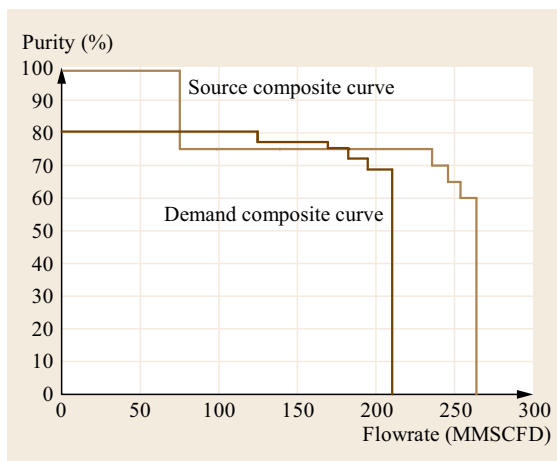


Fig. 25.6 Composite curve showing hydrogen flow and purity

ing units. When plotting hydrogen demands, remember the lesson on needs versus wants. Don't base your calculations on makeup purities!

By plotting hydrogen purity versus the area enclosed between the source and sink composites, a hydrogen surplus diagram is constructed (Fig. 25.7). This diagram is analogous to the grand composite curve in heat exchanger network synthesis and shows the excess surplus hydrogen available at each purity level. If the hydrogen surplus is positive throughout the diagram, there is some slack in the system.

The hydrogen generation flow rate can be reduced until the surplus is zero (Fig. 25.8). The purity at which

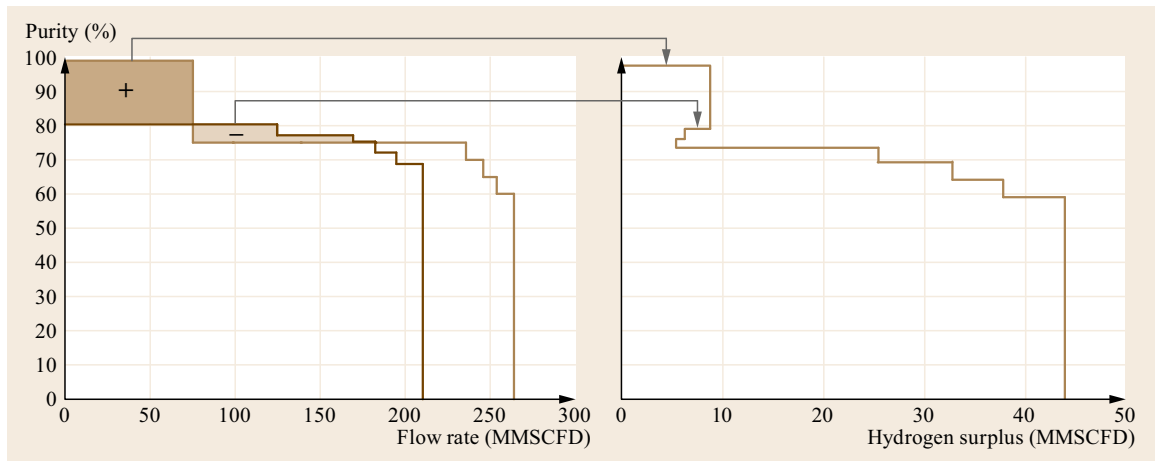


Fig. 25.7 Hydrogen surplus diagram

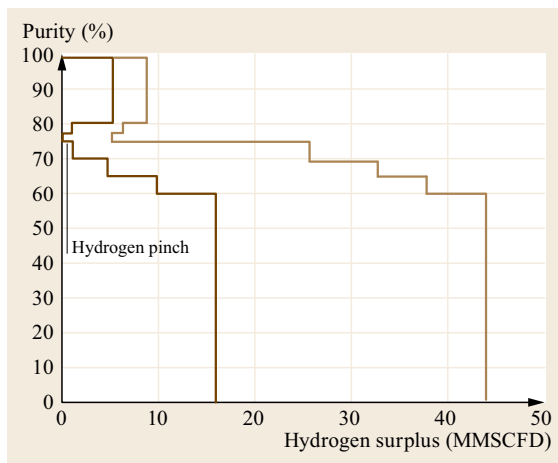


Fig. 25.8 Hydrogen surplus diagram showing pinch point

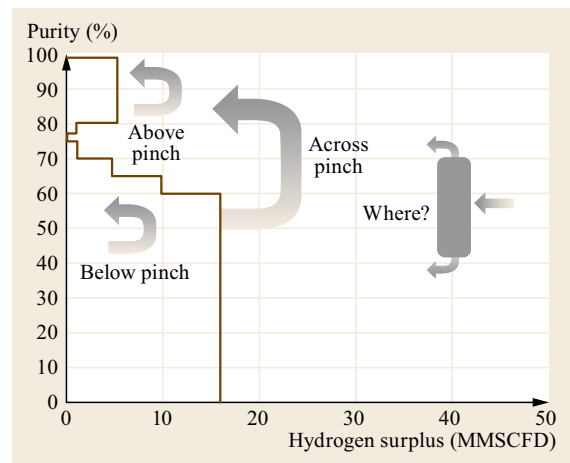


Fig. 25.9 Three ways of placing a purification unit relative to the pinch

this occurs is termed the *hydrogen pinch* and it is the theoretical limit on how much hydrogen can be recovered from the sources into the sinks. It is analogous to the heat recovery pinch [25.7]. The on-purpose hydrogen flow rate that produces a pinch is the minimum target and is determined *before* any network design analysis. With the appropriate software, a task that would have taken days, weeks or months can be accomplished in hours. If the gap between the target and the current use is large, it is worthwhile spending time reconfiguring the hydrogen network. The key is to avoid cross-pinch hydrogen transfer and to be especially careful about the above-pinch purity, as this is the region that is most tightly constrained. Hydrogen streams with purities greater than the pinch purity should not be used to feed consumers that can use hydrogen below the pinch purity. Also, hydrogen streams above the pinch purity should not be sent to the fuel system or flared. If the

gap is not large, your time would be better spent looking at other improvement options, such as purification.

There are three main options for purification. In case you are wondering, these are *not* PSAs, membranes and cryogenic systems. Those processes all do fundamentally the same thing, which is to split a feed stream into a product stream with a high purity and residue stream with a low hydrogen purity. The options we are talking about relate to the placement of the purifier relative to the pinch. As Fig. 25.9 shows, there are three possible placements: above the pinch, below the pinch and across the pinch.

Placing the purifier below the pinch is not a wise idea. This simply takes hydrogen from a region where it is in excess and purifies it before sending it back to the same region. In essence, you would be buying an expensive unit to purify hydrogen for burning!

The best option is to place the purifier across the pinch. This moves hydrogen from a region of excess to a region that is tightly constrained on hydrogen. It

freed up hydrogen from *on-purpose* sources and any hydrogen lost to residue would have ended up in the fuel system anyway.

25.5 Beyond Pinch

The pinch analysis approach discussed above is good for getting an immediate overview of the system, setting targets and even doing some initial screening of ideas. However, in our project work, we have found a number of limitations.

Firstly, it does not fully cope with all the complexities of network design. The two-dimensional representation only considers flow rate and purity, but does not incorporate other important practical constraints such as pressure, layout, safety, piping, operability and of course capital cost.

One of the more important constraints is stream pressure. The targeting method assumes that any stream containing hydrogen can be sent to any consumer, regardless of the stream pressure. In reality, this is only true if the stream has a sufficiently high pressure. Thus, pinch analysis targets usually are too optimistic. They can encourage refiners to waste time developing projects that are infeasible or far too expensive due to the need to install compressors. Compressors are among the most expensive capital items in any chemical or refining process. Therefore, a sound retrofit design should make best use of existing compression equipment. Often, the economic feasibility of a hydrogen recovery project is determined by bottlenecks in existing compressors and not by purity and flow rate constraints alone.

Obviously, direct reuse of hydrogen between consumers is only possible if the pressure is sufficient. However, it is certainly possible to reuse a low-pressure hydrogen stream indirectly, i. e., by routing it through an existing compressor, if certain conditions are met. Firstly, there has to be sufficient capacity in a compressor to accommodate the stream; reusing hydrogen will change the makeup and recycle flow rates throughout the system, so capacity might be available in one or more other compressors. Also, the pressure of the reused stream must satisfy the inlet-pressure requirements of the target compressor. In addition, the discharge pressure of the compressor should be high enough for use in the target consumer.

To account for pressure and other important constraints, a mathematical programming or optimization approach is required. Work on this was started at the University of Manchester Institute of Science and Technology (UMIST) and AspenTech took the lead in further development [25.8].

25.5.1 Multicomponent Methodology

At this point we should be able to begin process engineering of the proposed reuse project. However, if we were to do so we would find that the simulated benefits are very much lower than those predicted by the optimizer. This is due to another major limitation of the hydrogen pinch approach: its assumption of a binary mixture.

Consider two hydrogen streams, each of 85 mol% purity. The first is ethylene plant export, containing almost 15% methane. The second is catalytic reformer export, containing roughly equal amounts of methane, ethane and propane, plus small amounts of heavier material. Hydrogen pinch techniques cannot differentiate between these streams and would identify no penalty or benefit from switching between them as a source of makeup gas. Yet in reality the ethylene plant gas would require operation with a much higher purge rate, due to the tendency of methane to buildup in recycle loops. In fact, in certain circumstances it is more efficient to substitute a makeup supply with a lower purity hydrogen source (but lower methane content), while the hydrogen pinch methodology would lead you to do the opposite.

To meet this challenge, we developed a multiple-component optimization methodology that fully accounts for the behavior of individual components within the process reactors, separators and the recycle gas loop. While in the binary pinch approach the composition and flows of reactor feed and separator gas are fixed, our multiple-component approach allows these compositions to float, so long as constraints such as minimum hydrogen partial pressure and minimum gas-to-oil ratio are met. Simulation models for reactors, and high-pressure and low-pressure separators are used to correctly model overall process behavior. We also developed a network simulation tool based on AspenTech's Aspen Custom Modeler (ACM) software.

By extending our analysis to include components other than hydrogen, we can simultaneously optimize downstream amine scrubbers, liquefied petroleum gas (LPG) recovery systems and the entire fuel gas system. Our project experience shows that the benefits from increased LPG recovery can outweigh the value of hydrogen savings.

25.5.2 Hydrogen Network Optimization

In addition to methane and other light hydrocarbons, offgas hydrogen may contain toxic hydrogen sulfide (H_2S). H_2S is adsorbed in amine units, which usually are integrated in some way with the plantwide amine system; the amine system transfers the H_2S to a sulfur recovery plant. The H_2S -free offgases become refinery fuel gas for general use throughout the plant.

Keeping hydrogen out of fuel gas is beneficial for many reasons. Recovering hydrogen decreases the required amount of on-purpose hydrogen. Because hydrogen increases flame temperatures in fired heaters, it can limit heaters with tube temperature constraints.

Hydrogen network optimization identifies possible investment options and changes to operation, which recover and purify hydrogen before it reaches the fuel gas system. This activity is more complex than other utility optimization techniques, because in addition to consid-

ering flow and pressure, one must consider purity and the impact of composition.

While preparing the optimization software, we first set up a superstructure that connects every sink with every source, provided that the source pressure is greater than or equal to the sink pressure. Compressors are included as both sources and sinks. We formulate basic constraints such as balances on total flow rate and hydrogen flow rate, as well as any compressor limitations such as maximum power or maximum throughput. A whole host of other constraints can also be incorporated, such as limited space, no new compressors allowed and the old favorite: *I don't want to spend any capital!*

Next, we subjected the superstructure to mathematical programming that eliminates undesirable features while satisfying an objective function, which could be minimum hydrogen generation. There is actually no need to limit ourselves to minimizing hydrogen gen-

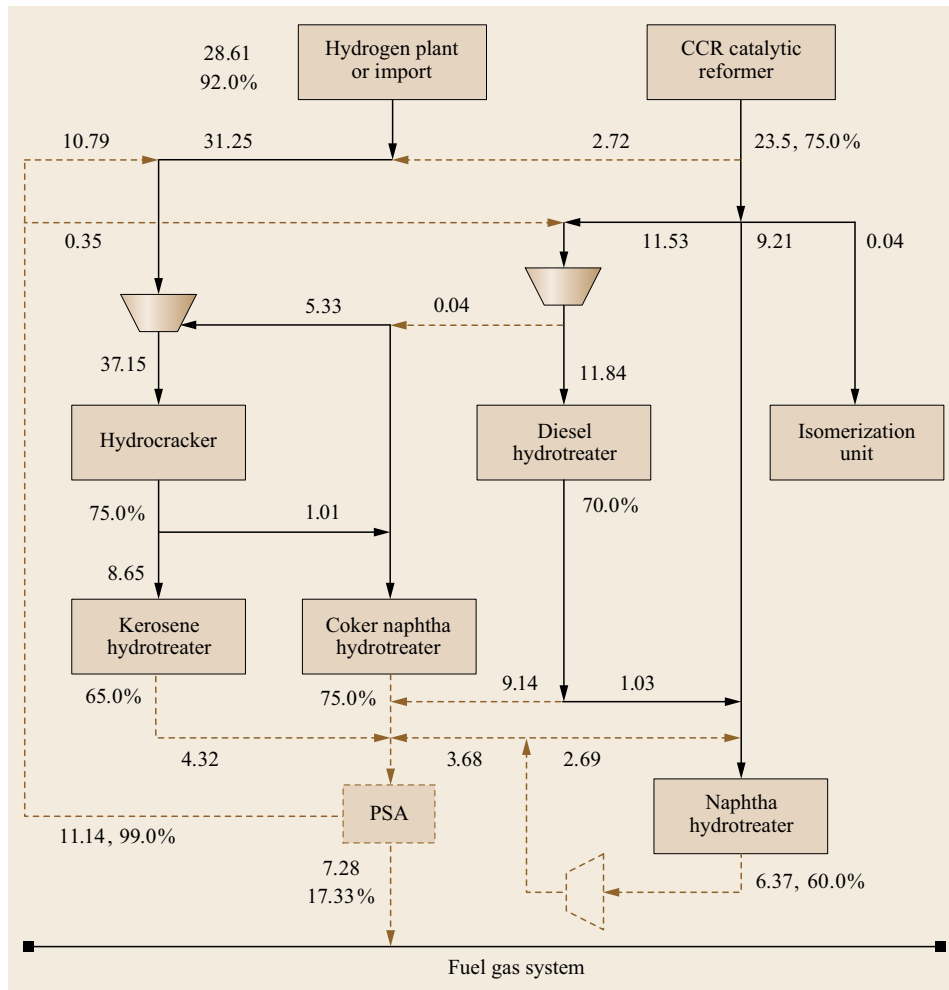


Fig. 25.10 Retrofit: Addition of PSA. New equipment shown with dotted lines

eration. For example, we could choose to minimize operating cost or total annual cost. All relevant costs can be considered, including hydrogen cost, compressor power cost, fuel gas credit and capital cost of new equipment. We will not bore you with all the details, as these can be provided by your front-end engineering contractor. Suffice it to say that the optimization tool uses a combination of linear and nonlinear programming.

The ability to add constraints at will means that all practical considerations can be built in. The cost of adding a constraint can also be determined. For example, an engineer may say he or she doesn't like the idea of running a long pipe across a road to connect two units. This option can be banned and the optimization carried out again. The difference in cost between the two solutions indicates how much his or her *not liking* the connection will cost. If it costs a million dollars per year, the engineer may decide that he or she doesn't actually mind it *that* much after all!

The other major limitation of pinch analysis is that it gives fundamental guidelines about purification placement, but does not always help with selecting which streams to purify or whether to use a PSA, membrane, cryogenic or other purification process. This is where know-how becomes vital. Purifier experts can rapidly assess different technologies for candidate feed streams, simulate their performance and give quick cost estimates. These experts can weigh the benefits of different options, recognizing that each application will be unique. For example, in a recent European study, a refinery was facing a large increase in hydrogen demand to meet upcoming sulfur-in-fuel specifications. In this case, hydrogen recovery was more important than product purity, so Air Liquide experts determined that, for a certain stream, a membrane would be a better choice than a PSA unit.

Another issue with purifiers is that different technologies have very different pressure requirements. A PSA unit gives a product pressure very close to the

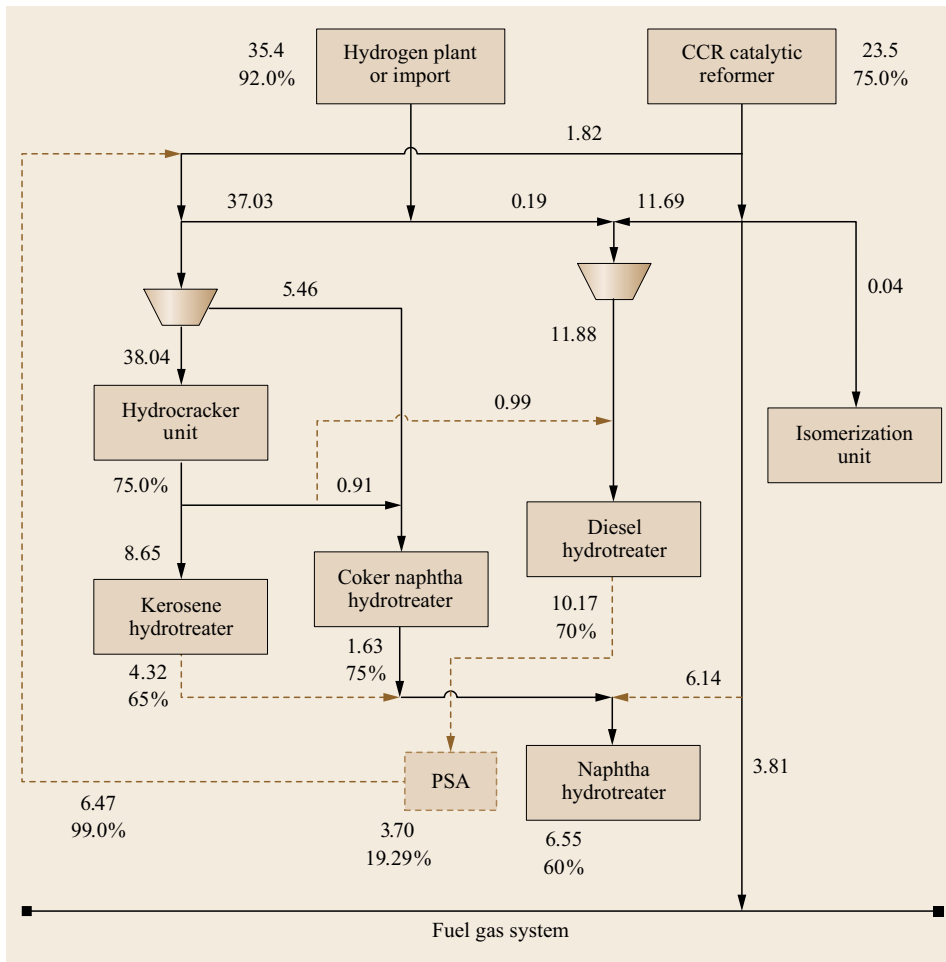


Fig. 25.11 Recommended changes if capital expenditure is limited to US\$ 5 million

feed pressure, but the PSA residue pressure is extremely low. On the other hand, a membrane requires a large pressure drop in order to perform properly, the product pressure is much lower than the feed pressure, and the residue pressure is almost the same as the feed pressure. These issues need to be considered in the specific context of the refinery and can be handled easily using the approach described above. Ultimately, economics should determine the optimum tradeoff between product purity, product pressure and hydrogen recovery.

Purification expertise also saves time. Hydrogen network analysis experts work in parallel with purification experts to rapidly assess options and develop a project flow sheet. This is much more time-effective than having one company generate a small number of options using pinch analysis and then sending the options to another company for cost quotes. With the parallel approach, more options are in less time and both the network analysis engineers and the purification engineers see the entire picture.

The following case study is representative of a real refinery system, but certain data have been disguised to maintain customer confidentiality. The existing hydrogen system is shown in Fig. 25.10. The objective of the study was to retrofit the network to minimize operating costs. Process and cost data are given elsewhere [25.9].

Several constraints were imposed by the refinery:

1. The existing compressors have 5% spare capacity
2. There is only space on the site for one new compressor and one new purification unit

3. A payback of more than two years will not be acceptable.

The network retrofit was designed by setting the objective function to be minimum operating cost while constraining the payback time (capital cost divided by annual operating cost savings) to be two years or less. Figure 25.10 shows the resulting design. Dotted lines indicate new equipment.

In the recommended project, both a new compressor and a PSA are used and substantial repiping is required. Notice that the new compressor accommodates the increased recycle requirement for the naphtha hydrotreater (NHT) as well as the need to compress one of the feeds to the PSA so that its product can be used in the hydrocracker.

The total capital investment of the retrofit is \$9.8 million and the operating-cost savings are \$6 million per year. The payback period is therefore 1.6 years, which is better than required.

Now, refineries often have limited capital budgets, so even modification with a good payback might be too expensive. It would be valuable to know the maximum savings achievable with a fixed capital budget, say US\$5 million. Adding capital expenditure as an additional constraint and re-optimizing gives the solution shown in Fig. 25.11. The best investment is a PSA unit requiring no new compressor. Notice too that fewer new pipes are installed. The operating cost savings are smaller (only \$3.5 million per year) but this is to be expected.

25.6 Investing versus Saving

Up to now, this article has addressed the issue of minimizing hydrogen supply, in other words, saving hydrogen. This is certainly a very real problem for refiners and many of our clients have specified this as their objective. After all, hydrogen is expensive and a few percent saved can mean millions of dollars per year. However, this is often not the most profitable course of action.

Let's go a step further and look at hydrogen consumers as investments. Instead of merely *saving* hydrogen, why not consider re-investing it where it will *make* money for you?

How do we re-invest hydrogen? By feeding more and/or purer hydrogen into the appropriate reactors. For example, the hydrogen freed up using the network design methods can be used to process cheaper feed stocks. It could also be used to boost partial pressures to enhance conversion, throughput, yields and catalyst life.

The important question is how do we know which units will be the most profitable ones to invest hydrogen in? When analyzing money investments, there are certain techniques that wise investors use. These include performing a due diligence and analyzing the financial statements and cash flows of the investment. A good return on investment is the goal. Nobody wants an investment that loses money and likewise a refiner should use hydrogen where it will provide a better return than simply saving it would give. We have our own techniques for analyzing hydrogen investments. They are reactor modeling and refinery LP modeling.

Rigorous kinetic modeling is used to obtain a good understanding of process operation under different feed hydrogen conditions. AspenTech has developed rigorous tools for modeling fixed-bed hydroprocessing units, such as hydrocrackers, reformers, FCC pretreaters and desulfurization units. They model kinetics for denitro-

genation, desulfurization, saturation and cracking and are capable of accurately predicting yields, hydrogen consumption and product properties for widely different feeds and operating conditions. These reactor models can easily be connected to rigorous fractionation models, creating a fully integrated model of the entire hydrotreater, reformer or hydrocracker complex.

The reactor models include a unique catalyst deactivation tool, which allows refiners to minimize catalyst life giveaway and to calculate future conversions, yields and product properties. Hydrocracking models can be used to optimize tradeoffs between feed rate, conversion, catalyst cycle life, feedstock severity, operating conditions and costs. For recycle hydrocracking units, there are tradeoffs between fresh feed rate and conversion-per-pass in single-stage units, or between first stage and second stage conversion in two-stage units.

It is not necessary to model every reactor and determine the benefits in a trial-and-error way. A combination of the LP model, understanding of current process operations and constraints and hydrogen network analysis can be used to develop a shortlist of key processes and potential changes to those processes. For example, the LP model will show the bottlenecks to increasing refinery profit. If increasing hydrogen partial pressure can eliminate one of these bottlenecks, then this unit will be a candidate for applying rigorous reactor modeling and subsequent process analysis.

Hydrogen network analysis can also give insights into process operations. Above a threshold hydrogen purity, hydrotreater operation is insensitive to hydrogen purity. If reducing the hydrogen partial pressure to a hydrotreating reactor gives a large saving in the overall refinery hydrogen target, this unit can be also be selected for rigorous modeling to determine the true impact on reactor operation.

All process changes need to be modeled, the impact on the hydrogen network evaluated and the final benefit established through the LP model. The reactor models can be linked to Aspen PIMS, a leading PC-based LP software package used by the petroleum and petrochemical industries. By providing automatic updates to Aspen PIMS vectors, the models can enhance detailed operations planning, economic evaluation and scheduling activities. In particular, they can help a refiner decide how best to apportion intermediate heavy distillate streams between different conversion units.

As an illustration, Fig. 25.12 shows case-study results from a rigorous model for a two-reactor hydrocracker with partial recycle of unconverted oil [25.9]. The unit runs at about 60% conversion-per-pass. A fixed flow of unconverted bottoms is recycled. The remainder

is exported to the FCC unit for heavy diesel blending. At present, the *export* comprises about half of the total unconverted oil.

For the case study, the purity of the makeup hydrogen was varied from the current value (89–100%). The feed rate, recycle oil flow rate and weighted average reactor temperature (WART) for both reactors was held constant. Under these conditions, the following effects were noted:

1. Full-range distillate yield increases from 52.8 to 54.6%
2. Heavy naphtha yield increases from 16.6 to 19.4%
3. Exported bottoms decreases from 17.8 to 11.3%.

According to the model, the net benefits of increasing the makeup-gas purity from 89–100% were on the order of \$2 million per year. But how much would it cost to make available the extra hydrogen needed? Using a simple marginal cost of hydrogen is not the way to answer this.

Figure 25.13 shows how our network design and analysis tools can fit into an overall profit optimization study. They identify quickly how much additional hydrogen can be made available for certain levels of cost. Typically, a few percent more hydrogen can be squeezed out with simple modifications requiring low or no cost, for example piping modifications. Then there will be a step-change where getting any more hydrogen will require a purification system. Finally, there will be another step-change where purification reaches its limit and any more hydrogen will have to be supplied from external sources, such as imports or a hydrogen plant. Knowing the true cost of providing additional hydrogen makes it easy to weigh it against the benefits that are suggested by process modeling and LP optimization.

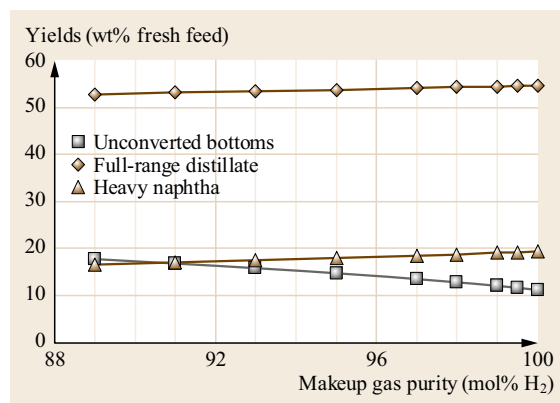


Fig. 25.12 Hydrocracker performance improves with increased hydrogen purity

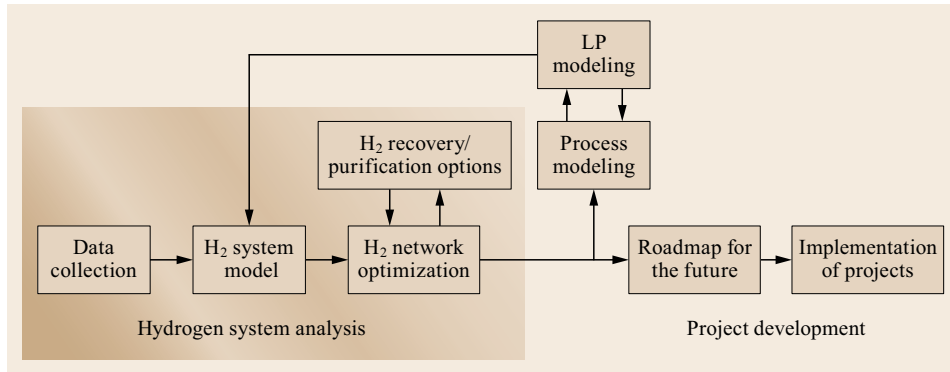


Fig. 25.13 Network design tools compare costs and benefits for project options

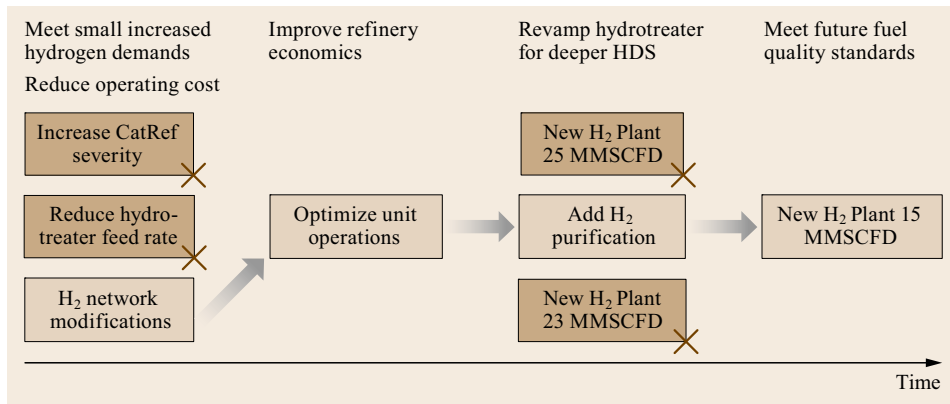


Fig. 25.14 Systematic tools are used to construct a roadmap for the future

Figure 25.14 shows a typical roadmap that can be drawn up, showing where the refinery is now and where it wants to be at different points in the future (e.g., in one year, five years, ten years). All of the tools described in this article give the refiner an eas-

ier job of planning how to tackle the future. They are used to systematically choose the best set of projects that achieve immediate objectives but also fit in with long-term goals. This avoids the *regret capital syndrome*.

25.7 Conclusion

In conclusion, several hidden opportunities typically are not addressed by refiners when developing plans for clean fuels. In our experience:

- Time spent in investigating the current balance pays back. This can identify substantial operating savings and it eliminates *unconscious over-design* in future investments.
- Make the best use of hydrogen purity. There is scope to reduce both capital investment and future operating costs by maximizing the benefits from high-purity hydrogen sources. Reactor modeling is an important part of evaluating these benefits and optimizing hydrogen use.
- Hydrogen is not the only consideration. A proper methodology for optimization must extend beyond the hydrogen system to include low-pressure purges, amine treating, LPG recovery and the fuel gas system. Purification upstream of LPG recovery units can debottleneck those units and increase their overall recovery efficiency, adding significantly to the value of the hydrogen-recovery project. Reducing hydrogen loss to fuel can have both positive implications (improved calorific value) and negative implications (increased fuel oil firing and hence increased SO_x emissions).
- New model-based network optimization methodologies allow the identification of no- and low-

capital-expenditure projects to improve current operations, particularly for refineries of types 2 and 3. As mentioned, these savings are often in excess of 1 million €/year, with payback times measured in months [25.2].

- If there is one conclusion you should take away with you, it should be that hydrogen is money. Stop thinking about it as merely an unglamorous utility and start looking at ways to make more money from it.

References

- 25.1 W. Hofer, I. Moore, P.R. Robinson: Hitting ULS targets through hydrogen management, *Petroleum Technol. Q. Spring*, 43–49 (2004)
- 25.2 N. Hallale, I. Moore, D. Vauk: Hydrogen optimization at minimum investment, *Petroleum Technol. Q. Spring*, 83–90 (2003)
- 25.3 D.A. Vauk, R. Gardner, D. Mercer: Managing hydrogen to achieve ULS targets, *Petroleum Technol. Q.* **10**(3), 89–95 (2004)
- 25.4 R.T. Cassidy, E. Petela: Life cycle utilities management, *Proc. NPRA Annu. Meet.* (2001), Paper No. AM-01-63
- 25.5 B. Linnhoff: Use pinch analysis to knock down capital costs and emissions, *Chem. Eng. Prog.* **90**(8), 33–57 (1994)
- 25.6 J. Alves: Analysis and Design of Refinery Hydrogen Distribution Systems, Ph.D. Thesis, (Univ. Manchester Institute of Science and Technology, Manchester 1999)
- 25.7 ProSim: Pinch Analysis, <http://www.prosim.net/en/page-pinch-analysis-17.php> (2016)
- 25.8 N. Hallale, F. Liu: Refinery hydrogen management for clean fuels production, *Adv. Environ. Res.* **6**, 81–98 (2001)
- 25.9 P.R. Robinson, J.M. Thiessen, P.J. Hanratty, D.R. Mudt, C.C. Pedersen: Plan for clean fuel specifications with rigorous models, *Proc. NPRA Comput. Conf.* (2000), Paper No. CC-00-143

26. Model-Predictive Control Fundamentals

Paul R. Robinson, Dennis Cima

Model-predictive control (MPC) improves the capability of process units by stabilizing operation, increasing throughput, improving fractionator performance, decreasing product quality giveaway, and reducing utility consumption. MPC provides real-time information to higher-level applications, such as planning models and process optimizers. MPC input comes from the distributed control system (DCS), advanced regulatory controllers (ARCs), and laboratory data. A well-implemented MPC controller responds once per minute – or in some cases more frequently – to changes in feedstock, ambient temperature, and so on, by moving several variables simultaneously. For major process units, returns on investment for

26.1	Useful Definitions	834
26.2	Overview of Economics	835
26.3	Sources of Benefits	836
26.4	Implementation	837
26.5	Costs versus Benefits	838
	References	839

MPC can exceed \$0.50 per barrel, not including collateral benefits, such as improving the efficiency of operators and engineers, and improving process safety.

At relatively low cost, model-predictive control (MPC) improves the capability of process units by stabilizing operation, increasing throughput, improving fractionator performance, decreasing product quality giveaway, and reducing utility consumption.

It is said that a well-implemented MPC application is like having your best operator on the control board 24/7. Operators are indispensable, certainly at critical times such as startup, shutdown and emergencies, but during normal operation, MPC can be more capable than any human.

Major process units are complex. A single change affects dozens of other variables, to one extent or another. For each variable, the response time is different. Constraints must be honored. Violating constraints can ruin products, damage equipment, and lead to loss of containment. In all hydrocarbon industries – gas processing, chemicals manufacturing, and every phase of petroleum production, transportation and processing – loss of containment can cause fires, damage the environment, and cause injuries and fatalities. Therefore, it's no surprise that during manual operation, human operators keep process variables in a comfort zone, well away from limits, leaving plenty of time to react if something changes.

In response to a change in the unit or process objectives, an operator makes small adjustments to one setting (or one group of settings) then waits until the process is steady before making subsequent changes. In contrast, MPC makes appropriate adjustments every minute – even more frequently in some cases – in response to multiple changes, all without violating operational, equipment, or product quality constraints.

A colleague cites a typical example to illustrate the benefits of MPC versus manual operation. On the US Gulf Coast, many units are limited on hot, humid days by air-cooler capacity. A sudden thunder storm can cool the ambient temperature by 10 °C within a few minutes. Under manual control, an operator might not respond at all, but MPC applications respond immediately, increasing feed rate and manipulating other variables to maintain conversion and product quality. As the storm passes and the heat and humidity return, the MPC adjusts to maximize production rates. For a 100 000 FCC unit, the incremental production could be 500 barrels – say, 125 barrels per hour for four hours – which could be worth \$10 000.

An MPC application gets input from the distributed control system (DCS), advanced regulatory control

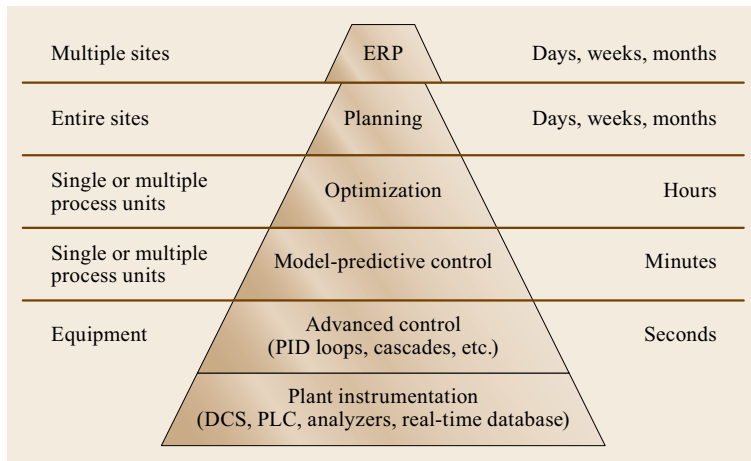


Fig. 26.1 Overview of computer control applications. ERP stands for enterprise resource planning, a software solution that integrates planning, manufacturing, sales, and marketing

(ARC), and laboratory data. It provides information to higher-level applications, such as planning models and process optimizers. For major process units, returns on investment for MPC can exceed \$0.50 per barrel, not including collateral benefits, such as improving the

efficiency of operators and engineers, and improving process safety.

Figure 26.1 presents an overview of refinery software applications and the frequency at which they typically run.

26.1 Useful Definitions

A *proportional-integral-derivative (PID)* controller is a feedback device. A *process value (PV)* is measured by a field transmitter. A controller compares the PV to its *setpoint (SP)* and calculates the required change – for example, a new *valve opening position (OP)*, expressed as a percentage – to bring the PV closer to the SP. The required change is calculated with a PID algorithm. In practice, proportional, integral, and derivative constants are parameters used for tuning.

Advanced process control (APC) and *advanced regulatory control (ARC)* applications employ control algorithms to improve process control compared to regulatory PID controllers. APC and ARC include loops or cascades, such as cascading a temperature controller to the fuel gas valve of a fired heater. They incorporate advanced control algorithms combined with regulatory control functions (i. e., lead/lag, ratio, high/low selectors, etc.) to implement a control strategy.

A *programmable logic controller (PLC)* is a small computer used to automate real-world processes. A PLC receives input from various sensors and responds to changes by manipulating actuator valves according to preprogrammed logic stored in the memory of the PLC.

A *distributed control system (DCS)* serves as the foundation of modern computer control. In a DCS, pro-

cess measurements and control functions, such as PID loops, and APC and ARC applications, are connected to processors, which are networked throughout the plant. A *graphical user interface (GUI)* makes it easier for operators to view data, create plots, change setpoints, and respond to alarms. In addition to process control, modern DCS software includes sophisticated trending and data storage.

A *real-time database* adds considerable capability to a DCS system. As the name implies, it stores historical data, but it does much more than that. It includes sophisticated graphics and real-time data trending, and it can be linked to external software, such as Microsoft Excel, planning software, or process optimizers.

Model predictive control (MPC) applications use multiple independent variables to control multiple dependent variables. If a variable is truly independent, its value is not affected by other process variables. There are two types of independent variables. *Manipulated variables (MVs)* can be changed by an operator to control the process. These include setpoints for regulatory PID controllers and valve positions. *Feed-forward (FF)* and *disturbance variables (DV)* affect the process but can't be manipulated. These include ambient temperature, the quality of an external feed, or the composition of fuel gas used by fired heaters.

The value of a dependent variable can be calculated using the values of independent variables and an appropriate dynamic model. *Controlled variables (CVs)* are maintained at a desired steady-state target. *Constraint variables* are maintained between high and low limits. Many variables are dependent, but not all dependent variables are important enough to be included in the MPC application.

MPC derives dynamic process models from past process behavior to predict future process behavior [26.1]. The dynamic models can be obtained during a series of manual step tests. Modern step tests are au-

tomated and/or rely on natural process variation. The predictions are used to control process units dynamically at optimum steady-state targets. MPC applications may also include the use of predicted product properties (*inferential analyzers*) and certain process calculations. Model-predictive controllers almost always include several independent variables, often several dozen.

In this chapter, when we say *APC (advanced process control)* we mean nonpredicting collections of cascades and control loops. In practice, *APC* and *MPC* are used interchangeably.

26.2 Overview of Economics

Table 26.1 presents typical benefits for applying model-predictive control to refinery units [26.2]. It is important to say that the benefits are not additive. For a combined MPC/optimization project, the costs are always lower and the benefits might be higher than if the projects are implemented separately. Conversely, the

advertised benefits of DCS and real-time database technology depend entirely on the applications for which they serve as platforms. Stabilizing a crude distillation unit with MPC will stabilize the feed to all downstream units, which decreases the impact of MPC on the other units.

Table 26.1 Typical benefits of multivariable model-predictive control

Process unit	Typical benefits (\$US/bbl)	Source(s)
Crude distillation	0.015–0.03	Higher feed rate Reduced product quality giveaway ^a Increased energy efficiency
Fluid catalytic cracking	0.15–0.30	Higher feed rate Reduced ΔP across slide valves Reduced product quality giveaway ^a Increased energy efficiency
Catalytic reformer	0.10–0.20	Higher feed rate Optimum coke on catalyst (CCR units) Reduced product quality giveaway ^a Increased energy efficiency
Hydrocracker	0.10–0.20	Improved safety Higher feed rate Increased stability Better conversion control Improved control of temperature profiles Better control of recycle gas purity Reduced product quality giveaway ^a Increased energy efficiency
Gas oil hydrotreater	0.02–0.10	Higher feed rate Increased stability Reduced product quality giveaway ^a Better control of recycle gas purity
Gas plant	0.05–0.10	Higher feed rate Reduced product quality giveaway ^a Increased energy efficiency
Product blending	0.10–0.20	Reduced product quality giveaway ^a

^a Equivalent to increased production of desired products

After installation of the requisite infrastructure – DCS, analyzers, real-time database software, operator terminals, process computer(s) – MPC projects on major petroleum refinery or chemical manufacturing units can be completed within 2–4 months. The return on investment is quite high; typical payback times usually are 4–12 months. For relatively simple gas processing plants, the costs are lower and the payback time can be shorter.

The applications that benefit most from model-predictive control have one or more of the following characteristics:

- High production capacity
- Competing control objectives
- Highly interactive processes

26.3 Sources of Benefits

The benefits of APC and model-predictive control come from one or more of the following:

- Reduced process variability
- Maximizing throughput against multiple process constraints
- Increased yield of high-value products
- Reduced product quality giveaway
- Reduced production losses [26.4].

Variability is a characteristic of all continuous processes. As shown in Fig. 26.2, simply reducing variability provides little (if any) benefit. Benefits start to accumulate when operators run the plant closer to true process constraints.

For example, if a hydrotreater must produce ultralow-sulfur diesel (ULSD) with ≤ 10 wppm sulfur

- Unusual dynamic behavior
- Day/night or seasonal variation
- A need to operate close to constraints
- A need to closely track optimization system targets
- A need to transition smoothly from one set of targets to another.

In refineries, the largest benefits of model-predictive control come from crude distillation units and gasoline blenders, for which the throughput is high, and from fluid catalytic cracking (FCC) and other conversion units, for which the difference in value between feeds and products usually is high. In all cases, benefits accrue from reduced product quality giveaway. In hydrocracking, MPC in conjunction with ARC can improve safety [26.3].

to meet product specifications, and if there is a severe economic penalty for exceeding the specification, the refiner may set a process target of 5 wppm to ensure that the plant never exceeds the limit. In this case, the difference between the target and the limit – i. e., the cushion – is 5 wppm. A cushion of this size is not atypical for coastal refineries where feed quality and/or hydrogen composition can change significantly from one day to the next, and where there is limited ability to correct a specification violation with blending. But a 50% cushion is expensive, resulting in higher operating cost and accelerated catalyst deactivation. If increased stability allows the process target to be raised from 5 to 8 wppm, hydrogen consumption will decrease, heater firing will decrease and catalyst cycle life will increase significantly. To achieve maximum bene-

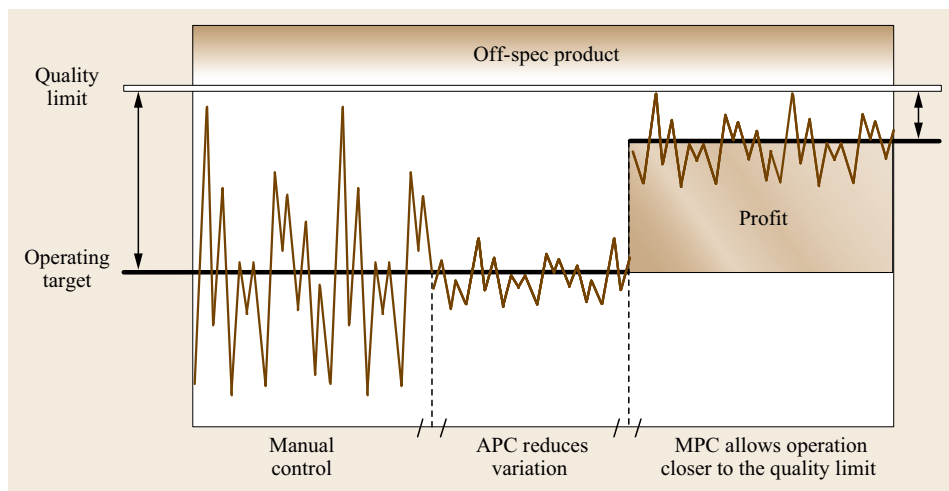


Fig. 26.2 Reducing variability with APC allows MPC to operate the process closer to a product quality limit

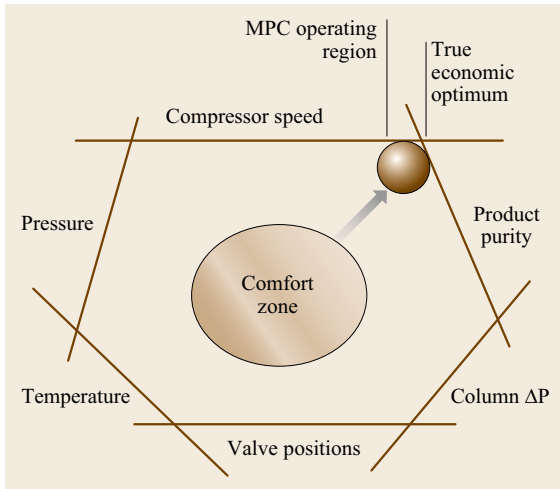


Fig. 26.3 Operating near the right constraints: a major source of MPC benefits

fits, automation requires good and timely information. Hydrotreaters equipped with online analyzers on both feed and product streams are in a much better position than those which rely on thrice daily laboratory measurements.

Speaking of measurements: Operating companies are always looking for ways to cut costs. In the recent past and even today, companies are reducing safety training budgets and analytical costs – with justification. Technology is improving the quality of training while allowing personnel to train when it’s most convenient. Automated training includes testing, which provides some assurance that an employee actually learned something. Automation of laboratories is improving the reliability of test results. Unfortunately, cutting tends to go too far. Deprived of laboratory information, inferential analyzers tend to degrade, sometimes so much that they become useless.

26.4 Implementation

The implementation of MPC requires four main steps – plant response testing, model analysis, commissioning, and training.

During plant response testing, independent variables are moved and dependent-variable responses are captured electronically. Obtaining good plant test data from which accurate models can be regressed is the key to a successful MPC project. For this reason, special care must be taken to ensure that the underlying instrumentation – meters, analyzers, and PID controllers – are properly tuned and calibrated. Traditionally, independent variables were moved manually and one at a time

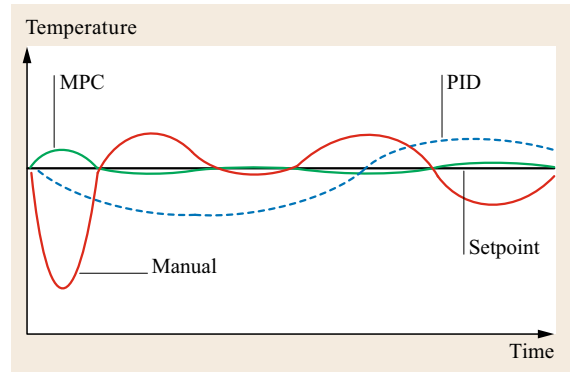


Fig. 26.4 Response to a disturbance: comparison between manual (red), PID (blue) and MPC (green) control

Figure 26.3 illustrates how model-predictive control can achieve additional benefits by pushing against process constraints, such as safe compressor speed, product purity specifications, temperature, pressure, and pressure drop across a column. A well-tuned model-predictive control application can move a unit out of the comfort zone of manual operation into more profitable operation, by pushing simultaneously against multiple process constraints. Special techniques, such as move suppression, are used to prevent the plant from moving too far too fast.

Model-predictive control diminishes the impact of disturbances and quickly returns the process to the desired setpoint. Figure 26.4 compares how response to a disturbance might differ between manual control versus feedback (PID) control versus model-predictive control (MPC). The red line shows open-loop (manual) response. The dotted line shows better response with a PID controller. The green line shows that MPC (1) detected the disturbance in advance and took immediate remedial action, and (2) was the first to return to stable operation at the setpoint.

during the plant response test, but with recently developed software, an engineer can obtain equivalent plant test data using closed loop testing methods. Proprietary identification software converts the data into dynamic models for the plant. Response-test models can be used to predict future plant behavior with the following control equation

$$\delta \mathbf{CV} = \mathbf{A} \times \Delta \mathbf{I}, \quad (26.1)$$

where $\delta \mathbf{CV}$ is the predicted change in a given $\mathbf{CV}(i, j)$, \mathbf{A} is the gain matrix obtained during the model analysis phase, and $\Delta \mathbf{I}$ is a matrix of independent variable.

Fig. 26.5 Example of the control equation in matrix form, where the predicted result is the product of the dynamic response gain matrix **A** and a matrix of independent variable changes $\Delta \mathbf{I}$ ▶

Figure 26.5 shows an example of the control equation in matrix form.

Model predictions are used to control the plant against constraints, as shown in Fig. 26.3. This is not a trivial matter, because the application must cope successfully with the following:

- Plant/model mismatch
- Instrument failure
- Unmeasured disturbances
- Input data error
- Diverse process dynamics
- Changing process objectives.

$$\delta \mathbf{CV} = \mathbf{A} \times \Delta \mathbf{I}$$

$$\begin{bmatrix} \delta CV_1 \\ \delta CV_2 \\ \delta CV_3 \\ \delta CV_4 \\ \delta CV_5 \\ \delta CV_6 \\ \delta CV_7 \end{bmatrix} = \begin{bmatrix} 1 & & & & & & \\ 4 & 1 & & & & & \\ 6 & 4 & 1 & & & & \\ 7 & 6 & 4 & & & & \\ 7 & 7 & 6 & & & & \\ 7 & 7 & 7 & & & & \\ 7 & 7 & 7 & & & & \end{bmatrix} \times \begin{bmatrix} \Delta I_1 \\ \Delta I_2 \\ \Delta I_3 \end{bmatrix} = \begin{bmatrix} 1 \\ 4 \\ 4 \\ -1 \\ -5 \\ -7 \\ -7 \end{bmatrix}$$

Despite these challenges, when implemented by qualified personnel, MPC applications provide considerable value for manufacturing plants throughout the world.

26.5 Costs versus Benefits

Figure 26.6 illustrates the infrastructure required for computer control. APC and model-predictive control software usually run on a separate process computer, which uses a *data highway* to communicate with the

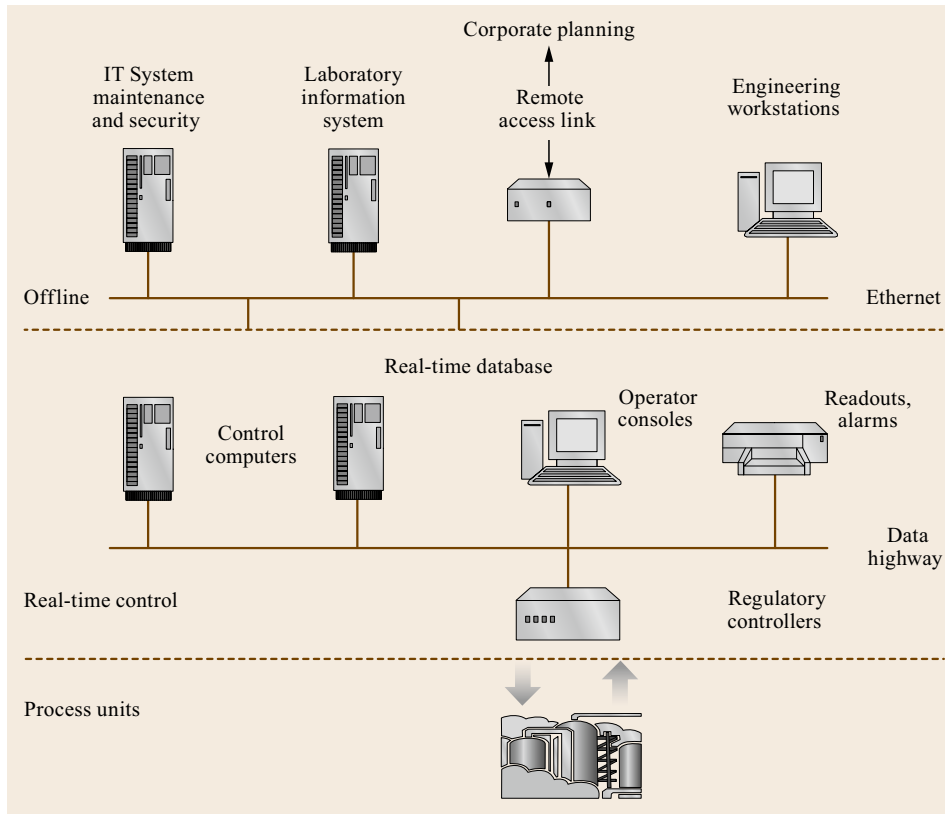
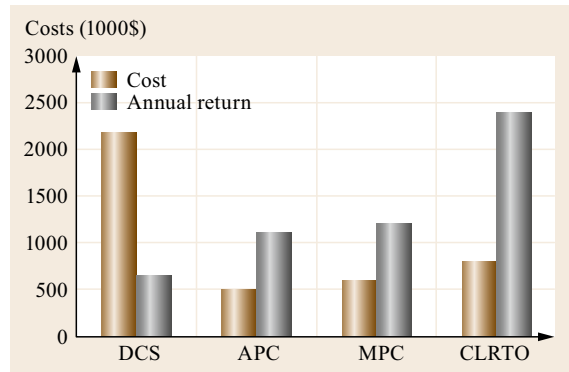


Fig. 26.6
Automation
infrastructure

Fig. 26.7 Relative costs and benefits of process computer applications. DCS = distributive control system, APC = advanced process control, MPC = model-predictive control, CLRTO = closed-loop real-time optimization ►

DCS, the laboratory information management system (LIMS), and a real-time database. Advanced applications receive process values from the DCS, calculate the sizes of MV moves, and send setpoints back to the DCS.

Figure 26.7 compares the relative costs and benefits of computer applications. As is the case for a personal computer, hardware accounts for most of the cost, but software provides the benefits.



References

- 26.1 C.R. Cutler, B.L. Ramaker: Dynamic matrix control – A computer algorithm, Proc. AIChE Natl. Meet., Houston (1979)
- 26.2 L.A. Richard, M. Spencer, R. Schuster, D.M. Tuppinger, W.F. Wilmsen: Austrian refinery benefits from advanced control, Oil Gas J. **93**, 70 (1995)
- 26.3 G.W. Hampton, P.R. Robinson: Controlling hydrocracker temperature excursions, Proc. NPRA Q&A Technol. Forum, San Antonio (2011), Paper PD-11-01
- 26.4 P.J. Vermeer, C.C. Pedersen, W.M. Canney, J.S. Ayala: Blend control system all but eliminates reblends for canadian refiner, Oil Gas J. **95**(30), 74 (1997)

Modeling Refining Processes

Teh C. Ho

Conversion of petroleum fractions and crude oils involves a vast number of chemical species. Modeling of such large reaction systems has been and will continue to be an active research area. There has been an array of approaches bearing on the subject scattered throughout the literature in different contexts. This chapter provides a brief, coherent overview of several selected approaches. The emphasis is on model simplification and mechanism reduction via heuristic concepts and formal mathematical techniques. Among the topics discussed are: top-down and bottom-up kinetic modeling, graph/matrix representation of chemical reactions, mechanistic versus pathways models, quantitative structure–reactivity relationships, asymptotic and optimization methods of dimension reduction, tradeoff between kinetics and hydrodynamics, continuum approximation, collective behavior, and overall kinetics of a large number of reactions. Some common features of dimension reduction approaches are discussed. The areas requiring further investigation are suggested.

27.1	Partition-Based Lumping	842
27.2	Composition-Based Modeling	843
27.2.1	Matrix Representation of Chemical Reactions	843
27.2.2	Splitting and Lumping	845
27.2.3	Mechanistic Modeling	847
27.2.4	Pathways Modeling	848
27.3	Mathematical Reduction of System Dimension	849
27.3.1	Time Scale Separation	849
27.3.2	Perturbation Analysis	850
27.3.3	Modal Analysis	851
27.3.4	Projective Transformation	851
27.3.5	Mathematical Programming	853
27.4	Kinetics–Hydrodynamics Tradeoff	854
27.5	Total Lumping: Continuum Approximation	855
27.5.1	Overall Lumped Kinetics	856
27.5.2	Long-Time Asymptotic Kinetics	857
27.5.3	Reactions in CSTR	858
27.5.4	Summary of Asymptotic Analysis	858
27.5.5	One-Parameter Model	859
27.6	Conclusions	859
	References	860

Petroleum refining is under increasing pressure to produce ultra-clean and high-value products with minimum capital outlays. A low-cost approach to meet this challenge is to develop robust process models capable of predicting how product quality is affected by feedstock composition, operating conditions, catalyst properties, and hardware configuration. Such models allow refiners to take full advantage of recent advances in analytical chemistry, computing, control, and optimization. This chapter provides an overview of modeling of petroleum refining.

Oil-refining processes are characterized by an astronomically large number of reacting species, each generating a complex reaction network. Traditionally, most kinetic models for oil refining have been developed along two lines. One is to divide a petroleum feedstock into a small number of kinetic lumps (or

pseudo-components) and the reactions among them are tracked. An example is the early 10-lump kinetic model for fluid catalytic cracking (FCC) of vacuum gas oil (VGO) [27.1]. Another is to lump all reactants into a single pseudospecies and determine the overall kinetic behavior of the feedstock as a whole. For instance, in hydrodesulfurization (HDS), only the reduction of total sulfur matters, not individual sulfur species. These two approaches may be called partition-based lumping and total lumping, respectively.

Recent developments in analytical chemistry and computing have made it possible to perform molecular speciation analyses on petroleum feedstocks and follow the reactions of a vast number of species computationally. Enormous efforts have been expended in developing detailed chemical kinetics for petroleum refining. To manage diverse refinery streams at a molec-

ular level calls for a bottom-up approach to kinetic modeling. The view is that it is the microscopic interactions at the molecular level that govern the macroscopic behaviors of petroleum fractions at the process scale. Thus, kinetic modeling starts with examining the feedstock at the molecular level, identifying mechanisms and pathways of individual reactions according to established reaction rules, and then working all the way up to the refinery level. To battle with the *curse of dimensionality*, one must sacrifice some exactness by judicious consolidation and pruning. The strategy is to develop high-fidelity, low-dimensional composition-based models through projection onto a subspace of the entire composition space.

Much progress has been made on using a multi-phase computational fluid dynamics (CFD) approach for modeling of hydrodynamically complex reactors. The problems needed to be solved become multidimensional and highly nonlinear. The result is that even with today's prodigious computing power, CFD-based process models can only accommodate rather simple

kinetics, thus, precluding the possibility of managing refinery streams at the molecular level. At the other end of the spectrum are composition-based models, which can accommodate a huge number of reactions but cannot portray the complexities of hydrodynamic effects. This state of affairs underlines the need for a hybrid approach aimed at striking a delicate balance between the kinetics-dominated and hydrodynamics-dominated approaches.

This chapter consists of six sections. The first is a brief account of the traditional top-down, partition-based lumping technique. Next is a discussion of some key features of the bottom-up, compositional modeling approach. Following this is a quick survey of mathematical techniques aimed at exorcising the curse of dimensionality. Then, the tradeoff between kinetics and hydrodynamics in process modeling is discussed using FCC as an illustrative example. The fifth section addresses total lumping. The concluding section points out some potentially fruitful areas for further research. Literature citations are illustrative rather than comprehensive.

27.1 Partition-Based Lumping

It has been a tradition to characterize petroleum feedstocks in terms of specific gravity, average molecular weight, boiling range, and solubility classes, rather than, say distinct individual gasoline molecules. For instance, the early paraffins, olefins, naphthenes, and aromatics (PONA) analysis divides countless number of molecules into just four lumps: paraffins, olefins, naphthenes, and aromatics. The literature abounds with kinetic and reactor models in terms of a small number of coarse lumps. These lumps, satisfying the conservation law and stoichiometric constraints, are usually selected based on measurability and gross properties (e.g., boiling range and solubility). For example, Fig. 27.1 shows an FCC four-lump kinetic model consisting of VGO, gasoline, gases, and coke [27.2].

Highly lumped models have also been developed based on functional groups (or structural moieties). An example is a three-lump model for the kinetics of heat release in hydroprocessing reactors [27.3, 4]. The extent of heat release is governed by three types of

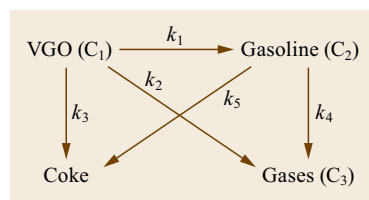


Fig. 27.1 Boiling point based-lump model for FCC; k_i 's are rate constants. (After [27.2])

carbon-carbon bonds: σ -paraffinic, π -aromatic, and π -olefinic.

Residual oils are commonly partitioned into solubility lumps. Figure 27.2 shows a simple lumped model for thermal cracking of residual oils [27.5]. Here, M and A are maltenes (n -heptane soluble) and asphaltenes (toluene soluble/ n -heptane insoluble) in the feed, \bar{M} and \bar{A} are maltene and asphaltene cores, respectively (pyrolysis products), and V is volatiles. All the reactions are first order. The model needs to account for an induction time for coke formation, arising from the separation of a second liquid phase formed from partially converted asphaltene cores. The maximum cracked asphaltene concentration in the solution, $\bar{A}_{\max} = S_L(M + \bar{M})$, is dictated by the solubility limit S_L , which is a fraction of total maltenes. When the excess asphaltene becomes positive, $\bar{A}_{\text{ex}} = \bar{A} - \bar{A}_{\max} > 0$ coke (toluene insoluble) forms instantaneously and separates out as a second

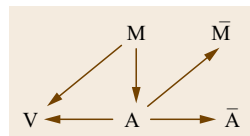


Fig. 27.2 Solubility-based lumped kinetic model for residua pyrolysis: M and A are maltenes and asphaltenes; \bar{M} and \bar{A} are maltene and asphaltene cores; V is volatiles. (After [27.5])

phase. With a single set of stoichiometric coefficients, the model predicts the observed induction period and product slates for pyrolysis of both maltenes and whole resid. This simple model can be used for modeling residuum coking process.

27.2 Composition-Based Modeling

There is a limit to what can be gained by pursuing the top-down lumping approach. For one, the lack of sufficient molecular details makes it very difficult to predict the effects of feedstock composition over a wide range of conditions. A more challenging task is to predict subtle changes in product qualities [27.7]. Against this backdrop, a bottom-up, compositional modeling approach has emerged, which tracks interactions among a huge number of individual reactions. This approach also requires considerable pruning and lumping to fold microscopic events into meso- or macroscopic models. Global lumping is done in the end to predict overall product quality from molecular composition [27.7]. The following sections briefly describe some key aspects of this approach.

27.2.1 Matrix Representation of Chemical Reactions

Individual hydrocarbon species, while enormous in numbers in any boiling cut, belong to a limited set of compound classes (e.g., paraffins, aromatics, and olefins) and structural moieties (e.g., sulfur-, nitrogen-, and oxygen-containing heterocycles). They give rise to a far smaller number of reaction families than that of species or reactions. This fortunate characteristic offers at least two benefits. First, it holds out the prospect for

Besides the solubility-based lumping, residua have also been lumped into several boiling point cuts. For instance, the thermal cracking of a heavy Arabian vacuum residuum in FCC is described by a six-lump model [27.6].

developing structure–reactivity relationships capable of grouping reactions of the same family involving similar transition states. Second, the bookkeeping and transformation of these species, involving breaking and forming bonds, can be automatically and algorithmically tracked by matrix operations.

In a structure-oriented-lumping (SOL) approach [27.8, 9], a hydrocarbon molecule is described by a vector whose components, referred to as structural increments, represent the number of specific structural features. These increments are building blocks for constructing molecules. For example, A6 represents a six-carbon aromatic ring present in all aromatics, whereas A4, a four-carbon aromatic ring, is an incremental structure that must be fused to an A6 or another A4. Figure 27.3 shows the structure vector and its 22 structural increments that comprise three aromatic (A6, A4, and A2) and six naphthenic (N6–N1) ring structures, a $-\text{CH}_2-$ group (R) to specify the carbon number of alkyl chains or paraffins, the number of branches in a chain (br), the number of methyl substituents (me) on rings, bridging between rings (AA), hydrogen deficiency (H), and heteroatom groups. Each group in the vector has carbon, hydrogen, sulfur, nitrogen, and oxygen stoichiometry and hence molecular weight. Also shown in Fig. 27.3 are examples of molecules represented by this type of vectors. The vector components

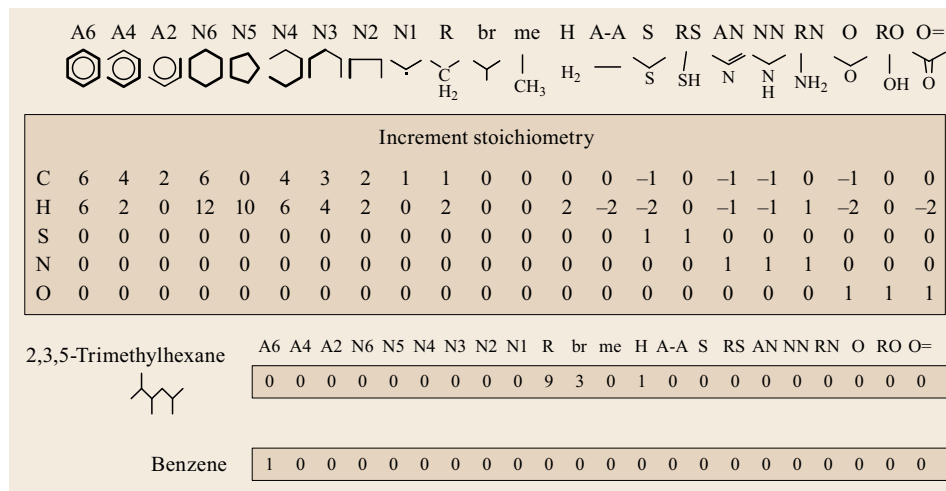


Fig. 27.3 Structure vectors and 22 structural increments defined in the structure-oriented lumping approach. Also shown are examples of SOL molecules. (After [27.8, 9])

indicate the number of increments in each group. Thus, benzene is represented by A6, with the first component of the vector having a value of one and all others zero. A homologous series is a set of vectors having identical structure increments except for the alkyl chain length and possibly the branching and methyl substituent indicators.

Graph theoretic concepts have been exploited to generate a reaction network by *Klein* and coworkers [27.10–12]. A molecule is represented by a graph whose nodes and edges are the atoms and bonds, respectively. This information can be contained in the associated connectivity matrix for a molecule, the numbers denoting the bond order for a bond between two atoms and the diagonal elements denoting an unpaired electron or ion associated with a particular molecule. Figure 27.4 shows an HDS reaction [27.13].

Hydrocarbons have also been represented by Boolean relation matrices [27.14, 15]. The matrix element on the *i*-th row and *j*-th column is *true* if there is

a bond between carbon atoms *i* and *j* in the molecule. Otherwise, a value of *false* is assigned. The number of ones on a row indicates whether a carbon atom is primary, secondary, tertiary, or quaternary. The presence and position of double bonds and a positive charge are provided by arrays. This scheme is illustrated in Fig. 27.5 for shifting methyl from the 2-methyl-3-heptyl carbenium ion to the 3-methyl-2-heptyl carbenium ion. The program searches all neighbors of the positively charged carbon atom and checks if they are linked to any methyl group. If so, the bond between the neighbor and the methyl group is broken and a bond between the methyl group and the positively charged carbon atom is formed.

With bookkeeping algorithms, reaction networks can be automatically generated by a computer based on known reaction rules. Such rules are generally obtained from experiments and sometimes from thermochemical considerations and/or computational chemistry.

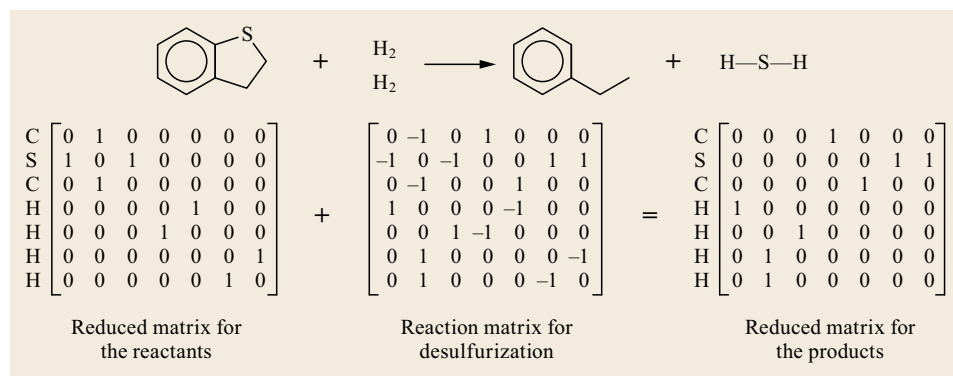


Fig. 27.4 Matrix representation of the HDS of benzothiophene. (After [27.13])

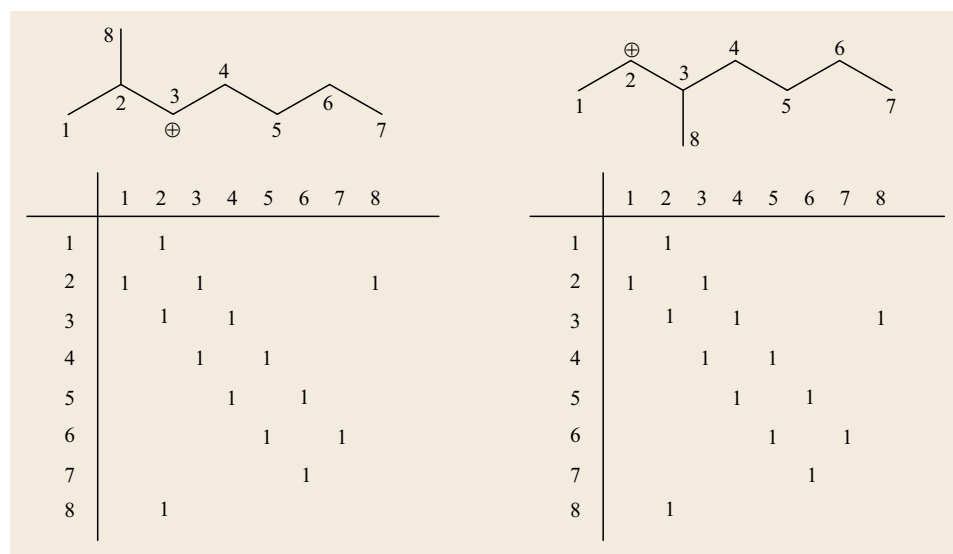


Fig. 27.5 Carbonation represented by Boolean relation matrices. (After [27.14, 15])

27.2.2 Splitting and Lumping

To split a complex mixture, one can take a mechanistic approach that describes reaction networks in terms of elementary steps, including transient intermediates such as adsorbed ions or free radicals in the bulk phase. If this splitting is not fine enough, each elementary step may be decomposed into single events to account for reaction path degeneracy [27.16]. An alternative approach is a pathways-level description that does not consider ions or radicals, as in Sect. 27.2.4.

Whenever possible, the rate and equilibrium constants are estimated from a variety of sources, such as analogies with liquid- and gas-phase reactions, transition state theory, semiempirical techniques, first principle quantum chemical calculations, statistical mechanics, empirical correlations, existing databases, and so on. Various conventional and quantum chemical methods for estimating thermochemical and reaction rate coefficients have been reviewed [27.17, 18]. Most theoretical methods of estimating rate parameters have been applied to homogeneous gas-phase reactions of relatively small molecules at low pressures. However, the majority of oil-refining reactions involve mixtures of large hydrocarbon molecules in the liquid phase at moderate or high pressures and temperatures lower than those used in combustion.

For manageability, the step following the splitting is the preprocessing of the huge number of reactions, which involves simplification and consolidation of the networks of elementary reactions or single events. That is, splitting and mechanism reduction work in tandem.

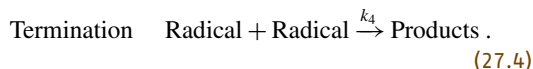
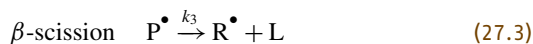
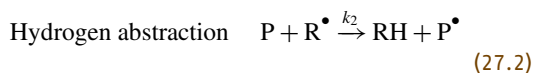
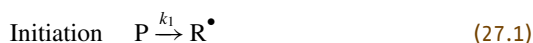
Mechanism Reduction

Kineticists have long used various mechanism reduction techniques [27.19–21] to simplify problems until they become manageable while capturing salient features of the underlying system. Examples of such techniques are as follows:

- Rate-determining step
- Irreversible step approximation
- Relative abundance of catalyst-containing species
- Quasi-equilibrium approximation (QEA)
- Quasi-steady-state approximation (QSSA)
- Long-chain approximation [27.22]
- Large activation energy [27.23]
- Sensitivity analysis [27.24]
- Principal component analysis [27.24]
- Reaction shortsightedness [27.20]
- Analogies with electrical circuits [27.25]
- Thermodynamic constraints and consistencies [27.26, 27].

Some of the above approaches at their core are based on the notion of time scale separation.

A laudable outcome of applying mechanism-reduction techniques is that a set of elementary reactions can be lumped into an overall rate expression capturing the essence of the underlying microscopic events. As an example, consider alkane pyrolysis with free radicals as intermediates. The essential features of this class of chain reactions can be explained by the Rice–Herzfeld mechanism [27.28]. The following elementary reactions are paradigmatic of hydrocarbon pyrolysis



Here, P and P[•] are the parent alkane and parent radicals, respectively, R[•] and RH are lower alkyl radicals and the corresponding alkanes, respectively, and L represents olefins. The hydrogen abstraction and β-scission reactions are the chain-propagation steps. Alkylaromatics and cyclic saturated compounds follow similar pathways, whether the reaction medium is vapor or liquid [27.29]. Invoking the QSSA, one finds that the overall disappearance rate $\bar{\tau}_P$ of the parent molecule obeys an *n*-th-order law

$$\bar{\tau}_P = \bar{k} c_P^n, \quad (27.5)$$

where c_P is the concentration of the parent molecule and $n = 0, 1/2, 1, 3/2, \text{ or } 2$, depending on the nature of the initiating and termination steps [27.28].

Sensitivity and Principal Component Analyses

A complex kinetic model generally has a multitude of interacting dependent variables and rate parameters. The effects of these rate parameters on a given measured dependent variable (concentration, overall rate, selectivity, etc.) vary greatly as the reaction proceeds. Sensitivity analysis can reduce the model by identifying which rate parameters can be lumped or removed from the model in different regions of the composition space [27.30, 31]. It also helps to explore correlations among model parameters and design critical experiments. Before formally eliminating any rate constant from a part of the reaction network, one needs to check if the reduced model retains the structural features of

the original model. For instance, if a branch of the reaction network is equilibrium controlled, the sensitivity coefficients for the forward and backward rate coefficients are small. However, removing this branch may not be desirable.

Using the principal component analysis (PCA) can vastly simplify the analysis of the mass of numerical information generated from the sensitivity analysis [27.32]. It identifies the dominant reactions and the interactions among constituent reactions. There are many examples of using the sensitivity analysis for contracting reaction networks. For catalytic cracking of isobutene, only 31 out of 367 steps are kinetically significant [27.33]. A 10-lump FCC model can be contracted to five coarser lumps [27.34]. Combining sensitivity analysis and PCA allows 46 elementary water–gas shift reactions on Pt to be lumped into an overall, one-step rate expression covering both the kinetics- and equilibrium-controlled regimes [27.24]. This one-step rate model is needed for a CFD-based reactor model. The success of the final reactor model crucially depends on how credible the overall, reduced kinetic model is.

Quantitative Structure–Reactivity Relationship

The size of the reduced model obtained from application of the above techniques may still be undesirably large, necessitating further reduction and parameterizations. This is usually accomplished by finding quantitative structure–reactivity relationships (QSRRs) for various reaction families. The term QSRR broadly means a correlation that quantitatively relates the response (e.g., reactivity and adsorptivity) of a group of chemical species to changes in certain common physicochemical characteristics (descriptors) of the constituent species. The behavior of the entire family is describable by a small set of parameters determined experimentally or theoretically. For instance, the hydrogenation of alkylbenzenes is a reaction family in which all member compounds share the same chemical moiety and undergo the same reaction. The reactivity varies systematically with the moiety's electronic density governed by the substituents.

A simple QSRR example is the semiempirical linear free energy relationship (LFER), which may take the simple form $\ln k_i = a + bz_i$, where k_i and z_i are the rate constant and descriptor value for molecule i , respectively [27.10]. The choice of descriptor z_i reflects the controlling mechanism of the reaction, such as the aromatics' electronic properties in hydrogenation, carbocation stability in catalytic cracking, or reaction enthalpy in pyrolysis. Once the constants a and b are known, which are experimentally determined in most cases, the rate constants for all members of the reaction family can be calculated from z_i . A complex system

may need multiple descriptors, which can be measured or computed.

The LFER approximation has been known for some time [27.35–37]. It is an essential tool for modeling oil-refining reactions. Typically, the number of independent rate constants for modeling individual gas oil reactions is of the order 10^4 [27.4], whereas that of LFER parameters is of the order 10 [27.38, 39]. Most QSRRs have been developed by means of theoretical or experimental methods. For instance, using the group contribution method can reduce the problem of establishing FCC kinetics for hundreds of species to one of determining two dozen parameters experimentally [27.40, 41]. Adsorption equilibrium constants have been estimated from an integrated form of Van 't Hoff's equation [27.42, 43]. Density-functional theory (DFT) calculations have shown that the hydrodenitrogenation (HDN) reactivities of cyclohexylamines and alkylpiperidines correlated with the negative Mulliken charges on the nitrogen atom [27.44].

For a simple homologous reaction family, one could probably identify what would be the dominant descriptors on intuitive grounds. For instance, it is reasonable to expect that chain length should be the most relevant descriptor when a linear paraffin's overall cracking rate is of primary concern. Indeed, the catalytic cracking rate scales as $N_c(N_c - 5)$, where N_c is number of carbon atoms in the chain [27.45]. The rate constants for olefin oligomerization on the ZSM-5 catalyst decrease with increasing N_c , based on diffusion considerations [27.46].

For more complex systems involving a large descriptor space, one faces the question of which descriptors from a long list of candidates are most relevant. There are many different types of descriptors. Some examples are as follows: constitutional (derived from atomic composition of compounds, e.g., counts of atoms and bonds), geometric (derived from three-dimensional atomic coordinates, e.g., molecular volume), topological (e.g., molecular connectivity), electrostatic (e.g., polarity indices), and quantum-chemical (e.g., bond orders). Some quantum-chemical descriptors can be calculated from available software (e.g., MOPAC and AMPAC). The following is an example of building a practical QSRR from a set of descriptors.

Organonitrogen species and polynuclear aromatic compounds are known to poison FCC catalysts through competitive adsorption. There are many different structural types of nitrogen compounds and aromatics. Candidate descriptors may include pK_a , proton affinity (PA), electron density around the nitrogen atom, various molecular connectivities, boiling point, molecular volume, to name a few [27.47]. In order not to miss any important descriptors, it pays to include all plausi-

ble descriptors at first, even though some of them show varying degrees of correlation. The result is a large descriptor space whose dimension must be drastically reduced for tractability and physical clarity. This is achieved by projecting the raw data onto a subspace with fewer orthogonal dimensions via the partial least squares (PLS) analysis [27.47–51]. The purposes are to eliminate data collinearity and gain insights into underlying fundamentals and therefore identify dominant descriptors. The thus-identified dominant descriptors are used to construct a compact correlation collapsing the data.

To illustrate, consider the poisoning effects of 32 nitrogen and aromatic compounds on FCC catalysts [27.47]. Let the poisoning power of the i -th poison (nitrogen or aromatic compounds) be y_i , a component of the vector \mathbf{Y} . For each poison, 24 descriptors are selected, hence the descriptor space is represented by a 32×24 matrix \mathbf{Z} . Each column contains the values of a particular descriptor for all 32 poison compounds, whereas each row contains all 24 descriptor values for a particular poison compound. If one uses conventional statistical regression methods (e.g., least squares) to find a linear correlation between \mathbf{Y} and \mathbf{Z} , the problem is ill-conditioned due to data collinearity. The resulting correlation would not be robust and has a large prediction variance. Using neural networks for constructing nonlinear models suffers from the same problem [27.52]. It is thus essential to eliminate data collinearity prior to model building. PLS achieves this by linearly combining all descriptors to form a new set of uncorrelated latent variables (LVs). The LVs are obtained in order of diminishing accountability: the first LV accounts for the largest amount of variation in \mathbf{Y} , the second LV explains the second largest amount of \mathbf{Y} variation, and so on. Dimension reduction is then accomplished by retaining only the first few LVs. Examining the major descriptors contributing to these dominant LVs helps reveal the physics of the system, which provide the basis for building a linear or nonlinear correlation in terms of these key descriptors. Such dominant descriptors are uncorrelated and their number is small [27.47–49]. The resultant correlation has clear physical meanings.

The PLS is more than just a tool for dimension reduction and model building, it should be used for gaining physical insights. For example, the PLS results indicate that of the 24 structural descriptors, the most influential one is molecular weight (MW) – followed by proton affinity. The best polynomial model is of the form [27.47]

$$y_i = 0.075 + 0.74(MW_i)^2(PA_i)^2 - 0.41(MW_i)^3, \quad (27.6)$$

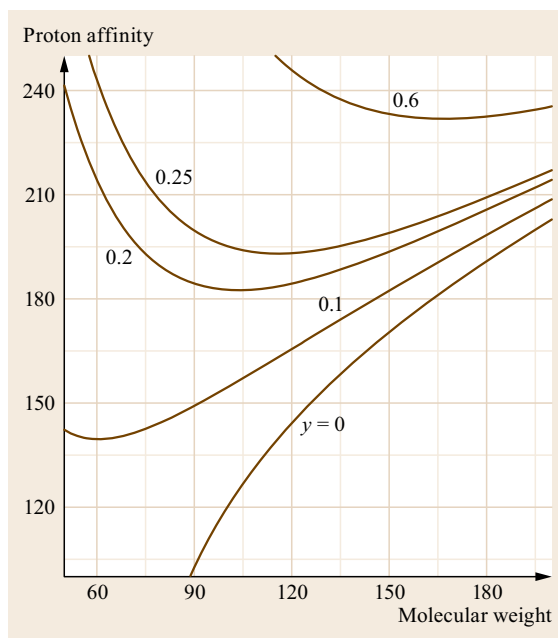


Fig. 27.6 Contour plot of poisoning value y_i versus MW_i and PA_i . (After [27.47])

where MW_i and PA_i are normalized values. That molecular weight (or size) is more important than PA counters conventional wisdom, which has held that basicity is the key determinant of poisoning potency. Moreover, the correlation reveals a pore diffusion effect: At a constant PA, poisoning increases with MW, but only up to a certain point beyond which poisoning starts to decrease, as shown in Fig. 27.6. Here, y_i can be viewed as a proxy for the apparent adsorption equilibrium constant. Then, MW and PA play the roles of adsorption entropy and enthalpy, respectively. This example demonstrates that in many cases a hydrocarbon processing system, complex as it is, can actually be governed by a small number of dominant physicochemical events once it is distilled to its essence.

27.2.3 Mechanistic Modeling

We now highlight approaches for developing fundamental models that include such mechanistic details as adsorbed ions or free radicals. Microkinetic analysis of surface reaction mechanisms helps developing a kinetic model for a network of elementary surface reactions [27.53]. By judiciously selecting a probe reaction, the analysis provides insights into the underlying mechanisms for a reaction family over a given catalyst type. This approach also provides a sensitive tool for characterizing a catalyst family. *Yaluris* et al. gave illustrative examples for isobutane cracking over zeo-

lite Y-based FCC catalysts from 733 to 773 K [27.54, 55]. Pruning the reaction network is an integral part of the analysis. An Evans–Polanyi type of correlation is used to parameterize the observed activation energies E_a based on known thermodynamic properties of gas phase hydrocarbons and carbocations. In so doing, the number of fitting parameters can be substantially reduced.

The single-event theory proposed by *Froment* [27.16] in essence is a structure-oriented approach. Its basic idea is to link rate constant to molecular structure, thereby, reducing the number of rate coefficients. This is done by factoring out the structure effect from the change of standard entropy associated with the reactant-to-product transformation through a transition state. The standard entropy consists of translational, vibrational, and rotational contributions. The last one can be considered as representative for the structure and written as

$$S_{\text{rot}} = \hat{S}_{\text{rot}} - R \ln \sigma,$$

where \hat{S}_{rot} is an intrinsic term and σ relates to the symmetry number of the species. If chirality needs to be considered, a global symmetry number $\sigma_{\text{gl}} = \sigma/2^{\tilde{n}}$ is introduced, where \tilde{n} is the number of chiral centers in the species. The change in the standard entropy due to symmetry changes in going from reactant (superscript r) to the transition state is

$$\Delta S_{\text{symm}} = R \ln \frac{\sigma_{\text{gl}}^r}{\sigma_{\text{gl}}^{\ddagger}}. \quad (27.7)$$

One can factorize the rate constant k into two terms, namely,

$$\begin{aligned} k &= \left(\frac{\sigma_{\text{gl}}^r}{\sigma_{\text{gl}}^{\ddagger}} \right) \left[\left(\frac{k_B T}{h} \right) \exp \left(\frac{\Delta \hat{S}}{R} \right) \exp \left(-\frac{\Delta H^{\ddagger}}{RT} \right) \right] \\ &= n_e \hat{k}. \end{aligned} \quad (27.8)$$

Here, $n_e \equiv \sigma_{\text{gl}}^r / \sigma_{\text{gl}}^{\ddagger}$, the number of single events for the elementary step, accounts for the structural effect, whereas \hat{k} is the single-event rate coefficient that is structure invariant. To calculate n_e requires information on species structure, which may be obtained from available quantum chemical software. This approach vastly reduces the number of single event rate coefficients. There are many oil-refining kinetic models based on the single event approach, as exemplified by FCC of VGO to which a massive consolidation of reactions is

essential [27.56]. Modeling of catalyst coking was also attempted [27.57].

27.2.4 Pathways Modeling

Applying the mechanistic modeling approach to refining processes is no easy task because of the sheer size of the reaction network, the more so when the kinetics must be combined with reactor hydrodynamics and heat transfer in attacking practical problems. These issues motivated the development of a simpler approach by neglecting transient intermediates (e.g., carbocations or free radicals) and focusing on dominant reaction pathways.

An example of pathways modeling is the SOL approach, which describes a petroleum mixture as a large set of structure vectors of different concentrations (e.g., weight percentages), with each vector being a molecule or a collection of isomers [27.8, 9]. Collections of reaction rules are defined for the thousands of representative hydrocarbon components. Typically, petroleum process chemistry is defined by 20–30 reaction families resulting in more than 50 000 reactions. Each refining process (e.g., FCC and HDS) has its own reaction rules, although all petroleum mixtures have the same vector representation. The isomers of a molecular class for a given carbon number are assumed to have similar physical, chemical, and thermodynamic properties. Lumping is largely done through consolidation of reaction types by invoking, for instance, the equal reactivity assumption and QSSRs.

The SOL approach has led to a number of oil-refining process models. For FCC applications, the approach applies reaction rules to more than 30 000 reactions involving over 3000 species [27.58]. These species include representative molecules, isomeric lumps, micro-lumps, and so on. The model can predict both product yields and composition for a range of feeds and catalysts with a single set of kinetic parameters and QSRRs. A more compact FCC model [27.59] involving 450 species and 5500 reactions was developed, featuring a stochastic approach for constructing molecular structures of gas oil feedstock. The model reveals that a significant protolytic cracking rate defines much of the product distribution for light catalytic cycle oil, whereas significant hydride-abstraction defines the gasoline product distribution. A hybrid approach is used to develop a molecule-based model for catalytic reforming [27.60]. The acid catalytic chemistry is described at the mechanistic level, whereas the metal chemistry at the pathways level. The assumption is that some exactness can be sacrificed for the metal chemistry with impunity.

27.3 Mathematical Reduction of System Dimension

This section is a very brief account of mathematical techniques for dimension reduction. The interested reader should consult the original references for details. In broad terms, an underlying theme in many of the techniques is to obtain a low-dimensional model by truncating an asymptotic expansion. This entails transforming the state variable (e.g., the vector function \mathbf{c}) into a new set of pseudostate variables with more desirable properties. For instance, the system behavior is expressed as a weighted sum of optimally selected basis functions (e.g., eigenfunctions or eigenvectors) – in descending order of influence. That is, the first term is the most influential. There then follows the second, the third term, and so forth. A low-dimensional model is therefore obtained by keeping only the first few terms. In so doing, one focuses only on the most essential part of the problem. This approach is also referred to as order reduction.

Let us consider an isothermal system governed by the following mass balance equation for N_s reacting species represented by the $N_s \times 1$ concentration vector \mathbf{c}

$$\frac{d\mathbf{c}}{dt} = \mathbf{f}(\mathbf{c}), \quad \mathbf{c}(0) = \mathbf{c}_f, \quad (27.9)$$

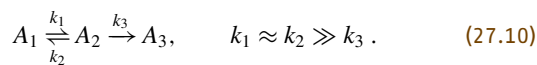
where t is space time (plug-flow reactor) or time (batch reactor) and \mathbf{c}_f is the feed concentration vector. The goal is to find a low-dimensional system that can at least approximately portray the behavior of the underlying full system. For first-order reactions $\mathbf{f} = \mathbf{K}\mathbf{c}$, where \mathbf{K} is the matrix of rate constants k_{ij} . Reference [27.61] is a brief review of some mathematical methods of dimension reduction.

27.3.1 Time Scale Separation

Although kinetically complex systems often have a multitude of widely disparate time scales, seldom does the need for considering all of them during the course of the reaction arise. This characteristic lends itself to dimension reduction. Suppose that the time window of interest is $\underline{t} \leq t \leq \bar{t}$. Species reacting with time scales much shorter than \underline{t} may be considered relaxed. The state of these fast-reacting species can be treated as initial conditions. On the other hand, species reacting on time scales much longer than \bar{t} remain dormant; their concentrations are essentially frozen and may be treated as system parameters.

The mathematical techniques considered here are the perturbation method, modal analysis, and projective transformation. To put them in perspective and illustrate the interplay of physical and mathematical viewpoints

in model reduction, we consider the quasi-equilibrium system of first-order reactions as



Here, A_1 and A_2 quickly reach equilibrium after which the system becomes one-dimensional, for it is governed by the slow depletion of the equilibrium pool of $(A_1 + A_2)$ due to the *leakage* reaction with rate constant k_3 . The time scale disparity is gauged by $\varepsilon = k_3/k_1 \ll 1$. (Throughout this chapter, ε denotes a small positive number, with its physical meaning depending on the context.)

Let c_1 and c_2 be the concentrations of A_1 and A_2 , respectively. The initial conditions are $c_1(0) = c_{1f}$ and $c_2(0) = c_{2f}$. With $\tilde{c}_1 = c_1/c_{1f}$, $\tilde{c}_2 = c_2/c_{1f}$, the system dynamics is described by

$$\frac{d\tilde{\mathbf{c}}}{dt} = \begin{bmatrix} -k_1 & k_2 \\ k_1 & -(k_2 + k_3) \end{bmatrix} \begin{bmatrix} \tilde{c}_1 \\ \tilde{c}_2 \end{bmatrix} = \mathbf{K}\tilde{\mathbf{c}}. \quad (27.11)$$

For $k_1 = 1$, $k_2 = 0.6$, and $k_3 = 0.05$, the eigenvalues of \mathbf{K} are -0.0309 and -1.6191 , hence the system has two well-separated time scales: $| -1/0.0309 | = 32.36$ versus $| -1/1.6191 | = 0.62$. If the short initial transient is not of interest, the system can be projected onto a one-dimensional subspace. Referring to Fig. 27.7, the subspace is invariant in that *once you get in, you cannot get out*. Regardless of their starting points, all trajectories get attracted to the common subspace (solid line)

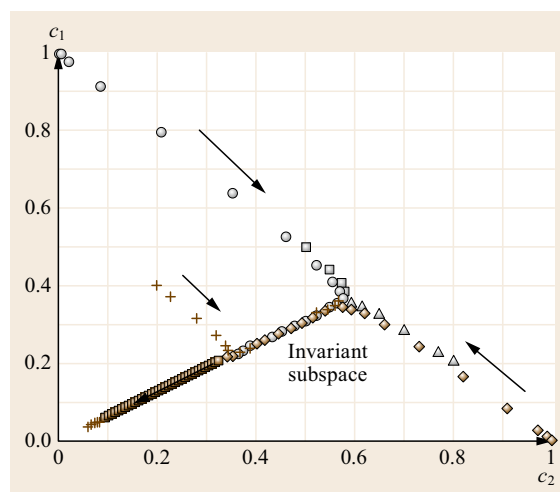


Fig. 27.7 A common invariant subspace (thick solid line) attracts reaction trajectories originated from different initial compositions for the reaction in (27.10); $k_1 = 1$, $k_2 = 0.6$, and $k_3 = 0.05$

after an exponentially fast transient. In this subspace, A_1 and A_2 are related to each other algebraically due to the quasi-equilibrium. The movement of the system toward equilibrium is governed by the slow motion within the invariant subspace, which is confined to a very small region of the composition space. Yet, it is this region that is of interest shortly after the startup of the reaction. In practice, process controllers are usually designed to operate a reactor around the invariant subspace.

27.3.2 Perturbation Analysis

To look at the system from a long-time perspective, we use a slow-time scale defined as $\tau = k_3 t$. Let $K = k_2/k_1$, (27.11) becomes

$$\varepsilon \frac{d\tilde{c}}{d\tau} = \begin{bmatrix} -1 & K \\ 1 & -(K + \varepsilon) \end{bmatrix} \begin{bmatrix} \tilde{c}_1 \\ \tilde{c}_2 \end{bmatrix}. \quad (27.12)$$

Given that $\varepsilon \ll 1$, one seeks the solution in the form $\tilde{c}_1 = \tilde{c}_{10}(\tau) + \varepsilon \tilde{c}_{11}(\tau) + O(\varepsilon^2)$ and $\tilde{c}_2 = \tilde{c}_{20}(\tau) + \varepsilon \tilde{c}_{21}(\tau) + O(\varepsilon^2)$. Substituting these series expansions into (27.12) and equating coefficients of like powers of ε , one obtains a set of equations for \tilde{c}_{1j} and \tilde{c}_{2j} ($j = 0, 1, 2, \dots$). For practical purposes, retaining only the leading-order terms (denoted by the subscript 0) of the expansion suffices because ε is sufficiently small. Then, the original problem is reduced to an algebraic equation coupled with a differential equation for a lumped species, namely

$$\tilde{c}_{10} = K\tilde{c}_{20} \quad (27.13)$$

$$\frac{d(\tilde{c}_{10} + \tilde{c}_{20})}{d\tau} = -\tilde{c}_{20}. \quad (27.14)$$

Thus, on the long-time scale, A_1 and A_2 are essentially in equilibrium (27.13) and move together as a lump (27.14). Solving (27.13) and (27.14) gives

$$\tilde{c}_{10} = Kb^* e^{-\tau/(1+K)}, \quad \tilde{c}_{20} = b^* e^{-\tau/(1+K)}, \quad (27.15)$$

where b^* is the yet-to-be-determined *initial* condition ($\tau = 0$) for the slow-time scale problem. Equation (27.15) describes the slow movement of the ($A_1 + A_2$) lump: It decays slowly with the time constant $(1 + K)/k_3 = 32$. The QEA is nothing but the leading-order term of the perturbation series, corresponding to the solution to the unperturbed problem ($\varepsilon = 0$).

The above reduced model, obtained from a long-time asymptotic analysis, is invalid over the initial

transient period. To examine the small- t dynamics requires a separate perturbation series on a short-time scale. Only when these two perturbation expansions are pieced together can one obtain a complete picture of the reaction trajectories for all t . This is done through matching in the regions of overlap between the small- t and large- t domains. This type of perturbation problems is called singular. A regular perturbation problem is easier to solve as it requires only one perturbation series for all t .

We now probe the short-time behavior (or the boundary-layer effect in perturbation parlance). To this end, we use a fast-time scale $\bar{\tau} = k_1 t$. The mass balances become $d\tilde{c}_1/d\bar{\tau} = -\tilde{c}_1 + K\tilde{c}_2$ and $d\tilde{c}_2/d\bar{\tau} = \tilde{c}_1 - (K + \varepsilon)\tilde{c}_2$ with $c_1(0) = c_1^*$ and $c_2(0) = c_2^*$, respectively. Adding these two equations yields $d(\tilde{c}_1 + \tilde{c}_2)/d\bar{\tau} = -\varepsilon\tilde{c}_2 \approx 0$, hence to leading order, $(\tilde{c}_1 + \tilde{c}_2) = \text{constant} = (c_1^* + c_2^*)$ over the initial period. This provides the needed initial condition for the large- t expansion; that is, setting $\tau = 0$ in (27.15) leads to $b^* = (c_1^* + c_2^*)/(1 + K)$, thus, completing the matching of the two expansions. Solving the unperturbed problem ($\varepsilon = 0$) reveals that during the initial period, A_1 and A_2 equilibrate at an exponentially fast rate, with a characteristic time scale of $1/[k_1(1 + K)] = 0.63$, to leading order.

The singular perturbation technique has often been used to attack nonlinear problems of high dimensionality [27.62]. Typically, the system in question is split into slow (subscript s) and fast (subscript f) subsystems in the following singularly perturbed form

$$\frac{dc_s}{dt} = f_s(c_s, c_f), \quad \varepsilon \frac{dc_f}{dt} = f_f(c_s, c_f), \quad (27.16)$$

where f_s and f_f are n_s -, n_f -dimensional vector functions, respectively, with $n_s + n_f = N_s$. The product $\varepsilon(dc_f/dt)$, symptomatic of a singular perturbation problem, cannot be dropped because dc_f/dt is sufficiently large (order of $1/\varepsilon$) for small t . In other words, the zeroth-order model $f_f(c_{s0}, c_{f0}) = \mathbf{0}$, obtained by setting $\varepsilon = 0$, cannot portray the rapidly changing behavior of c_f in the boundary-layer (small t) region of the composition space. So, the dc_f/dt term must be retained for small t by adopting a commensurately fast-time scale $t^* = t/\varepsilon$. An asymptotic solution for the small- t domain can be found through the expansion $c_f(t^*) = c_{f0} + \varepsilon c_{f1} + O(\varepsilon^2)$. A uniformly valid solution for all t can then be obtained by piecing together the short- and long- t expansions. This discussion is illustrative of an important tactic for dimensionality reduction: It is often necessary to divide the whole domain into several subdomains and develop a reduced model for each subdomain.

27.3.3 Modal Analysis

For linear systems represented by $d\mathbf{c}/dt = \mathbf{K}\mathbf{c}$, the approach is to decompose the original full system into dynamically independent modes. This is done through the decomposition $\mathbf{K} = \mathbf{X}^{-1}\mathbf{\Lambda}\mathbf{X}$, where $\mathbf{\Lambda}$ is the diagonal matrix of eigenvalues λ_i of \mathbf{K} . \mathbf{X} is taken as the modal matrix whose columns are the associated eigenvectors \mathbf{x}_i , and \mathbf{X}^{-1} is the inverse of \mathbf{X} . The modal system $\bar{\mathbf{c}}$ is obtained under the linear transformation

$$\bar{\mathbf{c}} = \mathbf{X}^{-1} \mathbf{c}, \quad (27.17)$$

which decouples the original system by virtue of the fact $d\bar{\mathbf{c}}/dt = \mathbf{\Lambda}\bar{\mathbf{c}}$ with $\bar{\mathbf{c}}(0) = \bar{\mathbf{c}}_f$. Hence, for $\bar{\mathbf{c}}(t) = \bar{\mathbf{c}}_f \exp(\mathbf{\Lambda}t)$, each mode \bar{c}_i moves independently with its own characteristic time scale $1/|\lambda_i|$. Back to the QEA case (27.10), the slow and fast eigenvalues are the roots of $\lambda^2 + (1+K+\varepsilon)\lambda + \varepsilon = 0$. Thus, $\lambda_s = -\varepsilon/(1+K) + O(\varepsilon^2) \approx -0.0313$ and $\lambda_f = -(1+K) + O(\varepsilon) \approx -1.6$. It follows that $\bar{c}_{s0} = \bar{c}_{10} + \bar{c}_{20} = \exp(-\lambda_s t) \approx \exp(-0.0313t)$ and $\bar{c}_{f0} = -\bar{c}_{10}/K + \bar{c}_{20} = \exp(-\lambda_f t) \approx \exp(-1.6t)$, reproducing the results from the perturbation method. The slow mode is the dominant one over much of the time period since the fast mode dies out rapidly during the transient period en route to the quasi-equilibrated state.

To recapitulate, suppose that λ_j 's are such that $|\lambda_1|, |\lambda_2|, \dots, |\lambda_k| \gg |\lambda_{k+1}|, |\lambda_{k+2}|, \dots, |\lambda_{N_s}|$ and we are interested only in events on time scales longer than $1/|\lambda_k|$. Then, dimensionality (or order) reduction is achieved by weeding out those fast, relaxed modes and projecting the system to a common $(N_s - k)$ dimensional subspace. This subspace, associated with slow time scales, is spanned by eigenvectors $\mathbf{x}_{k+1}, \mathbf{x}_{k+2}, \dots, \mathbf{x}_{N_s}$ as follows

$$\bar{\mathbf{c}} = \sum_{j=k+1}^{N_s} \bar{c}_{j,f} \exp(\lambda_j t) \mathbf{x}_j \quad t \gg \frac{1}{|\lambda_k|}. \quad (27.18)$$

Relaxing those fast modes provides algebraic relations among species, which can be substituted into the slow equations that govern the movement toward the equilibrium point. This linear analysis also forms the basis for attacking certain nonlinear systems through linearization and decoupling [27.62–64].

For more complicated situations, the system time scales vary with time. No clear distinction between fast and slow modes can be made. To circumvent the problem, a so-called computational singular perturbation (CSP) scheme has been developed [27.65]. The eigenvectors and associated adjoint eigenvectors are computed locally at any time. The CSP algorithm

then minimizes local mode coupling/mixing by deriving a progressively more *intelligent* set of basis vectors from any reasonable set of initial trial basis vectors. This is done on-the-fly as reactions proceed by using a recursive refinement procedure. The approach can distinguish fast and slow modes and account for the boundary-layer effect.

27.3.4 Projective Transformation

The approach here is to lump reacting species into a smaller number of pseudospecies through a linear transformation of the N_s -tuple vector \mathbf{c} into an \hat{N}_s -tuple vector $\hat{\mathbf{c}}$ ($\hat{N}_s < N_s$) with an $\hat{N}_s \times N_s$ constant matrix \mathbf{M} of the rank \hat{N}_s , that is,

$$\hat{\mathbf{c}} = \mathbf{M}\mathbf{c}. \quad (27.19)$$

Thus, the original N_s -dimensional space is projected onto a smaller \hat{N}_s -dimensional space. For first-order reaction system represented by $d\mathbf{c}/dt = \mathbf{K}\mathbf{c}$, the dynamics is dictated by the eigenvalues λ_i and eigenvectors \mathbf{x}_i of \mathbf{K} . The system is said to be exactly lumpable by the lumping matrix \mathbf{M} if an $\hat{N}_s \times \hat{N}_s$ matrix $\hat{\mathbf{K}}$ exists such that [27.66]

$$\frac{d\hat{\mathbf{c}}}{dt} = \hat{\mathbf{K}}\hat{\mathbf{c}}. \quad (27.20)$$

This is achievable if and only if

$$\mathbf{M}\mathbf{K} = \hat{\mathbf{K}}\mathbf{M}. \quad (27.21)$$

The consequence of the lumpability on the system's eigenspace is that the vector $\mathbf{M}\mathbf{x}_i$ either vanishes or is an eigenvector of $\hat{\mathbf{K}}$ with the same eigenvalue λ_i of \mathbf{K} , that is,

$$\mathbf{M}\mathbf{x}_i = \mathbf{0} \quad \text{or} \quad \hat{\mathbf{K}}(\mathbf{M}\mathbf{x}_i) = \lambda_i(\mathbf{M}\mathbf{x}_i). \quad (27.22)$$

The matrix $\hat{\mathbf{K}}$ has only \hat{N}_s eigenvectors derived from \mathbf{x}_i , $\hat{\mathbf{x}}_i = \mathbf{M}\mathbf{x}_i$. Thus, lumping amounts to crossing out some eigenvectors of \mathbf{K} , suggesting some degree of system decoupling. The fact that $\hat{N}_s < N_s$ means that we are solving an *underdetermined* problem. Finding $\hat{\mathbf{K}}$ from given \mathbf{M} and \mathbf{K} amounts to solving an optimization problem involving minimizing $\|\mathbf{M}\mathbf{K} - \hat{\mathbf{K}}\mathbf{M}\|^2$. A least-squares solution of (27.21) gives

$$\hat{\mathbf{K}} = \mathbf{M}\mathbf{K}\mathbf{M}^T (\mathbf{M}\mathbf{M}^T)^{-1}. \quad (27.23)$$

Determination of Lumping Matrices

\mathbf{K} defines the adjoint eigenvalue problem $\mathbf{K}^T \underline{x}_i = \lambda_i \underline{x}_i$. Transposing (27.21) gives

$$\mathbf{K}^T \mathbf{M}^T = \mathbf{M}^T \hat{\mathbf{K}}^T, \quad (27.24)$$

where \mathbf{M}^T and $\mathbf{M}^T \hat{\mathbf{K}}^T$ are both $N_s \times \hat{N}_s$ matrices. Equation (27.24) says that the mapping of \mathbf{K}^T on \mathbf{M}^T is to produce a matrix that still remains in the same vector space. The vector space represented by \mathbf{M}^T is said to be an invariant subspace of \mathbf{K}^T . The simplest \mathbf{K}^T -invariant subspace is the one-dimensional, straight line containing \underline{x}_1 : That $\mathbf{K}^T \underline{x}_1 = \lambda_1 \underline{x}_1$ means any vector $a \underline{x}_1$ (a , a constant) upon mapping by \mathbf{K}^T produces the vector $a \lambda_1 \underline{x}_1$ that remains on the same straight line. Thus, \mathbf{M} can be constructed from any of the invariant subspaces of \mathbf{K}^T . That is to say, \mathbf{M} can be determined from the modal matrix of \mathbf{K}^T , denoted by \mathbf{X} (i.e., $\mathbf{X}^{-1} \mathbf{K}^T \mathbf{X} = \Lambda$). Since $\mathbf{X}^{-1} = \mathbf{X}^T$, \mathbf{M} can also be determined from \mathbf{X}^{-1} . This says that lumping leverages optimization approaches to find the best invariant subspace capturing the essential features of the full system (more on this in Sect. 27.3.5).

Practitioners often perform lumping by summing up the concentrations of chemically similar species with equal weight. This direct sum is a special case of the so-called *proper lumping* [27.66], meaning that each column in \mathbf{M} is a canonical unit vector having a single nonzero entry of unity, for example,

$$\hat{c} = \mathbf{M}c = \begin{bmatrix} 1 & 1 & 0 \\ 0 & 0 & 1 \end{bmatrix} c. \quad (27.25)$$

For proper lumping, a *cluster analysis* can be used to determine $\hat{\mathbf{K}}$, which is based on an invariant response principle [27.67]. A mixture with innumerable components can be practically treated as a continuum (more on this later); the counterpart of (27.20) is available for continuous mixtures [27.68].

For perspective, let us return to the reaction system shown in (27.10) and (27.11). To leading orders, the eigenvectors of \mathbf{K}^T are $\underline{x}_{s0} [1, 1]^T$ and $\underline{x}_{f0} = [-1/K, 1]^T = [-1.67, 1]^T$. These approximate eigenvectors lead to the following lumping matrices: $\mathbf{M}_s = [1, 1]$ and $\mathbf{M}_f = [-1.67, 1]$, with the corresponding lumped species $\hat{c}_{s0} = c_1 + c_2$ and $\hat{c}_{f0} = -1.67c_1 + c_2$. The associated lumped rate constants can be calculated from (27.23). The resulting lumped models are

$$\frac{d\hat{c}_{s0}}{dt} = -0.031\hat{c}_{s0}, \quad \frac{d\hat{c}_{f0}}{dt} = -1.619\hat{c}_{f0}. \quad (27.26)$$

The trajectories in Fig. 27.8 are calculated from (27.26) for the same initial conditions as those for

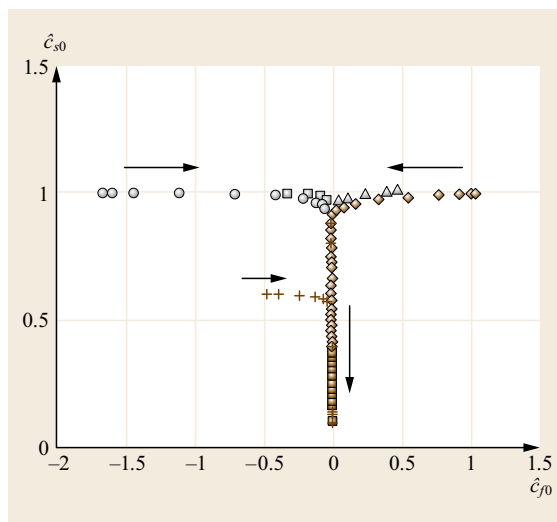


Fig. 27.8 Reaction trajectories calculated from lumped and full model for the reaction in (27.10) with different initial compositions. $k_1 = 1$, $k_2 = 0.6$, and $k_3 = 0.05$

Fig. 27.7. After a fast transient (horizontal trajectories), the system moves along a common one-dimensional vertical line, which is an exponentially attracting invariance subspace. As expected, the projective transformation method automatically decouples the system into two independent modes.

It must be noted that the lumped state variable \hat{c} in general has no clear physical meaning. This is especially true of large-scale reaction systems. In certain situations, one probably can gain physical insights from the weights (or coefficients) of the linear combination for a lumped variable. One may also be able to attach some physical meaning to \hat{c} by imposing a priori constraints on the lumping matrix. The caveat is that the accuracy requirement for the lumped model may have to be relaxed.

An example of the projective transformation approach is the reduction of a 10-lump FCC model to a 5-lump model with virtually the same predictive power for the product slate [27.69]. If gasoline is the only unlumped species, then three lumps suffice. Another example has to do with *nonane reforming*; the number of lumps can be reduced from 14 to 7 or possibly to 5 [27.70].

Approximate Lumping

Approximate lumping aims to minimize some measures of inconsistencies between the lumped and full system dynamics. Defining a lumping error $e(t) = \mathbf{M}c(t) - \hat{c}(t)$, one obtains $de(t)/dt = \hat{\mathbf{K}}e - (\hat{\mathbf{K}}\mathbf{M} - \mathbf{M}\mathbf{K})c$ implying $de/dt = \hat{\mathbf{K}}e(t)$ if $\mathbf{M}\mathbf{K} = \hat{\mathbf{K}}\mathbf{M}$. Thus, if $\hat{c}(0) = \mathbf{M}c(0)$, then $e(t) = 0$ for all t . This means that the reaction

trajectories for all initial conditions, upon projection onto a common subspace, are bunched together to lie within the subspace for all t . On the other hand, if $\hat{c}(0) \neq \mathbf{M}\mathbf{c}(0)$, $\mathbf{e}(t)$ asymptotes rapidly to zero. In this case, exact lumping is achieved asymptotically. If $\mathbf{M}\mathbf{K} \neq \hat{\mathbf{K}}\mathbf{M}$, one may choose \mathbf{M} such that some components of \mathbf{e} are zero and the nonzero components vanish quickly.

For most practical applications, $\mathbf{M}\mathbf{K} \neq \hat{\mathbf{K}}\mathbf{M}$. It is thus important to develop approximate lumping schemes that make $\mathbf{e}(t)$ as close to $\mathbf{0}$ as possible for all t [27.71, 72]. The part of system dynamics not projected onto the invariant subspace can be characterized by the error matrix $\mathbf{E} = \mathbf{M}\mathbf{K} - \hat{\mathbf{K}}\mathbf{M}$. Upper bounds on the maximum error for all t among all \hat{c}_i have been developed [27.71].

Nonlinear Kinetics

Nonlinear processes can be notoriously sensitive to initial conditions. The system represented by (27.9) is exactly lumpable by \mathbf{M} if an \hat{N}_s -dimensional system of the form $d\hat{\mathbf{c}}/dt = \hat{\mathbf{f}}(\hat{\mathbf{c}})$ can be found [27.73–76]. To realize this, the system must have some degree of *partial linearity* related to the properties of the Jacobian matrix $\mathbf{J}(\mathbf{c})$. Specifically, exact lumping can be achieved for the whole N_s -dimensional composition space if $\mathbf{J}^T(\mathbf{c})$ has nontrivial fixed (\mathbf{c} independent) invariant subspaces represented by \mathbf{M} . If exact lumping is desired only for a subdomain Ω of the composition space, then an additional necessary and sufficient condition is needed, namely that for any \mathbf{c} in Ω , the corresponding eigenvalues for $\mathbf{J}^T(\mathbf{c})$ and $\mathbf{J}^T(\overline{\mathbf{M}}\mathbf{M}\mathbf{c})$ are equal. $\overline{\mathbf{M}}$ is one of the generalized inverses of \mathbf{M} satisfying $\overline{\mathbf{M}}\mathbf{M} = \mathbf{I}_{\hat{N}_s}$, the \hat{N}_s -dimensional identity matrix. And there exists at least one point \mathbf{c}_o in Ω such that $\mathbf{c}_o = \overline{\mathbf{M}}\mathbf{M}\mathbf{c}_o$. The invariance of the eigenvalues can also be represented by $\mathbf{M}\mathbf{J}(\mathbf{c}) = \mathbf{M}\mathbf{J}(\overline{\mathbf{M}}\mathbf{M}\mathbf{c})$. The lumped system corresponding to (27.9) is

$$\frac{d\hat{\mathbf{c}}}{dt} = \hat{\mathbf{f}}(\hat{\mathbf{c}}) = \mathbf{M}\mathbf{f}(\overline{\mathbf{M}}\hat{\mathbf{c}}). \quad (27.27)$$

Whether or not a system is exactly lumpable depends on \mathbf{f} and \mathbf{M} . The number of the invariant subspaces is finite, but the number of the lumping matrices is infinite. The nonuniqueness of the lumping matrix does not affect the form of the lumped models. With the exception of first-order reaction mixtures, not all of the $\mathbf{J}^T(\mathbf{c})$ -invariant subspaces can be used to construct \mathbf{M} . Some of the resultant lumped kinetic equations may have different forms than the full system. Discussions on the determination of lumping matrices and nonlinear projective transformation can be found elsewhere [27.77–79].

27.3.5 Mathematical Programming

This section is about a computational optimization approach, based on the very fact that dimension reduction is essentially a matter of optimally reducing the number of reactions, reacting species, or a combination of the two. What follows is an illustrative example of reducing the number of reactions for a full kinetic model with N_r reactions in an isothermal plug flow reactor (PFR) or a batch reactor. The objective is to obtain a reduced model having the fewest number of reactions while retaining the salient features of the full model. The approach centers on an *on-off* binary variable ψ_i that signifies the presence ($\psi_i = 1$) or absence ($\psi_i = 0$) of a particular reaction. In this framework, the dimension reduction is cast as the following integer optimization problem [27.80]

$$\min_{\psi \in \Lambda^{N_r}} \sum_{j=1}^{N_r} \psi_j, \quad (27.28)$$

subjected to the constraints of satisfying required mass conservation and accuracy (as measured by ε shown below), that is,

$$J = \left[\sum_i \int_0^t \left(\frac{c_i^{\text{reduced}}(t) - c_i^{\text{full}}(t)}{c_i^{\text{full}}} \right)^2 dt \right]^{1/2} \leq \varepsilon \quad (27.29)$$

and

$$\begin{aligned} \frac{dc_i}{dt} &= \sum_{j=1}^{N_r} \psi_j (\overleftarrow{v}_{ij} - \overrightarrow{v}_{ij}) \\ &\times \left(\overrightarrow{k}_j \prod_{i=1}^{N_s} c_i^{\overrightarrow{v}_{ij}} - \overleftarrow{k}_j \prod_{i=1}^{N_s} c_i^{\overleftarrow{v}_{ij}} \right), \\ i &= 1, \dots, N_s, \end{aligned} \quad (27.30)$$

where v_{ij} , N_s , and Λ^{N_r} are stoichiometric coefficients, number of species, and the set formed by all possible N_r 's, respectively. In the same vein, the problem can be formulated as that of reducing the number of species. Solving the species reduction problem is in principle less demanding computationally because $N_s < N_r$ in most situations of interest.

Equations (27.28)–(27.30) define a class of optimization-integer-decision problems, which can be solved by means of Branch and Bound algorithms [27.80] or genetic algorithm [27.81]. One must be mindful of the fact that the resulting reduced model may be valid over only a limited region of the com-

position space. Hence, what is needed is an in-situ adaptive approach that performs mechanism reduction over different domains of the composition space as needed [27.82, 83].

Mentions should be made of another computational technique for dimension contraction, the so-called in-

trinsic low dimensional manifold method [27.83, 84]. It computes the low dimensional manifolds on which the slow chemistry evolves in the composition space and then tabulates the computed results in a lookup table. The table is incorporated into a CFD code for reactor simulation.

27.4 Kinetics–Hydrodynamics Tradeoff

As mentioned earlier, process modeling requires balancing kinetics and hydrodynamics. In this section, we use FCC as an illustrative example. Recent developments in FCC modeling fall into two broad categories. One is the one-dimensional, homogeneous plug-flow model [27.1, 2, 85], which can accommodate a large number of reactions and hence make it possible to develop a composition-based model using, say, the SOL approach. Such kinetics-dominated models pay little attention to hydrodynamic effects that affect the reaction time and the local catalyst-to-oil (CTO) ratio. In other words, the momentum conservation equations are either simplistic or ignored. Another approach is

the CFD-based models [27.86–89], which involves numerical solution of partial differential equations for multi-dimensional flow systems. Here, the allowable number of chemical reactions is necessarily small even with today's powerful computers. The CFD-dominated models would not be able to portray the complexities and subtleties of the underlying chemistry and catalysis. Nor do they enable refiners to manage FCC feedstocks and products at a molecular level.

Recently, attempts have been made to develop a hybrid approach aimed at striking a proper balance between the two aforementioned *asymptotic* approaches [27.90–93]. The tactic is to develop a phe-

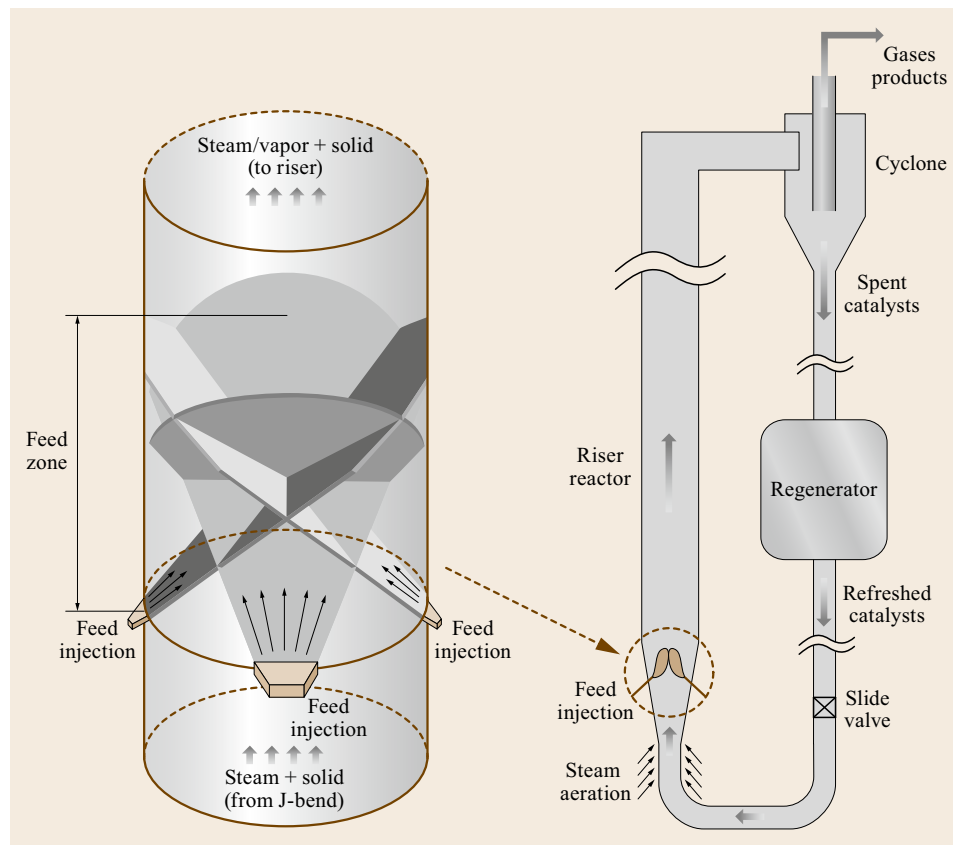


Fig. 27.9 FCC feed injection zone with four fan-shaped nozzles

nomenological model of momentum transfer without invoking the CFD. Also, there is a need to gain a predictive understanding of *entrance cracking* via the development of a quantitative treatment of the feed injection zone where temperature and catalyst activity/concentration are highest. These considerations led to the construction of one-dimensional heterogeneous riser models accounting for catalyst acceleration, catalyst–catalyst collision force, catalyst–gas interfacial force, and interactions of multiple feed injectors. What follows is an example.

A recent modeling study considers four symmetric, overlapping fan-shaped atomizing nozzles [27.93]. This type of nozzles provides a wide and fairly uniform feed coverage across the catalyst stream, thus, starting the vapor-phase cracking as early as possible [27.94, 95]. As Fig. 27.9 shows, a reactive, vaporizing spray will penetrate into the *territory* of another spray. The flows of gas and catalyst are accelerated by vaporization and cracking, both of which are driven by droplet–catalyst collision. The cracking reactions are described by the four-lump model shown in Fig. 27.1 because of the availability of commercial data [27.96].

Temperature and the CTO ratio are the dominant cracking intensity indicators and they behave similarly. The model divides the system into two zones: an entrance (feed injection) zone and a downstream fully developed riser zone. Inside the entrance zone, both indicators are very high and change rapidly, resulting in an immediate, sharp rise in VGO conversion. Outside the entrance zone, both indicators are low and become slowly varying, giving rise to a sluggish increase in VGO conversion. These two zones have very different physicochemical characteristics and need to be modeled separately. The behavior of the entrance zone sets the initial condition for the downstream zone. Here, an analogy may be loosely made with the boundary-layer theory in transport phenomena. The two-zone model

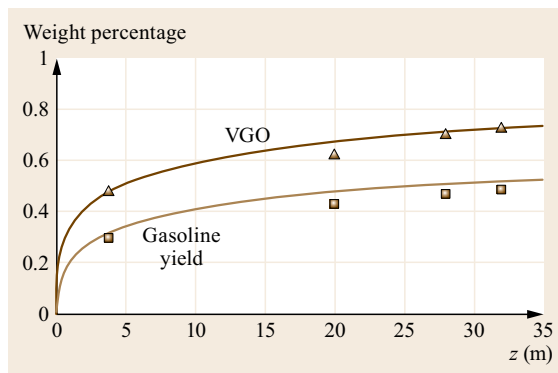


Fig. 27.10 Riser profiles of gasoline yield and VGO conversion, plant data versus model predictions. (After [27.93])

can accommodate a large number of reactions as each zone is described by a set of first-order ordinary differential equations.

The commercial data of *Derouin et al.* [27.96] indicate that the first 10% of the riser height accounts for more than 65% of the VGO conversion over the entire riser, signifying the dominance of *entrance cracking* and hence the need of predictive calculations for this region [27.97]. As detailed elsewhere [27.93], the two-zone model satisfactorily predicts both the VGO conversion and gasoline yield, as shown in Fig. 27.10.

In summary, the underlying chemistry and physics of the FCC process are such that the process has an inherent two-zone character. A key feature of the heterogeneous model is the consideration of catalyst–fluid interfacial momentum transfer. The model is computationally simple. As such, this model can be used for molecular management, on-line control, and real-time optimization. It is relevant to point out that the complexity of designing controller and the difficulty in its implementation scale with the complexity of the process model.

27.5 Total Lumping: Continuum Approximation

Total lumping is about determining the aggregate behavior and overall kinetics of a large number of reactions. As mentioned, in HDS, only the reduction of total sulfur really matters. The same is true of HDN and hydrodemetallation. FCC is designed primarily for the deep conversion of high-boiling ($> 340^\circ\text{C}$) to low-boiling ($< 340^\circ\text{C}$) fractions.

The problem of finding the aggregate behavior and overall, lumped kinetics of a large number of reactions can be stated as follows. Let $c_i(t)$ ($i = 1, 2, \dots, N \gg$

1) be the concentration of reactant i with rate constant k_i and $C(t) = \sum_i c_i$ be the total concentration of all reactants at time t . The concentration of reactant i in the feed is $c_{if} = c_i(0)$. Each reactant disappears at its own rate r_i . The aim is to predict the dependence of $C(t)$ on feed properties and reactor type. It is also of interest to know if an overall, lumped kinetics $\bar{r}(C)$ can be found for the large mixture as a whole [27.98]. Since petroleum feedstocks have an astronomically large number of species, a mathemati-

cally convenient approach is to treat the feedstock as a continuum [27.99–102]. That is, the sum \sum_i is replaced by an integral over a distribution function, which is parameterized by a small number of constants. In practice, the chemical–analytical characterization data for hydrocarbon mixtures can be obtained as a continuous function of such macroscopic properties as boiling point, molecular weight, molecular polarity, or hydrogen deficiency. Figure 27.11 shows the sulfur content of a gas oil over its boiling range [27.103]. In some refining processes, a feedstock’s reactivity is closely related to boiling point (or molecular size) and/or hydrogen deficiency.

Examples of continuum process models can be found elsewhere [27.104–106]. The continuum approach can also be used to solve an inverse problem: determining feedstock reactivity–composition spectra from the measured $C(t)$ [27.107]. When the total number of species N is very large, the total reactant concentration is approximated by the following integral [27.102]

$$C(t) = \int_0^{\infty} c(k, t) D(k) dk. \quad (27.31)$$

Here, each reactant is labeled by its reactivity k . The concentration of reactant k is $c(k, t)$. The slice $D(k)dk$ is the total number of reactant types with rate constant between k and $k + dk$. Thus, D is a reactant-type distribution function and acts as the Jacobian of the

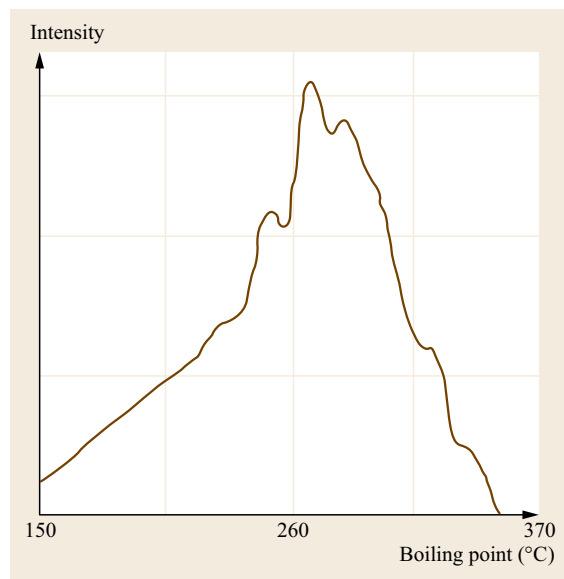


Fig. 27.11 Feed sulfur concentration as a function of boiling point. (After [27.103])

discrete-to-continuous (i -to- k) coordinate transformation. The construction of $D(k)$ requires analytical measurements [27.108, 109] combined with kinetics experiments using representative model compounds [27.110, 111]. A power-law expression for $D(k)$ is used in hydrocracking [27.104].

27.5.1 Overall Lumped Kinetics

For first-order reactions in a PFR,

$$c(k, t) = c_f(k) \exp(-kt)$$

and

$$C(t) = \int_0^{\infty} h(k) \exp(-kt) dk,$$

where $h(k) = D(k)c_f(k)$. To describe a wide variety of feed properties with just two parameters, *Aris* used the gamma distribution [27.100]

$$h(k) = \frac{\gamma^\gamma (k/\bar{k})^{\gamma-1} \exp(-\gamma k/\bar{k})}{\bar{k} \Gamma(\gamma)}, \quad \gamma > 0, \quad (27.32)$$

where Γ is the gamma function and γ a feed quality index; the smaller the γ value, the more refractory the feed. Substituting (27.32) into (27.31) gives

$$C(t) = \frac{1}{(1 + \bar{k}t/\gamma)^\gamma}. \quad (27.33)$$

This implies that $dC/dt = -\bar{r}(C) = -\bar{k}C^{\bar{n}}$ an overall reaction order $\bar{n} = 1 + 1/\gamma > 1$ with a rate constant \bar{k} .

For the design and development of hydrocarbon conversion catalysts and processes, it is essential to determine $C(t)$ and $\bar{r}(C)$ a priori, which requires complete information on feed properties and reactivity spectra. In practice, however, practitioners do not usually have the luxury of fully characterizing hydrocarbon feedstocks. A pragmatic approach is to find $C(t)$ and $\bar{r}(C)$ at high conversions (or long time) for partially characterized feedstocks [27.112–115]. Such an asymptotic approach provides a simple, unifying framework for gaining insights into a mixture’s behavior and explaining many perplexing behaviors observed in hydrocarbon processing [27.98]. Developing long-time asymptotic kinetics is commensurate with the growing need of refiners to achieve deep conversions, which is mainly driven by the ever-increasing demand for ultra-clean fuels. For example, the diesel sulfur specifications in a few countries

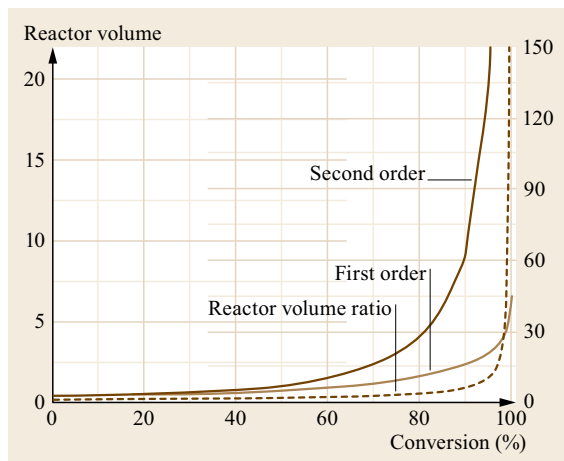


Fig. 27.12 Reactor volumes and reactor volume ratio versus percent conversion for first-order and second-order reactions

are now set at 10–15 ppmw. More countries will certainly follow suit in the future. The sulfur content of middle distillates (200–370 °C boiling range) typically ranges between 1 and 3 wt%. Desulfurizing a distillate from 1 wt% sulfur to 10 ppmw means an HDS level of 99.9%. A similar situation exists in hydrocracking that requires ultra-deep HDN. This may incur huge capital outlays because reactor volume is extremely sensitive to conversion at high conversions. This is shown in Fig. 27.12 for the first- and second-order reactions in an isothermal plug-flow reactor. Also shown is the reactor volume ratio for the two reactions versus percent conversion, which illustrates the importance of knowing the deep-conversion kinetics. In exploring or developing new catalysts for hydroprocessing, competing catalysts should be evaluated at high conversions.

27.5.2 Long-Time Asymptotic Kinetics

Developing long-time asymptotic kinetics can mostly be done with partially characterized feedstocks. Intuitively, one may expect that the feedstock's long-time behavior is governed by the most refractory part of the feed. Hence, we expand $D(k)$ and $c_f(k)$ as $D(k) \sim d_o k^\mu$ and $c_f(k) \sim c_o k^\nu$ near $k = 0$. Alternatively, $h(k) \sim h_o k^{\gamma-1}$, where $h_o = c_o d_o$ and $\gamma \equiv \mu + \nu + 1$. For the irreversible first-order reactions, $C(t) \sim h_o \Gamma(\gamma) / t^\gamma$ at large t , yielding an asymptotic (subscript a) overall kinetics $\bar{r}_a = \gamma [h_o \Gamma(\gamma)]^{-1/\gamma} C^{\bar{n}_a}$, where the asymptotic reaction order $\bar{n}_a = 1 + 1/\gamma > 1$ [27.112, 113]. *Ho* and *White* [27.116] determined the asymptotic power-law kinetics for deep HDS of a light cycle oil over three different catalysts, with $\bar{n}_a = 2.5$. *Sie* found that $\bar{n}_a = 2$ for both gas oil and prehy-

drotreated gas oil over a sulfided CoMo/Al₂O₃ catalyst [27.117].

Hydroprocessing catalyst and process exploratory studies involve rapid evaluation of various experimental catalysts with simple overall kinetics. For such studies, the continuum approach developed if–then rules that allow researchers to explain and predict the kinetic behaviors of reaction mixtures with incomplete feed information. Some examples include the following:

- The overall reaction order for HDS is higher than that for HDN.
- High-activity catalysts give rise to lower overall reaction order than low-activity catalysts.
- Refractory feeds show higher overall order than reactive ones.
- The overall HDS order decreases with increasing temperature.
- The overall order for plug flow reactors is higher than that for stirred tank reactors.
- Reactors with and without recycle in general have different overall kinetics.

Useful as it may be, the long-time asymptotic analysis based on the continuum theory has its limitation in some situations [27.116]. Consider first-order reactions in a discrete mixture as an example. After a sufficiently long time, one expects that the mixture behaves as if there were only one surviving reactant decaying exponentially because the concentrations of all other species are exponentially smaller. However, the corresponding continuous mixture at large times ($t \rightarrow \infty$) decays asymptotically as a second-order reaction [27.112, 113]. This apparent paradox arises from the fact that the long-time asymptotic kinetics is valid only over an intermediate time frame – one in which time is large enough for the asymptotic kinetics to be valid (and the mixture's behavior no longer depends on the details of feed properties), but short enough for the mixture remaining to be sufficiently crowded (hence second-order kinetics) [27.116]. Such intermediate asymptotics are common in engineering science [27.118].

Thus, there is a need to determine the condition under which the continuum theory and its long-time limit are both valid. The issue then boils down to the reaction mixture's granularity. A sufficiently fine granularity ensures the validity of the continuum approximation at long times. For first-order reactions, the condition is $1/\kappa \ll t \ll 1/\Delta$, where κ is a characteristic rate constant for a moderately refractory species and Δ is the maximum difference between the rate constants for two species whose reactivities are adjacent to each other. In many situations of practical interest, the above condition is not stringent [27.116]. For nonfirst-order

reactions, the condition becomes [27.119]

$$\frac{1}{\kappa} \ll t \ll \left(\frac{\kappa}{\Delta}\right)^y \frac{1}{\kappa} \quad \text{or} \quad \left(\frac{\kappa}{\Delta}\right)^y \gg 1. \quad (27.34)$$

The exponent y depends on reaction kinetics and feed properties. For irreversible first-order reactions, reversible first-order reactions, and bimolecular second-order reactions, $y = 1, 2,$ and $3,$ respectively.

For high-order reactions, the continuum approximation can be valid for arbitrarily long time. The large- t behavior of a reaction mixture with power-law kinetics is not necessarily dominated by the most refractory species. It can be dominated by species of intermediate reactivity, moderately refractory species, or all species. Zeroth- and certain fractional-order reactions are incompatible with continuum description [27.119]. The overall kinetics obtained from a PFR cannot be carried over to a continuous stirred tank reactor (CSTR). In general, backmixing widens the range of validity [27.120].

27.5.3 Reactions in CSTR

An advantage of the asymptotic analysis is that in many cases one needs only local information ($k \approx 0$) to determine the overall rate in a PFR. This is not necessarily true for reactions taking place in a CSTR. For first-order reactions in a CSTR, $c(k, t) = c_f(k)/(1+kt)$, hence $c(k, t) = O(1/t)$ at large t . $C(t)$ is of the form

$$C(t) = \int_0^{\infty} \frac{h(k)dk}{1+kt}. \quad (27.35)$$

Compared to the PFR, the system is more complex because for each reactant, there is an exponential distribution of residence times among all the molecules of that reactant. In this situation, the overall kinetics $\bar{\tau}_a(C)$ admits three possibilities [27.115]. The case $\gamma < 1$ (refractory feeds) is similar to the PFR in that the mixture's long-time behavior is dominated by the most refractory species and follows a power law: $C = O(1/t^\gamma)$ and $\bar{\tau}_a(C) \sim C^{1/\gamma}$ at large t . For $\gamma > 1$, the feed comprises primarily reactive species. Then, $\bar{n}_a = 1$ and $C \sim I/t$ at large t , with $I \equiv \int k^{-1}h(k)dk$. Hence, the mixture's long-time behavior is governed by all species.

The situation is very different for the transition case $\gamma = 1$, which gives rise to $C \propto \ln t/t$. Hence, the decay of C , although governed by the refractory species, is accelerated by the reactive species. The instantaneous asymptotic order $\bar{n}_a = d \ln \bar{\tau}_a / d \ln C$ decreases slowly with conversion, consistent with the experiment [27.121]. At high conversions, $1 < \bar{n}_a =$

Table 27.1 Asymptotic kinetics for PFR and CSTR

	PFR		CSTR	
	$\gamma > 0$	$\gamma > 1$	$\gamma < 1$	$\gamma = 1$
$\bar{\tau}_a(C) \sim$	$C^{1+1/\gamma}$	C	$C^{1/\gamma}$	$\frac{C}{ \ln C }$

$1 + 1/|\ln C| < 2$. Finally, \bar{n}_a for the PFR is always higher than that for the CSTR. The CSTR's size is larger than PFR's size at constant conversion [27.115].

The overall kinetics represents an averaging over the reactivity and composition spectra. Such averaging should be different in reactors with different residence time distributions. In consequence, the overall kinetics obtained from the PFR may not be directly carried over to the CSTR. It is therefore important to develop if-then guidelines for translating data from one reactor type to another. Table 27.1 is one such example. The asymptotic overall order for the PFR is higher than that for the CSTR.

Summarizing, the effect of lumping greatly manifests itself for the CSTR through the interactions between the reactivity/concentration spectra and the exponential residence time distribution. Although all reactants are slowed down compared to those in the PFR case, the fast-reacting ones are hampered more than the slow-reacting ones. Consequently, the disparities among the species become smaller, making the mixture more homogeneous. A relatively homogeneous feed (high γ) can be further homogenized in the CSTR to such an extent that its long-time behavior approaches that of a single reactant.

It has been observed experimentally that the overall kinetics of HDS, HDN, and hydrocracking of a coker gas oil are all first order in the CSTR free of mass transfer effects [27.122]. An overall order greater than one has been reported for HDS in a CSTR [27.123]. In the hydrodemetallization of a heavy residual oil that can be described by the gamma distribution with $\gamma = 1$, an overall order of two was observed with the PFR. For the CSTR, $C(t) = \exp(1/t)E_i(1/t)/t$, where E_i is the exponential integral, which can be fitted by a 1.5-order power law over the 20–80% conversion range [27.124].

27.5.4 Summary of Asymptotic Analysis

It is helpful at this point to wrap up the results of the asymptotic analysis. The preceding sections show that the asymptotic kinetics can be quite complex (e.g., 21 possibilities for reversible first-order reactions in a CSTR). Yet, the decay of $C(t)$ at suitably large t , for a variety of kinetics (n -th order, Langmuir-Hinshelwood, bimolecular reactions, etc.) and regardless of reactor type (PFR and CSTR), takes one of

following forms [27.114, 115, 118]

$$C(t) \sim \frac{1}{t^z}, \quad C(t) \sim \frac{\ln t}{t^z},$$

$$\text{or } C(t) \sim \frac{\exp(-\beta t)}{t^z} \quad \text{at large } t. \quad (27.36)$$

The most common behavior by far is the simple power law $C = O(1/t^z)$ for large t . The occurrence of $C = O(e^{-\beta t}/t^z)$ is restricted to first-order reversible reactions in a PFR. The parameters z and β are determined by (i) the most refractory species, (ii) all species, or (iii) species of intermediate reactivity.

27.5.5 One-Parameter Model

The foregoing asymptotic analysis indicates that in most cases $C(t) \sim \sigma/t^z$ at large t . This behavior gives rise to a one-parameter model that exactly calculates or estimates $C(t)$ for all t . The model is of the form [27.125]

$$C_q(t) = \frac{1}{(1 + t^z q / \sigma^q)^{1/q}} \quad q > 0, \quad (27.37)$$

where q is the model parameter determined experimentally at an intermediate time (say, between 45% and 60% conversions). The best result is obtained by measuring C at $t = t^* = \sigma^{1/z}$. Once $C(t^*)$ is known, then $q = -\ln 2 / [\ln C(t^*)]$. When $C(t^*)$ is not known, one may find q by nonlinear regression over a range of intermediate conversions. Numerical experiments show that

27.6 Conclusions

The past three decades have seen much progress on modeling of large-scale reaction systems. This is especially true for petroleum-refining processes. The molecule-based, bottom-up modeling approach is becoming increasingly important. Various useful QSSRs have been developed, some of which are based on computational chemistry. The continuum approximation has produced many useful results and guidelines. A recent development has been the application of mathematical programming to model reduction. It holds the promise of implementing in-situ adaptive algorithms for dimension reduction in different subdomains of the composition space.

Much remains to be done, however. One of the most challenging areas is to incorporate catalyst properties into kinetic models. For crystalline catalysts with well-characterized structures (e.g., zeolites), some limited progress has been made, but this is far from being the

the model has a remarkable ability to mimic the mixture behavior. In fact, if the overall kinetics are inherently of a power-law structure (e.g., gamma feeds with first-order reactions in a PFR), (27.37) mirrors $C(t)$ exactly by simply setting $q = 1/z$.

If the overall kinetics do not have an inherent power-law structure, it still pays to let $q = 1/z$: It results in a tight upper bound on C , or C_u , for all t ,

$$C(t) \leq C_u(t) \equiv \frac{1}{(1 + t/\sigma^{1/z})^z}. \quad (27.38)$$

C_u itself satisfies the power law

$$\frac{dC_u}{dt} = -z\sigma^{-1/z} C_u^{1+1/z} \quad (27.39)$$

and can be used as a tight, conservative estimate of $C(t)$. An accurate prediction needs an additional data point on $C(t)$ at an intermediate conversion by virtue of (27.37). Equation (27.38) suggests that $\bar{r}_a(C)$ in most practical situations can be described by a power law for nongamma feeds.

Both z and σ can be determined from information on the most refractory fraction of the feed. Thus, in developing process kinetics, in many cases, it is not necessary to characterize the whole feed. Instead, characterizing only the most refractory fraction and running the reaction at an intermediate conversion may suffice. In practice, it is easier to characterize the refractory species. After all, these species survive the reaction.

case for structurally complex catalysts such as highly disordered metal sulfides.

Extending catalyst life is an integral part of improving existing and developing new refining technologies. It is imperative to develop fundamentals-based model of coke formation, thereby, helping design mitigation means through control of feedstock composition and operating conditions. Coke on catalyst not only decreases activity, but also greatly affects selectivity. To complicate matters, there are many types of coke for a given process chemistry (e.g., FCC and coking). Catalyst deactivation caused by metal sintering or poisoning is also an issue of great concern. Reactor fouling caused by carbonaceous deposit remains an important operation issue in many cases. All these areas are fertile grounds for further modeling research.

The tradeoff between kinetics and hydrodynamics for hydrodynamically complex systems continues

to be a challenge. For instance, to address problems of fluid maldistribution in trickle bed reactors or the feed injection zone at the base of an FCC riser, one is compelled to sacrifice chemistry details. The same is true when one needs to solve control and optimization problems.

To make discovery and development faster and cheaper, many research laboratories have been engaged in developing high-throughput experimentation (HTE)

methodologies. Much effort has been focused on the design and development of parallel miniaturized reactors to which complex reaction mixtures are fed. If the results obtained from miniature-scale apparatus are not scalable, the HTE approach may well create a bottleneck. In order to reap the full benefit of HTE platforms, it is important to develop robust models from HTE units, aiming at extracting fundamental, scale-invariant information.

References

- 27.1 S.M. Jacob, B. Gross, S.E. Voltz, V.W. Weekman: A lumping and reaction scheme for catalytic cracking, *AIChE J.* **22**(4), 701–713 (1976)
- 27.2 L. Lee, Y. Chen, T. Huang, W. Pan: Four-lump kinetic model for fluid catalytic cracking process, *Can. J. Chem. Eng.* **67**(4), 615–619 (1989)
- 27.3 S.B. Jaffe: Kinetics of heat release in petroleum hydrogenation, *Ind. Eng. Chem. Proc. Des. Dev.* **13**, 34–39 (1974), <http://pubs.acs.org/doi/abs/10.1021/i260049a006>
- 27.4 S.B. Jaffe: Hot spot simulation in commercial hydrogenation processes, *Ind. Eng. Chem. Proc. Des. Dev.* **15**(3), 410–416 (1976), <http://pubs.acs.org/doi/abs/10.1021/i260059a011>
- 27.5 I.A. Wiehe: A phase-separation kinetic model for coke formation, *Ind. Eng. Chem. Res.* **32**(11), 2447–2454 (1993), <http://pubs.acs.org/doi/abs/10.1021/ie00023a001>
- 27.6 Z. Huang, T.C. Ho: Effect of thermolysis on resid droplet vaporization in fluid catalytic cracking, *Chem. Eng. J.* **91**(1), 4558 (2003), <http://www.sciencedirect.com/science/article/pii/S1385894702001146>
- 27.7 P. Ghosh, K.J. Hickey, S.B. Jaffe: Development of a detailed gasoline composition-based octane model, *Ind. Eng. Chem. Res.* **45**(1), 337–345 (2006), <http://pubs.acs.org/doi/abs/10.1021/ie050811h>
- 27.8 R.J. Quann, S.B. Jaffe: Structure-oriented lumping: Describing the chemistry of complex hydrocarbon mixtures, *Ind. Eng. Chem. Res.* **31**(11), 2483–2497 (1992), <http://pubs.acs.org/doi/abs/10.1021/ie00011a013>
- 27.9 R.J. Quann, S.B. Jaffe: Building useful models of complex reaction systems in petroleum refining, *Chem. Eng. Sci.* **51**(10), 1615–1635 (1996), <http://www.sciencedirect.com/science/article/pii/S009250996000231>
- 27.10 M.T. Klein, G. Hou, R.J. Bertolcini, L.J. Broadbelt, A. Kumar: *Molecular Modeling in Heavy Hydrocarbons Conversions* (CRC, Boca Raton 2006)
- 27.11 L.J. Broadbelt, S.M. Stark, M.T. Klein: Computer generated reaction networks: On-the-fly calculation of species properties using computational quantum chemistry, *Chem. Eng. Sci.* **49**(24), 4991–5010 (1994), <http://www.sciencedirect.com/science/article/pii/S009250994003262>
- 27.12 L.J. Broadbelt, S.M. Stark, M.T. Klein: Computer generated reaction modelling: Decomposition and encoding algorithms for determining species uniqueness, *Comput. Chem. Eng.* **20**(2), 113–129 (1998), <http://www.sciencedirect.com/science/article/pii/S009813549400009D>
- 27.13 R. Tanaka, C.A. Bennett, Z. Hou, M. Jones, M.T. Klein, G. Hou: Molecule-based kinetic modeling of naphtha hydrotreating, *Proc. ACS Nat. Meet.* (2006)
- 27.14 L.P. Hillewaert, J.L. Dierickx, G.F. Froment: Computer generation of reaction schemes and rate equations for thermal cracking, *AIChE J.* **34**(1), 17–24 (1988)
- 27.15 M.A. Baltanas, K.K.V. Raemdonck, G.F. Froment, S.R. Mohedas: Fundamental kinetic modeling of hydroisomerization and hydrocracking on noble metal-loaded faujasites. 1. Rate parameters for hydroisomerization, *Ind. Eng. Chem. Res.* **28**(7), 899–910 (1989)
- 27.16 G.F. Froment: Single event kinetic modeling of complex catalytic processes, *Catal. Rev.* **47**(1), 83–124 (2005)
- 27.17 S.E. Senkan: Detailed chemical kinetic modeling: Chemical reaction engineering of the future. In: *Advances in Chemical Engineering* (Academic, Boston 1992) pp. 95–196, <http://www.sciencedirect.com/science/article/pii/S0065237708601234>
- 27.18 L.J. Broadbelt, R.Q. Snurr: Applications of molecular modeling in heterogeneous catalysis research, *Appl. Catal. A* **200**(1/2), 23–46 (2000), <http://www.sciencedirect.com/science/article/pii/S0926860X00006487>
- 27.19 M. Boudart, G. Djega-Mariadassou: *Kinetics of Heterogeneous Catalytic Reactions* (Princeton Univ. Press, Princeton 1984)
- 27.20 F.G. Helfferich: *Kinetics of Homogeneous Multi-step Reactions* (Elsevier, Amsterdam 2001)
- 27.21 R.D. Cortright, J.A. Dumesic: Kinetics of heterogeneous catalytic reactions: Analysis of reaction schemes, *Adv. Catal.* **46**, 161–264 (2001)
- 27.22 G.R. Gavallas: The long chain approximation in free radical reaction systems, *Chem. Eng. Sci.* **21**(2), 133–141 (1966), <http://www.sciencedirect.com/science/article/pii/S009250966850042>

- 27.23 J.K. Bechtold, C.K. Law: The structure of premixed methane-air flames with large activation energy, *Combust. Flame* **97**(3/4), 317–338 (1994), <http://www.sciencedirect.com/science/article/pii/S0010218094900248>
- 27.24 A.B. Mhadeshwar, D.G. Vlachos: Is the water-gas shift reaction on Pt simple?: Computer-aided microkinetic model reduction, lumped rate expression, and rate-determining step, *Catal. Today* **105**(1), 162–172 (2005), <http://www.sciencedirect.com/science/article/pii/S0920586105002075>
- 27.25 I. Fishtik, C.A. Callaghan, R. Datta: Reaction route graphs. I. Theory and algorithm, *J. Phys. Chem. B* **108**(18), 5671–5682 (2004), <http://pubs.acs.org/doi/abs/10.1021/jp0374004>
- 27.26 M.A. Vannice: *Kinetics of Catalytic Reactions* (Springer, New York 2005)
- 27.27 A.B. Mhadeshwar, H. Wang, D.G. Vlachos: Thermodynamic consistency in microkinetic development of surface reaction mechanisms, *J. Phys. Chem. B* **107**(46), 12721–12733 (2003), <http://pubs.acs.org/doi/abs/10.1021/jp034954y>
- 27.28 K.J. Laidler: *Chemical Kinetics*, 3rd edn. (Harper Row, New York 1987)
- 27.29 M.R. Gray, W.C. McCaffrey: Role of chain reactions and olefin formation in cracking, hydroconversion, and coking of petroleum and bitumen fractions, *Energy Fuels* **16**(3), 756–766 (2002), <http://pubs.acs.org/doi/abs/10.1021/ef010243s>
- 27.30 J.T. Hwang, E.P. Dougherty, S. Rabitz, H. Rabitz: The Green's function method of sensitivity analysis in chemical kinetics, *J. Chem. Phys.* **69**, 5180–5191 (1978)
- 27.31 H. Rabitz: Chemical dynamics and kinetics phenomena as revealed by sensitivity analysis techniques, *Chem. Rev.* **87**(1), 101–112 (1987)
- 27.32 S. Vajda, P. Valko, T. Turanyi: Principal component analysis of kinetic models, *Int. J. Chem. Kinetics* **17**(1), 55–81 (1985)
- 27.33 M.A. Sanchez-Castillo, N. Agarwal, C. Miller, R.D. Cortright, R.J. Madon, J.A. Dumesic: Reaction kinetics study and analysis of reaction schemes for isobutane conversion over USY zeolite, *J. Catal.* **205**(1), 67–85 (2002), <http://www.sciencedirect.com/science/article/pii/S0021951701934190>
- 27.34 V.K. Pareek, A.A. Adesina, A. Srivastava, R.J. Sharma: Sensitivity analysis of rate constants of Weekman's riser kinetics and evaluation of heat of cracking using CATCRACK, *J. Mol. Catal. A* **181**(1/2), 263–274 (2002), <http://www.sciencedirect.com/science/article/pii/S138116901003715>
- 27.35 I. Mochida, Y. Yoneda: Linear free energy relationships in heterogeneous catalysis: III. Temperature effects in dealkylation of alkylbenzenes on the cracking catalysts, *J. Catal.* **8**(3), 223–230 (1967)
- 27.36 I. Mochida, Y. Yoneda: Linear free energy relationships in heterogeneous catalysis: I. Dealkylation of alkylbenzenes on cracking catalysts, *J. Catal.* **7**(4), 386–392 (1967), <http://www.sciencedirect.com/science/article/pii/S0021951767901674>
- 27.37 I. Mochida, Y. Yoneda: Linear free energy relationships in heterogeneous catalysis: II. Dealkylation and isomerization reactions on various solid acid catalysts, *J. Catal.* **7**(4), 393–396 (1967), <http://www.sciencedirect.com/science/article/pii/S0021951767901686>
- 27.38 A. Nigam, M.T. Klein: A mechanism-oriented lumping strategy for heavy hydrocarbon pyrolysis: Imposition of quantitative structure-reactivity relationships for pure components, *Ind. Eng. Chem. Res.* **32**(7), 1297–1303 (1993), <http://pubs.acs.org/doi/abs/10.1021/ie00019a003>
- 27.39 B.A. Watson, M.T. Klein, R.H. Harding: Catalytic cracking of alkylbenzenes: Modeling the reaction pathways and mechanisms, *Appl. Catal. A* **160**(1), 13–39 (1997), <http://www.sciencedirect.com/science/article/pii/S0926860X97001221>
- 27.40 D.K. Liguras, D.T. Allen: Structural models for catalytic cracking. 2. Reactions of simulated oil mixtures, *Ind. Eng. Chem. Res.* **28**(6), 674–683 (1989), <http://pubs.acs.org/doi/abs/10.1021/ie00090a005>
- 27.41 D.T. Allen: Structural Models of Catalytic Cracking Chemistry. In: *Kinetic and Thermodynamic Lumping of Multicomponent Mixtures*, ed. by G. Astarita, S.I. Sandler (Elsevier, Amsterdam 1991)
- 27.42 B. Sowerby, S.J. Becker, L.J. Belcher: Modeling of 2-methylpentane cracking: The application of adsorption equilibrium constants estimated using proton affinities, *J. Catal.* **161**(1), 377–386 (1996), <http://www.sciencedirect.com/science/article/pii/S0021951796901955>
- 27.43 B. Sowerby, S.J. Becker: Modeling catalytic cracking kinetics using estimated adsorption equilibrium constants. In: *Dynamics of Surfaces and Reaction Kinetics in Heterogeneous Catalysts*, ed. by G.F. Froment, K.C. Waugh (Elsevier, Amsterdam 1997)
- 27.44 M. Sun, A.E. Nelson, J. Adjaye: Correlating the electronic properties and HDN reactivities of organonitrogen compounds: An ab initio DFT study, *J. Mol. Catal. A* **222**(1/2), 243–251 (2004), <http://www.sciencedirect.com/science/article/pii/S138116904005722>
- 27.45 J. Abbot, P.R. Dunstan: Catalytic cracking of linear paraffins: Effects of chain length, *Ind. Eng. Chem. Res.* **36**(1), 76–82 (1997), <http://pubs.acs.org/doi/abs/10.1021/ie960255e>
- 27.46 R.J. Quann, F.J. Krambeck: Olefine oligomerization kinetics over ZSM-5. In: *Chemical Reactions in Complex Mixtures*, ed. by A.V. Sapre, F.J. Krambeck (Van Nostrand Reinhold, New York 1991)
- 27.47 T.C. Ho, A.R. Katritzky, S.J. Cato: Effect of nitrogen compounds on cracking catalysts, *Ind. Eng. Chem. Res.* **31**(7), 1589–1597 (1992)
- 27.48 T.C. Ho: Property-reactivity correlation for HDS of middle distillates, *Appl. Catal. A* **244**(1), 115–128 (2003), <http://www.sciencedirect.com/science/article/pii/S0926860X02005720>
- 27.49 T.C. Ho, G.E. Markley: Property-reactivity correlation for hydrodesulfurization of prehydrotreated distillates, *Appl. Catal. A* **267**(1/2), 245–250 (2004), <http://www.sciencedirect.com/science/article/>

- pii/S0926860X04001814
- 27.50 M.A. Sharaf, D.L. Illman, B.R. Kowalski: *Chemo-metrics* (John Wiley, New York 1986)
- 27.51 S. Wold, P. Geladi, K. Esbensen, J. Ohman: Multi-way principal components-and PLS-analysis, *J. Chemom.* **1**(1), 41–56 (1987)
- 27.52 S.J. Qin: A statistical perspective of neural networks for process modeling and control, Proc. 1993 IEEE Int. Symp. Intell. (1993) pp. 599–604, [10.1109/ISIC.1993.397629](http://dx.doi.org/10.1109/ISIC.1993.397629)
- 27.53 J.A. Dumesic, D.F. Rudd, L.M. Aparicio, J.E. Rekoske, A.A. Trevino: *The Microkinetics of Heterogeneous Catalysis* (Amer. Chem. Soc., Washington 1993)
- 27.54 G. Yaluris, J.E. Rekoske, L.M. Aparicio, R.J. Madon, J.A. Dumesic: Isobutane cracking over Y-zeolites: I. Development of a kinetic-model, *J. Catal.* **153**(1), 54–64 (1995), <http://www.sciencedirect.com/science/article/pii/S0021951785711074>
- 27.55 G. Yaluris, J.E. Rekoske, L.M. Aparicio, R.J. Madon, J.A. Dumesic: Isobutane Cracking over Y-zeolites: II. Catalytic cycles and reaction selectivity, *J. Catal.* **153**(1), 65–75 (1995), <http://www.sciencedirect.com/science/article/pii/S0021951785711086>
- 27.56 N.Y. Dewachtere, F. Santaella, G.F. Froment: Application of a single-event kinetic model in the simulation of an industrial riser reactor for the catalytic cracking of vacuum gas oil, *Chem. Eng. Sci.* **54**(15/16), 3653–3660 (1999)
- 27.57 T.M. Moustafa, G.F. Froment: Kinetic modeling of coke formation and deactivation in the catalytic cracking of vacuum gas oil, *Ind. Eng. Chem. Res.* **42**(1), 14–25 (2003)
- 27.58 G. Christensen, M.R. Apelian, K.J. Hicky, S.B. Jaffe: Future directions in modeling the FCC process: An emphasis on product quality, *Chem. Eng. Sci.* **54**(13/14), 2753–2764 (1999), <http://www.sciencedirect.com/science/article/pii/S0009250999000020>
- 27.59 P.V. Joshi, S.D. Iyer, M.T. Klein: Automated kinetic modeling of gas oil catalytic cracking, *Rev. Process Chem. Eng.* **2**, 111–140 (1998)
- 27.60 P.V. Joshi, M.T. Klein, A.L. Huebner, R.W. Leyerle: Automated kinetic modeling of catalytic reforming at the reaction pathway levels, *Rev. Process. Chem. Eng.* **2**, 169–193 (1999)
- 27.61 M.S. Okino, M.L. Mavrouniotis: Simplification of mathematical models of chemical reaction systems, *Chem. Rev.* **98**(2), 391–408 (1998), <http://pubs.acs.org/doi/abs/10.1021/cr950223l>
- 27.62 G. Li, A.S. Tomlin, H. Rabitz: Determination of approximate lumping schemes by a singular perturbation method, *J. Chem. Phys.* **99**, 3562 (1993)
- 27.63 R.J. Fisher, M.M. Denn: A modal approach to dynamics of nonlinear processes, *AIChE J.* **24**(3), 519–523 (1978)
- 27.64 C.C. Chen, H.C. Chang: Accelerated disturbance damping of an unknown distributed system by nonlinear feedback, *AIChE J.* **38**(9), 1461–1476 (1992)
- 27.65 S.H. Lam, D.A. Goussis: The CSP method for simplifying kinetics, *J. Chem. Kinet.* **26**(4), 461–486 (1994)
- 27.66 J. Wei, J.C. Kuo: Lumping analysis in monomolecular reaction systems. Analysis of the exactly lumpable system, *Ind. Eng. Chem. Fundamen.* **8**(1), 114–123 (1969)
- 27.67 P.G. Coxson, K.B. Bishoff: Lumping strategy. 2. System theoretic approach, *Ind. Eng. Chem. Res.* **26**101, 2151 (1987), <http://pubs.acs.org/doi/abs/10.1021/ie00070a037>
- 27.68 J.E. Bailey: Lumping analysis of reactions in continuous mixtures, *Chem. Eng. J.* **3**, 52–61 (1972), <http://www.sciencedirect.com/science/article/pii/0300946772850056>
- 27.69 G. Li, H. Rabitz: Determination of constrained lumping schemes for nonisothermal first-order reaction systems, *Chem. Eng. Sci.* **46**(2), 583–596 (1991)
- 27.70 G. Li, H. Rabitz: The direct lumping approach: An application to a catalytic reforming model, *Chem. Eng. Sci.* **48**(10), 1903–1909 (1993), <http://www.sciencedirect.com/science/article/pii/S0009250993803603>
- 27.71 J.C. Kuo, J. Wei: Lumping analysis in monomolecular reaction systems. Analysis of approximately lumpable system, *Ind. Eng. Chem. Fundamen.* **8**(1), 124–133 (1969), <http://pubs.acs.org/doi/abs/10.1021/i160029a020>
- 27.72 J.C. Liao, E.N. Lightfoot: Lumping analysis of biochemical reaction systems with time scale separation, *Biotech. Bioeng.* **31**(8), 869–879 (1988)
- 27.73 G. Li: A lumping analysis in mono- or/and bimolecular reaction systems, *Chem. Eng. Sci.* **39**(7-18), 1261–1270 (1984), <http://www.sciencedirect.com/science/article/pii/0009250984850873>
- 27.74 G. Li, H. Rabitz: A general analysis of exact lumping in chemical kinetics, *Chem. Eng. Sci.* **44**(6), 1413–1430 (1989), <http://www.sciencedirect.com/science/article/pii/0009250989850146>
- 27.75 G. Li, H. Rabitz: A general analysis of approximate lumping in chemical kinetics, *Chem. Eng. Sci.* **45**(4), 977–1002 (1990), <http://www.sciencedirect.com/science/article/pii/000925099085020E>
- 27.76 G. Li, H. Rabitz: New approaches to determination of constrained lumping schemes for a reaction system in the whole composition space, *Chem. Eng. Sci.* **46**(1), 95–111 (1991), <http://www.sciencedirect.com/science/article/pii/000925099180120N>
- 27.77 G. Li, H. Rabitz: A general analysis of exact nonlinear lumping in chemical kinetics, *Chem. Eng. Sci.* **49**(3), 343–361 (1994), <http://www.sciencedirect.com/science/article/pii/S0009250994870063>
- 27.78 G. Li, A.S. Tomlin, H. Rabitz, J. Toth: A general analysis of approximate nonlinear lumping in chemical kinetics. I. Unconstrained lumping, *J. Chem. Phys.* **101**, 1172 (1994)
- 27.79 A.S. Tomlin, G. Li, H. Rabitz, J. Toth: A general analysis of approximate nonlinear lumping in chemical kinetics. II. Constrained lumping, *J. Chem. Phys.* **101**, 1188 (1994)

- 27.80 I.P. Androulakis: Kinetic mechanism reduction based on an integer programming approach, *AIChE J.* **46**(2), 361–371 (2000)
- 27.81 I. Banerjee, M.G. Ierapetritou: Development of an adaptive chemistry model considering micromixing effects, *Chem. Eng. Sci.* **58**(20), 4537–4555 (2003), <http://www.sciencedirect.com/science/article/pii/S0009250903003439>
- 27.82 I. Banerjee, M.G. Ierapetritou: An adaptive reduction scheme to model reactive flow, *Comb. Flame* **144**(3), 619–633 (2006), <http://www.sciencedirect.com/science/article/pii/S0010218005002683>
- 27.83 S.B. Pope: Computationally efficient implementation of combustion chemistry using in situ adaptive tabulation, *Combust. Theory Model.* **1**(1), 41–63 (1997)
- 27.84 U. Mass, S.B. Pope: Simplifying chemical kinetics: Intrinsic low-dimensional manifolds in composition space, *Comb. Flame* **88**(3/4), 239–264 (1992), <http://www.sciencedirect.com/science/article/pii/S001021809290034M>
- 27.85 V.W. Weekman: *Lumps, Models, and Kinetics in Practice*, AIChE Monograph, Vol. 75 (AIChE, New York 1979)
- 27.86 I.S. Han, C.B. Chung: Dynamic modeling and simulation of a fluidized catalytic cracking process. Part II: Property estimation and simulation, *Chem. Eng. Sci.* **56**(5), 1973–1990 (2001), <http://www.sciencedirect.com/science/article/pii/S0009250900004942>
- 27.87 B.G.M. Van Wachem, J.C. Schowten, C.M. Van Den Bleek: Krishna, R., Sinclair J. L.: CFD modeling of gas–fluidized beds with a bimodal particle mixture, *AIChE J.* **47**(6), 1292–1301 (2001)
- 27.88 A.K. Das, J. De Wilde, G.J. Hegnderickx, G.B. Marin, J. Vierendeels, E. Dick: CFD simulation of dilute phase gas–solid riser reactors: Part I – a new solution method and flow model validation, *Chem. Eng. Sci.* **59**(1), 167–186 (2004), <http://www.sciencedirect.com/science/article/pii/S0009250903004433>
- 27.89 R.K. Gupta, K. Kumar, V.K. Srivastava: A new generic approach for the modeling of fluid catalytic cracking (FCC) riser reactor, *Chem. Eng. Sci.* **62**(17), 4510–4528 (2007), <http://www.sciencedirect.com/science/article/pii/S0009250907004046>
- 27.90 C. Zhu, Y. Jun, R. Patel, D. Wang, T.C. Ho: Interactions of flow and reaction in fluid catalytic cracking risers, *AIChE J.* **57**(11), 3122–3131 (2011)
- 27.91 R. Patel, D. Wang, C. Zhu, T.C. Ho: Effect of injection zone cracking on fluid catalytic cracking, *AIChE J.* **59**(4), 1226–1235 (2013)
- 27.92 R. Patel, P. He, B. Zhang, C. Zhu: Transport of interacting and evaporating liquid sprays in a gas–solid riser reactor, *Chem. Eng. Sci.* **100**, 433–444 (2013), <http://www.sciencedirect.com/science/article/pii/S0009250913000079>
- 27.93 P. He, C. Zhu, T.C. Ho: A two-zone model for fluid catalytic cracking riser with multiple feed injectors, *AIChE J.* **61**(2), 610–619 (2015)
- 27.94 T.C. Ho: On catalyst–oil interactions in fluid catalytic cracking, *J. Chin. Inst. Chem. Eng.* **37**(1), 25–35 (2006)
- 27.95 A.H. Lefebvre: *Atomization and Sprays* (Taylor Francis, Abingdon 1989)
- 27.96 C. Derouin, D. Nevicato, M. Forissier, G. Wild, J.R. Bernard: Hydrodynamics of Riser units and their impact on FCC operation, *Ind. Eng. Chem. Res.* **36**(11), 4504–4515 (1997), <http://pubs.acs.org/doi/abs/10.1021/ie970432r>
- 27.97 V. Kumar, A. Reddy: Why FCC riser is taller than model predictions?, *AIChE J.* **57**(10), 2917–2920 (2011)
- 27.98 T.C. Ho: Kinetic modeling of large-scale reaction systems, *Catal. Rev.* **50**(3), 287–378 (2008)
- 27.99 R. Aris, G.R. Gavalas: On the theory of reactions in continuous mixtures, *Phil. Trans. Roy. Soc. A.* **A260**, 351 (1966)
- 27.100 R. Aris: Prolegomena to the rational analysis of systems of chemical reactions, II. Some addendum, *Arch. Ratl. Mech. Anal.* **27**, 356–364 (1968)
- 27.101 G. Astarita, R. Ocone: Lumping nonlinear kinetics, *AIChE J.* **34**(8), 1299–1309 (1988)
- 27.102 M.Y. Chou, T.C. Ho: Continuum theory for lumping nonlinear reactions, *AIChE J.* **34**(9), 1519–1527 (1988)
- 27.103 S.S. Shih, S. Mizrahi, L.A. Green, M.S. Sarli: Deep desulfurization of distillates, *Ind. Eng. Chem. Res.* **31**(4), 1232–1235 (1992), <http://pubs.acs.org/doi/abs/10.1021/ie00004a040>
- 27.104 C.S. Laxminarasimhan, R.P. Verma, P.A. Ramachandran: Continuous lumping model for simulation of hydrocracking, *AIChE J.* **42**(9), 2645 (1996)
- 27.105 K. Basak, M. Sau, U. Manna, R. Verma: Industrial hydrocracker model based on novel continuum lumping approach for optimization in petroleum refinery, *Catal. Today* **98**(1/2), 253–264 (2004), <http://www.sciencedirect.com/science/article/pii/S0920586104004596>
- 27.106 I. Elizalde, M.A. Rodriguez, J. Ancheyta: Application of continuous kinetic lumping modeling to moderate hydrocracking of heavy oil, *Appl. Catal. A* **365**(2), 237–242 (2009), <http://www.sciencedirect.com/science/article/pii/S0926860X09004463>
- 27.107 J. Govindhakannan, J.B. Riggs: On the construction of a continuous concentration–reactivity function for the continuum lumping approach, *Ind. Eng. Chem. Res.* **46**(5), 1653–1656 (2007), <http://pubs.acs.org/doi/abs/10.1021/ie0607191>
- 27.108 K. Qian, W. Olmstead, J. English, L. Green, R. Saeger, S. Jaffe: Micro-hydrocarbon analysis, US Patent 20070114377 A1 (2007)
- 27.109 F. Bertocini, B. Celse, C. Dartiguelongue: Method of determining physico-chemical properties of a petroleum sample from two-dimensional gas chromatography, US Patent 8301397 B2 (2012)
- 27.110 M. Houalla, D.H. Broderick, A.V. Sapre, N.K. Ng, V.H.J. deBeer, B.C. Gates, H. Kwart: Hydrodesulfurization of methyl-substituted dibenzothiophenes catalyzed by sulfided Co–

- Mo/ γ -Al₂O₃, *J. Catal.* **61**(2), 523–528 (1980), <http://www.sciencedirect.com/science/article/pii/0021951780904005>
- 27.111 R. Stephan, G. Emic, H. Hoffman: On the kinetics of hydrodesulfurization of gas oil, *Chem. Eng. Process. Process Intensif.* **19**(6), 303–308 (1985), <http://www.sciencedirect.com/science/article/pii/0255270185850030>
- 27.112 F.J. Krambeck: Computers and modern analysis in reactor design, *Proc. ISCRE 8; IChemE Symp. Ser.* **87** (1984) pp. 733–754
- 27.113 T.C. Ho, Aris, R.: On apparent second-order kinetics, *AIChE J.* **33**(6), 1050–1051 (1987)
- 27.114 T.C. Ho, B.S. White, R. Hu: Lumped kinetics of many parallel n th-order reactions, *AIChE J.* **36**(5), 685–700 (1990)
- 27.115 T.C. Ho: Aggregate behavior and lumped kinetics of many reactions in backmixed and plug-flow reactors, *AIChE J.* **42**(1), 214–231 (1996)
- 27.116 T.C. Ho, B.S. White: Experimental and theoretical investigation of the validity of asymptotic lumped kinetics, *AIChE J.* **41**(6), 1513–1520 (1995)
- 27.117 S.T. Sie: Reaction order and role of hydrogen sulfide in deep hydrodesulfurization of gas oils: Consequences for industrial reactor configuration, *Fuel Process. Technol.* **61**(1/2), 149–171 (1999), <http://www.sciencedirect.com/science/article/pii/S0378382099000363>
- 27.118 G.I. Barenblatt: *Scaling, Self-similarity and Intermediate Asymptotics* (Cambridge Univ. Press, Cambridge 1996)
- 27.119 T.C. Ho, B.S. White: On the continuum approximation of large reaction mixtures, *AIChE J.* **56**(7), 1894–1906 (2010)
- 27.120 T.C. Ho, B.S. White: Continuum approximation of large reaction mixtures in reactors with backmixing, *AIChE J.* **61**(1), 159–165 (2015)
- 27.121 M.R. Gray: *Upgrading Petroleum Resids and Heavy Oils* (Marcel Dekker, New York 1994)
- 27.122 H.A. Rangwala, S.E. Wanke, F.D. Otto, D.I.G. Lana: The hydrotreating of coker gas oil: Effects of operating conditions and catalyst properties, *Proc. 10th Symp. Catal., Kinston* (1986) pp. 20–28
- 27.123 L.C. Trytten, M.R. Gray, E.C. Sanford: Hydroprocessing of narrow-boiling gas oil fractions: Dependence of reaction kinetics on molecular weight, *Ind. Eng. Chem. Res.* **29**(5), 725–730 (1990), <http://pubs.acs.org/doi/abs/10.1021/ie00101a003>
- 27.124 R.H. Van Dongen, D. Bode, H. van der Eijk, J. van Klinken: Hydrodemetallization of heavy residual oils in laboratory trickle-flow liquid recycle reactors, *Ind. Eng. Chem. Proc. Des. Dev.* **19**(4), 630 (1980), <http://pubs.acs.org/doi/abs/10.1021/i260076a021>
- 27.125 T.C. Ho: A simple expression for the collective behavior of a large number of reactions, *Chem. Eng. Sci.* **46**(1), 281–289 (1991), <http://www.sciencedirect.com/science/article/pii/000925099180136M>

Refinery-Wide

28. Refinery-Wide Optimization

Dale R. Mudt, Clifford C. Pedersen, Maurice D. Jett, Sriganesh Karur, Blaine McIntyre, Paul R. Robinson

Refinery-wide optimization (RWO) requires integration of several systems – regulatory control, the distributed control system (DCS), the laboratory information management system (LIMS), model-predictive control, online optimization based on rigorous models of individual units and process areas, and refinery planning linear program (LP) software. Project implementation requires communication between refinery personnel – managers, engineers, and operators – and outside modeling experts.

Starting in 1998, refinery-wide optimization was implemented at the Suncor refinery in Sarnia, Ontario, Canada. The model-predictive control system was DMCplus. The rigorous models were developed by Aspen Technology, Inc., using Aspen RT-Opt for conventional equipment, a rigorous hydrocracker model developed jointly by Sun Oil and

28.1	Overview of Suncor	865
28.2	Refinery-Wide Optimization (RWO)	866
28.3	Rigorous Models for Clean Fuels	868
28.3.1	Feedstock and Product Characterization	868
28.3.2	Aspen FCC Overview	868
28.3.3	Aspen Hydrocracker	870
28.3.4	Clean Fuels Planning.....	873
28.4	Conclusion	876
	References	877

AspenTech, and reactor models developed by AspenTech for the Houdry cracking unit (HCC) and a catalytic reformer. Benefits from implementation of an early version of the hydrocracker rigorous model exceeded US\$ 3000 per day.

One reason for writing this chapter is to report on the success of real-time, online refinery-wide optimization (RWO) at Suncor-Sarnia using rigorous process models. Another reason is to show how the same rigorous

models can be used offline to quantify key nonlinear relationships during the evaluation of project ideas, especially those related to the production of clean fuels.

28.1 Overview of Suncor

Suncor operates a 70 000 barrel/day refinery at Sarnia, Ontario, Canada. The refinery processes feeds from the following sources:

- Synthetic crude oil from Suncor's oils sands processing plant at Fort McMurray, Alberta
- Conventional crude oil
- Condensate
- Vacuum gas oil (VGO).

Figure 28.1 presents an outline of the plant, which started operation in 1953. Synthetic crude and conventional crude oil come to the refinery through the inter-provincial pipeline, which runs from Edmonton, Alberta to Sarnia, Ontario. The transit time is about one month. Other crudes are also available from nearby facilities.

The refinery includes the following major process units:

- Crude distillation (CDU) – 2 units
- Vacuum distillation (VDU)
- Houdry catalytic cracking unit (HCC)
- Catalytic reforming (CRU) – 2 units
- Alkylation unit
- Aromatics recovery unit
- Unsaturated gas plant
- Saturated gas plant
- Naphtha hydrotreater
- Diesel/gas oil hydrotreater
- Hydrocracker complex.

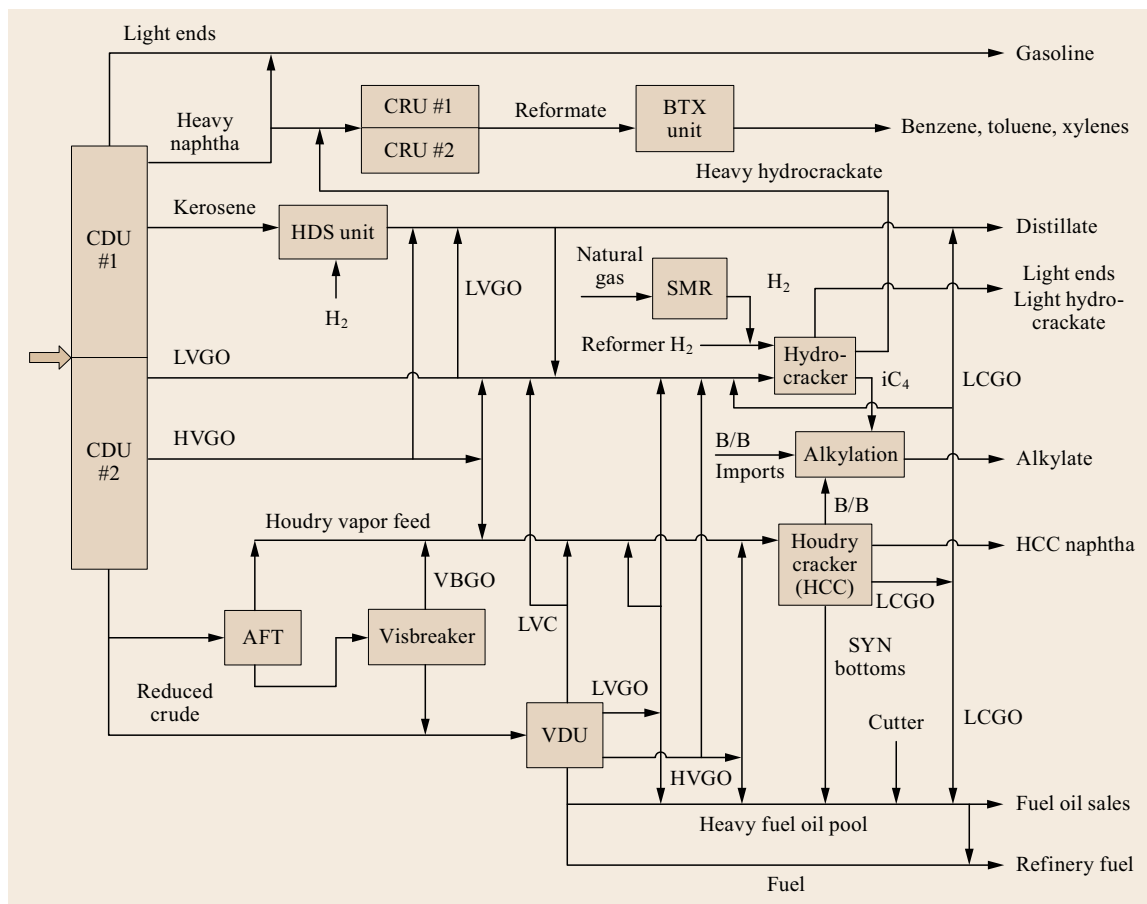


Fig. 28.1 Overview of the Suncor refinery in Sarnia, Ontario

28.2 Refinery-Wide Optimization (RWO)

The refinery-wide optimization (RWO) initiative began in July 1998. Three phases were defined for the project:

- Phase 1: Build a solid and sustainable advanced control and optimization foundation.
- Phase 2: Ensure model consistency between planning, scheduling, and real-time optimization.
- Phase 3: Integrate planning, scheduling, and real-time optimization by linking the optimization models to the refinery LP.

Expected benefits from the RWO initiative included:

- Increased refinery throughput
- Improved refinery yields
- Improved gas oil management

- Improved hydrogen management
- Optimum product recoveries
- Reduced energy costs
- Increased ability to respond to market changes.

Rigorous models for stand-alone units can also provide significant benefits. Previously [28.1], we reported benefits of US\$ 3000 per day (US\$ 0.15 per barrel) for the initial optimizer on the hydrocracking complex; these benefits were in addition to those provided by model-predictive DMC control. For RWO, a revised model based on Aspen Hydrocracker (AHYC) was developed. It included a catalyst deactivation block, which enhanced maintenance turnaround planning by predicting future catalyst activity, product yields and product properties for a variety of assumed feeds and specified operating conditions. This information

Table 28.1 Scope of refinery-wide optimization applications

Plant 1	Scope
Crude and HCC	Preheat train, crude heaters, crude tower, atmospheric flash tower, syn tower, HCC heaters, reactor, kiln, steam coils, air blower, cyclone, main fractionator, unsaturated gas plant
Plant 2	
Crude and vacuum reformer 2 and aromatics	Preheat train, heaters, atmospheric tower, vacuum tower heaters, compressors, pretreater, reactors, flash drums, depropanizer, naphtha splitter, absorber/deethanizer, aromatics complex
Plant 3	
Steam methane reforming (SMR), HYC, gas plant	H ₂ Plant, hydrocracker reactor section, preflash, main tower, absorber/stripper, debutanizer, jet tower, diesel tower, saturated gas plant

Table 28.2 Hardware and software for RWO

Item	Vendor
DCS systems	Honeywell TDC 2000/3000, Foxboro I/A
Online computers	DEC alpha with VMS software
Offline computers	Compaq (Windows NT)
Real-time database	Aspen infoplus, Honeywell PHD
Control software	DMCplus, Aspen IQ
Optimization software	Aspen RT-opt
Refinery LP	Haverly GRTMPS

is also used to impose constraints on daily operation.

The RWO initiative was driven in part by the need to upgrade or replace software applications that were not Y2K compliant. In addition, the project reduced application maintenance costs because the same software versions were used throughout the plant, and because modern control and optimization software is more user-friendly than it was in the 1980s, when Suncor first began implementing model-predictive control and online optimization.

Table 28.1 summarizes the scope of the major RWO applications. A large DMCplus application – 64 manipulated variables (MV) × 16 feed-forward variables (FF) × 168 controlled variables (CV) – controls Plant 1. For Plant 1, the process scope of the controller is equivalent to that of the optimizer, which sends 34 targets to the controller. In Plant 3, separate controllers are used for the hydrogen plant, the hydrocracker (HYC), the HYC gas plant, and low-sulfur diesel (LSD) tower, but a single optimizer sends targets to these controllers.

Table 28.4 Key integration points

Plants 2 (H ₂ from reformer) ⇒ Plant 3 (HYC)
Plants 1, 2, and 3 (reformates and HYC light naphtha) ⇒ Gasoline blender
Plant 3 (HYC heavy naphtha) ⇒ Plant 2 (Reformer 2)
Plant 3 (isobutane) ⇒ Plant 1 (alky feed)

Table 28.3 Integration point categories

Type of integration point	Time scale
Feed-forward information required by the model predictive controllers	Minutes
Steady-state information (inputs to and outputs from) the online optimizers	Hours
Higher level information (inputs to and outputs from) the refinery LP	Daily

The RWO initiative used the hardware and software listed in Table 28.2.

Each optimizer includes an offline version, which is periodically updated with live plant data. Offline models are used to tune and monitor the performance of the optimizers. They can also be used for maintenance planning and design studies.

The success of RWO depended heavily upon proper integration of the separate applications. Integration points fell into three categories (Table 28.3). Intermediate tanks presented special problems in part because they tend to stratify, but mostly because they complicate time-scale issues. For several critical tanks, open-equation models calculate tank compositions on a regular basis – about every 5 min – to provide feed-forward inputs to other optimizers or possibly DMCplus controllers. Special logic is used to compensate for stratification. To date, these tank composition models are performing well.

Other key integration points are shown in Table 28.4.

Integrating the real-time optimizers into Suncor's planning and scheduling methodology will require con-

sistency between the optimizers and the refinery LP in the following areas:

- Yields and product qualities
- Degrees of freedom
- Constraints.

Initially, data were transferred manually between the LP and the optimizers. This was beneficial because

28.3 Rigorous Models for Clean Fuels

As mentioned above, one purpose of this paper is to show how rigorous models can be used offline to quantify key nonlinear process relationships, including those related to manufacturing clean fuels.

At most North American refineries, including Suncor-Sarnia, most of the sulfur in the gasoline pool comes from a catalytic cracking unit. To make low-sulfur gasoline, an Axens Prime-G unit was installed to desulfurize gasoline from the Houdry catalytic cracker (HCC) and visbreaker units. Another option would have been to pretreat all of the HCC feed [28.3].

To summarize, our RWO experience has demonstrated the following:

- Rigorous optimizers provide significant economic benefits.
- Open-equation optimizers can be linked, and linked optimizers can successfully represent nonlinear interactions between process units.
- Aspen FCC (AFCC) (modified) and AHYC provide high-fidelity representations of Suncor's HCC and hydrocracker, respectively. We can conclude that linking AHYC with AFCC will enhance the industry's understanding of FCC feed pretreating, and eventually lead to the operation of FCC-plus-pretreater installations as a single, optimized complex.

28.3.1 Feedstock and Product Characterization

For any rigorous model, success requires detailed, accurate feedstock and product characterizations. For the HCC and hydrocracker, GC/MS, ^1H NMR, ^{13}C NMR, HPLC, and standard American Society for Testing and Measurement (ASTM) methods were used to analyze a battery of feedstock and product samples. The analytical results were used to generate base-case distributions for the components used in the models and to tune reaction kinetics.

In the real world, feedstock properties and product slates are changing continually. In AFCC and AHYC,

the models allowed us to increase the accuracy of LP shift vectors. A recent publication [28.2] describes the benefits of running steady-state models in recursion with Aspen PIMS, a widely used LP program. This method may offer the best of both worlds – the practicality of LP technology augmented by the rigor of nonlinear, unit-specific models.

It was expected that during RWO Phase 3, the transfer of data would be automated.

proprietary feed-adjust models skew the base-case component distribution to match the measured properties of feeds and products.

28.3.2 Aspen FCC Overview

Aspen FCC (AFCC) is an open-equation, flowsheet-based model designed for both online and offline applications. The model is constructed from individual blocks that represent the separate pieces of equipment – riser, standpipe, slide valve, cyclone, transfer line, etc. – found in commercial FCC units. Each building block is generic and can be configured with dimensions corresponding to a given commercial unit (Table 28.5).

A typical FCC unit configuration is presented in Fig. 28.2. The diagram shows a simple version of the actual blocks used to model the feed, feed adjust and preheat systems.

In the riser model, detailed hydraulics and heat effects are captured by linking flow equations to kinetics. The riser model can be configured vertically, horizontally, or at any angle of inclination. Multiple risers can be used. The individual risers can process different feeds or the same feed. In essence, any commercial riser/reactor configuration can be simulated with the modular components of AFCC.

Table 28.5 Aspen FCC building blocks

Riser model: hydrodynamics and kinetics
Reactor-vessel cyclones and plenum model
Reactor dilute-phase model
Reactor dense-bed model
Reactor stripping zone model
Catalyst stand-pipe model
Catalyst slide-valve two-phase flow model
Catalyst transfer-line model
Regenerator dense-bed model: coke burn kinetics
Regenerator freeboard model: coke burn kinetics
Regenerator cyclone model
Feed characterization, component-mapping model

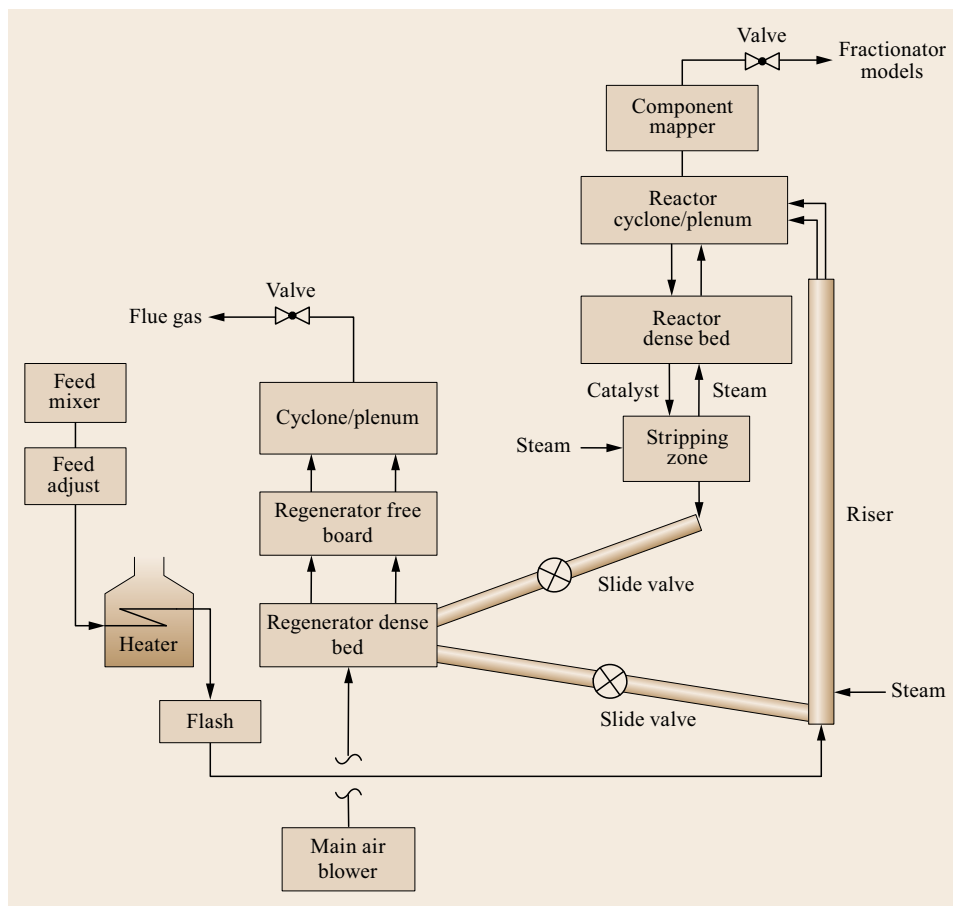


Fig. 28.2 Model components for Aspen FCC (riser/reactor/regenerator)

Hydrocarbon feed and regenerated catalyst models are connected to the inlet of the Riser model. The catalyst-stream model includes the mass flow, temperature, pressure, enthalpy of the catalyst/coke mixture, particle density of the catalyst/coke mixture, coke-on-catalyst weight fraction, and coke composition.

Pressure drop calculations are based on head, acceleration, and frictional effects. Pressure drop through the riser is modeled as a combination of pressure drop due to vapor and pressure drop due to solids. For the vapor, the frictional contribution is based on friction-factor correlations with the Reynolds number. For catalyst flow, frictional contributions are based on correlations for solid-vapor flow in a conduit. Proper prediction of pressure drop along the riser has a significant impact on predicted yields.

The riser model uses vertical or horizontal slip factor correlations (depending on the riser orientation) to determine the differential velocity between the vapor and the solid phases. The slip calculation is critical for determining bulk density profiles, which govern the path dependence of cracking profiles.

As coke is differentially produced along the length of the riser, additional solids are differentially transferred from the vapor to the catalyst surface. The physical effects of this transfer are described by continuity equations. The molar heat of adsorption for coke laydown is included in the heat balance. The heat of coke desorption is calculated in the regenerator model. Slip-factor correlations are based on fully developed flow. The model applies a correction for the turbulent, high-slip zone at the inlet of the riser.

The riser model effluent is connected to the reactor vessel models. These include the reactor dilute phase, the dense phase, and the cyclone system, which represents the segregation of effluent vapors and catalyst. The cyclone model performs a two-phase, loading-based ΔP calculation, for which cyclone inlet and body diameters are used. The cyclone model can be configured with one or two riser inlet ports.

The reactor dilute phase model is identical to the riser model without entry-zone and frictional effects. The reactor dense bed model can be configured to the exact geometry of an operating unit. It is used to represent

the inventory of spent catalyst above the stripping zone. For large vessels with significant holdup, this model can be configured as a fluidized bubbling bed system. For low holdup or riser-cracking systems, it is treated as a fluidized bed with a parameterized void fraction.

Spent catalyst and regenerator air are connected to the regenerator model. The regenerator includes three blocks, each of which can be configured for a specific unit. The first block (from the bottom up) is the regenerator dense bed. This model represents the bubbling, fluidized bed where the majority of coke burn occurs. The second block is the regenerator freeboard (disperse phase), which is the region between the surface of the bubbling bed (dense bed) and the inlet to the cyclones. The third block is the regenerator cyclone model.

The regenerator dense bed is modeled as a bubbling bed with heterogeneous coke burn and CO conversion to CO₂. Bulk density is modeled as a function of bed height and pressure. Promoters are modeled by updating selected coke-burn parameters. Combustion air composition is determined independently by the regenerator air model. Therefore, O₂ enrichment can be simulated and optimized.

The regenerator freeboard model represents the vessel region between the surface of the dense bed and the cyclone inlets. Inlets to the model are entrained, regenerated catalyst from the dense-bed model and the combustion-gas stream from the dense bed. Outlets from the model are the freeboard combustion-gas stream and the catalyst stream from the cyclones. The freeboard is modeled as a simple plug-flow reactor with homogeneous CO-to-CO₂ after-burn. Temperatures may rise rapidly in the presence of excess O₂.

The regenerator cyclone model performs a two-phase, loading-based ΔP calculation. Flue-gas compositions are calculated and reported on a standard dry mole percent basis for parameterization purposes. The flue gas stream can be connected to the valve model between the regenerator and CO boiler, or to a downstream power recovery system.

Inputs and outputs for the blocks described below are compatible with the vapor and catalyst streams used in the reactor/regenerator models.

The stripping zone model performs heat, mass and pressure balance calculations around the stripping zone. A tunable stripping efficiency curve is included. The stripping efficiency is related to the ratio of catalyst flow to stripping-steam flow.

The catalyst standpipes create a standing head that drives catalyst circulation. Different FCC designs make more or less use of standpipe technology. Standpipes typically end at a slide valve, which is used to control catalyst circulation. Standpipe diameter and length are variables in the standpipe model.

Table 28.6 Aspen FCC 21 reactive lumps

Gas lump
Gasoline lump
221–343 °C (P, N, As, Ar1, Ar2)
343–510 °C (P, N, As, Ar1, Ar2, Ar3)
510 °C-plus (P, N, As, Ar1, Ar2, Ar3)
Coke (2 lumps)

The catalyst transfer line model represents the pneumatic transport regime in the catalyst transfer line. Transfer-line diameter and length are configurable. Like the riser model, the catalyst transfer line model can be configured as vertical, horizontal, or inclined.

The slide valve model calculates ΔP for a two-phase, loading-based orifice. The valve coefficient is parameterized from measured slide valve position (percent open) and pressure differential across the slide valve.

Components with similar reaction kinetics are grouped into 21 lumps. These kinetic lumps are listed in Table 28.6. In practice, the 21 components provide sufficient granularity to model all of the important steady-state cause-and-effect relationships in the FCC reactor-regenerator complex. Kinetic parameters for the riser and reactor models are segregated from the hydraulics and heat balance relationships. This permits different FCC kinetic schemes to be implemented within the same rigorous riser/reactor models. The offline version of the model includes a simplified fractionator model and a product-property model.

The simplified fractionator includes a delumper model to convert the 21 kinetic lumps into > 80 pure- and pseudo-components, which are then divided into user-specified boiling fractions. A nonlinear distribution function generates ideal distillation curves with realistic fraction-to-fraction overlap. The fractionator can interconvert distillation methods, so a user can calculate D-86, D-1160, D-2887, and/or true boiling point (TBP) curves for gasoline and light cycle oil (LCO).

The product property model generates the product properties listed in Table 28.7. During projects, other product property calculations are added as needed. The online application at Suncor-Sarnia does not use the simplified fractionator model. Instead, it uses fully rigorous tray-by-tray models for the HCC fractionation section.

28.3.3 Aspen Hydrocracker

In many respects, AHYC is simpler than AFCC, mainly because it doesn't have to model the flow of a solid phase. Complexity arises for the following reasons:

- A separate reactor is used for each catalyst bed.
- The same set of reactions is used for both fixed-bed hydrotreating and fixed-bed hydrocracking units.

Table 28.7 Aspen FCC standard product properties

	API gravity	Specific gravity	Sulfur	Cloud point	RON	MON	PONA
As-fractionated product properties							
Gasoline	✓	✓	✓		✓	✓	✓
LCO	✓	✓	✓	✓			
HCO	✓	✓	✓				
Bottoms		✓	✓				
Standard-cut product properties							
Light naphtha	✓	✓	✓		✓	✓	✓
Heavy naphtha	✓	✓	✓		✓	✓	✓
LCO	✓	✓	✓	✓			
Bottoms	✓	✓	✓				

RON = research octane number, *MON* = motor octane number, *PONA* = paraffin/olefin/naphthene/aromatic ratio

- All recycle loops are closed.
- More components and reactions are required. The model employs 116 components and 195 reactions.
- Catalyst deactivation has a major impact on the economics of a fixed-bed hydrocracker.

AHYC is an update of SARCRACK, a hydrocracker model developed by Sun Oil Company [28.4], and modified by Suncor-Sarnia with assistance from DMC Corporation for online optimization. The component slate and reaction network for AHYC are consistent with publications by Klein et al. [28.4], Stangeland [28.5], Quann et al. [28.6, 7], Filiminov et al. [28.8], and Jacobs [28.9].

Figure 28.3 presents a diagram of the high-pressure reaction section of the hydrocracker at Suncor-Sarnia. The unit is a classical single-stage Unicracker with two reactors. In the first (R1), all three beds are loaded with high-activity hydrodenitrogenation (HDN) catalyst. In the second (R2), all four beds are loaded with a zeolite-based, distillate-selective hydrocracking catalyst.

For both reactors, the incoming gas is heated separately. The unit has two separator drums. The hydrogen-rich gas from the overhead of the high-pressure separator (HPS) is recycled. The HPS bottoms flow through a power-recovery turbine (PRT) to the low-pressure separator (LPS). LPS bottoms go through a preflash tower to the main fractionator.

Heavy naphtha from the main fractionator goes to the large catalytic reformer, which is used to produce both gasoline and feedstock for the aromatics plant. A portion of the bottoms from the main fractionator is recycled to R2. The remainder goes to the first of two distillation towers for recovery of middle distillate products.

AHYC is an open-equation, flowsheet-based model, which is used both online and offline at Suncor-Sarnia, where it was configured and tuned to rigorously represent the catalyst beds, quench valves, compressors, flash drums, heaters, exchangers, etc. in the commercial unit. A rigorous model for the hydrogen plant, a steam/methane reformer, was linked to the hydro-

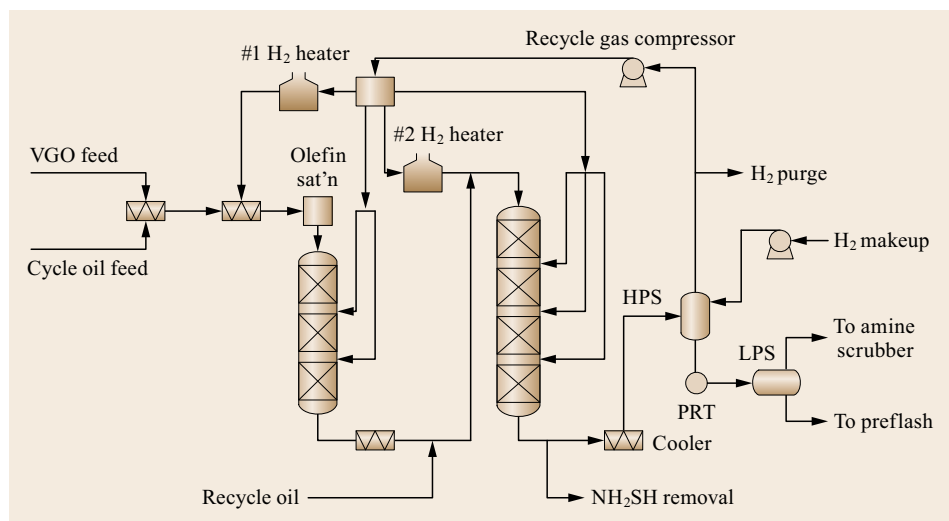


Fig. 28.3 AHYC model for the Suncor-Sarnia hydrocracker: Reaction section

cracker model. The entire fractionation section – comprising a preflash tower, main fractionator, all five gas plant towers, and two middle distillate recovery towers – was modeled rigorously.

After R1, a component-splitter model was used to simulate the removal of NH_4HS upstream from the HPS. This is a simplification, but it eliminates the need for a three-phase electrolytic flash model in the HPS, and it has no effect on reaction kinetics, the composition of recycle hydrogen, or the composition of the LPS bottoms.

A relatively simple extent-of-reaction model was used to simulate the saturation of olefins, including the associated consumption of hydrogen and generation of heat. It was assumed that 100% of the olefins in the feed are removed in the first bed of R1.

As mentioned above, each catalyst bed is modeled separately. Kinetic constituents are segregated from hydraulic and heat balance relationships, which permits different kinetic schemes to be implemented within the same mechanical framework.

Trickle-bed hydrodynamics are modeled with equations described by *Satterfield* [28.10]. Reaction rates and flash calculations are performed at multiple collocation points in each reactor bed. This enhances the ability of the model to perform an accurate heat-release calculation (Table 28.9).

A customized version of the Langmuir–Hinshelwood–Hougen–Watson (LHHW) mechanism is used both for reversible (28.1) and irreversible reactions (28.2). The main steps in this mechanism are:

- Adsorption of reactants to the catalyst surface
- Inhibition of adsorption
- Reaction of adsorbed molecules
- Desorption of products.

Several inhibitors are included in AHYC reaction kinetics. These include H_2S , ammonia, and organic nitrogen compounds. The inhibition of hydrodesulfurization (HDS) reactions by H_2S is modeled, and so is the inhibition of acid-catalyzed cracking reactions – dealkylation of aromatics, the opening of naphthenic rings, and paraffin hydrocracking – by ammonia and to a much greater extent by organic nitrogen.

$$\text{Rate} = A \cdot k \cdot \frac{((K_i C_i \cdot K_{\text{H}_2} \cdot (P_{\text{H}_2})^x K_{\text{eq}}) - K_j C_j) \cdot P F^y}{I_a \cdot I_b \cdot I_c}, \quad (28.1)$$

where A = catalyst activity, k = rate constant, K_i = adsorption constants for hydrocarbons, C_i = concentrations of hydrocarbons, K_{H_2} = adsorption constants for hydrogen, P_{H_2} = concentrations of hydrogen, K_{eq} = equilibrium constant, PF = pressure factor, I_a, I_b, I_c , etc.

= inhibition factors.

$$\text{Rate} = A \cdot k \cdot \frac{K_i C_i \cdot K_{\text{H}_2} \cdot (P_{\text{H}_2})^x \cdot P F^y}{I_a \cdot I_b \cdot I_c}, \quad (28.2)$$

where A = catalyst activity, k = rate constant, K_i = adsorption constants for hydrocarbons, C_i = concentrations of hydrocarbons, K_{H_2} = adsorption constants for hydrogen, P_{H_2} = concentrations of hydrogen, PF = pressure factor, I_a, I_b, I_c , etc. = inhibition factors.

Reaction Pathways

The following reaction types were modeled in SAR-CRACK:

- Hydrodesulfurization (HDS)
- Hydrodenitrogenation (HDN)
- Saturation of aromatics
- Ring opening
- Ring dealkylation
- Paraffin hydrocracking
- AHYC also models olefin saturation and (in an empirical way) paraffin isomerization.
- The AHYC reaction scheme has the following characteristics:
 - 45 reversible aromatics saturation reactions involving components in each major distillation range. The components include naphthene-aromatic compounds.
 - 19 irreversible olefins saturation reactions. The model assumes that olefin saturation is complete within the first catalyst bed.
 - Saturation and dealkylation for sterically hindered sulfur and nitrogen lumps. This allows AHYC to use different HDS and HDN rates for easy-to-treat and hard-to-treat sulfur and nitrogen compounds.

Recent publications [28.11–14] confirm that a hydrotreater removes sulfur from organic sulfides, disulfides, and mercaptans with relative ease. Thiophenes, benzothiophenes, unhindered dibenzothiophenes and hindered dibenzothiophenes are successively harder to desulfurize.

Figure 28.4 illustrates the so-called *direct* mechanism for the HDS of dibenzothiophene, and Fig. 28.5 shows a widely accepted mechanism for the HDS of hindered dibenzothiophenes. Note that the direct HDS

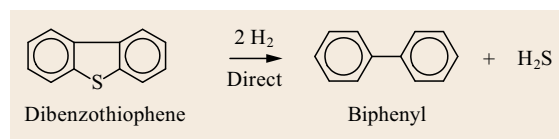
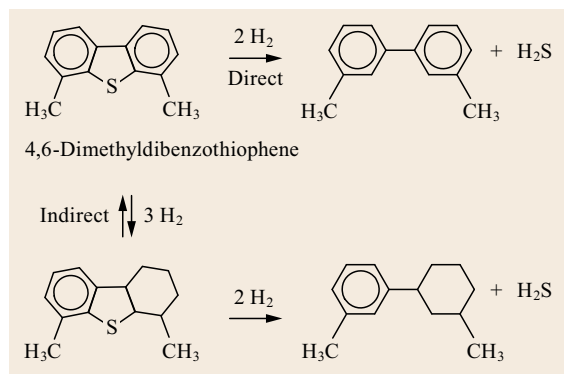


Fig. 28.4 Direct mechanism for the hydrodesulfurization of dibenzothiophene

Table 28.8 Relative reaction rates of hindered and unhindered sulfur compounds

Sulfur compound	Rel. HDS rate	Boiling point (°F)	Boiling point (°C)
Thiophene	100	185	85
Benzothiophene	30	430	221
Dibenzothiophene	30	590	310
Methyldibenzothiophene	5	600–620	316–327
Dimethyldibenzothiophene	1	630–650	332–343
Trimethyldibenzothiophene	1	660–680	349–360

**Fig. 28.5** Mechanism for the hydrodesulfurization of hindered dibenzothiophenes

of dibenzothiophene requires 2 moles of hydrogen per sulfur atom, while the HDS of hindered dibenzothiophenes requires 5 moles of H_2 per sulfur atom.

Structural differences between sulfur-containing compounds translate into significantly different HDS reaction rates. Table 28.8 shows pilot plant data for the HDS of small amounts of pure thiophenes in a clean-diesel solvent. The catalyst and temperature were the same for each compound. Note that HDS rates for the first three compounds, which are unhindered, are 30–100 times faster than rates for the last three compounds, which are hindered.

Catalyst Deactivation Model

In AHYC, the catalyst deactivation model calculates the deactivation rate as function of the following:

- Coke precursors in the feed
- Time on stream
- Average bed temperature for each catalyst bed
- H_2 partial pressure.

The model predicts future catalyst activity, required temperature, yields, hydrogen consumption, and product properties. Alternatively, if the catalyst cycle life is fixed, the model can compute the optimal changes in feed rate, feed properties, and/or conversion needed to reach the target end-of-run date.

Figure 28.8 shows how the deactivation model can be used to predict future temperatures required to hit

a user-selected process objective. The process objective can be sulfur removal, nitrogen removal, or hydrocarbon conversion – for example, the conversion of 650 °F-plus to 650 °F-minus (343 °C-plus to 343 °C-minus) material.

At the hydrocracker at Suncor-Sarnia, the deactivation model is applied to each catalyst bed. This enables the development of strategies to bring all catalyst beds to end-of-run at (roughly) the same time, and prediction of future yields, selectivity, and product properties.

AHYC Model Fidelity

Table 28.9 presents data from an AHYC project at a US East Coast refinery. The data show the excellent fit that can be achieved with the model. During that project, AHYC predictions were compared to step-test gains from a model-predictive controller. The optimizer matched most gains within $\pm 20\%$ (relative). This shows that the model does a good job of predicting process behavior under conditions well away from those at which it was tuned.

28.3.4 Clean Fuels Planning

Hydrogen Requirements for Deep Desulfurization

We ran a series of case studies to calculate the hydrogen requirements for deep desulfurization in a high-pressure gas-oil hydrotreater.

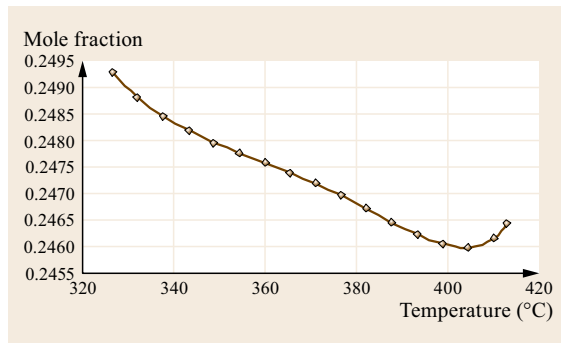
For the saturation of aromatics in a hydrotreating or hydrocracking unit, equilibrium effects, which favor formation of aromatics, start to overcome kinetic effects above a certain temperature. This causes a temperature-dependent *aromatics cross-over* effect, which explains the degradation of important middle distillate product properties – including kerosene smoke point and diesel cetane number – at high process temperatures near the end of catalyst cycles. The cross-over temperature is affected by feed quality and hydrogen partial pressure, so it can differ from unit to unit.

Figure 28.6 shows results from a case study in which the weighted average reactor temperature (WART) was changed over a wide range in a model based on the treating section of the Suncor-Sarnia hydrocracker. Even though the WART was changed, the

Table 28.9 Aspen hydrocracker model fidelity

Variable	Measured value		Predicted value		Offset
Conversion	63.6 wt% feed		63.54 wt% feed		0.057
R1 WART ^a	724 °F	384.4 °C	724 °F	384.4 °C	0.55 °F
R2 WART	723 °F	383.9 °C	723 °F	383.9 °C	-0.71 °F
N at R1 exit	61 wppm		59 wppm		2 wppm
N at R2 exit	3 wppm		3 wppm		0 wppm
S at R1 exit	300 wppm		299 wppm		1 wppm
S at R2 exit	33 wppm		33 wppm		0 wppm
H2 makeup	40.5 million scf/d		47 800 Nm ³ /h		-1 Mscf/d
R1B1 outlet temp	707 °F	375 °C	707 °F	375 °C	0.001 °F
R1B2 outlet temp	762 °F	405.6 °C	762 °F	405.6 °C	0.009 °F
R2B1 outlet temp	761 °F	405 °C	761 °F	405 °C	0.008 °F
R2B2 outlet temp	760 °F	404.4 °C	760 °F	404.4 °C	0.002 °F
R3B1 outlet temp	725 °F	385 °C	725 °F	385 °C	0.001 °F
R3B2 outlet temp	726 °F	385.6 °C	726 °F	385.6 °C	0.001 °F
R3B3 outlet temp	743 °F	395 °C	743 °F	395 °C	0.003 °F

^a WART = weighted average reactor temperature

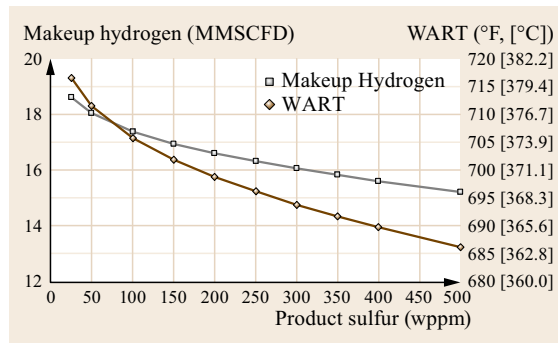
**Fig. 28.6** Product aromatics versus temperature

reactor temperature profile – equal outlet temperatures for the catalyst beds – was the same for every case.

The y-axis shows the mole fraction of total aromatics remaining in product. For this case study, the feed rate, feed type, and catalyst activity were kept constant, which means that deactivation effects were not included. With less-active end-of-run catalysts, the rates of forward (saturation) reactions are inhibited, so the aromatics cross-over effect is amplified.

Figure 28.7 shows results of a case-study in which the product sulfur was kept constant (fixed) at different levels between 500 and 15 wppm. Required WART and hydrogen makeup flow are plotted on the y-axis. Because the product sulfur was fixed, another normally fixed variable can be allowed to vary. For this study, the chosen variable was WART.

Again, we ran the case study using the hydrotreating portion of the Suncor-Sarnia hydrocracker model with an equal-outlet temperature profile. For 500 wppm sulfur in the product, the makeup H₂ flow

**Fig. 28.7** Aspen hydrocracker case study results: Hydrogen consumption and weighted average reactor temperature (WART) versus product sulfur content

is 15.2 MMSCFD. For 15 wppm, the makeup flow is 18.6 MMSCFD, more than 40% higher. Higher WART leads to increased conversion, increased HDN, and (up to a point) increased saturation of aromatics. This explains why the hydrogen consumption increased so much – and so nonlinearly – when the target product sulfur content went from 500 to 15 wppm.

We can also keep WART constant and achieve the desired level of HDS by allowing changes in liquid hourly space velocity (LHSV). When this is done, the effect on hydrogen consumption is less severe. But in the real world, decreasing the LHSV is equivalent to lowering feed rate or adding a reactor, both of which are expensive. The WART-based trend shown here is more relevant to an existing unit.

Figure 28.7 is consistent with the existence of both hindered and unhindered sulfur compounds in the feed. As mentioned above, the last traces of sulfur in diesel oil are locked inside highly hindered hydrocar-

bon molecules, which have to be cracked open before the sulfur can be removed.

Effects of Hydrotreating on FCC Performance

Many refiners include the hydrotreating of FCC feed in their plans to make clean fuels. To demonstrate the feasibility of running a rigorous model for an FCC-plus-pretreater complex, we connected AHYC to AFCC. To link the two, we created a component mapper model to compress the 97 reactive components from AHYC into the 21 lumps used in AFCC. We then connected the unconverted oil stream from the AHYC fractionator model to the feed-adjust block of AFCC.

Initially, the combined model was huge, containing more than 1.2 million nonzero terms in its matrix of variables. To allow the model to run in a reasonable amount of time on a Pentium III computer, we made some simplifications. In the reduced model, the four catalyst bed models are still fully rigorous. However, the hydrogen furnaces are represented with a heat-exchanger model, quench valves are modeled with mixers, a component splitter model is used for the wash-water system, and a group of component splitters is used for the fractionation section. These changes reduce the number of equations and nonzeros to 130 000 and 680 000, respectively. Despite these simplifications, the slimmed-down model remains, in our collective opinion, a useful tool for offline what-if studies and for economic comparisons of different process options.

We first looked at the effect of varying the amount of hydrotreated material in an FCC feed blend from 0.0 to 96.7 vol.%. Table 28.10 presents selected process conditions for the feed hydrotreater, which achieved 90% desulfurization and roughly 23 wt% conversion of vacuum gas oil to middle distillate and naphtha.

We modeled the effect of feed hydrotreating in two ways. The first and most logical approach was to

Table 28.10 Feed pretreater operating conditions

Variable	Units	Value
Feed rate	b/d	39 000.0
Number of catalyst beds		4.0
Weighted average reactor temperature	°F	720.0
	°C	382.0
LHSV	hr ⁻¹	1.2
Hydrogen partial pressure	psi	2000.0
	bar	136.0
Hydrotreater feed sulfur	wt%	1.95
Sulfur in hydrotreated FCC feed	wt%	0.195
Conversion of 343 °C-plus to 343 °C-minus	wt%	23.0

model the pretreating of the 100% of the FCC feed. We simply operated the pretreater model at several different severities and watched the response of the FCC model. Complications arose because upstream conversion in the pretreater affects the amount of feed going to the FCC model. When we compensated by increasing or decreasing the overall fresh feed rate to maintain a constant feed rate to the FCC, conversion in the pretreater changed due to the corresponding differences in LHSV. This is a classical – and very realistic – economic optimization problem, for which the combined AHYC/AFCC model is well suited. However, it doesn't easily lend itself to creating straight-forward graphs for publications.

In another approach to modeling the effects of FCC feed pretreating, the FCC model receives a blend of hydrotreated feed from AHYC with straight-run feed from a tank model. The latter case is discussed here.

Table 28.11 shows the properties of the four FCC feed blends that were used in the combined hydrotreater/FCC simulations. Table 28.12 presents FCC conversion and yield data. In each case, we held the FCC riser outlet temperature at 1030 °F (544 °C).

Table 28.11 FCC feed properties for blends of straight-run and hydrotreated feeds

Variable	Units	Case 1	Case 2	Case 3	Case 4
Straight-run VGO	b/d	30 000	20 000	10 000	1000
Hydrotreated VGO (90% HDS)	b/d	0	10 000	20 000	29 000
Total feed rate	b/d	30 000	30 000	30 000	30 000
API gravity	°API	22.60	24.57	26.58	28.44
Specific gravity		0.9182	0.9067	0.8951	0.8847
Sulfur	wt%	1.95	1.38	0.80	0.26
Basic nitrogen	wppm	417	380	344	310
Conradson carbon (CCR)	wt%	0.730	0.525	0.315	0.122
Vanadium	wppm	3.1	2.1	1.1	0.2
Nickel	wppm	5.2	3.5	1.8	0.3
Sodium	wppm	1.3	0.9	0.5	0.1
Iron	wppm	2.6	2.1	1.5	1.1
Copper	wppm	0.2	0.2	0.1	0.1
UOP K factor		11.67	11.79	11.92	12.03

Table 28.12 FCC conversion and yields

Variable	Units	Case 1	Case 2	Case 3	Case 4
Net conversion	Vol%	74.39	78.45	82.01	84.88
	Wt%	73.11	77.05	80.61	83.56
Yields					
Fuel gas (H ₂ -C ₂)	FOE*	5.68	5.83	5.95	6.03
C ₃	Vol%	16.48	17.07	17.55	17.90
C ₄	Vol%	25.38	26.71	27.90	28.88
C ₅	Vol%	0.85	0.93	1.00	1.06
Naphtha	Vol%	44.46	47.13	49.55	51.53
LCO	Vol%	19.13	16.56	14.15	12.20
Bottoms	Vol%	4.56	2.92	1.62	0.63
Coke	Wt%	5.30	5.30	5.30	5.30
Total liquid		116.54	117.16	117.74	118.23
Flue gas SO _x	wppm	390.0	296.0	180.0	60.0

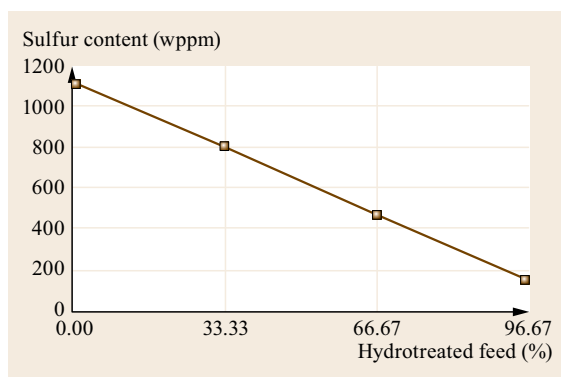
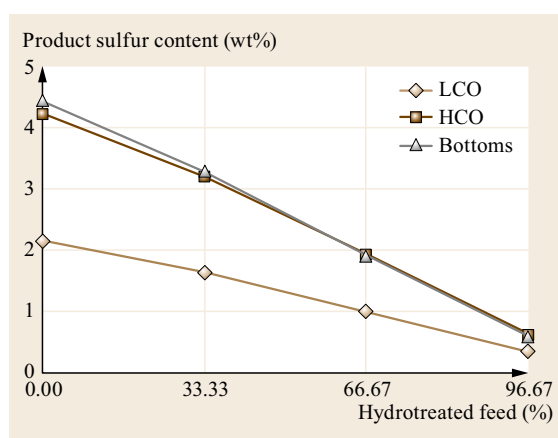
**Fig. 28.8** Sulfur in FCC gasoline versus percent hydrotreated oil in the FCC feed

Figure 28.8 shows that the sulfur content of FCC gasoline is essentially linear with respect to the percent of hydrotreated oil in the FCC feed blend. Figure 28.9 shows that relatively more sulfur goes into heavy FCC products (LCO, HCO, and slurry oil) at higher percentages of hydrotreated oil in the feed.

This is consistent with the easy-sulfur/hindered-sulfur hypothesis, which predicts that nearly all of the sulfur left behind after high-severity hydrotreating

**Fig. 28.9** Sulfur in heavy FCC products versus percent hydrotreated oil in the FCC feed

is encased in hindered compounds. These compounds contain multiple aromatic rings, so they are more likely (relative to other sulfur compounds) to be incorporated into the coke that forms on FCC catalysts. When the coke is burned away, the sulfur is converted into sulfur oxides (SO_x), which ends up in the regenerator flue gas.

28.4 Conclusion

Rigorous models are being used for closed-loop real-time optimization at the Suncor refinery in Sarnia, Ontario. Single-unit rigorous models – and combinations of models similar to those being used in Sarnia – can be used offline to quantify nonlinear relationships between important refinery units, such as the FCC and its associated feed pretreater. These relationships are important when planning for clean fuels, especially

when selecting and designing processes for hydrogen production and deep desulfurization.

Acknowledgments. We are pleased to thank the following people for their contributions to RWO and to the development of Aspen FCC or Aspen Hydrocracker: John Adams, John Ayala, Darin Campbell, Steve Dziuk, Fernando Garcia-Duarte, Steve Hendon, Nigel John-

son, Ajay Lakshmanan, Jiunnshyan Liou, Skip Paules, Rosalyn Preston, and Charles Sandmann. This chapter appeared originally as Chapter 23 Practical Advances in Petroleum Processing, C.S. Hsu, P.R. Robinson (Springer 2006). It is reprinted here with kind per-

mission from the lead author and the publisher. The abstract was added by the editors of this book, who also made minor corrections in the text. It is being reprinted here, because it describes one of the few examples of refinery-wide optimization in the industry.

References

- 28.1 C.C. Pedersen, D.R. Mudt, J.K. Bailey, J.S. Ayala: Closed loop real time optimization of a hydrocracker complex, Proc. NPRA Comput. Conf. (1995), Papers CC-95-121
- 28.2 K. English, M. Dunbar: Using steady state models to generate LP model inputs, Proc. NPRA Comput. Conf. (1997), Papers CC-97-131
- 28.3 S.W. Shorey, D.A. Lomas, W.H. Keesom: Improve refinery margins and produce low-sulfur fuels, World Refin., 41 (1999) World Refining Special Edition: Sulfur
- 28.4 A.T. Lapinas, M.T. Klein, B.D. Gates, A. Macris, J.E. Lyons: Catalytic hydrogenation and hydrocracking of fluorene: Reaction pathways, kinetics and mechanisms, Ind. Eng. Chem. Res. **30**(1), 42 (1991)
- 28.5 B.E. Stangeland: Kinetic model for the prediction of hydrocracker yields, Ind. Eng. Chem. Process Des. Dev. **13**(1), 71 (1974)
- 28.6 R.J. Quann: Hydrocracking of polynuclear aromatic hydrocarbons. Development of rate laws through inhibition studies, Ind. Eng. Chem. Res. **36**(6), 2041 (1997)
- 28.7 S.M. Jacob, R.J. Quann, E. Sanchez, M.E. Wells: Compositional modeling reduces crude-analysis time, predicts yields, Oil Gas J., 51 (1998)
- 28.8 V.A. Filimonov, A.A. Popov, V.A. Khavkin, I.Y. Perezhigina, L.N. Osipov, S.P. Rogov, A.V. Agafonov: The rates of reaction of individual groups of hydrocarbons in hydrocracking, Int. Chem. Eng. **12**(1), 21 (1972)
- 28.9 P.A. Jacobs: Hydrocracking of n-alkane mixtures on Pt/H-Y zeolite: Chain length dependence of the adsorption and the kinetic constants, Ind. Eng. Chem. Res. **36**(8), 3242 (1997)
- 28.10 C.N. Satterfield: Trickle-bed reactors, AIChE Journal **21**(2), 209 (1975)
- 28.11 M.A. Callejas, M.T. Martinez: Hydrocracking of a maya residue. Kinetics and product yield distributions, Ind. Eng. Chem. Res. **38**(9), 3285 (1999)
- 28.12 B.H. Cooper, K.G. Knudsen: Ultra low sulfur diesel: Catalyst and processing options, Proc. NPRA Annu. Meet. (1999), Paper No. AM-99-06
- 28.13 B.H. Cooper, K.G. Knudsen: What does it take to produce ultra-low-sulfur diesel? World Refin., 14 (2000)
- 28.14 B.L. Bjorklund, N. Howard, T. Heckel, D. Lindsay, D. Piasecki: The lower it goes, the tougher it gets, Proc. NPRA Annu. Meet. (2000), Paper No. AM-00-16

29. Rigorous Kinetics Modeling of Hydrogen Synthesis

Milo D. Meixell Jr

Closed-loop real-time optimization (CLRTO) with rigorous models improves the profitability of scores of process units in refineries and chemical plants. In addition to optimizing operations, the models serve as the basis for effective process monitoring and the identification of revamp opportunities. Rigor in every part of the plant – equipment, feed definition and reaction kinetics – is the key to success. Equipment constraints define the plant's capability, so CLROT models must include these too. Hydrogen synthesis online optimizers are part of several plant-wide optimizers.

This chapter describes the rigorous reaction kinetics employed for CLRTO in steam/hydrocarbon reforming plants. Kinetic relationships are shown for the core reactions, coking in different kinds of equipment, catalyst poisoning, heat transfer, and heat balances. Finally, comparisons are shown between model predictions and plant performance.

29.1	Steam Reforming Kinetics	880
29.1.1	Methane Steam Reforming Kinetic Relationships.....	881
29.1.2	Naphtha Steam Reforming Kinetic Relationships.....	882
29.1.3	Coking.....	885
29.1.4	Catalyst Poisoning.....	887
29.2	Heat Transfer Rates and Heat Balances	887
29.2.1	Firebox to Catalyst Tube.....	887
29.2.2	Conduction Across Tube Wall.....	889
29.2.3	Fouling Resistance.....	889
29.2.4	Inside Tube to Bulk Fluid.....	889
29.2.5	Bulk Fluid to Catalyst Pellet.....	889
29.2.6	Within the Catalyst Pellet.....	890
29.2.7	Convection Section.....	890
29.2.8	Fuel and Combustion Air System.....	890
29.2.9	Heat Losses.....	890
29.3	Pressure Drop	890
29.3.1	Secondary Reformer Reactions and Heat Effects.....	891
29.3.2	Model Validation.....	892
29.A	Appendix: Simulation Results	895
29.A.1	Primary Reformer.....	895
29.A.2	Adiabatic Prereformer.....	897
29.A.3	Oxo-Alcohol Synthesis Gas Steam Reformer.....	897
29.B	Appendix: Case Study of Effects of Catalyst Activity in a Primary Reformer	897
	References	900

Hydrogen for industrial use is manufactured by the steam reforming of hydrocarbons, or is available as a byproduct of refinery or chemical plant operations. Hydrogen demand can exceed the amount available as a byproduct. Often, hydrogen supply limits overall plant throughput. An operating plant can exploit untapped capacity in existing steam reformer and related equipment designs with rigorous models that employ kinetics. During plant design kinetics models are not necessarily used because experience and relatively simple models allow designers to build hydrogen plants to supply whatever hydrogen amount, purity, and pressure that is desired. The objective of suppliers of hydrogen plants is to establish an economically feasible design, given

these predetermined criteria. Additional hydrogen, or less expensive hydrogen can be manufactured from these facilities after construction, when rigorous models are used in online, closed-loop optimization systems. These systems manipulate independent operating conditions (degrees of freedom) and maximize or minimize an objective function (usually operating profit) while honoring numerous constraints, such as tube metal temperatures, pressure drops, pressures, damper and valve positions. A good kinetic model is the cornerstone of the predictive capabilities of such online optimization systems. An online optimization system exploits equipment under operating demands and constraints that were not necessarily anticipated during design.

The steam reformer and associated models represent the most significant models in an overall hydrogen or synthesis gas plant real-time, closed-loop optimization project. The reformer does the great majority of converting the feedstock (i.e., natural gas, butane or naphtha, plus steam) to the primary reactant for downstream synthesis reactors: hydrogen. Consequently, detailed modeling is required to predict the correct product yields from varying feedstock composition at various operating conditions. Additionally, the primary reformer is subject to numerous constraints, such as tube metal temperatures, that also demand detailed modeling to predict. The primary reformer consumes significant energy, and the methane slip or hydrogen purity from it affects operating conditions in downstream equipment. The optimization system must be able to exploit these opportunities if optimal plant operation is to be achieved.

The reformer reactions (reforming and water gas shift) are modeled using the best available heterogeneous kinetic relationships from the literature [29.1–4], and have been validated with industrial data and literature data [29.5] over a wide range of conditions. Equilibrium relationships are appropriately incorporated into the rate relationships, but the model does not use the empirical *approach to equilibrium temperature* as the basis for predicting outlet compositions. Nor does the model use *pseudohomogeneous* rate relationships.

The steam reformer model can handle feeds from methane to naphtha, with all the typical components that are present in natural gas, as well as recycled synthesis purge gas, or hydrogen recovery unit tail gases. Naphtha feed is characterized as about 30 chemical species, some of which are pure components, and some are hydrocarbon fractions (pseudocomponents). Each hydrocarbon species participates in a reaction that includes adsorption onto the catalyst, reforming, and desorption. The model includes diffusion effects within the catalyst, as well as heat transfer resistance from the bulk gas to the catalyst surface.

Since the model is based on mechanistic rate relationships, the composition profiles (as well as temperature and pressure) are calculated at positions from

the inlet of the catalyst tube to the outlet. The differential reaction rate relationships, as well as the mass balances, heat balances, and pressure drop relationships are solved simultaneously. A global spline collocation algorithm is used to pose the problem, and an SQP (SQP) algorithm solves the relationships.

The heat transfer rate from the primary reformer firebox to the catalyst tubes is calculated along the tube using radiant and convective heat transfer relationships. Heat transfer is also calculated from the tube outer surface, across the tube metal, through the inside tube surface film to the bulk fluid, and finally from the bulk fluid to the catalyst particles. Measurements of the catalyst temperatures at several positions along the tube, as well as measured tube skin temperatures provide feedback that is used to update heat transfer parameters, as well as to validate the model.

Pressure drop calculations are included, which use the *Ergun* relationship [29.6]. This relationship predicts the pressure drop through packed beds, such as the primary reformer catalyst tubes and the secondary reformer (autothermal) bed. Measurements provide feedback that is used to update appropriate parameters in this relationship.

The kinetics developed for natural gas and naphtha steam reforming in fired and autothermal reactors were put to more stringent tests by applying them to two other reactors. One is a *prereformer*, an adiabatic fixed bed typically used upstream of a fired tube reformer for debottlenecking. The other reactor is a fired furnace with high carbon dioxide content in the feed, making a 1:1 ratio hydrogen to carbon monoxide synthesis gas, at 3.5 bars (as opposed to the typical 40 bars pressure in many steam reformers), which is processed in downstream Fischer–Tropsch reactors, ultimately making oxo-alcohols. Calculated and measured yields and temperature profiles in these reactors, using the same kinetics, are in excellent agreement.

These rigorous models, developed from credible literature sources, and validated against industrial data over a wide range of conditions, are the foundation of several plant-wide optimization systems, including those for synthesizing hydrogen, ammonia, methanol, and oxo-alcohols.

29.1 Steam Reforming Kinetics

The reaction scheme and associated kinetics are based on methane reforming and *heavier hydrocarbon* reforming studies reported in the literature. The methane reforming relationships must be included in any model

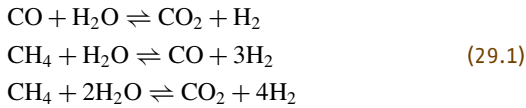
processing heavier hydrocarbons since methane is generated from these feeds, and subsequently reacts. The primary source of information used for methane reforming is *Xu* and *Froment's* most recent literature

articles on intrinsic kinetics and on using these along with diffusional resistance relationships to model industrial reformers [29.1, 2, 7]. The source of information for higher hydrocarbon steam reforming is based upon the work of *Rostrup-Nielsen* of Haldor Topsøe A/S, as well as that of others, whose work *Rostrup-Nielsen* has referenced extensively [29.3, 4, 8].

29.1.1 Methane Steam Reforming Kinetic Relationships

Numerous reaction mechanisms were investigated, and the best reaction scheme was determined by model discrimination methods described by *Froment* [29.1]. The kinetic expressions used for methane reforming account for adsorption of all the reacting species present (CO, H₂, CH₄, and H₂O), as well as reaction on the surface. The intermediate, adsorbed species concentrations, which are unmeasurable (at least in industrial equipment), are eliminated from the mechanistic steps (at steady-state), and only stable species concentrations (partial pressures) appear in the net reaction stoichiometry and the reaction rate expressions.

Net reaction stoichiometry



Reaction rate relationships

$$\begin{aligned} r_1 &= \frac{k_1}{p_{\text{H}_2}} \left(p_{\text{CO}} * p_{\text{H}_2\text{O}} - \frac{p_{\text{H}_2} * p_{\text{CO}_2}}{K_1} \right) \\ &\quad (\text{DEN})^2 \\ r_2 &= \frac{k_2}{p_{\text{H}_2}^{2.5}} \left(p_{\text{CH}_4} * p_{\text{H}_2\text{O}} - \frac{p_{\text{H}_2}^3 * p_{\text{CO}}}{K_2} \right) \\ &\quad (\text{DEN})^2 \\ r_3 &= \frac{k_3}{p_{\text{H}_2}^{3.5}} \left(p_{\text{CH}_4} * p_{\text{H}_2\text{O}}^2 - \frac{p_{\text{H}_2}^4 * p_{\text{CO}_2}}{K_3} \right) \end{aligned} \quad (29.2)$$

$$\begin{aligned} \text{DEN} &= 1 + K_{\text{CO}} * p_{\text{CO}} + K_{\text{H}_2} * p_{\text{H}_2} \\ &\quad + K_{\text{CH}_4} * p_{\text{CH}_4} + K_{\text{H}_2\text{O}} * \frac{p_{\text{H}_2\text{O}}}{p_{\text{H}_2}} \end{aligned}$$

The reaction rate *constants*, k_i s, are functions of temperature, activation energies, and frequency factors, in the classic Arrhenius form

$$k_i = A_i e^{-\left(\frac{E_i}{RT}\right)} \quad (29.3)$$

$i = 1$ to no. of reactions ($\cong 3$).

Similarly, the adsorption equilibrium constants are functions of temperature, heats of adsorption, and a fre-

quency factor

$$K_i = A_i e^{\left(\frac{\Delta H_i}{RT}\right)}, \quad i = \text{CO}, \text{H}_2, \text{CH}_4, \text{H}_2\text{O}. \quad (29.4)$$

The reaction equilibrium *constants* are functions of temperature. The equilibrium constants as a function of temperature are listed in [29.3, 4]. Those of [29.3] were used, and have been tabulated.

$$K_i = f(T) \quad (29.5)$$

$i = 1$ to no. of reversible reactions ($= 3$)

The kinetics discussed so far are intrinsic kinetics that are valid in the absence of diffusional or heat transfer resistances. Bulk phase concentrations (partial pressures) and temperatures are not present at the active sites within the catalyst pellets, since the pore structure offers very significant resistance to diffusion, and mild resistance to heat transfer exists between the bulk phase and the pellet surface. Little resistance to heat transfer exists within the pellets [29.4, p. 69].

The diffusional effects are accounted for using the classic *effectiveness factor* [29.2, 9–12].

$$\eta = \frac{\text{actual rate throughout pellet with resistances}}{\text{rate evaluated without resistances}}. \quad (29.6)$$

Evaluating the numerator of this expression requires simultaneous integration of the rate and diffusion relationships. *Froment* presents the results of that integration in [29.2, Fig. 6]. *Rostrup-Nielsen* lists results of Haldor-Topsøe's calculations in [29.4, p. 69]. These results are qualitatively similar, but differ in value due to numerous factors. Simplification of the effectiveness factor calculation can be applied for conditions that cause the diffusional resistance to be large [29.9, p. 431], and that simplification is implied in many of Haldor-Topsøe's equations [29.4, pp. 37, 69] [29.10]. The simplification [29.9, p. 434] is

$$\eta = \frac{3}{r_p} \sqrt{\frac{K(D_e)}{k(K+1)\rho_p}}. \quad (29.7)$$

Satterfield [29.11, p. 78] gives further insight to the simplification, when the diffusivities of the forward and reverse reactions are not equal.

Since the kinetics used in the DMCC model are from *Froment*, the effectiveness factor profiles in the primary reformer model are based upon his results. Rather than incur the computational burden of calculating the effectiveness factors for each reaction online,

they are entered as a function of length as constant profiles. Since the effectiveness factors are primarily functions of the catalyst pellet size, pore size, and pore size distribution, and since they are relatively weak functions of operating conditions over the normal range of these conditions, the effect of imposing them as constant profiles is very small. The results of reactor simulations with the effectiveness factor profiles fixed agree very well with measured results from industrial reformers, and with results presented in the literature. Offline calculations can be done to update the effectiveness factors if catalyst pellet size or pore size are changed significantly, or ultimately these calculations can be added to the online model. It is essential that effectiveness factors are used in conjunction with the intrinsic kinetic rate parameters, since the effectiveness factors account for phenomena that attenuate the intrinsic rates by factors on the order of 100. That is, effectiveness factors are on the order of 0.01.

The relationship among actual reaction rate, intrinsic rate, effectiveness factor, and catalyst activity is

$$r_{i,\text{observed}} = \eta_i \alpha r_{i,\text{intrinsic}}, \quad (29.8)$$

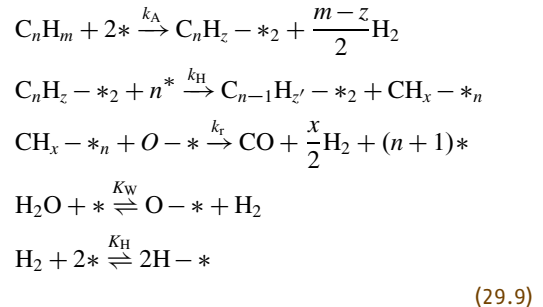
where η = effectiveness factor, α = relative catalyst activity (accounting for aging, sintering, pore closure, etc.), and $r_{i,\text{intrinsic}}$ = rate calculated with bulk fluid conditions. The catalyst activity is calculated as a parameter, updated from operating data.

29.1.2 Naphtha Steam Reforming Kinetic Relationships

Several intrinsic reaction-rate relationships have been derived for steam reforming of *higher hydrocarbons* (i. e., higher in carbon number than methane), based on Langmuir–Hinshelwood adsorption and reaction mechanisms [29.3, p. 118, 174] [29.4, p. 54]. These reaction rates (as with the reactions associated with the reforming of methane) are greatly attenuated in industrial tubular reactors by mass transfer resistance within the catalyst pellet and, to a lesser degree, by heat transfer resistance from the bulk fluid to the catalyst pellet surface. As with any intrinsic rate relationships, these rate expressions must be used in conjunction with a reactor model that accounts for these resistances for the model to be useful in assessing reformer performance, and predicting performance as independent conditions are manipulated. The relationship among intrinsic rates, observed rates, mass and heat transfer resistances, and catalyst activity has been shown in the

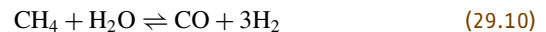
Methane Steam Reforming Kinetic Relationships section, Sect. 29.1.1.

One of the mechanisms [29.4, p. 54] is based on the following sequence of adsorption, reaction, and desorption.



The * symbol represents an active site on the catalyst surface. Concentration of $C_n H_z - *$ is generally assumed to be negligible, so the step 2 rate constant, k_H does not appear in the final rate expression. The rate constants k_A and k_r (adsorption and reforming) do appear in the rate expression. K_W and K_H are the adsorption equilibrium constants for water and hydrogen respectively.

The mechanisms account for chemisorption of the hydrocarbon and steam, followed by α -scission of the carbon-carbon bonds. The resulting adsorbed C_1 species react with adsorbed steam to form carbon monoxide and hydrogen. These mechanisms alone would result in no formation of methane, which is of course generated from naphtha feedstocks that are totally free of methane. Methane concentrations of 8–10 mol% (dry basis) are typical at the outlet of industrial naphtha steam reformers. Methane is generated when the hydrogen partial pressure is sufficiently high so that the reverse of the methane reforming reaction



is favored. This reaction, along with reforming to carbon dioxide, and the water gas shift reaction are solved simultaneously with the reforming reactions for the higher hydrocarbons. The mechanisms for these reactions are documented in the *Methane Steam Reforming* section, Sect. 29.1.1.

Competition between methane and the higher hydrocarbons for reactive sites on the catalyst surface is limited to a narrow axial position in the reactor tube, since the higher hydrocarbon species reform quickly, and since methane concentration buildup due to the reverse of the aforementioned methane reforming reaction is only significant after the great majority of the higher hydrocarbons are gone. The hydrogen partial pressure is only high enough to favor the reverse of

the methane reforming reaction when the higher hydrocarbon species have essentially disappeared. Therefore the denominator of the higher hydrocarbon rate relationships do not contain a methane adsorption term, nor does the denominator in the methane reforming reaction rate expressions have higher hydrocarbon adsorption terms. Rate expressions can be derived for the region in which the higher hydrocarbon and methane compete for active catalyst sites, however results of simulating a reactor with such a model will be essentially unchanged from the results obtained by applying the rate expressions discussed here.

The concentration profiles that result from solving the methane and the higher hydrocarbon reaction rates simultaneously agree well with the profiles reported by others [29.13, 14], and the reactor effluent species concentrations agree well with those observed from industrial reformers (Appendix 29.A). The effluent concentrations are fairly insensitive to reaction rates, since industrial reformers operate near equilibrium conditions. Effluent conditions will only be noticeably affected by reaction rates as the catalyst activity declines significantly. The temperature profile, especially in the first one third of the reactor, which is furthest from equilibrium, is affected significantly by reaction rates, and therefore is the most affected by the catalyst activity. The case study results in Appendix 29.B illustrate the concentration profiles, and the effects of catalyst activity on temperature profiles.

From [29.4],

$$r_i = \frac{k_A \cdot pC_nH_m}{\left(1 + \frac{n \cdot k_A}{k_r \cdot K_W} \cdot \frac{pC_nH_m}{pH_2} \cdot pH_2 + K_W \cdot \frac{pH_2O}{pH_2} + \sqrt{K_H \cdot pH_2}\right)^{2n}} \quad (29.11)$$

The exponent $2n$ in the denominator appears to be in error, since similarly derived rate expressions, listed below, have exponents of 2. Also, the $2n$ exponent leads to very unreasonable results for rates of reaction of higher carbon number hydrocarbons.

From [29.3, 14],

$$r_i = \frac{k_A \cdot pC_nH_m}{\left(1 + \frac{n \cdot k_A}{k_r \cdot K_W} \cdot \frac{pC_nH_m}{pH_2} \cdot pH_2 + K_W \cdot \frac{pH_2O}{pH_2}\right)^2} \quad (29.12)$$

From [29.3], including Boudart's interpretation of hydrogen and hydrocarbon site differences,

$$r_i = \frac{k_A \cdot pC_nH_m / pH_2^{y/2}}{\left(1 + \frac{n \cdot k_A}{k_r \cdot K_W} \cdot \frac{pC_nH_m}{pH_2} \cdot pH_2^{(1-y/2)} + K_W \cdot \frac{pH_2O}{pH_2}\right)^2} \quad (29.13)$$

The rate expression from *Catalytic Steam Reforming* (1984) [29.4] can be modified to include Boudart's hydrogen site interpretation, and can be solved in its original form, or the modified form by manipulating the value of y . A y value of zero restores the relationship to its original form. Additionally, that rate expression can be transformed into essentially the expression from *Steam Reforming Catalysts* (1975) by manipulating the value of K_H . A small value of K_H transforms the 1984 expression into the 1975 one. Generally, the final term in the denominator of the 1984 rate expression (the term including K_H) is much smaller than the other terms.

The rate expression from *Catalytic Steam Reforming* (1984) [29.4], modified to include the Boudart interpretation of the hydrogen site versus hydrocarbon site difference, is the relationship used in the model. The apparent error in the $2n$ exponent of the denominator has been corrected, and an exponent of 2 is used.

$$r_i = \frac{k_A \cdot pC_nH_m / pH_2^{y/2}}{\left(1 + \frac{n \cdot k_A}{k_r \cdot K_W} \cdot \frac{pC_nH_m}{pH_2} \cdot pH_2^{\frac{1-y}{2}} + K_W \cdot \frac{pH_2O}{pH_2} + \sqrt{K_H \cdot pH_2}\right)^2} \quad (29.14)$$

Each naphtha molecule is individually reformed, with its distinct set of rate constants, k_r and k_A . Each of these is a function of temperature and has its own pre-Arrhenius factor, as well as an activation energy (for k_r), and heat of adsorption (for k_A). The same K_H and K_W are used for each reaction. These too are functions of temperature, with their Arrhenius factors and heats of adsorption taken from *Froment's* most recent work [29.1]. The k_r and k_A values for each reforming reaction for hydrocarbons higher than methane are derived from rate data reported in the literature [29.3, 4, 15], and validated with overall reformer outlet compositions measured in industrial furnaces. Each reaction also has an effectiveness factor associated with it.

Naphtha is characterized as about thirty components, pure or pseudocomponents (several species of similar structure lumped together). The distribution of these components is chosen to best match measured specific gravity, volume average boiling fractions (ASTM-D86 method), and normal paraffinic, branched paraffinic (iso-paraffins), naphthenic, and aromatics (PINA) contents.

Numerous other rate expressions for steam reforming of higher hydrocarbons are listed in the literature [29.4, p. 55, 57]. Many of these are simplifications of the relationships shown here, with assumptions imposed on the relative contribution of the various terms. These assumptions may be valid for some operating

conditions, or for some catalysts. Many of the rate expressions are simple *power law* relationships that are difficult to relate to mechanistic pathways, and to physical attributes of the catalyst or the reacting species. The rate expression chosen for the model is one that has a broad range of applicability, for different catalyst types, and wide operating conditions.

Specific catalysts are characterized in part by their relative values of k_r , K_W , and k_A . The water adsorption equilibrium constant, K_W , is affected by the catalyst support. Alumina supports have lower values of K_W than magnesia supports [29.14]. Alkali content increases K_W . Increased alkali concentrations tend to decrease k_r , though. Catalysts' shape and size affect pressure drop and effectiveness factors. Their pore structure affects their effectiveness factors as well. Additionally,

the support affects the catalyst crush strength, and tendency to hold together under adverse conditions (i. e., wetting) that may be encountered during unplanned plant outages, severe operating conditions, or startup conditions. Migration of catalyst additives into equipment downstream of the reformers has caused fouling problems in some plants. Catalysts must maintain their activity and strength for several years to be commercially viable.

The following reactions are used in the primary reformer model, for butane and naphtha feeds. The model interprets the *StmReforming* qualifier, and determines the correct stoichiometry. The *User1* and *User2* qualifiers direct the model to use either the Froment reaction rate relationships, or the naphtha reaction rate relationships.

```

Reaction Mechanism = start
!
! USER1 REACTIONS:
!
! Water Gas Shift
CO          +   H2O => CO2 +   H2          :User1

! Methane Reforming to CO
CH4         +   H2O => CO  +   H2 :StmReforming :User1

! Methane Reforming to CO2
CH4         + 2*H2O => CO2 + 4*H2          :User1

!
! USER2 REACTIONS:
!
! Reforming of Higher Hydrocarbons to CO & H2 (Irreversible)
Ethane      +   H2O => CO  +   H2 :StmReforming :User2
Propane     +   H2O => CO  +   H2 :StmReforming :User2
Isobutane   +   H2O => CO  +   H2 :StmReforming :User2
N-Butane    +   H2O => CO  +   H2 :StmReforming :User2
Isopentane  +   H2O => CO  +   H2 :StmReforming :User2
N-Pentane   +   H2O => CO  +   H2 :StmReforming :User2
Cyclopentane + H2O => CO  +   H2 :StmReforming :User2

```

```

Iso-C6      + H2O => CO + H2 :StmReforming :User2
N-Hexane    + H2O => CO + H2 :StmReforming :User2
Cyclo-C6    + H2O => CO + H2 :StmReforming :User2
Benzene     + H2O => CO + H2 :StmReforming :User2
Iso-C7      + H2O => CO + H2 :StmReforming :User2
N-Heptane   + H2O => CO + H2 :StmReforming :User2
Cyclo-C7    + H2O => CO + H2 :StmReforming :User2
Toluene     + H2O => CO + H2 :StmReforming :User2
Iso-C8      + H2O => CO + H2 :StmReforming :User2
N-Octane    + H2O => CO + H2 :StmReforming :User2
Cyclo-C8    + H2O => CO + H2 :StmReforming :User2
Aromatic-C8 + H2O => CO + H2 :StmReforming :User2
Iso-C9      + H2O => CO + H2 :StmReforming :User2
N-Nonane    + H2O => CO + H2 :StmReforming :User2
Cyclo-C9    + H2O => CO + H2 :StmReforming :User2
Aromatic-C9 + H2O => CO + H2 :StmReforming :User2
Iso-C10     + H2O => CO + H2 :StmReforming :User2
Cyclo-C10   + H2O => CO + H2 :StmReforming :User2
N-Decane    + H2O => CO + H2 :StmReforming :User2
Aromatic-C10 + H2O => CO + H2 :StmReforming :User2

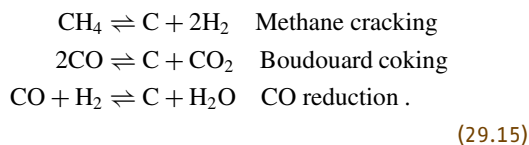
```

Reaction Mechanism = end

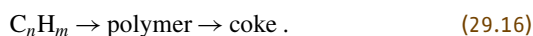
29.1.3 Coking

Coke deposition is a potential problem in steam reformers, and is favored by low steam-to-carbon ratio and high temperatures. High hydrogen composition also lowers the potential for carbon deposition. The following three reactions can deposit solid carbon, and the thermodynamic equilibrium relationships for these reactions, when carbon is graphite, are well known [29.3,

4, 14, 16–19].



Also, higher hydrocarbons can form carbon [29.3]



Equilibrium relationships with carbon of other forms have also been investigated and results reported in the aforementioned references. Whisker or filamental carbon is the form of carbon favored on nickel catalysts, and equilibrium of the aforementioned reactions with this form of carbon is reasonably well understood.

The first three carbon depositing reactions involve only methane and carbon monoxide, and are of particular interest in plants with methane feeds. These reactions can also occur in reformers with higher molecular weight feedstocks, since the reactants exist a short distance into the reformer tube, even when no methane exists in the feed. As mentioned in [29.19], *The mechanism of thermal cracking (pyrolysis) of higher hydrocarbons is more complicated*. Reference [29.14] highlights the relative risk of carbon laydown from several paraffinic, aromatic, and olefinic compounds.

Many literature articles imply that carbon deposition can be predicted and avoided by using equilibrium calculations. This implication is not correct, and several references acknowledge this fact. For methane feeds the equilibrium calculations provide reasonable guidelines, or *rules of thumb*, but still are not definitive in predicting whether coke formation will be encountered. For these feeds if the conditions (composition, temperature, and pressure) are constrained so that at equilibrium (with the appropriate carbon form) no carbon exists, then it is likely that none will deposit. As clearly stated in [29.4, p. 82],

The principle (of equilibrated gas) is no law of nature [...] It is merely a rule of thumb, indicating process conditions which are critical for carbon formation.

From [29.4, p. 85]:

The principle of equilibrated gas is no law of nature. Rates of carbon formation may be too slow. On the other hand, carbon formation may occur in spite of the principle, if the actual gas in the bulk phase, and thus the exterior of the catalyst pellet, shows affinity for carbon formation [...] Carbon formation is then a question of kinetics and the local approach to the reforming equilibrium.

Obviously, the defining relationships that would indicate whether carbon will deposit are the reaction rates associated with the actual gas (not the equilibrated gas), and include the carbon forming as well as the carbon gasifying reactions. These rates have been extensively studied [29.3, 4, 16] and are not presently well enough understood to justify including their reactions in the model. Reference [29.19] states [...] *the process conditions at which deposition (carbon) occurs can only be determined experimentally for each particular catalyst.*

Reference [29.4, Chap. 5] presents several mechanisms for coking reactions, for methane as well as higher hydrocarbons. The rate expressions presented cannot be directly and practically used in a reformer reactor model, since many of them are for *without steam present* conditions. Section 5.2.2 of Chap. 5 in [29.4] presents an empirical approach, which uses a critical steam-to-carbon ratio for each hydrocarbon species. Critical steam-to-carbon ratios must be established by experiment. This kind of simple empirical relationship can be added as a model and connected to the reformer model, if the need arises. Presently when applied online, operating conditions must be empirically constrained to avoid coke formation. Experience and advice from catalyst vendors can be used to establish the empirical guidelines. Consequently, operating conditions cannot as closely approach coking conditions as would be possible if the coking rates were well defined. Even if these rates were well defined, online analysis of reformer conditions (naphtha feed components of high coking potential, and down-the-tube temperatures) may still dictate that operating conditions be empirically established.

Some confusion may exist pertaining to how catalyst activity affects coke deposition, or the potential for coke deposition. There are three distinct effects of catalyst activity. First, an inactive catalyst can deliver a specified reformer outlet *methane slip* at only slightly higher outlet temperature compared to a catalyst that is significantly more active. Results in Appendix 29.B and [29.19, Fig. 12] show this significant rise of temperature. For the few furnaces with in-the-tube temperature measurements and the ability to control firing profiles, this rise of temperature can be avoided by automatically adjusting firing profiles. The allowable temperatures along the tube must be empirically determined, as mentioned. Results in Appendix 29.B illustrate this effect as well. Reformers without in-the-tube temperature measurements, or ones with limited capability of controlling firing profiles (i. e., top- or floor-fired) are at higher risk of coking due to inactive catalyst, since the rise in outlet temperature is subtle, and the rise in the process temperature near the tube inlet often goes unnoticed. The third effect of catalyst activity on coking is its influence on the coking reaction rates, which as shown are relatively poorly understood. It is clear that the first two effects of catalyst activity are captured well in this model, and that the effect on coking rate is not required to predict, and empirically avoids the higher temperatures near the tube inlet that arise due to inactive catalysts operated at a firing profile similar to that used for active catalysts.

Typical operating conditions in industrial reformers are sufficiently far from coking conditions so that significant benefits can be obtained by applying the model,

and constraining operating conditions empirically, as related to coking limits. Often, product values (hydrogen, ammonia or methanol) are sufficiently different from fuel values so that plant-wide optimum operating conditions are at a high steam-to-carbon ratio (where hydrogen production is favored, but at higher energy usage), and coking limits are not of concern. Plant operators, designers of steam reformers, and catalyst vendors often focus only on minimum steam-to-carbon ratios as being *optimum*, due to thermodynamic (energy per ton of product), and not economic objective functions.

29.1.4 Catalyst Poisoning

Catalyst *poisoning* is generally regarded as any process by which the number of catalyst active sites is reduced, and can occur due to sulfur coverage of active nickel sites, sintering of the nickel into fewer active sites, or coke deposition. The model lumps all those effects into the *activity* parameter.

The catalyst activity in the model can be a function of tube length, but typically is specified as uniform along the length. Measured data from an industrial reformer is essentially never available to allow the calculation of the activity profile. Even in reformers with in-the-tube temperature measurements, this information is usually insufficient to determine activity as a function of length. Process gas composition is required as a func-

tion of length to establish the activity profile. Clearly, such information can only be obtained in a laboratory environment.

References [29.19, 20] address sulfur poisoning in significant detail. Reference [29.19] illustrates the relative activity of a catalyst as a function of mean sulfur coverage. Also, that reference lists a Temkin-like adsorption isotherm for equilibrium sulfur coverage, as a function of temperature, hydrogen, and hydrogen sulfide mole fraction. As stated, it takes years to establish sulfur equilibrium in a reformer.

A reasonable approach might be to *enhance* the model by imposing an activity profile by incorporating the sulfur equilibrium, or an approach to the equilibrium isotherm, along the tube length. Without online, real time, or at least infrequent laboratory analysis of feed sulfur content, the model would have insufficient information to establish the sulfur isotherm, and subsequent activity profile. Sulfur levels in feedstocks may be very low (≈ 5 ppb) and difficult to detect. Also, it would be desirable to have feedback of sulfur content on the catalyst as a function of position in the tube, as well as feed sulfur history over the entire catalyst run length to properly validate the model. In view of these issues, and since the model with a uniform activity profile agrees well with measured conditions and outlet compositions, there appears little incentive to extend the modeling functionality in this area at this time.

29.2 Heat Transfer Rates and Heat Balances

Heat transfer rates are calculated to the catalyst tube from the firebox flue gas, through the tube wall, tube fouling, and inside tube film to the bulk fluid, as well as from the bulk fluid to the catalyst surface. As reported in the literature, the catalyst pellets are assumed to have a uniform temperature, since very little resistance to intrapellet heat transfer exists.

Heat balances are determined for all the reactor models discussed. Therefore the heat duties of the radiant tubes, convection section heaters, waste heat boilers, and associated steam drums are all explicitly calculated and reported. Heat losses are part of the models, as described in the *Heat Losses* section, Sect. 29.2.9. The enthalpies of all the streams entering and leaving each piece of equipment are calculated and reported. These streams include, for example, the process, fuel, air, and flue gas. Combustion, and all reaction-related heat effects, are handled in models using enthalpies of all species including heats of formation based on the elements at their standard states, so heats of reaction are avoided.

Heat balance terms such as furnace stack heat loss as a fraction of fired fuel heating value and furnace efficiency are not calculated, mainly since these *indices of performance* are not required in an optimization system that has the plant-wide operating profit as an objective function. These indices are remnants of local equipment or design *optimization* approaches. Typically a plant's operation should not be constrained nor its performance judged by these indices. Models can of course be easily used to calculate these indices, and *plant built* to the furnace models to perform these calculations online.

29.2.1 Firebox to Catalyst Tube

Firebox flue gas-to-catalyst tube heat transfer is primarily governed by radiation, but convection, although proportionally small, is included. The relationships used are derived from Chap. 19 of *Process Heat Transfer*, by *D.Q. Kern* [29.21, Chap. 19]

$$Q = \sigma F \alpha_{cp} (T_g^4 - T_{ff}^4) + h_c A_o (T_g - T_s), \quad (29.17)$$

where Q = total heat transferred, σ = Stefan-Boltzmann constant, F = overall view (exchange) factor (*Kern*, Fig. 19.15 in [29.21]), α = cold plane effectiveness factor (*Kern*, Fig. 19.11 in [29.21]), A_{cp} = cold plane area (of both sides of tube bank, or row), T_g = effective temperature of radiating gas, absolute, T_{ff} = temperature of tube front face (surface), absolute, h_c = convective heat transfer coefficient, A_o = outside area of tube, T_s = average outside tube surface temperature, absolute, $T_{ff} = T_s \cdot \text{PMDF}$, PMDF = peripheral maldistribution factor (accounts for circumferential heat flux maldistribution).

This equation is essentially Equation 19.9 from *Kern* [29.21], modified to allow variation of conditions along the tube length. The model integrates this heat transfer relationship along the length of the tube, while simultaneously solving the kinetics, pressure drop relationships, and all other equations related to the reformer (and the rest of the plant).

The effective gas radiating profile as a function of length is related to the burner placement in the firebox, as well as to the relative burner firing rates. The overall effective gas radiating profile is built up from the individual burner row profiles. The individual burner row profiles are similar to normal distributions of temperatures around the centerline location of the burners. The effects of adjacent burner rows overlap. Amplitudes of the temperature distributions are related to the firing rates of the burners. These amplitude-to-burner firing rate relationships have been derived from the steady-state gains of step response models relating *catalyst* temperatures (i. e., in the tube temperatures) to burner firing rates, and are included in the model. The chain ruling that may seem required to establish the relationship of the effective temperature profile amplitudes to the firing rates is implicitly done, since the steady-state gain relationships are added as constraints, and the amplitude variables then become dependent variables. Furthermore, the steady-state gain relationship intercept values are updated as parameters, for measured values of burner firing rates and measured *catalyst* temperatures. By this means the solution to the Parameter or Reconcile case (calculated prior to each Optimize case) can precisely match the measured down-the-tube temperatures, including the tube inlet (convection section heater outlet), in-the-tube *catalyst* temperatures, as well as tube outlet temperature. The Appendix 29.A simulation results and discussion illustrate that care must be taken so that the measured catalyst temperatures are not matched with unreasonable effective gas radiating and flux profiles.

Few plants have measured temperatures inside the catalyst tubes. When those temperatures are not avail-

able there may be little justification for building models that relate the individual burner profiles to an overall effective gas radiating profile. An overall effective radiating temperature profile is still justified, but without measured feedback its shape cannot be effectively updated online. A simpler gas temperature model can then be employed. Without in-the-tube temperature measurements it follows that temperature profile control in the tube is not practical. The absolute level of the radiating gas temperature, both in the case when the profile is built up from burner profiles and when it is not, is determined from actual operating conditions (namely measured or specified outlet temperature). The level of the temperature profile is that at which the resulting integrated heat transfer rate supplies the required heat to achieve the specified tube outlet temperature.

An important constraint on the effective gas radiating temperature profile is its relationship to the *bridgewall* temperature, which is the temperature of the flue gas leaving the radiating temperature after it has given up the total heat absorbed in the radiant section tubes and lost from the radiant section walls. This relationship is in many cases handled by a radiant section efficiency parameter. This model does not use that approach, but uses an offset between the length average effective gas radiating temperature and the *bridgewall* temperature as the analogous parameter. Others, such as *Wimpress* of C. F. Braun & Co. in [29.22] have used a similar approach. The offset parameter is updated online, and is determined by firebox heat balance determined from heat absorbed on the process side, fuel firing rate, and arch oxygen measurements. Heat balances using measured *bridgewall* temperatures from conventional thermocouples should not be attempted, due to the reasons explained in the *Convection Section* section, Sect. 29.2.7 of this report. The measured fuel flow, for the observed radiant duty, affects this parameter the most. The effective radiating gas temperature profile is not tied to the flue gas temperature at other than the *bridgewall* position, since the effective temperature (the radiation *source* temperature) is a result of all refractory as well as flue gas temperatures in line-of-sight of the tube front face temperature (radiation *sink* temperature) at any position. If the heat balance with the flue gas were calculated all along the tube, and if that temperature were used as the radiating source temperature, the resulting heat flux profile would not reflect the actual phenomena occurring, and would be significantly in error for most, if not all, industrial furnaces.

Figure 29.1 shows a typical net effective gas radiating temperature profile, along with the individual burner row by burner row profiles.

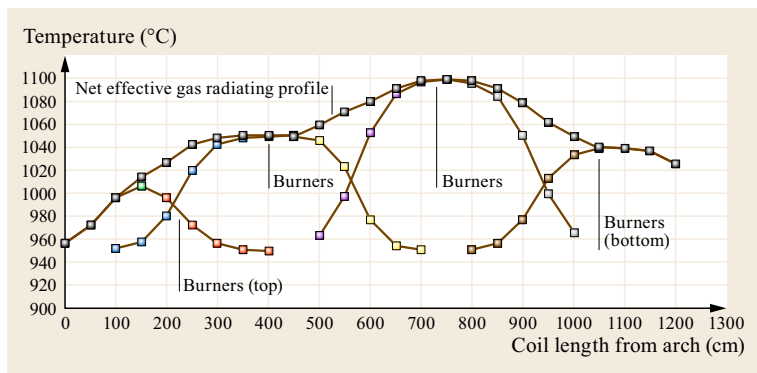


Fig. 29.1 Effective gas radiating temperature profile

29.2.2 Conduction Across Tube Wall

Heat transfer across the tube wall occurs by conduction. The one-dimensional form of Fourier's law of heat conduction [29.23, p. 245] is used as the governing relationship between heat flux, thermal conductivity, and temperature gradient. The tube wall thickness is an explicit *discretized* variable in the model. It therefore can vary with length, although most tubes are of uniform thickness. The thermal conductivity is also a model variable, but is considered constant as a function of length.

29.2.3 Fouling Resistance

A fouling (or *coke*) layer is included in the tube reactor model. Fouling thickness in the model can vary with length. The fouling thermal conductivity is a variable whose value can be specified, and is assumed invariant with length. Theoretically, measured tube metal temperatures at various lengths can be used to *back out* the apparent fouling profile, although inherent errors in pyrometer measurements make this impractical. With little or no fouling, the outside tube metal temperature profile approaches the shape of the process (inside-the-tube) temperature profile, and with appreciable fouling the outside metal temperature profile approaches the shape of the effective radiating gas profile. Hence, the fouling, even if assumed uniform, can be used as a parameter to more closely match tube metal temperatures close to the tube inlet, while the *peripheral maldistribution factor* can be used as a parameter to match the hottest measured tube metal temperature, usually near the tube outlet.

29.2.4 Inside Tube to Bulk Fluid

The inside tube surface to bulk fluid heat transfer coefficient is calculated using the Sieder–Tate correlation

for turbulent flow (similar to Dittus–Boelter), as listed in [29.24]

$$\frac{hD}{k} = 0.023 (\text{Re}^{0.8} \text{Pr}^{0.3}) \left(\frac{\mu}{\mu_0} \right)^{0.14}, \quad (29.18)$$

where h = inside heat transfer coefficient, D = inside tube diameter, k = process fluid thermal conductivity, Re = Reynolds number, Pr = Prandtl number, μ = bulk fluid viscosity, μ_0 = fluid viscosity at the tube wall.

29.2.5 Bulk Fluid to Catalyst Pellet

Heat transfer to the pellet is calculated by applying [29.25, Chap. 14, Eq. 28]

$$\Delta T_{\text{film}} = (T_{\text{gas}} - T_{\text{pellet surface}}) = \frac{L(-\text{rate})(-\Delta H_r)}{h_s}, \quad (29.19)$$

where the film temperature difference is between the catalyst surface temperature and the bulk fluid (gas) temperature. L is the characteristic length of the catalyst pellet (volume/arc), rate is the reaction rate occurring in the catalyst pores (moles/(time-volume)) and ΔH_r is the heat of reaction occurring in the catalyst pellet (energy/mole reacted). This relationship assumes that all the reactions occur inside the pellets, and that none occurs in the bulk fluid. This is a very good assumption in a steam reformer. The heat of reaction is backed out of the heat effects, since heats of reaction are not explicitly used elsewhere. Heats of formation are based on elements at their standard reference states, so the overall heat effects (sensible plus reaction) are included in enthalpies.

The bulk fluid to catalyst pellet heat transfer coefficient, h_s , is calculated as a function of fluid properties,

catalyst size, and fluid temperature using the heat transfer relationship from [29.12, p. 89, Table 4.2]

$$\frac{h_s D_p}{\lambda_f} = 2 + 1.1 \text{Pr}^{1/3} \text{Re}^{0.6} . \quad (29.20)$$

29.2.6 Within the Catalyst Pellet

Little resistance to heat transfer exists within the catalyst pellet [29.4, p. 69]. Consequently, the catalyst temperature is assumed to be uniform, at the catalyst surface temperature.

29.2.7 Convection Section

The convection section preheaters are modeled using standard heat exchanger models. Considerable differences between measured and calculated temperatures exist on the flue gas side, especially at the higher flue gas temperatures leaving the firebox, or just above the auxiliary burners. These discrepancies can be explained by the shortcomings associated with standard thermocouples employed in high-temperature service. The main problem with these thermocouples is that they cannot come close to thermal equilibrium with the very hot flue gas, so their measurements are consistently low. This problem is well understood, and documented in several heat transfer texts [29.26–28]. Reference [29.26] illustrates the large errors that can arise in high-temperature environments, and [29.27] highlights the futility of using temperatures measured with conventional thermocouples as the bases for heat balances. *Reed*, in [29.27], states,

[...] *experience shows that an attempt at heat balance where gas temperatures are taken from fixed thermocouples is largely a pointless exercise in calculation because of inaccuracy of gas temperature measurement and thus, gas heat content.*

Illustrations in [29.28, p. 33-17, 33-18] show thermocouples that are specially designed for high-temperature measurements.

The measured fuel flows, arch oxygen composition, and high pressure steam drum heat balance confirm that the heat duties calculated from the process side (as op-

posed to the flue gas side) are most accurate, as would be expected. The high-pressure steam system and boiler feed water measurements impact significantly on the convection section heat balance since boiler feed water preheat and steam superheat duties make up the majority of the convection section duty. The high-pressure steam import flow, and the expected versus measured and calculated synthesis gas compressor steam turbine performance further support the assertion that the process side, and not the flue gas side measurements are the most accurate.

29.2.8 Fuel and Combustion Air System

The fuel-air mixtures are combusted in *extent of reaction* models. Complete combustion to water vapor and carbon dioxide is assumed, with no residual carbon monoxide remaining. The model can be implicitly kept valid by lower bounding the flue gas oxygen content so complete combustion is maintained.

Combustion air preheat is modeled with standard heat exchanger models.

29.2.9 Heat Losses

The firebox model has a heat loss term that can be calculated as a parameter, however the loss term is essentially a small difference between large numbers (total heat fired minus total heat absorbed in radiant plus convection sections), so it is subject to large relative errors. Additionally, the heat *loss* may be calculated as a heat gain depending on the accuracy of the fired and absorbed heat duties. To keep the heat loss from the firebox reasonable, it is typically set to a small value, on the order of 1% of the heat fired.

There is also a heat loss term associated with the high-pressure steam drum. This term is typically used to understand the whether significant errors exist in boiler feed water flows, steam flows and temperatures, furnace convection section measurements, and fuel flow and composition measurements. During the optimization system commissioning, sensitivity of this term to the aforementioned measurements helps those commissioning the system eliminate the worst measurements, and establish the validity of the models.

29.3 Pressure Drop

Pressure drop calculations in the primary and secondary reformer models are based on the *Ergun* [29.6] relationship, as presented in [29.23]. Both the laminar flow and turbulent flow terms are included. The natural pa-

rameter that arises from the Ergun equation, which can be updated with measured pressure drop information, is the `TURBULENT_DP_COEF` term in the models of both the primary and secondary reformers. This term affects

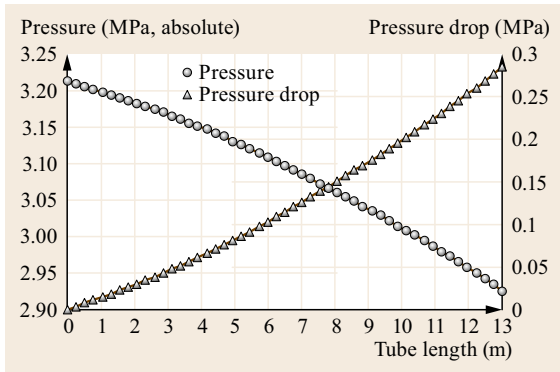


Fig. 29.2 Pressure and pressure drop profile

only the pressure drop, whereas another term, the bed void fraction, which might also have been used as the parameter to update with measure pressure drop, also affects all the reaction rates. The bed void fraction affects the amount of catalyst in a fixed-volume reformer tube, and is not an appropriate parameter to use in this case. The void fractions of typical packed beds are shown in [29.29, Fig. 5.70]. Void fractions of 0.4 to 0.6 are typical, and can be determined for specific catalysts sizes and shapes from vendor specification sheets, by measurement, or, with more difficulty, by calculation.

The `TURBULENT_DP_COEF` is the appropriate performance indicator for catalyst pressure drop, and is a better indicator than pressure drop itself, since it is independent of all the known effects of flow rate (both hydrocarbon and steam), gas density, viscosity, catalyst particle diameter, and void fraction. Pressure drop itself is important though, due to the stress it imposes on the catalyst (which raises the potential for crushing) and normally the optimization system has an upper bound on pressure drop. That bound may or may not be active at the solution, depending on the catalyst condition, and whether the solution is maximizing throughput. The pressure drop profile illustrated by Fig. 29.2 is for a pri-

mary reformer when the pressure drop across the catalyst was fairly high. The differential pressure indicator showed a 2.9 kg/cm^2 drop across the catalyst tubes.

29.3.1 Secondary Reformer Reactions and Heat Effects

Most steam reformers are process furnaces, transferring the required endothermic heat from a firebox to the process inside catalyst-packed tubes. Some steam reformers are *autothermal*, getting their heat from oxidation reactions occurring within the catalyst bed. Secondary reformers in ammonia plants are an example of autothermal steam reformers.

There are several categories of reactions and heat effects calculated in the secondary reformer model. First, the primary reformer effluent is mixed with the process air. Then, the effect of consuming the oxygen that is admitted with the process air is determined. This effect was investigated by simulating several possible reaction pathways. The results were insensitive to the pathway chosen, so the simplest, and also the most thermodynamically favored route was used. This assumes that all the oxygen preferentially reacts with primary reformer effluent hydrogen. Sufficient hydrogen exists under all reasonable operating conditions so oxygen is the limiting reactant, therefore no methane is oxidized. The model includes oxidation of methane as a possible pathway, however it is presently not activated. That pathway can be activated without modifying the model by just changing input data (extent of reaction). The adiabatic *flame* temperature is calculated for this oxidation set of reactions, and the outlet from this *extent of reaction* model is the inlet to the secondary reformer packed catalyst bed (Fig. 29.3).

This model assumes that the oxidation is complete before the top of the catalyst bed, and that only methane reforming as described by [29.1, 2] occurs in the reactor bed. The same kinetic rate expressions are used

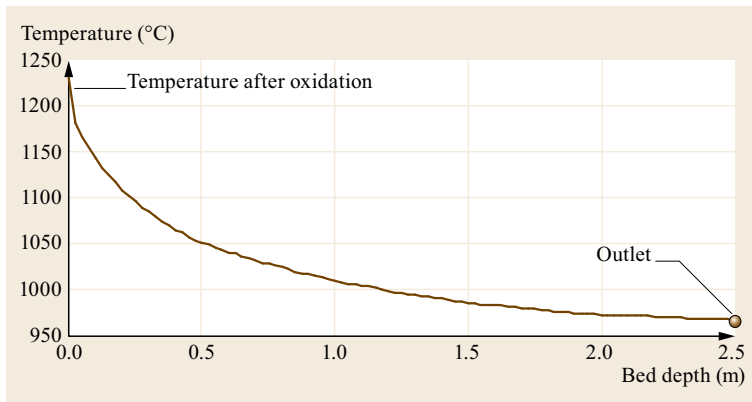


Fig. 29.3 Temperature profile as a function of bed depth

as in the primary reformer. The catalyst activity is of course different from the primary reformer activity, and is determined from operating data. An initial estimate of its value, relative to the primary reformer activity, was calculated as the primary reformer activity, times the nickel weight percent ratio, times the density ratio of the catalysts. This estimate assumes that the nickel mass in either catalyst supplies similar numbers of active sites. The activity calculated in this manner is close to the reconciled activity, based on measured compositions in the primary and secondary outlet, and operating conditions. Effluent compositions are very insensitive to assumptions concerning how the oxygen is reacted. For example, if some of the methane from the primary effluent is oxidized, rather than only hydrogen, the results are essentially unchanged. The high temperatures in the reactor cause the reaction rates to be relatively high, bringing the outlet near equilibrium. This near-equilibrium condition is a state, and not a path function, so it is not surprising that various reaction pathways affect the results so little.

The reactor bed is not assumed to be adiabatic, but loses heat from its walls. Presently a constant heat flux from the walls is assumed. A flux profile can easily be imposed, based on heat transfer driving force, but its effect will be negligible. In fact, if the reactor were assumed adiabatic the results would be essentially unchanged. The heat loss from the reactor walls was retained, so that the effects of the heat losses can be easily demonstrated.

29.3.2 Model Validation

The primary reformer models have been validated by comparing calculated to measured results, and by comparing predicted to observed results. Three cases of calculated versus measured results are presented, one for naphtha feed, and the other for butane feed. One case of predicted versus observed results is presented, for a naphtha feed. The online, closed-loop optimization system continuously supplies validation results, by reporting differences (biases) between calculated and measured results on every optimization cycle. These results, along with calculated parameters, can be monitored by trending their values as a function of time.

The first two validation cases are Parameter cases, while the third is a Reconcile case. In the first two cases only primary reformer calculations are done, while in the third case both primary and secondary reformer calculations are performed. The Parameter cases manipulate the process steam flow and outlet temperature to match observed outlet CO₂ and CH₄. In the Reconcile case the best values for the primary and secondary reformer catalyst activities are determined as well, us-

ing an objective function that minimizes the differences between calculated and observed outlet compositions of both reformers, calculated and observed primary outlet temperature, and calculated and observed process steam flow rate.

Validation Case 1 (Naphtha Feed Parameter Case)

For Validation Case 1, operating conditions, outlet composition, and feed composition are presented in Tables 29.1, 29.2, and 29.3, respectively. Figure 29.4 shows an outlet composition parity plot for dry gas with a naphtha feed. The feed composition used for this validation case was characterized as listed in Table 29.3, based on measured naphtha gravity, ASTM-D86 vol-

Table 29.1 Validation case 1 – operating conditions

Feed	Naphtha
Feed rate	17.7 t/h
Process steam rate	79.0 t/h (Parameterized to 82.92 to match effluent CO ₂)
Inlet temperature	470 °C
Outlet temperature	760 °C (Parameterized to 761.99 to match CH ₄)

Table 29.2 Validation case 1 – outlet compositions

Component	Calculated (Dry mol%)	Observed (Dry mol%)
Hydrogen	63.9077	63.6
Nitrogen	0.3675	0.4
Argon	0.0060	–
Carbon monoxide	9.0188	9.2
Carbon dioxide	16.4000	16.4
Methane	10.3000	10.3

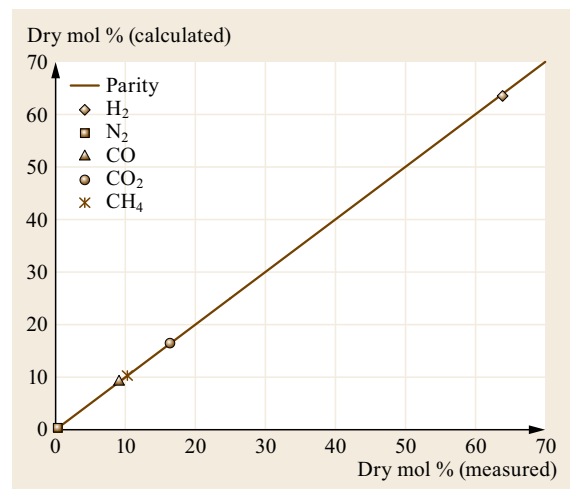


Fig. 29.4 Validation case 1 – outlet composition parity plot for dry gas with naphtha feed

Table 29.3 Validation case 1 – feed composition

Component	mol%
Hydrogen	13.807
Nitrogen	4.610
Argon	0.075
Carbon monoxide	0.000
Carbon dioxide	0.000
Methane	0.258
Ethane	0.000
Propane	0.000
Isobutane	0.932
<i>n</i> -Butane	1.792
Isopentane	17.142
<i>n</i> -Pentane	24.221
Cyclopentane	2.553
<i>iso</i> -C ₆	10.628
<i>n</i> -Hexane	7.386
Cyclo-C ₆	5.952
Benzene	2.064
<i>iso</i> -C ₇	2.639
<i>n</i> -Heptane	1.952
Cyclo-C ₇	1.441
Toluene	0.391
<i>iso</i> -C ₈	0.621
<i>n</i> -Octane	0.509
Cyclo-C ₈	0.314
Aromatic-C ₈	0.150
<i>iso</i> -C ₉	0.155
<i>n</i> -Nonane	0.103
Cyclo-C ₉	0.087
Aromatic-C ₉	0.066
<i>iso</i> -C ₁₀	0.048
Cyclo-C ₁₀	0.027
<i>n</i> -Decane	0.047
Aromatic-C ₁₀	0.030
Water	0.000

ume versus boiling point, and PINA (paraffin, isoparaffin, naphthinic, and aromatic content) information, plus recycle desulfurization hydrogen stream measurements. The feed is a mix of the naphtha and desulfurization hydrogen streams. This naphtha feed molecular weight is 65.923.

Validation Case 1a (Naphtha Feed Simulate Case)

Table 29.4 presents outlet compositions for Case 1a. This case is simulated at the same conditions as the Case 1 Parameter case, except at an outlet temperature of 778 °C, compared to 762 °C.

A comprehensive set of plant operating conditions was not available for this case, but the plant indicated a methane slip of about 8.5%, observed by the plant for this outlet temperature. The calculated outlet methane dry mole percent of 8.8% is very close to the 8.5%

Table 29.4 Validation case 1a – outlet compositions

Component	Calculated (Dry mol%)	Observed (Dry mol%)
Hydrogen	65.1413	Unavailable
Nitrogen	0.3550	Unavailable
Argon	0.0058	Unavailable
Carbon monoxide	9.8817	Unavailable
Carbon dioxide	15.8156	Unavailable
Methane	8.8006	≈ 8.5

Table 29.5 Validation case 2 – operating conditions

Feed	Butane
Feed rate	17.7 t/h
Process steam rate	70.3 t/h (Parameterized to 70.8 to match effluent CO ₂)
Inlet temperature	473 °C
Outlet temperature	773 °C Average (Range: 763 °C < T < 779 °C) (Parameterized to 779 to match CH ₄)

Table 29.6 Validation case 2 – outlet compositions

Component	Calculated (Dry mol%)	Observed (Dry mol%)
Hydrogen	63.6562	63.5
Nitrogen	0.2844	0.3
Argon	0.0046	–
Carbon monoxide	10.3548	10.4
Carbon dioxide	14.7	14.7
Methane	11.0	11.0

that was observed, and since all the independent conditions (feed rate, steam to carbon ratio, etc.) are not precisely known for this case, the *discrepancy* may be easily attributed to differences in simulated versus actual conditions.

Validation Case 2 (Butane Feed Parameter Case)

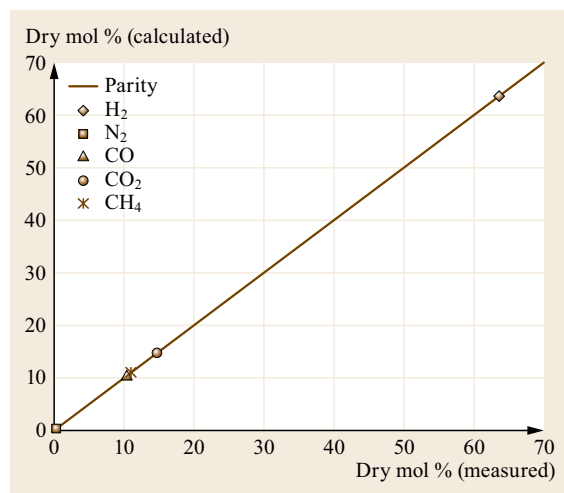
Tables 29.5, 29.6, and 29.7 present operating conditions, outlet compositions, and feed properties, respectively, for Case 2. Figure 29.5 shows the parity plot for this case. The feed composition used for this validation case was characterized as listed in Table 29.7, based on typical butane feed, plus recycle desulfurization hydrogen stream measurements. The feed is a mix of the butane and desulfurization hydrogen streams.

Validation Case 3 (Primary and Secondary Reformer Butane Feed Reconcile Case)

Tables 29.8, 29.9, and 29.10 show operating conditions, outlet compositions, and feed properties, respectively, for Case 3. Figure 29.6 shows the parity plot for this case. A Reconcile case was executed with the objective function minimizing the sum of the weighted

Table 29.7 Validation case 2 – feed composition

Component	mol%
Hydrogen	8.100
Nitrogen	2.806
Argon	0.046
Carbon monoxide	0.000
Carbon dioxide	0.000
Methane	0.157
Ethane	0.000
Propane	0.000
Isobutane	0.932
<i>n</i> -Butane	87.959
Isopentane	0.000
<i>n</i> -Pentane	0.000

**Fig. 29.5** Validation case 2 – outlet composition parity plot for dry gas with butane feed

squared differences between the calculated and measured primary outlet compositions, outlet temperature, and secondary reformer outlet compositions. Primary reformer catalyst activity, secondary reformer catalyst activity, primary outlet CO₂ measurement minus calculated value difference, and secondary outlet CH₄ measurement minus calculated value difference were the degrees of freedom (the independent manipulated variables). The degrees of freedom are bounded to assure the results are most reasonable. By posing the problem in this manner the insensitive nature of the catalyst activities (due to near equilibrium conditions) is handled as well as possible. By step bounding the catalyst activities, the errors or *noise* in the composition and process steam flow measurements are not all forced into the catalysts activities, as would be the case if a *square* Parameter case were posed. The best weighting of the terms in the objective function is determined during commissioning when many sets of data are pro-

Table 29.8 Validation case 3 – operating conditions

Feed	Butane
Feed rate	17.451 t/h
Process steam rate	73.556 t/h (Reconciled to 74.773)
Inlet temperature	464.2 °C
Outlet temperature	772.81 °C (Reconciled to 772.92)

Table 29.9 Validation case 3 – outlet compositions

Component	Calculated (Dry mol%)	Observed (Dry mol%)
Hydrogen	64.3261	66.4770
Nitrogen	0.4858	0.2608
Argon	0.0935	–
Carbon monoxide	9.9671	10.4600
Carbon dioxide	14.8347	14.896
Methane	10.2928	10.415

Table 29.10 Validation case 3 feed – composition

Composition	mol%
Hydrogen	10.8684
Nitrogen	4.5144
Argon	0.8692
Carbon monoxide	0.000
Carbon dioxide	0.000
Methane	2.9427
Ethane	0.000
Propane	0.000
Isobutane	0.8121
<i>n</i> -Butane	79.9885
Isopentane	0.000
<i>n</i> -Pentane	0.000

cessed in an open-loop mode. Over long time periods (months) the catalyst activities trend downward, since the step bounds are relative to the activity values from the last solution. Soft bounds (see DMO Users' Manual) may need to be employed if the data has significant error, causing otherwise (i. e., without soft bounds) infeasible problems to be posed.

This approach allows the relationship between firing duties and catalyst temperatures, if available, (derived from DMC controller steady-state gains) to be used, with all of the intercepts being updated as parameters, determined primarily by the measured catalyst temperatures. The catalyst temperatures are matched precisely at the solution of each Reconcile case.

The overall approach in determining the catalyst activities relies on reformer outlet compositions, which are near equilibrium to update rate parameters (catalyst activities). This kind of analysis is inherently problematic, but can be handled as described. Short-term trends of the catalyst activities (hourly, daily, or even over a week or so) will be subject to somewhat erratic, noisy behavior, but will not detract significantly from

the ability of the models to predict appropriate outlet compositions and reactor temperature profiles. As the catalysts become less active the aforementioned numerical problems diminish, and the activity trends will become smoother, for the same error in measurements, since the outlet conditions become further (but still not very far) from equilibrium.

The feed composition used for this validation case was characterized as listed in Table 29.10, based on typical butane feed, plus recycle desulfurization hydrogen stream measurements. The feed is a mix of the butane and desulfurization hydrogen streams.

As described, the secondary reformer model was solved along with the primary reformer model for validation case 3. The results are listed in Table 29.11.

The outlet methane concentration bias in the objective function was heavily weighted (to drive it toward zero, since the objective function is the sum of the weighted squares biases) and therefore explains the good agreement between calculated and observed values. The process air flow measurement bias (difference between measured and calculated) was a parameter, so the calculated nitrogen composition is precisely equal to the measured value. The air flow measurement bias was 4.4% of the measured value at the solution. The calculated outlet temperature is surprisingly close to the measured value. The heat balance around the high-pressure steam drum required only a 1.2% heat loss to close in this case. That balance is of course affected by numerous other measurements, so the calculated secondary reformer outlet enthalpy can only be said to be part of the overall consistent set of information.

29.A Appendix: Simulation Results

29.A.1 Primary Reformer

In Fig. 29.7, results are shown for naphtha and butane feeds. The naphtha feed case profiles are results from the *validation case 1*, and the butane feed results are from *validation case 3* described in the *Model Validation* section, Sect. 29.3.2.

The calculated versus outlet composition comparisons have been discussed. This section illustrates the profile results, and compares them to literature sources (for compositions), and to measurements (for temperatures). Only the key component concentrations are plotted, such as methane, hydrogen, carbon monoxide, carbon dioxide, and the main hydrocarbon species. The minor hydrocarbon species, nitrogen, and argon concentration profiles are not shown.

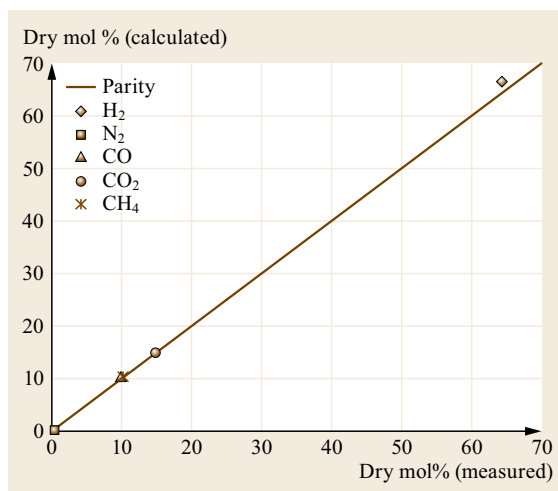


Fig. 29.6 Validation case 3 – outlet composition parity plot for dry gas with butane feed

Table 29.11 Validation case 3 – secondary reformer outlet conditions

Component	Calculated (Dry mol %)	Observed (Dry mol %)
Hydrogen	52.952	53.553
Nitrogen	22.254	22.254
Argon	0.327	–
Carbon monoxide	13.818	13.245
Carbon dioxide	10.164	10.583
Methane	0.4843	0.4843
Temperature (°C)	966.82	966.52

Both the naphtha and butane feed cases show the methane profile rising from very low inlet values to a maximum, and falling to the outlet composition. The hydrocarbon species compositions fall quickly, and are essentially zero at about 4–6 m from the tube inlet. These profiles are in close agreement with the profiles shown in [29.4, 14]. For more active catalysts, the hydrocarbon species disappear closer to the tube inlet. The simulated temperature profiles are also in good agreement with profiles in those references, but more importantly, they agree precisely with the measured profiles. Reference [29.19] shows that the temperature profile in a top-fired reformer is significantly different than in a wall-fired furnace.

Only one literature reference [29.13] was found that illustrated the hydrogen composition profile along the

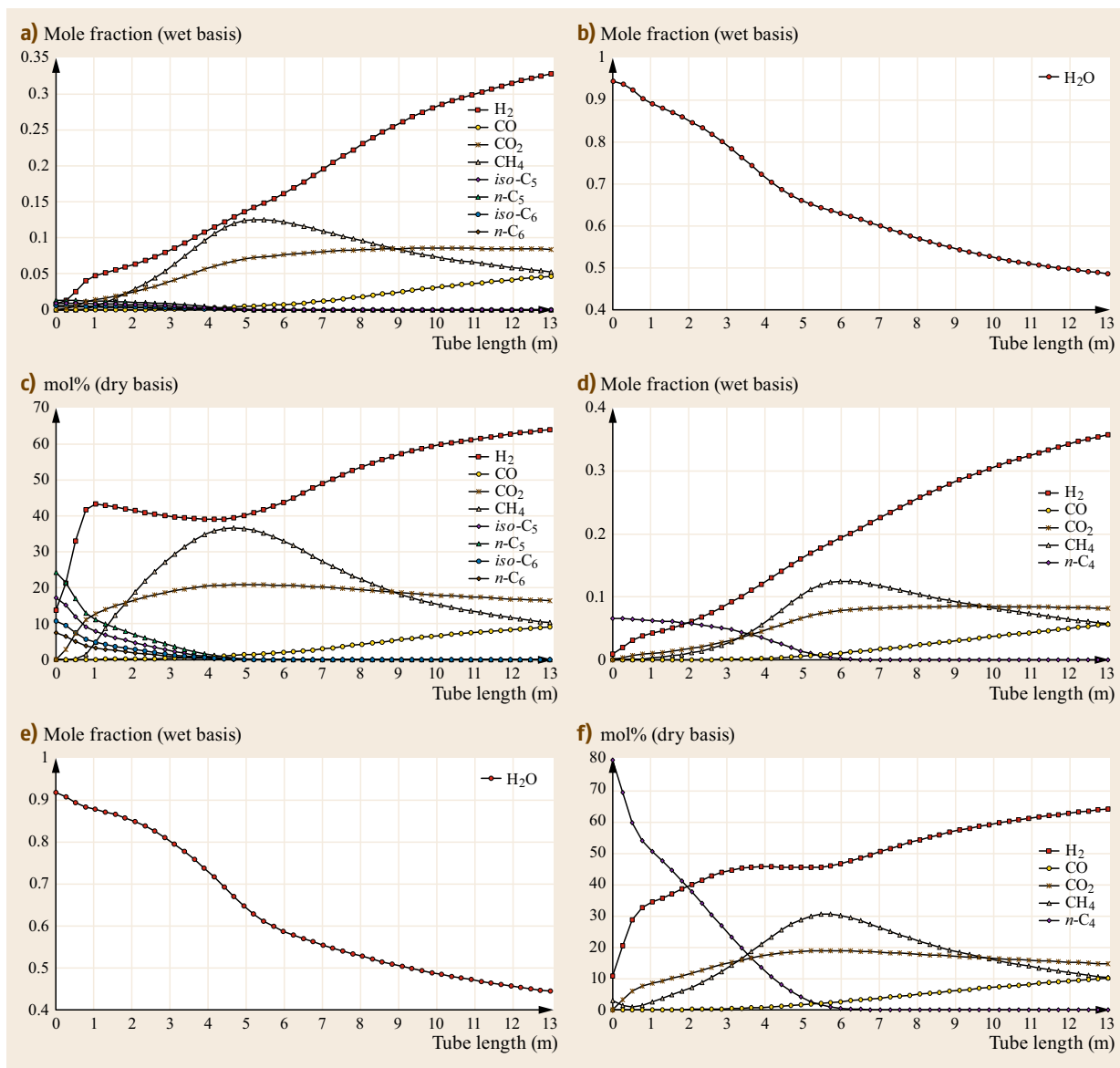


Fig. 29.7a-f Composition profiles for the naphtha (a-c) and butane (d-f) feed case

catalyst tube. The simulated results agree well with that reference's profile. At first the dry basis hydrogen composition profile appears strange, since it peaks at a position fairly close to the tube inlet (about 1–2 m), falls, then rises again. On a wet basis the profile is monotonic, and appears reasonable, since no decline occurs. The initial sharp rise in hydrogen concentration is due to the fast rates of reforming of the hydrocarbon species. As carbon dioxide concentration rises, it impedes hydrogen production via the water gas shift reaction, but as shown on the wet basis profile plots, the rate of change is still positive. Since water is a re-

actant, and not just a diluent of the hydrocarbon to prevent coking, dry basis profiles are misleading. The reference [29.13] dry basis hydrogen profile has the same peak and subsequent rise as the results plotted for naphtha feed. The hydrogen profile for butane feed, for the catalyst activity and firing profile representing late June 1994 operation, shows a much more subtle peak (Fig. 29.8).

The flux calculated at the top of the tube is quite small, but must be that small to allow the temperature to drop from the measured convection section feed/steam preheat exchanger outlet temperature to the uppermost

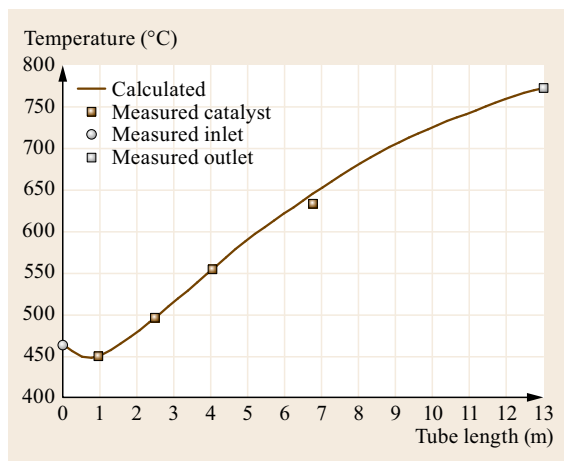


Fig. 29.8 Process temperature profiles measured versus calculated (butane feed)

measured catalyst temperature. The small flux is insufficient to supply all the net endothermic heat of reaction, so the temperature drops several degrees. Further down the tube the flux is sufficient to supply the reaction plus sensible heat, and the temperature rises. The flux profile is sensitive to the specified catalyst temperatures. Small discrepancies in the catalyst temperatures (or their position) require that the flux profile change significantly, if all the model and measured temperatures are required to match. Reconciliation of the measured temperatures, with shape constraints (rate of change or inflection point restrictions) on the flux profile can be used to assure a reasonable flux profile.

The measured tube metal temperature (TMT) is precisely matched at the solution of a Parameter or Reconcile case, since the *peripheral maldistribution factor* (Firebox to Catalyst Tube heat transfer section, Sect. 29.2.1) is used as a parameter to adjust the relationship between the average outside tube metal temperature, calculated assuming uniform heat flux distribution, and the front face tube metal temperature. The front face TMT is higher than the average TMT because

29.B Appendix: Case Study of Effects of Catalyst Activity in a Primary Reformer

Several cases were simulated to show the effects of catalyst activity. Plots of key operating conditions illustrate many effects that are unnoticed if only outlet compositions are examined. Table 29.12 shows how insensitive the outlet conditions are to catalyst activity, over a wide range. The plot of methane composition as a function of tube length for these cases is much more revealing. The

heat flux is not uniformly circumferentially distributed. The *peripheral maldistribution factor* is assumed constant in the Simulate or Optimize cases, which is a very good assumption. As mentioned in the *Fouling Resistance* heat transfer section (Sect. 29.2.3), the fouling can be used to match a measured TMT near the tube inlet.

29.A.2 Adiabatic Prereformer

An adiabatic prereformer was modeled with the same kinetics used in the previous models. A reactor bed was configured to represent an industrial reactor that was newly commissioned. Consequently the catalyst activity was assumed to be uniform, that is, no poisoned front had time to be established. The catalyst activity was reconciled so that one temperature in the nonequilibrium zone near the front of the reactor was matched. All other simulated temperatures then also matched the remaining measured temperatures, confirming that the kinetics were yielding appropriate heats of reaction, and compositions, all along the reactor bed. Effluent compositions were directly measured, and are plotted versus simulated compositions in the parity plot, showing excellent agreement.

Good agreement in this adiabatic reactor further confirms the validity of the kinetics. Issues related to heat transfer do not cloud the kinetics validity in this case.

29.A.3 Oxo-Alcohol Synthesis Gas Steam Reformer

A fired tube reactor was configured to match the dimensions and catalyst loading of an existing oxo-alcohol synthesis gas steam reformer. Simulation results at observed conditions (feed gas composition, outlet temperature, steam to carbon ratio, etc.) agree very well with observed results. Catalyst activity is first determined by matching an key effluent composition.

methane compositions for all the cases approach similar values near the tube outlet, but the methane composition profiles are significantly different at positions closer to the inlet.

The lower activity cases exhibit operating conditions (temperatures) that are likely to be unacceptable, as shown by the plots of the process temperatures. Both

Table 29.12 Effluent composition versus catalyst activity at constant inlet and outlet temperatures – naphtha feed cases. Inlet temperature = 462.0 °C. Outlet temperature = 761.8 °C. All cases have the same firing profile (not level)

Component	Catalyst activity					
	100%	90%	70%	50%	30%	20%
Hydrogen	63.9077	63.9072	63.9057	63.9029	63.8962	63.8872
Nitrogen	0.3675	0.3675	0.3676	0.3676	0.3677	0.3677
Argon	0.0060	0.0060	0.0060	0.0060	0.0060	0.0060
Carbon monoxide	9.0188	9.0186	9.0181	9.0171	9.0146	9.0109
Carbon dioxide	16.4000	16.4001	16.4004	16.4010	16.4026	16.4049
Methane	10.3000	10.3006	10.3022	10.3053	10.3130	10.3233

the overall temperature profile, as well as a *close up* of the first 3 m are shown. As discussed in the *Coking* section (Sect. 29.1.3), in the paragraph beginning with *Some confusion may exist...*, reformers with a less active catalyst operated at a similar outlet temperature as with an active catalyst, *at similar firing profiles*, exhibit higher, and likely unacceptable temperatures within the tube. The plotted profiles are similar in nature to those shown in [29.19]. The shapes are different due to top-firing [29.19] and wall-firing profile differences. The reason the temperature profiles change is because with a less active catalyst, less reaction heat sinks exist, and more of the heat input raises the sensible heat of the process fluid, and hence the temperature.

The unacceptable temperatures can be avoided. Two alternatives of avoiding them are simulated, one resulting in different unacceptable operating conditions (high methane slip), and the other with very acceptable conditions.

The first alternative focuses on the unacceptable temperatures encountered in the first few meters of the reactor, which may cause coking. In this alternative the temperature at approximately one meter from the inlet was the same temperature as the base, with 100% catalyst activity. This temperature was 449 °C. Table 29.13 and the accompanying plot (Fig. 29.9) show these results. To keep that temperature at 449 °C, and maintain the firing profile, the reactor outlet specification has to be relaxed. The independent operating condition is just moved from the reactor outlet, to the catalyst temperature. As illustrated, under these operating conditions, as the catalyst activity falls from 100% to 90%, and 70%, the methane slip rises dramatically. So does the reactor outlet temperature. As mentioned, this alternative is unacceptable, due to very high methane slip.

The second alternative is to minimize the tube outlet methane slip (dry basis), while modifying the firing profile, keeping the *CAT-I* temperature acceptable (in this case it was upper bounded at 449 °C), and while keeping the tube metal temperature (TMT) below acceptable limits. This was posed as an optimization problem. The objective in a plant-wide optimizer is not to minimize the reactor outlet methane content (profit is

Table 29.13 Effluent composition versus catalyst activity at constant upper bed catalyst temperature – naphtha feed cases. Inlet temperature = 462.0 °C. TI211-1 temperature = 449 °C. All cases have the same firing profile (not level)

Component	Catalyst activity		
	100%	90%	70%
Hydrogen	63.9077	63.1242	58.6711
Nitrogen	0.3675	0.3755	0.4209
Argon	0.0060	0.0061	0.0069
Carbon monoxide	9.0188	8.5117	6.1219
Carbon dioxide	16.4000	16.7405	18.3063
Methane	10.3000	11.2420	16.4730

maximized), but in this subplant problem it is the most realistic objective. The ability to modify the firing profile will depend greatly on the control system, burner design, fuel composition, and firebox design. In this case the range over which the optimizer could vary the firing was bounded simply by step bounding the amplitude changes for each burner row. In the overall furnace model the steady-state gain relationship between fuel fired and catalyst temperatures, as well as bounds on the duties that can be fired will constrain the range of firing. The amplitudes of the firing profiles will all be dependent variables, as described in the *Firebox to Catalyst Tube* heat transfer section, Sect. 29.2.1.

Results of this alternative for a catalyst activity of 90% show that the tube outlet temperature can be raised to 762.43 °C, slightly higher than the base (100% activity) case value of 761.8 °C, while not violating the *CAT-I* temperature limit, the TMT limit (of 884.92 °C, which is the same maximum as in the base case), nor the step bounds on the firing profile (shown in Fig. 29.10). The reason this case is at a slightly higher outlet temperature (and slightly lower methane slip) than even the base (100% activity) case is because the base case is not an optimized (profile) case. Had the base case been an optimized case, its methane slip would have been slightly lower than the optimized 90% activity case.

The optimized profile was reduced (to its lower step bound) for the top burner row, and increased (to the upper step bounds) for the next two burner rows. The

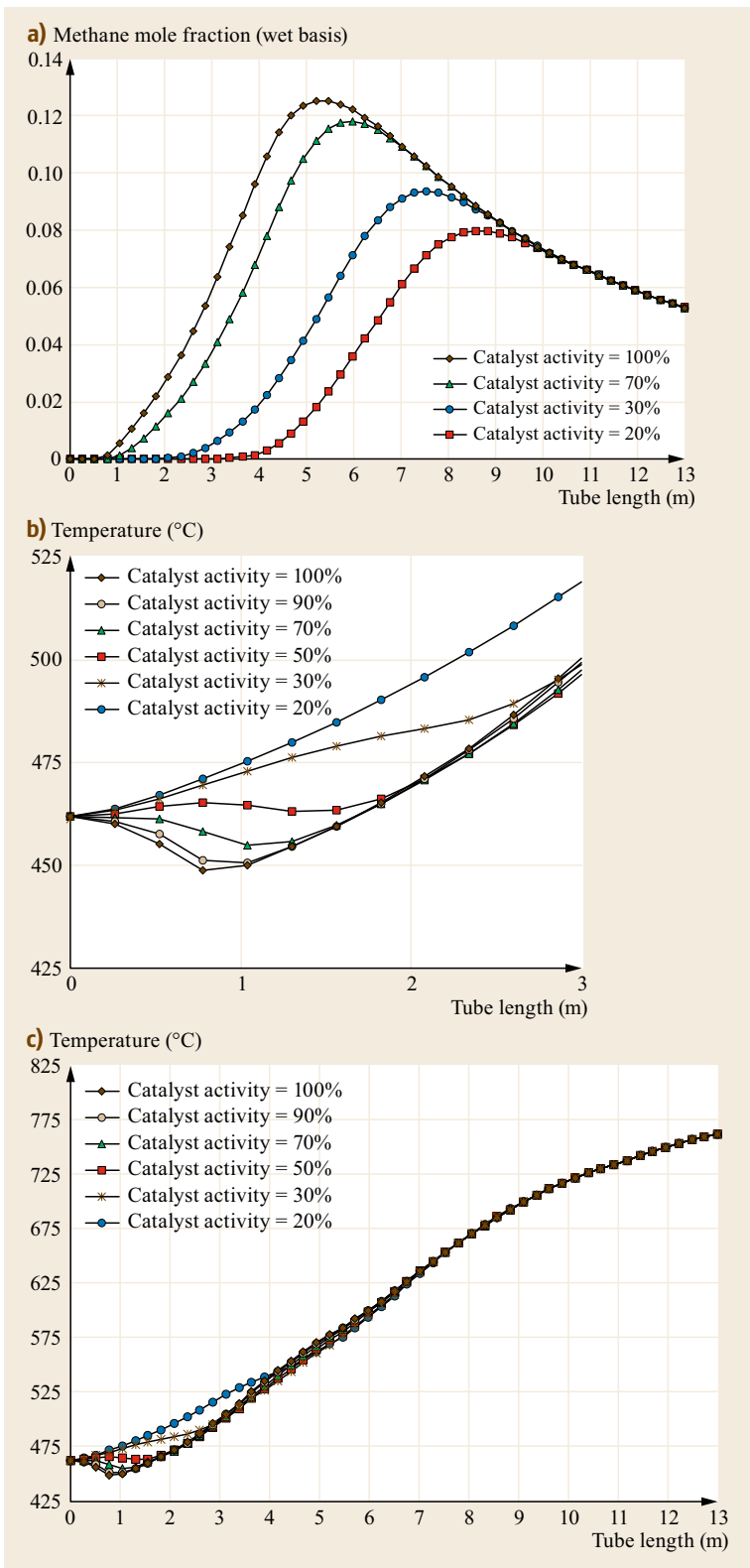


Fig. 29.9 (a) Methane composition profile as a function of catalyst activity. (b,c) Process temperature profile as a function of catalyst activity (at constant inlet and outlet temperatures, and firing profiles)

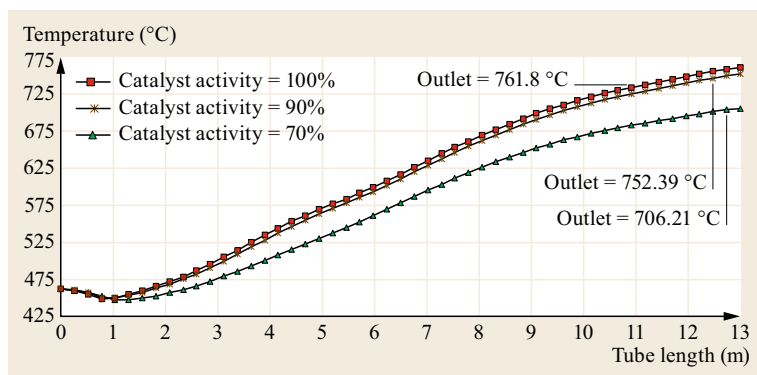


Fig. 29.10 Process temperature profiles for constant *CAT-I* temperature at 449 °C

bottom row firing was not at its limit, but the TMT in that section of the tube was at its maximum limit (884.92 °C). The resulting reactor outlet compositions show that the methane slip is slightly lower, and hydrogen composition slightly higher than the base case (Table 29.14). This is to be expected, even for a less active catalyst, for this system, which is close to equilibrium and at a slightly higher outlet temperature. This solution shows that profile control can essentially overcome the otherwise poor operating conditions that would accompany catalyst activity decline. The optimizer increases the heat flux to the part of the tube in which sufficient reaction heat sink exists, and decreases heat flux to the tube where insufficient reaction exists, and where temperature limits would otherwise be violated. Of course, at lower catalyst activities, and with less range of firing control, the debits associated with catalyst activity decline cannot be avoided. For

example, as the catalyst activity falls, the ability to reduce firing and maintain the *CAT-I* temperature below reasonable limits, while still maintaining a reasonable reactor outlet temperature, will cease to exist.

Table 29.14 Effluent composition for the maximize outlet temperature optimize case – naphtha feed cases. Inlet temperature = 462.0 °C. TI211-1 temperature upper limit = 449 °C. TMT temperature upper limit = 884.9 °C. There are step bounds on firing profile

Component	Catalyst activity 90%
Hydrogen	63.961
Nitrogen	0.3670
Argon	0.0060
Carbon monoxide	9.0552
Carbon dioxide	16.3755
Methane	10.2344

References

- J. Xu, G.F. Froment: Methane steam reforming, methanation and water-gas Shift: I. Intrinsic kinetics, *AIChE J.* **35**(1), 88 (1989)
- J. Xu, G.F. Froment: Methane steam reforming: II. Diffusional limitations and reactor simulation, *AIChE J.* **35**(1), 97 (1989)
- J.R. Rostrup-Nielsen: *Steam Reforming Catalysts, An Investigation of Catalysts for Tubular Steam Reforming of Hydrocarbons* (Teknisk Forlag AIS, Copenhagen 1975)
- J.R. Rostrup-Nielsen: *Catalytic Steam Reforming* (Springer, Berlin, Heidelberg, New York 1984)
- C.P.P. Singh, D.N. Saraf: Simulation of side fired steam-hydrocarbon reformers, *Ind. Eng. Chem. Process Des. Dev.* **18**(1), 1–7 (1979)
- S. Ergun: Fluid flow through packed columns, *Chem. Eng. Prog.* **48**(2), 89 (1952)
- S.S.E.H. Elnashaie, A.M. Adris, M.A. Soliman, A.S. Al-Ubaid: Digital simulation of industrial steam reformers for natural gas using heterogeneous models, *Can. J. of ChE* **70**, 786 (1992)
- M. Boudart: Two step catalytic reaction, *AIChE J.* **18**(3), 465 (1972)
- J.M. Smith: *Chemical Engineering Kinetics*, 2nd edn. (McGraw-Hill, New York 1970)
- J.R. Rostrup-Nielsen, J. Wristberg: Steam reforming of natural gas at critical conditions, Natural Gas Processing and Utilisation Conference, Dublin (1976)
- C.N. Satterfield, T.K. Sherwood: *The Role of Diffusion in Catalysis* (Addison-Wesley, Reading 1963)
- H.F. Rase: *Fixed-Bed Reactor Design and Diagnostics for Gas-Phase Reactions* (Butterworth, Boston 1990)
- G.W. Bridger: Design of hydrocarbon reformers, *Chem. Process Eng.* **53**, 38 (1972)
- J.R. Rostrup-Nielsen, T.S. Christensen, L.B. Dybkjaer: Steam reforming of liquid hydrocarbons, *Stud. in Surf. Sci. and Catal.* **113**, 81–95 (1998)
- J.R. Rostrup-Nielsen: Activity of nickel catalysts for steam reforming of hydrocarbons, *J. Catal.* **31**, 173–

- 199 (1973)
- 29.16 G.F. Froment, E.S. Wagner: Steam reforming analyzed, *Hydrocarb. Process.* **71**, 69 (1992)
- 29.17 J.W. Colton: Pinpoint carbon deposition, *Hydrocarb. Process.* **60**, 177–184 (1991)
- 29.18 J.R. Rostrup-Nielsen: Equilibria of decomposition reactions of carbon monoxide and methane over nickel catalysts, *J. Catal.* **27**, 343–356 (1972)
- 29.19 J.H.B. Hansen, L. Storgaard, P.S. Pedersen: Aspects of modern reforming technology and catalysts, *AIChE Ammonia Symposium, Safety in Ammonia Plants and Related Facilities*, Los Angeles (1991), *AIChE Paper No.* 279d
- 29.20 L.J. Christiansen, S.L. Andersen: Transient profiles in sulphur poisoning of steam reformers, *Chem. Eng. Sci.* **35**, 314–321 (1980)
- 29.21 D.Q. Kern: *Process Heat Transfer* (McGraw-Hill, New York 1950)
- 29.22 N. Wimpess: Generalized method predicts fired-heater performance, *Chem Eng.* **85**, 95 (1978)
- 29.23 R.B. Bird, W.E. Stewart, E.N. Lightfoot: *Transport Phenomena* (John Wiley, Hoboken 1960)
- 29.24 R.A. Greenkorn, D.P. Kessler: *Transfer Operations* (McGraw-Hill, New York 1972)
- 29.25 O. Levenspiel: *Chemical Reaction Engineering* (John Wiley, Hoboken 1972)
- 29.26 F. Krieth, R.M. Manglik: *Principles of Heat Transfer*, 8th edn. (Cengage Learning, Boston 2011)
- 29.27 R.D. Reed: *Furnace Operations* (Gulf, Houston 1976)
- 29.28 G.L. Tomei (ed.): *Steam – Its Generation and Use*, 42nd edn. (Babcock Wilcox, Charlotte 2015)
- 29.29 R.H. Perry, C.H. Chilton: *Chemical Engineers' Handbook*, 5th edn. (McGraw-Hill, New York 1973)

Delayed Coking

30. Delayed Coking

Keith Wisecarver

Thermal processing is the most common refining technique for heavy residues. Thermal processing techniques include delayed coking, fluid coking, flexicoking, and visbreaking; of these, delayed coking is by far the most common method of thermal processing, with the ability to produce motor fuels from vacuum tower bottoms with a minimum of capital expenditure. Delayed coking capacity has increased greatly in recent years, mostly due to the heavier crude slates being used in refineries. Although delayed coking is an old process, there are many challenges associated with it, especially as crude slates continue to change and greater throughput is required of delayed coking units.

30.1	History of Thermal Processing	903
30.2	Delayed Coking Process	904
30.2.1	Role of Delayed Coking in the Refinery	904
30.2.2	Process Description	904
30.2.3	Delayed Coking Reactions	907
30.2.4	Operating Variables	908
30.2.5	Coker Products	909
30.3	Other Thermal Processes	912
30.3.1	Flexicoking	912
30.3.2	Fluid Coking	912
30.3.3	Visbreaking	912
30.4	Future Challenges	913
	References	913

Delayed coking is the most common process for upgrading of vacuum residua as well as a primary method for upgrading tar sands for the production of syncrude. The delayed coking process begins with the heavy oil, usually a vacuum residuum, entering a furnace in conjunction with high-pressure steam and flowing at high velocities, reaching coking temperatures of approximately 900–930 °F at the exit of the furnace tubes. The feed proceeds through a transfer line to a coke drum. Cracking reactions begin in the furnace tubes and continue in the coke drum. Coke formation reactions are delayed in the sense that they take place in the drum rather than in the tubes.

The primary goal of delayed coking is usually carbon rejection, along with rejection of the metals, which can act as catalyst poisons in downstream processes, as well as rejection of a majority of the sulfur that is present in the feedstock. In other words, delayed coking produces lighter fuels with relatively high H/C ratios from heavier feedstocks with low H/C ratios, leaving behind carbon-rich coke and most of the metals. As such, it is the liquid fuels products that are the most valuable, and the coke can be considered a byproduct. However, there are exceptions, as in the production of anode-grade coke and especially of needle coke, where the coke can be quite valuable.

30.1 History of Thermal Processing

In early refineries, oil was boiled in small, iron stills to recover kerosene. After distillation was complete, the petroleum coke remaining in the still had to be dug out by hand. The first true thermal-cracking process, the Shukhov cracking process, was invented by Vladimir Shukhov in 1891 in Russia. The Burton process, developed by Standard Oil, Whiting, IN, USA, in 1912, was a method to convert gas oil to gasoline with the production of petroleum coke by thermal

cracking at temperatures of 700–750 °F and pressures of 90 psia. By gradual evolution of the art, it was found that heaters could be designed to raise residual stock temperature above the coking point without significant coke formation in the heaters. In 1919, the Dubbs process was invented. This process heated the oil to 900 °F at 150 psia at a low per-pass yield to prevent serious coke formation in the heating zone.

The first delayed coker was built by Standard Oil Whiting, IN, USA, in 1929, building upon the features of the previous thermal-cracking processes and separating the heater from the coke drum. The use of two coke drums in parallel enabled operation on a continuous basis.

In the years following World War II the drop in demand for heavy oil combined with the increased demand

for distillates resulted in a sharp increase in the number of delayed coking units, with more than a fivefold increase in coking capacity between 1950 and 1970. Since the 1980s, the production of heavier crudes has further increased the demand for coking. In 2014, the US delayed coking capacity, which accounts for about half the worldwide capacity, amounted to nearly 3 million bbl/day, an increase of almost 26% in the last decade.

30.2 Delayed Coking Process

30.2.1 Role of Delayed Coking in the Refinery

The most common feedstock to delayed cokers is the bottom product of the vacuum column, known as vacuum residuum. In a few cases, where the refinery lacks a vacuum unit, atmospheric residuum is sent to the delayed coker. Other feeds, such as aromatic gas-oils, tars, or cracked residua, are sometimes mixed with the main feed to influence the coker performance or to rid the refinery of certain unwanted products.

Delayed coking is the most popular method of upgrading residua. Hydrogen addition processes, such as resid hydrocracking and resid FCC, generally have higher capital and operating costs than thermal-cracking processes and have difficulty handling feeds with high contents of sulfur, nitrogen, and metals, as are commonly found in vacuum residua. Delayed coking is preferred due to its relative simplicity, high conversion rate to liquid products, and low operating and investment costs.

30.2.2 Process Description

Figure 30.1 shows the process flow diagram of a delayed coking unit. In some refineries, the vacuum residuum arrives at the coker unit hot, straight from the vacuum distillation unit. In most refineries, however, the vacuum residuum comes from storage tanks and is relatively cold. The feed is preheated by heat exchange with product streams, and then proceeds to the fractionator tower before going to the coker furnace. The coker feed enters the bottom of the fractionator at a temperature ranging from 680 to 750 °F (360–400 °C). Rarely, the coker feed is preheated in a tube furnace or in the convection section of the main coker furnace in order to achieve this temperature.

At the bottom of the fractionator tower, the fresh feed combines with some condensed product vapors to make up the feed to the coker heater. The addition of the feed at the bottom of the tower quenches the overhead vapor, helps to heat the feed, and condenses the heavier gas oils from the overhead vapor which are thus re-

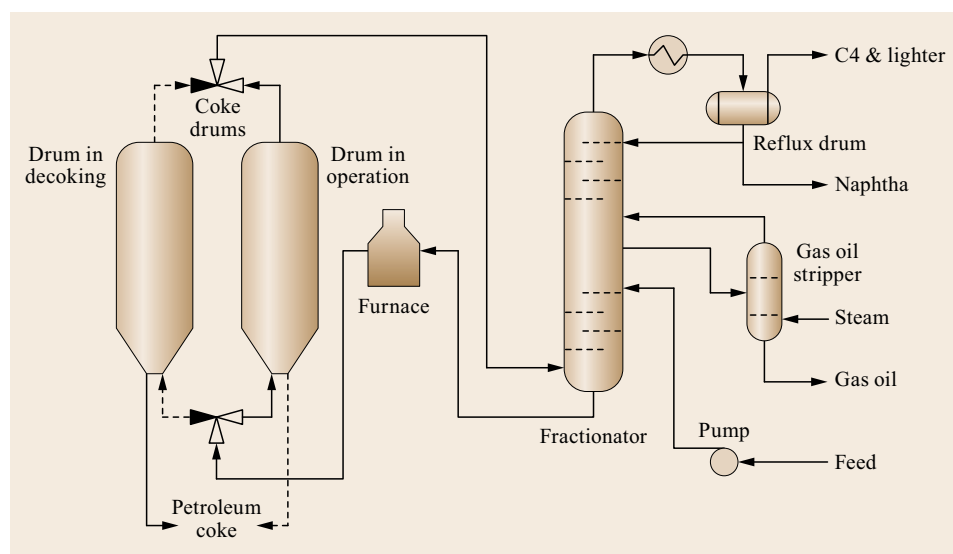


Fig. 30.1 Delayed coking process diagram

cycled through the coker. The fractionator bottom also provides some surge storage capacity for the incoming fresh feed.

The fractionator bottoms, including the recycled heavy gas oils, are then heated in a furnace whose outlet temperature typically ranges from 900 to 930 °F (480–500 °C). Cracking reactions begin when the feed reaches about 800 °F. The heated feedstock enters one of the pair of coking drums where the cracking reactions continue. The cracked products leave as overhead vapor, while coke deposits at the bottom of the drum. For continuous operation, two coke drums are used; while one is on stream, the other is being decoked. The temperature drops by about 100–110 °F (37–43 °C) between the bottom and top of the coke drum; coke drum pressures typically range from about 15–60 psig (1–4 barg). Overhead products go to the fractionator, where the cracked products are recovered.

Delayed coking drums are operated under a coking/decoking cycle whose length can vary from 10 to 24 h. Once the coke drum is filled with coke, the feedstock is redirected into an empty, prewarmed drum. The full coke drum must then be steam stripped (to decrease the amount of remaining volatile matter in the coke), water quenched and drained, unheaded (removal of top and bottom flanges), decoked, reheated, purged with steam, hydrostatically tested, and finally, prewarmed with gases coming from the drum on service. These steps are carried out in a while the adjacent drum is being filled with coke. During the steam stripping and quenching cycles, the overhead products are transferred to the blowdown system in order to separate, recover, and recycle the hydrocarbons stripped from the coke drum. The blowdown system is also designed to receive oil condensates produced in the coke drums while the warming operation is conducted.

Upon completion of the steam-stripping stage and before proceeding to cutting the coke bed, the drum must be quenched by injecting water at the bottom of the vessel. Continuous flow of water into the drum contributes to decreasing the average coke bed temperature from around 800 °F to around 195 °F. Afterward, the coke drum is drained to a pad or drain sump, where coke fines are separated from water discharged from the bottom of the drum.

Shorter coking cycles allow increased throughput in the delayed coking unit, but are difficult to maintain due to the minimum time requirements for each of the steps of the drum cycle. Table 30.1 shows the typical time required for each step in a 16 h coking cycle.

Furnace

The coker furnace is designed to achieve a constantly rising temperature gradient using a symmetrical piping

Table 30.1 Coking operations for a typical 16 h cycle. (After [30.1])

Operation	Hours
Fill drum with coke	16
Steam to fractionator	0.5
Steam to blow down	0.5
Depressure, Water quench and fill	4.5
Drain	2.0
Unhead Top and bottom	0.5
Coke cutting	3.0
Rehead, steam test, and purge	1.0
Drum warm-up	4.0
Total time	16.0

arrangement, while maintaining high in-tube velocities, minimum residence time in the furnace, and optimum heat flux rate in order to minimize fouling. Velocity steam is added at about 1 wt% of the feed to achieve high in-tube velocity. The furnace outlet feeds directly to a transfer line which is usually kept as short as possible in order to avoid coking in the line, as this can cause an increase the furnace pressure which will lead to an increase in the fouling of the furnace tubes.

Coker furnaces typically have two to four horizontal passes per furnace, with a 4 in inner tube diameter and 0.25–0.5 in tube wall thickness. The trend in recent years has been toward double-fired heaters as opposed to single-fired heaters, to provide a more uniform heat flux. At least a 9% chrome alloy is normally used for the tubes. The feed undergoes partial vaporization and mild cracking as it passes through the furnace. Typically 10–25% of the feed has been vaporized or cracked to lighter materials by the time the feed exits the furnace. Coker furnaces usually have a total liquid residence time of around 2 min [30.2] with a cold oil velocity of around 6 ft/s (1.8 m/s) [30.3].

Fouling in the furnace tubes is a significant problem in delayed coker units. Fouling deposits act as an insulating layer inside the tubes, hindering the heat transfer from the surface to the bulk of the fluid. Fouling deposits also decrease the effective tube diameter, increasing the pressure drop in order to maintain constant flow rates. Since the bulk temperature has to be maintained, the surface temperature has to be increased leading to increase in fuel costs. Once the maximum allowable outer tube wall temperature is reached, the tubes must be decoked. The trend toward heavier delayed coker feedstocks has caused increasing problems with furnace fouling. While run lengths of nine months used to be common, in recent years many refineries have experienced decreased run lengths. Species that tend to contribute toward fouling include suspended impurities such as dirt, clay, sand, and rust that attach to the surface; precursors such as reactive olefin that may

undergo bulk reaction with oxygen (which can enter into the feedstock due to exposure to the atmosphere in storage tanks) to form insoluble polymeric peroxide gum foulant which in turn may adhere to the surface; asphaltene destabilization due to various effects such as temperature, pressure, or change in the liquid composition; and the presence of sulfur, which can lead to accelerated corrosion fouling of the tube surface [30.4]. Fouling is also correlated with the presence of metals, especially sodium and calcium, which are commonly present in delayed coker feedstocks.

Some refiners add recycle or condensate to help prevent furnace fouling. Fouling can also be decreased by increasing velocity steam to the tubes; increasing cold oil velocity in the tubes; and by effective furnace design, to eliminate hot spots on the tubes by reducing peak heat flux rates and minimizing flame impingement. It is also helpful to monitor temperatures, minimize process upsets, and assure proper desalting of the crude. Downtime for delayed coker heaters can be reduced by the use of on-line spalling of the coker furnace tubes.

Coke Drums

In the coke drum, the liquid feed, partially cracked in the furnace tube, continues to crack and form vapors which disengage and leave the drum, while the remaining heavy liquid polymerizes to form coke. Foaming is a major issue in the coke drum for many delayed coking units. Coke drums are designed to provide enough volume for the accumulation of coke produced during the coking cycle, at the same time allowing the maximum allowable superficial velocity that will prevent entrainment of the liquid and prevent foam from carrying over. Generally, coke drums are designed to allow 0.3–0.4 ft/s (0.09–0.12 m/s) superficial vapor velocity at the top of the drum. Antifoam is usually added to prevent foam carry over.

Commercial coke drums generally range from 13 to 30 ft (4–9 m) in diameter. Lower coke drum pressures are preferred for increased liquid yield, but the minimum pressure is set by the pressure drop through the overhead system; in practice, it is difficult to operate at pressures lower than 15 psig (1 bar).

Figure 30.2 illustrates how coke is formed in the drum. Liquid, along with steam and cracked vapor products, enters the bottom of the drum through the transfer line as a two-phase mixture. The vapor disengages from the liquid and exits the overhead of the drum. The heavy liquid remaining behind cracks further, generating more vapor, and eventually polymerizes to form coke. The coke layer forms from the bottom up, with a layer of bubbly liquid on top of the coke and usually a foamy or frothy layer on top of the bubbly

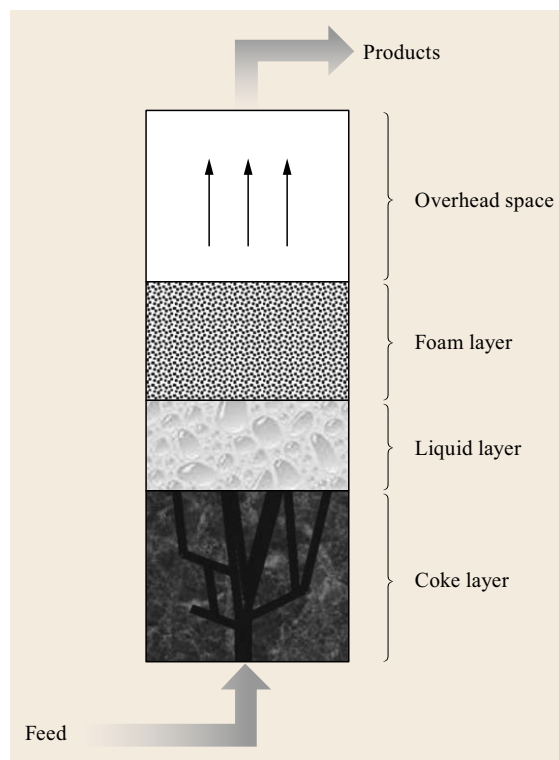


Fig. 30.2 Coke formation in the drum

liquid layer. Entrained liquid droplets disengage in the overhead space of the drum. The drum is switched out before the point is reached where liquid or foam will escape through the overhead line. In the modern refinery, the coke level and liquid level in the drum is usually determined through the use of nuclear backscatter devices mounted on the outside of the drum.

When the drum is full and switched out, the coke is steam stripped. Steam stripping must be done, not only to improve liquid recovery, but also to prevent the trapped liquid from plugging the channels in the coke bed, hence preventing the formation of *hot spots*. Hot spots are formed when steam (during stripping) and cooling water (during quenching) are not allowed to reach parts of the coke bed due to plugged channels or, in some cases (especially coke with a transitional morphology between sponge and shot), when the coke is too dense and lacks effective porosity. Steam must be flowing both before and immediately after the drums are switched, to prevent the unconverted liquid on top of the coke bed from flowing back down through the coke bed, where it can solidify to coke and plug the channels in the coke bed.

Steam stripping is usually carried out for 60 min, with steam typically flowing at the same rate as the velocity steam when the drum is online. When the steam

stripping is over, steam injection is increased for a short time, or in some cases water is immediately introduced at the bottom of the drum which instantly flashes to steam. Steam injection is then halted and the flow of cooling water is gradually increased. It is not uncommon to see a slight increase in the top vapor temperature in the drum right after the injection of water begins due to the increased flow of steam up through the coke resulting from water flashing. After that slight increase in temperature, cooling of the coke bed starts taking place. Once liquid water has filled the drum to the top of the coke level, the drum is drained and decoking can commence. The quench water rate must be carefully controlled to prevent cooling from taking place too rapidly, which can cause thermal stresses in the drum walls that can result in bulging of the drum.

Decoking

Removal of the coke drum top and bottom flanges, known as *unheading*, precedes the decoking or coke cutting step. Many delayed coker operations have moved to using deheader valves at the bottom of the drum. These are remotely operated, eliminating exposure risk to personnel, and providing isolation or control in the rare instance of a *drum dump*, in which there is a collapse of unstable and loose petroleum coke particles which flow freely out the bottom of drum upon deheading.

In the decoking step, high-pressure water (3500–4000 psig = 240–275 barg) is supplied by a jet pump during the cutting operation. Coke cuttings and water are discharged from the drum through a chute to the coke pad or pit. Simultaneously, petroleum coke piles up on the pad/pit, while water flows from this point to the settling maze. Once the cutting operation has concluded, dry coke is removed from the pad/pit area by front-end loaders (pad) or a clamshell (pit), transported to a crusher in order to reduce its particle size, and finally, transferred to coke piles by means of a belt or pipe conveyor.

An inappropriate quenching and/or decoking operation can lead to serious hazards for the operators, such as the presence of geysers when cutting water gets in contact with pockets of hot unconverted feed or *hot spots* embedded in the coke bed. Hot spots are also responsible for fires in the coke piles when hot volatile material in the coke burns when it is exposed to air.

Fractionator

The overhead vapors from the coke drum, consisting of steam and the products of the thermal-cracking reaction, are fed to the bottom of the fractionator. The fresh feed enters the fractionator two to four trays above the bottom vapor zone before proceeding to the coker fur-

nace. The introduction of fresh feed to the fractionator quenches the hot vapors from the coke drum, thus preventing any significant amount of coke formation in the fractionator. At the same time, it condenses a portion of the heavy ends of the coker product, which are then recycled back to the coker, while any lighter material in the fresh feed is stripped. Quenching the hot coke drum vapors also helps to preheat the feed, making the process more energy efficient. The amount of recycle is controlled by the fractionator pressure: higher pressure results in more recycle to the coker.

The hot vapors from the coke drum flow up through the quench trays where they contact the fresh feed. Above the fresh feed entry point, there are usually two or three additional trays below the gas-oil draw tray, which are refluxed with partially cooled gas oil. The gas oil is drawn off to a conventional side stripper having six to eight trays, with steam introduced under the bottom tray to vaporize the light ends and control the initial boiling point of the gas oil. Steam and vaporized light ends are returned from the top of the gas oil stripper to the fractionator one or two trays above the draw tray. A pumparound is also used to at the draw tray to provide better heat integration.

A heavy naphtha side draw is sometimes used. There are usually eight to ten trays between the gas-oil draw and the naphtha side draw or column top. If a naphtha side draw is employed, additional trays are needed above the naphtha draw tray.

The temperature of vapors rising to the gas oil draw-off tray is controlled to reach the desired gas oil end point. A higher temperature results in more heavies being drawn off in the gas oil, leaving less of the heavy gas oil to be recycled to the furnace.

The overhead condenser temperature is controlled to send most of the C_4 's and lighter to the gas stream and the C_5 's and heavier to the naphtha stream, which is then sent to a hydrotreater for sulfur removal and olefin saturation. The hydrotreated coker naphtha can be blended directly into the finished gasoline, but is often isomerized as the octane rating is poor.

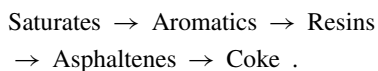
The gas oil fraction is usually split into light and heavy coker gas oils before further processing. The light coker gas oil is usually hydrotreated and used as diesel fuel, while the heavy coker gas oil is fed to the cat cracker or sent to a hydrocracker, or used as a heavy fuel oil. The off-gas from the condenser goes to the gas plant where C_3 and C_4 are recovered as LPG and the lighter end can be used as fuel gas in the refinery.

30.2.3 Delayed Coking Reactions

Vacuum residua are extremely complex mixtures of tens of thousands of compounds, so a complete char-

acterization of the delayed coker feed is impossible. However, there are several relatively simple analytical tests including the Conradson Carbon Residue (CCR) test (or, alternatively the Microcarbon Residue (MCR) test), which gives a rough idea of the coking propensity of the feed, as well as SARA (saturate-aromatic-resin-asphaltene) analysis. In a SARA analysis, the feed sample is separated into a saturate fraction consisting of linear, branched, and cyclic saturated hydrocarbons; an aromatic fraction, consisting of one or more aromatic rings; a resins fraction, consisting of large heterocyclic molecules which are completely miscible in oil; and an asphaltene fraction, which consists of very high-molecular weight molecules having large aromatic cores. Asphaltenes are defined as material that is insoluble in *n*-heptane (or, depending on the analysis being done, in *n*-pentane or *n*-octane) but soluble in toluene. The asphaltenes are thought to be kept solubilized in the oil due to the presence of the large resin molecules, which in turn are solubilized by the aromatic and saturate fractions. Asphaltenes are easily converted to coke, whereas the other components are generally thought to have to crack and condense to form asphaltenes before coke can be formed.

Cracking reactions in the delayed coking process are endothermic and occur as free radical reactions. There are three types of reactions involved in cracking: dehydrogenation, which involves the loss of a hydrogen atom from an aromatic hydrocarbon, resulting in the formation of an aromatic free radical intermediate; rearrangement reactions, in which thermal rearrangement usually leads to formation of more stabilized aromatic ring compounds; and polymerization of aromatic radicals to form coke. Reactions occur in both liquid and vapor phases, but since the vapors leave the coke drum quickly the vapor-phase reactions are quenched before the coke formation step. The progression to coke in the liquid phase is thus



Reactions occurring in the delayed coker have been described by *Wiehe* [30.5, 6] using a *pendant-core model* of the residuum molecules. Here the residuum macromolecules are modeled as having pendant chains that thermally crack from large aromatic cores. The pendants are volatile once broken off, while the large cores remain nonvolatile and convert to asphaltenes as the pendants are broken off. These asphaltene cores are unreactive as long as they remain dissolved in the resins. As the conversion is increased, the asphaltene core concentration increases and the nonvolatile resin concentration decreases until the solubility limit of as-

phaltene cores in the remaining resins is exceeded. At that point, asphaltene cores phase separate to form a second liquid phase. The asphaltene cores crack off nonvolatile heptane-soluble fragments and recombine to form solid coke.

As coke is formed, the asphaltene concentration decreases from its maximum value. As the unreacted asphaltenes become depleted, the asphaltene concentration approaches a constant ratio to the nonvolatile heptane-soluble fraction because of the solubility limit of the remaining asphaltenes in nonvolatile heptane solubles. An induction period for coke formation has been widely reported in the literature, but the evidence indicates that at the conditions in the delayed coker (temperatures greater than 840 °F (450 °C)) there is no measurable induction period [30.7, 8].

30.2.4 Operating Variables

The three most important operating variables that determine the yield in the delayed coker for a given feed are temperature, pressure, and recycle ratio. At constant pressure and recycle ratio, the coke yield decreases and the liquid yield and gas-oil end point increase as the drum temperature is increased. This is primarily because high temperatures favor the vaporization of more of the heavy gas oils, which leave the drum before reacting further. However, there is only a narrow range over which the temperature can be adjusted. Since delayed coking is an endothermic reaction, the heater outlet temperature is the control point for adjusting the coking reaction temperature. In actual practice, if the temperature is too low, the coking reaction does not proceed far enough resulting in the formation of pitch or high VCM (volatile combustible matter) coke. If the temperature is too high the coke formed will be excessively hard and difficult to remove from the drum with the hydraulic decoking equipment. In addition, at higher temperatures the possibility of prematurely coking the heater tubes and/or the transfer line increases. Generally, one reaches the temperature limit when the furnace run lengths become short, requiring more furnace decokes and unit startups and shutdowns, thus affecting unit safety and maintenance costs.

At higher temperatures, the extent of conversion of heavier products increases, thereby increasing the yield of the gas and light naphtha fractions. Increasing the temperature of the process also results in increased generation of olefinic and aromatic hydrocarbons both in coker naphtha and gas oil.

At constant temperature and recycle ratio, the effect of increased pressure is to retain more of the heavy hydrocarbons in the coke drum. This retention increases the coke yield and slightly increases the gas yield, while

decreasing the pentane and heavier liquid product yield. According to *Lieberman* [30.9] reducing the pressure of the coke drum by 8 psi decreases coke yield roughly by 1.3 wt%, while liquid yield increases by 1.3 vol.%. The recent trend in the design of delayed cokers has been to maximize the yield of liquid products by designing for lower pressures. The limitations on reducing the pressure of the unit are primarily system pressure drop losses, vapor velocity in coke drums, and possible increase in equipment size and cost [30.10]. In order to achieve low-pressure operation, the coke drum overhead pressure is controlled by a pressure controller located at the fractionator overhead separator, which is set to maintain a positive pressure of 1–2 psig (70–140 barg) at the compressor suction. The coke drum overhead pressure is equivalent to this controlled pressure plus the pressure drop in the piping and equipment between the coke drums and the compressor.

Recycle or throughput ratio (TPR) is defined as the ratio of the volumetric flowrate of feed to the furnace over the volumetric flowrate of the fresh feed to the delayed coking unit. Recycle ratio has a significant impact on product yields. Increasing the TPR by 10 vol.% reduces the liquid yield by roughly 1.5 vol.% [30.11]. As the TPR is increased, continuous condensation and recirculation of heavy coker gas oil from the main fractionator through the furnace causes *overcracking* and, consequently, production of coke and light compounds. Even though recycle lowers the yield of the valuable liquid products, it is often used because addition of recycle tends to reduce the coke deposition in the furnace tubes. The TPR used in commercial delayed cokers generally ranges from 1.0 to 1.2.

The quality of the products from delayed coking process is directly affected by the physicochemical properties of the feed. The effect of feedstock properties on the delayed coking process can be estimated from a SARA analysis of the feed. The saturate fraction determines how paraffinic a feed is: the higher the percentage of saturates, the higher the amount of paraffins. Coking reactions start with the thermal cracking of paraffins and their side chains to form olefins and paraffins of lower molecular weight. The more paraffinic the residue, the higher the formation of lower molecular weight compounds will be, resulting in a yield increase of distillates and gases. On the other hand, paraffinic-type feedstocks with some sodium present foam readily compared to aromatic feedstocks which tend to have smaller foam heights.

Aromatics play an important role in the coking process. Once the paraffin chains have been cracked into lower molecular weight molecules (paraffins and olefins), the polymerization reactions take place, which

are promoted by the dehydrogenation of some of the cracked paraffins, such as cycloparaffins (naphthenes). These reactions lead to the formation of aromatic molecules which in turn can be condensed into polynuclear aromatics, generating a mesophase which converts into coke. In other words, aromatics are precursors to mesophase formation, and therefore of coke formation.

Resins and asphaltenes are the heaviest, most aromatic and most polar compounds found in delayed coker feedstocks. Feeds that are high in asphaltenes will have higher coke yield than paraffinic or aromatic feeds.

The weight fraction of carbon present in the crude oil is another variable that greatly affects the overall yields of the process. This variable is strongly related to the amount of asphaltenes present in crude oil; the higher the weight fraction of asphaltenes, the higher the weight fraction of residual carbon. A widely used method to determine this variable is the CCR test or MCR test, which allow a preliminary estimate of the coke yield. As a rough rule of thumb, the coke yield is about 1.6 times the value of the MCR.

Other properties of the feed, such as metals, sulfur, and nitrogen, have no significant impact on the overall yields of delayed coking process; nonetheless, the quality of the products is highly affected by these properties.

In general, the kinetics of polymerization reactions are slower than for the thermal-cracking reactions. Therefore, coke drums provide the necessary residence time to proceed to coke formation. Short coking cycles do not allow completing cracking and polymerization reactions, so as a consequence, the concentration of VCM in the petroleum coke tends to increase when the coking cycle is shortened.

30.2.5 Coker Products

Coke Formation

Coke can exhibit a variety of morphologies, with the type of coke morphology dependent on feedstock properties and, to a lesser extent, on drum temperature and pressure. Needle coke, named for its needle-like structure, is produced from feedstocks without asphaltenes present. It is made from highly aromatic feedstocks such as FCCU decant oils, and requires carefully controlled coking conditions at high pressures (100 psig = 7 barg) and high recycle ratios (1 : 1). Needle coke, used in graphite electrode manufacturing, is considered a specialty product and commands a high price.

For delayed cokers running with vacuum resid as a feedstock, coke morphology is usually divided into two types: sponge coke and shot coke. Coke morphology can be correlated to the ratio of the C₇ asphaltenes of the feed (that portion of the feedstock that is in-

soluble in *n*-heptane) to CCR of the feed. Feedstocks with a C_7 asphaltene to CCR ratio of less than 0.5 tend to make sponge coke which, as the name implies, has a spongy, porous texture. On the other hand, feeds with a C_7 asphaltene to CCR ratio greater than about 0.65 tend to form shot coke. This morphology is characterized by small (0.06–0.25 in diameter) spheres, usually embedded in a matrix of coke material. In some cases, however, these shot clusters can grow large enough to plug the coke drum outlet. Asphaltene to CCR ratios between 0.5 and 0.65 generally form a transitional type coke, with some characteristics of both shot and sponge coke. Figure 30.3a,b shows typical looking examples of shot and sponge coke.

Shot coke is believed to form when droplets of asphaltene material, having separated out of solution from the feed, enter the coke drum at high velocities and quickly polymerize to form coke. Shot coke formation thus requires a high-asphaltene feedstock and is favored at higher temperatures, where coke formation occurs quickly, and low pressures, which causes in an increase in vapor velocity. The production of shot coke has increased greatly in recent years due to the heavier crudes being used in refineries.

Coke morphology can be affected by the recycle ratio used. Shot coke formation can sometimes be avoided by increasing the recycle ratio. This is probably due to the fact that the heavy coker gas oil has very little asphaltene content, so blending it with the fresh feed lowers the asphaltene content of the furnace charge. There is also thought to be a solubility effect in that recycle typically is a medium volatility, aromatic rich stream which has the ability to dissolve the heavy aromatics. In short, the higher the recycle ratio, the better the coke quality.

Coke that has been adequately steam stripped typically contains 5–15 wt% volatile matter.

Volatile Products

A number of investigators have developed correlations for delayed coking yields, including Gary and Handwerk [30.12], Castiglioni [30.13], Maples [30.14], Smith et al. [30.15], and Volk et al. [30.16]. The Gary and Handwerk, Castiglioni, and Maples yield correlations generally are based only on feedstock properties, mainly CCR, whereas the Smith et al. and Volk et al. are based on coker drum temperature and pressure as well as feedstock properties. Muñoz et al. [30.17] summarized these correlations and compared them to commercial operating data. The data came from 13 different commercial cokers, using feeds having CCR ranging from 15.6 to 31 and API gravity ranging from 0.1 to 10.3, run at temperatures between 900 and 930 °F (480–500 °C), pressures between 15 and 40 psig (1–3 barg), and TPR between 1.05 and 1.10. Their conclusion was that correlations that include the effect of operating conditions [30.15, 16] are more accurate than those that consider only feed properties [30.12–14]. Overall, the Volk et al. correlation exhibited the lowest errors. The average absolute error of all predicted yields were in the following increasing order: Volk et al. (10.14%) < Smith et al. (27.57%) < Castiglioni (28.03%) < Maples (41.63%) < Gary and Handwerk (49%).

The correlations of [30.16], obtained from microreactor data, were based on microcarbon residue (MCR, in wt%), temperature (T , in °F), pressure (P , in psig), and liquid space velocity (LSV, in min^{-1}). The range of operating conditions used to develop the correlations is 900–950 °F (480–510 °C), 6–40 psig, and MCR from

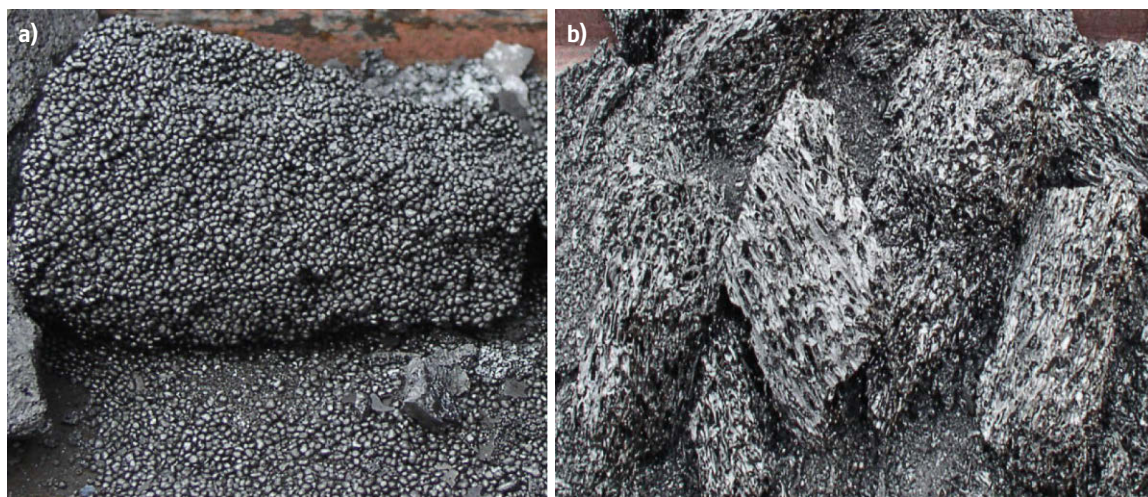


Fig. 30.3 (a) Shot coke morphology, (b) sponge coke morphology

16 to 29 wt%. The correlations are

$$\text{liquid (wt\%)} = -1.1139 \times \text{MCR} + 0.0419 \times T \\ - 0.2897 \times P + 1103.08 \times \text{LSV} \\ + 41.59 ,$$

$$\text{coke (wt\%)} = 0.9407 \times \text{MCR} - 0.0609 \times T \\ + 0.1529 \times P - 319.759 \times \text{LSV} \\ + 65.075 ,$$

$$\text{gas (wt\%)} = 0.1729 \times \text{MCR} + 0.0191 \times T \\ + 0.13646 \times P - 786.319 \times \text{LSV} \\ - 6.762 ,$$

$$\text{naphtha (wt\%)} = -0.3086 \times \text{MCR} + 0.0137 \times T \\ + 0.1571 \times P - 819.63 \times \text{LSV} \\ + 16.461 ,$$

$$\text{diesel (wt\%)} = -0.3339 \times \text{MCR} - 0.02635 \times T \\ - 0.0392 \times P + 70.957 \times \text{LSV} \\ + 50.452 ,$$

$$\text{gas oil (wt\%)} = -0.4714 \times \text{MCR} + 0.0546 \times T \\ - 0.4076 \times P + 1851.76 \times \text{LSV} \\ - 25.315 .$$

The correlations could not be used to predict yields from industrial cokers because of the lower liquid yields obtained in the microreactor, as compared to those observed in refineries, which becomes worse at the lowest feed rate. Also, the correlations include the effects of LSV, which has a different meaning for the microreactor than for commercial units. For these reasons, Volk et al. proposed the following correction to the above equations

$$\text{coke}^* (\text{wt\%}) = 0.91 \times \text{coke} ,$$

$$\text{gas}^* (\text{wt\%}) = 0.82 \times \text{gas} ,$$

$$\text{liquid}^* (\text{wt\%}) = 100 - (\text{coke}^* + \text{gas}^*) ,$$

$$\text{gasoline}^* (\text{wt\%}) = 0.75 \times \text{gasoline} \times (\text{liquid}^*/\text{liquid}) ,$$

$$\text{diesel}^* (\text{wt\%}) = 0.90 \times \text{diesel} \times (\text{liquid}^*/\text{liquid}) ,$$

$$\text{gas oil}^* (\text{wt\%}) = \text{liquid}^* - (\text{gasoline}^* + \text{diesel}^*) ,$$

where the * indicates a corrected value.

It is worth noting that none of the published correlations for delayed coker yields includes the effect of recycle.

Coke Usage

Petroleum coke is typically used as a source of energy, usually by burning but in some cases by gasification, or as a source of carbon for industrial applications. Fuel

grade coke represents nearly 80% of worldwide production and is a source of fuel for cement kilns and electric power plants. Calcining the coke, by heating it in a rotary kiln at temperatures over 2500 °F (1370 °C), increases the carbon content of the coke thus making it suitable, if it is sufficiently low in sulfur and metals (generally less than 2 wt% sulfur and less than 0.5% ash content), for use in the aluminum, graphite electrode, steel, titanium dioxide, and other carbon consuming industries.

More than 85% of all calcined petroleum coke is used to produce anodes for smelting alumina into aluminum via the Hall–Héroult process, and there is no other commercially viable method to produce primary aluminum. Although originally anthracite coal was used as the carbon source, calcined petroleum coke supplanted anthracite as soon as petroleum coke became commercially available due to its superior combination of electrical conductivity, resistance to chemical and physical degradation, higher carbon content, and low ash and sulfur content.

Calcined petroleum is also used in the production of titanium dioxide, and in the steel industry as a partial replacement for metallurgical coal as a feedstock for coke oven batteries, and as a partial substitute for pulverized coal directly injected into blast furnaces. All of these uses require high-quality sponge coke.

Needle coke is used to produce the electrodes used in electric arc furnace (EAF) steel production. No other material has needle coke's combination of electrical conductivity and physical properties required for EAF electrodes, making it a high-value product.

Calcined petcoke is also used in lime production and as a substitute for fuel oil in brick and glass manufacturing due to its low ash content as compared with coal.

Shot coke is unique in that the small spheres of shot each have a slick shiny exterior coating of needle-type coke, while the inside of each sphere contains isotropic or amorphous type coke. Shot coke cannot be used in making aluminum anodes because the outer needle coke layer of the shot sphere has a very low coefficient of thermal expansion while the inside of the sphere, being isotropic, has a very high coefficient of thermal expansion. When rapidly heated in a calcining kiln, the outer layer is cracked and pulled away from the center; thus when used in an anode with a coal tar binder, the binder adheres to the outer layer, resulting in cracks between the ball and the skin and thus causing the anode to crack in an aluminum smelter cell. The only significant use of shot coke is as a low quality fuel, especially in cement kilns where its generally high sulfur content is an advantage rather than a disadvantage.

30.3 Other Thermal Processes

30.3.1 Flexicoking

Flexicoking and fluid coking are similar processes that are sometimes used as an alternative to delayed coking. In this flexicoking process, hot feed, after contacting overhead effluent vapors for heat exchange, is sprayed on to a fluidized bed of hot coke particles. Here cracking takes place at much higher temperature than delayed coking (temperatures up to 1050 °F (565 °C)). Coke inventory is maintained by transferring bed coke from the reactor to a heater via a transfer line. Hot coke from the heater is circulated back to the reactor through a coke transfer line, supplying the heat necessary to maintain the reactor temperature. Excess coke is sent to a gasifier where the coke reacts with air and steam to produce a clean fuel gas. Approximately 97% of the coke generated in the reactor is consumed in the process, with a small amount of product coke recovered from the fines system. The fines are used in metallurgical, metals recovery, and fuels applications. Product fluid coke can be withdrawn from the heater to adjust the gasification level. This coke has a lower sulfur content compared to the coke produced in the reactor, making it more attractive for sale. Flexicoking produces a similar range of liquid products to delayed coking and provides an effective way of utilizing coke that might otherwise be difficult to dispose of. It has a considerably higher capital cost compared to delayed coking, however, and the greater complexity of the process can be a drawback. As of 2011, there were five commercial flexicoking installations with a total capacity of around 200 000 bbl/day.

30.3.2 Fluid Coking

Fluid coking is a simplified version of flexicoking. The Fluid Coking process burns only enough of the coke to satisfy the heat requirements of the reactor and the feed preheat. Typically, this is about 20–25% of the coke produced in the reactor. The rest of the coke is withdrawn from the burner vessel and is not gasified as it is in a flexicoker. As a result, there are only two fluid beds used in a Fluid Coker rather than three: a reactor and a burner which replaces the heater. Fluid coking has the advantage of its simplicity and reduced capital cost as compared to flexicoking. The main advantage of the flexicoker over the fluid coker is that most of the heating value of the coke product is made available as low sulfur gas which can be burned without an SO₂ removal system on the resulting stack gas, whereas SO₂ removal would be needed if coke containing 3–8 wt% sulfur is burned directly in a boiler. In addition, the coke gas can be used to displace liquid and gaseous hydrocarbon fu-

els in the refinery process heaters and need not be used exclusively in boilers as is the case with fluid coke.

As of 2014, the US fluid coking capacity was nearly 160 000 bbl/day.

30.3.3 Visbreaking

Visbreaking is a relatively mild thermal-cracking operation which is mainly used to reduce the viscosity and pour point of vacuum resid to meet No. 6 fuel oil specifications or to reduce the amount of cutting stock required to dilute the resid to meet these specifications. Refinery production of heavy fuel oils can be reduced from 20% to 35% and cutter stock requirements from 20% to 30% by visbreaking. The gas-oil fraction produced by visbreaking is also sometimes used as cat cracker feed.

In the visbreaking process, the goal is to crack off the long paraffinic side chains attached to aromatic rings in the vacuum resid, as these are the primary cause of high pour points and high viscosities. The amount of cracking is limited because if the operation is too severe, the resulting product can become unstable and form polymerization products during storage. The product improvement resulting from visbreaking is a function of the feed quality. Highly paraffinic feedstocks are easily cracked and a viscosity reduction of 25–75% can be achieved. For highly asphaltenic feeds, stability of the final product is a problem, so only smaller changes in fluid viscosity can be achieved.

The principal reactions occurring in visbreaking are: cracking of the side chains attached to cycloparaffin and aromatic rings at or close to the ring so the chains are either removed or shortened to methyl or ethyl groups; cracking of resins to lighter hydrocarbons and compounds which convert to asphaltenes; and (if temperatures above 900 °F (480 °C) are used) some cracking of naphthene rings.

There are two types of visbreaker processes: coil or furnace visbreaking, and soaker visbreaking. The coil or furnace visbreaking operation looks very much like a delayed coking operation, with furnace exit temperatures between 885 and 930 °F (475–500 °C), except that the feed is quenched upon exiting the furnace rather than being allowed to coke. In the soaker visbreaking process, feed leaves the furnace between 800 and 820 °F (426–438 °C) and passes through a soaker drum which provides additional reaction time at this temperature before quenching takes place.

Visbreaking is usually used in locations where motor fuel demand is relatively low and heavy fuel demand is relatively high. In areas such as the United States,

with high motor fuel demand and low demand for heavy fuel oil, visbreaking is rather rare. In 2014, vis-

breaking capacity in the United States was a mere 16 000 bbl/day.

30.4 Future Challenges

As crude slates have become heavier, the need for delayed coking has grown, creating a need to increase delayed coker throughput. This can sometimes be done by reducing the coking cycle time, but requires faster decoking and quench times. Heavier feeds also tend to make poor quality shot coke, sometimes leading to free flowing coke dumps or coke with hot spots, which create safety issues. Finding a market for shot coke can be difficult as well, which has created a problem with stockpiles of coke at some refineries.

Furnace fouling is a significant problem in delayed coking units. There is a need to develop ways to better understand causes of furnace fouling and find ways to prevent it.

Proper use of antifoam is important to prevent foamover events and to allow operating with a lower coke drum outage (the measured height of coke below the top head). Improvements are needed to foaming models in order to predict and understand severe foaming events and to optimize usage of antifoam. Overuse of silicon-based antifoam is not only costly but can cause poisoning of downstream units; for this reason, development of effective non-silicon-based antifoam is needed.

Finally, there are environmental issues with delayed cokers that are coming under increasing scrutiny. There is a need to understand and predict sour water quality from delayed cokers. Also, VOC emissions during the deheading and decoking steps are currently not well understood.

References

- | | |
|---|---|
| <p>30.1 P.J. Ellis, C.A. Paul: Tutorial: Delayed coking fundamentals, Proc. AIChE 1998 Spring Natl. Meet., New Orleans (1998), http://inside.mines.edu/~jjechura/Refining/DECOKTUT.pdf</p> <p>30.2 S. Skogestad, T. Gundersen, O. Johnsen: Compositional simulation of a refinery coker furnace, Model. Identif. Control 7, 25–44 (1986)</p> <p>30.3 R. DeBiase, J.D. Elliott: Delayed coking: Latest trends, Hydrocar. Process. 61, 99–104 (1982)</p> <p>30.4 A.P. Watkinson: Deposition of crude oils in heat exchangers, Heat Transfer Eng. 28, 177–184 (2007)</p> <p>30.5 I.A. Wiehe: The pendant-core building block model of petroleum residua, Energy Fuels 8, 536–544 (1994)</p> <p>30.6 I.A. Wiehe: A phase-separation kinetic model for coke formation, Ind. Eng. Chem. Res. 32, 2447–2454 (1993)</p> <p>30.7 P.E. Savage, M.T. Klein, S.G. Kukes: Asphaltene reaction pathways. 1. Thermolysis, Ind. Eng. Chem. Proc. Des. Dev. 24, 1169–1174 (1985)</p> <p>30.8 P.E. Savage, M.T. Klein: Asphaltene reaction pathways. V. Chemical and mathematical modeling, Chem. Eng. Sci. 44, 393–404 (1988)</p> <p>30.9 N.P. Lieberman: <i>Troubleshooting Process Operations</i>, 3rd edn. (PennWell Publishing Co., Tulsa 1991)</p> | <p>30.10 W.S. Louie, D. Ogren, G.L. Hamilton: Delayed coker projects – Design innovation and project execution, Proc. AIChE 1998 Spring Natl. Meet., New Orleans (1998)</p> <p>30.11 J.D. Elliott: Optimize coker operations, Hydrocar. Process. 9, 85–90 (2003)</p> <p>30.12 J.H. Gary, G.E. Handwerk: <i>Petroleum Refinery Technology and Economics</i> (Marcel Dekker, New York 1975)</p> <p>30.13 B.P. Castiglioni: How to predict coker yield, Hydrocar. Process. 9, 77–79 (1983)</p> <p>30.14 R.E. Maples: <i>Petroleum Refinery Process Economics</i> (PennWell Publishing Co., Tulsa 2000)</p> <p>30.15 M.J. Bagajewicz, A. Smith, M. Frow, J. Quddus, D. Howell, T. Reed, C. Landrum, B. Clifton: <i>Refinery Modeling, Advanced Chemical Engineering Design</i> (University of Oklahoma, Norman 2006)</p> <p>30.16 M. Volk, K. Wisecarver, C. Sheppard: <i>Fundamentals of Delayed Coking Joint Industry Project</i> (University, of Tulsa, Tulsa 2002)</p> <p>30.17 J.A.D. Muñoz, R. Aguilar, L.C. Castañeda, J. Ancheyta: Comparison of correlations for estimating product yields from delayed coking, Energy Fuels 27, 7179–7190 (2013)</p> |
|---|---|

31. Transitioning Refineries from Sweet to Extra Heavy Oil

Martin R. Gonzalez

A sweet-sour petroleum refinery shifting to heavy crude processing will face a number of challenges, many requiring investment to overcome. The difficulty in processing these feeds is related to the properties of extra-heavy oil, including a high aromatics content and a relatively high concentration of contaminants that pose a threat to reliability and product quality.

In this chapter, the relationship between feed composition and unit design is explored, with unit revamp and new-build strategies discussed for process units to adapt to the new crudes. Among other investments, significant scope is likely to include fractionation upgrading for improved removal of asphaltenes, volatile metals, and salts, as well as hydrotreaters modifications to deal with contaminants and counter the hydrogen deficiency of the oil.

31.1	The Evolving Refinery	915
31.2	Characterization of Extra-Heavy Crudes	917
31.3	Crude Desalting	917
31.4	Aromatics Content Affecting Diesel and Jet Fuel Production	918
31.5	High Aromatics Content Affecting Gas Oil Conversion	918
31.6	Vanadium and Nickel in Crude and Gas Oil	919
31.7	Asphaltene and Clay Precipitation	920
31.8	Fouling in Gas-Oil Hydrotreaters	921
31.9	Sulfur and Nitrogen in Bitumen-Derived Crudes	922
31.10	Hydrodesulfurization and Hydrodenitrogenation of Gas Oils	923
31.11	Production of ULSD and Jet Fuel	924
31.12	Fouling in Naphtha Hydrotreaters	925
31.13	Sulfur and Nitrogen Removal from Naphtha	926
31.14	Choice of Resid Conversion Technology	927
31.15	Other Investment	927
31.16	Conclusion	928
	References	929

31.1 The Evolving Refinery

The transition to extra-heavy Canadian crudes places unprecedented demands on the operating units within an existing refinery. Overcoming these challenges requires innovation as well as the effective utilization of familiar technology. In this section, technology hurdles for a transition to heavy oil are discussed, using a typical sweet-crude refinery configuration for illustration.

A block-flow diagram for a typical US refinery configured for gasoline production is shown in Fig. 31.1. Refineries such as this one are likely to employ the following main technologies:

- **Crude fractionation:** Many refineries have crude units designed for sweet- and medium-sour crudes, with some traditional heavy crude being processed.
- **Fluid-catalytic cracking (FCC) pretreat:** Refineries designed for the gasoline production in the United States tend to have FCC as their primary conversion technology. Some will have only partial FCC-feed hydrotreating, meaning that some of the sweeter straight-run gas oil is sent straight to the FCC without being pretreated.
- **FCC gasoline:** FCC naphtha must often be hydrotreated further to lower sulfur to acceptable level for the gasoline pool. However, many refiners do not

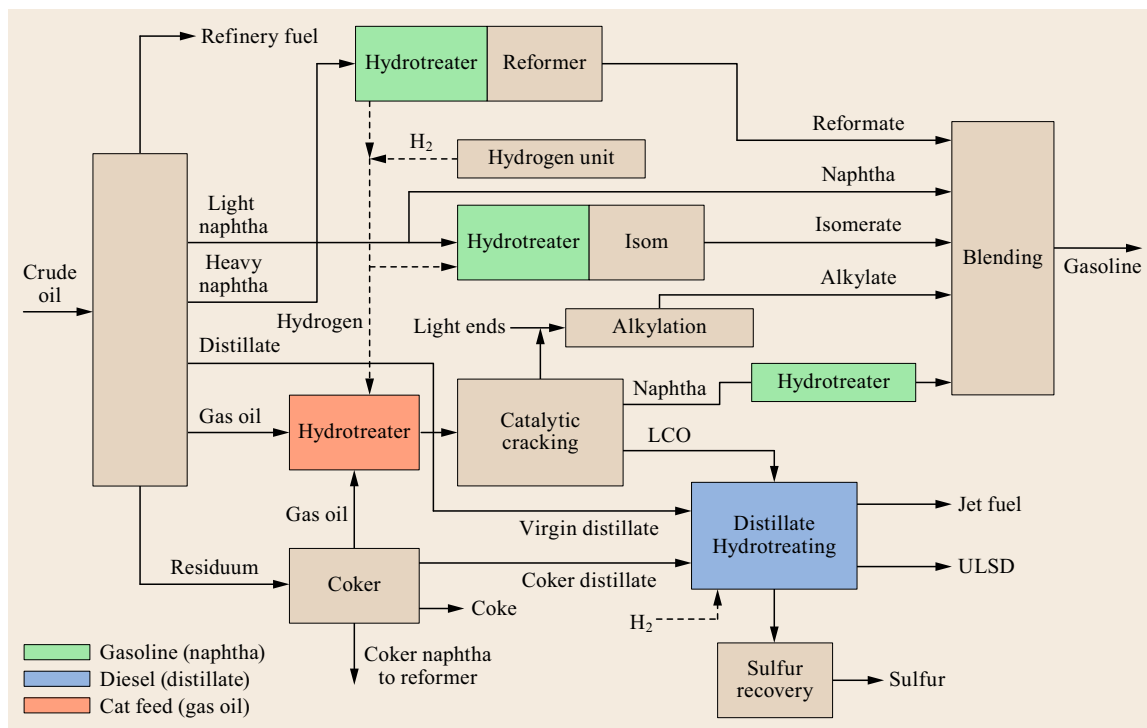


Fig. 31.1 Typical refinery configured for gasoline production. (Courtesy of BP)

have capacity to process the entire volume of FCC gasoline. They will instead desulfurize a smaller volume and let the rest go to blending without further processing. To be most effective, they may strategically segregate naphtha streams into *high* and *low* sulfur concentrations. Alternatively, or in addition, refiners may use fractionation to concentrate the difficult-to-remove sulfur into a *heavy* cut that will be hydrotreated more severely than the *light* cut [31.2].

- **Delayed coking:** Many refineries rely on thermal cracking technologies like delayed coking for residuum conversion. As they may not have open capacity to process the larger volume of residuum contained in bitumen-based crudes, they will need to consider investment in addition coking capacity, or in residuum hydrocracking technologies.
- **ULSD production:** The refinery may have a diesel unit that was designed to meet the prior sulfur requirement of 500 ppm, and has been repurposed for 15 ppm diesel, as was done by many to achieve the 2006 ultralow sulfur diesel (ULSD) specification [31.3]. Such a unit is likely to operate below 1000 psig in pressure, and may not have the severity to produce ULSD from higher sulfur intermediates. Further, the unit may not have the compressor capacity to provide the gas circulation rate necessary

for hydrogen-deficient feeds, having been designed for conventional crudes.

- **Octane-upgrade units:** Many refineries use light-duty hydrotreaters to desulfurize the feed to reformers and C₅/C₆ isomerization units. These units may not be configured for the effective removal of nitrogen and other poisons, or for handling a larger volume of olefinic naphtha, should the coker be expanded for bitumen processing. In addition, the volume of C₅/C₆ naphtha from these new crudes may exceed capacity of the isomerization unit. All these considerations will manifest as constraints to the refinery considering a shift to extra-heavy crudes.
- **Hydrogen supply:** Hydrotreating the new feedstocks and cracked intermediates is likely to require additional hydrogen, possibly a few times higher than that available in the refinery.
- **Treatment:** A refinery designed for medium-sour crudes may neither have the necessary sulfur recovery capacity, nor the amine circulation rate or sour water regeneration capacity needed.

An investment for Canadian crude at such a refinery would include conversion of the crude unit to enable processing of bitumen-derived crudes. This might imply metallurgy upgrades or even construction of new

furnaces and/or a bigger vacuum tower. Also, desalting capacity and efficiency may need to be improved to handle water-soluble impurities.

Coking capacity would need to be increased, or other residuum processing unit added such as a resid

hydrocracker. The downstream equipment would also need to be upgraded, to handle the change in quality of intermediates. This investment can be significant, owing to the differences between conventional and extra-heavy crudes.

31.2 Characterization of Extra-Heavy Crudes

Bitumen-derived crudes are characterized by the following qualities, relative to conventional crudes [31.4]:

- Low hydrogen content, in the range 10–11.5%, with a correspondingly high aromatics content.
- A high total acid number (TAN) likely to contribute to higher corrosion rates.
- Higher levels of sulfur in the gas oil and diesel range.
- High levels of asphaltenes. Blending with lighter *in-compatible* crudes can cause these species to lose solubility and deposit in crude trains.
- The presence of clays, which can aggravate asphaltene precipitation. Removal of clays and salts from crude depends on the effective desalter operation.

In addition, the crude may contain synthetic crude components, derived from bitumen having been upgraded through cracking and light hydrotreating, to stabilize the more reactive components. As such, the superficial concentrations of sulfur and nitrogen will seem low. However, it must be realized that the S and N species present and the way they are distributed will be different from conventional crudes [31.4].

The differences encountered in the type and concentration of sulfur, nitrogen, aromatics, and contaminants will drive the nature of the investment a refinery makes to accommodate processing of crude from the Canadian oil sands. These differences and their implications for design are discussed in the following sections.

31.3 Crude Desalting

The difficulty in removing chlorides, filterable solids, amines, and H₂S scavengers from heavy Canadian crudes is often underestimated. In fact, the desalting section of the crude complex can require significant investment to upgrade. The filterable solids are iron oxides, sulfides, sand, and clay, which can be held in a *rag layer* emulsion through the stabilizing force of the tramp amines and H₂S scavengers. Concentrations of filterable solids can vary tremendously, with some crudes having well under 50 ptb (pounds per thousand barrels) and others having close to 300 ptb [31.5, 6].

In desalted crude, the refiner transitioning to extra-heavy Canadian crude may experience 3–5 ptb of salt, where levels less than 1 ptb had been achieved before. Even worse, the desalter may have more frequent upsets, leading to excursions of very high salt concentrations for short periods of time. A high salt content can lead to a dramatic increase in crude unit corrosion. The problem can be aggravated by the organic and inorganic chlorides present in some extra-heavy crudes.

Chloride salts will hydrolyze in atmospheric and vacuum towers, forming corrosive HCl. It is common, with heavy Canadian crude processing, for corrosion and salt build-up of salts to increase in the vacuum tower.

For these reasons, a high-desalting efficiency is a critical aspect of Canadian extra-heavy oil processing. Desalters for this type of operation are sized larger than those for traditional crudes. Whereas the latter can be designed for settling based on gravity and viscosity, resolving the relatively stable interface emulsion formed from extra-heavy crudes requires a higher residence time. Additional expense may be required for the right mix valve design and to all a higher wash water rates so that appropriate droplet size may be achieved. In addition, new transformers may be needed that can supply a range of voltages for optimization, and the heat exchanger network may need to be redesigned to allow operation of the desalter at the optimal temperature.

31.4 Aromatics Content Affecting Diesel and Jet Fuel Production

Yui has published cetane numbers of diesel from synthetic crude oil, that is, crude derived through bitumen upgrading and lightly hydrotreated [31.7]. Cetane is a measure of the ignition delay during combustion [31.8].

The products generally had low cetane numbers – about 33, compared to a specification of 40 required in the United States. The poor combustion properties were associated with a high aromatics content of over 40%, although other factors, such as the degree of branching of paraffin side chains, were found to be significant [31.9].

Nevertheless, a commercial aromatics saturation process was shown to improve cetane number, producing a high-quality diesel that met all fuels specifications. Employing a noble metal or nickel–tungsten catalyst to saturate aromatic rings, the process achieves a total aromatics content as low as 5% by weight. In this way, a cetane improvement of up to 6 numbers is routinely achieved. Yui demonstrated a linear relationship between cetane number and aromatics content through this method. Aromatics saturation reached a maximum at about 572 °F [31.10].

It is important to note that typical ULSD units require much higher temperatures for sulfur removal. However, the maximum hydrogen uptake is generally lower at higher temperature due to equilibrium limitations for aromatics saturation reactions [31.11].

Similarly, jet fuel produced from the kerosene boiling range material of synthetic crude oils tends to have a high aromatics content. This can be problematic for meeting the aromatics specification itself, or for meeting smoke point [31.7]. Jet A and Jet A-1 have specifications of not more than 25% aromatics by volume [31.12].

However, *dilbit*-type crudes, which are typically produced by diluting bitumen with natural gas condensate, can have an aromatics content of 15–20%, the concentration depending partly on cut-point. In winter, the assays will tend toward a greater volume of low-aromatics material in the kerosene boiling range. With this in mind, the optimal volume of jet fuel to be produced by a heavy-oil refinery may be determined by crude mix, with dilbits favoring higher production.

31.5 High Aromatics Content Affecting Gas Oil Conversion

The shift from conventional crude to bitumen-derived crude can result in 20% lower conversion of gas oil in an FCC. This is not only because of the lower hydrogen content – from about 12.5% to about 10.5% by weight – but also because the primary upgrading processes used to produce any synthetic portion may result in aromatic species that have shorter side-chains [31.13].

Gas oils contain polynuclear aromatic species in concentrations as high as 60% by weight. Direct processing of multiring aromatics is associated with high cycle oil yield and low gasoline yield, with a gasoline quality that is paraffinic and olefinic. With hydrotreating, more mono-aromatic species are created, leading to a greater yield of higher octane gasoline.

Beyond this, it is possible to *over-hydrotreat*, creating a gas oil with a very high hydrogen content that is mostly naphthenic. Feeding a naphthenic feed to FCC can result in a high yield of gasoline that is lower in octane, and in a high dry gas yield. Depending on the nature of the starting gas oil, the optimal hydrotreating severity is one that achieves between 1 and 2% hydrogen uptake by weight. As a guideline, 1.5 wt% hydrogen content increase corresponds to approximately 1000 SCF/bbl chemical hydrogen uptake [31.13].

For these reasons, the refinery transitioning from sweet crudes to extra-heavy oils is likely to need an increase in gas-oil hydrotreating capacity and/or severity. Severity can be considered to be a combination of pressure, space velocity, and temperature. Temperature is usually limited on the high side by the onset of undesirable cracking and accelerated coke-laydown, and on the low side by the activation energy required to initiate desulfurization reactions. With the practical range of operating temperature constrained by these other factors, the design variables that determine the severity of a new unit are space velocity (i. e., catalyst volume) and unit pressure.

Space velocity and pressure will trade-off against each other in the sense that, at higher pressure, the necessary reactor size is smaller to achieve the same conversion objective. Starting with a higher pressure also leaves more options open for debottlenecking because additional reactors can be added later. Once a design pressure is determined, however, the design pressure rating of vessels and major equipment will be fixed, making a significant pressure increase nearly impossible at a later stage. A gas oil unit operating at a higher pressure may also be more ro-

bust in recovery from upsets and feed-quality excursions.

A higher pressure design has the disadvantage of requiring thicker reactor walls and compressors of greater horsepower, both of which may add significant capital and operating cost, and can make unit start-ups and shutdowns more complex. As design pressure increases significantly, it is also more likely that a higher flange rating will be required, making the cost of all the piping in the high pressure section significantly more expensive. A life-cycle cost analysis should always be performed when choosing operating pressure and reactor volume. As a practical matter, it may be optimal to design for the highest pressure possible without forcing the flange rating to the next higher class.

As with distillate hydrotreating, units that are designed for pretreating of FCC feed can have a very high hydrogen consumption of 1000 SCF/bbl or greater. Al-

though it is common for hydrogen consumption in ULSD units to decrease through the catalyst cycle, gas-oil hydrotreaters tend to exhibit much less variability, and may even have a higher consumption at end-of-run as reactor temperature is raised. This is partly owing to the higher deactivation rate of hydrodesulfurization (HDS) activity as compared to hydrogenation activity [31.14].

A further implication of high hydrogen consumption in gas oil and diesel hydrotreaters is that additional hydrogen generation capacity may need to be constructed to satisfy the increased demand. In this way, the transition from sweet to extra-heavy oils can double or triple the original refinery hydrogen requirement. To avoid the cost of capital, the refinery may have an option to contract a third-party gas supplier to construct the equipment, thereby transforming the refinery's investment into a long-term operating cost.

31.6 Vanadium and Nickel in Crude and Gas Oil

Vanadium occurs naturally in crude, and is concentrated in cuts at 800 °F and heavier. Canadian extra-heavy oils contain higher concentrations of vanadium. Gas oil produced in a crude or coking unit can entrain nondistillable residues that contain vanadium. This amount is in addition to volatile vanadium that boils in this range through the course of natural distillation [31.15].

The refiner transitioning to extra-heavy oils will desire to maximize the volume of gas oil produced, by operating at a very high 95% and final boiling point. Because vanadium is a severe hydrotreater poison, an optimized design may include scope to protect the hydrotreater, as well as scope on the crude and coking units to improve fractionation and minimize entrainment.

It is not uncommon for V in FCC feed streams to be as high as 5–10 ppm. In cases of severe entrainment, concentrations of V in heavy vacuum gas oil can reach 20 ppm. The volume of entrained residuum need to be very small for this to occur, as vacuum residuum can contain levels of over 800 ppm. Similarly, entrainment of residuum can also occur in atmospheric gas oil.

To minimize V in virgin cuts, the proper investment must be made in flash zone, wash section, and stripping section. The strategy for investment should be to reduce localized velocities that entrain residuum, while providing enough wash oil volume to prevent entrained residuum from reaching the gas oil draw. For volatile V, it is important to maximize stripping section efficiency rather than relying on vaporization in the vacuum heater to lift gas oil volume. The vacuum tower inlet

device may also need to be redesigned to reduce localized velocities. Because stripping steam may need to be increased while coil steam is added to combat furnace coking, the size of the vacuum ejector may also need to increase, and this can be a significant investment.

Some refiners may be surprised to learn that heavy coker gas oil (HCGO) vanadium may increase when processing extra-heavy crudes. HCGO vanadium goes up with vacuum residuum metals, vacuum unit cut point, and HCGO final boiling point. Further, entrained material from the coke drum can contain V at concentrations over 1000 ppm. Here, the factors governing entrainment are coke drum and main fractionator vapor velocities. Steaming of the hot coke drum may cause entrainment, in addition to that which occurs during normal operation. Lower operating pressure in coke drum and fractionator will make entrainment worse because superficial velocity increases.

Vanadium in crude exists mainly as vanadyl porphyrin species. Porphyrin rings, whose structure is shown in Fig. 31.2, are chelating agents that occur commonly in nature. Vanadyl porphyrins in crude tend to be associated with very large hydrocarbon molecules. As such, they are usually components of asphaltene micelles. In hydrotreating, vanadium is deposited on the catalyst surface as vanadium sulfide. Studies have shown that rates of vanadium and nickel removal are directly proportional to asphaltene conversion in gas-oil hydrotreating [31.16].

Because metals deposit in the catalyst pore near the external surface of the catalyst, they deactivate catalyst

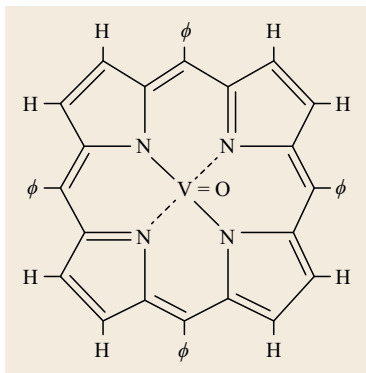


Fig. 31.2
Porphyrin ring

by preventing diffusion of the reactant to the active site. HDS activity is more susceptible to poisoning by nickel and vanadium than hydrodenitrogenation (HDN). As Ni and V levels of a hydrotreater feed increase, the addition of hydrodemetallization (HDM) catalyst to the

catalyst loading scheme becomes necessary. HDM catalysts have wide pores in the 100–300 nm range, which makes them effective for reactions involving large hydrocarbon structures, such as those that commonly contain nickel and vanadium in crude. Wide pores are also less likely to become blocked by metals that lay down at the pore mouth [31.14].

Because wide pore HDM catalysts have lower surface areas than catalyst designed for high HDS activity, the incorporation of HDM catalyst into a new design will require addition of a large catalyst volume, lest the sulfur removal capability be reduced. The sizing of metals guard beds or guard reactors must take into account the desired cycle length. It is not uncommon to design for 3–5 ppm Ni + V. For a 2–3 year catalyst cycle, the volume of such guard vessels can be 20–30% of the total catalyst volume. Both FCC pretreat hydrotreaters and hydrocracker first-stage hydrotreating sections need to be protected in this manner.

31.7 Asphaltene and Clay Precipitation

Asphaltenes are complex high-boiling point polyaromatic species. Although the structure of asphaltenes has been much debated and much studied, it is commonly agreed that they are comprised of the following components [31.16]:

- Sulfur in the form of benzothiophene rings
- Nitrogen in pyrroles and pyridine ring structures
- Groups of five or more aromatic rings joined by very long paraffin chains and having long side-chains
- Nickel and vanadium in a chelated form with porphyrin rings (whose main functional components are pyrrolic nitrogen)
- Oxygen in functional groups including carboxylic acids.

Asphaltenes are believed to have molecular weights over 1000 g/mol. In practice, asphaltenes are characterized by their tendency to precipitate from crude as black or brown solids that will decompose when heated, rather than melt. As such, determination of asphaltene concentrations is generally by mixing with *n*-pentane or *n*-heptane, for which there exist several ASTM methods [31.17].

The stabilization of asphaltenes in crude is thought to be through suspension with resinous and aromatic layers in the form of colloids. Although there are several factors known to bring about the onset of precipitation, the most concerning for a refinery transitioning to extra-heavy oils involves a change in the solvent power

of the resin layer. This can occur when a bituminous crude is mixed with a sweeter crude that has a lower aromatics content. For this reason, refiners have developed models to determine crude *compatibility*, based on viscosity, gravity, and other factors relating to mutual solubility [31.17].

Asphaltene precipitation from crudes can lead to fouling in heat exchangers, column internals, and fired heaters on crude units. Some refiners processing Northern Alberta bitumen restrict their vacuum furnace transfer line temperatures to 700 °F (≈ 370 °C) to avoid rapid coking of tubes. In some cases, run lengths longer than a year are difficult to achieve on atmospheric towers due to asphaltene precipitation on the stripping trays in atmospheric towers [31.18].

In a delayed coker, a high asphaltene content leads to the production of shot coke in a drum. Shot coke is a safety concern because water impacting a hot area during cutting may cause an eruption of small coke pellets to be propelled by the expansion of steam. To remove operating personnel from harm's way may require automatic *de-heading* devices for the top and/or bottom of the drums. Although costly, these valves improve availability by decreasing the time required to remove the head from a drum. Inclusion of a remote cutting station allows an operator to control drum de-heading and coke cutting from a safe distance [31.19].

Precipitation of asphaltenes often occurs along with other fine solids. This may include particles of pyrite or titanium oxide, or *ultrafine* clay platelets less than

< 0.3 μm in size. These clays tend to bind with organic matter that is both polar and aromatic. As such, they are often associated with water with which they can form emulsified droplets in oil [31.20].

The concentration of clay microfines in bitumen has been found to differ by production method [31.21]. Specifically, whereas bitumen produced through the

hot-water extraction process (HWEP) may contain up to 2% by weight of solids, that produced through steam-assisted gravity drainage (SAGD) can have a much lower concentration of clays and fines, in some cases nondetectable. However, it has been noted that nickel and vanadium concentrations can be greater in SAGD bitumen crudes [31.20].

31.8 Fouling in Gas-Oil Hydrotreaters

A phenomenon similar to crude incompatibility occurs in gas-oil hydrotreaters, leading to an accumulation of deposits in feed filters and in catalyst beds. Asphaltenes that may make their way into gas oil cuts by entrainment in crude units can lose suspension due to the chemical transformation of aromatic components during hydrotreating. Because of their aromatic nature and high nickel and vanadium content, asphaltene species can also suppress HDS reactions through competitive adsorption on active sites, and by blocking catalyst pores [31.16].

During hydrotreating, it is thought that asphaltenes lose aliphatic side-chains, while the maltenes holding them in suspension are hydrogenated. The net result is an increase in the aromatic nature of the asphaltene and a loss of solvency in the bulk fluid [31.22].

The deposition of particles comprised of asphaltenes, clays, and corrosion products has been known to occur in catalyst beds and even between beds, leading to high reactor pressure drop. Such particles tend to mass together in packed beds, taking up the space between individual pellets. The hydrodynamics are such that a greater mass of particles accumulates in the bed at a low liquid velocity, while at a higher velocity, more particles – especially smaller ones – will tend to pass through the bed [31.23].

Thus, although it may be counter-intuitive, over the course of the catalyst cycle of an operating unit, higher pressure drop may develop at low unit charge rates, compared to that which would develop at high rates.

Design of reactors in the pulsed flow regime, as is the practice of many licensors, may also help in this regard, as the celerity of the pulses can help to flush particles out of a catalyst bed. Factors that will affect flow regime include reactor dimensions, unit pressure, and gas flow rate and molecular weight [31.24, 25].

Risk of feed filter pluggage is higher for gas-oil hydrotreaters processing bitumen-derived crudes. In addition to mixture incompatibility causing asphaltenes to drop out of solution, some foulant-generating chemical mechanisms are introduced with bitumen derived gas oil. For example, it has been found that coker gas

oils from Canadian bitumen contain relatively high concentrations of pyrrolic nitrogen species that generate oil-insoluble filter deposits in hydrotreaters [31.26].

These pyrroles result from breakdown of porphyrin rings associated with the asphaltenes in bitumen, and they have a relatively low molecular weight. Such compounds oxidize easily, initiating the formation of insoluble polymers. The binding of these polymers with clay and other materials produces gummy material capable of plugging filters. The problem is worsened by the presence of corrosion products containing iron, as they can act as catalysts for polymer formation. Olefins are also present in coker gas oils, and these may participate in the reactions. Small concentrations of dissolved oxygen left in the coker products from steaming of coke drums will exacerbate the problem by accelerating the generation of free-radical chain initiators [31.27].

Figure 31.3 shows an example of deposits found in hydrotreaters that process gas oils derived from Cana-

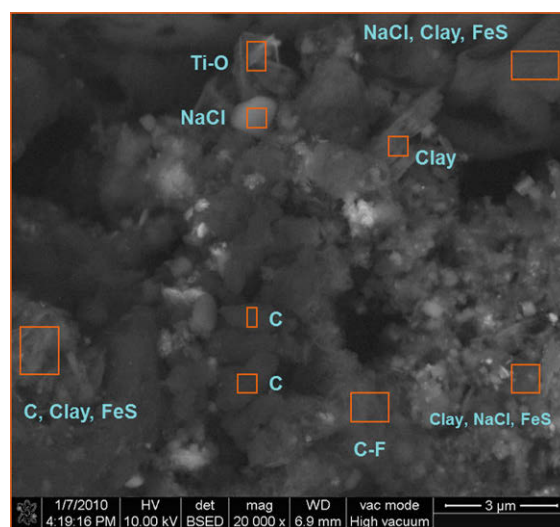


Fig. 31.3 Scanning electron micrograph of feed filter deposits collected at a gas-oil hydrotreater in a Canadian extra-heavy oil refinery. (Courtesy of BP)

dian extra-heavy oils. In this figure, the individual species have been identified using scanning electron microscopy. Clay, salt, and metal oxides can be observed, in addition to carbonaceous masses that are likely asphaltenes.

The presence of asphaltenes, clays, and components reactive for polymerization bears significant implications for the design of gas-oil hydrotreaters, including hydrocracker pretreat units. The presence of nickel and vanadium in the 3–5 ppm range will necessitate a large volume of demetallization catalyst. Coupled with exposure to asphaltenes and other foulants, the risk to unit availability may be such that dedicated guard reactors will be required. The advantage of this is that the reactors can be bypassed in the event that high pressure drop develops. Operation can continue, or the design can allow an on-line change-out.

To make this possible, the unit must generally incorporate high-pressure, tight shut-off valves with the proper redundancy and verification of zero energy. Even if the guard reactors are not to be taken out of service, provisions may need to be made to keep the bypassed

reactor warm by sweeping with hydrogen. In either case, the valves and piping can be complex and add significant cost. Such units have been designed to accommodate asphaltene levels as high as 500 ppm on a routine basis.

To prevent the foulant material from entering the unit, it is generally wise to install unit feed filters of adequate capacity, sized for a desired frequency of change-out. A pair of filter banks operating in parallel will help to reduce exposure of the unit to fouling material, as one bank can be changed while the other remains in operation. However, note that the unit will have to reduce feed rate if the filters develop high pressure drop faster than the refinery maintenance team can replace the elements.

Filters that back-wash automatically are commonly installed in high fouling services. For a refinery operating a large coker, it may be advantageous to install such *backwash* filters on coker gas oil because of the likelihood that coke fines will be present. In that situation, traditional cartridge-type filters may be installed on the feed to the gas-oil hydrotreater to reduce cost.

31.9 Sulfur and Nitrogen in Bitumen-Derived Crudes

The incentive for a refinery to process bitumen-based crudes is illustrated by the price differential between Western Canadian select (WCS) and West Texas intermediate (WTI) crudes, which averaged \$ 20–30 per bbl (US) in 2013–2014 [31.28]. The refinery investing to reposition for Canadian heavy crudes might expect to capture this margin.

Characterization of these crudes can be difficult because they are usually blends of oils with very different properties. Raw bitumen extracted from Canadian oil sands is too viscous to flow in a pipeline, so it must be diluted with a lighter oil to produce the final crude. If the diluent is natural gas condensate or a similar light naphtha, the resulting crude is called a *dilbit*. Alternatively, the diluent used may be a mix of lighter products generated from thermal cracking or hydrocracking of raw bitumen, that is, a synthetic crude. Bitumen diluted with synthetic crude produces a *synbit* crude [31.1].

Bitumen-based crudes have densities of 930–940 kg/m³ (API gravity 18–21°), compared to 825–840 kg/m³ (39–40° API) for light sweet crudes [31.29]. The difference in density reflects the highly aromatic nature of bitumen crudes.

Sulfur and nitrogen concentrations in crude go up dramatically with increasing crude density (decreasing API gravity). This is illustrated in Fig. 31.4, plotted from data gathered by Ball et al. for crudes of similar origin to Athabasca bitumen [31.30].

Canadian heavy crudes with API gravities in the 18–20° range can contain 3–4% sulfur, which is more than 10 times the sulfur level of WTI crude having an API gravity of about 40° [31.4, 29].

In addition to total sulfur and nitrogen levels being much higher than conventional crudes, the S and N distributions in dilbit and synbit also look very different. This is because cracking reactions form species

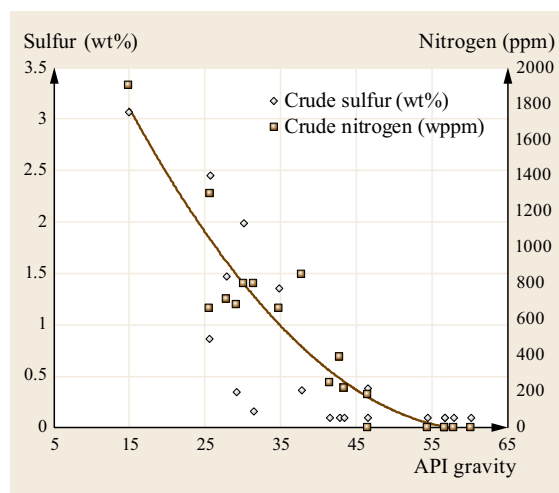


Fig. 31.4 Concentrations of sulfur and nitrogen by API gravity, for crudes of origin similar to Athabasca

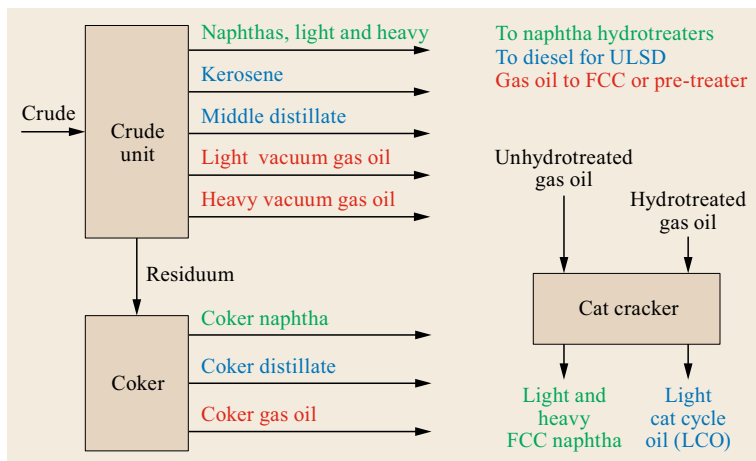


Fig. 31.5 Typical refinery intermediate streams to hydrotreaters. (Courtesy of BP)

that do not occur in nature. Also, thermal cracking processes (e.g., delayed coking) necessitate downstream hydrotreating to stabilize the products. Hydrotreating lowers the total sulfur and nitrogen content, while leaving behind the species that are hardest to convert. To further desulfurize and reduce nitrogen from these *upgraded* intermediate streams can be difficult.

Figure 31.5 illustrates the variety of intermediate products processed by hydrotreaters, including those

from other conversion processes such as FCC and coking. A strategy for processing must begin with consideration of the individual crude component sources, and an understanding of the species that will result by fractionation in each cut of crude. The demands for hydrotreating gas oil, diesel, and naphtha cuts of bitumen-based crudes and their derivatives are considered, in turn, in the following sections.

31.10 Hydrodesulfurization and Hydrodenitrogenation of Gas Oils

Desulfurization and denitrogenation of bitumen-derived gas oils, including heavy virgin gas oil and coker gas oil, have been studied by *Yui et al.* and others [31.4, 22, 31, 32]. While sulfur in heavy gas oil from conventional crude can be about 1.0%, straight-run gas oil from an Athabasca bitumen is 3.0–3.5%. Sulfur in heavy gas oil resulting from thermal cracking of Athabasca bitumen is typically in excess of 4.0%. Likewise, nitrogen can be 2000 ppm for Athabasca straight-run and 4000 ppm for coker gas oil, which is much higher than the 1000 ppm level of conventional crude.

Gas oil sulfur must be brought down to a few 100 ppm, so that FCC and hydrocracker naphthas will have a low enough sulfur level to allow blending into gasoline. Nitrogen removal is also important, for these units to achieve a high catalytic conversion.

Further, nitrogen removal is important for achieving adequate conversion in an FCC or hydrocracker. However, the nature of the nitrogen species – being largely pyrrolic and including substituted carbazoles – is such that they are difficult to remove and also inhibit sulfur removal by competing for active sites [31.32, 33].

Thus, desulfurization and denitrogenation of bitumen-derived gas oils require very high severity in a hydrotreater, including reactor pressures of 2000 psig (13 MPa) or higher, and liquid-hourly space velocities of 1.0/h or lower over high-activity catalysts.

Asphaltenes in gas oil have been found to inhibit desulfurization by adsorbing onto active sites and blocking catalyst pores. Hydrotreaters for bitumen gas oils often employ wide-pore demetallization catalysts to help convert asphaltenes. Interestingly, asphaltenes with high sulfur content tend to convert easier than those with low sulfur content, owing to breakage of the weaker carbon–sulfur bond as compared to a carbon–carbon bond [31.22].

In combination, high-activity desulfurization catalyst and wide-pore demetallization catalyst can total well over a million pounds in a 100 000 bbl/day gas-oil hydrotreater. Reactors, vessels, and flanges rated for the required pressure can all be very large and, therefore, costly to manufacture and install.

A concern for hydrotreaters processing a high-nitrogen feed is ammonium bisulfide (NH_4HS) corrosion in reactor effluent systems. Ammonium bisulfide condenses as a salt from the interaction of ammonia and

hydrogen sulfide gases in the reactor effluent stream. Solid NH_4HS can plug tubes in effluent heat exchangers or air coolers. The salt is hygroscopic and very corrosive when water wet [31.34].

For this reason, hydrotreaters taking high-nitrogen feeds commonly employ a water wash system. However, owing to the fact that wash water containing more than 2% by weight NH_4HS can be corrosive, high volumetric flow rates are sometimes required. A typical design point allowing mild corrosion can be 4% NH_4HS , concentration by weight in wash water effluent, for which a few hundred gpm *sweet water* may be needed.

A supply of such fresh water, and the means to treat the spent water will require additional equipment including wash-water feed drums, sour-water strippers, and the appropriate injection and mixing devices. Further, it is usually necessary to segregate the water systems used for hydrotreaters from those used in FCC in order to avoid cyanides that can accelerate the corrosive effects of NH_4HS .

Even at moderate concentrations of NH_4HS – between 2 and 8% – higher grades of steel may be needed for any piping or vessels in contact with this sour water, including piping for oil products that may contain

sour water carried over from separators. Concentrations above 8% are aggressively corrosive to carbon steel [31.34].

Ammonium salt corrosion can also attack stripper overhead systems. In this situation, ammonium chloride salts have also been implicated. Gas-oil hydrotreaters may be particularly at risk owing to the inclusion of hot low-pressure separators (HLPS) in the design. Small concentrations of chloride in oil may flash off in these drums, or strip off in strippers, operating in the 450–550 °F (230–290 °C) range. Sufficient cooling to form salts can take place in the small-bore piping of overhead handling systems, including lines for relief valves [31.35].

Once formed, these salts can corrode out piping rapidly in localized areas, where thinning can go undetected by a refinery inspection program, leading to an eventual release of light hydrocarbon with a high H_2S concentration.

Because the hydrotreating severity requires large vessels, while corrosion and fouling concerns demand more ancillary equipment and expensive metallurgy, a gas-oil hydrotreater can be very expensive to build and to maintain for a refinery processing bitumen-based crudes.

31.11 Production of ULSD and Jet Fuel

As with gas oil, the desulfurization of middle distillates from bitumen-based crudes can be difficult because of the high sulfur levels, the aromatic nature of the oil, and the presence of inhibiting nitrogen species. Although lighter species are generally easier to convert, the target sulfur levels are typically much lower, being 15 ppm sulfur for ULSD compared to 300–800 ppm for a typical gas oil unit. A solution often employed by refiners to accommodate Canadian heavy crude distillates in an existing ULSD unit is to revamp the hydrotreater by adding a reactor. Addition of a large tail reactor can be a relatively inexpensive way to reduce the space velocity of a unit by half.

It has been well established that the most difficult sulfur species to convert in ULSD are dibenzothio-phenes, particularly those with substitution at the 4- and 6-positions [31.14]. These species exist in feeds at levels of a few 100 ppm, and they are the usually last remaining sulfur species in ULSD product. Like any hydrotreated diesel, middle distillate from a synthetic crude or synthetic synbit fraction will have a disproportionate concentration of these difficult species, even though the total sulfur concentration may be relatively low [31.9].

As in gas oil, the nitrogen present in bitumen and coker distillates will contribute to corrosion of hydrotreater effluent systems and pluggage of air cooler tubes. Because sulfur is generally lower in this diesel-range cut, it is less likely that sour-water corrosion will be an issue. However, ammonium chloride accumulation has been known to result in localized corrosion and leaks. A water wash designed for NH_4HS removal may be ineffective for NH_4Cl removal, due to the salt's hygroscopic nature and its tendency to deposit further upstream in the effluent system [31.36].

A guideline commonly followed for water-wash design requires that at least 25% of the water introduced remain as unvaporized liquid water at the point of injection [31.37]. Thus, the necessary water flow rate will increase with hot high-pressure separator (HHPS) temperature requirement – which aids H_2S removal in the stripper – and hydrogen recirculation ratios. Temperature and hydrogen rate are, of course, variables of hydrotreating severity that a refinery will increase in order to remove refractory sulfur species.

Jet fuel production requires processing of kerosene-range distillates. Because the total sulfur specification

for jet fuel is fairly high at 3000 ppm, desulfurization has not been required by many refineries. Instead, the predominant technologies for jet fuel production have been based on *sweetening* of kerosene by reacting mercaptans to form disulfides, in order to satisfy the total mercaptan level specification [31.12].

However, the shift to a crude mix that results in a kerosene cut with more than 3000 ppm sulfur may require a refinery to hydrotreat jet fuel in order to remove sulfur. HDS severity need not be very high as sulfur re-

moval of about 50% is usually enough. Nevertheless, in lieu of a capital investment, the additional volume of oil to be hydrotreated means that the ULSD production must decrease, or another gasoline or diesel stream will to go unhydrotreated.

It should be noted that the fraction of the kerosene steam that is synthetic is likely to meet the total sulfur requirement for jet fuel. The aromatics content and smoke point may need to be upgraded as discussed in a previous section [31.7].

31.12 Fouling in Naphtha Hydrotreaters

A refinery that improves its bitumen-processing capability by installing more coking capacity may have to invest to mitigate risks to its naphtha hydrotreaters. These risks include a reduction of heat transfer in pre-heat exchangers, building of pressure drop in feed systems and reactors, poisoning of catalyst, and incomplete nitrogen conversion that could create availability problems for reforming and isomerization units.

The fouling tendency of coker naphtha owes to the relatively high concentration of olefins and diolefins, and especially to the presence of conjugated diolefins, which are prone to polymerizing once initiated by exposure to oxygen or by reactive pyrroles [31.38].

Watkinson et al. have studied the byproducts and initiation of fouling in naphtha [31.39]. The accumulation of fouling deposits can begin at temperatures as mild as 270 °F (130 °C). The first products of fouling are soluble gums, with molecular weights as high as 600 g/mol. As reaction continues, gums can concentrate and eventually become insoluble deposits.

At temperatures of about 370 °F (190 °C), deposits formed are more likely to adhere to heat-exchanger tubes, where they can hamper heat transfer or create high pressure drop. When this occurs in a hydrotreater, the unit may no longer be able to reach a target catalyst temperature or to maintain its maximum feed rate.

On a heat exchanger surface, the gum deposits can transform to thermally stable fines that are dark in color and have a high carbon content. Deposits have been identified with a hydrogen to hydrocarbon ratio that is only slightly greater than 1.

Deposits formed in the feed pre-heat section of a hydrotreater can carry through to the lead reactor, causing high pressure drop there. Once pressure drop develops, the unit may not be able to maintain a high feed rate or its target hydrogen circulation rate. An outage for catalyst replacement may be necessary, or a *skim* and replacement of the topmost portion of catalyst.

A technique sometimes used to delay the onset of pressure drop from fouling is to use of top bed grading with a high void fraction, to allow particulates to accumulate in a manner that will not immediately restrict flow [31.40].

The fouling potential of coker naphtha is about 300 times that of straight-run naphtha. To avoid a severe availability penalty, when increasing the volume of coker naphtha to an existing hydrotreater, it may be necessary to first stabilize the coker naphtha. Units designed for saturation of conjugated diolefins operate at mild temperatures (320–425 °F (160–220 °C)) and high space velocities (greater than 4.0 per h LHSV). Severity must be kept mild in such units, to avoid saturation of olefins, which can generate a large heat release and also lead to catalyst bed fouling via local hydrogen starvation [31.38].

Reduction of diolefins in a selective coker naphtha hydrotreater can be as great as 90%, with a starting concentration of about 4% by weight. Rates of diolefin saturation are maximized at about 350 °F (180 °C). However, sulfur and nitrogen removal are not performed below 400 °F (200 °C) [31.41].

A further advantage of a dedicated diolefin saturation unit is the opportunity to incorporate a guard catalyst that would otherwise take up space intended for active catalyst in the main naphtha hydrotreater. Silicon is present in coker naphtha in the form of tri- and tetrasiloxanes, which are products of the decomposition of silicon-based foam-control agents [31.38]. Such units are sometimes incorporated into the refinery's coker, a relatively convenient if a new coker is being built.

Exposure to oxygen from air has been shown to promote fouling of naphtha by free-radical chain initiation via formation of hydroperoxides. Concentrations of only a few ppm dissolved oxygen can lead to significant fouling [31.39].

Several strategies exist for mitigating or preventing oxygen-initiated fouling. Because dissolved O₂ is

usually introduced into naphtha by exposure to air in tankage, one option is to introduce nitrogen gas for blanketing tanks. However, it can be costly to run N_2 piping to a tank field and to maintain the system in reliable working condition.

Chemical additives can be effective for reducing gum formation in coker naphtha hydrotreaters. Here, a two-pronged approach is recommended, with an oxygen scavenger injected in the naphtha run-down line into tankage and a dispersant injected at the unit to prevent agglomeration of foulant species [31.42].

Some unit designs incorporate a stripping tower into the feed system, using hydrogen gas to strip out dissolved oxygen from oil entering the unit. With naphtha

serving as the *lean oil*, these towers can serve a second purpose by improving the purity of the hydrogen even as it is used for stripping. However, for fouling mitigation, this strategy is only effective for oils that have not already begun to react in feed tankage. For maximum effectiveness, the absorber–stripper design should allow stripping of straight-run naphtha only, with cracked naphthas coming to the unit directly and contacting the straight-run naphtha downstream of the stripper.

Utilization of a diolefin reduction unit has the added advantage of reducing the risk of gum formations, should the naphtha need to be stored in tankage, because the most reactive components in coker naphtha have been stabilized.

31.13 Sulfur and Nitrogen Removal from Naphtha

Sulfur and nitrogen must be removed from feeds to catalytic naphtha reforming units and C_5/C_6 isomerization units because they are poisons to the catalyst. Further, these units often use chlorided catalysts, and so, will have chloride present in the effluent system.

Organic nitrogen will convert to ammonia on precious metal catalysts, and the ammonia will combine with chloride to form corrosive ammonium chloride salts. The depositing of these salts in distillation towers and piping can make it difficult to maintain product quality, and can generate hydraulic restrictions. As a result, these units typically have hydrotreaters designed to reduce sulfur and nitrogen each to 0.5 ppm by weight or less.

The most common disposition for coker naphtha is feed to a reformer to improve stability and upgrade its octane for blending into gasoline. However, nitrogen in coker naphtha produced from Canadian bitumen can be in the 200–300 ppm range, as opposed to levels of a few ppm that are characteristic of straight-run naphtha. Hydrotreating of cracked stocks to produce a synthetic crude can bring the nitrogen level down to that of straight-run or even lower [31.43].

Sulfur inhibits the function of the precious metal on reforming and isomerization catalysts. Coker naphtha sulfur can be about 1.5% by weight, which is greater than straight-run naphtha by a factor of 6 or more. Sulfur is arguably a lesser problem than nitrogen because it is unlikely to form a corrosive salt in a reformer.

Nevertheless, an increased concentration of high-sulfur coker naphtha can lead to a product sulfur level above 0.5 ppm, because of a reaction between olefins and hydrogen sulfide that forms mercaptans at high reactor outlet temperatures [31.44].

Thus the need to remove nitrogen may necessitate an increase in severity of the naphtha hydrotreater. This can be accomplished by adding catalyst volume or enabling the feed furnace to achieve a higher temperature, as limited by mercaptan formation. A significant increase in pressure is rarely an option, as pressure will be limited by pressure rating of equipment and piping.

Removal of the heaviest fraction of feed by distillation can also be very effective for reducing nitrogen concentration, and eliminating from feed those heaviest ring species that are difficult to convert. This type of prefractionation will have the added benefit for a catalytic naphtha reformer that production of coke on catalyst will be slower for a feed containing fewer heavy aromatics.

Splitting of reformer feed in this way is most beneficial if performed on the combined desulfurizer product or feed to the desulfurizer rather than one component. However, distilling such a large volume can be energy intensive. Instead, a split performed on the coker naphtha only can capture nearly all the benefit requiring much less energy and smaller equipment. If the final boiling points of the straight-run fraction are not excessive, removal of the heaviest 20% of coker naphtha can be of greater benefit and will be more economical than removing the heaviest 10% of combined feed.

It should be recognized that such fractionation will remove volume from reformer feed, possibly resulting in a lower reformer total charge rate. If the split occurs on hydrotreated product, the diverted fraction can be sent directly to gasoline blending, thereby gaining total gasoline volume but at a lower octane, compared to

reforming. Otherwise, the rejected volume will generally need to be processed in another naphtha, diesel, or jet fuel hydrotreater to lower the sulfur level.

The higher olefin concentration that will accompany an increase in coker naphtha volume to a naphtha hy-

drotreater will result in an increased heat release that may need to be mitigated through addition of hydrogen quench between catalyst beds or between reactors. Depending on the starting configuration of the unit, this can be a costly modification.

31.14 Choice of Resid Conversion Technology

When adding capacity for conversion of bitumen to fuels and chemical feedstocks, the refiner has choice of technologies. The choices generally fall into two categories:

1. Carbon-rejection technologies, such as delayed coking
2. Hydrogen-addition technologies represented by the various forms of hydrocracking. Several studies have been performed to compare the merits of each, including analyses of the return on investment [31.4, 45–48].

The following general conclusions can be made:

- Total liquid yield from hydrocracking is over 100% by volume, when taking into account the density difference. Coking yield will be about 75% liquid.
- The ratio of gasoline to diesel production is greater with hydrocracking than with coking, although at least one study found that diesel yields by mass are approximately the same for both types of processes [31.49].
- Capital investment in a hydrocracker can be up to 50% greater than the investment in a delayed coking unit. Operating expenses will also be greater, owing in part to the cost of hydrogen compression.

- Coker products require stabilization by hydrotreating. The associated investment can be significant if newly build hydrotreating units are required. Alternatively, a large, complex refinery may be able to leverage the capacity of existing units to optimize cost while improving overall feedstock flexibility.
- A key consideration must be the refinery's solids handling capability, including access to markets for sale of petroleum coke and shipping infrastructure, by rail or truck.
- Hydrogen addition schemes are more attractive at low natural gas prices, methane being the primary feedstock for hydrogen production. Natural gas prices have declined to \$4–5 per million BTU with the recent boom in US tight oil production, having come down from highs above \$10 per million BTU a few years earlier. Nevertheless, prices are projected to rise again due to increasing production costs [31.50].

The discussion in this report has assumed residuum processing by coking process in order to highlight the difficult technical issues associated with processing of cracked intermediates. Further, a starting assumption included the revamp of a gasoline-based refinery with large FCC capacity, and the desire to maintain high utilization of existing cracking capacity.

31.15 Other Investment

The foregoing discussion has centered on the technology issues for bitumen-crude processing that directly trigger unit modifications or new builds. There are a number of other systems in a refinery that must be upgraded or supplemented in order to enable the new or modified kit to function as intended. As we have seen, the hydroprocessing units are impacted in a wide variety of ways, and this is likely to be the area with the greatest complexity of changes, even if not the greatest cost to modify. It is not surprising, then, that the majority of ancillary investment is

brought about by the new tougher hydroprocessing requirements.

A refinery processing 20–25% heavy crude, with the remainder being sweet and/or sour crudes, can shift its diet reliably to 75–85% heavy Canadian crude. In terms of hydrogen deficiency, it has been estimated that the difference in hydrogen content between a conventional crude and a raw bitumen is equivalent to about 1320 SCF/bbl [31.4]. In reality, a mix of synbit and dilbit crudes will be required to contain between 50 and 75% bitumen by volume. Thus, a large refinery bringing

in an incremental 250 kbd bitumen-based crudes may need on the order of 200 million standard cubic feet per day additional hydrogen supplied to its hydroprocessing units, in order to maintain the same volume and quality of final products as before.

The average sulfur content of the total crude mix can increase by 1.5–2.0 wt% by weight. For a 400 kbd refinery processing about 120 million lbs/day, this could mean that an increase in sulfur recovery capacity of about 1000 long ton/day is needed. To ensure environmental compliance, some investment in tail gas treating will also be necessary. Tail gas units ensure that the sulfur remaining in the sulfur recovery units' effluent gas is converted and captured.

The means by which sulfur is removed from individual crude cuts and intermediate streams involves transformation of the sulfur into H₂S in hydroprocessing units. The H₂S is picked up by amine flowing through absorber columns. Thus an increase in H₂S production rate will require a larger amine circulation system, with all of the infrastructure that entails. This is likely to include an investment in amine-stripping capacity of a few thousand gpm for the size of the refinery considered here.

As discussed above, there will be a greater demand for wash water in hydroprocessing and other units, to prevent build up of corrosive salts. In addition to needing new pumps and piping to supply the *sweet* water, sour water stripping capacity will need to be upgraded, likely through addition of a few thousand gpm for this hypothetical refinery.

31.16 Conclusion

The sustained price differential between conventional crudes and those derived from Canadian oil sands creates an attractive prospect for a sweet crude refinery to invest in crude repurposing. Investment will be driven by differences in crude composition, including a heavy fraction that is highly aromatic and a slew of contaminants that will interfere with processing, or that may negatively impact finished fuel quality.

Major components of investment may include residuum-processing capacity, crude fractionation including desalting, and a variety of hydroprocessing upgrades. If coking is chosen for residuum processing, the intermediate products must be hydrotreated, and this requirement triggers additional hydroprocessing scope.

Specifically, significant scope may include:

- Upgrading of crude unit and coker fractionation to avoid entrainment of asphaltenes and volatile met-

Not discussed in detail in this report is the potential for accelerated corrosion from a higher naphthenic acid content, as indicated by the TAN. The TAN of some bitumen-based crudes can be very high, such as 2.4 mg KOH/g for Peace River Heavy, compared to less than 0.5 for a typical light or medium sour crude [31.29].

However, some conventional US crudes also have a very high TAN. Further, it has been found that TAN by itself may not be the best indicator of crude corrosivity, due to the varied nature of organic acids in crude and the presence of other species that may passivate metal [31.50].

Nevertheless, crudes with high TAN will generally be offered at a discount. A refinery trying to gain feedstock flexibility by enabling Canadian heavy crude processing may not realize the full benefit of its investment without upgrading metallurgy of piping to accommodate a higher corrosion rate.

High TAN crudes put furnace transfer lines primarily at risk due to the temperature-dependency of acid-corrosion mechanisms. The risk will include pipe operating above 450 °F (232 °C) in and around hydroprocessing reactors on gas oil and diesel units. As an example, consider that the 80 kbd Suncor Sarnia refinery replaced 18 000 ft (≈ 5500 m) of pipe to accommodate a 2.4 mg KOH/g TAN crude mix in 2006. Carbon steel and chrome-enhanced piping was replaced with 316 and 3171 steel alloys to achieve a 15 year life [31.51, 52].

als (nickel and vanadium). In some cases, this may require construction of new large-diameter towers and higher duty furnaces. Crude desalting efficiency will also need to be improved, and piping upgraded in metallurgy to resist an increase in crude corrosivity.

- Addition of gas-oil hydrotreating capacity to improve FCC feed quality may be necessary if the refinery is configured for gasoline production. Gas oil will be high in asphaltenes, metals, and clay that can foul the unit and poison hydrotreating catalyst. Accommodating these contaminants may require inclusion of large guard reactors and feed filters.
- Improved diesel and jet hydrotreating capability including more reactor volume to improve qualities related to the aromaticity and sulfur content of the bitumen portion. Further, the synthetic portion is es-

entially lightly hydrotreated coker or hydrocracker product, containing refractory sulfur that must be removed.

- Improvements in naphtha hydrotreating severity to prevent nitrogen in cracked fractions from reaching sensitive reforming and isomerization units.
- Increased hydrogen supply as required by the hydroprocessing functions to produce fuels of the same quality as before.

- Supplemental sulfur recovery capacity, sour water stripping, and amine recirculation and regeneration, to enable the hydroprocessing units to reliably remove sulfur and nitrogen from intermediate cuts.

With careful consideration of the characteristics of bitumen-derived crudes, a sweet crude refinery can execute a successful design and achieve a high degree of reliability.

References

- 31.1 P. Swafford: Understanding the quality of Canadian bitumen and synthetic crudes, Proc. Crude Oil Quality Assoc. Meet., Long Beach (2009) pp. 1–32
- 31.2 S. Brunet, D. Mey, G. Perot, C. Bouchy, F. Diehl: On the hydrodesulfurization of FCC gasoline: A review, Appl. Catal. A **278**, 143–172 (2005)
- 31.3 US Department of Energy: *The Transition to Ultra-Low-Sulfur Diesel Fuel: Effects on Prices and Supply* (US Department of Energy, Washington DC 2001)
- 31.4 T. de Bruijn: *Critical Review of Existing and Emerging Approaches to Moderate Upgrading of Extra-Heavy Crudes* (National Centre for Upgrading Technology, Edmonton 2002)
- 31.5 T. Collins, T. Barletta: Desalting heavy Canadian crudes, Petroleum Technol. Q. Sour/Heavy, 23–26 (2012)
- 31.6 S. Bieber, L. Kremer: Rethink desalting strategies when handling heavy feedstocks, Hydrocarb. Process. **87**(9), 113–120 (2008)
- 31.7 S. Yui: Athabasca oil sands produce quality diesel and jet fuels, Oil Gas J. **98**(47), 58–66 (2000)
- 31.8 W. Dabelstein, A. Reglitzky, K. Reders, A. Schütze: Automotive fuels. In: *Ullmann's Encyclopedia of Industrial Chemistry*, ed. by B. Elvers (Wiley, Weinheim 2007)
- 31.9 S. Sato, Y. Sugimoto, K. Sakanishi, I. Saito, S. Yui: Diesel quality and molecular structure of bitumen-derived middle distillates, Fuel **83**, 1915–1927 (2004)
- 31.10 S. Yui, K.H. Chung: Syncrude upgrader revamp improves product quality, Oil Gas J. **105**(46), 52–62 (2007)
- 31.11 B.H. Cooper, B.B.L. Donniss: Aromatic saturation of distillates: An overview, Appl. Catal. A **137**, 203–223 (1996)
- 31.12 Exxon: *World Jet Fuel Specifications (ExxonMobil Aviation)* (International, Leatherhead 2005)
- 31.13 V.A. Gembricki, T.M. Cowan, G.R. Brierly: Update processing operations to handle heavy feedstocks, Hydrocarb. Process. **86**, 41–53 (2007)
- 31.14 T. Kabe, A. Ishihara, W. Qian: *Hydrodesulfurization and Hydrodenitrogenation: Chemistry and Engineering* (Wiley, Tokyo 1999)
- 31.15 S.W. Golden: Managing Vanadium from high metals crude oils, Petroleum Technol. Q. Revamps Oper., 26–33 (2003)
- 31.16 J. Ancheyta, F. Trejo, M.S. Rana: *Asphaltenes: Chemical Transformation During Hydroprocessing of Heavy Oils* (CRC, Boca Raton 2009)
- 31.17 J.G. Speight: *The Chemistry and Technology of Petroleum*, 4th edn. (CRC, Boca Raton 2007)
- 31.18 S. Golden, T. Barletta, S. White: Designing the CDU/VDU for opportunity crudes, Petroleum Technol. Q. Sour/Heavy, 17–21 (2012)
- 31.19 D. Mulraney, C. Stewart: State-of-the-art delayed coking structure for frontier refining, Proc. NPRA (2009), AM-09-66
- 31.20 S. Zhao, L.S. Kotlyar, B.D. Sparks, J.R. Woods, J. Gai, K.H. Chung: Solids contents, properties, and molecular structures of asphaltenes from different oilsands, Fuel **80**, 1907–1914 (2001)
- 31.21 J. Woods, J. Kung, D. Kingston, L. Kotlyar, B. Sparks, T. McCracken: Canadian crudes: A comparative study of SARA fractions from a modified HPLC separation technique, Oil Gas Sci. Technol. Rev. IFP **63**(1), 151–163 (2008)
- 31.22 I. Gawel, D. Bociarska, P. Biskupski: Effect of asphaltenes on hydroprocessing of heavy oils and residua, Appl. Catal. A **295**, 89–94 (2005)
- 31.23 R. Narayan, J.R. Coury, J.H. Masliyah, M.R. Gray: Particle capture and plugging in packed-bed reactors, Ind. Eng. Chem. Res. **36**, 4620–4627 (1997)
- 31.24 N.A. Tsochatzidis, A.J. Karabelas: Hydrodynamic properties of pulses in trickle beds, Proc. Exp. Heat Transfer Fluid Mech. Thermodyn., Amsterdam (1991) pp. 1515–1522
- 31.25 R.J.G. Lopes, R.M. Quinta-Ferreira: CFD modelling of multiphase flow distribution in trickle beds, Chem. Eng. J. **147**, 342–355 (2009)
- 31.26 X.A. Wu, K.H. Chung: Hydrotreater feed filter fouling and its remedy, Energy Fuels **21**, 1212–1216 (2007)
- 31.27 Z. Xu, Z. Wang, J. Kung, J.R. Woods, X.A. Wu, L.S. Kotlyar, B.D. Sparks, K.H. Chung: Separation and characterization of foulant material in coker gas oils from athabasca bitumen, Fuel **84**, 661–668 (2005)
- 31.28 B.G. Ector: *Q1 2014 Heavy Oil Pricing Update – April 8, 2014* (Baytex Energy, Calgary 2014)
- 31.29 Crude Quality: <http://www.crudemonitor.ca> (2014)
- 31.30 J.S. Ball, M.L. Whisman, W.J. Wenger: Nitrogen content of crude petroleum, Ind. Eng. Chem. **43**, 2577–2581 (1951)
- 31.31 S. Yui, T. Dodge: Catalyst deactivation, kinetics, and product quality of mild hydrocracking of bitumen-derived heavy gas oil, Petroleum Sci. Technol. **82**,

- 351–365 (2006)
- 31.32 W. Kanda, J. Adjaye, A.E. Nelson, M.R. Gray: Inhibition and deactivation of hydrodenitrogenation (HDN) catalysts by narrow-boiling fractions of athabasca coker gas oil, *Energy Fuels* **18**, 539–546 (2004)
- 31.33 P.L. Jokuty, M.R. Gray: Resistant nitrogen compounds in hydrotreated gas oil from athabasca bitumen, *Energ. Fuels* **5**, 791–795 (1991)
- 31.34 API: *Recommended Practice 571: Damage Mechanisms Affecting Fixed Equipment in the Refining Industry* (API Publishing Services, Washington 2003)
- 31.35 C.A. Shargay, G.E. Jacobs, M.D. Price: *Ammonium Salt Corrosion in Hydrotreating Unit Stripper Column Overhead Systems* (NACE International, Houston 1999), paper no. 392
- 31.36 A. Sun, D. Fan: *Prediction, Monitoring and Control of Ammonium Chloride Corrosion in Refining Processes* (NACE International, Houston 2010), paper no. 10359
- 31.37 J. Turner: *Design of Hydroprocessing Effluent Water Systems* (NACE International, Houston 1998), paper no. 593
- 31.38 R. Breivik, R. Egebjerg: Coker naphtha hydrotreating, *Petroleum Technol. Quarterly* **Q1**, 69–74 (2008)
- 31.39 Y. Li, P. Watkinson, P. Herrera, F. Fahimina, M. James: Formation of gum and deposits in an oxygenated naphtha system, *Proc. 7th Int. Conf. Heat Exchanger Fouling and Cleaning—Challenges and Opportunities*, ECI Symp. Ser. (Berkeley Electronic, Berkeley 2007) pp. 80–89
- 31.40 D.J. Podratz, K. Kleemeier, W.J. Turner, B.M. Moyses: Mixed-distillate hydrotreating reduces costs, *Oil Gas J.* **97**(20), 41–43 (1999)
- 31.41 S. Yui: Removing diolefins from coker naphtha necessary before hydrotreating, *Oil Gas J.* **97**(36), 64–70 (1999)
- 31.42 B. Wright, T. Hochheiser: Mitigation of heat exchanger fouling, *Petroleum Technol. Quarterly* **4Q**, 119–124 (2012)
- 31.43 S. Yui: Producing quality synthetic crude oil from Canadian oil sands bitumen, *J. Jpn. Petroleum Inst.* **51**(1), 1–13 (2008)
- 31.44 J.A. Anabtawi, K. Alam, M.A. Ali, A.S. Ali, M.A.B. Siddiqui: Performance evaluation of HDS catalysts by distribution of sulfur compounds in naphtha, *Fuel* **74**(9), 1254–1260 (1995)
- 31.45 D. Vartivarian, H. Andrawis: Delayed coking schemes are most economical for heavy-oil upgrading, *Oil Gas J.* **104**(6), 52–56 (2006)
- 31.46 L. Wisdom, E. Peer, P. Bonnifay: Resid hydrocracking better than delayed coking in case studies, *Oil Gas J.* **96**(7), 53–60 (1998)
- 31.47 F. Morel, J. Duddy, L. Wisdom: Consider new technologies to raise diesel yield in bottom-of-barrel products, *Hydrocarb. Process.* **91**, 61–70 (2012)
- 31.48 G.M. Sieli, N. Gupta: A winning combination, *Hydrocarb. Eng.* **14**(9), 42–48 (2009)
- 31.49 S. Sayles, S. Romero: Understand differences between thermal and hydrocracking, *Hydrocarb. Process.* **90**, 37–44 (2011)
- 31.50 US Department of Energy: *Annual Energy Outlook 2014* (US Department of Energy, Washington 2014)
- 31.51 J. Been: *Comparison of the Corrosivity of Dilbit and Conventional Crude* (Alberta Innovates – Technology Futures, Calgary 2011)
- 31.52 D. Chakraborty, M. Dunlop, R. Lun: Processing sour crude in conventional refinery – Conversion of suncor sarnia refinery, *Proc. 4th Upgrading and Refining of Heavy Oil, Bitumen, and Synthetic Crude Oil Conf.* (National Center for Upgrading Technology, Edmonton 2006) pp. 278–307

Carbon Dioxide

32. Carbon Dioxide Mitigation

Sultan M. Al-Salem, Xiaoliang Ma, Mubarak M. Al-Mujaibel

Stringent regulations on carbon dioxide (CO₂) emissions from industrial sources (in general) and petroleum refineries (in particular) are being enforced world wide. Low-sulfur clean fuels enhance the demand for petroleum refinery utility gases (e.g., hydrogen, H₂), which in turn leads to an increase in carbon-emission-intensive processes. This will ultimately force refineries to start implementing CO₂ mitigation measures, which are increasingly evident in the strategies of industrial countries. In this work, we describe the major processes that contribute to a typical petroleum refinery's global CO₂ emissions. Typical sources include unit utilities (i. e., heaters, boilers, and furnaces), fluid catalytic cracking units, hydrogen production (HP) units, flaring, and acid gas removal. A case study for a mega refinery structure is also given detailing a methodology for estimating CO₂ emissions from various processes. The carbon footprint and specific emissions of various sources being considered are also reported.

32.1	Main Sources of Carbon Dioxide (CO₂) Emission in Petroleum Refineries	933
32.1.1	Crude Oil Distillation	936
32.1.2	Atmospheric Residue Hydrodesulfurization (ARDS) Unit	938
32.1.3	Hydrogen Production (HP) Units	938
32.1.4	Hydrocracking	941
32.1.5	Fluid Catalytic Cracking (FCC) Unit	941
32.1.6	Catalytic Reforming.....	941
32.1.7	Acid Gas Removal (AGR).....	942
32.1.8	Estimated Amount of CO ₂ Emission from Petroleum Refineries.....	943
32.2	Case Study: CO₂ Emission Estimation from a Refinery in the State of Kuwait	944
32.2.1	Carbon Dioxide (CO ₂) Estimation.....	945
32.3	Challenges in Carbon Capture and Mitigation for Petroleum Refineries	950
32.4	Concluding Remarks	952
	References	952

Global warming is the increase in average temperature of the Earth's surface, air, and oceans, which will increase flooding and ice cap melting, and influence climate change. The Intergovernmental Panel on Climate Change (IPCC) concluded that the increase in greenhouse gases (GHGs) is dominantly the result of fossil fuel burning [32.1]. The major greenhouse gas is CO₂ and the major source of anthropogenic CO₂ emission is from fossil fuel combustion. A study has shown that industrial sectors account for 70% of global CO₂ emissions [32.2]. In particular, CO₂ emissions from refineries account for 5% of the global CO₂ emissions (≈ 1 billion metric tons of CO₂ per year) and ranks third among the world's stationary CO₂ producers behind the power sector and the cement industry [32.3]. It is estimated that for a 300 MBPD petroleum refinery, 0.8–4.2 million tons of CO₂ is emitted annually, depending on the refinery's configuration.

Carbon mitigation techniques and methods have become one of the most studied topics among engineering disciplines. Mitigation techniques and strategies can be

discussed in terms of the most influential contributing factors to the carbon load of an industrial facility or in this case petroleum refineries. The increasing demand for cleaner fuels gives rise to increased carbon emissions by increasing hydrogen and utilities demand in refineries. However, more stringent regulation of fossil fuels makes carbon management a priority research topic today. This is especially true when it comes to carbon capture and storage (CCS) implementation in oil refineries. The purpose of carbon capture is quite basic in theory, which is to produce a concentrated stream of CO₂ that can be readily transported to a CO₂ storage site. CCS involves three distinct processes [32.4]:

- Capturing CO₂ from the gas streams emitted during fuel and chemical conversion processing
- Compressing and transporting the captured CO₂ by pipeline or tankers
- Storing CO₂ underground in deep saline aquifers, depleted oil and gas reservoirs, or unmineable coal seams.

There are currently over ten capture projects worldwide demonstrating viable techniques for carbon capture, with over 74 geological storage projects [32.4]. In general, CO₂ can be captured from all industrial fossil-fuel-burning processes with substantial amounts of CO₂. Dispersed carbon sources (e.g., transportation, agricultural, service, and residential sectors) do not present themselves as a viable source. CO₂ can be captured either before or after combustion using a range of existing and emerging technologies. CO₂ capture can be allocated to the following categories [32.2]:

- *Postcombustion capture*: Defined as capture of CO₂ emitted from combustion of fossil fuels in air. This technique hosts a number of technologies and is commonly applied in a number of industrial processes. Postcombustion systems utilize well-known technologies for gas separation. Separation with sorbents or solvents is a prime example of such technology. This is achieved by passing CO₂-rich gas in intimate contact with solvents or sorbents capable of capturing CO₂. Application of a membrane (polymeric, metallic, or ceramic) is another common technology for postcombustion capture.
- *Oxy fuel combustion capture*: This method is suitable for burners in refineries, where pure oxygen is used instead of air in combustion processes to produce CO₂ and water, as air contains about 78 vol.% of N₂ as a diluent. If the fuel is burnt in pure oxygen, the flame temperature is excessively high. However, the produced CO₂- and H₂O-rich gas can be recycled to the combustor to reduce the concentration of oxygen.
- *Precombustion capture*: Physical or chemical absorption of CO₂ after producing syngas (CO + H₂) by reacting fuel and oxygen. The CO is then reacted with steam (catalytically) in a shift converter to produce CO₂ (later separated) and H₂O.

Much attention has been focused on postcombustion capture in recent years. Researchers have focused efforts on a number of solutions for effective CO₂ capture from postcombustion sources, including application of physical and chemical sorbents and amine-based solutions for gas treatment (details in later sections). CO₂ sorbents might rank highest in current research activities for CO₂ capture due to very promising results demonstrated in a number of systems with varying operating conditions. A variety of solid physical sorbents (physisorbents) may be used to remove CO₂ from flue gases including porous carbonaceous materials, zeolites, alumina, silica gels, and metal-organic frameworks (MOFs). Porous activated carbon (AC), graphene and carbon nanotubes (CNT) are common examples of carbon-based solid sorbents [32.5]. Pressure swing ad-

sorption (PSA), a common industrial process used in refineries to recover mainly hydrogen (H₂) from off-gases, has been reported to remove CO₂ by using AC as an adsorbent [32.6–8]. This seems to be a very promising technology for carbon capture and warrants further review and development. PSA is a process that is common in refineries and typically utilized for gas separation. AC was also used by *Do* and *Wang* [32.9] to demonstrate the adsorption isotherm of CO₂ at three different temperatures with pressures up to 20 kPa. CO₂-adsorption capacity using Ajax AC was reported to decrease drastically with increasing temperatures. The rising concern in relation to CO₂ and its impact on our future has warranted legislation in industrial countries regulating their emissions. After a number of summits and conventions that stated clearly that global warming is a manmade phenomenon due to greenhouse gas (GHG) emissions, research in CO₂ capture has been active. Petroleum refineries are definitely a source of CO₂ that could be viewed as a resource (rather than an economic burden). This is because of the vast array of possible applications for CO₂, which are described in the next section.

CO₂ has been recognized as a greenhouse gas that leads to warming effects on the environment. Carbon mitigation reduces emissions from fossil fuel burning. In refineries, it has been noted that a trade-off exists between product quality and carbon emissions. Effectively, the high demand for certain clean fuels increases carbon emissions from refineries. This is something that capture technologies can deal with in terms of reducing the carbon emissions. Implementing such technologies can significantly reduce the carbon footprint of a refining facility.

Carbon capture can also be useful in terms of enhanced oil recovery (EOR). EOR is applied in oilfields approaching the end of their life and can produce additional oil in the range 10% or more. These operations are applied in order to improve the oil flow in the reservoir, by altering its flow properties or its interaction with the rock. One of these techniques is EOR promoted by CO₂ injection [32.10]. A common way of storing CO₂ is underground aquifer storage. Storage of CO₂ in deep saline (subsea) aquifers has been demonstrated in a commercial-scale project in Sleipner, Norway. About 1 million tons of CO₂ has been stored in this site since 1996 with no leakage detected so far. Using CO₂ to enhance oil recovery has been demonstrated at the Weyburn project in Canada. About 2 million tons of CO₂ per year has been stored there since 2001. Pilot projects suggest that CO₂-enhanced coal-bed methane (ECBM) and enhanced gas recovery (EGR) may be viable, although these are still in developmental and research stages [32.4]. In the Gulf countries, most refineries are

close to the oil fields. This is a significant benefit for CO₂ storage and CO₂-injection EOR as it reduces the cost for transportation of the CO₂ captured from the refineries to the oil fields.

In order to mitigate CO₂ emission from refineries, it is essential to understand the major CO₂ emission sources and the composition and properties of the gases, from which CO₂ is emitted from a typical refinery. In this chapter, the major CO₂ emission sources from a typical refinery were assessed on the basis of an anal-

ysis of the typical refining processes and a literature review. A case study for estimation of CO₂ emission from a refinery in the State of Kuwait was conducted. The challenges for carbon capture and mitigation in relation to petroleum refineries were discussed. The objective of this study is to provide important information about CO₂ emission sources from a typical refinery and to help the petroleum refining sector in making strategic decisions in relation to CO₂ mitigation from petroleum refineries.

32.1 Main Sources of Carbon Dioxide (CO₂) Emission in Petroleum Refineries

Crude oil has less value in its original state and also limited applications before refining. Even after desalting, dewatering, and degassing, crude oil is still a complex mixture of hydrocarbons ranging from very light to heavy compounds. Hence, to achieve the prime objective of a petroleum refinery, i. e., to produce valuable products such as liquefied petroleum gas (LPG), gasoline, kerosene, jet fuels, diesel, fuel oil etc., crude oil has to go through a number of successive physical and chemical processes [32.11].

Petroleum refineries differ in complexity and configuration. Hence, each refinery is unique in its treated crude oils, operating conditions, location and product specifications. Refinery configuration is defined by the set of refining processes, unit throughputs and design capacities, which gives the refinery complex its classification [32.12] (Table 32.1). Low in complexity refineries are the ones that are commonly referred to as topping refineries, nominally physically processing the crude with distillation processes. When hydrotreating and catalytic reforming processes are added to the refinery's configuration, it is known as a hydroskimming one characterized with moderate complexity. Typically, when fluid catalytic cracking (FCC), Alkylation and/or hydrocracking is added to the configuration, the refinery will be called a high complexity one. When coking is added the refinery is a very high complexity one, and usually called a deep conversion one.

Refining processes could be classed based on the physical separation and chemical transformation of the throughput to each unit, as shown in Fig 32.1. The major processes can be summarized as follows:

- Crude distillation
- Conversion (cracking)
- Upgrading
- Treating
- Separation

- Blending
- Utilities.

Crude oil distillation is a process whereby the crude oil is separated based on boiling ranges of products into fractions or cuts for further processing. There are two types characterized by feed and operating conditions. These are atmospheric and vacuum distillation processes. Conversion processes are essentially concerned with the breakdown (cracking) of heavy crude fractions. Light refinery streams are produced from these processes for further processing and blending. Examples of these processes are: fluid catalytic cracking (FCC) and hydrocracking. Upgrading processes, such as catalytic reforming, isomerization and alkylation, rearrange molecular structures to improve the properties (mainly octane number) and value of gasoline and diesel components [32.13]. Separation processes either by physical or chemical means are concerned with quality control for further processing similar to the case in fractionation and aromatics extraction. While *treating* is the group of processes dedicated to sulfur, metal and aromatics removal from streams, including hydrotreating of FCC and reformer feedstock, hydrotreating of fuel and lubricant base oil products, and benzene saturation. *Blending* is the process whereby different streams are combined to produce finished products that meet the required specifications (gasoline, diesel, jet fuel, etc.). Finally, refinery utilities are required to provide power, water, and heat for the refinery operations. Typically fired heaters and boilers are employed to supply utilities for units. A large amount of electricity is also consumed for pumps, compressors, and processing control units.

The production and management of all the refinery complex products and their specification result in numerous activities that contribute to the total load of carbon dioxide (CO₂). A typical source of CO₂ in a petroleum refinery is the utilities required for the dif-

Table 32.1 Petroleum refineries configuration and main characteristics (after [32.13])

Refinery configuration	Complexity rank	Main definitions and comments	Characteristic process
Topping	Low	These refineries have only crude distillation units with no capabilities to alter the natural yield pattern of the crude they process These refineries separate crude oil to refinery gas, refinery fuel, naphtha, distillates (kerosene, diesel, jet fuel) and heavy fuels Product specifications are governed by the crude specifications	Crude distillation
Hydro-skimming	Moderate	In addition to crude distillation these refineries have catalytic reforming, hydrotreating units and product blending capabilities Naphtha is upgraded to gasoline and sulfur content is controlled in products These refineries are common in low gasoline demand regions	Crude distillation Catalytic reforming Hydrotreating
Conversion	High	Also known as cracking refineries, hence including catalytic cracking and/or hydrocracking Heavy crudes are converted into light streams Sulfur levels in product are controlled by hydrotreating process Substantial capability for yield and quality improvement	Crude distillation Catalytic reforming Hydrotreating FCC and/or hydrocracking Alkylation and other upgrading
Deep conversion	Very high	These refineries include all the above categories, in addition to coking units to convert the residual oil to light streams as additional feed to other conversion processes Maximum yields of high-value refined products Maximum capability for quality improvement	Crude distillation Catalytic reforming Hydrotreating FCC and/or hydrocracking Alkylation and other upgrading Coking

ferent unit operations, such as pumps and compressors and processing control in the refinery, which requires the burning of fuel gas or other carbon-rich sources of energy.

Other processes that emit CO₂ as part of their daily operational routine include (1) FCC, where CO₂ is emitted as a result of coke deposition burning on catalyst, (2) steam methane reforming (SMR), or gasification of heavy hydrocarbons, which are more commonly termed hydrogen production (HP) units, where the feedstock is treated with steam, or with both steam and oxygen, to produce hydrogen, CO₂ and other acid-gases as well as H₂S. CO₂ and H₂S are removed by absorption using amine solutions as a part of the petroleum refineries process scheme.

A comprehensive analysis of CO₂ emissions from various typical refining units is necessary to understand CO₂ emission sources. This should account for both direct and indirect emissions associated with a certain process. In general, the total CO₂ emission per year (Q_{CO_2} , tpa (tons per annum)) for a refining unit can be calculated as

$$Q_{CO_2} \text{ (tpa)} = Q_{\text{(feed/product)}} (\text{Em}_{\text{heating}} + \text{Em}_{\text{feed-conv}} + \text{Em}_{H_2} + \text{Em}_{\text{steam}} + \text{Em}_{\text{electricity}}), \quad (32.1)$$

where $Q_{\text{(feed/product)}}$ is the amount of feed (or product) treated in the refining unit per year (tpa), $\text{Em}_{\text{feed-conv}}$

(t CO₂/t feed) could be defined as the CO₂ emission from complete conversion of each ton of feed to product; and $\text{Em}_{\text{heating}}$ is the CO₂ emission from the combustion of the fuel for heating each ton of feedstock, which can be calculated as per the following equation

$$\text{Em}_{\text{heating}} = \left(\frac{\text{En}_{\text{heating}}}{\text{LHV}_{\text{fuel}}} \right) \text{Em}_{\text{fuel},f}, \quad (32.2)$$

where $\text{En}_{\text{heating}}$ (BTU/t-feed) is the energy required for heating one ton of the feed, LHV_{feed} (BTU/t fuel) is the lower heating value of the fuel, Em_{fuel} (t CO₂/t fuel) is the CO₂ emission factor of fuel combustion and f (in %) is the heating efficiency (due to heat loss). The LHV of some major fuels are listed elsewhere in *Staffell* [32.14] (Table 32.2) and the CO₂ emission factors for some refinery fuels could be found in the report of Hydrocarbon Publishing Company [32.15] (Table 32.3).

Em_{H_2} (t CO₂/t feed) is the CO₂ emission for the generation of hydrogen required for treating each ton of feed, which can be calculated as per the following

$$\text{Em}_{H_2} = \text{Cons}_{H_2} \times \text{Em}_{H_2,f}, \quad (32.3)$$

where Cons_{H_2} (wt%) is the hydrogen consumption based on weight to feed and $\text{Em}_{H_2,f}$ (t CO₂/t H₂) is the CO₂ emission factor for the production of hydrogen gas. The $\text{Em}_{H_2,f}$ value is in a range from 10 to 12 t CO₂/

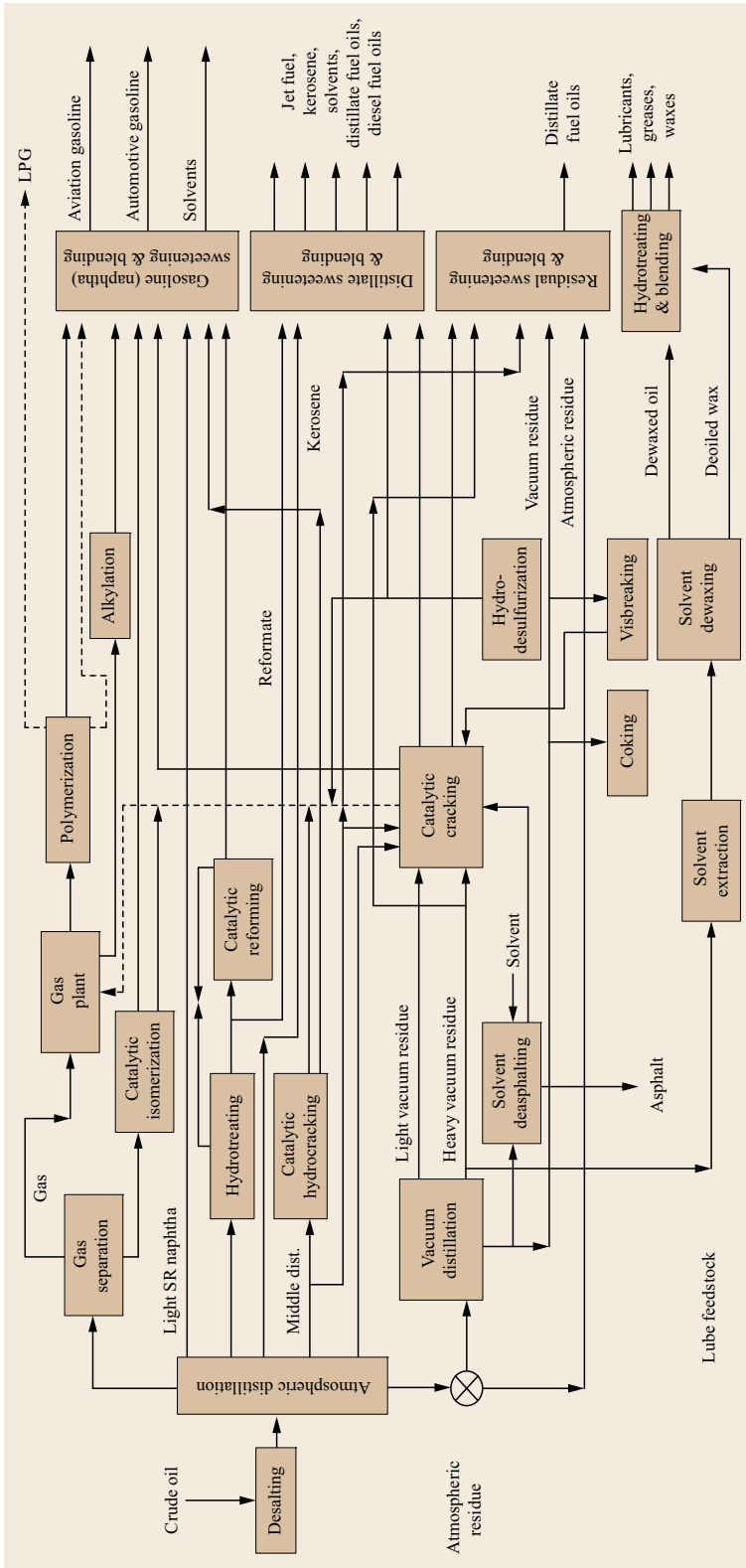


Fig. 32.1 Simplified modern refinery process flow diagram (after [32.16])

Table 32.2 The lower heating value (LHV) of some major fuels at standard temperature and pressure (STP) (after [32.14])

Fuel	Density at STP (g/m ³)	Net LHV (MJ/kg)
Crude oil	856	43.05
Petrol/gasoline	741	44.15
Diesel	837	42.91
Fuel oil	959	40.87
LPG	533	46.28
Kerosene	807	43.69
Coal	–	25.75
Natural gas	0.768	45.86
Hydrogen (1 atm)	0.0838	119.95

Table 32.3 CO₂ emission factors for some refinery fuels (after [32.15])

Fuel	CO ₂ emission factor (MM mt/EJ)
Natural gas	50.38
Refinery gas	60.80
Distillate fuel oil	69.37
Residual fuel oil	74.76
Coke	96.78
Coal	88.34

t H₂ for the production of H₂ from natural gas, according to *Bonaquist* [32.12]. Em_{steam} (t CO₂/t feed) is the CO₂ emission from the generation of steam required for treating each ton of feed. In many cases, Em_{steam} is estimated together with Em_{heating} and could be calculated as

$$Em_{\text{steam}} = Q_{\text{steam/feed}} \times Em_{\text{steam,f}}, \quad (32.4)$$

where $Q_{\text{steam/feed}}$ (t steam/t feed) is the amount of steam required for treating each ton of feed, Em_{steam,f} (t CO₂/t steam) is the CO₂ emission factor for generation of steam. The emission factor for steam is 88.18 kg/MM BTU as reported by the U.S. EIA (En-

ergy Information Administration) [32.18]. Em_{electricity} (t CO₂/t feed) is the CO₂ emission from the electricity power required for treating each ton of feedstock, which includes electric power for pumps, compressors, coolers, and separators. Em_{electricity} can be calculated as

$$Em_{\text{electricity}} = E_{kWh/feed} \times Em_{\text{electricity,f}}, \quad (32.5)$$

where $E_{kWh/feed}$ (kWh/t-feed) is the power required for treating each ton of feed, and Em_{electricity,f} (t CO₂/kWh) is CO₂ emission factor for generating electricity. The Em_{electricity,f} value suggested by the US EIA [32.17] for different fossil fuels and other fuels are shown in Table 32.4.

Below is analysis of the CO₂ emission from the individual refining processes, including crude oil distillation (COD), atmospheric residue hydrodesulfurization (ARDS), hydrocracking, hydrogen production (HP), fluid catalytic cracking (FCC), catalytic reforming, and acid gas removal (AGR).

32.1.1 Crude Oil Distillation

Crude oil distillation is a physical process that is considered as the front end of a petroleum refinery, regardless of configuration and complexity. The function of crude distillation is to separate raw crude oil into a number of intermediate refinery streams (more commonly termed *cuts*), characterized by their boiling ranges. The desalted crude oil is fed to an atmospheric distillation column. Each fraction leaving the crude distillation unit (CDU) is defined by a unique boiling point range. The fractions consist of hundreds or thousands of distinct hydrocarbon compounds. The atmospheric residue from this process is fed to a vacuum distillation tower for further separation of vacuum gas oil (VGO) from the atmospheric residue. CDU capacities typically range between 10–400 MBPD with a typical height of 50 m [32.16].

Table 32.4 CO₂ emission factor from electricity generation (after [32.17])

Fuel	Emission factor (kg CO ₂ /kWh)	Fuel	Emission factor (kg CO ₂ /kWh)
Anthracite	0.920	Crude oil	0.630
Coking coal	0.780	Natural liquids	0.480
Other bituminous coal	0.860	Refinery gas	0.400
Sub-bituminous coal	0.920	Liquefied petroleum gases	0.500
Coke oven coke	0.770	Kerosene	0.650
Coal tar	0.720	Gas/diesel oil	0.690
Brown coal briquettes (BKB)/peal briquettes	0.800–1.500	Fuel oil	0.670
Gas works gas	0.420	Petroleum cokes	1.000
Coke oven gas	0.420	Peat	0.760
Blast furnace gas	2.200	Industrial waste	0.400–2.000
Natural gas	0.400	Waste (nonrenewable)	0.450–3.500

Crude distillation could be summarized by a number of sequential processes in a petroleum refinery. These are desalting, the atmospheric distillation (topping) unit, and vacuum distillation. Energy management through optimal heat use for the different required processes is paramount for reducing the carbon emission from the distillation process. This should be achieved by minimizing the fired heaters duty while not compromising the products quality. The main utility of crude oil distillation is the crude oil furnace (direct fired heater or pipe still), which is responsible for heating the crude oil to a 75% vapor mixture with an outlet temperature between 350–380 °C.

The distillation process in refineries starts with desalting to remove the salt (expressed as NaCl) in the oil to minimize corrosion, fouling, and catalyst deactivation due to deposition. The basic principle is to wash the salt from the crude with water, which is typically achieved via a two-stage desalting process. The second desalter is cleaned (or under maintenance) whilst the first is in operation [32.16]. The typical power require-

ment for this process is between 0.01–0.02 kWh/bbl feed (0.0735–0.147 kWh/t).

Crude oils are preheated before and after the desalting unit at 120–150 °C and 228 °C, respectively, via a series of heat exchangers. A preflash drum is used to generate the vapor product which is then routed to the atmospheric crude distillation unit (CDU, Fig. 32.2). A furnace is employed in this stage to give the vapors the required temperature (343–399 °C) [32.11]. The heat required for separation in the distillation tower is provided according to the enthalpy of the feed. Heat is typically removed from the tower by an overhead condenser and pump-around streams. The latter is defined as a liquid stream withdrawn from a point below a side stream tray that is cooled by the cold crude feed as part of the preheat exchangers train.

Vacuum distillation units (Fig. 32.3) are employed in the last stage of the distillation processes, where residue from the atmospheric CDU is fed to a vacuum distillation unit typically under pressures of 25–40 mmHg. The distillates (cuts or products) of the

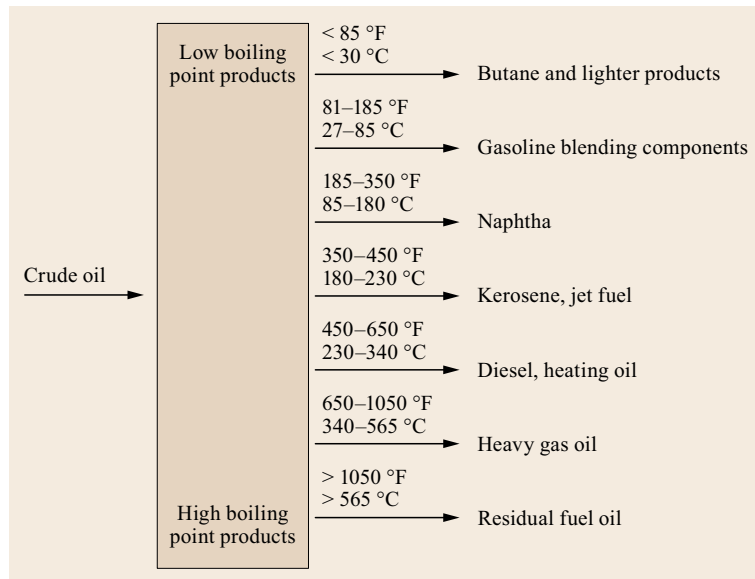


Fig. 32.2 Products from typical atmospheric distillation (after [32.19])

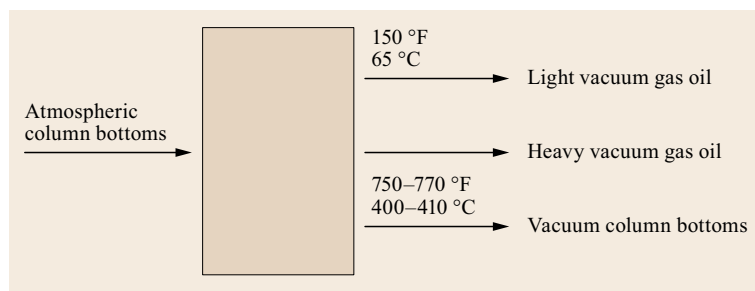


Fig. 32.3 Typical distribution of vacuum distillation products

vacuum unit are classified as light, middle, and heavy vacuum gas oil (LVGO, MVGO, HVGGO), respectively. After heat exchange in the crude preheat exchangers train, the atmospheric residues are fed to the vacuum unit (Fig. 32.3). The unit processes this feed to produce the required distillates in order to achieve maximum economic value for the crude oil barrel. Since the distillation units are not involved in chemical conversion and hydrogen consumption, according to (32.1)–(32.5), the total CO₂ emission per year (Q_{CO_2} (t/yr)) for the atmospheric/vacuum distillation of crude oil can be calculated as per (32.6) or (32.7)

$$Q_{\text{CO}_2\text{-CDU}} \text{ (t/yr)} = Q_{\text{feed}} (\text{Em}_{\text{heating}} + \text{Em}_{\text{steam}} + \text{Em}_{\text{electricity}}) \quad (32.6)$$

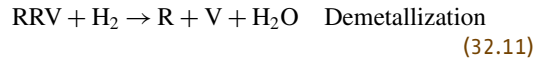
$$Q_{\text{CO}_2\text{-CDU}} \text{ (t/yr)} = Q_{\text{feed}} \left[\left(\frac{\text{En}_{\text{heating}}}{\text{En}_f} \right) \text{Em}_{\text{fuel},f} + Q_{\text{steam/feed}} \times \text{Em}_{\text{steam},f} + E_{\text{kWh/feed}} \times \text{Em}_{\text{electricity},f} \right] \quad (32.7)$$

Equation (32.7) clearly indicates that the annual CO₂ emission amount depends not only on the treated amount of the feed, but also on the CO₂ emission factor of fuel and the heating efficiency. Typical power required for the vacuum distillation unit is 0.3 kWh/bbl feed (2.206 kWh/t) and fuel of 0.03 MM BTU/bbl feed (0.2206 MM BTU/t) [32.20]. An industrial example is given for typical fired heater duty applied to CDU, showing process design capacity and heater duty for various throughputs (Table 32.5). There are a number of considerations when developing an emission factor for distillation processes. One should consider the type of fuel and utilities included, in addition to design requirements (actual throughput). We can estimate the CO₂ emissions from atmospheric and vacuum distillation of crude oil based on heating requirements (fired heaters duties using fuel oil) as 3.7 and 4.2 kg CO₂ per bbl (or 0.0272 and 0.0309 t CO₂/t feed) of feedstock, respectively.

32.1.2 Atmospheric Residue Hydrodesulfurization (ARDS) Unit

ARDS units (an application of hydrotreating) process the residue generated from crude atmospheric distillation units (CDU), commonly known as the bottom of the barrel, to produce fuel oil of certain specifications. The feed to ARDS units is typically hydrogenated catalytically to allow for the production of a low-sulfur fuel oil (LSFO) or other feedstock for further conver-

sion, as shown in Fig. 32.4. The following series of reactions take place in ARDS as depicted in (32.8), (32.9), (32.10), and (32.11).



Fixed-bed reactors are typically employed in this process along with a fractionating section. The feed is preheated by the reactor effluents then mixed with hydrogen. ARDS reactions are exothermic; hence the reactor effluent is quenched with cold recycle before entering the next reactor in the ARDS series. Representative feed and product properties are listed in Table 32.6 for a typical industrial ARDS unit of 218 m³/h. Other hydrotreating processes in a petroleum refinery include middle distillates and naphtha hydrotreating, in addition to gas oil and kerosene desulfurization.

Estimating the CO₂ emission from utilities in ARDS could be done by using the emission factor of 0.781 kg/bbl or 0.00512 t CO₂/t feed (based on design capacity). Since ARDS doesn't convert the feed to CO₂ and Em_{steam} is negligible, the total CO₂ emission per year ($Q_{\text{CO}_2,\text{ARDS}}$) for an ARDS unit can be calculated as

$$Q_{\text{CO}_2} \text{ (tpa)} = Q_{\text{feed}} (\text{Em}_{\text{heating}} + \text{Em}_{\text{H}_2} + \text{Em}_{\text{electricity}}) \\ Q_{\text{CO}_2} \text{ (tpa)} = Q_{\text{feed}} \left(\frac{\text{En}_{\text{heating}}}{\text{En}_f} \text{Em}_{\text{fuel}} \times f + \text{Cons}_{\text{H}_2} \times \text{Em}_{\text{H}_2} + E_{\text{kWh/feed}} \times \text{Em}_{\text{electricity},f} \right) \quad (32.12)$$

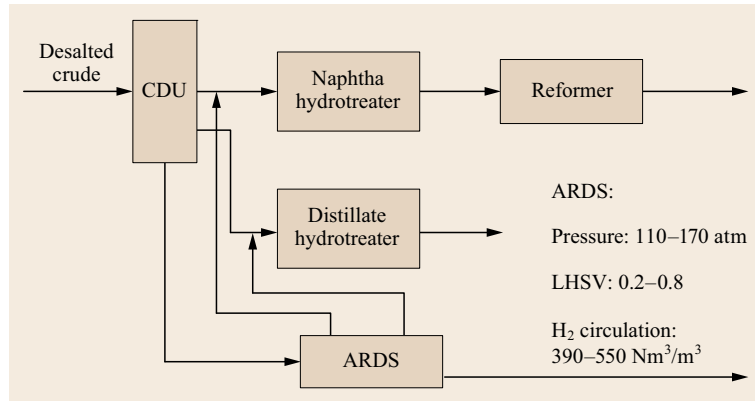
where Q_{feed} (tpa) is the amount of AR feed treated in the ARDS unit per year. Equation (32.12) indicates that the CO₂ emission is dependent on the heating and hydrogen consumption. The hydrogen consumption for ARDS is about 1–3 wt%. The heating duty for the fractionating section feed heater, recycle gas (after scrubbing) heater, and hydrogen charge heater in an ARDS unit with a design capacity of 36.3 MBPD used in different sections of the processing of fuel gas is shown in Table 32.7. The En_{heating} value estimated on the basis of the data shown in Table 32.7 is 0.417×10^9 J/t feed.

32.1.3 Hydrogen Production (HP) Units

Hydrogen production could be considered the core of utility production in refineries. The demand for hy-

Table 32.5 Industrial example of fired heater for CDU using fuel gas

Unit operation	Design capacity (MBPD)	Unit throughput (MBPSD)	Fired heater duty (MMGJ/yr)	En _{heating} (GJ/t-feed)	Furnace inlet temp. (°C)	Furnace outlet temp. (°C)	Stack gas outlet temp. (°C)
ACDU	120	110.2	3.5	639	177	322	239
ACDU	200	197.6	2.8	285	246	352	241
ACDU	122	107.7	1.5	280	272	355	332
ACDU	21	12.7	0.5	793	148	320	225
VCDU	85	66.1	1.3	396	298	362	189
VCDU	11	7.6	0.3	795	300	383	440

**Fig. 32.4** Schematic representation of the ARDS process as a part of the overall refinery scheme (after [32.21])**Table 32.6** ARDS feed and product properties reported in industry

Feed properties		
	Gravity (API) of oil (min.)	12.5
	Sulfur content in oil (max.) (wt%)	4.5
	Hydrogen Conc. (max.) (vol.%)	97
Product yield and properties		
ARDS off-gas (C ₁ –C ₄)	Yield (vol.%)	0.4
Naphtha (C ₅ –160 °C)	Gravity (API)	59
	Sulfur content (wt%)	0.003
	Yield (vol.%)	0.5
Distillate (160–360 °C)	Gravity (API)	33
	Sulfur content (wt%)	0.07
	Yield (vol.%)	17
LSFO (360 °C)	Gravity (API)	20.6
	Sulfur content (wt%)	0.7
	Yield (vol.%)	83.5
	Metal content (Ni+V) (ppm)	15

API – American Petroleum Institute

drogen in refineries is increasing due to the increase in demand for clean fuels. Refiners can use a number of feedstocks (refinery gas, liquefied petroleum gas, naphtha, and natural gas) to produce hydrogen. Deep

conversion refineries with a high level of bottom of the barrel conversion can have a H₂ demand of up to 2.7 wt% of total crude input. In general, refineries follow four steps in steam methane reforming (SMR) or hydrogen production (HP), these are [32.22]:

1. Feedstock treatment, where sulfur is removed with other contaminants
2. Steam methane reforming, where feedstock and steam is converted to syngas (CO + H₂) at high temperatures
3. Heat recovery for syngas and water/gas shift reaction incorporation to increase the hydrogen yield; and finally
4. Hydrogen purification, which is typically done with an amine scrubbing process or a pressure swing adsorption (PSA) process to achieve final product purity.

The reforming reaction between steam and hydrocarbon is an endothermic one. The reactions taking place in the process (as a whole) are summarized below.

For saturated hydrocarbons



Water/gas shift reaction for H₂ recovery

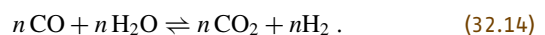


Table 32.7 Fired heaters for ARDS unit with a design capacity of 36.3 MBPD used in different sections of fuel gas processing

Heater no.	Heating section	Section throughput (BPSD)	Fired heater duty (GJ/yr)
Heater 1	Recycle gas (after scrubbing) heater	100 000	290.5×10^3
Heater 2	Hydrogen charge heater	36 300	488.2×10^3
Heater 3	Fractionating section feed heater	66 590	63×10^3
Total			841.7×10^3

According to the data shown in the above table, $En_{\text{heating}} = 0.417 \text{ GJ/t-feed}$

Thus, (32.13) + (32.14) result in (32.15)



In the adiabatic shift reactor vessel, the moderately exothermic water/gas shift reaction converts carbon monoxide (CO) and water (steam) to CO_2 and H_2 . The CO_2 is typically vented to the atmosphere after removal, which makes up for one of the major CO_2 hot spots in a petroleum refinery. In addition, HP units require utilities that add to the total load of carbon emissions from refineries (Table 32.8). The total CO_2 emission per year (Q_{CO_2-HP}) for HP units can be calculated as

$$Q_{CO_2-HP}(\text{tpa}) = Q_{H_2} \cdot (Em_{\text{heating}} + Em_{\text{feed-conv}} + Em_{\text{electricity}}), \quad (32.16)$$

where Q_{H_2} is the amount of hydrogen product per year from the hydrogen production plant, Em_{heating} is the CO_2 emission from the combustion of the fuel required for heating to produce each ton of hydrogen, which can be calculated as

$$Em_{\text{heating}} = \left(\frac{En_{\text{heating}}}{LHV_{\text{fuel}}} \right) Em_{\text{fuel}} \times f, \quad (32.17)$$

where En_{heating} is the energy required for heating to produce each ton of hydrogen, and LHV_{feed} is the lower heating value of the fuel. Using natural gas as fuel, the LHV_{feed} value is 45.86 MJ/kg feed, or 43.57 MM BTU/t feed (Table 32.2). $Em_{\text{fuel},f}$ is the CO_2 emission factor of fuel combustion. The CO_2 emission factor for natural gas is 2.768 t CO_2 /t fuel. According

Table 32.8 Utility requirements for HP units in refineries (after [32.15])

Utility type	Requirement	
Power	0.15 kWh/kg H_2	150 kWh/t H_2 , 0.512 MM BTU/t H_2
Fuel	105 MJ/kg H_2	99.8 MM BTU/t H_2
Feed Gas	0.26 mol/mol H_2	4.52 t feed/t H_2

to Table 32.8, En_{heating} is 99.8 MM BTU/t feed, thus, Em_{heating} can be calculated, being 3.17 t CO_2 /t H_2 , assuming a 50% heat loss. $Em_{\text{electricity}}$ can be calculated as

$$Em_{\text{electricity}} = E_{kWh/feed} \times Em_{\text{electricity},f}. \quad (32.18)$$

According to Table 32.8, the $E_{kWh/feed}$ value is 150 kWh/t H_2 . As defined previously, $Em_{\text{electricity},f}$ is the CO_2 emission factor for electricity generation. If we assume fuel oil is used for power generation, $Em_{\text{electricity},f}$ is 0.670×10^{-3} t CO_2 /kWh according to Table 32.4. Consequently, the $Em_{\text{electricity}}$ value is 0.101 t CO_2 /t H_2 . $Em_{\text{feed-conv}}$ (t CO_2 /t H_2) is CO_2 emission for complete conversion of feed to produce each ton of H_2 (complete conversion of carbon in the feedstock). It can be calculated thus

$$Em_{\text{feed-conv}} = Q_{\text{feed}/H_2} \times Em_{\text{feed} \times f}, \quad (32.19)$$

where Q_{feed/H_2} (t feed/t H_2) is the amount of feed required to produce each ton of hydrogen and $Em_{\text{feed} \times f}$ (t CO_2 /t feed) = the CO_2 emission for complete conversion of each ton of feed. Assuming that natural gas with 90 vol.% methane and 10 vol.% ethane is used as feed, Q_{feed/H_2} and $Em_{\text{feed} \times f}$ values can be calculated as 2.26 t feed/t H_2 and 2.768 t CO_2 /t feed, respectively. Thus, $Em_{\text{feed-conv}}$ value is 6.26 t CO_2 /t H_2 . The estimated results for hydrogen production are summarized in Table 32.9. The CO_2 emission factor for production of hydrogen is 9.53 t CO_2 /t H_2 . CO_2 emission for conversion of feed accounts for 65.7% as for heating and electric power, it accounts for 33.3 and 1.1%, respectively.

Table 32.9 CO_2 emission from hydrogen production plant

	CO_2 emission	
	t CO_2 /t H_2	%
Em_{heating}	3.17	33.3
$Em_{\text{feed-conv}}$	6.26	65.7
$Em_{\text{electricity}}$	0.101	1.1
Q_{CO_2-HP}/Q_{H_2}	9.53	100

32.1.4 Hydrocracking

By definition, hydrocracking is the treatment of feedstock with hydrogen (hydro) to convert higher molecular weight compounds to light molecular weight ones (cracking) using a catalyst. Hydrocrackers are used to produce middle distillates with low sulfur content such as kerosene and diesel (Table 32.10). The process was developed by I.G. Farben in 1927 for conversion of lignite to gasoline and ever since its development it has allowed operation at relatively low pressures with higher conversion to gasoline, jet fuel, naphtha, etc. [32.20].

Feedstocks are hydrotreated to saturate the olefins and remove the sulfur, nitrogen, and oxygen compounds. Metals are retained on the catalyst, and nitrogen and sulfur are removed by conversion to ammonia and H₂S, respectively. A number of reactions take place in the process, including olefin saturation and partially aromatic ring saturation. Desulfurization and denitrogenation reactions produce exothermic heat to the amount 65–75 BTU/SCF of hydrogen consumed. The saturation of olefins also provide additional exothermic heat (140 BTU/SCF of hydrogen consumed). The overall heat of reaction for typical hydrocracking feed preparation is 25 000 BTU/bbl of raw feed. On average, the required hydrogen is about 27–54 m³ [32.3] H₂/m³ feed. Operating temperatures and pressure vary according to the age of the catalyst. General utility requirements are given in Table 32.11.

The CO₂ emission (t CO₂/yr) from the hydrocracking unit can be calculated as

$$Q_{\text{CO}_2\text{-Hydrocracking}} = Q_{\text{feed}} (\text{Em}_{\text{heating}} + \text{Em}_{\text{H}_2} + \text{Em}_{\text{steam}} + \text{Em}_{\text{electricity}} + \text{Em}_{\text{cooling}}) \quad (32.20)$$

Table 32.10 Typical feedstocks and products in hydrocracking units

Feedstock	Product
Kerosene	Naphtha
SR diesel	Naphtha and/or jet fuel
Atmospheric gas oil	Naphtha, jet fuel and/or diesel
Vacuum gas oil	Naphtha, jet fuel and/or diesel
Deasphalted oil	Olefin plant feedstock

Table 32.11 Typical hydrocracker (10 621 BPD, 1604 t/day) utility requirements for petroleum refineries (after [32.15])

Item	Amount per day	Amount per ton of feed
Steam	797 mlb	0.225 t steam
Power	138 mkWh	86.0 kWh
Cooling water	3.3 mgal/min	11.2 m ³
Fuel	2124 MM BTU	1.324 MM BTU

32.1.5 Fluid Catalytic Cracking (FCC) Unit

The main objective of fluid catalytic cracking (FCC) is the conversion of feedstock to gasoline and other valuable products. FCC also minimizes the production of less valuable products (i. e., coke, clarified oil, etc.) [32.23]. However, due to current high energy costs and progressively tightening environmental regulations, refiners have recently been expanding their FCC focus to include improved energy efficiency and reduced CO₂ production [32.23–26].

FCC units supply their own fuel for the conversion of products and further downstream fractionation. This fuel is the by-product of the cracking reactions left on the catalyst, commonly referred to as coke. With heavier feeds that contain less hydrogen and inherently produce less liquid volume, higher coke burning capabilities are needed, or we need to find a way to increase coke production to improve product yields. The key is to produce enough coke to increase the conversion of the feed until the optimum yield pattern is achieved. A typical FCC unit is shown in Fig. 32.5.

Typically FCC accounts for 20–35% of a refinery's CO₂ emissions via its regenerator's stack. Most of the CO₂ produced in the FCC regenerator is required as a result of satisfying the FCC heat balance and is the result of the coke (carbon residue on catalyst) combustion. Hence, it is essential to control the FCC system to provide optimum performance by feedstock quality control, taking into consideration equipment limitations and environmental constraints [32.22].

The CO₂ emission for catalytic cracking each ton of feed can be calculated as

$$Q_{\text{CO}_2\text{-FCC}}(\text{tpa}) = Q_{\text{feed}} (\text{Em}_{\text{heating}} + \text{Em}_{\text{feed-conv}} + \text{Em}_{\text{electricity}}) \quad (32.21)$$

where Q_{feed} (t/yr) is the amount of FCC feed treated per year, $\text{Em}_{\text{heating}}$ (t CO₂/t feed) is the CO₂ emission from the combustion of the fuel added to heat each ton of FCC feed, $\text{Em}_{\text{electricity}}$ (t CO₂/t feed) is the CO₂ emission from the generation of electricity required to treat each ton of feed, $\text{Em}_{\text{feed-conv}}$ (t CO₂/t feed) is the CO₂ emission from the regenerator for burning coke formed from each ton of FCC feed. If assuming that f (4.6 wt%) is the coke content in the FCC product, $\text{Em}_{\text{feed-conv}}$ could be estimated as $f(44/12)$ which equals 0.169 t CO₂/t feed.

32.1.6 Catalytic Reforming

Catalytic reforming converts petroleum naphtha to high-octane gasoline pool components. These high-

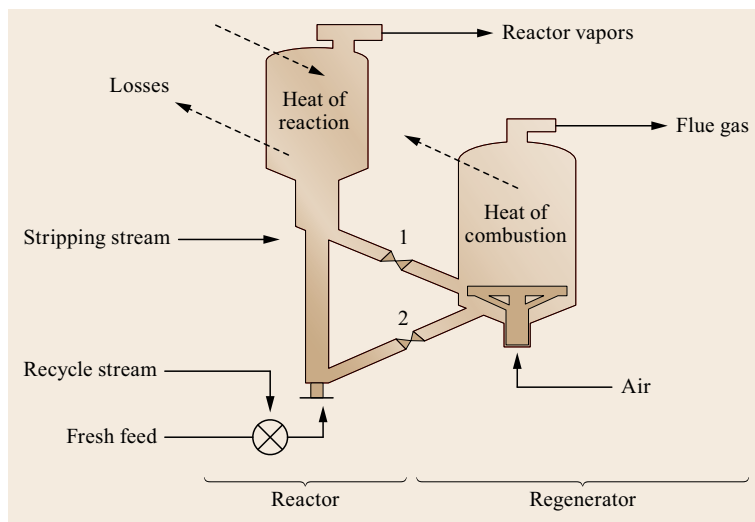


Fig. 32.5 A typical fluid catalytic cracking (FCC) unit showing the main energy balance elements of the reactor (left) and regenerator (right): 1. Spent catalyst throughput; 2. Regenerated catalyst throughput (after [32.26])

octane components are mainly branched and aromatic hydrocarbons which are less prone to ignite prematurely in internal combustion engines hence reducing the knocking effect [32.27]. The process transforms C₇–C₁₀ hydrocarbons to aromatics and *iso*-paraffins by selective reforming (catalytically). The process is highly endothermic and energy intensive. The main role of the process is to produce gasoline (about 37 wt%) to be added to the total pool of the refinery products [32.16]. Other units such as FCC, methyl *tert*-butyl ether (MTBE) production unit, alkylation unit, and isomerization unit all contribute to this pool. Reforming is operated in two modes in refineries. The first is a high severity mode which produces 80–90 vol.% aromatics. The second is a middle severity one, where a 70 vol.% aromatic content of high-octane gasoline is obtained [32.16]. The typical feedstocks for the process are heavy straight run (HSR) gasoline/naphthas (82–190 °C) and heavy hydrocracker naphthas. These are composed of what is known as PONA (paraffins, olefins, naphthenes, and aromatics). Typical feedstocks and reformer products (in terms of PONA) are summarized in Table 32.12.

A number of reactor configurations exist for this process, including axial and radial flow tubular and spherical reactors. Membrane reactors are also employed in this process consisting of a combination of

chemical reactor and membrane. They are used in reaction systems in which removal of reaction products from reaction media or addition of reactants along the reactor is beneficial. This effective configuration has various advantages such as increasing reaction rate, reducing by-product formation, lower energy requirements, and relatively safe operation. *Gary and Handwerk* [32.20] have detailed the utilities required in catalytic reforming per bbl feed: steam 30 lb, power 3 kWh, cooling water 600 gal, and fuel gas (LHV) 0.3 MM BTU. The CO₂ emission (t CO₂/yr) for catalytically reforming each ton of feed can be calculated as

$$Q_{\text{CO}_2\text{-reforming}} (\text{t CO}_2/\text{yr}) = Q_{\text{feed}} \times (\text{Em}_{\text{heating}} + \text{Em}_{\text{steam}} + \text{Em}_{\text{electricity}} + \text{Em}_{\text{cooling}}), \quad (32.22)$$

where $\text{Em}_{\text{cooling}}$ is the CO₂ emission from the generation of cooling water required to treat each ton of feed. It should be noted that the catalytic reforming can generate a significant amount of hydrogen gas, which can be used for hydroprocessing units, thus reducing the CO₂ emission (total carbon footprint) from the hydrogen production plant which should be considered in the CO₂ emission from the refinery.

32.1.7 Acid Gas Removal (AGR)

Acid gas removal processes are common in petroleum refineries and are a crucial part of the operations in gas treatment plants. Natural gas consists of hydrocarbons and acid gases (hydrogen sulfide, H₂S, and carbon dioxide). The process of removing hydrogen sulfide is commonly referred to as a sweetening process. Typ-

Table 32.12 Typical PONA analyses for reformer feedstock and product (after [32.20])

Component	Feed (vol.%)	Product (vol.%)
Paraffins	45–55	30–50
Olefins	0–2	0
Naphthenes	30–40	5–10
Aromatics	5–10	45–60

ical natural gas sold requires less than 5 ppmw H₂S with a heating value between 920 and 980 BTU/SCF. The actual specifications depend on the use and local country's regulatory requirements, which gives refiners added tasks of tailoring processes to meet demands.

Acid gas removal processes could be allocated to two main types: adsorption and absorption [32.28]. Adsorption is defined as a physiochemical phenomenon in which gas is concentrated on the surface of a solid or liquid to remove impurities. Usually, carbon is the adsorbing medium, which can be regenerated upon desorption [32.29]. What is adsorbed is typically in proportion to the surface area of the solid; hence, adsorbents are granular solids with large surface areas per unit mass. Conversely, absorption is achieved either by dissolution (a physical phenomenon) or by reaction (a chemical phenomenon). Typically, petroleum refineries employ a chemical absorption process (using solvents) in acid gas removal. Research and development are being undertaken in this area for more effective and efficient solutions with environmental benefits [32.29–32]. Chemical processes employ a solvent of alkaline nature such as amines or carbonates. Acid gases are stripped off the solvent in desorption by reducing pressure or increasing temperatures. Amines used in such processes can be categorized as primary, secondary or tertiary, depending on how many terminal nitrogen atoms are substituted by organic groups (Table 32.13).

The process of amine acid gas removal typically starts with sour gas entering through an inlet scrubber to remove entrained solid. The sour gas then enters the bottom of the absorber column and flows upward through the absorber in countercurrent contact with the aqueous amine solution, where the amine absorbs acid gas components from the gas stream.

The sweet gas exiting the top of the absorber passes through a separator and then flows to a dehydration unit before being ready for sale as a product. The rich amine solution from the bottom of the stripper column is pumped through an amine–amine heat exchanger to release the entrained acid gas and then through a cooler before being introduced to the top of the absorber column as a lean amine solution. The exiting gas from an accumulator contains H₂S and CO₂ which are typically

sent to sulfur recovery units and incinerators, respectively.

32.1.8 Estimated Amount of CO₂ Emission from Petroleum Refineries

Petroleum refineries convert crude oil to valuable products via a wide range of physical and chemical processes. CO₂ may be emitted via a number of sources in a refinery. Typically, these sources can be divided into [32.3, 33, 34]:

- **Furnaces and boilers:** They supply the heat required for separation of liquid feedstock and for the different utility units and combined represent 30–65% of refinery emission. Furnaces and boilers are typically referred to as utility sources.
- **Fluid catalytic cracking (FCC) unit:** This process is used to convert some heavier fractions, such as vacuum gas oil (VGO) or atmospheric residue (AR) into a more valuable product typically contributing to the gasoline pool of the refinery. It can be responsible for up to 35% of CO₂ produced in a refinery [32.3].
- **Hydrogen production (steam methane reforming, SMR):** Hydrogen production units produce hydrogen and CO₂ via reforming of natural gas or other hydrocarbon fuels. 20% of the total CO₂ emission in a refinery could be from hydrogen production.
- **Utilities production:** If a refinery produces steam or electricity (for pumps and compressors), CO₂ is a direct by-product of such a process which can contribute up to 50% of the total refinery CO₂ emission load.

The total CO₂ emission from a refinery can be estimated by summation of CO₂ emission from all processes in the refinery. According to the U.S. EPA [32.35], GHG emissions from petroleum refineries were estimated to be 214 million tons of CO₂ equivalents based on production rates in 2005. The majority of this estimate was from CO₂ emission rates. In the case of Europe, it was estimated that 114 refineries emitted about 155 million tons of CO₂ [32.36]. The specific emissions of a refinery can range from 0.02 to 0.82 t of CO₂/t of crude oil processed, depending

Table 32.13 Amine solvents used in acid gas removal

Amine solvent category	Primary amine	Secondary amine	Tertiary amine
Molecular weight	61	105	119
Examples	Monoethanolamine (MEA)	Diethanolamine (DEA)	Methyldiethanolamine (MDEA)
Max. acid gas flow (m ³ /d)	70 000	14 000	40 000
Notes	Reacts directly with H ₂ S, CO ₂ and COS ₂	Reacts directly with H ₂ S, CO ₂ and some COS ₂	Reacts directly with H ₂ S and indirectly with CO ₂

Table 32.14 CO₂ emission from refinery sources^a

Source (fuel used)	Number of units	CO ₂ emission (MM mt/yr)	Distribution (%)
Combustion, stationary devices		2.960	26.6
Steam boilers (refinery gas)	10	1.160	10.4
Process heaters (refinery gas)	40	1.130	10.2
FCCU CO boilers (refinery gas)	1	0.079	0.7
Internal combustion engines (natural gas)	12	0.036	0.3
Gas turbines (natural gas)	3	0.378	3.4
Flares	N.A.	0.154	1.4
Incinerator for sulfur recovery unit (SRU) and tail gas treatment		0.020	0.2
Combustion, indirect		0.033	0.3
Purchased electricity		0.033	0.3
Venting		2.570	23.1
Hydrogen plant (natural gas)	N.A.	0.367	3.3
Hydrogen plant (refinery gas)	N.A.	0.232	2.1
FCCU regenerator	1	1.970	17.7
Crude tanks	N.A.	–	
Maintenance and turnaround	N.A.		
Total		11.122	100

^a CO₂ emission factor for this refinery is 0.895 t CO₂/t feed (crude oil)

on the refinery configuration and quality of feedstock used.

The Hydrocarbon Publishing Company [32.15] noted a trend between refinery CO₂-equivalent emissions per barrel of gasoline produced and crude quality in terms of sulfur content and API (American Petroleum Institute) gravity. It is evident that the CO₂ emission increases with increasing sulfur content and decreasing API value. They also estimated the CO₂ emission from

various point sources at a hypothetical 250 Mbbl refinery with a hydrogen plant and an fluid catalytic cracking unit (FCCU). The results are depicted in Table 32.14. The CO₂ emission for heating and steam account for 21.3%; for the FCCU regenerator, 17.7%; for hydrogen production, 5.4%; for engines, turbines, and electricity, 4.0%; and for flares and incinerator, 1.6%. The CO₂ emission factor for this refinery is about 0.90 t CO₂/t feed (crude oil).

32.2 Case Study: CO₂ Emission Estimation from a Refinery in the State of Kuwait

In the following section, we demonstrate the methodology for assessing the CO₂ emissions from a refinery chosen in the State of Kuwait. Kuwait is an oil-producing country (member of OPEC (Organization of the Petroleum Exporting Countries) and OAPEC (Organization of Arab Petroleum Exporting Countries)) that refines about 1 million barrels of crude oil per day. Its economy is dependent on crude oil sales and petroleum-related activities. The methods of estimation are all up to date and are concerned with the processes carbon footprint (i.e., carbon dioxide emission from point source). The refinery dataset and process information is gathered from relevant parties and on-site data.

The refinery considered here is one of the largest on the Asian continent and has been in operation for over 60 years. Over its lifespan, a number of revamps

has been commissioned for this facility. It contains two sides; the first side is the refinery where crude oil is processed to produce a number of petroleum products (including naphtha, gasoline, diesel), the second side is a gas plant where natural gas and gas condensate is treated. The main objective of the gas plant side is to extract liquefied petroleum gas (LPG) products (propane and butane) from the treated gas. The refinery has a number of utility operations and consumes electric power purchased from the state's government.

The refinery's capacity is 460 MBPD with a total area of 10.5 km². The side hosts a number of topping units for crude oil distillation (atmospheric and vacuum) treating various grades. The side also hosts hydrotreating units (ARDS, kerosene desulfurization unit, gas oil desulfurization), conversion units (hydroc-

racking, FCC, naphtha reformers), and other supporting units (HP units, recovery units for various processes, etc.) The gas plant side as mentioned above is part of the refinery's overall scheme.

32.2.1 Carbon Dioxide (CO₂) Estimation

Hydrogen Production (HP) via Steam Methane Reforming

There are four steam methane reformers (SMR) for hydrogen production (HP) in the refinery (see Sect. 32.1.3 for process details). They are all of identical design in terms of capacity producing 49.5 MMSCFD hydrogen of 97% purity. Utilization capacity of each unit varies (according to 2012 average data) between 55 and 76%. Thus, the total hydrogen production rate by mass is 111.9×10^3 t H₂/yr.

The main function of the units is to meet the hydrogen demand for the refinery, and in particular the hydrocracking (HCR), atmospheric residue desulfurization (ARDS), kerosene desulfurization (KD), and gas oil desulfurization (GOD) units. Hydrogen is produced as per the reaction depicted in (32.13), (32.14), and (32.15). The CO₂ produced in the shift reaction is removed by a Benfield system.

The compositions of feed and typical products are shown in Table 32.15. The feed gas is desulfurized by absorption to remove all sulfur components using a di-*isopropanolamine* (DIPA) solution. The desulfurized gas is then mixed with steam (31.6 kg/cm²) and passed through the reformer cells to produce carbon monoxide (CO), carbon dioxide (CO₂), and hydrogen at 843 °C. A high-temperature shift convertor is used to convert the bulk of the CO to CO₂. A Benfield solution (K₂CO₃ + diethanolamine + water) is used to remove the CO₂ produced in the shift convertor from hydrogen. The solution is then regenerated and CO₂ is vented to atmosphere.

The four HP units in the refinery have identical capacity which was used to estimate the CO₂ vented to atmosphere. According to the discussion above (Sect. 32.1.3), the CO₂ emission (Em_{feed-conv}) for complete conversion of natural gas to produce each ton of H₂ without considering heating and utility is 6.26 t CO₂/t H₂. Thus, the CO₂ emission from the four HP

units without considering heating and utility is 700×10^3 t/yr, which is calculated by multiplying Em_{feed-conv} (6.26 t CO₂/t H₂) with the total hydrogen production rate (111.8×10^3 t H₂/yr).

Fluid Catalytic Cracking (FCC) Unit

The FCC unit has a design capacity of 40 000 BPD and processes feedstock to produce a number of products, mainly gasoline and liquefied petroleum gas (LPG). The olefin-rich LPG is further processed to produce propylene, alkylate, and MTBE. The FCC unit consists of the following sections:

1. Reactor/regenerator
2. Main fractionator
3. Gas concentration unit
4. Power recovery.

Figure 32.6 shows a simplified flowchart of the FCC unit in the refinery considered. The reactor/regenerator is where the cracking reactions, catalyst separation and regeneration take place. The feed to the unit is the preheated raw oil (220–265 °C) combined with the hot stream of regenerated catalyst introduced to the bottom of the reactor's riser. Table 32.16 shows the main product yields as per the design of the unit in the studied refinery, with typical operating conditions shown in Table 32.17.

The reactor vapor is sent to the main fractionator to be separated to heavy cycle oil (HCO), light cycle oil (LCO), distillate, heavy gasoline, and overhead vapors. The overhead vapors are partially condensed and collected in a receiver and both hydrocarbon liquids and gas are further processed in the gas concentration unit (GCU). The final products from the GCU can be summarized as:

1. Off-gas
2. LPG
3. Light gasoline.

The fluid catalytic cracking (FCC) unit has an operating capacity of 43 000 BPD; with a coke production of 4.62 wt% as per the unit's design with 89.2% utilization capacity. Consequently, the CO₂ emission from the FCC unit can be estimated as 339.4×10^3 tpa. On the basis of the average data for 2012, the FCC stack flue gas composition is reported in Table 32.18. The CO₂ composition is 15.2% of the stack, which gives an indication of a considerable quantity. The composition of the FCC stack flue gas is similar to the flue gas from a general coal-based power station. There is no carbon monoxide (CO) present in the FCC stack due to excess air pumped in to ensure complete combustion. There is about 0.05 vol.% of SO₂ in FCC flue gas, which may influence the performance of some sorbents

Table 32.15 Main feed and products qualities of HP units in the refinery being studied

Feed composition	mol% (dry)	Product composition	mol% (dry)
CO ₂	1.70	H ₂	97
C ₁	91.43	CH ₄	3
C ₂	6.61	CO+CO ₂	20 ppmv (max.)
C ₃	0.14	H ₂ O	Saturated

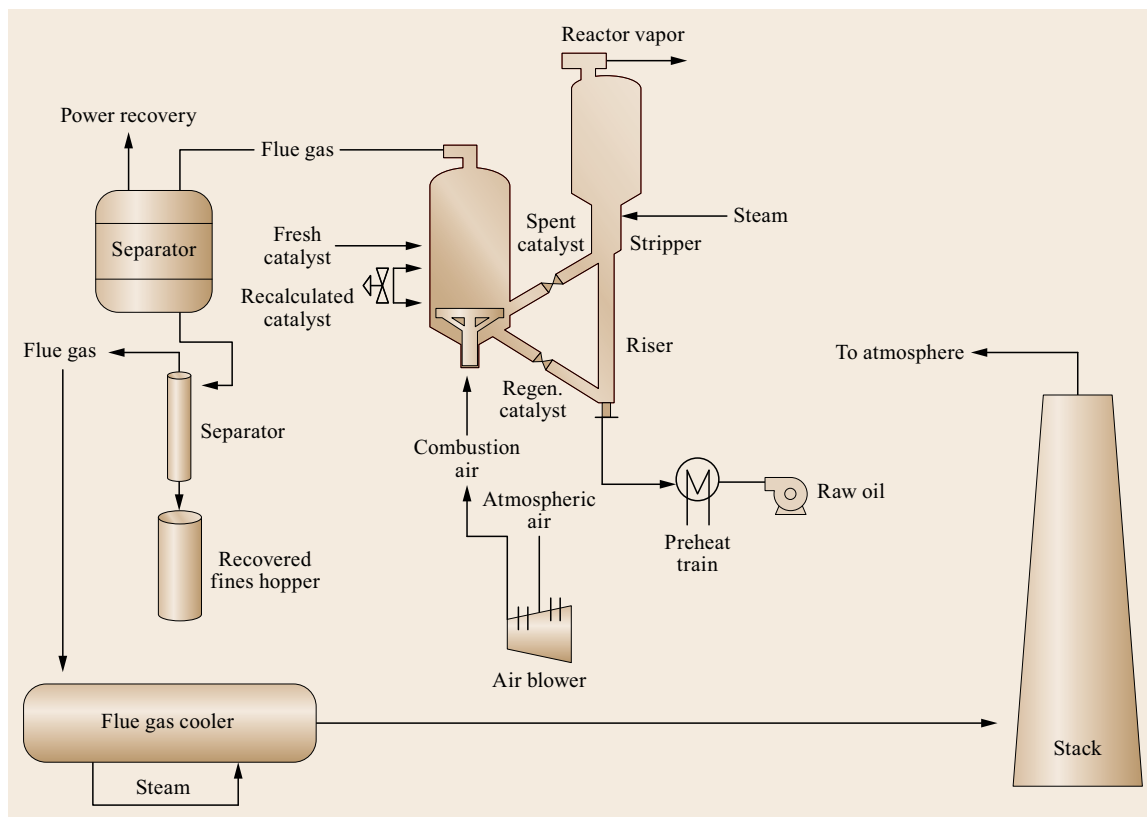


Fig. 32.6 Flow diagram of the fluid catalytic cracking (FCC) unit in the refinery

Table 32.16 Fluid catalytic cracking (FCC) unit product yield (wt%)

Product	wt%	Product	wt%
Off-gas	4.35	Distillate	15.94
LPG	20.40	LCO	0.64
Light gasoline	32.98	HCO	7.70
Heavy gasoline	13.37	Coke	4.62

and should be considered in the CO₂ capture from FCC flue gas.

Flaring

Flaring in refineries and other industrial facilities occurs as an alternative to venting hydrocarbons to the atmosphere. It is an important safety measure for controlling operation shutdowns and start-ups, in addition to controlling operating pressures. Flaring results in the combustion of hydrocarbons with CO₂ and steam as

products. The refinery considered in this study hosts 15 flares for control and release purposes on both the refinery and gas plant sides. According to the April 2013 data survey in the refinery, the main reasons for the flaring in this facility are as follows:

- Hydrogen header pressure fluctuation in ARDS
- Hydrogen make-up compressor seal pot valve passing in ARDS
- Overhead flaring of hydrocracker splitter
- Make-up gas compressor leaks in hydrocracker
- HP units compressor discharge
- Excess gas generation due to severe operating condition in ARDS unit
- Maintenance of crude column condensers
- Unit shutdowns and startups
- LPG storage flares
- LPG train flare.

Table 32.17 Typical operating conditions of the fluid catalytic cracking (FCC) unit

Reactor inlet temp.	243 °C	Regenerator pressure	2.32 kg/cm ²
Reactor temp.	529 °C	Combustion air flow	0.64
Reactor pressure	2.1 kg/cm ²	Catalyst circulation	1500 tph
Regenerator dense phase temp.	731 °C	Catalyst addition rate	1.5 tph

Table 32.18 Fluid catalytic cracking (FCC) flue gas composition

Gas component	(vol.%)
Hydrogen (H ₂)	0
C ₁ –C ₃ +	0
Nitrogen (N ₂) and air	83.3
CO	0
CO ₂	15.2
Oxygen	1.1
SO _x	0.05

Table 32.19 Flaring activities analysis and estimated CO₂ emission

Component	Amount
Flaring (total hydrocarbon amount reported in refinery)	76 650 MMtpa
Refinery capacity	460 × 10 ³ BPD
CO ₂ emitted from flaring activities	72 890 tpa

It is essential not to overlap between excess flaring activities and normal operations that might include CO₂ emissions as part of its composition. *Martin* et al. [32.37] reported a correlation based on emission inventory analysis that estimates the amount of GHG (CH₄ and CO₂) emitted by refineries flares. This was used in this study to estimate the amount of CO₂ (Table 32.18) emitted based on the following

$$FCE = 3.12 RT, \quad (32.23)$$

where FCE is the flares CO₂ emissions (kg) and *RT* is the refinery's throughput in tons. Kuwait's crude (more commonly termed Kuwait export crude, KEC) has been of 30.2 API in recent years with an estimated density of 875 kg/m³. Hence, a throughput of 23.34 million tpa for this refinery is calculated and 72 880 tpa is the estimated CO₂ emission (*Q*_{CO₂-flaring}) from flaring in this refinery (Table 32.19).

Acid Gas Removal (AGR)

On the gas plant side of this refinery, C₃, C₄, and gasoline are cryogenically extracted through extraction/dehydration, cooling/chilling, fractionation, and product treating. Moisture and liquids are removed from the entering gas to prevent freezing in the cold section of the plant. Natural gasoline recycle is used as an absorbent in the absorber to recover C₃ and C₄, amongst other products. Rich liquids that form at the absorber bottom are transferred to a stripper to reduce C₃ and C₄ content. The stripper bottom includes C₃, C₄, gasoline and associated C₂ and lighter gases. The stripper's condensate is fed to a fractionating plant comprising deethanizer, depropanizer, and debutanizer. The utilities of the fractionating plant will be discussed in the next section.

The gas plant contains an acid gas sweetening unit to remove H₂S and CO₂ from the gas feed. Diethanolamine (DEA) solution is used in this unit of 230 MMSCFD capacity. The gas feed enters an absorber where H₂S and CO₂ are absorbed using DEA. The treated gas is fed to a separator to separate the carried DEA. The design specifications reported for this unit are summarized in Table 32.20, which show the three cases of treated gas in this process. Using the absorber balance equation for CO₂, we can estimate the amount of CO₂ existing in the system as follows [32.38]

$$E(\text{CO}_2) = V_{\text{in}} \left(\frac{\text{vol}_{\text{in}} - \text{vol}_{\text{out}}}{1 - \text{vol}_{\text{out}}} \right). \quad (32.24)$$

When *vol*_{out} ≈ 0.0%, (32.24) becomes

$$E(\text{CO}_2) = V_{\text{in}} \times \text{vol}_{\text{in}}, \quad (32.25)$$

where *E*(CO₂) is the existing amount of CO₂ from the system in SCFD, *vol*_{in} is the mol fraction of CO₂ in the entering stream, and *vol*_{out} is the existing mol fraction taken as (1.2% maximum). Estimated amounts are also shown in Table 32.20.

Acid condensate is treated in a similar fashion but in a different unit in this refinery. The composition of the condensate is shown in Table 32.21. A density of 750 kg/m³ is assumed for this condensate [32.38]. Converting the flow rate of the entering stream to unit volume can allow the assessment of the total amount of moles. From the unit balance we can estimate the CO₂ emission amount (*Q*_{CO₂-ASC} (t CO₂/yr)) exiting the system taking CO₂ mol% (maximum out) as 0.5% (Table 32.21)

Utilities

Utilities play a major role in petroleum refineries. They supply through fired heaters and boilers the energy needed for units to operate at desired conditions. Fuel oil or gas is typically employed as a fuel for various

Table 32.20 Acid gas sweetening unit treated feed specifications showing entering main hydrocarbons and CO₂ (% mol) and estimated CO₂ existing (tpa) (*Q*_{CO₂-AGR} (t CO₂/yr))^a

Item	Case 1	Case 2	Case 3
Flow rate (MMSCFD)	149	230	89.2
C ₁	55.75	54.38	56.89
C ₂	19.13	18.63	17.98
C ₃	11.43	11.18	10.2
CO ₂	7.19	8.02	9.28
CO ₂ (Out) (tpa)	2.00 × 10 ⁵	3.5 × 10 ⁵	1.50 × 10 ⁵

^a Average *Q*_{CO₂-AGR} (tpa) = 4.2 × 10⁵

Table 32.21 Acid gas condensate treated in the refinery showing feed composition (mol%) and estimated CO₂ exiting the system (tpa). Average $Q_{\text{CO}_2-\text{ASC}}$ (t CO₂/yr) = 6.1×10^5

Item	Case 1	Case 2	Case 3
Flow rate (BPD)	34 700	39 000	11 100
C ₁ (mol%)	16.78	16.4	18.22
C ₂	18.42	17.94	19.54
C ₃	25.91	25.35	27.37
C ₄	18.66	18.43	17.59
C ₅	11.7	11.63	9.39
C ₆	3.3	3.27	0.69
O ₂	0	0	0
N ₂	0.06	0.06	0.1
H ₂ O	0.02	0.02	0.02
CO ₂	3.81	4.25	5.44
H ₂ S	1.36	2.64	1.64
Total mol in	95×10^6	108×10^6	32×10^6
CO ₂ (out) (tpa)	7.4×10^5	8.36×10^5	2.47×10^5

utility operations. Fuel oil was used in the estimation of CO₂ emitted in this work. Excluding the gas plant side, there are 45 fired heaters in operation in the refinery. Table 32.22 shows estimated CO₂ emission from the utilities of the refinery side.

The gas plant side contains nine fired heaters for the different LPG trains (deethanizer, depropanizer, and debutanizer). On the basis of a similar category for the past utility calculation for residual fuel oil. Table 32.23 summarizes the gas plant utilities duties and reports the

estimated CO₂ emission on the basis of an emission factor of 78.87 kg CO₂/MM BTU.

Analysis of Results and Discussion

The estimated CO₂ emissions from different sources in the refinery are listed in Table 32.24, and the CO₂ emission distribution per unit operation in the whole refinery is shown in Fig. 32.7. The results obtained for this refinery are discussed hereafter. The total amount of CO₂ emitted from the site is estimated between 4.91×10^6 tpa (without considering the CO₂ emission for consumption of electricity), depending on the AGR and condensate treatment units feed. As indicated in the previous sections, utilities represent the major source of CO₂ in refineries. Open literature is lacking in information regarding the distribution of CO₂ emission for utilities. However, as shown in Table 32.24 and Fig. 32.8, combined CO₂ emissions from the utility for heaters and boilers is 2.77×10^6 t CO₂/yr, which accounts for 56.3% of all CO₂ emissions from the refinery. Some unit operations in the refineries are quite energy intensive, such as 585×10^3 t CO₂/yr for atmospheric crude distillation, 414×10^3 t CO₂/yr for hydrogen production

Table 32.22 Fired heater (utilities) on the refinery side and CO₂ emissions based on fuel oil emission factor

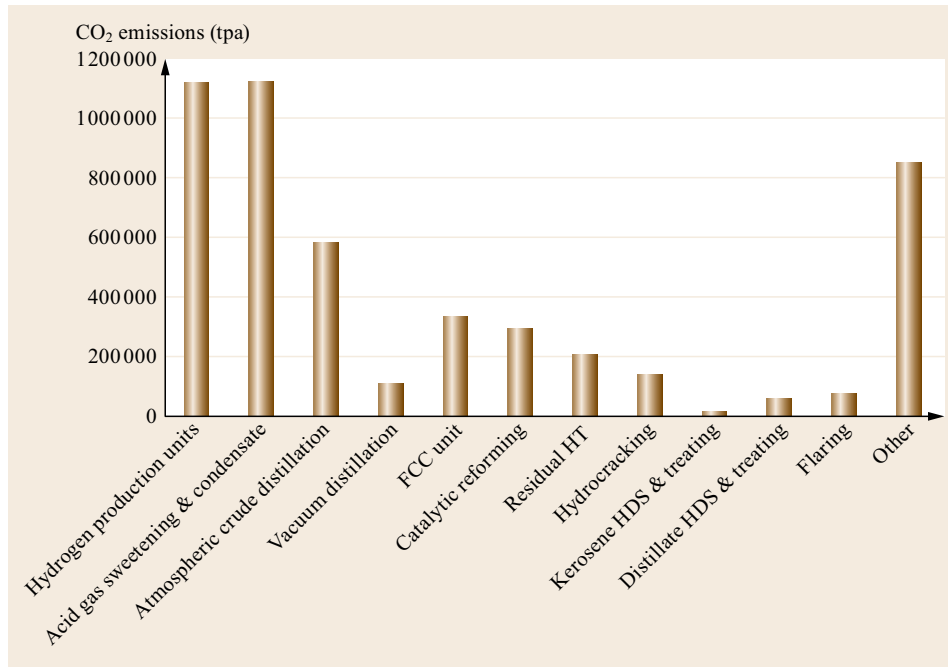
Process	CO ₂ emission (tpa)
Atmospheric crude distillation	5.85×10^5
Vacuum distillation	1.13×10^5
Hydrocracking	1.40×10^5
Catalytic reforming	2.94×10^5
Hydrogen generation	4.14×10^5
Residual desulfurization	2.06×10^5
Kerosene desulfurization and treating	1.21×10^4
Distillate desulfurization and treating	6.14×10^4
Other	8.46×10^5

Table 32.23 Fired heater (utilities) on the gas plant side and CO₂ emissions based on fuel oil emission factor

Fired heater	Function	Duty (MM BTU/hr)	CO ₂ emission (t/yr)
LPG train 1	Deethanizer reboiler	186	128 500
	Depropanizer reboiler	163	113 900
	Debutanizer reboiler	105	72 500
LPG train 2	Deethanizer reboiler	186	128 500
	Depropanizer reboiler	163	113 900
	Debutanizer reboiler	105	72 500
LPG train 3	Deethanizer reboiler	186	128 500
	Depropanizer reboiler	163	113 900
	Debutanizer reboiler	105	72 500
Total			944 700

Table 32.24 The estimated CO₂ emissions from different sources in the refinery

	Unit	Q_{feed} (t/yr)	$Q_{\text{CO}_2\text{-conv.}}$ (t CO ₂ /yr)	$Q_{\text{CO}_2\text{-heating}}$ (t CO ₂ /yr)	Q_{CO_2} (t CO ₂ /yr)	Q_{CO_2} distribution (%)
1	Hydrogen production units	111 886	700 403	414 000	1 114 403	22.7
2	Acid gas sweetening & condensate		1 030 000	94 470	1 124 470	22.9
3	Atmospheric crude distillation			585 000	585 000	11.9
4	Vacuum distillation			113 000	113 000	2.3
5	FCC unit	2 003 391	339 375		339 375	6.9
6	Catalytic reforming			294 000	294 000	6.0
7	Residual			206 000	206 000	4.2
8	Hydrocracking			140 000	140 000	2.9
9	Kerosene hydrodesulfurisation (HDS) & Treating			12 100	12 100	0.2
10	Distillate HDS & Treating			61 400	61 400	1.3
11	Flaring	23 359 088	72 880		72 880	1.5
12	Other			846 000	846 000	17.2
	Total		2 142 658	2 765 970	4 908 628	100.0
	Distribution, %		43.7	56.3	100.0	

**Fig. 32.7** CO₂ emissions from various utilities in the refinery. Note that CO₂ emission for the production of hydrogen in hydroprocessing is not included in the CO₂ emissions of the units

units, 294×10^3 t CO₂/yr for catalytic reforming, and 206 million t CO₂/yr for residual hydrotreating. Utilities on the gas plant side emitted 9.44×10^5 tpa of CO₂.

In comparison to the total CO₂ emission from different units, including feed-containing/feed-conversion CO₂ and CO₂ emission from utilities, the CO₂ emission from the acid gas sweetening and condensate ranked highest at 1.12×10^6 tpa, accounting for 22.9% of the whole CO₂ emission of the refinery. The CO₂ emission from the hydrogen production units is 1.11×10^6 tpa, ranking second. The third highest CO₂ emission is

from atmospheric crude distillation, being 5.85×10^5 t CO₂/yr. The CO₂ emission from the utility for all hydroprocesses, including residual hydrotreating, hydrocracking, kerosene HDS and treating and distillate HDS and treating, is about 4.20×10^5 tpa, accounting for 8.5%. The CO₂ emission from the FCCU for the generation of catalyst is 3.39×10^5 tpa, accounting for 6.9%. The CO₂ emission from flaring is very limited, accounting for only 1.5%.

Supporting units utilities (combined) are considered to be the largest emission source in the refinery. How-

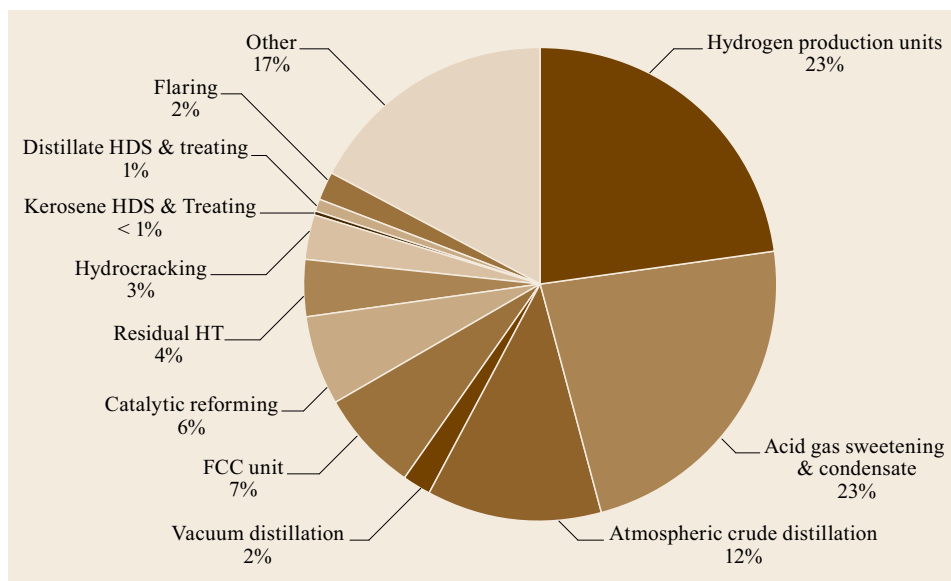


Fig. 32.8 Distribution by source of the total CO₂ emitted in the refinery

ever, it is very hard to manage such utility units and treat each individually for better energy management. Better energy management of hydrogen production, atmospheric crude distillation, catalytic reforming, and residual hydrotreatment will result in better carbon mitigation. It is estimated that by reducing the load of these units by 25%, the total carbon emissions of the refinery decrease by 7.6%. Hydrogen production is a major CO₂ emission source from the refinery. The whole refinery's CO₂ emission will be reduced by 5.7% if one reduces hydrogen consumption in all hydroprocesses by 25%.

CO₂ emission from acid gas removal (AGR, for both gas and condensate) ranks first (1.124×10^6 t/yr) with a contribution of 22.9%. Many past studies assessed refineries without considering AGR. This is

probably due to lack of data or the unit not being part of refinery operations. CO₂ is typically vented with a minimal hydrocarbon fraction to the atmosphere in this process [32.38]. Utilities represent 56.3% of the total refinery's emissions in this case study. *van Straelen et al.* [32.3] showed that utilities with furnaces and boilers can contribute up to 60% of the total refinery assessment with HP units reaching up to 20% in an electricity-producing refinery. The assessment conducted in this work agrees with their reports. A subdivision of two types of refineries was given by the IEA (International Energy Agency) [32.4], showing that an FCC refinery could have process heaters (utilities) contributing 44% of the CO₂ emissions total, while a hydrocracking refinery has 55% for utilities.

32.3 Challenges in Carbon Capture and Mitigation for Petroleum Refineries

Nominally, the main challenge in carbon capture is twofold: (1) The optimization of refineries utilities and energy consumption, and (2) capturing CO₂ from similar quality sources to be mixed in a single stream. Better energy management in a refinery leads to more cost-effective operation and a reduction in the total carbon footprint of the different processes. Emerging developments in the past few years have focused on developing technologies for capturing CO₂ from flue gas. This is mainly the case for FCC, where this process can contribute up to 20% of the total CO₂ load from a refinery. The amount of coke and subsequent CO₂ produced in

the reactor is a direct result of the quality of the FCC feed and the operating conditions imposed on the unit by the operator. The unit yields are directly related to the quality of the feed and the operating severity set by the enthalpy balance. *Wolschlag et al.* [32.23] discussed the opportunities for carbon emission reduction in FCC and suggested the following:

- *Improved energy optimization:* Gap analysis is suggested to identify root causes (insufficient maintenance, inefficient energy system design, inefficient process operation, procedures and control,

or outdated technology). This could be achieved by correlating the process parameters with process energy indicators. Hence, process conditions can be connected with energy-related parameters.

- *CO₂ reduction through energy efficiency revamps:* This is mainly concerned with power recovery in FCC units. An example of such is the five-body train of a hot-gas expander, main air blower, start-up steam turbine, motor/generator and gear box as necessary. In this configuration, the expander is coupled to the main air blower and provides a direct transfer of energy to the shaft to minimize power transfer losses to the air blower.

Legislation on refineries and environmental rules and regulations have given rise to CO₂ reduction planning in the past decade or so. This will drive operational changes to improve process efficiencies, which paves the way for simulation packages to have a front seat in carbon-reduction schemes. This is especially true nowadays where heavier crudes are considered to be the sole feedstock in many refineries (new or revamped). The use of a simulation package has led to a 50% reduction in flaring after implementing an on-line program [32.25]. The simulation package includes inferential fuel gas quality and volume imbalance prediction, and a furnace-monitoring and advisory system. Additional benefits reported include: improved furnace efficiencies, more consistent product qualities (for example, where the process furnace is a feed heater or re-boiler), and more reliable process operation. Coupled H₂ and CO₂ management has also been studied recently in refineries. By developing a mixed integer nonlinear program (MINLP), *Al-Hajri* [32.39] has optimized refinery operations by controlling fuel, FCC, and hydrogen reduction units.

Energy management in an oil refinery is an integral part of CO₂ reduction strategies, especially with recent new regulations governing sulfur content of gasoline and diesel. This leads to an increase in capacity and hydrogen consumption. It is estimated that the total amount of crude oil processed in U.S. refineries increased in comparison to the start of the 1990s by 5% to comply with gasoline and diesel specifications. In Brazil, an increase of 1.5 million tons of CO₂ was estimated due to a change in gasoline and diesel specifications in 2009. This leads directly to more energy-intensive operations that require more hydrogen for cleaner fuel production. It is estimated that a refinery uses 7–15% of its crude oil input in its processes in direct or indirect heat requirements [32.40]. To deal with energy management challenges, technologies that show potential include:

1. Alternatives for saving energy at refineries
2. Less severe alternatives for intensive process operations (e.g., hydrotreating)
3. Oil gasification and CO₂ removal at the refinery.

Szklo and *Schaeffer* [32.40] described the first two options as achievable in the near to medium term. However, the third option could be considered to still be in developmental stages. *Petrick* and *Pelegriano* [32.41] stated that a 15–20% target reduction of energy use is achievable for U.S. refining activities, with emphasis on waste heat recovery utilization in petroleum refineries.

Improvement of heat integration and waste heat recovery has been discussed in recent literature for more energy-efficient systems in refineries [32.38, 42, 43]. The following treatment options are possible:

- Use of waste heat in absorption refrigeration systems and utilizing heat to preheat feeds.
- Improvement of furnace efficiencies combined with computer-controlled combustion.
- Direct feed of intermediary products without storage to recover loss heat (omitting cooling stage).

Using solar energy to heat feed stock or generating steam to replace the hydrocarbon fuels is another option to reduce the CO₂ emission in refineries. It may be promising for refineries in hot areas, such as the Middle East.

Modern refineries have higher emissions because they can use heavier crudes and produce more light products, especially gasoline and diesel. Catalytic reformers, FCC units, and vacuum distillation unit (VDU) could also be equipped with combined heat and power (CHP) units with a CO₂ capture ability [32.4]. These units represent 30–40% of the refinery energy consumption. They are placed on top of the list of unit operations that require energy management and carbon mitigation strategies.

Development of new refining technologies that have low CO₂ emission is crucial for future refineries. This effort may focus on the following areas:

1. Development of more effective catalysts, which are able to improve processing performance significantly and reduce energy consumption in processing.
2. Development of non hydroprocesses for production of clean fuels, such as adsorptive desulfurization, adsorptive denitrogenation, and oxidative denitrogenation.
3. Development of separation processes with low energy consumption, such as membrane separation, adsorption and abstraction, instead of the energy-consuming processes applied in current refineries.

32.4 Concluding Remarks

It is paramount to consider carbon management strategies as an inherent part of petroleum refinery operation schemes. Capturable amounts of CO₂ can be successfully integrated into carbon capture plants which might result in high cost avoidance [32.44–46]. This might be a very efficient way to reduce the CO₂ emissions in a refinery, in addition to generating income and profit from the integration of carbon plants.

Utilities, as discussed earlier, can have a drastic effect on the CO₂ emissions rate from a refinery. Better energy management schemes can reduce the CO₂ emissions rates. Each refinery is unique in terms of its processes and configuration. This allows for more responsible operation and for green initiatives to be

integrated into such facilities making them more environmentally friendly.

The conventional refining technologies, including hydroprocesses and FCC, show higher CO₂ emission. The focus of research should be the development of new refining technologies that have low CO₂ emission rates.

Acknowledgments. The authors are grateful to the Kuwait Institute for Scientific Research (KISR) for funding project PF060K. The contribution from Dr. A.R. Khan of KISR (ELSRC) is gratefully appreciated. Parts of this chapter were previously published in *Al-Salem* [32.47].

References

- 32.1 C. Patel, P. Lettieri, S.J.R. Simons, A. Germanà: Techno-economic performance analysis of energy production from biomass at different scales in the UK, *Chem. Eng. J.* **171**, 986–996 (2011)
- 32.2 A. Thernesz, G. Szalmas, P. Dinka, T. Simon: CO₂ capture—new challenge in refinery industry, *MOL Scientific Mag. (Challenges)* **3**, 12–24 (2008)
- 32.3 J. van Straelen, F. Geuzebroek, N. Goodchild, G. Protopapas, L. Mahoney: CO₂ capture for refineries, a practical approach, *Int. J. Greenh. Gas Contr.* **4**, 316–320 (2010)
- 32.4 IEA: Prospects for CO₂ capture and storage. Energy technology analysis (International Energy Agency and Organization for Economic Co-operation and Development 2004)
- 32.5 A. Samanta, A. Zhao, G.K.H. Shimizu, P. Sarkar, R. Gupta: Post-combustion CO₂ capture using solid sorbents: A review, *Ind. Eng. Chem. Res.* **51**, 1438–1463 (2010)
- 32.6 F. Dong, H. Lou, M. Goto, T. Hirose: The petlyuk PSA process for separation of ternary gas mixtures: Exemplification by separating a mixture of CO₂-CH₄-N₂, *Sep. Purif. Technol.* **15**, 31–40 (1990)
- 32.7 E.S. Kikkindes, R.T. Yang: Concentration and recovery of CO₂ from flue gas by pressure swing adsorption, *Ind. Eng. Chem. Res.* **32**, 2714–2720 (1993)
- 32.8 R.V. Sirwardance, M.S. Shen, E.P. Fisher, J.A. Poston: Adsorption of CO₂ on molecular sieves and activated carbon, *Energy Fuels* **15**, 279–284 (2001)
- 32.9 D.D. Do, K. Wang: A new model for the description of adsorption kinetics in heterogeneous activated carbon, *Carbon* **36**, 1539–1554 (1998)
- 32.10 M. Andrei, M. De Simoni, A. Delbianco, P. Cazzani, L. Zanibelli: Enhanced oil recovery with CO₂ capture and sequestration. In: *Proc. 21st World Energy Congr., Montréal* (2010)
- 32.11 H. Al-Muslim, I. Dincer: Thermodynamic analysis of crude oil distillation systems, *Int. J. Energ. Res.* **29**, 637–655 (2005)
- 32.12 D. Bonaquist: *Analysis of CO₂ Emissions, Reductions and Capture for Large Scale Hydrogen Production Plants* (Prazair, Daubury 2010)
- 32.13 MathPro Inc.: An introduction to petroleum refining and the production of ultralow sulfur gasoline and diesel fuel, theicct.org (2011) Report prepared for the International Council on Clean Transportation (ICCT)
- 32.14 I. Staffell: *The Energy and Fuel Data Sheet* (Univ. Birmingham 2011) http://www.academia.edu/1073990/The_Energy_and_Fuel_Data_Sheet
- 32.15 Hydrocarbon Publishing Company: *Refinery CO₂ Management Strategies* (Hydrocarbon, Frazer 2010)
- 32.16 M.A. Fahim, T.A. Al-Sahaf, A.S. Elkilani: *Fundamentals of Petroleum Refining* (Elsevier, Amsterdam 2010)
- 32.17 EIA: *US Energy Information Agency Annex 4: IPCC Reference Approach for Estimating CO₂ Emissions from Fossil Fuel Combustion* (EIA, Washington 2011)
- 32.18 EIA: *US Energy Information Agency, Appendix N. Emission Factors for Steam and Chilled/Hot Water* (EIA, Washington 2013)
- 32.19 EIA: US Energy Information Agency, <http://www.eia.gov/todayinenergy/detail.cfm?id=9130> (EIA, Washington 2014)
- 32.20 J.H. Gary, G.E. Handwerk: *Petroleum Refining: Technology and Economics*, 3rd edn. (Marcel Dekker, New York 1994)
- 32.21 J. McKetta Jr.: *Petroleum Processing Handbook*, 1st edn. (Marcel Dekker, New York 1992)
- 32.22 G. Collodi, F. Wheeler: Hydrogen production via steam reforming with CO₂ capture, *Chem. Eng. Trans.* **19**, 37–42 (2010)
- 32.23 L.M. Wolschlag, K.A. Couch, F.X. Zhu, J. Alves: *UOP FCC Design Advancements to Reduce Energy Consumption and CO₂ Emissions* (UOP LLC, Des Plaines 2009)
- 32.24 K. Nillson, L. Zetterberg, M. Ahman: *Allowance Allocation and CO₂ Intensity of the EU15 and Nor-*

- wegian Refineries (IVL Swedish Environmental Research Institute, Stockholm 2005)
- 32.25 I. Moore: Reducing CO₂ emissions, *Pet. Technol. Q. Q2*, 1–6 (2005)
- 32.26 C.C. Wear: The concept of delta coke, *Catalagram* **106**, 3–9 (2009)
- 32.27 U.T. Turaga, R. Ramanathan: Catalytic naphtha reforming: Revisiting its importance in the modern refinery, *J. Scientific Ind. Res.* **62**, 963–978 (2003)
- 32.28 J.G. Speight: *Gas Processing: Environmental Aspects and Methods* (Butterworth Heinemann, Oxford 1993)
- 32.29 S. Mokhtab, W.A. Poe, J.G. Speight: *Handbook of Natural Gas Transmission and Processing* (Elsevier, Amsterdam 2006) pp. 261–294
- 32.30 B. Jiang, X. Wang, M.L. Gray, Y. Duan, D. Luebke, B. Li: Development of amino acid and amino acid-complex based solid sorbents for CO₂ capture, *Appl. Energ.* **109**, 112–118 (2013)
- 32.31 C. Wein, G. Puxty, P. Feron: Amino acid salts for CO₂ capture at flue gas temperatures, *Chem. Eng. Sci.* **107**, 218–226 (2014)
- 32.32 H. Mounzer: Reducing CO₂ emissions from refineries through amine chemistry upgrade. In: *Proc. 3rd Kuwait Chem. Conf., Kuwait City* (2014)
- 32.33 M. Stockle, T. Bullen: Integrating refinery CO₂ reduction strategies into your refinery. In: *Proc. 31st ERTC Sustainable Refining Conf., Brussels* (2008)
- 32.34 J. van Straelen, F. Geuzebroek, N. Goodchild, G. Protopapas, L. Mahoney: CO₂ capture for refineries: A practical approach, *Energ. Procedia* **1**, 179–185 (2009)
- 32.35 US EPA: Available and Merging Technologies for Reducing Greenhouse gas Emissions from the Petroleum Refining Industry (Office of air and radiation, Research Triangle Park 2010)
- 32.36 Ecofys: Methodology for the free allocation of emission allowances in the EU: ETS post 2012 (Sector report for the refinery industry 2009)
- 32.37 J. Martin, J. Lumberras, M.E. Rodríguez: Testing flare emission factors for flaring in refineries, <http://www.epa.gov/ttnchie1/conference/ei12/poster/martin.pdf> (2014)
- 32.38 Code of Federal Regulations: Calculating GHG emissions. Title 40, CFR 98.253, <http://www.law.cornell.edu/cfr/text/40/98.233>
- 32.39 I. Al-Hajri: *Integration of Hydrogen and CO₂ Management Within Refinery Planning*, Ph.D. Thesis (Chemical Engineering Department, Univ. Waterloo, Waterloo 2008)
- 32.40 A. Szklo, R. Schaeffer: Fuel specification, energy consumption and CO₂ emission in oil refineries, *Energy* **32**, 1075–1092 (2007)
- 32.41 M. Petrick, J. Pellegrino: *The Potential for Reducing Energy Consumption in the Refining Industry*, Report No. ANL/ESD/TM-158 (Argonne National Laboratory, Lemont 1999)
- 32.42 Liberty Gases: CO₂ fact sheet, <http://www.libertygases.com/carbon-dioxide.html> (2011)
- 32.43 IPIECA: Oil and gas industry guidance on voluntary sustainability reporting. Appendix D: Measurements units and conversion factors, 2014, http://www.ipieca.org/system/files/uploads/IPIECA_Reporting_Guidance_Measurement_units.pdf (London, 2014)
- 32.44 D. Johansson, P. Franck, T. Berntsson: CO₂ capture in oil refineries: Assessment of the capture avoidance costs associated with different heat supply options in a future energy market, *Energ. Convers. Manag.* **66**, 127–142 (2013)
- 32.45 D. Johansson, P. Franck, K. Pettersson, T. Berntsson: Comparative study of Fischer–Tropsch production and post-combustion CO₂ capture at an oil refinery: Economic evaluation and GHG (greenhouse gas emissions) balances, *Energy* **59**, 387–401 (2013)
- 32.46 D. Johansson, J. Rootze, T. Berntsson, F. Johnsson: Assessment of strategies for CO₂ abatement in the European petroleum refining industry, *Energy* **42**, 375–386 (2012)
- 32.47 S.M. Al-Salem: Carbon dioxide (CO₂) emission sources in Kuwait from the downstream industry: Critical analysis with a current and futuristic view, *Energy* **81**, 575–587 (2015)

Petroche

Part D

Part D Petrochemicals

33 Conventional Lube Base Stock

Brent E. Beasley, Laguna Woods, USA

34 Premium Lubricant Base Stocks by Hydroprocessing

Stephen K. Lee, Oakland, USA

John M. Rosenbaum, Santa Cruz, USA

Yalin Hao, Richmond, USA

Guan-Dao Lei, Richmond, USA

35 Synthetic Lubricant Base Stock

Margaret M. Wu, Annandale, USA

Suzzy C. Ho, Annandale, USA

Shuji Luo, Annandale, USA

36 Catalytic Processes

for Light Olefin Production

Genquan Zhu, Beijing, China

Chaogang Xie, Beijing, China

Zaiting Li, Beijing, China

Xieqing Wang, Beijing, China

37 Polyolefins

David Fiscus, Baytown, USA

Antonios Doufas, Baytown, USA

Sudhin Datta, Baytown, USA

38 Biomass to Liquid (BTL) Fuels

Gary Brodeur, Hillsboro, USA

Subramanian Ramakrishnan, Tallahassee,
USA

Chang Samuel Hsu, Tallahassee, USA,
Changping, China

39 Renewable Diesel and Jet Fuels

Henrik Rasmussen, Houston, USA

40 Small Scale Catalytic Syngas Production with Plasma

Adam A. Gentile, Clermont, USA

Leslie Bromberg, Cambridge, USA

Michael Carpenter, Research Triangle
Park, USA

41 Hydrocarbon Processing by Plasma

Robert J. Wandell, Tallahassee, USA

Bruce R. Locke, Tallahassee, USA

Conventional

33. Conventional Lube Base Stock

Brent E. Beasley

This chapter reviews the basic unit processes in modern conventional lube manufacturing. As this is a large subject area, this chapter will focus on giving the reader an overview of the major processes most frequently found in the lube-manufacturing plant. It will neither cover all technologies or processes nor will it discuss detailed plant design and operation as this would easily require another book. The reader should come away with a general understanding of the conventional lube-manufacturing process and key factors affecting the unit processes.

33.1	Lube Base Stock Manufacturing	958
33.2	Key Base Stock Properties	959
33.2.1	Lube Oil Feedstocks	959
33.3	Lube Oil Chemistry	960
33.4	Typical Lube Processes	960
33.4.1	Lube Vacuum Distillation Unit (VDU) or Vacuum Pipestill (VPS) – Viscosity and Volatility Control	960
33.4.2	Solvent Extraction – Viscosity Index Control	960
33.4.3	Solvent Dewaxing – Pour Point Control	960
33.4.4	Hydrofinishing – Stabilization	961
33.4.5	Solvent Desphalting	962
33.4.6	Refined Wax Production	962
33.5	Key Points in Typical Lube Plants	962
33.6	Base Stock End Uses	963
33.7	Lube Business Outlook	963
33.8	Feedstock Selection	963
33.8.1	Lube Crude Selection	963
33.9	Lube-Crude Assays	964
33.10	Vacuum Distillation	965
33.10.1	Feed Preheat Exchangers	967
33.10.2	Pipestill Furnace	967
33.10.3	Tower Flash Zone	967
33.10.4	Tower Wash Section	967
33.10.5	Wash Oil	967
33.10.6	Purpose of Pumps	967
33.10.7	Tower Fractionation	967
33.10.8	Fractionation Packing	967
33.10.9	Bottoms Stripping Section	968
33.10.10	Sidestream Strippers	969
33.10.11	Overhead Pressure	969
33.10.12	Tower Overhead Pressure with Precondensers	969
33.10.13	Tower Overhead Without Precondensers	969
33.10.14	Tower Pressure – Ejectors	969
33.10.15	Factors Affecting Lube Distillate Production	969
33.11	Pipestill Troubleshooting	970
33.11.1	Material Balance and Viscosity Measurements	970
33.11.2	Tower Pressure Survey	970
33.12	Solvent Extraction	971
33.12.1	The Characteristics of a Good Extraction Solvent	971
33.12.2	Extraction Process	972
33.12.3	Extraction Process Variables	973
33.12.4	Solvent Contaminants	973
33.12.5	Solvent Recovery	974
33.12.6	Minimizing Solvent Losses	975
33.13	Corrosion in NMP Plants	978
33.14	Analytical Tests for Extraction	978
33.15	Dewaxing	978
33.16	The Role of Solvent in Dewaxing	979
33.17	Ketone Dewaxing Processes	980
33.17.1	Incremental Ketone Dewaxing Plant	980
33.17.2	DILCHILL™ Dewaxing	981
33.17.3	Dewaxing Process Variables	981
33.18	Process Variable Effects	982
33.19	Solvent Composition	982
33.19.1	Miscible and Immiscible Operations	982
33.19.2	Effect of Viscosity on the Filtration Rate	983
33.19.3	Effect of the Chilling Rate on the Filtration Rate and Dewaxed Oil Yield	983
33.19.4	Effect of Temperature Profile	983
33.19.5	Effect of Solvent Dilution Ratio	984
33.19.6	Effect of Water	984

33.19.7	Effect of Increased Raffinate VI.....	984	33.29	Two-Stage Dewaxing	1002
33.19.8	Effect of Pour Point Giveaway on Product Quality and Dewaxed Oil Yield.....	985	33.30	Deoiling	1003
33.20	Scraped Surface Equipment	985	33.31	Propane Dewaxing	1005
33.20.1	Scraped Surface Equipment Suppliers	986	33.31.1	Effect of Water.....	1006
33.20.2	SSE Equipment Issues.....	993	33.32	Two-Stage Propane Dewaxing	1007
33.21	Filters	993	33.32.1	Propane Deoiling.....	1007
33.21.1	Operation.....	993	33.32.2	Propane Filter Washing with Hot Kerosene.....	1007
33.21.2	Filter Media.....	994	33.33	Analytical Tests in Dewaxing	1007
33.22	Cold Wash Distribution	997	33.34	Dewaxing Aids	1007
33.23	Wash Acceptance	998	33.35	DWA Mechanism	1008
33.24	Wash Efficiency	998	33.36	Asphaltene Contamination	1009
33.25	Filter Hot Washing	1000	33.37	Regulatory Requirements	1009
33.26	Dewaxed Oil/Wax-Solvent Recovery	1001	33.38	Glossary	1009
33.27	Solvent Dehydration	1001	References		1013
33.28	Solvent Splitter	1002			

33.1 Lube Base Stock Manufacturing

Lubes and specialties are high-value products that have a variety of end uses. Some end uses include:

- *Automotive*: engine oils, automatic transmission fluids (ATFs), gear oils
- *Industrial*: machine oils, greases, electrical oils, gas turbine oils
- *Medicinal*: food grade oils for ingestion, lining of food containers, baby oils
- *Specialty*: food grade waxes, waxes for candles, fire logs, cardboard.

Lube manufacturing is a complex process and it involves several processing steps. Crude is distilled and the bottoms, atmospheric resid, is sent to a vacuum distillation unit (VDU) sometimes called a vacuum pipestill (VPS) for further fractionation. Vacuum fractionation is used to separate the atmospheric resid into several feed streams or distillates. Conventional solvent processing uses selected solvents in physical processes to remove undesirable molecules (asphaltenes, aromatics, *n*-paraffins). Hydroprocessing is used to convert or remove the trace undesirables such as nitrogen, sulfur and multiring aromatics, or to enhance the base stock properties to make specialty, high-quality products.

The manufacture of lubes and specialty products makes a significant contribution to refining profitability, even though the yields and therefore volumes are relatively small.

The business drivers of the lube business are for increased production to reduce per barrel costs, to reduce

operating costs (OPEX), and for higher quality products to meet ever increasing product quality standards.

Refiners produce base stocks or base oils, and lube oil blenders produce finished oils or formulated products:

- Base stocks are products produced from the lube refinery without any additives in the oil or wax.
- Base oils are blends of base stock.
- Finished oils or formulated products are blends of base stock or base oil with special additives.

Lube base stocks are given various names. Some of the common names include:

1. Neutrals – from virgin distillates, for example, 100 N, 150 N, 600 N
2. Bright stock – from deasphalted oil (DAO), for example, BS150
3. Grades – for example, Society of Automotive Engineers (SAE) 5, 10, 30, etc.; ISO 22, 32.

The most common name is neutral (N) which was derived in the days when the lube distillates were acid treated (sulfuric acid) followed by clay filtration. After the clay treating, the oil was acid free or neutral. The viscosity number in this example, 150 N, is the approximate mid-point viscosity of the grade range in the ASTM (American Society for Testing and Materials)/BSI (British Standards Institution) Viscosity Classification System expressed in Saybolt seconds universal

(SUS) at 100 °F (≈ 38 °C). Bright stock is a heavy lube grade that is made from deasphalted resid. The name refers to the *bright* appearance of the product as compared to the resid feed. Bright stocks are very viscous. A typical bright stock, BS150, has a viscosity of 150 SSU at 210 °F (≈ 100 °C).

Grades may refer to the actual viscosity. For example, International Standards Organization (ISO) = cSt at 40 °C. Grades may be also be assigned arbitrarily, such as those assigned by the Society of Automotive Engineers (SAE).

There are many other grade names that are used to differentiate special products. These products may have special high-valued qualities that may make them very profitable, even though they tend to be lower volume products.

33.2 Key Base Stock Properties

Viscosity is a key lube oil property and is a measure of the fluidity of the oil. There are two measures of viscosity commonly used; kinematic and dynamic. The kinematic viscosity is flow due to gravity and ranges from approximately 4 to 20 cSt (centistokes) for solvent neutrals and about 30–32 cSt at 100 °C for bright stock. The dynamic viscosity is flow due to applied mechanical stress and is used to measure low-temperature fluidity. Brookfield viscosity for ATFs at -40 °C and cold cranking simulator (CCS) for engine oils at -25 °C are examples of dynamic viscosity measurements.

Lube-oil volatility is a measure of oil loss due to evaporation. NOACK volatility measures the actual evaporative loss which is grade dependent and can run 6–35 wt%.

The gas chromatographic distillation (GCD) can be used to measure the front end of the boiling point curve and may be used as an indication of volatility, for example, 10% off at 375 °C.

VI is based on an arbitrary scale that is used to measure the change in viscosity as a function of temperature. The scale was first developed in 1928 and was based on the *best* and *worst* known lubes at the time. The best paraffinic lube was assigned a value VI = 100 and the worst naphthenic was assigned a value VI = 0. The quality of base stock has been improved dramatically since 1928 with the VI of high-quality base stock in the 150+ range.

The pour point is the temperature at which the fluid ceases to pour and is nearly a solid. Typically, the pour point ranges from -6 to -24 °C for heavy to light neutrals.

The cloud point is the temperature at which wax crystals first appear.

Base stocks are assigned to five categories [33.1]:

1. Group I base stocks contain less than 90% saturates and/or greater than 0.03% sulfur and have a viscosity index (VI) greater than or equal to 80 and less than 120.
2. Group II base stocks contain greater than or equal to 90% saturates and less than or equal to 0.03% sulfur and have a VI greater than or equal to 80 and less than 120.
3. Group III base stocks contain greater than or equal to 90% saturates and less than or equal to 0.03% sulfur and have a VI greater than or equal to 120.
4. Group IV base stocks are polyalphaolefins (PAOs).
5. Group V base stocks include all other base stocks not included in Groups I–IV.

Saturates, aromatics, naphthenes are measures of these molecular types present in the base stock.

Color (appearance) and stability are the measure of color and change in the presence of light or heat.

Conradson carbon (CCR) or micro-carbon residue (MCR) is a measure of the ash left after flame burning. Additional base oil quality considerations may be found in [33.2].

33.2.1 Lube Oil Feedstocks

Lube oil feedstocks are taken from the bottom of the crude barrel (Fig. 33.1).

Lube crudes are generally paraffinic or naphthenic in composition. A paraffinic crude is characterized by a higher wax content. West Texas and Arab Light are good-quality paraffinic crudes. Naphthenic crudes are characterized by their low wax content, and they make low-to-medium quality lubes, for example, South Louisiana. In conventional solvent lubes, the atmospheric resid (bottoms from the crude distillation tower) is upgraded to lube products through the following processes:

- Vacuum distillation
- Solvent extraction (*n*-methyl-2-pyrrolidone (NMP), furfural, phenol)
- Solvent dewaxing (methyl ethyl ketone (MEK)/methyl isobutyl ketone (MIBK), MEK/toluene, propane)
- Hydrofinishing (may be integrated with extraction)
- Propane deasphalting
- Hydroprocessing for higher quality.

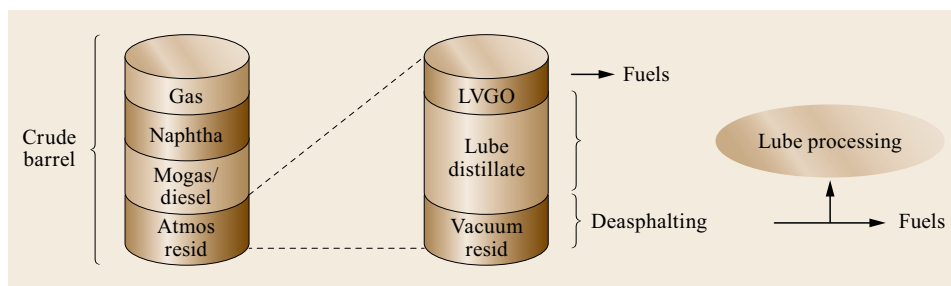


Fig. 33.1 Lube plant feedstocks are taken from the bottom of the crude barrel

Table 33.1 Lube oil molecules contribute to lube oil properties

Molecule	Base stock quality affected	Process involved
<i>n</i> -Paraffin	High pour, VI no S and CCR	Dewaxing
<i>i</i> -Paraffin	High VI and sats, med pour	
2 Ring naphthene	Mid VI, low pour, high acids	Extraction, hydrofinishing
1 Ring aromatic	Mid to high VI	Extraction
Multi-ring naphthene	Low VI, low pour, high acids	Extraction, hydrofinishing
Multi-ring aromatic	Low VI, low pour	Extraction
Organic sulfur	Good stability, antioxidant	Hydrofinishing
Organic nitrogen	Poor stability	Hydrofinishing
Organic sulfur and nitrogen	Removed by hydrofinishing	Hydrofinishing
Asphaltenes	High CCR, poor color	Distillation, deasphalting

33.3 Lube Oil Chemistry

Lube oil is produced from a wide variety of crude oil molecules. The molecular types and their effect on lube

oil quality are summarized in Table 33.1, along with the lube processes that act on them.

33.4 Typical Lube Processes

The typical lube process is depicted in Fig. 33.2 and 33.3. In the following, the individual process steps are explained. The impact of each step on the product quality is summarized in Table 33.2.

33.4.1 Lube Vacuum Distillation Unit (VDU) or Vacuum Pipestill (VPS) – Viscosity and Volatility Control

The VPS is generally the first process unit. The VPS's goal is to fractionate the atmospheric resid or reduced crude so that the base stock will have the desired viscosity. The fractionation also controls the volatility and it is required to meet base stock volatility specifications. Fractionation also controls the flash point. The boiling point separation is accomplished by using high-efficiency distillation/fractionation hardware. Secondary effects include asphalt segregation in the vacuum resid from the VPS (potential by-product), reduction in CCR, and color improvement.

33.4.2 Solvent Extraction – Viscosity Index Control

Extraction is typically the second process, although this is not always the case. The primary goal of extraction is to develop the VI that is required and to make the saturates content that is required. This is accomplished through solvent extraction of the aromatic fraction of the distillate using NMP, furfural, or phenol. The VI is raised by removing the aromatic (low VI) molecules. Secondary effects of extraction include reduction in the refractive index, density, and CCR, and improvement in color and oxidative stability.

33.4.3 Solvent Dewaxing – Pour Point Control

Solvent dewaxing is usually the last process unit, because the dewaxer is the most expensive to build, has the highest operating costs, and is the most complex

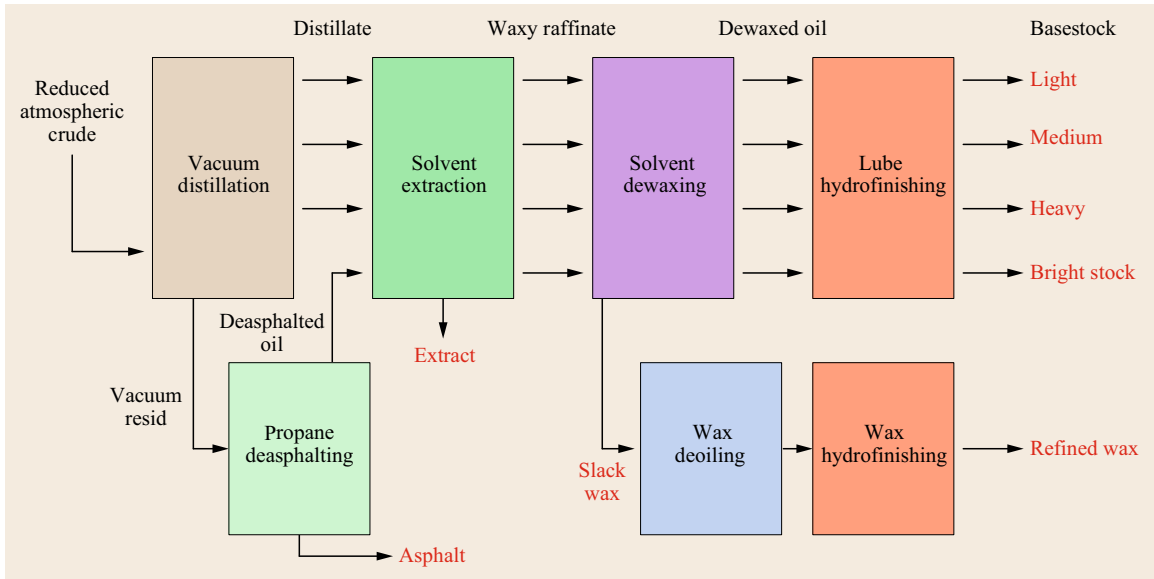


Fig. 33.2 Typical lube process flowchart

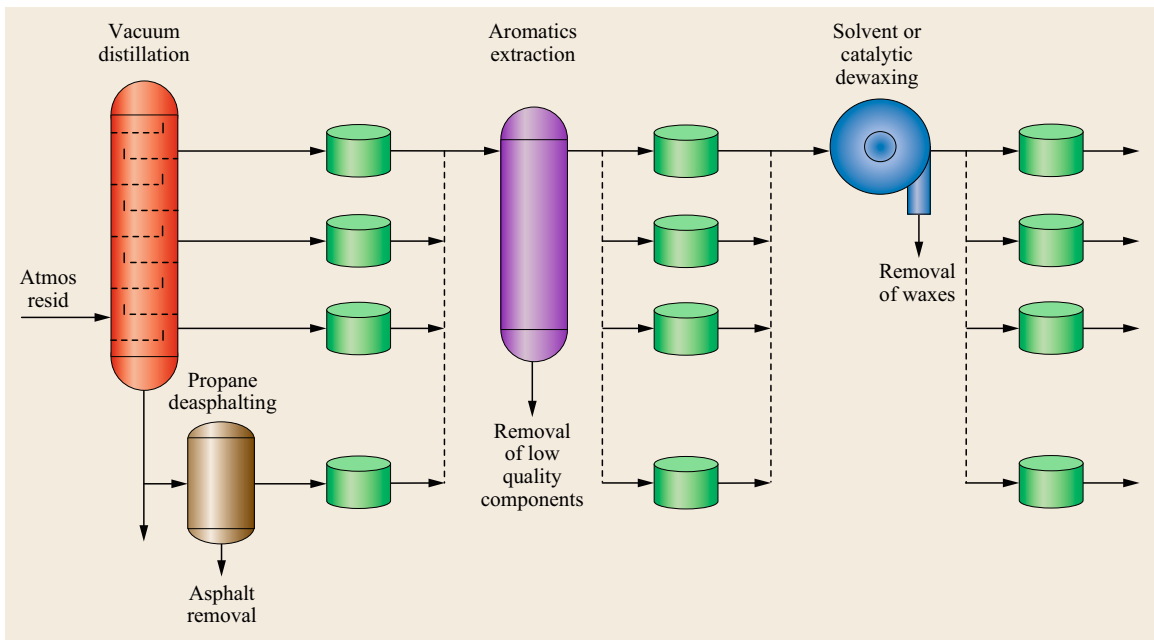


Fig. 33.3 Lube-manufacturing scheme

to operate. The primary goal of solvent dewaxing is to make the pour and cloud point requirements. This is accomplished by paraffin separation by the solubility of nonparaffins in cold solvent, fractional crystallization, and filtering the sold paraffins from the slurry. This may be done in *ketone* units which use MEK, MEK/MIBK, and MEK/toluene solvents, or in propane units which use liquefied propane as the solvent. Secondary effects

include viscosity increase, density increase, sulfur and CCR increase.

33.4.4 Hydrofinishing – Stabilization

Hydrofinishing follows extraction or dewaxing. The primary goal is to improve appearance (color and color-hold) and to remove impurities such as the solvent,

Table 33.2 Summary of lube process impact on product quality

	Distillation	Deasphalting	Extraction	Dewaxing	Hydrofinishing
Feed stock	Atmospheric resid	Vacuum resid	Distillate or deasphalted oil	Raffinate	Raffinate or dewaxed oil
Lube product	Distillate	Deasphalted oil	Raffinate	Dewaxed oil	H/F oil
By-products	Vacuum resid	Asphalt	Extract	Wax	Naphtha
Main lube quality improved	–	Con carbon ↓	VI ↑	Pour point ↓	Color improved
Secondary lube quality changes density (SG)	Varies	↓	↓	↑	↓
Gravity (API)	Varies	↑	↑	↓	↑
Viscosity	Varies	↓	↓	↑	↓
Viscosity index (VI)	–	↑	↑ ^a	↓	↑ (slightly)
Color (ASTM)	↓	↓	↓	–	↓ ^a
Pour point	–	–	–	↓ ^a	–
Cloud point	–	–	–	↓	–
Conradson carbon	↓	↓ ^a	↓	↑	↓
Sulfur	–	↓	↓	↑	↓
Nitrogen	–	↓	↓	↑	↓
Saturates	–	↑	↑	↓	↑ (slightly)
Hash point	↓	–	–	–	–
Refractive index	–	↓	↓	↑	↓

^a – Indicates main lube product quality improvement

nitrogen, acids, and sulfur to meet the required specification. This is accomplished by hydrogen saturation and chain breakage that uses hydrogen at mild pressures and temperatures in the presence of a catalyst. Secondary effects include slight improvement in VI, slight improvement in saturates, reduction in viscosity, lower acidity, reduction in CCR.

33.4.5 Solvent Desphalting

When used it always precedes extraction. The primary goal is to remove asphaltenes, which could be a possible by-product and to make the viscosity specification that is required. This is accomplished by asphaltenes separation by the solubility of nonasphaltenes in a solvent

and the precipitation of asphaltenes using, for example, propane as a solvent. Secondary effects include a reduction in CCR and metals, an increase in saturates and VI, and color improvement.

33.4.6 Refined Wax Production

Wax deoiling and hydrofinishing follow the dewaxing unit. The primary goal is to reduce the oil content of the wax and to meet melting point and needle penetration requirements. This is accomplished by soft wax solubility and physical separation in the deoiling equipment. Hydrofinishing's goal is hard wax saturation and chain breakage. Secondary effects include the removal of impurities, color improvement.

33.5 Key Points in Typical Lube Plants

- The majority of operations are *blocked operation* instead of *in-step*. Blocked operation requires intermediate tankage between units and allows the optimum operation of each unit on each viscosity grade.
- The dewaxing unit is usually the last unit in the manufacturing process. The dewaxer is the most expensive to build, has the highest operating costs, and is the most complex to operate.
- Bright stock is the most expensive conventional lube to manufacture and requires the addition of a deasphalting unit.
- Integration of extraction and hydrofinishing units saves energy, and the elimination of a hydrofiner furnace saves capital. However, this arrangement is less flexible than a stand-alone hydrotreater.

There are exceptions to the general flow. Some plants that process extremely high wax content crudes position dewaxing after vacuum distillation. Some plants position high-pressure hydrotreating upstream of dewaxing.

Hydroprocessed lubes will be covered in other chapters and include:

- Lubes hydrocracking
- Wax isomerization
- White oils hydrogenation
- Catalytic dewaxing.

Other processes include:

- Clay contacting or acid treating, both are older stabilization processes.
- Duo – Sol a process that combines propane deasphalting and solvent extraction.

33.6 Base Stock End Uses

Conventional lube base stocks are formulated into a multitude of finished products:

- Motor oils
- Transmission fluids
- Gear oils
- Turbine oils
- Hydraulic oils
- Metal working (cutting) oils

- Greases
- Paper machine oils.

Specialty products may include:

- White oils: foods, pharmaceuticals, and cosmetics
- Agricultural oils: orchard spray base oils
- Electrical oils: electrical transformers (heat transfer).

33.7 Lube Business Outlook

Lubricant base stocks are produced in approximately 170 refineries worldwide which have a total capacity of over 900kBD (kBD = kilo barrels per day). The average capacity utilization is somewhere around 80%, to meet an industry demand of just over 700kBD. However, almost all new capacity is hydroprocessing based, making Group II or Group III base stocks. Hydroprocessing quality and cost advantages continue to apply economic pressure on conventional lube manufacturing and additional rationalizations are expected with a subsequent loss of manufacturing share.

The lubricant market is roughly equally split between transportation lubricants (engine crankcase oils, transmission fluids, greases, etc.) and industrial process oils. Demand is growing at an average rate of 1%/yr, as

robust growth in the developing economies (e.g., China, India) is being partially offset by declining demand in the mature markets (North America, Europe) due to extended drain intervals for the higher quality engine oils. Engine builders tend to drive the transportation lubricant quality, as economic and environmental drivers push engine oils toward better oxidation stability, better low-temperature properties, lower volatility, and lower viscosity. These desired characteristics drive formulators to favor hydroprocessed base stocks which have higher VI. However, many other applications, such as most industrial and process oils, as well as older engine oils, still favor the characteristics of solvent-refined Group I base oils, which are expected to continue to play an important role in meeting the world's lubricant needs for years to come.

33.8 Feedstock Selection

Crude selection is extremely important for the profitable production of lubes. Downstream unit operability is affected by crude selection as are rates and yields. Typically, manufacturers would prefer operating at maximum throughput, thereby spreading costs over a larger volume. Poor crude selection can result in downstream bottlenecks reducing overall throughput.

33.8.1 Lube Crude Selection

Lube oil manufacturers may have a lube crude approval (LCA) process to assess the opportunity to manufacture base stocks from crudes available in the marketplace. The LCA process defines the detailed steps to qualify a new crude for purchase by

the refinery to make base stock and/or wax products.

The first step entails identifying economically attractive crudes. These crudes are characterized, or assayed, to quantify their lube yield and qualities. The assay process includes subjecting a small sample of the crude to an atmospheric distillation, vacuum distillation, extraction, and dewaxing to produce the desired base stock products. This information enables the manufacturer, through the use of modeling techniques, to predict the process response of the crude of interest to make the required base stock products. These modeling techniques may also allow the manufacturer to investigate process variables and operating optimization for distillation, extraction, and dewaxing to assess manufacturing flexibility. Not all crudes are acceptable for base stock manufacturing as yields may be too low or base stock products may not meet requirements.

With an acceptable assessment of the new crude, the refiner may elect to validate the crude for base stock manufacture. This may entail running a plant test to make base stock products from the new crude. The products made from the plant test are typically blended into formulated oils and subjected to testing to demonstrate acceptable product performance.

Results of the plant test are reviewed with a focus on lube plant manufacturing performance and base stock product quality to determine if the new crude can be approved for base stock manufacture:

1. Lube plant manufacturing performance – actual rate, yield, and operability. The actual operating conditions are compared to the predicted processing conditions to assess if the new crude processed as expected.
2. Base stock product quality – Plant testing protocol should be defined to ensure base stock products meeting acceptable quality specifications are made. Care should be taken to avoid making base stocks that may not be representative of how the crude will typically be processed to make base stocks. The range of acceptable base stock qualities should be defined by the test protocol. Plant test product disposition may need to be defined as part of the plant test.
3. Options may include blending the plant test products to dilute the new crude component or quarantining the product tank until product testing has been completed. Product testing failure will prevent the crude from being approved.
4. Results from the manufacturing test will determine if the crude will be accepted. The certification test must have been acceptable and the crude processed as expected. There must not be any evidence that base stock quality is unacceptable. If the above is completed successfully, the crude may be approved and added to the manufacturer's list of approved crudes.

The approval protocol may require periodic re-evaluation of the crude in recognition that the crude may change.

33.9 Lube-Crude Assays

A lube-crude assay is a laboratory process to measure the lube processing response from crude to base oil. It is an important step in a manufacturer's lube crude selection. A crude assay will include process yields for desired base oils at their quality specifications. The manufacturer can use the assay data to predict the process response for their refinery and to assess the desirability of purchasing particular crude. The assay results may be used to calculate the impact on profitability.

Key steps to complete a typical lube assay include:

1. Secure a representative sample of the crude. This may best be achieved by collecting a sample at a load port.
2. Fractionate the crude into discreet components first to separate the light, nonlubes boiling material. The bottoms are then sent to a high vacuum distillation.

The distillation produces several distillate blends for extraction. The distillates produced are sufficient to cover the base stock viscosity range.

3. The distillates are then extracted using a lab pilot unit and the preferred extraction solvent (e.g., furfural, NMP, or phenol). Waxy raffinates are produced from the extraction.
4. The waxy raffinates are then dewaxed using solvents of interest (MEK, MEK/MIBK, MEK/toluene, etc.) to produce a dewaxed oil and a slack wax.
5. The dewaxed oils will be characterized to quantify their properties and yields. This will enable an economic assessment to be made with respect to the crude's lube potential.

There are several lube assay objectives in distillation. One is to relate key lube properties such as

viscosity, sulfur, density, refractive index, etc. to boiling point. Another is to determine the yield of material boiling in the lube range and a third is to determine the yield of material boiling in the asphalt range.

The objectives of the lube assay extraction are to generate data that will determine the ability of the crude to produce base oil capable of meeting the base oil specifications. Obviously, this is of great importance in the selection of lube crudes for the plant. Key lube oil qualities related to process response are determined over the full lube oil viscosity range. Yields are used in manufacturing economic calculations. All crudes were not created equal, although there may be similarities

in a given region. For example, Middle Eastern crudes may contain high sulfur, high aromatics, and high isoparaffins, while North Sea crude may be low in sulfur, contain high saturates, and have a medium wax content. There are always outliers in every region. Crude production from a given *field* may change over time. If so, this may require that the assay is repeated to update the crude's relevant information to remain current.

In summary, the lube assay will characterize the potential of a crude to produce a specific base stock (viscosity, VI, saturates, wax, sulfur, basic nitrogen, etc.) and to determine the expected yields from distillation, extraction, and dewaxing.

33.10 Vacuum Distillation

Vacuum distillation is used to fractionate the heavier molecules in the crude. In the majority of plants, it is the beginning point for lube manufacturing. Vacuum distillation is applied to avoid the high-temperature fractionation, which would lead to undesirable coking and loss of lube oil yield.

Vacuum distillation equipment is often referred to as the VDU or VPS.

The objective of the VPS is to achieve test product quality for viscosity, volatility, and flash point. Maximizing the yield of the most valuable products requires using the right-cutting schemes. Steady control will minimize distillate variability. Good fractionation makes for sharp separation which is beneficial to good performance in downstream equipment. VPS per barrel costs can be minimized by operating the VPS at high capacity with long run lengths and making the best possible use of utilities and chemicals per barrel.

Fractionation is a separation by difference in boiling points of light and heavy components in the distillation tower achieved by the intimate contact between hot rising vapor with the cooler falling liquid. The hot vapor strips the lighter components from the liquid and the cold liquid condenses heavier components from the vapor. Stripping requires heat in order to vaporize the lighter components and the condensation of heavy components releases heat. Good contact between the phases is essential to achieve maximum fractionation efficiency. In the presence of vapor, the liquid may be carried upward in the form of a mist, foam, or spray, and may contaminate the desired distillates with heavy components. The contamination is known as entrainment and should be avoided.

The concept of a *theoretical stage* is a useful one and refers to the length of the VPS section required for the vapor and the liquid to reach equilibrium. The sharpness of the separation between adjacent streams

may be measured in theoretical stages or the minimum number of theoretical stages (N_s), which represents the number of theoretical stages at the infinite reflux to effect the separations.

Sidestreams from the distillation tower are typically named from the top (lighter products) down to the bottom (heavier streams). Typical atmospheric and vacuum sidestream nomenclature for a typical atmospheric and vacuum tower is shown in Table 33.3 (typical boiling point range of fractionated stream).

Cut points are used to describe the pipestill product. Volume cut points are the cumulative yield on the crude and is expressed as a liquid volume percent of the product. Temperature cut points are the boiling points that correspond to the volume cut point. A key objective of the VPS is to set the viscosity of the final product. This basic product property is set in the distillation by setting the cut points of the product streams. Nominal lube product boiling ranges are shown in Table 33.4. Volatility, another key product specification, is the amount of material removed at a certain temperature and is controlled in the distillation by cut point targets and front-end fractionation. It affects engine oil thickening and evaporative losses. The flash point is the

Table 33.3 Typical distillation tower sidestream names

Name	Description
AOH	Atmospheric overhead (−30–200 °C)
A1SS	Atmospheric 1, or first, sidestream (150–210 °C)
A2SS	Atmospheric 2, or second, sidestream (175–300 °C)
A3SS	Atmospheric 3, or third, sidestream (190–400 °C)
LVGO	Light vacuum gas oil, vacuum tower overhead (200–400 °C)
V1SS	Vacuum 1, or first, sidestream (350–425 °C)
V2SS	Vacuum 2, or second, sidestream (390–600 °C)
V3SS	Vacuum 3, or third, sidestream (450–620 °C)
VRES	Vacuum resid stream (500– > 900 °C)

Table 33.4 Nominal lube product boiling range

	Two product sidestreams (°C)	Three product sidestreams (°C)	Two product sidestreams (°F)	Three product sidestreams (°F)
Vacuum gas oil	345–385	345–370	650–725	650–700
Light neutral	385–455	370–425	725–850	700–800
Medium neutral	–	425–490	–	800–915
Heavy neutral	455–540	490–550	850–1005	915–1025
Overflash	540–580	550–580	1005–1075	1025–1075
Vacuum resid	580+	580+	1075+	1075+

ignition temperature above the liquid surface and affects engine oil thickening and is a safety concern for the storage of a liquid product. Cut point targets and fractionation in the main tower and stripper are used to control the product flash point.

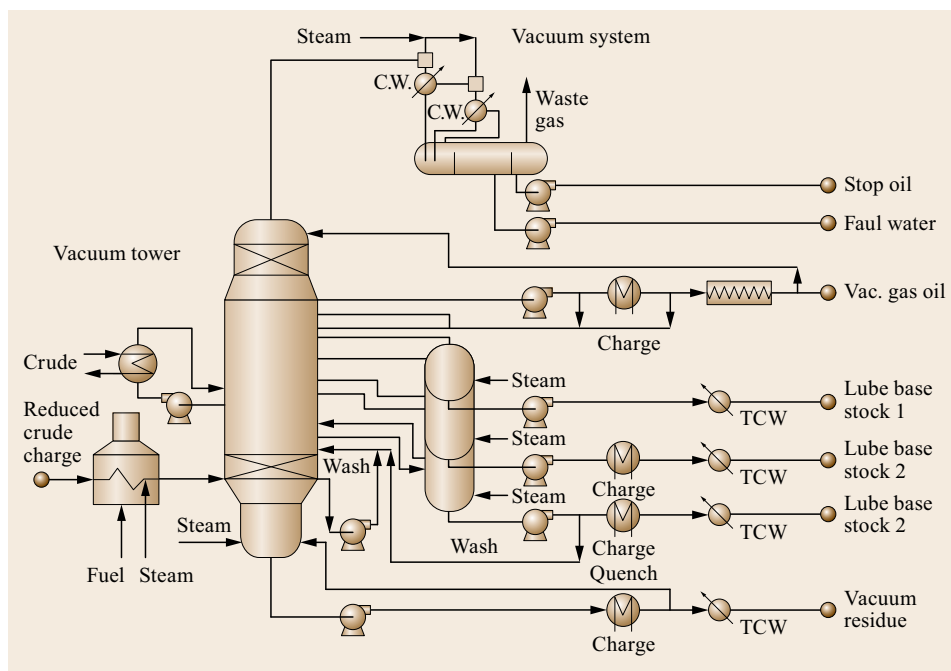
Distillate yields are affected by crude type, product viscosity and volatility specifications, the distillation tower-cutting scheme, fractionation efficiency, and the theoretical stages between the sidestreams. Poor fractionation efficiency can be caused by operating at feed rates above equipment design. If the feed is significantly lighter than the tower is designed to handle, fractionation efficiency may suffer. Mechanical damage such as dislodged or damaged internals, leaks or plugs in spray headers used to distribute liquids in the tower, leaking trays, etc. will degrade fractionation efficiency. Insufficient wash oil or reflux in the tower contributes to poor separation. The poor distribution of liquid or vapor reduces contact and leads to poor fractionation efficiency. When pumparound duties get out of balance fractiona-

tion efficiency is reduced. This can be caused by reflux rates being above or below design specifications and by flooding or entrainment occurring in overloaded sections of the tower.

Poor tower fractionation efficiency may adversely affect downstream lube operations. Insufficient separation of light grade front ends may result in light oil carryover in extraction, increasing solvent ratio requirements, possibly reducing throughput and will increase energy usage. Dewaxing throughput and yields are adversely affected across all grades by the presence of *tail ends*.

Crude oil was first distilled in batch distillation like a lab technique beginning in the 1850s. Advancements were made by increasing the size of the batch vessel. A continuous process was developed by using a series of batch stills – called a battery. The first continuous pipestill appeared in the 1920s and the *modern* pipestill came on the scene in the 1930s.

A typical lube VDU is shown in Fig. 33.4.

**Fig. 33.4** Typical lube vacuum tower design

33.10.1 Feed Preheat Exchangers

Feed preheat exchangers are used to recover heat from sidestreams and pumparounds and to make the overall distillation more energy efficient. Preheating minimizes the loss of heat to the atmosphere or cooling water. Heat integration reduces fuel consumption in the furnace and steam may be generated for stripping in the vacuum unit. Atmospheric and vacuum units may be heat integrated.

33.10.2 Pipestill Furnace

The furnace partially vaporizes the feed to the tower. A typical furnace has multiple parallel passes and the outlets are combined as feed to the distillation tower.

Steam may be injected into the vacuum furnace coil to increase the vaporization of feed at a lower temperature and to reduce the residence time. The vacuum cut points are set by the extent of the vaporization in the flash zone where temperatures may range from 390 to 420 °C. Furnace firing is controlled to achieve the desired vacuum cut point.

33.10.3 Tower Flash Zone

The flash zone is a large area in the tower that allows for the disengagement of liquid and vapor. The height of the zone affects the separation. The flash zone is designed to facilitate disengagement. Internals in this section consist of annular rings or vapor horns and collector rings for the bottoms stripping inlet.

33.10.4 Tower Wash Section

The wash section cleans entrained liquids from the flash zone vapor phase. Vapor in excess of the amount needed to meet distillate requirements is referred to as overflash. The wash section condenses the overflash. It also provides some fractionation between the heavy lube sidestream and the vacuum resid stream.

The wash zone may include a Glitsch grid or random packing. An open structure gives a low pressure drop while providing a high surface area to capture and retain resid. The resid is washed away by the wash oil that is applied through a spray header. The overflash, or spent wash, may be 40–50% resid and is removed and either sent to tankage as another sidestream or returned to the bottoms section for stripping. Maintaining wash oil flow is extremely important for efficient long-term operation. Loss of wash oil will result in rapid fouling.

33.10.5 Wash Oil

The wash oil that is used for de-entrainment is also important for improving the separation between the bottom sidestream and the resid stream. Separation is enhanced by the condensation of overflash by vaporizing the bottom sidestream. The amount of overflash that is required is affected by packing type, depth, and source of the wash oil. Overflash flow rates should be carefully monitored to make sure that there is no degradation in the bottom sidestream fractionation, there is no increase in pitch entrainment to the heavy solvent neutral stream, and there are no major increases in coking in the wash bed zone.

33.10.6 Purpose of Pumparounds

Pumparounds are used to remove heat from the tower and to adjust the vapor–liquid flow in the tower. They condense vapors rising in the tower and create an internal reflux for the fractionation stages below the pumparound. They also reduce vapor loads in sections of the tower above the pumparound. A pumparound takes liquid from the tower, cools it, and returns it higher up in the tower. The liquid condenses vapors in the pumparound section creating liquid reflux for fractionation lower in the tower. VPSs do not use overhead reflux seen in other distillation towers; a top pumparound is used instead.

33.10.7 Tower Fractionation

As mentioned earlier, fractionation is used to generate the various product sidestreams off the tower by condensing rising hot vapor with falling colder liquid. At each stage in the fractionation section, the highest boiling components are condensed, releasing heat that boils the highest liquid components putting them into the vapor phase. Contacting between the phases is needed for the heat and mass transfer. Contacting equipment may include bubble cap trays, sieve trays, Glitsch grid, structured packing, and many others. The number of theoretical stages between adjacent sidestreams typically varies from 1 to 3. The current trend is toward using packing.

33.10.8 Fractionation Packing

Packing used for fractionation can also reduce the pressure drop in a tower compared to trays. Tray designs are more limited in Delta P reduction. The packing surface allows intimate contact between vapor and liquid without having to have the vapor pass through the liquid. The liquid phase coats the packing surface as

a film so that the liquid phase movement is restricted only by the resistance of the packing surface. Packing has been used in high liquid loading service such as pumparounds and also in main fractionation sections. Packing is sensitive to liquid maldistribution, so spray rates, pan level control, and pumparound rate control are critical. A high-quality liquid distributor is preferred. Examples can be seen in Figs. 33.5 and 33.6.

If the liquid flow to the packing is low and a spray distributor is used, the sprays can collapse so that the liquid contact with the vapor degrades causing low viscosity and poor volatility of the stream below. If the pumparound rate is too high, liquid may be atomized at the spray distributor and the small liquid droplets may

be entrained upward. If the liquid stream is from the pumparound, the product above the pumparound will be contaminated with heavy components. If there is leakage or overflow from the sidestream draw off pan, the falling liquid does not contact the vapor, and it will reduce the viscosity of the stream below and also result in poor volatility.

33.10.9 Bottoms Stripping Section

The objective of the bottoms stripper is to strip distillate from the flash zone liquid, revaporize residual distillate that may be in the spent wash, and correction of bottoms flash. The bottom stripper typically has a design of

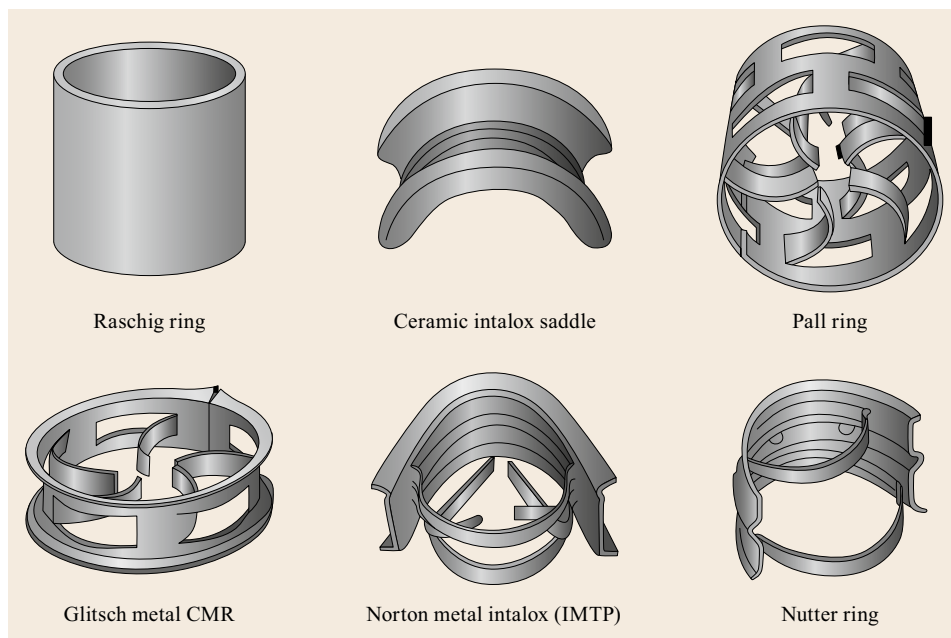


Fig. 33.5 Various types of random fractionation packing

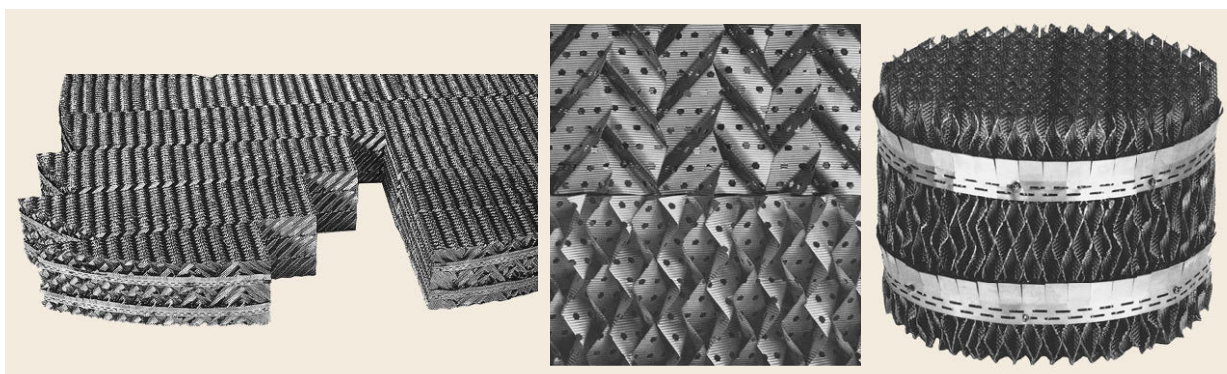


Fig. 33.6 Various types of structured fractionation packing. (Photos by Ted Sideropoulos, courtesy of ExxonMobil Research and Engineering)

4–6 bubble cap trays or sieve trays. Some of the newer designs use packing. Steam is used to reduce the hydrocarbon partial pressure to vaporize lighter molecules. A quench recycle is used to cool the stripped bottoms below 360 °C (680 °F) to reduce coking and cracking of the hydrocarbons.

33.10.10 Sidestream Strippers

Lube distillates are sent at their bubble points to sidestream strippers. Steam is injected, reducing the partial pressure of hydrocarbons which effectively removes lighter hydrocarbons, improving volatility beyond that obtainable without side stripping. About 10–30% of the stream may be removed in the stripper. If the heavier streams are not stripped, this will reduce the yield of lighter lubes. Stripping is an important part of the overall operation to achieve the best separation and produce the desired products. A stripper typically consists of 4–6 sieve trays but packing may also be used.

33.10.11 Overhead Pressure

Pressure has a very large effect. Low pressure (20–133 mbar overhead) is employed to reduce boiling points, allowing operation at temperatures low enough to minimize thermal degradation and cracking. The overhead vapors include steam, light hydrocarbons, and inerts. In the lower pressure (20–66 mbar) design, there is no precondenser before the first ejector. In higher pressure designs (53–133 mbar), a precondenser is employed and overhead pressure is dictated by condensing temperature (vapor pressure of water at the condensing temperature). Steam ejectors or vacuum pumps compress atmospheric pressure and pump away the noncondensable hydrocarbons and inerts. Precondensers will reduce the overall load on the compression system. Ejectors use steam for compression in two or three stages. Each ejector typically has an intercondenser. Secondary and tertiary ejectors may sometimes be replaced by a liquid ring vacuum pump.

33.10.12 Tower Overhead Pressure with Precondensers

In a precondenser design, the lower the cooling water temperature, the higher the achievable vacuum. The precondensers must operate below the water dew point to condense steam in the overheads. To achieve the lowest tower pressure, the tower should be operated at a low top temperature to minimize condensable hydrocarbons. Inerts should be minimized by reducing air

egress and by keeping the bottom temperature at or below 360 °C to avoid excess thermal cracking and the formation of light gases. Cooling water flow should be sufficient to minimize the cooling water outlet temperature which sets the equilibrium conditions in the precondenser and therefore the achievable tower vacuum.

33.10.13 Tower Overhead Without Precondensers

Towers without precondensers may operate at pressures lower than the vapor pressure of water at the condensing temperature. Lower pressure has both advantages and costs:

- Advantages:
 1. Higher distillate/resid cut point
 2. Less furnace coil and stripping steam required
 3. Pressure is controlled at a constant value (versus varying with cooling media temperature).
- Costs:
 1. Higher ejector steam rate
 2. Larger diameter tower.

33.10.14 Tower Pressure – Ejectors

The steam ejectors pump away the remaining vapor pressure of water, hydrocarbons, and inerts. Ejector systems typically have two stages or three by 50% ejectors. Because of the criticality for tower operation, most systems are overdesigned, and it may be possible for the tower to operate with one 50% ejector in each stage. Intercondensers (first stage) and after condensers (second stage) condense the steam from the ejectors, tower steam, and condensable hydrocarbons. Motive steam flow must be maintained for the best operation.

33.10.15 Factors Affecting Lube Distillate Production

- Crude type
- Equipment operation:
 1. Cutting scheme selected. Sidestream product viscosity and yield are shown for a two sidestream versus three sidestream cutting scheme in Table 33.5.
 2. Fractionation efficiency
 3. Pumparound heat removal capability
 4. Sidestream product stripper operation
 5. Equipment constraints
 6. Operational stability.
- Product inspection measurement precision.

Table 33.5 Two sidestream versus three sidestream product comparison. SUS: Saybolt universal seconds

Two sidestream products		Three sidestream products	
Viscosity (SUS at 100 °F/30 °C)	Yield on crude (vol.%)	Viscosity (SUS at 100 °F/30 °C)	Yield on crude (vol.%)
150	9.8	100	9.2
450	8.5	300	7.7
		700	5.3
Total	<u>18.3</u>	Total	<u>22.2</u>
Resid (1000 + °F) (538 + °C)	18.3	Resid (1075 + °F) (579 + °C)	16.8

33.11 Pipestill Troubleshooting

Steps of pipestill troubleshooting are described below.

33.11.1 Material Balance and Viscosity Measurements

1. Tabulate rates of crude feed, reduced crude, overhead condensate rate, and all VPS sidestream and bottoms rates for material balance calculations.
2. Take a sample of VGO and each sidestream and measure viscosities (100 °C) of all the VPS products.
3. Calculate yields, cumulative yield ranges, and mid-yield points for all the VPS products and combine with measured viscosities.
4. Compare viscosity to yield for each product. Compare to assay or lab-generated distillation cuts and viscosities.

33.11.2 Tower Pressure Survey

- Use the same vacuum gauge to measure tower absolute pressures. (Pressures are low and different gauges can have a calibration offset. Best results are obtained by moving the same gauge to the desired locations.):
 1. Make pressure measurement at the flash zone, tower top, and points in between.
 2. Determine Delta P across the strippers, both with steam on and with steam off.
 3. Measure ejector interstage pressures and condenser Delta P noting temperature differences between condenser liquid and vapor outlet as well as Delta T across the condensers.
 4. Determine pressure drop across spray nozzles.
 5. Transfer line pressure drop.
 6. Ejector motive steam pressure.
 7. Steam source pressure.
 - Inferences based on findings:
 1. If overall tower pressure drop is too low from the flash zone to the top, then there may be damage to the tower internals or hydraulic problems.
- If the pressure drop is too high, then flooding, plugging, or internal damage may be indicated.
2. Pumps typically have higher pressure drop than the fractionating sections.
 3. No or low Delta P in a tower section may indicate missing trays or the absence of liquid. High Delta P in a tower section may indicate that the drawoff is partially restricted or blocked, that may be due to high liquid rates in that section of the tower, flooding, or too much stripping steam.
 4. Check spray nozzle Delta P actual versus expected. If higher than expected, the spray nozzle may be plugged. If lower than expected, the header may be leaking or missing a nozzle(s).
 5. If stripper Delta P is too high, then this may be an indication that too much steam is being used. If the Delta P is too low, there may be too little steam being used of the trays or packing are damaged.
 6. If the precondenser Delta P is too high, this may be an indication of poor design, flooding, or fouling. If too low, equipment damage may be indicated.
 7. Review ejector interstage pressures versus design. Low interstage pressure may be an indication of the second stage overload.
 8. Tower pressure cycling may be due to steam ejector underload and high ejector discharge pressure.
 9. Condenser liquid and vapor temperatures should be about 3 °C apart. If the temperature difference is greater than this, it may be an indication of bypassing.
 10. Increase in cooling water temperature (in versus out) should be about 5–8 °C. If too low, this may indicate fouling or bypassing. If too high, the cooling water rate may be too low.
- Comparison to design – higher or lower rates:
 1. Cooling water
 2. Vacuum system
 3. Steam injection.

33.12 Solvent Extraction

The properties of the lube oil that are set by the extraction process are the VI, oxidation stability, and thermal stability. These properties are related to aromatics, sulfur, and nitrogen levels present in the base stock (Fig. 33.7).

Base stock VI has historically been used as a performance indicator for the base stock. The VI specification sets the extraction severity required to achieve the target. VI is also an indicator of relative stability from the same feed. VI is crude sensitive under constant extraction conditions.

Molecular structure affects lube quality. The impact of molecular type on lube oil VI and stability is shown in Table 33.6. Solvent extraction and dewaxing processes preferentially separate the molecules as shown in Fig. 33.8. Extraction separates *n*-paraffins, *i*-paraffins, naphthenes, and some aromatics from the distillate into the raffinate phase. Dewaxing rejects the *n*-paraffins and some *i*-paraffins from the raffinate to produce a dewaxed oil or base stock. The dewaxed oil will contain the *slice* of molecular types as shown in Fig. 33.8.

The extraction process is a physical separation that is used in all conventional lube plants. The solvent is added to the distillate to produce a raffinate, the desired product, and an extract that contains a higher percentage of aromatics and impurities. Typical solvents used are NMP, furfural, and phenol. Properties of the solvents are shown in Table 33.7. NMP solvent properties

relative to furfural and phenol are shown in Tables 33.8 and 33.9, respectively. The development of the NMP based EXOL N extraction process is described in [33.3–6].

33.12.1 The Characteristics of a Good Extraction Solvent

A good extraction solvent will have a high selectivity for the undesirable lube. The molecular weight of the oil affects its solubility. Solubility decreases with increasing molecular weight (Fig. 33.13a). Solubility increases with increasing solvent dosage (Fig. 33.13b). The solvent must also have good solvent power so that a low solvent to feed ratio may be used in the extraction plant. The solvent promotes rapid mass transfer. The solvent partitions between the raffinate and extract phases, and must be recovered; an easy recovery via distillation is desired. High density is also a characteristic of a good

Table 33.6 Impact of molecular type on lube oil VI and stability

	VI	Stability
Paraffins	Excellent	Good
Mono-naphthenes	Good	Fair
Polynaphthenes	Fair	Fair
Mono-aromatics	Good	Fair
Polyaromatics	Poor	Poor

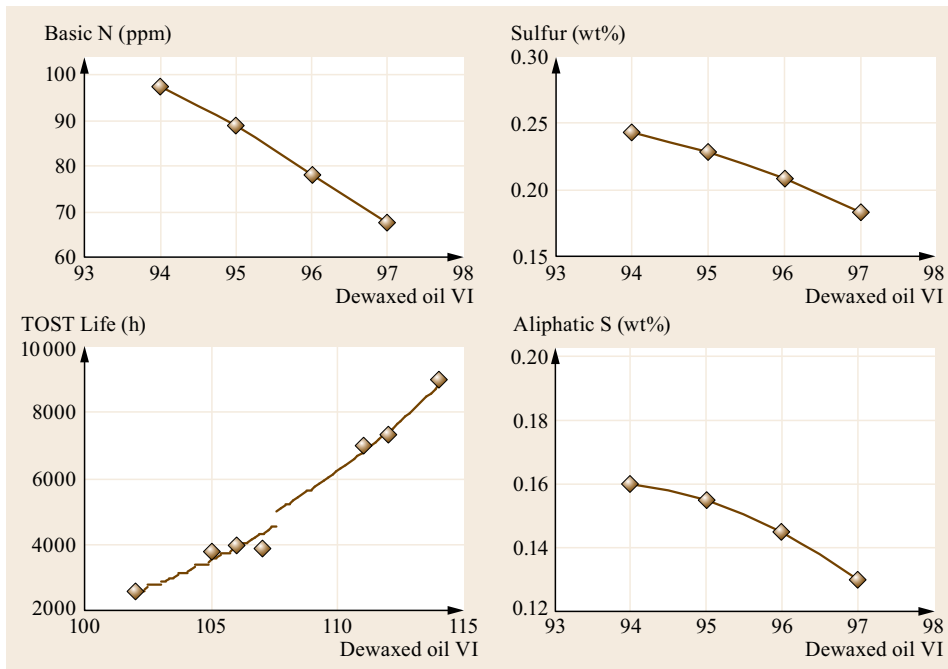


Fig. 33.7 Impact of extraction on VI and lube oil properties

	Molecule	Base stock quality affected	Process involved
Extraction	<i>n</i> -Paraffin	High pour, VI No S & CCR	Dewaxing
	<i>i</i> -Paraffin	High VI & sats, med pour	
	2 ring naphthene	Med VI, low pour, high acids	Extraction, hydrofinishing
	1 ring aromatic	Med to high VI	Extraction
	Multi-ring naphthene	Low VI, low pour, high acids	Extraction, hydrofinishing
	Multi-ring aromatic	Low VI, low pour	Extraction
	Organic sulfur	Good stability, antioxidant	Hydrofinishing
	Organic nitrogen	Poor stability	Hydrofinishing
	Organic sulfur & nitrogen	Removed by hydrofinishing	Hydrofinishing
	Asphaltenes	High CCR, poor color	Distillation, deasphalting

Dewaxing

Fig. 33.8 Principal molecular types and their effect on lube quality

Table 33.7 Physical properties of typical extraction solvents

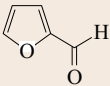
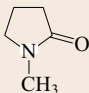
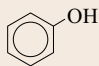
	Furfural	<i>N</i> -Methyl-2-pyrrolidone	Phenol
Structure			
Molecular weight	96	99.1	94.1
Specific heat (at 130 °F/54 °C)	0.42	0.47	0.56
Boiling point (at 1 atm)	323 °F/162 °C	399 °F/204 °C	359 °F/182 °C
(Flash point)	(137 °F/58 °C)	(187 °F/86 °C)	(175 °F/80 °C)
Melting point	-37 °F/-38 °C	-11.6 °F/-82 °C	105.6 °F/40 °C
Latent heat @ B.P., BTU/LB	194	187	206
Toxicity	Moderate	Low	High
Specific gravity (at 20 °C)	1.16	1.03	1.07

Table 33.8 NMP solvent properties relative to furfural

NMP solvent property	
Thermally stable	Heat integration with no measurable solvent decomposition
More selective	Higher yields at lower solvent treats
Lower latent heat	Requires less energy for solvent recovery
Chemically stable	Eliminates the need for feed deaerator for removal of oxygen
Higher boiling point	More efficient heat integration

extraction solvent as this allows the rapid separation of the oil and solvent phases. High demulsibility is needed for a rapid separation of the oil and solvent. The solvent must be chemically and thermally stable in the lube extraction

and recovery equipment. The ideal solvent would work for a wide range feedstocks that the refiner might process. Solvent must be available at a reasonable cost and noncorrosive to conventional materials of construction, and it must be environmentally safe.

33.12.2 Extraction Process

A simplified extraction flow diagram is shown in Fig. 33.9. Distillate is brought in contact with the solvent and aromatics, and polars are preferentially dissolved in the solvent phase. Saturates do not dissolve and remain in the hydrocarbon or dispersed phase. The hydrocarbon phase is lower in density than the solvent phase and rises as bubbles through the continuous

Table 33.9 NMP solvent properties relative to phenol

NMP solvent property	
Lower toxicity	Much safer
More selective	Higher yields and/or lower solvent treats
Lower latent heat	Less energy required for solvent recovery
Higher boiling point	More efficient heat integration
Lower melting point	Less steam tracing required, less chance of solidifying in piping
No hydrogen bonding effect with the oil	More efficient stripping, easier to achieve low-solvent concentration in product
No azeotrope	Simplifies water recovery

phase. After contact, the raffinate and extract solution are sent to their respective solvent recovery sections. Integration of a hydrofiner on the raffinate product is done in some lube plants for heat integration because this eliminates the need for an additional hydrofiner furnace.

There are several types of continuous treater tower designs used in conventional lube plants (Fig. 33.10). These include trayed towers, packed towers, and rotating disk contactors. The treater tower internals are designed to promote contact and separation of the oil and the solvent phases.

An example of a tray design is shown in Fig. 33.11.

An example of a typical rotating disk contactor is shown in Fig. 33.12.

There are several factors that affect extraction efficiency and in general the efficiency depends on the mixing/settling and coalescence characteristics of the system. Important factors include:

1. Hardware and staging
2. Throughput
3. Viscosity/gravity of oil/solvent
4. Solvent dosage and composition

5. Temperature and temperature gradient
6. Solvent quality
7. Dispersion energy.

33.12.3 Extraction Process Variables

Independent variables are controlled by the operator and include:

- Treat ratio – the volume ratio of the solvent to feed
- Solvent composition (water for NMP, phenol)
- Bottom and top treater temperature.

Dependent variables rely on the independent variables:

- Raffinate quality:
 - VI
 - Saturates content as an indicator of the degree of aromatic removal.
 - Sulfur.
- Raffinate yield – primarily dependent on the treat ratio at constant VI.

33.12.4 Solvent Contaminants

Water from steam stripping in the solvent recovery section must be removed. In the furfural solvent system, water is removed for process effectiveness and product quality. Water contamination in furfural reduces dewaxed oil (DWO) VI and leads to furfural degradation. In NMP and phenol systems, excess water is removed for process control.

Oil in the solvent results from incomplete solvent-oil separation and may be due to entrainment from flash vessels, volatilization, or stripper flooding. Characterization of the solvent contamination by GCD can be used to determine if contamination is occurring by light or heavy oil fractions. A light oil contamination suggests that there is an accumulation of distillate of the

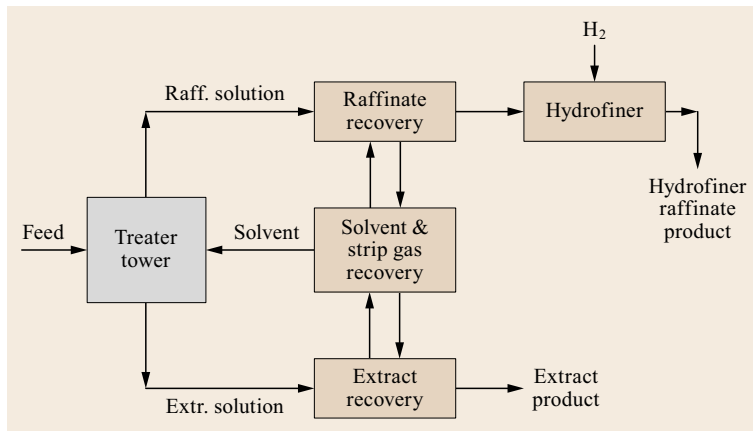


Fig. 33.9 Simplified extraction flow diagram

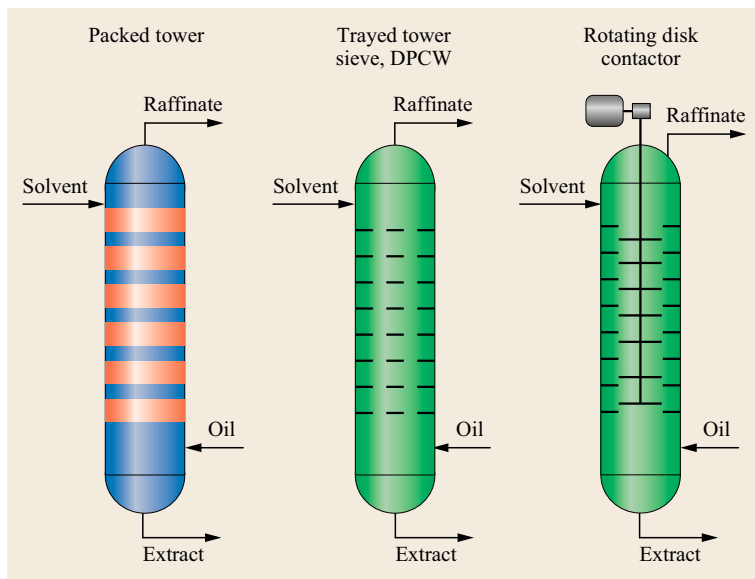


Fig. 33.10 Types of continuous extractors

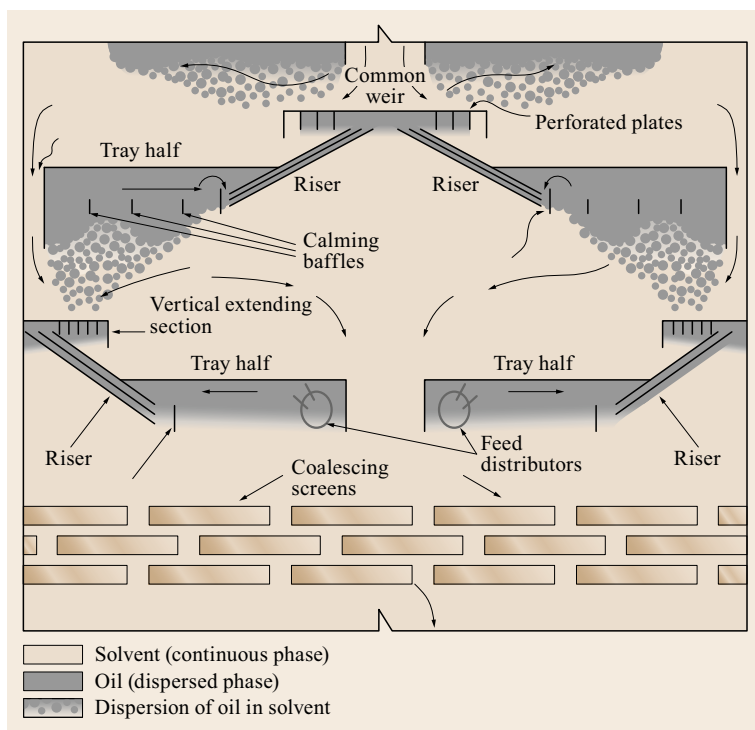


Fig. 33.11 ExxonMobil patented dual pass cascade weir tray [33.7]

front end. The presence of heavy oil suggests that the entrainment oil in the solvent can reduce the raffinate yield and increase the treat rate required.

33.12.5 Solvent Recovery

The objectives of solvent recovery sections are to:

1. Recover furfural/NMP/phenol from product streams
2. Purify furfural/NMP/phenol for recycle
3. Maximize energy efficiency while recovering solvent.

Simplified recovery sections are shown below.

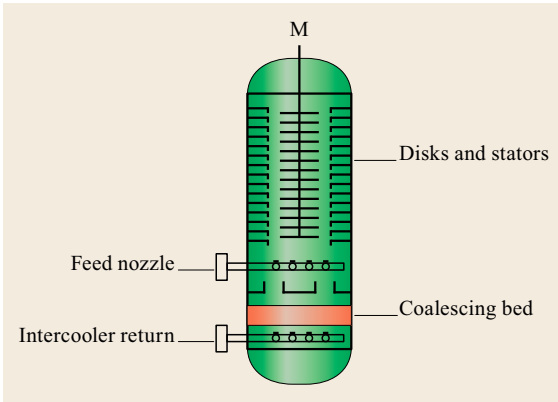


Fig. 33.12 Typical rotating disk contactor

Typical raffinate recovery flow diagrams are shown in Fig. 33.14.

Typical extract recovery flow diagrams are shown in Fig. 33.15.

33.12.6 Minimizing Solvent Losses

Recovery Sections

Excess solvent (NMP or furfural) in the product is costly. NMP and furfural concentrations can be reduced to < 20 ppm and < 50 ppm respectively, however, it requires additional energy during solvent recovery. The final concentration is an optimized balance of cost of solvent loss versus additional energy costs in recovery. The furnace coil outlet temperature (COT) is set based on the operating pressure. Typical furnace COTs are higher for NMP than furfural due to solvent boil-

ing points and the concern for furfural degradation. If fuel gas failure occurs at the furnace, the plant immediately goes on oil recycle. The solvent concentration in the product can rise to several percents if the COT is too low. Very high furnace temperature leads to an increase in solvent decomposition and premature furnace coking.

Other Contributors to Solvent Losses

1. Some solvent is lost through line flushing during product sampling. To reduce losses, end sample line flushes back to the unit.
2. Address miscellaneous leaks at flanges.
3. Startup and shutdown operation, typically will increase solvent losses in the year the shutdown is taken.
4. Check valves on bypass lines may not hold and may allow bypassing of solvent.
5. Water sent to the biox unit might contain a solvent.
6. Phenol will oxidize and form deposits in the unit. Effective management of solvent loss in lbs/BBL of feed is considered to be:

$$\begin{aligned} \text{NMP} &\leq 0.03 \\ \text{Phenol} &\leq 0.10 \\ \text{Furfural} &\leq 0.20. \end{aligned}$$

Furfural will decompose when exposed to oxygen or excessive temperatures.

Sources of oxygen ingress include:

1. Pump suction
2. Vacuum systems
3. Oil feed poorly deaerated
4. Poor/nonexistent inert gas blanketing.

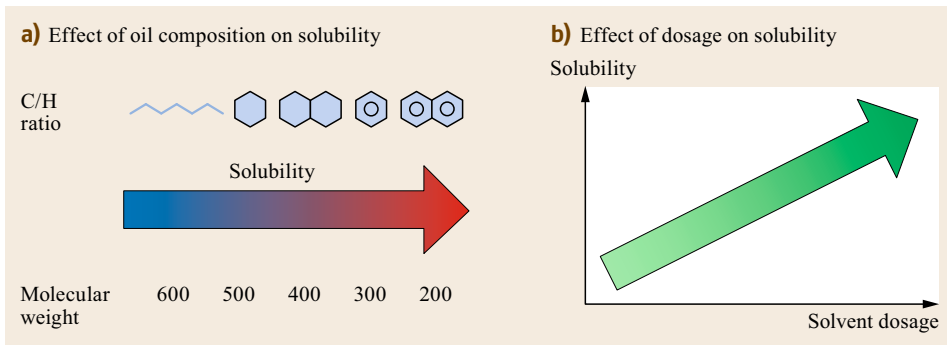


Fig. 33.13a,b Effect on oil composition (a) and dosage (b) on solubility

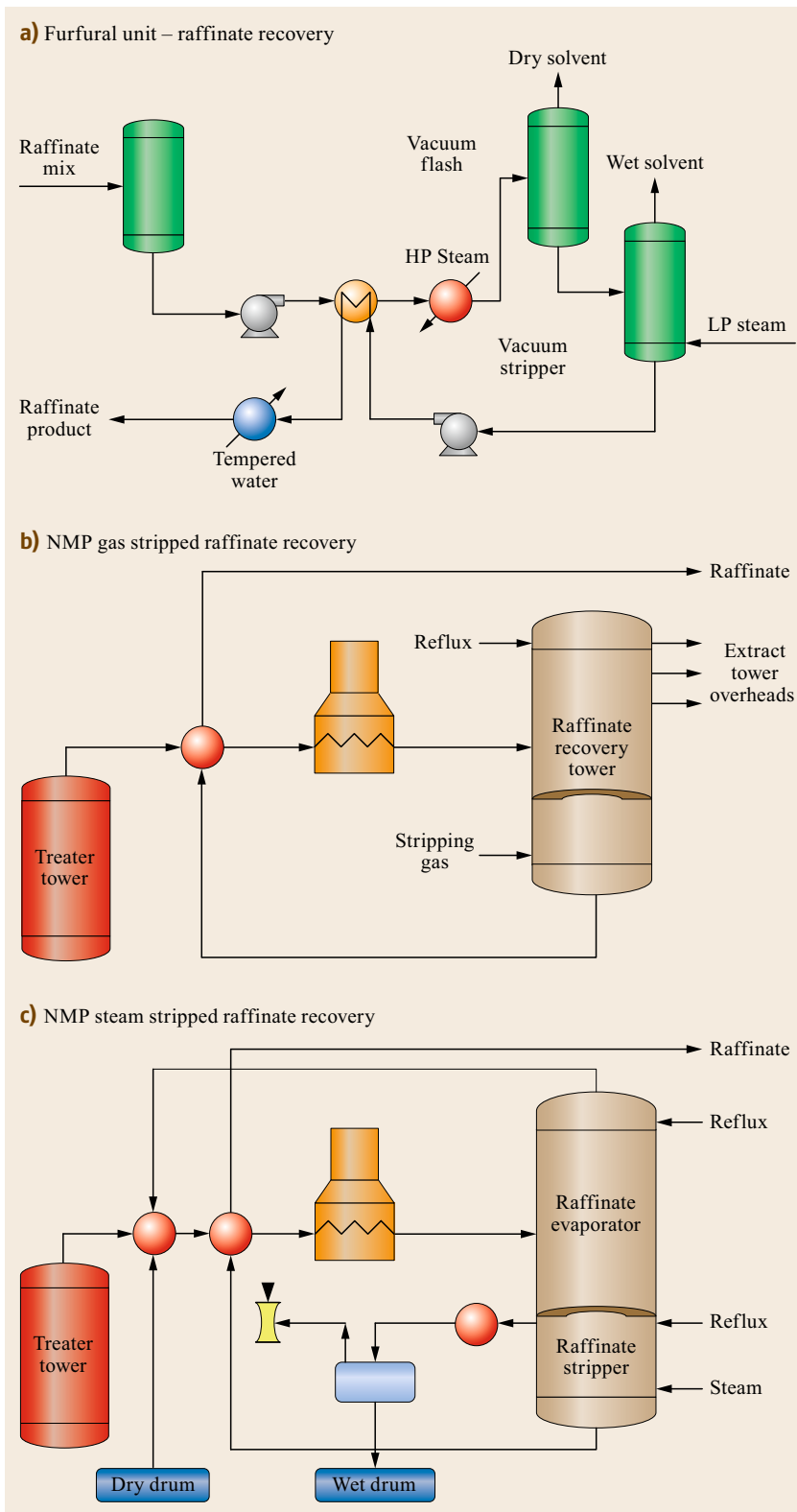


Fig. 33.14a–c Typical raffinate recovery flow diagrams. **(a)** Furfural unit – raffinate recovery flow diagram. **(b)** NMP gas stripped raffinate recovery flow diagram. **(c)** NMP steam stripped raffinate recovery flow diagram

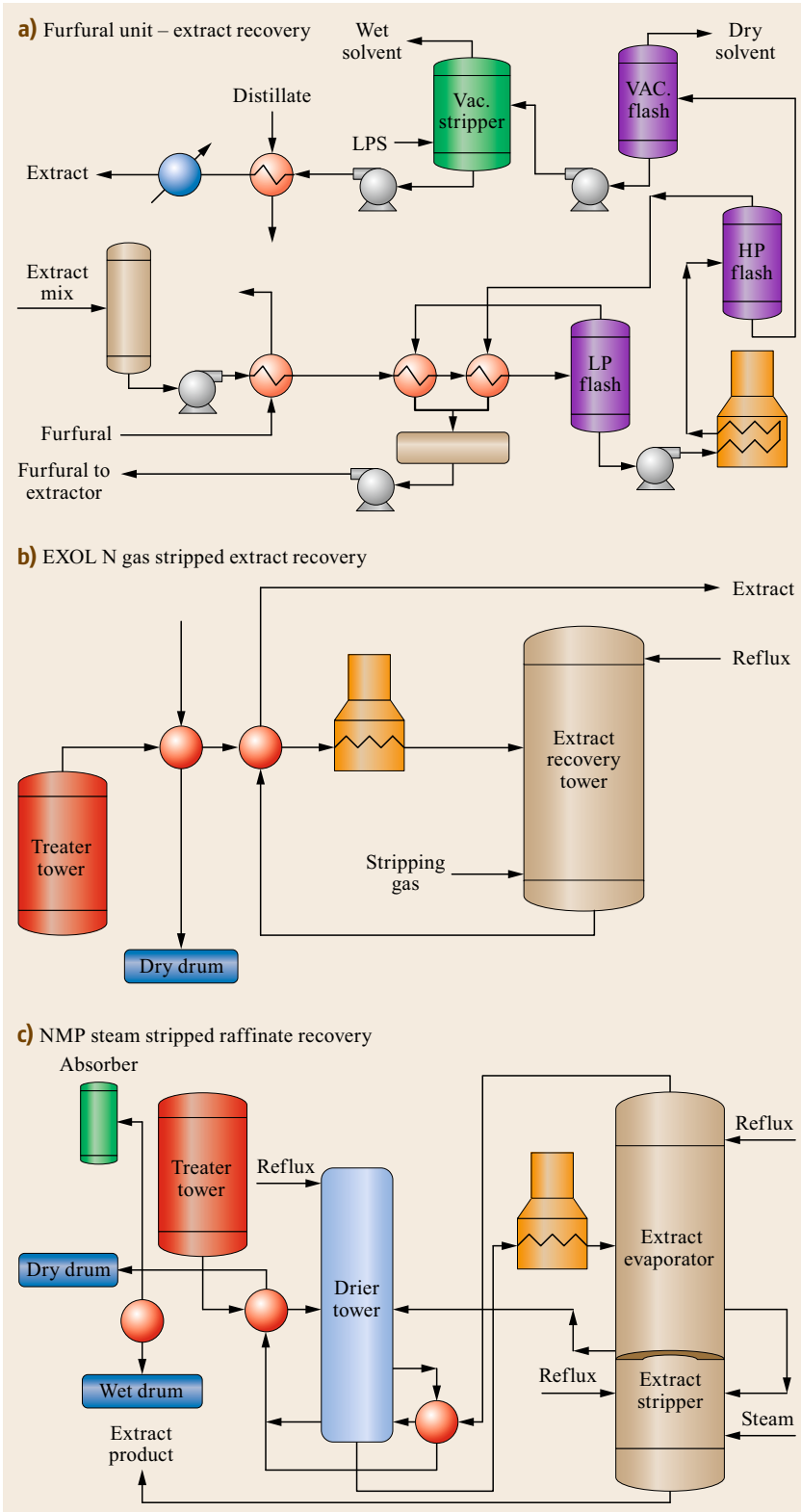


Fig. 33.15a-c Typical extract recovery flow diagrams. (a) Furfural unit – extract recovery flow diagram. (b) EXOL N gas stripped extract recovery flow diagram. (c) NMP steam stripped extract recovery flow diagram

33.13 Corrosion in NMP Plants

Pure NMP is not corrosive to carbon steel. However, because of NMP's high dielectric constant, other corrosive compounds will readily ionize in NMP and become very aggressive. The NMP condensing circuit may be at risk to accelerated corrosion from accumulated corrosive elements or corrosion/erosion from high velocities.

The refiner can take the following corrective actions. Firstly, avoid corrosive species ingress into the

circuit. Remove H₂S from recycle stripping gas with a ZnO bed. Neutralize acids with neutralizing additives or caustic injection. Consider alloy upgrade in areas of known corrosion or areas of known impingement or very high velocity such as 316 SS impingement baffles in exchangers. Insulate, overhead line to the first condenser to avoid premature condensation, leading to impingement issues.

33.14 Analytical Tests for Extraction

There are numerous analytical tests that are used to assess the extraction operation and to help optimize the

treater tower. A few of the most important tests are listed in Table 33.10.

Table 33.10 Typical analytical tests for extraction

Test	ASTM test no.	Application
Refractive index typically measured between 20–30 °C	D 1218	Correlation with dewaxed oil quality: VI, saturates, etc. Better for yield calculations than relying on process flow meters
Density at 15 °C	D 4052	Better for yield calculations than relying on process flow meters
Water in solvent by Karl Fischer	D 6304-3, E 203-1	Process optimization (NMP, phenol)
Treater carryunder		Measures the amount of distillate bypassing the treater and being downgraded from lubes to fuel
Oil in solvent 1. Percent 2. Characterization		Oil in solvent adversely affects raffinate yield
Dewaxed oil		
Test	ASTM test no.	Application
Viscosity VI	D 445, D 2270	Primary base stock specification
Molecular analysis	D 2007, D 2887 D 2140, D 2501	Troubleshooting Base stock quality

33.15 Dewaxing

Waxy raffinates from extraction are not useful as lubes because they contain too much wax. Referring to our molecular drawing (Fig. 33.8), we can see that the objective of dewaxing is to remove the paraffins from the raffinate to produce a final dewaxed oil base stock that when additized becomes the finished lube base oil.

Dewaxing is a physical process that adds a solvent to a raffinate (or distillate), and once the mixture is cooled, the *n*-paraffins drop out of the solution as solid wax crystals. The slurry is filtered to remove the wax crystals and to produce a dewaxed oil or base stock and a valuable wax by-product. Wax may be further refined to make hard wax by melting away the soft wax. Hard wax may meet U.S. Food and Drug Administration (FDA) standards for use in direct or indirect contact with food.

The majority of dewaxing processes today use methyl ethyl ketone (MEK), methyl isobutyl ketone (MIBK), mixtures of MEK and MIBK, or mixtures of MEK and toluene or propane. There are advantages and disadvantages of each solvent system.

Dewaxing sets the primary properties, as shown in Table 33.11.

A general flow plan for a dewaxing plant is shown in Fig. 33.16.

Table 33.11 Properties set by dewaxing

Dewaxed oil properties	Wax properties
Pour point	Oil content
Cloud point	Melting point
Low-temperature fluidity	Needle penetration

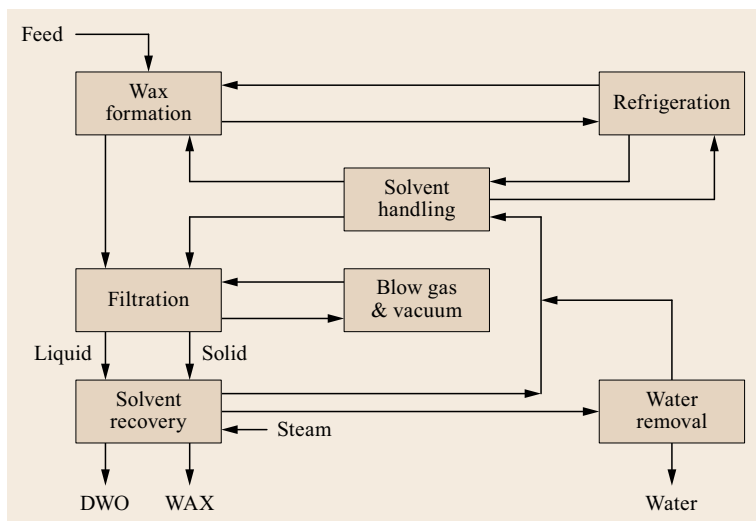


Fig. 33.16 Simplified dewaxing flow diagram

33.16 The Role of Solvent in Dewaxing

As soon as a solvent is added to the raffinate, the oil is diluted and the viscosity of the oil solvent mixture decreases, allowing filtration to take place more easily. The polarity of the oil–solvent mixture increases, decreasing the solubility of the wax and promoting the formation of more compact wax crystals. Also, as soon as a solvent is added, the resulting filtrate becomes more dilute, loading up filtrate pumps, and solvent recovery facilities. Properties to consider in selecting a dewaxing solvent:

1. Solubility
2. Selectivity
3. Solvent boiling point lower than the boiling point of the oil
4. Low heat capacity
5. Heat of vaporization
6. Low viscosity
7. Nontoxic
8. Noncorrosive
9. Low freezing point
10. Inexpensive
11. Readily available.

Ketone units typically use a dual solvent system consisting of MEK and either MIBK or toluene. The MEK acts as an antisolvent to reject wax molecules from the solution. This reduces refrigeration requirements but excessive MEK may cause oil phase separation. The second solvent keeps the oil in the solution, but it also dissolves some wax. MIBK and toluene act as pro-solvents.

The comparison of solvent properties are given in Table 33.12.

MEK/MIBK refrigeration requirements are lower than MEK/toluene because the pour–filter spread is smaller due to the lower wax solubility. The pour–filter spread is the difference between the dewaxed oil pour point and the filtration temperature required to meet the dewaxed oil pour point specification. Wax has a higher solubility in toluene than MIBK, and MEK/toluene systems will require a lower filtration temperature to achieve the same pour point. MEK/MIBK solvent mixture viscosity is lower than MEK/toluene. Filtration rates are higher for MEK/MIBK. Toluene costs less than MIBK.

Table 33.12 Typical dewaxing solvent properties

Solvent	Wax solubility (g/100 ml)	Viscosity at 0 °C (cSt)	BP (°C)	Latent heat of vaporization (cal/g)	Specific heat (cal/(g °C))
MEK	0.25	0.40	80	106	0.55
MIBK	0.90	0.61	116	87	0.46
Toluene	13.0	0.61	111	99	0.41

33.17 Ketone Dewaxing Processes

33.17.1 Incremental Ketone Dewaxing Plant

Incremental ketone dewaxing plants use a combination of scraped surface exchangers (SSEs) that use cold filtrate for cooling the slurry followed by scraped surface chillers (SSCs), which uses a refrigerant (propane, propylene, ammonia) to cool the slurry to the filtration temperature. A solvent may be added at the beginning or along the train in *increments*. A simplified incremental dilution dewaxing flow diagram is shown in Fig. 33.17.

The solvent may be mixed with the raffinate before the scraped service exchanger as primary dilution. The slurry passes through a feed heat exchanger to melt any crystals that may have formed in tankage. The slurry temperature is then reduced in a feed precooler. The slurry flows to the SSEs and through the tube side of the exchanger. Cold filtrate from the filters is used to cool the feed below the cloud point and initiate crystallization. Solvent may be added in increments to reduce the slurry viscosity and enhance heat transfer. Slurry flows to SSCs and through the tubeside. Propane, propylene,

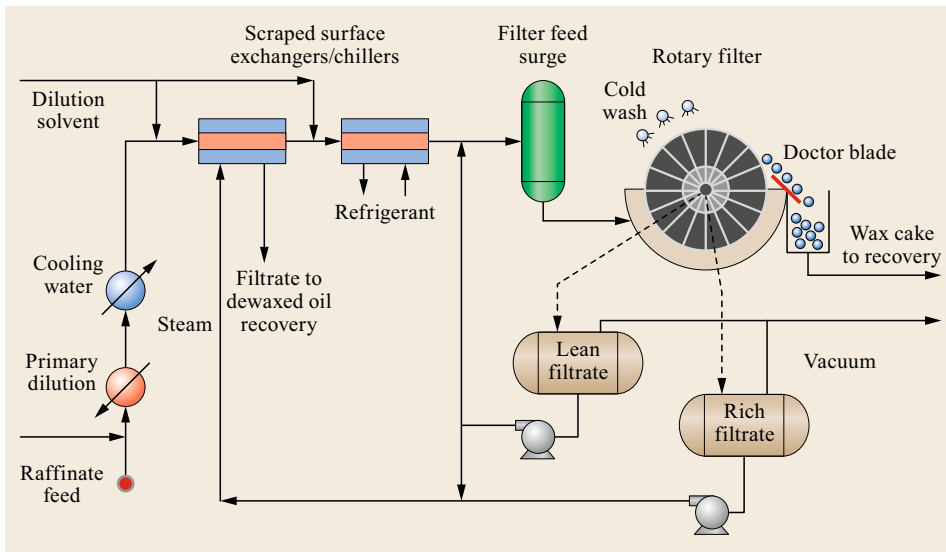


Fig. 33.17 Simplified incremental dilution dewaxing

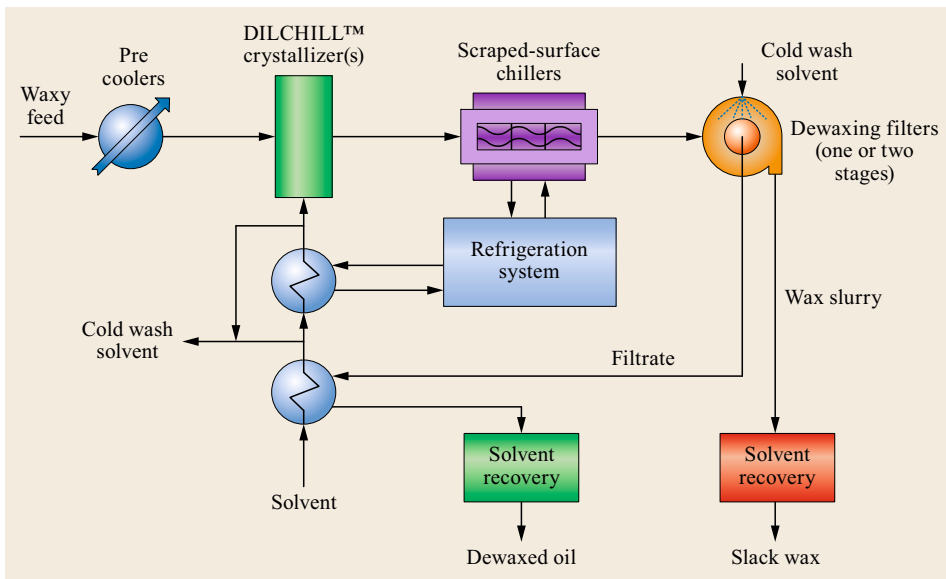


Fig. 33.18 Simplified DILCHILL™ dewaxing [33.8, p. 40], [33.9, Fig. 11.3] (courtesy of ExxonMobil Research and Engineering)

and ammonia are typical refrigerants used on the shell side. The slurry exits the last scraped surface temperature at filtration temperature and enters the filter feed drum. The slurry flows by gravity to the filters where the wax crystals are filtered across a rotary vacuum filter. Wax is removed from the filter and sent to the wax recovery section. Oil and solvent – filtrate – is collected and sent through the shell side of the SSEs on its way to the dewaxed oil recovery section. Filtrate may also be recycled back to the slurry to adjust the final dilution before filtering.

33.17.2 DILCHILL™ Dewaxing

In DILution CHILLing, the scraper surface exchangers (SSEs) are replaced with a multistage crystallizer. A simplified DILCHILL™ dewaxing flow diagram is shown in Fig. 33.18. A cold solvent is added at each stage and the slurry is mixed with an impeller. The crystallizer replaces all the SSEs with a single mixer. A simplified DILCHILL™ dewaxing crystallizer tower is shown in Fig. 33.19. The development and commercial experience of DILCHILL™ is described in [33.10–13].

The key features of DILCHILL are summarized below:

- Less oil is occluded in the wax crystal due to the vigorous *micromixing* in the crystallizer.
- Higher filtration rates and lower oil-in-wax are achieved as a result of compact, spherical crystals. Fig. 33.20a,b are micrographs that compare the wax crystals produced by DILCHILL™ and incremental dilution.
- Lower dilution solvent.

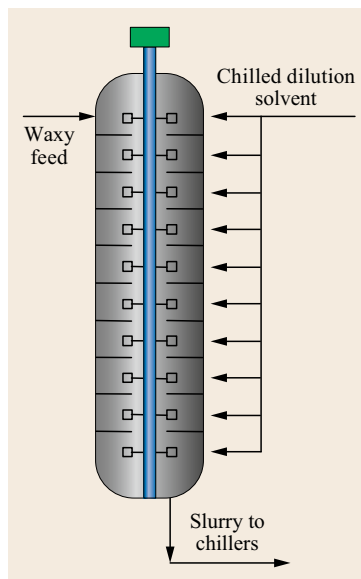


Fig. 33.19 Simplified DILCHILL™ dewaxing crystallizer tower [33.8, p. 38]

- Lower operating costs.
- Easier operation.
- Higher service factor.

33.17.3 Dewaxing Process Variables

Independent variables are controlled by the operator and include:

- Charge rate
- Solvent composition
- Precooler outlet temperature
- Dilution ratio (increments)
- Chilling rate

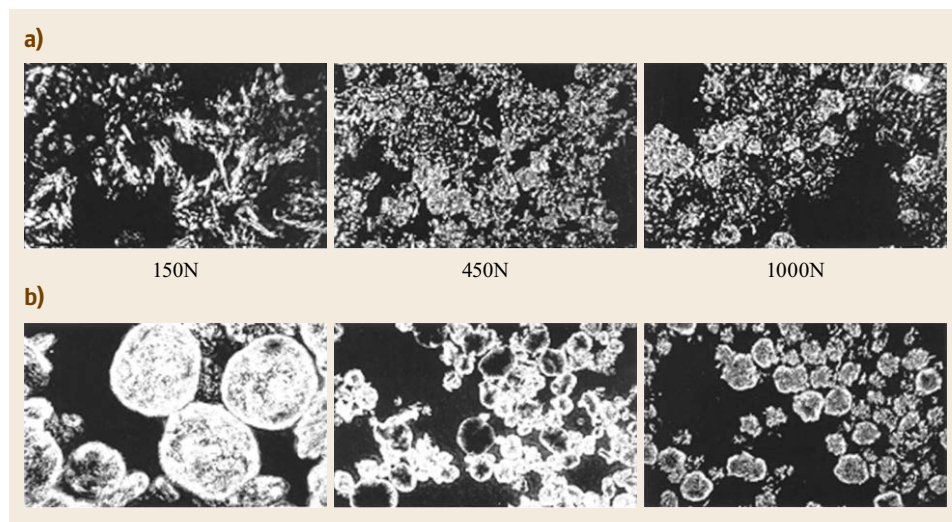


Fig. 33.20a,b Comparison of wax crystals formed in conventional incremental dewaxing (a) and in DILCHILL™ dewaxing (b). Optimum crystal formation leads to faster filter rates, lower solvent/oil ratios and lower oil-in-wax content [33.8, p. 38]

- Filter wash solvent ratio
- Wash temperature
- Mixing energy (DILCHILL™ only)
- Filtration temperature
- Filter speed
- Dewaxing aids.

Dependent variables rely on the independent variables:

- Filter feed rate

- Dewaxed oil quality:
 1. Cloud point
 2. Pour point
 3. Low-temperature properties
- Dewaxed oil yield
- Wax yield:
 1. Oil in wax
 2. Melting point
 3. Needle penetration.

33.18 Process Variable Effects

As mentioned earlier, crude selection can have an influence on downstream units. Table 33.13 shows the impact of the crude source on the dewaxed oil yield.

Table 33.13 Typical base stock yields. SUS: Saybolt universal seconds ►

Base stock	Minimum fluid point (°C)	Arab light Yield (vol%)	Statford Yield (vol%)
100 SUS	-18	81	79
300 SUS	-9	81	79
700 SUS	-7	85	80
Bright stock	-7	85	78

33.19 Solvent Composition

33.19.1 Miscible and Immiscible Operations

MEK is an antisolvent for the wax and helps to reduce its solubility. If the MEK content is too high, the base stock may become insoluble and a phase separation will occur. MIBK or toluene is added to help solubilize the oil. Both of these pro-solvents have a higher affinity for wax molecules than MEK. The higher the concentration of pro-solvent, the more wax stays in the solution and ends up in the filtrate. This raises the pour point of the dewaxed oil, and since the manufacturer must meet dewaxed oil pour point specification, the manufacturer is forced to reduce the filtration temperature to remove more wax. The reduction in filtration temperature increases the viscosity of the slurry, filtration rates are slower, and oil removal from the wax cake becomes more difficult. Thus, the objective is to use the maximum amount of MEK without having a phase separation. A plot of the phase separation temperature or miscibility temperatures versus solvent composition may be used to help set the optimum solvent composition. A typical miscibility curve for MEK and Toluene for heavy neutral lube oil is shown in Fig. 33.21.

The ideal would be to operate as close to the miscibility curve as possible. However, this curve shifts depending on the base stock. Wax molecules in heavier grades move out of the solution earlier and this has the effect of shifting the miscibility curve to the left.

Plants equipped with solvent splitters to separate the MEK from the MIBK or toluene, after it has been recovered in the DWO and wax recovery sections, may blend to the optimum solvent composition for each base stock. Manufacturers without the capability of changing solvent composition will set the plant solvent composition based on the heaviest grade to avoid immiscible operation. This increases the pour filler spread, because the pro-solvent composition is too high for the lighter grades. This will also affect plant processing capacity.

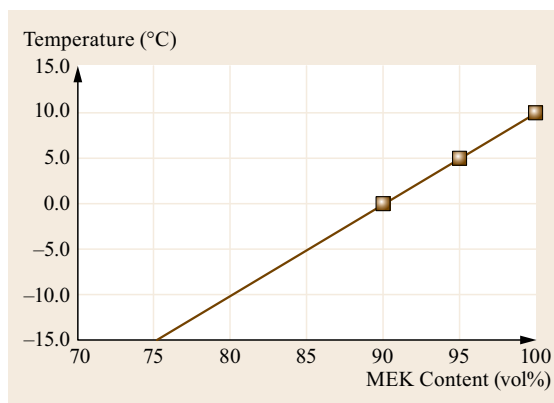


Fig. 33.21 Typical heavy neutral miscibility curve for MEK and toluene

The shift from miscible to immiscible operation occurs over a narrow range of solvent composition as can be seen in Fig. 33.23. When the plant moves deep into immiscible operation then phase separation occurs, the oily phase, containing the desirable high VI molecules, will hang up in the filter cake and be very difficult to remove, increasing the oil in the wax content of the wax and reducing the dewaxed oil yield. Dewaxed oil properties may be adversely affected and VI may decrease. Filtrates produced under miscible and immiscible operating conditions are shown in Fig. 33.22, where the clear filtrate was produced under miscible operating conditions. Interestingly, in severely immiscible operation, the dewaxed oil pour point may actually decrease as the waxy molecules remain in the wax cake.

33.19.2 Effect of Viscosity on the Filtration Rate

Higher viscosity base stocks will filter more slowly, as can be seen in Fig. 33.24. Increasing the MEK concentration in the solvent reduces the slurry viscosity, but the maximum amount of MEK is limited by miscibility considerations.

33.19.3 Effect of the Chilling Rate on the Filtration Rate and Dewaxed Oil Yield

Increasing the chilling rate forces wax molecules to come out of the solution quicker. When the wax molecules come out of the solution, they may either form a separate nuclei (nucleation) or attach onto an existing nucleus (growth). When the chilling rate is high, nucleation is favored over growth with the result



Fig. 33.22 Comparison of immiscible and miscible filtrates. (Photo by B.E. Beasley, courtesy of ExxonMobil Process Research)

that with the smaller average crystal size, the wax is more difficult to filter, and the wax retains a higher oil content. The effect of chilling rate on DWO yield and filtration rate shown in Table 33.14.

33.19.4 Effect of Temperature Profile

The preferred temperature profile for incremental and DILCHILL™ dewaxing is a linear profile. Both methods of dewaxing add solvent, either in increments along the SSE/scraped surface chiller/crystallizer (SSC) train or in stages in the crystallizer. Thus, the flow rate increases from the feed to the filters. Other tempera-

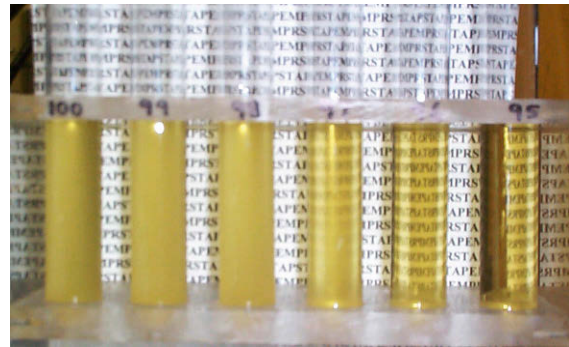


Fig. 33.23 Impact of change in solvent composition on miscibility. (Photo by B.E. Beasley, courtesy of ExxonMobil Process Research)

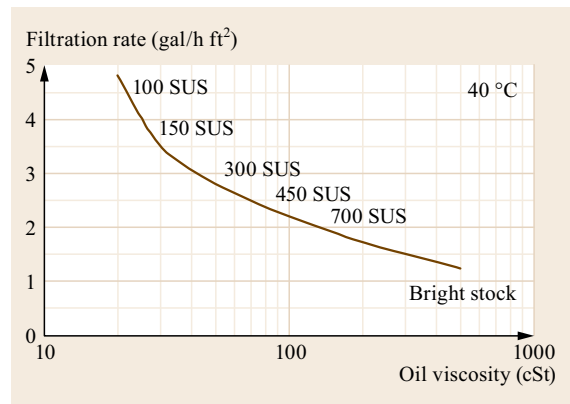


Fig. 33.24 Effect of oil viscosity on filtration rate

Table 33.14 Example of the effect of the chilling rate on the yield and filtration rate

Chilling rate (°C/min)	DWO yield (vol%)	Filtration rate (gal/(ft ² hr))
2.2	85.3	2.00
4.4	82.0	1.94
6.7	81.3	1.92
8.9	79.8	1.90

ture profiles are possible. Filtration rates in plants with a convex temperature profile are typically not as good as those with a linear profile. This may be due to the very high chilling rates in the SSC or last few DILCHILL™ stages, required to reach the filtration temperature, and which favors nucleation at the expense of growth and leads to a smaller average crystals. Typically, concave profiles offer no advantage over linear. In the rare case where a concave profile has produced improved filtration rates, it has been surmised that a high chilling rate at the beginning of the train, which will favor nucleation, was needed to establish *seed* crystals for growth.

33.19.5 Effect of Solvent Dilution Ratio

Filtration Rate

A solvent may be added in increments along the SSE/SSC train or in the DILCHILL™ crystallizer. The solvent reduces the slurry viscosity and facilitates filtration. When the dilution is too low, the slurry viscosity will be too high, and the slurry filtration will be reduced. This is often referred to as *viscosity limited*. When the dilution is too high, the volume of liquid to be filtered exceeds the capacity of the filter (filter cake resistance is limiting) and the filtration is said to be *hydraulically limited*. This balance results in an optimum dilution ratio dependent on the base stock being processed (Fig. 33.25), the solvent composition being used, and the crystallization which sets the filter cake resistance. Light base stock operations are more likely to be chilling or refrigeration limited rather than filtration limited because the light base stock pour points are typically lower than the heavy grades, while the average wax crystal size is larger, reducing wax cake resistance.

DWO Yield

Increasing the dilution ratio will reduce the oil in wax and increase the dewaxed oil yield.

33.19.6 Effect of Water

Water may enter with the feed from the extraction process or from tankage. Water may also enter the system from leaks in water coolers or condensers that are used in the dewaxing plant. Water may re-enter the solvent system through inadequate performance of the dehydrator section in the plant. Water is a strong antisolvent. Water reduces the solubility of wax and oil molecules so that they come out of a solution at a higher temperature. This has the effect of shifting the miscibility curve to the left. Typically, the increase in water concentration from the normal levels is an indication of a process/equipment problem and the root cause must be found and dealt with quickly.

Excessive water may drop out of the solution and form ice in the slurry or inside the scraped surface equipment. It may also flow downstream to the filters where it may be captured in the wax cake or on the filter cloth.

33.19.7 Effect of Increased Raffinate VI

Raffinate VI may be increased in extraction through more severe extraction. This increases wax concentration in the raffinate stream. These waxy molecules will come out of the solution in the dewaxer at a higher temperature, resulting in the miscibility curve shifting to the left. This will require the manufacturer to add more prosolvent to avoid immiscible operation.

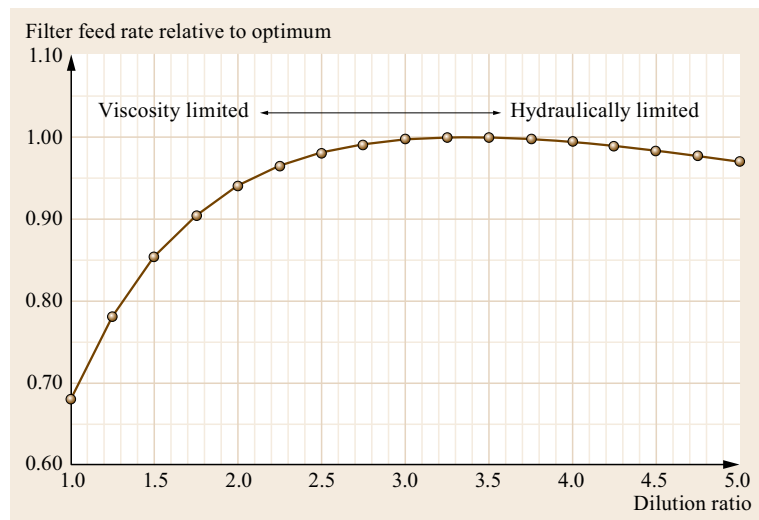


Fig. 33.25 Effect of dilution ratio on filtration rate, heavy neutral

33.19.8 Effect of Pour Point Giveaway on Product Quality and Dewaxed Oil Yield

When a base stock produces dewaxed oil with a lower pour point than the specification, the plant is *giving away* this product quality. Examples of quality giveaway are shown in Table 33.15. The economic penalty for pour point give away is a lower filtration rate and a lower throughput and a decreased dewaxed oil

Table 33.15 Examples of quality giveaway

Base stock	Pour point reduction (°C)	Typical VI loss	Typical yield loss (vol%)
Solvent neutrals	3	1	1.0
Bright stock	3	0.5	1.0

yield. Lower pour point also means that more wax has been removed and this will lower the dewaxed oil VI.

33.20 Scraped Surface Equipment

SSEs and SSCs are used in incremental dewaxing and SSCs in DILCHILL™ dewaxing. SSEs and SSCs are double pipe exchangers with slurry inside the central tube and the cooling media (filtrate or refrigerant) in the annular area around the inside tube (pipe). Typical installed SSEs are shown in Fig. 33.26.

The scraped surface continuous crystallizer is built as a double-pipe element, generally with a 6, 8, 10, or 12 in diameter inner pipe and a larger diameter outer pipe. The area between the inner pipe and the outer pipe is filled with cooling fluid. The inner pipe contains a rotating scraper blade element, which mixes the process fluid flowing through the inner pipe, and removes deposits which form on the inner pipe wall as cooling occurs.

The scraped surface continuous crystallizer is a heat exchanger, but quite an unusual one, because it generally functions as a cooling crystallizer. Heat transfer occurs across the wall in the inner pipe, with cold fluid outside, and process fluid inside. As cooling occurs,

crystals tend to form and foul the inner pipe wall. The scraper blades rotate on the inner pipe wall and remove these deposits that would inhibit heat transfer. The majority of crystallization takes place in the bulk of the fluid, as opposed to the wall, thus allowing growth of easily separable crystals. Generally, the scraper blades rotate at moderate speeds of 15–30 rpm. This speed promotes adequate heat transfer, consistent with good crystal growth and easy separation:

- Solvent and raffinate slurry are cooled by cold filtrate or refrigerant.
- Tubes may be stacked in stacks of 8, 10, or 12.
- Tube extends from 20 to 40 ft.
- Inner tubes may be configured for flow in either series or parallel.
- Spider bearings are used for shaft support.
- One double pipe assembly usually consists of four or five individual pipe shafts connected by spider shafts that run through the spider bearings



Fig. 33.26 Typical SSEs

which support the internals. Each pipe shaft is fitted with spring loaded scraping blades whose design is specific to the SSE supplier. A drive shaft extends through a seal or packing at the drive end.

- A sprocket is attached to the shaft outside the tube and the shaft is turned by the sprocket that is driven by lubricated chains which are connected to all the sprockets on one side of the tube bank.
- The chain is driven by a fixed speed drive motor or more commonly two motors mounted above the tube bank.
- Shaft speeds range from 2 to 30 rpm.

The scraped surface equipment removes wax from the wall by scraping. The internals are designed to maximize the open cross-sectional area in the tube in

order to reduce the pressure drop. Modern design uses 12 in inner pipe for optimum heat transfer and pressure drop. Over time, wax accumulates on the cold internals, such as the spider bearing and other cold surfaces affixed to the shaft. The build up of wax will increase the pressure drop across the tube. When the pressure drop begins limiting the equipment, it will either be cleaned on-line or off-line by washing with hot solvent. Lube plant operations developed procedures that optimize SSE cleaning with minimum impact on the process.

33.20.1 Scraped Surface Equipment Suppliers

BORSIG and Armstrong are the leading suppliers of scraped surface equipment.

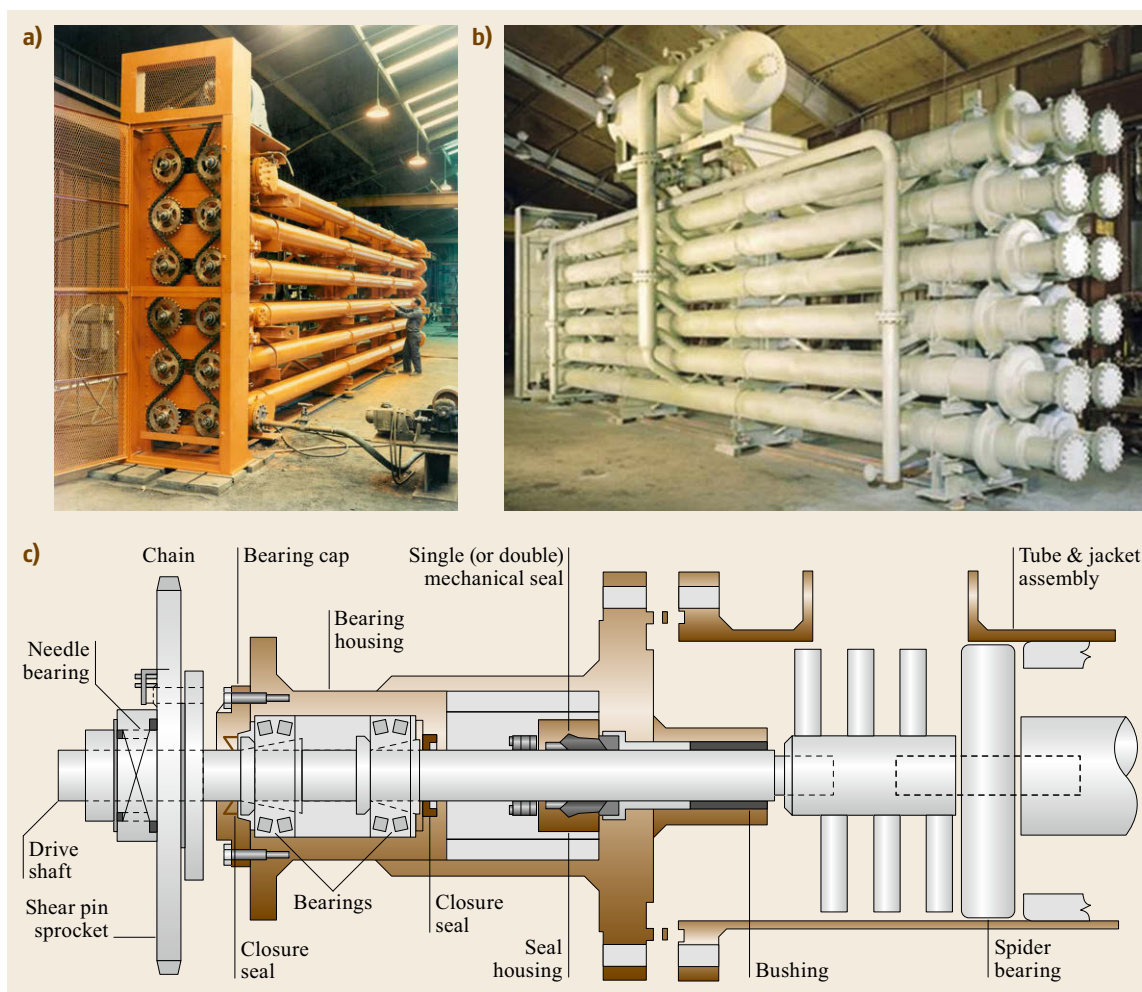


Fig. 33.27a-c Typical SSEs. View of SSE drive chain (a), view of chiller drum above SSE (b), SSE drive shaft bearing and seal assembly (c) (Photos courtesy of Armstrong)

Both Armstrong and BORSIG supply steel and bronze which are softer than the inner pipe wall. Each uses a spring to apply pressure on the scraper blade to push it against the tube wall so that it scrapes the wax off the wall as the internal shaft is turned.

Armstrong Scraped Surface Equipment

The drive end of a typical Armstrong SSE is shown in Fig. 33.27a. A chiller drum mounted on top of the tubes is shown in Fig. 33.27b. The Armstrong drive shaft assembly is shown in Fig. 33.27c. The design benefits of the drive unit:

- Rugged drive system.
- Easily understood by the maintenance personnel.
- Mechanical seals are frequently used to avoid leakage around the driven shaft.
- The drive staff is stabilized to avoid any bending which would reduce the life of the seal.
- The use of two heavy duty self-aligning bearings locks the drive shaft into place, and prevents any unwanted movement, which could cause leakage.
- The drive is bolted on which means that the unit must just be spaded off; there is no need for hot work. Once unbolted, the drive housing can be taken

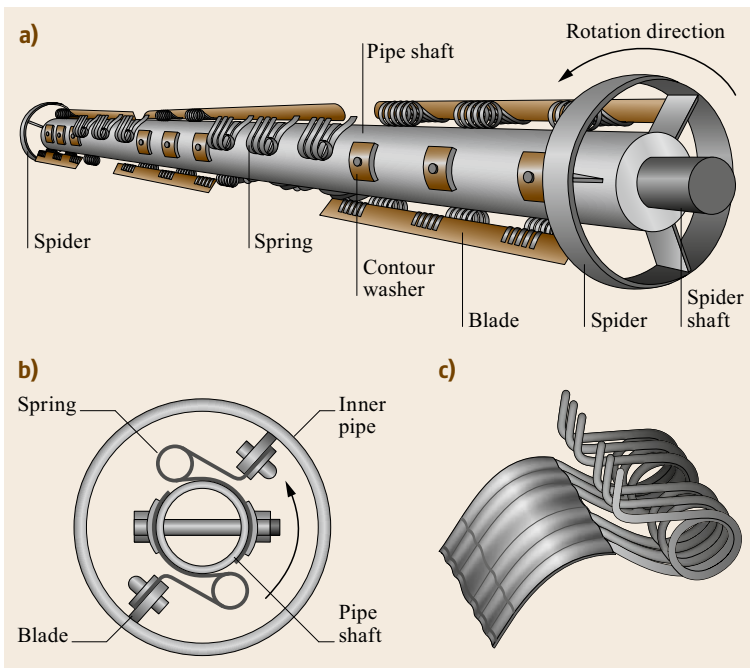


Fig. 33.28a,b Armstrong SSE internals – design views. Pipe shaft with leaf spring assembly and scraper blades (a), Cross-section of shaft showing leaf spring and scraper assembly (b), leaf spring (c) (courtesy of Armstrong)

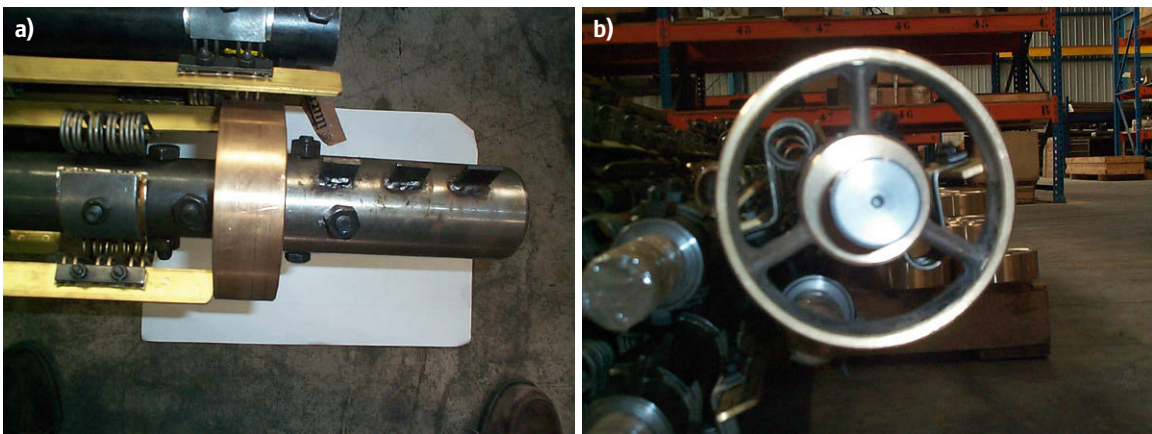


Fig. 33.29a,b Armstrong SSE internals – assembled views. Top end view of pipe shaft, leaf spring, scraper blade and spider bearing (a), end view of pipe shaft, spider bearing (b)

into the workshop for new mechanical seals to be fitted in a clean dry place. This reduces repair time and keeps the unit clean.

The design benefits of the scraper shaft:

- The drive system allows free turning off the drive shaft.
- The shaft is sealed against leakage of the process fluids.

An Armstrong pipe shaft with mounted springs and scraper blades is shown in Fig. 33.28a. Cross-section of the pipe shaft showing the leaf spring and scraper

blade assembly is shown in Fig. 33.28b. A six finger leaf spring is shown in Fig. 33.28c. Advantages of Armstrong springs:

- Extra long life – fatigue is minimized.
- Three springs per blade gives maximum scraping capability.
- Each spring made of 6 finger elements of either 316 SS or Monel.
- Lower pressure drop than plunger-type internals.
- Six elements per spring greatly reduces downstream damage from broken parts as the springs stay attached to the blade.

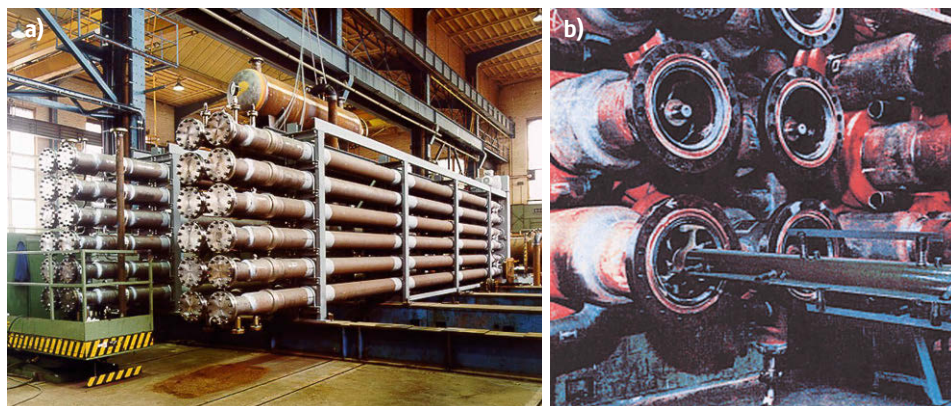


Fig. 33.30 Borsig SSE at the manufacturing site (a). Borsig internals being inserted into the tubes (b). (Photos courtesy of BORSIG)

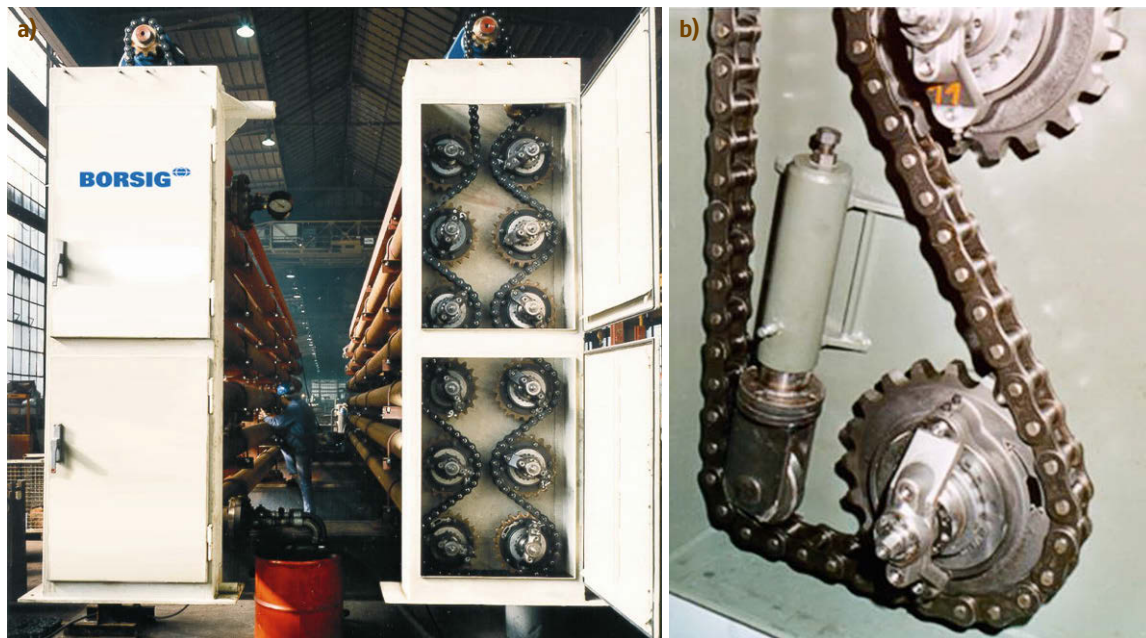


Fig. 33.31a,b Drive system and chain tightener of an SSE. End view of chain drive (a), close up view of chain tightener assembly (b) (Photos courtesy of BORSIG)

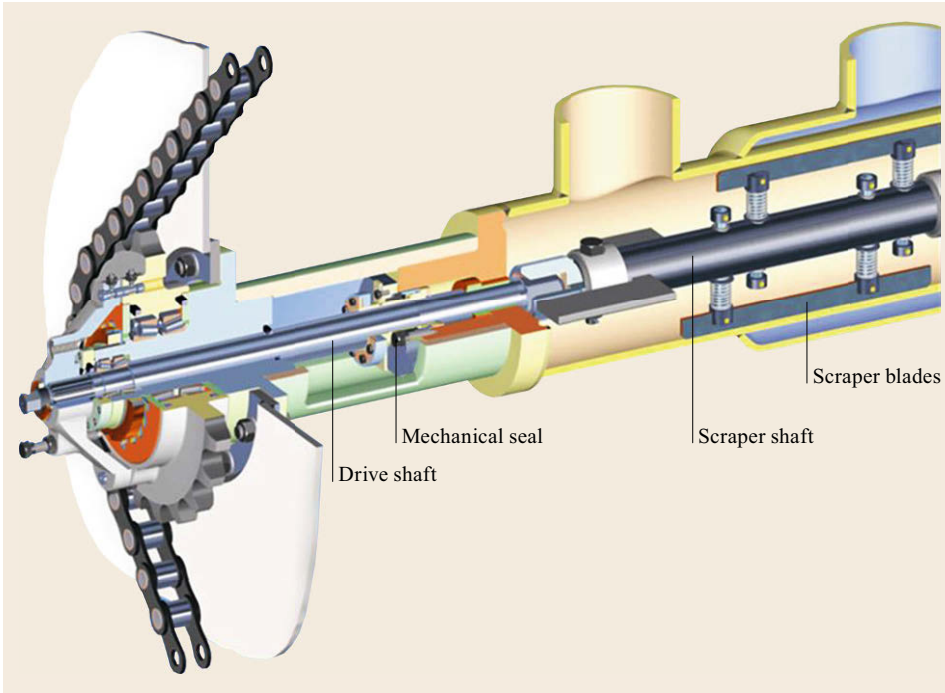


Fig. 33.32 Drive system with scraper shaft of an SSE. (Photo courtesy of BORSIG)

- Leaf springs consisting of one piece of stainless steel had a tendency to break across the radius as stress raisers were caused at every revolution. The Armstrong patented wire spring resolved this issue and offers better service life than the compression (plunger-type) spring. A major European refinery using these springs opened a chiller once, which had not been opened for 9 years, and it had less than a dozen broken springs. A fabricated Armstrong pipeshaft, leaf spring, scraper assembly and spider bearing are shown in Fig. 33.29a. A fabricated pipeshaft, spider bearing, leaf spring and scraper blade are shown in crosssection in Fig. 33.29b.

Borsig Scraped Surface Equipment

BORSIG supplies SSEs of 6, 8, 10, and 12 in inner pipe diameters to meet the volumetric flow rates and heat transfer needs which might be required. A typical Borsig SSE at the manufacturing site shown in Fig. 33.30a. Borsig internals being inserted into the tubes is shown in Fig. 33.30b. A typical scraper shaft ready for packing is shown in Fig. 33.34. Borsig SSE ready for shipment is shown in Fig. 33.39, installed SSEs in Fig. 33.40 and 33.41a–c.

The design benefits of the drive unit (see Fig. 33.31a end view of chain drive assembly and

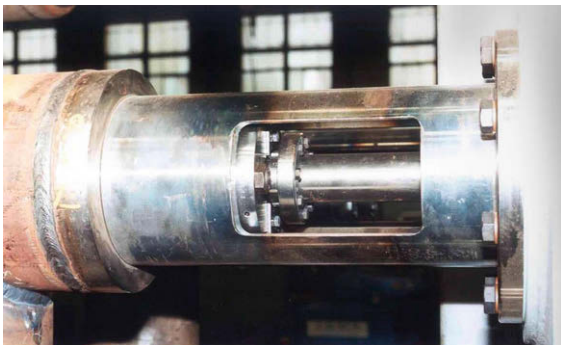


Fig. 33.33 Drive system – drive shaft and mechanical seal of an SSE. (Photo courtesy of BORSIG)

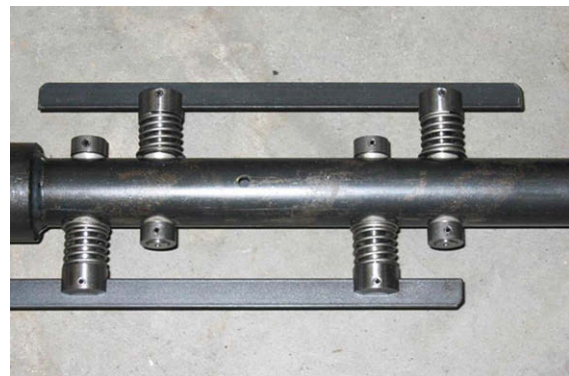


Fig. 33.34 Standard design of a scraper shaft as used for lube oil dewaxing in an SSE. (Photo courtesy of BORSIG)



Fig. 33.35 Scraper shafts ready for packing. (Photo courtesy of BORSIG)

Fig. 33.31b close up view of chain tightener assembly):

- The sprocket wheel is supported by a fixed bearing neck, which takes up the radial load caused by the chain pulling force. A critical alternating bending stress on the drive shaft is prevented.
- Owing to the absence of radial load on the drive shaft, a considerable improvement of the drive shaft seal is obtained.
- Potential bearing service life over 100 000 operating hours.

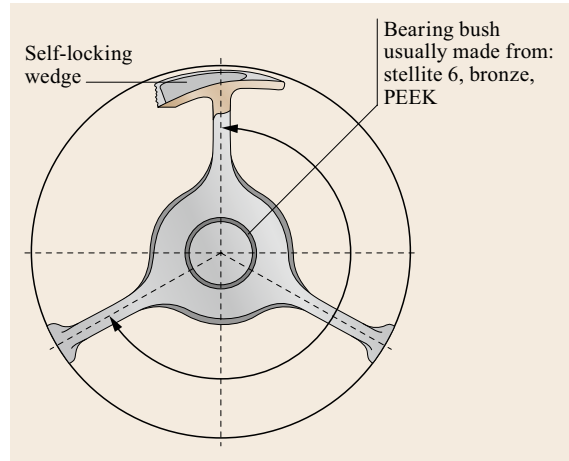


Fig. 33.36 Spider bearing in an SSE (courtesy of BORSIG)

- Gear housing for outdoor installation completely water- and dust-tight.
- In the case of shear pin failure, the sprocket wheel still rotates on main tapered roller bearings.
- Maintenance intervals more than 4 years.
- Removal of drive shaft, bearings, and drive shaft seal is possible without dismantling of chain drive (typical drive shaft and seal assembly shown in Fig. 33.33).
- Superior design for applying mechanical seal.

The design benefits of the scraper shaft and scraper blades are (Fig. 33.32):

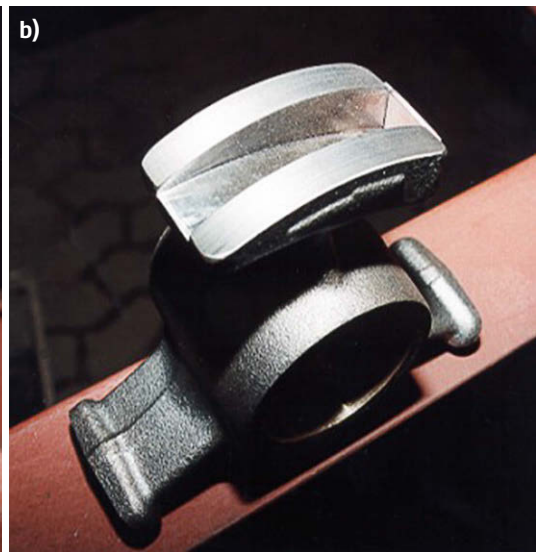


Fig. 33.37a,b Intermediate bearing design in an SSE. Side view of intermediate bearing (a), top view of intermediate bearing (b) (Photo courtesy of BORSIG)

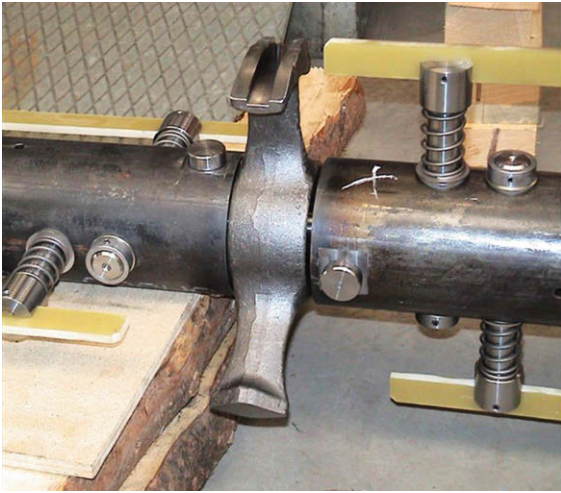


Fig. 33.38 Installed spider bearing in an SSE. (Photo courtesy of BORSIG) ◀



Fig. 33.39 SSE ready for shipment. (Photo courtesy of BORSIG)

- A stream-lined design especially with 10 and 12 in units (no intermediate pipe etc.) guarantees low-pressure drop due to low-flow resistance and less product deposition both resulting in longer running time of the units.
- Low wear of scraper blade due to optimum spring force.
- High blade/spring lift resulting in long service life of scraper blades.
- Robust design, also of the scraper blade holders, therefore insensitive to overloading.
- Running of the scraper shaft in the opposite direction presents no risk of breakage for spring and holders.

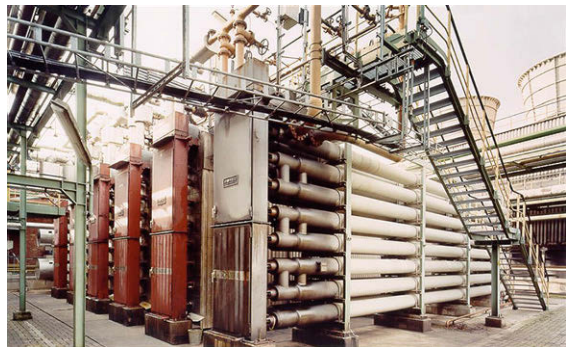


Fig. 33.40 Row of installed SSEs with access decking. (Photo courtesy of BORSIG)



Fig. 33.41 Two end views of installed SSE and one top view above the SSE (long tubes near the bottom of the picture). (Photo courtesy of BORSIG)



Fig. 33.42 Tube damage resulting from spider bushing failure. (Photos courtesy of Armstrong)



Fig. 33.43 Damage resulting from single leaf spring failure

- Coil springs (helical springs) affecting self-centering of the shafts, thus reducing the load on the bearings.
 - Corrosion resistant Monel K500 springs.
 - Rugged scraper shaft design.
 - Connection of each scraper shaft section with two solid bolts.
 - Plunger head design of the scraper blade holders (Fig. 33.34).
- Independent holders for each scraper blade.
 - No loose blades in the inner pipe should a spring brakes, blade is still held in position by the holder.
 - Damaging of inner pipe is excluded due to a special scraper shaft design, that is, stopping ring at the plunger prevents the plunger head to touch the inner pipe when the blade is worn out.



Fig. 33.44a-g Examples of damages in SSEs. (a) Damaged scraper blades, (b) damaged scraper leaf springs and blades, (c) broken chain link, (d) chain drive, (e) chain link wear, (f) bushing wear at chain link, (g) link and pin slack

- The scraper blade material is mild steel, brass, fibre-glass, or other material dependent on the product.

The design benefits of the spider bearing design (supports):

- Self-locking spider supports, not rotating with the shaft (wear in the inner pipe is excluded).
- Spider bearing supported scraper shaft is exactly fixed in the middle of the inner pipe. This guarantees equal load on all scraper blades and the scrapping is optimized.
- Spider-bearing-wedge design provides easy de-installation of the supports (Fig. 33.37a,b and Fig. 33.38).
- Spider-bearing design is stream-lined and guarantees low-pressure drop and less wax sticking (Fig. 33.36).
- Spider-bearing journals and drive shafts are hardened (i. e., with Colmonoy 6 or Wolfram Carbide).
- Support-bearing and drive shaft bushings can be made of bronze, stellite 6 or polyether ether ketone (PEEK).

33.20.2 SSE Equipment Issues

SSEs may require very high maintenance support as compared to other equipment in the lube plant. Excessive wax build up in the tubes may result in shear pins, which protect the internal shaft from damage, failing, and the shaft will stop turning. This reduces the ef-

fective heat transfer, which can further limit the plant on chilling limited base stocks. Seals and packing may leak contributing to solvent losses in the plant. Poorly lubricated chains will break or jump off the sprockets. Overall heat transfer coefficients may be low. Performance should be monitored, which is typically not an easy task. Internals must be overhauled when performance has permanently degraded.

Each SSE supplier uses a spring to apply pressure on the scraper blade to push it against the tube wall so that it scrapes the wax off the wall as the internal shaft is turned. Operators who buy cheap steel blades from local fabrication shops may save thousands of dollars compared with OEM equipment spare parts but in the end they will cost hundreds of thousands of dollars as the inner pipe wall wears beyond the corrosion allowance.

The internals weigh about 850 kg. Over a 40 ft scraped length when the spider bushings fail, the spider shafts wear and the resulting rotational ellipse just trepan the lower part of the inner pipe (Fig. 33.42).

An example of single leaf spring failures is shown in Fig. 33.43. Note that there are missing scrapers as well as twisted metal. Examples of SSE equipment damage may include damaged scraper blades (Fig. 33.44a), damaged scraper leaf sprongs and blades (Fig. 33.44b), broken chain links (Fig. 33.44c), broken chain drives (Fig. 33.44e), excessive wear at a chain link (Fig. 33.44e), excessive bushing wear at the chain link (Fig. 33.44f) and excessive chain link and pin slack (Fig. 33.44g).

33.21 Filters

Filters are used to separate the wax crystals from the slurry. The slack wax and filtrate are collected and sent to their respective recovery sections in the plant to recover and recycle solvent.

33.21.1 Operation

Rotary vacuum filters are used in ketone dewaxers and rotary pressure filters are used in propane plants. The principles of operation are the same. A typical filter is shown in Fig. 33.45.

The filter drum rotates at speeds from 0.2 to 1.6 rpm. The surface of the drum is divided into segments that run the length of the filter. Newer designs have 30 segments. Each segment has a lead and trail pipe connected to the segment at several locations running the length of the drum. The segment lead and trail pipes combine so that there are 30 lead and trail pipes, one for each segment, that carry filtrate to the mas-

ter valve, which is also called the trunnion valve. The master valve is stationary while the filter drum rotates. (A variable speed filter drive is shown in Fig. 33.47a.) The master valve has internal bridge blocks that effectively segregate the filtrate collected from the filter into as many as four distinct compartments or *pick-ups*. (Static master valve plate with bridge blocks shown on left of Fig. 33.46a. Rotating master valve plate shown on right in Fig. 33.46a. Typical piping at the master valve shown in Fig. 33.46b)

Starting from the deflector blade, the drum rotates into the slurry in the vat and filtration begins at the first *wet pick-up* port or No 1 vacuum. The filter segment continues its rotation into the *second wet pick-up* or No 2 vacuum. The rotation continues and the filter moves into the wash area or *first dry pick-up* and finally into the *drying area* or *second wet pick-up*. The drying area may also be washed with cold solvent. The filter rotates into the purge zone where N₂ blow gas is applied to the trail

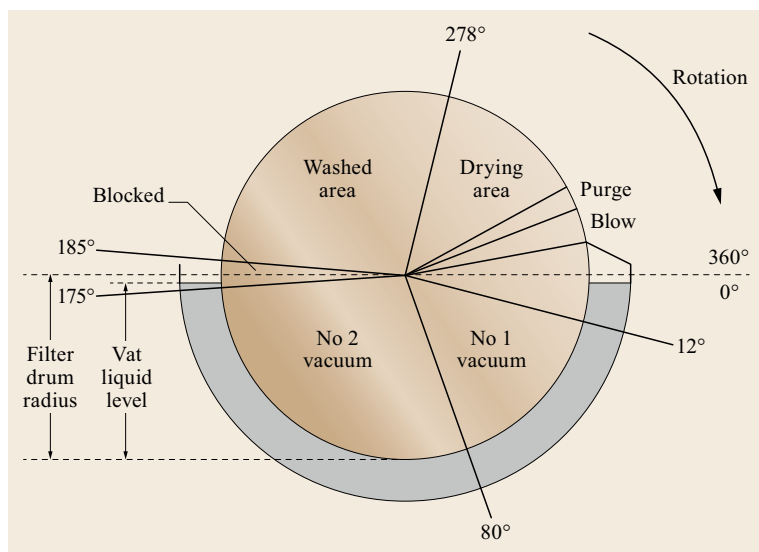


Fig. 33.45 Typical filter wash – dry segments

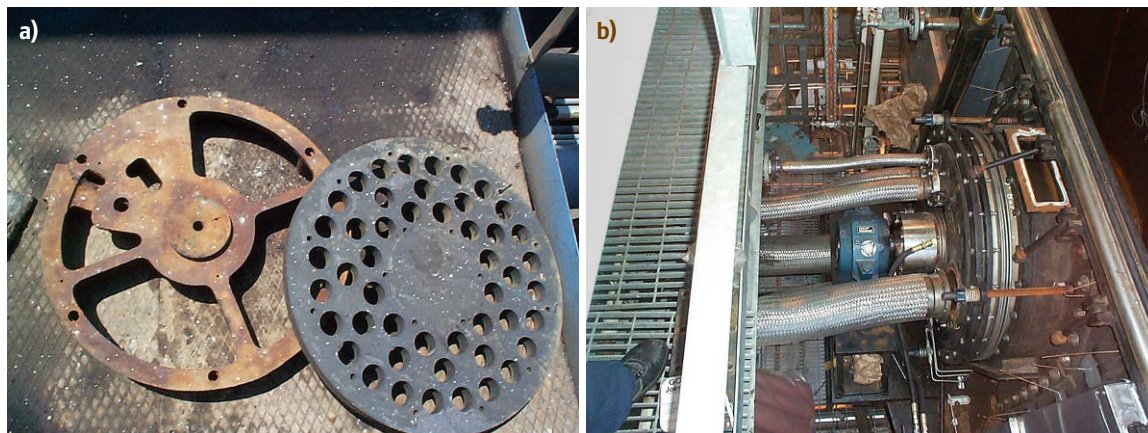


Fig. 33.46a,b Filter master valve. Static master valve plate (stator) with compartments shown on the *left* and rotating master valve plate (rotor) shown on the *right* (a). Installed master valve assembly with static piping attached to the static master valve plate (b). (Photos by B.E. Beasley, courtesy of ExxonMobil Process Research)

pipe while the lead pipe stays under vacuum. The purge zone clears out the filtrate in the pipes and increases the dewaxed oil yield by preventing the filtrate in the pipes from being blown back through the pipes and into the wax scroll with the wax. The segment moves into the blow gas zone and blow gas is applied to the lead and trail pipes and the cake *pops* off of the filter and slides across the Teflon deflector blade and into the wax scroll.

The scroll is an Archimedes screw (Fig. 33.47e) that moves slack wax from the outer ends of the filter to a center pipe. The slack wax falls down the pipe and may either proceed down a slide where it may be combined with slack wax from other filters into a slack wax drum or into a wax *boot* or vessel. This is a small drum dedicated to the filter. From the large wax drum

or the wax boot, the slack wax is pumped to either wax recovery, the second stage of dewaxing or de-oiling depending on the plant configuration.

33.21.2 Filter Media

The filter drums used in ketone dewaxing (rotary vacuum) and in propane dewaxing (rotary pressure) have filter cloths secured to the drum surface. The filter cloth retains the wax crystals while allowing the filtrate to pass through the filter cake or through the filter cloth and into the internals of the filter drum and eventually to the filtrate receiver drum.

Many different types of material have been used over the years. These include woven and nonwoven ma-



Fig. 33.47a–e Typical rotary vacuum filter. (a–b) Filter drum (c) solvent wash sprays and drip pipe (d,e) support grid and wax scroll. (Photos by B.E. Beasley, courtesy of ExxonMobil Process Research)

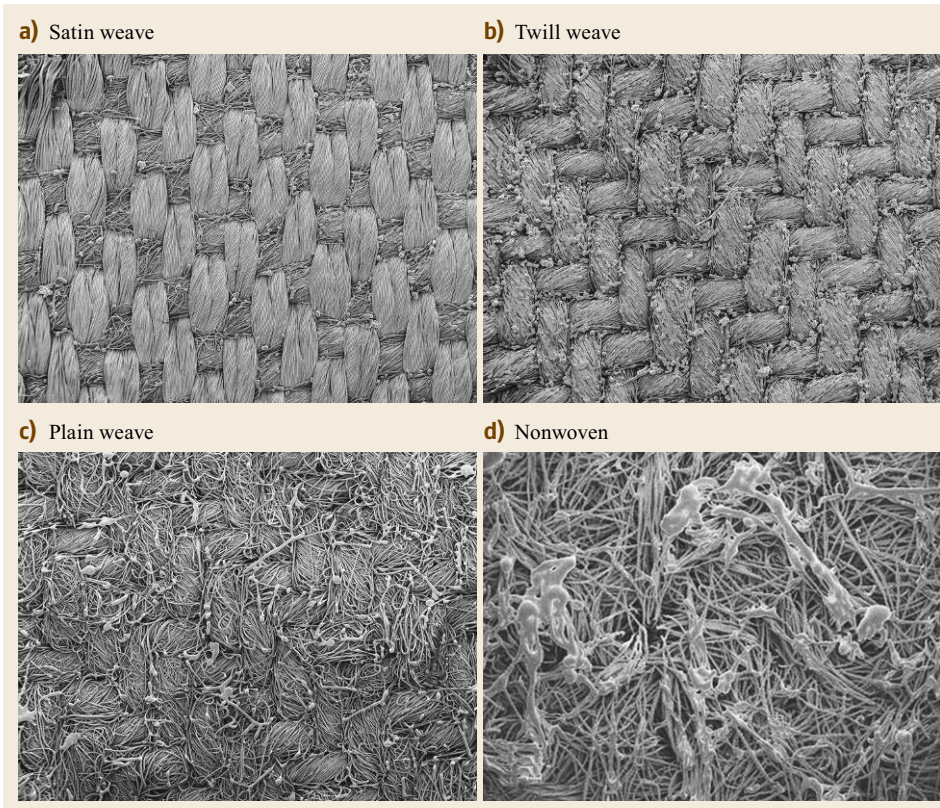


Fig. 33.48 SEM of typical filter medium. Stain weave (a), twill weave (b), plain weave (c), nonwoven (d). (Photos reprinted, courtesy of Madison U.S. Filter)

materials, single and dual layer cloths. A few examples are shown in Fig. 33.48.

The requirements of a good filter cloth are:

1. Low interfacial resistance for high filtration rates.
2. High filtration rates lead to high wash acceptance or lower filter speeds for increased dewaxed oil yields.

3. Elimination of wax bleed through and haze formation.
4. Thermally stable at hot wash temperature.
5. Chemically stable in ketone and propane service.

A comparison of typical filter cloth materials is given below.

Additional considerations include the mechanical stresses generated in vacuum and pressure filters that lead to fabric stretch and wear associated with filter blow gas. The filter cloth may suffer mechanical damage during installation, or from exposed deflector blades or other sharp or raised edges. The cost of the filter cloth is small as compared to the loss of production time incurred when a filter has to be re-clothed or when the dewaxed oil quality does not meet product specification.

Fiber selection, fabrication technique (woven, non-woven), and cloth finishing all play an important role in determining filter cloth performance.

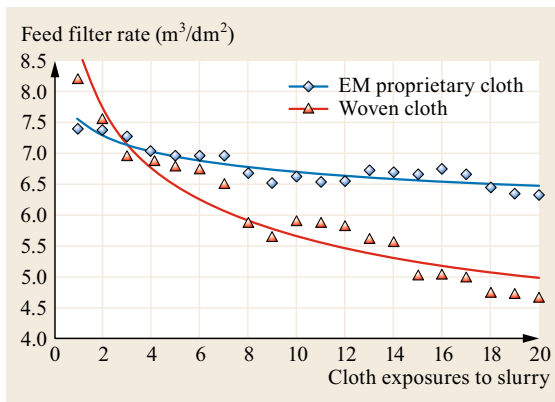


Fig. 33.49 Typical filter cloth fouling

The ExxonMobil patented proprietary filter cloth has been used in ketone and propane dewaxing processes for many years. It has higher resistance to



Fig. 33.50a–d Filter cloth installation. (a) Caulking bars hammered into caulking bar groove. (b) Removal of excess cloth. A small cloth strip is used in all grooves that do not have cloth overlap to provide tight fit. (c) Technicians tamp down the caulking bar as the wire is wound onto the drum. (d) Wire tension take up device. (Photos by B.E. Beasley, courtesy of ExxonMobil Process Research)

fouling due to several unique design features and has shown > 15% improvement in filtration relative to woven cloths can be achieved. Feed filter rate versus cloth exposures to slurry for ExxonMobil (EM) proprietary cloth and a typical woven cloth are shown in Fig. 33.49.

Filter cloth is cut to the length of the filter and depending on the width, several sections are required. The cloth sections are held in place on the surface of the

drum by a caulking bar, which is hammered into the caulking bar groove during the cloth installation. A steel wire is wrapped, under tension, around the drum to further secure the cloth. The wire will tend to migrate away from the drive end and many filters have installed a take-up tensioner device to extend the length of time before wire breakage occurs. Typical filter cloth installation shown in Fig. 33.50a–d. Filter cloth support grids are shown in Fig. 33.47b,d,e.

33.22 Cold Wash Distribution

Cold ketone wash is applied to the filters either through sprays or drip pipes or both. (A typical combination of sprays and drip pipes is shown in Fig. 33.47e.) There are advantages and disadvantages to both designs and both are in practice today. Cold wash is essential to reduce the oil in wax, increase dewaxed oil, and increase the wax product value. (Effect of filter–wash–dry sequence of DWO yield shown in Fig. 33.52.)

Good distribution is necessary to spread the wash completely over the wax cake and avoid dry sections. The wash must not impinge with excessive velocity onto the wax cake in order to avoid knocking it off or digging channels or grooves. The wash system should be resistant to fouling. Spray nozzles and drip pipes are the major wash distribution systems in use today. Both are acceptable provided the system is properly designed and operated within the design parameters.

ExxonMobil patented Drip Pipes provide excellent coverage and are capable of good turndown.

Wash falls by gravity onto the wax cake minimizing potential dislodging of the cake by wash impingement. Stainless construction and upstream filtration prevent fouling.



Fig. 33.51 Example of poor filter cold wash distribution. (Photo by D.S. Sinclair, courtesy of ExxonMobil Process Research)

Poor wash/spray distribution (example of poor wash distribution shown in Fig. 33.51):

- Poor wash distribution can result from collapsed sprays creating a wide area without coverage.
- If cold wash flow from the spray nozzles is too high wax may actually be blown off the filter cake. Evidence of this may be seen as an accumulation of wax on the filter windows.
- Conventional (not ExxonMobil) drip pipes may not be balanced, resulting in some areas with no flow and some areas with too much flow.
- Excessive wash flow rates through the spray nozzles may cut grooves in the cake and wash wax and solvent back into the vat resulting in recycling.
- Combinations of too high a flow through conventional drip pipes will collapse spray cones. Excess accumulation in a local area may cut grooves in the wax cake.

Drying out/compressing wax cake due to the lack of wash over portion of top pick-up zone not only affects DWO yield, but also drops filter feed rate (FFR):

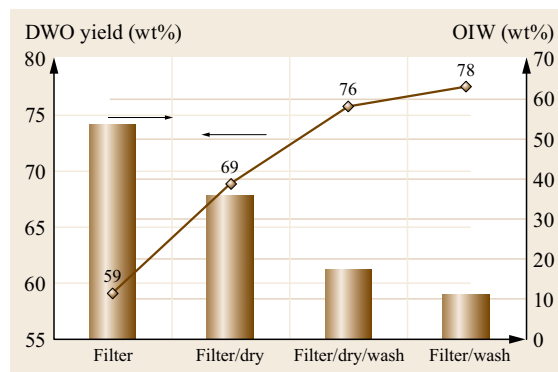


Fig. 33.52 Effect of filter–wash–dry sequence on oil yield. Bars show the oil in wax (OIW) by refractive index (RI) correlation with D3235, dots show the DWO yield in wt% by RI correlation with D3235

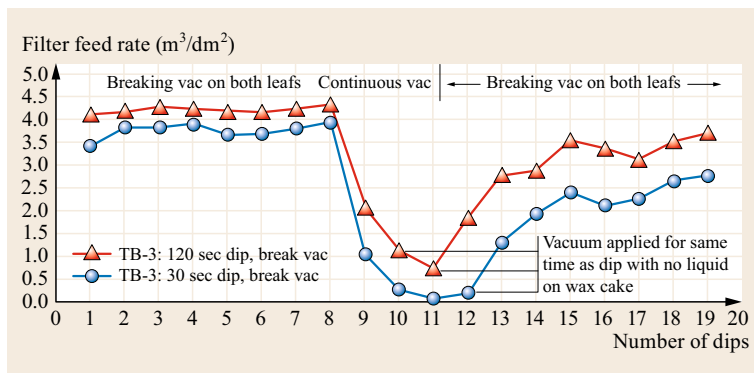


Fig. 33.53 Impact of wash application on FFR

- Recent plant test redistributed wash solvent to prevent large *dry* area on descending side of the filter and resulted in 15% increases in FFR.
- Figure 33.53 shows the effect of continuing to apply vacuum without wash and then reapplying wash – FFR improved again, but did not reach up to the previous level.

33.23 Wash Acceptance

Wash acceptance is the amount of wash that can be accepted through the wax cake before it begins to spill or run off the wax cake. The volume of filtrate collected as a function of time decreases in a square root relationship, for noncompressible wax cakes, until the end of the filtration step. At that point filtration is complete, the wax cake formation has stopped and the wash is applied to the cake. The flow of wash through the cake is at the same rate as the last increment of filtrate just

at the final moment of filtration (ignoring for the moment slight differences in liquid viscosity and wax cake compressibility). If too little wash is applied, the oil in wax will be higher than optimum and yield will be lower. If excess wash is applied, it will either roll off into the filter vat or into the scroll. Cumulative filtrate and wash volumes versus time are shown in Fig. 33.54. Normalized filtrate and wash rate versus time, shown in Fig. 33.55.

33.24 Wash Efficiency

Cold wash, distributed over the wax cake by drip pipes or sprays, will displace the cake liquids, reducing the oil in wax and increasing the yield. This occurs in two steps. The first step is a piston displacement where the wash liquid pushes out the cake liquids. In the second step, oil from within the wax crystal diffuses into the low oil concentration wash liquid. The theoretical reduction in oil content may be predicted by the Butler equation, which was developed by an Imperial Oil (Sarnia, Canada) researcher, Roger Butler, as a model for wash efficiency. Butler envisioned a cylindrical tube filled with oil being displaced by wash. Initially, its piston displaced up to 50% oil removal, and then the curve shifts to a parabola. The Butler equation can hence be formulated as $y = 1 - x$ for $x < 0.5$ and $y = 1/(4x)$ for $x > 0.5$. The efficiency of oil removal for any amount of wash is the comparison of the actually measured ratio *oil before wash* to *oil after wash* (A in Fig. 33.56)

and the prediction of the Butler curve (B in Fig. 33.56). Figure 33.56 shows various wash efficiencies in comparison to the Butler curve [33.14].

The wash efficiency is defined as the actual oil in wax obtained for a given amount of wash applied relative to that predicted by the Butler curve. Efficiencies may be less than 100%. This may be result from:

- Poor spray distribution
- Fouled, leaking, or missing spray nozzles
- Poor distribution along the drip pipe, *out of level* on older designs
- Fouled drip pipes
- Area of excessively fouled filter cloth may occur when *drying* is practiced
- Cracked filter cake, solvent flows through crack instead of cake
- Wash rate exceeding wash acceptance

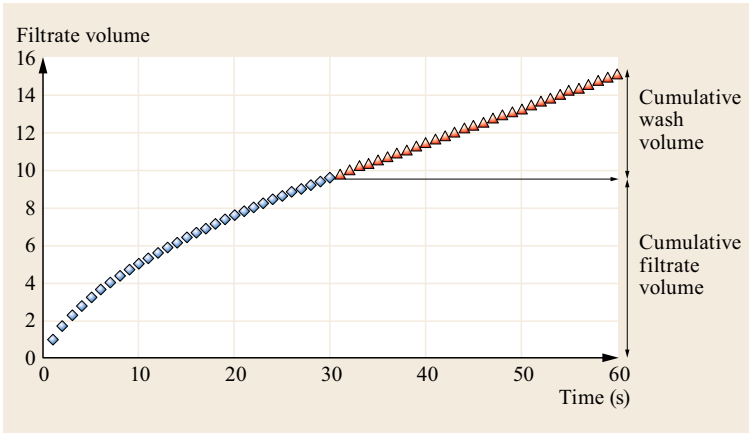


Fig. 33.54 Filtrate volume versus time. Wash acceptance (filtration time = wash time, incompressible cake)

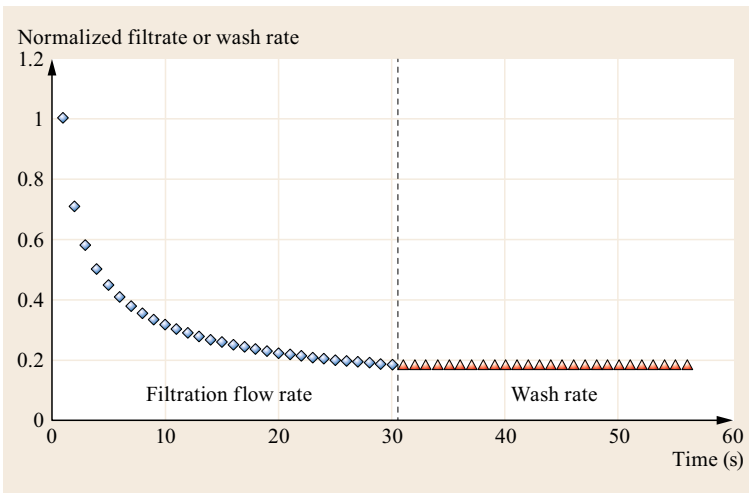


Fig. 33.55 Normalized filtrate or wash rate versus time. Wash acceptance (Filtration time = wash time, incompressible cake)

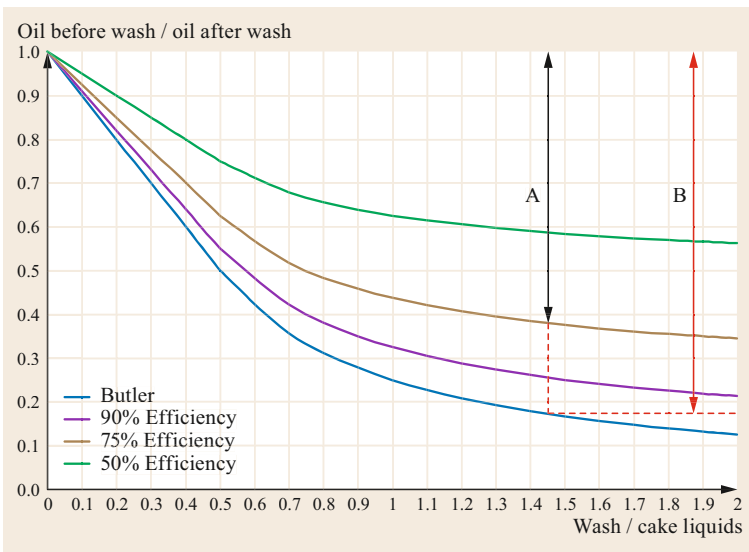


Fig. 33.56 Wash efficiency

8. Wash temperatures significantly lower than filtration temperature, which seals off wax crystals.

Wash efficiencies may be found to exceed 100%. This may be due to:

1. Hydraulic compression of the wax cake, *squeezing* oil out of the cake without using any wash solvent such as may occur in the drying section of the filter.
2. Higher crystal or wax cake compressibility in the presence of wash.

Some plants will dedicate a significant portion of the filter area to *drying* and will block or drips in this area. The intent is to reduce the oil in wax to increase yield and possibly debottleneck wax recovery. An unintended consequence is that the vacuum that remains on in this section will pull the wax cake into the filter cloth, accelerating the filter fouling, which will reduce wash acceptance and increase oil in wax. It will also require more frequent filter washing which will reduce plant throughput. These competing factors must be balanced by the manufacturer to achieve the optimum filter performance.

33.25 Filter Hot Washing

The filtration rate of a filter decays over time due to plugging of the filter cloth by small wax crystals. A typical decay curve is shown in Fig. 33.57. The feed rate measured by flow meter is plotted against the number of *dips* or exposures of the filter cloth to the wax slurry. The shape of the decay curve depends on the filter media, in this case an ExxonMobil proprietary cloth.

As the filtration rate decays throughout is lost and at some point the filter must be taken offline and washed to restore the filtration rate. The time during which the filter is off-line also represents lost production. The optimum time between washes is the economic balance between production lost due to the decay curve compared to the time to wash the filter and bring it back on line. An example of a series of decays and washes is shown in Fig. 33.58. If the shape of the decay curve is known and the wash time is known the optimum wash time may be determined analytically.

Hot ketone solvent is used to wash the filters. Cold wash solvent is blocked off and hot solvent flows through the same sprays or drip pipes, over the filter

cloth, melting the wax crystals, thereby cleaning the cloth. Filter washings are collected in a filter washing drum. The washings may be:

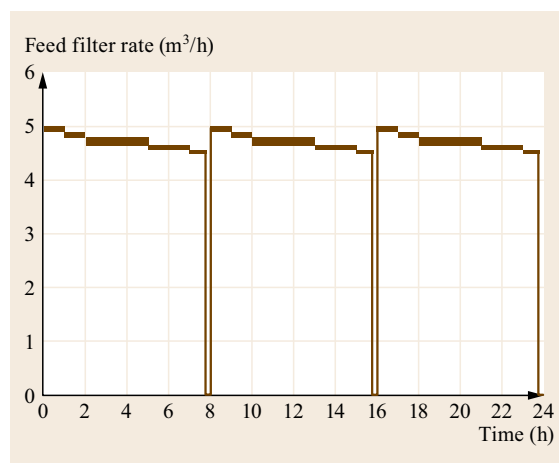


Fig. 33.58 FFR decay curves and filter washes

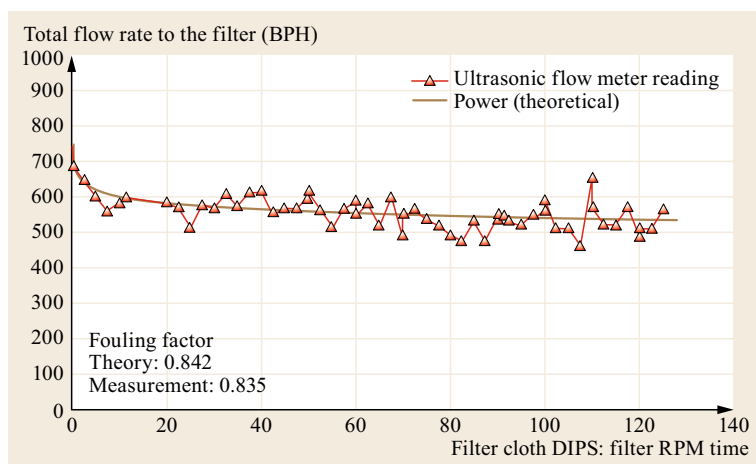


Fig. 33.57 The feed rate decay curve (light neutral) shows how the FFR decreases after several filter revolutions, the number of dips in rpm time

1. Injected with the feed as *predilution*
2. Injected between first and second filter stages
3. Injected into the appropriate stage of the DIL-CHILL™ crystallizer
4. Sent to wax recovery.

Hot wash temperature is controlled. If the temperature is too low, it may not adequately melt the wax crystals. If the wash temperature is too high, wire migration may occur resulting in reduced wire life and/or an increase in the frequency of wire retensioning.

33.26 Dewaxed Oil/Wax-Solvent Recovery

The objective of the dewaxed oil and wax recovery section is to remove solvent from the product stream for recycle back to the chilling train and the filters. This is done using low- and high-pressure flashes and a high-temperature flash followed by steam stripping and vacuum drying (dewaxed oil). Solvent concentrations are reduced to meet the product specification. High concentrations in the product represent avoidable solvent losses and increase operating expenses. In some cases, excessive high temperature operation in the recovery section can lead to light oil vaporization and accumulation in the solvent. This represents avoidable excess energy costs. The operation of the solvent recovery system becomes an economic optimization problem.

Dry *waxy solvent* from wax recovery should be segregated from the dry *clean* solvent recovered from the dewaxed oil recovery section. *Waxy solvent* tends to have wax in it and cannot be cooled to the same temperature as that of the *clean* solvent from the dewaxed oil recovery. It may be cooled and temperature blended with the *Clean* and used as filter wash. Flow restrictions may be set on flow to wax recovery to prevent wax carryover and downstream fouling.

Wet solvent from the stripper and the solvent from the low-pressure flash is sent to the dehydrator for solvent recovery.

A typical recovery section is shown in Fig. 33.59.

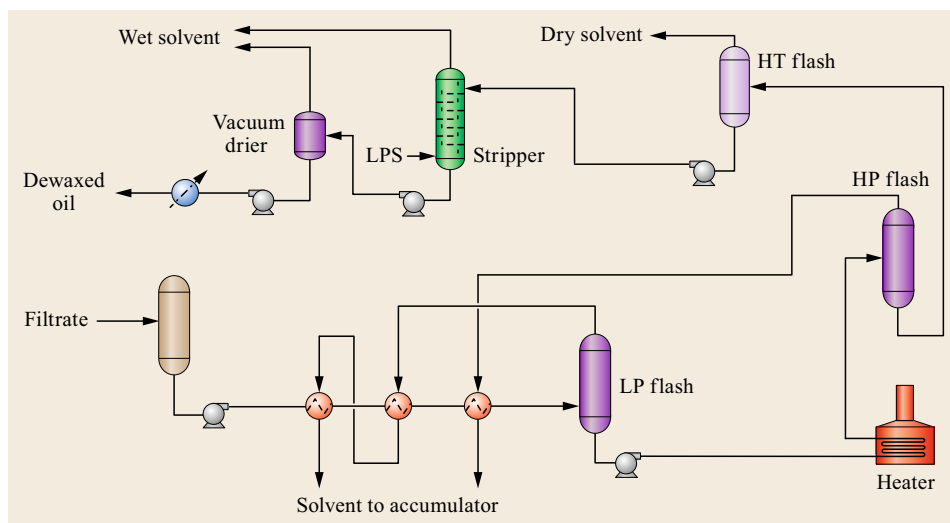


Fig. 33.59
Typical dewaxed oil recovery section flow diagram

33.27 Solvent Dehydration

Solvent from the low-pressure flashes is sent to the dehydrator tower. Overheads from the dehydrator tower are combined with stripper overheads and the overhead from the water tower is sent to the decanter. The solvent rich phase from the decanter is sent back to the dehydra-

tor. The water rich phase is sent to the water tower. Dry solvent from the dehydrator bottoms is returned to the unit. The water from the water tower is sent to waste water treatment. A typical solvent dehydration flow diagram is shown in Fig. 33.60.

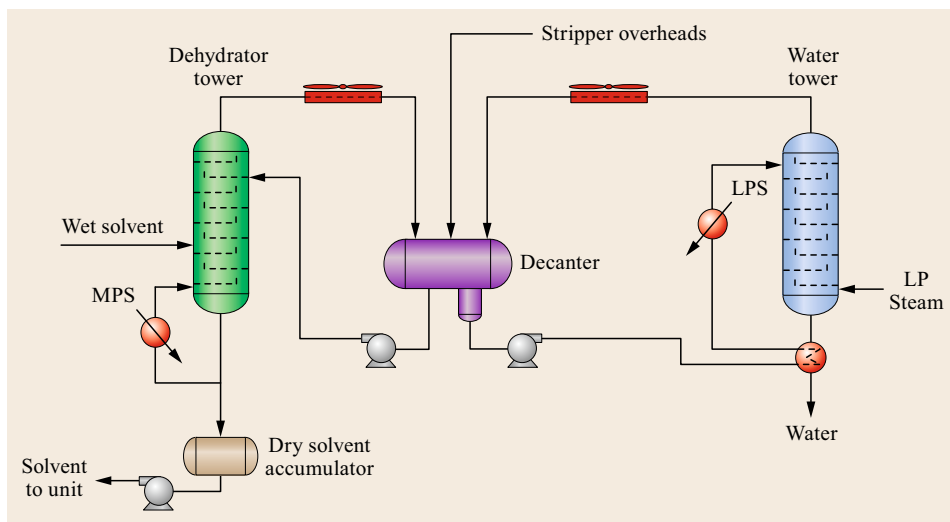


Fig. 33.60
Typical solvent
dehydration flow
diagram

33.28 Solvent Splitter

The solvent splitter allows the manufacturer to separate the solvent mixture back into MEK and MIBK or toluene which can then be added back to the solvent mixture in the plant to optimize the solvent composi-

tion and minimize the *pour-filter* temperature spread to achieve maximum throughput. A typical solvent splitter flow diagram is shown in Fig. 33.61.

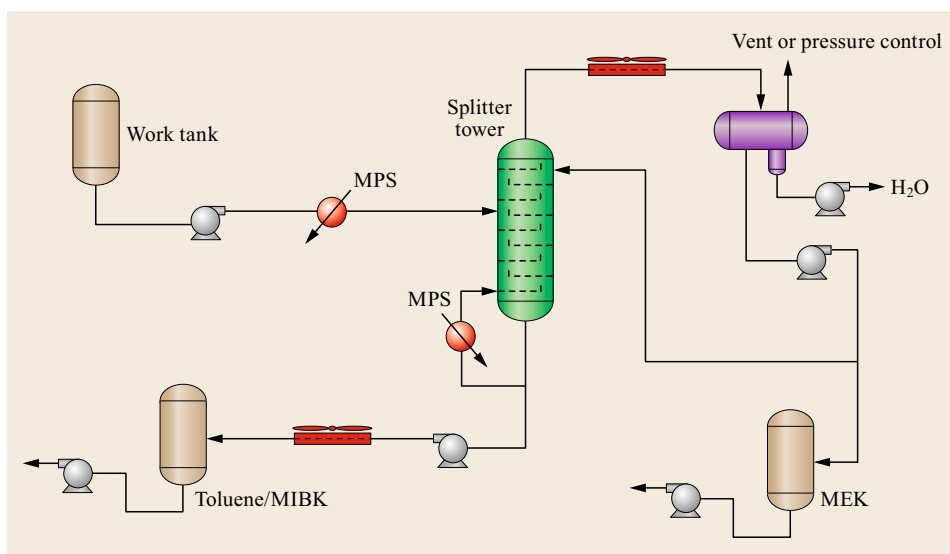


Fig. 33.61
Typical solvent
splitter flow
diagram

33.29 Two-Stage Dewaxing

A second stage of filtration can be used to reduce the oil in wax and to increase the dewaxed oil yield. Solvent (called repulp or repuddle) is added to the wax from

the first stage, typically in the wax scroll or wax boot depending upon the plant design, and pumped to a filter feed drum that feeds the second stage of filters.

Filtrate from the second stage is *lean* in oil and can be used in the first stage operation. It may be blended with *fresh* solvent and used as a first stage wash, or it

may be added as the final increment of dilution in an incremental plant. Recycling the second stage filtrate reduces the overall solvent usage.

33.30 Deoiling

The deoiling process is used to produce a hard wax containing a very low oil content. Waxes produced in deoiling have melting point and needle penetration specifications. Waxes intended for food grade use must also meet UV absorption specifications and require wax hydrotreating.

In recrystallization deoiling, lean solvent is added to the wax from the dewaxing plant and the resulting slurry is pumped through a heat exchanger where the wax crystals are melted. The wax is then recrystallized in SSEs and SSCs. Typically two stages of deoiling are used to meet the low oil in wax specification. Typical

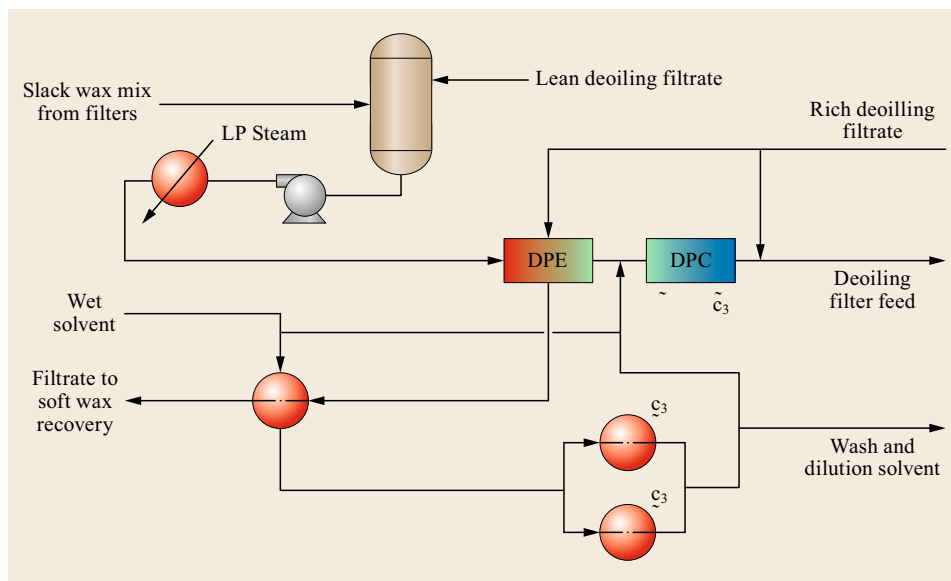


Fig. 33.62
Typical chilling section in recrystallization deoiling

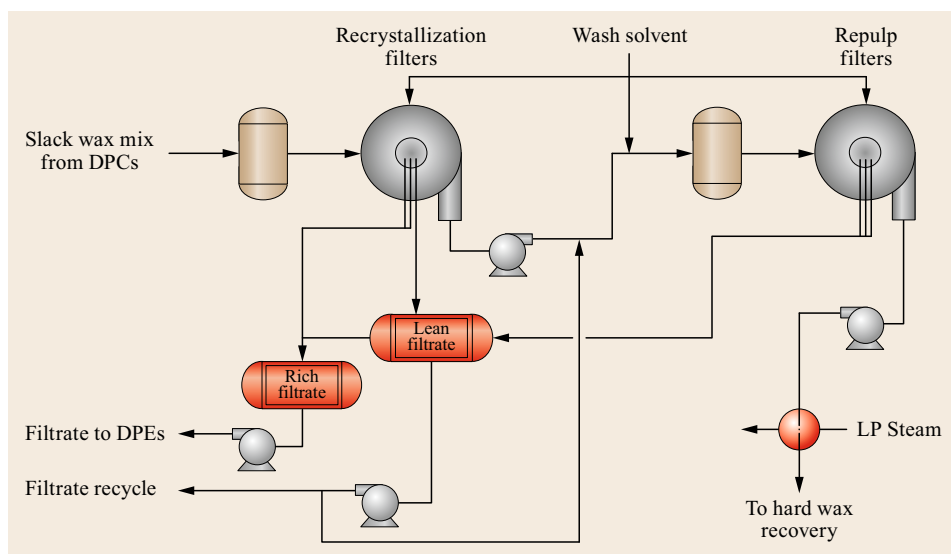


Fig. 33.63
Typical filtration section in recrystallization deoiling

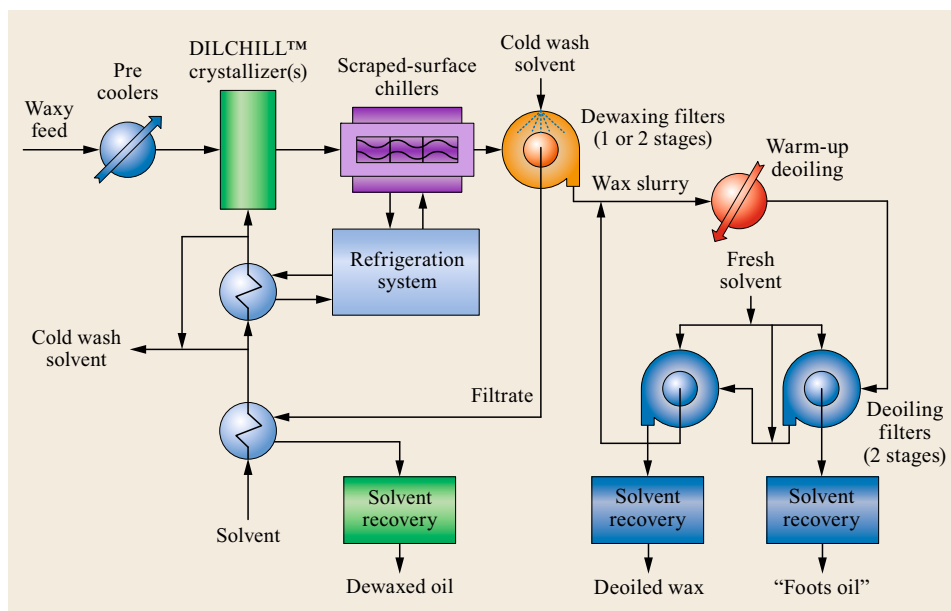


Fig. 33.64
Simplified
DILCHILL™
dewaxing/warm-
up deoiling flow
diagram [33.8,
p. 40]

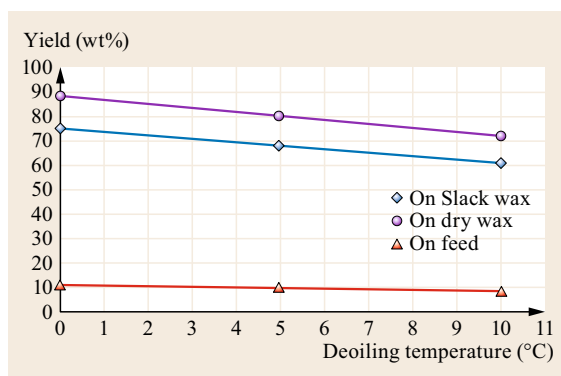


Fig. 33.65 Typical light neutral refined wax yields versus deoiling temperature

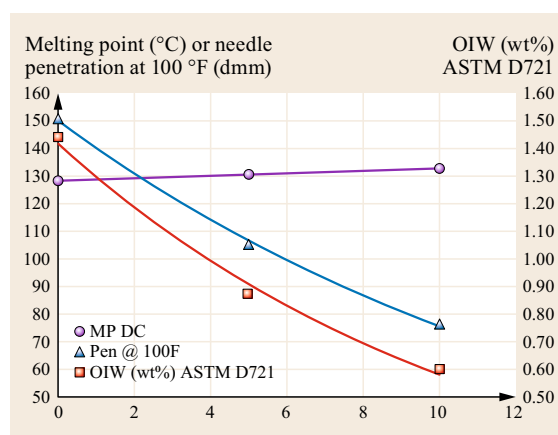


Fig. 33.66 Typical light neutral wax melting point and needle penetration versus deoiling temperature

chilling and filtration sections in recrystallization deoiling are shown in Fig. 33.62 and 33.63, respectively.

DILCHILL™ dewaxing is ideally suited for warm-up deoiling. The spherical nature of the crystals facilitates the melting of the soft wax and re-crystallization is not required. A simplified DILCHILL™ dewaxing/warmup deoiling flow diagram is shown in Fig. 33.64.

The deoiling (filtration) temperature in the deoiling plant is key to meeting final wax properties. As the temperature is increased, the soft wax melts and is removed leaving behind the higher melting, harder wax. A typical light neutral refined wax yields versus deoiling temperature is shown in Fig. 33.65. Typical light neutral wax melting point, needle penetration and DWO yield versus deoiling temperature are shown in Fig. 33.66.

Table 33.16 Typical yield comparison from dewaxing, two-stage dewaxing and deoiling of a heavy neutral

Yields (vol%)	One-stage dewaxing	Two-stage dewaxing	One-stage deoiling
Dewaxed oil	68	73	68
Slack wax	32	27	0
Soft wax (foots oil)	0	0	19
Finished wax	0	0	13

Needle penetration decreases whereas melting point increases. The melting point and needle penetrations define the specification *box* for the manufacturer. Usually the *box* is wide enough that a range of deoiling temperatures may be used that will produce a hard wax that

meets all product specifications. In this case, the manufacturer will select the lowest deoiling temperature that will achieve the desired product properties because this

will give the manufacturer the maximum yield. A yield comparison from dewaxing, two-stage dewaxing and deoiling of a heavy neutral is shown in Table 33.16.

33.31 Propane Dewaxing

Propane dewaxing uses liquid propane as the solvent. (A simplified propane dewaxing flow diagram is shown in Fig. 33.67.) Propane is normally a gas at ambient temperature and the vessels in the unit must be pressure vessels. This also includes the filter. Filtration in propane dewaxing is pressure filtration versus ketone dewaxing that uses vacuum filtration. The propane temperature depends on the pressure so that it is of paramount importance that the pressure must be controlled. It is often said that in propane dewaxing, propane is always either flashing or condensing. This adds an additional level of complexity that is not present in ketone dewaxing.

There are advantages and disadvantages to ketone versus propane dewaxing. A brief comparison is shown in Table 33.17.

Warm liquid propane is added to waxy raffinate and the slurry is prechilled in a shell and tube prechiller, with the slurry in the tube side. The warm dilution

ratio is controlled by the operator. Like the feed pre-cooler in ketone dewaxing, the outlet temperature of the prechillers is maintained just above the cloud point of the slurry to avoid fouling in the prechiller. Some newer designs use a prechiller tower.

The feed solution passes through the prechillers and into the warm solution drum. Up to this point, the propane dewaxing process is a continuous process. The warm solution drum alternatively feeds one of the two chillers and the process now becomes a batch process.

Large batch chillers cylindrical (older) or spherical in design accept prechilled slurry from the warm solution drum and batch chilling begins. Pressure on the chiller is slowly released and the liquid propane evaporates, cooling the batch of slurry in the chiller. A simplified propane dewaxer chilling section is shown in Fig. 33.68.

In older plants, control of the *vent gas* sets the chilling rate. This may be done with two pressure control

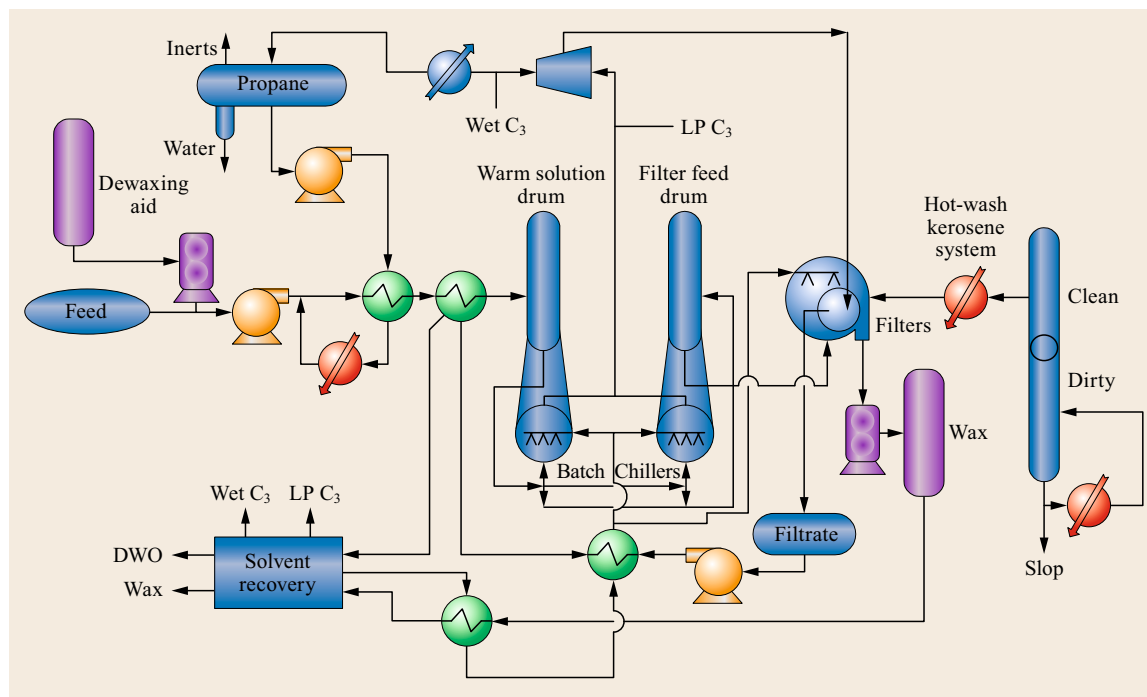


Fig. 33.67 Simplified propane dewaxing flow diagram (also see [33.9, Fig. 11.4], courtesy of Exxon Research and Engineering Company)

Table 33.17 Propane versus ketone dewaxing

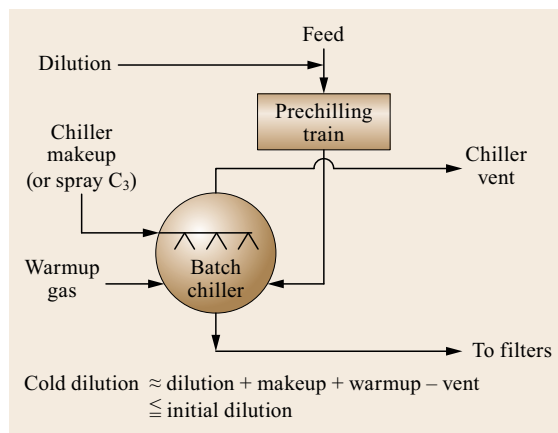
	Propane	Ketone
Higher filter rates		
150N	30–50	7–9
600N	18–30	4–5
Bright stock	10–15	2–3
Lower dilution ratios		
150N	1.2–1.6	2
600N	1.4–2.0	3
Bright stock	2–2.2	4
Economics		
Investment	40%	Base
Utilities	Less	Base
Operating costs	More	Base
Pour point	Limited to -15°C	
Two-stage	Yes	Yes
Deoiling	Yes	Yes

valves (chiller vent valves). Advanced control and valve design has been successfully applied to allow adequate pressure control using a single valve.

Make-up propane is added to replace the vented propane so that at the end of the cycle the dilution in the slurry, the cold dilution ratio (CDR) is at the desired target. Similar to ketone dewaxing where the filtration rate depends on the solvent dilution to the filters, the filtration rate in propane dewaxing is dependent on the CDR, which is also the dilution that will be seen at the filters. The CDR also has a large impact on the pour point. Wax molecules are highly soluble in propane, more than toluene. Increasing the CDR will carry more wax molecules into the filtrate and increase the pour point of the dewaxed oil. This requires the manufacturer to reduce the filtration temperature (by reducing the filtration pressure) to compensate. Because of the large pour-filter spread that exists in propane dewaxing, the base stock pour point is typically limited to -15 . This is a drawback for the propane dewaxing process.

Slurry in the chiller is cooled to the target conditions and then the bath is transferred to the filter feed drum that provides holding capacity for the filters.

Under ideal conditions, the transfer of the cold slurry would occur the moment after the chiller target temperature has been reached. In practice, two conditions may exist. If the chiller final chill temperature has been reached and the filters are not ready to accept the new batch, then the slurry is held in the chiller and the slurry *waits* for the filters. This is referred to as *wait time*. If the filters are ready to accept the next batch of feed but the chiller has not reached its final chill temperature so that it is ready for transfer, the filter levels will drop and the filters will be starved for feed. This is referred to as *starve time*. Chilled slurry is transferred

**Fig. 33.68** Simplified propane dewaxer chilling section

to the filters. After transfer has been completed, the chiller is warmed by pressuring with propane, which condenses on the walls of the chiller. The wall temperature is *warmed-up* to a high enough temperature such that when the prechilled slurry from the warm solution drum is fed to the chiller, shock chilling at the wall will not occur. Warm-up takes time which limits the production. The steps in the chiller cycle are:

1. Fill with prechilled slurry
2. Chill slurry to target temperature by venting propane, add make-up to make target CDR
3. Wait time for filters
4. Transfer slurry to filter feed drum
5. Warm-up.

Total cycle times may range from 20 to 30 min.

Rotary pressure filters are used to filter the slurry. Filtration rate is a function of the pressure drop across the filter. The temperature of the slurry also depends on the pressure. This requires carefully controlled pressure balance from the filter feed drum to the filters and to the filtrate drum. If the pressure in the filtrate drum is too high, the temperature will be high and the resulting dewaxed oil pour point will be too high. If the filter pressure is not increased to maintain the Delta P then filtration rate will also be reduced.

Wax and propane and oil and propane are sent from the filters to their respective recovery sections. High-pressure flash, low-pressure flash, stripper and drier vessels are used to recover propane from the product.

33.31.1 Effect of Water

Solvent *Drip Pipes* that are used to distribute the liquid propane wash over the wax cake in the filters, will

foul if the water content in the propane is too high. The water freezes and will reduce the wash flow and/or may change the wash distribution. The oil in wax will

increase and the overall dewaxed oil yield will drop. Methanol or acetone may be added to the propane to *de-ice* the drip pipes.

33.32 Two-Stage Propane Dewaxing

Two-stage dewaxing may be used to reduce the oil in wax and increase dewaxed oil yield and to reduce solvent requirements. Repulp/repuddle propane is added to the slack wax from the first dewaxing stage. The slurry is pumped to the second-stage filters. Control of the pressure balance is critical to avoid shock chilling and second-stage bog-downs that will limit plant throughput. The second-stage filtrate may be used as the first-stage wash or as dilution.

33.32.1 Propane Deoiling

Propane deoiling is accomplished using high-pressure filters that are required to handle the higher temperatures that must be used to melt the softwax. The finished

wax produced from deoiling is a valuable by-product and margins may at times exceed dewaxed oil margins.

33.32.2 Propane Filter Washing with Hot Kerosene

Temperatures required to successfully melt the wax from the filter cloth do not allow the use of liquefied propane as it requires very high pressure. Instead, kerosene is used to wash the filters. Kerosene wash temperature is typically controlled. If the wash temperature is too low, the wax crystals will not be melted and if the wash temperature is too high, wire migration will increase leading to reduced wire life and/or more frequent wire retensioning.

33.33 Analytical Tests in Dewaxing

There are numerous analytical tests used to assess and optimize the dewaxing operation. A few

of the most important tests are listed in Table 33.18.

Table 33.18 Analytical tests in dewaxing

Test	ASTM test no	Application
Pour point	D 97, D 5949, D 5950, D 5985, D 6749	Key specification for dewaxed oil
Oil-in-wax %	D 721, D 3235	Wax specification, measure of yield performance
RI at 20–30 °C	D 1218	Yield calculation, solvent composition
Miscibility curve		Used to set solvent composition for each stock to avoid immiscible operation
Gas chromatographic distillation	D 2887	GCDs may be for troubleshooting and predicting dewaxing performance
Feed cloud point	D 2500, D5551, D 5771, D 5772, D 7773	Helps set feed precooler outlet temperature
Water-in-solvent	D 6304-03, E 203-1	Excess water may lead to immiscible operation and icing of solvent chillers

33.34 Dewaxing Aids

DeWaxing aids (DWA) may be used in ketone dewaxing but are always used in propane dewaxing. Typically, the DWA doses used in propane plants are 2–3 times higher than those used in ketone plants. While DWAs are economically justified for use on all grades in the propane plant, performance on light neutrals in ketone plants has typically not been economically justified.

DWAs are expensive and may represent the single largest controllable operating expense in the propane plant. Filtration rates in the propane plant may be improved from a level that is almost inoperable to several times the highest rate experienced in the ketone dewaxing plant. Oil in wax may be greatly reduced increasing overall yield and enhancing the wax product value.

DWAs are required to achieve high filtration rates in propane dewaxing. Typically, a DWA consists of a polymer backbone with alkyl side chains. Factors affecting the DWA performance include:

1. Raffinate feed.
2. Polymer *backbone* chemistry.
3. Molecular weight, number distribution.
4. Side chain distribution.
5. Active ingredient.
6. DWA ratio (when combined with other additives) in blend. Feed filter rate as a function of DWA ratio for a light neutral is shown in Fig. 33.70.
7. DWA dose, the concentration used. Filtration rate improvement for a light neutral as a function of DWA dose is shown in Fig. 33.69.
8. Asphaltene contamination.
9. Regulatory requirements (FDA approval).

Major DWA polymer backbone chemistries include:

1. Polyalkyl methacrylate (PAMA)
2. Polyalkyl acrylate (PAA)
3. Copolymerization of PAMA, PAA
4. Dialkyl fumarate vinyl acetate (DAFVA)
5. Ethylene vinyl acetate (EVA)
6. Wax naphthalene condensate.

Molecular weights of the DWA may vary from 10000 to 1000000. Molecular number, the *branchiness*, may range from 7000 to 300000. Side chain lengths may vary from C₁₄ to C₂₆ and with various distributions. Active ingredient may range from 10% to 100% with 15–30% the most typical. Dewaxed oil (light or heavy neutral) or toluene may be used as diluent. DWA viscosity will depend on the active ingredient and the diluent and the viscosities can be quite high and may affect pumpability.

33.35 DWA Mechanism

The exact mechanism of how the DWA works is still being studied. Leading theories include:

1. Co-crystallization of the DWA into the wax crystal matrix that changes growth direction of crystal planes
2. Agglomeration mechanism
3. Wax crystal modifier that associates with the surface to change crystal growth plane.

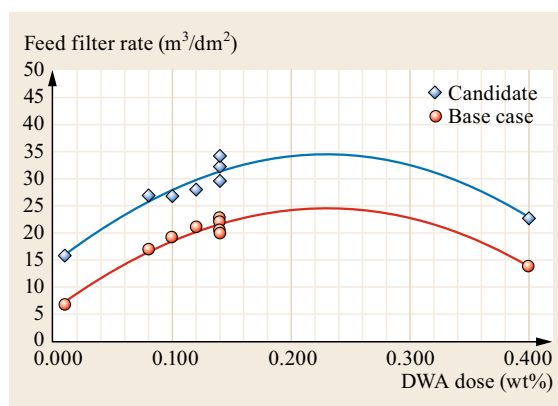


Fig. 33.69 Light neutral DWA dose response curve, DWA ratio 1 : 1

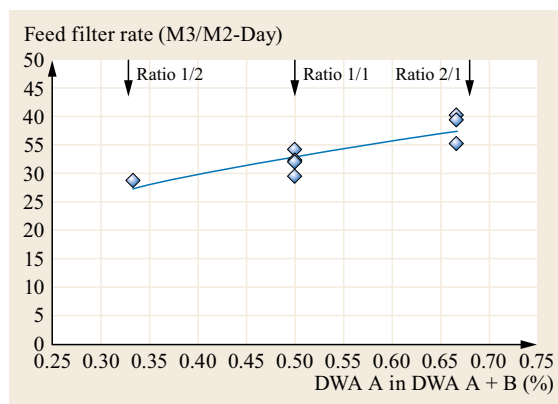


Fig. 33.70 Effect of DWA ratio on light neutral

Typically, DWA is stored at elevated temperatures. Positive displacement or centrifugal pumps are used for injection and various meters may be used to monitor the flow rate. Mass flow meters have been used with great success in the application.

Studies have shown that DWAs may be combined to give synergistic performance. Currently, because of the large number of variables (feed, DWA chemistry, etc.), it is not possible to predict DWA performance a priori and DWAs must be tested in a pilot plant that can simulate the propane dewaxing process. Laboratory and analytical tests typically over predict DWA performance due to favorable laboratory conditions and inability to simulate the plant.

33.36 Asphaltene Contamination

The presence of asphaltenes in the feed to the propane dewaxer or in the propane will significantly reduce the filtration rate and must be avoided. Asphaltenes may be present in the heavy neutral due to entrain-

ment from the VPS section below the heavy sidestream drawoff. Contamination may occur if the lube deasphalting unit (LDU) and propane dewaxer share propane.

33.37 Regulatory Requirements

The manufacturer using DWAs must determine if an FDA-approved DWA is required in their product market. The number of DWAs meeting FDA technical requirements is small and these DWAs command a premium in the marketplace. The qualification of new DWAs is expensive and takes a long time. DWA chem-

istry type, molecular weight (M_w), molecular number (M_n), polydispersity ($PDI = M_w/M_n$), unreacted monomer concentration, and concentration in the final product are some of the major factors the FDA considers and the candidate must pass technical specifications in these areas in order to obtain approval.

33.38 Glossary

- **API:** American Petroleum Institute.
- **Aromatic:** An unsaturated ring compound having a basic six-carbon-atom ring with either a hydrogen atom or a chain joined to each carbon atom.
- **ASTM:** American Society for Testing and Materials.
- **ATF:** Automatic transmission fluid.
- **Base oil:** A base oil is the base stock or blend of base stocks used in API licensed oil (see API 1509).
- **Base stock:** A base stock is a lubricant component that is produced by a single manufacturer to the same specifications (independent of feed source or manufacturer's location), that meets the same manufacturer's specification, and that is identified by a unique formula, product identification number, or both (see API 1509).
- **Base stock categories:** Base stock categories/base oil categories. The American Petroleum Institute (API) has categorized base oils into five categories. Groups I, II, III and are manufactured from refined crude oil. Group IV are fully synthetic (polyalphaolefin) oils. Group V are all those not covered in groups I–IV.
- **Base stock properties:** Key base stock properties may include properties such as viscosity, volatility, viscosity index (VI), pour point, cloud point, color and Conradson carbon (CCR).
- **Base stock slate:** A base stock slate is a product line of base stocks that have different viscosities but are in the same base stock grouping and from the same manufacturer (see API 1509).
- **Batch:** Any quantity of material handled or considered as a unit in processing.
- **Batch treat:** A treatment of a limited quantity of material with chemicals to improve quality.
- **Blowback:** The term applied to blow gas usage. Some call *blow gas* by a *blowback* or *blowback gas* term.
- **Blow gas:** Gas used to *blow* the wax cake from the filter cloth by being applied under pressure beneath the cloth.
- **Bright stock:** A vacuum distillation tower bottoms that has been deasphalted and extracted or hydrotreated and probably dewaxed as a heavy base stock.
- **BSI:** British Standards Institution
- **Caulking grooves:** The U-shape piece of metal welded to the drum deck. The resultant *grooves* are used to *caulk* the filter cloth into place. Also, lips on the grooves are used to retain the grid on which the cloth rests.
- **CCR:** Conradson carbon residue. A laboratory test that indicates the coke forming tendency of an oil. The amount of the residue remaining after evaporation and pyrolysis of the oil. Equivalent to micro carbon residue (MCR) test.
- **CCS:** Cold cranking simulator. A test used to determine the low temperature performance of lubricants when cranking a cold engine powered only by the battery and starter motor.
- **Controlled chillers:** SSE using cold filtrate to cool the slurry.
- **Carryover:** Entrainment of heavy phase into the light phase and out with the raffinate solution (essentially solvent at the tower top).

- *Carryunder*: Entrainment of light phase that has not settled from the heavy phase and exits with the extract solution (essentially feed at the tower bottom).
- *Centistoke*: The worldwide unit of kinematic viscosity.
- *Coalescence rate*: Relative rate at which fine, small droplets form larger droplets, which settle faster, forming a clarified oil layer.
- *Continuous phase*: Heavy, NMP-rich phase that forms an unbroken stream through the treater.
- *Corrosion*: The gradual eating away of metallic surfaces as the result of oxidation or other chemical action. It is caused by acids or other corrosive agents.
- *Crystallization*: May be defined as a phase change in which a crystalline product is obtained from a solution.
- *Cut*: The portion or fraction of a crude oil boiling within certain temperature limits.
- *Cut point*: The temperature limit of a cut or fraction, usually but not limited to a true boiling point basis.
- *DAO*: Deasphalted oil: The extract or residual oil from which asphalt and resins have been removed by an extractive precipitation process called deasphalting.
- *DAU*: Deasphalting unit: A process for removing asphalt from reduced crude or vacuum residua (residual oil) that utilizes the different solubilities of asphaltic and nonasphaltic constituents in light hydrocarbon liquids, for example, liquid propane.
- *Density*: The mass of a unit volume of a substance.
- *Deck pipes*: Each segment is drained by a series of pipes located along side each caulking groove.
- *DILCHILL™*: DILution CHILLing. ExxonMobil process where chilled solvent is added stagewise to an agitated tower. Mixing, cooling and crystallization occur in the tower.
- *Dilution ratio*: The ratio of solvent to waxy raffinate feed (vol/vol).
- *Dispersed phase*: Light, oil-rich phase which *bubbles* through continuous phase, then settles, and repeats the process on each tray.
- *Distillate*: Product of distillation collected by passing vapors through a condenser.
- *DPC*: Double pipe chiller.
- *DPE*: Double pipe exchanger.
- *Drum*: The horizontal drum on which the filter cloth is applied to its circumference surface.
- *Dry Wax*: The solid component present in a waxy feed at a certain oil pour point if all oil were removed from it.
- *DWO*: Dewaxed oil.
- *Entrainment*: Entrainment is the carryover of liquid by the vapor phase. Liquid may be in the form of a spray, foam or mist.
- *EXOLFINING*: An ExxonMobil extraction process used to extract aromatics from lube feedstocks to improve the VI and quality of lubricating oil base stocks, integrated with hydrofining.
- *Extract*: In solvent refining processes, that portion of the oil which is dissolved in and removed by the selective solvent; the solvent rich phase. Contains a low percentage of oil that is typically high in aromatic content.
- *Extraction*: The process of separating a material, by means of a solvent, into a fraction soluble in the solvent and an insoluble residue.
- *Feed retention drum*: Feed solution hold up drum.
- *Feed solution*: Waxy feed plus warm propane.
- *FFR*: Feed filter rate ($(\text{m}^3/\text{day})/\text{m}^2$ of filter cloth). Refers to feed only.
- *Filter cloth blinding*: The term applied to the reduction in filter rate due to wax or ice particles plugging up the flow paths in the filter cloth.
- *Filter hood*: The top part of the filter outer enclosure.
- *Filtrate (or wet) port*: The section or nozzle on the master valve that collects filtrate from the vat slurry.
- *Filtrate*: Liquid product (oil plus solvent).
- *Final dilution*: The last increment of solvent added after the shock chillers.
- *Foots oil*: The soft wax melted or dissolved/washed away during wax deoiling. In the old days, it was the oil drawn from the bottom (foot) or a pan separator for wax formed in a wax *sweater*.
- *Fractionation*: Fractionation is the separation of light and heavy fractions in the distillation tower.
- *Furfural*: An aldehyde obtained from corn shucks, wheat, or oat hulls, used in an extraction process for removing aromatic, naphthenic, olefinic, and unstable hydrocarbons from a lubricating oil charge.
- *GCD*: Gas chromatographic distillation (GCD). Chromatography technique used to separate and analyze compounds that can be vaporized without decomposition. A simulated distillation GC analysis using a gas chromatograph with a nonpolar column to determine the boiling-point distribution analysis of petroleum fractions.
- *Haze*: Visible, uncombined or flocculated, wax or water in dewaxed oil.
- *Hot wash*: The technique or the hot solvent used to periodically melt and dissolve wax out of the filter cloth.
- *Hydrofinishing*: The final step in base oil manufacturing uses H_2 and a catalyst to saturate the molecules, break undesirable molecular chain struc-

- tures, and improve the stability of the oil by removing oxygen and color bodies.
- **Immiscible:** Two phases, one oil rich and one solvent rich. Normally not desirable in solvent dewaxing.
 - **Incremental dilution:** Refers to the addition of solvent in increment to the waxy raffinate feed as it flows through the heat exchanger equipment.
 - **Internal reflux:** Portion of the light phase that springs from the heavy phase due to lower temperature at treater bottoms, and recycles back up the tower in the dispersed phase.
 - **ISO:** International Standards Organization.
 - **Kinematic viscosity:** The ratio of the absolute viscosity of a liquid to its specific gravity at the temperature at which the viscosity is measured.
 - **L/S:** Liquid-to-solid ratio in the wax cake. The liquids consist of oil and solvent or liquids to solids in the filter vat.
 - **LCA:** Lube crude approval process. A lube crude selection process used by base stock manufacturers that includes detailed steps to qualify a crude for purchase by the manufacturing organization.
 - **LHU:** Lube hydrofining unit to improve color stability of lube oils using hydrogen.
 - **Lead pipes:** The pipes on the leading side of each segment as the drum rotates.
 - **LPS:** Low pressure steam.
 - **Lube oil volatility – NOACK:** ASTM D-5800. A test method that provides an indication of the evaporation loss of lubricants in high temperature service.
 - **Lube oil volatility – capillary GCD:** An alternative to ASTM test methods D-5800 and D-5480 (withdrawn in 2003). The lubricant volatility is measured at 371 °C by capillary gas chromatography.
 - **Lubricant:** Any substance interposed between two surfaces in relation to motion for the purpose of reducing the friction and/or the wear between them.
 - **LVPS:** Lubes vacuum pipestill.
 - **Master valve:** Trunnion valve, the stationary sectioned casting in contact with the rotating end of the drum (i. e., the wear plate) at which the lead and trail pipe manifolds are dead ended.
 - **MCR:** Micro carbon residue. A laboratory test to determine the amount of residue remaining after evaporation and pyrolysis under specified conditions. Equivalent to Conradson carbon residue test.
 - **MEK:** Methyl ethyl ketone or loose term for ketone dewaxing unit.
 - **MEK OIW test:** Oil content of wax using ASTM D921 (MEK solvent at –25 °F).
 - **MIBK:** Methyl isobutyl ketone.
 - **Miscible:** One homogeneous phase. Usually preferred in solvent dewaxing. Refers to oil and solvent mixture.
 - **Miscibility temperature:** Temperature at which solvent and feed are completely miscible – all feed dissolved in solvent – and there is no phase separation in treater tower or in dewaxer slurry.
 - **MPS:** Medium pressure steam.
 - **NMP:** *N*-methyl-2-pyrrolidone, a solvent used as an alternate to furfural and phenol for the extraction of lubricating oil fractions.
 - **Naphthene:** A group of cyclic hydrocarbons also termed cycloparaffins. Polycyclic members are also found in the higher boiling fractions.
 - **Naphthenic crudes:** Class designation of crude oils containing predominantly naphthenes or asphaltic compounds.
 - **Neutral:** A VPS distillate, extracted, and dewaxed, made into a base stock.
 - **Normal paraffin:** A straight chain hydrocarbon in which no carbon atom is united with more than two other carbon atoms.
 - **OIW:** Oil in wax.
 - **OPEX:** Operating expenses.
 - **Pale oil:** A petroleum lubricating or process oil refined until its color is straw to pale yellow.
 - **Paraffin-base crudes:** Crude containing paraffin wax and practically no asphalt or naphthenes.
 - **Paraffinic:** Describing the paraffin nature or composition of crude petroleum or products therefrom.
 - **Paraffins:** A homologous series of open-chain saturated hydrocarbons of the general formula C_nH_{2n+2} of which methane (CH_4) is the first member.
 - **Paraffin wax:** A colorless wax extracted from paraffin-base lubricating oils.
 - **PDU:** Propane dewaxing unit to remove wax from oil using propane as a solvent.
 - **PNA:** Polynuclear aromatic: A compound composed of two or more aromatic rings (see aromatic). These compounds are under close scrutiny since they are generally considered to be carcinogens.
 - **Polarity:** A measure of the asymmetric distribution of a molecule's electrical charge. $MEK > MIBK > H_2O$.
 - **Polyalphaolefins (PAO):** Alpha-olefins are polymerized to make a polyalphaolefin (PAO). In an alphaolefin the carbon-carbon double bond is between the first and second carbon atoms. PAOs are useful basestocks in some synthetic lubes. PAOs are categorized by API as group IV and are fully synthetic.
 - **Pour point:** The temperature at which the oil will no longer pour.
 - **Predilution:** Solvent addition occurring before the precoolers. Sometimes called primary dilution.
 - **Prechillers:** In propane dewaxing, shell and tube exchangers that chill the feed solution before batch chillers.

- **Raffinate:** In solvent-refining practice, that portion of the oil which remains undissolved and is not removed by the selective solvent; the solvent lean phase. Contains a low percentage of solvent and typically a low aromatic content oil.
- **Rectification:** Rectification is the removal of heavy material from the vapor phase.
- **RI:** Refractive index.
- **SAE:** Society of Automotive Engineers.
- **Saybolt universal seconds (SUS):** A measure of kinematic viscosity, expressed as the time in seconds for 60 ml of fluid to flow through a standard Saybolt universal viscometer at a specified temperature. ASTM method D-88 describes the method and apparatus.
- **Scale wax:** Wax with an oil content of 1–5%, for example, wax from a two-stage dewaxer.
- **Segment:** Each drum segment is made up of a pair of the caulking grooves running longitudinally on the drum deck with the grid in between.
- **Selectivity:** A measure of the ability of a solvent to separate compounds of different structure, for example, aromatics from paraffins from naphthenes.
- **Service factor:** A quantity that relates the actual on-stream time of a process unit to the total time available for use of the unit. Frequently a ratio of the number of actual operating days divided by 365.
- **Settling Rate:** The rate at which droplets of the dispersed phase rise through and separate from the continuous phase.
- **Shock chillers:** Double pipe exchangers (see SSE) that use propane or propylene as a refrigerant.
- **Shock chilling:** Rapid cooling rates ($> 2\%/min$) shock the slurry resulting in smaller crystals and lower FFR. Rapid uncontrolled crystallization, characterized by high nucleation rates producing very small average crystal size.
- **Slack wax:** Wax with an oil content $> 5\%$, for example, wax from one-stage dewaxer.
- **Solubility:** Degree to which the oil (mainly aromatics) dissolves in the NMP. This is a function of aromatic type and concentration, changes from one grade to another as well as for the same grade from one crude to another.
- **Solvent deasphalting:** A process for removing asphalt from reduced crude or vacuum residua (residual oil) which utilizes the different solubilities of asphaltic and nonasphaltic constituents in light hydrocarbon liquids, e.g., liquid propane.
- **Solvent neutral oil (SNO):** A paraffinic base oil that has been solvent refined, dewaxed, and finished and is ready to be used in blending or compounding.
- **SSC:** Scraped surface chiller: Usually a double pipe design of 6, 8, and 12 in diameter with internal scrapers to remove wax from the cold walls. Typically, a refrigerant such as propane, propylene, or ammonia is used on shell side. Used in conventional dewaxing.
- **SSE:** Scraped surface exchanger. Usually a double pipe design of 6, 8, 12 in diameter with internal scrapers to remove wax from the cold walls. Typically cold filtrate is used on shell side. Used in conventional dewaxing.
- **SSU:** See Saybolt universal viscosity.
- **Stability:** Resistance to chemical change.
- **Stripping:** Stripping is the removal of light material from the liquid phase.
- **TAN:** Total acid number.
- **Third phasing:** Immiscible condition in a dewaxer where you have two liquid phases and a solid (wax phase).
- **Trail (or lag) pipes:** The pipes on the trailing side of each segment as the drum rotates.
- **Trunnion valve:** Master valve: The stationary sectioned casting in contact with the rotating end of the drum (i. e., the wear plate) at which the lead and trail pipe manifolds are dead ended.
- **Typical lube processes:** Typical lube processes include: Lube vacuum distillation (VDU) or vacuum pipestill (VPS) to control the viscosity and volatility of the oil. Solvent extraction of the aromatics to control the viscosity index. Solvent dewaxing to control the pour point of the oil. Hydrofinishing to stabilize the oil.
- **Vat:** The bottom part of the filter outer enclosure into which the filter feed slurry flows.
- **Viscosity, dynamic:** Measure of the internal resistance to deformation caused by shear or tensile stress.
- **Viscosity index:** A measure of the change in viscosity with temperature; ASTM D-2270.
- **Viscosity, kinematic:** The ratio of the absolute (dynamic) viscosity divided by the fluid mass density.
- **VPS (VDU):** Fractionation equipment, a vacuum pipestill (VPS) or vacuum distillation unit (VDU) is used to distill atmospheric bottoms into gas oil or lube distillate cuts.
- **VTB:** Vacuum lower (VPS) bottoms, or vacuum residue or vacuum resid.
- **Warm-up:** A step in the batch chiller sequence during which the chiller internal metal wall is warmed in preparation of accepting feed, and avoiding shock chilling at the wall.
- **Warm solution drum:** Drum containing prechilled feed solution.

- *Wash*: Generally the term used for the cold solvent applied to the wax cake.
- *Wax cake*: Solid product consisting of, generally, 2–10 liquids (solvent plus oil) to solids content in the discharged wax cake.
- *Wax doctor knife*: The deflector blade that rides against the filter cloth or winding wire. The blade keeps the wax cake from falling off the drum back into the feed slurry after the blow gas dislodges the cake.
- *Wax, Refined*: Wax of, usually, 0.5–2% oil-in-wax produced from deoiling.
- *Wax, Scale*: Wax of, usually, 2–10% oil-in-wax produced from two stage dewaxing.
- *Wax Scroll*: The screw conveyor rotating in the wax trough. All scrolls in dewaxing service are the center-discharge type.
- *Wax, Slack*: Wax of, usually, > 10% oil-in-wax produced from one stage dewaxing.

Acknowledgments. Special thanks to ExxonMobil employees and annuitants: Bob Aupperlee, Doug Boate, Joe Boyle, Mike Davis, Ken Del Rossi, Sasha Glivicky, Dave Mentzer, Chuck Quinlan, Evelino Ruibal, Dave Sinclair, Bernie Slade, and Howard Spencer and to Armstrong and Borsig Scraped Surface Equipment suppliers.

References

- 33.1 API: *API-1509 Engine Oil Licensing and Certification System Appendix E*, 17th edn. (American Petroleum Institute, Washington DC 2012)
- 33.2 B.C. Deane: Base oil quality. In: *Downstream, Modern Petroleum Technology*, Vol. 2 (Wiley, Chichester 2000), Chap. 25
- 33.3 J.D. Bushnell, R.J. Fiocco: Engineering aspects of the Exol N lube extraction process. In: *1980 Proc. – Refin. Dep. Am. Pet. Inst.*, Vol. 59 (1980) pp. 159–167
- 33.4 B.M. Sankey: A new lubricants extraction process, *Can. J. Chem. Eng.* **63**, 3–7 (1985)
- 33.5 M.B. Davis, D.S. McCaffrey, R.R. Savory: The EXOL N extraction process – Flexibility and high efficiency to meet modern lubes product requirements. In: *Advances in Production and Application of Lube Base Stocks, Indian Institute of Petroleum* (McGraw-Hill, New Delhi 1994) pp. 24–32
- 33.6 D.A. Gudelis, B.M. Sankey, J.D. Bushnell: EXOL N: New lubricants extraction process. In: *Proc. Tenth World Pet. Congr.*, Vol. 4 (1979) pp. 407–414
- 33.7 R.J. Fiocco: Development of the cascade weir tray for extraction. In: *New Dev. Liq.-Liq. Extr.*, *AIChE Symp. Ser.*, *ISEC 83*, Vol. 80 (1984) pp. 89–93
- 33.8 V.A. Citarella, E.A. Ruibal, S. Zaczepinski, B.E. Beasley: Crystallization technique to simplify dewaxing, *Pet. Technol. Q.* **Q1**, 37–40 (2000)
- 33.9 R.R. Savory: Base oil processes. In: *Downstream, Modern Petroleum Technology*, Vol. 2 (Wiley, Chichester 2000), Chap. 11
- 33.10 D.A. Gudelis, J.D. Bushnell, J.F. Eagen: Improvements in dewaxing technology, *API Proc. Div. Refin.* **53**, 725–737 (1973)
- 33.11 D.A. Gudelis, J.F. Eagen, J.D. Bushnell: New route to better wax, *Hydrocarb. Process.* **52**(9), 141–146 (1973)
- 33.12 J.D. Bushnell, J.F. Eagen: Commercial experience with DILCHILL™ dewaxing. In: *NPRA Fuels Lubr. Meet. 1975, Houston* (1975), paper F&L-75-50
- 33.13 J.F. Eagen, D.A. Gudelis, D.H. Shaw, J. Walker: Successful development of two new lubricating oil dewaxing processes. In: *Proc. Ninth World Pet. Congr.*, Vol. 5 (Applied Science, London 1975) pp. 345–357
- 33.14 R.M. Butler, J.L. Tiedje: The washing of wax filter cakes, *Can. J. Technol.* **3**(1), 455–467 (1957)

Premium Lub

34. Premium Lubricant Base Stocks by Hydroprocessing

Stephen K. Lee, John M. Rosenbaum, Yalin Hao, Guan-Dao Lei

This chapter discusses the manufacture of premium lubricant base stocks using hydroprocessing technology. After a brief introduction about base stock demand and key base stock properties, we discuss the benefits of premium base stocks versus solvent-refined base stocks and how premium stocks help to meet the stringent specifications of automotive engine oils. The focus of this chapter is on the chemistry and processing of base stocks by modern refining technology, which includes hydrocracking, hydroisomerization, and hydrofinishing. Also included is a brief discussion of syngas-to-liquids (STL), also called gas-to-liquids (GTLs).

34.1	Key Base Stock Properties	1016	34.6.4	Various Hydrocracker Process Configurations	1027
34.2	Base Stock Categories	1018	34.6.5	Block and Bulk Base Oil Hydrocracker Operation	1030
34.3	Why the Need for Premium Base Stocks?	1019	34.6.6	VI Droop	1031
34.4	Lube Base Stock Manufacturing Technologies	1020	34.6.7	Process Conditions	1032
34.5	All-Hydroprocessing Route for Lubricant Base Stocks	1021	34.7	Dewaxing	1033
34.6	Hydrotreating/Hydrocracking	1023	34.7.1	Current Dewaxing Technologies	1033
34.6.1	Hydrotreating and Hydrocracking Chemistry	1023	34.7.2	Conventional Catalytic Dewaxing – Wax Hydrocracking	1033
34.6.2	Crude Oil Selection for Base Stock Production	1025	34.7.3	Hydroisomerization Dewaxing	1034
34.6.3	Hydrocracker Catalyst	1026	34.7.4	Hydroisomerization Dewaxing Catalyst Poisons	1035
			34.7.5	Process Flow Diagrams	1036
			34.7.6	Bulk versus Block Dewaxing	1037
			34.7.7	Process Conditions	1038
			34.7.8	Comparison Between Solvent, Conventional Catalytic and Hydroisomerization Dewaxing	1038
			34.8	Hydrofinishing	1039
			34.8.1	Conventional Base Stock Finishing (Polishing) Process	1039
			34.8.2	Chemistry of Aromatics Saturation in Hydrofinishing	1039
			34.8.3	Hydrofinishing Catalysts	1040
			34.8.4	Process Conditions	1040
			34.9	Integrating Hydroprocessing with Solvent Plants – Hybrid Plants .	1040
			34.10	GTL Base Oils	1041
			References		1042

Base stocks are the core components for many lubricants and specialty products, including automotive engine oils, gear oils, industrial oils, turbine oils, greases, process oils, food-grade oils and medicinal oils. According to API 1509 Appendix E, a base stock is a lubricant component that is produced by a single manufacturer to the same specifications (independent of feed source or manufacturer's location); that meets the

same manufacturer's specifications; and that is identified by a unique formula, product identification number, or both. A base oil is a base stock or blend of base stocks used in an API-licensed oil [34.1]. The terms base oil and base stock are frequently used interchangeably in the industry. This is the case in this chapter. The specific functions for base stocks and additives in a lubricant oil are summarized in Table 34.1.

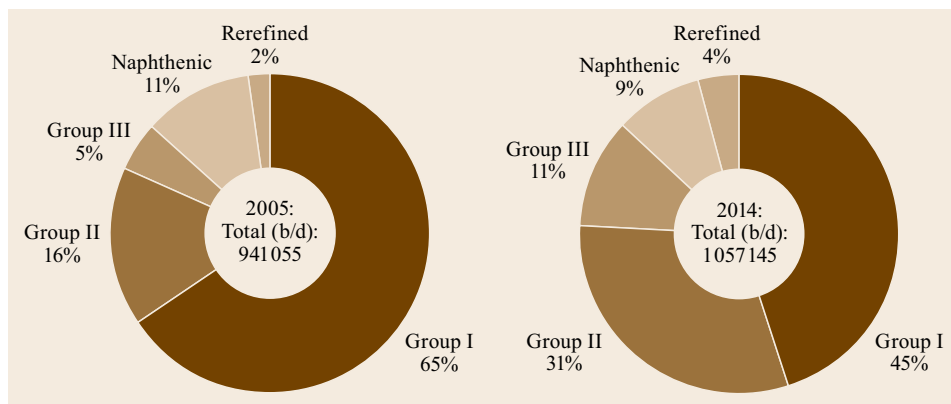


Fig. 34.1 Global base oils volume. Source: Lubes'n'Greases 2014 Lubricants Industry Factbook. Used with permission. May not equal 100 due to rounding [34.2]

Table 34.1 Functions of base oils and additives in a lubricant

Base oil contributions	Additive contributions
Viscosity grade	VI improvement
Low pour point	Corrosion resistance
High VI (Viscosity Index)	Low-temperature flow improvement
Stability	Dispersancy and detergency
Volatility	Oxidative and thermal stability
Solvency for additives	Antiwear improvement
	Extreme pressure improvement
	Friction modification
	Foam prevention

Total worldwide demand for lubricants is expected to rise only slightly for a number of years to come. As a result, the overall base oil demand is growing

slowly as well. Between existing plants, plant expansions, and new grassroots facilities, it is expected there will be adequate worldwide supply for the foreseeable future [34.2]. However, the demand for premium base stocks made from hydroprocessing is expected to continue growing significantly compared to base stocks made by solvent processing. API Groups II and III base stocks (hydroprocessed) are considered to be premium base stocks. Figure 34.1 shows the growth of premium base stocks globally. It increased from 21% of total base oil volume in 2005 to 42% in 2014 [34.2]. The growth of Groups II and III base stock volume virtually matches the decline in Group I (solvent-processed). Engine oils are by far the largest market for premium base stocks. Growth will be led by strong demand in the developing Asian countries, especially China and India.

34.1 Key Base Stock Properties

Some of the key base stock properties are viscosity, viscosity index (VI), pour point, volatility, and oxidation stability. A lube base stock must meet a viscosity specification within a narrow range, a maximum pour point specification, a volatility specification to limit the amount of low boiling molecules, and stability that is sufficient to meet the lubricant's required operating life.

Viscosity is the physical property that measures the fluidity of the base stock. Viscosity is a strong function of temperature. Two commonly used viscosity measurements are dynamic viscosity and kinematic viscosity.

Dynamic viscosity is the flow due to an applied mechanical stress. Cold-cranking simulator (CCS) viscosity at -25°C for engine oils and Brookfield viscosity at -40°C for automatic transmission fluids (ATF) are examples of dynamic viscosity measurements. The SI unit of dynamic viscosity is Pa s. The traditional unit

used is centipoise (cP), which is equal to 0.001 Pa s (or 1 mPa s). The industry is slowly moving to SI units.

Kinematic viscosity is the ratio of dynamic viscosity to density. The SI unit of kinematic viscosity is mm^2/s . The other commonly used units in industry are centistokes (cSt) at 40 and 100°C and Saybolt Universal Second (SUS) at 100 and 210°F . ASTM D445 (cSt) and ASTM D2161 (SUS) are the commonly used methods to measure kinematic viscosity. Conveniently, $1 \text{ mm}^2/\text{s}$ equals 1 cSt.

Typically, the naming of viscosity grades for neutral lube base stock, such as 100 Neutral and 600 Neutral, comes from the viscosity measured in SUS at 100°F . For the very heavy grades, such as 150 Bright Stock, the 150 viscosity is measured in SUS at 210°F .

Table 34.2 shows some typical viscosity grades for Groups II and III neutral oils.

Table 34.2 Typical base stock viscosity grades

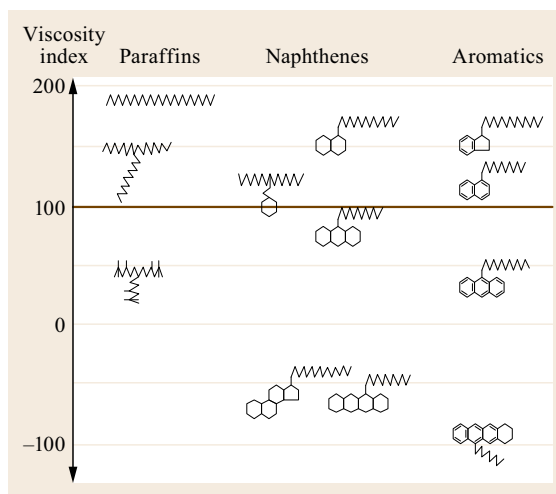
Group II base stocks			
Grade	Kinematic viscosity at 100 °C (KV100), cSt	Kinematic viscosity at 100 °F, SUS	Mid-boiling point, °F
Light Neutral – LN (100N–110N)	≈ 4.0–4.2	≈ 100–110	≈ 750–760
Medium neutral – MN (220N–225N)	≈ 6.3–6.6	≈ 210–220	≈ 820–840
Heavy neutral – HN (600N)	≈ 11.8–12.2	≈ 530–580	≈ 930–960
Group III base stocks			
Grade	Kinematic viscosity at 100 °C (KV100), cSt	Kinematic viscosity at 100 °F, SUS	Mid-boiling point, °F
4 cSt	≈ 4.2–4.3	≈ 100–105	≈ 790–810
6 cSt	≈ 6.0–6.5	≈ 165–195	≈ 850–880
8 cSt	≈ 7.6–8.0	≈ 235–260	≈ 900–920

Viscosity index (VI) is an empirical number used to measure the change in the base stock's kinematic viscosity as a function of temperature. It is based on an arbitrary scale first developed around 1928. At that time, the best paraffinic lube oil (Pennsylvania-grade crude) was assigned a VI of 100 and the worst naphthenic lube oil (Louisiana-grade crude) was assigned a VI of 0. The higher the VI, the less relative change in viscosity with temperature. High-VI base stocks are desired for most of the lubricant applications, especially in multigrade automotive engine oils and other automotive lubricants subject to large operating temperature variations. In addition to the VI from the base oil, VI improver additives are used to improve the VI of the finished lubricant. These are called VI improvers (VIIs) or viscosity modifiers (VMs). ASTM D2270 is a commonly accepted method to determine VI.

Figure 34.2 shows the VI for various classes of molecules in the base stock boiling range. Normal paraffins have the highest VI, naphthenes (cycloparaffins) have intermediate VI, and aromatics the lowest. Isoparaffins have slightly lower VI than normal paraffins. However, they also have lower pour points, which make them preferred molecules for base stocks.

Pour point is the lowest temperature at which movement of the test specimen is observed [34.3]. It is one of the most important properties for base stocks as most lubricants are designed to operate in the liquid phase. Low pour point is usually desirable, especially in cold weather lubrication. Typical maximum pour point specs for conventional petroleum base stocks range from -9 to -18 °C.

Normal paraffins are the hydrocarbon molecules with the highest pour point. They must be removed by solvent dewaxing or catalytic dewaxing, or converted to isoparaffins by hydroisomerization for the base stocks to achieve the target pour points.

**Fig. 34.2** Viscosity index of various chemical molecules

ASTM D97 is the standard manual method to measure pour point. It is being gradually replaced by automatic methods, such as ASTM D5950 and ASTM D6749.

Volatility is a measurement of oil loss from evaporation at an elevated temperature. It has become a very important specification due to emission and operating life concerns, especially for lighter-grade base stocks. Volatility is dependent on the oil's molecular composition, especially at the front end of the boiling point curve. The efficiency of the distillation step in the base stock manufacturing process can have a large impact on volatility. The VI of a base stock can also greatly impact the volatility, as for a given viscosity grade, a highly paraffinic base stock (higher VI) will usually have a higher boiling range than a base stock with a lower paraffin content (lower VI).

Noack (ASTM D5800) is a commonly accepted method to measure volatility for automotive lubricants. The Noack test method itself simulates evaporative loss in high-temperature service, such as in an operating internal combustion engine.

Simulated distillation by gas chromatography (GC) is also used as an indicator of volatility by measuring the front end of the boiling point curve, e.g., % distilled at 700 °F. ASTM D2887, ASTM D6352, and ASTM D7213 are commonly used GC methods. In comparison to Noack, they are faster and have excellent precision. However, Noack is still the generally accepted volatility specification for automotive engine oils and thus for base stocks. This is because the majority of global base oil volume is consumed in automotive lubricants, and these lubricants generally have more demanding performance requirements than most industrial lubricants, so base stock manufacturers tend to focus their specifications around the automotive industry.

Flash point (ASTM D92) is another indicator of volatility as it measures the temperature at which there

is sufficient vapor of a specimen to ignite, which also reflects the front end of the boiling point curve. Flash point is a required safety specification for many base stocks.

Stability is a broad term to describe the base stock's resistance to chemical reactions under heat and/or light in both storage and operating conditions. It can be measured in terms of the base stock's appearance and estimated from chemical composition. Because stability of a finished lubricant is so strongly dependent on additives, most stability specifications are based on finished lubricant performance tests. That being said, base stock stability is a strong contributor to finished lubricant stability.

ASTM D1500 is a commonly used color specification. Most premium base stocks have a D1500 reading of less than 0.5 when they are fresh. An increase in D1500 is an indication of formation of oxidation products. Many base stock manufacturers have their own proprietary test methods to measure oxidation and storage stability of base oils.

34.2 Base Stock Categories

All base stocks used for automotive engine oils are divided into five general categories based on API guidelines (Table 34.3). Groups I, II, and III base stocks are manufactured from paraffinic crudes in refineries. Sometimes they are referred to as mineral base stocks or petroleum base stocks to be differentiated from synthetic base stocks manufactured from well-defined chemical compounds through specific chemical processes, such as polyalphaolefins (PAOs, Group IV). Group V base stocks include all other base stocks not included in Groups I, II, III, or IV, such as pale oils (naphthenic base stocks), which are manufactured from naphthenic crudes, and various kinds of synthetic base stocks.

Groups I, II, and III base stocks are distinguished from each other in terms of sulfur and saturate contents, and viscosity index. Group I base stocks, which are also called conventional base stocks, are produced with solvent refining technology. Group II and Group III base stocks, often referred to as premium base stocks in

the industry, are manufactured through hydroprocessing technology. Groups I and II base stocks are used in the vast majority of lubricants.

As a side note, a 1999 decision by the National Advertising Division of the Better Business Bureau declared that automotive lubricants made using Group III base stocks could be labeled *synthetic*. That council ruled that the very severe processing conditions required to make Group III base stocks, resulted in most of the molecules being created in the processing from molecules which were in the original crude. Furthermore, the performance of Group III lubricants could be formulated as comparable to that provided by PAOs. This has led to Group III lubricants being marketed as *synthetic* in most of the world.

In recent years, these categories for marketing purposes have been informally expanded into Group I+, Group II+, and Group III+ and Group IV+, with classification based primarily on different VIs:

Table 34.3 API base stock categories

Group	Sulfur (wt%)		Saturates (wt%)	VI
I	> 0.03	and/or	< 90	80–119
II	≤ 0.03	and	≥ 90	80–119
III	≤ 0.03	and	≥ 90	≥ 120
IV	All polyalphaolefins (PAOs)			
V	All stocks not included in groups I–IV (pale oils and non-PAO synthetics)			

- Group I+ (103–108 VI)
- Group II+ (111–119 VI)
- Group III+ (130+ VI for light neutral base stocks)
- Group IV+ (5–15 higher VI than conventional PAOs made strictly from 1-decene).

34.3 Why the Need for Premium Base Stocks?

Automotive engine oils are by far the largest market for base oils. Figure 34.3 shows the typical components of engine oils, which contain 75–90 wt% base oils.

The engine oil performance specifications have become more stringent due to requirements for lower emissions, longer drain intervals, and better fuel economy. This has resulted in the demand for better performance base stocks. These performance traits include:

- Lower base stock viscosity, which increases fuel economy by improving cold start performance and reducing friction in engines.
- Lower volatility (e.g., Noack), which reduces the loss of oil from evaporation and emissions. This is very important to prevent the oil from thickening and requiring addition of oil between changes, and thus reduces oil consumption. The thickening of oil in the crankcase can reduce fuel economy and impair lubrication and cooling of critical engine parts.
- Improved oxidative and thermal stability, which give longer drain intervals.
- Improved lubricant performance at low and high temperatures, which meet the needs of modern engine designs. Engine oils must allow engines to crank and pump oil at arctic temperatures, and also provide lubrication at high operating temperatures.

Moreover, there is an increasing trend to lower sulfated ash, phosphorus, and sulfur (SAPS) specifications for automotive engine oils to protect the exhaust catalysts. Due to their high sulfur content, Group I base stocks are less likely to be used in formulations designed to meet these specifications.

In the past, PAOs were used in formulation to achieve the stringent requirements listed above. PAOs have excellent performance characteristics as lubricant base stocks, including high VI, low volatility, superior low-temperature fluidity, and great oxidation stability. However, they are more expensive than mineral base stocks due to their higher raw material and processing costs. Modern hydroprocessed base stocks, after careful formulation, can often rival the performance of PAOs in many applications. Today's refiner, by using hydroprocessing technology, can economically manu-

This chapter focuses on the discussion of producing Group II and Group III base stocks using hydroprocessing technology. Production of Group IV and other synthetic base stocks are covered in Chap. 35 of this book by Wu et al.

facture high-quality base stocks (Group II/III) derived from crude oil and refinery process streams such as vacuum gas oils (VGO), unconverted oil (UCO) and deasphalted oil (DAO). In addition, raffinate, foots oil and slack wax produced in existing solvent base oil facilities are excellent feeds to make premium Group III/III+ base stocks using hydroprocessing. Wax from a gas-to-liquids plant is an excellent feed to manufacture exceptionally high-quality base stocks (Group III/III+) when fed to a hydrocracker followed by a wax hydrosomerization and hydrofinishing unit.

Figure 34.4 shows that when formulated properly, Group II and Group III base stocks are sufficient (and required) to produce automotive engine oil products that meet the most stringent specifications [34.4]. This figure provides the screening process that an engine oil formulator will use to identify suitable base stocks when designing a new automotive lubricant. The first two parameters to be considered are viscosity and volatility. For a multigrade engine oil, the viscosity the formulator will first focus on is the cold-cranking simulator viscosity (CCS, ASTM D5293). The lighter the base stock, the lower the viscosity – including the CCS. On the other hand, as the base oil gets lighter, the Noack volatility increases.

Each curve in Fig. 34.4 is constructed by blending two or more base stocks from a single base stock slate. For example, the left side of the green curve shows the blend properties for a typical Group II 100N blended with 220N in varying proportions, and the right side

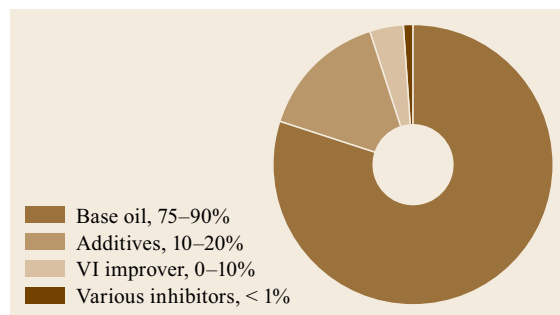


Fig. 34.3 Typical components in automotive engine oil

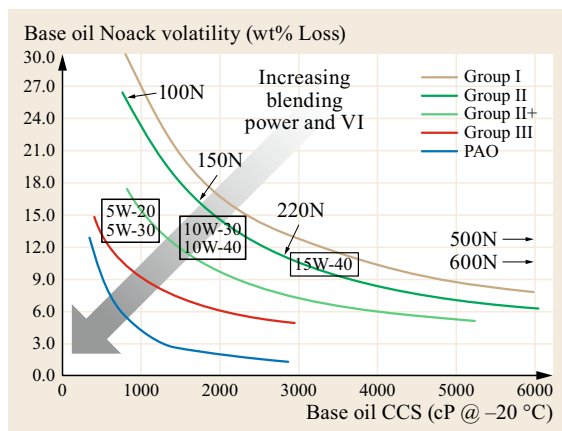


Fig. 34.4 Base stock suitability for blending premium engine oils (after [34.4])

continues the curve by blending increasing percentages of 600N with 220N. Likewise the Group II+, Group III and Group IV (PAO) curves are derived by blending base stocks from those groups. As one moves from the upper right to the lower left, the VI (and blending power) of the base stock group increases. But so, of course, does the cost of the oils. (Note: blending power is not to be confused with thickening power, but is rather a function of the viscosity index of a com-

ponent in an engine oil blend. Higher VI components are required to meet the critical low-temperature viscosity specifications while also meeting tight volatility requirements.)

Putting the rectangular blending spaces together with the blending curves shows graphically the strategy of blending various base stocks together to hit the viscosity and volatility requirements of various engine oils. If a rectangle falls below a particular curve, then that base stock group cannot be used to blend the viscosity grade(s) shown in the rectangle. Thus, the formulator can quickly see that a 5W-20 engine oil cannot be blended with a Group I or a Group II base stock. However, most North American 5W-20s can be easily blended with Group II+, a Group III, a Group IV, etc. Also noteworthy is that a Group II 220N is very close to the 15W-40 rectangle. This is the reason that essentially all 15W-40 heavy duty engine oils (HDEOs) with modern high-performance claims use almost 100% Group II 220N in their base stock blends.

Because Group III/III+ base stocks are more available and cheaper, they have replaced PAOs in many lubricant applications, except where PAOs are required for extreme lubricant starting and operating conditions. Currently, PAOs account for less than two percent of the total global base oil capacity. Most synthetic lubricants are predominantly Group III/III+ based.

34.4 Lube Base Stock Manufacturing Technologies

Today, there are two primary refining technologies used to manufacture lubricant base stocks from crude oil. The conventional technology is solvent refining, and the modern technology is hydroprocessing. Both technologies include the following basic steps in the manufacturing process: vacuum distillation, VI upgrading, dewaxing, and finishing (Fig. 34.5).

In the vacuum distillation step, a crude oil long residuum (or atmospheric column bottom) is distilled in a vacuum column to produce lube VGO cuts and residuum. The VGO cuts are used to manufacture neutral oils and the residuum is used to manufacture bright stock. These cuts are distilled to the proper viscosities that are optimum for the desired base stock products.

Conventional solvent refining and modern hydroprocessing technologies are fundamentally different in terms of molecular transformation in the VI upgrading and dewaxing steps. No chemical reactions and molecular transformations take place in the solvent refining processes except in the final hydrofinishing step. Molecules that are not friendly for lubricant applications, e.g., aromatics and sulfur compounds with low VI and normal paraffins with high pour point, are re-

moved by various chemical and physical separation techniques. In the VI upgrading step, low-VI molecules are extracted with a solvent such as *N*-methylpyrrolidone (NMP), phenol, or furfural. The upgraded lube oil is called raffinate (or waxy base stock) and the highly aromatic byproduct is called extract. In the following dewaxing step, raffinate is chilled in the presence of a solvent mixture (methyl ethyl ketone (MEK)-toluene and methyl ethyl ketone-methyl isobutyl ketone (MEK-MIBK) being the most common) and vacuum filtered for wax removal to meet a pour point specification. Because a considerable amount of aromatics and heteroatom compounds remain in the finished base stocks, solvent refining makes only Group I base stock, except in the very few plants with hybrid processes. This will be discussed in Sect. 34.9.

In hydroprocessing, molecules in the VGO cuts are rearranged and selectively cracked and converted into base stocks. Hydroprocessing gives higher total base stock yield than solvent refining from the same feed stock. Moreover, it leads to Group II and Group III base stocks with much improved purity and performances. Detailed discussions on base stock manufacture through

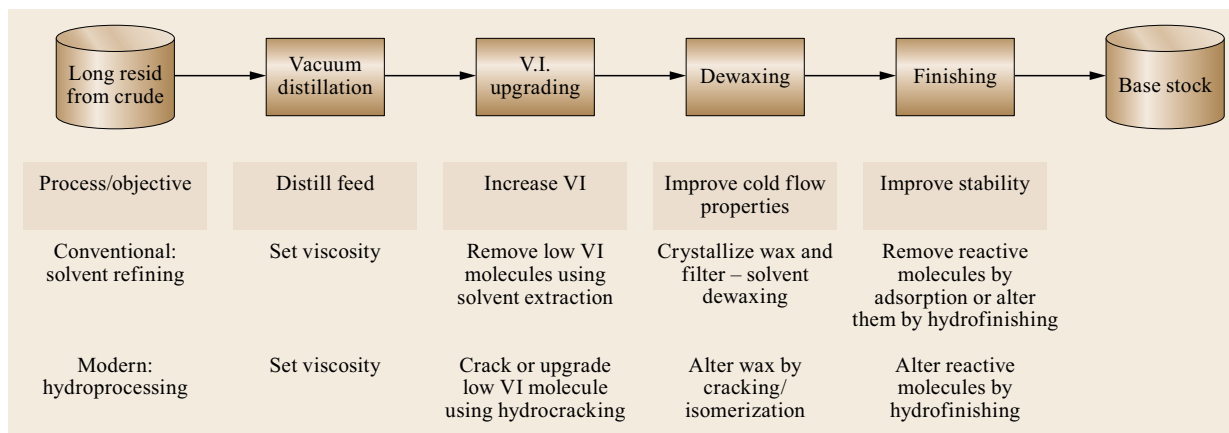


Fig. 34.5 Lube base oil simplified manufacturing steps

hydroprocessing technology are covered in Sects. 34.5–34.8.

Crude oil selection is critical for base oil economics. With solvent refining, the crude oil must have innate lube oil molecules to begin with. Therefore, a premium-grade crude oil, such as Arabian Light or other high-quality paraffinic crudes, must be used. The better the crude quality, the higher the lube stock yield. In contrast, refineries have much more flexibility to use a wider variety of crudes for base stock manufacture with hydroprocessing technology. This is one of the major advantages of hydroprocessing over solvent extraction technology. Hydroprocessing enables refiners to optimize crude selection around the entire refinery, not just around the base oil plant. Another advantage of hydroprocessing is that the byproducts are high value fuels while solvent processing produces a relatively low-value extract. It should be further noted that hydroprocessing frequently has lower capital and operating costs than solvent refining [34.5].

Bright stock is a very high viscosity base oil. Its major applications include automotive gear oils, marine lubricants, and heavy viscosity grade industrial oils. To manufacture bright stock, vacuum residuum must first be solvent deasphalted to obtain a deasphalted oil (DAO). Solvent deasphalting removes large, multiring compounds that cannot be handled by either the solvent extractor or the hydrocracker. Generally, propane is the

solvent used for deasphalting residuum. The DAO is then upgraded into a heavy base stock by either solvent processing (Group I bright stock) or hydroprocessing (generally Group II bright stock).

The majority of the world's bright stock supply is from solvent processing. With the demand for Group I neutral oils either declining or stagnant in all regions, bright stock capability has become a key economic driver to keep the solvent refining plants from rationalization. As the Group I plants with high operating costs continue to shut down, bright stock supply is expected to remain tight in the years to come.

Hydrotreating/hydrocracking DAO or a blend of DAO and VGO, followed by dewaxing and hydrofinishing produces a Group II bright stock with low levels of impurities. Group II bright stock offers a potential for high performance lubricants with its improved oxidation stability. However, due to its lower solvency, Group II bright stock cannot readily replace Group I base stock in many current formulations, especially for marine lubricants. Nevertheless, with advances in additive technology, formulations with Group II bright stocks are expected to be developed in the coming years because of the pressures for alternative bright stock supply and improved lubricant performance. Current Group II bright stock producers include IKC in Japan, SK in South Korea, Karamay in China, and IOCL in India.

34.5 All-Hydroprocessing Route for Lubricant Base Stocks

Lube hydroprocessing involves reactions of hydrocarbons and hydrogen at high pressure and moderate temperatures over various catalyst systems. The refinery processes to manufacture lube base stock using an integrated all-hydroprocessing route, as shown in

Fig. 34.6, consist sequentially of the processing steps hydrotreating/hydrocracking, catalytic dewaxing and hydrofinishing [34.6].

The purpose of the hydrotreater/hydrocracker is to upgrade the base stock to the target VI number. Cat-

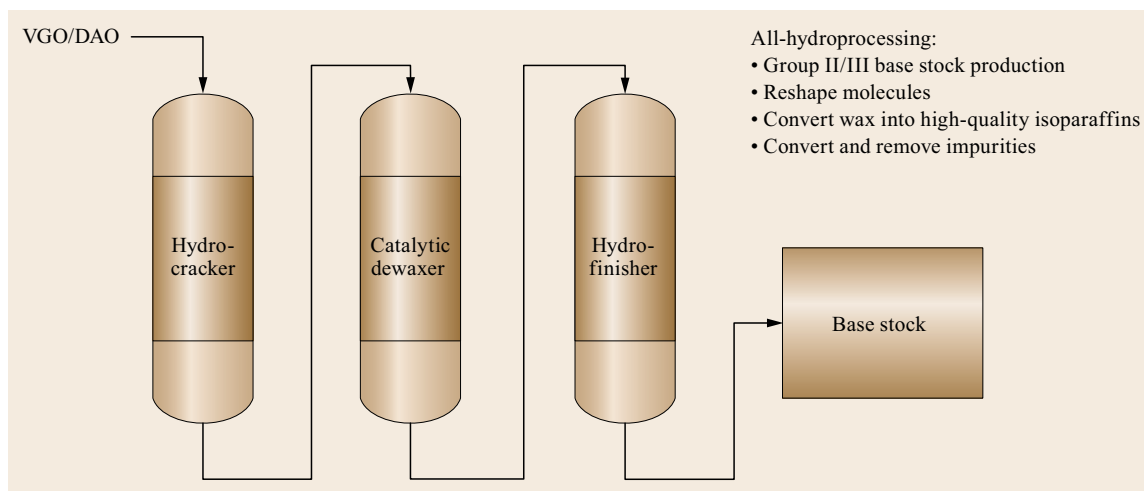


Fig. 34.6 Simplified all-hydroprocessing flow scheme for base oils

alytic dewaxing is the step that converts the waxy, high pour point hydrocrackate into a wax-free product at a target pour point. Hydrofinishing is the final polishing step to improve color and stability by saturation of trace aromatics and residual polar hydrocarbons.

Chevron's Richmond Refinery Lube Oil Plant (Fig. 34.7) was the world's first all-hydroprocessing plant to manufacture lube base oil. This plant has been operating since 1984.

As mentioned in the previous section, an all-hydroprocessing route provides a refinery much more flexibility to manufacture premium base stocks from a larger variety of crude oils and feed stocks than a solvent plant. In addition, the performance of these base stocks is superior to those from a solvent-refined plant for engine oils and many other applications. These are the principal reasons why virtually all base oil plants built in the past 20 years use hydroprocessing.



Fig. 34.7 Chevron's Richmond Refinery Lube Oil Plant

Figure 34.8 shows a comparison of the impurity levels in Group I and Group II light neutrals. The Group II LN sample is essentially free of sulfur and nitrogen. The aromatic content is below 1 wt%. For engine oils, lower impurity levels will result in a longer-lasting lubricant, and the higher saturate levels will give better soot dispersancy and enable other additives such as detergents and wear inhibitors to function better. This is the case for most internal combustion engines, with the exception of those marine diesel engines that burn fuels with high asphaltene contents. Although Group II base stocks with proper additives can still work well in marine engine oils, Group I base stocks still have an economic advantage as they are better able to keep highly aromatic and

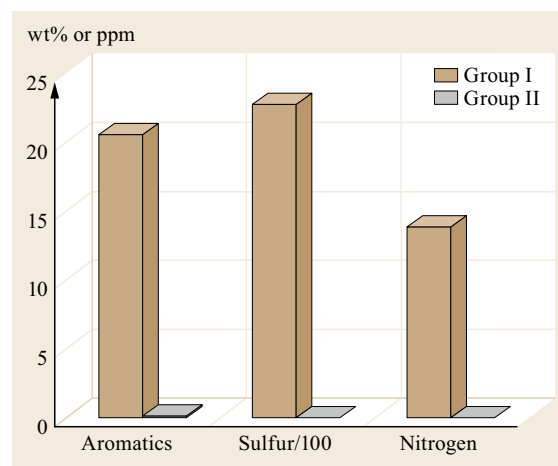


Fig. 34.8 Impurity levels in Group I and II base stocks (Ar and S, wt%; N, ppm)

polar compounds in solution with less detergent additives.

The all-hydroprocessing route also can make Group III base oils. This is done by increasing the severity of the hydrocracker operation to increase the VI of the base oil. Group III base oils via the all-hydroprocessing route have greatly improved oxidation stability and low temperature performance than conventional Group I base stocks. In addition to higher VI, they may exhibit better stability than Group II base stocks. Figure 34.9 shows the comparison of oxidation stability for the various classes of unadditized base stocks. The data is from a bench oxidation test designed to simulate a gasoline engine running at high temperature under high load. The time shown is the number of hours for the oil to consume a standard liter of oxygen. A longer duration means a higher quality and more stable base oil. The performance of Group III base stock in this test is close to the performance of PAOs, a big reason why lubricant

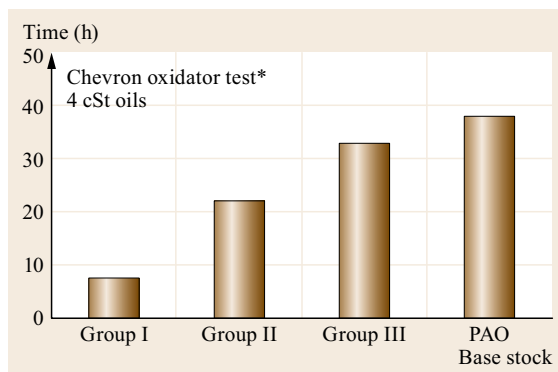


Fig. 34.9 Base oil oxidation stability tests.

* Data from Chevron proprietary oxidator test; longer time duration is better oxidation stability

companies are able to replace PAOs with Group III in some formulations [34.7].

34.6 Hydrotreating/Hydrocracking

Hydrocracking is the catalytic conversion process that converts heavy petroleum feedstocks (VGO, DAO, UCO, wax, etc.) into high-quality fuels and waxy base stock products. It is one of the two major heavy oil catalytic conversion processes used in modern refining, with the other being fluid catalytic cracking (FCC). There are two broad classes of reactions that take place in the hydrocracking process: (1) hydrotreating, in which impurities such as nitrogen, sulfur, oxygen, and metals are removed from the feedstock using base metal oxide catalysts; and (2) hydrocracking, in which carbon-carbon bonds are cleaved with hydrogen addition over bifunctional catalysts. When hydrocracking is used in a base oil plant, it is often referred to as lube hydrocracking, in comparison to fuel hydrocracking for the production of naphtha and mid-distillate fuels such as jet and diesel. Sometimes lube hydrotreating and lube hydrocracking are used interchangeably, which is the case for this chapter.

The lube hydrocracker does the following work to produce base stock hydrocrackates, which are the heaviest products from the hydrocracking reactions:

1. Increases the VI of the feedstock to the target VI.
2. Removes sulfur and nitrogen from the feedstock to produce a high-quality hydrocrackate to feed the isomerization dewaxer.
3. Saturates aromatics.

34.6.1 Hydrotreating and Hydrocracking Chemistry

Hydrocracking is the most severe step in the all-hydroprocessing process scheme. It usually consumes more hydrogen than the dewaxing and finishing steps combined. Some of the key reactions that occur in a hydrocracker include: hydrodesulfurization (HDS), hydrodenitrication (HDN), aromatic saturation, or hydrodearomatization (HDA), and hydrocracking/isomerization. They are summarized in Fig. 34.10 with increasing severity from top to bottom.

High sulfur content in the hydrocrackate is a poison to the noble metal catalysts in the catalytic dewaxing and hydrofinishing units and thus must be removed in the hydrocracker. During the HDS reactions, carbon-sulfur bonds in alkyl sulfides and thiophenes are broken readily through hydrogenolysis in the presence of base metal sulfide catalysts. The HDS reactions become much more difficult if the sulfur is hindered in substituted dibenzothiophenes, e.g., 4,6-dimethyldibenzothiophene. In this case, the molecule must be (at least partially) hydrogenated in order to free the sulfur atom from its aromatic ring and subsequently break the C-S bond. Deep HDS of a VGO feed reduces the sulfur content from roughly 1–3 wt% to less than 10–20 ppm in the waxy base stock.

Deep HDN faces the same dilemma as deep HDS. The rate-limiting step in the HDN reaction pathway

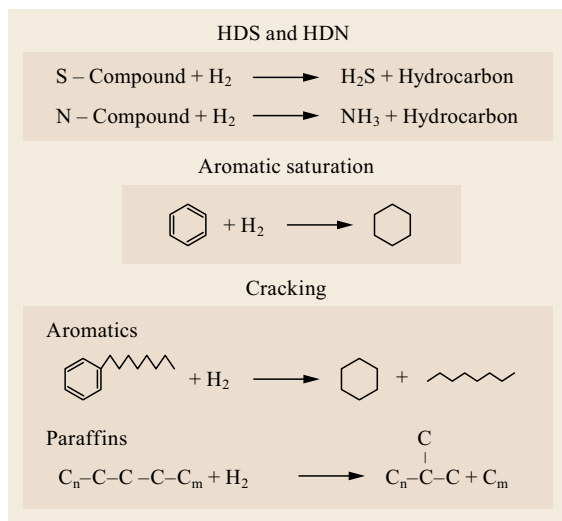


Fig. 34.10 Examples of chemical reactions occurring in a base oil hydrocracker

is the saturation of the aromatic ring. What makes this the slowest step is that the most refractory nitrogen molecules, such as substituted carbazoles, have the nitrogen atom embedded in the aromatic ring in a fairly inaccessible location [34.8]. As with sulfur, the aromatic ring containing the nitrogen atom must be saturated before the C–N bond can be broken. The nitrogen level is reduced to as low as < 2 ppm with the deep HDN. Nitrogen at an elevated level is a temporary poison that lowers the dewaxing catalyst activity, which will be discussed in detail later in this chapter.

HDA is a thermodynamically reversible process in which naphthenes can lose hydrogen to form aromatics if conditions are appropriate. Both hydrogen partial pressure and reaction temperature have a strong impact on the equilibrium constants. As the HDA reactions are exothermic, increasing reaction temperature would lead to higher aromatic contents at equilibrium. As higher temperature is required for the reaction to take place at a reasonable rate, aromatic saturation becomes a battle of kinetics against thermodynamics. If raising the reactor temperature decreases the product aromatic content, the reaction is described to be under *kinetic control*. Otherwise, it is under *thermodynamic control* [34.9]. Increasing hydrogen partial pressure can help to avoid undesirable thermodynamic control.

It is difficult to get total aromatics saturation as a hydrocracker because both the equilibrium and rate constants for the HDA reactions vary with aromatic types. Rates of saturation for monoaromatics are much smaller than those for diaromatics, which in turn are smaller than those for polycyclic aromatics (PCAs). Therefore, saturation of mono- and diaromatics are more

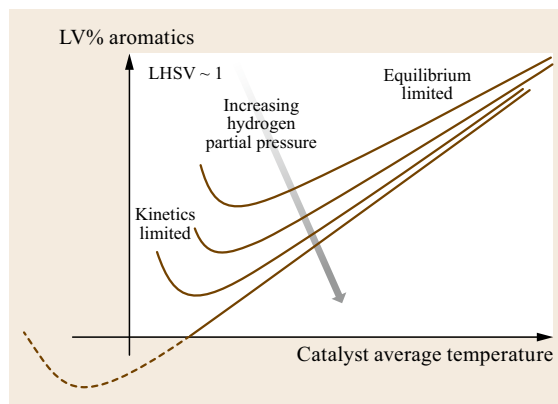


Fig. 34.11 Effect of temperature on aromatics at constant LHSV

favorable at a higher reactor temperature for a given hydrogen pressure. On the other hand, saturation of the PCAs are more favorable at lower temperatures because of the equilibrium constraint. Higher hydrogen pressure will favor the saturation of all types of aromatic molecules at a wider temperature range. Figure 34.11 shows that the hydrocracker reactor temperature drives the total product aromatics to a low level, but bumps up against equilibrium at high temperatures. At higher reaction temperatures, equilibrium competes against kinetics and dehydrogenation reactions become significant.

There are a couple of strategies to achieve near-complete aromatic saturation in an all-hydroprocessing lube plant. Building a plant that operates at a very high hydrogen pressure is one method. The very high hydrogen pressure results in a wider temperature range for the saturation of all aromatics. For example, with very high hydrogen pressure, as the temperature is raised to saturate the mono- and diaromatics, PCAs are also saturated to naphthenes. Building an all-hydroprocessing plant that operates at very high pressure, such as approaching 3000 psig, is very expensive, but in the early days of hydroprocessing, catalyst design expertise was limited and this was the only option aside from using solvent technology. A more cost-effective alternative is to design a lube plant to operate at a relatively lower pressure and do the aromatic saturation in two sequential temperature steps. The hydrocracker/hydrotreater and hydroisomerization dewaxer operate at higher temperatures and remove most of the mono- and diaromatics. The final-step hydrofinisher operates at a lower temperature and saturates the larger PCAs to improve the color and the oxidation stability of the base oil.

While HDS, HDN, and HDA convert impurities from the feedstock and modestly increase product VI,

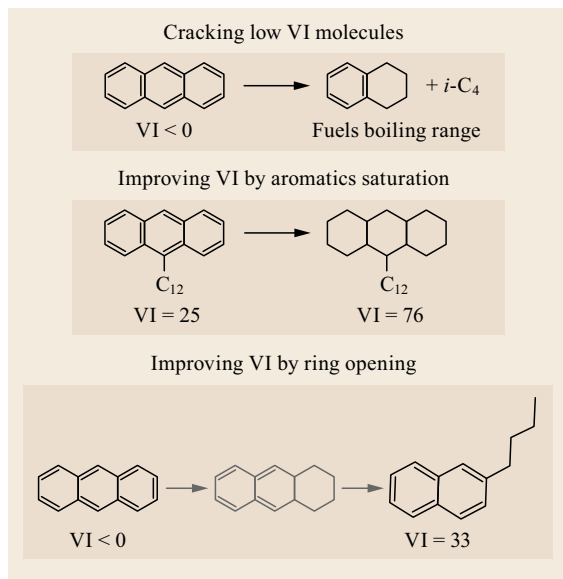


Fig. 34.12 VI improvement with hydrotreating and hydrocracking reactions

ring opening reactions that occur during hydrocracking significantly improve product VI by converting low-VI PCAs and polycyclic naphthenes to naphthenes that have fewer rings and much higher VI (Fig. 34.12). However, the reaction does not always stop after ring opening. The paraffinic side chain attached to the original aromatic molecule can easily break off (dealkylation), resulting in molecules (side chains and ring fragments) that shift into the fuels boiling range. In addition, some molecules can shift to a lighter waxy base stock. The ideal lube hydrocracker would severely hydrotreat the feed to remove organic nitrogen and sulfur molecules to low levels and improve VI through HDA and ring opening reactions with no appreciable cracking of the base stock into light products (fuels and gas). In reality, the conversion in a lube hydrocracker is typically 30–40% for Group II base stocks made from a typical Arabian Gulf crude. A conversion level greater than 60% is generally required for Group III base stocks. The impact of hydrocracking conversion on VI of 700 °F+ hydrocrackate is shown in Fig. 34.13.

Through HDA, ring opening, and cracking reactions, lube hydrocracking not only increases hydrocrackate VI, but also lowers its viscosity (Fig. 34.14, Table 34.4). Its pour point remains in the positive domain due to the high paraffinic content. Most of the normal paraffins present in the crude are very difficult to crack and go through the hydrocracker unaltered. Hydrocrackate is thus a waxy base stock.

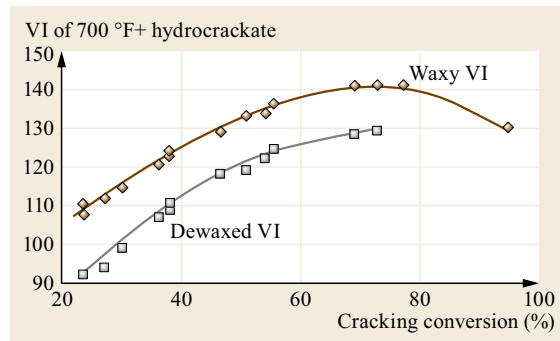


Fig. 34.13 VI improvement with increasing hydrocracker conversion – Arabian Heavy VGO

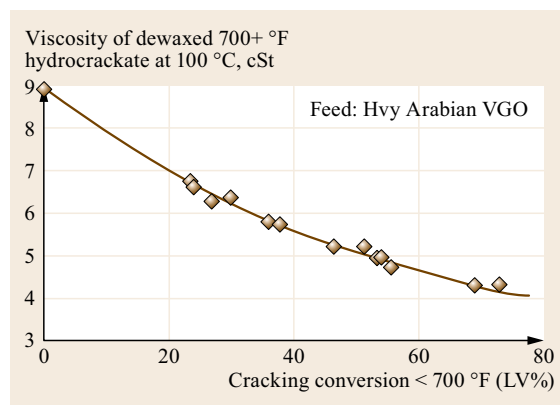


Fig. 34.14 Viscosity of hydrocrackate decreases as cracking conversion increases

Table 34.4 Summary of changes to base oil in the hydrocracker

Increase VI	Decrease viscosity
Reduce sulfur	Reduce nitrogen
Reduce aromatics	Increase naphthenes
Increase isoparaffins	Lower pour point
Produce transportation fuels	Reduce average molecular weight
Reduce carbon residue	Improve color

34.6.2 Crude Oil Selection for Base Stock Production

Hydrocracking permits the economic upgrading of VGOs with relatively low paraffin content, such as those from Alaskan North Slope crude, into base stocks. However, there are limits. Vacuum gas oils derived from very heavy refractory crudes oils cannot be economically used to manufacture base stocks. Figure 34.15 shows that VGO from San Joaquin Valley crude is essentially impossible to be upgraded to

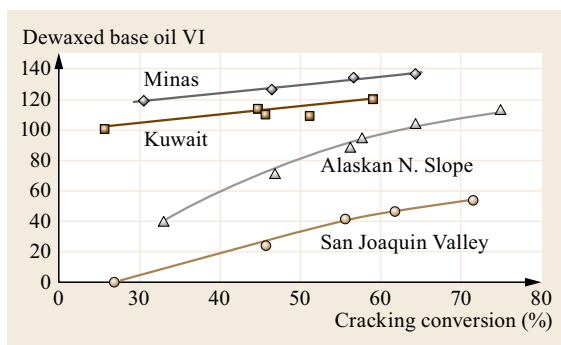


Fig. 34.15 Different crude oils require different conversion level to make base oils (solvent dewaxed VI)

lube base stock even at very high conversion levels, using typical lube hydrocracking catalysts and conditions.

The conversion of the base stock boiling molecules to fuels boiling molecules is generally low when using high-quality lube crudes, but can be as high as 30–40% for Group II base stocks depending on the feed and operating conditions of the hydrotreater/hydrocracker. Kuwait and other good-quality Middle East crudes are excellent for manufacturing Groups II and III base stocks using hydroprocessing. Minas (Sumatran Light) crude is not the ideal crude to make Group II base stocks because of its high wax content and the base stock VI will be too high. However, it is good for Group III base stocks. Most Group III base stocks are produced from fuels hydrocracking operations where the cracking conversion of heavy molecules to naphtha, jet and diesel frequently exceeds 70–80%, and the hydrocracker bottom product is sent to hydroisomerization and hydrofinishing. This is discussed more in Sect. 34.6.4. It should be noted that laboratory data and proprietary correlations were used to obtain the dewaxed oil VI data shown in Fig. 34.15.

34.6.3 Hydrocracker Catalyst

The lube hydrocracking catalyst system consists of both hydrotreating (pretreat) and hydrocracking catalysts. The design of the best catalyst system is dependent on the properties of the feed stock and the product specifications. Hydrotreating catalysts are typically composed of oxides of Group VIII (either Ni or Co) and oxides of Group VI (either Mo or W) metals supported on alumina. The metal oxides are reduced and converted to metal sulfides in the sulfiding process, which are the active forms for the hydrotreating reactions. Different combinations of metal sulfides and their functions are summarized in Table 34.5.

Hydrocracking catalysts are dual function catalysts. The hydrogenation function is provided by similar metal sulfides as those in the hydrotreating catalysts, mostly Ni and W sulfides. The cracking or acid function is typically provided by solid acid components in the catalyst support. They could be amorphous silica-alumina, crystalline zeolite, or a mixture of them. High zeolite content cracking catalysts are generally not used for lube hydrocracking as they tend to over-crack the molecules to the fuel boiling range.

The catalyst system designed for lube hydrocracking is generally different from a catalyst system designed to make maximum fuels. It is extremely important to not only to have the right catalysts but also the right ratio of hydrotreating to hydrocracking components to meet specific production targets. Lube hydrocracking is designed to do deep HDS, HDN, HDA, and crack only as needed to achieve the target VI. Thus, preserving molecules in the base stock boiling range is critical for a lube hydrocracker. Figure 34.16 shows that using a fuels hydrocracking catalyst system for a lube hydrocracker application can result in a significant penalty for both lube oil yield and VI.

Table 34.5 Hydrotreating and hydrocracking catalyst components

Function	Component	Activity
Hydrogenation	Cobalt-molybdenum sulfides	HDS
	Nickel-molybdenum sulfides	HDS and HDN
	Nickel-tungsten sulfides	Aromatic saturation
Cracking ^a	Alumina	Very weak
	Amorphous silica-alumina	Moderate
	Zeolite (crystalline Si-Al) ^b	Very strong ^c

Points to remember:

^a Acidity is the key difference between hydrotreating and hydrocracking catalysts.

^b Zeolites offer high acidity, plus their unique crystalline structures are resistant to carbon deposition reactions that shorten catalyst life.

^c Too much zeolite, or the wrong types of zeolite, can over crack, resulting in higher production of fuels byproducts and lower waxy base oil yield.

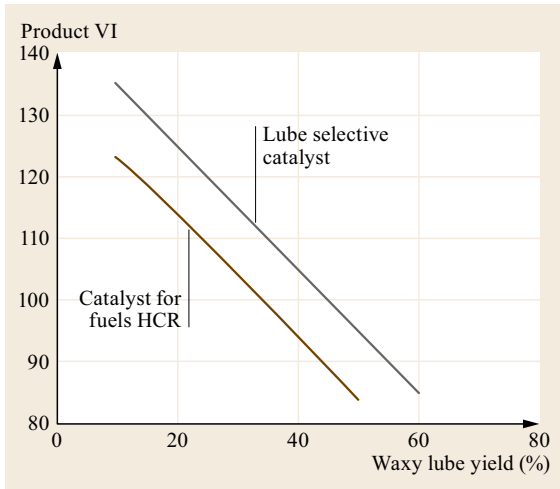


Fig. 34.16 A lube-selective hydrocracking catalyst provides much higher VI and lube oil yield

34.6.4 Various Hydrocracker Process Configurations

There are a number of hydrocracker configurations used commercially. The most common ones are:

1. Single-stage once-thru hydrocracker (SSOT)
2. Single-stage with recycle hydrocracker (SSREC)
3. Two-stage recycle hydrocracker (TSR).

All three configurations are used for fuels and lube oil hydrocrackers. When designing a hydrocracker for maximum base oil production, SSOT is generally the preferred configuration (Fig. 34.17). The hydrocracker is run to a conversion level needed to make waxy base

stocks that meet the VI specifications after dewaxing and hydrofinishing.

There are a number of high-conversion fuels hydrocrackers (SSREC or TSR units) operating globally that draw a UCO (unconverted oil) stream as base oil feed stock. As shown in Fig. 34.18, the hydrocracker yields about 80–95% fuels, the primary product, and about 5–20% UCO, the side product. The UCO stream typically has very high VI and is used to manufacture Group III base stocks. It is fractionated in a vacuum still into waxy base stock cuts, which are subsequently dewaxed and hydrofinished into finished base stocks.

It should be noted that not all hydrocracker UCO streams are good for making base stocks. UCO drawn from a hydrocracker feeding VGO from low-quality crudes and cracked stocks (like coker gas oil or heavy cycle oil from an FCC) most likely will not be good for base stocks due to the high concentration of polycyclic aromatic coke precursors. Also, a UCO drawn from a near-full/very high conversion fuels hydrocracker may be difficult to convert to high-quality base stocks when it contains PCAs with seven or more condensed aromatic rings. These compounds may be generated in a hydrocracker from the polymerization of three- and four-ring aromatics found in the feed [34.10].

SSOT Hydrocracker Process Flow Diagram

Figure 34.19 shows a simplified process flow diagram for a SSOT lube hydrocracker. Oil feed is mixed with makeup (MU) and recycle H_2 and preheated in the reactor feed/effluent exchangers and reactor feed furnace. The oil-gas mix then enters the fixed bed, down flow reactor. There are multiple catalyst beds in the reactor. For larger capacity plants, there will be multiple reactors in series. Because the chemical reactions

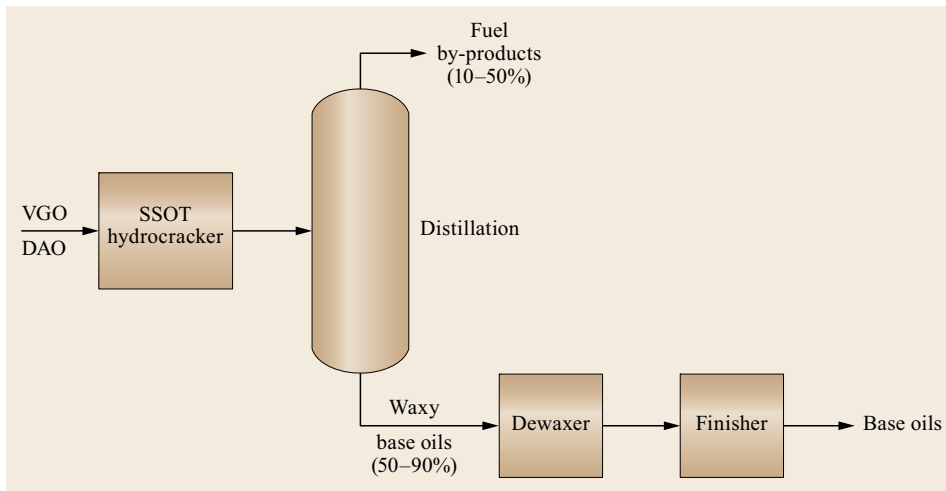


Fig. 34.17 SSOT base oil hydrocracker for maximum base oil yield

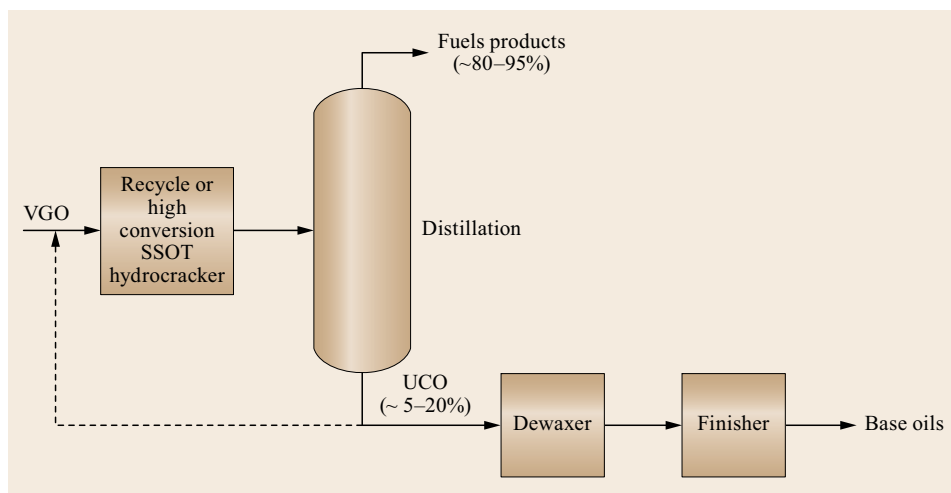


Fig. 34.18 Fuels hydrocracker making base oils as a byproduct

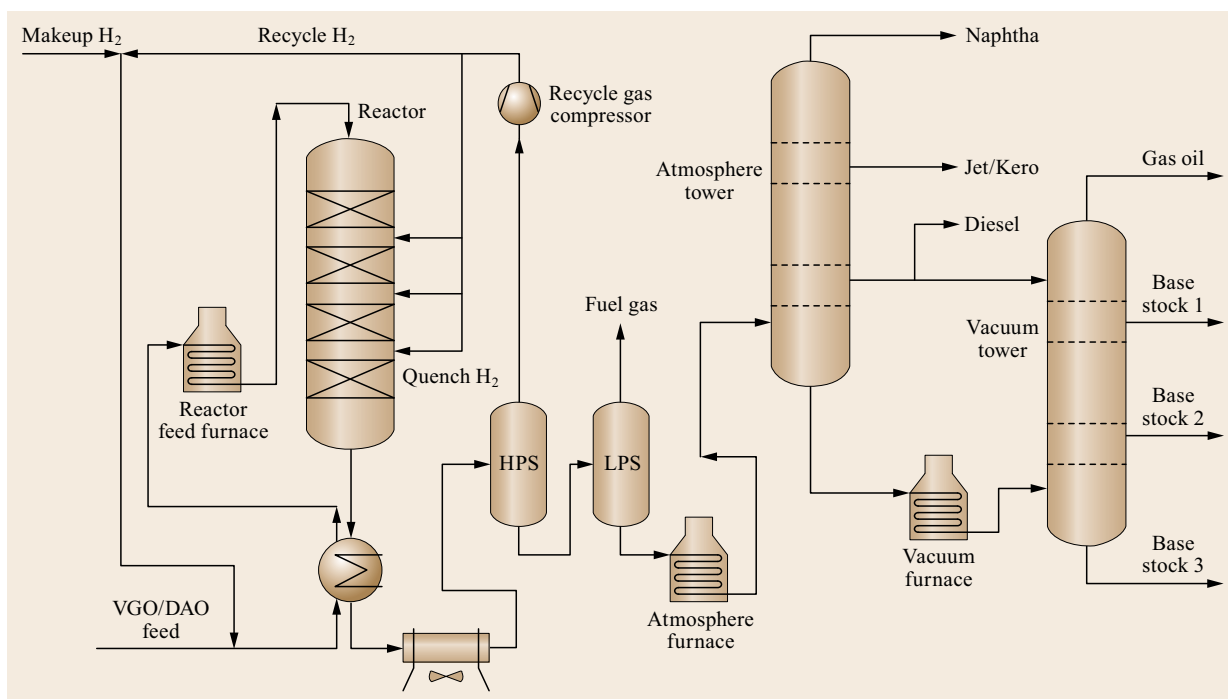


Fig. 34.19 SSOT lube oil hydrocracker

(HDS, HDN, HDA and cracking) in the reactor are highly exothermic, H_2 quench gas is injected between the catalyst beds to cool and control the reactor temperature. The effluent leaving the reactor is cooled and then enters a series of separators (high pressure and low pressure separators – HPS and LPS) to flash separate H_2 gas from liquid oil. The gas from the recycle compressor (mostly H_2 and some hydrocarbons) is sent to the reactor as quench gas. The remaining

gas is recycled and injected with the makeup H_2 into the fresh oil feed ahead of the feed/effluent exchangers. The liquid product from the LPS is sent to the atmospheric and vacuum columns to be fractionated into fuels products and waxy base stocks. The waxy base stocks must be distilled to the proper viscosity and cut points. They are subsequently sent to the hydrosomerization or solvent dewaxing plant for pour point reduction.

Fuels Hydrocracker Making Waxy Base Stocks as a Side Product

As previously discussed, globally there are a number of hydrocrackers that make fuels as their main product but also make waxy base stocks as a side product. The fuels hydrocrackers can be any of the previously mentioned designs: SSOT, SSREC, or a TSR.

Figure 34.20 shows a SSREC design in which a UCO stream is drawn for waxy base stock production. Depending on the VI of the UCO, this stream can

be converted to Group II or III base stocks after dewaxing and hydrofinishing.

Figure 34.21 shows a TSR hydrocracker in which a first-stage UCO is drawn to make Group II or III base stocks, depending on the VI of the UCO. The second-stage UCO is typically used to make Group III base stocks. The UCOs produced in these units are fractionated in a feed preparation unit (FPU) vacuum column to the correct viscosity and cutpoints. Each fractionated waxy lube cut is then individually dewaxed (block

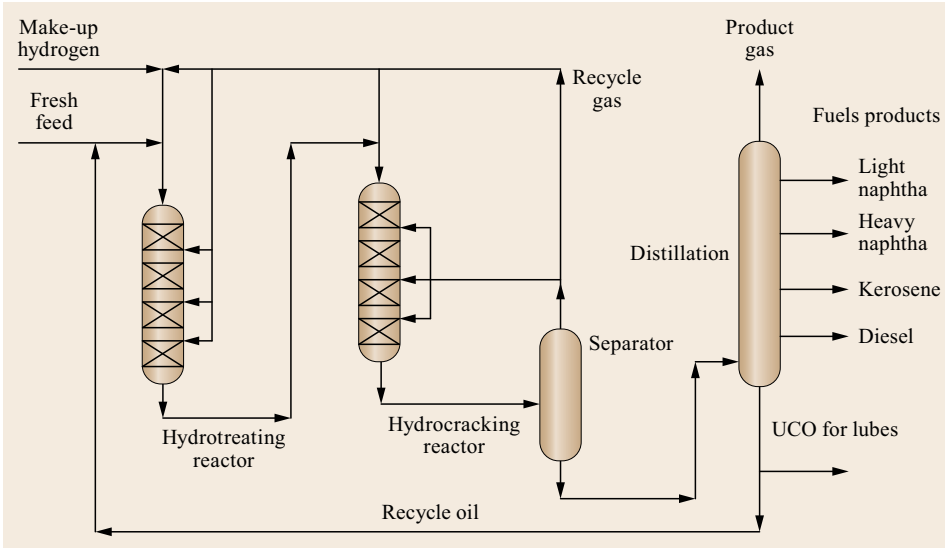


Fig. 34.20 Simplified SSREC fuels hydrocracker with base oil production

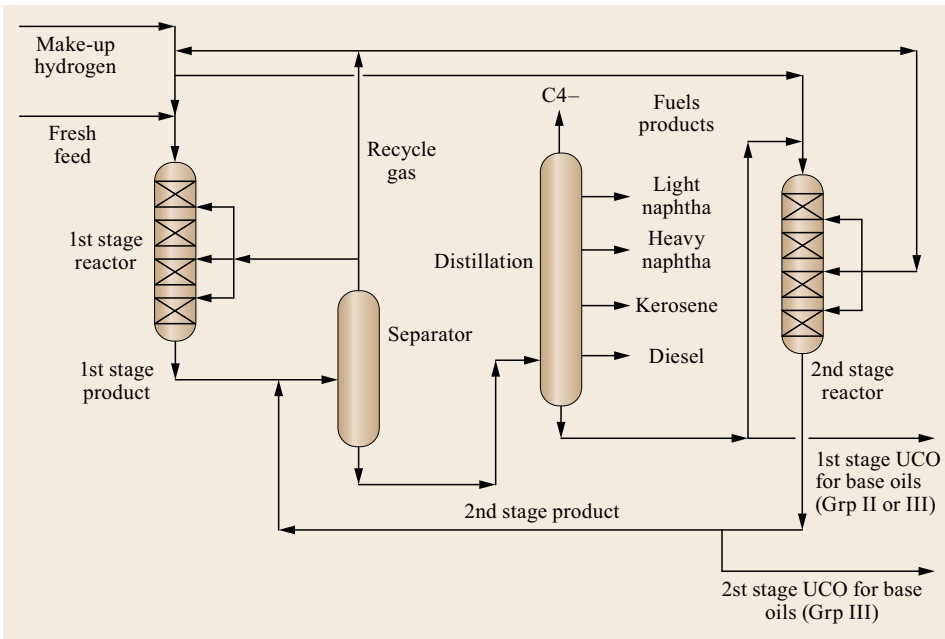


Fig. 34.21 Simplified TSR hydrocracker with base oil production

dewaxing) in the hydroisomerization dewaxer and hydrofinisher. A process option is to bulk dewax the entire UCO and then fractionate the dewaxed base oil into the desired viscosity grades. The merits of block and bulk dewaxing will be discussed in more detail in the dewaxing section.

34.6.5 Block and Bulk Base Oil Hydrocracker Operation

There are a couple of operating options to make waxy base stocks in a hydrocracker: block feed hydrocracking and bulk feed hydrocracking. There are pros and cons for each mode. The fractionation capability of the refinery's crude vacuum distillation unit, VDU, may have a large influence on which is the better mode. Sharply fractionated, narrow cut VGOs will provide the highest lube oil yield for a given feed. For an existing VDU in the refinery that has poor to mediocre separation efficiency, a capital expenditure to improve the VDU performance is money well spent, especially for a block operation mode. Also, new grassroots base oil plants are building high efficiency vacuum columns to prepare highly fractionated VGO feeds for the hydrocracker.

Block Hydrocracking

Figure 34.22 shows an example of a simplified flow scheme for block hydrocracking. The long residuum is fractionated in the VDU into three narrow lube VGOs plus a vacuum residuum. Each VGO cut must have the correct cut points and viscosity in order to make the desired base stock viscosity grades in the hydrocracker. The light, medium, and heavy VGOs make light neutral, medium neutral and heavy neutral oils respectively.

Block feeding each VGO will provide a primary base stock cut from the hydrocracker and possibly

a secondary base stock cut. For example, feeding a LN VGO can produce a waxy 100N (primary) and 60N (secondary). Feeding a HN VGO can produce a waxy 600N and possibly a small amount of lighter waxy base stock, depending on the boiling range of the HN VGO. However, the VI of the lighter base stock may be marginal in meeting the VI specifications because of VI droop. VI droop will be discussed in more detail later. Each of these primary base stock cuts are in turn blocked fed through the hydroisomerization dewaxer and hydrofinisher to make finished base stocks.

Note that the vacuum resid can be sent to a propane SDA plant to make feed for bright stock manufacture.

Bulk Hydrocracking

Feeding a broad-boiling-range VGO to a hydrocracker will result in multiple primary base stocks (of different viscosities) made simultaneously. In Fig. 34.23, a blend of the light and medium VGOs are fed to the hydrocracker to make waxy LN and MN base stocks simultaneously, and some light base stock such as a 60N. The ratio of the VGO blend will dictate the ratio of waxy LN and MN base stocks. Another scenario is to draw a combined light and medium VGO as a single VGO and feed it to the hydrocracker. This latter broad-boiling VGO will have a somewhat fixed ratio of LN and MN.

In Fig. 34.24, the medium and heavy VGOs are fed to make MN and HN waxy base stocks. In both scenarios, the hydrocrackate can either be fractionated into individual lube cuts (to a target viscosity) or fractionated into a broad-boiling base stock for dewaxing.

Advantages and Disadvantages of Block and Bulk Hydrocracking

The obvious advantages of bulk operation are fewer operating block changes on the hydrocracker with a sin-

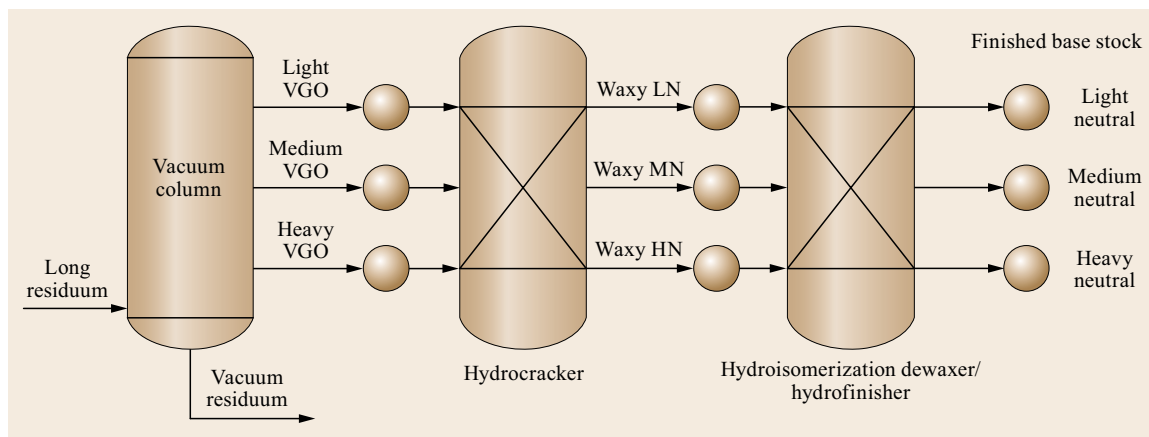


Fig. 34.22 Hydrocracker block feed operation

gle feed and possibly fewer and smaller intermediate tanks. However, there are some disadvantages. The hydrocracker vacuum column (Fig. 34.19) will be a more expensive and complex column to build and operate because at least two primary base stock draws are needed. An option is to not fractionate the lube hydrocrackate in the vacuum column, but to produce a wide-boiling waxy base stock fraction using a simple stripper. This wide-boiling fraction would then be bulk dewaxed followed by fractionation in a vacuum column to the various viscosity grades. Bulk dewaxing will be discussed in the dewaxing discussion.

It should be noted that for bulk hydrocracking the conversion must be sufficient to meet the target specifications of the limiting viscosity grade, which is generally the lighter grade. The VI and/or nitrogen level are usually the limiting specs for the waxy base stock. This will be better explained as we discuss VI droop. It could also result in much lower lube yield with VI giveaway.

With block hydrocracking, the unit is operated to meet the limiting specification(s) of a single waxy base stock grade instead of multiple grades. Very often, this is either VI or heteroatoms content, generally nitrogen. With the properties of only one base stock grade to achieve, this makes it easier to maximize/optimize the waxy base stock yield and base stock properties in the hydrocracker.

34.6.6 VI Droop

Because of the nature of bulk lube hydrocracking and due to the nonlinearity of the VI scale, the VI of the lighter base stock fraction will generally be lower than the VI of the heavier base stock fraction produced simultaneously. This has been referred to as VI droop and is explained in detail in a number of excellent articles [34.6, 11, 12]. In order to achieve the target VI for the lighter base stock, the hydrocracker must operate at a higher conversion, resulting in some

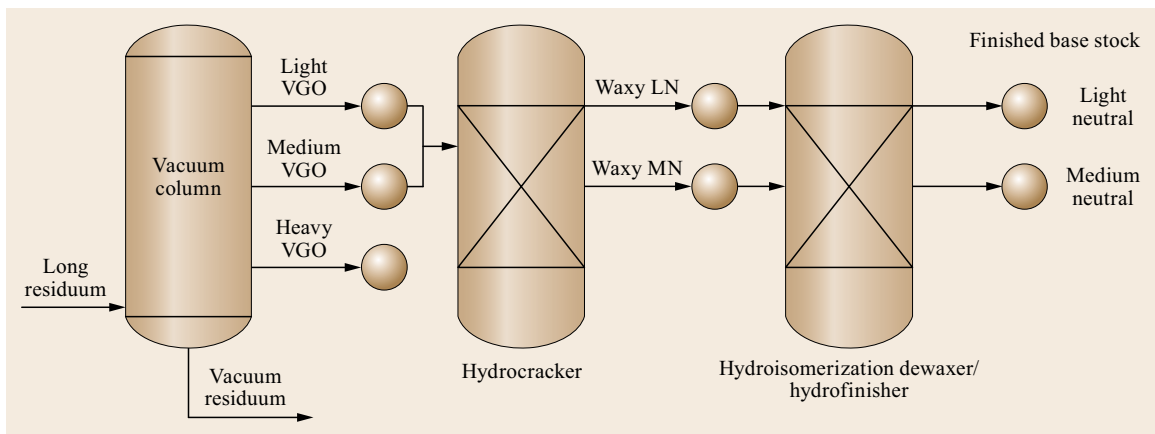


Fig. 34.23 Hydrocracker bulk feed operation – LN and MN block

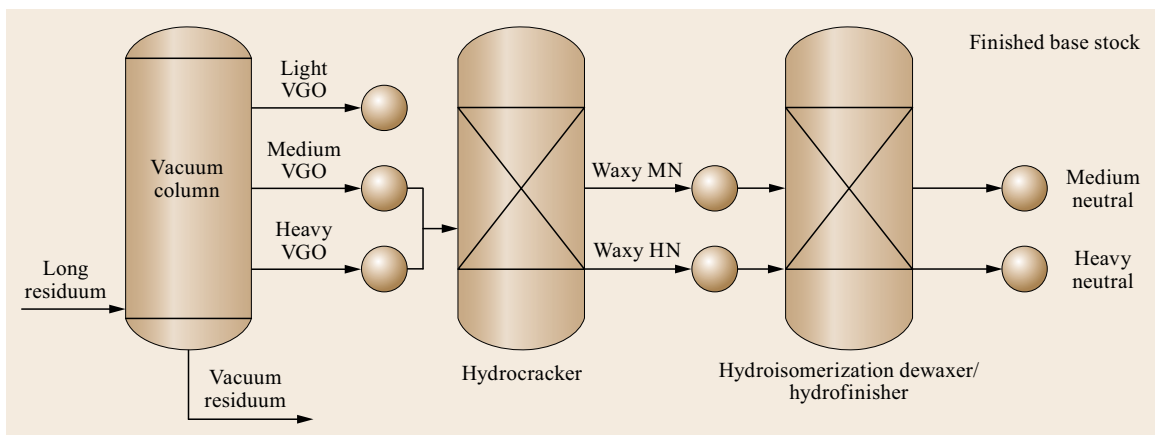


Fig. 34.24 Hydrocracker bulk feed operation – MN and HN block

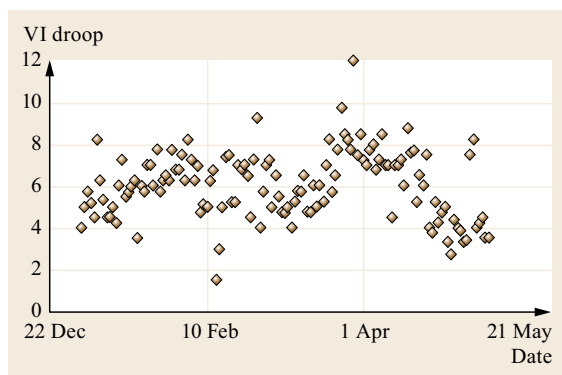


Fig. 34.25 VI droop in a hydrocracker feeding HVGO and making MN and HN base stocks – plant data

VI giveaway for the heavier lube cut. Thus, less total waxy base stocks are produced, and more fuels are made.

The VI droop between the adjacent base stock cuts typically ranges from two to ten VI numbers. The actual amount of droop depends on the viscosities of the adjacent base stock fractions, the hydrocracker conversion level and the feed VGO composition. Increasing the hydrocracker conversion generally results in a larger VI droop for a given feed. Also, increasing the severity (conversion of heavy molecules to lighter ones) results in more molecules cascading from the heavier to the lighter base stock fraction. The molecules that are converted to the lighter base stock fraction are frequently moieties with shorter alkyl chains and lower VI. Figure 34.25 shows commercial data in which the VI droop is about four to eight numbers for a hydrocracker feeding a broad-boiling-range HVGO to make MN and HN base stocks simultaneously.

Referring to Fig. 34.23, increasing the ratio of light VGO to medium VGO will directionally lower the VI droop between the LN and MN base stocks. This also holds true for the heavy block in Fig. 34.24 in which increasing the ratio of medium VGO to heavy VGO will directionally reduce the VI droop. The relationship between VI droop and feed VGO ratio generally must be determined experimentally or by a plant test run.

The parameters that affect the amount of VI droop in a bulk hydrocracker operation are:

- Blend ratio of LVGO:MVGO:HVGO, or boiling curve of the VGO feed
- Hydrocracker conversion level
- Distillation separation quality between the adjacent base stock cuts

Table 34.6 Typical hydrocracker process conditions

Process variable	Value
Pressure (psig)	1500–2500
Temperature (°F)	650–825
LHSV (1/hr)	0.5–1.2
Recycle hydrogen rate (scfb) ^a	3000–8000
Hydrogen consumption (scfb)	500–1800
Catalyst life (yrs)	2–3

^a scfb = std ft³/bbl feed

- Feed source (e.g., VGO, UCO, slack wax, raffinate, crude selection, etc.)
- Hydrocracker catalyst age.

34.6.7 Process Conditions

There are a number of process variables for designing a lube hydrocracker. The quality of the feed will dictate the process conditions for the hydrocracker design. A high-quality feed, such as Arabian Light VGO, will permit designing a higher reactor space velocity, while a poor-quality VGO from Alaskan North Slope crude will require a low reactor space velocity. Some typical process conditions are shown in Table 34.6.

These variables are interrelated in designing the hydrocracker. The reactor size (as determined by LHSV) must be designed to meet the desired catalyst run life for the design feed rate. There must be sufficient catalyst volume to make high-quality, on-specification base stocks throughout the entire run cycle. Generally, a 2–3 year run cycle is selected for the hydrocracker, although longer run cycles have been chosen. The catalyst operating temperatures at the start-of-run (SOR) and end-of-run (EOR) are defined and related to the reactor space velocity. The reactors and their internals must be designed properly to minimize reactor temperature maldistribution. The hydrogen pressure must be sufficient to make the desired product quality and control the catalyst fouling rate (coking) to meet the targeted run life. The recycle hydrogen rate must be set high enough to control the heat release in the reactor during normal operations and for potential temperature excursions and emergencies.

The hydrogen consumption in the lube hydrocracker will be a function of the feed properties (sulfur, nitrogen, and aromatics content) and the conversion level needed to achieve product VI. Generally, the more paraffinic the feed, the lower the hydrogen consumed in the process. The hydrogen consumption for a Middle East VGO is typically about 1000–1500 scfb of feed, depending on the conversion level.

34.7 Dewaxing

The pour points of the waxy base stocks coming out of the hydrocracker are lowered in the dewaxing step to meet the finished base stock low-temperature property specifications. This can be done by either physical removal of the wax or selective chemical reaction to alter or eliminate the wax. The wax is a mixture of hydrocarbons that separate out as a crystalline or semicrystalline solid material when the product is chilled, either alone or diluted by certain solvents. These hydrocarbons have the common feature of long normal paraffin chains. These chains can range from about 18 carbons to over 50 carbons long.

34.7.1 Current Dewaxing Technologies

The dewaxing technologies in commercial use today are solvent dewaxing and catalytic dewaxing. Solvent dewaxing is the conventional dewaxing technology. The wax in the waxy base stock is crystallized and precipitates when the solvent mixture, such as MEK and toluene, is chilled. It is then vacuum filtered to physically separate (extract) the wax from lube oil. A detailed discussion of solvent dewaxing can be found in other references [34.13, 14].

Catalyst dewaxing falls into two categories:

- Wax hydrocracking, referred to as conventional catalytic dewaxing
- Wax hydroisomerization.

Unlike solvent dewaxing, there is no slack wax byproduct from catalytic dewaxing. The byproducts are mostly LPG, naphtha and distillates. Refiners that want to continue to make refined and semirefined waxes must continue to use solvent dewaxing.

Figure 34.26 shows a simple schematic outlining the differences between solvent and catalytic dewaxing.

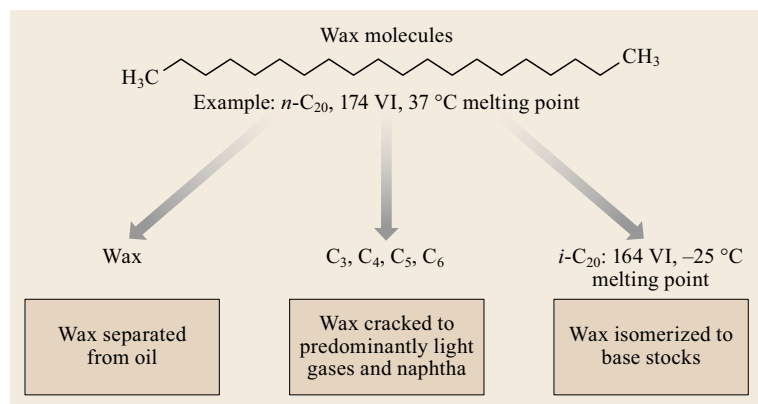


Fig. 34.26 Overview of dewaxing processes

34.7.2 Conventional Catalytic Dewaxing – Wax Hydrocracking

A number of catalytic dewaxing processes using wax cracking technology have been commercialized [34.13]. The most widely used was the Mobil Lube Dewaxing (MLDW™) process. ExxonMobil developed this technology in the mid-1970s as an alternative to using solvent dewaxing. The MLDW™ catalyst uses the ZSM-5 zeolite, a medium-pore zeolite, discovered in the late 1960s and patented by Mobil in 1972 [34.15]. The zeolite selectively cracks the undesirable wax while preserving the valuable base stock molecules. The primary cracking products include propane, butane, and light naphtha.

ZSM-5, as shown in Fig. 34.27, works on the principle of shape selective dewaxing. A constrictive, intersecting two-dimensional pore geometry ($5.4 \times 5.6 \text{ \AA}$ straight channel and $5.1 \times 5.5 \text{ \AA}$ sinusoidal channel) allows linear and the linear portions of some slightly branched alkanes to enter into the pore system while rejecting the low pour point, nonwaxy components (highly branched paraffins, naphthenes, and aromatics). The alkane molecules then get cracked to small hydrocarbons over the acid sites inside the zeolite pores.

Because of the shape selective nature of the ZSM-5 zeolite, it can withstand high nitrogen and sulfur levels in the waxy base stock. The large nitrogen and sulfur species cannot get deep inside the ZSM-5 pores and deactivate the zeolite. Therefore, the technology is robust and can be used to dewax a full range of raffinates ranging from spindle oil to bright stock from a Group I solvent plant, and all viscosity grades of hydrocrackate from a hydrocracker.

Depending on the operating pressure of the MLDW™, the dewaxing catalyst can lose activity from coke formation and carbonaceous deposits over time.

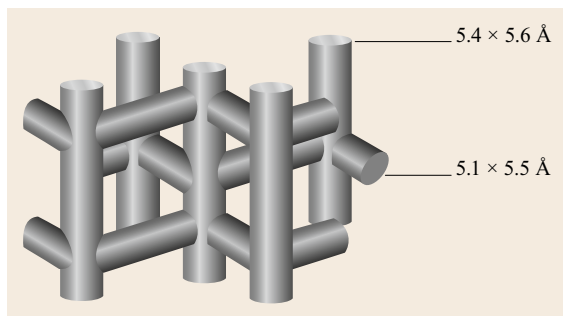


Fig. 34.27 ZSM-5 structure

Most of these contaminants form on the outside of the ZSM-5 crystals and plug the pore mouths. The catalyst is usually periodically reactivated with hot hydrogen gas stripping. The pressure of the MLDW™ units is generally designed between 500–3000 psig. The run length between hydrogen reactivation varies with the feed properties and operating pressure of the unit. A unit designed to operate at 2000 psig will run for years and not need a hot hydrogen reactivation. The ones designed around 500 psig will lose activity and must undergo periodic reactivation. The ZSM-5 zeolite was selected for the MLDW™ process because of its balance for wax reactant shape selectivity, reduced coking propensity, and resistance to poisoning from bulky nitrogen compounds [34.15].

Compared to solvent dewaxing, ZSM-5 removes more wax when achieving the same pour point on a common feed. The base stock yield is generally lower than solvent dewaxing, especially for the lighter viscosity grades such as LN and MN. However, the cold flow viscometrics for the formulated engine oils, such as cold crank simulator (CCS), mini-rotary viscosity (MRV), and scanning Brookfield viscosities, are better with base oil dewaxed with ZSM-5 because of more complete wax removal. In addition to wax molecules, some good base stock molecules, such as monobranched paraffins, may get cracked into fuels.

The VI of the ZSM-5 dewaxed base stocks can be 5–10 numbers lower than that of base stocks from solvent dewaxing, especially for the lighter grades. The high VI loss with the ZSM-5 catalyst can have a large ramification back to the solvent extractor and hydrocracker. Both of these units must operate at a higher severity to make up for the VI loss in the catalytic dewaxing step. Thus, for this type of catalytic dewaxing, there is an overall yield loss, which may be balanced out by less complex operations and better low-temperature performance for the base stocks. ZSM-5 performs better on heavy viscosity grades than lighter grades in terms of dewaxed oil yield and VI retention. For example, the dewaxed oil yield is higher for HN than LN. Also, the VI

losses on HN and bright stock are lower than for the LN and MN. In fact, the yield and VI for bright stock come close, or may even exceed that of solvent dewaxing as ZSM-5 is more selective for removing microcrystalline wax [34.15].

The wax cracking reaction causes the formation of a small amount of olefins. These intermediary olefins must be removed in the final hydrofinishing step to improve base stock stability. Hydrofinishing saturates all olefins and, depending on the pressure of the HDF, most aromatics. Catalytic dewaxing plants used for the manufacture of premium base stocks generally integrate catalytic dewaxing and hydrofinishing into a single plant with two reactors in series instead of two separate plants. This saves a considerable capital expenditure.

34.7.3 Hydroisomerization Dewaxing

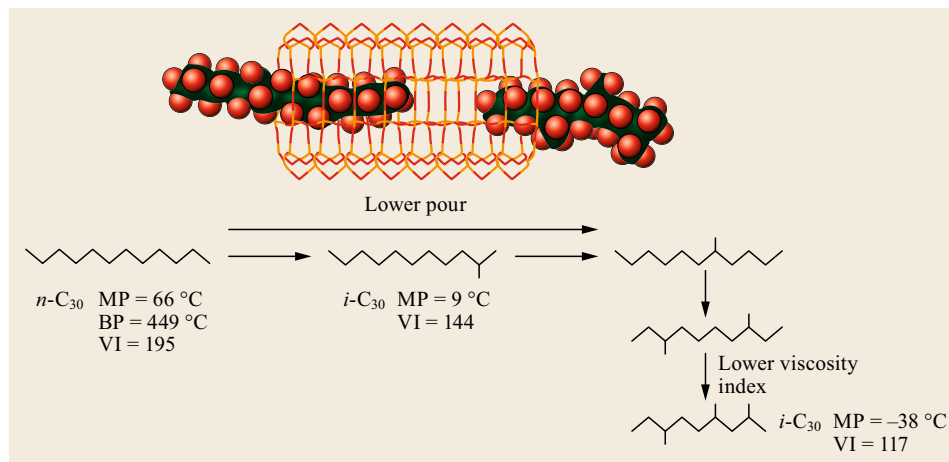
In the early 1990s, a new approach emerged for catalytic dewaxing. A breakthrough technology was invented by Chevron named ISODEWAXING®. Instead of solely cracking wax into relatively low value LPG and light naphtha, the ISODEWAXING® technology converts wax into high value products, including base stocks, middle distillates, and naphtha, by hydroisomerization. Table 34.7 shows an example of how hydroisomerization provides a high-VI, low-melting-point base stock molecule.

Chevron commercialized their ISODEWAXING® technology at its Richmond California Refinery in 1993. This technology is currently licensed by Chevron Lummus Global, LLC. Since then, ExxonMobil developed their version of a hydroisomerization dewaxing technology, MSDW™ (Mobil Selective Dewaxing). It was implemented into their Singapore-Jurong lube oil plant in 1997 [34.16]. Shell Criterion also has a hydroisomerization dewaxing technology that is used in their GTL Pearl Plant in Qatar [34.17].

The hydroisomerization dewaxing catalysts are composed of proprietary zeolitic or molecular sieve materials and at least one noble metal. The zeolite or molecular sieve typically utilizes a one-dimensional pore geometry, which has better selectivity for limiting primarily paraffins with long-straight chains to enter the catalyst pores than ZSM-5 [34.18]. As depicted in Fig. 34.28, the n -C₃₀ molecule enters the catalyst pore and gets isomerized to a lower melting point isoparaffin molecule by adding one or two methyl branches or, in some cases, an ethyl branch. There are a number of isomers that can form inside the catalyst pores. The more branching, the lower the melting point. However, as the melting point decreases, the VI is also lowered with the added side chains. The amount of branching

Table 34.7 Isomerizing $n\text{-C}_{30}$ (triacontane) lowers the melting point and provides a branched lube oil molecule [34.19]

Formula	Structure	Melting point ($^{\circ}\text{C}$)	VI
$n\text{-C}_{30}\text{H}_{62}$ triacontane		66.5	195
$\text{C}_{30}\text{H}_{62}$ squalane		-38	117

**Fig. 34.28**

Chevron's shape selective ISODE-WAXING® Catalyst – paraffins isomerize in the pores with minimal cracking (only partial C_{30} molecules are shown in the diagram)

and side-chain length is a function of the pore geometry of the sieve and process conditions. A balance must be achieved to get the correct amount of branching to achieve the base oil target pour point and not lose too many VI numbers. The byproducts are predominantly high-quality liquid transportation fuels, i.e., naphtha and mid-distillates for the jet and diesel pools.

The ideal hydroisomerization dewaxing catalyst will have selective acidic molecular sieve sites and active noble metal hydrogenation sites for enhancing isomerization reactions and for catalyst stability. The acidity of the isomerization sites is less than that of ZSM-5, thus there is less cracking of the wax to lighter species, and more preservation of species in the base stock range. The presence of a strong hydrogenation metal to rapidly saturate the olefins produced in the isomerization reaction prevents coke formation in the catalyst. This strong hydrogenation function is critical to maintain the catalyst activity and stability. It also contributes to improve the base stock stability. Final base stock stabilization occurs in the hydrofinishing step. Modern hydroisomerization catalysts are designed such that the two functions, hydroisomerization and hydrogenation, work together in balance to achieve superior cold flow properties with high lube oil yield and VI retention.

The catalyst temperature needed to dewax a waxy base stock is a function of the wax content (wt%).

The higher the wax content, the higher the temperature needed to achieve the target pour point. For typical Group II base stocks made from Arabian Light VGO, the wax content increases as the base stock gets heavier, and so does the dewaxing temperature: LN ($\approx 9\text{--}12\%$ wax) < MN ($\approx 13\text{--}18\%$ wax) < HN ($\approx 20\text{--}25\%$ wax).

34.7.4 Hydroisomerization Dewaxing Catalyst Poisons

Hydroisomerization and hydrogenation sites in the dewaxing catalysts are sensitive to nitrogen- and sulfur-containing molecules. Nitrogen compounds are responsible for poisoning the acid sites on the zeolite or molecular sieve, which results in the deactivation of the dewaxing catalyst. Nitrogen poisoning is mostly reversible. The dewaxing activity can be recovered by hot hydrogen gas stripping or by introduction of a cleaner liquid feed. High levels of nitrogen in the waxy feed will require the dewaxing catalyst to operate at higher than normal temperatures, which may cause an increase in unselective cracking. It should be noted the recent new generations of hydroisomerization dewaxing catalysts are much more tolerant to feeds with higher nitrogen.

Sulfur compounds can passivate the noble metal in the dewaxing catalyst and inhibit the dewaxing reaction.

The sulfur content in the feed must be kept low to prevent damage to the hydrogenation function of the noble metal.

The waxy lube oil feed to the dewaxer ideally should have a nitrogen level of no more than a few ppm and a sulfur level of no more than 10–20 ppm. This is generally not a problem as the hydrocrackate and UCO leaving the hydrocracker are clean with extremely low nitrogen and sulfur levels.

34.7.5 Process Flow Diagrams

To save capital costs, hydroisomerization dewaxing and hydrofinishing reactors are generally included in the same reactor loop. However, there are scenarios in which it may be economical to have separate dewaxing and hydrofinishing reactor loops operating at different pressures. Examples of these scenarios are beyond the scope of this chapter. For this discussion, these plants will be referred to as an isomdewaxer/hydrofinisher. Hydroisomerization dewaxing and isomdewaxing will be used synonymously. The process diagram for a lube oil isomdewaxer/hydrofinisher is essentially the same as a conventional hydrotreater.

There are two operating options for catalytic dewaxing base stocks. They are *block* dewaxing (Fig. 34.29), and *bulk* dewaxing, (Fig. 34.30). Block dewaxing is defined as dewaxing a single primary viscosity grade at a time. The waxy base stock is a narrow boiling range oil of a single viscosity grade. For example, a refiner that makes 100N, 220N and 600N base stocks

will have three individual dewaxing blocks. The waxy feeds for each viscosity grade are fractionated at the hydrocracker vacuum column or a vacuum feed preparation unit (FPU) to the correct viscosities and boiling ranges before dewaxing. This was previously depicted in Fig. 34.19.

Bulk dewaxing is defined as dewaxing a wide-boiling-range waxy oil followed by vacuum fractionation of the dewaxed oil into multiple viscosity grades at the tail-end.

As shown in Fig. 34.29, the waxy base stock is mixed with makeup and recycle hydrogen gas and heated in the reactor feed furnace. The heated oil and gas enter the isomdewaxing reactor where the waxy base stock is dewaxed. The isomdewaxing reactor temperature is set to achieve the desired dewaxed oil pour point. The chemical reactions in the isomdewaxing reactor generates a small amount of heat from aromatic saturation and cracking. Interbed hydrogen quenching between the catalyst beds is needed to cool the reactor and control the reactions. The dewaxed oil exits the isomdewaxing reactor, is cooled in an interreactor feed/effluent heat exchanger (not shown in Fig. 34.29) by exchanging heat with the cold feed, and then enters the hydrofinishing reactor.

In the hydrofinishing reactor, the remaining aromatics are saturated to stabilize the base stock. The hydrofinishing reactor must be set at the proper temperature to saturate the last remaining aromatics. The heat release in the hydrofinishing reactor is very small. Generally, no interbed hydrogen quenching is required for the hydrofinishing reactor.

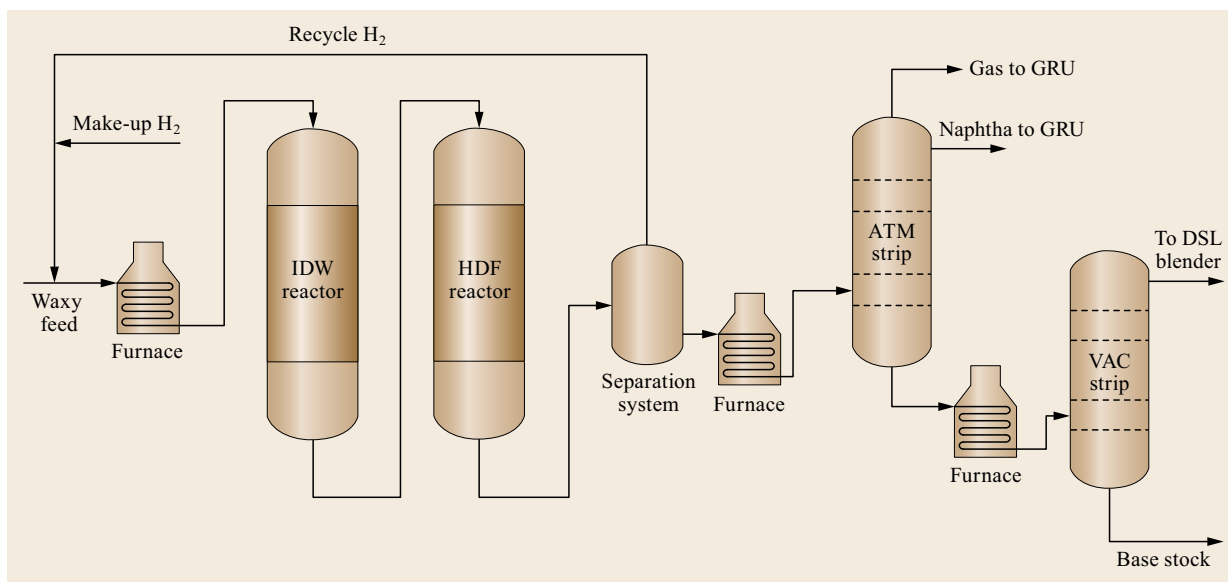


Fig. 34.29 Simplified process flow diagram for isomdewaxer/hydrofinisher – block dewaxing

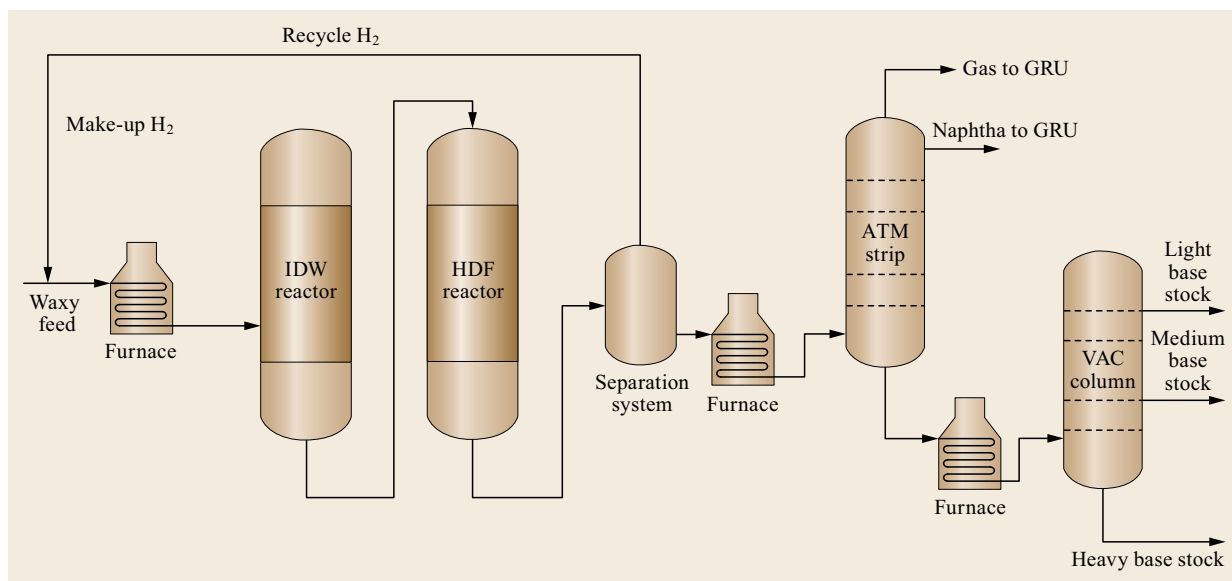


Fig. 34.30 Simplified process flow diagram for isom dewaxer/hydrofinisher – bulk dewaxing

The product exiting the hydrofinishing reactor then enters the separation system where hydrogen and light hydrocarbon gases are flash separated from the liquid oil. The liquid product is heated in the atmospheric furnace and enters the atmospheric stripper. Light gases and naphtha are removed overhead in the atmospheric stripper. The remaining product is heated in the vacuum furnace and sent to the vacuum stripper to separate the base stock and diesel.

The bulk dewaxer, as shown in Fig. 34.30, is essentially the same as the block dewaxer except the vacuum stripper becomes a vacuum column because of the need to boil up a greater percentage of the reactor effluent. The vacuum column fractionates the dewaxed oil into finished base stocks that meet viscosity specifications.

34.7.6 Bulk versus Block Dewaxing

There are a number of pros and cons with using bulk dewaxing compared to block dewaxing. The pros for bulk dewaxing include the following:

1. Less capital expenditure from:
 - a) Fewer and possibly smaller intermediate tanks
 - b) Less piping and other associated equipment
 - c) Possibly smaller reactors.
2. Simpler operation from fewer feed switches.
3. Smaller vacuum column in the hydrocracker or feed preparation unit.

The cons for bulk dewaxing include the following:

1. Less optimization of the viscosity grades to achieve the product specifications and the highest yield.
2. More complex vacuum column to fractionate the dewaxed oils to the target viscosities at the tail-end of the plant. This may be offset by item 3 in the pros.
3. Some VI loss in the lighter grade due to over-dewaxing.

The economics for bulk and block dewaxing needs to be properly evaluated before deciding which is preferred for a new lube oil plant. There can be a yield penalty with bulk dewaxing from not optimizing the product specifications. Figure 34.31 shows the pour

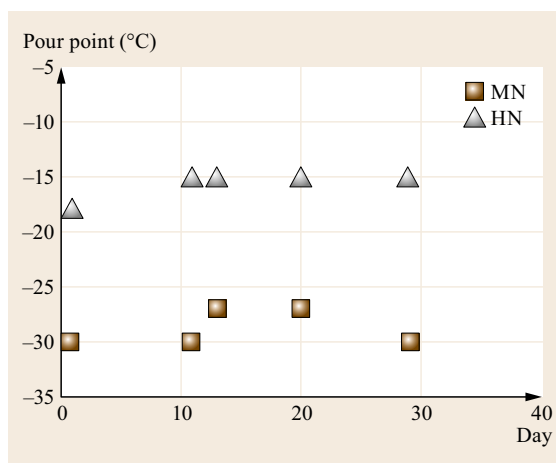


Fig. 34.31 Bulk dewaxing HN and MN – from Chevron data base

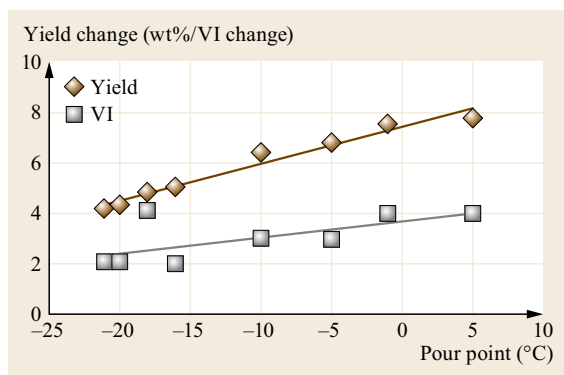


Fig. 34.32 Lube oil yield change and VI change versus pour point (after [34.20])

points for MN and HN with bulk dewaxing. The dewaxing reactor must operate at the temperature required to achieve the pour point target of the limiting oil that is HN. The MN is overdewaxed as its pour point is about 10–15 degrees lower than that of the HN. This leads to a lower MN yield in comparison to block dewaxing.

The amount of overdewaxing and potential yield loss between adjacent lube cuts depends on the feed properties and composition. Figure 34.32 shows the change in VI and yield for isomdewaxing a Group II 150N to various pour points. The yield loss is about 1 wt% for each 5 °C of pour point reduction for this particular product from block dewaxing. This can be different for other viscosity grades. The VI loss is about one VI number for each 10 °C reduction in pour point [34.20]. The yield and VI losses from over-dewaxing are not large from an absolute number standpoint. However, they can be significant when optimizing the finished base stock's volatility and cold flow properties for blending into premium engine oils as previously discussed in Sect. 34.3.

It should be noted that bulk dewaxing will result in a small amount of HN transitioning into MN from isomerization and cracking of wax, which is captured in

Table 34.8 Hydroisomerization dewaxing process conditions

Process variable ^a	Value
Pressure (psig)	1500–2500
Dewaxing temperature (°F)	600–700
LHSV (1/hr) ^b	0.5–2.5
Recycle hydrogen rate (scfb)	1500–5000
Hydrogen consumption (scfb) ^c	100–500
Catalyst life (yrs)	5–10+

^a Dewaxing and hydrofinishing reactors in series.
^b Dewaxing reactor only: oil volume rate/catalyst volume.
^c Includes both dewaxing and hydrofinishing hydrogen consumptions.

the final MN product. In block dewaxing, this portion of MN will not be captured as base stock unless the process distillation configuration is set up to do this.

Block dewaxing allows for optimization of the product specifications and yield for each grade of base stock. This can be especially important for the LN grades such as 100N and 150N. More interrelated specifications are required for these lighter base oils, including volatility (e.g., Noack), cold flow viscometrics (CCS, Brookefield, etc.), pour point, and VI. Block dewaxing makes it easier to meet all the specifications simultaneously, and provide the best base stock yield.

34.7.7 Process Conditions

The typical process conditions for dewaxing Groups II and III base stocks are shown in Table 34.8.

34.7.8 Comparison Between Solvent, Conventional Catalytic and Hydroisomerization Dewaxing

The technology transition from solvent dewaxing to conventional catalytic dewaxing to hydroisomerization dewaxing has been a dramatic evolution. The signifi-

Table 34.9 Comparison between solvent, conventional catalytic, and hydroisomerization dewaxing

Process/Item	Solvent dewaxing	Catalytic dewaxing	Hydroisomerization
Wax removal	Physical – wax crystallization and filtration	Chemical – wax cracking with shape selective catalyst	Chemical – wax isomerisation with shape selective catalyst
Product pour point	–10 to –15 °C	–10 to –50 °C	–10 to –50 °C
Yields	Base case	Same or lower	Same or higher
Drewaxed product VI	Base case	Generally 5–10 numbers lower	Generally 5–10 numbers higher
Byproducts	Slack wax	Gas, naphtha	Gas, naphtha, jet, diesel
Capital costs	Base (100%)	60–80%	65–85%
Operating costs	Base (100%)	50–60%	55–65%

cantly higher lube oil yield and higher retention of VI by the latest generation of hydroisomerization dewaxing catalyst has increased the efficiency and profitability for base stock manufacturers. Because base stocks are valued much higher than fuels, there is continuous, ongoing research by the technology licensors to improve the performance of their catalysts. Improvements in selectivity for more complete isomerization of wax to base stocks with minimum cracking to fuels is the major

goal of the catalyst researchers. As the catalyst performance improves incrementally by retaining more VI, the refiner is able to increase the yields in the hydrocracker and solvent extractor by running these plants at a lower severity.

Table 34.9 compares the various lube oil dewaxing technologies in terms of relative dewaxer yield, VI retention, byproduct slate, and capital and operating costs.

34.8 Hydrofinishing

The final processing step in the manufacture of premium base stocks is hydrofinishing. Without hydrofinishing, the residual aromatics in the base stock will oxidize, which results in oil darkening, sludge and varnish formation, and generation of corrosive compounds in engine and industrial oil applications. As previously discussed, a hydrofinishing reactor is generally included in the same reaction loop as the isomdewaxing reactor, giving a single, close-coupled hydroisomerization dewaxing/hydrofinishing plant. Today's modern hydrofinishing process virtually removes all polycyclic aromatics. This results in a dramatic improvement in color and high-temperature oxidation and storage stabilities.

34.8.1 Conventional Base Stock Finishing (Polishing) Process

Prior to the establishment of hydrofinishing as the final finishing step, base stocks were finished using sorbent beds of clay (Attapulgus clay was commonly used) or bauxite percolation treating to remove polycyclic aromatics. In the 1950s, lubricant formulators began to demand better quality base oils, and hydrofinishing

has progressively replaced adsorption treating for base stock manufacture. Besides providing superior quality base stocks, hydrofinishing is much more environmentally friendly than percolation adsorption treating, in which the exhausted clay must be thermally regenerated in a furnace or kiln to remove the adsorbed organic materials. After repeated regenerations, the clay loses adsorption efficiency and eventually must be replaced. The spent clay is a hazardous waste material requiring proper disposal.

34.8.2 Chemistry of Aromatics Saturation in Hydrofinishing

The chemistry and strategies for aromatic saturation were previously presented in the Hydrotreating and Hydrocracking Chemistry section, Sect. 34.6.1. Building a very high pressure hydrofinisher, say ≈ 3000 psig, will provide a wide temperature range to saturate all aromatics and overcome the thermodynamic equilibrium limitations. However, this is expensive. Thus, the two sequential temperature steps, as previously discussed, is the preferred strategy from a cost standpoint.

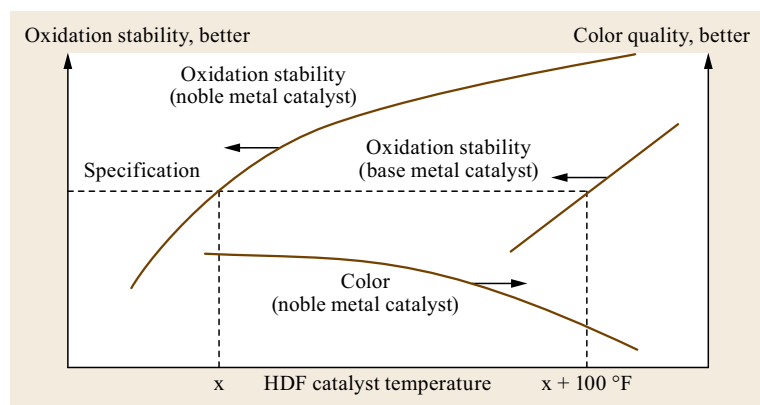


Fig. 34.33 Effect of HDF catalyst temperature on finished base oil qualities (after [34.21])

The hydrofinishing reactor is designed to run at lower temperatures, usually below 600 °F to saturate the polycyclic aromatics to naphthenes. Operating the hydrofinishing catalysts above 600 °F may work against saturating the polycyclic aromatics because of the thermodynamic equilibrium limitations, depending on the H₂ partial pressure and LHSV. This is depicted in Fig. 34.33 – the color of the base stock darkens at the higher HDF temperatures.

Today's modern noble metal hydrofinishing catalysts are so active that it is possible to saturate aromatics down to less than 1 wt%, and improve both color and oxidation stability significantly.

34.8.3 Hydrofinishing Catalysts

The early hydrofinishers were stand-alone units that typically fed Group I or Group II base stocks. The catalysts were base metal catalysts, such as Ni and Mo supported on alumina. Due to the catalysts' relatively low hydrogenation activity, the aromatics, sulfur and nitrogen levels of the hydrofinished base stocks were high when compared with today's all-hydroprocessing Group II and Group III base stocks.

Today's modern hydrofinishing catalysts contain noble metals and sometimes mixtures of noble metals, which provide deep saturation performance at low temperatures and low deactivation rate. These catalysts are significantly more active than the base metal hydrofinishing catalysts. The higher activity allowed

Table 34.10 Process conditions for lube oil hydrofinishing

Process variable ^a	Value
Pressure (psig)	1500–2500
Temperature (°F)	450–600
LHSV (1/hr) ^b	0.5–2.5
Recycle hydrogen rate (scfb)	1500–5000
Hydrogen consumption (scfb) ^c	50–500
Catalyst life (yrs)	5–10+

^a Dewaxing and hydrofinishing reactors in series.

^b Hydrofinishing reactor only: oil volume rate/catalyst volume.

^c Hydrofinishing hydrogen consumption.

the hydrofinishing step to operate at temperatures in the 450 °F range, where the equilibrium thermodynamics favor more complete aromatic saturation. This enables GpII/III base oil plants to almost completely remove aromatics and make products with superior color (practically water-white) and excellent oxidation stability. Chevron's ISOFINISHING® catalysts and ExxonMobil's MAXSAT™ catalysts, among others, offer high activity for Group II and Group III base stocks. The catalyst life can be as long as ten years or more.

34.8.4 Process Conditions

The typical process conditions for hydrofinishing Groups II and III base oils using noble metal catalysts are shown in Table 34.10.

34.9 Integrating Hydroprocessing with Solvent Plants – Hybrid Plants

There are a number of existing base oil plants that use a combination of solvent processing and hydroprocessing. These plants generally started out as a solvent refining plant, and added a hydrotreating step to improve the base stock quality and/or debottleneck the lube plant. Figure 34.34 shows some of the more common lube oil manufacturing process configurations.

Adding a hydrotreating step following the solvent extractor produces a more saturated raffinate with higher VI and better quality. The raffinate hydrotreater makes it possible to increase raffinate yield and flow rates from the extractor, as the extractor does not have to make a raffinate that achieves final base stock property targets such as VI [34.22]. There are several examples of existing solvent Group I lube plants that added a raffinate hydrotreater to their processing scheme. This permitted them to make Groups II and II+ base stocks. ExxonMobil's raffinate hydroconver-

sion technology (RHC) is an example of this processing scheme.

An alternative to hydrotreating the raffinate is to insert a hydrotreater upstream of the solvent extractor. In this scenario, the VGO from crude oil is upgraded before entering the solvent extractor. Hydrotreating the VGO upstream of the extractor removes sulfur, nitrogen and saturate aromatics, making it easier to upgrade the VGO in the solvent extractor. In addition, the VI of the VGO can be significantly upgraded in the hydrotreater. The more severe the VGO hydrotreating, the higher is the raffinate yield from the solvent extractor. Generally, a high-severity hydrotreater (i. e., higher pressure) is required for this configuration, which may be more costly. An economic study is needed to understand which is the better option for a specific refinery. Locating the hydrotreater upstream of the solvent extractor is not as common as locating it after the solvent extractor.

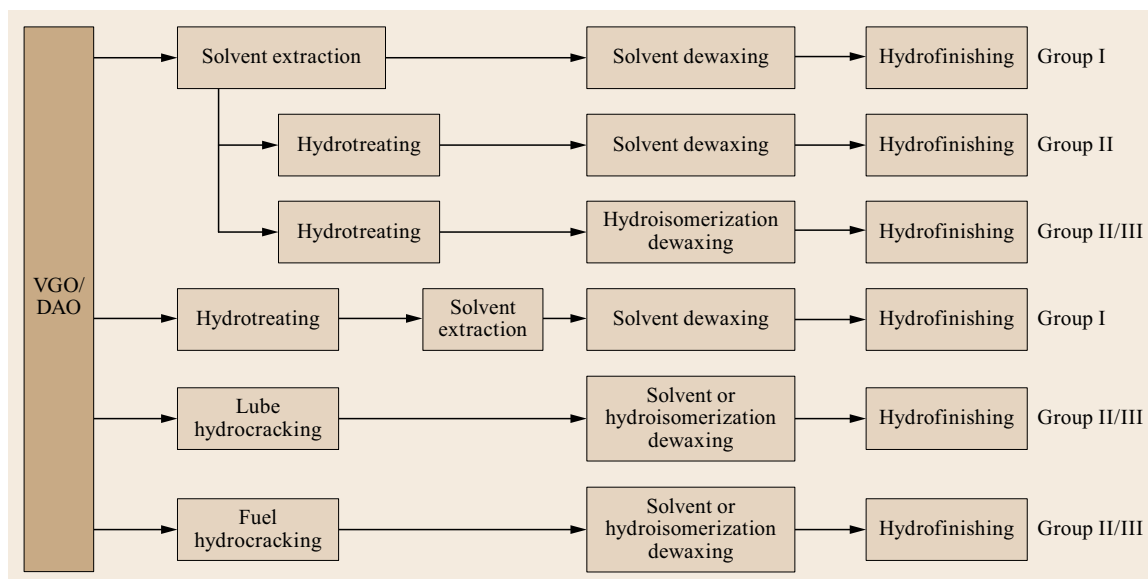


Fig. 34.34 Various base oil plant flow schemes

34.10 GTL Base Oils

Gas-to-liquid (GTL) is a process to convert natural gas or other gaseous hydrocarbons into longer chain hydrocarbon products, including fuels, base stocks, chemicals and wax. As shown in Fig. 34.35, a refinery process such as steam methane reforming (SMR), is used to convert natural gas into a mixture of carbon monoxide and hydrogen to make a synthesis gas. The syngas is then converted into paraffinic hydrocarbons over proprietary cobalt or iron catalysts in the Fischer–Tropsch (FT) process. The synthetic wax is subsequently upgraded using hydroprocessing to produce GTL fuels, naphtha, and base stocks. GTL base stocks are generally classified as Group III+. They are very-high-quality with virtually no contaminants, offering low pour point, low volatility, and high VI. Their performances are comparable to PAOs in many lubricant applications.

There are a total of five GTL plants globally:

1. PetroSA – Mossel Bay, South Africa
2. Shell – Bintulu, Malaysia
3. Sasol-Qatar – Oryx, Qatar
4. Shell-Qatar – Pearl, Qatar
5. Chevron-Sasol – Escravos, Nigeria.

Currently, the only two GTL plants that manufacture base stocks are Pearl, Qatar and Bintulu, Malaysia with capacities of 28 000 bpd and 1150 bpd respectively [34.23].

GTL plants are very expensive to build. They compete with LNG plants for monetizing natural gas. From an energy efficiency standpoint, LNG plants are more efficient. The carbon footprint of a GTL plant is high. The energy efficiency and large carbon footprint make

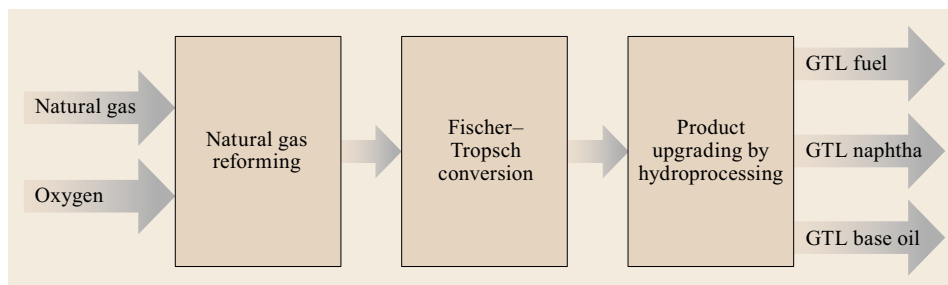


Fig. 34.35 GTL process scheme

GTL project economics challenging. A GTL plant becomes more attractive with low natural gas prices. There currently are a number of active GTL projects in development globally. Most of these projects are for

making liquid fuels. However, a project option to add hydroisomerization dewaxing to a GTL project is relatively simple and will permit manufacturing high-value Group III+ base stocks.

References

- 34.1 API: API 1509 Appendix E – API Base Oil Interchangeability Guidelines for Passenger Car Motor Oils and Diesel Engine Oils, September 2011.
- 34.2 Lubes'N'Greases: *Lubricants Industry Factbook* (LNG, Falls Church 2014)
- 34.3 ASTM: ASTM D97-12. In: *Annual Book of ASTM Standards*, Vol. 05.01 (ASTM, West Conshohocken 2014)
- 34.4 B.K. Lok: Group II base oils – An efficient route to formulating modern automotive lubricants, UELI Cong. Proc. (2009)
- 34.5 R.L. Howell, C. Hung, J. Xiao, J.F. Mayer: Hydroprocessing routes to improved base oil quality and refining economics, Proc. Asia Fuels and Lubes Conf. (2000)
- 34.6 J.A. Zakarian, R.J. Robson, T.R. Farrell: All hydroprocessing route for High-V.I. lubes, Energy Process **7**(1), 59–64 (1987)
- 34.7 G.-D. Lei, K. Krishna: All-Hydroprocessing route to base oil production – History and key process steps. In: *Encyclopedia of Lubricants and Lubrication*, ed. by T. Mang (Springer, New York 2014)
- 34.8 D.R. Cash, H.A. Yoon, M.M. Habib, A.S. Krishna, D.V. Law, U.K. Mukherjee: Partial Conversion ISO-CRACKING Process, Int. J. Hydrocar. Eng. **4**(44), 44–48 (1999)
- 34.9 T.R. Lynch: *Process Chemistry of Lubricant Base Stocks* (CRC, Boca Raton 2007), pp. 13, 24
- 34.10 R.F. Sullivan, M.M. Boduszynki, J.C. Fetzer: Molecular transformation in hydrotreating and hydrocracking, Energy Fuels **3**(5), 603–612 (1989)
- 34.11 J.A. Zakarian: The limitations of the viscosity index and proposals for other methods to rate viscosity-temperature behavior of lubricating oils, SAE Int. J. Fuels Lubr. (2012) doi:10.4271/2012-01-1671
- 34.12 J.A. Zakarian: The ASTM viscosity index and other systems for classifying lubricating oils, Proc. Nat. Petr. Ref. Assoc. Meet. (1982)
- 34.13 B.E. Beasley: Conventional lube basestock manufacturing. In: *Practical Advances in Petroleum Processing*, Vol. 2, ed. by C.S. Hsu, P.R. Robinson (Springer, New York 2006) pp. 31–78
- 34.14 A. Sequerira Jr.: *Lubricant Base Oil and Wax Processing* (Marcel Dekker, New York 1994)
- 34.15 T.E. Helton, T.F. Degnan, D.N. Mazzone, M.P. McGuinness, T.L. Hilbert, R.C. Dougherty: Mobil technology, catalytic hydroprocessing a good alternative to solvent processing, Oil Gas J. **96**(29), 58–67 (1998)
- 34.16 R.G. Wuest, R.J. Anthes, R.T. Hanlon, S.M. Jacob, L. Loke, C.T. Tan: Singapore all catalytic lube plant performs well, Oil Gas J. **97**(29), 70–73 (1999)
- 34.17 R. Szynekarczuk, M. Robinson, L. Huve: Dewaxing challenging paraffinic feeds, Pet. Technol. Q. **Q2**, 43–51 (2014)
- 34.18 S.J. Miller: Wax isomerization using catalyst of specific pore geometry, U.S. Patent 5 246 566 (1993)
- 34.19 L.Z. Pillon: *Surface Activity of Petroleum Derived Lubricants* (CRC, Boca Raton 2010) pp. 63–64
- 34.20 S. Bhattacharya, G. Lei, K.R. Krishna, J. Rogers: Next generation ISODEWAXING and ISOFINISHING catalysts, Proc. 15th Refin. Technol. Meet. (RTM) (2009)
- 34.21 J.N. Ziemer, K.R. Krishna: Lube oil hydrofinishing. In: *Encyclopedia of Lubricants and Lubrication*, ed. by T. Mang (Springer, New York 2014)
- 34.22 I.A. Cody: Selective hydroprocessing for new lubricant standards. In: *Practical Advances in Petroleum Processing*, Vol. 2, ed. by C.S. Hsu, P.R. Robinson (Springer, New York 2006) pp. 79–104
- 34.23 Lubes'N'Greases: *Non-Conventional Base Stock Guide* (LNG, Falls Church 2014)

Synthetic Lub

35. Synthetic Lubricant Base Stock

Margaret M. Wu, Suzy C. Ho, Shuji Luo

Conventional lubricants are formulated using mineral base stocks, which are refined from petroleum and contain many chemical species. Although mineral base stocks serve general-purpose lubricants well, they cannot be optimized for specific performance features. Modern machines and equipment are increasingly designed to operate under more severe conditions, to require less maintenance, to have improved longevity and better energy efficiency. Sometimes, conventional lubricants based on mineral base stocks fail to meet these elevated performance requirements. Synthetic lubricants using tailored synthetic base stocks are designed to meet these higher performance needs and can provide superior performance and economic benefits over conventional lubricants.

In this chapter, we briefly discuss the history of synthetic lubricant development to understand the fundamental driving forces behind the use of synthetic lubricants, which have synthetic base stocks as the main components. The major part of the chapter is devoted to discussing the key synthetic base stocks, polyalphaolefins (PAO), esters and polyalkyleneglycols (PAG) – their chemistries, manufacturing processes, product properties, per-

35.1	Background	1043
35.1.1	Why Use Synthetic Lubricants?	1044
35.1.2	What Is a Synthetic Base Stock?	1044
35.1.3	A Brief Overview of Synthetic Lubricant History	1045
35.2	Overview of Synthetic Base Stocks	1046
35.3	Synthetic Base Stock – Chemistry, Production Process, Properties, and Use	1047
35.3.1	PAO	1047
35.3.2	Dibasic, Phthalate, and Polyol Esters – Preparation, Properties, and Applications	1053
35.3.3	Polyalkylene Glycols (PAG)	1057
35.3.4	Other Synthetic Base Stocks	1058
35.4	Conclusion	1060
	References	1060

formance features, major applications and advantages compared with mineral base stocks. Additional discussions on less widely used synthetic base stocks, such as alkylaromatics, polyisobutylene and phosphate esters, are briefly reviewed for completeness.

35.1 Background

At the beginning of this chapter, we briefly discuss the background and motivation for using synthetic lubricants, followed by reviews of the products and processes for synthetic base stocks produced from chemicals of well-defined structures and tailored to optimize specific properties and performance features. These synthetic base stocks are major and critical components used in the formulation of many synthetic lubricants. In this chapter, we use *synthetic base stock* to represent the base fluid and *synthetic lubricant* to represent the formulated, finished lubricant product.

Many mineral oil manufacturers and marketers promote the use of Group II+ and Group III base stocks in the formulations of *synthetic lubricants*. However, Group II+ and Group III base stocks are usually produced from crude oil by hydroprocessing or hydrosomerization as part of a refining operation [35.1]. Discussion of these hydroprocessed base stocks can be found in other chapters of this book. In this chapter, we review only those synthetic base stocks produced from chemicals of well-defined composition and structures.

35.1.1 Why Use Synthetic Lubricants?

Synthetic lubricants are used for two major reasons:

1. When equipment demands specific performance features that cannot be met with conventional mineral oil-based lubricants. Examples are operations at extremely high or low temperatures, stability under severe conditions etc.
2. When synthetic lubricants offer economic benefits for overall operation, such as reduced energy consumption, reduced maintenance.

Conventional lubricants are formulated using mineral base stocks which are derived from petroleum. Mineral oil contains many classes of chemical components, including paraffins, naphthenes, aromatics, heteroatom species etc. Its chemical composition is pre-determined by the crude source and oil refining processes that have limited ability to substantially alter the initial oil compositions to fully optimize the hydrocarbon structures. Mineral oils of such complex compositions are good for general-purpose lubrication; they are not optimized for specific performance features. The major advantages of mineral oils are their low cost and user's familiarity due to their long history. However, this paradigm is changing.

Modern machines and equipment are increasingly designed to operate under more severe conditions, to last longer, to require less maintenance, and to improve energy efficiency. Synthetic lubricants are designed to maximize lubricant performance to meet the high demands of modern machines and equipment, and to offer tangible performance and economic benefits.

35.1.2 What Is a Synthetic Base Stock?

Most lubricant formulations contain 80 to 98% of base stock, and the choice of base stock mostly determines the performance level of the finished lubricant. Recognizing this importance, the American Petroleum Institute (API) classifies lubricant base stocks into five major groups, Group I to V in Table 35.1, depending on their physical properties and chemical compositions.

Conventional mineral base stocks are derived from crude oil by refining processes and typically contain sulfur and nitrogen compounds as well as naphthenes. Generally, these heteroatom-containing compounds promote the formation of sludge. All may act as poisons for catalytic converters and/or metal corrosives, during operation. Synthetic base stocks are classified as either Group IV or V and do not contain the sulfur or nitrogen compounds seen in mineral base stocks thereby eliminating the reaction pathways to harmful species and leading to better performance.

Synthetic base stocks are produced from carefully chosen and well-defined chemical raw materials and by specific chemical reactions. These base stocks are designed to have properties that significantly improve performance features to meet specific equipment demands. The most commonly optimized properties are described below.

Viscosity Index (VI)

VI (viscosity index) is a number used to gauge oil's viscosity change as a function of temperature. Higher VI, indicating less viscosity change as oil temperature changes, is a desirable property. Group I and II base stocks of 4 cSt generally have VIs in the range of 85 to 110, whereas most synthetic base stocks of similar viscosities have VIs greater than 120.

Viscosity

Fluid viscosity is one of the critical properties for lubrication. In this chapter, all fluid viscosities stated are kinematic viscosities in cSt measured at 100 °C according to the ASTM D445 method. Very low-viscosity fluids (2–4 cSt) offer advantageous energy or fuel efficiency for machine operation. Very high-viscosity fluids offer special lubrication and wear protection. Mineral oil viscosity is usually limited to less than 40 cSt. In contrast, synthetic base stock can be tailor-made to 1000 cSt or higher while maintaining low-temperature performance.

Pour Point and Low-Temperature Viscosities

Many synthetic base stocks have low pour points, –30 to –70 °C, and superior low-temperature fluidity. Combination of low pour and superior low-temperature fluidity ensures oil flow to critical engine parts during cold starting, thus, offering better lubrication and protection. Mineral oils typically have pour points in the range of 0 to –20 °C. Below these temperatures, wax crystallization or oil gelation can occur, preventing the flow of lubricant to critical machine parts.

Thermal/Oxidative Stability

When oil oxidation occurs during service, oil viscosity and acid content increase significantly, leading to corrosion of metal parts, generating sludge and reducing efficiency. These changes also exacerbate wear by preventing adequate oil flow to critical parts. Although oil oxidation can be controlled by adding antioxidants, the intrinsic oxidative stability of a base stock is an important factor in preventing oil degradation and ensuring proper lubrication after the depletion of antioxidant or in long-term service. Many synthetic base stocks are designed to have improved thermal oxidative stability, to respond well to antioxi-

Table 35.1 Definition of API category I to V lubricant base stock

	(Description)	% Saturates	% Sulfur	VI
Group I	(Conventional, solvent refined) ^a	< 90	> 0.03	80–119
Group II	(Hydroprocessed) ^a	≥ 90	≤ 0.03	80–119
Group III	(Severely hydroprocessed or isomerized wax) ^a	≥ 90	≤ 0.03	≥ 120
Group IV	Polyalphaolefins			
Group V	All other base stocks not included in Group I, II, III or IV (e.g., esters, PAG, alkylaromatics, etc.)	–	–	–

^a Comments in parentheses are not included in the original API definition

dants and to resist aging processes better than mineral oil.

Volatility

Synthetic base stocks can be designed to minimize oil volatility. For example, polyol esters have very low volatility because of their narrow molecular weight distribution (MWD), high purity, high polarity, and thermal stability. Similarly, careful selection of raw materials and processing conditions can influence the volatilities of polyalphaolefins (PAO).

Other Properties

Including friction coefficient, traction coefficient, biodegradability, resistance to radiation etc. can be optimized through selection of base stock structures.

35.1.3 A Brief Overview of Synthetic Lubricant History

Significant commercial development of synthetic lubricants started in the early 1950s with the increased use of jet engine technology [35.2]. Jet engines must be lubricated properly in extremely high- and low-temperature regimes where mineral lubricants could not function adequately. Esters of various chemical structures were synthesized and evaluated. Initially, dibasic esters were used as base stocks. Later, polyol esters with superior thermal/oxidative stability, lubricity, and volatility were developed to meet even more stringent demands. These polyol esters are still in use today.

Another early application that demanded the use of synthetic lubricants came in the mid-1960s during oil drilling in Alaska where mineral oil lubricants solidified and could not function in the severe Alaskan

cold weather [35.1–3]. Initially, a synthetic lubricant based on an alkylbenzene base stock of excellent low-temperature flow properties was used in the field. This base stock was soon replaced by polyalphaolefins (PAO) base stock with better overall properties.

Research on PAO began at Mobil in early 1949 [35.4, 5]. The researchers recognized PAO's unique viscometric properties could be attained by proper selection of starting olefins and reaction conditions. In 1973, after many years of continuous improvements, Mobil Corporation introduced the first PAO-based synthetic automotive engine oil, Mobil SHC in Europe, followed by the fuel-saving Society of Automotive Engineers (SAE) 5W-20 Mobil 1 in the US. The product was a commercial success and subsequent generations of Mobil 1 continue to be the leading synthetic automotive crankcase lubricant today [35.6].

Since the early introduction of synthetic lubricants in automotive and industrial applications, many products from numerous companies followed. In 2011, the total synthetic lubricant consumption amounted to about 1.1 million metric tons/year, approximately 2.9% of the total lubricant volume [35.6]. Although the volume of synthetic lubricant is relatively small compared to conventional lubricants, synthetic lubricant represents about 10% of the total value of the global lube oil market. Furthermore, synthetic base stock is estimated to have grown by 3.5% per year from 2011 to 2016, much higher than conventional lubricant which is estimated to grow at less than 1% per year or remain flat [35.6]. In addition, the overall economic impact from synthetic lubricants is much larger than just the volume number alone, since synthetic lubricants improve energy efficiency, productivity, reliability, and reduce waste.

35.2 Overview of Synthetic Base Stocks

Of the total worldwide synthetic base stock volume, over 80% are represented by three classes of materials [35.7]:

- PAO (45%)
- Esters, including dibasic ester and polyol esters (29%)
- Polyalkyleneglycol (PAG) (13%).

Other smaller volume synthetic base stocks are alkylbenzenes, alkylnaphthalenes (ANs), polyisobutylenes, phosphate esters, and silicone fluids. With the exception of phosphate esters and silicones, all synthetic base stocks are made from basic petrochemicals including ethylene, propylene, butenes, higher olefins, benzene, toluene, xylenes, and naphthalene, as illustrated in Fig. 35.1.

As expected, the major producers of the synthetic base stocks PAO, esters, PIB (polyisobutylene), and alkylaromatics are integrated petroleum or petrochemical companies that also supply mineral oil base stocks and/or petrochemicals. PAG, phosphate esters, and silicone fluids are manufactured by chemical companies that produce these fluids on a much larger scale mainly for other applications. Their use as synthetic lubricant base stocks accounts for only a fraction of the total volume. Table 35.2 summarizes the major synthetic base stock producers [35.7].

Synthetic base stocks, being produced from well-defined chemical compounds by specific chemical processes, have higher raw material and processing cost and are generally more expensive than mineral oils. Table 35.2 lists the price of these synthetic base stocks relative to conventional Group I base stock [35.6].

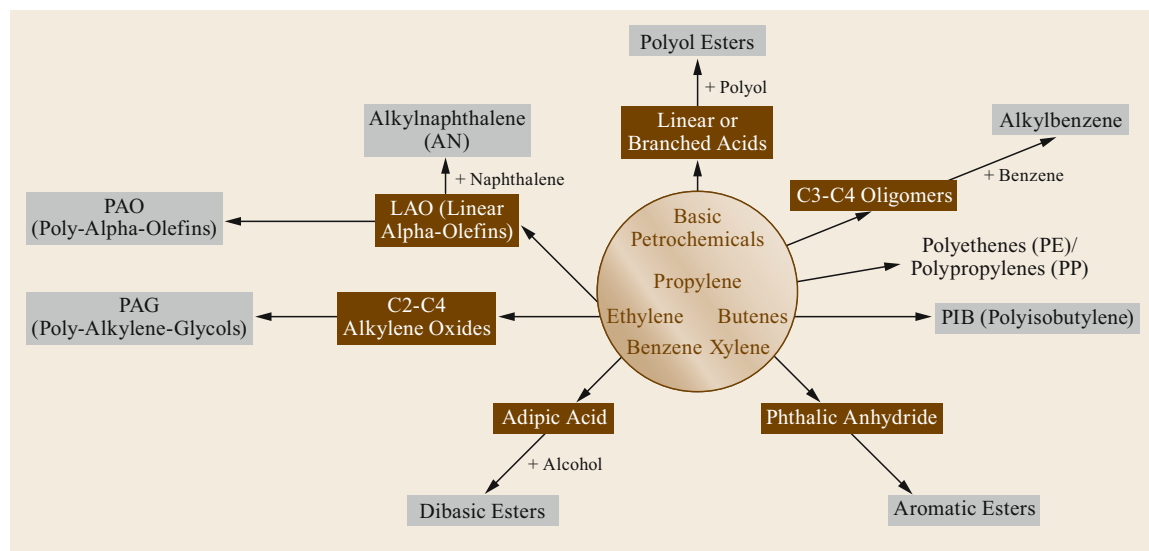


Fig. 35.1 Most synthetic base stocks are derived from petrochemicals

Table 35.2 Summary of major synthetic base stocks and producers

Synthetic base stock	Major manufacturers	Estimated relative price range ^a
PAO	Chemtura, Chevron Phillips Chemical Co., ExxonMobil Chemical Co., Idemitsu Petrochem., Ineos	2–4
Dibasic ester	Chemtura, Croda, ExxonMobil Chemical Co., Inolex Chemical Co.	2–6
Polyol ester	Chemtura, Croda, ExxonMobil Chemical Co., Inolex Chemical Co., Kao Corp.	2–6
PAG	BASF, Clariant, Dow Chemical Co.	2–3
Alkylaromatic	Chemtura, ExxonMobil Chemical Co., Huntsman LLC, King Industries, Inc., Pilot Chemical Co., Sasol North America Inc.	2–4
Polyisobutene (PIB)	INEOS, TPC group	1–3

^a Estimated relative price range (in dollars per kilogram) of synthetics versus low-viscosity Group I mineral oil in US

35.3 Synthetic Base Stock – Chemistry, Production Process, Properties, and Use

35.3.1 PAO

PAO is a class of base stock molecularly engineered to optimize viscosity index, pour point, volatility, oxidative stability, and other important lubricant base oil properties. PAO with viscosities of 2–150 cSt at 100 °C are currently produced and marketed commercially [35.8, 9]. The low viscosity PAO of 4–6 cSt account for more than 80% of the total PAO volume of 500 kta in 2010 [35.6]. The remaining are mainly medium to high viscosity fluids of 10–150 cSt.

Chemistry for PAO Synthesis

Historically, PAO is typically synthesized from 1-decene (Fig. 35.2). 1-Decene is produced from ethylene in an oligomerization process. This oligomerization process yields C_4 to C_{20} and higher linear alpha-olefins (LAO) according to the Schulz–Flory distribution [35.10]. 1-Decene is only one member of the many LAO products. Typically, 1-decene constitutes about 10–25% of the total LAO fraction, depending on the process technology. Recently, because of PAO's growth, 1-decene alone is not enough to meet demand. Other LAOs, especially mixtures of C_8 - and C_{12} -LAOs are also being used as starting materials for PAO synthesis.

In the typical PAO process, the linear 1-decene is polymerized using acidic Friedel–Crafts catalysts to give C_{20} , C_{30} , C_{40} , C_{50} , and higher olefin oligomers. Usually, C_{20} is too volatile for use as a high-performance base stock. It is removed by distillation or fractionation. The remaining fraction of C_{30} and

higher oligomers is further hydrogenated to convert the olefinic oligomers into fully saturated paraffinic hydrocarbons.

The degree of polymerization depends on the type of catalyst used and reaction conditions [35.11, 12]. Generally, BF_3 -type catalysts give a lower degree of polymerization. By careful choice of co-catalyst types and reaction conditions, the BF_3 process produces mostly oligomers of C_{30} to C_{50} range with fluid viscosities of 4–8 cSt. $AlCl_3$ -based catalysts are more suitable for the synthesis of higher viscosity PAO, 40–100 cSt because they produce oligomers with a higher amount of C_{60} , C_{70} and higher oligomers.

The choice of 1-decene as the starting material and the final base stock compositions were the results of extensive optimization. Early researchers at ExxonMobil systematically synthesized oligomers in the C_{30} to C_{40} range by BF_3 catalyst and compared their lubricant properties, as summarized in Table 35.3 [35.13].

These data show that the oligomers made from propylene, 1-hexene, and 1-octene have relatively low VI (70–106) and very high viscosity at -40 °C. This is because the oligomers have many short branches in the structures. Oligomers from 1-tetradecene have high VI but also have undesirable high pour points and are solid at -40 °C. Oligomers from 1-decene or mixtures of LAOs with an average branch length similar to 1-decene have the best combination of high VI, low pour points, and -40 °C viscosities.

Historically, the market dynamics of LAO supply and demand further drove the trend toward the use of 1-decene as a raw material [35.10]. Among all the ma-

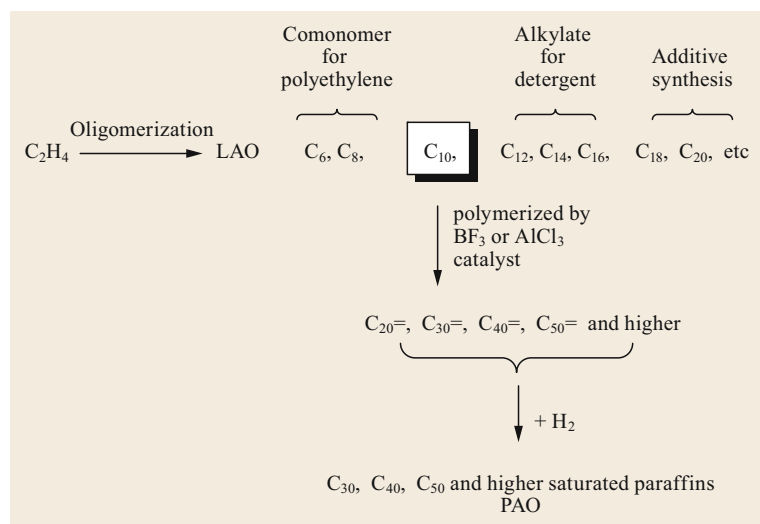


Fig. 35.2 Reaction scheme for converting ethylene into PAO

Table 35.3 Comparison of base stock properties for C₃₀–C₄₂ hydrocarbons made from different olefins

Name	Carbon number	Kinematic viscosity (cSt) at			Viscosity index	Pour point ^a (°C)
		100 °C	40 °C	–40 °C		
Propylene decamers	C ₃₀	7.3	62.3	> 99 000	70	–
Hexene pentamers	C ₃₀	3.8	18.1	7850	96	–
Octene tetramers	C ₃₂	4.1	20.0	4750	106	–75
Decene trimers	C ₃₀	3.7	15.6	2070	122	–78
Undecene trimers	C ₃₃	4.4	20.2	3350	131	< –55
Dodecene trimers	C ₃₆	5.1	24.3	13 300	144	–45
Decene tetramers	C ₄₀	5.7	29.0	7475	141	< –55
Octene pentamers	C ₄₀	5.6	30.9	10 225	124	–
Tetradecene trimers	C ₄₂	6.7	33.8	Solid	157	–20

^a By the ASTM D97 method

for LAO from the ethylene growth process (Fig. 35.2), C₆ and C₈ LAO were mainly used as co-monomer in the linear low-density polyethylene production; C₁₂ to C₁₆ LAO were mainly used in the production of linear alkylbenzene detergents; C₁₈ and C₂₀ LAO were used mainly in additive synthesis. 1-Decene was not in high demand for other chemical manufacturing. Its use as a raw material for synthetic base stocks made a perfect match. As PAO synthetic base stock grew, 1-decene supply became tight, and other LAO, such as C₈ and C₁₂, were successfully incorporated with 1-decene as the starting olefins for PAO production. Since 2001, the world's 1-decene supply has fluctuated with capacity as older plants have shut down and new technology has been developed to allow on-purpose production of specific LAOs such as 1-hexene, resulting in less side product LAOs [35.14, 15]. This fluctuation created uneven PAO growth rates, ranging from 3 to 7% per year, and sparked additional commercialization of mixed LAO base stocks [35.6]. Recent tight supply of LAO prompted the construction of new LAO facilities [35.6]. This new feed capacity is expected to sustain PAO growth.

The chemical composition of PAO from 1-decene is relatively simple. For example, a 4 cSt PAO is composed of ≈ 85% C₃₀ and ≈ 15% C₄₀ hydrocarbons. It has a narrow molecular weight distribution compared to typical 4 cSt mineral oils. The gas chromatogram in Fig. 35.3 shows that 4 cSt PAO has no low molecular weight components of less than C₃₀. In comparison, the mineral oil of same viscosity has many of these low molecular weight components which are highly volatile. They degrade oil volatility, flash and fire point. Therefore, PAOs outperform mineral oils by having low volatility and high flash or fire point.

Figure 35.3 also shows that the C₃₀ fraction of PAO is not a single compound but a mixture of many isomers. This is because the acidic BF₃ catalyst catalyzes the oligomerization reaction through a carbonium ion

intermediate which is well known to catalyze the isomerization of the double bonds, the backbone of the linear C₁₀ hydrocarbon chain, or the oligomer intermediates, thus, creating nonuniform connections between the monomers (Fig. 35.4). As a result, the PAO from the BF₃ process contains many isomers with different types of branching [35.16, 17]. This irregular branching is beneficial to imparting the very low pour point property for PAOs.

Manufacturing Process for PAO

Commercial production of PAO using a BF₃ or AlCl₃ catalyst generally involves a multistage, continuous stirred-tank reactor (CSTR) process [35.11, 12]. In early production technology, the catalyst was destroyed with diluted aqueous alkali after polymerization. More recent patents disclosed improved processes using BF₃ catalyst recycle to reduce catalyst usage, minimize process waste, and improve process economics [35.18].

Product Properties

The typical physical properties of some commercial PAO are summarized in Table 35.4 [35.8, 9]. PAO of different viscosity grades (VGs) and properties are available from different producers. Some PAO are produced with extra steps to meet specific performance criteria or to offer special performance advantages.

Comparison of PAO with Petroleum-Based Mineral Base Stocks

PAOs have different chemical compositions compared to mineral oil base stocks. The American Petroleum Institute (API) categorizes lubricant base stocks into five major categories, Group I to V, as shown in Table 35.1.

PAO is classified by itself as a Group IV base stock. Compared to Group I to III base stocks, PAO contains no naphthenes or aromatics, whereas Group I, II, and III base stocks contain different amounts of aromat-

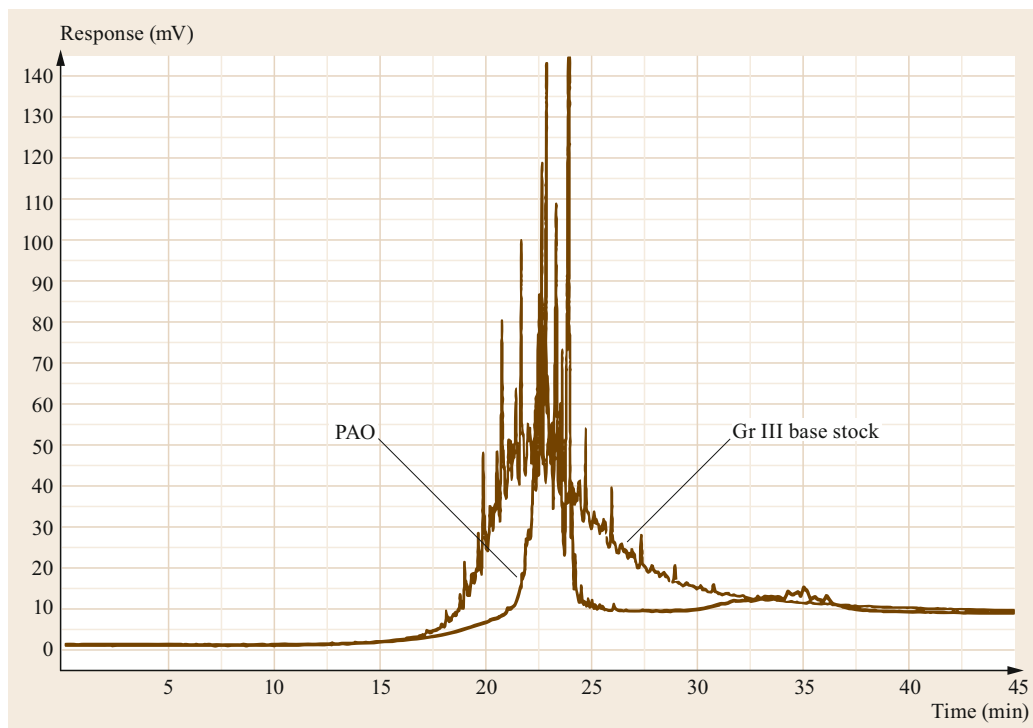


Fig. 35.3 Gas chromatograph comparison of a 4 cSt PAO with a 4 cSt Group III base stock

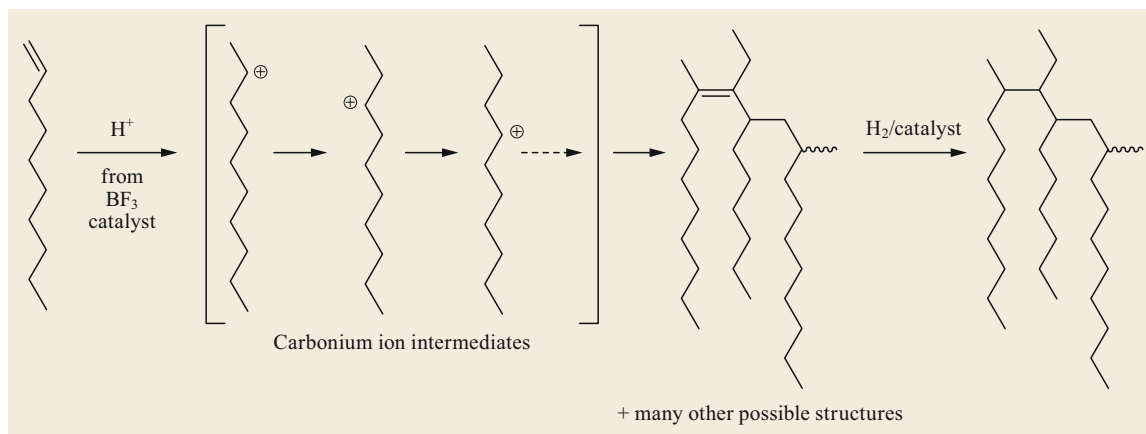


Fig. 35.4 Reaction chemistry responsible for the formation of many isomers in PAO synthesis using promoted BF_3 as the catalyst

ics ranging from < 1% to > 40% [35.19]. With the increasing presence of aromatics and/or naphthenes, oxidative stability and low-temperature properties of these fluids are typically degraded. Also, as shown earlier in Fig. 35.3, PAOs have discrete carbon numbers with relatively few low molecular weight fractions of lower than C_{30} hydrocarbons. In contrast, mineral base stocks contain significant amounts of these volatile, low molecular weight fractions. As a result, PAOs have lower volatility than mineral base stocks.

Table 35.5 compares the basic properties of low and high viscosity PAO versus Group I to Group III mineral oil base stocks. It is worth pointing out that the newer, next-generation PAOs have a wider range of viscosities and superior properties (see next section).

PAOs Have Superior Viscometric Properties Compared to Mineral Oil Base Stocks. Data in Table 35.5 show that PAO has higher VI and lower pour point than Group I and II base stocks. Compared to Group III

Table 35.4 General product properties of commercial PAO (courtesy of ExxonMobil Chemical Company)

Fluid type	2 cSt PAO	4 cSt PAO	6 cSt PAO	8 cSt PAO	10 cSt PAO	40 cSt PAO
Kinematic viscosity 100 °C (cSt)	1.7	4.1	5.8	8.0	10.0	39
Kinematic viscosity 40 °C (cSt)	5	19	31	48	66	396
Kinematic viscosity -40 °C (cSt)	262	2900	7800	19 000	39 000	–
Viscosity index	–	126	138	139	137	147
Pour point (°C)	-66	-66	-57	-48	-48	-36
Flash point (°C)	157	220	246	260	266	281
Specific gravity 15.6 °C	0.798	0.820	0.827	0.833	0.835	0.850

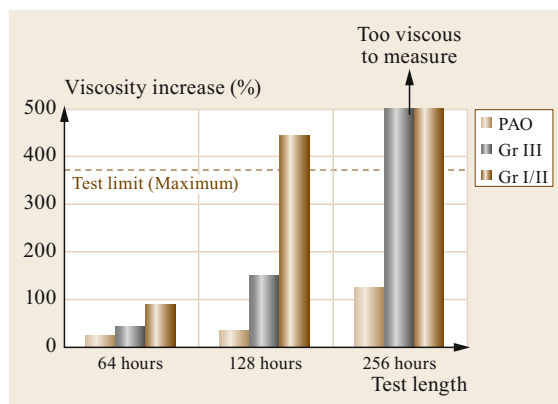
Table 35.5 Typical property comparison of PAO with Group I to III mineral oil

	Low viscosity				High viscosity		
	Group I	Group II	Group III	4 cSt PAO	Bright stock	40 cSt PAO	100 cSt PAO
Viscosity 100 °C (cSt)	3.8	4.6	4.1	4.1	30.5	39	100
Viscosity 40 °C (cSt)	18	23	19	19	470	396	1240
Viscosity index	92	117	127	126	94	140	170
Pour point (°C)	-18	-18	-15	-66	-18	-36	-30
Cold crank simulator -20 °C (cP)	–	–	750	620	–	–	–
Noack volatility (wt%), by ASTM D5800 method	32	15	14	< 12	–	–	–
Aniline point (°C), by ASTM D611 method	100	113	118	119	97	160	> 170

base stocks, PAO has comparable VI, but much lower pour point and improved low-temperature viscosity as measured by Cold Crank Simulator (CCS) viscosity at -20 °C. In the same engine oil formulation, this lower CCS viscosity observed with PAO results in a wider SAE cross-grade (5W-40) than with Group III base stock (10W-40) [35.20]. The lower low-temperature viscosity translates into better fuel economy during the engine warm-up period.

PAO Has Lower Volatility. Data in Table 35.5 show that PAO has lower volatility than Group I to III base stocks. This lower volatility is the result of the uniform molecular structure that is composed of branched paraffins with a narrow molecular weight distribution relatively free of low weight-average molecular weight (Mw) hydrocarbons of less than C₃₀ (Fig. 35.3). Low volatility is advantageous for decreased oil consumption and reduced emissions.

PAO Has Excellent Response to Antioxidant Additive Treatment, Resulting in Better Oxidative Stability than Mineral Oil Lubricants. It has been demonstrated that the un-formulated PAO base stock treated with 0.5 wt% antioxidant resists oxidation for more than 2500 min in a standard rotating pressure vessel oxidation test (RPVOT) per the ASTM D2272 method. In comparison, similarly treated Group II and III base stocks start to oxidize much earlier in less than 800 or 1700 min, respectively [35.21].

**Fig. 35.5** Comparison of viscosity increase in ASTM sequence IIIIE engine test for fully formulated lubricants based on PAO versus Group III or I/II base stocks (after [35.20])

This oxidative stability translates into performance advantages in actual engine oil tests (Fig. 35.5) [35.20].

Figure 35.5 shows that a fully formulated engine oil with PAO has a much lower viscosity increase than with Group III or with Group I/II base stocks in a standard length, 64 h, ASTM sequence IIIIE engine test. In an extended-length, 256 h test, the viscosity increase for the PAO-based lubricant is still much less than the maximum increase allowable for this test. In contrast, Group III- or Group I/II-based

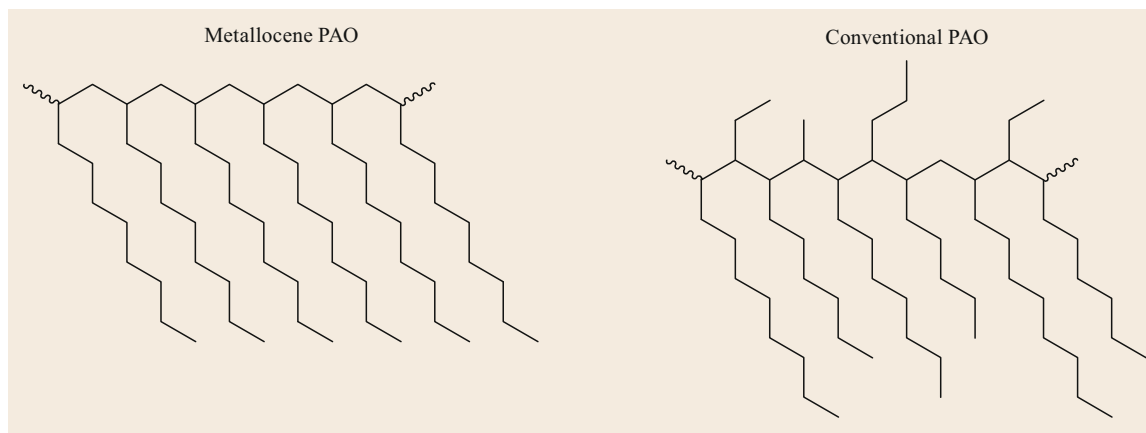


Fig. 35.6 Schematic representation of the molecular structures of mPAO versus conventional PAO made from 1-decene

engine lubricants become too viscous to measure. Because of this superior oxidative stability, PAO-based lubricants with performance advantages in fuel efficiency and oil consumption were reported in the literature [35.22].

PAOs Are Available in a Wide Viscosity Range. PAOs are available from 2 to 100 cSt at 100 °C. The high-viscosity PAOs maintain excellent VI and low pour point (Tables 35.4 and 35.5), in a manner that is superior to the highest viscosity mineral oil base stock – bright stock. High-viscosity PAOs are important as blend components with low-viscosity fluid to formulate high-viscosity-grade industrial oils. When used to blend with low-viscosity mineral oil, the high-viscosity PAO significantly improves the oxidative stability of the blended base stocks compared to using mineral bright stock [35.20].

PAOs Have High Aniline Point, Indicating Low Polarity. Table 35.5 shows that low-viscosity PAO has a higher aniline point than Group I mineral oils, 119 °C versus 100 °C. A more pronounced difference is observed for high-viscosity fluids (160 °C versus 97 °C). The higher aniline points of PAO mean that they are much less polar than Group I oils. Generally, lubricant additives and oil oxidation by-products are highly polar chemical species. They are not typically soluble in nonpolar fluids. As a result, additives and oxidation by-products have very poor solubility in PAO alone. To compensate for this, a polar co-base stock, such as ester or alkylnaphthalene, is usually added to the formulation to improve the solvency of PAO in a finished lubricant. These co-base stocks can also assist other performance features, such as seal compatibility and improved lubricity.

PAOs Possess Other Important Properties in Various Applications.

- Compatibility or miscibility with mineral oil at all concentration levels without phase separation or detrimental effects when cross-contamination occurs.
- Excellent hydrolytic stability.
- 10% higher thermal conductivity and heat capacity than comparable mineral oil, allowing equipment to run at lower temperature and improving wear performance [35.23, 24].
- Lower traction coefficients than conventional fluids, resulting in better energy efficiency for many industrial oil applications [35.8, 9].
- PAOs are nongreasy, have good skin feel, are non-irritant and noncomedogenic when used in the formulation of personal care products.

In summary, PAOs have superior VI, pour point, low-temperature viscosity, volatility, and oxidative stability and are available in a wider viscosity range compared to conventional Group I, II, or III mineral oils. Meanwhile, PAOs have poor solvency for additives due to their high hydrophobic/low polarity nature.

Recent Developments – SpectraSyn Elite – Next Generation PAO

Following the success of PAO, ExxonMobil Chemical Co. continues to develop new fluids with step-out performances [35.25–27]. In 2009, a new generation of PAO, SpectraSyn Elite was commercialized. SpectraSyn Elite is made from linear alpha-olefins using advanced metallocene catalyst technology, which produces polymers with a uniform, comb-like structure (Fig. 35.6). In contrast, conventional PAOs have short-chain branches due to the isomerizing nature of the

Table 35.6 Product properties of next-generation PAO – SpectraSyn Elite

Product	SpectraSyn Elite 65	SpectraSyn Elite 150
Kinematic viscosity 100 °C (cSt)	65	156
Kinematic viscosity 40 °C (cSt)	614	1705
Viscosity index	178	206
Pour point (°C)	−42	−33
Flash point (COC) (°C)	277	282
Specific gravity 15.6 °C	0.846	0.849

acidic catalysts, BF₃ or AlCl₃, used in their production processes (Fig. 35.4). The advanced metallocene catalyst technology enables production of high molecular weight PAOs with narrow molecular weight distribution. These structural differences are responsible for many of the properties and performance advantages for SpectraSyn Elite over other PAOs.

Table 35.6 summarizes the properties of commercial SpectraSyn Elite products [35.27]. Compared to conventional PAOs, SpectraSyn Elite mPAO have higher VI and lower pour points. They are available in higher viscosity ranges, up to 150 cSt. This unique class of fluid can be used in the formulation of automotive engine oil and industrial oil to provide improved shear stability, viscometric properties, and increased lubricant film thickness for better lubrication (see *Applications* below).

Overall, advantages for SpectraSyn Elite include:

- Wider viscosity range
- Improved shear stability for durability
- Higher viscosity index (VI) for low- and high-temperature performance
- Better low-temperature performance for increased flow in cold environments.

In addition to ExxonMobil Chemical Co., Chevron Phillips Chemical company introduced Synfluid high-viscosity mPAOs in the first quarter of 2011. The product is manufactured from a non-decene α -olefin feedstock (octene) using proprietary metallocene technology [35.6].

Applications

PAO is the workhorse base stock for most synthetic lubricants. Low viscosity PAO are used in high-performance synthetic automotive crankcase and gear lubricants, industrial oils and greases. High-viscosity PAOs have found great utility in high-performance industrial oils and greases. Both low- and high-viscosity PAOs are expected to grow at much higher rates than mineral oil base stocks in the future [35.6, 14, 15].

Synthetic Automotive Engine Lubricants. These consume the largest volume, \approx 50%, of all PAOs [35.6, 28–31]. They are typically formulated with 4–6 cSt PAO, ester or alkylated naphthalene and a balanced amount of additives such as antioxidants, antiwear additives, dispersants etc. Because of the choice of superior base stocks, the PAO-based synthetic engine lubricants have many performance advantages over mineral oil-based engine lubricants. These advantages are well documented in scientific and trade literature [35.28–31]. They include:

- Improved engine wear protection and durability
- Extended oil drain interval – less waste oil and reduced maintenance
- Improved fuel economy
- Better oil stability and hardware protection at high temperature
- Excellent cold-starting properties, low-temperature fluidity and pumpability – better low-temperature protection
- Better protection for the emission system due to low phosphorous and sulfur levels.

Many of these performance advantages are directly attributable to the intrinsically superior properties of PAO, such as high VI, low pour point, low-temperature fluidity, high oxidative stability, low volatility, and better lubricity.

The advantage of using synthetic engine oil is further supported by the fact that many automakers use synthetic lubricant as the *factory fill* lubricant for their high-performance cars. For example, in 2013, Mobil 1 synthetic engine oils were used as factory-fill lubricants for certain models of Corvette, Porsche, Mercedes-Benz, Nissan GT-R etc. [35.32].

PAO blended with mineral base stocks are also used in many partial synthetic lubricant formulations. In this case, PAOs are used as blending stocks to improve the volatility, high- or low-temperature viscosity, and oxidative stability etc. of the mineral base stocks.

Synthetic Industrial Lubricants and Greases. Synthetic industrial lubricants and greases formulated with PAOs are available in wider viscosity grades with improved performance because PAO base stocks are available in high viscosities with higher VI and lower pour point. For example, 150 cSt SpectraSyn Elite has 206 VI and a −33 °C pour point. In contrast, the highest mineral base stock is 40 cSt with 98 VI and a −18 °C pour point, which imposes limits on possible high-viscosity products or wide cross-grade products. Synthetic industrial lubricants have many documented performance and economic advantages over conventional lubricants [35.7, 33, 34]. For example, PAO-based in-

dustrial gear/circulation lubricants offer the following documented advantages:

- Energy savings, longer fatigue life, and lowered temperatures of operation due to lower traction coefficients
- Wider operating temperature range due to higher VI and better thermal-oxidative stability
- Reduced equipment down-time, reduced maintenance requirements, and longer oil life due to the excellent stability of PAO base stock.

When used as compressor lubricants, PAO-based lubricants have advantages due to their better chemical inertness and resistance to chemical attack. Some synthetic compressor oils are used in corrosive chemical environments, for example, in sulfuric acid or nitric acid plants. PAO-based lubricants are also used in refrigeration compressor applications due to their excellent low-temperature fluidity, lubricity, and generally wider operating temperature range.

When used in stationary gas turbines or wind turbines, PAO-based lubricants offer superior low-temperature performance and lubricant stability [35.25]. These performance features significantly increase the service life for these expensive turbines, and reduce equipment downtime and maintenance. PAO base stocks are approved for incidental food contact. When PAO-based synthetic lubricants are used in the gears of food-processing equipment, the lubricants provide excellent wear protection, extended service life, and reduced maintenance. Synthetic greases based upon PAOs are used in industrial equipment, aviation and automotive applications that take advantage of the wide operating temperature range, high degree of

stability, and other desirable properties and features offered by PAO base stocks.

The newer PAOs like SpectraSyn Elite 65 and 150 base stocks offer even more performance advantages. They are particularly suited for industrial lubricants requiring high stability under severe operating conditions. For example, when formulated into industrial gear lubricants of ISO viscosity grade (VG) 320, the lubricants based on SpectraSyn Elite 65 and 150 have significantly higher VI than the lubricant based on current PAO, SpectraSyn 100 (Fig. 35.7) [35.27]. Higher VI lubricants offer increased protection at high temperature while maintaining required performance level at low temperature. In another example, Fig. 35.8 shows that an ISO VG 460 circulating lubricant formulated with SpectraSyn Elite has much lower Brookfield viscosity at 0 °F (≈ -18 °C) and -20 °F (≈ -30 °C) than the similar lubricant based on PAO 100 [35.27]. This lower low-temperature viscosity is indicative of better lubrication function at low temperature or better energy efficiency. In addition, the new PAOs offer other advantages including outstanding shear stability and greater formulation flexibility.

PAO has found its way into personal care products such as shampoos, conditioners, and skin lotions because PAO provides emolliency, good skin feel, and is nongreasy and noncomedogenic. It is also used in off-shore drilling fluids because of its good lubricity. New applications for PAO are continuously emerging.

35.3.2 Dibasic, Phthalate, and Polyol Esters – Preparation, Properties, and Applications

Lard and vegetable oil, both ester-type compounds derived from natural sources, have been used as lubricants

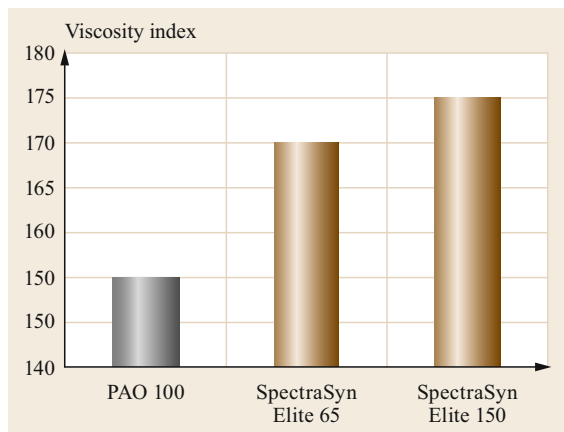


Fig. 35.7 Comparison of viscosity index of ISO VG 320 industrial gear lubricants based on SpectraSyn Elite 65 or 150 versus PAO 100

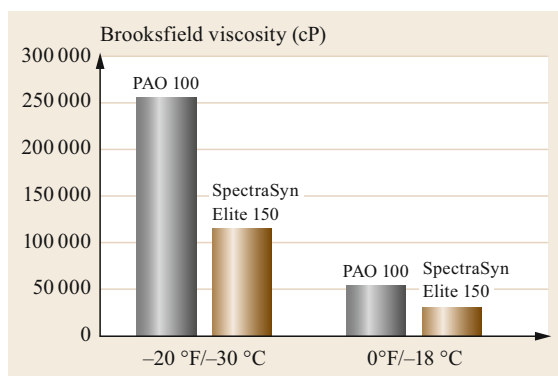


Fig. 35.8 Comparison of low-temperature Brookfield viscosity of ISO VG 460 circulating lubricant formulated with SpectraSyn Elite 65 or 150 versus conventional PAO 100

Table 35.7 Basic properties of ester base stocks

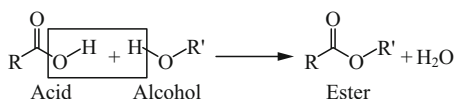
Acid	Alcohol	Viscosity (cSt)		VI	Pour point (°C)	Noack volatility ^a (wt%)	Biodegradability ^b
		100 °C	40 °C				
Dibasic ester							
Adipate	<i>iso</i> -C ₁₃ H ₂₇	5.4	27	139	-51	4.8	92
Sebacate	<i>iso</i> -C ₁₃ H ₂₇	6.7	36.7	141	-52	3.7	80
Polyol ester							
<i>n</i> -C ₈ /C ₁₀	PE ^c	5.9	30	145	-4	0.9	100
<i>n</i> -C ₅ /C ₇ / <i>iso</i> -C ₉	PE	5.9	33.7	110	-46	2.2	69
<i>n</i> -C ₈ /C ₁₀	TMP ^c	4.5	20.4	137	-43	2.9	96
<i>iso</i> -C ₉	TMP	7.2	51.7	98	-32	6.7	7
<i>n</i> -C ₉	NPG ^c	2.6	8.6	145	-55	31.2	97
Di- and mono-acids	NPG	7.7	40.9	160	-42	-	98
Aromatic esters							
Phthalate	<i>iso</i> -C ₁₃ H ₂₇	8.2	80.5	56	-43	2.6	46
Phthalate	<i>iso</i> -C ₉	5.3	38.5	50	-44	11.7	53
Trimellitate	<i>iso</i> -C ₁₃ H ₂₇	20.4	305	76	-9	1.6	9
Trimellitate	C ₇ /C ₉	7.3	48.8	108	-45	0.9	69

^a By ASTM D5800 method, ^b By CEC-L-33-A-96 test, % degradable in 21 days ^c PE: pentaerythritol, TMP: trimethylolpropane, NPG: neopentylglycol

throughout human history. After World War II, thousands of synthetic esters were prepared and evaluated as lubricant base stocks for jet engine lubricants [35.2].

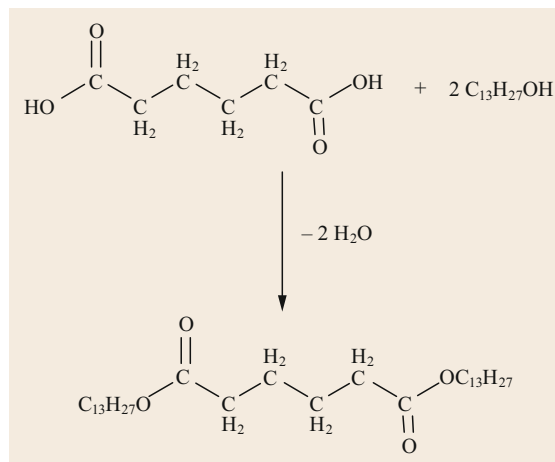
General Chemistry and Process

Esters are made by reacting carboxylic acids with alcohols with elimination of water, as shown by the following equation



The reaction proceeds by heating the mixture to 150 °C or higher with or without a catalyst [35.11, 12]. Catalysts such as *p*-toluenesulfonic acid or titanium (IV) isopropoxide, are typically used to accelerate reaction rates. The reaction is driven to completion by continuous removal of water from the reaction medium. Sometimes, one component is used in a slight excess to ensure complete conversion. The final product is purified over an adsorbent to remove trace water, catalyst and residual acids and alcohols, all of which are detrimental to base stock quality. Commercially, esters are generally produced by batch processes.

The choice of acid and alcohol determines the ester molecular weights, viscometric and low-temperature properties, volatility, lubricity, as well as the thermal, oxidative and hydrolytic stabilities [35.35–39]. The structure-property relationships of ester base stocks are

**Fig. 35.9** Synthesis of adipate ester

well documented in the literature. Compared to PAO and mineral oil, ester fluids have a higher degree of polarity, contributing to the following unique properties:

- Superior additive solvency and sludge dispersancy
- Excellent lubricity
- Excellent biodegradability
- Good thermal stability.

Three classes of esters are most often used as synthetic base stocks – dibasic ester, polyol ester, and aromatic ester. Some basic properties of these esters are summarized in Table 35.7.

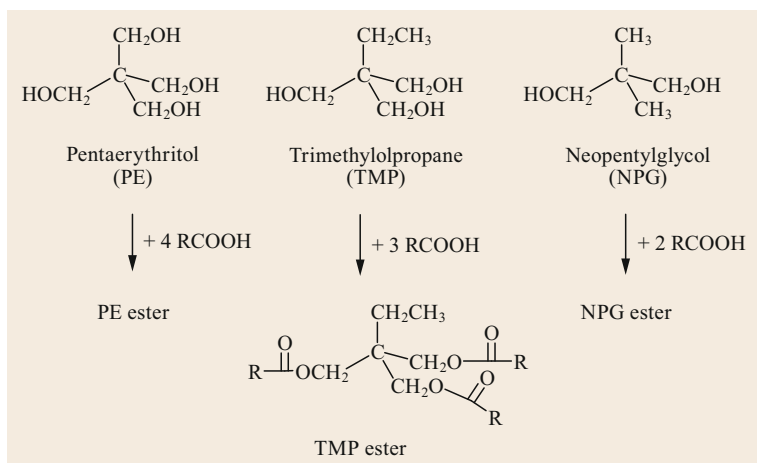
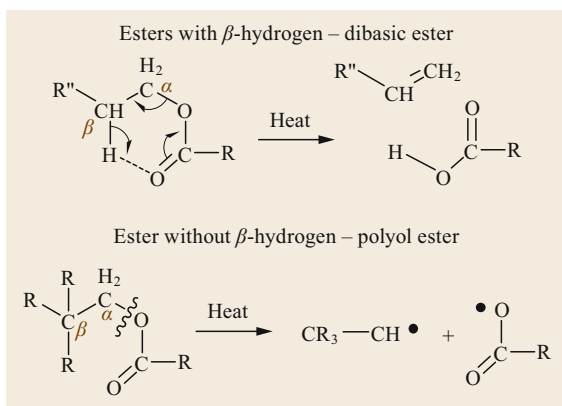


Fig. 35.10 Synthesis of polyol esters

Fig. 35.11 Cracking reaction mechanism for esters - β -H effect

Dibasic Esters

Dibasic esters are made from carboxylic diacids and alcohols. Adipic acid (hexanedioic acid) is the most commonly used diacid (Fig. 35.9). Because it is linear, adipic acid is usually combined with branched alcohols, such as 2-ethylhexanol or isotridecanols ($\text{C}_{13}\text{H}_{27}\text{OH}$) to give esters with balanced VI and low-temperature properties (Fig. 35.9). Dibasic ester is most often used as a co-base stock with PAO to improve solvency and seal swell properties of the final lubricants.

Polyol Esters

The most common polyols used to produce synthetic polyol ester base stocks are pentaerythritol (PE), trimethylolpropane (TMP) and neopentylglycol (NPG), (Fig. 35.10). By carefully choosing the degree of branching and size of the acid functions, polyol esters with excellent viscometric properties – high VI and very low pour points – can be produced (Table 35.7).

In addition to excellent viscometric properties, polyol esters have the best thermal resistance to cracking. This is because polyols lack β -hydrogen(s) adjacent to the carbonyl oxygen and thus cannot undergo the same facile β -H transfer reaction as the dibasic esters (Fig. 35.11) [35.35]. This cracking by β -H transfer leads to two neutral molecules and is a relatively low-energy process. Polyol esters can only be cracked by C–O or C–C bond cleavage, leaving two free radicals – a very high-energy process requiring extremely high temperature. Therefore, polyol esters are thermally stable up to 250 °C.

Among the three polyol ester types, the thermal stability ranking is

PE esters > TMP esters > NPG esters .

Aromatic Esters

Phthalic anhydride or trimellitic anhydride is converted into esters by reactions with alcohols as shown in Fig. 35.12. Phthalic anhydride is produced cheaply and in large volume from oxidation of *ortho*-xylene. The largest use of phthalate esters is in the plasticizer market. Only a small fraction of its production is consumed by the synthetic lubricants market. Phthalate esters generally have superior hydrolytic stability than adipic esters because the *ortho* di-ester groups are electronically less available and sterically more hindered [35.40]. However, they have lower VIs, 50–70, because of their high polarity and the presence of branched alcohol chains. They are used in special industrial oil applications where VI is not a critical parameter. Trimellitate esters are specialty products and relatively expensive. They are of high viscosity and usually are more resistant to oxidation than adipic esters.

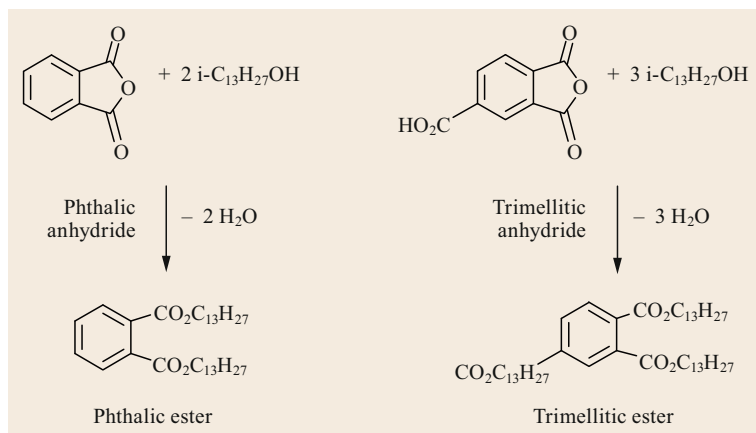


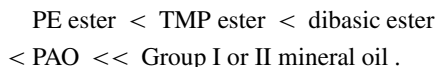
Fig. 35.12 Synthesis of phthalate and trimellitate esters

General Properties and Applications of Ester Fluids

Solvency and Dispersancy. Ester fluids are quite polar due to their high oxygen contents. They have high solubility for many commonly used additives. They also have high solubility for the polar acids and sludges generated by oxidation processes during service. This property makes ester-based lubricants *clean* compared to hydrocarbon-based lubricants, because of their better dispersancy and less sludge accumulation. Typically, low-viscosity ester fluids are soluble with nonpolar PAO base stocks. These properties make them excellent for use as co-base stocks with PAO in many synthetic automotive and industrial lubricants. Generally, 5–25% esters are used with PAO in finished lubricant formulations.

Hydrolytic Stability [35.40]. Hydrolysis of esters to give acids and alcohols is a facile reaction and can proceed at elevated temperatures in the presence of water. Hydrolysis of ester generates acid that can be very corrosive to metal components and can catalyze the base stock decomposition process. Therefore, hydrolytic stability of esters is an important issue. Much work has been carried out to improve the hydrolytic stability by varying the composition of acids and alcohols. Generally, esters made from aromatic acids or from more sterically hindered acids, such as 2-alkyl substituted acids or neo-acids, have improved hydrolytic stabilities. Proper branching of the acids protects the carbonyl ester function from the detrimental attack of water. The presence of an impurity, such as trace acid or metal, can catalyze the decomposition and hydrolysis of ester. Compared to PAO or alkylaromatic base stocks, ester hydrolysis is always an issue of concern in many lubrication applications.

Volatility. Ester fluids generally have lower volatility compared to PAO and mineral oil of comparable viscosities. A wt% volatility ranking for base stocks is as follows,



Lubricity. Polar ester fluids show mild boundary film protection at lower temperature. At lower temperature, esters interact with the metal surface via polar interaction, forming a chemisorbed surface film, which can provide better lubrication than the less polar mineral oil or nonpolar PAO. When esters decompose, they produce acids and alcohols. Higher molecular weight acids, can bind with the metal surfaces to form a film that can offer some degree of wear protection and friction reduction. However, none of these interactions are strong enough to persist when surface or oil temperature rises much above 100°C . At higher temperature, significant wear protection can only be achieved by the use of anti-wear or extreme-pressure (EP) additives. A drawback of the ester's high polarity is that esters can compete with a metal surface for polar additives, resulting in less efficient usage of anti-wear and EP additives. Therefore, in formulations using esters, it is important to choose the proper additives and concentration levels to obtain the full benefit of the lubricity from both the additives and esters.

Biodegradability. By carefully choosing the molecular compositions, esters of excellent biodegradability can be produced. Generally, esters from more linear acids and alcohols have better biodegradability [35.39].

Applications [35.41]. Esters, both dibasic and polyol esters, are used as co-base stocks with PAO or other

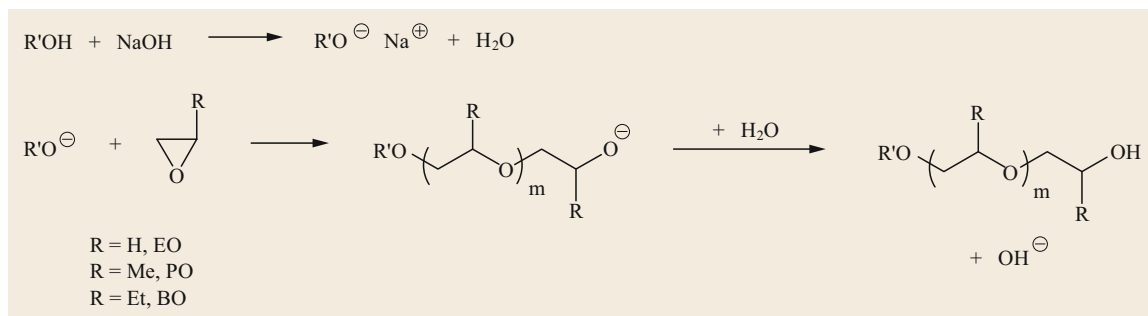


Fig. 35.13 Reaction scheme for PAG synthesis

hydrocarbon base stocks in synthetic automotive engine lubricants and industrial lubricants. Polyol esters are used in aircraft turbine oils due to their excellent thermal and oxidative stabilities, good lubricity, high VI, and excellent low-temperature properties ($< -40^{\circ}\text{C}$) [35.29]. Esters are also used in synthetic compressor oils for ozone-friendly refrigeration units. Because of their high biodegradability and low toxicity, esters are often the base oils of choice for many environmentally friendly lubricants or single-pass lubrication applications where ecological impact is critical [35.41].

Although ester chemistry has been studied extensively, new esters with unique performance improvements have continuously been reported in the literature [35.42, 43]. For example, esters with high stability were made from highly branched acids and polyols. Polyol esters formulated with ashless additives can be used as high-performance biodegradable hydraulic fluids.

35.3.3 Polyalkylene Glycols (PAG)

PAG is an important class of industrial chemicals. Its major use is in making polyurethanes. Outside of polyurethane applications, about 20% of the PAG is used in lubricant applications. Compared to PAO or esters, PAGs have very high oxygen content and hydroxyl end group(s). These unique chemical features give them high water solubility, high polarity, and excellent lubricity. PAG was first developed as fire-resistant, water-based hydraulic lubricants during World War II for military use [35.44]. Other applications such as textile lubricants, metal-working fluids etc. were developed subsequently to take advantage of their unique properties.

Chemistry and Process

PAGs are synthesized by oligomerization of alkylene oxides over a base catalyst with an initiator $R'OH$ (Fig. 35.13) [35.45]. When the initiator is water ($R' =$

H), the final PAG has two hydroxyl end groups. When the initiator is an alcohol ($R =$ alkyl group), one of the end groups is an alkoxy group (RO^{\ominus}). The most commonly used alcohol is *n*-butanol, although large alcohols have also been used for special applications. Phenol, thiols, or thiophenol are also used as initiators.

Ethylene oxide (EO), propylene oxide (PO), butylene oxides (BO), or combinations of these epoxides are used as starting materials for PAG syntheses. Longer chain alkylene oxides, such as butane oxide, hexene oxide or octene oxide, can be added to improve their compatibility with hydrocarbons. PAG with a wide range of viscosities, VIs, pour points, water solubilities and oil-compatibilities are produced by choosing the proper initiators, monomers, reaction conditions, and post treatments. The reaction is highly exothermic (22.6 kcal/mole) and heat removal is important to avoid side-reactions or broadening of the product molecular weight distribution.

Product Properties

Table 35.8 summarizes the typical lubricant properties of selected PAG produced from EO, PO, and BO with several different initiators [35.46].

EO-based fluids are typically waxy and have poor low-temperature properties. They have high water miscibility and are typically used to formulate water-based lubricants, especially fire-resistant hydraulic oil.

PO-based fluids are excellent lubricant base stocks with high VI and low pour point. They have lower solubility in water than EO-based fluids but are not oil miscible.

EO/PO-based fluids have a better combination of VI and low pour points than PO-based products. They are used as base stocks in industrial circulation/gear oils.

Pure BO-based PAG have improved oil solubility and are not less water-soluble. Recently, a wide range of oil-soluble PAG (OSP) base stocks have become available by co-polymerizing PO and BO [35.47].

Table 35.8 Lube properties of PAG fluids from EO, PO, and BO with different initiators

	AO type	End group	Average MW	KV _{100 °C} (cSt)	KV _{40 °C} (cSt)	VI	Pour point (°C)	Density (g/cm ³)	Solubility in oil ^a	Solubility in water ^a
E300	EO	OH/OH	300	5.9	36	1 [35.25]	-10	1.125	i	s
E600	EO	OH/OH	600	11.0	72	154	22	1.126	i	s
P425	PO	OH/OH	425	4.6	33	26	-45	1.007	-	-
P1200	PO	OH/OH	1200	13.5	91	161	-40	1.007	-	i
PB200	PO	Bu/OH	910	8.3	44	180	-48	0.9831	-	i
EP530	EO/PO	OH/OH	2000	25	168	192	-32	1.017	-	-
EPB100	EO/PO	Bu/OH	-	4.8	101	174	-57	1.0127	-	s
EPB260	EO/PO	Bu/OH	-	11.0	56.1	210	-37	1.0359	-	s
B100-500	BO	OH/OH	500	5.1	44.3	3	-30	0.975	s	s
B100-2000	BO	OH/OH	2000	24.7	234.7	142	-26	0.970	s	i
1500 MW poly BO Mono-ol	BO	Bu/OH	1500	15.8	117.1	153	-30	0.961	s	i

^a i = insoluble, s = soluble

Table 35.9 Lubricating properties of selected PAG fluids

Fluid type	Mol. Wt.	V100 °C (cSt)	V40 °C (cSt)	VI	Pour point (°C)	Four ball wear scar (mm) ^a	Four ball seizure load (kg) ^a	Friction coefficient ^b	Soluble in ^c
EO/PO	500	4.6	19	161	-46	0.53	120–140	0.15	Water
EO/PO	1300	15	76.0	218	-42	0.44	180–200	0.11	Water
PO	700	6.0	27	179	-44	0.53	160–180	0.19	Oil ^d
PO	1300	14.0	73	193	-35	0.57	120–140	0.12	None

^a By DIN 51 350 method, ^b Determined by oscillation of a steel ball on a steel disc at 30 °C under a load of 200 N, ^c Determined by mixing equal proportions of water and PAG or oil and PAG, ^d Partially soluble in oil

PAGs generally have excellent lubricity and low friction coefficients compared to mineral oil as shown in Table 35.9 [35.46, 48]. These properties result from the facile surface chemisorption of the oxygenate functions or through hydrogen bonding of the terminal OH groups with the metal surface.

Other unique properties for PAG include:

- Superior solvency – they dissolve additives, decomposition products, and sludges.
- Nonvarnishing and low ash – they leave little or no residue or carbon black upon decomposition.

Application

The major use of PAG is in industrial lube applications [35.48]:

- Fire-resistant hydraulic fluids. Water-soluble PAGs have fire resistancy, low toxicity, and excellent lubricity and anti-wear properties.
- Textile oils. PAG are nonvarnishing, nonstaining, and can be washed away with water.
- Compressor and refrigeration oils. Low solubility of many industrial gases, such as natural gas and ethylene, makes PAG suitable for gas compressor

applications. PAGs are compatible with new refrigerants (HFC-143a) and have excellent anti-wear properties.

- Metal working fluids. Some of the PAGs are nonvarnishing, have excellent lubricity, and anti-wear properties.
- Circulation/bearing/gear oil. Low friction coefficients and traction properties of PAG lead to lower operating temperature and energy consumption. They have good anti-wear properties and are low to nonvarnishing.

35.3.4 Other Synthetic Base Stocks

Polyisobutylene (PIB) fluids are produced by the oligomerization of isobutylene in a mixed C₄ stream over a BF₃ or AlCl₃ catalyst. PIBs are seldom used by themselves. They are typically used as blend stocks or as additives to increase lubricant viscosity. Table 35.10 summarizes the typical properties of selected PIB fluids [35.51]. The VI and pour points of PIBs are comparable to those of conventional mineral oil. PIBs usually have a lower flash point and decompose easily into monomer at 200 °C and higher. The advantages of PIB

Table 35.10 Typical physical properties of Indopol polyisobutylenes (PIB) available from Ineos (after [35.49, 50])

	H-25	H-50	H-100	H-300	H-1500
Kinematic viscosity 100 °C (cSt)	50	100	200	605	3000
Viscosity index	87	98	121	173	250
Pour point (°C)	−23	−13	−7	3	18
Bromine number ^a	27	20	16.5	12	8
Flash point ^b (°C)	171	193	232	274	307
Molecular weight ^c	635	800	910	1300	2200

^a By IP 129/87 method, ^b By Cleveland open cup ASTM D92 method, ^c By gel permeation chromatography

Table 35.11 Properties of alkylbenzene and alkylnaphthalenes base stocks

Fluid type Commercial source	Di-alkyl-benzene V-9050 from Vista Chem. Co	Di-alkyl-benzene Zero 150 from Chevron	Alkylnaphthalene Synesstic 5 from Exxon- Mobil Chem. Co.	Alkylnaphthalene Synesstic 12 from Exxon- Mobil Chem. Co.
Kinematic viscosity 100 °C (cSt)	4.3	4.4	4.7	12.4
Kinematic viscosity 100 °C (cSt)	22.0	33.5	28.6	109
Viscosity index	100	25	74	105
Pour point (°C)	−60	−40	−39	−36
Flash point (°C)	215	170	222	258
Aniline point ^a (°C)	78	–	33	90

^a By ASTM D611 method

are their high compatibility with most synthetic or mineral base stocks and their relatively low cost compared to other synthetic base stocks.

Alkylated aromatic base stocks include alkylbenzene and alkylnaphthalene. They are produced by the alkylation of benzene or naphthalene with olefins using Friedel–Crafts alkylation catalysts [35.49, 50]. Their typical properties are summarized in Table 35.11.

One unique feature of these alkylaromatic fluids is their very low pour points. Alkylbenzene was the first synthetic hydrocarbon used for engine lubricants in Alaska's oil production in the early 1960s because of its superior flow property at extremely low temperatures when mineral-based lubricants were frozen solid. Alkylbenzenes are mentioned in the patent literature as components for chlorofluorocarbon (CFC) or hydrochlorofluorocarbon (HCFC) refrigeration compressor oil. However, today, there is no reliable commercial supplier for alkylbenzene and it is rarely used in synthetic lubricant formulation.

In contrast to alkylbenzene, alkylnaphthalene (AN) is increasingly becoming an important class of polar synthetic base stock because of its many superior properties, especially its superior thermal, oxidative and hydrolytic stability [35.52]. Because of these outstanding stabilities, AN significantly improves lubricant service life and performance level when used to replace ester in the formulations of fully synthetic automotive engine lubricants or industrial lubricants. Figure 35.14 shows

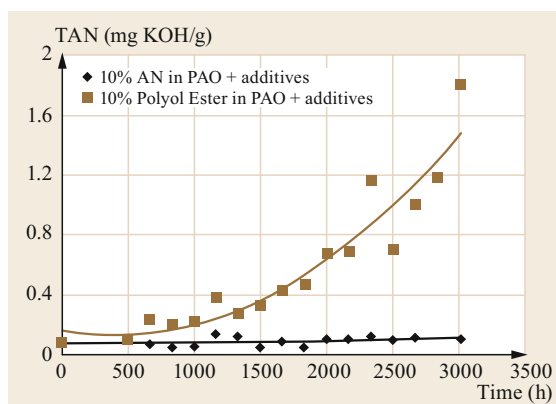


Fig. 35.14 Turbine lubricant formulated with 10% AN has much better stability than similar lubricant formulated with 10% polyol ester in an oxidative stability test (ASTM D943 method)

the results from an oxidative stability test (ASTM 943 method) (or turbine oil stability test, TOST). In this test, the oil sample is heated at 95 °C with oxygen in the presence of water and an iron-copper catalyst. The amount of oil degradation can be monitored by periodically measuring the total acid number (TAN). This graph shows that an industrial turbine lubricant containing 10% AN has no change in acid number throughout the test duration of 3000 h. In contrast, lubricant containing 10% polyol ester suffers significant degradation

with increasing total acid number after 1000 h of the test.

Phosphate esters are produced from phosphorus oxychloride with various alcohols or phenols, or combinations of these hydroxyl compounds [35.53]. These fluids generally have good thermal and oxidative sta-

bilities and fire-resistancy. However, because of their high polarity, poor VI-pour point balance, facile hydrolysis [35.54], and inferior elastomer and paint compatibility, their use in general lubrication is limited. The major use for phosphate esters is in fire-resistant hydraulic oils.

35.4 Conclusion

Finished synthetic lubricants have significantly raised the performance level of automotive and industrial lubricants with the help of high-quality synthetic base stocks and high-performance additive technologies. Equipment builders, industrial users, and general consumers have benefited from the enhanced performances of synthetic lubricants such as reduced maintenance and waste, lower emissions and pollution, higher reliability and efficiency. As a result, finished synthetic lubricant is projected to grow at 4% per year by volume from 2013 to 2023 [35.55], a range considerably greater than for conventional lubricants. Although part of this growth is based on the availability of high-quality Group II or Group III base stocks which are also used to formulate finished synthetic lubricants, a significant part of this growth is based on synthetic base stocks described in this chapter. From 2011 to 2016, the worldwide demand for all synthetic base stocks was projected

to grow at 3.5% annually [35.28–31]. The growth for PAO base stocks may be slowed temporarily due to competition from Group II or III base stocks or from gas-to-liquid base stocks. Recently, high-performance PAO base stocks were projected to grow at 7% annually through 2020 due to their well-documented advantages such as greater efficiency, reduced maintenance, lower emissions, and longer service life and wider viscosity range [35.14]. Further into the future, to meet the escalating performance demand of new equipment, lubricant industry leaders are expected to respond by developing and marketing next-generation, high-performance base stocks and lubricants.

Acknowledgments. The authors would like to thank Alex Lee, Bruce Harrington, Kathy Cooper, Angela Galiano-Roth, and Wenning Han for their valuable comments on this chapter.

References

- 35.1 J. Synthetic Lubr. **18**(4), 265–266 (2002)
- 35.2 G.J. Bishop: Aviation turbine lubricant development, *J. Synthetic Lubr.* **4**(1), 25 (1987)
- 35.3 E.A. Harlacher, R.A. Krenowics, C.R. Putnick: Alkylbenzene based lubricants, 86th AIChE Natl. Meet., Houston (1979)
- 35.4 W.E. Garwood: Synthetic lubricant, US Patent (Application) 2 937 129 (1960)
- 35.5 L.A. Hamilton, F.M. Seger: Polymerized olefins synthetic lubricants, US Patent (Application) 3 149 178 (1964)
- 35.6 M. Yoneyama, M. Hackett, S. Müller, V. Yang: *IHS Specialty Chemical Update Program Report Synthetic Lubricants* (IHS, London 2012)
- 35.7 W.R. Murphy, D.A. Blain, A.S. Galiano-Roth, P.A. Galvin: Synthetic basics – benefits of synthetic lubricants in industrial applications, *J. Synthetic Lubr.* **18**(4), 301 (2002)
- 35.8 ExxonMobil Chemical Synthetics: <http://www.exxonmobilsynthetics.com>
- 35.9 S. Reid-Peters: Group IV base stocks – PAO, UTS Semin. St Petersburg (2011)
- 35.10 G.R. Lappin: Routes to alpha olefins. In: *Alpha-Olefins Application Handbook*, ed. by G.R. Lappin, J.D. Sauer (Marcel Dekker, New York 1989) p. 35
- 35.11 M. Sacks: A Private Report of IHS Process Economic Program, Report no. 125, Synthetic Lubricant Base Stocks (1979)
- 35.12 R.E. Bolan: A Private Report of HIS Process Economic Program, Report no. 125A, Synthetic Lubricant Base Stocks (1989)
- 35.13 J.A. Brennan: Wide-temperature range synthetic hydrocarbons fluids, *Ind. Eng. Chem. Prod. Res. Dev.* **19**, 2–6 (1980)
- 35.14 B. Kamchev: Pace quickens for pao, Lubes-N-Greases (February), 28–32 (2013)
- 35.15 Strong demand for synthetic lubricants lead to increased investment in LAO production, *Industrial Lubr. Tribol.* **54**(1), 32 (2002)
- 35.16 A. Onopchenko, B.L. Cupples, N. Kresge: Boron fluoride-catalyzed oligomerization of alkenes: Structures, mechanisms, and properties, *Ind. Eng. Chem. Prod. Res. Dev.* **22**, 182 (1983)
- 35.17 R.L. Shubkin, M.S. Baylerian, A.R. Maler: Olefin oligomer synthetic lubricants: Structure and mech-

- anism of formation, Ind. Eng. Chem. Prod. Res. Dev. **19**, 15–19 (1980)
- 35.18 K.D. Hope, T.C. Ho, D.L. Archer, R.J. Bak, J.B. Collins, D.W. Burns: Process for recovering boron trifluoride from a catalyst complex, US Patent (Application) 6 410 812 (2002)
- 35.19 J. Cerny, M. Pospisil, G. Sebor: Composition and oxidative stability of hydrocracked base oils and comparison with a PAO, J. Synthetic Lubr. **18**(3), 199 (2001)
- 35.20 ExxonMobil Chemical Co. Sales Brochure. ExxonMobil Chemical Synthetics
- 35.21 Chevron Phillips Chemical Co.: PAO Problem Solver by Chevron Phillips Chemical Co., Lubes-n-Greases (March), 39 (2002)
- 35.22 L. Mattei, P. Pacor, A. Piccone: Oils with low environmental impact for modern combustion engines, J. Synthetic Lubr. **12**(3), 171 (1995)
- 35.23 L.R. Rudnick (Ed.): *Synthetics, Mineral Oils, and Bio-Based Lubricants – Chemistry and Technology* (CRC, Boca Raton 2013) p. 21
- 35.24 Chevron Phillips Chemical Co.: PAO problem solver by Chevron Phillips Chemical Co., Lubes-n-Greases (January), 39 (2003)
- 35.25 ExxonMobil Corporation: ExxonMobil superSyn ultra – A new generation of synthetic fluid, Soc. Tribol. & Lubr. Eng. Annu. Meet., Las Vegas (1999)
- 35.26 D. Mattran: SpectraSyn elite 65 joins ExxonMobil chemical's metallocene polyalphaolefin lineup, Tribol. & Lubri. Technol. **68**(11), 28 (2012), pp. 28–30
- 35.27 S. Mazzo-Skalski: SpectraSyn elite mPAO extends synthetic basestock performance range, Tribol. & Lubri. Technol. **66**(11), 40 (2010)
- 35.28 W.L. Maxwell: Environmental benefits of synthetic lubricants: Progress Since the 1998 Heroes of Chemistry Award for Mobil 1, Special Symp. Heroes of Chem. Mater. Adv. Appl. (2008) pp. 17–21
- 35.29 D.A. Law, J.R. Lohuis, J.Y. Breau, A.J. Harlow, M. Rochette: Development and performance advantages of industrial, automotive and aviation synthetic lubricants, J. Synthetic Lubr. **1**(1), 6–3 (1984)
- 35.30 R.J. Bergstra, D.J. Baillargeon, D.E. Deckman, J.A. Goes: Advanced low viscosity synthetic passenger vehicle engine oils, J. Synthetic Lubr. **16**(1), 51 (1999)
- 35.31 G. Bleimschein, J. Fotheringham, A. Plomer: On the road to new diesel regs – synthetic lubes push on with fuel to burn, Lubes-n-Greases (November), 22 (2002)
- 35.32 ExxonMobil Corporation: <http://www.mobil1.com> (2014)
- 35.33 D. Blain, A. Galiano-Roth, R. Russo, K. Harrington: Energy efficiency industrial gear lubricants, AGMA Fall Tech. Meet., Dearborn (2012)
- 35.34 D. Blain, A. Galiano-Roth, R. Russo, K. Harrington: Energy efficiency industrial gear lubricants, Gear-Solutions Mag. (June), 48–55 (2013)
- 35.35 J. Szydywar: Ester base stocks, J. Synthetic Lubr. **1**(2), 153 (1984)
- 35.36 F. Debuau, P. Hanssle: Aliphatic dicarboxylic acid esters for synthetic lubricants, J. Synthetic Lubr. **1**(4), 254 (1985)
- 35.37 A. Zeman, K. Koch, P. Bartle: Thermal oxidative aging of neopentylpolyol ester oils: Evaluation of thermal-oxidative stability by quantitative determination of volatile aging products, J. Synthetic Lubr. **2**(1), 2–21 (1985)
- 35.38 J. Denis: The relationships between structure and rheological properties of hydrocarbons and oxygenated compounds used as base stocks, J. Synthetic Lubr. **1**(3), 201 (1984)
- 35.39 L.R. Rudnick, R.L. Shubkin (Eds.): *Synthetic Lubricants and High-Performance Functional Fluids*, 2nd edn. (Marcel Dekker, New York 1999) pp. 63–101
- 35.40 S. Boyde: Hydrolytic stability of synthetic ester lubricants, J. Synthetic Lubr. **16**(4), 297 (2000)
- 35.41 K. Carnes: Ester? Ester who?, Lubr. World (October), 10 (2002)
- 35.42 R.H. Schlosberg, J.W. Chu, G.A. Knudsen, E.N. Suci, H.S. Aldrich: High stability esters for synthetic lubricant applications, Lubr. Eng. (February), 21 (2001)
- 35.43 C. Duncan, J. Reyes-Gavilan, D. Costantini, S. Os-hode: Ashless additives and new polyol ester base oils formulated for use in biodegradable hydraulic fluid applications, Lubr. Eng. (September), 18 (2002)
- 35.44 M. Greaves, D. Beatty: PAGs are rising to the top of the synthetic market, Mach. Lubr. Mag. (September), 36–40 (2006)
- 35.45 S. Kussi: Chemical, physical and technological properties of polyethers as synthetic lubricants, J. Synthetic Lubr. **2**(1), 63 (1985)
- 35.46 The Dow Chemical Co.: Dow Polyglycol product brochure, <http://www.dow.com>
- 35.47 M. Greaves: Oil soluble synthetic polyalkylene glycols – a new type of Group V base oil, Lube Mag. **104**, 21–24 (2011)
- 35.48 P.L. Matlock, W.L. Brown, N.A. Clinton: Polyalkylene glycols. In: *Synthetic Lubricants and High Performance Functional Fluids*, 2nd edn. ed. by L.R. Rudnick, R.L. Shubkin (Marcel Dekker, New York 1999) p. 159
- 35.49 M.M. Wu: Alkylated aromatics. In: *Synthetic Lubricants and High-Performance Functional Fluids*, 2nd edn., ed. by L.R. Rudnick, R.L. Shubkin (Marcel Dekker, New York 1999) p. 195
- 35.50 P.A. Brown, S.C. Ho, G.K. Dudley: Lubricant performance with alkylated naphthalene blendstocks, 14th Int. Colloq. Tribol. Esslingen (2004)
- 35.51 Ineos website: [http://www.ineos.com/Products/?bu=INEOS%20Ilgomers&m=Polybutene%20\(PIB\)&f=1](http://www.ineos.com/Products/?bu=INEOS%20Ilgomers&m=Polybutene%20(PIB)&f=1) (2014)
- 35.52 S. Mazzo-Salski: Alkylated naphthalene basestocks for incidental food contact, Tribol. & Lubri. Technol. **66**(11), 44 (2010)
- 35.53 M.P. Marino, D.G. Placek: Phosphate esters. In: *Synthetic Lubricants and High-Performance Functional Fluids*, 2nd edn., ed. by L.R. Rudnick, R.L. Shubkin (Marcel Dekker, New York 1999) p. 103
- 35.54 M.E. Okazaki, S.M. Abernathy: Hydrolysis of phosphate-based aviation hydraulic fluids, J. Synthetic Lubr. **10**(2), 107 (1993)
- 35.55 G. Gill: Synthetics market has spin to space, Lube'N'Greases **20**(9), 31 (2014)

36. Catalytic Processes for Light Olefin Production

Genquan Zhu, Chaogang Xie, Zaiting Li, Xieqing Wang

Up to now, the major process for light olefin production has been thermal steam cracking. The diversification of feedstocks from heavy oil fractions to light hydrocarbons as well as methanol led to the development of catalytic processes. Differing from the radical mechanism for olefin formation by the thermal process, there are two reaction mechanisms for the description of olefin formation in the catalytic process: the carbocation mechanism for hydrocarbon cracking and the hydrocarbon pool mechanism for methanol to light olefin.

Deep catalytic cracking (DCC), developed by the Research Institute of Petroleum Processing (RIPP) of Sinopec, is a fluidized catalytic cracking process that uses a proprietary catalyst for the selective cracking of a wide variety of heavy feedstocks to produce light olefins. The catalytic pyrolysis process (CPP), also developed by RIPP of Sinopec, is an extension of DCC that gives an increased ethylene yield while keeping propylene production at a reasonable rate. The commercial units run worldwide showing the success of the development of these processes.

The key process features, the representative catalysts, and the performance of PetroFCC, Propylur, SuperFLEX, propylene catalytic cracking, olefins

36.1	Fundamentals of the Cracking Mechanism for Light Olefin Production	1064
36.2	Catalysts	1066
36.3	New Technology	1068
36.3.1	Deep Catalytic Cracking	1068
36.3.2	Catalytic Pyrolysis Process (CPP).....	1069
36.3.3	PetroFCC	1071
36.3.4	Propylur	1072
36.3.5	SUPERFLEX.....	1072
36.3.6	Mobil Olefins Interconversion (MOI)....	1073
36.3.7	PCC (Propylene Catalytic Cracking).....	1074
36.3.8	Olefins Catalytic Cracking.....	1075
36.3.9	Olefins Conversion Technology (OCT) ...	1075
36.3.10	Propane Dehydrogenation	1075
36.3.11	Methanol to Olefin Process.....	1077
36.4	Prospects	1077
	References	1078

catalytic cracking, olefins conversion technology, propane dehydrogenation, and methanol-to-olefins are also briefly introduced.

In future, for the production of light olefin, catalytic processing is the key step to integrate the refining and petrochemicals plants.

Consumption of petroleum in the transportation fuel sector is expected to show only a modest rate of growth in the near future. Fuel specifications are becoming increasingly stringent due to new environmental regulations and energy sources such as biofuel, and especially fuel cells for vehicles, which are becoming increasingly attractive as environmentally friendly alternatives. In the petrochemical sector, however, the consumption of hydrocarbon raw materials is expected to grow more rapidly. The building blocks for the petrochemical industry are mainly light olefins, principally ethylene and propylene, and aromatics, including benzene, toluene, and xylenes (BTX). Steam cracking has been the major source of light olefins and aromatics for more than

half a century. The proportions of different steam cracking feedstocks used worldwide are shown in Fig. 36.1. Naphtha is currently the dominant feedstock, accounting for 40–50% of the total. It is expected that ethane, associate gas, condensates, and methanol will dominate as the major feedstock because they are easier to obtain at a lower price. In North America and the Middle East, ethane and shale gas and associated gas already make up 70–80% of the feedstock for steam cracking. This threatens to induce an imbalance in the ethylene-to-propylene ratio in the overall output from steam cracking because typical ethane pyrolysis gives 79% selectivity to ethylene and less than 1% selectivity to propylene at 70% conversion, whereas

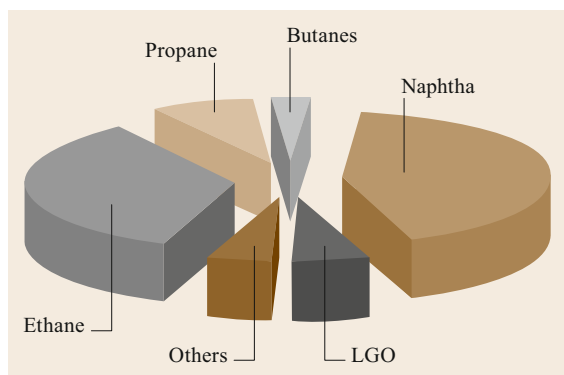


Fig. 36.1 Proportions of different feedstocks used in steam cracking

steam cracking of naphtha gives approximately 30% ethylene and 15% propylene. It is predicted that by 2020, the annual demand for ethylene and propylene will be 170 and 115 Mt respectively (a propylene-to-ethylene ratio of 0.68). The propylene stream from refineries currently accounts for one third of the total supply, and it is clearly necessary to develop new ways of increasing propylene production. A variety of new processes for modifying the propylene-to-ethylene ratio are emerging, such as transformation or product shift by isomerization, hydroisomerization, metathesis, interconversion, skeletal isomerization, and catalytic cracking.

Increasing the integration of petroleum refining with petrochemicals is an inevitable tendency not only for economic and environmental reasons but also because of an increasing reliance on deep upgrading of

crude oil. Statistics show that reserves of heavy crude are much larger than those of conventional crude, and deep upgrading of heavy crude for both refining and petrochemicals is attracting more and more attention from scientists and engineers. Integration will also lead to a rational development of both refinery product slates and petrochemical building blocks.

In the manufacture of the key building blocks for petrochemicals, i. e., ethylene, propylene and other olefins as monomers for polymerization, and BTX as the basic raw material for various synthetic pathways, thermal steam crackers currently still predominate. Catalytic processes such as fluid catalytic cracking (FCC), alkylation, isomerization, catalytic reforming, and hydroprocessing play a decisive role in the production of clean fuels and lubricants in refineries. The integration of refining with petrochemicals leads to the optimization of all the processes involved, and the development of processes with an adjustable ratio of ethylene-to-propylene production is now becoming possible. It can be expected that catalytic processes will play an increasingly significant role in the production of light olefins, especially when the feedstock for light olefins becomes diversified. Besides heavy or low grade oil, light hydrocarbon byproducts from refining and petrochemical plants, methanol and biomass are utilized to produce light olefins and aromatics in different catalytic processes. With the large-scale application of natural gas and shale gas, an agile portfolio of solutions is required to produce light olefins efficiently. This chapter introduces the latest progress toward the aim of increasing propylene production in FCC and related processes for light olefins.

36.1 Fundamentals of the Cracking Mechanism for Light Olefin Production

There are two routes for the production of light olefins by catalytic cracking, which differ according to whether heavy or light hydrocarbons are employed as feedstock. When heavy hydrocarbons are used, they undergo primary cracking. Light hydrocarbon feedstocks are byproducts from refining and petrochemical plants i. e., C₄ and C₅ fractions of relatively low added value, which are suitable for further cracking to ethylene and propylene. The reaction pathways involved for the two types of feedstock differ to some extent.

The complex composition of heavy feedstocks means that a large number of reactions can take place, both in parallel and consecutively, on the catalyst. The relative rates of the various reactions, taken together with the relative ease of the formation of various carbo-

cations from the parent molecules, lead to a bewildering array of possible reaction pathways. The matter is complicated by the presence of a variety of active sites on the heterogeneous catalysts. These sites not only differ in their acid strength but also in their nature. A variety of reactions of carbocations can take place on these acid sites, including cracking, isomerization, hydrogen transfer, alkyl transfer, and C–C bond formation as well as coke formation. Cracking reactions of large molecules tend to predominate, however.

In the FCC process using heavy feedstocks, light olefins are probably produced by the secondary cracking of primary olefins in the FCC naphtha fraction. The reaction proceeds readily over Zeolite Socony Mobil-5 (ZSM-5) zeolite-containing catalysts. It is widely ac-

cepted that olefin cracking over catalysts with Brønsted acidity involves the initial protonation of the double bond to form a tricoordinate carbenium ion, with subsequently scission of a carbon–carbon bond in the beta position, to form a free olefin and a smaller carbenium ion.

Anderson et al. [36.1] recently attempted to predict the optimum zeolite-based catalyst for the selective cracking of naphtha-range hydrocarbons by the pathway proposed by Haag and Dessau in 1984. According to this mechanism, light olefins are produced from alkanes via *protolytic cracking*, in which alkanes are protonated to form carbonium ion transition states that can undergo either C–C bond cleavage, yielding alkanes (including methane and ethane), or C–H bond cleavage, yielding dihydrogen and carbenium ions. These carbenium ions subsequently form alkenes via the back-donation of a proton to the zeolite. The formation of ethylene is probably via this pathway.

Weitkamp et al. [36.2] introduced a classification of carbenium ion beta scission processes. The process where the carbenium ions before and after scission are both tertiary is denoted as type A. Type B1 scission refers to the reaction of a secondary ion to give a tertiary ion, while type B2 involves a change from a tertiary to a secondary ion. Type C involves the conversion of a secondary ion to another secondary ion, and type D involves the transformation of a secondary ion to a primary ion. Buchanan [36.3] added an additional category of primary-to-tertiary ion transformation, designated as type E. Although the beta scission of primary carbenium ions can produce ethylene, the formation of other types of carbenium ions, which mostly produce propylene by terminating the reaction pathway, is more likely.

Cracking of the second category of feedstock – light hydrocarbons such as C₄ olefins – is likely to involve a bimolecular process and probably proceeds via initial oligomerization to form C₈ species, which then undergo

further cracking to form light olefins. Both the study of C₄ saturates and that of Wakui et al. [36.4] showed that butanes are difficult to crack directly. They must first be dehydrogenated to form butylenes, which are then consecutively cracked following the usual olefin reaction pathways.

It should be noted that, in addition to Brønsted acid sites, Lewis acid sites also play an important role in olefin production, although in fact these two types of acid sites can be interconverted at high temperatures. In general, heating the zeolite catalyst to a high temperature results in a loss of Brønsted acidity with a corresponding increase in Lewis acidity. This alters the activity and selectivity of the zeolite in favor of a high light olefin yield. We have found that it is of great importance to maintain an optimum Lewis-to-Brønsted (L/B) ratio in order to maximize ethylene yield under severe operating conditions.

Table 36.1 shows that when ZSM-5 zeolite is modified by treatment with silver (samples AGZ-1 and AGZ-2), both the number of Brønsted and Lewis acid sites increase, but the increase in the number of Lewis sites is much more marked. By using these zeolites as catalysts for the cracking of heavy oil at 650 °C, substantially higher yields of ethylene and propylene can be obtained compared with the reaction over quartz as a representative inert solid. Furthermore, increasing the number of acid sites, especially Lewis sites, leads to an enhanced ethylene yield. Our experimental data are summarized in Table 36.2.

Corma et al. [36.5] postulated that on highly dealuminated zeolites, the cracking reactions take place on extra-framework aluminum sites following a radical-type pathway, which will give more C₁ and C₂ hydrocarbons, mostly ethylene. The mechanism for the cracking reactions we observe at 650 °C (results shown in Table 36.2) may involve either carbenium ion or radical ion intermediates, but this still has to be determined.

The conversion of methanol-to-olefins (MTOs) over acidic zeolites (HZSM-5) or zeotype materials (HSAPO-34) has become an increasingly important catalytic process both in modern natural gas and coal chemical industries. HSAPO-34 was derived from (2x1x1)CHA supercell (24T), in which all Si atoms were substituted by P and Al atoms alternatively, and one P atom then is replaced by a Si atom to generate one Brønsted acid site per cage [36.6]. Due to its complex

Table 36.1 Acid sites in modified ZSM-5 zeolites (aging conditions: 800 °C for 4 h under 100% steam)

Sample	Acid amount (mmol/g)		L/B	L + B
	B-acid	L-acid		
ZSM-5	20.34	5.95	0.29	26.29
AGZ-1	32.20	48.81	1.51	81.01
AGZ-2	44.07	64.09	1.45	108.16

Table 36.2 Ethylene and propylene yields (in wt%) from heavy oil cracked over different catalytic materials

Zeolite	H ₂	Methane	Ethylene	Propylene	C ₇ ⁼ /C ₃ ⁼	C ₅ ⁼ + C ₃ ⁼
Quartz (inert)	0.08	2.12	4.74	4.01	1.18	8.75
ZSM-5	0.09	2.17	5.08	8.70	0.58	13.78
AGZ-1	0.27	2.61	8.23	11.78	0.70	20.01
AGZ-2	0.27	2.80	8.99	12.77	0.70	21.76

nature, the MTO reaction mechanism is still a hot area of dispute. It was traditionally believed that the MTO reaction proceeds through the hydrocarbon pool mechanism, and methylbenzenes (MBs) are the predominant hydrocarbon pool species. However, by extensive periodic density functional theory (DFT) calculations in the HSAPO-34 catalyst, Wang [36.7] proposed that olefins themselves rather than MBs are likely to be the dominating hydrocarbon pool species. A full reaction network is established, as depicted in Fig. 36.2, and the routes to produce olefins, alkanes, and aromatics are formulated. They find that light olefins such as ethene and propene are mainly produced through the scission of cracking precursors (carbenium ions, alkoxides, and higher olefins), and which are formed by the methylation of lighter olefins. The distribution of these cracking precursors as the number of carbon atoms in the pores of catalysts influences the product selectivity from the reaction point of view. A decrease trend in the cracking energy barriers is observed with the carbon atom number of cracking precursors. Hydride transfer between two olefins results in the formation of alkanes and dienes, and the latter are likely to be the precursors to forming aromatics, subsequently leading to the deactivation of catalysts.

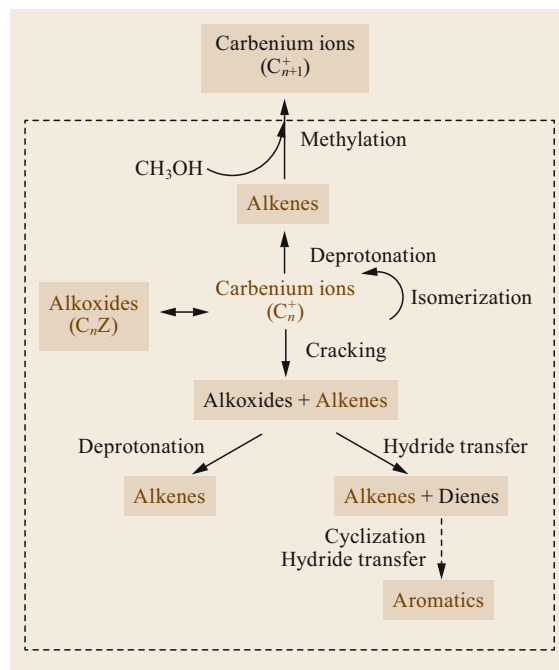


Fig. 36.2 Reaction network of the MTO conversion in acidic zeolites. (After [36.7])

36.2 Catalysts

In the FCC process, it is generally accepted that after vaporization the large molecules of heavy hydrocarbons undergo cracking on both the surface of the Y-zeolite and on the surrounding silica-alumina matrix as a primary reaction. The smaller molecules thus formed permeate into the pores of the Y-zeolite and reach the active sites of the catalyst where the desired catalytic cracking reactions take place. Great efforts have been made to redesign the catalyst formulation as well as to improve the process of catalyst manufacture in order to optimize the yield of light olefins.

As far as the improvement of catalyst formulation is concerned, there are two approaches to the goal of enhanced light olefin yields in the FCC process: incorporation of ZSM-5-containing additives into conventional FCC host catalysts or reformulation of the catalysts, especially for olefin production.

Both of these methods have their advantages and disadvantages. Mixing the conventional FCC catalyst with ZSM-5-containing additives gives the advantage of flexibility in fluid catalytic cracking unit (FCCU) operation according to changes in the market demand for gasoline or olefins. The disadvantage is the difficulty in providing the pore size distribution gradient in the mixed zeolite catalyst, which gives the desired

ratio of light olefins as products of primary cracking and secondary cracking. Furthermore, according to the accepted reaction mechanism, the intermediates from primary cracking should first be desorbed from the acid sites of the main catalyst and then enter the pores of the ZSM-5-containing additive. In the course of this migration, the intermediate species can undergo some undesired reactions. As a result, the yield of light olefins may be adversely affected. From the viewpoint of the physical properties of a mixed catalyst in an FCCU, the two kinds of solids should be closely matched in the density and attrition index in order to keep their relative proportions constant over time. This necessitates a careful choice by the user of both host catalysts and additives.

An especially formulated catalyst for maximizing the yield of light olefins can be tailored in light of the feed properties and target products by optimizing the composition of a mixture of different performances of zeolites. The pore-size distribution of the matrix should be such as to allow access to the large molecules of the feedstock, whilst the incorporation of large-pore Y-zeolite favors intermediate molecule formation and mesoporous ZSM-5 favors the production of light olefins. The gradient in the pore-size distribution allows

ready access to a series of reactants of different molecular sizes. Furthermore, the acidity of catalytic materials, as well as their strength and density, can be adjusted to give predominantly light olefins.

Modification of ZSM-5 is crucial if olefins are to be produced under much more severe operating conditions than those employed for conventional FCC. In the RIPP of Sinopec, there has been a long-term program aimed at enhancing the hydrothermal stability and selectivity of ZSM-5.

It is well known that the incorporation of rare earth cations can greatly improve the hydrothermal stability of Y-zeolite. *Shu et al.* [36.8] have reported the incorporation of rare earth ions into the ZSM-5 structure by a seeding method in which an REY-zeolite (Y zeolite modified by RE) is dispersed in a gel containing Si, Al, Na sources and water, and the mixture converted into an MFI-type zeolite (a kind of zeolite with mesopore). The resulting ZSM-5 zeolite containing rare earth ions was further modified under hydrothermal conditions and the final catalyst, denoted ZRP-1 (ZSM-5 modified by Fe), has outstanding hydrothermal stability as shown in Table 36.3.

Luo et al. [36.9] have reported the modified MFI-type zeolite ZSP (ZSM-5 modified by P and Fe), which was formed by the treatment of ZSM-5 with phosphorus and transition metal ions. When ZSP is used as the catalyst for *n*-C₁₄ cracking at 520 °C, the yield of propylene is increased compared with that obtained over the ZSM-5, as indicated in Table 36.4.

It was found that the introduction of phosphorus into the ZRP series of zeolites further stabilized the crystal structure and was successful in reducing dealumination at high reaction temperatures allowing a large

Table 36.3 Activity retention of ZRP-1 based catalyst in *n*-C₁₄ cracking. (After [36.10, 11])

Conditions	Conversion (wt%)
780 °C, 100% H ₂ O, 4 h	77.1
800 °C, 100% H ₂ O, 4 h	74.2
820 °C, 100% H ₂ O, 4 h	74.0

Table 36.4 Comparison of propylene yields obtained with modified MFI-type zeolites

MFI Zeolite	Conversion (%)	Propylene (wt%)	Propylene/LPG (wt%)
ZSM-5	75.00	9.14	31.11
ZSP-1	77.13	11.79	34.35

Table 36.5 Hydrothermal stability of the CEP-1 catalyst^a

Aging time (h)	4	8	12	16	20	24	28
Activity index	65	62	55	55	54	54	52

^a At 820 °C, 100% steam

fraction of the acidity, and hence activity, to be maintained. Based on this experience, a modified MFI-type catalyst CEP-1 [36.10, 11] was developed by RIPP, especially for the catalytic pyrolysis process (CPP) with the aim of giving high activity and selectivity for light olefins under severe operating conditions. The hydrothermal stability of the catalyst is shown in Table 36.5.

The stability of carbenium ions decreases in the order tertiary > secondary > primary, meaning that the yield of ethylene is generally much less than that of propylene. *Zhang et al.* [36.12] found that by adjusting the acid type, acid strength, and acid distribution, the ratio of ethylene-to-propylene can be altered in favor of ethylene. A modified MFI-type zeolite PMZ (ZSM-5 zeolite modified by Fe and alkaline earth metal) was formed by the treatment of ZRP-1 with alkaline earth metal ions. When PMZ is used as the catalyst for middle distillate cracking at 520 °C, the ratio of ethylene-to-propylene is increased, compared with that obtained over the ZRP-1 precursor, as indicated in Table 36.6.

It should be noted that in addition to the catalytic carbenium ion pathways for light olefin production, thermal reactions involving free radicals are also a sig-

Table 36.6 Comparison of ethylene yields obtained with modified MFI-type zeolites

MFI zeolite	Conversion (%)	Ethylene (wt%)	Ethylene/propylene
ZSM-5	44.06	0.82	0.13
ZRP-1	63.06	2.63	0.31
PMZ	63.01	3.30	0.49

Table 36.7 MAT (microactivity test) results with PMZ as a catalytically active material and quartz as an inert carrier

Reaction temperature (°C)	650		680	
	Quartz	PMZ	Quartz	PMZ
Catalyst				
Product yields (wt%)				
Cracked gas	17.05	37.94	30.68	45.08
In which, ethylene	5.19	8.48	9.31	11.20
Propylene	4.39	15.95	8.07	17.95
Butylenes	2.35	6.80	4.59	7.56
C ₅ + naphtha	23.21	18.22	25.10	18.33
LCO	49.02	37.40	34.92	26.31
HCO	7.66	5.20	5.33	3.41
Coke	0.12	0.98	0.49	1.80
Loss	2.94	0.26	3.48	4.35
Conversion (wt%)	43.32	57.40	59.75	70.28
C ₂ ⁼ +C ₃ ⁼ +C ₄ ⁼ (wt%)	11.93	31.23	21.79	36.71
Olefin selectivity (wt/wt)				
C ₂ ⁼	0.12	0.15	0.16	0.16
C ₃ ⁼	0.10	0.28	0.14	0.25
C ₄ ⁼	0.05	0.12	0.08	0.11

nificant source of ethylene and indeed predominate at higher temperatures. Table 36.7 gives a comparison of

the impact of such thermal reactions on the yields of ethylene and propylene at different temperatures.

36.3 New Technology

In the last few decades, great efforts have been made to produce light olefins by catalytic processes in order to achieve a rational utilization of heavy feedstocks or petrochemical byproducts. Some papers in this area presented at the 17th World Petroleum Council (WPC) drew considerable attention from both academic and industrial researchers. A variety of very promising processes have been developed, and some have already been commercialized. All of the new catalytic processes aim to tackle the problem of low propylene-to-ethylene ratio caused by the recent feedstock change for steam crackers.

36.3.1 Deep Catalytic Cracking

Deep catalytic cracking (DCC) [36.10, 11, 13, 14] is a new fluidized catalytic cracking process using a proprietary catalyst for the selective cracking of a wide variety of heavy feedstocks to give light olefins. The process, developed by RIPP of Sinopec, has been commercially proven with ten units built since 1990, seven in China and the others in Thailand, Saudi Arabia, and India. The DCC-I process is similar to that of conventional FCC with a modified reactor consisting of a riser plus fluidized dense bed. The dense bed at the end of the riser results in a longer residence time at a high catalyst-to-oil ratios, favoring the secondary cracking of primary intermediates, which is thought to enhance propylene production at the cost of gasoline yield. In the DCC-II system, the dense bed is removed in order to allow

flexibility in propylene and gasoline yields according to market demand. Table 36.8 shows a comparison of the key features of DCC with those of conventional FCC.

The experience accumulated over decades in four refineries and one petrochemical complex has shown that light olefin yields are greatly dependent on the feedstock properties as detailed in Table 36.9. Daqing paraffinic feedstock gives the highest propylene and isobutylene yields, with 23.0 and 6.9 wt% respectively. For intermediate base feeds, propylene yield is more than 18 wt% for DCC-I and 14.4 wt% for DCC-II operation with an FCC naphtha yield near 40 wt%.

The DCC gasoline fraction is rich in BTX, especially xylenes. Table 36.10 lists the BTX content in the DCC naphtha fraction and DCC 75–150 °C light gasoline range. Recovery of BTX from the narrow cut for petrochemical applications is economically viable.

A DCC unit with the capacity of 4600 kta has been put into commercial operation since May 2009 at Saudi Aramco-Sumitomo Chemical at their Rabigh, Saudi Arabia site. The production rates are 225 kta ethylene and 950 kta propylene. The DCC unit was integrated with the ethane steam cracking unit for recovering the ethylene.

The reactor of conventional DCC is a riser plus fluidized dense bed, which can enhance propylene production and can also bring out higher dry gas and coke yields due to the lower catalyst activity and an unreasonable temperature gradient in the DCC reactor. In order to improve the selectivity of the desired

Table 36.8 Comparison between DCC and FCC processes

Process	FCC	DCC
Feedstock	A wide range of heavy oils	A wide range of heavy oils preferably paraffinics
Catalyst	Various types of Y-zeolite	A modified pentasil structure zeolite and Y-zeolite
Hardware		
Reactor	Riser	Riser and bed
Regenerator	Base	Similar
Main fractionator	Base	Higher vapor-to-liquid ratio
Stabilizer/absorber	Base	Bigger
Compressor	Base	Larger capacity
Operating conditions		
Reaction temperature	Base	+30–50 °C
Regeneration temperature	Base	Similar
Catalyst-to-oil ratio	Base	1.5–2 times
Residence time	Base	More
Oil partial pressure	Base	Lower
Dilution steam	Base	More

Table 36.9 DCC light olefin yields

Refinery	Daqing	Anqing	IRPC	Jinan	Jinan
Operation mode	DCC-I	DCC-I	DCC-I	DCC-I	DCC-II
Feedstock	Paraffinic VGO+ ATB	Intermediate base VGO	Arabian HVGO+ DAO+WAX	Intermediate base VGO+DAO	
Reaction temperature (°C)	545	550	565	564	530
Olefin yields (wt%)					
Ethylene	3.7	3.5	5.3	5.3	1.8
Propylene	23.0	18.6	18.5	19.2	14.4
Butylenes	17.3	13.8	13.3	13.2	11.4
In which					
Isobutylene	6.9	5.7	5.9	5.2	4.8

Table 36.10 BTX content in DCC gasoline fraction

	DCC naphtha	75–150 °C cut
BTX content (vol%)	25.90	57.56
In which		
Benzene	2.41	5.36
Toluene	9.84	21.87
Xylenes	13.65	30.33

products, RIPP has developed a DCC-plus process, which can optimize the temperature and catalyst activity gradient along the reactor by introducing high temperature and activity catalysts into the fluidized-bed reactor through the second riser. A series of experiments for DCC-plus technology was carried out on the pilot plant unit [36.15]. The experimental results showed that as compared with DCC technology, the yields of liquid petroleum gas (LPG), propylene, and butylenes in DCC-plus process were enhanced significantly at the same time the yields of dry gas and coke were reduced.

A DCC-plus unit with the capacity of 1200 kta has been put into commercial operation since February 2014 at the CNOOC Hainan Dongfang Petrochemical Corporation limited.

The ethylene in the DCC dry gas can be recovered by means of cryogenic separation through integration with the steam cracking. On the other hand, the ethylene in the DCC dry gas can be converted into styrene, and some units have been put into commercial application in China.

It has been clearly demonstrated that increasing propylene production, even at the expense of gasoline yield, is a commercially economic proposition in an integrated refining-petrochemical complex.

36.3.2 Catalytic Pyrolysis Process (CPP)

The CPP [36.16], also developed by RIPP of Sinopec, is an extension of DCC that gives an increased ethylene yield while keeping propylene production at a reasonable rate. The key features of this process are as follows:

- A new catalytic material has been developed that reduces the activation energy required, thus allowing the reaction to be carried out at a significantly lower temperature compared with that required for steam cracking, and also favors the production of light olefins.
- The catalyst possesses excellent hydrothermal stability and attrition resistance.
- The operating conditions for CPP are more severe than that for residue fluid catalytic cracking (RFCC) to an extent that allows it to be operated in existing idle RFCC units without the risk of damage to the fabric of the plant.
- The heat required for the cracking reaction can be provided by burning coke in the regenerator, making the reaction fully self-supporting.
- An especially designed stripper located between the regenerator and reactor removes the flue gas carried over from the regenerator.
- Since the reaction temperature is higher than for conventional RFCC, a postriser quench has been introduced for heat recovery as well as termination of secondary reactions in order to prevent further thermal degradation of the target products.

Commercial trial runs were successfully completed in early 2001 at the PetroChina Daqing Refining and Chemical Co. using a revamped DCC unit with a capacity of 80 kta. Three sets of conditions were employed:

1. Mode 1 for the maximum propylene yield
2. Mode 3 for the maximum ethylene yield
3. Mode 2 – intermediate between the two.

Feedstock properties, product distribution, and major operating parameters can be seen in Tables 36.11–36.13. Across the three modes, the combined yield of ethylene and propylene ranges between 34 and 38 wt%, and the total yield of $C_2=C_4$ olefins is around 45 wt% in each case. The ethylene-to-propylene ratio can be adjusted by the variation of the operating conditions.

Table 36.11 Feedstock properties

Operating mode	Mode 1	Mode 2	Mode 3
Density (20 °C) (g/cm ³)	0.9002	0.9015	0.9012
CCR (wt%)	4.7	4.9	4.7
Hydrogen (wt%)	12.82	12.86	12.84
Sulfur (wt%)	0.16	0.16	0.16
Nitrogen (wt%)	0.29	0.26	0.25
Nickel (ppm)	5.8	6.2	6.3
Composition (wt%)			
Saturates	56.3	54.8	55.5
Aromatics	27.2	28.4	28.0
Resin	15.7	16.0	15.7
Asphaltene	0.8	0.8	0.8

We suggest that in order to optimize the use of crude oil as a petrochemical feedstock, a combination of steam cracking and CPP may be the best choice, as depicted in Fig. 36.3.

Key economic data for a CPP plant with the integrated steam cracker are shown in Table 36.14. Based on 500 kta of ethylene produced by CPP and 1000 kta of ethylene produced by steam cracking, the estimated net product revenue is 450 \$ MM/a.

A CPP unit with the capacity of 500 kta has been put into commercial operation since June 2009 at Shenyang Chemical Group Shenyang Paraffin and Chemical Company.

The plant producing ethylene and propylene from the Daqing atmospheric residue was composed of three parts: CPP system, ethane-propane tubular-cracking furnace, and pyrolytic gas purification and separation system. The flow diagram for this plant is shown in Fig. 36.4. The atmospheric residue is cracked in the CPP system's reactor, and the reactor effluents are cooled in the postriser quench and flow into the fractionator and direct cooling tower to be separated into cracked gas, naphtha, and LCO. The cracked gas is compressed and pumped into the pyrolytic gas purification and separation system to obtain poly-

Table 36.12 Product distribution and olefin yields

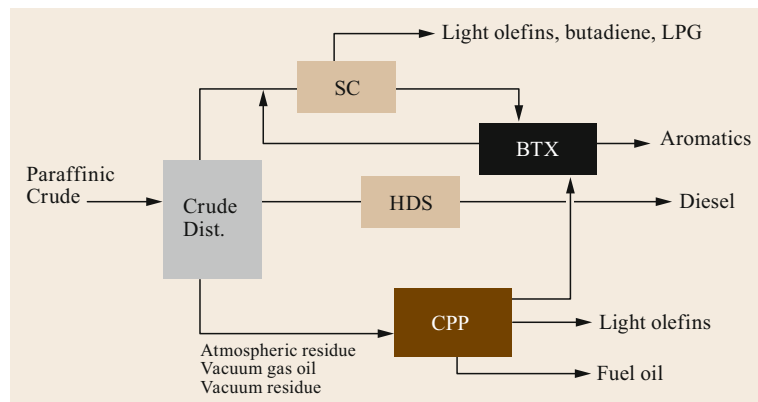
Operating mode	Mode 1	Mode 2	Mode 3
Product yields (wt%)			
C ₂ minus	17.64	26.29	37.13
C ₃ plus C ₄	43.72	36.55	28.46
C ₅ + naphtha	17.84	17.61	14.82
LCO	11.75	8.98	7.93
Coke	8.41	9.67	10.66
Loss	0.64	0.90	1.00
Olefin yields (wt%)			
Ethylene	9.77	13.71	20.37
Propylene	24.60	21.45	18.23
Butylenes	13.19	11.34	7.52

Table 36.13 Main operating parameters

Operating mode	Mode 1	Mode 2	Mode 3
Feed rate (t/h)	9.73	8.00	5.90
Reaction temperature (°C)	576	610	640
Reaction pressure (MPa (g))	0.08	0.08	0.08
Regeneration temperature (°C)	720	725	760
WHSV (h ⁻¹)	2.5	4.0	Zero level
Catalyst-to-oil ratio	14.5	16.9	21.1
Steam-to-oil ratio	0.30	0.37	0.51

mer levels of ethylene and propylene, and the separated ethane and propane, which are cracked into ethylene and propylene in the ethane-propane tubular cracking furnace. C₄ distillate is etherified to produce methyl *tert*-butyl ether (MTBE), and C₄ distillate after etherification is recycled to the CPP reactor. Naphtha is hydrotreated and extracted to produce BTX.

The results of the performance test [36.17] show that the ethylene and propylene yields reach 14.84 and 22.21 wt% respectively, at a reaction temperature of 610 °C by using the Daqing atmospheric residue as feedstock under the operation mode taking account of

**Fig. 36.3** The scheme of crude to petrochemicals

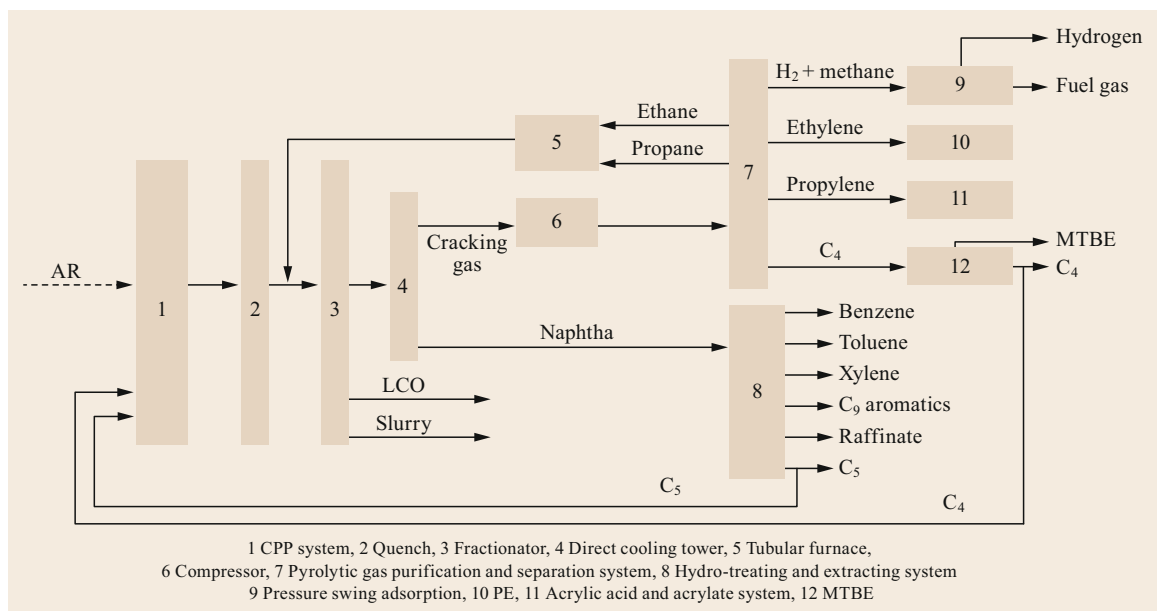


Fig. 36.4 The scheme of a plant producing petrochemicals from the atmospheric residue

Table 36.14 Key economic data for a CPP-integrated olefins plant. (Courtesy of C.P. Bowen of Stone and Webster, A Shaw Group Company)

Total input cost (TIC)	CPP/SC \$MM	SC	Δ
Catalytic pyrolysis process (CPP) (50 mbpd, 500 kta C ₂ H ₄)	150	–	–
Steam cracking (SC), recovery (1000 kta C ₂ H ₄)	600	650	–
(SC propylene/ethylene (P/E) 0.45)	750	650	100
	\$MM/a		
Operating cost (including catalyst)	30	20	10
Net product revenue	450	320	130
Δ TIC/revenue < 1 year pay out			

ethylene and propylene at the same time; the aromatics content in cracked naphtha is 82.46 wt%.

Since July 2014, a CPP unit with a capacity of 1500kta has been put into commercial operation at Yanchang Petroleum.

36.3.3 PetroFCC

The PetroFCC [36.18–21] process is licensed by UOP LLC and features RxCat technology. The process gives high yields of propylene, light olefins, and aromatics for petrochemical applications, from feedstocks that can include conventional FCC feeds and higher boiling or residual feeds. The feed comes into contact with the blended catalyst in the riser under very severe pro-

cessing conditions. The blended catalyst consists of the regenerated and coked catalysts.

The PetroFCC process uses a high-conversion, short-contact time reaction zone that operates at elevated reactor riser outlet temperatures and low partial pressures. It also incorporates a relatively high level of a shape-selective zeolite catalyst additive with a selected standard FCC catalyst as the balance. The PetroFCC process incorporates UOP's Optimix feed distribution system, vortex separation system (VSS), vortex separation technology, advanced fluidized (AF) spent catalyst stripping technology, and RxCat technology to enhance light olefin and/or aromatics production. RxCat is a key differentiating technology of the PetroFCC process when compared to alternate technology.

The PetroFCC process employs several measures to improve the yield and selectivity of propylene and lower the yield of dry gas:

- The PetroFCC catalyst has two components. The first component comprises a large-pore zeolite, such as a Y-type zeolite. The second component involves medium- or small-pore zeolites, such as ZSM-5 or ST-5, which have high coking resistance.
- The riser inlet temperature is reduced to about 620 °C by cooling the regenerated catalyst with the recycled coked catalyst. The ratio of the catalyst-to-feed can be increased to an extent without any adverse influence on the heat balance in the unit.
- The residence time for the feed in contact with the catalyst in the riser is less than or equal to 2 s. The

short residence time ensures that the target products are not further converted to undesired products. The diameter and height of the riser should be varied to give the desired residence time.

- To enhance light olefin production, low hydrocarbon partial pressures (70–210 kPa(a)) and elevated temperatures (540–620 °C) are employed.
- A second riser, which shares a common regenerator with the primary riser reactor, is provided for re cracking the naphtha-containing higher olefins.

The expected yield patterns for a typical vacuum gas oil (VGO) in a conventional FCC unit and a PetroFCC unit are compared in Table 36.15.

36.3.4 Propylur

The Propylur process [36.22–24] converts low-value light hydrocarbons enriched in olefins into petrochemicals such as propylene and is based on a shape-selective heterogeneous zeolitic catalyst of the ZSM-5 type.

The feedstock for the Propylur process can be C₄ cuts, Raffinate I, Raffinate II, or a gasoline fraction. Naturally, a feedstock with high olefin content is more favorable. Compounds such as paraffins, cycloalkanes, and aromatics are rarely converted when they pass through the reactor. The diolefin content should be limited to approximately 1.5% in order to reduce the formation of gum and coke during the reaction.

The Propylur reactor is an adiabatic fixed bed type, similar to that employed in a Claus unit. The operating temperature is approximately 500 °C and pressure is 100–200 kPa. The hydrocarbon partial pressure is reduced by diluting the feedstock with steam in order to shift the equilibrium toward the desired product (propylene). This also minimizes coking and gum formation. The reaction is endothermic and requires additional heat.

By cooling the reactor effluent, the steam is condensed and then separated together with some gasoline

Table 36.15 Yield patterns of conventional FCC and PetroFCC units

Component (wt%)	Conventional FCC	PetroFCC
H ₂ S, H ₂ , C ₁ , and C ₂	2.0	3.0
Ethylene	1.0	6.0
Propane	1.8	2.0
Propylene	4.7	22.0
Butanes	4.5	5.0
Butylenes	6.5	14.0
Naphtha	53.5	28.0
Distillate	14.0	9.5
Fuel oil	7.0	5.0
Coke	5.0	5.5

byproducts. The remaining vapor is compressed in order to allow C₃/C₄ separation at reasonable temperatures. Most of the C₄+ fraction is recycled to the reactor to increase the ultimate propylene yield and a portion of C₄+ is sent to the plant's furnace section to prevent excessive buildup of C₄+ paraffin recycle. Further separation of the C₃ fraction can be done in the ethylene plant. The single-pass propylene yield is 40–45%, and the ethylene yield is 10%. The ultimate yield of propylene is 60% and that of ethylene is 15%, with the butylenes recycled.

The catalyst lifetime is predicted to exceed 15 months based on the laboratory pilot-plant experience. The catalyst can be regenerated off-stream in situ by burning the coke deposited on it by controlled combustion with a nitrogen cycle and small air makeup.

When integrated with an ethylene plant, the Propylur plant can give increased propylene-to-ethylene ratios in a steam cracker. The typical yields of different products from the Propylur process are shown in Table 36.16.

36.3.5 SUPERFLEX

The SUPERFLEX process [36.25–31] is a proprietary technology patented by ARCO Chemical Technology, Inc. (now Lyondell Chemical Co.), and is exclusively offered for license by Kellogg Brown and Root (KBR). It uses an FCC system with a proprietary catalyst to convert low-value feedstock with high olefin content to petrochemical products such as propylene and ethylene.

The feedstock can be olefin-rich light hydrocarbons in the carbon range C₄–C₈, and the ideal feedstocks are C₄ and C₅ streams generated in the steam cracker. Diolefins and acetylenes in the feedstock can be partially hydrogenated to olefins, or the diolefins extracted for other petrochemical applications. Other possible feedstocks are MTBE raffinate-2, aromatics plant raffinate and refinery streams that are rich in olefins, such as light naphtha from an FCCU, coker or visbreaker. Refinery streams do not require pretreatment or hydrogenation of dienes – there is no limit on feed aromatic or diene content.

The SUPERFLEX FCC system is similar to that of a conventional FCC unit and consists of riser reactor, regenerator vessel and units for air compression, catalyst handling, flue gas handling and feed and effluent

Table 36.16 Typical yields from the Propylur process

	Typical yields (wt%)	
	Single pass	C ₄ recycle
Propylene	40–45	60
Ethylene	10	15
Butylenes	30	

heat recovery. The SUPERFLEX system should be integrated into an ethylene plant in order to minimize capital investment, with the feedstock obtained directly from the steam cracker and shared common product recovery. The cooled reactor effluent can be processed in a nearby existing ethylene plant recovery unit. Alternatively, the effluent can be processed in a partial recovery unit to recover recycle streams and olefin-rich streams concentrated for further processing in a nearby ethylene plant.

The SUPERFLEX process operates at approximately 500–700 °C and 100–200 kPa, and so it converts paraffins and naphthenes along with olefins. This allows it to operate in a total recycle mode and to produce higher yields of propylene and ethylene. The propylene-to-ethylene ratio is about 2 : 1 (wt/wt).

The conditions involve low hydrocarbon partial pressures, high temperatures, and low per-pass conversions in order to favor propylene production. The catalyst is very robust, and there is no need to pretreat for typical feed contaminants, such as sulfur, water, oxygenate, or nitrogen in feeds. The typical ultimate light olefin yields after the C₄–C₅ recycle operation are listed in Table 36.17. FCC light naphtha would make 30% propylene and a lesser amount of ethylene, whereas a typical C₄-raffinate-1 (butadiene has been extracted) yields half as much propylene and about the same amount of ethylene.

KBR also presents SUPERFLEX as a means of greatly increasing the production of propylene in a refinery by integrating it with the company's MAXOFIN process. When the two processes are synergistically combined to form a dual-riser version of SUPERFLEX, it is called SUPERFLEX plus.

36.3.6 Mobil Olefins Interconversion (MOI)

Mobil olefin interconversion (MOI) was developed by the Mobil Oil Corporation and converts light hydrocarbons containing C₄–C₇ olefins to more valuable light olefins by contacting the feed with a catalyst containing Mobil ZSM-5, which provides the acid activity and shape selectivity needed to help promote oligomerization, cracking, and disproportionation while limiting

coke formation and the production of polynuclear aromatics and dry gas [36.32].

The feedstocks will typically be low-value refinery or petrochemical streams, such as steam cracker byproducts rich in C₄s, which have poor propylene selectivity when recycled to the steam cracker. The feedstock can include raffinate, FCC naphtha, coker naphtha, and steam cracker pyrolysis gasoline, as well as synthetic chemical streams containing sufficient amounts of C₄–C₇ olefins. Dienes, sulfur, nitrogen, and oxygenates in the feeds are preferably selectively hydrotreated prior to the conversion process. However, feeds with low levels of dienes, sulfur, nitrogen, metal compounds, and oxygenates can be processed directly from FCC units, cokers, or steam crackers without any pretreatment.

The process uses a dense fluidized bed and the hydrocarbon feed containing the C₄–C₇ olefins is continuously passed through the bed under conversion conditions in the presence of the catalyst. The catalyst is continuously circulated between the fluidized bed and a regenerator. The fluidizable catalyst can transfer heat from the latter to the former, thereby helping to supply some of the thermal needs of the conversion reaction, which is endothermic. The operation of the process is similar to that of conventional FCC.

The dense fluidized-bed conversion conditions include temperature in the range 540–650 °C and pressure from 0.10 to 0.45 MPa, catalyst-to-oil weight ratio of 0.1–10, and a weight hourly space velocity (WHSV) of 1–10 h⁻¹. Because the catalyst used in the process has lower cracking activity relative to conventional FCC catalysts, a higher temperature compared with that for conventional FCC may be used in order to achieve a higher conversion to the desired light olefins.

The catalyst in MOI contains only ZSM-5 without any large-pore zeolites. The ZSM-5 preferably has a high initial silica/alumina molar ratio and is modified by phosphorus and metals such as gallium.

The products from MOI include light olefins such as propylene and ethylene. A higher yield of propylene is produced than is usually obtained in conventional catalytic cracking processes utilizing a ZSM-5 additive. The propylene-to-ethylene weight ratio is related

Table 36.17 SUPERFLEX product yields from various feeds^a

Yields (wt%)	C ₄ raffinate-1	Partially hydrogenation C ₅ S	FCC LCN	Coker LN
Dilute ethylene (C ₂ and lighter)	26.6	31.7	25.1	11.6
Propylene	44.4	39.5	30.5	19.8
Propane	4.8	6.1	5.1	38.7
Mixed C ₄ s	6.3	4.1	7.6	7.0
C ₆ + gasoline	17.9	18.6	31.7	22.9

^a The yields resulted from recycled C₄ and C₅

to the conversion and feed but almost always exceeds 3.0. The combined yield of ethylene plus propylene is about 20–30 wt%. Propylene purities of 85 wt% or greater can be achieved. In addition, only relatively small amounts of aromatics such as BTX are produced.

Table 36.18 shows the products obtained from the processing of FCC C₅–C₇ naphtha containing 51 wt% olefins and steam cracker byproduct using a single pass and a recycle configuration of the MOI process. Recycle of C₄ and C₅ olefins is used to increase ethylene and propylene yields. As shown in Table 36.18, conversion to propylene is higher with the steam cracker feed since it contains more olefins.

The use of MOI in the processing of C₄ steam cracking byproduct (typically 40% butadiene) results in the highest propylene yield. This option is compared in Table 36.19 against various upgrading alternatives. Hydrotreating is used in three of these options to either selectively convert butadiene to butylenes or to convert all of the butadiene and butylenes to butanes.

36.3.7 PCC (Propylene Catalytic Cracking)

The ExxonMobil PCC process [36.33–35] is a new fluid solid naphtha-cracking process to convert naphtha olefins to light olefins, such as propylene, which employs an optimum catalyst, reactor design, and patented combination of optimum operating conditions to achieve a high degree of reaction selectivity.

The feed can be obtained from cat naphtha, coker naphtha, and steam cracker's C₄s and pyrolysis gasoline. The largest source of olefinic feedstock molecules is cat naphtha, which contains 20–60% olefins. Most of the linear cat naphtha olefins are converted to light olefins, and at the same time an increased octane and reduced olefin content naphtha are produced by the concentration of higher octane aromatics, plus isomerization, and some additional aromatics formation.

A fluid solid reactor-regenerator configuration is designed for large-capacity units. Feed naphtha is preheated and is injected into the reactor of a fluid solids reactor-regenerator system. The hot, regenerated catalyst contacting the preheated feed supplies the necessary sensible heat to complete preheating the feed to reaction temperature, and supplies the heat of reaction. These fluid solids systems can use ZSM-5-containing fluid solids catalysts. In this way, coke made on the catalyst when cracking naphtha is low, therefore, a means to provide supplemental fuel to burn in the regenerator to supply the necessary sensible heat and heat of reaction is required. The regeneration of catalyst provides the flexibility to process a variety of feeds, which can contain diolefins, aromatics, or heavy ends to a certain degree.

Reactor effluent is cooled and vapors are compressed for product recovery. Once-through yields of ethylene and propylene typically are in the range of 10–20 and 30–40 wt% on feed olefin content, respectively. The propylene's concentration ranges from

Table 36.18 MOI yields when treating FCC and steam cracker products

Yields (wt%)	FCC light naphtha			Steam cracker byproduct		
	Fresh feed	Single pass	C ₄ –C ₅ recycle	Fresh feed	Single pass	C ₄ –C ₅ recycle
H ₂ +C ₁	–	2.7	5.1	–	0.9	1.4
Ethylene	–	6.4	9.7	–	7.9	11.1
Ethane	–	2.5	4.6	–	1.3	2.0
Propylene	–	17.4	26.3	–	25.5	35.7
Propane	–	3.8	4.6	0.1	4.0	5.6
Isobutylene	0.2	6.9	0.6	25.6	11.9	2.7
Butylenes	1.4	5.2	0.5	68.9	12.5	2.8
Butanes	0.4	2.1	2.6	4.9	9.2	10.9
C ₅ –C ₈ (no aromatics)	91.5	34.4	21.3	0.5	13.6	9.5
Benzene	2.1	2.5	2.7	–	1.7	2.4
Toluene	2.8	6.1	7.7	–	3.4	4.7
C ₈ aromatics	1.2	2.6	3.3	–	3.1	4.3
C ₉ + and coke	0.4	7.4	11.0	–	5.0	6.9

Table 36.19 MOI olefin yields compared to alternative technologies

	C ₇ ⁺ yield (wt%)	C ₄ ⁺ yield (wt%)	Propylene-to-ethylene ratio
Recycle cracking	12–14	16–17	1.3
Selective hydrotreating and recycle cracking	18–20	14–17	0.8
Full hydrotreating and recycle cracking	33–38	17–23	0.6
Selective hydrotreating and MOI	12–14	40–42	3.2

conversion and high selectivity toward the desired product. Regeneration is required because of coke formation on the dehydrogenation catalyst. PDH provides 85 wt% propylene and small amounts of hydrogen and ethylene byproducts, which can be used as fuel for the PDH process. Paraffin dehydrogenation reaction chemistry, although quite simple from a stoichiometric point of view, is very complex due to its strongly endothermic nature and significant conversion limitations caused by thermodynamic equilibrium. Side reactions include the cracking of hydrocarbons and hydrogenolysis, as well as oligomerization, cyclization, hydrogenation of olefins, deep dehydrogenation, and eventually the formation of coke and tar laid down on the catalyst, which requires frequent catalyst regeneration.

Two main catalytic systems have been identified and commercialized for light-paraffin dehydrogenation, the first being supported chromia catalysts (i. e., chromia on alumina support), which are doped with alkali metals to add alkalinity and suppress unwanted side reactions, and the second supported platinum or platinum-tin catalysts, with different support materials. These materials include alumina or zinc-/calcium-aluminate, and potentially further modifiers such as alkali metals, again to reduce the acidity of the support and suppress side reactions. Today, both catalyst systems are used in commercially available PDH processes (i. e., chromia catalyst in Lummus CATOFIN and platinum-tin catalysts in UOP Oleflex and Uhde's STAR process).

With the dehydrogenation reaction being favored by high temperatures and low hydrocarbon partial pressures, all commercially available technologies keep the

process temperature at or below approximately 650 °C, because higher temperatures would lead to a significant increase in side reactions and therefore a decrease in the selectivity of the main reaction for propylene production. Furthermore, the most significant side reactions are not limited by thermodynamic equilibrium. As a result, the higher retention times required to achieve higher per-pass conversions also have a strongly negative impact on propylene selectivity. At the same time, partial pressure is kept low by applying absolute pressures slightly above atmospheric pressure or even under vacuum, or by using a diluent to reduce the hydrocarbon partial pressure. As a result of these considerations, all the technical processes for PDH have limited conversion in the range of 32–55%, with selectivities to propylene in the range of 87–91 mol%. As the significant amount of coke laydown leads to a fairly quick deactivation of the catalyst (i. e., in the range of minutes to a few days), different reactor systems are applied to account for the regeneration needs. Continuous systems applied are moving-bed systems and fluidized-bed systems. Discontinuous (fixed-bed) systems applied are heated fixed-bed systems (as in Uhde's STAR process) and adiabatic fixed-bed systems.

Product work-up sections for all the PDH technologies are very similar, as the side products, and therefore the separation tasks are also similar. When comparing different PDH technologies, several key components need to be evaluated to find the differences and advantages of one technology over the other. Table 36.20 lists certain data generally available in the industry for commercial PDH technology.

Table 36.20 PDH process technology parameters

	UOP oleflex	Uhde STAR process	Lummus CATOFIN
Catalyst	Pt–Sn on alumina	Pt–Sn on zinc-/calcium-aluminate	Chromia on alumina
Reaction system	Fluidized bed system consisting of several radial-flow adiabatic reactors in series and an external regenerator (CCR)	Fixed-bed system consisting of an externally fired tubular reactor and an adiabatic reactor in series	Fixed-bed system consisting of a number of axial-flow adiabatic reactors connected in series
Main source for heat supply	Preheating of the feed and intermediate products before each reactor	External firing of the tubular reactor and selective hydrogen combustion in the adiabatic reactor	Heating the catalyst during catalyst regeneration
Operating mode	Continuous (5–10 days catalyst cycle time)	Discontinuous (7 h normal operation, 1 h regeneration)	Discontinuous (6–20 min reaction cycle)
Pressure (bars)	2	5	0.3–0.5
Temperature (°C)	580–650	570–590	560–650
Liquid hourly space velocity (h ⁻¹)	4	6	< 1
Per-pass conversion propane (%)	35	40	48–65
Selectivity propene (mol%)	89–91	89	88
The maximum capacity of commercial unit (kta)	460	350	455

Table 36.21 Overview of MTO and MTP pilots

Item	UOP MTO	DICP DMTO	Sinopec SMTO	Lurgi MTP
Scale (td ⁻¹)	0.75	50	100	0.36
Reactor	Fluidized bed	Fluidized bed	Fluidized bed	Fixed bed
Catalyst	SAPO-34	SAPO-34	SAPO-34	ZSM-5
Olefin yield (%)				
Ethylene	48.0	50	78.24	71
Propylene	33.0	30	78.24	71

36.3.11 Methanol to Olefin Process

The MTO process converts methanol to light olefins [36.47–50]. The process provides greater selectivity to ethylene and propylene versus C₄+ by-products.

The ethylene and propylene are produced from a dimethylether (DME) intermediate in the MTO process. Some byproducts such as butylenes and other higher olefins are also produced. The MTO reaction is exothermic. The coke deposited on the catalyst can be removed by combustion with air in a catalyst regenerator system in order to prolong the active life of the catalyst.

The MTO process utilizes the highly selective met-alloaluminophosphate molecular sieve catalyst, which is based on SAPO-34. The main olefin products are ethylene and propylene, but the catalyst is rapidly deactivated by aromatic coking. An alternative catalyst is the medium-pore zeolite ZSM-5 in the MTP process. In this case, the main olefin product is propylene, and the deactivation of the catalyst caused by aromatic coke is slower, but significant quantities of C₅+aromatic byproducts are formed.

In the MTO or MTP process unit, the methanol and DME come into contact with the catalyst in the reactor and are converted into light olefins. Residence times are very short and the reactor operates in a stable steady-state in the vapor phase at temperatures between 350 and 600 °C and pressures between 0.1 and 0.3 MPa. In

the process, the catalyst is deactivated by coke accumulation, and a part of the catalyst is transferred to the fluidized-bed regenerator in order to restore its activity.

Polymer-grade ethylene and propylene can be produced from the reactor effluent by a series of purification steps. The results from an MTO demonstration plant show that the conversion of methanol is 100%, selectivity to ethylene is above 40%, and selectivity to propylene is close to 40%. Table 36.21 lists certain data generally available in the pilots of MTO and MTP technologies.

A DMTO unit with a capacity of 500 kta ethylene and propylene has been put into commercial operation since January 2011 at Shenhua coal to olefin project in Baotou, China. And an SMTO unit with a capacity of 600 kta ethylene and propylene has been at final inspection and acceptance since January 2014 at Zhongyuan Petrochemical Co. Ltd. In the near future, 15 units with a capacity of about 10 000 kta ethylene and propylene will come on line in China.

In the MTO and MTP processes, a considerable quantity of light olefins such as butylenes and pentenes are also produced while acquiring ethylene and propylene. Discovering how to convert these light olefins into ethylene and propylene effectively will promote the profitability of the MTO and MTP process. So some new processes such as SMTO+OCC, UOP MTO+OCP, MTO+OCT, MTO+SUPERFLEX, and MTO+Omega have also been developed.

36.4 Prospects

The production of ethylene and propylene is one of the cornerstones of the petrochemical industry and developments in this area are key to progress in the industry as a whole.

According to reliable forecasts, the world's recoverable conventional oil resources amount to 310 billion tons [36.51] while nonconventional oil resources (including extra-heavy oil, oil sands, asphalt, and oil shale) total 400–700 billion tons. It is predicted that the output of conventional crude oil will be peak in 2030, and by 2060 the production of conventional and nonconven-

tional crude oil will reach 6.54 billion tons. Refineries will face the tough task of upgrading more heavy oils, not only for clean fuels, but also for the provision of petrochemical raw materials.

Olefin production technology can be separated into noncatalytic and catalytic processes. Nowadays, conventional pyrolysis of light hydrocarbons, a noncatalytic process, plays the dominant role in ethylene production and there have been significant advances in reaction selectivity through innovative designs as well as in energy saving. Catalytic processes have been de-

veloped rapidly in recent decades in an effort to extend the range of possible feedstocks in a variety including heavy hydrocarbons, byproducts from refineries and petrochemical streams and natural gas, as well as coal to olefins. Principal issues to consider in the selection of olefin technology for a grassroots plant or a revamped refining-petrochemical complex with expanded capacity are feedstock optimization, byproduct slate and markets, capital return, and environmental constraints. Many of these issues are site-specific, especially feedstock supply, which varies considerably from region to region. Feedstock preparation for olefin plants mainly involves the limited modification of the hydrogen-to-carbon ratio, either by hydrogen addition or carbon rejection. By virtue of the shortfall in light fraction supply as feedstock, integration of a steam cracker with FCC-modified processes, such as DCC, CPP, or PetroFCC is generally the best choice. Such a combination means making full use of crude by coupling a noncatalytic with a catalytic process.

To comply with the current or probable future clean gasoline specifications, the aromatic content as well as the olefin and sulfur content should be strictly limited. In order to increase the isoparaffin content of the gasoline pool, *Chen* [36.52] has proposed a new clean refinery system with the production and upgrading of light olefins at its heart. He proposed that the production of light olefins by catalytic hydrotreating be coupled with high-temperature catalytic cracking and upgrading of light olefins based on isomerization, oligomerization, and hydration or etherification. All of these processes lead to the manufacture of clean fuels and high-quality synthetic lubricants. *Furtado Ramos* [36.53] has also proposed that light olefins are a valuable raw material for the petrochemical industry, as well as for producing high-quality gasoline through alkylation, isomerization, and etherification.

Catalytic processing for the production of light olefins is the key step in the future towards the integration of refining and petrochemicals plants.

References

- 36.1 B.G. Anderson, R.R. Schumacher, R. Duren, A.P. Singh, R.A. Santen: An attempt to predict the optimum zeolite-based catalyst for selective cracking of naphtha-range hydrocarbons to light olefins, *J. Mol. Catal. A* **181**, 291–301 (2002)
- 36.2 J. Weitkamp, P.A. Jacobs, J.A. Martens: Isomerization and hydrocracking of C₉ through C₁₆ n-alkanes on Pt/HZSM-5 zeolite, *Appl. Catal.* **8**, 123–141 (1983)
- 36.3 J.S. Buchanan, J.G. Santiesteban, W.O. Haag: Mechanistic considerations in acid-catalyzed cracking of olefins, *J. Catal.* **158**, 279–287 (1996)
- 36.4 K. Wakui, K. Satoh, G. Sawada, K. Shiozawa, K. Matano, K. Suzuki, T. Hayakawa, Y. Yoshimura, K. Murata, F. Mizukami: Dehydrogenative cracking of n-butane using double-stage reaction, *Appl. Catal.* **230**, 195–202 (2002)
- 36.5 A. Corma, A.V. Orchilles: Formation of products responsible for motor and research octane of gasolines produced by cracking: The implication of framework Si/Al ratio and operation variables, *J. Catal.* **115**, 551–566 (1989)
- 36.6 L. Smith, A.K. Cheetham, R.E. Morris, L. Marchese, J.M. Thomas, P.A. Wright, J. Chen: On the nature of water bound to a solid acid catalyst, *Science* **271**(5250), 799–802 (1996)
- 36.7 C.M. Wang, Y.D. Wang, Z.K. Xie: Insights into the reaction mechanism of methanol-to-olefins conversion in HSAPO-34 from first principle: Are olefins themselves the dominating hydrocarbon pool species?, *J. Catal.* **301**, 8–19 (2013)
- 36.8 X. Shu, W. Fu, M. He, M. Zhou, Z. Shi, S. Zang: Rare earth-containing high-silica zeolite having pentasil type structure, US Patent (Application) 5 232 675 (1993)
- 36.9 Y.B. Luo, Y. Ouyang, X. Shu, M. He, D. Wang, B. Zong, M. Li: MFI structure molecular sieve containing phosphor and metal component and its use, US Patent (Application) 7 758 847 B2 (2004)
- 36.10 X.L. Hou: *Advances in Refining Technology in China* (China Petrochemical, Beijing 1997) pp. 12–25
- 36.11 X.L. Hou: *Advances in Refining Technology in China* (China Petrochemical, Beijing 1997) pp. 68–78
- 36.12 F.M. Zhang, X. Shu, Z. Shi, W. Wang, F. Qin, X. Wang: US Patent (Application) 6 080 698 (1998)
- 36.13 Z.T. Li, F.K. Jiang, E.Z. Min: DCC – A new propylene production process from vacuum gas oil, *Proc. NPRA Annu. Meet* (1990)
- 36.14 X.Q. Wang, Z.T. Li, F.K. Jiang, B.D. Yu: Commercial trial of DCC (deep catalytic cracking) process for gaseous olefins production, *Proc. AIChE 1991* (1991)
- 36.15 Z.G. Zhang, C.G. Xie, G.Q. Zhu: Experimental study of DCC-plus technology, *Petroleum Process. Petrochem.* **41**(6), 39–43 (2010)
- 36.16 G.Q. Wang, W.Y. Shi, C.G. Xie, Z.T. Li: Catalytic pyrolysis process (CPP) – An upswing of RFCC for ethylene and propylene production, *Proc. 5th Int. Conf. Refinery Processing, AIChE* (2002) pp. 241–249
- 36.17 X.Q. Zhu, C.G. Xie: Research and commercial application of CPP technology for producing light olefins from heavy oil, *China Petroleum Process. Petrochem. Technol.* **15**(3), 7–12 (2013)
- 36.18 D. Greer, M. Houdek, R. Pittman, J. Woodcock: *Proc. DGMK Conf. Creating Value from Light Olefins – Production and Conversion, Hamburg* (2001) pp. 31–43
- 36.19 R.M. Pittman, L.L. Upson: US Patent (Application) 6 538 169 (2003)
- 36.20 V. Rybkin, B. Ellis/UOP: Producing Propylene from FCC Unit. (2007), <http://core.theenergyexchange.co>

- uk/agile_assets/588/RYBKIN_UOP_-_eng.pdf
- 36.21 T. Brookes: New technology developments in the petrochemical industry publication. In: Proc. Echem./Petroleum Economist (2012) <http://www.petroleum-economist.com/pdf/TerryBrookes.pdf>
- 36.22 H.V. Bolt, S. Glanz: Increase propylene yields cost-effectively, *Hydrocarb. Process.* **81**(12), 77 (2002)
- 36.23 H.V. Bolt, H. Zimmermann: Proc. 13th Ethylene Producers Conf (American Institute of Chemical Engineers, New York 2001) pp. 518–547
- 36.24 H.V. Boelt, S. Glanz/Linde: Technology for propylene boosting in steamcrackers. (2003) <http://www.digitalrefining.com/data/articles/1000530>
- 36.25 M.J. Tallman, P.K. Niccum, M.F. Gilbert, C.R. Santner: Consider improving refining and petrochemical integration as a revenue-generating option, *Hydrocarb. Process.* **80**(11), 47–53 (2001)
- 36.26 D.W. Leyshon, G.E. Cozzone: Production of olefins from a mixture of cut olefins and paraffins, US Patent (Application) 5 043 522 (1991)
- 36.27 M.J. Tallman, C.N. Eng/KBR: Propylene on purpose. (2010) <http://www.kbr.com/newsroom/publications/articles/propylene-on-purpose.pdf>
- 36.28 KBR Technology: Superflex 74–Convert light olefinic feeds to propylene, <http://www.digitalrefining.com/data/literature/file/1618768792.pdf>
- 36.29 C. Eng: Producing propylene, *Hydrocarb. Eng.* **9**(7), P69 (2004)
- 36.30 M.J. Tallman, C. Eng: Propylene on purpose, *Hydrocarb. Eng.* **15**(12), 51 (2010)
- 36.31 C. Eng: Economic routes to propylene, *Hydrocarb. Asia* **14**(4), 36 (2004)
- 36.32 D.L. Johnson, K.E. Nariman, R.A. Ware: Catalytic production of light olefin rich in propylene, US Patent (Application) 6 222 087 (2001)
- 36.33 Catalagram Division: Special edition: propylene: opportunities, technologies, markets. (2004), <http://www.grace.com/about/businesses/Documents/Catalagram94SP.pdf>
- 36.34 Nexant: Propylene technology: the next generation. (2009) http://www.chemsystems.com/reports/search/docs/prospectus/MCO9_Propylene_Technology_pros.pdf
- 36.35 P.A. Ruziska, T.R. Steffens: AIChE Spring National Meeting, Technology Session of the 12th Ethylene Producers' Conference, Houston (2001)
- 36.36 J. Teng, Z.K. Xie: OCC process for propylene from C₄ olefins production, *Proc. Hydrocarbon Asia* (2006) p. 26
- 36.37 J. Teng, G. Zhao, Z. Xie, Q. Chen: Production of propylene from C₄ olefins by catalytic cracking – The effect of ZSM-5 crystal size, *Proc. 18th World Petroleum Congr., Johannesburg* (2005) pp. 25–28
- 36.38 J. Teng, R. Wang, Z. Xie, Y. Gan: New olefin production technologies in sinopec SRIPT, *Proc. 19th World Petroleum Congr., Madrid* (Institute of Petroleum, London 2008)
- 36.39 J. Teng, Z. Xie, W. Yang: Catalytic cracking of C₄-olefin to produce propylene over H-ZSM-5. Sinopec, *Proc. 15th Int. Zeolite Conf., Beijing* (2007)
- 36.40 J. De Barros: Olefins conversion technology application, *Proc. 17th World Petroleum Congr., Rio de Janeiro* (2002)
- 36.41 J. Cosyns, J. Chodorge, D. Commereuc, B. Tork: Maximize propylene production, *Hydrocarb. Process.* **77**(3), 61–65 (1998)
- 36.42 J.P. Laugier: Proc. 12th Ethylene Producers Conf. (American Institute of Chemical Engineers, New York 2000) pp. 123–138
- 36.43 CB&I: Olefins Conversion Technology, http://www.cbi.com/images/uploads/tech_sheets/Olefins-12.pdf
- 36.44 S. Kantotorowicz: The path to production, *Hydrocarb. Eng.* **11**(1), P89 (2006)
- 36.45 S. Wenzel. The Uhde STAR process: Oxydehydrogenation of light paraffins to olefins, <http://www.digitalrefining.com/data/literature/file/2130808091.pdf>
- 36.46 M. Heinritz-Adrian, S. Wenzel, F. Youssef/Uhde GmbH: Advanced propane dehydrogenation Oxdehydrogenation-based on-purpose propane dehydrogenation can close the propylene supply-demand gap, (2008) <http://www.digitalrefining.com/article/1000632>
- 36.47 S. Kvisle, H.R. Nilsen, T. Fuglerud, A. Gronvold, B.V. Vora, P.R. Pujado, P.T. Barger, J.M. Andersen: Methanol to Olefins (MtO): State of the art and perspectives, *Proc. DGMK Conf. Creating Value from Light Olefins – Prod. and Convers., Hamburg* (2001) pp. 73–84
- 36.48 P.T. Barger, B.V. Vora: Methanol to olefin process with increased selectivity to ethylene and propylene, US Patent (Application) 6 534 692 (2003)
- 36.49 Total R&D: MTO/OCP: A strategic research project, http://www.totalrefiningchemicals.com/SiteCollectionDocuments/Brochures/Thematic/brochure_mto_en.pdf
- 36.50 J. Zhu, Y. Cui, Y.J. Chen, H.Q. Zhou, Y. Wang, F. Wei: Recent researches on the process from methanol to olefins, *CIESC J.* **61**(7), 1674–1984 (2010)
- 36.51 R.W. Haddock: The Integration of Refining and Petrochemicals, (1999) NPRA, IPC-99-66
- 36.52 N.Y. Chen: An environmentally friendly oil industry?, *Chem. Innov.* **31**(4), 11–21 (2001)
- 36.53 J.G. Furtado Ramos, A. Pinho: Double riser FCC: An opportunity for the petrochemical industry, *Proc. NPRA* (2006)

Polyolefins

37. Polyolefins

David Fiscus, Antonios Doufas, Sudhin Datta

The petroleum refining industry produces small fractions of volatile olefins in addition to transportation fuels such as gasoline. In aggregate, these olefins represent very large quantities because of the huge scale of the primary refining industry. The availability of these olefins has given rise to a worldwide polyolefin industry which makes most of the common rubbers and plastics in use today. These olefins are converted to high polymers by the process of polymerization. The polymers span an unexpected range of thermal and mechanical properties. The introduction and the acceptance of these polymers arise from continuous innovation which improves the properties for use. The introduction of new fabrication processes allow the utilization of novel methods to produce forms with typical densities at or below 1.00 gm/cc, leading to lightweight materials.

37.1	Olefin Feedstocks and Derived Polymers	1082	37.6	Synthesis and Processing of Polyethylene	1088
37.1.1	Olefin Feedstocks.....	1082	37.6.1	Polyethylene.....	1088
37.1.2	General Polymerization Processes.....	1082	37.6.2	Historical Perspective.....	1089
37.2	Polymerization Mechanism	1083	37.7	Polyethylene Process and Catalysts ..	1090
37.2.1	Free Radical Polymerization.....	1083	37.7.1	High-Pressure Low-Density Polyethylene.....	1090
37.2.2	Ionic Polymerization.....	1083	37.7.2	Chromium Catalysts.....	1090
37.2.3	Coordination or Metal Complex Polymerization.....	1083	37.7.3	Ziegler-Natta Catalysts.....	1090
37.3	Polymerization Processes	1084	37.7.4	Supported Catalysts.....	1090
37.3.1	Bulk Polymerization.....	1084	37.7.5	Metallocene Catalysts.....	1090
37.3.2	Solution Polymerization.....	1084	37.7.6	Combined Processes.....	1091
37.3.3	Suspension Polymerization.....	1084	37.8	Structure of Polyethylene	1091
37.3.4	Emulsion Polymerization.....	1085	37.8.1	Morphology.....	1091
37.3.5	Gas-Phase Process.....	1085	37.9	Polyethylene Processing	1091
37.4	Postpolymerization Process	1085	37.9.1	Processing.....	1091
37.4.1	Mixing Equipment.....	1085	37.10	Synthesis and Processing of Polypropylene	1094
37.5	The Structure of Polymers	1086	37.10.1	Background.....	1094
37.5.1	Monomer Insertion.....	1086	37.11	Polypropylene Process and Catalysts	1094
37.5.2	Monomer Sequence in Copolymers ...	1086	37.11.1	Polymerization Processes.....	1094
37.5.3	Molecular Weight and Molecular Weight Distribution ...	1086	37.11.2	Extrusion and Finishing Processes ...	1097
37.5.4	Linearity and Branching.....	1087	37.12	Polypropylene Fabrication	1098
37.5.5	Mechanical Properties.....	1087	37.12.1	Polypropylene Rheology and Process Instabilities.....	1099
			37.12.2	Melt Fracture.....	1099
			37.12.3	Wall Slip.....	1100
			37.12.4	Processing Aids.....	1100
			37.12.5	Extrusion Surging.....	1100
			37.12.6	Compounding and Blending.....	1100
			37.12.7	Fibers and Nonwovens.....	1101
			37.12.8	Spunbond Nonwovens.....	1101
			37.12.9	Melt-Blown Nonwovens.....	1102
			37.12.10	Unoriented/Low-Orientation Films and Sheets.....	1103
			37.12.11	Thermoforming.....	1103
			37.12.12	Oriented Films.....	1103
			37.12.13	Injection Molding.....	1104
			37.13	Synthesis and Processing of Elastomers	1105
			37.13.1	Elastomer IUPAC Nomenclature.....	1105

37.14	Polybutadiene (BR)	1106	37.16.2	Structures of EPM and EPDM and Their Influence on Properties	1110
37.14.1	Synthesis.....	1106	37.16.3	Compounding of EPM and EPDM.....	1110
37.14.2	Structure of BR and Its Influence on Properties.....	1106	37.16.4	Processing of EPM and EPDM	1111
37.14.3	Compounding and Vulcanization of BR	1107	37.16.5	Properties of EPM and EPDM Vulcanizates	1111
37.14.4	Uses of BR	1107	37.17	Butyl (IIR) and Halobutyl Rubber	1112
37.15	Styrene–Butadiene Rubber (SBR)	1107	37.17.1	Synthesis.....	1112
37.15.1	Synthesis.....	1107	37.17.2	Structure of IIR and Its Influence on Properties.....	1112
37.15.2	Structure of SBR and Its Influence on Properties.....	1108	37.17.3	Properties of IIR Vulcanizates	1112
37.15.3	Compounding and Vulcanization of SBR.....	1109	37.17.4	Uses of IIR	1113
37.16	Ethylene–Propylene Rubber (EPR/EPDM)	1109	37.17.5	Synthesis CIIR and BIIR	1113
37.16.1	Synthesis.....	1109	37.18	Conclusion	1113
			References		1113

37.1 Olefin Feedstocks and Derived Polymers

37.1.1 Olefin Feedstocks

The feedstocks that are widely used for making polymers are described in Table 37.1. Most of the feedstocks are olefins and are derived as by-products of petroleum refining processes. These feedstocks are converted to polymers by the process of polymerization. Only a few polymers derived from these feedstocks are considered in this section, it is however exemplary that even for this small subset there are a number of manufacturing processes which lead to polymers and a larger number of fabrication processes for making products containing these polymers. The introduction and the acceptance of these polymers arise from continuous innovation to improve both properties and applications. The introduction of a new fabrication process allows the utilization of novel methods to produce forms with typical densities at or below 1.00 gm/cc, leading to lightweight materials.

37.1.2 General Polymerization Processes

A *polymer* (from Greek poly = many and meros = units) is a substance composed of macromolecules

Table 37.1 Olefin feedstocks

Olefin monomer	Chemical formula	Boiling point (°C)
Ethylene	C ₂ H ₄	−104
Propylene	C ₃ H ₆	−48
Butadiene	C ₄ H ₆	−5
Styrene	C ₈ H ₈	145
Isobutene	C ₄ H ₈	−7

built by covalently joining at least 50 monomer segments. The word polymer was introduced in 1832 by Jons Jacob Berzelius for substances that may have identical chemical composition but differ in molecular weight (MW) [37.1]. A polymer's chemical composition relates to the relative amounts of the constituent monomers while its molecular weight describes the number of monomers it contains and thus represents molecular size. Unlike typical discrete small molecules, polymer samples typically contain a distribution of molecular sizes arising from a corresponding distribution of individual molecular weights. This distribution of molecular weights is usually expressed as a number average or weight average value. A polymer's average molecular weight is an important factor in determining its performance and utility.

The polymerization of a petroleum-derived olefin monomer is dependent on the availability of double bonds, where the carbon atoms share both σ and π electrons. The π bonds can be broken under the influence of an external polymerization catalyst in a polymerization process and the result is the formation of two new σ bonds which link the monomers together at the expense of two π bonds. This process is highly exothermic. The representative polymerization of ethylene to polyethylene (PE) liberates 3.34 kJ/gm of heat. This chain growth process, repeated many times, leads to industrial polymers typically containing between 1000 and 15 000 monomer units. There are always three reaction steps in a polymerization:

- Initiation
- Propagation
- Termination.

Polymerization of high molecular weight polymers requires the propagation rates to be many times larger than the termination rates. Polymerization reactions can take place in a homogeneous phase such as bulk or solution or in a heterogeneous phase such as particle

forming or emulsion. A particularly common embodiment of the latter process for polyolefin thermoplastic is gas-phase polymerization where semicrystalline solid polymer is condensed from a gaseous mixture of olefins.

37.2 Polymerization Mechanism

37.2.1 Free Radical Polymerization

In free radical polymerizations, the homolytic dissociation of the π electrons in the double bond constitutes the initiation reaction. Dissociation occurs due to heat, light, electron transfer, or reaction with free radicals derived from agents such as peroxides. These agents initiate the polymerization. The most frequently used initiators are chemical electron transfer redox systems and free radical generation from peroxides. The initiation of the polymerization is followed by multiple propagation steps, where the polymer chain grows through stepwise addition of monomer molecules, until the polymerization reaction is terminated. Initiation, propagation, and termination are not temporally correlated but are each statistical time-dependent phenomenon. Thus, the lengths and composition of the chains do vary because of differences in degrees of polymerization, resulting in different distributions of molecular weight. The growing polymer chain can react with chain transfer agents whereby the current macromolecule is deactivated and a new polymer chain is initiated. Chain transfer reduces the molecular weight and modifies the branching character of the polymers. Thus, these modifications control the technological properties of polymers, such as processability. Free radical copolymers can be made by the copolymerization of two or more monomers. This follows the same pattern as the homopolymerization except that monomer radicals can be formed by all of the different monomers present. As a limiting example, one type of polyethylene (low density) is typically made by free radical polymerization [37.2]. In general, free radical polymerization leads to arboreal polymers with a mixture of short-chain branches (e.g., C_1 to C_6) and long-chain branches (e.g., up to several hundred carbon atoms). The architecture of the long-chain branches is similar to that of the polymer's backbone.

37.2.2 Ionic Polymerization

In ionic polymerization, electron pairs are asymmetrically allocated to the active polymerization intermediates to lead to anionic or cationic species. These initiators start the polymerization, which then propagates

as a chain reaction. While in a free radical polymerization, the initiator radical transfers the uncharged free radical to a monomer molecule, in ionic polymerizations, there is a transfer of charge from the initiator ion to the monomer. At the start of the polymerization, the initiator ion transfers the π -electrons of a monomer molecule to one or the other carbon atom, depending on the charge. Subsequently, the initiator attaches to the monomer, which then becomes the new initiator, attaching an additional polarized monomer molecule to form a growing polymer ion.

A cationic polymerization can be initiated by Bronsted or Lewis acids (e.g., H_2SO_4 , $AlCl_3$, BF_3), requiring typically, small amounts of cocatalyst, such as water or alcohol. Anionic polymerization initiators are most commonly alkyl lithium compounds. Since the activation energies for the initiation reactions are often significantly smaller for ionic than for free radical polymerizations, these polymerizations can often be carried out at low temperatures. Chain transfer reactions can also occur with cationic polymerizations. However, as the polymerization temperature is lowered, these reactions become less frequent and thus ionic polymerizations at low temperatures lead to high molecular weight polymers. Under these conditions, chain transfer reactions are almost eliminated with anionic polymerizations leading to very narrow molecular weight distributions. These polymerization sites are active even after all monomers are incorporated leading to *living polymers* that are capable of further growth on addition of fresh monomer. Block copolymers can be produced if a different kind of monomer is added partway through the polymerization process.

37.2.3 Coordination or Metal Complex Polymerization

In coordination polymerization reactions, the initiator is a metal complex, attached to the growing end of the polymer chain, and the chain reaction progresses by the insertion of monomer molecules into this complex. The most commonly used initiators are the Ziegler–Natta catalysts. These are reaction products of organometallic group I to III elements, and transi-

tion metal salts of group IV to VIII elements. Typical examples of Ziegler–Natta catalysts are mixtures of aluminum alkyls and halides of titanium, cobalt, nickel, vanadium or tungsten. The catalytic activity of these transition metal compounds may be due to their ability to form coordinate bonds with unshared pairs of π -electrons from olefins or dienes. This ability allows the catalysts to exchange one type of bond for another, and this exchange is the pertinent feature of the propagation (or insertion) reaction step at the transition metal ion. In contrast to both free radical and ionic polymerization as a monomer unit enters the polymer chain which is always connected to a metal center, it is possible to have a definite stereochemistry for this insertion to lead to a sterically controlled chain propagation, leading

to sterically configured (e.g., isotactic or syndiotactic) polymers.

These polymerization processes typically produce linear polymers. The catalysts determine the resin's chemical composition, the sequencing in copolymers, and molar mass distributions. For example, the linear low-density polyethylene produced using chromium and Ziegler–Natta catalysts have minor amounts of low-molecular-weight waxes and high-molecular-weight high-density components in conjunction with the predominate component, which has an intermediate density and molecular weight. Single-site catalysts produce resins with more uniform chemical composition and molar mass distributions than those produced using the chromium and Ziegler–Natta catalysts.

37.3 Polymerization Processes

37.3.1 Bulk Polymerization

In this process, the polymerization occurs in the pure, liquid, or gaseous monomer without solvent being present. The heat of polymerization is dissipated through refrigeration across the wall of the reactor or by evaporation followed by condensation of the liquid monomer. The first synthetic polymers nearly a 100 years ago were made in a bulk polymerization process.

37.3.2 Solution Polymerization

In solution polymerizations, the monomers are dissolved in a solvent which also acts as a solvent for the polymer. In solution processes, polymerization occurs at a temperature above the melting temperature of the polymer in hydrocarbon solvents, like cyclohexane or paraffinic hydrocarbon. The reactors are typically small continuous stirred tank reactors. The catalyst, reactants, and solvent are continuously added to the reactor. The solution is continuously removed from the reactor and the polymer recovered by removing the solvent. During polymerization the viscosity of the reaction medium rises with both the concentration of the polymer in solution and its molecular weight of polymerization, this limits the extent of polymerization as the viscosity of the solution becomes a limiting criteria. Solution polymerization is however an excellent process for polymerizing different monomers into the same polymer. The polymer content in steady state in solution is about 35% by weight for low molecular weight resins and less for higher molecular weight polymers. The reactor temperatures range between 120 and 300°C. The

reactor pressures range between 360 and 1500 psi. The residence time of the polymer in the reactor ranges between 1 and 30 min. The resin's molecular weight is controlled by the reactor conditions (temperature and pressure) or by adding transfer agents to the reactor. The process allows for short transition times between grades.

37.3.3 Suspension Polymerization

In suspension polymerization a liquified monomer is used as the medium and the other polymerization ingredients are added to it. In this process, polymerization occurs in the hydrocarbon medium at a temperature below the melting temperature of the polymer: thus the polymer is essentially insoluble. Typical reaction mediums are propane, isobutene, isopentane, and hexane. The catalyst, reactants, and solvent are continuously added to the reactor. The resulting high polymer is insoluble in the monomer, and remains suspended as a slurry in the reaction medium. The suspension/slurry is well agitated to prevent reactor fouling, i.e., the resin from sticking to the reactor's walls and limiting heat transfer. The slurry is constantly removed from the reactor and the polymer recovered by removing the solvent. Slurry processes are conducted in stirred tank or slurry loop reactors. In suspension polymerizations, the viscosity of the reaction medium increases only fractionally with either the increasing molecular weight or increasing weight fraction of the polymers. Thus, polymers with very high molecular weights can be made by this process with a high degree of conversion as well as a high concentration of polymer in the slurry ($\approx 60\%$ w/w). The polymer molecular weight is con-

trolled by controlling the reactor conditions or adding chain transfer agents to the reactor [37.3].

37.3.4 Emulsion Polymerization

Emulsion polymerization is an important example of free radical suspension polymerizations where water-insoluble monomers form water-insoluble polymers as latex. Emulsifiers or surfactants are required to maintain this morphology. The latex contains hydrocarbon droplets with a diameter of about 10^{-4} cm. Polymerization occurs within these suspended hydrocarbon latex particles. Compared to homogeneous polymerization the suspension or emulsion process has the following advantages:

- The continuous water media promotes easy removal of heat of polymerization.
- The diffusion of monomers into the latex is faster than polymerization, leading to uniform composition.
- The process is capable of a wide range of polymer viscosity.

37.3.5 Gas-Phase Process

In 1968, Union Carbide commercialized a fluidized-bed gas-phase process for polymerization utilizing low

temperatures and pressures. In this process, reactants, nitrogen, and catalyst are fed into a cylindrical reactor with constant and turbulent agitation in a flowing gas stream where polymerization takes place. The reaction components as gases and a diluent gas, typically nitrogen, are introduced into the bottom of the reactor through a distribution plate. The catalyst is added to the reactor above the distribution plate. The polymer particles that form are fluidized by the incoming gas stream. The polymer is continuously withdrawn from the reactor and recovered. The unreacted monomer and comonomer are separated and returned to the recycle stream. The gas-phase process is a very versatile process with low capital cost and broad polymer capability. These characteristics have made it the most widely used process for manufacturing polyethylene resins [37.4]. The inter-comonomer versus intra-comonomer distributions in resins produced in gas-phase processes are less uniform than those in resins produced in solution processes because of the differences in the mass transfer and reaction kinetics of the two processes.

Current gas-phase reactors have an L/D ratio of about 7. The reactor temperatures range between 60 and 110 °C, preferably less than about 80 °C. The reactor pressures are between about 200 and 500 psi. The residence time of the polymer in the reactor is several hours. The production rates are in excess of twice those obtained in the other processes [37.5].

37.4 Postpolymerization Process

Processing polymers has three component parts: the intimate mixing of ingredients, the fabrication of these mixtures, and a postfabrication annealing/vulcanization step for property enhancement. Ingredients can consist of low molecular weight additives as well as other polymers. Fabrication consists of shaping the mixtures to form fibers, sheets, laminates, and composites that are useful. In most processing applications there are additional, quiescent steps of heat treatment involved referred to as ageing, annealing, or vulcanization to induce irreversible physical or chemical changes in the polymer for better properties or durability.

37.4.1 Mixing Equipment

Addition of a portion of nonpolymeric ingredients, to improve the properties of polymers arises from the addition of fillers, plasticizers, protectants or vulcanizing agents, largely promoted by the need for tires [37.6]. The first internal processing equipment was by Werner & Pfleiderer GmbH [37.7]. The first enclosed batch

internal mixer with a ram closure was, and still is based on the subsequent design by *Banbury* [37.8]. This elliptical design with clamshell housing containing cooling–heating channels and bottom drop is largely the basis of commercial batch mixers to this day. The only major innovation was the invention of intermeshing rotor internal mixers by *Cooke* [37.9]. This allows high shear stresses to be applied to the compounds between the rotors as well as between the rotor and the mixing chamber wall. The Banbury internal mixers have industry standard performance. In comparing two-flight and four-flight rotors in Banbury design internal mixers *Cho* et al. [37.10] have showed the superior mixing ability of the latter rotors.

These batch mixers were soon supplanted by continuous mixers having similar mixing elements. The earliest description of a continuous mixer was by *Pfleiderer* [37.11] where two nonintermeshing counter-rotating shafts with sigma blade mixing elements and intermediate conveying screw sections were described. More sophisticated machine devices for mastication,

compounding, and blending include single-screw devices such as List's Buss Kokneter [37.12] and those with intermeshing counter-rotating kneading pumps such as from *Leistritz* and *Burghauser* [37.13]. In the last 50 years the development has been exclusively on twin-screw machines which are better continuous mixers. The concept of a self-wiping corotating twin-screw extruder dates to the beginning of the twentieth century with an intermeshing twin-screw extruder that was developed in 1939 by *Colombo* [37.14]. Several of these machines were purchased by IG Farbenindustrie and applied for polymer mixing and polymer dewatering [37.15]. This was followed by developments which are incorporated largely unchanged in today's continuous twin-screw extruders such as twin-

rotor kneading disc block mixing [37.16] and the twin-screw devolatilizer [37.17]. However, alternate designs of continuous mixers also evolved in parallel. An example of this is the nonintermeshing counter-rotating twin-screw extruder by *Farrell* [37.18], which has rotors consisting of screws feeding Banbury-like rotors. It has been widely used in the compounding and polymerization industries.

Modeling the performance and flow, both in individual modules and in composite modular machines [37.19] can predict fill factor and pressure and temperature profiles along the screws. Many efforts have been made to simulate the flow in individual modules of the machine as well as composite models of the mixing and metering section near the machine exit [37.20].

37.5 The Structure of Polymers

37.5.1 Monomer Insertion

Olefins can react in various ways in a polymerization and thus yield polymer molecules with significantly different structures. These differences arise from intrinsic *cis-trans* insertion of olefins during insertion and 1, 2 versus the less common 1, 3 or 1, 4 insertion. Specific conditions under which the polymerizations are carried out determine these insertion procedures. In addition to this insertion isomerization during polymerization various forms of stereoisomerization in the insertion of the monomer can also lead to differences in the polymer. Stereoisomerization is reflected in the geometry of the relationship of adjacent or nearby monomer units. In the case of polymerization catalyzed by coordination catalysts an additional isomeric form of insertion is in the mutual relationship of the adjacent monomer units. These differences lead to differences in tacticity from a *meso* to racemic structure in a pendant group.

37.5.2 Monomer Sequence in Copolymers

In copolymers an important difference is the repeat unit sequence. The statistical control of this sequence and sequence length is measured by the reactivity ratio $r_1 r_2$. This measure quantifies the statistics of the catenation sequence of the two monomers with low values indicating an alternating sequence while high values indicate a propensity to homologation. Copolymerization using several different monomers can lead to differences in the sequence distribution of monomers in the copolymer depending on the polymerization process [37.21]. Reactivity ratio values predict the statistics of the sequencing of the different monomers. This is exemplified

below in a hypothetical copolymer of A and B monomer units for certain limiting cases:

- $r_1 r_2 = 0$: Monomer sequence is strictly alternating since there are no A-A or B-B linkages and the polymer is -A-B-A-B-A-B-A-B-A-B-A-B-. Homopolymerization of either monomers is absent and the composition of the polymer is independent of the monomer feeds.
- $r_1 r_2 = 1$: Monomer sequence is completely random and determined by the feed composition and there are A-A or B-B linkages and the polymer is -A-B-A-A-B-A-B-B-B-A-B-. Homopolymerization of either monomers is present.
- $r_1 r_2 = \infty$: Monomer sequence is strictly a homopolymerization of two monomers since there are only A-A or B-B linkages and the polymer is -A-A-A-A-A-A-B-B-B-B-B-B- if a single A-B linkage is allowed kinetically. Homopolymerization of either monomers is present and the composition of the polymer is independent of the monomer feeds.

37.5.3 Molecular Weight and Molecular Weight Distribution

The distribution of molecular weights determines in great measure the processability of polymers. Polymers with a narrow molecular weight distribution soften only in a very limited range of temperatures, which has a negative influence on mixing processes. Because of their easy processing characteristics and better filler distribution, it is desirable to have polymers with a broad molecular weight distribution, where the low molecular weight portions behave somewhat like plasticizers.

If the molecular weight is too high, the processing of the resin is difficult because of the high viscosity. Such products either have to be degraded in molecular weight (*masticated*) prior to use, or they have to be extended with appropriate amounts of plasticizer. The latter improves the processability and it reduces the price of the product.

Today, very high molecular weight polymers, in particular rubbers which are extended with oil are commercially useful since in many cases the limited plasticizer extension does not impair the mechanical properties of the vulcanizate. A very high molecular weight-based polymer with a high tensile strength is used for this purpose, and the oil extension only reduces the processing viscosity to a practical level. Without oil extension the high strength properties of the base polymer cannot be exploited. Since the tensile behavior depends, amongst others, on the length of the primary polymer molecule, low molecular weight polymers are typically prone to mechanical failure.

37.5.4 Linearity and Branching

There are additional structural elements of the polymer molecule, such as linearity, short- or long-chain branching, and crosslinking (gel), which have a considerable influence on the processability as well as on the mechanical property spectrum. In most instances branching is welcome for processing advantages but gels are not since they lead to both optical and mechanical defects.

37.5.5 Mechanical Properties

The performance of a plastic part is greatly influenced by its resin's molecular architecture (molar mass, chemical composition, and long-chain branch content) and morphology (arrangement of crystalline and noncrystalline material) as fixed by the way the part is formed. All else being equal, a part's performance reflects that of its resin(s). A resin's stiffness increases with an increase in its density, while its strength and toughness (tear and impact resistance) increase with an increase in its molecular weight. The performance of resins is the same in all directions, i. e., isotropic. In general, extrusion and molding causes parts to be anisotropic – perform differently in one direction relative to another. Thicker parts are stronger than thinner parts.

A resin's strength is determined using a tensile test – a mechanical test measuring a material's response to an applied load/force. This test characterizes a resin's deformation behavior (elongation, deformation, and failure), allows comparing the performance of different resins, and determines how a resin's molec-

ular architecture affects its performance. Typically, an isotropic material of known dimensions (length and cross-sectional area, for example) is clamped by two *grips* with a known separation distance. One grip is moved away from the other grip, which is fixed. The force/energy required to separate the grips is transferred to the test specimen. The applied force is plotted against the distance the specimen deforms. The plot is called a load–displacement, stress–strain, or force–elongation curve (see the discussion below). The energy imparted to and dissipated by materials can be determined from these curves. This strain energy is proportional to the energy the materials dissipate during impact and tear testing.

Tensile tests are typically used to characterize a resin's stiffness, yield performance, plastic deformation/necking behavior, and ultimate properties.

Stiffness

Under a load, a polymer elongates reversibly until the applied force or elongation exceed threshold values, where upon the resin yields and deforms plastically, as discussed below. A resin's reversible elongation prior to yielding is referred to as stiffness. Stiffness describes a resin's resistance to deforming by elongation or bend processes. A material's stiffness is quantified as the ratio of the force required to elongate a sample reversibly to the amount the sample elongates under that load. A resin's stiffness is usually determined using up to the first 3% of its stress–strain curve.

Yield

The yield reaches a local maximum in the stress–strain curves for semicrystalline polymers. The local maximum becomes more pronounced as the resin's density increases, the strain rate of the test increases or the temperature at which the testing is conducted decreases.

Plastic Deformation/Necking

After yielding, semicrystalline polymers typically deform plastically: irreversibly and nonuniformly by thinning in the directions perpendicular to applied forces for several hundred percent without rupturing. The material thins over part of its length to form a constriction or *neck* in which the stretch is large and the sample's cross-sectional area is decreased relative to its initial cross-sectional area, while the rest of the sample is slightly stretched without a significant change. The constriction or *neck* can stabilize and travel along the material during tensile testing. As it travels, more of the sample is drawn into the necked region. This necking continues until the stretched region reaches the resin's natural draw, at which point no more sample is drawn into the necked region.

Ultimate Performance

Stretching a semicrystalline polymer beyond its natural draw results in irreversibly but uniformly drawing the necked region until the sample fails. This uniform stretching is called strain hardening, and the material's engineering strain increases with an increase in its engineering stress. The ratio of the material's force to elongation during strain hardening is referred to as its ultimate modulus. A linear resin's ultimate modulus and performance increase with an increase in the resin's molecular weight [37.22].

A stress-strain curve can be used to determine the energy dissipated by materials in a variety of tests and end-use applications. Simply stated, the energy a material dissipated during a tensile test is a measure of the energy it dissipates during other tests (tear and impact) and in end-use applications. Load-displacement curves allow one to determine the amount of work required to deform resins, i. e., the amount of energy consumed by resins under tensile testing conditions (strain rate and temperature). Increasing the amount of energy a resin consumes during a tensile test increases its strength and mechanical performance. Plastics dissipate energy differently at different strain rates with the energy dissipated at high strain rates being proportional to that dissipated at low strain rates. Low strain rates are used in tensile testing, while high strain rates are used in tear and impact testing. Increasing the amount of energy a resin consumes during a tensile test increases its strength, toughness, and mechanical performance like tear and impact resistance.

As mentioned above, extrusion and molding can create anisotropy in materials. The orientation causes

the material's tensile curves to deviate from those of corresponding isotropic materials. Increasing orientation shifts the material's tensile curve to appear like that of a higher molecular weight material. In this way, orientation alters the energy-absorbing capabilities of materials; increasing it in one direction and decreasing it in another.

Tear and Impact

In addition to strength, other key mechanical properties of resins are tear and impact resistance, i. e., the resin's toughness. Tear resistance is the tendency of a test specimen to resist the growth of a cut when the specimen is in tension. Increasing the strain energy in the direction of the test specimen perpendicular to the direction of the cut increases the specimen's tear resistance. Impact resistance is the tendency of a test specimen to resist a sudden impact. Balancing the strain energy in all directions of the test specimen increases its impact resistance.

In addition to the above, a resin's toughness, particularly its impact resistance, increases with an increase in the uniformity of its composition distribution and, for semicrystalline polymers, lamella thickness. Higher α -olefin comonomers (1-hexene and 1-octene) increased the toughness of polyethylene compared to lower α -olefins (propylene and butane). Increasing the size of the comonomer increases the amount of tie chains in a resin with the increase decreasing as the length of the chain increases. Further, a resin's toughness increases as the lamella become smaller, i. e., thinner and shorter. Smaller lamella convert into amorphous material more easily than larger lamella.

37.6 Synthesis and Processing of Polyethylene

37.6.1 Polyethylene

Polyethylene is a semicrystalline thermoplastic polymer made by polymerizing ethylene alone and with comonomers to form either linear chains or three-dimensional networks of polymer chains [37.23]. Ethylene is readily available from natural gas and as a by-product to the refining of crude oil into gasoline, fuel oils, lube oils, and industrial chemicals. Ethane is present in natural gas and as a by-product of the refining processes and is cracked to give ethylene. The forecast is for natural gas, which costs a fraction of crude oil (e.g., from shale), to provide the majority of ethylene for the foreseeable future. The comonomers are derivatives of ethylene, most of which are termi-

nal α -olefins, or more rarely, cyclic olefins or dienes. Most commercial polyethylene resins contain more than 2000 mer while those used for structural applications contain greater than 4000 mer. A resin's chemical composition is an important factor in determining its properties. Decreasing the comonomer content in a resin increases its stiffness at the expense of its toughness.

Polyethylene is the most widely used plastic with global annual consumption exceeding 80×10^3 MT/yr and growth rate increasing, depending on the source, in the high to low double digits per annum. It is clear that growth in developing economies exceeds that in the more mature regions. Polyethylene obtained its lead position in the plastics industry because of its cheap feed

stock, ease of manufacture and conversion into inexpensive articles of commerce having superior performance in applications, such as film, automotive, transportation, medical, electronic, computer, consumer product, packaging, coating, pharmaceuticals, pipe, conduit, tubing, foams, durable goods, and wire and cable. More than half of all polyethylene resins go into film applications.

Polyethylene resins are produced by over 30 major companies in over 35 countries using one of four manufacturing processes:

- High pressure
- Solution
- Slurry
- Gas-phase processes.

The various manufacturing processes make polymers with similar composition but different molecular architectures and thus properties. These differences are in both processing during fabrication (extrudability and drawability) and mechanical properties (stiffness, tensile strength, tear resistance, and impact resistance). The high-pressure processes employ exclusively free radical chemistry to produce resins that are slightly easier to process compared to those produced using the other processes which employ catalysts (Ziegler–Natta, chrome and single-site catalysts). These metal-catalyzed processes produce resins with superior mechanical properties. Each catalyst produces slightly different resins leading to the coexistence of all of these manufacturing processes.

37.6.2 Historical Perspective

Between 1890 and 1898, crystalline, high-density polyethylene was being made in laboratories via diazo methane polymerization [37.24]. In 1933, ICI in England started experimental work to produce polyethylene. In 1935, this work resulted in producing polyethylene using oxygen as the free radical initiator, followed in 1937 by the first high-pressure pilot plant and in 1939 by commercial production of low-density polyethylene. In 1940, BASF in Germany developed a high-pressure tubular reactor to produce high-pressure polyethylene resins, referred to as low-density polyethylene (LDPE) resins. The characteristic structure of LDPE resins is long-chain branches.

Using lower pressures, the Phillips slurry process alleviated some safety issues associated with high-pressure processes, and increased the production rates of polyethylene resins. This process, unlike the high-pressure process yielded linear resins with improved

physical properties over LDPE. Further, these processes allow one to control the amounts and types of comonomers incorporated into the polymer by addition of comonomer to the reactor. The development of new polyethylene resins centers on using dual metallocene catalyst systems in gas-phase reactors to provide tailored resins having both superior processability and toughness: easy processing with a superior balance of lifting ability, stiffness, tear resistance, and impact resistance. Commodity grades will be produced by gas-phase processes. Specialty grades will be produced by the other processes (high pressure, solution, and slurry).

The tubular process is different from the autoclave process, although both processes utilize free radical chemistry and have similar operating characteristics: pressures ranging between 2 and 50 kpsi (179–219 MPa), and temperatures ranging between 120 and 300 °C. Development of lower pressure processes for manufacturing polyethylene began in the late 1940s. These low-pressure processes alleviate some safety issues associated with the high-pressure processes, employ catalysts that increased the production rate for making resins, and yield linear resins with improved physical properties over the LDPE resins. The low-pressure processes operate at pressures less than 1.5 kpsi (10 MPa), temperatures less than 300 °C, and are conducted in solution, slurry, and gas-phase equipment. The chromium, Ziegler–Natta, and metallocene catalysts employed provide linear resins while introducing various amounts and types of comonomers into the polymer. The linear resins have improved physical properties over the LDPE resins. The comonomers are introduced and controlled by the amount of comonomers added to the reactor.

Currently, commercial grades of polyethylene resins are referred to as:

- Low-density polyethylene (LDPE)
- Linear low-density polyethylene (LLDPE)
- High-density polyethylene (HDPE)
- Very low-density polyethylene (VLDPE)
- Ultrahigh molecular weight polyethylene (UHMWPE).

These collectively ... *have bulk densities ranging between about 0.915 and 0.96 g cm⁻³, melting temperatures between 100 and 136 °C, and crystallinities between 40 and 90% ...* [37.25] (Table 37.2).

VLDPE resins or plastomers contain more than 10% by weight comonomer and can contain up to about 35% by weight comonomer. Plastomers incorporate the qualities of elastomers, such as rubber-like properties,

Table 37.2 Classification and properties of polyethylene resins

Classification	Density (g/cc)	Comonomer content (wt%)	Typical peak melting point (°C)	Crystallinity (%)	M_w (D)	Introduction
HDPE	> 0.95	< 2.5%	130–135	70–90	–	1957
LLDPE	0.91–0.95	< 10%	115–125	35–60	–	1965
LDPE	0.91–0.92	< 10%	108–115	45–65	–	1933
VLDPE	0.86–0.90	10–35%	–	20	–	–
UHMWPE	≈ 0.94	> 35%	N/A	–	> 3×10^6	–

into polyethylene resins. Specifically, elastomers undergo a permanent thinning in a direction perpendicular to an applied force with the extent of thinning in-

creasing with the applied load, but the resins recover a significant portion of their original shape once the applied force is removed.

37.7 Polyethylene Process and Catalysts

37.7.1 High-Pressure Low-Density Polyethylene

In high-pressure polyethylene manufacturing processes polyethylene resins are made in liquid ethylene at temperatures above the polymer melting point. Only about 30% of the ethylene is polymerized using a free radical initiator. The resin's molecular weight is controlled by regulating the reactor's pressure and temperature, and by using chain transfer agents. The polymerization is highly exothermic leading to temperature rises that if not controlled can result in reactor instabilities. The high-pressure processes are conducted in autoclave and tubular reactors which produce resins with densities between 0.920 and 0.927 g/cc. The crystallinity of the resins is between about 50 and 60%. Autoclave processes give resins with higher proportions of long-chain branches and greater amounts of low molecular weight components compared to the tubular process. In general, higher pressures lead to higher molecular weight resins, while higher temperatures increase branching in the resin. In these free radical processes, ethylene can be copolymerized with a wide range of comonomers, such as vinyl acetate and acrylates.

37.7.2 Chromium Catalysts

After World War II, Phillips Petroleum and Standard Oil Company of Indiana developed transition metal catalysts supported on metal oxides to polymerize ethylene into linear polyethylene in hydrocarbon liquids. In 1951, Phillips Petroleum used silica-supported chromium trioxide catalyst to produce a high-molecular-weight high-density polyethylene resin. The current Phillips slurry loop process pro-

duces resins with a broad range of molecular weights and densities greater than 0.95 g/cc.

37.7.3 Ziegler–Natta Catalysts

Ziegler–Natta catalysts are combinations of a transition metal catalyst (typically titanium tetrachloride) and organometallic activator (typically an aluminum alkyl). In 1953, commercial Ziegler–Natta catalysts were developed to make high-density polyethylene resins at atmospheric pressure and ambient temperature. Karl Ziegler began development of the Ziegler–Natta catalysts in 1940 using triethyl aluminum. Development of the Ziegler–Natta catalysts allowed increased incorporation of comonomers to densities below 0.92 g/cc. The early Ziegler–Natta catalysts were unsupported. In the 1960s, Ziegler–Natta catalyzed linear low-density polyethylene resins were commercialized.

37.7.4 Supported Catalysts

In the 1970s supported catalyst systems were developed. Ziegler–Natta catalysts were supported on magnesium chloride. Union Carbide supported chromium catalysts on other materials than the metal oxides that Standard Oil Company of Indiana used. These supported systems make the active centers of the catalysts more accessible to monomers which dramatically improves the catalyst's efficiency, meaning the catalyst does not have to be removed from the resin [37.26, 27].

37.7.5 Metallocene Catalysts

In the 1990s, Exxon and Dow Chemical Companies commercialized metallocene catalysts that produce low

density and plastomers. These catalysts have a single active site, unlike the chromium and Ziegler–Natta catalysts that have multiple active sites as discussed above. The metallocene resins are composed of one population of resin instead of a mixture of resins. The metallocene resins lack the low molecular weight waxes and high-molecular-weight high-density components inherent in the conventional linear low-density polyethylene resins.

Current efforts to develop metallocene-catalyzed resins centers on producing tailored resins having both superior processability and toughness:

- Easy processing with a superior balance of lifting ability
- Stiffness
- Tear resistance
- Impact resistance.

37.8 Structure of Polyethylene

37.8.1 Morphology

Conceptually, the solid state of polyethylene resins can be represented as composites of crystalline (lamella) and noncrystalline or amorphous materials. The crystalline material, called lamella, consists of orderly arrangements of the ethylene sequences in the polymer chains. Lamella form in a resin's melt spontaneously, via a process called self-nucleation, when the ethylene sequences in one or more chains align next to each other. Van der Waals forces cause the sequences to bond together to form nuclei that subsequently grow by addi-

tion of polymer chains via ethylene sequences of similar length to the lamella's thickness. A resin's morphology is determined by both its chemical structure and how it is processed. For example, the speed with which the resin is cooled greatly influences its morphology. During quiescent crystallization, lamella grow into larger space-filling structures, called super molecular structures with the most common type of structure being a spherulite – a ball-like structure [37.28]. Polyethylene spherulites can have diameters up to between 10 and 20 μm . These structures do not form when the resin is rapidly cooled, a process called quenching.

37.7.6 Combined Processes

All the manufacturing processes discussed above have particular advantages. Combining different processes can provide materials that exploit the advantages obtained from each process individually. Specifically, the different manufacturing processes can be tied together.

37.9 Polyethylene Processing

37.9.1 Processing

The semicrystalline nature of polyethylene resins enables the resins to become pliable and flow above a specific temperature and then return to a solid form on cooling below that temperature. These attributes make polyethylene resins thermoplastics. These attributes also allow easy and inexpensive conversion of polyethylene resins into usable parts. Polyethylene parts are formed by melting a polyethylene resin, molding the melt into a shape, and cooling the molten shape to below the resin's melting point, i.e., cooling the molten shape into a solid. In this way, thermoplastics can be extruded and molded into different articles of commerce. Thermoplastics can also be re-extruded and remolded.

Polyethylene is converted into end-use products by a variety of extrusion and molding methods such as film extrusion, sheet extrusion and fiber extrusion, blow molding, injection molding, and coating methods designed for specific product applications. In addition, there are two specialty fabrication methods: rotational molding and compression molding. The method selected to make parts is determined by the shape/dimension of the parts to be made, the applications of the parts, and the molecular weight of the resin used.

Extrusion

In the extrusion processes, polyethylene resins are melted in a plasticating extruder which is composed of heated barrels containing an Archimedean type screw.

The length-to-diameter ratios (L/D) of the extruders range from about 18 : 1 to about 30 : 1. The extruder's L/D ratio is determined by the quality of its products and the type of resin used. High-quality products require higher L/D screws of 24 : 1 to 30 : 1, which provide more extensive mixing of the melt. Medium-quality products employ screws with L/D ratios of about 20 : 1. Low-quality products employ screws with L/D ratios of at most 20 : 1. Additionally, extruders with L/D ratios of 24 : 1 or greater are typically smooth-bored extruders. Shorter extruders are typically grooved feed extruders, and are used to process higher density resins. The melts in these latter extruders have short time-temperature histories.

The extruder barrel and screw are divided into three sections, each providing a different function: advancing, melting, and mixing the melt. At the mouth of the extruder, the feed zone moves the resin along the barrel, and raises its temperature to near its melting point. The resin is a solid at the beginning of this section, but becomes a mixture of molten and solid resin by the time it reaches the end of the feed zone. The movement of the screw drags the pellets near the surface of the barrel across the barrel's surface which causes frictional heating to melt the resin. After the feed zone, the compression zone of the extruder further heats the melt bed by forcing it against the barrel. The compression forces needed are generated by reducing the depth of the flights in the screw. The melt phase changes from predominately solid to completely liquid over this section of the extruder. Once the resin is completely melted it is mixed or homogenized within the metering zone of the extruder. The depths of the flights in the metering section of the extruder are shallower than those in the other sections of the extruder, and are of uniform depth over the length of the mixing sections. The metering zones typically contain an advanced mixing section near the tip of the extruder to intensively shear the melt. Resin advancing within the extruder pressurizes the melt and enables extrusion from the extruder to an extrusion die or head which molds the melt into its final shape before being quenched to a solid product.

Blown Film

In blown film fabrication, the molten pressurized resins pass from an extruder to a die that redirects the melt 90° around a die pin to form a tube which is typically directed vertically upward. The tube is subsequently expanded in both the direction of extrusion (machine direction, MD) and transverse to that direction (transverse direction) by a process similar to inflating a balloon except the inflated melt resembles a tube. The expan-

sion causes the melt to become thinner in the direction perpendicular to both the film's machine and transverse directions, i.e., through the film. As the molten tube expands, it cools, begins to solidify, and eventually crystallizes. When the melt begins to crystallize it becomes opaque and the dimensions of the tube are fixed.

Polyethylene blown films are used in form-fill-and-seal applications, food packaging applications, shrink film applications, and thin-film applications like liners. Examples of form-fill-and-seal applications include heavy duty sacks such as resin bags, mulch bags, gravel bags, lawn and garden bags of different kinds, and bags for cement-like products. Polyethylene films are also used in flexible food packaging applications such as freezer films used to package frozen foods and ice. Freezer films are used to package vegetables, potato products, fish and seafood, meats, and ready meals. Other examples of flexible polyethylene film products are bread bags and fresh produce packaging. Nonfood packaging applications include shrink films such as shrink bundling films, industrial shrink film, retail shrink film, stiff high-clarity shrink film, pallet shrink film, collation shrink film, and light-duty shrink film.

Cast Film

In cast film fabrication, the molten resin is extruded vertically onto a chilled drum via a flat or coat hanger die that spreads the melt out to form a thin molten sheet or curtain. The curtain of molten resin is drawn in the direction of the extrusion (machine) direction by rotating the chilled drum. The drum quickly cools the melt and causes it to solidify. Cast polyethylene films are typically less than 1 mil thick and are used in stretch warp to unitize materials for shipping.

Blow Molding

In blow molding, the molten resins pass from an extruder to a forming head that redirects it 90° around a die pin within a manifold. The melt exits the head vertically downward in the form of a parison, which resembles a thick-walled hollow tube or pipe. The parison's length is matched to that of a clam shell mold that is closed around it. The mold seals the bottom of the parison and air is injected into the top of the parison forcing the resin against the mold. Inflating the parison expands the resin and thins its wall. Contact with the mold shapes and cools the thinned resin to produce the final blow-molded article. After being cooled, the mold is opened to collect the article as a product. This extrusion blow-molding process is used to make rigid packaging for dairy products and fruit juices, wa-

ter bottles, 55 gal drums, stadium seating, gas tanks, and beams as examples.

Sheet Extrusion and Thermoforming

In sheet extrusion and thermoforming, the molten pressurized resin is passed from an extruder to a flat or coat hanger die that spreads the melt out to form a molten sheet similarly to the sheet formed in cast film fabrication. However, in sheet extrusion and thermoforming operations the sheets can be very thick, 3 mm to greater than quarter of an inch and are extruded horizontally. They are not drawn in either the extrusion (machine) or transverse directions and are slowly cooled as they travel down a conveying system. The resultant thick flat sheets are cut to length and moved to the thermoforming stations, where they are heated and then brought into contact with a mold to form the final parts. The molding can be accomplished via draping the molten sheet over a male or female mold and then applying a vacuum or pressure to force it against the mold. Additionally, the molten sheet can be sandwiched between male and female molds. Sheet extrusion and thermoforming is used to produce large panels, housings, enclosures, truck bed liners, small rigid cups used in food packaging and pails as examples.

Wire and Cable

In wire and cable applications, the molten pressurized resins pass from an extruder to a cross head die that directs the melt's flow 90° around a die pin through which the wire and cable is pulled.

Pipe Extrusion

In pipe and tubing extrusion, the molten resin is extruded through an annular die to form a tube which passes through a sizer to fix the part's final dimensions before being quenched. The quenched tube is cut to length. These processes produce pipes up to a couple of meters wide with wall thicknesses up to inches.

Fiber Spinning

In fiber spinning, the molten pressurized resin is passed to a multiport die equipped with spinneret. The molten extrudate is caught in the high-speed air jet of the spinneret that elongates and cools the melt into a fiber.

Injection Molding

In injection molding, the molten pressurized resin is forced into the mold at very high pressure to form it

into a final shape that is quenched producing the molded part. Unlike in other processes, the screw serves a secondary function as a ram to fill the mold with the molten resin. Specifically, the barrel of the extruder is significantly longer than the screw. The screw is operated until the barrel is full of molten resin. Then, the screw is advanced forward and pushes the molten resin into the mold. After the mold is filled, the screw is returned to its original position to refill molten resin from the extruder. The temperature of the mold cycles between that of the melt and the quench temperature. After cooling, the mold is opened and the part collected. When foaming agents are included in the resin, the final part can be foamed. Injection molding is used to make small appliance housings, small electronic housings (telephone handsets, electrical switches, television cabinets, etc.), crates, medical devices, automotive dash boards, and bottle lids/closures, for example.

Injection Blow Molding

In injection blow molding, the injection-molding and blow-molding operations are combined.

Rotational Molding

In rotational molding, or rotomolding, polyethylene powder is introduced into a mold. The mold is closed, moved into an oven which is typically gas fired and rotated both vertically and horizontally. The powder melts and is flung onto the walls of the mold by centrifugal force where it forms a skin. The mold is removed from the oven, cooled, and the product collected. When the proper additives are included in the resin, the final part can be crosslinked. Rotomolding is used to make simple rigid hollow structures that can be processed further into final products, like children's toys, traffic cones and posts, canoes, and trash containers. It's most often used for very large articles and specialty products usually made in small quantities.

Compression Molding

In compression molding, polyethylene powder or resin is introduced into a square mold and then pressurized while being heated. After being heated with a specified time-temperature-pressure protocol, the formed part is cooled and collected. Parts are typically cut from the collected part, which is typically in the form of a sheet. Compression molding is typically used in making parts from resins that cannot be extruded, for example, ultra-high molecular weight polyethylene resins.

37.10 Synthesis and Processing of Polypropylene

37.10.1 Background

Polypropylene (PP) is a semicrystalline thermoplastic polymer made by polymerizing propylene, in the presence of catalysts which lead to isotactic or meso insertion of the pendant methyl groups of the propylene. This polymer is tough, hard plastic which can be shaped and fabricated by a variety of processes. Catalysts leading to a random racemic with meso mixture of soft, partly crystalline polypropylene are not the subject of this section. Polymerization may be by propylene itself leading to homopolypropylene or with other comonomers typically ethylene or other α -olefins, such as 1-butene, leading to random copolymers. In contrast to most other thermoplastics, the manufacture of polypropylene often also includes a variant in the propylene mixture with inclusion of ethylene and/or other α -olefins to be polymerized to form a copolymer which is a rubber. This rubbery copolymer is a distinct polymer compared to the polypropylene and exists within the matrix of

polypropylene as a separate phase. The mixture is often referred to as impact copolymer polypropylene (ICP) or heterophasic copolymer (HECO). The intent behind making these rubber-modified mixtures is improvement of the impact properties of the polypropylene at the expense of a reduced stiffness. A recent review summarizing the developmental history of ICPs and presenting options for the in-reactor design of these polymers and their modification by compounding with elastomers and fillers or reinforcements after polymerization can be found in *Gahleitner et al.* [37.29].

Polypropylene is a very useful plastic with an global annual consumption exceeding 53 MT/yr in 2012 making it the most produced single thermoplastic material [37.30], and a growth rate exceeding 9%. The reason polypropylene obtained its position in the plastics industry is the cheap feedstock derived from the refining of petroleum, and the ease of manufacture and conversion into inexpensive articles of commercial use.

37.11 Polypropylene Process and Catalysts

37.11.1 Polymerization Processes

Polypropylene is typically made with a single highly evolved titanium trichloride (TiCl_3)-based polymerization catalyst (Ziegler–Natta). The evolution of the catalysts over the last 60 years has led to greater tacticity or stereo regularity of the polymer. Increasing tacticity relates to higher stiffness and melting point of the polypropylene. The most recent evolution in the polymerization of propylene has been the discrete organometallic catalysts derived from metallocene which makes the polymer with a different error signature in terms of tacticity than the evolved Ziegler–Natta catalysts. A review highlighting the major evolutionary steps made in polyolefin catalyst systems in terms of productivity and possibilities to control the molecular architecture of both polypropylene and polyethylene can be found in *Gahleitner et al.* [37.31]. A comprehensive description of catalyst systems used for PP can be found in *Polypropylene Handbook* [37.32].

Most 1st-generation PP was produced commercially using Ziegler–Natta catalyst systems in a semi-batch slurry process (Montecatini and Hercules) with hexane or heptane as the diluent to suspend the crystalline polymer particles, remove the heat of polymerization, and dissolve the amorphous polymer fraction. The crystalline polymer product was separated from

the diluent by filtration or centrifugation and then dried [37.32]. Amorphous (atactic) polymer dissolved in the diluent was separated by evaporation. Slurry technologies require a section for the recovery of the diluent and segregation of the amorphous polymer, leading to extra costs in investment and operation of the plant. They are rarely used commercially today for the production of PP. The advances in catalyst technology (e.g., high yield and high stereospecific catalysts) and the continuous need for improved product performance have led to the development of new polymerization processes (typically bulk or gas phase) that are more cost effective than the early slurry processes. Polypropylene polymerization lines have been constructed with increased capacity, from about 5 kt/yr in the early 1960s to over 400 kt/yr today [37.30]. New products, such as ultrahigh melt flow rate (MFR) homopolymers and high melt flow, high impact copolymers can only be produced using advanced catalysts and processes [37.32].

Polypropylene is made commercially today with a variety of licensed polymerization processes [37.32] including:

- Novolen (NTH)
- Unipol (Dow)
- Spheripol (LyondellBasell)

- Hypol (Mitsui)
- Borstar (Borealis)
- Innovene (BP) etc.

Such processes eliminate the use of hydrocarbon diluent by using either liquid or gaseous monomer as the polymerization medium. Contrary to the slurry operations, in such processes, the removal of catalyst and atactic polymer are unnecessary.

The first commercial gas-phase propylene polymerization process was developed by BASF in the late 1960s [37.32]. The Novolen technology involves vertical stirred gas-phase reactors operating at pressures above 20 bar and temperatures of 70–90 °C [37.33]. Originally the design was that of a stirred autoclave with a bottom-mounted helical stirrer maintaining uniform conditions in the polymer bed. This stirrer is designed to convey the particles up the reactor wall and let them fall down through the center of the bed. The special design of the agitation system is considered to be responsible for forming sub segments in the reactor. By this it is claimed that the reactor behaves like a cascade of a large number of continuous feed stirred tank reactors (CSTRs) [37.30]. Unreacted monomer is condensed and recycled through an external heat exchanger to remove the heat of polymerization. By using mechanical agitation rather than fluidization to provide mixing, gas recirculation is minimized. Initially, the Novolen technology was used with a single reactor for the production of homopolymers. However, in the late 1970s, ICPs were produced with Novolen technology using two reactors in series.

The use of gas-phase fluidized-bed reactors for olefin polymerization was pioneered by Union Carbide with the development of the Unipol process for polyethylene in the late 1970s. The Unipol process was adapted for the production of PP in 1985 by incorporating Shell high-activity catalysts (SHAC) [37.32]. One feature of this Unipol process is the large fluid-bed reactor with a wider upper section that serves to separate the fluidized polymer from the recirculating gas. One reactor is required for the production of homopolymer or random copolymers; a second smaller reactor is used in series for the production of the ethylene-propylene rubber for impact-modified copolymers. The heat of reaction is removed by cooling with external water through a heat exchanger. Recycled propylene can thus be cooled to its dew point, allowing some liquid monomer to be fed in homopolymer production (condensing mode operation). The polymerization temperature is around 65 °C with operating pressures of 30 bar in the homopolymer reactor and 20 bar in the copolymer reactor. Plant capacities of Unipol PP plants are typically about 200 kt/yr [37.32].

Processes using liquid monomer as the polymerization medium are divided into two categories: those using continuous stirred reactors and those using loop reactors. Such processes are often used to produce homopolymer PP or random copolymer PP with less than about 5% ethylene [37.32]. However, processes using liquid monomer are not suitable for the production of the rubber phase of impact copolymer PPs due to the solubility of the rubber in the liquid monomer. Consequently, impact (heterophasic) copolymer polypropylenes today are mostly made with a hybrid process. In this process, the homopolymer or random copolymer matrix is made first in the liquid phase followed by copolymerization in the gas phase for the dispersed rubber.

The Spheripol process is the dominant hybrid process licensed by LyondellBasell. Roughly one third of today's world PP production is based on Spheripol technology [37.30]. In this process, catalyst components and monomers are fed into a loop reactor for homopolymerization as shown in Fig. 37.1. Operating conditions are typically in the range of 60–80 °C and 35–50 bar [37.34]. The use of spherically shaped catalysts with narrow particle size distribution in combination with the high liquid velocities avoids reactor fouling. Because of the large surface-to-volume ratio for loop reactors, the heat removal capacity is high and enables high specific outputs up to 450 kt/yr [37.32]. Upon exiting the loops, the PP slurry is depressurized and flashed at a pressure that allows for recycle of the vaporized monomer. External cooling water is used for cooling and condensation of the monomer mixture, which are required for gas-phase copolymerization. Impact copolymers are produced by using the granules made in the above process in a trailing fluidized-bed gas-phase reactor to produce ethylene-propylene rubber imbedded in the homopolymer spheres from the preceding loop reactors [37.32]. Typical operating conditions of the gas-phase reactor do not exceed 100 °C with a pressure of about 15 bar.

Borealis Borstar PP is another example of a hybrid process, where a combination of loop and gas-phase reactors in series is used for the production of homopolymer and random copolymer followed by one or two fluidized-bed gas-phase reactors for the production of rubber in the case of impact copolymers. The loop reactor of the Borstar process operates under sub- or supercritical conditions (80–100 °C and 50–60 bar pressure) resulting in increased hydrogen and comonomer concentration without the formation of gas bubbles.

Mitsui's Hypol first-generation process is an example of a hybrid process, where Montedison–Mitsui high yield, high stereospecificity catalysts and liquid propy-

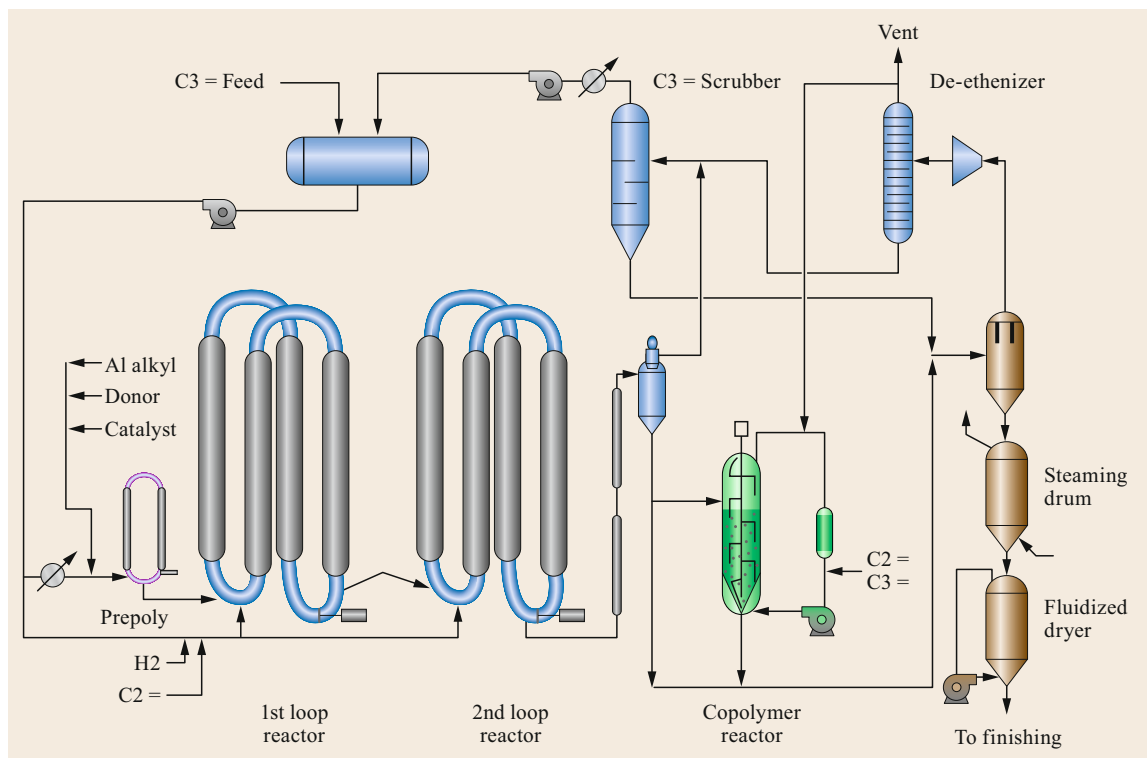


Fig. 37.1 Schematic of a polypropylene and impact copolymer polymerization process

lene are fed in a series of continuous stirred reactors (bulk polymerization), followed by gas-phase polymerization in a fluidized-bed reactor for the production of impact copolymer polypropylenes [37.32]. The latest generation of the Mitsui Hypol II process has replaced the continuous stirred tank reactors with a loop reactor configuration for homopolymer production.

The BP innovene process technology is based on a horizontal mechanically agitated multistage gas-phase reactor [37.35]. This process was commercialized by Amoco in 1979 for the production of homopolymer using TiCl_3 catalyst. The reactor design of the BP innovene process, where the polymer passes from one baffled zone to another, behaves as a series of stirred reactors providing a narrow overall residence time distribution [37.32]. As a result, polymer particle size and copolymer composition distributions can be significantly narrowed compared to those from single-stage stirred reactors. Additionally, molecular weight distributions can be broadened with the innovene process by varying the hydrogen feed to each section to produce a wide range of molecular weights. The residence time per reactor is typically 1 h. The reaction conditions are 65–85 °C for the homopolymer reactor and a pressure in the range of 25–30 bar. Producing the ethylene–propylene rubber in a sec-

ond gas-phase reactor can make heterophasic (impact) copolymers.

In the late 1980s, Basell developed the Catalloy technology which is a gas-phase, fluidized-bed process for the production of ex-reactor polypropylene-based blends [37.32]. Catalloy consists of three fluidized-bed reactors in series utilizing spherical-form controlled-morphology catalysts able to synthesize a wide range of polymer structures including homopolymer polypropylene and ethylene–propylene rubber. A unique feature of the Catalloy process is that each reactor can operate at its own temperature, pressure, gas composition and level avoiding cross contamination and allowing for accurate control of the desired amount of each polymeric phase [37.32]. Catalloy is targeted towards the specialties markets and as such the commercial plants are relatively small. The biggest Catalloy plant was built in 1997 in Moerdijk/The Netherlands with a capacity of 180 kt/yr.

In the early 2000s, Basell commercialized Spherizone, an innovative propylene gas-phase process. Spherizone consists of a multizone circulating reactor (MZCR) with two or more distinct zones, each operating under its own peculiar flow dynamic regime [37.32]. This reactor concept builds on the riser-tube design known from fluid catalytic cracking. The Spherizone

technology consists of two interconnected reaction zones, a riser and a downer, separated by a cyclone. In the riser (the first reaction zone) the gas velocity is high with the first zone acting as a fast-fluidized bed [37.30]. In the connected cyclone the polymer particles are separated from the gas, which then enter the second reaction zone (downer). The two sections of the reactor can be operated at different concentrations of hydrogen and comonomer, allowing for the production of bimodal composition polymers (in terms of molecular weight and/or comonomer concentration/type). This is achieved by introduction of a liquid or gas propylene stream on the top of the downer just below the polymer level, so that the riser gas is replaced by one with a different composition [37.28]. The fast circulation of the growing polymer particles between the different reaction zones makes the residence time per pass in each zone one order of magnitude smaller than the overall residence time. This leads to a very good homogeneity of the final product even for bimodal compositions [37.30].

37.11.2 Extrusion and Finishing Processes

The polymer made during the polymerization process is typically in granular or powder form and in most cases has to be converted into a stabilized pellet via the use of an extruder process. The direct sale of nonstabilized or (mostly) spray-stabilized PP where the antioxidant is sprayed on the surface of the granules of PP powder is rather limited [37.30]. In the 1990s, Himont (currently LyondellBasell) assumed that the spherical particle PP powders resulting from 4th-generation catalysts and the Spheripol process would be suitable in nonpelletized form for large parts of the PP market. Applications with powders are largely limited to rotomolding, melt-blown fiber spinning, and use as support for liquid additives like peroxides [37.30]. In particular, really low MW (high melt flow rate) PP used for melt-blown fibers (MFR on the order of 1000–1500 dg/min) is really difficult, if not impossible, to pelletize with current extruder/pelletizing technology due to the extremely low melt viscosity polymer *oozing out* from the die plate. Other alternate processing schemes have been proposed e. g. continuous mixer technology [37.32] for finishing of polypropylene, however they are rather limited commercially. Twin screw extruders coupled with underwater pelletizing system are almost universally used today to make pellets of polypropylene.

The type of extruder most often used in modern PP plants is the twin-screw corotating and fully intermeshing extruder due to its high flexibility and mixing/dispersion efficiency. Werner and Pfeiderer (Coperion), Japan Steel Works, and Kobe Steel are among the

lead manufacturers of twin-screw extruders. A typical L/D (screw length over diameter) of the extruder is 24–27, although a 32 L/D is used when devolatilization is required for the particular PP finishing process. During the extrusion process, different additives (usually in solid form) are fed directly at the extruder hopper without any significant premix with the PP powder. Typically, additives are added to the PP powder up to a level of 1 wt% (and most often in the range of ≈ 0.03 –0.5 wt%) on commercial extruders including primary and secondary antioxidants for polymer stabilization, UV stabilizers, nucleators, clarifiers, antistatic agents, slip and antiblocking agents etc. In special compounding processes, fillers, elastomers or other reinforcements can be mixed with PP pellets at concentrations of about 1–40 wt% [37.30].

A common practice in the PP industry is to use a postreactor reactive extrusion process. These modify the molecular weight (MW) and molecular weight distribution (MWD) of the resin produced in the reactor – which is often referred to as the *native* polypropylene. One example of PP reactive extrusion is the so-called visbreaking or controlled rheology (CR) process via the use of organic peroxides such as 2,5-di(*tert*-butylperoxy)-2,5-dimethylhexane [37.36, 37]. In the visbreaking process, the peroxide forms peroxy radicals, which attack the tertiary carbon items on the polymer backbone to form radicals. During the extrusion process, under the heat for a given residence time, the radicals undergo chain-scission reactions. The radicals abstract almost exclusively the tertiary hydrogen of the polypropylene. Since each tertiary carbon in the melt is equally likely to be abstracted, the longer polymer chains are more likely to be reacted. The unstable carbon centers are responsible for free radical chain *breakage* to form two lower molecular weight polymers in a process known as *chain scission* [37.32]. As a result, the visbreaking process lowers the weight-average molecular weight (MW) (thus increasing the PP melt flow rate MFR) and narrows the MWD (reduced Mw/Mn, where Mw is the weight average molecular weight and Mn is the number average molecular weight). In large-scale manufacturing plants, visbreaking allows the production of a multiplicity of grades from one reactor setting (one PP powder) with significant cost savings. Organic peroxides are usually added in liquid form to the extruder section where they can be premixed with the PP powder or, more typically, sprayed onto the pellets. The location for this addition is very close to the feeding screw elements in the hopper or in some cases, at the barrel feeding section. The visbreaking process can, in principle, be done in all kinds of PP including homopolymer, random copolymers, and impact (heterophasic) copolymers.

The visbreaking agent may be an organic peroxide, wherein at least a methyl group or higher alkyl or aryl is bound to one or both oxygen atoms of the peroxide. The visbreaking agent may also be a sterically hindered peroxide, wherein the alkyl or aryl group associated with each oxygen atom is at least a secondary carbon or a tertiary carbon. Nonlimiting examples of sterically hindered peroxides (*visbreaking agents*) include 2,5-bis(*tert*-butylperoxy)-2,5-dimethylhexane, 2,5-dimethyl-2,5-bis(*t*-butylperoxy)-hexyne-3,4-methyl-4-*t*-butylperoxy-2-pentanone, 3,6,6,9,9-pentamethyl-3-(ethylacetate)-1,2,4,5-tetraoxy cyclononane, α,α' -bis(*tert*-butylperoxy) diisopropyl benzene, and mixtures of these and any other secondary- or tertiary-hindered peroxides. As mentioned previously, a preferred peroxide is 2,5-bis(*tert*-butylperoxy)-2,5-dimethylhexane also known by the trade name Luperox 101 or Trigonox 101. Another common peroxide used as a visbreaking agent for polypropylene is di-*t*-amyl peroxide most commonly known by the trade name DTAP. Alternatively, the free radical initiator may include a diazo compound or any other compound or chemical that promotes free radicals in an amount sufficient to cause degradation.

The narrower MWD resulting from the CR process is particularly desirable in fiber spinning or cast film processes because the long chains resisting uniaxial deformation are preferentially reduced in molecular weight during this process. Therefore, in the case of fiber spinning, the spinnability (ability to produce fibers without or with a minimum amount of fiber breaks and with a fiber diameter of the order of 1 μm or even less) is significantly increased. While stiffness for reactor grades of PP (with broad MWD) increases with increasing MFR (lowering MW), it remains constant or is reduced for CR grades [37.30]. Additionally, transparency and surface gloss are improved via the visbreaking process.

37.12 Polypropylene Fabrication

Polypropylene (PP) is a thermoplastic material of great technological importance with a diversity of industrial applications including fibers, nonwoven spunbonding, injection molding, thermoforming, automotive compounding, film, foam extrusion, blow molding, and many others. A look at the global distribution of PP applications shows that the extrusion segments, including films and fibers but also coating and pipe extrusion, accounts for slightly more than 50% of the total volume, while injection and blow molding makes up less than

Pelletization can be achieved in strand form or in underwater systems. In a strand-cut pelletization process, several melt strands from the die plate are quenched in water for solidification and then chopped by high-speed cutters into 2–5 mm long cylinders. Strand-cut pelletizers are typically used for lab or semicommercial-scale extruders, while on the manufacturing scale underwater pelletizers are most often used. In underwater pelletizing systems, high-speed knives rotate against the extruder die plate to cut off short lengths of the molten extrudates. The insulated die plate is immersed in water which solidifies the lens-shaped pellets and also transports them to a sieving and drying device. Gala is a lead manufacturer of underwater pelletizers. While nitrogen has to be used for powder conveyance up to the extruder, air can be alternatively used for pneumatic pellet transport afterwards. *Neubauer* et al. [37.38] discussed the fundamental properties governing the underwater pelletizing process and confirmed their findings based upon actual observations during process and mechanical troubleshooting of high-capacity pelletizing systems. As the polymer melt becomes less elastic and less viscous (both properties reflected in the *Deborah* number), the ductility of the material increases, requiring relatively larger strains for the polymer to rupture (fracture). Therefore, the ability to obtain sharp and good cuts diminishes [37.38]. *Neubauer* et al. [37.38] reported that decreasing the cutting distance, increasing cutting velocity, increasing polymer viscosity, and increasing specific capillary flow rate all increase the cutting stresses being applied and help the polymer rupture as a brittle material versus a ductile material. This in turn makes the cutting process less difficult, thereby improving the overall performance of the underwater pelletizer. A description of common PP cut defects and a troubleshooting guide for their avoidance can be found in *Crumb* [37.39].

50% of the consumption [37.30]. A general trend towards material substitution has allowed PP to grow by replacing more costly polymers like polycarbonate (PC) and acrylonitrile–butadiene–styrene terpolymers (ABS) but also *traditional* materials like glass and metal.

A short description of some key PP fabrication processes is given below. For more details or descriptions of other processes, the interested reader is referred to [37.30, 32] or Handbook of Polypropylene and Polypropylene Composites [37.40].

37.12.1 Polypropylene Rheology and Process Instabilities

The rheological properties of PP are important because of the breadth of fabrication processes to which PP is subjected covering both extensional (e.g., fiber spinning, film extrusion) and shear (e.g., injection molding, extrusion/compounding) flow kinematics. A series of PP resins have been studied both in shear and extensional flow [37.41] and found to have a nonlinear correlation between the melt strength and fundamental shear flow properties including low-frequency loss tangent, crossover frequency and zero shear-rate viscosity. The study also modeled both the extensional (rheotens) and shear flow rheometric experiments with kinetic theory based on constitutive equations, demonstrating very good fitting and predictive capability. A comprehensive summary for the significance of melt strength was provided in several polymer processes, with the rheotens behavior of a variety of PP melts primarily from an experimental point of view [37.42]. A correlation of melt strength of several PPs with their sagging resistance in thermoforming processes was demonstrated [37.43].

High melt strength (HMS) refers to a melt that becomes stiffer and stronger (strain hardening) with an increase of the strain rate. Polymers with long-chain branches such as LDPE exhibit good melt strength or strain-hardening behavior. HMS PP is particularly useful in applications like blow molding, film blowing and thermoforming, where resistance of the melt to deformation for enhanced process stability or sagging under the influence of gravity become important. The melt strength of PP can be improved by increasing the average molecular weight, broadening the molecular weight distribution, and introducing long-chain branching (LCB). Different routes of producing HMS PP with introduction of LCB including irradiation of the polymer chains or by means of chemical, free-radical initiators (e.g., organic peroxides) are described in Polypropylene Handbook [37.32].

A principal problem in the extrusion of polyolefins is the phenomena of extrudate distortion, commonly known as melt fracture and wall slip [37.44]. Melt fracture usually appears when the wall shear stress exceeds a critical value, typically 0.13–0.15 MPa for polypropylenes [37.45]. Most of the previous studies on melt fracture of polymers examined the behavior of various types of polyethylenes (HDPE, LDPE, and LLDPE) and are summarized in *Hatzikiriakos and Migler* [37.44]. However, little is known about this phenomenon in the processing of PP and the relevant literature is summarized in this section.

37.12.2 Melt Fracture

Bartos [37.46] studied the melt fracture behavior of a series of polypropylenes to examine the critical conditions for the onset of extrudate distortions. He found that melt fracture occurs at a critical value of 8.5 MPa with a *melt fracture* number, which is defined as

$$N_{MF} = \frac{\eta_0 \dot{\gamma}_C}{PDI},$$

where η_0 is the zero-shear viscosity, $\dot{\gamma}_C$ is the critical shear rate for the onset of melt fracture, and PDI is the polydispersity index. *Kamide et al.* [37.47] reported a critical value of 10.9 MPa, while *Barnett* [37.48] found a critical value of 10.4 MPa for other series of polypropylenes. It would be desirable to have this information in terms of a critical shear stress, which unfortunately is lacking in these papers. *Ui et al.* [37.49] also studied the melt fracture behavior of a number of different polymers at various temperatures, including polypropylene. The flow curves obtained were smooth without any discontinuity similar to those found by *Kazatchkov and Hatzikiriakos* [37.45]. Such discontinuities are commonly observed in the flow curves of high-density and linear low-density polyethylenes. The type of melt fracture obtained for PP was fairly regular with a sharp transition from a smooth to a gross fracture appearance. Thus, small-amplitude periodic distortions which are obtained in the extrusion of linear low-density polyethylenes were not obtained for PP. Finally, *Ui et al.* [37.49] found that melt fracture occurs at a critical value of the wall shear stress in the range of 0.1–0.13 MPa, independent of temperature (180–260 °C), which is in agreement with findings reported by *Kazatchkov and Hatzikiriakos* [37.45]. The melt fracture of PP was also addressed in [37.50–53]. *Huang and Tao* [37.50] studied the melt fracture, shear rheology, extensional rheology, and die swell behavior of a fractional PP resin. They reported critical shear stresses for the onset of melt fracture ranging from 0.13–0.2 MPa, in agreement with other reported data in the literature. Finally, *Baik and Tzoganakis* [37.54] studied the melt fracture of a series of PP materials prepared by controlled rheology peroxide reactive extrusion. They found that PPs exhibit only gross melt fracture in agreement with other reports. They also reported that the critical shear stress for the melt fracture onset increases with decreasing molecular weight and polydispersity, and correlations have been developed between the critical stress values and the polymer polydispersity and shear compliance.

37.12.3 Wall Slip

It is known that molten polymers slip no matter how small the applied shear stresses [37.55]. Polypropylene was also found to obey this rule. Specifically, *Kazatchkov* and *Hatzikiriakos* [37.45] studied slip phenomena in the case of molten PPs using the Mooney technique in capillary flow. While diameter dependence was not observed directly via the Mooney technique, the authors explained that this is due to significant viscous heating. *Rosenbaum* and *Hatzikiriakos* [37.56] used a numerical technique to correct for the effect of viscous heating in order to calculate the slip velocity of PPs. *Mitsoulis* et al. [37.57] also studied the effect of slip on the flow of a branched polypropylene melt by using a visualization technique to directly deduce slip. Finally, *Kazatchkov* and *Hatzikiriakos* [37.45] carried out experiments in both sliding plate and capillary rheometers for a PP melt to determine the conditions for the onset of slip, surface and gross melt fracture.

37.12.4 Processing Aids

Athey et al. [37.58] and *Rudin* et al. [37.59] studied the melt fracture of a molten polypropylene and added a small amount of fluoropolymer to the resin to suppress this phenomenon. They found that this additive provided some benefits in the extrusion process such as reduction in extruder power and die pressure. *Kazatchkov* and *Hatzikiriakos* [37.45] also used a fluoropolymer-based processing aid to suppress the melt fracture phenomena in polypropylene. They reported that the presence of the fluoropolymer coating on the polymer–wall interface (i) improved the processability of polypropylene and (ii) significantly decreased the wall shear stress implying that it is a strong slip promoter. Melt fracture, shear rheology, extensional rheology, and die swell behavior of a fractional PP resin have been studied by several authors. *Huang* and *Tao* [37.50] studied this for capillary flow while *Baik* and *Tzoganakis* [37.54] studied the melt fracture of a series of PP materials prepared by controlled rheology peroxide reactive extrusion. *Kazatchkov* and *Hatzikiriakos* [37.45] carried out experiments in both sliding plate and capillary rheometers for a PP melt to determine the conditions for the onset of slip, surface and gross melt fracture.

37.12.5 Extrusion Surging

It has been reported that PP resins process on single-screw extruders at specific output rates that are about

30% less than those of linear low-density polyethylene (LLDPE) and that PP has a greater tendency for flow surging instabilities than LLDPE [37.60, 61]. In a single-screw extruder, the output rate is determined by the combined effectiveness of solid conveyance, melting, and melt metering [37.62]. Any imbalance of these three mechanisms can induce extrusion instability such as flow surging which is defined as the oscillatory variation of the output rate of the extruder under a given set of conditions. For PP, this has been attributed, among other factors, to the high melting temperature, high crystallinity, and low pellet compressibility of PP over other polymers. *Doufas* et al. [37.63] studied through experiments the extrusion instability surging phenomenon of a PP melt in a single-screw extruder with different screw designs and extruder conditions and found that a barrier screw yields considerably more stable extrusion performance relative to a metering screw.

37.12.6 Compounding and Blending

The modification of PP after the polymerization process via extruder compounding/blending plays a major role in enhancing the range of properties of PP compounds and blends. Besides the twin-screw extrusion and finishing processes to make pellets from powder/granules coming from the reactor discussed above, compounding is used for blending of PP pellets with fillers and elastomers/plastomers to create thermoplastic olefin (TPO) compounds with targeted stiffness/impact balance and other mechanical properties. A typical TPO formulation is 70 wt% ICP, 10 wt% talc, and 20 wt% plastomer (e.g., Engage of Dow Chemical Company or Exact of ExxonMobil Chemical) [37.64, 65]. HDPE additions in PP have been found especially suitable for the reduction of stress whitening or scratch sensitivity [37.30].

In the case of TPO compounding, special mixing elements/kneading blocks are used to maximize mixing and dispersion. For example, the Farrel kneader possesses a big blending chamber for adding EPR (ethylene–propene rubber), EPDM (Ethylene–propylene–diene terpolymer) and other elastomers in the form of bale, while the Buss cokneader allows a more gentle dispersion of glass fibers by combining rotating and pulsating melt movements [37.30]. Modifications of mechanical properties as well as shrinkage and thermal expansion are possible through the addition of fillers and reinforcements of mostly mineral nature. The respective effects are determined by the properties of the base polymer as well as by the quantity and nature of the filler [37.30, 66]. Talc with an average particle size of 0.6–10 μm is the most commonly

used filler, while calcium carbonate, kaolin, wollastonite, and mica are used to a lesser extent.

37.12.7 Fibers and Nonwovens

Fiber formation is one of the most demanding and delicate PP-fabrication processes because it requires the highest possible quality and consistency resin to enable production of very thin fibers (sometimes on the order of 1 μm) without occurrence of any breaks. Most often, PP fibers are produced via melt spinning, a process in which the polymer melt is extruded through a spinneret comprising a plurality of die holes (typically 0.3–0.8 mm in diameter) and the resulting extrudates are simultaneously cooled (via air flowing perpendicular to the filaments) and uniaxially stretched (either via mechanical or aerodynamic means) with an equivalent take-up speed in the range of 1000–5000 m/min. With the combination of extensional deformation, cooling, and flow-induced/enhanced crystallization (FIC), fibers are produced on the order of 1–20 dpf (denier per filament; where denier is grams of fiber per m^2) or equivalently about 10–55 μm .

A description of the melt-spinning process and fundamentals can be found in *Denn* [37.67] and *Ziabicki* [37.68]. A mathematical model for melt spinning with a two-phase constitutive/microstructural model for FIC that can be used for industrial product and process development is described in *Doufas et al.* [37.69]. Model validation in the case of PP melt spinning with on-line Raman crystallinity data and fiber tension measurements is discussed in *Patel et al.* [37.70] and *Paradkar et al.* [37.71]. As mentioned previously, narrow MWD (e.g., via peroxide visbreaking) enhances the spinnability performance stabilizing the spinline relative to both random disturbances and draw resonance [37.72, 73]. Overall, at a given MW (MFR) and spinning conditions, the fiber tensile strength (tenacity) increases and the elongation to break decreases [37.73, 74].

The three most common fiber-spinning processes for PP are:

- Continuous filament (CF)
- Bulk continuous filament (BCF)
- Staple fiber (SF) [37.30].

Because the holes in the die (spinneret) are quite small (0.3–0.8 mm), low melt viscosity is important. Therefore, high melt (die) temperature (230–280 $^{\circ}\text{C}$) and relatively high MFR (10–30 dg/min) are used. A relatively large extruder is usually equipped with a manifold to distribute a high throughput of molten

PP to a bank of 8–20 spinnerets. Each spinneret is equipped with a separate gear pump to regulate output through the spinhead, a filter pack supported by a *breaker plate* and the spinneret plate within the head [37.32]. The number of holes in the spinneret plate determines the number of filaments in a yarn and is typically in the range of 50–500. The holes can have round, annular, or rectangular patterns to help with good distribution of the quench airflow.

For the CF process, a *long spinline* is preferred which can combine spinning and finishing stages as well as out-of-line drawing options [37.30]. An air cooling gap of 2–5 m is needed between the die plate and the wind-up roll. Line speeds up to 1000 m/min at the spinning stage, increasing to 3000 m/min during solid drawing over hot rolls, call for complex and expensive haul off, drawing, and wind-up sections [37.30]. CF yarns typically range from 40–2000 denier (filaments ranging from 1–20 dpf) with spinning speeds ranging from 800–1500 m/min. The product is preferably sold as continuous yarns or tows having no texture or crimp. It can be used as is or textured and combined with other yarns [37.32]. PP BCF yarns are used mainly in carpet face yarns and upholstery fabrics. The BCF process is mostly used for carpet face and upholstery yarns and characterized by the addition of a *bulking* step after spinning or spinning and orientation [37.30]. The bulking or texturizing at 140–160 $^{\circ}\text{C}$ in a jet with compressed air has a similar effect as the crimping process used for other textile fibers, causing fibers to have a wavy to curly structure for higher volume. While the MFR range is the same as for CF (10–30 dg/min), broader MWD and higher crystallinity can give advantages for the BCF process [37.30].

37.12.8 Spunbond Nonwovens

In a spunbond process, filament spinning and web forming are integrated into a single process. Filament extrusion (from molten polymer), filament drawing (orientation of polymer molecules), filament laydown (collection of filaments on a screen or porous belt to form the fabric) are operations that are simultaneously controlled. A schematic of a spunbonding nonwoven process is given in Fig. 37.2.

The spunbonding process typically utilizes a slot drawing technique as described by *Geus* [37.75] and *Balk* [37.76]. Filament formation can be achieved with one large spinneret having several hundred holes. After exiting the spinneret, the molten filaments are quenched by a cross-flow air quench system, then pulled away from the spinneret and attenuated (drawn) by high-pressure air to an equivalent take up speed of up to

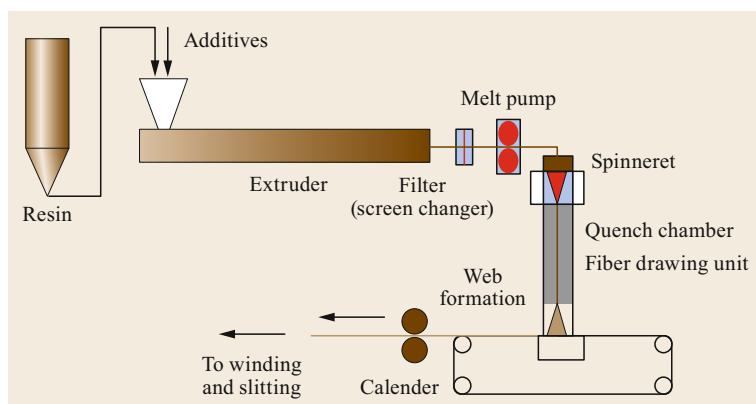


Fig. 37.2 Schematic for a spunbond nonwoven process for polypropylene

about 5000 m/min. There are two methods of air attenuation, both of which use the Venturi effect. The first draws the filament using an aspirator slot (slot draw) which runs the width of the machine. The second method draws the filaments through a nozzle or aspirator gun. Web-like structures are consolidated/bonded to form a nonwoven fabric. Thermobonding is the most usual technique to consolidate webs, while other techniques such as needle punching, chemical bonding, or water jetting may also be used [37.32]. In the case of thermobonding, the fabric is passed between heated calendar rolls to bond the fabric at points covering about 20 to 40% of its area in order to increase fabric integrity and strength. The choice of resin influences the bonding temperature window. A wide bonding temperature is desirable for the best combination of operability and properties.

The typical PP resin is homopolymer PP of 25–40 MFR with narrow MWD (e.g., achieved by visbreaking of a Ziegler–Natta resin and/or use of metallocene catalyst). The narrow MWD specifically improves spinnability and provides higher orientation (thus fiber tenacity) during the high drawdown of these fibers. Fine fibers on the order of 10–20 μm are formed. The advantages of finer fibers are improved fabric uniformity and better barrier properties. In fact, for the same base-weight nonwoven fabric (g/m^2 of fabric), the finer fabric leads to a greater number of filaments per unit area leading to enhanced uniformity and coverage. Following bonding, a topical finish can be applied to the fabric to make it hydrophobic, hydrophilic, antimicrobial, or antistatic, as desired. After bonding and treating, the fabric is slit into rolls of desired widths and lengths. PP spunbond nonwovens are used for a wide range of articles, such as, disposable hygiene goods including diapers, sanitary napkins, training pants, adult incontinence products, hospital gowns, baby wipes, moist towelettes, cleaner cloths, filters, geotextiles, furnishings and carpet backing.

37.12.9 Melt-Blown Nonwovens

In the melt blowing (MB) fiber process, a high temperature, high velocity gas (air) stream, impinging on the molten polymer stream as the polymer extrudes from the small capillary in the melt-blowing die, rapidly attenuates the filament from 500 μm diameter at the capillary down to diameters as small as 0.1 μm . This process occurs in about 200 μs over a distance of a few cm [37.32]. Die design is the key to producing a quality product efficiently. The major advantage of the MB process is that it can make very fine filaments and produce very lightweight fabrics with excellent uniformity. As a result, MB achieves soft fabrics with excellent barrier properties, meaning effective filtration characteristics and resistance to penetration by aqueous liquids. The melt-blown fabrics are poorer in tensile strength especially compared to spunbond fabrics. However, the finer filaments of the melt-blown fabrics provide better moisture barrier properties, and the optimum fabric is a laminated combination of spunbond and melt-blown fabric layers: spunbond for strength and melt-blown for barrier properties [37.32]. Typically two or three spunbonded (S) layers are combined with two or three melt-blown (M) layers, e.g., SSMMS is an example of combined nonwoven construction.

Melt blowing requires a very high MFR (> 200 dg/min up to about 1500 dg/min) to obtain the finest possible fibers. Some melt-blowing manufacturers purchase 35 MFR homopolymer PP and carry out peroxide-assisted (visbreaking) degradation during extrusion to achieve the required MFR. Commercial resins with MFR in the range of 400–1500 dg/min are available with the 4th-generation catalyst technology eliminating the need for peroxide visbreaking. Higher MFR resins allow lower melt and air temperatures resulting in energy savings. As with the spunbond nonwovens, MB fibers require narrow MWD for production of very thin fibers with enhanced orientation.

37.12.10 Unoriented/Low-Orientation Films and Sheets

Depending on the fabrication process employed, PP can be processed into film and sheets ranging in thickness from 5–2000 μm and converted further into a wide variety of products [37.77]. The more common processing step is film casting with an extrusion from a slit die onto a (relatively) cold roll. The so-called *chill roll* is kept at temperatures between 15 and 80 °C by liquid cooling or heating, depending on the polymer processed and its final destination [37.30]. If the film is applied directly after solidification in this step, in which only a limited degree of orientation in machine direction is achieved, cast film is produced which typically covers a thickness range of $\approx 30\text{--}300\ \mu\text{m}$. The rapid cooling leads to films of low crystallinity with excellent clarity, which can be influenced in performance both by a choice of polymer and additive package and by variation of the processing conditions [37.78]. Applications of these films are as diverse as bags for shirts and other textiles, stationery pocket pages for photos and collectibles and hard candy twist wrap [37.32]. For cast film, PP of MFR of 7–20 dg/min is typically used with preferably narrow MWD (e.g., visbroken grades). Film can be run from the chill/take-up roll further through a calendar-like arrangement of rolls for solidifying and annealing, and roll-stack films are produced with a primary thickness range of 300–2000 μm [37.30]. These films or sheets are primarily used for thermoforming applications described later.

37.12.11 Thermoforming

In the thermoforming process sheets of polypropylene are formed into complex shapes by a pressure-assisted die process. A variety of methods can be used depending on the desired shape and dimension. Both in-line and off-line processes are applied with two essential steps, heating and shaping, the former mostly by infrared irradiation and the latter either by mechanical force, air pressure, or vacuum. Thermoforming is the only film processing segment where nucleation is applied to a significant extent [37.79]. Thermoforming has the advantages of relatively low forming pressures, low mold costs, production of multilayer structures, and low-cost fabrication of large parts [37.32]. Critical process issues in thermoforming include sheet quality, thickness uniformity of formed parts, dimensional stability, part reproducibility, and regrind use. For thermoforming, PP with MFR of about 1.5–4 dg/min are typically used [37.30] and high melt strength is desirable to improve processability by reducing sagging [37.80]. A more detailed description about cast film and ther-

moforming processes is available in *Gahleitner* and *Paulik* [37.30] and *Pasquini* [37.32].

37.12.12 Oriented Films

Biaxially oriented PP (BOPP) processes are the most popular methods for manufacturing PP packaging films [37.32]. BOPP films can be made with two methods: the tubular process and the tenter process. Tubular (or double-bubble) is less capital intensive than the tenter process but requires more labor. Film thicknesses range from 8–50 μm , while line outputs are usually in the range of 100–550 kg/h. In the bubble process, a thick-walled tube is extruded downward from an annular die over a water-cooled large-sized mandrel and quenched further in a water bath. This is the first *bubble*. The tube is about 0.3–1.5 mm thick, i.e., 30–40 times thicker than the final product. Taking care to avoid putting a hard crimp in the sides of the flattened tube, it is reheated to a temperature of 140–160 °C and is then oriented in the second *bubble* by inflating it to about 7–8 times the tube diameter. Simultaneously, the tube is stretched in the machine direction. Cooling of the bubble during stretching aids in thickness as well as in uniformity and process stability. A substantial increase in crystallinity occurs during the bubble biaxial deformation resulting in a strain-hardening effect on the film which also improves thickness uniformity [37.32]. Because of the strain-hardening effect, the tubular process can manufacture very high-quality films with excellent gauge control, although minor bands of thickness, known as gauge bands, may still occur. For more information about postprocessing of BOPP film made with the tubular process, the reader is referred to *Propylene Handbook* [37.32].

Tenter is the most common process for production of BOPP because of its lower variable costs resulting from very high output rate and wider availability of this technology over the bubble process. Film ranging from 13–33 μm is produced with widths of 3–10 m at line speeds up to 300 m/min and output rates of over 3600 kg/h. The primary market for 13–25 μm film is for snack food packaging. Films of 25–30 μm are used primarily in adhesive tape constructions [37.32]. Extruders ranging in diameter from 110–300 mm are used in the tenter process [37.32]. The primary extruder melts the resin and transfers it to a secondary, usually larger, extruder that homogenizes the melt and precisely meters it to the die. The unoriented sheet is extruded from a flat sheet extrusion die with a die gap of 1.5–3 mm and a chill roll system is often used. A single, large diameter roll partially submerged in a water bath or two large chill rolls set at 20–30 °C are typical. As with flat film extrusion, an air knife and edge pinning

are used to provide intimate contact between melt and chill roll [37.32]. Downstream, the sheet is reheated to 125–150 °C by means of heated S-wrap rolls and then passed between closely spaced differential speed rolls to achieve machine direction (MD) orientation with restrained width. The lengthened and thinned sheet is cooled and passed to the tenter section of the line. The temperature in each oven section is controlled precisely to within 0.5 °C. At the desired temperature, the tenter chain diverges and stretches the sheet to the desirable film width. Oven temperatures range from 150–170 °C. In order to stabilize the molecular orientation achieved during stretching and increase heat stability (reduction in shrinkage), a heat-set stretching process can follow the stretching process [37.32]. The film is cooled, and the clips are released prior to edge trim, treatment (optional), and winding.

Contrary to the tubular process, in the tenter process the film generally undergoes sequential orientation (two-stage method). In the tenter process, extruded film is first drawn in the MD 4- to 6-fold, and then in the width or cross direction (CD) by about 7- to 10-fold with a total thickness reduction ratio of 40 : 1 to 55 : 1 [37.32]. Consequently, the extruded sheet can range from 0.6–3 mm in thickness. There are also available simultaneous biaxial stretching units, where machine and cross stretching are performed simultaneously. The two orientation methods (bubble and tented process) produce generally different physical film properties. Tubular film has balanced properties (MD versus CD), while the higher draw in the CD gives the tented films higher stiffness and strength in that direction. However, modern tenter lines can produce films with practically isotropic properties [37.32]. BOPP films are characterized by a much higher orientation, stiffness, gloss, and transparency in comparison to cast films. While in the packaging area, the low water vapor permeability and the excellent optical appearance are especially appreciated, the high mechanical and thermal resistance make BOPP also suitable for electrical capacitors.

PP resins with MFR values of 1.5–4 dg/min are used for BOPP with a relatively broad MWD to have sufficient melt strength and strain hardening for enhanced stability during stretching. The PP film resins have appropriate amounts of antiblock and slip additives to allow good film handling in production and high-speed converting operations downstream [37.32]. The BOPP film area is largely dominated by PP homopolymers and random copolymers with ethylene, but for sealing layers terpolymers with ethylene and butene are also used [37.30]. Impact copolymers are limited mostly to nontransparent applications with low-temperature toughness requirements, unless special polymer designs are applied which allow a combination of transparency

and toughness (e.g., *interpolymer* concept) with high propylene content in the EPR phase [37.32].

37.12.13 Injection Molding

Injection molding is a cost-effective fabrication process widely used for production of three-dimensional PP parts including rigid packaging containers and housewares, caps and closures, appliances and hand tools, medical articles and pharmaceutical packaging systems, consumer/industrial, etc. In injection molding, polymer (typically in pellet form) is softened, melted, and conveyed with a single screw. The melt is pushed through a runner system into a cavity or multiple cavities of a mold. The mold is cooled and eventually the solid parts are ejected and stacked. In thin-wall injection molding (TWIM) for rigid packaging container applications, the thickness does not usually exceed 25 mil and could often be considerably less than that [37.40].

Successful injection molding requires adequate product design, mold or tool design and construction, machine design and operation, and resin selection [37.32]. All these phases of product and process development and optimization frequently use computer-aided engineering (CAE) techniques. In particular, finite element analysis (FEA) can be used to simulate almost every mechanical and thermal condition such as static loads, impact events, thermal dilatation and creep, vibration and response to oscillatory loads, among others [37.30]. Thus, the design, dimensions, and thickness of injection-molded parts can be optimized. Details about injection-molding principles and design can be found in Injection Molding Handbook [37.81].

A typical range of PP MFR used for injection molding is 1–100 dg/min [37.30]. Increasing the MFR allows filling thin and narrow cavities over longer distances, however, the impact strength is greatly reduced. Use of random or impact copolymers can enhance impact strength. However, stiffness, heat resistance, and transparency, if targeted, will in turn be compromised. For TWIM, a typical reactor-based PP grade is approximately 35 dg/min MFR, although MFRs up to about 100 dg/min are used to permit more wall thinning and source reduction (downgauging). Both reactor and CR (Control rheology: a process of reducing molecular weight and molecular weight distribution of isotactic polypropylene (iPP)) PP resins are used, although reactor resins are generally more desirable for injection molding for two reasons. The broader MWD of a reactor resin over CR results in more shear thinning enhancing processability and a reactor resin has better organoleptics (taste and odor transfer characteristics) because of the absence of by-products of peroxide decomposition [37.40].

Typical PP injection-molding conditions are as follows [37.30]:

- Melt temperature T_m : 200–265 °C
- Injection pressure P_{inj} : 50–150 MPa
- Injection speed v_{inj} : 100–400 mm/s
- Mold (wall) temperature T_w : 30–60 °C.

Lower T_m will be used for higher MFRs, and lower levels of T_w for thinner parts. Molding machines for thin wall injection molding (TWIM) require fast injection speeds and high platen opening and closing speeds. Injection times of less than 0.20 s can be achieved for TWIM and cycles can vary between 7 and 20 min [37.32].

During PP injection molding, the formation of crystalline superstructures including shear-induced skin-core layers [37.82] affects both the solidification speed and the mechanical strength of molded parts. The presence of broad MWD resins containing a high molecular weight tail generally favors skin layer formation. Semicrystalline PP exhibits higher shrinkage and greater tendency for parts warpage than amorphous materials such as polystyrene (PS) and ABS. The resulting crystalline structure during injection molding determines the in- and post-parts shrinkage and anisotropy. Linear postmolding shrinkage of PP is 1.0–1.5%, of which 85% occurs within the first 24 h [37.30]. Distortion or warpage in molded products results from anisotropic shrinkage and both reflect internal stresses and crystal orientation. Higher MFR and/or narrow MWD typically reduce shrinkage and warpage of

parts [37.83]. Shrinkage and warpage can also be controlled by proper choice of processing conditions and part design. In general, the combination of resin attributes (e.g., M_w and MWD) and parts design and processing conditions affect the final parts properties.

A problem often encountered in injection molding of ICPs or thermoplastic olefin (TPO) compounds for long automotive parts is the formation of tiger marks. Tiger (flow) marking is defined as a viscoelastic melt flow instability that typically occurs in relatively long injection-molded parts, where alternate dull and glossy regions occur beyond a certain distance from the gate (onset distance to flow marks). Tiger marking is highly undesirable due to unacceptable appearance of the molded parts. Tiger marking fundamentals have been described in the literature [37.65, 84, 85]. It was found that the enhancement of melt elasticity at low shear rates effectively prevents the occurrence of flow marks on the molded parts [37.84]. As described in [37.64], a certain class of ICPs and TPOs with a high viscosity ratio (> 4) between ethylene–propylene rubber (EPR) and matrix phases (iPP) was reflected in a low value of loss tangent at 0.1 rad/s at 180 °C in a small-angle oscillatory shear (SAOS) experiment. These also exhibit either no tiger marks or significantly delayed onset of tiger marking. The ICP compositions made with a bulk/gas reactor process (nonslurry, solvent free) also exhibited significantly reduced amounts of gels/fish eyes despite the high viscosity ratio between matrix and rubber phases leading to excellence appearance and paintability of the molded parts [37.64].

37.13 Synthesis and Processing of Elastomers

37.13.1 Elastomer IUPAC Nomenclature

IUPAC nomenclature of elastomers is rigorous. It divides the materials into elastomers and rubbers, differing principally in their degree of crosslinking to create insoluble materials as well as hydrocarbon materials whose accepted acronyms end with M or R, corresponding to whether they are saturated in the backbone (M) or contain residual unsaturation (R). Nonhydrocarbon materials have spe-

cial designations such as Q for silicones. The common elastomers derived from petroleum which are described in this section are summarized in Table 37.3 [37.86].

Table 37.3 Common elastomers derived from petroleum

BR	Butadiene rubber (BR) (polybutadiene)
EPDM	Ethylene–propylene–diene terpolymer
IIR	Isobutylene–isoprene rubber (IIR) (butyl rubber)
SBR	Styrene–butadiene rubber (SBR)

37.14 Polybutadiene (BR)

37.14.1 Synthesis

The earliest polymerization of butadiene was with alkali metals in a bulk polymerization process. This technology using metallic sodium led to the development of the Buna grades. These early efforts were a technical demonstration without much commercial success. Subsequent efforts using either Ziegler coordination catalysts or alkyl lithium catalysts to produce solution polymers have led to a greater success in making BR. BR is composed of butadiene units which are joined by 1,4-addition (mostly in *cis*-1,4, but also *trans*-1,4-conformation) as well as by 1,2-addition. These geometric and stereo isomeric forms of monomer insertion lead to different polymeric properties ranging from amorphous to crystalline. The largest proportion of the globally produced BR is obtained by solution polymerization. The initiators used are primarily coordination catalysts, namely titanium [37.86], cobalt [37.87], nickel, and neodymium compounds [37.88]. Anionic polymerization using alkyl lithium compounds is also widely used since the BR rubber made in this process is structurally dissimilar to that obtained by the coordination polymerization. While with coordination catalysts the butadiene units in BR add linearly in greater than 92% *cis*-1,4-configuration, the alkyl lithium catalysts yield a BR with an intermediate *cis*-1,4-content and a higher 1,2-structure. The free radical emulsion polymerization in water of butadiene (emulsion or E-BR) yields a less uniform BR which although of great historical significance is not widely used today. However, a variant of this process where the polymerization is conducted as a coordination polymerization modification using a RhCl_2 catalyst in emulsion yields a predominantly *trans*-1,4-BR. The principal catalytic processes and thus the corresponding isomers of BR are listed below:

- **Titanium:** Originally, Phillips used titanium tetraoxide and aluminum tris(isobutyl) as catalysts. These formulations have now evolved to produce modified titanium catalysts to yield a BR which is easy to process.
- **Cobalt:** According to a process developed by Goodrich, CoCl_2 , Co-bis(acetylacetonate) or Co-bis(octanoate) in combination with diethyl aluminum chloride or ethylaluminum sesquichloride is used as catalyst [37.89].
- **Nickel:** A Bridgestone process [37.90] uses initiators such as Ni-bis(naphthenate)/boron trifluoride/ethylene oxide/aluminum trialkyl as a catalyst for the production of BR.
- **Neodymium:** A new Bayer development leads to a neodymium-based BR with high *cis*-1,4-content and correspondingly favorable mechanical properties in tread and sidewall compounds for car and truck tires due to improved fatigue resistance, abrasion resistance, and lower heat build-up compared to the conventional BR grades. Similar work has also been reported from the Chinese Academy of Sciences in Chanchung.
- **Lithium:** A process developed by Firestone uses alkyl lithium catalysts for the production of BR. The polarity of the solvent has a great influence on the microstructure and the vinyl content. The latter can be adjusted by the use of ethers or tertiary amines [37.91].
- **Alfin:** A process developed by Morton [37.92] for the production of BR with so-called Alfin catalysts, is an interesting specialty process with unique chemistry and polymer products. This catalyst consists of sodium salts of organic alkoxides in conjunction with sodium chloride. The polymerization is carried out in aliphatic hydrocarbon solvents. Contrary to the other processes, this process produces BR with high *trans*-1,4-content, and extremely high molecular weights. A unique facet of this polymerization process is that the high molecular weights persist through a range of process conditions including changes in the catalyst concentration.

37.14.2 Structure of BR and Its Influence on Properties

The average molecular weight of commercial BR grades is in the range of 250 000–300 000, corresponding to ML (1+4) Mooney viscosities at 100 °C of 35–55. The macrostructure of BR grades and the molecular weight distribution directly affects the properties and processability of the rubber both in the formation of compounds and the fabrication of the final article. These structural features depend on the polymerization process. Anionic lithium BR usually has a very narrow molecular weight distribution which leads to both poor processing and cold flow. Broader molecular weight distribution coordination polymerized BR is better. Broadening of the molecular weight distribution can be achieved using coupling or extensive branching which by extending the relaxation times leads to the same benefits in processing. With Li-BR, these branching reactions can be carried out by copolymerization with the difunctional monomer, divinyl benzene. Dramatic changes in the molecular weight distribution

are done with a coupling reaction. This coupling reaction uses an agent such as silicon tetrachloride or divinylchloride [37.93] and inorganic acid chlorides, such as POCl_3 , SOCl_2 , or S_2Cl_2 [37.94]. These very high molecular weight BRs are used for the production of oil-extended rubbers. Long-chain branching results in reduced cold flow, longer mixing cycles, better filler distribution, higher green strength, and higher extrusion rates.

Catalysts influence the microstructure of BR, and thus the vulcanized properties. The higher the *cis*-1,4-content of BR, the lower is its glass transition temperature T_g . Pure *cis*-1,4-BR grades have a T_g temperature of about -100°C , while commercial grades with about 96% *cis*-1,4-content have one below -90°C . Pure *cis*-1,4-BR has a subambient melting point and do not exhibit strain crystallization at room temperature. The glass transition temperature of BR rises monotonically as the concentration of 1,2-structure (vinyl content) increases. The tendency towards crystallization is determined by the 1,2-content.

37.14.3 Compounding and Vulcanization of BR

BR is mostly used in blends with natural rubber (NR) or SBR. Compared to BR alone, these blends in similar applications can be used with higher filler loading, higher extrusion rates, and higher green tensile strength. These attributes lead to lower cost and faster throughput in the manufacturing process. BR can be easily blended with all nonpolar diene rubbers. The blend ratio depends on the desired result, and ranges from about 30–50% for the BR elastomer.

The tensile strength of vulcanizates from BR with high *cis*-1,4 is much lower than desirable and cannot be used by itself in tires. However, blends with other rubbers show extremely low T_g with acceptable mechanical strength. These blends have a particularly high abrasion resistance, good low temperature flexibility, and

high resilience. Dynamic properties, such as heat generation during flexing and resistance to cracking, are also improved in general-purpose rubbers when they are blended with BR.

37.14.4 Uses of BR

- *Tires*: Over 90% of the total BR production is used in tires. The use of BR for specific tire components has changed in recent years due to the advances of radial tires. Originally BR had been widely used in tread compounds to improve the abrasion resistance. In radial tires, this rubber has found greater use in carcass, sidewall, and bead compounds because the tread of a radial tire already has an intrinsically higher abrasion resistance than that of bias tires. In winter tire treads, however, BR still plays an important role because of the improved ice traction.
- *Technical rubber goods*: In these products, and particularly in shoe soles or conveyor belting compounds, BR is preferred for its high abrasion resistance. Compounds containing BR also have improved flow properties, and for this reason, BR is recommended for compounds which are processed by injection molding. Successfully proven uses of BR are in compounds for shoe soles, bumpers, roll covers, conveyor belts, transmission belts, pads for chain tracks, shock absorber pads, and other products which require a reversion-resistant compound.
- *Liquid-reactive BR grades*: BR grades with a low molecular weight and reactive end groups (so-called telomers or reactive liquid polymers) can be converted into elastomers through a reaction with other suitable compounds in conventional methods for converting liquid polymers.
- *Impact modifiers for plastics*: Li-BR is used in considerable quantities as a modifier to improve the impact resistance of plastics.

37.15 Styrene–Butadiene Rubber (SBR)

37.15.1 Synthesis

In 1929, in a series of seminal experiments based on anionic polymerization and copolymerization of dienes and styrene, Tchunkur and Bock discovered that mixtures of butadiene and styrene can be copolymerized in emulsion [37.95]. These were called Buna S and had improved vulcanized properties compared to BR and were thus more widely accepted. Continuing re-

search and development lead to development of chain transfer agents for control of molecular weight and the development of redox initiators which allowed a reduction of the polymerization temperature as well as the development of easily processed SBR rubbers which still retained the excellent vulcanization characteristics [37.96]. Commercial production of emulsion SBR started in Germany in 1937, followed closely in 1942 in the United States as Government Rubber-Styrene. This

genesis led to the development of a very large commercial, worldwide SBR manufacturing industry based mostly on redox-initiated emulsion SBR with a growing amount of anionic or coordination solution SBR where the properties are more discretely variable. The styrene content in SBR ranges usually from about 23 to 40%. Since coordination catalysts have become available, stereospecific SBRs have also been produced in solution processes. An additional recent development is the block copolymers, composed of BR and PS blocks made by sequential anionic copolymerization of styrene and butadiene. These block polymers though isomers of SBR do not share the same properties. At room temperature, the styrene blocks separate into discrete phases, resulting in a physically crosslinked network structure and thermoplastic elastomers (TPEs).

In emulsion polymerizations, the rubber is obtained as latex which can be either used as such or further processed to yield solid rubber. The preferred emulsifiers for the dispersion of monomers during polymerization are, for instance, mixtures of sodium salts from fatty and rosin acids [37.97]. The ratio of butadiene to styrene is typically 76 to 23% by weight. The free radicals required for the initiation step are obtained by the reaction of iron(II) salts with *p*-menthane hydroperoxide or pinane hydroperoxide. *tert*-Dodecyl mercaptan is most frequently used as a chain modifier. With some SBR grades, extender oils and/or carbon black are added at the end of the polymerization stage. For oil extension, the rubber is usually produced to significantly higher molecular weights [37.98]. The oil, which is added to the latex, and which is recovered with the rubber from the latex, acts as a plasticizer during processing.

Solution copolymerization of butadiene and styrene in aliphatic or aromatic hydrocarbon solvents, using alkyl lithium catalysts produces the corresponding solution SBR [37.99]. Because of differential reactivity, the butadiene monomer polymerizes first, followed by the styrene, thus blocks of these monomers are found in the copolymer. Statistically random copolymerization occurs in the presence of modifiers such as ethers or tertiary amines. Although the overall composition of block copolymers and random copolymers can be the same, their physical properties differ significantly. Anionic polymerization is a living process which can be used to make multiblock butadiene and styrene block polymers by sequential and staged addition of monomers.

37.15.2 Structure of SBR and Its Influence on Properties

Emulsion SBR (E-SBR) is commercially available in ML (1+4) Mooney viscosities at 100 °C ranging from

30 to about 120, which correspond to average molecular weights of about 250 000–800 000. Emulsion SBR's differ in the amount of long-chain branching, thus in their processing and tensile characteristics, depending on the temperature of the polymerization. This emulsion process yields a rubber which may contain extremely high molecular weight gels, and their elimination requires a specific staged mode of addition of the chain transfer agent. Emulsion SBR's made by redox process at low temperatures have less long-chain branching and thus different processing characteristics than those made at a higher temperature with better tensile properties. At an equivalent viscosity, the low-temperature emulsion SBR can be more easily processed and form a smooth surface which is a consideration for tires. In the low-temperature redox polymerization SBR the butadiene component has, on average, about 9% *cis*-1,4-, 54.5% *trans*-1,4- and 13% 1,2-structures. At a 23.5% bound styrene level, the glass transition temperature (T_g) of SBR is about –50 °C. As the styrene content in the SBR increases, the glass transition temperature rises with loss of elastomeric properties like elastic recovery and resilience. However, the higher styrene content SBR also has an improvement in processability (extrusion rate, green strength, surface smoothness). Depending on the quantity of styrene in the butadiene chains, it is possible to adjust anywhere between these two extremes.

This rubber is supplied as gum, or extended with oil or carbon black, and can usually be processed directly. Since SBR cannot be readily masticated, the viscosity of the available material is of special importance regarding its processability. Low molecular weight SBR polymers are easily processed on rubber machinery, incorporate fillers and oil more readily, and can be fabricated by extrusion and calendaring. However, the higher molecular weight SBR rubbers have better green strength, and also accept higher filler and oil loadings.

Solution SBR affords entirely different structural, macrostructure, and butadiene insertion profile compared to emulsion SBR with a wide control using different catalysts and modifiers. By choosing appropriate polymerization systems and conditions, it is possible to custom-make solution SBRs with a wide range of specific properties. Solution SBR with a higher 1,2-content and thus a higher amount of pendant vinyl groups has largely the same effect on the polymer properties as the styrene with respect to T_g and interaction with fillers. Both lead to increase of T_g and the choice of concentrations of styrene and 1,2-butadiene units in the property of SBR rubbers can be tailored to suit the specific application. The spectrum of relaxation times of the rubbers is controlled by the breadth of molecular

weight distribution. This can be adjusted through the branching reactions. Solution SBR grades with a random distribution of styrene units are very similar to the emulsion polymers in composition except for the greater preponderance of the *cis*-1,4-structure and a narrower molecular weight distribution accompanied by less long-chain branching than the emulsion polymers. In segmented or blocky solution SBR, these polymers exhibit two distinct T_g at -85°C for the polybutadiene block and $+75^\circ\text{C}$ for the polystyrene block.

37.15.3 Compounding and Vulcanization of SBR

SBR can practically be blended with all nonpolar rubbers over the whole range of blend concentrations. Blends with BR or NR are of great importance in tire applications. In this example, the BR improves, for instance, the abrasion resistance and the hysteresis of the vulcanizates. Blends of SBR with polar rubbers, such as natural butyl rubber (NBR), are restricted to those NBR grades with low acrylonitrile.

Mechanical Properties

The tensile properties of E-SBR vulcanizates depend in great measure on the type and amount of filler in the compound. Gum vulcanizates have only poor tensile properties since the rubber lacks self-reinforcing qualities, and they are therefore of little interest. Instead, reinforcing fillers are usually required in SBR compounds. At optimum loadings with reinforcing carbon blacks, it is possible to reach virtually the same level of excellent tensile properties for SBR as for NR vulcanizates, but the tear resistance of the SBR vulcanizates is still inferior. The elastic properties of

E-SBR vulcanizates are also poorer than comparable ones of NR. The compression set of the vulcanizate, which is important for many applications, depends on the compound formulation, the cure conditions, and the specific test method. Through proper compounding and at optimum cure, it is, however, possible to obtain very low values of compression set for E-SBR vulcanizates.

Dynamic Properties, Aging Resistance, and Abrasion Resistance

E-SBR vulcanizates show surprisingly effective dynamic fatigue resistance, aging resistance, and heat resistance, surpassing NR vulcanizates. Without antioxidants the SBR vulcanizates are, however, not resistant to weathering and ozone degradation. Sulfur-free and low-sulfur vulcanization systems play an important role as well, and this also applies to NR. The heat resistance of optimized E-SBR vulcanizates allows service temperatures to be about 20°C higher than those for NR vulcanizates. E-SBR vulcanizates formulated with reinforcing fillers give a superior abrasion resistance than comparable ones from NR, which accounts for their predominance in passenger car tire treads. Since the E-SBR vulcanizates are so durable, they have replaced NR in many applications. The dynamic properties of E-SBR are inferior to those of NR, therefore, E-SBR vulcanizates give a higher heat buildup in dynamic applications. However, since they have a better heat resistance, E-SBR vulcanizates can also tolerate higher service temperatures. Nevertheless, in thick-walled rubber products, heat can build up because of the poor thermal conductivity of rubber, and this can lead to temperatures in excess of those tolerable by E-SBR vulcanizates.

37.16 Ethylene–Propylene Rubber (EPR/EPDM)

Polyethylene containing enough incorporated alpha olefin such as propylene can be essentially amorphous since the presence of statistically incorporated comonomer reduces both the melting point and the extent of the crystallinity. These amorphous materials are elastomeric and are thus resilient and recover from deformation over a wide range of temperatures. These resulting ethylene-propylene monomers (EPMs) do not contain unsaturation and can only be crosslinked to rubbers with peroxides. The incorporation of a third monomer during copolymerization of ethylene and propylene leads to sulfur-vulcanizable elastomer. The third monomer is a diene which retains one of the double bonds after polymerization as a pendant reactive

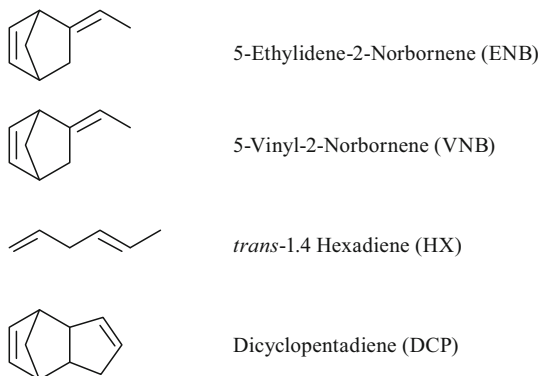
site. The terpolymers are EPDM which can be vulcanized using agents, depending on the reactivity of the double bond or atoms adjacent to them such as allylic hydrogens.

37.16.1 Synthesis

EPM and EPDM made by copolymerizing ethylene, propylene, and optional diene with Ziegler–Natta catalysts started in 1963. The majority of commercial EPM grades contain about 40 to 80% by weight corresponding to 45 to 85 mol% of ethylene, and the most important polymers contain about 50 to 70 mol%. The polymers at the higher end of the ethylene composi-

tion have some polyethylene-type crystallinity and are not amorphous. While many compounds are classified as dienes to make EPDM, commercial rubbers contain one of only four dienes. The choice of a suitable monomer depends on many criteria [37.100]. Firstly, the two double bonds of the diene should have different reactivities so that one will copolymerize with the second remaining unreacted in the polymer chain, enabling it to be used in subsequent vulcanization reactions. The other requirement is a high reactivity of the second double bond in sulfur vulcanization reactions.

These dienes are nonconjugated and in the final EPDM the retained double bond that did not participate in the Ziegler polymerization process is present as a pendant sidegroup to the main polymer chain. The four dienes are:



In commerce single-site catalysts such as vanadium or modern metallocene catalysts are used. The vanadium catalysts are formed in situ from a combination of VCl_4 and $VOCl_3$ along with the activating component $Al_2(ethyl)_3Cl_3$ or $Al(ethyl)_2Cl$. In the most common solution polymerization processes, the solvents are aliphatic hydrocarbons such as pentane or hexane. In suspension polymerization processes, an excess of propylene serves as the medium.

The key structural variations in the synthesis determine the properties of EPM and EPDM (in parenthesis, below):

- Composition: Ratio of ethylene and propylene (amorphous or semicrystalline)
- Co- or terpolymer (EPM or EPDM)
- Type and concentration of monomer (vulcanization kinetics, mechanical properties)
- Solution and suspension polymerization (highest obtainable molecular weight)
- Molecular weight distribution (processability)
- Oil extension (price).

37.16.2 Structures of EPM and EPDM and Their Influence on Properties

Sequence Distribution

Copolymers, which contain between 45 and 60 ethylene, are completely amorphous and are not self-reinforcing. At higher ethylene contents of 70–80%, the polymers contain long ethylene sequences, which are crystalline or crystallizable under deformation. These partially crystalline domains form thermally reversible physical crosslinks, which appear as high modulus prior to crosslinking.

Viscosity and Processability

The processability, which is both the ease of compound formation as well as fabrication of the final object prior to vulcanization, depends on their molecular structure [37.101]. Typically, a narrow distribution is adequate for average carbon-black dispersions, and a broad distribution for applications requiring excellent carbon-black dispersion. The molecular weights of most commercial grades are between 200 000 and 300 000 and the corresponding ML (1+4) Mooney viscosity at 100 °C lies between about 25 and 100.

Degree of Unsaturation

Since in both EPM and EPDM the polymer backbone is completely saturated having excellent resistance to oxygen and ozone even at elevated temperatures, EPM and EPDM vulcanizates are environmentally stable. The vulcanization properties, including rate and state of cure of EPDM, depend on the amount and type of double bonds from the monomer.

37.16.3 Compounding of EPM and EPDM

Blending EPM or EPDM with other polymers [37.102] improves the ozone resistance of other diene rubbers, such as BR and SBR. Since covulcanization of the components is difficult but highly desirable for high-ENB-EPDM grades, where ENB is 5-ethylidene-2-norbornene, the use of highly reactive accelerators or peroxides is common. EPDM grades with low unsaturation or EPM can also be used in blends with saturated polymers. Examples are blends of EPM or EPDM with polyolefins, sometimes already precrosslinked, to produce *thermoplastic elastomers* (TPE). The EPM or EPDM blend components also act as elastomeric modifiers to improve the impact strength, and since the modifiers have to be very elastomeric and often precrosslinked with peroxides, EPDMs are preferred in this application over EPMs.

Vulcanizing Agents

While EPM can only be crosslinked with peroxides, EPDM can use peroxides or sulfur. The methyl groups in polypropylene inhibit crosslinking reactions with peroxides, instead, they lead to chain scission. However, copolymer with 50 or greater mol% of ethylene can be crosslinked with peroxide. The termonomer also has an influence on the peroxide cure. For cable insulations, EPDM is frequently crosslinked with high-energy radiation as well. In this process no chemical curing agent is required. However, by using specific coactivators, a given degree of crosslinking can be obtained with a reduced dose rate. With sulfur cures, the required amount depends on the type and amount of termonomer in the polymer.

37.16.4 Processing of EPM and EPDM

Only compounds from low Mooney EPM or EPDM grades can be mixed on open mills. Therefore, EPM/EPDM compounds are almost exclusively mixed in internal mixers, and preferably by the so-called *upside down* technique. Since the EPM/EPDM is reversion resistant, high cure temperatures are generally used.

37.16.5 Properties of EPM and EPDM Vulcanizates

Mechanical Properties

The level of mechanical properties depends considerably on the type and amount of fillers in the compound. Optimized vulcanizates have lower levels of tensile properties as SBR. The mechanical properties of the partly crystalline, high ethylene content EPDM grades are particularly high, reaching the level of those for NR vulcanizates. Tear resistance, particularly at high temperatures, also compares with that achieved by NR vulcanizates. A wide range of hardnesses can be obtained with EPM or EPDM vulcanizates.

The elastic properties of EPM or EPDM vulcanizates are by far superior to those of many other SR vulcanizates, but they do not reach the level obtained with NR vulcanizates. The resistance to compression set of EPM or EPDM vulcanizates is surprisingly good, and this particularly applies to ENB-EPDM with a high ethylidene-norbornene (ENB) concentration, which is cured with either peroxides or sulfur in a highly active accelerator system. Compression set of sulfur-cured EPDM vulcanizates increases very rapidly with increasing temperatures in contrast to

peroxide crosslinked EPDM which remain relatively stable.

Dynamic Properties

The dynamic properties and the dynamic fatigue resistance of EPDM vulcanizates are also very good, comparable to those of SBR vulcanizates. This applies particularly to sulfur-cured vulcanizates.

Heat and Aging Resistance

The resistance to heat and aging of optimized EPM and EPDM vulcanizates is better than that of SBR or NBR vulcanizates. It is comparable to that of sulfur-cured IIR vulcanizates. Peroxide-cured EPM can, for instance, be exposed for 1000 h at 150 °C without significant hardening. The heat resistance of sulfur-cured EPDM vulcanizates is somewhat poorer. Therefore, because of the higher heat resistance of peroxide cures, combined with a very low compression set, this cure system is also widely used for EPDM. Under normal use conditions an oxidative degradation of the vulcanizates will not take place. The ozone resistance is also excellent. Even after an exposure for many months to ozone, the vulcanizates are not deteriorated. The ozone resistance of peroxide-cured EPM grades is best, followed by sulfur-cured EPDM. The ozone resistance of EPDM vulcanizates is still superior to that of CR and IIR. The resistance to weathering is also excellent, and follows the ozone resistance.

Resistance to Swelling and Chemicals

EPM and EPDM vulcanizates have an excellent resistance to chemicals. They are not attacked, and if so, only slightly, by dilute acids, alkalis, acetone, alcohol, and hydraulic fluids. Concentrated inorganic acids harden or destroy the vulcanizates. This is in contrast to the swelling resistance in aliphatic, aromatic, or chlorinated hydrocarbons. Since they are nonpolar, EPM and EPDM vulcanizates swell considerably in these media.

Electrical Properties

The electrical insulating and dielectric properties, or the breakdown and corona resistance, of EPM and EPDM vulcanizates are all excellent. In these respects, one should, however, differentiate between EPM and EPDM. EPM vulcanizates exhibit the best behavior. The electrical properties of these vulcanizates are also good at high temperatures and after heat aging of the vulcanizates. Because EPM and EPDM vulcanizates absorb little moisture, their electrical properties suffer minimally when they are submersed in water or buried underground.

37.17 Butyl (IIR) and Halobutyl Rubber

Isobutylene–isoprene rubber (IIR) is based on the BASF process of 1931 for making polyisobutylene. Standard Oil of New Jersey (now ExxonMobil) Chemical developed the commercial method for producing IIR in 1943. IIR consists of 97 to 99.5 mol% isobutylene and 0.5 to 3 mol% isoprene which provides the double bond required for sulfur vulcanization. More recently, chlorinated and brominated butyl rubbers (CIIR and BIIR, commercially known as chlorobutyl and bromobutyl) have also been produced to provide interfacial vulcanization of IIR and general purpose rubber (GPR) in tires.

37.17.1 Synthesis

IIR is produced by a cationic copolymerization of isobutylene and isoprene in methyl chloride suspension with AlCl_3 as a catalyst. The polymerization is conducted at -100°C with small amounts of water or HCl as cocatalysts. This low polymerization temperature is required to obtain high molecular weights for IIR. During the polymerization, which progresses to high conversion, high molecular weight IIR precipitate in discrete particles (precipitation polymerization), which are then separated from unreacted monomer and solvent, before drying. Cationic polymerization processes are dependable and reproducible only if the monomer is extremely pure. More recently, instead of AlCl_3 , $\text{Al}(\text{alkyl})_2\text{Cl}$ has been used as catalyst with a hexane solvent at higher polymerization temperatures of -40 – -50°C . This is a solution polymerization process which still leads to sufficiently high molecular weights [37.103].

37.17.2 Structure of IIR and Its Influence on Properties

Macrostructure

The average molecular weight of IIR is about 300 000–500 000, corresponding to ML (1+4) Mooney viscosities at 100°C of about 40–70. The molecular weight distribution of IIR is relatively broad most probably due to the inhomogeneous polymerization conditions.

Microstructure

The isobutylene monomer units polymerize predominantly in a head-to-tail arrangement, and the isoprene units are built into the polymer chains in *trans*-1,4-configuration.

Unsaturation

The largely saturated backbone of IIR contributes to its good resistance to oxidative and ozone degradation by

chemicals, while its density and chain dynamics determine the key attribute of low gas permeability. Among elastomers IIR is notable in having the lowest gas permeability and is thus principally used for air retention in tires and closures. The double bonds in the chain which are residues from isoprene permit sulfur vulcanization. At low levels of unsaturation, this vulcanization is slow. With increasing levels of unsaturation, vulcanization rates increase, but at the expense of thermal and chemical stability.

Blends

Since IIR cures relatively slowly, it does not covulcanize with other diene rubbers. For certain applications, blends with CIIR and chloro sulfonated rubber (CSM, up to 25% by weight) are used. CIIR and BIIR are important as blend partners with other diene rubbers.

37.17.3 Properties of IIR Vulcanizates

Mechanical Properties

With reinforcing fillers [37.104] very high tensile strengths can be obtained in IIR vulcanizates, corresponding to those of GPR vulcanizates. The vulcanized compounds characteristically exhibit very small rebound at room temperatures. Normally, IIR vulcanizates can be produced in hardnesses up to Shore A 85. For harder vulcanizates the use of resins or blending with CSM (up to 25% by weight) is recommended. As with other rubbers, the compression set of IIR vulcanizates depends primarily on the degree of vulcanization, and on the type and amount of filler and softener used in the compound formulation. In spite of the low rebound and stiffening of the vulcanizates at lower temperatures, the brittleness point is very low at -75°C .

Heat and Aging Resistance

The heat resistance of IIR vulcanizates, especially those cured with phenolic or halogenated phenolic resins, is excellent. Sulfur vulcanizates of IIR, however, have considerably poorer heat resistance compared with that of sulfur-cured EPDM vulcanizates. Because they contain a limited amount of unsaturation, IIR vulcanizates have an excellent resistance to weathering and ozone degradation.

Permeability

Vulcanizates from IIR have very low gas permeability, which is even lower than that of vulcanizates from high nitrile NBR.

37.17.4 Uses of IIR

The main applications of IIR are in cable insulations and jacketing, inner tubes of tires, inner liners of tubeless tires, curing bladders, pharmaceutical stoppers (mainly resin cured), and roofing membranes. However, tire treads based on IIR have not performed successfully.

37.17.5 Synthesis CIIR and BIIR

On adding chlorine or bromine to IIR in an inert organic solvent, a rapid electrophilic substitution reaction occurs, whereby one halogen atom is added per isoprene unit, mainly on the allylic positions [37.105]. Thus, only a relatively small number of halogen atoms are incorporated into the polymer chain. An addition of a pair of halogen atoms across the double bond hardly occurs. With chlorine, one obtains CIIR, and with bromine, BIIR:

- *Structures of CIIR and BIIR and their influence on properties:* Compared with IIR, the halogenated

IIRs have two advantages: the cure reactivity of the double bond is enhanced by both the halogen atom and allylic halogen structure. As a result, improvements occur in vulcanization rates, the states of cure, the reversion resistance, and interfacial covulcanization with other diene rubbers.

- *Compounding of CIIR and BIIR:* In addition to sulfur and phenolic crosslinking, crosslinking with ZnO or diamines is possible. BIIR gives faster vulcanization rates, and for the same cure systems, it gives a higher state of cure. Since with ZnO alone, the cure state is often inadequate, it is frequently used together with sulfur or sulfur donors.
- *Properties of CIIR and BIIR vulcanizates:* The properties of the CIIR and BIIR vulcanizates are better than those of IIR vulcanizates, such that BIIR vulcanizates have an even lower gas permeability, better weather and ozone resistance, higher hysteresis and better resistance to chemicals than the IIR parent.

37.18 Conclusion

Polymers derived from petroleum although composed of only a few major unsaturated building blocks occupy an increasing portion of the landscape and comprise of polymers which span the range of thermoplastics and elastomers. The efficiency of their manufacturing processes and the scale of the production of the monomers enable these polymers to be the biggest volumes in their respective fields. In addition, for these polymers their utility is greatly increased by the ease of the forma-

tion of binary or multicomponent blends. These blends, which typically have properties intermediate between the thermoplastics and the elastomers, are easily made by melt mixing. It is undoubtedly true that as the types of petroleum extricated changes in the future the nature of monomers available will change but the variety of petroleum-derived polymers ensures that under most conditions and scenarios this will continue to a productive and vibrant part of the economy.

References

- | | |
|---|--|
| <p>37.1 L.A. Utracki: <i>Commercial Polymer Blends</i> (Springer, Dordrecht 1988)</p> <p>37.2 R.J. Young, A.P. Lovell: <i>Introduction to Polymers</i>, 2nd edn. (Springer, Dordrecht 1991)</p> <p>37.3 J.D. Hottovy, B.E. Kreischer: Diluent recycle process, US Patent 6114 501 (2000)</p> <p>37.4 I. Burdett: <i>Hydrocarbon Engineering</i> (Palladian, Farnham 2008)</p> <p>37.5 E. Benham, M. McDanie: High Density Polyethylene. In: <i>Kirk-Othmer Concise Encyclopedia of Chemical Technology</i>, 5th edn., ed. by A. Seide (Wiley, Hoboken 2007) p. 590</p> <p>37.6 T. Hancock: Improvements in the method of manufacturing or preparing caoutchoc, either alone or in combination with other substances, English Patent 7549 (1838)</p> | <p>37.7 P. Pfeleiderer: German Patent 10164 (1880)</p> <p>37.8 F.H. Banbury: Machine for treating rubber and other heavy plastic material, US Patent 1200 070 (1916)</p> <p>37.9 R.T. Cooke: Rubber mixing or preparing machine, US Patent 215 618A (1934)</p> <p>37.10 J.W. Cho, P.S. Kim, J.L. White, L. Pomini: Flow visualization in an internal mixer using an adjustable rotor system comparison of double flighted and four flighted rotors, <i>Kautsch. Gummi. Kunstst.</i> 50, 496 (1997)</p> <p>37.11 P. Pfeleiderer: Innovations on kneading and mixing machines of Freyburger type, German Patent 18 797 (1882)</p> <p>37.12 H. Ahnhudt: Machine for producing patterned plastic materials, German Patent 397 961C (1924)</p> |
|---|--|

- 37.13 P. Leistritz, F. Burghauser: German Patent 682787 (1939)
- 37.14 R. Colombo: Italian Patent 370578 (1939)
- 37.15 R. Colombo: German Patent 895058 (1953)
- 37.16 R. Erdmenger: German Patent 813154 (1951)
- 37.17 W. Winkelmueller, R. Erdmenger, S. Neidhardt, E. Hirschberg, B. Fortuna: German Patent 813154 (1951)
- 37.18 E.H. Ahlefeld, A.J. Baldwin, P. Hold, W.A. Rapetzki, H.R. Scharer: US Patent 3154808 (1964)
- 37.19 Y. Wang, J.L. White, W. Szydowski: Flow in a modular intermeshing co-rotating twin screw extruder, *Int. Polym. Process.* **4**, 262 (1989)
- 37.20 D. Bang, J.L. White: Modular tangential counter-rotating twin screw extrusion: Non-Newtonian and non-isothermal simulation, *Int. Polym. Process.* **12**, 278 (1997)
- 37.21 F.R. Mayo, F.M. Lewis: Copolymerization. I. A basis for comparing the behavior of monomers in copolymerization: The copolymerization of styrene and methyl methacrylate, *J. Am. Chem. Soc.* **66**, 1594–1601 (1944)
- 37.22 R. Popli, L. Mandelkern: Influence of structural and morphological factors on the mechanical properties of the polyethylenes, *J. Polym. Sci. Part B.* **25**, 441–483 (1987)
- 37.23 R.J. Young: *Introduction to Polymers* (Chapman & Hall, London 1981)
- 37.24 H. von Pechmann: Pyrazol aus Acetylen und Diazomethan, *Ber. dtsch. chem. Ges.* **31**, 2950 (1898)
- 37.25 R. Kuhn, H. Kramer: Structures and properties of different low density polyethylenes, *Colloid Polym. Sci.* **260**, 1083–1092 (1982)
- 37.26 F.J. Karol: *Encyclopedia of Polymer Science and Technology*, Vol. 1 (Wiley, New York 1976) p. 120
- 37.27 J.P. Hogan: *Applied Industrial Catalysis*, Vol. 6 (Academic Press, New York 1983) p. 149
- 37.28 D. Maxfield, L. Mandelkern: Crystallinity, supermolecular structure and thermodynamic properties of linear polyethylene fractions, *Macromolecules* **10**, 1141–1153 (1979)
- 37.29 M. Gahleitner, C. Tranninger, P. Doshev: Heterophasic copolymers of polypropylene: Development, design, principles and future challenges, *J. Appl. Polym. Sci.* **130**, 3028–3037 (2013)
- 37.30 M. Gahleitner, C. Paulik: Polypropylene. In: *Ullmann Encyclopedia of Industrial Chemistry*, ed. by M. Bohnet (Wiley, Weinheim 2014)
- 37.31 M. Gahleitner, L. Resconi, P. Doshev: Heterogeneous Ziegler-Natta, metallocene and post-metallocene catalysis: Successes and challenges in industrial application, *Mater. Res. Soc. Bull.* **38**, 229–233 (2013)
- 37.32 N. Pasquini: *Polypropylene Handbook* (Carl Hanser, Munich 2005)
- 37.33 J.F. Ross, W. Bowles: An improved gas – Phase polypropylene process, *Ind. Eng. Chem. Prod. Res. Dev.* **24**, 149–154 (1985)
- 37.34 G. DiDrusco, R. Rinaldi: Polypropylene-process, selection criteria, *Hydrocarb. Process.* **63**, 113–117 (1984)
- 37.35 J.W. Shepard, J.L. Jezl, E.F. Peters, R.D. Hall: Divided horizontal reactor for the capor phase polymerization of monomers at different hydrogen levels, US Patent 3 957448 (1976)
- 37.36 C. Tzoganakis, J. Vlachopoulos, A. Hamielec: Modeling of the peroxide degradation of polypropylene, *Int. Polym. Process.* **3**, 141–150 (1988)
- 37.37 M. Xanthos: *Reactive Extrusion Principles and Practice* (Carl Hanser, Munich 1992)
- 37.38 A. Neubauer, S. Rhee, G. Smitherman: Troubleshooting underwater pelletizing processes, *SPE Tech. Papers, Proc. 61st Annu. Tech. Conf. Soc. Plast. Eng.* (2003) pp. 241–245
- 37.39 C. Crumb: http://www.er-we-pa.de/public_html/Company/pubs/EP_defects.html
- 37.40 H.G. Karian: *Handbook of Polypropylene and Polypropylene Composites* (Marcel Dekker, New York 2003)
- 37.41 A.K. Doufas, L. Rice, W. Thurston: Shear and extensional rheology of polypropylene melts: Experimental and modeling studies, *J. Rheology* **55**, 95–126 (2011)
- 37.42 A. Ghijsels, J. De Clippeir: Melt strength behavior of polypropylenes, *Int. Polym. Process.* **3**(9), 252–257 (1994)
- 37.43 H.C. Lau, S. Bhattacharya, G. Field: Melt strength of polypropylene: Its relevance to thermoforming, *Polym. Eng. Sci.* **38**, 915–923 (1998)
- 37.44 S. Hatzikiriakos, K. Migler: *Polymer Processing Instabilities: Control and Understanding* (Marcel Dekker, New York 2004)
- 37.45 I. Kazatchkov, S. Hatzikiriakos: Extrudate distortion in the capillary/slit extrusion of a molten polypropylene, *Polym. Eng. Sci.* **11**, 1864–1871 (1995)
- 37.46 O. Bartos: Fracture of polymer melts at high shear stress, *J. Appl. Phys.* **35**, 2767 (1964)
- 37.47 K. Kamide, Y. Inamoto, K. Ono: *Int. Chem. Eng.* **6**, 340 (1966)
- 37.48 S. Barnett: A correlation for melt fracture, *Polym. Eng. Sci.* **7**, 168 (1967)
- 37.49 J. Ui, Y. Ishimaru, H. Murakami, N. Fukushima, Y. Mori: Study of flow properties of polymer melt with the screw extruder, *Polym. Eng. Sci.* **4**(4), 295–305 (1964)
- 37.50 J.-C. Huang, Z. Tao: Melt fracture, melt viscosities and die swell of polypropylene resin in capillary flow, *J. App. Polym. Sci.* **1587**, 1594 (2003)
- 37.51 G. Akay: Unstable capillary flow of reinforced polymer melts, *J. Non-Newtonian Fluid Mech.* **13**(3), 309–323 (1983)
- 37.52 M. Fujiyama, Y. Kawasaki: Rheological properties of polypropylene/high-density polyethylene blend melts. I. Capillary flow properties, *J. Appl. Polym. Sci.* **42**(2), 467–480 (1991)
- 37.53 Z. Tao, J.-C. Huang: Observation of melt fracture of polypropylene resins in capillary flow, *Polymers* **44**, 719–727 (2003)
- 37.54 J. Baik, C. Tzoganakis: A study of extrudate distortion in controlled-rheology polypropylenes, *Polym. Eng. Sci.* **38**, 274–281 (1998)

- 37.55 S.G. Hatzikiriakos: Wall slip of molten polymers, *Progr. Polym. Sci.* **37**, 624–643 (2012)
- 37.56 E.E. Rosenbaum, S.G. Hatzikiriakos: Wall slip in the capillary flow of molten polymer subject to viscous heating, *AIChE J.* **43**, 598–608 (1997)
- 37.57 E. Mitsoulis, I.B. Kazatchkov, S.G. Hatzikiriakos: The effect of slip on the flow of a branched PP: Melt visualization experiments and simulations, *Rheologica Acta.* **44**, 418–426 (2005)
- 37.58 R. Athey, R. Thamm, R. Souffie, R. Chapman: *The processing behavior of polyolefins containing a fluoroelastomer additive*, SPE Tech. Pap, Vol. 21, (1986) pp. 1149–1153
- 37.59 A. Rudin, A.T. Worm, J.E. Blacklock: Fluorocarbon elastomer processing aid for LLDPE, HDPE and PP resins, *Proc. 1st Int. Conf. Process. Prop. Enhanc. Util. Modif. Addit. in Polym* (1985)
- 37.60 E. Strangland, J. Dooley, M. Spalding, E. Kim: Fundamental characterization on polypropylene extrusion, SPE ANTEC Tech. Pap., Annu. Tech. Conf. 2001 (2002) p. 302
- 37.61 C. Cheng: Effects of polypropylene crystallinity on extrusion, SPE ANTEC Tech. Pap., Soc. Plast. Eng., Vol. 1 (1995) pp. 98–106
- 37.62 C. Chung: *Extrusion of Polymers, Theory and Practice* (Hanser Gadner, Cincinnati 2000)
- 37.63 A.K. Doufas, E. Catalina, J. Avolio, R.J. Seung, K. Slusarz, B. Jonathan: Experimental studies of polypropylene extrusion instability, SPE ANTEC Tech. Pap., Proc. Annu. Tech. Conf. Soc. Plast. Eng. (2007) pp. 416–420
- 37.64 A.K. Doufas, E. Catalina, W. Thurston, R. Majewski: Propylene-based composition of enhanced appearance and excellent mold flowability, US Patent 20120157599A1 (2012)
- 37.65 K. Hirano, Y. Suetsugu, T. Kanai: Morphological analysis of the tiger stripe on injection molding of polypropylene/ethylene-propylene rubber/talc blends dependent on based polypropylene design, *J. App. Polym. Sci.* **104**, 192–199 (2007)
- 37.66 Y. Leong, M.A. Bakar, Z. Mohd-Ishak, A. Ariffin, B. Pukanszky: Comparison of the mechanical properties and interfacial interactions between talc, kaolin and calcium carbonate filled polypropylene composites, *J. App. Polym. Sci.* **91**, 3315–3326 (2004)
- 37.67 M. Denn: *Computational Analysis of Polymer Processing* (Applied Science, London 1983)
- 37.68 A. Ziabicki: *Fundamentals of Fiber Formation* (Wiley, New York 1976)
- 37.69 A.K. Doufas, A.J. McHugh, C. Miller: Simulation of melt spinning including flow-induced crystallization. Part I. Model development and prediction, *J. Non-Newtonian Fluid Mech.* **92**, 27–66 (2000)
- 37.70 R.M. Patel, A.K. Doufas, R.P. Paradkar: Raman spectroscopy for spinline crystallinity measurements. II. Validation of fundamental fiber-spinning models, *J. App. Polym. Sci.* **109**, 3398–3412 (2008)
- 37.71 R.P. Paradkar, R.M. Patel, E. Knickerbocker, A.K. Doufas: Raman spectroscopy for spinline crystallinity measurements. I. Experimental studies, *J. App. Polym. Sci.* **109**, 3413–3420 (2008)
- 37.72 W. Minoshima, J.L. White, J.E. Spruiell: Experimental investigations of the influence of molecular weight distribution on melt spinning and extrudate swell characteristics of polypropylene, *J. App. Polym. Sci.* **25**, 287–306 (1980)
- 37.73 S. Misra, F.-M. Lu, J. Spruiell, G. Richeson: Influence of molecular weight distribution on the structure and properties of melt-spun polypropylene filaments, *J. App. Polym. Sci.* **56**, 1761–1779 (1995)
- 37.74 E. Andreassen, O.J. Myhre, E.L. Hinrichsen, K. Grostad: Effects of processing parameters and molecular weight distribution on the tensile properties of polypropylene fibers, *J. App. Polym. Sci.* **51**, 1505–1517 (1994)
- 37.75 H. Geus, D. Frey, P. Schlag: Arrangement for the continuous production of a filament nonwoven fibrous web, US Patent 6 981 750B2 (2005)
- 37.76 H. Balk: Apparatus for making a spun-filament fleece, US Patent 4 820 142 (1989)
- 37.77 H. Bongaerts: *Flat Film Extrusion Using Chill-Roll Casting* (Hanser, Munich 1997)
- 37.78 K. Resch, G.M. Wallner, C. Teichert, G. Maier, M. Gahleitner: Optical properties of highly transparent polypropylene cast films: Influence of material structure, additives and processing conditions, *Polym. Eng. Sci.* **46**(4), 520–531 (2006)
- 37.79 N. Macauley, E. Harkin-Jones, W. Murphy: The influence of nucleating agents on the extrusion and thermoforming of polypropylene, *Polym. Eng. Sci.* **38**(3), 516–523 (1998)
- 37.80 K. McHugh, K. Ogale: High melt strength PP for melt phase thermoforming, SPE ANTEC Tech. Pap., Proc. Annu. Tech. Conf. Soc. Plast. Eng. (1990) pp. 452–455
- 37.81 D.V. Rosato, M.G. Rosato: *Injection Molding Handbook* (Springer, New York 2000)
- 37.82 G. Peters, L. Balzano, R. Steenbakkers: Flow-induced crystallization. In: *Handbook of Polymer Crystallization*, ed. by E. Piorkowska, G.C. Rutledge (Wiley, New York 2013) pp. 399–431
- 37.83 M. Gahleitner, P. Jääskeläinen, E. Ratajski, C. Paulik, J. Reussner, J. Wolfschwenger, W. Neibl: Propylene-ethylene random copolymers: Comonomer effects on crystallinity and application properties, *J. App. Polym. Sci.* **95**, 1073–1081 (2005)
- 37.84 S. Maeda, K. Fukunaga, E. Kamei: Flow mark in the injection molding of polypropylene/rubber/talc blends, *Nihon Reoroji Gakkaishi* **35**, 293–299 (2007)
- 37.85 B. Patham, P. Papworth, K. Jayaraman, C. Shu, M. Wolkowicz: Flow marks in injection molding of polypropylene and ethylene-propylene elastomer blends: Analysis of morphology and rheology, *J. App. Polym. Sci.* **96**, 423–434 (2005)
- 37.86 Phillips: GB Patent 848065 (1956)
- 37.87 B.F. Goodrich: DT Patent 1128143 (1958)
- 37.88 G. Marwede, B. Stollfuf: Actual state of butadiene rubber for tire application, *RubberCon* **87**, 112–116 (1987)

- 37.89 M. Grippin: *Ind. Eng. Chem. Proc. Res. Dev.* **4**, 160–165 (1965)
- 37.90 L. Furukawa: Mechanism of diene polymerization, *Pure Appl. Chem.* **42**, 495 (1975)
- 37.91 A.E. Oberster, T.C. Bouton, J.K. Valaitis: Balancing wear and traction with lithium catalyzed polymers, *Angew. Makromol. Chem.* **29**(1), 291–305 (1973)
- 37.92 A.A. Morton, E.E. Magat, R.L. Letsinger: Polymerization. VI. The alfin catalysts, *J. Amer. Chem. Soc.* **69**(4), 950–961 (1947)
- 37.93 H.L. Hsieh: Synthesis of radial thermoplastic elastomers, *Rubber Chem. Tech.* **49**(5), 1305–1310 (1976)
- 37.94 W. Ring, H.J. Cantow: Untersuchungen zur Molekulargewichtssprungreaktion von 1,4-*cis*-Polybutadien, *Makromol. Chem. Phys.* **89**(1), 138–155 (1965)
- 37.95 I.G. Farbenindustrie: DR Patent 570980 (1929)
- 37.96 I.G. Farbenindustrie: DR Patent 891 025 (1939)
- 37.97 A.L. Glasebrook, A.N. Hoffmann, J.B. Montgomery: Rosin hydrogenation, US Patent 2 776 276A (1953)
- 37.98 F.S. Rostler: *Rubber Age* **69**, 559 (1951)
- 37.99 J.M. Willis, W.W. Barbin: *Rubber Age* **100**, 53–56 (1968)
- 37.100 B.F.P. Baldwin, G. Verstrate: Polyolefin elastomers, based on ethylene and propylene, *Rubber Chem. Tech.* **45**, 709–781 (1972)
- 37.101 S. Shiga, M. Futura: Processibility of EPR in an internal mixer. II. Morphological changes in carbon black, *Rubber Chem. Tech.* **58**, 1 (1985)
- 37.102 A.Y. Coran: Blends of dissimilar rubbers – Cure rate incompatibility, *RubberCon* **87**, A32 (1987)
- 37.103 S. Cesca, M. Bruzzzone, A. Priola, G. Ferraris, P. Giusti: Copolymerization of isobutene and isoprene at high temperature with syncatalyst systems based on aluminum organic compounds, *Rubber Chem. Tech.* **49**(4), 937–959 (1976)
- 37.104 R.L. Zapp, P. Hous: Butyl and chlorobutyl rubber. In: *Rubber Technology*, 2nd edn., ed. by M. Morton (Van Nostrand Reinold, New York 1973) p. 249
- 37.105 A. van Tongerloo, R. Vucov: Butyl rubber-halogenation mechanisms, *Proc. IRC* (1979) p. 70

Biomass to L

38. Biomass to Liquid (BTL) Fuels

Gary Brodeur, Subramanian Ramakrishnan, Chang Samuel Hsu

We introduce a strategy for biomass fractionation and refinery co-processing. Some of the leading conversion technologies are reviewed, including pretreatment-hydrolysis (for 2nd-generation biofuels), gasification and Fischer-Tropsch (FT) synthesis, pyrolysis, and aqueous phase reforming (APR), along with some of the current challenges for commercialization. The main objective is to give an overview and recommendations in regard to the co-processing of biomass oil with crude oil that includes some of the developed technologies, as well as providing a new theoretical approach to the co-utilization of these raw materials. This new approach utilizes biomass to undergo 2nd-generation conversion processes where it is fractionated into relatively pure streams of soluble cellulosic/hemicellulosic sugars and residual solid lignin (non-sugar) fractions. The cellulose/lignin fractionation would also facilitate the development of new-generation characterization schemes to reduce interference between sugar and non-sugar components. Upgrading and reforming techniques such as gasification and Fischer-Tropsch (FT) synthesis, pyrolysis, or aqueous phase reforming (APR) can then be adopted for use with these fractions to generate feedstocks such as bio-oils that resemble those used within a petroleum refinery. If treated properly these

38.1	Lignocellulosic Biomass	1119
38.2	Biomass Processing Routes	1120
38.2.1	Pretreatment-Hydrolysis Pathway (Route 1).....	1120
38.2.2	Biomass-to-Liquid (BTL) Fuels (Route 2).....	1121
38.2.3	Pyrolysis (Route 3).....	1126
38.3	Biomass Oil and Petroleum Oil Co-processing	1127
38.3.1	Aqueous Phase Reforming (APR) – Virent.....	1128
38.3.2	Pretreatment-Hydrolysis/ Thermo-conversion Co-processing.....	1128
38.4	Conclusion	1130
	References	1130

biomass-derived oils have been shown to resemble crude-derived oil feeds and when supplemented in large quantities to process feeds can produce equivalent fuels and chemicals to that of petroleum crude oil. Consequently, dependence on fossil fuels will be reduced, among other advantages such as a reduction in greenhouse gas (GHG) emission, while still utilizing in-place technologies and with lower capital investments compared to earlier generations of biofuels.

Long-term success for a sustainable, clean energy source will require a new approach to the current biofuels trend that has focused on a comprehensive makeover of a billion-dollar industry, invested with trillions of dollars' worth of infrastructure and distribution networks, while having been completely integrated into our society. The goal should not be to merely replace the energy technologies that have been developed over time, but to supplement the feedstock (crude oil) with a cleaner and more sustainable resource that has similarities with regards to chemical make-up (e.g., biomass oil). The challenge with the current technologies lies

with the ability to break down the biomass, *cost effectively*, into its basic monomeric units and gaseous forms so that components may be upgraded or reformed into feedstocks that resemble those used within a petroleum or petrochemical refinery.

Recently, there has been a migration of research and technology from a petroleum foundation towards a more green (or alternative) approach to the energy and chemical industry. Environmental concerns are at the forefront of this need to transfer to a more carbon neutral platform in addition to economic and political backing providing a substantial push. The United States

Department of Energy (US DOE), among other national and international agencies, have laid out a goal to accelerate biomass-to-energy conversion research in order to make biofuels both possible and practical within the coming years [38.1]. There are a variety of pathways that are being considered for alternative routes including solar, wind, geothermal, etc., but the route that will be considered in this overview will be the biomass-to-liquids (BTL) fuel production pathway and how this method can be integrated into the current infrastructure of petroleum refineries.

The biomass used to generate biofuels can cover a broad range of materials that include: food crops (1st-generation biofuels), nonfood crops or nonedible portion of food crops (2nd-generation biofuels), and microalgae (3rd-generation biofuels). The 1st-generation biofuels have achieved a certain degree of success in terms of commercialization, especially under government subsidies or mandates. The bioethanol derived from corn and sugarcane, for example, is unable to replace gasoline completely without major modification to the internal combustion engine, and subsequently, must be blended with gasoline in order to be used within existing engines. Recently introduced biobutanol, which has a heat content close to gasoline and less water affinity, can be blended with gasoline at higher concentrations than bioethanol. Biodiesel produced from animal fats and vegetable oil has performed well in diesel engines, especially when blended with petroleum-derived diesel. However, all of the potential sources for 1st-generation fuels are associated with sustainability and affordability concerns, owing to the fact that they inherently compete with food sources considered to be limited in many regions of the world. The 3rd-generation biofuels that are currently under development have potential issues related to long time scales due to the slow growth-rate of the algae along with the need for an incredibly large photosynthesis area to support the large quantity of feedstock used to generate the extracted oils. Economic removal of excess water presents another challenge for algal fuel production.

The 2nd-generation biofuels can be categorized as a variety of products, namely: agricultural wastes (e.g., corn stover, sugarcane bagasse, etc.), municipal wastes, pulp milling by-products, recycled vegetable oils, as well as true feedstocks generated from under- or non-utilized forestry biomass. In essence, biomass is associated with such things as waste streams, pure feedstocks, recycled materials, as well as some materials that have not found a dedicated use. A large portion of biomass is in the form of lignocellulosics, which is a composite material particularly well suited for energy applications due to large-scale availability,

low costs, and the environmentally benign production. Many of the energy production and utilization cycles based on lignocellulosic biomass have low or near-zero greenhouse gas (GHG) emissions on a life-cycle basis [38.2–4]. This is owed to the fact that the CO₂ produced through the use of these fuels is utilized by the growth of other biomass. An added benefit of these new conversion routes is the generation of new employment opportunities in dwindling economies by consolidating and amplifying agricultural economy through energy crop cultivation as well as reinforcing long-standing industries such as sugar, paper, and forestry that can work synergistically with these conversion technologies.

A much overlooked concept that should increase the popularity of utilizing these biomass feedstocks is the idea of use within a fully integrated biorefinery, much like what has already been developed within petroleum refining [38.5, 6]. Biomass material can potentially integrate itself within existing petroleum refineries and be utilized as a feedstock for many of the products that petroleum has created a monopoly over. The integration could be considered as the 4th generation of biofuels as GHG emissions produced are reduced by sequestration techniques over standard refinery operations and biomass fuel production routes alone. This approach would not only be able to help alleviate the fuel industry but also that of plastics, chemicals, and other products that are derived from petroleum.

The primary obstacle impeding the more widespread production of energy from biomass feedstocks is the general absence of low-cost technology for overcoming the recalcitrance (difficulty to break down) of these materials. Currently, there are only a few lignocellulosic conversion methods that have been looked at for implementation into an adapted refinery. These include the generation of electricity by way of combustion, thermochemical treatment (gasification and/or pyrolysis), biochemical treatment, and a combined physicochemical treatment conversion pathway. A variety of chemicals, temperatures, and pressures are used separately or in combination with any of these processes to pretreat the feedstock and then break down the structures of the lignocellulosics into their monomeric, oligomeric, or gaseous forms so they can be further converted or upgraded into a usable product. Formation of these products can take the form of energy (heat and electricity), fuels (solid, liquid, or gaseous), and/or chemicals and materials. This paper will outline some of the technologies that are currently being investigated, along with a more detailed analysis of the utilization and implementation of gasification and pyrolysis into a fully integrated biorefinery (green refinery), and how these processes can be linked with current petroleum and petrochemical refineries.

38.1 Lignocellulosic Biomass

Before breaking down a complex material such as lignocellulosic biomass something must be known about how it is formed and what the structure is comprised of. Lignocellulose has three primary constituents which are cellulose, hemicellulose, and lignin, with smaller quantities of extractives, proteins, and inorganic materials. The largest of the constituents, cellulose, is a homopolymer composed of *D*-anhydroglucopyranose units (repeated glucose units), linked together by β -(1 \rightarrow 4)-glycosidic bonds. The cellulose chains are packed into microfibrils, stabilized by extensive hydrogen bonds (Fig. 38.1) [38.7]. These fibrils are attached to each other by hemicelluloses (amorphous polymers of various sugars) as well as other polymers such as pectin, and then encased by lignin. Hemicellulose is composed of mainly pentoses (xylose and arabinose) and hexoses (mannose, glucose, and galactose). Lignin is an amorphous polymer whose attributes include providing rigidity to the plant cell wall and resistance to microbial attack. The cellulose microfibrils present in the hemicellulose-lignin matrix are often associated in the form of bundles of macrofibrils.

Necessary information that could prove more important when dealing with some of the thermochemical processes is the ultimate analysis of various feedstocks that could be used (Table 38.1).

The ultimate analysis of the biomass materials is the chemical composition (e.g., carbon, hydrogen, oxygen content) of the feedstocks. A major factor that must be kept in mind during processing, as will be discussed later, is the oxygen content of these materials and its effect in various processing routes, especially when looking into integration within a refinery.

Fig. 38.1 Schematic representation of the matrix of polymers within lignocellulose that create the plant cells (after [38.7], courtesy of Genome Management Information System/ORNL) ▶

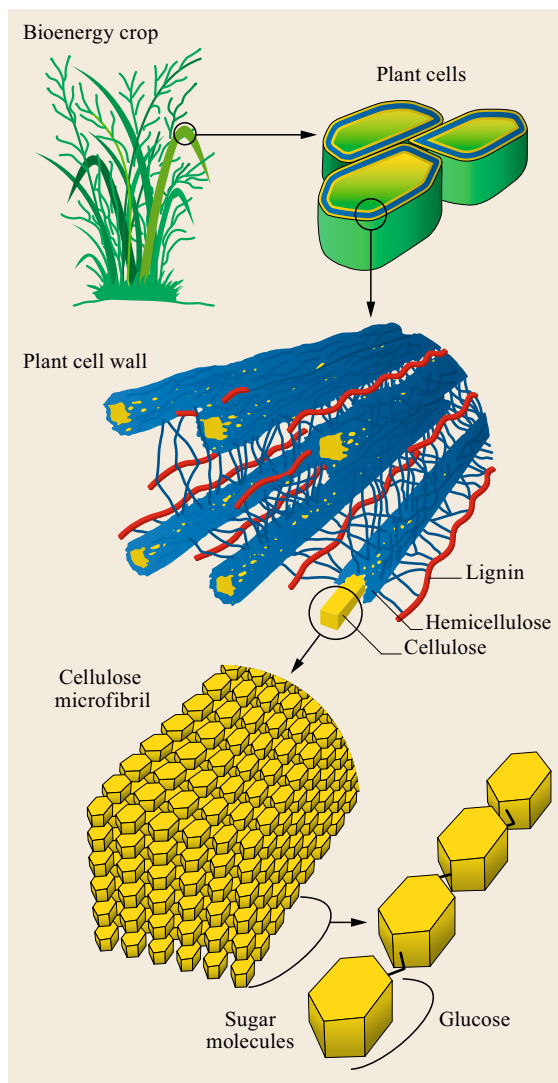


Table 38.1 Ultimate analysis of various feedstocks

Ultimate analysis (wt%)	Wood and woody biomass			Herbaceous and agricultural biomass			Processed biomass ^a		
	Mean	Low	High	Mean	Low	High	Mean	Low	High
C	52.1	48.7	57.0	49.9	45.2	58.4	53.6	45.4	70.9
O	41.2	32.0	45.3	42.6	34.2	49.0	37.0	16.4	46.1
H	6.2	5.4	10.2	6.2	3.2	9.2	7.3	6.0	11.2
N	0.4	0.1	0.7	1.2	0.1	3.4	1.7	0.2	6.1
S	0.01	0.01	0.42	0.15	0.01	0.60	0.46	0.01	2.33
C/O	1.26	1.52	1.26	1.17	1.32	1.19	1.45	2.77	1.54

^a Processed biomass includes: shredded currency, demolition wood, furniture waste, and wood yard waste [38.8].

38.2 Biomass Processing Routes

There are a few processing routes with regard to the break down of the lignocellulosic biomass into one of many potential products. The three routes that will be discussed herein are: (1) pretreatment-hydrolysis, (2) biomass-to-liquid (BTL) fuels via gasification and Fischer–Tropsch (FT) synthesis, and (3) pyrolysis. A schematic representation of these conversion routes along with the potential pathways that can be implemented for the production of biofuels can be seen in Fig. 38.2 [38.9].

In the pretreatment-hydrolysis route the recalcitrance of the biomass material is first reduced through some type of available pretreatment, followed by hydrolysis of the polymeric sugars into an easier-to-handle soluble fraction. This fraction can then be further treated by means of fermentation, dehydration, or hydrogenolysis to produce liquid fuel substitutes such as hydrocarbons or alcohols. Gasification has been looked at in conjunction with Fischer–Tropsch synthesis, combined as the Biomass-to-Liquid (BTL) fuel process, in order to gasify the feedstock and subsequently convert the gases formed into liquid fuels. Finally, pyrolysis will convert the biomass into a liquid fraction known as bio-oil that can be upgraded to hydrocarbon fuels by a variety of catalytic reactions, as well as having the potential to supplement various streams within a petroleum refinery.

38.2.1 Pretreatment–Hydrolysis Pathway (Route 1)

Ultimately, three distinct hurdles (Steps 2, 3, and 4 in Fig. 38.3) must be considered with this type of con-

version pathway that converts the lignocellulosic feed into a usable product, most notably ethanol and butanol, via biological processes. First, there must be some type of (1) pretreatment of the raw material to disrupt the fibrous structure by which the cellulose and hemicellulosic polymers will be made more accessible to be broken down into their monomeric sugars. This digestible lignocellulosic material can then be (2) hydrolyzed (acidically or enzymatically) into the individual subunits of the polymers or fermentable sugars. The fermentable sugars are then converted by one of the (3) oxygenate or alcohol formation pathways, such as fermentation in which microbial *bugs* are used to convert the sugars to products, such as alcohols [38.10].

The current bottleneck lies with the high cost of hydrolysis, owing to either the cost of enzymes or capital investment associated with acid hydrolysis. Currently, enzymatic hydrolysis is the preferred conversion route due to its ability to be specifically tailored to various feedstocks and the low operation costs linked with the reactors. Lowering the enzymatic loadings through the use of higher severity pretreatments without degradation of the feed is the focus of many research groups. The maximization of sugar production at the lowest possible cost can open up multiple routes for hydrocarbon/oxygenate formation [38.9–12].

The strategy that has recently received attention is the idea of fractionating the lignocellulosic biomass into its individual components so as to convert the material into the desired products more effectively [38.13–15]. Fractionation techniques have been used extensively in the pulp and paper industry in order to purify

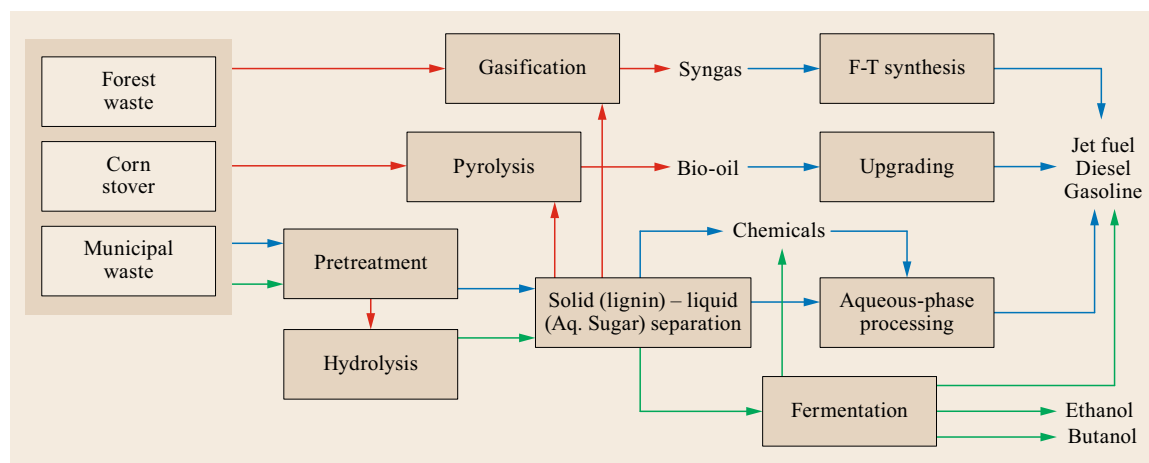


Fig. 38.2 Routes for the conversion of lignocellulosic biomass into liquid fuels. *Red arrows* refer to thermal routes, *green arrows* refer to biological routes, and *blue arrows* refer to catalytic routes (adapted from [38.7])

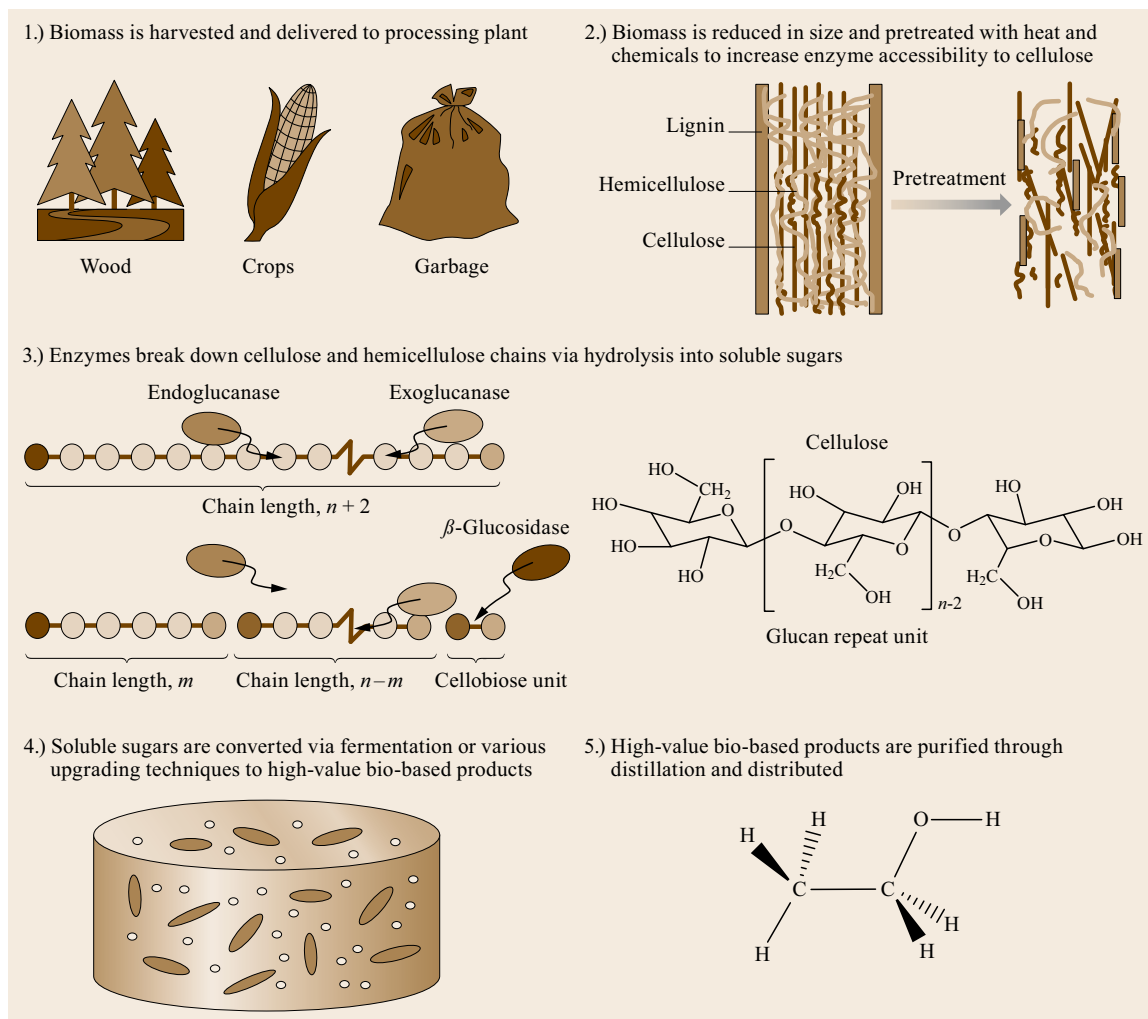


Fig. 38.3 Processing of 2nd-generation biofuels from biomass via the biological route

the cellulosic components of the feedstock, while the residual fraction is mostly burned to generate energy by combustion. However, this method does not effectively utilize the remaining biomass, making upwards of 70% of the total feedstock. These residual solids could potentially be used as feedstocks for gasification or pyrolysis where the material can be upgraded into higher value products.

38.2.2 Biomass-to-Liquid (BTL) Fuels (Route 2)

The BTL fuels route can be described almost equivalently to the much older technology of coal-to-liquids or gas-to-liquids (GTLs) conversion. These techniques involve the gasification of the feedstock, whether that is coal, gas, or biomass, followed by Fischer–Tropsch

(FT) synthesis for the production of liquid hydrocarbons.

Gasification

The idea of gasification has been around since the mid-19th century where it was originally utilized to convert coal to coal gas (or *town gas*) for lighting and heating purposes, and was used until just after WWII. Recently, the gasification pathway has shifted to producing more synthetic liquid chemicals and fuels through the use of integrated conversion operations. A relatively new approach to the utilization of gasification technology has been developed for use with biomass as a possible clean energy route with a lignocellulosic feed. This method preferentially converts organic-based carbonaceous material (e.g., biomass) into synthesis gas (*syngas* – a mixture of mainly CO and H₂) through the

use of high temperatures and the addition of a precise amount of air (or pure oxygen), and to a lesser extent, steam.

One of the attractive features of gasification is the fact that almost any biomass material can be used in this processing route; other routes such as ethanol or biogas production for example, can only use a select type of biomass material. This is due to the process's ability to break down the biomass into a gaseous form as opposed to the intermediates (monomeric sugars) required with the 1st-generation biofuels. A simplified scheme for which solid waste products (or potentially any carbonaceous material) are converted through a downdraft-type gasification system is shown in Fig. 38.4. The syngas produced from this system must first be treated to remove sulfur, nitrogen, and particulates before it can be further converted via FT synthesis. The generation of carbon-based co-products by gasification can be used for chemical upgrading or fertilization in soils (as 4th-generation biofuel production to provide a negative carbon budget in air), limiting waste generation. It is estimated that one ton of carbon (tar or char side-products) produced within this process scheme is equivalent to roughly 3–3.5 t of CO₂ that would normally be released by incineration, greatly reducing GHG emissions when implemented [38.16].

A more concrete definition for gasification would be the partial combustion (or partial oxidation, POX) of a solid fuel (biomass) that takes place at tempera-

tures of roughly 1000 °C in the presence of a controlled amount of oxygen. Complete combustion of the solid fuel will generally produce N₂, water vapor, CO₂, O₂, as well as small amounts of particulate matter considered harmful to both the atmosphere and humans. The *controlled* partial combustion of the biomass produces a preferred mixture of carbon monoxide (CO) and hydrogen (H₂) with traces of methane (CH₄) as well as some unwanted side products such as tars and chars, the latter being products of incomplete combustion. The key to a gasifier design is to create a situation in which biomass is reduced to charcoal and subsequently converted to syngas while also limiting the build-up of ash within the reactor. There are four unique processes (reaction zones) that can be considered to take place within a desired gasification process: dehydration, pyrolysis, combustion, and reduction. The break down of the biomass moving through these zones is illustrated in Fig. 38.4.

During the first stage (zone 1) of gasification the water is removed from the biomass feed (having a moisture content of roughly 10–30 % w/w) at temperatures of up to 200 °C, driven by the heat released from the lower zones of the gasifying unit. This is a necessary step as the water within the biomass can drive unwanted reactions during the following steps of gasification due to the presence of the molecular oxygen within the water. High oxygen content in biomass reduces the energy density of the material and for this reason must be removed (similar to the reasoning for the removal

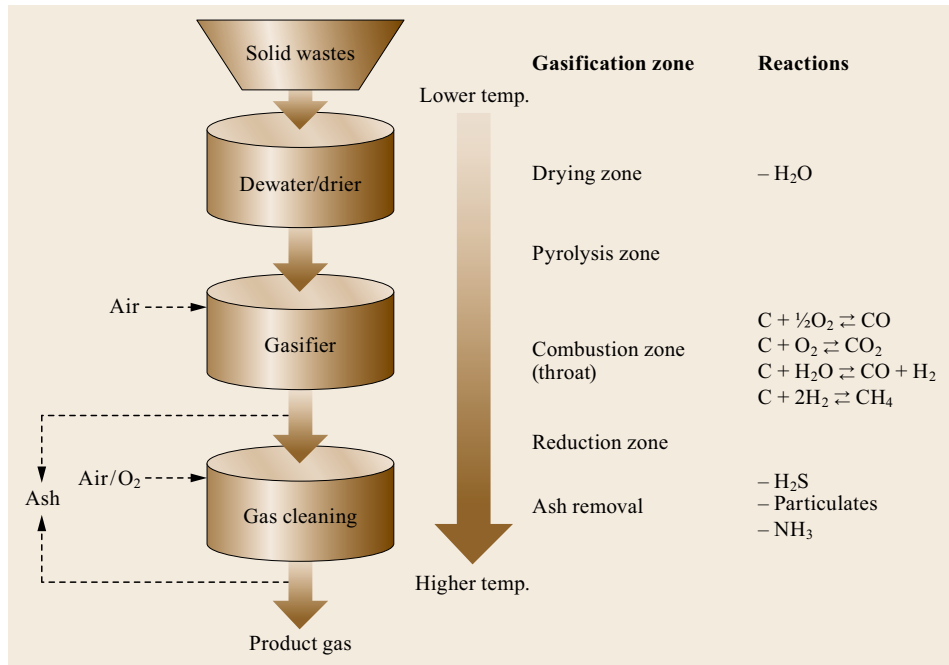


Fig. 38.4 Simplified schematic of a downdraft gasification unit along with some appropriate reactions and pathways

of oxygen in crude oil for petroleum transportation fuel production) in the form of either CO₂ or H₂O.

This dehydrated material is then mixed with a gas flow stream where it begins the process of pyrolysis (devolatilization). In this stage, the biomass is converted to large quantities of tars and gases containing carbon dioxide, as well as some methyl alcohols, as the carbonaceous particles are heated up at temperatures ranging from 280–500 °C. Although the gasification process is not necessarily synonymous with pyrolysis, it should be noted that pyrolysis will always occur to some degree within a gasifying reactor generating various condensable hydrocarbons as the material moves from the lower temperature zones to the higher temperature *gasifying* zones. Volatiles are released during this stage while the residual solids form the product char. The material properties of the products and the composition of the char formed during this particular step is highly dependent on the properties of the carbonaceous material that is being supplied to the system and will determine what type of gasification reactions these intermediate products will undergo. The possible reactions that occur during a gasification process can be seen in Table 38.2.

Combustion begins as the volatile products and char begin to react with O₂ to form CO₂ and CO, releasing heat for the subsequent gasification reactions. These reactions are effectively limited in this zone of the reactor by controlling the input rate of O₂. This limited flow of oxygen to the system will increase the amount of py-

rolysis that occurs in the zone above as the oxygen is consumed initially by the product from pyrolysis (char) that falls from the pyrolysis zone [38.18].

Gasification reactions will be introduced through the combined oxidation and reduction paths in which the carbon sources from the preceding zones are converted to the desired syngas. Solid-phase oxidation reactions will take place at temperatures ranging from 700–1000 °C where heterogeneous reactions (Table 38.2) between oxygen and the residual solid carbon fuel falling through the reactor form CO and H₂, as well as other by-products. As stated previously, another positive consequence of these reactions is the addition of heat that is necessary for processes within the system. The reduction reactions taking place will require high temperatures (up to 1100 °C) and consume the energy in the system, reducing the heat. Reduction reactions (Table 38.2) such as the Boudouard reaction, water-gas (WG) reaction, water-gas-shift (WGS) reaction, and the methane production reaction (Boudouard and WG preferred) will convert the available carbon to CO and CH₄ with the appropriate reacting material.

It is important to note that there is no distinct separation between the various zones throughout a gasification unit, but an overlap from one zone to the next. These zones may also vary in their order within the reacting system depending on where the air is fed, as well as the configuration of the gasifier. There are several configurations that have been used, most notably: updraft (air fed below gas outlet), downdraft (air fed above gas out-

Table 38.2 Main reactions during biomass gasification (after [38.17], courtesy of the International Energy Agency)

Reactants	Products	ΔH (kJ/mol)	Process
Primary devolatilization			
Biomass	Primary Tar (CH _x O _y) CO, CO ₂ , CH ₄ , C ₂ H ₄ , H ₂ O, C		
Tar cracking and reforming			
Primary Tar	Secondary Tar CO, CO ₂ , CH ₄ , C ₂ H ₄ , H ₂		
Homogeneous gas-phase-reactions			
Secondary Tars	C, CO, H ₂		
H ₂ + 0.5 O ₂	H ₂ O	−242	H ₂ – combustion (oxidation)
CO + 0.5 O ₂	CO ₂	−283	CO – combustion (oxidation)
CH ₄ + 0.5 O ₂	CO + 2H ₂	−110	CH ₄ – combustion (oxidation)
CH ₄ + CO ₂	2 CO + 2H ₂	+247	Dry reforming reaction
CH ₄ + H ₂ O	CO + 3H ₂	+206	Steam reforming methanization
CO + H ₂ O	CO ₂ + H ₂	−40.9	Water-gas-shift reaction
Heterogeneous reactions			
C + O ₂	CO ₂	−393.5	Oxidation of carbon
C + 0.5 O ₂	CO	−123.1	Partial oxidation
C + CO ₂	2 CO	+159.9	Boudouard equilibrium
C + H ₂ O	CO + H ₂	+118.5	Water-gas reaction (steam reforming)
C + 2 H ₂	CH ₄	−87.5	Methane production reaction

let), and cross-draft gasifiers (air fed at same level as the gas outlet). *Warnecke* [38.19] provides an extensive review of the various configurations of gasifiers along with their advantages and disadvantages.

Downdraft gasifiers are preferred when dealing with feedstocks such as wood and biomass residues as they tend to be smaller in scale, more affordable, and the tar that is developed during the process has a greater chance of being broken down as it descends through the combustion and reduction zones [38.19, 20]. Some of the other advantages and disadvantages of the various configurations have been highlighted in Table 38.3. Various geometrical configurations within a downdraft gasification unit (straight, single throat, or double throat) are also used depending on the application or feed [38.21].

Research has indicated that many parameters will affect the preferential production of syngas over the less-desired producer gas (mixture of CO, H₂, CO₂, CH₄, C_xH_y, and N₂). If producer gas is to form it can be further converted to syngas through other processes such as reforming or tar cracking, but this would add another costly operation step to an already complex process system. The controlling parameters of syngas production to note include the utilization of pure oxygen versus air feed, temperature range, particulate size, system pressure, residence times, as well as the feedstock to be used [38.9, 20]. The production of syngas from biomass for FT synthesis is normally associated

with high temperature, high oxygen content, small particle sizes, high pressure, and low residence times.

Co-firing of biomass with coal has been of recent interest in order to maximize the extent of the water-gas-shift reaction. *Kumabe* et al. observed that when a ratio of 0.5 (coal to biomass) was used, a maximum extent was observed [38.22]. If a further increase of the biomass ratio was introduced, an increase in the amounts of syngas and CO₂, along with decreases in char, tar, and H₂ were seen. Conversely, CO and hydrocarbon concentrations were left unchanged [38.23].

Syngas has the ability to be used in a variety of processing schemes for a variety of products. Some of the more common conversion routes are FT synthesis, combined heat and power (CHP) technologies, hydrogen production, catalytic synthesis of methanol (and other alcohols), and fermentation to ethanol. The catalytic synthesis of methanol is an interesting option for use with syngas due to the ability of methanol to be used for a range of products such as formaldehyde, dimethylether, and acetic acid. Methanol can also be converted to gasoline when used as the feedstock for methanol to gasoline (MTG) processes [38.24, 25]. FT synthesis however, will be the only option explained in-depth within the confines of this discussion.

Fischer–Tropsch (FT) Synthesis

FT synthesis is a technology that refers to the conversion of syngas to liquid hydrocarbons using a transition

Table 38.3 Advantages and disadvantages of various gasifiers (after [38.18])

Gasifier type	Advantage	Disadvantage
Updraft	<ul style="list-style-type: none"> ● Small pressure drop ● Good thermal efficiency ● Little tendency towards slag formation ● No carbon in ash 	<ul style="list-style-type: none"> ● Producer gas production ● Poor reaction capability with heavy gas load ● Relatively long time required for startup of internal combustion engine ● Great sensitivity to tar, moisture, and moisture content of fuel
Downdraft	<ul style="list-style-type: none"> ● Flexible adaption of gas production to load ● Small-scale applications ● Low sensitivity to charcoal dust and tar content of fuel 	<ul style="list-style-type: none"> ● Design tends to be tall ● Not feasible for very small particle size of fuel ● Producer gas production
Cross-draft	<ul style="list-style-type: none"> ● Short design height ● Very fast response time to load ● Flexible gas production 	<ul style="list-style-type: none"> ● Very high sensitivity to slag formation ● High pressure drop
Fluidized	<ul style="list-style-type: none"> ● Large-scale applications ● Feed characteristics ● Direct/indirect heating ● Can produce syngas 	<ul style="list-style-type: none"> ● Moderate tar yield ● Higher particle loading
Circulating fluid	<ul style="list-style-type: none"> ● Large-scale applications ● Feed characteristics ● Can produce syngas 	<ul style="list-style-type: none"> ● Moderate tar yield ● Higher particle loading
Entrained flow	<ul style="list-style-type: none"> ● Can be scaled ● Potential for low tar ● Can produce syngas 	<ul style="list-style-type: none"> ● Large amount of carrier gas ● Higher particle loading ● Particle size limits

metal catalyst. The products that are formed from this process (depending on the type of catalyst used – iron (Fe) and cobalt (Co) being predominant) can include transportation fuels (diesel or jet fuels) as well as higher value chemicals (waxes, lubricants, alcohols, etc.). The FT process can involve a variety of chemical reactions that produce multiple hydrocarbon molecules, however, primary reactions forming species with the formula $C_nH_{(2n+2)}$ (alkanes) are preferred. A block diagram of this FT synthesis pathway and the generalized products that form from the reactions can be seen in Fig. 38.5.

In order to avoid the production of methane ($n = 1$) the process temperature is normally kept below 400°C while pressures are kept in the range of $\approx 150\text{--}580$ psi. Lower temperature synthesis ($\approx 200\text{--}240^\circ\text{C}$ with Co catalyst) will yield high molecular waxes while higher temperatures ($\approx 300\text{--}350^\circ\text{C}$ with Fe catalyst) will yield low molecular weight olefins [38.26].

The generation of unreactive gases, short- and long-chain paraffins, olefins, and alcohols can all occur within the FT process. Paraffins produced tend to be straight-chain. However, the distribution of chain lengths (ranging from C_1 up to C_{50}) formed tends to be quite large. A positive fact to note with the production of these chains is that the chains will be predominately sweet (sulfur free) with low aromatic content, and can be further converted to automotive fuels through cracking, isomerization, or reforming. A route that has been taken to avoid the large distribution of chain lengths is to produce a more waxy material (larger carbon chains; $> C_{30}$) that can then be cracked into the diesel range by hydrocracking followed by purification using standard petroleum refining techniques. As an example, it has been shown that the syngas that has been converted during this process can be used as a feedstock for the generation of diesel and jet fuels using proprietary techniques developed by companies such as Syntroleum, Rentech, among others.

One of the major hurdles that accompanies BTL fuel processing is the fact that the syngas feed for FT synthesis must be free of impurities as the catalyst system is highly sensitive and is easily deactivated. Multiple, complex purification steps must be used in order to separate the unwanted species such as tars, volatile species (NH_3 and HCl), sulfur compounds, fine particles, and ashes that normally accompany the syngas produced. The volatile stream derived from biomass gasification will also have a much lower H_2/CO (≈ 0.5) ratio than what is normally preferred (≈ 2) during FT synthesis [38.9]. Consequently, the gas stream is usually co-fed to an intermediate reactor with water in order to increase the H_2/CO ratio (WGS reaction). Steam reforming may also be used in order to adjust

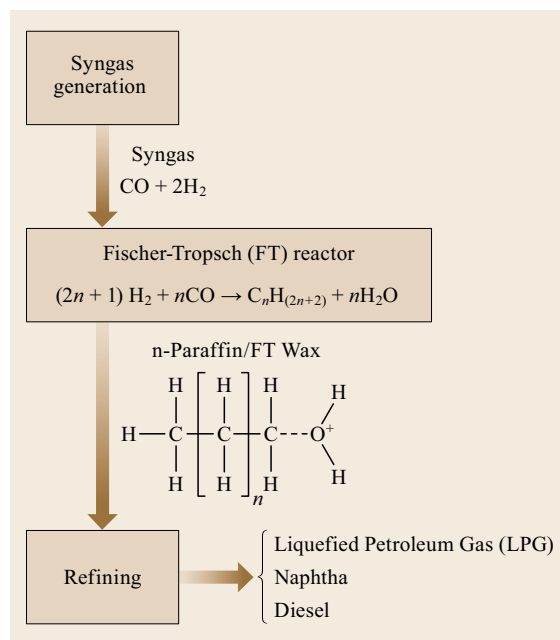


Fig. 38.5 FT synthesis schematic

the H_2/CO ratio if the CH_4 content is high. This reaction will convert CH_4 and H_2O to CO and H_2 (Table 38.2).

One example of a multistage gasification unit for biofuel production that is able to utilize a variety of biomass feedstocks is a process developed by Choren. Although this process has had difficulties becoming completely commercialized, it has shown the potential to be expanded upon and optimized in order to be fully functional. In this process, the biomass is first reduced in size, followed by dehydration, before being sent to a relatively low-temperature ($400\text{--}500^\circ\text{C}$) gasifier that forms the carbonization gas (syngas) along with tar and coke (solid state). This gas is then partially oxidized in a combustion chamber at high temperatures ($> 1400^\circ\text{C}$) with a precise amount of oxygen during coke addition, increasing the yield of CO and aiding in the break down of the material. After cooling, particulates that are not completely converted to gas are separated, followed by stripping of chlorides and sulfides. The gas stream will then be ready for FT synthesis and ultimately, fuel production [38.27].

Liu et al. [38.28] has shown evidence with performance and cost analysis that the co-generation of FT liquid fuels using coal alongside lignocellulosic biomass can be produced *cost effectively*. These synthetic fuels provide lower GHG emissions and capital investments than a standard fossil fuel power plant implemented with CO_2 capture. Fuels co-generated are also able to be produced cheaper than through a typical 1st-generation biofuels facility. The analysis shows that

it is possible to develop a scaled up biomass-derived FT fuel production facility with some further commercial optimization.

38.2.3 Pyrolysis (Route 3)

Pyrolysis differs from gasification by the fact that there is no air (specifically O₂) present during the break down of the carbonaceous material. The products that are formed during pyrolysis will also differ from that of gasification. However, the processes do show some similarities due to the overlap in reactions taking place. A lack of gasification within a pyrolysis reactor is usually never possible, as complete absence of oxygen is usually impossible as well as the fact that some oxygen is released from biomass during the reactions taking place. Consequently, some gasification occurs during pyrolysis just as some pyrolysis occurs during gasification. The desired product from pyrolysis is the liquid pyrolysis oils (bio-oils) that rapidly condense from the vapors released. Some other less desirable products will also form as solid residues containing carbon and ash, as well as producer gases.

In order to produce the bio-oil during processing, fast pyrolysis is preferred that utilizes moderate temperatures ($\approx 450\text{--}600\text{ }^\circ\text{C}$) at relatively high heating rates ($< 2\text{ s}$) followed by rapid quenching [38.29, 30]. Slow pyrolysis will produce char rather than bio-oil as the main product. Moisture content should also be strictly controlled, as too little moisture will simply form dust; conversely, too much moisture will form gases, owing to the presence of oxygen from the breakdown of compounds such as water, promoting gasification.

Pyrolysis Oil (Bio-Oil)

Pyrolysis oil (bio-oil) is a dark brown, viscous liquid product that is obtained from the pyrolysis of biomass. This bio-oil has a large variation of components dependent on pyrolysis conditions and the composition of the feedstock. A variety of highly oxygenated compounds make up the bio-oil and can be broken down into groups as acids, alcohols, aldehydes, esters, ketones, and aromatic species, along with some unreacted polymeric carbohydrates and lignin fragments [38.31–33]. The typical components of pyrolysis oil is shown in Table 38.4.

The highly complex bio-oil mixture is chemically unstable and can be altered or even degraded during storage due to thermal equilibrium shifts. The quality of the bio-oil is also highly dependent on the starting feedstocks and the pyrolysis reaction conditions need to be tailored to the characteristics of the feed [38.34]. It

Table 38.4 Typical component of pyrolysis oil (Bio-oil)

Component	(wt%)
Water	27
Ether-soluble organics (aldehydes, ketones, lignin monomers)	25
Volatile acids (mainly acetic)	5
Ether-insoluble organics (anhydrosugars, anhydro-oligomers, hydroxyacids)	28
Lignin derivatives, polymerization products and solids	15
Extractives (<i>n</i> -hexane soluble organics)	4

Table 38.5 Comparison of elemental composition of biomass-derived bio-oil and conventional crude oil (after [38.34, 36, 37])

Element (wt%)	Bio-oil	Crude oil
C	55–65	83–86
H	5–7	11–14
O	28–40	< 1
S	< 0.05	< 4
N	< 0.4	< 1

has been shown, however, that if the reaction conditions were tailored to each specific feedstock, the resulting compositions will have similar collections of cyclic hydrocarbons [38.35].

A comparison of the elemental compositions of bio-oil and crude oil has been made, shown in Table 38.5. Some observations can quickly be noted when comparing the elemental compositions of the two oil products. The conventional crude oils have extremely low oxygen content in comparison to the biomass-derived bio-oils that are intended to be co-fed. The high oxygen content within the biomass system can be attributed to the oxygenated functional groups that are prevalent within biomass. It is also estimated that roughly 15–30% of the components of the bio-oil is made up of water because of the high moisture content of the original biomass and the dehydration of the biomass that takes place during hydrolysis [38.38]. Accordingly, the high oxygen and water contents in the biomass-derived bio-oils will lower the heating values (half of that of hydrocarbon fuels) of the oil, and will also cause the streams to be immiscible when co-fed with petroleum-derived oils. For this reason, the products from pyrolysis must first be upgraded via hydrotreatment before being integrated into a petroleum refinery. This is similar to what petroleum-derived oils encounter when hydrotreatment is needed to remove impurities such as nitrogen and sulfur. In the case of biomass-derived bio-oils, however, the hydrotreatment will be used to remove oxygenated compounds.

38.3 Biomass Oil and Petroleum Oil Co-processing

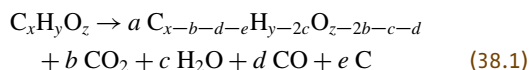
Biomass oils co-processed with petroleum cuts is a novel idea that has been formulated to overcome many of the hurdles that have been realized when developing processing routes that strictly use biomass for fuel production. If the pretreatment-hydrolysis route was simply used in conjunction with a fermentation-type process that converts the soluble sugars to alcohols many alterations would need to occur if the ties with petroleum were to be severed. The trillions of dollars that have been invested in infrastructure such as refineries, vehicles, and transportation networks would all be lost or have to be renovated. Work is still being conducted with regard to the thermochemical routes such as gasification and pyrolysis and being able to implement those technologies in more industrialized locations, as many undesired products are generated during the formation of the desired products.

In order to overcome these disadvantages it is theoretically possible to combine some of the newly developed technologies with the already-in-place petroleum infrastructure to develop biomass/crude co-processing. The idea would be to fractionate the biomass into its respective constituents (cellulose, hemicellulose, and lignin) and preferentially convert the materials by either liquefaction or catalytic conversion techniques. The products generated can then be combined with streams within the in-place petroleum or petrochemical refineries. The fact that biomass, once broken down, or pre-hydrotreated, has a very similar chemical composition and structure to the intermediate feed streams within a refinery makes this quite feasible.

This *co-processing* technique has the ability to add large quantities of feed to an already existent refinery stream with relatively low input in terms of capital costs as well as having a lower environmental impact compared to that which is normally synonymous with fossil fuels production. There are several options that can be used for co-processing that utilize the pretreatment-hydrolysis route, thermochemical route (gasification or

pyrolysis), or even a combination of the two, to generate a feedstock that can be supplemented into the refinery operations.

Fogassy et al. [38.39] has developed a representative reaction scheme (1) for the removal of oxygen in the bio-oil, forming the products CO₂, CO, C, and H₂O.



During this processing route a mixture containing 80 wt% vacuum gas-oil (VGO) and 20 wt% hydrodeoxygenated bio-oil was processed in a fluidized catalytic cracking (FCC) unit. The majority of the oxygen within the material was said to be removed in the form of CO₂ and H₂O by means of decarboxylation and dehydration reactions [38.39]. The impact of this release of CO₂ and CO that is produced during the co-hydrotreatment of petroleum gas oil and lignocellulosic biomass oil has been investigated and it was shown that it can be attributed to some inhibition within the hydrodesulfurization and hydrodenitrogenation reactions [38.40].

Elliot et al. [38.35] have shown that they can dramatically increase the C/O ratio (Table 38.6) over the course of various treatments of bio-oils that could be co-fed into a refinery. The lowest severity treatment, simply hydrotreating the bio-oil (A), focused on low temperatures with a palladium-on-carbon catalyst. The next two treatments made efforts to maximize the C/O ratio. In the first of these cases (B), the oil phase products of the hydrotreated bio-oil were subjected to hydrocracking, where lower pressures and higher temperatures were applied with a sulfide-form catalyst as opposed to directly hydrocracking the bio-oil products. In the second case, nonisothermal hydroprocessing (C) involves a low-temperature hydrotreatment followed by a high-temperature hydrocracking of the bio-oil products without an intermediary product phase separation

Table 38.6 Ultimate analysis of biomass feed (mixed wood, corn stover, oak, and poplar) and biomass-derived bio-oils, as well as three types of treatment: (A) Hydrotreated bio-oil, (B) Hydrocracked bio-oil, and (C) Nonisothermal hydroprocessed bio-oil (after [38.35])

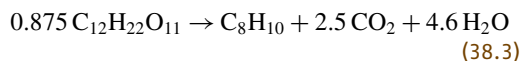
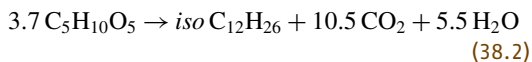
Ultimate analysis (wt%)	Biomass feed		Bio-oil (Moisture free)		(A) Hydrotreatment		(B) Hydrocracked		(C) Nonisothermal hydroprocessing	
	Average	+/-	Average	+/-	Average	+/-	Average	+/-	Average	+/-
C	43.6	9.4	57.9	8.2	75.4	1.5	87.0	0.5	87.6	0.2
H	7.4	0.5	6.2	0.5	9.2	0.6	12.3	0.4	11.7	0.2
O	46.8	7.9	31.9	4.5	14.1	2.3	0.5	0.2	0.4	0.2
N	0.5	0.4	0.6	0.5	1.3	1.1	0.4	0.2	0.2	0.2
S	0.1	0.1	n/a	n/a	0.1	0.1	0.0	0.0	0.0	0.0
C/O	0.93		1.81		5.33		174		202	

processing step. Work is ongoing with regards to optimization of the hydrodeoxygenation, catalytic cracking, and reforming techniques that would enable fully functional integration of the bio-oils into the refining process.

Al-Sabawi et al. [38.41, 42] reviewed co-processing of petroleum-derived and biomass-derived oils to produce clean transportation fuels via FCC [38.41] and hydroprocessing (such as hydrotreating and hydrocracking) [38.42]. The effect of biomass feedstocks on process operations, catalyst performance and deactivation, and product yield and quality were discussed. Even with the added benefit of the ability to use existing refining infrastructure and configurations that offer both economic and environmental advantages, many technical challenges remain. These include the low thermal stability of the bio-oil, compatibility of co-fed feedstocks, effects of the formed water on catalyst activity and stability, corrosion, mass and heat transfer properties, as well as quality and performance of fuels. Thermal stability is one of the biggest issues – the material cokes rapidly under reaction conditions or even in preheaters before reaching the reactor.

38.3.1 Aqueous Phase Reforming (APR) – Virent

Virent has developed reaction schemes for the conversion of sugars such as xylose and sucrose into hydrocarbons when utilizing their proprietary catalyst technologies [38.43]. These sugars can be derived from a multitude of biomass feeds by way of the pretreatment-hydrolysis technique, as has been noted. An efficient fractionation technology will be imperative for moving this technology further as it would be preferable to deal with a purified sugar source during these catalytic reactions. The following representative pathways (38.2) and (38.3) are used by Virent for the conversion of sugars, particularly xylose and sucrose, to hydrocarbons



As seen, the xylose $\text{C}_5\text{H}_{10}\text{O}_5$ sugars can be converted to branched C_{12} hydrocarbons and used as a product such as jet fuel, while the sucrose $\text{C}_{12}\text{H}_{22}\text{O}_{11}$ can be converted to the high-octane xylene (C_8) that can be used in gasoline blending [38.42]. The overall process that is in development consists of a multistage conversion for production of gasoline-range hydrocarbons: aqueous phase reforming (APR) of the carbohydrate sugars (glucose, xylose, etc.) and hydrolysates,

catalytic conversion, and fractionation into purified gasoline products. There are a multitude of reactions that are occurring during the APR process that include:

- Reforming to generate hydrogen
- Deoxygenation reactions – dehydration (alcohols), decarbonylation (ketones/aldehydes) and decarboxylation (acids/esters)
- Hydrogenolysis
- Cyclization.

Accordingly, the products formed can be further upgraded using a modified ZSM-5 catalyst to generate a high-octane gasoline, similar to that of the petroleum-derived reformat stream. What makes this processing ideal is the functionality of the products that are developed and the fact that these *drop-in* fuels can potentially replace over 90% of the products that come from a barrel of crude oil. Relatively little infrastructure will need to be implemented and almost none will need to be altered or replaced for the processing of the sugars (i. e., glucose via cellulose; primarily xylose, along with smaller quantities of arabinose, mannose, glucose, and galactose via hemicellulose – see Sect. 38.1) derived from biomass. This is because of the similar chemical compositions of the fuels derived from biomass to that of petroleum-derived fuels along with the in-place technologies that have the ability to upgrade these intermediary chemicals into the necessary feeds for refinery integration.

38.3.2 Pretreatment-Hydrolysis/ Thermo-conversion Co-processing

Now, a basis has been set for the idea of breaking down biomass material into purified fractions and then converting or upgrading these fractions through one of the aforementioned processing techniques. We can begin to think about how this can be done. A fractionation scheme that is currently in development utilizes a dual treatment of a lignocellulosic waste stream followed by enzymatic hydrolysis of that waste which is able to theoretically separate the majority of the constituents into three streams [38.44]. In applying this method, the biomass is first fractionated then the various thermochemical conversion techniques can be applied to upgrade these fractions individually where the products will begin to be representative of the crude streams within a petroleum refinery. It is at this point, that the biomass-derived oils and gases could potentially be co-processed with the streams within a refinery. An introduction of these methods will be discussed, followed by a generalization of the conversion method and results.

The first of the pretreatments is a dilute sulfuric acid (DA) treatment that is considered a well-established pretreatment technology within the biomass research community. This method of treatment has been extensively reviewed and refined by several groups and has been established as being able to not only enhance the ability of enzymatic hydrolysis, but also solubilize the majority of the short-chain hemicellulosic structure while leaving the long-chain cellulosic and lignin structures relatively intact for further processing due to the low severity of the treatment [38.10, 45–47]

Next, *N*-methyl morpholine *N*-oxide (NMMO) is used as a solvent to dissolve the DA-treated biomass for a short period of time (< 3 h) followed by an antisolvent regeneration step that will wash away the solvent and precipitate the biomass out of solution. The utilization of NMMO as a pretreatment is a relatively new technique, although it has been used predominately to treat purified cellulose within the fiber industry for several decades by generating Tencel fibers. The effects of this solvent on the lignocellulosic structure of biomass has been of recent interest. What has been discovered is the fact that NMMO is able to effectively and

efficiently decrystallize the cellulosic fibers and swell the lignocellulosic structure to increase the accessible hydrolyzable area for enzymatic attack. The result is that multiple groups have shown that the treatment of biomass with NMMO is able to enhance the rate of hydrolysis of cellulose by fungal enzymes [38.48–51]. However, the point of this discussion is the synergistic utilization of these two treatments to enhance the fractionation and conversion capabilities so that they can enhance the generation of intermediary products where one of the aforementioned conversion techniques will be employed to generate a feed ready for co-processing with crude oil.

The purified product streams generated from this dual treatment (dilute acid with NMMO treatment, or DAWNT) can be fractionated as follows: soluble hemicellulosic sugars (mixture of pentoses and hexoses), soluble cellulosic sugars (mainly glucose – hexose), and a residual solid lignin fraction according to the process design shown in Fig. 38.6. Fractionation is not new to biomass conversion practices, but the idea of a fractionation after enzymatic hydrolysis due to the highly digestible substrate may be considered a novel

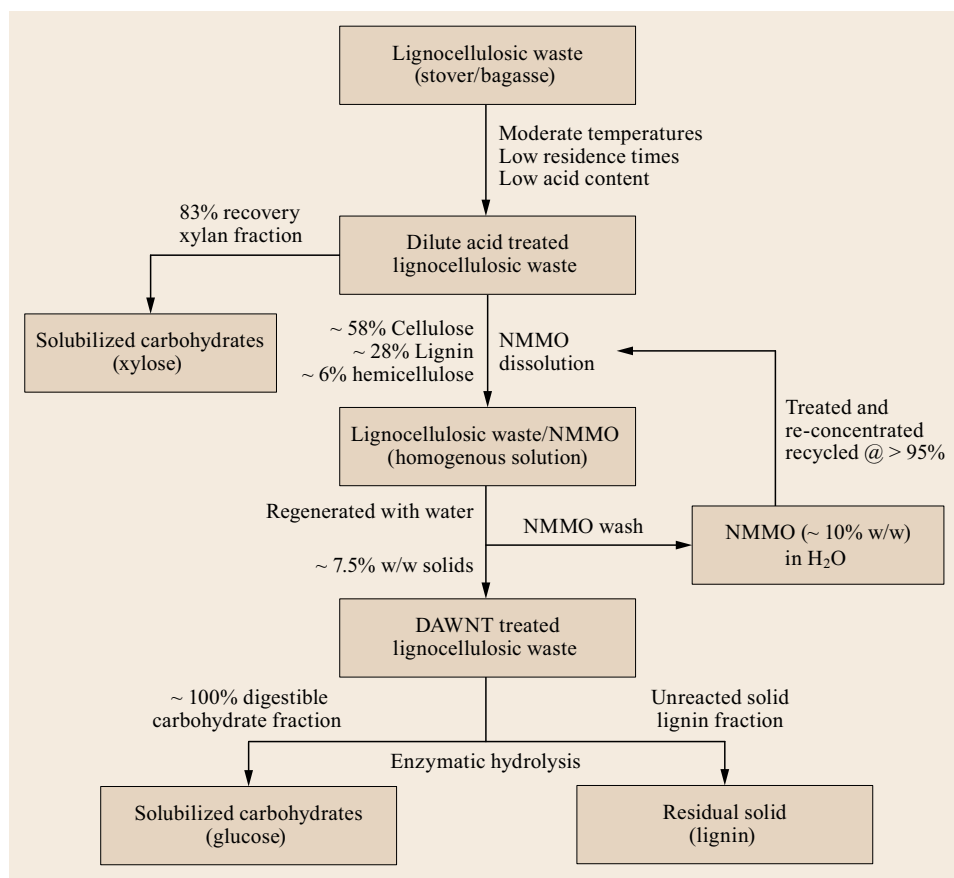


Fig. 38.6 Dilute acid with NMMO treatment (DAWNT) processing of lignocellulosic wastes (after [38.44])

technique. The DAWNT (dilute acid with NMMO treatment) method that uses this type of methodology can be summarized by the following criteria:

- DA Treatment [38.46]
 - $\approx 83\%$ of the hemicellulosic sugars will be solubilized and separated
 - Composition of processed solids: 58% cellulose, 28% lignin, and 6% hemicellulose
- NMMO Treatment [38.10, 44, 52, 53]
 - Unaltered solid composition
 - Highly digestible cellulosic fractionation
- NMMO swells cellulosic fibers enhancing enzymatic digestibility
- NMMO processing can be done at short time scales due to effects based solely on dissolution that occur rapidly due to the initial DA treatment
 - NMMO can be recycled at a rate of $> 95\%$ while keeping the same treatment efficiency
- Enzymatic Hydrolysis [38.10, 44]
 - $\approx 100\%$ cellulosic conversion to soluble sugars within 48 h at low enzyme concentrations (10 mg_{C_{Tec2}}/g_{glucan} enzyme loading)

- The remaining hemicellulosic fraction will also be converted here
- Residual solid lignin fraction and liquid sugar fraction can be easily separated.

This process is currently in development, but one can start to think about the potential applications when moving forward. Solubilized glucose, generated after enzymatic hydrolysis can easily be purified and used with either current 1st-generation conversion techniques or implemented into catalytic reforming processes, such as APR. The solubilized hemicellulosic-derived sugar fraction that is separated during the first treatment can potentially be used in an APR process, as was explained previously. The residual solid lignin fraction can be used in a thermo-conversion process such as gasification or pyrolysis after the solids are extracted post hydrolysis. If the pyrolysis route was to be used, bio-oil could be formed followed by mixing with the vacuum gas oil stream within a refinery process. Consequently, each of these methods will convert the starting biomass material into a usable hydrocarbon fuel, while utilizing the majority of the feedstock.

38.4 Conclusion

The majority of the conversion methods discussed here are still in their infancy and have not yet been fully investigated or refined. What can be taken away from this discussion is the fact that it is possible to convert biomass into a usable hydrocarbon fuel through co-processing without the need to convert the already in-place infrastructure and addition of significant capital investment to build independent continuous units (biorefineries). This is highly favorable over other alternative energy routes that would require alterations to an established billion dollar industry as well as an already developed trillion dollar infrastructure, but can simply be subsidized with biomass oil as a feedstock.

There appears to have been no significant breakthrough in 2nd-generation biomass-to-liquid processes in recent years [38.54]. Fractionation of biomass into digestible cellulosic sugars for fermentation and insoluble lignin for pyrolysis/gasification followed by Fischer-Tropsch and co-processing with petroleum oils might provide an alternative for further process development. Cellulose/lignin fractionation would also facilitate the development of new generation characterization schemes for detailed molecular compositional analyses of feedstock, process streams, and products of biofuel/chemical production.

References

- | | | | |
|------|---|------|--|
| 38.1 | R.D. Perlack, B.J. Stokes (Leads): <i>U.S. Billion-Ton Update: Biomass Supply for a Bioenergy and Bio-products Industry</i> , Vol. ORNL/TM-2011/224 (US Department of Energy, Oak Ridge National Laboratory, Oak Ridge 2011) p. 227 | 38.3 | A. Demirbas: Biofuels securing the planet's future energy needs, <i>Energy Conv. Manag.</i> 50 (9), 2239–2249 (2009) |
| 38.2 | M.A. Delucci: <i>Emissions of Greenhouse Gases from the Use of Transportation Fuels and Electricity</i> , Tech. Report (Argonne National Laboratory, Argonne 1991), ANL/ESD/TM-22 | 38.4 | L.R. Lynd, J.H. Cushman, R.J. Nichols, C.E. Wyman: Fuel ethanol from cellulosic biomass, <i>Science</i> 251 (4999), 1318–1323 (1991) |
| | | 38.5 | G.W. Huber, A. Corma: Synergies between bio- and oil-refineries for the production of fuels from biomass, <i>Angew. Chem.</i> 46 , 7184–7201 (2007) |

- 38.6 G.W. Huber, S. Iborra, A. Corma: Synthesis of transportation fuels from biomass: Chemistry, catalysis and engineering, *Chem. Rev.* **106**, 4044–4098 (2006)
- 38.7 S.K. Ritter: Genes to gasoline – Lignocellulose: A complex biomaterial, *C&E News* **86**(49), 10–17 (2008)
- 38.8 S.V. Vassilev, D. Baxter, L.K. Andersen, C.G. Vasileva: An overview of the chemical composition of biomass, *Fuel* **89**(5), 913–933 (2010)
- 38.9 J.C. Serrano-Ruiz, J.A. Dumesic: Catalytic routes for the conversion of biomass into liquid hydrocarbon transportation fuels, *Energy Environ. Sci.* **4**(1), 83–99 (2011)
- 38.10 G. Brodeur, E. Yau, K. Badal, J. Collier, K.B. Ramachandran, S. Ramakrishnan: Chemical and physicochemical pretreatment of lignocellulosic biomass: A review, *Enzyme Res.* **2011**, 1–17 (2011)
- 38.11 Y. Sun, J.Y. Cheng: Hydrolysis of lignocellulosic materials for ethanol production: A review, *Bioresour. Technol.* **83**(1), 1–11 (2002)
- 38.12 F. Carvalheiro, L.C. Duarte, F.M. Girio: Hemicellulose biorefineries: A review on biomass pretreatments, *J. Sci. Ind. Res.* **67**(11), 849–864 (2008)
- 38.13 N. Sathitsuksanoh, Z.G. Zhu, Y.H.P. Zhang: Cellulose solvent- and organic solvent-based lignocellulose fractionation enabled efficient sugar release from a variety of lignocellulosic feedstocks, *Bioresour. Technol.* **117**, 228–233 (2012)
- 38.14 W. Lan, C.F. Liu, R.G. Sun: Fractionation of bagasse into cellulose, hemicelluloses, and lignin with ionic liquid treatment followed by alkaline extraction, *J. Agric. Food Chem.* **59**(16), 8691–8701 (2011)
- 38.15 K.L. Kadam, C.Y. Chin, L.W. Brown: Continuous Biomass Fractionation Process for Producing Ethanol and Low-Molecular-Weight Lignin, *Environ. Prog. Sustain. Energy* **28**(1), 89–99 (2009)
- 38.16 F. Preto: Pyrolysis, Char and Energy. Presentation at The Canadian Biochar Initiative, Inaugural Meeting, CanmetEnergy: December 12, 2008, Ste Anne de Bellevue. <http://www.biochar.ca/files/Can%20Biochar%20Initiative%20Preto%20Dec08.pdf>
- 38.17 IES The Task 33/Thermal Gasification of Biomass. (accessed November 11, 2012) <http://www.ieatask33.org/>
- 38.18 A.K. Rajvanshi: *Biomass Gasification*, Vol. 2 (CRC Press, Maharashtra 1986)
- 38.19 R. Warnecke: Gasification of biomass: Comparison of fixed bed and fluidized bed gasifier, *Biomass Bioenergy* **18**, 489–497 (2000)
- 38.20 A. Kumar, D.D. Jones, M.A. Hanna: Thermochemical biomass gasification: A review of the current status of the technology, *Energies* **2**(3), 556–581 (2009)
- 38.21 J. Venselaar: *Design Rules for Down Draft Wood Gasifiers: A Short Review*, Project JTA–9A (Research Development at Institut Teknologi Bandung, Indonesia 1982) <http://elisa.tertso.nl/tertso/DRFGasifiers.pdf>
- 38.22 K. Kumabe, T. Hanaoka, S. Fujimoto, T. Minowa, K. Sakanishi: Co-gasification of woody biomass and coal with air and steam, *Fuel* **86**, 684–689 (2007)
- 38.23 M. Lapuerta, J.J. Hernandez, A. Pazo, J. Lopez: Gasification and co-gasification of biomass wastes: Effect of the biomass origin and the gasifier operating conditions, *Fuel Process. Technol.* **86**, 828–837 (2008)
- 38.24 S.L. Meisel, J.P. McCullough, C.H. Lechthaler, P.B. Weisz: Gasoline from methanol in one step, *Chemtech* **6**(2), 86–89 (1976)
- 38.25 J. E. Penick, W. Lee, J. Maziuk: Development of the methanol-to-gasoline process. In: *Chemical Reaction Engineering – Plenary Lectures*, ACS Symp. Ser. Vol. 226, ed. by J. Wei and C. Georgakis (Washington DC 1983) pp. 19–48
- 38.26 P. Spath, D. Dayton: Products from Syngas-Fischer-Tropsch Synthesis Products. *SunGrant BioWeb* <http://bioweb.sungrant.org/Technical/Bioproductions/Bioproductions+from+Syngas/Fischer-Tropsch+Synthesis/Default.htm>. (2008)
- 38.27 C. Kiener: Start-up of the first commercial BTL production facility – The beta-plant Freiberg, Proc. 16th Eur. Biomass Conf. Exhib., Valencia (2008)
- 38.28 G.J. Liu, E.D. Larson, R.H. Williams, T.G. Kreutz, X.B. Guo: Making Fischer-Tropsch fuels and electricity from coal and biomass: Performance and cost analysis, *Energy Fuels* **25**, 415–437 (2011)
- 38.29 L. Nan, G. Best, C. C. D. C. Neto: *Integrated energy systems in China – The Cold Northeastern Region Experience* (Natural Resources Management and Environment Department, Food and Agricultural Organization of the United Nations, Rome, Italy 1994) <http://www.fao.org/docrep/T4470E/T4470E00.htm>
- 38.30 D. Mohan, C.U. Pittman, P.H. Steele: Pyrolysis of wood/biomass for bio-oil: A critical review, *Energy Fuels* **20**(3), 848–889 (2006)
- 38.31 R.S. Karinen, A.O.I. Krause: New biocomponents from glycerol, *Appl. Catal. A Gen.* **306**, 128–133 (2006)
- 38.32 B. Kavalov, S. D. Peteves: *Status and Perspectives of Biomass-To-Liquid Fuels in the European Union*. (European Commission, Petten 2005) <http://www.mangus.ro/pdf/Stadiul%20actual%20si%20perspectivele%20bio-combustibililor%20in%20Europa.pdf>
- 38.33 A. Oasmaa, E. Kuoppala, A. Ardiyanti, R.H. Venderbosch, H.J. Heeres: Characterization of hydrotreated fast pyrolysis liquids, *Energy Fuels* **24**, 5264–5272 (2010)
- 38.34 Q. Zhang, J. Chang, T. Wang, Y. Xu: Review of biomass pyrolysis oil properties and upgrading research, *Energy Conv. Manag.* **48**(1), 87–92 (2007)
- 38.35 D.C. Elliott, T.R. Hart, G.G. Neuenschwander, L.J. Rotness, A.H. Zacher: Catalytic hydroprocessing of biomass fast pyrolysis bio-oil to produce hydrocarbon products, *Environ. Prog. Sustain. Energy* **28**(3), 441–449 (2009)
- 38.36 J. Holmgren, R. Marinangeli, P. Nair, D. Elliott, R. Bain: Consider upgrading pyrolysis oils into renewable fuels, *Hydrocarb. Process.* **87**(9), 95–113 (2008)
- 38.37 P.M. Mortensen, J.D. Grunwaldt, P.A. Jensen, K.G. Knudsen, A.D. Jensen: A review of catalytic up-

- grading of bio-oil to engine fuels, Appl. Catal. A Gen. **407**(1/2), 1–19 (2011)
- 38.38 A. Oasmaa, S. Czernik: Fuel oil quality of biomass pyrolysis oils – State of the art for the end user, Energy Fuels **13**(4), 914–921 (1999)
- 38.39 G. Fogassy, N. Thegarid, G. Toussaint, A.C. van Veen, Y. Schuurman, C. Mirodatos: Biomass derived feedstock co-processing with vacuum gas oil for second-generation fuel production in FCC units, Appl. Catal. B Environ. **96**(3/4), 476–485 (2010)
- 38.40 A. Pinheiro, N. Dupassieux, D. Hudebine, C. Geantet: Impact of the presence of carbon monoxide and carbon dioxide on gas oil hydrotreatment: Investigation on liquids from biomass cotreatment with petroleum cuts, Energy Fuels **25**, 804–812 (2011)
- 38.41 M. Al-Sabawi, J. Chen, S. Ng: Fluid catalytic cracking of biomass-derived oils and their blends with petroleum feedstocks: A review, Energy Fuels **26**(9), 5355–5372 (2012)
- 38.42 M. Al-Sabawi, J. Chen: Hydroprocessing of biomass-derived oils and their blends with petroleum feedstocks: A review, Energy Fuels **26**(9), 5373–5399 (2012)
- 38.43 P.G. Blommel, R.D. Cortright: *Production of Conventional Liquid Fuels from Sugars* (Virent Energy Systems, Madison 2008)
- 38.44 G. Brodeur, S. Ramakrishnan, C. Wilson, J. Telotte, J. Collier, J.J. Stickel: Combined dilute acid and solvent based pretreatment of agricultural wastes for efficient lignocellulosic fractionation and biofuels production, 245th ACS Natl. Meet. Exposition, New Orleans (2013)
- 38.45 B.C. Saha, L.B. Iten, M.A. Cotta, Y.V. Wu: Dilute acid pretreatment, enzymatic saccharification and fermentation of wheat straw to ethanol, Process Biochem. **40**(12), 3693–3700 (2005)
- 38.46 D.J. Schell, J. Farmer, M. Newman, J.D. McMillan: Dilute-sulfuric acid pretreatment of corn stover in pilot-scale reactor, Appl. Biochem. Biotechnol. **105–108**, 69–85 (2003)
- 38.47 C.E. Wyman, B.E. Dale, R.T. Elander, M. Holtzapple, M.R. Ladisch, Y.Y. Lee: Coordinated development of leading biomass pretreatment technologies, Bioresour. Technol. **96**(18), 1959–1966 (2005)
- 38.48 A. Jeihanipour, K. Karimi, M.J. Taherzadeh: Enhancement of ethanol and biogas production from high-crystalline cellulose by different modes of NMO pretreatment, Biotechnol. Bioeng. **105**(3), 469–476 (2010)
- 38.49 C.H. Kuo, C.K. Lee: Enhanced enzymatic hydrolysis of sugarcane bagasse by N-methylmorpholine-N-oxide pretreatment, Bioresour. Technol. **100**(2), 866–871 (2009)
- 38.50 P. Lennartsson, C. Niklasson, M. Taherzadeh: A pilot study on lignocelluloses to ethanol and fish feed using NMMO pretreatment and cultivation with zygomycetes in an air-lift reactor, Bioresour. Technol. **102**(6), 4425–4432 (2011)
- 38.51 S. Ramakrishnan, J. Collier, R. Oyetunji, B. Stutts, R. Burnett: Enzymatic hydrolysis of cellulose dissolved in N-methyl morpholine oxide/water solutions, Bioresour. Technol. **101**(13), 4965–4970 (2010)
- 38.52 C. Cuissinat, P. Navard: Swelling and dissolution of cellulose Part 1: Free floating cotton and wood fibres in N-methylmorpholine-N-oxide-water mixtures, Macromol. Symp. **244**, 1–18 (2006)
- 38.53 E. Yau: Enzymatic Hydrolysis of Cellulose Pretreated with Ionic Liquids and N-Methyl Morpholine N-Oxide, Master Thesis (Florida State University, Tallahassee 2012)
- 38.54 J. Regalbuto: An NSF perspective in next generation hydrocarbon biorefineries, Computer Chem. Eng. **34**, 1393–1396 (2010)

39. Renewable Diesel and Jet Fuels

Henrik Rasmussen

Hydroprocessing offers great potential for producing renewable diesel compatible with existing infrastructure and engine technology. This chapter discusses the catalyst technology and the process technology required to convert renewable feed sources such as triglyceride-based vegetable oil, used cooking oil, animal tallow and algae oils into transportation fuels.

39.1	Processing Renewable Feeds: Consequences for Hydrotreating	1134
39.2	Renewable Diesel: Feeds, Products and Reaction Pathways	1135
39.3	Development of Catalysts for Conversion of Renewable Feeds	1137
39.4	Choosing the Right Main Bed Catalyst when Coprocessing	1138
39.5	Simplified Process Diagram	1138
39.6	Catalysts for Dewaxing of Renewable Diesel	1139
39.7	Conclusion	1140
	References	1140

As a consequence of the general concern about fossil fuel resources and global warming from CO₂ emissions, the use of alternative, sustainable sources of energy for transportation has been increasing. Despite the growth in renewable fuels production, so far there has been little integration into existing petroleum refineries. There are two different classes of green fuels, namely first-generation *biofuels* and second-generation *renewable fuels*.

The two main biofuel products used in transportation fuels are bioethanol blended in gasoline and FAME (fatty acid methyl ester) used in or as diesel. FAME is a mixture of esters produced from chemical reactions between alcohols (typically methanol) and a renewable feedstock (typically a triglyceride-based compound). There are, however, several compatibility issues with the properties of FAME and the specifications of diesel, including a poor stability and filter plugging issues when blending FAME into the regular diesel fuel. For these reasons, only limited volumes of FAME can be blended into the fossil diesel fuel pool.

What is renewable diesel? The definition is a synthetic diesel fuel, produced from a renewable source that meets the ASTM D975 specifications for diesel fuel. Haldor Topsøe has commercialized a number of plants using our hydroprocessing technology desig-

nated HydroFlex for the production of renewable fuels such as diesel and jet fuel. In this process, the renewable organic material is reacted with hydrogen at elevated temperatures and pressure in a catalytic reactor. The obvious advantage of hydroprocessing compared to the use of FAME biodiesel is the fact that the final products, simple paraffins, from this simple process are the same components as those already present in fossil diesel.

Most of the existing FAME biodiesel can be characterized as first-generation biodiesel since it relies on the vegetable seed oils normally entering the human food chain; thus, this type of fuel may lead to escalating food prices and shortage of food supply. In contrast, renewable diesel from hydrotreating may be produced from a broad variety of sources, including waste animal fats and vegetable oils, but also from tall oil from the paper and pulp industry, pyrolysis oils, and other nonedible materials. The hydroprocessing of these feedstocks to renewable diesel utilizes the same types of catalysts as presently used for processing of fossil diesel streams to meet governing environmental specifications. Thus, a coprocessing scheme where fossil diesel and renewable feedstocks are mixed and coprocessed is possible, producing a clean and green diesel meeting all ASTM D975 specifications. The hydrotreating

Table 39.1 The advantages of renewable diesel over biodiesel

Property	Renewable diesel	Biodiesel	Advantages of renewable diesel
Storage stability	Months/years	Weeks	Easier to handle and distribute
Hydroscopic	No	Yes	Easier to handle and distribute
Cetane number	75+	48	Better blend stock
Energy content per volume	98–100% of fossil ultralow sulfur diesel (ULSD)	≈ 92% of fossil ultralow sulfur diesel (ULSD)	6–8% higher mileage per gallon

may also take place in a dedicated standalone unit that produces 100% renewable drop-in diesel. The new feed components, however, give rise to new reactions and to the formation of new byproducts, resulting in a series of challenges we have addressed by using optimized

catalysts and process design in our HydroFlex technology.

Table 39.1 compares some characteristics of renewable diesel and biodiesel, highlighting the advantage of renewable diesel over biodiesel.

39.1 Processing Renewable Feeds: Consequences for Hydrotreating

The refinery hydrotreaters play an important role in the production of transportation fuels. Before introducing even minor amounts of biomaterial into a diesel hydrotreater, it is important to know the implications and how all potential risk factors can be mitigated.

Virtually all naturally occurring oxygen-containing species are much more reactive than the sulfur compounds in fossil fuels. The challenge in industrial operation is mainly to control the very exothermic reactions and the large amounts of hydrogen consumed, which require higher makeup hydrogen rates and larger quench gas flows even when coprocessing smaller amounts of renewable feedstocks. Thus, the refinery hydrogen balance must be checked and the unit feed capacity may be lower than when only processing fossil diesel. The depletion of hydrogen from the treat gas, combined with high temperatures, directionally leads to accelerated catalyst deactivation and pressure drop buildup. To control these factors, tailor-made catalysts and a careful selection of unit layout and reaction conditions must be employed.

Another challenge is the often quite high content of contaminants such as phosphorous, sodium, and calcium. This may cause rapid pressure drop buildup and catalyst deactivation unless proper specialty guard beds are designed to prevent pressure drop buildup and to protect the downstream catalysts. When process-

ing other feed types, such as tall oil or vegetable oils with a high content of free fatty acids, severe corrosion of pipes and other equipment upstream of the reactor may take place if not properly addressed in the design.

High amounts of propane, water, carbon monoxide, carbon dioxide, and methane are formed as byproducts of the hydrotreating reactions. These gases must be removed from the loop either through chemical transformation, by a gas cleaning step (e.g., an amine wash), or more simply, by increasing the purge gas rate. If not handled properly, the gases will form buildup in the recycle gas loop and reduce the catalyst activity.

Due to these quite severe challenges, the present industrial practice involving coprocessing of fossil oil and renewable organic material is usually limited to blends with less than 5 vol.% renewable diesel. However, Haldor Topsøe has developed solutions to all of these issues that will result in a better economy of the coprocessing scheme and allow the proportion of renewable organic material in the feed to be increased up to 50 vol.% or more.

It is also possible using the HydroFlex technology to design the hydrotreating unit configuration and a catalyst system to process 100% renewable fuels; that is done commercially in a number of units around the world.

39.2 Renewable Diesel: Feeds, Products and Reaction Pathways

The purpose of hydrotreating biologically derived (i. e., renewable) feedstocks on an industrial scale is to produce hydrocarbon molecules, typically boiling in the diesel range, which are directly compatible with existing fossil-based diesel and which meets all current specifications for ULSD in ASTM D975. With the introduction of feedstocks stemming from renewable sources, new types of molecules are introduced with a significant content (10–15 wt%) of oxygen present. These molecules must be properly hydrotreated to eliminate the oxygen and contaminants.

Although a great variety of renewable feeds exist, the hydrotreating to produce diesel-type molecules is somewhat simplified by the fact that the chemistry of vegetable oils and animal fats is rather similar and based on triglycerides with a structure as shown in Fig. 39.1.

Since the paraffins produced from the fatty acid chains boils in the normal diesel boiling range, this means that a diesel hydrotreater is the preferred unit for coprocessing most feeds. Unlike fossil feedstocks, the content of sulfur and nitrogen species is very low in these feedstocks, thus the catalytic activity required for sulfur conversion (HDS) to make ULSD is reduced when coprocessing renewable feeds.

To investigate how the triglycerides react under typical hydroprocessing conditions, a pilot plant test with a NiMo catalyst was conducted using a blend of 75 vol.% Middle East straight-run light gas oil (SR LGO) and 25% rapeseed oil. Rapeseed oil is a triglyceride of fatty acids, mainly C₁₈ to C₂₂ acids. The conversion of triglycerides was confirmed to be 100%. Furthermore, yields of CO (0.6 wt%), CO₂ (1.2 wt%), and CH₄ (0.1 wt%) were observed. The total liquid product was analyzed by gas chromatography, and the results are shown in Fig. 39.2. The total conversion of rapeseed oil is confirmed by the fact that all high-boiling components (at retention times > 35 min) are not present in the product. Instead, four normal paraf-

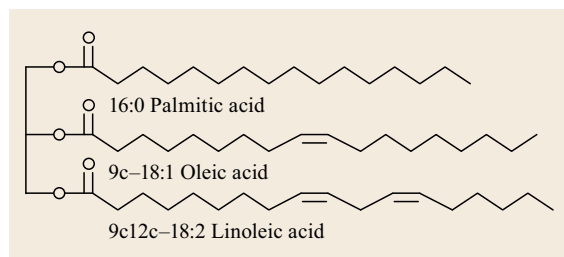


Fig. 39.1 Examples of some triglyceride structures in renewable feedstocks. 9c-18:1 is *cis*-9 oleic acid and 9c12c-18:2 is *cis*-9,12 linoleic acid

fins are formed with carbon chain lengths of 17, 18, 21 and 22 atoms respectively.

The conversion mechanism consists of several steps. The double bonds and the triglyceride are hydrogenated by one of at least two distinct reaction pathways (Fig. 39.3). The first pathway involves a complete hydrogenation. This pathway is usually called hydrodeoxygenation, or simply the HDO pathway. The other pathway involves a decarboxylation step, which means that CO₂ is split off.

The byproduct formation of both carbon dioxide and water influences the propagation of two additional reactions (also shown in Fig. 39.3); the reverse water gas shift (WGS, CO₂ + H₂ → CO + H₂O) and the methanation (CO + 3H₂ → CH₄ + H₂O), which will impact the overall hydrogen consumption.

Figure 39.4 shows gas chromatograms (GC) of liquid products from hydrotreating tests with 100% rapeseed oil as feed. The rapeseed oil is from a different source than that described above for the coprocessing test and consists mainly of C₁₈ fatty acids and minor amounts of C₁₆ fatty acids. The three catalysts were tested under identical conditions, but as Fig. 39.4 shows, the product distributions are quite different. Catalyst A converts the triglyceride mainly by the HDO route, producing mainly *n*-C₁₈. When using catalyst B, the HDO route is only slightly favored over the decarboxylation route, whereas catalyst C almost exclusively produces *n*-C₁₇ – the characteristic decarboxylation yield. The key is that Haldor Topsøe can catalytically control the reaction pathway, and by using the hydroprocessing catalyst A, we can increase the

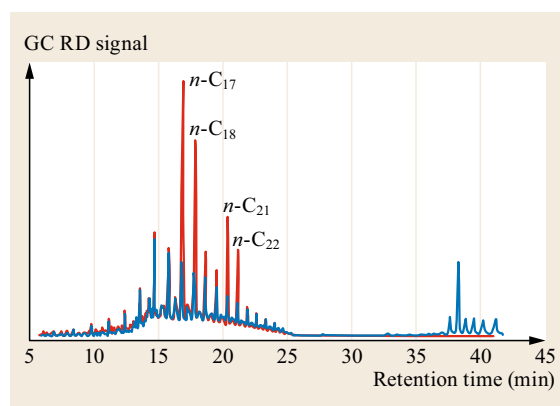


Fig. 39.2 Simulated distillation chromatogram of feed (blue) and product (red) from a pilot plant test of 25% rapeseed oil coprocessing. All rapeseed oil is converted into predominantly four normal paraffins with chain lengths of 17, 18, 21 and 22 respectively

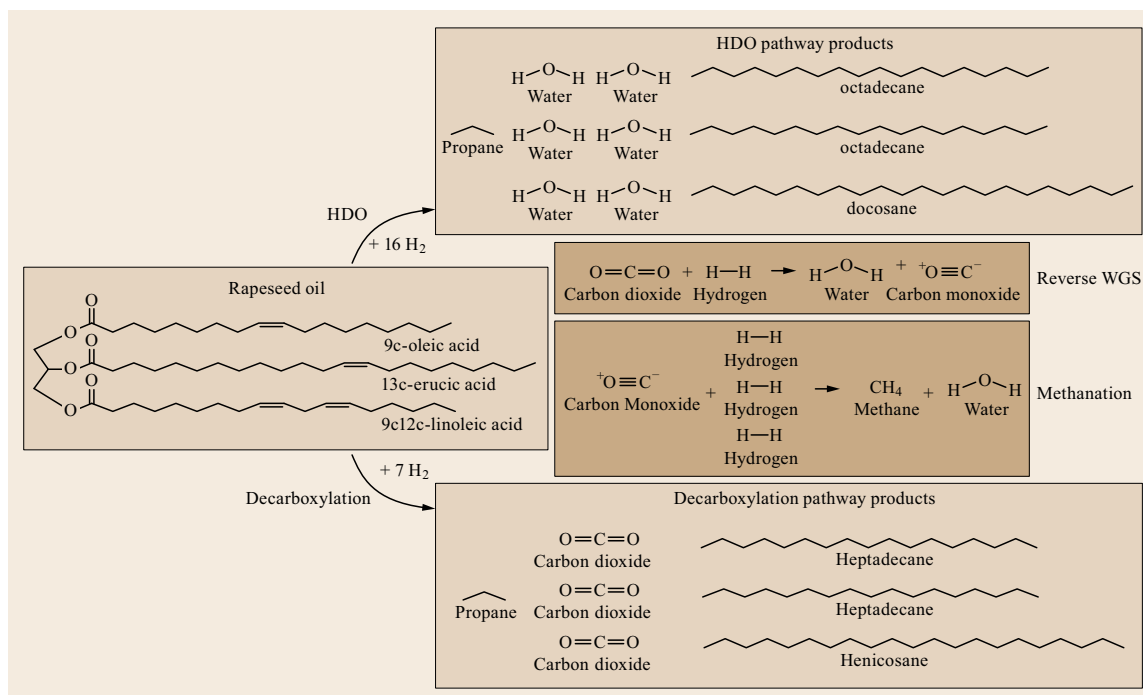


Fig. 39.3 Reactions occurring during the hydroprocessing of rapeseed oil

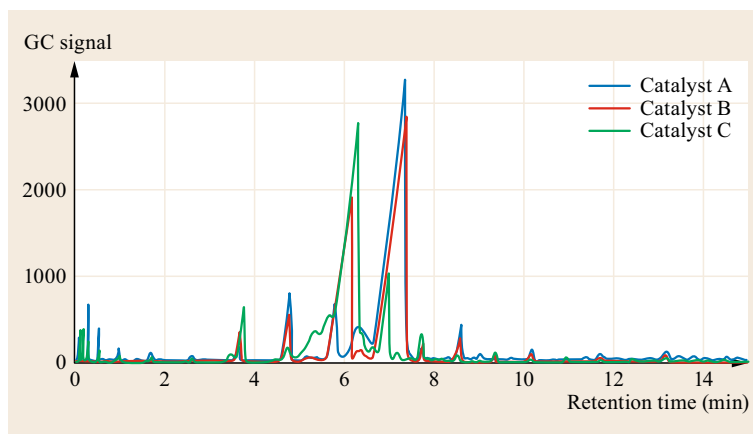


Fig. 39.4 Gas chromatograms of products from hydrotreating of 100% rapeseed oil. Large peaks at retention times of approximately 6 and 7 min are *n*-C₁₇ and *n*-C₁₈ respectively. The three catalysts have very different selectivities towards the decarboxylation and HDO pathways

liquid yield of diesel by about 4–5% because of the production of C₁₈ rather than C₁₇, which furthermore minimizes the CO₂ production.

The ability to control the reaction pathway away from the decarboxylation route and selectively toward the hydrogenation route will have advantages and disadvantages:

- Higher liquid diesel yield, which will have a very significant impact on the overall unit profitability.
- Practically eliminating the formation of CO₂, which also minimizes the formation of CO via the reverse

water gas shift reaction, which furthermore minimizes the methanation reaction.

- Higher recycle gas purity. Recycle gas purge is reduced. This is especially important in the coprocessing scenario because a lower hydrogen partial pressure (lower hydrogen purity) will impact the catalyst desulfurization abilities.
- Minimizing the formation of carbonic acid reduces the risk of corrosion in the downstream equipment.
- In a grassroots unit processing 100% renewable feedstock, the lack of CO₂ formation means that the amine scrubber can be eliminated. This will

- obviously reduce the installed cost for the plant and significantly increase the return on investment (ROI).
- In a coprocessing plant, the amine unit may become the limitation, because if CO_2 is formed, it will reduce the amount of H_2S that can be removed originating from hydrotreating the organic sulfur species in the conventional crude. Consequently, the feed rate of conventional crude barrels has to be reduced resulting in a reduced profitability from the asset.
 - The hydrogenation route typically consumes more hydrogen than the decarboxylation route, as can be seen in Fig. 39.3. This will result in a slightly higher operating cost when looking at the hydrogen only.

The higher cost of hydrogen, when utilizing the hydrogenation route, is easily justified due to many other advantages with this reaction route over the decarboxylation route, as described above.

39.3 Development of Catalysts for Conversion of Renewable Feeds

The complex reaction mechanism and the new challenges related to hydrotreating of renewable feeds must be taken into account when designing catalyst systems. If a catalyst is chosen that is not designed or tailor-made to handle coprocessing, the result may be poor desulfurization, hydrogen starvation, accelerated catalyst deactivation, and pressure drop buildup – depending on the amount and quality of the renewable material. Furthermore, the hydrotreated product may not meet the required targets for cold flow properties. The catalyst design for this service should, therefore, be based on solutions that address all of the challenges mentioned. In response to the challenges associated with the processing of renewable feedstocks, Topsøe has introduced a number of dedicated catalysts for the hydrodeoxygenation (HDO) of renewable feeds and isomerizing dewaxing catalysts for cold flow property improvement. In combination with specialized graded bed catalysts and conventional ULSD catalysts, these new products will extend the cycle length and ensure that an on-spec product with a renewable component is achieved without any operational problems. These

catalysts may be employed in both coprocessing and standalone units processing 100% renewable feeds.

These catalysts have already been employed in more than 15 industrial units, making renewable drop-in fuels in both coprocessing and neat (standalone 100% renewable) operating mode. Figure 39.5 shows the pressure drop in an industrial ULSD hydrotreater, which after two years of operation started to coprocess 3–5 wt% of vegetable oil. The original Haldor Topsøe catalyst loading was designed only for hydrotreating of a fossil feedstock, and when the refiner introduced the renewable feed, it was evident that the pressure drop increased quite dramatically. The pressure drop continued to increase, and as a result, the refiner was limited in how much renewable feed could be processed. At the next opportunity for a shutdown of the hydrotreater, the special optimized renewable fuels catalysts from Haldor Topsøe were installed. As illustrated in Fig. 39.5, with Haldor Topsøe catalysts, the pressure drop was low and stable while processing biofuels. In fact, the pressure drop was at the same very low level as before the introduction of renewable feeds [39.1, 2].

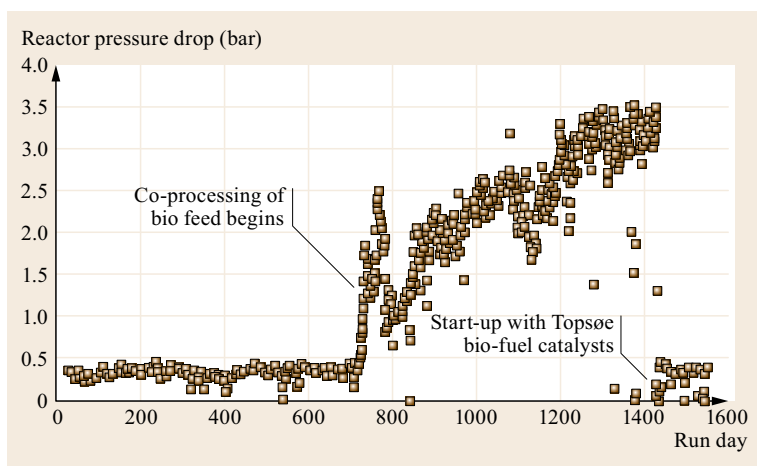


Fig. 39.5 Pressure drop development when coprocessing vegetable oil with and without Haldor Topsøe biofuel catalyst

39.4 Choosing the Right Main Bed Catalyst when Coprocessing

In the coprocessing scenario, the hydrotreater still needs to convert all the organic sulfur in the fossil diesel barrels to H_2S to be on-spec, so it is of utmost importance that the desulfurization (HDS) activity is maintained in the unit. In order to investigate the impact of a renewable fuel in a coprocessing mode, a number of pilot plant tests were conducted using both a nickel-molybdenum (NiMo) hydrotreating catalyst and a cobalt-molybdenum (CoMo) hydrotreating catalyst.

The first set of bars in Figs. 39.6 and 39.7 represents the HDS and HDN baseline activities when processing a 100% fossil light gas oil (LGO). The second set of bars represents the pilot plant test where the LGO is mixed with 15% rapeseed oil and tested at the exact same process conditions as when operating with pure LGO. The data clearly shows that the HDS and the HDN activity of the CoMo catalyst is severely inhibited by the rapeseed oil, but the NiMo catalyst is practically unaffected. In order to determine what component of the rapeseed oil is causing the severe inhibition, we

performed a third pilot plant test processing pure LGO with 1 vol.% CO mixed in the hydrogen treat gas. The data from this test is represented in the third set of bars in Figs. 39.6 and 39.7. The inhibition of the CO is very similar to the inhibition observed with coprocessing 15% rapeseed oil, which strongly indicates that the formation of the CO_2 , and consequently the CO formed via the reverse WGS reaction, is causing the inhibition. However, the NiMo catalyst is not affected by the CO in the recycle gas. This is clear evidence that a NiMo-type catalyst should be used as the main bed catalyst for the desulfurization of the fossil diesel when coprocessing. Even in the case where Topsøe's selective catalysts, which are going via the hydrogenation route, are used in the top of the reactor, we still recommend using a NiMo catalyst below these specialty catalysts. We want to prevent any inhibition issues in case the top part of the bed is poisoned to an extent that allows unconverted triglycerides to reach deeper into the bed, where the normal hydrotreating catalyst is located.

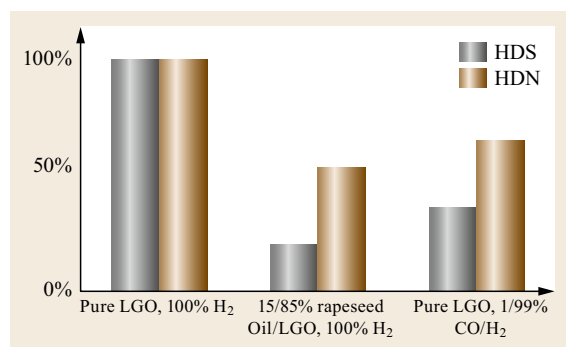


Fig. 39.6 The inhibition effect of CO on a CoMo hydrotreating catalyst on desulfurization (HDS) and denitri-fication (HDN) activity

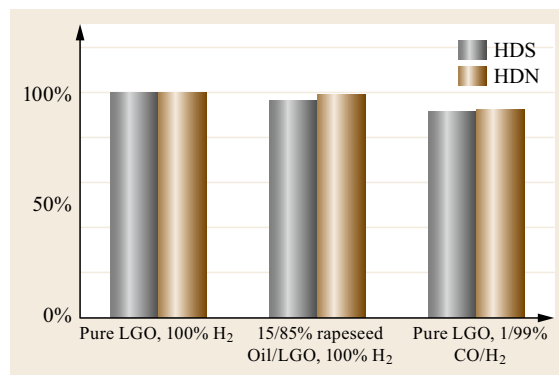


Fig. 39.7 The inhibition effect of CO on a NiMo hydrotreating catalyst on desulfurization (HDS) and denitri-fication (HDN) activity

39.5 Simplified Process Diagram

Haldor Topsøe has designed both grassroots renewable fuels units, as well as revamping existing hydrotreating units, to process sustainable fuels in coprocessing mode for 100% renewable feedstock. In the revamp case, we aim to utilize as much as possible of the existing equipment and the process layout can have a number of different configurations. In the grassroots scenario, we have the freedom to design the optimal process layout.

Figure 39.8 represents a typical process configuration of a grassroots renewable fuels unit. The unit consists of three reactors for hydrotreating. The lead reactor will be loaded with high void and active hydrotreating ring-shaped catalysts to minimize pressure drop buildup. The second reactor will have more demetallation (HDM) catalysts and typically some main bed HDO catalysts in the bottom part. The third reactor

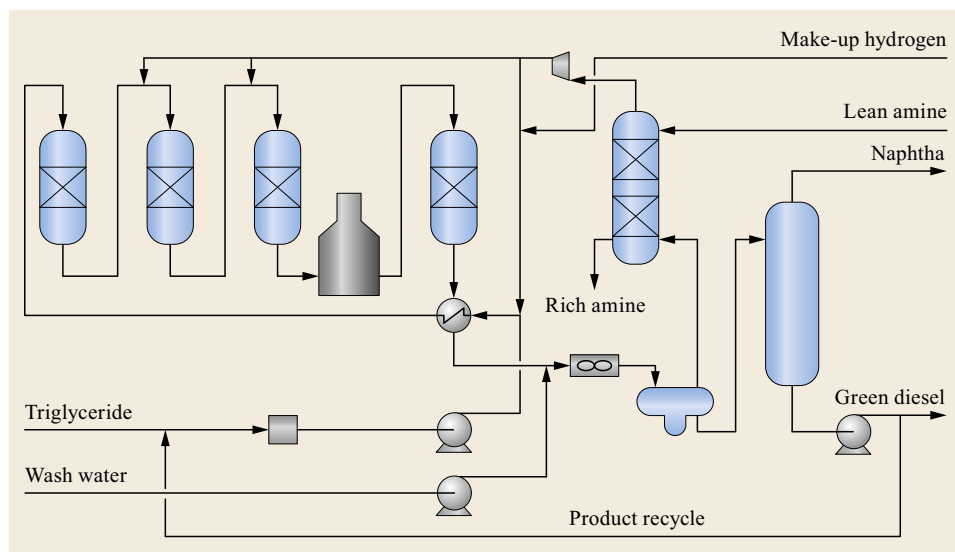


Fig. 39.8 Simplified process flow diagram for a grassroots renewable fuels unit for co-processing or 100% renewable feedstock

will be loaded with mainly HDO catalysts. Once the catalyst trains have converted the feedstock to long chain C_{17} – C_{22} , it is heated up before going through the fourth reactor for dewaxing – in other words, cold flow property improvement. The last reaction step can be eliminated if the renewable diesel product is used as blend stock in a larger fossil diesel pool, but is required if the renewable diesel is sold as a drop-in fuel.

In the case of a coprocessing unit, it is in most cases necessary to install an amine scrubber to remove the H_2S generated during the hydrotreating reactions. However, if the unit will be processing 100% renewable feedstock (standalone unit) and utilizing the catalyst selective for the hydrogenation route, the amine scrubber can be eliminated in the design, thus,

significantly reducing the equipment and installation cost.

Hydroprocessing units for renewable diesel will also typically be designed with product recycle used to quench the temperature rise in each reactor. This is especially important if processing 100% renewable feedstock as the temperature rise can be as high as $500^\circ F$ ($260^\circ C$), which is not manageable without a large amount of recycle used as a heat sink. The need for product recycle in a coprocessing unit will depend on the amount of renewable processed in the unit.

If the main purpose of the unit is to make a renewable jet fuel, the last reactor will also contain a hydrocracking catalyst to convert the long chain molecules into the jet boiling range and naphtha.

39.6 Catalysts for Dewaxing of Renewable Diesel

The most effective way of improving the cold flow properties of diesel fuels is catalytic hydrodewaxing. This technology improves the cold flow properties by selective isomerization to slightly branched paraffins. The hydrodewaxing catalysts are zeolitic-based, and they either selectively isomerize or crack mainly the normal paraffins. An inherent property of all dewaxing-type catalysts is the formation of smaller amounts of lighter products, mainly the formation of naphtha and some C_1 – C_4 gases.

Haldor Topsøe's dewaxing catalysts are sulfidic catalysts supported on an acidic carrier able to operate in a sour environment. Both have medium-high

HDS and HDN activity, and thus the reactor volume loaded is not lost in terms of desulfurization and hydrogenation capacity, when used in coprocessing mode. The hydrogenating activity will give slightly higher hydrogen consumption, which results in improved product properties such as lower density and higher cetane number. The dewaxing catalysts can advantageously be loaded close to the outlet of the reactor, thereby permitting the dewaxing function to be effectively switched on or off by temperature control in the last bed by use of quench and reactor inlet temperature control as illustrated in Fig. 39.8. To make use of the dewaxing function during wintertime oper-

ation, the reactor temperatures are simply increased. During summertime operation, the temperature inlet of the dewaxing catalyst is reduced by reducing the firing of the upstream furnace and/or by increasing quench.

The above plot in Fig. 39.9 illustrates that the cold flow properties of the diesel fuel can be improved by either cracking the molecules or by isomerizing normal alkanes into branched molecules. Cracking of the molecules, when producing diesel, should be minimized, as it will reduce the diesel yield and cetane number, and will produce jet and naphtha instead. Significant improvement in cold flow properties can be obtained through isomerization with only 1- or 2-branching as illustrated in Fig. 39.9.

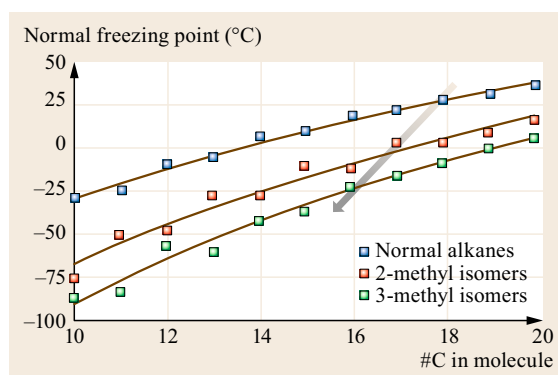


Fig. 39.9 Diesel dewaxing based on isomerization and cracking

39.7 Conclusion

Hydroprocessing of renewable diesel offers a unique opportunity to produce a sustainable hydrocarbon transportation fuel completely compatible with existing fuel infrastructure and engine technology. The process is very versatile in terms of feed type and thus offers great potential for future operation on e.g., algae oils or other high-yield feedstocks that cannot be used for human consumption.

Haldor Topsøe's HydroFlex technology and catalysts for both standalone 100% renewable feedstocks and coprocessing schemes with fossil fuels for the production of jet and diesel fuels are commercially proven. Haldor Topsøe's selective catalysts and unique technology will offer better diesel and jet yields, significantly improving the profitability of renewable fuels projects.

References

- 39.1 R.G. Egeberg, N.H. Egebjerg, S. Nystrom: Turning over a new leaf in renewable diesel hydrotreating. In: *Proc. NPRA Ann. Meet. 2010* (2010), Paper AM-10-158
- 39.2 P. Zeuthen, H. Rasmussen: Future fuels, *Hydrocarbon Eng.* 29-34 (2012)

40. Small Scale Catalytic Syngas Production with Plasma

Adam A. Gentile, Leslie Bromberg, Michael Carpenter

The production of syngas has been desired for nearly a century as a starting point towards an effort to achieve the synthesis of higher-energy liquid fuels. Methods that are utilized for obtaining syngas have undergone profound technological transformations over the years. The formation of plasma is one such concept capable of energizing molecular chains through dielectric manipulation in order to excite electrons and form radicals. Many types of plasma configurations exist under a range of variable parameters such as pressure, temperature, current, power intensity, and physical structure. Nonthermal plasma in conjunction with catalysis is a relatively new concept that takes a more subtle approach that eliminates the intensive energy requirement while maintaining high conversion efficiency. The technology and process presented in this book chapter will encompass a hybrid plasma/catalysis (PRISM) system having the ability to ionize and reform any vapor phase species with a focus on short to long chain hydrocarbons. The apparatus promotes reactions that would otherwise be disadvantageous from either a high activation energy standpoint or from the yield of unfavorable side products. Catalytic partial oxidation (CPOX) using a low-energy, nonthermal plasma is capable of nearly perfect conversion of a carbonaceous starting material into clean, homogeneous, hydrogen-rich syngas.

40.1	Plasma	1142
40.1.1	Introduction	1142
40.1.2	Types of Plasmas	1144
40.2	Partial Oxidation Reformation Using Cold Plasma	1147
40.2.1	Methane Reformation	1147
40.2.2	Plasma Catalysis	1151
40.2.3	Reactor Apparatus	1153
40.3	Cold-Plasma-Assisted Experimentation	1156
40.3.1	Steady State Operation	1156
40.3.2	Transients: Startup/Shutdown	1157
40.3.3	Conversion and Efficiency	1157
40.4	Analysis and Discussion	1159
40.4.1	Process Challenges	1159
40.4.2	Design Improvements	1159
40.4.3	Higher Hydrocarbon Reformation	1160
40.5	Synergistic Benefits of Plasma	1160
40.5.1	Chemical Processes	1160
40.5.2	Commercial Implementation	1160
40.6	Conclusion	1161
	References	1162

This chapter documents work done on small- to mid-scale plasma enhanced catalysis for platform-flexible fuel reformers in an effort to improve conventional (i. e., internal combustion) vehicle operation as well as the commercial standard reformation efficiency. Although industry has been focusing on methane, the system performs as a cost-effective method in the production of hydrogen-rich, process-ready syngas from any carbonaceous source/feedstock.

There exist several applications of stationary and onboard hydrogen production:

- Supplementation and augmentation of hydrogen into internal combustion engines (ICEs) for improved operation and pollutant elimination
- Diesel PRISM fuel reformation for after-treatment application
- Onboard hydrogen generation for fuel cell power production
- Clean-burn electrical generation (turbines, gen sets)
- Liquid drop-in fuel production.

The chapter is organized as follows: First, an introduction of plasma and its different forms and attributes are defined in Sect. 40.1. The primary reaction of interest is partial oxidation (POX) and this, along with the micro- and macrokinetics of the PRISM process in terms of theory, will be described in detail in Sect. 40.2. Section 40.3 details the experimental process from start to finish with a broad overview of operational perspec-

tive. In Sect. 40.4, we expound on a discussion of the data including process challenges, areas of improvement, and future development. Some of the synergistic effects of plasma over typical gas-phase processes can be found in Sect. 40.5, which leads to the conclusion of how and why plasma-assisted POX in a catalytic environment is a viable and cost-effective technology.

40.1 Plasma

40.1.1 Introduction

There are many different paths that lead to the production plasma, which is universally known as the fourth state of matter and also the most abundant state present in the universe. Some generally known devices and methods of generating plasma include the plasmatron, plasma jet or torch, spark, corona discharge, electrical or gliding arc, and glow discharge. For our purposes, plasma is regarded as a collection of freely charged particles in random motion that is, on average, electrically neutral [40.1]. Typically generated from a gaseous phase, application through an electrical field induces a temporary condition of a plasma state regardless of bulk medium temperature. Additional ways to accomplish this include, but are not limited to, a radio frequency (RF) treatment or a microwave treatment of the gas in a strong electromagnetic field. When utilized to augment a reaction, plasma adds substantial beneficial factors to the molecular interactions and kinetics of the reaction at hand.

Breakdown and Ionization

The standard gas molecule is stable in an environment when at or near a state of equilibrium with its surroundings. As intensive and extensive properties change, molecules begin to lose their stability. Electron movement rapidly increases and ionization is achieved when electrons gain enough energy to remove themselves from their respective orbitals unbound from their normal position within or around the molecule. Ionization

may also be achieved when temperatures rise beyond a distinct threshold level of the molecule. With less difficulty than applying extreme amounts of heat, ionization can be reached inside an electrical field supplied by an adequate voltage source. This approach causes a dielectric *breakdown* of the gas molecule into plasma consisting of charged species (electrons, ions, radicals) and neutral species (atoms, molecules, and excited particles). The plasma thus becomes a highly energetic state of matter characterized by an elevated electrical conductivity [40.2]. Strongly bonded molecules like hydrocarbons such as methane (CH_4) in a plasma-induced state have been documented to disassociate ($\text{C}_1\text{H}_4 \rightarrow \text{C}_1\text{H}_{[x<4]} + \text{H} + \text{H}_2$) then quickly recombine into intermediate compounds such as C_2H_2 , C_2H_4 , and C_2H_6 [40.3]. This can be achieved and maintained as long as the methane is exposed to the electrical field. The intermediate molecules are a short-lived species and will reform back into methane if not converted while yielding some amount of molecular hydrogen.

Generation of Plasma Field

Multiple methods exist to produce a viable plasma field, the most practical being two electrodes in close enough proximity supplied with a voltage creating an arc of electricity, or plasma, through the air gap between the electrodes. This can be seen in Fig. 40.1b using parallel conductive plates. The power supply drives the current between the conductive electrodes ionizing the gas flowing through it. Pressure plays an important role for the generation of the field. At pressures below

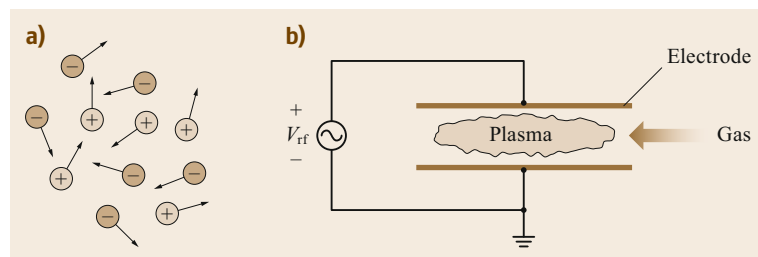


Fig. 40.1 (a) Visual of excited ion motion that makes up plasma. (b) Simple plasma discharge apparatus (after [40.1])

atmospheric and above vacuum, the electrical energy required to create a plasma field arc or glow discharge is reduced to a minimum. The augmentation of the dielectric strength of vacuum by matter and pressure is the primary function for sustaining the plasma field.

Another factor in field generation refers to the geometry of the electrodes. Industrially, these can vary from sharp singular points to infinitely long plates to annular arrangements physically similar in appearance to concentric pipe heat exchangers. In the case of processing gas, the annular apparatus is highly efficient and isolates the system from the surrounding environment. It is difficult to classify and analyze the plasma generated from an external electromagnetic field because of the inconsistent nature of the ionized particles. The generated plasma is on a very short time and space scale (10^{-7} – 10^{-9} s) as the excitation weakens, dissipating quickly upon departure from the applied electrical source. If not utilized properly, the plasma will return to a stable gaseous ground state.

Stability and Equilibrium

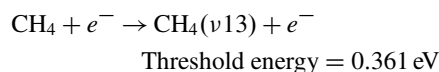
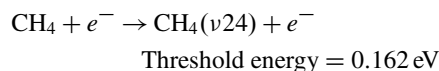
Plasma requires constant treatment via an external energy source in order to maintain its phase stability, making it a short-lived species at ambient conditions. In a continuous process, it's wise to consider the placement of the plasma generating field in order to optimize overall system efficiency. Ionization and dissociation are a requirement for the existence of plasma, but these induced conditions also cause a fluctuation in equilibrium. Plasma density, also defined as electron or ion density (n_i), is the number of free electrons per unit volume. Ion density can be used to determine the degree of fractional ionization (x_{iz}) of plasma represented by the equation

$$x_{iz} = \frac{n_i}{n_g + n_i}$$

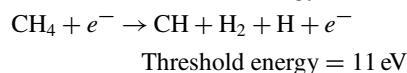
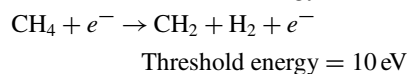
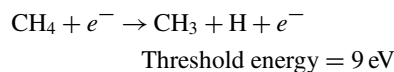
where n_g is neutral gas density. If the degree of ionization is ≈ 1 then the plasma can be considered fully ionized and if $x_{iz} \ll 1$, the plasma is weakly ionized. No matter how minute the presence of ionization in the gas phase, plasma characteristics still show to some degree [40.3]. Threshold levels for ionization exist during excitation of a gas-phase substance and depending on the amount of energy applied, different charged and neutral molecules will be produced that are of overall equal constituents to the original gas molecule. These excited forms consist of rotational excitation, vibrational excitation, disassociation, and full plasma ionization. Rotational and vibrational excited states are generally considered impractical for most processes due to their low threshold energy (< 2 eV) and short

lifetimes (nanoseconds) [40.1]. Electrical field energy is directly proportional to electron energy responsible for greater molecular decomposition from the electron-impact dissociation and ionization reactions. As an example, bonding energy of most hydrocarbons is between 3–6 eV. This range expresses C–H and C–C bond strength varying from molecule to molecule of any hydrocarbon in general. C–H bonds are stronger and closer to 6 eV in strength than that of C–C bonds, which reach the lower interval of 3 eV in strength. An electron-volt (eV) is energetically equivalent to about 1.6×10^{-19} J (Joules). The following electron-impact reactions of methane show the threshold energy barrier necessary to achieve specific levels of plasma excitation [40.3]:

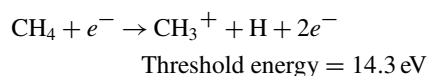
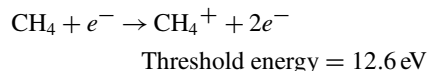
- Vibrational excitation



- Dissociation



- Ionization



Methane is a highly stable compound and, as a result, requires more energy to break the threshold barrier than most other hydrocarbons. This data can be used as an initial guide for determining the necessary energy requirement for any intended plasma application. Threshold levels affecting plasma stability lead to one possible reason as to why the plasma state is almost never in chemical or physical equilibrium with its surroundings. Since the discharges are electrically driven and weakly ionized, the applied power preferentially heats the mobile electrons while the heavy ions exchange energy through collisions with the background

gas [40.1]. At or below ambient pressure, the ion temperature (T_i) representing the overall temperature (T) is typically much less than the electron temperature (T_e). An immense amount of energy is required for neutral species and charged species to be in thermal equilibrium with each other ($T_e = T_i = T$). This is known as hot plasma and the requirement differs from element to element where, for example, a temperature of 20 000 K must be reached for complete thermal ionization of helium while around 4000 K is needed for cesium [40.1]. When not in thermal equilibrium ($T_e \gg T_i$), the phase state is considered cold plasma meaning that the overall temperature (T) of the plasma is at least equal to the ambient system process temperature.

40.1.2 Types of Plasmas

As stated before, there exist many different types of plasma, both natural and conventional (Fig. 40.2). The focus of this chapter is on one form of conventional plasma used in a reformation process; it is still worthwhile, however, to note other types. For instance, most plasma is naturally occurring in the universe from stars and interstellar matter. An example of hot plasma, also known as thermal plasma, is the Sun's surface or a bolt of lightning. A neon light can be considered nonthermal plasma or cold plasma. This classification depends on temperature, electronic density, and level of energy of the medium [40.2].

Conventional plasma is synthetic and every synthesized type carries different micro- and macroscopic benefits for process use. Plasma is also categorized by pressure in response to the method of ionization and the structure of the electrical field. For instance, in very low pressure environments plasma may always be considered nonthermal. The following is a list of conventional plasmas with descriptions grouped by pressure.

Low Field Pressure ($0 \text{ atm} < P_{\text{plasma}} < 1 \text{ atm}$)

Capacitive coupled plasma (CCP) and inductive coupled plasma (ICP) (Fig. 40.3a–d) are produced by high frequency RF electric fields where positive ion collisions are the dominant factor leading to electron dissociation. The bombarding ions are directly affected by the magnitude of frequency, typically at the MHz level, capable of causing an electron or Townsend avalanche cascading the electrons into a plasma state. CCP is generally used in material processing to enhance surface properties like that of integrated circuitry via etching or film deposition. A substrate is present upon one of the two interacting electrodes that are aided by a positive sheath material maintaining excess negative charges and directing them appropriately. ICP utilizes a coiled electrode (Fig. 40.3c,d) placed outside of the reactive zone in-

still an electromagnetic field that negates the direct current (DC) requirement necessary to reach efficient power in CCP. For analytical methods such as spectrometry, ICP provides a reliable detection limit over a wide range of sample elements. The RF power source can also be directed into the plasma gap itself as opposed to through the electrodes for both ICP and CCP.

Cascaded Arc

High-density, low-temperature cascaded arc is plasma in a relatively homogeneous thermal equilibrium. This creates an exception to the hot-thermal plasma classification since the gas, ions, and electrons are all thermally equal ($\approx 1 \text{ eV}$) at ambient conditions. The field is stabilized by cascaded plates with a floating voltage potential and is typically structured cylindrically. Operated under a DC supply, the power requirement is in the lower kW range (1–10 kW). This form of plasma and device is used in material deposition and surface treatment as well.

Electron Cyclotron Resonance (ECR) and Helicon Discharge

Electron cyclotron resonance (Fig. 40.3a) and helicon discharge (Fig. 40.3b) are produced by an axial varying DC magnetic field sustained by electromagnetic coils. The coils surround a cylindrical chamber in which microwaves are injected through a dielectric window propagating a rotating polarized wave. This generates the source plasma where it can be directed into the processing chamber. Electron cyclotron resonance (ECR) is operated with a strong magnetic field versus helicon discharge, which is much weaker by comparison. Helicon discharge uses an RF-driven antenna coupled with the weaker magnetic field to create a resonant helicon wave at the plasma source where it is believed that the particle-wave interaction is the cause of the wave energy transfer into the plasma. Conventional areas of interest for these plasma devices include semiconductor manufacturing, electric propulsion devices, or in advanced medical treatment.

Glow Discharge

Glow discharge is produced by a low frequency electrical field induced by DC or RF in the open area between interacting electrodes. Once adequate voltage is met, ionization occurs releasing a vibrant light based on the ionized gas. The system is usually enclosed in a non-conducting transparent tube. Known for its usage in fluorescent lamps and neon lights as well as plasma-screen television devices, glow discharge plasma also has applications in analytical chemistry via spectroscopy and mass spectrometry and in material surface treatment via a method known as sputtering.

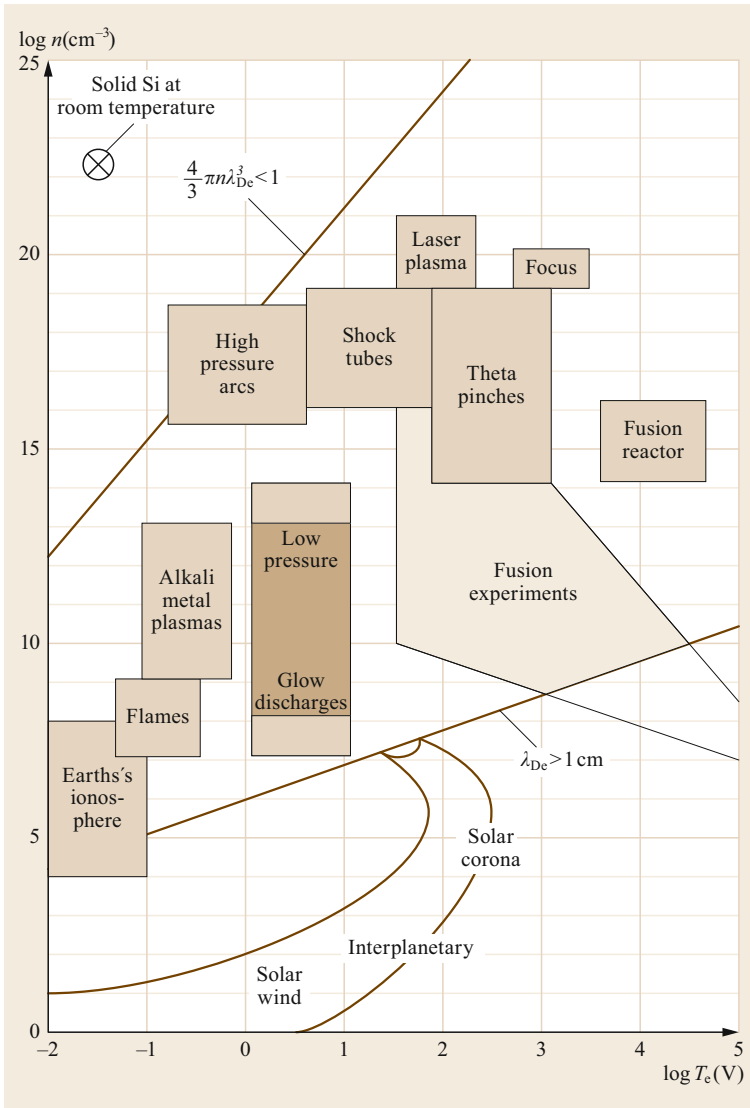


Fig. 40.2 Synthetic and universal plasma on energy (logarithmic temperature voltage equivalent) versus density plot. λ_{De} = Debye length – the distance scale over which charge densities can exist spontaneously or more simply, how far the electrostatic effects travel. As an example, low-voltage and undriven plasmas are generally a few Debye lengths wide (*middle portion* of figure) (after [40.1])

High Field Pressure ($P_{\text{plasma}} > 1 \text{ atm}$) Plasma Torch and Thermal Plasmatron

Plasmatron is a high-powered DC thermal plasma generated by electric resistive heating of a turbulent flow of gas molecules. The plasmatron provides highly controllable electrical heating, but requires resilient electrodes to withstand corrosion from the strong arcs and extreme heat. A relatively large amount of energy is required to harness a homogeneous field in thermal equilibrium due in part to the elastic collisions of the propagating energized electrons. Utilizing an annular configuration, the input gas is injected tangentially to produce a vortex that extends the plasma arc field inside of the ionization zone. Water is used as a heat sink to cool and control electrode temperature preventing thermal damage to the

components. The high power requirement pitfall limits widespread use of the thermal plasmatron in industry, but the plasma torch finds a niche in plasma cutting, pollution control and hydrocarbon reformation.

Corona Discharge

This form of nonthermal plasma is generated through finely pointed electrode tips at a voltage high enough to initiate a conductive field, but not so high to cause an electrical arc discharge to the grounded path. Although the corona charge can be positive or negative, the positive corona is undesirable due to the extremely high energy requirement to excite positive ions. This is not the case for a negative corona, in which electrons are much lighter and more easily ionized in a non-

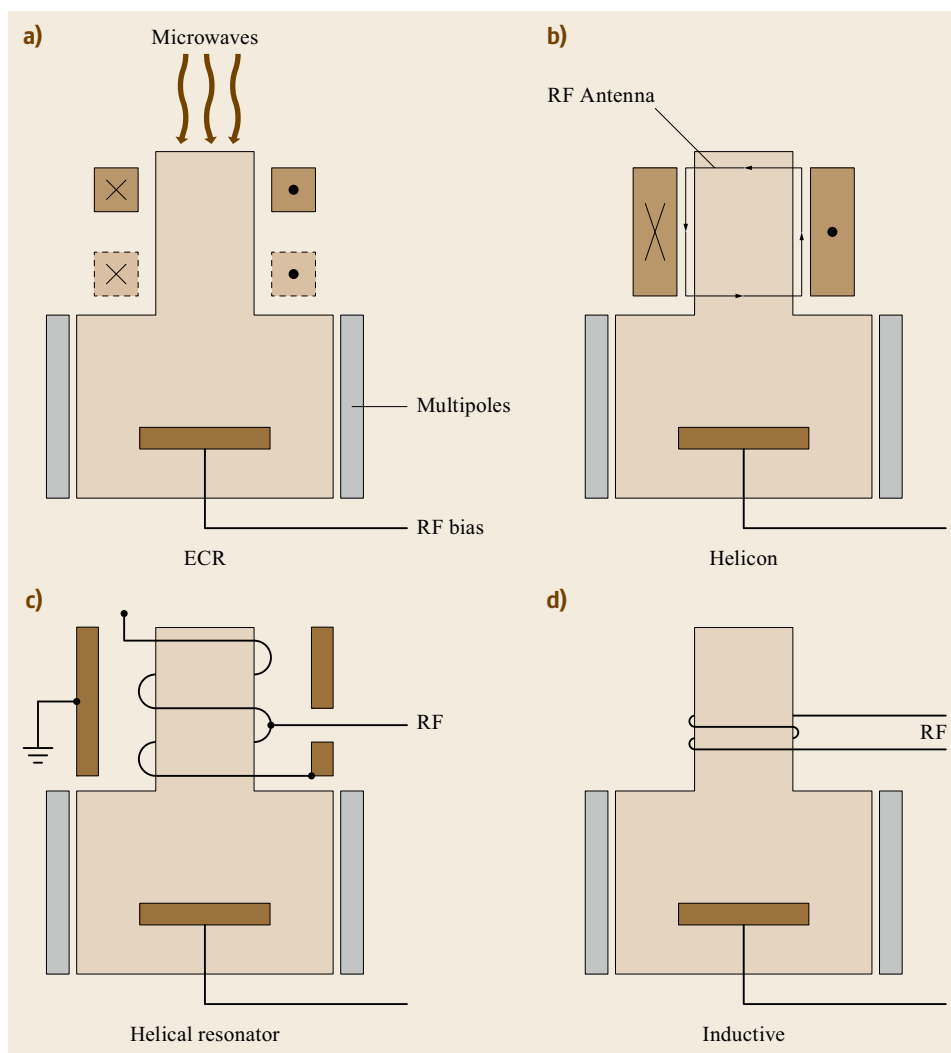


Fig. 40.3a–d
Example sources
of low-pressure,
high-density
plasma in basic
configurations
(after [40.1])

thermal low-pressure setting. The Townsend avalanche causes the highly energized and separated electrons to move radially in all directions creating a plasma cloud. As the electrons move further and further away from the voltage point, they lose energy and eventually are no longer able to force ionization as they begin to approach the grounded electrode. The field, or cloud of electrons, maintains ionization for as long as a voltage is supplied. Corona discharge is a method for ozone production, volatile organics (VOCs) removal, air clean-up, and water sanitization as well as for analytical techniques.

Dielectric Barrier Discharge (DBD)

An insulating dielectric barrier is used to separate, including the space gap, the field producing electrodes that uses low-RF or microwave frequency from a high voltage alternating current (AC) (1–10 kV)

power source. The material used for the dielectric barrier ranges from polymers to glass or ceramics, all nonconductive in nature. Planar or axial configurations may be utilized depending on flow applications and can be seen in Fig. 40.4. DBD is another form of nonthermal plasma that can be generated at ambient pressure and low temperature that is not in total particle equilibrium. Microdischarges occur at the dielectric surfaces and propagate like a glow discharge while maintaining homogeneity, but within a more pressurized environment. Originally designed for ozone generation, DBDs find use in catalysis enhancement, surface modification of materials, emissions control, excimer lamps, and silent-discharge CO₂ lasers.

Gliding arc

Gliding arcs are arc discharges that initiate from the point of shortest distance between parallel, but diverg-

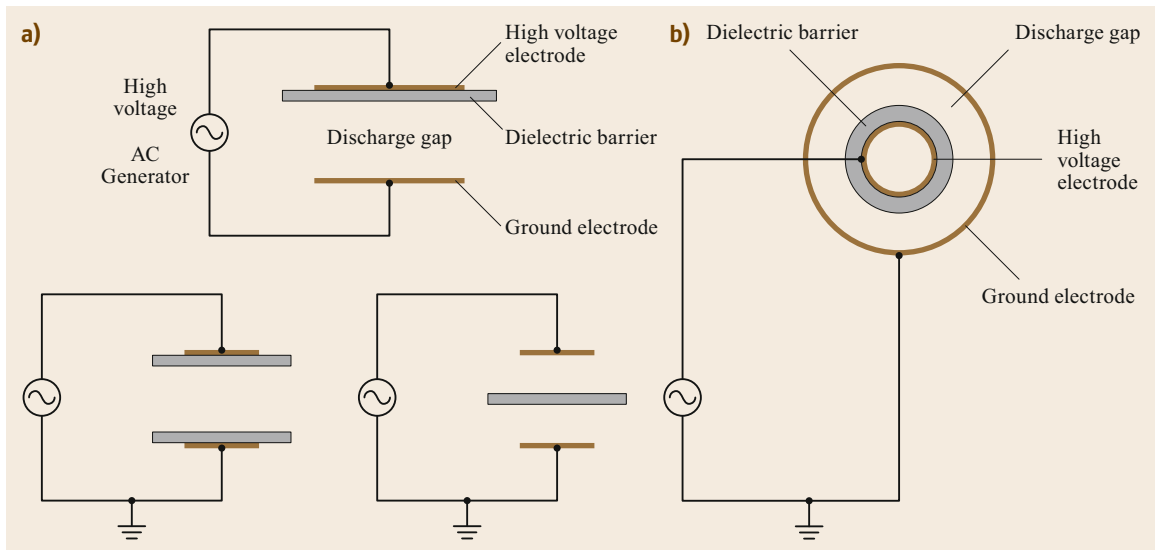


Fig. 40.4a,b Configurations of different DBD plasma devices (apparatus similar to other plasma devices minus the dielectric barrier) (after [40.4])

ing electrodes. The arcs travel along the length of the electrodes until complete breakdown of the arc occurs near the endpoints of the divergent electrodes [40.5]. As the gliding arc dissipates, the encompassing turbulent gas maintains a glow discharge plasma state. This continuous cycle is determined by the system parameters, which include characteristics of the electrical power source (AC or DC), range of current and voltage capacity, gas type, gas velocity, electrode geometry, and field pressure. Associated with a high level of current (≈ 50 A/arc discharge), this thermal plasma

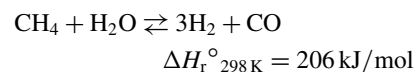
reaches extreme temperatures ($T > 10\,000$ K) energizing all the chemically active species (CAS) present in the medium. The power requirement varies from 1–10 kW based on the parameter conditions. Gliding arc can be considered a hybrid form of thermal and nonthermal plasma reaching only temporary equilibrium with traits similar to the plasmatron and glow discharge. Some of the many applications of gliding arc plasma include metallurgy, chemical reformation, reformation of flue gas, dissociation of CO_2 , and decontamination.

40.2 Partial Oxidation Reformation Using Cold Plasma

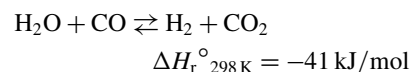
40.2.1 Methane Reformation

Industrial practices often vary in regards to reformation techniques as the end goal is unique to each process. Hydrocarbon reformation can be utilized as a supplement to larger-scale processes by making use of utility streams and side products that would otherwise be a detriment to overall system efficiency. For instance, when a surplus amount of steam is generated after primary and secondary cooling, it can be in the engineer's interest to make use of it. If a steady supply of natural gas is also available, then steam methane reforming (SMR) could be a source of additional revenue for a wide range of production applications, the most common and basic of these being the synthesis of hydrogen or methanol. Below are the ideal reactions that accompany the SMR process:

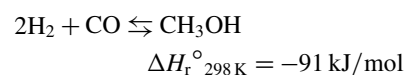
- Steam methane reformation (SMR)



- Water gas shift (WGS)



- Methanol synthesis



Being diverse in its usage and easily storable, methanol typically equates into a positive revenue

source. It is possible to deploy SMR as a primary process, but would require large-capacity equipment and a high rate of production to compensate for the high cost of generating steam given SMR's low conversion efficiency. The SMR process is well documented and currently used at the commercial level, but is only one method of methane reformation and the focus of this chapter is on partial oxidation reformation techniques.

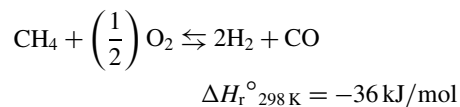
Reformation with the goal of hydrogen production has seen real promise for small-scale and on-hand applications like fuel cell technology or enhancement of internal combustion engines (ICEs). The advantages of hydrogen include fast flame speed and high octane (which enables high-pressure operation), allowing either high compression ratios or strong turbocharging with associated downsizing. The use of hydrogen-rich gas addition to spark-ignited (SI) engines allows for highly diluted operation. It is possible to extend the dilute-operation burn limits where nitrogen oxides are reduced to near nonexistent levels, eliminating the need for NO_x after-treatment (thus removal of the three-way catalyst). Dilution also allows for improved efficiency, from either reduced pumping losses at light load or lower in-cylinder temperature, thus reducing heat transfer to the cylinder walls. Running with hot hydrogen-rich gas further improves the flame speed as well as extends the dilution limit. Faster flame speed is another contributor to increased engine efficiency by enabling a more isochoric combustion zone.

Hydrogen is unfortunately a difficult molecule to store for extended periods of time. Aside from a high mass heating value, 120 kJ/g compared to methane (50 kJ/g), methanol (20 kJ/g), and gasoline (42.8 kJ/g), hydrogen is characterized by a low volumetric heating value due to its low density (2.016 g/mol): 11 kJ/l versus 16 MJ/l for methanol at standard temperature and pressure [40.2]. Volatility, flammability, and small molecule size all add to the storage difficulties of hydrogen. Some presented solutions to these issues are cryogenic and high-pressure containment, which have some validity but are not ideal due to further increase in efficiency losses and explosion hazards that are deemed high risk for mobile applications. Methanol has been used on occasion as a storage medium for utilities like fuel cells that are typically designed to operate on a source of hydrogen.

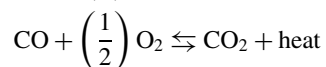
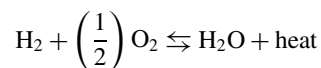
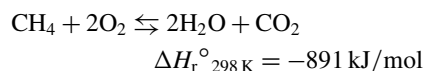
The integral step of methane reformation is the production of synthesis gas or syngas, a mixture of hydrogen and carbon monoxide. Often, realities of operation interfere, producing a syngas with adulterants such as carbon dioxide, methane, water, oxygen and nitrogen. Generally, these side constituents are unfavorable and limit overall efficiency in downstream processing requiring minimization when possible throughout oper-

ation. The methane POX reaction and other macroreactions of concern that are associated with methane POX (which include the SMR reactions above) are listed below. The following reactions can be considered competitive as well as reversible in nature:

- Methane partial oxidation

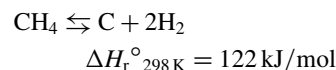


- Combustion reactions

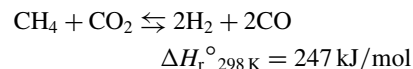


Other Possible Side Reactions

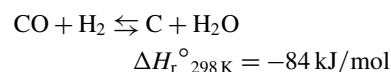
- Thermal decomposition



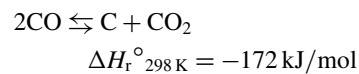
- Dry methane reformation



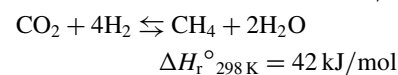
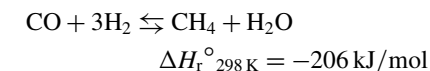
- CO reduction (undesired)



- Boudouard reaction (undesired)



- Methanation (undesired)



Partial oxidation is an exothermic reaction capable of producing an ideal syngas product of a 2 : 1 ratio of hydrogen to carbon monoxide. The reaction is able to reach temperatures in excess of 1300 °C that need to be levied and maintained through use of a catalyst in order to avoid nitrogen-based reactions. Nitrogen oxides (NO_x) are considered an emission that have, by orders of magnitude, a much greater environmental impact than unburned hydrocarbons and carbon oxides. Not only does NO_x cause the formation of ground-level ozone, but it also has negative effects upon the human respiratory system. The rate of formation of NO_x increases exponentially as temperatures rise in a lean and oxygen-rich flame zone during partial or total oxidation with air. Nitrogen, if not removed before reformation, must remain inert throughout the process. This factor is taken into consideration along with reactant conversion and hydrogen yield, all of which are influenced by thermal conditions.

Thermal Equilibrium

Not including plasma interaction, the factors that affect syngas production are reactor size, space velocity, flow dynamics, catalyst type, reactor and catalyst geometry, feed material and feed ratio, system pressure, and thermal equilibrium. Exothermic processes are controlled not only for safety reasons, but also for system efficiency and minimization of side products. Thermal equilibrium helps justify why the SMR reaction is inefficient and energy intensive while also explaining POX efficiency and NO_x formation.

The tubular reactor is commonly employed in industry and most often utilized for homogeneous gas-phase reactions. It is assumed that the reactants are consumed over the length of the reactor while experiencing some concentration variance both radially and in the direction of flow. This forces the rate of reaction to adjust accordingly as reactants are consumed and products are formed that become intermediate reactants themselves. In a POX reactor, the plug flow apparatus is selected to maximize production rate. The reactor can be used with, or without, a form of packed catalyst; when under a turbulent flow regime, equilibrium is maintained in a quasisteady state of operation creating a relatively stable, predictable thermal profile. As the process approaches completion under this configuration, different zones of the reactor experience a rise and fall in temperature due to the multitude of occurring reactions. This effect is more apparent in a shorter amount of reactor length using a packed-bed catalyst design and even more so if the reactor diameter is reduced. The thermal profile and reactions that take place are directly proportional to the ratio of fuel and oxidizer. More specifically, a carbon-to-oxygen atomic ratio of

1 correlates to stoichiometric POX while a ratio of 0.25 gives way to stoichiometric and complete combustion. Oxygen, within these stoichiometric bounds, is depleted quickly after injection due to its fast reaction rate and will not be present in the product stream. Oxygen can only be present postreactor if the system is not functioning properly or if lean operation is being conducted. Any ratio < 0.25 is considered lean (or fuel deficient) combustion and a ratio > 1.0 inactivates the reaction by extending the gas mixture past its flammability and reactive limits.

In order to lower reaction temperature, eliminate NO_x formation, and increase methane conversion, a catalyst is typically present inside the reactor. Currently, catalytic reformation is commonplace in the industry and as so, it is the most economically well-developed technique for hydrogen production. Typical POX catalysts include Pt, Rh, Ni, Co, Ir, Pd, or Ru metals that are supported on metal oxides, which include Al_2O_3 , CeO_2 , MgO , and TiO_2 in different proportions, mixtures, and geometric configurations [40.3,6]. Though difficult to fully model theoretically, the experimental reaction pathways using catalysis are consistent and repeatable. Initially, exothermic reactions of POX and combustion are activated together to provide heat to the reactor. This spike in temperature allows the intermediate products of H_2O , CO , and CO_2 to then immediately react via the SMR and WGS reactions with unconverted hydrocarbon as well as the hydrogen product. Due to the continuous nature of the plug flow reactor and high gas space velocity, the residence time of the reactive species is short (< 1.0 s). The short residence time in relation to the competing exothermic and endothermic reactions forces the process to reach completion that is not necessarily preferential to the best possible results.

Thermal equilibrium tends to develop in localized spots of the POX reactor and is contributed mostly from gas flow convection, downstream or upstream radiation, catalytic reaction, and heat conduction of the reactor and catalyst wall [40.7]. Even through well-controlled operation, the active species are always in a constant state of reactive flux. The bed temperatures along the length of the reactor help justify these claims, which have been seen through experimentation and are well documented in literature.

Maximization of hydrogen yield and selectivity can be achieved through manipulation of reactor temperature. Figure 40.5 shows this relationship and provides an example of thermal equilibrium influencing the product composition [40.7]. It is easy to see the asymptotic increase in conversion and the perfect selectivity that is achieved as temperatures rises in the reactor.

The syngas yield of purely two hydrogen molecules to each CO molecule from a 1.0 ratio of C/O would the-

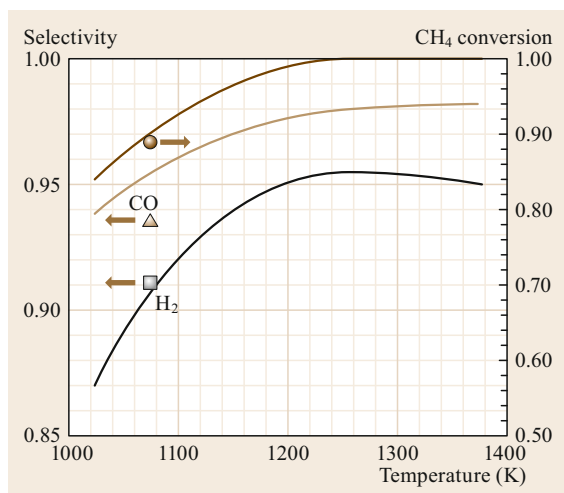


Fig. 40.5 Experimental POX using Rh-coated foam monolith catalyst. CH₄ conversion with H₂ and CO selectivity versus temperature (after [40.7])

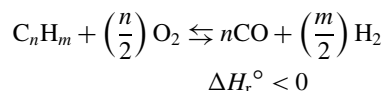
oretically be perfect for downstream applications like methanol production, but combustion is unavoidable during POX making this idealization next to impossible. It should be noted, that some CO₂ is necessary for methanol production as well, and though mostly viewed as a negative aspect to the process, combustion can be controlled to assist in reformation. As more oxygen is introduced to the feed, hydrogen yield tends to increase until a peak is reached (C/O ratio ≈ 0.85) where further addition of oxygen begins to lower hydrogen yield. Peak ratio is unique to each process with high dependency on reactor structure and plasma or catalysis assistance. The stability of feed ratio also contributes greatly to thermal equilibrium and, from a mechanical standpoint, reactor temperature provides a quick indication of syngas quality and possible system deficiencies. If the reaction is controlled solely by thermal activation then product selectivity is predictable, but will limit maximum product potential. When plasma becomes a dominant presence in the system, thermal equilibrium is overcome and the achievement of an even greater efficiency is then possible [40.8].

Chemical Kinetics

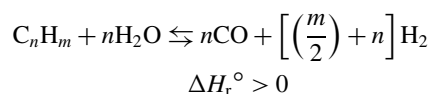
The reformation process can be summarized by the enthalpy changes exhibited throughout the system. Each reaction either imparts or removes heat in an effort to approach completion. The POX reaction itself has relatively slow kinetics and cannot initiate without the assistance of energy from an external source or an internal source such as combustion. Overall, the process of POX is still exothermic even with the multitude of associated competitive endothermic reactions. In the event

that the total net enthalpy change to the system is approximately zero ($\Delta H_r^\circ \approx 0$ kJ/mol), the process can then be considered autothermal. In order to compensate, some form of direct injection is required using water, CO₂, a process recycle stream, or simply the exhaust from an internal combustion engine:

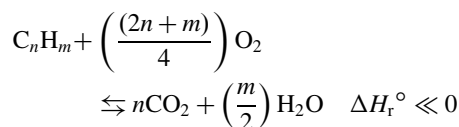
- Partial oxidation



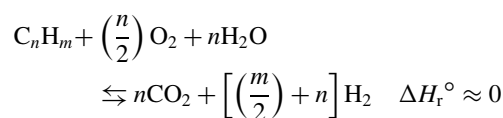
- Steam reformation



- Combustion



- Autothermal reformation (ATR)



The above global reactions give a straightforward overview and are the initial basis for modeling any reformation process. Reaction kinetics can then be utilized to help more thoroughly map the intrinsic system properties for determination of syngas product composition and yield. Temperature, pressure, and phase all play a role in the mechanism determining the pathway for reactions to follow. The homogenous gas phase reactions of POX do not inherently promote the formation of a high-quality syngas; this problem is partly resolved with the insertion of a durable and appropriate supported catalyst placed within the reactive zone [40.6]. The heterogeneous catalytic environment enhances the normal molecular pathway via active sites on the catalyst that reduce the energy barrier required for stoichiometric POX and lower the amount of combustion heat necessary for reaction stability. In a prior study, the CPOX of methane on a rhodium-coated catalyst has been indirectly modeled based on combustion, steam reformation, water gas shift, and dry methane reformation (DMR) kinetics. These equations, which are listed below, follow the Arrhenius model and have been

determined using empirical methods [40.9, 10].

$$R_{\text{Combustion}} = 2.119 \times 10^{10} \exp\left(\frac{-80}{RT}\right) p_{\text{CH}_4}^{0.2} p_{\text{O}_2}^{1.3}$$

$$R_{\text{SMR}} = 1.0 \times 10^{-9} T^5 \exp\left(\frac{-47.3}{RT}\right) \times \left(p_{\text{CH}_4} p_{\text{H}_2\text{O}} - K_{\text{eq,SMR}}^{-1} p_{\text{H}_2}^3 p_{\text{CO}}\right)$$

$$R_{\text{DMR}} = 7.0 \times 10^{-7} T^4 \exp\left(\frac{-32}{RT}\right) \times \left(p_{\text{CH}_4} p_{\text{CO}_2} - K_{\text{eq,DMR}}^{-1} p_{\text{H}_2}^2 p_{\text{CO}}^2\right)$$

For the WGS reaction ($r = \text{steam/CO ratio}$)

$$R_{\text{WGS}} = k \left(p_{\text{CO}} p_{\text{H}_2\text{O}} - K_{\text{eq}}^{-1} p_{\text{CO}_2} p_{\text{H}_2} \right)$$

$$k_{\text{HTSR}} = 1.78 \times 10^{22} (1 + 0.0097r - 1.1364r^2) T^{-8} \times \exp\left(\frac{-70}{RT}\right)$$

$$k_{\text{LTSR}} = 1.74 \times 10^{17} (1 + 0.154r + 0.008r^2) T^{-8.5} \times \exp\left(\frac{-35}{RT}\right)$$

Overall thermodynamic equilibrium constant (K_{eq})

$$K_{\text{eq}} = \exp\left(\frac{\Delta S^\circ}{R} - \frac{\Delta H^\circ}{RT}\right) (P_{\text{atm}})^{\sum_{j=1}^N \nu_j'' - \nu_j'}$$

The equilibrium constant (K_{eq}) takes into account the reversibility of each of the process reactions. This must be addressed due to the variability of conditions during operation. As an example, the WGS reaction approaches completion at two different temperature ranges. The high-temperature shift (HTSR) and low-temperature shift (LTSR) are performed in the ranges of 300–500 and 200–300 °C respectively. Lower temperatures support better CO conversion, but the kinetics favor an increased reaction rate at higher temperatures. The WGS reaction is always present, shifting the product composition towards thermodynamic equilibrium between CO, CO₂, H₂, and water. The subsequent production of hydrogen-rich syngas with minimal CO content, in particular to polymer electrolyte membrane (PEM) fuel cell application, is also based on WGS kinetics [40.11]. Industrial-scale applications looking to maximize hydrogen production tend to operate both HTSR and LTSR in separate reactors in series downstream of the reformation reactor. The use of both shift reactors as ancillary units downstream from the reformer allows for near-total conversion of CO into CO₂ and provides additional hydrogen from steam with

further intent to isolate the product hydrogen. This happens through the most economical form of separation possible and can be accomplished using one of the several following techniques: pressure-swing adsorption (PSA) to separate hydrogen, PSA to separate the CO₂ followed by condensation of the remainder of water, and membrane or sieve separation of the hydrogen [40.12]. With regards to the overall POX process, WGS is unavoidable and can be seen as neither beneficial nor detrimental to downstream application. This is especially true when engine combustion or electrical generation directly follows syngas production, as CO is also a suitable, burnable energy source.

40.2.2 Plasma Catalysis

Low-input energy capable of producing highly active species has become the focal point of potential for development of more efficient plasma reactors. In plasma catalysis, there exist a number of different configurations that rely upon location of the plasma field and catalyst zone. If the placement of the catalyst zone is prior to or much further downstream of the plasma field, then the process is a two-stage system (Fig. 40.7). Hot thermal plasma imparts extreme amounts of heat energy that cannot be used in conjunction with catalysis due to the structural limitations of catalytic material. The coating and the substrate are unable to withstand the high temperatures of the plasma field resulting in immediate thermal degradation as well as sintering of the coating material. In the immediate area surrounding the thermal plasma field, the cost of processing equipment and piping material would also rise in an effort to resist the high temperatures using higher durability equipment. This leads to applications in which thermal plasma has very limited appeal because of the inefficiency from the high energy demand and the inability to integrate into established chemical processes. For thermal plasma to have a role in catalysis, ample distance between the catalyst and plasma field is required, eliminating most of the potential synergy of the combined systems.

When the catalyst zone is located inside the plasma field or in close proximity postplasma generation, the process is known as a single-stage system (Fig. 40.6). In a single-stage plasma catalysis system, the effects of plasma and catalysis that contribute to the process become dependent on each other. This differs greatly from conventional catalysis due to the introduction of highly active species and the creation of a voltage potential and current flow by result of plasma discharge across the catalytic surface. The active species alter the status of the gas-phase reactions and associated reaction kinetics, which no longer ensues from the ground state. Elec-

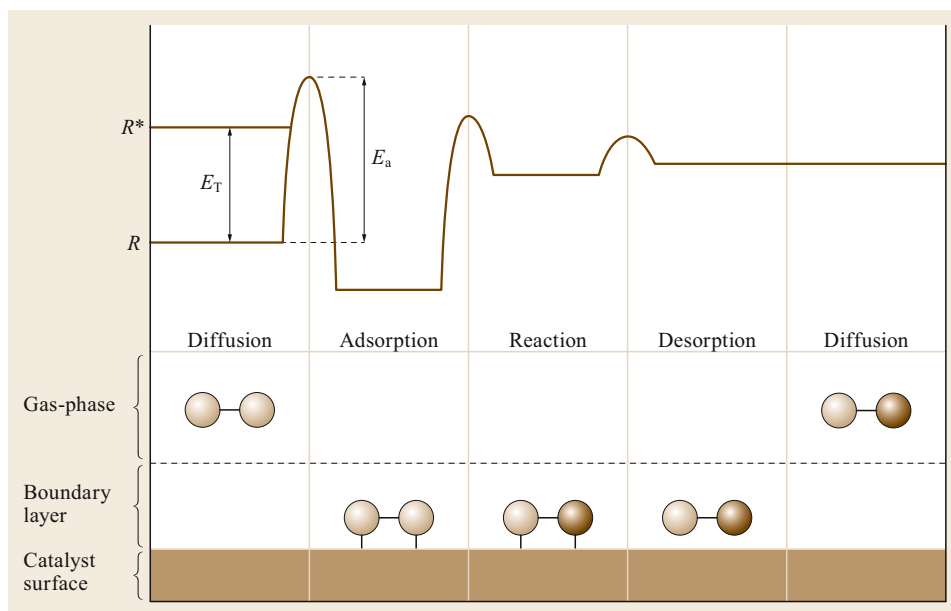


Fig. 40.6 Illustration of vibrationally excited species from a plasma-induced state accelerating a catalytic reaction. R represents the gas-phase molecule at ground state (uncharged) and R^* stands for the reactant in a vibrational state (charged). E_a is the activation barrier of chemisorption for R and E_T is the threshold energy for the formation of R^* through a plasma-induced electron-impact reaction (after [40.3]). The thermal energy required to initiate the catalytic process is now much less than the standard catalytic reaction and even further so than the reaction without catalyst

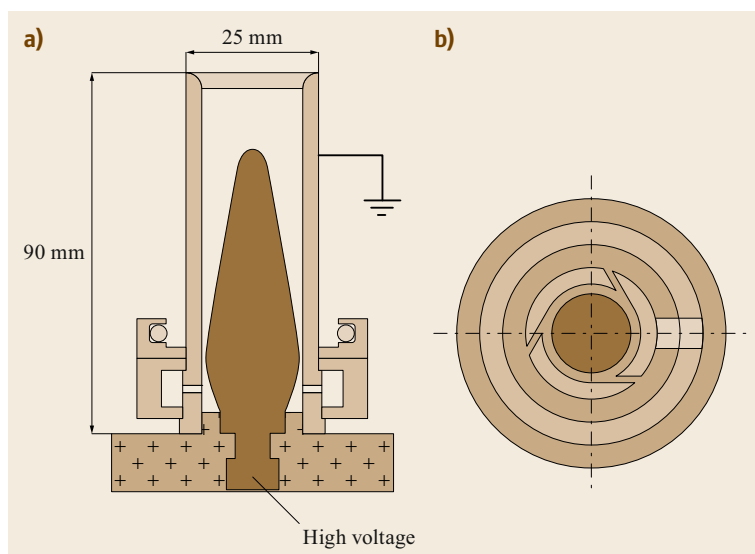


Fig. 40.7a,b Schematic drawing of rotating arc reactor used in a prior study conducted by Dae Hoon Lee et al. Side view (a) and overhead view (b) (after [40.13])

trical field enhancement depends on curvature, contact angle, and the dielectric constant of the packing pellets. Higher electric field leads to higher electron density promoting the electron-impact reactions responsible for hydrocarbon reforming. The decomposition of hydrocarbons is attributed to ionization and electron-impact dissociation of the excited molecules. Simply through

vibrational excitation it has been noted that activation energy is reduced in gas-phase reactions.

Physical adsorption and chemisorption are the methods where gas-phase molecules or ionized particles attach to the surface of the catalyst (Fig. 40.8). Physical adsorption is slightly exothermic and is mainly attributed to the weak Van der Waals attractive forces

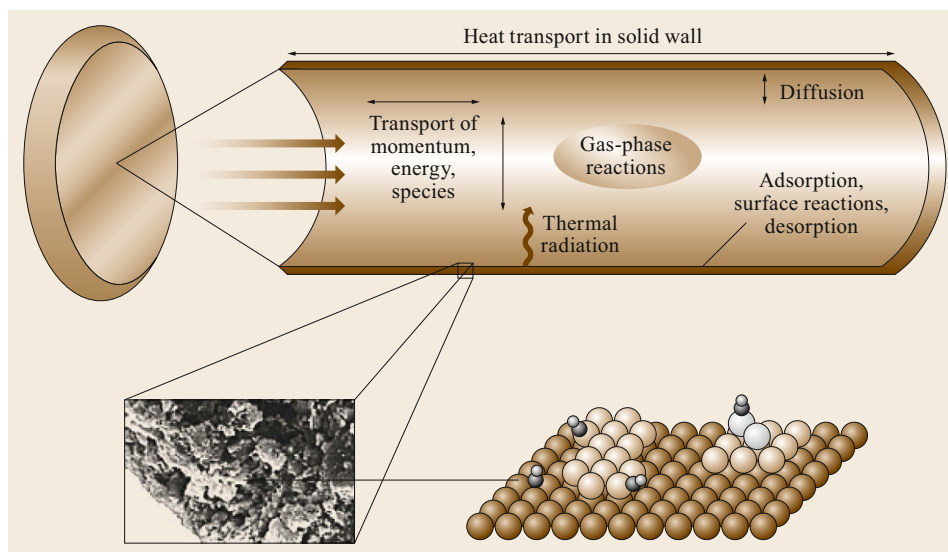


Fig. 40.8 Reaction effects flowing through a catalytic monolith, which include transport processes and a microscopic view at the nanoscale level (after [40.11], reproduced with permission of The Royal Society of Chemistry)

between the interactive surfaces. As the temperature profile surrounding the catalyst rises, the adsorption of particles steadily declines until critical temperatures are obtained in which physical adsorption no longer occurs. At this point, physical adsorption gives way to the sole influence of chemisorption. In the rate-influencing step of chemisorption, valence forces create highly reactive instances via bond stretching of the exposed and absorbed chemical species on the surface of the catalyst. Chemisorption produces heat comparable to the exotherm of the chemical reactions being performed. Atom and metastable compound formation along with electron multiplication cascade into the catalyst bed manipulating the normal conditions in which the catalyst performs. These effects are apparent and usually happen under very short electrical contact times. The heightened interaction between the surface and adsorbate then create new bonds, forming molecules that are specific to the catalyst and operating conditions.

40.2.3 Reactor Apparatus

In a lab setting, a reactor that imparts all of the above-listed chemical and physical effects has been constructed. The proprietary unit, known simply as PRISM and shown in Fig. 40.9, has demonstrated successfully the ability to reform methane gas into syngas at high efficiency and near perfect conversion using very little energy input. The process incorporates a three-step approach coinciding with intermediate stages that contribute to the final composition of the produced syngas.

At ambient or elevated temperatures, a stream of dry air or pure oxygen is introduced to a stream of natural gas and is well mixed prior to exposure of the plasma-

generating field within the plasma head. The plasma head is a precision-designed, stainless steel structure consisting of a tapered rod that acts as the anode, which is housed inside a cylindrical wall of like material (the cathode). The point of largest diameter along the length of the anode rod is where the plasma field initiates and can also be considered the choke point of the flowing element. The axial design makes use of the annular gap to hold steady the electrical field. This closely resembles that of a dielectric barrier discharge (DBD) apparatus, but without direct internal insulation while incorporating more of a coronal discharge approach to the plasma type utilized. In place of a fine-tipped point that is typically seen in a coronal design, the annular region is used to grant a larger volume coverage that increases the duration of electrical exposure to the gas molecules ensuring sufficient ionization. The plasma chamber of the PRISM mimics the flow patterns of the schematic shown in Fig. 40.9 for the rotating arc reactor, but differs in dimensionality and in orientation. The radial injection points allow for a toroidal arc that further increases residence time within the plasma head apparatus. As concentrated charges dissipate from the added rotational turbulence, both metal erosion and degradation upon the electrodes are reduced, extending their overall lifetime. An observation of the anode after long-term operation reveals minor impressions of spiral-type markings across its metal surface indicating the tangential path taken by the flowing gases.

The annular chamber provides uniform exposure to the incoming gas assisted by the well-mixed effect of the turbulent flow regime promoting molecular interactions and ion collisions, while the toroidal flow lengthens the space and time of the overall exposure.

These factors all contribute to the formation of the highly energized cold plasma state necessary for the reformation stage of the process.

An external power source is placed above the reactor providing voltage directly to the electrodes that are held inside a barrier of ceramic/quartz in order to maintain the uniform three-dimensional electric field throughout the annular gap. The power supply operates at high voltage (≈ 3 kV) and very low current expending no more than 100 W of combined processing power at maximum feed flow rate. Voltage to the plasma head is variable based on the fluid properties, which are primarily defined by gas density and velocity. The PRISM system operates with a 12+ kV compact transformer that allows for additional reserve voltage when fluid properties drastically change, and will adjust automatically without manual input control to sustain the plasma arc field.

Thermal expansion follows quickly after the gas stream is ionized by the plasma field. From there, the flow path continues by entering the main portion of the reactor that houses the proprietary catalyst crafted specifically for promoting the POX reaction. Catalyst composition is a mostly nickel-based coating prepared upon an alumina substrate. These monolithic, cylindrically sculpted blocks of catalyst remain stationary in a tightly packed fashion; these extend to the inner reactor wall.

In this chamber, the core of the partial oxidation reaction takes place. This is monitored through temperature readouts using multiple thermocouples drilled to the center of each catalyst. The external body of the reactor is 22" in length and roughly 8.5" in diameter. The inner wall of the reactor is lined by a nonconductive refractory material of high alpha alumina roughly 1" in thickness. This refractory participates as an insulator, but more importantly ensures containment of the electrical properties that were imparted to the incoming ionized gas stream. Figure 40.9 is an example schematic of an older generation model of the PRISM reactor.

Zonal Reactions

As listed in the section of methane modeling reactions that occur throughout the process (Sect. 40.2.1), each zone of the reactor and catalyst bed itself experience a fluctuation in primary reactions when favorable conditions arise during each reaction. This, however, can be manipulated through a well-controlled system. Initially, the plasma zone operates as an ignition source for the controlled combustion heating to the catalyst bed. When optimal bed temperature is achieved, the plasma field then takes responsibility for molecular breakdown by ionization and electron dissociation of the exposed compounds. Oxygen ionization into its atomic state and

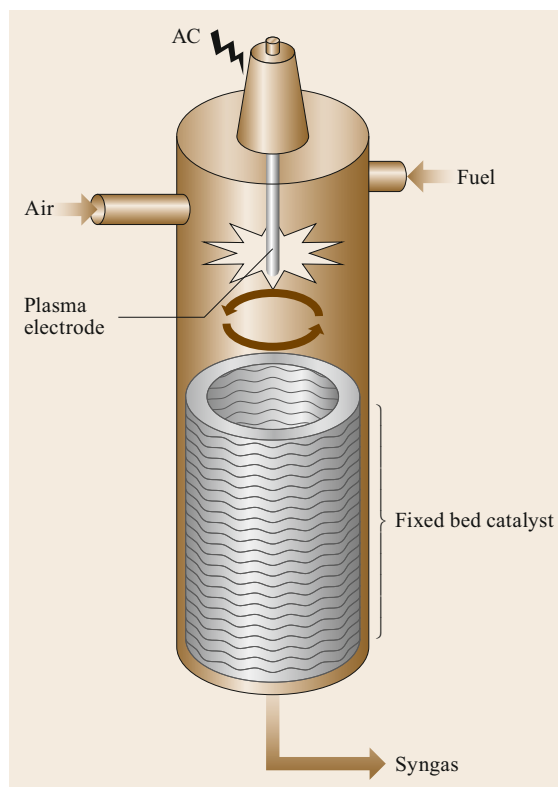


Fig. 40.9 PRISM reactor body and internals

the formation of ozone molecules are the first reactions to occur. Not only is ozone formed, but decomposition is also apparent in the complementing stream of hydrocarbons. These feed streams are well mixed and in a preferential syngas yielding ratio prior to introduction into the plasma zone. Hydrogen atoms released from C–H bond breakage and excited electrons that are initially released contribute to the reactions downstream as well as to the final syngas product. The remaining intermediate hydrocarbon compounds also react more readily in their hydrogen-depleted configurations. This first step helps drive the reaction rate of POX up to a level sufficient for effective overall system operation.

In the subsequent portion of the reactor, the diameter is increased to allow expansion of the gases granting longer exposure to the high surface area of the catalyst. Even distribution from turbulent flow of the particles onto the active sites of the catalyst is observed through stability of the temperature profile. Given a consistent feed composition at a specific ratio during steady-state operation, the specific zonal temperatures fluctuate at a ΔT near $\pm 1.0^\circ\text{C}$. This suggests all the participating reactions are held constant along the length of the reactor in their corresponding zones. As stated prior, oxygen atoms are the first particles to be consumed

and do not appear downstream of the reactor. If the oxygen atoms are not reduced with the carbon source into CO, then the atoms along with some CO will be fully oxidized into CO₂ before leaving the catalyst zone. The POX reaction not only produces the syngas mixture, but also releases sufficient enough heat to stabilize the reactor and perpetuate the overall reactionary process. Due to the fuel-rich environment and high process temperature, the unconverted methane tends to react with the steam side product via the SMR reaction also enhancing the syngas ratio [40.14]. The final stage falls to the WGS reaction and the reverse WGS reaction, which augment the CO₂ component forming either more hydrogen or more CO. The WGS reaction is not optimized in this configuration and purely participates as an indirectly controlled and closely monitored side reaction. Should the syngas ratio require more CO than hydrogen or vice versa, then a downstream WGS reactor can be implemented at a low additional capital cost to the system. The combination of reactions resulting in a net exothermic process leaves the product stream hot (> 600 °C) requiring heat exchange, if desired, to cool the syngas as well as condense any residual water.

Thermal Profile

With the operation of the plasma head being under a cold plasma configuration, there is not a significant enough generation of heat to give cause for thermal

readings of this zone. Temperature measurement for a predictable profile is thus only conducted in the main body of the reactor housing the fixed bed catalyst, which is monitored via eight equally spaced thermocouples. The thermocouples are placed in predrilled holes of appropriate dimensions and sealed tightly at the protruding ends that are connected to the wiring relay. The temperature of the catalyst bed is directly linked to the exo- or endothermicity of the reactions, and also to the conditions of the catalyst, plasma head activity, system pressure, and gas flow rate. As a comparative example that provides an accurate visual of catalyst temperature distribution, this noninduced flow in a laminar to transitional regime produces the temperature profile shown in Fig. 40.10.

The effect of modifying the flowrate through the catalyst suggests that at higher flows, the reaction encompasses a larger volume and initiates further downstream within the catalyst itself. The PRISM differs only slightly in flow path due to its transitional-to-turbulent regime reducing the radial variability of key parameters.

The thermal profile shown in Fig. 40.11 represents the consistency in occurring POX reactions down the length of the catalyst. In actual operation where flow rate and ratio are unaltered set points, the bed temperature and product composition do not deviate by more than the error present in the sensors-measurement equipment. The overall temperature drop within the

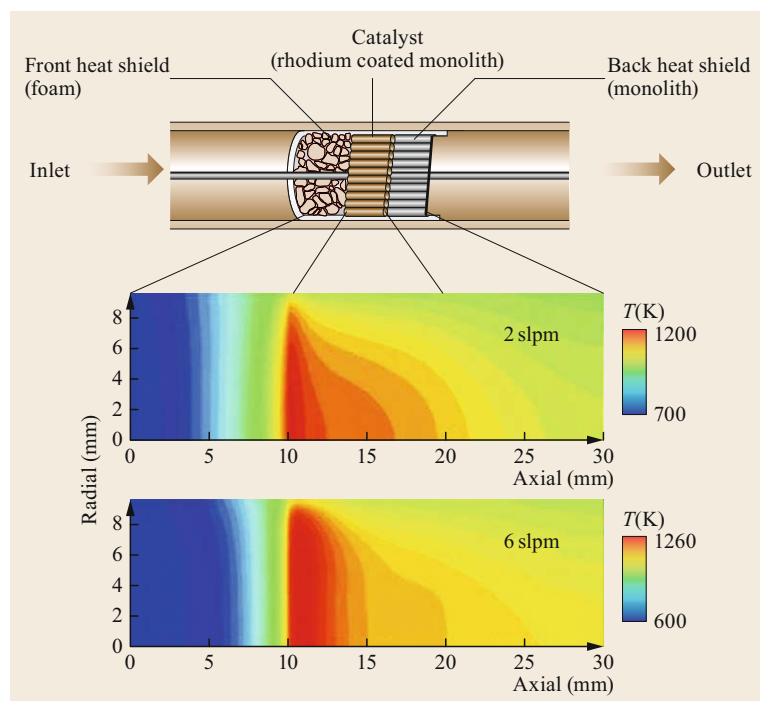


Fig. 40.10 Example POX catalyst temperature profile in laminar setting at differing flowrates. The catalyst coating is rhodium and the hydrocarbon is *iso*-octane (after [40.11], reproduced with permission of The Royal Society of Chemistry)

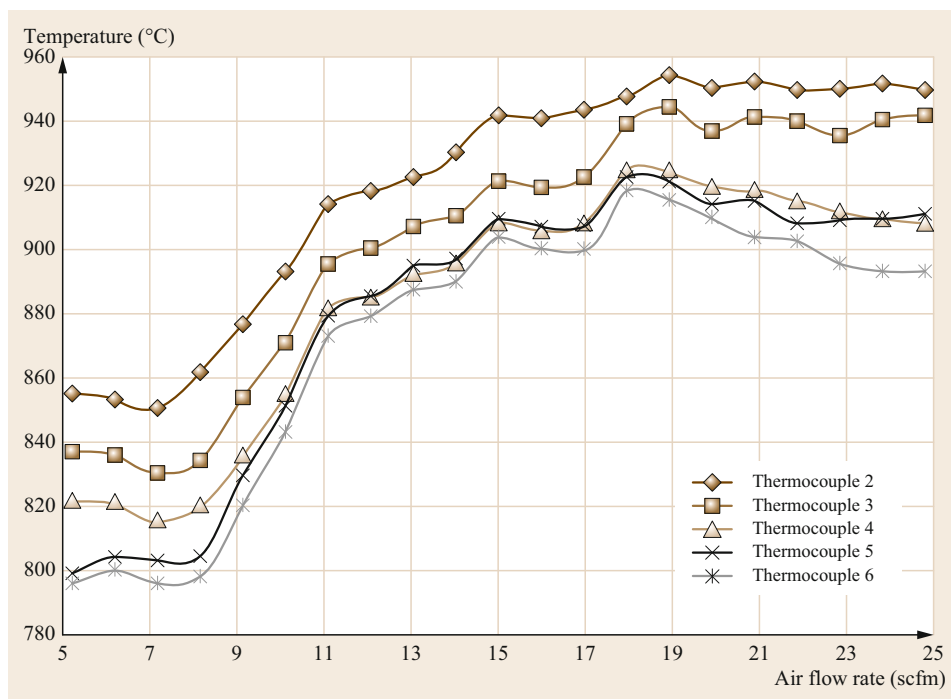


Fig. 40.11 Experimental operation of a PRISM reactor displaying average temperature readings for each catalyst zone over increasing rates of flow. The operational ratio was adjusted only to the automatic feedback control for the temperature rise in the system. The initial set point of the C/O atomic ratio was 0.55, which increased to 0.57 at the completion of the experiment

catalyst bed between thermocouples 2 and 6 is no more than 60°C translating to good thermal stability throughout reactor operation. The rise and fall of zonal temperatures correspond directly to each other and are dependent on the prior zone's temperature, and even more so the active zone temperature (thermocouple 2). At each discrete flow set point, an accurate representation of the PRISM's temperature profile can be observed if no manipulation of flow rate had been done. It should be noted that the PRISM under this experimental

scheme was operated closer to a combustion-oriented ratio at 0.55 of C/O species. As expressed previously in Sect. 40.2.1, *Thermal Equilibrium*, it was stated that peak hydrogen yield is achieved at ≈ 0.85 C/O ratio. While this holds true, results were more than adequate citing consistent results of over 99% methane conversion and a ≈ 1.8 H₂/CO product ratio. It stands to show that improvements can still be made on this already highly effective process, but are not necessary for viability of the technology in the field.

40.3 Cold-Plasma-Assisted Experimentation

40.3.1 Steady State Operation

Many experiments have been conducted at a facility in Brooksville, FL through research as well as trial and error. The PRISM system in a standalone configuration is ready for early-stage commercialization for stable, continuous production of usable clean syngas. Another experimental-phase application has been performed for syngas-hydrogen enhanced combustion in spark-ignited (SI) engines. The benefits of hydrogen fuel addition during combustion are well known to the scientific community, and the difficulties of its implementation have been discussed. A skid that consists of a General Motors 8.11 overhead valve/eight-cylinder

V configuration (OHV/V8) natural gas, turbocharged engine and a 100 kWe corresponding alternator have been integrated with a single PRISM unit for successful continuous slipstream engine operation.

The PRISM is a relatively simple system requiring a fuel valve, air valve, power source, and control system along with some corresponding instrumentation. In continuous operation, the system is stable under a well-controlled apparatus of a quick response ratio feedback loop based on system temperature. Attached are mass flow controllers that dictate the feed input based on ratio control and oxidizer flow rate. Adjustments can be allocated to either set point resulting in an automatic change in fuel flow. The feedback control loop

is responsive to changes in catalyst bed temperature, but focused on the main zone of operation, which is also the highest temperature zone of the process. This keeps reactor conditions favorable for higher hydrogen production and safe during long term operation. The control mapping has been optimized through many phases of testing on the PRISM unit. Manual control input is unnecessary when consistent homogeneous fuels are being used as the system will respond accordingly. This follows suit for the power supply, which operates within its voltage limits to always provide the electrically induced plasma field within the plasma head. The simplicity of the system and stability of the reactor make it possible for the need of only one operator overseeing the process. As syngas is being produced, it is then guided through heat exchange removing the formed water and lowering gas temperature to ambient levels. After a final water knockout point, the syngas is led to a low-tolerance oxygen sensor confirming the absence of oxygen before compression and then to storage of the syngas product. Excess syngas is sent to flare during experimentation.

When added to the 8.11 engine skid, the PRISM functionality remains the same; filtered air is either actively fed to the reactor or naturally pulled through the reactor via the engine requirement. The controls in place respond accordingly to either arrangement. In this case, the gen-set engine is brought to steady operation first, followed by the PRISM reactor, which is fully introduced to the engine fuel inlet. The natural gas valve is then slowly closed until the engine is no longer being fed with fuel other than freshly produced syngas. From this point, system operation will continue until shutdown. It must be noted that there is a drop in engine power return when fully supplied with only syngas, which is mainly due to the excess dilution of nitrogen from air being processed twice during the same system loop. Syngas can also be introduced hot or cold, eliminating the need for heat exchange if deemed unrequired. The main focus of this system is to eliminate NO_x production and the need for exhaust gas after-treatment. Using a five-gas analyzer, NO_x levels have been routinely recorded at less than 10 ppm prior to after-treatment while using slipstream syngas operation.

4.0.3.2 Transients: Startup/Shutdown

The startup sequence for operation of the PRISM begins with simply turning on the power supply and opening system flow. The plasma field is on at all times and initiates the process acting as a spark to ignite a very lean mixture of air to fuel. These gases are well mixed before introduction to the plasma head chamber. As temperatures rise, the fuel mapping for the controls ap-

proaches a fuel-to-air ratio that is richer in operation. Above 900°C the methane will flood the system and be too rich for any oxidation, thus cooling the catalyst bed and stabilizing the reactor conditions. At this point, the temperature of the system reaches its peak moment $\approx 1000^\circ\text{C}$ and will no longer approach this temperature range again under steady operation. The system is now self-sustained and very stable. Any adjustments to the fuel mapping at this point will only induce minor changes in temperature. If flow is increased, then the main reaction moves toward the next catalyst zone followed by the controls. Given added backpressure, a gas chromatograph (GC) analysis can be processed at any point during this time. In order to shut the system down, simply turn off the power supply and close the fuel valve. A slight air peak may cause a minor combustion instance with any remaining fuel in the system, but quickly subsides as shown by the drop in measured temperature. The reactor retains heat well and may require roughly 3 h to return to ambient levels.

In engine operation, many more transient situations must be considered. Startup ensues in the same manner, with normal engine startup first followed by PRISM startup. Once the temperature change in zone 1 approaches zero, syngas is being produced and can now give way to reduced fuel consumption on the engine's main line. Discontinuities from the piston's compression strokes do not affect the stability of the reactor even when air is being pulled through. This setup requires minimal manipulation to operate steadily, but additional instrumentation would be necessary in a real-life application using a motor vehicle where stops are frequent. A few ideas are in place to alleviate these potential transient issues. The most logical approach would be to implement the lowest possible flow through the reactor during engine idle. The system, though it retains heat well, would fluctuate more than desired since the unit is designed for continuous flow and not for on-off applications. If added to current motor vehicles, the benefit of the hydrogen-rich syngas can be used in a cursory manner; this makes the PRISM advantageous in highway situations. To shut the system down, fully open the engine fuel valve while shutting off the reactor fuel valve and power to the unit. After this, total shutdown is as simple as turning the ignition key.

4.0.3.3 Conversion and Efficiency

In order to achieve high conversion and efficiency, optimization on a working system is vital. True optimization requires experimentation, analysis of experiments, and adjustment thereafter from theory. This is a repeatable, stepwise process that demonstrates the versatility of the technology and potential for performance im-

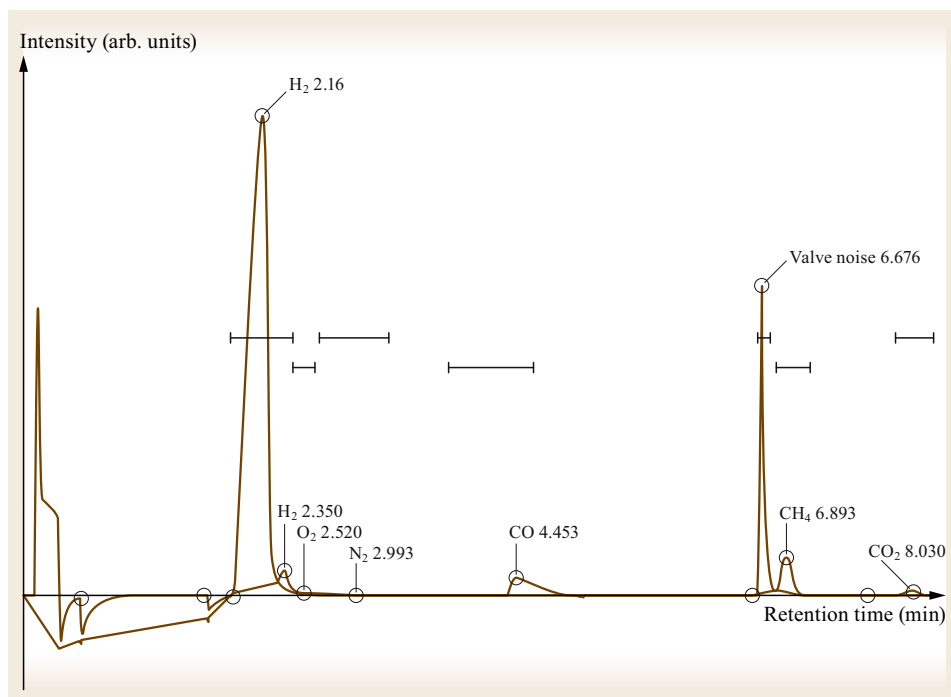


Fig. 40.12 GC results of PRISM operation with pure oxygen

provement. For instance, nonthermal plasma on its own does not provide enough energy or the environment to achieve any significant selectivity of hydrogen and carbon monoxide production. On the other hand, thermal plasma is capable of converting methane into hydrogen unassisted, but the high amount of energy required for thermal plasma generation coupled with the low methane conversion and low hydrogen selectivity is not an economically feasible path to any commercial application. There exists a point, between nonthermal and thermal plasma, which instills the necessary amount of energy required to fully convert the feed stream when coupled with other processes. Plasma does not simply exist in one form; it is affected by intensive properties just as any other phase of matter would by a change in its density or viscosity. The difference with plasma is the constant fluctuation of every property over short time intervals. Methane conversion into hydrogen using only a pure methane feed and nonthermal plasma is close to 6.0%, while thermal plasma with pure methane is near a 12.0% conversion. In an environment supportive of POX using air and methane, thermal and nonthermal plasma systems are capable of achieving a 99.0% conversion of starting material.

Conversion weighed against the energy input to the system is at its peak when nonthermal plasma is used in conjunction with catalysis. The active field of the system provides an ideal environment for the chemical species to react. Deviation from stoichiometry of

POX by decreasing the C/O ratio enhances the selectivity and yield of hydrogen (peaked curve) approximately around $C/O \approx 0.85$ and $T \approx 800^\circ\text{C}$. Efficiency is also increased at higher temperatures. The leaner partial oxidation ratios suggest that a little combustion initially assists in producing greater amounts of hydrogen through the side reactions (mainly steam reformation) immediately downstream in the reactor.

A number of reactions occur simultaneously along the length of the reactor while carrying the electrical properties of the plasma field throughout the process. The participating reactions are combustion, partial oxidation, steam methane reforming, and water gas shift. All of these reactions are reversible in nature, making it difficult to surmise and predict the product outcome from so many variables. The goal is to influence the outcome to the end user's needs, and this can be accomplished through manipulation of the necessary parameters. With a feedback control loop based on internal catalyst temperature and reactant ratio, stable reactor conditions are maintainable and adjustable. Through experimentation and analysis of these parameters at varied set points, a database is established for specific product yield. A production database also allows for early problem detection and error analysis.

Product Measurement

The product stream is analyzed via a small slipstream of gas into a high-precision SRI 1068C gas chromato-

Table 40.1 Volume/mole percentage display of GC results for air and oxygen

PRISM syngas product – GC analysis (% by volume)		
Compound	With air	With oxygen
H ₂	30.7%	58.5%
CO	15.9%	32.2%
CO ₂	3.3%	2.9%
CH ₄	1.3%	6.4%
O ₂	0.0%	0.0%
N ₂	48.8%	0.0%
Total	100.0%	100.0%

graph (GC) attached with Haysep D and Molesieve 13X columns. The GC uses a thermal conductivity detector (TCD) with the attachments to accurately measure the molecular content of the syngas that the unit is receiving. An algorithm has been implemented to the GC interface based on calibration gas at various compositions pertaining to the compounds of interest being synthesized. Based on the GC configuration, every compound known to be present in the gas product is accounted for and returned to the user in a percent volume composition. Refer to Table 40.1 and Fig. 40.12 for actual experimental GC results. The GC is maintained frequently and recalibrated on a three-month cycle. Third-party analysis of a process-derived fuel (PDF) from municipal solid waste (MSW) reformed into syngas from producer gas has also been performed resulting in high levels of hydrogen yield and a large

40.4 Analysis and Discussion

40.4.1 Process Challenges

The areas of concern that were encountered during design and operation of the PRISM process are system controls, modeling, catalyst durability, safety precautions, variable feedstock, and overall scale-up. The feedback control loop is responsive to changes in zonal reactor temperature where the fuel-to-air ratio set point adjusts accordingly to balance reaction heat, firstly preventing catalyst damage and secondly for safety in eliminating any potential runaway reaction. Though stable, the system must always be monitored. Plasma-assisted POX with catalysis provides a wide range of variables that are difficult to model at the atomic level. This limits the depth of process understanding to broader generalizations using separate macrolevel modeling techniques and theories that are well established. The catalyst is susceptible to thermal deactivation, coking, carbon deposition, chemical poisoning (typically sulfur), and deactivation after heavy usage over long periods of time.

Table 40.2 GC-MS results of producer gas composition directly after PRISM system reformation

Component	Mole percent	Weight percent
Oxygen and argon	1.995	2.787
Nitrogen	53.749	65.723
Methane	10.668	7.471
Hydrogen	17.789	1.565
Carbon monoxide	11.273	13.783
Carbon dioxide	4.488	8.622
Ethylene	ND	ND
Ethane	0.038	0.049
Acetylene	ND	ND
Propylene	ND	ND
Propane	ND	ND
Isobutane	ND	ND
<i>n</i> -Butane	ND	ND
<i>trans</i> -2-Butane	ND	ND
1-Butane	ND	ND
Isobutylene	ND	ND
<i>cis</i> -2-Butene	ND	ND
iso-Pentane	ND	ND
<i>n</i> -Pentane	ND	ND
1,3-Butadiene and methyl acetylene	ND	ND
C ₅ Olefins	ND	ND
Hexanes	ND	ND
Heptanes plus	ND	ND

percentage of tar reduction in the gas stream. Results from this experiment are shown in Table 40.2.

The transient issue is minor and ideas are in place to remedy these negatives, such as timing control to maximize the benefits of hydrogen supplementation.

40.4.2 Design Improvements

Startup requires short-term ignition in the form of a modified fuel-to-air ratio. This is viewed more as an unavoidable hindrance that has a greater affect on an operation with a high-frequency modulation between transient and steady-state operation. It is safe to assume that syngas is in full production from cold startup after approximately one minute; this dead time is lessened if system operation was recently shutdown due to the substantial thermal mass of the system. If possible, a more durable catalyst that has greater resistance to sulfur poisoning and thermal decomposition would be ideal for future experimentation and commercialization. This would loosen the restrictions that decrease the lifespan of the catalyst bed.

The system's flow capacity is high for the small footprint of the apparatus itself providing over 150 scfm of high-quality syngas per unit. Dimensions of each PRISM unit are 15" × 18" × 50", approximately. The limitation thus far is the capacity of the mass flow controllers, which reach maximum allowable flow rate before the reaction is extended beyond the catalyst bed. A safe assumption is that the PRISM is able to produce upwards of 200 scfm of syngas. This coincides with nitrogen displacement that reduces product output and system efficiency. Using pure oxygen from gas cylinders is not a viable avenue for long-term system operation, negating the low cost benefits of the process. Pressure swing adsorption (PSA) or vacuum pressure swing adsorption are both viable methods of producing > 95% oxygen content from air in a continuous manner at low operating costs. The physical footprint of the systems tend to be large, but even a small separation of oxygen from nitrogen would provide dramatic improvements in production efficiency and power recovery.

40.4.3 Higher Hydrocarbon Reformation

Longevity tests showing system durability are conducted regularly and for months at a time. Under stable operation, process efficiency does not diminish over time and, in fact, results tend to improve slightly. Under a previous control schema, a fluctuation in syngas product yields and conversion is observed in the range of ±2% of the average data acquired over time. For ex-

ample, average hydrogen percent by volume of syngas was 30% with low-end results being 28% and high-end results being 32% by volume. Some variance could also be attributed to the inconsistent composition of the natural gas pipeline. This range of syngas composition is observed for all components of the product stream during short-term operation as well as month-long continuous experimentation. Data have been logged and thoroughly examined to show stable production of high volume and quality syngas. Reformation efficiency versus stoichiometrically perfect conversion is high in the 80% range for air operation and in the 90% range for oxygen operation. Methane conversion efficiency has been recorded to > 99% at higher process flows while generally in the ≈ 98% range otherwise.

It has been deemed plausible to reform all chains and types of hydrocarbons using the PRISM reactor. Given a vapor phase of feeds such as heptane or aromatics like benzene in stoichiometric proportions with oxygen for POX, a product that consists of mostly hydrogen and carbon monoxide can be achieved. The plasma field imparts enough energy and the heated catalyst bed allows for activation of the POX reaction that could result in near-perfect conversion comparable to the use of methane. Higher hydrocarbon reformation results in a ratio of H₂ to CO much closer to 1.0 than 2.0, which would inhibit downstream processing, but again could be alleviated by a PSA unit to increase hydrogen content. The reformation of waste has also been successfully observed at the facility.

40.5 Synergistic Benefits of Plasma

40.5.1 Chemical Processes

In gasification, a portion of potential product is lost through tar buildup, which consists of higher carbon chained molecules that are condensable, but only at high temperatures up to 400 °C. Not only is it a loss in production, if not properly removed before downstream processing, the tars will obstruct process flow and cause eventual shutdown. These concerns can be dealt with by a plasma-induced field in a catalytic environment supportive of partial oxidation of the hydrocarbons into syngas (Fig. 40.13).

The production of hydrogen is possible through many processes, as it is such an abundant element. The various methods of obtaining hydrogen are energy intensive and also typically involve the destruction of another compound that could hold value on its own. In processes that create excess side hydrocarbons or hydrogen-containing compounds, there is little to no

value in them unless further processing is done. This is true for a side product such as dirty glycerol, which is difficult to handle and costly to remove as well. The PRISM is able to make these side products useful for additional heating to primary processes or for a valuable side product such as methanol. Because of its low operating expense, the PRISM can be utilized in any process looking to maximize its hydrogen potential. PEM and solid oxide fuel cells that run directly on hydrogen are another potential beneficiary of this technology.

40.5.2 Commercial Implementation

This process has the flexibility to create numerous market-worthy products, allowing the user to choose their path of profitability. Syngas, once synthesized, can be taken down any processing path that would use the H₂ and CO molecules as building blocks for the product. Olefins are the raw material for most plastics

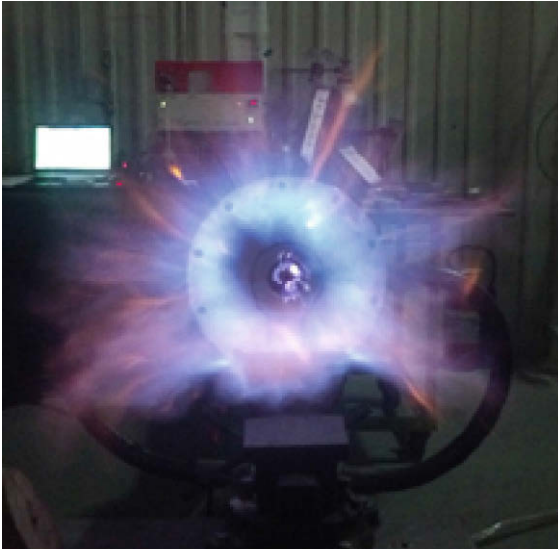


Fig. 40.13 Operation and view of the ionized plasma field exposed to the air (pre-catalysis)

and can be produced in a high-pressure, temperature-controlled environment when provided with the proper catalyst. Methanol, ammonia, and diesel fuel are just some of the many other products that can be made from feedstock derived of syngas.

Decreasing emissions from motor vehicles and increasing engine efficiency is a necessary step toward improving air quality and decreasing greenhouse gases. Internal combustion engines for transportation constitute as one of the largest consumers of imported oil and are also a major source of ozone-eliminating gases such as NO_x . A variety of potential improvements are presently being investigated: lean-burn engines, engines designed with increased compression ratios, improved catalyst formulations, use of close-coupled catalysts,

new types of exhaust treatment, electric and fuel-cell powered vehicles, and alternative fuels.

One outlet for plasma reforming technology, which also presents a solution to the negatives of internal combustion in transportation, is for onboard vehicular implementation. In a fully integrated system, the generation of hydrogen as syngas into an ICE allows for lower combustion temperatures, better flame speed and propagation, increased sparkplug life, and decreased NO_x emissions during engine operation. Onboard production of hydrogen may be attractive for reduction of cold-start emissions and minimizing engine cranking during cold start. This is beneficial for catalyst regeneration and posttreatment as well. The robust, compact design of the PRISM unit can be used with a variety of fuels to provide a rapid response without the necessity of reformed gas storage. Complete integration of the vehicle operating system with the PRISM reactor would call for an intuitive approach to achieve a seamless, well-controlled operation. This would factor in startup, shutdown, ratio control, valve timing, and additional temperature sensors, but would otherwise not require further manipulation of either new or old standard vehicle engine designs.

Upon total oxidation or combustion of fuel with or without syngas, large quantities of water and CO_2 are produced in the exhaust. The hydrogen-rich gas may be useful during cold start, both minimizing the cranking, as well as potentially decreasing the hydrocarbon emissions due to cold-start ignition. In an exhaust gas recycle (EGR) process the dry reforming reaction plays a major role in altering the stoichiometry of the system. The main goal of EGR is to lower peak combustion temperature in the piston chamber. This provides a smoother cycle of operation reducing NO_x and ensuring maximum conversion while boosting thermal-to-mechanical efficiency.

40.6 Conclusion

Very few configurations exist, outside highly specialized areas of use, which allow thermal plasma to be implemented in a profit-worthy system. A low energy, nonthermal plasma creates a better source for utilization of resources, providing efficient production of high quality syngas. Nonthermal plasma also requires assistance from catalysis in the form of a tailored reaction as opposed to simple decomposition. If unassisted, gaseous carbon and hydrogen atoms in a heated environment will preferentially recombine into methane instead of separating into hydrogen and carbon monoxide molecules. Plasma-assisted catalytic

POX has great potential to address many environmental concerns while maintaining profitability for the end user. In its present design, PRISM is a viable tool for implementation into small- to middle-scale syngas production plants. Expending roughly 100 W of energy in a robust system configuration built for extended operation, nonthermal single-stage plasma catalysis has proven to be a viable technology for reforming. Full integration of the PRISM reactor into future commercial endeavors is possible with only minor adjustments to the current benchmark operation.

Acknowledgments. This chapter was written with the assistance of Dr. Leslie Bromberg from MIT and Michael Carpenter of RTI International. Leslie has over 40 years of plasma and reformation experience most of which was spent in conducting research, educating students, and writing a vast number of published documents for the field of plasma science and plasma engineering. Michael has degrees in both physics and chemistry with a focus on nanoscience at NCSU. He has participated first-hand in key developments of the PRISM system and successful downstream processing of our fresh syngas product. His insight has been invaluable towards the growth of our technology. We would like to thank Leslie and Michael for their time and contributions to our research and to this book chapter. A kind thank you to all previous studies on reformation and plasma technology, especially to the authors and

contributors whose works were incorporated and cited as an influence to the completion of this chapter. I'd like to thank Shiva Wilson and Nat Mundy of Freedom Energy Tech, LLC and Mr. Larry Bell for their tireless efforts and dedication to the company as well as lending their wisdom and expertise to the technology and the opportunity. Freedom Energy Tech, LLC has the exclusive license on the PRISM Plasma technology. I would also like to acknowledge Chet Staron and Mike Wirthman of TopLine Automotive Engineering, Inc. Finally, I would like to acknowledge the Chemical and Biomedical Engineering Department of the University of South Florida for the thorough education provided to me and every student involved with the department. The credit goes to the well-established curriculum and one-of-a-kind faculty devoted to the wellbeing of each individual and to the engineering society as a whole.

References

- 40.1 M.A. Lieberman, A.J. Lichtenberg: *Principles of Plasma Discharges and Materials Processing* (Wiley-Interscience, Hoboken 2005)
- 40.2 J.D. Rollier, A. Darmon, D. Gonzalez-Aquilar, R. Mekemeijer, L. Fulcheri, G. Petitpas: A comparative study of non-thermal plasma assisted reforming technologies, *Int. J. Hydrogen Energ.* **32**, 2848–2867 (2007)
- 40.3 H.M. Lee, S.H. Chen: *Yu. Chao, M.B. Chang, H. Chen: Review of plasma catalysis on hydrocarbon reforming for hydrogen production – Interaction, integration and prospects* (*Appl. Catalysis B* 85, 1–9 2008)
- 40.4 U. Kogelschatz, B. Eliasson, W. Egli: Dielectric-barrier discharges, principle and applications, *J. Phys. IV* **7**(C4), 47–66 (1997)
- 40.5 A. Czernichowski: Gliding arc – Applications to engineering and environment control, *Pure Appl. Chem.* **66**(6), 1301–1310 (1994)
- 40.6 P.K. Cheekatamarla, C.M. Finnerty: Synthesis gas production via catalytic partial oxidation reforming of liquid fuels, *Int. J. Hydrog. Energ.* **33**, 5012–5019 (2008)
- 40.7 O. Deutschmann, L. Schmidt: Two-dimensional modeling of partial oxidation of methane on rhodium in a short contact time reactor, 27th Symp. (Int.) on Combustion/The Combustion Institute, Naples (1998) pp. 2283–2291
- 40.8 S. Jo, D. Lee, Y. Song: Effect of gas temperature on partial oxidation of methane in plasma reforming, *Int. J. Hydrog. Energ.* **38**, 13643–13648 (2013)
- 40.9 W.H. Chen, T.W. Chiu, C.I. Hung: Hysteresis loops of methane catalytic partial oxidation under the effects of varied reynolds number and Damköhler number, *Int. J. Hydrog. Energ.* **35**, 291–302 (2010)
- 40.10 W.H. Chen, T.W. Chiu, C.I. Hung: Hydrogen production from methane under the interaction of catalytic partial oxidation, water gas shift reaction and heat recovery, *Int. J. Hydrog. Energ.* **35**, 12808–12820 (2010)
- 40.11 O. Deutschmann: Catalytic reforming of logistic fuels at high-temperatures, *Catalysis* **24**, 48–82 (2012) doi:10.1039/9781849734776-00048
- 40.12 L. Maier, M. Hartmann, S. Tischer, D. Deutschmann: Interaction of heterogeneous and homogeneous kinetics with mass and heat transfer in catalytic reforming of logistic fuels, *Combust. Flame* **158**, 796–808 (2011)
- 40.13 D.H. Lee, K.T. Kim, M.S. Cha, Y.H. Song: Plasma-controlled chemistry in plasma reforming of methane, *Int. J. Hydrog. Energ.* **35**, 10967–10976 (2010)
- 40.14 S.A. Al-Sayari: Recent developments in the partial oxidation of methane to syngas, *Open Catalysis J.* **6**, 17–28 (2013)

Hydrocarbon

41. Hydrocarbon Processing by Plasma

Robert J. Wandell, Bruce R. Locke

Nonthermal plasma processes have been successfully utilized commercially in air pollution control, ozone generation, polymerization processes, and microelectronics processing. The addition of a liquid phase that contacts the plasma has given rise to a wide range of other potential applications in materials synthesis, biomedicine, and chemical synthesis. Applications in the petroleum and energy fields utilizing organic chemistry plasma processes have been investigated as well, for example, in hydrogen generation, gas reforming, and partial oxidation. Partial oxidation of hydrocarbons is a longstanding challenge in organic chemistry, and recent work with plasma and plasma contacting liquids have demonstrated the formation of alcohols and other oxygenated species from a range of hydrocarbons. This review focuses on the functionalization of hydrocarbons with radical species produced by nonthermal plasma discharges primarily in oxygen and argon gases with liquid water. Since the types of chemical reactions that can be induced by plasma depend strongly on the composition of the gases utilized, the reactor configuration, and the plasma properties, we address two major ways of functionalizing hydrocarbons with plasma; 1) utilization of oxygen radicals from molecular oxygen and 2) utilization of hydroxyl radicals from liquid water. Both methods supply oxidants that lead to similar reaction product distributions and such plasma processes have the potential to produce value-added products efficiently and with reduced environmental impact.

41.1	Historical Aspects	1164
41.2	Properties of Plasma – Thermal versus Nonthermal	1164
41.3	Commercial Viability of Plasma Processes	1165
41.4	Challenges in Performing Selective Organic Reactions with Plasma	1165
41.5	Strategies to Induce Selectivity	1166
41.6	Radical Chemistry in Various Plasma Discharges	1167
41.7	Pure Organic Compounds in Direct Contact with Plasma Discharge	1168
41.8	Functionalization of Hydrocarbons with Plasma-Generated Radical Species	1168
41.9	Functionalization of Liquid Hydrocarbons with Oxygen Plasma	1169
41.10	Functionalization of Liquid Hydrocarbons with Water Plasmas	1173
41.11	Conclusions and Future Trends	1174
	References	1175

The functionalization of saturated hydrocarbons is a fundamental problem in industrial organic chemistry because there are very limited ways to induce selective reactions into the relatively strong and localized C–H and C–C bonds of these molecules [41.1, 2]. Hydrogen abstraction of alkanes at high temperature, mostly for combustion, has been studied [41.3–11]. However, various catalysts must be employed, and the harsh conditions often lead to over oxidation of the

initially formed alcohols. Enzymes exist and synthetic inorganic catalysts have been developed that selectively oxidize alkanes, typically with hydrogen peroxide addition, but these catalytic methods can be impractical due to the high cost, limited availability of the catalysts, and the relatively slow reaction rates [41.12–14]. Conventional high temperature thermal cracking can generate valuable products; however, the energy costs are significant and the process leads to the generation

of unsaturated hydrocarbons which present additional challenges. Therefore, there is a significant need for new methods that can be used to capitalize on valuable hydrocarbon natural resources to make useful chemical products efficiently and with low environmental impact [41.1, 2, 15]. The use of plasma discharge to induce these reactions has the potential to provide such

an alternative; however, significant challenges must be overcome to facilitate this application. The goal of this review is to provide the current status of plasma processes focusing primarily on hydrocarbon partial oxidation, and to consider this application within the context of other applications of chemical synthesis by plasma processes.

41.1 Historical Aspects

Chemical reactions induced by electrical discharge, including sparks and arcs, have long been of interest since the early observations in the Netherlands on the formation of oily condensed products from ethylene in spark discharges at the end of the 18th century [41.16–19]. Development of commercial ozonizers by Siemens led to an increased interest in chemical synthesis (including ozone and nitrogen oxides) at the end of the 19th century. During the early to middle 20th century, studies on chemical synthesis by electric discharge included ammonia synthesis [41.20–22], acetylene production from methane and hydrogen [41.23], formation of nitrogen oxides [41.24–33], synthesis of other organics (e.g., cyanhydric acid) [41.34–43] and work on nitric acid reactions with water vapor [41.44, 45]. A landmark study of amino acid formation by elec-

tric discharge under atmospheric conditions simulating the earth before the origin of life led to extensive work on electrical discharge-induced chemical synthesis and chemical evolution [41.46–48]. Reviews of the wide range of other organic compounds synthesized by plasma have been published [41.16–18, 49] with more recent work focusing on hydrogen formation and methane conversion due to increased interest in processing of natural gas and the hydrogen fuel cycle [41.50–56].

This review will focus on work dealing with hydrocarbon processing with nonthermal plasma with particular emphasis on the role of water and hydroxyl radicals to induce functionalization into organic molecules and to form high value added products rather than complete oxidation or polymerization.

41.2 Properties of Plasma – Thermal versus Nonthermal

Plasma is an ionized gas containing both positive and negative ions, as well as free electrons. The overall volume of the plasma is electrically neutral because charge is not lost to the surroundings [41.57]. Many types of plasmas exist in nature and technology. They are primarily distinguished by the density of ions and electrons and the energy of those species. Thermal plasmas have very high energies as well as densities, and in such plasma the energy of the free electrons is of the same order of magnitude as the ions and molecules (temperatures > 10 000 K). In nonthermal, or cold plasma, the free electrons have much higher energies than the ions and molecules; here the temperature of the background gas can be close to ambient while the electron temperatures range from 10 000–100 000 K (1–10 eV) [41.58].

A key factor in utilizing a plasma process to perform chemical synthesis is to suppress reactions that destroy the desired products through degradation reactions with ions, radicals, and other species formed in the plasma. Some thermal plasma processes can utilize high quenching rates (i. e., steep spatial or temporal

gradients of plasma conditions) to partially suppress these back reactions [41.49]. In contrast, nonthermal plasma offers the potential to perform useful chemistry by utilizing primarily the higher energy electrons to initiate reactions through electron collisions with the background gases to produce radicals, ions, and excited species which can react with the targets, and because of the low ambient background gas temperature less energy is utilized in thermal processes and less heat is lost.

One of the most common and effective ways of making nonthermal or cold plasma for technological applications is to use electrical discharges by AC (alternating current), DC (direct current), or pulsed electric fields [41.60]. Microwave and radiofrequency plasmas are also used. A large number of reactor configurations utilizing various electrode arrangements and plasma contacting schemes have been investigated for a variety of applications [41.61]. Figure 41.1 shows an example of the commonly studied gliding arc plasma discharge [41.55, 59].



Fig. 41.1 Images of plasma processes. Gliding arc plasma discharge over water. Reprinted with permission from [41.59]. Copyright (2008) American Chemical Society

41.3 Commercial Viability of Plasma Processes

The major commercial successes of chemical synthesis with plasma are in ozone generation, plasma polymerization, and the fabrication of semiconductor devices [41.19, 62, 63]. It is noteworthy that the application of plasma processing in semiconductor manufacturing has contributed to the success of the \$ 300 B worldwide market in computer technology [41.19]. It can also be noted, that pilot- and commercial-scale plasma processes have been successful in air pollution control [41.64–70] and some pilot-scale systems for water pollution control have been developed [41.71].

The commercial success of ozone generation with oxygen plasma discharge is due to the key factor of reaction selectivity. To generate ozone with a plasma discharge, only one chemical feed to the system is necessary, molecular oxygen. Not only can oxygen be easily separated from air, but this single feedstock limits the chemical reactions that are possible to ones that only contain oxygen species [41.72–75]. In turn, this significantly narrows the number of possible stable products which can be generated, the most dominant

being ozone, making the process commercially viable. Ozone generation by plasma discharge does not require catalyst due to the relatively simple chemistry, and only compressed oxygen is needed as a chemical feed with no separation or purification of the products generated required. It can be noted that in practical applications the tradeoff between using pure oxygen and air requires consideration of the cost of the oxygen relative to the formation of by-products from air and lower ozone generation efficiency. More complicated systems of chemical reactions occur in plasma polymerization and plasma processing in microelectronics where process control by variation of feed gas composition and other plasma properties can be used to facilitate the desired reactions and both of these applications feature plasma interactions with substrate surfaces. It is possible that a deep understanding of the underlying chemistry, physics, and engineering principles involved in initiating chemical reactions with electrical discharges will lead to the development of new plasma chemical synthesis applications to petroleum-based technologies.

41.4 Challenges in Performing Selective Organic Reactions with Plasma

The reactions of organic compounds in plasma discharges have been investigated for a wide range of applications and conditions including plasma discharge in pure organic liquids, oxidation of dilute organic compounds in liquid water for pollution control [41.76–81], and the more commonly studied and commercialized case of plasma polymerization [41.63]. However, there

are important differences between the functionalization of hydrocarbons to produce small intermediate products by plasma and the intensively studied case of plasma polymerization. It is because of these differences that polymerization with plasma has become commercially viable, while selective functionalization with plasma has not. In plasma polymerization, the desired goal is to

form a surface polymer coating using gas phase plasma which contains the precursor molecules. In such cases, a large conversion is required to form the coating. In order to produce large conversions, high plasma energy is required which leads to complete dissociation of the precursor compounds into small organic fragments. The resulting recombination reactions are not significantly selective due to the large distribution of compounds generated and the large number of possible chemical reactions which can occur [41.63]. While this does not pose a problem for surface coating, a significant challenge in chemical synthesis of smaller nonpolymeric compounds with plasma discharge is the requirement for higher selectivity. Although selectivity may come at the cost of lower conversion, this cost can often be compensated in synthetic chemistry by component recirculation as well as series or parallel reactor designs [41.82].

A second major issue relates to the location where the reactions occur. In plasma polymerization there is still debate on whether the main polymerization reac-

tions occur in the gas phase or on the substrate surface. While both cases are predicted to lead to the *irregular structure* of the polymer, it has been shown that the reactor pressure and plasma pulsing can influence the location of these reactions [41.63]. In gas–liquid plasma systems the physical location of the plasma chemical synthesis will depend, in part, on the volatility of the precursor molecule. Under conditions of low volatility, the plasma radicals may directly impinge on the liquid surface initiating reactions at the interface or even generating some radicals in the liquid phase. For high volatility cases, the organic liquid is fully vaporized and can react directly in the gas phase. Different product distributions are expected in these different conditions. A third issue relates to modification of reactor/reaction conditions including pulse generation by the power supply. For example, shorter plasma pulses (of order μs) (or with superimposed pressure pulses) have been shown to control chain propagation in plasma polymerization, but again at the cost of yield [41.63].

41.5 Strategies to Induce Selectivity

As previously stated, a major hurdle in the development of viable bulk phase chemical synthesis with plasma discharge which greatly complicates commercialization is that overall production is limited by degradation of the desired product by electron or radical attack before it can be collected. This issue is a fundamental problem in that many synthetic processes are dominated by endothermic reactions where electron impact dissociation of the parent compound is rapidly followed by a series of radical chain reactions leading to the product, which itself is susceptible to additional attack by radical species [41.83]. Thus, one must control or stop the plasma-induced radical reactions in order to promote reaction selectivity.

Typical strategies to suppress plasma degradation reactions are to impose strong spatial and temporal gradients between the plasma and the surroundings so as to limit the degradation reactions and/or to rapidly quench undesired radical species [41.83–86]. Partial selectivity can be achieved by the addition of gas and/or liquid phase radical quenchers which prevent undesired reactions and potentially enhance desired ones. While it is desirable to introduce completely inert quenching media it is difficult to find any such compounds that do not to some degree participate in the plasma reactions. Additional selectivity can also be achieved by:

1. Decreasing residence time of all species by adjusting reactor geometry and flow rates

2. Imposing large spatial or temporal gradients on the plasma
3. Adjusting characteristics of the applied electric field
4. Imposing large cooling gradients in the system.

Another strategy is to sequester the desired product in an environment that protects it or removes it from the plasma [41.87, 88]. This concept is analogous to the chemical engineering processes that utilize simultaneous reaction and separation [41.82, 88–91]. The addition of a liquid phase in which the desired product is highly soluble was a significant advancement in chemical synthesis with plasma, and well studied in the synthesis of hydrazine from ammonia where it was shown that the introduction of a liquid ethylene glycol solution can significantly increase the energy yield for hydrazine [41.92]. In that study, the liquid phase was sprayed in to the gas phase discharge and acts only as an absorbent which sequesters and protects the hydrazine molecule after it has been formed in the gas phase.

Water can also be used as an absorbent in plasma systems. It has been shown that formaldehyde, methanol, and hydrogen peroxide can be synthesized from methane–water vapor mixtures [41.93]. This situation provides a unique advantage in that the liquid water acts not only as an absorbent but also as a source of reactive species (hydroxyl radicals, $\bullet\text{OH}$). Significant work has been conducted to investigate various reactor designs which increase the gas–liquid interfacial area to

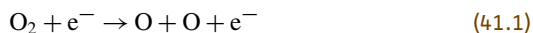
take advantage of this duality, particularly in the generation of hydrogen peroxide from liquid water [41.87, 94, 95]. The large solubility of hydrogen peroxide in liquid water is one of the primary reasons the energy yield for hydrogen peroxide is high in liquid water/gas plasma systems [41.87]. The thermodynamics of such phase equilibrium are extensively covered in the literature [41.96]. However, it should be noted that the nature

of the gas–liquid equilibrium and component solubility becomes significantly more complicated in systems with more complex chemistry such as those where hydrocarbons are present. Nonetheless, some selectivity has been demonstrated in a gas phase microwave plasma with *n*-hexane vapor in flowing argon through changes in the plasma input power, feed flow rates, and location of the feed [41.97].

41.6 Radical Chemistry in Various Plasma Discharges

Because of difficulties in analyzing the diverse distributions of reactive species formed when a large number of complex reactants such as hydrocarbons are subjected to plasma, studies have been made in situations with limited chemical complexity, where some degree of selectivity can be achieved and analysis simplified. These studies are essential towards understanding the fundamental factors involved in generating reactive species with plasma discharges before more complicated situations can be understood. As already mentioned, of these simplified cases, electrical discharges with pure oxygen gas are among the simplest.

When pure oxygen is subject to a plasma discharge the dissociation of diatomic oxygen occurs through direct electron impact as shown in reaction (41.1).



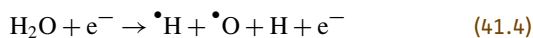
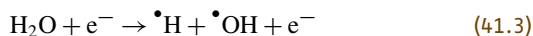
The O resulting from reaction (41.1) may be of the form ^3P , ^1D , and ^1S . In the case of ozone generation the plasma parameters can be adjusted to favor the recombination of O to form O_3 through reaction (41.2), where M is a third collision partner [41.74].



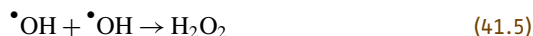
Alternatively, the plasma and reactor parameters, particularly pressure, can be adjusted to favor the generation of $\text{O}(^3\text{P})$. This highly reactive species can then be utilized to oxidize other components in the plasma system [41.98].

Other studies utilizing liquid or vaporized water and noble gases have established that the major reactive species formed when electrical discharges contact liquid water are hydroxyl radicals ($^{\bullet}\text{OH}$) and hydrogen peroxide (H_2O_2) [41.76, 87, 99–104]. Other species, including molecular hydrogen (H_2), molecular oxygen (O_2), and reducing compounds such as O_2^- and $^{\bullet}\text{H}$, can also be formed [41.102, 105, 106]. When liquid water contacts a plasma channel a portion of the liquid is vaporized into the gas phase where it then undergoes reaction. Many reactions with water can occur in the gas

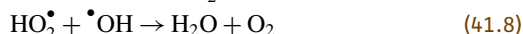
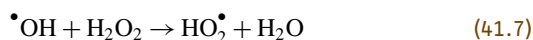
phase including electron dissociation reactions (41.3) and (41.4) [41.107, 108].



Generally, the hydroxyl radical density in gas–liquid plasmas is sufficient to produce hydrogen peroxide by hydroxyl radical recombination through reaction (41.5), and H recombination forms H_2 by reaction (41.6).



Limitations on hydrogen peroxide formation generally come from reactions that either degrade it by radical attack (reaction (41.7)) or limit the hydroxyl radical density through recombination to make water (reactions (41.8) and (41.9)). Therefore, strategies to increase the formation of hydrogen peroxide require means to suppress reactions (41.7)–(41.9). At high temperature, thermal degradation of hydrogen peroxide can also occur.



It is for the above reasons that the energy yield for hydrogen peroxide is significantly higher for cases with liquid water rather than for vaporized water alone [41.87]. In gas phase systems, the hydrogen peroxide produced can quickly undergo further degradation by the plasma. However, when liquid water is present, the liquid phase acts as an absorbent to collect and protect the chemical species generated in the plasma phase. Liquid water also provides a continuous source of water molecules transferring into the plasma by evaporation. In these cases, the plasma is pulsed and of low energy so as to not completely evaporate the liquid phase and this leads to quite large energy yields for H_2O_2 [41.109].

41.7 Pure Organic Compounds in Direct Contact with Plasma Discharge

When organic molecules such as hydrocarbons are directly subject to plasma discharge the chemistry can become significantly more complicated due to the likelihood of breaking carbon–carbon and carbon–hydrogen bonds. Generally, in alkanes, the C–C bonds are much weaker than the C–H bonds. For example, the C–C bond dissociation energy in *n*-hexane is 338.9 kJ/mol, while the C–H bond energy is 410.03 kJ/mol. Thus, when vaporized hydrocarbons are directly subject to a plasma discharge one would expect the C–C bond to break more easily than the C–H bond resulting in fragmentation of the molecule [41.110].

Plasma generated directly in an organic liquid phase has been demonstrated to form diamond coatings [41.111] and other carbonized materials such as nanofibers [41.112]. Gas phase plasma (spark discharge: 3–12 W) generated with argon over heavy oils (*n*-C₁₀ to *n*-C₂₅ hydrocarbons) has been shown to lead to significant chain breakage forming one to four carbon-containing compounds with ethylene and hydrogen being the predominant species [41.113, 114]. Liquid *n*-hexadecane was studied as a model compound for hydrocarbon oil and was cracked into C₆ to C₁₅ hydrocarbons using a dielectric barrier discharge with a methane carrier over the liquid hydrocarbon [41.115]. In another example, crude oil was treated with a dielec-

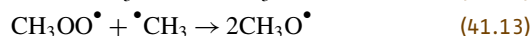
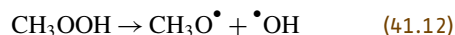
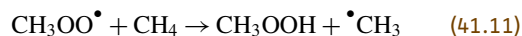
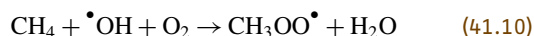
tric barrier discharge for various carrier gases (H₂, CO₂, CH₄) where rheological analysis showed a decrease in viscosity of the crude oil treated by plasma, and nuclear magnetic resonance (NMR) analysis showed that the plasma treatment primarily led to water extraction from the naturally occurring emulsified water in the crude [41.116]. Further, an 80 W microwave plasma with water vapor over an aromatic heavy oil liquid (viscosity: 2–8 cSt, density: 1100 kg/m³, distillation interval: 280–500 °C) demonstrated a series of reaction products including long-chain aromatics, linear and shorter aromatic rings, and also, syngas, CO₂, and small alkanes and alkenes. Trace amounts of other carbonaceous products were also reported [41.117]. Clearly at high enough plasma power and exposure time, a wide range of hydrocarbons, even heavy oils, can be cracked to relatively small compounds. On the subject of smaller gaseous hydrocarbons, extensive literature also exists on methane conversion in dry gas plasma reactors into higher hydrocarbons [41.118–120]. Key issues that will make these types of applications useful for chemical synthesis of valuable products are controlling or stopping plasma-induced radical reactions and promotion of reaction selectivity, which, as previously discussed, is an extremely difficult task when fragmentation and polymerization are predominant reactions in the system.

41.8 Functionalization of Hydrocarbons with Plasma-Generated Radical Species

In order to avoid the fragmentation and polymerization seen when pure organic compounds are subject directly to plasma discharge studies have been performed with organic molecules mixed with other easily ionized compounds such as oxygen or water. The strategy here is to not ionize, dissociate, or otherwise activate the organic molecule directly with the free electrons in the plasma. Instead, reactive chemical species are produced from the other major components in the mixture, which are then able to attack the organic molecules present in the system.

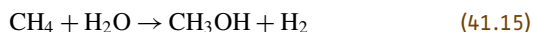
One of the simplest of these plasma systems is the oxidation of methane with reactive species formed in oxygen or carbon dioxide plasma discharges. Gas to liquid conversion of methane to methanol has been demonstrated in these systems [41.121–127]. Research efforts have also been devoted towards methane to methanol and/or formaldehyde conversion with water vapor and or liquid water films [41.93, 125, 128–130]. As with the formation of hydrogen peroxide [41.131–

133] and hydrazine [41.134–138], the formation of methanol may be optimized under conditions where degradation reactions with radicals are minimized and over oxidation to CO and CO₂ is suppressed [41.130]. The reaction kinetics of methane oxidation have been extensively studied [41.139–141] and include the main reactions (41.10)–(41.14) [41.141].



In plasma discharge with humid gas, *Okazaki* [41.129] suggests that the direct conversion of methane to methanol, reaction (41.15), proceeds by the direct reaction of methyl radicals, CH₃·, with hydroxyl radicals

produced from water.



Using a 500 Hz pulsed discharge reactor at approximately 400 °C with a relatively low pressure of 10–40 Torr and 2–6 W power, they found a methanol yield of approximately 0.8% with energy yields of up to 10 g/kWh (8.68×10^{-8} mol/J) for glow-like discharge. However, with a high-voltage spark-like discharge with lower power (5 mW) they claim approximately 100 times better efficiency at 1 kg/kWh (8.68×10^{-6} mol/J). In addition to methanol, formaldehyde and formic acid were also formed. While the yield was relatively small, the energy efficiency is extremely high and would be economically competitive.

Larger hydrocarbons can also be successfully oxygenated by oxygen radicals produced from oxygen plasmas to form predominantly alcohols and ketones [41.18, 98, 142–160]. However, functionalization

of organic compounds with hydroxyl radicals formed from water plasma systems has been less studied. Oxidation with water plasma discharges has mostly been limited to water pollution control and biomedical applications such as sterilization where the goals are larger degrees of mineralization [41.94, 161]. Recent reviews on the chemistry and physics of plasma discharges in contact with liquid water discuss hydroxyl radical reactions with various organic compounds including those of interest in biology such as cell membrane components [41.61, 94, 162, 163]. It can also be noted that plasma oxidation in water has significant similarities with supercritical water oxidation for both chemical destruction and hydrogen formation [41.164–174]. In addition, the functionalization, or partial oxidation, of hydrocarbons such as *n*-hexane, cyclohexane, and cyclohexene with radicals produced from water by plasma discharges has been demonstrated, with results similar to that of oxygen plasmas [41.109, 175].

41.9 Functionalization of Liquid Hydrocarbons with Oxygen Plasma

Because of the ease of generating $\text{O}(^3\text{P})$ radicals with oxygen plasma discharges, significant work has been conducted to utilize the high reactivity of this species to oxygenate various types of hydrocarbons. A schematic of an apparatus frequently employed to perform such experiments is shown in Fig. 41.2 [41.142]. In this system, $\text{O}(^3\text{P})$ produced by the gas phase oxygen plasma impinge directly on the surface of the liquid hydrocarbon under investigation, which is well mixed and cooled to a temperature close to its freezing point. The cooling prevents vaporization of the hydrocarbon into the gas phase plasma (8–40 W) which would create the potential for fragmentation and polymerization. Here the goal is to control the plasma conditions so that radical chain reactions that would normally form a polymer film are not favored. Thus, the relative amount of alkyl radical must be low compared to the plasma formed $\text{O}(^3\text{P})$ so that fragmentation and polymerization can be suppressed in favor of oxygenation. It is for this reason that cooling of the liquid hydrocarbon is an essential aspect of this system.

Utilizing the system shown in Fig. 41.2, functionalization has been demonstrated for a variety of short- and long-chain normal alkanes (*n*-hexane – 1.02×10^{-8} mol/J, *n*-heptane, *n*-octane, *n*-dodecane – 1.11×10^{-8} mol/J, and *n*-tridecane – 7.48×10^{-8} mol/J) as well as branched alkanes such as 4-methyl-heptane (9.77×10^{-8} mol/J) and squalane (2,6,10,15,19,23-hexamethyltetracosane) (4.87×10^{-8} mol/J) [41.98, 158].

In the experiments with normal alkanes, the predominant products generated were secondary alcohols and ketones. One of the most interesting results of these experiments is that functionalization of the primary carbons of these molecules did not occur. An explanation for this lies in the fact that previous research has suggested simple hydrogen extraction is the dominant mechanism in the reaction of saturated hydrocarbons with $\text{O}(^3\text{P})$ and this results in the generation of an alkyl and a hydroxyl radical as shown in reaction (41.16) [41.158].



With this information, the preferential attack on the secondary and tertiary carbons in these experiments can be accounted for by the different energies of the various C–H bonds found in saturated hydrocarbons as illustrated in Fig. 41.3. This hypothesis is supported by results with 4-methyl-heptane where the major product was found to be 4-methyl-4-heptanol (52.6%), the result of hydrogen abstraction of the single tertiary carbon in the molecule as shown in the reaction in Fig. 41.4 [41.98].

These experiments also demonstrated that the pressure of the system, the temperature of the liquid hydrocarbon, and the total reaction time significantly impact overall conversion of the hydrocarbons. In the case of temperature, maximum conversion of the hydrocarbon

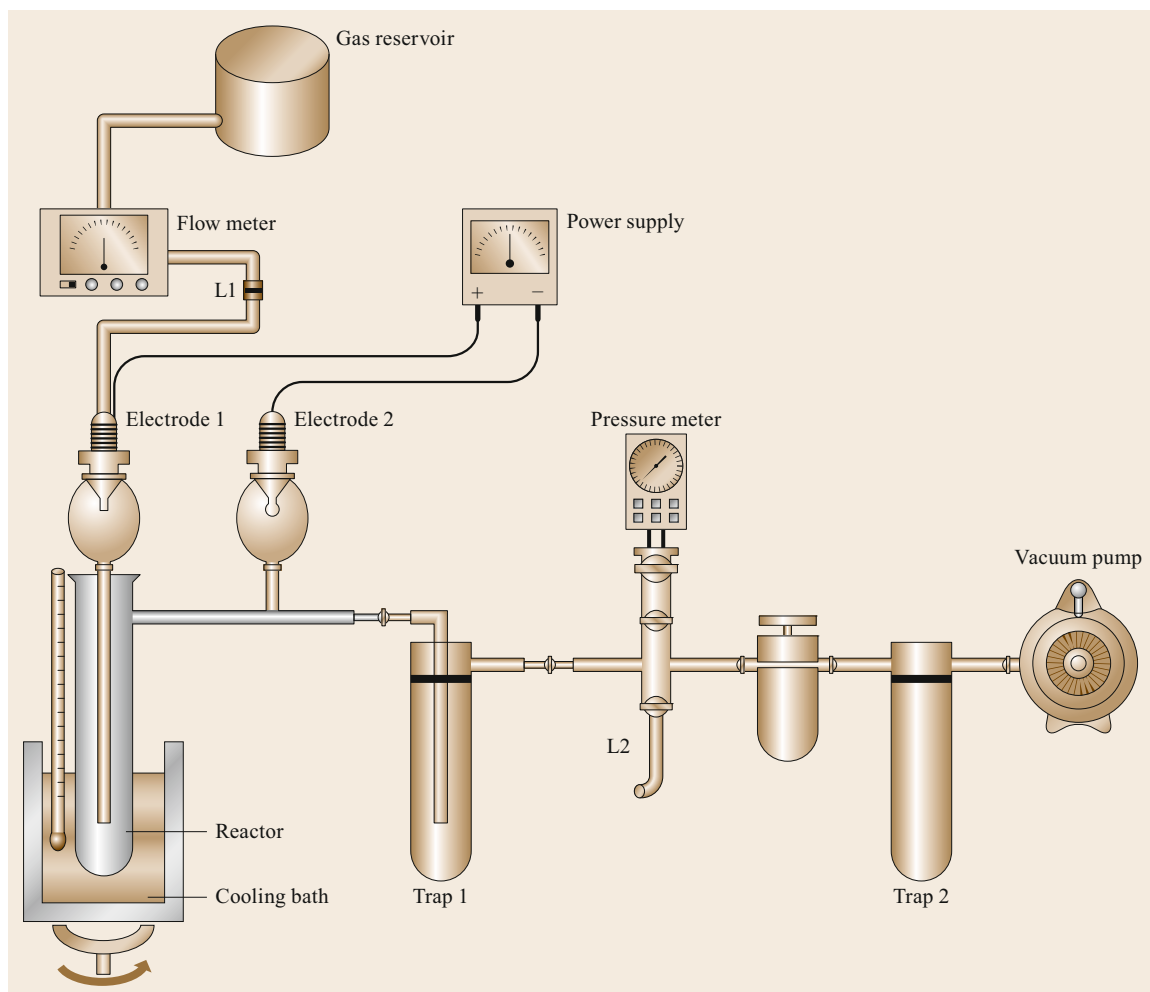


Fig. 41.2 Low-pressure oxygen plasma system (reprinted (adapted) with permission from [41.142], Copyright (2002) American Chemical Society)

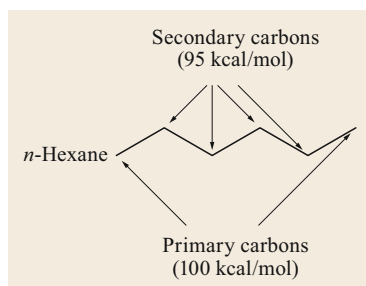


Fig. 41.3 Various bond dissociation energies for a *n*-hexane molecule

was found at temperatures closest to the pure component freezing point of the liquid hydrocarbon. Once the freezing point was reached and solidification of the pure liquid hydrocarbon commenced, conversion sharply decreased because the reactivity of active oxygen species and solid particles is negligible. Pressure

was found to significantly impact the density of $O(^3P)$ atoms. An optimum pressure was found to maximize the $O(^3P)$ population, which resulted in the highest conversions [41.158]. Higher conversions were also achieved with longer total reaction times. However, it was also shown that the reaction time has an additional effect on the selectivity of the reaction products [41.98]. This is apparent in the case of squalane, where increasing the reaction time increased the ratio of ketones to alcohols generated. An explanation for this can be found in the fact that the reactions to produce the ketone products are a result of interaction between $O(^3P)$ and the previously generated alcohols, an example of which can be found in Fig. 41.5.

In addition to these alkanes, functionalization of various liquid olefins using the system described in Fig. 41.2 has also been investigated [41.98, 159]. The

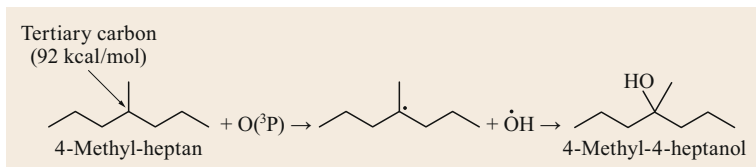


Fig. 41.4 Oxidation of 4-methyl-heptane to an alcohol by attack with $O(^3P)$

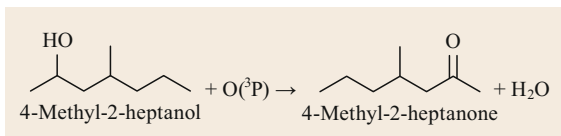


Fig. 41.5 Oxidation of 4-methyl-heptanol to a ketone by attack with $O(^3P)$

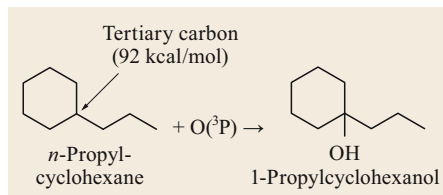


Fig. 41.6 Oxidation of *n*-propyl-cyclohexane to 1-propylcyclohexanol

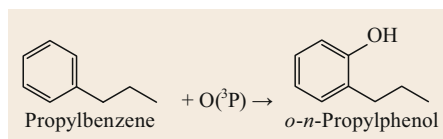


Fig. 41.7 Oxidation of propylbenzene to *o*-*n*-propylphenol

trends of overall conversion with the temperature of the liquid hydrocarbon and reactor pressure are the same as those seen for alkanes. However, in the case of reaction time versus product distribution, significantly higher conversions were found at much shorter reaction times with olefins than with alkanes. This is a result of the higher reactivity and faster rate of reaction between the $O(^3P)$ atoms and the hydrogen bound to the unsaturated carbons. Because of the change in chemistry, intermediate epoxide products are generated before the alcohols or ketones are formed. When the results for 1-dodecene are examined the epoxide and aldehyde products dominate for short reaction times. However, when the reactions are allowed to proceed, these compounds further oxidize into alcohol and ketone products, which dominate the product distribution for long reaction times [41.98]. From a commercial viability standpoint, comparison of the product distributions found for *n*-dodecane and 1-dodecene are significant, wherein if reactions are allowed to proceed for long periods with these differing starting materials the same products can be generated because oxidation beyond the ketone does not appear to be favored. This suggests that under certain conditions the same product distributions can be achieved for a mixture of an alkane and alkene of the same carbon number, a result which could prove important due to the difficulty of separating such chemically similar components from a mixture.

When various branched cyclic hydrocarbons were investigated it was found that the predominant products resulted from $O(^3P)$ reactions with the branched carbon in the ring, Fig. 41.6 [41.142]. In contrast, when branched aromatics were examined, the dominant products were a result of alcohol addition to an unbranched carbon in the conjugated ring [41.160], Fig. 41.7. With this information, combined with data from the oxidation of other more complex branched hydrocarbon species, as well as mixtures, it is possible to rank the reactivity of $O(^3P)$ with the various types of hydrocarbons

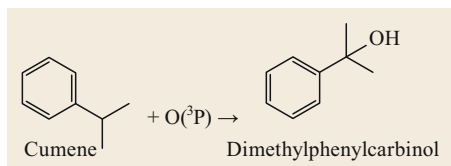
in the following manner: olefins are the most reactive, followed by branched alkanes, then normal alkanes, aromatics, and finally naphthenes [41.143].

Other work conducted with a different type of oxygen plasma reactor system (i.e., dielectric barrier discharge, DBD) illustrates the reactivity trends of various hydrocarbons with $O(^3P)$ in an alternate manner [41.145]. In this work, oxygen saturated with various hydrocarbons (*n*-hexane, cyclohexane, cyclohexene, and cumene) flowed through a dielectric barrier discharge reactor. The following trend in energy yield (moles of functionalized products generated/mean discharge energy) for conversion of these species was found: cyclohexene (3.64×10^{-7} mol/J) > cumene (2.77×10^{-7} mol/J) > cyclohexane (1.99×10^{-7} mol/J) > *n*-hexane (1.09×10^{-7} mol/J). When the major products for each hydrocarbon are compared with these energy yields, shown in Table 41.1, similar trends for the reactivity of $O(^3P)$ with various types of hydrocarbons can be seen for the DBD reactor system as was found with the system shown in Fig. 41.2.

The high energy yield for cyclohexene with the DBD system can be attributed to unsaturated hydrocarbons having the highest reactivity with $O(^3P)$, in that the dominant product was a result of oxidation of the double bond in the ring structure. The major product from cumene was dimethylphenylcarbinol, a result of oxidation of the tertiary carbon of the branch off the aromatic ring, Fig. 41.8. Therefore, the high energy yield for cumene can be attributed to the high reactivity of $O(^3P)$ with the tertiary carbon of branched alkanes. Following suit, the oxidation of cyclohexane was less energy efficient due to it being an unbranched naphthene, which

Table 41.1 Product distribution and energy yields for oxidation of hydrocarbons in DBD with oxygen. G is the energy consumption for the conversion of the starting hydrogen. Note: G is the inverse of energy yield (after [41.145])

Compound	G (kWh kg ⁻¹)	Products	Proportion (wt %)
Hexane	29.14	Hexanal	22.06
		Hexanone-3, hexanone-2	21.45
		Hexanol-3	27.49
		Hexanol-2	19.90
		Hexanol-1	7.74
		Other	1.34
		Cyclohexane	16.57
		Cyclohexanone	47.66
		Other	0.23
Cyclohexene	9.29	Epoxy cyclohexane	61.87
		Cyclohexanone	12.46
		Cyclohexen-2-ol-1	10.15
		Cyclohexen-2-one-1	7.40
		Cyclopentylmethanal	4.81
		Bicyclohexenyl	2.17
		Other	1.14
		Cumene	8.33
		Acetophenone	21.07
		Other	13.53

**Fig. 41.8** Oxidation of cumene to dimethylphenylcarbinol

contains only the less reactive, secondary carbons. It is interesting to note that the product distribution was significantly narrowed in the case of cyclohexane when compared to the other hydrocarbons investigated in this study. With cyclohexane, the distribution was narrowed to only two major products. This displays a unique quality of unbranched cyclic hydrocarbons, where all the carbons of the molecule are chemically indistinguishable and attack on any one of them would result in the same product.

On the basis of the results from the previously discussed work, one would expect the energy yield for *n*-hexane to be equal or greater than cyclohexane. However, the energy yield for the functionalization of *n*-hexane was almost half of what was found for cyclohexane when both molecules were studied in the same DBD reactor system. A possible explanation for this difference is oxidation of the primary carbon of the *n*-hexane molecule did not occur in the low-pressure oxygen system described in Fig. 41.2, which is likely due to its higher bond dissociation energy. However, in the experiments performed with the DBD reactor, hexanal was one of the predominant products. While it is

still unclear why oxidation of the primary carbon occurred in one system and not the other, the higher bond dissociation energy of the primary carbon is a likely explanation for the lower energy yield.

While the reactivity trend in the DBD system is mostly in line with that of the low-pressure oxygen system, it should be noted that the energy yields for total conversion with the DBD reactor are approximately an order of magnitude higher. One major difference between the two systems that could be attributed to this is the fact that the hydrocarbon was vaporized into the oxygen gas feed in the DBD reactor in low concentration (≈ 10 ppm), while a liquid hydrocarbon was used in the low-pressure oxygen system. The difference in discharge power and operating pressure are other possible explanations. Lower discharge power has been shown to result in higher energy yields in other plasma systems [41.176]. Discharge power for the DBD system was 10.6 W, whereas the discharge power for the low-pressure oxygen plasma system was 29 W. Additionally, an interesting advancement in the DBD reactor system discussed above should be noted, where it was shown that the energy yield for cyclohexane and *n*-hexane could be significantly increased (1.99×10^{-7} mol/J $\rightarrow 4.03 \times 10^{-7}$ mol/J for cyclohexane and 1.09×10^{-7} mol/J $\rightarrow 1.51 \times 10^{-7}$ mol/J for *n*-hexane) with the addition of a condensed phase of the liquid hydrocarbon [41.150]. As previously discussed, this liquid phase acts as an absorbent to collect the generated products, protecting them from the gas phase discharge.

Table 41.2 Properties of LCGO before and after treatment with oxygen plasma (after [41.143])

Property	Original	Original treated −40 °C, 120 min	Simulated	Simulated treated −90 °C, 60 min
Alkanes (vol.%)	62.1	73.9	61.4	73.9
Aromatics (vol.%)	34.8	26.1	34.1	26.1
Olefins (vol.%)	3.1	0.0	4.5	0.0
Carbonyl index (%) ^a	0.0	6.0	0.0	2.4
Alcohols and epoxide index (%) ^a	0.0	4.4	0.0	6.5

^a Calculated from NMR spectra

In order to demonstrate the potential commercial application of these oxygen–hydrocarbon plasma systems, actual and simulated mixtures of LCGO (light cycle gas oil) were prepared and treated with the low-pressure oxygen plasma reactor system. An assay of the mixtures both pre- and post-treatment can be found in Table 41.2 [41.143]. This table shows that the olefins in the mixtures were completely converted in both plasma-

treated samples, a result which is attributed to their high reactivity. In contrast, while there were no alcohols or carbonyl (ketone) compounds in the untreated mixtures, treatment with plasma demonstrated significant oxygenation of both samples. It should also be noted that the percent volume of alkanes increased in the samples after treatment while that of the aromatics decreased.

41.10 Functionalization of Liquid Hydrocarbons with Water Plasmas

While significant work has been performed to investigate the use of oxygen plasmas for the functionalization of hydrocarbons, the use of radicals produced from water has been limited primarily to pollution control where the objective is more complete oxidation [41.76]. Only a limited number of studies have explored the high reactivity of the radicals produced when water is introduced into a plasma discharge (reactions (41.3) and (41.4)) in order to functionalize the organic molecules to produce partially oxidized products. Of these studies, one subjects vaporized water molecules to a low-pressure plasma discharge to generate reactive species and utilized a system almost identical to that shown in Fig. 41.2 [41.175], while a second system utilized a plasma discharge in direct contact with liquid water to generate the reactive radical species [41.109]. In addition to work already cited previously on methane conversion in humid gases, other work involved the functionalization of methane with a pulsed corona discharge using oxygen gas, water vapor and discharge over a liquid film of water [41.141].

In the study utilizing low-pressure water vapor, it was shown with emission spectroscopy that the relative abundance of active species in the plasma was significantly affected by the flow rate of the water vapor, Fig. 41.9 [41.175]. It was shown that some reaction selectivity can be achieved by exploiting this relationship through the fact that $\cdot\text{H}$ radicals would hydrogenate an olefin while O and $\cdot\text{OH}$ would lead to oxidation. To explore this, cyclohexene was utilized to

test if the reaction conditions with various water vapor flow rates favor either oxidation or hydrogenation. It was found that at low water vapor flow rates hydrogenation dominates, thus cyclohexane was found to be the predominant product generated (50.94%), a result

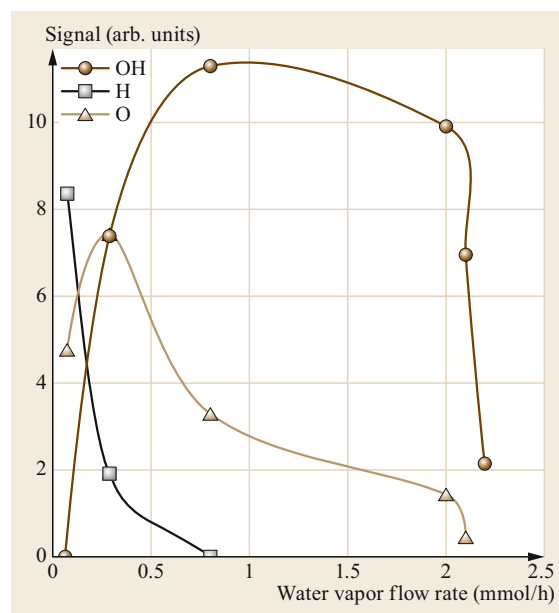


Fig. 41.9 Relative abundance of active species in water vapor plasma. Reprinted with permission from [41.175]. Copyright (2002) American Chemical Society

which coincides with the high abundance of $\cdot\text{H}$ radicals found under these conditions. In contrast, at higher water vapor flow rates oxidation dominated, shifting the product distribution towards ketone and alcohol products. At a discharge power of 100 W, the energy yield for the conversion of cyclohexene with this system was found to be 1.89×10^{-9} mol/J when hydrogenation dominated and 1.62×10^{-9} mol/J when oxidation dominated [41.175].

In a study utilizing plasma directly impinging on a liquid water surface, the functionalization of *n*-hexane and cyclohexane was investigated [41.109]. Here, the hydrocarbons were vaporized at low concentration (approximately 10 ppm) into the gas phase. This low concentration was essential to avoid fragmentation and polymerization of the hydrocarbon. In this system, the liquid water acted not only as a source of radical species but also as a sink to collect the functionalized products. The product distributions in this study are similar to those found for the oxygen plasmas previously discussed [41.150]. For the case of *n*-hexane, the major product identified were 3-hexanol (26%), 2-hexanol (21%), 3-hexanone (17%), 2-hexanone (17%), 1-hexanol (11%), and hexanal (8%). For cyclohexane the major products found were cyclohexanone (47%), cyclohexene (20%), cyclohexanol (19%), hexanal (11%), and 2-cyclohexenone (2%).

When the distribution of products generated from the oxidation of *n*-hexane in this system is examined, the radical species appear to preferentially attack

the C-2 and C-3 carbons of the *n*-hexane molecule. This is indicated by the lower ratios of 1-hexanol and hexanal in comparison to the ketones and secondary alcohols, and these results are consistent with those in the previous study with oxygen plasmas. When the distribution of the products generated from the oxidation of cyclohexane is examined, the product distribution is significantly narrowed when compared to the oxidation of *n*-hexane, as evident from the large portion of cyclohexanone, 47%, found relative to the other products. The fact that there is no distinction between carbons in the cyclohexane molecule again leads to the increase in selectivity. Detailed reaction pathways for this system using both density functional theory and experiments have also been reported [41.177].

The energy yield for products generated from *n*-hexane in this study was found to be 8.6×10^{-9} and 9.0×10^{-9} mol/J for the products of cyclohexane. These values are approximately an order of magnitude lower than those found for the conversion of *n*-hexane and cyclohexane by oxygen plasma in the DBD system previously discussed [41.150]. However, it should be noted that this does not represent the total energy yield for all generated products, because hydrogen peroxide was also produced with an energy yield of 0.54 mol/kWh (1.5×10^{-7} mol/J). Therefore, it may be possible to significantly increase the energy yield for the oxygenated products in this system by capitalizing on the unutilized hydroxyl radicals which generate the hydrogen peroxide.

41.11 Conclusions and Future Trends

The main factors which limit the commercial viability of functionalizing hydrocarbons with plasma discharge are percent conversion, energy yield, and product distribution. It has been demonstrated that for a given experimental apparatus, yield and selectivity for a particular compound can be optimized by varying parameters such as pressure, discharge power, and reaction time. However, the structure of the starting material itself also plays a large role in these factors as well as the resulting distribution of products. One of the major complicating factors in assessing the viability of these processes is that there are many different plasma reactor configurations as well as resulting plasma properties which can be employed to study these processes. This makes drawing general conclusions for various systems difficult to formulate.

In order to develop a more complete understanding of which factors dominate these plasma systems, more data is needed for various experimental condi-

tions in a single reactor system. Studies which include variation in the oxygen–water vapor content to determine differences in oxidation while utilizing various radicals are needed. In addition, because there are numerous reactor configurations available to study plasma processes it is necessary to report more detailed information on the various plasma properties of these systems such as electron density, gas temperature, and electron energy to allow for more relevant comparison.

Nonetheless, these systems show particular promise in improving the quality of mixtures of fuel oil or gas by oxygenation. A one-step plasma oxidation process may provide similar results as the current commercially practiced oxygenation method where oxygenate compounds are separately added to these fuels in order to improve performance and reduce exhaust emissions. Because olefins have been shown to be the most reactive chemical species in these plasma processes, mixtures

with high concentrations of these molecules would be particularly suited to this method.

Acknowledgments. This work was partially supported by the National Science Foundation grant CBET

1236225 and Florida State University. We would also like to thank Prof. Igor Alabugin and Mr. Stefan Bresch for collaboration on studies dealing with electrical discharges and hexane and Prof. Sam Hsu for discussion and encouragement to prepare this chapter.

References

- 41.1 J.A. Labinger, J.E. Bercaw: Understanding and exploiting C–H bond activation, *Nature* **417**(6888), 507–514 (2002)
- 41.2 C.G. Jia, T. Kitamura, Y. Fujiwara: Catalytic functionalization of arenes and alkanes via C–H bond activation, *Acc. Chem. Res.* **34**(8), 633–639 (2001)
- 41.3 G. Suss-Fink, L. Gonzalez, G.B. Shul'pin: Alkane oxidation with hydrogen peroxide catalyzed homogeneously by vanadium-containing polyphosphomolybdates, *Appl. Catal. A-Gen.* **217**(1/2), 111–117 (2001)
- 41.4 Y.N. Kozlov, L. Gonzalez-Cuervo, G. Suss-Fink, G.B. Shul'pin: The kinetics and mechanism of cyclohexane oxygenation by hydrogen peroxide catalyzed by a binuclear iron complex, *Russ. J. Phys. Chem.* **77**(4), 575–579 (2003)
- 41.5 G.B. Shul'pin, C.C. Golfeto, G. Suss-Fink, L.S. Shul'pina, D. Mandelli: Alkane oxygenation with H_2O_2 catalysed by $FeCl_3$ and 2,2'-bipyridine, *Tetrahedron Lett.* **46**(27), 4563–4567 (2005)
- 41.6 M. Jannini, L.S. Shul'pina, U. Schuchardt, G.B. Shul'pin: Hydrogen peroxide oxidation of alkanes catalyzed by the vanadate ion-pyrazine-2-carboxylic acid system, *Pet. Chem.* **45**(6), 413–418 (2005)
- 41.7 D. Mandelli, A.C.N. do Amaral, Y.N. Kozlov, L.S. Shul'pina, A.J. Bonon, W.A. Carvalho, G.B. Shul'pin: Hydrogen peroxide oxygenation of saturated and unsaturated hydrocarbons catalyzed by montmorillonite or aluminum oxide, *Catal. Lett.* **132**(1/2), 235–243 (2009)
- 41.8 E.W. Wilson, W.A. Hamilton, H.R. Kennington, B. Evans, N.W. Scott, W.B. DeMore: Measurement and estimation of rate constants for the reactions of hydroxyl radical with several alkanes and cycloalkanes, *J. Phys. Chem. A* **110**(10), 3593–3604 (2006)
- 41.9 A. Monod, J.F. Doussin: Structure-activity relationship for the estimation of OH-oxidation rate constants of aliphatic organic compounds in the aqueous phase: Alkanes, alcohols, organic acids and bases, *Atmospheric Environ.* **42**(33), 7611–7622 (2008)
- 41.10 R. Sivaramakrishnan, J.V. Michael: Rate constants for OH with selected large alkanes: Shock-tube measurements and an improved group scheme, *J. Phys. Chem. A* **113**(17), 5047–5060 (2009)
- 41.11 M.M. Sprengnether, K.L. Demerjian, T.J. Dransfield, J.S. Clarke, J.G. Anderson, N.M. Donahue: Rate constants of nine C6–C9 alkanes with OH from 230 to 379 K: Chemical tracers for OH, *J. Phys. Chem. A* **113**(17), 5030–5038 (2009)
- 41.12 J.N. Baptist, R.K. Gholson, M.J. Coon: Hydrocarbon oxidation by a bacterial enzyme system. 1. Products of octane oxidation, *Biochim. Biophys. Acta* **69**(1), 40 (1963)
- 41.13 P. Battioni, J.P. Renaud, J.F. Bartoli, M. Reinaartiles, M. Fort, D. Mansuy: Monooxygenase-like oxidation of hydrocarbons by H_2O_2 catalyzed by manganese porphyrins and imidazole – Selection of the best catalytic system and nature of the active oxygen species, *J. Am. Chem. Soc.* **110**(25), 8462–8470 (1988)
- 41.14 M.G. Clerici: Oxidation of saturated-hydrocarbons with hydrogen-peroxide catalyzed by titanium silicalite, *Appl. Catal.* **68**(1/2), 249–261 (1991)
- 41.15 R.A. Periana, G. Bhalla, W.J. Tenn, K.J.H. Young, X.Y. Liu, O. Mironov, C.J. Jones, V.R. Ziatdinov: Perspectives on some challenges and approaches for developing the next generation of selective, low temperature, oxidation catalysts for alkane hydroxylation based on the CH activation reaction, *J. Mol. Catal. a* **220**(1), 7–25 (2004)
- 41.16 H. Suhr: Organic syntheses in plasma of glow discharges and their preparative application, *Angew. Chem. Int. Ed. Engl.* **11**(9), 781 (1972)
- 41.17 H. Suhr: Applications of nonequilibrium plasmas to organic chemistry. In: *Techniques and Applications of Plasma Chemistry*, ed. by J. Hollahan, A. Bell (Wiley, New York 1974) pp. 57–111
- 41.18 H. Suhr: Organic syntheses under plasma conditions, *Pure Appl. Chem.* **39**(3), 395–414 (1974)
- 41.19 M.R. Wertheimer: Plasma processing and polymers: A personal perspective, *Plasma Chem. Plasma Process.* **34**(3), 363–376 (2014)
- 41.20 E. Briner, E. Durand: Action of the electric spark on a low temperature nitrogen-oxygen mixture, *C. r. hebd. séances Acad. Sci.* **145**, 248–250 (1907)
- 41.21 E. Briner, E. Mettler: Formation of ammonia gas from its elements under the influence of electric sparks: Influence of power, *C. r. hebd. séances Acad. Sci.* **144**, 694–697 (1907)
- 41.22 E. Briner, A. Baerfuss: Contribution to the study of the formation of ammonia by means of electric discharge, *Helv. Chim. Acta* **2**, 95–100 (1919)
- 41.23 E. Briner, J. Desbaillets, J.P. Jacob: Research on the chemical effect of electrical discharges. XVII. Production of acetylene in mixtures of methane and hydrogen by electric arcs at varying frequencies, *Helv. Chim. Acta* **21**, 1570–1578 (1938)
- 41.24 E. Briner, A. Rivier: A: Studies on the chemical action of electrical discharge I. Influence of the

- nature of electrodes on the production of nitrogen oxide in the electric arc, *Helv. Chim. Acta* **12**, 881–893 (1929)
- 41.25 E. Briner, J. Corbaz, C. Wakker: Research on the chemical activity of electric discharges V. The influence of the type of electrode on the production of nitrogen oxide in the electrical arc, *Helv. Chim. Acta* **14**, 1307–1314 (1931)
- 41.26 E. Briner, B. Siegrist, H. Paillard: Research on the chemical effect of electric discharges XI The production of nitrogen oxide by an electric arc at high flowing frequency in nitrogen–oxygen mixtures in depression, *Helv. Chim. Acta* **19**, 1074–1079 (1936)
- 41.27 E. Briner, C.H. Wakker, H. Paillard, G. Carrisson: Research on the chemical activity of electric discharge IX Influence exerted on production in nitrogen oxide in industrial ovens by the addition of metal alkali earth–alkali electrodes, *Helv. Chim. Acta* **19**, 308–320 (1936)
- 41.28 B. Siegrist, C.H. Wakker, E. Briner: Research on the chemical activity of electric discharge VIII Production of nitrogen oxide by electric arc at different frequencies, *Helv. Chim. Acta* **19**, 287–308 (1936)
- 41.29 C.H. Wakker, E. Briner: Research on the chemical activity of electric discharges X Effect exercised on production yield of nitrogen oxide by increasing the frequency associated with the addition of lithium to electrodes and enriching the air in oxygen mix, *Helv. Chim. Acta* **19**, 320–322 (1936)
- 41.30 E. Briner, B. Siegrist, B. Susz: Researches on the chemical action of the electrical discharges. XIII. Note on the spectroscopic examination of the nitrogen–oxygen mixture (air) subjected to the action of the electric arc at different frequencies, *Helv. Chim. Acta* **21**, 134–137 (1938)
- 41.31 E. Briner, J. Desbaillets, F. Richard, H. Paillard: Research on the chemical action of electric discharges XVIII Production of nitrogen oxide thanks to the high frequency arc – Corrections and new results, *Helv. Chim. Acta* **22**, 1096–1107 (1939)
- 41.32 E. Briner, G. Papazian: Researches on the chemical action of electric discharges XXIV Entry on the formation of nitrogen oxides by effluvation of the industrial oxygen, *Helv. Chim. Acta* **24**, 919–921 (1941)
- 41.33 W.J. Cotton: Electric activation of chemical reactions production of nitrogen oxides. 2. Chemical reaction frequencies, *Trans. Electrochem. Soc.* **91**, 419–436 (1947)
- 41.34 E. Briner, A. Baerfuss: On nitrogen fixation in the form of hydrocyanic acid by means of electric arc, *Helv. Chim. Acta* **2**, 663–666 (1919)
- 41.35 E. Briner, J. Desbaillets, H. Paillard: Researches on the chemical action of the electrical discharge. XII. Production of the cyanhydric acid by the electric arc at different frequencies, *Helv. Chim. Acta* **21**, 115–133 (1938)
- 41.36 E. Briner, J. Desbaillets, B. Susz: Researches on the chemical action for electrical discharges. XIV. Note on the examination of the mixtures of methane–nitrogen–hydrogen subjected to the electric arc at different frequencies, *Helv. Chim. Acta* **21**, 137–140 (1938)
- 41.37 E. Briner, J. Desbaillets, M. Wertheim: Research on the chemical effects of electrical discharge. XVI The production of cyanhydric acid by the electric arc, at different frequencies, spurting in vapour hydrocarbon–azote–hydrogen mixes, *Helv. Chim. Acta* **21**, 859–862 (1938)
- 41.38 E. Briner, H. Hoefler: Research on the chemical effect of electric discharges. XX. Conditions of the obtaining of raised energetic output in the synthesis of cyanhydric acid by means of an electric arc, *Helv. Chim. Acta* **23**, 1054–1062 (1940)
- 41.39 E. Briner, H. Hoefler: Research on the chemical effect of electrical discharges. XIX. The production of cyanhydric acid and ammoniac by the electrical arc in high and low frequencies sending out in nitrogen–oxide mixtures of carbon hydrogen at ordinary pressure and at low pressure, *Helv. Chim. Acta* **23**, 826–831 (1940)
- 41.40 E. Briner, H. Hoefler: Research on the chemical effect of electrical discharges. XVIII. The production of formic aldehyde by means of the electric arc in high and low frequency, *Helv. Chim. Acta* **23**, 800–806 (1940)
- 41.41 E. Briner, H. Hoefler: Researches on the chemical action of electric discharges. XXV. On the production of cyanhydric acid and of ammoniac by means of high frequency arch gushing out in a gas of distillation of hard coal, *Helv. Chim. Acta* **24**, 1006–1010 (1941)
- 41.42 E. Briner, H. Hoefler: Researches on the chemical action of the electric discharges. XXI. Variation, with the molecular size of treated hydrocarbon, of the yield of production of cyanhydric acid by means of the high frequency arch, *Helv. Chim. Acta* **24**, 188–190 (1941)
- 41.43 E. Briner, H. Hoefler: Research on the chemical reactions of electrical discharges. XXVII. Notice on the production of hydrazine by means of the arc, in high and low frequency, sprouting out in the mixture of hydrogen nitride or ammonia, *Helv. Chim. Acta* **25**, 96–97 (1942)
- 41.44 E. Briner, H. Hoefler: Studies on the chemical effect of electric releases. XXVIII. The effect of the electric arc in high and low frequency on the azote–vapour and water vapour systems of water, *Helv. Chim. Acta* **25**, 530–538 (1942)
- 41.45 B.P. Susz, H. Hoefler, E. Briner: Studies on the chemical effect of electric discharge. XXIX. A note on some characteristics of electric arc spectrum spurting in high and low frequency in a gas mix enclosed in water vapour, azote and oxygen, *Helv. Chim. Acta* **25**, 889–892 (1942)
- 41.46 S.L. Miller: Production of some organic compounds under possible primitive earth conditions, *J. Am. Chem. Soc.* **77**, 2351–2361 (1955)
- 41.47 S.L. Miller: The mechanism of synthesis of amino acids by electric discharges, *Biochim. Biophys. Acta* **23**(3), 480–489 (1957)
- 41.48 J. Oro: Synthesis of organic compounds by electric discharges, *Nature* **197**(487), 862 (1963)

- 41.49 A. Fridman: *Plasma Chemistry* (Cambridge Univ. Press, Cambridge 2008)
- 41.50 H. Kabashima, H. Einaga, S. Futamura: Hydrogen generation from water, methane and methanol with nonthermal plasma, *IEEE Trans. Industry Applications* **39**(2), 340–345 (2003)
- 41.51 X.Z. Liu, C.J. Liu, B. Eliasson: Hydrogen production from methanol using corona discharges, *Chin. Chem. Lett.* **14**(6), 631–633 (2003)
- 41.52 B. Sarmiento, J.J. Brey, I.G. Viera, A.R. Gonzalez-Elipse, J. Cotrino, V.J. Rico: Hydrogen production by reforming of hydrocarbons and alcohols in a dielectric barrier discharge, *J. Power Sources* **169**(1), 140–143 (2007)
- 41.53 R. Burlica, K.Y. Shih, B.R. Locke: Formation of H_2 and H_2O_2 in a water-spray gliding arc nonthermal plasma reactor, *Ind. Eng. Chem. Res.* **49**(14), 6342–6349 (2010)
- 41.54 R. Burlica, K.Y. Shih, B. Hnatiuc, B.R. Locke: Hydrogen generation by pulsed gliding arc discharge plasma with sprays of alcohol solutions, *Ind. Eng. Chem. Res.* **50**(15), 9466–9470 (2011)
- 41.55 M.A. Malik, D. Hughes, A. Malik, S. Xiao, K.H. Schoenbach: Study of the production of hydrogen and light hydrocarbons by spark discharges in diesel, kerosene, gasoline and methane, *Plasma Chem. Plasma Process.* **33**(1), 271–279 (2013)
- 41.56 C. Du, J. Mo, H. Li: Renewable hydrogen production by alcohols reforming using plasma and plasma-catalytic technologies: Challenges and opportunities, *Chem. Rev.* **115**, 1503–1542 (2015)
- 41.57 M.A. Lieberman, A.J. Lichtenberg: *Principles of Plasma Discharges and Materials Processing* (Wiley, New York 1994) p. 572
- 41.58 M. Lieberman, A. Lichtenberg: *Principles of Plasma Discharge and Materials Processing*, 2nd edn. (Wiley, Hoboken 2005)
- 41.59 J.L. Brisset, D. Moussa, A. Doubla, E. Hnatiuc, B. Hnatiuc, G.K. Youbi, J.M. Herry, M. Naitali, M.N. Bellon-Fontaine: Chemical reactivity of discharges and temporal post-discharges in plasma treatment of aqueous media: Examples of gliding discharge treated solutions, *Ind. Eng. Chem. Res.* **47**(16), 5761–5781 (2008)
- 41.60 H. Conrads, M. Schmidt: Plasma generation and plasma sources, *Plasma Sources Sci. Technol.* **9**(4), 441–454 (2000)
- 41.61 B.R. Locke, P. Lukes, J.L. Brisset: Elementary chemical and physical phenomena in electrical discharge plasma in gas-liquid environments and in liquids. In: *Plasma Chemistry and Catalysis in Gases and Liquids*, ed. by V.I. Parvulescu, M.M.P. Lukes (Wiley, Weinheim 2012)
- 41.62 J. Tynan, V.J. Law, P. Ward, A.M. Hynes, J. Cullen, G. Byrne, S. Daniels, D.P. Dowling: Comparison of pilot and industrial scale atmospheric pressure glow discharge systems including a novel electro-acoustic technique for process monitoring, *Plasma Sources Sci. Technol.* **19**(1), 15015 (2009)
- 41.63 J. Friedrich: Mechanisms of plasma polymerization – Reviewed from a chemical point of view, *Plasma Process. Polym.* **8**(9), 783–802 (2011)
- 41.64 S.A. Nair, A.J.M. Pemen, K. Yan, F.M. van Gompel, H.E.M. van Leuken, E.J.M. van Heesch, K.J. Ptasinski, A.A.H. Drinkenburg: Tar removal from biomass-derived fuel gas by pulsed corona discharges, *Fuel Process. Technol.* **84**(1–3), 161–173 (2003)
- 41.65 G.J.J. Winands, K.P. Yan, A.J.M. Pemen, S.A. Nair, Z. Liu, E.J.M. van Heesch: An industrial streamer corona plasma system for gas cleaning, *IEEE Trans. Plasma Sci.* **34**(5), 2426–2433 (2006)
- 41.66 M. Okubo, T. Kuroki, S. Kawasaki, K. Yoshida, T. Yamamoto: Continuous regeneration of ceramic particulate filter in stationary diesel engine by nonthermal-plasma-induced ozone injection, *IEEE Tran. Ind. Appl.* **45**(5), 1568–1574 (2009)
- 41.67 K. Yoshida, T. Yamamoto, T. Kuroki, M. Okubo: Pilot-scale experiment for simultaneous dioxin and NO (x) Removal from garbage incinerator emissions using the pulse corona induced plasma chemical process, *Plasma Chem. Plasma Process.* **29**(5), 373–386 (2009)
- 41.68 H. Fujishima, T. Kuroki, T. Ito, K. Otsuka, T. Yamamoto, K. Yoshida, M. Okubo: Performance characteristics of pilot-scale indirect plasma and chemical system used for the removal of NOx from boiler emission, *IEEE Trans. Ind. Appl.* **46**(5), 1707–1714 (2010)
- 41.69 H. Fujishima, A. Tatsumi, T. Kuroki, A. Tanaka, K. Otsuka, T. Yamamoto, M. Okubo: Improvement in NOx removal performance of the pilot-scale boiler emission control system using an indirect plasma-chemical process, *IEEE Trans. Ind. Appl.* **46**(5), 1722–1729 (2010)
- 41.70 D. Gerrity, B.D. Stanford, R.A. Trenholm, S.A. Snyder: An evaluation of a pilot-scale nonthermal plasma advanced oxidation process for trace organic compound degradation, *Water Res.* **44**(2), 493–504 (2010)
- 41.71 I.R.A.L. Enterprises: Zebra Mussel Control Alternative Plasma Sparker Technology for the Pilot Plant Project, Report to the City of St. Alban and the Wergemnes-Panton Water District (1996)
- 41.72 B. Eliasson, U. Kogelschatz: Basic Data for Modelling of Electrical Discharges in Gases: Oxygen, Ph.D. Thesis (ABB Asea Brown Boveri, Baden 1986), Research Report KLR 86-11C, No. 11
- 41.73 B. Eliasson, U. Kogelschatz: Electron impact dissociation in oxygen, *J. Phys. B.* **19**, 1241–1247 (1986)
- 41.74 B. Eliasson, M. Hirth, U. Kogelschatz: Ozone synthesis from oxygen in dielectric barrier discharges, *J. Phy. D Appl. Phys.* **20**, 1421–1437 (1987)
- 41.75 Y. Kogelschatz, B. Eliasson: Ozone generation and applications. In: *Handbook of Electrostatic Processes*, ed. by J.S. Chang, A.J. Kelly, J.M. Crowley (Marcel Dekker, New York 1995) pp. 581–605
- 41.76 B. Locke, M. Sato, P. Sunka, M. Hoffmann, J. Chang: Electrohydraulic discharge and nonthermal plasma for water treatment, *Ind. Eng. Chem. Res.* **45**(3), 882–905 (2006)
- 41.77 T. Sugai, T. Abe, Y. Minamitani: Improvement of efficiency for decomposition of organic com-

- pounds in water using pulsed streamer discharge in air with water droplets by increasing of residence time. In: *IEEE Pulsed Power Conference* (IEEE, Washington DC 2009) pp. 1053–1057
- 41.78 T. Kobayashi, T. Sugai, T. Handa, Y. Minamitani, T. Nose: The effect of spraying of water droplets and location of water droplets on the water treatment by pulsed discharge in air, *IEEE Trans. Plasma Sci.* **38**(10), 2675–2680 (2010)
- 41.79 T. Suzuki, Y. Minamitani, T. Nose: Investigation of a pulse circuit design and pulse condition for the high energy efficiency on water treatment using pulsed power discharge in a water droplet spray, *IEEE Trans. Dielectr. Electr. Insulation* **18**(4), 1281–1286 (2011)
- 41.80 M.A. Malik, A. Ghaffar, S.A. Malik: Water purification by electrical discharges, *Plasma Sources Sci. Technol.* **10**(1), 82–91 (2001)
- 41.81 M.A. Malik: Water purification by plasmas: Which reactors are most energy efficient?, *Plasma Chem. Plasma Process.* **30**(1), 21–31 (2010)
- 41.82 R. Aris: *Introduction to the Analysis of Chemical Reactors* (Prentice-Hall, New Jersey 1965)
- 41.83 J.D. Thornton: Chemical engineering aspects of chemical synthesis in electrical discharges, *Adv. Chem. Ser.* **80**, 372–389 (1969)
- 41.84 B.R. Locke, S.M. Thagard: Analysis of chemical reactions in gliding-arc reactors with water spray into flowing oxygen, *IEEE Trans. Plasma Sci.* **37**(4), 494–501 (2009)
- 41.85 A.A. Fridman: *Plasma Chemistry* (Cambridge Univ. Press, Cambridge 2008) p. 978
- 41.86 J.D. Thornton: Applications of electrical energy to chemical and physical rate processes, *Rev. Pure Appl. Chem.* **18**, 197 (1968)
- 41.87 B.R. Locke, K.Y. Shih: Review of the methods to form hydrogen peroxide in electrical discharge plasma with liquid water, *Plasma Sources Sci. Technol.* **20**(3), 15 (2011)
- 41.88 J.L. Degarmo, V.N. Parulekar, V. Pinjala: Consider reactive distillation, *Chem. Eng. Prog.* **88**(3), 43–50 (1992)
- 41.89 S. Balakrishna, L.T. Biegler: A unified approach for the simultaneous synthesis of reaction, energy and separation systems, *Ind. Eng. Chem. Res.* **32**(7), 1372–1382 (1993)
- 41.90 A. Nisoli, M.F. Malone, M.F. Doherty: Attainable regions for reaction with separation, *Aiche J.* **43**(2), 374–387 (1997)
- 41.91 R.A. Schmitz, N.R. Amundson: An analysis of chemical reactor stability and control. 5B. 2-phase gas liquid and concentrated liquid-liquid reacting systems in physical equilibrium 2, *Chem. Eng. Sci.* **18**(7), 391–414 (1963)
- 41.92 J.D. Thornton, W.D. Charlton, P.L. Spedding: Hydrazine synthesis in a silent electrical discharge, *Adv. Chem. Ser.* **80**, 165–175 (1969)
- 41.93 R. Sergio, J.D. Thornton: Synthesis of formaldehyde and methanol from methane and water in an electrical discharge 2-phase reactor, *J. Appl. Chem.* **17**(11), 325–328 (1967)
- 41.94 P. Lukes, B.R. Locke, J.L. Brisset: Aqueous-phase chemistry of electrical discharge plasma in water and in gas-liquid environments. In: *Plasma Chemistry and Catalysis in Gases and Liquids*, ed. by V.I. Parvulescu, M.M.P. Lukes (Wiley, Weinheim 2012)
- 41.95 P. Bruggeman, C. Leys: Non-thermal plasmas in and in contact with liquids, *J. Phys. D Appl. Phys.* **42**(053001), 1–28 (2009)
- 41.96 J. Prausnitz, R. Lichtenthaler, E. de Azevedo: *Molecular Thermodynamics of Fluid-Phase Equilibria*, 2nd edn. (Prentice Hall, Englewood Cliffs 1986)
- 41.97 M. Mora, M.C. Garcia, C. Jimenez-Sanchidrian, F.J. Romero-Salguero: Selectivity control in a microwave surface-wave plasma reactor for hydrocarbon conversion, *Plasma Process. Polym.* **8**(8), 709–717 (2011)
- 41.98 G. Gambus, P. Patino, B. Mendez, A. Sifontes, J. Navea, P. Martin, P. Taylor: Oxidation of long chain hydrocarbons by means of low-pressure plasmas, *Energy Fuels* **15**(4), 881–886 (2001)
- 41.99 A.A. Joshi, B.R. Locke, P. Arce, W.C. Finney: Formation of hydroxyl radicals, hydrogen-peroxide and aqueous electrons by pulsed streamer corona discharge in aqueous solution, *J. Hazard. Mater.* **41**(1), 3–30 (1995)
- 41.100 D.R. Grymonpre, A.K. Sharma, W.C. Finney, B.R. Locke: The role of Fenton's reaction in aqueous phase pulsed streamer corona reactors, *Chem. Eng. J.* **82**(1–3), 189–207 (2001)
- 41.101 P. Lukes, A.T. Appleton, B.R. Locke: Hydrogen peroxide and ozone formation in hybrid gas-liquid electrical discharge reactors, *IEEE Trans. Ind. Appl.* **40**(1), 60–67 (2004)
- 41.102 M. Sahni, B. Locke: Quantification of hydroxyl radicals produced in aqueous phase pulsed electrical discharge reactors, *Ind. Eng. Chem. Res.* **45**(17), 5819–5825 (2006)
- 41.103 M. Sahni, B.R. Locke: The effects of reaction conditions on liquid-phase hydroxyl radical production in gas-liquid pulsed-electrical-discharge reactors, *Plasma Process. Polym.* **3**(9), 668–681 (2006)
- 41.104 S. Mededovic, B.R. Locke: Primary chemical reactions in pulsed electrical discharge channels in water, *J. Phys. D* **40**(24), 7734–7746 (2007)
- 41.105 M. Sahni, B. Locke: Quantification of reductive species produced by high voltage electrical discharges in water, *Plasma Process. Polym.* **3**(4/5), 342–354 (2006)
- 41.106 M. Kirkpatrick, B. Locke: Hydrogen, oxygen and hydrogen peroxide formation in aqueous phase pulsed corona electrical discharge, *Ind. Eng. Chem. Res.* **44**(12), 4243–4248 (2005)
- 41.107 Y. Itikawa, N. Mason: Cross sections for electron collisions with water molecules, *J. Phys. Chem. Reference Data* **34**(1), 1–22 (2005)
- 41.108 D.X. Liu, P. Bruggeman, F. Iza, M.Z. Rong, M.G. Kong: Global model of low-temperature atmospheric-pressure $He + H_2O$ plasmas, *Plasma Sources Sci. Technol.* **19**(2), 25018 (2010)

- 41.109 R.J. Wandell, S. Bresch, K. Hsieh, I.V. Alabugin, B.R. Locke: Formation of alcohols and carbonyl compounds from hexane and cyclohexane with water in a liquid film plasma reactor, *IEEE Trans. Plasma Sci.* **42**(5), 1195–1205 (2014)
- 41.110 H. Taghvaei, A. Jahanmiri, M.R. Rahimpour, M.M. Shirazi, N. Hooshmand: Hydrogen production through plasma cracking of hydrocarbons: Effect of carrier gas and hydrocarbon type, *Chem. Eng. J.* **226**, 384–392 (2013)
- 41.111 S.M. Thagard, K. Takashima, A. Mizuno: Electrical discharges in polar organic liquids, *Plasma Process. Polym.* **6**(11), 741–750 (2009)
- 41.112 M.A. Malik, M. Ahmed: Preliminary studies on formation of carbonaceous products by pulsed spark discharges in liquid hydrocarbons, *J. Electrostat.* **66**(11/12), 574–577 (2008)
- 41.113 G. Prieto, M. Okumoto, K. Shimano, K. Takashima, S. Katsura, A. Mizuno: Reforming of heavy oil using nonthermal plasma, *IEEE Trans. Ind. Appl.* **37**(5), 1464–1467 (2001)
- 41.114 G. Prieto, M. Okumoto, K. Takashima, S. Katsura, A. Mizuno, O. Prieto, C.R. Gay: Nonthermal plasma reactors for the production of light hydrocarbon olefins from heavy oil, *Braz. J. Chem. Eng.* **20**(1), 57–61 (2003)
- 41.115 M.R. Khani, S.H.R. Barzoki, M.S. Yaghmaee, S.I. Hosseini, M. Shariat, B. Shokri, A.R. Fakhari, S. Nojavan, H. Tabani, M. Ghaedian: Investigation of cracking by cylindrical dielectric barrier discharge reactor on the n-hexadecane as a model compound, *IEEE Trans. Plasma Sci.* **39**(9), 1807–1813 (2011)
- 41.116 H.D.A. Honorato, R.C. Silva, C.K. Piumbini, C.G. Zucolotto, A.A. de Souza, A.G. Cunha, F.G. Emmerich, V. Lacerda, E.V.R. de Castro, T.J. Bonagamba, J.C.C. Freitas: ¹H low- and high-field NMR study of the effects of plasma treatment on the oil and water fractions in crude heavy oil, *Fuel* **92**(1), 62–68 (2012)
- 41.117 J.L. Hueso, V.J. Rico, J. Cotrino, J.M. Jimenez-Mateos, A.R. Gonzalez-Elipe: Water plasmas for the revalorisation of heavy oils and cokes from petroleum refining, *Environ. Sci. Technol.* **43**(7), 2557–2562 (2009)
- 41.118 C. De Bie, T. Martens, J. van Dijk, S. Paulussen, B. Verheyde, S. Corthals, A. Bogaerts: Dielectric barrier discharges used for the conversion of greenhouse gases: Modeling the plasma chemistry by fluid simulations, *Plasma Sources Sci. Technol.* **20**(2), 24008 (2011)
- 41.119 C. De Bie, B. Verheyde, T. Martens, J. van Dijk, S. Paulussen, A. Bogaerts: Fluid modeling of the conversion of methane into higher hydrocarbons in an atmospheric pressure dielectric barrier discharge, *Plasma Process. Polym.* **8**(11), 1033–1058 (2011)
- 41.120 A. Indarto: A review of direct methane conversion to methanol by dielectric barrier discharge, *IEEE Trans. Dielectr. Electr. Insulation* **15**(4), 1038–1043 (2008)
- 41.121 T. Nozaki, A. Hattori, K. Okazaki: Partial oxidation of methane using a microscale non-equilibrium plasma reactor, *Catal. Today* **98**(4), 607–616 (2004)
- 41.122 T. Nozaki, S. Kado, A. Hattori, K. Okazaki, N. Muto: Micro-plasma technology – Direct methaneto-methanol in extremely confined environment. In: *Natural Gas Conversion VII*, Vol. 147, ed. by X. Bao, Y. Xu (Elsevier B.V., Amsterdam 2004) pp. 505–510
- 41.123 A. Agiral, T. Nozaki, M. Nakase, S. Yuzawa, K. Okazaki, J.G.E. Gardeniers: Gas-to-liquids process using multi-phase flow, non-thermal plasma microreactor, *Chem. Eng. J.* **167**(2/3), 560–566 (2011)
- 41.124 T. Nozaki, A. Agiral, S. Yuzawa, J. Gardeniers, K. Okazaki: A single step methane conversion into synthetic fuels using microplasma reactor, *Chem. Eng. J.* **166**(1), 288–293 (2011)
- 41.125 T. Nozaki, V. Goujard, S. Yuzawa, S. Moriyama, A. Agiral, K. Okazaki: Selective conversion of methane to synthetic fuels using dielectric barrier discharge contacting liquid film, *J. Phys. D* **44**(27), 274010 (2011)
- 41.126 T. Nozaki, K. Okazaki: Innovative methane conversion technology using atmospheric pressure non-thermal plasma, *J. Jpn. Petroleum Inst.* **54**(3), 146–158 (2011)
- 41.127 V. Goujard, T. Nozaki, S. Yuzawa, A. Agiral, K. Okazaki: Plasma-assisted partial oxidation of methane at low temperatures: Numerical analysis of gas-phase chemical mechanism, *J. Phys. D–Appl. Phys.* **44**(27), 274011 (2011)
- 41.128 J.D. Thornton, R. Sergio: Synthesis of formaldehyde from methane in electrical discharges, *Nature* **213**(5076), 590–591 (1967)
- 41.129 K. Okazaki, T. Kishida, K. Ogawa, T. Nozaki: Direct conversion from methane to methanol for high efficiency energy system with exergy regeneration, *Energy Convers. Manag.* **43**(9–12), 1459–1468 (2002)
- 41.130 K. Hijikata, K. Ogawa, N. Miyakawa: Methanol conversion from methane and water vapor by electric discharge (effect of electric discharge process on methane conversion), *Heat Trans. Asian Res.* **28**, 404–417 (1999)
- 41.131 B.R. Locke, K.Y. Shih: Review of the methods to form hydrogen peroxide in electrical discharge plasma with liquid water, *Plasma Sources Sci. Technol.* **20**, 34006 (2011)
- 41.132 R. Burlica, K. Shih, B. Locke: Formation of H_2 and H_2O_2 in a water-spray gliding arc nonthermal plasma reactor, *Ind. Eng. Chem. Res.* **49**(14), 6342–6349 (2010)
- 41.133 R. Burlica, K.Y. Shih, B.R. Locke: Formation of H_2 and H_2O_2 in a water-spray gliding arc nonthermal plasma reactor, *Ind. Eng. Chem. Res.* **52**(37), 13516–13516 (2013)
- 41.134 G. Bredig, A. Koenig: Electrical synthesis of hydrazine, *Naturwissenschaften* **16**, 493–493 (1928)
- 41.135 J.C. Devins, M. Burton: Formation of hydrazine in electric discharge decomposition of ammonia, *J. Am. Chem. Soc.* **76**(10), 2618–2626 (1954)

- 41.136 J.D. Thornton, W.D. Charlton, P.L. Spedding: Hydrazine synthesis in a silent electrical discharge, *Adv. Chem. Ser.* **80**, 165 (1969)
- 41.137 A. Hickling, G.R. Newns: The synthesis of hydrazine by glow discharge electrolysis of liquid ammonia, *Proc. Chem. Soc.* **11**, 368–369 (1959)
- 41.138 B.A. Brown, C.R. Howarth, J.D. Thornton: The synthesis of hydrazine from ammonium using pulsed electrical discharge technique. In: *Engineering, Chemistry and Use of Plasma Reactors*, Vol. 67, ed. by J. Flinn (American Institute of Chemical Engineers, New York 1971) pp. 28–36
- 41.139 C.L. Rasmussen, P. Glarborg: Direct partial oxidation of natural gas to liquid chemicals: Chemical kinetic modeling and global optimization, *Ind. Eng. Chem. Res.* **47**(17), 6579–6588 (2008)
- 41.140 H.D. Gesser, N.R. Hunter, C.B. Prakash: The direct conversion of methane to methanol by controlled oxidation, *Chem. Rev.* **85**(4), 235–244 (1985)
- 41.141 W. Hoeben, W. Boekhoven, F. Beckers, E.J.M. van Heesch, A.J.M. Pemen: Partial oxidation of methane by pulsed corona discharges, *J. Phys. D* **47**(35), 10 (2014)
- 41.142 P. Patino, M. Mendez, J. Pastran, G. Gambus, J. Navea, O. Escobar, A. Castro: Oxidation of cycloalkanes and diesel fuels by means of oxygen low pressure plasmas, *Energy Fuels* **16**(6), 1470–1475 (2002)
- 41.143 P. Patino, A. Mejia, P. Rodriguez, B. Mendez: Upgrading of diesel fuels and mixtures of hydrocarbons by means of oxygen low pressure plasmas: A comparative study, *Fuel* **82**(13), 1613–1619 (2003)
- 41.144 M. Tezuka, T. Yajima: Oxidation of aromatic hydrocarbons with oxygen in a radiofrequency plasma, *Plasma Chem. Plasma Process.* **16**(3), 329–340 (1996)
- 41.145 S.V. Kudryashov, G.S. Shchegoleva, E.E. Sirotkina, A.Y. Ryabov: Oxidation of hydrocarbons in a barrier discharge reactor, *High Energy Chem.* **34**(2), 112–115 (2000)
- 41.146 S.V. Kudryashov, A.Y. Ryabov, E.E. Sirotkina, G.S. Shchegoleva: Transformations of n-hexane and cyclohexane by barrier discharge processing in inert gases, *High Energy Chem.* **35**(2), 120–122 (2001)
- 41.147 S.V. Kudryashov, G.S. Shchegoleva, A.Y. Ryabov, E.E. Sirotkina: Simulation of the kinetics of cyclohexane oxidation in a barrier discharge reactor, *High Energy Chem.* **36**(5), 349–353 (2002)
- 41.148 S.V. Kudryashov, A.Y. Ryabov, E.E. Sirotkina, G.S. Shchegoleva: Oxidation of cyclohexene in the presence of alkanes in a barrier discharge plasma, *High Energy Chem.* **37**(3), 184–186 (2003)
- 41.149 S.V. Kudryashov, A.Y. Ryabov, E.E. Sirotkina, G.S. Shchegoleva: Oxidation of propylene and isobutylene in a reactor with barrier discharge, *Russ. J. Appl. Chem.* **77**(11), 1904–1906 (2004)
- 41.150 S.V. Kudryashov, A.Y. Ryabov, G.S. Shchegoleva, E.E. Sirotkina, L.M. Velichkina: Oxidation of hydrocarbons in a bubble plasma reactor, *Pet. Chem.* **44**(6), 438–440 (2004)
- 41.151 S.V. Kudryashov, A.Y. Ryabov, G.S. Shchegoleva, V.Y. Savinykh, A.I. Suslov: Oxidative conversion of cyclohexane in discharge plasma maintained with different high-voltage power sources, *High Energy Chem.* **42**(1), 51–55 (2008)
- 41.152 S.A. Perevezentsev, S.V. Kudryashov, S.E. Boganov, A.Y. Ryabov, G.S. Shchegoleva: Transformations of benzene–argon mixture in barrier discharge, *High Energy Chem.* **45**(1), 62–65 (2011)
- 41.153 S.V. Kudryashov, A.N. Ochered'ko, G.S. Shchegoleva, A.Y. Ryabov: Oxidation of propylene with air in barrier discharge in the presence of octane, *Russ. J. Appl. Chem.* **84**(8), 1404–1407 (2011)
- 41.154 S.V. Kudryashov, S.A. Perevezentsev, A.Y. Ryabov, G.S. Shchegoleva, E.E. Sirotkin: Study of the products of benzene transformation in the presence of argon, hydrogen and propane–butane mixture in barrier discharge, *Pet. Chem.* **52**(1), 60–64 (2012)
- 41.155 D.W. Lee, J.H. Lee, B.H. Chun, K.Y. Lee: The characteristics of direct hydroxylation of benzene to phenol with molecular oxygen enhanced by pulse DC corona at atmospheric pressure, *Plasma Chem. Plasma Process.* **23**(3), 519–539 (2003)
- 41.156 H. Sekiguchi, M. Ando: Direct hydroxylation of benzene using micro plasma reactor, *Kagaku Kagaku Ronbunshu* **30**(2), 183–185 (2004)
- 41.157 M. Tezuka, T. Yajima: Oxidation of cycloalkanes in a radiofrequency plasma, *Bull. Chem. Soc. Japan* **64**(3), 1063–1065 (1991)
- 41.158 P. Patino, F.E. Hernandez, S. Rondon: Reactions of O(P–3) with secondary C–H bonds of saturated hydrocarbons in nonequilibrium plasmas, *Plasma Chem. Plasma Process.* **15**(2), 159–171 (1995)
- 41.159 P. Patino, N. Sanchez, H. Suhr, N. Hernandez: Reactions of nonequilibrium oxygen plasmas with liquid olefins, *Plasma Chem. Plasma Process.* **19**(2), 241–254 (1999)
- 41.160 P. Patino, M. Roper, D. Iacocca: Reactions of O(P–3) with aromatic compounds in the liquid phase, *Plasma Chem. Plasma Process.* **16**(4), 563–575 (1996)
- 41.161 R.P. Joshi, S.M. Thagard: Streamer-like electrical discharges in water: Part II. Environmental applications, *Plasma Chem. Plasma Process.* **33**(1), 17–49 (2013)
- 41.162 P. Bruggeman, B.R. Locke: Assessment of potential applications of plasma with liquid water. In: *Low Temperature Plasma Technology: Methods and Applications*, ed. by P.X.L. Chu (CRC, Boca Raton 2013)
- 41.163 P. Lukes, J.L. Brisset, B.R. Locke: Biological effects of electrical discharge plasma in water and in gas–liquid environments. In: *Plasma Chemistry and Catalysis in Gases and Liquids*, ed. by V.I. Parvulescu, M.M.P. Lukes (Wiley, Weinheim 2012)
- 41.164 T.D. Thornton, P.E. Savage: Phenol oxidation in supercritical water, *J. Supercrit. Fluids* **3**, 240–248 (1990)
- 41.165 T.D. Thornton, D. LaDue, P.E. Savage: Phenol oxidation in supercritical water: Formation of dibenzofuran, dibenzo-p-dioxid and related com-

Important Conversion Factors in Petroleum Technology

Table 1 Oil volume and mass

To convert Into				
	Tonnes (metric)	Kiloliters	Barrels	US gallons	Tonnes/yr ^b
Tonnes (metric)	1	1/SG ^a	6.2898/SG ^a	264.17/SG ^a	–
Kiloliters	1 SG ^a	1	6.2898	264.17	–
Petroleum barrels	0.159 SG ^a	0.159	1	42	–
US gallons	0.0038 SG ^a	0.0038	0.0238	1	–
Barrels/day ^b	–	–	–	–	58.03 SG ^a

^a SG = specific gravity of the oil @ 15.55 °C

^b For converting between mass and volume, some sources use an assume or average density. That can be misleading and is not best practice

Table 2 Flow/consumption ratios

To convert Into	Multiply by
Standard cubic feet per barrel (scf/bbl)	Normal cubic meters per cubic meter (Nm ³ /m ³)	0.178

Table 3 Geothermal gradients

To convert Into	Multiply by
°C/100 m	°F/100 ft	0.549

Table 4 Density

To convert Into	Use the formula
API gravity	Specific gravity @ 60 °F (sp.gr.)	API gravity = (141.5/sp.gr.) – 131.5
Specific gravity @ 60 °F (sp.gr.)	API gravity	sp.gr. = 141.5/(API gravity + 131.5)

Table 5 Volume

To convert Into	Multiply by
Standard cubic feet (scf) of gas @ 60 °F and 14.73 psi	Standard cubic meters (Sm ³) @ 15 °C and 101.325 kPa	0.0283058
Standard cubic meters (Scm) of gas @ 15 °C and 1.0325 kPa	Normal cubic meters (Nm ³) @ 0 °C and 101.325 kPa	1.0549000

In considering industrial gases, especially when negotiating contracts, it is crucial to know the difference between *standard* and *normal*.

Table 6 Temperature

To convert Into			
	°C	°F	K	R
	Use the Formula			
Celsius (°C)	–	Multiply by 1.8, then add 32	Add 273.15	Convert to °F, then add 459.67
Fahrenheit (°F)	Subtract 32, then divide by 1.8	–	Convert to °C, add 273.15	Add 459.67
Kelvin (K)	Subtract 273.15	Subtract 273.15, then convert to °F	–	Add 273.15, then convert to °F, then add 459.67
Rankine (R)	Subtract 459.67, then convert to °C	Subtract 459.67	Subtract 459.67, then convert to °C, then add 273.15	–

Table 7 Temperature difference

To convert Into	Multiply by
°C	°F	1.8

Table 8 Pressure

To convert Into					
	bar	atm	MPa	psi	Torr	mmHg
	Multiply by					
bar	1	0.986923	0.1	14.5038	750.062	750.062
Atmospheres (atm)	1.01325	1	0.101325	14.6959	760	760
Megapascals (Mpa)	10	9.86923	1	145.038	7500.6	7500.6
Pounds/square inch (psi)	0.06895	0.06986	0.006895	1	51.7149	51.7149
Torr	0.001333	0.001316	0.0001333	0.0193368	1	1
mmHg	0.001333	0.001316	0.0001333	0.0193368	1	1

Table 9 Masses and energy

- 1 metric tonne = 2204.62 lb = 1.1023 short tons = 1000 kg
- 1 kilolitre = 1 cubic meter = 6.2898 barrels
- 1 kilocalorie (kcal) = 4.187 kJ = 3.968 Btu
- 1 kilojoule (kJ) = 0.239 kcal = 0.948 Btu
- 1 British thermal unit (Btu) = 0.252 kcal = 1.055 kJ
- 1 kilowatt-hour (kWh) = 860 kcal = 3600 kJ = 3412 Btu

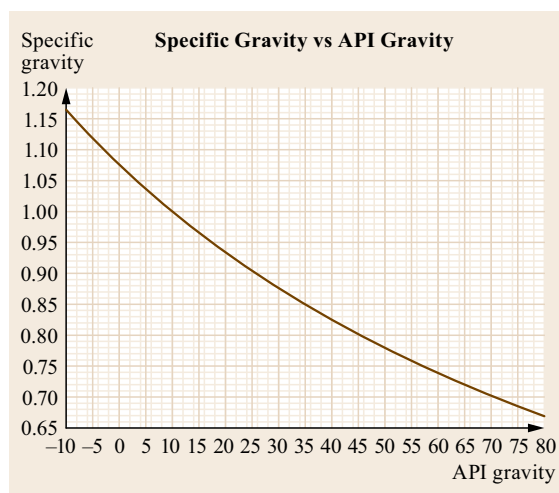
Table 10 Energy equivalencies^a

One tonne of oil equivalent equals approximately:	
Heat units	10 × 10 ⁶ kcal 42 GJ 40 × 10 ⁶ Btu
Solid fuels	1.5 tonnes of hard coal 3 tonnes of lignite
Electricity	12 MWh

10⁶ tonnes of oil or oil equivalent produces about 4400 GWh of electricity in a modern power station.
^a BP Statistical Review of World Energy (2016)

Table 11 Greek and Roman prefixes

Prefix	Factor	Power
atto		10 ⁻¹⁸
femto		10 ⁻¹⁵
nano		10 ⁻¹²
nano		10 ⁻⁹
micro	0.000001	10 ⁻⁶
milli	0.001	
centi	0.01	
deci	0.1	
deca	10	
hecto	100	
kilo	1000	
mega	1 000 000	10 ⁶
giga	1 000 000 000	10 ⁹
tera		10 ¹²
peta		10 ¹⁵
exa		10 ¹⁸



Glossary of Defining Terms

A

Absorbent

A material (solid or liquid) able to take in and hold (absorb) a gas or liquid. Examples include alkanolamine solutions, which absorb H₂S and CO₂ from sour gas, and absorbent clays, which pick up oil by incorporating the oil into their structure

Absorption tower

A column or tower in which absorption of selected components from mixtures occurs

Acid gas

Natural gas or a gas mixture containing high concentrations of hydrogen sulfide (H₂S) and/or carbon dioxide (CO₂). Acid gas is a more general term than ► *sour gas*, which contains H₂S but does not always contain CO₂

Acid number

► *total acid number (TAN)*

Adsorbent

A material like activated charcoal, alumina, or silica gel that is used in an adsorption process. Impurities selectively attach to its surface

Adsorption

A process of removing selected components from a stream by adherence to an adsorbent

Alcohol

A chemical compound composed of an alkyl group and an –OH group. Examples include methanol (CH₃OH) and ethanol (CH₃CH₂OH). In the oil industry, ethanol is used as gasoline additive and isopropanol as a solvent

Aldehyde

A chemical compound in which one carbon atom is bound to both =O and –H. Examples include formaldehyde, H(C=O)H, and acetaldehyde, CH₃(C=O)H. Formaldehyde is a building block in the synthesis of many other compounds of specialized and industrial significance. Acetaldehyde is mainly used as a chemical precursor, for example to make acetic acid, resin, pyridine derivatives, etc.

Alkanes

► *Hydrocarbons, paraffins*

Alkenes

► *Hydrocarbons, olefins*

Alkylate

The main product from an alkylation process unit. Alkylate is a high-octane gasoline blending component with many desirable properties, such as zero sulfur, olefins and benzene

Alkylation

A refining process in which isobutane reacts with C₃ to C₅ olefins to produce alkylate – a mixture of C₆ to

C₉ isoparaffins. The process is catalyzed by strong acids such as sulfuric acid or hydrofluoric acid.

American Petroleum Institute (API)

The largest trade association for the oil and gas industry in the United States. API publications include technical standards and online products designed to help users improve the efficiency and cost-effectiveness of operations, to comply with legislative and regulatory requirements, to safeguard health, to improve safety, and to protect the environment

Amine treating (amine washing)

Used in petroleum refineries, natural gas processing plants and other industrial facilities to remove acidic components, such as hydrogen sulfide and carbon dioxide, from gas streams by treatment with an alkanolamine

Aniline point

The lowest temperature at which aniline is soluble in a specified amount of oil. The aniline point is proportional to aromatics content; a low value indicates high aromatics. The aniline point is a specification for certain refining processes

Anticline

A type of fold with an arch-like shape resembling an inverted bowl, with the oldest beds at its core. Some of the world's largest oil fields, including many of those in the Middle East and the East Texas oil field, reside within anticlines

Antiknock index (AKI)

► *Octane number*

API gravity

Used for expressing density of crude oil. API gravity is defined as $^{\circ}\text{API} = 141.5 / (\text{specific gravity at } 60^{\circ}\text{F}) - 131.5$

Aquifer

A subsurface rock formation (stratum), such as permeable rock, sand, or gravel, which holds water. An aquifer often underlies a petroleum reservoir

Archie's law

Named after Gus Archie, this empirical equation relates the electrical conductivity of sedimentary rock to its porosity and brine saturation. It is used to relate borehole electrical conductivity measurements to hydrocarbon concentration of the material

Aromatics or aromatic hydrocarbons

► *Hydrocarbons, aromatic*

Asphalt

(1) A dark brown or black cement-like material precipitated from atmospheric residue with aliphatic solvents, usually propane. (2) Often used as a synonym for bitumen. (3) Also used as a feed for coking to increase the yields of more valuable products

Asphaltene structures

Archipelago and continental (pericondensed) structures. Surrogate molecules used to model asphaltenes are commonly classified based on their resemblance to archipelagos and continents

Asphaltenes

Polar fraction of petroleum that is insoluble in light alkanes, e.g., pentane or heptane, but soluble in aromatic solvents. Asphaltenes do not dissolve in crude oil but exist as a colloidal suspension

Asphaltic crudes (Naphthenic crude)

► *Crude oil, asphaltic*

ASTM

ASTM International, formerly known as the American Society for Testing and Materials, develops and publishes consensus standards for materials, products and processes.

Atmospheric distillation

► *Distillation, atmospheric pressure*

Atmospheric equivalent boiling point (AEBP)

Calculated based on observed boiling points at a reduced pressure, the atmospheric equivalent boiling point (AEBP) is relevant to compounds for which the atmospheric boiling point cannot be measured because they decompose before they boil

Autothermal reforming (ATR)

An alternative to traditional steam methane reforming (► *SMR*). ATR does not require external heat. It processes mixtures containing hydrocarbon gases (primarily methane), steam, and oxygen. In a combustion zone, partial oxidation generates syngas and heat. The syngas flows to a catalyst zone, where reforming reactions occur, producing mainly hydrogen. The product can also be syngas with a specific composition

Aviation gasoline (Avgas)

A high-octane blend of hydrocarbons and additives, which meets ASTM Specification D910 or Military Specification MIL-G-5572. Used primarily in airplanes with piston-driven propellers. Often contains tetraethyl lead (TEL)

B**Barrel (bbl)**

In petroleum, a unit of volume equal to 42 US gallons, 33.6 Imperial gallons, or 158.9873 liters

Barrels per calendar day (BPCD)

The average daily amount of oil produced, transported or processed in a petroleum facility during one calendar day. BPCD is less than BPSD, because BPCD includes downtime for maintenance

Barrels per stream day (BPSD)

The maximum daily amount of oil produced, transported or processed in a petroleum facility when the facility is running under normal operating conditions, with referal to the feedstock quality, process operating conditions, and product objectives

Base oil

A blend of one or more basestocks

Base stock (Basestock)

Products produced from the lube refinery without any additives in the oil. Group I: with saturates < 90%, sulfur > 0.03%, and viscosity index 80–120. Obtained from solvent processing (solvent refining). Group II: with saturates > 90%, sulfur < 0.03%, and viscosity index 80–120. Obtained from hydroprocessing. Group III: with saturates > 90%, sulfur < 0.03%, and viscosity index > 120. Obtained from severe hydroprocessing, isodewaxing or gas-to-liquid processes. Group IV: made from polyalpha olefins (PAO). Group V: Basestocks not included in Groups I–IV, such as synthetic lubricant oils

Basins (sedimentary basins)

Large-scale region of the earth where long-term subsidence has created a depression. Provides space for infilling by sediments and oils

Batch processing

A noncontinuous process in which material is loaded into a vessel and given time to react. When the reaction is complete, the vessel is opened and products are removed. Examples include delayed coking, digestion, batch polymerization, and the roasting of ores

Batch reactor

A typical batch reactor consists of a large, sturdy canister or vessel with its own heating and cooling mechanisms. Sometimes includes a rotating agitator inside the vessel to facilitate mixing

Benfield process

A process for removing acid gases (CO₂ and H₂S) from natural gas or manufactured hydrogen. The acid gases are adsorbed into molten potassium carbonate then recovered in concentrated form during thermal regeneration of the carbonate

Biodiesel

A fuel comprised of monoalkyl esters. Derived from the long-chain fatty acids found in vegetable oils or animal fats

Biogenic

Material derived from biological sources, such as bacteria, algae, and vegetables

Biomarkers (petroleum biomarkers)

Organic compounds contained in rocks and petroleum whose carbon skeletons remain after paleotransformation stages and can be linked to known biological precursors

Biomass

Biological organic matter

Biomass to liquid (BTL)

A process to produce liquid biofuels from biomass, which may include the Fischer-Tropsch process, pyrolysis or catalytic depolymerization

Biopolymer

High molecular weight polymers, such as

carbohydrates, proteins, lipids, and lignin, in living organisms

Bitumen

A naturally occurring thick, sticky form of hydrocarbon found in pits or associated with oil sand. It will not flow unless heated or diluted with lighter hydrocarbons. It is also the British term for asphalt or extra heavy crude oil

Blending terminal

A facility used for intermediate storage of refinery products and for blending them with additives. Gasoline additives might include oxygenates such as ethanol and detergents to mitigate intake valve deposits. Additives for diesel might include cetane improvers and antioxidants. Oil trucks (lorries) are loaded at blending terminals, from which they transport the products to retail filling stations

Blending unit

A facility in a refinery where streams are mechanically blended to make finished products. In the case of US gasoline, the main product is RBOB reformulated blendstock before gasoline blending

Blowout

Uncontrolled escape of oil or gas from a well

BHCI (Bureau of Mines Correlation Index)

A method of petroleum classification.
 $BHCI = 48,640/TB + 473.7G - 456.8$, where TB is mean average boiling point in K and G is specific gravity at 60 °F. Also called CI. CI for straight-chain paraffins is 0 and for benzene it is 100. 0–15 indicates a predominance of paraffinic hydrocarbons; 15–50 indicates a predominance either of naphthenes or of mixtures of paraffins, naphthenes, and aromatics. > 50 indicates the predominance of aromatic character. For a petroleum fraction, CI correlates with many characteristics, such as crackability, steam cracking feed quality, and aromaticity

Borehole logging

► *Well log*

Bottoms

The product coming out of the bottom of a distillation column

Brent crude oil

An important group of crude oils produced in North Sea, which is used as a reference crude for international crude trading

Bright stock

A heavy lube basestock derived from vacuum resid after dewaxing

British Thermal Unit (BTU)

The quantity of heat required to raise the temperature of 1 pound of water by 1 °F

Bromine number

The grams of bromine absorbed in 100 g of oil. Correlates to the percentage of double bonds in the oil sample

BTX

A mixture of benzene (C_6H_6), toluene ($C_6H_5CH_3$),

and xylenes ($C_6H_4(CH_3)_2$). Commonly used as a solvent or feedstock to chemical plants

Bunker oil (Bunker fuel)

Fuel oil used in engines aboard ships. Bunker A corresponds to No. 2 fuel oil, Bunker B corresponds to No. 4 or No. 5 fuel oil, and Bunker C corresponds to No. 6 fuel oil

Butanes: A mixture of two isomers

normal butane and isobutane. Normal butane was used as a RVP booster during cold weather prior to the use of ethanol. It is isomerized to isobutane. Isobutane is an important (key) feed for alkylation
 (► *Hydrocarbons*)

Butene (butylene)

A colorless alkene with the formula C_4H_8 generated in refineries or olefin plants by cracking
 (► *Hydrocarbons, olefins*)

Butyl rubber

A synthetic rubber. Specifically, it is a copolymer consisting of about 98% isobutylene with about 2% isoprene. Butyl rubber and halogenated rubber are used for the impervious inner liner of tubeless tires

C

Calcining (calcination)

Decomposition of a solid with heat below the melting or fusing point. Causes loss of moisture and the decomposition of carbonates and other compounds

Cap rock (seal rock)

Impermeable rock that serves as a cap to stop petroleum migration. A key component of a petroleum and/or natural gas reservoir

Carbene

The pentane or heptane insoluble fraction that is insoluble in benzene or toluene but soluble in carbon dioxide or pyridine

Carboid

The pentane or heptane insoluble fraction that is insoluble in benzene or toluene but also insoluble in carbon dioxide or pyridine

Carbon Preference Index (CPI)

The ratio obtained by dividing the sum of the odd carbon-numbered n -alkanes to the sum of the even carbon-numbered n -alkanes between C_{25} and C_{34}

$$CPI = 1/2 [(C_{25} + C_{27} + C_{29} + C_{31} + C_{33}) / (C_{24} + C_{26} + C_{28} + C_{30} + C_{32})] + [(C_{25} + C_{27} + C_{29} + C_{31} + C_{33}) / (C_{26} + C_{28} + C_{30} + C_{32} + C_{34})]$$
 It can also be used to estimate thermal maturity of organic matter

Carbon rejection

Upgrading processes in which coke and other hydrogen-deficient products are formed. Examples include FCC and coking. Carbon rejection is accompanied by the formation of light products. The heavy products contain less hydrogen than the feed, while the light products contain more hydrogen than the feed. Often, molecular hydrogen is one of the products

Carrier rock

Permeable rock that allows oil and gas to migrate from source to reservoir

Catagenesis

A process that consolidates sediment containing dead organic material, water, minerals, and numerous living organisms, providing conditions that convert biopolymers to geopolymers (kerogen)

Catalyst

A substance that increases the rate of a chemical reaction without itself undergoing any permanent change

Catalyst acidity

For heterogeneous catalysts, acidity refers to the number and strength of acid sites per unit of weight or volume. Includes both Lewis and Brønsted sites; generally, the Hammett function is used instead of pH to indicate strength. Relative acidity is determined by adsorption of ammonia or other volatile bases with known acidity. For homogeneous systems, acidity can refer either to the strength of the acid itself or to the concentration of acid in the system

Catalyst activity

Relative rate at which a catalyzed reaction proceeds

Catalyst coke

Carbonaceous material that deposits on catalysts

Catalyst deactivation

Loss of catalyst activity due to routine fouling, attrition, or agglomeration (► *Catalyst poisoning*)

Catalyst fouling

Plugging of catalyst beds with particulates or gums. Sometimes used as a synonym for deactivation due to coking (► *Catalyst deactivation*)

Catalyst impregnation

A method for adding active metals to a solid catalyst support

Catalyst poisoning

Partial or total deactivation of a catalyst caused by exposure to a range of chemical compounds

Catalyst regeneration

Restoration of catalyst activity. Heterogeneous refining catalysts for FCC, hydroprocessing, and catalytic reforming are regenerated by controlled combustion, which removes accumulated coke, sulfur, nitrogen, and other volatile or flammable materials

Catalyst rejuvenation

Further restoration of catalyst activity via chemical treatment of a regenerated catalyst. Used (for example) to redispense active metals on catalysts in which agglomeration has occurred

Catalyst selectivity

Percentage of desired product from a catalyzed reaction

Catalytic cracking

The conversion of high-boiling feedstocks into lower-boiling products over a catalyst. Occurs in fixed beds or fluid beds, in the absence of excess hydrogen (as in FCC) or in the presence of external hydrogen (as in hydrocracking)

Catalytic dewaxing

Catalytic process for converting normal paraffins to isoparaffins, usually with a heterogeneous catalyst in a fixed-bed reactor

Catalytic hydrocracking

(► *Hydrocracking*)

Catalytic hydrotreating

(► *Hydrotreating*)

Catalytic reforming

A catalytic refining process in which C6 to C12 naphthenes and paraffins are converted into aromatics while producing hydrogen. The liquid product (► *reformate*) serves as high-octane gasoline blendstock or as a feedstock to aromatics production units. Hydrogen purities range from 80–90 vol%. This hydrogen goes primarily to hydroprocessing units. The three main catalytic reforming processes are semiregen, cyclic, and CCR. In *semiregen* units, the catalyst occupies fixed-bed reactors and slowly deactivates. When liquid yields and hydrogen purity become unacceptably low, due to increased formation of C1–C5 hydrocarbons, operators shut the unit down and regenerate the catalyst. Typical semiregen cycles last six to 12 months. *Cyclic* reformers include four to six reactors. The reactors deactivate sequentially. Every week or so, a reactor goes down for regeneration as a regenerated reactor returns to service. With this strategy, a unit can run for years without a total shutdown. The most profitable option is CCR – *continuous catalyst regeneration* – in which the catalyst moves through several reactors before circulating through an online regeneration section and back to the lead reactor. CCR liquid yields are greater, because they operate continuously, and at lower pressure, which favors dehydrogenation. For semiregen units, catalysts usually contain both platinum (Pt) and rhenium (Rh), where the Rh improves stability. For CCR units, Rh is not needed, but promoters such as tin (Sn) are added to improve selectivity. To provide acidity, chloride is injected into the unit at prescribed rates. Chloride promotes important reactions, but too much chloride can lead to excessive cracking

Caustic Wash

The process of treating a product with a caustic soda solution to remove minor but especially undesired impurities

Cetane index

Used as an alternative for cetane number. Based on density and distillation range.

$$CI = -420.34 + 0.016 G^2 + 0.192 G \log M + 65.01(\log M)^2 - 0.0001809 M^2$$

where G = API gravity at 60 °F and M = D86 temperature at 50% volume, in °F

Cetane number (CN)

A measure of the tendency of a diesel fuel to knock and undergo ignition delay. It is measured in a standard diesel engine according to ASTM D613. Originally, the CN of a test fuel was compared to

standard mixtures that knocked with the same intensity as the test fuel. The original standards were prepared by mixing *n*-hexadecane (CN = 100) with *a*-methyl-naphthalene (CN = 0). In 1962, *a*-methyl-naphthalene was replaced with 2,2,4,4,6,8,8-heptamethyl-nonane, which has a CN of 15

Characterization factor (UOP K or Watson K, K_w)

A method of petroleum classification.

$K_w = (TB)1/3/G$, where *TB* is mean average boiling point in K and *G* is specific gravity at 60 °F. K_w ranges from 10.5 for highly naphthenic crude to 12.9 for highly paraffinic crudes

Chemical injection

A tertiary recovery or enhanced oil recovery method. It involves injecting water-soluble polymers, surfactants or alkaline solutions into rock to flood the formation and drive oil to production wells for recovery

Claus process

Converts hydrogen sulfide into sulfur in a two-step process. (1) The thermal step entails combustion of a mixture containing H₂S and air in which the H₂S: oxygen molar ratio is 2 : 1. The products are SO₂, water, and unreacted H₂S. (2) The catalytic step entails the reaction of SO₂ from step 1 with unreacted H₂S to form elemental sulfur. Named after Carl Friedrich Claus

Cloud point

Temperature at which a haze appears in a sample due to the formation of wax crystals. Determines the plugging tendency of a fuel as it flows through small orifices. Particularly important for jet fuel and diesel at cold operating temperatures

Coal

A combustible black rock. A solid fossil fuel comprised of 65–95% carbon and different amounts of hydrogen, sulfur, oxygen, nitrogen, and ash. It is a sedimentary rock formed from peat that is buried under rocks

Coal bed methane

Natural gas extracted from natural coal beds. Contains fewer C₂+ hydrocarbons than natural gas from conventional reservoirs

Coke (petroleum coke)

Carbonaceous product generated in refineries by coking processes

Coke, anode grade

Calcined petroleum coke, low in sulfur and metals. Primarily used to produce electrodes for steel and aluminum (► *Coke, needle*)

Coke, catalyst

Undesired carbonaceous material that deposits on catalysts

Coke, fuel grade

Calcined sponge coke or shot coke from a delayed coker, with lower quality than anode-grade coke due to excessive ash or trace metals. Suitable as a replacement for coal in fired boilers in power plants. Can be a feedstock for gasification with partial

oxidation. In power plants, some form of sulfur capture is required to meet current North American emission standards

Coke, green

Uncalcined raw coke from a delayed coker

Coke, needle

Premium highly crystalline petroleum coke used in the manufacturing of graphite electrodes of low thermal expansion for arc furnaces in the steel, aluminum and titanium industries (► *Coke, anode grade*)

Coke, shot

Lowest quality coke from a delayed coker. Typically, shot coke is comprised of small round pellets ranging 1.5–4 or 5 mm in diameter, which are loosely bound together in structures roughly the size and shape of ostrich eggs. Shot coke can disrupt coke drum operations by causing blowbacks during the cutting of coke from drums, plugging of the bottom nozzle of a coke drum, and fouling of coke handling equipment

Coke, sponge

Sponge-like coke from a delayed coker with a relatively uniform consistency

Coking

A thermal process for continuous conversion of reduced crude, straight-run residua or cracked residua into hydrocarbon gases, H₂S, NH₃, naphtha, gas oils and petroleum coke. The most common processes are ► *delayed coking* (batch), ► *fluid coking* and ► *Flexicoking* (continuous)

Coking, delayed

A semicontinuous (semi-batch) process by which residue and other heavy fractions, such as FCC decant oil or coal tar, are thermally decomposed to produce coke and cracked products. The feed is heated to ca. 500 °C and sent to large coking (soaking) drums. Usually, four or more drums are used so that operation can be staggered. Drums are switched every 18–24 h. Hot oil is added until a drum is full. Cracking begins immediately, generating coke and hot cracked vapor. The oil stays in the drum for several hours (hence the term delayed) until coking is complete. Vapors rise to the top, from whence they are sent to a fractionator for separation and recovery. Coker gases and liquids contain sulfur and olefins. The liquids must be stabilized by hydrotreating or hydrocracking. The coke can be used either as a fuel or in other applications such as the manufacturing of anodes for steel or aluminum production

Coking, Flexi-

A combination of continuous fluid coking and oxidative steam reforming, which can upgrade virtually any pumpable feed including residual, pitch or total crude. Approximately 95 wt% conversion of feed can be achieved. Products include coke and a full range of gas and liquid products. Some of the coke is heated and circulated back to the reactor to supply process heat. Excess coke goes to a gasifier, where it reacts with air and steam to produce Flexigas. After treatment to remove particulates and hydrogen sulfide,

the Flexigas is ready for use as fuel in refinery boilers and furnaces and/or for steam and power generation

Coking, fluid

A continuous thermal cracking process for converting residua to more valuable products, such as gases, a full range of liquids, and coke. The coke is burned or gasified and returned to the main reactor to provide some of the heat required for cracking

Combined feed ratio (CFR)

In a process where unconverted feed is recycled, the combined feed ratio = $(FF + RO)/FF$, where FF = fresh feed rate and RO = recycle oil rate

Compression ratio

The ratio of the volumes in an internal combustion engine when the piston is at the bottom of the stroke and the top of the stroke

Condensate

Liquids produced during the processing of natural gas. Also referred to as gas condensate, and (historically) natural gasoline. Includes pentanes and heavier hydrocarbons

Conradson carbon residue (CCR)

Also known as Concarbon. A quantitative measurement of carbonaceous residue remaining after evaporation and pyrolysis of oil from a sample under controlled conditions. An indication of the coke-formation tendency of the oil being tested

Conversion

In refining, conversion means boiling point reduction. That is: transforming material that boils above a product cutpoint into material that boils below that cutpoint. Most conversion is accomplished by breaking C–C bonds. Depending on the feedstock, up to 15% conversion of material that boils above 700 °F (370 °C) can be achieved by other reactions: saturating aromatics and removing heteroatoms

Correlation index (CI)

► *BMC1*

Crack spread

Expressed as $X : Y : Z$ where X = price of X barrels of crude, Y = price of Y barrels of gasoline, and Z = price of Z barrels of distillate fuel oil (diesel, etc.). By convention, $X = Y + Z$. Corresponds roughly with refinery profitability

Cracked gas

The gas from thermal crackers, steam crackers, catalytic crackers and cokers. Depending on the process and reaction conditions cracked gas is often rich in hydrogen and olefins

Cracking

Breaking down large molecules into smaller molecules by heat. Thermal cracking includes steam cracking and coking. Catalytic cracking includes FCC and hydrocracking

Crude assay (crude oil assay)

A collection of the results of physical tests, which determine key properties (boiling point, density, viscosity, heteroatom contents, acid number, etc.) of a crude oil and its fractions. Important for determining the value and processability of crude oil

Crude oil

Liquid form of petroleum. A mixture of naturally occurring hydrocarbons in (or produced from) underground ► *reservoirs*. It is formed from the bodies of dead microorganisms, which accumulated millions of years ago in sediments at the bottoms of ancient seas and lakes. Deep underground, the sediments were subjected to heat and pressure, which converted them into sedimentary rock via diagenesis. During diagenesis, the organic matter was transformed into fossil hydrocarbons. Depending on local conditions, including time, diagenesis produces natural gas, petroleum, heavy oil, bitumen, or coal. Crude oil in reservoirs is associated with dissolved hydrocarbon gases, water, salt, dirt, dissolved light natural gas, CO_2 , H_2S , and trace metals such as Fe, Ni, V, As, and Hg. When brought to the surface, dissolved gases desorb and are collected and processed in associated facilities. Widely construed, the term crude oil also includes other fossil hydrocarbons: bitumen recovered from tar pits by conventional mining, bitumen recovered from tar sands (oil sands), and liquids produced from the kerogen in oil shale. Liquids from natural gas processing plants are often included, especially when they are back-blended with crude oil prior to transportation. Crude oil is refined into a wide array of fuels and other products

Crude oil, asphaltic

also called naphthenic crudes, containing higher concentrations of naphthenes and aromatics than paraffinic crudes

Crude oil, conventional

Oil extracted from the ground by conventional drilling methods. Includes oil produced with primary, secondary, and tertiary recoveries

Crude oil, paraffinic

Paraffinic (waxy) crude oils contain relatively high concentrations of long-chain n -paraffins. In comparison, naphthenic crudes contain relatively low concentrations of paraffins. Waxy crudes cause problems due to their high viscosity and tendency to leave deposits in equipment

Crude oil, synthetic

Crude oil produced from coal, bitumen or shale oil; in this context, shale oil comes from retorted oil shale. To make so-called synthetic bitumen (synbit), bitumen is upgraded by a coker, visbreaker, or hydroprocessing unit. To make so-called diluted bitumen (dilbit), the bitumen is diluted with cutter stock. The quality of synbit is much higher than the quality of dilbit

Crude oil, unconventional

Unconventional crude oils include oil and natural gas condensates that are not recovered by conventional means, such as primary to tertiary recoveries. These include oil sand bitumen and syncrude, extra heavy crude oil, and shale oil

Cut

The portion or fraction of a crude oil boiling within

certain temperature limits. Also called ► *distillate* in distillation

Cut point

The temperature limit of a cut or fraction, usually (but not always) specified on a true boiling point basis

Cyclic steam stimulation (CSS)

A thermal recovery method for heavy oils, also known as the Huff and Puff method, consisting of three stages: steam injection, soaking, and production

D

Deasphalted oil (DAO)

The extract or residual oil from which asphalt and resins have been removed by an extractive precipitation process called deasphalting

Deasphalting

A refinery process for removing asphalt from reduced crude or vacuum residua (residual oil) by light alkanes (propane, pentane, heptane, etc.)

Deep catalytic cracking (DCC)

A modified catalytic conversion technology that uses heavy hydrocarbon feedstocks, such as VGO, VR or VGO, blended with DAO to produce light olefins (ethylene, propylene and butylenes), LPG, gasoline, middle distillates, etc

Delayed coking

► *Coking, delayed*

Desalting

Removal of salts and other material, such as particulates, from crude oil. Usually the first step in crude oil refining. The process entails: (1) adding and dispersing water, (2) forming an emulsion to expedite the dissolution of salts in the water, and (3) separating the emulsion into oil and water phases by electrostatic and/or chemical methods

Desulfurization

Removal of organic sulfur compounds by scrubbing, mercaptan oxidation, or catalytic hydrotreating via hydrodesulfurization (HDS)

Dewaxing

A lubricant plant process to remove wax (higher-boiling normal paraffins) from oil after extraction of aromatics. Solvent dewaxing often employs methylethyl ketone (MEK) mixed with toluene or propane

Dewaxed oil (DWO)

The oil remaining after dewaxing processes for lubricant oil production

Diagenesis

Formation of sedimentary rocks from sediments or from different sedimentary rocks at high temperature and pressure. Diagenesis occurs at depths reaching several kilometers. When the sediments contain enough organic matter, kerogen forms. Over time, the kerogen starts evolving into liquid petroleum, various ranks of coal, and gases (mostly methane)

Dibenzothiophenes

A class of sulfur-containing aromatic compounds. They are difficult to remove, especially when they

have alkyl groups adjacent to the sulfur atom or when they include fused aromatic rings (► *Hydrocarbons, heteroatom-containing*)

Diesel

Fuel used in compression-ignition (diesel) engines. Most diesel (petro diesel) is produced in petroleum refineries from distillation of crude oil and by conversion processes such as hydrocracking. Other sources include biomass, biogas or natural gas. Diesel is produced from synthesis gas with the Fischer-Tropsch process. No. 1 diesel is lighter than No. 2 diesel (close to kerosene) and with high cetane number and volatility, it is better suited for cold temperatures. No. 2 diesel is less volatile than No. 1 (containing heavy gas oil), enabling it to carry heavy loads for long distances at sustained speed. No. 4 diesel fuel is used for low- and medium-speed diesel engines and conforms to ASTM Specification D 975

Dilbit (diluted bitumen)

Bitumen diluted with cutter stock to facilitate transportation. In refineries, dilbit is processed as if it were a conventional heavy crude oil

Distillate

An overhead or side-draw distillation fraction from a distillation column after cooling

Distillate fuel oil

A collective term referring to heating oils for which the distillation endpoint is less than about 400 °C (750 °F). No. 1, No. 2, and No. 4 fuel oils are similar to No. 1, No. 2, and No. 4. diesel respectively, but with different (fewer) additives. Used primarily for space heating and electric power generation

Distillation

Process of selective evaporation and condensation to separate substances from a liquid mixture. Primary means of separation in oil refineries

Distillation, atmospheric

Distillation at atmospheric pressure up to 700 °F or 370 °C. In petroleum refining, atmospheric distillation separates crude oil into fractions, which are subsequently transformed into finished products. Typical fractions include C1–C4 gases, naphtha, middle distillates, atmospheric gas oil, and atmospheric residue

Distillation, vacuum

Distillation of crude oil under vacuum or reduced pressure, such as 40 mmHg (50 mbar), up to 700 °F or 370 °C. Recovers components that thermally decomposed before they vaporize under atmospheric pressure

Donor solvent process

A hydrogenation process, such as donor-solvent coal liquefaction, in which a hydrogen-rich liquid solvent such as tetralin replaces gaseous molecular hydrogen. Much of the hydrogenated coal liquefies; the coal liquids are easier to transport and process than solid coal. Due to the modest pressure of the coal section, construction and processing costs are relatively low.

The dehydrogenated solvent is removed by distillation, rehydrogenated, and recycled

Downhole fluid analysis (DFA)

Technique to characterize reservoirs and the distribution of reservoir-fluid properties using optical spectroscopy

Downstream

Business sector in the oil industry for refining crude oils and purifying natural gas. Includes the marketing and distribution of refined products

Drilling engineering

A branch of petroleum engineering for designing and implementing procedures to drill wells safely and economically

Dry gas

Natural gas or refinery gas that does not contain significant amounts of C₂+ components

E

Ebulated bed (e-bed) hydrocracking

► *Hydrocracking*

Ebulated bed (e-bed) reactor

Key part of an ebulated bed unit

Engine oils

Lubricant oils for internal combustion engines

Enhanced oil recovery (EOR)

► *Tertiary recovery*

Entrainment

Entrainment is the carryover of liquid by the vapor phase or of gas by the liquid phase. Liquid may be in the form of a spray, foam or mist

Epimers

Stereoisomers with different configurations of atoms around one of several asymmetric carbon atoms (chiral centers). Important isomeric molecule for maturity assessment through petroleum biomarkers

EST (ENI Slurry Technology)

A slurry-phase hydrocracking process licensed by ENI

Exploration (discovery)

Searching for oil and gas deposits under the Earth's surface. A branch of the petroleum upstream business

Extract

For solvent refining in general, the extract is the stream rich in impurities. In solvent extraction for preparing lube basestocks, the extract is rich in aromatics and other undesirable components. In wax deoiling, the extract is rich in oil (► *Raffinate*)

Extraction

In general, extraction is the process of separating a mixture into a fraction soluble in a solvent and an insoluble residue. In solvent refining for lube oil production, the aromatic portion of an oil is separated from the paraffinic and naphthenic portions. This improves the viscosity index, oxidation resistance, and color of the basestock. It also reduces carbon and sludge formation. Solvents used include furfural, phenol or *N*-methylpyrrolidone (NMP)

Extra heavy crude oil

Crude oil with °API gravity less than 10 (specific gravity > 1.0). The heaviest of *heavy crude oils*

F

Facies

Characteristics of a rock expressed by its morphology, composition, and fossil content. *Fasces* is a Latin term for the bundles of sticks carried by lictors in Ancient Rome

Fatty acid methyl ester (FAME)

Primary constituent of biodiesel, resulting from the transesterification of fats with methanol

Fault

Natural fracture in stratum caused by plate tectonics. Serves as a conduit for petroleum migration or as a reservoir in the presence of cap rock

Fold (geological)

A permanent deformation caused when flat sedimentary strata are bent or curved by geological forces

Fischer-Tropsch process

A series of chemical reactions to convert a mixture of carbon monoxide and hydrogen into liquid hydrocarbons. The key process in the production of synthetic lubricants or fuels in gas-to-liquid (GTL) technology

Flash point

The lowest temperature at which vapor of a volatile material will ignite

Flexicoking

► *Coking, Flexi-*

Flue gas

The exhaust gas from a furnace, boiler, reactor, etc.

Fluid catalytic cracking (FCC)

Catalytic cracking in a fluidized bed reactor. The cracking reaction occurs on high-acidity zeolite catalysts, which have the consistency of sifted flour. Reaction products include gases, predominantly C₃+, which are highly olefinic; high-octane FCC gasoline; highly aromatic cycle oils; and coke. The coke goes to a regenerator, where it is burned in air (or oxygen-enriched air) to produce CO₂, H₂O, and heat. Hot catalyst is mixed with fresh feed and returned to the reactor. FCC produces a significant portion of the world's gasoline

Fluid coking (fluidized bed coking)

► *Coking, fluid*

Fluidized bed reactor

A reactor in which the catalyst bed is fluidized by upflowing gas. Used in fluid catalytic cracking and fluid coking

Foots oil

The oil washed out of slack wax

Formation (geological)

Stratified sedimentary bed. The fundamental unit of petrostratigraphy in geology

Formulated oil

A blend of base oils with special additives

Fouling

The deposition and accumulation of unwanted materials such as scale, algae, suspended solids and insoluble salts on the internal or external surfaces of processing equipment including boilers and heat exchangers

Fracking

► *Hydraulic fracturing*

Fractional distillation

Primary means of separating crude oils at refineries into fractions with different boiling ranges

Fracture

A natural or man-made crack in reservoir rock

Frasch Process

Method to extract sulfur from underground deposits, where superheated water is pumped into the formation to melt the sulfur. Compressed air is used to froth the sulfur and bring it to the surface

Froth treatment

A process of eliminating the aqueous and solid contaminants from bitumen froth to produce a clean bitumen product

Fuel ethanol

Ethanol intended for fuel use, as in reformulated gasoline. Fuel ethanol in the United States must contain less than 1 wt% water and be denatured with > 2 vol% C5+ paraffins or conventional gasoline

Fuel oils (heating oils)

A range of oils used for heating or for locomotion in ships and locomotives. No. 1 fuel oil is a volatile distillate oil with a boiling range similar to that of kerosene, but a higher pour point and an end point that is adjusted to suit vaporizing pot-type burners. No. 2 fuel oil is a distillate home heating oil, similar to No. 1. It may contain hydrotreated cracked stock. The chain length of the hydrocarbons ranges from 10 to 20. No. 3 fuel oil is for burners requiring low-viscosity heating oil, merged with No. 2 in specifications. No. 4 fuel oil is usually a light residual oil used in a furnace that can atomize the oil and is not equipped with preheater. The chain length of the hydrocarbons ranges from 12 to 70. No. 5 fuel oil has higher viscosities than No. 4. In use, it requires preheating to 170–220 °F for atomizing and handling. Also known as Bunker B oil. The chain length of the hydrocarbons ranges from 12 to 70. No. 6 fuel oil is a high-viscosity residual oil that requires preheating to 220–260 °F for storage, handling and atomizing. Also specified by navies as Bunker C oil for ships. The chain length of the hydrocarbons ranges from 20 to 70. *Residual fuel oils* are the heaviest, including No. 5 and No. 6 fuel oils

G**Gas hydrate**

Solid ice-like form of water cage that contains gas

molecules inside its cavity. In nature, the gas is mostly methane

Gas injection (for oil recovery)

Gas injection is used both in secondary recovery for artificial lift of the oil, and in tertiary recovery. In the latter, carbon dioxide or nitrogen is introduced through an injection well to sweep the formation for remaining oil

Gas oils

Distillation fractions boiling between heavy naphtha and kerosene and atmospheric residue. They are obtained from atmospheric distillation as atmospheric gas oils (AGOs), vacuum distillation as vacuum gas oil (VGOs) and coker as coker gas oils (KGOs). Also known as middle distillates. After subsequent processing, gas oils become suitable for blending into finished fuel oil and transportation fuel

Gas oils, heavy coker (HKGO)

Heavy gas oil fraction from coker with boiling points > 650 °F (340 °C), which contains very high concentrations of polycyclic aromatic compounds and other contaminants, such as metals. If used as a hydrotreating or hydrocracking feed, it is crucial to control endpoint, CCR, and metals to avoid shortening catalyst cycle life.

Gas oils, heavy straight run (HGO or HAGO)

Liquid petroleum distillates from atmospheric distillation heavier than kerosene with boiling points between 600 °F and 800 °F (315–420 °C) in the diesel range

Gas oils, light coker (LKGO)

Highly olefinic middle distillates produced by coking units, with boiling points that range from about 400 °F to 650 °F (200–340 °C). Highly reactive with air. Hydroprocessing transforms light coker gas oils into diesel blendstocks or heavy naphtha

Gas oils, light straight run (LGO or LAGO)

Liquid petroleum distillates from atmospheric distillation heavier than naphtha with boiling points between 400 °F and 600 °F (200–315 °C) in the kerosene and jet fuel range. Also called middle distillates

Gas oils, vacuum (VGO)

Overhead and side-streams from a vacuum distillation unit. Include light vacuum gas oil (LVGO) and heavy vacuum gas oil (HVGO). A typical VGO boiling range is 650–1050 °F (340–560 °C). They are feedstocks for catalytic cracking or hydrocracking

Gasohol

A mixture of gasoline and ethyl alcohol used as fuel in internal combustion engines

Gasoline

A mixture of C5–C12 hydrocarbons used as fuel in spark-ignition internal combustion engines. A high-octane naphtha blend with additives to meet official specifications for octane number, RVP, and other properties as described by ASTM D4814, EN 228, JIS K2202, China V, etc.

Gasoline, blending

Mechanical mixing of motor gasoline blending

components from refinery process units with additives, including oxygenates when required. Final blends must meet official specifications for octane number, RVP, sulfur, and other properties

Gasoline, blending components

Refinery streams containing C5-C12 hydrocarbons with suitable properties for blending into gasoline. Typically, the streams include straight-run naphtha, reformate, FCC gasoline, alkylate, isomerate, polymer gasoline, and others. Oxygenates and other additives are included as required or needed

Gas-to-liquids (GTL)

A process for converting natural gas into liquid hydrocarbons

Gravity drainage

The movement of oil in a reservoir due to gravity

Grease

A semisolid lubricant usually prepared by emulsifying a lubricant basestock with soap. Greases are highly viscous when first applied, but they undergo sheer thinning (their viscosities fall) during operation. Because they are semisolid, greases stay in place where liquid lubricants will not. Bearings are typically lubricated with grease instead of with less-viscous oil. Some greases act as sealants or waterproofing agents

Green coke

Unprocessed raw coke from a delayed coker (► *Coke*)

H

Heating oil

No. 2 to No. 4 fuel oils (► *Fuel oil*)

Heavy coker gas oil (HKGO)

► *Gas oils, heavy coker*

Heavy crude oil

Crude oil with °API gravity ranging from 10 to 20

Heavy gas oil (HGO)

Petroleum distillates with an approximate boiling range from 500 to 750 °F (260–400 °C)

H-Oil

An ebullated-bed hydrocracking process licensed by Axens

Houdry process

A process invented by Eugène Houdry, a French chemist. Revolutionized thermal cracking with the use of a moving bed of catalyst integrated with oxidative regeneration. Produced less gas, higher liquid yields, and gasoline with higher octane

Huff and Puff

► *Cyclic steam stimulation*

Hydraulic fracturing (fracking)

Injecting fluid (about 90% water, 9.5% proppant, and chemical additives) under controlled pressure intermittently over a short period (three to five days) to create fractures in a targeted rock formation. The fracture permits oil or natural gas to flow to the wellbore. The proppants are small grains of sand, ceramic, aluminum oxide or other particulates to keep the fracture open

Hydrocarbons

Molecules that contain carbon and hydrogen. The term is loosely used in the oil industry to include all compounds containing carbon and hydrogen, including those that also contain heteroatoms. Hydrocarbons are classified into the following groups: saturates (paraffins and cycloparaffins), olefins, aromatics (monoring and polyring) and heteroatom-containing

Hydrocarbons, acetylene

Acetylenes have a formula of C₂H₂ with a carbon-carbon triple bond. They are not found in petroleum or natural gas due their high reactivity, but can be manufactured from the hydrolysis of calcium carbide, and the partial oxidation of methane, coke, or coal. Acetylene has mainly been used in oxyacetylene welding and as a feedstock for a variety of plastics and acrylic acid derivatives

Hydrocarbons, aromatics

Aromatics are hydrogen-deficient ring compounds with the general formula C_nH_{2n} + z, where z = -6 for benzenes, -8 for indans, -10 for indenenes, -12 for naphthalenes, etc. The rings are stabilized with resonance energy, making them difficult to open with cracking processes. Aromatics are dense and have higher boiling points than other hydrocarbons with the same number of carbon atoms. Important examples include benzene (C₆H₆), toluene (C₇H₈), and four isomers of C₈H₁₀: *o*-xylene, *m*-xylene, *p*-xylene, and ethylbenzene

Hydrocarbons, diolefins

Diolefins have two carbon-to-carbon double bonds, which are usually conjugated. Butadiene is an important monomer for making petrochemicals. In refining, due to their high reactivity, diolefins cause storage and processing problems as well as gum formation in gasoline engines. Coking units produce significant butadienes and pentadienes, which can polymerize at the top of hydroprocessing reactors, producing gums that increase pressure drop and can shut a unit down

Hydrocarbons, heteroatom-containing

Strict definitions of hydrocarbons exclude compounds that contain heteroatoms. However, they are included with hydrocarbons in much of the literature because their hydrocarbon backbones are the main interest. The most common heteroatom compounds contain sulfur, nitrogen, and oxygen. They are *bad actors*, i. e., they cause equipment problems and poison catalysts. The sulfur compounds include mostly thiols, sulfides, thiophenes, benzothiophenes, dibenzothiophenes, etc. The nitrogen compounds include pyrroles, pyridines, carbazoles, etc. The oxygen compounds include acids, phenols, furans, etc. Trace metal compounds include nickel and vanadyl porphyrins, the removal of which is the subject of intensive research

Hydrocarbons, naphthenes (cycloparaffins or cycloalkanes)

Naphthenes have the general formula C_nH_{2n+z} where

$z = -((\text{number of rings}) \times 2 - 2)$. They contain a fully saturated ring comprised of five or six carbons. Cyclopentane and cyclohexane are the simplest naphthenes. Commercially, naphthenes can be prepared by saturating aromatics with hydrogen. Cyclohexane (C_6H_{12}) is an important solvent and petrochemical

Hydrocarbons, naphthoaromatics (hydroaromatics)

Naphthoaromatics contain at least one aromatic ring fused to at least one naphthene ring. One example is tetralin ($C_{10}H_{12}$). Alkyl naphthoaromatics are highly isomeric. The isomers tend to have similar chemical and physical properties and are very difficult to separate from each other

Hydrocarbons, olefins

Olefins (alkenes) have the general formula C_nH_{2n} and contain one carbon-to-carbon double bond. Olefins are rare in nature, but they are produced in large quantities by thermal cracking and steam cracking. Examples include ethylene (ethane), propylene (propene), 1-butene, 2-butene (butylenes), and isobutylene (2-methylpropylene). Far more reactive than paraffins, olefins have a tendency to polymerize. They serve as building blocks of polyethylene, polypropylene, and hundreds of other important polymers

Hydrocarbons, paraffins

Paraffins (alkanes) have the general formula $C_nH_{(2n+2)}$. They can be divided into normal paraffins, where chains of carbon atoms are straight (linear) and isoparaffins, containing at least one branch. The lightest paraffins are methane (CH_4), ethane (C_2H_6) and propane (C_3H_8). There are two stable isomers of butane (C_4H_{10}), three stable isomers of pentane (C_5H_{12}), five for hexane (C_6H_{14}), 75 for decane ($C_{10}H_{22}$), and many, many thousands for $C_{34}H_{70}$. Light paraffins are highly flammable. Large normal paraffins are waxy. Large isoparaffins are excellent lube basestocks

Hydrocarbons, polynaphthenes (polycycloparaffins)

Polynaphthenes contain more than one fully saturated five- or six-membered ring, where at least two of the rings are fused. At high temperatures, polynaphthenes readily lose hydrogen to form naphthoaromatics and/or polyaromatics. Examples include cis- and transdecalin ($C_{10}H_{18}$). Polynaphthene structures can be three-dimensional, as diamondoid hydrocarbons

Hydrocarbons, polynuclear aromatic (PNA or PAH)

Polynuclear aromatics (PNA) are also known as polynuclear aromatic hydrocarbons (PAH). They contain more than one aromatic ring, and at least two of the rings are fused. They are more hydrogen deficient than benzene. Important examples include naphthalene ($C_{10}H_8$), anthracene ($C_{14}H_{10}$), chrysene ($C_{18}H_{12}$), pyrene ($C_{16}H_{10}$), perylene ($C_{20}H_{12}$), coronene ($C_{24}H_{12}$), and ovalene ($C_{32}H_{14}$). Large polyaromatics are difficult to crack and readily form coke. Many of them are carcinogenic or mutagenic

Hydrocracking

A group of upgrading processes that convert heavy oils into light products in the presence of high-pressure hydrogen. Hydrocracker (HC) products are low in sulfur and nitrogen. HC light naphtha can be blended into gasoline. HC heavy naphtha is an excellent feedstock for catalytic reforming. With certain feeds, HC middle distillates can meet sales specifications for jet and diesel fuels. HC unconverted oil (UCO, also called hydrowax) is a superb FCC feed. In some locales, UCO serves as a feedstock for olefin production plants. For lubricant basestock production, hydrocracking replaces the aromatic extraction step by saturating aromatics to naphthenes and converting the naphthenes into isoparaffins (► *Isodewaxing*)

Hydrocracking, ebullated-bed (e-bed)

Ebullated-bed (e-bed) hydrocracking employs bifunctional catalysts. E-bed processes can achieve significant conversion of vacuum residue. A mixture of catalysts, hydrogen, and resid-containing oil is pumped upwards through a reactor into a reaction zone at high temperature and pressure. The mixture expands as hydrocracking reactions generate light molecules. At the top of the reactor, the catalyst is separated from the product gases and liquids, which pass through a series of separators. Hydrogen is scrubbed to remove H_2S and recycled. Reaction products go through a stripper to a fractionator. The catalyst is returned to the reactor with a recirculation pump at a rate that maintains equilibrium flow inside the reactor

Hydrocracking, fixed-bed catalytic

Fixed-bed catalytic hydrocracking produces C_3+ hydrocarbons from vacuum gas oil and other distillates with similar boiling points. The catalysts are bifunctional, providing both acid-derived cracking activity and metal-derived hydrogenation activity. Hydrocracking catalysts are protected by hydrotreating upstream

Hydrocracking, slurry-phase (thermal)

Slurry-phase hydrocracking is thermal, employing small-diameter additives, which might or might not be catalytic. In combination with a fixed-bed second stage, slurry-phase processes can achieve 95 wt% conversion of vacuum residue, FCC slurry oil, and coal

Hydrodemetalation (HDM)

Removal of trace metals, such as Fe, Ni, V, As, Hg, and Si, in a hydroprocessing unit. HDM is accompanied by HDS, HDN, and saturation reactions

Hydrodenitrogenation (HDN)

Conversion of organic nitrogen compounds into hydrocarbons and ammonia in a hydroprocessing unit. HDN is accompanied by HDO, HDS, and saturation reactions

Hydrodeoxygenation (HDO)

Conversion of organic oxygen compounds into hydrocarbons and water in a hydroprocessing unit.

HDO is accompanied by HDN, HDS, and saturation reactions

Hydrodesulfurization (HDS)

Conversion of organic sulfur compounds into hydrocarbons and hydrogen sulfide in a hydroprocessing unit. HDS is accompanied by HDN, HDO, and saturation reactions

Hydrofinishing

A high-pressure hydrotreating process to improve the color and oxidation stability of lubricant oils

Hydrogen

The lightest chemical element. Molecular hydrogen is H₂. In petroleum processing, H₂ streams might contain different amounts of CO, CO₂, N₂, Cl₂, CH₄, H₂S, and higher hydrocarbons. On-purpose hydrogen is manufactured by steam-hydrocarbon reforming, colloquially called ► *steam-methane reforming* (SMR). Coproduced hydrogen comes from catalytic reformers, olefin manufacturing plants (steam crackers), and electrolytic chlorine-production plants. H₂ is consumed in large quantities in hydroprocessing units

Hydrogen purification

Processes for recovering and purifying hydrogen. Pressure-swing adsorption (PSA) units produce hydrogen with 99.99% purity. In hydrotreaters and hydrocrackers, membrane units can recover > 90% of the hydrogen in high-pressure offgas streams, achieving purities > 95%. Benfield units remove CO₂ and H₂S with potassium carbonate. Amine units remove CO₂ and H₂S with diethanolamine (DEA), methyldiethanolamine (MDEA), or similar compounds. Lean-oil adsorption units remove C₃+ hydrocarbons. Turboexpanders can separate H₂ and methane from other hydrocarbons, and cryogenic units can separate H₂ from everything

Hydroisomerization

Isomerization under hydrogen, also known as isodewaxing in lubricant base oil manufacturing

Hydroprocessing

A general term for refining processes in which hydrogen is consumed. Includes catalytic hydrotreating (to remove sulfur, nitrogen, oxygen, and trace contaminants), catalytic hydrocracking (to convert heavy hydrocarbons into lighter hydrocarbons), catalytic saturation of aromatics (to produce cyclohexane from benzene), and noncatalytic thermal hydrocracking (to convert vacuum residue)

Hydrotreating

A refining process for removing contaminants from petroleum fractions in the presence of catalysts and excess hydrogen. Required pressures depend of feedstock properties. Naphtha hydrotreaters may operate at 300 psig (about 20 barg) while residue hydrotreaters require 2000–3000 psig (about 140–200 barg). Most hydrotreaters employ fixed-bed reactors. Hydrotreating reactions include saturation of olefins and aromatics, HDS, HDN, HDO, and HDM

Isobutylene (C₄H₈)

2-methylpropene, also known as isobutylene. An important feedstock for polyisobutylene, butyl rubbers, ethers (e.g., methyl-*t*-butylether) and antioxidants (e.g., butylated hydroxytoluene).

► *Hydrocarbons*

Isocracking

A fixed-bed hydrocracking process licensed by Chevron Lummus Global (CLG)

In situ

In the original place, as within a reservoir or inside a reactor

Inhibitor

A substance that prevents chemical reactions from happening

Isodewaxing

A fixed-bed hydrocracking process licensed by Chevron Lummus Global (CLG). Specifically designed to catalytically isomerize *n*-paraffins with minimal cracking, thereby reducing the wax content and pour point of lube basestocks and serve as a replacement for solvent dewaxing

Isomerate

High octane product from an isomerization unit. Excellent for blending into gasoline

Isomerization

Refinery processes for isomerizing linear paraffins. C₅/C₆ isomerization converts low octane *n*-pentane and *n*-hexane into high octane *i*-C₅ and *i*-C₆ compounds, which are excellent blendstocks for gasoline. C₄ isomerization converts normal butane into isobutane, which is a necessary feedstock for alkylation units

Isomers

Chemical compounds with the same formula but different structures

Jet and turbine fuels

Middle distillate fuels with boiling ranges of 350 to 550 °F (175–285 °C). Must meet specifications for Jet A, Jet A-1, JP-5, JP-8 and JP-50, and others. Prepared from hydrotreated straight-run kerosene and hydrocracking. Naphtha-based jet fuel (Avjet) is mainly for military usage. *Jet A and Jet A-1 (Commercial)* have been used in the US since the 1950s. Jet A-1 is used in the rest of the world. The freezing point of Jet A is –40 °C, while the freezing point of Jet A-1 is –47 °C. Both Jet A and Jet A-1 have a flash point higher than 38 °C (100 °F) with an autoignition temperature of 210 °C (410 °F). Kerosene-type jet fuel has a carbon number distribution between 8 and 16, similar to JP-8. *Jet B (Commercial)* is a fuel comprising about 70% naphtha-range material and 30% kerosene-range material. It is used for its enhanced cold-weather performance. Its lighter composition makes it more

dangerous to handle. Hence, it's rarely used except in very cold climates. Naphtha-type jet fuel has a carbon number distribution between 5 and 15, similar to JP-4. *JP-4 (Military)* is a turbine or propeller fuel, and a wide-cut fuel (kerosene-gasoline blend) for broader availability. *JP-6 (Military)* is a turbine or propeller fuel and a higher cut than JP-4 with fewer impurities. *JP-7 (Military)* is a turbine fuel and a high-flashpoint specialty kerosene used in advanced supersonic aircraft. *JP-8 (Military)* turbine fuel is kerosene modeled on the Jet A-1 fuels used in civilian aircraft

K

Kerogen

A mixture of complex organic compounds and minerals found in sedimentary rocks. Geologically, kerogen is a precursor to petroleum and natural gas. When heated above 510 °C (950 °F), kerogen decomposes into a full range of hydrocarbon gases and liquids, leaving behind trapped oil/gas, undecomposed geopolymers and minerals. *Type I kerogen (sapropelic)* has a H : C ratio > 1.25 and an O : C ratio < 0.15. It has a great tendency to produce liquid hydrocarbons. *Type II (planktonic) kerogen* has a H : C ratio < 1.25 and an O : C ratio 0.03–0.18. It tends to produce a mix of gas and oil. *Type III (Humic) kerogen* has a H : C ratio < 1 and an O : C ratio 0.03–0.3. It tends to produce coal and gas. *Type IV (residue) kerogen* has a H : C ratio < 0.5. It has no potential to produce hydrocarbons

Kerosene

A fuel with a boiling range between about 150 °C and 275 °C. Historically, due to its use as an illuminant, it was called lamp oil. At present, kerosene is widely used to fuel turbine engines, primarily those that power jet aircraft. It is also a fuel for domestic heaters or furnaces (▶ *Fuel oil* and ▶ *Jet fuel*)

Kerosene-type jet fuel

▶ *Jet fuel*, *Jet A* and *Jet B*

L

LC fining

An ebullated-bed hydrocracking process licensed by CB&I and Chevron Lumms Global (CLG). It is a hydrocracking process capable of desulfurizing, demetallizing and upgrading a wide spectrum of heavy feedstocks. It allows the processing of heavy feedstocks, including atmospheric resids, vacuum resids and bitumen

LC MAX

A CLG process that combines LC-fining and solvent ▶ *deasphalting* (SDA) in an integrated hydroprocessing configuration. Vacuum residue conversions ranging from 80 up to 90% can be attained, even when processing very difficult high-sediment feeds

Lean oil

An absorbing liquid (oil) entering the absorption tower

LHSV

An acronym for liquid hourly space velocity. LHSV is the ratio of the hourly volume of oil processed to the volume of catalyst

Light coker gas Oil (LKGO)

▶ *Gas oil*, *light coker*

Light cycle oils (LCO)

Highly aromatic light middle distillate produced by FCC units, with boiling points that range from about 200 to 400 °C (400–750 °F). Hydrotreaters saturate much of the aromatics and reduce the amounts of sulfur and nitrogen. A typical cetane number for LCO is < 25, and the sulfur content can exceed 0.5 wt%. With severe hydrotreating, LCO can be made suitable for blending into diesel. In hydrocrackers, LCO is converted into naphtha. LCO is commonly used as a *cutter stock* to decrease the viscosity of heavy fuel oils

Light ends

The lowest boiling (lightest) fractions of crude oil. Note: light ends of oil are not referred to as gases

Light gas oils

Liquid petroleum distillates heavier than naphtha, with boiling ranges similar to kerosene

Liquefied natural gas (LNG)

Natural gas, mainly methane, which has been liquefied under pressure and supercooling. The removal of carbon dioxide is critical for dry-ice formation during transportation

Liquefied petroleum gases (LPG)

Liquefied hydrocarbon gases, mainly propane and butanes. Usually sold as fuels

Liquefied refinery gases (LRG)

Hydrocarbon gas liquids produced in refineries, liquefied with pressurization and/or refrigeration. LRG might include ethane, propane, butanes, and refinery olefins (ethylene, propylene, butylene, and isobutylene)

Lithology

The physical characteristics of rocks

Lube assay

Similar to a crude assay. Specifically for crude oils or distillates intended for production of lube basestocks. Includes atmospheric distillation, vacuum distillation, aromatics content, naphthene content, wax content, viscosity, and sulfur content

Lubricant (lube)

A substance that reduces friction between surfaces in contact, which ultimately reduces the heat generated when surfaces move against each other. The finished product is a blend of basestocks with special additives. *Lubricant base oil* is a blend of one or more
▶ *basestocks*

M

Magnaforming

A semiregenerative catalytic reforming process developed by Engelhard and Atlantic Richfield (now a part of BP). Its characteristic feature is a split flow of recycled hydrogen, with about half going to the first

two reactors, which operate at mild conditions, and the other half going to the third reactor, where conditions are more severe (i. e., temperatures are higher). Initially, it employed a monometallic-supported platinum catalyst. More recently, most units contain Pt-Re catalysts for enhanced stability (► *Catalytic reforming*)

Maltenes

Solvent-soluble fraction from deasphalting

MEK

Methyl ethyl ketone, a commonly used solvent in lubricant dewaxing units

Mercaptan

► *Thiols*

Merox

A mercaptan oxidation process developed by UOP for the removal of odorous mercaptans from LPG, propane, butane, naphthas, kerosene, and jet fuel. Mercaptans are converted to liquid disulfides, which can be processed with hydrotreating

Metagenesis

A process that occurs when sedimentary rocks are exposed to the influence of magma and hydrothermal effects (metamorphism). At this physicochemical paleotransformation stage, the only remaining carbon-containing molecules are methane and a carbon residue

Metalloporphyrins

Organometallic compounds in which metals such as nickel and vanadium are bound by chelation within a tetrapyrrolic structure

Methanol (CH₃OH)

The simplest alcohol. An important source of petrochemicals. An intermediate to synthetic gasoline from the Fischer–Tropsch process

Methanol-to-gasoline (MTG)

A process that converts methanol to gasoline via the initial formation of dimethyl ether (DME) by dehydration, followed by DME dehydration over a zeolite catalyst, ZSM-5

Methanol-to-olefin (MTO)

A process that converts methanol to olefins via the initial formation of dimethyl ether (DME) followed by dehydration over an acidic zeolite catalyst, such as H-SAPO-34, to yield ethylene and propylene

MIBK

Methyl isobutyl ketone, a commonly used solvent in wax deoiling units

Microcrystalline wax

Wax derived from vacuum resids, which contains mostly cycloparaffins with *n*-alkyl and isoalkyl sidechains

Middle distillates

Fractions boiling between about 200 and 400 °C (400–700 °F). Middle distillates include kerosene, jet fuel, diesel, and fuel oils

Midstream

Business sector in the oil industry that involves bulk transportation, storage, and distribution of crude oil,

LNG, natural gas, and refined petroleum products. In some companies, midstream includes trading, marketing, and/or retail sales

Motor gasoline (Mogas)

► *Gasoline*

Motor octane number (MON)

► *Octane number*

MTBE (methyl tertiary butyl ether, (CH₃)₃COCH₃)

An oxygenate initially used in reformulated gasoline. Banned in the United States after it leaked into groundwater from some filling station storage tanks. Still used in Europe, where filling station storage tanks are properly maintained

N**Naphtha**

The lowest-boiling liquid fractions from petroleum distillation

Naphtha, heavy (HN)

Heavy naphtha boils between 90 and 200 °C. Constituents have carbon numbers ranging from 6 to 12. The octane rating is usually too low for direct blending into gasoline. Therefore, after sulfur removal, HN is generally conveyed to a catalytic reforming unit, which converts it into high-octane reformate (► *Catalytic reforming*). Small amounts of hydrotreated HN are used as solvents

Naphtha, light (LN)

Light naphtha boils between 30 and 90 °C. Constituents have carbon numbers ranging from 5 to 6. The octane rating of straight-run LN is often suitable for blending into gasoline, usually after treating to remove sulfur compounds (► *Merox*). Treated LN can be used as a solvent

Naphtha, petrochemical (PCN)

Full-range low-sulfur naphtha that is converted into olefins in steam-cracking plants. Paraffinic naphthas are preferred

Naphthenes

► *Hydrocarbons, naphthenes*

Naphthenic crudes (asphaltic crudes)

Contain more naphthenes than paraffinic crudes. Good for producing certain lubricant basestocks

Natural gas

A mixture of naturally occurring hydrocarbon gases, primarily methane. Used for fuel and to make petrochemicals. Merchant natural gas must contain less than 2 vol% CO₂ and less than 4 ppmv hydrogen sulfide

Natural gas liquids (NGL)

Components of natural gas other than methane, including ethane, propane, butane, isobutane and pentanes. Separated from methane by absorption, condensation or other methods in a field facility or in a gas processing plant

Natural gasoline

A mixture of hydrocarbons, mostly pentanes and heavier, which are extracted from natural gas. To be

transported in common-carrier pipelines, it must meet specifications on vapor pressure, endpoint, and composition set by the Gas Processors Association or similar organizations

Needle coke

▶ *Coke, needle*

Normal paraffin

▶ *Hydrocarbons, paraffins*

O

Octane number

A measure of the burning quality of gasoline (petrol) in a spark-ignition internal combustion engine. A higher octane number (ON) means a fuel is less susceptible to knocking (premature ignition). Specifically, ON is the percentage by volume of isooctane in a combustible mixture containing isooctane (ON = 100) and normal heptane (ON=0) for which the knocking characteristics match those of the fuel being tested. The octane number tested in a standard engine at 900 rpm to compare with highway driving conditions is the *Motor octane number (MON)*. The *Research octane number (RON)* is tested in a standard engine at 600 rpm to compare with low-speed or city driving conditions. The *Posted octane number (PON)* is defined as $(RON + MON)/2$ and is posted on pumps in gasoline filling stations in North America, where it is also referred to as the antiknock index (AKI)

Oil sand (tar sand)

Loose sand or partially consolidated sandstone containing mixtures of sand, clay, water, and bitumen

Oil shale

Organic-rich fine-grained sedimentary rock containing kerogen from which liquid hydrocarbons can be recovered

Olefins

▶ *Hydrocarbons, olefins*

Organization of Petroleum Exporting Countries (OPEC)

An intergovernmental organization, founded in 1960, whose stated objective is to *coordinate and unify the petroleum policies of member countries*. Founding members include Iran, Iraq, Kuwait, Saudi Arabia, and Venezuela. Other members now include Algeria, Angola, Ecuador, Libya, Nigeria, Qatar, and the United Arab Emirates. Former members are Gabon and Indonesia. It is not true that Alberta, a Province of Canada, is a member of OPEC

Outcrop

A visible exposure of bedrock or ancient superficial deposits on the surface of the Earth

Overburden rock

Rock that overlies the source rock, seal rock, and reservoir rock of a petroleum system. The weight of the overburden affects the pressure and temperature in a reservoir

P

PAH

▶ *Polynuclear aromatic hydrocarbon*

Paraffinic (waxy) crudes

▶ *Crude oil, paraffinic*

Paraffins

▶ *Hydrocarbons, paraffins*

Partial oxidation (POX)

Process for converting coke, coal, or resid into a mixture of CO and H₂ (synthesis gas) in the presence of substoichiometric oxygen and steam

Petrol

A term commonly used in some countries as a synonym for gasoline

Petrolatum

Petroleum jelly derived from dewaxing heavy lube basestocks. Its color is translucent white, amber or yellowish. It has no odor or taste. It can be used in medicines, ointments and cosmetics, as well as in polishes and greases

Petroleum

Generally includes liquid crude oils and condensates. Sometimes includes natural gas and synthetic petroleum. Synthetic petroleum, also known as synthetic crude or syncrude, is liquid obtained from the processing of oil shale, oil sands, and biomass (▶ *Crude oil*). Physical properties of petroleum include boiling point, density, viscosity, heteroatom contents, etc., measured by crude assay tests

Petroleum classification

Petroleum (crude oil) is broadly classified as paraffinic, asphaltic or mixed crudes by Watson Characterization Factor for paraffinic or Correlation Index for aromaticity (▶ *Crude oil*)

Petroleum coke

▶ *Coke, petroleum*

Petroleum components (chemical composition)

Petroleum is mainly composed of hydrocarbons, which may include heteroatoms of sulfur, nitrogen, oxygen and metals. Hydrocarbons include saturates, such as paraffins and naphthenes, and aromatics

Petroleum engineering

A field of engineering related to the production of crude oil and natural gas, including drilling engineering, reservoir engineering, production engineering, etc.

Petroleum gas

Hydrocarbons that are gases at ambient temperature and pressure. Includes natural methane and ethane along with C₂–C₄ olefins from refining processes. May include small amounts of propane and butanes

Petroleum system (hydrocarbon system)

The petroleum system is a unifying concept that encompasses all of the disparate elements and processes of petroleum geology, including the essential physical elements: source rock, in which oil and gas were formed; reservoir rock, in which oil and

gas accumulate; impermeable seal rock (cap rock), which prevents oil and gas from escaping the reservoir; and overburden rock (► *Overburden*). It also includes the processes that form traps and enable petroleum formation, migration, and accumulation. Finally, it includes mechanisms for the movement of petroleum from reservoirs and other sources into shows, seeps, or accumulations

PIONA Analysis

► *PONA analysis*

Pipe still

A distillation apparatus composed of a series of pipes used to fractionate petroleum. Synonym for atmospheric distillation unit

Plastics

Materials made of organic compounds, typically polymers of high mass. Plastics are malleable and can be molded into solids

Play or petroleum play

A group of oil fields or prospects in a geographic region that are controlled by the same set of geological circumstances. Usually refers to an area with conditions favorable for hydrocarbon accumulation, including a specific source, reservoir, and trap type

PNA

► *Polynuclear aromatic hydrocarbon*

Polyalphaolefin (PAO)

Star-shaped polymer (oligomer) with a central carbon atom connected to four arms (alkyl groups). Derived from alpha olefins and used as high-viscosity index lube basestock

Polyester

Polymer with units linked by ester groups. Mainly used as a resin for making synthetic textile fibers

Polymer gasoline

Gasoline product from polymerization of light olefins

Polymerization

A chemical reaction in which two or more small molecules combine to form larger molecules that contain repeating structural units of the original molecules. In oil refining, catalytic polymerization (Catpoly) converts propylene (and sometimes isobutylenes) into high-octane C6–C12 isoparaffins suitable for gasoline blending. The most common catalyst is solid phosphoric acid (SPA). In the petrochemical industry, polymerization is the key process for producing high polymers, such as polyethylenes and polypropylenes

Polynuclear aromatic hydrocarbon (PAH or PNA)

Molecules that include at least two fused aromatic rings (► *Hydrocarbons*)

Polyolefins

High polymers derived from olefins, such as polyethylenes, polypropylenes, ethylene/propylene copolymers, polyisobutylenes, etc.

Polyol Esters

Esters made from polyols (pentaerithritol, trimethylol propane or neopentyl glycol) with acid. Due to their high viscosity indexes (VIs), they are excellent Group V lube basestocks

PONA or PIONA analysis

Distributions of paraffins, isoparaffins, olefins, naphthenes, and aromatics

Pour point

The lowest temperature at which an oil loses fluidity. Determined as 3 °C above the temperature at which a sample no longer moves when inverted. Important parameter for pipeline transportation and diesel fuel

Powerforming

A semiregenerative catalytic reforming process developed by Esso (now ExxonMobil) (► *Catalytic reforming*)

Pressure swing adsorption (PSA)

An adsorbant-based process in which a gas is purified by differential pressure. In refining, PSA is used for hydrogen purification. Applications include removal of CO and CO₂ from ► *SMR* product gas, and purification of refinery offgas streams. PSA employs adsorbents, usually activated carbon, silica gel, alumina, and zeolite molecular sieves. The process steps are as follows: 1. At high pressure, *dirty* gas containing hydrogen, CO, CO₂, N₂, Ar, light hydrocarbons, and sometimes H₂S, passes over a clean bed of adsorbents. The adsorbents remove most of the nonhydrogen components. The hydrogen continues on to a subsequent reactor. 2. In the first low-pressure step, the reactor is depressured under concurrent flow, i. e., the gases continue to flow in the original direction. 3. During the second low-pressure step, clean hydrogen flows across the loaded adsorbent in the opposite direction, sweeping the contaminants into a tail gas stream. When the bed is clean, the reactor is repressured with dirty gas. PSA can achieve 80–90% hydrogen recovery while producing hydrogen with 99.99 vol% purity

Primary migration

The expulsion of newly generated hydrocarbons from a source rock and movement into carrier rock

Primary recovery

Oil recovery by natural underground pressure, usually supplied by associated natural gas and evolution of dissolved gas (gas drive), or driven by hydrostatic pressure, liquid expansion and expansion of reservoir water (water drive)

Process control

A system of valves, instruments, controllers, and computer programs that are used to operate an industrial process unit. *Advanced process control (APC)* describes a broad range of techniques that enhance process control. Applications can reside within a DCS computer or supervisory computer. *Advanced regulatory control (ARC)* describes techniques including feed-forward, override, adaptive gain, switching logic, and inferentials. It is a catch-all term for customized DCS-resident techniques that do not fall into any other category. ARCs are typically implemented in the DCS computer. *Inferential control* calculates a stream property from process measurements. Inferentials are developed and verified

with laboratory measurements. They are used to replace online analyzers when suitable analyzers do not exist or are deemed to be too expensive to install and maintain. *Model predictive control (MPC)*, also called *multivariable predictive control (MVPC)*, manipulates several MVs simultaneously to achieve multiple objects. It is based on a matrix of important independent variables (MVs and DVs), a matrix of controlled variables, and a third matrix that captures dynamic relationships between the other two. Proper matrix identification, for example with manual or automated step tests, is the key to success. An MPC controller executes on a predetermined schedule, typically every minute; some controllers in the glass industry execute far more frequently

Process control, distributed control system (DCS)

A system in which control elements (controllers) are located in many places throughout a system. In modern facilities, operators in a central control room can operate important control elements from a single location. Computerized DCS systems include the ability to host computer programs, including ARC and APC applications

Process control, proportional–integral–derivative (PID)

A common type of feedback controller, which continuously calculates the difference between a measurement and a setpoint. The controller calculates how to minimize the error based on P, I, and/or D algorithms. It then adjusts the relevant MV accordingly

Process control, time to steady state (TSS)

The time it takes for a CV to reach a steady value after an MV is changed

Process control, variables

The *Controlled variable (CV)* is the process target achieved by adjusting manipulated variables. The *Disturbance variable (DV)* is an independent variable, such as ambient temperature, which cannot be manipulated. The *Manipulated variable (MV)* is an independent variable that can be used to manage process performance. The change in the value of a CV divided by a unit change in an MV is called *Gain*

Production

A branch of upstream petroleum business that recovers gas or oil from reservoirs

Production engineering

A branch of petroleum engineering that includes a combination of manufacturing technology, engineering practices, and management principles related to oil and gas production. A production engineer is engaged in reviewing seismic and other data, designing and executing drilling plans, selecting drilling technology (mud weight, bits, piping, centralizers, motors, etc.) and well completion technology, and the handling of produced oil and gas at the well head

Propane (C₃H₈)

A three-carbon alkane used as a chillant in sulfuric

acid-catalyzed alkylation, a solvent in deasphalting, or a diluent in catalytic polymerization of propylene

► *Hydrocarbons*

Propylene (C₃H₆)

► *Hydrocarbons*

Prospect

An individual exploration target. A specific trap that has been identified and mapped but has not yet been drilled

Pseudocomponents

Hypothetical components used to model petroleum during the design and optimization of equipment and processes. The properties of pseudocomponents are averages of the properties of many individual compounds with similar boiling ranges. Traditional pseudocomponents do not include molecular information, such as hydrocarbon types or concentrations of heteroelements. This makes them ill-suited for kinetic reaction models, in which conversion, HDS, HDN, and saturation are important parameters

PVT measurements

The pressure, volume and temperature of a material, usually a gas

Pyrolysis

Thermochemical decomposition of organic material at elevated temperatures in the absence of oxygen

Q

Quantitative structure-activity relationship (QSAR)

Correlation or classification that quantitatively relates the response (activity, adsorptivity, etc.) of a group of chemicals to changes in certain common physicochemical characteristics (descriptors) of the constituent species, usually by modeling

Quench

A relatively cool stream (liquid or gas), which is mixed with hot reactants to control reaction temperatures

R

Raffinate

In general, the raffinate in a solvent extraction process is the stream from which undesired components have been removed. In lube basestock preparation, the raffinate is the dearomatized oil. In extractive wax deoiling, the raffinate is the oil-free wax

Raffinate hydroconversion

Hydroconversion of raffinate from solvent extraction processes to produce lubricant basestock with a high viscosity index and low volatility

Reboiler

A heater or heat exchanger at the bottom of an atmospheric distillation tower, which vaporizes a portion of the liquid and introduce it several trays above the bottom to assure some of light components not carried out with the bottom product

Recycle cut point (RCP)

In hydrocracking, the recycle cutpoint (RCP) is the final boiling point of the heaviest product of conversion. If it were possible for a fractionator to give square-cut distillation with no overlap, the RCP would be the initial boiling point of unconverted oil (UCO). In many units, the hydrocracker UCO is recycled. The analogous term for once-through units, in which there is no recycling, is *conversion cutpoint*. RCP has been applied to delayed coking units in which heavy liquids are recycled to improve separation in the fractionator

Refinery

An installation that manufactures finished petroleum products from crude oil, unfinished oils, natural gas liquids, other hydrocarbon streams, and oxygenates. Refinery operations include: planning and scheduling, crude blending, preprocessing in desalting units, separation with distillation or extraction, treating (including chemical treatment, mercaptan oxidation, and hydrotreating) conversion (breaking C–C bonds) with thermal and catalytic cracking, catalytic reforming (dehydrogenation of naphthenes and formation of ring compounds; no C–C bond breaking), alkylation and polymerization (making high-octane C6 to C12 molecules from C3 to C5 molecules), catalytic isomerization, lubricant manufacturing, sulfur removal and recovery, hydrogen production, product blending, and environmental protection

Refinery, hydroskimming

A refinery with atmospheric distillation, hydrotreating and reforming units designed to produce desulfurized fuels, petrochemical naphtha, and high-octane gasoline. In many modern hydroskimming refineries, the atmospheric residue goes to an asphalt plant

Refinery, integrated

A refinery integrated with a petrochemical manufacturing plant

Refinery, topping (simple)

A simple refinery that consists of tankage, an atmospheric distillation unit, recovery units for gas and light hydrocarbons and necessary utility systems (steam, power and water treatment plant). Due to tight restrictions on product quality, very few of these are left in developed countries

Refinery yield

The amount of finished product from a refinery divided by the sum of feedstocks (crude oil and other imported unfinished oils), expressed either as volume percent or weight percent. The calculation generally excludes produced sulfur, natural gas liquids, oxygenates and other imported blending components

Reflux

That portion of the condensed top stream from an atmospheric distillation tower that is returned to the tower to provide cooling. Reintroduction of the condensed liquid reduces the amount of heavy components that otherwise would be carried out with

the top product. Reflux is an essential manipulated variable (MV) for controlling tower temperature

Reflux ratio

The ratio of the portion of condensed liquid returning to the distillation tower to the portion collected as top product

Reformate

Liquid product from a catalytic reformer. Reformate is highly aromatic, and has a high octane number and a low vapor pressure (RVP). It can be blended into gasoline or converted into solvents and chemical precursors in an aromatics plant

Reforming, catalytic

A catalytic process for dehydrogenating naphthenes into aromatics. Also converts acyclic paraffins to alkyl cyclopentanes and alkyl cyclohexanes, which then undergo dehydrogenation. The products are high-quality hydrogen and reformate (► *Reformate* and ► *Catalytic reforming*)

Reforming, thermal

A process to convert low-octane naphtha to high-octane gasoline

Reformulated gasoline

Low-emissions gasoline that meets regulations promulgated by the US Environmental Protection Agency (EPA) under Section 211(k) of the Clean Air Act. Specifications include upper limits on RVP, olefins, sulfur, air toxics such as benzene, and lower limits on oxygen. A gasoline can be designated as reformulated if it meets or exceeds EPA emissions and benzene content standards in engine tests, even though it may not meet all composition requirements (e.g., oxygen content). This category includes Oxygenated Fuels Program Reformulated Gasoline (OPRG). Reformulated gasoline excludes Reformulated Blendstock for Oxygenate Blending (RBOB) and Gasoline Treated as Blendstock (GTAB)

Refractive Index

The ratio of the velocity of light of a specific wavelength in air to the velocity in a test sample. Used to estimate polynuclear aromatic (PNA) content

Regenerator

► *Catalyst, regeneration*

Reid vapor pressure (RVP)

Common measure of the volatility of gasoline determined at 100 °F (≈ 38 °C) of vapor pressure of the liquid by ASTM D-323

Research octane number (RON)

► *Octane number*

Reserve

Oil and gas accumulations that have been drilled and can be produced economically

Reservoir (petroleum)

Subsurface pool of oil or gas contained in porous or fractured rock formation, broadly divided into conventional and unconventional reservoirs. In *conventional reservoirs* buoyant forces keep hydrocarbons in place below a sealing caprock. The term *unconventional reservoir* is used for any reservoir that requires special recovery operations.

These include tight shale, tight sands, oil shales, coalbed methane, heavy oil, oil sands, and gas-hydrate deposits

Reservoir engineering

A branch of petroleum engineering concerned with characterizing and defining oil and gas reservoirs. Reservoir engineers work closely with production engineers as they develop drilling and production plans. It also deals with drainage problems or other challenges arising during development and production

Resid

A term commonly used in the oil industry as a synonym for *residue* or *residuum*. Specifically refers to the residue at the bottom of a distillation after all light fractions distill off

Resid FCC (RFCC)

A version of ► *FCC* designed to process resid. Includes provisions to deal with both the high metals content of resid and its high propensity to form coke. Typically, most metals are removed in an upstream resid hydrotreater. Remaining metals are accommodated with metal-resistant catalysts. When burned in the regenerator, the excess coke on the FCC catalysts produces more than enough heat to run the unit. The excess heat can be removed with catalyst coolers (steam coils) in the regenerator. Another solution is to burn off part of the coke in a primary regenerator and the rest of the coke in a secondary regenerator

Resid hydrocracking (RHC)

Hydrocracking processes that convert resids (► *Hydrocracking, e-bed* and ► *Hydrocracking, slurry-phase*)

Resid upgrading

Processes for upgrading resids, either thermally, catalytically, or with extraction (► *Coking* ► *Hydrocracking, e-bed* ► *Hydrocracking, slurry-phase* and ► *deasphalting*). The choice of technologies depends upon both the quality of the resid stream and the desired quality of the naphtha, diesel, and VGO products. Products from coking and solvent extraction require hydroprocessing to remove sulfur, nitrogen, metals, Conradson carbon residue (CCR), and any remaining asphaltene

Residual oil supercritical extraction (ROSE)

A process for extracting oil from atmospheric and vacuum resids with supercritical propane, butane or pentane, leaving behind resins and asphaltenes

Residuum

► *Resid*

Resin

Polar fraction of petroleum isolated by solvent fractionation, containing relatively high-molecular-weight, polar, polycyclic, aromatic ring compounds

RFCC

Resid FCC or reduced crude cracking (► *FCC*)

Rheniforming

A semiregenerative reforming process developed by Chevron, which employs bimetallic platinum-rhenium

catalysts. The rhenium improves catalyst stability (► *Catalytic reforming*)

Rich oil

The absorbing liquid (oil) containing selectively absorbed components

Rock-Eval pyrolysis

An analytical method used in petroleum exploration to measure the quantity, quality, and thermal maturity of organic matter in rock samples

S

Scrubber

An apparatus to remove particulates and/or gases from process streams, including industrial exhaust streams. Examples include amine scrubbers, which remove H₂S and CO₂, and flue-gas scrubbers, some of which remove SO_x and NO_x

Secondary migration

After primary migration, further movement of the hydrocarbons in carrier rock into reservoir rock in a hydrocarbon trap or other area of accumulation (reservoir)

Secondary recovery

When the natural pressure of a reservoir is low and not sufficient for oil recovery, surface or submerged pumps are used. Alternatively, it is possible to increase reservoir pressure by water injection (water flood) and gas injection (gas flood). Chemicals are often applied to free up oils

Selective catalytic reduction (SCR)

A catalytic process for removing nitrogen oxides from flue gas. The nitrogen oxides are reacted with ammonia to produce N₂ and water

Selectivity

The amount (percentage) of a desired product in the total product

Shale gas

Natural gas trapped within shale formations and recovered by unconventional means, such as hydraulic fracturing

Shale oil

Oil trapped within shale formations and recovered by unconventional means, such as hydraulic fracturing. Also refers to oil produced by thermally cracking the kerogen in oil shale

Shell Claus Offgas Treatment (SCOT)

The sulfur compounds in Claus tail gas are converted to H₂S by hydrotreating over a Co-Mo catalyst. The gas is cooled and contacted with di-isopropanolamine (DIPA) to recover the H₂S. The sulfur-rich DIPA is sent to a stripper, where H₂S is removed and sent back to the Claus plant. The lean DIPA is recycled to the absorber

Slack wax

Raw wax containing oil. A byproduct of solvent dewaxing during lubricant oil manufacturing

Slurry Reactor

Slurry reactors process mixtures of solids, mixtures, and gases, where the solids are so finely divided that

they behave as part of the liquid. Bubble-point gas is introduced at the bottom of the reactor and reacts with the slurry as the mixture moves toward the top (► *Hydrocracking, slurry-phase*)

Smoke point

A test (ASTM D1322) performed to determine the smoke-forming tendency of jet fuels and kerosene. It is the maximum flame height at which a test fuel will burn without smoking in a standard smoke point lamp and a circular wick made of woven cotton. Smoke points are highest for paraffins and lowest for aromatics

Solubility

The amount of a compound or liquid that can be dissolved in a specific amount of solvent

Sour crude

Crude oil containing > 0.5 wt% total sulfur

Sour gas

Natural gas and any other gas containing more than 5.7 mg of H₂S per cubic meter (equivalent to 4 ppmv in methane)

Source rock

Rocks containing kerogens that could generate hydrocarbons

SO_x

The sum of SO₂ and SO₃

Sponge oil

The liquid used in an absorption tower to soak up the constituents to be extracted

Stabilizer

A fractionator used to stabilize products by removing volatile or reactive lighter components. A prominent example is removal of butane from gasoline range streams

Steam-assisted gravity drainage (SAGD)

An enhanced oil recovery technology for producing heavy crude oil and bitumen. A pair of horizontal wells is drilled into the oil reservoir. Steam is pumped through the top well, where it mobilizes oil with heat. The oil flows down to the bottom well, a few meters below, where it is collected and brought to the surface

Steam cracking

A process for converting saturated gaseous or liquid hydrocarbons – such as ethane, LPG, naphtha, and hydrocracker UCO – into olefins. The feed is diluted with steam and heated to ≈ 1050 °C in Cr-Ni reactor tubes, where the hydrocarbons crack into smaller compounds, primarily olefins; at such high temperatures, olefins are more stable than paraffins. Reaction time is measured in milliseconds. The cracked products exit at around 850 °C and are rapidly quenched to 300 °C to improve yields and avoid coke formation. Steam cracking is the principal industrial means of producing ethylene, propylene, and other olefins, which are converted into polyolefins (polyethylenes, polypropylenes, etc.)

Steam-hydrocarbon reforming

(► *Steam-methane reforming, SMR*).

Steam-hydrocarbon reforming is a more accurate term

than SMR, because some feeds contain up to 20% nonmethane hydrocarbons

Steam-methane reforming (SMR)

The most common method for producing high-quality hydrogen from methane. The reaction between steam and methane (1 : 1 mole ratio) occurs at 1500 °F (815 °C) over a nickel catalyst. The main reaction products are hydrogen and carbon monoxide (3 : 1 ratio). In a downstream high-temperature shift reactor, CO reacts with water via the water-gas reaction to form CO₂ and more hydrogen. In modern units, CO and CO₂ are removed from the product with a PSA unit, which makes hydrogen with a purity > 99.9%. It is common now to send refinery offgas streams to SMR units; in addition to methane, these offgas streams contain hydrogen and C2–C3 gases

Still gas (refinery gas)

A general term for gases produced in refineries by strippers or distillation units. Depending on composition, still gas is used as a refinery fuel, a source of recoverable hydrogen, or a petrochemical feedstock

Straight-run

A fraction taken directly from the atmospheric distillation unit and not from a conversion process

Strategic petroleum reserve

Petroleum stocks maintained by the US government for use during periods of major supply interruption

Stratum

A layer or a series of layers of rock in the ground

Surfactant

A chemical that reduces interfacial resistance for the mixing of oil and water. In oil production, surfactants change the wettability of reservoir rock

Sweet crude

Crude oil containing < 0.5 wt% total sulfur

Sweet gas

Natural gas with a low sulfur content (< 4 ppm by volume under standard temperature and pressure)

Sweetening

A process for improving odor and color in petroleum products by oxidizing or removing sulfur-containing compounds

Syncrude (synthetic crude oil)

Crude oil produced from coal, bitumen or shale oil; in this context, shale oil comes from retorted oil shale. To make so-called synthetic bitumen (synbit), bitumen is upgraded by a coker, visbreaker, or hydroprocessing unit

Syngas (synthetic gas)

A mixture of CO and hydrogen produced by steam-methane reforming, partial oxidation, or Fischer–Tropsch synthesis

Synthetic gasoline (note: not syngas)

Gasoline produced from biomass, coal and heavy oil fractions with Fischer–Tropsch or methanol-to-gasoline (MTG) processes

Synthetic lube basestock (synlube)

Basestock synthesized from polyalphaolefins. Used to make lubricants of very high quality, with high

viscosity index (VI), low pour point, low volatility, and high thermal and oxidation stability

T

Tail ends

The highest boiling components of a mixture

Tank farm

A collection of tanks at a given location for storing crude oil and products

Tanker and barge

Tankers transport crude oil and products over oceans and seas. The largest supertankers can carry more than three million barrels of crude. Barges transport smaller quantities on rivers or lakes

Tar sand

► *Oil sand*

Tertiary recovery (enhanced oil recovery)

Tertiary recovery or enhanced oil recovery (EOR) is designed to reduce viscosity of the crude oil in low-permeability carbonate reservoirs that respond poorly to conventional secondary recovery. Three primary techniques for EOR are gas injection, chemical injection, and thermal recovery

Tetraethyl lead (TEL)

A nearly extinct gasoline additive used to enhance the octane number of gasoline. It is used in avgas and in some countries with loose environmental regulations

Thermal cracking

Breaking C–C bonds with thermal energy (heat). Modern thermal cracking processes include visbreaking, delayed coking, fluid coking, and one particular brand of slurry-phase hydrocracking. Compared to catalytic cracking, thermal cracking makes far more undesirable light ends (methane, ethane) and olefinic naphtha. The advantage of noncatalytic thermal hydrocracking is the ability to achieve up to 95 wt% conversion of vacuum resid

Thermal recovery

Thermal recovery introduces heat into a reservoir with steam, hot water, or hot gas. This increases pressure and reduces the viscosity of oil in the reservoir, allowing it to make its way to a production well. In situ combustion, supported by pumping air into an injection well, is another thermal recovery method

Thermofor catalytic cracking (TCC)

An obsolete catalytic cracking process, which contained a moving bed to which regenerated catalysts were added and from which spent catalysts were removed. Catalysts were transported by baskets on elevators

Thermoplastic

Synthetic resin that becomes plastic on heating and hardens on cooling

Thiols (mercaptans)

Organosulfur compounds containing an –SH group. Many have strong odor. Some mercaptans, especially *t*-butyl mercaptan, are used as odorants in natural gas for leak detection

Toe-to-heel air injection (THAI)

An in situ combustion method for producing heavy oil, also known as *fireflooding*. Air is introduced through a vertical injection well. Oil is produced from a horizontal well having its *toe* in close proximity to the air-injection well. Combustion supported by air injection generates a flame front, which pushes oil through the horizontal well to its *heel*, where a production well conveys the oil to the surface

Toluene (C₆H₅CH₃)

An aromatic hydrocarbon, used as a solvent or petrochemical feedstock (► *Hydrocarbons*)

Topped crude

The bottoms of atmospheric distillation of crude oil after the removal of gas oil and lighter fractions

Topping

Removal of light fractions from crude oil by distillation (► *Refinery*, *topping*)

Total acid number (TAN)

The acidity of a crude oil determined by titration with potassium hydroxide. Results are expressed as milligrams of KOH required to neutralize the acids in a gram of oil

Total boiling point (TBP) curve

A distillation curve in which accumulated yield is plotted against boiling point. Determined from atmospheric and vacuum distillation, where vacuum distillation boiling points are converted to atmospheric equivalent boiling points (AEBP)

Trap

Impermeable rock that enables the accumulation of petroleum. Typical petroleum traps include anticline traps, faults and salt-domes (► *Petroleum system*)

Trickle bed reactor

A fixed-bed reactor containing a packed bed of catalyst, in which reacting fluids flow concurrently downwards. Typically used in catalytic hydrogenation, hydrotreating, and hydrocracking processes

True boiling point (TBP) curve

A distillation curve in which accumulated yield is plotted versus boiling point, determined from atmospheric and vacuum distillation with vacuum distillation boiling points converted to atmospheric equivalent boiling points (AEBP)

U

Ultraforming

A cyclic semiregenerative reforming process developed by Standard Oil of Indiana (Amoco, now a part of BP) in 1954

Ultralow sulfur diesel (ULSD)

Diesel fuel with sulfur content < 10 ppmw in North America, Europe and many other countries. As of January 1 2017, ULSD in populous regions of China must contain < 10 ppmw sulfur

Unicracking

A collection of hydrocracking processes designed and licensed by UOP

Uniflex

A slurry-phase hydrocracking process licensed by UOP that achieves higher than 90 wt% conversion of vacuum residue and other low-quality feeds. Achieves > 60 vol% diesel yield. Uniflex VGO can go to a conventional refinery unit, such as FCC or a hydrocracker

Upstream

Business sector in the oil industry. Includes discovery (exploration) and recovery (production) of crude oils and natural gases. Commonly known as exploration and production (E&P)

Urea dewaxing

Using urea to dissolve waxy paraffins for producing low-pour-point oils

V**Vacuum distillation**

► *Distillation, vacuum*

Vacuum gas oil (VGO)

► *Gas oil, vacuum*

Vacuum residue or vacuum resid (VR)

Resid from a vacuum distillation unit; typically everything that boils above about 1050 °F (≈ 565 °C) (AEBP). Contains the highest boiling and nonboiling components in crude oil

Van Krevelen diagram

Plots the hydrogen-to-carbon ratio as a function of the oxygen-to-carbon ratio. Used to assess kerogens and petroleum

Vapor lock

A condition under atmospheric conditions of high temperature that causes excessive gasoline vaporize in fuel lines, disabling the fuel pump and shutting down the engine

Veba Combi-Cracking (VCC)

A two-stage hydrocracking process developed by Veba (now BP) and licensed by KBR. Vacuum residue, FCC slurry oil, coal tar, and coal are converted into finished gasoline, finished diesel, and high-quality unconverted oil. Total conversion of 1050 °F-plus (565 °C-plus) can exceed 95 wt%. Slurry-phase hydrocracking occurs in the first stage. The slurry is a mixture of oil, hydrogen, and a finely divided additive. Thermal cracking generates light products and intermediate microcoke, which deposits on the additive and undergoes hydrogenation. First stage products then go to the second stage, which is a conventional fixed-bed hydrocracking unit. The hydrogen pressure for both stages is 200 bar. Temperature in the first stage is about 465 °C. Second-stage temperatures are lower
 (► *Hydrocracking, slurry-phase*)

Visbreaking

A mild thermal cracking process, which operates at 470–490 °C (880–920 °F) and at 3.4–13.8 bar (50–200 psi), and reduces the viscosity of fuel oil to acceptable levels. Conversion is not the prime

purpose. The residence time is low to avoid coke formation. The cracking reaction is quenched before completion to minimize overcracking

Visbreaking, coiled cracking

Occurs in furnace tubes (coils). The quench is provided by heat exchange with feed or a stream of cold oil. Compared with soaker visbreaking, it has higher outlet temperatures (885–930 °F or 473–500 °C) and shorter reaction time (1–3 min)

Visbreaking, soaker cracking

Occurs not in the furnace, but in a soaker drum after the furnace. Oil is held in the drum for a predetermined time prior to quenching to allow cracking to occur. Compared with coiled visbreaking, it has lower outlet temperatures (800–830 °F or 427–433 °C) and longer reaction time

Viscosity

Resistance of a fluid to shear and/or tensile stress. The dynamic viscosity is the resistance of a fluid against shearing flows, where adjacent layers move with different speeds, parallel to each other. Kinematic viscosity is the ratio of the absolute viscosity of a liquid to its specific gravity at the temperature at which the viscosity is measured

Viscosity index (VI)

A measure of kinematic viscosity as a function of temperature. Higher VI lubricant oils are superior, because for them the relative change in viscosity with temperature is lower

W**Water flooding**

The injection of water into a reservoir to displace oil for secondary recovery

Water gas shift (WGS) reaction

Reaction of carbon monoxide (CO) with steam to produce carbon dioxide and hydrogen. The second reaction step in a steam-methane (steam-hydrocarbon) reformer

Watson (or UOP) characterization factor (K_w)

► *Characterization factor*

Wax (petroleum wax)

A solid or semisolid material consisting of a mixture of hydrocarbons obtained or derived from petroleum fractions, or through a Fischer–Tropsch-type process, in which straight-chained paraffins with high carbon numbers predominate

Wax deoiling

A process for making food-grade wax from low-sulfur slack wax, which is a byproduct of solvent dewaxing during lube basestock preparation. Oil is extracted from the slack wax with solvents such as MIBK (methylisobutyl ketone). The wax is crystallized in a chiller and recovered by rotary drum filtration

Weathered crude oil

Crude oil that has lost an appreciable quantity of more volatile components during transportation, handling and storage

Weight hourly space velocity (WHSV)

Weight of feed flow per hour divided by catalyst weight. Units: 1/hr

Well completion

In petroleum production, the process of making a well ready for oil recovery or fluid injection. Wells are completed by casing the well bore with steel pipe and cementing the casing into place

Well log

A record of chemical and physical measurements along the depth of a well bore. Well logs can be updated in real time with signals transmitted via wire to the surface. An *Acoustic well log (Aonic)* is a record of the speed of sound as it travels through rock, and is useful in determining porosity. *Electric resistivity well logging* records the resistivity of the rock. The downbore measurement of various physical properties, such as porosity, resistivity, mineral contents, etc., versus depth is also often described as electric resistivity well logging. Well logs augment other geological information and hence are important in defining a reservoir. Oil-filled sand has higher resistivity than water-filled sand. A *Gravity well log* (or radioactivity well log) is a record of the absorption of gamma radiation through the rock, used to determine the rock density. A *Magnetic well log* is a record of the mineral content of rock formations, especially ferromagnetic minerals

Well stimulation

Performed on oil or gas wells to increase the flow of hydrocarbons for higher production

Wellhead

Equipment at the surface of an oil or gas well that provides the structural and pressure-containing interface for the drilling and production equipment

West Texas Intermediate (WTI)

An important group of crude oils produced in Texas

and southern Louisiana, which is used as a reference crude for domestic trading

Wet gas

Natural gas containing C₄+ and natural gasoline that has not been removed

White oil

Kerosene or treated kerosene used for pharmaceutical purposes or in the food industry

wppm

Parts per million by weight

X**Xylene (C₆H₄(CH₃)₂)**

An important aromatic molecule (► *Hydrocarbons*), used as a solvent or petrochemical feedstock

Y**Yen–Mullins model (modified Yen model)**

Describes the predominant molecular and colloidal structure of asphaltenes in crude oil, whether the asphaltene molecules form nanoaggregates or clusters. The model provides a foundation for the development of the first asphaltene equation of state for predicting asphaltene gradients in oil reservoirs

Z**Zeolites, synthetic**

Microporous, crystalline aluminosilicates used as commercial adsorbents and molecular sieves, and as catalyst components in petroleum refining

ZSM-5

Important shape-selective aluminosilicate patented by Mobil in 1975. Used in numerous heterogeneous catalytic processes, including FCC, catalytic dewaxing, and the conversion of methanol to gasoline

About the Authors



Hendratta N. Ali

Fort Hays State University
Dept. Geosciences
Hays, USA
h_ali@fhsu.edu

Chapter B.9

Hendratta Ali obtained her PhD in Geology from Oklahoma State University-Stillwater in 2010. Prior to this, she obtained a Diplôme D'études Approfondie (DEA), MSc in Soil Science, and a BSc in Earth Sciences, from the University of Yaoundé I, Cameroon. She teaches Geosciences and coordinates the Petroleum Geology Program at Fort Hays State University, Kansas, USA.

Mubarak M. Al-Mujaibel

Kuwait Institute for Scientific Research (KISR)
Environment & Life Sciences Research Center
Safat, Kuwait
mmojbel@kisir.edu.kw

Chapter C.32

Mubarak Al-Mujaibel is a Research Technician with over 15 years of experience in various petroleum downstream processes, including pilot unit commissioning for hydro-cracking and distillation. He graduated from the Technical Studies College of Kuwait, Chemical Engineering Department and before joining the Kuwait Institute for Scientific Research, where he is still affiliated to this day.

Adel Al-Mutairi

Kuwait Institute for Scientific Research
Petroleum Research Center
Safat, Kuwait
amutairi@kisir.edu.kw



Chapter C.21

Adel Al-Mutairi received his BSc from Clarkson University in 2001. He works as a Chemical Engineer, focused on heavy oil (AR and VR) pre-treatment and hydroprocessing using pilot plants at the Petroleum Research Centre (PRC), Kuwait Institute for Scientific Research (KISR).

Sultan M. Al-Salem



Kuwait Institute for Scientific Research (KISR)
Environment & Life Sciences Research Center
Safat, Kuwait
ssalem@kisir.edu.kw

Chapter C.32

Sultan Al-Salem is a Chemical Engineer with degrees from Kuwait University and a PhD from University College London. His work experience at a number of institutions has linked him with a strand of projects in the crude oil refining and petrochemicals area, air pollutants monitoring, dispersion, and chemical mass balance modeling. He is currently an Associate Research Scientist at the Environment and Life Sciences Research Center of KISR.

Jan T. Andersson



University of Münster
Inst. of Inorganic and Analytical Chemistry
Münster, Germany
anderss@uni-muenster.de

Chapter A.5

Jan Andersson obtained his PhD from the University of Lund, Sweden, and moved to Germany after 2 years of postdoctoral research in USA. He obtained his Habilitation degree in Analytical Chemistry from the University of Ulm and was appointed Professor at the University of Muenster in 1991. His research interests center on separation techniques of supercomplex mixtures like petroleum.

A. Ballard Andrews

Schlumberger-Doll Research
Sensor Physics
Cambridge, USA
bandrews@slb.com



Chapter A.6

A. Ballard Andrews received his PhD in Condensed Matter Physics from the University of Texas at Austin, where he investigated the electronic structure of magnetic thin films. His postdoctoral research at Los Alamos National Laboratory concentrated on heavy fermions. He worked at Brookhaven National Laboratory in computation and scientific visualization. He now works on laser applications in spectroscopy and asphaltene science.

Brent E. Beasley

Brent E. Beasley and Associates, LLC
Consulting, Contracting and Engineering
Laguna Woods, USA
brentbeasley@brentbeasleyllc.com



Chapter D.33

Brent Beasley worked in various capacities for ExxonMobil over a 34-year career, including a decade in conventional lube research, pilot plant operations, manufacturing plant troubleshooting, and technical licensing support. Brent is President and CEO of Brent. E. Beasley and Associates, LLC, a consulting contracting and engineering company.

F. Emmett Bingham

Haldor Topsoe, Inc.
Orange, USA

Chapter C.23

Emmett Bingham is the Manager of Hydroprocessing Technology for Haldor Topsoe Inc. He has more than 40 years of experience. He has worked for Topsoe for 10 years, Unocal for 20 years, and Dow Chemicals for 10 years.

Gary Brodeur

Intel Corp.
Logic Technology Development
Hillsboro, USA
gary.brodeur@intel.com

Chapter D.38

Gary Brodeur received his PhD from Florida State University in 2013. He worked at the National Renewable Energy Laboratory in Golden, CO, within the National Bioenergy Center division. He now works as a Senior Process Development Engineer at Intel Corporation in Hillsboro, OR.

Leslie Bromberg

Massachusetts Institute of Technology
Plasma Science and Fusion Center and
Sloan Automotive Laboratory
Cambridge, USA
brom@psfc.mit.edu



Chapter D.40

Dr Bromberg received his BS and PhD from the Massachusetts Institute of Technology. He worked at MIT in plasma physics, first on fusion and recently on industrial applications of plasmas and microwave based sensors. He has over 70 issued patents and started three companies in the automotive market.

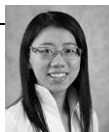
Michael Carpenter

RTI International
Energy Technology
Research Triangle Park, USA
mcarpenter@rti.org



Chapter D.40

Michael Carpenter received degrees in physics and chemical engineering in 2011 from North Carolina State University. His work at RTI International focuses on catalysis relevant to the natural gas industry such as GTL and ammonia synthesis. He also has interest and experience in modeling physical systems and chemical synthesis.

Shengnan Chen

University of Calgary
Dept. Chemical and Petroleum
Engineering
Calgary, Canada
snchen@ucalgary.ca

Chapter B.14

Shengnan Chen is an Assistant Professor in the Department of Chemical and Petroleum Engineering at the University of Calgary. Her major interests include the development of unconventional reservoirs, reservoir simulation, and production optimization. Chen holds BSc and MSc degrees in Petroleum Engineering from China University of Petroleum and a PhD degree in Petroleum Systems Engineering from the University of Regina, Canada.

Dennis Cima

Aspen Technology, Inc.
Houston, USA

Chapter C.26

Cortis K. Cooper

Chevron Energy Technology Company
San Ramon, USA
cortiscooper@alum.mit.edu



Chapter B.15

Dr Cooper is a Chevron Fellow, one of 27 scientists and engineers recognized by Chevron for their contributions. His primary job is providing wind, wave, and current criteria for Chevron's worldwide operations. He received a PhD from the University of Maine in 1987, has published 44 papers, co-authored 8 books, served on 7 National Academy of Sciences committees and Boards, and advisory panels to Federal agencies.

M. Andrew Crews

Chicago Bridge and Iron
Houston, USA
andyc6362@yahoo.com



Chapter C.24

M. Andrew Crews received his degree in Chemical Engineering from the University of Arkansas in 1991. He has held various management positions at Chicago Bridge and Iron over the last 25 years. His most recent assignment was as the Vice President of Operations for CB&I India and he is currently assigned as the Regional Vice President of Engineering for the Americas.

Sudhin Datta

ExxonMobil Chemical Co.
Global Chemical Research
Baytown, USA
sudhin.datta@exxonmobil.com



Chapter D.37

Sudhin Datta received his PhD in Chemistry from Harvard University in 1978. He has been at ExxonMobil Chemical Company developing new polyolefin polymers and their blends for the last 35 years. He has authored 118 US patents and 13 review chapters on polyolefins. Sudhin Datta is the recipient of the 2015 Charles Goodyear Medal of the Rubber Division of the American Chemical Society.

Geoffrey E. Dolbear

Katy, USA
geoffd41@gmail.com



Chapter C.22

Geoff Dolbear is a Physical Chemist with a BSc from UC Berkeley and a PhD from Stanford. After 24 years in industrial research, he became an independent consultant in 1989, retiring in 2014. His publications and patents describe catalysts and processes, with particular strengths in hydrocracking, heavy oil, and coal. He is a Fellow of the American Chemical Society.

Antonios Doufas

ExxonMobil Chemical Co.
Global Polymer Technology
Baytown, USA
antonios.k.doufas@exxonmobil.com



Chapter D.37

Antonios K. Doufas received his PhD in Chemical Engineering at the University of Illinois at Urbana-Champaign in 2000. He worked at the corporate R&D laboratories of the Dow Chemical Company and later in polypropylene product development at Sunoco Chemicals and Braskem Americas. He is currently a Technical Leader in Global Polymers Technology at the ExxonMobil Chemical Company with interests in structure properties, rheology, and flow-induced crystallization.

Rudraksha Dutta Majumdar

University of Toronto Scarborough
Dept. Physical and Environmental
Sciences
Toronto, Canada
r.duttamajumdar@utoronto.ca



Chapter A.6

Rudraksha Dutta Majumdar received his PhD from the University of Lethbridge, Canada, in 2015, working on asphaltene structure elucidation using NMR spectroscopy. His current position as a Postdoctoral Research Associate at the University of Toronto Scarborough is focused on developing novel comprehensive multi-phase NMR and *in vivo* NMR spectroscopic techniques for materials and organisms of environmental relevance.

David Fiscus

ExxonMobil Chemical Co.
Global Research Product Development
Baytown, USA
david.m.fiscus@exxonmobil.com



Chapter D.37

David M. Fiscus received his PhD from the Ohio State University in 1985. He has run technical programs in research, manufacturing, and customer support positions mainly related to polyethylene resins and products. He currently works for ExxonMobil Chemical Company in Global Product Research supporting the development of new metallocene catalyzed polyethylene resins.

Go Fujisawa

Schlumberger Gould Research
Cambridge, UK
gufujisawa@slb.com



Chapter A.7

Go Fujisawa received his Master's degree in Applied Physics from Osaka University. Since he joined Schlumberger in 1999, he has worked on various projects related to spectroscopic downhole fluid analysis for oil field wellbore applications as Engineer, Scientist, and Project Manager in engineering and research organization.

Graham Ganssle

Sandstone Oil&Gas
New Orleans, USA
graham@ganssle.com



Chapter B.12

Graham Ganssle received his PhD from the University of New Orleans. He is the Owner and Principal Geoscientist of Sandstone Oil & Gas, a petroleum exploration company operating in the North America, South America, and Africa. His research interests are in the fields of acoustic imaging and digital signal processing, specializing in optimization methods for seismic data migration.

Adam A. Gentile

Freedom Energy Tech, LLC
Clermont, USA
agentile@mail.usf.edu



Chapter D.40

Adam A. Gentile has served as Lead Research Analyst of the Prism cold plasma catalytic partial oxidation technology for use with various hydrocarbon feed stocks producing high quality synthesis gas for the purpose of synthetic fuel production using Fischer–Tropsch processes. He currently works as a Scientist and Analyst in a GLP compliant bioanalytical laboratory on the development and validation of immunoassays for clinical and non-clinical drug studies.

Pierre–Yves le Goff

Axens SA
Rueil–Malmaison, France
pierre-yves.le-goff@axens.net



Chapter C.18

Pierre le Goff holds a PhD from the Ecole de Chimie de Mulhouse and an MBA from Sorbonne University. He started his career in the field of inorganic chemistry. He joined Axens in 2000 and was involved in reforming and hydrotreating activities. Since 2013 he has been in charge of the R&D program covering reforming, isomerization, and aromatics.

Martin R. Gonzalez

BP
Refining Technology and Engineering
Naperville, USA
martin.gonzalez@bp.com



Chapter C.31

Martin R. Gonzalez received his PhD in Chemical Engineering from the University of Wisconsin, with research in heterogeneous catalysis. In his 20-year career with Amoco and BP, he has held positions in R&D, process design, and refinery operations, including commissioning and start-up of hydrotreaters for BP's North American heavy-oil project. He is currently Discipline Leader for Hydroprocessing and Reforming technologies.

Lamia Goual

University of Wyoming
Dept. Petroleum Engineering
Laramie, USA
lgoual@uwyo.edu



Chapter A.6

Lamia Goual received her PhD in Petroleum Engineering from Imperial College, UK, in 2003. She worked at the University of Alberta and the Enhanced Oil Recovery Institute. She is currently an Associate Professor of Petroleum Engineering at the University of Wyoming. Her research interests include interfacial phenomena with applications to energy and environment. She holds an NSF CAREER award on remediation of oil-contaminated aquifers.

Nick Hallale

AspenTech
Warrington, UK
hallalen@gmail.com



Chapter C.25

Nick Hallale holds BSc and PhD degrees in Chemical Engineering from the University of Cape Town. He has experience across the academic, consulting, and industrial sectors.

Thomas Hantschel

Schlumberger Aachen Technology Center
Aachen, Germany
thantschel@slb.com



Chapter B.11

Thomas Hantschel is the Manager of the Schlumberger Technology Center for Exploration Geology, in Aachen, Germany. He is a physicist with a focus on basin modeling simulations related to heat flow, pore pressure and stress evolution, and multiphase fluid-flow. He has worked as a peer reviewer for more than 100 exploration projects and applications worldwide related to petroleum systems modeling and geomechanics.

**Yalin Hao**

Chevron Lubricants
Chevron Base Oils
Richmond, USA
yalinhao@chevron.com

Chapter D.34

Yalin Hao joined Chevron as a Research Engineer after receiving her PhD from University of California, Davis in 2008. Her work focused on process/catalyst studies for base oil and fuel hydroprocessing. Since she joined Chevron Base Oils in 2012, she has been responsible for providing technical support for Chevron's Group II Base Oil Slate and other key marketing activities.

Paul Hazendonk

University of Lethbridge
Dept. Chemistry and Biochemistry
Lethbridge, Alberta, Canada
paul.hazendonk@uleth.ca



Chapter A.6

Paul Hazendonk is an Associate Professor at the University of Lethbridge. He obtained his MSc at the University of Manitoba and received his PhD from McMaster University. An expert in NMR spectroscopy, Paul specializes in solid-state NMR, developing experimental techniques particularly suited to complex organic-inorganic mixtures and fluorine containing systems. His current projects include the investigation of nano-structural motifs in fossil fuel materials.

Donald G. Hill

University of Southern California
Walnut Creek, USA
dgh@hillpetro.com



Chapter B.13

Donald G. Hill is a Consulting Petrophysicist and Adjunct Professor of Petrophysics at the University of Southern California. He holds a PhD in Geology and Exploration Geophysics. Over 40 years he has been in developing and conducting innovative projects in petroleum, mining, and geothermal exploration and production worldwide.

Suzzy C. Ho

Exxon Mobil Research & Engineering Co.
Corporate Strategic Research Department
Annandale, USA
suzzy.c.ho@exxonmobil.com

Chapter D.35

Suzzy Ho is a Senior Research Associate at ExxonMobil's Corporate Strategic Research. She received her PhD in Organic Chemistry from the California Institute of Technology in 1986. After a postdoctoral position at Princeton University, she joined ExxonMobil and has worked primarily in the area of lubricant base stocks ranging from research to product, processes, and new market development.

**Teh C. Ho**

Bridgewater, USA
tehcho@yahoo.com

Chapter C.27

Teh C. Ho received a BSc degree from Tunghai University, Taiwan, and a PhD in Chemical Engineering from the University of Delaware. He is an independent consultant, having retired from ExxonMobil's Corporate Strategic Research Labs. in 2013. He received Wilhelm and Evans Awards of the American Institute of Chemical Engineers and is a member of the National Academy of Engineering.

Allegra Hosford Scheirer

Stanford University
Dept. Geological Sciences
Stanford, USA
allegras@stanford.edu



Chapter B.11

Allegra Hosford Scheirer is a Research Geophysicist at Stanford University specializing in basin and petroleum system modeling. Allegra's obtained her PhD degree from the MIT-Woods Hole Oceanographic Institution Joint Program in Oceanography. Prior to joining Stanford, Allegra was a member of the Geophysical Unit of Menlo Park and the Energy Resources Program at the US Geological Survey, where she constructed three-dimensional geologic models for use in the resource assessment process.

Chang Samuel Hsu

Chapters 1, A.3, A.4, C.16, C.17, D.38

For biographical profile, please see the section "About the Editors".

Manhoi Hur

Iowa State University
Genetics, Development and Cell Biology
Ames, USA
mhhur@iastate.edu



Chapter A.4

Manhoi Hur received his BS from PaiChai University, Korea, in 2002. At the Korea Basic Science Institute he improved the performance of FT-ICR mass spectrometers. Since 2008, his research focuses on the development of novel statistical models and software for petroinformatics. His work at the Iowa State University also includes bioinformatics and big-data integrative analysis of multi-omics data.

**Maurice D. Jett**

Chapter C.28

BP Refining
Refining Technology & Engineering
Houston, USA
mdjett1@gmail.com

Maurice Jett received his PhD in Chemical Engineering from Rice University in 1991. He spent more than 19 years at Aspen Technology executing reactor modeling and real-time optimization projects for a wide range of refinery and petrochemical processes. He is currently employed by BP, building and deploying high fidelity operator training simulators.

**Sriganesh Karur**

Chapter C.28

Katy, USA
srikarur@gmail.com

Sriganesh Karur received his DSc in Chemical Engineering from Washington University in Saint Louis. He worked with Aspen Technology Inc. as Optimization Engineer for 10 years before joining Shell Global Solutions (US) Inc., where at present he heads the Process Engineering and Supply Chain Applications group.

Sunghwan Kim

Chapter A.4

Kyungpook National University
Dept. Chemistry
Buk-Gu Daegu, Korea
sunghwank@knu.ac.kr



Sunghwan Kim received his PhD from the Ohio State University in 2003. He has worked at the National High Magnetic Field Laboratory at Florida State University and at the Korea Basic Science Institute. He is an Associate Professor at Kyungpook National University. His research focusses on understanding the chemical composition of crude oil at the molecular level.

William Kostka

Chapter C.18

Axens North America
Houston, USA
bkostka@axensna.com



Bill Kostka received his PhD from Purdue University in 1981. He worked at Mobil Research and Development Corporation in Paulsboro, NJ and ExxonMobil Research and Engineering Company in Fairfax, VA. After retirement from ExxonMobil, he came to Axens North America in Houston, TX as a Technical Advisor for reforming and isomerization.

**Stephen K. Lee**

Chapter D.34

Lee Associates
Oakland, USA
stephen.lee9@comcast.net

Stephen Lee has a BS and an MS in Chemical Engineering. He worked 36 years at Chevron Corporation in process engineering, project engineering, refinery planning and operations, capital projects, and new technology development. Stephen is an expert in the manufacture of premium lube base oils using hydroprocessing technology. He has extensive experience in technical consultation and process design of base oil plants.

**Guan-Dao Lei**

Chapter D.34

Chevron Energy Technology Company
Downstream Technology and Service
Richmond, USA
guandao.lei@chevron.com

Guan-Dao Lei received his PhD from the University of Houston. He worked at Honeywell International, in Illinois, US and Süd-Chemie Inc. in Kentucky, US. He now works on hydroprocessing catalyst and process development at the Chevron Energy Technology Company in California, US.

Zaiting Li

Chapter D.36

Research Institute of Petroleum Processing
Beijing, China
leitsaiting@sina.cn



Zaiting Li studied Chemical Engineering at Tsinghua University and Petroleum Processing at China University of Petroleum. She worked at the Research Institute of Petroleum Processing, SINOPEC. She is the inventor of the deep catalytic cracking (DCC) technology for the production of low-carbon olefins from heavy oil.

Bruce R. Locke

Florida State University
Dept. Chemical and Biomedical
Engineering
Tallahassee, USA
blocke@fsu.edu



Chapter D.41

Bruce Locke earned his degrees in Chemical Engineering from Vanderbilt University, University of Houston, and North Carolina State University. He serves on the Faculty of Chemical and Biomedical Engineering as a Distinguished University Research Professor at Florida State University. His research interests include plasma reaction engineering for chemical synthesis and environmental pollution control.

Shuji Luo

Exxon Mobil Research & Engineering Co.
Corporate Strategic Research Department
Annandale, USA
shuji.luo@exxonmobil.com



Chapter D.35

Shuji Luo received her PhD in Organometallic Chemistry from the University of Chicago in 2007. Since 2009, she has worked in the Corporate Strategic Research Laboratory of ExxonMobil Research and Engineering company in Clinton, NJ, conducting research related to performance fluids and polymers. She currently holds the position of Research Associate.

Xiaoliang Ma

Kuwait Institute for Scientific Research
(KISR)
Petroleum Research Center
Safat, Kuwait
maxiaoliang@kisir.edu.kw



Chapter C.32

Xiaoliang Ma received his PhD from Kyushu University in 1995. He has worked at the China Coal Research Institute, the National Institute for Resources and Environment in Japan, Pennsylvania State University, and the Kuwait Institute for Scientific Research. He works on petroleum refinery processes and fuel science, focusing on hydrotreating, adsorption, and separation in clean fuel production.

Ekaterina V. Maksimova

University of South Florida
College of Marine Science
St. Petersburg, USA
maksimova@mail.usf.edu



Chapter B.15

Dr Maksimova is an NSF Postdoctoral Fellow affiliated with the University of South Florida and Florida State University (FSU). Her interests are in fundamental physical processes that govern ocean dynamics. She is a recipient of several prestigious awards, including the Gold Medal for Academic Excellence from Moscow State University, an O'Brien Graduate Fellowship from FSU, and an Ocean Sciences Postdoctoral Fellowship from NSF.

Abdulazeem M. J. Marafi

Kuwait Institute for Scientific Research
Petroleum Research Center
Safat, Kuwait
amarafi@kisir.edu.kw



Chapter C.21

Abdulazeem M.J. Marafi received his PhD from the University of Oklahoma in 1996. He works as a Senior Research Scientist, focused on petroleum refining (heavy oil hydroprocessing) and kinetics at the Petroleum Research Center (PRC), Kuwait Institute for Scientific Research (KISR).

Blaine McIntyre

Calgary, Canada

Chapter C.28

Milo D. Meixell

Aspen Technology, Inc.
Professional Service
Houston, USA
milo.meixell@aspentech.com



Chapter C.29

Milo D. Meixell, Jr. is a chemical engineer. He worked with Exxon Chemical Company in the area of agricultural chemicals and with Dynamic Matrix Control Corporation, before joining Aspen Technology, Inc. in 1996. His area of expertise is real time and plant-wide optimization using large-scale, high-fidelity models, reactor modeling, kinetics, simultaneous, matrix-based modeling, and optimization.

Isao Mochida

Kyushu Environmental Evaluation
Association
Fukuoka, Japan
mochida@keea.or.jp



Chapter C.21

Isao Mochida received his PhD from the University of Tokyo in 1968. He was Professor at Kyushu University for 22 years and has been Professor Emeritus since 2004. He is now a consultant to Kyushu Environmental Evaluation Association and works in applied chemistry on petroleum refining, **coal conversion** and carbon materials for environmental protection.

Ian Moore

Jacobs Consultancy
Power and Energy
Stockport, UK
ian.moore@jacobs.com



Chapter C.25

Ian Moore has over 30 years' experience in engineering services, modeling, optimization, and capital project development for the refining and petrochemicals industries. He has led hydrogen management studies in North America, Europe, and Asia. He is an expert in the application of pinch analysis in energy-intensive industries, and executes energy improvement, power generation, carbon management, and GHG reduction studies worldwide.

Daniel Morton

Haldor Topsoe Inc.
Refinery and Chemicals
Houston, USA
dim@topsoe.com

Chapter C.23

Daniel Morton received his degree in Mechanical Engineering from Auburn University. He worked in various industries, including paper-mills, steel fabrication, and building maintenance and construction. In 2009 he joined Topsoe and has since been involved in the design and sale of much of the proprietary hardware in the company's refinery and chemical business.

Dale R. Mudt

Suncor Energy Products Partnership
Sarnia Refinery
Sarnia, Canada
dmudt@suncor.com

Chapter C.28

Dale R. Mudt is the Process Automation Manger at the Suncor Energy Products Refinery. For the last 30 years he has implemented and maintained DMC controllers and closed-loop real-time optimizers, and managed the Process Automation group at the Sarnia Refinery. Dale was a key contributor to the development of the online version of Sun Oil Company's hydrocracker model, which is now marketed worldwide as AspenHydrocracker.

Oliver C. Mullins

Schlumberger–Doll Research
Cambridge, USA
mullins1@slb.com



Chapters A.6, A.7

Dr Oliver C. Mullins, Science Advisor at Schlumberger, is the primary originator of downhole fluid analysis (DFA) in well logging. Dr Mullins also leads an active research group leading to the Yen–Mullins model of asphaltenes and the Flory–Huggins–Zuo EoS. His current interests include utilizing DFA technology and new asphaltene science for reservoir evaluation and clarifying reservoir fluid geodynamic processes.

Douglas E. Nelson

Haldor Topsoe, Inc.
Orange, USA



Chapter C.23

Douglas E. Nelson is the Engineering Manager for Haldor Topsoe Inc. He has worked for more than 38 years in refinery hydroprocessing for Unocal, Fluor, and now at Haldor Topsoe. Doug has a BSc in Chemical Engineering from Oregon State University.

Joo-II Park

Kuwait Institute for Scientific Research
Petroleum Research Center
Safat, Kuwait
jpark@kisir.edu.kw

Chapter C.21

Joo-II Park received his PhD from Kyushu University in 2012. He worked at Kyushu University as an Associate Professor from 2012–2015. Since 2015 he has been researching heavy oil upgrading, focused on the advanced characterization and catalysis of heavy oil at the Petroleum Research Center (PRC), Kuwait Institute for Scientific Research (KISR).

**Clifford C. Pedersen**

Chapter C.28

Pedersen Enterprises Inc.
Sarnia, Canada
cliffpedersen@sympatico.ca

Clifford (Cliff) C. Pedersen is regarded as one of the pioneers of computer process control in the oil refining industry. His career in the oil refining industry has spanned technical and management leadership positions with NWR, Suncor Energy, Shell Canada, and Imperial Oil in plant automation and information technology. He is currently President of Pedersen Enterprises Inc., an independent consulting agency specializing in advanced process control, real-time optimization and systems interoperability.

Kenneth E. Peters

Chapter B.11

Schlumberger
Mill Valley, USA
Stanford University
Geological Sciences
Stanford, USA
kpeters2@slb.com



Ken Peters is Science Advisor for Schlumberger, where he uses geochemistry and basin modeling to study petroleum systems and teach or consult with external clients. He has 37 years of experience with Chevron, Mobil, ExxonMobil, USGS, and Schlumberger and teaches geochemistry and basin modeling throughout the industry and at various universities, including UC Berkeley and Stanford. Ken has a PhD in Geochemistry from UCLA.

Andrew E. Pomerantz

Chapter A.6

Schlumberger–Doll Research
Cambridge, USA
apomerantz@slb.com



Andrew E. Pomerantz received a PhD in Chemistry from Stanford University in 2005. His research focuses on developing and applying novel techniques to characterize the structure of kerogen and asphaltenes, including methods in mass-spectroscopy, and IR-spectroscopy. That information is used to understand fundamental processes in petroleum such as asphaltene compositional grading and hydrocarbon transport in shales.

Subramanian Ramakrishnan

Chapter D.38



Florida A&M University/Florida State
University
Dept. Chemical and Biomedical
Engineering
Tallahassee, USA
sramakrishnan@fsu.edu

Subramanian Ramakrishnan received his PhD from the University of Illinois at Urbana Champaign in 2001. After a postdoctoral appointment at Princeton and then at the University of Illinois, he joined FAMU-FSU College of Engineering in 2005, where he currently works on biofuels production and processing of complex fluids. In 2016 he was a Visiting Professor at Harvard University.

Henrik Rasmussen

Chapter D.39



Haldor Topsoe Inc.
Houston, USA
hwr@topsoe.com

Henrik Rasmussen graduated from the University of Copenhagen in 1989 with a degree in Chemical Engineering before relocating to the US in 1991. He has worked at Haldor Topsoe for over 25 years, holding numerous technical and management positions for all Topsoe's business units. Mr Rasmussen is currently Vice President of Catalyst and Technology and responsible for catalyst and license technology business for USA, Canada, and the Caribbean.

Paul R. Robinson

Chapters 1, .2, C.16, C.17, C.20, C.22, C.25, C.26, C.28

For biographical profile, please see the section "About the Editors".

John M. Rosenbaum

Chapter D.34

Chevron Lubricants
Chevron Base Oils
Santa Cruz, USA
energyengineerjohn@gmail.com



John Rosenbaum has a PhD in Materials Science and Mineral Engineering from UC Berkeley and retired in 2015 after 34 years working for various Chevron Companies in minerals processing, petroleum hydroprocessing, catalyst development, and lubricant base oil product technology.

Joseph Ross

Axens North America
Princeton, USA
jross@axensna.com



Chapter C.18

Joseph Ross is a graduate from Princeton University with a degree in chemical engineering. He has over 30 years of commercial experience in the field of transportation fuels including engineering design, R&D, and process licensing. He is a Technology and Marketing Manager for Axens North America specializing in fluid solid systems, heavy oil upgrading, FCC, and catalytic reforming.

Yosadara Ruiz-Morales

Mexican Petroleum Institute
Mexico City, Mexico
yruiz@imp.mx



Chapter A.6

Yosadara Ruiz-Morales received her PhD in Theoretical Chemistry from the University of Calgary in 1998. Since 1999, she has been working at the Mexican Petroleum Institute. She is a pioneer in the application of electronic structure calculations to elucidate the asphaltenes' aromatic core and inventor of the Y-rule for asphaltene stability. In her current research on oil rheology, she investigates asphaltene interfacial activity using particle dynamics.

Marco A. Satyro (deceased)

Chapter A.8

Oliver Schenk

Schlumberger Aachen Technology Center
Aachen, Germany
oschenk@slb.com



Chapter B.11

Oliver Schenk is a Geologist and received his PhD from RWTH Aachen University (2006), focusing on the influence of fluids on recrystallization and the deformation behavior of rocks. Since 2006 he has been working for Schlumberger, specialized on multi-dimensional applications of basin and petroleum system modeling (BPSM). Since 2007, he has been Research Affiliate at Stanford University, lecturing and mentoring graduate students in BPSM.

John M. Shaw

University of Alberta
Dept. Chemical and Materials Engineering
Edmonton, Canada
jmshaw@ualberta.ca



Chapter A.8

John M. Shaw obtained his PhD from the University of British Columbia in 1985 and was a Professor at the University of Toronto, before joining the University of Alberta, in 2001, where he holds a Natural Sciences and Engineering Research Council of Canada Industrial Research Chair in Petroleum Thermodynamics. His research focuses on experimental methods development, and thermophysical property measurement and prediction of hydrocarbon resources.

B. Gregory Shumake

CB & I
Engineered Products
Tyler, USA
gshumake@cbi.com



Chapter C.24

Greg Shumake is the Director of Engineering for the Engineered Products business group within CB&I. He has over 20 years of experience in the hydrogen and synthesis gas industry. He has a BS in Chemical Engineering from the University of Arkansas. He has published several articles on various aspects of hydrogen plants.

James G. Speight

CD&W Inc.
Laramie, USA
jamesp8@aol.com



Chapter C.19

Dr James G. Speight has degrees in Chemistry, Geological Sciences, and Petroleum Engineering and is the author of more than 60 books in petroleum science, petroleum engineering, and environmental sciences. He has more than 45 years of experience in the petroleum industry and has taught at various universities worldwide. Among other honors, he received the Scientists without Borders Medal of Honor (Russian Academy of Sciences) and the Einstein Medal.

**Dennis Vauk**

Chapter C.25

Phillips 66
Refining Business Improvement
Houston, USA
dennis.a.vauk@p66.com

Dennis Vauk received a Chemical Engineering degree from the University of Idaho. He worked as Senior International Expert for Air Liquide, where he conducted hydrogen optimization studies for refineries worldwide. He is currently Hydroprocessing Technology Director for Phillips 66. He started his career doing research, process design, and technical services for hydrotreaters and hydrocrackers at Unocal.

Clifford C. Walters

Chapter B.10

ExxonMobil Research & Engineering Co.
Corporate Strategic Research
Annandale, USA
clifford.c.walters@exxonmobil.com



Clifford C. Walters received his PhD in Geochemistry from the University of Maryland in 1982. Since then, he has been a Research Geochemist with Gulf, Sun, Mobil, and ExxonMobil with efforts focused on petroleum biomarkers, models of generation and reservoir transformations, and geomicrobiology.

Robert J. Wandell

Chapter D.41

Florida State University
Dept. Chemical and Biomedical
Engineering
Tallahassee, USA
rjw05c@my.fsu.edu



Robert J. Wandell studied Chemical Engineering at Florida State University. His research interests include the study and development of electrical discharge plasma reactors for synthesis of useful chemical species, as well as transfer of university technologies into commercial markets.

Xieqing Wang

Chapter D.36



Research Institute of Petroleum Processing
Beijing, China
wangxieqing.ripp@sinopec.com

Xieqing Wang received his PhD in Chemical Engineering from Merseburg University of Applied Sciences in 1961. His work at SINOPEC's Research Institute of Petroleum Processing concentrates on petroleum refining, with a special focus on catalytic cracking.

Keith Wisecarver

Chapter C.30



University of Tulsa
Dept. Chemical Engineering
Tulsa, USA
keith-wisecarver@utulsa.edu

Keith Wisecarver is Professor of Chemical Engineering at the University of Tulsa. He received his PhD from the Ohio State University in 1987 and has been on the faculty at Tulsa since that time. He has been doing research in the field of delayed coking since 1999, as co-PI of the Tulsa University Delayed Coking Joint Industry Project.

Margaret M. Wu

Chapter D.35

Exxon Mobil Research & Engineering Co.
Corporate Strategic Research Department
Annandale, USA
margaret.m.wu@exxonmobil.com



Margaret Wu received her PhD from the University of Rochester at Rochester in 1976. She worked at ExxonMobil Research & Engineering Co. for 32 years, conducting research related to synthetic lubricant products and processes and was the author or co-author of numerous patents and publications. Since her retirement in 2009, she holds the position of Emeritus Senior Scientific Advisor for the same organization.

Björn Wygrala

Chapter B.11

Schlumberger Aachen Technology Center
Aachen, Germany
bwygrala@slb.com



Björn Wygrala received his PhD in Petroleum Geology from the University of Cologne in 1989. He has worked for Uranerz in Australia, for Integrated Exploration Systems (IES) in Germany, and for Schlumberger in Germany. He currently works on global business development for software and services related to exploration risk and resource assessments.

Chaogang Xie

Chapter D.36



Research Institute of Petroleum Processing
Beijing, China
xiecg.ripp@sinopec.com

Chaogang Xie received his MSc from Tianjin University in 1987. He works at the SINOPEC Research Institute of Petroleum Processing. His research centers around catalytic cracking processes, focusing on the production of light olefins.

**Harvey W. Yarranton**

Chapter A.8

University of Calgary
Dept. Chemical and Petroleum
Engineering
Calgary, Canada
hyarrant@ucalgary.ca

Harvey Yarranton is a Professor of Chemical and Petroleum Engineering and the NSERC Industrial Research Chair in Heavy Oil Properties and Processing. He received his PhD degree from the University of Alberta in 1997. His research interests are the phase behavior and properties of heavy oils and the fundamentals water-in-oil emulsions, with application to heavy oil and oil sands processes.

Richard N. Zare

Chapter A.6

Stanford University
Dept. Chemistry
Stanford, USA
rnz@stanford.edu; zare@stanford.edu



Richard (Dick) Zare is the Marguerite Blake Wilbur Professor in Natural Science at the Department of Chemistry of Stanford University. He works in the area of physical and analytical chemistry with an emphasis on the development of new methods and new instrumentation.

Genquan Zhu

Chapter D.36

Research Institute of Petroleum
Processing
Beijing, China
zhugq.ripp@sinopec.com



Genquan Zhu received his PhD from China University of Petroleum in 2001. He works at the SINOPEC Research Institute of Petroleum Processing. His research centers around catalytic cracking processes, focusing on the production of light olefins.

Subject Index

1-D BPSM 385
 2-D BPSM 387
 4,6-dimethyldibenzothiophene
 (4,6-DMDBT) 728
 4-methyldibenzothiophene (4-MDBT)
 699
 5-ethylidene-2-norbornene (ENB)
 1110
 5-lump FCC model 852

A

abatement technology 135
 absolute permeability 344
 acceptor 681
 acetone-butanol-ethanol (ABE) 584
 acid
 – deposition 665
 – gas 656
 – gas enrichment 660
 – gas removal (AGR) 936, 942
 – mine drainage (AMD) 669
 – rock drainage (ARD) 669
 – -soluble oil (ASO) 44, 576
 acidity 684, 696
 – control 603
 acoustic borehole imager 489
 acoustic impedance 427
 acrylonitrile (AN) 87
 – –butadiene–styrene terpolymer
 (ABS) 1098
 – styrene (AS) 87
 activated carbon 700
 active continental margin 351
 activity
 – catalytic 634
 – coefficient 301
 additive 630
 adiabatic prereformer 897
 adsorption 289, 675, 685, 698, 931
 advanced
 – fluidized (AF) 1071
 – process control (APC) 834, 835
 – regulatory control (ARC) 768,
 833
 aggregate
 – asphaltene 682
 – behavior 855
 – model 679
 aggregation 679
 air induction system 553
 air quality 77
 air/fuel ratio (AFR) 553
 airgun 421
 airlift thermofor catalytic cracking
 625, 640
 algae 1118
 alkane 327
 alkyl substitution 688
 alkylated aromatic base stock 1059
 alkylation (ALKY) 43, 59, 575,
 676, 717
 all glass heated inlet system (AGHIS)
 155
 alumina 684, 694, 698, 705
 – support 705
 American Petroleum Institute (API)
 328, 385, 447, 526, 722, 939, 1044
 American Society for Testing and
 Materials (ASTM) 34, 164, 186,
 563, 639, 868, 958
 amine treating 657
 amine unit 818
 aminocyclopentene dithiocarboxylic
 acid (ACDA) 211
 ammonia destruction 661
 ammonia formation 806
 ammonium nitrate explosion 103
 Amoco Cadiz 103, 140
 amorphous silica alumina (ASA)
 43, 713, 734
 amplitude variations with offset
 (AVO) 426
 analytical instrumentation 151
 angular unconformity 341
 annular flow 504
 anticline trap 26
 anti-knock index (AKI) 563
 API 309
 – gravity 328
 apparent conversion 722
 apparent water resistivity R_{wa} 488
 appearance 332
 APPI data 179
 APPI mode 180
 approximate lumping 852
 aqueous phase reforming (APR)
 1117, 1128–1130
 – model 299
 AR hydrotreatment 700
 Arabian
 – heavy gas oil (AH-GO) 678
 – light gas oil (AL-GO) 678
 – medium gas oil (AM-GO) 678
 Archie formation factor 462
 Archie resistivity index 462
 Archie's equations 451, 462
 Archimedes buoyancy 262
 archipelago model 230, 371
 ARDS process 939
 aromatic 327, 676, 700, 918
 – content 684
 – ester 1055
 – ring 687, 696
 – species 693
 aromaticity 684
 aromatics 559, 1017
 – alkylation 598
 – complex 592
 – saturation (ASAT) 23
 Arps relationships 460
 array laterolog tool (ALT) 483
 array sonic log (AST) 448
 arsenic 682
 artificial lift 508
 Aspen Custom Modeler (ACM)
 825
 Aspen hydrocracker 870
 asphalt 72
 – residual treating (ART) 642
 asphaltene 152, 162, 225, 621, 675,
 679, 702
 – cluster 240
 – cluster accumulation 241
 – contamination 1009
 – Hansen solubility parameter 244
 – Hildebrand solubility parameter
 244
 – intermolecular interaction 243
 – molecule 226, 228
 – nanoaggregate 236

- polymer 681
 - precipitation 920
 - Yen–Mullins model 222, 252, 262, 371, 681
 - ASTM D1655-15 34
 - ASTM D4814–14b 34
 - Athabasca bitumen 277
 - Athabasca vacuum residue (AVR) 277
 - atmospheric
 - distillation 545, 937
 - distillation unit (ADU) 541, 656, 717
 - equivalent boiling point (AEBP) 544
 - gas oil (AGO) 21
 - pressure chemical ionization (APCI) 160, 163, 174
 - pressure chemical ionization mass spectrometry (APCI MS) 243
 - pressure gas chromatography (APGC) 163
 - pressure ionization 159, 160
 - pressure laser ionization (APLI) 213
 - pressure photo ionization (APPI) 160, 163, 174
 - residue (AR) 21, 546, 679, 683, 705, 717, 943
 - residue hydrodesulfurization (ARDS) 936
 - atomic emission detector (AED) 154, 214
 - automatic transmission fluid (ATF) 958, 1016
 - automation infrastructure 838
 - automotive engine oil 1019
 - autothermal reformation (ATR) 793, 879
 - plant 794
 - autothermal reforming (ATR) 787, 1150
 - average
 - absolute relative deviation (AARD) 308
 - bed bottom temperature 724
 - bed top temperature 724
 - molecular weight (AMW) 230
 - aviation gasoline 552
- B**
-
- Bakken Formation 409
 - barrel of oil equivalent (boe) 325
 - barrels per day (BPD) 590
 - basal heat flow 394
 - base metal catalyst 1040
 - base oil oxidation stability test 1023
 - base stock 1015
 - categories 959, 1018
 - group II 1017
 - group III 1017
 - impurities 1022
 - properties 959
 - basic sediment and water (BSW) 722
 - basin
 - fill 382
 - modeling 74
 - basin and petroleum system modeling (BPSM) 381
 - three-dimensional model 387
 - two-dimensional model 387
 - workflow 382
 - Beavon sulfur removal (BSR) 662
 - bed axial temperature rise
 - average 724
 - max 724
 - bed pressure drop 723
 - Benfield process 659
 - benzene, toluene, and xylene (BTX) 591, 1063, 1069
 - benzothiophene 202, 688, 689, 692
 - best available control technology (BACT) 805
 - Bhagyam field 268
 - biaxially oriented PP (BOPP) 1103
 - bimolecular second-order reactions 858
 - binder 61
 - biochemical 1130
 - process 151
 - biodiesel 1118
 - bioethanol 1133
 - biofuel 1117, 1130
 - 1st generation 1118
 - 2nd generation 1117, 1121, 1130
 - 3rd generation 1118
 - 4th generation 1118, 1122
 - catalyst 1137
 - biogas 1122
 - biogenic methane 395
 - biomarker 359, 372
 - analysis 155
 - biomass 1117, 1121, 1126–1128, 1130
 - conversion 1118
 - feed 1127
 - fractionation 1117, 1120, 1127–1130
 - lignocellulosic 1118, 1127–1130
 - processing routes 1120
 - -to-liquid (BTL) 1118, 1120, 1125, 1130
 - bio-oil (biomass oil) 1117, 1120, 1126, 1130
 - hydrotreated 1127
 - lignocellulosic 1127
 - biorefinery 1117, 1130
 - Biot coefficient 391
 - bitumen 20
 - -derived crude 922
 - diluted (Dilbit) 29
 - non-Newtonian behavior 275
 - blending optimization 585
 - blendstock 552
 - block dewaxing 1037
 - block hydrocracking 1030
 - blowout preventer (BOP) 28, 354
 - blowout well failure 27
 - boiling
 - point reduction 23
 - range 676, 683, 700
 - -water reactor (BWR) 105
 - Boolean relation matrix 844
 - borehole
 - compensated (BHC) 447
 - diameter 469
 - environment 252
 - fluid 470
 - gravity meter (BHGM) 448
 - imager 488
 - televiewer (BHTV) 443
 - bottom dead center (BDC) 554
 - bottom-hole temperature (BHT) 384
 - bottom-of-the-barrel cut 32
 - bottoms stripping section 968
 - boundary conditions 395
 - Branch and Bound algorithm 853
 - branched hydrocarbon 1171
 - breakdown
 - petroleum product 4
 - British Petroleum (BP) 12, 324
 - Texas City isomerization unit 114
 - British Standards Institution (BSI) 958
 - British thermal unit (BTU) 325

Brønsted acid (B-acid) 1065
 brominated butyl rubbers (BIIR)
 1112
 brown coal briquettes (BKB) 936
 BSR reaction 662
 BSR-Beavon sulfur removal 662
 bubble cap 541
 bubble flow 504
 bulk
 – compressibility 390
 – dewaxing 1037
 – hydrocracking 1030
 – kinetic model 398
 – polymerization 1084
 – properties (petroleum) 153
 – property 722
 bulked continuous filament (BCF)
 1101
 butadiene rubber (BR) 1105
 Butler equation 999
 butyl rubber 1112
 butylene oxide (BO) 1057

C

C_5/C_6 isomerization 569
 calcination 653
 calcining 739
 caliper (CAL) 443
 capacity 685
 capillarity 347
 carbenium ion 696
 carbohydrate sugars (xylose, sucrose,
 glucose) 1119, 1128
 carbon
 – –carbon (C–C) 714
 – deposition 698
 – dioxide 931
 – –hydrogen–nitrogen–sulfur
 contents (CHNS) 153
 – mitigation technique 931
 – monoxide (CO) 89, 631, 666,
 763, 940
 – nanotube (CNT) 932
 – number 681, 707
 – on regenerated catalyst 632
 – preference index (CPI) 373
 – sequestration 659
 – storage 931
 carbon capture 950
 – and sequestration (CCS) 659
 – and storage (CCS) 29, 931
 carbonate compensation depth
 (CCD) 392
 carbonate mineral 332
 carbonyl sulfide (COS) 659
 cascaded arc 1144
 catagenesis 326, 367, 395
 catalyst 1066
 – acidity 603
 – activity 684, 699, 703
 – aggregation 704
 – average temperature (CAT) 724
 – capacity 694
 – characterization 700
 – coking 848
 – contact time 629
 – coordination 683
 – cycle 614, 740
 – cycle life 724
 – deactivation 635, 686, 873
 – deactivation rate 724
 – degradation 682
 – demetalization 683
 – design 632
 – manufacture 634
 – –oil ratio 628, 635
 – poisoning 887
 – reclamation 745
 – regeneration 57, 571, 590, 599,
 613, 744
 – regenerator 624
 – rejuvenation 744
 – relative activity 882
 – residence time 629
 – stripping 636
 – support 704
 – testing 639
 – –to-oil (CTO) 854
 – transfer line model 870
 – treatment 636
 – weight ratio 629
 – Ziegler–Natta 1090
 catalytic
 – conversion 1127
 – dewaxing (CDW) 60, 717
 – hydrocracking 731
 – hydrotreating 777
 – NO_x removal 47
 – oxidation (Cat-Ox) 136
 – partial oxidation (CPOX) 1141
 – pyrolysis process (CPP) 1063,
 1069–1071, 1078
 – selective reduction (SCR) 47,
 137, 657, 805
 catalytic cracking 617, 619, 676,
 1128
 – airlift thermoform 625, 640
 – batch reactor 618
 – catalyst 617
 – chemistry 617, 619
 – deep (DCC) 640, 1063, 1078
 – feedstock 617
 – fluid 618
 – heavy oil 617
 – Houdry process 618
 – orthoflow fluid-bed process 639
 – process options 617
 – reactor design 617
 – resids 617
 – S and W process 643
 – suspensoid 626, 641
 – Thermoform 580, 640
 – thermoform 618
 catalytic reforming 44, 57, 589,
 818, 848, 941
 – commercialization 607
 – cyclic 608
 – main reaction 590
 – reaction 595
 – semiregenerative 572, 608
 – unit (CRU) 717, 865
 caustic scrubbing 46
 cellulose 1117, 1119, 1129
 cementation exponent 451
 characterization 707
 – heavy oil 287
 – scheme 1130
 Chemec 986, 989
 chemical
 – engineering 151
 – ionization (CI) 160
 – kinetic 1150
 – process 151
 – property 152, 332
 chemical reaction
 – hydrocracking 731
 – matrix representation 843
 chemistry
 – heavy oil 288
 Chernobyl 104
 chilling rate 983
 chloride control 615
 chloride trapping 615
 chloriding roasting 653
 chlorin 682
 chlorinated butyl rubbers (CIIR)
 1112
 chlorine plant 818

- chloro sulfonated rubber (CSM) 1112
- chlorofluorocarbon (CFC) 91, 134, 666, 1059
- chromatography 153, 207, 222
- chromium catalyst 1090
- circumferential acoustic scanning tool (CAST) 449, 489
- clarified slurry oil (CSO) 629
- Claus
 - process 46, 78, 660
 - tail gas recovery 46
- clean air acts 128
- clean fuel 830
 - rigorous model 868
- Cleveland open-cup method (COC) 1052
- closed-loop real-time optimization (CLRTO) 879
- cluster analysis 852
- CO₂
 - emission factor 936
 - recycle 794
 - sequestration 1118
- coal 9, 19
 - asphaltene 226
 - bed methane (CBM) 374
 - mining 102
 - -to-liquids 1121
- co-hydrotreatment 1127
- coil outlet temperature (COT) 975
- coke 71, 607
 - deposition 885
 - drum 906
 - formation 599, 621, 909
 - formation induction time 842
 - sponge 909
- coker 590
 - furnace 905
 - naphtha 593
 - naphtha hydrotreating 593
- coking 36, 598, 682, 685, 707, 885
 - /decoking cycle 905
 - cycle 905
 - drum 905
 - flexi- 51, 903, 912
 - fluid 903, 912
- cold
 - -bed adsorption (CBA) 654, 662
 - box 795
 - crank simulator (CCS) 959, 1016, 1034, 1050
 - dilution ratio (CDR) 1006
 - heavy oil production with sand (CHOPS) 512
 - high-pressure separator (CHPS) 723
 - wash distribution 997
- collisional activated dissociation (CAD) 230
- combination trap 348
- combined feed ratio (CFR) 722
- combined heat and power (CHP) 951, 1124
- combustion
 - air preheat unit (CAP) 790
 - product 684
- comfort cooling tower (CCT) 134
- common midpoint (CMP) 424
 - gather 424
- CoMo 676, 685, 700
- compact microimager (CMI) 491
- compaction 389
 - correction 452
- compensated neutron logs (CNL) 475
- completion 356
- component lumping 74
- composition
 - -based modeling 843
 - petroleum 7
- compound
 - identification 160, 166
 - -type analysis 159, 166
 - -type separation 159
- comprehensive two-dimensional gas chromatography (GC×GC) 154, 157, 676
- computational fluid dynamics (CFD) 842, 854
- computer-aided engineering (CAE) 1104
- condensate 655
- connected pores 344
- Conradson carbon residue (CCR) 705, 722, 875, 908, 959
 - catalytic reforming 574
- consumer gas 655
- contaminant 604, 675
 - removal 623
- continental drift hypothesis 350
- continuous
 - filament (CF) 1101
 - stirred tank reactor (CSTR) 761, 858, 1048, 1095
- controlled rheology (CR) 1097
- conventional hydrocarbon potential 521
- conversion 934
 - parameter 722
 - processes 153
- copolymer
 - monomer sequence 1086
- co-processing, biomass oil and petroleum oil 1117, 1127, 1129, 1130
- core measurement 460
- corona discharge 1145
- correlation 309
 - diagram 184
 - study 183
- corrosion 695
- cracking unit 818
- critical clustering concentration (CCC) 240
- critical nanoaggregate concentration (CNAC) 238
- cross cutting 338, 339
- cross direction (CD) 1104
- crude
 - compatibility 920
 - desalting 917
 - distillation tower troubleshooting 970
 - extra heavy 917
 - fractionation 915
 - gas oil 919
 - vanadium nickel 919
- crude assay 153
 - fraction 22
 - lube 964
 - report 21
- crude oil 20, 327, 533
 - assay 72
 - bulk physical property 20
 - bulk property 22
 - complex 223
 - cracking catalyst 632
 - distillation (COD) 47, 541, 936
 - distillation unit (CDU) 35, 533, 865, 936
 - property 328
 - selection 1025
 - sour 329
 - sulfur-containing compound 692
 - sweet 329
- crustal thinning 352
- cubic equation of state (CEOS) 293, 297
- cubic plus association (CPA) 294

Cyber Service Unit (CSU) 448
 cyclic
 – catalytic reforming 608
 – hydrocarbon 1171
 – steam stimulation (CSS) 100
 cyclization 621, 1128

D

Dalton's law 537
 Darcy flow migration 399
 Darcy's law 502
 deactivation 676, 682, 684
 dead oil 277
 – density 283
 – heavy 283
 – viscosity 309
 deasphalted oil (DAO) 49, 292, 548, 958, 1019
 deBoer plots 276
 decarbonylation 1128
 decarboxylation 1127, 1128
 decoking 907
 decompaction 392
 deep
 – catalytic cracking (DCC) 640, 1063, 1068, 1078
 – conversion 934
 – desulfurization 873
 Deepwater Horizon 116
 degradation 686
 dehydration 1120, 1122, 1127
 dehydrocyclization 602
 dehydrogenation 602, 621
 delayed coking 50, 903, 916
 – process diagram 904
 – reactions 907
 – unit (DCU) 740
 demet 637
 demetalization 702
 denitrification 1138
 density 283
 – functional theory (DFT) 846, 1066
 – logs 472
 deoiling 1003
 deoxygenation 1128
 deposition 686, 694
 depositional environment 155, 359, 363
 desalter 717
 desalting 36, 542, 682
 desorption 681

desulfurization 205, 645, 1138
 – reactivity 689
 desulfurizer 643
 dewaxed oil (DWO) 973
 dewaxing 978, 1033
 – aids (DWA) 1007
 – catalytic (CDW) 60, 717
 – cloth 994
 – DILCHILL™ 981
 – filter media 994
 – ketone 980
 – VI reduction 1034
 diagenesis 326, 365, 395
 dialkyl fumarate-vinyl acetate (DAFVA) 1008
 dibasic ester 1055
 dibenzothiophene (DBT) 202, 678, 685, 688–690
 dichlorodiphenyltrichloroethane (DDT) 88
 dielectric barrier discharge (DBD) 1146, 1171
 diesel 67
 – additive 67
 – cetane 918
 – deep hydrodesulfurization 699
 – fuel 1133
 – renewable 1135
 diethanolamine (DEA) 136, 657, 943
 diffusion limited aggregation (DLA) 240
 diffusivity 707
 diglycolamine (DGA) 657
 di-isopropanolamine (DIPA) 945
 diluent phase behavior 278
 dilute sulfur acid (DA) treatment 1129
 diluted bitumen (Dilbit) 29
 dilution 363
 – ratio 984
 dimension reduction 847
 dimethyl disulfide (DMDS) 736, 744
 dimethyl ether (DME) 77, 582, 1077
 dimethyl terephthalate (DMT) 87
 dimethyldibenzothiophene (DMDBT) 685
 dimethylsulfide 206
 Diophantine algorithm 166
 dip moveout correction (DMO) 426
 direct current (DC) 164, 1144, 1164

direct digital logging (DDL) 448
 disconformity 340
 DISTACT fraction 162
 distillate 675, 681, 687, 708
 – chemical composition 676
 – fuel 549
 distillation 36, 537
 – data 290
 – fraction 153
 – ideal 537
 – yield 22, 548
 distillation tower 48
 – sidestream 965
 distributed control system (DCS) 833, 834, 865
 disturbance variables (DV) 834
 disulfide 662
 donor 681, 697
 double-bond equivalent (DBE) 174, 184, 681, 692
 double-focusing sector mass spectrometry 164, 165
 down-draft gasification unit (system) 1122
 downhole fluid analysis (DFA) 251
 – hardware 257
 – operation 260
 downhole plunger pump 508
 downstream 14, 151–153, 167
 drill stem test (DST) 385
 driller's logs 436
 drilling 354
 drillship 525
 droplet–catalyst collision 855
 dry methane reformation (DMR) 1150
 dual treatment (DAWNT) 1129
 Dubbs process 903
 dynamic porosity 344
 dynamite source 421

E

ebullated bed (e-bed) 55, 713
 – hydrocracking 55, 761
 eccentric shaft 557
 effective
 – gas radiating 889
 – permeability 344
 – porosity 344
 – stress 390
 effectiveness factor 881

- elastomer 1105
 – thermoplastic (TPE) 1108, 1110
 electric arc furnace (EAF) 911
 electrical
 – microimaging (EMI) 490
 – submersible pump (ESP) 509
 – survey (ES) 451
 electron
 – cyclotron resonance (ECR) 1144
 – impact ionization (EI) 156, 160
 – spin resonance (ESR) 683
 electronic fuel injection (EFI) 553
 electrospray ionization (ESI)
 160–163, 174
 electrostatic desalting 543
 emergency depressuring (EDP) 52,
 110
 emulsion polymerization 1085
 EN 590 67
 engine oil blending 1019
 enhanced coal-bed methane (ECBM)
 932
 enthalpy 304
 – hydrotreating 745
 entropy 304
 environmental 151, 167
 – agencies 126
 – laws 88
 enzymatic hydrolysis 1120, 1129
 enzyme 1129
 Eocene 268
 eon 342
 equation of state (EoS) 222, 251
 – cubic 293, 297
 – Flory–Huggins–Zuo (FHZ) 222,
 246, 251, 262
 – Langmuir 222
 – Peng–Robinson 298
 – statistical associating fluid theory
 (SAFT) 294
 – van der Waals 222, 252
 equilibrium 688
 – composition 282
 equivalent NaCl salinity 460
 Ergun relationship 880, 890
 E-shaft 557
 ethanol 1121, 1122
 ethyl tertiary butyl ether (ETBE) 64
 ethylene 1064, 1072, 1077
 – /propylene ratio 1063
 – glycol (EG) 87
 – oxide (EO) 87, 1057
 – propylene monomer (EPM)
 1109
 – propylene rubber (EPR) 1100,
 1105
 – propylene–diene terpolymer
 (EPDM) 1100
 – vinyl acetate (EVA) 1008
 ethylene–propylene rubber (EPR)
 1109
 Euro V automotive 67
 eustatic correction 393
 euxinic conditions 363
 Evans–Polanyi correlation 848
 evaporative low-angle light scattering
 detector (ELSD) 154
 exploration 322, 353
 – and production 152, 433
 exponential residence time
 distribution 858
 export steam 798
 – credit 813
 expulsion model 370
 extended legal continental shelf
 521
 extinction 343
 extraction 704
 – process variable 973
 – solvent 972
 extra-heavy crude
 – characterization 917
 – processing 917
 extratropical storm 526
 extrusion surging 1100
 Exxon Valdez 109
- F**
- fabric 346
 fatty acid methyl ester (FAME)
 1133
 fault 26
 faunal succession 339
 feed
 – aggregation 707
 – -forward (FF) 834, 867
 – polymerization 707
 – preheat exchanger 967
 – preparation unit (FPU) 1029
 feed/effluent exchanger (F/E) 122
 feedstock 683, 707
 – characteristics 592
 – hydrotreating 623
 – molecule 719
 – quality 622
 feel 332
 Fenske equation 539
 fermentation 1120, 1124, 1127,
 1130
 fiber industry 1129
 field desorption (FD) 155, 160, 164
 field ionization (FI) 159–161
 filler 61
 filter 993
 – cloth 996
 – drip pipe 995
 – feed rate (FFR) 997
 – hot washing 1000
 – master valve 994
 – media 995
 – spray 995
 – support grid 995
 – wax scroll 995
 filtration rate 984
 finite element analysis (FEA) 1104
 first pretreat (PT) 55
 Fischer–Tropsch (FT) 19, 1041,
 1120
 – synthesis 1117, 1120,
 1124–1126, 1130
 five-stacked sand reservoir 268
 fixed-bed
 – catalytic hydrocracking 54
 – hydrocracker 713
 – hydrocracking 754, 758, 760
 – hydroprocessing 755, 777
 – trickle-flow reactor 572
 – unit 743
 flame ionization detector (FID) 73,
 154, 156, 174, 290
 flares carbon emission (FCE) 947
 flash point 1018
 flexicoking 51, 903, 912
 flexural subsidence 382
 floating
 – liquid natural gas (FLNG) 525
 – production system (FPS) 524
 – production, storage and offloading
 (FPSO) 524
 – storage and offloading system
 (FSO) 525
 – storage unit (FSU) 525
 Flory–Huggins–Zuo (FHZ) 222,
 243, 251
 – equation of state 222, 246, 252,
 262
 flow
 – distribution 804
 – induced crystallization (FIC)
 1101

- -path migration modeling 400
- time 502
- flue gas
 - desulfurization 135
 - emission 804
 - scrubbing 657
- fluid
 - -bed 624
 - coking 903, 912
 - saturation 346
- fluid catalytic cracking (FCC) 15, 36, 49, 51, 89, 549, 581, 590, 618, 637, 656, 677, 713, 818, 836, 841, 915, 933, 941, 1064, 1127
- 5-lump model 852
- 10-lump model 841
- catalyst 637
- chemical composition 637
- conversion 876
- entrance cracking 855
- feed injection zone 855
- feedstock 623
- gasoline 915
- hydrotreating performance 875
- nomenclature 638
- organonitrogen poisoning of catalyst 846
- pretreat 915
- process 1066
- process flow 51
- properties 638
- reactor 631
- residue (RFCC) 162, 582, 622, 641, 715, 1069
- Shell process 643
- SO_x transfer additives 136
- two-zone model 855
- unit (FCCU) 944, 1066
- zeolite 638
- fluidization 706
- fluorapatite 664
- flushed zone 470
- fold associated trap 348
- fold change (FC) 187
- formation
 - evaluation (FE) 435
 - micro-imager (FMI) 448
 - tester (FT) 443
- Forristall distribution 527
- fouling 905
 - resistance 889
 - resistance, steam reforming 879
- Fourier-transform ion cyclotron resonance (FT-ICR) 675

- Fourier-transform ion cyclotron resonance mass spectrometry (FT-ICR MS) 154, 160, 165, 173, 200, 224, 275, 679, 690
- fracking 14, 100
- fraction 679, 707
- fractional conversion 393
- fractionation 1120, 1127, 1129
 - packing 967
- fractionator 907
- fracturing fluid 514
- Frasch sulfur 652
- free radical polymerization 1083
- friction theory 310
- fuel delivery system 552
- fuel gas 818
- fuel/air equivalence ratio 553
- fugacity coefficient 296
- fugitive emission 79, 100
- functionalization 1163, 1168, 1173
- fused aromatic ring (FAR) 226

G

- gamma
 - distribution 856
 - ray (GR) 443
 - ray neutron tool (GNT) 447, 475
- gas
 - composition 723
 - concentration unit (GCU) 945
 - hydrates 374
 - lift 501, 506
 - oil desulfurization (GOD) 945
 - slippage 504
 - sour 326, 655
 - sweet 326
 - -to-liquid (GTL) 19, 1015, 1041, 1121
- gas chromatographic distillation (GCD) 959
- gas chromatography (GC) 73, 153, 174, 223, 268, 289, 677, 704, 1018, 1135, 1157
 - atomic emission detection (GC-AED) 675
 - flame ionization detection (GC-FID) 206
 - inductively coupled plasma-mass spectrometry (GC-ICP-MS) 675
 - mass spectrometry (GC-MS) 155, 157, 163, 174, 200, 223, 289
 - specific detector 154
- -tandem mass spectrometry (GC-MS-MS) 156
- -time of flight (GC-TOF) 675
- gas oil conversion
 - high aromatics content 918
- gas oil hydrotreater (GOHT) 34
 - fouling 921
- gaseous hydrocarbons 326
- gasification 1117, 1120–1123, 1126, 1129
- gasifier 1124
- gasifying zone 1123
- gasoline 64, 551
 - additive 65, 584
 - blend stock 64, 552, 567
 - engine 552
 - pool composition 591
 - production 564
 - property 559
 - specification 563
- gas-to-oil ratio (GOR) 224, 251, 385, 723
 - crude oil 246
- gel permeation chromatography (GPC) 208
- general purpose rubber (GPR) 1112
- genetic algorithm 853
- geocatalysis 370
- geochemical information 152, 155
- geochronology 341
- geophone 421
- geophysical well logging 353
- geopolymer 365
- glow discharge 1144
- glucose 1129
- grain shape 346
- grain size 346
- graphical user interface (GUI) 834
- gravity-based structure (GBS) 524
- grease 71
- greek fire 9
- green river oil shale 19
- greenhouse gas (GHG) 92, 931, 1117
- Gulf oil 324
- Gulf residuum process 640

H

- halobutyl rubber 1112
- hazardous air pollutant (HAP) 129
- health and safety (H&S) 476

- health, safety, environment (HSE) 87
- heat
- balance 630, 887
 - capacity 284, 304
 - conduction 394
 - convection 394
 - flow 384
 - flux 802
 - loss 890
 - transfer rate 887
 - -up rate 698
- heating oil 69
- heavy
- coker gas oil (HCGO) 50, 919
 - crude processing 915
 - cycle oil (HCO) 51, 581, 945, 1067
 - duty engine oil (HDEO) 1020
 - feedstock 707
 - HC fraction 328
 - key 540
 - naphtha (HN) 66, 717
 - straight run (HSR) 942
 - vacuum gas oil (HVGO) 21, 938
- heavy oil 20, 273, 278
- equilibrium composition data 282
 - rheology 285
 - treating (HOT) 642
- helicon discharge 1144
- Helmholtz energy 300
- hemicellulose 1117, 1119, 1128–1130
- Henry's Law 805
- heteroatom 676, 679, 681, 683, 691
- ring-compound 721
- heterophasic copolymer (HECO) 1094
- hexose 1119, 1129
- hierarchical clustering analysis (HCA) 173, 175
- high
- -density polyethylene (HDPE) 1089
 - field pressure 1145
 - melt strength (HMS) 1099
 - molecular weight nonvolatile material 622
 - -pressure low-density polyethylene 1090
 - pressure separator (HPS) 871
 - -Q ultrasonic 238
 - -resolution mass spectrometry 164
 - -resolution transmission electron microscopy (HRTEM) 242
 - -temperature shift (HTSR) 1151
 - -temperature shift converter (HTSC) 799
 - -throughput experimentation (HTE) 860
 - -voltage EI (HVEI) 165
- higher hydrocarbon reformation 1160
- Hildebrand solubility parameter 243
- Hingle plot 488
- homogeneous model 504
- homologous series 844
- hopane (triterpane) 156
- hot
- high-pressure separator (HHPS) 924
 - low-pressure separator (HLPS) 924
 - spots 906
 - -water extraction process (HWEP) 921
- Houdresid catalytic cracking 641
- process 626
- Houdriflow catalytic cracking 641
- process 626
- Houdry cracking unit (HCC) 865
- Hue-gamma ray zone (Hue-GRZ) 404
- hybrid migration 400
- hydraulic
- fracturing 29, 514
 - jet pumping 511
 - piston pumping 511
- hydride abstraction 848
- hydrocarbon 322, 620, 676, 677, 681, 695–697
- analysis 160
 - aromatic 677
 - fossil origin 18
 - ring compound 720
 - saturated 1163
- hydrocarbon reservoir fluid
- Vis/NIR spectroscopy 254
- hydrochlorofluorocarbon (HCFC) 1059
- hydrocracker (HYC) 715, 867
- catalyst 1026
 - conversion 1025
 - fixed-bed 713
 - performance 829
 - process condition 1027, 1032
- hydrocracking (HC) 23, 55, 590, 597, 676, 695, 697, 706, 713, 856, 941, 1127, 1128
- catalytic 731
 - chemical reaction 731
 - chemistry 1023
 - ebullated bed 55, 761
 - fixed-bed 54, 754, 758, 760
 - poly-ring compound 732
 - process variable 722
 - selective 695
 - thermal 766
 - unit (HCU) 33, 714, 740
 - zeolite-containing catalyst 738
- hydrodearomatization (HDA) 684, 1023
- hydrodemetalation (HDM) 36, 40, 582, 675, 683, 684, 694, 698, 700–706, 708, 725, 730, 920, 1138
- activity 694
 - catalyst capacity 704
 - chemistry 694
 - reaction rate 683
 - residual 704
- hydrodenitrogenation (HDN) 23, 36, 39, 110, 675, 725, 730, 846, 857, 871, 920, 1023, 1127, 1138
- reaction 694
- hydrodeoxygenation (HDO) 36, 40, 675, 725, 730, 1128, 1135
- rate constant 702
 - reaction 694
- hydrodesulfurization (HDS) 23, 36, 37, 202, 590, 622, 641, 675, 676, 684, 687, 688, 699, 725, 727, 841, 856, 872, 873, 919, 949, 1023, 1127, 1135
- chemistry 687
 - continuum model 856
 - inhibition 691
 - rate constant 701
 - sulfide catalyst 686
 - two-stage process 699
- hydrodynamic trap 348
- hydrofinishing 676, 717, 961, 1039
- catalyst 1040
- hydrofluoric acid (HF) 513, 575
- alkylation (HFA) 44, 576
- hydrogen
- and CO co-production (HYCO) 794
 - available on demand 819
 - bonding 681
 - composite curve 823

- consumption 818
- feedstock 787
- generation flow rate 823
- index (HI) 365, 385, 475
- long 819
- network optimization 826
- partial pressure 723
- pinch point 824
- pressure 1024
- production 787, 818, 938, 939
- purification 799, 818
- purity 723
- short 819
- source 818
- spillover 686, 697
- supply 916
- surplus diagram 824
- thermodynamics 788
- to-carbon (H/C) 41
- to-oil ratio (H2OR) 723, 741
- hydrogen sulfide (H₂S) 90
 - desorption 693
 - explosive range 90
 - removal 136
- hydrogenation 676, 684, 687, 691, 694–696, 702, 704
 - olefin 36, 725
- hydrogenolysis 598, 685, 689, 694, 696, 1120, 1128
- hydroisomerization dewaxing 1034
 - catalyst poison 1035
- hydrolysis 1117, 1120, 1126, 1128–1130
- hydrophone 422
- hydroprocessing 52, 676, 700, 714, 1128
 - catalyst 736
 - flow scheme 1022
 - fuel production 718
 - kinetic 747
 - reaction 748
 - reactor design 777
 - thermochemistry 745
 - unit 715
- hydroskimming 934
- hydrostatic pressure 343
- hydrotreater 715
- hydrotreating (HDT) 37, 53, 590, 675, 676, 730, 1023, 1127
 - AR 700
 - catalytic 777
 - chemical reaction 725
 - coker naphtha 593
 - enthalpy 745

- FCC performance 875
- process 676, 683
- process variable 722
- residue 698
- unit (HTU) 31
- hydrotreating catalyst 684
 - activity 686
 - deactivation 686, 698
 - regeneration 686
- hydroxyl radical (\bullet OH) 1167

I

- igneous rock 331
- ill-defined heavy oil 282
- immiscible operation 982
- in situ fluid analyzer (IFA) 258
- inclusion 338
- inductively coupled plasma-mass spectrometry (ICP-MS) 676
- inflow performance relationship (IPR) 501
 - curve 502
 - partial two-phase oil reservoir 503
 - single-phase reservoir 502
 - two-phase reservoir 503
- infrared (IR) 93
 - spectroscopy 153
- initial boiling point (IBP) 546
- injection molding 1104
- injection production well 29
- inlet diffuser device 777
- inside-battery limits (ISBL) 762
- in-situ adaptive model reduction 854
- instantaneous mean effective cylinder pressure (IMEP) 561
- instantaneous shut-in pressure (ISIP) 515
- insulator catalysts 632
- integration point 867
- Intergovernmental Panel on Climate Change (IPCC) 4, 92, 931
- interlocking crystal 331
- intermediate asymptotics 857
- intermediate fuel oil (IFO) 70
- internal combustion engine (ICE) 551, 1141
- internal rate of return (IRR) 810
- International Energy Agency (IEA) 6, 324, 950

- International Organization for Standardization (ISO) 34, 563, 959
- intrinsic low dimensional manifold method 854
- intrusion 338
- invaded zone 470
- invariant subspace 850
- invasion percolation (IP) 387, 402
- ion mobility analyzer 166
- ion trap 166
- ionic polymerization 1083
- ionic-liquid alkylation 578
- ionization technique 154, 160
- island model 230, 371
- isobutane-to-olefin (I/O) 44
- isobutylene–isoprene rubber (IIR) 1105, 1112
- isolated pores 344
- isomerization (ISOM) 58, 676, 685, 688, 717, 818
- isostatic subsidence 382
- isotactic polypropylene (iPP) 1104
- isotope pattern computation 166

J

- jacket 522
- jack-up 523
- Jacobian matrix 853
- jet fuel 918, 1128
 - production 924

K

- Kendrick mass scale 160
- kero hydrotreater (KHT) 33
- kerogen 19, 361, 365
 - decomposition 369
 - formation 365
 - oil interaction 370
 - type 367
- kerogen decomposition
 - kinetic model 369
- kerosene desulfurization (KD) 945
- kerosene jet fuel 68
- kinetic
 - analysis 700
 - lumping/aggregation 841
 - modeling 167
- kinetic relationship
 - methane steam reforming 881

- naphtha steam reforming 882
 - steam reforming 879
 - kinetics
 - -hydrodynamics tradeoff in FCC 854
 - optimization 398
 - steam reforming 880
 - Kuwait export crude (KEC) 700, 947
 - Kyoto Protocol 127
-
- L**
- laboratory information management system (LIMS) 839, 865
 - Lakeview blowout 102
 - Langmuir
 - -Blodgett film 229
 - equation of state 222
 - -Hinshelwood adsorption 882
 - -Hinshelwood/Hougen–Watson (LHHW) 749, 872
 - Larson–Miller equation 807
 - laser desorption ionization (LDI) 174, 230
 - mass spectrometry (LDI MS) 229, 243
 - laser desorption, laser ionization mass spectrometry (L²MS) 225
 - laser induced acoustic desorption (LIAD) 163
 - mass spectrometry (LIAD-MS) 230
 - laser-assisted ionization 163
 - laterolog (LL) 443
 - LBC correlation 309
 - Le Chatelier principle 596
 - lean oil recovery (LOR) 818
 - length-to-diameter ratio (L/D) 1092
 - levelness sensitivity 780
 - Leverett J-function 463
 - levigation 653
 - Lewis acid (L-acid) 1065
 - ligand 683, 704
 - ligand-exchange chromatography (LEC) 209
 - light
 - coker gas oil (LCGO) 50, 1173
 - crude oil 328
 - cycle oil (LCO) 51, 581, 676, 870, 945, 1067
 - -emitting diode (LED) 258
 - key 540
 - naphtha (LN) 66, 717
 - olefin cracking 1064
 - vacuum gas oil (LVGO) 21, 938
 - -water reactor (LWR) 105
 - light gas oil (LGO) 1138
 - hydrocarbon type 752
 - lignin 1117, 1119, 1129, 1130
 - limited steam export 790
 - linear
 - alkyl benzene (LAB) 87
 - alpha-olefin (LAO) 1047
 - free energy relationship (LFER) 846
 - low-density polyethylene (LLDPE) 1089, 1100
 - paraffin cracking 846
 - paraffin isomerization 597
 - program (LP) 32, 819, 865
 - liquefaction 1127
 - liquefied natural gas (LNG) 655
 - liquefied petroleum gas (LPG) 6, 64, 549, 564, 627, 643, 655, 717, 825, 933, 1069
 - liquid
 - chromatography (LC) 153
 - chromatography-mass spectrometry (LC-MS) 154, 158, 163
 - distribution tray design 778
 - feed rate 722
 - holdup 504
 - hourly space velocity (LHSV) 722, 874
 - hydrocarbon 1169, 1173
 - infusion 162
 - injection field desorption/ionization (LIFDI) 164
 - -liquid extraction 206
 - -liquid–vapor (LLV) 281
 - petrol 327
 - phase Newtonian viscosity correlation 307
 - redistribution tray 778
 - space velocity (LSV) 910
 - water plasma 1173
 - lithodensity identification (LID) 482
 - lithodensity matrix identification (LID) trimineral plot 482
 - lithology tool 480
 - lithospheric thickening 352
 - lithostatic pressure 343
 - live oil 277
 - density 283
 - sample preparation 283
 - viscosity 286, 309
 - loading
 - sedimentary 352
 - volcanic 352
 - local grid refinement (LGR) 387
 - logging while drilling (LWD) 435, 441
 - loil train derailment 118
 - London force 679
 - long-chain branching (LCB) 1099
 - long-time asymptotic kinetics 856
 - low
 - -density polyethylene (LDPE) 1089
 - -dimensional model 849
 - field pressure 1144
 - GOR fluid 246
 - -GOR reservoir 263
 - -pressure separator (LPS) 871
 - -sulfur diesel (LSD) 867
 - -sulfur fuel oil (LSFO) 938
 - -temperature shift (LTSR) 1151
 - -temperature shift converter (LTSC) 799
 - temperature viscosity 1044
 - -voltage EI (LVEI) 165
 - lower far crude (LFC) 701
 - lower heating value (LHV) 792, 936
 - lube
 - base 70
 - base stock manufacturing 958
 - crude approval (LCA) 963
 - crude assay 964
 - crude selection 963
 - deasphalting unit (LDU) 1009
 - oil 959, 960, 972
 - lubricant base oils 153
 - lubricant base stock
 - all-hydroprocessing route 1021
 - lumping
 - continuum approximation 855
 - matrix 852
 - nonlinear kinetics 853
 - structure-oriented (SOL) 74, 167, 750, 843
-
- M**
- maceral 332, 365
 - macrofossil 340
 - magnetic resonance imaging log (MRIL) 478

- magnetic roasting 654
 makeup gas compressor (MUGC)
 759
 maltene 292
 – asphaltene 842
 – fraction 292
 manipulated variable (MV) 834,
 867
 marine diesel oil (MDO) 70
 marine gas oil (MGO) 70
 mass chromatogram 156
 mass spectrometer
 – component 154
 – magnet sector 164
 mass spectrometry (MS) 73, 152,
 154, 164, 679
 – data interpretation 166
 – reference spectra 154, 160, 166
 – resolution 707
 – tandem (MS/MS) 156, 164
 material safety data sheet (MSDS)
 127
 mathematical programming 853
 matrix 61
 – acidizing 512
 – -assisted laser
 desorption/ionization (MALDI)
 163, 164, 208
 – component 202
 – representation of reactions 843
 maximum recording thermometer
 (MRT) 471
 maya crude oil 277
 McCabe–Thiele method 538
m-chloroperbenzoic acid (MCPBA)
 204
 McKenzie thermal model 394
 mean average boiling point (MABP)
 623
 mean diameter formula 807
 measurements while drilling (MWD)
 25, 435, 441
 mechanism reduction 845
 mechanistic modeling 847
 medium cycle oil (MCO) 677
 melt flow rate (MFR) 1094
 melt-blown nonwoven 1102
 mercaptan conversion 662
 mercaptopropyl silica gel (MPSG)
 213
 mercury 207, 682
 Merichem LO-CAT process 661
 Merox reaction 662
 metagenesis 326, 365, 395
 metal 681, 684, 694, 702–704, 708
 – capacity 675, 703, 705
 – complex polymerization 1083
 – deposition 698
 – extraction 683
 – function dehydrogenation catalyst
 602
 – ion 683, 694, 698, 704
 – porphyrin 682
 – product 705
 – removal capacity 704
 – support 708
 metallocene catalyst 1090
 metal–organic framework (MOF)
 932
 metamorphic rock 331
 metamorphism 326
 methane
 – hydrates 374
 – production reaction 1123
 – reformation 1147
 methanol-to-gasoline (MTG) 7,
 582, 1124
 methanol-to-olefin (MTO) 1065,
 1077
 methyl
 – diethanolamine (MDEA) 136,
 657, 943
 – ethyl ketone (MEK) 50, 959,
 1020
 – isobutyl ketone (MIBK) 50, 959,
 1020
 – isocyanate (MIC) 103
 – isocyanate leak 103
 – *tert*-butyl ether (MTBE) 7, 129,
 567, 942, 1070
 methylation 205
 methylcyclohexane (MCH) 695
 methylcyclohexanethiol (MCHT)
 695
 methylcyclohexene (MCHE) 695
 methylcyclo-hexylamine (MCHA)
 694
 methylcyclopentadienyl manganese
 tricarbonyl (MMT) 562
 metric matrix identification (MID)
 482
 met-x 637
 micro-carbon residue (MCR) 722,
 908, 959
 microcylindrically focused tool
 (MCFT) 484
 microfibrils 1119
 microfossil 339
 microkinetic modeling 847
 microlaterolog (MLL) 443
 microresistivity scanner (MRS) 488
 microscale sealed vessel pyrolysis
 (MSSV) 398
 microspherically focused log
 (MSFL) 443, 492
 middle vacuum gas oil (MVGO)
 938
 middle-of-run (MOR) 755
 mid-infrared spectroscopy (MIR)
 254
 million standard cubic feet per day
 (MMSCFD) 820
 million tonnes of oil equivalent
 (Mtoe) 325
 Mina Abdulla spill 109
 minimum export steam 792
 mini-rotary viscosity (MRV) 1034
 Miocene 268
 miscible operation 982
 mist flow 504
 mixed integer nonlinear program
 (MINLP) 951
 mixed oxide 633
 mixing equipment 1085
 Mobil Lube Dewaxing (MLDW™)
 1033
 mobile offshore drilling unit
 (MODU) 522
 modal analysis 851
 model IV fluid-bed catalytic cracking
 639
 modeling
 – Darcy flow 403
 – flow-path 403
 – hybrid migration 403
 – invasion percolation 403
 model-predictive control (MPC) 1,
 833, 835
 modified Claus process 660
 modular formation dynamic tester
 (MDT) 252
 Mohr circle 411
 molecular
 – -based modeling 151, 167
 – characterization 152–154, 166
 – composition 152, 676, 679, 722
 – engineering 151, 167
 – level 676, 681
 – management 151, 167
 – orbital calculation 227
 – structural vector 167
 – structure 151–153

– type 972
 – weight (MW) 847, 1082, 1097
 – weight distribution (MWD) 1045, 1097
 molecule characterization 679, 707
 monoethanolamine (MEA) 657, 799, 943
 monomer insertion 1086
 montmorillonite clay 632
 Montreal Protocol 91
 Moody friction factor 505
 motor octane number (MON) 64, 559, 871
 moving
 – -bed process 625, 640
 – -belt LC-MS interface 159
 mud acid 513
 mud logs 439
 mudcake 470
 Mukluk prospect 405
 multi-azimuthal seismic data recording geometry 422
 multicomponent kinetic model 397
 multicomponent methodology 825
 multiple-reaction monitoring (MRM) 165
 multizone circulating reactor (MZCR) 1096
 mutual diffusion coefficient 286

N

NaCl equivalent concentration 460
 nanoaggregate (NA) 237
 – asphaltene 236
 naphtha 618, 624, 717
 – light (LN) 66, 717
 – nitrogen 926
 – properties 592
 – side draw 907
 – sulfur removal 926
 naphtha hydrotreater (NHT) 592, 828
 – fouling 925
 naphtha, kerosene and distillate fuel oil (NKD) 34
 naphthene 327, 560, 1017
 – dehydrogenation 595
 – isomerization 597
 naphthenic 620
 naphthenoaromatic 328
 natural
 – butyl rubber (NBR) 1109

– ratio range 794
 – rubber (NR) 1107
 natural gas 326
 – dry gas 19
 – processing 655
 – sour gas 19
 – water removal 656
 needle coke 909
 neopentylglycol (NPG) 1055
 net
 – effective overburden (NEO) 461
 – present value (NPV) 810
 – reaction stoichiometry 881
 neural network 847
 neutron lifetime logs (NLL) 447
 neutron porosity log 474
 Newtonian viscosity correlation
 – full phase 309
 NH₃ desorption 685
 nickel 681, 700, 704
 NiMo 685, 696
 nitric oxide (NO) 90
 nitrogen 675, 681, 684, 688, 693, 698, 703
 – chemiluminescence 676
 – chemiluminescence detector (NCD) 154, 676
 – oxides (NO_x) 47, 90, 1149
 – phosphorus detector (NPD) 154
 – slip (N slip) 722
 nitrogen, sulfur and oxygen (NSO) 382
N-methyl morpholine *N*-oxide (NMMO) 1129
 – pretreatment 1129
N-methylpyrrolidone (NMP) 50, 959, 1020
 – plant corrosion 978
 noble metal catalyst 1040
 noble metal hydrocracking catalyst 744
 nonane reforming 852
 nonconformity 340
 noncubic equations of state 299
 non-Newtonian behavior
 – bitumen 275
 non-noble-metal catalyst 743
 nonrandom two liquid (NRTL) 294
 nonwoven filter media 995
 normal moveout (NMO) 424, 430
 normal paraffinic, branched paraffinic (iso-paraffins), naphthenic, and aromatic (PINA) 883

nuclear instrument module (NIM) 453
 nuclear magnetic resonance (NMR) 73, 153, 175, 205, 222, 441, 443, 599, 1168
 – logs 477
 numeric dating 341

O

ocean current 528
 octane 64
 – rating 559
 – -upgrade unit 916
 octane number 559
 – motor 559
 – prediction 158
 – research 559
 offshore drilling 517
 – mobile unit (MODU) 522
 offshore oil
 – collection 519
 – main production region 522
 oil
 – /wax-solvent recovery 1001
 – abiogenic 359
 – -based mud (OBM) 254, 256, 479
 – biogenic 359
 – clarified slurry (CSO) 629
 – composition 372
 – deasphalted (DAO) 49, 292, 548, 958, 1019
 – dewaxed (DWO) 973
 – -gas contact (OGC) 347
 – heating 69
 – heavy duty engine (HDEO) 1020
 – industry sector 151
 – -oil and oil-rock correlation 155
 – origin of 359
 – -soluble PAG (OSP) 1057
 – unconverted (UCO) 6, 713, 757, 1019
 – -water contact (OWC) 268, 347
 – well logging 255
 oil spill 100
 – clean up 137
 olefin 199, 559, 676, 679
 – catalytic cracking (OCC) 1075
 – conversion technology (OCT) 1075
 – cracking mechanism 1064
 – feedstock 1082
 – hydrogenation 36, 725

- production plant 818
 - thermoplastic (TPO) 1100
 - oligomerization 621
 - on-stream catalyst replacement (OCR) 705
 - opening position (OP) 834
 - operating
 - cost (OPEX) 958
 - mode 1070
 - stability 780
 - optical density (OD) 254
 - optical spectroscopy 227
 - optimization-integer-decision problem 853
 - orbitrap 166
 - order reduction 849
 - organic
 - carbon redox cycle 364
 - -rich sediments 362
 - sulfur 664
 - Organization of the Petroleum Exporting Countries (OPEC) 13, 324, 520, 944
 - orthorhombic sulfur 650
 - oscillatory shear 285
 - Otto-cycle engine 554
 - overall lumped kinetics 855
 - overburden rock 361
 - over-cracking 628
 - overhead pressure 969
 - overhead valve (OHV) 1156
 - oxidation 203, 1171
 - oxo-alcohol synthesis gas steam reformer 897
 - oxone 205
 - oxy fuel combustion capture 932
 - oxychlorination 614
 - oxygen 675, 681, 683, 693, 703
 - content 1119
 - enrichment 660
 - plasma 1169
 - ozone generation 1165
-
- P**
- paleobathymetry 392
 - paleomagnetism 350
 - paleowater depth 387
 - paraconformity 340
 - paraffin 620, 1017
 - cracking 846
 - dehydrocyclization 596
 - dehydrogenation process (PDH) 1075
 - isomerization 46, 597
 - paraffins, olefins, naphthenes, and aromatics (PONA) 842, 871, 942
 - parametric effect 599
 - paraxylene (PX) 591
 - partial combustion 1122
 - partial least squares (PLS) 256, 847
 - partial oxidation (POX) 787, 793, 818, 1122, 1142
 - catalyst 1149
 - plant 794
 - reaction 789
 - particulate matter (PM) 89, 135, 665
 - partition-based and total lumping 841
 - passivation 645
 - passive continental margin 351
 - pathways modeling 848
 - pendant-core model 908
 - Peng–Robinson equation of state 298
 - pentaerythritol (PE) 1055
 - pentose 1119, 1129
 - peracid 204
 - period 342
 - periodate 204
 - Perkins–Kern–Nordgren (PKN) 515
 - permanent poison 607
 - permeability 343
 - permeability, porosity, saturation (KPS) 461
 - permissible exposure limit (PEL) 127
 - peroxyacetyl nitrate (PAN) 90
 - peroxybenzoyl nitrate (PBN) 90
 - personal protection equipment (PPE) 125, 763
 - PetroFCC 1071, 1078
 - petroinformatics 173
 - petroleomics 158, 167, 174, 225, 359, 371
 - petroleum 675, 676, 681, 694, 700, 707
 - accumulation 343
 - asphaltene 236
 - biomarker 152, 155
 - cycle 322
 - engineering 151
 - exploration 419
 - geology 322
 - mass spectrometry 152
 - middle distillate 857
 - migration accumulation 399
 - nonfuel product 6
 - origin 326, 359
 - preindustrial use 323
 - product 63, 694
 - refining chemistry 36
 - research and development 152
 - system 359
 - trap 347, 361
 - trap assessment 348
 - wax 71
 - petroleum production
 - pollution 89
 - petroleum refinery 715, 1118, 1127
 - CO₂ emission 943
 - petrophysics 435
 - Phanerozoic 343
 - phase behavior 277
 - correlation 294
 - prediction 303
 - phase composition measurement 277
 - photodetector (PD) 258
 - photo-electric factor (PEF) 441, 473, 481
 - photoionization (PI) 160
 - phytane (Ph) 156
 - Pickett plot 488
 - pinch analysis 823
 - pinch point
 - hydrogen 824
 - PIONA-type characterization 295
 - pipe corrosion 682
 - pipe failure analysis 113
 - pipestill furnace 967
 - pipestill troubleshooting 970
 - piston engine 554
 - plant performance 808
 - plantwide system 817
 - plasma
 - catalysis 1151
 - discharge 1167
 - -generated radical species 1168
 - polymerization 1165
 - processing 1163, 1165
 - properties 1164
 - radical chemistry 1167
 - torch 1145
 - type 1144
 - plate tectonic 349
 - platform as a service (PaaS) 194
 - point adjustment 23

- polar–polar interaction 681, 698
 polyalkyl acrylate (PAA) 1008
 polyalkyl meth acrylate (PAMA) 1008
 polyalkyleneglycol (PAG) 1043, 1057
 polyalphaolefin (PAO) 71, 959, 1018, 1043, 1047
 polyaromatic condensation 727
 polybutadiene (PBR) 87
 – synthesis 1106
 polychlorinated biphenyl (PCB) 108
 polycyclic aromatic (PCA) 1024
 – hydrocarbon (PAH) 204, 221, 254, 257, 681
 – sulfur heterocycle (PASH) 202
 polydispersity index (PDI) 1009, 1099
 polyethylene (PE) 87, 1082, 1088
 – processing 1091
 – ultrahigh molecular weight (UHMWPE) 1089
 – very low-density (VLDPE) 1089
 polyethylene terephthalate (PET) 7, 87, 591
 polyisobutylene (PIB) 1046, 1058
 polymer electrolyte membrane (PEM) 1151
 polymeric molecule 681
 polymerization 579
 – free radical 1083
 polyol ester 1055
 polyolefin 1081
 polypropylene (PP) 87, 1094
 – fabrication 1098
 – injection-molding conditions 1105
 – rheology 1099
 polystyrene (PS) 87, 1105
 polyvinyl chloride (PVC) 7, 87, 138
 pore diffusion effect 847
 pore-pressure formation 391
 porosity 343
 – tool 471
 porphyrin 682, 702, 704
 postcombustion capture 932
 pot still 534
 pour point 329, 1017
 – giveaway 985
 – reduction 1038
 power-recovery turbine (PRT) 871
 precipitation 739
 precombustion capture 932
 precondenser 969
 predistillation processing 541
 premium base stock performance 1019
 prereforming 879
 pressure 628
 – drop (dP) 723, 725, 1137
 – drop calculation 869
 – filter 993
 – prediction 388
 – swing adsorption (PSA) 42, 795, 801, 818, 932, 1151
 pressure, volume, temperature (PVT) 387, 460
 pressurized heavy-water reactor (PHWR) 105
 pressurized water reactor (PWR) 105
 pretreatment 1117, 1120, 1127, 1129
 – -hydrolysis 1120
 primary
 – energy 3
 – migration 370
 – porosity 344
 – productivity 362
 – reformer 895
 principal component
 – analysis (PCA) 173, 175, 845, 846
 – regression (PCR) 256
 PRISM reactor 1154
 pristane (Pr) 156
 – /phytane ratio 373
 process
 – controller 850
 – -derived fuel (PDF) 1159
 – value (PV) 834
 product 683
 – cracked 679
 – hydrogenated 697
 – specification 675
 programmable logic controller (PLC) 834
 progressing cavity pump 511
 projective transformation 851
 propane
 – dehydrogenation 1075
 – deoiling 1007
 – dewaxing 1005
 – filter hot wash 1007
 proportional-integral-derivative (PID) 834
 proppant 514
 propylene 1064, 1072, 1077
 – catalytic cracking (PCC) 1074
 – oxide (PO) 1057
 propylur process 1072
 protolytic cracking 848
 proton affinity (PA) 846
 proton precession magnetometer (PPM) 477
 pseudo first-order approximation (PFOA) model 747
 pseudomolecular ion 160
 pseudosteady-state flow 502
 pulp and paper industry 1121
 pumaround 967
 purge stream 818
 purification 824
 purified terephthalic acid (PTA) 87
 P-wave 419
 pyrolysis 1117, 1120, 1125–1127, 1130
 – catalytic (CPP) 1063, 1069, 1078
 – fast 1126
 – oil 1126
 – slow 1126
-
- Q**
-
- quadrupole mass analyzer or spectrometer (QMS) 164
 quadrupole time-of-flight mass spectrometer (QTOF MS) 165
 quantitative comparison (QC) 190
 quantitative structure–reactivity relationship (QSRR) 846
 quasi-equilibrium approximation (QEA) 845
 quasi-steady state approximation (QSSA) 845
 quench
 – injection device 778
 – mixing chamber 778, 781
 – temperature difference 724
 quinolone 729
-
- R**
-
- R2R process 643
 Rackett equation 297
 radial flow reactor 573, 609
 radial temperature difference 724, 784
 radioactivity 341

- radiogenic heat 394
- radiological dispersion device (RDD) 477
- raffinate hydroconversion (RHC) 1040
- Raman spectroscopy 153
- Raney nickel 205
- Raoult's law 537
- rapeseed oil 1135
 - hydroprocessing 1136
- rapid sedimentation 394
- rate
 - constant 687, 702
 - of penetration (ROP) 435
- Raymer–Hunt–Gardner (RHG) porosity 492
- reactant-type distribution function 856
- reaction
 - catalytic reforming 572
 - limited aggregation (RLA) 240
 - network 599
 - rate relationships 881
 - rules 844
 - time 629
 - trajectory 852
- reactivity 151, 152
- reactor
 - apparatus 1153
 - average pressure 723
 - axial temperature rise 724
 - CAT 724
 - dilute phase model 869
 - effluent air cooler (REAC) 754
 - inlet temperature (RIT) 57, 573
 - pressure drop 723
 - temperature 628, 723
 - WABT 724
 - wall corrosion 706
- reactor design 624
 - hydroprocessing 777
- reactor internal
 - performance 783
 - revamp 783
- real-time optimizer (RTO) 74, 747
- recommended exposure limits (REL) 127
- recycle gas compressor (RGC) 120, 755, 759
- recycle rate 628
- reduced crude 624
 - conversion (RCC) 643
- reduction roasting 653
- refined wax production 962
- refinery
 - fuel gas 717
 - gasoline-production 915
 - intermediate stream 923
 - software 834
 - solid wastes 141
 - wastewater treatment 137
 - -wide optimization (RWO) 865
- refining 322, 675, 699
 - process 152, 167, 1021, 1128
 - research and development 153
- reflection coefficient 427
- reformat yield 594
- reforming 676, 684, 1128, 1130
 - catalyst contaminants 605
 - Motor Gasoline Pool 590
 - reaction 594, 880
- reformulated gasoline 65, 583
 - before oxygenate blending (RBOB) 65
- refractive index (RI) 154
- refractory 685, 688, 691, 693, 701, 703
 - character 629
- regeneration 686
- regenerator
 - air rate 631
 - cyclone model 870
 - freeboard model 870
 - model 870
- regular solution theory 294
- Reid vapor pressure (RVP) 59, 64, 129, 561
- relative
 - catalyst activity 882
 - dating 338, 340
 - permeability 344
- remotely operated vehicle (ROV) 421, 525
- removal of nickel by hydrotreatment (HDNi) 702
- removal of vanadium by hydrotreatment (HDV) 702
- renewable diesel
 - dewaxing 1139
 - feed 1135
 - product 1135
 - reaction pathway 1135
- renewable feed
 - catalyst 1137
 - hydrotreating 1134
 - triglyceride structure 1135
- renewable fuel 1133
- research octane number (RON) 56, 559, 592, 871
- reservoir crude oil 223
- reservoir rock 329, 361
- resid conversion 927
- resids (residua) 152, 163
- residual HDM 704
- residual oil 842
- residue fluid catalytic cracking (RFCC) 162, 582, 622, 641, 715, 1069
- residue hydrotreatment 703
- resonance enhanced multiphoton ionization (REMPI) 234
- retrofit 826
- return on investment (ROI) 1137
- revolutions per minute (RPM) 558
- Rice–Herzfeld mechanism 845
- rigorous kinetic modeling 828
- rigorous model
 - clean fuel 868
- ring-opening 694–696
 - hydrocracking 695
- Rio Earth Summit 134
- riser 627
 - model 868
 - outlet temperature (ROT) 51, 581
 - pipe cracking 627, 639
 - reactor 627
- risk analysis 388
- rock
 - deformation 351
 - failure 410
 - poroelastic stress modeling 409
 - stress 388
- Rock–Eval measurement 365
- rotary
 - engine 556
 - gas lift system 507
 - vacuum filter 993
- rotating pressure vessel oxidation test (RPVOT) 1050
- roundness 346
- Royal Dutch 324
 - Shell 12
- rubber
 - butadiene (BR) 1105
 - butyl 1112
 - chlorinated butyl (CIIR) 1112
 - ethylene–propylene (EPR) 1100, 1105, 1109
 - natural (NR) 1107

- natural butyl (NBR) 1109
- styrene–butadiene (SBR) 1105
- RxCat technology 1071

S

- S and W catalytic cracking process 643
- safety critical reactor axe man (SCRAM) 107
- salt 332
 - -dome trap 27
- sandstone 336
- saturated hydrocarbon 1163
- saturates, aromatics, resins, and asphaltenes (SARA) 175, 208, 282, 382, 679, 702, 908
 - analysis 291
 - kinetic model 397
- saturation
 - exponent 451
 - pressure 299
 - reaction 36, 725
 - tool 483
- Saybolt universal seconds (SUS) 959, 970, 982, 1016
- Schlumberger 449
- scraped surface
 - chiller (SSC) 980, 983
 - exchanger (SSE) 980, 985, 993
 - supplier 986
- seal 347
 - rock 361
- secondary
 - energy 3
 - migration 370
 - porosity 344
 - reformer reactions 891
- sedimentary
 - basin 382
 - rock 331, 334, 336
 - structure 335
- seismic
 - activity 419
 - method 353
 - wave 419
- seismic data
 - acquisition 420
 - deconvolution 423
 - interpretation 426
 - processing 423
- selective catalytic reduction (SCR) 47, 137, 657, 805
- selective hydrocracking 695
- selectivity
 - catalytic 634
 - strategy 1166
- self-contained breathing apparatus (SCBA) 90
- semiregenerative catalytic reforming 608
- semi-submersible 524
- semisynthetic catalysts 633
- sensitivity analysis 846
- separated flow model 505
- sequential quadratic programming (SQP) 880
- SETatWork 4
- shale 337
 - gas 374
- Shell FCC process 640, 643
- shielding cone (SC) 237
- shift converter 796
- shot coke 909
- Si–Al ratio (SAR) 734
- side wall core (SWC) 443
- side-stream stripper 969
- silica-alumina phosphate (SAPO) 46, 713
- silicate mineral 332
- silicon 682
- silver ion 207
- simulated distillation (SimDist) 291
- single photon ionization (SPI) 230
- single-event theory 848
- single-phase reservoir IPR 502
- single-stage once-thru hydrocracker (SSOT) 1027
- single-stage with recycle hydrocracker (SSREC) 1027
- singlet oxygen 205
- singular and regular perturbation methods 850
- sinter roasting 654
- sintering 686, 698, 703
- SiO₂ 685
- skin factor 502
- sludge 142
- slug flow 504
- slurry-phase 706
 - distillate (SPD) 19
 - hydrocracking 57, 761
- small angle
 - neutron scattering (SANS) 236
 - oscillatory shear (SAOS) 1105
 - x-ray scattering (SAXS) 236, 279
- sodium lauryl sulfate (SLS) 664
- sol-gel process 686
- solid
 - -phase oxidation 1123
 - phosphoric acid (SPA) 579
 - waste handling 79
 - waste recovery 141
- solubility 289
 - -based lumping 843
- solution polymerization 1084
- solvent 704, 708
 - and hydroprocessing comparison 1020
 - contaminant 973
 - deasphalting 49
 - deasphalting (SDA) 57
 - dehydration 1001
 - desphalting 962
 - dewaxing 50, 960, 979, 1033
 - extraction 50, 960, 971
 - fractionation 289
 - loss 975
 - neutral oil (SNO) 1012
 - plant with hydroprocessing 1040
 - recovery 974
 - -refining processes 153
 - splitter 1002
- sorting 346
- sour crude oil 329
- sour gas 326, 655
- source rock 329, 359, 361
 - generative potential 367
- sour-water stripper (SWS) 659
- space velocity 629, 722
- spacing density 780
- spar 524
- spark-ignited (SI) 1148
- Spearman's rho 183
- special core analysis laboratory (SCAL) 461
- speciality oil 71
- sphericity 346
- split-flow enrichment 660
- sponge coke 909
- spontaneous polarization (SP) 480
- stability 1018
- standard (temperature and pressure) original gas in place (SCFOGIP) 436
- Standard Oil Company 11, 324
- standard temperature and pressure (STP) 460, 746, 936
- staple fiber (SF) 1101
- start-of-run (SOR) 741, 1032

- statistical associating fluid theory (SAFT) 294
 – equations of state 301
 steady-state heat flow 394
 steam
 – /carbon ratio 802
 – -assisted gravity drainage (SAGD) 1, 27, 100, 274, 921
 – ejectors pump 969
 – methane reforming (SMR) 19, 42, 740, 787, 790, 799, 818, 867, 934, 939, 1041, 1147
 – methane reforming combined with oxygen secondary reforming (SMR/O₂R) 793
 – reformer model 880
 – stripping 906
 steam reforming 879, 1123, 1125
 – kinetic relationship 879
 sterane 156
 steric hindrance 687, 688, 694, 700
 stock tank original oil in place (STOOIP) 435
 straight run (SR) 592
 – gas oil (SRGO) 677
 – light gas oil (SR LGO) 1135
 Stratco effluent refrigeration process 578
 strategic petroleum reserve (SPR) 13
 stratigraphic trap 348
 stratospheric ozone 91
 strike-slip fault 348
 strip logs 436
 stripper 627
 structural trap 347
 structural vectors (for molecules) 167
 structure-based lumping (SBL) 750
 structure-oriented lumping (SOL) 74, 167, 750, 843
 – kinetic modeling 167
 study-state flow 502
 styrene
 – butadiene resin (SBR) 87
 – -butadiene rubber (SBR) 1105, 1107
 – monomer (SM) 87
 subduction zone 350
 subsea system 525
 substitution 688, 690, 694
 – nucleophilic 694
 sucker rod pumping 508
 sucrose 1128
 sulfated ash, phosphorus, and sulfur (SAPS) 1019
 sulfide catalyst 698
 sulfiding 736
 sulfur 681, 683, 687–689, 691, 694, 699–701, 703
 – chemiluminescence 676
 – chemiluminescence detector (SCD) 154, 676
 – compound 199, 201
 – -containing polycyclic aromatic compound (S-PAC) 212
 – coordination 688, 693
 – extraction 688
 – oxides (SO_x) 54, 642, 876
 – pollution 665
 – production 651
 – recovery 78, 928
 – recovery unit (SRU) 654
 – refractory species 684, 693
 – slip (S slip) 722
 – source 651
 – strategy 654
 sulfur removal 654
 – capacity 699
 – rate 687
 sulfuric acid alkylation (SAA) 43, 577
 – unit (SAAU) 576
 sum frequency generation (SFG) 245
 Suncor refinery 866
 supercritical
 – fluid chromatography (SFC) 153
 – fluid extraction (SFE) 141
 – -water reactor (SCWR) 105
 SUPERFLEX 1072
 support 676, 684, 695, 698, 704, 708
 – alumina 684
 – material 685
 supported catalyst 1090
 surface-assisted laser desorption ionization (SALDI) 235
 suspension polymerization 1084
 suspensoid catalytic cracking 626, 641
 S-wave 419
 sweet
 – crude oil 329
 – gas 326
 – -sour petroleum refinery 915
 syngas 19, 1121, 1124
 – -to-gasoline plus (STG+) 582
 – -to-liquids (STL) 1015
 synthesis 1106
 – gas 19
 synthetic 1018
 – automotive engine lubricant 1052
 – base stock 1043
 – catalyst 633
 – diesel fuel 1133
 – fuel 1125
 – gasoline 582
 – industrial lubricant 1052
 – lubricant 1043
 – seismogram 428
 synthetic crude (syncrude) 1
 – hydrocarbon type 752
 – production 903
-
- T**
-
- tail-gas treating 662
 – unit (TGTU) 47, 654, 662
t-amyl methyl ether (TAME) 64
 tandem mass spectrometry (MS/MS) 156, 164
 tandem triple-stage quadrupole mass spectrometer 165
 teletype (TT) 447
 temperature gain 724
 temperature indicator (TI) 111, 723
 temporary poison 604
 – coke 607
 tension-leg platform (TLP) 524
 Terzaghi rock stress modeling 389
 Terzaghi-compressibility 390
 tetraethyl lead (TEL) 65, 551
 Texaco 324
 thermal
 – conductivity 394
 – conductivity detector (TCD) 1159
 – conversion 1128, 1130
 – cracking 41, 618, 842, 903
 – hydrocracking 766
 – modeling 393
 – partial oxidation (POX) 793
 – plasmatron 1145
 – process 676
 – processing 903
 – reforming 618
 – stability 1128
 – subsidence 382

thermal/oxidative stability 1044
 thermochemical route 1127
 thermodynamic
 – analysis 261
 – constraints and consistencies 845
 – equation 296
 Thermofor catalytic cracking (TCC)
 580, 640
 thermoforming 1103
 thermogenesis 370
 thermophysical property
 measurement 283
 thermoplastic elastomer (TPE)
 1108, 1110
 thermoplastic olefin (TPO) 1100
 thermospray (TSP) 162
 thin-layer chromatography (TLC)
 209
 thin-wall injection molding (TWIM)
 1104
 thiol 202
 thiophene 202, 678, 687–690
 third-stage separator (TSS) 135
 threshold limit values (TLV) 127
 Tianjin 118
 tight oil plays 374
 time
 – interval 343
 – -of-flight (TOF) 679
 – -of-flight mass spectrometry (TOF
 MS) 165
 – -resolved fluorescence
 depolarization (TRFD) 226
 – scale separation 849
 – to steady state 724
 TiO₂ 686
 tons per annum (tpa) 934
 top dead center (TDC) 554
 top liquid distribution tray 778
 topping 934
 tornado diagram 388
 tortuosity coefficient 451
 Tosco Avon Hydrocracker 110
 total
 – acid number (TAN) 20, 153, 183,
 186, 199, 722, 917, 1059
 – depth (TD) 441
 – dissolved solids (TDS) 487
 – isomerization process (TIP) 59,
 571
 – organic carbon (TOC) 365, 385
 tower
 – flash zone 967
 – fractionation 967

– overhead pressure 969
 – pressure survey 970
 – wash section 967
 TPR model 504
 trace contaminant 720
 transformation 322
 – ratio (TR) 387, 397
 transient flow 502
 transient heat flow 394
 trap 343
 – anticline 26
 – salt dome 27, 332
 – stratigraphic 348
 – structural 347
 treatment 916
 – catalyst 636
 trimethylolpropane (TMP) 1055
 truck tape recorder (TTR) 448
 true
 – boiling point (TBP) 67, 718, 870
 – conversion 722
 – vertical depth (TVD) 263
 tube metal temperature (TMT) 897
 turbine 557
 – oil stability test (TOST) 1059
 two-dimensional heteroatom single
 quantum coherence (HSQC) 228
 two-phase reservoir
 – IPR 503
 two-stage dewaxing 1002
 two-stroke engine 555

U

ultra-deep hydrodenitrogenation for
 hydrocracking 857
 ultra-deep hydrodesulfurization of
 diesel 856
 ultrahigh molecular weight
 polyethylene (UHMWPE) 1089
 ultra-low-sulfur diesel (ULSD) 38,
 729, 836, 916, 1134
 – production 916
 ultra-stable (US) 61
 unconformity 341
 unconverted oil (UCO) 6, 713, 757,
 1019
 uninvasion zone 470
 unit of measure (UOM) 722
 UOP
 – fluid-bed catalytic cracking 640
 – Mercox process 662
 – Selectox process 661

upflow 706
 upgrading process 151
 upstream 14, 151–153, 167
 USY 696
 utility 931

V

vacuum
 – distillation 546, 965
 – distillation unit (VDU) 541, 568,
 717, 865, 951, 958, 960
 – gas oil (VGO) 22, 167, 548, 568,
 622, 713, 841, 865, 936, 1019,
 1072, 1127, 1130
 – pipestill (VPS) 958, 960
 – residue (VR) 21, 36, 546, 679,
 684, 706, 717
 – residue upgrading 716
 – residuum 904
 – -ultraviolet laser light (VUV) 164
 validity condition for asymptotic
 lumped kinetics 858
 van der Waals
 – condition 297
 – equation of state (EoS) 222, 252
 van Krevelen diagram 192, 368
 vanadium 681, 700, 704
 vapor pressure osmometry (VPO)
 163, 226
 vapor-lift tray (VLT) 780
 – distributor performance 781
 vapor-liquid equilibrium (VLE)
 538
 vertical seismic profiling (VSP)
 448
 very low-density polyethylene
 (VLDPE) 1089
 vibrational spectroscopy 153
 vibroseis 421
 vinyl acetate monomer (VAM) 87
 vinyl chloride monomer (VCM) 87
 Vis/NIR spectroscopy 252
 – hydrocarbon reservoir fluid 254
 visbreaking 50, 903, 912
 viscosity 1016, 1044
 – blend index (VBI) 308
 – dynamic 959
 – grade (VG) 1048, 1053
 – heavy oil 307
 – kinematic 959
 – modifier (VM) 1017

viscosity index (VI) 70, 329, 959,
1016, 1044
– droop 1031
– loss 1038
visible ultraviolet (UV) spectroscopy
683
vitrinite reflectance 397
volatile organic compound (VOC)
65, 90, 130, 563, 665, 1146
volatile products 910
volatility 1017, 1045
volatilizing roasting 653
vortex separation system (VSS)
1071

W

Wankel engine 556
wash
– acceptance 998
– efficiency 998
– oil 967
waste heat recovery (WHR) 801
waste product 322
wastewater 100, 806
– treatment 79
water gas reaction (WG) 1123
water gas shift (WGS) 789, 1123,
1135, 1147
– reaction 789, 1124
water phase behavior 280
water-based mud (WBM) 253
wax 1125
– crystal 982
– hydrocracking 1033
weight hourly space velocity
(WHSV) 722, 1073
weighted average bed temperature
(WABT) 724, 784
weighted average reactor temperature
(WART) 829, 873
well
– bore 501
– completion 28
– failure blowout 27
– log 436, 445, 466
– log analysis 435
– site 465
– stimulation 512
West Texas intermediate (WTI) 30,
922
wet
– flue-gas desulfurization 657
– gas 655
– -gas scrubbing (WGS) 135
– sulfuric acid 663
wetting 347
whole-oil
– gas chromatograms 372
wide angle x-ray scattering (WAXS)
279
wireline formation tester 491

wireline log 439
World Petroleum Council (WPC)
1068
Wyllie's time-average equation 452

X

x-ray fluorescence spectrometry
(XRF) 637, 639
x-ray powder diffraction (XRD)
639
xylose 1128

Y

yankee whaling 9
Yen–Mullins 371
– model 252, 262, 681

Z

zeolite 61, 685, 695
– catalyst 633
– catalyzed alkylation 579
Zeolite Socony Mobil-5 (ZSM-5)
1033, 1064, 1128
Zero-Zero-Zero campaigns 86
Ziegler–Natta catalyst 1090
zig-zag mechanism 727
zinc/calcium-aluminate 1076
zonal reaction 1154